Talanta, Vol. 39, No 1, pp 1–7, 1992
Printed in Great Britain

0039-9140/92 $5.00 + 0.00
Pergamon Press plc

APPLICATION OF THE H-POINT STANDARD ADDITIONS METHOD BY USING ABSORBANCE INCREMENT VALUES AS ANALYTICAL SIGNALS

PILAR CAMPINS FALCO,* FRANCISCO BOSCH REIG and JORGE VERDU-ANDRES
Department of Analytical Chemistry, Faculty of Chemistry, University of Valencia, 46100, Burjassot, Valencia, Spain

(*Received* 27 *May* 1991. *Revised* 18 *July* 1991. *Accepted* 26 *July* 1991)

Summary—This paper demonstrates how the absorbance increment (ΔA) between two wavelengths selected according to the fundamental criteria for application of the H-Point standard additions method (HPSAM) are only related to the analyte concentration. A procedure for calculation of the unknown analyte concentration with no bias error by applying HPSAM to ΔA values in much the same way as the method of standard additions (MOSA), is reported. The method was also applied to a calibration with a single standard. The results obtained on 6 samples with maximal separations between 65 and 0 nm are reported. Finally, the proposed method was applied to the resolution of different phenol-*o*-cresol mixtures.

The selectivity of virtually all analytical methods reported lately is normally studied either on the basis of experimental measurements or by using mathematical algorithms taking due account of the potential mutual interferences of the different species involved; all these studies have resulted in significant gains in the knowledge and performance of analytical separation methods.

A number of methods aimed at increasing analytical selectivity by using algebraic expansions have been reported lately thanks to the rapidity with which results can be obtained and to the vast amount of information they provide. Many of these developments have emerged from the spectroscopic field; such is the case with:

(*a*) The application of derivative spectroscopy to real problems subject to constant systematic errors and to the resolution of multi-component mixtures with fairly overlapped absorption spectra.[1,2]

(*b*) The use of multi-variate calibration, whether direct (when the spectra of all the components are known) or indirect (which calls for no individual interference data but requires the use of standards including all the components to be determined and the content in each interferent to be varied over a sufficiently wide range for the algorithm used to succeed in evaluating its effect).[3–7]

(*c*) The implementation of deconvolution methods, which isolate the spectrum of the analyte from the overall sample spectrum, thereby allowing it to be quantified.[5–7]

Despite the remarkable achievements in this field, the obtainment of reliable results is rendered difficult by samples including components with strongly overlapped or unknown spectra and/or unknown concentrations.

The H-Point Standard Additions method[8–10] was developed as an alternative to existing methods for solving the above-mentioned problems. It allows the analyte concentration to be calculated free from all constant systematic and proportional errors even in the presence of a direct interferent in the sample to be assayed. It relies on the use of the analytical signals obtained at two wavelengths where the absorbance is the same for the interferent and different for the analyte; the application of the Method of Standard Additions (MOSA) under these conditions thus leads to two straight lines at each wavelength which intercept at the so-called H-point, defined by the coordinates $(-C_H, A_H)$, where C_H is the analyte concentration and A_H is the analytical signal yielded by the interferent, which can thus be quantified as well.

The foundation of the HPSAM was described in two earlier papers.[8,9] A third, more recent paper, reported its application to the resolution of mixtures of two components with extensively or completely overlapped spectra.[10]

*Author for correspondence

This paper shows how the application of the HPSAM can be simplified by using a single calibration graph when only the analyte concentration must be calculated or only the overall sample spectrum is available; it is also of use in applying the single-standard calibration method.[11]

As shown below by solving several major analytical problems, the analytical signal used (ΔA) is only dependent on the analyte concentration and should therefore be preferred to the absorbance.

The proposed modified HPSAM allows the determination of the analyte concentration with no systematic errors in the presence of a direct interferent and any constant systematic error, thereby making any preliminary separation step dispensable and enhancing selectivity.

THEORETICAL BACKGROUND

The consideration about the HPSAM made in earlier papers[8,9] are applicable here in using ΔA as the analytical signal as described below.

Consider a sample containing two compounds X (analyte) and Y (interferent). The equations resulting from application of the MOSA to the two HPSAM wavelengths, λ_1 and λ_2, will be:

$$A_1 = b_0 + b + M_1 C_i + \text{TYB} \quad (1)$$

$$A_2 = A_0 + A' + M_2 C_i + \text{TYB} \quad (2)$$

where A_1 and A_2 are the absorbances measured at the two selected wavelengths for the different solutions assayed, b_0 and A_0 bear the same meaning for the analyte of the solution containing sample alone and b and A' for the interferent, M_1 and M_2 denote the slope of the MOSA plots and TYB stands for the Total Youdan Blank, which will normally be the same at the two wavelengths, especially taking into account their closeness (for other information, refer to reference 9). C_i denotes the different added concentrations of pure analyte ($i = 0, 1, \ldots, n$).

Application of the HPSAM under the condition that the absorbance values of the interferent at the two wavelengths are the same ($b = A'$), yields:

$$A_1 - A_2 = \Delta A_{1,2} = b_0 - A_0 + (M_1 - M_2)C_i \quad (3)$$

According to this equation, the absorbance increment depends exclusively on the analyte concentration, so the plot of $\Delta A_{1,2}$ *vs.* C_i will be a straight line of ordinate $b_0 - A_0$ and slope $M_1 - M_2$ (Fig. 1). The analyte concentration can thus be calculated from ΔA values by applying the HPSAM to the intercept of the straight line, at the H-point of which

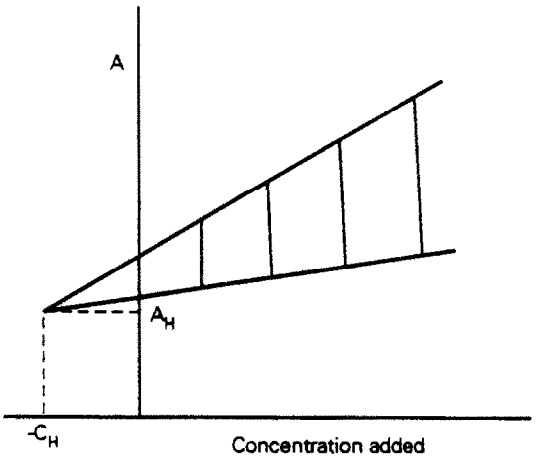

Fig. 1. The plot of the HPSAM.

$$-C_i = -C_H = (b_0 - A_0)/(M_1 - M_2) \quad (4)$$

The ΔA value obtained after each addition will be exclusively related to the analyte concentration as the interferent absorbance will be the same at the two wavelengths, so its contribution to ΔA will be zero even if the intensity of its analytical signal changes on successive analyte additions because of interaction with the analyte. Therefore, the analytical signals will be free from constant systematic errors (and also from proportional errors thanks to the features of the MOSA).

Consequently, when only the analyte concentration must be calculated or only the sample matrix spectrum is known, a single calibration plot of ΔA against the added analyte concentration allows one to calculate the unknown concentrations free from any bias error from the intercept of the line in the same way as with

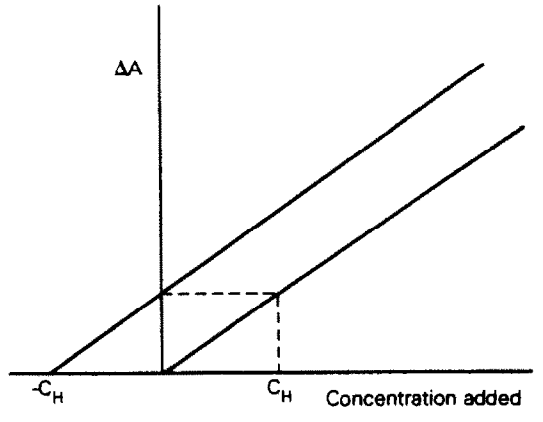

Fig. 2. The plot of the HPSAM with ΔA values.

the MOSA, but with no systematic errors. Figure 2 illustrates the two possibilities of using the HPSAM plots to calculate the analyte concentration.

On the other hand, routine work usually involves determining the analyte in a given sample by using the single-calibration method, which requires the sample signal (A_s), the analytical signal (A_r) and the concentration of standard used (C_r) to be known. Thus, the analyte concentration can be calculated from spectroscopic data by using the equation:

$$C_s = (A_s/A_r)C_r \quad (5)$$

The variables required to obtain unbiased results by applying the MOSA are A_s and the analytical signal (A_t) yielded by a solution containing the sample plus a certain known added concentration of pure analyte (C_a). The equation to be applied in this case is:

$$C_s = (A_s/A_a)C_a = [A_s/(A_t - A_s)]C_a \quad (6)$$

Applying the HPSAM to ΔA values requires them to be known for the original sample and the solution including the added pure analyte at the two selected wavelengths, as well as the analyte concentration added. The equation to be used will thus be:

$$C_s = [\Delta A_s/(\Delta A_t - \Delta A_s)]C_a \quad (7)$$

We applied the HPSAM to various mixtures of dyes, and phenol plus *o*-cresol featuring spectral maximum differences between 65 and 0 nm by using ΔA values to check the performance of the proposed method in terms of accuracy and precision in determining the analyte concentration only. The results showed the HPSAM based on the use for ΔA values to be a viable alternative to the obtainment of unbiased results wherever the working conditions allow for its application.

EXPERIMENTAL

We prepared aqueous solutions of Carmine Indigo, Thymol Blue, Methyl Red, Congo Red and Arsenazo III by weighing appropriate amounts of the indicator-grade reagents, as well as phenol/*o*-cresol mixtures form ACS phenol (Merck) and *o*-cresol (Merck). The required pH was adjusted with hydrochloric acid or sodium hydroxide.

Sample spectra were recorded on a Shimadzu UV-240 spectrophotometer and absorbances were measured at each wavelength by means of the OPI-2 unit used.

RESULTS AND DISCUSSION

Table 1 lists the results obtained by applying the HPSAM to six dye mixtures (the corresponding analyte is underlined in each case). It also gives the equations of the HPSAM plots for each replicate and the results obtained from them, as well as the average and precision. The results were satisfactory in all instances and consistent with those obtained by applying the unmodified HPSAM.

The homogeneity of the variance of the straight lines obtained at each wavelength for all the mixtures assayed was checked by applying Bartlett's test.[12] We also checked the coincidence of such lines by the ANOVA method.[12] As χ^2_{tab} was greater than χ^2_{cal} for all the sets of straight lines obtained (Table 2), the corresponding variances were thus homogeneous. The ANOVA method revealed F_{tab} to be greater than F_{cal}, so the different lines were coincident for all the mixtures assayed.

Figure 3 shows the HPSAM plots obtained with ΔA values for all the mixtures assayed. Their slopes vary with the absorbance at the two wavelengths; however, their intercepts yield the correct analyte concentration in each case. For $\Delta A = 0$, the abscissa represents the analyte concentration estimated by applying the HPSAM with ΔA values.

The mean relative errors in the analyte concentrations are listed in Table 3, which also gives the average slope for each mixture assayed, the interferent absorbance at the two selected wavelengths and the separation between maxima. As can be seen, the relative error does not depend on the interferent absorbance, but rather on the slope of the calibration graph. The results are all quite satisfactory.

These data were processed by applying equation (7) to a single-standard calibration plot. The results obtained by carrying out several additions and using ΔA values are listed in Table 4, which also gives the analyte concentration found in each replicate, the average concentration, the standard deviation and the relative error made in the determination.

The results obtained were accurate and precise for all the mixtures assayed, so the HPSAM based on ΔA can be safely applied to routine work.

As shown above, when only the analyte concentration is to be calculated, the HPSAM

Table 1. Results obtained by the HPSAM with ΔA values for the mixtures of dyes tested. See conditions in Fig. 3

Mixture	$\Delta\lambda_{max}$	λ selected	Parameter	H-point standard additions method: Replicates 1	2	3	Analyte concentration, M ($\times 10^6$): Found (C_H), CI* 4	5	Added	1	2	3	4	5
Thymol Blue *Indigo Carmin*	65 nm	555, 535 nm	*a*	0.139 ± 0.002	0.135 ± 0.002	0.136 ± 0.002	0.138 ± 0.001	0.137 ± 0.002	38	43	39	40	41	40
			b	3230 ± 30	3470 ± 80	3430 ± 70	3380 ± 40	3400 ± 50		2	4	3	2	3
			syx	2.8×10^{-3}	3.3×10^{-3}	2.9×10^{-3}	1.5×10^{-3}	2.2×10^{-3}						
			t-Test	linear	linear	linear	linear	linear						
									$\bar{x}$	4.0×10^{-5}				
									s	0.2×10^{-5}				
Methyl Red Congo Red	50 nm	558, 578 nm	*a*	0.142 ± 0.003	0.139 ± 0.003	0.141 ± 0.004	0.141 ± 0.002	0.149 ± 0.005	7.9	7.9	8.0	8.0	7.6	8.2
			b	17900 ± 200	17500 ± 250	17700 ± 300	18500 ± 300	18100 ± 400		0.4	0.5	0.7	0.8	0.9
			s_{yx}	3.9×10^{-3}	5.0×10^{-3}	6.7×10^{-3}	6.2×10^{-3}	7.3×10^{-3}						
			t-Test	linear	linear	linear	linear	linear						
									$\bar{x}$	7.9×10^{-6}				
									s	0.2×10^{-6}				
Methyl Red *Thymol Blue*	27 nm	528, 508 nm	*a*	0.073 ± 0.002	0.075 ± 0.002	0.080 ± 0.003	0.078 ± 0.004	0.075 ± 0.002	11.2	11.3	12	12	11.6	10.8
			b	6490 ± 70	6400 ± 100	6700 ± 100	6700 ± 100	6920 ± 80		0.7	1	1	0.9	0.8
			s_{yx}	2.6×10^{-3}	3.8×10^{-3}	4.1×10^{-3}	3.7×10^{-3}	3.1×10^{-3}						
			t-Test	linear	linear	linear	linear	linear						
									$\bar{x}$	1.15×10^{-5}				
									s	0.05×10^{-5}				
Methyl Red *Arsenazo III*	16 nm	528, 508 nm	*a*	0.052 ± 0.001	0.054 ± 0.001	0.050 ± 0.001	0.050 ± 0.001		5.96	5.79	5.9	5.7	5.7	
			b	9010 ± 20	9160 ± 45	8740 ± 70	8740 ± 50			0.08	0.2	0.3	0.3	
			s_{yx}	3.1×10^{-4}	8.6×19^{-4}	1.4×10^{-3}	1.0×10^{-3}							
			t-Test	linear	linear	linear	linear							
									$\bar{x}$	5.78×10^{-6}				
									s	0.06×10^{-6}				
Thymol Blue Arsenazo III at pH 0.90	11 nm	544, 524 nm	*a*	0.051 ± 0.001	0.055 ± 0.001	0.054 ± 0.002	0.056 ± 0.001	0.054 ± 0.001	8.4	8.4	8.4	8.3	8.8	8.7
			b	6060 ± 70	6500 ± 100	6500 ± 200	6400 ± 90	6200 ± 90		0.5	0.7	0.9	0.5	0.6
			s_{yx}	1.4×10^{-3}	2.4×10^{-3}	4.0×10^{-3}	1.6×10^{-3}	1.7×10^{-3}						
			t-Test	linear	linear	linear	linear	linear						
									$\bar{x}$	8.5×10^{-6}				
									s	0.2×10^{-6}				
Thymol Blue Arsenazo III at pH 12.00	0 nm	555, 635 nm	*a*	0.042 ± 0.001	0.042 ± 0.001	0.042 ± 0.001	0.042 ± 0.001	0.043 ± 0.001	5.6	5.2	5.3	5.4	5.4	5.5
			b	8010 ± 30	7989 ± 40	7950 ± 40	7780 ± 50	7840 ± 40		0.3	0.4	0.4	0.5	0.5
			s	7×10^{-4}	9×10^{-4}	9×10^{-4}	1.2×10^{-3}	1.0×10^{-3}						
			t-Test	linear	linear	linear	linear	linear						
									$\bar{x}$	5.4×10^{-6}				
									s	0.1×10^{-6}				

*Confidence interval of the analytical result.

Table 2. Study of the homogeneity of the variance and coincidence of lines for the six sets of straight lines obtained for the six tested mixtures of dyes

Maxima separation of the mixtures, *nm*	Mixture	Bartlett's χ^2 (s^2_{yx} homogeneity)			Snedecor's F (coincidence of lines)
65	Thymol Blue Indigo Carmin	1.77			1.76
	Tabulated values ($\alpha = 0.05$) $\mu_o = 4$	9.49	$\mu_d = 8$	$\mu = 18$	2.51
50	Methyl Red Congo Red	2.60			2.18
	Tabulated values ($\alpha = 0.05$) $\mu_o = 4$	9.49	$\mu_d = 8$	$\mu = 24$	2.36
27	Methyl Red Thymol Blue	1.33			0.10
	Tabulated values ($\alpha = 0.05$) $\mu_o = 4$	9.49	$\mu_d = 8$	$\mu = 28$	2.29
16	Methyl Red Arsenazo III	4.64			0.70
	Tabulated values ($\alpha = 0.05$) $\mu_o = 3$	7.82	$\mu_d = 6$	$\mu = 12$	3.00
11	Thymol blue Arsenazo III at pH 0.9	9.00			2.19
	Tabulated values ($\alpha = 0.05$) $\mu_o = 4$	9.49	$\mu_d = 8$	$\mu = 29$	2.28
0	Thymol blue Arsenazo III at pH 12	1.11			2.33
	Tabulated values ($\alpha = 0.05$) $\mu_o = 4$	9.49	$\mu_d = 8$	$\mu = 20$	2.49

μ = No. of degrees of freedom.

based on ΔA values is equally applicable provided the spectrum yielded by one or several compounds in the presence or absence of matrix effects is known because the HPSAM compensates for constant bias errors and proportional errors, and converts uncorrectable errors introduced by a direct interferent into constant, correctable bias errors. Then, the analyte concentration is calculated from the intercept of the straight line obtained in the plot of ΔA *vs.* added analyte concentration, or from equation (7) if a single-standard calibration is made.

Finally, we applied the HPSAM based on ΔA values to various synthetic mixtures of

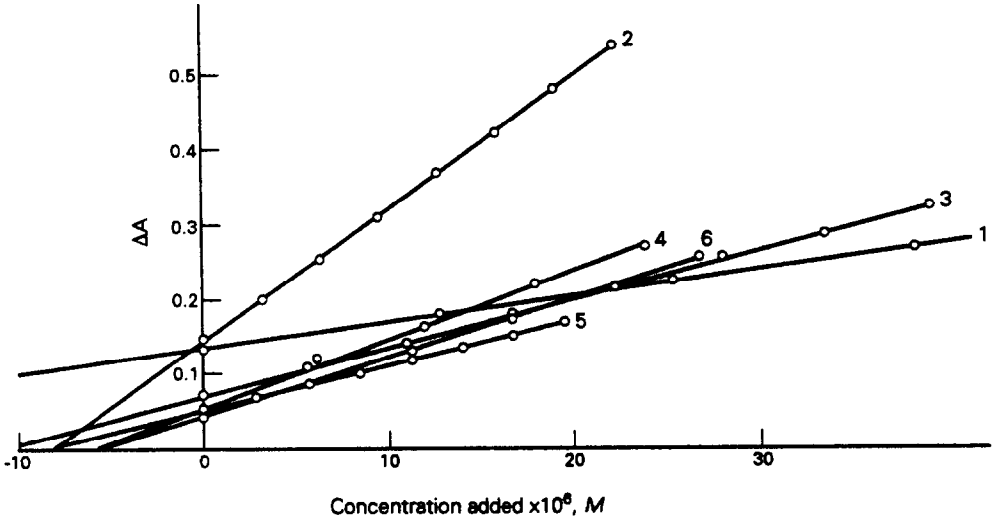

Fig. 3. The plots of the HPSAM with ΔA values for the mixtures tested, being: 1. pH 0.90, $1.82 \times 10^{-5}M$ Thymol Blue, $3.80 \times 10^{-5}M$ Indige Carmin and $8.88 \times 10^{-5}M$ maximum added analyte. 2. pH 2.00, $2.5 \times 10^{-5}M$ Congo Red, $7.9 \times 10^{-6}M$ Methyl Red and $2.98 \times 10^{-5}M$ maximum added analyte. 3. pH 0.90, $7.85 \times 10^{-6}M$ Methyl Red, $1.12 \times 10^{-5}M$ Thymol Blue and $13.88 \times 10^{-5}M$ maximum added analyte. 4. pH 0.90, $4.25 \times 10^{-6}M$ Methyl Red, $5.96 \times 10^{-6}M$ Arzenazo III and $29.80 \times 10^{-6}M$ maximum added analyte. 5. pH 0.90, $4.54 \times 10^{-6}M$ Arsenazo III, $8.37 \times 10^{-6}M$ Thymol Blue and 27.90×10^{-6} maximum added analyte. 6. pH 12.00, $4.54 \times 10^{-6}M$ Arsenazo III, $5.58 \times 10^{-6}M$ Thymol Blue and 33.48×10^{-6} maximum added analyte.

Table 3. % Relative Error obtained on applying the HPSAM with ΔA values for the six mixtures tested

Maxima separation, *nm*	A_H	Average slope	% E_R
65	0.400	3382	5.3
50	0.354	17940	0.0
27	0.401	6642	2.7
16	0.176 0.230	8913	−3.0
11	0.139	6332	1.2
0	0.097	7912	−3.6

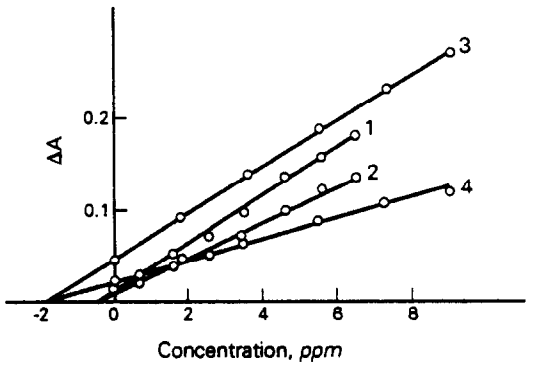

Fig. 4. The plots of the HPSAM with ΔA values for the 82 commercial grade of phenol (1, 2) and for the 50 commercial grade of *o*-cresol (3, 4). Chosen wavelengths (nm): 1 226,241; 2. 238,230; 3. 229,243 and 4 234, 239.

commercially available phenol and *o*-cresol, 82% commercial grade phenol (84.0:16.0 w/w phenol/*o*-cresol), and 50% commercial grade *o*-cresol (49:49.2 phenol/*o*-cresol/*m*- and *p*-cresol + 2,6-xylenol). Neither *m*-, nor *p*-cresol or 2,6-xylenol were used as their contribution to the interferent spectrum in the spectral region of interest was small and constant as a result of their extreme dilution.

The spectrophotometric resolution of the phenol/*o*-cresol mixtures was rendered difficult by the closeness of the absorption maxima of the two components in 0.1*M* sodium hydroxide (234 and 287 nm for phenol, and 237 and 289 for *o*-cresol) and the similarity between their absorptivities.

To determine the commercial grade phenol, the MOSA was applied to a sample containing 3.1 mg/l. phenol and concentrations of *o*-cresol (the analyte) between 0.6 and 6.5 mg/l. The commerical grade *o*-cresol was determined similarly in a sample containing 2.0 mg/l., to which phenol concentrations in the range 2.0–9.1 mg/l. were added. All the solutions were 0.1*M* in sodium hydroxide. The absorbance of the solutions was monitored over the wavelength range 244–224 nm. The slit width used was 1 nm and three replicates were run in each case.

Figure 4 shows the HPSAM plots obtained by using ΔA values. Two wavelength pairs were selected for each commercial grade; the experiments were conducted by considering phenol and *o*-cresol as respective interferents in the determinations of the 82 and 50% commercial grade compounds. The results were quite good in all instances (see Table 5). As can

Table 4. Results obtained from the HPSAM with ΔA values using the calibration method with a unique standard for the six mixtures tested

Maxima separation, *nm*	$C_{added} \times 10^6/M$	$C_{found} \times 10^6/M$					$\bar{C} \times 10^6$	$s \times 10^6$	% E_R
65	25 4	43	36	36	40	39	39	3	2.6
	38 1	42	37	38	40	39	39	2	2.6
	50.8	44	38	39	41	40	40	2	5.3
50	6.3	8.0	8.6	8.4	8.0	7.2	8.0	0.5	1.3
	9 5	8.3	8.5	8.2	7.9	7.6	8.1	0.3	2.5
	12.6	8.1	8.5	8.3	8.3	7.8	8.2	0 3	3.8
27	5.5	11.2	12.2	11.6	10.2	10.6	11.2	0.8	0.0
	11 0	11.5	11.5	10.6	10.6	11.0	11.0	0.5	−1.8
	16 6	11.4	11.6	11.4	10.2	10.8	11.1	0.6	−0.9
16	6 0	6.2	6.0	6.0	6.1		6.1	0.1	1.7
	11 9	5 7	6.0	5.9	5.9		5.9	0.1	−1.7
11	5.6	7.8	9.0	9.0	8.6	7.9	8.5	0 6	1.2
	8.4	8.1	8.4	7.9	8.4	8.2	8.2	0.2	−2.3
	11.2	8.2	8.9	7.9	8.3	8.3	8.3	0.4	−1.2
0	5 6	5.4	5.4	5.5	5.7	5.6	5.5	0.1	−1.8
	11.2	5.4	5.3	5.5	5.7	5.5	5.5	0.1	−1.8

Table 5. Results obtained by the method for the mixtures of aromatic compounds

Commercial grade	Analyte	wt%	Measurement wavelengths	$C_{found} + S$
82	*o*-cresol	16.0	238, 230	16 ± 1
			226, 241	14.5 ± 0.6
50	phenol	49.0	234, 239	49.5 ± 0.5
			229, 243	49.0 ± 0.5

be seen from Fig. 4, the wavelengths 226 and241 nm, and 229 and 243 nm used for the former and latter grade, respectively, provided steeper slopes—and hence better results—than the other two pairs used (238 and 230 nm for the 82% grade, and 234 and 239 nm for the 50% grade).

The average percent relative error in the analyte concentration was always less than 10% in analysing the two commercial grades with single-standard calibration.

Therefore, the HPSAM based on the use of ΔA values provides good results, however close the absorption maxima and similar the absorptivities of the two components of the mixture, and however high the interferent/analyte concentration ratio may be.

CONCLUSIONS

As shown above, the HPSAM can be applied by using absorbance increments as analytical signals whenever only the analyte concentration must be determined. ΔA values are directly (and exclusively) related to the analyte concentration and thus allow this to be calculated free from bias errors from the intercept of the straight line obtained by plotting ΔA against the analyte concentration.

The proposed method is also applicable to routine analyses by using single-standard calibration.

Acknowledgement—The authors are grateful to the DGICYT for financial support (Project no. PB88-0495)

REFERENCES

1. T. C. O'Havier, *Anal. Chem.*, 1979, **51**, 91A.
2. F. Sanchez Rojas, C. Bosch Ojeda and J. M. Cano Pavon, *Talanta*, 1988, **35**, 753.
3. H. Martens. Dr. Techn. Thesis, University of Trondheim, Norway, 1985.
4. B. E. H. Saxberg and B. R. Kowalski, *Anal. Chem.*, 1979, **51**, 1031.
5. J. A. Howell and L. G. Hargis, *ibid.*, 1986, **58**, 108R.
6. L. G. Hargis and J. A. Howell, *ibid.*, 1988, **60**, 131R.
7. S. D. Brown, T. O. Barker, R. J. Larivee, S. L. Monfre and H. R. Wilk, *ibid.*, 1988, **60**, 252R.
8. F. Bosch Reig and P. Campins Falcó, *Analyst*, 1988, **113**, 1011.
9. *Idem*, *ibid.*, 1990, **115**, 111.
10. P. Campíns Falcó, F. Bosch Reig and A. Molina Benet, *Fresenius J. Anal. Chem.*, 1990, **338**, 16
11. M. J. Cardone, Ph J. Palermo and L. B. Sybrandt, *Anal. Chem.*, 1980, **52**, 1187.
12. Commissariat à l'energie Atomique, *Statistique appliquée à l'exploitation des mesures*, Masson, Paris 1978.

Talanta, Vol. 39, No. 1, pp 9–15, 1992
Printed in Great Britain

0039-9140/92 $5.00 + 0.00
Pergamon Press plc

RAPID DECOMPOSITION OF ORGANIC MATERIALS WITH ACIDIC LITHIUM SULPHATE FLUX CONTAINING CATALYSTS, OXIDIZING AGENTS OR REDUCING AGENTS, AND KJELDAHL DETERMINATION OF NITROGEN

NOBUTAKA YOSHIKUNI
Laboratory for Analytical Chemistry, Faculty of Engineering, Chiba University, Yayoi-cho, Chiba, Japan

(*Received* 27 *March* 1991. *Revised* 3 *July* 1991. *Accepted* 3 *July* 1991)

Summary—Organic compounds and natural materials such as dimethylglyoxime, *p*-nitrophenol, α-nitroso-β-naphthol, 4-(2-pyridylazo)-resorcinol, phenylhydrazine hydrochloride, monopyrazolone, residual fuel oil and coal can be rapidly decomposed in the melting state with various ratios of sulphuric acid–lithium sulphate (v/w) mixture containing catalysts, oxidizing agents or reducing agents such as elemental selenium powder, cupric sulphate, ceric sulphate and stannous sulphate. The quantitative recovery of nitrogen in the melting medium can be obtained with the Kjeldahl method.

It is well known that the apparatus and operation of the Kjeldahl method are very simple, which readily allows the determination of nitrogen in a large number of samples. Thus, in analogy with the Dumas method,[1] the Kjeldahl method has been widely used for the determination of nitrogen in various organic materials, but the classical Kjeldahl method suffers the disadvantage that the decomposition time is long[2–4] and complete recovery of nitrogen cannot be obtained from certain organic materials.[5]

It is actually impossible to determine nitrogen in organic compounds that contain azo, diazo, nitro, nitroso, oxime, hydrazine and pyrazolone groups with the classical Kjeldahl method. Compounds with the first six groups can of course be converted into amino compounds with catalysts[5] such as Zn–Fe powder in hydrochloric acid media, and then Kjeldahl determination of nitrogen is possible. This is not possible with heterocyclic N–N groups.[5] The gas volumetric method for determining N–N groups by oxidative fusion with chromic acid has been successfully employed to determine the heterocyclic nitrogen in indazolinone derivatives.[6]

Previous studies[7–8] have shown that a liquid medium of sulphuric acid–lithium sulphate (20 ml, 10 g) mixture can easily decompose refractory oxides such as hafnium oxide, titanium dioxide, zirconium oxide, and if a strong oxidizing reagent such as ceric sulphate, manganese dioxide, potassium permanganate or potassium periodate is added, the more refractory chromium(III) oxide can be decomposed in a few minutes. However, decomposition of organic compounds takes a long time in a liquid medium.

However, if more lithium sulphate is added to the sulphuric acid–lithium sulphate mixture, for example, changing to molten acidic lithium sulphate (ALS) flux at a $H_2SO_4 : Li_2SO_4 . H_2O$ ratio of 15 ml : 30 g instead of liquid medium (20 ml, 10 g) many organic compounds can be completely decomposed with ease. This paper demonstrates the rapid decomposition of organic compounds such as dimethylglyoxime, *p*-nitrophenol, α-nitroso-β-naphthol, 4-(2-pyridylazo)-resorcinol, phenylhydrazine hydrochloride and monopyrazolone, and natural samples such as residual fuel oil and coal in this melting medium and the quantitative recovery of nitrogen with the Kjeldahl method.

EXPERIMENTAL

Reagents

Boric acid, lithium sulphate monohydrate, potassium hydroxide, hydrochloric acid, sulphuric acid, selenium metal powder and stannous sulphate were analytical grade from Wako Pure Chemical Co. Ceric(IV) sulphate tetrahydrate (min. 98%) was from Merck. All other reagents were analytical grade. Demineralized distilled water was used throughout. The mixed

indicator was prepared by dissolving bromocresol green (0.075%) and methyl red (0.050%) in ethanol.

Organic samples

Dimethylglyoxime (DMG), p-nitrophenol and phenylhydrazine hydrochloride were from Kanto Chemical Co., Inc., analytical grade. Monopyrazolone (1-phenyl-3-methyl-5-pyrazolone) and α-nitroso-β-naphthol were analytical grade from Wako Pure Chemical Co. 4-(2-Pyridylazo)-resorcinol (PAR) was Dojindo Laboratories dotite reagent. The Standard Reference Material 1632b of Coal (bituminous) was from the National Institute of Standards and Technology of the U.S.A. The standard sample of nitrogen in residual fuel oil was from Japan Petroleum Institute.

Apparatus

The Kjeldahl distillation apparatus used was of the Parnas-Wagner type of Sibata Scientific Technology Ltd.

Decomposition procedures

Decomposition of organic materials with molten ALS flux. Weigh out roughly 30 g of $Li_2SO_4.H_2O$ into a dry 100-ml Kjeldahl flask. Add 11 or 15-ml of concentrated sulphuric acid to the flask in such as way that any solid caught in the neck is washed down. Place a small short-stemmed funnel in the neck of the flask and heat the flask with a Bunsen burner in a well ventilated fume-hood, with the flask at 45° from the vertical. Start with a strong flame, rapidly increasing the temperature until the acid begins to fume after hydrate water is boiled off. Continue heating for about 10 min until a clear melting medium (molten ALS flux) is obtained, then cool the flask, rotating gently until the melt solidifies (solid ALS flux) into thin sheets or cakes on the bottom or sides. When the ALS flux from the $H_2SO_4/Li_2SO_4.H_2O$ (15 ml, 30 g) mixed system is cooled, accurately weigh approximately 10–100 mg of organic sample such as DMG, monopyrazolone, α-nitroso-β-naphthol and PAR, and transfer into the flask without a catalyst. For a 0.1-g coal powder sample or residual fuel oil sample, the decomposition requires a catalyst such as 1.0 g of elemental selenium powder and concentrated sulphuric acid (15 ml). For the ALS flux from the $H_2SO_4/Li_2SO_4.H_2O$ (11 ml, 30 g) mixed system, accurately weigh approximately 50 mg of *p*-nitrophenol with a catalyst of about 0.1 g of selenium metal powder, transfer into the flask and add 4 ml of concentrated sulphuric acid to the flask in such a way that any solid caught in the neck is washed down. Natural samples such as coal powder or residual fuel oil were decomposed by addition of about 1.0 g of elemental selenium powder and 19 ml of concentrated sulphuric acid to the ALS flux of the H_2SO_4–$Li_2SO_4.H_2O$ (11 ml, 30 g) mixture.

Fix the flask on a stand, and start with a gentle flame for 5 min. When the contents have melted, after 5 min increase to a strong flame and continue the heating for about 10 min. Immediately before the molten ALS flux has cooled off add 30 ml of concentrated sulphuric acid to the flask and swirl gently. Let the flask stand for a few minutes, then cautiously add about 50 ml of water little by little. After cooling to room temperature with tap water, transfer the contents into a 200-ml standard flask and dilute to the mark with water. An aliquot of this sample solution is analysed by the Kjeldahl method for nitrogen.

Decomposition of organic compounds with the molten state of powdery ALS flux. Weigh out roughly 100 g of $Li_2SO_4.H_2O$ and transfer to a 500-ml beaker. Add 50 ml of concentrated sulphuric acid, cover the beaker with a watch glass, and heat with a Bunsen burner on a wire-gauze with asbestos. Begin with a strong flame, rapidly increasing the temperature until the acid begins to fume, after hydrate water is boiled off continue the heating for about 20 min. Pour the clear melted medium (ALS flux) onto a glass plate and allow to cool to room temperature.

Grind the cooled solid with a mortar and pestle, and store the powdered material of ALS flux in a desiccator. For decomposition of the organic compound, weigh out roughly 50 g of the powdered and cooled ALS flux and 0.1 g of selenium metal powder, and then add them to a dry 100-ml Kjeldahl flask. Rotate and shake the flask in order to blend the powders. Accurately weigh approximately 50 mg of finely powdered organic compound, and transfer into the flask. Mix the powders in a shaker and swirl gently. Fix the flask on a stand and place a small short-stemmed funnel in the neck of the flask. Start with a strong flame, rapidly increasing the temperature until the contents begin to melt, and continue heating for about 15–20 min. Before the ALS flux cools, add 30 ml of concentrated sulphuric acid to the flask and shake until the solution is completely mixed. Transfer to a

200-ml standard flask and dilute to volume with water.

Decomposition of coal with molten ALS flux containing $CuSO_4$. Weigh out 30 g of $Li_2SO_4.H_2O$ and transfer into a dry 100-ml Kjeldahl flask. Add 2.5 g of $CuSO_4.5H_2O$ to the flask and then 20 ml of concentrated sulphuric acid in such a way that any solid caught in the neck is washed down. Place a small short-stemmed funnel in the neck of the flask and heat with a Bunsen burner. Continue the heating with a strong flame for about 10 min until a clear green melting ALS flux is obtained, and then cool the flask.

When the contents are cool, accurately weigh approximately 0.1 g of coal powder and 5.0 ml of concentrated sulphuric acid, by pipette, and transfer into the flask. Fix the flask on a stand and heat with a gentle flame for 5 min. When the contents become a clear green melted ALS flux after 5 min, increase to a strong flame and continue the heating for about 15 min. Immediately before the ALS flux is cool, add 30 ml of concentrated sulphuric acid to the flask, mix the contents completely and dilute to 200 ml with water by the method stated above.

Decomposition of phenylhydrazine with molten ALS flux containing $SnSO_4$. Accurately weigh approximately 15 mg of phenylhydrazine hydrochloride and transfer into a dry 100-ml Kjeldahl flask. Weigh out roughly 30 g of $Li_2SO_4.H_2O$ and 0.2 g of tin(II) sulphate and add to the flask. Shake the flask to blend the powders. Add 20 ml of 13.5*M* sulphuric acid to the flask in such a way that any solid caught in the neck is washed down. Place a small short-stemmed funnel in the flask and fix the flask on a stand at 45° from the vertical. Start with a gentle flame and continue heating for about 30 min. Then heat with a strong flame until the acid begins to fume after all water is boiled off, and continue the heating for about 20 min. Before the clear molten ALS flux is cool, add 30 ml of concentrated sulphuric acid to the flask, mix the contents completely, and dilute to 200 ml with water by the method stated above.

Kjeldahl determination of nitrogen

Take 20–50 ml portions (accurately measured) of the sample solutions and transfer to the Kjeldahl distillation apparatus. Generate ammonia with sodium hydroxide solution and absorb the ammonia in 30 ml of saturated boric acid solution. Continue the steam distillation until about 100 ml of liquid have passed over so that all the ammonia may be recovered. Add a few drops of indicator to the ammonia absorption media and titrate the H_3BO_3–NH_3 solution with standard 0.1*M* hydrochloric acid, using a 1-ml microburette.

RESULTS AND DISCUSSION

Organic compounds having groups of azo, diazo, nitro, nitroso, hydrazine, oxime and pyrazolone are among the most difficult to rapidly decompose and quantitatively recover nitrogen with the classical Kjeldahl method.[5] However, if a melting ALS flux such as H_2SO_4–Li_2SO_4, H_2SO_4–Li_2SO_4–Se, H_2SO_4–Li_2SO_4–$CuSO_4$ or H_2SO_4–Li_2SO_4–$SnSO_4$ is used, these organic compounds can be rapidly decomposed and the nitrogen content quantitatively recovered. Fusion[6,9] and catalysts[4,10–16] are effectively utilized in the Kjeldahl method. The molten state of the ALS flux is analogous to that of a fusion flux.

Decomposition of DMG, monopyrazolone, α-nitroso-β-naphthol, PAR and p*-nitrophenol*

Organic compounds such as DMG, monopyrazolone, α-nitroso-β-naphthol, and PAR can be rapidly and easily decomposed by heating for 10–30 min with the molten state of ALS flux from H_2SO_4–$Li_2SO_4.H_2O$, without a catalyst. However, elemental selenium powder seems to be one of the most effective catalysts in the decomposition system and reduces the decomposition time of α-nitroso-β-naphthol (from 20 to 15 min) and PAR (from 10 to 7 min). The complete decomposition of these organic compounds with the concentrated sulphuric acid and lithium sulphate monohydrate (15 ml, 30 g) mixture requires heating for long periods such as 30–60 min because the coordinated water of lithium sulphate gives rise to bubbles in the flask. Therefore, before decomposing the organic compounds, the hydrate water in the mixture of H_2SO_4–$Li_2SO_4.H_2O$ should be completely removed by heating. After the organic compounds are decomposed, concentrated sulphuric acid (30 ml) must be added to the hot melting ALS flux to prevent the solidification of the liquid state. The solidifying medium, ALS flux in other words, cannot be rapidly dissolved with water or dilute sulphuric acid at room temperature. DMG, α-nitroso-β-naphthol and PAR can be completely decomposed with molten ALS flux from the H_2SO_4–$Li_2SO_4.H_2O$ (15 ml, 30 g) mixture without a catalyst in the

Table 1. Determination of nitrogen in dimethylglyoxime

Decomposition systems		Sample (Nitrogen content %)	Sample taken, mg	Nitrogen found, mg	Nitrogen found, %	Decomposition time, min
ALS flux	Additional reagents					
From H_2SO_4–$Li_2SO_4.H_2O$ (15/30, v/w)	no addition	DMG (24.1)	21.2	5.04	23.8	10
			23.8	5.48	23.0	10
			25.9	6.24	24.1	15
			24.7	5.78	23.4	15
			26.0	6.31	23.3	15
					(average 23.7, S.D. 0.47)	

Volume in ml, weight in g, S.D. standard deviation.
H_2SO_4: concentrated sulphuric acid.

Table 2. Determination of nitrogen in α-nitroso-β-naphthol

Decomposition systems		Sample (Nitrogen content %)	Sample taken, mg	Nitrogen found, mg	Nitrogen found, %	Decomposition time, min
ALS flux	Additional reagents					
From H_2SO_4–$Li_2SO_4.H_2O$ (15/30, v/w)	no addition	α-Nitroso-β-naphthol (8.09)	90.2	7.52	8.34	20
			83.7	6.62	7.91	20
			82.7	6.89	8.33	20
Powder (50 g) of H_2SO_4–Li_2SO_4 solid cake*	elemental selenium powder (0.1 g)	α-Nitroso-β-naphthol (8.09)	85.3	6.97	8.17	15
			103.6	8.26	7.97	15
					(average 8.14, S.D. 0.18)	

Volume in ml, weight in g, S.D. standard deviation.
*Solid cake from H_2SO_4–Li_2SO_4 H_2O (50/100, v/w).
H_2SO_4: concentrated sulphuric acid.

Table 3. Determination of nitrogen in 4-(2-pyridylazo)-resorcinol

Decomposition systems		Sample (Nitrogen content %)	Sample taken, mg	Nitrogen found, mg	Nitrogen found, %	Decomposition time, min
ALS flux	Additional reagents					
From H_2SO_4–$Li_2SO_4.H_2O$ (15/30, v/w)	no addition	PAR (19.5)	40.6	7.71	19.0	10
			46.8	8.70	18.6	10
Powder (30 g) of H_2SO_4–Li_2SO_4 solid cake*	elemental selenium powder (0.1 g)	PAR (19.5)	26.4	5.20	19.7	10
			37.0	7.25	19.6	7
			42.0	8.17	19.5	7
					(average 19.3, S.D. 0.42)	

Volume in ml, weight in g, S.D. standard deviation.
*Solid cake from H_2SO_4–$Li_2SO_4.H_2O$ (50/100, v/w).
H_2SO_4: concentrated sulphuric acid.

Table 4. Determination of nitrogen in monopyrazolone

Decomposition systems		Sample (Nitrogen content %)	Sample taken, mg	Nitrogen found, mg	Nitrogen found, %	Decomposition time, min
ALS flux	Additional reagents					
From H_2SO_4–$Li_2SO_4.H_2O$ (15/30, v/w)	no addition	Monopyrazolone (16.1)	46.8	7.03	15.0	15
			46.4	6.97	15.0	20
			42.4	6.66	15.7	30
			32.0	4.97	15.5	30
			45.7	6.81	14.9	30
			10.7	1.70	15.9	30
					(average 15.3, S.D. 0.39)	

Volume in ml, weight in g, S.D. standard deviation.
H_2SO_4: concentrated sulphuric acid.

Table 5. Determination of nitrogen in *p*-nitrophenol

Decomposition systems						
ALS flux	Additional reagents	Sample (Nitrogen content %)	Sample taken, *mg*	Nitrogen found, *mg*	*%*	Decomposition time, *min*
From H_2SO_4–$Li_2SO_4.H_2O$ (15/30, v/w)	no addition	*p*-nitrophenol (10.1)	30.1	1.78	5.91†	15
From H_2SO_4–$Li_2SO_4.H_2O$ (11/30, v/w)	elemental selenium powder (0.1 g) and H_2SO_4 (4 ml)	*p*-nitrophenol (10.1)	39.6	4.09	10.3	20
				3.91	9.87	
			51.3	5.02	9.79	20
				5.05	9.84	
				(average 9.95, S.D. 0.20)		

Volume in ml, weight in g., S.D. standard deviation.
†Did not account for the values of average and standard deviation.
H_2SO_4: concentrated suphuric acid.

Kjeldahl flask for 10–20 min and the nitrogen content in the samples can be quantitatively recovered (Tables 1, 2 and 3). The decomposition time for monopyrazolone is about 30 min, but the nitrogen can only be recovered quantitatively heating for 10 min longer with a strong flame. The decomposition method for determining N–N groups in monopyrazolone with molten ALS flux and no catalyst, oxidizing agent or reducing agent was successfully employed to determine the heterocyclic nitrogen (Table 4). For the complete decomposition of *p*-nitrophenol, the catalyst and a few milliliters of concentrated sulphuric acid need to be added to the ALS flux from the H_2SO_4–$Li_2SO_4.H_2O$ (11 ml, 30 g) system before the melt. Furthermore, the ratio of H_2SO_4/Li_2SO_4(ml/g) in the melting ALS flux is very important for complete decomposition of these organic compounds. After the *p*-nitrophenol (~50 mg), elemental selenium powder (~0.1 g) and concentrated sulphuric acid (4 ml) are added the ALS flux H_2SO_4–$Li_2SO_4.H_2O$ (11 ml, 30 g) in the Kjeldahl flask, the mixture should be gently heated for about 10 min and after melting of the ALS flux, it can be heated rapidly up to a high temperature. The organic compound can be decomposed in about 20 min and the quantitative recovery of nitrogen in *p*-nitrophenol can be obtained with the procedure, with a standard deviation of 0.20% nitrogen at the 10% level (Table 5).

Decomposition of phenylhydrazine hydrochloride

The quantitative recovery of the nitrogen content in phenylhydrazine hydrochloride cannot be obtained with the decomposition systems of ALS flux and powdery ALS flux containing

Table 6. Determination of nitrogen in phenylhydrazine hydrochloride

Decomposition systems						
ALS flux	Additional reagents or mixtures	Sample (contains nitrogen, %)	Sample taken, *mg*	Nitrogen found, *mg*	*%*	Decomposition time, *min*
From H_2SO_4–$Li_2SO_4.H_2O$ (15/30, v/w)	no addition	phenylhydrazine hydrochloride (19.4)	30.8	2.37	7.69†	60
Powder (50 g) of H_2SO_4–Li_2SO_4 solid cake*	elemental selenium powder (0.1 g)	phenylhydrazine hydrochloride (19.4)	36.5	2.37	6.49†	20
	H_2SO_4–$Li_2SO_4.H_2O$–$SnSO_4$ mixture (15/30/0.2, v/w/w)	phenylhydrazine hydrochloride (19.4)	36.2	4.98	13.8†	60
			34.5	4.22	12.2†	90
	H_2SO_4–H_2O–$Li_2SO_4.H_2O$–$SnSO_4$ mixture (15/5/30/0.2, v/v/w/w)	phenylhydrazine hydrochloride (19.4)	10.3	1.94	18.8	60
			15.2	2.82	18.6	60
			11.7	2.22	19.0	60
			16.5	3.38	20.5	60
				(average 19.2, S.D. 0.75)		

Volume in ml, weight in g, S.D. standard deviation.
*Solid cake from H_2SO_4–$Li_2SO_4.H_2O$ (50/100, v/w).
†Did not account for the values of average and standard deviation.
H_2SO_4: concentrated sulphuric acid.

Table 7. Determination of nitrogen in residual fuel oil*

Decomposition systems		Sample (certified value of nitrogen, %)	Sample taken, *mg*	Nitrogen found,		Decomposition time, *min*
ALS flux	Additional reagents			*mg*	%	
From H_2SO_4–$Li_2SO_4.H_2O$ (11/30, v/w)	elemental selenium powder (1.0 g) and H_2SO_4 (19 ml)	residual fuel oil (0.589 ± 0.08)	129.9	0.77	0.59	10
				0.75	0.58	
			137.6	0.81	0.59	9
				0.82	0.60	
				(average 0.59, S. D. 0.01)		

Volume in ml, weight in g, S.D. standard deviation.
*Standard sample of nitrogen in residual fuel oil (Lot No. 88N5006) of The Japan Petroleum Institute.
H_2SO_4: concentrated sulphuric acid.

selenium. The solid ALS flux and the powdery ALS flux cannot be used for decomposing phenylhydrazine hydrochloride because the nitrogen in this compound appears to be volatilized before the ALS flux is completely melted. Therefore, a suitable reductant, such as tin(II) sulphate and water are required for decomposition of phenylhydrazine. A recovery of only 60–70% of the nitrogen content in phenylhydrazine hydrochloride is obtained with the decomposition system of a H_2SO_4–$Li_2SO_4.H_2O$–$SnSO_4$ (15 ml, 30 g, 0.2 g) mixture in the Kjeldahl flask at 60 or 90 min. However, a quantitative recovery is obtained by adding a little water. The phenylhydrazine hydrochloride (~15 mg) can be decomposed by heating with a gentle flame for about 30 min with the H_2SO_4–H_2O–$Li_2SO_4.H_2O$–$SnSO_4$ (15 ml, 5 ml, 30 g, 0.2 g) mixture, followed by heating with a stronger flame for about 10 min to boil off the

Table 8. Determination of nitrogen in coal*

Decomposition systems		Sample (Nitrogen content %)	Sample taken, *mg*	Nitrogen found,		Decomposition time, *min*
ALS flux	Additional reagents			*mg*	%	
From H_2SO_4–$Li_2SO_4.H_2O$ (15/30, v/w)	no addition	Coal powder (1.56 ± 0.07)	134.0	1.81	1.35†	30
From H_2SO_4–$Li_2SO_4.H_2O$ –Ce $(SO_4)_2$ $4H_2O$ (15/30/5, v/w/w)	H_2SO_4 (10 ml)	Coal powder (1.56 ± 0.07)	109.4	1.49	1.36†	30
From H_2SO_4–$Li_2SO_4.H_2O$ (15/30, v/w)	elemental selenium powder (1.0 g) and H_2SO_4 (15 ml)	Coal powder (1.56 ± 0.07)	120.3	1.90	1.58	9
				1.91	1.58	
			110.6	1.72	1.56	8
				1.67	1.51	
				1.74	1.57	
			217.3	3.15	1.45	10
				3.22	1.48	
			104.2	1.74	1.67	8
				1.67	1.60	
From H_2SO_4–$Li_2SO_4.H_2O$ (15/30, v/w)	elemental selenium powder (1.0 g) and H_2SO_4 (20 ml)	Coal powder (1.56 ± 0.07)	103.5	1.13	1.09†	8
			105.2	1.26	1.20†	8
From H_2SO_4–$LI_2SO_4.H_2O$ (11/30, v/w)	elemental selenium powder (1.0 g) and H_2SO_4 (19 ml)	Coal powder (1.56 ± 0.07)	114.2	1.74	1.52	8
				1.73	1.51	
From H_2SO_4–$Li_2SO_4.H_2O$– $CuSO_4.5H_2O$ (20/30/2.5, v/w/w)	H_2SO_4 (5 ml)	Coal powder (1.56 ± 0.07)	112.8	1.77	1.57	20
				1.70	1.51	
From H_2SO_4–$Li_2SO_4.H_2O$– $CuSO_4.5H_2O$ (20/30/2.5, v/w/w)	H_2SO_4 (10 ml)	Coal powder (1.56 ± 0.07)	117.2	1.62	1.38†	20
				1.59	1.36†	
				(average 1.55, S.D. 0.06)		

Volume in ml, weight in g, S.D. standard deviation.
*NIST standard Reference Material 1632b (bituminous) of U.S.A
†Did not account for the values of average and standard deviation.
H_2SO_4: concentrated sulphuric acid.

water, and then continuing for about 20 min. Consequently, the H_2SO_4–H_2O–$Li_2SO_4.H_2O$–$SnSO_4$ mixture for the decomposition of phenylhydrazine hydrochloride is considered best for recovery of nitrogen (Table 6).

Decomposition of residual fuel oil and coal

Table 7 gives the results obtained for analysis of a standard sample of nitrogen in residual fuel oil of the Japan Petroleum Institute. The residual fuel oil (~ 0.1 g) can be rapidly decomposed by addition of about 1.0 g of elemental selenium powder and 19 ml of concentrated sulphuric acid to the ALS flux from the H_2SO_4–$Li_2SO_4.H_2O$ (11 ml, 30 g) system. The certified value of nitrogen in the standard sample of residual fuel oil is $0.589 \pm 0.08\%$ and the determination value of nitrogen under the recommended conditions is 0.59% (S.D. 0.01). Therefore, the decomposition of samples and the recovery of nitrogen in the residual fuel oil under the recommended procedure is complete. Table 8 gives the results obtained for analysis of NIST standard reference material of coal under the various decomposed conditions. Decomposition with the molten state of the ALS flux from the H_2SO_4–$Li_2SO_4.H_2O$ (15 ml, 30 g) mixture without catalyst gave low recovery of nitrogen in coal. Similarly, the decomposition with the H_2SO_4–Li_2SO_4–$Ce(SO_4)_2$ system gives lower than the certified value of nitrogen in coal. Hence, a suitable catalyst, such as elemental selenium powder or cupric sulphate, is required for complete recovery of nitrogen in coal by the ALS flux decomposition system. Heating with the ALS flux from H_2SO_4–$Li_2SO_4.H_2O$ (15 ml, 30 g), elemental selenium (1 g) and concentrated sulphuric acid (15 ml) decomposes 0.1 g of coal powder in about 8 min and the recovery of nitrogen in coal is complete. However, more addition of concentrated sulphuric acid (such as 20 ml) to the ALS flux gave low results. Heating with the ALS flux from H_2SO_4–$Li_2SO_4.H_2O$–$CuSO_4.5H_2O$ (20 ml, 30 g, 2.5 g) and concentrated sulphuric acid (5 ml) decomposes 0.1 g of coal powder in about 20 min and the determined value of nitrogen in coal is exactly equal to the certified value, but more addition of concentrated sulphuric acid, such as 10 ml, to the ALS flux gave a lower value than the certified value. It is suggested that the ratio of H_2SO_4/Li_2SO_4 (ml/g) in the melting state of the ALS flux is very important for complete decomposition of coal samples and quantitative recovery of nitrogen.

This decomposition system comprises many variations from mixing the ALS flux with various ratios of $H_2SO_4/Li_2SO_4.H_2O$ and catalysts, oxidizing agents[8] or reducing agents. Therefore, this is a potentially widely useful and rapid decomposition method for various organic, biological and environmental materials.

REFERENCES

1. W. J. Kirsten and K. H. Jansson, *Anal. Chem.*, 1986, **58**, 2109.
2. S. Moldoveanu, *J. Chromatog. Sci.*, 1988, **26**, 12.
3. L. J. Lennox and M. J. Flanagan, *Water Res.*, 1982, **16**, 1127; *Anal Abstr.*, 1983, 5H41.
4. M. Minagawa, D. A. Winter and I. R. Kaplan, *Anal. Chem.*, 1984, **56**, 1859.
5. H. Hamaguchi, *Bunseki Kagaku Binran*, Maruzen, 1981.
6. P. Kozak, M. Jurecek and J. Sramakova, *Mikrochim. Acta*, 1976 **II**, 423.
7. N. Yoshikuni, *Talanta*, 1989, **36**, 709.
8. *Idem*, *ibid.*, 1991, **38**, 515.
9. G. Adelantado, J. V. Bosch and F. Reig, *Quim. Anal.* 1988, **7**, 289; *Anal. Abstr.*, 1989, 5C7.
10. B. T. Croll, T. Tomlinson and C. R. W. Whitfield, *Analyst*, 1985, **110**, 861.
11. J. Alvarado, M. Marquez and L. E. Leon, *Anal. Lett.*, 1988, **21**, 357.
12. E. Florence, W. M. Harris and D. F. Milner, *Analyst*, 1985, **110**, 971.
13. M. N. Jones and H. D. Bradshaw, *Commun. Soil Sci. Plant Anal.*, 1989, **20**, 1513; *Anal. Abstr.*, 1990, 9D25.
14. I. Pichl, M. Burianova and K. Rezek, *Chem. Listy*, 1988, **83**, 311; *Anal. Abtr.*, 1988, 9G20.
15. E. Florence and W. M. Harris, *Analyst*, 1987, **112**, 317.
16. C. F. H. Liao, *J. Assoc. Off. Anal. Chem.*, 1982, **65**, 786.

Talanta, Vol. 39, No. 1, pp. 17–19, 1992
Printed in Great Britain

0039-9140/92 $5.00 + 0.00
Pergamon Press plc

APPLICATION OF ELECTRON PROBE MICRO-ANALYSIS TO THE ESTIMATION OF CHLORINE IN ALUMINA-BASED HETEROGENEOUS CATALYSTS

V. J. KOSHY,* K. V. RAO, G. KALPANA and V. N. GARG

Research Centre, Indian Petrochemicals Corporation Limited, PO: Petrochemicals, 391 346, Vadodara, Gujarat, India

(*Received* 24 *July* 1990. *Revised* 2 *July* 1991. *Accepted* 3 *July* 1991)

Summary—Chlorine in alumina-based catalysts has been determined with a scanning electron microscope attached to an energy dispersive x-ray analyser (SEM–EDX). The method is less time consuming compared to conventional methods involving sample dissolution followed by titrimetry, absorption spectrophotometry or ion chromatography. The spectrometer is calibrated with laboratory prepared standards. This technique is found suitable for the estimation of chlorine in the range 0.1–1.0% (w/w) with a relative standard deviation < 10% for chlorine levels above 0.2%.

Noble metal catalysts, mainly platinum supported catalysts, are employed in several petrochemical processes like dehydrogenation, reforming and isomerization. It is well known that the chlorine ion which gets incorporated during impregnation of platinum into the alumina support has profound influence on the physicochemical properties of the catalyst.[1] Chlorine balance in the catalyst is critically important for optimum activity, selectivity and stability of the catalyst during reforming operations.[2–4] It is therefore important to monitor the level of chlorine in the catalysts during their preparation as well as usage in commercial plants.

Argentometric titration,[1] x-ray fluorescence spectrometry,[5] absorption spectrometry[6] and ion-chromatography[7] are the techniques reported for the estimation of chlorine in catalysts. In the present study, the possibility of using the Scanning Electron Microscope in conjunction with an Energy Dispersive X-ray Analyser (SEM–EDX) is investigated. This technique has been widely used for qualitative identification of elements, but rarely for their quantitative estimation in catalysts. The accurate quantification of elements by x-ray emission methods is based on availability of reference materials whose matrix and composition match fairly well with those of the samples to be analysed.[8] Since these standards were not available, they were prepared in our laboratory and their chlorine content was ascertained by spectrophotometry.

EXPERIMENTAL

A Scanning Electron Microscope (JEOL, JSM-35C) in conjunction with an energy dispersive x-ray analyser (Kevex, model 7000-77) was employed for this study. EDX spectra were recorded on a Hewlett–Packard 7015 B X-Y recorder. Absorbance measurements were recorded on a Varian Superscan-3 spectrophotometer with matched 1-cm silica cells.

All reagents used were of GR grade. γ-Alumina pellets (3.2 mm) from Alfa Products were used as the support material for preparation of standards. Doubly distilled water was used in all the experiments.

Preparation of standard samples

Sodium chloride was dried at 100° for 4 hr. About 1.65 g was weighed accurately into a 100-ml standard flask and made up with water to prepare a stock solution containing 10 mg/ml chloride. A 5.0-g portion of finely powdered and dried (<210 mesh, 200° for 12 hr) γ-alumina was taken in six separate 100-ml round bottom flasks. To each of them was added 0, 1, 2, 3, 4 and 5 ml, respectively, of sodium chloride solution. The total volume of solution in each flask was adjusted to 15 ml with water and the contents were kept at 40° for 4 hr with constant stirring. Subsequently, the samples were dried

IPLC Communication No.: 173.
*Author for correspondence.

with a Buchi Rotavapor and the final drying was carried out in an air oven at 100° for 4 hr. These samples were cooled and transferred into airtight containers and preserved in a desiccator. The chlorine contents of laboratory-prepared standards were estimated by the spectrophotometric method,[6] using Fe(III)–$Hg(SCN)_2$ reagent.

Preparation of samples for SEM–EDX measurements

All standards and catalyst samples were ground to pass through a 210-mesh sieve. Pellets of 13-mm diameter and 2-mm thickness were prepared with a hydraulic press at a pressure of 10 tons/cm^2 and a retention time of 2 min. The flat surfaces of the spacers that came into contact with the pellet were mirror-polished so that the specimen (pellet) had a very smooth surface. The pellet was cut into four quadrants and one quadrant was mounted on a carbon stub with silver conducting paste with the smooth surface facing upwards. Since all the specimens were non-conducting, a carbon layer of 400 Å thickness was coated by using a JEOL JEE-4X vacuum evaporator in order to avoid charge build-up and specimen heating during the analysis.

Spectra acquisition

The sample, after mounting and carbon coating, was kept in the specimen chamber of the scanning electron microscope. The electron flux was kept constant by maintaining the x-ray count rate of 4000 cps on a clean aluminium stub. The count rate did not change throughout the spectral acquisition, indicating that there was no loss of surface chlorine due to electron beam impingement. The other conditions used in operating the x-ray analyser are given in Table 1.

RESULTS AND DISCUSSION

The spectra obtained from the various samples have been analysed by different computer programs like ASAP, ZAF and LSQ supplied by Quantex software. The LSQ program was found to be the most suitable in the present case. It uses a background filtering routine and determines the area of peak in terms of counts per second in the range of interest, *i.e.*, 2.62 keV for chlorine K_α emission. Figure 1 shows the x-ray emission spectrum of alumina samples in the presence and absence of chlorine.

Table 1. Operating conditions for the acquisition of EDX spectrum of chlorine on γ-Alumina

Operating voltage	18 KV
Specimen surface area	2 mm^2
Specimen tilt	zero degree
Magnification	100 ×
Spectrometer range	10 eV/channel
Acquisition time	200 sec
Dead time	20%

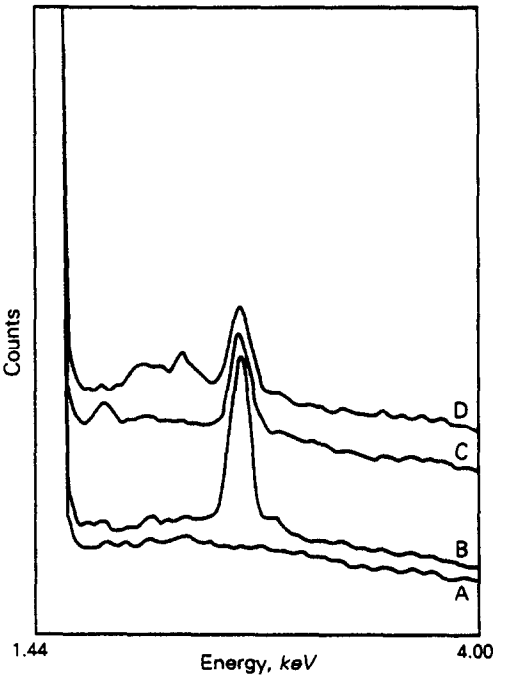

Fig. 1. EDX spectra of (A) support (γ-Al_2O_3), (B) standard (0.95% Cl/γ-Al_2O_3) (C) catalyst (Cl/Pt/γ-Al_2O_3—3 in Table 2) and (D) catalyst (Cl/Pt–Re/γ-Al_2O_3—5 in Table 2).

Evaluation of standards

The uniformity as well as stability of the laboratory-prepared standards have been tested by recording their EDX spectra and analysing them by the LSQ method. Four standard samples having chlorine contents of 0.14, 0.36, 0.61 and 0.95% (w/w) were chosen and six spectra were acquired from different portions of each sample. This exercise was carried out on the basis of the assumption that non-uniformity of chlorine distribution in the sample would result in a difference in the analyte signals obtained from different portions of the same sample specimen. The variation in the results was less than 3%, suggesting that the samples were uniform. The chlorine peak intensity measurement of each standard sample was performed over a period of three months and the variation observed from time to time was 5–8%

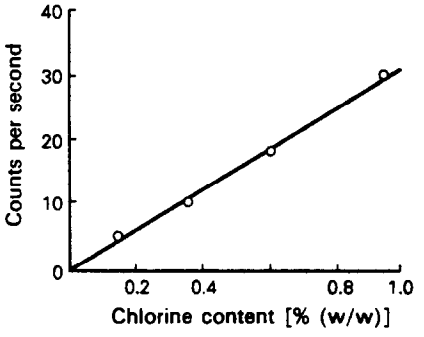

Fig. 2. Relationship between counts per second and chlorine content with LSQ program.

Table 2. Chlorine content of various laboratory-prepared Alumina supported Pt–Re catalysts with different composition

Sample No.	Chlorine content (% w/w) by SEM–EDX	Spectrophotometry
1	0.13 ± 0.04	0.11 ± 0.01
2	0.15 ± 0.03	0.13 ± 0.01
3	0.60 ± 0.02	0.65 ± 0.02
4	0.78 ± 0.02	0.77 ± 0.02
5	0.69 ± 0.03	0.66 ± 0.01
6	0.77 ± 0.03	0.74 ± 0.01

when each of the standards was analysed with the stored calibration graph. Hence it is considered essential to acquire fresh standard spectra and construct a calibration graph each day, before sample analysis. The calibration graph obtained on a particular day is presented in Fig. 2.

Analysis of alumina-based catalyst samples

The EDX spectrum A in Fig. 1 shows the absence of any x-ray emission in the region of 2.62 keV energy. The chlorine peak is clearly shown in spectrum B corresponding to the calibration standard. Spectra C and D show the well-defined chlorine peak sufficiently separated from all concomitant emission lines, enabling accurate computation. Catalyst samples, designated 1 through 6, were analysed by the LSQ routine and the results are presented in Table 2. The standard deviations in the order of 0.04% in chlorine content show good reproducibility of the method. The mean values of chlorine obtained by SEM–EDX agree well with the spectrophotometric results.

The method has been applied successfully in the case of platinum on alumina as well as platinum–rhenium on alumina catalysts. However, under the experimental conditions employed, *i.e.*, channel width of 10 eV, Ru ($L_\alpha = 2.56$ keV) and Rh ($L_\alpha = 2.70$ keV) can cause interferences.

CONCLUSION

A simple, rapid and direct method has been developed for the estimation of chlorine in catalysts with Quantex software LSQ method. Laboratory prepared standards are suitable for calibration purposes. It is essential that spectra of calibration standards be acquired prior to the analysis of catalyst samples. Noble metals like Ru and Rh can cause interference by virtue of their L_α emission. The spatial resolutions of this technique make it useful for profiling studies, an objective in our laboratory.

Acknowledgements—The authors wish to thank Dr I. S. Bhardwaj, Director (R&D), IPCL for encouragement and permission granted to publish this paper. They also thank Dr K. R. Krishnamurthy for the supply of catalyst samples. The skilled assistance of Mr A. R. Shah, Mr H. N. Vaidya and Ms R. H. Patel is gratefully acknowledged.

REFERENCES

1. A. A. Castro, O. A. Scelza, E. R. Benvenuto, G. T. Baronetti, S. R. De Miguel and J. M. Parera, in *Preparation of Catalysts III*, G. Poncelet, P. Grouge and P. A. Jacobs (eds), p. 47. Elsevier, Amsterdam, 1983.
2. R. J. Verderoane, C. L. Pieck, M. R. Sad and J. M. Parera, *Appl. Catal.*, 1986, **21**, 239.
3. M. N. Edgar, in *Applied Industrial Catalysts*, B. E. Leach (ed.), Vol. 1, pp. 141, 147. Academic Press, New York, 1983.
4. M. Sittig, *Handbook of Catalyst Manufacture*, p. 230. Noyes Data Corporation, New Jersey, 1978.
5. J. P. Bouronville and G. Martino, in *Catalyst Deactivation*, B. Delmon and G. F. Froment (eds), p. 159. Elsevier, Amsterdam, 1980.
6. V. J. Koshy and V. N. Garg, *Talanta*, 1987, **34**, 905.
7. R. P. Singh, K. Alam, D. S. Redwan and N. M. Abbas, *Anal. Chem.*, 1989, **61**, 1924.
8. J. Goldstein, D. Newbury, P. Echlin, D. Joy, E. Fiori and E. Lifshin, *Scanning Electron Microscopy and X-ray Microanalysis*, Plenum Press, New York, 1981.

Talanta, Vol. 39, No. 1, pp. 21–27, 1992
Printed in Great Britain.

0039-9140/92 $5.00 + 0.00

SIMULTANEOUS DETERMINATION OF ALUMINIUM AND BERYLLIUM BY FIRST-DERIVATIVE SYNCHRONOUS SOLID-PHASE SPECTROFLUORIMETRY

FERMÍN CAPITÁN, ELOISA MANZANO, ALBERTO NAVALÓN, JOSÉ LUIS VILCHEZ and LUIS FERMÍN CAPITÁN-VALLVEY*

Department of Analytical Chemistry, University of Granada, E-18071 Granada, Spain

(*Received* 15 *November* 1990. *Revised* 3 *June* 1991. *Accepted* 11 *June* 1991)

Summary—A method for the simultaneous determination of aluminium and beryllium in mixtures by first-derivative synchronous solid-phase spectrofluorimetry has been developed. Aluminium and beryllium reacted with morin to give fluorescent complexes, which were fixed on a dextran-type resin. The fluorescence of the resin, packed in a 1-mm silica cell, was measured directly with a solid-surface attachment. The constant wavelength difference chosen to optimize the determination was $\Delta\lambda = \lambda_{em} - \lambda_{ex} = 75$ nm. Aluminium was measured at $\lambda_{ex}/\lambda_{em} = 445/520$ nm and beryllium at $\lambda_{ex}/\lambda_{em} = 430/505$ nm. The range of application is between 0.5 and 5.0 ng/ml for both aluminium and beryllium. The accuracy and precision of the method are reported. The method has been successfully applied to the determination of aluminium and beryllium in synthetic mixtures and natural waters.

Several organic ligands have been proposed for the separate determination of aluminium(III) and beryllium(II) that take advantage of the fact that these two ions, and other cations with empty *d* and *f* orbitals, give sensitive fluorogenic reactions with a wide range of organic reagents,[1,2] particularly in coordination processes. One of these reagents, morin, is especially suitable for the determination of beryllium given its high sensitivity.

Spectrofluorimetry is often used, even in routine laboratory work, to determine both aluminium and beryllium alone. However, differentiating them in mixtures is more difficult because of their broad and featureless emission spectra, and because their spectra strongly overlap. This fact is usually found in fluorescent complexes of inorganic ions with organic reagents that generally show spectral characteristics of the reagent alone, slightly modified by the inorganic ion.

Synchronous spectrofluorimetry in combination with derivative techniques has been shown to be useful (even in routine analysis by giving advantages of speed and simplicity) in the analysis of mixtures of fluorescent compounds in solution when their spectra show strong overlapping.

In relation to the analysis of mixtures of inorganic compounds by derivative synchronous spectrofluorimetry, the following have been described: binary and/or ternary mixtures of titanium, zirconium and hafnium, through the formation of fluorescent complexes with diacetyl monoxime nicotinylhydrazone,[3] gallium in the presence of aluminium with di-2-pyridinylmethylen-2-furoylhydrazone,[4] gallium and zinc mixtures with salicylaldehyde thiocarbohydrazone,[4,5] aluminium and zinc with 8-hydroxyquinoline-5-sulphonic acid, in the presence of hexadecyltrimethylammonium bromide,[6] beryllium and aluminium with morin[7] and molybdenum and tungsten with carminic acid.[8]

The solid-phase spectrofluorimetry technique combines the measurement of solid-surface fluorescence with the use of a solid support, (*e.g.*, a dextran-type resin), to preconcentrate the analyte, rendered fluorescent by the use of an appropriate reagent. This approach is useful for the analysis of very dilute solutions, such as in water analysis.[9–13]

In this paper we combine the solid-phase spectrofluorimetry methodology with first-derivative synchronous spectrofluorimetry. Hence, the aluminium and beryllium mixtures are resolved by complexation of both ions with morin and later adsorption on a dextran-type resin, using the above technique.

*Author for correspondence.

EXPERIMENTAL

Apparatus

All the spectrofluorimetric measurements were conducted with a Perkin–Elmer LS 5 luminescence spectrometer, equipped with a Xenon discharge lamp (9.9 W) pulsed at line frequency, Monk-Gillieson F/3 monochromators, a Quantic Rhodamine 101 counter to correct the excitation spectra, a Hamamatsu R928 photomultiplier, and a variable-angle solid–surface accessory designed and constructed by the authors.[14–16] In order to compare all spectrofluorimetric measurements and to ensure reproducible experimental conditions, the LS 5 spectrometer was checked daily. A fluorescent polymer standard of *p*-terphenyl ($10^{-7}M$) gave a relative fluorescence intensity of 90% at $\lambda_{em} = 340$ nm, $\lambda_{ex} = 295$ nm, slit widths of 2.5 and 2.5 nm and a sensitivity factor of 0.594. For synchronous excitation measurements, both excitation and emission monochromators were locked together and scanned simultaneously.

The LS 5 spectrometer was interfaced to an IBM PC XT-286 microcomputer, using RS 232C connections for spectral acquisition and subsequent calculation of the excitation–emission matrices and of the derivative spectra.[16,17] Smoothed and derivative spectra were calculated by the Savitzky and Golay method[18,19] and contour plots in the excitation–emission plane were produced, linking points of equal fluorescence intensity. An Olivetti DM 100 printer was used for graphical representation.

Further, we used a Braun Melgunsen Thermomix 1441 thermostatic water-bath circulator for temperature control, a Crison 501 digital pH-meter with a combined glass-calomel saturated electrode and an Agitaser 2000 rotating agitator.

Reagents

All reagents were of analytical-reagent grade unless stated otherwise.

Sephadex G-15 resin (Pharmacia Fine Chemicals). Used without pre-treatment to prevent contamination.

Morin (2′,3,4′,5,7-pentahydroxyflavone) (Merk) solution, 0.02% w/v in absolute ethanol. More dilute solutions were prepared by appropriate dilution with absolute ethanol. Morin was purified following the procedure described by Laitinen and Kivalo.[20] The dilute morin solutions were prepared fresh every other day and the concentrated solutions were prepared weekly.

Aluminium(III) stock solution, 0.1 mg/ml. Prepared from aluminium nitrate [$Al(NO_3)_3 \cdot 9H_2O$] (Merck) and gravimetrically standardized with oxine.[21] Solutions of lower concentration were obtained by dilution with doubly-distilled water.

Beryllium(II) stock solution, 0.1 mg/ml. Prepared from beryllium sulphate ($BeSO_4 \cdot 4H_2O$) (Merck) and standardized by the phosphate method.[22] Working solutions were prepared by appropriate dilutions with doubly distilled water.

Buffer solutions. Solutions of the required pH were prepared from $0.1M$ acetic acid and $0.1M$ sodium acetate.

Fluorescence measurements

The measured relative fluorescence intensity (RFI) of the resin beads, containing the fluorescent products and packed in a 1-mm silica cell, was the diffuse transmitted fluorescence (DTF) emitted from the resin at the unirradiated face of the cell. The optimal angle between the cell plane and the excitation beam was 45° in all instances.

Procedures

Basic procedure. A 500-ml water sample containing between 0.25 and 2.5 μg of aluminium and between 0.25 and 2.5 μg of beryllium, was transferred into a 1-litre polyethylene bottle and 7 ml of 6.2×10^{-3}% morin solution, 10 ml of pH 5.75 acetic acid/acetate buffer solution and 100 mg of Sephadex G-15 resin were added. The mixture was shaken mechanically for 15 min. Afterwards, the resin beads were collected by filtration under suction and with the aid of a pipette, packed in a 1-mm cell together with a small volume of the filtrate. A blank solution containing all the reagents except both aluminium and beryllium was prepared and treated in the same way as described for the sample. We recorded the synchronous spectra (at $20.0 \pm 0.5°$) with the following fixed instrumental parameters: $\Delta\lambda = \lambda_{em} - \lambda_{ex} = 75$ nm; with a scan speed of 120 nm/min, and a spectrometer response time of 1 sec. The spectra were then stored on a disk file, corrected for the blank signal, and the first-derivative spectra with an interval of 15 nm were calculated.

First-derivative analytical signals were measured as the vertical distance from the first-derivative synchronous spectrum at

$\lambda_{ex}/\lambda_{em} = 445/520$ nm to the base line for aluminium and from $\lambda_{ex}/\lambda_{em} = 430/505$ nm to the base line for beryllium, respectively.

Calibration graphs were constructed in the same way with aluminium(III) and beryllium(II) solutions of known concentrations.

Procedure for natural waters. The above-mentioned reagents were added to a volume of natural water sample containing an adequate amount of Al(III) and Be(II) levelled off at 500 ml with doubly-distilled water and placed in a one-litre polyethylene bottle, as described above. The standard addition method was used for calibration.

Reference method. Determination of both aluminium and beryllium by AAS with a dinitrogen oxide–acetylene flame after extraction with oxine–MIBK was used as a reference method.[23]

Treatment of the sample. Natural waters (preserved by addition of 0.25 ml of concentrated nitric acid per litre) were filtered through a 0.45-μm membrane filter paper (Millipore) into a polyethylene container carefully cleaned with nitric acid.[23]

RESULTS AND DISCUSSION

Effect of experimental variables

Morin forms fluorescent complexes with aluminium(III) and beryllium(II) that are retained on ion-exchanger resins. The 1:1 aluminium complex is fixed in cationic Sephadex (SP C-25) with optimum pH being 5.3,[10] whereas the 1:1 beryllium complex is retained on anionic Sephadex (QAE A-25) at pH 11.5.[9] Given the different charges of these complexes, the simultaneous fixation of both complexes on ion-exchangers is not possible. We have selected a dextran-type resin without fixed ionic groups (Sephadex G-15) in order to adsorb both complexes.

Sorbed on Sephadex G-15 resin, morin has an excitation maximum at 443 nm and an emission maximum at 497 nm. The aluminium complex shows an excitation maximum at 430 nm and exhibits maximum fluorescence at 506 nm. The beryllium complex has its excitation maximum at 441 nm and exhibits maximum fluorescence at 519 nm. At these wavelengths the reagent fluorescence is low.

The fixation mechanism of both complexes on Sephadex G-15 resin is different due to its non ionic-exchanger nature. It might take place through the ligand molecules because of possible hydrogen-bond formation, as demonstrated by the fixation of morin alone on this resin.

The fluorescence emission of the aluminium complex fixed on Sephadex G-15 resin is maximum at around pH 5, and that of the beryllium complex at about pH 12. The shape of pH influence on RFI differs from what is observed in solution: optimum pH for the Al complex is 3.5, and 12.0 for the Be complex. In the latter complex a slight maximum at pH 5.5 is observed. In order to simultaneously obtain a fluorescence signal for both complexes, a pH of 5.75 was selected (pH value of equal fluorescence intensity for both complexes). Acetic acid/acetate was used as buffer solution, see Fig. 1.

The fluorescence of both complexes decreases with an increase in buffer concentration. A $0.002M$ concentration of pH 5.75 buffer was selected to obtain an adequate buffering capacity without excessive loss of sensitivity.

A $2.4 \times 10^{-6}M$ (8.1×10^{-5}%) reagent concentration was chosen as optimum in order to have an appropriate reagent excess ([morin]/[metal] molar ratio of around 22 for Al and 7 for Be). Lower molar ratios reduce the fluorescence intensity of both complexes while higher molar ratios increase the blank signal.

The RFI decreases when the temperature of measurement increases [-0.4%/°C between 5 and 70° for the Al(III) complex and -0.6%/°C

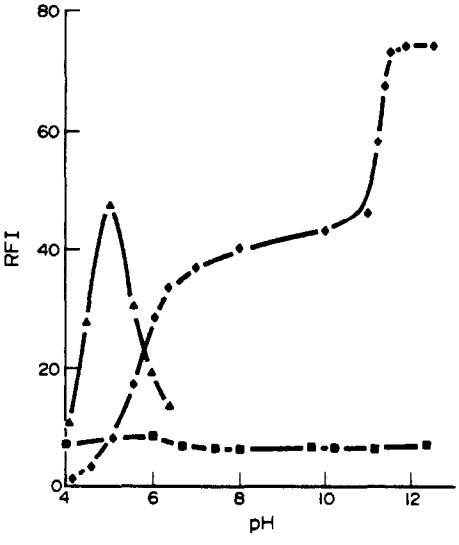

Fig. 1. Influence of pH on RFI in resin phase. (▲) Aluminium–morin complex. (◆) Beryllium–morin complex. (■) Morin alone. [morin] = $7.3 \times 10^{-7}M$, [Al(III)] = 3 μg/l., [Be(II)] = 2.5 μg/l., 500 ml of sample, 100 mg of Sephadex G-15.

for the Be(II) complex], but this effect is completely reversible for both complexes. All RFI measurements reported here were taken at $20.0 \pm 0.5°$.

The stirring time necessary for maximum RFI development was 15 min for both complexes. For stirring times longer than 25 min, RFI decreases slightly (19% at 35 min) for the Be complex. The Al complex remains unaltered with an increase in stirring time. Fluorescence for both complexes is developed immediately, remaining constant for at least 2 hr before equilibration. Variation in the order of addition of reactants was shown to have no effect on the emission intensity.

Selection of the optimum $\Delta\lambda$ for synchronous scanning

The extent of the overlap of these complexes has been examined by obtaining total fluorimetric information available in the excitation–emission matrix. Suitable plots of excitation *vs.* emission wavelengths have been drawn from the three-dimensional spectra. This allows us to select the most suitable trajectory in the excitation–emission matrix to obtain synchronous fluorescence spectra for the complete resolution of overlapping component peaks. The optimum scan path for determining aluminium and beryllium in mixtures seems to be a $\Delta\lambda$ of 75 nm, because it passes near the maximum of both complexes, allowing the determination without a considerable loss of sensitivity.

Figure 2 shows synchronous spectra of aluminium and beryllium complexes with morin fixed on Sephadex G-15 and of a mixture of both complexes, corrected for the blank signal, and maintaining a constant interval between the emission and excitation wavelengths of 75 nm.

Because of the large overlap of the spectra, the determination of aluminium and beryllium by synchronous spectro-fluorimetry is subject to considerable difficulties. This overlap has been resolved by taking the first-derivative of the spectrum. Figure 3 shows the first-derivative synchronous fluorescent spectra of aluminium and beryllium complexes with morin fixed in Sephadex G-15 and of a mixture of both complexes.

Assuming that the derivative of a spectral band is equivalent to the sum of the derivatives of its individual bands, we have chosen suitable wavelengths to take measurements proportional

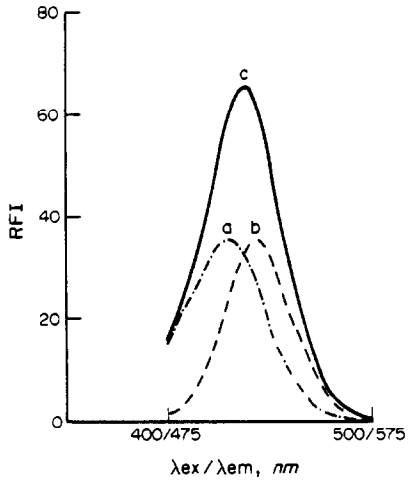

Fig. 2. Synchronous fluorescence spectrum of (*a*) aluminium–morin complex, (*b*) beryllium–morin complex and (*c*) a mixture of both complexes. ($\Delta\lambda = 75$ nm).

to the concentration of aluminium and beryllium for the preparation of the calibration graphs.

When the first-derivative spectrum of one of the two components is zero, the total derivatives spectrum is only a function of the concentration of the other component and *vice versa*. In fact, the height $h_2(\lambda_{ex}/\lambda_{em} = 445/520$ nm) is proportional to the aluminium concentration, whereas h_1 ($\lambda_{ex}/\lambda_{em} = 430/505$ nm) is proportional to the beryllium concentration (Fig. 3).

Instrumental parameters

For recording the first-derivative spectra, a scan speed of 120 nm/min and a response time of the spectrometer of 1 sec were chosen. It was

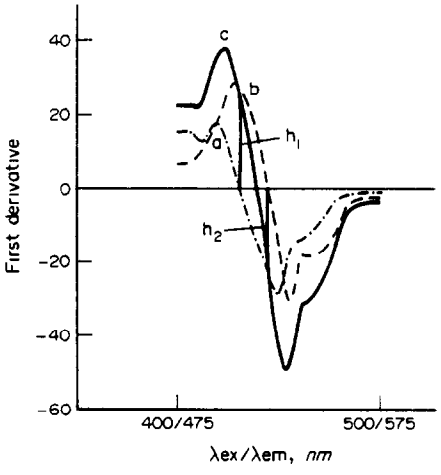

Fig. 3. First-derivative synchronous spectrum of (*a*) aluminium–morin complex, (*b*) beryllium–morin complex and (*c*) a mixture of both complexes. ($\Delta\lambda = 75$ nm).

Table 1. Statistical analysis of the determination of aluminium (0.5–5.0 μg/l.) and beryllium (0.5–5.0 μg/l.) in mixtures by first-derivative synchronous solid-phase spectrofluorimetry

Element determined	Other element present	μg/l.	Slope	Intercept	Correlation coefficient
Al(III)	Be(II)	—	6.33	1.57	0.997
		2.0	6.13	1.67	0.996
		4.0	6.09	1.74	0.997
Be(II)	Al(III)	—	7.88	1.65	0.997
		2.0	7.69	1.82	0.998
		4.0	7.58	2.04	0.996

found that these values did not appreciably affect the derivative signal obtained, because the differentiation was accomplished numerically and not electronically. An interval of 15 nm was selected for the calculation by the Savitzky and Golay[18,19] method, as this gives the best signal-to-noise ratio.

Analytical parameters

In order to test the mutual independence of the analytical signals for aluminium and beryllium, *i.e.*, to show that h_1 and h_2 are independent of aluminium and beryllium concentrations, respectively, three calibration graphs were obtained from height (h) measurements for standards containing between 0.5 and 5.0 μg/l. aluminium, in the absence of beryllium and in the presence of 2.0 and 4.0 μg/l. beryllium, respectively.

Following the same procedure, three calibration graphs were prepared for standards containing between 0.5 and 5.0 μg/l. beryllium, in the absence of aluminium and in the presence of 2.0 and 4.0 μg/l. aluminium, respectively.

The analytical parameters for all the calibration graphs are summarized in Table 1.

The IUPAC detection limits ($K = 3$)[24] are 0.1 μg/l. for Al(III) and 0.06 μg/l. for Be(II). The quantification limits ($K = 10$)[25] are 0.4 μg/l. for Al(III) and 0.2 μg/l. for Be(II). The relative standard deviations (RSD %) ($P = 0.05$, $n = 10$) are 4.6% for 2.0 μg/l. Al(III) and 3.6% for 2.0 μg/l. Be(II).

Effect of foreign ions

A systematic study was made of the effect of the ions commonly found in natural waters on the determination of 3.0 μg/l. Al(III) and 3.0 μg/l. Be(II). An 8000-μg/l. level of each potentially interfering ion was tested first. If interference occurred, the ratio was reduced progressively until interference ceased. The tolerance level was defined as the amount of foreign ion producing an error not exceeding ±5% in the determination of the analyte. The results are summarized in Table 2.

It is important to note that the interference level can be reduced by sample dilution. Taking into account the concentration range for the method proposed here and the average level for aluminium to be higher than that for beryllium in water, a minimum of five-fold dilution is required.

Applications

Determination of aluminium and beryllium mixtures in synthetic samples. The proposed method has been applied to the analysis of several synthetic mixtures of aluminium and beryllium in different ratios. Table 3 summarizes the results calculated from the calibration graphs.

Table 2. Effect of foreign ions on the simultaneous determination of 3.0 μg/l. aluminium and 3.0 μg/l. beryllium

Foreign ion or species	Tolerance level (μg/l.) Aluminium	Beryllium
NO_3^-, SiO_3^{2-}, CO_3^{2-}	>8000	>8000
Cl^-	1200	>8000
SO_4^{2-}	600	4000
PO_4^{3-}	60	800
F^-	15	400
Ca(II)	900	500
Cu(II)	45	150
Mg(II)	50	30
Fe(III)	60	20

Table 3. Determination of aluminium and beryllium in binary mixtures

Ratio	Al(III), μg/l.			Be(II), μg/l.		
Al/Be	Taken	Found	Error, %	Taken	Found	Error, %
4:1	4.0	4.1	+2.5	1.0	1.0	0.0
2:1	2.0	2.1	+5.0	1.0	1.1	+10.0
2:1	4.0	4.2	+5.0	2.0	2.1	+5.0
1:1	1.0	1.1	+10.0	1.0	1.1	+10.0
1:1	2.0	2.1	+5.0	2.0	2.1	+5.0
1:1	4.0	4.1	+2.5	4.0	3.9	−2.5
1:2	1.0	1.1	+10.0	2.0	2.0	0.0
1:2	2.0	2.1	+5.0	4.0	4.1	+2.5
1:4	1.0	0.9	−10.0	4.0	4.1	+2.5

Table 4. Recovery study of aluminium and beryllium in natural waters

Sample	Al(III), μg/l. Taken	Found*	Recovery, %	Be(II), μg/l. Taken	Found*	Recovery, %
Mineral water†	—	2.9	—	—	<0.2	—
	1.0	3.8	97.4	1.0	1.0	100.0
	1.5	4.5	102.3	2.0	1.9	95.0
	2.0	4.8	98.0	3.0	3.1	103.3
Raw water‡	—	2.2	—	—	<0.2	—
	1.0	3.2	100.0	1.0	0.9	90.0
	1.5	3.6	97.3	2.0	2.1	105.0
	2.0	4.3	102.4	3.0	2.9	96.7

*Data are the average value of three determinations.

†From Ortigosa del Monte. The content of aluminium found was 14.5 μg/l. (by AAS 15.0 μg/l.) The content of beryllium was lower than the quantification limit in this instance.

‡From Genil River. The content of aluminium found was 22.0 μg/l. (by AAS 22.5 μg/l.). The content of beryllium was lower than the quantification limit in this instance.

Determination of aluminium and beryllium in natural waters. The method was applied to the determination of both aluminium and beryllium in water samples by the standard additions method. Raw water from Granada City supply (Genil River) and mineral water from the Ortigosa del Monte (Segovia) spring were selected as representative samples. The volume of water used for the determination was 50 ml for raw water and 100 ml for mineral water.

The loss of sensitivity by a matrix effect can be evaluated by the slope's ratio between the standard calibration graph and the standard-additions calibration graph. The ratios found were 1.01 for aluminium and 0.98 for beryllium in Ortigosa del Monte water and 0.85 for aluminium and 1.34 for beryllium in raw water.

The average aluminium and beryllium contents in the samples studied, based on three determinations, are shown in Table 4.

Recovery studies were carried out to check the accuracy of the proposed method: various amounts of aluminium(III) and beryllium(II) were added and recovery percentages were determined. Table 4 shows the results obtained.

In conclusion, the present paper provides a practical application of derivative synchronous spectrofluorimetry in combination with the solid-phase spectrofluorimetry methodology to multicomponent analysis. The combination of both techniques allows the simultaneous determination of aluminium and beryllium in low level mixtures, without previous pre-concentration nor separation.

Acknowledgement—This research was supported by the Dirección General de Investigación Científica y Técnica (DGICYT) del Ministerio de Educación y Ciencia of Spain (Project No. PS88–0101).

REFERENCES

1. Z. Holzbecher, L. Divis, M. Kral, L. Sucha and F. Vlacil, in *Handbook of Organic Reagents in Inorganic Analysis*, R. A. Chalmers (ed.), Ellis Horwood, Chichester, 1976.
2. A. Fernández Gutierrez and A. Muñoz de la Peña, in *Molecular Luminiscence Spectroscopy: Methods and Applications*, S. G. Schulman (ed.), Part I, Chap 4, Wiley, New York, 1985.
3. S. Rubio, A. Gómez-Hens and M. Valcárcel, *Anal. Chem.*, 1985, **57**, 1101.
4. M. Salgado, M. E. Ureña, A. García de Torres and J. M. Cano Pavón, *J. Mol. Struct.*, 1986, **143**, 477.
5. M. E. Ureña, A. García de Torres and J. M. Cano Pavón, *Anal. Chem.*, 1987, **59**, 1129.
6. A. Muñoz de la Peña, F. Salinas, M. E. Sánchez and J. A. Murillo, *Analyst*, 1988, **113**, 1435.
7. F. García Sánchez, J. C. Márquez Gómez and M. Hernández López, *ibid.*, 1987, **112**, 649.
8. F. Salinas, A. Muñoz de la Peña, L. F. Capitán-Vallvey and A. Navalón, *ibid.*, 1989, **114**, 1297.
9. F. Capitán, E. Manzano, A. Navalón, J. L. Vilchez and L. F. Capitán-Vallvey, *ibid.*, 1989, **114**, 969.
10. F. Capitán, E. Manzano, J. L. Vilchez and L. F. Capitán-Vallvey, *Anal. Sci.*, 1989, **5**, 549.
11. *Idem*, *Talanta*, 1990, **37**, 193.
12. F. Capitán, J. P. De Gracia, A. Navalón, L. F. Capitán-Vallvey and J. L. Vilchez, *Analyst*, 1990, **115**, 849.
13. E. Manzano, *PhD Thesis*, University of Granada, 1989.
14. M. J. Blanch, *Tesis de Licenciatura*, University of Granada, 1986.
15. R. Escoz, *Tesis de Licenciatura*, University of Granada, 1988.
16. J. P. De Gracia, *Tesis de Licenciatura*, University of Granada, 1989.
17. M. T. Oms, V. Cerdá, F. García Sánchez and A. L. Ramos, *Talanta*, 1988, **35**, 671.
18. A. Savitzky and M. J. E. Golay, *Anal. Chem.*, 1964, **36**, 1627.
19. J. Steiner, Y. Termonia and J. Deltour, *ibid.*, 1972, **44**, 1906.
20. H. A. Laitinen and P. Kivalo, *ibid.*, 1952, **24**, 1467.
21. F. D. Snell and L. S. Ettre (eds.), *Encyclopedia of Industrial Chemical Analysis*, Vol. 5, Interscience, New York, 1971.

22. N. H. Furman (ed.), *Standard Methods of Chemical Analysis*, Sixth Edition, Vol. 1, Van Nostrand, Princeton, NJ, 1962.
23. *Standard Methods for the Examination of Water and Wastewater*, *APHA-AWWA-WPCF*, 15th Ed., Washington, 1980.
24. IUPAC, *Nomenclature, Symbols, Units and Their Usage in Spectrochemical Analysis*, *Pure Appl. Chem.*, 1976, **45**, 105.
25. *Guidelines for Data Acquisition and Data Quality Evaluation in Environmental Chemistry*, *Anal. Chem.*, 1980, **52**, 2242.

Talanta, Vol. 39, No. 1, pp. 29–34, 1992
Printed in Great Britain.

0039-9140/92 $5.00 + 0.00

AN ION-EXCHANGE SEPARATION OF METAL CATIONS ON A C-18 COLUMN COATED WITH DODECYLSULPHATE

PAVEL JANOŠ
The Research Institute of Inorganic Chemistry, 400 60 Ústí nad Labem, Czechoslovakia

KAREL ŠTULÍK* and VĚRA PACÁKOVÁ
Department of Analytical Chemistry, Charles University, Albertov 2030, 128 40 Prague 2, Czechoslovakia

(*Received* 4 *March* 1991. *Revised* 3 *June* 1991. *Accepted* 24 *June* 1991)

Summary—The retention mechanism was studied for the cations of the alkaline earth metals and Zn^{2+}, Ni^{2+}, Co^{2+}, Cd^{2+} and Bi^{3+} on a C_{18} column permanently coated with sodium dodecylsulphate, with aqueous mobile phases containing cupric chloride or sulphate, or cerous nitrate. The dependencies of the logarithm of the capacity ratio on the logarithm of the eluent concentration were linear, demonstrating that ion-exchange was the predominating separation mode; the slopes of these dependencies were in good agreement with the values predicted from the ion-exchange theory. Indirect UV photometric detection yielded limits of detection (LOD) of 21, 44, 120 and 275 ng in the volume injected, 20 μl, for Mg^{2+}, Ca^{2+}, Sr^{2+} and Ba^{2+}, respectively, with the $10^{-2}M$ copper(II) chloride mobile phase; the respective LOD values decreased to 0.8, 1.6, 3.0 and 6.7 ng with the $5 \times 10^{-4}M$ cerium(III) nitrate eluent. The method was found to be primarily suitable for determination of the alkaline earths and was applied to analyses of surface and mineral waters.

Ionic substances are often separated by ion-exchange chromatography, especially by the method known under the name, ion chromatography.[1] The mechanism of ion exchange is primarily characterized by linear dependences between the logarithm of the analyte capacity ratio and the logarithm of the concentration of the eluting ion.[2–8] The linearity of this dependence has often been confirmed in separation of cations,[3–7,9–11] but there may be considerable differences between their experimental and predicted slopes.[5,7,12,13] The slope is determined by the ratio of the electric charges carried by the analyte and the eluent ion and it has been pointed out[5] that the effective charges may vary owing to steric effects preventing interaction of the cations with a stoichiometric number of the exchange sites on a low-capacity cation exchanger. Some considerations of the effective charge on metal ions in ion-exchange chromatography have been summarized by Lederer.[14]

In addition to fixed-site cation exchangers, reversed-phase stationary phases can also be employed for separations of cations when suitable hydrophobic ion-pairing agents are present in the system (*e.g.*, alkyl sulphates or sulphonates). An ion-pairing agent can be added to the mobile phase, but it has been shown[15] that some of these agents that contain a sufficiently long alkyl chain are strongly adsorbed on the stationary phase and thus can be pre-adsorbed, so that they need not be present in the mobile phase during separations. It is assumed that ion exchange occurs at these modified stationary phases.

The mechanism of ion-pair separation of various organic substances with octyl, decyl and dodecyl sulphonates was studied by Knox and Hartwick.[16] Hori *et al.*[17] recently discussed the relationships between the hydrophobicity of analytes and their retention in separation systems with C_{18} stationary phases, in the presence of sodium dodecyl sulphate which was either present in the mobile phase or used to pre-coat the stationary phase.

Columns containing C_{18} stationary phases permanently coated with dodecylsulphate were used for separations of alkali metals and alkaline earths,[18] the rare earths[19] and also organic anions employing an ion-exclusion mechanism.[20] The mechanism of the retention of cations has not been studied, except for the finding that the dependence of the logarithm of the capacity ratio of Na^+ on the logarithm of

*Author for correspondence

the concentration of the NH_4^+ eluent is linear, suggesting that ion-exchange takes place.[20] Therefore, we studied the mechanism of retention of the alkaline earths, Zn^{2+}, Ni^{2+}, Co^{2+}, Cd^{2+} and Bi^{3+} on a C_{18} column permanently coated with sodium dodecylsulphate (SDS). The mobile phases contained Cu^{2+} or Ce^{3+} eluent ions that permitted indirect UV photometric detection.[9,10,21–23]

EXPERIMENTAL

Apparatus

The liquid chromatograph consisted of a HPP 5001 pump, an LCI 30 injection valve with a 20-μl sampling loop, a TZ 4261 chart recorder (all from Laboratorní Přístroje, Prague, Czechoslovakia) and the model 732 870 variable-wavelength UV/Vis photometric detector (Knauer, Berlin, Germany). Glass columns 150 × 3 or 30 × 3 mm, Separon SGX C 18, 5 μm, were obtained from Tessek, Prague, Czechoslovakia and were precoated with a sodium dodecylsulphate (SDS) solution. A short guard column, 30 × 3 mm, packed with Separon SGX, 7 μm (Tessek) was placed between the pump and the injection valve. Separon SGX C_{18}, is based[24] on totally porous, spherical silica gel with an average specific surface area of 500 m^2/g and a pore volume of 1 ml/g. The average mass of the material in a 150 × 3 mm column is 0.4 g. The carbon content corresponding to the octadecyl modifier is 18%, which corresponds to a surface concentration of bound octadecyl groups of 2.03 μmoles/m^2. The dead volume equals about 0.3 ml for the 150 × 3 mm column.

The mobile phases were deaerated in an ultrasonic bath. The mobile phase flow-rate was 0.3 ml/min and the measurements were carried out at laboratory temperature (20 ± 2°).

Chemicals

All the chemicals used were of reagent-grade purity (Lachema, Brno, Czechoslovakia). The SDS substance was research grade, obtained from Serva, Heidelberg, Germany. The solutions were prepared in demineralized water. The eluents involved $CuCl_2$, $CuSO_4$ and $Ce(NO_3)_3$; the working solutions were prepared by diluting 1M stock solutions (0.1M cerium nitrate stock solution). Stock solutions of the test metal cations were prepared from the corresponding chlorides or nitrates, at a concentration of 0.1M. For quantitative analyses, these solutions were standardized by complexometric titrations. The metal ion stock solutions were appropriately diluted with water immediately before the measurements.

Column preparation

The method was analogous to one described previously.[19] The columns were washed first with methanol for 2 hr at a flow-rate of 0.1 ml/min, briefly with water and then with a $5 \times 10^{-3}M$ SDS at the same flow-rate followed again by a brief washing with water. The capacity of the column was measured dynamically, with a cerium nitrate mobile phase, using the retention of the La^{3+} and Pr^{3+} ions. As these ions exhibit the same retention characteristics, it can be assumed that the selectivity coefficient for the La^{3+}–Ce^{3+} and Pr^{3+}–Ce^{3+} ion exchange is close to unity. The ion-exchange capacity can then be calculated as the product of the column dead volume, the mobile phase concentration and the capacity ratio for the La^{3+} ion.[20]

The column capacity, at given SDS concentration and flow-rate, depends on the time of washing with the SDS solution and the shape of the dependence corresponds to the Langmuir isotherm. For the 30 × 3 mm column, the dependence of the capacity Q (μeq) on the time of washing with SDS (hours) can be expressed by the linearized equation,

$$Q^{-1} = 9.76 \times 10^{-3} + 30.54 \times 10^{-3}/t, \quad (1)$$

with a correlation coefficient of $r = 0.9996$, for a flow-rate of 0.1 ml/min, a SDS concentration of $5 \times 10^{-3}M$ and within a time interval of $t = 0.5$–3 hr. The amount of SDS bound to the stationary phase in the 150 × 3 mm column is *ca.* 70 μmoles. This corresponds to an SDS surface concentration of 0.35 μmoles/m^2 and a C_{18}-to-SDS ratio of *ca.* 6:1. The optimal time of washing the 150 × 3 mm column with the SDS solution is 2 hr; the column capacity is then *ca.* 65 μeq. The exchange capacity of SDS apparently approaches 100%.

The prepared column is stable for several weeks. Prior to use, it must be washed with the mobile phase until the baseline stabilizes (*ca.* 1–2 hr). The column is highly stable when aqueous mobile phases are used: With 10^{-3}–$10^{-2}M$ copper(II) chloride or copper(II) sulphate and 10^{-4}–$10^{-3}M$ cerium(III) nitrate, no change in the retention characteristics was observed during continuous use for at least two weeks.

RESULTS AND DISCUSSION

Separation

It is assumed that the retention on a reversed-phase column coated with SDS is governed by the ion-exchange equilibrium,

$$yM_m^{x+} + xE_s^{y+} \rightleftarrows yM_s^{x+} + xE_m^{y+}, \qquad (2)$$

where M^{x+} is the analyte, E^{y+} is the eluent cation and the subscripts m and s refer to the mobile and stationary phase, respectively.

The capacity ratio, k_M, is given by

$$\log k_M = \frac{1}{y}\log K_{M,E} + \frac{x}{y}\log\frac{Q}{y} + \log\frac{w}{V_M} - \frac{x}{y}\log[E^{y+}]_m \qquad (3)$$

in the simplest case without side equilibria,[7] where $K_{M,E}$ is the selectivity coefficient, Q is the ion exchange capacity of the column, w is the weight of the stationary phase and V_M is the volume of the mobile phase in the column.

Equation (3) predicts a linear relationship between $\log k_M$ and the logarithm of the concentration of the eluting ion in the mobile phase; the slope of this dependence is given by the ratio of the charges of the analyte and the eluting ion. This equation yields the slopes in the absence of complexation reactions of the analyte and eluting cations with the mobile phase anions; Haddad and Foley[7] reported more complex relationships considering these side equilibria.

The slopes of the experimental dependences of $\log k_M$ *vs.* $\log c_E$, obtained over ranges of 2×10^{-3}–$2 \times 10^{-4}M$ for copper chloride and copper sulphate and 1×10^{-4}–$5 \times 10^{-3}M$ for cerium nitrate, are given in Table 1. The slopes are in very good agreement with the values calculated from equation (3), except for Cd^{2+} and the copper chloride eluent, where the experimental value is greater than the predicted slope due to complexation between Cd^{2+} and chloride.[25] The ion-exchange interaction then involves both the Cd^{2+} and $CdCl^+$ ions.

Table 1. The slopes of the $\log k_M$ *vs.* $\log c_E$ plots

Cation	Eluent $CuCl_2$	$CuSO_4$	$Ce(NO_3)_3$
Mg^{2+}	−0.951	−0.908	−0.675
Ca^{2+}	−0.978	−0.906	−0.676
Sr^{2+}	−0.964	−0.914	−0.660
Ba^{2+}	−1.022	−0.920	−0.669
Zn^{2+}, Ni^{2+}, Co^{2+}	−0.958	−0.907	−0.671
Cd^{2+}	−1.212	−0.950	−0.674
Bi^{3+}	—	—	−0.946

The theoretical slopes are −1.000 for the divalent analytes and the Cu^{2+} eluent ion and −0.667 for the same analytes and the Ce^{3+} eluent ion.

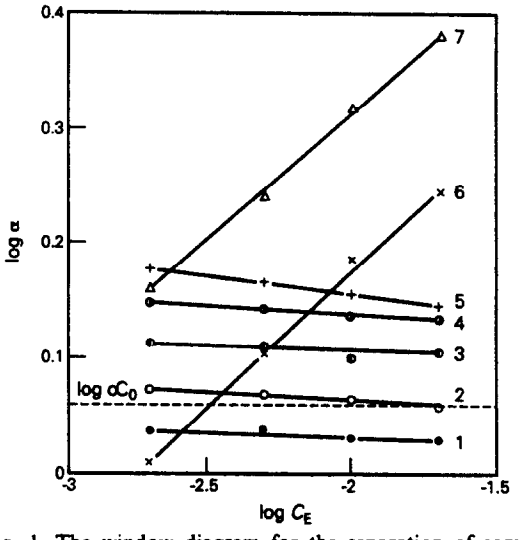

Fig. 1. The window diagram for the separation of some divalent cations with the $CuCl_2$ eluent. For conditions see Fig. 2. The analyte couples: 1—Mg^{2+}, Zn^{2+}; 2—Sr^{2+}, Ca^{2+}; 3—Ca^{2+}, Zn^{2+}; 4—Ca^{2+}, Mg^{2+}; 5—Ba^{2+}, Sr^{2+}; 6—Mg^{2+}, Cd^{2+}; 7—Ca^{2+}, Cd^{2}.

In separations of the alkaline earth cations on low-capacity, fixed-site cation exchangers, the slopes of the $\log k_M$ *vs.* $\log c_E$ plots were significantly dependent on the radii of the hydrated cations.[5,12] We did not observe this dependence in our measurements. The apparent reason for this is the fact that the adsorbed SDS molecules are not rigidly bound to the C_{18} stationary phase and their functional groups can be oriented in such a way that steric hin-

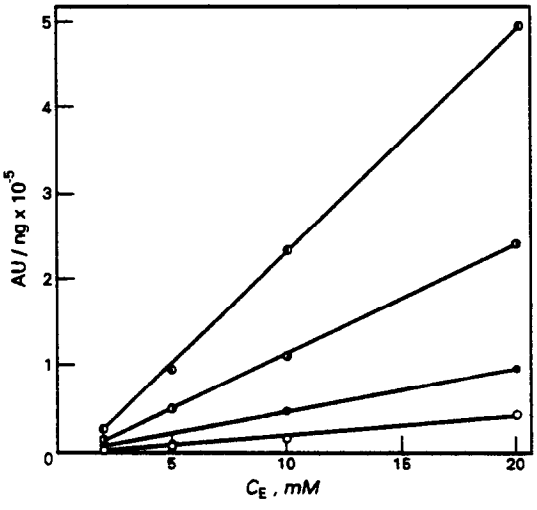

Fig. 2. Dependence of the sensitivity of measurement on the concentration of the $CuCl_2$ eluent. The 150 × 3 mm column, coated with $5.10^{-3}M$ SDS for 2 hr at a flow rate of 0.1 ml/min. 1—Ba^{2+}, 2—Sr^{2+}, 3—Ca^{2+}, 4—Mg^{2+}.

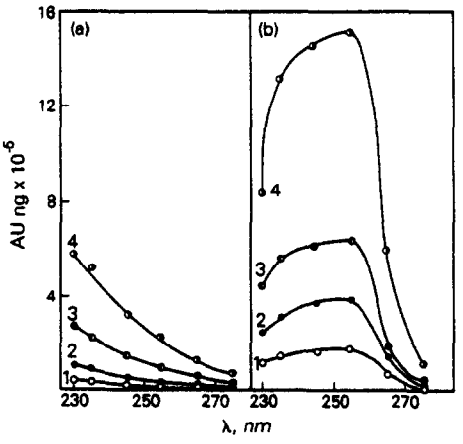

Fig. 3. Dependence of the sensitivity of measurement on the wavelength. For the conditions see Fig. 2; (*a*) $10^{-2}M$ $CuCl_2$, (*b*) $5 \times 10^{-4}M$ $Ce(NO_3)_3$. 1—Ba^{2+}, 2—Sr^{2+}, 3—Ca^{2+}, 4—Mg^{2+}.

drance causing a decrease in the effective charge of the analyte in ion exchange on fixed-rate stationary phases, does not occur.

The alkaline earths are resolved well with all the mobile phases used. On the other hand, Zn^{2+}, Ni^{2+} and Co^{2+} exhibit virtually identical retention characteristics The Cd^{2+} ion has a different retention with the copper chloride eluent.

The separation was optimized with window diagrams,[26] with relative retention, α_{21},

$$\alpha_{21} = k_{M2}/k_{M1} \quad (4)$$

as the criterion. The window diagram for the separation of some divalent cations with the copper chloride eluent is given in Fig. 1. Only the Ca^{2+}–Cd^{2+} and Mg^{2+}–Cd^{2+} couples exhibit a pronounced dependence of the relative retention on the eluent concentration, due to the complexation between Cd^{2+} and chloride, mentioned above. In view of the given efficiency of the separation system, the value of $\alpha_{21} = 1.15$ was selected as the critical relative retention (it is given by the dashed line in Fig. 1). Under the given conditions, magnesium cannot be adequately resolved from Zn^{2+}, Ni^{2+} and Co^{2+}. Cadmium is not resolved from calcium when the eluent concentration is less than *ca.* $3.2 \times 10^{-3}M$. The resolution of calcium and strontium deteriorates at high concentrations of the copper chloride eluent. When using $10^{-2}M$ copper chloride eluent, a mixture of Cd^{2+}, Zn^{2+}, Ca^{2+}, Sr^{2+} and Ba^{2+}, for example, can be readily separated.

Detection

The sensitivity of indirect photometric detection is independent of the mobile phase concentration,[4,27] but detectability of the analytes can be affected by the changes in the retention characteristics and consequent variations in the elution curve shape caused by changing the eluent concentration. Figure 2 depicts the sensitivity (AU/ng) dependence on the concentration of the copper chloride eluent for the Mg^{2+}, Ca^{2+}, Sr^{2+} and Ba^{2+} ions. Similar dependences were also obtained for the cerium nitrate eluent.

The sensitivity dependences on the wavelength are given in Fig. 3 for the copper chloride and cerium nitrate eluents. With copper chloride, the sensitivity increases with decreasing wavelength in accordance with the shape of the Cu^{2+} absorption spectrum;[22] however, at wavelengths of less than *ca.* 230 nm, the baseline

Table 2. The limits of detection and the calibration plot parameters for determination of the alkaline earth metals

Cation	Limit detection *ng*	Calibration plot parameters: Slope, AU/*ng*	Intercept, AU	Correlation coefficient, $n = 9$
		$10^{-2}M$ $CuCl_2$ eluent		
Mg^{2+}	20.8	2.26×10^{-5}	1.20×10^{-4}	0.9997
Ca^{2+}	43.7	1.08×10^{-5}	1.46×10^{-4}	0.9995
Sr^{2+}	116.8	0.41×10^{-5}	-1.13×10^{-4}	0.9977
Ba^{2+}	274.6	0.17×10^{-5}	1.73×10^{-4}	0.9946
		$5 \times 10^{-4}M$ $Ce(NO_3)_3$		
Mg^{2+}	0.78	22.76×10^{-5}	1.59×10^{-4}	0.9981
Ca^{2+}	1.59	11.81×10^{-5}	-1.88×10^{-4}	0.9984
Sr^{2+}	3.00	6.36×10^{-5}	-1.39×10^{-4}	0.9996
Ba^{2+}	6.70	2.97×10^{-5}	1.61×10^{-4}	0.9990

The Separon SGX C_{18} column, 150 × 3 mm I.D.; flow-rate 0.3 ml/min. Indirect photometric detection at 254 nm. The limit of detection corresponds to the analyted absolute amount injected into the column that produces a signal of three times the baseline noise; 20-μl samples.

Table 3. Determination of the alkaline earth metals in mineral and surface waters (mg/l.)

	Sample (confidence limits, $x \pm s.t/\sqrt{n}$; $n = 7$; $\alpha = 0.05$)					
	S – 1		S – 2		S – 3	
Element	HPLC	AAS	HPLC	AAS	HPLC	AAS
Mg	13.2 ± 0.4	10.4	72.5 ± 3.1	71.5	12.4 ± 0.4	11.4
Ca	63.3 ± 4.5	58.6	58.4 ± 7.2	54.0	10.1 ± 0.3	7.5
Sr	<DL	0.21	<DL	0.07	3.22 ± 0.06	3.5
Ba	0.61 ± 0.06	0.42	0.55 ± 0.05	0.69	1.55 ± 0.06	1.85

Mg and Ca were determined with the $10^{-2}M$ $CuCl_2$ eluent, Sr and Ba with the $5 \times 10^{-4}M$ $Ce(NO_3)_3$ eluent.

noise greatly increases with a consequent increase in the limits of detection. When using the cerium nitrate eluent, the highest sensitivity is attained around 255 nm, again in agreement with the absorption spectrum of Ce^{3+} (a value of 253.6 nm was recommended for a spectrophotometric determination).[28]

The detection characteristics for Mg^{2+}, Ca^{2+}, Sr^{2+} and Ba^{2+} at 254 nm are summarized in Table 2. The sensitivities of detection (the slopes of the calibration plots) are by about one order of magnitude higher with the cerium nitrate eluent, owing to the higher absorption coefficient of the Ce^{3+} ion.[25] The limits of detection obtained with the cerium nitrate eluent are comparable with those reported earlier,[23] while the values obtained by us with the copper chloride eluent are somewhat lower.

Ion-exchange chromatography with indirect photometric detection is commonly associated with the appearance of system peaks.[29,30] However, these peaks need not necessarily appear or be detected. We only observed system peaks in some cases and their retention times were always shorter then those of the analytes, so that there were no problems in repeated determinations.

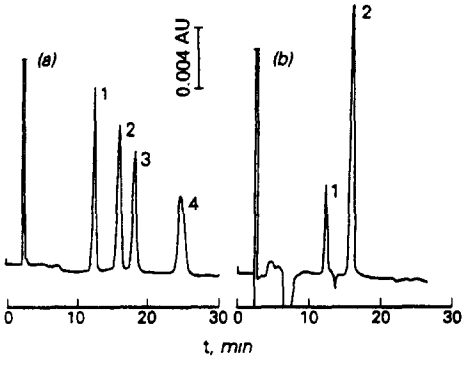

Fig. 4. Determination of the alkaline earths with the $10^{-2}M$ $CuCl_2$ eluent. For the conditions see Fig. 2. (*a*) Standard mixture: 1—Mg^{2+} (0.5 μg), 2—Ca^{2+} (0.8 μg), 3—Sr^{2+} (1.7 μg), 4—Ba^{2+} (2.7 μg). (*b*) Mineral water sample S-1.

Application

The method was applied to determination of the alkaline earth metals in mineral and surface waters; the $10^{-2}M$ copper chloride eluent is suitable for analyses involving analyte concentrations of the order of tens of mg/l., while $5 \times 10^{-4}M$ cerium(III) nitrate should be used when the analyte concentrations are from tenths to units of mg/l. Examples of the chromatograms are given in Figs. 4 and 5, the results are listed in Table 3 and compared with the values obtained by atomic-absorption spectrometry; the agreement is satisfactory. As can be seen from Fig. 6, rapid and sufficiently efficient separations of the alkaline earths can also be attained with the short 30 × 3 mm column.

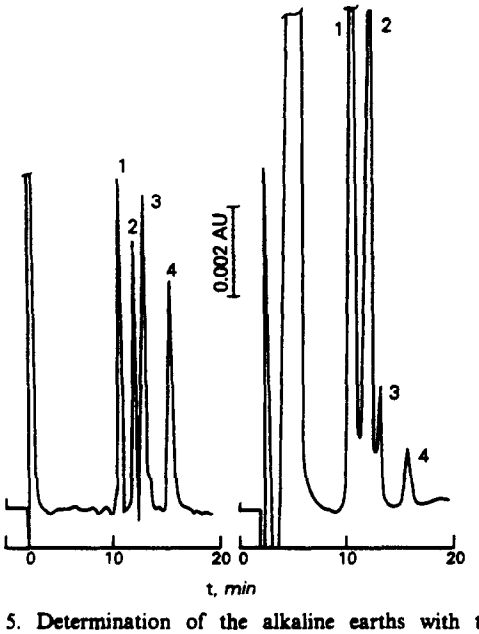

Fig. 5. Determination of the alkaline earths with the $5 \times 10^{-4}M$ $Ce(NO_3)_3$ eluent. For the conditions see Fig. 2. (*a*) Standard mixture: 1—Mg^{2+} (48 ng), 2—Ca^{2+} (80 ng), 3—Sr^{2+} (175 ng), 4—Ba^{2+} (275 ng). (*b*) Surface water sample S-3.

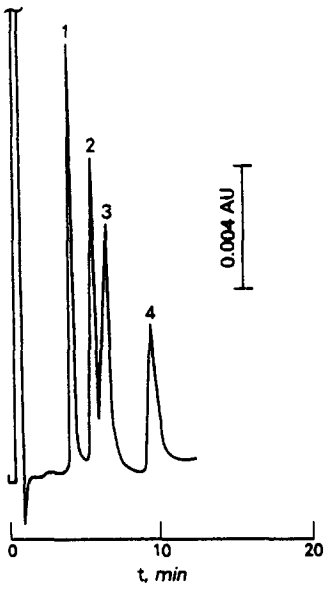

Fig. 6. Separation of the alkaline earths on the 30 × 3 mm column, using the $10^{-2}M$ $CuCl_2$ eluent at 254 nm. 1—Mg^{2+}, 2—Ca^{2+}, 3—Sr^{2+}, 4—Ba^{2+}.

REFERENCES

1. H. Small, *Ion Chromatography*, Plenum Press, New York, 1989.
2. P. Jandera and J. Churáček, *J. Chromatog.*, 1974, **91**, 207.
3. G. J. Sevenich and J. S. Fritz, *Anal. Chem.*, 1983, **55**, 12.
4. R. C. L. Foley and P. R. Haddad, *J. Chromatog.*, 1986, **366**, 13.
5. D. T. Gjerde, *ibid.*, 1988, **439**, 49.
6. R. D. Rocklin, A. M. Rey, J. R. Stillian and D. L. Campbell, *J. Chromatog. Sci.*, 1989, **27**, 474.
7. P. R. Haddad and R. C. Foley, *J. Chromatog.*, 1990, **500**, 301.
8. J. Hradil, F. Švec, A. A. Aratskova, L. D. Belyakova and V. I. Orlov, *ibid.*, 1990, **509**, 369.
9. M. Miyazaki, K. Hayakawa and S. G. Choi, *ibid.*, 1985, **323**, 443.
10. Y. S. Rho and S. G. Choi, *Arch. Pharm. Res.*, 1986, **9**, 211.
11. P. Hájos, T. Kecskeméti and J. Inczédy, *Reactive Polymers*, 1988, **7**, 239.
12. G. J. Sevenich and J. S. Fritz, *J. Chromatog.*, 1986, **347**, 361.
13. P. Janoš, K. Štulik and V. Pacáková, *Talanta*, submitted for publication.
14. M. Lederer, *J. Chromatog.*, 1988, **452**, 265.
15. R. M. Cassidy and S. Elchuk, *Anal. Chem.*, 1982, **54**, 1558.
16. J. H. Knox and R. A. Hartwick, *J. Chromatog.*, 1981, **204**, 3.
17. S. Hori, K. Ohtani-Senuma, S. Ohtani, K. Miyasaka and T. Ishikawa, *ibid.*, 1990, **515**, 67.
18. W. Schmidt and F. Fuchtner, *Z. Chem.*, 1988, **28**, 453.
19. V. Kubáň and D. B. Gladilovich, *Coll. Czech. Chem. Commun.*, 1988, **53**, 1664.
20. K. Šlais, *J. Chromatog.*, 1989, **469**, 223.
21. H. Small and T. E. Miller, *Anal. Chem.*, 1982, **54**, 462.
22. Z. Iskandarani and T. E. Miller, *ibid.*, 1985, **57**, 1591.
23. J. H. Sherman and N. D. Danielson, *ibid.*, 1987, **59**, 490.
24. Chromatography Products A-E, *Catalogue Tessek 1990–1991.*
25. S. Kotrlý and L. Šůcha, *Handbook of Chemical Equilibria in Analytical Chemistry*, Horwood, Chichester, 1985.
26. D. R. Jenke and G. K. Pagenkopf, *Anal. Chem.*, 1984, **56**, 85.
27. P. R. Haddad, *Chromatographia*, 1987, **24**, 217.
28. H. L. Greenhaus, A. M. Feibush and L. Gordon, *Anal. Chem.*, 1957, **29**, 1531.
29. P. E. Jackson and P. R. Haddad, *J. Chromatog.*, 1985, **346**, 125.
30. H. Sato, *Anal. Chem.*, 1990, **62**, 1567.

Talanta, Vol. 39, No. 1, pp. 35–44, 1992
Printed in Great Britain.

0039-9140/92 $5.00 + 0.00

REDUCTION OF INJECTION VARIANCE IN FLOW-INJECTION ANALYSIS

BEVERLY F. JOHNSON,* ROBERT E. MALICK and JOHN G. DORSEY†
Department of Chemistry, University of Cincinnati, Cincinnati, Ohio 45221-0172, U.S.A.

(*Received* 31 *December* 1990. *Revised* 26 *June* 1991. *Accepted* 26 *June* 1991)

Summary—In order to achieve maximum sensitivity in flow-injection analysis, sample dispersion must be kept to a minimum. This dispersion process, however, is not well understood. Studies of the dispersion process have concentrated on dispersion within the flow manifold while dispersion due to the injection process has been largely ignored. Here sample injection loops packed with inert glass beads and a Serpentine II (distorted) empty loop were constructed and compared to traditional empty sample loops. Digitization of the response curves and subsequent calculation of the statistical moments were used to compare the contribution of each sample loop type to the total system dispersion. Both packed and Serpentine II sample loops were shown to decrease dispersion and increase throughput in flow-injection systems. Plots of peak variance *vs.* injection volume show variance increasing 1.67 times faster with traditional open sample loops compared to packed loops. When combined with other peak width minimization techniques, this method should further lower concentration limits of detection.

Flow-injection analysis has become an extremely popular alternative to manual solution handling, and offers more rapid analysis, with greater precision, higher sample throughput, and lower reagent consumption.[1,2] The only aspect of flow injection that suffers in comparison to manual alternatives is the limit of detection. Flow injection is (as is chromatography) a dilution technique. From the moment of sample injection, the sample is continuously diluted until it passes through the flow detector. The minimization of this dilution process would then improve the limit of detection, and by decreasing the peak width, would also improve throughput. We have been interested in both chemical and physical ways of decreasing peak dispersion.[3,4]

The dispersion coefficient, D, introduced by Růžička and Hansen[5] is a simple descriptor for the dispersion process in flow-injection analysis. It does not, however, contain information in the time domain nor does it provide any information about the peak shape and is therefore of limited use for guiding the design of flow manifolds. The dispersion coefficient is defined as C^0/C^{max} where C^0 is the original solute concentration and C^{max} is the solute concentration at the peak maximum recorded after dilution. Since it is a purely physical descriptor, D was not intended to be used in the presence of a chemical reaction.

The use of peak shape and peak width as descriptors to gain more information about dispersion has been applied less often. Poppe first reported the similarity between chromatographic and flow-injection systems in terms of the system contributions to band broadening.[6] As with chromatographic systems, the total variance of the system is affected by the individual variance contributions from the injection device, manifold tubing and connectors and the detector volume and electronic time constants. The total band broadening in a non-reacting system is due to the sum of these individual variance contributions:[7]

$$\sigma^2 \text{ peak} = \sigma^2 \text{ injection} + \sigma^2 \text{ transport} + \sigma^2 \text{ detection} \quad (1)$$

If the detector is well designed, the variance contribution from the detector will be at least five times less than the variance caused by the injection device and transport phenomena. If modern LC detectors with fast electronics and small volume flow cells are used, this condition is usually met and the band broadening due to the detector can be neglected.

The effect of a chemical reaction upon peak broadening is also of importance but has been studied less. Painton and Mottola were the first to study the influence of a chemical reaction on peak broadening in a flow-injection system.[8–10]

*Present address: AMOCO Corporation, P.O. Box 3011, Naperville, IL 60566.
†Author for correspondence.

Since that time additional reports have appeared.[11-14] It is generally concluded that at reasonable flow velocities the contribution to overall peak broadening from the reaction kinetics is negligible compared to the transport contribution.

Ramsing *et al.* first suggested the use of variance (second statistical moment) as a measure of peak width and for study of the relationship between peak width and dispersion.[15] Reijn *et al.* suggested the use of statistical moments in order to gain fundamental information about the dispersion process.[11] Since the determination of statistical moments requires extensive manual calculations or the use of digital data acquisition, their application to peak analysis has been limited. Foley and Dorsey, using an exponentially modified gaussian (EMG) peak shape model, developed simple empirical equations allowing manual calculation of statistical moments based simply on peak width measurements.[16] Jeansonne and Foley recently reviewed the use of the EMG peak shape model in chromatography and flow-injection analysis.[17] Brooks and Dorsey recently verified the applicability of the EMG model for real flow-injection peaks over a wide range of flow rates for coiled, knitted and Serpentine II manifolds, single-bead string reactors and a coiled reactor with a single confluence point.[3]

In the vast majority of cases, the dispersion due to the injection process is ignored. In the theoretical models developed for dispersion, delta functions are assumed for the injection profiles and variance due to transport (and chemical reaction in some cases) is taken as the only dispersion process. Ramsing *et al.* have concluded, however, that the starting point of dispersion in an empty sample loop is located at the middle of the sample zone prior to its injection.[15] Reijn *et al.*[7] and Coq *et al.*[18] have discussed injection variance and demonstrated that the mode of injection can have a large influence on dispersion profiles in chromatography and flow-injection analysis and that this effect becomes worse as the injection volume is increased. Injection variance is a potentially worse problem in flow injection, however, as in chromatographic analysis sample focusing typically occurs, or concentration occurs at the top of the column.

Typically the sample loop on the injection device is a piece of empty tubing in which laminar flow profiles dominate during the injection process. The laminar flow profiles make it impossible to obtain the plug injections desired. Using a coiled configuration for the sample loop helps to overcome some of the band broadening but coiling is not possible for small sample loops and thus laminar flow profiles prevail causing the associated band broadening.

Timed injections have been used in order to achieve plug injection profiles at the cost of needing computer control to obtain reproducible injection volumes.[18] In this method a loop twice as large as the desired injection volume is used. Only the front half of the loop is injected into the system thereby avoiding the region of the sample loop where the carrier stream has replaced some of the sample because of the developing laminar flow profiles.

The use of packed sample loops decreases the injection variance by blunting the edges of the laminar flow profiles, and has been recommended for chromatographic systems.[18] The increased radial mixing caused by the packing causes a decrease in the axial dispersion and should provide a more plug-like injection profile. This paper discusses the use of packed sample loops to minimize band broadening and produce near plug injection profiles for flow-injection analyses. In addition, a single Serpentine II empty sample loop was constructed and its performance compared to a single packed loop of the same volume. Two solutes were tested, one non-reacting solute (methyl ethyl ketone) and one that underwent an on-line reaction to give a detectable product (oxidation of pyridoxal in the presence of cyanide). Statistical moments were used to evaluate and compare the response curves for empty and packed sample loops.

EXPERIMENTAL

Apparatus

The flow-injection apparatus consisted of a TosoHaas (Philadelphia, PA) Model TSK-6010 dual piston reciprocating HPLC pump, an ABI Analytical Kratos Divison (Ramsey, NJ) Spectroflow 757 variable wavelength absorbance detector and a Recordall (Fisher Scientific, Fairlawn, NJ) Series 5000 recorder. The flow manifold was made of 0.5 mm i.d. Teflon tubing in either a linear configuration (approximately 30 cm) or a coiled configuration (150 cm coil wound around a 1.3 cm core, total length approximately 230 cm). Temperature control was maintained with a water bath equipped

with an Allied Model 73 (Fisher Scientific) Circulator.

The samples were introduced with a modified Rheodyne (Cotati, CA) Model 5020 sample injection valve with 0.8-mm i.d. Teflon sample loops. The injection volumes were determined by "injecting" a loop of standardized 6*M* hydrochloric acid into a flask and titrating with standardized sodium hydroxide. For the smallest injection volumes (12.74 μl packed and 23.16 μl empty) the valve was modified (Fig. 1) in order to give the smallest volumes possible from the 0.8 mm i.d. Teflon tubing. The Serpentine II loop was produced from 0.5 mm i.d. Teflon tubing, constructed on an epoxy/fiberglass electronic breadboard according to the procedure given by Curtis and Shahwan.[19]

Nonporous glass beads (150–212 μm; Sigma Chemical Co., St. Louis, MO) were used to fill the packed loops. The packing was performed with a HPLC pump with a reservoir containing the glass beads placed at the pump outlet. For the smallest packed loop [constructed as in Fig. 1(a)] a piece of FISHERbrand Quantitative Grade, 5–10 μm filter paper (Fisher Scientific) was placed between the cap and stator with small holes cut out at the flanged ends of the loop "Fill" line and the nearest end of the sample loop. The injector was assembled in the FILL position so that one of the grooves on the rotor was between the two holes in the filter paper. The sample loop "Fill" line was attached to the outlet of the glass containing reservoir and the pump was started. The glass beads moved through the "Fill" line and sample loop until they were stopped by the filter paper. For the larger loops, the sample loop tubing was cut in half and each end was flanged. Each half of the loop was filled with glass beads (filter paper again used to keep the glass in the loop) and the flanged ends were joined with a 1/4 28 union and flanged fittings (Upchurch Scientific, Ann Arbor, MI).

After a loop was completely packed, the injector cap was removed and a new piece of filter paper installed. Flow in the FILL position is from the "Fill" port, across the the groove in the rotor to the loop inlet, through the loop to loop outlet, across rotor, and to "Waste" [Fig. 1(b)]. In order to reduce the amount of back pressure experienced when the sample loop was filled with sample, two holes were cut into the filter paper at the positions of loop "Fill" and "Waste". The glass beads were held in the loop

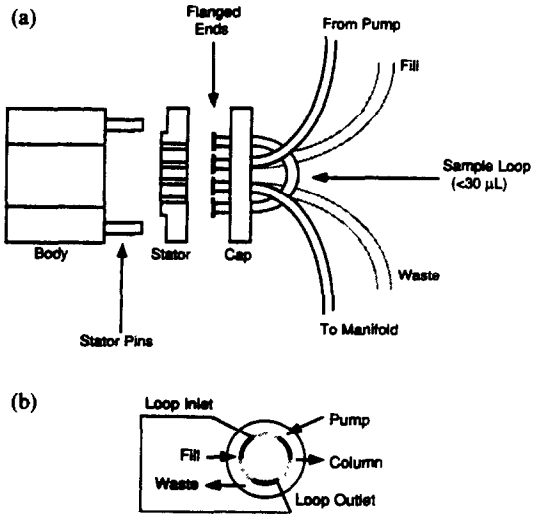

Fig. 1. (a) Modified Rheodyne 5020 Teflon rotary injection valve. (b) Flow diagram for modified Rheodyne 5020 Teflon rotary injection valve. Solid line represents the rotor in FILL position and shaded line represents the rotor in INJECT position.

by the filter paper at loop inlet and outlet. The valve was then reassembled for injections.

Solutions

Class 1B methyl ethyl ketone (Fisher Certified) and potassium cyanide (Certified A.C.S.) were obtained from Fisher Scientific. Pyridoxal was purchased from Sigma Chemical Co. All chemicals were used as received. All solutions were made with water purified by a Barnstead (Milford, MA) Nanopure system equipped with a 0.2-μm filter.

The carrier stream and sample solvent for the methyl ethyl ketone studies were both water. The carrier stream for the pyridoxal studies was 0.015*M* potassium cyanide in 0.06*M* (pH 6.74) phosphate buffer. The pyridoxal sample solvent was 0.06*M* (pH 6.74) phosphate buffer. The standards were prepared fresh daily.

The methyl ethyl ketone studies were carried out at ambient temperature in an unregulated laboratory and the methyl ethyl ketone was detected at 254 nm. The pyroxidal studies were conducted either at room temperature (unregulated) or at 49° by immersing the reaction coil in a water bath. The reaction product, 4-pyridoxolactone, was detected at 355 nm.

Procedure

The flow-rate was set at 1.0 ml/min for all studies. Each sample was injected at least three times and the results averaged. For the statistical moment determinations, the chart speed was

set at 20 cm/min to facilitate digitization and measurement. The digitization was performed with a Houston Instruments (Houston, TX) HIPAD Plus 11" × 17" digitizing tablet and the data were collected with an IBM PC XT Compatible. The statistical moments were calculated on an IBM PC AT 286 Compatible.

RESULTS AND DISCUSSION

Statistical moments

The statistical moments in units of time are defined by the following equations:[20]

zero-th moment

$$M_0 = \int_0^\infty h(t)\,dt \tag{2}$$

first central moment

$$M_1 = \frac{\int_0^\infty (t)\,h(t)\,dt}{M_0} \tag{3}$$

higher central moments

$$M_n = \frac{\int_0^\infty (t - M_1)^n\,h(t)\,dt}{M_0} \tag{4}$$

where $h(t)$ is the peak height at time t and the notation "central" indicates that the moment is taken around the first moment. If the peak is not normalized, the zero-th moment of the peak is the peak area. The first moment is the peak centroid or center of gravity which corresponds to the time of appearance of peak maximum for a Gaussian peak profile. The second moment is the variance and when taken around the first moment is a measure of the peak width. The third moment is the skew and is a measure of the magnitude and direction of the peak's asymmetry. The fourth moment is the kurtosis or excess and is a measure of the peak flattening relative to a Gaussian profile. All higher odd moments provide information on the peak symmetry while the higher even moments give information similar to that provided by the fourth moment.

The standard method for statistical moment determinations is the summation method. The peak is divided into small vertical slices and summation of the terms within the integrals of equations (2)–(4) is performed:

$$M_n = \frac{\sum_{\text{all } i} t_i^n y_i}{\sum_{\text{all } i} y_i} \tag{5}$$

where y_i is the peak height "count" in the ith interval.[20] This method makes no assumptions about peak shape and can be used for peaks which cannot be fit by Gaussian or modified Gaussian functions for which simple manual methods are available for moment calculations.

Digital data are necessary for the moment calculations. Digital data acquisition is often used but presents some problems. One of the major drawbacks is the need to rely on the computer system to appropriately assign the peak start and peak stop times. This is difficult for the system to achieve if there is a noisy or drifting baseline. Some work has been conducted on measuring the error in the statistical moments due to peak sensing capabilities, random noise, baseline position and baseline drift.[20–22] Chesler and Cram have detailed criteria for selecting the limits for peak area integration and the number of data points required for precision and accuracy in the calculated moments.[21]

Here the analog response curves recorded by the strip chart recorder were subjected to manual peak tracing and computer digitization. The digitization for each peak was started on the baseline about an inch before the rising portion of the response curve and was ended about an inch after the peak tail had leveled off after the decreasing portion of the response curve. In this way, it can be assumed that the entire peak area was covered in the digitization and errors associated with the start–stop algorithms should be minimized.

The digitized data were then processed by the computer with the summation method and the zero-th, first and second statistical moments were calculated. It should be noted that while interesting information may be contained in the higher moments, the error associated with moments higher than M_2 causes significant inaccuracies in the results. Since the value of the first moment is used in the calculations of all the higher moments, any error in the first moment is amplified as the moments increase. Additionally, as the higher moments are calculated, the leading and tailing portions of the response curves figure into the calculations to a greater extent. Thus any drift or noise in the baseline will have a serious effect on the accuracy of the calculated moments. However, it is possible to use these higher moments to identify trends in the data.

Non-reacting solute

One commonly used application for flow-injection is simply automated sample handling where the controlled dispersion aspect of the technique is used to reproducibly introduce a solute to a flow detector. For these non-reacting solutes, physical dispersion should be the only band broadening process present. The decrease in dispersion due to the packing in the sample loop should be evident at the detector if the manifold remains the same for the packed and empty sample loop situations. A short, linear manifold was chosen for the non-reacting solute since the manifold was used only to facilitate reproducible transport of the solute from the injector to the detector.

The response curves for similar injection volumes with packed and empty sample loops are shown in Figs 2 and 3 for relatively small and large injection volumes respectively. The injection volumes for the packed and empty loops are not exactly the same since the lengths of tubing used to make the packed loops were approximated based on the volume of the empty loops and assuming that the packing material would occupy approximately 60% of the tubing volume. The volumes used for Fig. 2 represent typical FIA injection volumes, and it is clear that even though curve *a* represents 5 μl more volume than *b*, the peak is actually narrower! Figure 3 shows the curves representing much

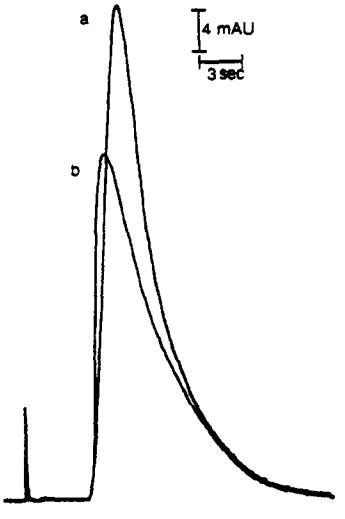

Fig. 2. Response curves for 1.0 mg/ml methyl ethyl ketone with small packed and empty sample loops. Peak (*a*) corresponds to the 28.20-μl packed sample loop and peak (*b*) corresponds to the 23.16-μl empty sample loop. (Manifold 30 cm linear; detection wavelength 254 nm; carrier stream water; flow-rate 1.0 ml/min; room temperature. Other conditions as in experimental section.)

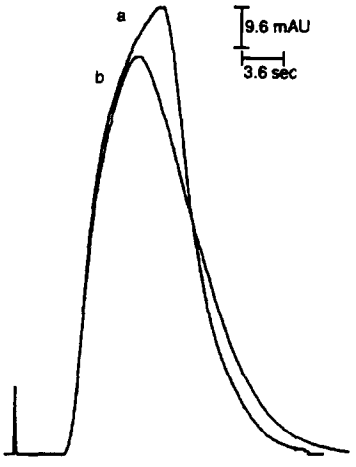

Fig. 3. Response curves for 1.0 mg/ml methyl ethyl ketone with large packed and empty sample loops. Peak (a) corresponds to the 123.3-μl packed sample loop. Peak (*b*) corresponds to the 115.6-μl empty sample loop. (Manifold 30 cm linear; detection wavelength 254 nm; carrier stream water; flow-rate 1.0 ml/min; room temperature. Other conditions as in experimental section.)

larger volumes, as would be used to try to obtain the lowest possible concentration limits of detection. It is evident that the response curves cannot be fit by Gaussian or modified Gaussian functions. Thus it is inappropriate to rely on the derived equations, which assume these functions, for accurate statistical moment calculations.

The average values of the peak height and the calculated moments for both the packed and empty sample loops are given in Table 1. When the peak area is plotted against the injection volume the relationship is linear for both the packed and empty sample loops over the considered injection volume range. It was expected that for a non-reacting system, the slopes and y-intercepts of the peak area versus injection volume plots would be the same regardless of the injection profile and this was found to be true.

The relationship between the peak centroid and the injection volume is linear for both empty and packed sample loops. As the injection volume is increased, the centroid of the peak occurs at larger volumes. As the injection volume is increased in a non-reacting system, the rising edges of the response curves coincide but the tailing becomes more extreme. This peak broadening with increasing injection volume causes the center of gravity to occur at larger volumes. Figure 4 shows the relationship between the peak variance (second moment) and the injection volume for both types of sample

Table 1. Peak characteristics for 1.0 mg/ml methyl ethyl ketone comparing packed and empty sample loops. (Manifold, 30 cm linear; detection wavelength, 254 nm; carrier stream, water; flow-rate, 1.0 ml/min; room temperature. Other conditions as in experimental section.)

	Volume injected, μl				
Packed loops	12.74	28.20	74.35	123.3	169.4
Peak height (mAU)	21.98	52.86	99.28	114.0	127.5
Peak area (mAU ml)	1.706	4.297	11.86	16.99	23.62
Peak centroid (μl)	126	144	179	198	228
Peak variance (μl^2)	2700	2700	3400	4600	5200
Empty loops	23.16	51.13	115.6	171.6	
Peak height (mAU)	36.48	62.75	97.15	113.2	
Peak area (mAU ml)	3.379	7.361	16.35	23.22	
Peak centroid (μl)	155	185	225	249	
Peak variance (μl^2)	3200	3800	5700	7400	

loops. The results show that packed sample loops are clearly superior to empty loops in terms of the injection device's contribution to total dispersion, with the ratio of the slopes being 1.67. This has important implications for the ability to improve the concentration limit of detection by increasing the injection volume. Furthermore, this also improves the throughput of the system, as

$$S_{max} = 60\,Q/k\sigma_v \qquad (6)$$

where S_{max} is the maximum throughput (samples/hr), Q is the flow-rate (ml/min) k is a factor depending on acceptable carryover and is generally taken to be 4 and σ_v is the volume standard deviation of the peak (the square root of the second moment).[1]

Prompted by a reviewer's suggestion, we also compared a Serpentine II empty loop to the packed loop. As this was performed at a later time, the flow system and detector were different, and these values should not be directly compared to those in the Tables. The Serpentine II empty loop ($V = 149.7$ μl) displayed a peak height of 138.0 mAU, a peak area of 24.98 mAU ml, a peak centroid of 256 μl, and a peak variance of 6691 μl^2. The packed loop ($V = 149.4$ μl) employed in the same system displayed a peak height of 141.3 mAU, a peak area of 25.09 mAU ml, a peak centroid of 265 μl, and a peak variance of 6325 μl^2. For packed and Serpentine II loops of the same volume, there is no real difference in any of these calculated moments.

Reacting solute

As with the non-reacting solute, the response curves for the reacting system cannot be fit to a Gaussian or modified Gaussian function and thus digitization of the analog signal was necessary for moment determinations. The peak characteristics for all injection volumes are given in Table 2. The relationship between peak area and injection volume for both types of sample loops is shown in Fig. 5. The peak areas are relatively independent of sample loop type and, within experimental error, follow the same curve. Unlike the non-reacting solute,

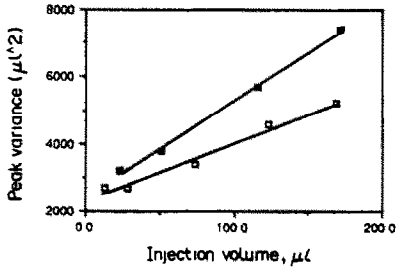

Fig. 4. Peak variance *vs.* injection volume for 1.0 mg/ml methyl ethyl ketone comparing packed and empty sample loops. The open squares represent packed sample loops (correlation coefficient = 0.9800) and the solid squares represent empty sample loops (correlation coefficient = 0.9977). (Manifold, 30 cm linear; detection wavelength, 254 nm; carrier stream, water; flow-rate, 1.0 ml/min; room temperature. Other conditions as in experimental section.)

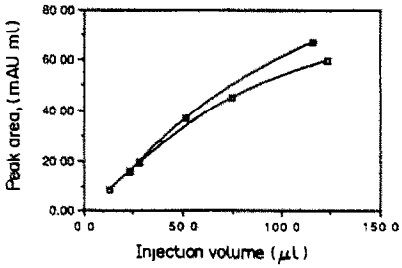

Fig. 5. Peak area *vs.* injection volume for 0.1 mg/ml pyridoxal comparing packed and empty sample loops. The open squares represent packed sample loops and the solid squares represent empty sample loops. (Manifold 230 cm coiled; detection wavelength 355 nm; carrier stream 0.05*M* KCN in 0.06*M* (pH 6.74) phosphate buffer; flow-rate 1.0 ml/min; temperature 49°. Other conditions as in experimental section.)

Table 2. Peak characteristics for 0.10 mg/ml pyridoxal comparing packed and empty sample loops. (Manifold 230 cm with a 150-cm coil; detection wavelength 355 nm; carrier stream 0.015*M* KCN in 0.06*M* (pH 6.74) phosphate buffer; flow-rate 1.0 ml/min; temperature 49°. Other conditions as in experimental section.)

	Volume injected, μl				
Packed loops	12.74	28.20	74.35	123.3	169.4
Peak height (mAU)	36.89	76.95	164.6	191.7	---*
Peak area (mAU ml)	8.553	19.36	44.84	59.54	---
Peak centroid (μl)	333	330	350	370	---
Peak variance (μl^2)	9500	11,000	11,600	13,200	---
Empty loops	23.16	51.13	115.6	150.7†	171.6
Peak height (mAU)	68.89	147.2	201.0	---	---
Peak area (mAU ml)	15.51	36.41	66.81	---	---
Peak centroid (μl)	342	335	366	---	---
Peak variance (μl^2)	8700	10,700	16,400	---	---

*Dashed lines represent situations in which no data could be collected due to peak splitting.
†This empty loop was in the Serpentine II configuration.

the relationship between peak area and injection volume was not linear for pyridoxal. The pyridoxal reaction follows pseudo-first order kinetics in the presence of excess cyanide[23] and thus the reaction rate decreases as the amount of cyanide is decreased. At large injection volumes, the amount of cyanide present in the center of the sample zone is small and the reaction is slowed. Since the time between injection and detection remains constant, a slower reaction produces a smaller amount of product which yields a smaller peak area.

The relationship between the peak centroid and the injection volume is also complicated by the presence of the reaction. Since the amount of product formed as the injection volume is increased does not follow a linear relationship, it is not surprising that the change in the center of gravity of the detected product peak is nonlinear as well.

Figure 6 shows the trends of the variance as the injection volume is increased. The crossover in the curves for the packed and empty loops was unexpected but may be explained as follows. Due to the decreased injection variance with the packed sample loops, the reaction comes closer to completion compared to the empty loop situation. The reagent is able to reach the center of the sample zone sooner when packed loops are used and thus a longer reaction time is available. For the same reason, the reaction comes closer to completion for small injection volumes than for large injection volumes. Brooks *et al.*[14] have found that a chemical reaction actually causes a decrease in peak broadening relative to a non-reacting system. Thus the extent of reaction attained before the detector is reached determines whether the chemical reaction or the physical flow processes control the final peak width. If the reaction is near completion the sample may behave more like a non-reacting solute and the decrease in dispersion due to the reaction will be lost.

For the small packed sample loops, the reaction approaches completion throughout the sample plug before that in the empty sample loop and the solute begins to act like a non-reacting solute. This translates into a larger dispersion for the packed loop compared to the empty loop. For the large sample volumes, however, the reaction does not come as close to completion and the decrease in dispersion due to the packed sample loop is augmented by the decrease in dispersion due to the reaction. This translates into larger dispersion with empty loops compared to the packed loops.

The moment analysis on the peaks produced from the Serpentine II empty loop is also shown in Table 2. The Serpentine II loop produced

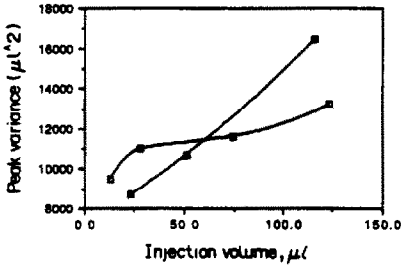

Fig. 6. Peak variance *vs.* injection volume for 0.1 mg/ml pyridoxal comparing packed and empty sample loops. The open squares represent packed sample loops and the solid squares represent empty sample loops. (Manifold 230 cm coiled; detection wavelength 355 nm; carrier stream 0.05*M* KCN in 0.06*M* (pH 6.74) phosphate buffer; flow-rate 1.0 ml/min; temperature 49°. Other conditions as in experimental section.)

split peaks, and no determination of these values could be made. In an effort to resolve the situation, the volume of the loop was reduced. A sample of response curves under varying conditions is shown in Fig. 7. Response curve (*a*) was obtained by replacing the reaction coil with the 30-cm linear manifold used for the methyl ethyl ketone. Response curve (*b*) was obtained after removing the reaction coil from the water bath and equilibrating to room temperature. Response curve (*c*) was obtained with the same conditions as for the pyridoxal reaction given above. Curve (*c*) exhibits a flat-topped peak with a maximum at 0.89 AU. Reducing the temperature (and thereby the extent of reaction) leads to a smaller peak, 0.30 AU, without a flat top. Reducing the length of tubing also leads to a smaller peak, curve (*a*), which is slightly larger (0.39 AU) than curve (*b*), again without a flap top. The sample zone produced by the Serpentine II loop allows for complete reaction to take place, yielding a steady-state response.

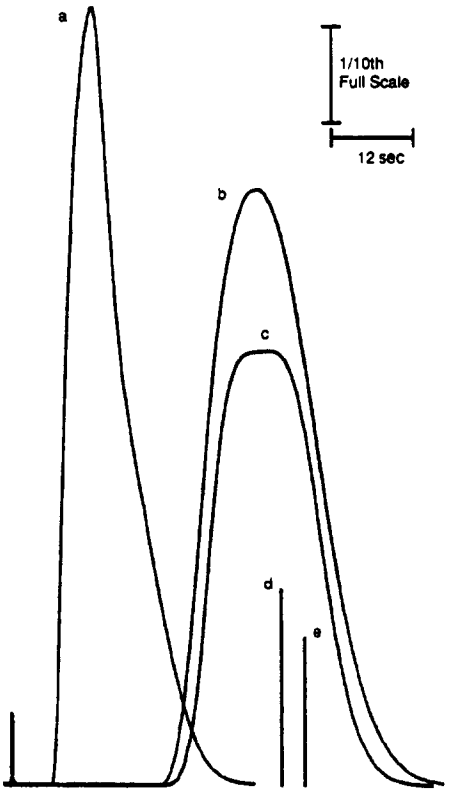

Fig. 7. Response curves for 1.0 mg/ml pyridoxal with 108.4 μl Serpentine II sample loop. Peak (*a*) corresponds to the 30-cm linear manifold at 22°, peak (*b*) corresponds to the 200-cm coiled manifold at 22°, and peak (*c*) corresponds to the coiled manifold at 49°. [Peaks (*a*) and (*b*) were 0.5 AUFS while peak (*c*) was 2.0 AUFS. Bars (*d*) and (*e*) correspond to the heights of peaks (*a*) and (*b*), respectively, scaled to the same full scale as peak (*c*). Other conditions as in experimental section.]

Figures of merit

In order to determine the effect of packed sample loops on the figures of merit, calibration plots were prepared for both the non-reacting and reacting systems with packed and empty sample loops. The results are given in Tables 3 and 4 for the non-reacting and reacting systems respectively. It can be seen that by decreasing the injection variance there is improvement in the limit of detection, especially as the injection volume is increased.

Table 3. Figures of merit for methyl ethyl ketone determination with packed and empty sample loops. (Detection wavelength 254 nm; carrier stream water; flow-rate 1.0 ml/min; room temperature. Other conditions as in experimental section.)

	Volume injected, μl				
Packed loops	12.74	28.20	74.35	123.3	169.4
Sensitivity (mAU/μg)*	2.06	2.13	1.31	0.939	0.751
Correlation coefficient	0.9999	0.9999	0.9993	0.9996	0.9976
Limit of detection (ng)†	76	73	130	150	190
Limit of detection (μg/ml)	5.95	2.59	1.74	1.19	1.13
LDR lower limit (μg)	0.255	0.564	0.372	1.23	1.70
LDR upper limit (μg)	637	846	1490	1230	1700
Empty loops	23.16	51.13	115.6	171.6	
Sensitivity (mAU/μg)*	1.70	1.33	0.756	0.579	
Correlation coefficient	0.9992	0.9978	0.9997	0.9996	
Limit of detection (ng)†	78	120	210	290	
Limit of detection (μg/ml)	3.35	2.29	1.85	1.69	
LDR lower limit (μg)	0.232	1.02	2.31	3.43	
LDR upper limit (μg)	1160	1530	2310	1720	

*Slope of calibration plot: detector response (mAU) *vs.* amount methyl ethyl ketone injected (μg).

†Calculated as LOD = $3s_B/m$ where s_B is the standard deviation of the blank and m is the analytical sensitivity taken as the slope of the calibration curve.

Table 4. Figures of merit for pyridoxal determination with packed and empty sample loops. (Detection wavelength 355 nm; carrier stream 0.015*M* KCN in 0.06*M* (pH 6.74) phosphate buffer; flow-rate 1.0 ml/min; temperature 49°. Other conditions as in experimental section.)

	Volume injected, μl				
Packed loops	12.74	28.20	74.35	123.3	169.4
Sensitivity (mAU/μg)*	0.0297	0.0237	0.0195	0.0124	---†
Correlation coefficient	0.9997	0.9996	0.9969	0.9980	---
Limit of detection (ng)‡	18	19	23	48	---
Limit of detection (μg/ml)	1.40	0.681	0.314	0.389	---
LDR lower limit (μg)	0.0318	0.0282	0.0372	0.0616	---
LDR upper limit (μg)	25.5	42.3	74.4	123	---
Empty loops	23.16	51.13	115.6	150.7§	171.6
Sensitivity (mAU/μg)*	0.0267	0.0227	0.0137	---	---
Correlation coefficient	0.9993	0.9991	0.9970	---	---
Limit of detection (ng)‡	20	20	33	---	---
Limit of detection (μg/ml)	0.855	0.393	0.288	---	---
LDR lower limit (μg)	0.0579	0.0256	0.0578	---	---
LDR upper limit (μg)	46.3	25.6	116	---	---

*Slope of calibration plot: detector response (mAU) *vs.* amount pyridoxal injected (μg).

†Dashed lines represent situations in which no data could be collected due to peak splitting.

‡Calculated as LOD = $3s_B/m$ where s_B is the standard deviation of the blank and m is the analytical sensitivity taken as the slope of the calibration curve.

§This empty loop was in the Serpentine II configuration, see text for values and discussion.

A single Serpentine II loop was also compared to a packed loop. As these data were taken on a different flow system with a different detector, these data should not be directly compared to the Tables. The figures of merit calculated for the Serpentine II empty loop were sensitivity = 0.866 mAU/mg ($r^2 = 0.9999$), limits of detection = 13.8 ng and 0.0922 μg/ml, and LDR limits of 0.749–1490 μg. The figures of merit calculated for the same volume packed loop were sensitivity = 0.895 mAU/mg ($r^2 = 0.9998$), limits of detection = 20.0 ng and 0.134 μg/ml, and LDR limits of 1.49–1490 μg. The Serpentine II loop for a non-reacting solute exhibited similar sensitivity to the same volume packed loop. The LOD both as an amount and as a concentration was somewhat improved in the Serpentine II loop. This is due to the absence of the increased pressure drop across the packed loop. This pressure drop leads to a pressure pulse and refractive index gradient, both of which act to increase the standard deviation of the blank signal. This also allowed an improved lower LDR limit.

CONCLUSIONS

It has been shown that the use of injection devices equipped with packed or Serpentine II (distorted) sample loops significantly decreases the dispersion and resulting peak width in both reacting and non-reacting systems. For a non-reacting system, sample throughput and limits of detection are correspondingly improved. The effect of increased injection volume has been studied and it is shown that the improvements obtained with packed sample loops are especially great at large injection volumes. This advance, especially when combined with other peak width minimization techniques such as highly distorted flow manifolds[3] and solute focusing[4] should allow for extremely low limits of detection for most flow injection applications.

Acknowledgements—The authors thank Dr T. Ridgway for the use of his digitizing equipment and computer expertise. They also wish to thank an anonymous reviewer for the suggestion of evaluating Serpentine II loops. They are also grateful for support of this work by NSF CHE-8704403 and gratefully acknowledge TosoHaas for a gift of the TSK-6010 pump.

REFERENCES

1. J. Růžička and E. H. Hansen, *Flow-Injection Analysis* 2nd Ed., John Wiley & Sons, New York, 1988.
2. M. Valcarcel and M. D. L. d. Castro, *Flow-Injection Analysis: Principles and Applications* Ellis Horwood Ltd., Chichester, 1987.
3. S. H. Brooks and J. G. Dorsey, *Anal. Chim. Acta*, 1990, **229**, 35.
4. B. F. Johnson and J. G. Dorsey, *Anal. Chem.*, 1990, **62**, 1392.
5. J. Růžička and E. H. Hansen, *Anal. Chim. Acta*, 1978, **99**, 37.
6. H. Poppe, *ibid.*, 1980, **114**, 59.
7. J. M. Reijn, W. E. Van der Linden and H. Poppe, *ibid.*, 1980, **114**, 105.
8. C. C. Painton and H. A. Mottola, *Anal. Chem.*, 1981, **53**, 1713.
9. *Idem*, *Anal. Chim. Acta*, 1983, **154**, 1.

10. *Idem*, *ibid.*, 1984, **158**, 67.
11. J. M. Reijn, H. Poppe and W. E. Van der Linden, *Anal. Chem.*, 1984, **56**, 943.
12. J. F. Tyson, *Anal. Chim. Acta*, 1986, **179**, 131.
13. J. M. Hungerford and G. D. Christian, *ibid.*, 1987, **200**, 1.
14. S. H. Brooks, D. V. Leff, M. A. Hernández Torres and J. G. Dorsey, *Anal. Chem.*, 1988, **60**, 2737.
15. A. U. Ramsing, J. Růžička and E. H. Hansen, *Anal. Chim. Acta*, 1981, **129**, 1.
16. J. P. Foley and J. G. Dorsey, *Anal. Chem.*, 1983, **55**, 730.
17. M. S. Jeansonne and J. P. Foley, *J. Chromatogr. Sci.*, 1991, **29**, 258.
18. B. Coq, G. Cretier, J. L. Rocca and M. Porthault, *ibid.*, 1981, **19**, 1.
19. M. A. Curtis and G. J. Shahwan, *LC · GC*, 1988, **6**, 158.
20. E. Grushka, M. N. Myers, P. D. Schettler and J. C. Giddings, *Anal. Chem.*, 1969, **41**, 889.
21. S. N. Chesler and S. P. Cram, *Anal. Chem.*, 1971, **43**, 1922.
22. D. J. Anderson and R. R. Walters, *J. Chromatogr. Sci.*, 1984, **22**, 353.
23. M. A. Hernández Torres, M. G. Khaledi and J. G. Dorsey, *Anal. Chim. Acta*, 1987, **201**, 67.

Talanta, Vol. 39, No. 1, pp. 45–50, 1992
Printed in Great Britain.

0039-9140/92 $5.00 + 0.00

AMPEROMETRIC FLOW-INJECTION ANALYSIS OF HYDRAZINE BY ELECTROCATALYTIC OXIDATION AT COBALT TETRAPHENYLPORPHYRIN MODIFIED ELECTRODE WITH HEAT TREATMENT

WEIYING HOU, HUAMIN JI and ERKANG WANG*

Laboratory of Electroanalytical Chemistry, Changchun Institute of Applied Chemistry, Chinese Academy of Sciences, Changchun, Jilin 130022, People's Republic of China

(*Received* 4 *April* 1991. *Revised* 25 *May* 1991. *Accepted* 3 *June* 1991)

Summary—Chemically modified electrodes prepared by treating the cobalt tetraphenylporphyrin modified glassy-carbon electrode at 750° (HCME) are shown to catalyze the electrooxidation of hydrazine. The oxidation occurred at +0.63 V *vs.* Ag/AgCl (saturated potassium chloride) in pH 2.5 media. The catalytic response is evaluated with respect to solution pH, potential scan-rate, concentration dependence and flow-rate. The catalytic stability of the HCME is compared with that of the cobalt tetraphenylporphyrin adsorbed glassy-carbon electrode. The stability of the HCME was excellent in acidic solution and even in solutions containing organic solvent (50% CH_3OH). When used as the sensing electrode in amperometric detection in flow-injection analysis, the HCME permitted sensitive detection of hydrazine at 0.5 V. The limit of detection was 0.1 ng. The linear range was from 50 ng to 2.4 μg. The method is very sensitive and selective.

Hydrazines represent an important family of organic compounds with wide use in a number of industrial and pharmacological applications. Their detection and quantitation have attracted considerable analytical interest. As a consequence, recent activity has been directed toward the development of sensitive and selective analytical methods for the determination of hydrazines in a variety of sample matrices.

In recent years, electrochemical techniques have been shown to provide a sensitive and selective approach for the detection of numerous compounds following high-performance liquid chromatography.[1,2] The major requirement for the useful application of such electrochemical methods to liquid chromatography (LCEC) is that the analyte of interest should be oxidizable or reducible at a comparatively low potential. Unfortunately, many compounds of considerable analytical interest undergo electrolysis only at electrode potentials substantially different than their thermodynamic redox potentials. For these compounds, detection by LCEC usually cannot provide optimum levels of sensitivity and selectivity and extreme cases can provide no useful quantitation at all. One promising approach for minimizing overpotential effects is the use of electrocatalytic chemically modified electrodes (CMEs).

Baldwin's group and others have reported application of CMEs in high-performance liquid chromatography (HPLC)[3–16] or flow-injection analysis (FIA). Hydrazine has a large overpotential toward electrooxidation at ordinary carbon surfaces, and a high potential (>1.0 V) was essential for the detection of hydrazine in acidic solution. Therefore, it is not suited for quantitation via conventional electrochemical approaches. Baldwin's group used electrochemically treated glassy-carbon electrodes for the oxidative detection of hydrazine compounds in LC.[17] They also used carbon paste modified electrodes containing cobalt phthalocyanine (CoPC) for the oxidative detection of hydrazine in FIA.[3] Wang *et al.* used cobalt phthalocyanine/cellulose acetate (CoPC/CA) CMEs for oxidative detection of hydrazine and other compounds in FIA.[12] They also used glassy-carbon electrodes coated with mixed-valent ruthenium(II,III) cyanide films for oxidative detection of hydrazine compounds.[16] Dong *et al.* found that the metal (Fe, Co) tetraphenylporphyrin (FeTPP, CoTPP) modified glassy-carbon electrodes with heat treatment (HCME) exhibited excellent electrocatalytic stability towards the reduction of oxygen in

*To whom correspondence should be addressed.

acidic solution.[18,19] In this paper, we found firstly that the HCME exhibited strong electrocatalytic activity and excellent stability for the oxidation of hydrazine in acidic solution, and used the HCME for electrocatalytic and flow-injection–amperometric detection of hydrazine. We also examined the catalytic behaviour of hydrazine at the CoTPP adsorbed glassy-carbon electrode (CoTPP/GC).

EXPERIMENTAL

Reagents

The synthesis and purification of cobalt tetraphenylporphyrin were the same as in the literature.[19] Hydrazine sulphate was from the Beijing Institute of Chemical Reagents. Other reagents were analytical grade. Solutions were prepared with doubly-distilled water unless otherwise stated. Hydrazine sulphate solutions for use in flow-injection were prepared with the mobile phase.

Apparatus

A laboratory-built cyclic voltammetric analyser was used for cyclic voltammetry. A three-electrode cell system with a glassy carbon (GCE) or HCME working electrode, a silver-silver chloride (saturated potassium chloride) reference electrode, and a platinum auxiliary electrode was employed in the conventional electrochemical experiment.

The flow-injection system consisted of a JASCO LCP-350 pump, an injection valve (made in China) with a 10-μl sample loop, and a laboratory-built thin-layer flow-through electrochemical detector. A laboratory-built bipotentiostat[20] was used to control the detector. The injector and detector were connected by a 44-cm length of 0.5-mm inner diameter Teflon tube. The mobile phase was 0.1M potassium dihydrogen phosphate (containing 1mM EDTA). The flow-rate was 0.5 ml/min.

Electrode preparation

HCME. Glassy-carbon electrodes (GCE) (10 mm × 10 mm) were polished with 300-mesh magnesium oxide powder to a bright finish. The electrodes were then cleaned with distilled water and acetone respectively in an ultrasonic bath. These electrodes are referred to as the fresh bare electrodes. After drying, a small amount of CoTPP (about 0.5 mg CoTPP for six GCEs) was placed on the GC surface and the GC electrode was ground on another GC electrode, then placed into a 15-ml quartz tube filled with nitrogen gas. The latter was placed in a horizontal quartz furnace with autocontrol temperature equipment under a continuous flow of N_2. The temperature was increased slowly to 750°, held for one hour, and cooled to room temperature. The electrodes were then removed for electrochemical measurement. The resulting electrodes are referred to as the HCMEs.

CoTPP/GC electrode. A glassy-carbon electrode was polished with 0.3 μm of α-Al_2O_3 powder, added to $10^{-3}M$ CoTPP for several minutes and then cleaned with distilled water. The electrode is referred to as the CoTPP/GC electrode.

Fabrication of thin-layer flow-through electrochemical cell

The laboratory-built thin-layer electrochemical detector was similar to a conventional thin-layer electrochemical detector.[2] The effective cell volume is 1 μl. A saturated calomel reference electrode was employed.

RESULTS AND DISCUSSION

Cyclic voltammetric behaviour of hydrazine at the HCME

Figure 1 shows the cyclic voltamperograms in a conventional cell obtained for a GCE and a HCME (12.6 mm^2) immersed both in blank solution and containing 10mM hydrazine sulphate solution with different pH values. The cyclic voltamperograms of 10mM hydrazine in 0.2M potassium nitrate + 0.05M potassium dihydrogen phosphate (pH 2.5) shows that no obvious oxidation peak was obtained at a GCE in the potential range 0.2–1.2 V, while a well-defined oxidation peak with peak potential (E_p) of 0.63 V was observed at the HCME. Even after the reverse of the potential sweep, the catalytic oxidation peak still appears at the same E_p value, and no reduction wave was observed. The oxidation of hydrazine at the HCME is irreversible. In the reports of using a CME for electrocatalytic oxidation of hydrazine,[21–26] the catalytic oxidation peak still often appears after the reverse potential sweep.[23–26] From Fig. 1, the overpotential of hydrazine oxidation is greatly reduced and the oxidation current of hydrazine is enhanced by the use of the HCME. Also as shown in Fig. 1, when the pH of the supporting electrolyte increased, the E_p was shifted negatively and the peak current (i_p) increased. This suggests that hydrogen ions were produced in this reaction.[22,24] No obvious peak was observed when the pH was larger than 7.0.

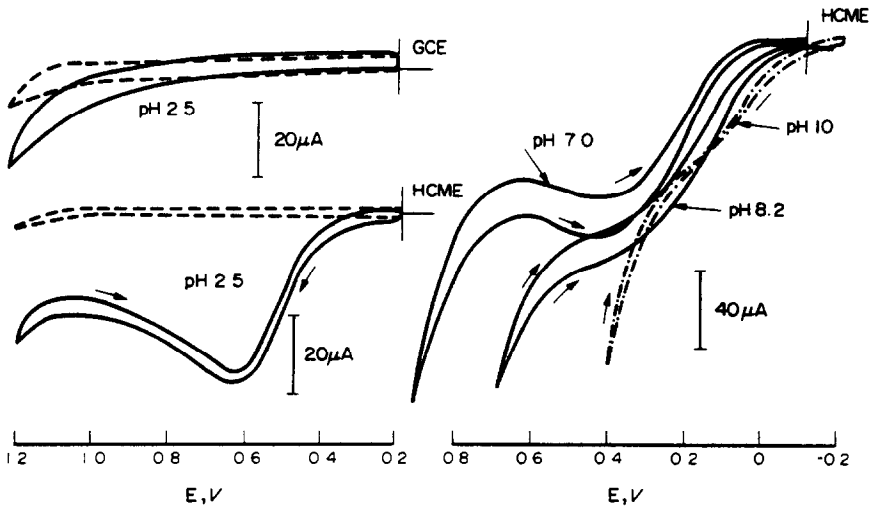

Fig. 1. Cyclic voltamperograms of hydrazine sulphate at a GCE and a HCME in 0.2*M* KNO_3 + 0.05*M* KH_2PO_4 solution with different pH values. (– – –): blank solution, (— · — · —): containing 10 m*M* hydrazine sulphate solution, scan-rate, 100 mV/sec.

The effect of the scan-rate, v, on i_p and E_p of cyclic voltammetry of hydrazine was examined over the 10–400 mV/sec range. The resulting i_p and E_p were not changed. So the oxidation process of hydrazine at a HCME was controlled by the kinetics of the catalytic reaction.

The catalytic stability of the HCME for the oxidation of hydrazine was examined in acidic and neutral electrolyte solution. After the HCME was scanned potentially for seven thousand cycles at 2 V/sec over the 0.2–1.2 V range in 0.2*M* potassium nitrate + 0.05*M* potassium dihydrogen phosphate solution (pH 2.5) containing 10m*M* hydrazine, the E_p, i_p and peak shape of the cyclic voltamperogram which was recorded at a scan-rate of 100 mV/sec were not changed. If the HCME was scanned over the 0–1.0 V range (2 V/sec) in pH 7.0 solution with the same conditions for five thousand cycles, the i_p was reduced to 70% of the initial value, and E_p moved slightly to a more positive potential. Moreover, the hydrazine oxidation on the HCME at both pH values produces gas, as can be observed from the numerous small bubbles on the surface of the HCME when the solution containing hydrazine was scanned potentially for many continuous cycles. We suggest that the gas is probably nitrogen gas, produced by 4-electron oxidation of hydrazine.

The above results show that the HCME exhibited strong electrocatalytic activity and excellent stability to the oxidation of hydrazine in acidic media.

We also examined the electrochemical behaviour of some other compounds [ascorbic acid, cysteine, oxalic acid, glucose, $NaNO_2$, KSCN and $K_4Fe(CN)_6$] at the HCME. The results of experiments indicated that the HCME did not exhibit electrocatalytic characteristics for these compounds. Otherwise, CoPC/CA modified glassy-carbon electrodes exhibited electrocatalytic activity to N_2H_4 at about 0.6 V, oxalic acid, ascorbic acid and cysteine,[12] while carbon paste modified electrodes containing CoPC exhibited electrocatalytic activity to N_2H_4 at −0.1 V,[3] cysteine,[4] oxalic acid,[5] carbohydrates,[6] and glassy-carbon electrodes coated with mixed-valent ruthenium(II,III) cyanide films exhibited electrocatalytic activity to N_2H_4[16] at 0.88 V, SCN^-[27] and cysteine.[28] The electrochemically pretreated glassy-carbon electrodes exhibited electrocatalytic activity to N_2H_4[17] at about 0.2 V, ascorbic acid[29] and oxalic acid.[29] It can be seen that the HCME exhibited higher selectivity toward the oxidation of hydrazine than the reported papers.[3,12,16,17] The specific modification scheme of the HCME which results in the different catalytic mechanisms from the CoPC modified carbon paste electrode is probably the reason for the highly selective reaction for hydrazine. Moreover, the stability of the HCME was better than in the reported papers[3,12,16,17] from the results of cyclic voltammetric experiments.

Cyclic voltammetric behaviour of hydrazine at a CoTPP/GC electrode

To make a comparison with the HCME, we examined the electrocatalytic behaviour of the

CoTPP/GC electrode toward the oxidation of hydrazine. Figure 2 shows cyclic voltamperograms obtained for a CoTPP/GC electrode immersed both in a blank solution and one containing 10mM hydrazine sulphate. A well-defined oxidation peak with an E_p of 0.69 V was observed at the CoTPP/GC electrode. After the reverse of the potential sweep, the catalytic oxidation peak also appears at the same E_p value, but the peak current was small. The twentieth cyclic voltamperogram was recorded in the potential range of 0.2 to 1.2 V at 100 mV/sec. The 650th cyclic voltamperogram was recorded at 100 mV/sec after 650 cycles at 2 V/sec. It can be seen that i_p decreased quickly before the tenth cycle and then decreased slowly. When the CoTPP/GC electrode was scanned for 10, 20 and 650 cycles, the i_p was respectively reduced to 47, 35 and 26% of the initial value. However, after the CoTPP/GC electrode was scanned for 10 cycles in the range 0–1.2 V at 100 mV/sec, it lost its electrocatalytic activity. This indicated that the CoTPP/GC electrode easily lost its electrocatalytic activity at high potentials (> 1.0 V).

The effect of the scan rate, v, on the i_p was evaluated over the 10 mV/sec–400 mV/sec range. The resulting dependence of i_p versus $v^{1/2}$ is linear, indicating diffusion control.

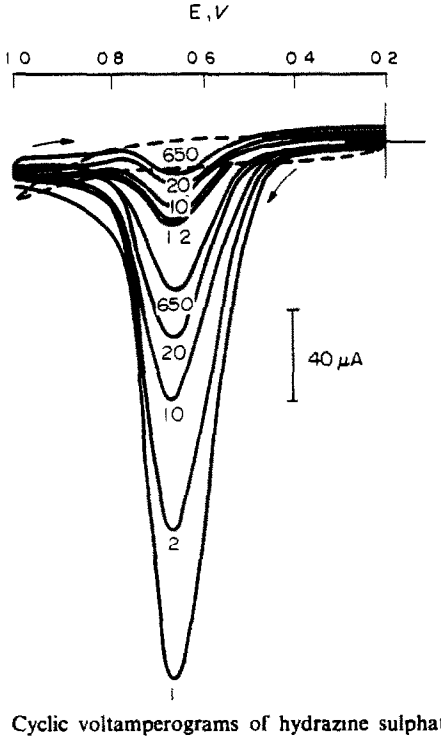

Fig. 2. Cyclic voltamperograms of hydrazine sulphate at CoTPP/GC electrode in 0.2M KNO_3 + 0.05M KH_2PO_4 (pH 2.5) solution. Scan rate, 100 mV/sec; (– – –): blank solution, (——): containing 10mM hydrazine sulphate solution; Figures refer to number of cyclic scans.

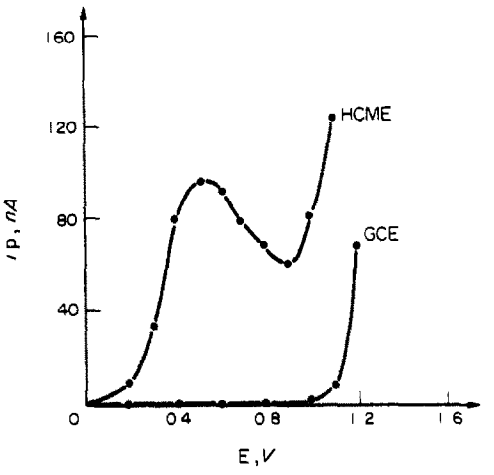

Fig. 3. Hydrodynamic voltamperograms of 20 ng/μl hydrazine sulphate at the GC electrode and 5 ng/μl hydrazine sulphate at HCME electrode. Mobile phase, 0.1M KH_2PO_4 (containing 1 mM EDTA), pH 4.5; flow-rate, 0.5 ml/min.

It can be seen that the electrocatalytic oxidation process of hydrazine was controlled by the kinetics of catalytic reaction at the HCME and was controlled by a diffusion reaction at a CoTPP/GC electrode. The HCME was very stable and reproducible to the electrocatalytic oxidation of hydrazine.

Flow injection amperometric detection of hydrazine

Despite some uncertainty concerning the catalysis mechanism, it was apparent that hydrazine oxidation at relatively low potentials produced by the use of the HCME should make its use attractive in a number of analytical applications. One area where their use could be of particular advantage is as sensing electrodes for the detection and determination of hydrazines in flowing systems. To this end, the response of the HCME placed in a laboratory-built thin-layer flow-through cell was examined.

Hydrodynamic voltamperograms (HDVs) obtained for hydrazine sulphate via flow-injection are shown in Fig. 3. The bare electrode (GCE) requires extremely high operating potentials to detect the hydrazines, and hence it exhibited large background currents and potential interferences. The HCME-based detector exhibits peak-shape HDVs with marked decreases in overpotentials. Such a peak-shaped response was observed previously at CoPC modified carbon paste electrodes.[4,5] An anodic

wave reached a maximum at approximately +0.5 V *vs.* SCE and rapidly decreased at higher potentials. Also provided for comparison is the HDV obtained at the bare glassy-carbon electrode which, as in CV, showed no response at potentials lower than +1.0 V. On the basis of the HDVs, it was apparent that the optimum potential for FIA detection of hydrazine sulphate at the HCME should be chosen at +0.5 V *vs.* SCE. The peaks in FIA are shown in Fig. 4 with a detection potential at +0.5 V. As expected, a well-formed oxidation peak was obtained at +0.5 V only when the HCME was employed and not for glassy-carbon electrodes.

The effect of the flow-rate on the i_p was evaluated over the 0.2–1.3 ml/min range. When the flow-rate was increased from 0.2–0.4 ml/min, the i_p decreased. When the flow-rate was increased from 0.4 ml/min to 1.3 ml/min, the i_p increased.

Stability problems often characterize the electrocatalytic response at the HCME-based detector. With a series of 40 replicate injections of a standard solution containing 20 ng/μl hydrazine sulphate within 1 hr, and 10 replicate injections within 6 hr, the coefficients of variation of peak current were found to be 2.2 and 4.5% respectively; the peak height after 6 hr was 83% of its initial value.

The concentration dependence of the HCME-based detector was evaluated for successive injections of hydrazine solutions of increasing concentration, 50 ng–2.4 μg (operating potential, +0.5 V). The electrocatalytic peak current increased linearly with increasing concentrations of hydrazine; the slope of the resulting calibration plot corresponded to a sensitivity of 2.2 nA/ng (correlation coefficient, 0.999). Similar injections of 1 ng/μl hydrazine solution were used to estimate the detection limit. The signal-to-noise characteristics (S/N = 3) indicated a detection limit of 0.01 ng/μl, *i.e.*, 0.1 ng in the 10 μl sample.

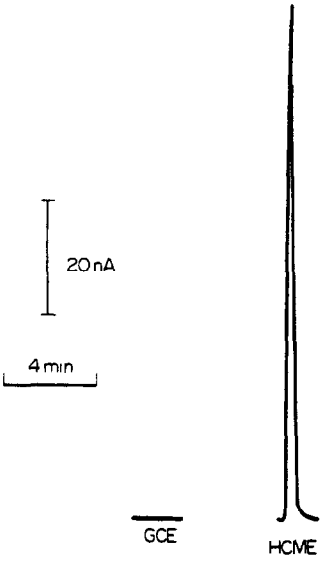

Fig. 4. Flow-injection responses of 5 ng/μl hydrazine sulphate at the GCE and the HCME at 0.5 V. Other conditions were the same as in Fig. 3.

Because practical chromatographic applications often required the use of a binary mobile phase containing substantial amounts of organic modifiers, it was important to establish whether the HCMEs were stable and retained their electrocatalytic properties in the presence of common organic solvents. Consequently, the effect of moderate fractions of methanol on the performance of the electrode in LCEC was also examined. This was accomplished by performing flow-injection experiments. During continuous flow-injection runs using 50% (v/v) CH_3OH/0.1*M* potassium dihydrogen phosphate (containing 1m*M* EDTA), 40 replicate injections within 1 hr and 14 replicate injections of 5 ng/μl hydrazine sulphate within 7 hr yielded coefficients of variation of 1.0 and 4.8% respectively; the peak height after 7 hr was 80% of its initial value, indicating that the HCME was stable even in the solution containing organic solvent.

From the above results, it can be expected that the HCME is especially suitable for electrochemical detection with liquid chromatographic separation because the HCME was stable in acidic solution and the solution containing organic solvent. Without question, the detection and quantitation of hydrazine in the flow-injection or LCEC context are greatly facilitated by the use of the cobalt tetraphenylporphyrin modified glassy-carbon electrode with heat treatment. In the wider sense, this work clearly illustrated some of the advantages which can be expected by use of judiciously selected electrocatalytic CMEs in flowing systems for the quantitation of high overpotential analytes. It would seem that, by use of electrocatalytic CMEs, the current range of applicability of FIA and LCEC technique might be considerably increased.

Acknowledgement—The support of the National Natural Science Foundation of China is gratefully acknowledged. We thank Lijuan Xu very much for her help in experimental equipment.

REFERENCES

1. L. R. Snyder and J. J. Kirkland, *Introduction to Modern Liquid Chromatography*, 2nd Ed, pp. 153–158. Wiley-Interscience: New York, 1979.
2. P. T. Kissinger, *Laboratory Techniques in Electroanalytical Chemistry*, P. T. Kissinger, W. R. Heineman (eds.), pp. 611–635. Dekker, New York, 1984.
3. K. M. Korfhage, K. Ravichandran and R. P. Baldwin, *Anal. Chem.*, 1984, **56**, 1514.
4. M. K. Halbert and R. P. Baldwin, *ibid.*, 1985, **57**, 591.
5. L. M. Santos and R. P. Baldwin, *ibid.*, 1986, **58**, 848.
6. *Idem*, *ibid.*, 1987, **59**, 1766.
7. S. V. Prabhu and R. P. Baldwin, *ibid.*, 1989, **61**, 2258.
8. A. M. Tolbert and R. P. Baldwin, *Anal. Lett.*, 1989, **22**, 683.
9. *Idem*, *Electroanalysis*, 1989, **1**, 389.
10. K. N. Thomsen and R. P. Baldwin, *Anal. Chem.*, 1989, **61**, 2594.
11. M. R. Gregg, *Chromatographia*, 1985, **20**, 129.
12. J. Wang, T. Golden and R. Li, *Anal. Chem.*, 1988, **60**, 1642.
13. G. G. Wallace, M. Meaney, M. R. Smyth and J. G. Vos, *Electroanalysis*, 1989, **1**, 357.
14. J. Wang and R. Li, *Talanta*, 1989, **36**, 279.
15. J. Wang and T. Golden, *Anal. Chim. Acta*, 1989, **217**, 343.
16. J. Wang and Z. Lu, *Electroanalysis*, 1989, **1**, 517.
17. K. Ravichandran and R. P. Baldwin, *Anal. Chem.*, 1983, **55**, 1782.
18. S. Dong and R. Jiang, *Ber. Bunsenges. Phys. Chem.*, 1987, **91**, 479.
19. P. Rothemund and A. R. Menotti, *J. Am. Chem. Soc.*, 1948, **70**, 1808.
20. H. Ji and E. Wang, *Anal. Chem.*, (*Chin.*), 1991, **19**, 976.
21. J. Zagal, E. Muñoz and S. Ureta-Zanartu, *Electrochim. Acta*, 1982, **27**, 1373.
22. S. Antoniadou, A. D. Jannakoudakis and E. Theodoridou, *Synthetic Metals*, 1989, **30**, 295.
23. J. Zagal, S. Lira and S. Ureta-Zañartu, *J. Electroanal. Chem.*, 1986, **210**, 95.
24. S. Autoniadou, A. D. Jannakoudakis, P. D. Jannakoudakis and E. Theodoridou, *Synthetic Metals*, 1989, **32**, 309.
25. J. Zagal and S. Ureta-Zañartu, *J. Electrochem. Soc.*, 1982, **129**, 2242.
26. T. Yiang and M. Wang, *Molecular Catalysis*, 1989, **3**, 218.
27. J. A. Cox, T. J. Gray and K. R. Kulkarni, *Anal. Chem.*, 1988, **60**, 1710.
28. J. A. Cox and T. J. Gray, *Electroanalysis*, 1990, **2**, 107.
29. K. Ravichandran and R. P. Baldwin, *J. Liq. Chromatog.*, 1984, **7**, 2031.

Talanta, Vol. 39, No. 1, pp. 51–53, 1992
Printed in Great Britain.

0039-9140/92 $5.00 + 0.00
Pergamon Press plc

DETERMINATION OF TRACE AMOUNTS OF GOLD IN WASTE WATER BY GRAPHITE FURNACE ATOMIC-ABSORPTION SPECTROPHOTOMETRY WITH PRECONCENTRATION ON TRIOCTYLPHOSPHINE OXIDE CHEMICALLY MODIFIED TUNGSTEN WIRE MATRIX

LU GUANGHAN
Department of Chemistry, Central China Normal University 430070, Wuhan, People's Republic of China

XU JINYA
Department of Chemistry, Zhe Jiang Normal University Hangzhou, People's Republic of China

XU TONGMING, JIN LITONG and FANG YUZHI
Department of Chemistry, East China Normal University, Shanghai, People's Republic of China

(*Received* 3 *January* 1991. *Revised* 21 *May* 1991. *Accepted* 4 *June* 1991)

Summary—Preconcentration on a trioctylphosphine oxide (TOPO) chemically modified tungsten wire matrix followed by graphite furnace atomic-absorption spectrophotometry measurement is described for the determination of trace gold in waste water. The TOPO modified tungsten wire matrix, after accumulating the gold, is placed in a graphite cup for direct atomization and measurement. Under the selected conditions, the absorbance is proportional to the concentration of gold over the range 0.4–18 ng/ml and the detection limit is 0.2 ng/ml. This method is sensitive and convenient. It has been applied to some waste waters with satisfactory results.

The determination of trace Au(III) is significant in the exploration of gold mines and the recovery of gold. There are several methods for the determination of gold. For example, atomic-absorption spectrometry,[1–7] liquid chromatography,[8] anodic-stripping voltammetry,[9,10] polarography,[11,12] ion-selective electrodes[13,14] and spectrophotometry[15–18] have been employed for the determination of traces of gold. However, some of these methods require strictly controlled experimental conditions while the sensitivity of others is not high enough for determining trace amounts of gold. In this work, TOPO is adsorbed onto a tungsten wire matrix. Traces of gold are preconcentrated on the TOPO modified tungsten wire matrix which is then transferred into a graphite cup for direct atomization and measurement by atomic-absorption spectrometry. The entire procedure is very simple, including the preparation of the TOPO–tungsten wire matrix.

EXPERIMENTAL

Apparatus

A Hitachi 180-80 polarized Zeeman atomic-absorption spectrophotometer was used. In the preconcentration step, the solution was stirred with a Teflon-covered stirring bar, rotated by a magnetic stirrer (78-HW).

Reagents

All solutions were prepared from doubly-distilled water. A stock standard solution containing 1 mg/ml of gold in 1*M* hydrochloric acid was used to prepare secondary standard solutions. Trioctylphosphine oxide (TOPO) $5 \times 10^{-3}M$ was prepared in ethanolic solution.

Procedure

Preparation of TOPO modified tungsten wire matrix. Wind the tungsten wire (diameter 0.5 mm) into a coil (diameter 3 mm, Fig. 1) and add 6 μl of $5 \times 10^{-3}M$ ethanolic TOPO onto the tungsten wire coil with a micro-syringe. Dry under an IR lamp for 2 min. TOPO melts in the process and attaches itself firmly onto the tungsten wire coil.[19]

General procedure. Transfer measured amounts of standard Au(III) solution or 2 ml of waste water sample into a 50-ml standard flask, add 10 ml of 5*M* hydrochloric acid, and dilute to the mark with water. Transfer it into a

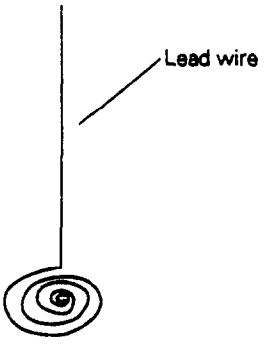

Fig. 1. Tungsten wire coil.

beaker. Submerge the TOPO modified tungsten wire coil in the solution, start the magnetic stirrer, and preconcentrate for 2 min. Then remove the TOPO modified tungsten wire coil from the beaker and blot with filter paper. The TOPO modified tungsten wire coil is then transferred to the graphite cup (Fig. 2). The lead wire (Fig. 1) is near the side of the cup wall to avoid the light path. After this, start the atomization procedure and measure the absorbance under the conditions given in Table 1.

Table 1. Atomization conditions

Gold lamp current	10 mA
Wavelength	243 nm
Bandpass	1.3 nm
Sheathing gas (Ar) flow-rate	200 ml/min
Drying temperature and time	80–120°, 10 sec
Ashing	400°, 20 sec
Atomization temperature and time	2700°, 7 sec
Cleaning temperature and time	2800°, 3 sec

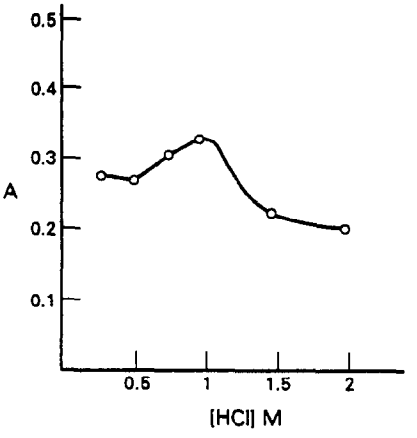

Fig. 3. Relationship between the absorbance and concentration of hydrochloric acid. Au(III), 10 ng/ml.

RESULTS AND DISCUSSION

Effect of the concentration of hydrochloric acid

Comparative tests of various media, such as acetic acid, sulphuric acid and potassium chloride were studied. Among these media, hydrochloric acid was found to be best. Variation of the concentration of hydrochloric acid from 0.3 to 2*M* was investigated. The result indicated that the optimum condition for the determination of gold is to have a medium of 1*M* hydrochloric acid. (Fig. 3).

Effect of amount of TOPO

Figure 4 shows the dependence of absorbance on the amount of TOPO solution used. Because of the strongly polar nature of the P-O groups in TOPO, the extraction of gold from acidic solutions by TOPO is very effective. Au(III) can form a complex with TOPO in 1*M* hydrochloric acid. The reaction can be expressed as follows:[20]

$$HAuCl_4 + TOPO = [TOPO \cdot H]\,[AuCl_4]$$

Figure 4 shows that, between 0 and 6 μl, the more TOPO on the surface of the tungsten wire coil, the larger the absorbance. Without TOPO modification, a pure tungsten wire coil does not preconcentrate gold. When TOPO is above 6 μl, the absorbance varies only slightly. Therefore 6 μl of TOPO solution is recommended.

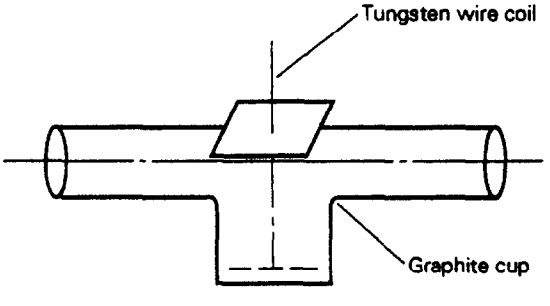

Fig. 2. Position of tungsten wire coil in graphite cup.

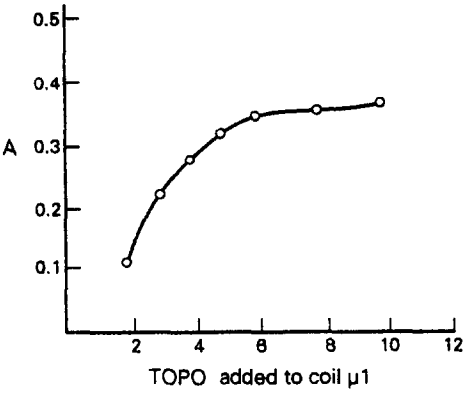

Fig. 4. Dependence of absorbance on the modification amount of TOPO. Au(III), 10 ng/ml.

Table 2. Results for the recovery of gold from waste water

Sample	Au(III) added, *ng*	Au(III) found, *ng*	Recovery, *%*
1	—	2.7	
	2.0	4.9	110
2	—	2.6	
	2.0	4.5	95
3	—	1.5	
	2.0	3.7	110

Effect of preconcentration time

The longer the preconcentration time, the more gold is adsorbed, and the longer the absorbance. With times above 8 min, the preconcentration quantity would tend to saturate, so the absorbance varies slightly with preconcentration time. It takes only 2 min to preconcentrate because preconcentration for 2 min can meet the requirement when the sample is determined. Higher sensitivity with less critical timing can be reached by using longer preconcentration time.

Relationship between concentration of Au(III) and absorbance

Under the selected conditions, a linear relation was obtained between absorbance and concentration of Au(III) in the range of 0.4–18 ng/ml, the detection limit is 0.2 ng/ml for 2 min preconcentration time.

Reproducibility

A tungsten wire coil was treated with TOPO 8 times, under previously selected conditions and the absorbance for each modification was measured to give a coefficient of variation of 1.8%. This shows that the results obtained with the TOPO tungsten wire are in good agreement with each other.

Effect of foreign ions

The experimental results show that amounts of 1000-fold Ca(II), Mg(II), 100-fold Zn(II), Al(III), Cu(II), Pb(II), Fe(III), Ti(IV), Cr(III), Co(II), Cd(II), Ba(II), K^+, NO_3^-, SO_4^{2-}, 50-fold As(III), Hg(II), Na^+, Ag^+, PO_4^{3-}, 20-fold Bi(III), Ni(II) do not interfere in the determination of gold.

Sample analysis

The recovery of gold added to three different waste water samples (2 ml) is shown in Table 2. Recoveries at the 1 ng/ml level were 95–110%.

REFERENCES

1. T. Pal and A. Ganguly, *Indian J. Chem., Sect. A*, 1988, **27A**, 987.
2. J. Fazakas, *Rev. Roum. Chim.*, 1982, **27**, 685.
3. E. D. Prudnikov, Yu. S. Shapkina, *Zh. Anal. Khim.* 1983, **38**, 2019.
4. J. M. Vermeulen, *J. Anal. At. Spectrom.*, 1989, **4**, 77.
5. Zhicheng Ma and Fan Zhang, *Fenxi Huaxue*, 1988, **16**, 713.
6. Guangzhang Ma and Yahui Wang, *Fenxi Shiyanshi*, 1988, **7**, 11.
7. Le Houillier and C. Deblois, *Analyst*, 1986, **111**, 291.
8. P. R. Haddad and N. E. Rochester, *Anal. Chem.*, 1988, **60**, 536.
9. Zhang Y. X. and Wang C. M., *Mikrochim. Acta*, 1984 **I**, 291.
10. M. Lintern, A. Mann and D. Longman, *Anal. Chim. Acta.*, 1988, **209**, 193.
11. Yilong Ma, Peibiao Li and Zaofan Zhao, *Fenxi Shiyanshi*, 1986, **5**, 1.
12. T. D. Gornostaeva and S. V. Longunova, *Zavod. Lab.*, 1983, **49**, 5.
13. Dezhong Dan and Peifang Xu, *Fenxi Huaxue*, 1987, **15**, 706.
14. Wenfang Zhang, Yong Du and Fengjun Zou, *ibid.*, 1987, **15**, 565.
15. Zhicheng Ma, Xiaoning Zhu, Yiguo Tian and Jian Ye, *ibid.*, 1983, **11**, 759.
16. Guofo Zhang, *Lihua Jianyan*, 1987, **23**, 297.
17. S. G. Nagarkar and M. C. Eshwar, *Anal. Chim. Acta.*, 1974, **71**, 461.
18. Xinmin Li and Changsong Liu, *Fenxi Huaxue*, 1983, **11**, 30.
19. Tongmin Xu, Zhujun, Zhuping Bai and Litong Jin, *Fenxi Shiyanshi*, 1988, **7**, 1.
20. K. Kalcher, H. Greschong and R. Pietsch, *Z. Anal. Chem.*, 1987, **327**, 513.

Talanta, Vol. 39, No. 1, pp. 55–62, 1992
Printed in Great Britain.

039-9140/92 $5.00 + 0.00

STUDY OF HETEROGENEOUS EQUILIBRIA IN SATURATED SOLUTIONS OF SOME SPARINGLY SOLUBLE 8-HYDROXYQUINOLINES

TOMISLAV J. JANJIĆ* and LIDIJA B. PFENDT
Faculty of Chemistry, University of Belgrade, P.O., Box 550, 11001 Belgrade, Yugoslavia

MIRJANA B. ALEKSIĆ
Faculty of Pharmacy, University of Belgrade, 11001 Belgrade, Yugoslavia

(*Received* 15 *April* 1991. *Revised* 25 *June* 1991. *Accepted* 25 *June* 1991)

Summary—Heterogeneous equilibria in saturated aqueous solutions of 8-hydroxyquinoline (A), 2-methyl-8-hydroxyquinoline (B) and 5-chloro-8-hydroxyquinoline (C) were investigated at constant ionic strength (1*M* sodium chloride), at 25.0 ± 0.1°, by the application of the following methods: the formation function method, the method of bound protons, the method of free proton sites and the solubility method. The following equilibrium constants were determined: $K_{s1} = [H_2A^+]/[H_3O^+]$, $K_{s2} = [HA]$ and $K_{s3} = [H_3O^+][A^-]$. Their mean *pK* values are: −2.88, 2.42 and 12.09 for A, −3.27, 2.71 and 12.73 for B, and −0.34, 3.88 and 12.75 for C. In addition, the acidity constants of investigated 8-hydroxyquinolines were determined by pH-metric titrations. The values obtained for these constants were consistent with those calculated on the basis of corresponding equilibrium constants determined in heterogeneous systems.

Heterogeneous equilibria in saturated solutions of sparingly soluble protolytes have been poorly investigated to date. Besides other applications, such investigations offer the possibility of calculating the distribution of the equilibrium species as a function of pH in corresponding heterogeneous systems and consideration of the buffer properties of these systems which represent two-phase buffers.[1–6] All this is of particular interest for such analytical reagents and pharmacologically active substances which are sparingly soluble protolytes.

In our previous papers we have investigated systems in which the solid phase was a sparingly soluble acid[1–4] or base.[5,6] Continuing these investigations, in this work we have studied equilibria in systems containing sparingly soluble ampholytes, namely: 8-hydroxyquinoline, 2-methyl-8-hydroxyquinoline and 5-chloro-8-hydroxyquinoline. All these compounds are important analytical reagents.[7]

The methods used in this study are described in our previous papers but when necessary they were adapted for investigation of ampholytes. Among the aforementioned ampholytes only heterogeneous equilibria of 8-hydroxyquinoline[8–10] have hitherto been investigated, but by other methods and under different experimental conditions.

EXPERIMENTAL

The following apparatus was used: a PHM-62 pH meter (Radiometer) with a glass-calomel electrode assembly; a TTT-60 titrator with an ABU-12 autoburette (Radiometer) and a Beckman DU-2 spectrophotometer.

All reagents used were of analytical reagent grade from Merck. Stock solutions of sodium hydroxide and hydrochloric acid were standardized pH-metrically and the solutions of investigated ampholytes were prepared by weighing dry substances and dissolving them in hydrochloric acid. The investigations were carried out at constant ionic strength (1*M* sodium chloride) and at 25 ± 0.1°. The calibration of the pH-meter and the measurement of hydronium ion activity are described in our previous paper.[5] The pc_H and pc_{OH} values were calculated from measured pH values (pH_{GE}) by using the following equations: $pc_H = pH_{GE} + 0.10$, $pK_w^c = pc_H + pc_{OH} = 13.74 \pm 0.01$. Stock solutions for the determination of equilibrium constants in heterogeneous systems were $1 \times 10^{-1}M$ relative to 8-hydroxyquinoline and 2-methyl-8-hydroxyquinoline in $1 \times 10^{-1}M$ hydrochloric

*Author for correspondence.

acid, and $1 \times 10^{-2}M$ relative to 5-chloro-8-hydroxyquinoline in $1.5 \times 10^{-2}M$ hydrochloric acid.

Aliquots of 20 ml of these solutions were made alkaline with sodium hydroxide solution on account of solid phase separation, and were kept at constant temperature with vigourous stirring. The equilibration time was followed pH-metrically and amounted to 3–5 min. From pH_{GE} values measured at equilibrium state, the formation function, *i.e.*, the mean number of protons bound per mole of the ampholyte, was calculated. Solutions were then separated from the insoluble part by centrifugation. Aliquots of these solutions were titrated pH-metrically with sodium hydroxide or hydrochloric acid and from data obtained the concentration of protons which are or can be bound to species originating from the investigated ampholytes in the solution, was calculated. From other parts of these solutions the stoichiometric solubility of investigated ampholytes was determined. Solutions were acidified with hydrochloric acid until pH = 1.0 and the actual concentration of the corresponding 8-hydroxyquinolines was determined spectrophotometrically. Measurements were made at 355, 350 and 375 nm, *i.e.*, at the absorption maxima of 8-hydroxyquinoline, 2-methyl-8-hydroxyquinoline and 5-chloro-8-hydroxyquinoline, respectively; the validity of Beer's law was verified previously. The acidity constants were determined by the classical pH-metric titration of the corresponding hydrochlorides with standard sodium hydroxide. The concentrations of titrated solutions were: 8-hydroxyquinoline, $2.5 \times 10^{-3}M$; 2-methyl-8-hydroxyquinoline, $1 \times 10^{-3}M$; and 5-chloro-8-hydroxyquinoline, $2 \times 10^{-4}M$.

In the processing of experimental data, corrections were made for volume changes; the data were processed by means of suitable programs with a Texas Instrument TI-66 programmable calculator.

RESULTS AND DISCUSSION

In saturated aqueous solutions of investigated ampholytes, the following equilibria may take place between the solid phase and (HA)s and the solution:

$$(HA)_s + H_3O^+ \rightleftharpoons H_2A^+ + H_2O$$

$$K_{s1} = \frac{[H_2A^+]}{[H_3O^+]} \qquad (1)$$

$$(HA)_s \rightleftharpoons HA$$

$$K_{s2} = [HA] \qquad (2)$$

$$(HA)_s + H_2O \rightleftharpoons H_3O^+ + A^-$$

$$K_{s3} = [H_3O^+]\,[A^-] \qquad (3)$$

The corresponding equilibrium constants were determined by the application of the formation function method, the method of bound protons and the method of free proton sites, as well as by the stoichiometric solubility method. These methods were described in our previous papers,[1-6] but in this work they were adapted for the study of heterogeneous equilibria of sparingly soluble ampholytes. In view of the fact that acid–base processes in ampholyte solutions are separated since $pK_{a2} > (pK_{a1} + 4)$, in the solution in which $pH < (pK_{a2} - 2)$ it may be assumed that $[A^-] \rightarrow 0$, whereas in the solution of $pH > (pK_{a1} + 2)$, it may be taken that $[H_2A^+] \rightarrow 0$.

In addition, the acidity constants of investigated ampholytes K_{a1} and K_{a2} ($K_{a1} = [H_3O^+][HA]/[H_2A^+]$; $K_{a2} = [H_3O^+][A^-]/[HA]$) were determined according to the Rossotti–Rossotti method.[11]

Formation function method

This method is based on the determination of the mean number of protons bound per mole of the ampholyte:

$$\bar{n}_{tot} = \frac{2[H_2A^+] + [HA] + [HA]_s}{C_{tot}^{app}} \qquad (4)$$

In equation (4) $(HA)_s$ corresponds to the number of moles of the ampholyte which are precipitated from one litre of the solution, and C_{tot}^{app} denotes the apparent stoichiometric concentration of the ampholyte, *i.e.*, the concentration which would be present in the solution, provided the total amount of the precipitate is dissolved.

From mass-balance it follows that:

$$C_{tot}^{app} = [H_2A^+] + [HA] + [A^-] + [HA]_s \qquad (5)$$

The combination of equations (1) and (3) with equations (4) and (5) gives the following relation:

$$C_{tot}^{app}(\bar{n}_{tot} - 1) = K_{s1}[H_3O^+] - \frac{K_{s3}}{[H_3O^+]} \qquad (6)$$

In case $[A^-] \rightarrow 0$ we find:

$$C_{tot}^{app}(\bar{n}_{tot} - 1) = K_{s1}[H_3O^+] \qquad (7)$$

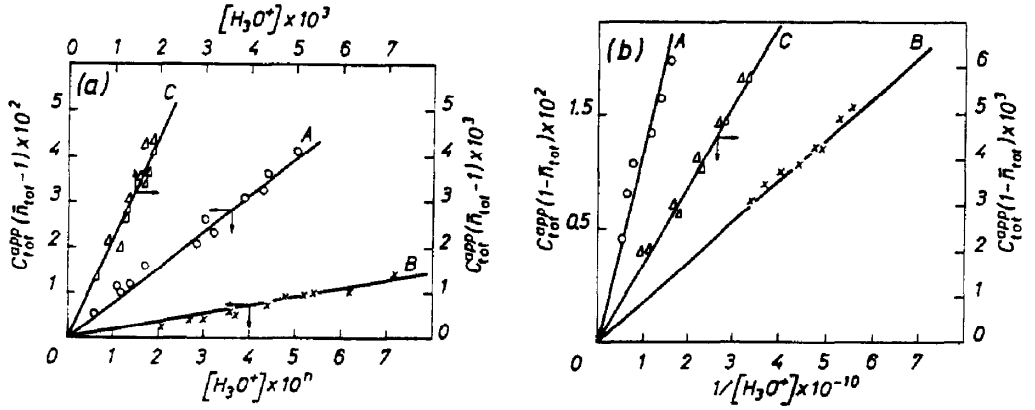

Fig. 1. Plots of (a) $C_{tot}^{app}(\bar{n}_{tot}-1)$ *vs.* $[H_3O^+]$ and (b) $C_{tot}^{app}(1-\bar{n}_{tot})$ *vs.* $1/[H_3O^+]$, used for the determination of equilibrium constants by the formation function method. A denotes 8-hydroxyquinoline ($C_{tot}^{app}=1\times10^{-1}M$), B 2-methyl-8-hydroxyquinoline ($C_{tot}^{app}=1\times10^{-1}M$), C 5-chloro-8-hydroxyquinoline ($C_{tot}^{app}=1\times10^{-2}M$); $I=1M$ (NaCl), $t=25°$; $n=5$ for A and 6 for B.

whereas in case $[H_2A^+]\to0$ we obtain the relation:

$$C_{tot}^{app}(1-\bar{n}_{tot})=\frac{K_{s3}}{[H_3O^+]} \tag{8}$$

From the dependences given by equations (7) and (8) the corresponding equilibrium constants K_{s1} and K_{s2} for all three investigated ampholytes were calculated by linear regression analysis (Fig. 1). For the calculation of $\bar{n}_{tot}$ from experimental data the following relation was used:

$$\bar{n}_{tot}=\frac{C_{tot}^{app}+[Cl^-]+[OH^-]-[H_3O^+]-[Na^+]}{C_{tot}^{app}} \tag{9}$$

where $[Cl^-]$ and $[Na^+]$ denote the concentrations of Cl^- and Na^+ ions originating from added hydrochloric acid and sodium hydroxide, respectively. The concentration of H_3O^+ ions was calculated from measured pH_{GE} values, and the concentration of OH^- from the corresponding ion product of water.

Method of bound protons and method of free proton sites

The concentration of bound protons, $[H_b^+]$, in saturated solutions of ampholytes is given by the following equation:

$$[H_b^+]=2[H_2A^+]+[HA] \tag{10}$$

By combining equations (1), (2) and (10) we obtain:

$$[H_b^+]=2K_{s1}[H_3O^+]+K_{s2} \tag{11}$$

Equation (11) offers the possibility of calculating K_{s1} and K_{s2} in acidic solutions. $[H_b^+]$ is experimentally determined from data obtained by pH-metric titration of saturated acidic solutions of ampholytes with sodium hydroxide by means of the following dependence:

$$[H_b^+]=[Na^+]-[H_3O^+] \tag{12}$$

The concentration of free proton sites, $[H_f^+]$, in saturated solutions is given by the following relation:

$$[H_f^+]=[HA]+2[A^-] \tag{13}$$

The combination of equations (2), (3) and (13) gives:

$$[H_f^+]=K_{s2}+2\frac{K_{s3}}{[H_3O^+]} \tag{14}$$

Equation (14) makes the calculation of equilibrium constants K_{s2} and K_{s3} in alkaline solutions possible. Experimentally $[H_f^+]$ is determined by the pH-metric titration of saturated alkaline solutions of ampholytes with hydrochloric acid according to the following relation:

$$[H_f^+]=[Cl^-]-[OH^-] \tag{15}$$

By applying the linear regression analysis to the corresponding dependences expressed by equations (11) and (14) all three equilibrium constants in heterogeneous systems of investigated ampholytes were calculated (Fig. 2).

Solubility method

This method is based on the spectrophotometric determination of the stoichiometric solubility, S, of investigated ampholytes at different pH values:

$$S=[H_2A^+]+[HA]+[A^-] \tag{16}$$

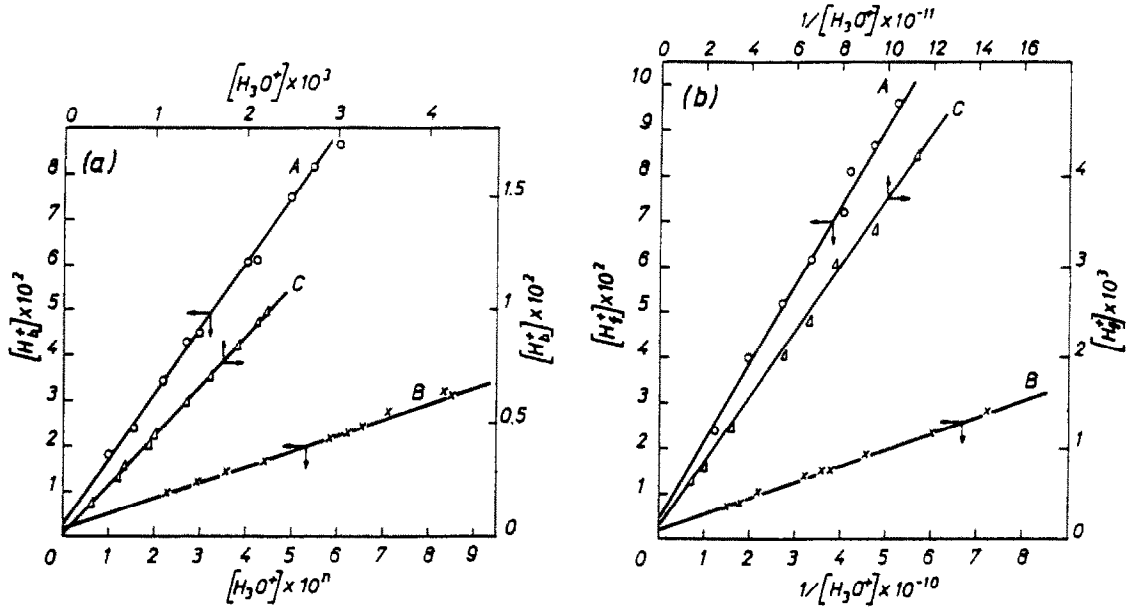

Fig. 2. Plots of (a) $[H_b^+]$ *vs.* $[H_3O^+]$ and (b) $[H_f^+]$ *vs.* $1/[H_3O^+]$, used for the determination of equilibrium constants by the methods of bound protons and of free proton sites, respectively. $I = 1M$ (NaCl), $t = 25°$; $n = 5$ for A and 6 for B; A, B and C as in Fig. 1.

From equations (1)–(3) and equation (16) the following dependence is obtained:

$$S = K_{s1}[H_3O^+] + K_{s2} + \frac{K_{s3}}{[H_3O^+]} \qquad (17)$$

When $[A^-] \to 0$

$$S = K_{s1}[H_3O^+] + K_{s2} \qquad (18)$$

and when $[H_2A^+] \to 0$ the following relation is obtained:

$$S = K_{s2} + \frac{K_{s3}}{[H_3O^+]} \qquad (19)$$

On the basis of dependences expressed by equations (18) and (19) all three equilibria constants were calculated by linear regression analysis (Fig. 3).

Determination of acidity constants

The acidity constants were experimentally determined by the pH-metric titration of solutions according to the Rossotti–Rossotti method.[11] Since the protolytic processes of investigated ampholytes are separated, the acidity constants can be determined independently

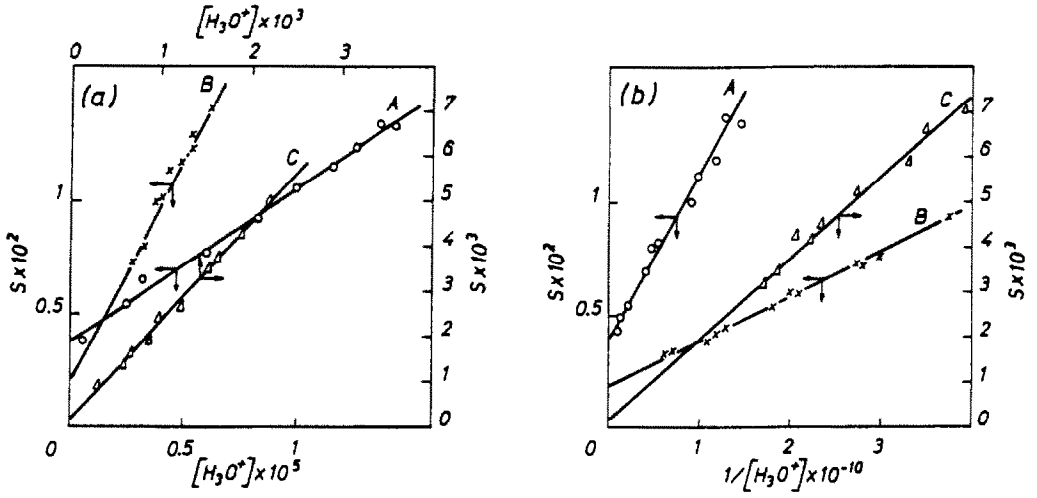

Fig. 3. Plots of (a) S *vs.* $[H_3O^+]$ and (b) S *vs.* $1/[H_3O^+]$ used for the determination of equilibrium constants by the solubility method. $I = 1M$ (NaCl), $t = 25°$; A, B and C as in Fig. 1.

Table 1. Concentration equilibrium constants ($\bar{x} \pm \sigma/\sqrt{n}$) in the heterogeneous and homogeneous systems studied. $I = 1M$ (NaCl); $t = 25°$

Investigated ampholyte	Equation employed	Heterogeneous systems			Homogeneous systems			
					Calculated*		Found†	
		pK_{s1}	pK_{s2}	pK_{s3}	pK_{a1}	pK_{a2}	pK_{a1}	pK_{a2}
8-Hydroxyquinoline	(7)	-2.95 ± 0.01						
	(8)			12.07 ± 0.06				
	(11)	-2.87 ± 0.05	2.44 ± 0.05		$5\,30 \pm 0.08$			
	(14)		2.42 ± 0.06	12.06 ± 0.06		9.63 ± 0.08		
							5.22 ± 0.01	9.60 ± 0.02
	(18)	-2.83 ± 0.01	2.41 ± 0.02		5.24 ± 0.02			
	(19)		2.40 ± 0.02	12.14 ± 0.01		9.73 ± 0.02		
2-Methyl-8-hydroxyquinoline	(7)	-3.27 ± 0.04						
	(8)			12.74 ± 0.05				
	(11)	-3.24 ± 0.01	2.70 ± 0.05		5.94 ± 0.04			
	(14)		2.70 ± 0.02	12.74 ± 0.02		10.04 ± 0.02		
							5.93 ± 0.04	9.96 ± 0.04
	(18)	-3.31 ± 0.02	2.7 ± 0.1		6.02 ± 0.06			
	(19)		2.73 ± 0.02	12.70 ± 0.07		9.99 ± 0.07		
5-Chloro-8-hydroxyquinoline	(7)	-0.33 ± 0.02						
	(8)			12.76 ± 0.06				
	(11)	-0.34 ± 0.04	3.9 ± 0.1		4.24 ± 0.1			
	(14)		3.82 ± 0.01	12.75 ± 0.01		8.93 ± 0.01		
							4.19 ± 0.02	8.95 ± 0.02
	(18)	-0.34 ± 0.05	3.9 ± 0.1		4.24 ± 0.09			
	(19)		3.89 ± 0.05	12.75 ± 0.05		8.88 ± 0.09		

*Calculated according to equation (23) and (24), respectively.

†By pH-metric titration in a homogeneous system.

from one another. For their calculation the following equations were used:

$$K_{a1} = [H_3O^+]\frac{2-\bar{n}_H}{\bar{n}_H - 1}, \quad (\bar{n}_H > 1) \qquad (20)$$

$$K_{a2} = [H_3O^+]\frac{1-\bar{n}_H}{\bar{n}_H}, \quad (\bar{n}_H < 1) \qquad (21)$$

The value $\bar{n}_H$ was calculated from experimental data according to the following expression:

$$\bar{n}_H = \frac{C_{tot} + [Cl^-] + [OH^-] - [H_3O^+] - [Na^+]}{C_{tot}} \qquad (22)$$

where C_{tot} denotes the stoichiometric concentration of ampholytes.

In addition, the acidity constants of investigated ampholytes were calculated from the corresponding equilibrium constants in heterogeneous systems, with the following dependences:

$$pK_{a1} = pK_{s2} - pK_{s1} \qquad (23)$$

$$pK_{a2} = pK_{s3} - pK_{s2} \qquad (24)$$

The equilibrium constants determined in this paper are summarized in Table 1, which shows that there is a good agreement among the constants determined by different methods. Small differences among them, as well as the differences in the range of standard deviations of individual mean values, can be understood if we take into account the fact that the equilibria in a heterogeneous system are affected by the quality of the separated precipitate which, as it is known, depends on a number of factors being not easily controlled.[12] However, a good accordance between the acidity constants determined in the solution by the pH-metric titration method and those calculated from equilibrium constants determined in the corresponding heterogeneous systems, point not only to the correctness of the equilibria assumed, but also to the reliability of the constants determined. This is of a particular interest for indirect determination of acidity constants in cases where, on account of a small protolyte solubility and similarities in absorption spectra of various protolyte species, the application of the classical pH-metric and spectrophotometric methods are not possible.

As already mentioned heterogeneous equilibria have so far been investigated only for 8-hydroxyquinoline. In all cases the method used was the bromometric determination of its solubility at 25°. Stone and Friedman[8] found $pK_{s2} = 2.21$ (0.1M borax–sodium carbonate buffers), whereas Irving *et al.*[9] reported 2.32 (various buffers, $I = 0.1M$). Klygin and Kolyada[10] found $pK_{s1} = -2.71$, pK_{s2} 2.35 and pK_{s3} 12.10 (ionic strength is not specified). The

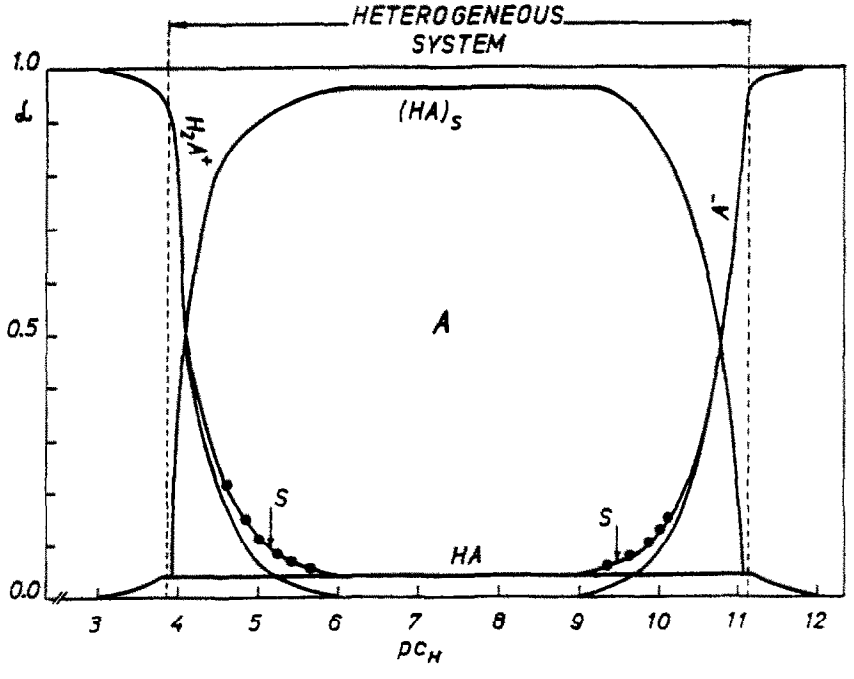

Fig. 4(A).

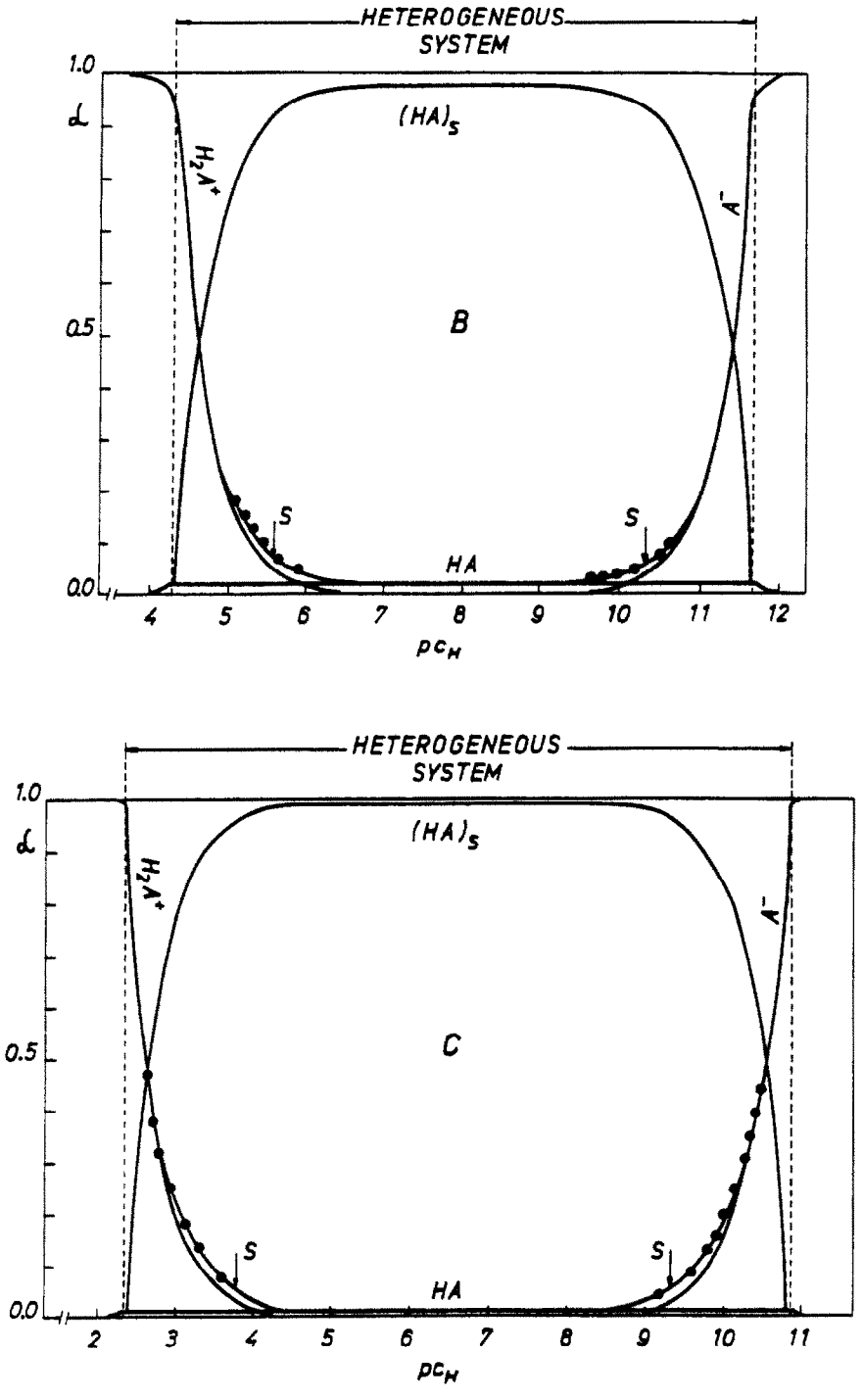

Fig. 4. Distribution diagrams and solubility curves (S) in the function of pc_H; (●●●●) experimental data; A, B and C as in Fig. 1.

results reported by these authors, although obtained from the solutions of different electrolytes and ionic strengths, are in relatively good accordance with our results.

On the basis of pK-values determined, the distribution of all equilibrium species in the function of pc_H was calculated by the usual procedure[13] (Fig. 4.) In addition, by differentiating equation (17) and by setting $dS/dpc_H = 0$ we obtained the equation for the calculation of the pc_H value at which the solubility of the investigated ampholytes is the lowest:

$$(pc_H)_{min_S} = \frac{pK_{s3} - pK_{s1}}{2} \quad (25)$$

By using equation (25) the $(pc_H)_{min_S}$ values were calculated for 8-hydroxyquinoline, 2-methyl-8-hydroxyquinoline and 5-chloro-8-hydroxyquinoline to be 7.48, 8.00 and 6.54, respectively.

The equilibrium constants determined in this work, in addition to other applications, are indispensable for the calculation of buffer characteristics of two-phase buffer systems consisting of a sparingly soluble ampholyte as the solid phase and its saturated solution (buffered phase), which will be a subject for our further investigation.

Acknowledgement—The authors are grateful to the Serbian Republic Research Fund for financial support.

REFERENCES

1. T. J. Janjić, L. B. Pfendt and M. B. Ćelap, *J. Inorg. Nucl. Chem.*, 1979, **41**, 1019.
2. T. J. Janjić, L. B. Pfendt and M. B. Pasulj, *Glasnik Hem. Društva Beograd*, 1980, **45**, 443.
3. *Idem*, *Monatsh. Chem.*, 1984, **115**, 125.
4. *Idem*, *ibid.*, 1984, **115**, 705.
5. L. B. Pfendt, D. M. Sladić, T. J. Janjić and G. V. Popović, *Analyst*, 1990, **115**, 383.
6. L. B. Pfendt, T. J. Janjić and G. V. Popović, *ibid.*, 1990, **115**, 1457.
7. J. M. Korenman, *Organicheskie Reagenty v Neorganicheskom Analize*, *Spravochnik*, 1st Ed., p. 150. Khimiya, Moskva, 1980.
8. K. G. Stone and L. Friedman, *J. Am. Chem. Soc.*, 1947, **69**, 209.
9. H. Irving, J. A. D. Ewart and J. T. Wilson, *J. Chem. Soc.*, 1949, 2672.
10. A. E. Klygin and N. S. Kolyada, *Zh. Neorgan. Khim.*, 1958, **12**, 2767.
11. F. J. C. Rossotti and H. Rossotti, *The Determination of Stability Constants*, 1st Ed., p. 110. McGraw-Hill, New York, 1961.
12. L. Sůcha and S. Kotrlý, *Solution Equilibria in Analytical Chemistry*, 1st Ed., p. 211. van Nostrand, London, 1972.
13. *Idem*, *ibid.*, 1st Ed., p. 74. van Nostrand, London, 1972.

Talanta, Vol. 39, No 1, pp. 63–68, 1992
Printed in Great Britain.

0039-9140/92 $5.00 + 0.00

CALCON-MODIFIED SILICA GEL SORBENT. APPLICATION TO PRECONCENTRATION OR ELIMINATION OF TRACE METALS

R. KOCJAN and S. PRZESZLAKOWSKI
Department of Inorganic and Analytical Chemistry, Medical Academy, 20-081 Lublin, Poland

(*Received* 17 *November* 1990. *Revised* 10 *June* 1991. *Accepted* 10 *June* 1991)

Summary—Silica gel impregnated with a mixture of Aliquat 336 and Calcon was used as chelating sorbent for preconcentration of metals from dilute aqueous solutions and their separation as well as for additional purification of analytical grade sodium and potassium salts from other metals. The relative capacities of sorbent towards 33 metal ions were determined in the pH range 1–9 as well as the concentrations of hydrochloric and perchloric acid eluting the retained metals. It was found that Calcon was not eluted from sorbent with 5*M* perchloric and 10*M* hydrochloric acids. The rate of sorption for Mg, Ca, Cu, Zn, Al, Cr(III) and Fe(III) was also studied and it was found that relatively high flow-rates (up to 5 ml/min) can be used for solutions passed through the column. The sorbent was used for preconcentration of traces of some metals from aqueous solutions before their determination by AAS, for separation of metal ion mixtures by column extraction chromatography and for additional purification of potassium chloride solutions used as supporting electrolyte in determination of some heavy metals by anodic stripping voltammetry.

The determination of trace elements often requires their preconcentration and separation from a matrix of macroamounts of other metals.[1] On the other hand, the use of very sensitive analytical methods for metals requires the reagents of a very high purity which are used in preliminary chemical operations. One of the most commonly used methods for preliminary concentration of metals from aqueous solution is based on the utilization of chelating sorbents and many such materials containing different chelating groups have been proposed.[2] However, the synthesis of such sorbents is difficult and except the chelating resin containing aminoacetic groups (known as Chelex), others are not commercially available. The chelating sorbents can be obtained in a very simple manner by the impregnation of silica gel with a mixture of Aliquat 336 (methyltricaprylammonium chloride) and chelating reagent containing sulphonic groups,[3] since it was found that many such reagents are very strongly extracted into solutions of liquid anion exchangers in organic solvents.[4–9] Several silica gels modified in this way with nitroso-R-salt,[10,11] thorin,[12] Eriochrome Black T,[13,14] Chromotrope 2B[15] and calconecarboxylic acid[16] have been described but the disadvantage of them (except the last one) was the partial elution of the chelating reagent with perchloric or hydrochloric acid solutions of the concentration required for elution of metals forming very stable chelating complexes which makes impossible the use of the same column in several sorption–elution processes.

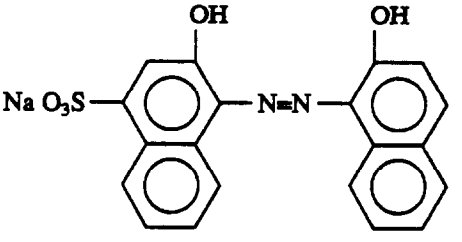

A molecule of Calcon (a reagent used as indicator in complexometric titrations[17] and in colorimetric determination of calcium and magnesium[18]) is more hydrophobic than the molecules of chelating reagents used earlier and therefore the properties of silica gel modified with Calcon and some applications of this sorbent are described in this paper.

EXPERIMENTAL

All experiments were done at room temperature (21 ± 2°).

Reagents

Aliquat 336 (Fluka, Switzerland) was purified to remove iron. Calcon (Merck, FRG) was used as supplied without further purification. Silica

gel 100, 0.063–0.2 mm (Merck, FRG) previously fractionated (the fraction of particle size 0.1–0.2 mm being collected) and purified from iron in the manner described previously[10] was used as a support for the stationary phase.

Aqueous metal ion solutions

Aqueous metal ion solutions were prepared by dilution of Titrisol standard metal salt solutions (Merck, FRG) or were prepared from appropriate analytical grade reagents (nitrate of Ag, Hg(I), U(VI), Ga, In, Bi, La, Th or $K_2Cr_2O_7$ and K_2TeO_3). Working solutions were freshly prepared from standard metal salt solutions by dilution with doubly-distilled water and adjusted to an appropriate pH with a mixture of hydrochloric acid and potassium chloride (pH 1 and 2), tartrate buffer (pH 3–6) or borax buffer (pH 9). Solutions of perchloric and hydrochloric acids (Suprapur, Merck, FRG) were used as eluents.

Apparatus

A single beam AAS 1N (Zeiss, GDR) atomic-absorption spectrophotometer was used for determination of Ca, Mg, Sr, Cu, Fe, Co, Ni, Zn, Cd, Mn, Ag, Pb and Hg; barium, sodium and potassium were determined by flame emission spectrometry. Other metals were determined spectrophotometrically with a UV–Vis VSU 2P spectrophotometer (Zeiss, GDR). All pH measurements were made with a Mera-Elwro N 517 (Poland) direct reading pH meter with a glass-calomel electrode assembly. A voltammetric analyser UPE-2a (Radius, Poland) was used in determination of traces of lead, cadmium, copper and zinc in potassium chloride or sodium chloride solutions by anodic stripping voltammetry. A graphite electrode, impregnated with epoxy resin and coated with a mercury film *in situ* was used as a working electrode with a working area of 12.5 mm^2. The details of the preparation of this electrode were described by Sykut *et al.*[19]

Procedure

The impregnating solution was prepared by shaking an appropriate volume of 0.01*M* Aliquat 336 in freshly distilled chloroform with 5 volumes of 0.001*M* aqueous Calcon. After separating the phases, the organic phase was filtered through a cellulose filter to remove the remaining aqueous solution. Silica gel was impregnated with a chloroform solution of Aliquat 336 plus Calcon in the following manner. A 200-ml volume of the organic solution (containing 1 mmole of Calcon and 2 mmoles of Aliquat 336) was mixed with 8.63 g of silica gel. The diluent was then evaporated with a vacuum evaporator on a water bath. The chelating sorbent obtained contained 0.1 mmoles of Calcon and 0.2 mmoles of Aliquat 336.

Small glass columns (110 × 5 mm) dry packed with 0.4 g of sorbent were used for the determination of the relative capacities of the sorbent toward metal ions. A 10-ml volume of the solution containing 1 mg of the metal ion to be tested (previously adjusted to an appropriate pH) was passed through the column over a period of 10 min, and unretained metal was determined in the eluate by AAS or spectrophotometrically.

The influence of the contact time on the relative capacity of the sorbent towards some chosen metal ions was investigated by the static method. The sorbent (0.4 g) was then shaken with 5 ml of the metal salt solution (previously adjusted to pH 6 except iron where the pH was adjusted to 1) containing 0.3 mg of the metal ion investigated. The mixture was subsequently centrifuged and the metal ion in the solution was determined.

The influence of the flow-rate on the capacity of the sorbent was investigated by using small columns packed with 0.4 g of the sorbent. A 5-ml volume of the solution containing 0.3 mg of the metal ion being tested was then passed through the column and unretained metal was determined in the eluate. The flow-rate was regulated with a syringe pump.

In a similar manner column experiments were performed under conditions where the relative capacity of the sorbent was somewhat higher (about 25%) than the amount of metal ion in the solution being passed through the column. Columns packed with 0.5 g of the sorbent were then used and 5-ml volumes of the solution were passed through the column.

Glass columns (249 × 8 mm) dry packed with 5 g of sorbent were used for the separation of metal ion mixtures. After the column had been washed with 10 ml of pH 5 buffer solution, a 10-ml volume of the synthetic solution of pH 5 containing 100 μg of each metal ion separated was passed through the column. The metals were eluted with perchloric acid solutions, 5-ml fractions being collected. Elution under hydrostatic pressure (head pressure 380 mm H_2O) was used. Metals were determined in single fractions by AAS or spectrophotometrically.

Voltammetric determination of metals was performed in the following manner. Volumes of 10 ml of 0.5*M* potassium chloride (analytical grade) to which mercuric nitrate was subsequently added [the concentration of $Hg(NO_3)_2$ in the resulting solution was $10^{-4}M$] were passed through the column packed with 5 g of the sorbent. The column packed with 1 g of sorbent was used only when doubly distilled water or sodium chloride Suprapur solution was analysed. Into one previously purified potassium chloride solution 2 μl volumes of standard Cu^{2+}, Cd^{2+}, Pb^{2+} and Zn^{2+} ions of 100 ppm concentration were introduced (concentration of each metal ion added in the solution was then 20 ppb). Oxygen was removed from analysed solutions with a stream of argon of a special purity. The solutions were (except one sample) electrolysed for 3 min at -1.2 V. Anodic oxidation of metals was subsequently performed at the following conditions: amplitude 1.2 V; potential change of 10 mV/sec.

RESULTS AND DISCUSSION

The relative affinities of inorganic and simple organic anions to strongly basic solid or liquid anion exchangers have been described in many papers and apparent equilibrium constants were collected in several monographic books,[20,21] the highest affinity always being found for perchlorate ions. Since extraction of chelating reagents containing sulphonic groups by Aliquat 336 can be described with simple anion exchange reactions, the relative affinities of anions of sulphonated chelating reagents to Aliquat 336 can be at least qualitatively compared on the basis of displacement of these anions from the ion-pair by anions of strong mineral acids: stripping the reagents from their organic solutions or elution of these coloured anions from impregnated silica gels. Several such quantitative data for Alizarin Red S, stripped or eluted with different acids have been estimated recently[22,23] and it has been found that, in both cases, the ability of anions displacing this reagent increased in the following order: $CH_3COO^- < SO_4^{2-} < Cl^- < NO_3^- < ClO_4^-$. In preliminary experiments performed presently it was found that Calcon is very strongly extracted from aqueous solutions into Aliquat 336 in chloroform and a partial elution of this chelating reagent from silica gel impregnated with a mixture of Aliquat 336 and Calcon required high concentrations of 5*M* perchloric or 10*M* hydrochloric acids which suggested a very high stability of this ion pair.

The concentrations of both acids at which partial elution of various sulphonated chelating reagents from modified silica gels (6, 11–15, 24) begins are collected in Table 1. The data are comparable since each sorbent contained 0.1 mmoles of the reagent per g and 0.2 mmoles (reagents containing one sulphonic group) or 0.4 mmoles (other reagents) of Aliquat 336. These results suggest that the stabilities of ion-pairs composed with an alkylammonium cation and an anion of the reagent increase in the following order: ferron < nitroso-R-salt < Chromotrope 2B ~ Alizarin Red S < Calmagit < Titan yellow < calconecarboxylic acid < Calcon; the hydrophobicity of these reagents increase in the same order.

The relative capacities of silica gel modified with Calcon toward some chosen metal ions (estimated by the static method) depended on shaking time: maximal values of the capacity for magnesium, calcium and zinc were reached relatively quickly whereas for aluminium and chromium longer shaking times (60 and 75 min) were required. Maximal capacity values toward aluminium and chromium distinctly decreased with increasing flow-rate of the solution passed through the column packed with sorbent (maximal values at very low flow-rates—up to 0.2 ml/min—were reached), contrary to magnesium, calcium and zinc, when the sorbent capacities remained constant even at a high flow-rate of 5 ml/min. These results suggest that the main factor determining the sorption kinetics is the speed of complex formation which is especially low

Table 1. Concentrations (*M*) of hydrochloric and perchloric acids to give elution of the chelating reagent from silica gel impregnated with a mixture of Aliquat 336 and sulphonated chelating reagent (sorbents contained 0.1*M* of the reagent per g)

	Ferron	Nitroso-R-salt	Chromotrop 2 B	Alizarin Red S	Calmagit	Titan Yellow	Calone-carboxylic acid	Calcon
HCl	0.1	0.5	2	2	5	5	10	10
$HClO_4$	0.005	0.005	0.005	0.005	0.07	0.5	2.5	5

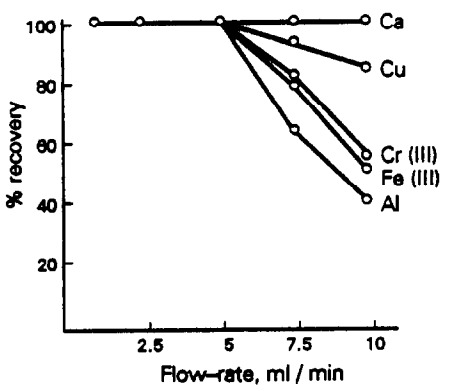

Fig. 1. Percent recovery of some metals as a function of flow-rate of the solution passed through the column packed with silica gel modified with Calcon.

for inert aquocomplexes of aluminium and chromium.

However, when the concentrations of metals in aqueous solution were lower than the maximal capacities of the sorbent, the quantitative retention even for chromium and aluminium was reached at high flow-rates of the solution passed through the column, up to 5 ml/min^{-1}, see Fig. 1.

The relative capacities of silica gel modified with Calcon toward metal ions are differentiated and for all metals increase with the pH of the aqueous metal salt solution. It should be added that relative capacities toward such metals as aluminium and chromium should be somewhat higher than the values given in Table 2 since the capacities were estimated at relatively high elution rates (1 ml/min).

All retained metals can be eluted from the sorbent with dilute solutions of mineral acids (0.1*M* perchloric acid or 1*M* hydrochloric acid, see Table 2) which do not elute Calcon from the sorbent, making it possible to repeat the sorption–elution process many times in the same column. The column can be regenerated in a simple manner; by washing with doubly distilled

Table 2. The relative capacities of silica gel modified with Calcon toward metal ions (micromoles/g) and minimal concentrations of acid (*M*) required for elution (1 g of the chelating sorbent contained 0.1 mmoles of calcon and 0.2 mmoles of Aliquat 336)

	Sorption at pH									Elution	
Metal	1	2	3	3.5	4	4.5	5	6	9	HCl	$HClO_4$
Na	0	0	0	0	0	—	—	0	0	—	—
K	0	0	0	0	0	—	—	0	0	—	—
Mg	0	0	0	0	0.2	2.8	4.3	18.2	32.7	0.001	0.0005
Ca	0	0	0	0	0.2	2.1	4.1	17.4	30.2	0.001	0.0005
Sr	0	0	0	0	0.1	1.7	3.2	11.2	21.0	0.001	0.0005
Ba	0	0	0	0	0.1	1.6	3.1	10.4	16.2	0.001	0.0005
Al	0	0	2.3	3.0	4.4	—	—	6.6	*	0.05	0.01
Ga	2.6	5.4	*	*	*	—	—	*	*	1.0	0.1
In	0.7	1.5	2.5	*	*	—	—	*	*	1.0	0.1
Tl(I)	1.2	2.4	4.5	6.3	7.6	—	—	10.8	17.0	1.0	0.1
Pb	0	0	2.0	2.8	4.1	—	—	5.8	9.7	—	0.01
As(III)	0	0	1.5	2.2	3.1	—	—	5.1	7.2	0.05	0.01
Sb(III)	1.5	*	*	*	*	—	—	*	*	1.0	0.1
Bi(III)	1.7	*	*	*	*	—	—	*	*	1.0	0.1
Se(IV)	0	0.7	4.1	4.7	5.5	—	—	8.1	12.4	0.1	0.05
Te(IV)	0	1.3	3.3	3.8	4.3	—	—	6.0	10.1	0.1	0.05
Ti(IV)	1.3	2.6	5.1	5.6	6.1	—	—	7.4	16.8	1.0	0.1
V(V)	1.8	2.5	3.8	4.0	4.3	—	—	6.1	10.1	1.0	0.1
Cr(III)	0	0.9	4.7	5.2	6.3	—	—	8.3	12.3	0.1	0.05
Cr(VI)	0	1.0	4.9	5.3	6.5	—	—	9.2	14.8	0.1	0.05
Mo(VI)	0	2.2	6.9	6.3	7.9	—	—	10.1	17.0	0.1	0.05
W(VI)	0	2.2	4.8	5.4	6.4	—	—	9.6	17.1	0.1	0.05
Mn(II)	0	0	6.5	10.0	12.6	—	—	11.2	23.0	0.05	0.01
Fe(III)	4.6	*	*	*	*	—	—	*	*	0.5	0.1
Co	0	1.2	3.6	4.8	6.1	—	—	10.1	16.7	0.1	0.05
Ni	0	1.3	3.8	5.4	7.9	—	—	11.2	17.0	0.1	0.05
Cu	0.8	2.9	6.6	8.1	10.1	—	—	14.5	25.0	0.5	0.1
Ag	0	0.7	1.8	2.0	2.2	—	—	4.3	8.4	—	0.01
Zn	0	0	1.0	1.5	3.2	—	—	6.2	12.5	0.05	0.01
Cd	0	0	0.9	1.6	2.8	—	—	5.3	10.2	0.05	0.01
Hg(I)	0	0	0.5	0.9	1.5	—	—	2.6	5.0	—	0.01
Hg(II)	0	0	0.8	1.2	1.9	—	—	3.0	6.1	0.05	0.01
La	0	0	1.2	1.7	2.1	—	—	3.9	5.6	0.05	0.01
Th	0	0	1.7	2.1	2.9	—	—	4.4	9.5	0.05	0.01
U(VI)	0	0	1.3	1.8	2.4	—	—	3.7	8.6	0.05	0.01

*Hydrolysis or metal hydroxide precipitate.

water to remove the mineral acid solution used as eluent.

Although in the experimental conditions used some metals could be retained by a sorbent containing an excess of quaternary alkyl-ammonium chloride relative to the amounts of Calcon also in the form of simple anions (SeO_3^{2-}, TeO_3^{2-}, MoO_4^{2-} and $Cr_2O_7^{2-}$ or CrO_4^{2-}) or chloride complexes [some metals retained from solutions of pH 1 and 2 buffered with a mixture of HCl and KCl are Fe(III), Bi, Sb, In], the increase of the relative capacity of the sorbent with pH for other metal ions indicate their retention in the form of metal complexes with Calcon.

Different concentrations of mineral acids eluting various retained metals from the sorbent can be utilized for the separation of metal ion mixtures and some examples extractive–chromatographic separations performed are illustrated by Fig. 2. It should be added that the chromatographic bands were relatively sharp even for metals [Bi, Fe(III) and Sb] which should hydrolyse in the pH 5 solutions introduced into the column—recoveries for these metals were higher than 96%.

One experiment was performed for separation of traces of some metals from macroamounts of alkali or alkaline earth metals. A 100-ml volume of the synthetic aqueous solution was adjusted to pH 3.5 with tartrate buffer. The solution contained 1% Na, 0.14% Mg, 0.04% Ca and K, and 5×10^{-5}% Zn, Cu and Fe(III). This solution was passed through the column packed with 5 g of the sorbent. After the column had been washed with 15 ml of doubly distilled water, the unretained metals (Ca, Mg, Na and K) were found in the collected eluate. The retained metals (Cu, Zn and Fe) were then eluted with 5 ml of 0.5*M* perchloric acid and determined in the eluate by AAS. Recoveries higher than 95% were found for each retained metal ion. Thus the proposed sorbent can be utilized for preconcentration of traces of heavy metals from aqueous solutions and for elimination of the matrix effect of alkali and alkaline earth metals in the determination of heavy metals by conventional analytical methods.

Since all metals except alkali metals are retained from aqueous solutions of pH $\geqslant 4$ on silica gel modified with Calcon, it was expected that this sorbent can find application in additional purification of alkali metal salts. Voltamperograms for potassium chloride solutions illustrated by Fig. 3 confirmed this supposition: it was found that analytical grade

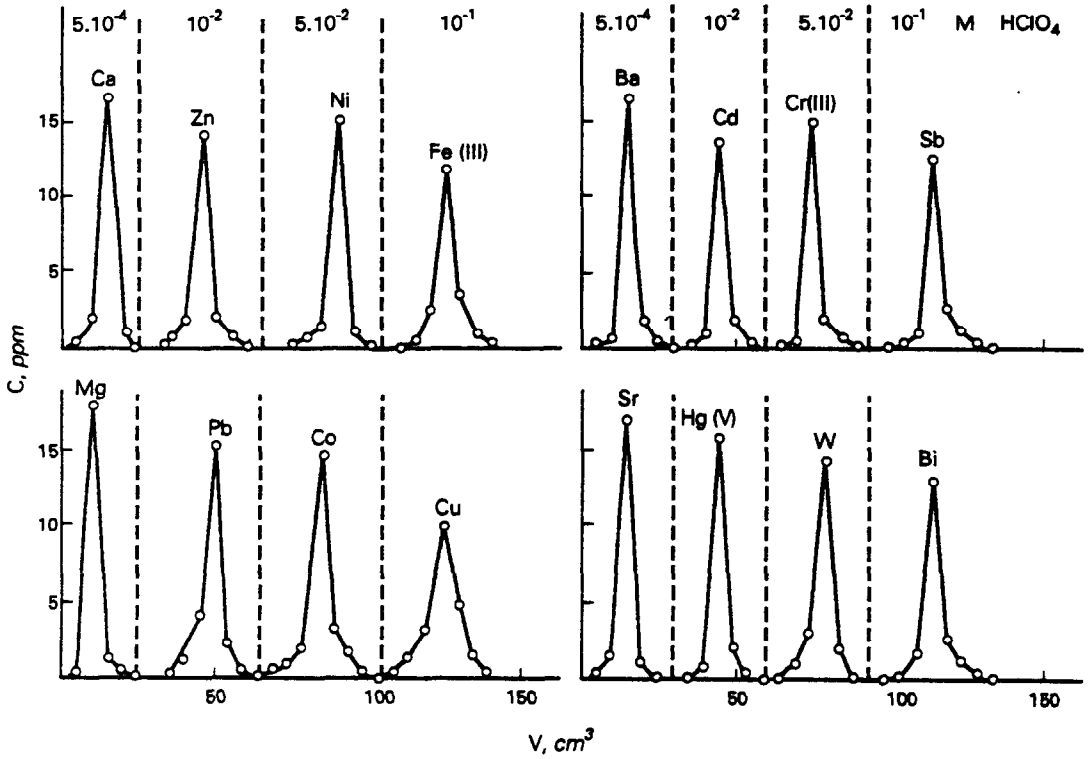

Fig. 2. Separations of some synthetic mixtures of metals containing 100 μg of each metal ion to be separated. Mean flow-rate 1 ml/min.

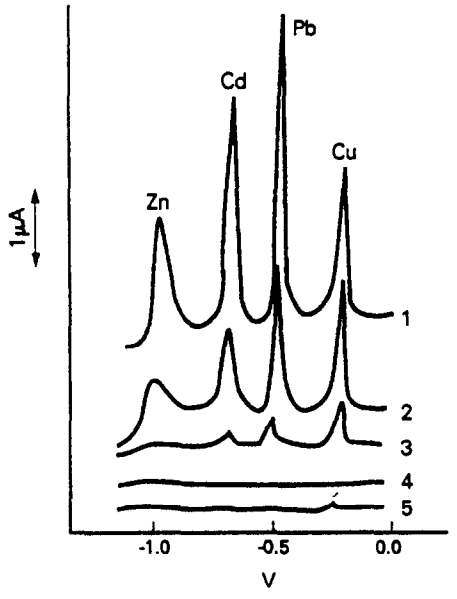

Fig. 3. Voltamperograms for 10-ml volumes of 0.5*M* potassium chloride solutions after 3 min electrolysis at −1.2 V. Curves:
1—solution of KCl containing 20 ppb of Cu, Pb, Cd and Zn
2—unpurified solution of analytical grade KCl
3—9 ml of doubly distilled water + 1 ml of purified KCl solution
4—KCl solution after passing through the column packed with silica gel modified with Calcon
5—as in curve 4 but after 10 min electrolysis.

potassium chloride solution which is usually used as a supporting electrolyte in polarography and anodic stripping voltammetry, contained considerable amounts of Cu, Cd, Pb and Zn. It was also found that even doubly distilled water (to which a purified solution of potassium chloride was added) and aqueous solutions of sodium chloride Suprapur contained traces of these metals, especially copper and lead. After passing potassium chloride solutions through the column packed with modified silica gel, these metals were removed and only traces of copper were found after elongated electrolysis (10 minutes instead normally used 3 minutes). Thus, in author's opinion, columns packed with silica gel modified with Calcon can be useful for simple purification of supporting electrolyte solutions used in determination of several metals (especially of Pb and Cd) by ASV in various materials which makes it possible to utilize the very high sensitivity of this method which is normally limited by impurities present in supporting electrolyte and in doubly distilled water.

Acknowledgement—This work was supported by the Institute of Chemistry of the Maria Curie-Skłodowska University in Lublin/Grant No. PR.I.08/.

REFERENCES

1. A. Mizuike, *Enrichment Techniques for Inorganic Trace Analysis*, Springer Verlag, 1983.
2. G. V. Myasoedova and S. B. Savvin, *Khelatoobrazuyushchie sorbenty*, Nauka, Moscov, 1984.
3. S. Przeszlakowski, E. Soczewiński, R. Kocjan, J. Gawecki and Z. Michno, *Polish Patent 128 743*, November 1985.
4. S. Przeszlakowski and H. Wydra, *Chromatographia*, 1981, **14**, 685.
5. *Idem, ibid.*, 1982, **15**, 301.
6. S. Przeszlakowski and E. Habrat, *Analyst*, 1982, **107**, 1320.
7. S. Przeszlakowski and H. Wnuk, *Chem. Anal. (Warsaw)*, 1985, **30**, 535.
8. S. Przeszlakowski, *ibid.*, 1988, **33**, 617.
9. R. Kocjan and S. Przeszlakowski, *ibid.*, 1988, **33**, 753.
10. S. Przeszlakowski and R. Kocjan, *Chromatographia*, 1982, **15**, 717.
11. R. Kocjan and S. Przeszlakowski, *Chem. Anal. (Warsaw)*, 1988, **33**, 419.
12. S. Przeszlakowski and R. Kocjan, *Chromatographia*, 1984, **17**, 266.
13. *Idem, Analyst*, 1985, **110**, 1077.
14. S. Przeszlakowski, R. Kocjan and I. Cukrowski, *Chem. Anal. (Warsaw)*, 1986 **31**, 735.
15. R. Kocjan, *ibid.*, in the press.
16. R. Kocjan and S. Przeszlakowski, *Sep. Sci. and Technol.*, 1989, **24**, 291.
17. K. L. Cheng, *Chemist Analyst*, 1956, **45**, 79.
18. C. N. Railley and G. P. Hildebrandt, *Anal. Chem.*, 1959, **31**, 1763.
19. K. Sykut, I. Cukrowski and E. Cukrowska, *J. Electronal. Chem.*, 1980, **115**, 137.
20. B. Trémillon, *Les Separations par les Resines Exchangeuses d'Ions*, Gauthier Villars, Paris, 1965.
21. A. S. Kertes, Y. Marcus and E. Yanir, *Equilibrium Constants of Liquid–Liquid Distribution Reactions, Part 2. Alkylammonium Salts Extractants*, Butterworths, London, 1974.
22. S. Przeszlakowski, *Chem. Anal. (Warsaw)*, in the press.
23. S. Przeszlakowski and M. Maliszewska, *ibid.*, in the press.
24. R. Kocjan, *unpublished results.*

Talanta, Vol. 39, No. 1, pp 69–72, 1992
Printed in Great Britain.

0039-9140/92 $5.00 + 0.00
Pergamon Press plc

OXIDANTS FOR THE COLORIMETRIC DETERMINATION OF PINDOLOL

M. S. MAHROUS, A. S. ISSA and N. S. AHMED

Department of Pharmaceutical Chemistry, Faculty of Pharmacy, University of Alexandria, Alexandria, Egypt

(*Received* 22 *May* 1991. *Revised* 24 *April* 1991. *Accepted* 23 *May* 1991)

Summary—A simple, sensitive and accurate colorimetric method is described for the quantitative determination of pindolol either in the pure form or in its tablets. The method is based on the oxidation of the indole moiety in pindolol with potassium persulphate or hydrogen peroxide—in acid medium—to give a highly coloured product that exhibits maximum absorption at 535 nm and 570 nm, respectively. Beer's law is obeyed over concentrations ranging from 0.07–0.35 mg/10 ml for potassium persulphate and 0.1–0.5 mg/10 ml for hydrogen peroxide with mean recoveries of 99.6 ± 0.6 and 99.8 ± 0.9%, respectively. The method is applied for the assay of pindolol tablets without any interference due to tablet fillers.

Pindolol is a B-adrenergic receptor blocking agent. It is used in the treatment of hypertension and to reduce the incidence of attacks in angina pectoris.

Pindolol has been determined by a non-aqueous titration method.[1] It was also determined spectrophotometrically,[2–4] colorimetrically[5,6] and fluorimetrically where excitation is at 263 nm and emission at 305 nm.[7] Thin-layer chromatography was also used for pindolol determination.[8]

The present work is concerned with the ability of pindolol, which is an indole derivative, to be oxidized with potassium persulphate or hydrogen peroxide. The oxidation leads to the development of a highly coloured oxidation product that can be used for the quantitative colorimetric determination of pindolol.

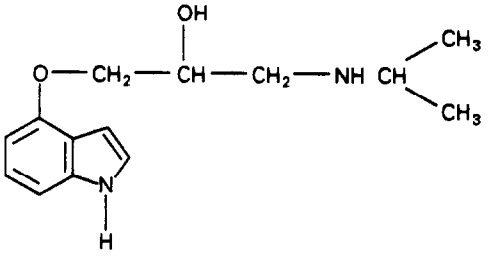

Scheme 1

EXPERIMENTAL

Instrumentation

Perkin–Elmer Model 550S spectrophotometer with matched 1-cm quartz cells was used.

Reagents

Potassium persulphate solution, 0.1% w/v.
Hydrogen peroxide solution, 5% w/v.
3-Sulphuric acid (AR), 96% w/v.

Materials

Pharmaceutical grade pindolol (Sandoz Co.).
Visken tablets, 5 mg pindolol/tablet (Sandoz Co.).

Preparation of calibration curves

A series of 1–5 ml portions of an alcoholic solution containing 0.07 mg/ml pindolol for potassium persulphate or 0.1 mg/ml for hydrogen peroxide was transferred to 10-ml measuring flasks. Each solution was diluted to about 5 ml with ethanol, treated with 1 ml of potassium persulphate or hydrogen peroxide reagent, cooled in ice for 5 min, then 2 ml of sulphuric acid were added dropwise while mixing and cooling. The flasks were left at room temperature for 40 min then diluted to volume with water. The developed colours were measured at 535 nm for potassium persulphate and at 570 nm for hydrogen peroxide against a reagent blank treated similarly (Fig. 1).

Analysis of pindolol tablets

Twenty tablets of the drug were weighed and powdered. A quantity of the powdered tablets equivalent to 8 mg of pindolol was transferred to a 100-ml measuring flask, followed by the addition of about 50 ml of alcohol. The mixture was shaken for 15 min, then the flask was made

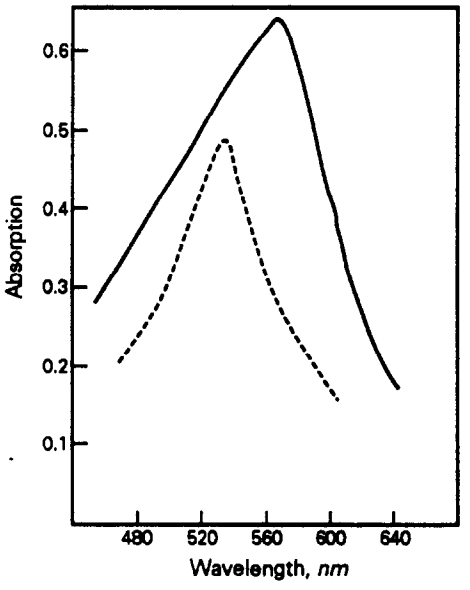

Fig. 1. Absorption curves for pindolol oxidation products.

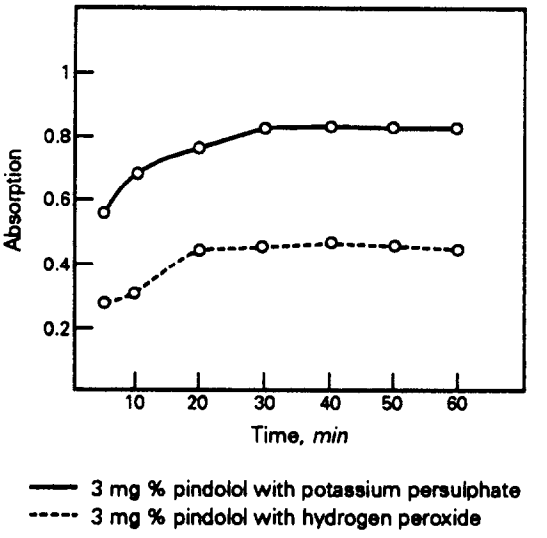

Fig. 2. Colour development and stability of pindolol oxidation products.

up to volume with alcohol and the solution mixed and filtered (1 ml = 0.08 mg/ml pindolol). The filtrate was used for the determination of pindolol, applying the procedure described under the preparation of calibration curves.

RESULTS AND DISCUSSION

Houlihan *et al.*[9] reported that indole is readily oxidized by a variety of oxidants and the extent of oxidation depends on the oxidant and the experimental conditions. Indoxyl is frequently observed as an intermediate in the oxidation process. Thus oxidant converts indole to indoxyl, which is then reoxidized, mainly to indigo. This can be illustrated as follows:

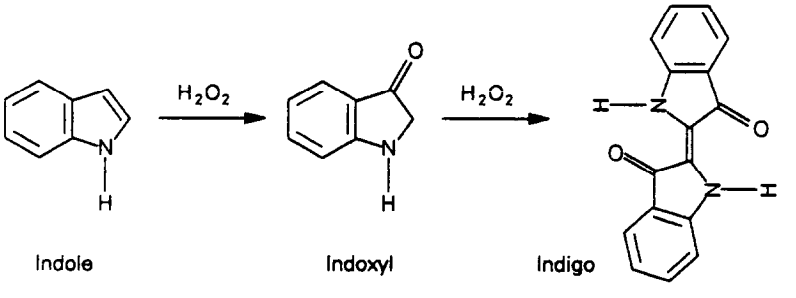

Scheme 2

In this work, this reaction was utilized for the colorimetric determination of pindolol as an indole derivative, using potassium persulphate and hydrogen peroxide. The colour formed was measured at 535 nm for potassium persulphate with a quantity ranging from 0.07–0.35 mg/10 ml and at 570 nm for hydrogen peroxide with a quantity ranging from 0.1–0.5 mg/10 ml pindolol. The molar absorptivities were 0.7×10^3 $l.mole^{-1}.cm^{-1}$ and 3.7×10^3 $l.mole^{-1}.cm^{-1}$, respectively.

The influence of various factors on the colour development was studied to determine the optimal conditions. Potassium persulphate was maximally effective when using 1 ml of 0.1% w/v solution and hydrogen peroxide was most effective when using 1 ml of 5% w/v solution. The intensity of the colour was found to increase with time and the colour reached its maximum intensity after 40 min and then remained stable for more than 1 hr (Fig. 2). Also, the most effective volume of sulphuric acid was found to be 2 ml.

Table 1. Determination of pindolol powder by the proposed and non-aqueous titration methods

Potassium persulphate mg Taken, %	Recovery, %	Hydrogen peroxide mg Taken, %	Recovery, %	Non-aqueous titration[1] mg Taken	Recovery, %
1.4	100.0	2.4	98.8	50	99.5
	99.3		100.0		98.5
	100.0		99.6		100.7
2.1	96.6	3.2	99.1	100	98.5
	99.5		99.7		99.8
	99.0		99.1		99.6
2.8	100.0	4.0	99.3	150	99.0
	100.4		102.0		99.5
	100.0		100.3		99.6
Mean % and S.D.	99.6 ± 0.6		99.8 ± 0.96		99.4 ± 0.7

Table 2. Determination of pindolol in its tablets* by the proposed and non-aqueous titration methods[1]

Potassium persulphate mg Taken, %	Recovery, %	Hydrogen peroxide mg Taken, %	Recovery, %	Non-aqueous titration[1] mg Taken	Recovery, %
1.4	100.7	2.4	101.7	50	102.8
	101.4		101.7		101.6
	101.4		101.3		102.2
2.1	100.4	3.2	100.0	75	102.0
	101.0		102.2		101.3
	100.7		101.6		101.6
2.8	102.0	4.0	101.3	100	100.5
	101.6		101.3		100.5
	100.0		100.3		101.0
Mean % and S.D.	101.0 ± 0.6		101.3 ± 0.7		101.5 ± 0.8

*Visken tablet, 5 mg/tablet (Sandoz Co.).

These proposed reagents gave good recoveries and reproducibility. The results obtained were compared with the non-aqueous titration method[1] and were found to show the same reproducibility. The mean percentage recoveries show no difference when compared with the non-aqueous titration[1] demonstrating the accuracy of the method (Table 1).

The regression equations and regression coefficients were derived with the least squares method:[10]

$$A = 0.003 + 0.283C,\ r = 0.999,$$

and

$$A = 0.003 + 0.1583C,\ r = 0.996$$

for potassium persulphate and hydrogen peroxide, respectively, where C is in mg%. These equations were utilized for computation of different unknown drug concentrations.

Pindolol was also analysed in its tablets and the results obtained were compared with the non-aqueous titration method[1] and found to show the same reproducibility (Table 2). The results in Table 2 show that tablet fillers formulated with pindolol do not interfere with these methods.

The proposed methods are sensitive and specific compared with the non-aqueous technique.[1]

REFERENCES

1. H. Auterhoff and R. Stank, *Dt. Apoth. Ztg.*, 1976, 116, 1596.
2. M. E. Mohamed, M. S. Tawakkol and H. Y. Aboul-Enein, *Spectrosc. Lett.*, 1982, **15**, 609.
3. A. S. Issa, M. S. Mahrous and N. S. Ahmed, *Talanta*, 1987, **34**, 670.
4. N. M. Sanghavi, N. G. Jivani, *ibid.*, 1980, **27**, 591.

5. F. A. Elyazbi, M. A. Korany and M. H. Abdel-Hay, *Ind. J. Pharm. Sci.*, 1984, **46**, 183.
6. M. S. Mahrous, A. S. Issa and N. S. Ahmed, *Alex. J. Pharm. Sci.*, 1987, **1**, 46.
7. M. E. Mohamed, M. S. Tawakkol and H. Y. Aboul-Enein, *J. Assoc. Off. Anal. Chem.*, 1983, **66**, 273.
8. A. Brantner, M. G. Lukacs, *Gyogyyszereszet*, 1976, **20**, 369.
9. W. Houlihan, W. Remers and R. Brown, *The Chemistry of Heterocyclic Compounds*, p. 153, 1972.
10. M. R. Spiegel, *Theory and Problems of Probability and Statistics*, McGraw-Hill, 1975.

Talanta, Vol. 39, No. 1, pp. 73–76, 1992
Printed in Great Britain.

0039-9140/92 $5.00 + 0.00

THE CHEMISTRY OF IRON IN BIOSYSTEMS—V†

STUDY OF COMPLEX FORMATION BETWEEN IRON(III) AND TARTARIC ACID IN ALKALINE AQUEOUS SOLUTIONS

V. SALVADO and X. RIBAS
Departament de Química, Collegi Universitari de Girona (UAB), Pça. Hospital 6, 17071 Girona, Spain
M. VALIENTE‡
Química Analítica, Universitat Autònoma de Barcelona, 08193 Bellaterra, Barcelona, Spain

(*Received* 30 *May* 1990. *Accepted* 24 *May* 1991)

Summary—Complex formation between Fe(III) and tartaric acid (H_2L) has been studied in 0.5*M* $NaNO_3$ medium at 25° by potentiometry at pH 4.5–11. The following complex species and corresponding values of the stability constants (charges omitted) are proposed:

$$2Fe + 2L + 5H_2O \rightleftharpoons Fe_2(OH)_5L_2 + 5H^+; \quad \log^* \beta_{-522} = 4.95$$

$$Fe + L + 3H_2O \rightleftharpoons Fe(OH)_3L + 3H^+; \quad \log^* \beta_{-311} = -1.55$$

$$Fe + L + 5H_2O \rightleftharpoons Fe(OH)_5L + 5H^+; \quad \log^* \beta_{-511} = -21.2$$

These results are in good agreement with those reported for this system in acid. The results may be presented as the degeneration of the "core + link" mechanism observed in the acidic zone. Structures are suggested for the complex species formed.

Systematic investigations of complex formation in aqueous solutions between Fe(III) and various carboxylate ligands have been carried out in our laboratory.[1–4] Tartrate (L) is a ligand that can prevent precipitation of hydrated ferric oxide in aqueous solutions. The complex formation between Fe(III) and tartaric acid in the acid pH range 1.5–4.5 was studied earlier.[1] The results obtained in the present work indicate that the species FeL, $Fe_2(OH)_3L_2$ and $Fe_3(OH)_6L_3$ are formed by stepwise polynuclear complex formation of the "core + links" type, a mechanism proposed by Sillén.[5] In the Fe(III)–tartrate system, the species FeL is the "core" and the polynuclear species result from stepwise addition of the "link" group $Fe(OH)_3L_2$. The "link" group was not detected as an individual species in the acidic range studied.

No literature data for Fe(III)–tartrate system have yet been reported for alkaline aqueous solutions. The present work attempted to investigate the behaviour of this system in alkali in order to extend the previous information from acidic conditions.

†Part IV—V. Salvadó, X. Ribas and M. Valiente, *Polyhedron*, 1990, **9**, 2675.
‡Author for correspondence.

EXPERIMENTAL

Free hydrogen-ion concentrations at equilibrium, *h*, were measured for solutions prepared from stock solutions of ferric nitrate, tartaric acid, nitric acid and sodium nitrate. The potentiometric technique used was that described previously.[1] Values of *h* are obtained from the Nernst equation:

$$E_i = E_i^0 + 59.16 \log h + E_j \qquad (1)$$

where E_i^0 is a constant and E_j is the liquid-junction potential. Both these parameters were determined by a Gran titration[6] when no ferric and tartrate ions were present in the test solution. This was done in both the acidic and basic pH regions, and is the calibration of the system.

A computer system[7] was employed to monitor the titration experiments. The emf measurements utilized a glass electrode (Metrohm 1028) and a double-junction reference electrode (Orion 9002) containing 0.5*M* sodium nitrate as outer filling solution, which also served as a salt bridge.

For the different experiments the analytical concentrations of Fe(III), B, and tartrate, C, were in the range 2.0–6.0mM and 5.0–20.0mM respectively and kept constant within each experiment. The pH values ranged from 4.0 to 11.0. Particular care was needed because of the low buffer capacity of the solution, and the well known difficulty of obtaining accurate emf measurement in the alkaline range. The measured potentials were considered to be stable when their variation was less than 0.1 mV in 10 min. All solutions were kept under an atmosphere of nitrogen.

The data indicated that equilibrium conditions had been achieved, because reproducible results were obtained in back-titration experiments, see Fig. 1.

The experiments were done at $25 \pm 0.1°$.

RESULTS

Figure 1 shows the experimental data obtained in the pH range 4.5–11.0, plotted as Z *vs.* $-\log h$ for the various concentrations B and C. Z represents the number of hydrogen ions bound per ligand entity, defined by:

$$Z = (A - h + K_w/h)/C \qquad (2)$$

where A represents the analytical concentration of hydrogen ions. Full symbols in Fig. 1 represent back-titration data. The good agreement between direct titration and back-titration results indicates that no irreversible processes interfere with the complexation reactions.

As reported before,[1] the formation of complexes between Fe(III) and tartaric acid can be expressed by the general equation:

$$p\mathrm{H} + q\mathrm{Fe} + r\mathrm{L} \rightleftharpoons \mathrm{Fe}_q\mathrm{H}_p\mathrm{L}_r; \quad {}^*\beta_{pqr} \qquad (3)$$

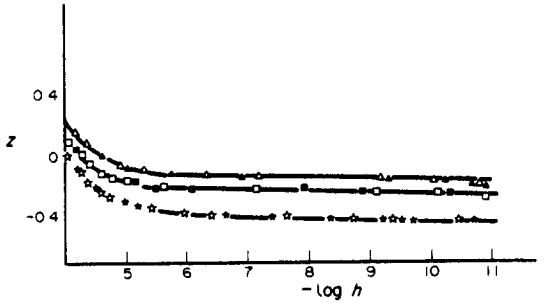

Fig. 1. Z plotted *vs.* $-\log h$ for the various experiments. Filled points represent back-titrations. Solid lines were calculated for model III of Table 1. ☆ [Fe] 4.8mM, [L] 31mM; □ [Fe] 1.8mM; [L] 30mM; △ [Fe] 1.5mM, [L] 48mM.

where ${}^*\beta_{pqr}$ represents the formation constant of the species formed. Charges are omitted throughout, for simplicity.

The stoichiometry of the complexes and the constants ${}^*\beta_{pqr}$ were determined by numerical analysis of the experimental data with the computer program LETAGROP–NYTIT.[8] The treatment is based on the minimization of the error square sum, U, defined by:

$$U = \sum_{N_p} (E_{calc} - E_{exp})^2 \qquad (4)$$

where E_{exp} represents the experimental emf values, E_{calc} is the corresponding value calculated by the program for the model with corresponding stability constants, and N_p is the number of experimental points. In our case, the program is also fed with the information corresponding to the binary systems, *i.e.*, hydrolysis of Fe(III),[3] the protolytic equilibria of tartaric acid and the information for this ternary system in the acidic zone.[1] In the present case, the calculation starts by testing the fit of the previous results in the acidic range to the new experimental information. The results of these calculations are given in Table 1. In model I, ${}^*\beta_{pqr}$ for the complexes FeL and $Fe_2(OH)_3L_2$, which are present in low concentration only at pH > 4.5, were fixed while the stability constant for the predominant $Fe_3(OH)_6L_3$ was varied. A large deviation of this model from the experimental data, reflected by the U and σ values, is observed. Therefore, models II and III were proposed by adding new species, including polynuclear and mononuclear complexes,

Table 1. Resumé of the results obtained from numerical treatment of the experimental data for the system Fe(III)–tartrate in the alkaline region†

Model	(p, q, r)	U	σ, mV	log ${}^*\beta_{pqr}$
(I)	(0, 1, 1)	0.36×10^5	82.0	Fixed
	(−3, 2, 2)			Fixed
	(−6, 3, 3)			13.95 Max. 14.47
(II)	(−6, 3, 3)	0.15×10^3	1.46	14.00 ± 0.08
	(−5, 2, 2)			4.95 ± 0.17
	(−3, 1, 1)			-1.54 ± 0.10
	(−4, 1, 1)			Rejected
	(−5, 1, 1)			-21.21 ± 0.10
(III)‡	(−6, 3, 3)	0.10×10^3	1.16	14.00 ± 0.05
	(−5, 2, 2)			4.95 ± 0.04
	(−3, 1, 1)			-1.55 ± 0.034
	(−5, 1, 1)			-21.21 ± 0.10

†The standard deviation σ (mV) is defined as $(U/(N_p - N_k\beta))^{1/2}$. N_k is the number of constants adjusted. The error in the constants is given as $\pm 3\sigma(\log {}^*\beta)$. When $\sigma(k) > 0.2\beta$, the "best" value of log ${}^*\beta$ and the maximum value, Max. = log $[{}^*\beta + 3\sigma({}^*\beta)]$ are given.

‡After correction for possible analytical errors.

e.g., $Fe_2(OH)_5L_2$, $Fe(OH)_3L$ and $Fe(OH)_5L$, in addition to complexes formed in the acidic range. Model III provides the best fit to the experimental data and can be expressed by the following reaction equations:

$$2Fe + 2L + 5H_2O \rightleftharpoons Fe_2(OH)_5L_2 + 5H; \quad \log {}^*\beta_{-522} = 4.95 \quad (5)$$

$$Fe + L + 3H_2O \rightleftharpoons Fe(OH)_3L + 3H; \quad \log {}^*\beta_{-311} = -1.55 \quad (6)$$

$$Fe + L + 5H_2O \rightleftharpoons Fe(OH)_5L + 5H; \quad \log {}^*\beta_{-511} = -21.2 \quad (7)$$

Figure 2 shows the individual values of the differences $E_{calc} - E_{exp}$ (in mV) over the pH range studied. It can be seen that the proposed model shows no systematic deviations from the experimental data.

Figure 3 represents the distribution diagram of the species, calculated by the program HALTAFALL.[10]

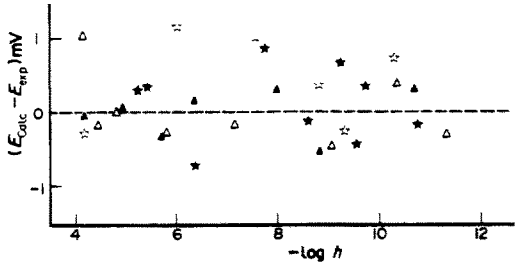

Fig. 2. $E_{calc} - E_{exp}$ (mV) *vs.* $-\log h$. E_{calc} corresponds to the emf values calculated by the program on the basis of the proposed model III. ☆ [Fe] 4.8m*M*, [L] 31m*M*; △ [Fe] 1.8m*M*, [L] 30m*M*; filled points represent back-titrations.

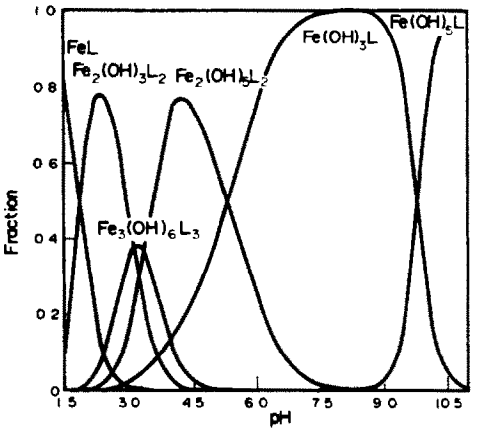

Fig. 3. Distribution diagram for the Fe(III)–tartrate complex species as a function of $-\log h$, including the species previously obtained in the acid range.[1] $[Fe^{3+}] = 2.0mM$ and $[L] = 20mM$.

DISCUSSION AND CONCLUSIONS

Equations 5–7 correspond to complex formation between Fe(III) and tartrate ions in aqueous 0.5*M* sodium nitrate as ionic medium in the pH range 4.5–11.0.

In Fig. 1, the full lines represent theoretical values of Z *vs.* $-\log h$ calculated on the basis of the proposed model. The observed agreement with the experimental data gives a high confidence level to this model.

The model is also in agreement with the behaviour of this system in acid solutions.[1] Complex formation between Fe(III) and tartaric acid can be explained as occurring by a "core + link" mechanism where the species FeL represents the "core" and the species $Fe(OH)_3L$ is the "link". That is, the mechanism of formation of polynuclear species can be represented by the following equations:

$$FeL + Fe(OH)_3L \rightleftharpoons Fe_2(OH)_3L_2 \quad (8)$$

$$Fe_2(OH)_3L_2 + Fe(OH)_3L \rightleftharpoons Fe_3(OH)_6L_3 \quad (9)$$

The result of this study in the alkaline region includes the species $Fe(OH)_3L$ which was formulated as a "hypothetical link" in the acidic region. As observed in Fig. 3, this species predominates only at pH > 5, which may explain why it was not detected in the previous study. On the other hand, the species $Fe_2(OH)_5L_2$ may correspond to a first step in the hydrolytic degradation of the polynuclear species $Fe_3(OH)_6L_3$ which predominates at pH 4.0.

Such a hydrolytic process could be expressed by the reaction:

$$2Fe_3(OH)_6L_3 + 3H_2O \rightleftharpoons 3Fe_2(OH)_5L_2 + 3H \quad (10)$$

In accordance with Fig. 3, the hydrolytic process can be assumed to proceed by further steps to produce the mononuclear species $Fe(OH)_3L$ and $Fe(OH)_5L$ as suggested by the equations:

$$Fe_2(OH)_5L_2 + H_2O \rightleftharpoons 2Fe(OH)_3L + H \quad (11)$$

$$Fe(OH)_3L + 2H_2O \rightleftharpoons Fe(OH)_5L + 2H \quad (12)$$

$Fe(OH)_3L$ is the most stable of those species in the pH range studied, as shown by Fig. 3. Possible structures for the species present in the acid range have been suggested.[1] Figure 4 shows structures proposed for the species present at pH > 5.

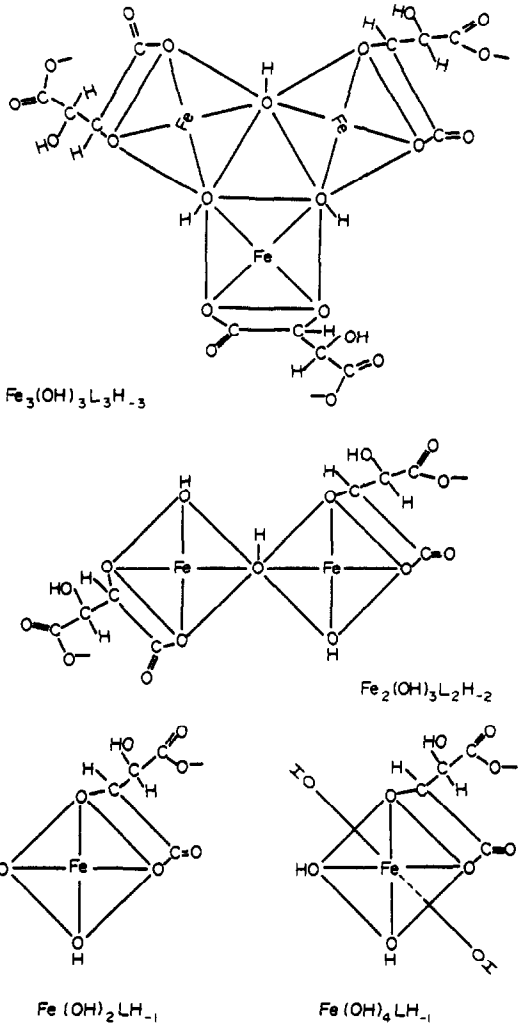

Fig. 4. Structures suggested for the complex species found in the alkaline region of the Fe(III)–tartaric acid system. (L_nH_{-n} means co-ordination of n tartrate anions L, each of which has lost a proton from a hydroxy group.)

The species $Fe_3(OH)_6L_3$, considered as the end product of the nucleation process in the acidic range, is now the origin for the degenerate species, $Fe_2(OH)_5L_2$, $Fe(OH)_3L$ and $Fe(OH)_5L$. The denucleation process should therefore be written as:

$$2Fe_3(OH)_3L_3H_{-3} + 3H_2O \rightleftharpoons 3Fe_2(OH)_3L_2H_{-2} + 3H$$

$$Fe_2(OH)_3L_2H_{-2} + H_2O \rightleftharpoons 2Fe(OH)_2LH_{-1} + H$$

$$Fe(OH)_2LH_{-1} + 2H_2O \rightleftharpoons Fe(OH)_4LH_{-1} + 2H$$

This model suggests that the species $Fe(OH)_3LH_{-1}$ should be rejected, since it would have an asymmetric structure, which should favour the formation of $Fe(OH)_4LH_{-1}$.

REFERENCES

1. V. Salvadó, X. Ribas, M. Blanco and M. Valiente, *Inorg. Chim. Acta*, 1987, **137**, 155.
2. X. Ribas, V. Salvadó and M. Valiente, *J. Chem. Res.*, (S) 1989, 332.
3. V. Salvadó, X. Ribas, V. Zelano, G. Ostacoli and M. Valiente, *Polyhedron*, 1989, **8**, 813.
4. V. Salvadó, X. Ribas and M. Valiente, *ibid.*, 1990, **9**, 2675.
5. L. G. Sillén, *Acta Chem. Scand.*, 1954, **8**, 299.
6. G. Gran, *Analyst*, 1952, **77**, 661.
7. X. Ribas, *Doctoral Thesis*, Col. Univ. Girona (UAB), 1987.
8. L. G. Sillén and B. Warnquist, *Ark. Kemi*, 1970, **31**, 377.
9. X. Ribas, V. Salvadó, V. Zelano, G. Ostacoli and M. Valiente, unpublished data.
10. N. Ingri, W. Kakołowicz, L. G. Sillén and B. Warnquist, *Talanta*, 1967, **14** (errata, *Talanta*, 1968, **15**, No. 3, ix).

Talanta, Vol 39, No. 1, pp 77–80, 1992
Printed in Great Britain.

0039-9140/92 $5.00 + 0.00

EXTRACTIVE–SPECTROPHOTOMETRIC DETERMINATION OF TRACE IRON(II) WITH DI-2-PYRIDYLMETHANONE 2-(5-NITRO)PYRIDYLHYDRAZONE

TOSHIHIRO TAKAOKA, TOSHIKI TAYA and MAKOTO OTOMO
Department of Applied Chemistry, Nagoya Institute of Technology, Gokiso, Showa, Nagoya 466, Japan

(*Received* 14 *May* 1991. *Accepted* 16 *July* 1991)

Summary—The optimum conditions for the extractive–spectrophotometric determination of trace iron(II) with di-2-pyridylmethanone 2-(5-nitro)pyridylhydrazone have been established. Iron(II) reacts with this reagent at pH 2.0–7.5 to form an uncharged 1:2 (metal-to-ligand) complex, which can be extracted with toluene. Beer's law is obeyed over the range up to 0.84 μg/ml of iron(II) at 505 nm. The molar absorptivity of the extracted species is 5.83×10^4 l·mole^{-1}·cm^{-1}. The proposed method is extremely sensitive and reproducible, and has been satisfactorily applied to the determination of total iron in freshwater samples by adding ascorbic acid to reduce iron(III).

Di-2-pyridylmethanone 2-pyridylhydrazone (DPPH), a *NNN*-tridentate heterocyclic hydrazone ligand, has been used for the spectrophotometric determination of several metal ions, including cobalt(II)[1] and iron(II).[2] Iron(II) reacts with this reagent in acidic media to form a dipositively charged bis complex, $Fe(HL)_2^{2+}$ (HL is a neutral form of the ligand), which undergoes successive deprotonation to monocationic [$Fe(HL)L^+$] and uncharged bis (FeL_2) complexes with a decrease in the acidity of the solution. Although all of the complex species can be used for the spectrophotometric determination of iron(II), the $Fe(HL)_2^{2+}$ species [1.40×10^4 l.mole^{-1}.cm^{-1} at 540 nm in 28% (v/v) aqueous dioxane] has the highest molar absorptivity.[3]

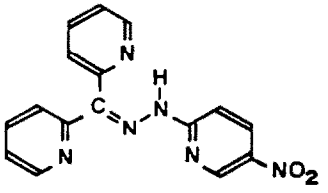

(I)

In a previous paper[4] we have introduced an improved ligand, di-2-pyridylmethanone 2-(5-nitro)pyridylhydrazone (DPNPH, I)—a nitration derivative of DPPH—as a useful and extremely sensitive chromogenic reagent for certain transition metal ions, including palladium(II). The greatly enhanced sensitivity of the new ligand obtained by introducing a strongly electron-withdrawing nitro group to the 5-position of the pyridine ring in the hydrazine moiety, was explained by a prolonged conjugated system (quinoid structure) of the metal complex resulting from the redistribution of the electron-pair previously shared by the imino nitrogen. This paper describes a highly sensitive and precise method for the extractive spectrophotometric determination of iron(II) with DPNPH. The proposed method, which permits the determination of sub-ppm levels of iron(II), can be applied to the determination of total iron in freshwater samples in the presence of ascorbic acid without a tedious preconcentration step.

EXPERIMENTAL

Apparatus

Spectrophotometric measurements were made with a Hitachi Model 150-20 spectrophotometer with matched 1.00-cm quartz cells. A Toa Dempa HM-30S pH meter was used for pH adjustments. All measurements were performed at 25°.

Reagents

All solutions were prepared with analytical-grade chemicals and doubly distilled water unless otherwise stated. Toluene was distilled before use.

Iron(II) solution. Iron(II) standards were obtained by dilution of 0.01*M* ammonium iron(II) sulphate acidified with sulphuric acid

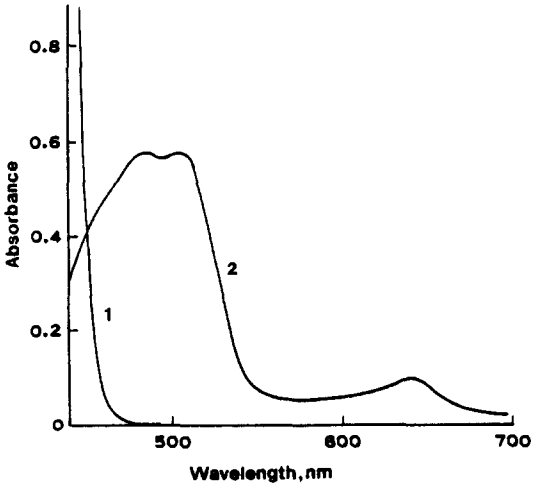

Fig. 1. Absorption spectra of DPNPH and its iron(II) complex extracted into toluene. Fe(II) $1.0 \times 10^{-5}M$, pH 4.60, DPNPH $2.0 \times 10^{-3}M$. (1) DPNPH *vs.* toluene, (2) Fe(II)–DPNPH complex *vs.* reagent blank.

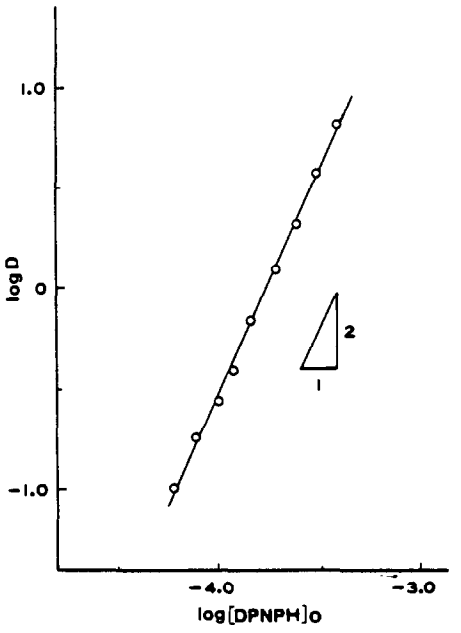

Fig. 2. Logarithmic plot for iron(II) distribution. Fe(II) taken $1.0 \times 10^{-5}M$, pH 4.60, measurement at 505 nm.

standardized against a standard potassium permanganate solution.

DPNPH. The ligand was synthesized as previously described[4] by diret interaction of equimolar portions of di-2-pyridyl ketone and 2-hydrazino-5-nitropyridine. The acid–base characteristics of the ligand were also described previously.[4] A $2.0 \times 10^{-3}M$ DPNPH in toluene was freshly prepared daily.

General procedure

Into a 50-ml separating funnel, transfer a suitable aliquot of sample solution containing up to 8.4 μg of iron(II, III) with 1 ml of 1% ascorbic acid and 2 ml of $1M$ acetate buffer adjusted to pH 4.6. Dilute to 10 ml with water and equilibrate with exactly 10 ml of $2.0 \times 10^{-3}M$ DPNPH in toluene by mechanical shaking for 30 min. Measure the absorbance of the organic phase at 505 nm against a reagent blank.

RESULTS AND DISCUSSION

Characteristics of the complex

The iron(II) complex formed with the reagent is sparingly soluble in water, but readily soluble in various organic solvents such as aromatic hydrocarbons, partially halogenated aliphatic

Table 1. Effect of foreign ions on determination of 5.6 μg of iron(II)

Tolerance limit ([ion]/[Fe(II)])	Ion
10,000 (at least)	Br^-, Cl^-, NO_3^-, SCN^-, SO_3^{2-}, SO_4^{2-}, $S_2O_3^{2-}$, tartrate, thiourea
5000	PO_4^{3-}
1000	citrate
100 (at least)	Ag^+, Cd^{2+}, Co^{2+}*, Cu^{2+}†, Hg^{2+}‡, In^{3+}§, Mg^{2+}, Mn^{2+}, Mo(VI), Ni^{2+}, Os(VIII), V(V)§
100	Al^{3+}, Bi^{3+}, Pb^{2+}, W(VI), oxalate
50	Ga^{3+}, Pd^{2+}‖, Pt^{4+}
10	Au^{3+}, Ir^{3+}, Rh^{3+}, U(VI), NTA
5	Zn^{2+}††, Ru^{3+}

*Preliminarily separated by anion exchanger (Dowex 1-X8, 50–100 mesh, 9 × 60 mm resin bed).[10]
†In the presence of $0.1M$ sodium thiosulphate.
‡In the presence of $0.2M$ sodium hydrogen sulphite.
§In the presence of $0.2M$ tartrate adjusted to pH 4.6.
‖In the presence of $0.04M$ thiourea.
††In the presence of $1 \times 10^{-4}M$ NTA.

hydrocarbons, acetic esters and ketones. Toluene was chosen as the extracting solvent, because it gave negligibly low blank absorbance at the selected wavelength. Under the optimum conditions of the reagent concentration, pH and shaking period, iron(II) can be quantitatively extracted from aqueous solution with a single 10-ml portion of DPNPH in toluene over the concentration range studied. The intensity of the colour thus obtained remains unchanged for at least 18 hr. Figure 1 illustrates the visible absorption spectrum of the iron(II) complex extracted into toluene, along with that of the reagent blank. The absorption spectrum is characteristic for iron(II), three absorption maxima being located at 485, 505 and 640 nm. Iron(III) did not react with DPNPH and should be reduced by ascorbic acid.

Effects of experimental conditions

A pH study for the formation and extraction of the iron(II) complex was performed between pH 1.5 and 9.0, using 4.2 μg of iron(II). The absorbance of the organic phase as a function of the pH of the aqueous phase was maximal and constant over the pH range 2.0–7.5. Below pH 2, unextractable complex species [possibly $Fe(HL)_2^{2+}$ and/or $Fe(HL)L^+$ species] remained in the aqueous phase.

A maximal and reasonably constant absorbance was obtained by using more than $7.5 \times 10^{-4}M$ DPNPH in the organic phase.

Addition of 1.0 ml of 0.1% ascorbic acid was sufficient for preventing oxidation of iron(II) to the trivalent state. It was also found that a shaking period of 15 min is sufficient for complete equilibrium, provided the volume ratio of aqueous to organic phase is between 0.5:1 and 4:1.

Conformance to Beer's law and comparison of sensitivity

The analytical species of interest obeys Beer's law over the concentration range up to 0.84 μg/ml iron(II) in the organic phase. The molar absorptivity (ϵ) of the complex was 5.83×10^4 $l.mole^{-1}.cm^{-1}$ at 505 nm (it was 6.23×10^4 $l.mole^{-1}.cm^{-1}$ at 510 nm in *o*-dichlorobenzene), which is higher than or comparable with those of the respective complexes with DPPH in aqueous solution ($\epsilon = 1.53 \times 10^4$ $l.mole^{-1}.cm^{-1}$ at 538 nm),[2] di-2-pyridylmethanone 2-quinolylhydrazone in benzene ($\epsilon = 3.14 \times 10^4$ $l.mole^{-1}.cm^{-1}$ at 504 nm),[5] 2-pyridyl-3′-sulphophenylmethanone 2-pyridylhydrazone in aqueous solution ($\epsilon = 4.79 \times 10^4$ $l.mole^{-1}.cm^{-1}$ at 379 nm),[6] 2-pyridylmethanone 2-pyridylhydrazone in chloroform ($\epsilon = 5.00 \times 10^4$ $l.mole^{-1}.cm^{-1}$ at 405 nm)[7] and 2-pyridylmethanone 2-(5-nitro)pyridylhydrazone in benzene ($\epsilon = 6.54 \times 10^4$ at 496 nm[8]; benzene is highly toxic and appropriate precautions should be taken). The reproducibility of the proposed method, expressed as the standard deviation of the absorbance, was 0.13% for 5.6 μg of iron(II) (10 replicates).

Composition of the complex

The extraction method,[9] where metal distribution is followed in the presence of a reasonable excess of ligand, was used to find the composition of the extracted species. The plot of log D against log $[DPNPH]_{org}$ at pH 4.60, where D denotes the distribution ratio of iron(II) between the two phases and $[DPNPH]_{org}$ is the equilibrium concentration of DPNPH in the organic phase, is shown in Fig. 2. A straight line with a slope equal to about 2 demonstrates a 1:2 metal-to-ligand ratio complex being extracted.

Effect of diverse ions

The effect of diverse ions on the determination of 5.6 μg of iron(II) is summarized in Table 1. The tolerance limit of foreign ions was taken as that value which caused an error of not more than $\pm 2\%$ in the absorbance. For some interfering ions, suitable masking agents were used together as indicated in the table.

Determination of iron in freshwater

The proposed method was applied to the determination of the total iron in tap-water and lake water samples. The sample solution was acidified (pH 1.5) with hydrochloric acid immediately after sampling. Five or ten millilitre portions of the sample were analysed for iron without a preconcentration process. The results shown in Table 2 are in good agreement with

Table 2. Determination of total iron in freshwater samples

Sample	Iron found, *mg/l.*	
	Proposed method	ICP–AES*
Tap-water† (Nagoya City)	0.383 ± 0.003 0.383 ± 0.004‡	0.380 ± 0.003
Lake water§ (Lake Biwa)	0.200 ± 0.002	0.210 ± 0.002

*Analytical line: 238.04 nm (Japan Jarrell-Ash ICAP-575 spectrometer).
†Sample taken = 5.0 ml.
‡Combination with the standard addition.
§Sample taken = 10.0 ml.

each other and with those obtained by inductively coupled atomic emission spectrometry (ICP–AES) performed for comparison.

In conclusion, the tridentate hydrazone ligand, DPNPH, is worthy of use as a chromogenic reagent for the spectrophotometric determination of iron(II) at sub-ppm levels.

REFERENCES

1. G. S. Vasilikoitis, Th. Kouimtzis, C. Apostolopoulou and A. Voulgaropoulos, *Anal. Chim. Acta*, 1974, **70**, 319.
2. H. Alexaki-Tzivanidou, *ibid.*, 1975, **75**, 231.
3. M. Otomo, T. Taya, K. Doi and C. Umeda, *Anal. Sci.*, 1991, **7**, 383.
4. T. Kanetake and M. Otomo, *ibid.*, 1988, **4**, 411.
5. M. Otomo, S. Ano and H. Kako, *Microchem. J.*, 1981, **26**, 228.
6. T. Aita, T. Odashima and H. Ishii, *Analyst*, 1984, **109**, 1139.
7. M. A. Quddas and C. F. Bell, *Anal. Chim. Acta*, 1968, **42**, 503.
8. H. Ishii, T. Odashima and T. Hashimoto, *Anal. Sci.*, 1987, **3**, 347.
9. J. Inczédy, *Analytical Applications of Complex Equilibria*, p. 260. Wiley, New York, 1976.
10. P. R. Haddad, P. W. Alexander and L. E. Smythe, *Talanta*, 1976, **23**, 275.

Talanta, Vol. 39, No. 1, pp. 81–84, 1992
Printed in Great Britain

0039-9140/92 $5.00 + 0.00

A NEW SPECTROPHOTOMETRIC METHOD FOR DETERMINING THE EXTRACTION CONSTANT OF QUATERNARY COMPLEXES

J. L. MARTINEZ-VIDAL, A. R. FERNANDEZ-ALBA and D. CERVANTES OCAÑA

Departamento de Química Analítica de Almería, Facultad de Ciencias de Almería, Universidad de Granada, 04120, Almería, Spain

F. SALINAS

Departamento de Química Analítica, Facultad de Ciencias de Extremadura, Universidad de Granada, 04120, Almería, Spain

(*Received* 11 *October* 1990. *Revised* 7 *June* 1991. *Accepted* 10 *June* 1991)

Summary—A new spectrophotometric method for determining the extraction constants of quaternary complexes is described. The method has been applied to a study of the distribution between water and toluene in the V(V)–salycylhydroxamic acid–nitrate–trioctyl methyl ammonium system, determining its conditional extraction constant in toluene for several pH values.

In previous works[1–4] a graphical method has been proposed, based on the effect of dilution on the degree of dissociation of the complexes, for determining extraction constants as well as differentiating mono- and poly-nuclear complexes.[2,3]

In the present paper this method has been extended to determination of the solvent extraction constant of a mixed ligand complex forming a quaternary system in the organic phase. The method has been applied to the determination of the apparent extraction constant of an ion-pair association complex formed between a mixed ligand complex and an ammonium quaternary salt as extractant agent.

THEORY

Let us consider the formation of a mixed ligand complex and its extraction forming a quaternary complex by means of the equilibria:

$$M(w) + nX(w) \overset{k_{1n}}{\rightleftharpoons} MX_n(w)$$

$$MX_n(w) + mY(m) \overset{k_{nm}}{\rightleftharpoons} MX_nY_m(w)$$

$$MX_nY_m(w) + qB(o) \overset{K_e}{\rightleftharpoons} MX_nY_mB_q(o)$$

where 'w' is the aqueous phase, 'o' the organic phase and $m, n, q \geq 1$. Where X, Y and B are three different ligands on the coordination sphere, and M the metallic ion.

The conditional extraction constant, K_c, when only one metallic complex is extracted, for a particular pH value is:

$$K_c = \frac{[MX_nY_mB_q](o)}{[MX_nY_m](w)[B]^q(o)} \quad (1)$$

and

$$k_{1n} = \frac{[MX_n](w)}{[M](w)[X]^n(w)} \quad k_{nm} = \frac{[MX_nY_m](w)}{[MX_n](w)[Y]^m(w)}$$

where K_{1n} and K_{nm} are respectively the formation constants of the binary and ternary complexes in the aqueous phase.

$$P_c = \frac{[MX_nY_mBq](o)}{[MX_nY_mBq](w)} \quad E_B = \frac{[B](o)}{[B](w)}$$

where P_c and E_B are respectively the partition coefficient of the quaternary complex and the extraction coefficient of the ligand.

C_M, C_X C_Y and C_B are the initial concentrations of ligand X, Y and B respectively and C_M is the initial concentration of the cation.

Let us consider a 1:1 phase volume ratio and the initial conditions; C_x, $C_Y \gg C_M$ and $C_B/C_M = q$ and only one extractable species —$MX_nY_mB_q$ (o)—in the operational conditions.

Under these conditions we can define the molar ratio of MX_nY_m in the aqueous phase as:

$$\Phi = \frac{[MX_nY_m](w)}{C_M - [MX_nY_mB_q](o)} \quad (2)$$

And by material balance

$$\Phi = \frac{K_{1n}K_{nm}[X]^n(w)[Y]^m(w)}{1 + K_{1n}[X]^n(w) + K_{1n}K_{nm}[X]^n(w)[Y]^m(w)}$$

it is noted that $\Phi = f$ (X) (w), (Y) (w) and so is a constant in the conditions mentioned above. By substitution of [B](o) (from material balance) and MX_nY_m(w) [from equation (2)] in (1)

$$K_e^* = \frac{K_e \Phi E_B^q}{(E_B + 1)^q} = \frac{[MX_nY_mB_q](o)}{q^q(C_M - [MX_nY_mB_q](o))^{q+1}} \quad (3)$$

in the operational conditions the degree of extraction of the metal α_e is

$$\alpha_e = \frac{[MX_nY_mB_q](o)}{C_M} = \frac{A}{A_o}$$

where A is the absorbance of the complex and A_o the absorbance when the complexation and extraction of the cation is complete ($\alpha_e = 1$)

Substituting the values of $[MX_nY_mB_q](o)$ in equation (3)

$$A/A_o C_M^q = q^q K_e^* (1 - A/A_o)^{q+1} \quad (4)$$

Provided that the Beer-Lambert law is obeyed, when an initial concentration of metallic ion "b_o" is diluted by a factor β the corresponding value of $A_o(b_o)$ is decreased by the same factor, *i.e.*, $b = b_o/\beta$ and $A_o(b) = A_o(b_o)/\beta$.

Substitution of b and $A_o(b)$ into equation (4) gives

$$Y = \frac{(\beta A)^{1/q+1}}{(b_o/b)^{q/q+1}} \quad [q^q K_e^* A_o(b_o)]^{1/q+1} \times [1 - A/A_o(b_o)] \quad (5)$$

A plot of Y against βA gives a straight line. When

$$b_o/\beta \to \infty, \quad Y \to 0 \quad \text{and} \quad \beta A \to A_o(b_o).$$

Thus the intersection of the straight line with the abcissa provides the value of $Ao(bo)$. The slope of the straight line is

$$\frac{(q^q K_e^*)^{1/q+1}}{A_o(b_o)^q}$$

which allows the calculation of the extraction constant. In order to plot Y, the left hand side of equation (4), against βA, it is necessary to know the complex stoichiometry and to make an approximation, since the unknown term $A_o(b_o)$ appears in the ordinate. This can be effected if $A_o(b_o)$ is considered as the greatest experimental value obtained for βA.

The precision of the method will depend on the value of α_e

$$K_e^* = \frac{\alpha_e}{q^q(C_M^q(1 - \alpha_e)^{q+1})}$$

this equation can be differentiated to give

$$\frac{dK_e^*}{K_e^* d\alpha_e} = \frac{(1 - \alpha_e)^q(1 + q\alpha_e)}{\alpha_e(1 - \alpha_e)^2}$$

and by approximation to finite increments

$$\frac{\Delta K_e^*}{K_e^*} = \frac{(1 - \alpha_e)^q(1 + q\alpha_e)}{\alpha_e(1 - \alpha_e)^2} \Delta\alpha_e$$

If a reasonable value of $\Delta\alpha_e$ such as ± 0.01 is accepted, the relative error can be calculated as a function of α_e and q. So, the highest precision of $\log K_e^*$ (± 0.03) is obtained, when $q = 1$, for α_e values between 30–70%.

EXPERIMENTAL

Reagents and apparatus

Salycylhydroxamic acid (SHA) solution ($10^{-2}M$) was prepared by dissolving 1.5314 g of the acid (Jenssen) and diluting to one litre with demineralized water. A $1.89 \times 10^{-3}M$ vanadium(V) solution was prepared by diluting ammonium monovanadate (Merck) solution standardized gravimetrically with silver nitrate. A $1M$ potassium nitrate solution was prepared by dissolving 202.22 g of potassium nitrate (Merck) in one litre of demineralized water. Samples are buffered with acetic acid/sodium acetate solution. A trioctylmethylammonium

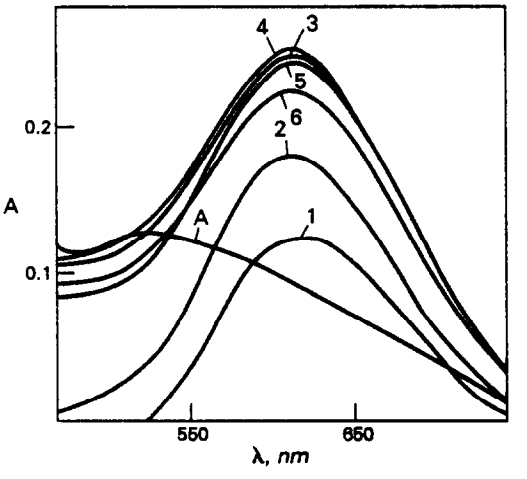

Fig. 1. Absorption spectra of SHA–V(V)–NO_3 complex extracted in toluenic trioctylmethylammonium chloride solution at different pH values. pH = (1) 2.5; (2) 3.0; (3) 3.5; (4) 4.5; (5) 5.0; (6) 5.5. (A) Absorption spectrum of SHA–V(V) complex in TOMA–toluene. pH = 4.5.

Table 1. Data for V(V)–SHA_2–NO_3^-–TOMA system at different pH values for 1:1 complex by application of equation (5)

C_v(V)	βA				Y			
M	pH = 4.2	pH = 4.5	pH = 5.0	pH = 5.3	pH = 4.2	pH = 4.5	pH = 5.0	pH = 5.3
3.78×10^{-5}	0.287	0.447	0.411	0.363	87.2	108.7	104.3	98.1
5.67×10^{-5}	0.332	0.495	0.468	0.423	79.3	93.4	90.9	86.3
9.45×10^{-5}	0.397	0.557	0.532	0.492	72.5	76.8	75.0	72.1
1.32×10^{-4}	0.468	0.590	0.567	0.522	59.5	66.8	65.6	62.9
1.51×10^{-4}	—	0.599	0.575	0.534	—	62.9	61.7	59.5

chloride (TOMA) solution $9.45 \times 10^{-4}M$ was prepared by dissolving 0.3819 g of $C_{25}H_{54}N^+Cl^-$ (Serva) and diluting to one litre with toluene. All reagents were of analytical reagent grade.

A Baush Lomb Spectronic 2000 spectrophotometer and an Orion 801 pH-meter were used.

Procedure

Into a 100-ml separating funnel, 0.5 ml of $10^{-2}M$ SHA solution, 3 ml of $1M$ potassium nitrate, 1 ml of HAc/AC^- buffer solution (pH 4.2–5.3 and $C = 0.2M$), suitable aliquots of V(V) of 3.78×10^{-4}–$1.32 \times 10^{-4}M$ were transferred, diluted to 10 ml with demineralized water and mixed well. Then 10-ml of trioctylmethylammonium chloride toluene solution of identical concentration to the one of V(V) were added and shaken vigorously for 3 min before the phases were allowed to separate. The organic phase was transferred to a flask containing anhydrous sodium sulphate. The absorbance of each extract was measured at 620 nm against a reagent blank prepared with the same reagent concentration, but no vanadium(V). It is convenient to increase the cell path length by a factor equal or proportional to the dilution factor. In this fashion, the value of βA is obtained directly.

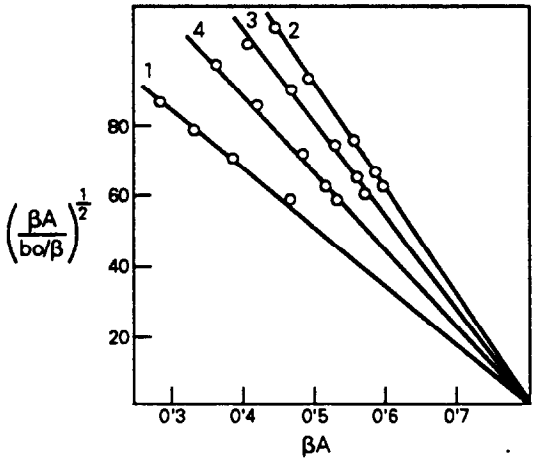

Fig. 2. Determination of K_c^* at several pH values for the V(V)–SHA–NO_3–TOMA system. pH = (1) 4.2; (2) 4.5; (3) 5.0; (4) 5.3.

RESULTS AND DISCUSSION

Vanadium–SHA–nitrate–TOMA system

The study of the A *vs.* pH curves (Fig. 1) and the application of the Job, Joe-Yones and Asmus methods to determine the stoichiometry, showed that for pH values in the aqueous phase between 3.0–5.5 a single complex is extracted into the organic phase. The stoichiometry of this complex is 1:1:2:1 for V(V):NO_3:SHA:TOMA. This implies that the extraction occurs through the ion-pair formation between the anionic complex $[V(V)NO_3(SHA)_2]^-$ and the TOMA cation. Both the ion-pair formation and the extractions were almost instantaneous with only 30 sec of shaking required for complete extraction of the complex. The absorbance of the extract remains stable for at least 15 min and the spectra show a maximum at 620 nm. The degree of extraction (αe) of the metal is ≈ 1 in the same pH interval when the ratio TOMA/V(V) ≥ 10.

Determination of conditional extraction constants at different pH values

The conditional extraction constants were determined for an initial metallic ion concentration of $1.51 \times 10^{-4}M$ at different pH values (4.2, 4.5, 5.0 and 5.3). Table 1 shows the results obtained. In all cases the corresponding plots (Y *vs.* βA) shown in Fig. 2 are straight lines (Table 2) when the stoichiometry TOMA/mixed ligand complex is 1:1, which confirms this

Table 2. Regression parameters for straight lines shown in Fig. 2

pH	4.2	4.5	5.0	5.3
r	0.996	0.999	0.991	0.996
m (slope)	−152.1	−294.1	−262.5	−223.8
Y intercept	124.8	239.8	214.9	181.2

Table 3. Log K_e^* values at several pH values for the V(V)–SHA-NO_3–TOMA system

pH	4.2	4.5	5.0	5.3
Log K_e^*	8.07	8.66	8.56	8.43

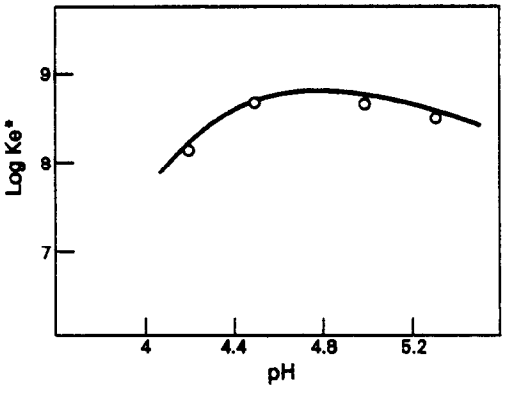

Fig. 3. Relationship between log K_e^* and pH.

value. These straight lines intersect the abcissa to give a value of 0.815 which leads to a molar absorptivity, ϵ^*, of $5{:}40 \times 10^3$ l.mole^{-1}.cm^{-1}. The same value is obtained when calculated by the Beer-Lambert law. The data obtained by application of equation (5) are given in Table 3, and Fig. 3 shows the relationship between log K_e^* and pH, resulting in a maximum value of about pH = 4.5 (log $k_e^* = 8.66$ at 20°).

CONCLUSION

The present method allows the spectrophotometric calculation of extraction constants as well as the verification of stoichiometries of different ligand complexes containing four components. It is based on the effect of dilution on the degree of dissociation of the complexes. The calculation is performed on spectrophotometric measurements of the quaternary complex formed in the organic phase, using the stoichiometric ratio of extractant ligand and metallic ion ($C_B/C_M = q$). The method used does not require a complex mathematical model, which simplifies the expressions used as well as the data processing. Because of the complexity of these quaternary systems, previous experimental work is required to ensure adequate extraction conditions where only one metallic complex is present in the organic phase, and to ensure the absence of spectral overlapping with other components which could be present in the solution.

REFERENCES

1. T. Toman Galan, A. Arrebola Ramirez and M. Roman Ceba, *Talanta*, 1980, **27**, 545.
2. J. J. Berzas Nevado, A. Arrebola Ramirez and M. Roman Ceba, *Anal. Chim. Acta*, 1981, **124**, 201.
3. M. Roman Ceba, A. Arrebola Ramirez and T. Roman Galan, *Anal. Quim.*, 1983, **79B**, 413.
4. F. Salinas, J. L. Martinez-Vidal and A. R. Fernandez-Alba, *Anal. Lett.*, 1989, **22**, 147.

Talanta, Vol. 39, No. 1, pp. 85–90, 1992
Printed in Great Britain.

0039-9140/92 $5.00 + 0.00
Pergamon Press plc

INDIRECT DETECTION METHOD FOR FLOW SYSTEMS BASED ON PERTURBATION OF OXYGEN REDUCTION AT GOLD AND GOLD CHLORIDE ELECTRODES

M. S. TUNULI*

Department of Chemistry, California State University Northridge, Northridge, CA 91330, U.S.A.

(*Received* 11 *September* 1990. *Revised* 8 *March* 1991. *Accepted* 24 *March* 1991)

Summary—A simple scheme for potential indirect electrochemical detection in flow analyses (liquid chromatography and ion chromatography) with experimental examples is presented. The proposed scheme exploits the influence of the analyte on the reduction current of an intrinsic mobile phase additive—oxygen—at the detector electrode, and utilizes the resulting changes in background current as an analytical signal. Several analytes: chloropromazine, ascorbic acid, nitrate and sulfate, cause a shift in the oxygen reduction peak, particularly at the AuCl electrode, that results in a cathodic or anodic shift in the current at a fixed potential.

Liquid chromatography (LC) with electrochemical (EC) detection, LCEC, is a highly sensitive and selective tool used in a myriad of analyses relating to agricultural, environmental and clinical samples. However, reductive LCEC is plagued by the well-known interference from oxygen reduction. Although this interference can easily be "tuned-out" by saturating both the sample solution to be injected and the mobile phase (which also acts as the supporting electrolyte in LCEC) with a suitable inert gas, the resulting increase in analysis time is usually undesirable. The objective of initiating the work reported here was to extract analytical advantages out of this misfortune of reductive electroanalyses. The idea was to explore the possibility of interference of the analyte species in the process of oxygen reduction and to use the resulting changes in reductive current as an analytical signal.

In recent times several procedures for the indirect detection of analytes after their separation on a chromatographic column have been reported.[1–13] These methods exploit the displacement of a signal generating species (deliberately added to the mobile phase) at the detector with the concomitant changes in the background signal (baseline) acting as an analytical signal. Depending on the nature of the mobile phase additive, one of the conventional methods (such as UV–VIS, fluorescence, electrochemical, *etc.*) is used for the detection of the background signal. Of particular interest to us are those methods which rely upon the signal generated by an electroactive mobile phase additive.[10–12] In these methods the analyte interferes with the electroactivity of the additive at the detector electrode and gives rise to an easily detectable change in the background current. The trouble and time spent in adding an additive to the mobile phase can be saved by realizing the fact that a universal additive is always present in almost all the solutions. This intrinsic additive is oxygen which is highly electroactive and provides a large and stable reductive background signal. Clearly, a novel detector for LC and IC (ion chromatography) can be developed if a change in this background current via interference caused by the analyte can be realized in practice.

In this paper we present our preliminary data demonstrating that the indirect electrochemical detection via interference of analyte with the phenomenon of oxygen reduction is a reality. This has the following advantages over other indirect detection methods: (i) no additive is required because an intrinsic species, oxygen, serves this function and (ii) the need for oxygen removal is eliminated which offers the advantage of reduced analysis time.

*Present address: Department of Chemistry, California State Polytechnic University, Pomona, CA 91768-4032, U.S.A.

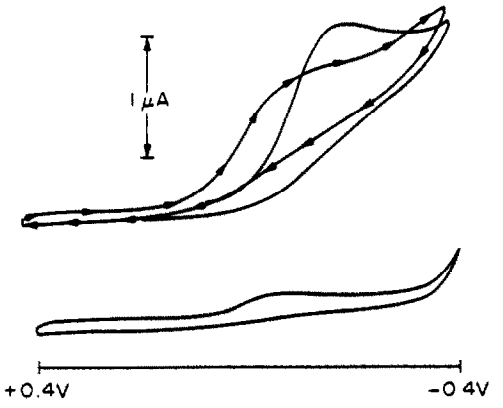

Fig. 1. Cyclic voltamperograms at the Au electrode in air equilibrated MP-1 in the absence (upper CV with arrows) and presence (upper CV without arrows) of 1m*M* chloropromazine. The lower CV was obtained in deaerated MP-1. The scan rate for all CVs was 20 mV/sec.

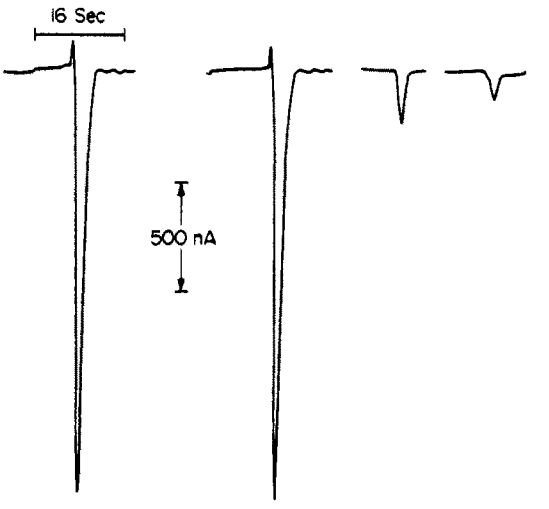

Fig. 3. Two successive FI traces of 1 nmole of chloropromazine under an applied potential of −0.3 V at Au (two smaller traces on the right hand side) and at AuCl (two larger traces on the left hand side) electrode. The MP-1 flow rate was 0.3 ml/min.

EXPERIMENTAL

Apparatus

Cyclic voltammetry measurements were made with a PAR model 173 potentiostat–galvanostat in conjunction with a PAR model 175 universal programmer. A BAS voltammetry gold electrode (0.02-cm^2 area), a BAS model RE-1 Ag/AlCl electrode and a platinum wire electrode were used as working, reference and counter electrodes, respectively.

The flow injection, FI, system consisted of a Beckman model 110 pump; an Altex model 210 injector with 20-microliter loop and a BAS model LC4B/17AT electrochemical detector. The EC transducer employed a BAS gold working electrode, a BAS model RE-4 Ag/AgCl/gel reference electrode, a stainless steel counter electrode and a BAS model TG-2M Teflon gasket. The mobile phase and supporting electrolyte (MP-1) for ascorbic acid and chloropromazine consisted of 0.05*M* chloroacetic acid containing 15 mg/l. sodium octyl sulfate and 150 mg/l. disodium EDTA. For anions we used a 2.5 m*M* aqueous solution of potassium hydrogen phthalate (KHP) as the mobile phase (MP-2). The detector temperature was held at 25°.

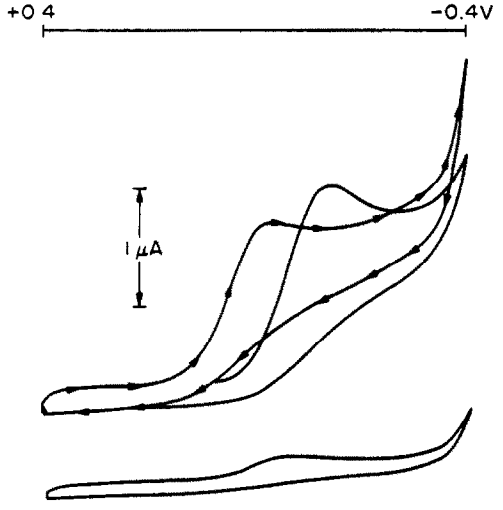

Fig. 2. Cyclic voltamperograms at AuCl electrode in air equilibrated MP-1 in the absence (upper CV with arrows) and presence (upper CV without arrows) of 1m*M* chloropromazine. The lower CV was obtained in deaerated MP-1. Scan rate for all CVs was 20 mV/sec.

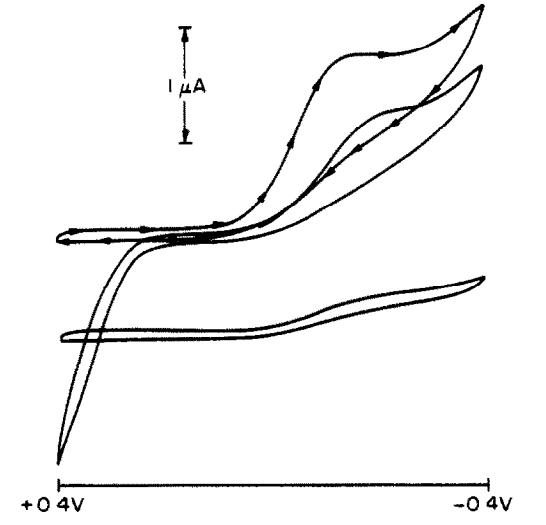

Fig. 4. Cyclic voltamperograms of Au in air equilibrated MP-1 in the absence (upper CV with arrows) and presence (upper CV without arrows) of 1m*M* ascorbic acid. Lower CV was obtained in deaerated MP-1. Scan rate for all the CVs was 20 mV/sec.

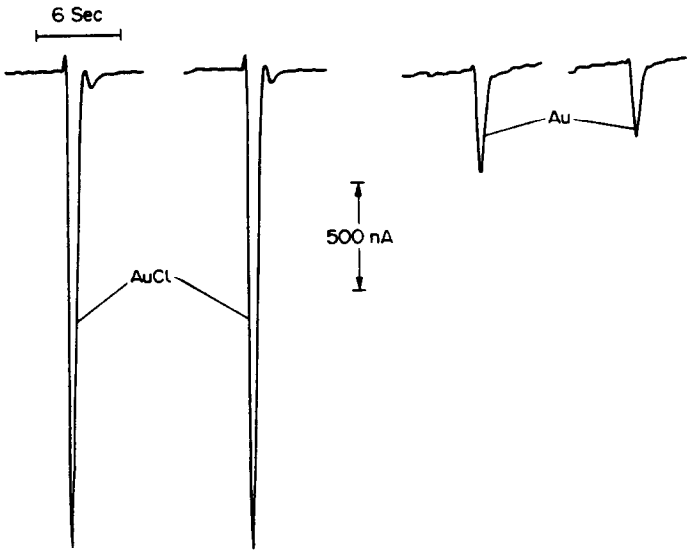

Fig. 5. Two successive FI traces of 10 nmole ascorbic acid under an applied potential of −0.1 V at Au (right) and at AuCl (left) electrodes. The MP-1 flow rate was 1 ml/min.

Reagents

Sodium octyl sulfate (Sigma), *L*-(+)-ascorbic acid (MC/B), chloropromazine (Sigma) and disodium EDTA (Fisher) were used as received. All solutions prepared by dissolving the reagents in the appropriate mobile phase were freshly prepared before use.

Preparation of gold-chloride electrode

Prior to their use the gold electrodes were hand polished on a pad of microcloth (Buehler) to a mirror finish by sequentially using 1-micron and 0.3-micron alumina suspensions (Buehler micropolish II). These electrodes were then ultrasonically cleaned for 10 min with frequent water replacement. Polished electrodes were either used unmodified or were subjected to the following electrochemical modification procedure in 0.37*M* hydrochloric acid for 300 sec.[14,15] The potential program used for this purpose consisted of oxidation–reduction cycles, from 0.0 to 1.15 ± 0.05 V (anodic limit cannot be extended beyond 1.2 V because the onset of chlorine evolution prohibits the formation of a smooth and reproducible chloride film) at a scan rate of 100 mV/sec in the anodic direction, and at a scan rate of 1100 mV/sec in the cathodic direction. The first cycle initiated, and the last cycle terminated, at +0.4 V. Since the chloride deposition mainly takes place at higher positive potentials, *i.e.*, towards the end of the anodic scan, a slow forward (anodic) scan

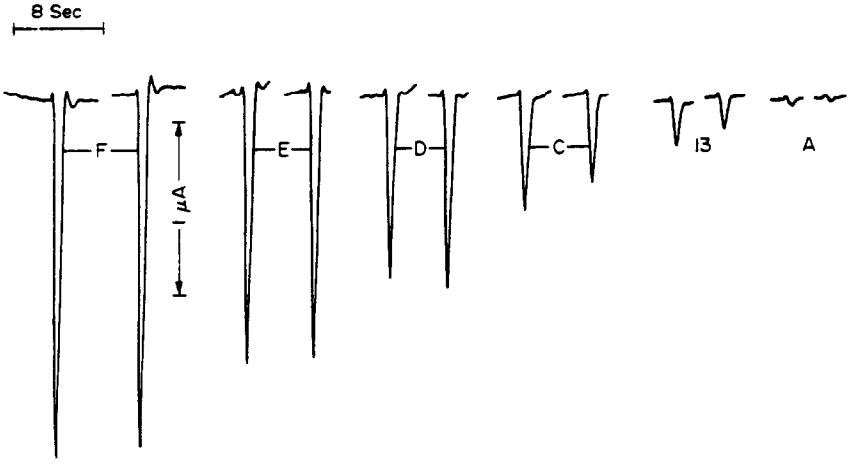

Fig. 6. Two successive FI traces of 10 nmole ascorbic acid at the Au electrode at each of the following applied potentials: 0.00 V(A), −0.10 V(B), −0.15 V(C), −0.20 V(D), −0.25 V(E), −0.30 V(F). The MP-1 flow rate was 1 ml/min.

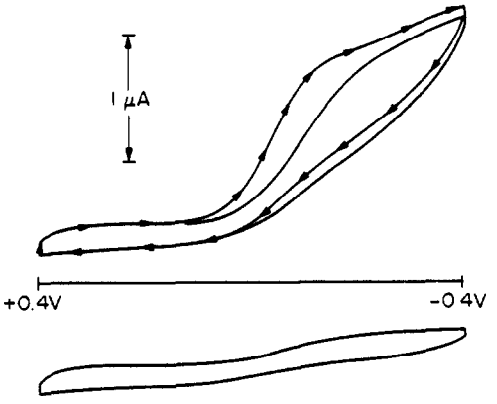

Fig. 7. Cyclic voltamperograms of AuCl electrode in air equilibrated MP-2 in the absence (upper CV with arrows) and presence (upper CV without arrows) of 10m*M* nitrate ions (sodium salt). The lower CV was obtained in deaerated MP-2. Scan rate for all the CVs was 20 mV/sec.

ensures a fixed deposition time and a fast cathodic reversal reduces the desorption time. The net result of this procedure is the formation of a smooth and reproducible chloride film on the Au electrode. This film is visible to the eye as a glassy, copper color layer.

RESULTS AND DISCUSSION

If the redox potential of an analyte is equal to or more cathodic than the redox potential of oxygen, then the faradaic activity of such an analyte would make its indirect detection quite difficult. Thus, our first consideration in demonstrating the indirect electrochemical detection via interference of an analyte with the oxygen reduction process was the selection of a few species that are electroinactive at potentials corresponding to oxygen reduction. With this restriction in view, we otherwise arbitrarily selected two organic species (L-ascorbic acid and chloropromazine) and three inorganic ions (nitrate, sulfate, and ferrous) for preliminary tests. For organic species, we used MP-1 as supporting electrolyte in cyclic voltammetric and FI studies. For similar experimentation involving anions, we used MP-2 as the supporting electrolyte. The compositions of these mobile phases are given in the experimental section. These mobile phases were selected merely on the basis of their successful use in other studies for LC (MP-1) and IC (MP-2).

Cyclic voltamperograms, CVs at the Au electrode in the absence and presence of 1m*M* chloropromazine are shown in Fig. 1. The lower CV in this figure was obtained in the nitrogen saturated MP-1 containing no additives. This CV, when contrasted with the upper CVs, clearly establishes that the reductive waves in the latter CVs arise from the electroreduction of oxygen. Further, a comparison of the upper CVs reveals that chloropromazine strongly interferes with the oxygen electroactivity as evidenced by a large cathodic shift in the oxygen reduction wave. The corresponding interference at gold chloride electrode is shown in Fig. 2. Description of various CVs in this figure is the same as that outlined above for the Au electrode. A comparison of appropriate CVs in Fig. 1 and Fig. 2 establish a stronger interference of chloropromazine with oxygen reduction at the gold chloride electrode. These observations indicate that: (i) an indirect signal for LC detection can be obtained by injecting the analyte species in a flow stream moving past the detector electrode held at a potential corresponding to the oxygen reduction process and (ii) the signal obtained at the gold chloride electrode will be much stronger as compared to that which can be generated at the gold electrode. Flow injection traces of 1 nanomole of chloropromazine (obtained at an applied potential of -0.3 V) shown in Fig. 3 give evidence of the soundness of these conclusions. Notice that the signal at the gold chloride electrode is more stable and larger (about ten times) than that at the gold electrode.

Cyclic voltamperograms at the Au electrode in the absence and presence of 1m*M* ascorbic acid, AA, are shown in Fig. 4. The lower CV in this figure pertains to nitrogen saturated MP-1 in the absence of AA. Like chloropromazine, AA interferes with the redox activity of oxygen (compare upper CVs). The anodic wave shown by one of the upper CVs is due to the oxidation of AA and it lies in a potential region outside the oxygen reduction regime. Hence, the electrochemical oxidation of AA does not interfere with oxygen reduction and the observed signal is attributable to the influence of AA on the oxygen current. The FI traces shown in Fig. 5 indicate that this interaction is strong enough to give a large signal. Further, as expected, the performance of the gold chloride electrode is superior to that of the gold electrode.

For a given concentration of an analyte and a given mobile phase flow rate, we expect a profound influence of changing electrode potential upon the magnitude of the observed indirect signal. This expectation is based on the oxygen reduction trend shown in Fig. 4. Observe that the background signal increases with cathodic

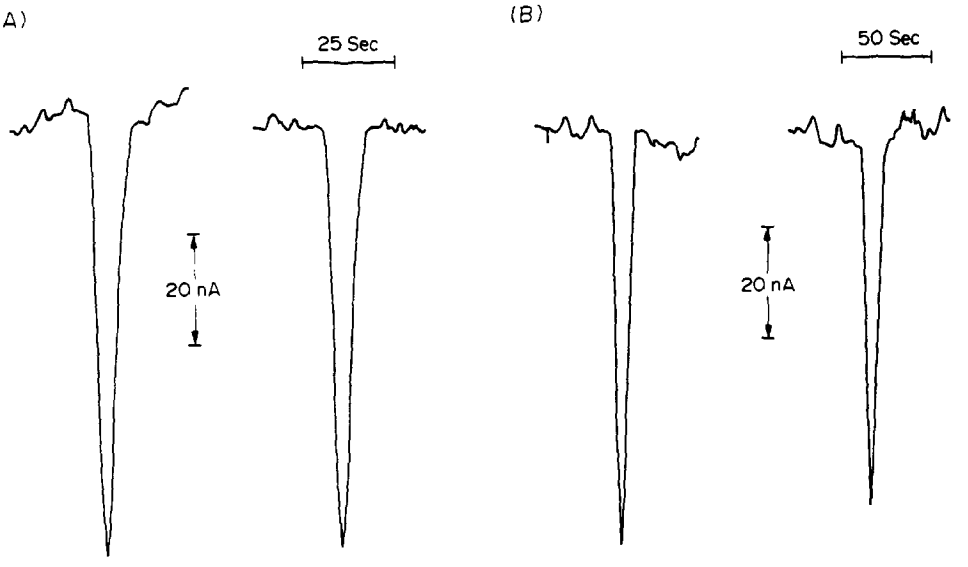

Fig. 8. Two successive FI traces of (A) 10 nmole sulfate ions and (B) 20 nmole nitrate ions under an applied potential of −0.1 V at AuCl electrode. The MP-2 flow rate was 0.1 ml/min.

potential, indicating that in the flow-injection work an increasingly larger anodic change in the background current in the presence of ascorbic acid will result at higher (more cathodic) applied potentials. This trend is clearly seen in Fig. 6 which displays two successive FI traces for 10 nmolar AA at various applied potentials.

Additional experimental observations extending the application of the proposed indirect electrochemical detection scheme are presented in Figs. 7 and 8. Shown in Fig. 7 are the CVs of the gold chloride electrode in the absence and presence of 10m*M* nitrate (sodium salt). The lower CV in this figure obtained in the absence of nitrate in deaerated MP-2 establishes that the reductive waves in upper CVs belong to the process of oxygen reduction. Similar CVs were obtained for other ions (sulfate and ferrous) investigated. For all species tested, we found a strong interference (of these species) with the oxygen reduction wave and they were all indirectly detected in our FI experiments. Two successive FI traces for 10 nmolar sulfate ions [Fig. 8(A)] and 20 nmolar nitrate ions [Fig. 8(B)] are shown in Fig. 8 (both ionic species were injected as their sodium salts). These traces were obtained at the gold chloride electrode and the corresponding traces obtained at the gold electrode were much weaker.

In conclusion, with ample examples we have clearly demonstrated that the influence at the detector electrode of the analyte molecules or ions on the oxygen reduction signal provides an indirect signal for their detection, providing this interaction disturbs the process of oxygen reduction. The proposed scheme has the potential for designing a novel EC detector for flow analyses such as ion chromatography and liquid chromatography. The only limitation of this scheme is the requirement that the analyte must affect the oxygen reduction process and be electroinactive in the potential regime corresponding to the electroactivity of oxygen. Interaction of analyte species with the signal generating mobile phase additive (oxygen) seems to be a universal property. In many cases, the effect can be enhanced through the selection of an appropriate electrocatalyst (the detector electrode) for oxygen reduction. Our recent CV experiments in 0.5*M* sulphuric acid have clearly indicated substantial anodic and cathodic shifts in the oxygen reduction onset potential, respectively, at the AuCl and AuBr electrodes, as compared with the Au electrode. Further, using a dual electrode configuration, the electroactivity of the analyte species at the detector electrode can be eliminated by its electrolysis at the upstream electrode. The catalytic behaviour of the AuCl electrode towards oxygen and other species is probably due to the well known inner-sphere electron transfer via the metal ligand bridge. These bridges are known to provide a lower activation energy barrier to electron transfer as compared to the corresponding solvent assisted path. Similar work with a large number of other species is continuing and will be published in the near future.

Acknowledgement—This work was supported by the California State University Foundation at the California State University Northridge.

REFERENCES

1. H. Small and T. E. Miller, Jr., *Anal. Chem.*, 1982, **54**, 462.
2. P. G. Rigas and D. J. Pietrzyk, *ibid.*, 1986, **58**, 2226.
3. C. A. Chang, Q. Wu and C. Sheu, *J. Chromatog.*, 1987, **404**, 282.
4. S.-I. Mho and E. S. Yeung, *Anal. Chem.*, 1985, **57**, 2253.
5. J. E. Parkin, *J. Chromatog.*, 1984, **287**, 457.
6. *Idem*, *ibid.*, 1984, **303**, 436.
7. Gy. Vigh and A. Leitold, *ibid.*, 1984, **312**, 345.
8. S. Banerjee and M. A. Castrogivanni, *ibid.*, 1987, **396**, 169.
9. S. Banerjee, *Anal. Chem.*, 1985, **57**, 2590.
10. J. Ye, R. P. Baldwin and K. Ravichandran, *ibid.*, 1986, **58**, 2337.
11. G. Horvai, J. Fekete, Zs Niegreisz, K. Tóth and E. Pungor, *J. Chromatog.*, 1987, **385**, 25.
12. H. Hojabri, A. G. Lavin, G. G. Wallace and J. M. Rivielle, *Anal. Chem.*, 1987, **59**, 54.
13. P. R. Haddad, *Chromatographia*, 1987, **24**, 217.
14. M. S. Tunuli and L. Armendariz, *J. Electrochem. Soc.*, 1987, **134**, 2641.
15. M. S. Tunuli, *Talanta*, 1988, **35**, 697.

Talanta, Vol. 39, No. 1, p. 91, 1992
Printed in Great Britain

0039-9140/92 $5.00 + 0.00
Pergamon Press plc

LETTER TO THE EDITORS

CORRECTION FACTORS FOR THE GLASS ELECTRODE REVISITED

SIR,

When a pH meter is calibrated with aqueous buffers and the pH measurement is made in mixed solvent solutions, the absolute error in pH is given by[1]

$$pH^* - B = \log U_H^0 \quad (1)$$

where pH^* is $-\log a_H$ in the mixed solvent and B is the reading of the pH meter. The term $\log U_H^0$ is usually called the *correction factor* which is applied to the glass electrode.[2-4] If the stoichiometric concentration C of a strong acid in a mixed solvent is known, the pH^* value may be readily calculated as

$$pH^* = -\log C - \log f_H^* \quad (2)$$

where f_H^* is the activity coefficient for the hydrogen ion in the studied medium. From equations (1) and (2), we obtain

$$\log U_H^0 = -\log C - \log f_H^* - B \quad (3)$$

which allows the direct calculation of the correction factors.

Since the landmark work of van Uitert,[2] the experimental way for determining $\log U_H^0$ has essentially remained the same. This consists of preparing mixed solvent solutions containing final concentrations, C_{HR} of a strong acid and C_{NaR} of its sodium salt (that fulfill $C_{HR} + C_{NaR} = 0.02$), in a temperature-controlled system, and then measuring the steady pH meter reading B. Values for $\log f_H^*$ at this ionic strength are computed by using Debye–Hückell relationships.[5] However, this procedure leads to a correction factor for only the given B value in the mixed solvent considered. Accordingly, the constant nature of the correction factor in a given solvent mixture along the pH scale should be considered with caution. Moreover, Douhert[6] showed that the correction factors for several organic aqueous mixtures depend on the measured pH of the solvent mixture. Accordingly, the reported data on correction factors for solvent mixtures should be re-examined for the whole empirical pH scale in order to avoid biased results when these are applied to the evaluation of pK_a values.[7-12]

We have recently proposed a straightforward method for evaluating correction factors covering the whole pH meter readout range.[13] In the case of dioxane–water mixtures, the correction factors are pH dependent which will cause a bias in the evaluation of, say, acidity constants in non-aqueous media. Our investigation of several other solvent mixtures is now in progress and we expect to find similar behaviour with regard to the non-constant nature of pH of the correction factors to be made to the glass electrode.

REFERENCES

1. G. Gonzalez, D. Rosales, J. L. Gomez Ariza and A. Guiraum Perez, *Talanta*, 1986, **33**, 105.
2. L. G. van Uitert, *Ph. D. Thesis*, Pennsylvania State University, 1952.
3. L. G. van Uitert and C. G. Haas, *J. Am. Chem. Soc.*, 1953, **75**, 451.
4. H. M. N. H. Irving and U. S. Manhot, *J. Inorg. Nucl. Chem.*, 1968, **30**, 1215.
5. M. Galus, S. Glab, G. Grekulak and A. Hulanicki, *Talanta*, 1979, **26**, 169.
6. G. Douheret, *Bull. Soc. Chim. France*, 1968, 3122.
7. Y. K. Agrawal and S. G. Tandon, *Talanta*, 1972, **19**, 700.
8. J. T. Rubino and W. S. Berryhill, *J. Pharm. Sci.*, 1986, **75**, 182.
9. J. P. Shukla, R. S. Sharma and M. R. Patil, *Monatsh. Chem.*, 1978, **118**, 931.
10. A. G. Gonzalez, D. Rosales, J. L. Gomez Ariza and J. Fernandez Sanz, *Anal. Chim. Acta*, 1990, **228**, 301.
11. A. G. Gonzalez, M. C. Mochon, J. L. Gomez Ariza and A. Guiraum Perez, *ibid.*, 1989, **224**, 109.
12. A. G. Gonzalez, M. A. Herrador and A. G. Asuero, *ibid.*, 1991, **246**, 429.
13. A. G. Gonzalez and F. Pablos, *ibid.*, 1991, **251**, 321.

26 September 1991

Department of Analytical Chemistry,
University of Seville,
41012 - Seville, Spain

A. GUSTAVO GONZALEZ
F. PABLOS
AGUSTIN G. ASUERO

Talanta, Vol. 39, No. 1, pp 93–94, 1992
Printed in Great Britain

0039-9140/92 $5.00 + 0.00
Pergamon Press plc

BOOK REVIEWS

Unified Separation Science: J. C. GIDDINGS, Wiley Interscience, New York, 1991. Pages xxiv + 320. £43.65.

This book is a distillation of the work of the author and others, on the multifaceted subject of molecular separation which impinges on nearly all the scientific disciplines from the biological to the physical sciences. Although it is clearly written it is by no means for the beginner, but for the graduate with a mathematical background knowledge of physical phenomena. Its stated objective is that it is 'for the purpose of education and not necessarily to train'.

After a general introduction the book is divided essentially into two sections. Chapters one to six review comprehensively the theoretical basis of separation, covering transport, flow and equilibrium phenomena. Many of the concepts and terms pertaining to separation, diffusion, capillary and packed bed flow, viscosity, zone formation, random walk processes, *etc.*, are developed mathematically, although this treatment is balanced with a readable narrative.

A bridging chapter rationalizes and classifies the various separation methods, concentrating initially on codification and then on the categorization of flow-assisted separation. Having classified the various techniques, the last five chapters deal with specific classes, utilizing the theoretical concepts developed earlier. Techniques described include electrophoresis, sedimentation, field flow fractionation and an in-depth consideration of chromatography, which covers molecular migration, plate-height and optimization.

At the end of each chapter are graded exercises to facilitate the reinforcement of the concepts. Fortunately answers are also provided. Each chapter is well referenced and there is also a comprehensive bibliography containing the author's publications.

In this advanced text the author has succeeded, as the title states, in presenting a unified approach to this complex subject in that the inter-relationships of the mechanisms involved in molecular separations have been examined effectively in detail.

G. G. SKELLERN

HPLC in Clinical Chemistry: I. N. PAPADOYANNIS, Dekker, New York, 1990. Pages x + 488. $115.00 (US and Canada), $138 (elsewhere).

This reference text offers a prominent contribution to the literature on clinical analysis by HPLC and covers a wide range of drugs and biological components. The chapters, which include the subject groups alkaloids, antiobiotics, steroids and proteins, contain considerable experimental detail of literature methodologies reported in relatively recent publications. These aspects cover the topics of clinical sample preparation, multicomponent separation and moreover in some instances, the inclusion of a typical pharmaceutical preparation assay. Additionally there are useful introductory sections, prior to the HPLC text, which discuss other spectroscopic and chromatographic methods and point to advantages and disadvantages of these techniques.

Preceding the major text the author has included a preliminary section of introductory information on "Instrumentation in HPLC". Although this section is generally useful, segments such as septum injection, pneumatic and motor-driven pumps are rather outmoded in modern HPLC. It is considered that micro and narrow bore HPLC columns, multichannel detection, method optimization and automation of clinical assay would have provided useful enhancements. Additionally further discussion in mass spectrometry to include "soft" ionization techniques and reference to quadruple analysers and MS-MS would have been beneficial. However, this is a minor criticism of the book and does not detract from its overall usefulness as a practical reference text.

B. J. CLARK

Multivariate Calibration: H. MARTENS and T. NAES, Wiley, Chichester, 1989. Pages xvii + 418. £75.00 (Hardback), £29.50. (Softback).

The adoption of chemometric methods (statistical procedures which allow otherwise unavailable or non-obvious conclusions to be drawn from the multivariate data typical of modern analytical instruments) is a striking feature of modern analytical science. These methods, like all computer-based procedures, have many pitfalls for the naive or unwary, but the overall effect of their introduction has undoubtedly been positive, and nowhere more so than in the field of calibration. This book covers the methods of multi-variate calibration developed up to 1987–8, including virtually all those now in general use.

The book begins with an excellent, often humorously written, chapter on the need for calibration methods; this is worth reading, even by those who do not wish to face the rigours of linear algebra as outlined in the second chapter. The basic principles of matrix and vector manipulation are covered in only a dozen or so pages; this is a little too compressed for the many chemists who will start with little or no knowledge of this area, and I have seen better summaries in other chemometrics texts. The same chapter outlines the basics of statistics as applied to calibration methods. The third chapter, no less than 160 pages long, contains the meat

Talanta, Vol. 39, No. 1, pp 93–94, 1992
Printed in Great Britain

0039-9140/92 $5.00 + 0.00
Pergamon Press plc

BOOK REVIEWS

Unified Separation Science: J. C. GIDDINGS, Wiley Interscience, New York, 1991. Pages xxiv + 320. £43.65.

This book is a distillation of the work of the author and others, on the multifaceted subject of molecular separation which impinges on nearly all the scientific disciplines from the biological to the physical sciences. Although it is clearly written it is by no means for the beginner, but for the graduate with a mathematical background knowledge of physical phenomena. Its stated objective is that it is 'for the purpose of education and not necessarily to train'.

After a general introduction the book is divided essentially into two sections. Chapters one to six review comprehensively the theoretical basis of separation, covering transport, flow and equilibrium phenomena. Many of the concepts and terms pertaining to separation, diffusion, capillary and packed bed flow, viscosity, zone formation, random walk processes, *etc.*, are developed mathematically, although this treatment is balanced with a readable narrative.

A bridging chapter rationalizes and classifies the various separation methods, concentrating initially on codification and then on the categorization of flow-assisted separation. Having classified the various techniques, the last five chapters deal with specific classes, utilizing the theoretical concepts developed earlier. Techniques described include electrophoresis, sedimentation, field flow fractionation and an in-depth consideration of chromatography, which covers molecular migration, plate-height and optimization.

At the end of each chapter are graded exercises to facilitate the reinforcement of the concepts. Fortunately answers are also provided. Each chapter is well referenced and there is also a comprehensive bibliography containing the author's publications.

In this advanced text the author has succeeded, as the title states, in presenting a unified approach to this complex subject in that the inter-relationships of the mechanisms involved in molecular separations have been examined effectively in detail.

G. G. SKELLERN

HPLC in Clinical Chemistry: I. N. PAPADOYANNIS, Dekker, New York, 1990. Pages x + 488. $115.00 (US and Canada), $138 (elsewhere).

This reference text offers a prominent contribution to the literature on clinical analysis by HPLC and covers a wide range of drugs and biological components. The chapters, which include the subject groups alkaloids, antiobiotics, steroids and proteins, contain considerable experimental detail of literature methodologies reported in relatively recent publications. These aspects cover the topics of clinical sample preparation, multicomponent separation and moreover in some instances, the inclusion of a typical pharmaceutical preparation assay. Additionally there are useful introductory sections, prior to the HPLC text, which discuss other spectroscopic and chromatographic methods and point to advantages and disadvantages of these techniques.

Preceding the major text the author has included a preliminary section of introductory information on "Instrumentation in HPLC". Although this section is generally useful, segments such as septum injection, pneumatic and motor-driven pumps are rather outmoded in modern HPLC. It is considered that micro and narrow bore HPLC columns, multichannel detection, method optimization and automation of clinical assay would have provided useful enhancements. Additionally further discussion in mass spectrometry to include "soft" ionization techniques and reference to quadruple analysers and MS-MS would have been beneficial. However, this is a minor criticism of the book and does not detract from its overall usefulness as a practical reference text.

B. J. CLARK

Multivariate Calibration: H. MARTENS and T. NAES, Wiley, Chichester, 1989. Pages xvii + 418. £75.00 (Hardback), £29.50. (Softback).

The adoption of chemometric methods (statistical procedures which allow otherwise unavailable or non-obvious conclusions to be drawn from the multivariate data typical of modern analytical instruments) is a striking feature of modern analytical science. These methods, like all computer-based procedures, have many pitfalls for the naive or unwary, but the overall effect of their introduction has undoubtedly been positive, and nowhere more so than in the field of calibration. This book covers the methods of multi-variate calibration developed up to 1987–8, including virtually all those now in general use.

The book begins with an excellent, often humorously written, chapter on the need for calibration methods; this is worth reading, even by those who do not wish to face the rigours of linear algebra as outlined in the second chapter. The basic principles of matrix and vector manipulation are covered in only a dozen or so pages; this is a little too compressed for the many chemists who will start with little or no knowledge of this area, and I have seen better summaries in other chemometrics texts. The same chapter outlines the basics of statistics as applied to calibration methods. The third chapter, no less than 160 pages long, contains the meat

of the book, including lengthy discussions of principal components regression and partial least squares. Some illustrative chemical examples are given, and if the reader is by this stage fully conversant with matrix notation, *etc.*, this central section of the book will be extremely rewarding.

The remainder of the text is also excellent. Chapter 4 deals with the crucial but frequently neglected question of method validation. Chapter 5 covers outlier detection, and it is notable that the authors are not enthusiasts for robust regression methods. Chapter 6 covers the design of calibration experiments, a topic which might seem to have merited earlier treatment, but which in practice sits nicely at this juncture. Chapter 7 is an equally successful account of data pre-treatments such as linearization. The book concludes with an illustrative example studied in some detail, and there is also a bibliography, a glossary of symbols and terms, and—for once—an excellent index. Computer programs are not provided, or even recommended, despite the authors' association with the well-known UNSCRAMBLER package.

This book is not, nor is it expected to be, an easy read. However, it covers a complex and crucial area of data handling supremely well, and must take its place on the bookshelves of all serious analytical scientists.

J. N. MILLER

Statistical Methods in Applied Chemistry: J. CZERMINSKI, A. IWASIEWICZ, Z. PASZEK and A. SIKORSKI, Elsevier, Amsterdam, 1989. Pages xviii + 493. US$ 179.50, Dfl. 350.00

This is a thorough mathematical treatment of the science of statistics as applied to chemistry. It covers all the major topics of parametric and non-parametric statistics, *e.g.*, random variables, the various distribution functions, parameter estimation, hypothesis testing, analysis of variance, correlation and regression (multiple linear and non-linear regression are included). Chemical data are used in all the examples.

A chapter on "Methodological Guidelines" gives details of the statistical procedures used in particular chemical problems, covering areas such as limit of detection and sensitivity, precision and accuracy, propagation of errors, the effects of rounding errors, and sampling. The final chapter gives two extended examples of data analysis, one for a technological problem and the other for an analytical one.

Fourteen useful tables of statistical data are included, and also a collection of computer programs written in Turbo Pascal, together with some tables of test data.

This will be a useful book for the serious research worker, but the mathematics is probably too advanced to make it suitable as a student text-book, even at postgraduate level. The translation is adequate, but could have been greatly improved by a translation editor.

M. MASSON

of the book, including lengthy discussions of principal components regression and partial least squares. Some illustrative chemical examples are given, and if the reader is by this stage fully conversant with matrix notation, *etc.*, this central section of the book will be extremely rewarding.

The remainder of the text is also excellent. Chapter 4 deals with the crucial but frequently neglected question of method validation. Chapter 5 covers outlier detection, and it is notable that the authors are not enthusiasts for robust regression methods. Chapter 6 covers the design of calibration experiments, a topic which might seem to have merited earlier treatment, but which in practice sits nicely at this juncture. Chapter 7 is an equally successful account of data pre-treatments such as linearization. The book concludes with an illustrative example studied in some detail, and there is also a bibliography, a glossary of symbols and terms, and—for once—an excellent index. Computer programs are not provided, or even recommended, despite the authors' association with the well-known UNSCRAMBLER package.

This book is not, nor is it expected to be, an easy read. However, it covers a complex and crucial area of data handling supremely well, and must take its place on the bookshelves of all serious analytical scientists.

J. N. MILLER

Statistical Methods in Applied Chemistry: J. CZERMINSKI, A. IWASIEWICZ, Z. PASZEK and A. SIKORSKI, Elsevier, Amsterdam, 1989. Pages xviii + 493. US$ 179.50, Dfl. 350.00

This is a thorough mathematical treatment of the science of statistics as applied to chemistry. It covers all the major topics of parametric and non-parametric statistics, *e.g.*, random variables, the various distribution functions, parameter estimation, hypothesis testing, analysis of variance, correlation and regression (multiple linear and non-linear regression are included). Chemical data are used in all the examples.

A chapter on "Methodological Guidelines" gives details of the statistical procedures used in particular chemical problems, covering areas such as limit of detection and sensitivity, precision and accuracy, propagation of errors, the effects of rounding errors, and sampling. The final chapter gives two extended examples of data analysis, one for a technological problem and the other for an analytical one.

Fourteen useful tables of statistical data are included, and also a collection of computer programs written in Turbo Pascal, together with some tables of test data.

This will be a useful book for the serious research worker, but the mathematics is probably too advanced to make it suitable as a student text-book, even at postgraduate level. The translation is adequate, but could have been greatly improved by a translation editor.

M. MASSON

Talanta, Vol. 39, No. 2, pp. 95–99, 1992
Printed in Great Britain.

0039-9140/92 $5.00 + 0.00

APPLICATION OF A MULTICHANNEL DROPPING DISPENSER IN SEGMENTED CONTINUOUS FLOW ANALYSIS

V. KUBAN*
Department of Analytical Chemistry, Masaryk University, CS-61137 Brno, Czechoslovakia
L.-G. DANIELSSON and F. INGMAN
Department of Analytical Chemistry, The Royal Institute of Technology, S-100 44 Stockholm, Sweden

(*Received* 1 *May* 1991. *Revised* 3 *July* 1991. *Accepted* 29 *July* 1991)

Summary—A simple dual channel dropping dispenser has been used for the simultaneous introduction of aqueous solutions of sample and reagent directly into a continuous flow of an organic solvent. Each aqueous segment forms an enclosed reaction system, completely surrounded by a film of the organic phase, which prevents any carry over between segments. An analytical signal is measured directly on the moving segments of precisely defined volumes of the homogenized reaction mixture. The applicability of this "microbatch" technique for the determination of light-absorbing species, for sample dilution and one-standard calibration, and for providing acid–base titrations on a microlitre scale is demonstrated with simple examples.

The automation of liquid sample and reagent processing was greatly facilitated by the introduction of flow analysis (FA) with a great variety of working principles. All but the simplest of manifolds for FA includes one or more confluence points. Many designs have been presented and claimed to give improved mixing.[1–6] Regardless of the angles between the channels, the flow is strictly laminar under the conditions used in one phase FA (flow rates and channel i.d.) thus, no turbulence will aid the mixing.[3,4] The two streams leaving the confluence point mix through diffusion during transport in the following tubing. This is a relatively slow process requiring a long residence time for acceptable mixing. Coiling, knitting or otherwise introducing a number of points where the direction of flow is changed creates a radial flow and mixing is improved.[6]

In an air-segmented continuous flow analyser[1] (SCFA) with the sample, gas for segmentation, and reagents sequentially introduced into the flow system by peristaltic pumping at fixed flow rates, each segment is intensely mixed due to the intensive intrasegmental flow. If a second stream is merged with the segmented flow the contents of this flow is rapidly mixed into segments of the same phase. This is the standard procedure in air segmented systems and has also been used in liquid–liquid segmented flow.[7] However, if the added flow is too large, the original segmentation pattern might be disturbed by the new flow forming segments of its own.

In an "encapsulated chemistry" technology[5,6] system marketed by Technicon, CHEM I, precisely defined volumes of the sample and reagent(s), sequentially introduced into the system together with a capsulating fluorocarbon liquid, intercalate with air bubbles of two different sizes. The smaller bubbles separate individual reaction components prior to their mixing and forming segments of reaction mixture in a "vanishing zone" (a widening of the tube diameter over a short length[5]). A drawback with this system is the very complicated mechanism needed for creating a suitable segment pattern and the presence of a compressible phase obviating the attainment of a stable flow.

The air-carrier continuous analysis system[8] (ACCAS) allows the mixing of a fixed volume of the sample with fixed volumes of one or more reagents, introduced either simultaneously or sequentially with an electronically controlled system of valves. The complex valve system seems to limit the practical value of the method.

During our studies of the segmentation process in liquid–liquid extraction flow-injection analysis (FIE), it was found that the multichannel coaxial segmentor[9,10] allows the operations performed by a dispenser, a confluence

*Author for correspondence.

point, a mixing coil and a segmentor to be combined in one unit. The theory behind the formation of droplets, and other processes in these systems have been outlined in previous papers.[9-11] When applying this theory to the present system it must be kept in mind that here droplets of the aqueous phase are formed at the junction of the inlet capillaries drilled in a lipophilic material. Such a system could be useful not only for FIE but also for fundamental chemistry studies involving kinetic measurements since the starting point is better defined than in systems based on the slow mixing in unsegmented flow and there is practically no dispersion. The idea of concurrently starting a reaction and creating a reaction "vessel" in a segment flow was the basis for this work in which its applicability is demonstrated with simple examples.

EXPERIMENTAL

Chemicals and apparatus

Air, chloroform (E. Merck, FRG, analytical grade) and Freon 113 (1,1,2-trichloro-1,2,2-trifluoroethane, technical quality) saturated with water were tested as carrier fluids. Aqueous $1\mu M$–$1.5mM$ solutions of Bromocresol green (BCG) or Neutral Red (NR) were used. All other chemicals were of analytical grade and used without purification. Distilled water and all other solvents and solutions were degassed in a Branson 2200 ultrasonic bath (Branson, USA) before use.

The multichannel dropping dispenser (Fig. 1) comprises two parts, a polyvinylidenedifluoride (PVDF)/glass main part and a PVDF screw with the inlet capillaries. The main part is constructed from a 14-mm long thick-walled glass tube (6 mm i.d., 9 mm o.d.) clamped between two PVDF pieces with 4 screws. The glass tube allows visual checking of the droplet formation process and the homogenization of the reaction mixture. The lower of the two PVDF parts is threaded to accommodate the screw containing the inlet capillaries and has an inlet (0.7 mm) for the organic carrier fluid. The upper part has an extension which fits tightly into the glass tube. The end of this extension has a conical chamber with an outlet (0.7 mm) for the segmented flow in its apex. Connections to the rest of the flow system is made with flanged 1/16″ o.d. Teflon tubing. The screw with inlets for the aqueous solutions has two capillary channels (0.3 mm dia., 5 mm long, $\approx 20°$ angle) meeting right at the surface of the screw. In order to simplify the machining of this part a much wider bore (1.6 mm) was used for the rest of the connection and the Teflon tubing was drawn into this bore and tightened with an O-ring seal. The on-tube detector and the data handling procedure have been described previously.[9,10] For this work a transparent FEP tubing of 1.5 mm i.d. was used in the detector because it gives higher measurement precision and sensitivity.

In this work three different measuring modes have been used: signal height, the absorbance recorded for an aqueous segment as compared to the absorbance of an organic segment; signal area, the integrated signal over the length of the segment; relative signal area, signal area divided by the length of the segment (in seconds). The last mode should be favourable as it uses as many measurements of the signal as possible and compensates for the slight variation in segment length. However, there are some problems connected with the determination of the end-points of segments with low signals.

RESULTS AND DISCUSSION

Repeatability of the droplet formation

The repeatability of droplet formation was slightly better for Freon-113/water than for the chloroform/water system, thus Freon-113 was subsequently used as the carrier fluid. The lower toxicity of this solvent was also taken

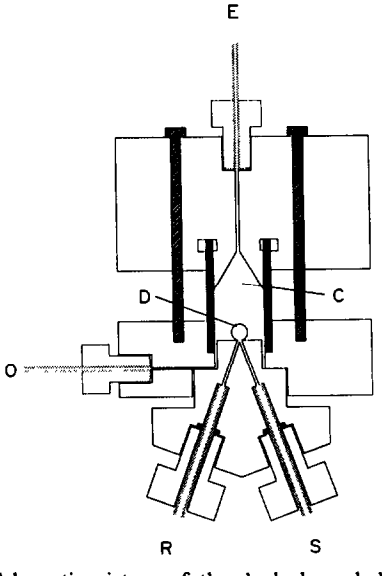

Fig. 1. Schematic picture of the dual channel dropping dispenser. R–reagent, S–sample, O–organic phase, E–segmented outflow, C–conical chamber, D–droplet.

into account. The segmentation repeatability was not satisfactory ($s_r \approx 10\%$) with air as the carrier, although the droplet formation was seemingly very regular. Serious pulsation of the resulting segmented flow occurred because of the compressibility of the air segments. Also, the baseline noise was worse by one order of magnitude than when the carrier fluid was Freon-113. The small droplets of aqueous phase clinging to the walls of the measuring tube were not completely removed by the air segments. Their appearance in the light path, and their movement, was accompanied by a serious increase both in the baseline signal and in the baseline noise.

To establish regular film formation the segment length of the organic phase cannot be reduced indefinitely, thus the lowest organic phase flow rate (Q_o) used was 0.2 ml/min.

Direct determination of light absorbing species

The determinations of the blue alkaline (L^{2-}, 627 nm) and yellow acidic (LH^-, 420 nm) forms of Bromocresol green (BCG) and of copper(II) ions in acidic solution were chosen as examples. The aqueous solution was pumped through both inlet capillary channels to eliminate effects of eccentricity of the junction, and the analytical signal was measured on the aqueous phase segment at 600 and 420 nm, respectively. The organic phase flow was stopped after some preselected time (usually after 10 segments have passed through the detector) and the analytical signal was then also measured for a continuously pumped solution of the analyte at "steady state" to compare the signal levels.

The analytical signal increases linearly with the analyte concentration from negative to positive values passing through an area with signals of the same order as the baseline noise ($S_0 < 10s_0$). The calibration graphs are linear in the range 6.2–154μM BCG and 0.01–0.8M copper(II) ions. The correlation coefficients were good for signal height and signal area *vs.* concentration but considerably worse for the calibration based on relative signal area. This is due to a large spread in the values for samples with signals close to zero. For these samples the measurement of segment length is difficult and this shows up as errors in the relative signal area (Fig. 2).

The values agree well with those obtained by continuous pumping of the analyte solutions without segmentation through the measuring tube as demonstrated by the slopes and intercepts of the Youden graphs: ($y = 1.02x - 0.06$, $0.992x + 0.08$ and $1.01x + 0.02$ with correlation coefficients of 0.993, 0.989 and 0.997, respectively).

Dilution and one solution calibration

Pumping an aqueous solution containing either 30.8μM BCG or 0.1M Cu simultaneously with water into the inlet capillary channels at constant flow-rate ratio $Q_1/Q_2 = 1$ or 2 keeping the total flow-rate constant at $Q_t = 0.5$ ml/min, makes it possible to dilute the sample solution, the degree of the dilution depending on the Q_1/Q_2 ratio. The resulting signal values differ by less than 3 and 2% from those obtained by continuously pumping a corresponding non-segmented aqueous phase.

Data obtained by changing the phase flow-rate ratio Q_1/Q_2 in steps from 0.5 : 0 to 0 : 0.5 of the sample solution (154μM BCG) and water at a constant total flow-rate $Q_t = 0.5$ ml/min was used in order to construct a calibration graph from dilution experiments. A linear dependence was obtained between the analytical signal and analyte concentration which fits well with graphs obtained by pumping aqueous phase only and also with graphs obtained earlier, using a series of solutions of different concentration.

Indirect determination of analyte concentration

As an example of a fast reaction, BCG in its alkaline form was pumped together with 0.1M hydrochloric acid at a constant total flow-rate $Q_t = 1.6$ ml/min and $Q_1/Q_2 = 1$ and 0.5 into the inlet capillary system. This example is suitable for studying the mixing efficiency and the influence of the reaction rate. The analytical signal

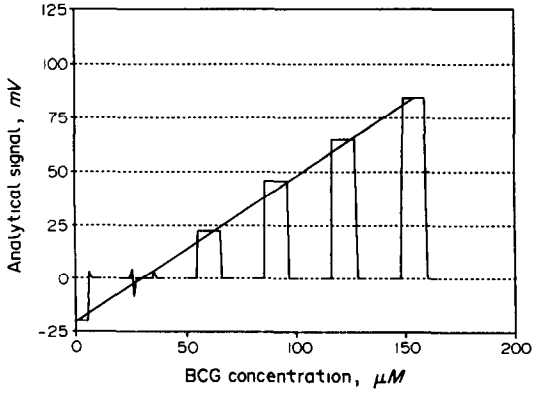

Fig. 2. Calibration graph for the direct determination of the blue alkaline form of BCG (at 600 nm) with the signal shape indicated at the different levels.

was measured at the absorption maximum of the acid form LH^- of BCG at 420 nm.

The solutions are very rapidly mixed and the yellow acidic form of BCG is generally formed quantitatively already during the droplet formation, especially at the higher total flow-rate and when the flow-rate ratio is close to 1. No significant difference in the analytical signal was found when the signal was measured 10 or 60 cm downstream from the dropping device ($y = 1.00x + 0.03$ for the Youden graph). Consequently, the reaction seems to be quantitative already at the beginning of the measuring tube. The calibration graph is linear in the range 3.1–154μM BCG.

Acid–base titration

A sodium hydroxide solution ($c = 0.1M$) containing 92.4μM BCG or 80μM Neutral Red (NR) as an indicator was titrated with 0.1M hydrochloric acid by changing the flow-rate ratio between the two solutions stepwise at a constant total flow-rate $Q_t = 1.6$ ml/min. The analytical signal was measured at the absorption maximum of the blue and red forms of the indicator (600 and 560 nm, respectively) and a titration curve with a very sharp change of the analytical signal at the equivalence point at $Q_1/Q_2 = 0.93 \pm 0.08$ and 0.96 ± 0.08 ($n = 5$) was obtained (Fig. 3). The repeatability of the procedure is relatively poor ($s_r = 8.5$ and 7.3%) as a result of experimental factors influencing the measurement precision (flow-rate, flow-rate ratio, pulsation *etc.*).

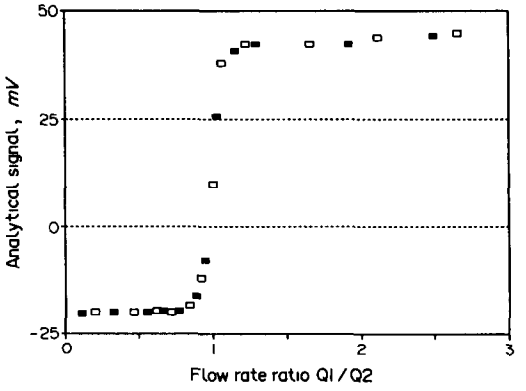

Fig. 3. Titration of 0.1M NaOH with 0.1M HCl in the presence of 92.4μM BCG (600 nm) by varying the flow-rate ratio Q_1/Q_2. Filled squares represents data obtained when the flow-rate ratio was changed from 0.1 to 2.5. Open squares represents results obtained when the flow-rate ratio was changed back to 0.1.

CONCLUSIONS

The system presented is based on the simultaneous formation and mixing of small aqueous droplets of the reaction mixture in a flowing organic fluid, immiscible with the aqueous phase. The concentration of a particular component in each droplet of the reaction mixture is governed by the flow-rate ratio of the component streams of aqueous phase and by the actual concentration of the component in each solution. The droplets form closed reaction systems completely isolated from each other by segments of organic phase, and by a film of organic phase on the tubing wall, which prevent any analyte and reagent carry-over during the transport through the capillary system of the analyser. The reaction yield is determined by the experimental conditions in each individual closed reaction system and by the kinetics of the reaction.

The rapid mixing taking place during drop formation and the fact that the system provides negligible dispersion in a flow of incompressible media makes the system suitable for kinetic studies. It can also be useful for the application of slow reactions because no dispersion occurs during transport through even very long capillaries.

With the low flow-rate of the organic phase ($Q_o = 0.2$–0.5 ml/min) used to form segments, the total consumption of the organic solvent does not exceed the volume of 25 ml/hr. This fact together with the completely closed measuring system and recycling of the organic solvent minimizes the environmental hazards connected with the use of Freon-113 or chloroform.

The use of a fast reading "on-tube" detection system makes it possible to measure the analyte concentration in each aqueous segment in a liquid/liquid segmented flow. Both direct and indirect analytical methods can be used. The sensitivity of the technique may be improved by integrating the analytical signal over the whole period when the segment passes through the transparent tubing. The precision of measurement is good due to the use of a larger number of segments for mean value calculations.

Sample introduction could most easily be obtained with the aid of a conventional loop injector and a carrier stream. However, since very little sample is actually needed to obtain a measurement (2–5 μl) a direct introduction of the sample into the forming droplet seems possible. Titrations could be performed by

connecting a perfusor pump to one of the capillaries of the dispenser and introducing the sample for short periods at different flow-rate ratios relative to the titrator flowing through the other capillary. With such a system, under computer control, a titration curve could rapidly be obtained with as little as 1–2 ml of sample.

Acknowledgements—This work was financially supported by the Swedish National Board for Technical Development and, in the form of a fellowship, by the Swedish Institute.

REFERENCES

1. L. T. Skeggs, Jr., *Am. J. Clin. Pathol.* 1957, **28**, 311.
2. R. W. Frei, *Chemical Derivatization in Analytical Chemistry, In Modern Analytical Chemistry*, R. W. Frei and J. F. Lawrence (eds.), Vol. 1, p. 211. Plenum Press, New York, 1981.
3. G. D. Clark, J. M. Hungerford and G. D. Christian, *Anal. Chem.*, 1989, **61**, 973.
4. C. Silfwerbrand-Lindh, L. Nord, L. G. Danielsson and F. Ingman, *Anal. Chim. Acta*, 1984, **160**, 11.
5. M. Valcárcel and M. D. Luque de Castro, *Automatic Methods of Analysis, in Techniques and Instrumentation in Analytical Chemistry*, Vol. 9, Chaps. 5 and 6. Elsevier Scientific Publisher, 1988.
6. J. Růžička and E. H. Hansen, *Flow-Injection Analysis*, p. 12. Wiley, New York, 1988.
7. L-G. Danielsson and Z. Huazhang, *J. Pharm. Biomed. Anal*, 1989, **7**, 937.
8. K. Petersen and P. K. Dasgupta, *Talanta*, 1989, **36**, 49.
9. V. Kubán, L-G. Danielsson and F. Ingman, *Anal. Chem.*, 1990, **62**, 2026.
10. V. Kubán and F. Ingman, *Anal. Chim. Acta*, 1991, **245**, 251.
11. V. Kubán and F. Ingman, *CRC Crit. Rev. Anal. Chem.*, 1991, **22**, 491.

Talanta, Vol. 39, No. 2, pp. 101–111, 1992
Printed in Great Britain.

0039-9140/92 $5.00 + 0.00

FLOW INJECTION AND SOLVENT EXTRACTION WITH INTELLIGENT SEGMENT SEPARATION. DETERMINATION OF QUATERNARY AMMONIUM IONS BY ION-PAIRING

CHERRYLEEN C. LINDGREN and PURNENDU K. DASGUPTA*
Department of Chemistry and Biochemistry, Texas Tech University, Lubbock, TX 79409-1061, U.S.A.

(*Received* 27 *June* 1991. *Revised* 17 *July* 1991. *Accepted* 17 *July* 1991)

Summary—Organic solvent segments are introduced into a premixed stream of the sample and an ion-pairing dye by a 3-way valve at regular intervals. The major mechanism of "extraction" in such a system appears to be the adsorption of the ion-pair on conduit walls and subsequent elution by the organic solvent. Following passage through the conduit, the immiscible organic segment is isolated in the loop of a 6-port valve; loop filling is sensed by a pair of conductivity sensors located respectively at the fill and drain ports of the loop and appropriate logic circuitry. The isolated segment is then injected into a purely organic carrier and detected by a suitable optical detector. Results are reported for a number of parametric studies that characterize this system. With immobilized adsorbents on conduit walls for preconcentration, a limit of detection of $<10^{-7}M$ tetrabutylammonium ion can be obtained with bromothymol blue as the ion-pairing agent.

In-line solvent extraction procedures play an important role in the current practice of flow-injection analysis.[1,2] There are many approaches to the introduction of extractant segments and their separation; this has been summarized and attendant advantages/disadvantages pointed out.[3] In many cases it is possible to perform an optical measurement of the extractant segment without physical separation of the phases; Kuban *et al.*[4] demonstrate a recent example of this. However, if post-extraction chemistry must be carried out, a physical separation of the phases is mandatory.

From the point of view of robustness and reliability for long-term unattended operation, an approach was developed in this laboratory to introduce the extractant segment by a loop injector. Further, for aqueous extractants introduced into nonaqueous sample streams, the extractant segment was automatically isolated downstream by a second loop injector.[3,5] To perform intelligent switching of this valve, the conductivity across its loop is measured. When the valve is completely filled with the aqueous extractant, the conductivity between the probes placed between the fill and drain ports of the loop rises abruptly and the loop contents are injected into a purely aqueous carrier stream. Unfortunately, the reverse task of isolating a nonconductive organic segment intercalated in an aqueous sample cannot be directly accomplished in this manner. Even a partial filling of the loop with the nonconductive segment indicates lack of conductivity between the probes placed across the loop. In this paper, we demonstrate a reliable means for accomplishing this task in conjunction with a wall-preconcentration technique. The determination of cationic surface active agents is chosen as an example; the rationale for this choice and a review of the relevant ion-pair extraction literature is given below.

The annual production of cationic surfactants is projected to be 863.1 million lbs by the year 2000.[6] Cationic surfactants are commonly used in fabric softeners and conditioners, hair rinses, oil-based petroleum drilling muds and as foam controllers in laundry detergent. Quaternary ammonium compounds, the most important group of cationic surfactants, have biocidal properties and are used as disinfectants/sanitizers (*e.g.*, in alcohol-free mouthwash) and algaecides. Their presence in discharged water is a major problem because they are lethal to a variety of microorganisms at micromolar levels.[7,8]

Auerbach[9] was the first to introduce a method of measuring cationic surfactants involving the

*Author for correspondence.

addition of an optically absorbing lipophilic dye anion, such as bromophenol or bromothymol blue (BTB) and extraction of the resulting ion-pair into an organic solvent followed by photometric measurement of the latter. Dyes of this family, including bromocresol green, continue to be particularly popular for this application;[10-12] ternary ion-aggregates involving the analyte cation, the dye and a protonated quinine cation have also been used for some applications.[13,14] Other absorbing anionic pairing agents have included Orange II,[15,16] $[Co(SCN)_4]^{2-}$,[17,18] picrate,[19,20] Erdmann's salt,[21] the anionic oxidation product of diphenylcarbazide by chromate,[22] Methyl Orange,[23] thiocyanate,[24] Brilliant Red S,[25] 2,6-dibromophenolindopenol,[20] eosin,[26] the anionic complex of Chrome Azurol S with Fe,[27] and Bengal Red.[28] Fluorescent pairing agents used include anthracenesulfonate,[29,30] Rosin, Erythrosin and Bengal Pink B,[31] and 2,4,5,7-tetrabromo-3,6-dichlorofluorescein.[32]

Bromothymol Blue was regarded as a convenient and adequately sensitive ion-pairing agent for the purpose of this study. At pH below 7, it exists predominantly as the yellow sulfonate monoanion (BTB^-). In alkaline solutions, a phenolic proton also ionizes, resulting in the blue dianion (BTB^{2-}, pK 7.1).[33] The following parameters were available from preliminary studies[34] for $(n\text{-}C_4H_9)_4N^+$ as the surface active ion Q^+ for the ion-pair extraction with BTB^-. The extracted ion-pair displays a broad band absorption maximum at 415–430 nm; ϵ_{430} for $Q^+.BTB^-$ in $CHCl_3$ is 1.8×10^4. The extraction can be made reasonably selective for quaternary ammonium ions (over, for example, trialkyl- and dialkylammonium ions) by extracting from mildly alkaline solutions; extraction efficiency (in the $Q^+.BTB^-$ form) decreases in strongly alkaline solutions. If the extraction constant K_{ex} is defined to be $[Q^+.BTB^-]_{org}/[Q^+]_{aq}[BTB^-]_{aq}$, $K_{ex} \simeq 10^7$ at pH 8.6 with $CHCl_3$ as the extractant. Extraction efficiencies observed with other aliphatic halogenated solvents, *e.g.*, CH_2Cl_2 or 1,2-dichloroethane are not markedly different. The magnitude of the extraction constant indicates that in the presence of a large excess of the ion-pairing agent, extraction efficiencies in typical manual extraction systems should be nearly quantitative. Very recently, Yamamoto and Motomizu[35] have examined the extraction behavior of a large number of sulfonephthalein dyes with a variety of quaternary ammonium ions. They find that K_{ex} values are the highest with BTB and their quantitative findings are in good agreement with the above data.

EXPERIMENTAL

Reagents

Bromothymol Blue (Kodak) and tetrabutylammonium sulfate (Aldrich) were used without further purification. Aqueous solutions of BTB were maintained at a pH of 8.5–8.8. Technical grade chloroform was used as the extractant. Before use, solutions were generally ultrasonicated for 10 min to avoid bubble formation in the manifolds.

Apparatus

Six-port injector valves were electropneumatically driven rotary devices (type 5020 P, Rheodyne Inc., Cotati, CA) and 3-way valves used were fast-acting (<25 msec), low internal volume (7.4 μl per passage) elastrometric-tubing solenoid valves (type LFYA 1203032H 12 V, 2 W, ~25 msec actuation time, The Lee Company, Westbrook, CT). Wetted parts for both valves are fluoropolymers. Pumping was provided by pneumatic pressure or by a multichannel peristaltic pump (Minipuls 2, Gilson International), as indicated. Except as noted, connecting or conduit tubing was polytetrafluoroethylene (PTFE, type SW, Zeus Industrial Products, Raritan, NJ). The photometric detector used was a Spectromonitor III with a 6.5-mm path length cell (Laboratory Data Control, Riviera Beach, FL) set at 430 nm.

Design of conductivity probes

The present instrumental design consisted of one pair each of conductivity probes placed at the fill and drain ports of the segment isolation valve (*vide infra*). The design of the probes is critical. In each pair of probes, the electrodes must be as close to each other as practical without significant problems from wall films bridging them. Probes based on inserted tubular metal segments or metallic fittings placed on each side of a nonmetallic union represent significant hold up volumes; these devices lead to frequent segment breakage as well. The best arrangement devised involved two fine nichrome wires (32 ga., 0.23 mm dia) placed 2 mm apart through small bore holes drilled through the walls of the tubing connected to the valve, one pair each immediately adjacent to the drain and fill ports. The exterior of the

PTFE-tube was etched with a sodium/naphthalene etchant (Chemgrip, Norton Performance Plastics, Akron, OH) so that the inserted wires can be sealed in place with a graphite epoxy adhesive (Dylon Industries, Berea, OH).

Extractant segment isolation valve controller

The necessary circuitry is shown in Fig. 1. Conductivity sensors S1 and S2 are components of a bridge circuit with each sensor status being monitored by respective halves of a dual operational amplifier (A, B) used here as voltage comparators. The 5 mΩ potentiometers provide a "sensitivity adjust" control for each sensor. When the resistance in the sensor becomes high, the comparator output becomes high causing the transistor (Q1, Q2) to conduct and sensor tripped status is indicated by the corresponding light emitting diode (LED), L1 and L2. The high output status is also transmitted to the inputs (1, 2) of the NAND gate N. Only when *both* sensors are tripped does the NAND gate output become low, triggering timer T on the falling edge. Valve inject status LED (L3) is illuminated and the air solenoids (S) governing the pneumatically driven valve are turned on by relay K via optocoupler C. The latter is used to couple the timer output for driving the solenoids because

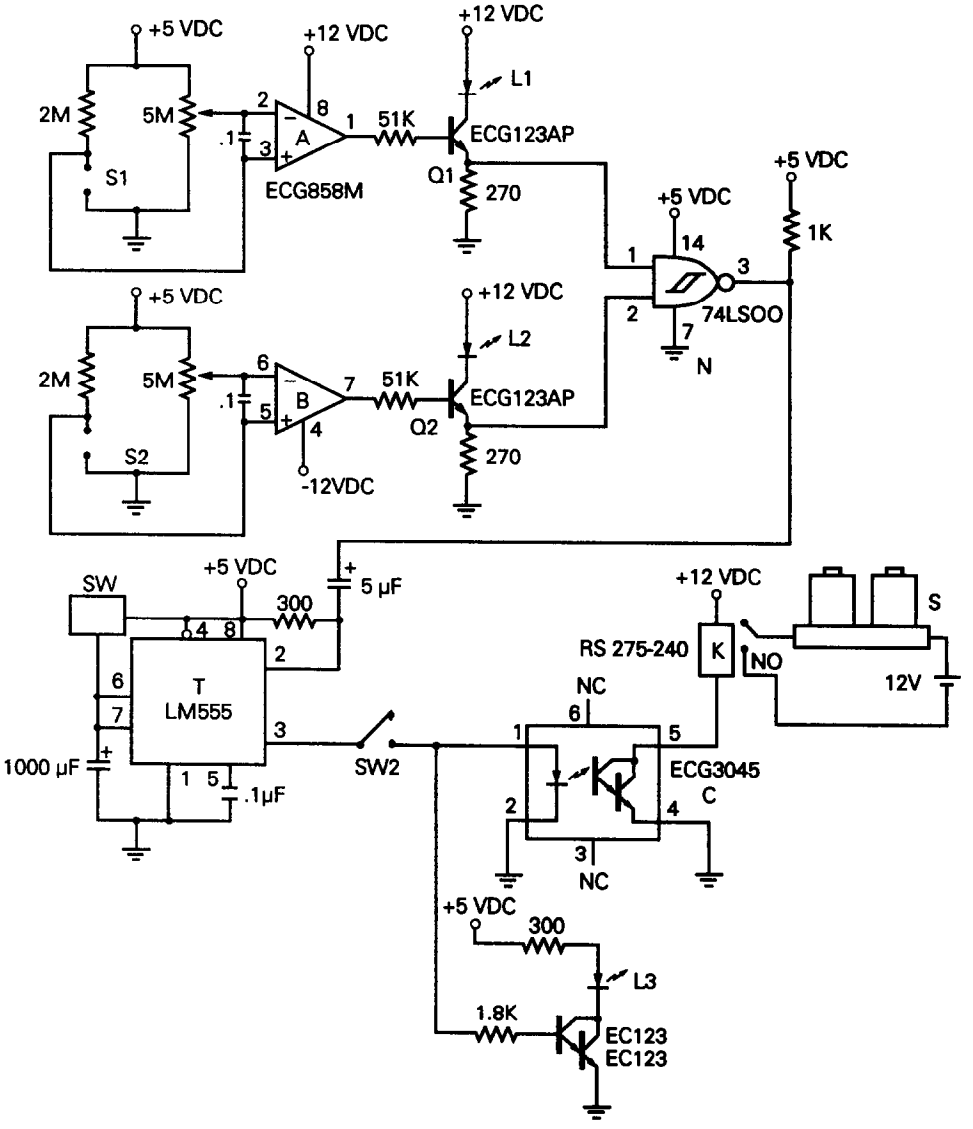

Fig. 1. Conductivity based intelligent valve controller. S1, S2: conductivity sensors; A, B: operational amplifier; N: NAND gate; Q1, Q2: transistors driving sensor status LEDs L1, L2; T: timer; SW: period selection switch; L3: valve inject status LED; C: optocoupler; K: relay; S: solenoid valves.

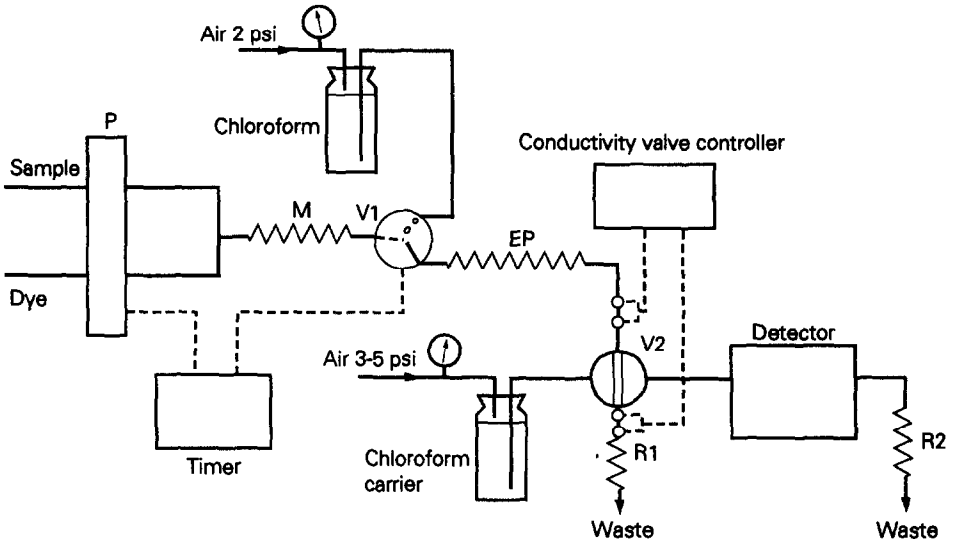

Fig. 2. Manifold design. P: peristaltic pump; V1: 3-way valve for segmentation; M: mixing conduit; EP: extraction/preconcentration conduit; V2: segment isolation valve; R1, R2: restriction tubing.

the major current spikes produced by the solenoids otherwise interfere with reliable operation of the logic circuitry. Timer T remains in the inject position for a period selected by switch SW, a 12-position switch that connects a resistor (4.7–56.4 kΩ in increments of 4.7 kΩ) at this junction, resulting in timer periods of 5–60 sec in increments of 5 sec, and then returns to the load position again.

Manifolds

Three variations of the basic manifold design shown in Fig. 2 were used. In system 1, the sample and the BTB reagent are pumped peristaltically with polyvinylcholoride (PVC) pump tubing, merged at a PTFE tee, mixed in conduit M (knotted, 0.86 × 700 mm) and flow through segmentation valve V1, extraction conduit EP and load/drain ports of segment isolation valve V2. Valve V1 and pump P are alternately powered by a double pole double throw relay, programmed by a microprocessor controlled timer (LS 100, Minarik Electric, Los Angeles, CA) such that pump P is on only when V1 and chloroform flow are off. Chloroform is introduced when V1 is turned on; the segment volume is controlled by the pneumatic pressure on the chloroform reservoir or more conveniently by V1 on-time. Restrictors (R1, R2, 0.46 × 1000 mm) are placed at the waste outlet of V2 and the detector exit to inhibit bubble formation. Chloroform flows from the second reservoir by pneumatic pressure as a carrier through valve V2 and the detector. The detector output was recorded on a strip-chart recorder (Omniscribe, Houston Instruments, Houston, TX) and the data processed manually. Experiments conducted with this manifold included parametric studies on the effects of conduit diameter, segment length, conduit length, flow-rate, extent of conduit wall adsorption and the geometrical configuration of the conduit. All of the above experiments were conducted with $10^{-5}M$ $(n\text{-}C_4H_9)_4N^+$ and $2 \times 10^{-5}M$ BTB.

System 2 was adopted to work at trace sample concentrations at which it was necessary to avoid perceived sample loss on PVC tubing. In this configuration, only the dye was pumped (at a flow-rate, f_1) by pump P. The PTFE sample conduit was merged with the dye as before but the sample channel was not pumped by positive pressure. Rather, a second pump P2 aspirated the waste stream from the drain port of V2 at a flow-rate, f_2 (Vilton® pump tubing). The sample flow-rate is given by $f_2 - f_1$. Segmenting chloroform flow also occurs by aspiration of pump P2 when V1 is on. Mixing conduit M (0.86 × 1000 mm) was used in the serpentine-II configuration[36] for enhanced mixing. The extraction/preconcentration conduit consisted of flexible wall tubing with adsorbent imbedded on the wall. Macroreticular poly(styrenedivinylbenzene) (Amberlite XAD-2, TosoHaas) was ground into a fine dust with a grinding mill. Polyethylene (1.67 mm i.d., Clay-Adams, Inc., New York, NY) or Tygon® tubing (1.5 mm i.d., Norton Performance Plastics) was inserted in a glass tube to prevent major deformation,

packed with the powdered absorbent and placed in an oven (170–200°) for a very short period (20–60 sec). The tube walls soften to such a degree that some of the adsorbent becomes heat-embedded in the walls of the tube. A similar technique for embedding porous glass in conduit walls has been previously reported by Gosnell *et al.*[37] Excess loosely held absorbent is removed by blowing compressed air through it and followed by thorough washing with water. Experiments conducted with this system included parametric studies on the preconcentration conduit configurations and injection frequency.

In system 3, we sought to combine the simpler aspects of system 1 with the preservation of sample integrity provided by system 2. This was achieved by keeping the configuration of system 1 but replacing the usual PVC pump tubes with modified PTFE-lined pump tubing. Very thin wall heat-shrink PTFE tubes (Zeus Industrial Products) which just fit inside a PVC pump tubing are taken. The inside of the PVC pump tubes are sprayed with a silicone spray lubricant (Slipicone, Dow-Corning) to facilitate insertion of the above PTFE tubes. Approximately 1 cm of the PTFE tubes are allowed to protrude out of the PVC tube termini, and then standard wall thickness PTFE tubes are forcibly inserted inside the thin wall PTFE tubes and crimped in-place with nichrome wire crimps. Any liquid (from organic solvents to concentrated sulphuric acid) can be pumped with these tubes; however, flow-rate remains constant over a shorter period than standard PVC tubes pumping dilute aqueous solutions. Experiments conducted with this system included the evaluation of performance at low analyte concentrations with the Tygon preconcentration conduit and the determination of the limits of detection (LOD).

RESULTS AND DISCUSSION

Segmentation and segment isolation

Highly reproducible and reliable segmentation was provided very conveniently by the 3-way valve. Kuban and Ingman[38] reported similar experience with such devices. Although they found that the performance deteriorates at flow-rates >2.5 ml/min, such flow-rates are not commonly used.

Probe placement and strategy of isolation of a conductive segment in a nonconductive solvent by conductivity sensing and the associated electronic circuitry have previously been described.[5] The reasons for the failure of this strategy to work in the present experiment have been outlined earlier. In a typical arrangement for intelligent valve control, once the sensor(s) indicate that the loop is filled with the desired segment, the valve is switched. The isolated segment is thus injected into a miscible carrier which transports it to a detector; further chemistry can be performed en route if desired. The valve remains in the inject position for some preset period of time adequate to complete the injection and then returns to the load position. For the present system, it may seem at first that placing a single pair of probes at the drain port of the loop should be adequate. As long as the extractant segment is sufficiently greater in volume than the isolation loop, loop-filling will be indicated by the excess nonconductive extractant triggering the sensor. The problem with this concept appears at the next stage of operation: when the valve switches back to the load position, the aqueous stream flushes small portions of the organic carrier liquid remaining in the rotor grooves of the valve, which triggers the sensor again, this time falsely. It is possible to formulate a scheme with a flip-flop[39] such that the valve will switch every alternate time the sensor is tripped. Experience showed that the pitfall of this approach is that if it once triggers on the wrong event, it remains locked on the erroneous sequence. An alternative approach studied was to provide a second delay time after the valve returns to the load position; during this period the sensor output is ignored such that small amounts of organic solvent that quickly exit after each switching of the valve are ignored as well. The system took long periods to be initialized and even then did not prove reliable. The use of two pairs of electrodes, constituting two independent conductivity sensors located at the fill and the drain ports of the loop, proved to be a robust approach. This design and the associated logic circuitry as described in the experimental section provided reliable performance in isolation of the segment and its injection into a miscible carrier.

Parametric studies

In conventional flow-injection extraction systems, the typical situation involves very short extractant segments ($\leqslant$1 cm in length) and extraction occurs largely at the interface film of the phase that wets the conduit wall. The wall film thickness varies as a function of fluid velocity and the bridging of the individual

extractant segments by the wall film is the principal cause for dispersion;[40-42] air-segmented systems behave similarly.[43,44] In the present study, the extractant segment length is typically $\geqslant 10$ cm and more often than not there is only one extractant segment resident in the conduit at any given time. Clearly, the concept of wall films bridging individual extractant segments is inappropriate in this case. As will be apparent in the following, adsorption of the ion-pair on the walls of the conduit (or solvent film left thereon) and its subsequent removal by the extractant segment constitutes a major "extraction" mechanism beyond extraction through the phase boundaries. The relative importance of the two factors is dependent on the frequency of injection of the extractant segment, *i.e.*, the period over which the material is allowed to accumulate or preconcentrate on the wall. Because of these basic differences, fundamental studies of the experimental variables are needed for this system; lessons from the more conventional extraction systems, thorough as some of these studies are,[40-42] are not directly applicable. For brevity, the following symbols are used in the description below for the respective parameters: conduit diameter (d), length (l), extractant segment length (l_e), extractant segment volume (V_e), residence time (t_R), flow-rate (f) and injection cycle period (p). Unless otherwise specified to be coiled, knotted or serpentine, the conduit is linear (bend radius $\geqslant 50$ cm).

Variation of extractant conduit diameter (constant $V_e t_R$, f, p)

Different tube lengths were taken to provide the same residence volume. Two separate sets of experiments were conducted: (a) $d = 1.35$, 0.86, 0.56 mm; $f = 1.5$ ml/min, $t_R = 36$ sec; and (b) $d = 1.5$, 0.86, 0.46 mm; $f = 1.0$ ml/min, $t_R = 46$ sec. In this and the following experiments, the injection cycle period is relatively small ($p = 2$ min) and $V_e = 90$ μl, except as stated. The extractant segment can be approximated by a right circular cylinder; for the long segments used in this work, the surface area of the segment is essentially its lateral surface area, the area of the menisci can be neglected. Thus, the surface area is approximately equal to $4V_e/d$. Figure 3 shows that the relationship between the observed signal and $1/d$ is approximately linear and the best fit lines through each data set are roughly parallel. The residence volume in the conduits of set (a) are only about 17% larger than those in (b); relative to this, the signal is much higher in (a). This could not solely be attributed to higher flow velocities; because the flow velocities in the two smallest tubes in cases (a) and (b) are essentially the same. Circulation within the segment, which renews the interfacial boundary layer depends both on the flow velocity and the conduit diameter in a complex manner.[45,46]

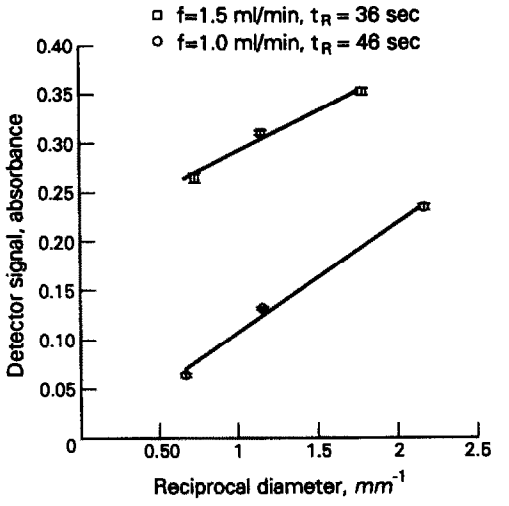

Fig. 3. Effect of the conduit diameter on analytical sensitivity. In this and all subsequent figures, ± 1 standard deviation is indicated by the error bar.

Variation of extractant segment length (constant d, l, t_R, f, p)

For $d = 0.86$ mm, and $f = 1$ ml/min, l_e was varied from 10.0 to 29.0 cm. V_e is linearly related to l_e and if essentially the same amount is extracted by each segment regardless of its length, the detector signal is expected to increase linearly with $1/l_e$. The results are shown in Fig. 4. A linear relationship between $1/l_e$ and the detector signal is observed for all but the shortest segment; saturation at the interface may have commenced for this situation—the precision in this case is also the poorest. It is interesting to note that the abscissa intercept for the extrapolated line corresponds to a finite value (corresponding to a length of ~ 55 cm). Indeed, this intercept should occur at a finite positive value because the extraction conduit length is finite and increasing amounts of extractant displaces corresponding amounts of sample. Thus, increasing l_e systematically decreases the amount of sample in contact with the conduit.

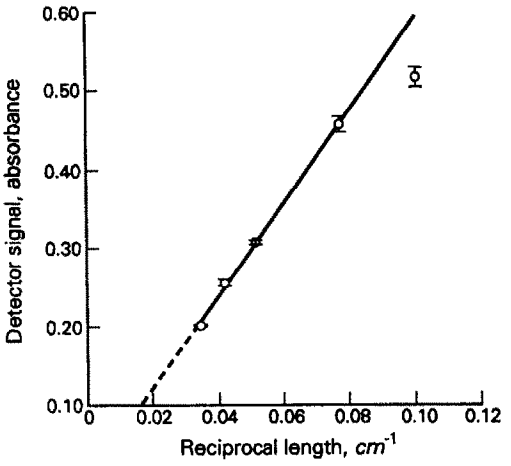

Fig. 4. Effect of the extractant segment length on analytical sensitivity. The straight line is the best fit line drawn through the lower four points and the dotted portion is extrapolated.

Variation of extractant conduit length (*constant* d, v_e, f, p)

The detector outputs obtained for $l = 3.21$, 3.71, 4.21, 4.71, 5.21 and 6.21 m ($d = 0.86$ mm, $l_c = 16$ cm, $f = 1.5$ ml/min) are shown in Fig. 5. For $p = 2$ min and the stated values of d and f, two segments will be present in the conduit at $l \geqslant 5.2$ m (at which point, the intersegment distance is 4.9 m). Interestingly, the signal increases essentially linearly up to $l = 4.7$ m and thereafter becomes constant. The latter should not be construed as saturation of the extractant segment, greater signals can be obtained if p is increased (*vide infra*). Increasing the length of the conduit increases both the residence time and the available surface area for adsorption. An unambiguous determination of the effect of the individual factors on the signal is difficult. Similarly, the available sample volume for extraction increases linearly with conduit length, at least up to $l = 5.2$ m (at this point, the second segment is introduced before the first leaves the system). Can the increase in signal be attributed simply to greater sample volume available for extraction? Intuitively, it does not seem plausible that the presence of additional sample at distances of $\geqslant 3$ m from the segment can make much difference to the overall extraction yield via direct interphase mass transfer; it is not likely that axial mass transport within the aqueous phase is that efficient. On the other hand, if we extrapolate to zero conduit length, a finite signal is suggested—this ordinate intercept is an indirect measure of the extraction yield via direct interphase mass transfer. Note that with increasing conduit length, the attainment of a plateau response is rather abrupt and also coincides approximately with the entrance of a second segment into the system. We believe that these observations are consistent with the hypothesis that the signal increases with increasing conduit adsorption area. The effective upper limit of the available conduit length ahead of any segment is set in the above experiments by the chosen values of p, d and f to be ~ 5 m regardless of the actual conduit length. Note that t_R continues to increase with l throughout, even though the signal does not increase beyond $l \geqslant 5$ m. This supports the adsorption hypothesis; t_R in this case is not a critical parameter.

Variation in flow-rate (*constant* l, v_e, p)

The results of flow-rate variations for three different tube diameters are shown in Figs. 6 and 7. Qualitatively, the signal increases with increasing fluid velocity within each class of tube diameter but the slopes are different from one diameter to another. At very high fluid velocities, standard deviation abruptly increases and shortly thereafter frequent segment breakage has been observed to occur. The extraction yield may actually decrease past a certain point as observed in the results for $d = 0.86$ mm. As previously noted for the experiments with variations in d at constant t_R (Fig. 3), a higher velocity promotes greater circulation within the segment and may thus improve mass transfer at the interfacial boundary. Certainly the data in Fig. 6 indicate that the effect of a greater flow-rate overshadows the effect of the corresponding decrease in residence time. The considerable difference in response between the

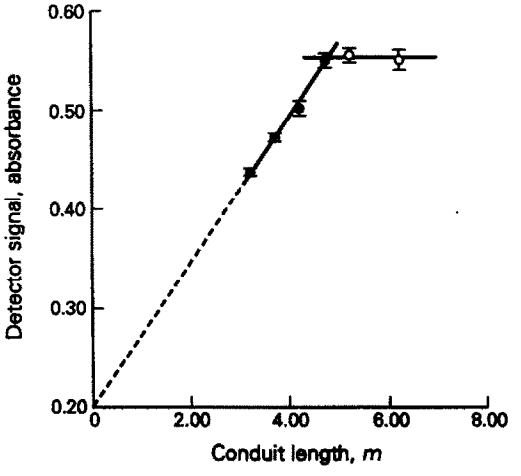

Fig. 5. Effect of conduit length on analytical sensitivity. The injection cycle period used limits the effective upper length to ~5 m.

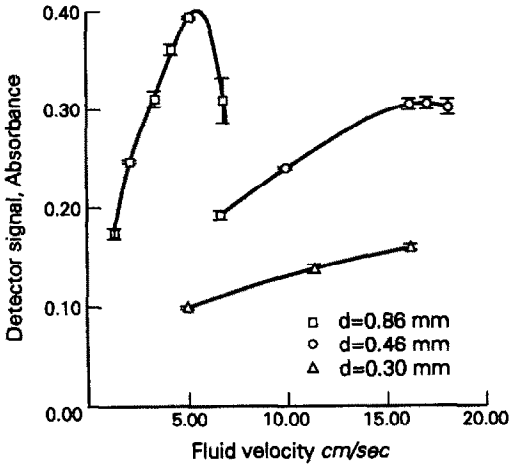

Fig. 6. Effect of flow-rate shown in terms of fluid velocity on analyical sensitivity.

different tube diameters at comparable velocities, however, imply that the velocity is not the only factor. Since essentially the same conduit length ($l = 2.21$ m for $d = 0.86$, 0.46 mm, $l = 2.0$ m for $d = 0.30$ mm) was used for the experiments, the total sample volume theoretically available in the conduit for direct extraction through interfacial transfer is dependent on the square of the diameter. The differences in the actual signal observed at any given velocity for the three different tube diameters are significantly lower than that suggested by a d^2 dependence. More importantly, considerations based solely on the velocity dependence and sample volume availability cannot explain why the curves for the three different tube diameters as a function of flow-rate are virtually parallel (Fig. 7). An alternative explanation is as follows. For a given value of p, the amount of sample passed through the conduit before the introduction of an extractant segment is linearly related to f. Given that a fixed fraction of the influent ion-pair may adsorb on the wall (until saturation occurs), the observed dependence on flow-rate can be due to adsorption of the ion-pair on the conduit wall and its subsequent elution by the organic solvent.

Variations of injection cycle period (all other parameters constant)

The walls of an extruded PTFE conduit are smooth and offer a relatively small adsorption area. Typically it is considered to be inert and adsorption effects are seldom regarded to be of importance. Nonetheless, much of the foregoing results strongly suggest that adsorption on conduit walls may play a major role in the present system. The definitive experiment in this regard is to vary the injection cycle period while keeping all other parameters constant. The results are shown in Fig. 8 ($l = 4.50$ m, $d = 0.86$ mm, $f = 1.0$ ml/min). Observed signals increase well beyond an injection period equal to t_R. This can only be explained by adsorption on the conduit wall. At low cycle periods, the signal increases linearly with the period, characteristic of preconcentration systems; saturation eventually occurs at $p \geqslant 7$ min. It is interesting to note that if the linear pattern is extrapolated, the ordinate intercept is essentially zero, suggesting that the great majority of the "extraction" may be occurring via the adsorption/elution pathway. However, we have also observed that the magnitude of this intercept

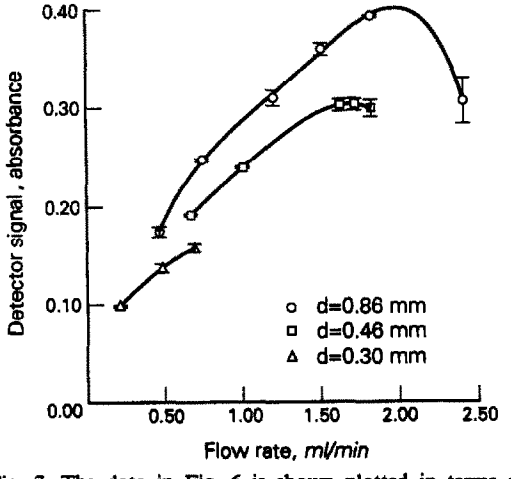

Fig. 7. The data in Fig. 6 is shown plotted in terms of flow-rate.

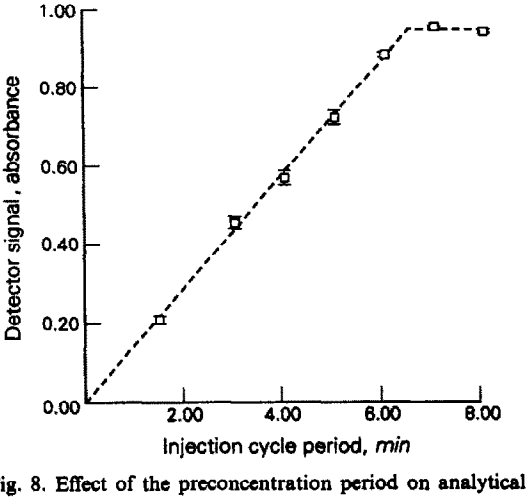

Fig. 8. Effect of the preconcentration period on analytical sensitivity.

increases at higher flow rates: either preconcentration is less efficient because the efficiency of mass transfer to the wall under laminar flow conditions decreases with increasing flow-rate (see, for example, the Gormley–Kennedy equation[47]) or higher fluid velocities increase the magnitude of direct interfacial extraction. In either case, the relative importance of the latter process is enhanced. Nevertheless, the results shown in Fig. 9 indicate that the system behaves most like a conventional adsorbent-based preconcentration system in that although total available surface area (conduit length) has an influence on the onset of saturation and the plateau absorbance at saturation, the behavior is largely governed by the total volume "preconcentrated".

It is not possible to determine from the available data as to the details of the adsorption process. From the magnitude of the "extraction" yield, we estimate that more than monolayer coverages are involved. This suggests that solvent films play a role; but this could not be unequivocally established. Amankwa and Cantwell[48] have recently examined the adsorption of tetrahexyl-ammonium-BTB ion-pairs at a chloroform water interface. Their data indicate that BTB^- competes with $Q^+.BTB^-$ for adsorption at the interface and the adsorption of the ion-pair is decreased by an excess of BTB^-.

Variation in geometrical configuration of the conduit

Relative to a linear configuration, geometrically deformed configurations promote greater mass transport to the wall and may thus improve preconcentration efficiency. For 3–4-m conduits ($d = 0.86$ mm, $f = 1.5$ ml/min), the gain was marginal ($\leqslant 15\%$), however, upon coiling the conduit to a coil of diameter ~ 1 cm. No further increase in efficiency was observed in knitting the conduit on a perforated board in crisscross and serpentine II configurations,[36] even though these configurations promote better radial mass transport than coiled conduits. On the other hand, these highly deformed configurations led frequently to segment breakage and were not further pursued.

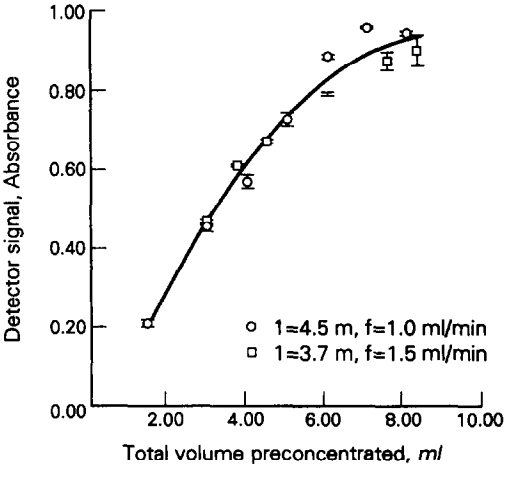

Fig. 9. Analytical sensitivity as a function of total volume passed through the conduit prior to extractant introduction. The data represent two different combinations of conduit length and flow-rate.

Wall-imbedded adsorbent preconcentration conduits

Because it was apparent after the foregoing studies that the present system essentially operates in a preconcentration mode via wall adsorption, it was deemed advantageous to use conduits with greater available surface area for adsorption. This was accomplished with imbedding adsorbent on the walls of the conduit. It is also necessary at this point to consider the merits of such a system as opposed to using a packed column filled with adsorbent[49] and eluting the adsorbed analyte with a miscible solvent (immiscible solvent segments cannot be used with a packed column without disintegrating the segment). While the latter system is obviously simpler, trace analysis by optical detection methods is inhibited by major refractive index disturbances. It may be possible in the future to completely correct for refractive index changes,[50] the present system meanwhile offers a practical alternative with low flow resistance and can deal with real samples without scrupulous filtration. The latter is an important advantage with many real samples in that the potential analyte loss is minimized.

The addition of a single 16-cm polyethylene conduit containing wall-imbedded adsorbent to an existing 3.3-m PTFE extraction conduit increased the signal by over 40%, clearly indicating that it is advantageous to have a greater surface area available for adsorption. Using a 24-cm absorbent imbedded polyethylene tubing, a coiled (*ca.* 1.5-cm coil diameter) configuration proved to be $\sim 18\%$ more efficient than the linear configuration, essentially the same increase observed with PTFE conduits upon coiling. Using $2\mu M$ $(n\text{-}C_4H_9)_4N^+$ as the analyte, the detector output is shown as a function of injection cycle period for a 2-m Tygon conduit in Fig. 10. The conduit is resistant to saturation up

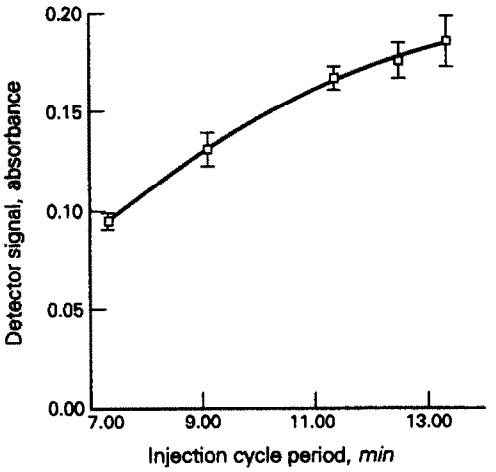

Fig. 10. Analytical sensitivity for the determination of $2\mu M$ $(n\text{-}C_4H_9)_4N^+$ for a 2-m long coated wall Tygon conduit as a function of preconcentration period (flow-rate 1.2 ml/min).

to very substantial preconcentration periods. Using a practical preconcentration period of 4.3 min ($f = 1.2$ ml/min), the response of the system in the $0\text{–}2\mu M$ analyte concentration range was studied. The response equation can be summarized as:

$$\text{Signal (abs)} = 3.64(\pm 0.14) \times 10^{-2}\, C(\mu\text{M}) + 0.0019 \pm 0.0013, r^2 = 0.9977$$

The computed blank absorbance agrees well with the observed value of 0.0024 ± 0.0001 (note that uncertainty in this measurement is equal to the intrinsic noise level of the detector used). Based on the uncertainty of the blank, an LOD of $\sim 8 \times 10^{-8} M$ was computed. In comparison, a sample containing $2 \times 10^{-8} M$ $(n\text{-}C_4H_9)_4N^+$ was experimentally indistinguishable from the blank while a sample containing $7 \times 10^{-8} M$ analyte produced a mean absorbance signal of 0.0029.

The ultimately attainable LOD depends, of course, on the detectability of the ion-pairing dye itself, as long as a reasonably low and reproducible blank can be maintained. With an experimental arrangement identical to that used above, we have observed that the use of 3-hydroxy-2-napthoic acid (3H2NA) as the pairing agent ($4\mu M$, pH 10) provides ultralow detection limits; for example, with detection at 250 nm, $(n\text{-}C_4H_9)_4N^+$ concentrations of 0 and $7nM$ respectively produced absorbance signals of 0.144 ± 0.001 and 0.176 ± 0.001. This compound is also intensely fluorescent and further work may provide an attractive means to measure ultratrace amounts of cationic surfactants with this reagent, albeit the response may be nonlinear over a large range.

The present system operates in the sample preconcentration mode; the sample is aspirated or pumped for fixed periods of time rather than a fixed volume being introduced by a loop injector. The large sample volumes used and wall adsorption leads to significant carryover; however, it is completely eliminated when samples are alternated with wash solutions as in segmented flow analyzers.

CONCLUSIONS

If hydrophobic organic solvent extractable adducts/ion-pairs/chelates can be formed from aqueous analytes upon addition of appropriate reagents, they can be preconcentrated on conduit walls. Such adsorption is promoted by coating the conduit walls with suitable nonpolar adsorbents. The preconcentrated analyte is then detected after elution with an immiscible organic solvent. For trace analysis of real samples where sample availability is not a problem and the necessity of filtration can be a nuisance, this approach can be particularly attractive, whether the technique of segment isolation presented in this paper is used, or direct measurement is made with an on-tube detector.[4,42,51]

Acknowledgements—This research was supported partially by the Office of Basic Energy Sciences, U.S. Department of Energy, through DE-FG05-84ER13281. However, this manuscript has not been subjected to review by the DOE and no endorsement should be inferred. We thank Steve Gluck, Dow Chemical Company, for educating us on the importance of trace measurements of cationic surface active agents, especially quaternary ammonium ions. Jorge L. Lopez is acknowledged for his help with electronic design. This manuscript benefited significantly from the constructive criticism offered by an anonymous reviewer.

REFERENCES

1. J. Ruzicka and E. H. Hansen, *Flow Injection Analysis* 2nd Ed., Wiley, New York, 1988.
2. B. Karlberg and G. E. Pacey, *Flow Injection Analysis, A Practical Guide*, Elsevier, New York, 1989.
3. P. K. Dasgupta and W. Lei, *Anal. Chim. Acta*, 1989, **226**, 255.
4. V. Kuban, L.-G. Danielsson and F. Ingman, *Anal. Chem.*, 1990, **62**, 2026.
5. W. Lei, P. K. Dasgupta, J. L. Lopez and D. C. Olson, *ibid.*, 1989, **61**, 496.
6. B. F. Greek, *Chem. Eng. News*, 1990, **68**(5), 37.
7. R. S. Boethling, *Water Res.*, 1984, **18**, 1061.
8. G. Roederer, *Arch. Environ. Contam. Toxicol.*, 1987, **16**, 291.

9. M. E. Auerbach, *Ind. Eng. Chem., Anal. Ed.*, 1943, **15**, 492.
10. G. Schill, *Acta Pharm. Suec.*, 1965, **2**, 13.
11. H. M. N. H. Irving and J. J. Markham, *Anal. Chim. Acta*, 1967, **39**, 7,
12. V. P. Toryanik, Z. M. Zhikhareva and S. M. Velichko, *Khim. Prom.-st., Ser.: Khlornaya Prom.-st.*, 1981, **1**, 9.
13. T. Sakai, *Analyst*, 1983, **108**, 608.
14. T. Sakai and N. Ohno, *Chem. Lett.*, 1982, 107.
15. A. B. Few and R. H. Ottewell, *J. Colloid. Sci.*, 1956, **11**, 34.
16. G. V. Scott, *Anal. Chem.*, 1968, **40**, 768.
17. A. W. Ashbrook, *Analyst*, 1959, **84**, 177.
18. A. LeBihan and J. Courtot-Coupez, *Analusis*, 1976, **4**, 58.
19. K. Gustavii and G. Schill, *Acta Pharm. Suec.*, 1966, **3**, 241.
20. S. Tsurubo, N. Ohno and T. Sakai, *Nippon Kagaku Zasshi*, 1980, 828.
21. H. M. N. H. Irving and A. D. Damodraran, *Analyst*, 1965, **90**, 180.
22. T. M. Florence and Y. I. Farrar, *Anal. Chim. Acta*, 1973, **63**, 255.
23. M. Nishida, M. Kanamori, S. Ooi and S. Miyagishi, *Yukagaku*, 1976, **25**, 21.
24. M. Malat, *Z. Anal. Chem.*, 1979, **297**, 417.
25. A. S. Maslennikov and N. A. Shikina, *Lesokhim. Podoschka*, 1979, **9**, 10.
26. A. I. Zhebentyaev, *Gig. Sanit.*, 1981, **10**, 67.
27. Z. Marzcenko and H. Kalowska, *Anal. Chim. Acta*, 1981, **123**, 279.
28. J. Lengyel and J. Krtill, *Vodni Hospod. B.*, 1987, **37**, 244.
29. R. Modin and G. Schill, *Acta Pharm. Suec.*, 1967, **4**, 301.
30. B. Zapior, A. Kellner and J. Czapkiewics, *Anal. Chem. (Warsaw)*, 1975, **20**, 823.
31. A. T. Pilipenko, G. N. Peshinko, A. I. Zhebentyaev, A. I. Volkova and V. P. Denisenko, *Khim. Tekhnol. Vody*, 1980, **2**, 130.
32. A. I. Zhebentyaev and I. E. Talut, *Gig. Sanit.*, 1989, **5**, 56.
33. G. Schill, *Acta Pharm. Suec.*, 1964, **1**, 169.
34. C. C. Garcia, *Solvent Extraction–Flow Injection Analysis of Quaternary Ammonium Ions Through Ion-Pairing*, M.S. Thesis, Texas Tech University, Lubbock, TX, 1991.
35. K. Yamamoto and S. Motomizu, *Talanta*, 1991, **38**, 477.
36. M. A. Curtis and G. J. Shahwan, *LC·GC*, 1988, **6**, 158.
37. M. C. Gosnell, R. E. Snelling and H. A. Mottola, *Anal. Chem.*, 1986, **58**, 1585.
38. V. Kuban and F. Ingman, *Crit. Revs. Anal. Chem.*, 1991, **22**, 491.
39. P. Horowitz and W. Hill, *The Art of Electronics*, 2nd Ed., Cambridge University Press, New York, 1989.
40. L. Nord and B. Karlberg, *Anal. Chim. Acta*, 1984, **164**, 233.
41. L. Nord, K. Bäckström, L.-G. Danielsson, F. Ingman and B. Karlberg, *ibid.*, 1987, **194**, 221.
42. C. A. Lucy and F. F. Cantwell, *Anal. Chem.*, 1989, **61**, 101.
43. L. R. Snyder and H. J. Adler, *ibid.*, 1976, **48**, 1017.
44. *Idem*, *ibid.*, 1976, **48**, 1022.
45. H. S. Lew and Y. C. Fung, *Biorheology*, 1969, **6**, 109.
46. G. Bugliarello and G. C. Hsiao, *ibid.*, 1970, **7**, 5.
47. P. G. Gormley and M. Kennedy, *Proc. Ir. Acad. Sci.*, 1949, **52A**, 163.
48. L. Amankwa and F. F. Cantwell, *Can. J. Chem.*, 1991, **69**, 88.
49. B. F. Johnson and J. G. Dorsey, *Anal. Chem.*, 1990, **62**, 1392.
50. C. N. Renn and R. E. Synovec, *ibid.*, 1990, **62**, 558.
51. P. K. Dasgupta, J.-S. Rhee and E. L. Loree, *Spectroscopy*, 1987, **2**(10), 39.

Talanta, Vol. 39, No. 2, pp. 113–117, 1992
Printed in Great Britain

0039-9140/92 $5.00 + 0.00
Pergamon Press plc

TRACE METAL ANALYSES IN OCTOCORALS BY MICROWAVE ACID DIGESTION AND GRAPHITE FURNACE ATOMIC-ABSORPTION SPECTROMETRY

RUDOLF JAFFE and CARMEN A. FERNANDEZ
Laboratorio de Geoquímica y Química Ambiental, Universidad Simón Bolívar, Departamento de Química, Apartado 89000, Caracas 1080-A, Venezuela

JOSE ALVARADO
Laboratorio de Espectroscopía Atómica, Universidad Simón Bolívar, Departamento de Química, Apartado 89000, Caracas 1080-A, Venezuela

(*Received* 29 *January* 1991. *Revised* 9 *July* 1991. *Accepted* 10 *July* 1991)

Summary—Eight octocoral species from two reefs off the Venezuelan coast were analyzed to determine their Cd, Cu, Ni, Pb and Zn content. A microwave sample work-up procedure, including drying and acid digestion, was developed and found to be faster and more convenient than conventional methods. Accurate and precise results were obtained for the determination of the metals of interest, using graphite furnace atomic-absorption spectrometry (GFAAS) with L'vov platforms. The accuracy of the results was checked against synthetic standards prepared to simulate the matrix of the analyzed octocoral species. Standard deviation values for synthetically prepared standards were less than 1% in all cases. On the other hand, standard deviations for sample results were considerably higher due to heterogeneity of the samples and environmental conditions at the sampling sites.

The quality of the marine environment has been severely affected by the discharge of a great variety of pollutants. Therefore, marine organisms such as mussels, fish and others, which are known to accumulate contaminants, have found great use as biological indicator organisms of marine pollution.[1,2]

One of the various marine environments which have been found to be particularly threatened by pollution are the coral reefs,[3–5] which are considered amongst the most productive but also most vulnerable marine ecosystems. It is therefore of great importance to monitor pollutants such as heavy metals in coral reefs, and to investigate their potential effects upon them. The accurate analysis of heavy metals in different coral species could also help to determine the possible uses of corals as biological indicator organisms of marine pollution. As such, corals have recently been used as chronological indicators of heavy metal pollution in the ocean.[6–8] These studies required the use of skeletarian corals, which are generally low in organic carbon (0.1–6%), and therefore show a low tendency to accumulate heavy metals. Octocorals on the contrary, have a much higher organic carbon content (40–80%), and have been found more useful as bioindicators of pollution.[9,10]

Relatively few reports have appeared in the literature concerning the analysis of heavy metals in octocorals.[9,10] However, their use as bioindicators of marine pollution seems very promising and needs to be investigated further. With this in mind, the present study was aimed at developing a relatively simple, accurate and precise method for the sample preparation and analysis of heavy metals in octocorals.

In this report, we describe such a procedure for the determination of Cd, Cu, Ni, Pb and Zn in octocoral samples by means of microwave drying and digestion followed by graphite furnace atomic-absorption spectrometry. Microwave heating has been used for drying[11,12] and acid digestion[13–19] of various types of samples in order to increase the efficiency of the sample treatment. Conventional drying and digestion procedures were also used for sample preparation in this work. Due to contamination problems, samples obtained in this way were not used for final analysis. However, the tests with the conventional approach were useful for comparison of both sample treatment procedures in respect of speed of drying and dissolution of the octocoral samples.

EXPERIMENTAL

Sampling

Eight octocoral species (see Table 1) were sampled from two coral reefs. One of these was

Table 1. Heavy metal concentrations in octocoral species

Octocoral species	Cd, μg/g		Cu, μg/g		Ni, μg/g		Pb, μg/g		Zn, μg/g		TOC
	L.B.	I.L.	L.B.	I.L.	L.B.	I.L.	L.B.	I.L.	L.B.	I.L.	%
P.H.	2.4 ± 0.3	0.4 ± 0.07	1.9 ± 0.3	2.8 ± 0.3	5.7 ± 0.3	6.4 ± 0.3	5.03 ± 0.02	7.0 ± 0.9	66 ± 12	59 ± 3	58 ± 8
P.Am.	1.2 ± 0.3	0.6 ± 0.1	1.5 ± 0.3	1.9 ± 0.1	3.0 ± 1.3	23 ± 5	4 ± 1	4.8 ± 0.2	98 ± 20	256 ± 35	75 ± 3
P.D.	1.3 ± 0.3	0.3 ± 0.2	1.9 ± 0.9	1.1 ± 0.2	10 ± 1	6.5 ± 1.0	3 ± 0.9	2.6 ± 0.7	34 ± 8	25 ± 6	54 ± 5
P.F.	1.4 ± 0.2	0.3 ± 0.03	1.2 ± 0.02	1.1 ± 0.05	13 ± 2	6.2 ± 0.7	5.7 ± 0.9	5.7 ± 0.9	152 ± 26	70 ± 22	56 ± 3
P.Ac.	0.9 ± 0.2	1.7 ± 0.04	3.1 ± 0.1	2.3 ± 0.2	13 ± 2	7.5 ± 0.3	9.42 ± 0.01	17.5 ± 0.9	48 ± 18	159 ± 19	63 ± 8
G.V.	0.9 ± 0.1	1.5 ± 0.03	2.1 ± 0.3	2.6 ± 0.6	38 ± 2	11.5 ± 1.4	2.3 ± 0.2	5.1 ± 0.3	59 ± 18	264 ± 57	64 ± 3
PF.sp.	0.8 ± 0.2	0.6 ± 0.08	2.3 ± 0.05	2.0 ± 0.2	11 ± 3	38 ± 7	14.9 ± 0.5	3.8 ± 0.2	63 ± 3	37 ± 11	78 ± 5
E.sp.	0.9 ± 0.1	0.1 ± 0.01	1.5 ± 0.8	0.9 ± 0.07	5 ± 3	12 ± 3	3.4 ± 0.2	2.6 ± 0.1	24 ± 5	17 ± 2	40 ± 14

*P.H.: *Plexaura homomalla*; P.Am.: *Pseudoterogoria americana*; P.D.: *Plexaura dichotoma*; P.F.: *Plexaura flexuosa*; P.Ac.: *Pseudoterogoria acerosa*; G.V.: *Gorgonia ventalina*; PF.sp.: *Pseudoflexaura sp.*; E.sp.: *Eunicea sp.*; L.B.: *La Blanquilla*.; I.L.: *Isla Larga*.; TOC: *Total organic carbon*.

located between the bays of Falucho and Caño Martin on the Isla de La Blanquillas' southern shore, located about 200 km north of the Venezuelan coast at Barcelona. The second sampling station was a coral reef located on the central bay of Isla Larga, located about 0.8 km north of the Venezuelan coast at Puerto Cabello. The eight octocoral species were selected based on their abundance in Venezuelan coastal waters. Each species was sampled in triplicate. Both sampling sites are basically unpolluted particularly the Isla de La Blanquilla, which has no permanent inhabitants, and no tourism.

Samples were collected by divers, at a maximum depth of 6 m. Pieces between 10 and 20 cm in length were cut off with stainless steel scissors and immediately collected in acid cleaned[20,21] zip-lock plastic bags. The samples were not in direct contact with the divers hands at any time. The bags were opened under water and inverted over the diver's hand, leaving the pre-cleaned surface to the outside. This "inverted glove" was used to hold on to the coral while it was cut off with stainless steel scissors. The bag was then re-inverted over the sample, the seawater was decanted, and the sample immediately placed on dry ice and kept frozen at $-10°$ until analysis. All glassware and plastic materials were purified before use according to reported procedures.[20,21]

Microwave drying and sample dissolution

Subsamples of approximately one gram (dry weight) were cut off the original samples with stainless steel scissors, placed in precleaned glass beakers and immediately covered with a watch glass. The samples were then microwave predried at "medium low" (40% total power) during time intervals of between 20 and 50 min, depending on the water content of the octocoral species. After this pre-drying step, the samples were taken to constant weight by leaving them in a precleaned, nitrogen pressure flushed (to remove small dust particles) oven, at 120° overnight. During this period the oven was kept closed at all times.

Since octocorals contain a flexible but very dense interior support, consisting almost exclusively of organic matter, dried samples could not be crushed and homogenized with a mortar. Therefore, the whole dried sub-sample was weighed and transferred to a 200-ml thick-walled, acid cleaned[20,21] Pyrex glass reusable test tube containing 10 ml of concentrated nitric acid and immediately sealed with a specially

designed screw cap. Details of the modified tubes used for sample digestion are described elsewhere.[22] The sample was then irradiated at 40% total power for 4–6 periods of one minute each. Each heating cycle was followed by cooling of the tubes in a water bath to room temperature. Once cool, the dissolved sample developed a supernatant layer of greasy appearance. The sample was then set aside for a period of about 5 hr to allow the greasy layer to separate. This suspension was removed by filtration through acid-cleaned glass wool. Once filtered, the sample filtrates were made up to 25 ml and stored in sealed polyethylene containers at room temperature for GFAAS analysis.

In order to establish whether the greasy layer contained significant amounts of metals, it was analyzed as follows. Since this material was insoluble in concentrated acids and hydrogen peroxide, the organic phase which was retained in the glass wool was first rinsed with distilled demineralized water and then dissolved in a minimum amount of analytical grade ethanol. The ethanol phase was collected in a clean glass container. After allowing the ethanol to evaporate at room temperature, 10 ml of analytical reagent grade nitric acid were added to the glass container and the solution was analyzed by GFAAS. No appreciable difference in heavy metal content could be observed between these samples and those of the pure acid. Therefore, it was concluded that the greasy layer contained insignificant amounts of metals compared to the octocoral samples and could be discarded.

Conventional drying and sample dissolution

Samples, contained in beakers covered with a watch glass, were pre-dried in a water bath for periods of at least 8 hr. Once dried, these samples were taken to constant weight in an oven at 120° overnight as described previously. For acid digestion, 10 ml of nitric acid were added to the beakers which were then heated on a water bath for at least three days. As the volume of acid decreased, more acid was added to maintain a constant level. Further steps were similar to those described in the previous paragraph, including filtering of the greasy layer that formed upon cooling the digest.

Sample analysis

Samples were analyzed for their cadmium, copper, lead and nickel content by GFAAS, using electrothermal atomization and L'vov platforms. Zinc was analyzed by flame atomic-absorption spectrometry (FAAS) with a fuel-lean air-acetylene flame. Prior to the analyses by GFAAS, the wavelength, the carrier gas flow, and the temperatures and time of drying, ashing and atomization steps were optimized. Starting with the standard conditions recommended by the instrument manufacturer, each parameter was then varied, keeping the others fixed, until the highest absorption signal for each analyte was obtained. The best set of instrumental conditions obtained is shown in Table 2. Matrix interference was checked by comparison of the slopes of calibration graphs with those using standard addition methods. Since matrix effects were apparent for the GFAAS measurements, quantitation was performed with the standard addition method.

Instrumentation

A commercial domestic National Panasonic Model NE 6660 microwave oven, provided with a variable timing cycle, a variable heating cycle with power settings from "warm" to "high" (60–600 W) and a rotary tray, was used for the microwave sample treatment. The use of the rotating tray allowed a more homogeneous and uniform exposure of the samples to the incoming radiation, thus leading to a more efficient drying and digestion process. Details of the sample containers for microwave irradiation have been given elsewhere.[22]

For AA analyses, graphite furnace atomic-absorption measurements were made on a Perkin–Elmer Model 503 spectrometer equipped with a HGA-2100 graphite furnace atomiser, using pyrolytic graphite coated graphite tubes and pyrolytic graphite L'vov platforms. Samples were manually injected onto the

Table 2. Optimized analytical conditions for the determination of Cd, Cu, Ni and Pb in octocorals by GFAAS

Element	Wavelength, *nm*	Gas flow, *ml/min*	Drying Temp, *°C*	Drying time, *sec*	Ashing temp, *°C*	Ashing time, *sec*	Atomization temp, *°C*	Atomization time, *sec*
Cadmium	228.8	65	100	40	350	25	1900	5
Copper	324.8	60	100	45	800	25	2600	5
Nickel	232.0	65	100	45	450	40	2500	7
Lead	217.0	60	100	45	500	40	2250	6

platform by means of micropipettes with disposable plastic tips.

Flame atomic-absorption measurements were made on a Perkin-Elmer Model 2380 spectrometer, with an air-acetylene flame. Both spectrometers were provided with deuterium-arc background correction systems.

Recovery study and blanks

Since octocorals possess a highly complex matrix and since no certified standard material was available to match this matrix, a synthetic standard was prepared for this study. To simulate the matrix of the octocorals, an exactly known amount of microwave dried NIES mussel standard material was combined with the appropriate amount of a calcium carbonate solution required to obtain a final mixture of 61% organic matter, represented by the NIES mussel standard, and 39% calcium carbonate. This organic/carbonate ratio is representative of the ratios of the species studied. Triplicates of this mixture (0.5 g) were placed inside the modified glass tubes and microwave digested in the presence of 10 ml of nitric acid.

The synthetic solutions containing certified amounts of the analytes of interest were used to carry out recovery studies. Precision and accuracy were determined based on comparisons of the reported metal contents of the standard reference material used with experimentally determined values.

The calcium carbonate solution used for the preparation of the synthetic reference material was previously purified by extraction with HPLC grade chloroform after the addition of a 1% APDC solution and an acetic acid–ammonium acetate buffer solution to keep the pH at 4.5. The APDC and buffer solutions were also purified prior to use.[23–25]

Triplicates of blanks, prepared in a similar way as the samples, but having no NIES mussel material, were also analyzed for the trace elements of interest.

Reagents

Standard solutions for calibration and optimization of the analytical conditions were prepared by conventional dilution of stock solutions containing 1000 μg/ml of the analytes as nitrates. Nitric acid was of analytical-reagent grade. Distilled, demineralized water (specific resistivity of 18 Mohm/cm) from a Millipore water purification system was used for the preparation of samples, blanks and standards.

RESULTS AND DISCUSSION

It has been reported in the literature that microwave drying significantly decreases the time required for the process,[11,12] and should certainly minimise the possibilities of sample contamination. In the case of the octocorals, conventioanl pre-drying and final drying to constant weight conditions required at least 8 and 12 hr, respectively, while the microwave pre-drying required 20–50 min, depending on the moisture content of the samples, followed by a 12-hr final drying period to constant weight. In addition, microwave pre-dried and digested blanks consistently presented substantially lower metal concentration levels than those prepared by conventional pre-drying in the open on the water bath followed by microwave digestion. This was particularly the case for lead, where for conventional drying followed by microwave digestion, the concentrations in the blanks were 90–95% of those in the samples. Copper, cadmium and nickel levels in the blanks were 50–70% of those in the samples. In contrast, heavy metal concentrations in blanks, pre-dried and digested with the microwave oven, were at parts per billion levels, with the highest concentration corresponding to Zn, 120 ppb, and the lowest corresponding to Cd, 0.1 ppb. This range of blank values can be considered negligible in comparison to the concentrations found for the metals of interest in the octocoral samples analyzed (see Table 1).

These results show that microwave heating greatly reduces the time of sample drying, and minimises significantly the possibility of sample contamination during preparation for AA analysis.

Our results also show, as in previous work, that microwave heating should apply to the acid digestion process. In fact, samples were completely digested in only 4–6 min of microwave heating, while conventional digestions could take up to 4 days.[9] Therefore, as expected, the use of microwave heating for acid digestions significantly reduces the time for sample preparation. In addition, the method not only minimises the amounts of chemicals required for the digestion, and therefore contamination *via* impurities in reagents, but also reduces the risks of sample contamination and sample loss when the samples are treated in sealed tubes.

Table 1 shows the data obtained for the determinations of Cd, Cu, Ni, Pb and Zn in the eight octocoral species. Each column represents the

average concentration obtained in three samples analyzed in triplicate for each sampling site. For all species, the lowest concentration levels were observed for cadmium, while the highest were those for zinc. Standard deviations were, in most cases, relatively high. This could be attributed to the heterogeneous character of this type of sample. In addition, variations in metal concentrations within one species, between sites, and between species are likely to be due to environmental and biological factors which will be discussed and published elsewhere.

Cadmium and copper levels in Venezuelan octocorals were similar to those reported for the Great Barrier Reef.[9] Cadmium concentrations were somewhat higher, while copper concentrations were lower, than those reported for the northern Florida reef tract.[10] Concentrations of Ni, Pb and Zn in the Venezuelan octocorals were, in all cases, one to two orders of magnitude higher than those reported for the Australian octorals, and in the case of lead, for the Florida octocorals. These differences are likely to be due to differences in the environmental conditions of the sampling sites.

Accuracy studies were carried out to check the reliability of the measurements. The analysis of synthetically prepared certified standards, whose matrix closely simulates that of the octocoral samples, produced recovery efficiencies of 98.9, 99.6, 95.4, 99.7 and 99.4% for Cd, Cu, Ni, Pb and Zn, respectively. These results indicate that microwave drying of the NIES standard reference material and the microwave digestion procedure used to bring the synthetically prepared standard into solution, allow for accurate determinations of Cd, Cu, Ni, Pb and Zn in the studied samples.

In conclusion, a fast, efficient, precise and accurate procedure was developed for the analysis of octocorals, making use of microwave heating for the drying as well as acid digestion of the samples, and graphite furnace atomic-absorption spectrometry with L'vov platforms for the measurement of their metal content. The use of microwave heating significantly reduces the time of drying and acid digestion process when compared to conventional methods, and minimises the contamination of samples during handling in the laboratory.

Acknowledgements—The authors wish to thank F. Lozada, D. Boone, E. Mosquera, M. Figueroa and P. Gardinali for assistance during sampling and species identifications. Special thanks to the Venezuelan Navy and the Fundación Terra-Mar for logistic help during the Blanquilla sampling trip, and the Universidad Simón Bolivar and CONICIT for financial assistance.

REFERENCES

1. J. W. Farrington, E. D. Goldberg, R. W. Riesenbrough, J. H. Martin and V. T. Bowen, *Environ. Sci. Technol.*, 1983, **17**, 490.
2. D. J. H. Phillips, *Environ. Poll.*, 1978, **16**, 167.
3. R. E. Johannes, *Tropical Marine Pollution*, E. T. Ferguson Wood and R. E. Johannes, pp. 13–51. Elsevier, Amsterdam, 1975.
4. P. W. Glynn, L. S. Howard, E. Corcoran and A. D. Freay, *Mar. Poll. Bull.*, 1984, **15**, 370.
5. B. E. Brown, *ibid.*, 1987, **18**, 9.
6. R. E. Dodge and R. T. Gilbert, *Mar. Biol.* 1984, **82**, 9.
7. R. T. Shen and E. A. Boyle, *Earth and Planetary Sci. Letters*, 1987, **82**, 298.
8. G. T. Shen, E. A. Boyle and D. W. Lea, *Nature*, 1987, **328**, 794.
9. G. R. W. Denton and C. Burdon-Jones, *Mar. Poll. Bull.*, 1986, **17**, 209.
10. P. W. Glynn, A. M. Szmant, E. F. Corcoran and S. V. Cofer-Shabica, *ibid.*, 1989, **20**, 568.
11. T. S. Koh, *Anal. Chem.*, 1980, **52**, 1978.
12. E. S. Beary, *ibid.*, 1988, **60**, 742.
13. P. Barret and L. J. Davidovski, *ibid.*, 1978, **50**, 1021.
14. S. Tsukada, R. Demura and I. Yamamoto, *Elsei Kagaku*, 1985, **31**, 37.
15. *Idem.*, *ibid.*, 1985, **31**, 405.
16. P. J. Lmothe, T. L. Fries and J. J. Consul, *Anal. Chem.*, 1986, **58**, 1882.
17. M. Burguera and J. L. Burguera, *Anal. Chim. Acta*, 1986, **179**, 351.
18. C. S. E. Papp and L. B. Fisher, *Analyst*, 1987, **12**, 337.
19. K. I. Mahan, T. A. Foderaro, T. L. Garza, R. M. Martinez, G. A. Mariney, M. R. Trivisonno and E. M. Willing, *Anal. Chem.*, 1987, **59**, 938.
20. J. R. Moody and R. M. Lindstrom, *ibid.*, 1977, **49**, 2264.
21. D. P. H. Laxen and R. M. Harrison, *J. Am. Chem. Soc.*, 1981, **12**, 132.
22. J. Alvarado, M. Marquez and L. E. León, *Anal. Lett.*, 1988, **21**, 357.
23. L. G. Danielsson, B. Magnisson and S. Westerlund, *Anal. Chim. Acta*, 1978, **98**, 47.
24. R. E. Sturgeon, S. S. Bergman, A. Desaulniers and D. S. Russell, *Talanta*, 1980, **27**, 85.
25. B. Magnisson and S. Westerlund, *Anal. Chim. Acta*, 1981, **131**, 63.

Talanta, Vol. 39, No. 2, pp. 119–122, 1992
Printed in Great Britain.

0039-9140/92 $5.00 + 0.00

A NEW CATALYTIC POLAROGRAPHIC SYSTEM FOR DETERMINATION OF TRACE AMOUNTS OF TUNGSTEN

DEZHONG DAN
Department of Applied Chemistry, Chengdu College of Geology, Chengdu, Sichuan, People's Republic of China

JUN RE
103 Factory, Chengdu Branch, Bureau of Chinese Civil Airplane Administration, Chengdu, Sichuan, People's Republic of China

(*Received* 24 *May* 1988. *Revised* 20 *July* 1991. *Accepted* 1 *August* 1991)

Summary—A new catalytic polarographic system for the determination of trace amounts of tungsten is described. It is found that the tungsten–2-mercaptobenzothiazole (MBT) complex yields a sensitive catalytic hydrogen wave at −1.10 V (*vs.* SCE) in strongly acidic medium. The peak height is a linear function of tungsten concentration over the range 0.004–1.4 μg/ml in 0.9*M* H_2SO_4–20 mg/ml NaCl–0.01 μg/ml MBT medium. The method can be applied for determination of trace amounts of tungsten in geochemical materials.

Several catalytic polarographic systems for tungsten, mainly involving the sulphuric acid–benzilic acid–potassium chlorate–cetyltrimethylammonium bromide and sulphuric acid–hydrocyanic acid–potassium chlorate systems have been used for the determination of trace amounts of tungsten.[1–4] Recently these systems have been improved, but the organic reagent used is still benzilic acid.[5,6]

We have found 2-mercaptobenzothiazole (MBT) to be an excellent reagent for the determination of tungsten by linear sweep polarography (LSP). MBT can cause a catalytic hydrogen wave in polarography.[7] This paper reports the polarographic behaviour of MBT in strongly acid medium. There is a sensitive and well-defined catalytic hydrogen wave in a solution of 0.9*M* sulphuric acid–20 mg/ml sodium chloride. The peak height is enhanced by the presence of tungsten, and is a linear function of tungsten concentration over the range 0.004–1.4 μg/ml in 0.9*M* sulphuric acid–20 mg/ml sodium chloride–0.01 μg/ml MBT medium. Interferences can be eliminated by heating to fuming with sulphuric acid, cooling, diluting, and neutralizing with sodium hydroxide. The procedure has been successfully used for the determination of tungsten in geochemical standard materials.

EXPERIMENTAL

Reagents

All chemicals used were of analytical-reagent grade. The MBT (Third Reagent Factory of Shanghai), was used without further purification.

Tungsten stock solution, 2 mg/ml. This was made by dissolving 3.590 g of sodium tungstate dihydrate in demineralized water, adding about 50 mg of sodium hydroxide and diluting accurately to 1000 ml with demineralized water. Working solutions were prepared by further dilution.

Apparatus

A Model JP-1A oscillopolarograph (Chengdu Instrumental Factory, China) was used. For derivative linear sweep polarography (derivative LSP), the operating conditions were drop-time 7 sec, scan-rate 250 mV/sec, scan from −0.8 to −1.3 V, mercury head 55 cm, and mercury flow-rate 0.5 mg/sec. The three-electrode system comprised a dropping mercury electrode (DME), platinum counter-electrode, and saturated calomel electrode (SCE) as reference. All potentials were referred to the SCE. The electrolytic cell was a 10 ml-beaker.

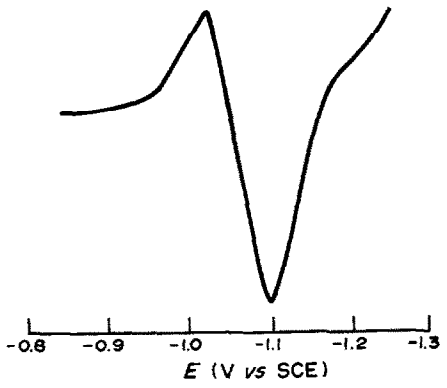

Fig. 1. Derivative polarogram: 0.9*M* H_2SO_4–20 mg/ml NaCl–0.01 μg/ml MBT–0.5 μg W.

Procedures

To the tungsten standard solution in a 25-ml standard flask, add 2.5 ml of sulphuric acid (1 + 1), 2.5 ml of 20% sodium chloride solution and 0.25 ml of 1 μg/ml MBT solution, dilute to volume with demineralized water, and let stand for about half an hour. Record the derivative linear sweep polarogram from −0.8 to −1.3 V (*vs.* SCE).

Analysis of samples. Weight 0.1–0.25 g of geochemical sample into a 50-ml PTFE crucible, add 10 ml of concentrated hydrochloric acid, and heat gently for a few minutes on a hot-plate. Add 3 ml of concentrated nitric acid, 5 ml of 47% hydrofluoric acid and 2 ml of 60% perchloric acid, and heat. Evaporate the solution until no more fumes are evolved. Cool, add 1 ml of hydrochloric acid (1 + 1) to dissolve the residue, then transfer the solution to a 25-ml beaker, rinsing the crucible with demineralized water. Add 2 ml of sulphuric acid (1 + 1), heat the solution until the yellow colour disappears,

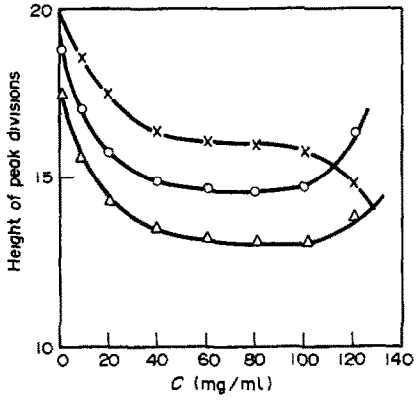

Fig. 2. Effect of supporting electrolytes on the peak height: 0.9*M* H_2SO_4–0.01 μg/ml MBT–0.5 μg W. ○, NaCl; △, KCl, ×, NH_4Cl.

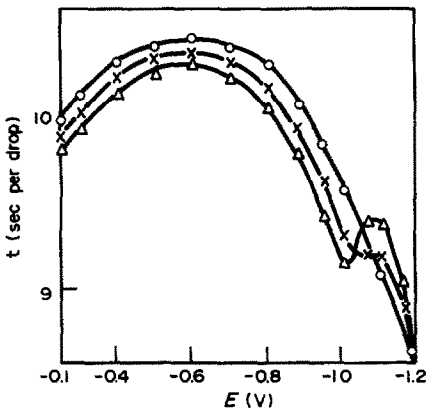

Fig. 3. Electrocapillary curves: ○, 0.9*M* H_2SO_4–20 mg/ml NaCl; ×, 0.9*M* H_2SO_4–20 mg/ml NaCl–0.01 μg/ml MBT; △, 0.9*M* H_2SO_4–20 mg/ml NaCl–0.01 μg/ml MBT–0.5 μg W.

transfer the solution to a 25-ml standard flask, dilute to volume with 5% sodium hydroxide solution and mix. Allow the precipitate to settle. Pipette 10 ml of the clear solution into a 25-ml standard flask, add the reagents as described above, and dilute to volume. Let stand for half an hour, then polarograph as described.

Calibration graph. Add 2 ml of sulphuric acid (1 + 1) to portions of standard tungsten solution (to cover the range 0.004–1.4 μg/ml). Evaporate the solutions till fuming and heat for 2 min longer. Cool, dilute to volume in 25-ml standard flasks with 5% sodium hydroxide solution and mix. Pipette 10 ml of a solution into a 25-ml standard flask, add 3.2 ml of sulphuric acid (1 + 1), and polarograph as described above. Run a blank and apply a correction for it.

RESULTS AND DISCUSSION

Optimum condition for catalytic system

Tungsten can give a sensitive catalytic wave at about −1.10 V (*vs.* SCE) in presence of MBT

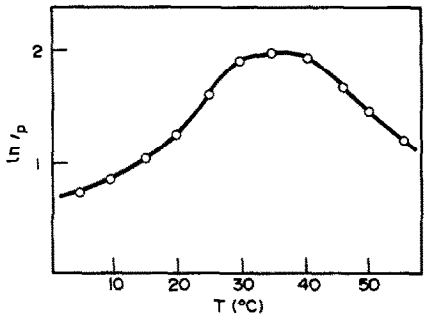

Fig. 4. Effect of temperature on peak height. Conditions as for Fig. 1.

Table 1. The effect of foreign ions

Ions, X	Maximum concentration ratio tolerated, [X]/[W]
Alkali and alkaline-earth metals	no interference
Fe(II), Fe(III), Cu(II), Cd(II) Bi(III), Sb(III), Ga(III)	500–800
Ag(I), Co(II), Ni(II), Zn(II) Pt(IV), Ti(IV), Se(IV), Ta(V) Mo(VI)	40–80
Hg(II), Mn(II), In(III), Ge(IV) Te(IV), V(V), Os(IV)	1–5
Pd(II), As(III), Ru(III), Rh(III) Au(III), Cr(VI), NO_3^-	interfere seriously

in acidic medium, in LSP (Fig. 1). The peak potentials depend on the species of acid used. A well-defined peak is obtained with sulphuric acid medium, and the peak height is constant over the range 0.9–2*M* sulphuric acid. At low acidity the peak height decreases and at pH > 5, the wave disappears.

If the supporting electrolyte concentration is not high enough, it is difficult to obtain a stable catalytic wave. Potassium, sodium and ammonium chlorides were tested and the sodium salt was found the most suitable, as the sensitivity was reasonably high and the peak height did not change much with salt concentration in the range 20–100 mg/ml (Fig. 2).

MBT is a key factor for the catalytic wave, as the background current increases with MBT concentration, but the peak height is considerably enhanced by the presence of tungsten (VI). It was found that 0.01 μg/ml MBT was sufficient to give reasonable sensitivity, low background, and wide linear range. To sum up, the optimum composition of the catalytic system was found to be 0.9*M* sulphuric acid, 20 mg/ml sodium chloride, 0.01 μg/ml MBT.

Once the test solution had been prepared, the peak height obtained with it decreased slightly during the first 30 min, then remained unchanged for a day. The peak current was a linear function of tungsten concentration over the range 0.004–1.4 μg/ml, and different sensitivities could be used for different ranges.

Table 2. Determination of tungsten in six Chinese standard reference materials

Sample	Recommended value, $\mu g/g$	This method, $\mu g/g$
GBW07302	24.4 ± 2.7	23.7; 24.0; 22.7
GBW07303	2.9 ± 0.7	3.3; 3.3; 3.4
GBW07304	2.5 ± 0.8	3.0; 1.9; 1.8
GBW07305	3.2 ± 0.6	3.3; 3.2; 3.8
GBW07306	25 ± 3	26; 26; 26
GBW07308	1.95 ± 0.44	1.79; 1.77; 1.79

Characteristics of the catalytic wave

The electrocapillary curves are shown in Fig. 3. When MBT and MBT plus tungsten were present the surface tension of the mercury drop was decreased and a sharp change in drop time appeared at between −1.0 and −1.2 V.

The peak height changed with temperature over the range 5–55° (Fig. 4), the temperature coefficient being +7% per degree at <30°, and −6% per degree at >40°. The peak height was almost constant over the temperature range 30–40°. The behaviour of the background current is similar to that of the tungsten-enhanced wave.

The effect of surfactants on the peak current was examined. The peak height is considerably decreased by the addition of 1 or 2 drops of solutions (at the concentrations given in parentheses) of surfactants such as sodium lauryl sulphate (1 mg/ml), gelatin (1 mg/ml), tetrabutylammonium iodide (0.1 mg/ml), Triton X-100 (0.1 mg/ml) to the medium used. The peak height is greatly increased by the presence of 0.1 mg/ml poly(vinyl alcohol), but the reason for this enhancement effect is not known.

The peak height is proportional to the height of the mercury head.

These results indicate that the catalytic wave has adsorption characteristics. Hydrogen bubbles can be observed at the surface of the dropping mercury electrode, if large amounts of MBT or tungsten are present in the system. It is clear that the current is due to catalytic discharge of hydrogen ions. On the basis of these observations, it may be deduced that MBT can yield a catalytic hydrogen wave, the catalysis being enhanced by presence of tungsten.

Effect of foreign ions

More than forty ions were examined for possible interference in the determination of tungsten. The results of Table 1 show that the system has good selectivity. Most common metal ions have little effect. Of the ions tested, only As(III), Ru(III), Rh(III), Au(III), Pd(II) and Cr(VI) interfered seriously, the last five causing a decrease in the peak current, and As(III) causing the wave to split. Of the anions tested, only nitrate was found to interfere. Prior

separation is unnecessary since the sample solution is prepared by fuming with sulphuric acid, followed by the addition of sodium hydroxide to precipitate interfering species.

Application

Six Chinese standard stream-sediment reference materials were analysed by the method. These samples are used throughout China as primary-control standards for the trace-element analysis of geological-exploration samples. They are well homogenized and have a particle size of 200 mesh. The results (Table 2) compare well with the recommended values.[8]

Acknowledgement—We are grateful to Prof. Peifan Xu for his help with the experimental work.

REFERENCES

1. Jiaqi Deng, *Huaxue Shijie*, 1963, **17**, 565.
2. Jinsen Zhou, *Polarog. Anal. Lett.*, 1974, **1**, 38.
3. Jingru An and Jiayi Lin, *Fenxi Huaxue*, 1981, **9**, 263.
4. Riyun Zheng, *Fenxi Shiyinshi*, 1983, **2**, No. 2, 5.
5. Sunkai Yang and Liyi Chen, *Fenxi Huaxue* 1984, **12**, 84.
6. Baichong Shu, *ibid.*, 1984, **12**, 331.
7. V. F. Toropova, G. K. Budnikov, E. P. Medyantseva and V. P. Frolova, *Zh. Obshch. Khim.*, 1977, **47**, 154.
8. *Catalogue of Standard Materials of People's Republic of China*, Chinese Academy of Metrology, 1985.

Talanta, Vol. 39, No. 2, pp. 123–126, 1992
Printed in Great Britain

0039-9140/92 $5.00 + 0.00
Pergamon Press plc

POLAROGRAPHIC DETERMINATION OF ATMOSPHERIC NITROGEN OXIDES

LU GUANGHAN and HE ZHIKE
Department of Chemistry, Central China Normal University, Wuhan, 430070, People's Republic of China
LIU YULING
Shan Dong Lin Yi Education College, Ji Nan, People's Republic of China

(*Received 2 August* 1990. *Revised* 3 *March* 1991. *Accepted* 13 *March* 1991)

Summary—A new polarographic method is described for the determination of nitrite/nitrogen oxides. The nitrite is first diazotized with *p*-aminobenzoic acid, followed by coupling to 8-hydroxyquinoline to produce an azo dye. This azo dye is adsorbable on a mercury drop electrode and its reduction is reversible. The linear response range is 6×10^{-9}–3×10^{-7} g/ml. The detection limit is 4×10^{-9} g/ml. This method has been applied to the determination of nitrogen oxides in the air.

The oxides of nitrogen found in air consist mainly of nitrogen monoxide and nitrogen dioxide, most of which results from the combustion of fossil fuels, the exhaust gas from internal-combustion engines, and waste gas released by steelworks, metal smelters, and factories that produce and use nitric acid. Experiments with animals show that oxides of nitrogen can affect the respiratory organs,[1] and cause the extension of bronchial asthma and other diseases. Therefore, it is important to monitor and determine the oxides of nitrogen in the air.

Many methods have been introduced for determination of nitrite/nitrogen oxides.[2–10] Spectrophotometric methods are often used, but some suffer from poor sensitivity. However, the polarographic and adsorptive cathodic stripping voltammetry methods can give greater sensitivity.[11,12] The method proposed in this paper uses a tube filled with chromium trioxide to oxidize nitrogen monoxide to nitrogen dioxide, which is then absorbed in alkaline sodium arsenite solution to produce nitrite, followed by diazotization of *p*-aminobenzoic acid and coupling to 8-hydroxyquinoline (oxine) to form an azo dye. The azo dye can be reduced at the dropping mercury electrode in pH-7.5 medium. The content of nitrogen oxides in the air can thus be determined.

EXPERIMENTAL

Apparatus

A JP-1A oscillopolarograph, a voltammetric analyser and a model 883 D.C. polarograph were used, in a three-electrode configuration, with an *x*–*y* recorder. A dropping mercury working electrode was used, except for the cyclic voltammetry, for which a hanging drop mercury electrode was used. The counter-electrode was a platinum wire. All potentials were measured against a saturated calomel electrode (SCE). The electrolytic cell was a 10-ml beaker.

For sampling, a commercially available gas sampling device was used, fitted with an oxidizing tube containing chromium trioxide and a trap for interferents (Fig. 1). The trap contained cotton wool impregnated with lead acetate. The oxidizing tube contained about 8 g of the oxidizing agent, between two plugs of cotton wool. The oxidizing agent[13,14] was prepared by making a paste of 5 g of chromium trioxide (CrO_3) with a little water, mixing this with 95 g of 14–16 mesh silica, and drying the mixture at 105°.

Reagents

A 1-mg/ml nitrite stock solution was prepared from sodium nitrite which had been dried at 105–110° for 2 hr, and a working standard solution was obtained by diluting the stock solution with triply distilled water.

p-Aminobenzoic acid solution (1 mg/ml) was prepared by dissolving 0.10 g of *p*-aminobenzoic acid in 10 ml of ethanol and diluting to 100 ml with water.

8-Hydroxyquinoline (oxine) solution, 10 mg/ml, was prepared by dissolving 1.00 g of oxine in 2 ml of 6*M* hydrochloric acid and diluting to 100 ml with water.

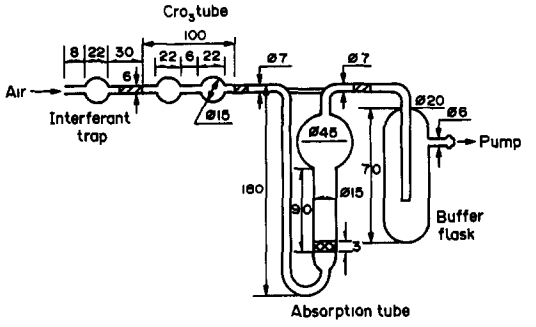

Fig. 1. Sampling device for nitrogen oxides (dimensions in mm).

Alkaline sodium arsenite solution[6] was prepared by dissolving 1.0 g of arsenious oxide and 5.2 g of sodium hydroxide in water and diluting to 2 litres.

Sodium hydroxide solution (0.1*M*) was also prepared. Triply distilled water was used throughout.

Procedure

Pipette an aliquot of the standard solution of nitrite into a 10-ml beaker, add 0.5 ml of the *p*-aminobenzoic acid solution (giving a pH of ~1.5) and after about 1 min add 0.3 ml of the oxine solution followed by 1.0 ml of 0.1*M* sodium hydroxide. The solution turns orange. Dilute to 10 ml with water and mix thoroughly. Let stand for 2 min and record the derivative polarogram from −0.40 to −0.90 V (*vs.* SCE), starting the potential scan at −0.40 V (Fig. 2). Figure 3 shows the D.C. polarogram.

For air analysis, place 6 ml of the alkaline sodium arsenite solution in the absorption tube, and draw air through the sampling apparatus at 400 ml/min for 50 min. Transfer into a 10-ml beaker 1 ml of the sample solution thus obtained, add 0.5 ml of *p*-aminobenzoic acid solution, adjust the pH to *ca.* 1.5, then proceed as above by adding the oxine *etc.*

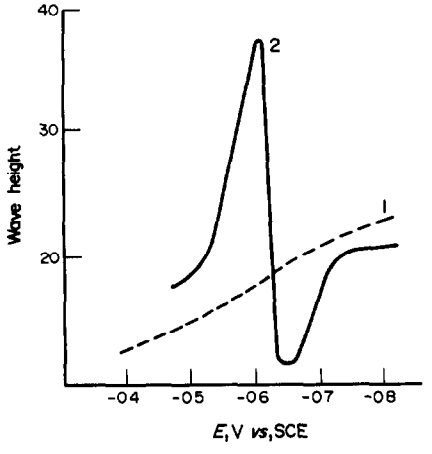

Fig. 2. Derivative single sweep polarogram of azo dye. 1, Oxine, 0.3 mg/ml; *p*-aminobenzoic acid, 0.05 mg/ml; pH 7.5. 2, 1 + 0.3 μg/ml NO_2^-.

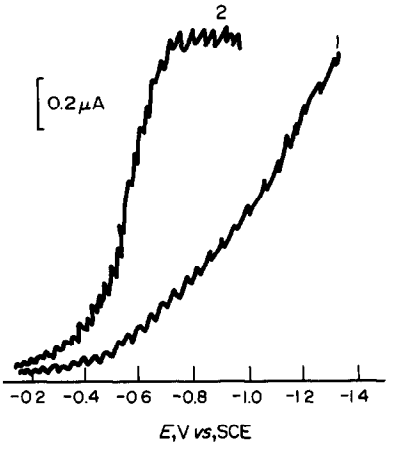

Fig. 3. D.C. polarogram of azo dye, conditions as for Fig. 2, except for NO_2^-, 0.5 μg/ml.

RESULTS AND DISCUSSION

Optimum conditions

The effects of the *p*-aminobenzoic acid and oxine concentrations and pH on the peak height are shown in Fig. 4. The optimum final concentrations are 0.05 and 0.3 mg/ml respectively and the optimum pH is about 7.5.

Linear range and reproducibility

Under the optimum conditions chosen, the peak height is proportional to the nitrite concentration in the range 6×10^{-9}–3×10^{-7} g/ml and the detection limit is 4×10^{-9} g/ml. A relative standard deviation of 4.1% was obtained for seven determinations of 1×10^{-8} g/ml nitrate.

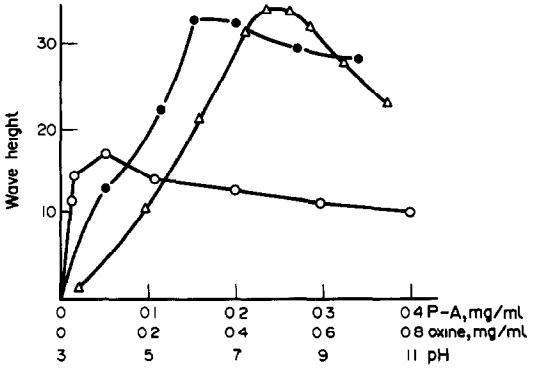

Fig. 4. Effect of reagent concentrations and pH on peak height for azo dye. NO_2^-, 0.05 μg/ml; ○, *p*-aminobenzoic acid (P-A); ●, oxine; △, pH.

Effect of other ions

It was found that a 1000-fold NO_3^- or SCN^-, 500-fold SO_4^{2-}, $S_2O_3^{2-}$, F^- or Hg(II), 200-fold PO_4^{3-} or Mo(IV), 60-fold Bi(III), 50-fold Pb(II), Zn(II), Co(II) or Ti(IV) and 30-fold Al(III) or Cd(II) concentration ratio to NO_2^- has no effect on the determination of nitrite. In addition, arsenite does not interfere.

Effect of height of the mercury column

The peak height is directly proportional to the mercury column height, indicating adsorption of the azo dye on the dropping mercury electrode, and that an adsorption wave is obtained.

Electrocapillary curves

The drop times (t, sec/drop) at various potentials were investigated (Fig. 5). From curve 3, it can be seen that the electrocapillary curve was considerably lowered by the presence of the azo dye, which was adsorbed very strongly at the electrode, resulting in the surface tension of the mercury drop being reduced.

Cyclic voltammetry

Figure 6 shows single sweep voltamperograms measured at the hanging mercury drop electrode. A reduction peak is formed when the potential is scanned between −0.4 and −0.9 V (*vs.* SCE), and arises from reduction of the —N=N—group in the azo dye. The reduction is apparently reversible, as there is only a small difference between the reduction and the oxidation potentials when the scan direction is reversed. The number of electrons (n) transferred in a reversible surface reaction can be calculated from the peak width at half height, $W_{1/2}$, by the equation[15] $n = 3.52\ RT/FW_{1/2}$. We found that $W_{1/2}$ (Fig. 6) was 50 mV (at 23°). From this value, $n = 2$, confirming that the reduction peak is due to reduction of the azo group (—N=N—) to a hydrazo group (—NH—NH—).

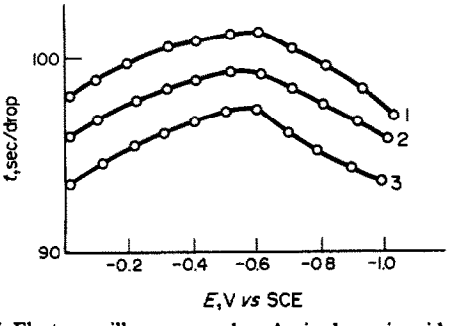

Fig. 5. Electrocapillary curves. 1. *p*-Aminobenzoic acid. 0.05 mg/ml, pH 7.5. 2. 1 + oxine (0.3 mg/ml). 3. 2 + NO_2^- (0.1 μg/ml).

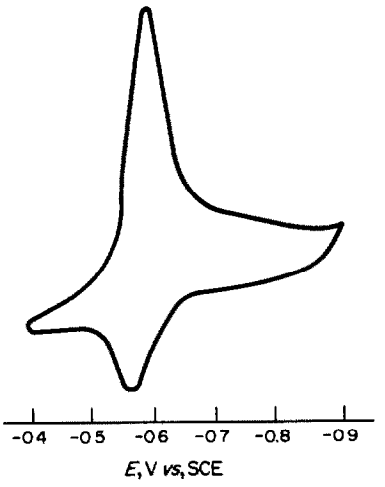

Fig. 6. Cyclic voltamperogram. Experimental conditions as for Fig. 2, except for NO_2^-, 0.5 μg/ml. Scan-rate, 250 mV/sec; X, 100 mV/cm; Y, 5 mV/cm.

Sampling

Christie *et al.*[16] have reported that nitrogen dioxide is trapped in alkaline sodium arsenite with an efficiency of ~95%, so alkaline sodium arsenite solution was chosen as the absorption solution. The oxidation efficiency[13,14] can reach 99% when nitrogen monoxide in air is oxidized by chromium trioxide at a relative humidity of 30–80%, ambient temperature and a flow-rate of 500 ml/min. No interference results from the presence of a 5-fold amount of O_3 (relative to NO_x) but the presence of a 3-fold amount of H_2S or 20-fold amount of SO_2 will cause interference. The interference can be overcome by fixing a trapping tube filled with cotton-wool impregnated with lead acetate upstream of the oxidizing tube (Fig. 1).

Typical results, together with those obtained by a standard method,[5] are given in Table 1. The agreement is satisfactory.

Table 1. Determination of nitrogen oxides in the air (calculated as the NO_2^- obtained in the absorption solution after sampling of 20 litres of air)

Sample	NO_2^- found,* mg/ml	
	Present method	Reference method[5]
1	0.216	0.224
2	0.242	0.256
3	0.219	0.201
4	0.172	0.163

*Means of 3 determinations.

REFERENCES

1. J. R. Foster, R. C. Cottrell, I. A. Herod, H. A. C. Atkinson and K. Miller, *Br. J. Exp. Pathol.*, 1985, **66**, 193.
2. Y. Fang, L. Jin and T. Xu, *Environmental Surveillance and Analysis* (in Chinese), p. 44. East China Normal University Press, Shanghai, 1987.
3. A. Bhatt and V. K. Gupta, *J. Indian Chem. Soc.*, 1980, **57**, 1056.
4. S. Hong, *Methods of Analysis of Environmental Pollution* (in Chinese), p. 373. Science Press, Beijing, 1987.
5. American Society for Testing and Materials, *1979 Annual Book of ASTM Standards*, Part 31: *Water*, p. 463. ASTM, Philadelphia, 1979.
6. V. Raman and M. S. Dabbas, *Microchem J.*, 1989, **40**, 242.
7. J. B. Fox, *CRC Crit. Rev. Anal. Chem.*, 1983, **15**, 283.
8. S. Flamerz and W. A. Bashir, *Analyst*, 1985, **110**, 1513.
9. A. Chaube, A. K. Baveja and V. K. Gupta, *Talanta*, 1984, **31**, 391.
10. D. Krochmal, M. Rzeminski and L. Gorski, *Chem. Anal. (Warsaw)*, 1987, **32**, 581.
11. Z. Zhao and X. Cai, *J. Electroanal. Chem.*, 1988, **252**, 361.
12. C. M. G. van den Berg and H. Li, *Anal. Chim. Acta*, 1988, **212**, 31.
13. D. Levaggi, E. L. Kothny, T. Belsky, E. de Vera and P. K. Mueller, *Environ. Sci. Technol.*, 1974, **8**, 348.
14. S. Sao and J. Cui, *Methods of Monitoring the Polluted Atmosphere* (in Chinese), p. 722. Chemical Industry Press, Beijing, 1984.
15. J. Wang, C. Sun and W. Jin, *J. Electroanal. Chem.*, 1990, **291**, 59.
16. A. A. Christie, R. G. Lidzey and D. W. Radford, *Analyst*, 1970, **95**, 519.

Talanta, Vol. 39, No. 2, pp. 127–136, 1992
Printed in Great Britain

0039-9140/92 $5.00 + 0.00
Pergamon Press plc

DETERMINATION OF GALLIUM BY ANODIC STRIPPING SQUARE-WAVE VOLTAMMETRY

DETECTION OF A Ga–Zn INTERMETALLIC COMPOUND AND ITS DESTRUCTION BY Sb IN AN NaSCN–$NaClO_4$ SUPPORTING ELECTROLYTE

PABLO COFRÉ* and KARIN BRINCK
Facultad de Química, Pontificia Universidad Católica de Chile, Vicuña Mackenna 4860, Santiago, Chile

(*Received* 3 *October* 1990. *Revised* 28 *December* 1990. *Accepted* 13 *January* 1991)

Summary—Reproducibility for successive determinations with a hanging mercury drop electrode is assessed in relation to solution stirring, drop size and back-diffusion to the mercury thread. The effect of experimental parameters such as drop size, deposition time and gallium concentration on the observed stripping current is investigated. The interference of zinc present in a $0.5M$ NaSCN + $4.2M$ $NaClO_4$ supporting electrolyte on the gallium detection limit and calibration plots is described. Formation of an intermetallic compound with a Zn:Ga ratio of 2:3 and its destruction by co-deposition of zinc with Sb are reported. A detection limit of $10^{-8}M$ gallium was obtained in the presence of $10^{-5}M$ Sb(III).

The determination of trace amounts or trace concentration levels of gallium is of interest in different fields. The discovery of the special affinity of gallium for specific tissues and the anti-tumor activity in either radioactive or non-radioactive isotope form has stimulated studies of its cytotoxicity and retention by tissues and revealed a need for precise and rapid methods for trace determinations of this metal.[1,2] In the semiconductor industry gallium is used as one of the doping elements. Determination of trace amounts of gallium present as GaAs in ZnS·CdS powders and films requires the measurement of 10^{-8}–10^{-6} g of the metal in microscopic weighed samples.[3] More recently, exposure to gallium arsenide particulates in the air has been identified as a potential health hazard in the semiconductor industry and therefore methods for the determination of nanogram and sub-nanogram levels of gallium in blood, tissues and other biological materials are required for investigation of the distribution characteristics of this element.[4] Anodic stripping voltammetry appears to be a good choice for this application.

The electroanalytical determination of gallium by voltammetric (including stripping) techniques is faced with the problem of the irreversibility of the electrode process in acidic media.[5] Different supporting electrolyte compositions have been tried in polarographic studies[6] in order to obtain a reversible process and studies in thiocyanate or salicylic acid based electrolytes[7a] are of special interest. An NaSCN-based supporting electrolyte, together with the high ionic strength (normally obtained with $NaClO_4$) essential for electrochemically reversible behaviour,[8,9] has been used in thorough studies on phase-selective anodic stripping analysis (PSAS) for trace concentrations of gallium.[10,11] A $0.5M$ NaSCN + $4.5M$ $NaClO_4$ supporting electrolyte allowed the detection of gallium down to $8.55 \times 10^{-8}M$, but linear dependence of the PSAS current on concentration was obtained only above $10^{-6}M$.[10] Linear dependence of PSAS current on electrode area has been reported,[10] but its theoretical substantiation was based on equations derived for chronopotentiometric stripping[12] rather than PSAS. The dependence of PSAS current on deposition time has been studied for $8.55 \times 10^{-6}M$ gallium in $0.5M$ NaSCN + $4.5M$ $NaClO_4$ supporting electrolyte[10] and for $9.72 \times 10^{-6}M$ gallium in $1M$ NH_4SCN.[11] Both studies showed a negative deviation from linearity for long deposition times, but neither reported experiments at lower gallium concentrations.

Reproducibility studies based on ten determinations in a $1M$ NH_4SCN electrolyte at 60°

*Author for correspondence.

produced a 4.4% relative standard deviation for a $9.72 \times 10^{-7}M$ gallium solution.[11] However, the results showed a gradual increase in the PSAS current with run sequence, on which the authors made only minor comments.

Several metal ions can interfere in potentiometric stripping analysis for gallium. Zinc can hinder the gallium stripping signal in a pH 4.0 acetate buffer[13] and has been recognized as a potential interferent in thiocyanate-based electrolytes.[10] Attempts to obtain a Zn-free $NaSCN–NaClO_4$ supporting electrolyte have led to the use of glass-immobilized 8-hydroxyquinoline for sequestering trace metals[14] which appears to be an effective but slow procedure.

This work is focused on the use of square-wave voltammetry for the stripping step. A thorough study of different experimental parameters has been performed in order to understand all the observed deviations from ideal behaviour. The problem of back-diffusion into the mercury thread, the effect of the Zn(II) present in the supporting electrolyte on the calibration plots and detection limit and the presence of a Zn–Ga intermetallic compound and its elimination by Sb are discussed.

EXPERIMENTAL

Apparatus

All the experiments were carried out with an EG & G Princeton Applied Research model 384B polarographic analyser provided with a model 303A static mercury drop electrode, glass cells and a silver/silver chloride (saturated KCl solution) reference electrode (SSCE). Modified cells with a side-tube at the bottom for the collection of mercury drops[15] were used, except for experiment *A* in Table 1. All the stripping currents were plotted on a Houston Instruments model DMP-40 plotter.

The 303A electrode was modified by inserting a toggle switch to allow manual on/off control of the solenoid valve which dispenses the mercury drops. The switch, together with the dislodge-adjustment potentiometer at the rear, allowed the execution of several strippings from a single drop or strippings from consecutive drops. In the normal mode, the 303A electrode will dispense and dislodge two mercury drops between runs. Solutions were degassed with high-purity argon presaturated with an aqueous solution of the supporting electrolyte and stirred with an EG & G 305 magnetic stirrer, at its "slow" rate (nominally 400 rpm).

The different gallium concentrations were obtained by spiking with a stock solution dispensed from Gilson Pipetman micropipettes, models P20 and P200.

Reagents

Sodium thiocyanate was Fluka *purum* p.a. Sodium perchlorate was made by neutralization of Merck *pro analysi* sodium carbonate with Baker Analyzed perchloric acid. Gallium stock solutions were made by dissolution of Strem Chemicals 99.999% pure gallium(III) oxide in the smallest amount of Merck *pro analysi* concentrated hydrochloric acid. Zinc(II) sulphate and antimony(III) chloride were Merck *pro analysi*. Pierce Chemical Co. glass-immobilized 8-hydroxyquinoline was used in our attempts to purify a $0.5M$ NaSCN + $4.2M$ $NaClO_4$ supporting electrolyte, as was constant-potential electrolysis at a stirred mercury pool electrode. However, all the experiments reported in this paper were conducted with chemicals used without further purification. Distilled water was obtained from a high-performance automatic self-flushing still,[16] which ensured purity for trace analysis.

Procedure

All the glassware was soaked in $6M$ nitric acid for 24 hr prior to use. The $0.5M$ NaSCN + $4.2M$ (or $0.85M$) $NaClO_4$ supporting electrolyte was adjusted to pH 2.0 and 10 ml were placed in a dry cell and degassed for 300 sec before measurement. This solution was then spiked with the corresponding stock solution to give the desired concentration and degassed for another 30 sec. The presence of Zn in the supporting electrolyte was confirmed and quantified by spiking with a $0.1M$ $ZnSO_4$ solution and use of a built-in standard addition program.

Gallium was preconcentrated on the mercury drop at different constant deposition potentials (E_d) and for different deposition times (t_d) with constant solution stirring. This was followed by a 5-sec rest period prior to stripping, which was carried out by using square-wave voltammetry with a 100 Hz 2 mV step. Peak stripping currents (i_p) were automatically measured by a tangent fit program and the peak potentials (E_p), referred to the SSCE, were also recorded.

The dispensing and dislodging of single mercury drops was obtained under manual control with the additional toggle switch and the dislodge-adjustment knob at the rear of the 303A electrode.

RESULTS AND DISCUSSION

Reproducibility

After several deposition–stripping cycles had been run with the same gallium solution, each on a different mercury drop, an apparent stabilization of the stripping current was obtained. Ten successive cycles performed from that point on provided the results for reproducibility.

Experiment *A* in Table 1 allowed the accumulation of mercury drops on the cell bottom, which was apparently accompanied by a gradual decrease in average stripping current, possibly because of a progressive change in stirring efficiency. Experiment B, however, was performed with evacuation of the mercury drops into the side-arm between each run. This meant that the cell position on the magnetic stirrer was not exactly the same for each run. The results show a higher average stripping current, presumably because of more efficient stirring. The poorer reproducibility is probably due to the use of a star-shaped stirrer bar which does not spin around a single axis but tends to precess in a fashion which is irreproducible and very dependent on the stirrer position. The smaller relative standard deviation (rsd) in experiment *A* was due to more reproducible stirring, since the cell position was not altered between runs. The difference between the currents for the first drop in experiments A and B could be due to the larger rsd of the latter.

Several trial experiments starting with a fresh charge of mercury in the 303A electrode always showed an initial steady increase in stripping current for successive runs on the same solution, in spite of the use of a new drop for each cycle. This was further investigated by using a more negative deposition potential which also allowed the deposition of any zinc present in the supporting electrolyte. Figure 1 shows that the gallium (a) and zinc (b) stripping currents gradually increase with run sequence, but tend to level off. A plot of the ratio of the gallium and zinc stripping currents (c) shows a fairly constant value, with a 3% relative standard

Table 1. Reproducibility of gallium stripping currents for successive deposition–stripping cycles on fresh mercury drops (medium size): [Ga] = $2 \times 10^{-6} M$; t_d = 360 sec; E_d = −0.900 V; slow stirring rate

	i_p, *nA*	
Run	Exp. A*	Exp. B†
1	1714	1923
2	1688	1906
3	1688	2032
4	1702	1907
5	1662	1685
6	1652	2017
7	1677	2039
8	1641	1945
9	1665	1861
10	1753	2081
Average	1684	1940
% Std. Dev.	1.9	5.6

*With accumulation of mercury drops on the cell bottom.

†With evacuation of mercury drops from the cell bottom.

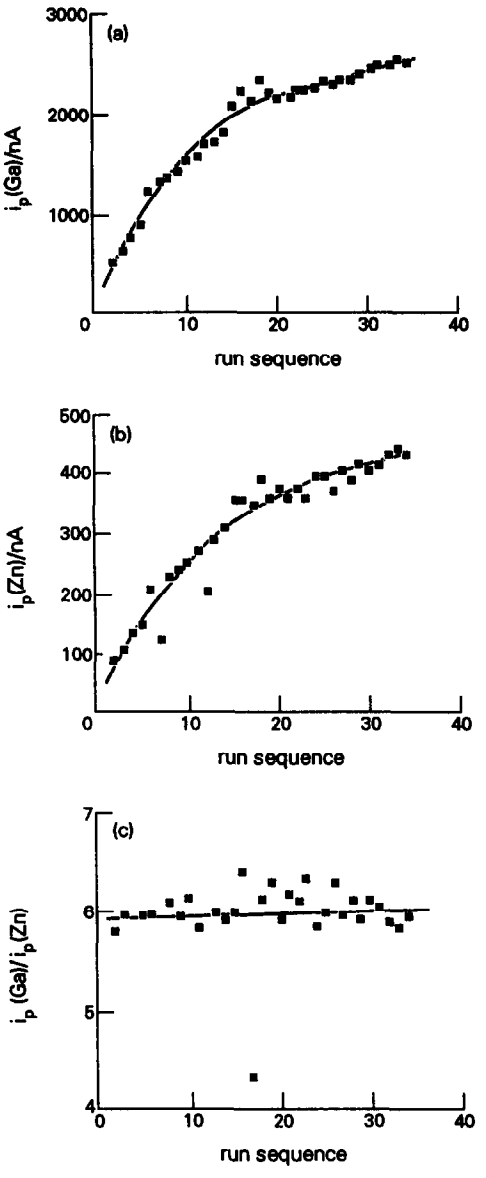

Fig. 1. Gallium (a) and zinc (b) stripping currents and their ratio (c) for successive deposition–stripping cycles on a freshly-charged electrode, using a fresh (medium size) mercury drop for each run. [Ga] = $2 \times 10^{-6} M$; [Zn] = $1.3 \times 10^{-7} M$; t_d = 360 sec; E_d = −1.100 V; slow stirring rate.

deviation. This suggests that the phenomenon responsible for the curvature in (a) and (b) is not specific for gallium.

Our first concern was whether successive mercury drops differed in area. An experiment was run in which each mercury drop was collected and weighed after stripping. The results in Table 2 show that the stripping current increases at a rate much greater than the electrode area, which eliminates changes in electrode size as an explanation for the results in Fig. 1.

A more likely cause could be the presence of residual metals (zinc or gallium) remaining in the mercury drop electrode, owing to incomplete stripping. After one deposition step on a small drop, several consecutive strippings were run on the same drop. The results in Fig. 2 show the change in zinc (a) and gallium (b) stripping currents with stripping sequence. A gradual decrease was observed for zinc whereas an abrupt current drop was obtained for gallium. This is consistent with the zinc diffusion coefficient in mercury being higher than that for gallium.[7b] The non-zero and constant stripping current is due to deposition occurring during the time elapsed in going from the initial potential to the stripping potential during the stripping step, even in the absence of any programmed deposition step. These results suggest that some residual metals may be present in the mercury. However, the 303A electrode will dispense and dislodge two mercury drops between runs and any metals remaining in the first drop after a stripping cycle should be flushed away. The question, therefore, is whether the metals could have diffused into the mercury thread in the capillary, as reported by Neeb *et al.*[17]

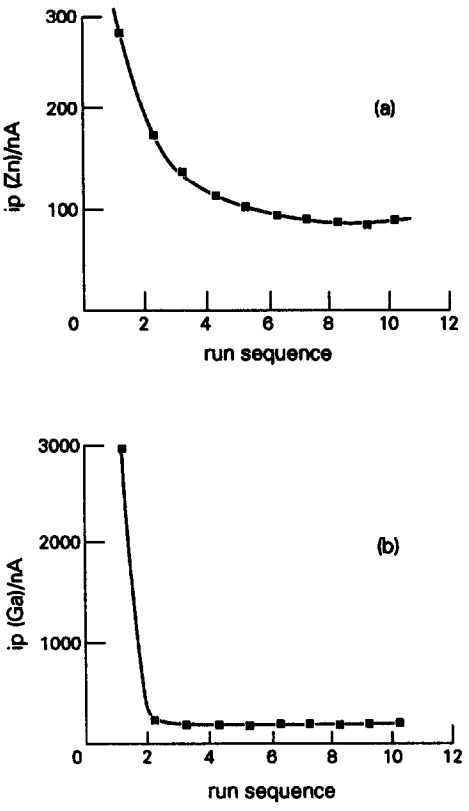

Fig. 2. Zinc (a) and gallium (b) stripping currents after a single deposition step on a single mercury drop (small size) as a function of consecutive stripping steps on the same drop. [Ga] = $2 \times 10^{-6}M$; [Zn] = $1.3 \times 10^{-7}M$; $t_d = 360$ sec; $E_d = -1.100$ V; slow stirring rate.

Table 2. Gallium stripping current a nd electrode area for successive deposition–stripping cycles on fresh mercury drops (medium size): [Ga] = $2 \times 10^{-6}M$; $t_d = 360$ sec; $E_d = -0.900$ V; slow stirring rate

Run	i_p(Ga), *nA*	Drop area*, mm^2
1	1334	1.73
2	1275	1.96
3	1820	2.04
4	1979	2.00
5	1633	2.11
6	1710	2.14
7	1762	2.11
8	2137	1.96
9	2249	2.04
10	2268	2.07

*Electrode area (S) was obtained from $S = 0.8505\ W^{2/3}$, where W is the drop weight in mg.

An experiment consisting of a single deposition step followed by successive strippings from the end of the capillary after consecutive drops had been dislodged was run in order to detect any concentration profile in the mercury capillary. Figure 3 shows the results obtained for zinc (a) and gallium (b) stripping peaks. The maximum observed after drop number five was dislodged proves that back-diffusion occurs.

Now we can explain the results in Fig. 1. When starting with a fresh mercury electrode, there is always a certain amount of metal (zinc or gallium) lost during the deposition step due to diffusion into the mercury capillary thread. This is maximal when the mercury thread is free from metals (zinc or gallium in this case), *i.e.*, when the concentration gradients that develop are maximal. After the first deposition–stripping cycle is completed, a fraction of the deposited metal remains in the mercury thread, although two mercury drops have been dispensed and

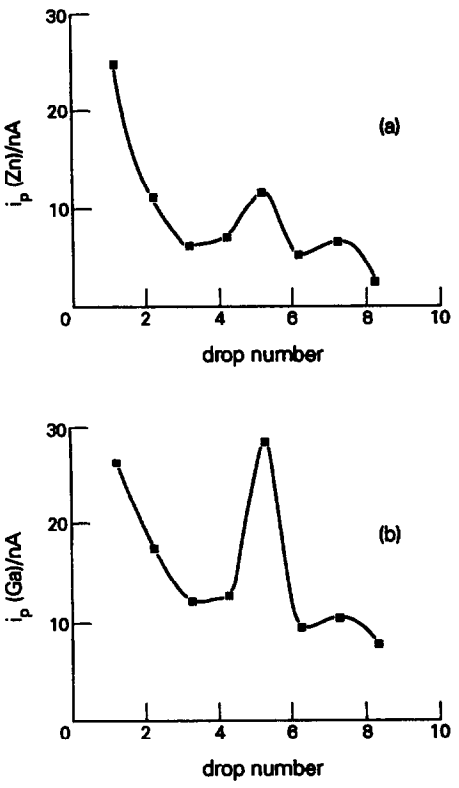

Fig. 3. Zinc (a) and gallium (b) stripping currents after a single deposition step as a function of drop sequence after drop dislodgement. [Ga] = $2 \times 10^{-6} M$; [Zn] = $1.3 \times 10^{-7} M$; t_d = 360 sec; E_d = −1.100 V; slow stirring rate.

dislodged. Therefore, the loss of metal due to back-diffusion is lower during the next cycle because the concentration gradient along the capillary is lower, and a higher stripping current is observed. An equilibrium between the amount of metal being deposited and the amount of metal lost can eventually be obtained after several consecutive runs, leading to a constant stripping current.

The appearance of the maximum shown in Fig. 3 can be explained as follows. The dimensions of the capillary of the 303A instrument, as reported by the manufacturer, are length 12.7 cm, internal diameter 0.15 mm, giving a volume of 2.24 mm^3 for the mercury thread. As the volume of a medium size drop (2 mm^2 surface area) is 0.26 mm^3, the capillary can hold the equivalent of almost nine drops of this size. The consequence of back-diffusion of deposited metal into the mercury thread from the mercury drop will be an exponential-type profile for the metal concentration in the thread. During the stripping step a corresponding profile will develop in the opposite direction in the thread, resulting in a maximum in the concentration distribution along the capillary. When a new mercury drop is extruded, this maximum will move along the capillary in the direction of the drop. Its relative position in the thread (and hence the drop number at which it reaches the end of the capillary) will depend on a number of time-dependent factors.

Drop size

The effect of drop size on the magnitude of the stripping current when back-diffusion occurs cannot be easily predicted. The results in Table 3 were obtained with a fresh mercury electrode and with this condition the currents are not maximal. However, the observed trend is that higher currents are obtained with smaller drops. A common mistake, which can even be found in the manufacturer's 303A operating manual, is to think that sensitivity varies directly with drop area. On the contrary, a simple theoretical analysis based on the following equations

$$V = (4/3)\pi R^3;\ S = 4\pi R^2;\ C = \frac{I_l t_d}{nFV};\ I_l = kS$$

leads to the conclusion that the metal concentration C obtained in a spherical mercury drop of radius R, surface area S and volume V, during a deposition time t_d under conditions of constant limiting current I_l will be proportional to $1/R$. However, the impact of loss by back-

Table 3. Effect of drop size on stripping currents: [Ga] = $2 \times 10^{-6} M$; [Zn] = $1.3 \times 10^{-7} M$; t_d = 360 sec; E_d = −1.100 V; slow stirring rate

	Small drop	Medium drop	Large drop
Volume ratio*	1	2	4
Area ratio*	1	1.6	2.5
Area ratio/volume ratio	1	0.80	0.62
i_p(Zn)†, *nA*	435	292 (348)§	145 (270)§
i_p(Ga)†, *nA*	786	553 (629)§	329 (487)§

*From model 303A operating manual.

†Average of three measurements.

§Calculated by multiplication of the current for the small drop by the area ratio/volume ratio for the larger drop.

diffusion on the metal concentration in the mercury drop is higher for a smaller drop because the ratio of capillary cross-sectional area to drop volume is higher.

The results in Table 3 show that higher stripping currents were observed with smaller drops, *i.e.*, the effect of a higher area/volume ratio predominated over the increased loss by back-diffusion.

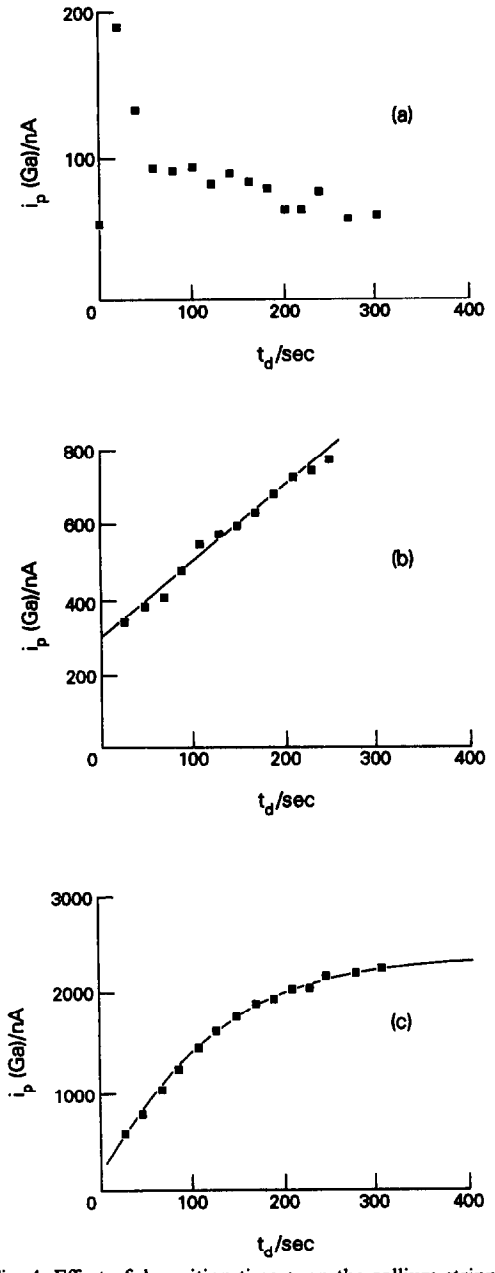

Fig. 4. Effect of deposition time t_d on the gallium stripping current for (a) $10^{-7}M$ (b) $2 \times 10^{-7}M$ and (c) $5 \times 10^{-7}M$ gallium. [Zn] = $1.3 \times 10^{-7}M$; $E_d = -0.900$ V; medium size drop; slow stirring rate.

Deposition time

Experiments were performed in order to determine the effect of deposition time (t_d) on the gallium stripping currents at different concentration levels. Figure 4 shows three different types of behaviour. For the lowest gallium concentration (a), an initial current rise is followed by a gradual decay for longer times. This is due to use of a deposition potential ($E_d = -0.900$ V) only slightly more negative than and too close to the rest potential for that particular concentration. After the first amount of gallium is deposited, a gallium amalgam is formed, resulting in a negative shift of the rest potential so that no further deposition occurs. The gradual decay in stripping current is a consequence of increasing loss by back-diffusion with time.

For the medium gallium concentration (b), the rest potential is more positive, so that deposition is not interrupted and an almost ideal linear dependence is observed. Deposition times longer than those plotted result in a negative deviation. The positive intercept is due to the amount of gallium deposited, even for a programmed deposition time $t_d = 0$, during the time elapsed from the start of the stripping cycle (E_i) to the point of actual stripping.

For the highest gallium concentration (c), the plot increases non-linearly and then tends to level off. This is due to increasing loss by back-diffusion as the metal concentration builds up in the mercury drop. For sufficiently long deposition times, the stripping current becomes independent of deposition time as a steady state between the rate of deposition and rate of back-diffusion is reached.

From these experiments we concluded that a more negative deposition potential ($E_d = -1.100$ V instead of -0.900 V) and a deposition time at the plateau ($t_d = 360$ sec) should be used.

Calibration graphs

The effect of gallium concentration on the stripping current was explored from 10^{-8} to $10^{-5}M$ and is shown in Fig. 5(a) and (b). No change in peak shape with concentration was detected in this range. Figure 5(a) shows a linear calibration plot for the range $3–10 \times 10^{-7}M$ but curving at lower concentrations. No stripping current was observed for concentrations lower than $2 \times 10^{-7}M$. We found later that this was due to the presence of zinc in the electrolyte.

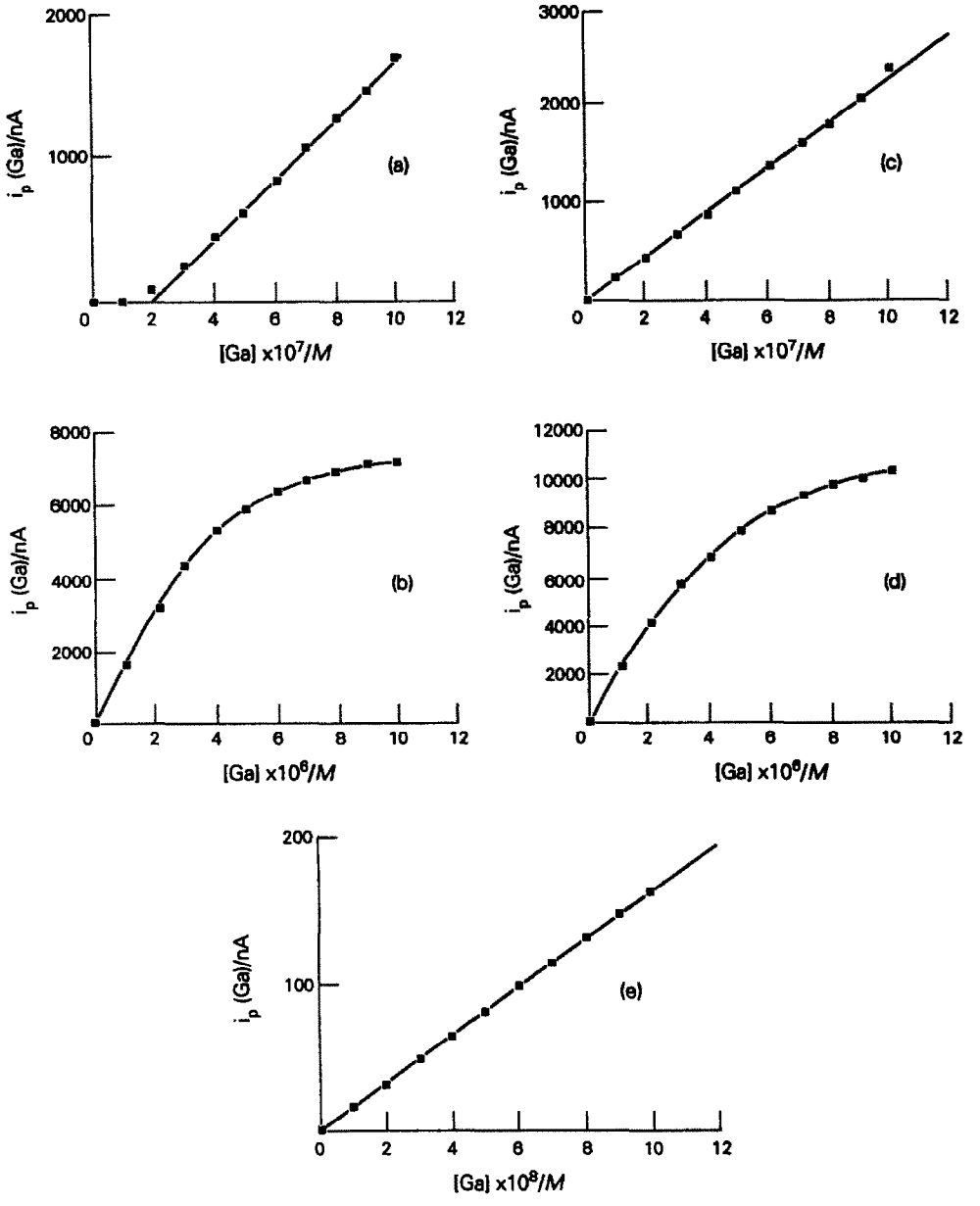

Fig. 5. Effect of gallium concentration on the gallium stripping currents in the absence (a, b) and presence (c, d, e) of $10^{-5}M$ Sb(III). $t_d = 360$ sec; $E_d = -1.100$ V; small drop size; slow stirring rate.

Similar curvature had previously been described but no explanation was given.[10] A higher concentration range of $1–10 \times 10^{-6}M$ is shown in Fig. 5(b), where the calibration plot is linear up to $2 \times 10^{-6}M$, with a negative deviation at higher concentrations. This resembles the curvature in Fig. 4(c) for long deposition times. Again this is due to loss by back-diffusion. The higher the gallium bulk concentration, the higher the concentration gradient that develops within the mercury, with a consequently greater loss of gallium. For sufficiently high bulk concentrations, the stripping current will eventually become independent of gallium concentration as a balance between the rates of deposition and back-diffusion is reached.

A study of different metal interferences[18] showed that some degree of "current enhancement" was obtained in the range $10^{-8}–10^{-7}M$ for gallium stripping currents in the presence of a tenfold molar ratio of Sb(III) to Ga(III). Calibration curves were obtained in the presence of $10^{-5}M$ Sb(III), as in Fig. 5(c)–(e). Stripping currents were detected down to $10^{-8}M$ and, as shown in Fig. 5(c), a straight line which goes through the origin was obtained for the range

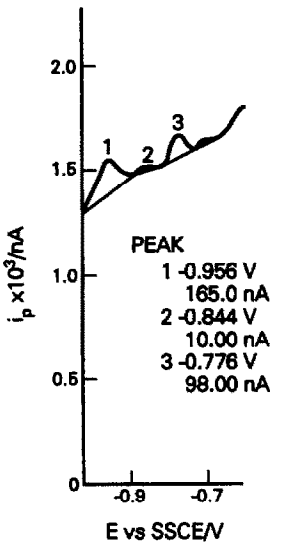

Fig. 6. Stripping peaks for gallium ($E_p = -0.776$ V), zinc ($E_p = -0.956$ V) and Zn–Ga intermetallic compound ($E_p = -0.844$ V) in a $0.5M$ NaSCN + $4.2M$ $NaClO_4$ supporting electrolyte (pH 2.0) containing $3.2 \times 10^{-7}M$ gallium and $1.3 \times 10^{-7}M$ zinc; $t_d = 150$ sec; $E_d = -1.030$ V; small drop size; slow stirring rate.

$1–10 \times 10^{-7}M$, in contrast to Fig. 5(a). Figure 5(d) shows a plot for the range $1–10 \times 10^{-6}M$ very similar to that in Fig. 5(b), although the stripping currents are somewhat higher. A straight line was also obtained for the range $1–10 \times 10^{-8}M$, as shown in Fig. 5(e), provided that the gallium stripping currents were previously normalized with the zinc stripping peak as an internal standard (thus correcting for minor differences in stirring rate) and a blank subtraction was applied.

Zn–Ga versus Zn–Sb intermetallic compounds

The absence of stripping currents for gallium concentrations below $2 \times 10^{-7}M$, the curvature in Fig. 5(a) and the effect of Sb(III) led us to the conclusion that zinc present in the supporting electrolyte was responsible for this behaviour. Even if a deposition potential was chosen so that no zinc was deposited, its interfering action persisted. If the Zn:Ga concentration ratio in solution and the deposition potential E_d were carefully adjusted (Fig. 6), an intermediate peak between the gallium (−0.776 V) and zinc (−0.956 V) stripping peaks was observed. This intermediate peak was not observed if an excess of either zinc or gallium was present.

Experiments were performed with a $0.5M$ NaSCN + $0.85M$ $NaClO_4$ electrolyte. The lower $NaClO_4$ concentration results in a lower zinc concentration and residual current. Figure 7 shows the observed stripping peaks for different deposition potentials, E_d. For $E_d = -1.000$ V, no zinc (−0.990 V) was deposited and only the gallium stripping peak (−0.798 V) was observed (a). For $E_d = -1.030$ V, an intermediate stripping peak was observed at −0.896 V and the gallium peak was somewhat lower (b), but no zinc deposit was observed. When E_d was

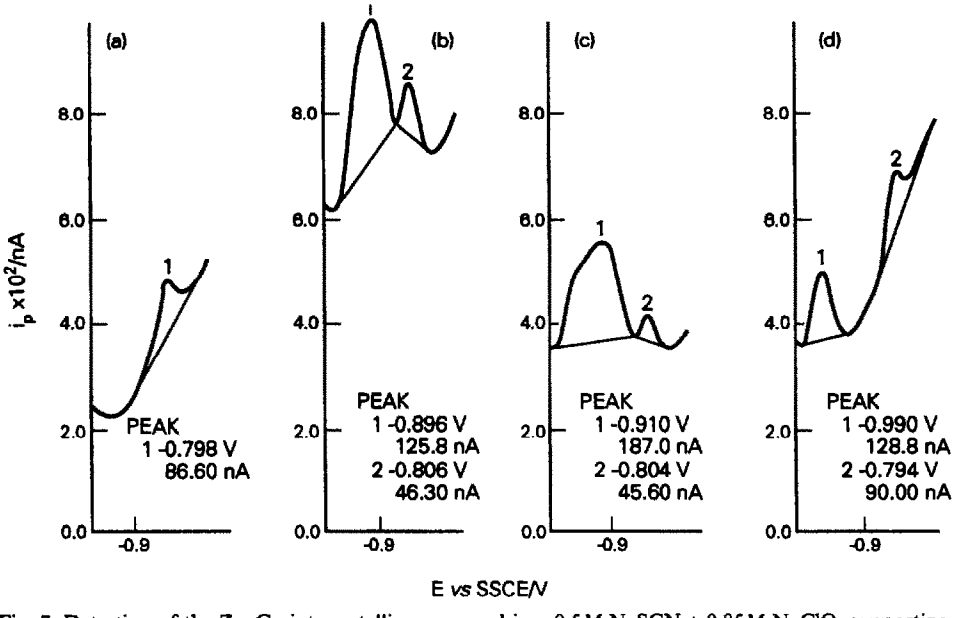

Fig. 7. Detection of the Zn–Ga intermetallic compound in a $0.5M$ NaSCN + $0.85M$ $NaClO_4$ supporting electrolyte (pH 2.0) containing $10^{-7}M$ gallium and $2.5 \times 10^{-8}M$ zinc by adjusting the deposition potential (E_d) to (a) −1.000, (b) −1.030, (c) −1.050 and (d) −1.060 V. $t_d = 360$ sec. Medium drop size; slow stirring rate.

-1.050 V, the intermediate peak was still observed at a slightly more negative potential (-0.910 V), while a shoulder corresponding to the zinc stripping appeared at a more negative potential (c). With $E_d = -1.060$ V, the intermediate peak was no longer observed and the zinc and gallium stripping peaks were completely resolved (d). The observed intermediate peak is attributed to a Zn–Ga intermetallic compound. As the deposition potential was made more negative, the Zn:Ga concentration ratio in the amalgam increased, until the stoichiometric ratio for the intermetallic compound was obtained and a distinct peak was observed, as in Fig. 7(b). For more negative potentials, zinc in excess of the stoichiometric ratio was deposited and the intermetallic compound was no longer detected, as in Fig. 7(d). Attempts to avoid the formation of the Zn–Ga intermetallic compound by using $E_d = -1.000$ V, at which no zinc deposit was detected, rather than $E_d = -1.1$ V [as used for Fig. 5(a)] did not produce a zero intercept. This is an indication that the intermetallic compound was being deposited at a lower potential close to that of gallium.

An estimate of the Zn–Ga intermetallic compound stoichiometry can be inferred from Fig. 5(a), which is equivalent to a titration curve with an equivalence point at $2 \times 10^{-7}M$ Ga(III) for a $1.25 \times 10^{-7}M$ Zn(II) concentration. If the Zn^{2+} concentration in the electrolyte was increased by spiking with a $10^{-4}M$ stock solution, the equivalence point was observed at a higher Ga(III) concentration. If the metal concentrations in the amalgam are assumed to be proportional to their bulk solution concentrations, Zn:Ga = 2:3 is obtained for the intermetallic compound. This kind of titration has been applied for determining the stoichiometry of a Ga–Ni intermetallic compound.[13]

The Zn–Ga intermetallic compound will hinder gallium detection at low concentrations in electrolytes containing Zn(II). However, the addition of Sb(III) to a Zn(II)-containing electrolyte will destroy the Zn–Ga intermetallic compound by formation of the well-known Zn–Sb intermetallic compound, which has a higher formation constant.[7c]

$$Zn_2Ga_3 + 2Sb \rightarrow 2ZnSb + 3Ga$$

This explains why gallium concentrations down to $10^{-8}M$ could be detected, as shown in Fig. 5(e), and linear calibration plots were obtained [Fig. 5(c) and (e)] for 10^{-8}–$10^{-6}M$ Ga in the presence of added Sb(III).

The destruction of the Zn–Ga intermetallic compound by Sb was confirmed by performing a plating–stripping cycle with and without added Sb(III) in a $10^{-7}M$ gallium solution in a Zn(II)-containing electrolyte. Figure 8(a) shows the intermetallic compound stripping peak at -0.884 V, together with the gallium stripping peak at -0.804 V in the absence of Sb(III). The addition of $10^{-5}M$ Sb(III) completely suppressed the Zn–Ca intermetallic compound peak while the gallium peak was enhanced as shown in Fig. 8(b).

Attempts to obtain a completely Zn(II)-free supporting electrolyte by constant-potential electrolysis on a mercury cathode or by using glass-immobilized 8-hydroxyquinoline[14] either failed or proved to be too time-consuming. The effect of adding Sb(III) to Zn(II)-containing supporting electrolytes appears to be a very simple and attractive alternative for overcoming interference by zinc. Zn–Ga intermetallic compound formation and its interfering action are thus suppressed.

CONCLUSIONS

Better reproducibility can be obtained with an aged rather than a fresh 303A mercury drop

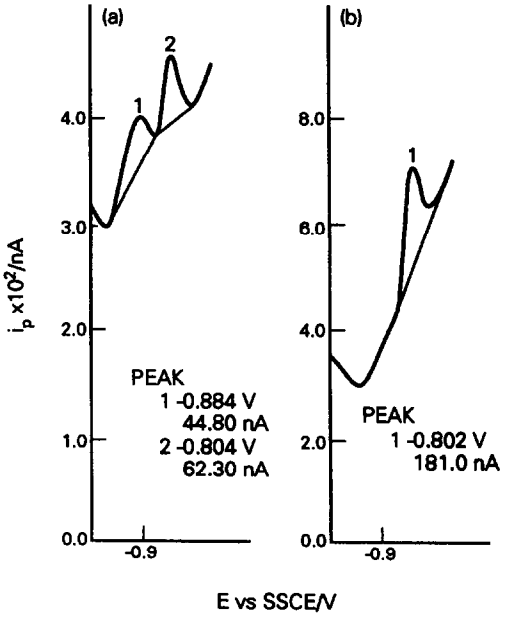

Fig. 8. Detection of the Zn–Ga intermetallic compound in a $0.5M$ NaSCN + $0.85M$ $NaClO_4$ (pH 2.0) supporting electrolyte containing $10^{-7}M$ gallium and $2.5 \times 10^{-8}M$ zinc (a) without Sb(III) and (b) with $10^{-5}M$ Sb(III). $t_d = 360$ sec; $E_d = -1.020$ V; medium drop size; slow stirring rate.

electrode, because of the problem of back-diffusion. The use of a standard addition method is recommended over the use of calibration plots. If a deposition potential, E_d, of -1.100 V is used, the simultaneous deposition of Zn and Ga will allow the use of the zinc stripping peak as an internal standard. This is especially useful in the lower concentration range $1–10 \times 10^{-8}M$, which will give linear calibration plots if an excess (*e.g.*, $10^{-5}M$) of Sb(III) is added. The formation of a Ga:Zn = 3:2 intermetallic compound has been recognized as the cause of the Zn interference, but it can easily be eliminated by addition of Sb(III) to the Zn(II)-containing electrolyte. The choice of a deposition potential of -1.000 V, although it would prevent the deposition of Zn metal, does not prevent deposition of the Ga–Zn intermetallic compound.

A deposition time, t_d, of 360 sec has been found appropriate for the range 1×10^{-8}–$2 \times 10^{-6}M$ and the use of a small mercury drop rather than a medium or large size drop, gives the highest sensitivity and lowest residual currents.

Acknowledgements—This work was supported by the United Nations Development Programme UNDP, Codelco-Chile and Pontificia Universidad Católica de Chile under grant PNUD CHI/87/029 and by Dirección de Investigación PUC under grant DIUC 082/88.

REFERENCES

1. P. H. Davis and E. D. Moorhead, *Anal. Lett.*, 1975, **8**, 387.
2. E. D. Moorhead and W. H. Doub, Jr., *ibid.*, 1977, **10**, 673.
3. A. A. Kaplin and N. T. Rud, *J. Anal. Chem. USSR*, 1980, **35**, 730.
4. N. Scott, D. E. Carter and Q. Fernando, *Anal. Chem.*, 1987, **59**, 888.
5. K. Asada, P. Delahay and A. K. Sundaram, *J. Am. Chem. Soc.*, 1961, **83**, 3396.
6. T. I. Popova, I. A. Bagotskaya and E. D. Moorhead, in *Encyclopedia of the Electrochemistry of the Elements*, Vol. 8, A. J. Bard (ed.), pp. 207–62. Dekker, New York, 1978.
7. F. Vydra, K. Štulík and E. Juláková, *Electrochemical Stripping Analysis*, (*a*) pp. 197–199; (*b*) p. 60; (*c*) p. 62. Horwood, Chichester, 1976.
8. E. D. Moorhead and P. H. Davis, *Anal. Lett.*, 1974, **7**, 781.
9. E. D. Moorhead and G. A. Forsberg, *Anal. Chem.*, 1975, **47**, 2313.
10. E. D. Moorhead and P. H. Davis, *ibid.*, 1975, **47**, 622.
11. E. D. Moorhead and G. A. Forsberg, *ibid.*, 1976, **48**, 751.
12. W. H. Reinmuth, *ibid.*, 1961, **33**, 185.
13. S. V. Psaroudakis and C. E. Efstathiou, *Analyst*, 1987, **112**, 1587.
14. E. D. Moorhead and P. H. Davis, *Anal. Chem.*, 1974, **46**, 1879.
15. J. Wang and T. Peng, *ibid.*, 1987, **59**, 2014.
16. E. Bishop and J. R. B. Sutton, *Anal. Chim. Acta*, 1960, **22**, 590.
17. R. Neeb, G. Willems and I. Kiehnast, *Z. Anal. Chem.*, 1970, **249**, 86.
18. P. Cofré and K. Brinck, unpublished results.

Talanta, Vol. 39, No. 2, pp. 137–144, 1992
Printed in Great Britain.

0039-9140/92 $5.00 + 0.00

A FIELD-INDUCED POISING TECHNIQUE FOR PROMOTING CONVERGENCE OF STANDARD ELECTRODE POTENTIAL VALUES OF THERMALLY OXIDIZED IRIDIUM pH SENSORS

MICHAEL L. HITCHMAN* and SUBRAMANIAM RAMANATHAN†

Department of Pure and Applied Chemistry, University of Strathclyde, 295 Cathedral Street, Glasgow, G1 1XL, U.K.

(*Received* 18 *June* 1991. *Revised* 17 *July* 1991. *Accepted* 17 *July* 1991)

Summary—An electrochemical technique based on reversible charge ejection/injection is shown to be an effective procedure for bringing about the convergence of standard electrode potential values in a batch of thermally prepared iridium oxide pH sensors. Such a convergence simplifies electrode calibration procedures. The rationale for the technique and the results obtained are discussed in terms of adjustment of the proportions of iridium(III) and iridium(IV) oxides at the electrode surface.

In an investigation of thermally oxidized iridium electrodes for pH monitoring we noticed that a batch of electrodes, prepared at the same time and under the same conditions, showed a wide variation in equilibrium potential values (*e.g.*, as much as 120 mV) in aqueous buffer solutions even though their potential–pH responses were all essentially Nernstian (*i.e.*, 59 mV/pH). When the electrodes were subjected to highly corrosive acid electrolytes[1] or high temperature buffer solutions[2] the effect could be even more pronounced. Furthermore, we found that the time for any given electrode to reach a stable equilibrium potential value in an aqueous buffer also showed a large variation, *e.g.*, from a matter of hours to many days. This state of affairs is clearly quite unsatisfactory if solid state sensors such as iridium oxide electrodes are to be used routinely for pH monitoring because of the need for each individual electrode to be calibrated frequently. Of course, a batch of glass electrodes is also known to have a spread of equilibrium potential values, particularly if the batch comprises sensors from different manufacturers. However, for a batch from the same supplier, modern manufacturing techniques ensure close agreement between electrodes (*e.g.*, usually within a few millivolts) and certainly settling down times are rapid (*e.g.*, typically within a few minutes after immersing in a buffer solution).[3] Therefore, if thermally prepared iridium oxide electrodes are to be considered as robust sensors for pH monitoring it is obviously desirable that interelectrode agreement and stabilization times be improved so that calibration procedures are simplified.

In our studies of iridium oxide electrodes prepared by potential cycling[4,5] we have reported that the apparent standard electrode potential of such electrodes is very dependent on whether the electrode surface is left in an "oxidized" or "reduced" state immediately prior to measurements in aqueous buffer solutions; here "oxidized" means the electrode potential was scanned to the anodic voltammetric peak observed in 0.5*M* sulphuric acid while "reduced" indicates that the scan was terminated at a cathodic potential corresponding to the onset of hydrogen evolution. It thus occurred to us that closer agreement between equilibrium potentials for different thermally oxidized electrodes in the same buffer solutions could be achieved by adjusting the state of oxidation of the electrode surfaces and hence the apparent standard electrode potentials. From our experience with the potential cycled electrodes we would also expect this to lead to better control of stabilization times.

In this paper we consider the mechanism of pH response that could be operating for thermally oxidized iridum electrodes and we report on a field-induced poising technique for the enhancement of the behaviour of thermally oxidized electrodes for use as pH sensors.

*Author for correspondence.
†Present address: Singapore Science Centre, Science Centre Road, Singapore 2260.

EXPERIMENTAL

Iridium oxide electrodes were made from iridium wires of length 1 cm, diameter 0.5 mm and purity 99.9% (Goodfellow Metals). An electroactive coating was formed by soaking the wire in $2M$ sodium hydroxide and then heating the wetted wire at 800° in a furnace for 30 min.[6] This process was repeated three times in order to obtain a uniform blue-black coating. The electrode was then cooled in air and immersed in doubly distilled water for two days. This step ensured that the iridate coating formed by the thermal treatment was converted to iridium oxide. A small area of the oxide coating was then scraped off at one end of the wire in order to expose the base metal and on to this a length of platinum wire (Johnson Matthey Chemicals Ltd.) was spot welded to form an ohmic contact. This junction as well as the platinum wire was encapsulated with heat-shrink PTFE tubing (Farnell Electronics) such that only the iridium oxide surface was exposed to the solution. When not in use the electrode was stored in distilled water.

All reagents used were of AnalaR grade and solutions were made up in water which had been twice distilled in glass. Buffers were prepared according to standard recipes.[7] The pH values of the buffers were checked with a glass electrode calibrated in Corning precision buffers with pH values of 4.000 and 7.000.

A Corning 150 pH/ion meter was used for potentiometric measurements. It had an impedance of $10^{12}\ \Omega$ and the current drawn was typically 1 pA. A voltage output from the pH meter was fed to a Keithley Model 175 DVM which was used for logging the potentiometric data. A PAR model 363 potentiostat/galvanostat, controlled by a PAR model 175 universal programmer, was used for electrochemical charge injection and ejection treatment of the electrodes with an appropriate waveform. Cyclic voltamperograms were recorded on a Houston Omnigraphic 2000 X-Y plotter.

An Ingold combination glass electrode containing $3M$ potassium chloride and saturated with silver chloride was used to check the pH of the buffer solutions. An Ingold double junction saturated calomel electrode (SCE) containing saturated potassium chloride as inner electrolyte and potassium nitrate as outer electrolyte was used to provide a stable reference potential during open circuit potential measurements of the iridium oxide electrodes in buffer solutions. During cyclic voltammetric experiments and charge injection and ejection treatments the outer electrolyte was the same as that in the cell.

Two principal procedures were used for investigating the behaviour of the thermal iridium oxide electrodes. The first procedure was that associated with the study of the mechanism of pH response of the electrodes. For this a three electrode configuration was used with a thermal oxide as the working electrode, an iridium counter electrode and the SCE reference described above. Initially the open circuit potential in $0.5M$ sulphuric acid was allowed to stabilize and then a voltage ramp with a sweep rate of 1 mV/sec was used to perturb the oxide/electrolyte interface with either an anodic or cathodic sweep. At the end of the potential sweep the oxide electrode was disconnected from the potentiostatic circuit and its open circuit potential was monitored in the same electrolyte for one hour. For this part of the investigation four electrodes which had previously been used in various electroanalyses,[1,2] and which showed a wide span of equilibrium potentials for identical measuring conditions, were selected.

The second procedure, used for promoting the convergence of apparent E^0 values, was similar to the first procedure in that oxide electrodes in a three electrode configuration were treated with a voltage sweep of 1 mV/sec from the rest potential in $0.5M$ sulphuric acid. Here, though, the end potential was always 600 mV *vs.* SCE; the reason for choosing this potential is discussed below. The same four electrodes as used in the first procedure were again used. For some experiments the effect of a period of potential holding at the end of the sweep was explored. In all cases after the potential treatment the open circuit potential of the electrode was monitored in pH 4 buffer.

All measurements were made at $25 \pm 0.1°$.

RESULTS AND DISCUSSION

Figure 1 shows the variation with time of the apparent standard electrode potentials ($E^{0'}$), as determined from Nernst plots, for four freshly prepared iridium oxide electrodes. The wide range of initial $E^{0'}$ values from $\sim$760 to $\sim$930 mV is apparent as is the very slow drift towards a common value of *ca.* 730 mV. Plot A in Fig. 2 shows the wide spread of equilibrium potential values, from 289 mV to 425 mV, for measurements made in pH 4 buffer with the four

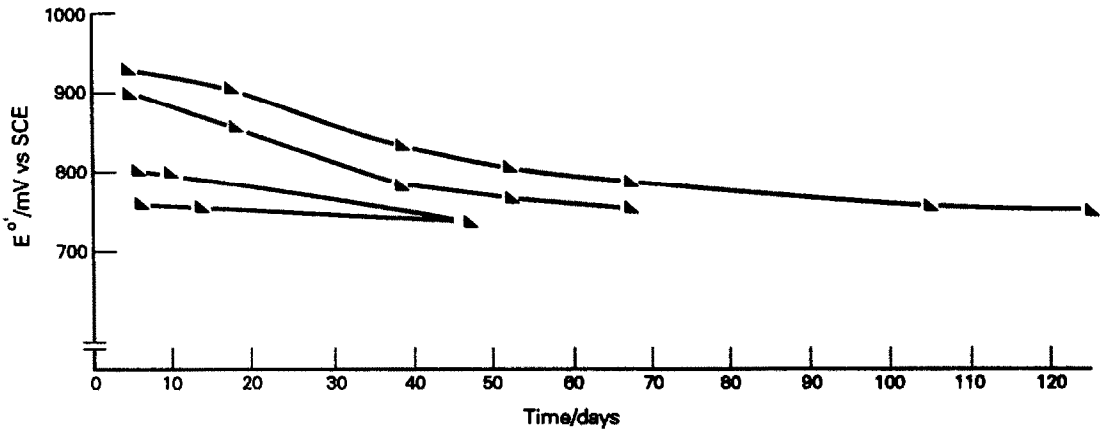

Fig. 1. Variation in apparent standard electrode potentials ($E^{0'}$) with time for thermally oxidized iridium electrodes. Measurements made in buffer solutions pH 2–12.

electrodes which had previously been routinely used in various electroanalyses.[1,2] The corresponding range of $E^{0'}$ values from ~525 to ~661 mV was calculated on the assumption of a 59 mV/pH dependence; such a dependence was always found in this work (*cf.* Table 2) and has been observed by others under a variety of conditions.[8–10] Table 1 gives $E^{0'}$ values which have been calculated from literature data for thermally oxidized iridium electrodes. A wide variation in $E^{0'}$ values is also seen. From these results it is evident that not only is it necessary to individually calibrate electrodes when they are used initially, but also over a long period of time due to the slow drift in $E^{0'}$ values. It is significant in this context to note that the $E^{0'}$ values for the four freshly prepared electrodes all tend to the same value with time, and this leads one to consider what is occurring during this period of drift.

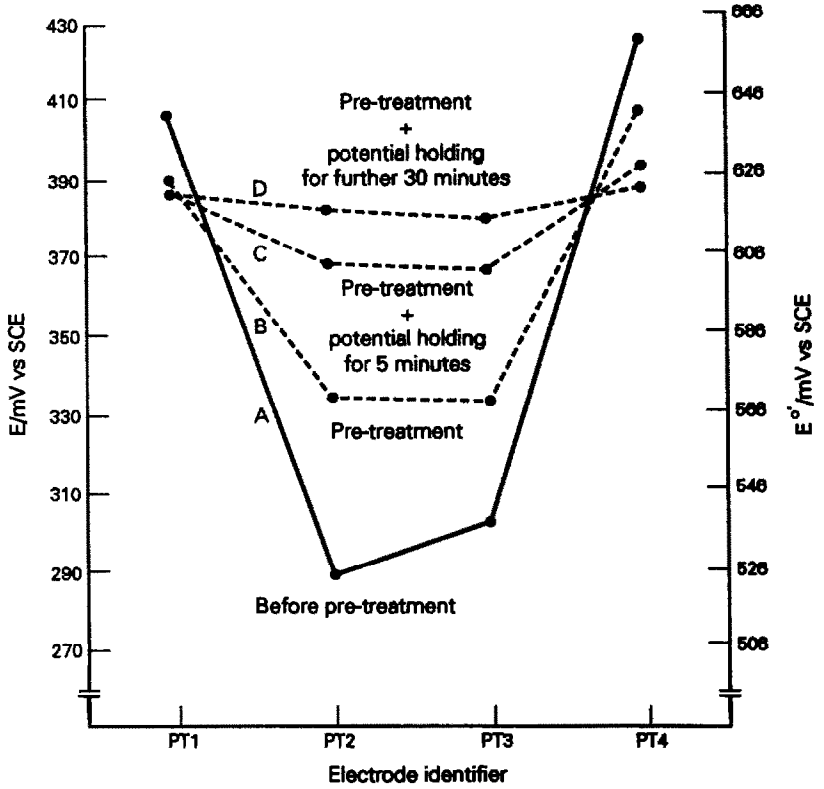

Fig. 2. Equilibrium and apparent standard electrode potential values of electrodes before and after electrochemical pretreatments (cf. Fig. 4).

Table 1. $E^{0'}$ values for thermally oxidized iridium electrodes at 25°

$E^{0'}/mV$ vs. SCE	Remarks	Reference
727.2	Calculated from tabulation of E vs. pH results	6
672.3	Calculated from data at 4°. A temperature coefficient of −1.27 mV per °C was assumed	8
618.7	Calculated from open circuit potential response at pH 6.84 and pH 7.38 at 37°. A temperature coefficient of −1.27 mV per °C was assumed	9
516.7	Interpolated from E vs. pH graph	10

Pourbaix[11] gives three equilibria involving iridium oxide and protons:

$$Ir_2O_3 + 6H^+ + 6e^- \leftrightharpoons 2Ir + 3H_2O \quad (1)$$

$$IrO_2 + 4H^+ + 4e^- \leftrightharpoons Ir + 2H_2O \quad (2)$$

$$2IrO_2 + 2H^+ + 2e^- \leftrightharpoons Ir_2O_3 + H_2O \quad (3)$$

For each of the three reactions it is apparent that there would be a Nernstian response of 59 mV/pH but what is a little surprising is that the theoretical standard electrode potential given by Pourbaix for each equilibrium is also identical with a value of 681 mV *vs.* SCE. Which of the three equilibria is responsible for the pH response of thermally oxidized iridium electrodes is therefore not immediately obvious. Macur[6] has proposed that reactions (1) and (2) are both involved while Papeschi *et al.*[8] have proposed reaction (2) as the potential determining equilibrium. Other workers though, notably Burke *et al.*,[12] Ardizzone *et al.*[13] and Kinoshita and Madou,[14] all using iridium oxide deposited on a titanium substrate, have suggested that reaction (3) is the dominant equilibrium. On purely theoretical grounds the equilibrium with the highest exchange current density would be expected to be the dominant one, but for equilibria with comparable degrees of reversibility mixed control of the rest potential could be expected. However, on more empirical grounds the fact that the thick oxide formed on iridium by thermal oxidation is known to be a highly impervious overlayer[6] would suggest that the involvement of the underlying metal in an equilibrium with protons in solution would be more unlikely. Therefore reactions (1) and (2) are not likely to be significant contributors to the rest potential and we concentrate solely on reaction (3).

Table 2. Nernstian slopes for thermally oxidised electrodes before and after electrochemical pretreatment

Electrode number	Nernstian slope, *mv/pH*	
	Before pretreatment	After pretreatment
PT1	59.0	58.8
PT2	58.0	58.2
PT3	58.4	58.7
PT4	59.2	59.1

The dependence of the equilibrium potential on the activities of the various species in reaction (3) can be represented by

$$E = E^0 + \frac{2.303RT}{2F} \log_{10} \frac{[IrO_2]^2 [H^+]^2}{[Ir_2O_3]} \quad (4)$$

or, in terms of pH, by

$$E = E^0 + \frac{2.303RT}{2F} \log_{10} \frac{[IrO_2]^2}{[Ir_2O_3]} - 0.591 \text{ pH}$$

$$= E^{0'} - 0.0591 \text{ pH} \quad (5)$$

The Nernstian dependence of potential observed under a variety of conditions[2,8–10] is clearly in accord with equation (5). However, what can also be seen is that the apparent standard electrode potential $E^{0'}$ obtained by extrapolation of the Nernst plot to pH = 0 will depend on the relative mole fractions of Ir(IV) and Ir(III) oxides. This is analogous to the mixed oxidation states one gets with anodically oxidized iridium electrodes[5] and with hydrogen tungsten bronzes.[15] It now becomes apparent why a wide range of $E^{0'}$ values is found for thermally oxidized iridium electrodes where there has been no careful control over the degree of oxidation. It is interesting to note in this context that in Fig. 1 all of the initial values of $E^{0'}$ are higher than the final values. Although there was no careful control of the extent of oxidation of the iridium, nevertheless the strong oxidizing conditions would suggest a greater tendency to form the Ir(IV) oxide than the Ir(III) oxide. Therefore any subsequent adjustment in solution of the ratio of the two oxides present in the surface of the oxide film to achieve equilibrium values would be expected, according to equation (5), to lead to a diminution of $E^{0'}$. If this hypothesis is true then any deliberate redistribution of the relative activities of the two oxide species in an oxidized layer would be expected to shift the value of $E^{0'}$ and hence the measured value of an equilibrium potential. Using the first electrochemical procedure described above an electrode with a rest potential of 549.6 mV in 0.5*M* sulphuric acid

was anodically oxidized to 700 mV. The rest potential of 658 mV of the electrode in 0.5*M* sulphuric acid after this treatment was more positive, as would be expected if the proportion of IrO_2 in the oxide layer had been increased. Conversely, an electrode with an initial rest potential of 621.5 mV in 0.5*M* sulphuric acid had a rest potential of 511.8 mV after a cathodic sweep to 470 mV, *i.e.*, a more negative value as would be expected if the amount of Ir_2O_3 had been increased. Thus the ejection of charge from or injection of charge into a thermally oxidized iridium electrode with corresponding anodic or cathodic conversion of the oxide layer, together with the previously noted imperviousness of such a layer, would seem to support the mixed oxidation state hypothesis for a mechanism of pH response, similar to that found previously for hydrous oxide electrodes.[5] Other explanations for the behaviour of oxide electrodes have been suggested by Fog and Buck,[16] but they concluded that the "pronounced potential drifts in the presence of redox reagents seem to show that a variable composition (non-stoichiometry) of the solid phases influences the potential..." and this is consistent with our observations and hypothesis. A more direct technique, such as XPS as used by Hall and Sherwood[17] for the study of anodically formed oxides, could possibly help to clarify the mechanism of the field-induced poising technique.

We can now turn to considering the possibility of improving interelectrode agreement and stabilization times for thermally oxidized iridium electrodes. Before doing that, though, one should note a further point about the charge ejection/injection procedure. The mild potential perturbation condition of 1 mV/sec was deliberately chosen to ensure near equilibrium conditions were maintained at the electrode/electrolyte interface and that hydrous oxide formation did not occur.[18] This precautionary measure seemed to have been successful as any significant amount of hydrous oxide formed with involvement of the water in the potential determining equilibrium would have resulted in a super-Nernstian dependence of equilibrium potential on pH.[5] This was not observed after the anodic or cathodic treatment of the two electrodes. The Nernst plots still showed a slope close to 59 mV/pH (*cf.* Table 2).

If we wish to electrochemically pretreat a thermally oxidized iridium electrode in order to improve its comparability to other electrodes and its temporal stability then it would seem appropriate to aim for conditions which would bring about the achievement of the thermodynamic equilibrium ratio of iridium(IV) oxide to iridium(III) oxide. A potential close to the theoretical value of E^0 of 681 mV *vs.* SCE might be expected to be appropriate. The results in Fig. 3 indicate this is not an unreasonable assumption since electrode Y treated with a sweep end potential of 700 mV shows much less potential drift than electrodes X and Z which were treated with end potentials of 800 mV and 100 mV respectively. Further investigations

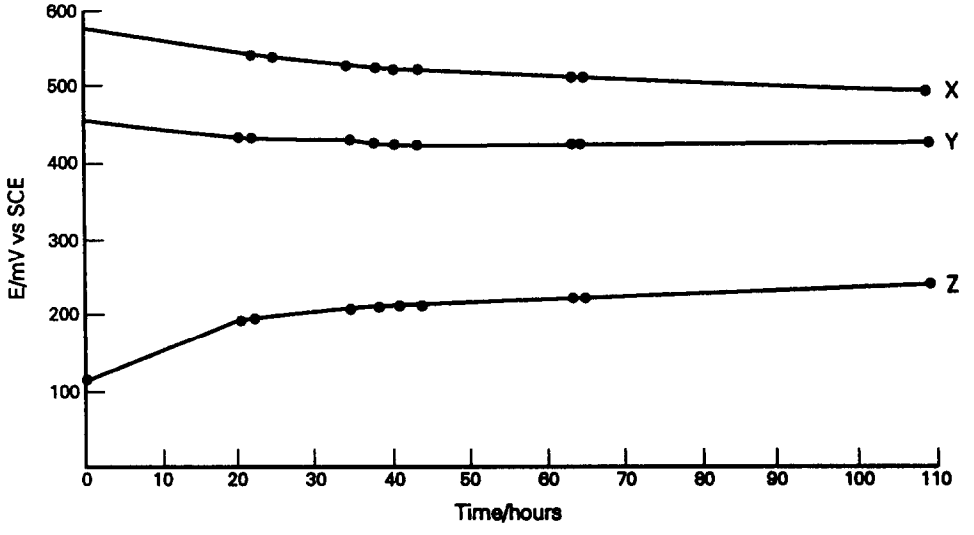

Fig. 3. Open circuit potential decay of electrodes in pH 4 buffer after exploratory pretreatment to different end potentials in 0.5*M* H_2SO_4. X—pretreatment to 800 mV; Y—pretreatment to 700 mV; Z—pretreatment to 100 mV.

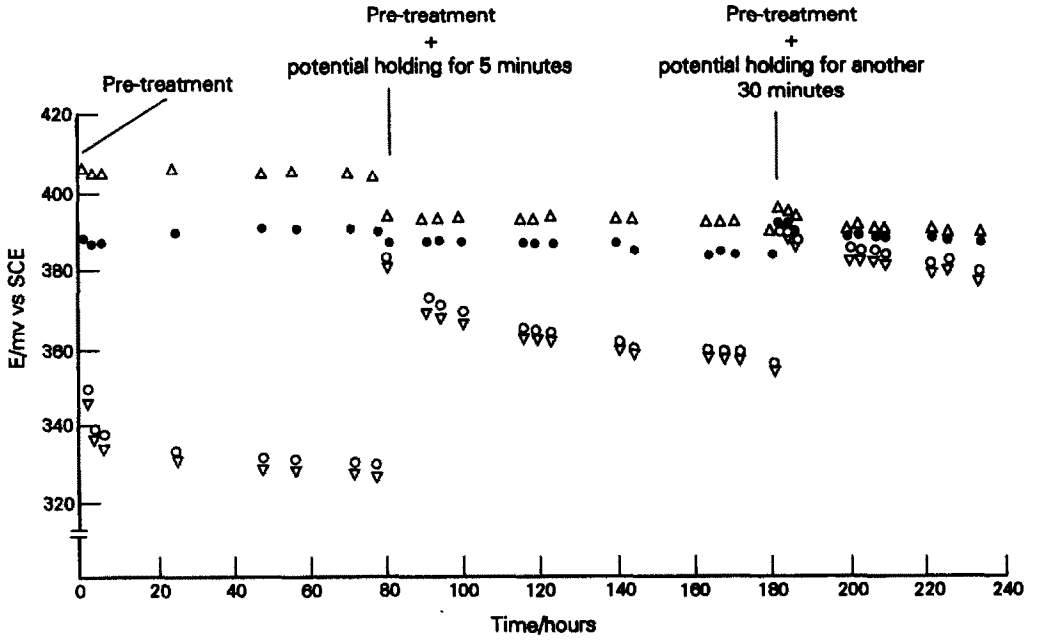

Fig. 4. Open circuit potential decay of electrodes in pH 4 buffer after pretreatment to 600 mV in 0.5*M* H_2SO_4 and different holding times.
● PT1 ○ PT2 ▽ PT3 △ PT4

showed that a sweep end potential of about 600 mV *vs.* SCE for treatment in 0.5*M* sulphuric acid was very effective. Plot B in Fig. 2 shows that electrochemical treatment according to the second procedure described above of four electrodes with initially very disparate values of $E^{0'}$, and hence equilibrium potentials, leads to a greater comparability. A significant reduction in potential drift is also observed (Fig. 4). However, there are still quite significant potential differences between the four electrodes after the slow potential sweep treatment. This probably arises from some degree of kinetic irreversibility associated with the interconversion of the two forms of iridium oxide. Certainly there is some evidence of this when cyclic voltamperograms are run with increasing anodic reversal excursions (Fig. 5). The current does not immediately decay to zero as it would for a truly reversible Faradaic process but instead an anodic current

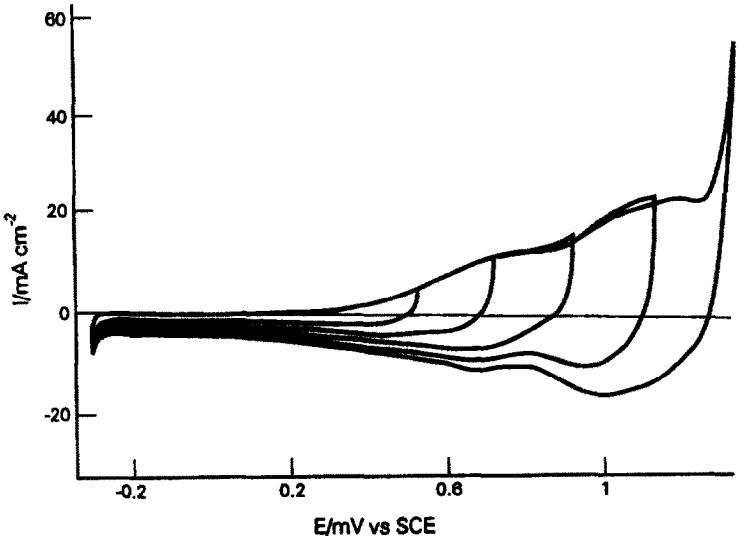

Fig. 5. Cyclic voltammetry of a thermally oxidized iridium electrode in 0.5*M* H_2SO_4. Scan rate 50 mV/sec.

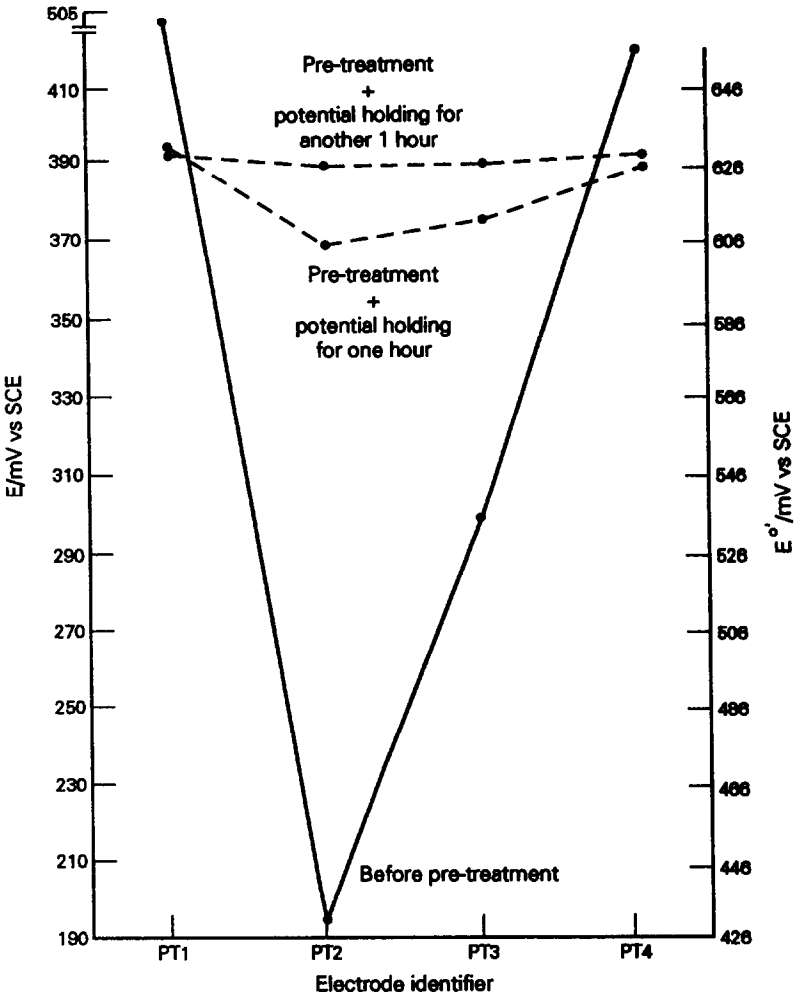

Fig. 6. Equilibrium potential values of electrodes in pH 4 buffer before and after "correcting" pretreatment in 0.5*M* H_2SO_4. Before the "correcting" pretreatment, the electrodes were electrochemically modified with different end potentials: PT1—800 mV; PT2—100 mV; PT3—450 mV; PT4—700 mV. The "correcting" pretreatment was applied with an end potential of 600 mV.

prevails at the initial stages of the cathodic sweep. Therefore it seemed reasonable to assume that a more effective poising of the electrode would be achieved by a potential scan followed by a holding of the end potential. During such potential holdings the current flowing was observed to decay to residual levels and afterwards much closer agreement between both equilibrium potentials and $E^{0'}$ values was found (Plots C and D in Fig. 2). Furthermore, as shown in Fig. 4, the potential drift was reduced to no more than 2–3 mV per day. Figure 6 further illustrates the efficacy of the field induced poising technique for here the four electrodes were first electrochemically treated so that their rest potentials and $E^{0'}$ values were even more divergent than previously. The "correcting" procedure of sweeping to 600 mV and holding was then applied. The very good inter-electrode agreement is apparent. Table 2 shows also that the poising technique, while improving electrode comparability and reducing potential drift, does not disturb the Nernstian $(\partial E/\partial \mathrm{pH})_T$ response of the electrodes.

CONCLUSIONS

We have suggested that the pH response of thermally oxidized iridium electrodes involves an equilibrium between a higher and lower valent oxide. On this basis a simple electrochemical treatment technique has been devised to vary the relative activities of the two oxides and to allow poising of the apparent standard electrode potential at a value close to that of

true equilibrium. Thus the chemical potentials of electrons in the oxide overlayer tend to converge to very similar values in a batch of sensors and comparable pH responses can be achieved. Also because the electrode interface is in a near equilibrium state there is little potential drift over many hours. It may be that an investigation of other treatment potentials and treatment procedures would narrow the spread of equilibrium potential values even further and confer even greater potential stability on the electrodes. It may also be that the poising could be brought about by the choice of a suitable redox couple in solution. Whichever of the three equilibria, reactions (1), (2) or (3), applies, it has to be remembered that they are only half reactions and implicit in any adjustment of equilibrium position is the presence of a redox couple to constitute the other half reaction. The slow potential drifts observed for newly prepared oxide electrodes suggest a rather irreversible redox system with a very low exchange current for electron transfer with the oxide electrodes; a likely candidate would be the water/oxygen couple. A redox system with a higher exchange current might therefore also be suitable to use for poising the electrode potential. However, a redox couple method of poising would probably not be as convenient or as flexible as the field induced poising method which we have described and which does certainly provide the basis for initial quality control of a batch of sensors and also for reducing the need for frequent calibration. It is a technique which could also probably be used for other electrodes with equilibria involving two oxidation states of a solid component.

Acknowledgements—The support of an ORS award for SR is gratefully acknowledged. We are pleased to acknowledge financial support for this work from Ingold Messtechnik AG, and many useful discussions with Drs. R. Bucher and H. Buehler of that company. We also thank the referee of this paper for constructive and helpful comments about the effect of redox couples on oxide electrodes.

REFERENCES

1. M. L. Hitchman and S. Ramanathan, *Analyst*, in press.
2. *Idem*, in preparation.
3. R. G. Bates, *Determination of pH: Theory and Practice*, p. 334. Wiley, New York, 1973.
4. M. L. Hitchman and S. Ramanathan, *Analyst*, 1988, **113**, 35.
5. *Idem*, *Electroanalysis*, in the press.
6. R. A Macur, *US Patent 1348912*, 1974.
7. R. C. Weast (ed.), *CRC Handbook of Chemistry and Physics*, p.D149. Chemical Rubber Publishing Co., Florida, 1985.
8. G. Papeschi, S. Bordi, C. Beni and L. Ventura, *Biochim. Biophys. Acta*, 1976, **453**, 192.
9. G. Papeschi, S. Bordi, M. Carla, L. Criscione and F. Ledda, *J. Med. Eng. Tech.*, 1981, **5**, 86.
10. E. Gianazza, P. G. Righetti, S. Bordi and G. Papeschi in B. J. Randola and D. Graesslin, *Electrofocussing Istachophoresis, Proc. Int. Symp.*, p. 173. Gruyter, Berlin, 1977.
11. M. Pourbaix, *Atlas of Electrochemical Equilibria in Aqueous Solutions*, p. 374. Pergamon Press, Oxford, 1966.
12. L. D. Burke, J. K. Mulcahy and D. P. Whelan, *J. Electroanal. Chem.*, 1984, **163**, 117.
13. S. Ardizzone, A. Carugati and S. Trasatti *ibid.*, 1981, **126**, 287.
14. K. Kinoshita and M. J. Madou, *J. Electrochem. Soc.*, 1984, **131**, 1089.
15. M. L. Hitchman, *J. Electroanal. Chem.* 1977, **85**, 135.
16. A. Fog and R. P. Buck, *Sensors and Actuators*, 1984, **5**, 137.
17. H. Y. Hall and P. M. A. Sherwood, *J. Chem. Soc. Faraday Trans I*, 1984, **80**, 135.
18. B. E. Conway and J. Mozota, *Electrochim. Acta*, 1983, **28**, 9.

Talanta, Vol. 39, No. 2, pp. 145–147, 1992
Printed in Great Britain.

0039-9140/92 $5.00 + 0.00

DETERMINATION OF DISSOLVED OXYGEN BY CATALYTIC REDUCTION ON NAFION–METHYL VIOLOGEN CHEMICALLY MODIFIED ELECTRODE

JIN LITONG, JIN PING, YE JIANNONG and FANG YUZHI
Department of Chemistry, East China Normal University, 3663 Zhong Shan Road (N), Shanghai, 200062, People's Republic of China

(*Received* 12 *February* 1991. *Revised* 3 *July* 1991. *Accepted* 3 *July* 1991)

Summary—A small size Nafion–methyl viologen chemically modified electrode (Nafion–MV CME) together with a small size electrolytic cell were constructed for the purpose of dissolved oxygen (DO) determination. The catalytic reduction of DO on Nafion–MV CME results in fast and sensitive DO determination. The mechanism of such detection is also considered.

Determination of DO can be accomplished by several methods such as chemical,[1] electrochemical[2] and EPR[3] approaches. However, some of these methods are time-consuming or suffer from high limits of detection. To our knowledge, determination of DO by using CMEs is relatively rare.[4,5] Not long ago, Xu and Dong[6] reported an approach for DO determination by cyclic voltammetry with iron tetraphenyl porphyrin and cobalt tetraphenyl porphyrin CMEs. Unfortunately, the construction of such CMEs is rather complicated and time-consuming. In the present work, DO is determined by using a Nafion–MV CME, which can be constructed conveniently and reproducibly. Because of the catalytic effect of a Nafion–MV CME toward DO, this method is also very sensitive. The results of DO quantitation in water samples by this method are in good agreement with those of Winkler's method. This method, therefore, provides a good alternative for the determination of DO.

EXPERIMENTAL

Reagents

Nafion 117 methanol solution (5%) was from Aldrich and was diluted to 0.1% with ethanol. Methyl viologen dichloride (Aldrich) was used as received. All other chemicals used were analytical grade or better.

Apparatus

All voltammetry experiments were performed with a model XJP-821 polarographic analyser (Jiangsu Electroanalytical Instrument Factory). All experiments employed a homemade plexiglass electrolytic cell with a Teflon electrode supporter (Fig. 1). The three-electrode system consists of a Nafion–MV CME working electrode, a saturated Ag/AgCl reference electrode and a platinum wire auxiliary electrode.

Nafion-MV CME construction

The glassy-carbon electrode (1 mm diameter) was polished with alumina paste and rinsed with water, then further cleaned ultrasonically in 1:1 nitric acid, acetone and doubly distilled water, successively. Next, the clean glassy-carbon electrode was dried under an IR lamp. Nafion was coated on the electrode by pipetting 5 μl of ethanol diluted Nafion (0.1%) onto the electrode surface, which was then dried under an IR lamp. Finally, the electrode was immersed in 0.1*M* methyl viologen aqueous solution for 20 min and then rinsed with doubly distilled water.

General procedure

Adjust 0.1*M* sodium chloride solution to pH 3 with hydrochloric acid, scan the applied potential from 0 to −0.8 V (*vs.* Ag/AgCl) at a rate of 80 mV/sec, and record the resulting voltamperogram. The electrocatalytic reduction peak of oxygen is found at −0.5 V (*vs.* Ag/AgCl), and the oxygen quantitation is achieved by measuring the current of this reduction peak.

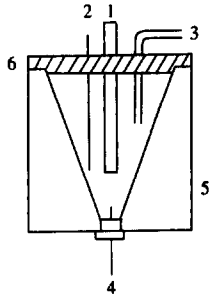

Fig. 1. Schematic drawing of the electrolytic cell: 1, Nafion–MV CME; 2, reference electrode; 3, degassing tube; 4, auxiliary electrode; 5, plexiglass; 6, Teflon. Cell size: 2.8 cm × 3.5 cm.

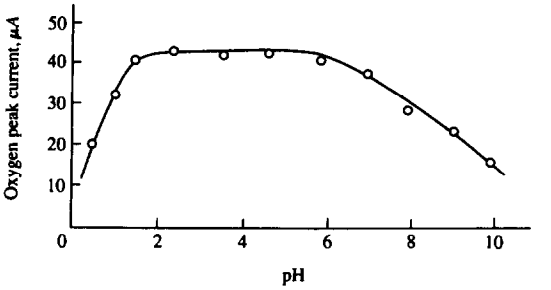

Fig. 3. Peak currents of oxygen reduction obtained at Nafion–MV CME in solutions with different acidity. Scan rate: 80 mV/sec.

RESULTS AND DISCUSSION

Catalytic reduction of oxygen at Nafion–MV CME

Figure 2 shows the voltamperogram of oxygen reduction at both the Nafion–MV CME (curve *a*) and a bare glassy-carbon electrode (curve *b*) in the same solution. The oxygen reduction peak is higher in curve *a* than that in curve *b*. Also, the peak potential of oxygen reduction is shifted anodically about 150 mV if the Nafion–MV CME is employed. These phenomena could be explained by the catalytic effect of the Nafion–MV CME towards oxygen reduction as described below:

$$[(SO_3^-)_2MV^{2+}] + e = [(SO_3^-)_2MV^+] \text{ (electrode reaction)}$$

$$[(SO_3^-)_2MV^+] + H^+ + 1/2O_2 = [(SO_3^-)_2MV^{2+}] + 1/2H_2O_2 \text{ (chemical reaction)}$$

Effect of scan rate

When keeping other conditions the same as described in the general procedure, the peak current of oxygen reduction increases with an increase in the scan rate. However, the background noise also increases accordingly. It was found that the optimum scan rate is 80 mV/sec in terms of maximum signal-to-noise ratio.

Effect of solution acidity

Supporting electrolytes with pH values ranging from 0.5 to 10.0 were prepared by adding different amounts of sodium hydroxide solution to 0.5*M* hydrochloric acid/sodium chloride solution. As can be seen from Fig. 3, the oxygen peak current reaches its maximum value at pH 1.5, then levels off until pH 6.0, and finally decreases when the pH value is higher than 6.0. Because of this feature, we used pH 3.0 supporting electrolyte in our subsequent experiments for DO determination.

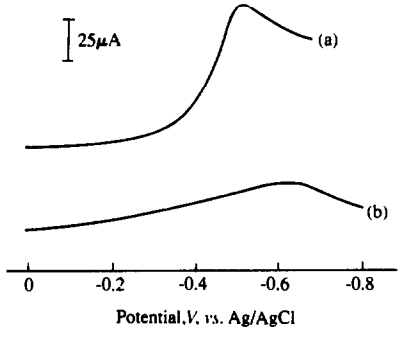

Fig. 2. Voltamperogram of oxygen reduction at both Nafion–MV CME (curve *a*) and bare glassy-carbon electrodes (curve *b*) in pH 3 0.1*M* NaCl/HCl solution (DO concentration: 7.5 ppm). Scan rate: 80 mV/sec.

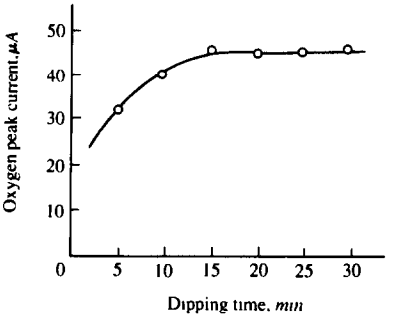

Fig. 4. Peak currents of oxygen reduction obtained in pH 3 0.1*M* NaCl/HCl solution at Nafion–MV CMEs constructed by dipping in 0.1*M* methyl viologen aqueous solution for different time period. Scan rate: 80 mV/sec.

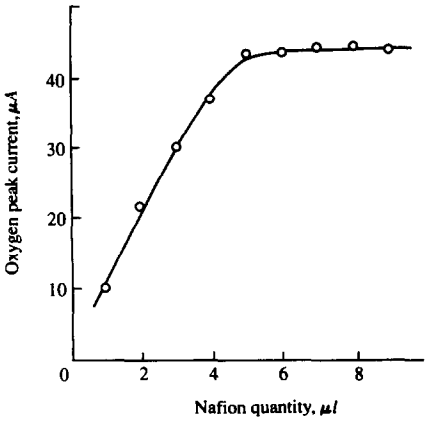

Fig. 5. Peak currents of oxygen reduction obtained in pH 3 0.1*M* NaCl/HCl solution at Nafion–MV CMEs constructed by applying different amounts of 0.1% Nafion ethanol solution. Scan rate: 80 mV/sec.

Effect of dipping time in MV solution

Sulphonic groups in the Nafion film possess strong electrostatic attraction towards MV^{2+}. It was found that the amount of MV^{2+} binding to sulphonic groups is a function of dipping time of Nafion coated electrode in MV solution. As shown in Fig. 4, the oxygen peak current reaches a plateau region when the dipping time is longer than 15 min. It is assumed that the binding sites of the Nafion film become saturated by MV^{2+} within 15 min. We use 20 min as the dipping time for Nafion–MV CME construction.

Effect of Nafion quantity

Nine different Nafion–MV CMEs were prepared by applying different amounts (1–9 μl) of 0.1% Nafion solution onto the glassy-carbon surfaces, followed by dipping into 0.1*M* MV solution for 20 min, and the resultant electrodes were then used for DO determination. As shown in Fig. 5, the oxygen response curve levels off when more than 5 μl of Nafion solution was employed. For this reason, we select 5 μl of Nafion solution in Nafion–MV CME construction.

Reproducibility and calibration curve

After choosing the optimum experimental conditions, the reproducibility of DO determination by catalytic reduction was examined. For ten parallel DO measurements, the relative standard deviation is 1.7%. The linear range of DO calibration is from 1.0 to 8.4 ppm (typical DO content in an oxygen saturated water at room temperature) with a correlation coefficient of 0.995.

Table 1. DO measurement in water samples

Sample	Nafion–MV CME method, *ppm*	Winkler's method, *ppm*	Relative error,* %
Doubly demineralized water	7.65	7.51	1.9
Demineralized water	7.15	7.11	0.6
Tap water	2.35	2.49	−5.6
Campus river water	2.20	2.38	−7.6

*Take the DO values by Winkler's method as standards.

Sample analysis

Four water samples were analysed for DO content by the Nafion–MV CME method[7,8] and also by Winkler's method.[9] The results listed in Table 1 demonstrate that the DO contents obtained by both methods are quite comparable.

CONCLUSION

The success of DO determination by the Nafion–MV CME is a good example of the analytical use of chemically modified electrodes. It appears that this method is a good alternative for DO quantitation because of its sensitivity, reproducibility, simplicity and reliability.

REFERENCES

1. S. A. Robin and S. H. Mohamed, *Talanta*, 1978, **25**, 519.
2. B. S. Smolyakovet and L. P. Pogodina, *Khim. Nank.*, 1977, **5**, 20; *Anal. Abstr.*, 1979 **36**, 1H26.
3. D. F. Bocian and F. W. Findsen, *Inorg. Chem.*, 1984, **23**, 800.
4. N. Oyama, N. Oki, H. Ohuo, Y. Ohnaki, H. Matsuda and E. Tsuchida, *J. Phys. Chem.*, 1983, **87**, 3642.
5. S. Dong and T. Kuwana, *Electrochim. Acta*, 1988, **33**, 667.
6. L. Xu and S. Dong, *Fenxi Huaxue*, 1988, **16**, 511.
7. J. F. Stargardt, *Anal. Chem.*, 1978, **50**, 930.
8. R. W. Murray, *ibid.*, 1987, **59**, 379A.
9. Y. Fang, L. Jin and B. Xu *Environmental Analysis and Monitoring*, East China Normal University Publishing House, 1987.

Talanta, Vol. 39, No. 2, pp. 149–154, 1992
Printed in Great Britain.

0039-9140/92 $5.00 + 0.00

POLYCHLOROBIPHENYLS DIFFERENTIATION AND IDENTIFICATION BY GAS CHROMATOGRAPHY/FOURIER TRANSFORM INFRARED SPECTROSCOPY

P. DOUMENQ, M. GUILIANO and G. MILLE

Faculté des Sciences et Techniques de St Jérôme, Centre de Spectroscopie Moléculaire, URA 1409 CNRS, Avenue Escadrille Normandie-Niemen, 13397 Marseille Cedex 13, France

(*Received* 25 *October* 1990. *Revised* 13 *March* 1991. *Accepted* 21 *March* 1991)

Summary—Reference infrared vapour phase spectra of 20 polychlorobiphenyls (PCBs) have been obtained by gas chromatography/Fourier transform infrared spectroscopy (GC/FTIR). These spectra are consistent with those of PCB obtained by diffuse reflectance IR spectroscopy (DRIFT) and with those of more simple molecular structures (iodochlorobenzenes, 1-bromodichlorobenzenes). The IR frequencies of the GC/FTIR spectra of PCB are assigned in terms of substitution patterns. This work shows that GC/FTIR can be a good approach for differentiation and identification of PCB in complex mixtures.

Since the work of Jensen[1] which showed the effects of polychlorobiphenyls (PCBs) in biological chain contamination, the PCB isomers have become a high-priority concern in industry, because of their potential toxicity and their persistence (non-volatility).[2–4]

The exceptional dielectric and physico-chemical properties of this class of compounds (thermal stability, resistance to acids, bases and corrosive agents, high boiling point, *etc.*) have led PCBs to be used in many industrial applications as heat-conductors, transformers, capacitors, *etc.*[2] Since being made commercial, about two million tons of PCB materials have been produced.

Polychlorobiphenyls are synthesized in industry by reaction of chlorine with biphenyl. The substitutions are non-selective and consequently a very complex mixture is obtained. Theoretically there are 210 isomers, but only 103 are sterically probable. The analytical techniques most widely used to study such complex mixtures are gas chromatography (GC) and gas chromatography coupled with mass spectroscopy (GC/MS).[5]

In the environment PCBs can be partially or totally degraded by microorganisms.[6] This degradation is dependent (even when it occurs in the laboratory under optimal temperature and aerobic conditions) on the number and the position of chlorine atoms on the aromatic rings. Enzymatic degradation methods (specific dioxygenases) occur in a preferential fashion. The initial attacks occur principally at non-chlorinated adjacent or adjoining carbons: -2,3 (-5,6) or -3,4 (-4,5). Before being able to understand the complexity of PCB mixtures, the specificity of the attacks and the degradation products variety, a PCB biodegradation study requires a good structural knowledge of the different isomers.

We had shown that mass spectroscopy, could not always differentiate some PCB isomers.[7] The mass spectra of certain isomers are so similar that they cannot be distinguished even when the reference spectra are in the data base.

This fact leads us to enter upon a study of PCB mixtures by GC coupled with Fourier transform infrared spectroscopy (GC/FTIR). This analytical technique combines the separation capabilities of GC with the possibilities of IR spectroscopy to differentiate aromatic isomers.[8–22] The advantage of IR is that it can readily differentiate isomeric compounds because of finite differences in their vibrational spectra, particularly in the "*fingerprint*" range. The ability of the IR data to distinguish isomers varying in the position of subtituents leads to unambiguous identification.

Even in the case of badly resolved peaks of the IR reconstructed chromatogram[23] it has been shown that data manipulation by special computer software allows the IR spectrum of each compound to be obtained.[22]

EXPERIMENTAL

GC/FTIR spectra were recorded with a 20 SXB Nicolet spectrometer interfaced with a

6180 Vega Carlo-Erba chromatograph (on-column injector, FID detector). Chromatographic separations were achieved with a fused-silica capillary column (0.4μM, SE 52 film, 30 m × 0.32 mm) at a helium flow-rate of 1 ml/min. A helium make-up of 2 ml/min was used. The oven was ramped at 5°/min from 70 to 270°. The end of the capillary column was passed through a transfer line maintained at 275°.

Vapour-phase infrared spectra were performed at 8 cm^{-1} resolution with a MCT detector (4000–650 cm^{-1}) by co-adding 16 interferograms. The chromatograms were reconstructed with the Gram-Schmidt algorithm.[23]

Gas chromatography/Fourier transform infrared spectra were obtained by injecting pure compounds (Interchim, Supelco, Altech) (between 100 and 500 ng per compound) and a standard mixture (DCMA PCB mixture, Supelco).

RESULTS AND DISCUSSION

Library

Before starting to analyse PCB mixtures by GC/FITR, it was necessary to create a specific library. This library (Table 1), although very incomplete (20 PCB), contains representative derivatives with one to seven chlorine atoms.

The limitation for the extension of this library is purely financial. Gas chromatography/Fourier transform infrared spectra of PCBs are given in Figs. 1 and 2. The signal to noise ratios of these spectra are good enough to allow their utilization for identification problems. The IR Gram-Schmidt (IR reconstructed chromatogram) of the DCMA PCB mixture is given in Fig. 3.

Table 1. Polychlorobiphenyls analysed by GC/FTIR

	Compounds
	Biphenyl
1	2-Chlorobiphenyl
2	3-Chlorobiphenyl
3	4-Chlorobiphenyl
4	2,2′-Dichlorobiphenyl
5	3,3′-Dichlorobiphenyl
6	4,4′-Dichlorobiphenyl
7	2,4-Dichlorobiphenyl
8	2,5-Dichlorobiphenyl
9	2,4,4′-Trichlorobiphenyl
10	2,4,5-Trichlorobiphenyl
11	2,2′,3,3′-Tetrachlorobiphenyl
12	2,2′,4,4′-Tetrachlorobiphenyl
13	2,2′,5,5′-Tetrachlorobiphenyl
14	3,3′,4,4′-Tetrachlorobiphenyl
15	2,2′,4,5,5′-Pentachlorobiphenyl
16	2,2′,4,4′,6-Pentachlorobiphenyl
17	2,3′,4,5′,6-Pentachlorobiphenyl
18	2,2′,4,4′,5,5′-Hexachlorobiphenyl
19	2,2′,3,3′,6,6′-Hexachlorobiphenyl
20	2,2′,3,4,5,5′,6-Heptachlorobiphenyl

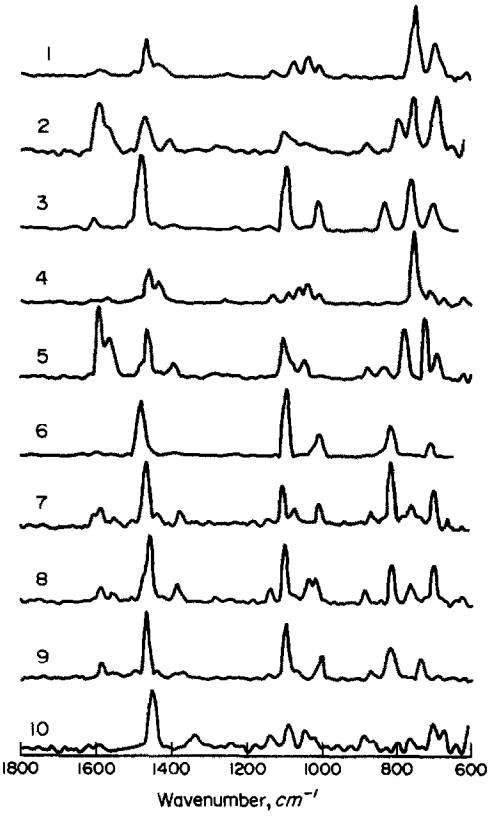

Fig. 1. GC/FTIR spectra between 1800 and 600 cm^{-1} of mono, di and trichloro PCB (spectra 1–10 correspond to PCB with the same number in Table 1).

Previous works

There are many IR studies of chlorobenzenes but only a few concerning polychlorobiphenyls.[24–26]

Nyquist *et al.*[24] studied many pentachlorobiphenyl isomers by FTIR with a diffuse reflectance accessory (DRIFT). Spectra were performed on solid samples obtained after evaporation of the solvent on potassium bromide powder.[24]

Barret and Steele[25] and Eaton and Steele[26] have analysed IR spectra of biphenyl and 4,4′-dichlorobiphenyl under different physical states (solid, liquid and vapour). They concluded that the molecules were not planar and they determined that the dihedral angle between the two aromatic rings was about 30–45°.[25,26]

Only two studies of PCBs by GC/FTIR have been done.[27,28] In these works, spectra were achieved with a matrix isolation technique.

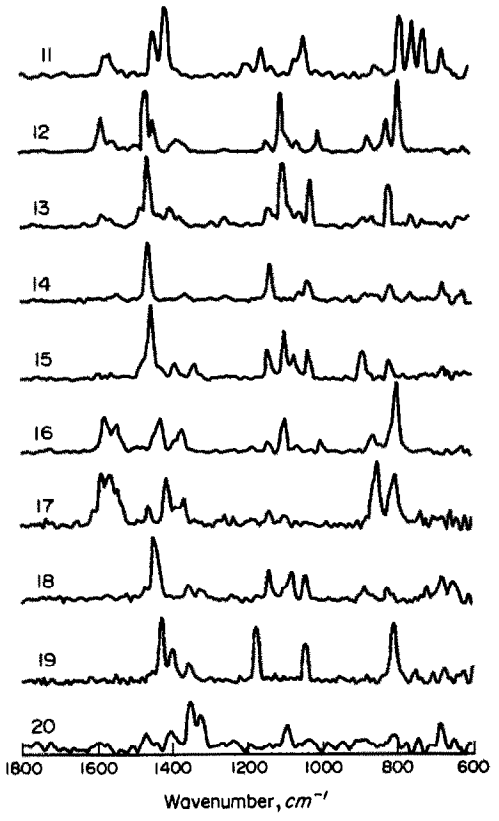

Fig. 2. GC/FTIR spectra between 1800 and 600 cm^{-1} of tetra, penta, hexa and heptachloro PCB (spectra 11–20 correspond to PCB with the same number in Table 1).

Results

The interpretation of PCB IR spectra is very difficult because group frequencies and intensities are influenced by several factors as follows:

(i) high number of IR bands (60 vibrations are theoretically expected in a PCB spectrum).

(ii) mass and substitution effects of the chlorine atoms.

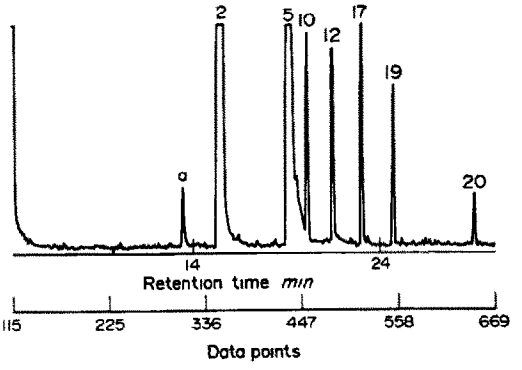

Fig. 3. Gram-Schmidt of the DCMA PCB mixture (Supelco). Peaks 2, 5, 10, 12, 17, 19, 20: see Table 1 for the compound names. a: biphenyl.

(iii) molecular symmetry effects on the vibration activities.

(iv) vibrational coupling effects (the υCCl stretching mode may be coupled with one aromatic ring vibration to generate 2 vibrations, one of which appears between 900 and 700 cm^{-1} (out-of-plane CH aromatic bending vibrations range).

We have attempted two different approaches in interpreting PCB IR spectra: comparison of a GC/FTIR PCB isomer spectrum with (i) the IR spectrum of the same compound obtained by the classical technique and (ii) the IR spectra of simple homologous chlorobenzenes.

Table 2 compares the IR frequencies of the 2,3′,4,5′,6-pentachlorobiphenyl spectrum obtained by Nyquist *et al.*,[24] who used the DRIFT technique, with the corresponding one achieved by GC/FTIR. This GC/FTIR spectrum has been obtained by injecting a standard mixture of 10 PCBs and corresponds to an injected quantity of 600 ng of 2,3′,4,5′,6-pentachlorobiphenyl. Table 2 shows that the two results are very similar, in spite of the GC/FTIR analytical conditions (8 cm^{-1} resolution, low injected quantity, number of scans limited to 16 which lead to a signal to noise ratio decrease). Moreover, the change in physical state of the sample in DRIFT and GC/FTIR techniques

Table 2. GC/FTIR and DRIFT bands between 1800 and 650 cm^{-1} for 2,3′,4,5′,6-pentachlorobiphenyl (S = strong, m = medium, w = weak and sh = shoulder)

GC/FTIR	DRIFT[24]
1588 S	1590 S
	1575 sh
1562 S	1560 S
1542 m	1542 S
1458 w	1459 m
1412 S	1411 S
1388 sh	1386 m
1365 m	1368 S
1259 w	1269 w
1233 w	1233 w
1185 w	1183 w
1142 w	1142 w
	1131 w
1098 w	1099 m
	1040 w
	855 sh
849 S	849 S
	815 sh
804 sh	805 sh
803 S	797 S
733 w	729 m
	689 m

(solid state *vs.* vapor state) leads only to very small shifts in IR wavenumbers.

Consequently, previous data concerning PCB IR spectra, and more particularly the work of Nyquist *et al.*,[24] may be directly used to identify a PCB isomer via its GC/FTIR spectrum.

In Table 3, symmetrical dichlorobiphenyl GC/FTIR spectra are compared with IR spectra of *ortho*, *meta* and *para* homologous iodochlorobenzenes.[29–35] The comparison between GC/FTIR spectra of 2,2',3,3'-; 2,2',4,4'-; 2,2',5,5'- and 3,3',4,4'- biphenyls and IR spectra of homologous 1-bromodichlorobenzenes are given in Table 4.[36] In these two tables the absorptions assigned to C—I or C—Br bonds and the weak intensity absorptions of chlorobenzenes are omitted. Tables 3 and 4 show that the spectrum of a PCB isomer can be directly deduced from that of a homologous chlorobenzene derivative.

The case of assymetrical PCBs requires the comparison of two different chlorobenzene derivatives as shown by Nyquist *et al.* for pentachlorobiphenyl isomers.[24]

Assignment of the principal bands

The bands due to stretching vibrations of the CH aromatic bonds appear in the 3100–3000 cm^{-1} spectral range. These absorptions, often weak, are not very useful for structural identification and will not be examined in this work.

In the 1650–1400 cm^{-1} range, the C=C aromatic stretching vibrations which are sensitive to the substitution appear. Four bands are expected in this range.[29–36] A doublet is located between about 1620–1585 cm^{-1} and 1590–1540 cm^{-1}. These bands are generally weak in PCB spectra; the second component is not always observed. On the other hand, two strong bands are observed at 1590 and 1560 cm^{-1} and at 1589 and 1562 cm^{-1} respectively for 3-chlorobiphenyl and 3,3'-dichlorobiphenyl. These two strong bands are then characteristic of a 3-chloro structure. We also find two strong absorptions between 1585 and 1540 cm^{-1} in GC/FTIR spectra of 2,3', 4,5', 6- and 2,2', 4,4', 6-pentachlorobiphenyls as in DRIFT spectra of 2,2',4,6,6',- and 2,3',4,4',6-pentachlorobiphenyls.[24] These two bands can be used to characterize the 2,4,6-trichloro structure.

The second doublet appears between 1485 and 1409 cm^{-1}. We also observe one or two absorptions between 1400 and 1325 cm^{-1} in all the PCB spectra.

The 1200–1000 cm^{-1} range exhibits five principal bands at 1152 ± 21 cm^{-1}, 1060 ± 15 cm^{-1}, 1030 ± 10 cm^{-1}, 1006 ± 4 cm^{-1} and 1088 ± 15 cm^{-1}. This last band can be assigned to a CCl stretching vibration.[29–36]

Between 900 and 650 cm^{-1}, out-of-plane bending vibrations of CH aromatic bonds (γCH) are expected, which are highly characteristic of the ring substitution. For all PCBs we find one isolated hydrogen CH band at 879 ± 9 cm^{-1}. This band is shifted slightly in the case of a 2,4,6-trichloro structure from 879 to 855 ± 5 cm^{-1}. Two adjacent hydrogen atoms give a CH band at 810 ± 6 cm^{-1}. This band is observed at a slightly higher frequency (830 cm^{-1}) for 4-chlorobiphenyl. A structure with three adjacent hydrogen atoms is charac-

Table 3. Comparison of GC/FTIR frequencies of symmetrical dichlorobiphenyls with IR frequencies of homologous iodochlorobenzenes

ortho		*meta*		*para*	
2,2'-Dichlorobiphenyl	Iodochlorobenzene[29,30]	3,3'-Dichlorobiphenyl	Iodochlorobenzene[31,32]	4,4'-Dichlorobiphenyl	Iodochlorobenzene[33–35]
		1589 S	1565 S	1596 w	
1568 w	1566 w	1562 m	1551 w		
1459 m	1448 S	1463 S	1456 S	1481 S	1472 S
1434 m	1432 m	1394 w	1403 w	1389 w	1387 m
1128 w	1127 w				
1087 w	1115 m				
1061 w	1100 m	1102 S	1096 m	1095 S	1091 S
1038 w	1033 w	1047 m	1058 m		
1007 w	1013 S	1003 w	993 m	1008 w	1006 S
		878 w	868 m		
				815 m	810 S
		777 S	771 S		
749 S	746 S				
	719 sh	722 S	742 S		722 w
		688 m	672 S		

Table 4. Comparison of GC/FTIR frequencies of symmetrical tetrachlorobiphenyls with IR frequencies of homologous 1-bromodichlorobenzenes[36]

2,2′,3,3′-Tetrachloro biphenyl	1-Bromo 2,3-dichloro benzene	2,2′,4,4′-Tetrachloro biphenyl	1-Bromo 2,4-dichloro benzene	2,2′,5,5′-Tetrachloro biphenyl	1-Bromo 2,5-dichloro benzene	3,3′,4,4′-Tetrachloro biphenyl	1-Bromo 3,4-dichloro benzene
		1581 m	1562 m	1580 w	1569 m		1561 m
1560 w	1558 S	1552 w	1553 m	1560 w	1555 m	1542 w	1554 m
1441 m	1431 S	1461 S	1450 S	1457 S	1454 S	1458 S	1452 S
1409 S	1411 S	1442 m	1413 w	1395 w	1409 w		
		1380 w	1368 m	1373 w	1369 m	1358 w	1369 m
1195 w	1190 m			1251 w	1241 w		
1153 m	1155 m	1141 w	1141 m	1134 m	1139 w	1134 S	1137 S
	1144 w		1124 w		1115 w		
	1078 w		1094 w		1108 w		1089 w
		1103 S	1088 S	1098 S	1097 S		
				1055 w	1078 w	1056 w	1075 m
1041 m	1040 w	1003 m	1019 S	1025 S	1027 S	1032 m	1031 S
		870 w	865 m	880 w	870 m	879 w	869 m
		818 m	811 w	813 S	811 S	811 m	809 S
782 S	770 S						
749 S	749 w	787 S	805 S	755 w	792 m	756 w	791 m
719 m	728 m						
671 w	693 m					671 m	675 m

Table 5. Significant absorption assignment of GC/FTIR spectra of PCB

PCB	Aromatic C=C				C—C and C—Cl			CH	CCl	Ring	
biphenyl	1595 m	1481 m				1069 w	1009 w	738 S		700 S	
		1434 w									
2	1592 w	1467 m		1129 w	1074 w	1036 m	1009 w	748 S	748 S	695 m	
		1435 w									
3	1590 S	1485 S	1394 m		1100 m	1051 m	1006 w	878 m			
	1560 S	1465 S				1020 w		780 m			
								760 S		690 m	
4	1603 w	1481 S	1397 w	1138 w	1095 S		1010 m	830 m	759 S	698 m	
		1446 w						759 S			
2,2′	1568 w	1458 m		1128 w	1087 w	1060 w	1007 w	749 S	708 w		670 w
		1434 m				1038 w					
3,3′	1589 S	1463 S	1394 w		1102 S	1047 w	1003 w	878 w	722 S	688 m	
	1562 m							777 w			
4,4′	1596 w	1481 S	1389 w		1095 S		1008 w	815 m	706 w		
2,4	1587 m	1466 S	1378 w	1143 w	1103 S	1073 w	1009 m	871 w	762 m	697 m	
	1550 w	1436 w						816 S			
2,5	1584 m	1458 S	1381 m	1135 m	1098 S	1035 m		886 w	763 m	698 S	
						1018 m		812 S			
2,4,4′	1587 w	1466 S	1372 w	1142 w	1096 S	1060 sh	1003 m	871 w	734 m		
								818 m			
2,4,5		1450 S	1339 w	1140 m	1087 m	1048 m		887 m		699 m	675 m
						1025 w		763 m			
2,2′,3,3′	1560 w	1441 m		1153 m		1041 m		782 S	748 S	719 m	671 m
		1409 S									
2,2′,4,4′	1581 m	1461 S	1380 w	1141 w	1103 S	1058 w	1003 m	870 w	787 S		
	1552 w	1442 m						818 m			
2,2′,5,5′	1580 w	1457 S	1395 w	1134 w	1098 S	1055 w		880 w	755 w		671 m
	1560 w		1373 w			1025 S		813 S			
3,3′,4,4′	1542 w	1458 S	1358 w	1134 S		1056 w		879 w	756 w		671 m
						1032 m		811 m			
2,2′,4,5,5′		1450 S	1387 w	1141 m	1096 S	1072 m		887 m			671 w
						1033 m		816 m			
2,2′,4,4′,6	1575 m	1427 m	1368 w	1140 w	1097 S	1064 w	1002 w	859 w	795 S		
	1543 m										
2,3′,4,5′,6	1583 S	1458 w	1388 sh	1142 w	1098 w			850 S	733 w		
	1562 S	1412 S	1366 m					804 S			
	1542 m										
2,2′,4,4′,5,5′		1448 S	1356 w	1141 m	1081 m	1045 m		887 w	825w/717w		678 m
2,2′,3,3′,6,6′		1472 S	1399 m	1176 S		1046 S		809 S	749 w		672 w
			1357 m								
2,2′,3,4,5,5′6		1466 w	1351 S		1095 S	1041 m		808 w	748 w		679 m
		1405 w	1326 m								

terized by a CH vibration between 782 and 777 cm^{-1} and by a ring vibration near 700 cm^{-1}. In the case of four or five adjacent hydrogen atoms, we observe the CH vibration at 750 ± 13 cm^{-1} and a ring vibration, for a mono-substituted ring only, at 697 ± 3 cm^{-1}.

The second coupled CCl vibration gives IR bands which are variable in frequency (between 800 and 700 cm^{-1}) and in intensity.

Significant absorption bands of GC/FTIR PCB spectra and their assignments are given in Table 5.

CONCLUSION

The GC/FTIR technique is a good approach for studying PCB complex mixtures because of on-line separation and generation of a unique spectrum for each of the individual PCB isomers.

Specific IR group frequencies correlated with subsitution patterns allow the differentiation between PCB isomers which is of great importance for environmental studies. The interest of such analysis had been previously demonstrated by Grainger and Gelbaum for tetrachlorodibenzo-*p*-dioxines.[37]

To continue this study, the library of GC/FTIR spectra of PCB must be extended. However, this work shows that previous IR work concerning PCB or chlorobenzenes may be used for interpreting GC/FTIR spectra which are not included in the library.

In order to separate and identify specific PCB isomers in environmental complex samples, the GC/FTIR technique appears to be very complementary to GC and GC/MS ones.

REFERENCES

1. S. Jensen, *J. Chromatog.*, 1972 **68**, 345.
2. B. L. Sawhney in *PCBs and the Environment*, J. S. Waid (ed.), Vol. 1, Chap. 2, CRC Press, Boca Raton, 1986.
3. K. Ballschmiter and M. Zell, *Fresenius Z. Anal. Chem.*, 1980, **302**, 20.
4. O. Hutzinger, S. Safe and V. Zitko, in *The Chemistry of PCBs*, CRC Press, Cleveland, 1974.
5. T. Cairns, G. M. Doose, J. E. Froberg, R. A. Jacobson and E. G. Siegmund, in *PCBs and the Environment*, J. S. Waid (ed.), Vol. 1, Chap. 1, CRC Press Boca Raton, 1986.
6. K. Furukawa in *ibid.*, J. S. Waid (ed.), Vol. II, Chap. 6, CRC Press, Boca Raton, 1986.
7. P. Doumenq, M. Guiliano and G. Mille, *Intern. J. Environ. Anal. Chem.*, 1989, **37**, 235.
8. P. R. Griffiths, J. A. de Haseth and L. V. Azarraga, *Anal. Chem.*, 1983, **55**, 1361 A.
9. K. S. Chiu, K. Biemann, K. Krishnan and S. L. Hill, *ibid.*, 1984, **56**, 1610.
10. D. F. Gurka, *Appl. Spectrosc.*, 1985, **39**, 827.
11. J. R. Cooper and L. T. Taylor, *ibid.*, 1984, **38**, 366.
12. K. H. Shafer, T. L. Hayes, J. W. Brasch and R. J. Jakobsen, *Anal. Chem.*, 1984, **56**, 237.
13. J. R. Cooper and L. T. Taylor, *ibid.*, 1984, **56**, 1989.
14. S. L. Smith, S. E. Garlock and G. E. Adams, *Appl. Spectrosc.*, 1983, **37**, 192.
15. L. V. Azarraga and C. A. Potter, *J. High Resolut. Chromatogr. Chromatogr. Commun.*, 1981, **4**, 60.
16. K. S. Kalasinsky, *J. Chromatog. Sci.*, 1983, **21**, 246.
17. D. F. Gurka, M. Hiatt and R. Titus, *Anal. Chem.*, 1984, **56**, 1102.
18. D. F. Gurka, M. Umana, E. D. Pelizzari, A. Moseley and J. A. de Haseth, *Appl. Spectrosc.*, 1985, **39**, 297.
19. R. E. Fields and R. L. White, *Anal. Chem.*, 1987, **59**, 2709.
20. D. F. Gurka and S. M. Pyle, *Environ. Sci. Technol.*, 1988, **22**, 963.
21. M. Guiliano, P. Doumenq, A. Jawad and G. Mille, *Appl. Spectrosc.*, 1989, **43**, 571.
22. P. Doumenq, M. Guiliano and G. Mille, *Analusis*, 1989, **17**, 39.
23. J. A. de Haseth and T. L. Isenhour, *Anal. Chem.*, 1977, **49**, 1977.
24. R. A. Nyquist, C. L. Putzig and D. P. Peterson, *Appl. Spectrosc.*, 1983, **37**, 140.
25. R. M. Barrett and D. Steele, *J. Mol. Struct.*, 1972, **11**, 105.
26. J. Eaton and D. Steele, *J. Chem. Soc. Faraday Trans. II*, 1973, **69**, 1601.
27. J. F. Schneider, G. T. Reedy and D. G. Ettinger, *J. Chromatog. Sci.*, 1985, **23**, 49.
28. J. F. Schneider, J. C. Demirgian and J. C. Stickler, *ibid.*, 1986, **24**, 330.
29. M. Brigodiot and J. M. Lebas, *J. Chim. Phys.*, 1965, **62**, 347.
30. J. H. S. Green, *Spectrochim. Acta*, 1970, **26A**, 1913.
31. C. Garrigou-Lagrange, M. Chehata and J. Lascombe, *J. Chim. Phys.*, 1966, **63**, 552.
32. J. H. S. Green, *Spectrochim. Acta*, 1970, **26A**, 1523.
33. C. Garrigou-Lagrange, J. M. Lebas and M. L. Josien, *ibid.*, 1958, **12**, 305.
34. A. Stojiljkovic and D. H. Whiffen, *ibid.*, 1958, **12**, 57.
35. J. H. S. Green, *ibid.*, 1970, **26A**, 1503.
36. R. A. Nyquist, B. R. Loy and R. W. Chrisman, *ibid.*, 1981, **37A**, 319.
37. J. Grainger and L. T. Gelbaum, *Appl. Spectrosc.*, 1987, **41**, 809.

Talanta, Vol. 39, No. 2, pp. 155–158, 1992
Printed in Great Britain.

0039-9140/92 $5.00 + 0.00

DETERMINATION OF SULPHA-DRUGS WITH A PIEZOELECTRIC SENSOR

L.-H. NIE, T.-Q. WANG and S. Z. YAO*

New Material Research Institute, Department of Chemical Engineering, Hunan University, Changsha 410082, People's Republic of China

(*Received* 30 *June* 1989. *Revised* 29 *March* 1991. *Accepted* 23 *April* 1991)

Summary—A piezoelectric sensor is used for the determination of sulpha-drugs, as pure substances and in their dosage forms, by an indirect micro method based on reaction of the sulpha-drug with bromine and reduction of the resultant *N*-bromoderivative with iodide to form iodine, which after extraction is monitored with a piezoelectric quartz sensor. The response of the sensor is linear from 2×10^{-5} to $4 \times 10^{-4} M$ sulpha-drug.

Sulpha-drugs are widely used in the treatment of infections, especially for patients intolerant to antibiotics. The nitrite titration method[1–3] has been recommended for the determination of most pharmacopoeial sulpha-drugs and their dosage forms, but diazo salts and nitrous acid are unstable and the diazotization reaction may be affected by a number of factors, and measures have to be taken to avoid erroneous results. Recently a new method has been proposed for the determination of sulpha-drugs by conversion into an *N*-bromoderivative which is then determined iodometrically.[4] A piezoelectric sensor has been proposed for the determination of iodide in aqueous solution,[5] and in the present work, these two techniques are combined for the determination of medically important sulpha-drugs, as the pure substances and in their dosage forms. As proposed by Amin and Shaba,[4] the *N*-bromoderivative is formed by reaction with bromine water and is reduced with iodide to produce an equivalent amount of iodine. The iodine is then extracted and measured with a silver-plated piezoelectric quartz crystal.

*Author for correspondence.

EXPERIMENTAL

Apparatus and reagents

The apparatus used for the determination was as reported previously.[5] The piezoelectric crystal was a 9-MHz cut quartz crystal 12.5 mm in diameter, with a silver-plated electrode (6 mm in diameter) on each side. The electrode holder was directly connected to an oscillator built with an *IC* circuit powered by a d.c. voltage regulator.

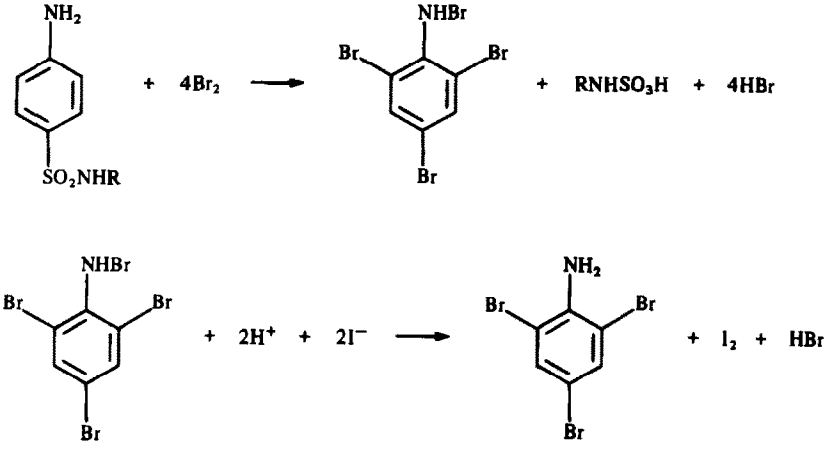

Frequency changes produced by adsorption were measured with a digital counter (model 72, Shijiazhong Electronic Factory No. 4). All chemicals used were of analytical-reagent grade. Doubly distilled water was used throughout.

Standard solutions of sulpha-drugs (0.01*M*) were prepared by dissolving 86.1 mg of sulphanilamide, 107.1 mg of sulphacetamide, 125.1 mg of sulphadiazine or 126.6 mg of sulphamethoxazole in about 15 ml of ethanol (for sulphadiazine and sulphamethoxazole 1*M* hydrochloric acid was added dropwise until complete dissolution was achieved) and then diluting to volume with water in a 50-ml standard flask. Less concentrated solutions were prepared by serial dilution.

Potassium iodide was dissolved in deaerated water to give a 0.01*M* solution, which was kept in an amber-glass bottle.

A saturated solution of bromine water, 90% formic acid solution and 0.5*M* sodium acetate were also prepared.

Procedure

Mix a known volume of the sample solution (not exceeding 3 ml) and 2 ml of saturated bromine water in a separatory funnel (flushed with nitrogen), let stand for 20 min, then add 2 ml of 90% formic acid solution to destroy the excess of bromine. Five min after the solution has become colourless, add 1 ml of 0.01*M* potassium iodide, shake the mixture for 5 min, then add 10 ml of carbon tetrachloride and shake for 1.5 min. Allow the phases to separate, transfer the organic layer into a measuring cell marked at 10 ml, and add carbon tetrachloride to the mark. Start the magnetic stirrer and immerse the piezoelectric quartz crystal (initial oscillation frequency F_1 in air). After exactly 5 min, remove the crystal, dry it with an electric blower and record the frequency (F_2). Run a reagent blank under the same conditions. After each measurement, wash the crystal with ammonia solution (1 + 5), rinse with water and dry it with the electric blower. Correct the frequency change ($\Delta F = F_1 - F_2$) for the blank. Prepare a calibration plot by use of the standard solutions.

Determination of sulphamethoxazole in co-trimoxazole tablets

Weigh 20 tablets and grind them to a fine powder. Accurately weigh a portion of the powder and triturate it with a minimum amount of 1*M* sodium hydroxide at 60° to dissolve the sulphamethoxazole. After cooling, transfer the mixture into a 50-ml standard flask and dilute to volume with water. Leave for 2 hr to let the undissolved trimethoprim settle. After filtration, analyse the filtrate for sulphamethoxazole as described above.

Determination of sulphacetamide in ophthalmic solution

Dilute the ophthalmic solution with distilled water to give a *ca.* $10^{-4}M$ solution. Pipette 2 ml and proceed as described above.

RESULTS AND DISCUSSION

The effect of the reaction medium has been examined for the determination of sulpha-drugs. Water was found to be the most appropriate medium, resulting in a higher frequency change at the same concentration of the sulphonamide compound, e.g., for 0.4m*M* sulphanilamide the frequency change with water as the reaction medium was 819 Hz, whereas in 0.5*M* sodium acetate it was only 104 Hz (a 10-ml sample solution was used). The effect of dilution was also investigated by adding different amounts of water to 1 ml of sample solution. No significant effect is caused by the dilution when the total volume of the diluted sample does not exceed 8 ml, but above this the frequency change tends to decrease. In the present work, the sample solution was diluted to 2–3 ml.

Effect of bromination conditions on the frequency change

A 1-ml sample of 0.2*M* sulphanilamide was used to test the effect of bromination time on the determination of sulpha-drugs. The result is shown in Fig. 1. The frequency change becomes maximal and constant after about 15 min. Up to 68 μg of sulphanilamide (or 100 μg of sulphadiazine) reacts completely with 1.2 ml of saturated bromine water. Use of up to 2 ml of saturated bromine water has no significant effect on the result, but less than 1.2 ml gives smaller frequency changes (Fig. 2). To remove the excess of bromine, 2 ml of 90% formic acid solution is sufficient.

Factors affecting the liberation of iodine

Iodine is liberated on addition of potassium iodide to the reaction system containing the *N*-bromoderivative. There was no significant change in the amount of iodine liberated when 0.75–1.25 ml of 0.01*M* potassium iodide was

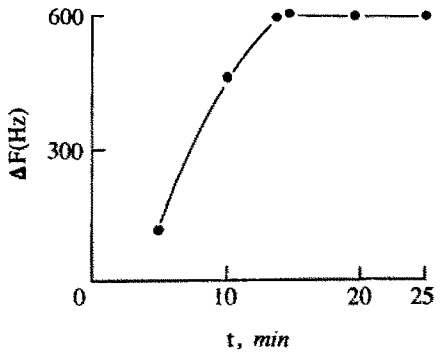

Fig. 1. Effect of bromination time on the determination of $2 \times 10^{4}M$ sulphanilamide.

added. Less than this gave low results in the determination of the sulpha-drug. The frequency change remained virtually unvaried for an iodine-liberation time of 3-9 min. A shorter time resulted in a smaller frequency change.

Factors affecting the iodine extraction

A number of organic solvents were examined as extractants for the iodine produced. A 10-ml volume of carbon tetrachloride was sufficient for quantitative extraction, whereas smaller volumes gave poorer results. Complete extraction was achieved within 30 sec. Chloroform, methylene chloride, benzene and n-heptane can also be used, but are either more volatile or highly flammable, and the first three are regarded as carcinogenic.[6] Diethyl ether and di-isopropyl ether gave much smaller frequency changes and so are unsuitable.

Factors affecting the frequency change

The frequency change increases with the length of time the piezoelectric crystal is immersed in the extract. Sufficient sensitivity can be achieved in 5 min for the determination of microgram levels of the sulpha-drugs. For sub-microgram levels, a longer immersion time is proposed. Varying the temperature from 8 to 35° had no significant influence on the frequency change.

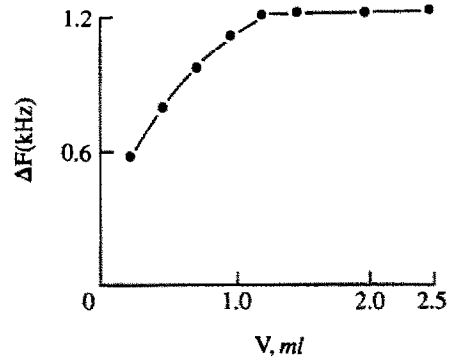

Fig. 2. Effect of the amount of saturated bromine water added to $4 \times 10^{4}M$ sulphanilamide.

Restoration and life-span of the piezoelectric crystal

In the present work, ammonia solution (1 + 5) is proposed for removal of the iodine adsorbed on the crystal surface. Other reagents can also be used, e.g., 10 mg/ml sodium hydrogen sulphate solution or $1M$ sodium carbonate, but a longer immersion time is required. Sodium hydroxide solutions are unsuitable because they cause etching of the quartz crystal, which increases its oscillation frequency and hence affects the sulpha-drug determination.

The life-span of the piezoelectric quartz crystal varies from *ca.* 80 to 300 measuring cycles, depending on the quality of the silver-plated electrode and the amount of iodine adsorbed.

Calibration and reproducibility

The frequency change of the crystal is in direct proportion to sulpha-drug concentration over the range 2×10^{-5}–$4 \times 10^{-4}M$. The standard deviation was 20.4 Hz for 6 determinations of $2 \times 10^{-4}M$ sulpha-drug, corresponding to a relative standard deviation of 3.7%.

The iodine liberated in the reaction is stoichiometrically equivalent to the amount of sulpha-drug. Most commercially available piezoelectric quartz crystals are coated with silver, hence, crystals with silver-plated electrodes were used in the present work, but gold-plated quartz crystals can also be used.

The sensitivity and precision of the sulpha-drug determination in this paper are poorer than those in the analytical system for iodide, based on use of the Leipert multiplication reaction.[5] In addition, the relative magnitude of the blank is large, which also impoverishes the sensitivity.

Table 1. Measurement of sulpha-drugs

	Concentration, $10^{-4}M$	
Sulpha-drug	Taken	Found
Sulphanilamide	4.00	4.06
	0.200	0.194
Sulphadiazine	4.00	4.16
	0.200	0.205
Sulphacetamide	4.00	3.92
	0.400	0.387
Sulphamethoxazole	2.00	2.06
	0.200	0.204

Table 2. Analysis of pharmaceutical preparations

Pharmaceutical preparation	Nominal content	Found	
		Piezoelectric	Pharamacopeial[3]
Sulphacetamide sodium ophthalmic solution	10% (sulphacetamide sodium)	9.82; 9,35; 9.62; 9.77; 10.06; 10.07% (9.78 ± 0.27)%*	(9.88 ± 0.21)%*
Co-trimethoprim tablets†	0.4 g/tablet (sulphamethoxazole)	432; 421; 439; 424; 420; 437 mg per tablet (428 ± 9) mg per tablet*	(419 ± 8) mg per tablet*

*Mean and SD.
†Each tablet contains 0.08 g of trimethoprim and 0.4 g of sulphamethoxazole.

Interferences

Various ions were added to a $2 \times 10^{-4}M$ sulphanilamide solution to examine interference in the technique. Alterations in the frequency change by more than 5% were considered to result from interferences. No significant interferences were caused by 50-fold molar ratio (to sulpha-drug concentration) of potassium, ammonium, sodium, nitrate, bromide, chloride, sulphate, phosphate, carbonate, oxalate, formate and sulphamate, 5-fold ratio of benzoate, tartrate, citrate, salicylate, phthalate, glucose, atropine, benzhexol, glycine, scopolamine and alanine, 3-fold ratio of aspartate and glutamate, equimolar amounts of chlorpheniramine and cocaine, and 0.1% of starch. Trimethoprim, toluidine, xylidine, aniline, phenetidine, procaine and benzocaine interfere. Other oxidants will oxidize iodide to iodine and cause interference if they are not destroyed by formic acid, but such oxidants would seldom be present along with sulpha-drugs.[3]

Analytical applications

The method was applied to the determination of sulpha-drugs (Table 1). It can be applied to the determination of sulpha-drugs in pharmaceutical preparations. The results (Table 2) are in agreement with those obtained by the pharmacopoeial method.[3]

REFERENCES

1. *United States Pharmacopeia, 20th Revision*, 1980, pp. 744–751, 925.
2. *British Pharmacopoeia*, 1980, pp. 432–439.
3. *Chinese Pharmacopoeia*, 4th Ed., Vol. II, 1985, pp. 637–648.
4. D. Amin and B. Shaba, *Microchem. J.*, 1988, **37**, 30.
5. S. Z. Yao, Z.-H. Mo and L.-H. Nie, *Anal. Chim. Acta*, 1988, **215**, 79.
6. M. Sittig, *Handbook of Toxic and Hazardous Chemicals*, pp. 75, 140, 166, 440. Noyes, Park Ridge, NJ. 1981.

Talanta, Vol. 39, No. 2, pp. 159–171, 1992
Printed in Great Britain

0039-9140/92 $5.00 + 0.00
Pergamon Press plc

ANALYSIS OF ANIONS BY SOLID-STATE SPOT-TESTS

ALI MOHAMMAD,* NAIM FATIMA and SHARAD TIWARI
Analytical Laboratory, Department of Applied Chemistry, Z.H. College of Engineering and Technology, Aligarh Muslim University, Aligarh 202002, India

(*Received* 24 *March* 1989. *Revised* 23 *May* 1991. *Accepted* 22 *July* 1991)

Summary—Trituration and capillary solid-state spot-tests for 25 anions with a number of organic and inorganic reagents have been examined. A comparative study of the corresponding reactions in solution has also been made. Incorporation of a glass-wool plug in the capillary improves the selectivity. Schemes are presented for possible use of the technique.

The capillary solid-state spot-test technique reported by this laboratory[1] offers a simple and inexpensive tool for identification of many organic and inorganic solids, and in some cases for their determination.[2–4] The screening procedure can easily be adapted for use by mobile laboratories in the field. The choice of indicative parameters in this technique, such as the colour, length and direction of movement of the coloured boundary leads to selective or even specific detection, even of chemically closely related compounds. The tests can also be applied by trituration of the test compound and the reagent on a spot-plate.

Another novel feature of capillary solid-state spot-tests is that the boundary between the product and reactants can be clearly distinguished even when their colours are similar. Coloured anions such as CrO_4^{2-}, $Cr_2O_7^{2-}$, $Fe(CN)_6^{3-}$ *etc.* can be clearly detected in a glass capillary even if the product is yellow or orange. Likewise, coloured reagents can be easily utilized for detection purposes in a glass capillary. The enhanced selectivity due to the surface contact of the reactants is an added advantage. Reactivity in the solid state depends not only on the chemical nature of the crystal, but also on the positions occupied by ions, atoms or molecules in it.[5]

Earlier studies[2] showed that the colour produced by a reaction in solution is not always the same as that for the same reaction in the solid state, since the latter occurs with a minimum of atomic and molecular movement. Considerable work has been done on the detection and determination of anions in solution,[6,7] but none on systematic detection of anions in the solid state.

The present work summarizes our efforts to utilize the capillary solid-state spot-test technique for selective detection and systematic analysis of anions. It has already proved useful for common cations.[2] The technique has been modified by use of a glass-wool plug to make the test more selective or even specific.

EXPERIMENTAL

Reagents

All reagents used were of BDH analytical or laboratory reagent grade, and ground to 50–100 mesh size. The reagents used were *p*-dimethylaminobenzaldehyde (p-DAB), *p*-dimethylaminocinnamaldehyde (p-DAC), diphenylamine (DPA), *p*-toluidine (p-TD), benzidine (BD), benzidine hydrochloride (BDHC), diethylamine hydrochloride (DEAHC), barbituric acid (BTA), chromotropic acid (CA), sodium nitroprusside (SNP), phenolphthalein (PPL), potassium hydrogen sulphate (PHS), ferric chloride ($FeCl_3$), silver nitrate ($AgNO_3$), and 50% w/w intimate mixtures of p-DAB, DPA, p-DAC, p-TD, BTA, CA, KI, Na_2MoO_4, $FeCl_3$, $FeSO_4(NH_4)_2SO_4$ and $AgNO_3$ with PHS, and of SNP and PPL with NH_4Cl.

For detection in solution, ethanol or demineralized water, or a mixture of the two when required, was used as the solvent, and PHS and ammonium chloride were replaced by dilute hydrochloric acid and ammonia solution respectively.

*Author for correspondence.

Procedures

Solid-state detection. About 5–10 mg of the powdered test material was triturated with several mg of reagent in a depression on a white spot-plate with a glass rod. The colours developed at 30 or 40° and on heating to a higher temperature (60–100°) were recorded.

Detection in solution. One or two drops of an aqueous solution of the test material were mixed with a few drops of a concentrated solution of the reagent in a depression on the spot-plate. The colours developed at 40° and at higher temperatures were recorded.

Solid-state detection in capillaries. A 10-cm length of graduated capillary (3 mm internal diameter) was partly filled with powdered reagent from one end with the help of two iron rods, and the powdered sample was similarly packed from the other end. Care was taken to make the packing reproducible and that the two materials were in close contact in the middle of the capillary. The colour of the product formed at the junction, and the length and direction of movement of the coloured boundary at the desired temperature after specified time intervals were recorded.

Solid-state detection in capillaries modified with a glass-wool plug. An air gap between the reagent and the test material was created by placing a glass-wool plug (4–8 mm) in the middle of the capillary before filling it with the reactants. The test material and the reagent were then added from opposite ends of the capillary as usual. The capillary was kept at the desired temperature in an electrically heated oven. The colour formed either at the glass-wool/reagent junction or the glass-wool/test material junction was observed after a fixed time interval and the thickness of the coloured boundary was also recorded.

RESULTS AND DISCUSSION

The results obtained for the trituration reactions are summarized in Table 1. They were compared with those obtained in solution, and in many instances these colours were entirely different. For example, VO_3^- reacts with p-DAB + PHS to give a brown product in the solid state but a red precipitate in solution. Similarly, $Fe(CN)_6^{3-}$ gives an orange-yellow product with p-DAB + PHS at 60° in the solid state, and a brown product in solution. With the same reagent in the solid state $Fe(CN)_6^{4-}$ yields a green product which changes to blue-green, while in solution a yellow colour is observed. At 40°, $Cr_2O_7^{2-}$ reacts with p-DAB + PHS to give a red product in the solid state, which is immediately converted into a dark brown product, but at 60° only a dark brown product appears. A red colour does not occur in solution at any temperature. It appears that the red product is unstable and its formation is only possible in the solid state at lower temperature.

DPA can be used for the specific detection of CrO_4^{2-} in the solid state because this is the only one of the anions studied that gives any colour (green-yellow at 40°). In solution DPA forms a bright yellow product with CrO_4^{2-}, orange with $Cr_2O_7^{2-}$ and green-yellow with $Fe(CN)_6^{3-}$. The colours produced by DPA + PHS with NO_2^-, BrO_3^-, IO_3^-, SO_4^{2-} and $Cr_2O_7^{2-}$ are different in the solid state from those in solution. When BrO_3^- reacts with DPA + PHS the initial blue colour changes to green within a few minutes. In solution only a yellow-brown precipitate is obtained. IO_3^- behaves similarly in the solid state but in solution gives a green product. IO_4^- gives a green colour which changes into yellow in the solid state, and in solution a stable green product is formed. DPA + PHS reacts with MoO_4^{2-} only in solution, to give a green product. With $Cr_2O_7^{2-}$ and $Fe(CN)_6^{4-}$ it gives a yellow colour in the solid and green in solution.

p-DAC produces a green-yellow product with most anions in solution. The brown species formed with SCN^- in the solid state differs from that formed in solution (green-yellow). SO_3^{2-} gives an orange colour in the solid state but does not react in solution. SO_4^{2-} and NO_3^- produce a light orange colour in the solid at 40° but in solution both anions give a greenish yellow colour. For the detection of most anions on a spot-plate p-DAC + PHS was not suitable because of its own colour. However, the colours formed with S^{2-}, MoO_4^{2-}, $Fe(CN)_6^{4-}$, VO_3^- and $Fe(CN)_6^{3-}$ in the solid state differ from those formed in solution. p-TD + PHS gives coloured species with NO_2^- (light yellow), NO_3^- (red-brown). I^- (red-black), IO_3^- (blue-black), IO_4^- (red-violet), MoO_4^{2-} (blue-violet), VO_3^- (violet) and $Fe(CN)_6^{4-}$ (pink) in solution but does not react with these anions in the solid state. In the solid state, CrO_4^{2-} and $Cr_2O_7^{2-}$ give pale yellow and orange-yellow colours respectively with p-TD + PHS whereas in solution they produce violet and brown colours respectively. $Fe(CN)_6^{3-}$ gives a brown-yellow product in the solid state, but a red-violet product in solution.

With BD only two anions, $Cr_2O_7^{2-}$ and $Fe(CN)_6^{3-}$, react in the solid state at 40°, giving brown-yellow and green-yellow colours respectively, allowing their selective detection. In solution $Cr_2O_7^{2-}$ and $Fe(CN)_6^{3-}$ give violet and green-yellow products respectively, and $Fe(CN)_6^{4-}$ produces a brown precipitate. CrO_4^{2-} forms a green-yellow precipitate in solution, which interferes in the detection of $Cr_2O_7^{2-}$, whereas in the solid state it does not interfere, because of its complete inertness. At 80° BD reacts with $S_2O_8^{2-}$ (yellow solution), IO_3^- (yellow precipitate) and IO_4^- (brown precipitate) only in solution. NO_2^- produces a beautiful red precipitate with BDHC at 80°, which can be utilized for its selective detection. IO_3^- and IO_4^- give yellow and green-yellow precipitates respectively at 40°, whereas at 80° they produce brown and blue precipitates respectively, indicating formation of different species at the two temperatures. CrO_4^{2-} gives a blue-violet precipitate at 40° but at 80° it produces a dark brown precipitate along with a green solution. However, in the solid state only a green product is obtained at both temperatures. $Cr_2O_7^{2-}$ gives a brown product in the solid state but in solution gives brown-violet (40°) and brown (80°) precipitates. $Fe(CN)_6^{4-}$ does not react in the solid but gives light blue and yellow precipitates at 40 and 80° respectively. BDHC reacts to give coloured species with only three anions, CrO_4^{2-} (green), $Cr_2O_7^{2-}$ (brown) and $Fe(CN)_6^{3-}$ (orange-yellow) in the solid state at 40° and can be used for their selective detection.

DEAHC was found to be much less reactive towards anions both in the solid state and in solution. However, it can be used for the selective detection of CH_3COO^- and $S_2O_3^{2-}$ which produce yellow products in the solid state at 40°. At 80°, NO_2^- gives a yellow product, and I^- and SCN^- give light pink products.

BTA can be used for the selective detection of SCN^- and VO_3^- at 40°. SCN^- does not give any colour in solution but gives a pink colour in the solid state. VO_3^- gives a brown colour in the solid state and a yellow colour in solution. None of the other anions studied gives any colour in the solid state with BTA at this temperature. However, in solution the selectivity of BTA is reduced and seven anions produce coloured products at 40°; NO_2^-, producing a violet solution, can be distinguished from the rest of the anions. At 80°, $Fe(CN)_6^{4-}$ gives a green-yellow solution but does not react in the solid state.

Solid-state colour reactions of BTA + PHS can be used for the selective detection of Br^- (orange-yellow), I^- (yellow), SCN^- (violet), $Cr_2O_7^{2-}$ (brown), $Fe(CN)_6^{3-}$ (red) and $Fe(CN)_6^{4-}$ (blue). $Fe(CN)_6^{3-}$ can be distinguished from $Fe(CN)_6^{4-}$, and $Cr_2O_7^{2-}$ from CrO_4^{2-} in the solid state. Cl^- gives no colour with BTA + PHS and hence does not interfere in the detection of I^- and Br^- in the solid state. SCN^- gives a red-violet colour with aqueous BTA + PHS, but no coloured species was observed in solution when PHS was replaced by dilute hydrochloric acid. $Cr_2O_7^{2-}$ produces a blue-green colour with aqueous BTA + PHS, which changes to blue. Similarly, the yellow colour initially formed with $Fe(CN)_6^{3-}$ changes to green, but $Fe(CN)_6^{4-}$ gives only a green-blue colour. With an aqueous solution of BTA containing hydrochloric acid, NO_2^- produces a violet colour which is quickly converted into yellow. A red-brown precipitate is obtained with I^-. $Cr_2O_7^{2-}$ and $Fe(CN)_6^{4-}$ give very stable blue species whereas the green-yellow colour formed with $Fe(CN)_6^{3-}$ changes to green-blue. BrO_3^-, VO_3^-, SO_3^{2-} and $S_2O_3^{2-}$ also give coloured species with BTA in the presence of hydrochloric acid, but these anions do not react with aqueous BTA + PHS. CA is a selective reagent for the detection of $Fe(CN)_6^{3-}$. The colours obtained in the solid state with NO_2^- (brown), CO_3^{2-} (brown), and $Fe(CN)_6^{3-}$ (red-yellow) are different from those obtained in solution. At 80°, $S_2O_8^{2-}$ and $Fe(CN)_6^{4-}$ give light blue and yellow colours respectively, but only in solution. $Cr_2O_7^{2-}$ does not react in the solid state but in solution it gives a dark brown colour at 80°. CA + PHS gives colour reactions with many anions, and hence it can be used as a general reagent for detection of anions. It gives a brown colour with VO_3^-, yellow with $Fe(CN)_6^{3-}$ and light yellow with $Fe(CN)_6^{4-}$ in the solid state, but in solution gives a yellow colour with VO_3^-, green-yellow with $Fe(CN)_6^{3-}$ and blue with $Fe(CN)_6^{4-}$. Thus $Fe(CN)_6^{3-}$ can be distinguished from $Fe(CN)_6^{4-}$ in solution.

SNP can be used as a selective reagent for the detection of CrO_4^{2-}, $Cr_2O_7^{2-}$, I^- and $Fe(CN)_6^{3-}$ in the solid state, and in solution SO_3^{2-} can be detected selectively by means of the red colour formed. NH_4Cl + SNP can be used for the selective detection of I^-, $S_2O_8^{2-}$, CrO_4^{2-} and $Cr_2O_7^{2-}$ in the solid state at 40°. $Fe(CN)_6^{3-}$, $Fe(CN)_6^{4-}$ and $S_2O_3^{2-}$ can also be selectively detected at 80°. In solution this reagent produces coloured products with most of the anions and can be used as a general reagent.

It is also clear from Table 1 that PPL, which produces a pink colour with most anions in solution, can be used for the selective detection of CO_3^{2-} (pink), CrO_4^{2-} (green-yellow), $Cr_2O_7^{2-}$ (orange) and $Fe(CN)_6^{3-}$ (yellow) in the solid state. Amongst all the anions tested, only CO_3^{2-} and HCO_3^- give coloured products, violet and pink respectively, in the solid state at 100°, leading to their specific detection.

In solid-state spot-tests PHS has been used as a source of hydrogen ions.[8] We have observed that it is a good reagent for the selective detection of a few anions, in particular SCN^-, VO_3^-, CrO_4^{2-}, $Cr_2O_7^{2-}$, $Fe(CN)_6^{3-}$ and $Fe(CN)_6^{4-}$. It produces an unstable violet product with SCN^- at 30°. With VO_3^- an orange colour in the solid state and a dark brown precipitate in solution are observed. CrO_4^{2-} shows an interesting pattern of colour changes with PHS at 30°. It gives an orange product which changes through yellow to brown in the solid state, whereas in solution a stable orange-yellow colour is obtained. However, at 80°, a green-yellow colour appears in solution. $Fe(CN)_6^{3-}$ forms a yellow product in the solid state and a green one in solution. $Fe(CN)_6^{4-}$ gives a blue product in both the solid state and in solution.

KI + PHS does not react with NO_3^- in the solid state but gives a red colour with it in solution. Cl^- and I^- react only in solution, to give a yellow colour and a dark brown precipitate respectively. BrO_3^- gives a blue precipitate in solution at 30°, and in the solid state reacts to give an orange-red product. Other anions which react only in solution are SO_4^{2-} (red-yellow), CO_3^{2-} (yellow), $C_2O_4^{2-}$ (yellow), PO_4^{3-} (yellow) and $Fe(CN)_6^{3-}$ (red-yellow). The colours formed with IO_3^-, VO_3^-, S^{2-}, SO_3^{2-}, $S_2O_8^{2-}$, $Cr_2O_7^{2-}$ and $Fe(CN)_6^{4-}$ are different in the solid state from those in solution. At 30°, $S_2O_8^{2-}$ gives a brown precipitate along with a violet gas but at 80° a red solution. Similarly, MoO_4^{2-} gives a blue precipitate along with a brown gas at 30°, and a green solution at 80°.

Na_2MoO_4 + PHS produces yellow-brown and violet products with I^- and SCN^- respectively in the solid state, whereas in solution it gives a green-blue colour with I^- and yellow with SCN^-. In the solid state HCO_3^- produces a colourless gas and no colour, whereas CO_3^{2-} gives a light yellow product along with evolution of a colourless gas. Br^- does not give any colour in solution, but in the solid state gives a yellow-brown (30°) or blue-yellow (80°) product. VO_3^- produces a blue-red product at 30° and a red-brown one at 80°, but only a yellow colour in solution. $Cr_2O_7^{2-}$ gives yellow and blue products at 30° and 80° respectively in the solid state, and an orange-yellow colour in solution. At elevated temperature Na_2MoO_4 + PHS cannot be used satisfactorily as a solid-state reagent, because of possible interference by its own colour.

$FeCl_3$ and $FeCl_3$ + PHS can be used as general reagents because they produce coloured species with most of the anions, but they require special care to ensure non-hygroscopic conditions. Furthermore, their utility in analytical solid-state spot-tests is restricted because of their own colour. The colour reactions of $FeCl_3$ with Br^-, I^-, SCN^-, VO_3^-, SO_3^{2-}, $Fe(CN)_6^{3-}$ and $Fe(CN)_6^{4-}$ in the solid state differ from those obtained in solution. $Fe(CN)_6^{3-}$ and $Fe(CN)_6^{4-}$ react with $FeCl_3$ + PHS to give brown and green products respectively in the solid state, and in solution both give a blue precipitate. I^- and SCN^- give a red precipitate in solution, whereas in the solid state I^- produces dark brown (30°) and green-yellow (80°) products. SCN^- gives a violet product in the solid state. $S_2O_8^{2-}$ gives a blue colour in solution at 30° and a yellow product in the solid state at 80°.

$FeSO_4(NH_4)_2SO_4$ + PHS can be used for the selective detection of VO_3^- (buff), $Fe(CN)_6^{3-}$ (blue) and $Fe(CN)_6^{4-}$ (blue) in the solid state at 30°. At this temperature, I^-, IO_3^-, IO_4^-, $C_2O_4^{2-}$, CrO_4^{2-}, $Cr_2O_7^{2-}$ and MoO_4^{2-} do not react in the solid state but produce colours in solution.

$AgNO_3$ reacts with I^- to give a light yellow colour in the solid state, which changes to black, but in solution a grey precipitate is obtained. $S_2O_8^{2-}$ shows similar behaviour in the solid state but produces an orange brown precipitate in solution. With $S_2O_3^{2-}$ the red product initially formed becomes dark-brown and then black. $AgNO_3$ + PHS gives violet and yellow-brown products with SCN^- at 30° and 80° respectively, but only a white precipitate is formed in solution. I^- gives light yellow (30°) and grey (80°) products in the solid state whereas in solution only a grey precipitate (30°) is produced. $Fe(CN)_6^{4-}$ gives light yellow (30°) and green (80°) products in the solid state and a grey precipitate in solution.

Capillary solid-state tests

In the solid-state spot-tests, the test material is triturated with the reagent to form an intimate mixture but in the capillary solid-state spot-tests the reactants are only in contact at the interface.

Table 1. Solid-state spot-test reactions of anions with some reagents at room temperature (38°)

	1	2	3	4	5	6	7	8	9	10	11	12	13	14	15	16	17	18	19	20	21	22	23	24	25	26
NO_2^-	−	+	−	+	−	+	−	−	−	−	−	−	−	+	+	−	−	−	−	+	−	+	+	−	−	−
NO_3^-	−	+	−	+	+	+	−	−	−	−	−	−	−	−	+	−	−	−	−	−	+	+	+	−	−	−
Cl^-	−	+	−	+	−	−	−	−	−	−	−	−	−	−	−	−	−	−	−	−	−	+	+	−	−	−
Br^-	−	+	−	+	−	−	−	−	−	−	−	−	+	−	+	−	−	−	+	+	+	+	+	−	−	+
I^-	−	+	−	+	−	+	−	−	−	−	−	−	+	−	+	−	+	−	+	−	+	+	+	−	+	+
CH_3COO^-	−	+	−	−	−	−	−	−	−	−	+	−	−	−	−	−	−	−	−	−	−	+	+	−	−	−
HCO_3^-	−	+	−	+	−	+	−	−	−	−	−	−	−	−	−	−	−	−	−	+	−	+	+	−	−	−
BrO_3^-	−	+	−	+	−	+	−	+	−	−	−	−	−	−	+	−	−	−	+	−	+	+	+	−	−	−
IO_3^-	−	+	−	+	−	+	−	−	−	−	−	−	−	−	+	−	−	−	+	+	−	+	−	−	−	−
IO_4^-	−	+	−	+	−	+	−	−	−	−	−	−	−	−	+	−	−	−	−	+	−	+	−	−	+	−
SCN^-	−	+	−	+	+	+	−	+	−	−	−	+	+	−	+	−	−	−	+	−	+	+	+	−	−	+
VO_3^-	−	+	−	+	+	+	−	−	−	−	−	+	−	−	+	−	−	−	+	+	+	+	+	+	+	+
S^{2-}	−	+	−	+	+	+	−	−	−	−	−	−	−	−	−	−	−	−	−	+	+	+	+	−	−	−
SO_3^{2-}	−	+	−	+	+	+	−	−	−	−	−	−	−	−	+	−	−	−	−	+	−	+	−	−	−	−
SO_4^{2-}	−	+	−	+	+	+	−	−	−	−	−	−	−	−	−	−	−	−	−	−	−	+	+	−	−	−
$S_2O_3^{2-}$	−	+	−	+	−	+	−	−	−	−	+	−	−	−	+	−	−	−	−	+	+	+	+	−	+	+
$S_2O_6^{2-}$	−	−	−	+	−	+	−	−	−	−	−	−	−	−	−	−	+	−	−	+	+	+	−	−	+	+
CO_3^{2-}	−	−	−	+	−	−	−	−	−	−	−	−	−	+	+	−	−	+	−	−	+	+	−	−	−	−
$C_2O_4^{2-}$	−	+	−	+	−	+	−	−	−	−	−	−	−	−	+	−	−	−	−	−	−	−	−	−	−	−
CrO_4^{2-}	−	+	+	+	−	+	+	+	−	+	−	−	−	+	+	+	+	+	+	+	+	+	+	−	+	+
$Cr_2O_7^{2-}$	+	+	−	+	+	+	+	+	+	+	−	−	+	−	+	+	+	+	+	+	+	+	+	−	+	+
MoO_4^{2-}	−	+	−	−	−	+	−	−	−	−	−	−	−	−	+	−	−	−	+	+	−	+	+	−	−	−
PO_4^{3-}	−	−	−	−	−	−	−	−	−	−	−	−	−	−	−	−	−	−	−	−	+	+	+	−	−	−
$Fe(CN)_6^{3-}$	−	−	−	+	−	+	+	+	+	+	−	−	+	+	+	+	−	+	+	−	+	+	+	+	+	−
$Fe(CN)_6^{4-}$	−	+	−	+	−	+	+	−	−	−	−	−	+	−	+	−	−	−	+	−	+	+	+	+	−	+

1 p-DAB
2 p-DAB + PHS
3 DPA
4 DPA + PHS
5 p-DAC
6 p-DAC + PHS
7 p-TD
8 p-TD + PHS
9 BD
10 BDHC
11 DEAHC
12 BTA
13 BTA + PHS
14 CA
15 CA + PHS
16 SNP
17 NH_4Cl + SNP
18 PPL
19 PHS
20 KI + PHS
21 Na_2MoO_4 + PHS
22 $FeCl_3$
23 $FeCl_3$ + PHS
24 $FeSO_4(NH_4)_2SO_4$ + PHS
25 $AgNO_3$
26 $AgNO_3$ + PHS

Thus, many colour reactions which occur on trituration are usually not noticed in the glass capillary tests. Therefore, the anions that give colour reactions by the trituration method were selected for further study in glass capillaries. Tables 2 and 3 summarize some of the results obtained for the glass capillary reactions. It is observed that many anions giving a colour reaction on the spot-plate do not react in the glass capillary, showing the greater selectivity of the latter technique. For example, CrO_4^{2-}, $Cr_2O_7^{2-}$, $Fe(CN)_6^{3-}$ and $Fe(CN)_6^{4-}$ do not react with p-DAB in the glass capillary but form coloured products on the spot-plate. Thus, p-DAB can be used for the specific detection of SCN^- by the capillary test (Table 3). It gives a yellow product at the junction, which moves towards the reagent, giving a 6-mm length of colour (after 1 hr at 60°).

p-DAC can be used for the specific detection of S^{2-} (yellow product) at 80° and for the selective detection of NO_3^- (pink-brown product) or SO_3^{2-} (yellow product) at 120° by the capillary method. Furthermore, NO_3^- can be clearly distinguished from SO_3^{2-} on the basis of the length of the coloured boundary: NO_3^- gives a 4.0-mm boundary length and SO_3^{2-} only 1.0 mm after 1 hr at 140°. In both cases the coloured boundaries move towards the test material, showing that p-DAC is the only species diffusing. SCN^-, SO_3^{2-}, SO_4^{2-} and $Cr_2O_7^{2-}$ do not react in the glass capillary.

p-TD can be used for the selective detection of CrO_4^{2-} and $Fe(CN)_6^{4-}$ by means of the products, green and buff respectively, obtained at the junction in capillaries. The boundary zone moves towards the test material in both cases, but is twice as long for CrO_4^{2-} as for $Fe(CN)_6^{4-}$. Interestingly, $Cr_2O_7^{2-}$ and $Fe(CN)_6^{3-}$ do not react in capillaries and hence CrO_4^{2-} can be detected in the presence of $Cr_2O_7^{2-}$. Similarly, $Fe(CN)_6^{4-}$ can be detected in the presence of $Fe(CN)_6^{3-}$.

BTA is found to be the most suitable reagent for the specific detection of NO_2^- by the capillary method. None of the anions which give coloured products in the trituration spot-test produces any colour at the junction in the capillary, except NO_2^-. It forms a pink boundary which moves towards the test material, to give a length of 4.0 mm after 3 hr at 120°.

$Fe(CN)_6^{3-}$ can be specifically detected by observing the orange product formed at the junction by reaction with BDHC. NO_2^- and SCN^- can be selectively detected at 80° with DEAHC as reagent. I^-, $Fe(CN)_6^{3-}$, CrO_4^{2-} and $Cr_2O_7^{2-}$ do not react in the capillary at this temperature but at 120°. CrO_4^{2-} gives a 1.0-mm red-brown boundary and $Fe(CN)_6^{3-}$ a 2.0-mm dark green boundary after 1 hr. In all cases the reagent is the diffusing species, since the coloured boundary always extends towards the test material.

Of all the anions which produce coloured products with CA on the spot-plate, only NO_2^- gives a red-orange ring at the junction in the capillary within 10 min at 30°, leading to its specific detection. This colour reaction is also specific at 80°. At this temperature NO_2^- gives a violet boundary which develops away from the reagent. However, at 120° VO_3^-, MoO_4^{2-} and $Fe(CN)_6^{3-}$ also react with CA to give thin black, red-brown and brown-black rings, respectively, at the junction, within 3 hr. Under these conditions NO_2^- gives a 6.0-mm red-violet boundary which is specific.

NO_2^- and NO_3^- react with p-DAB + PHS to give yellow-orange products at the junction. In the case of NO_3^- the product changes to green-brown on keeping for half an hour at 60°, giving a boundary length of 2.0 mm on the reagent side, and NO_2^- can be distinguished from NO_3^- on the basis of either boundary length or colour. Similarly, Br^- and I^- can be distinguished from each other by the colour of the junction; I^- and Br^- give orange and yellow products respectively (Cl^- does not produce a colour). IO_4^- gives an unstable yellow product which at 60° changes to brown within half an hour, whereas IO_3^- forms a quite stable orange product, which distinguishes it from IO_4^-. The red-brown boundary (4.0 mm) formed by BrO_3^- at 60° within half an hour with p-DAB + PHS can be utilized to distinguish BrO_3^- from VO_3^- (thin ring), IO_4^- or IO_3^- (0.5 mm). Similarly, CrO_4^{2-} (thin orange ring) can be distinguished from $Cr_2O_7^{2-}$ which gives a red boundary 4 mm in length. $Fe(CN)_6^{3-}$ reacts with p-DAB + PHS to give a transient orange colour which quickly changes to greenish-blue, whereas $Fe(CN)_6^{4-}$ gives only a blue product. The boundary length after half an hour at 60° is 3.0 mm for the former and 4.0 mm for the latter. In all cases the coloured boundaries move towards the reagent, showing that the test materials are the only diffusing species.

p-DAC + PHS gives coloured products at the junction only with SCN^- (violet), CrO_4^{2-} (dark brown) and $Fe(CN)_6^{3-}$ (dark brown) within 10 min at 30°. Amongst these only SCN^- shows a boundary length of 10.0 mm. Therefore, SCN^-

can be selectively detected. Cl^- reacts at 80° to give a dark brown product (2.0 mm) towards the reagent and a pink product (6.0 mm) towards the test material after 1 hr; I^- and Br^- do not form coloured species, however. Thus, Cl^- can be detected in the presence of I^- or Br^-. NO_2^- and NO_3^- both react with p-DAC + PHS, NO_2^- to give a brown boundary (2.0 mm) towards the reagent and NO_3^- a violet boundary (2.0 mm) towards the test material. Thus, NO_2^- can be distinguished from NO_3^- by means of the position of the boundary.

DPA + PHS gives a violet boundary with SCN^-, yellow with $S_2O_3^{2-}$ and blue with $Fe(CN)_6^{4-}$. NO_3^-, BrO_3^-, IO_3^-, CrO_4^{2-} and $Cr_2O_7^{2-}$ all produce green products. However, the green boundary moves only in the case of NO_2^- (1.0 mm) towards the reagent. Thus, NO_2^- can be selectively detected on the basis of boundary length. The coloured boundary formed with SCN^- gives the greatest length, leading to the selective detection of SCN^-.

Capillary solid-state spot-tests can be utilized for the specific detection of SCN^- and $Fe(CN)_6^{4-}$ with BTA + PHS and SNP + NH_4Cl respectively as reagents. Similarly, PPL + NH_4Cl can be used for the specific detection of CO_3^{2-} or HCO_3^-, which form pink products at 120°.

PHS can be utilized for the specific detection of VO_3^- at 40° and the selective detection of $Fe(CN)_6^{3-}$ or $Fe(CN)_6^{4-}$ at 80°. The coloured boundaries formed with VO_3^- (brown) and $Fe(CN)_6^{3-}$ or $Fe(CN)_6^{4-}$ (blue) do not show any movement during 1 hr at 80°. It is interesting to note that of 11 anions which produce coloured products with $AgNO_3$ on trituration, only $S_2O_3^{2-}$ and $S_2O_6^{2-}$ form black-brown products at the junction within 10 min at 40°. The coloured boundary formed with $S_2O_6^{2-}$ shows no movement, whereas $S_2O_3^{2-}$ gives a 2.0-mm boundary length, which distinguishes between them. At 80°, $AgNO_3$ gives coloured products with $Fe(CN)_6^{3-}$ (red), PO_4^{3-} (black-brown), I^- (black-brown), CrO_4^{2-} (black) and $Cr_2O_7^{2-}$ (black) at the junction. The coloured boundary moves only in the case of PO_4^{3-} (2.0 mm, 1 hr).

Ferrous ammonium sulphate can be utilized for the selective detection of NO_2^- and MoO_4^{2-}. NO_2^- gives a red ring (80°, 1 hr) and a red-brown boundary 1.0 mm in length (1 hr at 100°). Amongst all the anions which produce coloured products (Table 2) at 80°, only MoO_4^{2-} gives a boundary length of 2.0 mm, which can be used for its selective detection.

I^- can be selectively detected with Na_2MoO_4 + PHS on the basis of the length or direction (which is towards the test material) of the yellow-brown boundary formed at the junction. In all cases the coloured boundaries move towards the test material. $S_2O_6^{2-}$ forms a brown-black boundary (4.0 mm) at 100° which moves towards the reagent. Thus, $S_2O_6^{2-}$ can be distinguished from I^- on this basis, but not from the colour. VO_3^- gives a red ring at 40° but a brown ring at 80 or 100°. Of all the anions tested only SO_3^{2-} forms a blue ring at 40 or 80°. Therefore, it can be selectively detected. However at 100°, PO_4^{3-} also forms a blue ring at the junction.

At 40°, SCN^- reacts with KI + PHS to give a violet boundary (8.0 mm) towards the test material within 10 min. The other anions which give coloured products at the junction such as NO_2^- (red), BrO_3^- (yellow), IO_3^- or IO_4^- (orange), $S_2O_3^{2-}$ (red), $Fe(CN)_6^{4-}$ (blue) and CrO_4^{2-} (brown) show no boundary movement. Thus, SCN^- can be selectively detected on the basis of the boundary length. At 80° the formation of a 10.0-mm thick blue boundary by $Fe(CN)_6^{4-}$ allows its selective detection.

It is apparent from Table 2 that the colour reactions of some anions are temperature-dependent. For example $S_2O_3^{2-}$ gives only a red product with KI + PHS at 40°, whereas at 80°, it gives two coloured species. The red product formed at 40° shows no movement. However, at 80°, in addition to the red ring, a yellow product (2.0 mm) is also formed which moves towards the test material, and gives selective detection of $S_2O_3^{2-}$.

$FeCl_3$ can be used for the specific detection of SCN^- which gives a red-violet ring at 40°. Cl^-, Br^- and I^- can be distinguished from each other at 80° on the basis of the boundary length measured after half an hour (Table 2). NO_3^- can be detected in the presence of NO_2^- because at 80° a red ring appears only with NO_3^-. At 80°, CrO_4^{2-} gives a light brown boundary (3.0 mm) after 1 hr, but $Cr_2O_7^{2-}$ does not react. Thus, CrO_4^{2-} can be detected in the presence of $Cr_2O_7^{2-}$ and SO_3^{2-}. S^{2-} gives a red ring and SO_3^{2-} forms a yellow ring with $FeCl_3$.

It is clear from the discussion above that the capillary solid-state spot-tests are more selective than the conventional solid-state spot-tests and many anions can be selectively or specifically detected by performing the tests in a capillary. Table 3 summarizes the results obtained for the selective/specific detection of some anions by the capillary method. The selectivity of the

Table 2. Capillary solid-state spot-tests for some anions [reagent 27 is $Fe(NH_4)_2(SO_4)_2.6H_2O$]

Reagent	2	6		20		22	25	27
Anion	60°, 30 min CDB/DM, *l*	30°, 10 min CDB/DM, *l*	80°, 1 hr CD/DM, *l*	40°, 10 min CDB/DM, *l*	80°, 1 hr CDB/DM, *l*	80°, 30 min CDB/DM, *l*	80°, 1 hr CDB/DM, *l*	80°, 1 hr CDB/DM, *l*
NO_2^-	Y(Y–O) / 0.5	NC	DBr / TR,2.0	R / NM	DBr / NM	NC	—	R / NM
NO_3^-	G–Br (Y–O) / TR,2.0	NC	V / TM,2.0	—	—	R / NM	—	—
Br^-	Y / TR,1.0	NC	NC	NC	O / NM	DBr / NM	—	—
Cl^-	—	NC	DBr / TR,2.0	—	—	O–Y / TM,4.0	—	—
I^-	O / TR,1.0	NC	NC	—	—	Br / TM,10.0	BK–Br / NM	Y–Br / NM
BrO_3^-	R–Br / TR,4.0	NC	NC	Y / NM	Br / NM	—	—	—
IO_3^-	O / 0.5	NC	NC	O / NM	Br / NM	—	NC	LBr / NM
IO_4^-	Br(Y) / 0.5	—	—	O / NM	Br / NM	—	NC	—
SCN^-	PK / TR,1.0	V / TM,10.0	—	V / TM,8.0	—	R–V / NM	NC	—

VO_3^-	R–Br / NM	NC	Y / TM,1.0	NC	DBr / NM	—	—	DBr / NM
SO_4^{2-}	LY(M)	NC	Y / TM,1.0	—	—	NC	—	—
SO_3^{2-}	—	NC	NC	NC	NC	Y / NM	—	—
MoO_4^{2-}	—	NC	NC	NC	DBr / NM	Br / TM,2.0	—	Br / TR,2.0
S^{2-}	—	NC	Y / TM,2.0	NC	NC	R / NM	—	—
$S_2O_3^{2-}$	NC	NC	Y / NM	R / NM	Y with R ring / TM,2.0	NC	BK(M)	—
$S_2O_6^{2-}$	NC	NC	V / NM	NC	NC	NC	BK–Br / NM	—
CrO_4^{2-}	O / NM	DBr / NM	DBr / NM	Br / NM	DBr / TM,2.0	LBr / TM,3.0	BK / NM	Br / NM
$Cr_2O_7^{2-}$	R(O–R) / TR,4.0	NC	NC	NC	NC	NC	BK / NM	—
$Fe(CN)_6^{3-}$	G–Bl(O) / TR,3.0	DBr / NM	Bl / NM	NC	NC	G / NM	R / NM	NC
$Fe(CN)_6^{4-}$	Bl / TR,4.0	NC	DBr / NM	Bl / NM	Bl–Br / TM,10.0	G / NM	NC	Bl / NM

Table 2. *Continued*

Table 2. *Continued*

Reagent	4		11	14	19	21	
Anion	40°, 5 min CDB/DM, *l*	30 min CDB/DM, *l*	120°, 1 hr CDB/DM, *l*	120°, 3 hr CDB/DM, *l*	80°, 1 hr CDB/DM, *l*	40°, 10 min CDB/DM, *l*	80°, 1 hr CDB/DM, *l*
NO_2^-	G / NM	G / TR,1.0	—	R–L / TM,6.0	—	NC	NC
I^-	NC	NC	NC	NC	NC	Y / TM,2.0	Y–Br / TM,5.0
BrO_3^-	G / NM	G / NM	—	—	NC	NC	NC
IO_3^-	G / NM	G / NM	—	—	—	NC	NC
SCN^-	V / TR,2.0	V / TR,4.0	R–Br (M)	—	—	V / NM	V / 1.0
VO_3^-	NC	NC	—	BK / NM	Br / NM	R / NM	Br / NM
SO_3^{-2-}	NC	NC	—	—	—	Bl / NM	Bl / NM
MoO_4^{2-}	NC	NC	—	R–Br / NM	—	—	—
$S_2O_3^{2-}$	Y / NM	Y / NM	—	—	—	NC	NC
$S_2O_6^{2-}$	NC	NC	—	—	—	NC	DBr / NM
CrO_4^{2-}	NC	G / NM	R–Br / TM,1.0	NC	NC	NC	NC
$Cr_2O_7^{2-}$	NC	G / NM	—	—	NC	NC	NC
$Fe(CN)_6^{3-}$	NC	NC	DG / TM,2.0	Br–BK / NM	Bl / NM	NC	NC
$Fe(CN)_6^{4-}$	DBr / NM	Bl / NM	—	NC	Bl / NM	NC	NC

CDB = colour of the developed boundary at the junction. DM = direction of movement of the boundary. *l* = Length of the coloured boundary (*mm*). TR = towards reagents, TM = towards the test material. NC = no colour, NM = no movement, O = orange, Br = brown, — = not done, M = melted, D = dark, Bl = blue, W = white, P = pale, G = green, R = red, L = light, Y = yellow, BK = black, V = violet, PK = pink.

NO_3^-, Cl^-, Br^-, HCO_3^-, IO_4^-, SO_4^{2-}, S^{2-} do not react with reagents 4, 11, 14, 19, 21 in the glass capillary.

Other abbreviations as in Table 1. Information within brackets refers to the coloured product initially formed at the junction.

Table 3. Specific/selective capillary solid-state spot-test for some anions

Anion	Reagent	Temperature, °C	Time	Colour of boundary	Direction of movement	Length, mm
SCN^-	1	60	1 hr	Y	TR	6.0
S^{2-}	5	80	1 hr	Y	NM	—
SO_3^{2-}	5	100	1 hr	LY	NM	—
NO_3^-	5	120	1 hr	RBr	TM	4.0
CrO_4^{2-}	7	40	12 hr	G	TM	4.0
$Fe(CN)_6^{4-}$				Buff	TM	2.0
$Fe(CN)_6^{3-}$	10	100	1 hr	O	TM	4.0
NO_2^-	11	80	1 hr	Y	NM	—
SCN^-				V	TM	2.0
NO_2^-	12	120	3 hr	PK	TM	4.0
SCN^-	13	30	10 min	PK	NM	—
		120	1 hr	PK	TR and TM	16.0 10.0
NO_2^-	14	80	1 hr	V	TM	4.0
$Fe(CN)_6^{4-}$	17	80	1 hr	Bl–BK	NM	—
I^-	17	120	1 hr	O	NM	—
VO_3^-	19	40	10 min	Br	NM	—
SCN^-	22	40	10 min	R–V	NM	—
$S_2O_3^{2-}$	25	40	10 min	BK–Br	TM	2.0
$S_2O_6^{2-}$				BK–Br	NM	—
CO_3^{2-}	28*	120	1 hr	LPK	TM*	—
HCO_3^-				LPK	TM*	—

*Reagent 28 is NH_4Cl + PPL. The portion of the tube filled with the test material becomes completely pink. All abbreviations as in Table 2.

capillary technique can be further enhanced by introducing a glass-wool plug into the middle of the capillary, between the reactants. In this way the reactants do not come into direct contact and the reaction, if any, proceeds by vapour phase diffusion of the reagent or test material through the glass-wool plug. Such reactions may be termed solid–vapour phase reactions rather than solid–solid reactions. The glass-wool technique was applied to the anions which gave coloured products in glass capillaries, and the colour reactions observed are shown in

Table 4. Glass-wool plug modified capillary solid-state spot-test for some anions

Anion	Reagent	Temperature, °C	Time, hr	Colour of boundary	Length, mm
NO_2^-	2	65	8	G at GW/R	1.0
NO_2^-	4	40	8	G → Bl at GW/R	—
Br^-	2	65	8	Y at GW/M	2.0
HCO_3^-	28	120	1	LPK* at GW/M	—
HCO_3^-	20	80	0.5	Y at GW/M	—
		80	1	O at GW/M	—
BrO_3^-	2	65	8	G at GW/R	5.0
IO_4^-	2	65	2	DBr at GW/M	2.0
		65	8	DBr at GW/M	6.0
SCN^-	2	65	0.5	O at GW/R	—
	20	80	0.5	O at GW/M	2.0
VO_3^-	21	80	1	Y → Br at GW/M	—
		100	1	Y → Br at GW/M	—
CO_3^{2-}	28	120	1	LPK* at GW/R	—
MoO_4^{2-}	2	65	0.5	O at GW/R	—
		65	2	Y at GW/M	4.0
PO_4^{3-}	25	80	1	BK at GW/R	2.0
$Fe(CN)_6^{3-}$	2	65	2	G at GW/M	—
		65	8	G at GW/M	6.0
$Fe(CN)_6^{4-}$	2	65	8	Bl at GW/M	—

GW/R = glass wool/reagent junction.
GW/M = glass wool/test material junction.
* = Whole tube containing test material (CO_3^{2-} or HCO_3^-) becomes pink.
→ indicates a change in colour.
Other abbreviations as in Table 2. For reagent 28 see Table 3.

Table 4 and show that the glass-wool technique is superior to the ordinary capillary technique in terms of selectivity and specificity.

Applications

For obvious reasons (the main one being the complexity of the work that would be involved) the investigation was restricted to the sodium and potassium salts of the anions involved. It is a fairly simple matter to devise a systematic scheme for identification of one of these salts in the absence of the others, as shown in Scheme 1. It is also possible to devise a systematic scheme for analysis of a mixture containing almost all the anions examined in this work. The major problem in devising such schemes is that in contrast to schemes based on physical separation by precipitation or extraction, each test is applied to a portion of the original sample, so all the components are present in every test

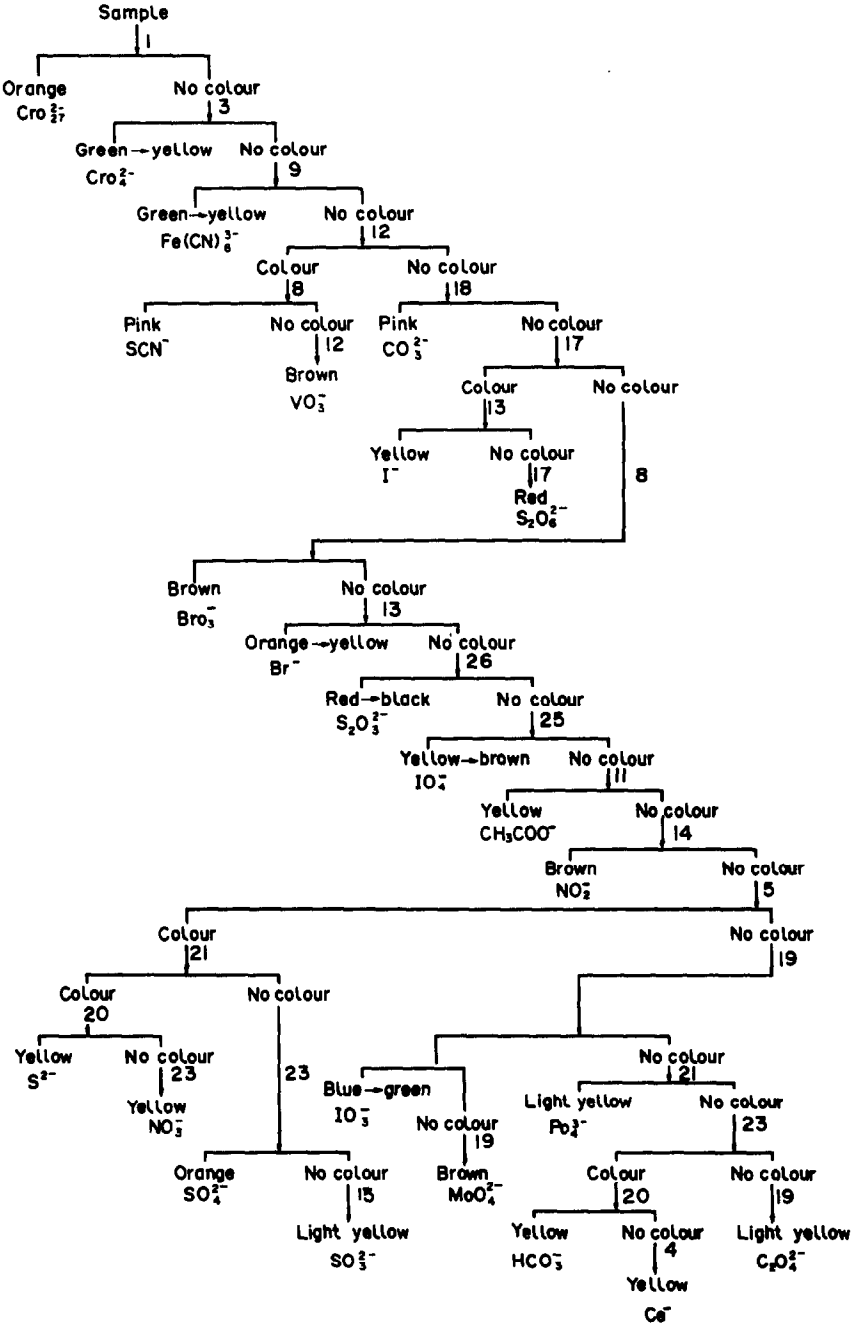

Scheme 1.

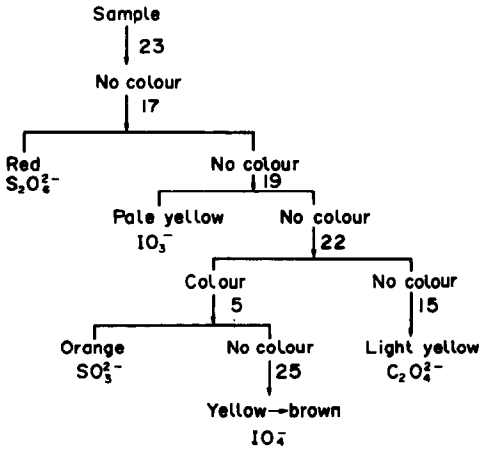

Scheme 2.

performed. Hence the classification is based on elimination of groups of anions from consideration, by their failure to give a colour with a particular group reagent. For instance, if no colour is obtained with DPA + PHS in the trituration test, acetate, molybdate and phosphate are the only anions (of the 25 in the scheme) that may be present. However, if a colour *is* obtained, these three anions may also be present in subsequent tests, so their reactions with all subsequent reagents have to be taken into account in working out the scheme.

On the other hand, it is comparatively easy to use Table 1 to find small groups of anions that do not give a colour with a given reagent, and then to devise identification schemes such as that in Scheme 2.

The capillary tests can similarly (and more easily) be organized into a detection scheme, since additional information is provided by boundary movement of the products. Devising such schemes is an excellent exercise in logical thinking, as a part of student training.

As far as we are aware, this is the first attempt at systematic solid-state analysis for anions. Further publications will be concerned with the chemistry of the new reactions described.

Acknowledgements—The authors thank Professor K. T. Nasim for providing research facilities, and the University Grants Commission (India) for providing financial assistance.

REFERENCES

1. M. Qureshi, H. S. Rathore and A. Mohammad, *Talanta*, 1976, **23**, 874.
2. M. Qureshi, A. Mohammad and G. G. Raju, *ibid.*, 1981, **28**, 817.
3. M. N. Akhtar, H. S. Rathore and M. Qureshi, *ibid.*, 1978, **25**, 235.
4. A. Mohammad and N. Fatima, *Microchem. J.*, 1988, **37**, 161.
5. M. D. Cohen and B. S. Green, *Chem. Brit.*, 1973, **9**, 490.
6. F. Feigl, *Spot Tests in Inorganic Analysis*, 6th Ed., Elsevier, Amsterdam, 1972.
7. W. J. Williams, *Handbook of Anion Determination*, Butterworths, London, 1979.
8. P. I. Voskresenskii, *Talanta*, 1965, **12**, 11.

Talanta, Vol. 39, No. 2, pp. 173–178, 1992
Printed in Great Britain.

0039-9140/92 $5.00 + 0.00
Pergamon Press plc

CAPILLARY ZONE ELECTROPHORESIS SEPARATION AND LASER-INDUCED FLUORESCENCE DETECTION OF ZEPTOMOLE QUANTITIES OF FLUORESCEIN THIOHYDANTOIN DERIVATIVES OF AMINO ACIDS

SHAOLE WU* and NORMAN J. DOVICHI†
Department of Chemistry, University of Alberta, Edmonton, Alberta T6G 2G2, Canada

(*Received* 3 *June* 1991. *Revised* 15 *July* 1991. *Accepted* 15 *July* 1991)

Summary—Capillary zone electrophoresis, when combined with laser-induced fluorescence, is a very powerful technique for the separation and determination of minute amounts of labeled amino acids. This paper presents the determination of the fluorescein thiohydantoin derivative of 17 amino acids which takes 13.5 min. The detector, based on laser-induced fluorescence, is optimized with respect to laser power to produce detection limits, three standard deviations above background, ranging from 1 to 2 zeptomoles (1 zeptomole = 1 zmole = 10^{-21} = 600 analyte molecules) injected onto the capillary.

The Edman degradation reaction, based on phenylisothiocyanate (PITC), is the main technique used to elucidate the amino acid sequence of proteins and peptides.[1,2] Although the classic methodology allows the amino acid sequence determination from picomole amounts of proteins, many proteins of biological interest can only be isolated in much smaller amounts.[3] In order to obtain amino acid sequence information from the small amounts of proteins, a modified Edman-type reagent, fluorescein isothiocyanate (FITC), was introduced by Kawauchi and co-workers.[4,5] Under basic conditions, the molecule couples with the *N*-terminus amino acid to form the thiocarbamyl derivative (FTC) and under acidic conditions the terminal amino acid is cleaved as the thiohydantoin derivative (FTH). That is, to sequence proteins with FITC, it is necessary to determine FTH amino acids. These fluorescein amino acid derivatives are detectable in femtomole quantities by use of conventional technologies. The few reports of protein sequencing using this reagent have employed liquid chromatography separation and fluorescence detection.[3,6] The highly fluorescent reagent produces improvements in the minimum concentration of amino acid and protein that can be analyzed.

Additional improvements in the mass of protein required for analysis will follow from reduction in the size of sequencing instrumentation. A capillary-scale separation scheme is important in miniaturizing the sequencing instrumentation. This research group has developed a very sensitive detector for the capillary zone electrophoresis separation of nanoliter solutions of FTC and FTH derivatives of amino acids. Preliminary results for the capillary electrophoresis separation of the FTH amino acids were summarized elsewhere.[7] Detailed discussion of the separation of FTC amino acids has also been presented,[8,9] including separation conditions and photobleaching effects. FTC amino acids have been studied at the zeptomole level by Sweedler *et al.*[10] and Monning and Jorgenson.[11] In the former paper, a charged-coupled device was used to record the emission spectrum of minute samples eluted from the capillary whereas the latter paper reported a novel sample injector based on photobleaching of FTC amino acids.

In this manuscript, we present, for the first time, a simplified preparation of FTH amino acids; a comparison of different acids for conversion of FTC to FTH amino acids; the effect of pH on separation of FTH amino acids; a compilation of interferences in FTH amino acid separation by capillary zone electrophoresis (CZE); the absorbance and emission spectra of fluorescein with both FTH and FTC amino acid derivatives; the fluorescent quantum yield of

*Present address: Chemistry Division, Alberta Environment Centre, Vegreville, Alberta T0B 4L0, Canada.
†Author for correspondence.

FTC and FTH amino acids; the photobleaching characteristics of FTH amino acids; the detection limits for FTH amino acids; and the noise characteristics in high sensitivity fluorescence detection. It is not the purpose of this paper to present protein sequencing at the sub-attomole level. Rather, we are interested, at this point, in developing instrumentation that can be used to characterize the FTH derivatives with the highest possible sensitivity. Further work will address applications of this separation and detection technology to sequencing samples.

EXPERIMENTAL

Fluorescein thiohydantoin derivatives of amino acids were prepared in micro-scale with a method similar to that reported by Maeda *et al.*[4] Stock amino acid (Fluka) solutions, $5 \times 10^{-3}M$, were prepared in pH 9.1 carbonate buffer ($0.2M$) and stored at 4°. Stock $1.3 \times 10^{-3}M$ fluorescein isothiocyanate (Sigma) was prepared in pure (99.9%, HPLC grade) acetone and also stored at 4°. One milliliter of each amino acid solution was mixed with 0.1 ml of the FITC solution in a 1.5-ml disposable centrifuge vial and allowed to react for four hours at room temperature in the dark to produce the thiocarbamyl derivative. Next, 0.5 ml of each thiocarbamyl solution was mixed with 0.5 ml of trifluoroacetic acid and allowed to react for 15 hr in the dark to form FTH amino acids. These FTH amino acid solutions were stored at 4° until use. The FTH amino acids were diluted at least 4000-fold in $0.01M$ pH 7 phosphate buffer before injection.

Capillary electrophoresis separation of the FTH amino acids was performed in a 1.0-m long, 50-μm inner diameter fused silica capillary, Polymicro. A $10mM$ pH 7.0 phosphate buffer was used for the separation. The sample was injected electrokinetically at 0.5 kV for 10 sec, manually timed and the separation proceeded at 30 kV. The fluorescence detector was identical to that described before.[7-9,12] The detection end of the capillary was placed within the flow chamber of a sheath flow cuvette. A ~25-mW beam from an argon ion laser, $\lambda = 488$ nm, was focused into the cuvette. Fluorescence was collected at right angles to the radiation source, using a microscope objective of numerical aperture 0.65. The collected light was passed through a spectral band-pass filter to reject scattered laser light. The fluorescence was imaged onto a pinhole matched in size to the illuminated sample stream and detected with a high quantum yield photomultiplier tube. A 0.3-sec time constant electronic filter was used to smooth the photomultiplier output before display on a strip chart recorder.

Absorption spectra of FTH and FTC amino acids were measured with a Hewlett–Packard diode array spectrophotometer model 8451A. The uncorrected emission spectra were measured with a Turner Spectrofluorometer model 430.

RESULTS AND DISCUSSION

Separation

Several points can be made concerning the preparation and separation of these derivatives. We found that the precipitation of FTC amino acids before the cyclization reaction reported by Kawauchi *et al.*[5] can be eliminated, greatly simplifying the procedure. Although unreacted amino acids remain in the sample, they interfere with neither the separation by electrophoresis nor the detection by laser-induced fluorescence. Concentrated trifluoroacetic acid (TFA), 50% trifluoroacetic acid, $6N$ hydrochloric acid and $6N$ hydrochloric acid:acetic acid (1:1) were used for the cyclization reaction of FTC-arg in a 1:1 volume ratio for 15 hr at room temperature in the dark. The relative peak heights observed for the FTH-arg samples are listed in Table 1, normalized to the peak height produced for the mixed hydrochloric acid:acetic acid reaction. Concentrated TFA gave the highest sensitivity and was used for the cyclization reaction. The following abbreviations are used for the amino acids: alanine (ala), arginine (arg), asparagine (asn), aspartic acid/aspartate (asp), cysteine (cys), glutamine (gln), glutamic acid/glutamate (glu), glycine (gly), histidine (his), hydroxyproline (hpro), isoleucine (ile), leucine (leu), lysine (lys), methionine (met), phenylalanine (phe), proline (pro), serine (ser), threonine (thr), tryptophan (trp), tyrosine (tyr) and valine (val).

Table 1. Relative sensitivity *vs.* reaction acids used to form FTH–arginine

Reaction acids	Relative peak height
Concentrated trifluoroacetic acid	4
50% trifluoroacetic acid	2
$6N$ HCl	2.3
$6N$ HCl:acetic acid (1:1)	1

FTH amino acids are dianions under basic conditions. These derivatives possess low interaction with fused silica at pH greater than 7 and may be separated with high efficiency in capillary zone electrophoresis. A pH range of 6.5–10 of the eluting buffer (5–10m*M*) was tested. At pH lower than 7.0, the FTH amino acid peaks were broad and strongly tailed, presumably due to the interaction of the less negatively charged species with the wall of the capillary. At pH 8 and higher, multiple peaks corresponding to both the FTH and FTC derivatives, along with some unidentified peaks, were found for arg, ala and phe, presumably due to the decyclization reaction at high pH. The peak height of the FTH amino acids was usually lower than that of the corresponding FTC amino acids. Thus the pH range of the eluting buffer applicable to the separation of FTH amino acids in the capillary zone electrophoresis is rather narrow: 7.0–7.5. In this range most of the FTH amino acids show a single, well-resolved peak on the electropherogram.

Rather surprisingly, the retention time of some of the neutral amino acids depends upon the pH of the eluting buffer. For example, the eluting order is histidine followed by leucine at pH 7.0 but the order was reversed at pH 7.5. Presumably, the electron withdrawing properties of the particular side-chain of the amino acid can influence the ionization constant of the carboxylic acid group of fluorescein. Thus, reproducible pH is required to obtain consistent separations. Relatively low ionic strength buffers are used in the capillary zone electrophoresis separations to minimize the effect of Joule heating on the separation. It was necessary to take care in the preparation of the FTH solutions so that the sample was at the same pH and similar ionic strength as the separation buffer. Most simply, the trifluoroacetic acid can be driven off by passing nitrogen gas through the solution and the pH adjusted with the separation buffer.

Individual FTH amino acids were analyzed by capillary electrophoresis. Under the experimental conditions most of the FTH amino acids show one major peak except serine, threonine, glutamine and asparagine. FTH-ser and FTH-thr both contain a hydroxyl group and both show two peaks, as observed by Kawauchi *et al.*[5] in thin-layer chromatography, which may be caused by decomposition into the FTH-dihydro-derivatives.[4] The two serine peaks had similar heights. The first threonine peak is nearly twice as high as its second peak. FTH-gln has one major peak and two minor peaks with a peak height ratio of approximately 3:1:1. FTH-asn also has one major peak and two minor peaks with height ratio 3.5:1:1.

Several of the other FTH-amino acids show minor peaks in addition to one major peak, presumably due to degradation of the molecule under the derivatization conditions. FTH-arginine, which bears two amino groups, has one major peak and two minor peaks appearing right after the major peak and forming its tailing part, with peak height ratio 14:2:1. Alanine has one major peak and two minor peaks also with a peak height ratio of 14:2:1. Tyrosine has one major peak and one minor peak with peak height ratio 6:1. After reaction for 15 hr, FTH-cys, similar to FTC-cys, showed two peaks, presumably because the sulfhydryl group of cysteine was involved in the reaction with FITC. However, the first peak vanished and left only one peak after reaction for about 30 hr.

Under the conditions employed, the following sets of FTH amino acids cannot be separated: FTH-arg and FTH-lys; FTH-phe, FTH-met, and FTH-thr; FTH-cys and FTH-ser; and FTH-ile and FTH-trp. The separation of a mixture of 21 FTH-amino acids in an aqueous, low ionic strength buffer is shown in Fig. 1. The separation produces $\sim 1 \times 10^6$ plates for these analytes at this pH. A total of 17 peaks, including one reagent peak, are obtained and 12 amino acids may be identified unambiguously.

We have considered elsewhere the separation of the fluorescein thiocarbamyl derivatives of amino acids.[8,9] The FTC derivatives have an additional negative charge, as compared with the FTH derivatives, and consequently have higher electrophoretic mobility. However, the FTC derivatives migrate at lower net velocity than do the FTH derivatives (*e.g.*, 390 sec for FTH-arg *vs.* 518 sec for FTC-arg eluted in 94.5-cm capillary at 29 kV with 5m*M* pH 7.0 phosphate buffer). In both cases, electro-osmosis produces bulk flow in the capillary that is greater in magnitude but opposite in direction from electrophoresis. This electro-osmosis is due to the excess in positive charge in the free solution near the electric double layer at the surface of the fused silica capillary. Because the electro-osmosis opposes the electrophoretically induced motion of the analyte, the FTC molecules, with high electrophoretic mobility,

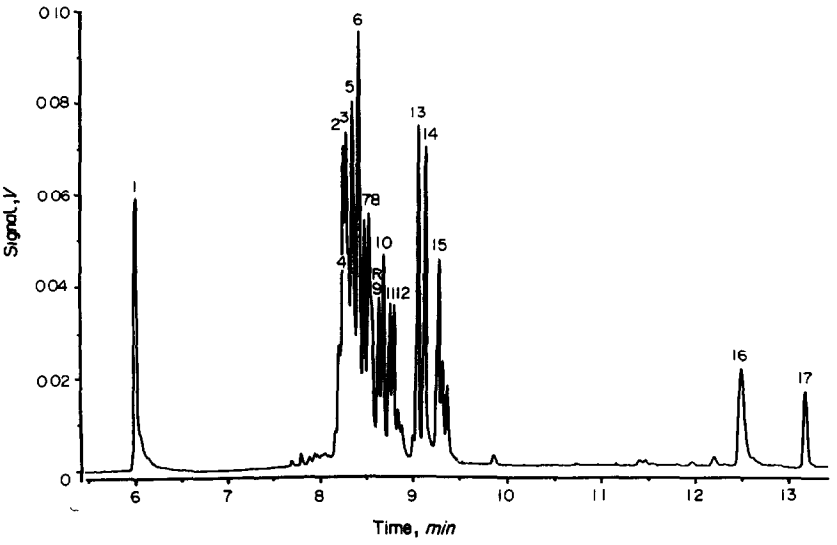

Fig. 1. Determination of FTH amino acids. Peak 1, arg; 2, his; 3, leu; 4, try; 5, ile and tyr; 6, met, phe and thr; 7, val, 8, hpro; 9, asp; 10, pro; 11, thr and ser; 12, ala; 13, gly; 14, cys and ser; 15, gln; 16, glu; 17, asp. Injected concentration was $2.2 \times 10^{-9}M$ for his, leu and gly, and $1.5 \times 10^{-9}M$ for glu and asp, and $1.1 \times 10^{-9}M$ for the others.

will move at lower net velocity than the FTH derivatives.

While FTC-leu and FTC-ile are not easily separated in CZE, the corresponding FTH derivatives can be separated. Similarly, while FTC-arg and FTC-lys are well separated, their FTH species cannot be separated. Thus, complete analysis of amino acids might be achieved by performing two separations, one with the FTC amino acids and one with the FTH amino acids. Alternatively, micellar chromatography may be applied to the separation of thiohydantoin derivatives of amino acids.[13]

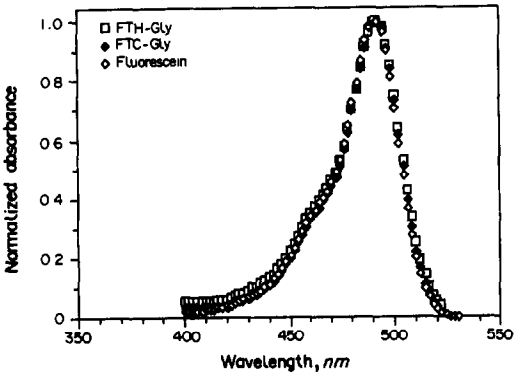

Fig. 2. The normalized absorption spectra of Fluorescein (◇), FTH-gly (□) and FTC-gly (◆). The measurements were performed on a Hewlett-Packard spectrophotometer model 8451A. The fluorescein solution contains $1.12 \times 10^{-6}M$ fluorescein in $0.1N$ NaOH. The FTC-gly solution was prepared by diluting the original reaction product (which contained $1.18 \times 10^{-4}M$ FTC-gly and 5×10^{-3} glycine in $0.2M$ of pH 9 carbonate buffer) with $5mM$ carbonate buffer (pH 10) to $1.18 \times 10^{-6}M$. The FTH-gly solution was prepared by diluting the original reaction product which contained $5.9 \times 10^{-5}M$, FTH-gly and $2.5 \times 10^{-3}M$ glycine in strong acidic solution (trifluoroacetic acid) with $0.1N$ NaOH first (to pH = 5) and then $0.2M$, pH 9 carbonate buffer and finally $10mM$ phosphate buffer (pH 7) to the concentration of $\sim 2 \times 10^{-6}M$.

Detection

The shapes of the absorption spectra of FTH-gly, FTC-gly, and fluorescein in the visible spectral range (400–600 nm) are very similar, with a slight enhancement in the blue absorbance of the thiohydantoin derivative (Fig. 2). The molar absorptivities of FTH-gly (pH 7), FTC-glycine (pH 10 and 7) and fluorescein (pH 13) at 488 nm and 322 nm (the latter wavelength was used as the excitation wavelength in the measurement of the emission spectrum) are listed in Table 2. Despite the

Table 2. Molar absorptivity*

Analyte	Molar absorptivity, $l.\mu mole^{-1}.cm^{-1}$ $\lambda = 322$ nm	$\lambda = 488$ nm
Fluorescein (pH 13)	120,000 ± 10,000	85,000 ± 2500
FTH-Gly (pH 7)	150,000 ± 20,000	82,000 ± 4000
FTC-Gly (pH 7)		77,000 ± 1000
FTC-Gly (pH 9)	150,000 ± 20,000	85,500 ± 2500
FTH-Tyr (pH 7)		59,000
FTC-Tyr (pH 9)		61,000
FTH-Ala (pH 7)		68,000
FTC-Ala (pH 9)		78,000

*Assuming FITC used was 100% pure and each reaction went to completion.

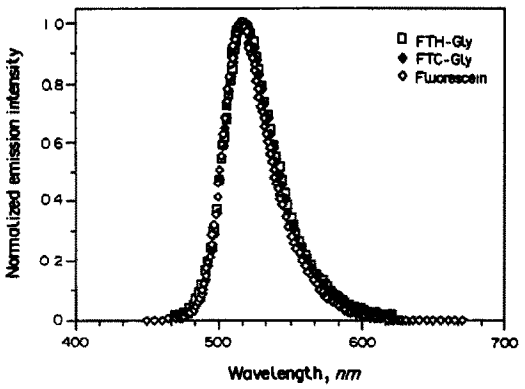

Fig. 3. The normalized emission spectrum of Fluorescein (◇), FTH-gly (□) and FTC-gly (◆). The measurements were performed on a Turner spectrofluorometer model 430, with an excitation wavelength of 322 nm, slit of 15 mm, range of × 100 and high sensitivity. The fluorescein solution contains $1.12 \times 10^{-7}M$ fluorescein in $0.1N$ NaOH. The FTC-gly solution was prepared by diluting the solution stated in Fig. 2 with 5mM carbonate buffer (pH 10) to $1.18 \times 10^{-7}M$. The FTH-gly solution was prepared by diluting the solution stated in Fig. 1 with 10mM (pH 7) phosphate buffer to $\sim 2 \times 10^{-7}M$.

differences in pH and ionic strength of the solvent, the molar absorptivities of fluorescein FTH-gly and FTC-gly at $\lambda = 488$ nm are similar. The differences of the molar absorptivities at $\lambda = 322$ nm are probably due to the presence of reaction byproducts for FTH-gly and FTC-gly but not in the sample of fluorescein. The molar absorptivities of FTH and FTC-tyr and -ala are somewhat lower than that of fluorescein. Similarly, the peak-heights for FTC-gly and FTH-gly are higher than the other derivatized amino acids.

The normalized emission spectra of fluorescein, FTH-gly, and FTC-gly are also very similar, Fig. 3, and the relative quantum yields of FTH-gly and FTC-gly, Table 3, can be estimated by comparison of their emission intensities with the emission intensity of fluorescein ($\Phi_{fluor} = 0.95$ for fluorescein in $0.1N$ sodium hydroxide).[14,15] The fluorescence quantum yield and emission spectra are similar for the other FTC and FTH amino acids that were studied. As a result, it is possible to tune the fluorescence detector of the capillary electrophoresis instrument to very high sensitivity for these derivatives.

Table 3. Fluorescence quantum yields of FTH-gly and FTC-gly*

Analyte	Quantum yield
FTH-Gly (pH 7)	0.4 ± 0.1
FTC-Gly (pH 7)	0.4 ± 0.1
FTC-Gly (pH 10)	0.5 ± 0.1

*Taking the quantum yield of fluorescein ($10^{-6}M$) in $0.1N$ NaOH solution as 0.95.[14,15]

See Fig. 3 for the preparation and concentration of the samples.

We have noted elsewhere that the fluorescence signal of FTC–amino acid derivatives does not increase linearly with laser power due to photodegradation.[9] Figure 4 shows the peak height and the detection limit of FTH amino acids as a function of the laser power. With increasing laser power, the fluorescent signal first increases and then, when the laser power is higher than 30 mW, becomes nearly constant. However, the background noise increased with laser power. As a result, the best detection limit was obtained at the laser power of about 25 mW.

Table 4 lists the detection limits of some FTH amino acids under capillary zone electrophoresis separation; detection limits range from 1 to 2 zeptomole (1 zeptomole = 1 zmole = 10^{-21} mole[16]). Generally speaking the detection limits for FTH–amino acids (except arginine) are about 1.5–2 fold superior to those obtained

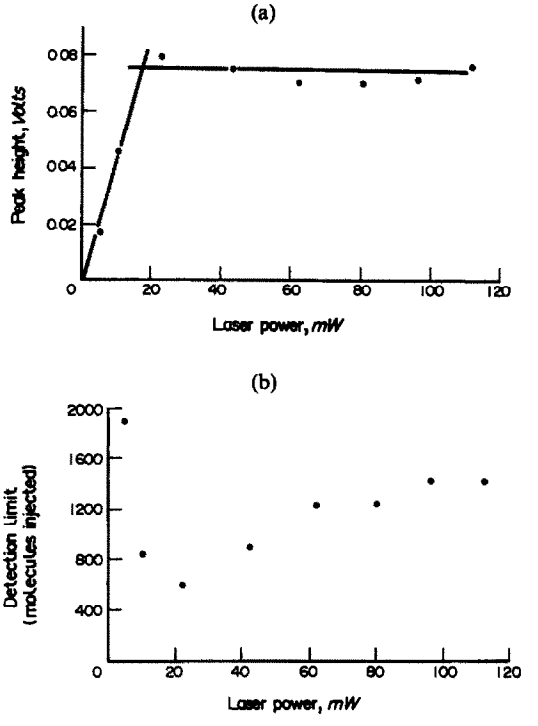

Fig. 4. The fluorescence signal of FTH amino acid by capillary zone electrophoresis and detected by laser induced detector as a function of the laser power applied. (a) Fluorescence signal (the straight lines give a guide); (b) detection limits (3σ) in units of number of analyte molecules injected.

Table 4. Detection limits of FTH amino acids

FTH amino acid	Injection volume, *nl*	Detection limit*		
		Concentration, $10^{-12}M$	Amount, *zmole*[16]	Molecules injected
Ala	0.59	2.5	1.4	800
Arg	0.76	2.6	2.0	1200
Asn	0.60	1.6	1.0	600
Asp	0.48	2.9	1.4	800
Glu	0.49	2.8	1.4	800
Gly	0.58	1.7	1.0	600
Hpro	0.60	1.8	1.1	650
Ile	0.62	2.1	1.2	700
Leu	0.62	1.9	1.2	700
Val	0.61	1.8	1.0	600

*Detection limits refer to the amount of analyte injected into the capillary that produces a signal three times larger than the standard deviation of the background signal.

for FTC–amino acids, both run with 10m*M* phosphate buffer at pH 7 elution buffer in electrophoresis, although their spectroscopic properties are similar as discussed above. This difference in detection limit arises because the retention time of the FTH amino acid is typically three-quarters of the retention time of the corresponding FTC amino acid. The peak height produced in the sheath-flow detector in capillary electrophoresis is inversely proportional to the retention time.[12]

It is interesting that the detection limit is not due to shot noise in the number of detected photons. Shot noise, governed by Poisson statistics, predicts that the noise in the measurements will scale as the square root of signal. Instead, a measurement of noise in the background signal as a function of laser power demonstrated a linear dependence of noise on signal; that is, the relative noise in the signal was constant, 0.5%. We presume that variations in the laser power, specified at 0.5%, are the major source of noise in this experiment. It is reasonable to assume that use of a more stable laser will produce a corresponding improvement in detection limit. The state of the art in ion laser stability is 0.1%. The use of this highly stable laser should result in a five-fold reduction in detection limits, from 600 analyte molecules to 120.

REFERENCES

1. P. Edman, *Acta Chem. Scand.*, 1950, **4**, 277.
2. P. Edman and G. Begg, *Eur. J. Biochem.*, 1967, **1**, 80.
3. S. Kent, L. Hood, R. Aebersold, D. Teplow, L. Smith, V. Farnsworth, W. Cartier, P. Hines, P. Hughes and C. Dodd, *Bio Techniques*, 1987, **5**, 314.
4. H. Maeda, N. Ishida, H. Kawauchi and K. Tuzimura, *J. Biochem.*, 1969, **65**, 777.
5. H. Kawauchi, K. Tuzimura, H. Maeda and N. Ishida, *ibid.*, 1969, **66**, 783.
6. H. Muramoto, H. Kamiya and H. Kawauchi, *Anal. Biochem.*, 1984, **141**, 446.
7. K. C. Waldron, S. Wu, C. W. Earle, H. R. Harke and N. J. Dovichi, *Electrophoresis*, 1990, **11**, 777.
8. Y. F. Cheng and N. J. Dovichi, *Science*, 1988, **242**, 562.
9. S. Wu and N. J. Dovichi, *J. Chromatog.*, 1989, **480**, 141.
10. J. V. Sweedler, J. B. Shear, H. A. Fishman and R. N. Zare, *Anal. Chem.*, 1991, **63**, 496.
11. C. A. Monnig and J. W. Jorgenson, *ibid.*, 1991, **63**, 802.
12. Y. F. Cheng, S. Wu, D. Y. Chen and N. J. Dovichi, *ibid.*, 1990, **62**, 496.
13. K. Otsuka, S. Terabe and T. Ando, *J. Chromatog.*, 1985, **332**, 219.
14. S. Wu and N. J. Dovichi, *J. Appl. Phys.*, 1990, **67**, 1170.
15. J. H. Brannon and D. Magde, *J. Phys. Chem.*, 1978, **82**, 705.
16. G. R. Freeman, *Private Communication*; zepto, $z = 10^{-21}$ and yocto, $y = 10^{-24}$ were accepted as prefixes by the Comité International des Poids et Mesures in October 1990 to be put forward to the Conférence Générale des Poids et Mesures for adoption in October 1991.

Talanta, Vol. 39, No. 2, pp. 179–185, 1992
Printed in Great Britain.

0039-9140/92 $5.00 + 0.00

DECOMPOSITION OF $Cu(PCD)_2$ EXTRACTED INTO IBMK AND DIBK PHASES FROM HYDROCHLORIC ACID MEDIA

MASAHIKO MURAKAMI,* HIROSHI TADANO† and TAKEO TAKADA

Department of Chemistry, College of Science, Rikkyo (St. Paul's) University, Nishi-Ikebukuro, Toshima-Ku, Tokyo 171, Japan

(*Received* 5 *October* 1990. *Revised* 30 *April* 1991. *Accepted* 8 *May* 1991)

Summary—The decomposition of the bis(1-pyrrolidinedithiocarbamato) copper(II) complex [$Cu(PCD)_2$] extracted into isobutyl methyl ketone (IBMK) and di-isobutyl ketone (DIBK) from hydrochloric acid solution (0.01–8*M*) has been studied with UV-visible and ESR spectrometry. The mixed-ligand complex CuCl(PCD) is formed as an intermediate and $CuCl_2$ or $CuCl_3^-$, are formed as final products, in the decomposition of $Cu(PCD)_2$. The concentration of free hydrochloric acid dissolved in the extract has also been determined, and the effect of the free acid on the decomposition has been studied. The decomposition reaction of $Cu(PCD)_2$ extracted from hydrochloric acid solution can be thought of as a ligand substitution by Cl^-, and occurs with both IBMK and DIBK extraction.

Ammonium 1-pyrrolidinecarbodithioate (APCD) is one of the most widely used reagents for solvent extraction of metal chelates, since it forms stable and extractable chelates with a large number of elements in a relatively low pH region. Although dithiocarbamates, including APCD, are decomposed in acidic solution, APCD shows the highest stability amongst them.[1,2] We have studied the extraction of Cu(II) from highly acidic solution (0.01–8*M* hydrochloric acid) into isobutyl methyl ketone (IBMK)[3,4] or di-isobutyl ketone (DIBK)[5] with APCD. It was defined that the copper chelate is quantitatively extracted from such a media provided a large excess of reagent was used; DIBK is preferred for such a purpose.

In these studies, we observed the characteristic decomposition behaviour of the chelate extracted into both solvents; the copper chelate is stable for a certain period of time but then, it suddenly begins to decompose. As stated earlier, preventing the decomposition of the chelate is important for its extraction in strongly acidic media. It was also reported that the decomposition of the metal–PCD chelate extracted into IBMK causes problems in analysis; however, although several reports commented on the kinetic stability and decomposition of the metal–PCD chelate extracted into IBMK, they have merely discussed the practical point of view, and have not reported its behaviour in detail.[6–8]

Therefore, we have systematically studied the decomposition of the Cu(II)–PCD chelate extracted into IBMK and DIBK via UV-visible and ESR spectrometry, and have discussed its mechanism.

EXPERIMENTAL

Reagents

All chemicals used were of reagent grade. Water was redistilled from an all-glass apparatus. The standard stock solution (1000 μg/ml) of copper was prepared from 99.99% pure metal. The solution was appropriately diluted with water to give a desired working solution concentration. All solvents were used without further purification.

Procedure

Extraction. A 20-ml portion of hydrochloric or nitric acid of desired concentration and 2.5 ml of copper working solution were transferred to a 100-ml separating funnel, and 10 ml of IBMK or DIBK as well as 2.5 ml of APCD solution were added. Combinations of $1.6 \times 10^{-4}M$ copper and $8.0 \times 10^{-4}M$ APCD solutions, and $8.0 \times 10^{-4}M$ copper and $4.0 \times 10^{-3}M$ APCD solutions were chosen to give extracts containing $4.0 \times 10^{-5}M$ and $2.0 \times 10^{-4}M$ copper chelate, respectively.

*Author for correspondence.
†Deceased.

Through the present study, relatively dilute solutions of APCD (in both cases corresponding to about a 5-fold ratio to copper) were used, in order to hasten the point of time at which the chelate decomposes. After the mixture was mechanically shaken virogously, the aqueous phase had been withdrawn and the extract was filtered through a phase separation filter paper (Whatman 1PS "phase separators").

UV-visible measurements. All UV-visible spectra were measured with a Shimadzu model UV-240 spectrophotometer equipped with a water-surrounded cell holder and micro stirrer. A 10-mm and a 5-mm quartz cell were used for measurement of the samples containing $4.0 \times 10^{-5}M$ and $2.0 \times 10^{-4}M$ copper chelate, respectively. The spectrum was measured in the range 350–500 nm, at 45-sec intervals against IBMK or DIBK as reference. The sample was kept in the cell compartment of the spectrophotometer throughout the period, and the temperature was kept constant at 25°, with a Yamato CTE-22W "Coolnics" and a water-bath. Timing was started when the reagent was added to the mixture.

ESR measurements. ESR measurements were made with a JEOL model JES-ME-3X spectrometer and a 1-mm i.d. quartz capillary cell. A magnetic field was applied at 3300 ± 500G with 100 KHz modulation; and the modulation amplitude of 6.3G was used for the majority of the measurements. The magnetic field was calibrated with a JEOL model JES-FC-2 NMR marker and a Takeda Riken model TR-5766 frequency counter.

Formation of CuCl(PCD). The mixed ligand complex, CuCl(PCD), was formed from the reaction of $Cu(PCD)_2$ and $CuCl_2$ as follows. Into a centrifuge tube was transferred 5-ml of $Cu(PCD)_2$, $1 \times 10^{-4}M$ IBMK solution and 5 ml of $1 \times 10^{-4}M$ $CuCl_2$ IBMK solution, and the mixture was shaken vigorously for 2 min. To remove the remaining $CuCl_2$, 10 ml of water was added to the tube and it was mechanically shaken for 2 min. After the mixture had separated into layers, the upper phase was filtered through a phase separation filter paper.

Determination of free hydrochloric acid in the extract. The free hydrochloric acid dissolved in the DIBK and IBMK phase was determined as follows. A 25-ml volume of hydrochloric acid of the desired concentration and 10 ml of IBMK or DIBK were transferred to a 100-ml separating funnel and the mixture was mechanically shaken vigorously for 300 sec. It was then allowed to stand until the layers separated clearly. After they had separated, a suitable portion (1–5 ml) of the upper phase and 10 ml of water were transferred to a 100-ml separating funnel, and again the mixture was mechanically shaken vigorously for 120 sec. After the layers had separated, the pH of the lower phase was measured with a pH meter. Blanks for acidic impurities in the solvents and absorbed atmospheric carbon dioxide were obtained by pH measurements of water which had been shaken with fresh solvents.

RESULTS AND DISCUSSION

Analysis of the decomposition reaction of $Cu(PCD)_2$

UV-visible spectrum. The decomposition behaviour of $Cu(PCD)_2$ extracted from hydrochloric acid solution and its dependence on the acid concentration of the aqueous phase have been studied with UV-visible spectrophotometry. The change in absorbance of $Cu(PCD)_2$ extracted into IBMK at 433.5 nm is shown in Fig. 1, and the change in the absorption spectrum, at 45-sec intervals, of $Cu(PCD)_2$ extracted into IBMK is shown in Fig. 2; in both cases, the initial concentration of the chelate was $4.0 \times 10^{-5}M$. The absorbance of $Cu(PCD)_2$ extracted from both $2M$ [Fig. 1(a)] and $4M$ [Fig. 1(b)] hydrochloric acid were constant for a certain time and then suddenly decreased. The shape of the absorbance–time curves change with the acid concentration.

When $4.0 \times 10^{-5}M$ chelate extracted from $\leqslant 2M$ hydrochloric acid, it was shown that an inflection point is observed in the absorbance–time curve, and after that the rate of decrease in the absorbance declines with time. In

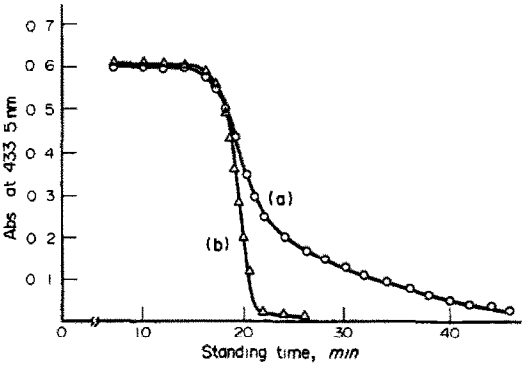

Fig. 1. Change in absorbance of Cu(II)–PCD chelate in IBMK phase: (a) extracted from $2M$ HCl, (b) extracted from $4M$ HCl; [APCD] $8 \times 10^{-5}M$.

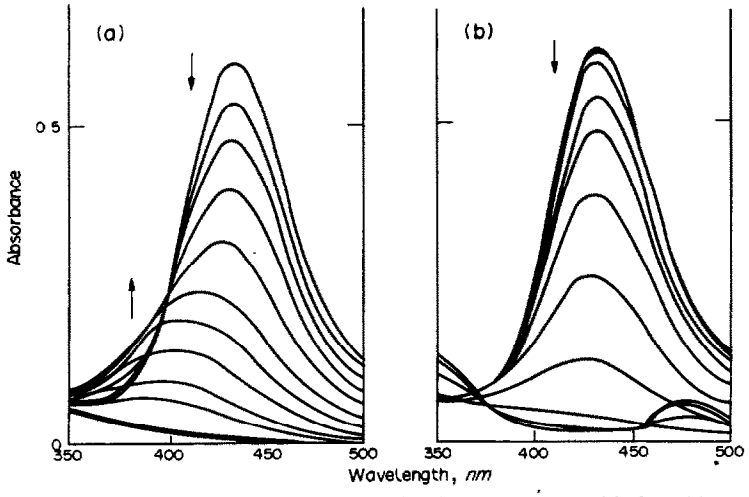

Fig. 2. Change in UV-visible spectra of Cu(II)–PCD chelate in IBMK phase with time: (a) extracted from $2M$ HCl, (b) extracted from $4M$ HCl; time intervals 45 sec; [APCD] $8 \times 10^{-5}M$.

the case of $2M$ [Fig. 1(a)], the inflection point is shown in the curve at the point when the absorbance is reduced to about 50% of its initial value (20–22 min of the standing time), and after that the slope of the curve becomes less steep. Such a profile of decreasing the absorbance was observed when the chelate was extracted from $\leqslant 2M$ hydrochloric acid. As the acid concentration of the aqueous phase was decreased to $\sim 0.01M$, the same profiles as that shown in Fig. 1(a) were observed, although the inflection point became obvious at an earlier stage of the decrease in the absorbance and although the rate of decrease in the absorbance was very slow.

The typical profile of the change in the absorbance spectrum for the above case is shown in Fig. 2(a); it shows the change in the absorbance spectrum of $4.0 \times 10^{-5}M$ $Cu(PCD)_2$ extracted into IBMK from $2M$ hydrochloric acid, at 45-sec intervals. The peak of the spectrum which initially existed at about 433.5 nm is gradually shifted to shorter wavelengths as the absorbance decreases. In this case, an isosbestic point was observed at about 400 nm in the early stages of the spectrum change. However, it shifted to a shorter wavelength with a decrease in absorbance, and then was no longer observed. Such a spectral change suggests the presence of an intermediate product and that the greater part of its spectrum is overlapped with that of $Cu(PCD)_2$. After the initial peak had disappeared, no absorption peak remained in the visible region, although a weak band was observed below about 400 nm [Fig. 2(a)]. This type of spectrum was observed when the copper chelate had been extracted from $\leqslant 2M$ hydrochloric acid.

When $4.0 \times 10^{-5}M$ $Cu(PCD)_2$ was extracted from $\geqslant 3M$ hydrochloric acid, the absorbance drops more steeply than when extracted from $2M$, as shown in Fig. 1(b). As shown in our previous studies,[4,5] such a drop in the absorbance was observed when $Cu(PCD)_2$ was extracted from 4–$8M$ hydrochloric acid solution into IBMK or DIBK phase, regardless of the amount of APCD. The change in the absorption spectrum for such a case is shown in Fig. 2(b) which shows the results for $4M$ acid. Although it is less marked than for $2M$ acid, the shift of the peak to shorter wavelength with a decrease in its absorbance was also observed, regardless of the acid concentration. The isosbestic point was slightly observed only in the very early stages of the decomposition, and little increase in absorbance was observed below about 400 nm.

However, the spectra of the final products are altered with the acid concentration. In contrast to the case of $2M$, an absorption peak was in the end observed with $4M$ acid at about 480 nm, ϵ being in the order of $1.5–2.0 \times 10^3$ $l.mole^{-1}.cm^{-1}$; a stronger absorption band than that shown in Fig. 2(a) appears in the region below 350 nm [Fig. 2(b)]. Such a spectrum was observed when the copper chelate was extracted from 3–$8M$ hydrochloric acid solution. However, in the case of $3M$ acid, the final spectrum was almost the same as Fig. 2(b), but its absorbance at 480 nm was lower than that shown in Fig. 2(b). It suggests that the final species shown in the case of $4M$ acid forms only partly at $3M$ concentration. The above results

for the change in the UV-visible spectrum suggest that the behaviour of the decomposition is gradually changed when the concentration of hydrochloric acid in the aqueous phase is increased from 2 to $4M$, when the initial concentration of $Cu(PCD)_2$ in the IBMK extract is $4.0 \times 10^{-5}M$.

On the other hand, when the initial concentration of $Cu(PCD)_2$ is increased to $2.0 \times 10^{-4}M$, similar profiles of a decrease in the absorbance and similar spectral changes as above were also observed. However, the acidity ranges, in which each profile was observed, shifted to higher values than those in the case of $4.0 \times 10^{-5}M$. When the chelate was extracted from $3M$ or below, the same profile as that in Fig. 1(a) and the same final spectrum as that shown in Fig. 2(a) were observed. It was observed, however, that a small peak due to the intermediate product remains at about 400 nm. The intensity of the remaining peak increased as the acid concentration was decreased which suggests that in these conditions the extent of progress in the decomposition reaction depends on the acid concentration. When the chelate was extracted from $\geqslant 4M$ hydrochloric acid, the absorbance dropped steeply with the same profile as shown in Fig. 1(b), and in the case of $5M$ or above, the same final spectra was observed as those shown in Fig. 2(b), whereas in the case of $4M$ these spectra were only partly observed. Thus, when the initial concentration of $Cu(PCD)_2$ is $2.0 \times 10^{-4}M$, the behaviour of the decomposition is gradually changed when the concentration of hydrochloric acid in the aqueous phase is increased from 3 to $5M$.

ESR spectrum. Figure 3(a) shows the initial ESR spectrum of $2.0 \times 10^{-4}M$ $Cu(PCD)_2$ extracted into IBMK from $4M$ hydrochloric acid, measured 12 min after the extraction. There were four split absorption bands, with ESR parameters of $g = 2.048 \pm 0.002$ and $a = 79 \pm 1G$. This spectrum agrees with those of the series of bis(N,N'-disubstituted-dithiocarbamato)copper(II) complexes in various organic solvents.[9,10] With the decomposition of $Cu(PCD)_2$ chelate, a decrease in intensity of this band and the appearance of a new absorption band were observed. Figure 3(b) shows the spectrum measured at 33 min after the extraction. ESR parameters of this band are determined as $g = 2.077 \pm 0.002$ and $a = 75 \pm 2G$. The line width, defined as the peak-to-peak separation in a splitting line, of the new absorption band is relatively broad

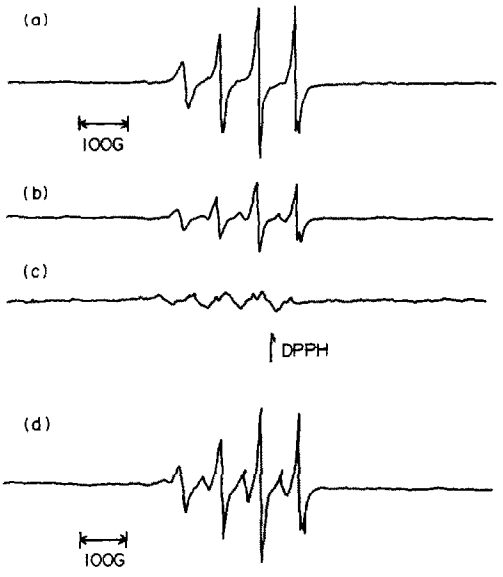

Fig. 3. Change in ESR spectra of Cu(II)–PCD chelate extracted in IBMK phase from $4M$ HCl [(a) 12 min, (b) 33 min and (c) 45 min after extraction, respectively] and (d) ESR spectrum observed in the reaction between $Cu(PCD)_2$ and $CuCl_2$ in IBMK.

(about $25G$). The intensity of the initial absorption band considerably decreased, and the new four splitting bands were overlapped with the initial band. Although the intensity of the new band once increased with decreasing that of the initial band [Fig. 3(c)], and soon it also decreases with time.

The appearance of this new band in the ESR spectrum corresponds to the existence of an intermediate species which is expected from the observations of the change in the UV-visible spectrum. Furthermore, when the chelate was extracted from $1M$ hydrochloric acid, it was found that the decomposition is stopped halfway and both bands remain, and it agrees with the behaviour observed in the UV-visible study on $2.0 \times 10^{-2}M$ $Cu(PCD)_2$. As mentioned above, it was observed that when the chelate was extracted from the aqueous phase of such an acidity the absorption spectrum due to the intermediate product remains. Therefore, it is taken that this new absorption band is due to the intermediate species.

Identification of the intermediate and the final product

Intermediate product. ESR spectra and parameters are similar to those of mixed-ligand copper(II) dithiocarbamate complexes with chloride, CuCl(dtc). Yordanov and Shopov[11] reported the ESR study on the formation of

these mixed ligand complexes by the reaction of some bis(N,N'-disubstituted-dithiocarbamato) copper(II) complexes with $CuCl_2$ in various organic solvent media, as follows:

$$Cu(dtc)_2 + CuCl_2 \rightleftharpoons 2CuCl(dtc) \qquad (1)$$

and the following parameters are reported for CuCl(dtc): $g = 2.073 \pm 0.002$ and $a = 72 \pm 2G$ in acetone, and $g = 2.076 \pm 0.002$ and $a = 69 \pm 2G$ in benzene. Although these parameters can be altered with a certain kind of solvent, they remain virtually unaltered with a substituent on the nitrogen atom in dithiocarbamic acid.

Hence, to identify the species of the intermediate, CuCl(PCD) complex was formed by the reaction of $Cu(PCD)_2$ with $CuCl_2$ in IBMK and its UV-visible and ESR spectra were measured, and compared with those which appear in the course of the decomposition of $Cu(PCD)_2$. Figure 3(d) shows the ESR spectrum which was observed with the reaction mixture of $Cu(PCD)_2$ and $CuCl_2$ in IBMK solution. Similar, to the spectrum which had been observed in the course of the decomposition of $Cu(PCD)_2$ [Fig. 3(b)], the four splitting absorption bands were overlapped with the absorption band of $Cu(PCD)_2$. The ESR parameters were determined to be $g = 2.075 \pm 0.002$ and $a = 74 \pm 1G$, values which closely agree with those of the intermediate. Furthermore, in the UV-visible spectrum of this reaction mixture, the absorption maximum appeared at about 420 nm, and it is similar to that observed in the course of the decomposition of $Cu(PCD)_2$ (Fig. 2). From these facts, it can be concluded that the intermediate product of the decomposition reaction of $Cu(PCD)_2$ extracted from hydrochloric acid media was CuCl(PCD).

Final products. UV-visible spectra of final products and their spectral change with hydrochloric acid concentration in the extract are similar to those of copper(II) chloride, $CuCl_2$, and the trichloro copper(II) complex, $LiCuCl_3$, in non-aqueous solution. Sawada *et al.* studied the equilibrium of copper(II) chloride with lithium chloride in acetic acid;[12] and in their paper, it was reported that when lithium chloride was added to a solution of copper(II) chloride, the $LiCuCl_3$ complex was formed, and this caused the following spectral change: the characteristic spectrum of $CuCl_2$, which shows an absorption maximum at 300 nm (ϵ is about 4×10^3 $l.mole^{-1}.cm^{-1}$), was changed to that of $LiCuCl_3$, which shows a maximum at about 310 nm (ϵ being of the order of several thousands) and at about 450 nm (ϵ being about 1×10^3 $l.mole^{-1}.cm^{-1}$).

On the basis of this report, it was attempted to measure the absorption spectrum of $CuCl_2$ dissolved in IBMK or DIBK. Although the value of ϵ could not be determined since $CuCl_2$ was sparingly soluble in both solvents ($10^{-4}M$ at most), a spectrum similar to that in acetic acid solution was observed. Furthermore, a spectrum similar to $LiCuCl_3$ and to the final product in the case of the copper chelate extracted from $3M$ or above hydrochloric acid solution, was observed when $CuCl_2$ was dissolved in the IBMK containing free hydrochloric acid. Hence, it was concluded that the final products of the decomposition of $Cu(PCD)_2$ extracted from hydrochloric acid media are copper(II) chloride complexes, and it was expected that the composition of the complex depends on the concentration ratio of the free hydrochloric acid to the initial copper(II) in the organic phase.

Effect of initial copper and free acid concentrations

From the results of above studies, it is noted that the decomposition profile and the final copper species depends on both the initial copper concentration and the hydrochloric acid concentration of the aqueous phase. It should be concluded that it is due to a change in the concentration ratio of the free hydrochloric acid to total copper in the extract. Hence, the free hydrochloric acid in the extract was determined, and the effect of the free acid on the decomposition behaviour was studied.

In the preceding paper,[5] we determined the free hydrochloric acid dissolved in the IBMK and DIBK phase with potentiometric titration. However, the titration could not be used in the present study since it was shown that the titration method could not be applied to the case in which the acidity of the aqueous phase is lower than 2 and $4M$ for IBMK and DIBK, respectively. In the previous study, it was also observed that when the extract is shaken with an aqueous phase the free acid can be almost completely transferred to the aqueous phase. Hence, we have tried to determine the free acid in the extract from the pH of the aqueous phase which had been used for washing the extract. To estimate the effectiveness of the method, the free acid concentrations in the DIBK phase which

Table 1. Comparison of titration and back extraction

Conc. of HCl in aq. phase (M)	Conc. of free acid in DIBK(M)	
	Titration	Back extraction
10	2.3×10^{-1}	3.4×10^{-1}
8	3.2×10^{-2}	3.1×10^{-2}
6	3.8×10^{-3}	3.7×10^{-3}
4	4.3×10^{-4}	2.9×10^{-4}

Aqueous phase 25 ml, organic phase 10 ml, shaking time 5 min.

had been determined by this method were compared with those of the titration. Table 1 shows that the values obtained with the present method closely agreed with that obtained by the potentiometric titration method. It indicates that the present method can be applied for determining a wide range of the free acid, and that it is a simpler and more rapid method compared to the titration.

The results of the determination of free acid dissolved in IBMK had been shaken with 0.1–5M hydrochloric acid shown in Table 2. It was observed that the free acid concentration of the extract is about 10^{-5}–$10^{-3}M$ in these conditions, and it corresponds to about 0.3–30-fold and 0.06–5.5-fold ratio to the total copper concentration of $4.0 \times 10^{-5}M$ and $2.0 \times 10^{-4}M$, respectively. Based on the free acid concentration obtained as above, the decomposition behaviours can be roughly classified by the ratio of the concentration of free acid to initial copper in the extract, as follows: (1) When the concentration of free acid is considerably higher than that of copper, the absorbance drops steeply as shown in Fig. 1(b), and the trichloro complex should be formed as the final product. (2) When the concentration of free acid is little more than that of copper, *i.e.*, about 2–3-fold, the absorbance again drops steeply [Fig. 1(b)]. However, the trichloro complex is only partly observed in the final products, the dichloro complex being the main species. (3) When the concentration of free acid is lower than that of copper, the decomposition is very slow and almost stops halfway.

Table 2. Free acid concentration in IBMK phase

Conc. of HCl in aq. phase (M)	Conc. of free acid in IBMK phase (M)
5	1.1×10^{-3}
4	3.4×10^{-4}
3	1.3×10^{-4}
2	4.5×10^{-5}
1	2.0×10^{-5}
0.1	1.3×10^{-5}

Aqueous phase 25 ml, organic phase 10 ml, shaking time 5 min, with filtration.

For example, in the case of an initial copper concentration of $4.0 \times 10^{-5}M$, the above decomposition behaviour [(1), (2) and (3)] was observed when the chelate was extracted from 4M or above; about 3M; and 2M or below hydrochloric acid solution, and they corresponded to 8.5-fold or above; about 3.3-fold; and 1.1-fold or below ratio to copper, respectively. Such a relationship as above between the decomposition and the concentration ratio of the free hydrochloric acid to the initial copper(II) is also observed when the initial copper(II) concentration is altered to $2.0 \times 10^{-4}M$. In this case, behaviour (1), (2) and (3) was observed when the chelate was extracted from 5M or above, 4M and 3M or below hydrochloric acid, and they corresponded to a 5.5-fold or above, 1.7-fold, and 0.65-fold or below ratio to copper, respectively. Thus, it was concluded that the decomposition behaviour and species of the final product are mainly determined by the relation between the copper concentration and the free acid concentration.

Difference between IBMK and DIBK

The decomposition behaviours of the chelate extracted into DIBK were compared with those of IBMK. On the whole, no difference in the behaviour of both solvents was found in both the UV-visible and ESR studies. In the case of DIBK, however, the same behaviour was observed as in the case of IBMK at higher acid concentration. For example, the same shape of the UV-visible spectra of the final products as that observed in up to $\sim 3M$ in IBMK extract [Fig. 2(b)] was observed in DIBK extract up to 6M. These facts indicate the difference in the amount of free hydrochloric acid remaining in each extract. As previously reported, the free acid in DIBK extract is much smaller than that in IBMK extract.[5]

CONCLUSIONS

Each species found in the respective steps in this reaction indicate that the decomposition reaction of $Cu(PCD)_2$ in the organic phase can be concluded to be the ligand exchange reaction of the copper complex with chloride. Based on the species in each step and considering the

effect of both concentrations of the free acid and the total copper on the decomposition behaviour, the following reaction scheme was assumed:

$$\begin{aligned} Cu(PCD)_2 + HCl &\rightarrow CuCl(PCD) \\ &\quad + C_4H_9N + CS_2 \\ &\quad \times CuCl(PCD) + (x-1)HCl \\ &\quad \rightarrow CuCl_x^{(2-x)} \ (x = 2 \text{ or } 3) \\ &\quad \rightarrow C_4H_9N + CS_2 \end{aligned} \qquad (2)$$

It is assumed that the free PCD^- ligand dissociated from the copper chelate reacts with a proton and is decomposed; Aspila and co-workers[13,14] made systematic studies on the decomposition mechanism of some dithiocarbamates, and concluded that only the acid form of the DTC molecule was decomposed into a corresponding amine [in this case, pyrrolidine (C_4H_9N)] and a carbon disulphide.

Such a decomposition of the dissociated PCD^- ligand is assumed as the "motive force" of decomposition of the copper chelate. In the present case, it seems that the PCD^- ligand is only slightly substituted with Cl^- if the ligand is not decomposed immediately after its dissociation from the copper chelate, since the formation constants of series of Cu(II) dithiocarbamato complexes are considerably larger than those of Cu(II) chloro complexes. Of course, it is expected that there are various other factors which affect the decomposition of $Cu(PCD)_2$ *i.e.*, decomposition of the ligand by its oxidation by air, presence of water dissolved in the extract, and so on. However, provided that the concentration of the free acid is sufficiently higher than that of the copper chelate, They are negligible and the above mechanism can be assumed.

In the present study, the same behaviour was observed in both solvents on the whole. Therefore, it was concluded that the above mechanism can be assumed in IBMK or DIBK system. To discuss the above mechanism in detail, the kinetics would need to be investigated. Some kinetic studies on the decomposition of $Cu(PCD)_2$ extracted from hydrochloric acid solution into IBMK or DIBK phases is in progress.

REFERENCES

1. A. Hulanicki, *Talanta*, 1967, **14**, 1371.
2. R. J. Everson and H. E. Parker, *Anal. Chem.*, 1974, **46**, 1966.
3. T. Takada, *Talanta*, 1982, **29**, 799.
4. M. Murakami and T. Takada, 1985, *ibid.*, **32**, 513.
5. *Idem*, *ibid.*, 1990, **37**, 229.
6. I. Dellien and L. Persson, *ibid.*, 1979, **26**, 1101.
7. R. F. Roberts, *Anal. Chem.*, 1977, **49**, 1862.
8. K. S. Subramanian and J. C. Meranger, *Analyst*, 1980, **105**, 620.
9. T. Vänngård and S. Åkerström, *Nature*, 1959, **184**, 183.
10. R. Pettersson and T. Vänngård, *Ark. Kemi.*, 1961, **17**, 249.
11. N. D. Yordanov and D. Shopov, *J. Inorg. Nucl. Chem.*, 1976, **38**, 137.
12. K. Sawada, H. Ohtaki and M. Tanaka, *ibid.*, 1972, **34**, 3455.
13. K. I. Aspila, V. S. Sastri and C. L. Chakrabarti, *Talanta*, 1969, **16**, 1099.
14. S. J. Joris, K. I. Aspila and C. L. Chakrabarti, *J. Phys. Chem.*, 1970, **74**, 860.

Talanta, Vol. 39, No. 2, pp. 187–190, 1992
Printed in Great Britain.

0039-9140/92 $5.00 + 0.00

SPECTROPHOTOMETRIC STUDY OF THE REACTION OF ZINC WITH *O*-HYDROXYBENZENEDIAZOAMINOAZOBENZENE AND ITS APPLICATION

WEI-FENG YANG, WAN-RU CHEN,* CHUNG-GIN HSU and WEI WANG

Department of Chemistry, East China Normal University, 3663 Zhong-Shan Road (N), Shanghai 200062, People's Republic of China

(*Received* 25 *July* 1989. *Revised* 23 *July* 1991. *Accepted* 24 *July* 1991)

Summary—A highly sensitive and selective procedure for spectrophotometric determination of zinc has been developed. At pH 10.6, in the presence of emulsifier *p*-octylpolyethyleneglycol phenylether (OP), zinc forms an orange–red complex with *o*-hydroxybenzenediazoaminoazobenzene (HDAA) which has an absorption maximum at 525 nm. The molar absorptivity is 1.50×10^5 l.mole^{-1}.cm^{-1}. Beer's law is obeyed for zinc in the range 0–13 μg/25 ml. The method has been applied to the spectrophotometric determination of trace amounts of zinc in aluminium alloy and in human hair. The proposed method is simple, rapid and accurate. No heating or separation is required.

Numerous methods for the spectrophotometric determination of zinc have been reported,[1] but few of them give high sensitivity and simple operation. *o*-Hydroxybenzenediazoaminoazobenzene (HDAA), a derivative of benzenediazoaminoazobenzene,[2,3] synthesized in our laboratory, with the following structure

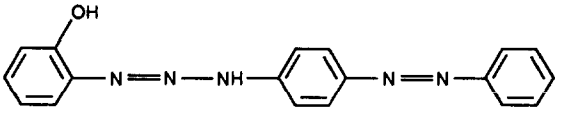

gives sensitive reaction with cadmium.[4,5] It was found that HDAA also gave a sensitive colour reaction with zinc in borax buffer of pH 10.6. The sensitivity for determination of zinc is superior to that of other triazenediyl reagents. In this work, the conditions for the zinc–HDAA complex formation were studied in detail. In the presence of the nonionic surfactant emulsifier OP, HDAA reacts instantaneously with zinc to form an orange–red 1:3 complex. The zinc–HDAA complex exhibits an absorption maximum at 525 nm with a molar absorptivity of 1.50×10^5 l.mole^{-1}.cm^{-1}. Beer's law is valid over the concentration range of 0–13 μg of zinc per 25 ml of solution. Using the masking agents, the colour reaction is free from interference by more than thirty ions investigated. The proposed method has been applied to the spectrophotometric determination of trace amounts of zinc in aluminium alloy and in human hair and offers the advantages of high sensitivity, simplicity, rapidity and high stability of the coloured solution, without heating or separation.

*Author for correspondence.

EXPERIMENTAL

Apparatus

Absorption spectra and absorbance were recorded with a Beckman DU-7HS spectrophotometer and a model 721 spectrophotometer (Shanghai Third Analytical Instruments Factory) with 1.0-cm cells. A Model pH S-2 pH meter (Shanghai Second Analytical Instruments Factory) was used to measure the pH values of the solutions.

Reagents

All reagents were of analytical reagent grade unless otherwise stated.

Standard zinc solution. Dissolve zinc oxide (99.99%) in sufficient concentrated hydrochloric acid, dilute to volume in a 100-ml calibrated flask and mix well. Dilute further to obtain a 5 μg/ml working standard solution.

HDAA solution. Dissolve 100 mg of HDAA in 500 ml of ethanol.

Borax buffer solution (pH 10.6). Add sodium hydroxide dropwise to a 0.05*M* borax solution to the required pH.

Emulsifier OP solution. A 5% w/v aqueous solution of OP (Shanghai First Reagent Factory) was used.

Recommended procedures

Procedure for study of the colour reaction of zinc. Take a test solution containing not more than 13 μg of zinc in a 25-ml calibrated flask, add 5 ml of pH 10.6 borax buffer, 2.5 ml of 5% emulsifier OP and 2.5 ml of 0.02% HDAA solution, successively dilute to the mark with water and mix well. Measure the absorbance at 525 nm in a 1.0-cm cell against a reagent blank.

Procedure for the determination of zinc in aluminium alloy. Take 0.2 g of a sample of alloy into a 100-ml beaker, add 10 ml of 20% sodium hydroxide and 3 drops of 30% hydrogen peroxide. Heat until the sample has been completely dissolved, then add 30 ml of distilled water. Heat the solution again to boiling and cool. Transfer the solution into a 100-ml calibrated flask, dilute to volume with distilled water and mix well. Filter the solution into a 200-ml beaker. Pipette 2.0 ml of the filtrate into a 25-ml calibrated flask and add hydrochloric acid (1 + 3) dropwise with swirling until a precipitate just appears and dissolves again. Finally, add 2.0 ml of 2% sodium fluoride, 1.0 ml of 0.5% thiourea solution, 2.0 ml of 1% sodium potassium tartrate and a few drops of 2% sodium hydroxide. Then follow the recommended procedure described above.

Procedure for the determination of zinc in human hair[6,7]

Place the hair sample, *ca.* 1.0 cm in length, in a 100-ml beaker, introduce sufficient 1% detergent solution to cover it and soak for 30 min at 60°. Pour out the detergent solution and wash the hair with distilled water until the foam completely disappears. Then add acetone and soak for 2 hr. Pour out the acetone and wash the hair three times with distilled water, dry for 90 min at 120° and store in a desiccator.

Place 0.2 g of treated human hair in a 100-ml beaker, add 5.0 ml of concentrated nitric acid, heat at a low temperature to decompose the sample and evaporate to almost 1.5 ml (the colour of the solution is bright orange–yellow). After cooling, add two portions of 1 ml of 30% hydrogen peroxide and each time heat continuously until the solution becomes colourless. Transfer the solution into a 50-ml calibrated flask, dilute to volume with distilled water and mix well. Pipette 1.0 ml of the solution into a 25-ml calibrated flask and add 1–2 drops of 2*M* sodium hydroxide, 2.0 ml of 1% sodium potassium tartrate and then follow the above recommended procedure for the determination of zinc.

*Tween-20; polyoxyethylene sorbitan monolaurate (Shanghai Chemical Reagent Supply Centre).

RESULTS AND DISCUSSION

Absorption spectra

The absorption spectra of HDAA and the zinc–HDAA complex are shown in Fig. 1. The absorption maximum of the reagent is at 436 nm and of the complex at 525 nm.

Conditions for complex formation

Since a surfactant should be used as a solubilizing agent, various surfactants were tried for this purpose. Of the eight surfactants tried, namely cetylpyridinium chloride, polyvinyl alcohol, sodium dodecylbenzenesulphonic acid, polyvinyl pyrrolidone, polyethylene glycol 10,000, Tween-20,* Triton X-100 and emulsifier OP, it was found that Triton X-100 and emulsifier OP gave a remarkable increase in sensitivity of the zinc–HDAA complex, hence emulsifier OP was chosen for all subsequent work. The optimum amounts of 5% emulsifier OP solution added were 1.0–4.0 ml in 25 ml of solution. An addition of 2.5 ml was recommended.

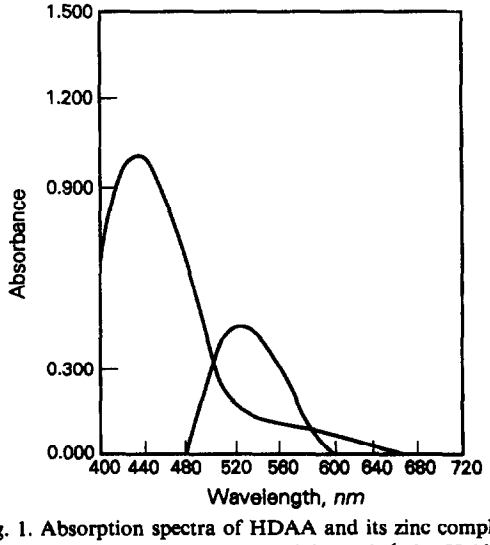

Fig. 1. Absorption spectra of HDAA and its zinc complex (1) HDAA against water HDAA, $3.02 \times 10^{-6}M$; pH 10.6; emulsifier OP, 0.6%. (2) Zn (10 μg)–HDAA complex against reagent blank HDAA, $3.02 \times 10^{-6}M$; pH 10.6; emulsifier OP, 0.6%.

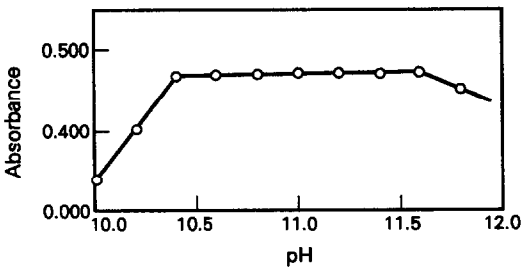

Fig. 2. Effect of pH. Absorbance of complex measured against corresponding reagent blank.

The absorbance of the complex depends on the pH of the solution, as shown in Fig. 2. The maximal and constant absorbance was attained in the pH range 10.4–11.6. Therefore a pH of 10.6 was chosen for the determination.

Addition of 2.0–7.0 ml of borax buffer gave maximal and constant absorbance of the complex for 5.0 μg of zinc. Hence an addition of 5.0 ml was appropriate.

Under the conditions employed, the volumes of 0.02% HDAA solution required to obtain maximal and constant absorbance for 5.0 μg of zinc were 2.0–5.0 ml, therefore 2.5 ml of HDAA solution were introduced.

Characteristics of the complex

In pH 10.6 borax buffer, the absorbance reached its maximum instantaneously and remained stable for at least 24 hr. Normal variations in laboratory temperature will have no effect on the complex, but the solution becomes turbid above 50°.

Adherence to Beer's law and sensitivity

The absorbance is a linear function of zinc concentration in the range 0–13 μg in 25 ml of solution. The apparent molar absorptivity of the complex is 1.50×10^5 l.mole^{-1}.cm^{-1}.

Composition of the complex

The composition of the complex was determined by the continuous variation method and the mole-ratio method. A ratio of zinc to HDAA was found to be 1:3 in the complex by both methods.

Effect of foreign ions

The effects of various ions on the determination of zinc was studied and their tolerance limits are listed in Table 1. If an error of 5% in the absorbance reading is considered tolerable, as shown in Table 1, most of the interfering ions can be masked and the selectivity of the method will be improved. Therefore, the method can be applied to the determination of trace amounts of zinc without separation.

Table 1. Tolerance limits of foreign ions in the determination of 5.0 μg of zinc

Foreign ion	Tolerance limit, μg	Ion/Zn(II)
NH_4(I)	350	70
K(I)	45,000	9000
Na(I)	45,000	9000
Ag(I)	10	2
Au(I)	10	2
Ca(II)	100	20
Sr(II)	100	20
Ba(II)	30	6
Mg(II)	1000	200
Cu(II)*	20	4
Ni(II)†	10	2
Mn(II)	8	1.6
Pd(II)	10	2
Co(II)†	25	5
Hg(II)†	80	16
Cd(II)†	20	4
Pb(II)†	50	10
Fe(III)‡	20	4
Bi(III)	100	20
Ga(III)	10	2
Cr(III)	2	0.4
Al(III)§	150	30
Ce(III)	10	2
In(III)	20	4
Ti(IV)	2.5	0.5
Sn(IV)†	5	1
Zr(IV)	10	2
V(V)	100	20
W(VI)	10	2
Mo(VI)	5	1
Chloride	10,000	2000
Nitrate	10,000	2000
Sulphate	10,000	2000
Phosphate	500	100
Silicate	300	60
Sodium potassium tartrate	1%, 2.0 ml	‖
Sodium fluoride	2%, 3.0 ml	‖
Sodium diethyldithiocarbamate (DDTC)	0.1%, 3.0 ml	‖
Thioures	0.3%, 1.0 ml	‖

*Add 1.0 ml of 0.5% thiourea. †Add 3.0 ml of 0.1% DDTC. ‡Add 2.0 ml of 1% sodium potassium tartrate. §Add 2.0 ml of 2% sodium fluoride. ‖No interference.

Application to aluminium alloy and human hair

The method has been applied to the determination of zinc in real samples. The results obtained for standard samples of aluminium alloys, given in Table 2, agreed well with the certified values. The recovery of zinc was in the range 95.8–101.7%.

The results obtained for several human hair samples, presented in Table 3, agreed well with those obtained by atomic-absorption spectrometry. The recovery of zinc is in the range 99.92–101.2%.

Table 2. Determination of zinc in standard aluminium alloys

Alloy	LF2	LT1	ZL9
Certified composition, %	Cu, 0.11; Mg, 2.97; Mn, 0.36; Fe, 0.47; Si, 0.50; Ti, 0.0029; Zn, 0.20; Ni, 0.0027;	Cu, 0.11; Mg, 0.055; Mn, 0.080; Fe, 0.49; Si, 5.55; Ti, 0.012; Zn, 0.16; Ni, 0.0061; Pb, 0.017	Mg, 0.72; Mn, 0.12; Fe, 0.63; Si, 12.98; Zn, 0.11; Cu, 0.30; ΣRE, 1.02
Certified value zinc, %	0.20	0.16	0.11
Zn found, %*	0.202	0.166	0.106
Relative standard deviation, %	0.47	0.36	1.45
Zn added, μg	2.0	2.0	—
Zn found, μg†	1.95	1.99	—
Recovery, %	95.8–99.2	96.8–101.7	—

*Mean of nine determinations.
†Mean of four determinations.

Table 3. Results for determination of zinc in hair

Sample*	Zinc found, *ppm*		Relative standard deviation, %
	Atomic-absorption spectrophotometry	Present method†	
A	247	247	0.5
B	216	216	1.0
C	241	241	0.5

*A—The hair sample of a pregnant woman. B—The hair sample of an old woman. C—The hair sample of a young woman.
†Mean of five determinations.

Table 4. Sensitivities of methods for the spectrophotometric determination of zinc

Reagent	Medium or solvent	λmax, *nm*	$\epsilon \times 10^{-4}$ ($l.mole^{-1}.cm^{-1}$)	Reference
PAN, Triton X-100	pH 8.0–9.5	555	5.6	8, 9, 10
PAR, CTMAB	pH 9.2–10.2	505	8.21	11
5-Br-PADAP, Triton X-100	pH 7.8–9.0	565	12.0	12
3,5-di-Br-PADAP	pH7.0–10.0	570	13.0	13
Phenylfluorone	pH 7.7–8.2	585	8.0	14
Malachite Green, SCN^-	pH 5.8, C_6H_6 or CCl_4, C_6H_{12} (5 + 1) extraction	626–632	10.0	15
Tetrabromofluorescein, Phenanthroline	pH 7.0–8.0 $CHCl_3$ extraction	540	12.0	16
Dithizone	pH 4.0–11.0	530	9.6	17
Cadion 2B; Triton X-100	pH 8.5–9.8	524	10.0	18
HDAA, emulsifier OP	pH 10.4–11.6	525	15.0	Present method

Comparison with other reagents

HDAA in the presence of emulsifier OP is one of the most sensitive reagents available for the spectrophotometric determination of zinc. The proposed method is simple, rapid and accurate as compared with the published methods. The sensitivities of various reagents are listed in Table 4 for comparison.

REFERENCES

1. Z. X. Wang, *Yejing Fenxi*, 1987, **7**, 51.
2. L. P. Yang, J. M. Pan and H. M. Guo, *Huaxue Shiji*, **167**, 1988.
3. L. P. Yang, J. M. Pan, C. G. Hsu, W. Wang and Y. Ye, *Journal of East China Normal University (Natural Science)*, 1988, **4**, 55.
4. C. G. Hsu, W. Wang, L. P. Yang, J. M. Pan and Y. F. Wang, *Lihua Jianyan*, 1989, **25**, 76.
5. *Idem*, *Mikrochim. Acta*, 1989 **I**, 313.
6. G. Xie, *Huanjing Huaxue*, 1989, **8**, 58.
7. S. J. Li, W. B. Zhang and J. Z. Yan, *Lihua Jianyan*, 1983, **24**, 230.
8. Shanghai Institute of Materials, *ibid.*, 1978, **14**, 6.
9. H. Watanabe and Y. Sakai, *Bunseki Kagaku*, 1974, **23**, 396.
10. H. Watanabe and H. Tanaka, *Talanta*, 1973, **25**, 535.
11. W.-B. Qi and L-Z. Zhu, *ibid.*, 1985, **32**, 1013.
12. X. T. Lin, *Fenxi Huaxue*, 1981, **9**, 198.
13. T. Zhe and S. S. Wu, *Talanta*, 1984, **31**, 624.
14. S. Sakuraba, *ibid.*, 1984, **31**, 840.
15. P. P. Kish, I. I. Zimomrya and Y. A. Zolotov, *Zh. Anal. Khim.*, 1973, **28**, 252.
16. M. M. Tananaiko and N. S. Bilenko, *Zavod. Lab.*, 1976, **42**, 1161.
17. J. M. Pan and Y. S. Chen, *Chromogenic Reagents and Their Applications in Metallurgical Analysis*, p. 272. Shanghai Publishing House of Science and Technology, Shanghai, 1984.
18. N. K. Shen, W. T. Chu, Z. Y. Chen, W. L. Xiao and Y. R. Zhu, *Analyst*, 1987, **112**, 301.

Talanta, Vol. 39, No. 2, pp. 191–193, 1992
Printed in Great Britain.

0039-9140/92 $5.00 + 0.00

ANALYTICAL NOTE

ERBIUM DETERMINATION IN PREFORMS OF OPTICAL FIBRES BY INDUCTIVELY COUPLED PLASMA–ATOMIC EMISSION SPECTROMETRY

A. LOPEZ-MOLINERO,* A. VILLAREAL and J. ANZANO
Department of Analytical Chemistry, Science Faculty, University of Zaragoza, 50009 Zaragoza, Spain

(*Received* 6 *November* 1990. *Revised* 25 *July* 1991. *Accepted* 2 *August* 1991)

Summary—Erbium which is used in the composition of heavy metal fluoride optical fibres was determined in preforms of these materials by inductively coupled plasma–atomic emission spectroscopy (ICP–AES). The new analytical procedure developed comprises: solid sample dissolution, via an alkaline fusion with sodium carbonate, and acid leaching with dilute hydrochloric acid, and measurements of emission intensities of 337.276 nm. This method has a detection limit of 31 ng/ml and a reproducibility of 0.90% r.s.d.

Optical fibre cables are now used extensively for telecommunications applications. In this field, the development of heavy metal fluoride (HMF) glasses for use in a new generation of low loss optical fibres is receiving considerable attention. The basic composition of HMF fibres includes fluorides of: metallic transition elements, alkaline, alkaline earth and rare earth elements. This last group includes erbium.

Control of the fibre composition is of great importance because the performance such as attenuation loss is expected to depend on the presence of impurities and the element concentration.

One of the characteristics of optical fibres is the extreme difficulty in decomposing and dissolving these inorganic solids. For the direct analysis of the solid, AAS with electrothermal atomization and hot hollow-cathode emission spectrometry[1] or by NAA[2] has been proposed. Nevertheless, several dissolution procedures have been published. They are based principally on acid attack ($HF–H_2SO4$),[3] but all are very time-consuming and require considerable experimental experience.

In this report we present the determination of erbium in preforms from which the HMF optical fibers are obtained. As dissolution procedure we propose a decomposition based on alkaline fusion and as determination method we measure the erbium ionic emission (at 337.276 nm) in solution by inductively coupled plasma–atomic emission spectroscopy (ICP–AES).

*Author for correspondence.

EXPERIMENTAL

Apparatus

A Perkin–Elmer P 40 plasma spectrometer, consisting of a 40-MHz free running generator operating at 1.0 kW and containing a dismountable torch was used. The observation height was 15 mm above the coil. Gas feed pressure to the plasma was 5 bar. The flow of gases were: nebulizer gas (0.7 l./min), intermediate gas (0.6 l./min) and outer gas (12 l./min). Solutions were introduced into the plasma by a cross-flow nebulizer at 1 ml/min solution uptake rate, utilizing a peristaltic pump.

Reagents

Standard erbium solution (1000 μg/ml) was prepared by dissolving 0.1143 g of erbium trioxide (Er_2O_3) in the least quantity of concentrated hydrochloric acid and subsequently dilution with demineralized water in a 100-ml standard flask. Another standard Er solution was prepared from 0.1322 g of erbium fluoride (ErF_3) and fusion with 0.92 g of sodium carbonate in a platinum crucible. The melt was dissolved in 25 ml of 1*N* hydrochloric acid and subsequently diluting with demineralized water in a 100-ml standard flask.

Solutions of other elements present in the fibre composition (Al, Ba, Cd, La, Li, Mg, Na and Zn) were prepared at a concentration of 1000 μg/ml from the corresponding nitrate (analytical grade quality). Solutions of other reagents were prepared by dissolution and/or dilution with demineralized water.

Standardization of erbium compounds

The erbium compounds (oxide and fluoride) were standardized by complexometric titration with EDTA, using Xylenol Orange as indicator.[4]

Preparation of the real samples

The sample was ground in an agate mortar to produce a powder with a particle size under 150 μm. This powder (0.1726 g) is mixed intimately with sodium carbonate. The proportion of sample to 'flux' is 1 : 7. The mixture is placed in a platinum crucible and heated appropriately. Then the solidified melt is dissolved in diluted hydrochloric acid (1*M*) and diluted with demineralized water in a 100-ml standard flask to give an acidity of 0.1*M* hydrochloric acid.

Analysis procedure

The standards for the calibration graph are prepared in a 100-ml standard flask from the standard erbium solution (Er_2O_3) diluting to volume with 0.1*M* hydrochloric acid. The erbium content of these solutions ranges from 0.10 to 100.00 μg/ml. The emission of the real samples at 337.276 nm is interpolated on the linear graph obtained.

RESULTS AND DISCUSSION

Choice of analysis line

The bibliography gives a list of the atomic and ionic emission lines of erbium which are potentially of use,[5,6] but only ionic lines are analytically useful. Their sensitivity and the possible interferences due to the main elements (as matrix effect or concomitant elements, and spectral interferences) that make up the sample and the fusion reagent were evaluated. As a result of this study, the ionic line at 337.276 nm with a 31-ng/ml detection limit is proposed as the analytical line.

Analysis conditions

Important matrix effects in the ICP are found to be due to variations in the acid content.[7,8] For that reason and because hydrochloric acid is necessary in the dissolution procedure, we studied the influence of the concentration of hydrochloric acid. We found that 1*M* hydrochloric acid depresses the intensity of erbium, by about 11%, as compared to aqueous solution, while 0.1*M* only results in a 6% decrease of the signal. Therefore, as a compromise, 0.1*M* hydrochloric acid was used to prepare the standards.

Table 1. Analysis of the artificial preform of optical fibre sample solution

Er added	Er found	% recovery	% r.s.d.
0.40	0.388	97.0	4.95

number of determinations = 10

composition of the artificial sample solution (μg/ml):

element	concentration	element	concentration
Na	3900	Cd	430
Ba	370	Zn	270
La	70	Al	20
Li	10		

Analysis of real samples

Reference materials with certified contents of erbium were not available. The accuracy of the method was therefore tested by analysis of an artifical solution prepared with the same content as that of real optical fibre samples. The results are shown in Table 1. The procedure was verified by standard addition to a solution obtained after real sample decomposition. The results obtained in this last solution by both calibration graph and standard addition methods are given in Table 2. The results are satisfactory and a *t*-test applied to compare the means of two determinations[9] revealed no significant difference at $P = 0.05$.

CONCLUSION

An alternative, rapid and simple procedure to analyse the preforms of optical fibres is proposed. It includes an alkaline fusion with dissolution of the melt in 1*M* hydrochloric acid. The obtained solution can be analysed by ICP–AES. Concomitant elements effects have not been detected but acid matrix matching is necessary.

Table 2. Determination of Er in preform materials of optical fibres

Parameter	Calibration graph	Standard addition
Er content (% w/w)	0.32	0.34
No. of determinations	10	10
% r.s.d.	6.57	2.84

REFERENCES

1. J. B. Headridge, *Anal. Proc.*, 1983, **20**, 207.
2. K. Kobayashi, *Chem. Lett.*, 1987, **8**, 1499.
3. Q. Xiong, *Fenxi Huaxue*, 1987, **15**, 1025; *Anal. Abstr.*, 1988, 6B142.
4. V. Mach, S. Kotrly and K. Vytras, *Chem. Pap.*, 1989, **43**, 377; *Anal. Abstr.*, 1990, 5B34.
5. C. H. Corliss and W. Bozman, *Experimental Transition Probabilities of Spectral Lines of Seventy Elements*, NBS monographs, Washington, 1962.
6. R. K. Winge, V. J. Peterson and V. A. Fassel, *Appl. Spectrosc.*, 1979, **33**, 206.
7. E. Yoshimura, H. Suzuki, S. Yamazaki and S. Toda, *Analyst*, 1990, **115**, 167.
8. S. Greenfield, H. McD McGeachin and P. B. Smith, *Anal. Chim. Acta*, 1976, **84**, 67.
9. J. C. Miller and J. N. Miller, *Statistics for Analytical Chemistry*, 2nd Ed., Ellis Horwood, Chichester, 1988.

Talanta, Vol. 39, No. 3, pp. 195–200, 1992
Printed in Great Britain.

0039-9140/92 $5.00 + 0.00

MICELLAR ENHANCED SPECTROFLUOROMETRIC DETERMINATION OF CHLOROPHYLL *a* AND CHLOROPHYLL *b* IN FRESH WATERS*

JOSE J. SANTANA,† MARYANN GUNSHEFSKI and JAMES D. WINEFORDNER‡
Department of Chemistry, University of Florida, Gainesville, FL 32611, U.S.A.

(*Received* 23 *May* 1991. *Revised* 31 *July* 1991. *Accepted* 31 *July* 1991)

Summary—The enhancement of the fluorescence of chlorophyll *a* and chlorophyll *b* in a non-ionic micellar media is used for the establishment of a new analytical method for the determination of these pigments. After optimization of the variables, including concentration of surfactant, pH, temperature and percentage of organic solvent, the analytical figures of merit are determined. High recovery percentages are found when the method is applied to the simultaneous determination of chlorophyll *a* and *b* in synthetic mixtures. Finally, the method is used for the determination of both chlorophylls in local fresh waters, finding excellent agreement with the results obtained by an HPLC/fluorescence method.

Determination of chlorophylls, as an indicator of phytoplankton biomass, is one of the most important measurements in oceanography and liminology. Measurement of chlorophyll concentration, above all, chlorophyll *a* and *b*, helps us to understand natural systems and is important in studies aimed at assessing the impact of pollution or other disturbances.

The standard analytical methods for chlorophyll determination are based on spectrophotometry[1–3] or spectrofluorometry.[4–6] In the last several years, high-performance liquid chromatographic (HPLC) methods have largely been used for the analysis of plant pigments.[7–10]

In the case of the determination of chlorophyll *a* and chlorophyll *b* in natural waters (sea water and fresh water), after filtration these pigments are extracted from phytoplankton with an organic solvent (normally 90% acetone) and are detected in this extract by any of the previously mentioned methods. However, it is possible that very small concentrations of chlorophyll *a* and chlorophyll *b* remain in the aqueous filtrate, despite the low solubility of these compounds in water. Because of the very low absorbance and fluorescence signals of the chlorophylls in aqueous medium, it is very difficult to determine "residual" amounts of chlorophyll *a* and chlorophyll *b* with standard methods.

However, in aqueous medium, the fluorescence of these pigments is enhanced in a micellar solution. The reasons for the reduction of non-radiative processes in the presence of a surfactant include the reduced motion of the fluorophore molecules (less dynamic quenching) and the reduction of quenching effects of oxygen or other species.[11] Micellar media and fluorescence techniques have been used previously to study the photochemical properties of chlorophylls.[12,13]

In this work, we present a study of the fluorescent characteristics of chlorophyll *a* and chlorophyll *b* in different media, including an anionic surfactant, sodium dodecyl sulphate (SDS), a cationic surfactant, dodecyltrimethylammonium chloride (DTMACl), and several non-ionic surfactants, isooctylphenoxypolyethoxyethanol (Triton X-100) and polyoxyethylene-23-lauryl-ether (Brij-35). Triton X-100 is chosen as the best surfactant for the enhancement of the fluorescence of chlorophyll *a* and chlorophyll *b*. The method is applied to the determination of these species in fresh waters, and the results are compared with those obtained by HPLC with fluorescence detection.

EXPERIMENTAL

Apparatus

A Perkin-Elmer LS-5 luminescence spectrophotometer (Perkin-Elmer, Norwalk, CT),

*Research supported by NIH 5R01-GM11373-28.
†On leave from the Dept. of Chemistry, University of Las Palmas de G.C., Las Palmas de G.C., Spain.
‡Author for correspondence.

fitted with a xenon discharge lamp and interfaced with a model CLS-3600 data station was used in the fluorescence mode for the collection of all room-temperature fluorescence spectra and intensity measurements. The excitation slit was set at a 10-nm band pass and the emission slit was set at a 5-nm band pass. A 505-nm long-pass filter was placed in front of the emission monochromator in order to minimize second-order scatter. Quartz cuvettes with a 1-cm path length were used.

The HPLC system consisted of an Altex (Berkely, CA) model 110A pump used with an Altex model 210 valve and a 20-μm sample loop. The Alltech column (Alltech Associates, Inc., Deerfield, IL) was 50 mm × 4.6 mm i.d., and filled with Spherisorb ODS (5-μm particle diameter). Fluorescence measurements were obtained with the LS-5 spectrophotometer with a cell volume of either 8 or 25 μl.

The Perkin-Elmer PECLS Application program, in the LC mode, was used to obtain the respective chromatograms and the calculation of peak area (or height).

Reagents

Spectrograde acetone (Eastman Kodak Co., Rochester, NY) was used for extraction and preparation of the stock solutions of chlorophyll *a* and *b*. HPLC-grade methanol (Fisher Scientific, Fair Lawn, NJ) was degassed with helium before use, and "nanopure" demineralized water (Barnsted System, Sybron Corp., Boston, MA) was used throughout.

Stock solutions (0.1*M*) of Triton X-100 (Fisher Scientific, Fair Lawn, NJ), sodium dodecyl sulfate (SDS) (Sigma Chemical Co., St. Louis, MO), dodecyltrimethylammonium chloride (DTMACl) (Eastman Kodak Co., Rochester, NY) and Brij-35 (Aldrich Chemical Co., Inc., Milwaukee, WI) were all prepared in "nanopure" water.

Standards of chlorophyll *a* and *b* were obtained from Aldrich Chemical Co., Inc. (Milwaukee, WI) (Product Codes: 25,825-3 and 25,826-1 respectively). Stock solutions in 90% acetone were stored at about 5° in the dark.

Procedures

Determination of chlorophyll a *and* b *with Triton X-100 and fluorescence detection.* A known volume of sample or stock solution (containing 2–1000 ng of either chlorophyll *a* or *b*), 3.0 ml of 0.01*M* Triton X-100, and an adequate volume of acetone to produce a final solution of 1% acetone, was placed in a 10-ml standard flask. The fluorescence measurements were made with an excitation wavelength (λ_{ex}) of 431 nm and an emission wavelength (λ_{em}) of 673 nm for chlorophyll *a*, and a λ_{ex} of 462 nm and a λ_{em} of 654 nm for chlorophyll *b*. The analytical calibration curves were obtained from standard solutions prepared in the same manner.

Determination of chlorophyll a *and* b *using HPLC with fluorescence detection.* A known volume of sample or stock solution (containing 2–1000 ng of either chlorophyll *a* or *b*) and an adequate volume of acetone to produce a final solution of 90% acetone was placed in a 10-ml standard flask. A volume of 20 μl of each sample was then injected onto the HPLC column and eluted with a 97:3 methanol:water mixture for 5 min at a flow-rate of 1 ml/min. The respective chromatograms were obtained with an LC program with a λ_{ex} of 429 nm and a λ_{em} of 669 nm for chlorophyll *a*, and a λ_{ex} of 458 nm and a λ_{em} of 652 nm for chlorophyll *b*. The analytical calibration curves were obtained following the same procedure.

Determination of chlorophyll a *and* b *in fresh waters with fluorescence detection.* A volume of 500 ml of local lake water was prefiltered through Whatman filters (# 4) to remove any large particulate matter. This filtrate was then vacuum-filtered through a 47-mm Whatman glass microfiber filter (GF/C). Chlorophyll *a* and *b* were then extracted from the filter by pulverization and ultrasonication of the filter in 10 ml of cold (0–5°) solvent (90% acetone) in subdued light. The extracts (previously separated from the particulate residue by centrifugation), and the aqueous residual samples (2nd filtrate) were analyzed with both the above-mentioned techniques.

RESULTS AND DISCUSSION

Fluorescence characteristics of chlorophyll a *and* b *in different media*

In Table 1 the fluorescence characteristics of these pigments in different media and in the presence of different types of surfactants are given. Several conclusions can be made from these results:

(1) With a low percentage of organic solvent (1% acetone) present, the wavelengths of both chlorophylls (Fig. 1) are different than when a high percentage of organic solvent (90% acetone) is present.

Table 1. Fluorescence characteristics of chlorophyll *a* and *b* in the presence of different media*

Medium		Chlorophyll *a* λ_{exc}†	Chlorophyll *a* λ_{em}†	Chlorophyll *a* Rel.int.	Chlorophyll *b* λ_{exc}†	Chlorophyll *b* λ_{em}†	Chlorophyll *b* Rel.int
acetone:water	90:10	429	669	402.2	458	652	224.8
acetone:water	1:99	394	726	0.14	462	715	0.07
acetone:water +Triton X-100	1:99	431	673	275.3	462	654	214.4
acetone:water +Brij-35	1:99	414	673	47.2	464	655	42.8
acetone:water +SDS	1:99	433	673	—‡	466	656	—‡
acetone:water +DTMACl	1:99	433	673	—‡	465	656	—‡

*Results using 100 ng/ml of chlorophyll and 0.01*M* surfactant.
†Wavelengths are all ±2 nm.
‡No enhancement of the fluorescence signal was observed.

(2) The relative intensities of fluorescence of chlorophyll *a* and *b* are much lower in "aqueous" medium (1% acetone) than in "organic" medium (90% acetone).
(3) The fluorescence behavior of chlorophyll *a* and *b* in aqueous medium (1% acetone) varies as a function of different types of surfactants. While an anionic surfactant (SDS) and a cationic surfactant (DTMACl) do not enhance the fluorescence of these pigments, non-ionic surfactants (like Triton X-100 and Brij-35) greatly increase the fluorescence signal. There is a different degree of enhancement from different non-ionic surfactants. The enhancement of the fluorescence is greater when using Triton X-100 than when using Brij-35. In addition, the excitation and emission wavelengths of chlorophyll *a* and *b* in non-ionic surfactants are practically the same as in organic medium (90% acetone), except in the case of Brij-35 where the excitation wavelength for chlorophyll *a* shifts to a shorter wavelength (15 nm). According to these results, Triton X-100 was chosen as the surfactant best suited for the determination of low concentrations of chlorophyll *a* and *b*.

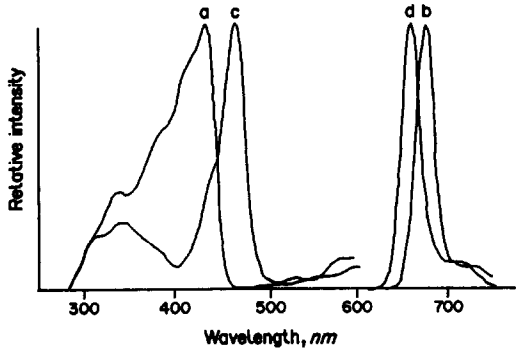

Fig. 1. Fluorescence spectra of chlorophyll *a* and *b* with Triton X-100 in 1% acetone. (*a*) Chlorophyll *a* excitation, (*b*) chlorophyll *a* emission, (*c*) chlorophyll *b* excitation, (*d*) chlorophyll *b* emission.

Optimization of variables

Figure 2 shows that the fluorescence intensities of both chlorophyll *a* and *b* change sharply with the concentration of Triton X-100 when it is close to the critical micellar concentration (cmc) (0.6m*M* for chlorophyll *a* and 0.4m*M* for chlorophyll *b*). For concentrations of surfactant higher than 1.0m*M* (believed to be the cmc of Triton X-100 in 1% acetone), the fluorescence intensity remains practically constant. According to these results, a post cmc concentration of 3.0m*M* of Triton X-100 was used for all other studies.

The study of the influence of pH shows that the relative fluorescence intensity remains constant from pH 2.5 to 12 for chlorophyll *a*, and from pH 3 to 12 for chlorophyll *b*. In more acidic media, the fluorescence signal rapidly decreases with decreasing pH. This last behavior

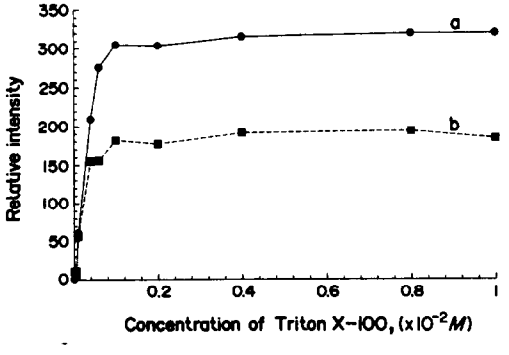

Fig. 2. Influence of concentration of Triton X-100 on the fluorescence intensity of chlorophyll *a* and *b* in 1% acetone. (*a*) Chlorophyll *a*, (*b*) chlorophyll *b*.

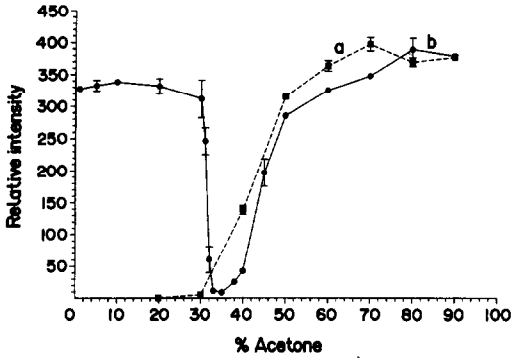

Fig. 3. Influence of the % acetone on the fluorescence of chlorophyll *a* and *b* with and without 0.003*M* Triton X-100. (*a*) Chlorophyll *a* without Triton, (*b*) chlorophyll *a* with Triton.

Table 2. Influence of temperature on fluorescence intensity of chlorophyll *a* and *b*

Temperature, °C	Relative intensity, (1% acetone)* chl *a*	chl *b*	Relative intensity, (90% acetone)† chl *a*	chl *b*
5	286.8	158.8	94.6	46.3
15	300.6	154.5	91.0	44.3
25	313.4	146.1	87.2	43.1
40	323.0	136.5	79.8	41.5
65	319.9	134.2	74.5	38.3

*Conditions: 3m*M* Triton X-100; 0.1 ppm chlorophyll; Perkin-Elmer LS-5 fluorimeter; λ_{ex} 431, λ_{em} 673 for chlorophyll *a*; λ_{ex} 462, λ_{em} 654 for chlorophyll *b*.

†Conditions: 50 ppb chlorophyll; Perkin-Elmer MPF-44A fluorimeter; λ_{ex} 429, λ_{em} 669 for chlorophyll *a*; λ_{ex} 458, λ_{em} 652 for chlorophyll *b*.

is a result of formation of decomposition products (pheophytins, pheophorbides) of chlorophyll *a* and *b* in the presence of a strong acid.

The influence of the % acetone on the fluorescence intensity of chlorophyll *a* is shown in Fig. 3. Since the solubility of chlorophyll *a* and *b* in water is very low, standard solutions in water could not be made, therefore in this work a concentration of 1% acetone is used as the initial point for the study. For both chlorophylls, the fluorescence signal does not vary with the % acetone in the range 1–30%. From 30–40% acetone, the relative fluorescence intensity drops suddenly and then slowly increases at higher percentages of acetone. This increase is similar to the behavior of chlorophyll *a* and *b* without surfactant, which suggests that this enhancement of the fluorescence signal is due to the acetone and not the surfactant. It is believed that at about 31% acetone the micelles begin to dissappear due to the higher polarity of the organic solvent.

The influence of temperature on fluorescence intensity of chlorophyll *a* and *b* has been carried out between 5 and 65° (Table 2). The results show that for chlorophyll *a* (1% acetone), the fluorescence increases slightly until 20°, remaining constant until 65°. However, for chlorophyll *b* (1% acetone), increasing the temperature decreases the fluorescence very slowly over the entire range of the study. Also, a study of the stability of chlorophyll *a* and *b* in the presence of Triton X-100, at each temperature, was performed; the fluorescence intensity did not vary with time for times less than one hour.

Table 3. Analytical figures of merit for the determination of chlorophyll *a* and *b* using Triton X-100 with fluorescence detection

Pigment	LDR*, *ng/ml*	Slope† log–log	Correlation coefficient	LOD‡, *ng/ml*	Precision§, %
chl *a*	0–100	0.97	0.999	0.04	5.0
chl *b*	0–100	1.00	0.999	0.09	2.9

LDR: linear dynamic range obtained from using 7 different analyte concentrations (ng/ml).

†Slope was calculated from the curve log fluorescence *vs.* log concentration.

‡LOD: limit of detection calculated by $3s_{blank}/m_{linear}$; s_{blank} = standard deviation of blank (16 values); m_{linear} = slope of linear coordinates calibration curve.

§Precision for the method was obtained by the following formula:

$$P_{method} = \frac{\sqrt{(s_{A+B}^2 + s_B^2)}}{I_{A-B}} 100$$

Sixteen determinations of 50 ng/ml analyte and their respective blanks were utilized to determine s_{A+B}, standard deviation of analyte and blank intensity; s_B, standard deviation of blank intensity; and I_{A+B}, average net analyte intensity.

Table 4. Determination of chlorophyll *a* and *b* in synthetic mixtures

Ratio (*a* : *b*)	*ng/ml* Added chl *a*	chl *b*	*ng/ml* Measured* chl *a*	chl *b*	% Recovery chl *a*	chl *b*
1 : 1	10	10	10.2	10.1	102.0	101.0
1 : 2	10	20	10.0	19.3	100.0	96.5
1 : 3	10	30	10.8	32.2	108.0	107.3
2 : 1	20	10	20.1	9.7	100.5	97.0
3 : 1	30	10	31.2	9.4	104.0	94.0
4 : 1	40	10	42.1	9.8	103.0	98.0
5 : 1	50	10	51.5	9.8	103.0	98.0
6 : 1	60	10	61.8	9.8	103.0	98.0
8 : 1	80	10	81.4	9.9	101.8	99.0
10 : 1	100	10	103.7	10.2	103.7	102.0
15 : 1	15	1	14.9	1.0	99.3	98.0
20 : 1	20	1	20.1	1.0	100.5	98.0
50 : 1	50	1	52.7	1.1	105.4	110.0

*Mean value of two determinations.

Analytical figures of merit

Table 3 shows the analytical characteristics of this new method for the determination of chlorophyll *a* and *b* with Triton X-100 as the fluorescence enhancer. For a range between 0–100 ng/ml, there a linear relationship exists between the fluorescence signal and the concentration of both chlorophylls with high correlation coefficients. The limits of detection for chlorophyll *a* and chlorophyll *b* were 0.04 ng/ml and 0.09 ng/ml, respectively. These detection limits compare favorably with the previous most sensitive HPLC/fluorescence detection method for the determination of these pigments. Sixteen samples, each containing 50 ng/ml of either chlorophyll *a* or *b*, were determined; and 5.0 and 2.9% RSD values were obtained, respectively.

The selectivity of this new method was determined by using solutions containing different ratios of chlorophyll *a* and chlorophyll *b*. The results show that chlorophyll *a* can be determined in the presence of chlorophyll *b* up to a ratio of 3:1 (*b* : *a*), and chlorophyll *b* in the presence of chlorophyll *a* up to a ratio of 50:1 (*a* : *b*) without interference. In environmental samples (algae, natural waters), the chlorophyll *a* pigment is normally in excess with respect to chlorophyll *b*, therefore, our method can be applied to these types of samples.

Application to the determination of chlorophyll a *and* b *in synthetic mixtures and fresh waters*

The surfactant method was applied to the simultaneous determination of both chlorophyll *a* and *b* in synthetic mixtures. The results (Table 4) show an excellent recovery (96–108%) for different ratios and concentrations of chlorophyll *a* and *b*.

Table 5 shows the results obtained from the analysis of local fresh water samples (Newnans Lake, Gainesville, FL). The concentrations of chlorophyll *a* and *b* from the phytoplankton were determined with the surfactant method and the HPLC/fluorescence method mentioned previously. Figure 4 illustrates the chromatogram obtained for sample # 1. Excellent agreement was found between both methods.

Also, the soluble chlorophyll *a* and *b* in the residual water samples (2nd filtrate) was determined with the surfactant method in combination with the internal standard method. This procedure was used due to the limited sensitivity of the HPLC/fluorescence method. The results show that, even though chlorophylls are highly insoluble in water, a low concentration of

Table 5. Determination of chlorophyll *a* and chlorophyll *b* in fresh waters

Sample #	Surfactant method (phytoplankton), *μg/ml** chl *a*	chl *b*	HPLC method (phytoplankton), *μg/ml** chl *a*	chl *b*	Surfactant method (residual water), *ng/ml** chl *a*	chl *b*
1	0.74	0.03	0.72	0.02	5.10	0.96
2	0.47	0.02	0.47	0.02	6.46	0.94

*Mean value of two determinations.

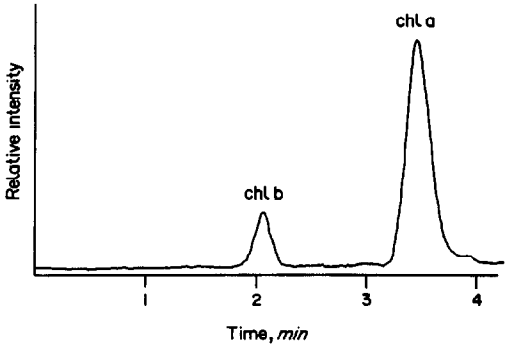

Fig. 4. Chromatogram of sample # 1. Eluent: 97 : 3 methanol : water, $\lambda_{ex} = 429$ nm, $\lambda_{em} = 669$ nm for chlorophyll *a*, $\lambda_{ex} = 458$ nm, $\lambda_{em} = 652$ nm for chlorophyll *b*.

chlorophyll *a* and *b* can be determined by the micellar enhanced fluorescence method (see Table 4).

CONCLUSIONS

It is known that chlorophyll *a* and *b* are highly fluorescent in organic solvents (acetone, methanol, *etc.*). The study carried out in this work show that these pigments produce practically no fluorescence when the percentage of organic solvent present is low (<40%). However, under the same solvent conditions, the addition of a non-ionic surfactant greatly enhances the fluorescence of both chlorophyll *a* and *b*. This allowed us to present a new, very sensitive and selective method for the determination of chlorophyll *a* and *b* in environmental samples with Triton X-100 as the fluorescence enhancer. With this new method, determination of the concentrations of chlorophyll *a* and *b* in the phytoplankton was performed without prior chromatographic separation of the extract, and determination of the concentration of chlorophyll *a* and *b* in the residual water was also possible.

Acknowledgements—José J. Santana would like to thank the Spanish Education and Science Ministry for the grant which made possible his stay at the University of Florida.

REFERENCES

1. F. A. Richards and J. G. Thomson, *J. Mar. Res.*, 1952, **11**, 156.
2. J. D. H. Strickland and T. R. Parsons, *A Practical Handbook of Seawater Analysis*, Fisheries Research Board of Canada Bulletin 167, 2nd Ed., 1972.
3. S. W. Jeffrey and G. F. Humphrey, *Biochem. Physiol. Pflanz.*, 1975, **167**, 194.
4. C. S. Yentsh and D. W. Menzel, *Deep Sea Res.*, 1963, **10**, 221.
5. M. E. Loftus and J. H. Carpenter, *J. Mar. Res.*, 1971, **29**, 319.
6. O. Holm-Hansen, C. J. Lorenzen, R. W. Holmes and J. D. H. Strickland, *J. Cons., Const. Int. Explor. Mer.*, 1965, **30**, 3.
7. J. K. Abaychi and J. P. Riley, *Anal. Chim. Acta*, 1979, **107**, 1.
8. R. F. C. Mantoura and C. A. Llewellyn, *ibid.*, 1983, **151**, 297.
9. S. W. Wright and J. D. Shearer, *J. Chromatog.*, 1984, **294**, 281.
10. D. P. Sartory, *Water Res.*, 1985, **19**, 605.
11. H. Sing and W. L. Hinze, *Anal. Lett.*, 1982, **15**, 221.
12. K. Csatorday, E. Lehoczki, and L. Szalay, *Biochim. Biophys. Acta*, 1975, **376**, 268.
13. E. Lehoczki and K. Csatorday, *ibid.*, 1975, **396**, 86.

Talanta, Vol. 39, No. 3, pp. 201–206, 1992
Printed in Great Britain

0039-9140/92 $5.00 + 0.00
Pergamon Press plc

RELATIVE RESPONSE RATIOS FOR DUAL-ISOTOPE MEASUREMENTS VIA COELUTION AND GC/MS

LAWRENCE C. THOMAS and WALTER WEICHMANN
Department of Chemistry, Seattle University, Seattle, Washington 98122, U.S.A.

(*Received* 15 *May* 1991. *Revised* 14 *August* 1991. *Accepted* 14 *August* 1991)

Summary—Dual-isotope internal standard measurements by GC/MS which mimic isotope dilution may suffer from non-linear response relations, irreproducibilities or unduly large uncertainties because of variations in ionization efficiences for the respective isotopic forms in the MS source. Such variations may sometimes be avoided via extensive pretreatments, high resolution GC separations and careful control of instrumental parameters. However, an alternative approach is feasible which instead exploits advantages of decreasing GC resolution. By forcing both forms of each analyte to coelute, their relative ionization efficiencies in the MS source should be nearly constant, thereby effectively allowing for constant relative sensitivities over several orders of magnitude in concentration. Thus, constant relative response ratios, required for internal standard calculations, may be attained as a consequence of dramatically lowered GC resolution. Coelution results described herein show linear relative sensitivity relations over much broader ranges than observed for corresponding conventional calibrations with separated components. Coelution methods for dual-isotope GC/MS determinations are compatible with internal standard calculations and thereby offer a powerful alternative to the conventional approach of requiring expensive and labor-intensive additional pretreatments and separations to assure resolution of measured eluates.

Recently dual-isotope internal standard methods which mimic isotope dilution have become increasingly popular. Some GC/MS approaches have been adopted for use in important environmental measurements, *e.g.*, Methods 1624 and 1625 from the U.S. Environmental Protection Agency (EPA).[1] The general approach is to add known amounts of isotopically labelled compounds, otherwise identical to each target analyte, to samples prior to pretreatment. For each target analyte, both of its forms undergo identical treatment because they coexist in the same mixtures throughout the procedures. The isotopically labelled internal standard added prior to pretreatment, chromatographic separation and detection allows for compensation of pretreatment variables as well as injection variations if the two forms of the target analyte are chemically identical but isotopically different. The prepared sample is analyzed by GC/MS according to recommended protocols, with each target analyte and its isotopically labelled form typically eluting separately and being measured via their respective ion currents at their characteristic m/z values, often by selected-ion detection (SID).[1] The direct proportionality between relative sensitivities for the two forms and their relative concentrations is an important condition for valid use of the dual-isotope internal standard methods for quantitative analyses by chromatography.

Dual-isotope techniques using mass spectrometry of equilibrated mixtures of target analytes with appropriate isotopically labelled compounds have been used for many years to help ensure reliable analyses.[2] However, even dual-isotope methods are not always accurate, and it has been recommended that other quantitative methods be used if the two forms do not show baseline separation between themselves and from all potential interferants.[1] The excellent selectivity of MS measurements enhances discrimination from interferences, but MS is not always sufficient for reliable determinations. Moreover, the special sensitivity dependencies of MS upon a variety of variables, *e.g.*, pressure and coeluting species, may complicate GC/MS measurements considerably.[3] Unfortunately, requiring improved separations to be achieved via special pretreatments and modified instrumental variables can be unacceptably expensive and labor-intensive,[4,5] making valid optional approaches desirable.

Alternatively, procedures which exploit the special advantages of dual-isotope internal standard techniques but are not appreciably affected by potential interferences are attractive. Herein we describe an alternative approach which

requires coelution of respective labelled pairs and offers potential improvements in quantitative data quality. As shown herein, the coelution alternative for dual-isotope analyses may yield linear relative calibration relations, *i.e.*, constant relative sensitivities over several orders of magnitude of eluted analyte masses. Consequently, for appropriate situations, ensuring coelution may obviate many restrictive sample pretreatment and GC separation requirements, thereby potentially decreasing analysis costs for internal standard GC/MS methods which mimic isotope dilution.

THEORY

If an isotopically-labelled, *e.g.*, deuterated or ^{13}C-labelled, form d of a target analyte i is added to sample n prior to pretreatment, then the peak area for its elution and measurement by GC/MS and SID may be modelled as:

$$A_{\text{ind}} = \frac{V_{sn} C_{ind} E_{ind} V_{\text{col},n} S_{ind} V_{\text{inj},n}}{V_{cn}(V_{\text{col}} + V_{\text{split}})_n V_{cn}} \int_{\text{RT}-bw}^{\text{RT}+bw} k_{ind}(I_{ind})_t \, \text{d}t \quad (1)$$

with $(I_{ind})_t = (E_{\text{ion},ind})_t (E_{\text{ext},ind} E_{\text{sel},ind} P_{\text{mult},id} f_p)_t$

where A_{ind} is the peak area for analyte i from sample n and isotopic label d, V_s and V_c correspond to original sample volume and the volume after pretreatment, C is the concentration of the specified analyte in the sample, E is the efficacy of the pretreatment as the fraction of the specified substance recovered, V_{col} and V_{split} respectively correspond to carrier volumes which flow to the column and out of the split vent during the time the analyte resides in the injector, S is the fraction of the analyte which is in the carrier during the time the analyte resides in the injector, V_{inj} is the volume of pretreated sample injected, RT is the retention time of the analyte, bw is some selected multiple of the analyte's peak width, k relates electrometer current to the monitored response, E_{ion} is the ionization efficiency in the source for the target analyte at the specified time t, E_{ext} and E_{sel} are efficiencies of extraction from the source and delivery to the first stage of the electron multiplier through the m/z selector, and $P_{\text{mult}} f_{\text{p}}$ defines the response of the electron multiplier to incident selected ions.

Relative response factors (RRF) for naturally occurring analyte, i, indicated here as h, relative to its chemically identical isotopically labelled internal standard form, d, can be defined for the overall pretreatment and measurement, using known amounts of both forms in a reference sample, r:

$$\text{RRF}_{irhd} = (\text{A}_{\text{irh}}/\text{C}_{\text{irh}})(\text{A}_{\text{ird}}/\text{C}_{\text{ird}})^{-1} \quad (2)$$

In subsequent determinations, a known amount of the isotopically labeled form is added to each sample before analysis and the relative response factor is typically assumed to be invariant; thus, for sample m, using a relative response factor determined from reference sample r, *i.e.*, assuming $\text{RRF}_{imhd} = \text{RRF}_{irhd}$

$$C_{imh} = (C_{imd} A_{imh})(\text{RRF}_{imhd} A_{imd})^{-1}$$
$$= (C_{imd} C_{irh} A_{imh} A_{ird})(C_{ird} A_{imh} A_{irh})^{-1} \quad (3)$$

Unfortunately, measured areas are not always proportional to subsample concentrations, *i.e.*, the GC/MS sensitivity for a selected analyte typically is not constant over wide ranges in injected masses of analyte. Correspondingly, linear concentration *vs.* measured-area relations for GC/MS typically span only 1–2 orders of magnitude.[4,5] Consequently, relative response ratios also may fluctuate. Worse, if the injected mass of added reference substance varies, relative response ratios may become even more unreliable because of mathematical interactions between the two variable sensitivity relations. Therefore, unless typical dual-isotope internal standard methods which mimic isotope dilution are extremely well-controlled, calculations based upon relative response factors may be excessively imprecise or incorrect.[1]

Much of the nonlinearity in concentration *vs.* response relations for a given eluate may be caused by fluctuations in the MS ionization efficiencies which typically change dramatically in GC/MS as the eluates' effective concentrations and the source pressures change along with variations in the mass of eluate entering the source per unit time. Thus, $E_{\text{ion},inx}$ may change throughout elution of a component, typically diminishing as the rate of eluates entering the source increases. Baseline separation of the components, as is recommended,[1] therefore may exacerbate the undesirable effects of response *vs.* concentration non-linearities.

If instead, the components are coeluted rather than separated, then the relative ionization efficiencies of both the labelled and non-labelled forms will be essentially constant, because they coexist in the same environment at the same time. Consequently, if the relative extraction efficiencies of the ions from the source and their

relative efficiencies through the selector are reproducible, then the components' relative response factor should be invariant. For example, if only one reference solution r is used for assessing RRF, then

$$C_{\text{imh}} = \text{constant}(C_{\text{imd}})\frac{\int(I_{imh})_t\,\text{dt}}{\int(I_{imd})_t\,\text{dt}} \qquad (4)$$

Fortunately, if there are no SID interferences, coelution may thereby cause the quantitative calculation of analyte concentrations to follow a simple proportionality to relative areas, despite variations in sensitivities for specific components, *i.e.*, the relative sensitivities for the components are the same from run-to-run. With identical ionization efficiencies and other MS parameters stabilized, the relative currents detected for the two forms should vary directly with the relative concentrations of the two forms in the source, thereby allowing for valid internal standard calculations.

This alternative to assuring baseline separation is attractive, *i.e.*, ensuring coelution so that both forms of the target analyte are concurrently present in the same ionizing environment. With coelution of differently labelled forms of each analyte, relative GC/MS ionization efficiencies of the two forms should be constant, neglecting tiny differences at electron energies near their ionization potentials due to differences in ground-state vibrational and rotational energies because of their different reduced masses. For moderate-to-high resolution gas chromatography, the different forms typically separate. Effects of increased interferences due to lowered GC resolution must be considered and weighed against possible benefits of forced coelution. Consequently, despite tradition, for appropriate situations one might purposely decrease GC resolution in order to cause coelution of labeled and nonlabeled forms of the target analytes to achieve extended ranges of constant relative sensitivities, thus allowing for reliable quantitative analyses in dual-isotope internal standard GC/MS procedures.

EXPERIMENTAL

Reagents

Anthracene and decadeuteroanthracene were purchased from Aldrich Chemical Co., both at 99% purity. All solvents were Mallinkrodt ChromAR grade, and helium carrier gas was 99.9995% pure.

Apparatus

A Hewlett–Packard Model 5971A Mass Selective Detector interfaced to a Hewlett–Packard Model 5890 Series II GC was used, controlled and monitored by a Hewlett–Packard Model QS-20 Vectra Computer. Helium carrier gas was used with a 15-kPA pressure in the split/splitless inlet, yielding 1.0 ml/min carrier gas flow at 25°. A split ratio of 60:1 at 25° was used with a 1.0-min splitless period following injection. Injections of 1.0 μl were used unless otherwise stated.

Procedures

Mixed solutions of anthracene and decadeuteroanthracene were made in methanol, varying the molar concentrations from 10^{-5} to $2 \times 10^{-3}M$, with relative concentrations, [anthracene]/[d_{10}-anthracene], spanning 2000:1 to 0.01:1. Replicate ($n = 4$) 1-μl injections of each solution were made over several days, retuning the MS intermittently. They eluted isothermally at 160° over a 12-m by 0.2-mm i.d. fused silica capillary column with 0.33-μm thick cross-linked methyl silicone stationary phase. Selected ions, $m/z = 178$ and $m/z = 188$, were monitored over the elution duration of the two forms of anthracene. Peak areas were calculated by provided algorithms, and statistical calculations were made by conventional techniques.

RESULTS AND DISCUSSION

Decadeuteroanthracene and normal anthracene essentially coeluted via the isothermal elution (see Figs. 1 and 2). Sensitivities for each form, measured via parent ions, varied with concentration, as expected when several orders of magnitude are spanned (see Figs. 3 and 4). Uncertainties in sensitivities varied widely, *e.g.*, ±25% (rsd) for both anthracene and d_{10}-anthracene.

Relative sensitivities, however, varied proportionally, *i.e.*, linear log–log plot with slope = 1.0, for relative concentrations over more than three orders of magnitude (see Fig. 5), despite making measurements over several days and retuning the MS intermittently, *i.e.*,

$$\frac{C_{imh}}{C_{imd}} = \text{constant}\,\frac{\text{Area}_{imh}}{\text{Area}_{imd}} = \text{constant}'\,\frac{\int(I_{imh})_t\,\text{dt}}{\int(I_{imd})_t\,\text{dt}} \qquad (5)$$

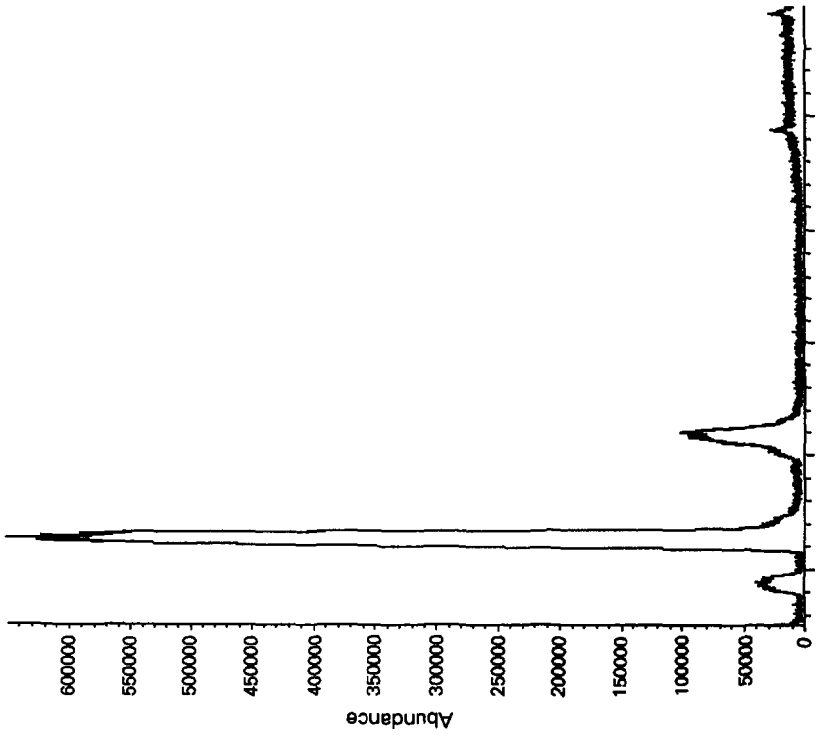

Fig. 1. GC/MS total ion chromatogram for isothermal (160°) coelution of decadeuteroanthracene and normal anthracene with a retention time of about 6.2 min; for a 1-μl injection containing 1.1×10^{-7} g of anthracene and 2.6×10^{-7} g of d_{10}-anthracene, along with dihydroanthracene at 4.4 min and anthraquinone at 10.8 min.

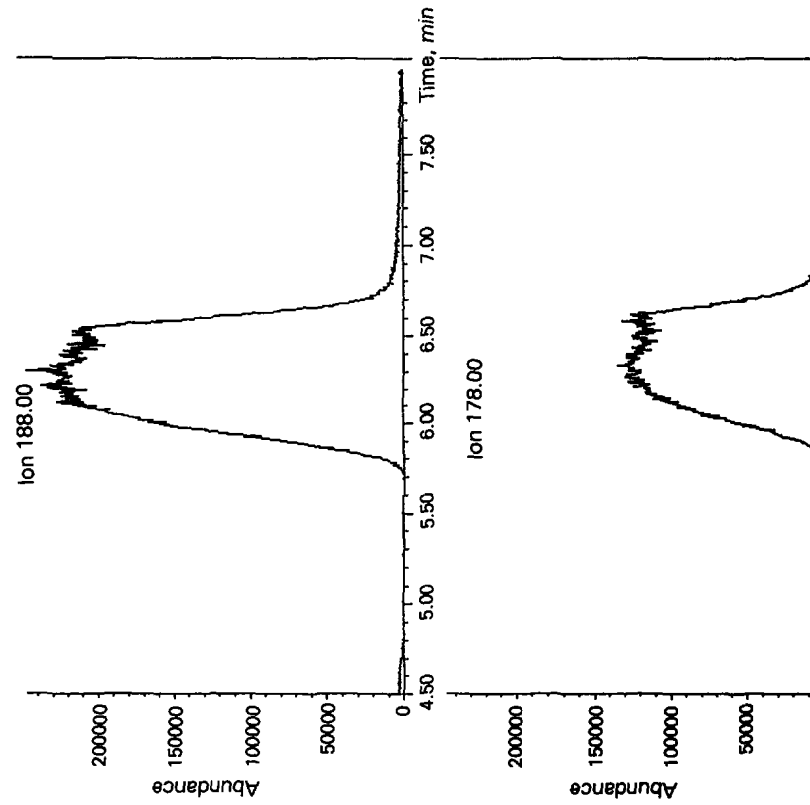

Fig. 2. GC/MS selected ion chromatograms for isothermal (160°) coelution of decadeuteroanthracene ($m/z = 188$) and normal anthracene ($m/z = 178$); relative concentrations for this result of a 1-μl injection was 2:1, respectively, in a total of 10^{-9} moles of combined anthracene and d_{10}-anthracene.

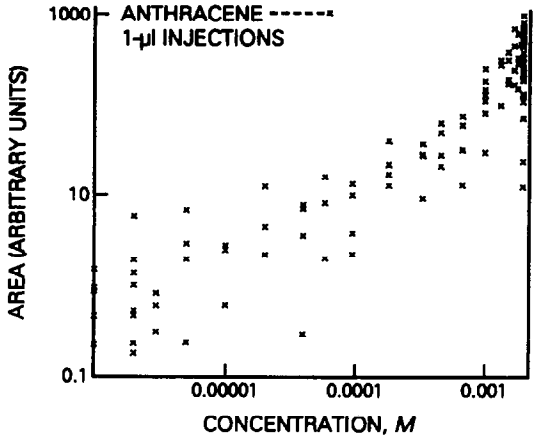

Fig. 3. Integrated response *vs.* concentration relationships for 124 1-μl injections of normal anthracene ($m/z = 178$), measured by selected-ion GC/MS, spanning concentrations from 10^{-6} to $2 \times 10^{-3} M$.

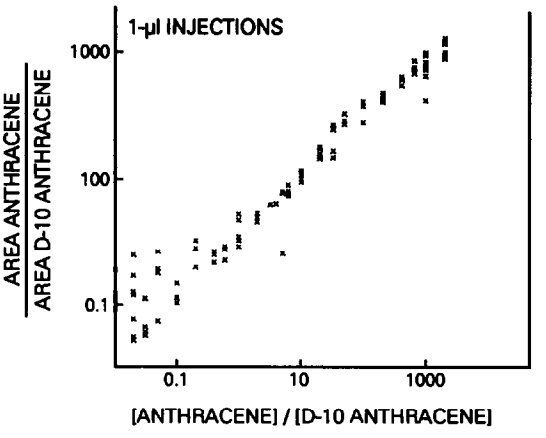

Fig. 5. Relative integrated response *vs.* relative concentration relationship for 124 1-μl injections of decadeuteroanthracene and anthracene. Each datum corresponds to the ratios ($A_{m/z=178}/A_{m/z=188}$) and ($C_{\text{anthracene}}/C_{\text{decadeuteroanthracene}}$), for a single 1-$\mu$l injection.

Moreover, uncertainties in relative sensitivities varied only about $\pm 10\%$ (rsd) for relative concentrations between 1 and 10^3, being somewhat larger when the concentration of one or the other form of analyte approached limits of detection. Consequently, adding a known amount of d_{10}-anthracene to samples containing normal anthracene target analyte is compatible with internal standard quantitative calculations for GC measurements. Moreover, coelution of the two forms helps ensure the required bases for valid use of internal standard techniques. Coelution of d_{10}-anthracene concurrently with normal anthracene caused their relative sensitivities to be constant, thereby compensating for fluctuations in measurement sensitivities resulting from variables such as GC/MS source pressures, and noninterfering coeluates.

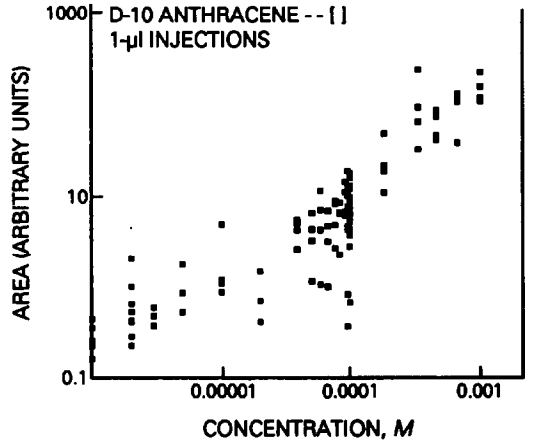

Fig. 4. Integrated selected ion response *vs.* concentration relationships for 124 1-μl injections of d_{10}-anthracene ($m/z = 188$), measured by GC/MS, spanning concentrations from 10^{-6} to $10^{-3} M$.

These results indicate that GC/MS measurements of isotopically labelled internal standards coeluting with corresponding normal target analytes are compatible with dual-isotope procedures which mimic isotope dilution. Of course, effects of increased interferences, reduced sensitivities and worse selectivities due to lowered GC resolution must be considered along with possible resulting benefits of forced coelution. However, by adding a small-but-reliably-measured amount of an isotopically labelled form of each target analyte to the samples, one may expect the labelled form to work as a reliable internal and recovery standard over a wide dynamic range, making accurate and precise determinations feasible. Also, coelution of the two forms should compensate for potential variations in relative sensitivities caused by variations in ionization efficiencies due to changes in source pressures, effective analyte concentrations in the source or the presence of many potential interferents.

The direct proportionality between relative sensitivities and relative concentrations is an important condition for use of internal standard methods for quantitative analyses by chromatography: dual-isotope internal standard procedures can be especially reliable for such determinations, and coelution can help ensure validity in their use. Consequently, in some circumstances, lowering GC resolution may improve quantitative GC/MS measurements when higher resolution separations become unreliable.

Acknowledgements—We thank the National Institutes of Health for their support of this and earlier work via grant number 1R15 GM36273-01A1.

REFERENCES

1. *Method 1624, Rev. C and Method 1625, Rev. C*, U.S. Environmental Protection Agency, Washington, D.C., 1988.
2. A. V. Grosse, S. G. Hindin and A. D. Kirshenbaum, *Anal. Chem.*, 1949, **21**, 386.
3. F. W. McLafferty, *Interpretations of Mass Spectra*, W. A. Benjamin, Inc., New York, 1966.
4. W. D. MacLeod, Jr., A. J. Friedman and D. W. Brown, *Marine Envir. Res.*, 1988, **26**, 209.
5. W. D. MacLeod, Jr., P. G. Prohaska, D. D. Genero and D. W. Brown, *Anal. Chem.*, 1982, **54**, 386.

Talanta, Vol. 39, No. 3, pp. 207–209, 1992
Printed in Great Britain.

0039-9140/92 $5.00 + 0.00

CATALYTIC POLAROGRAPHIC DETERMINATION OF TOTAL SELENIUM IN TEA LEAVES

LIU XUNJIAN,* TU YEFENG, ZHAO YANG, ZHU LING, LIU HSIAOYAN,† YU HONG, DING YUANCHEN and REN YUBEI

Department of Chemistry, Suzhou University, Suzhou 215006, People's Republic of China

(*Received* 29 *November* 1989. *Revised* 24 *August* 1991. *Accepted* 2 *September* 1991)

Summary—The catalytic polarographic determination of selenium(IV) by use of the $SeSO_3^{2-}$–KIO_3 system is sensitive, accurate, rapid and requires only small quantities of sample. The detection limit for selenium(IV) is 0.04 ng/ml in the final solution. The working range of the calibration is 0.04–2.5 ng/ml. Se(VI) present can be reduced with hot hydrochloric acid to Se(IV), allowing determination of the total selenium.

Selenium is one of the trace elements necessary in the human body, and there are numerous methods for its determination; examples include fluorimetry,[1] neutron-activation,[2] gas and liquid chromatography,[3] cathodic stripping voltammetry,[4] and a catalytic polarographic method.[5] Speciation of selenium in biomaterials and water samples has also been reported.[6–9] This paper reports the determination of total selenium in tea by the catalytic polarographic method. Only small quantities of sample are required and the tea leaves need not be ground before decomposition. It is not necessary to deaerate the solution before the polarography.

EXPERIMENTAL

Apparatus

A JP-2 type oscillographic polarograph with a three-electrode system was used. Dropping mercury and saturated calomel electrodes were used as the working and reference electrodes respectively. The auxiliary electrode was made of platinum. An automatic electric digestor and a micro-injector were also used.

Reagents

Standard solution of Se(IV). Dissolve 0.500 g of selenium powder with 10 ml of concentrated nitric acid in a beaker, on a boiling water-bath, dilute the solution to volume in a 100-ml standard flask and dilute it further as required.[8]

*Sodium sulphite solution, 1.3*M. Dissolve 8.2 g of anhydrous sodium sulphite in 50 ml of water. Discard the solution when it is three days old.

Buffer solution (pH 10). Add 40.2 g of ammonium chloride to 150 ml of concentrated aqueous ammonia solution and dilute to 200 ml with water.

Potassium iodate solution. Dissolve 4.2 g of potassium iodate in 100 ml of water.

Preparation of selenium-free sulphuric acid. Add 15 ml of concentrated hydrobromic acid to 100 ml of analytical-reagent grade sulphuric acid. Heat on an electric heater until fumes appear and then for half an hour longer. Store in a glass bottle after cooling.

Mixed-acid digestion solution. Mix selenium-free concentrated sulphuric acid and 70% perchloric acid in 3:4 v/v ratio.

Ammonium molybdate solution. Dissolve 5 g of $(NH_4)_6Mo_7O_{24}\cdot 4H_2O$ in 100 ml of water.

Use analytical grade reagents or better, and water that has been doubly distilled in fused-silica apparatus.

Calibration

Prepare a series of calibration solutions in 20-ml standard flasks, by mixing appropriate volumes of standard Se(IV) solution with 0.40 ml of 70% perchloric acid and 2.0 ml of 1.3*M* sodium sulphite, letting stand for 20 min at room temperature, then adding 4.0 ml of the pH-10 buffer solution and 2.0 ml of potassium iodate solution and diluting to volume with

*Author for correspondence.

Table 1. Precision of determination (relative standard deviation, RSD)

No.	Se found, μg/g				Mean, μg/g	RSD, %
1	0.727	0.768	0.768	0.727	0.74_8	3.2
2	0.727	0.743	0.727	0.768	0.74_1	2.6
3	0.849	0.849	0.849	0.809	0.83_9	2.4

water. Place the flasks in a thermostatic bath at 25° for 10 min. For each solution record the first derivative polarogram over the voltage range from −0.6 to −1.1 V (*vs.* SCE). Measure the peak height of the catalytic wave at −0.87 V (*vs.* SCE) and plot the calibration graph.

Analysis of tea samples

Weigh 0.2 g of dried tea into a Kjeldahl flask, add 5.0 ml of mixed acid and 0.40 ml of the ammonium molybdate solution, and heat in an automatic digestor (set at 213°), until the solution becomes yellow. Remove the flask from the digestor, allow it to cool, and make the solution up to volume in a 25-ml standard flask.

Place an aliquot of the solution in a beaker, add 0.1 ml of 6*M* hydrochloric acid and 0.2 ml of 12*M* perchloric acid, and heat on a boiling water-bath for 20–30 min, until the volume is about 0.2 ml. Rinse the wall of the beaker with a small quantity of water, add 2.0 ml of 1.3*M* sodium sulphite and let stand at room temperature for 20 min. Continue as for preparing the calibration graph, to obtain the total selenium content.

RESULTS AND DISCUSSION

Se(IV) is reduced to Se by sulphurous acid in acid solution. In a pH-10 ammonia buffer Se forms $SeSO_3^{2-}$ with sulphite, and this produces a sensitive catalytic polarographic wave in the presence of potassium iodate. When standard additions of Se(IV) were made to aliquots of digest, the wave form and peak potential of the catalytic polarographic waves obtained were the same as for a standard solution, showing that the signal was due to the initial presence of Se(IV). If standard additions of Se(VI) were made, no increase in peak height was observed.

Table 2. Determination of recovery

Se present, μg/g	Se added, μg/g	Total Se found, μg/g	Recovery, %
0.75	0.50	1.21	92
	0.50	1.29	108
	0.50	1.21	92
0.74	0.50	1.29	110
	0.50	1.29	110
	0.52	1.21	94
0.84	0.50	1.45	90
	0.50	1.54	106
	0.50	1.54	90

The results in Tables 1–3 show that the coefficient of variation is less than ~5% and the average recovery between 95 and 105%.

In principle it is possible to determine both Se(IV) and Se(VI) in the same sample provided that no change in the proportions of the two oxidation states occurs during dissolution of the sample. The Se(IV) is determined in an aliquot of sample solution as described for calibration, and the total selenium is then determined in a second aliquot as described for the analysis of tea, the Se(VI) content being obtained by difference.

In the digestion procedure used for the tea samples, however, it is not certain that the proportions of Se(IV) and Se(VI) will remain constant, so only total selenium can be determined in this case. Various digesting agents were tested, including nitric acid/hydrogen peroxide mixtures, nitric acid/perchloric acid

Table 3. Total selenium in tea leaves

	Se(IV)			Total Se		
Sample	Found, μg/g	Mean, μg/g	RSD, %	Found, μg/g	Mean, μg/g	RSD, %
1	0.778	0.75	2.7	1.101	1.08	2.1
	0.738			1.063		
	0.738			1.104		
	0.738			1.063		
2	0.731	0.74	5.4	0.934	1.00	4.1
	0.731			1.016		
	0.772			1.016		
	0.731			1.016		
3	0.849	0.84	2.4	1.145	1.18	3.3
	0.849			1.226		
	0.849			1.145		
	0.809			1.185		

Table 4. Comparison of results for total selenium

Sample	Se found	
	Present method	Flourimetry
Tea leaves	0.996 μg/g	0.952 μg/g
Well water	0.150 μg/ml	0.170 μg/ml
Standard sample*	0.313 μg/ml	

*Reference value = 0.300 μg/ml.

mixture with or without ammonium molybdate, and the 5 ml of 3:4 v/v mixture of sulphuric acid and perchloric acid plus 0.4 ml of 5% ammonium paramolybdate solution, and only the last of these gave satisfactory decomposition of the tea samples. Various heating times and temperatures were tried and heating at 213° until the solution becomes yellow (about 35 min) is recommended. Use of higher temperature resulted in loss of some selenium.

It was found that though the total selenium found in the tea leaves by this method was reproducible, the ratio of Se(IV) to Se(VI) in the digest varied considerably, depending on the time and temperature of the digestion. Hence for samples that require use of the digestion mixture for decomposition, only the total selenium should be determined. For samples that are already in solution, or can be brought into solution readily in the cold, the Se(IV) and Se(VI) present may both be determined.

It was established experimentally that Se(VI) is not reduced by heating with sulphurous acid at 60° for 20 min, so the Se(IV) determination is free from interference by Se(VI). The amount of paramolybdate added is not critical—addition of 0.1 ml of the 5% solution gives practically the same result as addition of 0.4 ml.

The calibration graph was found to be linear over the selenium range 2–10 ng in the 20 ml of solution used for the polarography.

The precision of determination of total selenium at a level corresponding to 1.0–1.2 μg/g in a sample of tea was found to be about 3% (relative standard deviation) and the recovery of an amount of standard corresponding to an addition of 0.5 μg/g ranged from 90 to 110% in individual determinations.

Analysis of various samples by the method for total selenium and by a fluorimetric comparison reference method gave the results shown in Table 4.

Acknowledgements—The authors are very grateful to Professor Pan Jiali for helpful advice.

REFERENCES

1. T. Westermarck, P. Raunu, M. Kirjarinta and L. Lappalainen, *Acta Pharmacol. Toxicol.*, 1977, **40**, 465.
2. H. K. J. Hahn, R. V. Williams, R. E. Burch, J. F. Sullivan and E. A. Novak, *J. Lab. Clin. Med.*, 1972, **80**, 718.
3. J. W. Young and G. D. Christian, *Anal. Chim. Acta*, 1973, **65**, 127.
4. Z. Shen, R. Lu and Q. Shi, *Chin. J. Appl. Chem.*, 1987, **1**, 78.
5. X. Liu, Y. Tu, W. Cheng and Z. Wu, *Shengwu Huaxue Yu Shengwu Wuli Jinzhan*, 1987, **14**, No. 6, 52; *Chem. Abstr.*, 1988, **108**, 218519w.
6. K. Kurahashi, S. Inoue, S. Yonekura, Y. Shimoishi and K. Tôei, *Analyst*, 1980, **105**, 690.
7. Y. Shimoishi, *Bull. Chem. Soc. Japan*, 1974, **47**, 997.
8. X. Zhang, C. He and C. Xu, *Beijing Daxue Xuebao, Ziran Kexueban*, 1985, No. 1, 1; *Chem. Abstr.*, 1986, **104**, 192778v.
9. G. A. Gutter, *Anal. Chim. Acta*, 1978, **98**, 59.
10. C. A. Parker and L. G. Harvey, *Analyst*, 1962, **87**, 558.

Talanta, Vol. 39, No. 3, pp. 211–214, 1992
Printed in Great Britain.

0039-9140/92 $5.00 + 0.00

ENHANCED SEPARATION OF TRIVALENT LANTHANOIDS BY SOLVENT EXTRACTION WITH 18-CROWN-6 AND EDTA COMPLEXONATE

ROBERT FRAZIER and C. M. WAI*
Department of Chemistry, University of Idaho, Moscow, Idaho 83843, U.S.A.

(*Received* 12 *August* 1991. *Accepted* 29 *August* 1991)

Summary—The selectivities during solvent extraction of lanthanoids with macrocycles can be modified with complexonates in the aqueous phase. In the case of solvent extraction of lanthanoids with 18-crown-6 and trichloroacetic acid (TCA), addition of EDTA to the aqueous phase enhances the selectivities of lanthanoids by 3–7 times compared to those without the complexonate. This is due to the fact that the stability of lanthanoid–EDTA complexes increases in the opposite direction to the crown–TCA complexes across the lanthanoid series. The selectivities observed in this system are among the largest reported for the light lanthanoids. The effect of the complexonate on lanthanoid extraction can be explained by a simple model presented in this paper.

Macrocyclic polyethers (crown ethers) are known to form stable complexes of different stoichiometry with trivalent lanthanoids.[1] The stability of crown complexes in solvent extraction depends generally on the following four factors: crown cavity to cation diameter ratio, the counter anion, ligand flexibility, and the type of donor atoms (N, O or S) in the macrocyclic host.[2] Using 18-crown-6 to extract lanthanoid ions in aqueous solution with trichloroacetate (TCA) as counter anions, selectivities as good as the best commercial extractant, di-2-ethylhexyl-phosphoric acid (HDEHP) were obtained by Samy *et al.*[3] The relative stability constants of the lanthanoid complexes in this case decrease by three orders of magnitude from La^{3+} to Eu^{3+}. The large selectivity observed in this macrocyclic system has been attributed to the steric hindrance of the lanthanoid complex with TCA. The decrease in stability across the lanthanoid series with 18-crown-6-TCA complexes is significant, because it is opposite to many known lanthanoid complexonates in aqueous solution. Therefore, by choosing a proper complexonate, the two opposite trends may compliment each other resulting in enhanced selectivity for the extraction of lanthanoids by 18-crown-6. It is known that lanthanoid–EDTA complexes show increased stabilities from La^{3+} to Lu^{3+} and the complexation depends on pH.[4] This paper reports the enhanced lanthanoid selectivity in solvent extraction, using 18-crown-6 as an extractant, TCA as the anion and EDTA as a complexonate with 1,2-dichloroethane solvent. Hydrogen ion is used as a displacer to release lanthanoids complexed with EDTA in the aqueous phase.

*Author for correspondence.

EXPERIMENTAL

The 18-crown-6 extractant was purchased from Aldrich. The EDTA was Aldrich gold label and dried four days at 80° according to Schwartzenbach.[5] The La, Eu and Lu solutions were purchased as standard solutions from Aldrich and Thiokol. Lanthanoid solutions of Ce, Nd and Ho were prepared from their nitrates obtained from Aldrich. Praseodymium was prepared from its oxide obtained from Baker and Adamson. The solvent, 1,2-dichloroethane, was purchased from EM Science. Demineralised water was used in all experiments.

Radioisotope tracer techniques were used in the extraction experiments. Usually, lanthanoid solutions were irradiated in a TRIGA nuclear reactor with a steady flux of 6×10^{12} $n \cdot cm^{-2} \cdot sec^{-1}$ for one hour. An aliquot of this radioisotope solution was placed in a pyrex tube (50 ml), containing TCA, 18-crown-6, EDTA, and lanthanoids of known concentration in a total aqueous volume of 10 ml with a phase ratio (organic/aqueous) of 1.0. The pH of the solution was adjusted with lithium hydroxide or

nitric acid and measured with an Orion model 701A digital analyzer and Orion 8103 semi-micro combination electrode. The mixture was shaken for 45 min, which was determined to be equilibrium by a series of time dependent experiments, at 25.0 ± 0.5°, using a Burrell model 75 wrist-action shaker. After phase separation, samples of the organic and aqueous phases were taken with disposable pipettes and counted in polyvials on a large volume EG&G Ortec Ge(Li) detector with a resolution of 2.3 keV at 1332 keV. The following radioisotopes and characteristic gamma energies were used for the identification and quantification of the lanthanoids: ^{140}La (40.2 hr, 328, 487, 815, 1596 keV), ^{141}Ce (32.5 d, 145 keV), ^{143}Ce (33.7 hr, 293 keV), ^{142}Pr (19.2 hr, 1575 keV), ^{147}Nd (11.1 d, 91, 531 keV), ^{152m}Eu (9.3 hr, 121, 344, 841 keV), ^{166}Ho (26.8 d, 82 keV), and ^{177}Lu (6.7 d, 208 keV). The multichannel analyzer was an EG&G ADCAM model 950A. EG&G software was used to set visually-adjusted peak and background regions. A program was written to reduce data, correcting exactly for decay during counting. The details of neutron irradiation and gamma spectroscopy are described elsewhere.[6]

RESULTS AND DISCUSSION

Preliminary experiments showed the lanthanoid–EDTA complexes were insoluble in 1,2-dichloroethane. Calculations of the effective stability constants of La and Lu with EDTA also indicated that the lanthanoid ions would be released in the pH region 2–3. The distribution coefficients (D) of La^{3+}, Ce^{3+}, Pr^{3+}, Nd^{3+}, Eu^{3+}, Ho^{3+} and Lu^{3+} in the pH range 1.9–2.8 and the experimental conditions are given in Table 1. The percent error is one-sigma counting statistic.

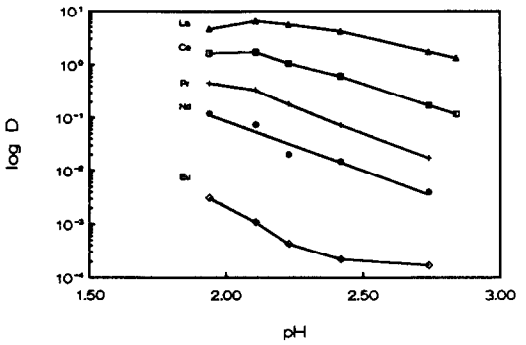

Fig. 1. Graph of log D versus pH. Experimental conditions: [TCA] = 1.1M [18-C-6] = 0.017M, Ln^{3+} = 1 × $10^{-4}M$ [EDTA] = 0.002M, 25 ± 0.5°, solvent = 1,2-dichloroethane, phase ratio = 1.0.

The D values for Ho are very small ($< 10^{-3}$) with relatively large errors and those for Lu are virtually unmeasurable. A significant observation of this system is the large selectivities for the light lanthanoids, *e.g.* the selectivities of La/Ce, La/Pr and La/Eu are 10.2, 101 and 1.04 × 10^4, respectively, at pH 2.74. These values are 3 to 7 times greater than the best selectivities reported by Samy *et al.*[3]

A graph of log D *vs.* pH for La^{3+}, Ce^{3+}, Pr^{3+}, Nd^{3+} and Eu^{3+} is shown in Fig. 1. The graph is linear in the pH region 2.1–2.8, which can be accounted for by the following model. The complexation of a cation (M^{n+}) with a macrocycle (L) and a counter anion (A^-) can be generally expressed by the following equation:

$$M^{n+} + mL + nA^- = ML_mA_n \quad (1)$$

The extraction constant K is given by equation 2.

$$K = [ML_mA_n]_{org}/[M^{n+}][L]^m[A^-]^n \quad (2)$$

or

$$K = D'/[L]^m[A^-]^n \quad (3)$$

Table 1. Distribution coefficients of lanthanoids with number of measurements (in parentheses) and per cent error

	pH 1.94	pH 2.11	pH 2.23	pH 2.42	pH 2.74	pH 2.84
La	4.58 (4)	6.49 (3)	5.53 (4)	4.15 (4)	1.75 (7)	1.34 (3)
	2.8%	2.4%	2.0%	1.9%	1.6%	1.4%
Ce	1.65 (2)	1.73 (2)	1.07 (2)	0.613 (2)	0.172 (4)	0.118 (2)
	8.3%	6.0%	5.2%	6.2%	6.7%	5.9%
Pr	0.457 (1)	0.342 (1)	0.183 (1)	0.0729 (1)	0.0173 (1)	
	3.8%	3.9%	4.2%	6.0%	11.9%	
Nd	0.121 (2)	0.0748 (2)	0.0202 (2)	0.0148 (2)	3.97 × 10^{-3} (1)	
	7.8%	9.5%	24%	28%	50%	
Eu	3.13 × 10^{-3} (2)	1.09 × 10^{-3} (3)	4.31 × 10^{-4} (3)	2.17 × 10^{-4} (2)	1.69 × 10^{-4} (2)	
	2.0%	3.9%	7.2%	18%	26%	
Ho	4.65 × 10^{-4} (1)					
	35%					

Experimental conditions: [TCA] = 1.1M, [18-C-6] = 0.017M, Ln^{3+} = 1 × $10^{-4}M$ each, [EDTA] = 0.002M, solvent = 1,2-dichloroethane, temp = 25.0 ± 0.5°.

where D' is the distribution coefficient without EDTA. If two cations M_1 and M_2 have the same stoichiometry in the extraction process, the selectivity α is related to the relative extraction constants K_1 and K_2 by the following equation.

$$\alpha = K_2/K_1 = D_2/D_1 \quad (4)$$

If a complexonate such as EDTA (YH_4) is present in the aqueous phase, lanthanoid ions can displace one or more protons in the complexonate to form different water-soluble complexes. In the pH range 2–3, H_4Y and H_3Y^- are the two EDTA species present in water with the latter being the predominant one and having almost constant concentration in this region. The reaction of lanthanoid ions with the complexonate can be represented by the following reactions:

$$Ln^{3+} + H_3Y^- = LnH_2Y^+ + H^+ \quad (5)$$

$$Ln^{3+} + H_3Y^- = LnHY + 2H^+ \quad (6)$$

$$Ln^{3+} + H_3Y^- = LnY^- + 3H^+ \quad (7)$$

These reactions are of the following general form.

$$Ln^{3+} + H_3Y^- = LnH_{(3-n')}Y^{(2-n')} + n'H^+ \quad (8)$$

The distribution coefficient in the presence of complexonate is given by the following equation.

$$D = [LnL_mA_n]_{org}/([Ln^{3+}] + [LnH_{3-n'}Y^{(2-n')}]) \quad (9)$$

$$= [Ln_mA_n]_{org}/[Ln^{3+}](1 + K'[H_3Y^-]/[H^+]^{n'}) \quad (10)$$

$$= D'/(1 + K'[H_3Y^-]/[H^+]^{n'}) \quad (11)$$

where D' is the distribution coefficient without complexonate and K' is the equilibrium constant for reaction (8). Since excess EDTA is used, $[LnH_{3-n'}Y^{(2-n')}]/[Ln^{3+}]$ or $K'[H_3Y^-]/[H^+]^{n'} \gg 1$, and equation (11) can be simplified as the following.

$$D = D'/(K'[H_3Y^-]/[H^+]^{n'}) \quad (12)$$

Therefore,

$$\log D = \log D' - \log K'[H_3Y^-] - n'\text{pH} \quad (13)$$

In the pH range 2–3,$[A^-]$ is practically a constant because the pK_a value of TCA is very small, about 0.65. Since [L] ($1.7 \times 10^{-2}M$) is much larger than $[Ln^{3+}]$ ($1 \times 10^{-4}M$) in our experiments, it can also be considered as a constant. Consequently, D' should be a constant in this pH range, as observed experimentally by Samy *et al.*[3] It was pointed out previously that $[H_3Y^-]$ is also near a constant in this pH range. Therefore, log D should be linearly related to pH as shown in equation (14).

$$\log D = \text{constant} - n'\text{pH} \quad (14)$$

According to Fig. 1, the slopes for La^{3+}, Ce^{3+}, Pr^{3+} and Eu^{3+} are -1.2, -1.6, -2.1 and -2.8, respectively, indicating less protonated complexes are favored with the heavier lanthanoids. Consequently, the differences in relative D values increase with pH as shown in Fig. 1. At pH 2.7, the α value for La^{3+}/Ce^{3+} is 10.2 and for La^{3+}/Pr^{3+} is 101. With each unit increase in the Z number of the lanthanoids, the D value appears to decrease by approximately one order of magnitude from La^{3+} to Nd^{3+} at pH 2.8. We did not extend our experiments at pH higher than 3 because the D values for most of the lanthanoids studied became so small and could not be measured accurately.

According to equation (12) the selectivity with complexonate (α) is enhanced by the factor $(K_1'/K_2')([H^+]^{n_2'-n_1'})$ with respect to (α'), the selectivity without complexonate, for two metals as shown in equation (15).

$$\alpha = \alpha'(K_1'/K_2')([H^+]^{n_2'-n_1'}) \quad (15)$$

Since lanthanoid ions form protonated complexes with EDTA and their stability constants are not available in the literature, it is not possible to calculate the selectivity with equation (15). However, it is known that at pH > 3, lanthanoids form unprotonated complexes (LnY^-) with EDTA. Using the stability constants of LnY^- from Martell and Smith[7] and the D values obtained without EDTA as given in Table 2, the calculated selectivity of La/Ce ($\alpha_{La/Ce}$), and Ce/Pr ($\alpha_{Ce/Pr}$) are 11 ± 1 and 12 ± 1, respectively. Our measured values at pH 3.1 were 15 ± 1 for ($\alpha_{La/Ce}$) and 15 ± 3 for ($\alpha_{Ce/Pr}$), in reasonable agreement with the calculated values.

A comparison of the D values obtained without complexonate is given in Table 2. Data reported by Samy *et al.*, as taken from a figure,[3] are also given in the table. Their D values are for slightly different TCA and 18-crown-6 concentrations and should be about 20% greater than ours. After normalization, our data without EDTA agree well with those reported by Samy *et al.*[3] within experimental uncertainties. Furthermore, our experimental

Table 2. Distribution coefficients of lanthanoids without EDTA complexonate at 25.0 ± 0.5°

	D values	
	Literature*	This work†
La^{3+}	7.6	5.8
Ce^{3+}	2.0	1.6
Pr^{3+}	0.56	0.36
Nd^{3+}	0.10	0.096
Eu^{3+}	0.004	0.0039

*[TCA] = 1.0M, [18-crown-6] = 0.01M, $Ln^{3+} = 1 \times 10^{-5}M$ each, pH 3.0. (Ref. 3)

†[TCA] = 0.9M, [18-crown-6] = 0.011M, $Ln^{3+} = 1 \times 10^{-4}M$ each, pH 3.1.

results indicate that in the absence of EDTA, the D value for La^{3+} decreased by nearly a factor of 40 from pH 2 to 0.7. Other lanthanoids such as Pr^{3+}, Nd^{3+}, Eu^{3+} and Ho^{3+} showed a similar decrease in D at low pH. This decrease at low pH suggests that the lanthanoid-18-crown-6-TCA complex in 1,2-dichloroethane can be back-extracted with an acid solution. Experimentally, we have verified that lanthanoids extracted into 1,2-dichloroethane in this system can be stripped from the organic phase with 0.3M nitric acid. This reversibility is important for the recovery of lanthanoids in practical applications.

The model given has also been experimentally verified as follows: Substituting $K[A^-]^n[L]^m$ [equation (3)] for D' in equation (12) and taking the log gives the following linearization.

$$\log (D/[H^+]^{n'}) = \log K + n \log [A^-] + m \log [L] - \log K'[H_3Y^-] \quad (16)$$

Figure 2 shows the variation of $\log(D/[H^+]^{n'})$ with respect to log[L] in the pH region 2.1–2.9 using the n' values determined from Fig. 1. As

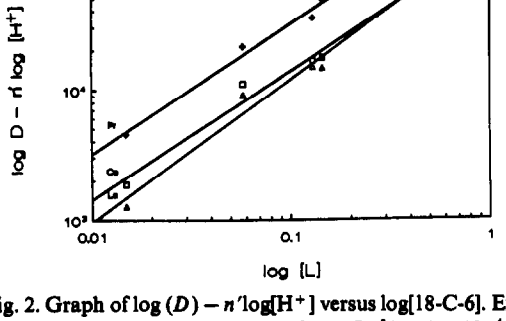

Fig. 2. Graph of $\log (D) - n'\log[H^+]$ versus log[18-C-6]. Experimental conditions: [TCA] = 0.93M, $Ln^{3+} = 1 \times 10^{-4}M$ each, [EDTA] = 0.002M, 25 ± 0.5°, solvent = 1,2-dichloroethane, phase ratio = 1.0.

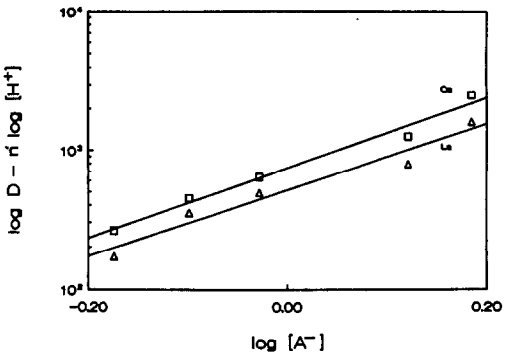

Fig. 3. Graph of $\log (D) - n'\log[H^+]$ versus $\log[A^-]$. Experimental conditions: [18-C-6] = 0.017M, $Ln^{3+} = 1 \times 10^{-4}M$ each, [EDTA] = 0.002M, 25 ± 0.5°, solvent = 1,2-dichloroethane, phase ratio = 1.0.

shown in Fig. 2, La^{3+}, Ce^{3+} and Pr^{3+} gave linear plots. The slope for La^{3+} was 1.1 and the slopes for Ce^{3+} and Pr^{3+} were 1.0, suggesting a 1:1 complex for the lanthanoids with 18-crown-6.

Figure 3 offers further support, showing a linear $\log(D/[H^+]^{n'})$ *vs.* $\log[A^-]$ plot. Slopes of 2.5 for La^{3+} and Ce^{3+} were obtained, which imply three TCA anions in the complex. Samy *et al.*[3] obtained slopes of 2.15 and 2.41 for La^{3+} and Ce^{3+}, respectively, without EDTA.[3] They explained these values as being a result of the decreasing activity coefficient with ionic strength.

In conclusion, EDTA showed enhanced selectivities for lanthanoids in solvent extraction with 18-crown-6 and TCA. The effect of the complexonate on lanthanoid extraction can be explained by a simple model presented in this paper. The selectivities observed in this system are among the largest reported in the literature for the light lanthanoids.

Acknowledgements—This work was supported, in part, by the Idaho EPSCoR Program of the National Science Foundation (Grant No. RII-8902065) and by the Idaho State Board of Education.

REFERENCES

1. J. G. Bunzli and D. Wessner, *Coord. Chem. Rev.*, 1984, **60**, 191.
2. I. M. Kolthoff, *Anal. Chem.*, 1979, **51**, 1R.
3. T. M. Samy, N. Suzuki and H. Imura, *J. Radioanal. Nucl. Chem. Letters*, 1988, **126**, 153.
4. T. Moeller, *Inorganic Chemistry, An Advanced Textbook*, Wiley, New York, 1965.
5. G. Schwarzenbach and H. Flaschka, *Complexometric Titration*, Methuen & Co., London, 1969.
6. W. M. Mok and C. M. Wai, *Anal. Chem.*, 1987, **59**, 233.
7. A. E. Martell and R. M. Smith, *Critical Stability Constants, Vol. 1: Amino Acids*, Plenum Press, New York, 1974.

Talanta, Vol. 39, No. 3, pp. 215–219, 1992
Printed in Great Britain.

0039-9140/92 $5.00 + 0.00

SIMPLE APPROACH FOR ELIMINATION OF BLANK PEAK EFFECTS IN FLOW-INJECTION ANALYSIS OF SAMPLES CONTAINING TRACE ANALYTE AND AN EXCESS OF ANOTHER SOLUTE

TAKESHI YAMANE* and MASAE SAITO
Department of Chemistry, Faculty of Education, Yamanashi University, Takeda-4, Kofu 400, Japan

(*Received* 17 *June* 1991. *Revised* 1 *August* 1991. *Accepted* 1 *August* 1991)

Summary—A blank peak effect in FIA systems often found for samples containing an excess of solute other than the analyte has been studied. Emphasis has been given to trace level determinations and a simple approach for elimination of this effect is presented. The present approach is based on the use of a large sample injection volume, which results in a portion of the sample plug being undiluted with carrier and hence prevents the formation of refractive index gradients in the undiluted portion. The quantitative performance of this approach was demonstrated with the determination of iron in the presence of 0.20*M* sodium chloride and cobalt in the presence of 0.10*M* glucose. No significant difference in the accuracy, precision, and limit of detection was observed between samples for iron both in the presence and absence of sodium chloride and for cobalt in the presence and absence of glucose. Despite using a large sample volume (0.89 ml for a 400-cm sample loop), the sample throughput was about 25/hr.

Flow-injection analysis (FIA) has proved to be a suitable tool for rapid, simple and reproducible determinations with rather inexpensive apparatus. Absorption spectrophotometry is the most widely used mode of detection in FIA because it can be applied to a wide variety of analytical problems. A blank peak appears where there is a difference in refractive index between the carrier solution and the injected sample solution. Such a situation can be illustrated by injecting a salt solution into the stream of distilled water as carrier. Despite the excellent stability of recent commercially available photometric detectors, this perturbation in the refractive index affects the real signal response and consequently causes deterioration of accuracy, precision, and limit of detection, especially in the case of determinations at trace levels.

Few reports[1–4] have mentioned this blank peak effect and its study is of analytical interest. Betteridge *et al.*[1] have discussed the origin of the blank peak and suggested two possible ways to compensate the refractive index problem: the first is to make the refractive index of the carrier equal to that of the sample by adding an inert solute, and the second one is to measure the absorbance on the over-all peak at the point where the "refractometric" peak passes the zero baseline. The first solution, however, requires extra manipulations and is troublesome. Success is not always achieved in finding the suitable salt and its concentration which can give the same refractive index as the sample solutions which may have large variations, because different solutes even at the same concentration may yield different refractive indexes. The second case requires a precisely timed pin-point measurement of absorbance when the signal is sharply decreasing or increasing. This is not easy and the analytical value is subject to operator error unless special equipment is used.

In this paper, the blank peak effect on trace level determinations with FIA has been studied extensively and a simple approach is presented to eliminate the refractive index problem by employing a large volume of sample. The usefulness of this approach is demonstrated with experiments for the determination of iron and cobalt with spectrophotometric detection with 1,10-phenanthroline (PHEN) and 2-(5-bromo-2-pyridylazo)-5-(N-propyl-N-sulphopropylamino)-phenol (PAPS), respectively.

THEORETICAL BACKGROUND

The origin of refractive index perturbation arises from the dispersion (dilution) of the sample plug in the carrier stream, resulting in

*Author for correspondence.

the formation of refractive index gradients. Therefore, a simple way to solve this refractive index problem should be provided by the measurement of the absorbance corresponding to a non-dispersed portion of the sample plug. The present approach for eliminating the refractive index problem is based on the provision of a non-dispersed zone in the sample plug and using this zone for measurement, in contrast to the use of larger dispersion with smaller volume samples as found in ordinary FIA systems.

The dispersion (D) occurring in an FIA system can be considered as the sum of the dispersions originating in the three main parts (D_i, D_t, and D_d) of the system:[5] D_i is concerned with the sample volume and the geometric aspects of the system, D_t is related to the reactor geometry, and D_d is related to the flow-cell geometry contribution to the dilution. According to Růžička and Hansen,[6] changing the injected sample volume is an effective way of changing the dispersion. The present study has mainly focused on the sample volume in order to provide a non-dispersed zone designated as "steady state" by Růžička and Hansen.[6]

EXPERIMENTAL

Reagents

Unless otherwise noted, all reagents were of analytical grade and were used as received. The standard solutions of iron and cobalt were prepared from a 100 μg/ml stock solution (Wako Pure Chemical Industries, Osaka, Japan) by suitable dilution, in which $1.0 \times 10^{-3}M$ ascorbic acid was added to the working standard solution of iron. The PHEN solution ($2.5 \times 10^{-3}M$) was prepared by dissolving the reagent (Dojindo Laboratories, Kumamoto, Japan) in 2.5 ml of $0.50M$ sulphuric acid with small amounts of water and then diluting to 250 ml with water. The working solution of PHEN ($2.5 \times 10^{-4}M$, pH 5.9) was prepared by mixing 25 ml of $2.5 \times 10^{-3}M$ PHEN solution, 0.0176 g of ascorbic acid, 25 ml of $1.0M$ sodium acetate solution and 1.6 ml of $1.0M$ acetic acid solution, followed by dilution to 250 ml with water. The PAPS solution ($5.0 \times 10^{-4}M$) was prepared by dissolving the reagent (Dojindo Laboratories) in water and then diluting to 250 ml. The working solution of PAPS ($1.0 \times 10^{-4}M$, pH 4.7) was prepared by mixing 50 ml of $5.0 \times 10^{-4}M$ PAPS, 20 ml of $1.0M$ sodium acetate solution, and 20 ml of $1.0M$ acetic acid solution, and finally diluting to 250 ml with water.

Manifold and apparatus

The flow system used consists of two channels, carrier C (distilled water) and chromogenic reagent R ($2.5 \times 10^{-4}M$ PHEN for iron or $1.0 \times 10^{-4}M$ PAPS for cobalt). The flow-rate of both streams was 0.75 ml/min. The sample solution is introduced into the carrier stream with a Daiflon six-way rotary valve with sample loop. The injected sample meets downstream with the reagent R and the metal complex formed during the merged zone is transported through the reaction coil (100-cm long) to the flow-cell (35-μl volume). The absorbance is monitored at 526 nm for iron or at 562 nm for cobalt. A Jasco Uvidec-320 spectrophotometer equipped with a flow-cell, a Sanuki DM2M-1024 pump, and a Toa-Dempa EPR-221A chart recorder were used. All pieces of tubing and sample loops were of 0.5 mm i.d. and made of Teflon.

RESULTS AND DISCUSSION

The effect of the presence of excessive salt on the signal response due to trace analyte was studied by injecting the 0.20-ppm iron solution with a 40-cm sample loop considered of normal size in ordinary FIA procedures. Sodium chloride was used as solute in order to produce a high refractive index in the sample solution. Distilled water was used as carrier. As shown in Fig. 1(a), when the solution containing only $0.20M$ sodium chloride was injected, a blank peak appeared as a set of sharp negative and sharp positive peaks. Peak heights increased

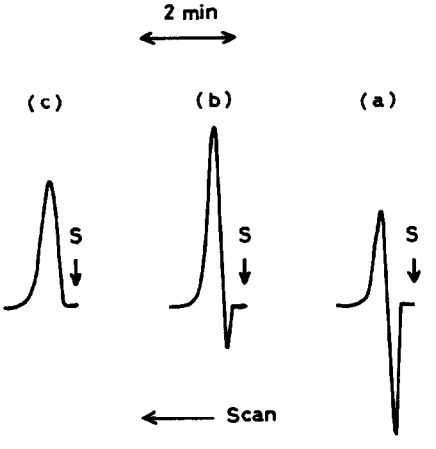

Fig. 1. Typical signal response with a 40-cm sample loop for injecting solutions containing (a) $0.20M$ sodium chloride, (b) 0.20 ppm iron and $0.20M$ sodium chloride in a mixture, and (c) 0.20 ppm iron. S denotes injection of sample.

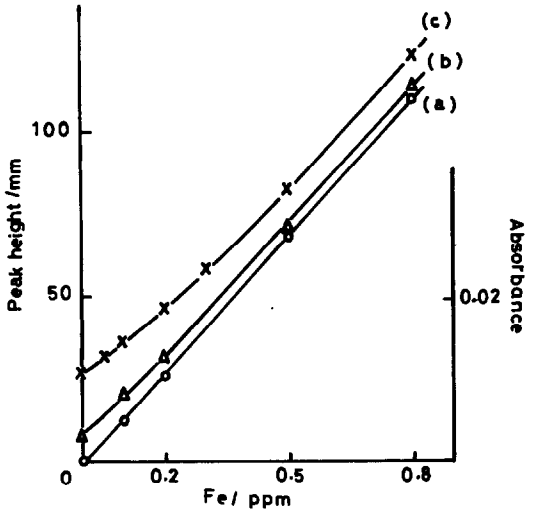

Fig. 2. Calibration graphs with a 40-cm sample loop for injection of (a) iron only, (b) iron in the presence of 0.10*M* sodium chloride, and (c) iron in the presence of 0.30*M* sodium chloride.

with an increase in salt concentration. Judging from the peak of the iron solution without sodium chloride, the peak for iron was evidently affected by the presence of sodium chloride. The peak for a mixture of iron and excess sodium chloride can well be understood as a result of contributions of refractometric and absorptiometric nature. This indicates that the refractometric response perturbs the shape of the analyte signal peak and thus obscures the absorptiometric response, especially for low concentrations of analyte. Figure 2 shows calibration graphs for sample injection with a 40-cm loop obtained by plotting the peak height, measured as the difference between the positive peak maximum and baseline absorbance, as a function of iron concentration. For the iron solution without sodium chloride a linear relationship was observed, but the graphs in the presence of sodium chloride did not pass through the origin due to the presence of the blank peak and showed a slight deviation from linear dependence at the lower concentration range. It can also be seen that the larger the concentration of sodium chloride, the larger the deviation of the slope from that of the linear calibration graph for iron only. This suggests that the additivity is not always guaranteed in the total contribution of refractometric and absorptiometric response, which is combined with a large blank value to control the limit of detection generating larger values than without a high concentration salt. Figure 3 shows the dependence of the shape of signal response on sample loop length with a reaction coil of 100-cm and a constant flow rate. In the blank signal, a plateau, close to the zero baseline, was observed with a sample loop larger than 300-cm, suggesting the presence of a steady state and the occurrence of no refractive index gradient in a limited portion of the sample plug. This was accompanied by a leading and a tailing peak still showing the presence of refractive index gradients at both ends of the sample plug. Also in the signal response for a solution containing 0.20 ppm iron together with 0.20*M* sodium chloride, there is good resolution for the response in the "steady state" zone of the sample plug if the sample loop is longer than 300-cm. This can be recognized as a plateau

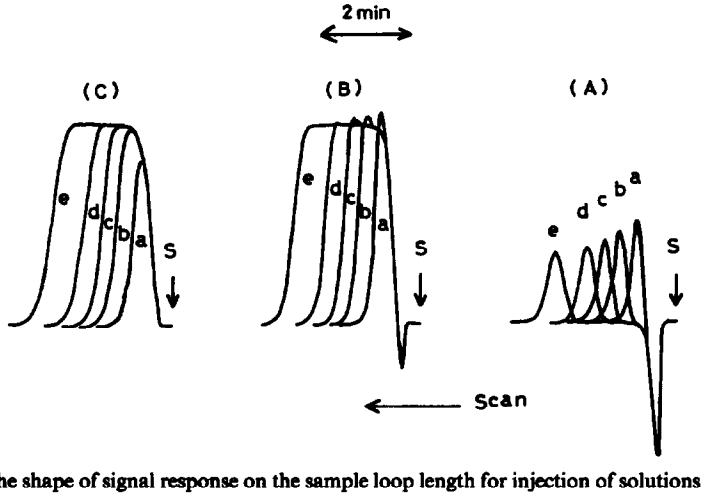

Fig. 3. Dependence of the shape of signal response on the sample loop length for injection of solutions containing (A) 0.20*M* sodium chloride, (B) 0.20 ppm iron and 0.20*M* sodium chloride in a mixture, and (C) 0.20 ppm iron. Sample loop length: (a) 100-cm, (b) 200-cm, (c) 300-cm, (d) 400-cm, (e) 600-cm.

(or as a shoulder) on the upper side of the ascending signal. The height of this plateau from the baseline was found to be independent of the sample loop length. There was no considerable difference in the height of this plateau for solutions of 0.20 ppm iron containing 0.10, 0.20 and 0.30*M* sodium chloride, even though the blank peak due to the refractive index of the sodium chloride solution proportionally increased with its concentration. This evidently shows that there is a portion of the sample plug which is unaffected by the carrier stream. In addition, no change in the height of this plateau was found even when the flow-rate was varied from 0.45 to 0.75 or even 1.0 ml/min.

The effect of the reaction coil length on the signal response for solutions containing 0.20 ppm iron and 0.30*M* sodium chloride in a mixture was studied with a 400-cm sample loop. No significant change in signal response (both in shape and in the height of the plateau) was observed by changing the reaction coil from 100 to 500-cm, although the plateau region tended to become smaller as a result of increased dispersion with increasing reaction coil (this became apparent with a 700-cm reaction coil). Similar results were observed for solutions containing only 0.20 ppm iron. Linear calibration graphs for iron solutions both in the presence and in the absence of 0.20*M* sodium chloride were obtained by plotting the height of this plateau against iron concentration ranging from 0 to 0.80 ppm. The equations for both linear graphs obtained by least squares are as follows: $Y = 0.892X$ and $Y = 0.894X$ (Y: peak height absorbance, X: iron concentration in ppm) for solutions in the presence and absence of 0.20*M* sodium chloride, respectively. The slopes for both linear graphs passing through the origin were in good agreement with each other. In the case of 0.10*M* sodium chloride and iron in a mixture, similar results were also obtained. These results show that real signal response due to the analyte, even in the presence of an excessively high concentration of salt, can easily be recognized and measured by employing a large sample volume, large enough to prevent the formation of refractive index gradients within a limited portion of the sample plug. It should be noticed that the use of a larger sample volume offers an additional advantage by improving sensitivity. In the present case, for instance, the peak height for 0.20 ppm iron increases by *ca.* 70% when increasing the sample loop from 40 to 400 cm.

Longer sample loops at a fixed flow-rate would appear more desirable for achieving better resolution of the non-dispersed zone and an easy and reliable measurement of real signal response due to analyte. This, however, would lengthen the determination time and consume more sample and reagents.

Dispersion and refractive index are also subject to variation by temperature changes, and the present approach would also serve to suppress signal fluctuations originating from temperature changes, although this is not at all effective for preventing the error that would arise from a change in reaction rate.

The recorded signal noise in the plateau for 0.20*M* sodium chloride solution was found to be almost the same as that in the baseline. The limits of detection, estimated as the signal equal to three times the standard deviation of the average blank signal, were 0.008 and 0.009 ppm for iron solutions in the presence and absence of 0.20*M* sodium chloride, respectively. In addition, good reproducibility could be obtained for iron solutions (0.20 ppm), both in the presence and in the absence of 0.20*M* sodium chloride, with relative standard deviations of 0.5 and 0.7%, respectively. Despite using a

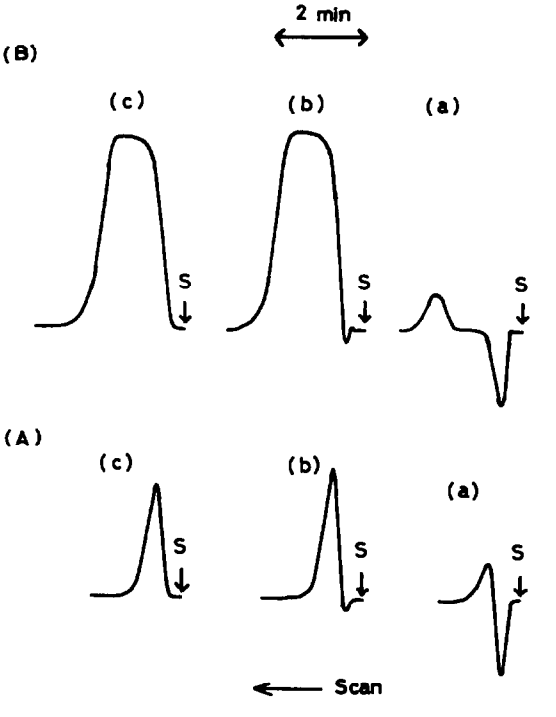

Fig. 4. Typical signal responses with (A) 40-cm sample loop and (B) 400-cm sample loop for solutions containing (a) 0.10*M* glucose, (b) 0.050 ppm cobalt and 0.10*M* glucose in a mixture, and (c) 0.050 ppm cobalt.

400-cm sample loop, the sample throughput was *ca.* 25/hr at a flow-rate of 0.75 ml/min.

In order to assess the feasibility of the present approach, the determination of traces of cobalt with PAPS as a chromogenic agent was performed with solutions containing glucose in place of sodium chloride. It is interesting to compare the characteristics of the two solutes: glucose is an undissociated species in aqueous solution, whereas sodium chloride is a strong electrolyte. Figure 4 shows typical signal traces for solutions containing 0.050 ppm cobalt, 0.050 ppm cobalt plus 0.10*M* glucose, and 0.10*M* glucose, with sample loops of 400 and 40-cm, respectively. A similar blank peak for solutions in the presence of 0.10*M* glucose as in the case of sodium chloride solution was clearly observed. By using the 400-cm sample loop, a plateau, showing that there was a portion of the plug which has undergone no dilution with carrier, was also obtained for glucose solutions both in the presence and in the absence of cobalt. The height of the plateau for 0.050 ppm cobalt in the presence of 0.10*M* glucose (measured as the difference from the baseline obtained for 0.10*M* glucose solution without cobalt) was in good agreement with the plateau observed for 0.050 ppm cobalt solution without glucose. Two linear calibration graphs passing through the origin and having the same slope were obtained for cobalt solutions, both in the presence and absence of 0.10*M* glucose. Table 1 illustrates the results for determination of trace iron added to the 0.20*M* sodium chloride solution and trace cobalt added to the 0.10*M* glucose solution, by using different sample loops of 40 and 400 cm with the FIA system as described above. Each metal concentration was calculated with reference to the calibration graph prepared by standard iron solutions without sodium chloride or standard cobalt solutions without glucose and by the respective use of 40–400-cm sample loops. It can be seen that considerable errors were observed for solutions containing a high concentration of solutes when using ordinary sample injection with a 40-cm loop. In contrast, no considerable blank peak effect on the analytical result was observed by use of a large sample volume with the 400-cm loop.

Table 1. Determination of iron and cobalt in the presence of sodium chloride and glucose, respectively, with use of 40- and 400-cm sample loops

Sample loop, *cm*	NaCl or glucose, *M*	Fe(Co) added, *ppm*	Fe(Co) found,* *ppm*
40	0.10 NaCl	0.10 Fe	0.15 Fe
	0.10	0.20	0.23
	0.10	0.50	0.52
	0.30	0.05	0.23
	0.30	0.10	0.27
	0.30	0.20	0.34
	0.30	0.50	0.61
400	0.20	0.10	0.10
	0.20	0.20	0.20
	0.20	0.50	0.51
40	0.10 Glucose	0.010 Co	0.022 Co
	0.10	0.030	0.041
	0.10	0.050	0.059
	0.10	0.080	0.086
400	0.10	0.010	0.009,
	0.10	0.030	0.031
	0.10	0.050	0.050
	0.10	0.080	0.081

*Results of 3 to 5 determinations.

In conclusion, the use of a large sample volume has proved to be a simple and attractive approach in order to eliminate the blank peak effect, especially at trace level determinations. The present approach was also found to provide advantages in improving the sensitivity by *ca.* 70% and stabilizing the signal response both for analyte and for the blank which may result in improved sensitivity and accurate and reproducible determinations, even when the analyte is present with a large excess of another solute.

REFERENCES

1. D. Betteridge, E. L. Dagless, B. Fields and N. F. Graves, *Analyst*, 1978, **103**, 897.
2. J. Thomsen, K. S. Johnson and R. L. Petty, *Anal. Chem.*, 1983, **55**, 2378.
3. K. S. Johnson and R. L. Petty, *ibid.*, 1982, **54**, 1185.
4. R. A. Leach, J. Růžička and J. M. Harris, *ibid.*, 1983, **55**, 1669.
5. M. Valcarcel and M. D. Luque de Castro, *Flow-Injection Analysis, Principles and Applications*, Ellis Horwood, Chichester, 1987.
6. J. Růzička and E. H. Hansen, *Flow-Injection Analysis*, 2nd Ed., Wiley, New York, 1988.

Talanta, Vol. 39, No. 3, pp. 221–227, 1992
Printed in Great Britain

0039-9140/92 $5.00 + 0.00
Pergamon Press plc

DETERMINATION OF THALLIUM IN SOILS BY FLOW-INJECTION–DIFFERENTIAL PULSE ANODIC STRIPPING VOLTAMMETRY

ZENON LUKASZEWSKI and WLODZIMIERZ ZEMBRZUSKI
Institute of Chemistry, Technical University of Poznan, PL-60-965 Poznan, Poland

(*Received* 17 *November* 1990. *Revised* 8 *July* 1991. *Accepted* 26 *July* 1991)

Summary—A relatively simple and quick method for the determination of thallium in soils is described. The method does not require any separation prior to determination. Total decomposition of the sample was performed in a teflon bomb. The interferences of iron, aluminum and manganese were removed by media exchange performed in a flow-injection measuring system, and the other interferences were removed by the use of the base electrolyte consisting of 0.15*M* EDTA and 0.1*M* ascorbic acid. The contents of thallium in the examined samples of soil were between 100 and 350 ppb.

Thallium is a highly toxic element, however, it has not commanded a lot of attention from investigators because of its low content in the environment, owing to its low crystal abundance (0.7 μg/g).[1,2] On the other hand, the antropogenic sources of pollution with this metal exist and occasional ecological catastrophies caused by thallium arise (*e.g.*, Chernovcy, 1988). It is reported that thallium which is preconcentrated in the soil can dampen the vitality of soil microorganisms.[1] That is why the content of thallium in the environment, its speciation, circulation *etc.*, has a certain importance and should be systematically controlled.

A more extensive investigation of thallium in the environment cannot be performed because of the lack of quick and cheap methods for its determination which are resistant to interferences. This situation occurs because of the very low abundance of the element and the numerous interferences which are very difficult to overcome. That is why the majority of methods combines the final measurement with a preconcentration procedure, *e.g.*, extraction with spectrophotometry[3,4] or volatilization of thallium in the form of hydride with AAS.[5,6] Detection limits for different methods for determination of thallium are compared in a report by IUPAC.[7] Liem *et al.*[5] critically compared the detection limits of methods for determination of thallium also. The potential for stripping voltammetric methods is promising although both reports[5,7] differ very much in evaluation of detection limits of different methods. The lowest detection limit was achieved for the differential pulse mode. Also, the use of a mercury film electrode (MFE) gives a lower detection limit than HMDE. Extremely low concentration of thallium (10 ng/l.) was achieved when the mercury film was used together with a rotating disc.[8] Such a low detection limit is sufficient for the determination of thallium in environmental samples but interferences are the main problem.

The main interferences with thallium in voltammetry are caused by lead, tin and cadmium.[9] Also indium interferes with thallium under the conditions of a MFE,[10] but this interference can be removed by the use of a proper voltage scan-rate. The signals of thallium, lead and cadmium can be separated by the use of certain base electrolytes having alkaline pH.[11] However, in the matrices having practical importance the separate determination of thallium seems to be a more practical solution because of the great difference in the level of thallium on the one hand and the interferents (*e.g.*, lead) on the other hand. Dieker and van der Linden[12] proposed a method for the determination of thallium in the presence of a 10^5-excess of lead with an MFE produced *in situ*. The use of complexons as the base electrolytes is a very effective measure against the interferences. EDTA solution together with acetates, tartrates or citrates is used.[8,13,14] If surfactants are used together with the complexons the excess of lead against the thallium can be substantially increased (to 10^5–10^7).[15,16] The interference of copper can also be removed in this way.[17]

The interferences caused by the presence of iron and titanium turned out to be very difficult to overcome, although these metals do not accumulate in the mercury. These elements are present in many matrices at very high concentrations and their presence causes such problems that the determination is frequently impossible.[18,19] The interferences discussed can be limited by the use of properly selected surfactants. However, the simultaneous presence of several interferents is difficult to overcome, *e.g.*, the use of EDTA which limits the interference of lead involves the appearance of the peak of titanium which does not appear in the non-complexing electrolytes.[19]

Removing the interferents which do not undergo deposition in the form of an amalgam (iron, titanium, *etc.*) seems to be possible by means of media exchange performed after the preconcentration has been completed. Simple removal of analyte containing interferents, after deposition of thallium is completed and its replacement by the pure electrolyte, is possible only in a flow-injection measuring system in which such an operation is possible without breaking the electric contact in the circuit. If these interferents were not present during the stripping stage their interfering influence would be eliminated. A similar solution has recently been used for removing the surfactant from the measuring system after the deposition of cadmium, lead and copper is complete but before the stripping step[20] or for improving determination of copper.[21] The measuring system in these works was very similar to the flow-injection system.[22]

The aim of this paper is to develop a highly selective method for the determination of trace thallium, using media exchange in a flow-injection measuring system and proper selection of base electrolyte for removing interferences. Such a method should be sufficient for the determination of thallium in complicated environmental matrices. Soil seems to be a very good example of such a complicated environmental matrix which has large amounts of possible interferences. Limited deposition time, connected with the volume of analyte is a certain drawback in using a flow-injection system, but can be simply overcome by using circulation of the analyte during the time necessary for effective preconcentration of thallium.

Information on thallium content in soil is comparatively scanty. Chattopadhyay and Jervis have determined 0.17–0.22 ppm in garden soil[23] (the detection limit of this method is only 0.15 ppm) and Ure and Bacon 0.27 ppm.[24] Smith and Carson have reported 0.02–2.8 ppm in surface soils of the USA.[25] The largest antropogenic source of thallium is related to coal combustion.[1]

The normal level of lead in soil should not exceed 70 ppm,[1] although in polluted soils can be much higher. Iron, aluminum, titanium and manganese have the most common range from 0.5 to 5%, from 0.45 to 10%, from 0.1 to 0.9% and from 200 to 800 ppm, respectively.[1] The influence of antimony, bismuth and copper should also be taken into account. The content of antimony and bismuth does not exceed 1–2 ppm but copper can be several hundred ppm.[1] Such a ratio of these interferents should be expected in the solution obtained after the decomposition of the soil sample. The presence of iron(III) in the determined solution obtained after the decomposition of soil is extremely troublesome. Iron(III) causes the dissolution of the mercury film making the determination impossible. The use of supporting electrolyte consisting of EDTA and ascorbic acid can overcome this problem. The results of the determination of thallium in the soil with the use of such electrolyte and media exchange were preliminarily reported.[26,27]

EXPERIMENTAL

Apparatus

A Telpod (Poland) pulse polarograph model PP-04 was used. Voltamperograms were displayed on an Endim (GDR) 620.02 XY-recorder. The differential pulse amplitude was 50 mV and the scan-rate was 11.1 mV/sec. The flow-injection voltammetric system shown in Fig. 1 was used. A wall-jet type three-electrode flow-through cell was used. This cell consisted of: a mercury film electrode based on the epoxy resin impregnated graphite (manufactured in Maria Sklodowska-Curie-University), saturated calomel electrode (SCE) and platinum wire auxiliary electrode. The geometrical surface of MFE was 3.14 mm^2. The mercury film was deposited over 10 min from the solution consisting of 50μM mercury(II) nitrate and 0.1M potassium nitrate, and was washed with potassium nitrate solution. Only one mercury film was required for a whole day of measurements. The peristaltic pump 372.C (Elpan, Poland) was used with a flow-rate of 15 ml/min. During the

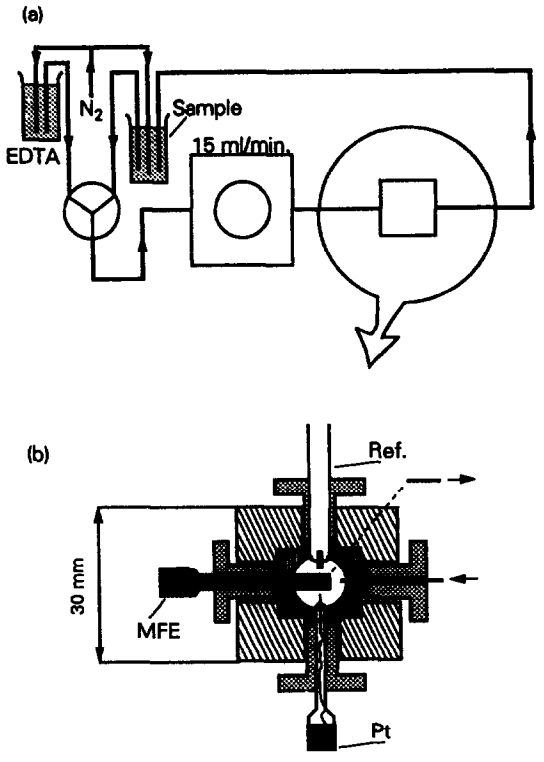

Fig. 1. The voltammetric flow-injection measuring system (a) with flow-through cell of wall-jet type (b). MFE—mercury film electrode based on epoxy resin impregnated pyrolitic graphite, Ref.—reference electrode (SCE), Pt—auxiliary electrode (Pt wire).

measurement, circulation of measured solution was used by junction of the outlet from the measuring system with an analysed sample in the beaker.

Another flow-injection voltammetric system was used for part of the experiments. This system was the first version of the final system and was characterized by the lower hydrodynamic effectiveness of the cell and, as a result, weaker analytical signal.

Reagents

The supporting electrolyte was 0.15*M* EDTA containing 0.1*M* ascorbic acid (pH 4.5), which was prepared from the analytical grade reagents (POCh). The pH of this solution was adjusted with sodium hydroxide solution (Merck). The carrier solution was 0.05*M* EDTA solution which was continuously deaerated with the purified nitrogen. The standard solution of Tl(I) was prepared from thallium(I) nitrate.

All solutions were prepared in triply distilled water in a fused-silica apparatus. Suprapure nitric and hydrochloric acids (Merck) and the analytical grade hydrofluoric acid and hydrogen peroxide (POCh) were used. The samples of soil were received from the Institute of Soil Science and Cultivation of Plants, Pulawy, Poland together with the determined contents of lead, iron and manganese.

Decomposition of soil

The soil sample (approx. 0.5 g) was transferred to the beaker of a teflon bomb and moistened with water. Hydrofluoric acid (2.5 ml) and 3.5 ml of a mixture of hydrochloric and nitric acids (3:1) were added. The teflon bomb was closed and put in the drying-oven for 3 hr (135°). The obtained solution was transferred into a teflon beaker and heated on a graphite heater until evaporated. In the final stage of the evaporation, 2 ml of hydrogen peroxide was added in a few portions, for decomposition of residual organic substances originating from soil. The residue was dissolved in 1 ml of hot hydrochloric acid. The solution of ascorbic acid in the amount corresponding to the final concentration of 0.1*M* was added and after a few minutes the corresponding amount of EDTA solution was added. The pH was adjusted to 4.5 and the volume was supplemented to 25 ml with water in the measuring flask.

Extraction of soil (slightly modified procedure of Wolf et al.*[28])*

The sample of soil (*ca.* 5 g) was placed in the conical flask equipped with a reflux condenser and treated with 20 ml of a mixture of hydrochloric and nitric acids (3:1) and put aside for 48 hr. Then the sample was heated for 2 hr and filtered. The filter was washed with 2*M* nitric acid and the filtrates were mixed. The obtained solution was evaporated. In the final stage of evaporation 2.5 ml of hydrogen peroxide were added in a few portions to completely destroy any organic matter. The residue was dissolved in 1 ml of hydrochloric acid and the procedure was continued as for decomposition of soil.

Measuring procedure

A portion of the solution (8 ml) was transferred to the beaker and was introduced into the flow-injection system. The solution was directed to the measuring cell and then back to the beaker with the sample. In this way the solution was in circulation. Now the preconcentration was started by application of a preconcentration potential. In all experiments preconcentration was carried out at a potential of −0.850 V with the exception of the experiments in which the

influence of preconcentration potential on the peak height was examined. The preconcentration time was 1–3 min depending on the thallium concentration. After the deposition stage was complete the valve was switched off and the analysed solution was replaced by the deaerated carrier solution (0.05*M* EDTA). Then the flow was stopped and the voltamperogram recorded after 15 sec of quiescent time. The evaluation of the concentration of thallium was performed by the method of two additions of standard. The pH remained constant throughout the measuring cycle and so did not require correction.

RESULTS AND DISCUSSION

The presence of ascorbic acid in the base electrolyte transforms iron(III) into iron(II), which highly improves possibilities for the measurement. However, it is still insufficient for the sensitive determination of thallium because of too high a base-line current. This is visible in Fig. 2(a), which shows the voltamperogram of a solution containing EDTA, ascorbic acid, aluminum, iron(II) [introduced in the form of iron(III)] and 10n*M* thallium. Aluminum and iron are present here in the ratio typical of their contents in the soil. Only a small bulge resulting from thallium is visible on this voltamperogram. Media exchange for pure 0.05*M* EDTA removes iron(II) as well as other interferents which do not form amalgams, and in this way radically improves the conditions for the determination of thallium [see Fig. 2(b)].

The correct selection of a deposition potential is very important. On the one hand, a sufficiently negative deposition potential guarantees a stable peak height of thallium (if it is located on the plateau of dependence of the peak height on the deposition potential). On the other hand, with the shifting of potential towards negative direction, the lead signal increases. Thus the selection of deposition potential is the compromise between these two tendencies. This is shown in Figs 3(a) and 3(b). Figure 3(a) shows the dependence of height of the peak of thallium on the deposition potential both in the pure EDTA solution (circles) and in the solution containing additionally iron(II) and aluminum(III) in the ratio typical of the solution obtained after decomposition of soil[25] (crosslets). Iron was introduced in the form of iron(III) for the control of effectiveness of its reduction. These two dependences are identical and their plateau is located starting from a potential of −0.850 V *vs.* SCE. The discussed

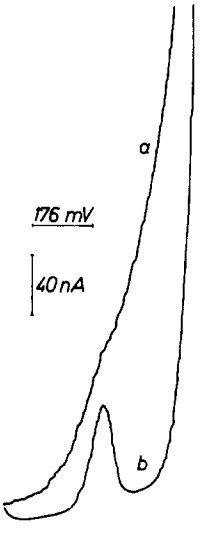

Fig. 2. The voltamperograms with signals of thallium in the presence of iron(II) (before medium exchange) (*a*) and in the absence of iron(II) (after the medium exchange) (*b*). The base electrolyte for the case (*a*) whole cycle and for the deposition stage in the case (*b*) 0.15*M* EDTA + 0.1*M* ascorbic acid + 70m*M* of aluminum(III) + 20m*M* of iron(II) (pH 4.5). The base electrolyte for stripping stage in the case (*b*) 0.05*M* EDTA (pH 4.5). Concentration of thallium: 10n*M*. Preconcentration potential: −0.900 V *vs.* SCE; preconcentration time: 180 sec.

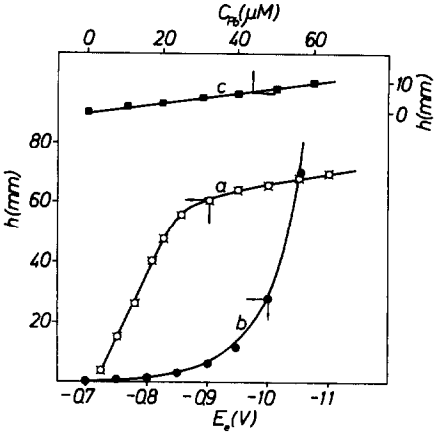

Fig. 3. The dependence of the peak height of thallium (a) and lead (b) on the deposition potential and the peak height of lead on its concentration (c) under conditions of the medium exchange. The base electrolyte for the deposition stage: 0.15*M* EDTA (pH 4.5) [Fig. 3(a)—circles] or 0.15*M* EDTA + 0.1*M* ascorbic acid + 70m*M* of aluminum(III) + 20m*M* of iron(II) (pH 4.5) (other cases). The base electrolyte for stripping stage (all cases): 0.05*M* EDTA (pH 4.5). Concentration of thallium: (a) 10n*M*, (b, c) 0; concentration of lead: (a) 0, (b) 10μ*M*, (c) variable. Preconcentration potential: (a, b) variable, (c) −0.850 V *vs.* SCE. Preconcentration time: (a, b and c) 300 sec.

dependence is shifted toward more negative values in the comparison with similar dependence measured with the use of HMDE.[16] The potential peak of thallium is also located at about −150 mV more negative than when using HMDE (−0.600 V *vs.* SCE). The dependence of the peak height of lead on the deposition potential under these conditions is shown in Fig. 3(b). It is obvious from this picture that the lead peak appears at a potential of −0.850 V *vs.* SCE which is necessary for the determination of thallium. The dependence of the peak height of lead on the concentration of this metal is shown in Fig. 3(c).

This dependence makes possible the evaluation of the positive error of determination of thallium caused by the presence of a certain concentration of lead. This error is negligible for $< 10\mu M$ lead which corresponds to 100 ppm lead in a 0.5-g soil sample.

The masking of the lead signal is caused by the presence of EDTA and the question arises as to whether the excess of free EDTA, *i.e.*, nonbounded with iron, aluminum, *etc.* is necessary for the effective masking of lead. The dependence of the peak height of lead on the preconcentration potential was examined under the following conditions: pure EDTA solution, a solution with an EDTA to iron ratio of 1:1 and a solution with an excess of iron *vs.* EDTA. The results are shown in Fig. 4 and the representative voltamperograms are shown in Fig. 5. The results shown in Fig. 4 were performed with the first version of a measuring system which

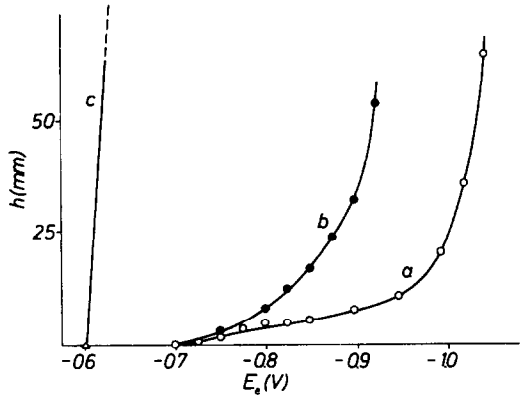

Fig. 4. The dependence of the peak height of lead on the preconcentration potential under conditions of absence (a) or in the presence of iron in the sample (b, c). The ratio of iron *vs.* EDTA: (a) 0, (b) 1, (c) 1.1. The base electrolyte for the deposition stage: $0.1M$ EDTA + $0.1M$ ascorbic acid + 0.1mM of lead(II) (pH 4.5). The base electrolyte of stripping stage: $0.05M$ EDTA. Preconcentration time: 180 sec.

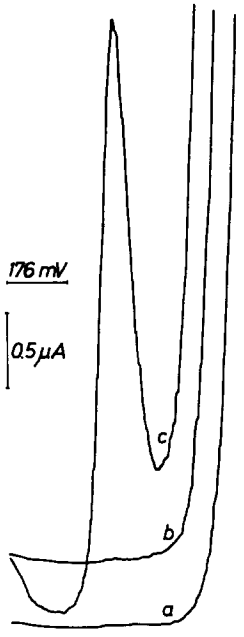

Fig. 5. The effect of excess or deficit of nonbounded EDTA on the tolerance of the system on the presence of lead. The ratio of EDTA *vs.* iron: (*a*) 7.5:1, (*b*) 1:1, (*c*) 1:2. The base electrolyte of deposition stage: $0.15M$ EDTA + $0.30M$ ascorbic acid (pH 4.5). Concentration of lead (deposition stage): 0.01mM. Concentration of iron (deposition stage): (a) 20mM, (b) 150mM and (c) 300mM. The base electrolyte of stripping stage: $0.05M$ EDTA (pH 4.5). Preconcentration potential: −0.850 V; preconcentration time: 900 sec.

was less sensitive and the results were further checked with the system finally used (Fig. 5). The higher concentration of ascorbic acid was used in the last case for more effective reduction of introduced amounts of iron(III) to iron(II). It is clearly visible in Fig. 4 and supported in Fig. 5, that if the concentration of iron and aluminum exceeds EDTA concentration lead is no more effectively masked and a huge peak arising from this metal appears. Thus the ratio of the weight of soil sample to the EDTA concentration must be synchronized and an excess of EDTA in the measured solution is necessary.

The possible interferences of antimony, bismuth and copper with the determination of thallium were predicted.[5] For this reason the tolerated excess of these metals was checked. Antimony or bismuth ($0.1\mu M$) or $1\mu M$ of copper was added to the 10nM thallium solution. Such a ratio is required because of the reported highest level of these elements in the soil.[1] The results of these experiments are shown in Fig. 6. The peaks of considered metals are located at (−0.240), (−0.240) and (−0.200) V *vs.* SCE respectively, under the

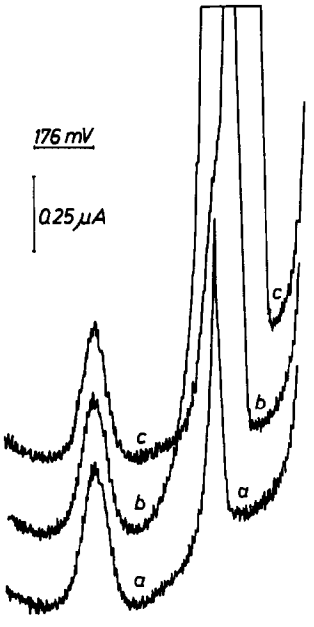

Fig. 6. The voltamperograms of solution containing thallium in the presence of an excess of antimony (a), copper (b) and bismuth (c). Concentration of thallium: 10n*M*. Concentration of antimony or bismuth: 100n*M*, concentration of copper: 1μ*M*. The base electrolyte of deposition stage: 0.15*M* EDTA + 0.1*M* ascorbic acid (pH 4.5). The base electrolyte of stripping stage: 0.05*M* EDTA. Preconcentration potential: −0.850 V *vs.* SCE; preconcentration time: 600 sec.

experimental conditions (deposition from 0.15*M* EDTA + 0.1*M* ascorbic acid solution at −0.850 V and stripping from 0.05*M* EDTA solution). No serious interferences of the investigated metals at such a ratio are observed.

Removal of interferences makes the determination of thallium in the real soil samples possible. The recovery and precision of such a determination has been checked. The representative soil sample (No. 126D8437—see Table 1) contained 1.07% iron, 270 ppm manganese and 8.5 ppm lead. It was analysed according to the described procedure, both alone as well as spiked with 250 ppb thallium. A 213-ppb concentration of thallium was found in the analysed soil (7 independent measurements, $S = 30.5$ ppb, $S_r = 14.3\%$). The spiked thallium was recovered in 94% (6 independent measurements, $S = 31.5$ ppb, $S_r = 7.2\%$). Such results seem to be satisfactory for such a complicated matrix and difficult decomposition procedure. Precision of measurement is satisfactory because it is typical of measurement on such a concentration level.

A concentration of 1n*M* thallium can be comparatively easily determined with 10–15 min preconcentration. Hence, the detection limit of 10 ppb (with 0.5 g of soil) can be achieved, and, if necessary, improved by prolonging deposition time. Lead is tolerated up to 100 ppm but higher contents cause a small positive error.

The developed method was used for the determination of thallium in several samples of soil. Parallel samples were totally decomposed or extracted with a mixture of nitric and hydrochloric acids according to the procedure described above. The results are given in Table 1, together with the content of iron, manganese and lead in the soil samples. It is visible that the content of thallium in the totally decomposed samples is roughly located between 100 and 350 ppb. The extraction of thallium leads to much lower results, which indicates only partial extraction (21–74%). Thus the extraction is the unproper way for the evaluation of total thallium content in the soil in contrast to the determination of zinc, lead, cadmium and copper in the soil,[25] where extraction is complete. The contents of thallium seem to be correlated with the content of iron and manganese. Of course, such a conclusion should be supported with much extensive examination.

Table 1. The results of the determination of thallium in different soil samples performed after the total decomposition of the samples and after the extraction of samples with the mixture of nitric and hydrochloric acids

Sample number	Content of iron, manganese and lead			Thallium content (average)		
	Fe, %	Mn, *ppm*	Pb, *ppm*	Total decomposition, *ppb*	Extraction, *ppb*	Extraction, %
99D8448A	0.23	120	9.0	97	27	28
127D8446	0.44	210	32	175	37	21
26D8321B	0.58	750	240	203	150	74
126D8437	1.07	270	8.5	213	74	35
29D8325B	1.36	400	31	353	148	42
36D8309F	2.91	710	29	355	176	50

The promising results for the determination of thallium in the soil, *i.e.*, sample having silicium, aluminum, iron, titanium, manganese and lead indicate that this element can also be determined in geological samples of similar composition, by means of a very similar procedure.

Acknowledgements—This work was supported by Research Program CPBP 01.17. We thank Professor A. Kabata-Pendias of the Institute of Soil Science and Cultivation of Plants, Pulawy, Poland for providing the soil samples with determined contents of iron, manganese and lead and for valuable discussion. We are grateful to Miss Anna Piela for her technical assistance in the measurements.

REFERENCES

1. A. Kabata-Pendias and H. Pendias, *Trace Elements in Soils and Plants*, CRC Press, Boca Raton, Florida, 1984.
2. R. D. Reeves and R. R. Brooks, *Trace Element Analysis of Geological Materials*, Wiley, New York, 1978.
3. M. Sager and G. Tolg, *Mikrochim. Acta*, 1982 **II**, 231.
4. Z. Marczenko, W. Kalowska and M. Mojski, *Talanta*, 1974, **21**, 93.
5. I. Liem, G. Kaiser, M. Sager and G. Tolg, *Anal. Chim. Acta*, 1984, **158**, 179.
6. J. Aznarez, J. Vidal, L. Marco and J. Galban, *Euroanalysis VI*, Paris 1987.
7. IUPAC Report, *Pure Appl. Chem.*, 1982, **54**, 1565.
8. J. E. Bonelli, H. E. Taylor and R. K. Skogerboe, *Anal. Chim. Acta*, 1980, **118**, 243.
9. G. Henze and R. Neeb, *Elektrochemische Analytik*, Springer-Verlag, 1986.
10. K. Wikiel and Z. Kublik, *J. Electroanal. Chem.*, 1984, **165**, 71.
11. R. Neeb and I. Kiehnast, *Z. Anal. Chem.*, 1968, **241**, 142.
12. J. Dieker and van der Linden, *ibid.*, 1975, **274**, 97.
13. V. Gemmer-Colos, I. Kiehnast, J. Trenner and R. Neeb, *ibid.*, 1981, **306**, 149.
14. R. G. Dhaneshwar and L. R. Zarapkar, *Analyst*, 1980, **105**, 386.
15. N. You and R. Neeb, *Z. Anal. Chem.*, 1983, **314**, 394.
16. A. Ciszewski and Z. Lukaszewski, *Talanta*, 1983, **30**, 873.
17. *Idem*, *ibid.*, 1985, **32**, 1101.
18. Z. Lukaszewski, A. Ciszewski and A. Szymanski, *Chem. Analit. (Warsaw)*, 1987, **32**, 903.
19. A. Ciszewski and Z. Lukaszewski, *Talanta*, 1988, **35**, 191.
20. F. Wahdat, Z. Lukaszewski and R. Neeb, *Anal. Chem.*, 1990, **338**, 163.
21. Z. Lukaszewski, F. Wahdat and R. Neeb, *ibid.*, 1990, **337**, 885.
22. T. Frank and R. Neeb, *ibid.*, 1987, **327**, 670.
23. A. Chattopadhyay and R. E. Jervis, *Anal. Chem.*, 1974, **45**, 1630.
24. A. M. Ure and J. R. Bacon, *Analyst*, 1978, **103**, 807.
25. I. C. Smith and B. L. Carson, *Trace Metals in the Environment*, Vol. 1, Ann Arbor, Michigan, 1977.
26. Z. Lukaszewski and W. Zembrzuski, *ElectroFinn-Analysis*, Turku, 1988.
27. Z. Lukaszewski and W. Zembrzuski, 11th International Symposium on Microchemical Techniques, Wiesbaden, 1989; *Z. Anal. Chem.*, 1989, **334**, 624.
28. A. Wolf, P. Schrammel, G. Lill and H. Hohn, *ibid.*, 1984, **317**, 512.

Talanta, Vol. 39, No. 3, pp. 229–234, 1992
Printed in Great Britain.

0039-9140/92 $5.00 + 0.00

THE INFLUENCE OF COMPLEXING AGENTS ON THE EFFECTIVENESS OF ELECTROCHEMICAL MASKING WITH ANIONIC SURFACTANTS IN ANODIC STRIPPING VOLTAMMETRY

J. OPYDO
Institute of Chemistry, Technical University of Poznań, 60-965 Poznań, Poland

(*Received* 2 *May* 1991. *Revised* 25 *July* 1991. *Accepted* 2 *August* 1991)

Summary—The influence of sodium dodecyl sulphate, sodium dodecyl sulphonate and sodium stearinate on the anodic stripping peaks of Tl(I), Pb(II), Cd(II), Cu(II) and In(III) was investigated. The supporting electrolytes were 0.5*M* sodium sulphate solution, 0.2*M* citrate solution (pH 3.7, 4.6 and 7.3), 0.5*M* tartrate solution (pH 4.4) and 0.1*M* solution of EDTA (pH 4.4). The composition of complex compounds forming in a solution under experimental conditions was defined. The conditions of ion reduction of metals on hanging mercury electrode during the electrolytical deposition were investigated. The investigation included an analysis of voltammetric curves of the metal ions. The obtained results suggest that "electrochemical masking" is much stronger in electrolytes containing a complexing agent than in the sodium sulphate solution. The influence of the complexing agent may not be explained in terms of the interaction between the form of the complex and the charge of the adsorbed surfactant particles; rather the complexing process is connected with indirect inhibition, *i.e.*, by decreasing the rate of charge transfer reaction.

The influence of surfactants on the processes of metal ion electroreduction in electrochemical methods depends to a significant extent on the supporting electrolyte. There is an opinion that in the case of a simultaneous presence of surfactants and complexing agents the effect of "electrochemical masking" is stronger.[1,2] The literature describes many good examples of "electrochemical masking" performed in the presence of both these components.[3–11] It is also suggested that this phenomenon results from the character of actions between the form of a metal ion in a given solution and a charge of adsorbed particles of surfactants. This problem has been signaled by Jacobsen and co-workers[12,13] in relation to polarography waves. According to the mentioned authors the electrode processes of negatively charged metal ion complexes are strongly modified by an adsorbed layer of anionic surfactants, whereas cationic surfactants exert a large influence on the electrode processes of cationic metal complexes.

The present paper deals with the influence of complexing process while "electrochemical masking" of the peaks of Tl(I), Pb(II), Cd(II), Cu(II) and In(III) by anionic surfactants in dc anodic stripping voltammetry (ASV); the influence of nonionic polyethylene glycols and cationic surfactants on metal ion peaks in different supporting electrolytes was investigated in earlier papers.[14,15] The supporting electrolytes were 0.5*M* sodium sulphate solution, 0.2*M* citrate solution (pH 3.7, 4.6 and 7.3), 0.5*M* tartrate solution (pH 4.4) and 0.1*M* EDTA solution (pH 4.4). The anionic surfactants: sodium dodecyl sulphate (SDS), sodium dodecyl sulphonate (DS) and sodium stearinate (S), were applied at different concentrations. With the aim to determine the composition of complex compounds occurring in the solution we calculated a percentage portion of metal ions in individual complex forms arising in the solution under experimental conditions, *i.e.*, at a definite pH and concentration of the supporting electrolyte. The conditions of ion reduction of metals on the hanging mercury electrode during the electrolytic deposition were investigated. The investigation included an analysis of voltammetric curves of the metal ions.

EXPERIMENTAL

Apparatus

Voltammetric measurements were carried out with the Radelkis OH-105 polarograph with a voltage scan-rate of 400 mV/min. A hanging

mercury drop electrode was used as working electrode and SCE as a reference electrode. The surface area of the hanging mercury drop was 2.1 mm^2.

Reagents

Sodium dodecyl sulphate and sodium dodecyl sulphonate (Merck), sodium stearinate (POCh), were used without additional purifications. The supporting solutions were prepared from the analytical grade reagents: sodium sulphate, sodium tartrate, sodium hydrogen tartrate, sodium citrate, citric acid and EDTA. Standard solutions of Tl(I), Pb(II), Cu(II) and In(III) were prepared by dissolving the metals in nitric acid. Solutions with concentrations below 1m*M* were prepared just before use. Water was doubly distilled in a quartz still.

Procedure

The solutions examined were deaerated by a passage of purified nitrogen and were brought to $20 \pm 0.2°$ before measurement. In all the experiments preconcentration was done at a potential of -0.9 V *vs.* SCE for 180 sec, with the solution stirred. After switching off the stirrer, a stripping voltamperogram was recorded after a rest period of 1 min. Each measurement was made with a new drop.

Registration of cathodic voltammetric curves

The studied solution was deaerated and brought to $20 \pm 0.2°$ as above. Then, the $i - E$ curves of the cathodic metal ion reduction in the chosen supporting electrolytes were registered [in the case of Cu(II) the potentials ranged from $+0.2$ to -1.0 V, while the remaining ions ranged from 0.0 to -1.0 V *vs.* SCE]. The solution was uniformly stirred during these studies. The scan-rate of the electrode polarization amounted to 900 mV/min.

RESULTS AND DISCUSSION

The influence of anionic surfactants on the height of the anodic stripping peak of Tl(I) is not significant. The degree of thallium peak damping in all electrolytes, within the range of concentration of surfactants under investigation, does not exceed 20%.

The influence of anionic surfactants on the heights of the anodic stripping peaks of Pb(II), Cd(II), Cu(II) and In(III) in different supporting electrolytes is presented in Figs. 1–4, respectively. All the studies were carried out under identical conditions, *i.e.*, while performing deposition electrolysis for 180 sec at a potential of -0.9 V *vs.* SCE; this is a potential localized in the vicinity of that of a maximum adsorption of applied surfactants,[16,17] and on the "plateau" of most there is a dependence of the peak height on the deposition potential.[16] Concentration of the studied ions was 1μM (only that of Pb in EDTA was 1m*M*), and that of surfactants was changed in the range of 0.1–10 ppm in the case of S and in the range of 0.1–100 ppm in the case of other surfactants. The obtained results were presented as dependences of the relative peak heights (i_s/i_o) on surfactant concentrations (c), where: i_s is the peak height of a metal ion in the presence of a surfactant and i_o is the peak height of a metal ion in the absence of a surfactant. The studies did not cover only ions of Cd(II) and In(III) in EDTA solution, since the obtainment of Cd and In peaks in that electrolyte is connected to the performance of deposition electrolysis beyond the maximum adsorption range of the applied surfactants.

A percentage portion of metal ions in particular complex forms was calculated from the equations of complex formation equilibrium discussed previously.[18] Results of these calculations are summarized in Table 1; column 5 contains the corresponding pK values.[19] Thallium (I) was omitted in these calculations because it is a weakly or not at all complexing ion with the used supporting electrolytes.

Results presented in Figs. 1–4 evidently show that the peak damping of metal ion by the applied surfactants as a rule is significantly stronger in complexing electrolytes than in sodium sulphate solution. Doubts arise when analysing data of Table 1, whether the effectiveness of "electrochemical masking" may be related to a charge sign of the dominant complex in a solution or even to a complex stability. Anionic EDTA complexes, characterized by the largest stability, are in fact damped most strongly, but there are too many exceptions to this rule. In citrate basic electrolyte at pH 7.3, Pb has an anionic form ($Pb\,citr^-$) characterized by p$K = 6.3$, while in citrate electrolyte at pH 4.6 there dominates a neutral form (Pb citr) at p$K = 5.7$, in basic tartrate solution a neutral form (Pb tart) at p$K = 3.4$ was also dominant. Damping is smaller in citrate solution at pH 7.3 than at pH 4.6, and it is also smaller in tartrate solution. Similarly in sodium sulphate solution Cd(II) occurs mostly in the form of $[Cd(SO_4)_2^{2-}]$

Table 1. Characteristics of complex compounds formed under experimental conditions

Metal ion	Supporting electrolyte	Complex form	Ion content	pK
Pb(II)	0.2M citr. at pH 3.7	Pb citr$^-$	3.07	6.30
		PbHcitr	96.93	5.70
	0.2M citr. at pH 4.6	Pb citr$^-$	20.10	6.30
		PbHcitr	79.90	5.70
	0.2M citr. at pH 7.3	Pb citr$^-$	100.00	6.30
	0.5M tart. at pH 4.4	Pb tart	99.89	3.40
		Pb^{2+}	0.11	
	0.1M EDTA. at pH 4.4	Pb EDTA^{2-}	96.65	18.00
		PbHEDTA-	3.35	10.60
Cd(II)	0.5M Na_2SO_4	Cd SO_4	9.10	2.10
		$Cd(SO_4)_2^{2-}$	90.75	3.40
		Cd^{2+}	0.15	
	0.2M citr. at pH 3.7	Cd citr$^-$	14.88	3.75
		CdHcitr	52.84	2.20
		CdH_2citr^+	18.73	0.97
		Cd^{2+}	13.55	
	0.2M citr. at pH 4.6	Cd citr$^-$	66.99	3.75
		CdHcitr	29.90	2.20
		CdH_2citr^+	1.36	0.97
		Cd^{2+}	1.75	
	0.2M citr. at pH 7.3	Cd citr$^-$	99.82	3.75
		CdHcitr	0.09	2.20
		Cd^{2+}	0.09	
Cu(II)	0.2M citr. at pH 3.7	Cu citr$^-$	62.60	5.90
		CuHcitr	26.10	3.42
		CuH_2citr^+	10.90	2.26
		Cu^{2+}	0.40	
	0.2M citr. at pH 4.6	Cu citr$^-$	94.75	5.90
		CuHcitr	4.97	3.42
		CuH_2citr^+	0.26	2.26
		Cu^{2+}	0.02	
	0.2M citr. at pH 7.3	Cu citr$^-$	100.00	5.90
	0.5M tart. at pH 4.4	Cu tart	1.70	3.10
		$Cu(tart)_2^{2-}$	29.70	4.80
		$Cu(tart)_3^{4-}$	68.60	5.60
	0.1M EDTA at pH 4.4	Cu EDTA^{2-}	92.01	18.80
		CuHEDTA-	7.99	11.80
In(III)	0.5M Na_2SO_4	$InSO_4^+$	13.56	1.85
		$In(SO_4)_2^-$	38.15	2.60
		$In(SO_4)_3^{3-}$	47.91	3.00
		In^{3+}	0.38	
	0.2M citr. at pH 3.7	In citr	99.67	6.20
		In^{3+}	0.33	
	0.2M citr. at pH 4.6	In citr	99.99	6.20
		In^{3+}	0.01	
	0.2M citr. at pH 7.3	In citr	100.00	6.20
	0.5M tart. at pH 4.4	In tart$^+$	100.00	4.48

characterized by pK = 3.4. Peaks in that solution are damped by SDS, DS and S like in citrate solution at pH 3.7, in which there dominates a neutral form (CdHcitr) with a lower stability. In sulphate solution In(III) also has mostly the form of anionic complexes, *i.e.*, $[In(SO_4)_3^{3-}]$ (pK = 3.0) and $[In(SO_4)_2^-]$ (pK = 2.6). In all considered citrate solutions In(III) occurs in the form of a neutral complex (In citr) (pK = 6.2), and in tartrate solution it has a cationic form (In tart$^+$) (pK = 4.48). The peak of In(III) in the solutions characterized by dominance of neutral (citrates) and cationic (tartrates) forms is damped considerably more strongly than in sulphate supporting electrolyte, where it has an anionic form.

In the considered solution, Cu(II) occurs mainly in anionic forms of complexes, which suggests a small comparative value of these systems.

An inhibiting effect of surfactants is related to a decrease in the electrode process constant rate.[20-22] This decrease, however, immediately causes a fall in the current of reduction or oxidation only in the case when the electrode process is controlled by the rate of charge

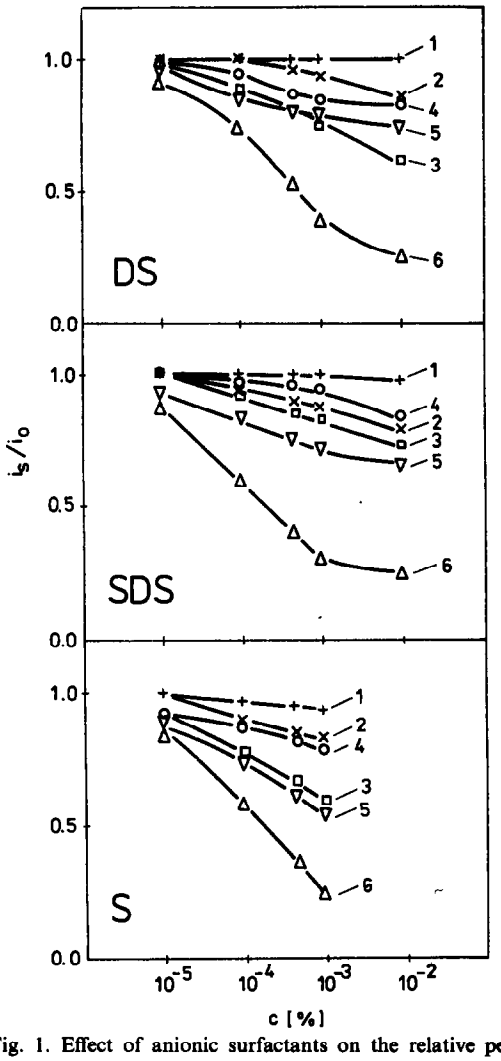

Fig. 1. Effect of anionic surfactants on the relative peak height of Pb(II) in 0.5*M* Na_2SO_4 (1), 0.2*M* citrate at pH 3.7 (2), 0.2*M* citrate at pH 4.6 (3), 0.2*M* citrate at pH 7.3 (4), 0.5*M* tartrate at pH 4.4 (5) and 0.1*M* EDTA at pH 4.4 (6). Concentration of Pb was 1m*M* in EDTA and 1μM in the remaining solutions. Deposition potential −0.9 V *vs.* SCE. Deposition time 180 sec.

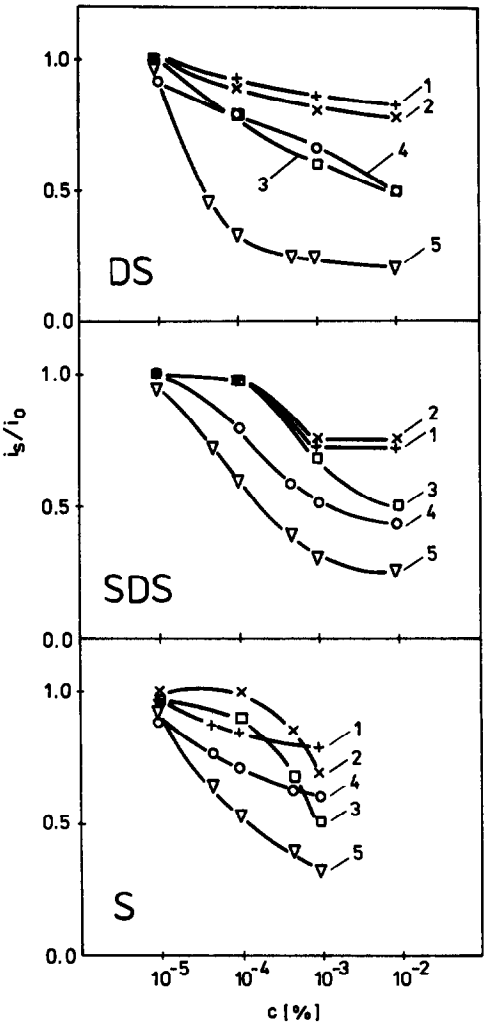

Fig. 2. Effect of anionic surfactants on the relative peak height of Cd(II). Concentration of Cd was 1μM. The supporting electrolytes, deposition potential and time as for Fig. 1.

transfer. When the electrode process is controlled by a slow depolarizer transport rate, a decrease of the electrode process constant rate may remain unnoticed. For that reason electrode processes with deviations from reversibility should be significantly more susceptible to the action of surfactants than reversible processes. The procedure used for investigation of metal ion electroreduction reversibility was the accepted rotating disc method[23] (under conditions of rotating fluid movement the electrolytical deposition stage in ASV assimilates with the rotating disc method). The obtained $i - E$ curves have the shape of polarography waves with well-developed limiting current. A logarithmic analysis of these waves permitted to present results in the form of the dependence $\log[(i_g - i)i^{-1}] = f(E)$, where i_g is a limiting current, i is the current at any point on the wave, and E is potential. Then directional coefficients γ as a criterion of electrode process reversibility were determined in the function $\log[(i_g - i)i^{-1}] = f(E)$. Results are presented in Table 2. It follows from this table that many considered systems containing a complexing agent show significant deviations from the curves of the reversible electrode process (*i.e.*, the process controlled by a slow rate of charge transfer). It may, therefore, be inferred that the complexing process is related to peak inhibition indirectly, *i.e.*, through a decrease in the rate of charge transfer reaction. Decreasing the

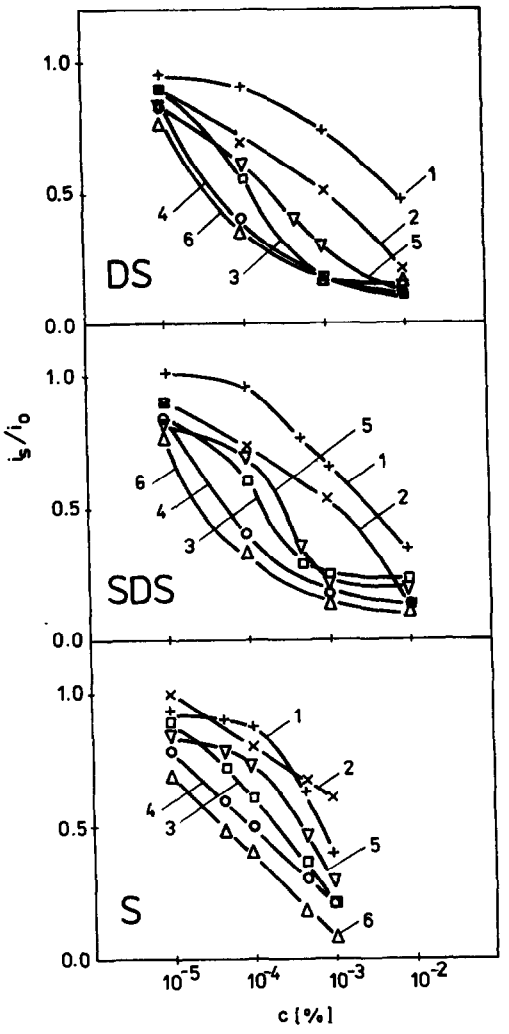

Fig. 3. Effect of anionic surfactants on the relative peak height of Cu(II). Concentration of Cu was 1μM. The supporting electrolytes, deposition potential and time as for Fig. 1.

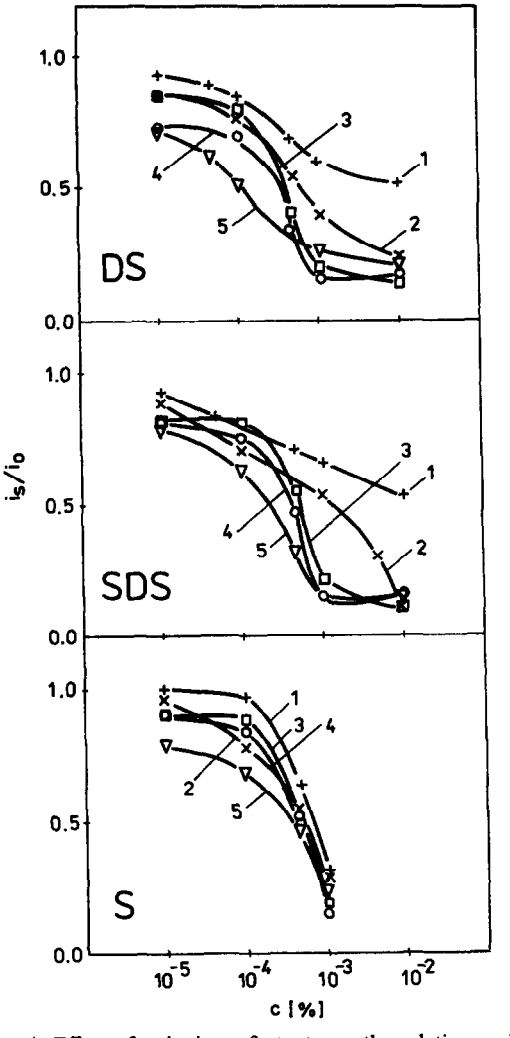

Fig. 4. Effect of anionic surfactants on the relative peak height of In(III). Concentration of In was 1μM. The supporting electrolytes, deposition potential and time as for Fig. 1.

Table 2. Directional coefficients γ of the dependence $\log[(i_g - i)i^{-1}]$ *vs.* E

Metal ion	Supporting electrolyte	γ
Tl(I)	0.5M Na_2SO_4	59
	0.2M citr. at pH 4.6	60
	0.5M tart. at pH 4.4	60
Pb(II)	0.5M Na_2SO_4	30
	0.2M citr. at pH 4.6	39
	0.5M tart. at pH 4.4	79
	0.1M EDTA at pH 4.4	114
Cd(II)	0.5M Na_2SO_4	35
	0.2M citr. at pH 3.7	34
	0.2M citr. at pH 4.6	62
	0.2M citr. at pH 7.3	61
	0.5M tart. at pH 4.4	62
Cu(II)	0.5M Na_2SO_4	27
	0.2M citr. at pH 4.6	62
	0.2M tart. at pH 4.4	44
	0.1M EDTA at pH 4.4	143
In(III)	0.5M Na_2SO_4	45
	0.2M citr. at pH 4.6	50
	0.5M tart. at pH 4.4	50

rate of the charge transfer reaction, a complex formation has the same effect as a surfactant, *i.e.*, contributes to peak damping.

In studies on the influence of surfactants upon anodic stripping peaks a significant role is also played by such parameters as concentration and the kind of applied surfactant as well as the kind of determinable ion.

As may be observed in Figs. 1–4, substances present in 0.1 ppm concentration either have no influence on the peak heights at all or cause only insignificant reduction. A concentration increase in the range 0.1–10 ppm causes a great increase in the influence of anionic surfactants. A concentration increase to 100 ppm has mostly no influence on an already more significant intensification of peak damping.

The influence of the kind of applied surfactants is not submissive to distinct rules. Comparatively small differences may be observed in the action of DS and SDS. This seems to indicate that a hydrophobic group has a greater inhibiting effect than a hydrophilic group.

More pronounced and regular differences were observed in the peak damping of individual ions in the order Tl < Pb < Cd < Cu < In which agrees with that of ionic potentials of particular metals. The values of the ionic potential after acceptance of ionic radius[24] are: Tl(I)–0.74, Pb(II)–1.59, Cd(II)–2.02, Cu(II)–2.50 and In(III)–3.26, respectively. A similar agreement has also been obtained for the influence of cationic surfactants and polyethylene glycols.[15,25]

REFERENCES

1. R. W. Schmid and C. N. Reilley, *J. Am. Chem. Soc.*, 1958, **80**, 2087.
2. I. M. Kolthoff and Y. Okinaka, *ibid.*, 1959, **81**, 2296.
3. Z. Łukaszewski, M. K. Pawlak and A. Ciszewski, *Talanta*, 1980, **27**, 181.
4. A. Ciszewski and Z. Łukaszewski, *ibid.*, 1983, **30**, 873.
5. N. You and R. Neeb, *Z. Anal. Chem.*, 1983, **314**, 394.
6. A. Ciszewski, *Talanta*, 1985, **32**, 1051.
7. A. Ciszewski and Z. Łukaszewski, *ibid.*, 1985, **32**, 1101.
8. Z. Łukaszewski, A. Ciszewski and A. Szymański, *Chem. Analit.* (Warsaw), 1987, **32**, 903.
9. A. Ciszewski and Z. Łukaszewski, *Talanta*, 1988, **35**, 191.
10. J. Opydo, *Mikrochim. Acta*, 1989, **2**, 15.
11. A. Ciszewski, *Talanta*, 1990, **37**, 995.
12. E. Jacobsen and G. Kalland, *Anal. Chim. Acta*, 1964, **30**, 240.
13. E. Jacobsen and G. Tandberg, *ibid.*, 1969, **47**, 285.
14. M. K. Pawlak, *Doctoral Thesis*, Technical University of Poznań, 1977.
15. A. Ciszewski and Z. Łukaszewski, *Anal. Chim. Acta*, 1983, **146**, 51.
16. J. Opydo, *Doctoral Thesis*, Technical University of Poznań, 1982.
17. H. Jehring, *Electrosorptionanalysis with A.C. current Polarography*, p. 123. Akademie-Verlag, Berlin, 1974.
18. J. Inczedy, *Analytical Applications of Complex Equilibria*, Ellis Horwood, 1976.
19. J. Kragten, *Atlas of Metal-Ligand Equilibria in Aqueous Solutions*, Ellis Horwood, 1978.
20. J. Lipkowski and Z. Galus, *J. Electroanal. Chem.*, 1979, **98**, 91.
21. G. Pyzik and J. Lipkowski, *ibid.*, 1981, **123**, 351.
22. R. Guidelli, M. L. Foresti and M. R. Moncelli, *ibid.*, 1980, **113**, 171.
23. Z. Galus, *Fundamentals of Electrochemical Analysis*, p. 245. Ellis Horwood, 1976.
24. Yu. Yu. Lur'e, *Spravochnik po analiticheskoi khimii*, Izdat Khimiya, Moscow, 1962, p. 382. Leningrad-Moscow, 1963.
25. Z. Łukaszewski, A. Ciszewski, M. K. Pawlak and J. Opydo, Euroanalysis IV, Helsinki, 1981, p. 203.

Talanta, Vol. 39, No. 3, pp. 235–242, 1992
Printed in Great Britain.

0039-9140/92 $5.00 + 0.00

AMPEROMETRIC DETECTION OF CATECHOLAMINES WITH LIQUID CHROMATOGRAPHY AT A NOVELLY CONSTRUCTED PRUSSIAN BLUE CHEMICALLY MODIFIED ELECTRODE

JIANXUN ZHOU and ERKANG WANG*

Laboratory of Electroanalytical Chemistry, Changchun Institute of Applied Chemistry, Chinese Academy of Sciences, Changchun, Jilin 130022, People's Republic of China

(*Received* 20 *February* 1991. *Revised* 8 *July* 1991. *Accepted* 10 *July* 1991)

Summary—A novel Prussian blue chemically modified electrode (CME) was constructed and characterized for liquid chromatography electrochemical detection (LCEC) of catecholamines. Both anodic and cathodic peaks could be obtained by monitoring at constant applied potential at anodic and slightly cathodic potential ranges (0.3–0.7 and −0.2–0.1 V *vs.* SCE), respectively. When arranged in a series configuration, using the modified electrodes as generating and collecting detectors, extremely high effective collection efficiencies of 0.91 (for norepinephrine) and 0.58 (for dihydroxyphenylacetic acid) were achieved in dual-electrode LCEC for catecholamines; and a linear response range over 3 orders of magnitude and a detection limit of 10 pg were obtained with a downstream CME as the indicating detector.

Liquid chromatography with electrochemical detection (LCEC) continues to grow in popularity for the sensitive determination of trace compounds in complex samples,[1] and is most highly publicised for its applications in neurochemistry. Up to 1986, over 800 papers had been published dealing with LCEC to solve neurochemical problems which would otherwise have been more time-consuming or even impossible to attack.[2] Among electrochemical flow detectors, amperometric detection at constant potentials has proved to be the most popular tool for solving a wide variety of practical analytical problems in neurochemical research by virtue of the facility in operation, sensitivity and excellent selectivity;[3] and catecholamines have been the primary target compounds among the major neurotransmitter groups penetrated by LC amperometric detection procedures. Single-electrode detectors at a constant applied potential have been widely employed for the determination of catecholamines in biological fluids,[4–10] including catecholamines in plasma[4–7] and brain tissue homogenate.[7–10] Amperometric dual-electrode detectors have recently become popular in LCEC monitoring of catecholamine-related species, which have three configurations termed parallel–adjacent, series, and parallel–opposed dual-electrode detectors,[11] according to the orientation of the electrodes with respect to the flow axis. Parallel–opposed dual-electrode detection has been explored to improve detectability of catecholamines in blood plasma[12] and serum.[13] Parallel–adjacent detectors have been employed to aid in identification of catecholamines in brain tissue.[14,15] Series dual-electrode configurations have been applied mainly to substantially enhance the selectivity for the determination of catecholamines,[16–20] because the system which is routinely operated in oxidative–reductive mode discriminates against chemically irreversible reactions upstream.

For series dual-electrode detectors, the fraction of upstream products that are converted at the downstream detector, termed collection efficiency (N), is the governing parameter for analytical applications of the downstream signal. The N value is highly dependent on the electrodes' size, shape and the configuration with respect to one another,[2,12] as well as the cell designs. Although as high as 60% collection efficiency would be obtained theoretically with horseshoe cell configuration,[2] series dual-electrode detection with N values less than 40% is the typical occasion encountered in LCEC procedures of catecholamines and other redox species.[12,20] High performance collection of catecholamines (N of 0.5–0.6) with LC amperometric detection has recently been achieved with an interdigitated microarray electrode (IDAE).[21]

*Author for correspondence.

This paper reports the attempts on LC amperometric monitoring of catecholamines with a chemically modified electrode (CME). A number of unique features were obtained compared with conventional LCEC procedures of catecholamines. These include extremely high collection efficiencies that could be readily obtained with series dual-electrode configuration which are highly recommended for the CMEs analytical applications in LCEC of catecholamines and perhaps other neurotransmitters.

EXPERIMENTAL

Reagents

Analytical reagent potassium ferricyanide was from Beijing Chem. Co. Epinephrine (E) was from Serva. Norepinephrine (NE), dopamine (DA) and 3,4-dihydroxyphenylacetic acid (DOPAC) were purchased from Fluka A.G. All these chemicals were used as received. Other chemicals were of analytical grade. Doubly distilled water was used for the preparation of all solutions. Catecholamines stock solutions (1 mg/ml) were prepared with 0.1*M* perchloric acid, stored at 4° in the dark. The mobile phase was always 0.1*M* phosphate buffer (pH 5.0) containing 1m*M* EDTA delivered at 1 ml/min, unless stated otherwise.

Apparatus

The instrumentation used was the same as in the previous report.[22] The electrochemical detector was a TL-5A thin-layer cell (BAS, U.S.A.) incorporating two glassy carbon electrodes of the same size. The auxiliary electrode was positioned across the thin-layer channel from the working electrodes to minimize ohmic losses for adequate potential control,[11] when the series dual-electrode arrangement was utilized. All potentials were measured and reported against a saturated calomel electrode (SCE), unless stated otherwise.

Working electrodes

Prussian blue chemically modified electrode (PB–CME). A glassy carbon (GC) electrode was modified with the procedure similar to that described earlier.[23] Prior to modification, the GC electrode was polished with a 0.5-μm alumina suspension on a smooth cloth, thoroughly ultrasonicated in a water bath and rinsed with water. The GC electrode was then subjected to potential cycling between −0.4 and 1.5 V *vs.* SCE at 1 V/sec for 30 min in 1m*M* ferricyanide solution in 0.5*M* potassium chloride.

Electrochemically pretreated GC electrode (EPGC). The polished and washed GC electrode was subjected to potential cycling as in the above procedure in 0.5*M* potassium chloride containing no ferricyanide.

RESULTS AND DISCUSSION

CME electrochemistry

On removal of the electrode from the ferricyanide solution after the modification was completed, no obvious changes of the electrode surface was observed. However, cyclic voltamperograms (CVs) similar to the ferro/ferricyanide redox couple were obtained (Fig. 1) when the electrode was washed and examined in 0.5*M* potassium chloride devoid of the redox species. Sharp and narrow peaks for oxidation and reduction exhibited characteristics of a surface reaction, with the peak currents, both anodic (i_{pa}) and cathodic (i_{pc}), increasing linearly with scan-rates (5–100 mV/sec). This indicated that such a modified electrode did incorporate a stably bound redox group characteristic of the adsorption type.

The nature and mode of the modification of the ferro/ferricyanide redox couple is not immediately clear yet. On extending the anodic sweep limit to +1.3 V *vs.* Ag/AgCl during the potential cycling with the CME in 0.5*M* potassium chloride, a second redox couple with E_p of *ca.* +1.0 V was repeatedly observed (not

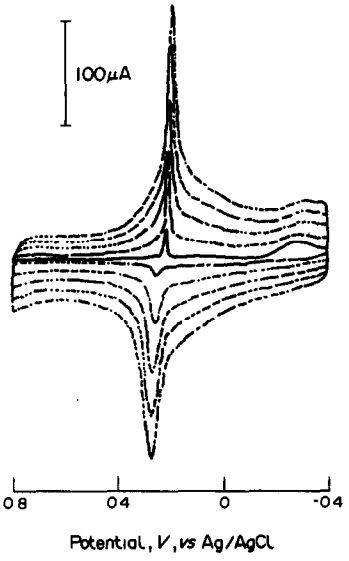

Fig. 1. Cyclic voltamperograms (CVs) with the CME in 0.5*M* KCl at a scan-rate of 5, 25, 50, 75 and 100 mV/sec.

shown), which is suggested to correspond to the Prussian blue/Berlin green redox couple on the electrode surface.[23] Based on evidence of the occurrence of this second redox couple, it was established that the incorporated species corresponded to Prussian blue (PB).[23]

Figure 2B shows the effect on the cyclic voltamperograms (CVs) obtained at the CME in 0.5*M* potassium chloride upon addition of dopamine to the blank supporting electrolyte. In the presence of dopamine, no changes of the background peaks at the CME was observed, but another pair of redox waves (with E_{pa} and E_{pc} of 0.40 and 0.34 V *vs.* Ag/AgCl at 100 mV/sec, respectively) appeared, corresponding to the dopamine redox group itself. Compared with CVs of dopamine at the bare GC electrode (Fig. 2A), the peak potential separation ΔE_p was significantly reduced (from 600 mV at the bare GC to 60 mV at the CME at 100 mV/sec), and the peak currents increased, indicating a greatly improved reversibility of the dopamine electrode process. In view of the fact that the CME modification procedure has in effect involved an electrochemical treatment process by alternative anodic and cathodic polarization at high speed, the effect of such electrochemical pretreatment on CVs of dopamine at the bare GC was determined with an EPGC electrode and is shown in Fig. 2C. Interestingly it was found that the CV behaviour of dopamine at the EPGC electrode was nearly the same as that at the CME, which might suggest that the redox couple (Prussian blue) sustained on the CME had little effect on the electrode process of dopamine. The small and smooth redox couple with E_p of *ca.* 0.20 V *vs.* Ag/AgCl observed on CVs at the EPGC corresponded to quinone groups bound at the GC surface.[24–26]

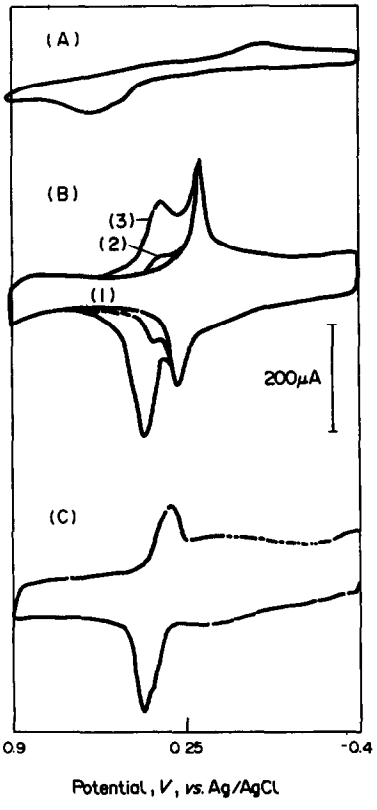

Fig. 2. Cyclic voltamperograms of dopamine at the bare GC (A), CME (B) and EPGC (C) electrodes. Scan-rate, 100 mV/sec. Dopamine concentration is 60 ppm for (A) and for (C); 0 ppm for curve 1 in (B), 10 ppm for curve 2 in (B) and 60 ppm for curve 3 in (B).

Flow-through amperometric detection

Single electrode detection. Figure 3(A) shows the hydrodynamic voltamperograms (HDVs) for catecholamines at the single PB modified CME, with 0.1*M* phosphate buffer (pH 5.0) containing 1m*M* EDTA as mobile phase. In the anodic potential region, a plateau response level was achieved at +0.45 V *vs.* SCE and beyond. Cathodic currents, however, arose in the cathodic potential range (more negative than 0.20 V), reaching maximal levels at around +0.05 V. The absence of 1m*M* EDTA in the mobile phase had little effect on the HDV behaviour of the analytes in the anodic response region; however, the cathodic currents decreased to a certain degree (20% at the maximum response level) in this EDTA free solution.

The flow-rate dependence on the anodic peak current of LC amperometric detection of catecholamines was studied and is shown in Fig. 4. It is clear that the current response always decreased with increasing flow rate, contrasting sharply with theoretical predictions,[27,28] with practical considerations for conventional LCEC of catecholamines with unmodified electrodes.[29] This unique flow-rate dependence is of advantage for the compatibility with microbore HPLC, high sensitivity being attained at rather low flow-rate of the mobile phase.

All these observations indicated that the detector response is not controlled by the process of direct electron transfer between the analytes and the GC surface. The specification of actual mechanism for the appearance of both anodic and cathodic peaks with LCEC of catecholamines, using the single CME working electrode remains difficult. There would be a possibility that the detector response was governed by the complexation of the solutes with iron ions

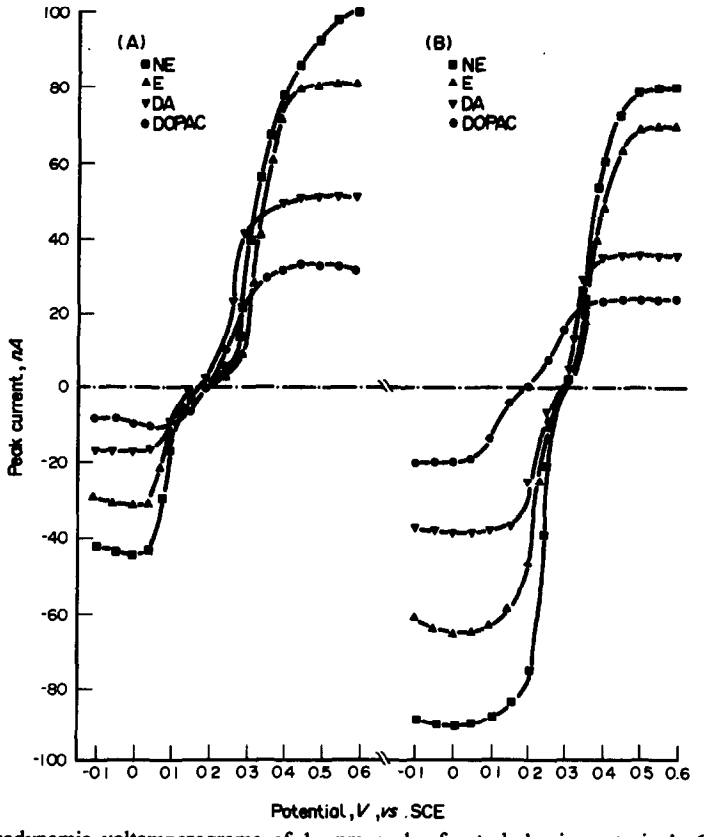

Fig. 3. Hydrodynamic voltamperograms of 1 ppm each of catecholamines at single CME (A) and downstream CME in series configuration (B) with the upstream CME monitored at 0.60 V *vs.* SCE. Column, Nucleosil C_{18} (7 μm) 200 × 4 mm i.d. Mobile phase, 0.10*M* phosphate buffer (pH 5.0) containing 1m*M* EDTA at a flow-rate of 1 ml/min. Injection volume, 10 μl.

[Fe(II) or Fe(III), determined by operating potential] present in the PB molecule.[30] The current response at the CME might result from the differences in solubility and electroactivity of complexes between the components in the mobile phase (EDTA, *etc.*) and the ligands (analytes) injected with Fe(II) or Fe(III) sustained on the CME surface. Eluted catecholamines may form more or less favoured soluble and electroactive iron complexes than the mobile phase components with Fe(III) or Fe(II), respectively, while monitoring the detector at either anodic or cathodic potential regions, and thereby resulting in an increased or a decreased current for iron ion redox reactions, and hence in amperometrically positive or negative peaks. Considering the EDTA effect on the HDV behavior of the analytes, these complexation kinetics would more likely occur in the cathodic response region.

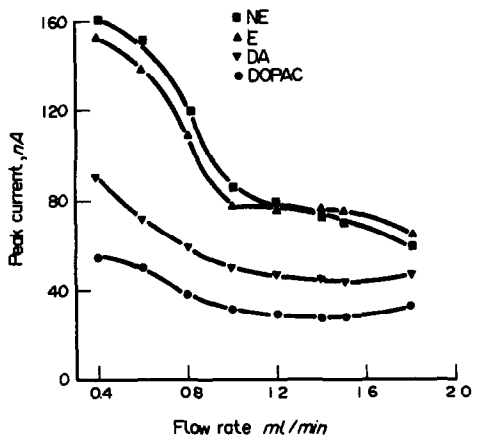

Fig. 4. Effect of mobile phase flow-rate on current response in LCEC of catecholamines at the CME. Potential, 0.45 V *vs.* SCE. Chromatographic conditions as in Fig. 3.

Figure 5 shows the dual-electrode chromatograms of catecholamines with parallel–adjacent configuration, using a bare GC electrode and a CME as indicator detectors, respectively. Distinct cathodic peaks of adequate sensitivity were observed with the CME at the applied potential of 0.0 V *vs.* SCE which exhibited a moderate amount of tailing compared with those obtained at the bare GC electrode.

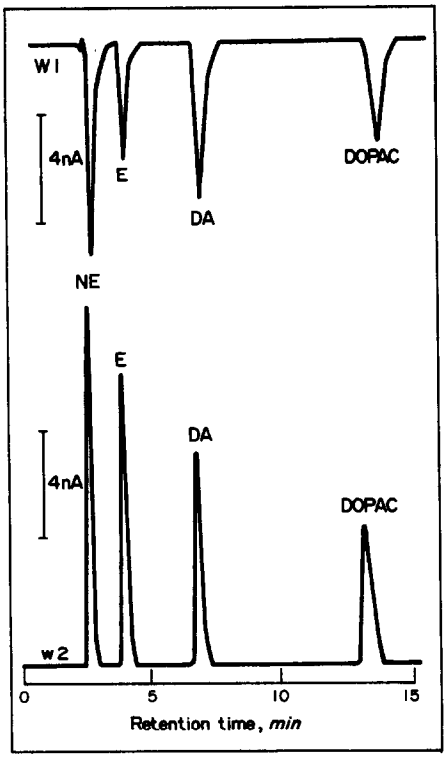

Fig. 5. Parellel–adjacent dual-electrode chromatograms of catecholamines at a bare GC (W1) and the CME (W2). Potential, 0.60 V for W1 and 0 V for W2. Flow parameters as in Fig. 3.

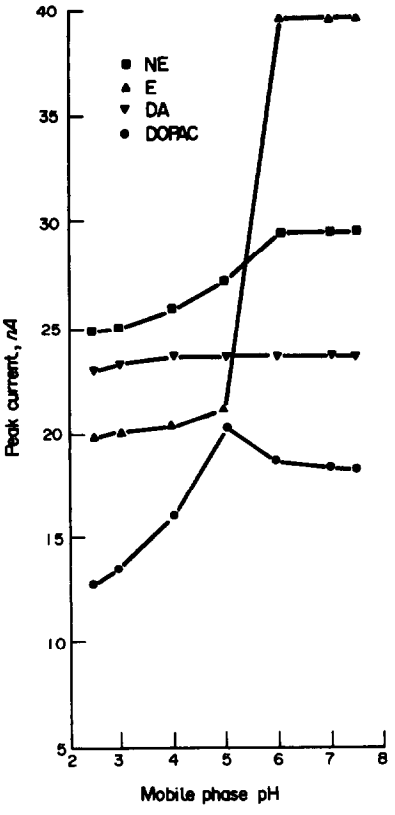

Fig. 6. Effect of mobile phase pH on the peak current in LCEC of catecholamines at the bare GC electrode. Potential, 0.60 V *vs.* SCE. Analyte concentration: 1 ppm for NE and E, 1.5 ppm for DA and 2 ppm for DOPAC. Other conditions as in Fig. 3.

The effects of the mobile phase pH on peak current with the LCEC of catecholamines at the bare GC and the CME are shown in Figs. 6 and 7, respectively. With the bare GC electrode, the current response of epinephrine at higher pH (>6) was double that at lower pH (2.5). Increasing pH had less effect on current response for norepinephrine and negligible change for dopamine. This is due to the dramatic effect of pH on the electrode mechanism involving ECE reactions.[1] Higher pH favoured the indoline form of the epinephrine molecule which has the known high rate of nucleophilic addition, resulting in a net four electron transfer and thereby the detector response may double. All these observations were consistent with previous work.[1] DOPAC exhibited maximum current response at pH 5.0. Lowering the pH is disadvantageous for DOPAC oxidation due to a more positive half-wave potential,[1] whereas higher pH is also unfavourable for DOPAC oxidation probably due to the lower heterogeneous electron transfer rate constant at higher pH.

With the CME, however, the case is quite different. As shown in Fig. 7, catecholamines (except for NE) exhibit maximal current response at pH 5.0. This unique pH dependence was ascribed to the altered electrode mechanism involved at the CME compared with that on the bare GC electrode. It should be noted that the response sensitivity was greatly improved with the CME in the LCEC of catecholamines.

Series dual-electrode configuration. Figure 3(B) shows the hydrodynamic voltamperograms of catecholamines at the downstream CME in a series dual-electrode configuration, monitoring the upstream CME at constant potential of 0.60 V *vs.* SCE. It is clearly seen that the anodic plateau response levels were lower than those at the upstream CME [Fig. 3(A)], indicating that the latter depleted a significant portion of the analyte in the diffusion layer before the mobile phase arrived at the downstream detector. However, the cathodic current response levels dramatically increased at the downstream CME in a series arrangement, reaching maximal response levels at an identical potential of 0 V. The enhancement of current responses should

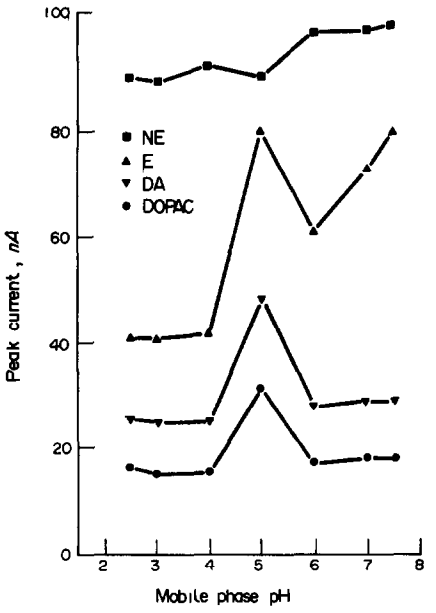

Fig. 7. Effect of mobile phase pH on LCEC of 1 ppm each of catecholamines at the CME. Potential, 0.50 V *vs.* SCE. Flow conditions as in Fig. 3.

be ascribed to the reduction of catecholamine oxidation products upstream.

Figure 8 shows dual-electrode chromatograms of catecholamines with generation (oxidation)–collection (reduction) mode, using bare GC electrodes, PB modified electrodes and EPGCs as working electrodes, respectively. The current measurements at the CMEs and EPGCs, both anodic and cathodic, were much higher than those obtained at bare GC electrodes. The effective collection efficiency (*Ne*) (determined from the ratio of the current at the downstream electrode to the current at the upstream electrode measured under given experimental conditions) for catecholamines was no more than 30% with bare GC electrodes (see Table 1). *Ne* values, however, were greatly increased at EPGCs due to the improved reversibility of catecholamines in the electrode process, as mentioned above. With CMEs, extremely high collection efficiencies were readily obtained, with the maximal value of 91% for NE, resulting from the total contributions of the complexation reaction between the analytes and Fe(II) ion sustained at the CME surface and the reduction of catecholamine oxidation products upstream.

Figure 9 shows the series dual-electrode chromatograms of catecholamines with the same oxidative–reductive mode, using EPGC (or CME) and CME (or EPGC) as generating and collecting electrodes, respectively. It was interestingly found that extremely high *Ne* values were always obtained with the CME as collecting electrode, whether the CME or EPGC was used as the generating electrode, indicating that it was the reduction of upstream oxidation products of catecholamines that contributed a significant portion to the high collection efficiencies, and not the upstream complexation reaction between the analytes and Fe(III) ion sustained on the CME surface.

Table 1 summarizes the effective collection efficiencies of catecholamines obtained with the series oxidative–reductive operation mode, using various electrodes in the upstream–downstream arrangements. It is essential that the CME be used as the collecting electrode in order to obtain highly enhanced effective collections.

Using the PB modified electrodes as generating and indicating detector in a series configuration and the oxidative–reductive mode (at constant applied potentials of 0.60 and 0.0 V *vs.* SCE), LCEC of catecholamines gave linear response range over 3 orders of magnitude, with a correlation coefficient greater than 0.99, and detection limits (S/N = 3) of 10 pg (for NE) and 50 pg (for DOPAC), readily obtained, which are much lower than those obtained at the interdigitated microarray electrode.[21]

In the past few years, a number of investigations have appeared[30–36] concerning the preparation, electrochemical properties and analytical applications of chemically modified electrodes based on the mixed-valence hexacyanides (Prussian blue and its analogues). Li and Dong[31] and Neff[32] prepared thin adherent films of PB on platinum substrate by controlled current electrolysis and studied the electrochromism of the resultant PB CMEs. Cox and co-workers[33,34] and Kulesza *et al.*[35] designed PB analogue CMEs for the electrocatalysis and determination of inorganic ions and organic compounds, including ruthenocyanide CMEs[33,34] and a nickel ferrocyanide CME.[35] All these PB CMEs and analogues were reported to possess good stability under pH less than *ca.* 5.5; higher pH conditions would destroy the films sustained on the electrode surfaces.[31] Recently, Hou and Wang[36] applied the simple adsorption procedure to the glassy carbon electrode to construct a PB/GC CME and used it in flow amperometry by electrocatalytic oxidation for hydrazine. It was found that such a PB/GC electrode was not stable in flow system at high

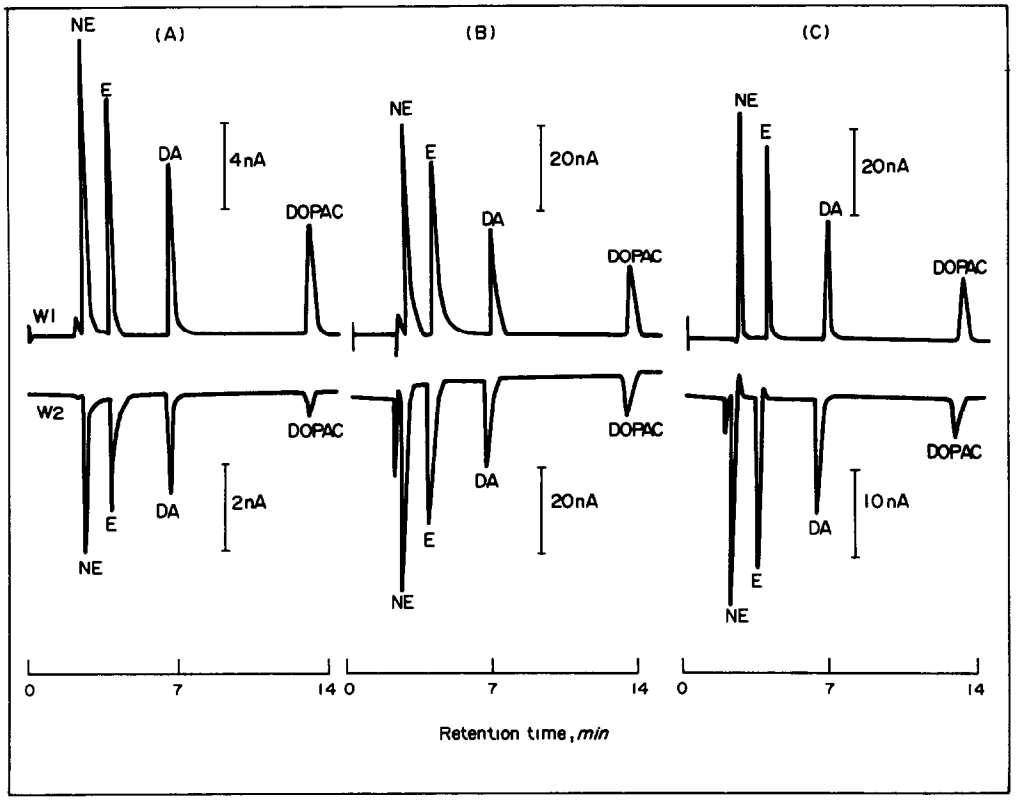

Fig. 8. Series dual-electrode chromatograms of 1 ppm each of catecholamines with bare GC electrodes (A), CMEs (B) and EPGCs (C) as working electrodes. Potential, 0.60 V for upstream W1, 0.0 V (B and C) and −0.20 V (A) for downstream W2. Other conditions as in Fig. 3.

positive applied potentials (0.9 V and beyond). In view of the fact that electrocatalysis is the fundamental point of all these previous works,[33-36] and not the case in our research, from an analytical point of view the stability of the PB CME designed should be our primary concern. It should be noted that the PB/GC CME made in this work possesses favoured stability over those mentioned above.[30-36] This is evidenced by three factors: (*a*) the CME permits hundreds of potential cycles with the anodic scan limit up to +1.5 V *vs.* Ag/AgCl, without any obvious changes in the peak potentials and peak currents; when used in a flowing stream, the cathodic and anodic peak currents of catecholamine responses retained more than 90% of their initial levels after two days of continuous service, even with high positive applied potentials (1.0 V and beyond); (*b*) the CME can be normally operated over a wide pH range (typically 1.5–8.0), examined by batch (CV) and flow (FIA) experiments. This makes the CME completely compatible with conventional reversed-phase liquid chromatography systems. Finally, the CME appears to possess excellent chemical and mechanical stability, as immersing the electrode in concentrated nitric acid for several minutes or submitting it to an ultrasonic water bath and polishing for a long period of time (typically more than 10 min) could not completely destroy the CME examined by cyclic voltammetry in a blank supporting electrolyte.

Table 1. Effective collection efficiencies for catecholamines with series dual-electrode LCEC*

	Upstream W1 Downstream W2	Bare GC Bare GC†	CME CME	EPGC EPGC	EPGC CME	CME EPGC
Ne (ic/ia)	NE	0.27	0.91	0.47	0.88	0.35
	E	0.26	0.82	0.44	0.79	0.35
	DA	0.30	0.80	0.51	0.82	0.50
	DOPAC	0.12	0.58	0.34	0.59	0.16

*Potential: 0.60 V for W1 and OV for W2 *vs.* SCE.
†Potential: −0.20 V *vs.* SCE.

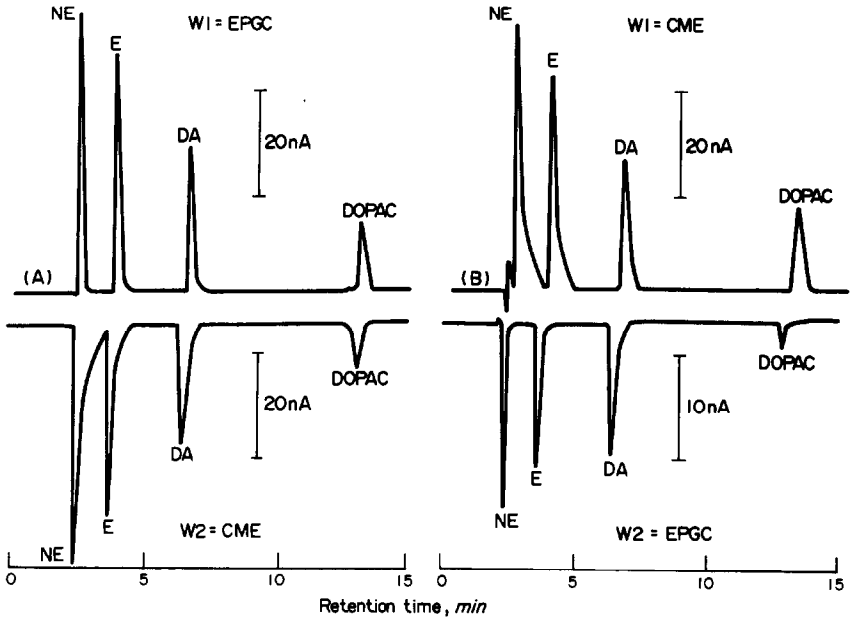

Fig. 9. Series dual-electrode chromatograms of 1 ppm each of catecholamines with EPGC and CME as generating and collecting electrodes (A) and vice versa (B). Potential: 0.60 V for upstream W1 and 0.0 V for downstream W2. Flow conditions as in Fig. 3.

This confirms that modification readily occurred in depth at the GC surface. When a fresh electrode surface is needed, the old CME surface could be effectively depleted by performing several potential cycles between −0.40 and +1.5 V *vs.* Ag/AgCl in 0.1*M* potassium hydroxide.

Acknowledgements—The support of the National Natural Science Foundation of China is gratefully appreciated.

REFERENCES

1. P. T. Kissinger, K. Bratin, G. C. Davis and L. A. Pachla, *J. Chromatogr. Sci.*, 1979, **17**, 137.
2. R. E. Shoup, in *High-Performance Liquid Chromatography*, p. 91–194. Academic Press, New York, 1986.
3. D. C. Johnson, S. G. Weber, R. M. Wightman, R. E. Shoup and I. S. Krull, *Anal. Chim. Acta*, 1986, **180**, 187.
4. P. Hjemdahl, M. Daleskog and T. Kahan, *Life Sci.*, 1979, **25**, 131.
5. G. C. Davis, P. T. Kissinger and R. E. Shoup, *Anal. Chem.*, 1981, **53**, 156.
6. R. C. Canson, M. E. Carruthers and R. Rodnight, *Anal. Biochem.*, 1981, **116**, 223.
7. P. Y. T. Lin, M. C. Bulawa, P. Wong, L. Lin, J. Scott and C. L. Blank, *J. Liq. Chromatogr.*, 1984, **7**, 509.
8. S. K. Salzman, C. L. Eckman and E. Hirofuji, *ibid*, 1985, **8**, 345.
9. C. F. Saller and A. Salama, *J. Chromatogr.*, 1984, **309**, 287.
10. M. H. Joseph, *ibid.*, 1985, **342**, 370.
11. D. A. Roston and P. T. Kissinger, *Anal. Chem.*, 1982, **54**, 429.
12. R. J. Fenn, S. Siggia and D. J. Curran, *ibid.*, 1978, **50**, 1067.
13. M. Goto, G. Zou and D. Ishii, *J. Chromatogr.*, 1983, **268**, 157.
14. G. S. Mayer and R. E. Shoup, *ibid.*, 1983, **255**, 533.
15. D. A. Roston, R. E. Shoup and P. T. Kissinger, *Anal. Chem.*, 1982, **54**, 1417A.
16. C. L. Blank, *J. Chromatogr.*, 1976, **117**, 35.
17. L. C. Lunte, P. T. Kissinger and R. E. Shoup, *Anal. Chem.*, 1986, **57**, 1541.
18. M. Goto, T. Nakamura and D. Ishii, *J. Chromatogr.*, 1981, **226**, 33.
19. *Idem, ibid.*, 1982, **238**, 357.
20. Ji Huamin and Wang Erkang, *Chinese J. Chromatogr.*, 1988, **6**, 137.
21. A. Aoki, T. Matsue and I. Uchida, *Anal. Chem.*, 1990, **62**, 2206.
22. Zhou Jianxun and Wang Erkang, *Anal. Chim. Acta*, 1990, **236**, 293.
23. H. Gomathi and G. P. Rao, *J. Appl. Electrochem.*, 1990, **20**, 454.
24. R. C. Engstrom and V. A. Strasser, *Anal. Chem.*, 1984, **56**, 136.
25. T. Nagaoka and T. Yoshino, *ibid.*, 1986, **58**, 1037.
26. I. Hu, D. H. Karweik and T. Kuwana, *J. Electroanal. Chem.*, 1985, **188**, 59.
27. S. G. Weber and J. T. Long, *Anal. Chem.*, 1988, **60**, 903A.
28. S. V. Prabhu and J. L. Anderson, *ibid.*, 1989, **59**, 157.
29. Ji Huamin and Wang Erkang, *J. Chromatogr.*, 1987, **410**, 111.
30. Li Fengbin and Dong Shaojun, *Scientia Sinica (Series B)*, 1987, **30**, 367.
31. *Idem, Chinese J. Appl. Chem.*, 1986, **3**, 42.
32. V. D. Neff, *J. Electrochem. Soc.*, 1978, **125**, 886.
33. J. A. Cox and P. J. Kulesza, *Anal. Chem.*, 1984, **56**, 1021.
34. J. A. Cox and T. J. Gray, *ibid.*, 1989, **61**, 2462.
35. P. J. Kulesza, K. Brajter and E. Dabek-Zlotorzynska, *ibid.*, 1987, **59**, 2776.
36. Hou Weiying and Wang Erkang, *Anal. Chim. Acta*, in the press.

Talanta, Vol. 39, No. 3, pp. 243–247, 1992
Printed in Great Britain

0039-9140/92 $5.00 + 0.00
Pergamon Press plc

DETERMINATION OF FLUORIDE IN ZINC CONCENTRATES, PROCESSING PRODUCTS AND SOLUTIONS WITH AN ION-SPECIFIC ELECTRODE

R. RAGHAVAN,* B. L. GUPTA† and SUBHIR RAHA†

*Hindustan Zinc Limited, Rampura Agucha Mines, Agucha—311029, Rajasthan, India and
†Hindustan Zinc Limited, Zinc Smelter, Udaipur—313024, Rajasthan, India

(*Received* 20 *March* 1989. *Revised* 6 *June* 1991. *Accepted* 22 *July* 1991)

Summary—Determination of fluoride in hydrometallurgical zinc-plant processing products and solutions with a fluoride-ion electrode is described. Various types of buffers were tested, to find a suitable common buffer for use in analysis of all types of substances generated at the zinc plant. The method involves decomposition of samples either by fusion with sodium hydroxide or by leaching with perchloric acid to bring fluoride into solution. The fluoride concentration is measured directly with a fluoride-specific electrode. In standard addition tests 100% recovery was obtained when a citric acid/sodium nitrate buffer was used. Validation tests gave satisfactory results.

In an integrated hydrometallurgical zinc plant various process solutions flow to the main circuit so that maximum recovery of zinc and various valuable by-products is achieved. Fluoride build-up in these process solutions has been found to occur, depending on the operating conditions of the plant. It has been observed that a high concentration of fluoride will cause difficulties[1] in removal of the zinc deposit from the aluminium cathode, and corrosion[2,3] of the cathode and anode, resulting in reduced life of the electrodes and in effluents from the bleed-off process that can cause environmental hazards. It is therefore essential to determine the fluoride levels accurately at various stages in the process, for effective quality-control operation of the plant as well as to provide a clean environment.

The determination of fluoride in zinc plant products and solutions has changed with the change in technology in this field. During the 1960s the fluoride was separated by the Willard and Winter steam-distillation method[4] and then determined spectrophotometrically by means of its decolourization of the zirconium–Alizarin complex. Though this is a standard reference method, it is tedious, requires constant watch on the temperature range and control, and produces a large volume of distillate.

After the introduction of the fluoride-specific electrode, the steam distillate could be analysed directly for fluoride after addition of TISAB (total ionic-strength adjustment buffer) as for water samples. Later, various decomposition/dissolution[5–8] methods were adopted to bring the fluoride into solution for potentiometric measurement with the fluoride electrode.

At Hindustan Zinc Limited, the aim has been to find a single buffer system suitable for determination of fluoride in all types of sample. Depending on the nature of the sample, the sample preparation step involves either leaching with 2*M* perchloric acid or fusion with sodium hydroxide in a zirconium crucible followed by extraction with water. The solution is then buffered and measured, with a single-point standard addition to provide the calibration data. Highly acidic process solutions are brought to an appropriate pH before addition of the buffer and measurement. A citric acid/sodium nitrate buffer has been found the most suitable for analysis of all types of complex materials arising in the zinc plant operation. The method is simple, rapid, reliable and accurate.

EXPERIMENTAL

Reagents

All reagents used were of analytical grade.

Standard fluoride solution (0.1 mg/ml). Weigh 0.221 g of sodium fluoride, previously dried at 120° for 2 hr. in water, and dilute accurately to 1000 ml.

Sodium citrate/potassium nitrate buffer (Buffer I). Dissolve 294 g of sodium citrate dihydrate

and 20.2 g of potassium nitrate in 600 ml of water. Adjust the pH to 5.5 with 5*M* hydrochloric acid, dilute exactly to 1000 ml with water.

Sodium chloride/sodium citrate buffer (Buffer II). Dissolve 58 g of sodium chloride in 500 ml of water, add 0.3 g of sodium citrate dihydrate and 57 ml of glacial acetic acid, adjust the pH to 5.5 with sodium hydroxide, dilute exactly to 1000 ml with water.

TISAB (Buffer III). Dissolve 58 g of sodium chloride in 500 ml of water, add a slurry of 5 g of diaminocyclohexane-*N,N,N',N'*-tetra-acetic acid, and 125 ml of 6*M* sodium hydroxide to dissolve the acid. Add 57 ml of glacial acetic acid, adjust the pH to 5.5 with 6*M* sodium hydroxide and dilute to exactly 1000 ml with water.

Sodium citrate/sodium nitrate buffer (Buffer IV). Dissolve separately, in 100 ml portions of water, 20 g of citric acid, 68 g of sodium nitrate and 28 g of sodium hydroxide. Mix these solutions, along with 24 ml of glacial acetic acid, adjust the pH to 5.5 with 6*M* sodium hydroxide or hydrochloric acid, and dilute exactly to 1000 ml with water.

Perchloric acid, 2M.

Apparatus

A Metrohm model E 510 precision pH-meter, fluoride-ion electrode (6.0502.050), silver chloride electrode (6.0711.100), a swing-out magnetic stirrer with built-in speed regulator (2.504.0014) and Teflon-coated paddles (6.1903.000) were used.

Sample preparation

Sulphide concentrates. To a 1.000-g sample in a 50-ml nickel/zirconium crucible add 5 g of sodium hydroxide pellets. Place the crucible in a cold muffle furnace and raise the temperature slowly to 500°. Keep the sample at this temperature for 30 min. Cool, digest the fusion cake with 30–40 ml of water, adjust the solution to pH 5.5 with acetic acid, filter through a Whatman No. 41 filter paper into a standard flask. Make up to the mark and mix.

Roasted products and other leached residues. To a 1.000-g sample in a 100-ml polythene beaker add 50 ml of 2*M* perchloric acid, and stir on the magnetic stirrer at controlled speed for 30 min. Filter the solution into a standard flask and make up to volume.

Highly acidic process solutions. Treat with zinc oxide powder to bring to pH 5.5, and filter. Use the filtrate for fluoride estimation.

Other types of process solution. For solutions at pH 4.0–5.5 no preliminary treatment is necessary.

Measurement

To a known volume (10 ml) of prepared sample solution add 25 ml of buffer, stir on the magnetic stirrer and measure the fluoride content potentiometrically with the fluoride electrode. Add a known volume of standard fluoride solution and measure again. From the data thus obtained, calculate the concentration of fluoride in the sample.

RESULTS AND DISCUSSION

The method was tested by analysing various important types of sample generated at the zinc smelter plant. Tables 1–3 show the results, together with those obtained by the standard reference spectrophotometric method. Table 4 shows the results of recovery experiments. The method can be applied to fluoride sample concentrations between 1 μg/g and 6 mg/g, and to even higher concentrations by suitable dilution of the sample solution.

The value of 4.10% for the standard reference sample of zinc–tin–copper–lead ore (MP-1) is slightly higher than the provisional official value[9] of 4.04%. The higher value and the better response may be due to a more effective fusion technique obtained by use of the citric acid/sodium nitrate buffer.

Different sample preparation techniques were used to bring fluoride into solution, depending on the nature of the sample. For sulphide concentrates a fusion technique similar to that reported by Rajan *et al.*[10] was adopted. For oxide and other leached residues a simple acid leaching technique has been found useful for bringing the fluoride into solution. Though fusion can also be applied, we prefer the leaching technique because it gives complete dissolution effectively. The pH of the solution should be adjusted to 5–5.5 before addition of the buffer acid. All the potentiometric measurements have to be made at pH 5.5.

Zinc oxide powder was used to neutralize highly acidic plant solutions. It is preferred to other neutralizing agents such as sodium hydroxide or sodium carbonate, because it has effective neutralizing capacity without any precipitation of zinc at pH 5–5.5, and it also provides the same matrix with no loss of fluoride.

Table 1. Results obtained for total fluoride in zinc concentrates by specific ion-electrode and spectrophotometry (means of 4 replicates)

Sample	Nominal composition, %							F^- found, $\mu g/g$				
	Zn	Pb	Fe	Cu	S	SiO_2	Al_2O_3	Buffer I	Buffer II	Buffer III	Buffer IV	Spectrophotometric method
Zinc ore. CZN-1	44.74	7.45	10.93	0.144	30.2	1.0	0.25	150	148	158	162	—
Zinc–tin–copper–lead ore MP1	15.9	1.88	5.68	2.09	11.8	19.4 as Si	3.63 as Al	4.07×10^4	4.01×10^4	4.09×10^4	4.10×10^4	—
Zinc concentrate												
Indian	52.5	1.5	5.8	0.05	30.2	1.8	1.00	88	87	90	92	92
Canadian	51.9	0.7	5.6	0.68	31.6	5.5	1.0	58	55	60	62	61
Mexican	56.4	0.5	5.6	1.00	32.0	2.0	1.0	48	45	48	51	51
Peruvian	55.8	1.8	5.1	0.28	30.2	2.0	1.0	118	115	120	122	122
Australian	52.6	0.9	10.7	0.12	31.6	2.6	1.5	57	55	58	62	62
Irish	53.8	2.2	3.3	0.06	29.6	3.9	1.0	75	70	75	82	82
Swedish	53.9	1.4	7.3	0.50	30.0	2.8	1.2	95	92	98	103	103

Table 2. Results obtained for total fluoride in roasted product/oxide by specific ion-electrode and spectrophotometry (means of 4 replicates)

Sample	Nominal composition, %							F^- found, $\mu g/g$				
	Zn	Pb	Fe	Cu	S	SiO_2	Al_2O_3	Buffer I	Buffer II	Buffer III	Buffer IV	Spectrophotometric method
Calcine	59.24	3.10	5.60	0.06	3.60	4.0	1.20	80	78	82	85	85
Drum cake	18.7	4.7	21.7	0.10	10.1	7.0	2.0	160	155	160	162	164
Jarosite	4.0	4.5	16.8	0.12	6.2	10.2	6.0	112	110	115	118	122
Waelz slag	2.5	1.0	20.0	0.02	2.8	20.0	6.0	120	120	122	124	125
Bag filter product	58.8	8.0	4.5	0.04	3.0	3.0	1.0	220	210	240	242	242
Clinkered oxide	62.5	6.0	5.5	0.10	0.5	8.0	2.5	100	105	108	108	110
Lead oxide	20.5	28.0	2.0	0.05	1.5	8.5	1.5	6.00×10^3	6.00×10^3	6.01×10^3	6.02×10^3	6.02×10^3
Lead sulphate	7.5	36.8	3.0	0.06	8.0	18.0	1.8	1.20×10^3	1.20×10^3	1.21×10^3	1.22×10^3	1.22×10^3
Magnesium bleed cake	8.5	—	—	—	—	1.5	0.8	155	150	158	160	160

Table 3. Results obtained for total fluoride in process solutions by specific-ion electrode and spectrophotometry

Sample	Nominal composition, *g/l.**							F^- found, *μg/ml*				
	pH	H^+	Zn	Fe	Cu	Mn	Mg	Buffer I	Buffer II	Buffer III	Buffer IV	Spectrophotometric method
Acid overflow	—	1.1	100	1.0	0.02	3.5	6.5	4.2	4.2	4.5	4.55	4.6
Conversion overflow	—	35	90	10	0.35	3.5	8.0	30.0	28.8	30.0	30.5	30.5
Spent electrolyte	—	180	50	Tr	Tr	6.2	7.5	14.0	13.5	14.0	14.8	15.0
Plant effluent before treatment	—	1.5	1.5	Tr	Tr	—	—	12.8	12.0	12.7	12.9	13.0
High acid–high iron zinc sulphate solution	—	130	15	35	0.750	2.0	1.0	34.0	33.5	34.0	35.0	35.0
Neutral overflow	4.8	—	135	0.001	0.25	3.5	8.5	6.0	5.8	6.2	6.5	6.7
Neutral solution	5.0	—	135	0.001	Tr	3.5	8.7	6.0	5.8	6.1	6.2	6.2
Solution after removal of Mg	8.5	—	0.05	—	Tr	2.8	0.2	26.5	26.0	26.8	27.0	27.2
Plant effluent after treatment	9.2	—	0.005	0.001	Tr	0.1	0.2	0.9	0.8	0.9	0.9	1.0

*Except pH; Tr = trace.

Table 4. Recovery of added fluoride by the proposed method

	F^-, *μg*		Buffer I		Buffer II		Buffer III		Buffer IV	
	Present	Added	F^- found, *μg*	Recovery, %	F^- found, *μg*	Recovery, %	F^- found, *μg*	Recovery, %	F^- found, *μg*	Recovery, %
Zinc concentrate MP1	20.5		20.4	99.3	20.0	97.8	20.5	99.8	20.5	100
		20.0	38.3	94.6	34.3	84.6	38.5	95.1	40.5	100
Zinc concentrate (Indian)	9.2		8.8	95.7	8.7	94.6	9.0	97.8	9.2	100
		10.0	18.5	96.4	16.9	88.0	18.8	97.9	19.1	99.5
Calcine	8.5		8.0	94.1	7.8	91.8	8.2	96.5	8.5	100
		10.0	17.6	95.1	16.7	90.0	18.1	97.8	18.4	99.5
Drum cake	16.4		16.0	97.6	15.5	94.5	16.0	97.6	16.2	98.8
		20.0	35.3	97.0	34.3	94.2	35.4	97.3	35.9	98.6
Jarosite cake	12.2		11.2	91.8	11.0	90.2	11.5	94.3	11.8	96.7
		20.0	29.6	91.9	30.8	93.2	31.4	97.5	31.8	98.8
Mg bleed cake	8.0		7.8	97.5	7.5	93.8	7.9	98.8	8.0	100
		10.0	17.6	97.8	16.9	93.9	17.8	98.9	18.0	100
Conversion overflow	30.5		30.0	98.4	28.8	94.4	30.0	98.4	30.5	100
		40.0	69.1	66.3	68.0	96.5	69.8	98.6	70.5	100
Spent electrolyte	150.0		140	93.3	135	90.0	140	93.3	148	98.7
		100	235	94.0	232	92.8	238	95.2	248	99.2
Neutral overflow	67.0		63.8	95.2	62.0	92.5	64.0	95.5	66.5	99.3
		100	160	95.8	154	92.2	164	98.2	167	99.4
Natural solution	62.0		60.0	96.8	58.0	93.5	61.0	98.4	62.0	100
		100	157	96.9	155	95.7	160	98.8	162	100

The Ag/AgCl electrode is used as reference electrode and is found to provide satisfactory results.

Various buffers were tested for their efficiency in measurement of fluoride and elimination of interferences. It was found that the sodium citrate/sodium nitrate/sodium acetate buffer was more effective than the other types of buffer tested. When this buffer was used, the response was very fast with minimum time needed for stabilization, 100% recovery of standards was obtained, and the system was effective in the presence of interfering elements such as Al^{3+}, Fe^{3+}, and soluble silica. A maximum of 5 min was needed for stabilization of the potentials whereas with the other buffers 15 min or more was needed and the recovery of a standard addition varied between 85 and 95%. Use of this buffer gave more accurate results than those obtained with the citrate/DCTA buffer,[11] and also quicker stabilization and response.

Acknowledgements—The authors wish to thank the management of Hindustan Zinc Limited for their kind permission to publish the work done in the process control laboratory of Zinc Smelter.

REFERENCES

1. E. G. Parker, Cominco Ltd, Trail, Canada, Personal communication.
2. C. H. Mathewson (ed.), *Zinc: The Science and Technology of the Metal, its Alloys and Compounds*, p. 224. Reinhold, New York, 1970.
3. Kirk-Othmer *Encyclopedia of Chemical Technology*, 3rd Ed., Vol. 24, p. 821. Wiley, Chichester, 1984.
4. H. H. Willard and O. B. Winter, *Ind. Eng. Chem., Anal. Ed.*, 1933, **5**, 7.
5. R. L. Clements, G. A. Sergeant and P. J. Webb, *Analyst*, 1971, **96**, 51.
6. B. L. Ingram, *Anal. Chem.*, 1970, **42**, 1825.
7. M. A. Peters and D. M. Ladd, *Talanta*, 1971, **18**, 655.
8. D. Jagner and V. Pavlova, *Anal. Chim. Acta*, 1972, **60**, 153.
9. D. S. Russell, H. B. MacPherson and V. P. Clancy, *Talanta*, 1980, **27**, 403.
10. S. C. S. Rajan, L. M. Bhandari and B. R. L. Row, *ibid.*, 1985, **32**, 1064.
11. A. Hulanicki, M. Trojanowicz and J. Sztandor, *Chem. Anal. (Warsaw)*, 1979, **24**, 617.

Talanta, Vol. 39, No. 3, pp. 249–254, 1992
Printed in Great Britain.

0039-9140/92 $5.00 + 0.00

THE STABILITY OF THE METAL COMPLEXES OF CYCLIC TETRA-AZA TETRA-ACETIC ACIDS

SILVIA CHAVES, RITA DELGADO and J. J. R. FRAUSTO DA SILVA
Centro de Química Estrutural, Instituto Superior Técnico, Lisbon, Portugal

(*Received* 25 *April* 1991. *Revised* 12 *July* 1991. *Accepted* 26 *July* 1991)

Summary—The stability constants of the complexes formed by three tetra-aza macrocyclic complexones (DOTA, TRITA and TETA) with Mn^{2+}, Fe^{2+}, Co^{2+}, Ni^{2+}, Cu^{2+}, Zn^{2+}, Cd^{2+} and Pb^{2+} were determined with an automated titration instrument with data acquisition and the calculations were performed with the Superquad program, confirming and extending the range of values previously available. Both 1:1 and 2:1 metal-to-ligand complexes were now considered including their protonated species.

The results show that DOTA is a powerful but unselective ligand whereas TETA, although not so powerful as DOTA, is an interesting selective ligand for pairs of metal ions, *e.g.*, Cd^{2+} and Pb^{2+}.

In a previous paper[1] we reported the results of a study of the complexation properties of a series of *N*-acetate derivatives of tetra-aza macrocycles (**I–III**).

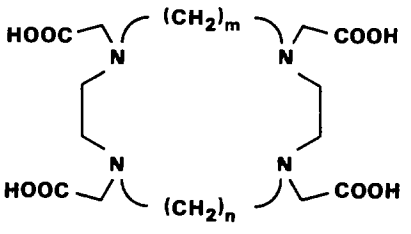

I—$m = n = 2$—1,4,7,10-tetra-azacyclododecane-1,4,7,10-tetra-acetic acid (DOTA);

II—$m = 3$; $n = 2$—1,4,7,10-tetra-azacyclotridecane-1,4,7,10-tetra-acetic acid (TRITA);

III—$m = n = 3$—1,4,8,11-tetra-azacyclotetradecane-1,4,8,11-tetra-acetic acid (TETA).

They are all strongly complexing ligands, particularly DOTA, which was reported to give the most stable Ca^{2+} complex in aqueous solution.[2,3] In our paper we confirmed this finding and extended the work to include the other alkaline-earth metal ions and a group of transition metals, namely Co^{2+}, Ni^{2+} and Cu^{2+} as well as Zn^{2+}. We have demonstrated that although the stabilities of the complexes of the alkaline-earth ions decrease steeply with the increase of the size of the tetra-aza ring of the ligands, the stability constants of the complexes that DOTA forms with these ions are 10^4–10^6 orders of magnitude higher than those of the classic complexones, *e.g.*, EDTA, whereas the stability constants of the complexes of the three ligands with the transition metal ions are very close and of the same order of magnitude of those formed by the linear complexones. This was in agreement with the suggestion that in the cyclic complexones not all donor atoms are able to coordinate to the transition metals[4] and with the X-ray structures of the Cu^{2+} and Ni^{2+} complexes of ligands **I** and **III**.[5–7] In contrast, for the complexes of the alkaline-earth metal ions, the stability constants are critically dependent on the size of the internal cavity of the ligand, but all potential donor atoms may be implicated, as shown by the X-ray structures and NMR studies of similar metal complexes, namely the complexes of some trivalent lanthanides.[8–11]

Subsequently to this work we determined the thermodynamic functions corresponding to the formation of the complexes of the alkaline-earth and transition metal ions in aqueous solution,[12] studied the protonation sequence of these ligands[13] and carried out a ^1H NMR study of the conformation in solution of some lanthanide(III) complexes of the ligand **II**.[14] The results of these studies confirmed the conclusions tentatively presented in our first paper.

The interest in this group of ligands and other similar *N*-functionalized tri- and tetra-azamacrocycles has been steadily growing in the last few years due to their potential usefulness in various fields, *e.g.*, analytical methods[1,15] and medical applications with their Gd^{3+} complexes as magnetic resonance imaging contrast

agents,[16,17] the ^{67}Ga, ^{111}In, ^{99m}Tc and ^{55}Co complexes in radioimmunoimaging and the ^{90}Y and ^{67}Cu complexes in radioimmunotherapy.[18–20] Notwithstanding, it does not seem that other determinations of stability constants of complexes of these ligands have been carried out, with the exception of those of some lanthanide ions[21,22] and that of yttrium.[23,24] This omission limits the evaluation of analytical and other possible applications, hence we decided to complete our first report by studying the formation of the complexes of Mn^{2+}, Fe^{2+}, Cd^{2+} and Pb^{2+}. To ensure the consistency of the results, we have repeated the determinations of the protonation constants and of the formation constants of the complexes of Co^{2+}, Ni^{2+}, Cu^{2+} and Zn^{2+} in the same experimental conditions, but with an automated titration equipment with data acquisition, followed by the calculations with the Superquad program.[25]

EXPERIMENTAL

Reagents

Ligands **II** and **III** were synthesized in our laboratories.[1] DOTA was supplied by Guerbet (Aulnay-sous-Bois, France). Analytical grade metal nitrates were used and the metal content of the solutions checked by titration with EDTA. The CO_2-free potassium and tetramethylammonium hydroxide solutions were prepared as described in a previous paper;[26] tetramethylammonium nitrate, necessary for the work with DOTA, was prepared by neutralizing the hydroxide with nitric acid.

Dimethyl sulphoxide, for the study of the protonation constants of DOTA, was purified by fractional distillation, discarding the first 20% of the distillate. This procedure ensures desiccation analogous to that obtained with molecular sieves.[27]

Equipment

A Crison Digilab 517 measuring instrument was used together with an Ingold U1330 glass electrode and a Radiometer K401 saturated calomel reference electrode with a Wilhelm-type salt bridge containing the inert-salt solutions (0.1*M* potassium nitrate or Me_4NNO_3).[26] Titrations were carried out in a thermostated cell at $25.0 \pm 0.1°$ and the ionic strength of the solutions was kept at 0.10*M* with potassium nitrate or Me_4NNO_3. A nitrogen atmosphere was maintained above the working solution to avoid any contact with carbon dioxide.

Determination of the constants

The protonation and the stability constants were determined from the potentiometric titrations with the Superquad program.[25]

As referred in our previous papers,[1,12] the reactions of metal complexation are sufficiently rapid for the automatic titration to be feasible. The equilibration is too slow only in the case of nickel, hence we have taken the data from our previous work obtained by batch ("out-of-cell") titrations.[28–30] In the case of cobalt automated titrations were still possible but with large intervals between each addition of base (5–10 min in the case of DOTA). For the other metal ions the intervals were 2–3 min and the mixture of metal and ligand were left to equilibrate for 1–2 hr before the titration was started.[1,12]

The results were obtained from a minimum of three titrations for which the $C_M:C_L$ ratios were 1:2, 1:1 and 2:1. The errors quoted are the standard deviations given directly by the program running with the data of three or more titration curves (minimum 200 points).

RESULTS AND DISCUSSION

The results obtained in the present work are summarized in Table 1 and may be compared with the values presented previously.[1] For the protonation constants the agreement is excellent for the three ligands. Since the value of log K_1 of DOTA previously published[1] raised some doubts because it is too high to be accurately determined by a direct potentiometric technique in aqueous solutions, we have repeated its determination in five different mixtures of DMSO/H_2O with the same instrumental set-up and extrapolated the straight line obtained to zero fraction of DMSO when log K_1 *vs.* X_j[31] is plotted (X_j being the mole fraction of the DMSO in the solution). The equation for the straight line is $\log K_1 = 12.14 + 4.631X_j$. The value now obtained, $\log K_1 = 12.1 \pm 0.2$ (*cf.* Table 2), is very close to the 12.09 previously reported and was therefore adopted.

As to the formation constants of the metal complexes, the agreement is, generally, quite good, particularly since a larger number of experimental data was dealt with, and a fuller description of the systems was achieved, including species that were not taken into account in our first paper, namely those involving the coordination of two metal ions to the same molecule of the ligand, already found in the

Table 1. Protonation* (log β_{H_iL}) and stability† constants of metal complexes (log β_{mlh}) of DOTA, TRITA and TETA

		$T = 25.0 \pm 0.1°$; $\mu = 0.10M$		
Ions	Species	DOTA‡	TRITA§	TETA
H^+	HL	12.09 ± 0.04	11.35 ± 0.04	10.520 ± 0.008
	H_2L	21.853 ± 0.006	21.08 ± 0.03	20.695 ± 0.004
	H_3L	26.409 ± 0.009	25.24 ± 0.03	24.780 ± 0.008
	H_4L	30.499 ± 0.006	28.56 ± 0.06	28.127 ± 0.006
Mn^{2+}	ML	20.202 ± 0.008	16.74 ± 0.02	11.272 ± 0.007
	MHL	24.351 ± 0.005	20.65 ± 0.08	—
	M_2L	22.60 ± 0.08	20.07 ± 0.08	—
	M_2HL	26.83 ± 0.07	24.03 ± 0.07	—
Fe^{2+}	ML	20.22 ± 0.06	17.56 ± 0.03	13.09 ± 0.01
	MHL	24.48 ± 0.02	21.94 ± 0.01	—
	M_2L	—	—	15.55 ± 0.06
	ML-H	—	—	4.16 ± 0.02‖
Co^{2+}	ML	20.27 ± 0.02	19.84 ± 0.08	16.38 ± 0.01
	MHL	24.35 ± 0.01	24.04 ± 0.06	20.42 ± 0.01
	MH_2L	27.73 ± 0.05	27.02 ± 0.02	—
	M_2L	—	—	19.25 ± 0.04
	M_2HL	—	—	23.07 ± 0.08
Ni^{2+}	ML	20.03‡‡	20.821‡‡	19.83 ± 0.03
	MHL	23.54‡‡	24.99‡‡	23.97 ± 0.03
	MH_2L	28.26‡‡	28.26‡‡	27.14 ± 0.03
	M_2L	—		22.01 ± 0.1
Cu^{2+}	ML	22.25 ± 0.03	21.13 ± 0.05	20.49 ± 0.03
	MHL	26.03 ± 0.05	25.00 ± 0.04	24.26 ± 0.04
	MH_2L	29.80 ± 0.04	27.90 ± 0.03	—
	M_2L	24.48 ± 0.06	—	24.9 ± 0.1
	M_2HL	29.33 ± 0.02	—	27.9 ± 0.1
Zn^{2+}	ML	21.099 ± 0.009	19.13 ± 0.08	16.395 ± 0.004
	MHL	25.277 ± 0.008	23.39 ± 0.05	20.494 ± 0.008
	MH_2L	28.79 ± 0.01	26.53 ± 0.03	—
	M_2L	—	—	18.48 ± 0.07
	M_2HL	—	—	22.77 ± 0.06
Cd^{2+}	ML	21.31 ± 0.03	19.60 ± 0.02	18.02 ± 0.01
	MHL	25.70 ± 0.02	24.26 ± 0.01	22.06 ± 0.01
	MH_2L	28.73 ± 0.04	27.30 ± 0.02	24.5 ± 0.1
	M_2L	25.16 ± 0.04	23.27 ± 0.03	20.95 ± 0.03
	M_2HL	28.44 ± 0.09	27.25 ± 0.04	24.81 ± 0.05
Pb^{2+}	ML	22.69 ± 0.03	19.11 ± 0.02	14.319 ± 0.002
	MHL	26.55 ± 0.03	23.266 ± 0.008	19.07 ± 0.02
	MH_2L	—	—	23.32 ± 0.02
	M_2L	25.99 ± 0.04	22.83 ± 0.09	18.01 ± 0.01
	M_2HL	29.66 ± 0.07	26.32 ± 0.04	21.42 ± 0.07

*Protonation constants $\beta_{H_iL} = [H_iL]/([H_iL](H)^i)$.
†Stability constants $\beta_{mlh} = [M_mL_lH_h]/([M]^m[L]^l(H)^h)$.
‡$\mu = 0.10M$ Me_4NNO_3.
§$\mu = 0.10M$ KNO_3.
‖$\beta_{ML\text{-}H} = \beta_{ML(OH)} \times K_w$, where $\beta_{ML(OH)} = [ML(OH)]/([M][L][OH])$ and $K_w = [H][OH]$.
‡‡Values from Ref. 1, determined by "out-of-cell" titrations.[28-30]

Table 2. Protonation constants (log β_{HiL}) of DOTA, obtained in different mixtures of DMSO/H_2O

		$T = 25.0 \pm 0.1°$, $\mu = 0.10M$ Me_4NNO_3				
% DMSO	X_j*	log K_W	log β_1	log β_2	log β_3	log β_4
10	0.02739	−14.01	12.23 ± 0.02	21.86 ± 0.03	26.50 ± 0.03	30.64 ± 0.03
20	0.05959	−14.29	12.43 ± 0.03	22.00 ± 0.04	26.76 ± 0.04	31.07 ± 0.03
30	0.09797	−14.59	12.61 ± 0.03	22.11 ± 0.04	26.98 ± 0.04	31.41 ± 0.04
40	0.14453	−14.98	12.82 ± 0.03	22.20 ± 0.04	27.24 ± 0.04	31.88 ± 0.04
50	0.20219	−15.50	13.05 ± 0.01	22.31 ± 0.02	27.59 ± 0.02	32.48 ± 0.02

*X_j = mole fraction of DMSO.

solid state,[5-7] *i.e.*, M_2H_iL ($i = 0$–2) species, for which the formation constants obtained are quite reasonable. The formation of these species is almost negligible when the metal is not in considerable excess, as can be seen in a species distribution diagram such as that of Fig. 1 for the Cu^{2+}/DOTA system.

The availability of data for an extended series of ions allows a better comparison of the coordination tendency and capacity of each member of the series. We have already commented on the fact that the Irving–Williams natural order of stability does not appear to be followed in the cases of DOTA and TRITA and less so for the complexes of other polyoxa–polyaza cyclic complexones,[26,32] but Fig. 2 illustrates the differences more clearly.

Besides the "anomalous" behaviour of the above-mentioned compounds, which is fairly common for these constrained ligands,[26,32] other interesting features are apparent, namely the appreciable difference in stability of the TETA complexes of Cd^{2+} and Pb^{2+}, compared with the corresponding complexes of DOTA and TRITA, and the almost invariant value of the stability constants of the Mn^{2+}, Fe^{2+}, Co^{2+},

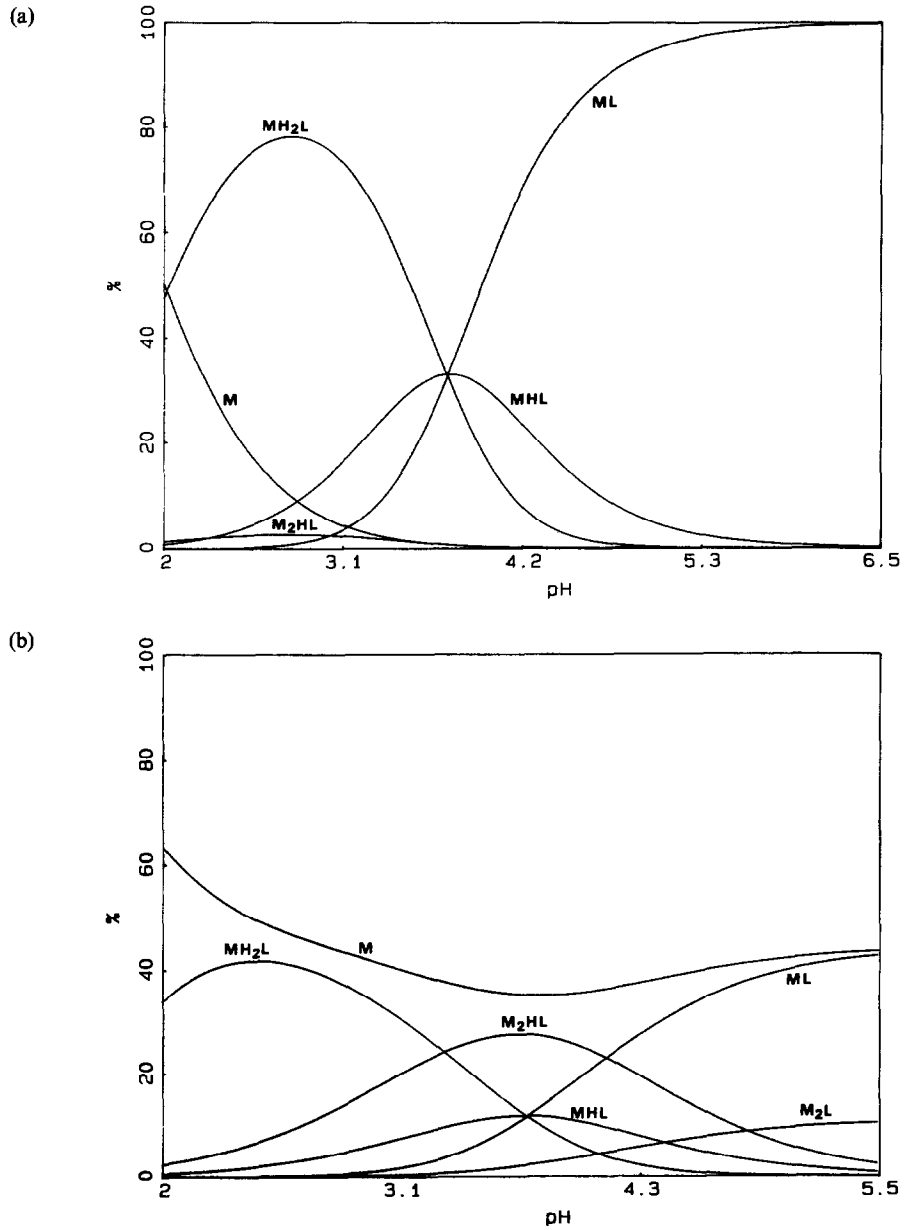

Fig. 1. Calculated distribution of the equilibrium species for the Cu^{2+}/DOTA system as a function of pH. $T = 25.0°$, $\mu = 0.1M$. (*a*) $C_{Cu} = C_{DOTA} = 8.33 \times 10^{-4}M$ (*b*) $C_{Cu} = 1.67 \times 10^{-3}M$, $C_{DOTA} = 8.33 \times 10^{-4}M$.

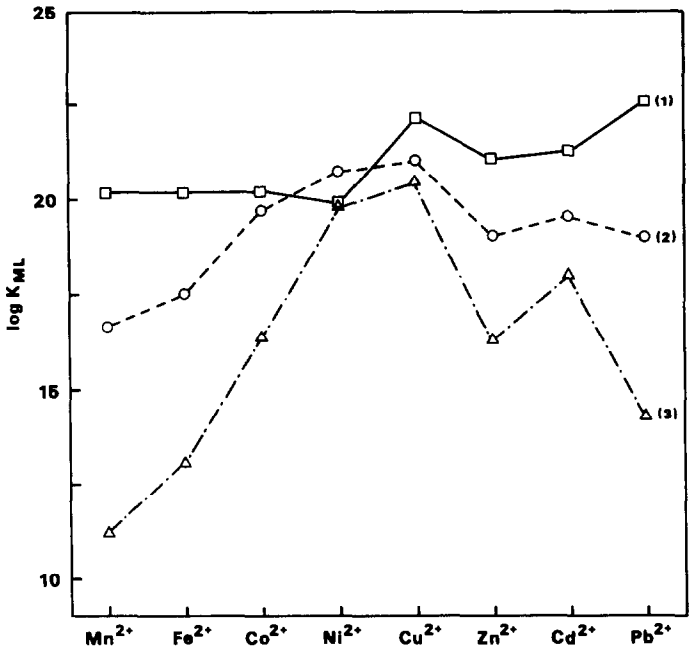

Fig. 2. Stability constants of the metal complexes of the tetra-aza macrocyclic complexones (log K_{ML}) along the first transition series metal ions, Zn^{2+}, Cd^{2+} and Pb^{2+}. (1) DOTA; (2) TRITA; (3) TETA.

Ni^{2+}, complexes of DOTA, not too different, either, from those of Zn^{2+} and Cd^{2+}.

Indeed, it seems that this ligand acts like a rigid "cage" of such conformation (*i.e.*, orientation of the lone-pair of electrons of the nitrogen atoms,[12] that the size of the transition metal ion, Zn^{2+} or Cd^{2+} does not make much difference; the ligand is quite unselective.

For the TRITA and particularly the TETA complexes, the increased flexibility of the ligand molecules allows a better discrimination of the metal ions; TETA behaves like a normal acyclic complexone and follows the Irving–Williams' series, but the selectivity ratio of its cadmium to lead complexes, contrary to the usual trend for the complexone type of ligands, is so large (4 log units) that it may allow useful analytical and other applications. The same may be said for the pairs Ni^{2+}, Co^{2+} and Cu^{2+}, Zn^{2+}, although the orders of stability are the normal ones and high selectivity ratios not so uncommon.

Acknowledgements—The authors thank the Instituto Nacional de Investigação Científica (INIC) for permanent financial assistance and the Junta Nacional de Investigação Científica e Tecnológica (JNICT) for financing the present research project.

REFERENCES

1. Rita Delgado and J. J. R. Fraústo da Silva, *Talanta*, 1982, **29**, 815.
2. H. Stetter and W. Frank, *Angew Chem. Int. Ed. Engl.*, 1976, **15**, 686.
3. H. Stetter, W. Frank and R. Mertens, *Tetrahedron*, 1981, **37**, 767.
4. H. Häfliger and T. A. Kaden, *Helv. Chim. Acta*, 1979, **62**, 683.
5. A. Riesen, M. Zehnder and T. A. Kaden, *ibid.*, 1986, **69**, 2067.
6. *Idem*, *ibid.*, 1986, **69**, 2074.
7. *Idem*, *Acta Cryst.*, 1988, **C44**, 1740.
8. J. F. Desreux, *Inorg. Chem.*, 1980, **19**, 1319.
9. M.-R. Spirlet, J. Rebizant, J. F. Desreux and M.-F. Loncin, *Inorg. Chem.*, 1984, **23**, 359.
10. *Idem*, *ibid.*, 1984, **23**, 4278.
11. J. F. Desreux and M.-F. Loncin, *Inorg. Chem*, 1986, **25**, 69.
12. Rita Delgado, J. J. R. Fraústo da Silva and M. Cândida T. A. Vaz, *Inorg. Chim. Acta*, 1984, **90**, 185.
13. J. R. Ascenso, Rita Delgado and J. J. R. Fraústo da Silva, *J. Chem. Soc. Perkin Trans. II*, 1985, 781.
14. *Idem*, *J. Chem. Soc. Dalton Trans.*, 1986, 2395.
15. Rita Delgado, J. R. R. Fraústo da Silva and M. Cândida T. A. Vaz, *Talanta*, 1986, **33**, 285.
16. R. B. Lauffer, *Chem. Rev.*, 1987, **87**, 901.
17. D. Meyer, M. Schaffer and B. Bonnemain, *Inv. Radiology*, 1988, **23**, S232.
18. R. W. Konzack, T. A. Aldman, R. W. Atcher and O. A. Gansow, *Trends of Biotechnology*, 1987, **4**, 259.
19. S. V. Deshpande, S. J. DeNardo, C. F. Meares, M. J. McCall, G. P. Adams, M. K. Moi and G. L. DeNardo, *J. Nucl. Med.*, 1988, **29**, 217.
20. A. Reisen, T. A. Kaden, W. Ritter and M. R. Măcke, *J. Chem. Soc., Chem. Commun.*, 1989, 460.
21. M. F. Loncin, J. F. Desreux and E. Merciny, *Inorg. Chem.*, 1986, **25**, 2646.
22. W. P. Cacheris, S. K. Nickle and A. D. Sherry, *ibid.*, 1987, **26**, 958.

23. J. P. L. Cox, K. L. Jankowski, R. Kataky, D. Parker, N. R. A. Beeley, B. A. Boyce, M. A. W. Eaton, K. Millar, A. T. Millican, A. Harrison and C. Walker, *J. Chem. Soc., Chem. Commun.*, 1989, 797.
24. C. J. Broan, J. P. L. Cox, A. S. Craig, R. Kataky, D. Parker, A. Harrison, A. M. Randell and G. Ferguson, *J. Chem. Soc. Perkin Trans. 2*, 1991, 87.
25. P. Gans, A. Sabatini and A. Vacca, *J. Chem. Soc. Dalton Trans.*, 1985, 1195.
26. Rita Delgado, J. J. R. Fraústo da Silva and M. C. T. A. Vaz, *Polyhedron*, 1987, **6**, 29.
27. D. R. Burfield and R. H. Smithers, *J. Org. Chem.*, 1978, **43**, 3966.
28. L. J. Zompa, *Inorg. Chem.*, 1978, **17**, 2531.
29. A. Evers and R. D. Hancock, *Inorg. Chim. Acta*, 1989, **160**, 245.
30. V. J. Thöm and R. D. Hancock, *J. Chem. Soc. Dalton Trans.*, 1985, 1877.
31. G. Papanastasiou, I. Ziogas and I. Mountzis, *Anal. Chim. Acta*, 1986, **186**, 213.
32. Rita Delgado, J. J. R. Fraústo da Silva, M. C. T. A. Vaz, P. Paoletti and M. Micheloni, *J. Chem. Soc. Dalton Trans.*, 1989, 133.

Talanta, Vol. 39, No. 3, pp. 255–257, 1992
Printed in Great Britain

0039-9140/92 $5.00 + 0.00
Pergamon Press plc

GRAVIMETRIC DETERMINATION OF FLYASH CONTENT IN BLENDED CEMENT

SAU-MO FAN, WAI-MING FOK and SHIU-FAI LUK*
Laboratory, China Cement Company Ltd, Tap Shek Kok, Tuen Mun, N.T., Hong Kong

(*Received* 20 *May* 1991. *Revised* 27 *August* 1991. *Accepted* 28 *August* 1991)

Summary—A simple gravimetric method is devised to determine the percent flyash in flyash blended cement. Insoluble residue of the sample was determined by the British Standard method. The flyash content was calculated by taking the insoluble residue in ordinary Portland cement and flyash to be 0.46% and 70.74%, respectively. The accuracy and precision are good and the standard deviation of the method is less than 1% for three determinations.

Flyash blended cement is formed by blending ordinary Portland cement (OPC) with flyash (FA). Such blending improves the sulphate resistance and reduces the water demand as well as the heat of hydration. It also offers the advantages of reduced cost and a reduction in the amount of flyash to be disposed by the power plant.

The ASTM suggests no method to determine the amount of flyash in the blended cement. According to the British specification (BS 6588:1985) the percent flyash is required to be reported to the nearest 1%. This method is based on the titration of soluble calcium oxide in the sample.[1] Its accuracy is limited by the variation of calcium oxide in both OPC and FA. As original samples of OPC and FA are not available, it has to be assumed that the calcium oxide in OPC and FA is 64.5% and 2%, respectively. Other methods include gamma ray spectrometry,[2] natural radioactivity measurement[3], leaching by picric acid[4] and EDTA titration in alkaline medium.[5] Instruments involved in these methods are too specialized. The picric acid method is not suitable for samples with high ash content and the EDTA method takes a long time to complete the extraction. In this paper a method is proposed based on the determination of the insoluble residue of the sample. Results indicate that the accuracy is comparable to that of the BS method and is less affected by the variation in the quality of the OPC.

*Author for correspondence.

EXPERIMENTAL

Analytical-reagent grade chemicals and demineralized water were used throughout the procedure.

Procedure

A 1.000-g sample was accurately weighed into a 250-ml beaker and 10 ml of demineralized water was added. Then 10 ml of concentrated hydrochloric acid was added and the solution was diluted to 50 ml with hot demineralized water. The beaker was covered and the solution kept at boiling for 15 min to digest the sample. The solution was cooled and filtered through a low retention ashless filter paper. The residue was washed several times with hot demineralized water to remove the soluble salt.

The filter paper was then transferred to the original beaker and 100 ml of 1% sodium hydroxide was added. The mixture was covered and heated to boiling. After 15 min, several drops of 0.1% methyl red indicator was added. The solution was neutralized with 12*M* hydrochloric acid and was further acidified with 4–5 drops of hydrochloric acid. The mixture was then filtered through low retention ashless filter paper and the residue was washed several times with hot 2% ammonium nitrate solution.

The residue in the combined filter papers was then transferred to a preweighed platinum crucible and heated to 400° for 15 min and then to 900° for another 45 min. The crucible was cooled in a desiccator and weighed. Then the mass of insoluble residue was calculated. The

percent flyash in the sample was calculated from the following relationship:

Mass (g) insoluble residue in flyash + Mass (g) insoluble residue in OPC = Mass (g) insoluble residue in blended cement − Mass (g) blank

$$A \times \frac{\%FA}{100} + C \times \frac{(100 - \%FA)}{100} = \frac{W - b}{m} \times 100$$

From which may be derived:

$$\% \text{ flyash} = \frac{\left(\frac{W \times 100}{m}\right) - B - C}{A - C} \times 100$$

W = mass (g) of insoluble residue
m = mass (g) of sample used
A = % insoluble residue of flyash, taken as 70.74%
b = mass (g) blank
B = % insoluble residue found in the blank determination (=[b/m] × 100)
For simplicity it is taken as 0.07 ± 0.03% (by the average of 20 determinations)
C = % insoluble residue of OPC, taken as 0.44%

RESULTS AND DISCUSSION

The calcium oxide contents of OPC & FA sampled from a market and a cement plant during the past six months are shown in Table 1. For 10% flyash in blended cement the calculated deviation of % FA caused by one standard deviation of calcium oxide in OPC can be as high as 1.0%, thus the BS method is not always an accurate method. On the other hand, flyash is known to be high in insoluble residue. Flyash samples from two power plants with coal sources from Australia and China were found to have insoluble residue values of 70.36 ± 4.79 and 75.63 ± 3.30%, respectively. This is a great contrast to that of cement (Table 1). Determining the insoluble residue in a sample may be a reliable alternate means to determine the flyash content. As seen from Table 1, the variation of insoluble residue for cement is much less than the calcium oxide, which is revealed from both manufactured and market samples. A similar calculation as above shows that the deviation of flyash content caused by one standard deviation of insoluble residue in OPC is about 0.5%, which is less than that calculated by calcium oxide. Taking cement standard NBS 634 (%FA = 0) as an example, its calcium oxide content is 62.58%. By the BS method, the calculated flyash content will be around 3% but in case of insoluble residue, its flyash content is expected to be less than 0.5%. Hence to determine the flyash content by means of insoluble residue measurement is expected to have better accuracy where it is less affected by the variation of composition in OPC.

More than 40 samples of blended cement were prepared with flyash from the two power plants and analysed by the proposed method. In the plot of insoluble residue *vs.* percent flyash, the correlation is found to be 0.9961. Therefore a linear relationship exists between the insoluble residue and the flyash content, it is feasible to determine the flyash in blended cement by insoluble residue measurement. To compare the accuracy and precision of the method with the BS method, blended cement samples prepared by mixing different sources of flyash (Australia, China, United States) with ordinary Portland cement were analysed by both methods. The results are summarised in Table 2. It is shown that the source of flyash does not have significant effect on the accuracy. The BS method is more affected by the variation of the calcium oxide content as shown by samples 13–15 in Table 2. By the matched pairs technique, the calculated t value was found to be 1.71, which shows that there is no significant difference between two methods. In fact from Table 2, the average difference of results of the proposed method and the known values is smaller. With

Table 1. Chemistry of ordinary Portland cement

Sample type	CaO (%)	Insoluble residue (%)
Cement plant	64.37 ± 0.65	0.44 ± 0.38
Market	63.93 ± 0.97	0.52 ± 0.25

Table 2. % Flyash determination by different methods

Sample no.	% Flyash Known	BS method Found	BS method Difference	Proposed method Found	Proposed method Difference
1	5.62	6.12	0.50	7.81	2.19
2	11.77	11.64	−0.13	10.74	−1.03
3	14.82	14.83	0.01	14.03	−0.79
4	7.96	8.62	0.66	8.48 ± 0.32	0.52
5	22.76	25.03	2.27	21.31	−1.45
6	30.72	32.47	1.75	30.03	−0.69
7	40.16	43.67	3.51	39.59	−0.57
8	25.7	29.23 ± 0.42	4.10	23.19 ± 0.59	−1.88
9	16.07	17.40	1.26	17.91	1.84
10*	5.73	6.31	0.58	6.32	0.49
11*	16.63	18.60	1.87	17.65	1.02
12	17.94	18.60	0.59	18.60	0.66
13†	9.04	13.13	4.09	8.63	−0.41
14†	12.60	11.98	−0.62	12.13	−0.47
15†	41.06	44.78	3.72	41.59	0.53
16	14.35	13.44	−0.91	14.75	0.40
17	14.34	14.26	−0.08	15.75	1.41
18	13.71	14.26	0.55	13.67	−0.04
19	20.41	19.61	−0.80	19.83	−0.58
20	14.35	14.49	0.14	14.38	0.03

*Flyash used for samples 10 and 11 were flyash standard SRM 1633a and ASCRM 010, respectively.

†CaO in OPC component of samples 13, 14 and 15 were 62.0, 66.6, 63.2, respectively.

triplicate analyses, the standard deviation is less than 1% (Table 2). In addition its accuracy and precision is better than that by gamma spectrometry.[2] The time required is less than the EDTA extraction method and the skill required by this method is less demanding than for the instrumental methods.

CONCLUSION

The proposed method to determine the flyash content in blended cement is an alternative method to the classical method. It does not involve any special instrumentation. It is more accurate than the BS method and is less subject to variation of the chemistry of the OPC, as shown in the previous calculation and result. Since insoluble residue is required to be determined in concrete laboratories, the procedure is expected to be well established. The technique should be easily mastered by technicians.

REFERENCES

1. British Standard, *British Standard Institution, B.S. 6588*; 1985.
2. J. S. Chinchon, A. Lopez-Soler, A. Sanchez Reyes, M. Ginjaume, E. Vazquez and A. Yague, *Cem. Concr. Res.*, 1989, **19**, 173.
3. L. Baranyai, *Appl. Radiat. Isot.*, 1986, **37**, 1111; *Anal. Abstr.*, 1987, **49**, 4B190.
4. S. S. Rehsim and S. K. Garg, *J. Indian Chem. Soc.*, 1974, **51**, 837; *Anal. Abstr.*, 1975, **29**, 3B182.
5. H. C. Erntroy, *ZKG International*, 1987, **40**, 270.

Talanta, Vol. 39, No. 3, pp. 259–263, 1992
Printed in Great Britain.

0039-9140/92 $5.00 + 0.00

A SELECTIVE SPECTROPHOTOMETRIC METHOD FOR DETERMINATION OF QUERCETIN IN THE PRESENCE OF OTHER FLAVONOIDS

HASSAN F. ASKAL and GAMAL A. SALEH
Department of Pharmaceutical Chemistry, Faculty of Pharmacy, Assiut University, Assiut, Egypt

ENAAM Y. BACKHEET*
Department of Pharmacognosy, Faculty of Pharmacy, Assiut University, Assiut, Egypt

(*Received* 13 *March* 1991. *Revised* 4 *July* 1991. *Accepted* 4 *July* 1991)

Summary—A simple, rapid and highly selective method for determination of quercetin in the presence of other flavonoids was developed. The method is based on the oxidation reaction of quercetin in neutral aqueous solution with *N*-bromosuccinimide (NBS) in the presence of phenol to give a violet chromogen measurable at 510 nm. Beer's law was valid within a concentration range of 2.5–30 μg/ml with a good correlation coefficient ($r = 0.9990$). All variables were studied to optimize the reaction conditions. The method is highly selective for quercetin. Other investigated flavonoids do not interfere. Mixtures of flavonoids were also analysed through native UV measurements of absorbance readings at 370 nm and then at 510 nm after adopting the proposed procedure. The method could also be utilized for the quantitative determination of quercetin in some plant extracts. Moreover, the proposed procedure could be considered as a good tool to follow the hydrolysis of quercetin glycosides.

The quantitative analysis of flavonoids by ultraviolet absorption is well known.[1–6] Other methods for their determination include fluorimetry,[7] polarography,[8] densitometry[9] and HPLC.[10–15] Few colorimetric methods have been reported for their determination.[16–21] Most colorimetric methods cannot be used to distinguish between the different flavonoids. When interfering flavonoids are to be present, quercetin must first be isolated chromatographically[1] but this requires an empirical correction for adsorption of quercetin.

Recent studies have shown that, flavonoids have mutagenic activity.[22–24] Quercetin is the most mutagenic; it also acts as a carcinogenic agent towards rats.[25]

There has been a need for a selective colorimetric method which could best be utilized in detecting and distinguishing between quercetin and other flavonoids without the need for any pretreatments or prior separation. *N*-Bromosuccinimide (NBS) has been previously used for the analysis of hydroxy compounds.[26,27] However, no report is available on its use for quantitative determination of flavonoids.

In the present work, the applicability of NBS for the quantitative determination of quercetin in the presence of other flavonoids has been investigated and has resulted in a selective, simple and rapid spectrophotometric method.

EXPERIMENTAL

Apparatus

Uvidec-320 (Jasco, Tokyo, Japan) and SP 1750 (Pye-Unicam) spectrophotometers were used.

Reagents

A 0.2% w/v solution of freshly recrystallized *N*-bromosuccinimide (NBS, obtained from Aldrich, Germany) was prepared in distilled water, the solution was freshly prepared before use and standardized iodometrically.[28]

Phenol, a 1% w/v solution was prepared in methanol. Flavonoids were obtained from Fluka, Koch Light, Aldrich, Eastman Organic Chemicals and Sigma. Solutions containing 0.5 mg/ml of quercetin were prepared in methanol and diluted quantitatively with the same solvent to obtain dilutions between 20–300 μg/ml.

Solvents used were of analytical reagent grade.

*Author for correspondence.

Procedures

Quercetin. Transfer 1 ml of working quercetin solution into a 10-ml standard flask, add 1 ml of phenol solution and 1 ml of NBS solution and make up to volume with distilled water. Mix and measure the absorbance at 510 nm against a reagent blank.

Quercetin and kaempferol. Into 2 sets of 10-ml standard flasks, transfer 0.5-ml aliquots (to the first set) and 1-ml aliquots (to the second set) of a mixture containing different proportions from quercetin and kaempferol (Table 3). Dilute the first set to volume with methanol, mix and measure the absorbance at 370 nm. To the other set, add 1 ml of phenol solution followed by 1 ml of NBS solution. Make up to volume with distilled water, mix and measure the absorbance at 510 nm against a reagent blank.

Stoichiometric study. A series of 5-ml quantities of mixtures containing master equimolar solutions ($2 \times 10^{-4} M$) in different complementary proportions (from 0:5 to 5:0 inclusive) were made up in 10-ml standard flasks containing 1 ml of phenol solution. After the flasks have been made up to volume with water, absorbances were measured at 510 nm against a blank treated in the same manner.

Monitoring of the hydrolysis of quercetin glycosides (Rutin). Into a 50-ml round-bottom flask, weigh accurately 18 mg of rutin (equivalent to 7.5 mg quercetin), dissolve in 5 ml of methanol, add 2.5 ml of distilled water and 7.5 ml of hydrochloric acid to produce a final solution of 5*N*. Reflux the resulting solution and at different time intervals, withdraw a 1-ml volume, transfer to a 50-ml separating funnel, extract with ethylacetate (three times, each of 10 ml). Pass the collected organic layer over anhydrous sodium sulphate and evaporate ethylacetate under reduced pressure. Dissolve the residue in methanol to produce 5 ml in a 5-ml standard flask and use 1 ml from this solution for the procedure for quercetin.

Determination of quercetin in plant. A 30-g sample of either leaves and stems, or flowers (dried and ground to 40 mesh) of *Cassia didymobotrya* Fres. was heated under reflux with 100 ml of 70% ethanol for 2 hr. The extract was concentrated to 25 ml and extracted with ethylacetate. After evaporation of the solvent under reduced pressure, the residue was dissolved in methanol to produce 10 ml in a 10-ml standard flask. Apply the procedure for quercetin, using 1 ml of the final extract solution in the blank.

RESULTS AND DISCUSSION

Optimization of conditions

Addition of an aqueous solution of NBS to a methanolic solution of different flavonoids resulted in the formation of an instantaneous violet colour only with quercetin, the other investigated flavonoids fail to give any coloured product. The violet colour is developed immediately at room temperature and in the presence of phenol remains stable for at least 15 min. Higher temperatures produce lower absorbance values. No increase in the absorbance reading (0.540 at 510 nm) was obtained upon increasing the temperature from 20 to 30° while a further 10°-increase decreases the absorbance by 6.9%. After that a regular 10° increase in the temperature up to 80° produces a 4% decrease in the corresponding absorbance readings. The absorption spectra for the quercetin reaction product exhibits three absorption peaks at 305, 375 and 510 nm (Fig. 1). Quercetin and NBS both have negligible absorbances at 510 nm.

A 1.0-ml volume of 1.5–3 mg/ml NBS was found to be optimum. Use of 1.0 ml of 5–15 mg/ml phenol solution in the total volume of 10 ml gives maximum absorbance readings. Various reducing substances such as phenol, hydrogen peroxide, salicylic acid, salicylamide, sulphanilamide, sodium nitrite and aniline sulphate were tested to try to increase the stability of the colour formed. Phenol was found the best as it gives the highest absorbance readings as well as the higher stability time. This effect might be explained on the basis of interacting the excess NBS with phenol thus preventing its destructive effect on the formed chromogen.

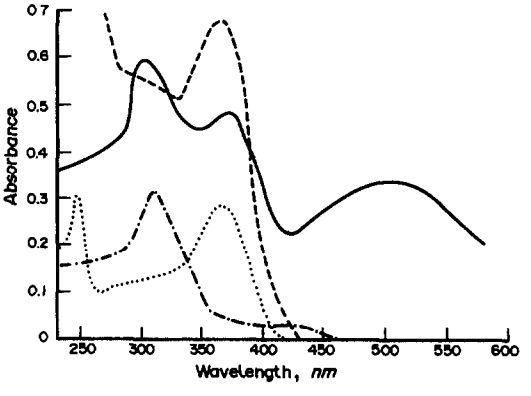

Fig. 1. Absorption spectra of: (---) quercetin, 12.4 μg/ml; (···) kaempferol 3.2 μg/ml (——) quercetin–NBS (12.4 μg quercetin and 20 mg NBS/ml and (-·-·-·) kaempferol–NBS (3.2 μg kaempferol and 20 mg NBS/ml).

The violet colour is not developed in acidic or alkaline media and the effect of pH was so studied. Tests with acetate and phosphate buffers, showed that, the maximum colour intensity and stability were obtained with phosphate buffer of pH 7 but this system was still inferior to the phenol procedure, with regard to colour intensity and stability.

Dilution of the developed coloured product by different solvents brings about bathochromic shifts with dimethylsulphoxide dimethylformamide, methanol, ethanol, n-propanol and isopropanol relative to water whereas absorption intensity was only slightly influenced (Table 1). Water was used throughout this work as it is the cheapest. These findings are in agreement with the fact that, in n-π^* transition peaks, a hypsochromic shift occurs with increasing polarity of the solvent (expressed as dielectric constant). This is due to stabilization of the ground state through hydrogen bonding.[29]

Stoichiometry

As assessed by the continuous molar variation method[30] quercetin was found to interact with NBS in a ratio of 1:4.

Reaction mechanism

The reaction does not seem to depend only on the catechol function, since rutin (which has the same catechol function as quercetin but sugar moiety at C-3 and luteolin (which lacks the 3-hydroxyl group) does not form such colour with NBS. Also a hydroxyl group at C-5 is necessary, as quercetin-5-glucose gives no such colour. Kaempferol failed to give a positive response indicating the necessity for orthodihydroxyl groups at C-3′ and 4′ in addition to the 3-, 5- and 7-hydroxyl groups. Morin (which has hydroxyl groups at C-3, 5, 6, 2′ and 4′) produces no such colour under the specified reaction conditions indicating that *m*-dihydroxyl groups at ring B (see structure below) are not suitable for such interaction. In conclusion, hydroxyl groups at C-3, 5, 7, 3′ and 4′ are necessary for this reaction.

Table 1. Effect of diluting solvents on the absorption intensity of the developed colour

Solvent	Absorbance*	λ_{max}†	Dielectric constant (E)‡
Water	0.540	510	78.3
Dimethylsulphoxide	0.560	518	47.0
Dimethylformamide	0.294	522	37.0
Methanol	0.459	525	33.0
Ethanol	0.490	525	25.0
n-Propanol	0.540	528	21.8
Iso-Propanol	0.523	532	19.9

*Final concentration 20 μg/ml.
†Average of three determinations.
‡Reference 33.

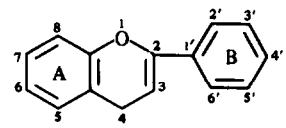

Quercetin = 3,5,7,3',4' - pentahydroxyflavone
Kaempferol = 3,5,7,4' - tetrahydroxyflavone
Rutin = 3-glucose-rhamnose quercetin
Luteolin = 3-deoxy - quercetin
Apigenin = 3-deoxy-kaempferol
Isorhamnetin= quercetin-3'-methylether
Morin = 3,5,6,2' and 4'-pentahydroxyflavone

Evidence for the oxidation of 3-, 5-, 3′- and 4′-hydroxyl groups in the proposed procedure is the failure of aluminium chloride alone or with hydrochloric acid to induce any bathochromic shifts when added to the reaction product indicating the absence of these hydroxyl groups (*cf.* quercetin gives bathochromic shifts due to the presence of 3-, 5-, 3′- and 4′-hydroxyl groups).[31]

Unfortunately, all trials made to isolate the formed chromogen were unsuccessful as it is destroyed during different isolation steps even under reduced pressure.

From the aforementioned observations as well as similar reports on the oxidation of catecholamines[26,27] it could be concluded that a polyquinone structure of quercetin may be formed.

Determination range

At 510 nm, a linear correlation was obtained between absorbance of the coloured product and concentration of quercetin over the range of 2.5–30 μg/ml with good correlation coefficient and small intercept, the regression equation was:

$$A_{510} = 0.019 + 0.026\ C_Q\ (r = 0.9990, n = 9)$$

The molar absorptivity was 8.14×10^3 l. mole^{-1}. cm^{-1}.

Selectivity of the colour reaction

Selectivity of the method was checked by examining the effect of NBS on various

flavonoids having hydroxyl groups in different positions such as kaempferol, rutin, isorhamnetin, luteoline, apigenin and morin.

No violet colour was produced with any of these compounds inspite of their observed interaction with NBS as shown in Fig. 1, for kaempferol as an example.

Precision

The mean of 10 replicate analyses of a solution of quercetin at a concentration of 20 μg/ml was assayed with a coefficient of variation of 1.02%. This level of precision is adequate for quality control analysis of quercetin in natural sources.

Analysis of mixtures

Eleven synthetic mixtures containing 2.5–20 μg kaempferol/ml and 2.5–25 μg quercetin/ml with a quercetin/kaempferol ratio of 0.125–10 were subjected to analysis with the proposed procedure and the results are shown in Table 2 with a mean recovery of $98.88 \pm 0.88\%$ for kaempferol and $99.54 \pm 0.45\%$ for quercetin.

The method depends upon the fact that, under the specified reaction conditions, only quercetin reacts with NBS to give a coloured product measurable at 510 nm. The other flavonoids give zero absorbance at this wavelength. Measurements at 370 nm determine the total flavonoids.

Concentration of quercetin could be directly calculated from the regression equation derived from the NBS-reaction product ($A_{510} = 0.019 + 0.026\ C_Q$). On the other hand, concentration of other flavonoids—calculated as kaempferol—could be calculated through measurement of the native absorbance at 370 nm before carrying out the reaction, then at 510 nm after the reaction, and, using the following equation:

$$A_k = 2A_{370} - 2.08A_{510} = 0.004 + 0.086\ C_k$$

from which,

$$C_k = \frac{(2A_{370} - 2.08\ A_{510}) - 0.004}{0.086}$$

where C_k is the concentration of flavonoids other than quercetin (calculated as kaempferol) in μg/ml, $2A_{370}$ is the total absorbance of the solution at 370 nm, 2.08 is a factor relating the absorbance of quercetin at 370 and 510 nm before and after the reaction, A_{510} is the absorbance of the quercetin reaction product, 0.004 and 0.086 are the intercept and slope of the regression equation of kaempferol at 370 nm respectively.

Table 2. Determination of synthetic mixtures of kaempferol and quercetin

Mixture taken, $\mu g/ml$		Recovery, % ± SD*	
Kaempferol	Quercetin	Kaempferol	Quercetin
20.0	0.0	97.28 ± 0.71	—
17.5	2.5	97.17 ± 0.92	99.69 ± 1.29
15.0	5.0	99.81 ± 0.67	100.62 ± 1.38
12.5	7.5	99.53 ± 0.78	98.97 ± 1.09
10.0	10.0	99.32 ± 0.61	99.46 ± 1.07
10.0	15.0	99.49 ± 0.53	99.49 ± 0.55
7.5	12.5	98.72 ± 0.60	99.94 ± 1.18
5.0	15.0	99.15 ± 0.68	99.37 ± 0.83
5.0	20.0	98.79 ± 0.91	99.00 ± 0.75
5.0	25.0	99.25 ± 0.53	99.57 ± 0.68
2.5	17.5	99.18 ± 1.22	99.43 ± 0.55
0	20.0		99.39 ± 0.71
Mean %		98.88	99.54
±SD		0.88	0.45

*Average of five determinations.

Table 3. Monitoring the hydrolysis of rutin and its subsequent determination as quercetin

Time, *hr*	Quercetin produced, % ± SD*
0.5	22.76 ± 2.32
1.0	40.08 ± 2.51
1.5	66.17 ± 2.13
2.0	83.36 ± 1.87
2.5	98.14 ± 0.93
3.0	97.34 ± 2.17

*Average of three determinations and calculated with reference to quercetin treated in the same manner as rutin.

Hydrolysis of quercetin glycosides

The proposed procedure would be valuable as a tool for quantitative monitoring of the hydrolysis of quercetin glycosides. When rutin is subjected to hydrolysis with 5*N* hydrochloric acid under reflux for 4 hr a gradual increase in the concentration of quercetin was observed, Table 3.

Analysis of plant extracts

To check the validity of the proposed procedure, assay of quercetin in *Cassia didymobotrya* Fres. in which quercetin has been described[32] was carried out. Quercetin could be determined quantitatively in ethylacetate extract without the need for preseparation steps and without interference from other constituents. Interference from any trace absorption from the extract could be eliminated by taking the same volume of extract in the blank and the results obtained are shown in Table 4.

Accuracy of the method was confirmed by the good recovery of added quercetin to the plant extracts (Table 4).

Table 4. Determination of quercetin in *Cassia didymobotrya* Fres.

Extract	Quercetin		
	Found, *mg*	Added, *mg*	Recovery, % ± SD*
Leaves and stems	1.86	2.0	99.59 ± 1.56
Flowers	2.37	2.5	99.18 ± 1.99

*Results based on three determinations per sample.

In conclusion, the proposed procedure is simple, time saving and selective for quercetin, moreover, it could be considered as a new highly-selective shift reagent for quercetin in the presence of other related flavonoids as well as a stability-indicating assay for quercetin glycosides.

In addition, it reports a good method for the selective analysis of quercetin in the presence of other flavonoids.

REFERENCES

1. L. E. Dowd, *Anal. Chem.*, 1959, **31**, 184.
2. D. H. Charles, H. W. Margref and T. E. Weichselbaum, *ibid.*, 1960, **32**, 122.
3. L. Jurd and T. A. Geissman, *J. Org. Chem.*, 1956, **21**, 1395.
4. N. M. Akhmedkhodzhaeva, A. N. Svechnikova, V. A. Bandyukova and D. M. Kambarova, *Farmatsiya*, 1986, **35**, 60.
5. Z. P. Kostennikova, G. A. Panova and R. Dambrauskiene, *ibid.*, 1984, **33**, 33.
6. G. A. Fetkhullina and T. I. Bulenkov, *ibid.*, 1984, **33**, 38.
7. J. Peinado and J. Florindo, *Analyst*, 1988, **113**, 555.
8. L. Xu, A. Liu and X. Zhang, *Yaoxue Xuebao*, 1987, **22**, 208; *Anal. Abstr.*, 1987, **49**, E16.
9. Y. Zhang, J. Cui and S. Zhao, *Yaoure Fenxi Zazhi*, 1984, **4**, 1; *Anal. Abstr.*, 1985, **47**, E18.
10. H. Wagner, G. Tittel and S. Bladt, *Dtsch. Apoth. Ztg.*, 1983, **123**, 515.
11. D. J. Diagle and E. J. Conkerton, *J. Liq. Chromatogr.*, 1983, **6**, 105.
12. D. J. Diagle and E. J. Conkerton, *ibid.*, 1988, **11**, 309.
13. K. Hostettmann, B. Domon, D. Schaufelberger and M. Hostettmann, *J. Chromatogr.*, 1984, **283**, 137.
14. E. Revilla, E. Alonso and M. I. Estrella, *Chromatographia*, 1982, **22**, 137.
15. K. H. Law and N. P. Das, J. Chromatogr., 1987, **388**, 225.
16. I. S. Bhatia, J. Singh and K. L. Bajaj, *Mikrochimica Acta*, 1974, **5**, 909.
17. J. A. Delcour and D. Janssens de Varebeka, *J. Inst. Brew.*, 1985, **91**, 37; *Anal. Abstr.*, 1985, **47**, 8F77.
18. Y. Liang and Q. Zhang, *Yaowu Fenxi Zazhi*, 1987, **7**, 347; *Anal. Abstr.*, 1988, **50**, 7E23.
19. H. Glasl, *Z. Anal. Chem*, 1985, **321**, 325.
20. H. Ogura, Y. Shikiba and Y. Yamazaki, *J. Pharm. Sci.*, 1968, **57**, 705.
21. R. Neu, *Z. Anal. Chem.*, 1961, **42**, 335.
22. J. T. MacGregor and L. Jurd, *Mutat. Res.*, 1978, **54**, 297.
23. G. Tamura, C. Gold, A. Ferro-Luzzi and B. N. Ames, *Proc. Natl. Acad. Sci.*, 1980, **77**, 4961.
24. M. Nagao, N. Morita, T. Yahagi, M. Shimizu, M. Kuroyanagi, M. Fukuoka, K. Yoshihira, S. Natori, T. Fujino and T. Sugimura, *Environ. Mutagen.*, 1981, **3**, 401.
25. A. M. Panukcu, J. Hatcher, H. Taguchi and G. T. Bryan, *Proc. Am. Assoc. Cancer Res.*, 1980, **21**, 74.
26. M. I. Walash, A. Abou Ouf and E. B. Salem, *J. Assoc. Off., Anal. Chem.*, 1982, **65**, 1445.
27. *Idem, Analyst*, 1981, **106**, 949.
28. M. Z. Barakat and M. F. Abdel-Wahab, *Anal. Chem.*, 1973, **26**, 1954.
29. K. A. Connors, *A Textbook of Pharmaceutical Analysis*, 3rd Ed., p. 206. Wiley-Interscience, New York, 1982.
30. J. Rose, *Advanced Physico-Chemical Experiments*, p. 54. Pittman, London, 1964.
31. J. B. Harborne, T. J. Mabry and H. Mabry, *The Flavonoids*, Chapman and Hall, London, 1975.
32. S. M. El-Sayyad, A. M. Abdel-Baky, E. Y. Backheet and K.-W. Glombitza, *Bull. Pharm. Sci.*, Assiut University, 1989, **12**, 195.
33. J. A. Riddick, W. B. Bunger, *Organic Solvents*, 3rd Ed., Wiley Interscience, New York, London, 1970.

Talanta, Vol. 39, No. 3, pp. 265–271, 1992
Printed in Great Britain.

0039-9140/92 $5.00 + 0.00

SIMULTANEOUS SPECTROPHOTOMETRIC DETERMINATION OF THYMOL BLUE, SEMI-METHYLTHYMOL BLUE AND METHYLTHYMOL BLUE

S. KICIAK* and M. A. MEHDI

Department of Physical Chemistry, Institute of Chemistry and Technical Electrochemistry, Politechnika Poznańska, PL-60-965, Poznań, Poland

(*Received* 11 *September* 1989. *Revised* 17 *August* 1991. *Accepted* 29 *August* 1991)

Summary—A direct spectrophotometric method for the simultaneous determination of Thymol Blue, Semi-Methylthymol Blue (SMTB) and Methylthymol Blue (MTB) in mixtures in the presence of other components usually found in synthetic SMTB and commercial MTB is presented. The method for selecting the most advantageous conditions for the spectrophotometric determination of the three dyes in different mixtures is given. A graphical version of the method is useful for monitoring syntheses of SMTB and MTB.

The mixtures obtained in the syntheses[1,2] of Methylthymol Blue (MTB) and Semi-Methylthymol Blue (SMTB) usually contain Thymol Blue (TB) and colourless substances such as formaldehyde, acetic acid and iminodiacetic acid (IDAA).[2–5] The last three compounds do not interfere in the spectrophotometric determination of the three dyes. A method for determination of MTB, SMTB and TB is needed for control of the synthesis of MTB and SMTB, the separation of MTB, SMTB and TB, and for monitoring the ageing of MTB in SMTB reagents.

The analysis of two-component mixtures of MTB and SMTB (transformed into the acid form) by potentiometry, reported by Yoshino and co-workers[3,4] gives good results only in the absence of other acids such as acetic acid, iminodiacetic acid and Thymol Blue in the acid form. These authors used the method only for analysing relatively pure MTB and SMTB reagents.

The spectrophotometric method given for simultaneous determination of MTB and SMTB by Kosenko and Mal'kova[6] utilizes the difference in the molar absorptivities of the aluminium MTB and SMTB complexes at 475 and 590 nm at pH 5.0, but does not take into consideration the presence of TB in mixtures of MTB and SMTB. Such mixtures containing TB are often met in analytical practice and particularly in the mixtures obtained during synthesis of MTB or SMTB. TB has a relatively high molar absorptivity at 475 nm and pH 5.0 and does not absorb at 590 nm. Its presence can therefore cause positive errors in determination of SMTB and relatively smaller negative errors in determination of MTB (Fig. 1).

The results of spectrophotometric determinations of *o*-Cresol Red, Semi-Xylenol Orange and Xylenol Orange,[7–10] and the initial results of

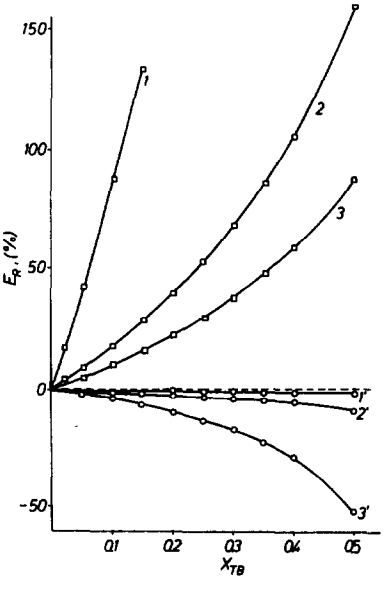

Fig. 1. Relative error (E_R) of SMTB (□) and MTB (○) determination *vs.* molar fraction of TB (x_{TB}) for ratio of molar concentrations $C_{SMTB}/C_{MTB} = 1/9$ (curves 1 and 1'), 1/1 (2 and 2') and 9/1 (3 and 3').

*Author for correspondence.

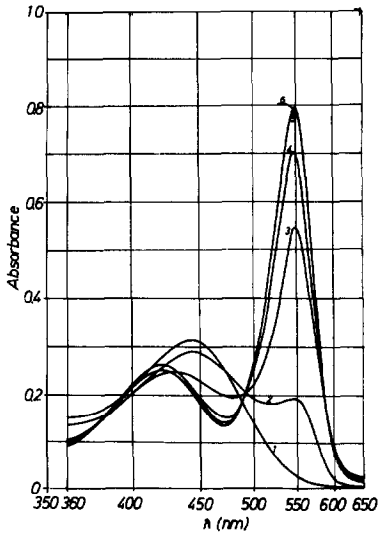

Fig. 2. Absorption spectra of $2.0 \times 10^{-5}M$ MTB for different sulphuric acid concentrations: $1.0M$ (curve 1), $4.0M$ (2), $5.5M$ (3), $7.0M$ (4), $10.0M$ (5) and $12.0M$ (6).

experiments with TB, SMTB and MTB in dilute sulphuric acid suggest that a corresponding determination of TB, SMTB and MTB is possible.

EXPERIMENTAL

Apparatus

The absorption measurements were made with a Zeiss-Jena spectrophotometer (Specord M40) with 1-cm cells. The potentiometric experiments were done with a Mera (Poland) type N517 pH-meter.

Reagents

MTB (Merck) containing ~90% of the dye was purified by extraction in a dilute sulphuric acid–1-butanol system. A mixture containing ~35% of SMTB, obtained from E. Krzyżanowska of the Organic Chemistry Department, Technical University, Poznań, was purified in small quantities (~25 mg) in the way given by Yoshino and coworkers[3,4] and in greater amounts by extraction in a water–butanol system. The latter method will be reported in a subsequent paper. The resulting MTB or SMTB were over 99.5% pure and free from TB. A commercial sample of TB was recrystallized from ethanol. All other reagents were of analytical grade.

Standard solutions of the three dyes ($0.001M$) were prepared in $0.01M$ sulphuric acid for MTB and SMTB, and in 1:1 v/v ethanol–$0.01M$ sulphuric acid mixture for TB.

Procedure

Dissolve 10–50 mg of the sample (accurately weighed) in 5 ml of water or ethanol, and dilute it to the mark with water in a 50-ml standard flask (solution I). Dilute 1 ml of this solution to 50 ml with $5M$ sulphuric acid (to obtain solution II) and measure its absorbance at 548 nm (1-cm path-length). Dilute x ml of solution I to the mark with water in a 50-ml standard flask to obtain solution III, the value of x being 25.0, 10.0, 5.0 and 2.0 when the absorbance of solution II is <0.3, 0.3–0.8, 0.8–1.5 and >1.5 respectively. Add 5-ml aliquots of this solution, with cooling) to 20.0 ml of 1.25, 5.0 and $8.75M$ sulphuric acid in 25-ml standard flasks, and make up to the marks with water, to obtain three solutions, designated S_1, S_4 and S_7, the subscript indicating the molarity of sulphuric acid in the solution. Measure the absorbances of these solutions at 548 nm (1-cm path-length cells). Calculate the concentrations of the components as shown below. The molar absorptivities of pure samples of the three dyes should be determined with the equipment used, and substituted for those quoted, if there is a difference.

RESULTS AND DISCUSSION

Molar absorptivities of TB, SMTB and MTB in sulphuric acid

The absorption spectra of MTB (Fig. 2), SMTB (Fig. 3) and TB (Fig. 4) in sulphuric acid have two peaks, at wavelengths depending on

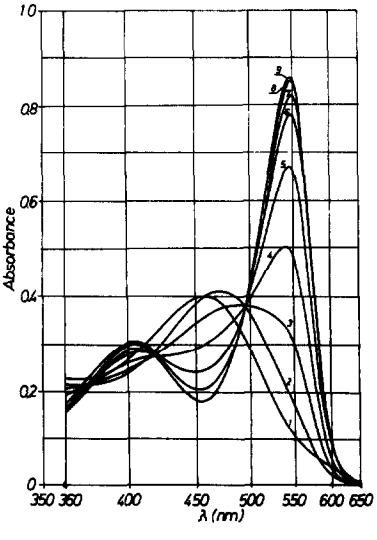

Fig. 3. Absorption spectra of $2.2 \times 10^{-5}M$ SMTB for different sulphuric acid concentrations: $0.001M$ (curve 1), $0.2M$ (2), $1.0M$ (3), $2.0M$ (4), $3.0M$ (5), $4.0M$ (6), $5.0M$ (7), $7.0M$ (8) and $10.0M$ (9).

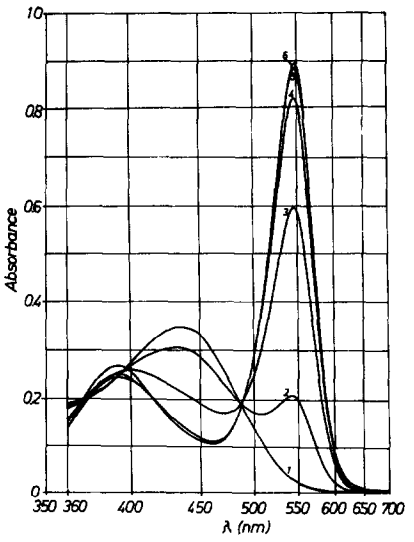

Fig. 4. Absorption spectra of $2.35 \times 10^{-5}M$ TB in buffer solutions of pH 4.0 (curve 1), 2.0 (2) and for different sulphuric acid concentrations: $0.05M$ (3), $0.5M$ (4), $4.0M$ (5) and $7.0M$ (6).

the acidity. The one near 435 nm is greatest at low concentrations of the acid, and is blue-shifted and decreased in magnitude with an increase in the acid concentration. The shift is relatively large, so the absorbance at 435 nm is not suitable for determination of the dyes. The peak at about 548 nm does not change position with an increase in the sulphuric acid concentration, but changes considerably in amplitude. The molar absorptivities of MTB, SMTB and TB differ very much from each other over almost the whole acidity range from pH 4 to $10M$ sulphuric acid (Fig. 5), and this is utilized for determination of the three dyes.

In accordance with the detailed potentiometric and spectrophotometric investigations conducted by Yoshino and co-workers[2-4] symbolic formulae such as H_6MTB, H_4SMTB and H_2TB can be assigned to the undissociated (yellow) molecules of MTB, SMTB and TB. Red protonated molecules, H_3TB^+, H_5SMTB^+, H_7MTB^+ and H_8MTB^{2+} are formed in acidic media. H_3TB^+ begins to form at pH 2, H_5SMTB^+ requires more concentrated sulphuric acid ($>1M$) and the protonated forms of MTB form if the concentration of sulphuric acid exceeds $4M$.

The blue-shifts of curve 1 (Fig. 2) for MTB and curve 1 (Fig. 3) for SMTB can be ascribed to the beginning of formation of the anionic forms of the dyes.

The ranges of sulphuric acid concentration in which the greatest changes in the spectra take place are 0.005–$1.0M$ for TB, 2–$4M$ for SMTB and 4–$7M$ for MTB.

Two-component systems

System TB–SMTB. To select the optimum concentration of sulphuric acid for the simultaneous determination of TB and SMTB the molar absorptivities at the absorption maximum (548 nm) were determined precisely and their differences ($\Delta\epsilon$) were plotted against sulphuric acid concentration (Fig. 6). It can be seen that the optimum acid concentration (greatest value of $\Delta\epsilon_{548}$) is $\sim 1.0M$.

In contrast, very small values of $\Delta\epsilon_{548}$ were obtained for $7M$ and greater concentrations of the acid. Therefore the second sulphuric acid concentration chosen for use in determination of TB and SMTB was $7.0M$.

The molar absorptivities of TB and SMTB in $1M$ and $7M$ sulphuric acid (at 548 nm) are $\epsilon_{TB_1} = 36.0 \times 10^3$, $\epsilon_{SMTB_1} = 13.0 \times 10^3$, $\epsilon_{TB_7} = 37.6 \times 10^3$ and $\epsilon_{SMTB_7} = 35.4 \times 10^3$ l.mole^{-1}.cm^{-1}. Beer's law is obeyed and the absorbances of TB and SMTB are additive over the concentration range $0.5–25 \times 10^{-6}M$, so for a path-length of 1 cm the absorbances A_1 and A_7 (in $1M$ and $7M$ sulphuric acid) are

$$A_1 = 36.0 \times 10^3 C_{TB} + 13.0 \times 10^3 C_{SMTB} \quad (1)$$

$$A_7 = 37.6 \times 10^3 C_{TB} + 35.4 \times 10^3 C_{SMTB} \quad (2)$$

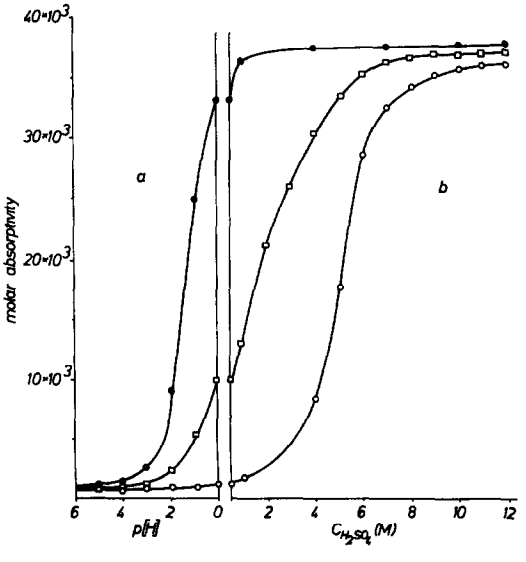

Fig. 5. Molar absorptivities (at 548 nm) of TB (●), SMTB (□) and MTB (○), (a) *vs.* p[H] (below pH = 2, calculated as p[H] = $-\log 0.5C_{H_2SO_4}$), (b) *vs.* sulphuric acid concentration.

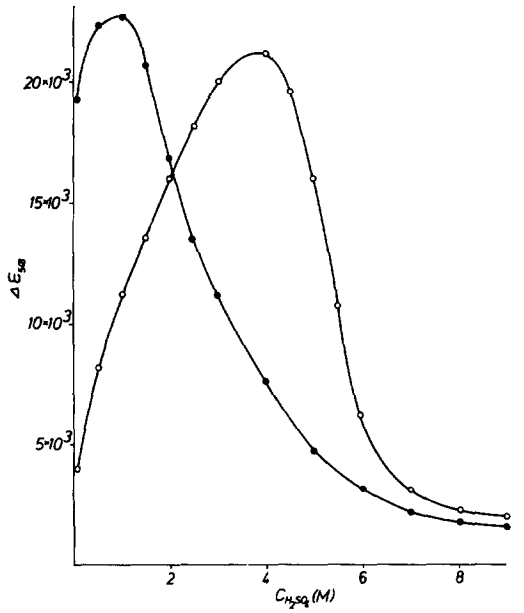

Fig. 6. Differences of molar absorptivities at 548 nm ($\Delta\epsilon_{548}$) *vs.* sulphuric acid concentration: $\Delta\epsilon = \epsilon_{TB} - \epsilon_{SMTB}$ (●) and $\Delta\epsilon = \epsilon_{SMTB} - \epsilon_{MTB}$ (○).

Rearranging gives

$$C_{TB} = (45.06A_1 - 16.55A_7) \times 10^{-6}M \quad (3)$$

$$C_{SMTB} = (45.82A_7 - 47.86A_1) \times 10^{-6}M \quad (4)$$

Table 1 shows the same experimental results for given TB and SMTB concentrations.

It is necessary to remark that even a small amount of MTB causes significant errors in determination of SMTB and TB. For example, for a mixture containing 10 μmole of TB, 10 μmole of SMTB and 0.4 μmole of MTB, from the absorbances of 1 and 7*M* sulphuric acid solutions of the mixture, the results obtained are 10.55 μmole of SMTB and 9.82 μmole of TB. In such a case better results

Table 1. Results for simultaneous spectrophotometric determination* of TB and SMTB

Taken†, μM		Found‡, μM	
TB	SMTB	TB	SMTB
2.0	18.0	$1.9_5 \pm 0.1_6$	$18.1_2 \pm 0.1_7$
5.0	15.0	$4.9_7 \pm 0.1_7$	$14.9_7 \pm 0.2_2$
10.0	10.0	$10.1_0 \pm 0.1_3$	$10.0_2 \pm 0.2_1$
15.0	5.0	$14.9_6 \pm 0.1_4$	$5.1_4 \pm 0.1_6$
18.0	2.0	$18.2_3 \pm 0.1_1$	$2.0_8 \pm 0.1_8$

*Absorbances measured at 548 nm in 1 and 7*M* sulphuric acid media.
†With error of $\pm 0.05\mu M$.
‡Means and standard deviations for 5 measurements.

Table 2. Results for simultaneous spectrophotometric determination* of SMTB and MTB

Taken†, μM		Found‡, μM	
SMTB	MTB	SMTB	MTB
2.0	18.0	$2.1_2 \pm 0.0_9$	$17.8_8 \pm 0.1_2$
5.0	15.0	$4.9_6 \pm 0.0_8$	$14.9_6 \pm 0.0_9$
10.0	10.0	$10.0_4 \pm 0.1_5$	$9.9_5 \pm 0.1_2$
15.0	5.0	$15.1_3 \pm 0.1_8$	$5.1_0 \pm 0.1_7$
18.0	2.0	$18.2_0 \pm 0.1_6$	$1.9_9 \pm 0.1_1$

*Absorbances measured at 548 nm in 4 and 7*M* sulphuric acid media.
†With error of $\pm 0.05\mu M$.
‡Means and standard deviations for 5 measurements.

can be obtained by using a solution in 4*M* instead of 7*M* sulphuric acid, and then

$$C_{TB} = (50.54A_1 - 22.24A_4) \times 10^{-6}M \quad (5)$$

$$C_{SMTB} = (61.58A_4 - 63.29A_1) \times 10^{-6}M \quad (6)$$

The results for the same mixture are then 10.12 μmole of SMTB and 9.98 μmole of TB.

System SMTB–MTB. It is similarly shown (Fig. 6) that 4*M* and 7*M* are the optimum sulphuric acid concentrations for simultaneous determination of SMTB and MTB. In this case the molar absorptivities at 548 nm are $\epsilon_{SMTB_4} = 29.6 \times 10^3$, $\epsilon_{MTB_4} = 8.2 \times 10^3$, $\epsilon_{SMTB_7} = 35.4 \times 10^3$ and $\epsilon_{MTB_7} = 32.4\,1.\text{mole}^{-1}.\text{cm}^{-1}$. Beer's law is obeyed and the absorbances are additive in the same range of dye concentration $0.5 - 25.0 \times 10^{-6}M$ as that for the TB–SMTB system, so

$$C_{SMTB} = (48.45A_4 - 12.26A_7) \times 10^{-6}M \quad (7)$$

$$C_{MTB} = (44.26A_7 - 52.94A_4) \times 10^{-6}M \quad (8)$$

Typical values for C_{SMTB} and C_{MTB} are given in Table 2.

System TB–MTB. This system is not met in practice (SMTB is always also present)—so it will not be described except for the equations:

$$C_{TB} = (29.49A_1 - 1.64A_7) \times 10^{-6}M \quad (9)$$

$$C_{MTB} = (32.77A_7 - 34.22A_1) \times 10^{-6}M \quad (10)$$

Three-component system (TB, SMTB, MTB)

Figures 5 and 6 show that in sulphuric acid solutions of TB, SMTB and MTB the dominant influence on the change of absorption at 548 nm is the concentration of the acid: for TB up to 1*M*, for SMTB up to 4*M* and for MTB up to 7*M*. Therefore solutions with these concentrations of sulphuric acid were chosen for the simultaneous determination of the three dyes.

Table 3. Results for simultaneous spectrophotometric determination* of TB, SMTB and MTB

Taken†, μM			Found‡, μM		
TB	SMTB	MTB	TB	SMTB	MTB
1.0	4.0	15.0	$1.0_6 \pm 0.0_9$	$4.0_3 \pm 0.2_7$	$15.1_7 \pm 0.2_6$
2.0	6.0	12.0	$2.0_8 \pm 0.1_4$	$5.9_4 \pm 0.3_0$	$12.2 \pm 0.2_0$
2.0	10.0	8.0	$2.1_4 \pm 0.1_3$	$9.8_9 \pm 0.2_9$	$8.0_9 \pm 0.2_2$
6.0	7.0	7.0	$6.0_7 \pm 0.2_0$	$7.1_1 \pm 0.2_4$	$7.1_3 \pm 0.2_0$
10.0	5.0	5.0	$10.0_2 \pm 0.1_8$	$5.0_8 \pm 0.2_2$	$4.9_2 \pm 0.1_8$
10.0	8.0	2.0	$9.9_6 \pm 0.2_3$	$7.9_0 \pm 0.2_8$	$2.1_1 \pm 0.2_1$
16.0	3.0	1.0	$16.1_5 \pm 0.2_9$	$3.0_1 \pm 0.3_2$	$1.1_2 \pm 0.1_7$
16.0	2.0	2.0	$15.9_1 \pm 0.2_7$	$2.0_8 \pm 0.2_0$	$2.1_4 \pm 0.2_4$
16.0	1.0	3.0	$16.0_8 \pm 0.2_3$	$0.9_8 \pm 0.1_9$	$2.9_6 \pm 0.1_8$
18.0	1.0	1.0	$18.2_0 \pm 0.3_0$	$1.0_6 \pm 0.1_8$	$1.0_8 \pm 0.2_0$

*Absorbances measured at 548 nm in 1.0, 4.0 and 7.0M sulphuric acid media.

†With error of $\pm 0.05 \mu M$.

‡Means and standard deviations for 5 measurements.

The additional molar absorptivities at 548 nm needed are $\epsilon_{TB_4} = 37.0 \times 10^3$ and $\epsilon_{MTB_1} = 1.8 \times 10^3$ l.mole^{-1}.cm^{-1}.

Beer's law is obeyed and the absorbances of the three dyes are additive from 0.5–25μM, so for a path-length of 1 cm the absorbances of the 1, 4 and 7M sulphuric acid solutions are

$$A_1 = 36.0 \times 10^3 C_{TB} + 13.0 \times 10^3 C_{SMTB} + 1.8 \times 10^3 C_{MTB} \quad (11)$$

$$A_4 = 37.0 \times 10^3 C_{TB} + 29.6 \times 10^3 C_{SMTB} + 8.2 \times 10^3 C_{MTB} \quad (12)$$

$$A_7 = 37.6 \times 10^3 C_{TB} + 35.4 \times 10^3 C_{SMTB} + 32.4 \times 10^3 C_{MTB} \quad (13)$$

Rearranging gives

$$C_{TB} = (52.03A_1 - 27.81A_4 + 4.15A_7) \times 10^{-6} M \quad (14)$$

$$C_{SMTB} = (-69.20A_1 + 85.40A_4 - 17.75A_7) \times 10^{-6} M \quad (15)$$

$$C_{MTB} = (15.30A_1 - 61.05A_4 + 45.44A_7) \times 10^{-6} M \quad (16)$$

Some results thus obtained for synthetic mixtures of TB, SMTB and MTB are collected in Table 3. Results obtained for some commercial samples of MTB and for mixtures obtained during synthesis of SMTB are collected in Table 4.

Graphical method for the three-component system (TB, SMTB and MTB)

A graphical version of the method for the three-component system has also been worked out, and is very useful for monitoring the changes during synthesis of SMTB or MTB. In

Table 4. Results for the simultaneous spectrophotometric determination of TB, SMTB and MTB in commercial MTB and mixtures obtained during synthesis of SMTB

		Found‡, μM					
		Present method			Kosenko and Mal'kova method[6]		
Sample	Taken	TB	SMTB	MTB	ΣC_i	SMTB	MTB
MTB (Merck, FRG)	16.60 mg/l. (19.7μM)†	0	1.0_7	17.9_4	19.0	1.1_9	18.1_6
MTB (Aldrich, USA)	16.90 mg/l. (20.0μM)†	0.1	3.6_2	16.0_9	19.3	3.7_7	15.6_9
MTB (POCH, Poland)	16.80 mg/l. (19.9μM)†	0.8_1	3.1_2	9.4_1	13.3	3.8_6	9.2_7
MTB (POCH, Poland)	16.95 mg/l. (20.1μM)†	0.3_0	2.1_6	11.3_7	13.8	2.4_1	11.2_5
SMTB (1 hr)*	20.2μM	18.6_0	1.6_2	0.1_7	20.4	6.6_4	0
SMTB (2 hr)*	20.0μM	16.1_7	3.1_7	0.4_4	19.8	9.9_4	0
SMTB (4 hr)*	20.3μM	14.1_0	4.4_2	1.5_1	20.0	12.7_4	0.8_2
SMTB (6 hr)*	20.6μM	13.0_3	4.3_4	2.8_7	20.2	12.4_9	2.1_3
SMTB (36 hr)*	20.4μM	11.6_6	2.1_8	6.4_0	20.2	10.8_4	6.0_3

*Time elapsed from start of synthesis.

†Equivalent concentration of pure MTB.

‡Mean of three determinations.

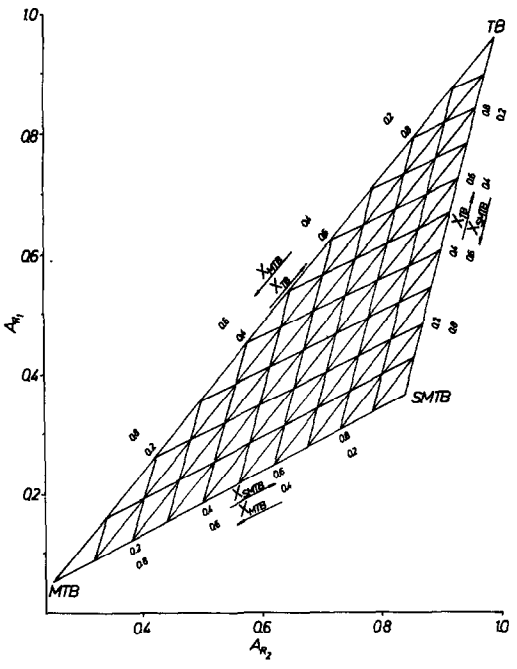

Fig. 7. Dependence of molar fractions of TB, SMTB and MTB on relative absorbances, $A_{R_1} = A_1/A_7$ and $A_{R_2} = A_4/A_7$ where A_1, A_4 and A_7 are the absorbances at 548 nm for 1, 4 and 7*M* sulphuric acid solutions.

this version the absorbance ratios are used (see Appendix for derivation):

$$A_{R_1} = \frac{A_1}{A_7} = \frac{36.0 - 23.0\,X_{SMTB} - 34.2\,X_{MTB}}{37.6 - 2.2\,X_{SMTB} - 5.2\,X_{MTB}} \quad (17)$$

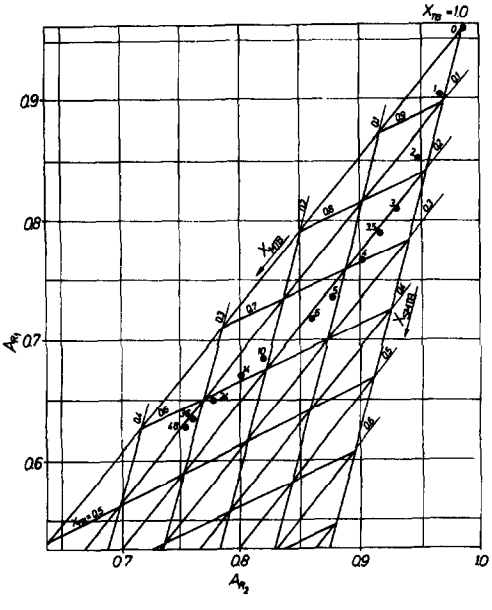

Fig. 8. Dependence of molar fraction of TB, SMTB and MTB on relative absorbances A_{R_1} and A_{R_2}. Changes in the composition of the mixture during the synthesis of SMTB are shown by the points (●) numbered with the time (hr) elapsed from the beginning of the reaction.

$$A_{R_2} = \frac{A_4}{A_7} = \frac{37.0 - 7.4\,X_{SMTB} - 28.8\,X_{MTB}}{37.6 - 2.2\,X_{SMTB} - 5.2\,X_{MTB}} \quad (18)$$

Equations (17) and (18) allow construction of Fig. 7. From which the composition of the mixture can be directly read by using only the relative values of the absorbances without calculation of the concentrations of the three dyes.

Figure 8 shows an example of use of the graphical version of the method for observation of progress during synthesis of SMTB. It is easy to see that the largest molar fraction of SMTB in the mixture is obtained 4 hr from the beginning of the synthesis.

APPENDIX

It follows from the equations for A_1, A_4 and A_7 that

$$A_{R_1} = \frac{A_1}{A_7} = \frac{(36.0\,C_{TB} + 13.0\,C_{SMTB} + 1.8\,C_{MTB}) \times 10^3}{(37.6\,C_{TB} + 35.4\,C_{SMTB} + 32.4\,C_{MTB}) \times 10^3}$$

and

$$A_{R_2} = \frac{A_4}{A_7} = \frac{(37.0\,C_{TB} + 29.6\,C_{SMTB} + 8.2\,C_{MTB}) \times 10^3}{(37.6\,C_{TB} + 35.4\,C_{SMTB} + 32.4\,C_{MTB}) \times 10^3}$$

The molar fractions of TB, SMTB and MTB are:

$$X_{TB} = \frac{C_{TB}}{\Sigma C_i}, \quad X_{SMTB} = \frac{C_{SMTB}}{\Sigma C_i}$$

and

$$X_{MTB} = \frac{C_{MTB}}{\Sigma C_i}$$

where $\Sigma C_i = C_{TB} + C_{SMTB} + C_{MTB}$ and $X_{TB} + X_{SMTB} + X_{MTB} = 1$.

Division of the numerators and denominators of both equations by ΣC_i gives

$$A_{R_1} = \frac{36.0\,X_{TB} + 13.0\,X_{SMTB} + 1.8\,X_{MTB}}{37.6\,X_{TB} + 35.4\,X_{SMTB} + 32.4\,X_{MTB}}$$

and

$$A_{R_2} = \frac{37.0\,X_{TB} + 29.6\,X_{SMTB} + 8.2\,X_{MTB}}{37.6\,X_{TB} + 35.4\,X_{SMTB} + 32.4\,X_{MTB}}$$

Because $X_{TB} = 1 - X_{SMTB} - X_{MTB}$, we obtain

$$A_{R_1} = \frac{36.0 - 23.0\,X_{SMTB} - 34.2\,X_{MTB}}{37.6 - 2.2\,X_{SMTB} - 5.2\,X_{MTB}}$$

and

$$A_{R_1} = \frac{37.0 - 7.4\,X_{SMTB} - 28.8\,X_{MTB}}{37.6 - 2.2\,X_{SMTB} - 5.2\,X_{MTB}}.$$

REFERENCES

1. J. Körbl, *Chem. Listy*, 1957, **51**, 1304.
2. T. Yoshino, H. Imada, T. Kuwano and K. Iwasa, *Talanta*, 1969, **16**, 151.
3. T. Yoshino, S. Murakami and M. Kagawa, *ibid.*, 1974, **21**, 199.

4. T. Yoshino, H. Imada, S. Murakami and M. Kagawa, *ibid.*, 1974, **21**, 211.
5. N. F. Kosenko, T. V. Mal'kova and K. B. Yatsimirskii, *Zh. Analit. Khim.* 1975, **30**, 2245.
6. N. F. Kosenko and T. V. Mal'kova, *Khim. Khim. Tekhnol.*, 1981, **24**, 54.
7. M. Murakami, T. Yoshino and S. Harasawa, *Talanta*, 1967, **14**, 1293.
8. S. Kiciak and H. Gontarz, *ibid.*, 1986, **33**, 341.
9. S. Kiciak, *ibid.*, 1989, **36**, 1101.
10. *Idem*, *ibid.*, 1990, **37**, 1197.

Talanta, Vol. 39, No. 3, pp. 273–280, 1992
Printed in Great Britain

0039-9140/92 $5.00 + 0.00
Pergamon Press plc

STUDIES ON THE EXTRACTION AND SPECTROPHOTOMETRIC DETERMINATION OF Ni(II), Fe(II), Fe(III) AND V(IV) WITH BIS(4-HYDROXYPENT-2-YLIDENE)DIAMINOETHANE

F. I. NWABUE* and E. N. OKAFO†
Department of Pure and Industrial Chemistry, University of Nigeria, Nsukka, Nigeria

(*Received* 24 *March* 1989. *Revised* 10 *September* 1991. *Accepted* 18 *September* 1991)

Summary—The extraction of Ni(II), Fe(II), Fe(III) and V(IV) with bis(4-hydroxypent-2-ylidene)-diaminoethane from various acids and buffer solutions has been studied. The golden yellow Fe(II) and wine-red Fe(III) complexes have maximum absorption at 445 and 435 nm respectively, and the yellow–green Ni(II) chelate shows two maxima, at 373 and 560 nm. The blue–green V(IV) chelate also has two maxima, at 580 and 660 nm. These characteristics can be used for the determination of these species. Iron, nickel and vanadium have been separated and determined in the presence of one another and of many other elements.

Since the work of Combes on the preparation of a tetradentate β-ketoamine complex of copper,[1] a considerable literature has appeared on the subject. Much of it concerns the synthesis and structural elucidation of β-ketoamine analogues,[2–4] and the gas chromatographic,[5–7] thermogravimetric[5] and spectrometric[8–10] determination of some of their metal complexes. Although these compounds have not found much use either as metal extractants or as spectrophotometric reagents, they have been noted[11–13] as promising for the purpose.

We have found bis(4-hydroxypent-2-ylidene)-diaminoethane (BHPDE) to be suitable for the extraction and spectrophotometric determination of iron, vanadium and nickel in the presence of each other and of many other elements.

EXPERIMENTAL

Reagents

All reagents and solvents used were of analytical grade. All aqueous solutions were prepared in distilled demineralized water. Working solutions were prepared by dilution as required.

Standard iron solution (0.1 mg/ml). Iron(II) and iron(III) solutions were prepared by dissolving the requisite amounts of ferrous or ferric ammonium sulphate (as appropriate) in dilute sulphuric acid, and were standardized by the permanganate method.[14]

Standard nickel solution (0.1 mg/ml). Prepared from nickel sulphate hexahydrate.

Standard vanadium(IV) solution (0.1 mg/ml). Freshly prepared from vanadyl sulphate pentahydrate.

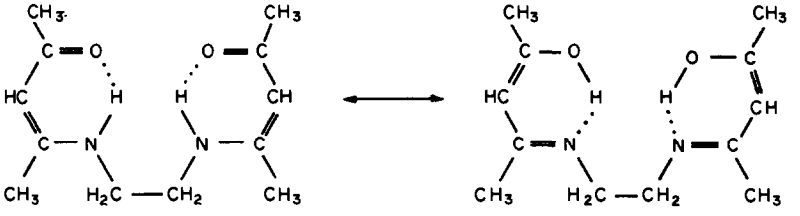

BHPDE

*Author for correspondence.
†Department of Foundation and Remedial Studies, University of Jos, Makurdi Campus, Makurdi, Nigeria.

Synthesis of BHPDE. Ethylenediamine (6.00 g) is added gradually with stirring to 20.0 g of acetylacetone in a 250-ml beaker, both liquids having previously been chilled in an ice–salt mixture for 30 min. If the ethylenediamine solidifies during the cooling, it should be liquefied by very gentle warming. The reaction is exothermic. Initially a whitish solid forms, but as more ethylenediamine is added the reaction mixture becomes hot and deep golden yellow. Stirring is continued until crystallization starts, leading to a cream-coloured cake. The product is recrystallized twice from carbon tetrachloride, to give whitish crystals (96% yield, m.p. $108 \pm 1°$). The reagent is used as a freshly prepared 0.1 g/ml aqueous solution, dissolution being effected by warming.

Buffer solutions. Clark and Lubs buffers[15] for pH 1–10, and as described by Kolthoff *et al.*[15] for pH 11–13, were prepared.

Protonation and acid dissociation constants of the reagent

A 0.01*M* aqueous solution of the reagent gave a pH value of 8.3 ± 0.1. The protonation constants were determined by titration of the reagent with 0.01*M* hydrochloric acid, as log K_1, 4.40 ± 0.10 and log $K_2 = 3.20 \pm 0.15$. These values suggest stepwise protonation of the two nitrogen sites in the ligand, H_2B, to give H_3B^+ and H_4B^{2+} respectively. The acid dissociation constants were obtained by titration with 0.01*M* sodium hydroxide, and were found to be $pK_{1D} = 9.70 \pm 0.10$ and $pK_{2D} = 10.80 \pm 0.10$, corresponding to the formation of HB^- and B^{2-} respectively.

Measurement of distribution ratios

Equal volumes (5 ml) of the aqueous and organic phases were shaken mechanically [for 3 min for iron(II), 10 for vanadium and iron(III), and 20 for nickel at pH 13, but 60 at pH 5] in glass-stoppered bottles at $28 \pm 1°$. The phases were centrifuged and separated, and analysed spectrophotometrically after acid decomposition.

Iron was determined with 1,10-phenanthroline after reduction with hydroquinone,[16] nickel with dimethylglyoxime,[16] and vanadium with oxine after reduction with solid sodium dithionite.[17]

Colour stability

The stability of the colour of the complexes was studied at room temperature ($28 \pm 1°$). Maximum absorbance of the chloroform extract was obtained after 10 min standing of the aqueous phase before extraction. The absorbance of the iron(II) and iron(III) complexes was constant for at least 3 days, while that of the nickel(II) and vanadium(IV) complexes was stable for up to 1 day.

Temperature effect. The temperature was varied from 18 to 40°: the absorbance is at a maximum and constant between 24 and 30°. All determinations were done at room temperature ($28 \pm 1°$).

Phase volume ratio. Variation in volume of the aqueous phase from 3 to 40 ml had little or no effect on the absorbance of the chloroform extract or on the extraction efficiency: a working volume of 5 ml is recommended for ease of manipulation.

Recommended procedures for iron, vanadium and nickel

Iron. To 2 ml of sample solution containing 5–30 μg of iron(II), add 0.25 ml of 0.1*M* perchloric, sulphuric or hydrochloric acid, and 0.5 ml of 5 mg/ml hydroquinone solution to reduce any iron(III) to iron(II); for iron(III), add 0.25 ml of 0.1*M* perchloric acid or 0.5 ml each of 0.1*M* nitric acid and potassium nitrate but no hydroquinone. Add 1 ml of BHPDE solution, make up to about 5 ml with water, let stand for 10 min, shake with 5 ml of chloroform for 3 min, and measure the absorbance of the extract at 445 nm for iron(II) or 435 nm for iron(III), against a reagent blank.

Vanadium. Adjust 2 ml of sample solution containing 50–500 μg of vanadium(IV) to pH 10–11 with dilute ammonia solution and buffer. Add 1 ml of BHPDE solution, make up to about 5 ml with water, let stand for 10 min, shake with two 5-ml portions of chloroform for 10 min each time, and measure the absorbance of the combined extracts at 660 nm against a reagent blank.

Nickel. Adjust 2 ml of sample solution containing not less than 15 μg of nickel to pH 13 with dilute ammonia and sodium hydroxide solutions. Add 1 ml of BHPDE solution, make up to about 5 ml with water, let stand for 10 min, shake with 5 ml of chloroform for 20 min and measure the absorbance of the extract at 375 nm against a reagent blank.

Separation of iron from nickel or vanadium

Extract the iron from acid solution, then the nickel at pH 13, or vanadium at pH 10–11.

Separation of nickel and vanadium

Extract the nickel at pH 5 (triple extraction is needed) and then the vanadium at pH 10–11.

Determination of iron, nickel and vanadium together

Extract the iron from acid solution, then the nickel after adjustment of the pH to 5 (triple extraction) and finally the vanadium at pH 10–11.

Analysis of plant matter

Samples of *colocasia antiquorum* prepared from the air-dried pulp of the edible cormel were used as a model.

Ash (at 400–450°) a weighed sample sufficient to give about 0.1 g of ash. Dissolve the ash in 2*M* hydrochloric acid, dilute to a convenient volume, and then evaporate an aliquot to dryness. Take up the residue in dilute acid and determine the iron and nickel as already described.

RESULTS AND DISCUSSION

Figure 1 shows the extraction of iron(II), iron(III), nickel(II) and vanadium(IV) into chloroform with BHPDE as a function of pH. There is quantitative extraction of iron(II) in the pH range 2–5, but at pH 1 the extraction is negligible. At above pH 5 the extraction decreases, suggesting formation of an unextractable hydroxo species, which becomes more pronounced at above pH 12. The extraction of iron(III) increases from zero at below pH 1 and reaches a maximum of about 90% in the pH range 3–5. Quantitative extraction at pH 3 would be expected from the results obtained with unbuffered acid media, as shown later in Fig. 3. The shortfall could be attributed to complexation by the phthalate in the buffer at pH 3–5, as well as to hydrolysis at above pH 4.[18] This was confirmed by increase of the extraction up to 100% at pH 3–4 when phthalate was replaced by tartrate in the buffer. The partial extraction observed at above pH 11 could be due to formation of extractable complexes formed with HB^- or B^{2-} or with hydroxyl ions. The extraction of nickel(II) into chloroform, which attains equilibrium slowly at pH below 9, probably owing to kinetic factors, is incomplete at low pH but becomes quantitative and much faster at pH above 11. Vanadium(IV) is not extracted at all over the pH range 1–5, but

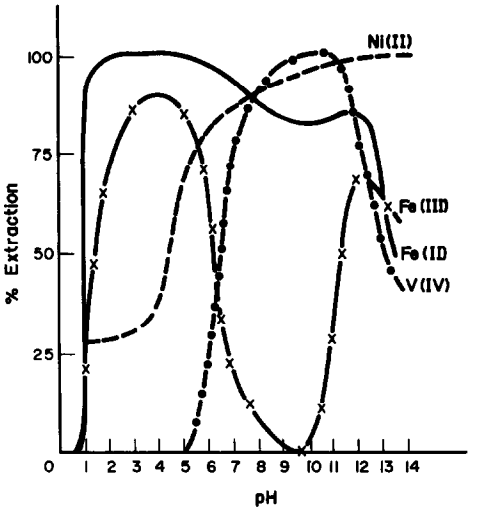

Fig. 1. Extraction of —— Fe(II), ×——× Fe(III), ●——● V(IV), and --- Ni(II) from aqueous pH buffer with an equal volume (5 ml) of 20-mg/ml BHPDE/$CHCl_3$ solution at 28 ± 1°.

its extraction increases gradually with pH > 5, becoming quantitative at pH 10–11 before decreasing sharply at higher pH. The decrease could be due to formation of the hydrous oxide,[18] $VO(OH)_2$.

The extraction of iron(II) and iron(III) from unbuffered acid media with 2% BHPDE and an equal volume of chloroform is shown in Figs. 2 and 3 respectively. Iron(II) is quantitatively extracted from all four acids when these are present in the concentration range 0.001–0.005*M*. At higher acidity a sharp decrease in extraction is observed at 0.005*M*

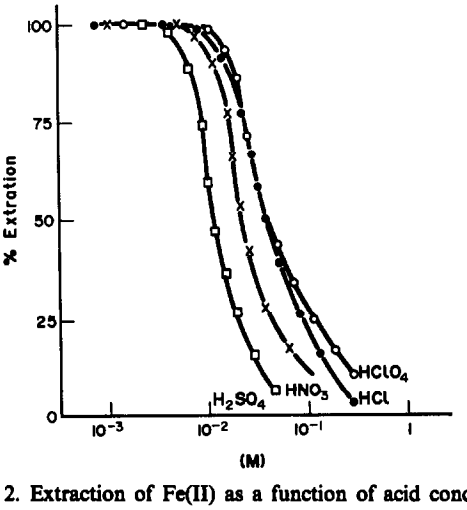

Fig. 2. Extraction of Fe(II) as a function of acid concentration: ●——● HCl, ×——× HNO_3, O——O $HClO_4$, □——□ H_2SO_4. Equal volumes (5 ml) of aqueous phase and 20-mg/ml BHPDE/$CHCl_3$ solution, contact time of 3 min, at 28 ± 1°.

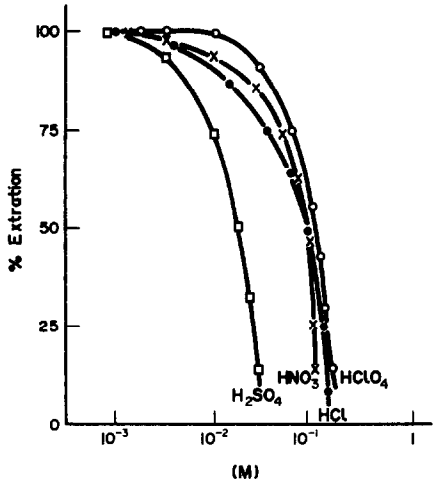

Fig. 3. Extraction of Fe(III) as a function of acid concentration: ●——● HCl, ×——× HNO_3, ○——○ $HClO_4$, □——□ H_2SO_4. Equal volumes (5 ml) of aqueous phase and 20-mg/ml BHPDE/$CHCl_3$ solution, contact time 10 min, at 28 ± 1°.

for sulphuric and nitric acids, and 0.01M for hydrochloric and perchloric acids, as a result of protonation of the ligand, H_2B, according to the equations:

$$H_2B + H^+ \rightleftharpoons H_3B^+; \quad \log K_1 = 4.40 \qquad (1)$$

$$H_3B^+ + H^+ \rightleftharpoons H_4B^{2+}; \quad \log K_2 = 3.20 \qquad (2)$$

At >1.0M acid concentration, an unextractable pinkish complex is formed but was not investigated.

The extraction of iron(III) from various acids follows a trend similar to that of iron(II) for perchloric acid, and for the other acids quantitative extraction is achieved only at 0.001M acid concentration. The extraction of iron(II) and iron(III) shown in Figs 2 and 3 shows a general decrease with increasing acidity of the aqueous phase, according to the equation:

$$M^{n+} + mH_3B^+ + nX^- \rightleftharpoons M(H_2B)_m^{n+} \cdot nX^- + mH^+ \qquad (3)$$

Hence the extraction constant is given by

$$K_{ex} = \frac{[M(H_2B)_m^{n+} \cdot nX^-][H^+]^m}{[M^{n+}][H_3B^+]^m[X^-]^n} \qquad (4)$$

where $X^- = NO_3^-$, Cl^-, ClO_4^- or HSO_4^-.

Hence

$$\log D = m \log[H_2B] + n \log[X^-] + m \log K_1 + \log K_{ex} \qquad (5)$$

Plots of log D *vs.* log[H_2B] at pH 4–6 and at constant ionic strength 0.1, maintained by chloride, perchlorate or nitrate ion, are linear with slopes of 2 and 1 for iron(II) and iron(III) respectively. Similar plots of log D *vs.* log[X^-] at 0.1M H_2B concentration and pH 4–6 are also linear, with slopes of 2 and 1 for iron(II) and iron(III) respectively. These results suggest formation of ion-association complexes of the type $[Fe^{II}(H_2B)_2^{2+}] \cdot 2X^-$ and $[Fe^{III}(H_2B)(OH)_2^+] \cdot X^-$ as the predominant species at low acidity, whereas at high acid concentration the equilibrium in equation (3) shifts to the left, preventing complex formation. The log K_{ex} values obtained from these plots are 13.85 and 6.05 for iron(II) and iron(III) respectively.

The extraction of nickel(II) and vanadium(IV) from unbuffered acid media is low, but increases with increasing pH according to the equations:

$$M^{n+} + xH_2B \rightleftharpoons M(HB)_x^{(n-x)+} + xH^+ \qquad (6)$$

$$M^{n+} + xH_2B \rightleftharpoons MB_x^{(n-2x)+} + 2xH^+ \qquad (7)$$

Hence

$$\log D = x \log[H_2B] + y\text{pH} + \log K_{ex} \qquad (8)$$

where $y = x$ and $2x$ for equations (6) and (7) respectively.

Plots of log D *vs.* log[H_2B] at constant ionic strength 0.1 and 0.15 are linear with a slope of 1 in the pH range 5–10 for nickel and vanadium, and 2 in the pH range 11–13. This suggests the extraction of $Ni(HB)_2$ and $VO(HB)_2$ complexes at pH below 10 and of NiB and VOB at pH

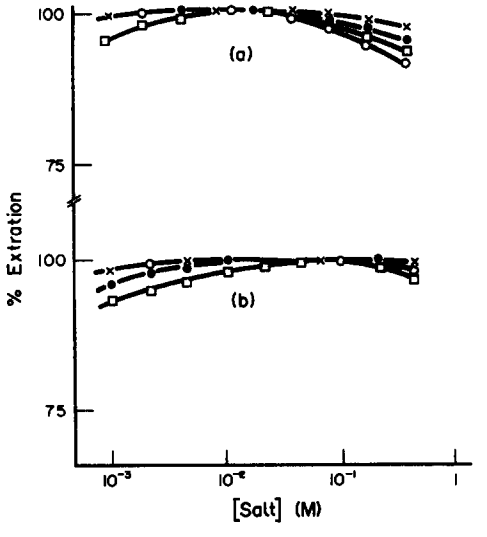

Fig. 4. Effect of added salts on the extraction of (A) Fe(II) and (B) Fe(III) from 0.05M HCl, HNO_3, $HClO_4$ and 0.01M H_2SO_4; ●——● NaCl, ×——× KNO_3, ○——○ $NaClO_4$, □——□ Na_2SO_4. Equal volumes (5 ml) of aqueous phase and 20-mg/ml BHPDE/$CHCl_3$ solution, contact time 3 min for Fe(II), 10 min for Fe(III), at 28 ± 1°.

above 11. The log K_{ex} values obtained on the basis of equation (7) are −20.82 and −20.18 for nickel and vanadium respectively.

Other extraction variables

The extraction of iron(II) and iron(III) with a 20-mg/ml BHPDE solution in chloroform is not quantitative from 0.05*M* acid, as shown in Figs 2 and 3. Under these conditions, the addition of various amounts of the sodium salts of the corresponding acids, and of sodium sulphate to 0.01*M* sulphuric acid results in quantitative extraction, as shown in Fig. 4 for iron(II) and iron(III). For both iron species this is consistent with the equilibrium suggested in equation (3).

The extraction of iron(II) from 0.005*M* hydrochloric acid is influenced by the presence of various complexing agents as shown in Fig. 5. Cyanide (0.001–0.1*M*) and trace amounts of oxalate, fluoride and thiocyanate ions have negligible effects on the extraction, even though partial masking is observed as the concentrations of fluoride and thiocyanate ions are increased, and complete masking of iron(II) is achieved at oxalate concentrations above 0.1*M*. At 0.001*M* concentration EDTA masks about 50% of the iron(II), but at higher concentrations only about 40%.

The stripping of iron(II), iron(III), nickel(II) and vanadium(IV) with various acids from chloroform extracts was studied. Two back-extractions of iron(II) and iron(III) with 3*M* hydrochloric acid (equilibration for 2 min) gave quantitative recovery, but equilibration for 3 min was needed for the complete recovery of nickel(II) and vanadium(IV) with 1*M* hydrochloric or sulphuric and 4*M* hydrochloric acid respectively.

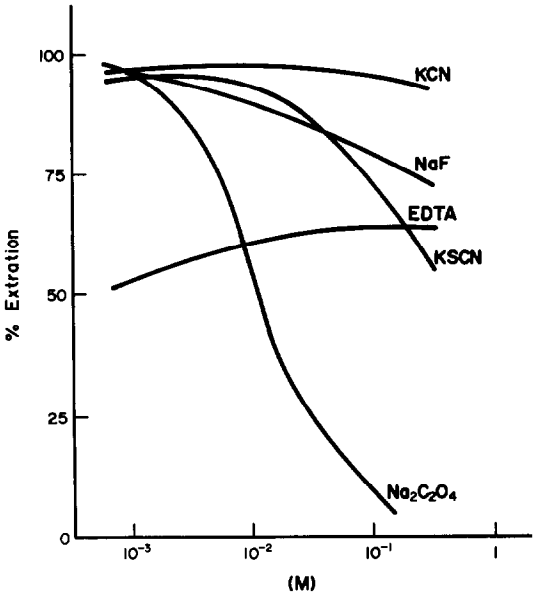

Fig. 5. Effect of complexing agents on the extraction of Fe(II) from 0.005*M* HCl with an equal volume (5 ml) of 20-mg/ml BHPDE/$CHCl_3$ solution, contact time 3 min, at 28 ± 1°.

Spectral studies

The absorption spectra of BHPDE and of chloroform extracts of its iron(II), iron(III),

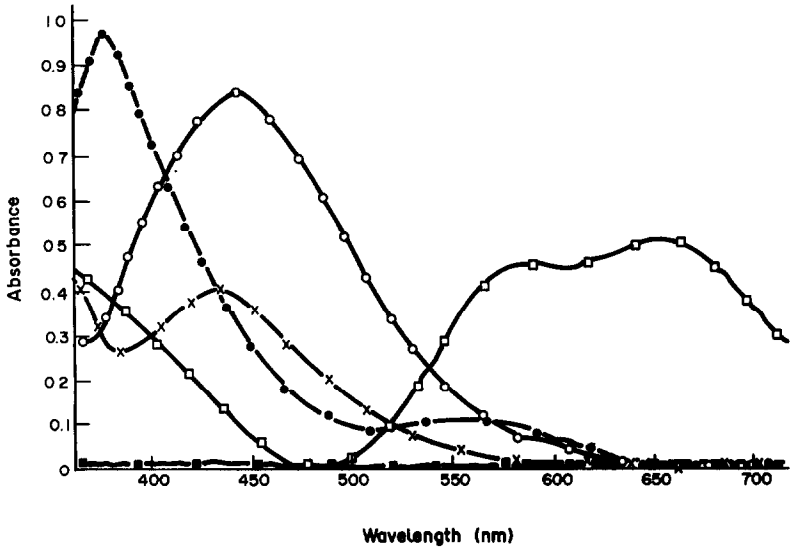

Fig. 6. Absorption spectra of chloroform solutions of BHPDE and its complexes: O——O Fe(II), ×——× Fe(III), ●——● Ni(II), □——□ V(IV), ■——■ 20-mg/ml BHPDE solution.

nickel(II) and vanadium(IV) complexes, measured against a reagent blank, and also those of the copper(II), mercury(II), palladium(II) and gold(III) complexes (which are also extracted) are shown in Fig. 6. The spectra of the golden yellow iron(II) and wine-red iron(III) complexes are similar, with maxima at 445 and 435 nm respectively. The yellow–green nickel(II) chelate shows two maxima, at 375 and 560 nm, as does the blue–green vanadium(IV) chelate (at 580 and 660 nm). The molar absorptivities of these two complexes are highest at 375 nm (Ni) and 660 nm (V), and these wavelengths are therefore used for their determination. Of the co-extracted complexes, only the violet–blue copper(II) complex shows an absorption maximum in the visible region at 540 nm.

Choice of solvent

Chloroform, carbon tetrachloride, benzene, toluene, methyl isobutyl ketone (MIBK) and n-butyl acetate were tried as solvents. BHPDE is readily soluble in chloroform, but sparingly in the rest. Iron(II) and vanadium(IV) are quantitatively extracted by all six solvents, and iron(III) by all except n-butyl acetate and MIBK. Nickel(II) is quantitatively extracted only into chloroform and toluene. Chloroform gives a clean separation and the highest absorbance for all the complexes and is therefore used in all the determinations.

Reagent concentration

The effect of varying the concentration of the BHPDE solution was examined over the range 1–50 mg/ml. Complete extraction of iron(II), iron(III) and vanadium(IV), without variation in absorbance, was obtained with 17.5–25-mg/ml reagent, corresponding to about 550–800-fold molar ratio of reagent to metal, and the range for nickel was 15–25 mg/ml. A 20-mg/ml solution (600-fold molar ratio to metal) is recommended. The order of addition of the reagents is not critical.

Spectral data

Table 1 summarizes the calibration and other data. The use of hydroquinone in the iron(II) determination ensures complete reduction of any iron(III) to iron(II).[16] For freshly prepared iron(II) solutions hydroquinone has no effect on the absorbance during the determination, whereas for solutions kept for more than one day, a lower absorbance is observed if no hydroquinone is present. The decrease is due to the presence of iron(III) [from aerial oxidation of iron(II)], which forms a complex having lower molar absorptivity at 445 nm.

Effect of diverse ions

The separation factors of various metal ions with respect to iron(II) and iron(III), nickel(II) and vanadium(IV), for extraction with 20-mg/ml BHPDE/$CHCl_3$ solution are given in Table 2. Alkali and alkaline earth metal ions, Mn(II), Ti(III), Ti(IV), La(III), Nb(V) and W(VI) are not extracted under the conditions used. Copper is quantitatively co-extracted with vanadium and iron, and palladium, mercury and gold are quantitatively co-extracted with iron. Vanadium and nickel are not co-extracted with iron, and can be separated from it in very dilute acid solution. Vanadium and nickel are co-extracted with each other under the conditions used for vanadium. However, vanadium is not extracted below pH 5, whereas nickel is about 70% extracted at this pH. A triple extraction of nickel at this pH gives practically complete separation from vanadium. These separation methods were tested with mixtures of iron and vanadium or nickel, and of vanadium and nickel. Recovery was quantitative and the results were reproducible, as shown in Table 3.

The effect of some ions in the determination of iron(II), nickel(II) and vanadium(IV) by the recommended photometric procedures was examined. Chloride, sulphate, perchlorate, nitrate, alkali and alkaline earth metal ions in up to 5000-fold amount (w/w), and Zr(IV),

Table 1. Spectral data for the complexes with BHPDE

Parameter	Fe(II)	Fe(III)	Ni(II)	V(IV)
λ_{max}, *nm*	445	435	375	660
ε, 10^3 *l.mole*$^{-1}$.*cm*$^{-1}$	4.65	3.40	4.82	0.67
Linear range, *μg/ml*	1–20	1–20	1–20	5–500
Optimum range, *μg/ml*	2–15	2–15	2–15	20–300
Relative standard deviation*, %	1.1 (8)	1.1 (8)	1.3 (5)	1.1 (100)

*Concentration measured (μg/ml) is shown in parentheses.

Table 2. Separation factors of various metal ions (Me) with respect to iron(II) and iron(III) extracted from 0.005*M* $HClO_4$, nickel(II) extracted at pH 13, and vanadium(IV) extracted at pH 11 with 20-mg/ml BHPDE/$CHCl_3$

Iron	Concentration, M	Separation factors		
		$D_{Fe(II,III)}/D_{Me}$	D_{Ni}/D_{Me}	D_V/D_{Me}
Fe(II)	1.43×10^{-4}	—	4.1×10^2	1.9×10^2
Fe(III)	1.43×10^{-4}	—	5.2×10^2	2.7×10^3
Ni(II)	1.36×10^{-4}	10^6	—	20.4
V(IV)	1.57×10^{-4}	10^6	6.9×10^2	—
Pd(II)	9.39×10^{-5}	1	4.0×10^2	5.2×10^2
Cu(II)	1.00×10^{-3}	1	4.1×10^3	1
Mn(II)	1.82×10^{-4}	10^6	10^6	10^6
Hg(II)	4.99×10^{-5}	1	4.1×10^2	5.3×10^2
Cs(I)	6.01×10^{-5}	10^6	10^6	10^6
Sr(II)	9.13×10^{-5}	10^6	10^6	10^6
Ti(III)	1.67×10^{-4}	10^6	10^6	10^6
Ti(IV)	1.67×10^{-4}	5.1×10^5	10^6	10^6
La(III)	5.76×10^{-5}	10^6	10^6	10^6
Au(III)	1.02×10^{-4}	1	12.5	12.5
U(VI)	8.40×10^{-5}	1.4×10^2	10^6	1.7×10^3
Zr(IV)	8.77×10^{-5}	8.2×10^5	10^6	10^6
Nb(V)	8.61×10^{-5}	10^6	10^6	10^6
W(VI)	4.35×10^{-5}	10^6	10^6	10^6

Hf(IV), Nb(V), Ta(V), Pt(IV), Al(III), Sn(II), Mo(VI) and W(VI) up to 1000-fold amount relative to iron(II), nickel(II), and vanadium(IV) do not interfere. The tolerance limits for other ions are given in Table 4. In the presence of cyanide (0.1*M*) the tolerance limit for copper is increased to 250-fold (w/w) relative to iron, nickel and vanadium.

Table 3. Analysis of synthetic mixtures of iron and vanadium or nickel, and of vanadium and nickel, by the recommended procedures

Element	Taken, *m*M	Found, *m*M	Relative standard deviation, %
Fe(II)	0.143	0.142	1.3
		0.143	
		0.139	
		0.140	
V(IV)	0.157	0.154	1.1
		0.154	
		0.155	
		0.151	
Fe(II)	0.143	0.141	1.0
		0.144	
		0.141	
		0.142	
Ni(II)	0.136	0.134	1.4
		0.136	
		0.136	
		0.132	
V(IV)	0.157	0.156	0.8
		0.155	
		0.155	
		0.153	
Ni(II)	0.136	0.134	1.3
		0.135	
		0.131	
		0.132	

Composition of the complex

Job's method indicates a 1:2 and 1:1 metal:ligand mole ratio for the iron(II) and iron(III) complexes respectively. For the nickel-(II) and vanadium(IV) complexes a 1:2 mole ratio is observed in the pH range 5–10 and a 1:1 ratio at pH 11–13. This supports the $Fe^{II}(H_2B)_2.2X^-$, $Fe^{III}(H_2B)(OH)_2.X^-$, $Ni(HB)_2$, $VO(HB)_2$, NiB and VOB stoichiometries postulated from the log–log plots of

Table 4. Effect of diverse ions on the determination of 40 μg/5 ml iron(II) or nickel(II) and 100 μg/5 ml vanadium(IV) with 20-mg/ml BHPDE/$CHCl_3$

Ion added	Tolerance limit* (mg/5 ml) relative to:		
	Fe(II)	Ni(II)	V(IV)
Fe(II)	—	0.1	10.0
Ni(II)	0.5	—	0.5
V(IV)	0.5	0.07	—
Cu(II)	0.2	0.2	0.5
Mn(II)	20.0	20.0	20.0
Be(II)	0.1	0.1	0.1
Cd(II)	20.0	20.0	20.0
Zn(II)	20.0	20.0	20.0
Pd(II)	5.0	1.0	5.0
Co(II)	0.5	0.1	10.0
Hg(II)	10.0	10.0	10.0
Pb(II)	10.0	10.0	10.0
Y(III)	0.5	1.0	1.0
La(III)	20.0	20.0	20.0
Pr(III)	20.0	20.0	20.0
Cr(III)	0.1	0.1	10.0
Au(III)	1.5	0.1	5.0
U(VI)	0.4	1.0	10.0

*Average of 7 determinations, <1% error.

Table 5. Determination of iron, vanadium and nickel in various synthetic matrices by the recommended procedures

Contents per ml	Found,* μg/ml		Relative standard deviation, %
8 μg Fe(II) + 8 μg Ni(II) + 20 μg V(IV)	Fe(II)	7.98	1.1
	Ni(II)	8.01	1.2
	V(IV)	19.87	1.1
8 μg Fe(II) + 10 μg Ni(II) + 30 μg V(IV)	Fe(II)	8.06	0.6
+ 4 mg Zn(II) + 2 mg W(VI) + 2 mg Zr(IV)	Ni(IV)	20.91	0.8
5 μg Fe(II) + 8 μg Ni(II) + 0.2 mg Pd(II) + 2 mg Zn(II)	Fe(II)	4.97	1.3
+ 4 mg Mn(II) + 1 mg Mo(VI) + 2 mg Ti(IV)	Ni(II)	7.89	1.1
10 μg Fe(II) + 50 μg V(IV) + 0.5 mg Cu(II) + 2 mg Pt(IV)	Fe(II)	9.82	1.0
+ 2 mg Zr(IV) + 4 mg Cd(II) + 4 mg Sr(II)	V(IV)	50.00	0.8

*Average of 8 determinations.

distribution ratio *vs.* ligand concentration at constant ionic strength. The structure suggested for the extracted iron(II) complex is octahedral, probably distorted, in which the two neutral BHPDE molecules lie in an equatorial plane, with two water molecules *trans* to each other. It is possible, of course, that the complex is not an ion-association species, but a mixed-ligand compound, in which case the two X^- ions would occupy the *trans*-positions on the octahedron. The structure of the iron(III) complex is more difficult to predict: it could be an ion-association complex analogous to that proposed for iron(II), or a mixed-ligand complex $Ni(HB)_2$ and NiB are possibly octahedral and square complexes with the ligand exhibiting terdentate and quadridentate co-ordination respectively. These geometries have been reported[11,19] for some copper(II) complexes prepared with analogous reagents in non-aqueous solvents. A square pyramidal structure is suggested for both the $VO(HB)_2$ and the VOB complexes.

Applications

The recommended procedures were tested with synthetic solutions and the pulp of the cormel of an edible cocoyam species, *Colocasia antiquorum*, in which 0.053–0.054% iron and 0.330–0.332% nickel were found present in air-dried samples. The relative standard deviations for seven replicates were 0.8 and 1.0% for iron and nickel respectively. The results agreed with those obtained by the 1,10-phenanthroline and dimethylglyoxime methods,[16] (0.052–0.054% iron and 0.331–0.334% nickel, relative standard deviations 1.1 and 1.2% for seven replicates). The results for the synthetic solutions are given in Table 5.

Acknowledgements—The authors gratefully acknowledge the assistance of Messrs C. Duru, C. Onwuachu, O. Eneh, P. Ukoha and E. Ezike in some of the laboratory work.

REFERENCES

1. A. Combes, *Compt. Rend.*, 1899, **108**, 1252.
2. N. H. Cromwell, F. A. Miller, A. R. Johnson, R. L. Frank and D. J. Wallace, *J. Am. Chem. Soc.*, 1949, **71**, 3337.
3. K. Ueno and A. E. Martell, *J. Phys. Chem.*, 1955, **59**, 998.
4. R. H. Holm, G. W. Everett, Jr. and A. Chakravorty, *Prog. Inorg. Chem.*, 1966, **7**, 83.
5. R. Belcher, M. Pravica , W. I. Stephen and P. C. Uden, *Chem. Commun.*, 1971, 41.
6. R. Belcher, K. Blessel, T. Cardwell, M. Pravica, W. I. Stephen and P. C. Uden, *J. Inorg. Nucl. Chem.*, 1973, **35**, 1127.
7. S. Dilli and E. Patsalides, *J. Chromatog.*, 1977, **130**, 251.
8. G. W. Everett, Jr. and R. H. Holm, *J. Am. Chem. Soc.*, 1965, **87**, 2117.
9. G. T. Morgan and J. D. M. Smith, *J. Chem. Soc.*, 1925, **127**, 2030.
10. N. K. Dutt and K. Nag, *J. Inorg. Nucl. Chem.*, 1968, **30**, 3273.
11. J. Aggett and R. A. Richardson, *Anal. Chim. Acta*, 1970, **50**, 269.
12. D. G. Gambarov, S. B. Bilalov and A. K. Babaev, *Zh. Analit., Khim.*, 1976, **31**, 1731.
13. E. C. Okafor, *Talanta*, 1980, **27**, 887.
14. A. I. Vogel, *A Textbook of Quantitative Inorganic Analysis*, 3rd Ed., p. 293. Longmans, London, 1961.
15. I. M. Kolthoff, E. B. Sandell, E. J. Meehan and S. Bruckenstein, *Quantitative Chemical Analysis*, 4th Ed., pp. 1161–1164. Macmillan, London, 1969.
16. E. B. Sandell, *Colorimetric Determination of Traces of Metals*, 3rd Ed., pp. 541, 672. Interscience, New York, 1959.
17. V. Yatirajam and S. P. Arya, *Talanta*, 1976, **23**, 596.
18. F. Cotton and G. Wilkinson, *Basic Inorganic Chemistry*, pp. 389, 401. Wiley, New York, 1976.
19. G. R. Clark, D. Hall and T. N. Waters, *J. Chem. Soc. A*, 1968, 223.

Talanta, Vol. 39, No. 3, pp. 281–284, 1992
Printed in Great Britain.

0039-9140/92 $5.00 + 0.00

SPECTROPHOTOMETRIC DETERMINATION OF VANADIUM IN DIFFERENT OXIDATION STATES WITH PYROGALLOL

N. IRANPOOR, N. MALEKI, S. RAZI and A. SAFAVI
Department of Chemistry, College of Sciences, Shiraz University, Shiraz, Iran

(*Received* 23 *August* 1989. *Revised* 17 *August* 1991. *Accepted* 29 *August* 1991)

Summary—Determination of vanadium at low concentrations is easily performed with pyrogallol as a ligand which forms a bluish-violet complex with vanadium(III), (IV) or (V). The colour of the bluish-violet complex (λ_{max} = 580 nm) contrasts well with the colour of both pyrogallol and vanadium. The complexes are stable for several hours. Beer's law is obeyed over the range 0–14 μg/ml vanadium at pH 6. The apparent molar absorptivity at 580 nm is $(7.75 \pm 0.25) \times 10^3$ l.mole^{-1}.cm^{-1}. The effects of diverse ions on the determination of vanadium have been fully studied. Only Mo(VI) and W(VI) interfere seriously. The method is selective, sensitive and can be applied to the determination of total vanadium in a variety of samples.

Although there are a number of methods proposed for the spectrophotometric determination of vanadium,[1–7] only a few are sufficiently selective to be useful[4] and most can determine only one oxidation state. Determination of total vanadium often requires converting all the oxidation states to a single state.

Reagents with suitably located nitrogen and/or oxygen donor atoms can be useful chelating agents for vanadium determination.[4] It has been proposed[8] that pyrogallol forms a complex with V(V) and this was made the basis for determination of up to 2 μg/ml of V(V). During our studies on the use of organic reagents in analysis, we observed that pyrogallol gives a bluish-violet complex with vanadium in oxidation states (III), (IV) and (V) at pH 6. This observation led us to develop the method described below.

EXPERIMENTAL

Reagents

*Pyrogallol solution, 1*M. Prepared on the day of use (to minimize aerial oxidation) by dissolving 12.6 g of pyrogallol (Merck) in triply distilled water and diluting to 100 ml.

Vanadium(V) solution, 1000 μg/ml. Prepared by dissolving 2.296 g of ammonium metavanadate (Merck) in distilled water and diluting to one litre, and standardized.[9,10]

Vanadium(IV) solution, 1000 μg/ml. Prepared by dissolving 1.776 g of vanadyl sulphate monohydrate (Merck) in distilled water and diluting to 500 ml, and standardized.[9,10]

Vanadium(III) solution, 1000 μg/ml. Prepared by dissolving 1.545 g of vanadium trichloride (Merck) in 500 ml of distilled water, and standardized.[9,10]

Standard stock solutions of other metal ions (10 mg/ml) were prepared by dissolving the nitrate or chloride in water or dilute hydrochloric acid.

An acetic acid–sodium acetate buffer solution (pH 6) was used.

Apparatus

The absorption spectra were recorded on a Varian Cary-118 instrument, with one-cm glass cells. The absorbances at a fixed wavelength were measured with a Bausch and Lomb Spectronic 70 spectrophotometer.

Procedure

A known volume of sample containing 10–350 μg of vanadium (in oxidation state III, IV or V) is placed in a 25-ml standard flask, 5 ml of buffer (pH 6) and 10 ml of 1*M* pyrogallol solution are added, and the solution is made up to the mark with distilled water and mixed. The absorbance at 580 nm is measured against a reagent blank solution.

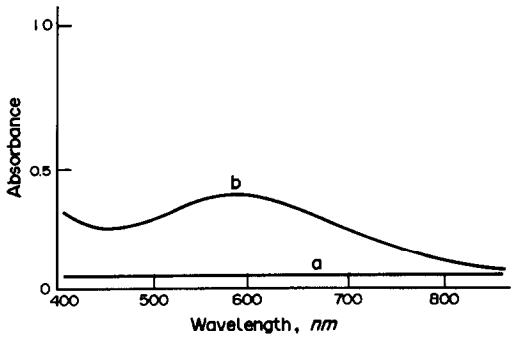

Fig. 1. Absorption spectra of (a) pyrogallol, (b) pyrogallol–vanadium complex (10 μg/ml vanadium).

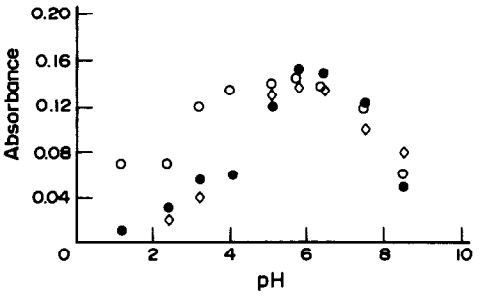

Fig. 2. Effect of pH on complex formation: (○) V(III), (●) V(V), (△) V(IV).

RESULTS AND DISCUSSION

The absorption spectra of the complex and the reagent blank are shown in Fig. 1. As neither vanadium nor the ligand show absorption at 580 nm, this wavelength was chosen for absorbance measurement of the complex.

Optimization of conditions

The absorbances of the complexes at 580 nm were found to be maximal in the pH range 5–6.5 (Fig. 2). The absorbances were found to be practically unaffected by changes in temperature or ionic strength.

A final pyrogallol concentration of at least 0.4*M* was found necessary for practically complete complexation.

Beer's law and molar absorptivity

The formation of the complex is instantaneous and its absorbance remains constant for at least 6 hr irrespective of the vanadium oxidation state. The calibration graph is linear with the regression equations

$$A = 0.043 + 0.115\,[\mathrm{V(V)}]$$
$$A = 0.016 + 0.116\,[\mathrm{V(IV)}]$$
$$A = 0.040 + 0.113\,[\mathrm{V(III)}]$$

where the concentration is expressed in μg/ml. Beer's law is obeyed for vanadium concentrations up to 14 μg/ml in the final solution, and the molar absorptivity is $(7.75 \pm 0.25) \times 10^3$ $\mathrm{l.mole^{-1}.cm^{-1}}$ for all three vanadium oxidation states. The detection limit (defined as the concentration corresponding to the average absorbance of the blank plus 3 times its standard deviation) was found to be 47 ng/ml vanadium in the final solution. By this method the three oxidation states of vanadium can be determined without a preliminary oxidation or reduction step. The analytical figures of merit for determination of vanadium by the proposed method and some other spectrophotometric methods are compared in Table 1.

Composition of the complex

The ratio of vanadium to pyrogallol was determined by the mole ratio[11] and continuous variation methods.[12] The results obtained show the formation of a 1:2 (metal:pyrogallol) complex. This is the case for all three oxidation states of vanadium at ph 6. It is assumed that

Table 1. Comparison of the proposed method with some other spectrophotometric methods

Characteristics	*N*-Hydroxy-*N*-*p*-chlorophenyl-*N*-(3-chloro-4-methylphenyl)-*p*-toluamidine[5]	3-Hydroxy-1,3-diphenyltriazine[1]	Ferron[6]	Proposed method
Conc. range (Beer's law), μg/ml	0.6–8.4	0.25–10	0–5	0–14
ε, $l.mole^{-1}.cm^{-1}$	5.7×10^3	5.88×10^3	—	$7.7 \pm 0.25 \times 10^3$
Detection limit, ng/ml	—	—	—	47
Interferences	W, Fe	Fe(III), Pd(II), Mo(IV), Cr(III), Ti(IV), oxalate, fluoride, EDTA	Mo(IV), Ti(IV), Zr(IV), Bi(V), Sn(II)	Mo(VI), W(VI)
Oxidation state of vanadium determined	(V)	(V)	(III)	(V), (IV), (III)
Stability constant	—	1.67×10^4	—	7.54×10^6

Table 2. Effect of anions on the absorbance of the vanadium–pyrogallol complex (10 μg/ml vanadium)

Ion	Concentration, mg/25 ml	Relative error, %
F^-	250	—
Cl^-	250	—
Br^-	250	—
I^-	250	—
NO_2^-	125	—
NO_3^-	125	—
SO_3^{2-}	25	+0.7
CH_3COO^-	125	—
ClO_4^-	250	—
Tartrate	125	—
$C_2O_4^{2-}$	125	+0.7
Phthalate	250	+0.5
Citrate	250	—
SO_4^{2-}	250	−0.5
CN^-*	125	−0.7
S^{2-}*	75	−0.4

*After removal as ferrous ferrocyanide and zinc sulphide respectively.

vanadium(III) is oxidized to vanadium(IV) by dissolved oxygen and that vanadium(V) is reduced by the pyrogallol [the maximum in the Job plot occurs at a mole fraction of 0.74 for pyrogallol, corresponding to a 1:2 complex and reduction of two V(V) by one pyrogallol molecule].

Interferences

The criterion for interference was a change of ±2% in the absorbance of 10 μg/ml vanadium(V) in the presence of a large excess of pyrogallol.

The effects of various anions and complexing agents on the absorbance of the complex were studied, as shown in Table 2. No interference was observed from 10^4 μg/ml concentrations of most of the common anions and complexing agents studied. Only sulphide and cyanide interfere with the determination of vanadium. Sulphide interference is removed by precipitation of zinc sulphide. Cyanide forms a precipitate with Fe(II).[13] These precipitates were filtered off before the addition of pyrogallol.

Table 3. The efficiency of the procedure recommended for removing the interfering effects of foreign ions in the determination of vanadium (10 μg/ml) in the presence of 2 mg/ml interfering ion

Ion	Relative error, %
Fe(II)	—
Fe(III)	—
Au(III)	—
Cr(III)	—
Pb(II)	−0.7
Ag(I)	−0.5
Hg(I)	−0.7
Bi(III)	—
Th(IV)	−1.0
Zr(IV)	−1.3
Sb(V)	—

Table 4. Results for determination of total vanadium

Taken, μg/ml			Total vanadium found, μg/ml
V(III)	V(IV)	V(V)	
1.0	1.0	1.0	2.90
1.0	1.0	1.6	3.61
1.5	1.0	1.0	3.24
1.0	1.0	2.0	4.00
1.0	2.0	1.0	3.91
1.0	2.0	1.5	4.45
2.0	2.5	2.5	7.02

The tolerance limits for various cations in the determination of 10 μg/ml vanadium(V) were studied. Levels of 2000 μg/ml of Mg(II), Ca(II), Sr(II), Ba(II), Zn(II), Cd(II), Hg(II), Co(II), Cu(II), Cu(I), Ni(II), Pd(II), Al(III), Tl(I), La(III), Mn(II), Ce(III), Te(IV), Sb(III), Y(III) did not show any interference. Au(III), Ag(I), Pb(II), Fe(II), Fe(III) and Cr(III) at concentrations >500 μg/ml interfered with the determination. Their effects were removed by adding 5–10 ml of saturated ammonium thiocyanate solution to the test solution (Table 3). Fe(III) and Fe(II) complexes of thiocyanate can be extracted into MIBK. The interfering effects of Zr(IV) and Th(IV) can be removed by the addition of ammonia solution to give pH 8. The precipitated hydroxides are separated before adjustment of the pH to 6 and addition of pyrogallol. Hg(I) and Bi(III) are removed from the solution by precipitation with saturated sodium fluoride solution.[14] Although Sb(III) does not have any interfering effects, Sb(V) interferes seriously. The effect of this interference is easily removed by the addition of sodium dithionite to the solution to reduce Sb(V) to Sb(III) prior to the addition of pyrogallol. Of the 30 metal ions studied, only molybdenum and tungsten are found to interfere.

Determination of total vanadium

Since pyrogallol reacts with the three oxidation states of vanadium(III, IV, V) to give the same complex, which absorbs at $\lambda_{max} = 580$ nm, attempts were made to determine total vanadium in mixtures of the three forms. The result in Table 4 shows that the recommended procedure can be applied to the determination of total vanadium wthout any pretreatment.

Table 5. Analysis of samples by the proposed method

Matrix*	V added, μg	V found, μg	Recovery, %
Ni^{2+} (50), Fe^{3+} (20), Co^{2+} (50)	250	250, 249	99.8
Al^{3+} (60), Ce^{3+} (50)	200	200, 200	100
Sb^{5+} (30), Pd^{2+} (50), Cd^{2+} (50)	300	300, 298	99.7
Al^{3+} (40), Zn^{2+} (7), Cu^{2+} (2.5), Fe^{3+} (0.35)†	100	100, 100	100
Fe^{2+} (5), Ni^{2+} (2.3), Cr^{3+} (2), Mn^{2+} (0.1)‡	100	100, 101	100.5
Low alloy D§	—	0.29%, 0.32%, 0.305%	

*The number in parentheses indicates mg of the element in the aliquot taken for analysis.
†Analogous to V-alloy.
‡Analogous to Nichroloy (cast).
§Vanadium present 0.29%.

Applications

The applicability of the method is shown by the satisfactory analysis of a variety of synthetic samples (Table 5).

Acknowledgement—The authors are thankful to Shiraz University Research Council for support of this work.

REFERENCES

1. D. Chakraborti, *Anal. Chim. Acta*, 1974, **71**, 196.
2. R. S. Kharsan, K. S. Patel and P. K. Mishra, *Talanta*, 1979, **26**, 254.
3. K. A. Abdullah, A. G. M. Al-Dahar and W. A. Bashir, *Analyst*, 1985, **110**, 409.
4. V. Yatirajam and S. P. Arya, *Talanta*, 1979, **26**, 60.
5. R. S. Kharsan, K. S. Patel and P. K. Mishra, *ibid.*, 1979, **26**, 50.
6. V. Yatirajam and S. P. Arya, *Anal. Chim. Acta*, 1976, **86**, 209.
7. P. Bermejo-Barrera, A. Bermejo-Barrera and F. Bermejo-Martinez, *Microchem. J.*, 1980, **25**, 458.
8. K. Sugawara, K. Tanino and J. Seki, *Bunseki Kagaku*, 1973, **22**, 1559; *Anal. Abstr.*, 1975, **29**, 1B15.
9. N. H. Furman (ed.), *Standard Methods of Chemical Analysis*, Vol. 1, 6th Ed., pp. 1205–1227. Van Nostrand, Princeton, 1962.
10. I. M. Kolthoff, R. Belcher, V. A. Stenger and G. Matsuyama, *Volumetric Analysis*, Vol. III, p. 634. Interscience, New York, 1957.
11. J. H. Yoe and A. L. Jones, *Ind. Eng. Chem., Anal. Ed.*, 1944, **16**, 111.
12. P. Job, *Ann. Chim. (Paris)*, 1928, **9**, 113.
13. A. I. Vogel, *A Text Book of Micro and Semimicro Qualitative Inorganic Analysis*, 4th Ed., p. 260. Longmans, London, 1954.
14. J. R. Partington, *General and Inorganic Chemistry*, 3rd Ed., p. 640. Macmillan, London, 1961.

Talanta, Vol. 39, No. 3, pp. 285–292, 1992
Printed in Great Britain

0039-9140/92 $5.00 + 0.00
Pergamon Press plc

FLOW-INJECTION COULOMETRIC TITRATIONS*

RICHARD H. TAYLOR, JAROMIR RŮŽIČKA† and GARY D. CHRISTIAN†
Center for Process Analytical Chemistry, Department of Chemistry, BG-10, University of Washington, Seattle, WA 98195, U.S.A.

(*Received* 4 *March* 1991. *Revised* 29 *March* 1991. *Accepted* 12 *April* 1991)

Summary—A flow-injection analysis technique based on stop flow coulometric titrations is described, utilizing a gradient chamber, reagent generation chamber, and detector flow cell integrated into a single unit. The use of stop flow allowed for automated sample dilution up to a factor of 100 times. The system has been used to titrate samples of sodium hydroxide in the range 5×10^{-4}–$4M$, and nitric acid ranging from 5×10^{-3}–$15M$. Analyses over the entire range of concentrations yielded a relative standard deviation of less than 3%. A correlation coefficient of 0.999 was obtained for all comparisons with manual titrations. Remote spectrophotometric detection was performed with optical fibers. No frit or membrane is required to separate the generating and counter electrodes within the system, yet the advantages of conventional coulometric titration, which eliminate the problems of reagent and calibration solution handling, storage or degradation, are retained.

Flow-injection analysis (FIA) titrations represent a well known and widely used technique, especially in the field of industrial process monitoring.[1–5] This technique has gained acceptance due to its relative simplicity and good accuracy. Although these titrations are often used in FIA, the area of coulometric titration has gained very little attention. Feher and co-workers coulometrically generated a reagent which was subsequently merged with a carrier stream to perform triangle titrations of phenothiazine compounds.[6] Ruttinger and Spohn incorporated a coulometric titration cell and a flow through detector into a single component.[7] Ilcheva and Dakahev reported a coulometric detection cell for use in an FIA system.[8] Liang described a method of performing Karl Fischer titrations coulometrically in a close loop system.[9] In this paper we describe a novel stopped flow technique which is applicable to a wide variety of chemistries and incorporates a method of automated dilution. A gradient chamber and a detector flow cell are integrated into a single unit, allowing for detection at the site at which dilution and chemical reaction occurs (Fig. 1).

In conventional FIA titrations a pair of equivalence points, located on the leading and trailing edge of a dispersed sample zone, is identified (Fig. 2). The distance between these points (measured in time, Δt) at a constant flow-rate (Q) has been shown to be a function of the concentration of the sample,[1] such that

$$\Delta t = (V_m/Q) \ln 10 \log \{C_s^0/(C_T^0 n)\} + (V_m/Q) \ln 10 \log \{S_v/V_m\} \quad [1(a)]$$

where V_m is the volume of the mixing chamber, C_T^0 is the concentration of the titrant, C_s^0 is the concentration of the injected sample, n is the stoichiometric factor of the reacting components, and S_v is the volume of the injected sample (Fig. 1). In a system with a carrier of constant concentration, and a fixed sample and flow volume, the peak width (Δt) is related to the sample concentration (C_s) by the equation

$$\Delta t = (k_1) \log C_s + k_2 \quad [1(b)]$$

where k_1 and k_2 are constants. Thus, in conventional FIA titrations the peak width is directly proportional to the logarithm of the sample concentration.

The relationship described above is due to the concentration gradient produced by the zone dispersion within a mixing chamber, the volume (V_m) of which dominates the volume of the flow system. By injecting a sample, the concentration of which (C_s) is much higher than that of the titrant (C_T) in the carrier stream, the elements of the dispersal zone are gradually neutralized, until an equivalence point is reached at the leading and the trailing edge of the dispersal

*Presented at Winter Conference on Flow-Injection Analysis, Scottsdale, AZ, USA January 6–9, 1991.
†Authors for correspondence.

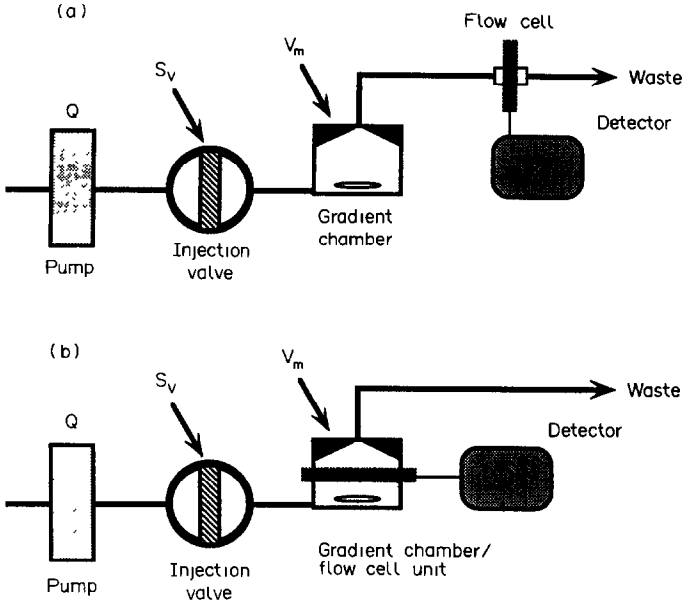

Fig. 1. FIA system for titration. In a conventional FIA titration system (1A) detection occurs downstream of the gradient chamber. For the stop flow coulometric titration technique, detection occurs at the gradient chamber (1B) where titrant is produced and chemical reaction takes place. Q = volumetric flow-rate, S_v = sample volume, V_m = chamber volume.

zone (Fig. 2). This approach, though widely used, has two disadvantages: (1) the distance between the points (Δt) is a logarithmic function of the sample concentration; and (2) the bulk of the injected sample (shaded area, Fig. 2) remains untitrated. It was Pardue and Fields[10,11] who first pointed out the second disadvantage, which seriously limits the accuracy and operational range of the flow-injection titration, since it necessitates the use of a diluted (and therefore less stable) titrant when extending to less concentrated samples.

It is proposed here to eliminate the above disadvantages by introducing a combination of stopped flow with the coulometric technique.

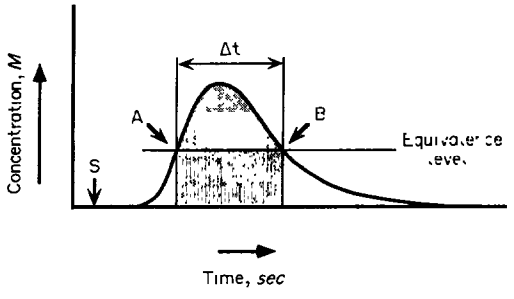

Fig. 2. Conventional FIA titration. The dispersed zone contains two equivalence points (A and B). The distance between them (Δt) is the measured parameter and is proportional to the logarithm of the sample concentration. The shaded portion of the zone represents the portion of the sample which is not titrated.

By stopping the flow at a suitable delay time following sample injection the sample zone will be arrested within the mixing chamber. If the detection and coulometric reagent generation are performed within the mixing chamber, all sample material will be reacted, as in conventional titrimetry. In addition, by selecting an appropriate delay time, a desired trailing section of the dispersal zone can be captured within the chamber, thus allowing automated dilution prior to titration, *i.e.* a selected portion of the injected sample is titrated.

In a coulometric titration,[12] reagent is produced by the application of a current at an appropriate electrode to an electrolyte. Through control of the current and time a precise amount of reagent is produced at a specified rate. The amount of reagent produced may be calculated with Faraday's Law of Electrolysis, which states that the quantity of electricity passed through a cell is directly proportional to the quantity of chemical change that occurs at the cell electrode.[13] The mathematical expression of this law, when applied to a constant current system, is

$$N = Q/nF = it/nF \qquad [2(a)]$$

where N = moles of substance, Q = total charge passed (coulombs, C), n = number of electrons transferred per molecule (equivalents, eq), i = current (amps), t = time (sec), and F = Faraday's constant (96,485 C/eq). By

measuring the time required to reach the titration endpoint and knowing the value of the constant current applied, the amount of reagent generated and reacted to reach the endpoint can then be calculated. Thus the measured parameter, Δt, the time from the initiation of electrolysis to the titration endpoint, is directly proportional to the sample concentration, as seen by rearrangement of equation [2(a)] to

$$\Delta t = NnF/i = C_s S_v nF/i = kC_s \quad [2(b)]$$

where k is a constant.

In this study the electrolysis of water was used to generate reagent for acidobasic titrations. The half reactions which occur are, at the anode

$$2H_2O \rightarrow O_2 + 4H^+ + 4e^-$$

and, at the cathode

$$2H_2O + 2e^- \rightarrow H_2 + 2OH^-$$

When a very large degree of mixing of a segment of a flow system is required, it may be achieved by using a mixing chamber. The chamber allows for the homogeneous dispersion of a flow segment into a much larger portion of the system fluid. This is achieved through the use of an externally driven mechanical stirring mechanism inside the chamber.

The gradient chamber has long been implemented in FIA systems.[1] Previously, the gradient chamber was used to form a reproducible concentration gradient at the outlet of the chamber. This implies that the portion of the sample remaining in the gradient chamber at a specific time is reproducible. Therefore, instead of placing a detector downstream of the gradient chamber, detection at the chamber itself would allow for detection of the homogeneous zone of the system and would result in a simplified system where the mixing chamber and detector flow cell are integrated into a single component. The dilution possibilities presented by the concentration gradient are retained through the use of stop flow, which provides the ability to isolate a predetermined portion of the sample within the chamber by stopping the flow at a specific time.

An FIA system has been viewed as following the tanks-in-series model,[14] introduced by Dankwerts.[15] The volume of the mixing chamber (V_m) completely dominates the system volume, and therefore the system behaves as a single mixing tank while the volume of the injected sample (S_v) is small. At any time t after the point at which the entire sample has entered the chamber (t_0), the concentration of a component of the fluid (C) is represented by the equation

$$C = (1/T_i)e^{-t/T_i} \quad (3)$$

where T_i is the mean residence time of a component of fluid in the tank. For a gradient chamber, the mean residence time is dependent upon the volume of the chamber and the volumetric flow-rate, such that

$$T_i = V_m/Q \quad (4)$$

Previously in FIA, equation (3) was used to model the concentration of an analyte at the effluent of a gradient chamber.[1] In the present case, however, the portion of the sample remaining inside the gradient chamber will be titrated. A representation of the area under the curve of the concentration profile produced (Fig. 3) is therefore needed. The area under this

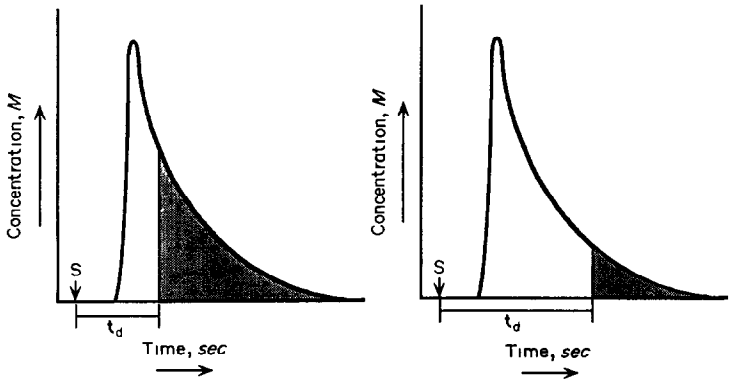

Fig. 3. Detector response to sample concentration within a gradient chamber. Response after all the sample has entered into the chamber conforms to a single tank in the tanks-in-series model. By selecting an appropriate delay time (t_d), a desired trailing section (shaded) of the zone may be arrested within the chamber and analyzed, thus providing a method of automated dilution.

curve can be integrated for any time interval after time = t_0, as

$$\int_t^{\infty} (1/T_i)\, e^{-t/T_i}\, dt \qquad [5(a)]$$

which yields the equation

$$C_t = e^{-t/T_i} \qquad [5(b)]$$

The dilution which occurs in the system can be described by the inverse mole ratio (X^{-1}), introduced by Whitman and Christian,[16] which is defined as

$$X^{-1} = n^0/n_{det} \qquad (6)$$

where n^0 is the number of moles injected and n_{det} is the number of moles detected.

By defining n as a product of molar concentration and volume, then at a constant sample volume (S_v), X^{-1} can be redefined as the ratio of molar concentrations

$$X^{-1} = C^0 S_v / C_{det} S_v = C^0/C_{det} \qquad (7)$$

By substituting equation [5(b)] into equation (7), where $C^0 = C_t$ when $t = 0$ and $C_{det} = C_t$ when $t \geq t_0$, the result is

$$X^{-1} = C^0/C_{det} = e^{-0/T_i}/e^{-t/T_i} = e^{t/T_i} \qquad (8)$$

Thus the portion of a sample remaining in the gradient chamber and the inverse mole ratio can be easily calculated at any time during which the response curve follows the given model. The degree of dilution obtained can be predetermined by calculation and controlled through the use of the stop flow technique.

EXPERIMENTAL

Reagents

The carrier for all titrations was an aqueous solution of 0.5M Na_2SO_4 (Mallinckrodt) containing bromothymol blue (BTB) (Merck) as the indicator at a concentration of 0.04% (w/v). For titrations of base, the carrier was made slightly basic with sodium hydroxide and for titrations of acid it was made slightly acidic with nitric acid. This was done to prevent any neutralization of the sample by the carrier. Appropriate dilution of concentrated nitric acid (J. T. Baker) with demineralized water was used to prepare nitric acid samples for titration. Appropriate dilution of a 5M sodium hydroxide (J. T. Baker) solution with demineralized water was used for all sodium hydroxide samples. Potassium acid phthalate (Allied Chemical) was used as a primary standard for manual titrations. For experiments determining the effects of flow-rate and chamber volume the carrier was 0.01M sodium borate (J. T. Baker) and 0.40% (w/v) BTB was injected as sample.

Apparatus

A single line FIA manifold (Fig. 4) was used in all experiments. The pump was an Alitea C4-XV peristaltic pump with a remote controller. A Rheodyne Type 5701 pneumatic actuator was used with a Rheodyne Type 50 4-way injection valve furnished with a 19-μl sample loop.

The PTFE tubing connecting the mixing chambers and the chamber containing the counter electrode had an inner diameter of 1.3 mm, while all other tubing had an internal diameter of 0.82 mm.

Stirring in the gradient chamber was performed by means of a TRI-R model MS-7 magnetic stirrer. The gradient chamber was 10-mm inner diameter glass tubing with end caps constructed of PTFE, equipped with a miniature stirring bar (Fig. 5). The net chamber volume could be varied by adjustment of the end cap positions.

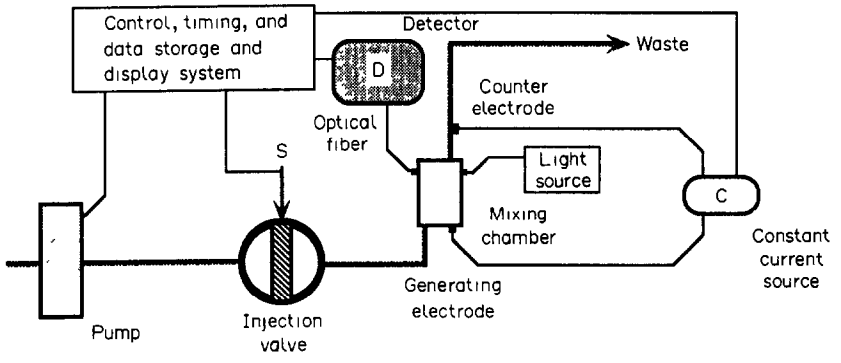

Fig. 4. Stop flow coulometric titration system. Light is transmitted from the light source, across the gradient chamber, and to the detector via optical fibers. The injection valve, pump, and constant current source are controlled by computer.

The generating and counter electrodes were 1.2-mm diameter platinum wire. The 3.4-cm generating electrode was coiled at the bottom of the mixing chamber (Fig. 5), with a total surface area of 1.3 cm^2. The counter electrode was placed in a separate chamber downstream of the mixing chamber. The connecting tubing was 4 cm long. The electrodes were connected to a laboratory built constant current source with four current settings (0.78–3.90 mA, current densities of 0.60–3.0 mA/cm^2). Current was continuously measured with a Dynascan 2830 Digital Multimeter connected in line in the constant current source circuit. Current was switched by a relay between the electrodes and a variable resistor which was used as a "dummy cell" in order to have continuous current flow in the current source.

The detector was a Bausch & Lomb Spectronic Mini 20 spectrophotometer. The output was directed to an electronic low-pass filter and a linear amplifier and then through the DACA interface board to the computer where the transmittance signal was converted to absorbance. A Volpi Intralux 4000 external light source with a variable intensity control was used. Light was directed from the external light source via a 45-cm long, 5.56-mm diameter optical fiber bundle (Volpi), across the chamber, and collected and directed to the spectrophotometer via a 45-cm long, 3.18-mm diameter optical fiber bundle (Twardy) (Fig. 5).

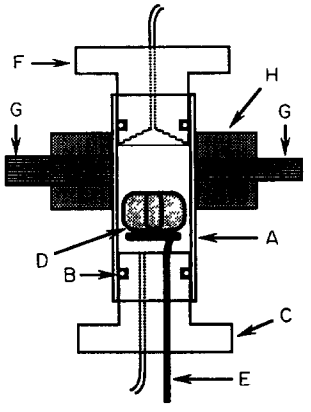

Fig. 5. Integrated flow cell, gradient chamber, and reagent generation chamber. The body of the chamber (A) is 10 mm i.d. glass tubing. The PTFE end caps (C & F) are sealed with O rings (B). The chamber is mounted vertically with the inlet cap (C) on the bottom. The star-shaped stirring bar (D) rests atop the coiled generating electrode (E). The outlet cap (F) is domed to prevent any air bubbles which may enter the chamber from becoming trapped. Light is transmitted across the chamber and collected by optical fiber bundles (G) which are held in place by the chamber mounting bracket.

The pump controllers, injection valve actuator, and constant current source were controlled and data were collected with an IBM Data Acquisition and Control Adapter (DACA) in conjunction with an IBM XT computer.

General procedure

The following steps were performed for each titration: (1) a sample or blank (H_2O) was injected into the carrier containing electrolyte and indicator; (2) at a specified delay time the flow was stopped, causing a selected portion of the sample to be arrested in the chamber; (3) at that time a current was applied, electrochemically producing reagent for the titration; (4) a titration endpoint was reached and the current stopped; (5) after sufficient time for the endpoint to have been reached, the flow was resumed to flush out the chamber. This automated sequencing was controlled by an IBM XT computer with the

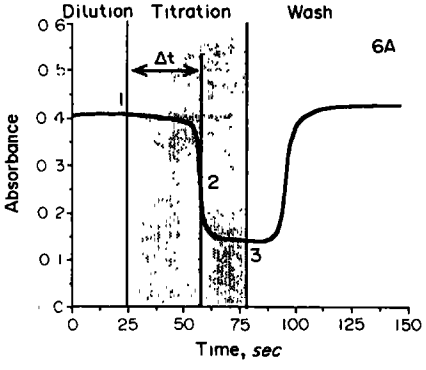

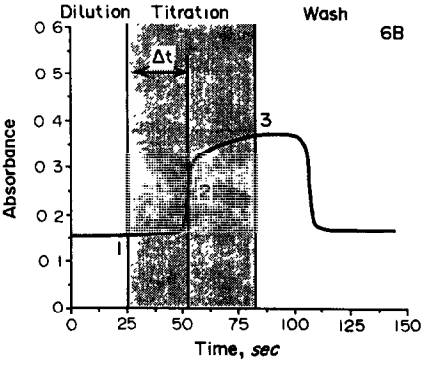

Fig. 6. FIA profiles of titrations of 0.0500M sodium hydroxide (6A) and 0.0600M nitric acid (6B), at a current of 0.78 mA each, with Sv = 19 μl, Vm = 0.930 ml, and Q = 4.23 ml/min. At the delay time after injection (25 sec) at which the desired dilution has been obtained (X^{-1} = 4.78), the flow is stopped and current is applied to begin titration (1). After an endpoint (2) is reached and titration is completed, current is turned off and flow is resumed to flush the chamber (3). The titration curve, corresponding to that obtained in conventional titrations, is indicated by the shaded area. The time from start of reagent production to the inflection point (Δt) is the parameter measured from the FIA profile.

general FIA control software of Clark *et al.*[17] This software could also display the first derivative of the FIA profile, which was used to determine the titration curve inflection point, and thus Δt. The FIA profiles for an acid and a base titration are shown in Fig. 6. The end-point was detected at a wavelength of 620 nm.

RESULTS AND DISCUSSION

The initial set of experiments was performed to determine the parameters of the single mixing tank model for our system and to enable the calculation of the dilution achieved at any specific delay time. Samples of BTB dye ($S_v = 19$ μl) were injected into a 0.01M borax carrier stream, at different flow-rates (2.83–4.88 ml/min), with a chamber volume of 0.900 ml, and at a carrier stream flow-rate of 2.9 ml/min with various chamber volumes (0.64–1.10 ml). The area under the absorbance profile at various delay times where $t_d > t_{max}$ was ratioed with the area at the peak maximum (t_{max}) to give X^{-1},

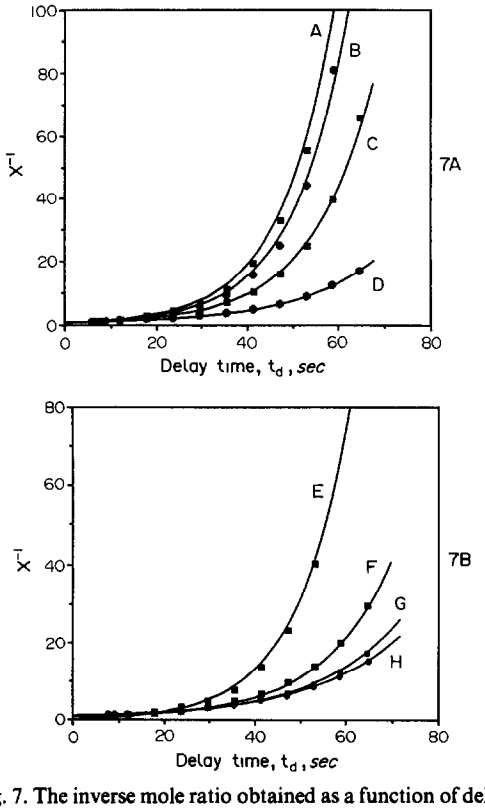

Fig. 7. The inverse mole ratio obtained as a function of delay time for various values of volumetric flow-rate and chamber volume. In 7A the chamber volume was 0.900 ml with flow-rates of (A) 4.88 ml/min, (B) 4.24 ml/min, (C) 3.95 ml/min and (D) 2.83 ml/min. In 7B the flow-rate was 2.83 ml/min with chamber volumes of (E) 0.635 ml, (F) 0.780 ml, (G) 0.900 ml, (H) 1.10 ml.

Table 1. Comparison of the mean residence times calculated ($T_{i,cal}$) with the mean residence times experimentally determined ($T_{i,exp}$)

Q, ml/min	Vm, ml	$T_{i,cal}$, sec	$T_{i,exp}$, sec
4.88	0.900	11.1	11.3
4.24	0.900	12.7	12.5
3.95	0.900	13.7	14.0
2.83	0.900	19.1	19.8
2.83	1.10	23.2	22.8
2.83	0.900	19.1	19.8
2.83	0.780	16.5	16.8
2.83	0.635	13.6	13.4

which was then plotted against delay time for each combination of flow-rate and chamber volume (Fig. 7). The equation of each of the resulting curves was of the form

$$X^{-1} = k_1 e^{k_2 t_d} \tag{9}$$

The mean residence time, which is $1/k_2$ [as seen from equation (8)], from each curve ($T_{i,exp}$) was in close agreement with the values calculated from the measured values of the flow-rate and the chamber volume ($T_{i,cal}$) (Table 1). The value of k_2 is dependent upon the flow-rate and the chamber volume. Each equation also included a constant, k_1, which was a factor to correct for the time required for the trailing portion of the injected sample to enter the gradient chamber, where the detection profile deviates from the ideal of the model, which assumes that the entire sample is in the mixing tank at time zero. The value of k_1 is dependent upon the flow-rate, the chamber volume, the sample volume and all other factors governing the dispersion of the sample zone prior to entering the chamber. It is thus observed that the shape of the X^{-1} curve does follow the single tank of the tanks-in-series model and, after all of the sample has entered into the chamber, is dependent only upon the chamber volume and the system flow-rate. Thus the amount of dilution obtained at a specific stop time can easily be predicted and controlled by adjustment of either of these two parameters.

Once determined for a given set of conditions (V_m, Q, S_v, *etc.*), the equation defining X^{-1} can be used to determine the degree of dilution obtained at a delay time after all the sample has entered into the chamber. The X^{-1} is used in conjunction with Faraday's law to calculate the amount of analyte in the injected sample, obviating the need for standards.

For all further experiments the flow-rate was 4.23 ml/min and the chamber volume of 0.930

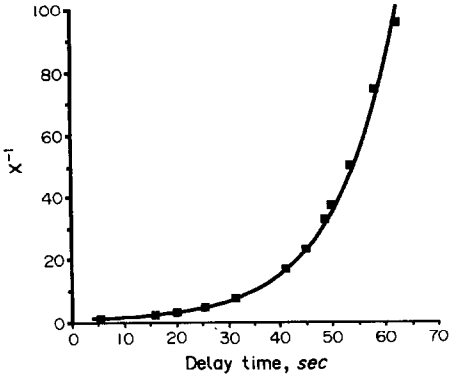

Fig. 8. The inverse mole ratio obtained as a function of delay time for the titration of 0.0200*M* NaOH. The system flow-rate was 4.23 ml/min and the chamber volume was 0.930 ml.

ml was used. Demineralized water was used as a blank for all titrations. Current values ranged from 0.7 to 4 mA. It should be noted that at high current densities, generating electrode reactions involving gases, as here, may result in increased noise levels if the gas solubility level is exceeded, which would allow bubble formation. Bubble formation was observed at currents of approximately 20 mA.

Samples of 0.0200*M* sodium hydroxide ($S_v = 19$ μl) were injected and titrated with various delay times. The resulting X^{-1} values were plotted versus their respective delay times (Fig. 8). The equation of this plot had the form of equation (9), demonstrating compliance with the given model. The greatest portion of the sample arrested in the chamber was 92%, or an X^{-1} of 1.086, at a delay time of 5.02 sec.

The results of a series of titrations performed on the described system were compared with the corresponding manual titrations. For the manual titrations, a sodium hydroxide solution was standardized against potassium acid phthalate and was used as a titrant for all acid samples. For titrating all base samples, a nitric acid solution was standardized with respect to the sodium hydroxide secondary standard solution. Titrant solutions were standardized daily prior to use.

Titration of samples ranging in concentration from 5×10^{-4}–$8 \times 10^{-2}M$ sodium hydroxide was performed with a stop time of 5.25 sec. A linear relationship was obtained from plotting the results against the equivalent manual titration, with an intercept of 1.9×10^{-3}, a slope of 0.989 and $R^2 = 0.999$.

Additional samples at concentrations up to 4.14*M* sodium hydroxide were titrated using

Table 2. Experimental data of the coulometric titration of nitric acid (see Fig. 6). For all samples: $S_v = 19$ μl, $V_m = 0.930$ ml, $Q = 4.23$ ml/min. t_d = delay time, Δt = titration time, i = current, Conc. = concentration, rsd = relative standard deviation

t_d, sec	Δt, sec	i, mA	Conc, M	rsd, %
5.27	14.97	0.785	0.00760	1.1
5.27	37.78	2.28	0.0539	1.2
5.27	44.70	3.84	0.110	0.6
16.79	37.28	3.59	0.182	0.3
28.51	27.11	3.58	0.420	1.9
40.23	19.18	3.85	0.851	1.6
50.00	14.02	3.84	1.43	0.5
50.00	21.83	3.88	2.24	1.3
62.50	6.38	3.85	3.44	1.8
62.50	8.59	3.87	4.66	2.8
62.50	14.45	3.78	8.65	1.9
62.50	17.24	3.80	9.16	1.9
62.50	19.95	3.83	10.7	2.8
62.50	23.37	3.82	12.5	2.9
62.50	27.28	3.83	14.6	2.5

various stop times such that the entire analysis time, including flushing the chamber, was 180 sec. The time allotted to flush the chamber was 70 sec for all titrations, which was slightly greater than five times the mean residence time for the flow-rate and the chamber volume used. When compared with the manual titration results, the resulting plot was again a straight line with an intercept of 1.5×10^{-2}, a slope of 1.033 and with $R^2 = 0.999$.

By changing polarity of the constant current source, hydroxide ions were produced in the mixing chamber, allowing titrations of an acid. Samples with concentrations up to 14.7*M* nitric acid were titrated (Table 2), with no physical modification of the system. The analysis time was increased to 240 sec for samples with concentrations greater than 5.0*M*. The delay time for all samples with concentrations greater than 3.0*M* was 62.50 sec. When the results were compared with manual titrations, the plot was linear with an intercept of -5.39×10^{-2}, a slope of 0.999 and with $R^2 = 0.999$.

Multiple analyses (≥ 3) were performed for all samples. The relative standard deviation was less than 1.5% for samples with a delay time of 5.02 sec and was less than 3% for samples at a delay time of 62.5 sec. The relative standard deviation tended to increase with an increase in delay time (Table 2). This occurs since any error in stopping the flow had a greater effect on the portion of the sample arrested within the chamber for those samples with the larger delay times, as can be seen in Fig. 8. All comparisons

between the manual and coulometric titrations produced correlation coefficients of 0.999.

CONCLUSIONS

A stop flow coulometric titration technique has been developed and tested. It has been shown to be capable of accurately performing titrations over a wide range of sample concentrations with good precision. The concentration profile produced within the gradient chamber has been shown to follow the tanks-in-series model, allowing for sample dilution of a preselected degree through the use of stop flow. For the first time an actual titration curve is an integral part of an FIA profile (Fig. 6).

The stop flow coulometric titration system has several advantages which enhance its appeal for application in process analysis. In industrial processes analyte concentrations are often very high or may vary over a wide dynamic range. The stop flow coulometric titration system can be used to perform a wide range of dilutions without the need for physical reconfiguration.

The direct proportionality of the measured parameter (Δt) to the concentration of the portion of the sample analyzed, instead of the logarithm of the sample concentration, enhances the precision of the analysis.

The system is mechanically simple, another advantage for use in the industrial environment. It is a single line system, incorporating only one valve and one pump. The gradient chamber, reagent generation chamber, and the detector flow cell are combined into a single component, and the system contains no frits or membranes which are prone to fouling.

The titrant is produced within the system during analysis, thus eliminating the problems of reagent handling, storage and stability. Since unstable reagents can also be produced by electrolysis, a wide range of chemistries can be exploited. Also, calibration solutions are not needed once the system has been characterized, since titrant is produced by electrolysis and the amount of titrant produced for any given current over a given period of time can be calculated. By varying the intensity of the constant current, reagent can be produced at different rates.

The system has been shown to be easily automated and controlled by computer software. The stop flow coulometric titration technique has been demonstrated to be precise and versatile. In the future, a variety of chemistries and detection schemes will be investigated with the aim to exploit them for both laboratory and process control applications.

Acknowledgements—The authors thank Camilla Winbo for her technical assistance. We also thank the Electronic and Machine Shops of the Department of Chemistry, University of Washington, for their advice and assistance on materials and construction.

REFERENCES

1. J. Růžička and E. H. Hansen, *Flow Injection Analysis*, 2nd Ed., John Wiley & Sons, New York, 1988.
2. C. B. Ranger, *Autom. Stream Anal. for Process Control*, 1982, **1**, 39.
3. K. K. Stewart and A. G. Rosenfeld, *J. Autom. Chem.*, 1981, **3**, 30.
4. J. G. Williams, M. Holmes and D. G. Porter, *ibid.*, 1982, **4**, 176.
5. R. K. Gilpin and L. A. Pachla, *Anal. Chem.*, 1989, **61**, 191R.
6. Z. Feher, I. Kolbe and E. Pungor, *Z. Anal. Chem.*, 1988, **332**, 345.
7. H. H. Ruttinger and U. Spohn, *Anal. Chim. Acta*, 1987, **202**, 75.
8. L. I. Ilcheva and A. D. Dakashev, *Analyst*, 1990, **115**, 1247.
9. Y. Y. Liang, *Anal. Chem.*, 1990, **62**, 2504.
10. H. L. Pardue and B. Fields, *Anal. Chim. Acta*, 1981, **124**, 39.
11. *Idem*, *ibid.*, 1981, **124**, 65.
12. G. W. C. Milner and G. Phillips, *Coulometry in Analytical Chemistry*, Pergamon Press, London, 1967.
13. G. D. Christian and J. E. O'Reilly, *Instrumental Analysis*, 2nd Ed., Allyn and Bacon, Boston, 1986.
14. O. Levenspiel, *Chemical Reaction Engineering*, 2nd Ed., Wiley, New York, 1972.
15. P. V. Dankwerts, *Chem. Eng. Sci.*, 1953, **2**, 1.
16. D. A. Whitman and G. D. Christian, *Talanta*, 1989, **36**, 205.
17. G. D. Clark, G. D. Christian, J. Růžička, J. A. van Zee and G. F. Anderson, *Anal. Instrumentation*, 1989, **18**, 1.

Talanta, Vol. 39, No. 3, pp. 293–297, 1992
Printed in Great Britain.

0039-9140/92 $5.00 + 0.00

INVESTIGATION OF TURBOMIXERS IN CONTINUOUS FLOW ANALYSIS

T. L. SPINKS and G. E. PACEY*
Department of Chemistry, Miami University, Oxford, OH 45056, U.S.A.

L. FABIAN, S. LEE and B. P. BUBNIS
Novatek, Oxford, OH 45056, U.S.A.

(*Received* 17 *April* 1991. *Revised* 2 *July* 1991. *Accepted* 3 *July* 1991)

Summary—This paper describes an investigation of turbomixers as replacements for mixing coils in FIA. The turbomixer is a device that will efficiently mix three streams simultaneously. Although the traditional FIA gradient is not produced, the data shows that the reproducibility of a turbomixer continuous flow system is comparable to a standard FIA system.

For almost two decades, research with continuous flow analysis has followed three basic approaches to automation: segmented flow, non-segmented flow and discrete analysis. Non-segmented or flow-injection analysis (FIA) has become particularly popular because of its ease of operation, speed and flexibility in automating a variety of methods and/or techniques. The basic cornerstones of flow injection are sample injection, reproducible timing and controlled sample dispersion. The most intriguing of the three and the least analytically exploited is the control concept of controllable dispersion and the sample gradient. There have been numerous papers describing the virtues of using the gradient.[1–3] In fact, the gradient has been used to perform many operations and methods unique to FIA.

In reality, few analyses utilize the potential of the gradient. In many cases, the gradient does not offer any significant advantage in terms of increased sensitivity or detectability. Why then should the gradient be formed in situations where it is not needed? This work supports the view that the gradient need not be formed to a large extent in non-segmented systems to be analytically useful in FIA.

For discussion purposes, it is important to recall why the gradient exists in an FIA system. Unlike air-segmented analyzers where the primary objective is to limit dispersion or sample carryover from one segment to a succeeding segment, the objective in FIA is to control the extent and reproducibility of sample zone spreading inside a reaction manifold. Traditionally, this has been accomplished with tubing coils of various lengths and diameters. Thus, dispersion is largely dependent on the physical design of the manifold. The coils also perform two additional functions: (*a*) their shapes help to create mixing currents and (*b*) they create a time delay necessary for some reaction chemistries to develop a measurable product.

The degree of mixing inside an FIA system has been discussed in detail and with very little agreement between practising FIA users. However, if generation of the gradient is not a priority, the primary issue becomes one of how to provide optimal mixing as rapidly as possible.

In retrospect, classical stopped-flow kineticists have been using rapid mixing techniques for several decades and have designed numerous systems to achieve their objectives. It appears that the incorporation of a design we call "turbomixer" provides excellent mixing. These turbomixing cells were incorporated into several non-segmented continuous flow manifolds. This paper presents the observations made comparing classical FIA mixing and turbomixing in non-segmented continuous flow manifolds.

EXPERIMENTAL

All flow rates were generated with standard peristaltic pumps. The turbomixers were fabricated in-house as previously described,[4,5] with

*Author for correspondence.

Table 1. Manifold characteristics

Chemistry	Injector volume*	Coils,† cm	Flow rate, ml/min	Technique
Ozone	200 μl	30	1.0(R) 1.0(C)	FIA
	200 μl	1 mixer	1.0(R) 1.0(C)	TM
Chlorite	200 μl	30, 100	1.5(C) 1.5(R_1 & R_2)	FIA
	200 μl	2 mixers	1.5(C) 1.5(R_1 & R_2)	Both TM
Chlorate	200 μl	2000, 3000	1.5(C) 1.5(R_1 & R_2)	FIA
	200 μl	2 mixers	1.5(C) 1.5(R_1 & R_2)	Both TM
TKN‡	40, 200 μl	100 (0.7 mm i.d.)	1.4(C) 1.8(R_1) 0.9(R_2)	FIA
	40, 200 μl	1 mixer	1.4(C) 1.8(R_1) 0.9(R_2)	TM
Nitrite	200 μl	30, 60	1.0(C) 0.9(R_1 & R_2)	FIA
	200 μl	2 mixers	1.0(C) 0.9(R_1 & R_2)	Both TM
Phosphate	200 μl	30, 30, 60	1.0($C_{1\&2}$) 0.9(R_1 & R_2)	Both TM

*All injections were made into a carrier stream.
†All tubing and coils were 0.5 mm i.d. Teflon unless otherwise noted.
Tecator Chemifolds III were used for all FIA methods.
In multiple turbomixer systems 10-cm 0.5-mm i.d. tubing was used to connect the mixers.
‡A Tecator Chemfold IV was used in addition to the Chemifold III in the FIA system and with the turbomixer.
R = Reagent, C = Carrier, TM = Turbomixer.

the dimensions given previously,[4,5] using 90° angle jets. The four jet ports may or may not be used, depending on the chemistry. The chemistries tested, except chlorite ion and chlorate ion analysis used standard/accepted protocols. Reagents, concentrations and flow rates were as described previously.[6] The FIA conditions established for chlorite ion and chlorate ion analyses were as described in the literature.[7] Table 1 gives all the dimensions for the manifolds. The turbomixer was simply substituted for the usual FIA reaction coils and manifolds or tees in mixer experiments. Tecator 5020 and 5023 FIA and Spectrophotometer units were used throughout the study. Tecator chemifold three and five were the manifold blocks used in these experiments.

RESULTS AND DISCUSSION

The turbomixer used here was termed a ball mixer by Berger and co-workers.[4,5] The ball is at the confluence of a curved Y mixer, and turbulence is created on the downstream side of the ball, moving back against the ball as the flow increases.[4]

The chemistries tested were chosen to show the relationship between complete mixing and chemistry. The glycerin data is included to show that complete mixing is indeed accomplished with the turbomixing system. A relatively fast ozone chemistry with indigo trisulfonate is presented as a baseline to measure doable, easy to automate chemistries. Nitrite ion measurement with the sulfanilamide/NED chemistry are included to better understand chemistries where measurement requires the formation of an intermediate prior to the formation of a measurable reaction product. Total Kjeldahl nitrogen (TKN) data were gathered to investigate the effect that turbomixing has on neutralizing a highly acidic acid digestion matrix prior to raising the pH of the system for determining the digested organic nitrogen content. *Ortho*-phosphate measurements were made for two reasons: (*a*) to determine if turbomixing prior to heat addition has an effect on product development and (*b*) to investigate whether turbomixing would provide a needed lower detection limit for this chemistry. The oxychlorine measurements were carried out as part of an on-going investigation to improve methods for measuring very low concentrations of disinfection by-products associated with the use of chlorine dioxide for water treatment. These tests require tight pH control, excellent mixing and time for product development as the chlorate ion measurement is second order with respect to acid.

The data presented compare standard FIA manifolds, turbomixing manifolds, and turbomixing manifolds incorporated into a stopped-flow FIA program. For these experiments all stopped-flow experiments mean that the sample plug was stopped external to the flow cell. These conditions were chosen since reaction coils in standard FIA manifolds act both as mixers and time delay devices. The turbomix data demonstrate the mixing capability while the turbomixer stopped-flow data represent optimized

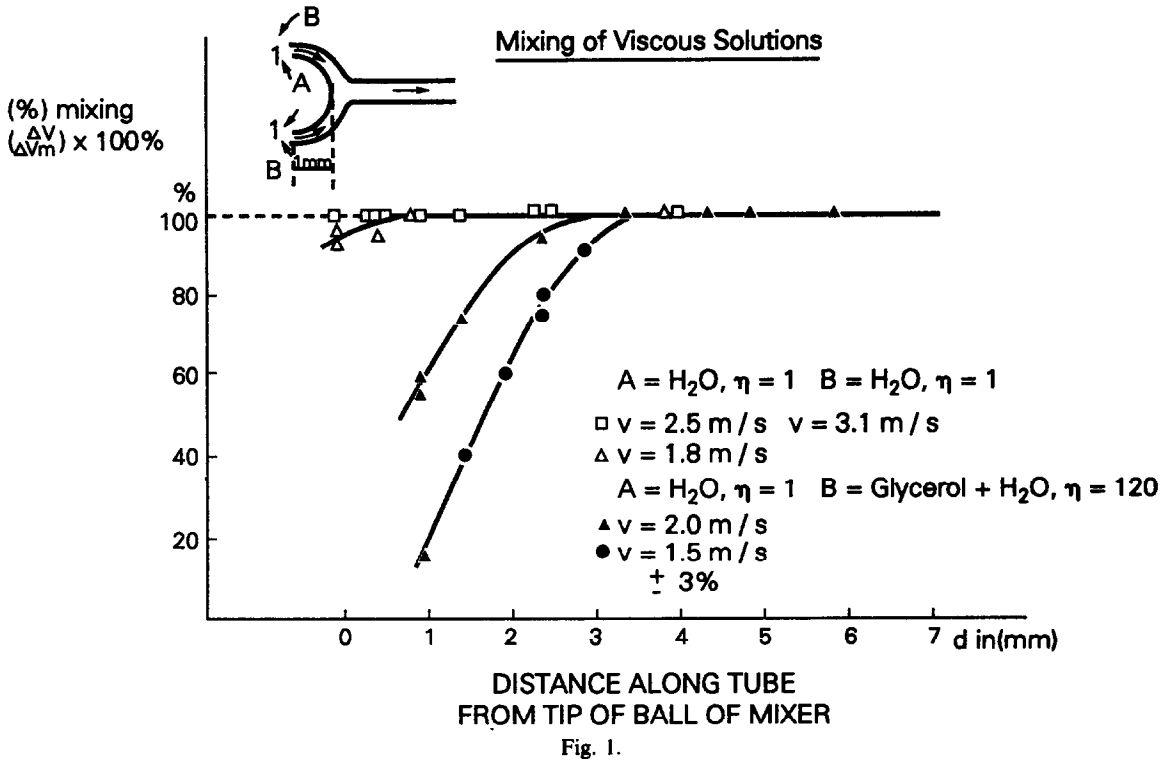

Fig. 1.

reaction conditions. The data in Table 1 represent the best available detection limits and sensitivities obtained for the conditions tested.

Mixing data—glycerin

A good test of mixing is whether the mixer can homogenize two very different solvents. In particular, solvents with viscosity differences seem to be the most difficult to mix in a FIA manifold. The turbomixers have been tested with water and glycerin.[5] Figure 4 (from reference 5) shows that complete mixing is accomplished within the first three millimeters of the turbomixer.

Fast chemistry—ozone

The reaction between ozone and potassium indigo blue is extremely fast. The working range tested was 0.01–1 mg/l. If turbomixers are to provide improved detection limits, it will most likely be observed in a fast reaction where physical mixing is the slow step. The data in Table 2 shows that the turbomixer does provide improved detection limits compared to a straight FIA system. The precision and y-intercepts are comparable. Since the selectivity of the indigo reaction is related to the amount of time the indigo is in contact with the interferent, the selectivity enhancement created by kinetic discrimination is improved by a factor of five.

Chemistries involving intermediate formation—nitrite ion

Nitrite ion data were gathered over the 1–100 mg/l. range. The data clearly show that a time delay is required to form the diazo intermediate by reacting sulfanilamide under acid conditions with nitrite ion before fully developing the measurable product as indicated by the slope and method detection limit values. All three arrangements can be used but the turbomix/stopped-flow combination provides improved sensitivity and correlation. The high RSD calculated with the turbomix set-up could be a result of the absence of time delay (needed for intermediate formation) normally incorporated with coil arrangements.

Complex matrix chemistry—TKN

TKN measurements by gas diffusion were gathered over the 1–10 mg/l. range for the 40-μl injection loop and 0.2–2 mg/l. for the 200-μl injection loop volumes, respectively. Turbomix with stopped-flow was not tested. For both loop volumes the slopes are relatively constant, indicating that both manifolds are efficient in neutralizing the acid matrix. The data also show that the smaller sample volume tends to give

Table 2. Comparison of FIA and turbomixer systems for several methods. (All data is based on five injections per concentration)

	Slope	y-intercept	Correlation coefficient	Detection limit	RSD
Ozone					
FIA	0.056	3.2e-3	0.9994	0.25 ppm	1.8%*
Turbomixer	0.068	3.0e-3	0.9970	0.03 ppm	1.2%*
Chlorite ion					
FIA	0.160	8.11e-4	0.9999	0.017 mg/l.	0.3%†
Turbomixer	0.196	3.00e-3	0.9998	0.015 mg/l.	1.2%†
Turbomix + SF	0.182	5.23e-3	0.9999	0.004 mg/l.	0.9%†
Chlorate ion					
FIA	0.093	1.05e-2	0.9995	0.215 mg/l.	1.1%†
Turbomixer	0.101	3.20e-3	0.9991	0.025 mg/l.	1.2%†
Turbomix + SF	0.144	1.72e-2	0.9986	0.120 mg/l.	0.5%†
Total Kjeldahl nitrogen					
40 μl injection					
FIA	0.0247	7.6e-3	0.9996	0.20 mg/l.	1.4%‡
Turbomixer	0.0253	4.7e-3	0.9993	0.10 mg/l.	1.3%‡
200 μl injection					
FIA	0.132	1.5e-3	0.9999	0.017 mg/l.	2.3%‡
Turbomixer	0.136	9.0e-5	0.9999	0.064 mg/l.	2.1%‡
Nitrite ion					
FIA	0.0046	9.6e-3	0.9983	0.70 μg/l.	1.4%§
Turbomixer	0.0027	1.2e-2	0.9984	0.80 μg/l.	9.3%§
Turbomix + SF	0.0068	1.8e-2	0.9999	0.70 μg/l.	2.9%§
Phosphate					
FIA	0.626	2.7e-3	0.9999	0.01 mg/l.	2.3%‖
Turbomixer	0.648	8.8e-3	0.9999	0.007 mg/l.	4.8%‖
Turbomix + SF	0.675	3.6e-3	0.9993	0.02 mg/l.	2.1%‖

Detection limit was determined as 3 times the signal to noise ratio.
SF = Stopped-flow.
*RSD at 1.0 ppm.
†RSD at 1.2 mg/l.
‡RSD at 2 mg/l.
§RSD at 10 μg/l.
‖RSD at 0.05 mg/l.

better precision data. This is understandable since the amount of acid contained in a 40-μl volume of digest is 5 times less than that in a 200-μl sample injection volume.

Temperature dependent chemistry—phosphorus

Ortho-phosphorus was measured over the 0.01–1 mg/l. range with ascorbic acid phosphomolybdate chemistry. In this experiment, the four parts of one mixer took the place of two coils. The reduction by ascorbic acid is temperature dependent. The data clearly indicate that turbomixing with or without stopped-flow has no analytical advantage. If the chemistry was measured without temperature control, it is highly possible that data similar to that of the nitrite ion would be generated.

Higher order reaction—chlorite and chlorate ions

The chlorite ion measurement chemistry involves the reaction between iodide ion and chlorite ion at pH 1.5. The manifold requires two reagents, a pH buffer followed by the addition of potassium iodide. The resulting iodine is detected spectrophotometrically at 360 nm.

The stopped-flow system maintained flow for 7 sec with a 10-sec stop period before the resumption of flow. The y-intercepts increased slightly between the FIA system and turbomixer and turbomixer stopped-flow systems. This effect is probably due to an impurity in the reagent which increases the background iodine measurement. The correlation coefficient for the calibration curves were comparable. The relative standard deviations at the 1.2 mg/l. level were all under 1.2%, which is acceptable. The detection limits based on three times the signal to noise ratio were 0.017, 0.015 and 0.004 mg/l. respectively. The lower detection limit value of the turbomix/stopped flow data does not give higher detection limits based on the larger y-intercept that is seen in standard FIA manifolds.

Chlorate ion measurement uses the KI chemistry described for chlorite ion except for the pH adjustment. The chlorate manifold requires the use of 12*M* hydrochloric acid to promote the reaction. This chemistry was the slowest chemistry tested. The FIA manifold requires over 3 meters of coil to reach the desired detection limits, indicating that time delay is important.

The chlorate data are shown in Table 2. The stopped flow period was 15 sec after injection with a duration of 4 sec. The *y*-intercepts are comparable for the FIA and the turbomixer stopped-flow but significantly lower for the turbomixer only system. The sensitivity increases from the FIA to the turbomixer stopped-flow. The relative standard deviations at 1.2 mg/l. ranged from 0.5–1.2%. The detection limit was slightly better for the turbomixer only system.

The data presented in Table 1 show that the use of mixing coils and the creation of dispersion is not a prerequisite for non-segmented continuous flow analysis. In fact, when dispersion coefficients are measured for turbomix stopped-flow manifolds, values between 1.5 and 3 are typical even for reactions requiring dispersion coefficients of 5–9 under normal FIA conditions.

Turbomixers remove the need for circular, serpentine or knotted coils in FIA systems. Further, the mixers can be made of Teflon or other materials, making them ideal for organic solvents and process control applications.

CONCLUSIONS

The need to create a gradient and dispersion in non-segmented continuous flow analysis systems was eliminated in the chemistries tested in this study. Turbomixing in situations where the sample and reagent are mixed instantaneously has proven to be an effective way to perform automated analysis. Time delays created by reaction coils are simply handled by stopped-flow periods. In these experiments the optimal FIA flow-rate conditions were used to make the comparison. No attempt was made to optimize the conditions for the turbomixers. In reality the optimized turbomixers do offer improved analytical performance for some chemistries. The potential for turbomixers in extraction and fast reactions with chemiluminescence is not presented but experiments have shown significant improvements associated with their use. The lower detection limits are related to the improved slopes. Lower noise was not seen. Sample throughput is about 10% higher for turbomixers. The combination of stopped flow and turbomixers are perfect for the FIA systems of the future where peristaltic pumps will not be the pump of choice. The alternative low cost pumps will need less flow line restriction (*i.e.*, less tubing length).

REFERENCES

1. J. Růžička and E. H. Hansen, *Flow Injection Analysis*, 2nd Ed., Wiley Interscience, New York, 1988.
2. D. Betteridge and B. Fields, *Anal. Chem.*, 1978, **50**, 654.
3. E. H. Hansen, *Flow Injection Analysis*, Polyteknisk Forlag, Copenhagen, Denmark (D.Sc. Dissertation), 1986.
4. R. L. Berger, *Biophysical Journal*, 1978, **24**, 2.
5. R. L. Berger, B. Baka and H. Chapman, *Rev. Sci. Instr.*, 1968, **39**, 493.
6. *Standard Methods for the Examination of Water and Waste Water*, American Public Health Association, 17th Ed., Washington D.C. 1990.
7. G. Gordon, K. Yoshino, D. G. Themelis, D. Wood and G. E. Pacey, *Anal. Chim. Acta*, 1989, **224**, 383.

Talanta, Vol. 39, No. 3, pp. 299–312, 1992
Printed in Great Britain.

0039-9140/92 $3.00 + 0.00

SPECTROPHOTOMETRIC METHOD FOR DETERMINATION OF SULFIDE WITH IRON(III) AND NITRILOTRIACETIC ACID BY FLOW INJECTION

MICHAEL D. KESTER, PAUL M. SHIUNDU and ADRIAN P. WADE*

Laboratory for Automated Chemical Analysis, Department of Chemistry, University of British Columbia, Vancouver, B.C., Canada, V6T 1Z1

(*Received* 14 *April* 1991. *Revised* 26 *June* 1991. *Accepted* 26 *June* 1991)

Summary—A manual colorimetric method for determination of sulfide has been adapted to flow injection, systematically optimized, and more fully characterized. Its intended application is for measurement of sodium sulfide reagent strength in pulp process streams, and sulfide contamination in effluent from Kraft pulp mills. In the flow-injection method developed, a sample solution containing sulfide is reacted with a mixture of iron(III) and nitrilotriacetic acid under ammoniacal conditions. The absorbance of the intensely-colored green product of this reaction is measured at 636 nm. Excess sulfite is present as a color stabilizer. A linear dynamic range of 20–100 ppm sulfide is readily achieved; the relative standard deviation is less than 1.2% ($n = 10$) throughout this range, and 0.37% ($n = 10$) midrange at 60 ppm. The usable dynamic range is 8–250 ppm sulfide. Long-term stability of the method is ensured by periodically performing an automatic cleaning cycle using a hydrochloric acid wash solution. This prevents tube discoloration and removes any precipitates which are formed under strongly alkaline conditions. The sample throuhput rate is at least 30/hr, given alternate acid wash cycles.

Production of pulp and paper is one of Canada's most important industries. The most common process by which wood chips are converted into pulp for high quality, high brightness papers is the Kraft process.[1] The principal chemical reagent solution for this pulping process contains high concentrations of sodium hydroxide and sodium sulfide, and is known as "white liquor". Wood chips are digested in this liquor at elevated temperature (160–180°) to remove lignin. During reaction, the concentrations of hydroxide and sulfide decrease, while organics and dissolved solids in the liquor greatly increase. It is vital to the economy of the process that reagent chemicals are recovered from the resulting "black liquor", and re-used. This involves their chemical regeneration in another part of the pulp mill. Adequate process control requires that the liquors are analyzed for sodium sulfide and sodium hydroxide at several points in the digestion and recovery process. Presently, both analyses are typically performed by manual titration of the liquor with hydrochloric acid;[2] this results in a doubly inflected plot (pH *vs.* equivalents of acid added). The titration procedure is a slow and tedious procedure which requires considerable human skill, and the quality of results obtained is highly operator dependent. Thus, there was an obvious need for development of a semi-automated method for analysis of sulfide in several streams in a Kraft pulp mill, which would be suited to on-line and at-line process-control measurements. This would improve accuracy and precision, and decrease reagent consumption. Further uses in monitoring mill effluent can be readily envisaged.

Flow injection[3] (FI) is a fast and very versatile methodology for automated chemical analysis. Its advantages and capabilities were compatible with the aforementioned analytical requirements. At least four flow-injection methods for sulfide appear in the literature. These are based on colorimetry (methylene blue method[4]), potentiometry (silver sulfide ion selective electrode[5]), atomic-absorption spectrophotometry (AAS) (precipitation as cadmium sulfide and detection by AAS[6]) and, more recently, gas diffusion (conversion to hydrogen sulfide and subsequent colorimetric detection[7]).

An alternative manual colorimetric method for sulfide determination, reported by Rahim and West,[8] appeared to be particularly suited to the highly basic nature of Kraft mill streams, and was of special interest to us. It was known[8] that their method could tolerate 100-fold molar

*Author for correspondence.

excess levels of key potential interferents such as chloride and sulfate. It involves reaction of iron(III) and nitrilotriacetic acid (NTA) with sulfide under ammoniacal conditions. Sulfite is present in excess to maintain constant ionic strength and provide color stabilization. Rahim and West suggest that the green complex formed is a colloidal basic form of Fe(OH)S. This chemistry will be discussed in more detail below and reference will be made to literature which indicates that other reaction products may also be possible under these conditions.

Preliminary evidence suggested that the iron(III)/NTA method could be more sensitive than the methylene blue procedure. Furthermore, it was felt that several questions regarding the nature of this chemistry could be uniquely addressed by use of an automated flow-injection analyzer.[9] We decided to adapt the iron(III)/NTA chemistry to flow injection, systematically optimize the method, and multivariately characterize the reaction in an automated manner.[10]

EXPERIMENTAL

Reagents

Stock solutions of 10 and 20% w/v sodium sulfite were prepared by dissolving 100.0 or 200.0 g, respectively, of anhydrous sodium sulfite (BDH Inc., Toronto, Ontario) in one litre of distilled water. These were freshly prepared each day as required, due to the possibility of oxidation of sulfite to sulfate.

A stock solution of 1000 ppm sulfide was prepared by dissovling 0.7490 g of analytical-reagent grade sodium sulfide nonahydrate (BDH Inc., Toronto) in 100 ml of 10% w/v sodium sulfite solution. This was prepared fresh daily and standards of lower concentration were made by appropriate dilution with 10% w/v sodium sulfite solution.

A solution containing 3.98m*M* iron(III) and 10.0m*M* NTA was prepared for the preliminary experiments. First, 1.92 g of ammonium ferric sulfate dodecahydrate (BDH Chemicals Ltd., Poole, England) was dissolved in 25 ml of distilled water containing 1 drop of 1*M* sulfuric acid. Then, while heating, 1.91 g of NTA (Fisher Scientific Co., Toronto) was dissolved in 25 ml of 1*M* sodium hydroxide. These two solutions were mixed, while stirring, and diluted with distilled water to 100 ml in a standard flask. Automated optimization studies required an iron(III)/NTA solution which contained 4.00m*M* iron(III) (1.93 g/25 ml) and 40.0m*M* NTA (7.64 g/25 ml). This was made in the same way. Experiments carried out at optimized conditions required a more concentrated solution which contained 6.98m*M* iron(III) and 69.8m*M* NTA. First, 1.68 g of ammonium ferric sulfate dodecahydrate was dissolved in 80 ml of distilled water containing 1 drop of concentrated sulfuric acid. Then, while warming, 6.67 g of NTA was dissolved in 50 ml of 1*M* sodium hydroxide. This solution was diluted with distilled water to *ca.* 400 ml and the iron(III) solution was then added slowly, while the solution was stirred. Using this procedure, it was possible to prepare this solution without precipitation, and the solution was found to be stable for at least one month.

Ammonia solutions were prepared by diluting 6, 10, 17 and 25-ml aliquots of concentrated ammonia (Analytical Reagent, BDH Inc.) to 100 ml with distilled water. Solutions of sodium hydroxide (AnalaR, BDH Inc.), nitrate (Analytical Reagent, BDH Inc.), chloride (Reagent grade BDH Inc.) and thiosulfate (Analytical Reagent, BDH Inc.) were prepared in distilled water from the solids, as needed. A cleaning solution (hydrochloric acid, 50% v/v) was prepared by slow addition of 50 ml of concentrated hydrochloric acid (Analytical Reagent, BDH Inc.) to 50 ml of distilled water. Early experiments used a less effective cleaning solution containing 10% v/v hydrochloric acid and 30% v/v nitric acid (iron oxides form in the presence of strong oxidizing agents such as nitric acid or dichromate).

Apparatus

Manual experiments. Absorption spectra were obtained with a diode-array spectrophotometer (Hewlett-Packard 8452A, Hewlett-Packard, Palo Alto, CA) which was controlled by a 12-MHz Intel 80286-based computer (NORA Systems, Vancouver, B.C.). The computer was equipped with an Intel 80287 math coprocessor, 40 Mb hard drive and EGA color graphics adapter card. Communication was across a Hewlett-Packard Interface Bus (HP-IB). Data acquisition software was as provided by Hewlett-Packard. Experiments used a standard quartz cell (Hellma, Model 110-QS, Fisher Scientific, Vancouver, B.C.) with a 1-cm pathlength.

Flow-injection experiments. Polytetrafluoroethylene tubing (0.5 mm i.d.) and 1/4″ inert, low pressure fittings (Omnifit, New York, NY) were used throughout.

The automated flow injection analyzer which was used for the majority of the studies has been described in detail elsewhere.[9] Its principal detector is the same diode-array spectrophotometer as used above. Specialized data acquisition routines used were written in-house and have been described elsewhere.[11] The several types of pumps interfaced to the computer include five independent stepper-motor driven, variable-speed peristaltic pump heads (Type mini-micro 2/6, Ismatec, Chicago, IL) and two high-precision variable speed peristaltic pumps (Models C-4V and C-6V, Alitea U.S.A., Seattle, WA). Sample injection is via 1–3 six-port air-driven, solenoid-actuated injection valves (Type 5020P, Rheodyne Inc., Cotati, CA), each equipped with a 70-μl sample loop. The quartz flow cell (Type P 5061-3394, Hewlett-Packard, Richmond, B.C.) used was of 30-μl volume and 1-cm path length.

A simplified flow-injection analyzer was then constructed and used for coil length optimization, sulfide calibration curves, interference studies and analysis of real samples. All components were controlled by another computer which was identical to that used for the automated analyzer. The control software for this apparatus was a modified version of that used for the automated analyzer detailed above, and is discussed elsewhere.[9–11] Stream propulsion was by three high-precision, variable speed peristaltic pumps (Models C-4V or C-6V, Alitea USA). Samples were injected with a six-port, air-driven solenoid-actuated injection valve (Type 5020P, Rheodyne) equipped with a 70-μl sample loop. A second six-port valve of the same design was used as a switching valve for the cleaning solution. Both valves could be triggered either manually or by computer, using custom-built electronic controllers.[9] The flow-through cell was of quartz, and had a 30-μl volume and 1-cm pathlength. The photometric detector used with this analyzer was a two-channel design based on the work of Patton *et al.*,[12] and was built in-house. Its output, the log of the photoresistor voltage ratio (sample to reference), was read by a Data Acquisition and Control Adapter (DACA) board (IBM Instruments; from Mendelson Electronics, Dayton, OH). The detector design was modified so as to provide a five-fold increase in the output voltage over the original design. This maximizes measurement precision by providing an optimal match between the detector output voltage level and the 0–10 V dc input required by one of the DACA's 12-bit analog-to-digital convertors. The detector's light sources were two bi-color light-emitting diodes (LED's) (Cat. No. 276-012, Radio Shack, Richmond, B.C.), one for the sample channel and the other for the reference channel. The color emitted by the LED's, red (635 nm) or green (565 nm), is selected according to the polarity of the applied potential. The emission spectra for similar diodes have been published[13] and indicate a bandwidth of 30–40 nm. Initially the LED's were powered by a 6 V lantern battery and a simple circuit incorporating one double-pole, double-throw (DPDT) switch to reverse the polarity, one 10 kΩ variable resistor to control the brightness of both LED's and one 200 Ω current-limiting resistor in series with each diode. The most recent detector modification has been to add circuitry to power and control the LED's, without external batteries. Analyzer control software was written in this laboratory in Microsoft QuickBASIC® version 4.0. This sampled the detector log-ratio output at a rate of 5 Hz and with 12-bit (1 part in 4095) resolution, and displayed a plot of peak shape on the screen in real-time. The data were subsequently stored on disk for later processing.

Further data processing was undertaken with a commercial spreadsheet (Lotus 123), a graphing program (SigmaPlot version 4.0, Jandel Scientific, Corte Madera, CA) and a three-dimensional plotting program (SURFER version 3.0, Golden Software, Golden, CO).

Procedures

Preliminary manual studies. These studies were to determine the order of addition of reagents (which inevitably determines the flow-injection manifold) and confirm the wavelength of maximum absorption (λ_{max}). Initially, the manual experiment as described by Rahim and West[8] was attempted. To each of six 50-ml standard flasks was added 0.2–1.2-ml aliquots of the 1000 ppm sulfide standard. Then 20 ml of 20% sodium sulfite solution, 1 ml of concentrated ammonia solution and 0.5 ml of the iron(III)/NTA composite solution were added in sequence, with mixing between each step. The solutions were diluted to the mark with distilled water. Aliquots from these solutions were transferred to a 1-cm quartz cell and a full UV-visible absorption spectrum from 190 to 820 nm was taken with the diode array spectrophotometer. The λ_{max} was found to be 636 nm.

The effect of the iron(III)/NTA ratio was then ascertained. Composite iron(III)/NTA solutions

were prepared where NTA ranged from equal to 10-fold molar excess relative to iron(III). The iron concentration was maintained at 2.5m*M* in all ten composite solutions while the NTA concentration was varied from 2.5–25m*M*. The absorbance (at 636 nm) of each solution was measured in a 1-cm quartz cell with the diode-array spectrophotometer.

Baseline noise and solvent effect on flow injection manifold. Once the preliminary investigations were complete, an initial manifold [Fig. 1(a)] was assembled on the automated flow injection analyzer.[10] The baseline noise was studied by varying the reaction coil length and inserting post-pump damping coils. The effects of potential color-formation enhancers were studied with sodium sulfide dissolved in: 0.5*M* sodium chloride, 0.01*M* sodium hydroxide, 10% (w/v) sodium nitrate, and 10% (w/v) sodium sulphite. The effect of distilled water was also tested.

Automated simplex optimization. Simplex optimization[14] is an efficient way to search for the values of several experimental variables which produce a maximum response. Optimization was carried out, without operator intervention, on the automated flow-injection analyzer in the same manner as has been reported previously.[10] The method used was the composite modified simplex.[15,16] Initially, we attempted to optimize all three (variable) concentrations simultaneously [sulfite, ammonia and iron(III)/NTA]

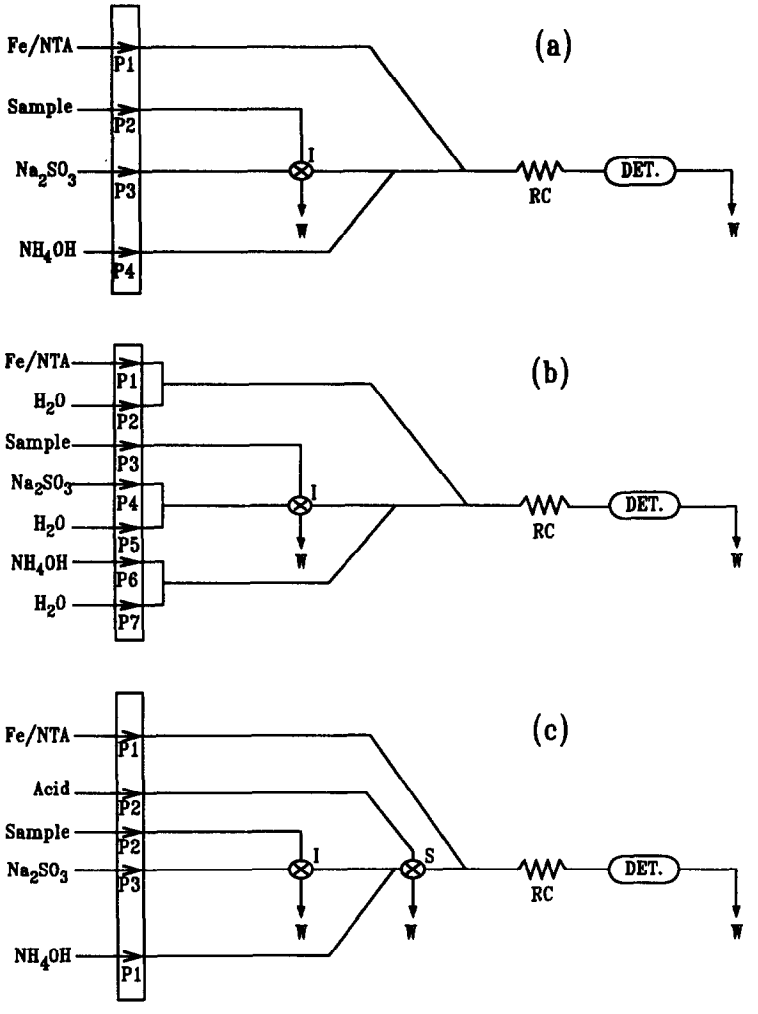

Fig. 1. Schematic diagram of the flow-injection manifolds used. Shown are variable speed pumps (P1 to P7), sample injection valve (I), wash switching valve (S), reaction coil (RC), detector (DET), and the waste lines (W). (*a*) Manifold used for preliminary flow-injection experiments. The reaction coil was 1.0 m in length. (*b*) Manifold used for automated simplex optimizations. The reaction coil was 1.0 m in length. (*c*) Simplified optimized flow-injection manifold. Flow-rates used were P1 = 0.5 ml/min, P2 = 4.5 ml/min (maximum rate), and P3 = 0.8 ml/min. The reaction coil was 80 cm in length.

while measuring absorbance at 636 nm. The automated analyzer specified reaction conditions by use of appropriate flow-rates and the stock solutions. The flow manifold used is shown in Fig. 1(b). Several optimizations were carried out. In each, the variable flow-rate reagent streams were "buddied"[10] to distilled water streams to give predetermined total flow-rates, but variable reagent concentration. In this way, each of the reagents could assume a concentration that ranged from full strength down to zero while maintaining a constant total flow-rate (and sample residence time) through the manifold. The absorbance recorded was the average of duplicate experiments at each set of conditions. On completion of each optimization, the reagent flow-rates which resulted in the largest response were reported.

Automated response surface mapping using grid search. For chemical systems with two variables, response surface mapping[10] provides a useful means of characterizing the effects of these variables, and their interactions, on the system response(s). Reagent flow-rates for iron(III)/NTA and ammonia solutions were each varied independently in seven steps from 0.1–1.0 ml/min, using a regularly-spaced square experimental design of 7 × 7 points (a total of 49 experiments, with each in duplicate). The sulfite flow-rate was kept constant. Response surface maps of these data were produced using the SURFER® graphics program.

Simplified manifold. Once optimum conditions had been established, a simplified analyzer and manifold [Fig. 1(c)] were constructed for routine analysis. The concentrations of the reagents were those determined to be optimum in the previous studies. A second automated valve (S) was placed immediately before the reaction coil to allow flushing of the manifold with acid. This removed any high pH precipitates automatically. When engaged, the valve allowed the acid cleaning solution to pass through the coil while briefly diverting the reagents to the waste bottle. A two channel pump simultaneously refilled the sample loop and propelled cleaning solution through the reaction coil and flow cell. When this pump stopped, valve s was switched back to allow pasage of the reagent stream, and the baseline absorbance reading was allowed to re-equilibrate before injection of the next sample by valve i. A calibration curve was produced for 6, 8, 10, 12, 14, 16, 18, 20, 40, 50, 60, 80, 100, 250, 500, 750 and 1000 ppm S^{2-}. In each case, the mean and sample standard deviations were calculated from 10 replicate peaks.

Coil length optimization. For this, the flow-manifold shown in Fig. 1(c) was used at the flow-rates and reagent concentrations found to be optimal. Some 20 different coil lengths were used, in the range 10–300 cm. The detector output was adjusted manually to read 0.2 V before each injection. A response surface map and contour plot was obtained which showed the effect of reaction coil length on peak shapes obtained for 50 ppm S^{2-}. The response readings were plotted in analog-to-digital convertor (adc) units and were directly proportional to absorbance.

Time dependence of absorption spectra. Manual experiments were carried out to determine the time dependence of absorption spectra, both with and without sulfide present. For this, 5.0 ml of 17% ammonium hydroxide, 8.0 ml of 10% sodium sulphite, 2.0 ml of 100 ppm S^{2-} in 10% sulfite and 5.0 ml of 6.98m*M* iron(III)/69.8m*M* NTA solution were mixed, in that order, and transferred to a 1-cm quartz cell within 30 sec of adding the iron(III)/NTA reagent. The blank contained all reagents except for sulfide. Visible spectra were recorded at a rate of one per minute for 40 min (400–800 nm; spectra taken relative to distilled water). The results were plotted as three-dimensional surfaces and contour plots.

RESULTS AND DISCUSSION

Reaction chemistry

Complete characterization of the reaction mechanism and kinetics is beyond the scope of this present study. However, some discussion of the chemical form of reagent and reaction product(s) is warranted.

It is known that under acidic conditions (pH 0.5–3.5), six coordinate iron(III) forms a 1:1 complex with tetradentate NTA.[17–20] As the pH is raised to 3.5–7.0, progressive hydrolysis[17,18,20,21] and subsequent olation[18,21] of the complex are known to occur. As the pH is raised above 9 the complex becomes unstable,[17,20] and precipitation occurs. From this we infer that formation of iron(III) sulfide complexes which retain the NTA is unlikely at high pH.

Initially the iron(III)/NTA reagent solution is at *ca.* pH 3: therefore the iron(III)/NTA complex then exists primarily in its monomeric form. The flow manifold designed for this study merges this acidic reagent stream with a highly

basic stream (pH ≈ 12) of ammonium hydroxide and sodium sulphite. This then meets the injected "sulfide plus sulfite" sample. This process has the effect of quickly raising the pH of the iron(III)/NTA reagent solution from pH 3 to approximately pH 11 in the presence of sulfide. Hydrolysis and olation may now occur if the reaction kinetics are suitably fast. However, the instability of the iron(III)/NTA complex at this pH is likely to result in rapid release of hydrolyzed iron(III) by the NTA. This would allow immediate reaction with sulfide, and explain the instantaneous color formation which is observed.

It has been shown[22] that, at pH 6.5, iron(III) and HEDTA (a similar ligand to NTA) can form an intensely colored soluble dimeric iron-sulfur complex which is bridged by one sulfide ion in the presence of H_2S. Thus, the presence of iron(III)/NTA dimer has also been suggested. However, we feel this is unlikely at pH 11, as the iron(III)/NTA complex itself is unstable.

Other researchers have suggested that a variety of reaction products can exist at elevated pH's. Morozov and Rozanov[23] reported that iron hydroxide reacted with sulfide at pH 9.5 (in the presence of sodium) to eventually precipitate as $Na_x[Fe^{III}(OH)_yS_z]$. In this x, y and z were dependent on relative reagent concentrations. They found that, in the absence of sodium, mixtures of this nature remain as a colloidal solution. Coagulation is observed when sodium chloride is added. The charged hydroxothioferrite is the likely cause of the transient green color in our reaction mixture. Precipitation of the ammonium or sodium salt of the hydroxothioferrite could follow soon afterwards [in addition to $Fe(OH)_3$ and possibly Fe_2S_3]. Morozov and Rozanov[23] also reported that the ratio of S/Fe in this complex increases if sulfide is limiting. This would explain the deviation from Beer's law which we observe at low sulfide concentrations.

The possibility of sulfide reduction of iron(III) to iron(II) via the formation of zero-valent sulfur can be ruled out as this redox effect has been shown to be minimal at high pH.[23–25] Moreover, a deep green solution has been noted under basic conditions by combining ferric chloride, potassium hydroxide, and sulfide;[24] elemental analysis of this solution and the co-existent precipitate revealed that no ferrous iron or zero-valent sulfur was present. Other workers[23] have shown that iron(III) is reduced by sulfide only if the pH is lower than 9.5. Reduction of iron(III)–NTA by sodium sulphite has been studied[25] and has been shown to decrease steadily from pH 5 to pH 8. Again, this suggests minimal formation of iron(II) at the high pH of our final reaction mixture.

From the above, we presently conclude that the (colloidal) color body is an initially soluble form of hydroxothioferrite of variable composition. Subsequent precipitation of the sodium or ammonium salts of this ion is likely. Formation of the black ferric sulfide is seen in manual experiments, but this occurs significantly later than formation of the intense dark green color (which is instantaneous). We note that, in the absence of sulfide, excess iron(III) precipitates as ferric hydroxide. This is via replacement of NTA with hydroxide when the iron(III)/NTA reagent is merged with the basic stream of sodium sulfite and ammonia.

Preliminary manual studies

It was found that the method would only work when the reagents were mixed in the order listed by Rahim and West[8] [*i.e.*, sulfide, sulfite, ammonia and then iron(III)/NTA]. A spectrum from 190 to 820 nm confirmed that maximum absorbance is at 636 nm, and absorption by the reagent is (initially) minimal in this region. Color formation was strongest and occurred instantaneously only if iron(III)/NTA was added last. From this we concluded that a flow manifold in which all reagents were merged (or otherwise combined) before sample injection was not feasible.

The effect of iron(III)/NTA concentration ratio was then determined. The iron(III) reagent was kept in at least 5-fold molar excess relative to sulfide. Under these conditions, the same amount of color development was achieved for an equal to ten-fold excess of NTA relative to iron(III). Thus the iron(III)/NTA ratio is not critical to color formation within this range. However, it was felt that free iron(III) could result in precipitation of ferric hydroxide (or sulfide or hydroxosulfide when a sulfide-containing sample plug passes through) and, to help avoid this, NTA was kept in a 10-fold molar excess relative to iron(III) for all subsequent experiments.

Baseline noise characteristics

Figure 2 shows peak shapes obtained with different coil lengths in the initial manifold [Fig. 1(a)]. The baseline noise observed was significant and periodic. From this it was

assumed that the peristaltic action of the pumps was responsible for the fluctuating response at the detector. The noise magnitude decreased as longer coil lengths were used. However, long reaction coils result in a low sample throughput rate, increased dispersion and decreased sensitivity. Rather than use a long reaction coil, the noise was minimized by lengthening the lines between the pumps and the merging tees to one meter for all subsequent experiments. The baseline noise thereafter was minimal.

Evaluation of potential color formation enhancers

The presence of 10% sodium sulfite was known to enhance color formation. Various other sodium compounds, and water, were evaluated to see if they produced the same effect.

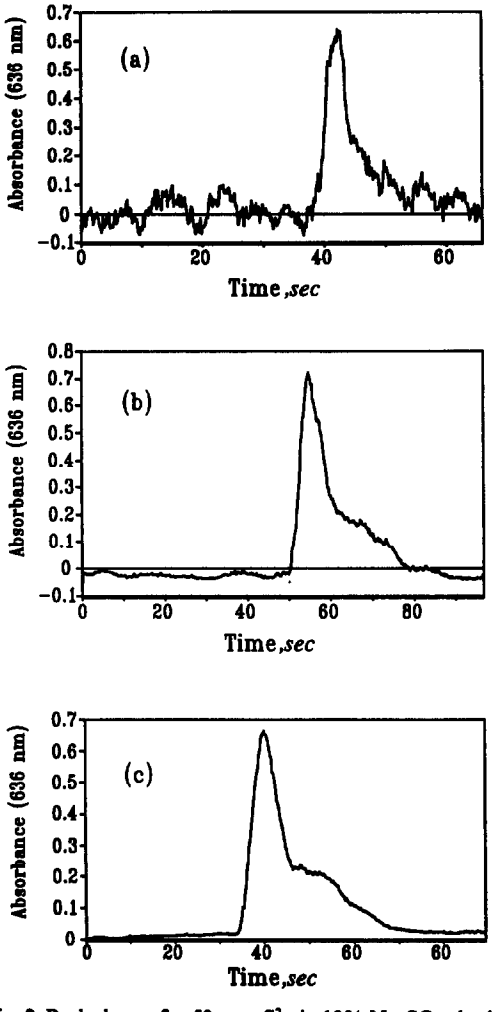

Fig. 2. Peak shapes for 50 ppm S^{2-} in 10% Na_2SO_3 obtained with the manifold shown in Fig. 1(a). The reaction coil length used was (*a*) 0.2 m, (*b*) 1.0 m and (*c*) 2.0 m. Reagent streams were 20% w/v sodium sulfite, 3.98m*M* iron(III)/10.0m*M* NTA and 25% v/v NH_4OH, each flowing at 1.0 ml/min.

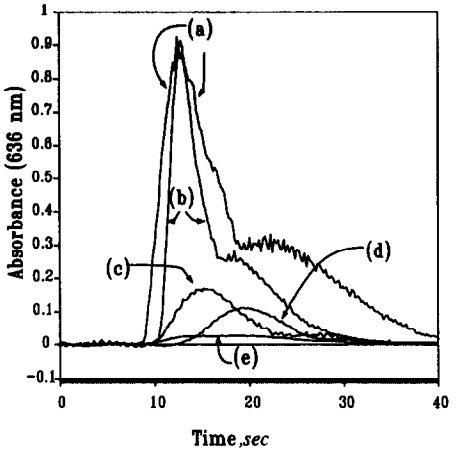

Fig. 3. Peak shapes for solutions containing 50 ppm S^{2-} and concentrations of selected sodium salts. These were obtained with the manifold shown in Fig. 1(*a*). Reagent streams were 20% w/v sodium sulfite, 3.98m*M* iron(III)/10.0m*M* NTA and 25% v/v NH_4OH (each flowing at 1.0 ml/min). The salt solutions used were: (*a*) 10% w/v sodium nitrate; (*b*) 10% w/v sodium sulfite; (*c*) 0.5*M* sodium chloride; (*d*) 0.01*M* sodium hydroxide, (*e*) water.

The peaks shown in Fig. 3 indicate that both 10% sodium sulfite and 10% sodium nitrate enhanced the peak absorbances. Water, 0.01*M* sodium hydroxide and 0.5*M* sodium chloride provided no such enhancement. The peaks for sulfite and nitrate exhibited distinct "tailing", which was proven in subsequent experiments to be due to refractive index fluctuations over the injection zone. The carrier stream being used was of 20% sodium sulfite; thus, in both cases a sulfite concentration gradient existed across the dispersed sample zone. The refractive index fluctuations caused by this gradient resulted in light scattering, which was confirmed by recording transmission spectra (190–820 nm) at a rate of 1 Hz as a sodium sulfite concentration gradient passed through the cell of the diode-array spectrophotometer. As would be expected for a scattering phenomenon, these spectra showed that transmitted radiation decreased at all wavelengths (despite the solution appearing optically colorless). Peak tailing completely disappeared when the sulfite concentration gradient was removed. In all subsequent studies, sample and carrier stream contained equal concentrations of sulfite and the observed peak heights were smaller since they no longer had a contribution from light scatter.

Automated optimization studies

Simplex methods[15,16] have been widely used in chemistry and successfully applied in flow-

Table 1. Simplex optimization of flow-injection method for sulfide

	Optimization A	Optimization B
Ammonia		
Maximum rate (ml/min)	1.0	1.0
Initial rate (ml/min)	0.3	0.3
Optimum rate (ml/min)	0.48	1.0
Iron(III)/NTA		
Maximum rate (ml/min)	1.0	1.5
Initial rate (ml/min)	0.3	0.3
Optimum rate (ml/min)	1.0	1.5
Maximum absorbance found	0.284	0.258
Experiment # (optimum conditions)	8	8
Total # of experiments performed	16	13
Total flow rate (ml/min)	3.5	4.0
Absorbance corrected to total flow rate of 3.5 ml/min	0.284	0.295

Both optimizations used 25 ppm sulfide in 10% sulfite solution.
Peak absorbance values listed are average values from two injections.
The sulfite flow rate was maintained at 1.5 ml/min.
Stock solution concentrations used were sulfite 10%, ammonia 25% and 4.00m*m* iron(III)/40.0m*M* NTA.

injection analysis.[9,10] Simplex optimization involves sequentially evaluating the responses obtained under sets of experimental conditions predicted by its algorithm. Values of several system variables are changed simultaneously.

Figure 1(a) shows the optimization manifold assembled on the automatic flow-injection analyzer. Initially, an attempt was made to optimize all three reagents [iron(III)/NTA, NH_4OH and sulfite] simultaneously. Unfortunately, interference due to the aforementioned sulfite concentration gradient resulted in unsatisfactory results.[26] Hence, a two-variable simplex optimization was attempted by maintaining a constant sulfite concentration (10% w/v). Table 1 shows the results from two such optimizations. Optimization A concluded that it was best to run iron(III)/NTA at its maximum rate (1.0 ml/min), therefore, the maximum allowable rate was increased to 1.5 ml/min for optimization B. At the high concentrations predicted by optimization B (maximum of both reagents), a brown precipitate was observed on the walls of the tubes and flow cell. This was principally of $Fe(OH)_3$ but could also contain small amounts of the black Fe_2S_3, and possibly the other species discussed above. The precipitate was easily removed by flushing the system with acid. It was assumed that the peak height measurements obtained under these conditions contained a contribution from the precipitate, and so simplex optimization was not pursued further. At this stage in the method development it was felt that better system characterization could be achieved by univeriately optimizing the sulfite concentration, and then undertaking a more detailed automated surface mapping study of the remaining two variables.

Optimization of sulfite concentration

A limited univariate study (Fig. 4) determined that the optimum concentration for sulfite was greater than 5% (w/v). A 10% (w/v) sulfite concentration was used in all experiments thereafter. This level was considered as optimal since

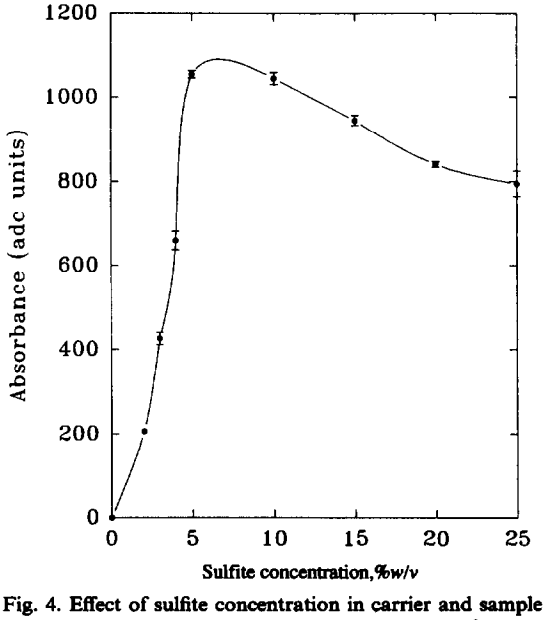

Fig. 4. Effect of sulfite concentration in carrier and sample solutions on absorbance at 636 nm for 50 ppm S^{2-}. The sulfite concentration was varied from 0 to 25% w/v. The carrier was at 0.8 ml/min. Other streams were 6.98m*M* iron(III)/69.8m*M* NTA and 17% NH_4OH, each flowing at 0.5 ml/min.

it was far enough removed from the steep absorption decrease at values below 5% sulfite, and higher concentrations would incur increased reagent costs without improving analytical performance.

Automated response surface mapping

A response surface map and a contour plot were produced by allowing the 8.00m*M* iron(III)/80.0m*M* NTA and 25% ammonia flow-rates to vary independently over the range 0.1–1.0 ml/min in seven steps. The surface map obtained (Fig. 5) confirms the findings of simplex optimization B in that maximum absorbances are obtained when the reagents are flowing at or near their maximum allowed rates. Again, precipitation was observed under these conditions. The increased absorbance found in the highest corner of the surface map was from precipitation and not increased green color complex formation. Values of 0.85 ml/min of the 8.00m*M* iron(III)/80.0m*M* NTA and 0.66 ml/min of 25% ammonia were chosen as optimum, since they lie on a high plateau, but are not in the region where most precipitation occurs (the back corner). In terms of concentration, these correspond to 6.98m*M* iron(III), 69.8m*M* NTA and 17% ammonia—and it is these concentrations which were used in all later studies, and for routine analysis. Such a choice ensured high method sensitivity and minimal effects due to small changes in the concentrations of the reagents.

Simplified flow-injection manifold

With the required concentrations of all three reagents now optimized, a simplified flow-injection manifold was assembled as shown in Fig. 1(c). In order to improve the sensitivity by decreasing the system's sample dilution factor, the pump speeds were changed so that the injection stream (sodium sulfite) ran slightly faster (0.8 ml/min) than the merging reagent streams (0.5 ml/min). The concentrations of reagents were then adjusted to match the optimum found above. An additional valve was incorporated into the manifold immediately before the reaction coil to facilitate automatic cleaning of the reaction coil and flow cell. This resulted in long-term stable operation of the system and excellent repeatability. As well, this allowed efficient removal of any lingering substances introduced from real sample matrices.

Coil length optimization

Figure 6 shows a three-dimensional surface map and contour plot that are made from 20 compiled peaks that resulted from coil lengths of 10–300 cm. These surfaces exhibit several important features. As coil length decreases, peak width decreases, time to peak maximum decreases, and baseline noise increases (note the instability in the lower right hand corner of the contour plot). Since both ammonia and the iron(III)/NTA reagent are merged with the sample carrier stream, the color forms

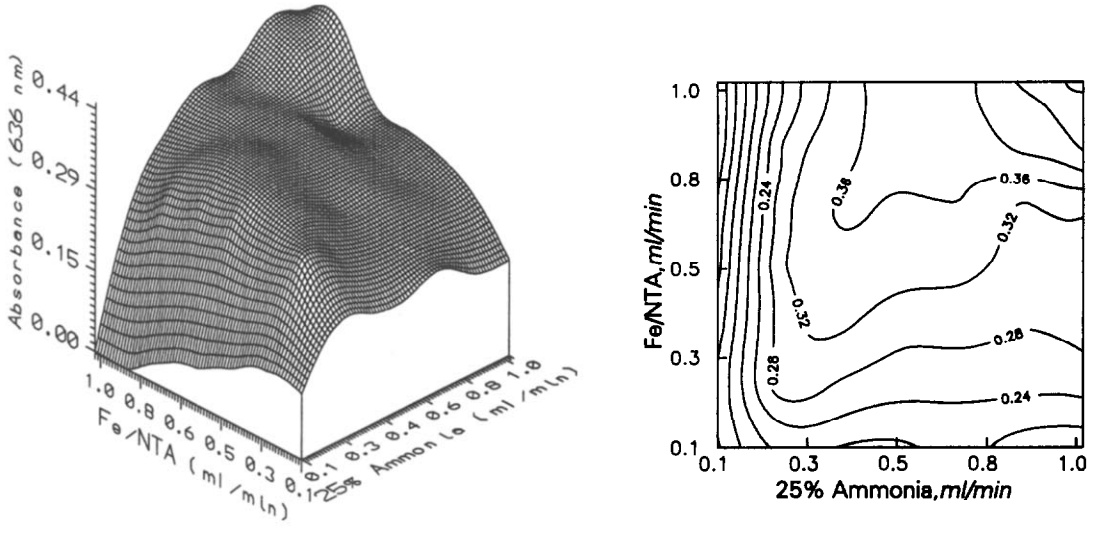

Fig. 5. Absorbance response surface map and contour plot for 50 ppm S^{2-} in 10% Na_2SO_3. This was produced by the automated flow injection analyzer using the flow manifold as shown in Fig. 1(*b*). Reagent streams were 10% Na_2SO_3 (fixed 1.5 ml/min) 8.0m*M* iron(III)/80.0m*M* NTA (variable) and 25% NH_4OH (variable).

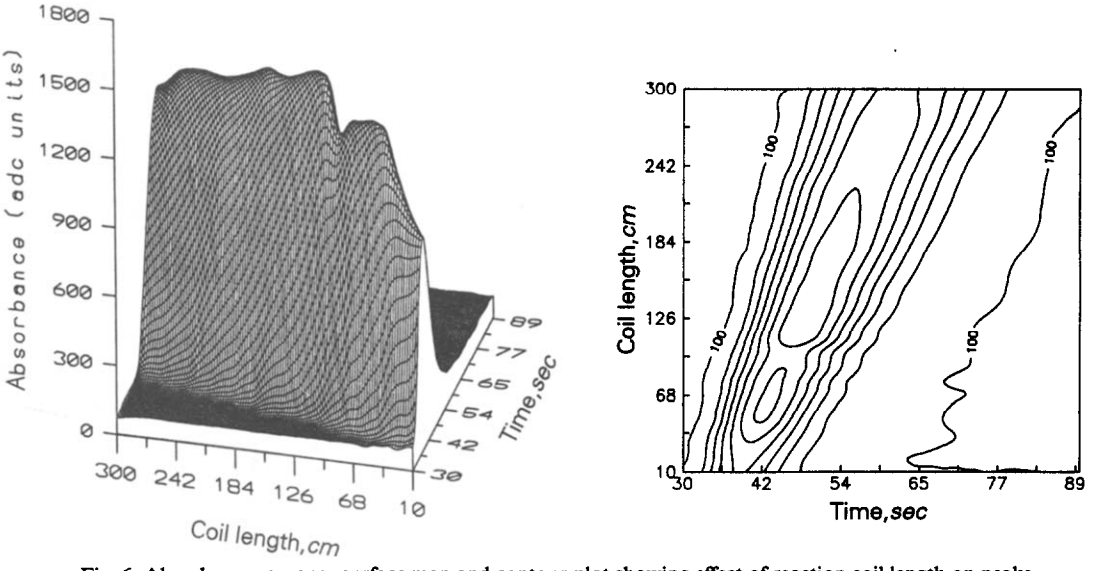

Fig. 6. Absorbance response surface map and contour plot showing effect of reaction coil length on peaks obtained for 50 ppm S^{2-}. The plot is composed of 20 peaks, observed at 636 nm. There are 300 data points across each peak, sampled at a rate of 5 Hz. The flow manifold used was as shown in Fig. 1(*c*). The flow rates and reagent concentrations were found to be optimal. Coil lengths used were 10–300 cm, in 10-cm increments from 10–130 cm, and then in 25-cm increments from 150–300 cm.

instantaneously. Without an intermittent acid wash, a gradual build-up of precipitate is seen for the longest tube lengths.

In addition to these expected observations, and the expected skewed Gaussian peak shape, there is an unexpected dip in peak height at *ca.* 100 cm. This effect is not an artifact, since it appears over 4–5 compiled peaks, which were recorded with a coil length resolution of 10 cm. Its origin posed something of a puzzle, and one possible interpretation is discussed below.

The reaction rate for precipitate formation is significant, but is much slower than that for the sulfide color body. The increased peak height seen for coil lengths of 120 cm or greater cannot be due to unassisted precipitation, since the geometry of the flow system is such that this would be seen at all times, especially for the longer coil lengths. Thus, clearly, the signal observed can only have been caused by the presence of sulfide in the sample zone (see our comments re sulfide-containing precipitates).

An 80-cm reaction coil was chosen as optimum for subsequent analytical use of the manifold, since this has low baseline noise, avoids the dip and minimizes the possibility of precipitate formation. However, before proceeding with this, further discussion of the kinetics of color body formation and precipitation is appropriate.

Time-dependence of absorption spectra

Figures 7(a) and (b) show the time-dependent absorption spectra of the reaction mixture (with and without sulfide) in a standard 1-cm cell, over a period of 40 min. When sulfide is present [Fig. 7(a)], the colored body is seen to form rapidly. Its largest absorbance maximum is at 636 nm, and it exhibits smaller maxima at 434 nm and 532 nm. At longer times, absorption was found to increase across the entire visible spectrum, a behavior typical of precipitate formation (where light is absorbed at all wavelengths, and scattered). The data shown in Fig. 7 confirmed that formation of the precipitate was the much slower of the two processes, but dominates at times greater than 3 min.

Figure 7(c) shows that the 636 nm absorbance rises rapidly over a period of *ca.* 1 min. At times between 1 and 3 min a small decrease in absorbance is seen. The absorbance increased rapidly over the next 20 min and readings became much more noisy. Thereafter, absorbance was seen to decrease as the precipitate began to settle to the bottom of the cell. After several hours the solution above the precipitate was clear.

These results suggest that the kinetic effects observed in the flow system are of the same nature to those seen under static conditions, but operate faster. This is likely because of the much greater degree of mixing which occurs

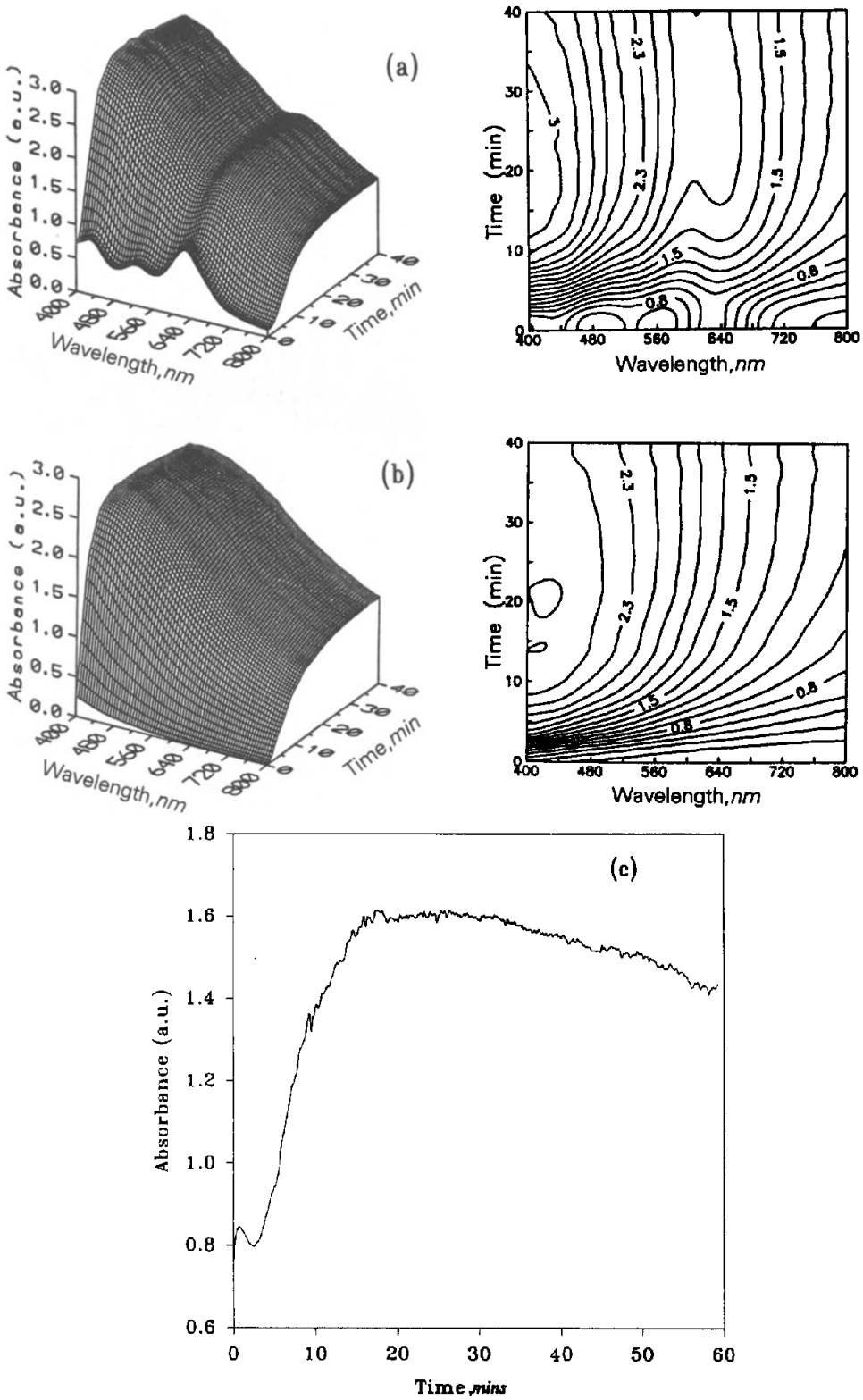

Fig. 7. Time dependence of reagent mixture absorption. Reagent solutions were comprised of 8.0 ml of 10% Na_2SO_3, 5.0 ml of 17% NH_4OH, and 5.0 ml of 6.98m*M* iron(III)/69.8m*M* NTA, and either (i) 2.0 ml of 100 ppm S^{2-} in 10% Na_2SO_3 or (ii) 2.0 ml of 10% Na_2SO_3. (*a*) Time-resolved absorption spectra (400–800 nm) for reagent mixture (i) (with sulfide), shown as 3D surface and contour plot; (*b*) Time-resolved absorption spectra (400–800 nm) for reagent mixture (ii) (without sulfide), shown as 3D surface and contour plot; (*c*) Absorbance of reagent mixture (i) at 636 nm. Measurements were taken at a rate of 0.1 Hz for 60 min.

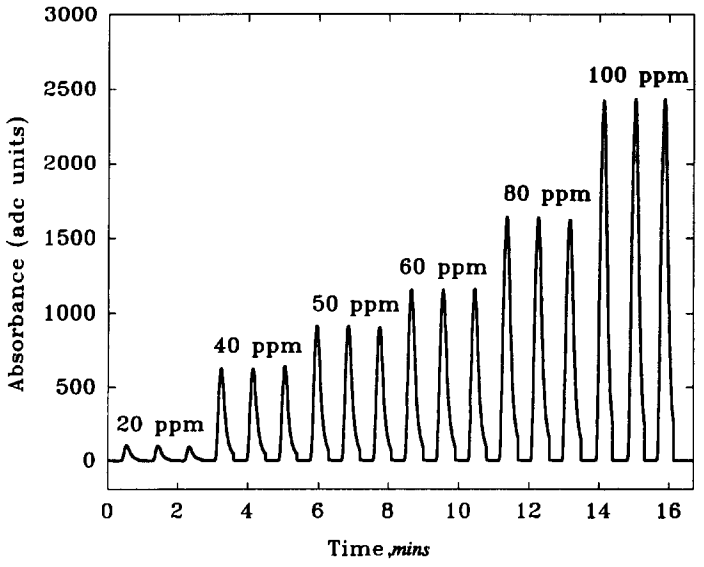

Fig. 8. Typical replicate calibration peaks for 20–100 ppm S^{2-}, obtained using the optimized manifold [Fig. 1(c)]. Reagent streams were 10% Na_2SO_3 (0.8 ml/min), 6.98m*M* iron(III)/69.8m*M* NTA (0.5 ml/min), and 17% NH_4OH (0.5 ml/min). The figure has been reconstructed from multiple data files. Tails of the peaks appear truncated in the figure as data acquisition for each peak is terminated shortly after the peak maximum is detected.

within the small bore tubing at the flow-rate used. Furthermore, it is possible that the hydroxothioferrite formed may itself have a colloidal nature.[8] Formation of the colloid would explain the small drop in product absorbance at 3 min [Fig. 7(c)], and subsequent action of the colloidal particles to increase the rate of formation of the colloid salt and/or ferric hydroxide, ferric sulfide (or hydroxothioferrites) would perhaps explain the behavior seen for coil lengths of 120 cm and above. In any case, use of the 80-cm coil length and total flow-rate of 1.8 ml/min avoids these problems.

Analytical performance

Figure 8 shows typical replicate peaks obtained at several points within the linear dynamic range of the developed method. The response is linear over the range 20–100 ppm; this range of concentration has a slope of 28.2 adc units per ppm, an intercept of −508 adc units, and a correlation coefficient of 0.996. The precision of the system is good; the relative standard deviation was less than 1.2% ($n = 10$) at all concentrations from 20–100 ppm, and was 0.37% ($n = 10$) midrange at 60 ppm. At lower concentrations, the calibration curve is unusual in that the slope decreases with decreasing concentration (Fig. 9). This effect most likely results from an uncharacterized chemical equilibrium at low sulfide concentration, possibly due to a change in the stoichiometry of the reaction product as previously mentioned. For the

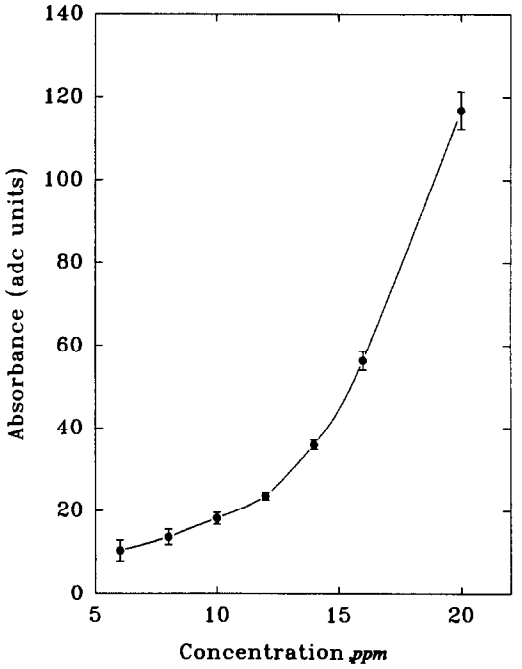

Fig. 9. Calibration curve and error bars (±1 sec) which were obtained from injections of 6–20 ppm S^{2-} ($n = 10$), using the optimized manifold [Fig. 1(c)]. Reagent streams were 10% Na_2SO_3 (0.8 ml/min), 6.98m*M* iron(III)/69.8m*M* NTA (0.5 ml/min), and 17% NH_4OH (0.5 ml/min). Beyond this range the curve is highly linear from 20 to 100 ppm S^{2-}, and then shows a negative (asymptotic) deviation from linearity at higher concentrations.

Table 2. Evaluation of effects of potential interferents

Potential interferent	Concentration of interferent	$[S_{2-}]$, *ppm*	Peak height, *adc units*	RSD, %
None	—	0	0.0	0.00
None	—	50	276.7	0.60
Cl^-	542m*M*	0	9.8	8.90
Cl^-	542m*M*	50	283.8	0.34
$Na_2S_2O_3$	156m*M*	0	−26.7	2.70
$Na_2S_2O_3$	156m*M*	50	258.0	0.39

Chloride was tested at (*ca.*) its concentration in sea water. Thiosulfate was tested at a 100-fold molar excess relative to sulfide. All samples were made up in 10% sulfite. In each case, 10 replicate injections were considered.

calibration plot shown in Fig. 9, quantitation would only be accurate to about 8 or 10 ppm since the slope decreases rapidly beyond this point. The usable dynamic range was 8–250 ppm sulfide. This may be extended somewhat (at the expense of measurement precision) if the amplifier gain is reduced.

Interference studies

Rahim and West[8] reported that the following anions did not interfere at 100-fold molar excess relative to sulfide: SO_3^{2-}, SO_4^{2-}, SeO_4^{2-}, NO_3^-, CO_3^{2-}, ClO_3^-, Cl^-, Br^-, I^-, CH_3COO^-, PO_4^{3-} and OH^-. They also reported that oxalate, citrate, tartrate and chromate could be tolerated at less than 10-fold molar excess. The interference of $Na_2S_2O_3$ (at 100-fold molar excess), and chloride at the concentration at which it is found in sea water (*ca.* 350-fold molar excess), were found to be acceptable (Table 2). Refractive index fluctuations over the sample zone were the major source of interference.

Real samples

Table 3 shows data collected on liquor and waste water samples obtained from facilities where Kraft pulping is practiced. Peak shapes were exactly as expected. Baseline noise and other causes of peak height irreproducibility were minimal, as indicated by the relative standard deviation values obtained ($n = 10$). The developed method had more than adequate sensitivity for the real samples, including the dilute pulp wash water taken from an intermediary stream. The liquor samples all required substantial dilution in order to ensure that they fell within the linear dynamic range of the method. The pulp wash water sample was analyzed as received.

Further work

This method will be applied to a variety of sample matrices obtained from different sampling locations at different mill sites. On-site performance comparisions of this with other methods should be made. On-line application of the method will require development of an automated sample dilution stage. Flow injection manifolds for such purposes have appeared in the literature.[27,28] The kinetics and chemical interactions of the colored product formed warrant further spectrochemical attention.

Table 3. Real sample data for pulp liquors and wash waters

Sample	Source	Dilution ratio	Peak height, *adc units*	$[S^{2-}]$ *ppm*	RSD, %
Blank (10% sulfite)	UBC Chemistry Department	None	0.0	0.0	0.00
Green liquor # 1	Prince George, B.C.	1:500	131.7	13,300	1.77
Green liquor # 2	Prince George, B.C.	1:250	395.5	17,900	0.46
Green liquor # 3	Paprican, Vancouver, B.C.	1:100	714.1	12,600	0.56
Dilute pulp wash water	Paprican, Vancouver, B.C.	None	240.6	45.2	0.73

Samples were as provided by industry, without details of actual source or any prior pretreatment. With the exception of the dilute pulp wash water, all samples were diluted with 10% sodium sulfite. In each case, 10 replicate injections were considered.

CONCLUSIONS

A flow-injection method for determination of sulfide has been developed, optimized and characterized. Use of an automated flow-injection apparatus allowed problems caused by refractive index effects and precipitation to be rapidly determined and eliminated.

Although the actual chemistry is complex, the analytical method developed is fast, relatively simple to use, and is well suited to the needs of the pulp and paper industry. The precision was good, and the detection limit and sensitivity adequate for the type of samples for which it was designed.

The time-dependence of this reaction makes it better suited to flow injection than as a manual analysis, since the reproducible timing from injection to detection afforded by flow injection circumvents most of the problems associated with precipitation.

Acknowledgements—The authors thank James T. Wearing (PAPRICAN) for helpful discussions, John Ball (Prince George, B.C.) and James Wearing for providing test samples and allowing these results to be published, and Richard J. Kerekes (UBC Pulp and Paper Centre) for encouragement to address such problems.

The automated flow-injection analyzer was constructed with assistance from UBC-NSERC equipment grant 5-80885. MDK acknowledges support from a MacMillan Bloedel Graduate Fellowship. PMS acknowledges support from the UBC University Graduate Fellowship program.

REFERENCES

1. J. P. Casey, *Pulp and Paper, Chemistry and Chemical Technology*, Vol. 1, 3rd Ed., Wiley, Toronto, 1980.
2. Chemical Methods Committee of the Process and Product Quality Division, *TAPPI*, T625 cm-85, 1984.
3. J. Růžička and E. H. Hansen, *Flow-Injection Analysis*, 2nd Ed., Wiley, New York, 1988.
4. D. J. Leggett, N. H. Chen and D. S. Mahadevappa, *Anal. Chim. Acta*, 1981, **128**, 163.
5. J. F. van Staden, *Analyst*, 1988, **113**, 885.
6. B. O. Petersson, Z. Fang, J. Růžička and E. H. Hansen, *Anal. Chim. Acta*, 1986, **184**, 165.
7. K. Sonne and P. K. Dasgupta, *Anal. Chem.*, 1991, **63**, 427.
8. S. A. Rahim and T. S. West, *Talanta*, 1970, **17**, 851.
9. P. D. Wentzell, A. P. Wade, P. M. Shiundu, R. M. Ree, M. Hatton, T. J. Sly and D. Betteridge, *J. Automatic Chem.*, 1989, **11**, 227.
10. A. P. Wade, P. M. Shiundu and P. D. Wentzell, *Anal. Chim. Acta*, 1990, **237**, 361.
11. P. M. Shiundu and A. P. Wade, *J. Automatic Chem.*, 1991, **13**, 83.
12. C. J. Patton and S. R. Crouch, *Anal. Chim. Acta*, 1986, **179**, 189.
13. J. R. Clinch, P. J. Worsfold and H. Casey, *ibid.*, 1987, **200**, 523.
14. K. W. C. Burton and G. Nickless, *Chemometrics and Intelligent Laboratory Systems*, 1987, **1**, 135.
15. D. Betteridge, A. G. Howard and A. P. Wade, *Talanta*, 1985, **32**, 709.
16. *Idem*, *ibid.*, 1985, **32**, 723.
17. V. V. Vekshin, V. I. Kernev, I. P. Doinikova and A. V. Elenskii, *Russian J. Inorg. Chem.*, 1983, **28**, 1448.
18. R. L. Gustafson and A. E. Martell. *J. Phys. Chem.*, 1963, **67**, 576.
19. G. Anderegg, *Inorg. Chim. Acta*, 1986, **121**, 229.
20. M. Morin and J. P. Scharff, *Anal. Chim. Acta*, 1973, **66**, 113.
21. H. Schugar, C. Walling, R. B. Jones and H. B. Gray, *J. Amer. Chem. Soc.*, 1967, **89**, 3712.
22. C. V. Philip and D. W. Brooks, *Inorg. Chem.*, 1974, **13**, 384.
23. A. A. Morozov and A. G. Rozanov, *Russian J. Inorg. Chem.*, 1979, **24**, 1781.
24. H. N. Stokes, *J. Amer. Chem. Soc.*, 1907, **29**, 304.
25. E. Sada, H. Kumazawa and H. Machida, *Ind. Eng. Chem. Res.*, 1987, **26**, 2016.
26. M. D. Kester, B.Sc. Honours Thesis, Chemistry Department, University of British Columbia, 1990.
27. G. D. Clark, J. Růžička and G. D. Christian, *Anal. Chem.*, 1989, **61**, 1773.
28. Y. Israel and R. M. Barnes, *Analyst*, 1991, **116**, 489.

Talanta, Vol. 39, No. 3, pp. 313–318, 1992
Printed in Great Britain.

0039-9140/92 $3.00 + 0.00

AUTOMATED MEASUREMENT OF DYE COVERAGE IN PHOTOGRAPHIC NEGATIVES BY FLOW-INJECTION ANALYSIS

TERRENCE P. TOUGAS* and KATHLEEN M. HOBBS
Polaroid Corporation, Waltham, Massachusetts 02254, U.S.A.

(*Received* 24 *May* 1991. *Revised* 21 *June* 1991. *Accepted* 22 *June* 1991)

Summary—A system was designed to automate the determination of three image dyes in an instant photographic material. The method involves extracting negative samples with dimethylsulfoxide and filtering the extract, followed by quantitating the dye coverage (dye per unit area of negative) through a spectrophotometric flow-injection procedure. Significant spectral overlap exists among the dyes, and as a result calculation of coverage requires solving three simultaneous equations. A microcomputer and data acquisition system were employed for controlling the detector and flow-injection system, acquiring and integrating the detector response, calculating coverage, producing and displaying control charts, and automatically transferring results to a VAX based corporate database. In addition to automating sample preparation and measurement steps as much as possible, the goal of this project was to automate the data manipulation and transfer steps.

In general, the process of performing a routine chemical determination is a set of well-defined sequential steps. For a given determination, the process might include; (*a*) generating a request for measurement, (*b*) obtaining the appropriate sample(s), (*c*) preparing the samples, (*d*) performing the measurements, (*e*) analyzing the data (including data quality assurance), (*f*) reporting the results and (*g*) archiving the results. The decision to automate a determination generally rests with an analysis of the benefits of automation relative to the cost. The consequence of the sequential nature of the determination process is that any step might be the rate determining step. Any analysis in consideration of automating a determination should examine all steps. In general the greatest benefit will be realized by focusing the automation effort on these slow steps. Different technologies are required for automating the various aspects of a determination. As chemists, we tend to focus on the chemical steps, *i.e.*, sample preparation and measurement, but the overall automation problem requires strategies involving information management and computer networking, as well as novel chemistries and chemical instrumentation.[1]

The present work arose from a need to automate the determination of three image dyes coated on a photographic negative. Samples are generated by a pilot coating operation that supports product development. In this particular case, the photographic material is part of an instant integral film. There are three major subsystems in this type of film; photographic negative, receiving sheet and reagent pod.[2] After exposure the entire film structure is ejected from the camera between a pair of rollers. The rollers serve to break a seal on the reagent pod, and spread reagent between negative and sheet. This initiates the development process which ultimately results in the transfer of image dyes from the negative to the receiving sheet.

There is a need to routinely monitor dyes coated on negatives as an amount per unit area (coverage). These dyes are responsible for the final photographic image and the amount of dyes coated is crucial to the quality of the image. The actual measurement is used for, among other things, process control during a coating run. Thus, rapid turnaround of results is essential. The manual spectrophotometric determination is a time intensive and tedious operation. Previous to this work, a robot based system was used to automate this determination. When this system failed after several years of use, the issues surrounding automating this determination were re-examined. As a result, we have replaced this manual/robotics procedure with an automated procedure based on flow-injection analysis (FIA), and integrated this automated chemical procedure with an evolving computer

*Author for correspondence.

network composed of hardware and software from many different vendors.

EXPERIMENTAL

Dye spectra were obtained individually with a conventional spectrophotometer (AVIV model 14DS) with a 1-cm cell. Dyes were dissolved in dimethylsulfoxide (DMSO) to concentrations similar to those expected in the negative extracts. Dimethylsulfoxide (HPLC grade) was used throughout as extraction solvent for negative samples and carrier stream for FIA experiments. Samples were prepared for measurement by extracting 8.65 cm^2 of coated negative with 10 ml if DMSO. The negative extracts were filtered through 0.45-μm glass microfiber filters (Xydex, Autovial Syringeless Filters) into sampling vials for FIA with Xydex Processor (automated filtration station capable of filtering 18 samples simultaneously).

System

A requirement for the flow-injection system (FIS) was that it be integrated with the computing environment illustrated in Fig. 1. All the users of analytical information have access to a corporate-wide VAX-based network of minicomputers. The strategy within the analytical group was to connect microcomputers via a Novell based local area network (LAN) to each other and the corporate network. In this configuration, a microcomputer potentially serves as (*a*) a laboratory automation system (LAS), and (*b*) a terminal to both VAX and HP minicomputer, and a local computing resource. With respect to this work, LAS denotes a system for instrument control, data acquisition and data reduction. A decision was also made to implement an Oracle based laboratory information management system (LIMS) in a client-server configuration within the LAN. An additional requirement for the LAN was that it should integrate with an HP-1000 used to automate a chromatography laboratory.

Based on the above requirements, an FIS was configured with an HP Vectra QS/16 as the microcomputer-LAS, a Control Equipment Corporation (now part of Leeman Laboratory) AMI-103 FIA and an Applied Biosystem 783a UV/Vis detector. The AMI-103 has a pressure driven pumping system which results in pulseless flow and excellent flow stability. Crucial to the present work are two features of this system. The AMI-103 can be controlled either through a keyboard on the unit or by an external computer via an RS-232 port. A consequence of the pressure driven design is that wetted parts are all chemically inert (Teflon, glass). This proved important since the carrier stream was DMSO. Previous experiences with peristaltic pumps and this solvent were unsatisfactory because of chemical incompatibility with the pump tubing. The detector was a conventional HPLC detector equipped with the optional preparatory cell (3-mm pathlength) and tungsten lamp. The features of this detector critical to this work were: (*a*) control of wavelength and sensitivity by an external computer (RS-232) and (*b*) operability to at least 700 nm. Figure 2 provides an overview of the hardware and

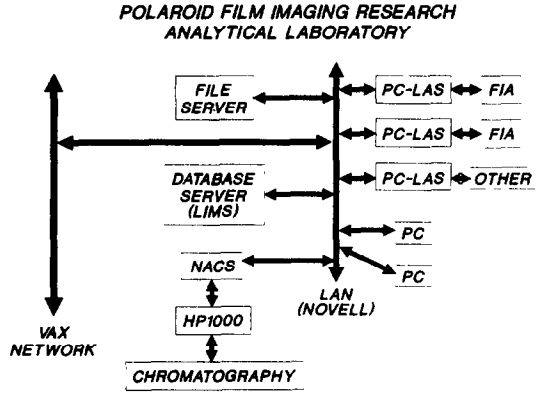

Fig. 1. Analytical laboratory computing environment designed for laboratory automation with MS-DOS microcomputers (PC) based laboratory automation systems (PC-LAS). NACS: Novell Asynchronous Communications Server, HP1000: Hewlet-Packard HP1000 minicomputer used as LAS for a chromatography laboratory.

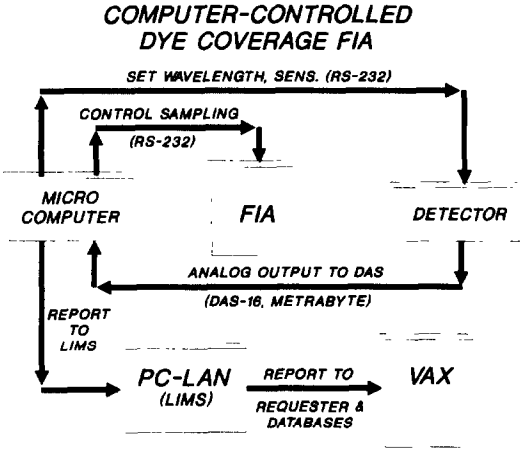

Fig. 2. Overview of equipment used to automate dye coverage determination. Illustrated are electronic paths among the computer, flow-injection system, detector local area network and wide area network.

its relationship to the computing environment. Serial communication is used to control both the flow-injection system and the detector. The analog signal from the detector is digitized (Metrabyte DAS-16) and analyzed within the local PC. Calculated results and reports are output to the LAN or VAX environments.

Operation of the flow-injection system

The operator controls the entire dye coverage determination through a microcomputer system. An MS-DOS batch file controls the overall process by executing the appropriate software (Fig. 3). Sample information is entered into a spreadsheet (Quattro Pro). This information is used by the computer to control the flow-injection system and the detector. The analog signal from the detector is digitized and converted to a concentration of analyte. The calculations require solving a set of three simultaneous equations which compensates for spectral overlap of the three dyes. This is done automatically with routines written in Asyst. The coverage information produced in Asyst is automatically passed to a Quattro spreadsheet, where a report is generated (printed locally) and transferred electronically to the LIMS. The LIMS is used to transfer chemical information based on the coverage data to VAX nodes on the corporate network. Data quality assurance is supported through automatic generation of control charts and flagging spurious controls in the reports.

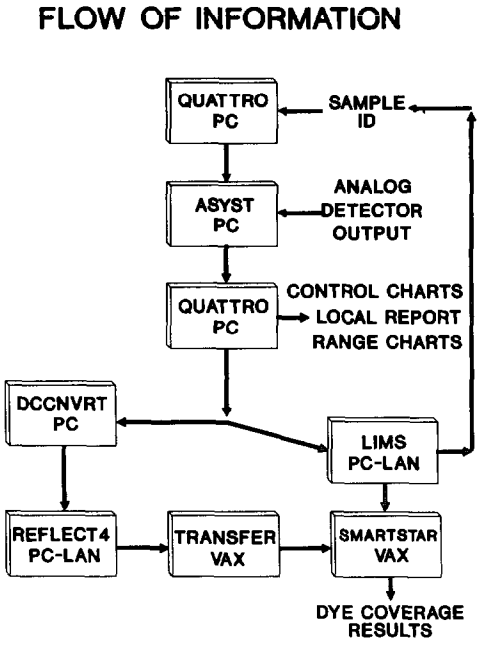

Fig. 3. Overview of software used to automate dye coverage determination. Illustrated is flow of data/information from one process to another, ultimately populating a corporate-wide database and transferring reports electronically to the individual requesting the determination. Shaded arrows indicate final configuration. DCCNVRT is a PASCAL program used to convert a report from Quattro to the format required by Smartstar database.

RESULTS AND DISCUSSION

The manual and robotics methods for dye coverage used absorbance measurements at 459, 554 and 608 nm. As can be seen in the visible spectra (Fig. 4), the former two values correspond to maxima for the yellow and magenta dyes, respectively. In the case of the cyan dye, an intense absorbance maximum occurs at about 678 nm. The dynamic range of the absorbance detector allows the use of the latter wavelength in conjunction with the other two. As a result 459, 554 and 678 nm were selected for subsequent work. The advantages

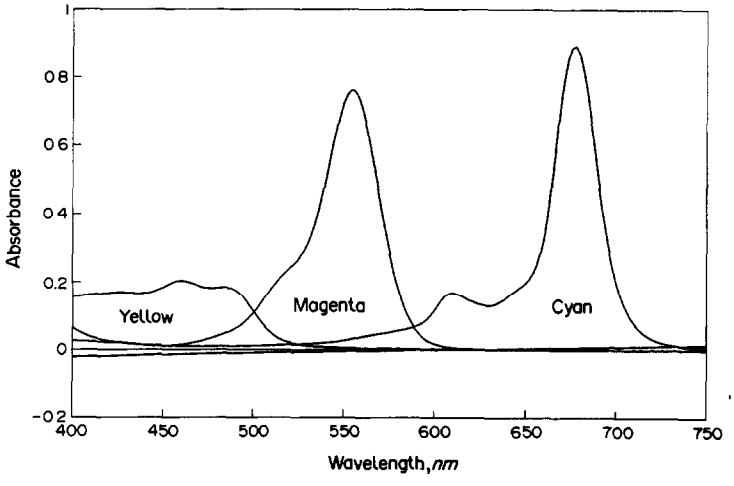

Fig. 4. Visible spectra of three image dyes determined by dye coverage methods.

are increased sensitivity and less spectral overlap with the magenta dye.

The standard negative sample is a disk with area of 8.65 cm^2 punched from a larger section of negative. Extraction and dissolution of the dyes is performed with dimethylsulfoxide (DMSO). Two aspects of the sample preparation were examined. These were the issue of filtering sample extracts *vs.* centrifuging, and the time required for complete extraction of the image dyes. The former issue arises because the centrifugation step in the manual procedure is time consuming and imposes constraints with respect to batch size. A study was performed to compare centrifuging samples extracted in DMSO to filtering these same extracts through 0.45-μm glass microfiber filters. The results indicate (based on *t*-tests) that there is no significant difference between the absorbance of sample extracts filtered *vs.* those centrifuged. On this basis, filtering was adopted for sample preparation.

The optimum time for complete extraction of the negative was examined by extracting three different negative sections for 5, 15 and 30 min and then determining dye coverage by FIA. The results were compared to results obtained by the manual method where samples were extracted for 1–2 hour, and the ratio of these results was defined as the percent extracted. These samples ranged in age from 4 days to 2 years. Previous work had indicated that 30 min was sufficient time for extracting a freshly coated negative. The purpose of this study was to see if the age of the negative had a significant impact on extraction of the dyes. The results of this study are summarized in Table 1. They indicate that 30 min is sufficient for complete extraction for the fresh and 8 month old negative. The cyan result for the 2 year old negative was 94.4%, indicating there may be incomplete extraction of this dye in the old negative.

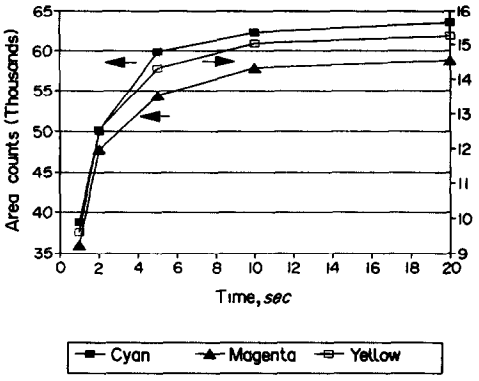

Fig. 5. Flow-injection response (peak area) to image dyes as injection time is varied.

The experimental variables which can be controlled in FIA include manifold dimensions, flow rates, carrier stream(s) and injection volume.[3] Conditions for low dispersion and minimum analysis time were selected because of the need for rapid sample turnaround. Since the extraction of sample required DMSO, this solvent was selected for the carrier stream. Two instrumental variables (injection time and sampling time) were optimized by measuring response (peak area) as a function of each variable. Sampling time is the length of time sample is pumped through the loop prior to injection and injection time is the length of time the carrier stream is flushed through the filled sample loop. In both cases, the response should reach some limit as the variables are increased. Each was varied up to a maximum of 20 sec. In the case of injection and sampling time, the response of a standard mixture was examined. The operating values selected were values well into this limiting plateau of response. Figures 5 and 6 illustrate the results of these studies. Final operating conditions were: carrier flow-rate, 1.5 ml/min; sample loop volume, 100 μl; sampling time, 12 sec; sampling flow-rate, 4 ml/min; injection time, 12 sec. This yielded a sampling

Table 1. Study of extraction efficiency *vs.* time for fresh and aged negative

	Time extracted, *min*	% Extracted relative to 2 hr Cyan	Magenta	Yellow
Fresh negative (4 days after coated)				
	5	60.8	93.2	97.4
	15	97.9	101.9	99.6
	30	98.9	103.4	100.5
Aged negative (8 months after coated)				
	5	44.1	82.8	97.6
	15	97.7	102.4	102.3
	30	99.5	102.8	99.9
Aged negative (2 years after coated)				
	5	36.0	73.6	86.6
	15	76.1	95.5	95.9
	30	94.4	99.5	100.0

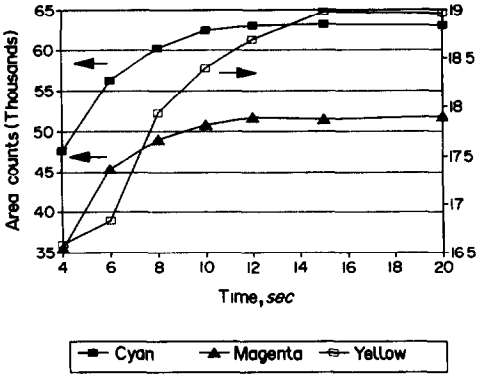

Fig. 6. Flow-injection response (peak area) to image dyes as sampling time is varied.

Table 2. Precision of peak area *vs.* peak height measurement

	Relative standard deviation, %		
	Cyan	Magenta	Yellow
Height	7.7	8.0	5.8
Area	1.0	1.2	1.2

Based on 10 replicate injections

Table 3. Comparison of overall precision based on the determination of a control sample

	Precision: mg/m² (%) as ±1 standard deviation		
	Cyan	Magenta	Yellow
FIA	7.9 (1.8)	7.4 (2.1)	20.8 (2.0)
Manual	5.9 (1.4)	6.2 (1.8)	19.3 (1.9)

frequency of 80 inj/hr. In principle, either peak height or area is proportional to concentration. Since it is practical to obtain either in this system, the precision of these two modes of measurements was considered. A control negative was extracted and injected repeatedly. The results in Table 2 indicate that the precision of peak areas is significantly better than of peak height. As a result, peak area has been adopted as the mode for measurement.

Precision was evaluated both in an overall sense and in an attempt to quantitate individual contribution to method variability. The FIA procedure has been in use in its working environment for over a year. As part of the standard operating procedure, a sample of negative used as a laboratory control is analyzed with every batch of samples. Recently, control limits was established for this control sample. A comparison of these statistics with the control limits established for the manual procedure form a good basis for comment on the overall precision of the new procedure. Table 3 compares the precision (as a sample standard deviation) of the FIA method to the manual method. Data used to estimate precisions were collected over about a two-week period for each case (manual and FIA). They therefore include any contributions due to daily set-up of instruments or any other day-to-day factors. Note that all results (both manual and FIA) are reported as the mean of duplicate determinations. Thus the quoted standard deviation is really a standard error. While in all three cases the estimated precision is slightly larger for the FIA, an *F*-test indicates that the differences are not statistically significant. One must also keep in mind the newness of the FIA method and anticipate that the precision will improve with increasing experience. The laboratory control was run twelve times by FIA and nineteen times by the manual method over a period of two weeks. The results for the three dyes are contained in Table 4. A comparison of means via *t*-test suggests that there is no significant difference in the results from either method.

The use of a single standard solution assumes not only that the response is linear, but also that the intercept is zero in the concentration-response curve. If a non-zero intercept exists, then accuracy will be a function of the concentration difference between sample and standard. To evaluate the correctness of these assumptions, a control negative extract was spiked with various levels of a standard dye solution. The experiment was repeated for each image dye. Knowing the coverage of the control and the amount of dye spiked into the extract, the amount found by the FIA dye coverage method was compared to a calculated coverage. The latter is the hypothetical coverage

Table 4. Comparison of laboratory control results: accuracy of FIA *vs.* manual dye coverage

		Cyan		Magenta		Yellow	
	Count	Mean, mg/m²	S.D.	Mean, mg/m²	S.D.	Mean, mg/m²	S.D.
FIA	12	425.5	9.2	356.5	8.8	1011	33
Manual	19	423.7	10.6	354.9	6.6	1021	16
$t_{v,0.05}$		0.474		0.588		0.920	

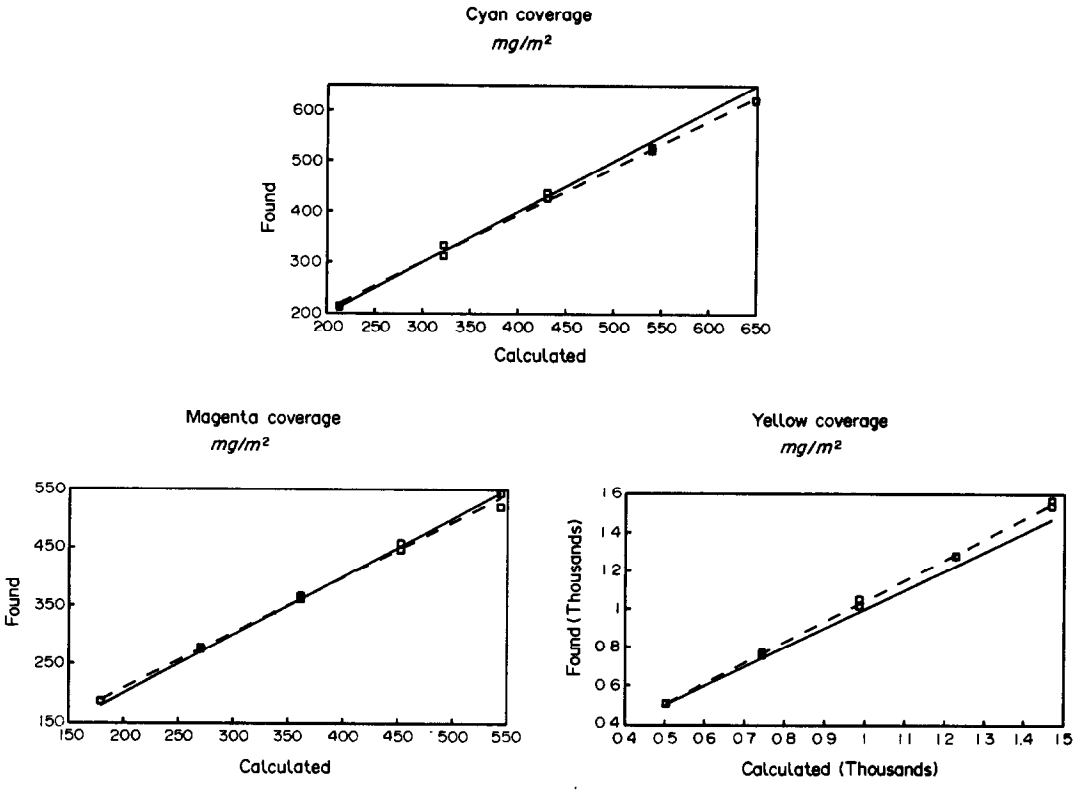

Fig. 7. Results of spiking negative extract with various level of the image dyes. Comparison of calculated dye coverage to measured dye coverage. Solid line represents a slope of one (perfect recovery) and dashed line represents best fitting line.

corresponding to the concentrations of dyes in the spiked extracts. The results of this study are contained in Fig. 7 as a plot of calculated *vs.* measured dye coverages. They indicate a slight bias at the extremes of the conditions tested. The conclusion reached is that for the best accuracy, standard and sample concentrations should be as close as possible.

An analysis of our laboratory operations related to this determination showed that the operators spent most of their time calculating results, preparing and distributing reports, and updating control charts. This was true of either the manual or the robotics version of the determination. It was clear that major time savings could be realized by automating these operations. These aspects of the project were solved with several different software packages in the MS–DOS environment. These included a spreadsheet program (Quattro Pro) used as the operator interface, data acquisition/reduction software (Asyst), communications software (Reflections 4), and database/data management software (Oracle). The result was a system which automated all of the above operations.

CONCLUSIONS

The FIA procedure for determining dye coverage has many advantages over the manual and robotics procedures. These include: (*a*) reduced labor requirements (>70%), (*b*) decreased solvent consumption (65%), (*c*) high sample throughput (80 inj/hr), (*d*) automation of data handling and quality control procedures, and (*e*) 1/3–1/4 the cost of a robotics system. It was optimized and in its present form is equivalent to the older procedures with respect to accuracy and precision. With existing hardware and software, it is practical to integrate flow-injection systems into electronic based information networks.

REFERENCES

1. J. G. Liscouski, *Anal. Chem.*, 1988, **60**, 95A.
2. V. K. Walworth and S. H. Mervis, in J. Sturge, V. Walworth and A. Shepp, *Imaging Processes and Materials*, Ch. 6, p. 181. Van Nostrand Reinhold, New York, 1989.
3. J. Růžička and E. H. Hansen, *Flow-Injection Analysis*, Ch. 2, p. 6–29. John Wiley & Sons, New York, 1981.

Talanta, Vol. 39, No. 3, pp. 319–324, 1992
Printed in Great Britain.

0039-9140/92 $3.00 + 0.00

CROSS-CORRELATION IN FLOW-INJECTION ANALYSIS WITH PARALLEL FLOW STREAMS AND AMPEROMETRIC DETECTION

R. E. McKEAN* and D. J. CURRAN†
Department of Chemistry, University of Massachusetts, Amherst, MA 01003, U.S.A.

(*Received* 9 *April* 1991. *Revised* 21 *May* 1991. *Accepted* 21 *May* 1991)

Summary—Cross-correlation was implemented for flow-injection analysis by using two parallel flow lines, each with amperometric detectors, and driven by peristaltic pumps. One flow line was used to generate the reference signal for an analog correlator circuit and the other to generate the analyte signal. Cross-correlation was performed by multiplying these signals together at a time delay of zero, followed by low pass filtering. Using dopamine as a test system, improvements in signal-to-noise ratios of about two orders of magnitude were found for the correlation signal over the direct measurement of the electrode current.

Electrochemical detectors are well known for their excellent detection limits in flow-injection analysis. Further improvement in their performance in this regard can be pursued in terms of approaches which reject noise. Correlation techniques[1–4] are powerful methods to improve signal-to-noise ratios and their use in flow-injection analysis is developed in this work.

Correlation approaches have been used in inductively coupled plasma atomic-emission spectrometry,[5–8] infrared absorption spectroscopy,[9,10] flame spectrometry,[11,12] interferometry in the UV–VIS region,[5,13] chromatography[14–26] and electrochemistry.[27–34] Much of this work has focussed on improving selectivity or providing peak identification. An example of the latter is the work of Mann and co-workers who cross-correlated IR spectra of lipid samples with a reference spectrum containing only the peaks of interest.[9,10] Betty and Horlick used cross-correlation to improve the selectivity of ICP–AES spectra.[6] Blanc *et al.*[27] analysed noise generated at an electrochemical interface by an autocorrelation method similar to that of Brown and Twiss.[35] Van Rooijen and Poppe[36] used cross-correlation to identify the predominant noise source in coulometric and amperometric detectors used in HPLC and FIA. A strong correlation was found between the measured noise and the working electrode area.

We report here on the use of cross-correlation in real time, to improve the electrochemical response of a thin layer amperometric detector used in flow-injection experiments. Two independent flow-injection systems were constructed in parallel. A high concentration of analyte was injected into one stream to produce the necessary reference signal and the sample of interest was injected into the other stream. The two detector responses were then cross-correlated by an analog correlation circuit and the correlation output was plotted on a strip chart recorder.

When two signals are similar but their noise components are different, correlation can be utilized to extract the coherence of the two signals while discriminating against the noise. The correlation function is expressed by equation (1):

$$R_{xy}(\tau) = \lim_{T\to\infty} \frac{1}{2T} \int_{-T}^{+T} V_x(t)V_y(t \pm \tau)\,dt \quad (1)$$

where the time averaged or time integrated product of two power signals, $V_x(t)$ and $V_y(t)$, is evaluated at relative displacements (τ) and $R_{xy}(\tau)$ represents the correlation function. Cross-correlation was used at a single time displacement in this work and time averaged continuously by a first order low pass filter.

EXPERIMENTAL

Instrumentation

A schematic diagram of the experimental set-up is shown in Fig. 1. Teflon tubing was used throughout the FIA system (0.05 cm i.d.) and

*Present address: Rhone-Poulenc Rorer, 680 Allendale Road, Building No. 10, King of Prussia, Pennsylvania 19406, U.S.A..
†Author for correspondence.

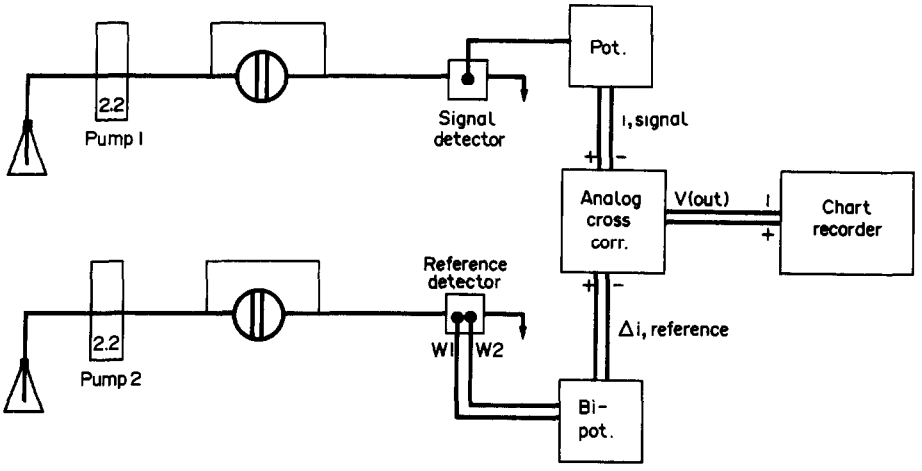

Fig. 1. Diagram of the instrumentation for parallel stream flow-injection analysis with cross-correlation in real time. The outputs from the potentiostat and the bipotentiostat are cross-correlated with analog circuitry and the correlation signal measured on a strip chart recorder.

connectors were flangeless low pressure fittings (Upchurch Scientific Inc., Oak Harbor, WA). The length of tubing connecting the injector to the detector was 30 cm for both flow systems. Two Rainin Rabbit peristaltic pumps (Rainin Instruments, Woburn, MA) were used to avoid the cross-correlation of synchronized pump noise, which occurs when a two channel pump is used. The flow-rate of each pump was set at 2.2 ml/min. A piece of silicone rubber tubing (0.15 cm i.d., Rainin, Woburn, MA) was placed after the pump to act as a pulse dampener. Low pressure Teflon injection valves (Rheodyne, type 5020, Berkeley, CA) were pneumatically actuated simultaneously with a Rheodyne 5701 and 38-931 assembly (Berkeley, CA) and control circuitry constructed in the laboratory.

A single carbon electrode thin layer amperometric detector (Bioanalytical Systems, West Lafayette, IN) was used in the sample stream and a dual carbon electrode thin layer amperometric detector (MF-1000, Bioanalytical Systems) was used in the reference stream. These detectors contain stainless steel auxiliary electrodes and silver–silver chloride reference electrodes. An applied potential of +600 mV was used in all experiments for each working electrode. Both electrochemical cells, two waste containers and a battery operated potentiostat were placed in a metal tool box which served as a Faraday cage. There was no electrolytic contact between the two flow streams.

The single electrode cell voltage was controlled by a conventional adder type potentiostat constructed in the laboratory. Battery power was used to eliminate the ac ripple present in line-operated power supplies. The applied potential was also battery supplied. The working electrode current was measured with a Keithley 427 current-to-voltage converter (Keithley Instruments Inc., Cleveland, OH). Additional functions available with the Keithley 427 are: current nulling capabilities and a second order low pass filter. Due to the low power consumption, and small electrochemical currents, nine volt batteries were employed to power operational amplifiers. High quality operational amplifiers (Burr-Brown Corp., OPA128JM, Burlington, MA) were used to achieve minimum noise and low power consumption.

The circuit shown in Fig. 2 was used to operate the dual electrode electrochemical cell and calculate the difference current between the upstream electrode and the downstream electrode when both working electrodes were held at the same potential. This is a modification of a circuit for a bipotentiostat reported by McClintock and Purdy.[37] Operational amplifiers 5 and 8 were used to supply a nulling current.

A diagram of the cross-correlation circuit is shown in Fig. 3. All resistors were 1.4 mΩ 1% precision resistors and the low pass filter capacitor was 0.94 μF. Power was provided by a Philbrick Research PR-300 ± 15 V power supply. Operational amplifiers were Burr-Brown OPA128JM (Burlington, MA) and the multiplier was an Analog Devices AD534J (Norwood, MA). Data were recorded on a dual pen strip chart recorder (Microscribe 4500, Fisher Scientific, Medford, MA).

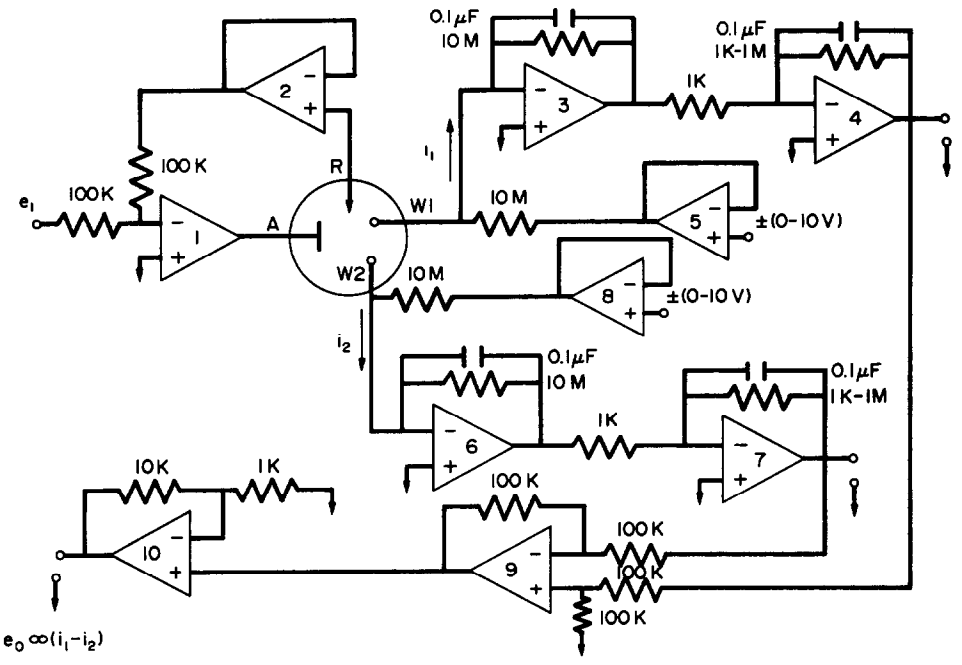

Fig. 2. Circuit digram of the bipotentiostat.

Reagents

A carrier solution of 0.1*M* sodium acetate (reagent grade, Fisher, Fairlawn, NJ) was adjusted to pH 5.1 with hydrochloric acid (Fisher, Fairlawn, NJ). Dopamine was purchased from Sigma (St. Louis, MO). Demineralized water was further purified with a Barnstead Nanopure System (Boston, MA). All dopamine solutions were prepared in 0.1*M* acetate buffer.

RESULTS AND DISCUSSION

A complete correlation operation requires multiple time delays, which is difficult to implement in real time. As a compromise a single time delay was selected. It is clear that the maximum correlation response will occur between the reference signal and the measurement signal in an FIA experiment at a time delay of zero, since the correlation process involves a multiplication and time averaging. All measurements were therefore made with zero time delay.

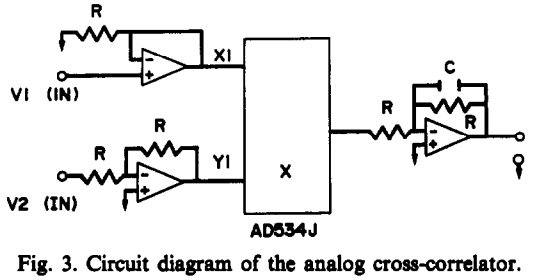

Fig. 3. Circuit diagram of the analog cross-correlator.

A zero mean baseline is necessary for the reference signal. To achieve this, a dual electrode amperometric cell with a series electrode arrangement was employed to subtract the downstream electrode current from the upstream electrode current. Figure 4 shows the

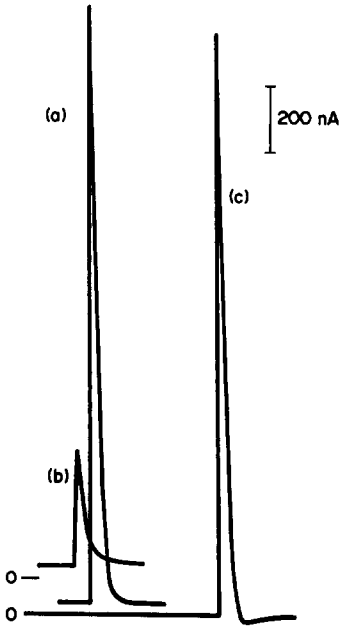

Fig. 4. Current-time response curves under bipotentiostatic control for the series electrode arrangement to illustrate peak height and background current. Zero current baseline is indicated by (0). (*a*) Upstream electrode, (*b*) downstream electrode, (*c*) difference current [(*a*) − (*b*)]. Each electrode was held at +600 mV *vs.* Ag/AgCl.

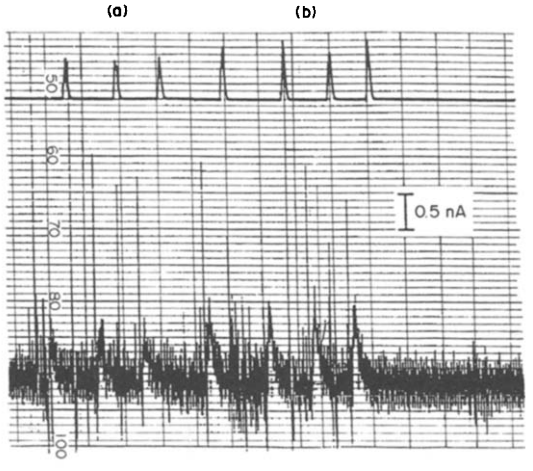

Fig. 5. Strip chart recording of noisy electrode current response signal (bottom) and cross-correlated signal (top), for injections of (*a*) 7.4n*M* and (*b*) 15n*M* dopamine in pH 5.4, 0.1*M* acetate buffer carrier solution.

response for an injection of 10μM dopamine at (*a*) the upstream electrode; (*b*) the downstream electrode and (*c*) the difference current.

For clarity, the (*a*) and (*b*) curves have been displaced on the horizontal (time) and vertical (current) axes and do not show their true time relationship. Note that both signals (*a*) and (*b*) have a nonzero baseline. After subtraction of the downstream current from the upstream current, the baseline current was reduced to zero. The advantage of this technique over simply nulling the background current is that the difference current compensates for drifting baselines while a nulled baseline cannot. Because the collection efficiency is not high, a small current is subtracted from a large current leading to a substantial difference current. The difference current can also be ampified by operational amplifiers 10 (Fig. 2), to increase the magnitude of the reference signal.

By maintaining the same flow-rate of 2.2 ml/min in each FIA system and using 30 cm of tubing between each injector and its corresponding detector, simultaneous injections of dopamine resulted in simultaneous detection. One-hundred μl of 10μM dopamine were injected into the reference stream and the same volume of dopamine with concentrations ranging from 7.4 to 240nM were injected into the sample stream. The direct electrochemical response, without cross-correlation, showed severe baseline noise as illustrated by the lower stripchart recording shown in Fig. 5. The correlated output, recorded simultaneously, is shown in the upper trace in Fig. 5. The reduction in baseline noise is very evident and the peaks are recovered nicely from the noise. The correlated response signal was converted to current and plotted versus concentration. The result was linear with a correlation coefficient of 0.997. It is important to note that the experimental configuration was such that cross-correlation of the noise was accomplished, but the choice of time constant for the low pass filter was such that the signal was not time averaged. In fact, correlation was implemented recursively, with a time constant of 1.3 sec over the entire FIA experiment. As seen in Fig. 5, the cross-correlated signal retains a peaked shape. Had the

Table 1. Cross-correlation response

Conc., nM	Peak height, *nA* 1	2	3	Mean, *nA*	St. dev.	% RSD	S/N
7.4	0.53	0.53	0.56	0.54	0.02	3.2	180
15	0.73	0.77	0.77	0.76	0.03	3.3	253
30	1.40	1.38	1.35	1.38	0.03	1.8	460
59	2.27	2.31	2.29	2.29	0.02	0.9	763
120	4.74	4.63	4.74	4.70	0.06	1.3	1570
240	8.36	8.42	8.24	8.34	0.09	1.1	2780

$Noise_{rms}$ = 0.003 nA Reference peak height = 5.5 V.

Direct current from electrode

Conc., nM	Peak height, *nA* 1	2	3	Mean, *nA*	St Dev.	% RDS	S/N
7.4	0.50	0.45	0.34	0.43	0.08	19.0	1.4
15	0.62	0.72	0.74	0.69	0.06	9.2	2.3
30	1.82	1.52	1.60	1.65	0.15	9.3	5.5
59	2.88	2.79	2.90	2.85	0.06	2.1	9.5
120	6.25	6.34	6.13	6.24	0.10	1.6	21
240	11.5	11.6	11.3	11.5	0.14	1.2	38

$Noise_{rms}$ = 0.3 nA.

signal also been time averaged, the data would appear in the form of the integral of the peaks shown in the upper trace of Fig. 5.

Signal-to-noise ratios (S/N) were determined by dividing the mean peak height of three replicates by the root mean-square (rms) noise. The rms noise of the baseline current, as measured at the output of the current-to-voltage converter was 0.3 nA, while that at the correlator output was 0.003 nA after converting the voltage outputs of the respective circuits to current. Table 1 shows the data for triplicate determinations for both the I/E converter output and the correlator output, along with the calculated means, standard deviations and signal-to-noise ratios. The improvement in relative standard deviation and S/N of the correlation results over the electrode current measurements is substantial. The electrode current signal for the lowest concentration is essentially buried in noise (S/N = 1.4), but the correlation result for the same concentration had a S/N of 180. The improvement in S/N for the lower concentrations studied is over two orders of magnitude.

Choosing a S/N of 3 to correspond to the detection limit, the correlation results should yield a detection limit of 0.12nM dopamine, or about 2 picograms for 100-μl injections. This is over two orders of magnitude better than the detection limit for the measurement without cross-correlation. Attempts to achieve these detection limits in practice were inhibited by two problems which were identified. The first is the presence of false response peaks due to the pressure surge created when the injection valve is turned. Their shape and timing is identical to that of analyte peaks and they produce a blank response when carrier stream solution is injected into the carrier stream. Peak heights for these blanks had an average value of 0.031 nA which would correspond to an apparent concentration of 0.83nM. The second problem relates to the use of a reference signal obtained in real time. The precision of the reference peak maximum is subject to the experimental variation inherent in the injection and measurement process. The experimental variability in the reference signal manifests itself in the precision of the correlation signal. Solutions to these problems have been investigated. The false peak has been separated in time from the analyte peak and computer storage and playback of the reference peak were used. The detection limit was improved by a factor of four. Details will be presented elsewhere.

CONCLUSIONS

It has been demonstrated that cross-correlation techniques produce improvements in S/N of over two orders of magnitude for flow-injection analysis with amperometric detection. The correlation operation was performed in real time in the analog domain. Its implementation is simple, straightforward and inexpensive. In addition, the approach is not limited to electrochemical detectors and could be applied to any type of flow stream detector.

Acknowledgement—Partial funding for this work has been provided by Merck Sharp & Dohme Research Laboratories, West Point, PA. Presented at the Third Winter FIA Conference, Scottsdale, AZ, January, 1991.

REFERENCES

1. G. M. Hieftje, *Anal. Chem.*, 1972, **44**, 81A.
2. Y. W. Lee, T. P. Cheatham Jr and J. B. Wiesner, *Proc. IRE*, 1950, **38**, 1165.
3. K. Doerffel, A. Wundrack and S. Tarigopula, *Z. Anal. Chem.*, 1986, **324**, 507.
4. F. H. Lange, *Correlation Techniques*, pp. 1–90. Van Nostrand, Princeton, New Jersey, 1967.
5. R. C. L. Ng and G. Horlick, *Appl. Spectrosc.*, 1985, **39**, 834.
6. K. R. Betty and G. Horlick, *ibid.*, 1978, **32**, 31.
7. R. M. Belchamber and G. Horlick, *Spectrochim. Acta.*, 1982, **37B**, 1037.
8. R. C. L. Ng and G. Horlick, *ibid.*, 1981, **36B**, 529.
9. L. L. Tyson, U. Ling and C. K. Mann, *Appl. Spectrosc.* 1984, **38**, 663.
10. C. K Mann, J. R. Goleniewski and C. A. Sismanidis, *ibid.*, 1982, **36**, 223.
11. G. Hieftje, R. I. Bystroff and R. Lim, *Anal. Chem.*, 1973, **45**, 253.
12. G. Horlick, *ibid.*, 1973, **45**, 319.
13. R. C. L. Ng and G. Horlick, *Appl. Spectrosc.*, 1985, **39**, 841.
14. K. Izawa, K. Furuta, T. Fujiwara and N. Sayama, *Ind. Chim. Belge.*, 1967, **32**, 223.
15. H. C. Smit, *Chromatographia*, 1970, **3**, 515.
16. *Idem, J. Res. Natl. Bur. Stand.*, 1985, **90**, 441.
17. J. M. Laeven, H. C. Smit and J. C. Kraak, *Anal. Chim. Acta*, 1983, **150**, 253.
18. H. C. Smit in *Trace Residue Analysis*, D. A. Kurtz, (ed.), pp. 101–113. American Chemical Society, Washington, D.C., 1985.
19. H. C. Smit, *TRAC*, 1983, **2**, 1.
20. R. Annino and J. Leone, *J. Chromatog. Sci.*, 1982, **20**, 19.
21. H. C. Smit, T. T. Lub and W. J. Vloon, *Anal. Chim. Acta*, 1980, **122**, 267.
22. H. C. Smit, C. Mars and J. C. Kraak, *ibid.*, 1986, **181**, 37.
23. R. B. Lam, D. T. Sparks and T. L. Isenhour, *Anal. Chem.*, 1982, **54**, 1927.
24. R. Annino, *Chromatogr. Sci.*, 1976, **14**, 265.

25. J. M. Laeven, H. C. Smit and J. C. Kraak, *Anal. Chim. Acta*, 1987, **194**, 11.
26. M. Kaljurand and E. Kullik, *J. Chromatogr.*, 1979, **186**, 145.
27. G. Blanc, C. Gabrielli and M. Keddam, *Electrochim. Acta*, 1975, **20**, 687.
28. M. Ichise, Y. Nagayanagi and K. Tsugio, *J. Electroanal. Chem. Interfacial Electrochem.*, 1974, **49**, 187.
29. M. C. Lorenzo, P. Canas and A. Aldaz, *Anal. Chim. Acta*, 1987, **201**, 295.
30. R. L. Birke, *Anal. Chem.*, 1971, **43**, 1253.
31. S. C. Creason and D. E. Smith, *J. Electroanal. Chem.*, 1972, **40**, 1.
32. S. C. Creason and D. E. Smith, *Anal. Chem.*, 1973, **45**, 2401.
33. D. E. Glover and D. E. Smith, *ibid.*, 1973, **45**, 1869.
34. S. C. Creason and D. E. Smith, *J. Electroanal. Chem. Interfacial Electrochem.*, 1972, **36**, App 1.
35. R. M. Brown and R. Q. Twiss, *Proc. R. Soc. A.*, 1957, **291**, 243.
36. H. W. Van Rooijen and H. Poppe, *J. Liq. Chromatogr.*, 1983, 2231.
37. S. A. McClintock and W. C. Purdy, *Anal. Lett.*, 1981 791.

Talanta, Vol. 39, No. 3, pp. 325–327, 1992
Printed in Great Britain

0039-9140/92 $5.00 + 0.00
Pergamon Press plc

ANALYTICAL DATA

SPECTROPHOTOMETRIC DETERMINATION OF THE ACIDITY CONSTANTS OF 2-AMINO CYCLOPENTENE-1-DITHIOCARBOXYLIC ACID AND SOME OF ITS DERIVATIVES

M. B. GHOLIVAND and A. SAFAVI*
Department of Chemistry, Shiraz University, Shiraz, Iran

(*Received* 3 *June* 1991. *Accepted* 9 *August* 1991)

Summary—The acidity constants of 2-amino cyclopentene-1-dithiocarboxylic acid (ACDA) and some of its derivatives have been determined spectrophotometrically, at 25° and at different mole fractions of ethanol in water. In all solvent mixtures used, the acidity constants vary in the order ACDA > *N*-methyl-ACDA > *N*-ethyl-ACDA > *N*-butyl-ACDA.

Recently, there has been increasing interest in the compounds of 2-amino cyclopentene-1-dithiocarboxylic acid (ACDA) and its derivatives.[1,2] These compounds act as ligands to form different complexes with metal ions.[3–7] The importance of these complexes lies in the fact that they are used as models of sulphur metal proteins.[1] Moreover, there are reports on the use of some of these compounds as antifungal substances.[8]

Evaluation of the acidity constants of organic reagents is of great value in planning analytical work,[9] *e.g.*, the acidity constants can be employed in the design of titration procedures and in examining the possibility of the separation of mixtures of compounds by extraction. The complexing properties of a molecule depend on the number and steric disposition of its donor centres as well as on its acid–base properties. The study of the analytical behaviour of ACDA and its derivatives has been undertaken in this laboratory. In this paper we report the acidity constant of some of these compounds in mixed solvents.

EXPERIMENTAL

Chemicals

Hydrochloric acid (Merck) and sodium hydroxide (Merck) were used without any purification. ACDA and its derivatives were synthesized according to the work of Takashima and Yokoyama[10] and Bordas *et al.*[11] These compounds were further recrystallized from methanol.

Apparatus

A Corning 130 pH meter and a Cary 118 spectrophotometer with a temperature control were used.

Procedure

The procedure of Asuero *et al.* was used.[12] In this procedure the absorbance of $9.8 \times 10^{-5}M$ ACDA was measured in highly acidic and basic media, and at pH values close to p*K*a, in different mole fractions of ethanol in water. A similar procedure was used for *N*-methyl-2-amino cyclopentene-1-dithiocarboxylic acid (*N*-methyl-ACDA), *N*-ethyl-2-amino cyclopentene-1-dithiocarboxylic acid (*N*-ethyl-ACDA) and *N*-butyl-2-amino cyclopentene-1-dithiocarboxylic acid (*N*-butyl-ACDA). All experiments were performed at 25°.

RESULTS AND DISCUSSION

Water, with its particular relevance to the biological systems, is the best solvent for determination of acidity constants. But owing to the low solubility of ACDA and its derivatives in aqueous media, the acidity constants were also

*Author for correspondence.

Table 1. The pKa values of ACDA and its derivatives (pKa ± 0.03)

X_{EtOH}	ACDA	*N*-methyl-ACDA	*N*-ethyl-ACDA	*N*-butyl-ACDA
0	6.18	6.39	6.50	*
0.07	6.24	6.40	6.82	*
0.17	6.54	6.77	7.20	7.44
0.32	7.28	7.50	7.61	7.71
0.55	8.16	8.23	8.31	8.44

*The acid was not soluble.

determined in mixed solvents. Ethanol was chosen as the non-aqueous solvent, because the structure of ethanol is very similar to the water structure. The pKa values of mentioned compounds were determined and are shown in Table 1. The variation in pKa values of 2-amino-cyclopentene-1-dithiocarboxylic acids containing different substituents on nitrogen atoms can be explained in terms of factors such as inductive effect due to alkyl substituents, strain factors associated with bonding at the nitrogen atom, and various degrees of solvation of ligand and the ligand anion.

As can be seen from Table 1, the presence of electron releasing groups such as methyl, ethyl and butyl decreases the acidic properties of these acids. This is expected since by replacing one of the hydrogen atoms of the NH_2 group by alkyl groups, the electron releasing property of the amino function to the ring is increased and this inductive effect results in a larger negative charge on the sulphur atoms, which attracts the proton. Thus addition energy is required for the dissociation of the acid, making ΔG° less negative and, hence, larger values of pKa are obtained. Therefore, the ionic property of the S—H bond in four acids varies in the order ACDA > *N*-methyl-ACDA > *N*-ethyl-ACDA > *N*-butyl-ACDA.

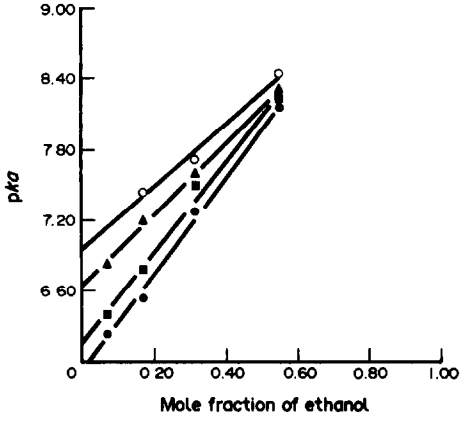

Fig. 1. Variation of pKa values of acids with X_{EtOH} in binary mixtures for ACDA (●), *N*-methyl-ACDA (■), *N*-ethyl-ACDA (▲) and *N*-butyl-ACDA (○).

The data shown in Table 1 clearly illustrate the important influence of the nature of the solvent in the dissociation reaction. The acidity constants of four acids decreases rapidly with increasing the mole fraction of ethanol in the mixed solvents. It has been shown that the solvating ability[13] (as expressed by the Gutmann donicity scale) and dielectric constant of the solvent play a fundamental role in dissociation reactions. Water is a solvent of high solvating ability [*i.e.*, donor number (DN) = 33[14] and dielectric constant (ϵ) = 78] which can dissociate the acid and stabilize the produced anion and hydrogen ion. Thus it is expected that addition of ethanol with lower donor number and dielectric constant (DN = 18.5, ϵ = 24.3) to water, decreases the extent of interaction between the ligand anion and proton with solvent, and this decreases the acidity constant of the acids.

It is interesting to note that there is actually a linear relationship between the pKa value of each acid and the mole fraction of ethanol (X_{EtOH}) in the binary mixed solvents used (Fig. 1).

It is clear that, the dissociation of an uncharged acid in a solvent requires the separation of two ions of opposite charges. The work required to separate these charges is inversely proportional to the dielectric constant of the solvent. The energy required for dissociation is supplied by solvation of the ions and also an additional energy is supplied by the proton transfer from acid to the solvent molecule. If the dielectric constant and the solvating ability of the solvent is decreased, more energy will be required to separate the anion and cation and consequently the extent of dissociation of acid will be lowered. Therefore, the increase in pKa value of each acid is due to increasing the mole fraction of ethanol in the binary mixed solvent.

Another interesting point that is seen in Fig. 1 is the differentiating property of water. Water is an amphiprotic solvent that acts as differentiating solvent. By addition of ethanol to water the basicity of mixed solvent will be increased, so that the solute acids become much stronger

proton donors than the protonated solvent. The dissociation reaction then goes to completion, and the acid is said to be levelled to the strength of the solvated proton. Therefore, although transfer of the proton is complete, because of lower dielectric constant of the mixed solvent, the equilibrium involves an ion-pair rather than the solvated ions. This causes an increase in the levelling effect of solvent by increasing the mole fraction of ethanol, or decreasing the dielectric constant of the binary mixed solvent. This is clearly shown in Fig. 1.

REFERENCES

1. D. M. Baird, *J. Chem. Educ.*, 1985, **62**, 168.
2. M. B. Gholivand and A. Safavi, *submitted for publication.*
3. K. Nag and D. S. Joarder, *Inorg. Chim. Acta*, 1975, **14**, 133.
4. *Idem, Z. Naturforsch*, 1975, **30b**, 107.
5. *Idem, Can. J. Chem.*, 1976, **54**, 2827.
6. S. M. Mondal, R. S. Mondal and K. Nag, *Indian J. Chem.*, 1981, **20A**, 982.
7. S. K. Mondal, D. S. Joarder and K. Nag, *Inorg. Chem.*, 1978, **17**, 191.
8. G. Matolcsy, B. Bordas, M. Hamran and M. Tiborez, *Acta, Phytopathologica Academiae Scientiarm Hungaricae*, 1971, **6**, 381.
9. C. Crevoisier and P. Buri, *Pharm. Acta Helv.*, 1971, **51**, 193.
10. T. Takeshima and M. Yokoyama, *J. Org. Chem.*, 1969, **34**, 730.
11. B. Bordas, D. Sohar, G. Matolcsy and P. Berencsi, *ibid.*, 1972, **37**, 1727.
12. A. G. Asuero, M. J. Naras and J. L. Jimenez-Trillo, *Talanta*, 1986, **33**, 195.
13. V. Gutmann, *Coordination Chemistry in Nonaqueous Solutions*. Springer-Verlag, New York, 1960.
14. P. H. Erlich and A. I. Popov, *J. Am. Chem. Soc.*, 1971, **93**, 5620.

Talanta, Vol. 39, No. 4, pp. 329–339, 1992
Printed in Great Britain

0039-9140/92 $5.00 + 0.00
Pergamon Press plc

APPLICATION OF HYDRIDE GENERATION TO ATOMIC-ABSORPTION SPECTROMETRIC ANALYSIS OF WINES AND BEVERAGES: A REVIEW

C. BALUJA-SANTOS* and A. GONZALEZ-PORTAL
Department of Analytical Chemistry, Nutrition and Bromatology, Faculty of Chemistry, University of Santiago de Compostela, Santiago 15706, Spain

(*Received* 4 *February* 1989. *Revised* 14 *September* 1991. *Accepted* 27 *September* 1991)

Summary—The use of hydride-generation systems for atomic-absorption spectrometry and other spectrometric methods for the determination and control of As, Sb, Bi, Pb, Sn, Se and Te in wines and beverages is reviewed.

Methods based on atomic-absorption spectrometry (AAS) and inductively-coupled plasma atomic-emission spectrometry (ICP/AES) are widely used for chemical characterization of wines and beverages, investigation of their adulteration, and study of the changes that take place during vinification and the preparation of beverages. Of more than 20,000 papers published on these techniques in less than 25 years, over 300 are concerned with their application to the major, trace and ultratrace elements in wines and beverages, and of these over 100 are devoted solely to the determination of calcium and magnesium.[1]

The analytical potential of hydride generation systems in atomic-absorption spectrometry (HG–AAS) is apparent from earlier reviews,[2–8] systematic studies of interferences,[9,10] and papers on hydride generation and atomization mechanisms.[11,12] However, of the more than 600 articles published on this subject since 1970, very few are devoted to the application of HG–AAS to wines and beverages.

The aim of the present review, based in part on a paper presented in 1986 at the International Viticultural and Oenological Congress (OIV) in Santiago (Chile),[13] is to describe the hydride-generation technique, decide which of the various spectrometric methods are best fitted for use with hydride-generation systems, and compare the results obtained by their use with those of other techniques used in the analysis of wine and beverages, with special attention to determination of As, Sb, Bi, Pb, Sn, Se and Te.

*Author for correspondence.

FUNDAMENTALS

Covalent hydrides are volatile compounds in which hydrogen is bound to elements of Groups IIIb–VIb. So far, only eight of these elements are determined by atomic-absorption or emission photometric methods by means of the hydrides: Ge, Sn, Pb, As, Sb, Bi, Se and Te.

Levels of As, Sb, Bi, Pb, Sn, Se and Te in wine

According to Bowen's classification,[14] As, Sb, Bi, Pb, Sn, Se and Te are elements of unknown biological function that are regarded as toxic because they accumulate in the human organism. In fact, many of the elements found at very low concentrations in living beings have toxic effects at concentrations that are only slightly higher than normal. The problems posed by these elements for oenology, toxicology and physiological biochemistry are similar.

The mineral elements contained in wine depend on numerous factors, including kind of soil, variety of grape, climatological conditions, pollution and viticultural practices. The primary natural mineral content is to be distinguished from the secondary contaminants derived from the use of pesticides and fertilizers or acquired during vinification (in spite of the overall reduction in mineral content during this process). Table 1 summarizes the levels of various elements in man and in wine.

Table 1. Levels of certain elements in wines

Element	Level in man, *mg*	Level in wine, *mg/l.* Primary	Secondary	Limit[a]
As	1	—	1[b]	0.2
Sb	8	—	(A)	—
Bi	—	None	3[c]	—
			0.1–0.2[d]	
Pb	100–400	0.1	0.4–1.0 (B)	0.4
Sn	17	0.1–0.9	(C)	0.2
		0.3 (mean)	0.2–0.7[e], 0.1[f]	
Se	3.15	—	1.0	—
Te	(?)[h]		(D)	—

[a] Limit fixed by Office Internationale de la Vigne et du Vin (OIV).

[b] Higher levels are considered dangerous. Possible sources of As include additives such as citric or tartaric acid, agar-agar, bentonite or tannins.[15]

(A) In contact with old rubber hose, Sb levels rose tenfold after 3 hr and more than 60-fold after 48 hr.[16]

[c] A problem with Australian wines.[17]

[d] Fortified Spanish wine.[18]

(B) Contamination from lead alloys, plastics, paints and ambient air.[19]

(C) The source of tin may be tinplate containers[20,21] or the storage of wine in untreated PVC bottles.

[e] Average level measured in 8 Moselles.[21]

[f] Wine and brandy from Moldavia.[23]

[g] Selenium levels higher than about 100 μg can produce symptoms of chronic poisoning.[24]

[h] Probably 550–600 μg.

(D) The source of Te in wine is contamination.

Methods used in the analysis of wine and beverages

Among the most widely used techniques for the determination of mineral elements in wine and beverages are atomic-absorption spectrometry (AAS) and electrothermal AAS (ET–AAS), but it is generally necessary to subject samples to pretreatments that vary from one element to another. The choice of method is influenced by the desired selectivity and sensitivity, the number of samples to be analysed, the interferences present, the need to use standards or reference methods, and the cost of apparatus. A general discussion of these factors has been published elsewhere.[1] Table 2 offers a comparative summary of various methods used.

Hydride generation

Initially, "nascent" hydrogen produced by metal–acid reactions was used to generate hydrides for quantitative analysis; the most widely employed are listed in Table 3. However, these reactions all have some drawback, such as low reaction rate, presence of excess of hydrogen, or (last but not least) the small number of hydrides generated, which limits the number of elements that can be determined in a single sample.

To avoid these problems, Braman *et al.*[28] introduced use of sodium borohydride (also called sodium tetrahydroborate), which has been found applicable to determination of eight elements.[29–31] The stability of stock solutions of $NaBH_4$, which was initially a problem, was increased by using a 0.45 μm filter to remove the cloudy carbonaceous precipitate produced by alkalization with potassium hydroxide[32] or sodium hydroxide.[33] To avoid interference

Table 2. Comparative summary of the methods for analysis of wines and beverages

Method	No. of elements determinable	Cost factor	Selectivity	Sensitivity, μg	Precision, %
POL or VOL	30	1	poor	1.0	3
S (vis–UV or F)	60	0.5	poor	0.1	1
AES	60	—	medium	1.0	2
AAS	60	1	good	0.1	1
ET–AAS	60	2	good	0.0001	3
ICP	75	6	good	0.01	2
XRF	80	4	medium	1.0	10
SSMS	80	10	good	0.001	5
NAA*	75	1.5	medium	0.001	5

POL or VOL = polarography or voltammetry.
S (vis–UV or F) = spectrophotometry in the vis–UV region or by fluorescence.
AES = atomic-emission spectrometry.
AAS = atomic-absorption spectrometry.
ET–AAS = electrothermal atomic-absorption spectrometry.
ICP = inductively coupled plasma.
XRF = X-ray fluorescence spectrometry.
SSMS = spark-source mass spectrometry.
NAA = neutron-activation analysis.
*With Ge(Li) detector.

Table 3. Metal–acid reactions for hydride generation

Metal	Acid	No. of hydrides generated	Rate of reaction	Reference
Zn*	HCl	2	Slow	25
$Zn/TiCl_3$	H_2SO_4 and/or HCl	2	Slow	26
$Mg/TiCl_3$	H_2SO_4 and/or HCl	5	5–10 min	26
Al†	HCl	3	—	27

*Prior reduction of As(V), Se(VI) and Se(VI) with $SnCl_2$–KI.
†For As determination, prior reduction with $SnCl_2$–KI.

from nickel in the determination of arsenic and selenium, use of sodium cyanoborohydride ($NaBH_3CN$) has been proposed,[34] but the risk of release of HCN and the consequent need for strict safety measures make this method inadvisable for routine work, and the $NaBH_4$ reaction is currently the most widely used. Most authors recommend storing the reductant solution in glass containers under refrigeration.

A wide variety of designs have been proposed for the hydride-generation apparatus.[7,35–37]

Collection of the hydride

Various systems have been devised for collection of the hydrides generated and their transport to the atomizer.

Liquid-nitrogen trap. This was the first system employed.[38] The hydride is collected in a U-tube which is then closed with a stopcock to prevent back-diffusion. One end of the U-tube is then connected to the premix chamber of the instrument used, and the other to a nitrogen or argon flow to carry the hydride to the atomizer. This technique was further developed by Braman *et al.*[39] and modified by Crecelius,[40] but is sometimes considered too slow for routine work.

Absorption solutions. Madsen[41] proposed generating AsH_3 (by reduction with zinc in sulphuric acid) in a 125-ml conical flask and collecting it in 5 ml of 0.01*M* silver nitrate in a 10-ml measuring cylinder. The absorption solution is then aspirated into an argon–hydrogen flame in an AAS apparatus. For sampling in the field, the hydrides of As, Sb, and Se can be absorbed on solid supports impregnated with silver nitrate or mercuric chloride, which are then transported to the laboratory for analysis.[42]

The balloon method. The collector described by Fernandez and Manning[43] has been modified for use as a closed system.[44] This has become the most popular method of hydride collection and has been commercialized by Perkin–Elmer. Its main drawback is the frequency with which the balloon must be changed; the useful life of a balloon has been variously estimated as 50,[44] or as few[45] as 15–20 determinations.

Other collector systems. Glass or plastic[46] flasks have been used as an alternative to balloons.

Direct introduction. It is not always necessary to collect the hydride released, though this is the procedure followed in the only commercial system currently available. Many authors have used systems in which collection of the hydride is not required.[28,30,46,47]

Atomization techniques

Tubes heated by flames. This is the most widely used method. The air–acetylene flame employed by Holak[38] has been replaced by the argon–hydrogen flame, which is currently the most highly recommended of all the various methods of heating the tube by a flame or electrically. To aid combustion for atomization of the hydride, Siemer and Hagemann[46] added a small quantity of oxygen to the stream of hydrogen used to carry the hydride (released by $NaBH_4$) to the silica tube. Thompson and Thomerson[30] were the first to employ a special open tube having the advantages of not requiring a collector and of removing virtually all background absorption by the flame. Both air–acetylene and argon–hydrogen flames were tried, better sensitivity being obtained with the latter. The tube is fixed to the head of the burner.

Electrically heated tubes. Chu *et al.*[45] used an electrically heated tube as an alternative to a flame. The carrier gas used was argon. The absence of a flame reduces background absorption, and the relatively great length of time for which the atoms to be determined remain in the tube considerably improves the sensitivity relative to that of flame techniques. This system is used for the determination of arsenic. The great advantage of these atomizers is the ease with which the temperature can be controlled

Table 4. Atomization systems

Method	Reductor	Carrier gas	Flame	Elements	Reference
AFS*	$NaBH_4$	Argon	$Ar-H_2$	As, Bi	50
AFS*	$NaBH_4$	Argon	$Ar-H_2$	Bi	51
AFS†	Zn powder	Argon	$Ar-H_2$	Sb, As, Se, Te	52
DC-arc	$NaBH_4$	Helium	—	As, Sb	53
MIP	Zn	Argon	—	As‡	53, 54
MECA	$NaBH_4$	§	—	As, Sb	55
ICP	$NaBH_4$	#		As	56

AFS = atomic-fluorescence spectrometry (*undispersed system; †dispersed system).
DC arc = arc or plasma spectrography.
MIP = microwave induced plasma.
MECA = molecular emission cavity analysis.
ICP = inductively coupled plasma.
‡Comparison with molybdenum blue method.
§Gas chromatography separation.
#Hydride preconcentration apparatus.

provide the optimal temperature for each hydride.

A detailed investigation was made of the system to optimize the sensitivity for the individual elements. The stability of the hydrides was also investigated and decided which hydrides should be introduced directly into the cell (Sb, Pb, Te, Sn) or could be collected in a gasometer and subsequently transferred to the cell (As, Bi, Se).[48]

Deterioration of the inner surface of the silica tube has been observed.[34,49]

Other atomization systems. Table 4 summarizes other systems employed, which range from atomic-fluorescence spectrometry (AFS) to the inductively-coupled plasma (ICP) and microwave-induced plasma (MIP) techniques. The latter two are particularly valuable for multielemental analysis, since they considerably widen the working range.

Light sources

The most commonly used light source is the hollow-cathode lamp (HCL), but it is not advisable for the determination of As or Se, for which the signal-to-noise ratio in single-beam apparatus is rather small. For these elements, Fernandez[31] has obtained good sensitivities and detection limits with an electrodeless discharge lamp (EDL) in conjunction with $NaBH_4$, a balloon collector and an argon–hydrogen flame. The AFS and ICP techniques naturally need no light source.

Automatic systems

Various articles on the design and application of automatic and semi-automatic systems have been published.[47,57] Two groups may be distinguished: methods which use a peristaltic pump and those in which the reagent is transported under pressure. Those in the former group are the more highly automated because they involve less manipulation, but those in the latter group have the advantage of allowing very strict control of the hydride generation conditions.

Flow-injection analysis

The flow-injection hydride generation methods coupled with AAS are characterized by high efficiency, low sample and reagent consumption, and improved tolerance of interferences.[58-60] High throughput, of over 200 samples/hr, is feasible with relative sensitivities and detection limits comparable with those of conventional HG–AAS methods but consuming only μl volumes of sample. Such samples have to go through tedious preconcentration procedures to achieve 10–50-fold enrichment before the hydride-generation determination. Ion-exchange preconcentration has been combined with flow-injection HG–AAS to produce an efficient system for ultratrace determination of hydride-forming elements.[61]

Sample preparation

It is usually necessary to subject samples to wet or dry ashing. The methods used are summarized in Table 5.

Dry ashing. This is not the most usual method, since As, Sn, Sb, and Se tend to undergo loss through volatilization. Tam and Lacroix[62] have none the less obtained 100% recovery for As and Se determined by HG–AAS, from samples subjected to dry ashing

Table 5. Methods of sample preparation

Method	Elements	Remarks
Dry ashing		
$Mg(NO_3)_2$	As, Sb, Se	HCl solution
MgO	As, Se	HCl solution
Wet digestion		
$HNO_3 + H_2SO_4$	As, Sb	
$HNO_3 + HClO_4$	Se, As, Sb	
$HNO_3 + HClO_4 + H_2SO_4$	Se, As, Se	Often utilized

with a magnesium nitrate and oxide mixture as an alternative to wet ashing by digestion with a mixture of nitric, perchloric and sulphuric acids. The optimal Mg^{2+} concentration in the ashing aid is 0.6–6.0 mg/ml; higher concentrations lead to low results.

Wet digestion. Because of the volatility of the chlorides of the elements to be determined, the samples are decomposed with nitric acid, sulphuric acid, hydrogen peroxide and/or perchloric acid. Each of these reagents has its advantages and drawbacks, and normally they are used in combination. Among the reviews on the preparation of samples, that of Gorsuch[63] is particularly noteworthy, and for the digestion of biological samples that of Nève *et al.*[64]

Bomb digestion. Digestion with acid in a Teflon bomb considerably reduces losses. Alkaline media are not used for HGS work, nor is hydrofluoric acid, which gives rise to fluoride complexes of As, Sb and Sn. The bomb method is limited by the volume of sample and by the critical nature of the volume of acid and the temperature and duration of heating.

Microwave oven. Digestion by microwave oven, first used by Koirtyohann and colleagues at the University of Missouri[65] and later popularized by Kingston and Jassie,[66] is one of the most recent methods. The technique has a wide range of applications, and has excellent speed and reproducibility.[67]

Wine and beverage sampling. The preparation of samples of wines and beverages for analysis by HG–AAS is not particularly difficult. It is generally sufficient to subject the sample to degasification and acidification, followed by reduction of the analyte with potassium iodide (for As or Sb) or hydrogen (for Se and Te). The mineralization of wines and beverages has been comprehensively discussed by Baluja-Santos *et al.*,[1] Godden and Thomerson,[7] and others.[68–73]

Interferences

The interferences affecting HG–AAS may be classified in two groups, those arising during preparation of the hydrides and those arising during atomization.

Factors causing interferences during hydride generation

Oxidation state. The initial oxidation state of the element to be determined has a considerable influence on the absorption signal. The signals produced by Se(VI) and Te(VI), for example, are negligible compared with those of Se(IV) and Te(IV). After boiling for 15 min with 3:1 v/v nitric acid–hydrochloric acid mixture and subsequent cooling and dilution, Te(VI) is completely reduced to Te(IV) by the hydrochloric acid, but application of the same procedure to Se(VI) reduces only 50% of the selenium.[30]

As and Sb can be reduced to hydrides from both their (III) and (V) oxidation states. The selective determination of As(III) in presence of As(V) by suitable adjustment of the acidity before addition of $NaBH_4$ has been proposed by Aggett and Aspell[37] and Nakashima.[74]

Concentration of acid. When $NaBH_4$ is used as the hydride generation agent, the absorption signals of the As, Bi, Se and Te hydrides remain constant when the acid concentration is increased.[31] These findings have been corroborated by other studies, except that the Te signal has been observed to increase when the acid concentration is increased from 1 to 4*M*.[75]

When the acidity is maintained at pH 4–5, As(III) can be determined in presence of As(V), and total arsenic determined after increasing the acidity to 5*M* (hydrochloric acid).[37,74,76]

Pettersson and Olin[77] studied the reduction of Se(VI) to Se(IV) in 4, 5, and 6*M* hydrochloric acid at temperatures between 50 and 95° with continuous-flow hydride-generation AAS. Their results indicate that the addition of chloride to an acid digest should be limited to a concentration of about 2.5*M*.

Organic bonds. As with biological media, in analysis of wines and beverages it is necessary to take into account bonds between the element to be determined and organic groups. Fernandez and Manning consider that when the sample may contain such bonds, a preliminary oxidation is necessary.[43]

Factors causing interferences during atomization

Interference by other elements may produce a signal that is greater or smaller than the true signal of the element to be determined. Among other isolated results, it may be noted that Braman *et al.*[28] found that Cu and Ag interfere

Table 6. Interferences observed for the determination of hydrides generated with sodium borohydride (argon–hydrogen flame). (Reproduced by permission from A. E. Smith, *Analyst*, 1975, **100**, 300; Copyright Royal Society of Chemistry.)

	Interference (suppression of signal)		
Element	Severe to moderate (>50% suppression)	Moderate to slight (10–50% suppression)	Not significant (<10% suppression)
As (1 μg)	Au, Ge, Ni, Pt, Pd, Rh, Ru	Ag, Bi, Co, Cu, Sb, Se, Sn, Te	Al, B, Ba, Be, Ca, Cd, Cr, Cs, Fe, Ga, Hf, Hg, In, Ir, K, La, Li, Mg, Mn, Mo, Na, Pb, Rb, Re, Si, Sr, Ti, Tl, V, W, Y, Zr, Zn
Bi (0.5 μg)	Ag, Au, Co, Cu, Ni, Pd, Pt, Rh, Ru, Se, Te	As, Cd, Cr, Fe, Ge, Ir, Mo, Sb, Sn	Al, B, Ba, Be, Ca, Cs, Ga, Hf, Hg, In, K, La, Li, Mg, Mn, Na, Pb, Rb, Re, Si, Sr, Ti, Tl, V, W, Y, Zn, Zr
Ge (2 μg)	As, Au, Cd, Co, Fe, Ni, Pd, Pt, Rh, Ru, Sn, Sb, Se	Bi, Cu, Ir, Te	Al, Ag, B, Ba, Be, Ca, Cr, Cs, Ga, Hf, Hg, In, K, La, Li, Mg, Mn, Mo, Na, Pb, Rb, Re, Si, Sr, Ti, Tl, V, W, Y, Zn, Zr
Sb (1 μg)	Au, Co, Ge, Ni, Pt, Pd, Rh, Ru	Ag, As, Cr, Cu, Re, Se, Sn	Al, B, Ba, Be, Bi, Ca, Cd, Cs, Fe, Ga, Hf, Hg, In, Ir, K, La, Li, Mg, Mn, Mo, Na, Pb, Rb, Si, Sr, Te, Ti, Tl, V, W, Y, Zn, Zr
Se (2 μg)	Ag, Cu, Ni, Pd, Pt, Rh, Ru, Sn	Au, As, Cd, Co, Fe, Ge, Pb, Sb, Zn	Al, B, Ba, Be, Bi, Ca, Cr, Cs, Ga, Hf, Hg, In, Ir, K, La, Li, Mg, Mn, Mo, Na, Rb, Re, Si, Sr, Ti, Tl, V, W, Y, Zr (Te)
Te (10 μg)	Ag, Au, Cd, Co, Cu, Fe, Ge, In, Ni, Pb, Pd, Pt, Re, Rh, Ru, Se, Sn, Te	As, Bi, Ir, Mo, Sb, Si, W	Al, B, Ba, Be, Ca, Cr, Cs, Ga, Hf, Hg, K, La, Li, Mg, Mn, Na, Rb, Sr, Ti, V, Y, Zn, Zr

*Results for tin are not quoted because of the high blank.

with arsine and stibine generated in alkaline media with NBH_4, and nitric acid has been found to cause considerable interference in the determination of antimony.[7]

The most comprehensive study of interferences in hydride-generation work was made by Smith,[9] who investigated the effects of 48 elements on the determination of As, Sb, Bi, Ge, Se and Te by hydride generation with $NaBH_4$ and AAS with an argon–hydrogen flame. Table 6 summarizes his results. In another valuable study, Pierce and Brown[10] found significant differences between the results of manual and automatic hydride generation when they compared the effects of various anions, cations and acids on the determination of As and Se in a system with a graphite atomization furnace.

Verlinden and Deelstra[78] studied the effects of other hydride-forming elements on the determination of selenium, and found them to be in the order Bi < As < Te < Ge < Se < Sn.

Castillo *et al.*,[79] studied the interference by 27 ions.

Elimination of interferences

For the determination of As by HG–AAS with an argon–hydrogen flame, Kirkbright and Taddia[80] have developed a method for the elimination of interferences from Cu, Ni, Pt and Pd, by means of thiosemicarbazide and/or 1,10-phenanthroline. Co-precipitation with lanthanum hydroxide has been used to remove interference from the matrix metal in the determination of As, Sn, Se and Te.[81] It has been proposed that interference from nickel may be

Table 7. Sensitivities of some spectroscopic methods

	Sensitivities, μg/l.						
Method	As	Sb	Bi	Pb	Sn	Se	Te
ET–AAS	0.3	0.2	0.2	5	0.2	1.0	0.2
AAS	630	60	44	17	150	230	44
HG–AAS	0.1	0.02	0.02	0.6	0.04	0.01	0.02
AFS	100	50	5	10	50	40	5
HG–AFS	0.1	0.1	0.005	—	1.2	0.6	0.08
ICP	40	200	50	8	300	30	80
HG–ICP	0.8	1.0	0.8		1	0.8	1.0
MIP	—	—	—	—	—	3.2*	—
HG–MIP	0.35	0.5	—	—	2.0	1.25	—
APAN†	0.2	1.0	0.1	5	20	5	50

*In aqueous medium.

†APAN = atmospheric-pressure active nitrogen.[87]

Table 8. Experimental parameters and performance of hydride generation*

Element	Oxidation state	Volume of reaction system, *ml*	Acid	Volume (concentration) of $NaBH_4$ soln. injected, *ml*	λ, *nm*	Carrier gas (N_2), *l./min*	Flame	Range, *μg/l.*	Content, *μg*	Precision,† %
As	(III) and (V)	30	1.5*M* (HCl)	2 (3%)	196.0	1.25	H_2	0.5–3.0	2 [As(V)]	4.2
Sb	(III)	30	1.5*M* (HCl)	2 (1%)	217.6	1.20	Air–C_2H_2	—	—	20
Bi	(III)	50	1.5*M* (HCl)	2 (1%)	223.1	1.20	Air–C_2H_2	500	—	29
Pb	‡		0.1*M* (HCl)	3 (2.5%)	283.3§		Air–C_2H_2	0.7	0.1	5.5
Sn	(IV)	50	0.5*M* (HCl)	2 (1%)	224.6	1.20	Air–C_2H_2	—	—	—
Se	(IV)‖	50	0.6*M* (H_2SO_4)	2 (3%)	197.2	3.0	H_2	—	1.0	28
Te	(IV)	50	1.5*M*	2 (1%)	214.3	3.0	Air–C_2H_2	0.4	—	—

*Light-source HCL except for As and Se, for which an EDL is used.
†Twenty measurements.
‡Metastable Pb(IV) compounds stabilized with lactic acid.
§Measurement at 217.0 nm gives better sensitivity.
‖Reduction of Se(VI) by boiling with 4*M* HCl for 10 min.
¶Injection at intervals of 30 sec for As (6 times) and 2 min for Se (4 times).

Table 9. Applications of hydride-generation spectroscopic methods to wines and beverages

Technique	Elements	Matrix	Concentration	Remarks	Reference
HG–AAS	Sn	Wines	White (5) 0–3.6 ng/ml Red (3) 10.1–18.8	Samples digested in a Buchi 445 digestor with NHO_3 and H_2SO_4 (DL = 3.3 μg/ml)	68
	As	Wine with "Appellation of origin"	Red (14) 5.0 ± 3.2 ng/ml Rosé (14) 2.7 ± 0.1 ng/ml	Comparison with molecular absorption photometry (DL = 3.0 μg)	88
	Pb	Wine of Rioja	0.1 μg/ml	Comparison of several decomposition methods	89
	Pb	Wine	0.10 ± 0.03* μg/ml	Samples pretreated with 0.5*M* HNO_3. Lactic acid used to stabilize Pb(IV)	90
	Se	Grapes	Seeds 3.2–5.4 ng/g Skin 2.4–2.9 ng/g Flesh 0.53–0.74 ng/g	Decomposed with $HNO_3/HClO_4$ mixture. Determination based on a publication by Piwonka *et al.* (DL = 20 pg)[91]	69
	As Sb Sn	Beverages	106% recovery 97% recovery 98% recovery	Wet-oxidation procedure	70
	As	Sugar beet, pulp, molasses	0.05–0.1 μg/g	Comparison with AAN and colorimetry, levels of As considerably below EEC limits	92
	As	Beers	Spanish 3.1–8.2 ng/g Foreign 4.8–11.2 ng/g Canned 1.8–11.2 ng/g Bottled 2.0–8.2 ng/g Standard 1.8–11.2 ng/g Special 3.1–8.2 ng/g Extra 2.0–7.0 ng/g	Samples dry-ashed at 450°. Ash dissolved in HCl, and arsine generated by addition of $NaBH_4$ prior to atomization in a flame-heated silica cell. (DL = 0.1 ng/g)	71
DCP	Sn	Canned juice	Pineapple 62.6 ± 1.3 Orange 75.0 ± 0.6 Grape 32.0 ± 0.3 Apple <0.075	Digestion with concentrated HNO_3–H_2SO_4 (9:1 v/v). Recoveries of spikes ranged from 98 to 108%	72
Flow injection HG–AAS	As, Sb, Bi, Pb, Sn, Se, Te	Fruit juices, soft drinks	—	Flow injection combined with HG	93

*The method did not give satisfactory results, mainly owing to ethanol interference, which substantially reduces the lead signal.

eliminated by using $NaBH_3CN$ to generate the hydrides,[34] but this method involves a high risk of poisoning for personnel.

Speciation

The determination of the particular form of an element in its natural environment, *speciation*, is the most fascinating and rapidly developing area of application of atomic spectroscopy to have emerged in recent years.

Knowledge of the speciation in some types of samples is important because to relate the toxicity, bioaccumulation and transport of a particular element to its oxidation state, the nature of the ligand needs to be considered.[82] As an example, different forms of arsenic greatly vary in toxicity: arsenite > arsenate > monomethylarsonic acid > dimethylarsinic acid > arsenobetaine. Branch *et al.*[83] have stated that arsenite is the most toxic; arsenobetaine[84,85] is relatively non-toxic.

Organotin compounds are used as biocides, mainly in antifouling paints and wood preservatives; tributyltin oxide and its derivatives are commonly used for this purpose. These materials are both irritant and toxic.[24] Krull and Panaro[72] have discussed the speciation of methyltin species in beverages. The speciation of selenium present in beers has been described by Robberecht *et al.*[73]

Optimal conditions for the use of HG–AAS

When using hydride generation in the analysis of wines and beverages, the following points should be borne in mind.

(*a*) Organic matter should be totally oxidized, and the elements to be determined should be present in a single appropriate oxidation state.

(*b*) Interferences and other sources of error should be guarded against as carefully as possible. Factors to be considered include the acids and oxidizing agents employed, the "cross effect" of interfering ions,[86] the delay involved in collecting the hydride, the concentration of $NaBH_4$ used, the aging of stock solutions and the storage of samples.

(*c*) All operating conditions should be carefully optimized. The acidity, for example, is critical in the determination of Pb, Sn and Se, temperature in that of Ge, and hydride collection-time in that of Pb, Se and Te.

Table 7 lists the sensitivities of spectroscopic methods with and without use of hydride-generation systems. Table 8 summarizes the optimal conditions for the determination of As, Sb, Bi, Pb, Sn, Se and Te with hydride generation.

CONCLUSIONS

The procedures that should be followed in order to avoid errors and reduce interferences when using hydride-generation systems in AAS may be summed up in the following ten points. (*i*) Samples should be highly diluted. (*ii*) High acidities or a mixture of acids should be used. (*iii*) The quantity to be measured is the area of the absorption peak. (*iv*) Hydride collection-time should be optimized. (*v*) The hydride should be collected at low temperature (liquid-nitrogen bath) and then rapidly released. (*vi*) Interferences should be eliminated by addition of masking agents, precipitation, or other means. (*vii*) Hydrides should be collected in suitable absorbents and determination performed whenever possible by ET–AAS with a graphite furnace. (*viii*) The residence time in the optical path of the detector should be optimized. (*ix*) Blanks should be used. (*x*) The standard-addition method should be used.

The hydride-generation technique can give correct results if the proper digestion and hydride-generation conditions are used. A summary of their principal applications to analyse wines and beverages is given in Table 9.

Acknowledgement—The authors are thankful to Dr R. A. Chalmers for his keen interest, valuable suggestions and criticism.

REFERENCES

1. C. Baluja-Santos, A. Gonzalez-Portal and F. Bermejo-Martinez, *Analyst*, 1984, **109**, 797.
2. *Idem*, Communication No. 114, Analyticon-84, London, 1984.
3. M. Ihnat and H. J. Miller, *J. Assoc. Off. Anal. Chem.*, 1977, **60**, 813.
4. *Idem, ibid.*, 1977, **60**, 1414.
5. J. R. Castillo, J. M. Mir and M. C. Martínez, *Quim. Anal.*, 1987, **6**, 33.
6. W. B. Robbins and J. A. Caruso, *Anal. Chem.*, 1979, **51**, 889A.
7. R. G. Godden and D. R. Thomerson, *Analyst*, 1980, **105**, 1137.
8. M. Ihnat and B. K. Thompson, *J. Assoc. Off. Anal. Chem.*, 1980, **63**, 814.
9. A. E. Smith, *Analyst*, 1975, **100**, 300.
10. F. D. Pierce and H. R. Brown, *Anal. Chem.*, 1976, **48**, 693; 1977, **49**, 1417.
11. B. Welz and M. Schubert-Jacobs, *J. Anal. At. Spectrom.*, 1986, **1**, 23.
12. B. Welz, *Chem. Brit.*, 1986, **22**, 130.

13. C. Baluja-Santos and A. Gonzalez-Portal, *XIX^e Congres International de la Vigne et du Vin*, 1986, **III**, 347.
14. H. J. M. Bowen, *Trace Elements in Biochemistry*, Academic Press, London, 1966.
15. L. G. Gomes, *Anais Vinho Porto*, 1959, **20**, 1; 1960, **21**, 1; *Rev. Port. Farm.*, 1963, **13**, 159.
16. H. Eschnauer, *Z. Lebensm.-Untersuch.-Forsch.*, 1966, **128**, 337.
17. B. Rankine, *Aust. Wine Brew. Spirit Rev.*, 1962, **80**, 14.
18. H. Eschnauer, *Wein u. Rebe*, 1958, **39**, 492.
19. F. Bermejo, A. Gonzalez and C. Baluja, *Estudio y determinación de plomo en los vinos de Galicia*, Anque, Madrid, 1980.
20. E. Kielgofer and H. Aumann, *Mitt. Kosterneuburg*, 1955, **5A**, 127.
21. H. Eschnauer, *Spurenelemente in Wein and anderen Getränken*, p. 184, Verlag Chemie, Weinheim, Bergstr., 1974.
22. U. Rüdt and D. Stoll, *Wein u. Rebe*, 1968, **50**, 1048.
23. S. Ya. Raik and E. Kh. Kryzhanovskaya, *Sadovod. Vinograd. Vinodel. Mold.*, 1970, **25**, No. 12132.
24. F. A. Patty (Ed.) *Industrial Hygiene and Toxicology*, 2nd Ed., p. 886. Wiley, New York, 1967.
25. E. F. Dalton and A. J. Malanoski, *At. Absorpt. Newsl.*, 1971, **10**, 92.
26. E. N. Pollock and S. J. West, *ibid.*, 1972, **11**, 104; 1973, **12**, 6.
27. P. D. Goulden and P. Brooksbank, *Anal. Chem.*, 1974, **46**, 1431.
28. R. S. Braman, L. L. Justen and C. C. Foreback, *ibid.*, 1972, **44**, 2195.
29. F. J. Schmidt and J. L. Royer, *Anal. Lett.*, 1973, **6**, 17.
30. K. C. Thompson and D. R. Thomerson, *Analyst*, 1974, **99**, 595.
31. F. J. Fernandez, *At. Absorpt. Newsl.*, 1973, **12**, 93.
32. J. R. Knechtel and J. L. Fraser, *Analyst*, 1978, **103**, 104.
33. M. Verlinden, J. Baart and H. Deelstra, *Talanta*, 1980, **27**, 633.
34. R. M. Brown, S. J. Northway and R. C. Fry, 30th Pittsburgh Conf. Anal. Chem. Appl. Spectroscopy, Atlantic City, 10–14 March 1980.
35. D. E. Fleming and G. A. Taylor, *Analyst*, 1978, **103**, 101.
36. J. R. Liddle, R. R. Brooks and R. D. Reeves, *J. Assoc. Off. Anal. Chem.*, 1980, **63**, 1175.
37. J. Aggett and A. C. Aspell, *Analyst*, 1976, **101**, 341.
38. W. Holak, *Anal. Chem.*, 1969, **41**, 1712.
39. R. S. Braman, D. L. Johnson, C. C. Foreback, J. M. Ammons and J. L. Bricker, *ibid.*, 1977, **49**, 621.
40. E. A. Crecelius, *ibid.*, 1978, **50**, 826.
41. R. E. Madsen, Jr., *At. Absorpt. Newsl.*, 1971, **10**, 57.
42. R. J. Watling and H. R. Watling, *Spectrochim. Acta*, 1980, **35B**, 451.
43. F. J. Fernandez and D. C. Manning, *At. Absorpt. Newsl.*, 1971, **10**, 86.
44. D. C. Manning, *ibid.*, 1971, **10**, 123.
45. R. C. Chu, G. P. Barron and P. A. W. Baumgarner, *Anal. Chem.*, 1972, **44**, 1476.
46. D. D. Siemer and L. Hagemann, *Anal. Lett.*, 1975, **8**, 323.
47. P. N. Vijan and G. R. Wood, *Talanta*, 1976, **23**, 89.
48. J. F. Chapman and L. S. Dale, *Anal. Chim. Acta*, 1979, **111**, 137.
49. D. B. Hatfield, *Anal. Chem.*, 1987, **59**, 1887.
50. K. Tsuji and K. Kuga, *Anal. Chim. Acta*, 1978, **97**, 51.
51. S. Kobayashi, *Talanta*, 1979, **26**, 951.
52. K. C. Thompson, *Analyst*, 1975, **100**, 307.
53. F. E. Lichte and R. K. Skogerboe, *Anal. Chem.*, 1972, **44**, 1480.
54. W. B. Robbins, J. A. Caruso and F. L. Fricke, *Analyst*, 1979, **104**, 35.
55. R. Belcher, S. L. Bogdanski, E. Henden and A. Townshend, *Anal. Chim. Acta*, 1977, **92**, 33.
56. R. J. Watling and A. R. Collier, *Analyst*, 1988, **113**, 345.
57. J. A. Fiorino, J. W. Jones and S. G. Capar, *Anal. Chem.*, 1976, **48**, 120.
58. O. Åström, *ibid.*, 1982, **54**, 190.
59. Z. Fang, S. Xu, X. Wang and S. Zhang, *Anal. Chim. Acta*, 1986, **179**, 325.
60. X. Wang and Z. Fang, *Kexue Tongbao*, 1985, **30**, 1958.
61. S. Zhang, S. Xu and Z. Fang, *Quim. Anal.*, 1989, **8**, 191.
62. G. K. H. Tam and J. Lacroix, *J. Assoc. Off. Anal. Chem.*, 1982, **65**, 647.
63. T. T. Gorsuch, *Analyst*, 1959, **84**, 135.
64. J. Nève, M. Hanocq and L. Molle, *Mikrochim. Acta*, 1980, **I**, 259.
65. A. Abu-Samra, J. S. Morris and S. R. Koirtyohann, *Anal. Chem.*, 1975, **47**, 1475.
66. L. B. Jassie and H. M. Kington, *Introduction to Microwave Sample Preparation: Theory and Practice*, ACS, Washington D.C., 1988.
67. A. C. Grillo, *Spectrosc. Intern.*, 1990, **2**, 14.
68. G. P. Molinari, M. Trevisan, P. Natali and A. M. del Re, *J. Agric. Food Chem.*, 1987, **35**, 727.
69. F. Alt, J. Messerschmidt and G. Tölg, *Z. Anal. Chem.*, 1987, **327**, 233.
70. W. H. Evans, F. J. Jackson and D. Dellar, *Analyst*, 1979, **104**, 16.
71. M. L. Cervera, A. Navarro, R. Montoro, R. Catala and N. Ybañez, *J. Assoc. Off. Anal. Chem.*, 1989, **72**, 282.
72. I. S. Krull and K. W. Panaro, *Appl. Spectrosc.*, 1985, **39**, 960.
73. H. Robberecht, O. van Schoor and H. Deelstra, *J. Food Sci.*, 1984, **49**, 30.
74. S. Nakashima, *Analyst*, 1979, **104**, 172.
75. T. Nakahara, *Prog. Anal. At. Spectrosc.*, 1983, **6**, 163.
76. E. J. Knudson and G. D. Christian, *Anal. Lett.*, 1973, **6**, 1039.
77. J. Pettersson and A. Olin, *Talanta*, 1991, **38**, 413.
78. M. Verlinden and H. Deelstra, *Z. Anal. Chem.*, 1979, **296**, 253.
79. J. R. Castillo, J. M. Mir and M. T. Gomez, *Microchem. J.*, 1989, **39**, 213.
80. G. F. Kirkbright and M. Taddia, *Anal. Chim. Acta*, 1978, **100**, 145.
81. M. Bedard and J. D. Kerbyson, *Can. J. Spectrosc.*, 1976, **21**, No. 3, 64.
82. R. J. A. van Cleuvenbergen, W. E. van Mol and F. C. Adams, *J. Anal. At. Spectrom.*, 1988, **3**, 169.
83. S. Branch, K. C. C. Bancroft, L. Ebdon and P. O'Neill, *Anal. Proc.*, 1989, **26**, 73.
84. J. F. Lawrence, P. Michalik, G. Tam and H. B. S. Conacher, *J. Agric. Food Chem.*, 1986, **34**, 315.
85. C. Baluja-Santos and A. Gonzalez-Portal, *Hydride Generation Atomic Spectrometry in the Environment-I, Waters*, Sisipa, Lisbon, 1989, **III**, 253.
86. A. Meyer, Ch. Hofer, G. Tölg, S. Raptis and A. Knapp, *Z. Anal. Chem.*, 1979, **296**, 337.

87. A. P. D'Silva, G. W. Rice and V. A. Fassel, *Appl. Spectrosc.*, 1980, **34**, 578.
88. M. V. Aguilar-vilas, M. del C. Martinez-Para and T. A. Masoud, *An. Bromatol.*, 1988, **40**, 97.
89. J. Sanz, P. Basterra, J. Galban and J. R. Castillo, *Mikrochim. Acta*, 1989, **I**, 271.
90. Y. Madrid, J. Meseguer, M. Bonilla and C. Cámara, *Anal. Chim. Acta*, 1990, **237**, 181.
91. J. Piwonka, G. Kaiser and G. Tölg, *Z. Anal. Chem.*, 1985, **321**, 225.
92. A. W. M. Huijbregts, D. Hibbert, R. T. Phillipson, H. Schiweck and G. Steinle, *Inst. Sugar J.*, 1985, **87**, 163.
93. Y. Yamamoto, M. Yamamoto and M. Yasuda, *3rd China-Japan Symposium Anal. Chemistry*, Hefei, China, 1988.

Talanta, Vol. 39, No. 4, pp. 341–347, 1992
Printed in Great Britain

0039-9140/92 $5.00 + 0.00
Pergamon Press plc

DETERMINATION OF BROMIDE BY LOW POWER SURFATRON MICROWAVE INDUCED PLASMA AFTER BROMINE CONTINUOUS GENERATION

M. D. CALZADA, M. C. QUINTERO, A. GAMERO and J. COTRINO*
Department of Applied Physics, Faculty of Science, University of Cordoba, Spain

J. E. SANCHEZ URÍA and A. SANZ-MEDEL†
Department of Physical and Analytical Chemistry, Faculty of Chemistry, University of Oviedo, Spain

(*Received* 11 *July* 1991. *Revised* 7 *October* 1991. *Accepted* 7 *October* 1991)

Summary—A simple continuous flow generation of volatile bromine is described for the determination of low concentrations of the element by atmospheric-pressure argon microwave induced plasma (MIP) surfatron. Bromine is continuously generated by mixing the bromide with sulphuric acid and hypochlorite solutions. The bromine vapour is separated from the aqueous phase by a gas–liquid separator and is desiccated by passing it through concentrated sulphuric acid. The detection limit attained was 2 μg/l. and the precision was $\pm 0.7\%$ (at the 80 μg/l. level). The proposed determination is very selective if oxidizing/reducing agents are absent. The procedure has been tested for bromide determination in two drug preparations. Good agreement between the experimental results and the certified values has been obtained.

Since McCormack *et al.*[1] introduced microwave induced plasma (MIP) for the element selective detection in gas chromatography, MIPs operated at relatively low paper levels (< 150 W), with helium or argon as the plasma support, have provided sensitive excitation for non-metals and some metals in the vapour phase.[2–5] Unfortunately the low kinetic temperature of such plasmas is inadequate for direct aspiration of liquid solutions into the MIP which should be desolvated before atomization/excitation of the elements of interest. In spite of this fact we are witnessing a revival of interest in MIP as excitation source, particularly for the analysis of non-metals, using both the TM_{010} Beenakker cavity[6–7] and surfatron type devices as those first proposed by Moissan *et al.*[8,9] It appears that the surfatron type coupling is more easily tuned and more resistant to detuning by solvent and solute loading than are conventional resonant-cavity devices.[10]

The determination of bromide by MIP–AES has been reported on several occasions[11–15] using different approaches for sample introduction: chemical generation of hydride or bromine,[11,14] electrothermal vaporization[12,15] and gas-chromatography techniques.[16] However, to the best of our knowledge, only one publication deals with the detection of bromide using a surfatron-MIP:[13] a glass-frit nebulizer is used for sample introduction along with a desolvation system to reduce the amount of water vapour entering the plasma. The detection limit reported was 4 μg/ml at 889.8 nm, in the NIR spectral region where most promising analytical lines appear.

We are reporting here on the improvement of Ar-MIP surfatron detection capability for bromide just by continuous chemical generation of bromine swept into the MIP by the Ar plasma gas. The technique is applied to the determination of bromide in some real samples.

EXPERIMENTAL

The basic configuration of the instrumentation used has been published elsewhere.[17] The different components of our instrumental set-up are listed in Table 1.

Relevant details of the main components of our Ar-surfatron-MIP analytical system are as follows:

Sample introduction device

The bromide samples were introduced into the plasma as chemically generated bromide. The bromine was produced in a continuous mode using a gas–liquid continuous separation

*Present address: Department of Atomic, Molecular and Nuclear Physics, University of Seville, Spain.
†Author for correspondence.

Table 1. Description and specifications of the major components of the analytical system

Instrument component	Description and specification
Microwave generator	Microtron 200 Mark III, 2450 ± 25 MHz 0–200 W, (Electro Medical Supplies, Wantage, U.K.)
Microwave Launcher	Surfatron. The microwave power is supplied to the surfatron through a coaxial line using an N-type connector
Monochromator	Jobin-Yvon THR-1000s, 1-m focal length, Czerny-Turner mount with a grating of 1200 grooves/mm. Reciprocal linear dispersion of 0.83 nm/mm in the range 500–1000 nm.
Optical arrangement	Surfatron and monochromator mounted on the same optical rail. Plasma viewed axially and imaged 1:1 on the entrance slit with a fused silica lens.
Read-out system	R-212 Hamamatsu PMT. Jobin-Yvon Spectralink system controlled by a Computer.
Argon flow control	Brooks R-2-25C.
Discharge tubes	Fused silica capillary 1 mm i.d.

system previously described for arsenic determinations and iodine generation.[17,18] The sample solution (or blank solution), the oxidant (hypochlorite) solution and the diluted sulphuric acid solution are pumped via a three channel peristaltic pump and generation, separation and desiccation of bromine formed occurs in a continuous manner, according to Fig. 1 scheme.

Surfatron-MIP source

The experimental measurements were carried out with the MIP set-up described previously.[17] The plasma was produced within 1-mm i.d. silica fused capillary tubes through the propagation of a surface wave at 2.45 GHz. The generator microwave power was coupled to the wave through a surfatron.[19] The plasma tube was surrounded by a cylindrical metallic waveguide, coaxial with it, and enclosing it completely. Forward and reflected power levels were measured with an external thermistor.

The optical resolution/detection system

The optical resolution/detection systems used have been described elsewhere.[17]

Reagents

A 1000-μg/ml stock solution of potassium bromide was prepared by direct dissolution of 1.000 g of the salt in a 1000-ml flask with redistilled water. A $4.32 \times 10^{-3}M$ solution of

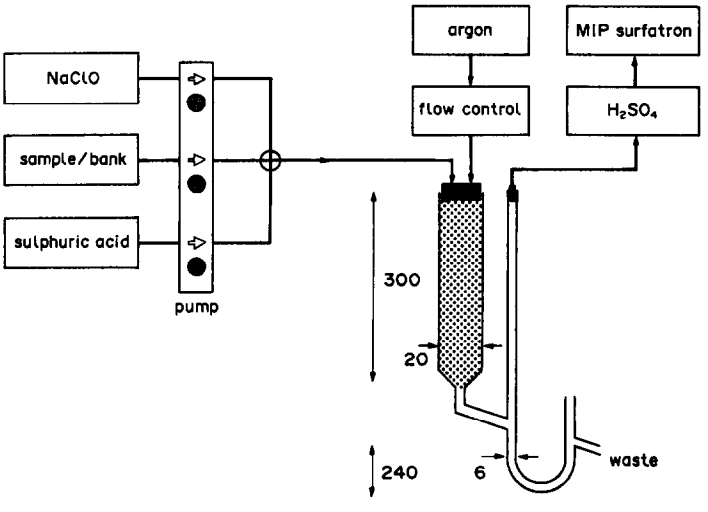

Fig. 1. Diagram of the gas–liquid continuous separation device (lengths in nm).

sodium hypochlorite, was prepared by diluting 2 ml ($7 \pm 2\%$ of active chlorine) in 250 ml of redistilled water. A $3M$ solution of sulphuric acid was also used. The salts used for interference studies were all of analytical reagent grade.

General procedure

The solution containing the bromide sample (0.020–20.000 μg/ml bromide) and the $4.32 \times 10^{-3}M$ hypochlorite and sulphuric acid solutions are pumped with the aid of a peristaltic pump towards a "T-piece" (Fig. 1). The corresponding optimum flows are 3.80 ml/min for the sample and 1.23 ml/min for the reagents. The bromine, dissolved in the resulting solution, goes into the gas-liquid continuous separator where a mild stream of argon (the plasma gas) carries the volatile Br out of the aqueous solution (which is discarded via the "U" tube). The bromine volatile species and the argon plasma gas are desiccated by passing them through concentrated sulphuric acid before entering the microwave plasma formed in the discharge tube by the surfatron device.

The operating conditions are summarized in Table 2. The atomic emission at 827.24 nm of bromine was then measured for the optimization of bromine generation conditions and of instrumental set-up parameters.

Under the operating conditions shown in Table 2, the bromine emission signal begins to rise from the baseline rather slowly. Thus, only after stabilization (around 10 min), the emission intensities are integrated for 0.5 sec. Longer integration intervals did not improve the S/N ratio.

Table 2. Optimum operating conditions for the determination of bromine with the 827.244 nm emission line

Plasma	
Forward Power	100 W
Reflected Power	< 5 W
Generator frequency	2450 MHz
Inner Diameter (Plasma Tube)	1 mm
Argon flow rate	0.5 l./min
Monochromator	
Photomultiplier voltage	1200 V
Integration time	500 msec
Slit Widths (entrance and exit)	50 μm
Sequential scanning (bandpass)	<0.03 nm
Bromine generation	
H_2SO_4 concentration	$3M$
NaClO concentration	$4.32 \times 10^{-3}M$
H_2SO_4 solution flow	1.23 ml/min
NaClO solution flow	1.23 ml/min
Sample solution flow	3.81 ml/min

RESULTS AND DISCUSSION

Wavelength selection

There are several emission lines lying in the UV-visible or IR regions which have been recommended for bromine determination by MIP–AES at atmospheric pressure.[11,12,14,20–22] Among published analytical lines, we have selected those in the long wavelength region, where the sensitivity of the detector of our instrument is still adequate. Thus the 889.80 nm, 827.24 nm and the 888.90 nm emission lines were tested. We verified the signal to background ratios of bromine at the above-mentioned emission lines in our analytical system with continuous generation of bromine. The atomic line at 824.27 nm was finally selected for subsequent measurements because it produced the most intense emission and highest signal to background ratio for bromine.

Bromine generation conditions

The conditions for optimum chemical generation of bromine in a continuous mode from potassium bromide solutions were studied by using a 10 μg/ml solution of the salt as reference and then following the general procedure proposed previously.

Three different oxidant systems for chemical generation of bromine were investigated, namely: (a) $KBrO_3$–H_2SO_4, (b) H_2O_2–H_2SO_4 and NaClO–H_2SO_4. The latter system proved to be the most efficient for bromine generation. It was faster and the intensity of emission observed was 5 times higher than that obtained with the other oxidant systems. Once selected the most convenient method for chemical vapour generation of bromine, optimum concentrations and flows of sulphuric acid and sodium hypochlorite solutions were investigated by following a univariant search. The results observed in these experiments using flows of 1.23 ml/min have been plotted in Fig. 2 (sulphuric acid) and Fig. 3 sodium hypochlorite. As shown in Figs 2 and 3, optimum concentrations for sulphuric acid are above $1M$ (a plateau is observed above $1M$ sulphuric acid concentrations), while for sodium hypochlorite solutions, the emission intensity of bromine was constant above $0.5 \times 10^{-3}M$. Concentrations of $3M$ sulphuric acid and of $4.3 \times 10^{-3}M$ sodium hypochlorite were finally selected.

Optimum flows of sample and reagents were also investigated with selected reagent concentrations in order to obtain maximum intensity

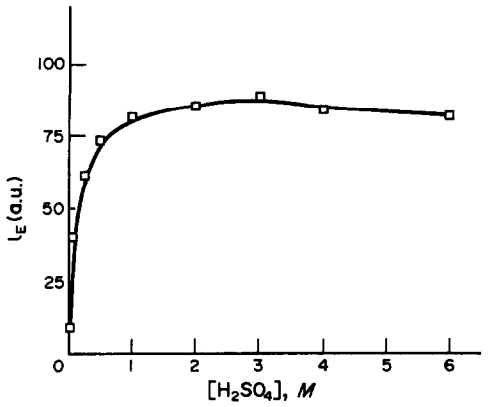

Fig. 2. Optimization of the analytical signal. Effect of the H_2SO_4 concentration. Sample and reagents flows 1.23 ml/min. Concentrations of 10 μg/ml KBr and of $1.08 \times 10^{-3}M$ NaClO.

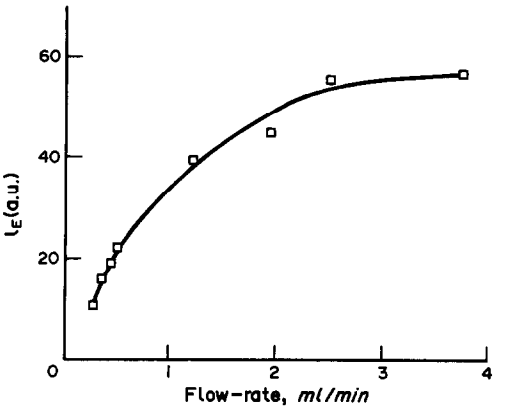

Fig. 4. Optimization of the analytical signal. Influence of sample and reagents flows (the same flow of sample and of reagents). Concentration of 4 μg/ml KBr. Other experimental conditions as in Table 2.

of bromine emission at 827.24 nm. The flow-rates of each of the three channels of the peristaltic pump were varied from 0.27 to 3.80 ml/min (the same flow-rates for the three channels in each experiment). The results observed for the emission intensity of a solution of 4 μg/ml of bromide, using $3M$ sulphuric acid and $4.3 \times 10^{-3}M$ sodium hypochlorite solutions, versus the flow-rates (of sample reagents) have been plotted in Fig. 4. As shown by Fig. 4, higher flows led to higher emission signals. The observed emission, however, tends to level off at flows higher than 2.5 ml/min of sample and reagents (Fig. 4).

In a second optimization experiment, sulphuric acid and oxidant solution flow-rates were fixed at 1.23 ml/min (intermediate level of emission intensity of Fig. 4) and sample solution flow-rates were varied from 1.23 to 3.81 ml/min. The results obtained generating bromine from 4 μg/ml potassium bromide solution show a linear increase in the analytical signal with sample solution flow-rate. We selected for subsequent experiments the reagents and sample flow-rates detailed in Table 2.

Temperature effect in bromine separation

To test the possibility of a faster separation/volatilization of bromine, and thus to attain a quicker signal stabilization, a study of the effect of the bromine separation temperature was carried out. A heating mantle connected to an electrical unit (allowing for control and measurement of the temperature with a precision of $\pm 1°$) was wrapped around the gas–liquid separator to investigate the effect of heating on the bromine generated signal. The results obtained are shown in Fig. 5, which

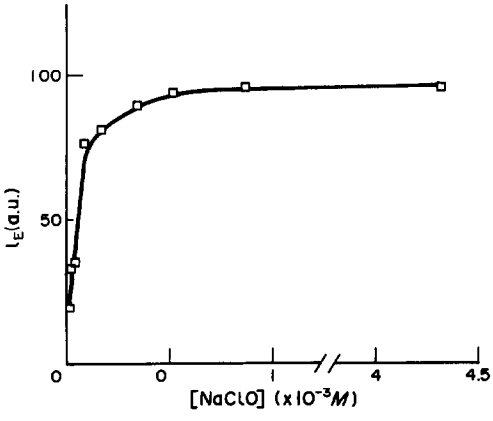

Fig. 3. Optimization of the analytical signal. Effect of the NaClO concentration. Sample and reagents flows 1.23 ml/min. Concentrations of 10 μg/ml KBr and of $3M$ H_2SO_4.

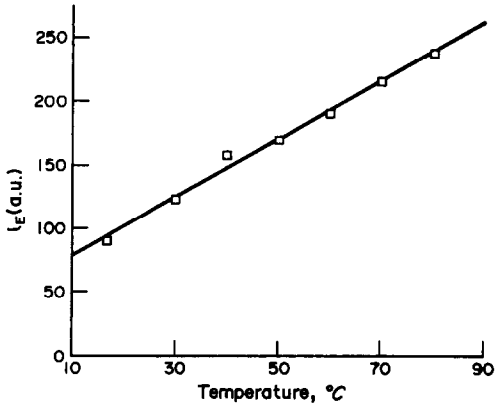

Fig. 5. Effect of temperature on bromine generation (and emission signal). Concentration of 4 μg/ml KBr. Other experimental conditions as in Table 2.

documents how temperature increases brought about an enhancement of emission intensities (due to an increased inflow of bromine into the plasma). Unfortunately, as described previously,[17] the increasing water load deteriorates the desiccator properties of concentrated sulphuric acid (see Fig. 1) in a few minutes. Therefore, working above 70° causes serious instability of the plasma which can eventually be extinguished. As improvements in bromine generation with higher temperatures are not dramatic, room temperature is recommended for bromine generation in routine operation.

Optimization of instrumental parameters

The most critical MIP instrumental parameters (including microwave power, internal diameter of quartz discharge tube and Ar plasma gas flow) affecting the bromine atomic emission have been optimized with a univariant search.

The microwave power was varied from 25 to 200 W at fixed values of the inner diameter of the plasma tube and the argon flow-rate given in Table 2. As can be seen in Fig. 6, the emission intensity turned out to be constant above 150 W. It has to be pointed out, however, that at microwave power values above 100 W, a higher reflected power and background were observed degrading reproducibility of our measurements. Therefore, a 100 W microwave power was finally selected (see Table 2).

It is well known that the internal diameter of the quartz discharge tube has a great influence on the geometry of the MIP plasma: big tube diameters originate filament-like plasmas (resulting in poor sample excitation due to inadequate contact between the sample and the plasma). Thus, we tested three different discharge tubes having 4.5, 3 and 1-mm internal diameters. Results showed that the most favourable one for atomization/excitation of bromine in our Ar plasma was the 1-mm i.d. tube.

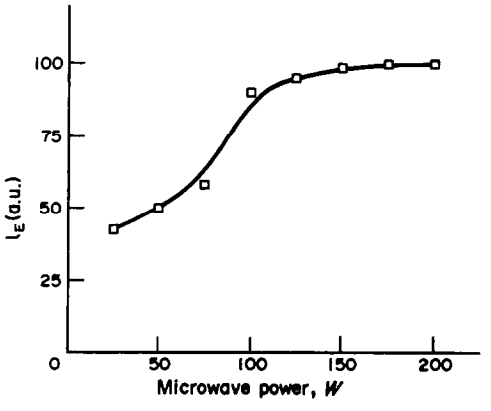

Fig. 6. Effect of microwave power on the intensity of the bromine emission. Concentration of 4 μg/ml KBr. Other experimental conditions as in Table 2.

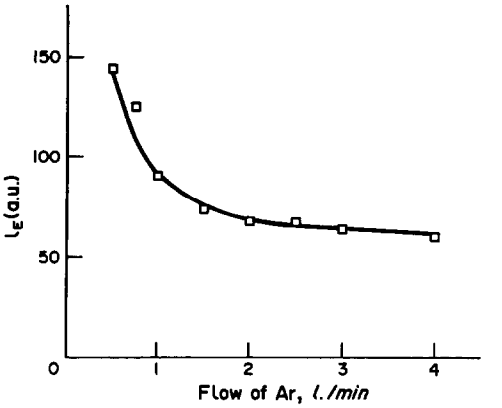

Fig. 7. Effect of the variation of plasma gas flow on the analytical signal. Concentration of 4 μg/ml KBr. Other experimental conditions as in Table 2.

The influence of plasma gas flow-rate on the analytical signal was studied by varying the plasma Ar flow between 0.5 and 4.0 l./min. The results obtained have been plotted in Fig. 7. As could be expected, increasing the flow-rate of Ar gave a decreasing bromine emission intensity because the time of residence for the analyte in the plasma decreases accordingly. A compromise value of 0.5 l./min Ar flow-rate was selected.

Analytical characteristics

Optimum conditions finally selected according to results from the above mentioned experiments are summarized in Table 2. Using such optimum conditions and the proposed general

Table 3. Selectivity achieved in the determination of 5 μg/ml of bromine at the 827.244 nm emission line

Compound added	Tolerance ratio
$NaIO_4$	500:1
KIO_3	500:1
NaCl	500:1
$NaClO_4$	500:1
$NaClO_3$	500:1
$KBrO_3$	500:1
NaF	500:1
$C_2O_4^{2-}$	500:1
Sodium tartrate	500:1
EDTA	500:1
CO_3^{2-}	500:1
KI	250:1

Table 4. Drug preparations and recovery of bromide obtained in each case

Drug	Weight taken, *mg*	ml Taken	Br^- expected, *ppm*	Br^- found, *ppm*	Recovery, %
"Magnesium Pyre"	100	1	0.036	0.034	94.4
Salvat		2	0.089	0.086	96.6
		5	0.178	0.172	96.6
Spain				Mean recovery	95.9
				R.S.D.	1.32%
"Otogen"	50	1	0.349	0.364	104.3
Rifamar, S. A.		2	0.698	0.745	106.7
		5	1.745	1.847	105.8
Spain				Mean recovery	105.6
				R.S.D.	1.21%

procedure we evaluated the detection limit attainable for bromine in our instrumental set-up. The limit of detection (3σ IUPAC criterion) was 2 μg/l. of bromide at room temperature. If the determination was carried out at 70° the detection limit became 0.8 μg/l.

The linear range observed (intensity of emission, I_E, *vs.* potassium bromide concentration) extended from the detection limit up to 20 mg/l. potassium bromide (regression coefficient 0.9999).

The precision of the proposed method was evaluated by analysing eleven replicates of a solution containing 80 μg/l. potassium bromide. The observed standard deviation was $\pm$ 0.7%.

Interference studies

In order to evaluate the extent of potential interferences particularly in the generation of bromine aqueous samples (containing 5 μg/ml potassium bromide and various amounts of foreign anions which would be compatible with bromide in aqueous solution and could be present in real samples) were analysed for Br^- by following the recommended procedure. Results obtained are summarized in Table 3 and they show that the proposed method is very selective for bromide analysis as the presence of different types of anions do not interfere.

Applications

The analytical performance of the proposed method for the determination of low levels of bromide was tested by analysing bromide in two drug preparations: "Magnesium Pyre" ($MgCl_2$ 500 mg, $MgBr_2$ 20 mg, MgF_2 0.5 mg, MgI_2 0.1 mg, Excp. c.s.) and "Otogen" (KBr 175 mg, Li_2CO_3 20 mg, KI 15 mg, Tiamine 0.2 mg, Excp. c.s.).

For sample preparation, three tablets of each drug preparation (Magnesium Pyre and Otogen) were weighed and finely ground to assist its final water dissolution. The resulting solutions were filtered and made-up to 500 ml in a standard flask, with diluted sulphuric acid (3*M* final concentration) before their final aspiration into the continuous bromine generator system.

Recovery studies were conducted along with actual analysis of the samples. To do so, 1, 2 and 5 ml of the 500-ml sample solution were delivered in three different 100-ml standard flasks and made-up to volume with 3*M* sulphuric acid (final magnesium bromide concentration in each standard flask should then be 0.041, 0.103 and 0.205 mg/l. for the "Magnesium Pyre" sample and 0.52, 1.04 and 2.6 mg/l. for the "Otogen" sample).

Good agreement between the expected amount of magnesium bromide and potassium bromide (values reported in the drug vials) and the MIP-Surfatron found values was observed as shown by Table 4. At the same time, the recoveries observed (tied to the accuracy of expected values, taken as "true" values) and the good precision for different dilutions demonstrate the excellent performance of the proposed method for this type of sample.

Acknowledgement—The authors wish to acknowledge the financial support of this work by CICYT (PA86-0091-C02-00/01).

REFERENCES

1. A. J. McCormack, S. S. C. Tong and W. D. Cooke, *Anal. Chem.*, 1965, **37**, 1470.
2. R. H. Skogerboe and G. N. Coleman, *ibid.*, 1976, **48**, 611A.
3. C. I. M. Beenakker, P. W. J. M. Boumans and P. J. Rommers, *Phillips Tech.*, 1980, **Rev. 39**, 65.
4. A. T. Zander and G. M. Hieftje, *Appl. Spectrosc.*, 1981, **35**, 357.
5. J. P. Matousek, B. J. Orr and M. Selby, *Prog. Anal. Atom. Spectrosc.*, 1984, **7**, 275.
6. C. I. M. Beenakker, *Spectrochim. Acta.*, 1976, **31B**, 483.
7. C. I. M. Beenakker and P. W. J. M. Boumans, *ibid.*, 1978, **33B**, 53.

8. M. Moisan, P. Leprince, C. Beandry and E. Bloyet, U. S. Patent No. 4. 049.940.
9. M. Moisan, C. Beandry and P. Leprince, *IEEE Trans. Sci.*, 1975, **55**, PS-3.
10. M. Selby and G. M. Hieftje, *Spectrochim. Acta.*, 1987, **42B**, 258.
11. M. M. Abdillahi, W. Tschanen and R. D. Snook, *Anal. Chim. Acta*, 1985, **172**, 139.
12. M. M. Abdillahi and R. D. Snook, *Analyst*, 1986, **111**, 265.
13. L. J. Galante, M. Selby and G. M. Hieftje, *Appl. Spectrosc.*, 1988, **42**, 559.
14. N. W. Barnett, *J. Anal. Atom. Spectrom.*, 1988, **3**, 969.
15. M. Wu and J. W. Carnahan, *Appl. Spectrosc.* 1990, **44**, 673.
16. C. I. M. Beenakker, *Spectrochim. Acta.*, 1977, **32B**, 173.
17. M. C. Quintero, J. Cotrino, M. Saez, A. Menendez Garcia, J. E. Sanchez Uria and A. Sanz Medel, *ibid.*, in the press.
18. A. Menendez Garcia, J. E. Sanchez Uria and A. Sanz Medel, *J. Anal. Atom. Spectrom.*, 1989, **4**, 581.
19. M. Moisan, Z. Zakrzewski and R. Pentel, *J. Phys. D: Appl. Phys.*, 1979, **12**, 219.
20. S-K. Chan and A. Montaser, *Spectrochim. Acta.*, 1987, **42B**, 591.
21. K. S. Hughes and R. C. Fry, *Anal. Chem.*, 1981, **53**, 1111.
22. J. E. Freeman and G. M. Hieftje, *Spectrochim. Acta.*, 1985, **40B**, 653.

Talanta, Vol. 39, No. 4, pp. 349–354, 1992
Printed in Great Britain.

0039-9140/92 $5.00 + 0.00

CATALYTIC DETERMINATION OF IODIDE BY CONTINUOUS ADDITION OF CATALYST TO A REFERENCE SOLUTION WITH PHOTOMETRIC PROBE MONITORING

G. López-Cueto,* J. M. Santiago and N. Grané
Analytical Chemistry Division, Faculty of Science, University of Alicante, Spain

(*Received* 15 *March* 1991. *Revised* 11 *July* 1991. *Accepted* 26 *July* 1991)

Summary—Probe photometry is proposed as a simple monitoring technique for catalytic determinations by continuous addition of catalyst to a reference solution. The approach has been tested on the catalytic determination of iodide which, in the concentration range of 10–100 ng/ml, can be determined with a relative error usually lower than 4–5% and relative standard deviations of 4.6 and 4.0% for 9.98 and 79.92 ng/ml, respectively. Two alternative techniques of measuring the analytical signal (the intersection time) are suggested to improve the reproducibility: the "initial signal preadjustment" and the "two-intersection point" techniques. The method has been applied to determination of iodide in table salt samples.

Kinetic catalytic methods are comparative methods, as are many other instrumental methods of analysis, because their application requires comparison of some kinetic parameter with a calibration plot. This may be avoided by continuous addition of catalyst to a reference solution.[1] This is a new unconventional method of catalytic analysis, one of its main features is that reaction kinetics are monitored in two different solutions: the sample solution, that contains the analyte (catalyst) and the reference solution, to which a standard solution of catalyst is added at a constant rate. Theory for a second-order catalysed reaction (first-order in both the catalyst and one of the reagents)[1] predicts that, once the kinetic curves from both the sample and the reference solutions have been recorded together on the same coordinate axes, they cross at a certain time, designated as the intersection time (t_x), which is the analytical variable to be measured. From here, two approaches may be followed to obtain the concentration of analyte: either the comparative procedure, based on an empirical calibration curve, or the pseudostoichiometric procedure, in which the concentration of analyte $[C]_x$ is calculated directly from the following non-empirical equation, which is valid provided dilution in the reference solution is negligible:

$$[C]_x = \frac{m[C]_s}{2V_0} t_x \qquad (1)$$

where the parameters m (addition rate), $[C]_s$ (concentration of the standard solution of catalyst) and V_0 (initial volume of the reference solution) are known. A certain formal similarity can be found between this approach and the null-point method developed by Malmstadt *et al.*[2–4] Nevertheless the foundations of the two types of method are very different, the principal difference being that, while the null-point method refers to an equilibrium situation, the method of continuous addition of catalyst to a reference solution is kinetic in nature.

In a previous paper,[1] the theoretical basis of the new method was reported and the method was tested by using the iodide-catalysed Ce(IV)–As(III) reaction.[5–9] Reaction kinetics were monitored amperometrically by means of a rotating disk platinum electrode. Amperometry is a suitable technique to take continuous measurements from a reaction medium, but a source of error arises from the poor reproducibility of currents measured with solid electrodes. This drawback was partially overcome by normalizing both the sample and the reference kinetic curves,[1] that is to say, by dividing the current measured at each time by its initial value. This procedure is, nevertheless, cumbersome and time-consuming, and therefore some simple alternatives have been searched for.

*Author for correspondence.

Photometric techniques are usually more reproducible than solid-electrode amperometry, a foreseeable feature of the use of these techniques is that kinetic curves do not need to be normalized. Continuous photometric monitoring of the reaction kinetics in the sample and reference solutions may be easily followed by using a fibre-optic probe.

In this paper the predictions above have been examined by using a fibre-optic probe photometer for the catalytic determination of iodide by continuous addition of catalyst to a reference solution. In order to test the reliability of this operating method, the method has been applied to iodide determination in table salt samples.

EXPERIMENTAL

Reagents and solutions

Ceric sulphate ($2.5 \times 10^{-2}M$) in $1.8M$ sulphuric acid, $0.100M$ As(III) (prepared from arsenious oxide), $1.8M$ sulphuric acid and $1.023 \times 10^{-2}M$ potassium iodide (standardized by titration with silver nitrate) were used.

All reagents were of analytical grade. Demineralized distilled water was used throughout.

Apparatus

Photometric monitoring of the reaction kinetics was carried out with a E-616 Metrohm photometer provided with a fibre-optic probe that allows measurements to be taken in the reaction vessel. The analog output for connecting the strip chart recorder (a E-536 Metrohm potentiograph) gives transmittance rather than absorbance values, so that kinetic plots were recorded as transmittance–time curves. A Metrohm EA 876-20 temperature-controlled titration vessel was used as the reaction cell. The temperature was kept constant at $25.0 \pm 0.1°$ with a Haake K circulation bath and a 620/3 Crison probe thermometer. The catalyst solution was continuously added to the reference solution by means of an E-655 Metrohm Dosimat electronic burette. A 2–10 ml Brand Dispensette dispenser was used for the sample addition to the sample cell.

Procedure

All the reagents must be maintained at $25.0 \pm 0.1°$ before preparing the solutions. To prepare the reference solution take, directly in the reaction cell (kept at $25.0 \pm 0.1°$), 10 ml of the arsenic(III) solution, 13 ml of the sulphuric acid solution, 25 ml of demineralized water, and 2 ml of the cerium(IV) solution. Start the continuous addition of a potassium iodide standard solution ($[C]_s$ from 2.948×10^{-5} to $1.018 \times 10^{-4}M$) with an addition rate m from 1.083×10^{-3} to 1.000×10^{-2} ml/sec. The reaction rate is monitored by continuously measuring the transmittance at 410 nm. Both the recorder and the electronic burette must be switched on simultaneously. This has been easily achieved because the E-655 Metrohm burette operates in a synchronous way with the E-536 Metrohm potentiograph.

To prepare the sample solution, the same volumes of As(III), sulphuric acid and Ce(IV) solutions have to be taken, plus $(25 - V_s)$ ml of demineralized water and V_s ml of the analyte solution (containing 4.356×10^{-8}–$1.102 \times 10^{-6}M$ iodide). The addition order has to be the same as in the preparation of the reference solution. The recorder will be switched on at the same time as the sample solution is added. The temperature is maintained constant at $25.0 \pm 0.1°$.

Once obtained, superpose together the reference and the sample curves and measure the intersection time t_x, that is to say, the time elapsed until the curves cross.

Determination of iodide in table salt. The required amount of dry sample (about either 1 g for iodized salt or 20 g for non-iodized salt respectively) was weighed accurately, dissolved in demineralized water and diluted to a final volume of 500 or 100 ml, respectively. Finally, a 20-ml aliquot was transferred to the sample cell, which contained the above cited volumes of arsenic(III), sulphuric acid and cerium(IV) solutions, and 5 ml of demineralized water. On the other hand, a $4.104 \times 10^{-5}M$ potassium iodide standard solution was continuously added to the reference solution at a rate of 1.667×10^{-3} ml/sec.

RESULTS AND DISCUSSION

Testing of the sample and the reference curves

According to the theory derived in a previous paper,[1] the transmittance–time curves for the sample and the reference solutions (provided the uncatalysed reaction is sufficiently slow and dilution of the reference solution is negligible) may be written respectively as:

$$T_s = T_0^{[\exp(-k_d[C]_x t)]} \qquad (2)$$

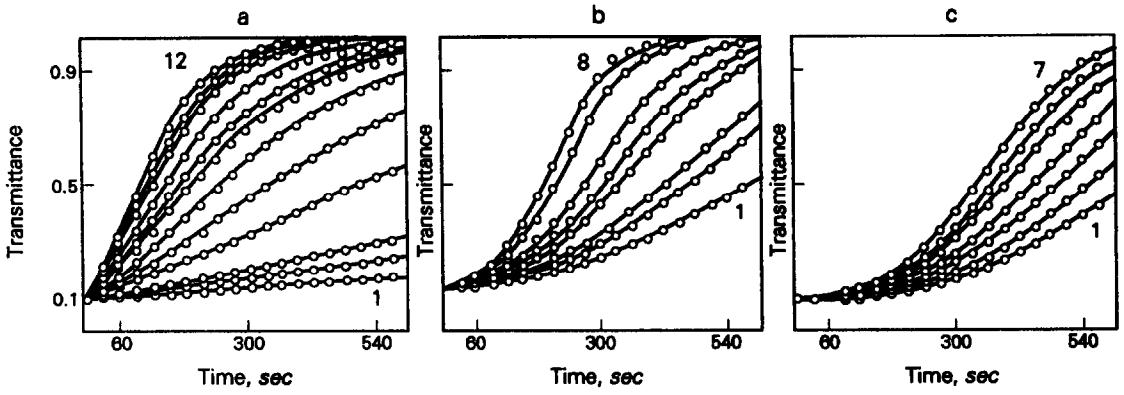

Fig. 1. Experimental (○) and simulated (——) transmittance–time curves. Ce(IV), $10^{-3}M$; As(III), $10^{-2}M$; H_2SO_4, $0.54M$; T, 25°; V_o, 50 ml. (a) Sample curves. $[I^-]$: (1) 4.356×10^{-8} (2) 6.534×10^{-8} (3) 1.043×10^{-7} (4) 2.087×10^{-7} (5) 3.101×10^{-7} (6) 4.172×10^{-7} (7) 5.216×10^{-7} (8) 5.993×10^{-7} (9) 7.303×10^{-7} (10) 8.615×10^{-7} (11) 9.389×10^{-7} (12) $1.102 \times 10^{-6}M$. (b) Reference curves for $[C]_s = 2.29 \times 10^{-5}M$; m: (1) 1.083×10^{-3} (2) 1.667×10^{-3} (3) 2.000×10^{-3} (4) 3.333×10^{-3} (5) 4.170×10^{-3} (6) 5.000×10^{-3} (7) 8.333×10^{-3}. (8) 1.000×10^{-3} ml/sec. (c) Reference curves for $m = 8.333 \times 10^{-3}$ ml/sec; $[C]_s$: (1) 2.948×10^{-5} (2) 4.033×10^{-5} (3) 5.186×10^{-5} (4) 6.339×10^{-5} (5) 7.096×10^{-5} (6) 9.241×10^{-5} (7) $1.078 \times 10^{-4}M$.

and

$$T_r = T_o^{[\exp(-k_c(m[C_s]/V_o)t^2)]} \qquad (3)$$

where T_s and T_r are, respectively, the sample and the reference transmittance, T_o is the transmittance measured at zero time and k_c is the rate coefficient (second-order constant) for the catalysed reaction. According to the equations (2) and (3), straight lines will be obtained by plotting $\ln(-\log T)$ *vs.* t and $\ln(-\log T)$ *vs.* t^2 for the sample and the reference solutions, respectively.

A series of 12 sample curves for $[C]_x$ in the range 4.356×10^{-8}–$1.102 \times 10^{-6}M$ were obtained and linearized in the indicated way. By plotting the measured slopes *vs.* the $[C]_x$ values a straight line was obtained, from whose slope the pseudo-second order rate constant k_c was measured $k_c = (1.195 \pm 0.012) \times 10^4$ $1.\text{mole}^{-1}.\text{sec}^{-1}$).

On the other hand, two series of reference curves have been obtained. In the first one, different values of $[C]_s$ from 2.948×10^{-5} to $1.078 \times 10^{-4}M$ have been used and m was kept constant. In the second one, $[C]_s$ was kept constant and different values of m from 1.083×10^{-3} to 1.000×10^{-2} ml/sec were used. Values of $(1.189 \pm 0.011) \times 10^4$ and $(1.194 \pm 0.003) \times 10^4$ $1.\text{mole}^{-1}.\text{sec}^{-1}$, for k_c are obtained from each of the series, and are in good agreement with those obtained from the sample curves.

In Fig. 1, experimental and simulated curves are compared for both sample and reference solutions. As can be seen, experimental curves fit fairly well to the theoretical equations.

Determination of iodide

Catalytic determination of iodide in pure solutions has been carried out by measuring the intersection time t_x from the crossing between the sample and the reference curves obtained separately, and then by applying the pseudo-stoichiometric procedure, that is to say, by using equation (1) directly. This is why the analytical results are shown by means of tables of the "taken–found" type. The results obtained by this "standard" technique for the t_x measurement are shown in Table 1. Relative standard deviations of 4.6 and 4.0% were obtained for 9.98 and 79.92 ng/ml iodide, respectively (ten determinations). Alternatively, linear calibration curves are obtained when the intersection times (all obtained by using the same

Table 1. Catalytic determination of iodide by continuous addition of catalyst to a reference solution. Ce(IV), $10^{-3}M$; As(III), $10^{-2}M$; H_2SO_4, $0.54M$; V_o, 50 ml; T, 25°

[I] *ng/ml*			Error,
Taken	Found	Difference	%
10.45	9.89	−0.86	−5.4
21.49	21.26	−0.22	−1.0
27.00	27.27	0.27	1.0
32.96	31.99	−0.97	−2.9
45.07	47.26	2.19	4.9
54.94	56.71	1.77	3.2
65.74	68.35	2.61	4.0
75.13	73.25	1.00	−2.5
104.23	98.61	−5.62	−5.4

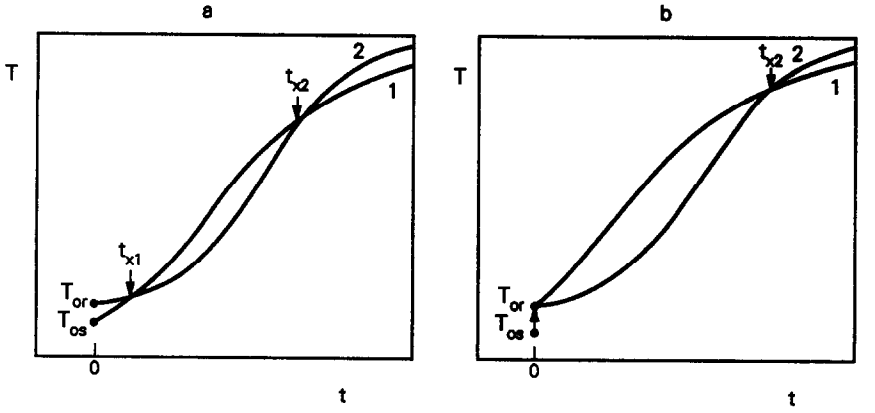

Fig. 2. Schematic drawing of crossing of (1) the sample and (2) the reference curves in (a) the two-intersection point technique and (b) the initial signal preadjustment technique.

reference curve) are plotted *vs.* the iodide concentration of standard iodide solutions, so that the comparative procedure could also be used.

To overcome the effect of possible random differences in the initial transmittance values between the two solutions, two alternative t_x measurement techniques were introduced, from which a somewhat higher precision can be expected. The "initial signal preadjustment" technique uses a sample solution that contains a cerium(IV) initial concentration higher than the one of the reference solution, so that the initial transmittance of the sample solution is lower than that of the reference solution. The reference curve is recorded first. Afterwards, the reaction is started in the sample solution, but at the beginning of the reaction the recorder remains switched off. As the reaction proceeds in the sample solution, its transmittance increases and, just when it reaches the initial value of the transmittance of the reference solution, the recorder is switched on [Fig. 2(a)].

The "two-intersection point" technique also requires that the sample solution must contain initially a cerium(IV) concentration higher than the reference solution, so that the superposition of the sample and the reference curves yields two intersection points [Fig. 2(b)]. Because the initial transmittances are not now equal, equations (2) and (3) will then be transformed into

$$T_s = T_{os}^{[\exp(-k_c[C]_x t)]} \tag{4}$$

and

$$T_r = T_{or}^{[\exp(-k_c(m[C_r]/V_o)t^2)]} \tag{5}$$

where T_{os} and T_{or} are the initial transmittance values of the sample and the reference solutions, respectively. The sample and reference transmittance values will be equal in each of the two intersection points. If t_{x1} and t_{x2} symbolize the values of the two intersection times, the following relationships can be obtained by equating (4) and (5):

$$[C]_x = \frac{m[C]_s}{2V_o} t_{x1} - \frac{B}{k_c}\frac{1}{t_{x1}} \tag{6}$$

and

$$[C]_x = \frac{m[C]_s}{2V_o} t_{x2} - \frac{B}{k_c}\frac{1}{t_{x2}} \tag{7}$$

where

$$B = \ln\frac{\log T_{or}}{\log T_{os}}$$

Finally, by solving the system of equations (6) and (7) for $[C]_x$, it can be deduced that

$$[C]_x = \frac{m[C]_s}{2V_o}(t_{x1} + t_{x2}) \tag{8}$$

According to this last expression, when two intersection points are produced, the analytical variable is the sum of the two measured intersection times.

Results of iodide determinations obtained by the pseudostoichiometric procedure by using both the initial signal preadjustment and the two-intersection point techniques are shown in Table 2. Iodide concentrations lower than about 25 ng/ml are difficult to determine by the two-intersection point technique, because the two points are very close and the measurements of the intersection times become poorly precise. Relative standard deviations of 0.9 and 1.6% (ten replicate) have been obtained for the initial signal preadjustment (69.73 ng/ml) and the two intersection point (56.93 ng/ml) techniques, respectively.

Table 2. Catalytic determination of iodide by continuous addition of catalyst to a reference solution. (a) Initial signal preadjustment technique. (b) Two-intersection point technique. Ce(IV), $10^{-3}M$; As(III), $10^{-2}M$; H_2SO_4, $0.54M$; V_o, 50 ml; T, 25°

(a)				(b)			
[I] *ng/ml*			Error,	[I] *ng/ml*			Error,
Taken	Found	Difference	%	Taken	Found	Difference	%
10.8	11.3	0.5	4.6	27.0	29.8	2.8	10.4
28.6	28.9	0.3	1.1	33.0	32.9	−0.1	−0.3
43.2	43.3	0.1	0.2	45.1	46.1	1.0	2.2
57.8	57.2	−0.6	−1.0	54.9	56.9	2.0	3.6
71.4	71.8	0.4	0.6	56.9	57.4	0.5	0.9
87.6	90.6	3.0	3.4	65.7	64.2	−1.5	−2.3
102.2	104.0	1.8	1.8	66.7	67.3	0.6	0.9
				70.8	71.1	0.3	0.4
				75.1	77.8	2.7	3.6
				79.9	77.5	2.4	3.0
				86.2	85.7	−0.5	−0.6
				104.2	108.1	3.9	3.7

The variances of the three different techniques for measuring the intersection time have been compared by applying the F-test. The variance of the standard technique is proved to be significantly higher than the variances of both the initial signal preadjustment and the two intersection point techniques at the 95% confidence level, although no significant difference has been found between the variances of these latter measurement techniques.

Since a single-beam photometer has been used, it can be expected that the differences in the initial transmittance values between the sample and the reference solutions are due to fluctuations in the power supply voltage to a certain extent. In order to avoid such fluctuations, a voltage stabilizer was used and the standard technique to measure the intersection time was applied. A series of determinations of different amounts of iodide was carried out. Relative errors of 4.1 and 0.36% were found for 13.55 and 138.6 ng/ml iodide, respectively. A relative standard deviation of 0.9% was obtained for 70.90 ng/ml (ten replicates). A statistical comparison between these results and those obtained by the initial signal preadjustment and by the two-intersection point measurement technqiues showed that their variances are not significantly different (99% confidence level). It can be seen, therefore, that the use of a voltage stabilizer allows us to obtain results as precise as obtained by the initial signal preadjustment and the two-intersection point techniques.

Determination of iodide in table salt

According to Dubravčić,[10] an excess of chloride may interfere with the catalytic determination of iodide because chloride exerts a low catalytic effect on the cerium(IV)–arsenic(III) reaction. As a previous test, it has been proved that chloride concentrations up to at least $7 \times 10^{-3}M$ do not affect the reaction kinetics significantly.

The proposed method has been applied to the determination of iodide in several samples of both iodized and non-iodized table salt (theoretical contents in the range from 0.01 to 6 ng/100 ml of iodine). Table 3 shows the results obtained by applying the pseudostoichiometric procedure to three samples of iodized and one sample of non-iodized table salt, before and

Table 3. Catalytic determination of iodide in table salt samples

	Iodide, mg/100 g					Recovery,
Sample	Specified	Found	Added	Total found	Recovered	%
Iodized salt "Carmencita"	6	5.43	5.30	10.66	5.23	98.7
		5.56	5.30	10.93	5.37	101.3
Iodized salt "Bueno"	6	3.71	5.30	9.01	5.30	100.0
		4.07	5.30	9.34	5.27	99.4
Iodized salt "Bevia"	6	5.41	5.30	10.76	5.35	100.9
		5.54	5.30	10.99	5.45	102.8
Non-iodized salt "Prodiet"	0.01	0.0097	0.0085	0.018	0.0083	97.6
		0.0098	0.0085	0.018	0.0082	96.5

after spiking with standard potassium iodide. Satisfactory recoveries between 96.5 and 102.8% were achieved.

It may be concluded that photometric probe monitoring proves to be a valuable alternative to amperometric monitoring for catalytic determinations by continuous addition of catalyst to a reference solution. Unlike amperometric monitoring with a rotating disk platinum electrode, normalization of the experimental kinetic curves is not necessary when photometric monitoring is used, owing to the higher signal reproducibility. Moreover, the simplicity, robustness and low price of the photometric instrumentation which may be used in these determinations is another point to be borne in mind.

Acknowledgements—This work was supported by CAICIT (Spain), Grant No. 955/84. The reported material has been presented at the Third Symposium on Kinetics in Analytical Chemistry, Dubravnik-Covtet, Yugoslavia, 1989, P.S. 111-25.

REFERENCES

1. G. López-Cueto and A. Cueto-Rejón, *Anal. Chem.*, 1987, **59**, 645.
2. H. V. Malmstadt and J. D. Winefordner, *Anal. Chim. Acta*, 1959, **20**, 283.
3. H. V. Malmstadt and W. E. Chambers, *Anal. Chem.*, 1960, **32**, 225.
4. H. V. Malmstadt and H. L. Pardue, *ibid.*, 1960, **32**, 1034.
5. A. Lein and N. Schwart, *ibid.*, 1951, **23**, 1507.
6. H. V. Malmstad and T. P. Hadjioannou, *ibid.*, 1963, **35**, 2157.
7. J. J. Moran, *ibid.*, 1952, **24**, 378.
8. P. A. Rodriguez and H. L. Pardue, *ibid.*, 1969, **41**, 1369.
9. *Idem*, *ibid.*, 1969, **41**, 1376.
10. M. Dubravčić, *Analyst*, 1955, **80**, 296.

Talanta, Vol. 39, No. 4, pp. 355–360, 1992
Printed in Great Britain

0039-9140/92 $5.00 + 0.00
Pergamon Press plc

DETERMINATION OF TOTAL INORGANIC IODINE IN SEAWATER BY CATHODIC STRIPPING SQUARE WAVE VOLTAMMETRY

GEORGE T. F. WONG* and LING-SU ZHANG
Department of Oceanography, Old Dominion University, Norfolk, VA 23529–0276, U.S.A.

(*Received* 13 *June* 1991. *Revised* 15 *August* 1991. *Accepted* 26 *August* 1991)

Summary—A method has been designed for the reduction of iodate to iodide in seawater and subsequent determination of total dissolved iodine as iodide by cathodic stripping square wave voltammetry. The pH of the sample is lowered to about 1–2 and iodate is reduced to iodide with sodium sulfite under this acidic condition. The pH of the sample is then raised to 8–9 before the concentration of iodide is measured.

Dissolved inorganic iodine is found in seawater primarily as iodate and iodide.[1–3] The concentration of total iodine in seawater is about 0.5μM.[4] In estuarine waters, the concentration of total iodine generally decreases with decreasing salinity, reaching undetectable concentrations at times.[5–7] Total iodine in seawater has been determined directly without any preconcentration step by converting one of these two forms of inorganic iodine to the other form and then measuring total iodine either as iodide or iodate.[4] In most reported studies, the detection limit is about 20nM.

Recently, a method has been described for the direct determination of iodide in seawater by cathodic stripping square wave voltammetry (CSSWV) and the detection limit can reach 0.1nM.[8] In this method, iodide is deposited onto the surface of a hanging mercury drop electrode (HMDE) as mercurous iodide under an applied potential for a specified period of time. This deposited mercurous iodide is later reduced by a cathodic potential scan and it gives rise to a current peak at about −0.33 V. The magnitude of the current peak is related to the concentration of iodide in the solution. However, before the deposition of the iodide from the sample, oxygen, which gives rise to an interfering current peak, must first be quantitatively removed from the sample by bubbling it with an inert gas such as nitrogen or argon. This step is frequently the most time consuming step in the analytical scheme. We have reported that, instead of bubbling the sample with an inert gas, sulfite may be used as an effective agent for removing the oxygen from the sample chemically at the natural pH of seawater while leaving the speciation of dissolved inorganic iodine unchanged.[9] As a result, the time required for analyzing a sample for iodide may be reduced by a factor of two. We have also observed that while sulfite does not reduce iodate at the pH of seawater, it reduces iodate to iodide readily under acidic conditions. Thus, CSSWV can also be used for the determination of total inorganic iodine in seawater after iodate has been reduced to iodide with sulfite. The resulting method is simple, fast and reliable. With the low detection limit, the required sample volume can be reduced to a milliliter or less, if necessary. Furthermore, if total inorganic iodine is determined as iodate by oxidizing all iodine species to iodate with an oxidizing agent such as hypochlorite,[10] some as yet unknown fraction of organic iodine, if it is present, may also be oxidized to iodate and be included as inorganic iodine.[11] In the voltammetric method, since a reduction rather than an oxidation step is used, it is less likely that organic iodine will be destroyed and be included as part of the inorganic iodine. We have also investigated the optimization of the operational parameters that may affect the determination of iodide or total inorganic iodine in seawater by CSSWV. Our results are reported in this paper.

EXPERIMENTAL

Apparatus

A Princeton Applied Research Model 384B polarographic analyzer system, equipped with a

*Author for correspondence.

Model 303A static mercury drop electrode (SMDE) in the HMDE mode, a Model 305 stirrer and a digital plotter, was arranged as described by Luther *et al.*[8] and used for square wave voltammetry. A platinum wire acted as the auxiliary electrode. The Ag/AgCl reference electrode supplied with the instrument was not used as the reference electrode in order to avoid any reaction between iodide and silver. This electrode was isolated from the sample in an empty reference electrode jacket. In its place, a standard calomel electrode was used as the reference electrode through a salt bridge in a Model K0065 reference electrode bridge tube filled with a 1*M* sodium carbonate solution. A small hole was drilled near the top of each glass polarographic cell for adding various reagents to the sample since the port for adding reagent had already been occupied by the reference electrode bridge tube.

Reagents

Nitrogen was purified by passing it through an alkaline pyrogallol trap.[12] The Triton X-100 was prepared from a Fisher brand concentrated stock solution.

All other chemicals used were of ACS reagent-grade.

Procedures

Pipette 5 ml of seawater into a 50-ml standard flask and dilute to volume with distilled, deionized water. Pipette 5 ml of this diluted seawater to a polarographic cell which contains 0.05 ml of a 0.2% Triton X-100 solution and a small magnetic stirring bar. Position the cell in the polarographic analyzer. Blanket the solution in the cell with a positive pressure of purified nitrogen to prevent the dissolution of atmospheric oxygen into the sample. Add 0.2 ml of 1*M* sodium sulfite and 1 ml of 2*N* sulfuric acid to lower the pH of the sample to 1–2. Stir the solution for about 30 sec and then add 1 ml of 1 + 4 ammonium hydroxide to raise the pH of the sample to about 8. Stir the mixture for about 30 sec. Analyze the sample by CSSWV under the following settings: deposition potential, −0.15 V; deposition time, 60 sec; equilibration time, 5 sec; scan range, −0.15 to −0.6 V; scan increment, 2 mV; pulse height, 20 mV; frequency, 100 Hz; mode, square wave voltammetry; drop size, large; reference electrode, standard calomel electrode via a salt bridge. The concentration of iodide in the sample is estimated by the method of standard internal addition by recording the height of the current peak of iodide after consecutive additions of 0.1 ml of a standard 2000n*M* potassium iodide solution to the sample. A reagent blank, if present, should be corrected for. The reagent blank is determined by substituting distilled deionized water for the sample. It is usually less than 5n*M*.

RESULTS AND DISCUSSION

Reduction of iodate with sulfite

The reduction of iodate by sulfite follows the stoichiometry of:

$$IO_3^- + 3SO_3^{-2} = I^- + 3SO_4^{-2}$$

The concentration of iodate in seawater is no more than 0.5μM.[4] After the dilution of the sample and the addition of reagents, the concentration of iodate in the analyte is reduced to 35n*M* or less. The added sulfite will also react with oxygen dissolved in the analyte.[9] Even if the analyte is saturated in oxygen with respect to the atmosphere, its concentration of oxygen should only be in the order of several hundred micromoles per liter. In the proposed procedure, the concentration of sulfite in the analyte is about 28m*M*. Thus, a large excess of sulfite is maintained to ensure that the iodate is reduced quantitatively to iodide and oxygen is absent from the analyte.

While sulfite does not reduce iodate to iodide at basic pH, it will do so readily under acidic conditions. The effect of pH on the reduction of iodate to iodide by sulfite was studied by adding sulfite to a NaCl-KBr-$NaHCO_3$ solution (0.375*M* in sodium chloride, 1m*M* in potassium bromide and 5m*M* in sodium hydrogen carbonate) with a known concentration of iodate, adjusting the pH of the solution to a specified value by adding 1*M* hydrochloric acid and/or 1*M* sodium hydroxide, allowing the reduction to occur for 30 sec, raising the pH to about 9 by adding 1*M* ammonium hydroxide and then determining the concentration of iodide formed by CSSWV. (Seawater is about 0.5*M* in sodium chloride, 0.8m*M* in Br^-, 2m*M* in HCO_3^- and 10m*M* in K^+.) The concentration of added iodate in the solution analyzed ranged from 25 to 100n*M*. The recovery of iodate as iodide at various pH values is shown in Fig. 1. Above a pH of about 7.5, there was no detectable formation of iodide. Below this pH, the recovery of iodate as iodide increased with decreasing pH. Quantitative recovery was achieved at pH below

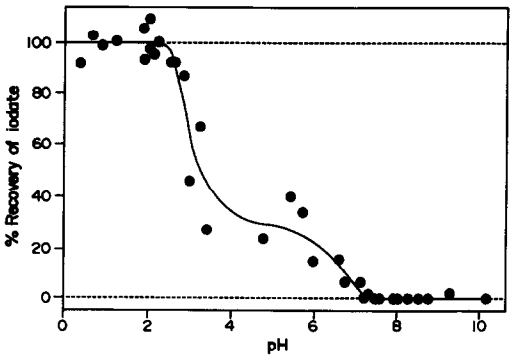

Fig. 1. The effect of pH on the reduction of iodate to iodide with sodium sulfite.

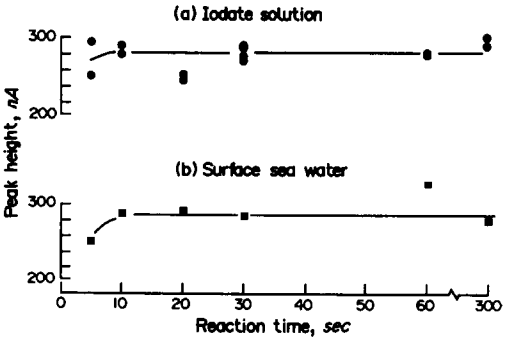

Fig. 2. Time required for the reduction of iodate to iodide (*a*) in a 519n*M* iodate solution and (*b*) in surface seawater with sulfite at a pH of 1.8.

2.3. We have chosen a pH of 1–2 for the reduction of iodate to iodide with sulfite.

The time required for the reduction of iodate to iodide with sulfite in the NaCl–KBr–$NaHCO_3$ solution and in surface seawater were studied at a pH of 1.8. Sulfite was added to the sample and the pH of the sample was adjusted to the prescribed value. After a specified amount of time ranging from 5–300 sec, 1 ml of 1 + 4 ammonium hydroxide was added to raise the pH to about 9 to stop the reaction. The peak height of the current peak of the iodide formed was then measured and the results are shown in Fig. 2. Within the analytical uncertainty, a constant peak height was reached after the reaction was allowed to proceed for 10 or more seconds. We have chosen a reaction time of 30 sec to ensure that the reaction is complete.

During the reduction of iodate to iodide, volatile iodine species with intermediate oxidation states such as molecular iodine and hypoiodous acid may be formed. Potentially, these iodine species may be lost to the atmosphere by volatilization. This possibility was tested by comparing the concentration of added iodate found in sub-samples of the NaCl–KBr–$NaHCO_3$ solution that were undisturbed, stirred with a magnetic stirrer or bubbled with nitrogen while sulfite was allowed to react with iodate at a pH of about 1. The results are shown in Table 1. The concentrations of iodate determined as iodide by these three methods for treating the sub-samples were indistinguishable from each other within experimental uncertainty.

The pH of the solution must be raised to above 7 before the concentration of total dissolved inorganic iodine can be determined as iodide by CSSWV because sulfite gives rise to a sharp current peak at about −0.6 V[13] under acidic conditions (Fig. 3). With the large amount of excess sulfite present, the residual current of the current peak of sulfite can mask the peak of iodide at −0.33 V. At pH above 7, the peak of sulfite disappears. Renard[14] suggested that the current peak of sulfite is due to the bisulfite ion. The pK_2 of sulfurous acid in a pure solution is 7.21.[15] Its value in seawater is not well known. However, it is expected to be lower as the ionic strength of seawater is high. Thus, the concentration of bisulfite may become minimal at pH above 7. We have adopted a pH of 8–9 in our analytical

Table 1. Possible loss of volatile iodine species during the reduction of iodate to iodide

	Iodate as iodide, *n*M				Avg. ± 1 SD,* *n*M
Sample 1.					
No N_2-bubbling	86.5	86.3	91.3	87.6	88 ± 2
With N_2 bubbling	90.9	86.0	86.9		88 ± 3
Sample 2.					
No stirring	57.4	53.4	51.9		54 ± 3
Slow stirring (2 min)	55.8	53.0			54 ± 2
Fast stirring (5 min)	50.7	52.3	50.5	50.6	51 ± 1

*SD—Standard deviation.

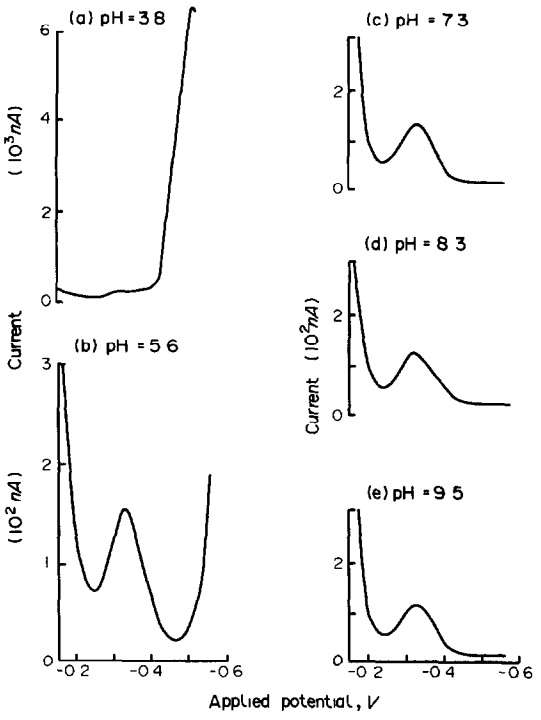

Fig. 3. The effect of pH on the voltamperogram of iodide in the presence of sulfite.

scheme to insure that the interference by sulfite may be circumvented.

Optimization of voltammetric parameters

A number of adjustable operational parameters are involved in CSSWV. Luther *et al.*[8] have studied some of them for the determination of iodide in seawater. In their study, sulfite was not added to the sample. In the presence of a large excess of sulfite, we have shown that the optimal depositional and initial stripping potential for the determination of iodide should be changed from -0.1 to -0.15 V.[9] This depositional and initial stripping potential should also be used for the determination of total iodine as iodide.

The dynamic range of the method, which can be controlled by the length of the deposition time, was studied. The results are shown in Fig. 4. At each given concentration of iodide, the peak height of the current peak of iodide increased with increasing deposition time [Fig. 4(a)]. The increase was especially pronounced at deposition times that were shorter than 35 sec. Thus, at these short deposition times, the peak height may vary significantly if the deposition time cannot be controlled with a high degree of accuracy and precision. As a result, the precision of the method will be lowered. At deposition times of longer than 50 sec, the increase in peak height was minimal. In order to maximize the sensitivity and precision of the method, a deposition time of 60 sec was chosen. At each deposition time, the peak height increased with increasing concentration of iodide. The highest concentration below which a linear relationship between peak height and concentration was observed decreased with increasing deposition time from about 150n*M* at 45 sec of deposition time to 75n*M* at 80 sec of deposition time [Fig. 4(b)]. At the proposed deposition time of 60 sec, the peak height was linearly related to concentration up to about 130n*M*. Given that a calibration curve is constructed for each sample by internal additions in 3 to 4 stepwise increases in the concentration of iodide of about 25n*M* in each step, the concentration of iodide in the analyte should not exceed about 75n*M* so that the concentration of iodide in the analyte plus the added iodide does not exceed 130n*M*. The

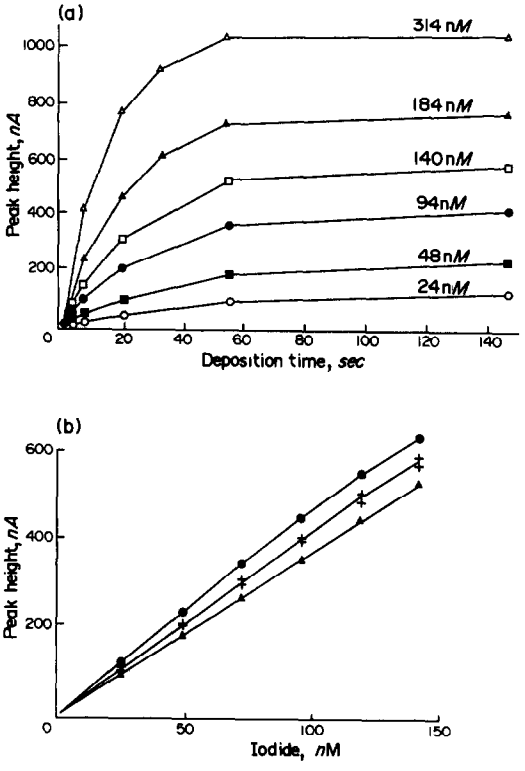

Fig. 4. (*a*) The influence of deposition time on the height of the current peak of iodide at various concentrations of iodide. (*b*) The relationship between peak height and the concentration of iodide at deposition times of 45 sec (▲), 60 sec (+) and 80 sec (●). Duplicate runs were made at a deposition time of 60 sec.

concentration of total inorganic iodine is usually about 0.5μM. A ten-fold dilution before the analyses would bring the concentration of the analyte within the dynamic range of the method. Since only 5 ml of the diluted seawater is needed for each analysis, even 0.5 ml of sample would be sufficient for the analysis. If this method is used for the determination of total inorganic iodine in other kinds of natural waters with substantially different concentrations, the dilution step and the deposition time should be adjusted accordingly to bring the concentration of total iodine in the analyte to within the dynamic range of the method. The concentration of iodide in seawater may range from less than 10nM to 300nM.[4] In most cases, it can be analyzed directly by CSSWV by varying the deposition time between 30 and 180 sec as described by Luther *et al.*[8] With a deposition time of 180 sec, a detection limit of 0.1nM can be reached.[8] However, at the high end of the concentration range, a dilution of the sample before it is analyzed may yield more precise results than shortening the deposition time alone.

Recovery and intercomparison of results from three independent methods

Aliquots of the NaCl–KBr–$NaHCO_3$ solution containing various known concentrations of added iodide, iodate or both iodide and iodate together were analyzed by the proposed method and the results are summarized in Table 2. In three solutions that were analyzed in duplicate, the concentration of added iodide ranged from 19.6 to 58.7nM and the amount of iodide recovered as total iodine averaged to 102 ± 3%. In the case of iodate, four solutions were analyzed in duplicate. The concentration of added iodate varied between 18.8 and 56.4nM and the averaged recovery of iodate as total iodine was 100 ± 3%. When both iodate and iodide were added, the average recovery in five analyses was 99 ± 3%. The recoveries in all cases were quantitative within the analytical uncertainties.

Five samples of seawater collected at various depths from the Sargasso Sea were stored frozen and later analyzed in a shore-based laboratory in triplicate according to published methods for iodide by CSSWV,[8] for iodate by differential pulse polarography (DPP),[16] and for total dissolved iodine by DPP.[10] They were also analyzed in triplicate for total inorganic iodine by the method described here. The results are shown in Table 3. The standard deviation of the triplicates determined by CSSWV ranged from 1.3 to 6.9% (one standard deviation). The concentrations agreed well with those determined by DPP or by summing the concentration of iodide and iodate. There was no detectable systematic difference between the concentration given by CSSWV and the other two methods. In all cases, the values obtained by CSSWV and one of the other two methods agreed to within ±3% of the mean value of the results from the two methods compared.

Table 2. The recovery of iodide and/or iodate by the proposed method

Iodine species added, nM			Total I measured, nM	Recovery, %	Avg. Rec.* ±1 SD, %
I	IO_3^-	$(I + IO_3^-)$			
19.6	—	19.6	20.6	105	102 ± 3
19.6	—	19.6	19.4	99	
39.1	—	39.1	38.4	98	
39.1	—	39.1	41.6	106	
58.7	—	58.7	58.5	100	
58.7	—	58.7	60.7	103	
—	18.8	18.8	19.6	105	100 ± 3
—	18.8	18.8	18.6	99	
—	32.8	32.8	32.0	98	
—	32.8	32.8	33.2	101	
—	37.6	37.6	36.3	97	
—	37.6	37.6	37.1	99	
—	56.4	56.4	58.2	103	
—	56.4	56.4	56.5	100	
9.8	9.4	19.2	18.3	95	99 ± 3
9.8	9.4	19.2	18.4	96	
19.6	18.8	38.4	38.7	101	
19.6	18.8	38.4	38.2	100	
29.4	28.2	57.6	58.4	101	

*Avg. Rec.—Average Recovery.
SD—Standard deviation.

Table 3. The determination of total iodine in seawater by three independent methods

Sample	I^-, nM	IO_3^-, nM	$(I^- + IO_3^-)$, nM	Total iodine CSSWV,* nM	Total iodine DPP,† nM
1	32°00.0′N, 75°00.0′W; Depth: 150 m				
	21.5	428.8	450.3	445.6	477.1
	23.5	420.5	444.0	457.7	462.0
	20.2	426.0	446.2	450.9	469.3
Avg.	22	425	447	451	470
SD‡ (nM)	2	4	3	6	8
SD (%)	8	1	1	1	1
2	32°11.5′N, 76°00.0′W; Depth: 50 m				
	163.1	326.5	489.6	479.3	496.1
	166.5	310.1	476.6	467.7	481.3
	162.0	307.9	469.9	474.4	477.1
Avg.	164	315	479	474	485
SD‡ (nM)	2	10	10	6	10
SD (%)	1	3	2	1	2
3	32°33.0′N, 77°46.0′W; Depth: 200 m				
	0.0	462.1	462.1	453.7	465.6
	0.0	469.3	469.3	481.8	486.4
	7.9	459.8	467.7	509.9	479.9
Avg.	3	464	466	482	477
SD‡ (nM)	5	5	4	28	11
SD (%)	177	1	1	6	2
4	32°53.5′N, 78°02.5′W; Depth: 10 m				
	160.7	310.7	471.4	461.4	470.2
	158.7	313.0	471.8	456.6	472.6
	160.6	320.7	481.3	470.8	476.3
Avg.	160	315	475	463	473
SD‡ (nM)	1	5	6	7	3
SD (%)	1	2	1	2	1
5	32°53.5′N, 78°02.5′W; Depth: 100 m				
	9.3	481.3	490.6	507.1	467.0
	9.3	471.2	480.4	545.4	474.3
	8.7	464.0	472.7	475.2	476.0
Avg.	9	472	481	509	472
SD‡ (nM)	0.3	9	9	35	5
SD (%)	3	2	2	7	1

*CSSWV—Cathodic stripping square wave voltammetry.
†DPP—Differential pulse polarography.
‡SD—Standard deviation.

Acknowledgement—This work was supported by the National Science Foundation under grant OCE-8910956.

REFERENCES

1. S. Tsunogai, *Deep-Sea Res.*, 1971, **18**, 913.
2. G. T. F. Wong and P. G. Brewer, *Geochim. Cosmochim. Acta*, 1977, **41**, 151.
3. G. T. F. Wong, K. Takayanagi and J. F. Todd, *Mar. Chem.*, 1985, **17**, 177.
4. G. T. F. Wong, *Rev. Aquat. Sci.*, 1991, **4**, 45.
5. J. D. Smith and E. C. V. Butler, *Nature*, 1979, **277**, 468.
6. K. Takayanagi and D. Cossa, *Can. J. Earth Sci.*, 1985, **22**, 644.
7. W. J. Ullman, G. W. Luther, R. C. Aller and J. E. Mackin, *Mar. Chem.*, 1988, **25**, 95.
8. G. W. Luther, C. B. Swartz and W. J. Ullman, *Anal. Chem.*, 1988, **60**, 1721.
9. G. T. F. Wong and L.-S. Zhang, *Mar. Chem.*, 1992, in the press.
10. K. Takayanagi and G. T. F. Wong, *Talanta*, 1986, **33**, 451.
11. G. W. Luther, T. Campbell and E. Tsamakis, *Deep-Sea Res.*, 1991, **38**, Suppl. 2A, S875.
12. M. Zief and J. W. Mitchell, *Contamination Control in Trace Element Analysis*, Wiley, New York, 1976.
13. G. W. Luther, A. E. Giblin and R. Varsolona, *Limnol. Oceanog.*, 1985, **30**, 727.
14. J. J. Renard, G. Kubes and H. I. Bolker, *Anal. Chem.*, 1975, **47**, 1347.
15. I. M. Kolthoff and V. A. Stenger, *Volumetric Analysis*, Vol. 1, p. 282. Interscience, New York, 1942.
16. J. R. Herring and P. S. Liss, *Deep–Sea Res.*, 1974, **21**, 777.

Talanta, Vol. 39, No. 4, pp. 361–366, 1992
Printed in Great Britain.

0039-9140/92 $5.00 + 0.00

THE USE OF A PIEZOELECTRIC CRYSTAL TO DETERMINE SULPHUR DIOXIDE IN GASES

RUDOLF PŘIBIL*
Faculty of Sciences, Charles University, Albertov 6, Prague 2, Czechoslovakia

EVA BÍLKOVÁ
Institute of Physics of the Atmosphere, Czechoslovak Academy of Science, Boční II/1401, Prague 4, Czechoslovakia

(*Received* 24 *May* 1991. *Revised* 2 *August* 1991. *Accepted* 23 *September* 1991)

Summary—This work describes the detection of sulphur dioxide with a piezoelectric crystal, at a resonance frequency of 9 MHz, covered with an active coating containing trioctylmethylammonium dichromate which irreversibly bonds sulphur dioxide in an oxidation–reduction reaction. The decrease in the vibration frequency of the crystal is directly proportional to the mass of sulphur dioxide bonded. The detector works on the basis of integration of the decrease in the frequency over a given time interval (at least 10 min), resulting in a high measuring sensitivity. The calibration curve is linear for sulphur dioxide concentrations from a few to 500 $\mu g/m^3$. Partial exhaustion of the capacity of the active coating, occurring after prolonged use, appears as nonlinearity of the detector concentration response. This nonlinearity can be compensated by a simple mathematical correction that permits the lifetime of the active coating to be lengthened by several orders of magnitude.

The ever-increasing interest in environmental protection throughout the world has led to the need for reliable, inexpensive methods of studying pollution of the atmosphere. This work, dealing with determination of the sulphur dioxide concentration in the air with piezoelectric phenomena, is a contribution to this effort.

The piezoelectric phenomenon, constituting a connection between the mechanical and electrical properties of substances, can be used to determine small mass increases in special types of microscales. Quartz piezoelectric crystals with suitable mechanical properties have been used most widely for this purpose. Sauerbrey[1] first described the dependence between the mass on the oscillating crystal surface and the change in the resonance frequency of the crystal. The above principle has been employed in a number of procedures for measuring gaseous pollutants and aerosols, but their use in practice has been complicated by a number of difficulties. Gases can be detected with piezoelectric resonators consisting of a thin quartz plate, on both sides of which fine metallic, circular electrodes are vacuum-plated. The surfaces of these electrodes are covered with a layer that, ideally, selectively absorbs the test gas. The increased mass of the electrode coating leads to a decreased resonance frequency of the crystal which is thus a measure of the amount of gas absorbed. The type of interaction between the active coating and the detected gas determines the character of the frequency response of the detector. Most of the detectors so far described utilize reversible sorption and desorption of the detected gas on the active electrode surface, leading to establishment of equilibrium between the amount of sorbed analyte and its instantaneous concentration in the gas phase.[2,3] The requirements of high detector sensitivity and simultaneous reversibility are in a certain sense contradictory and the use of reversible detectors to measure the concentrations of gaseous pollutants in the atmosphere is thus limited. An irreversible detector is better suited for highly sensitive measurements, involving irreversible sorption of the analyte from a gas stream passing through the measuring cell and thus integration of the frequency response over a certain time interval. This approach has the disadvantage of gradual exhaustion of the active electrode surface, which must thus be periodically renewed.

The composition of the active coating strongly affects the detector function. A number of substances[2–8] have been proposed for the detection of sulphur dioxide. Study of the

*Author for correspondence.

literature led us to the conclusion that the most promising substance would be a homogeneous coating with the consistency of a highly viscous liquid that would react with sulphur dioxide throughout its volume while retaining its original properties and high reactivity. Consequently, we studied two high-molecular mass amines that are employed in analytical chemistry in the extraction of anionic metal complexes, trioctylamine and trioctylmethylammonium chloride (TOMA). These substances are clear, highly viscous oils that behave as liquid ion exchangers and can be combined with various anions. About 20 different coatings were prepared from these substances, several of which exhibited acceptable activity. The complex of TOMA with dichromate ions had by far the best properties (TOMA–Cr_2O_7). This is a dark yellow substance with the consistency of honey, and is soluble in a number of organic solvents. It reacts readily with sulphur dioxide, with reduction of chromium(VI) to chromium(III). The reduced substance is green and stable to oxidation. The detailed study of the reaction mechanism was not performed but in the reduced coatings the presence of chromium(III) was established. In the experiments with greater volumes of the active substance it was confirmed that due to the sulphur dioxide diffusion the reaction passes throughout the whole volume of the substance. The bonding of sulphur dioxide in the coating is completely irreversible and the frequency response of the detector corresponds directly to the mass of the sorbed sulphur dioxide.

This work deals with the use of TOMA–Cr_2O_7 for the determination of sulphur dioxide in an irreversible detection system.

EXPERIMENTAL

The detectors consisted of AT-type quartz crystals with a characteristic resonance frequency of 9 MHz and a negligible temperature dependence in laboratory conditions. The active coatings were prepared from a 5% (vol.) solution of TOMA in carbon tetrachloride, shaken manually in a separating funnel with a four-fold volume of a saturated aqueous solution of potassium dichromate. The separated organic phase containing TOMA–Cr_2O_7 was diluted five-fold with carbon tetrachloride and sprayed onto both the electrodes of the crystal. The thickness of the coating was adjusted electronically by controlling the spraying time. The crystals were dried in a drying box at 70° for one hour. The measurements were carried out in teflon cells[2] of commonly used design with a volume of about 1.5 ml, in which the analysed gas was introduced by two inlets directed against both electrodes of the crystal plate. The oscillator frequency was read with a counter with a precision of ± 1 Hz (gate time 1 sec) and the whole measuring apparatus was computer-controlled.

A sulphur dioxide mixture with defined concentration for model experiments was prepared with standardized sulphur dioxide permeation sources (Chemoprojekt, Prague) or in a mixing apparatus.[9] The carrier gas was technical nitrogen which was not purified. The sulphur dioxide concentration was controlled analytically with the standard colorimetric method of West and Gaeke.[10]

Real atmospheric samples were measured with two identical measuring cells in series or in parallel; a membrane filter with a pore diameter of 0.4 μm (Synpor, Synthesia, Czechoslovakia) was placed at the entrance to the sampling unit to remove aerosol particles.

RESULTS AND DISCUSSION

Determination of the optimal amount of the active coating and the gas flow rate through the measuring cell

The amount of the active coating used should ensure the highest possible sensitivity and lifetime of the detector and also its reliable and reproducible functioning. It follows from Fig. 1 that the capacity of the active coating, *i.e.*, the amount of sulphur dioxide that a given coating can absorb, increases linearly with the amount of the active substance. The mass of the coating is directly proportional to the decrease in the resonance frequency of the crystal occurring after application to the electrode, and is thus expressed in the figures in terms of frequency units. Figure 2 depicts the dependence between the mass of the active substance and the detector sensitivity. It can be seen that the detector sensitivity increases with increasing mass of the active substance up to a frequency decrease of about 20 kHz, after which it no longer increases. The maximal load on the electrodes, *i.e.*, about 100 μg, corresponds to a frequency decrease of 40–45 kHz[4] (the crystal ceases to oscillate at larger loads) and the maximal amount of sulphur dioxide which the active coating can absorb corresponds to a frequency decrease of

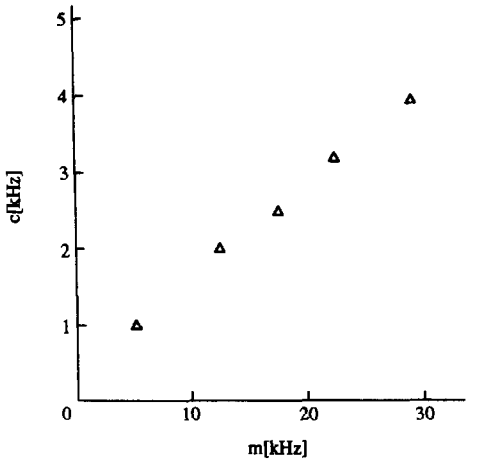

Fig. 1. Effect of the mass of the active coating, m, on its capacity, c, *i.e.*, the maximum mass of SO_2 that the given coating can absorb. Both the mass of the coating and the mass of SO_2 are expressed in terms of the frequency decrease on the crystal. Gas flow-rate through the measuring cell was 200 ml/min, SO_2 concentration was about 43 $\mu g/m^3$.

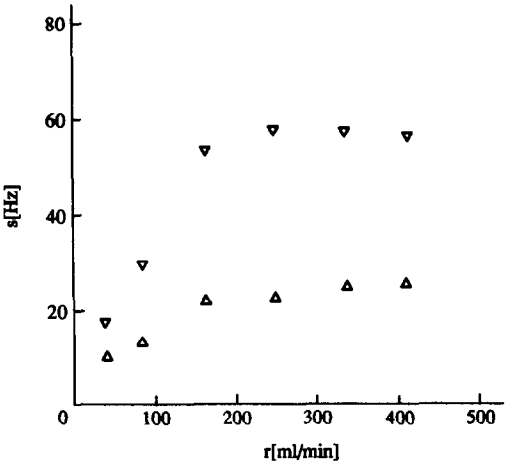

Fig. 3. Effect of the gas flow-rate through the measuring cell, r, on the detector sensitivity, s, *i.e.*, on the frequency decrease over a time interval of 10 min, for the SO_2 concentrations △: 50 $\mu g/m^3$; ▽: 100 $\mu g/m^3$.

about 5 kHz. Consequently the optimal amount of the active substance was considered to be that corresponding to a frequency decrease of 30 kHz, when a high sensitivity was ensured, with a sufficient reserve for reliable detector functioning. It also follows from Fig. 2 that the reproducibility of the active coating weight (up to ±10%) does not affect the detector sensitivity.

The experiments were carried out at a gas flow-rate of 200 ml/min, see Fig. 3, which was supposed to be the most suitable in regard to sufficient detector sensitivity for claims on the pump performance in the case of a portable instrument development.

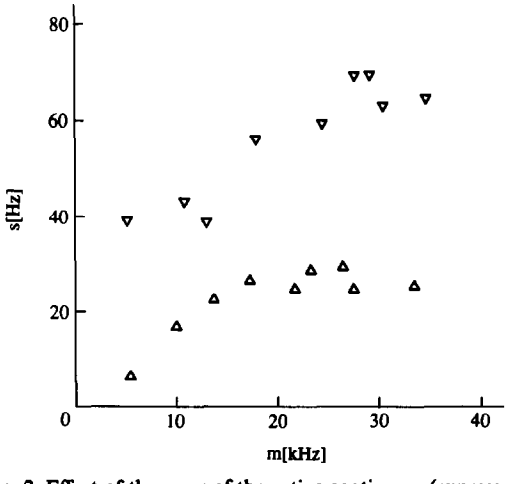

Fig. 2. Effect of the mass of the active coating, m (expressed in terms of frequency decrease), on the detector sensitivity, s, *i.e.*, on the frequency decrease over a time interval of 10 min. Gas flow-rate through the measuring cell was 200 ml/min, SO_2 concentration △: 50 $\mu g/m^3$; ▽: 200 $\mu g/m^3$.

The dependence of the detector response on the sulphur dioxide concentration

It was found that this dependence is linear in the studied concentration range up to 500 μg SO_2/m^3 and can be approximated by a straight line given by the relationship

$$f = 0.30c + 9, \quad (1)$$

where f is the frequency decrease over a time interval of 10 min (Hz). The sulphur dioxide concentration is then given by

$$c = 3.33f - 30 \quad (2)$$

where c is the concentration in $\mu g/m^3$. The correlation coefficient of the equations is equal to 0.998. It thus follows that the detector sensitivity is sufficient for measuring the sulphuric dioxide concentration in the atmosphere and that the piezoelectric crystal can reproducibly detect concentrations at the level of several μg SO_2/m^3, *i.e.*, of the order of units of ppb; this sensitivity has also been confirmed by other model experiments. The intercept of the straight line on the ordinate was observed in all the experiments with coated and even with uncoated crystals when the nitrogen or purified air were used as the carrier gas. This constant change in frequency can be explained by an increase in the crystal load but its true nature is so far not clear.

The analytical accuracy and the precision of the piezoelectric detector

The exact assessment of the measuring accuracy and precision in detectors of atmospheric pollutants is a relatively complex problem. It is difficult to compare the performances of the individual detectors because of their different operating conditions, sampling requirements and calibration procedures.

The variations in the frequency response of piezoelectric detector are basically a consequence of the lack of uniformity of the individual manufactured crystals and of the variations in the detector temperature. In model experiments, the measurements will also reflect errors in the preparation of a defined sulphur dioxide concentration in the gas dilution apparatus. The use of the common spectrophotometric method of West and Gaeke[10] as a standard procedure for checking sulphur dioxide concentrations is not completely satisfactory, especially at low concentrations where a long sampling time (up to several tens of hours) is necessary. In our work the evaluation of the piezoelectric detector performance was based on the used certified permeation devices (Chemoprojekt, Prague) that were employed in model experiments. The overall precision of the measuring system in the range from tens to hundreds of μg SO_2/m^3 over a time interval of 10 min is approximately $\pm 10\%$ as can be seen in Table 1. The precision can be improved by increasing the measuring time interval.

Table 1. Precision and accuracy of the SO_2 determination in model experiments

SO_2 concentration Prepared, $\mu g/m^3$	Found,* $\mu g/m^3$	Recovery, %
20	18	90
30	24	80
40	41	103
50	51	102
100	124	124
200	183	92
300	302	101
400	395	99
500	504	101
	Average	100
	Standard deviation	±12
	Relative deviation	±12%

*Mean of 3 or 4 results.

The detector lifetime and measuring procedure

One of the drawbacks of irreversible detectors is the gradual depletion of the capacity of the active coating, leading to a decrease in the detector sensitivity. Consequently, the change in the detector response with time was studied. Figure 4 depicts the changes in the detector response for a given constant sulphur dioxide concentration over 24 hr. It follows from the dependence for various sulphur dioxide concentrations that a linear detector response can be expected only in the beginning, up to a frequency decrease resulting from sorption of sulphur dioxide of about 500 Hz, where the slope of the tangent to the curve is directly proportional to the sulphur dioxide concentration. However, the detector sensitivity is still sufficient in the curved region and the use of a suitable mathematical approximation to the dependence of the detector sensitivity on time permits a several-fold lengthening of the detector lifetime. The approximation was carried out with a rational fractional function in the form

$$y = k_1 \cdot x/(k_2 + x), \tag{3}$$

where y is the frequency decrease from the beginning of the measurement to time $t = x$ (given in minutes).[11] The coefficient k_1 corresponds to the maximal sorption capacity of the active coating, expressed as the frequency decrease and given by the mass of the coating alone. Fraction k_1/k_2 equals the slope of the frequency decrease df/dt and corresponds to the experimentally established values for the frequency decrease in the linear response region. The validity of the approximation function was confirmed in 24-hr experiments for various sulphur dioxide concentrations. The results are

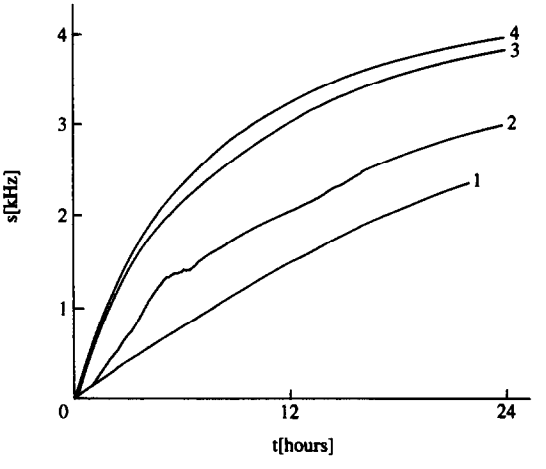

Fig. 4. The time dependence of the detector sensitivity, s, *i.e.*, of the frequency decrease over a time interval, for SO_2 concentrations: 1–47 $\mu g/m^3$, 2–116 $\mu g/m^3$, 3–370 $\mu g/m^3$, 4–428 $\mu g/m^3$. Gas flow-rate through the measuring cell was 200 ml/min.

given in Table 2. It can be seen that coefficient k_1 actually expresses the experimentally established sorption capacity of the coating. The only exception was the detector response for a concentration of 47 μg SO_2/m^3, where the detector response was almost linear over the whole 24-hr period and thus the calculated k_1 value is subject to a considerable computing error and is not in agreement with the expected sorption capacity. Nevertheless the k_1 computed for higher concentrations can be applied for the whole range of the studied concentrations (10–500 μg SO_2/m^3). Fraction k_1/k_2 is directly proportional to the sulphur dioxide concentration. The relationship between the frequency decrease f and the sulphur dioxide concentration c,

$$f = 0.27c + 19, \tag{4}$$

$$c = 3.70f - 70, \tag{5}$$

calculated on the basis of the above approximation is in relatively good agreement with the experimentally obtained calibration equations given above [equations (1) and (2)].

The practical importance of this approximation lies in the fact that the relative change in the detector sensitivity can be determined during its entire lifetime. It was experimentally confirmed that this sensitivity change is dependent solely on the total mass of sulphur dioxide that has already been absorbed by the coating, which is quantitatively reflected in the overall frequency decrease recorded during the detector lifetime. Thus, when we know the resonance frequency of the crystal with fresh coating, the change in sensitivity can be easily compensated, for instance by a series of correction coefficients to the detector response. The tangent of the frequency decrease corrected in this way corresponds to the value of the tangent that would be obtained if measurements were carried out in the linear response region and is proportional to the sulphur dioxide concentration read off the linear calibration graph. The values of the correction coefficients for the practically exploitable frequency interval are given in Table 3. The simple compensation of the sensitivity loss outlined above demonstrates the general approach and can be modified.

It can be found theoretically that the crystal can be used for continuous measurement at a concentration of 20 μg SO_2/m^3 for approximately 110 hr and at a concentration of 150 $\mu g/m^3$ for approximately 30 hr.

Table 2. The values of the coefficients of the approximation function related to the SO_2 concentration

SO_2 concentration, $\mu g/m^3$	k_1	k_2	k_1/k_2
50	10,070*	3930	2.6
120	4960	910	5.8
250	5600	620	8.5
340	5130	470	11.3
370	5540	430	12.4
430	5150	410	13.0
Average	5300		
Standard deviation	±280		
Relative deviation	±5.3%		

Experimentally established sorption capacity equaled to 5200 Hz frequency decrease.

*This value was not included in calculation of the average.

Practical monitoring of the sulphur dioxide concentration does not usually necessitate continuous measurement; it is usually sufficient to carry out the measurements at given time intervals. The measuring interval and frequency must be selected according to the expected variations in the sulphur dioxide concentration and the requirements of the measuring instrument. This method has been tested on model samples and it has been found that it is useful to alternate measurement on the test and on a blank reference gas, leading to considerable lengthening of the detector lifetime.

Continuous measurement over 100 hr was carried out to determine whether any other time-dependent processes occur in the crystal active coating that would affect its sensitivity and lead to its ageing. The sensitivity of the crystal to a mixture with a defined sulphur dioxide concentration was then tested. The crystal response corresponded to that expected on the basis of the degree of exhaustion of the coating and thus the crystal sensitivity was not affected by any processes of ageing of the active coating and the lifetime of the detector is given by the amount of sorbed sulphur dioxide alone.

Table 3. Values of correction coefficients

Overall frequency decrease (Hz)	Correction coefficient	Overall frequency decrease (Hz)	Correction coefficient
0	1.00	1800	2.30
200	1.08	2000	2.59
400	1.17	2200	2.94
600	1.27	2400	3.36
800	1.39	2600	3.88
1000	1.52	2800	4.53
1200	1.67	3000	5.36
1400	1.85	3200	6.44
1600	2.06	3400	7.89

Interferences

Orientative measurements were carried out to determine the effect of gases that could interfere in the determination of sulphur dioxide by reaction with the active coating. Those investigated were HCl, H_2S, CO, CO_2, NH_3, NO_x, $CH{\equiv}CH$, C_4H_{10} and O_3. As expected, these gases did not interfere even at high concentrations, as they cannot undergo redox reactions with the active surface.

The greatest interference in the measurement of sulphur dioxide was produced by changes in the test gas humidity. As it was not possible in model experiments to ensure a constant humidity of the test gas without affecting the sulphur dioxide concentration, real atmospheric samples were measured, using a method with a reference crystal. These reference crystals were resonators whose active coating was saturated in sulphur dioxide. It was found that the response of the reference crystal was completely independent of the sulphur dioxide concentration but depended very strongly on the humidity of the atmosphere. The sulphur dioxide concentration was found as the difference between the frequency decrease of the measuring and reference crystals over the given time interval according to the calibration dependence. We know of course that the problem of removing the humidity interferences is very complicated and the use of the method suggested is limited especially when fast changes of humidity in the atmosphere occur. Practical use of the piezoelectric detector will necessitate more detailed study of this question.

CONCLUSIONS

The above experiments have demonstrated that the detection method employing irreversible reaction of the analyte with the active coating of the piezoelectric crystal can be used to measure the sulphur dioxide concentration in gases. The method has been tested on model experiments for sulphur dioxide concentrations of 10–500 $\mu g/m^3$. The detector is simple, inexpensive, and exhibits high sensitivity and a wide measuring range with sufficient selectivity and a relatively short measuring time. The whole measurement can be automated. The integration method of measurement is a disadvantage, as it is accompanied by a limited capacity of the active coating. The lifetime of the active coating depends on the procedure employed and the measured sulphur dioxide concentrations. After depletion of the active surface, the crystal must be exchanged. The depleted coating can be readily washed off with a suitable solvent, *e.g.*, CCl_4 or $CHCl_3$, and application of a new coating makes the crystal ready for use again.

The applicability of this method for measurement in the atmosphere is complicated by humidity interferences. The suggested compensation method with the reference crystal is not completely satisfactory and the problem of humidity requires further study.

Acknowledgement—The authors would like to thank Prof. T. S. West for providing the initial stimulus for this work.

REFERENCES

1. G. Sauerbrey, *Z. Phys.*, 1959, **155**, 206.
2. K. H. Karmarkar and G. G. Guilbault, *Anal. Chim. Acta*, 1974, **71**, 419.
3. M. Janghorbani and H. Freund, *Anal. Chem.*, 1973, **45**, 325.
4. J. Hlavay and G. G. Guilbault, *ibid.*, 1977, **49**, 1890.
5. H. Beitnes and K. Schroder, *Anal. Chim. Acta*, 1984, **158**, 57.
6. F. W. Karasek and J. M. Tiernay, *J. Chromatogr.*, 1974, **89**, 31.
7. D. Humphreys, Dissertation, 1973.
8. M. W. Frechette, J. L. Fasching and M. R. Douglas, *Anal. Chem.*, 1973, **45**, 1765.
9. R. Přibil and Černá, *Chem. Listy*, 1979, **3**, 653.
10. P. W. West and G. C. Gaeke, *Anal. Chem.*, 1956, **28**, 1816.
11. O. Školoud, unpublished results.

Talanta, Vol. 39, No. 4, pp. 367–369, 1992
Printed in Great Britain.

0039-9140/92 $5.00 + 0.00

ELECTROCHEMICALLY-CONTROLLED GENERATION OF SMALL AMOUNTS OF CARBON MONOXIDE

FRANTIŠEK OPEKAR* and JAN LANGMAIER

UNESCO Laboratory of Environmental Electrochemistry, J. Heyrovský Institute of Physical Chemistry and Electrochemistry, Czechoslovak Academy of Sciences, Dolejškova 3, 182 23 Prague 8, Czechoslovakia

(*Received* 10 *June* 1991. *Accepted* 14 *September* 1991)

Summary—The generation of carbon monoxide is based on oxidation of carbon at a temperature of 920–950° by electrolytically generated oxygen. The rate of production of CO is a linear function of the oxygen generating current over a range of 5–60 mA and corresponds to the theoretical value. By the method described it is possible to obtain CO concentrations from 0.0075 to 2.5% in an inert gas (nitrogen, argon and helium).

Permeation devices containing liquefied gases are very advantageous for calibrating gas analysers, testing sensors and have many other uses when a continuous supply of small amounts of gases and vapours is required. Carbon monoxide cannot be liquefied under the conditions permitting the preparation and use of these permeation devices. A permeation device containing gaseous CO under pressure has been described.[1] The CO permeates through a hole in a pressure vessel covered by a silicone rubber membrane. However, the production from this source varies with variation in the CO pressure in the vessel, *i.e.*, with the time of the use of the source. Therefore, gaseous mixtures containing defined amounts of carbon monoxide are mostly prepared by the method of volumetric gas dilution.[2,3]

Many gases can be generated electrolytically, usually at a constant current.[4,5] An advantage of this approach is the fact that the gas is only generated when required and that the rate of its production (and thus also its concentration in a carrier gas) is readily controlled through the magnitude of the generating current. The production rate can be determined from Faraday's law for a given generating current, provided that the current efficiency is known.

In this work carbon monoxide generation by oxidation of carbon with electrolytically generated oxygen at an elevated temperature is described. The oxidation takes place under conditions analogous to those for oxygen determination in elemental analysis of organic substances (the Unterzaucher method).[6]

EXPERIMENTAL

The apparatus used is shown in Fig. 1. The carrier gas (helium, argon or nitrogen) was supplied from a pressure cylinder, at flow-rates from 0.3 to 1.0 ml/sec adjusted by valve 1 and measured by flowmeter 2.

The electrolysis cell was made of plexiglass and contained separate anodic and cathodic compartments (3 and 4). The two compartments, with volumes of *ca.* 5 ml, were conductively connected by an ion-exchange membrane (5) (Nafion 117). Perchloric acid (1*M*) was used as electrolyte. A glass tube (3 mm in internal diameter) was cemented in the upper part of the anodic compartment and provided with a gas inlet and outlet, so that the carrier gas only passed over the meniscus of the electrolyte solution and thus its humidity was not much increased. A 0.2-mm platinized platinum wire served as the anode (6); the part immersed in the electrolyte was *ca.* 5 mm long. The position of the meniscus in the tube was adjusted with a syringe (7) containing the electrolyte solution. Cathodic compartment 4, containing the platinum cathode (8) was open to the atmosphere. Oxygen was generated by a constant current of 0 to 60 mA, produced by the galvanostat (9).

Carbon was oxidized in a reaction tube made of sintered corundum (400 mm long, with a bore of 5 mm and a wall thickness of 1 mm) heated to a working temperature of 920–950° by an

*Present address: Department of Analytical Chemistry, Charles University, Albertov 2030, 128 40 Prague 2, Czechoslovakia.

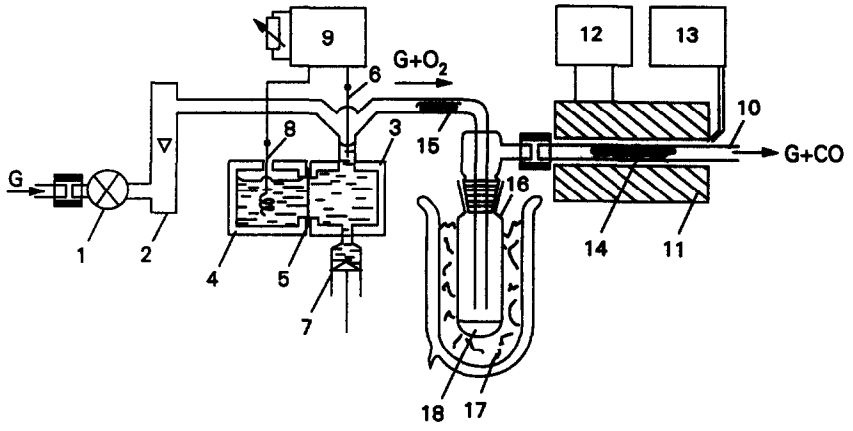

Fig. 1. A scheme of the apparatus for the CO generation. For description see the text (G = He, Ar or N_2).

electric oven (11). The temperature was adjusted by the regulating transformer (12) and measured with a thermometer (13) with a Pt–Pt/Rh thermocouple.

The reaction tube was packed into a 50-mm length with pieces of carbon (14) of 0.5–2 mm size, obtained by crushing spectrographic electrodes (Electrocarbon Topolčany, Czechoslovakia). The carbon particles were fixed in the tube with glassy carbon wool wads. After heating the reaction tube to the working temperature, the apparatus was ready for operation within an hour. A constant stream of carrier gas was passed through the apparatus when standing overnight. After a long period without operation, the apparatus can be filled with an inert gas at a small overpressure,[6] to keep out air, but this procedure is not absolutely necessary. If air enters the apparatus, the only consequence is a somewhat longer time required for preparation of the apparatus for operation and it is advisable to employ a special procedure for heating the reaction tube, see below.

The gas from the electrolyser passed through the glass wool filter (15) prior to entering the reaction tube, in order to remove any electrolyte droplets, and was dried by freezing in trap 16, cooled with dry ice in chamber 17 and by passage over a layer of phosphorus pentoxide (18).

The individual parts of the apparatus were connected by glass tubes. To prevent penetration of atmospheric oxygen, only the three joints that could be disassembled were used in the apparatus. The gas supply from the pressure cylinder and the connection of the cold trap to the reaction tube were attained by placing the tubes close together and covering the joint with thick tygon tubing. A ground-glass joint was used in the cold trap, permitting removal of the trapped moisture and replenishment of the phosphorous pentoxide packing.

Carbon monoxide was determined by gas chromatography.[7]

RESULTS AND DISCUSSION

The dependence of the CO production on the reaction tube temperature at a constant oxygen concentration in the carrier gas is plotted in Fig. 2A. This dependence was analogous to when other forms of carbon were used (*e.g.*, graphite, several kinds of active charcoal and glassy carbon wool). When using the spectrographic carbon electrode, the background production, *i.e.*, the production of CO at zero generating current, was lowest at a given

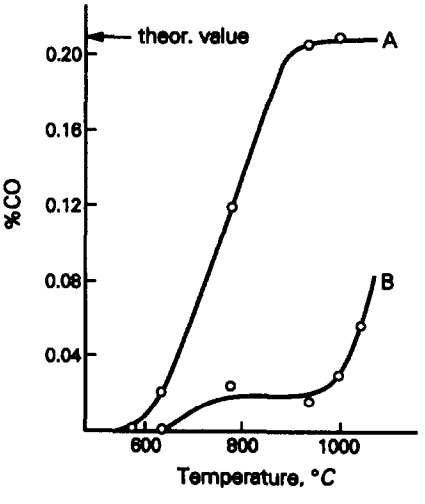

Fig. 2. Temperature dependence of the CO production (helium carrier gas, 0.6 ml/sec, spectrographic carbon electrode). A—generating current of 10 mA (the background production subtracted); B—background production.

working temperature, as can be seen in Fig. 2B. It is obvious from Fig. 2 that the optimal reaction temperature lies between 920 and 950° for the given experimental arrangement, as the production of CO is virtually 100% and the background production is low.

It has been found that the background production primarily stems from reaction of the carbon with the reaction tube walls. It is higher than the value corresponding to the oxygen content in the carrier gas which was below 5 vppm. The background production was unaffected by: using two cold traps (elimination of the carrier gas humidity), disconnecting the electrolysis cell (elimination of oxygen diffusion through the electrolyte solution), placing the reaction tube inside an auxiliary tube filled with an inert gas (elimination of possible diffusion of oxygen through the reaction tube walls at higher temperatures). On the other hand, the background production depended on the kind of carbon used and it was somewhat higher when a quartz reaction tube was employed.

To attain a constant background production more rapidly when preparing the apparatus for operation, especially when atmospheric oxygen has penetrated the apparatus, heating the reaction tube at a higher temperature (*ca.* 1150°) is recommended, for about 20 min, followed by decreasing the temperature to the working value.

The rate of production, R, of carbon monoxide (ng/sec) is a linear function of the oxygen generating current, I (mA). The equation of a regression straight line obtained from seven measurements within an interval of 5–60 mA has the form, $R = a.I + b$, where $a = (149.7 \pm 1.7)$ $ng.sec^{-1}.mA^{-1}$ and $b = (92.2 \pm 45.4)$ ng/sec, with a standard deviation of 31.9 ng/sec and a correlation coefficient of 0.999. The theoretical rate of production, obtained from Faraday's law assuming a 100% current efficiency and a 100% conversion ($O_2 = 2CO$), is $R_{theor} = 145.1\ I$ ng/sec. Slope a corresponds to (103.2 ± 1.1)% of the theoretical value. Intercept b expresses the value of the background production; here it is equivalent to the production at a generating current of about 0.6 mA.

The carbon monoxide concentration, C_{CO} (vppm), in the carrier gas flowing at a velocity of v (ml/sec) can be found for various generating currents I (mA) from the relationship, $C_{CO} = 125\ I/v$ (for 20° and 101.3 kPa). The CO production was constant over the studied flow-rates, 0.3–1.0 ml/sec. The highest CO concentration for $I = 60$ mA and $v = 0.3$ ml/sec is 25,000 vppm (2.5%). The lowest concentration is determined by the background production value, here *ca.* 75 vppm (0.0075%) for $v = 1.0$ ml/sec.

At generating currents higher than 60 mA, the contact between the anode and the electrolyte solution was periodically disconnected owing to intense evolution of oxygen. The electrolysis cell would have to be designed differently for higher generating currents.

With a change in the generating current, the rate of change in the outlet CO concentration is determined virtually only by the transport delay in the apparatus.

REFERENCES

1. D. Brocco and M. Possanzini, *Anal. Lett.*, 1974, **7**, 153.
2. B. E. Saltzman, *Anal. Chem.*, 1961, **33**, 1100.
3. L. Angely, E. Levart, G. Guiochon and G. Poslerbe, *ibid.*, 1969, **41**, 1446.
4. P. A. Hersch, *J. Air Pollut. Control Assoc.*, 1969, **19**, 164.
5. Z. Tocksteinová and F. Opekar, *Talanta*, 1986, **33**, 688.
6. *Standard Methods of Chemical Analysis*, N. H. Furman (ed.), Vol. 1, p. 780. D. Van Nostrand Comp. Inc., 1962.
7. P. G. Jeffery and P. J. Kipping, *Gas Analysis by Gas Chromatography*, p. 102. Pergamon Press, Oxford 1972.

Talanta, Vol. 39, No. 4, pp. 371–382, 1992
Printed in Great Britain.

0039-9140/92 $5.00 + 0.00

ELECTROCHEMICAL INVESTIGATION OF ACID–BASE PROPERTIES OF ORDERED LIQUID SYSTEMS

ALAIN BERTHOD* and OSCAR SALIBA
Laboratoire des Sciences Analytiques, Universite de Lyon 1, U.A. CNRS 435, 69622 Villeurbanne cedex, France

(*Received* 15 *October* 1990. *Revised* 8 *April* 1991. *Accepted* 1 *July* 1991)

Summary—Acid–base properties of ordered media were investigated via potentiometry, polarography and electrochemical probes. Electrochemical probes have a pH-dependent reduction potential and their oxidized and reduced forms have a different affinity for aqueous and organic phases. Solutions of anionic, cationic and nonionic surfactants were investigated. One anionic and one cationic surfactant stabilized emulsion were studied. A water–dodecane–pentanol–anionic surfactant microemulsion and a water–heptane–butanol–cationic surfactant were also investigated for several compositions. In micellar solutions and emulsions, it was possible to standardize and use the classical glass electrode for pH values in the range 1–12. The hydrogen electrode was required in the microemulsion systems. The reduction of electrochemical probes was studied by polarography. It is shown that in the ordered media studied, the aqueous phase played the most important role in micellar solutions and in O/W emulsions, as far as acid–base properties were concerned. In microemulsions, the acid–base properties of the aqueous phase were very different to those of water. The alizarin probe could be reduced at a "local" pH of about 12 when the aqueous phase pH was only 6.

Ordered systems are defined as liquid systems with some micro-organization. These systems contain surfactant molecules. A surfactant molecule is composed of two parts of very different polarity, a hydrophilic part (polar or ionic head) and a hydrophobic part, most often a hydrocarbon chain. The two main properties of such molecules are the trend to adsorb at any interface and the ability to form micelles. In order of increasing complexity, the studied systems were: micellar solutions that are two component mixtures (water + surfactant), six emulsions, that are three component mixtures (water + hydrophobic oil + surfactant), and two microemulsion systems that are four component mixtures (water + oil + surfactant + a long chain alcohol or cosurfactant[1]). The surfactants used were anionic, cationic and nonionic surfactants non-sensitive to pH changes. Carboxylate surfactants (soaps) were excluded because they are salts of a weak acid. For example, sodium stearate is a soap which is protonated to stearic acid when the pH is lowered. Stearic acid is a wax without any surfactant property.

In ordered media, the pseudo-phase model[2] is very useful for explaining many results. The ordered medium is separated in two pseudo-phases: the aqueous phase and the organic phase. The interface between the two phases is stabilized by adsorbed surfactant. Figure 1 shows an oversimplified view of the pseudo-phase representation of the three ordered media used in this work. In micellar media, normal and reversed micelles exist with diameters in the low nanometer range. An emulsion can be oil in water (O/W) or water in oil (W/O) type. Emulsion droplet diameters range from a tenth of a micrometer to some tens of a micrometer. Due to light scattering by these droplets, an emulsion has a milky appearance. The structure of a microemulsion is complex. An L1 water-rich microemulsion corresponds to an O/W system. The L1 microemulsion structure has a water phase in which oil droplets are suspended. The oil droplet diameter is smaller than 100 nanometers. An L2 oil-rich microemulsion corresponds to a W/O system. The L2 microemulsion structure has an oil phase in which water droplets are suspended (Fig. 1). In intermediate compositions, bicontinuous systems (Fig. 1) can exist.[1] The droplets are smaller than visible wavelengths and so a microemulsion is transparent. Any composition change can induce a change in the physico-chemical structure of the ordered medium. Addition of one drop of water can turn a clear L1 microemulsion into a turbid

*Author for correspondence.

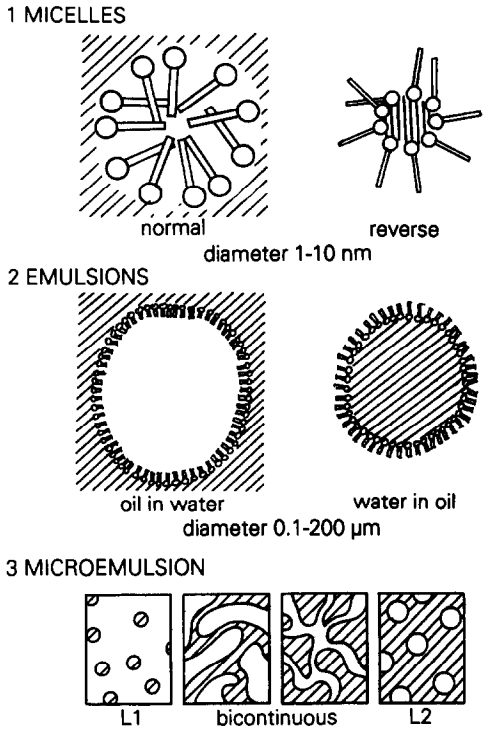

Fig. 1. Simplified view of the physicochemical structures of liquid ordered systems. 1—Normal and reverse micelles (lifetime in the microsecond range); 2—W/O and O/W emulsion droplets (lifetime ranging from few seconds to the year); 3—L1, bicontinuous, and L2 microemulsion structures (lifetime in the microsecond range). Hatched area: aqueous phase. ⊂⊃ Surfactant molecule.

W/O emulsion. Phase maps are used to understand the physicochemical structure of emulsions and microemulsions. Another important point to know is that the lifetime of a micelle or a microemulsion droplet is in the microsecond range, with continuous destruction–formation producing a macroscopically stable system. The lifetime of an emulsion droplet ranges from seconds to years depending on the emulsion stability.[1-3]

Ordered systems are widely used. Their main interest is the aptitude for associating apolar and hydrophilic molecules in the same medium in fields as different as paints and dyeing, pharmaceutical and cosmetics, pesticides and fertilizers, and enhanced oil recovery.[2-5] In many applications of these systems, the acidic strength must be known. Usually, to measure the pH of an ordered medium, a glass electrode is used.[6,7] Alternatively, the pH of the aqueous phase is measured before the preparation of a W/O emulsion or microemulsion.[8] Several theories have shown that the pH of the aqueous phase can be different from the interphase pH.[9,10] In experimental studies, the known concentrations often refer to the total volume of the studied system. We thought it might be useful to study the acid–base properties of ordered systems considered as solvents.

This work presents a theoretical approach to the acid–base properties of ordered systems by using the classical pseudo-phase model described, for example, by Fendler and Fendler.[3] Experimental results obtained in micellar solutions, O/W emulsions and microemulsions are presented. All experiments were performed by using potentiometry and polarography. To get an insight into some "local" pH values occurring in ordered media, we have used electrochemical probes. These are electroactive apolar organic molecules which need protons to be reduced. They are localized in the apolar phase of ordered systems. Their half-wave reduction potentials, $E_{1/2}$, are pH-dependent. This experimental $E_{1/2}$ value can be related to the "local" pH of the solubilization site of the electroactive probe.

EXPERIMENTAL

Chemicals

Sodium dodecylsulphate (SDS) ($C_{12}H_{25}SO_4^-$ Na^+, m.w. 288.3), cetyltrimethylammonium bromide (CTAB) ($C_{16}H_{33}N(CH_3)_3^+$ Br^-, m.w. 364.5) and polyoxyethylene 23 dodecylether (Brij 35) ($C_{12}H_{25}(OC_2H_5)_{23}OH$, m.w. 1200) were surfactants supplied by Merck. Pentanol, butanol and heptane were from Prolabo (Rhone-Poulenc, France). Dodecane was purchased from Fluka. All chemicals were analytical grade and were used without further purification. All solutions were prepared with demineralized, distilled water.

Table 1 introduces the electrochemical probes that were obtained from Rhone Poulenc. These quinones need two electrons and two protons to be reduced to the corresponding hydroquinones. Alizarin is also a diphenol whose phenol functions are ionized at elevated pHs (Table 1). Vitamin K3 has no ionizable functions.

Apparatus

Potentiometric measurements were performed with a digital reading pH-meter/millivoltmeter (Solea-Tacussel, Villeurbanne, France). The glass electrode was a TBC 112/HS or a TBC 170/HS (Tacussel). The hydrogen electrode was home-made by covering a platinum wire with platinum-black and working

Table 1. The electrochemical probes

Electrochemical probe	2-Methyl-1,4-naphthoquinone	1,2-Dihydroxi-anthraquinone
Common name	Vitamin K3 Menadione	Alizarin
M.w.	172.2	240.2
Water solubility (M)	8.6×10^{-4}	2.5×10^{-6}
Electrochemical reduction	Quinone + $2H^+ + 2e \rightarrow$ Hydroquinone	
pH properties	not ionizable	$AH_2 \rightarrow AH^- + H^+$ $pK_1 = 6.4$ $AH \rightarrow A^{2-} + H^+$ $pK_2 = 11.7$

with hydrogen bubbling under atmospheric pressure. The platinum-black coverage was obtained by electroreduction of a chloroplatinic acid glycol solution in a platinum crucible. The reduction time was 15 min, the reduction current was 300 μA. When the response of the hydrogen electrode became slow, it was cleaned with an abrasive paste and a new platinum-black coverage was performed. The reference electrode was a saturated calomel electrode (SCE) with a double junction RDJ/C8 (Tacussel). The junction was filled with a gel of agar-agar (2%) and 0.1M sodium chloride. The gel junction between the sample and the SCE was made necessary to minimize any leakage of electrolyte solution in the sample, to avoid any precipitation that would disrupt the junction, and to avoid any junction potential change during an experiment.

Polarographic measurements were performed with a PAR-174 polarographic analyser (Princeton Applied Research). The working electrode was a dropping mercury electrode, the counter electrode a platinum wire and the reference electrode the SCE described above. Emulsions were prepared with an Ultra-Turax homogenizer (Cole Palmer). All solutions were deaerated by bubbling with nitrogen saturated in water vapour (micellar solutions), oil and water vapours (emulsions) or oil, alcohol and water vapours (microemulsions). All experiments were performed in a thermostatic bath at 25°. All pH values referred to H^+ concentrations in the aqueous phase volume. Other concentrations are given in moles per litre of ordered medium (total volume).

Titration in an ordered medium

To avoid any change in the composition of the ordered system under investigation, the following procedure was used for titration. A 30-ml sample of the ordered medium was prepared including the electrochemical probe (10^{-5}–$5 \times 10^{-4}M$) and divided in two parts to perform acid–base titration. For example, if a study with increasing pH values had to be performed, the first part (10 ml) was made acidic by addition to pure acid to get a proton concentration of 0.1 moles/(litre of aqueous phase). The second part (20 ml) was made basic by addition of a concentrated base, to get a hydroxide concentration of 0.1 moles/(litre of aqueous phase). Using microsyringes and adding the basic ordered medium to the acidic one, it was possible to increase the pH without modifying the composition, that is to say without producing any structure change.

pK_s Determinations

The autoprotolysis constant or ionic product, K_s, in a given ordered medium was determined with a procedure established for K_s measurements in non-aqueous solvents.[11] First, a dilution of the ordered medium containing sodium chloride 0.1M, with the same medium, but containing 0.1M hydrochloric acid, was performed from $-\log [H^+] = 5$ to $-\log [H^+] = 1.2$. The curve $E_A = f(-\log [H^+])$, potential of the pH sensitive electrode (glass or hydrogen electrode) *vs.* the calculated pH ($= -\log [H^+]$), was drawn [Fig. 2-(1)]. The equation is

$$E_A = -A \log [H^+] + B = A\,\mathrm{pH} + B \quad [1(a)]$$

A similar dilution of the same composition of ordered medium, with sodium chloride in the aqueous phase, by the corresponding ordered medium, but with sodium hydroxide in the aqueous phase, was performed from $-\log [OH^-] = 5$ to $-\log [OH^-] = 2$ [Fig. 2-(2)]. The equation is

$$E_B = -D \log [OH^-] + F = D\ \mathrm{pOH} + F \quad [1(b)]$$

The coefficients A and D are the slopes of the straight lines and B is the theoretical electrode potential at $\log [H^+] = \mathrm{pH} = 0$. The term F is the theoretical potential at $\log [OH^-] = \mathrm{pOH} = 0$ (Fig. 2). In all studied cases, the

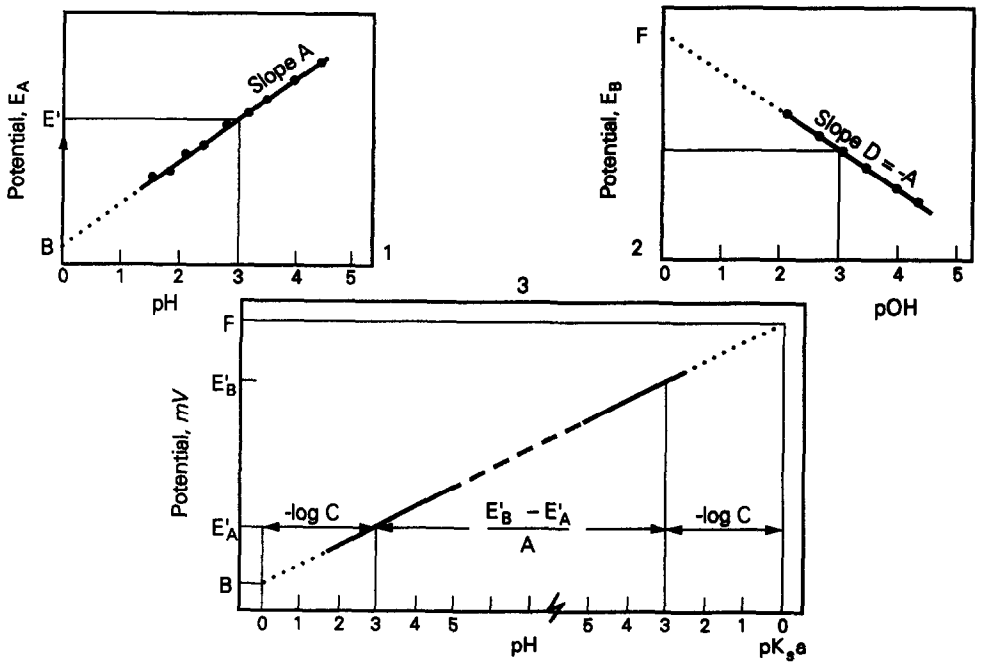

Fig. 2. The pK_s determination. 1—The acid standardization line: electrode potential versus $pH = -\log [H^+]$. 2—The basic standardization line with $pOH = -\log [OH^-]$. 3—Combining both curves allows the pK_s determination. A geometrical illustration of equation (7) is given with $C = 10^{-3}M$ ($pH = pOH = 3$).

absolute values of the slopes of the two curves were similar if not equal:

$$|A| = |D| \tag{2}$$

Because the signs of A and D were different, we wrote [Fig. 2-(2)] $A = -D$. Combining activity and concentration, the ionic product (or autoprotolysis constant) of water, K_s, is defined as:

$$K_s = [H^+]\,[OH^-] \tag{3}$$

and

$$pK_s = -\log K_s = -\log [H^+] - \log [OH^-] = pH + pOH \tag{4}$$

Theoretically, when the pH moves from $pH = 0$ to $pH = pK_s$ (or $pOH = 0$), the electrode potential moves from B (mV) to F (mV). In Fig. 2-(3), we plotted together the two curves obtained in acidic media [Fig. 2-(1)] and in basic media [Fig. 2-(2)]. These two curves were obtained with the same electrodes, so they belong to the same E *vs.* pH curve, with the unique slope A. Since the potential B corresponds to $pH = 0$ and the potential F corresponds to $pH = pK_s$, we can write

$$pK_s = \frac{F - B}{A} \tag{5}$$

The ionic strength was constrained to 0.1 and the pH ranged from 1 to $(pK_s - 1)$. For a concentration $[H^+] = [OH^-] = C$, the electrode potentials in acid and basic medium were E'_A and E'_B, respectively [Fig. 2-(3)]. Using equations [1(a)], [1(b)] and (2) [Fig. 2-(2)], we form

$$E'_B - E'_A = 2A \log C + F - B \tag{6}$$

and, with equation (5),

$$pK_s = \frac{E'_B - E'_A}{A} - 2 \log C \tag{7}$$

RESULTS AND DISCUSSION

Theory

In any medium the acidic strength is defined as the solvated proton activity. In experimental studies, people usually take a litre of say an emulsion, and add say 0.1 mole of an acid to make a $0.1M$ acidic emulsion. This means that with ordered media, the known concentrations refer to the whole volume of the system. The problem is that in an ordered system, the whole system is not of the same concentration because of the microheterogeneous nature illustrated by Fig. 1. By electrochemical investigations in ordered media, we have shown that ions are excluded from the oil phase and are mainly

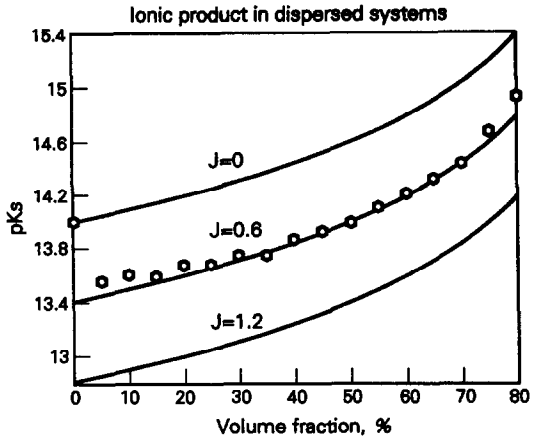

Fig. 3. Theoretical pK_s values of an organized medium plotted versus the organic volume fraction, ϕ, using equation (12) with the J values 0, 0.06 and 1.2. Open hexagons correspond to the experimental results of Ref. 15.

located in the aqueous phase with some ion-exchange with the interphase or with the micelle surface.[12–14] Hydroxide (OH^-) and hydronium (H_3O^+) ions are very hydrophilic ions and are mainly located in the aqueous phase.

Introducing $[H^+]_a$, the hydronium concentration in moles per litre of aqueous phase, and ϕ, the volume fraction of organic phase from which H^+ and OH^- ions are excluded, it is clear that the $[H^+]_a$ concentration in the aqueous phase is higher than the $[H^+]$ concentration in the total medium. The concentrations in aqueous phase (volume fraction $1-\phi$) and in the whole system are linked by:

$$[H^+]_a = [H^+]/(1-\phi) \qquad [8(a)]$$

The hydroxide ions are equally excluded out of the organic phase

$$[OH^-]_a = [OH^-]/(1-\phi) \qquad [8(b)]$$

The ionic product (autoprotolysis constant) of water in the ordered media [equation (3)] can be expressed by equations [8(a)] and [8(b)],

$$K_s = [H^+]_a[OH^-]_a(1-\phi)^2 \qquad (9)$$

The important question in ordered media studies with the pseudo-phase model is whether or not the aqueous phase of ordered systems behaves like water. The ionic product $[H^+][OH^-]$ corresponds to the autoprotolysis constant, $K_s a$, of water whose value is 10^{-14} mole^2/l.^{2} at 25°. If the aqueous phase of a given ordered system behaves like pure water, the ionic product $[H^+]_a[OH^-]_a$ should also be equal to 10^{-14}. To emphasize the acid–base behaviour of the aqueous phase of ordered media, we introduce a J value such that

$$[H^+]_a[OH^-]_a = 10^{-14+J} \qquad (10)$$

If $J = 0$, the aqueous phase behaves like water. If not, the aqueous phase cannot be regarded as pure water. Ion-exchange phenomena or electrical interactions with the organic interphase and/or modification of the aqueous phase by cosurfactant solubilization may act on the ion localization in the aqueous phase inducing non-zero J values.

The pK_s value is defined as

$$pK_s = -\log K_s \qquad (11)$$

with equations (9), (10) and (11), we form

$$pK_s = 14 - J - 2\log(1-\phi) \qquad (12)$$

Let us develop the example of a concentrated emulsion ($\phi = 0.8$) whose aqueous phase has a pure water behaviour ($J = 0$). The emulsion pK_s value is 15.4. It means that when 0.01 moles of acid is added to a litre of such an emulsion, the proton concentration is $[H^+] = 0.01M$, and the apparent hydroxide concentration is $[OH^-] = 10^{-13.4} = 3.8 \times 10^{-14}M$. However, the actual proton concentration in the aqueous phase is $[H^+]_a = [H^+]/(1-\phi) = 0.05M$ (pH = 1.3), that is five times more concentrated than in the whole emulsion. If this emulsion is a cosmetic product, such a high acidity of the water phase may have disastrous effects.

Figure 3 presents three theoretical curves obtained by using equation (12) with the three J values, 0, 0.6, 1.2. The points represent the pK_s data measured by Bahri and Letellier[15] in a microemulsion system of water–toluene–SDS–pentanol. For $\phi > 5\%$, our equation (12) seems to fit their experimental results with $J = 0.6$. It must be noted that the J value is not necessarily a constant for any composition of a given ordered system. In any system, a low ϕ value means a water-rich composition. The limit, $\phi = 0$, corresponds to water. Then, for any system

$$\lim_{\phi \to 0} J = 0. \qquad (13)$$

Micellar solutions

In all anionic, cationic and nonionic micellar solutions containing 1% w/w surfactant, the J values were nil. Given the high water content of such solutions (>99% v/v), the aqueous phase plays the predominant role as far as acid–base properties are concerned[16] (Table 2). However,

Table 2. Slope and intercept of the curves $E = f(\text{pH})$ for the reduction of Vitamin K3 in micellar media

Medium	Electrolyte	ϕ	Slope, mV/pH	Intercept mV at pH = 1	Correlation coefficient	J
Water	Phosphate buffer	0	−55.3	86	0.999	0
SDS 1%	NaCl 0.1M	0.0085	−58.7	61	0.981	0
SDS 1%	Phosphate buf.	0.0085	−59.9	55	0.992	0
CTAB 1%	NaCl 0.1M	0.010	−52.3	48*	0.998	0.1
CTAB 1%	Phosphate buf.	0.010	−53.0	86*	0.995	0
Brij 35 1%	NaCl 0.1M	0.0087	−55.8	89	0.998	0

*Extrapolated value. The bromide ions restricted the working potential range with the mercury electrode. Oxidation of mercury, enhanced by bromide ions, occurred at −0.1 V(SCE), that corresponded to a pH value of about 4 for the half-wave potential of Vitamin K3 reduction.
All pH values refer to the aqueous phase volume = $(1 - \phi) \times$ total volume.

the study of an oil-soluble electroactive compound (Vitamin K3) showed the importance of the micellar phase. The half-wave reduction potential of Vitamin K3 was linearly related to the aqueous pH with a slope of about 55 mV/pH (Table 2). The electrolyte, used to buffer the ionic strength, seems to have some influence. With sodium chloride, and titrating with sodium hydroxide and hydrochloric acid, as described in Experimental, the straight lines $E = f(\text{pH})$ were shifted toward less acidic values compared to the water line. For example, for a pH value of 1, the Vitamin K3 reduction occurred at a half-wave potential of 0.061 V(SCE) in a SDS 1% solution. The corresponding value in water was 0.086 V(SCE) (Table 2).

If the micelle binding constants of the oxidized and reduced forms of alizarin are different, a potential shift must be observed. This is the first explanation of the observed results. However, such a potential shift should not be dependent on the salt used to buffer the aqueous phase. Table 2 shows a 40-mV potential difference when sodium phosphate or sodium chloride were used in CTAB solutions.

Micellar ion exchange is the second parameter that can be responsible for potential shifts. The pH value at the probe location during the reduction step is called "local" pH. In the case of CTAB, the cationic surface of the micelles attracts some hydroxide ions inducing a "local" pH higher than the bulk pH. The opposite should be observed in the case of anionic SDS micelles. This is not the case. The ion-exchange process is more complex. Quina and Chaimovich[17] introduced an affinity constant $K_{x/y}$ to quantify the affinity of the ion x for the micelle surface when competing with the ion y. If $K_{x/y}$ is higher than 1, x ions have more affinity for the micelle surface than y ions. They determined $K_{H/Na}$ to be 0.8 for SDS micelles,[18] which means protons have less affinity for the SDS micelle surface than sodium ions, which can explain our results.

When a phosphate buffer was used (0.1M phosphoric acid) titrated with sodium hydroxide, the CTAB line shift disappeared, but the SDS line shift remained unchanged (Table 2). These observations are a further point showing the role of the ion-exchange process on the ionic micellar surface.[9,10,17,18] Phosphate ions had a high affinity for the cationic micelles. The CTAB micelle surface was buffered by the phosphate ions. These ions have no affinity for the

Table 3. Compositions, acid-base properties and slope of $E = f(\text{pH})$ for alizarin reduction in heptane-water emulsions

#	Composition: Heptane, % w/w	Water, % w/w	Surfactant, % w/w	ϕ	pK_a	J	Slope, mV/pH
1	49	50	SDS 1%	0.592	14.7	0.1	62.8
2	25.3	74	SDS 0.7%	0.337	14.4	0	62.8
3	5	94	SDS 1%	0.080	13.8	0.3	61.5
4	49	50	CTAB 1%	0.593	14.6	0.2	58.8
5	25.3	74	CTAB 0.7%	0.337	14.4	0.0	65.4
6	5	94	CTAB 1%	0.080	13.9	0.2	*

*Too low currents.
The confidence limits on the pK_aa and pK_a values were 0.1 unit. The accuracy on the slope determination was 3%.
All pH values are referred to the aqueous phase volume $(1 - \phi)$.

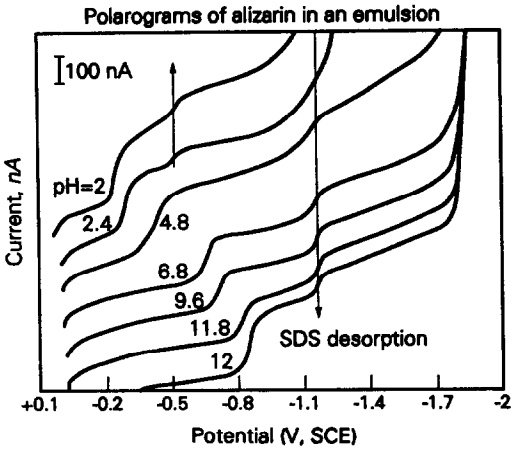

Fig. 4. D.c. polarograms of alizarin ($10^{-4}M$) in an emulsion of water (50% w/w), heptane (49% w/w) and SDS (1% w/w). The first arrow shows a wave appearing in acidic media at −0.53 V(SCE) due to a rearrangement of the SDS layer adsorbed on the mercury electrode. The second arrow shows a pseudowave [−1.2 V(SCE)] due to the desorption of SDS out of the mercury electrode (see text and Ref. 21). Mercury drop time: 1 sec. Potential scan rate 10 mV/sec.

anionic SDS micelles whose surface was not buffered. The ion-exchange process could not occur with nonionic Brij 35 micelles as observed on the data of Table 2 (no potential shift).

With the assumption that the reduction potential of Vitamin K3 was only dependent on the pH value, 0.061 V(SCE) corresponded to a pH of 1.45 in water (Table 2). In the 1% SDS solution, the "local" pH, at the Vitamin K3 location during the reduction step, seems to be 0.45 pH unit higher than the aqueous bulk pH. The 0.048 V(SCE) value in CTAB solution with sodium chloride at pH = 1, corresponded to a pH of 1.76 in water. In CTAB micelles, Vitamin K3 seems to be located in an environment with a "local" pH about 0.75 unit higher than the aqueous bulk pH.

Emulsions

Water–heptane emulsions were prepared with a homogenizer. SDS and CTAB could stabilize such emulsions for more than five hours. Water–heptane emulsions, prepared with the emulsifying agent Brij 35, were stable for only 30 min. Alizarin (Table 1) was more soluble in water–heptane emulsions than Vitamin K3, and gave reproducible results. Compositions and acid–base properties of the studied O/W emulsions are listed in Table 3.

Figure 4 shows a typical set of polarograms obtained in an emulsion with a 60% v/v organic phase content (emulsion # 1). The half-wave reduction potential was shifted toward more negative values as the pH increased from 2 to 12. The slopes of the curves $E_{1/2} = f(\text{pH})$ were not significantly different in water (Table 2) from those in emulsions (Table 3). Arrows on

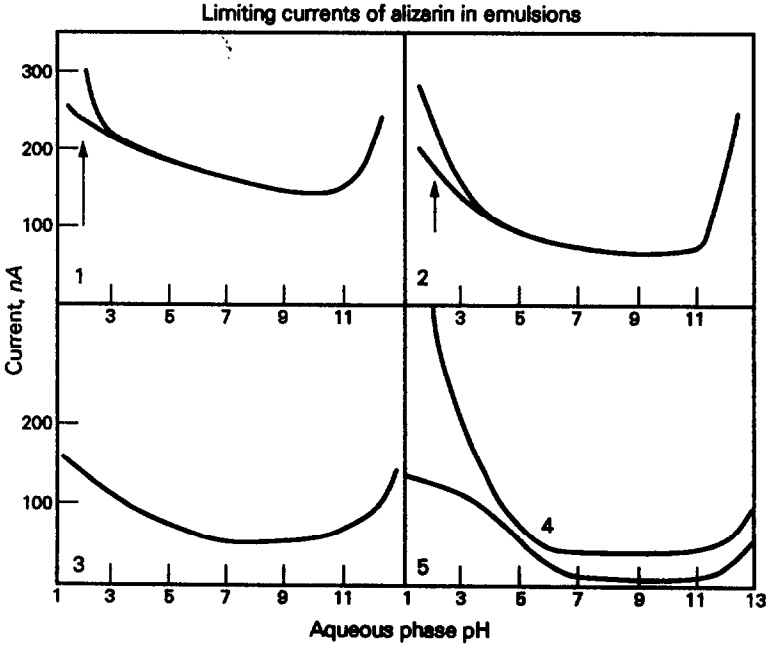

Fig. 5. Limiting currents of alizarin ($10^{-4}M$) reduction in emulsions. The figures correspond to the emulsion compositions given in Table 3. For emulsions # 1 and # 2, the arrow corresponds to the appearance of a rearrangement wave due to the electrode-adsorbed SDS layer (see Fig. 4 and Ref. 21).

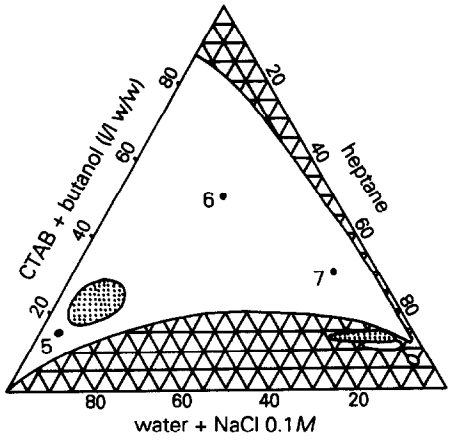

Fig. 6. Phase map of the cationic microemulsion system. Dotted areas correspond to liquid-crystal phases. ●: points studied in this work (see Table 4).

Fig. 4 point out two pseudo-waves due to SDS surfactant adsorbed onto the mercury electrode. At −0.53 V(SCE), a rearrangement of the adsorbed SDS layer induces a change in the alizarin limiting diffusion current. At −1.2 V(SCE), the mercury electrode becomes negative enough to repel adsorbed anionic SDS ions.[21] This produced the second non-pH-dependent wave shown in Fig. 4.

Figure 4 shows that, at constant alizarin concentration, the limiting diffusion current is pH-dependent. At −0.9 V(SCE), the reduction current was higher at pH 2.0 than at pH 7.0. This change was observed for all emulsions studied. Figure 5 presents the limiting diffusion current *vs.* pH for the five emulsions of Table 3. The higher the water content, the lower the reduction current. The reduction current of alizarin ($10^{-4}M$), in the water-rich CTAB emulsion # 6, was so low that it was not possible to obtain reproducible results.

The release of the oil-soluble alizarin was linked to the oil-phase volume as studied by Georges and co-workers.[13,19] The limiting current was dependent on the ionic state of alizarin. At high pH values (>11.5), the two phenol groups of alizarin were ionized and the dianion gave high reduction current due to a high diffusion coefficient. At intermediate pH values, the monoanion existed and seems to have a lower diffusion coefficient than the dianion. The alizarin molecule, existing at low pH values (<6), gave high reduction currents in both studied emulsion systems.

The J values, in SDS and CTAB emulsions, were very low, which means the acid–base properties of such emulsions are mainly those of the aqueous phase. The heptane phase excludes the hydroxide and hydronium ions in the aqueous phase. To be reduced at the mercury electrode surface, alizarin must leave the oil phase (heptane droplets) and the reduction process must take place in the water phase, or in a water-rich surfactant layer adsorbed on the electrode, according to a chemical–electrochemical (CE) process as already described.[13,19] Given the straight lines $E = f(\text{pH})$ (Table 3), during the reduction process, the pH environment of alizarin was proportional or equal to the aqueous phase pH over the whole pH range studied (from pH 1 to pH 13) with both an anionic and cationic surfactant.

Table 4. Compositions, acid–base properties and slope of $E = f(\text{pH})$ for alizarin reduction in two microemulsion systems

	Composition*						
#	Oil, % w/w	Water, % w/w	Active blend	ϕ	pK_a†	J†	Slope,‡ mV/pH
1	5	80	15	0.225	13.6	0.6	58.7
2	25	25	50	0.780	14.4	0.9	55.5
3	5	15	80	0.863	15.0	0.7	56.9
4	60	10	30	0.919	14.9	1.3	57.0§
5	5	80	15	0.231	13.9	0.3	83; 38‖
6	25	25	50	0.787	14.3	0.8	195; 40‖
7	60	10	30	0.924	14.6	1.6	195; 0‖

*Composition # 1, # 2, # 3, # 4: oil = dodecane; active blend = SDS + pentanol (1/2 w/w). Compositions # 5, # 6, # 7: oil = heptane; active blend = CTAB + butanol (1/1 w/w).

†Confidence limits 0.1 unit.

‡Slope of the pH-dependent wave. Accuracy 5%.

§Taking in account only two points: pH = 12 and pH = 8, see Fig. 9.

‖See Fig. 10.

All pH values refer to the aqueous phase volume [total volume × $(1-\phi)$].

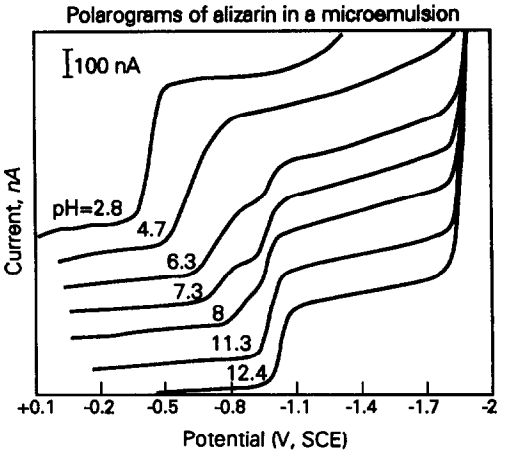

Fig. 7. Polarograms of alizarin ($5 \times 10^{-4}M$) in a pentanol-rich microemulsion (# 3). Mercury-drop time: 1 sec; potential scan rate: 10 mV/sec.

Microemulsions

In micellar solutions and emulsions, the classical glass electrode gave correct, stable and reproducible responses. That was not the case in microemulsions: the signals produced by the glass electrode were very unstable and non-reproducible. Furthermore, the glass-electrode response was strongly dependent on the stirring of the microemulsion. The use of the hydrogen electrode was necessary.[20] Two microemulsion systems were investigated. The phase map of the system water–dodecane–SDS–pentanol can be found in the literature.[20,22] The phase map of the system water–heptane–CTAB–butanol was established for this study and is presented in Fig. 6. Seven compositions in both microemulsion systems were studied (Table 4).

The results obtained in the microemulsion were very different from those obtained in micellar solutions and emulsions. Table 4 shows that the J values differ significantly from zero. The lower the water content, the higher the J value. The aqueous phases of microemulsion systems do not behave as pure water. Previous studies[4,5] have shown that, in microemulsion systems, a considerable fraction of the water is bound water, especially in low water content microemulsions. Also, a significant amount of cosurfactant (pentanol and butanol in SDS and CTAB systems, respectively) can be dissolved in the aqueous phase. However, given the proportionality of the hydrogen electrode response to the proton concentration in the aqueous phase (slope between 57.1 and 58.3 mV/pH for the H_2 potential E *vs.* pH[20]), the aqueous phase still played the most important role in acid–base properties.

A typical set of polarograms in a microemulsion (# 3) is shown in Fig. 7. Figure 8 shows the limiting current of alizarin plotted *vs.* pH for the four anionic microemulsions studied. There was only one polarographic wave in microemulsion compositions # 1, # 5 and # 6, over the pH range 1–13. In microemulsion

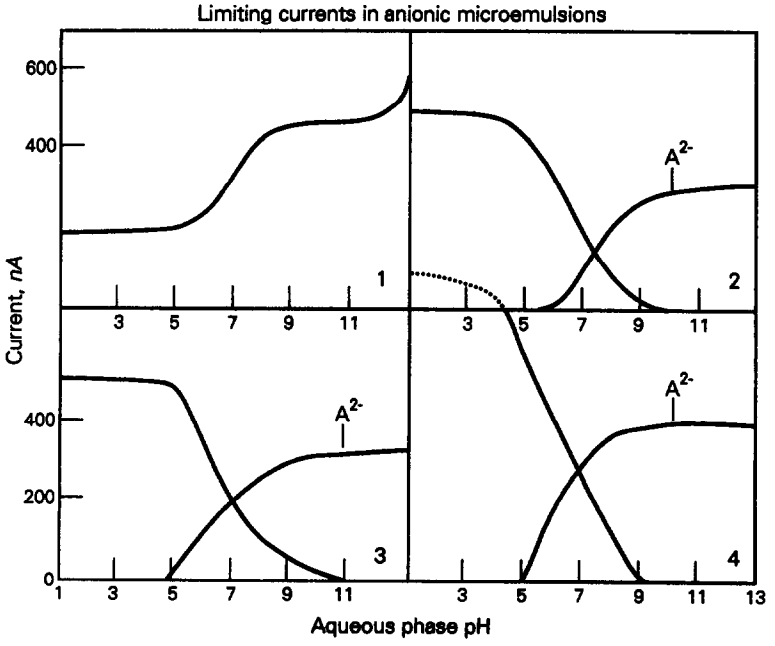

Fig. 8. Limiting currents of alizarin ($5 \times 10^{-4}M$) reduction in microemulsions. The figures correspond to microemulsion composition given in Table 4.

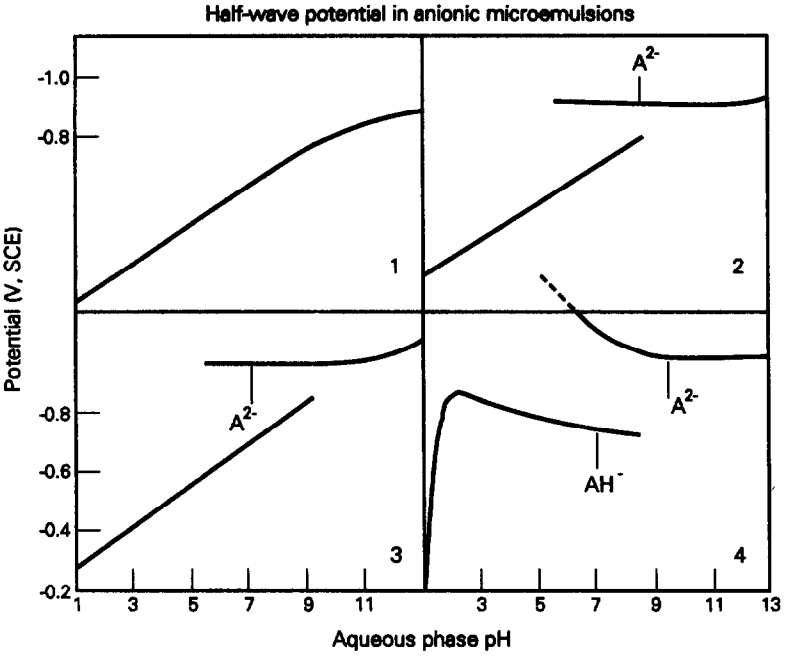

Fig. 9. Half-wave potential of alizarin reduction in anionic microemulsions. Compositions 1–4 given in Table 4.

compositions # 2, # 3, # 4 and # 7, at intermediate pH values, the reduction of alizarin occurred with two polarographic waves. Only the first wave was pH dependent. The second wave appeared at pH values higher than 5 (Fig. 7). Between pH 5 and 9, the two waves were present. Above pH 9, only the second wave remains.

It is interesting to note that the alizarin reduction occurred following a similar pattern in both cationic and anionic microemulsions of similar physico-chemical structure. In water-rich microemulsions (compositions # 1 and # 5, Table 4), the reduction process occurred in one step whatever the aqueous pH. This reduction pattern was similar to the one observed

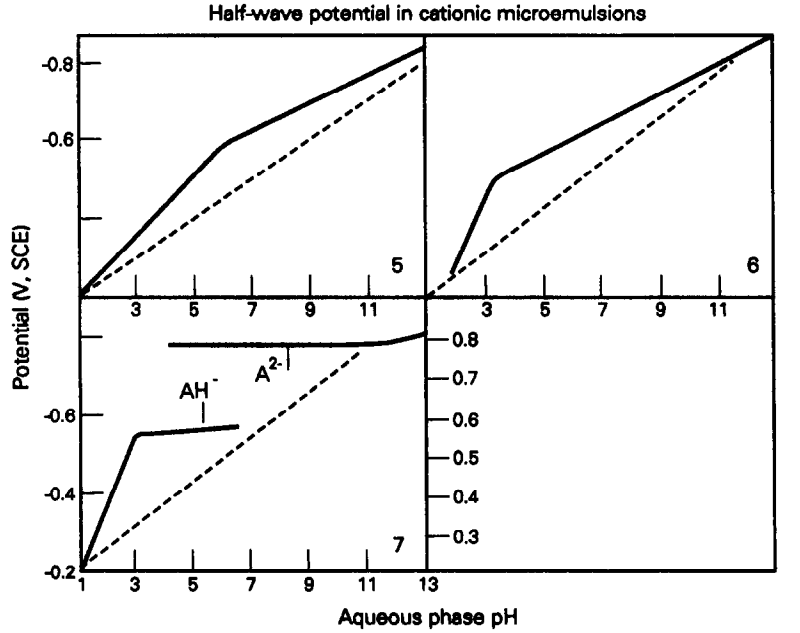

Fig. 10. Half-wave potential of alizarin reduction in cationic microemulsion. Compositions 5–7 given in Table 4. The dotted lines indicate a theoretical slope of 59 mV/pH.

in classical O/W emulsions (Fig. 4). The L1 structure of microemulsion # 1 and # 5 was the closest to the O/W emulsion structure (Fig. 1). However, the dynamic nature of the microemulsion droplets (lifetime in the microsecond range) with continuous destruction–creation, differs fundamentally from the static nature of emulsion droplets. The two L2 structure microemulsions (compositions # 4 and # 7, Table 4) gave a similar reduction pattern. Such similarities between very differing microemulsion systems allow the rejection of surfactant adsorption as a possible explanation for the two waves observed. It seems that the solute is responsible for the two waves. Alizarin has pH-dependent forms: AH_2 at low pH values, AH^- at intermediate pHs, and A^{2-} at elevated pH values (Table 1). Figures 9 and 10 show the half-wave potential of the polarograhic waves plotted *vs.* the aqueous phase pH for the SDS and CTAB microemulsion systems, respectively.

Water-rich microemulsions # 1 and # 5. In these L1 systems, the alizarin reduction occurred in one step. The limiting diffusion current was constant at low pH values, and increased from pH 6 to 9 (Fig. 8). A pH of 5 corresponds to the first ionization ($pK_{a1} = 6$) of alizarin. Above pH 10, the limiting current did not increase anymore. The J values were low, 0.6 and 0.3 in SDS and CTAB L1 systems, respectively. The aqueous phase of L1 systems has acid–base properties similar to those of water.

Oil-rich microemulsions # 4 and # 7. In these L2 oil-rich microemulsions, the alizarin reduction occurred following different routes: at high pH values (pH > 9) there was only one non pH-dependent step that seems to correspond to the dianion reduction (labelled A^{2-}, Figs 9 and 10). At intermediate pH values (4 < pH < 9), the alizarin reduction occurred in two non pH-dependent steps that may correspond to the dianion and monoanion reduction. The dianion was reduced at a constant potential [−0.98 V(SCE) and −0.78 V(SCE) for SDS # 4 and CTAB # 7, respectively] between pH 5 and 13. The monoanion, AH^-, was reduced at a constant potential [0.75 V(SCE) and 0.56 V(SCE) for SDS # 4 and CTAB # 7 systems, respectively].

We note that a pH increase induced an increase in the second wave and a simultaneous decrease of the first wave (Figs 8, 9 and 10). If the attribution of the first and second non-pH-depending waves to AH^- and A^{2-}, respectively, is correct, is seems logical to think that a pH increase depletes the AH^- form to convert it to A^{2-}. The polarity change is likely to induce a change in the probe location. The polar A^{2-} form of alizarin was certainly not located in the oil phase.

Assuming the alizarin reduction potential can be linked to a pH value, the constant potential −0.98 and −0.75 V(SCE) for A^{2-} and AH^-, respectively, in the SDS microemulsion # 4, corresponded to pH 13 and pH 7, respectively. In the CTAB microemulsion # 7, −0.78 and −0.56 V(SCE) corresponded to pH 12 and pH 7, respectively. It seems that the "local pH" at the A^{2-} dianion location was around 12 and the "local pH" at the AH^- monoanion location was around 7 even if the aqueous phase pHs of both systems were as low as 3.

Intermediate microemulsion compositions # 2, # 3 and # 6. These compositions contain a large amount of active blend surfactant–alcohol. They probably have the bicontinuous structure (Fig. 1). In anionic systems # 2 and # 3, two waves were observed, a pH-dependent and a non pH-dependent wave (Fig. 7). Since the non pH-dependent wave occurred at elevated pH values, it was attributed to the A^{2-} alizarin form reduction. The potentials of the non-pH-dependent waves were −0.85 and −0.95 V(SCE) in microemulsion # 2 and # 3, respectively. These potentials corresponded to pH values around 11. In the cationic system # 6, only one pH depending wave was observed (Fig. 10). Although the physicochemical structure of microemulsions # 2 and # 6 were similar, the acid–base properties were different. The pentanol–SDS active blend may act differently from the butanol–CTAB active blend as far as acid–base properties are concerned.

For cationic microemulsions, # 5, # 6, and # 7, the dotted lines in Fig. 10 represent the theoretical reduction potential proportional to the aqueous phase pH (59 mV/pH unit). The actual reduction potential was higher than this theoretical potential. This can be explained if the "local" pH, at the alizarin reduction location on the mercury electrode, was higher than the aqueous phase pH. It seems that the positively charged interphase was richer in anionic hydroxide ions than the aqueous phase. Electrostatic interactions and ion-exchange with bromide ions may explain this hydroxide ion enrichment.

CONCLUSION

The aqueous phase plays the most important role in acid–base properties of micellar solutions and O/W emulsions. The J value is an empirical parameter introduced to compare the acid–base properties of the aqueous phase of an ordered medium with water. If $J = 0$, the aqueous phase behaves as pure water. If J is different from zero, aqueous phase cannot be assimilated to water.

From an analytical point of view, it must be pointed out that the glass electrode can be used in ordered liquid systems. However the pH value obtained corresponds to the aqueous phase pH. The classic indicator dyes or coloured papers, used for pH determinations, must not be used in ordered media: most often a micellar effect shifts the pKa values of the dyes. Surfactants can also induce spectral changes. That is why the use of a pH indicator paper can lead to errors as high as 3 pH units when plunged into an ordered media.[16,20] Before using a glass electrode in a microemulsion system, its response must be checked (stability and reproducibility).

REFERENCES

1. A. Berthod, *J. Chim. Phys.*, 1983, **80**, 407.
2. S. C. Stinson, *Chem. & Eng. News*, 1987, 21.
3. J. H. Fendler and E. J. Fendler, *Catalysis in Micellar and Macromolecular Systems*, Academic Press, New York, 1975.
4. K. L. Mittal and E. J. Fendler (eds.), *Solution Behavior of Surfactants*, Vol. 2, Plenum Press, New York, 1982.
5. K. L. Mittal and B. Lindman (eds.), *Surfactants in Solution*, Vol. 3, Plenum Press, New York, 1984.
6. R. A. Mackay, K. Jacobson and J. Tourian, *J. Colloid Interface Sci.*, 1980, **76**, 515.
7. A. Honnorat and P. Martinet, *Electrochim. Acta*, 1983, **28**, 1703.
8. O. A. El Seoud, in *Reversed Micelles*, P. L. Luisi and B. E. Straub (eds.), pp. 81–93. Plenum Press, New York, 1984.
9. H. Chaimovich, R. M. V. Aleixo, I. M. Cuccovia, D. Zanette and F. M. Quina, in *Solution Behavior of Surfactants*, K. L. Mittal and E. J. Fendler (eds.), Vol. 2, p. 949. Plenum Press, New York, 1982.
10. L. S. Romsted, in *Surfactants in Solution*, K. L. Mittal, K. L. and B. Lindman (eds.), Vol. 3, p. 1015. Plenum Press, New York, 1984.
11. R. G. Bates, in *The Chemistry of Non Aqueous Solvents*, J. J. Lagowski (ed.), pp. 97–128. Academic Press, New York.
12. A. Berthod and J. Georges, *J. Chim. Phys.*, 1983, **80**, 245.
13. J. Georges and A. Berthod, *J. Electroanal. Chem.*, 1984, **175**, 143.
14. A. Berthod and J. Georges, *J. Colloid Interface Sci.*, 1985, **106**, 194.
15. H. Bahri and P. Letellier, *J. Chim. Phys.*, 1985, **82**, 1010.
16. A. Berthod and C. Saliba, *Analusis*, 1985, **13**, 437.
17. F. H. Quina and H. Chaimovich, *J. Phys. Chem.*, 1979, **83**, 1844.
18. F. H. Quina, M. J. Politi, I. M. Cuccovia, E. Baumgarten, M. M. Franchetti and H. Chaimovich, *ibid.*, 1980, **84**, 361.
19. J. Georges and S. Desmettre, *J. Dispersion Sci. Technol.*, 1986, **7**, 21.
20. A. Berthod and C. Saliba, *Analusis*, 1986, **14**, 414.
21. N. Framkin and B. B. Damaskin, *J. Electroanal. Chem.*, 1962, **3**, 36.
22. M. Clausse, J. Peyrelasse, C. Boned, J. Heil, L. Nicolas-Morgantini and A. Zradba, in *Surfactants in Solution*, K. L. Mittal and B. Lindman (eds.), Vol. 3, p. 1583. Plenum Press, New York, 1984.

Talanta, Vol. 39, No. 4, pp. 383–390, 1992
Printed in Great Britain.

0039-9140/92 $5.00 + 0.00

THE DETERMINATION OF TRACE AMOUNTS OF TIN BY FLOW-INJECTION HYDRIDE GENERATION ATOMIC-ABSORPTION SPECTROMETRY WITH ON-LINE ION-EXCHANGE SEPARATION AND PRECONCENTRATION

ZHAOLUN FANG and LIJING SUN
Flow-injection Analysis Research Centre, Institute of Applied Ecology, Academia Sinica, Box 417, 110015 Shenyang, China

ELO H. HANSEN, JES E. OLESEN and LINA M. HENRIKSEN
Chemistry Department A, Technical University of Denmark, Building 207, DK-2800 Lyngby, Denmark

(*Received* 25 *June* 1991. *Revised* 31 *July* 1991. *Accepted* 31 *July* 1991)

Summary—A hydride generation atomic-absorption spectrometric (AAS) method with flow-injection (FI), aimed at developing a practical routine assay for the determination of tin in food digests, is described. In order to modify the sample matrix and to achieve optimized and reproducible conditions for the hydride generation reaction, the analyte is initially converted into its chlorostannate-complex thereby allowing it to be separated and preconcentrated on-line on an incorporated micro-column packed with a strongly basic anion exchanger and subsequently to be eluted by diluted nitric acid under strictly controlled conditions. Optimum acidic conditions for the FI hydride generation AAS system was found to be 0.01–0.05*M* nitric acid. At a consumption of 2.7-ml sample volume, aspirated by time-based injection, the procedure resulted in an enrichment factor of 3.5 and yielded a detection limit of 0.08 μg/l. (3σ) at a sampling frequency of 72/hr. The precision was 2.5% rsd at the 10 μg/l. level. Potential interferents, such as Ni(II), Co(II), Zn(II) and Fe(III) could, at a Sn level of 10 μg/l., be tolerated at an excess of 1000 times without impairing the assay, while a 100–1000-fold excess of Cu(II) decreased the signal by 10–15%. Recoveries in the range 94–102% were obtained for canned food sample digests spiked with 10 μg/l. Sn.

Recently, the performance of hydride generation atomic-absorption spectrometric (HGAAS) methods has been enhanced significantly through the application of flow-injection (FI) techniques. Sample and reagent consumption are decreased substantially, while the absolute sensitivities are increased. Because of the inherent precise and reproducible timing of flow-injection systems, FI-HGAAS methods are generally also much more tolerant to interferents compared to batch HGAAS procedures.[1] The application of the technique has been quite successful for the assay of a number of hydride forming elements including selenium, arsenic, bismuth, and antimony in waters, environmental and metal samples.[1] However, to the authors best knowledge, so far no application of the technique for the determination of tin has been reported. Difficulties in the HGAAS determination of tin in the batch mode, owing to the strong influence of acidity on the sensitivity, have been described by several groups.[2–4] Thus, in contrast to most of the other hydride forming elements where a fairly wide range of acidity can be tolerated without impairing the hydride generation process, formation of stannane requires rigorously controlled conditions. In fact, preliminary experiments in the present study revealed that the effects of the acidity were even more crucial in the FI mode; this obviously being the reason for the lack of successful reports on the determination of tin by FI–HGAAS.

In this investigation an attempt was made to optimize the acidity conditions for the determination of tin [*i.e.*, Sn(II) and Sn(IV)] by FI–HGAAS. On-line ion-exchange separation was used to modify the acid matrix of the sample in order to obtain optimal acidity conditions for the ensuing hydride generation procedure and, as an added benefit, to allow sample preconcentration. Thus, tin was collected in the form of anionic chlorostannate-complexes in 2*M* hydrochloric acid medium on a strongly basic anion exchanger and subsequently eluted by diluted nitric acid before being mixed with

the borohydride reductant. In this manner, the acidity level of the hydride generation procedure could reproducibly and repeatedly be maintained. Sources of potential interference are discussed and quantified, and the practical applicability of the method is demonstrated by the assay of tin in canned food digests.

EXPERIMENTAL

Apparatus

A Perkin-Elmer Model 2100 atomic-absorption spectrometer was used with the Model FIAS-200 flow-injection system and hydride generation accessories. A tin hollow cathode lamp was used at a wavelength of 286.3 nm and operated at 30 mA. The temperature of the quartz atomizer cell was set to 900°, and the argon carrier flow was fixed at 90 ml/min as recommended by the instrument manufacturer. The injection valve of the instrument was modified by drilling an extra channel on the rotor so that four channels remained open at both loading and injection positions (cf. Fig. 2). The signals were processed with a time constant of 0.5 sec in the peak height mode, and recordings from the graphic screen were printed out by a Model FX-850 printer.

The ion-exchange column used for preconcentration was made by packing 90 mg of 80–100 mesh Dowex 1-X8 strongly basic anion exchange resin into a conical plastic Eppendorf pipette tip. The construction of the conical column was as described previously.[5] According to the manufacturer, the exchange capacity of the ion-exchanger (Cl-form, wet) is 1.33 meq/ml or 1.9 meq/g. In a later stage in this study, a larger column reactor (3 mm i.d. and 45 mm long[6]), was also used to obtain better recoveries for some samples. The latter column accommodated about 140 mg of resin.

All reaction coils and connections were made with 0.7 mm i.d. PTFE tubing.

Reagents

All reagents were of analytical grade and demineralized water was used throughout. Sodium borohydride solutions [0.2% (w/v)] were freshly prepared twice every day. The appropriate volume of 2.0*M* sodium hydroxide, made by diluting Titrisol standards (Merck, Darmstadt), was added to the borohydride solution to create the necessary base concentrations for maintaining optimum acidity in the final reaction mixture (for details see Results and Discussion). Hydrochloric, nitric and sulphuric acid eluents and carrier solutions were made by dilutions of 2*M* Titrisol acid standards (Merck, Darmstadt).

Standard series solutions for tin used in the preconcentrations were prepared by two-stage dilutions of a 10 mg/l. stock solution of Sn(II) (made from $SnCl_2$ $2H_2O$) in 2*M* hydrochloric acid (diluent) [the signal outputs for Sn(II) and Sn(IV) are identical; hence, the use of the Sn(II) salt for preparing the standards was merely dictated by convenience]. Tin solutions (10 μg/l.) used to study the effects of acidity for various acids were made in acid solutions with concentrations identical to those in the carrier solution. When solutions of low acidity, that is, of below 0.1*M*, were studied, dilutions were made shortly before the experiments to avoid loss of tin through hydrolysis.

Operational procedures

Studies on the effects of acidity. The FI manifold shown in Fig. 1 was used for the study of

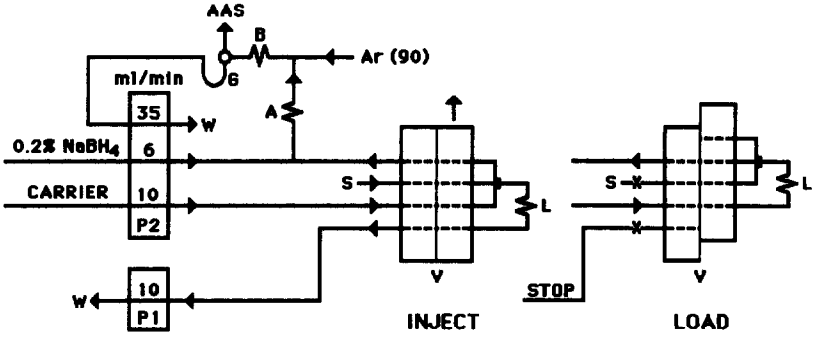

Fig. 1. FI manifold for the study of acid conditions in hydride generation AAS. L, sample loop; V, injection valve; P1, P2, peristaltic pumps; W, waste; G, gas-liquid separator; Ar, argon gas flow 90 ml/min; S, sample; A, B, 0.7 m i.d. 30 cm PTFE coils; AAS, atomizer cell, heated to 900°. Sample solution was aspirated for 10 sec corresponding to a total sample volume of 1.67 ml.

effects of the acid concentration in the carrier stream and sample solutions. The sample loading time and injection times were 10 and 15 sec respectively. The sodium hydroxide concentration in the borohydride solution during this study was maintained at 0.01*M* in all cases. The neutralization effect of this solution was taken into account when computing the acid concentration in the final reaction mixture.

On-line ion-exchange preconcentration. The FI on-line ion-exchange preconcentration manifold is shown in Fig. 2. In the loading sequence, the sample in 2*M* hydrochloric acid was propelled by pump 1 through the column at 8 ml/min, entering the column at the narrow end, and delivered to waste. Simultaneously the acid eluent was pumped through the by-pass on the rotor into the hydride generation system. In this stage the baseline for the final readout was established. At the end of the loading period, normally 20 sec, the valve was actuated automatically, directing the eluent flow to the column and entering from the wider end. The absorbed chlorostannate-complex was eluted into the hydride generation manifold and merged with the borohydride reductant solution, both eluent and reagent being propelled at 11 ml/min by pump 2. After passing through a 30 cm length of reaction coil (A), the stannane formed was stripped from the solution by a steady argon carrier flow of 90 ml/min. The gas-liquid mixture was guided into the gas-liquid separator where the waste was pumped out at a flow-rate of 35 ml/min. The separated hydride was transported by the carrier gas together with the evolved hydrogen into the atomizer cell and the absorption signal recorded. The elution sequence was 30 sec. During this stage the sample line operated by pump 1 was programmed to pump at a reduced rotation speed (30 rpm) to expel the previous sample in the pump tube to waste and to introduce the next sample.

Sample pretreatment. The canned food samples were treated by a nitric–hydrochloric acid digestion procedure according to details described previously.[7] Homogenized sample (5 g) was dried in an oven at 120° in a 250-ml flask. Concentrated nitric acid (30 ml) was added, the mixture was gently heated on a hot-plate to initiate digestion, and then boiled down to about 5 ml. Hydrochloric acid (25 ml) was added, and gently boiled down to 10–15 ml. The digest was cooled, transferred into a 100-ml standard flask and diluted to volume with water. In order to satisfy the analytical range of the hydride generation determination and conditions for the ion exchange, 10 ml of digest was taken and diluted further to 100 ml with 2*M* hydrochloric acid. In the spiking experiments, aliquots of tin-standards were added to the food samples prior to initiating the wet digestion procedure.

RESULTS AND DISCUSSION

Effects of types of acid species, and their concentration, on the HGAAS signal response for tin

At a preliminary stage in this work an attempt was made to find the acid matrix conditions which could ensure sensitive and reproducible determination of tin directly in the sample solution. Such conditions have been approached to a reasonable extent in batch methods. In one case, this involved almost complete removal of acid in a food digest, except for a very small amount of residual sulphuric acid, and then making up the solution in 0.12*M* hydrochloric acid, which gave optimum sensitivity for the subsequent HGAAS determination of tin.[3] In another application of the batch HGAAS method by Legret and Divet for the determination of tin in sediments, it was found that in

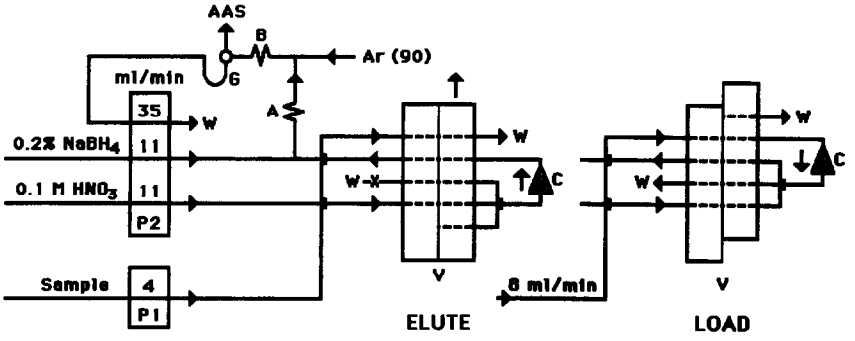

Fig. 2. FI manifold for on-line ion-exchange separation hydride generation AAS. Symbols are the same as for Fig. 1. C, conical column. Aspirated sample volume 2.67 ml. For details, see text.

nitric acid medium the signal output varied merely 10% within a wide range of acid concentrations extending from 0.05—0.6*M*, whereas variations of 50% or more were observed for hydrochloric and sulphuric acids of similar strengths.[2] Thus, using a 0.4*M* nitric acid medium it was feasible for these authors to determine tin reproducibly.

When the effects of various concentrations of hydrochloric, nitric, and sulphuric acids were studied with the FI manifold in Fig. 1, more pronounced influences from the acids were observed. The results are shown in Fig. 3, and are compared to results obtained in the batch mode for hydrochloric and nitric acids in a boric acid medium.[4] Since a reliable method would necessitate that a region of stable and reproducible signals could be established, these results appear to constitute a major disadvantage of the FI approach, because an absolutely precise control of the final acidity would be very difficult to achieve. The situation seemed to be especially unfortunate for the hydrochloric and sulphuric acids where virtually no stable region of influence on sensitivity could be found. Although control of nitric acid in the 0.01*M* range in the final reaction mixture may be feasible, with careful balancing of the flow-rates and of the acid/base concentrations in the carrier, sample and reagent solutions, the procedure would obviously lack the robustness of a good routine analytical method.

An attempt was therefore made to use buffering systems to control the pH of the reaction mixture in the 1.5–2.5 pH range. However, when oxalic acid and malonic acid buffer systems were used instead of the strong acids, the signals for tin decreased drastically, that is, to 10–20% of those obtained with the strong acids at identical molar concentrations. The use of boric acid together with the strong acids, recommended in the batch mode,[4] was also tested in the FI system, but produced no improvements in the performance. Nitric acid medium within the 0.01–0.05*M* range therefore appeared to be the best condition achieved in this study. However, hydrolysis of tin(IV) is reported to be rapid in solutions with less than 0.7*M* hydrochloric acid or 0.1*M* sodium hydroxide, producing insoluble hydrolysis products which polymerize and are difficult to redissolve.[8] For this reason, samples should not be expected to be stored in acid concentrations lower than 0.7*M* for extended periods, which is obviously in contradiction with the requirements of the FI hydride generation procedure.

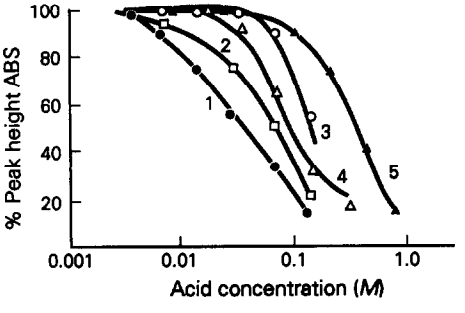

Fig. 3. Effect of acid concentrations on the Sn-signal expressed in % peak heights with peak absorbance at 0.003*M* acid concentration taken as 100% for all the acids studied, using the FI-HGAAS system in Fig. 1. 1, HCl; 2, H_2SO_4; and 3, HNO_3. Curves 4 and 5 are for HCl and HNO_3 respectively, obtained by batch procedures in boric acid medium [reconstructed from relative sensitivity (%) data in ref. 5].

Therefore a method was sought in this work for on-line modifying of the acid matrix of the sample solutions by using an incorporated ion-exchange column which, in addition to preconditioning the samples for the hydride generation process, potentially would also provide the extra advantage of removing interferences as well as effecting an enhancement in sensitivity through preconcentration.

The optimization of experimental parameters for on-line ion-exchange preconcentration HGAAS determination of tin

Ion-exchange separation and preconcentration of tin has been used successfully in combination with flame AAS in the determination of tin in copper.[9] The operation was performed off-line in the batch mode with a column packed with a Dowex 1-X8 strongly basic anion exchanger. The sample was prepared in 2*M* hydrochloric acid before being passed through the column. The tin retained as the chlorostannate-complex-anion was later eluted with 1*M* nitric acid and determined by flame-AAS. In the present work the anion-exchange preconcentration system was adapted for on-line use in a FI system, using the same ion-exchange material, resulting in the FI manifold shown in Fig. 2.

According to experiences gained in using similar anion-exchange columns for the on-line preconcentration of selenium,[10,11] a sample loading rate of 8 ml/min seemed to be a good compromise between concentration efficiency (preconcentration factor achieved in unit time) and retention efficiency (percentage of analyte collected on the column).[6] This was therefore

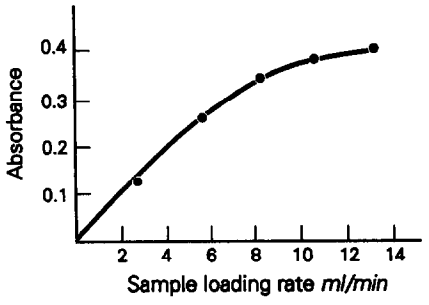

Fig. 4. Effect of sample loading flow-rate on peak absorbance. FI–HGAAS system in Fig. 2. 10 μg/l Sn; 0.1*M* HNO_3 eluent; loading period 20 sec.

used as a starting point for the optimization of other parameters. The preliminary choice was later confirmed using the optimized conditions as shown in Fig. 4. With a 20-sec loading period, the 8 ml/min loading rate appeared to be the upper limit for maintaining a close to linear relationship between loading time and signal. The lowering of the slope of the curve beyond this point implies a substantial increase of break-through due to insufficient time for arriving at ion-exchange equilibrium. Although better enrichment factors could definitely be achieved with loading rates higher than 8 ml/min, the tolerance to interferences may be considerably weaker, and is therefore not recommended.

Intuitively it might be expected that the chlorostannate-complex of Sn(IV) would be differently withheld on, and eluted from, the column as compared to that of Sn(II). However, this was found not to be the case, as verified by injecting standards of the two species. Entirely identical results were obtained, which validates the preparation of standards from Sn(II) salts.

The elution flow-rate was considered to be the most important experimental parameter in the preconcentration system because it not only influenced the rate of release of the analyte, and hence the peak width and height of the elution peak, but also the hydride generation reaction itself. The feasibility and necessary compromise in combining the on-line preconcentration with the hydride generation system have been discussed previously.[10,11] As 1*M* nitric acid was used successfully in the batch mode as an eluent,[9] this was used as a starting concentration for optimization of eluent flow-rate. The borohydride reductant flow was always made identical to that of the eluent flow-rate. This was found to be convenient in controlling the final acidity of the reaction mixture which was maintained as close as possible within 0.025–0.05*M* nitric acid (*cf.* Fig. 3), through adjustments of the sodium hydroxide concentration in the borohydride solution. While lower reductant flow-rates with higher borohydride and acid concentrations were feasible, the sensitivity was not improved although the sample was less diluted, becuase in the hydride generation system the total mass of hydride produced rather than the analyte concentration determines the magnitude of the absorption signal.[1,12] Furthermore, adjustments of acidity, using higher base concentration with lower flow-rates would become more critical and difficult to control.

As seen in Fig. 5, the recorded peak signal became increasingly higher with increase in eluent flow-rate up to a flow-rate of 11 ml/min (Fig. 5), after which a gradual drop in signal was observed. The 11 ml/min was therefore taken as the optimum eluent flow rate.

Subsequently, the effect of the acid concentration in the eluent was investigated. In these experiments the concentration of sodium hydroxide in the borohydride solution was adjusted to maintain an acid concentration of 0.05*M* in the reaction mixture, while the concentration of nitric acid in the eluent stream was gradually decreased from 1.0*M*. Surprisingly, it was found that the peak height increased and the peak width decreased with a decrease in acid concentration. This tendency continued when using demineralized water or dilute alkaline solutions as eluent (Fig. 6). This phenomenon implies that the release of the chloro-complex might be effected through mechanisms other than ion-exchange. Presumably, uncharged hydrolysis products might be formed with the decrease in acidity, giving rise to the formation

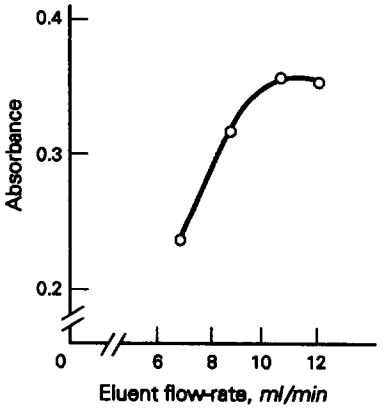

Fig. 5. Effect of 0.2*M* HNO_3 elution flow-rate on peak absorbance. FI-HGAAS system in Fig 2. 10 μg/l. Sn; loading period 20 sec.

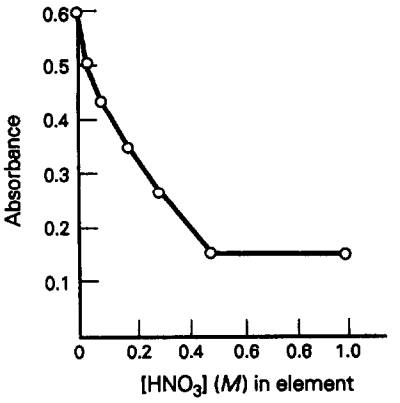

Fig. 6. Effect of nitric acid concentration on peak absorbance. FI–HGASS system in Fig 2. 10 μg/l. Sn; 20 sec loading.

of a colloidal solution which could be readily eluted. An explanation for the response under alkaline eluent conditions is that the acid conditions for the hydride generation reaction may be provided by the residual acidified sample solution remaining in the column following sample loading.

The low acidity of the eluent created, in fact, an extremely beneficial condition for optimizing the acid concentration of the hydride generation reaction. Thus the control of acid concentration within 0.025–0.05*M* proved to be quite simple by using a 0.1*M* nitric acid eluent and merging with a reductant containing 0.05*M* sodium hydroxide. Eluents with lower acid concentrations, although producing higher sensitivities, are generally not recommended since alkaline concentrations in the borohydride would also have to be decreased to maintain the acid conditions for reduction.

An alkaline concentration which is too low would affect the stability of the reductant. In fact, with a sodium hydroxide concentration of 0.05*M* in the borohydride reagent, it is strongly recommended to make this solution freshly every day and to protect it from the ambient air by means of a carbon dioxide trap. Furthermore, with eluents of lower acidity the acid conditions for reduction would be predominated by the acid in the above mentioned residual sample in the column following sample loading. This residual sample bolus forms an acid concentration gradient which presumably overlaps eluted analyte. Under hydride generation conditions, where gases are produced in this overlapping gradient of acid, hydride generation will not be very reproducible. This may explain the increase of noise in the baseline signal at lower acid concentrations for the eluent (particularly below 0.01*M*).

The effect of increasing the sample loading time was investigated with the optimized conditions, that is 0.1*M* nitric acid as eluent and 0.05*M* sodium hydroxide in the borohydride solution. The relationship between time and absorbance was not linear above a loading period of 20 sec. Although higher enrichment factors may be achieved by increasing the loading time, one has to be careful of enhanced interference effects when working with real sample solutions. The increase in loading time naturally also would imply a decrease in the sampling frequency. A relatively short loading period of 20 sec is therefore recommended.

Characteristic data for the performance of the ultimately adopted on-line preconcentration HGAAS system (*cf.* Fig. 1) are reproduced in Table 1, with a 20-sec loading period and using the optimized reagent concentrations. The good reproducibility shows an effective control over the acid conditions through the ion-exchange matrix modification.

In on-line ion-exchange procedures, the column design and capacities both strongly influence the performance of the methods.[6] The conical column used in this study appears to provide a reasonable compromise between sensitivity, sampling frequency, and tolerance of interferences. However, the anion exchanger exhibited non-ideal kinetic properties in the release of the adsorbed complex, producing elution curves with relatively long tailing (the time to reach peak maximum was *ca.* 6 sec while total elution required an additional *ca.* 20–25 sec). This tailing phenomenon was further enhanced when larger column capacities, such as the 3 × 45 mm columns, were used for separation, although that slightly better recoveries could be achieved (*cf.* analysis of practical samples where spiking experiments with the smaller columns generally yielded slightly less than 100% recovery). Within the concentration range of standards used (0–15 μg/l.), both column sizes yielded strictly linear calibration

Table 1. Characteristic data of the on-line preconcentration FI–HGAAS system

Enrichment factor	3.5
Analysis cycle (sec)	50
Sampling frequency (samples/hr)	72
% r.s.d. ($n = 10$) (10 μg/l.)	2.5
L.o.d. (μg/l.) (3σ)	0.08
Calibration curve (0–15 μg/l.): $A = 0.030 + 0.032\,C$ ($r = 0.997$)	

curves. The sensitivity of the larger column was *ca.* 20% lower than that of the short one, whereas the tolerance to interferences was better, but the back pressure was somewhat increased. However, an elution period of more than 1 min was necessary for complete elution of the analyte using the larger column, which lowered the sampling frequency, compared to that of the smaller conical column. If indeed the recovery is solely to be ascribed to the incorporated column, an alternative approach for improving recoveries would be by decreasing the sample load by diluting the sample digest or shortening the loading period, with some sacrifice in sensitivity.

Evaluation of potential interferences

In the proposed procedure there are potentially three types of interferences which should be considered, that is, (1) chlorocomplexes of other metal ions (and possibly also the presence of certain anions) which might compete with the stannate-complex ions for the sites on the ion-exchanger; (2) chlorocomplexes of metal ions which are retained on the column and which, when eluted along with the stannate ions, might interfere in the hydride generation process itself; and (3) chlorocomplexes of metal ions which are so tightly bound to the active sites of the ion-exchanger that they prevent the regeneration of the column from cycle to cycle.

It is well known that Cu(II) and Ni(II) are potential interferents for hydrides, particularly in batch procedures, because, being reduced to oxidation state zero by the borohydride, they act effectively as catalyst for the degradation of the hydrides formed so that these are at risk of being decomposed before they reach the measuring cell. It is precisely in order to eliminate, or at least to suppress, this type of side reaction that FI with its inherent accurate timing has proven itself such an ideal vehicle for hydride generating procedures. Considering the stability constant of the chlorocomplexes of these two species and the acidity/chloride concentration prevailing in the 2*M* hydrochloric acid matrix used, it should not be anticipated that they would consititute any serious problems. Indeed it was verified experimentally, that up to 1000 times excess of Ni(II) and 100 times of Cu(II) could be tolerated without any significant adverse effect on the readout (*cf.* Table 2). Thus, these two constituents do not appear to have a negative influence on either the ion-exchange process or on the hydride generation itself.

Table 2. Effect of various potentially interfering species on the recovery of Sn. All samples contained 10 μg/l. Sn and were measured with interferents added at 1, 5 and 10 mg/l. levels. If results for the two first levels are not reported, it signifies that the recovery was 100 ± 2%. All measurements are an average for $n = 5$

Ionic interferent added	Concentration, *mg/l.*	Recovery, %
Cu^{2+}	1	91
	5	85
	10	84
Ni^{2+}	1	95
	5	96
	10	97
Co^{2+}	10	101
Zn^{2+}	10	98
Fe^{3+}	10	102
MoO_4^{2-}	10	96
PO_4^{3-}	10	104

Furthermore, the levels of tolerance should amply suffice for the intended use of the analytical procedure, that is, for the determination of tin in food digests. Iron(III), which is ubiquitously expected in canned foods, forms stronger chlorocomplexes than Cu and Ni, but is not known to interfere seriously in the hydride generation process as such. When tested experimentally, it was indeed verified that this species readily could be tolerated at a 1000 times excess. The same was true for Zn(II) at the same concentration level, although with chloride it forms highly stable complexes and therefore could be expected to create difficulties particularly in regeneration of the column. However, the diluted nitric acid eluent appears to very effectively reconstitute the column so that no additional wash cycle is needed, which from a practical viewpoint is very convenient. The possible interference of two species of anions, that is, molybdate and phosphate were also tested, and neither of these gave, at the 1000 excess level tested, rise to any adverse effect.

Practical performance of the optimized on-line preconcentration HGAAS system

The practical feasability of the proposed system was tested on three canned food digests. Since standard reference biological materials with certified tin values were not available, the specificity and accuracy of the method was tested by spiking the sample digests. As shown in Table 3, the recoveries were between 94 and 102%, which demonstrates the general reliability of the method.

Table 3. Recoveries of canned food sample digests spiked with 10 μg/l. Sn

Sample	Sn found in digest, μg/l.	Sn found in sample, mg/kg	Recovery, %	rsd, % ($n = 3$)
Ham	13.1	2.62	94	1.0
Stewed beef	8.8	1.76	94	3.5
Mackerel in tomato sauce*	10.9	1.10	102	1.0

*10 g sample and 3 × 45 mm column used.

Acknowledgements—The authors are grateful to Bodenseewerk Perkin-Elmer & Co. GmbH, Überlingen for partial financial support to FIARC, and for the loan of ASS and FI equipment to their respective laboratories. Mr. Liping Dong's assistance in the analysis of the canned food samples is greatly acknowledged. One of us (ZF) expresses his appreciation to the Julie Damm's Foundation for providing the economic basis for a one-month stay in Denmark.

REFERENCES

1. Z-L. Fang, *Flow-Injection Atomic Spectroscopy*, J. L. Burguera (ed.), Ch. 4. Marcel Dekker, 1989.
2. M. Legret and L. Divet, *Anal. Chim. Acta*, 1986, **189**, 313.
3. G. H. Alvarez and S. G. Capar, *Anal. Chem*, 1987, **59**, 530.
4. B. Welz, *Atomic Absorption Spectrometry*, 2nd Ed., VCH, 1985.
5. Z-L. Fang and B. Welz, *J. Anal. Atom. Spectrom.*, 1989, **4**, 543.
6. Z-L. Fang, S-K. Xu and S-C. Zhang, *Anal. Chim. Acta*, 1987, **200**, 35.
7. R. W. Dabeka, A. D. McKenzie and R. H. Albert, *J. Assoc. Off. Anal. Chem.*, 1985, **68**, 209.
8. J. D. Smith, *Anal. Chim. Acta*, 1971, **57**, 371.
9. J. D. McCrackan, M. C. Vecchione and S. L. Longo, *At. Absorp. Newslett.*, 1969, **8**, 102.
10. S-C. Zhang, S-K. Xu and Z-L. Fang, *Quim. Anal.*, 1989, **8**, 191.
11. Z-L. Fang, Z-H. Zhu, S-C. Zhang, S-K. Xu, L. Guo and L-J. Sun, *Anal. Chim. Acta*, 1988, **214**, 41.
12. A. Meyer, C. Hofer, G. Tolg, S. Raptis and G. Knapp, *Z. Anal. Chem.*, 1979, **296**, 337.

Talanta, Vol. 39, No. 4, pp. 391–396, 1992
Printed in Great Britain.

0039-9140/92 $5.00 + 0.00

VOLTAMMETRIC DETERMINATION OF MERCURY(II) AT A CARBON PASTE ELECTRODE IN AQUEOUS SOLUTIONS CONTAINING TETRAPHENYLBORATE ION

IVAN ŠVANCARA and KAREL VYTŘAS
Department of Analytical Chemistry, University of Chemical Technology, Pardubice 532 10, Czechoslovakia

CHI HUA and MALCOLM R. SMYTH*
School of Chemical Sciences, Dublin City University, Dublin 9, Ireland

(*Received* 18 *June* 1991. *Revised* 2 *September* 1991. *Accepted* 4 *September* 1991)

Summary—The determination of mercury(II) ions can be achieved by monitoring the decrease in the oxidation peak of the tetraphenylborate ion in the presence of this metal ion at a carbon paste electrode. The reaction between mercury(II) and the tetraphenylborate ion results in the formation of diphenylmercury, thus providing the method with good selectivity over other metal ions. Using anodic stripping voltammetry in a neutral electrolyte, a linear dependence of the decrease of peak height was observed on increasing the mercury(II) concentration in the range 1×10^{-6}–8×10^{-9}*M* mercury(II). Zinc(II), cadmium(II), lead(II), nickel(II), cobalt(II), tin(II), potassium(I) and ammonium(I) ions did not interfere at a 1000-fold concentration excess. Iron(III) and chromium(III) did not interfere at a 250-fold and 50-fold concentration excess, respectively. Following masking procedures, copper(II), bismuth(III) and silver(I) did not interfere at a 100-fold concentration excess. The method can be used to determine the concentration of mercury(II) in natural waters contaminated by this metal.

Mercury(II) and organomercury compounds are very harmful for most living organisms even in very low concentrations, and considerable attention has therefore been devoted to the determination of mercury(II) in environmental samples. The voltammetric approaches to mercury(II) determination usually involve the use of solid graphite electrodes,[1] where the mercury(II) ion is plated on the surface of the electrode and then stripped off by imposition of an anodic scan.[2] Gold electrodes, in association with either stationary or flow systems, have also often been exploited for the analysis of mercury(II) in environmental samples.[3–6] Since a number of sensitive reactions of organic compounds with Hg(II) are known, chemically modified solid electrodes have been used to determine Hg(II) by differential pulse voltammetry, often in connection with an accumulation step.[7–10] The use of a carbon-paste electrode (CPE) has also been reported for the determination of mercury(II) in the presence of copper(II) by Ulrych and Ruegsegger.[11] The CPE has the advantages of surface renewal and very low background currents, mainly in positive potential ranges.[1] This approach suffers, however, from interferences from other metal ions forming intermetallic compounds.[1] An approach to incorporate various ligands into the paste has been exploited to improve the selectivity of the determination step compared to using an unmodified CPE.[12,13]

In potentiometry, the reaction between mercury(II) and the tetraphenylborate ion has been previously exploited.[14] A carbon paste ion-selective electrode containing sodium tetraphenylborate has been described for the determination of the potassium(I), rubidium(I) and tetralkylammonium(I) ions, respectively.[15] The electrochemical behaviour of sodium tetraphenylborate (NaTPB) has been previously reported by Turner and Elving.[16] The electrochemical oxidation in aqueous solutions proceeds in three steps:

$$B(Ph)_4^- = B(Ph)_2^+ + Ph - Ph + 2e^- \quad (1)$$

$$B(Ph)_2^+ + H_2O = B(Ph)_2OH + H^+ \quad (2)$$

$$B(Ph)_2OH + 2H_2O = B(OH)_3 + Ph - Ph + 2H^+ + 2e^- \quad (3)$$

*Author for correspondence.

NaTPB may be chemically oxidized with iridium(IV), cerium(IV), and iron(III) to form similar products.[17] Turner and Elving[16] demonstrated that two waves were obtained corresponding to these changes. The first wave was well-defined and pH-independent, whereas the second wave arose at more positive potentials, and was deformed and pH-dependent. The electrochemical activity of NaTPB has also been successfully applied in the amperometric titration of potassium(I).[18] If mercury(II) is present, the following reaction with NaTPB occurs:

$$3Hg^{2+} + 2B(Ph)_4^- + 4H_2O = 3(Ph)_2Hg + 2PhB(OH)_2 + 4H^+ \quad (4)$$

and insoluble diphenylmercury is formed. Commonly occurring heavy metals, such as silver and copper, also react with NaTPB, forming insoluble silver(I) tetraphenylborate [$AgB(Ph)_4$] and copper(I) tetraphenylborate [$CuB(Ph)_4$], respectively.[19] It is required therefore to mask these ions prior to determination of mercury(II).

EXPERIMENTAL

Chemicals and reagents

All chemicals were of analytical reagent grade unless stated otherwise. The supporting electrolytes and other solutions were prepared from doubly-demineralized water obtained by passing distilled water through a Millipore Milli-Q water purification system. Dilute solutions ($\leq 1 \times 10^{-3} M$) of NaTPB, Hg(II), and other ions were prepared fresh daily.

Apparatus

All measurements were carried out using an EG&G Princeton Applied Research Model 264A polarographic analyser connected to an XY-recorder (Lloyd Instruments, Model PL-3). The electrochemical behaviour of NaTPB was monitored by cyclic voltammetry and differential pulse anodic stripping voltammetry (DPASV). A three-electrode cell involving a CPE as the working electrode, a Ag/AgCl reference electrode, and a Pt-wire counter electrode were used for all investigations. During the accumulation step a mechanical stirrer (Heidolph, Model RZR 1) was used. Oxygen was removed by bubbling of nitrogen gas through the electrolyte solution for 10 min. Sample volumes of metal ion solutions were introduced into the cell with an Oxford-sampler system micropipette.

Fabrication of carbon paste electrode

The paste was prepared by thorough mixing of 2.50 g of graphite powder (Aldrich Chemical Co., Ltd) and 1.50 ml of Nujol oil (Aldrich). The electrode body was fabricated from a plastic pipette, which had both ends removed. The paste was packed carefully into the pipette tip to avoid possible air gaps, which often enhance electrode resistance. The contact was made with a copper wire, which was passed through a glass tube. The glass tube served also as a piston for extrusion of the paste. The paste was then smoothed on wax paper.

Determination of mercury(II) in natural waters

To a 20-ml sample of river or sea water was added 100 μl of 0.001M NaTPB and 5 ml of 0.5M sodium sulphate. The current responses of NaTPB were then recorded for each sample. To check the reproducibility, five succesive scans were carried out. The same procedure was then employed for a reference solution containing 20 ml of distilled water + 5 ml of sodium sulphate + 100 μl of 0.001M NaTPB, using the same electrode surface. Subsequently, successive additions of known concentrations of mercury(II) were introduced into the reference solution to obtain the dependence between peak heights and the concentration of mercury(II) (calibration plot). Finally, the NaTPB peak heights of samples were compared with a calibration plot obtained for the reference solution.

RESULTS AND DISCUSSION

Cyclic voltammetry of tetraphenylborate ion at the CPE

The cyclic voltamperogram of NaTPB obtained with the CPE in 0.1M sodium sulphate electrolyte is shown in Fig. 1. In accordance with the results of Turner and Elving,[16] two peaks were observed. However, the second peak was badly formed, because its peak potential lay at high positive potentials, where the CPE showed a large background current. The first peak was therefore further investigated for analytical purposes. The choice of sodium sulphate supporting electrolyte was made since it gave rise to lower background currents than other acidic or basic electrolytes investigated. The first well-defined peak was pH-independent, but using a CPE, its potential occurred at a more positive potential ($E_p = +0.53$ V *vs.* Ag/AgCl) than Turner and Elving had reported

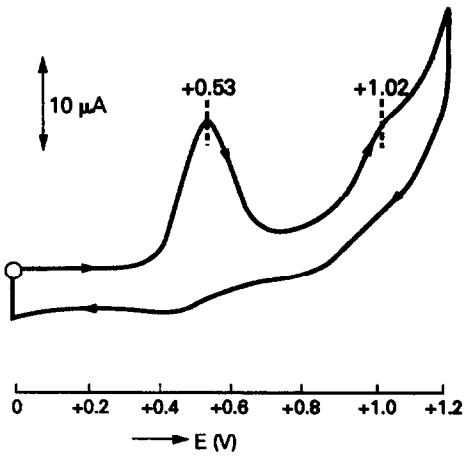

Fig. 1. Cyclic voltamperogram of tetraphenylborate ion obtained at a carbon-paste electrode. Supporting electrolyte, 0.1M Na_2SO_4; scan-rate 20 mV/sec. Concentration of NaTPB, $1 \times 10^{-5}M$. Arrows indicate scan direction.

($E_p = +0.20$ V *vs.* SCE) with the pyrolytic graphite electrode.[16] The favourable response of the CPE was obtained at a scan-rate of 20 mV/sec. Lower values resulted in lower sensitivity and higher values showed distorted curves.

Anodic stripping voltammetry

The sensitivity of the NaTPB response was enhanced by using anodic stripping voltammetry in conjunction with stirring the solution. It was found that the NaTPB peak height was essentially independent of deposition time, and for deposition times longer than 10 sec, the peak size became constant. This can be explained by the fact that NaTPB adsorbed on the electrode surface forms a compact film due to the surfactant properties of the tetraphenylborate ion.[16,19] Hence, from this it was thought that the anodic stripping detection of NaTPB itself could be a sensitive approach for the indirect determination of mercury(II).

Dependence of NaTPB peak on the presence of mercury(II)

In the presence of mercury(II), the oxidation peak of NaTPB rapidly decreases and disappears completely at high relative concentrations of mercury(II). This is illustrated in Fig. 2(A) for a $1 \times 10^{-6}M$ concentration of NaTPB in the presence of 8.3×10^{-8}–$6.7 \times 10^{-7}M$ mercury(II). It was shown that this decrease was

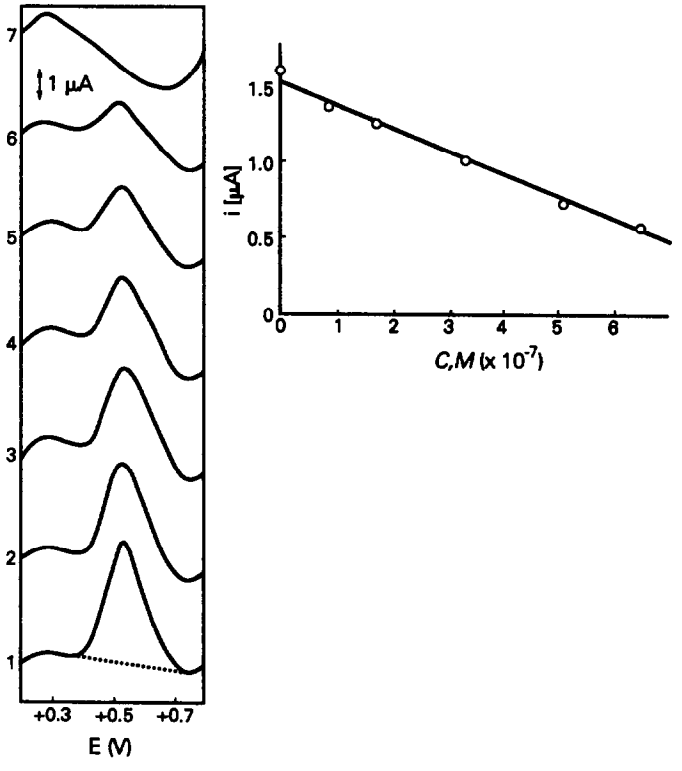

Fig. 2. (A) Effect of varying concentration of mercury(II) upon DPSAV behaviour of tetraphenylborate ion, (B) resultant calibration plot for concentration range $8.3 \times 10^{-8}M$–$6.7 \times 10^{-7}M$ mercury(II). (1) $1 \times 10^{-6}M$ NaTPB, (2–6) successive additions: 25, 50, 100, 150, 200 and 300 μl of $1 \times 10^{-4}M$ mercury(II). Supporting electrolyte, 0.1M Na_2SO_4; scan-rate 20 mV/sec. Deposition time, 10 sec; initial potential, +0.20 V. Dotted line represents base-line for evaluation.

essentially linear [Fig. 2(B)]. Despite the fact that background currents varied slightly during successive scans, especially in the lower concentration ranges, a good reproducibility was obtained for this oxidation peak. For instance, the standard deviation for twenty successive scans of $1 \times 10^{-7}M$ NaTPB was found to be 7%, whereas the standard deviation for ten successive scans of $1 \times 10^{-6}M$ NaTPB was less than 4%. It was also observed that medium exchange of solutions containing the same amount of mercury(II) had practically the same response size even in different electrolytes. The fact that the response of the NaTPB peak was reproducible during these medium exchanges is important for practical applications, which will be discussed later. In order to use this reaction for practical analyses, it is necessary to choose a suitable ratio between the concentrations of NaTPB and mercury(II). Approximately, a 10-fold excess of NaTPB against mercury(II) concentration was found to be optimal for concentrations in the range 1×10^{-8}–$1 \times 10^{-6}M$ mercury(II).

Interferences from other ions

During optimization of the voltammetric parameters for detection of mercury(II), the possibility of interferences from some heavy metals was investigated. As expected, the formation of the oxidation peak and the resultant peak decrease owing to the presence of mercury(II), was not influenced by heavy metals such as zinc(II), lead(II), cadmium(II), nickel(II), cobalt(II) and tin(II) in 1000-fold excess in concentrations, because their anodic reactions proceed in a more negative potential range than the oxidation of NaTPB. Iron(III) interferes at a 250-fold excess in concentration and chromium(III) ions interfere at a 50-fold excess, owing to their anodic oxidations proceeding near to the peak potential of NaTPB. Any incidental anodic redepositions of such metal ions were particularly restricted by the choice of a positive initial potential ($E_i = +0.20$ V). It was then noticed that the anodic peaks due to copper(II) and bismuth(III) at the CPE were small and badly formed, and that these ions influenced the peak of NaTPB at a 100-fold excess in concentrations when mercury(II) was analysed. This again supports the assumption about a coverage of the electrode surface by the compact film, which hinders other redox processes.[20] The undesirable interference of bismuth(III), whose anodic detection at the CPE is considerably sensitive,[21] was suppressed by the choice of a neutral electrolyte, where the bismuth(III) ion irreversibly hydrolyses. However, large difficulties were observed due to the interference of silver(I), if a $0.1M$ sodium sulphate electrolyte was used. This can be overcome if either $0.05M$ sodium sulphate + $0.05M$ sodium bromide or $0.05M$ sodium sulphate + $0.05M$ sodium chloride electrolytes were chosen, probably owing to the formation of both silver chloride and silver bromide precipitates, respectively. A similar paper[23] using the same masking procedure has appeared more recently. The effectiveness of this masking procedure can be seen in Fig. 3. The first set of voltamperograms 1–4 represents interferences from Ag(I) ions in $0.1M$ sodium sulphate electrolyte, where, due to the presence of these ions, the peak of NaTPB rapidly decreases. If $0.05M$ sodium sulphate + $0.05M$ sodium chloride or

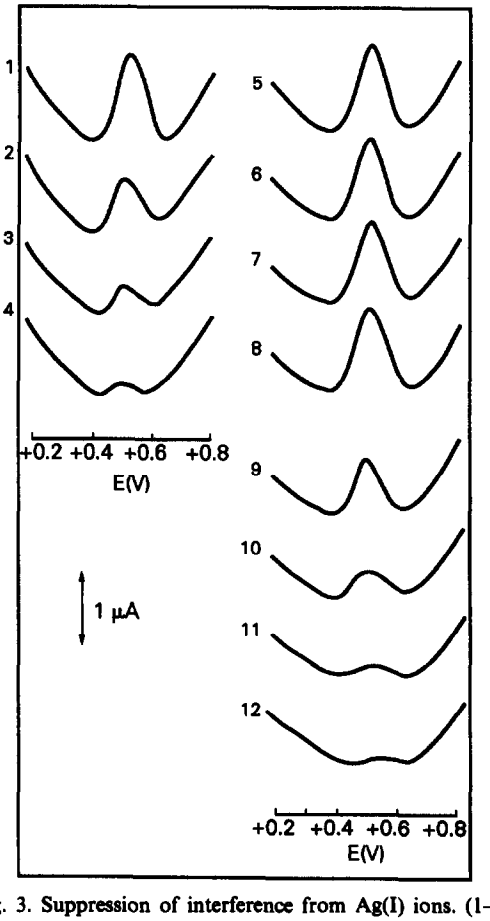

Fig. 3. Suppression of interference from Ag(I) ions. (1–4) $0.1M$ Na_2SO_4 electrolyte; successive additions: 0, 50, 100 and 200 μl $1 \times 10^{-4}M$ silver(I). (5–8) $0.05M$ Na_2SO_4 + $0.05M$ NaCl electrolyte; successive additions: 0, 50, 100 and 200 μl $1 \times 10^{-3}M$ silver(I). (9–12) Successive additions: 50, 100, 150 and 200 μl $1 \times 10^{-4}M$ mercury(II). Experimental conditions: see Fig. 2.

0.05*M* sodium sulphate + 0.05*M* sodium bromide electrolytes were used, silver(I) ions did not interfere (voltamperograms 5–8), although their concentration had been 10-fold higher than in the sulphate electrolyte. However, after successive additions of mercury(II) ions, the oxidation peak of NaTPB diminished immediately (voltamperograms 9–12). No oxidation of bromide ions was observed in the potential range studied. Potassium(I) and ammonium(I) ions, whose reactions with NaTPB are often employed in potentiometry,[15,22] did not interfere with the decrease of the NaTPB peak even in a 1000-fold excess.

A determination employing this approach would, however, be affected by the presence of strongly oxidizing agents, such as chromate or permanganate anions, or bromine water, which oxidize the tetraphenylborate ion. No interferences of organic compounds have been investigated in this work.

Analytical applications

The usable concentration range in which the decrease of NaTPB peak in the presence of mercury(II) could be employed was investigated. For appropriate NaTPB concentrations in both 0.1*M* sodium sulphate and 0.05*M* sodium sulphate + 0.05*M* sodium chloride electrolytes, the decrease in response of NaTPB due to mercury(II) was proportional in the range 1×10^{-6}–$8 \times 10^{-9}M$. The detection limit was estimated as $6 \times 10^{-9}M$ mercury(II) (by means of 3:1 current-to-noise ratio) using an appropriate amount of NaTPB in connection with highest-possible analyser sensitivity. A calibration plot for the concentration range of 8.3×10^{-8}–$6.7 \times 10^{-7}M$ mercury(II) (correlation coefficient, $r = 0.989$) was linear as shown in Fig. 2(B). Similar plots for both concentration ranges of 8.3×10^{-7}–$5 \times 10^{-6}M$ Hg(II) ($r = 0.994$) and 8.3×10^{-9}–$6.7 \times 10^{-8}M$ Hg(II) ($r = 0.984$) were also obtained (not shown). For the latter concentration range it was observed that due to high background currents, relatively distorted voltamperograms were obtained.

The determination of mercury(II) was then carried out in both river and sea water. However, as expected, this method is not sensitive enough to determine the concentration of mercury(II) at its base level in these matrices, which has been quoted to be extremely low (*e.g.*, in sea water about $1 \times 10^{-11}M$).[4] Hence, the determinations were carried out in "spiked" water samples. No pretreatment of samples to remove any matrix component was carried out. The results of these analyses are given in Table 1.

Both water samples were made $5 \times 10^{-7}M$ in mercury(II), assuming that the original content of these ions was negligible compared to the concentration that was spiked in. Peak heights were computed in a manner as shown in Fig. 2A. The standard deviations for both reference and sample solutions were less than 4% in all cases.

The responses of the NaTPB peak in both river and sea water samples were essentially the same size, and the difference between the results shown in Table 1 can probably be explained due to the effect of the different organic and inorganic constituents in each matrix. The calibration plots for reference solutions were linear, with correlation coefficients from 0.983 to 0.995. Original river and sea water samples yielded the same size of peaks as for reference solutions. The procedure of successive additions was also applied for solutions of samples, and it was observed that linear calibration plots had practically the same slopes. These observations and results have confirmed that the method employing the indirect determination approach reported in this paper can be used for practical analysis; its application would, however, be limited to heavily polluted water systems.

Table 1. Results of determinations in natural waters containing $5.0 \times 10^{-7}M$ mercury(II) (added)

Sample (place)	Number of determinations	Concentration found (mean)	CV*
River water (Royal Canal, Dublin)	5	$5.65 \times 10^{-7}M$	5.2%
Sea water (Malahide Beach, Dublin)	5	$4.70 \times 10^{-7}M$	3.5%

*Coefficient of variation

CONCLUSIONS

The oxidative voltammetric behaviour of NaTPB at the CPE has been shown to be dependent upon the presence of mercury(II). As a linear response was obtained for mercury(II) over a wide concentration range, this approach was first examined for the indirect determination of mercury(II) in aqueous solution. This method can be used for the determination of mercury(II) in the concentration range between 1×10^{-6}–$1 \times 10^{-8} M$. This is superior to the detection limits offered by potentiometric methods of analysis,[15,22] and is similar to those reported by other authors using stripping voltammetry.[8–10]

This indirect determination is, however, accompanied by a poorer precision compared to common direct methods.[8,10,12] However, on the other hand, a simple preparation of working electrode (compared to either the fabrication of modified solid electrodes[7,8] or expensiveness of gold electrodes), together with the exploitation of very short deposition times (in contrast to other procedures[7,8]) can be advantageous. Even so, the considerable sensitivity and selectivity towards mercury(II) can be useful for routine analysis. It was found that the electrochemical behaviour of the tetraphenylborate ion was practically not affected by the presence of other metal ions such as zinc(II), cadmium(II), lead(II), nickel(II), cobalt(II), tin(II), iron(III), copper(II), bismuth(III) and potassium(I) ions. The interference of the silver(I) ion was overcome by application of an appropriate masking procedure. The determination is unfavourably affected by the presence of higher concentrations of chromium(III), and particularly, by the presence of strongly oxidizing agents.

This method can also be used as a relatively simple and quick method to determine mercury(II) in polluted and industrial waste water.

Acknowledgements—Financial grants under the EC TEMPUS Programme (Contract Nos. IMG-CZS-0014-90 and IMG-CZT-0107-90) are gratefully acknowledged.

REFERENCES

1. J. Wang, *Stripping Analysis*, VCH Publishers Inc., Florida, 1985.
2. I. Tanase, J. Vartires, N. D. Torir and I. Ioneci, *Rev. Roum. Chim.*, 1985, **30**, 679.
3. G. J. Svoboda, J. P. Sottery and W. C. Anderson, *Anal. Chim. Acta*, 1984, **166**, 297.
4. I. Gustavsson, *J. Electroanal. Chem.*, 1986, **214**, 31.
5. M. Lev and H. Seiler, *Z. Anal. Chem.*, 1985, **321**, 479.
6. F. S. Chagonda Lameck and J. S. Millership, *Analyst*, 1988, **113**, 243.
7. M. D. Imisides, D. M. T. O'Riordan and G. G. Wallace, *Anal. Lett.*, 1988, **21**, 1969.
8. J. Labuda and V. Plaskoň, *Anal. Chim. Acta*, 1990, **228**, 259.
9. M. D. Imisides and G. G. Wallace, *J. Electroanal. Chem.*, 1988, **246**, 181.
10. J. Lexa and K. Štulík, *Talanta*, 1989, **36**, 843.
11. L. Ulrych and P. Ruegsegger, *Z. Anal. Chem.*, 1975, **277**, 349.
12. J. Wang and M. Bonakdar, *Talanta*, 1988, **35**, 277.
13. S. V. Prabhu, R. P. Baldwin and L. Kryger, *Electroanalysis*, 1989, **1**, 13.
14. A. Heyrovský, *Z. Anal. Chem.*, 1960, **173**, 301.
15. A. A. Pendin and P. K. Leontevskaia, *Zh. Anal. Khim.*, 1979, **34**, 2113.
16. R. W. Turner and P. J. Elving, *Anal. Chem.*, 1965, **37**, 207.
17. E. Negishi, in G. Williamson (ed.), *Comprehensive Organometallic Compounds*, Vol. 1, pp. 323–336. Pergamon Press, Oxford, 1982.
18. D. L. Smith, D. R. Jamieson and P. J. Elving, *Anal. Chem.*, 1960, **32**, 1253.
19. H. Flaschka and A. J. Barnard, in C. N. Reilley (ed.), *Advances in Analytical Chemistry and Instrumentation*, Vol. I, pp. 1117, Interscience, New York, 1960.
20. I. Švancara, *Thesis*, University of Chemical Technology, Pardubice, 1988.
21. I. Švancara and F. Renger, unpublished results, University of Chemical Technology, Pardubice.
22. M. L. Ruberte Sanchez and K. Vytřas, *Analyst*, 1988, **113**, 959.
23. E. D. Jeong, M. S. Won and Y. B. Shim, *J. Korean Chem. Soc.*, 1991, **35**, 545; *Chem. Abstr.*, 1991, **222**, 293e.

Talanta, Vol. 39, No. 4, pp. 397–403, 1992
Printed in Great Britain.

0039-9140/92 $5.00 + 0.00

A QUANTITATIVE INVESTIGATION OF PROTON– AND LEAD(II)–DITHIOERYTHRITOL COMPLEX EQUILIBRIA UNDER PHYSIOLOGICAL CONDITIONS

NOUKPO GNONLONFOUN

INSERM U305, Equipe "Bioréactifs: Spéciation et Biodisponibilité", Laboratoire de Synthèse et d'Etudes Physico-chimiques Organiques (SEPO), Université François Rabelais, Parc de Grandmont, 37200 Tours, France

LUC LAMBS and GUY BERTHON†

INSERM U305, Equipe "Bioréactifs: Spéciation et Biodisponibilité", Université Paul Sabatier, 38, Rue des Trente-six Ponts, 31400 Toulouse, France

(*Received* 5 *March* 1990. *Revised* 21 *September* 1991. *Accepted* 27 *September* 1991)

Summary—Dithioerythritol (DTE) is frequently employed as a reducing agent or a protective reagent for thiol groups in biological assays. Owing to its known inhibiting properties in enzyme catalysis reactions, lead is also commonly used in such experiments, and often simultaneously with DTE. Given the potential affinity of these two reactants, their measured individual effects may well depend on their interactions in the medium used. Any quantitative assessment of these interactions necessitates, however, that the complex equilibria between lead and DTE be investigated beforehand. To test this hypothesis, the formation constants of lead(II) complexes with DTE under physiological conditions (37°, NaCl 0.15M) have been calculated from the results of glass electrode potentiometry, with the help of the MINIQUAD and ESTA computer programs. The pK values for dissociation of DTE have been found equal to 8.926 ± 0.003 and 9.840 ± 0.003. The following lead–DTE species have been characterized: ML (12.774 ± 0.037), MLH_{-1} (2.858 ± 0.037), M_2LH_{-1} (13.349 ± 0.025) and M_6L_5 (86.586 ± 0.099); the log $*\beta$-values are given in the parentheses. Appropriate computer simulations effectively show that the interactions of the two reactants are indeed quite significant within the concentration ranges commonly used in *in vitro* biological assays. They should thus be taken into account in interpretation of the effects observed.

Dithioerythritol (DTE), the erythro isomer of 2,3-dihydroxy-1,4-dithiobutane, has as low a redox potential as dithiothreitol (DTT) (−0.33 V at pH 7), and is thus capable of maintaining monothiols completely in the reduced state as well as of reducing disulphides quantitatively.[1] DTE has thus gained wide acceptance as a reducing agent or protective reagent for —SH groups in biochemical systems.[2,3] Owing to its capacity to inhibit certain enzyme catalysis reactions, lead is also frequently used in biological assays, and often simultaneously with DTE. Since, like some transition metal ions,[4] lead is expected to display some affinity for DTE, the individual effects attributed to each of these reactants may, to some extent at least, be affected by interactions between the two of them when both are present in the system. It was thus of interest to test this possibility on quantitative grounds. However, any reliable assessment of these interactions required that the formation constant of the lead–DTE complexes be determined under appropriate conditions.

Accordingly, in parallel to a study on lead(II)–DTT co-ordination with respect to lead/5-aminolevulinic acid dehydratase/DTT interactions,[5] the present work reports a quantitative investigation into proton– and lead(II)–DTE complex equilibria under physiological conditions (37°, NaCl 0.15M). First, the stoichiometries and stabilities of all the species potentially formed between lead(II) and DTE were determined, then distribution profiles for each of these two reactants were simulated for concentrations commonly used in *in vitro* biological investigations.

EXPERIMENTAL

Reagents

Dithioerythritol and lead(II) chloride were purchased from Aldrich Chemical Co. Fresh solutions were systematically prepared every day by dissolving the crystals in doubly-demineralized water distilled from potassium

†Author for correspondence.

permanganate, and kept under a nitrogen atmosphere.

Carbonate-free sodium hydroxide solutions were prepared by diluting BDH standard volumetric concentrates with freshly distilled water of the above quality under a constant flow of nitrogen. The alkali titre and absence of carbonate were periodically checked by use of appropriate Gran plots[6] and Merck *p.a.* potassium hydrogen phthalate. The hydrochloric acid used to acidify initial solutions to be titrated was a Prolabo R. P. Normapur product. The sodium chloride used as background electrolyte was a Merck *p.a.* reagent.

Potentiometric measurements

Potentiometric titrations were performed with use of a Beckman 4500 mV-meter equipped with Ingold glass and calomel electrodes. The electrode system was calibrated on the concentration scale in the presence of 0.15*M* sodium chloride at 37°; the corresponding pK_w determined was 13.22.

The titration vessel consisted of a thermostated Ingold Cell System in which anaerobic conditions were imposed by constant passage of nitrogen through the solution. Successive aliquots of sodium hydroxide were added by means of a Radiometer Autoburette.

The initial solution to be titrated was made sufficiently acidic for all donor groups to be substantially protonated. Proton–ligand as well as metal–ligand concentration ratios were varied over the largest possible range so as to favour the characterization of all possible complexes. Each experiment was repeated at least twice.

Table 1 summarizes the corresponding analytical data.

Calculation techniques

Estimates of the stability constants derived from protonation and formation curves were refined with MINIQUAD[7] and with the optimization module of the ESTA program library.[8] A first selection between the possible sets of constants was made by comparing numerical goodness-of-fit parameters (sum of squared residuals, Hamilton *R* factors). The ultimate discrimination among the several sets displaying almost equally favourable numerical fits was made on graphical grounds, based on pseudo-experimental curves calculated with the simulation module of the ESTA library.[9] The final constants were refined with MINIQUAD.[7]

Distribution profiles of Pb^{2+} ions and DTE under the concentration conditions commonly used in biological investigations were plotted by means of the SPEC module of the ESTA library.[9]

RESULTS AND DISCUSSION

The DTE molecule displays only two active protonation sites in water, which correspond to the thiol groups according to the following equilibria:

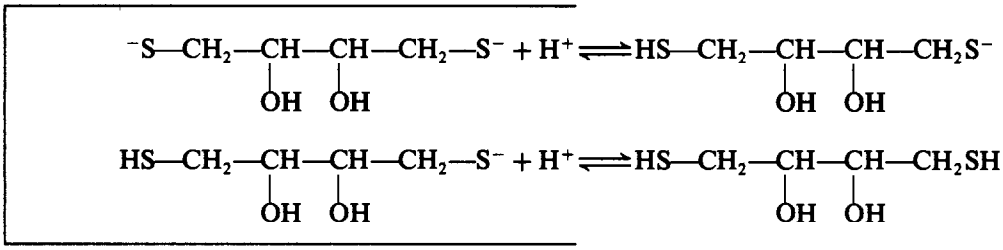

The corresponding protonation constants shown in Table 2 are in good accordance with those reported by Zahler and Cleland[10] (9.0, 9.9) and by Loechler and Hollocher[11] (9.14, 9.94) though determined under different experimental conditions.

Figure 1 shows the experimental protonation curves obtained in the presence of different concentrations of lead, put in perspective by the reference protonation curve calculated from the two constants above. Figure 2 shows the corresponding experimental formation curves obtained over the whole range of concentrations investigated.

As can be seen from Fig. 2, complex formation is not expected to be limited to simple mononuclear species in this system; otherwise all the experimental curves obtained would have indeed been statistically regular and superimpossible regardless of the reactant concentrations. In the present case, on the contrary, all the curves are "tail-shaped" above average coordination numbers of *ca.*1, except for the 2:1 metal–ligand ratio experiment, where there is a "curl back" near 0.5. Since formation curves are

Table 1. Summary of the titration data used for calculating formation constants [the initial total concentrations of DTE (C_L) and metal ion (C_M), mineral acid (C_H) in the titrand, and the sodium hydroxide concentration (C_{OH}) in the titrant are expressed in mmole/l.; N represents the number of experimental observations in each titration]

System	C_L	C_M	C_H	C_{OH}	pH* range	N
Proton–DTE	4.83			100.3	5.98–10.77	47
	10.00			100.3	5.93–10.99	47
	15.00			100.3	5.64–11.09	46
	19.28			100.3	5.76–11.11	51
Lead(II)–DTE	2.01	0.200	2.10	99.6	3.26–9.46	36
	4.27	0.400	4.20	99.6	3.58–8.94	33
	2.01	0.400	2.19	99.6	2.66–10.25	55
	2.01	0.600	2.29	99.6	2.77–10.07	47
	2.01	0.800	2.39	99.6	2.80–9.76	41
	1.01	0.500	1.24	99.6	3.53–9.95	30
	2.01	1.000	2.48	99.6	2.59–9.84	50
	1.01	0.800	1.39	99.6	3.43–9.27	30
	1.01	1.000	1.48	99.6	2.83–8.80	41
	1.00	2.000	1.96	100.0	2.69–3.98	16

*To be understood as $-\log [H^+]$ (see text).

deduced from apparent free ligand concentration calculated by supposing the existence of only simple mononuclear complexes, the shifts observed with respect to Bjerrum's theoretical definition are characteristic of species not explicitly considered. Thus, the present "tails" may *a priori* express: (*i*) the formation of metal–ligand hydroxo species, (*ii*) the additional deprotonation of ligand side-chain hydroxyl groups in one or several complexes formed at lower pH, or (*iii*) the formation of metal hydroxides.

Metal hydrolysis is taken into account in the calculations, the corresponding constant (extrapolated from Sylva and Brown's work[12]) being kept constant during the refinements. In addition, its influence can be directly appreciated by simulating the formation curves as they would have been if metal hydroxides were the only species present in solution. In this respect, the comparison of Fig. 2 with Fig. 3 suggests that strong lead–DTE complexes exist before hydrolysis becomes predominant at very high pH-values, where pseudo-experimental points tend to coincide with experimental ones.

Regarding the formation of hydroxo complexes or the possible deprotonation of hydrated lead–DTE species formed at lower pH values (both phenomena being strictly equivalent from the chemical point of view), MLH_{-1} and

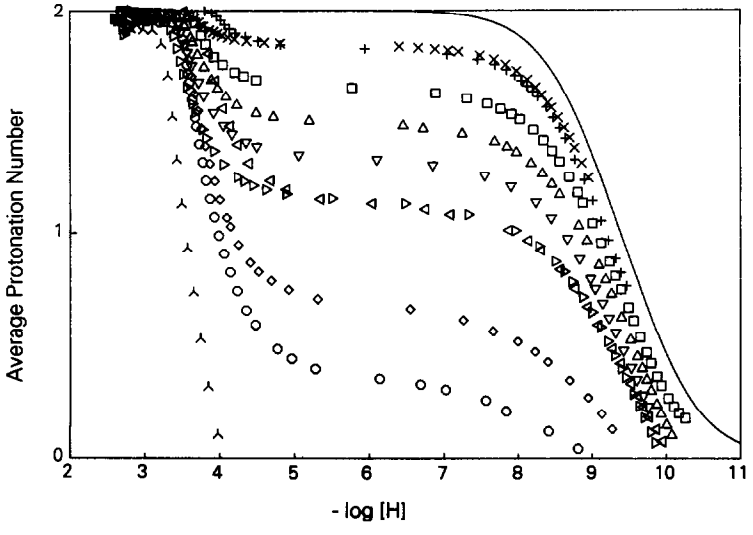

Fig. 1. Experimental protonation curves for DTE in the presence of various lead concentrations. Experiments are given in the order of Table 1 with the following symbols: +, ×, □, △, ▽, ◁, ▷, ◇, ○, ⅄. The solid line represents the reference curve calculated from protonation constants in Table 2.

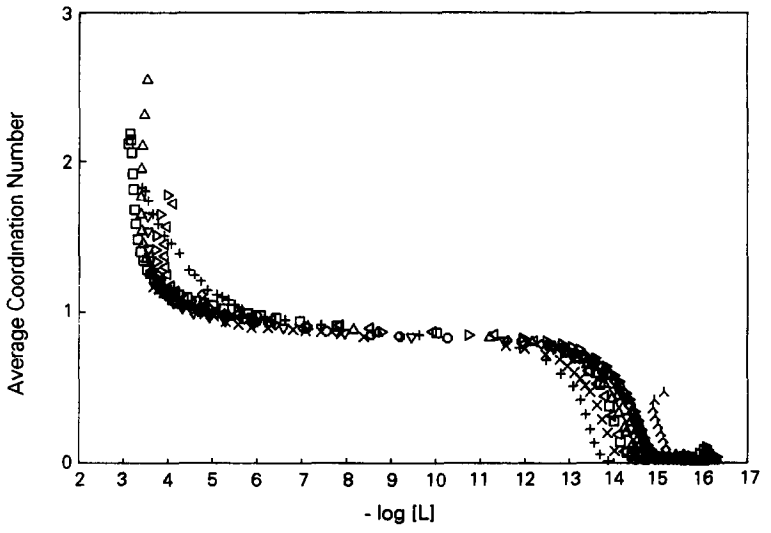

Fig. 2. Experimental formation curves for the lead(II)–DTE system. Key to symbols as for Fig. 1.

M_2LH_{-1} were easily selected on numerical as well as graphical grounds (Fig. 4). However, taking these two species into account in the set of constants likely to describe the experimental data proved insufficient for satisfactory graphical fits to be obtained.

The systematic deviations observed near the two bends of the inflexion at average co-ordination numbers of about 1 may indicate the existence of polynuclear complexes. As was done in the parallel study of lead–dithiothreitol (DTT) equilibria,[5] corresponding constants were successively introduced in the refinement, in accordance with Sillen's "core + links" theory.[13] Of all the species tested during this research, which led us to consider more than 50 different combinations of constants involving M_2L_2, M_3L_3, M_4L_4, M_5L_5, M_6L_6, M_3L_2, M_4L_3, M_5L_4, M_6L_5 and their hydroxo counterparts, several polynuclear complexes gave rise to similarly acceptable goodness-of-fit parameters, but only two of these, namely $M_3L_2H_{-1}$ and M_6L_5, led to satisfactory graphical comparisons.

A priori, the formation of such polynuclear complexes may stem from the known ability of sulphur to accept electrons from a metal by π-bonding.[14] The size of the donor atom may also be a facilitating factor. In this regard, the two species above may respectively result

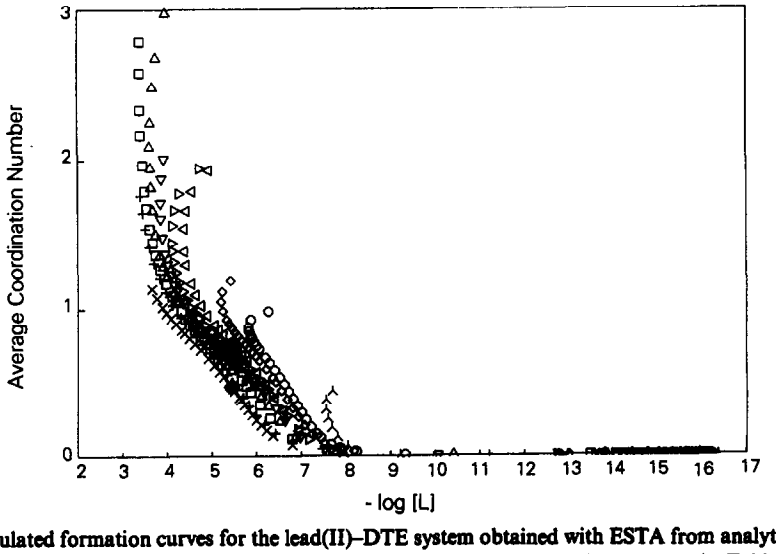

Fig. 3. Simulated formation curves for the lead(II)–DTE system obtained with ESTA from analytical data in Table 1, supposing the exclusive formation of hydroxides (see hydrolysis constants in Table 2). Key to symbols as for Fig. 1.

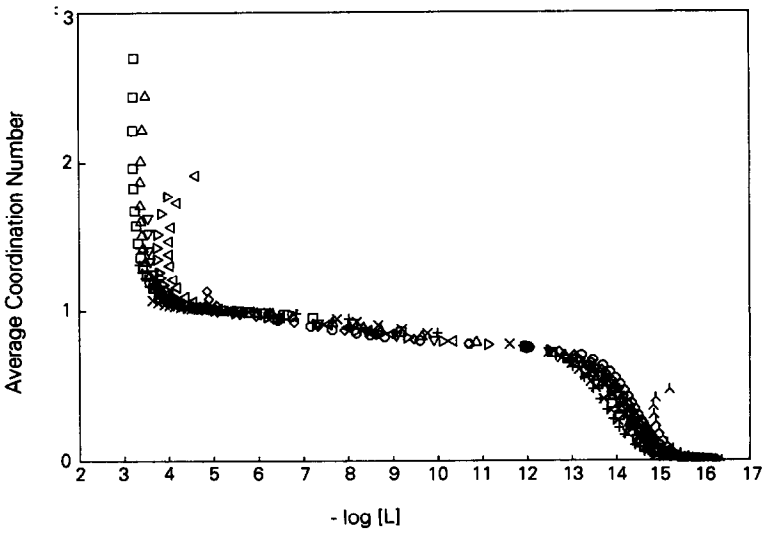

Fig. 4. Simulated formation curves for the lead(II)–DTE system obtained with ESTA from analytical data in Table 1, supposing the formation of ML (12.63), MLH_{-1} (2.71), M_2LH_{-1} (13.44), and lead hydroxides (see hydrolysis constants in Table 2). Key to symbols as for Fig. 1.

from a favourable displacement of the hydroxyl ions of the $M_3(OH)_5$ and $M_6(OH)_8$ species by deprotonated DTE molecules.

The final selection of the "best" set of constants was made extremely difficult by the fact that, like the goodness-of-fit parameters, simulated formation curves resulting from the addition of $M_3L_2H_{-1}$ or M_6L_5 to the basic model (ML, MLH_{-1} and M_2LH_{-1}) were very similar. Table 2 reports the two corresponding possibilities, with stability constants ultimately refined with MINIQUAD.

Considering, however, that (*i*) the *S* and *R* values are slightly more favourable in the case of M_6L_5, (*ii*) the graphical coincidence between the experimental and simulated formation curves is slightly better with M_6L_5 (Fig. 5) than with $M_3L_2H_{-1}$ (curve not shown here), (*iii*) the standard deviations of the constants for ML, MLH_{-1} and M_2LH_{-1} are significantly lower

Table 2. Formation constants (mean ± standard deviation) for the lead(II)–DTE complexes at 37° in 0.15*M* aqueous NaCl: the general constant is $\beta_{pqr} = [M_qL_pH_r]/[M]^q[L]^p[H]^r$; *S* is the sum of squares, *R* the Hamilton *R*-factor,[7] and *N* the total number of experimental observations used in the calculations. log*β values given in parentheses

System	*p*	*q*	*r*	log*β	*S*	*R*	*N*
Proton–DTE	1	0	1	9.840 ± 0.003	1.46E-06	0.00396	191
	1	0	2	18.766 ± 0.003			
Lead(II)-DTE	1	1	0	12.731 ± 0.051	2.41E-07	0.00613	379
	1	1	−1	(2.850 ± 0.044)			
	1	2	−1	(13.259 ± 0.044)			
	2	3	−1	(30.430 ± 0.072)			
	1	1	0	12.774 ± 0.037	2.28E-07	0.00597	379
	1	1	−1	(2.858 ± 0.037)			
	1	2	−1	(13.349 ± 0.025)			
	5	6	0	86.586 ± 0.099			

†Lead-hydroxide equilibria were taken into account in these determinations. The following formation constants (extrapolated from Sylva and Brown[12] for the present experimental conditions) were used in the calculations:

MH_{-1} (−8.0)
M_3H_{-4} (−24.5)
M_3H_{-5} (−32.5)
M_4H_{-4} (−21.1)
M_6H_{-8} (−44.8)

For definition of *β see J. Bjerrum, G. Schwarzenbach and L. G. Sillén (eds.), *Stability Constants of Metal Ion Complexes*, Part II, *Inorganic Ligands*, p.xiii, Chemical Society, London, 1958.

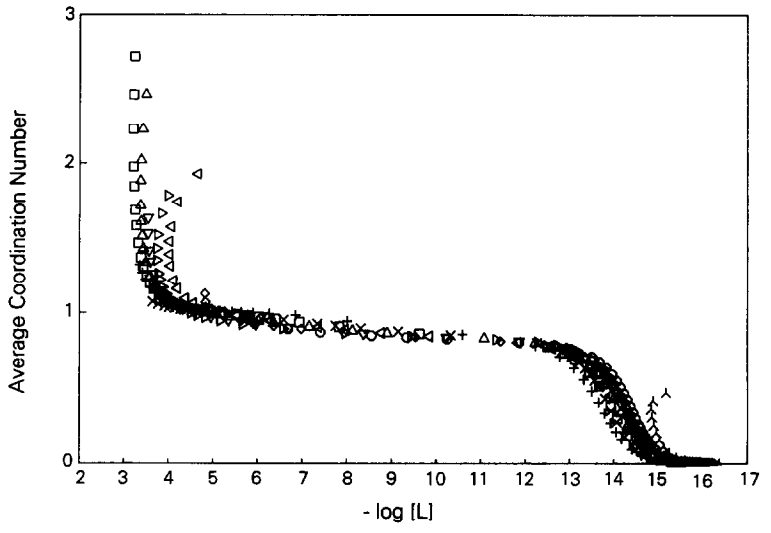

Fig. 5. Simulated formation curves for the lead(II)–DTE system obtained with ESTA from analytical data in Table 1 and formation constants in Table 2 (model with M_6L_5). Key to symbols as for Fig. 1.

with M_6L_5 than with $M_3L_2H_{-1}$, (*iv*) all species distribution percentages obtained from MINIQUAD calculations over the experimental conditions reported in Table 1 are almost exactly the same with use of M_6L_5 and $M_3L_2H_{-1}$, (*v*) M_6L_5 may well result from the dimerization of $M_3L_2H_{-1}$, the co-ordination of an additional ligand molecule at the expense of two hydroxyl ions being a supplementary factor inducing stability, we finally chose M_6L_5 as the most likely species.

As an application of the selected constants, Fig. 6 shows the distribution profile of lead from pH 2 to 11 under concentration conditions chosen within the range commonly used for *in vitro* biological systems. As can be seen, the concentration of free Pb^{2+} ions becomes negligible at pH 6 and above. This indicates that a strong competition is to be expected from DTE with respect to the lead–enzyme interactions involved in the biological process. In other words, DTE appears as a very potent agent for restricting the inhibitory capacity of lead towards the enzyme system. In contrast, the distribution of the free and protonated forms of DTE is not significantly influenced by the presence of lead at such concentration ratios (simulations not shown here).

The overall influence of DTE complexation on the distribution of lead can be still better appreciated from Fig. 7, where variations of the concentration of free Pb^{2+} ions are plotted as a

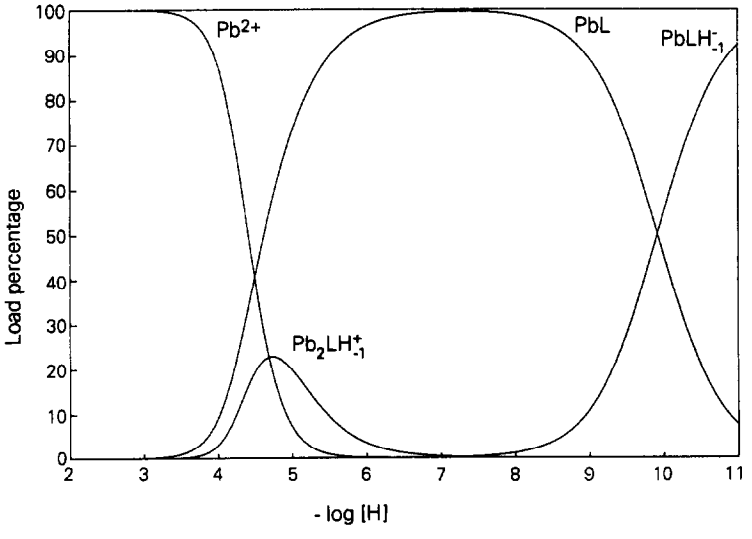

Fig. 6. Simulated distribution of Pb^{2+} ions in the presence of DTE with $C_{Pb} = 5\mu M$ and $C_{DTE} = 1mM$.

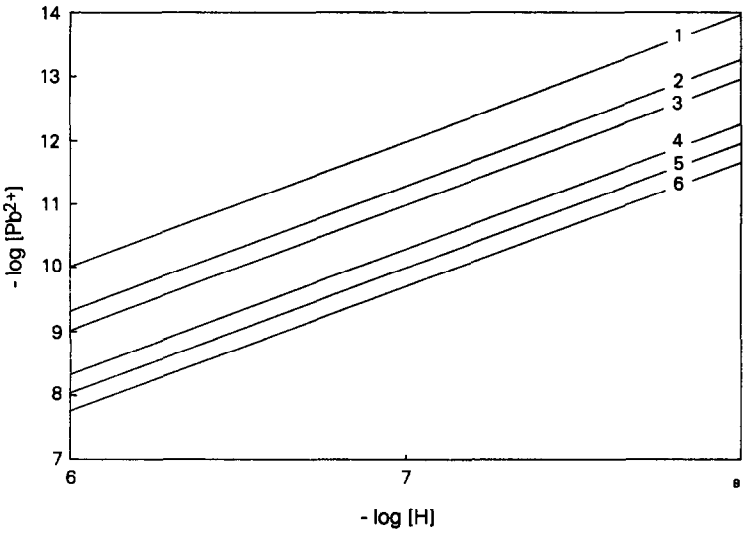

Fig. 7. Variation of the free concentration of lead in the presence of 1m*M* DTE as a function of total lead concentration within the pH range 6–8 (curves 1, 2, 3, 4, 5, 6 correspond to $C_{Pb} = 0.1$, 0.5, 1, 5 and 10μM, respectively).

function of total lead concentration within the pH interval 6–8. The family of curves drawn on this figure gives direct access to the maximum free lead concentrations present in solutions used for enzyme assays.

REFERENCES

1. R. O. Burns and M. H. Zarlengo, *J. Biol. Chem.*, 1968, **243**, 178.
2. E. L. Loechler and Th. C. Hollocher. *J. Am. Chem. Soc.*, 1975, **97**, 3235.
3. G. M. Whitesides, J. Houk and M. A. K. Patterson. *J. Org. Chem.*, 1983, **48**, 112.
4. H. N. Po, K. D. Legg and S. S. Kuwahara, *Anal. Lett.*, 1973, **8**, 659.
5. N. Gnonlonfoun, M. Filella and G. Berthon, *J. Inorg. Biochem.*, 1991, **42**, 207.
6. F. J. C. Rossotti and H. Rossotti, *J. Chem. Educ.*, 1965, **42**, 375.
7. A. Sabatini, A. Vacca and P. Gans, *Talanta*, 1974, **21**, 53.
8. P. M. May, K. Murray and D. R. Williams, *ibid.*, 1988, **35**, 825.
9. *Idem, ibid.*, 1985, **32**, 483.
10. W. L. Zahler and W. W. Cleland, *J. Biol. Chem.*, 1968, **243**, 716.
11. E. L. Loechler and Th. C. Hollocher, *J. Am. Chem. Soc.*, 1980, **102**, 7312.
12. R. N. Sylva and P. L. Brown, *J. Chem. Soc. Dalton*, 1980, 1577.
13. L. A. Sillén, *Acta. Chem. Scand.*, 1954, **8**, 299.
14. D. D. Perrin and I. G. Sayce, *J. Chem. Soc. A*, 1968, 53.

Talanta, Vol. 39, No. 4, pp. 405–408, 1992
Printed in Great Britain

0039-9140/92 $5.00 + 0.00
Pergamon Press plc

EXTRACTION AND SEPARATION STUDIES OF TELLURIUM(IV) WITH TRIS-(2-ETHYL HEXYL) PHOSPHATE

G. S. DESAI and V. M. SHINDE*
Analytical Laboratory, The Institute of Science, 15 Madam Cama Road, Bombay 400 032, India

(*Received* 13 *May* 1991. *Revised* 28 *August* 1991. *Accepted* 28 *August* 1991)

Summary—A method is proposed for the extraction of microgram levels of tellurium(IV) from halide media with tris-(2-ethyl hexyl) phosphate dissolved in toluene as extractant. The optimum conditions have been evaluated from a critical study of acid concentration, extractant concentration, period of equilibration and effect of solvent. Tellurium ion from the organic phase is stripped with water and determined spectrophotometrically with stannous chloride. The method affords binary separation of tellurium from copper, bismuth, gold and selenium and is applicable to the analysis of alloy samples and synthetic mixtures. The method is fast, accurate and precise.

Tellurium is an important component of thermoelectric couples used for power generating and cooling. The compound Bi_2Te_3 is widely used in the preparation of semiconductors. The addition of tellurium to stainless steel increases its machinability. Tellurium has also been used in the ceramics industry for the manufacture of glasses and porcelains of various colours. In view of this, separation of tellurium from associated elements is desired. Very few extraction methods of tellurium(IV) are available in the literature. Solvent extraction methods, using polar solvents such as tributyl phosphate (TBP), methyl isobutyl ketone (MIBK), trioctylphosphine oxide (TOPO) and di-(2-ethyl hexyl) phosphoric acid have been reviewed by Havezov and Jordanov[1] and by Sekine and Hasegawa[2] in their monographs. A novel extractant, tris-(2-ethyl hexyl) phosphate (TEHP), has been used as an extractant for the extraction of uranium(VI)[3] and thorium(IV)[4] in our laboratory. An extension of this work has shown that TEHP could also be used for the extraction of tellurium from halide media. The method is rapid and provides separation of tellurium from copper, bismuth, gold and selenium.

EXPERIMENTAL

Apparatus

Absorbance measurements were made on a Spectronic 20 (Bausch and Lomb) and pH was measured on a Control Dynamics digital pH meter with combined glass electrode.

*Author for correspondence.

Reagents and chemicals

A stock solution of tellurium(IV) was prepared by dissolving 0.435 g of sodium tellurite in distilled water and diluting to 250 ml. The solution was standardized gravimetrically[5] and diluted as required to obtain working solutions. A 70% (v/v) solution of tris-(2-ethyl hexyl) phosphate (TEHP) (97%, Aldrich) dissolved in toluene was used as an extractant. A 20% (m/v) solution of stannous chloride in 2*M* hydrochloric acid was used for the determination of tellurium.[6] All other reagents used were analytical reagent grade.

General extraction procedure

To an aliquot of solution containing 100–200 μg of tellurium(IV), add hydrobromic or hydrochloric acid so that the solution concentration is in the range 3.5–7.0 or 6.0–8.5*M*, respectively, in a total volume of 10 ml. Transfer the solution into a separating funnel and extract with 5 ml of 70% TEHP in toluene for 15 sec. After separating the aqueous layer, strip tellurium from the organic phase with 5 ml of water and estimate spectrophotometrically with stannous chloride at 400 nm.[6]

RESULTS AND DISCUSSION

Extraction conditions

The extraction of tellurium(IV) was studied at various concentrations of hydrobromic (1.0–7.0*M*) and hydrochloric acid (2.0–8.5*M*) with different concentrations of TEHP (20.0–70.0%). The results showed that 70% TEHP in toluene

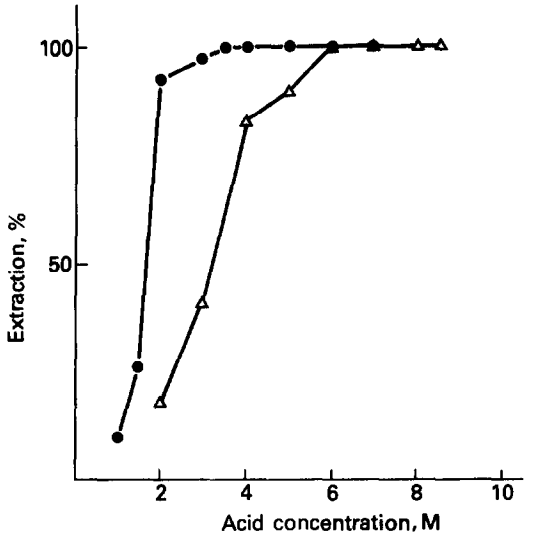

Fig. 1. Extraction behaviour of tellurium(IV) as a function of hydrobromic acid (●) and hydrochloric acid (△) concentration.

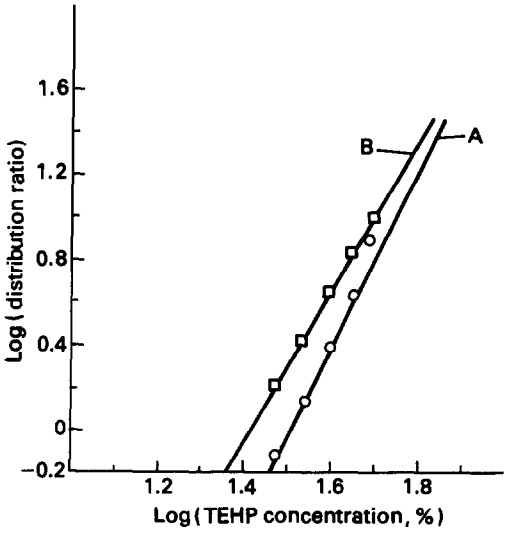

Fig. 2. Plot of log (distribution ratio) *vs.* log (TEHP concentration, %) at 4*M* hydrobromic acid concentration (A) and 6*M* hydrochloric acid concentration (B).

extracts tellurium quantitatively either from 3.5–7.0*M* hydrobromic acid or 6.0–8.5*M* hydrochloric acid (Fig. 1).

Period of extraction

Variation of the shaking period from 5 to 60 sec showed that a 15-sec equilibration time was adequate for quantitative extraction of tellurium from bromide or chloride media. However, prolonged shaking had no adverse effect on the extraction.

Effect of organic phase

The suitability of several solvents such as benzene, toluene, xylene, chloroform and carbon tetrachloride for the extraction of tellurium from bromide or chloride media, using the proposed method was investigated. It was found that a 70% (v/v) solution of TEHP in toluene, xylene or benzene provides quantitative extraction of tellurium. The extraction of tellurium was incomplete if TEHP is dissolved in other solvents. Inert diluents such as toluene, xylene, benzene, *etc.*, do not participate in the actual extraction process. However, TEHP causes solvation of the tellurium–chloro or bromo complexes and promotes extraction.

Nature of extracted species

The nature of the extracted species was established with log-log plots. The log-log plot of distribution ratio *vs.* TEHP concentration (at 4.0*M* hydrobromic acid or 6.0*M* hydrochloric acid) gave a slope of 2.2 and 1.7, respectively, indicating a molar ratio of 1:2 with respect to the extractant (Fig. 2). Hence, the extracted species is either an ion-association complex $H_2TeX_6 \cdot 2TEHP$ or solvated halo salt $TeX_4 \cdot 2TEHP$, where X stands for Cl^- or Br^- and TEHP represents tris-(2-ethyl hexyl) phosphate.

Effect of foreign ions

Varying amounts of foreign ions were added to a fixed amount of tellurium(IV) (200 μg) to study their interference in the recommended procedure in bromide and chloride media. The tolerance limit was set at the amount required to cause $\pm 2\%$ error in tellurium recovery. The results are reported in Table 1.

Binary separation of tellurium(IV) from copper(II), bismuth(III), gold(III) and selenium(IV)

The method permits separation and determination of tellurium(IV) from binary mixtures containing either copper, bismuth, gold or selenium.

Tellurium is separated from copper and selenium by its extraction with 70% TEHP in toluene from 6*M* hydrochloric acid. Under this condition both copper and selenium remain quantitatively in the aqueous phase where they are determined sepectrophotometrically with 1-(2-pyridylazo)naphth-2-ol (PAN)[7] and 3,3′-diaminobenzidine,[6] respectively. Tellurium is stripped from the organic phase with water and estimated spectrophotometrically with stannous chloride.

Table 1. Effect of foreign ions on the extraction of 200 μg of tellurium(IV) from 4*M* HBr or 6*M* HCl with 70% tris-(2-ethyl hexyl) phosphate dissolved in toluene

Ions	Tolerance limit, μg Bromide media	Chloride media	Ions	Tolerance limit, μg Bromide media	Chloride media
Ba(II)	6000	6000	Ce(IV)	2000	2000
Ca(II)	6000	6000	Zr(IV)	2000	2000
Mg(II)	6000	6000	Ti(IV)	2000	2000
Cu(II)	4000	5000	V(V)	2000	2000
Bi(III)	4000	2000	Ge(IV)	2000	2000
Pb(II)	4000	4000	Oxalate	2000	2000
Zn(II)	4000	4000	Nitrite	2000	2000
Co(II)	4000	4000	Thiourea	2000	500
Ni(II)	4000	4000	EDTA	2000	2000
Mn(II)	4000	5000	Citrate	2000	2000
Th(IV)	4000	4000	Tartrate	2000	2000
Cd(II)	4000	5000	Ascorbic acid	2000	2000
Al(III)	4000	4000	Se(IV)	1000	700
Sulphate	4000	5000	Mo(VI)	1000	1000
Phosphate	4000	5000	Cr(VI)	1000	400
Nitrate	4000	5000	W(VI)	800	100
Chloride	4000	5000	Thiosulphate	800	100
As(III)	2000	2000	Pd(II)	400	500
Ag(I)	2000	2000	Sb(III)	400	400
Au(III)	2000	500	Hg(II)	200	400
U(VI)	2000	2000	SN(II)	100	50
FE(III)	2000	1500			

Tellurium and bismuth are separated by extracting bismuth from 0.2*M* hydrobromic acid solution with 70% TEHP as an extractant. Tellurium remains in the aqueous phase quantitatively; the extracted bismuth is subsequently stripped with 0.2*M* nitric acid and determined spectrophotometrically with thiourea.[8]

Similarly gold and tellurium are separated by extracting gold from 0.5*M* hydrobromic acid solution with 25% TEHP in toluene. The unextracted tellurium is estimated in the aqueous phase while the extracted gold is estimated spectrophotometrically in the TEHP phase itself by measuring the absorbance of the yellow–orange complex at 400 nm.

While Bi(III) and Au(III) do not interfere in the Te(IV) extraction or determination from 3.5–7.0*M* hydrobromic acid, the above procedure allows their separation and separate determination.

The recovery of tellurium and that of the added ions was ⩾99.0%. The results are reported in Table 2.

Table 2. Binary separation of tellurium(IV) from copper(II), bismuth(III), gold(III) and selenium(IV)

Metal ions, μg	Amount found,* μg	Recovery, %	Standard deviation	Coefficient of variation, %
Te(IV), 200	199.7	99.4	0.09	0.04
Cu(II), 200	199.6	99.8	0.10	0.05
Te(IV), 200	199.8	99.9	0.14	0.07
Bi(III), 200	199.6	99.8	0.10	0.05
Te(IV), 200	199.6	99.8	0.10	0.05
Au(III), 200	199.4	99.7	0.14	0.07
Te(IV), 200	199.8	99.9	0.14	0.07
Se(IV), 200	198.2	99.1	0.22	0.11

*Average of six determinations.

Analysis of synthetic mixtures

The proposed method was applied to the extraction and determination of tellurium from bromide media in various synthetic mixtures. The results are reported in Table 3.

Analysis of alloys

Since standard alloy samples containing tellurium were not available, we analyzed synthetic alloy and leaded brass (BCS 385) samples,

Table 3. Analysis of synthetic mixtures

Composition, μg	Tellurium found,* μg	Recovery, %	Standard deviation	Coefficient of variation, %
Te, 200; Au, 1000; Ag, 1000; Bi, 1000	199.6	99.8	0.10	0.05
Te, 200; Ge, 1000; Pb, 1000; Bi, 1000; Cd, 1000	198.2	99.1	0.22	0.11
Te, 200; Bi, 1000; Cu, 1000; Pb, 1000; Fe, 1000	199.0	99.5	0.14	0.07

*Average of six determinations.

Table 4. Analysis of alloys

Alloy	Composition, %	Tellurium found,* mg	Recovery, %	Standard deviation	Coefficient of variation, %
Synthetic alloy†	Te, 51.86; Se, 6.55; As, 31.91; Ge, 9.68	15.54‡	99.9	0.009	0.06
Leaded brass (BCS 385)	Cu, 58.7; Pb, 2.24; Fe, 0.15; Zn, 38.5; Sn, 0.27; Ni, 0.13; Al, 0.005; Mn, 0.005; Sb, 0.005 + 2.0 mg Te.	1.98	99.0	0.014	0.71

*Average of six determinations.

†Composition of synthetic alloy was determined using Inductively Coupled Plasma–Atomic Emission Spectrophotometer. (ICP–AES: Plasmalab 8440, Labtam).

‡30 mg of synthetic alloy containing 15.56 mg of Te(IV) was taken for analysis.

BCS—British Chemical Standard.

to which a known amount of tellurium had been added. The tellurium was recovered from bromide media by the proposed method. The procedures are given below.

A 30-mg sample of synthetic alloy was dissolved in 3 ml of *aqua regia* and diluted to 100 ml with water. A 1-ml aliquot of this solution was taken for the extraction and determination of tellurium by the proposed method.

A 50-mg sample of leaded brass (BCS 385) was dissolved in 3 ml of concentrated nitric acid and evaporated to almost dryness. The residue was taken up in water and the precipitated metastannic acid was filtered off. To the filtrate solution, 2 mg of tellurium was added and the solution diluted to 25 ml with water. An aliquot of 2.5 ml of filtrate containing 200 μg of tellurium was taken for extraction and determination of tellurium by the proposed method. The results of the analysis are reported in Table 4.

The method is selective and permits rapid separation and determination of micro amounts of tellurium. The average recovery of tellurium was $\geqslant$99.0%. Each determination took a total of 15–20 min.

Acknowledgements—The authors are grateful to the University of Bombay for awarding "The Pandit Bhagwandin Dube and Mrs Ramdulari Dube Scholarship in Science" to one of them (G.S.D.).

REFERENCES

1. I. Havezov and N. Jordanov, *Talanta*, 1974, **21**, 1013.
2. T. Sekine and Y. Hasegawa, *Solvent Extraction Chemistry: Fundamentals and Applications*, p. 632. Marcel Dekker, New York, 1977.
3. N. M. Sundaramurthi, G. S. Desai and V. M. Shinde, *J. Radioanal. Nucl. Chem. Letters*, 1990, **144**, 439.
4. G. S. Desai and V. M. Shinde, *ibid.*, 1991, **154**, 227.
5. A. I. Vogel, *A Textbook of Quantitative Inorganic Analysis*, 3rd Ed., p. 508. Longmans, London, 1961.
6. Z. Marczenko, *Separation and Spectrophotometric Determination of Elements*, pp. 522 and 476. Ellis Horwood, Chichester, 1976.
7. B. F. Pease and M. B. Williams, *Anal. Chem.*, 1959, **31**, 1044.
8. E. B. Sandell, *Colorimetric Determination of Traces of Metals*, 3rd Ed., p. 337. Interscience, New York, 1961.

Talanta, Vol. 39, No. 4, pp. 409–413, 1992
Printed in Great Britain

0039-9140/92 $5.00 + 0.00
Pergamon Press plc

COLOUR REACTION OF GOLD WITH 5-(4-SODIUM SULPHONATEPHENYLAZO)-8-AMINOQUINOLINE AND ITS ANALYTICAL APPLICATION

ZENG ZUOTAO*
Kunming Baimamiao Medical Institute, Kunming, 650032, People's Republic of China

XU QIHENG
Department of Chemistry, Yunnan University, 650091, People's Republic of China

(*Received* 28 *May* 1991. *Accepted* 24 *July* 1991)

Summary—The synthesis of 5-(4-sodium sulphonatephenylazo)-8-aminoquinoline (SPAQ) is described, and a simple, rapid, selective and sensitive new spectrophotometric method for determination of gold is developed. SPAQ reacts with gold(III), and in the presence of cetyl trimethyl ammonium bromide cationic surfactant and upon making the solution alkaline, forms a blue-green 1:3 (metal:ligand) with an absorption maximum at 605 nm. Beer's law is obeyed over the concentration range 0–2 μg/ml gold. The molar absorptivity and Sandell's sensitivity of the method are 1.48×10^5 l.mole^{-1}.cm^{-1} and 0.0013 μg/cm^2, respectively. The interference of various ions has been studied and the method has been used for the determination of microamounts of gold in ores and anode slimes.

Both 8-hydroxy- (8HQ) and 8-mercaptoquinoline (8MQ) are well-known reagents widely used as chelating agents in analytical chemistry.[1] However, the 8-amino derivative of quinoline (8AQ) has received little analytical attention, resulting in only a few published papers.[2,3] Because 8AQ has (N,N) as its chelating atom, it is more selective than 8HQ(N,O) and 8MQ(N,S). In recent years, some 8-aminoquinoline derivatives have been synthesized and used in the fluorimetric analysis of copper[4] and cobalt,[5] and spectrophotometric determination of platinum.[6]

Gold may usually be determined with various chromogenic agents such as diethyldithiocarbamate,[7] 8-mercaptoquinoline,[8] 2-quinolylaldoxime,[9] thiomides,[10] aniline,[11] ethylxanthate,[12] 2-pyridinealdoxime,[13] anthranilic acid,[14] di-2-thienyl ketoxime,[15] chromophryozole[16] or phenothiazine.[17] In most of the methods, the sensitivity is very poor and the colour fades after a few minutes. In some instances the complex is formed only after heating for a long time and requires extraction with an organic solvent, whereas others suffer from interferences from other metal ions. A thorough survey of the literature showed that no previous attempt has been made to employ 8-aminoquinolines for the spectrophotometric determination of gold. Hence, in this paper, 5-(4-sodium sulphonatephenylazo)-8-aminoquinoline (SPAQ) is proposed as a reagent for the spectrophotometric determination of gold(III) in aqueous solution. Various parameters such as pH, reagent concentrations, equilibration time and interference of foreign ions have been studied. This method has been applied to the determination of gold(III) in ores and anode slimes. The reagent has been found to be sensitive and selective compared with other chromogenic agents.

EXPERIMENTAL

Apparatus

A 751GW spectrophotometer (Analytical Instruments Factory, Shanghai) with 1-cm pathlength cells, wavelength range 200–1000 nm, was employed for all absorbance measurements.

Reagents

Synthesis of SPAQ. Sulphanilic acid (2.1 g) was dissolved in 2 ml of ice-cold concentrated hydrochloric acid, 10 ml of ice-cold distilled water and slowly diazotized with a solution of 0.8 g of sodium nitrite in 8 ml of water. The diazotized solution was then added dropwise

*Author for correspondence.

with stirring to an ice-cold solution of 8AQ (1.6 g) in 50 ml of 2*M* acetic acid, 2*M* sodium hydroxide being added to keep the pH constant, and the mixture was left for 1.5 hr, with stirring in the ice-bath, then neutralized with sodium hydroxide and filtered. The red precipitate was recrystallized and salted out with sodium chloride several times from water to give needle-shaped crystals (decomposed above 325°) with a yield of 76%. Elemental analysis was as follows: calculated, C 48.87, H 3.53, N 15.20, S 8.68%; found, C 49.11, H 3.50, N 15.15, S 8.70%. The data obtained from thermogravimetry, infrared and nuclear magnetic resonance spectra confirmed the structure of SPAQ to be as shown in Fig. 1. The acid dissociaton constant of SPAQ was obtained by Perisic-Janjic's method,[18] the pK_{a3} value being 3.65 ± 0.03.

Colour reagent solution. A 0.0368 g amount of SPAQ was dissolved in 500 ml of distilled water ($2.0 \times 10^{-4}M$). The solution is stable for one year at least.

Standard gold(III) solution, 100 μg/ml. A stock solution of gold(III) was prepared by dissolving the requisite amount of pure gold in *aqua regia*. A working standard solution, 5 μg/ml, was prepared by diluting this solution.

Cetyltrimethyl ammonium bromide (CTMAB) solution (0.2%). Prepared by dissolving the substance in water.

Sodium hydroxide solution, 0.5% in water. All other reagents were of analytical grade.

Procedures

Determination of microgram amounts of gold. Take a known volume of solution containing not more than 50 μg of gold(III) in a 25-ml standard flask, add 3.0 ml of CTMAB solution, 4.0 ml of SPAQ solution and 2.5 ml of sodium hydroxide solution, in that order, dilute to the mark with distilled water, mix and let stand for about 15 min. Measure the absorbance at 605 nm against a reagent blank prepared similarly but without gold.

Determination of gold in anode slimes. Take 0.1 g of sample into a beaker, add 10 ml of concentrated hydrochloric acid and 5 ml of concentrated nitric acid to dissolve the sample by heating on a boiling-water bath, evaporate the solution mixture to incipient dryness, add 4 ml of concentrated hydrochloric acid and evaporate until nitrogen dioxide ceases to evolve. Allow to cool to room temperature (about 25°), add 10 ml of 0.1*M* hydrochloric acid to dissolve the soluble salts, filter off the residue and wash it with distilled water three times, collect the filtrate and washings and dilute to 50 ml. (For most accurate results, the residue should be fused with Na_2O_2 and combined with the main solution.) Pipette out 1.0 or 4.0 ml of the solution, add 1 ml of 5% sodium fluoride solution to mask iron(III) and complete the determination as above.

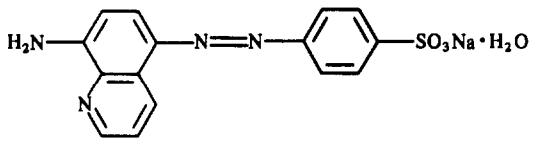

Fig. 1. Structure of SPAQ confirmed by data obtained from TG, IR and NMR spectra.

Determination of gold in ores. A 5–10 g amount of sample is transferred into a 200-ml beaker and 50 ml of concentrated hydrochloric acid is added. The beaker is covered and heated gently to dissolve the sample. About 50 ml of distilled water is added and the mixture is filtered. The residue is dissolved in *aqua regia* and heated twice to incipient dryness with distilled water to reduce the acidity. If the residue does not completely dissolve, fusion may be required as above. *Aqua regia* dissolution fails to extract all gold present in ores that have high sulphide content, high organic content, and some "Black Shale" materials. Also, it may be necessary to add sodium chloride to avoid precipitation of gold. The solutions are then transferred into 50-ml calibrated flasks and diluted to the mark with distilled water. Take 3 ml of the solution in a 25-ml standard flask, add 1 ml of 5% sodium fluoride solution, complete the determination as above.

RESULTS AND DISCUSSION

Reactivity of SPAQ

The reactivities of SPAQ with various metal ions at pH 4, 7 and 10 were investigated. In acidic medium, SPAQ reacts with gold(III), palladium(II), iridium(III), rhodium(III), platinum(IV), silver(I) and copper(II) to give coloured or precipitable complexes; in alkaline solution, the reagent is found to react with mercury(II), cobalt(II), nickel(II), gold(III) and palladium(II) to give coloured complexes, and reacts with copper(II) to give a fluorescent complex ($\lambda em/\lambda ex = 370$ nm/325 nm). The study suggested the usefulness of the synthesized SPAQ for the determination of gold, and there-

fore the conditions for this colour reaction were examined in subsequent studies.

Absorption spectra

Absorption spectrum of the reagent blank shows a maximum absorption at 459 nm. The Au–SPAQ–CTMAB system shows a maximum absorption at 605 nm, where the reagent blank gives almost zero absorption (Fig. 2). Hence in all instances the absorption was measured at 605 nm against a corresponding reagent blank.

Reaction conditions

The optimum pH for the Au–SPAQ–CTMAB system is in the strongly alkaline region and addition of 1.0–5.0 ml of sodium hydroxide solution to an approximately neutral test solution was found to give essentially a constant absorbance, addition of 2.5 ml is recommended. See below for order of reagent addition.

In the absence of surfactant or the presence of nonionic or anionic surfactants, the coloured system gives a low absorbance but the presence of a cationic surfactant, the absorbance increases markedly. Various cation surfactants enhance the absorbance in the following order: CTMAB > cetyl pyridinium bromide > tetradecyl dimethylbenzyl ammonium chloride > *N*-cetyl pyridinium chloride > tetradecyl pyridinium bromide. CTMAB is the best additive, 2.0–6.0 ml of 0.2% CTMAB solution gives good results; a volume of 3.0 ml is recommended.

In order to study the influence of cationic surfactants on the reaction of the metal ion with

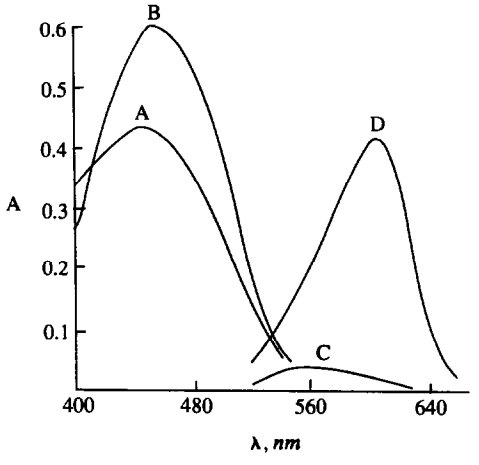

Fig. 2. The absorption spectra of: A, SPAQ alone; B, SPAQ-CTMAB; C, Au-SPAQ; D, Au-SPAQ-CTMAB. Conditions: Au (III) = $3 \times 10^{-6} M$; SPAQ $\times 3 \times 10^{-5} M$.

Table 1. Tolerance limits in the determination of 10 μg of Au(III) with SPAQ

Ion added	Amount tolerated, μg
F^-, NO_3^-	50,000
Cl^-, EDTA	10,000
PO_4^{3-}, SO_4^{2-}, V(V)	2000
Cr(VI), Ba(II), Mo(VI)	1500
Cu(II)*	1000*
Fe(III)†	800†
Ca(II), Cr(III), Ag(I), Ce(IV)	500
Cd(II), Zn(II), Y(III), Ga(III)	300
Al(III)	250
Ge(IV), Hg(II), Ni(II), Zr(IV)	200*
Pb(II), W(VI), Co(II)	100
Mn(VII), Mg(II)	80
In(III), Rh(III)	60
Bi(III), Pd(II), Pt(IV)	50

*Masked with 5 mg of EDTA.
†Masked with 50 mg of NaF.

the reagent, we synthesized a series of reagents which have a methoxyl (CH_3O-), acetyl (CH_3CO-), nitro (-NO_2), carboxyl (-COOH), or arsono-group (-AsO_3H_2) instead of a sulphonyl-group (-SO_3H_2) on the benzene ring, separately. The reactivity of gold(III) with the reagents which have the different substitute-groups was investigated. It was found that cationic surfactant only affects the complexation reaction between gold(III) and the reagents which have an anionic substitute-group (-SO_3^-, -AsO_3^{2-} or -COO^-), with an increase in the absorbance of the solution, but does not affect the reaction of the metal ion with the reagents which have a nonionic substitute-group (CH_3O-, CH_3CO- or O_2N-). This therefore, suggests the ion-association between the anionic group of the reagent and cationic surfactant is advantageous to the colour reaction.

Maximum and stable absorbance is attained with 2.0–5.0 ml of $2 \times 10^{-4} M$ SPAQ solution, and use of 4.0 ml is selected as optimal.

At room temperature, the maximum absorbance is obtained 10 min after the mixing of the components, and is stable for 48 hr at least. The order of addition of reagents seriously affects the system, however. Addition in the order Au(III), sodium hydroxide solution, CTMAB solution and SPAQ solution produces metal hydroxide precipitation. The order

Table 2. Determination of gold in ores and anode slimes

Sample	Au content*	Gold found
Ore 1	34.2 (g per tonne)	33.9 (g per tonne)
Ore 2	14.7 (g per tonne)	14.9 (g per tonne)
Anode slime 1	0.241%	0.25%
Anode slime 2	0.18%	0.19%

*Values obtained by atomic-absorption spectrometry.

Table 3. Comparison of reagents for the spectrophotometric determination of gold

Reagents	λ_{max}, nm	ε, $l.mole^{-1}.cm^{-1}$	Medium	Comments	Reference
Azide	330	1.32×10^3	Butanol	Color stable for 15 min	19
Thiocaprolactam	400	3.7×10^3	$CHCl_3$	—	20
Triisooctylamine	325	5.8×10^3	CCl_4	—	21
Mepazine hydrochloride	514	2.18×10^4	Aqueous	Color stable for 30 min	22
Rhodamine	562	3.2×10^4	Aqueous	Heat, colour stable for 30 min	23
Acetylpryidyl thiosemicarbazide	460	1.5×10^4	—	—	24
Anisaldehyde-4-phenyl-3-t-hiosemicarbazone	365	2.12×10^4	Ethyl acetate	Shaking for 60 sec	25
Rhodamine B	555	9.7×10^4	Diisopropyl-ether	Color stable for 30 min	23
Methylene blue	657	1.08×10^5	$C_2H_2Cl_2$		26
4,4'-Bis(dimethylamino) thiobenzophenone	540	1.2×10^5	Aqueous	30 mins required for color development	27
SPAQ	605	1.48×10^5	Aqueous		This work

Au(III), CTMAB, SPAQ and sodium hydroxide solution gives the best result.

Analytical characteristics

A calibration graph was constructed under the optimum conditions described above. The system obeys Beer's law over the concentration range 0–50 μg of gold in 25 ml of final solution. The molar absorptivity and Sandell's sensitivity of the method are 1.48×10^5 l.mole^{-1}.cm^{-1} and 0.0013 μg cm^2, respectively. The standard deviation for ten replicate determinations of 20 μg of gold was 0.015 μg.

The composition of the complex was established by Job's method of continuous-variation and the molar-ratio method, and found to be 1:3 (metal:ligand).

Interferences

The influence of 34 diverse ions on the determination was examined. The ions tested were added individually to a solution containing 20 μg of gold(III). A maximum error of 2% in the absorbance reading was considered tolerable. The tolerance limit of foreign ions is given in Table 1. The interference from Fe^{3+} can be eliminated by masking with sodium fluoride, and the interference of Cu^{2+} and Hg^{2+} was eliminated by masking with EDTA. Thus the data in Table 1 indicate the reasonable selectivity of the method in the presence of associated ions.

Applications

In order to confirm the usefulness of the proposed spectrophotometric method, it has been applied to the determination of microamounts of gold in ores and anode slimes. The results are shown in Table 2, along with the value found by atomic-absorption spectrometry.

CONCLUSION

The comparison (in Table 3) of the SPAQ method with others shows the proposed method for spectrophotometric determination of gold is sensitive, simple and rapid, it does not require heating and extraction with organic solvents, and may be used to determine microamounts of gold in small samples directly in aqueous solution.

REFERENCES

1. K. Burger, *Organic Reagents in Metal Analysis*, Pergamon Press, Oxford, 1973.
2. S. Maspoch, J. Bartroli and M. Blanco, *Mikrochimica Acta*, 1983 **III**, 95.
3. M. Blanco and S. Maspoch, *ibid.*, 1983 **III**, 11.
4. Zeng Zuotao and Xu Qiheng, *Metallurgical Analysis (China)*, 1990, **6**, 1.
5. Zeng Zuotao and Xu Qiheng, *Fenxi Huaxue*, 1991, **2**, 134.
6. Zhao Jianwei and Xu Qiheng, *Talanta*, 1991, **38**, 909.
7. A. K. De, S. M. Khopkar and R. A. Chalmers, *Solvent Extraction of Metals*, p. 143. Van Nostrand Reinhold, New York, 1970.
8. V. I. Suprunovish and Yu. I. Shevchenko, *Zh. Anal. Khim.*, 1979, **34**, 1738.
9. N. K. Dutta and S. N. Dhar, *J. Inst. Chem. Calcutta*, 1978, **50**, 83.
10. A. V. Radhusev and B. V. Golomolzin, *Zh. Anal. Khim.*, 1979, **34**, 742.
11. W. Rzeszutko and T. Kopec, *Z. Anal. Chem.*, 1977, **285**, 125.
12. E. M. Donaldson, *Talanta*, 1976, **23**, 411.

13. E. Gagliardi and P. Presinga, *Mikrochim. Ichnoanal. Acta*, 1965, 791.
14. M. E. Makovsch, *Talanta*, 1969, **16**, 443.
15. W. J. Holland and J. Gerard, *Anal. Chim. Acta*, 1968, **43**, 71.
16. A. I. Busev, L. N. Simonova, T. A. Misharina and N. D. Zayukova, *Zh. Anal. Khim.*, 1972, **27**, 298.
17. I. Nemcova, P. Rychlovsky and E. Kleszczewska, *Talanta*, 1990, **37**, 855.
18. N. U. Perisic and Janjic, *Anal. Chem.*, 1973, **45**, 798.
19. R. G. Clem and E. H. Huffman, *ibid.*, 1965, **37**, 1155.
20. H. Sikorska Tomicka, *Mikrochim. Acta*, 1970, 1006.
21. M. Y. Mirza, *Talanta*, 1980, **27**, 101.
22. H. Sanke Gowda and K. N. Thimmaiah, *Indian J. Chem.*, 1976, **14**, 632.
23. Z. Marczenko, *Spectrophotometric Determination of Elements*, p. 282. Wiley, New York.
24. C. K. Bhaslare and S. Devi, *Indian J. Chem.*, 1985, **24**, 901.
25. K. M. M. S. Prakash, L. D. Prabhakar and D. V. Reddy, *Analyst*, 1986, **111**, 1301.
26. T. Koh, T. Okazaki and M. Ichikawa, *Anal. Sci.*, 1986, **2**, 249.
27. T. Sukhara, *Talanta*, 1977, **24**, 633.

Talanta, Vol. 39, No. 4, pp. 415–418, 1992
Printed in Great Britain.

0039-9140/92 $5.00 + 0.00

SPECTROPHOTOMETRIC DETERMINATION OF PLATINUM IN GLASS AFTER EXTRACTION WITH POLYURETHANE FOAM

DIPALI KUNDU and S. K. ROY*
Central Glass and Ceramic Research Institute, 196 Raja S.C. Mullick Road, Calcutta 700 032, India

(*Received* 21 *July* 1989. *Revised* 7 *August* 1991. *Accepted* 19 *August* 1991)

Summary—A spectrophotometric method has been developed for determination of trace amounts of platinum in glass. The method is based on the extraction of platinum(II) from 1*M* hydrochloric acid containing 0.2*M* stannous chloride and $4 \times 10^{-4}M$ dithizone onto polyurethane foam, elution with acetone (containing 3% v/v concentrated hydrochloric acid) and measurement of the absorbance of the eluate at 530 nm. Beer's law is obeyed up to 10.0 μg/ml Pt. The minimum platinum level in the eluate that can be determined by this method is 0.1 μg/ml.

Platinum vessels are often used when melting special types of glasses, which results in traces of platinum being introduced into the glass matrix and affecting the expected properties of the glass. Therefore, determination of platinum in such glasses is often necessary for evaluation and quality control. The most commonly applied spectrophotometric method[1] involves reduction of Pt(IV) to Pt(II) with stannous chloride in fairly concentrated hydrochloric acid medium and extraction of the yellow-orange Pt(II)–$SnCl_2$ complex with diethyl ether, ethyl acetate and similar solvents.

Numerous spectrophotometric methods are available,[2] in which various reagents have been used, including dithizone.[3–5] Marczenko and co-workers[6,7] have reported two methods for the separation and spectrophotometric determination of palladium and platinum by extraction with chloroform containing dithizone.

Bowen[8] pioneered the work on the extraction of metals from aqueous solution by polyurethane foam. Moore and Chow[9] have reported a method in which iridium and platinum are extracted from organic solvents with polyurethane foam. The extraction of platinum and palladium from thiocyanate solution with polyether-type polyurethane foam has also been reported.[10] Koch and co-workers[11–13] have made a critical study of the extraction of the Pt(II)–$SnCl_2$ complex by polyurethane foam. Here we describe the extraction of platinum(II) from aqueous medium containing stannous chloride and dithizone by polyurethane foam, and its use for spectrophotometric determination of platinum.

*Author for correspondence.

EXPERIMENTAL

Apparatus

A Spectromom 360 spectrophotometer was used.

Reagents

All reagents used were of analytical grade. The solutions were prepared with doubly distilled water.

Standard platinum solution. Dissolve 0.63 g of hexachloroplatinic acid in water, add 2 ml of 2*M* hydrochloric acid, dilute accurately to 250 ml and standardize the solution. Store the solution in a polythene bottle. Prepare a working solution (10 μg/ml Pt) by further dilution with water.

Stannous chloride solution. Dissolve 23 g of stannous chloride dihydrate in 16.7 ml of concentrated hydrochloric acid by heating, cool, and dilute to 100 ml with water.

Dithizone solution. Dissolve 0.060 g of dithizone in 100 ml of methanol and store the solution in a dark bottle. Standardize the solution by extractive titration with standard silver solution.[6]

Eluent. Add 3 ml of concentrated hydrochloric acid to 97.0 ml of acetone and store in a glass bottle. Freshly prepared solution should be used.

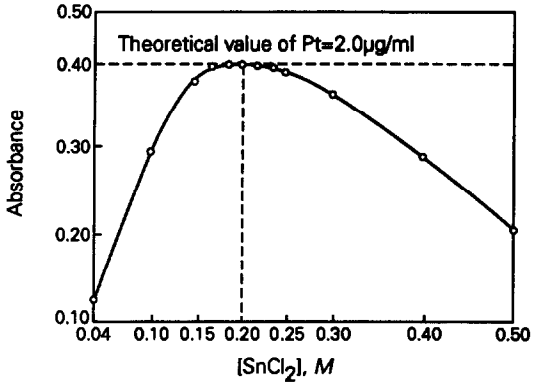

Fig. 1. Effect of stannous chloride concentration on the extraction of platinum dithizonate: $[H_2Dz] = 3.5 \times 10^{-4}M$, $[HCl] = 1.0M$.

Foam preparation[14]

Cut a sheet of polyether-based polyurethane foam into small cylindrical pieces (each ~2 cm long and ~0.5 cm in diameter, and weighing ~0.01 g). Soak the pieces in $3M$ hydrochloric acid for 24 hr, occasionally squeezing them with a plunger. Wash them several times, first with water, in a syringe, then with acetone, dry them at room temperature, place them in a vacuum desiccator for a few hours and finally store them in a plastic container in the dark.

Preparation of sample solution

Weigh accurately 1 g of sample (−200 mesh and dried at 110°) in a Teflon dish. Add 10 ml of concentrated hydrofluoric acid and 5 ml of concentrated nitric acid. Place the basin on a heated sand-bath and evaporate the acid until the residue is just moist. Repeat the acid treatment and evaporation twice more. Then add 5 ml of concentrated hydrochloric acid and evaporate the solution nearly to dryness, and repeat this twice more. Finally add 8.5 ml of concentrated hydrochloric acid and 20 ml of water, and heat to dissolve the residue. Transfer the solution to a 100-ml standard flask and dilute to the mark with water.

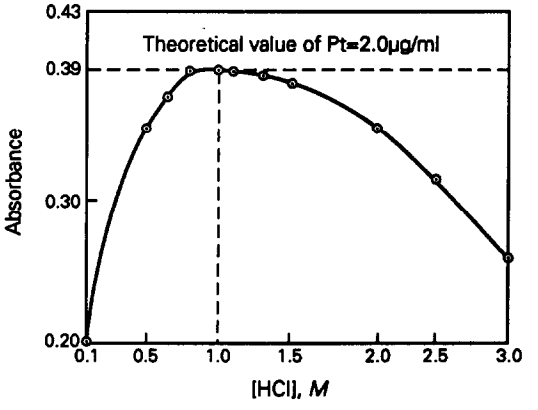

Fig. 2. Effect of hydrochloric acid concentration on the extraction of platinum dithizonate: $[SnCl_2] = 0.2M$, $[H_2Dz] = 3.5 \times 10^{-4}M$.

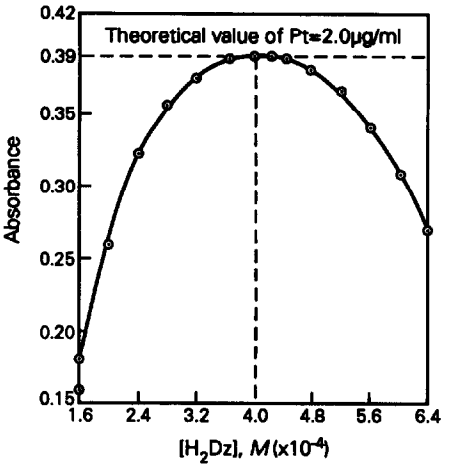

Fig. 3. Effect of dithizone concentration on the extraction of platinum dithizonate: $[SnCl_2] = 0.2M$, $[HCl] = 1M$.

Procedure

Transfer 5 ml of sample solution to a 50-ml glass beaker. Add 7.5 ml of $2M$ hydrochloric acid and 5 ml of $1M$ stannous chloride, dilute to 20 ml with water and after allowing the mixture to stand for 25–30 min, add 5 ml of the dithizone solution. Extract the platinum dithizonate onto the polyurethane foam by placing 6 pieces of foam in the solution. Squeeze the foam with a glass plunger 15 times every 15 min over a period of an hour. Transfer the foam chips into a disposable 5-ml plastic syringe. Wash the foam first with water to remove acid, then with ammonia solution (1 + 9) to remove excess of dithizone and finally with water, by repeated

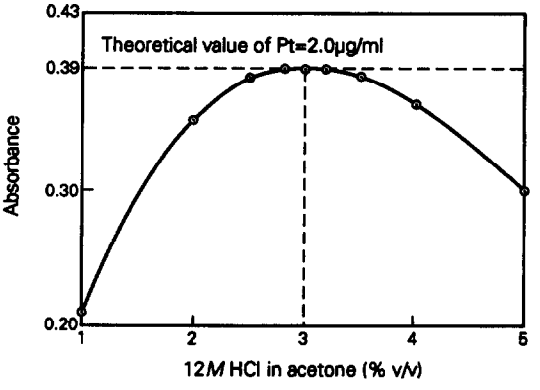

Fig. 4. Effect of hydrochloric acid concentration on the elution of platinum dithizonate with acetone.

Table 1. Determination of platinum (5 μg) with dithizone in solutions containing copper and mercury

Added, μg		Pt found,
Cu	Hg	μg
0.50		4.9; 5.1
1.0*		4.7; 5.3
3.0*		4.8; 4.9
5.0*		5.1; 4.7
10.0*		4.9; 5.2
	10.0	5.3; 4.8
	15.0	4.9; 5.1
	25.0	5.2; 4.9

*Decomposition time was 1 hr before extraction with polyurethane foam.

operation of the syringe. Elute the platinum dithizonate in the same way, with small portions of the hydrochloric acid–acetone mixture (to give a total volume of 10 ml), transferring the eluate into a 10-ml standard flask. After allowing 1 hr for full colour development, measure the absorbance at 530 nm against a reagent blank to which the whole procedure has been applied.

Calibration

Prepare a calibration graph to cover the range up to 5 μg/ml Pt, by the same procedure.

RESULTS AND DISCUSSION

Platinum(IV) in 0.1–4*M* hydrochloric, sulphuric or perchloric acid does not form a dithizonate, nor does Pt(II) if produced by reduction of Pt(IV) with ascorbic acid or sulphite. With stannous chloride as the reductant, however, a brown-yellow Pt(II) dithizonate is rapidly formed and can be extracted with suitable solvents.[6] The stannous chloride first reduces Pt(IV) to Pt(II) and then reacts (as $SnCl_3^-$) with the latter to form a labile Pt(II) complex[6] which can react with dithizone to form a Pt(II)-dithizonate complex that can be quantitatively sorbed on polyurethane foam and eluted with acidified acetone under the optimized conditions.

To optimize the concentration of stannous chloride a series of 25-ml solutions containing 20 μg of Pt(IV), $4 \times 10^{-4}M$ dithizone, 1.0*M* hydrochloric acid and different amounts of stannous chloride were equilibrated with foam chips according to the procedure given. It was found (Fig. 1) that the yield of platinum dithizonate was maximal at 0.17–0.22*M* stannous chloride concentration, and hence formation of the platinum chlorostannate(II) complex was also maximal with this reagent concentration.

The hydrochloric acid concentration was similarly optimized, by equilibrating a series of 25-ml solutions containing 20 μg of Pt(IV), 0.2*M* stannous chloride, $4 \times 10^{-4}M$ dithizone, and various amounts of hydrochloric acid, with foam chips, and the extraction of platinum dithizonate was found to be maximal and quantitative at 0.8–1.1*M* hydrochloric acid concentration (Fig. 2).

The optimal concentration of dithizone was similarly found and was in the range $3.8–4.5 \times 10^{-4}M$ (Fig. 3). The decrease in absorbance at higher dithizone concentration is attributed to competition for adsorption sites on the foam.

In all these experiments, the equilibration time for quantitative extraction of platinum dithizonate by the foam was found to be 1 hr and the elution was quantitative only with acidified acetone and not with acetone alone. The optimum eluent composition was found to be 2.8–3.2 ml of concentrated hydrochloric acid diluted to 100 ml with acetone (Fig. 4).

This observation suggests that the sorbed species is not neutral $Pt(HDz)_2$, because if it were, acetone should be able to elute it. From the reports[11–13] that the species sorbed by polyurethane foam from a solution containing platinum(II) and stannous chloride is mainly $Pt(SnCl_3)_5^{3-}$ and the observation that a complex of this type is involved in the formation of $Pt(HDz)_2$,[6] it seems a distinct possibility that an anionic mixed-ligand complex such as $Pt(HDz)_2SnCl_3^-$ or $Pt(HDz)_2Cl^-$ may be the species sorbed. Furthermore, from the report

Table 2. Determination of platinum in synthetic glasses

Nature of sample	Pt found, %
Glass No. 1 (0.0020% Pt)	0.0019; 0.0021; 0.0020
Soda-lime glass (0.0060% Pt)	0.0059; 0.0063; 0.0061
Borosilicate glass (0.0040% Pt)	0.0042; 0.0038; 0.0041
Flint glass (0.0030% Pt)	0.0029; 0.0031; 0.0033
Optical glass (0.0080% Pt)	0.0078; 0.0084; 0.0084

Glass compositions: Fe_2O_3, 0.02–0.44%; Al_2O_3, 0.82–1.28%; B_2O_3, 0.07–8.12%; CaO, 0.52–20.73%; MgO, 0.03–1.70%; Bao, 0–0.59%.

Table 3. Determination of platinum in laser glass samples

Sample	Pt found %	
	Present method	Reference method[15]
LG-N-1	0.00450; 0.00449; 0.00453	0.00490
LG-N-2	0.00751; 0.00746; 0.00750	0.00750
LG-N-3	0.00500; 0.00497; 0.00505	0.00520
LG-N-4	0.00581; 0.00577; 0.00580	0.00605
LG-N-5	0.00316; 0.00309; 0.00310	0.0030
LG-N-6	0.00071; 0.00080; 0.00076	0.00075
LG-N-7	0.00110; 0.00108; 0.00097	0.00110
LG-N-27	0.00457; 0.00466; 0.00436	0.00468
LG-N-29	0.00299; 0.00281; 0.00290	0.00310

that $Pt(SnCl_3)_5^{3-}$ is not readily desorbed from the foam,[12] a hot ethanolic hydrochloric acid solution being required for desorption, it seems likely that the elution with acidified acetone involves ion-exchange and/or ligand displacement. A test for tin in the final eluate proved negative, which suggests that $Pt(HDz)_2Cl^-$ may be the species finally eluted from the foam. As the mechanism was not of direct interest in the work, however, the matter was not pursued further.

From the observations above, a spectrophotometric method has been developed for the determination of traces of platinum. Beer's law is obeyed from 0.1 to 10.0 μg/ml Pt. The molar absorptivity is 3.80×10^4 l.mole^{-1}.cm^{-1} at 530 nm.

Silver, mercury and copper also form dithizonates in acidic media and can be extracted with polyurethane foam, but silver does not form any dithizonate complex in the presence of chloride, so silver has no effect on the method. Mercury(II) and copper(II) are reduced to their lower oxidation state by stannous chloride, and it was observed that mercury up to 25 μg/ml and copper up to 0.5 μg/ml (Table 1) can be tolerated under the experimental conditions. However, copper(I) can be displaced from its dithizone complex by platinum and a decomposition time of 1 hr is sufficient for thus eliminating the adverse effect of up to 10.0 μg/ml Cu (Table 1). After the mixture has stood for 1 hr only the platinum complex is extracted onto the polyurethane foam.

The method developed has been applied to some synthetic and laser glass samples. The results are presented in Tables 2 and 3.

REFERENCES

1. T. D. Rees and S. R. Hill, *Talanta*, 1968, **15**, 1312.
2. Z. Marczenko, *Separation and Spectrophotometric Determination of Elements*, Horwood, Chichester, 1986.
3. R. S. Young, *Analyst*, 1951, **76**, 49.
4. V. G. Goryushina and E. Ya. Gailis, *Zavodsk. Lab.*, 1954, **20**, 14.
5. W. Kemula, W. Brachaczek and A. Hulanicki, *Chem. Anal. (Warsaw)*, 1958, **3**, 913.
6. Z. Marczenko, S. Kuś and M. Mojski, *Talanta*, 1984, **31**, 959.
7. Z. Marczenko and S. Kuś, *Analyst*, 1985, **110**, 1005.
8. H. J. M. Bowen, *J. Chem. Soc. A*, 1970, 1082.
9. R. A. Moore and A. Chow, *Talanta*, 1980, **27**, 315.
10. A. Chow and S. L. Ginsberg, *ibid.*, 1983, **30**, 620.
11. K. R. Koch and I. Nel, *Analyst*, 1985, **110**, 217.
12. K. F. G. Brackenberry, L. Jones and K. R. Koch, *ibid.*, 1985, **112**, 459.
13. K. F. G. Brackenberry, L. Jones, I. Nel, K. R. Koch and J. M. Wyrley-Birch, *Polyhedron*, 1987, **6**, 71.
14. M. P. Maloney, G. J. Moody and J. D. R. Thomas, *Analyst*, 1980, **105**, 1087.
15. A. Simonsen, *Anal. Chim. Acta*, 1970, **49**, 368.

Talanta, Vol. 39, No. 4, pp. 419–428, 1992
Printed in Great Britain

0039-9140/92 $5.00 + 0.00
Pergamon Press plc

DEVELOPMENT OF FIELD SCREENING METHODS FOR TNT, 2,4-DNT AND RDX IN SOIL

THOMAS F. JENKINS and MARIANNE E. WALSH
U.S. Army Cold Regions Research and Engineering Laboratory, Hanover, New Hampshire, U.S.A.

(*Received* 13 *June* 1991. *Revised* 8 *September* 1991. *Accepted* 10 *September* 1991)

Summary—Simple field-screening methods are presented for detecting 2,4,6-TNT, 2,4-DNT and RDX in soil. A 20-g portion of soil is extracted by manually shaking with 100 ml of acetone for three minutes. After the soil settles, the supernatant is filtered and divided into three aliquots. Two aliquots are reacted with potassium hydroxide and sodium sulfite to form the red-colored Janowsky complex when 2,4,6-TNT is present or the blue–purple complex when 2,4-DNT is present. The third aliquot of the extract is passed through a strong anion exchange resin to remove nitrate and nitrite. Then the extract is acidified and RDX is reduced with zinc to nitrous acid, which is reacted with a Griess reagent to produce a highly colored azo dye. Concentrations of TNT, 2,4-DNT and RDX are estimated from their absorbances at 540, 570 and 507 nm, respectively. Detection limits are about 1 μg/g for 2,4,6-TNT and RDX and about 2 μg/g for 2,4-DNT. Concentration estimates from field analyses correlate well with laboratory analyses.

One of the most serious environmental problems facing the Army is the presence of soil contaminated with residues of high explosives and propellants at sites where the munitions were formerly manufactured, stored, used or demilitarized. The residues TNT (2,4,6-trinitrotoluene) and RDX (hexahydro-1,3,5-trinitro-1,3,5-triazine) are most commonly encountered in munition-contaminated soils because these explosives were extensively produced and used by the military. A major impurity in production grade TNT[1] is 2,4-DNT (2,4-dinitrotoluene), which is a component of several propellant compositions. These compounds do not rapidly decompose in the environment, and, since they leach through the unsaturated zone in water, they pose an immediate problem to ground water.[2] Thus contaminated soil must be located and treated or isolated. Though laboratory methods for determining munitions residues in soil and water have been developed,[3,4,5] reliable field methods are also desirable. Use of field methods would enable efficient identification of zones of high contamination during initial surveys and the interface between clean soil and contaminated soil during clean-up. These methods can also be used for selection of samples for in-depth laboratory examination. The objective of this work was to develop rapid field methods based on simple color-forming reactions for the detection of 2,4,6-TNT, 2,4-DNT and RDX.

As early as 1891 Janowsky[6] observed that colored reaction products were formed when polynitroaromatic compounds reacted with alkali such as potassium hydroxide. Meisenheimer[7] and Jackson and Earle[8] independently proposed a quinoidal structure to explain this phenomenon. In general, Jackson–Meisenheimer anions for dinitroaromatics are blue to purple in color and those from trinitroaromatics are red.[9]

When sulfite ion is present along with hydroxide, addition of sulphite to the aromatic ring can also occur.[10] This anion is more stable than the anion formed from hydroxide alone,[11] with stabilities extended from about 30 min for the hydroxide[12] complex to at least six hours.[11]

When the base catalyzed reaction takes place in a ketone solution such as acetone (Janowsky reaction), addition of the carbanion can also occur, with resulting production of a Janowsky complex (Fig. 1).[13]

These reactions have been used analytically for a number of applications. Yinon and Zitrin[14] give examples of their use for forensic detection of TNT in post-blast debris. Heller *et al.*[15] used the reaction of strong base with TNT as the basis of a field kit for detection of low levels of TNT in water. The use of this kit was later extended to estimation of TNT in soil extracts.[16] In general, their kit provides a field method to detect the presence of TNT in soil, but is less useful for estimating concentration.[17] These

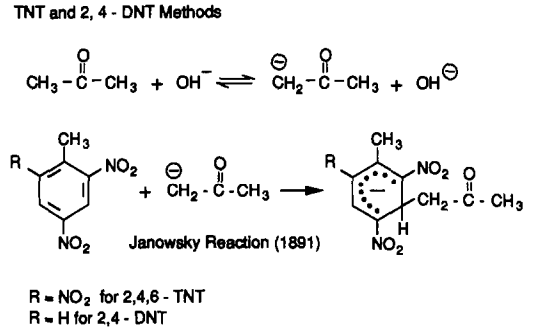

Fig. 1. Reactions used for colorimetric determination of 2,4,6-TNT and 2,4-DNT.

color-forming reactions have not been used to detect 2,4-DNT in soil.

Colorimetric chemical methods have also been developed for RDX for forensic applications.[14] These procedures generally rely on sequential reactions where RDX is first converted to nitrous acid with the Franchimont reaction (Fig. 2). The nitrous acid is used to nitrosate an aniline derivative such as sulfanilic acid and the resulting diazo cation couples to a naphthylamine to form a highly colored azo dye (Griess Reaction). Several pairs of reagents may be used to produce azo dyes.[18] A reagent containing procaine and *N,N*-dimethyl–naphthylamine was initially used for the procedure described in this paper. This choice was based on the work of Wyant,[19] who tested several reagents and found this combination to be best in terms of detection capability and shelf life. However, this liquid reagent was cumbersome to work with in the field since it is sensitive to sunlight. Also, we were concerned about the possible cancer risk associated with *N,N*-dimethylnaphthylamine. Subsequently, we found

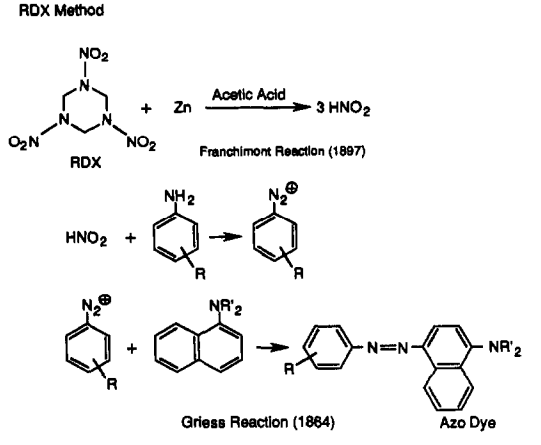

Fig. 2. Reactions used for colorimetric determination of RDX.

that a Hach NitriVer3 powder pillow, which is specifically designed for the determination of nitrite in the field, and distilled water can be substituted for the liquid Griess reagent. The powder pillow contains sodium sulfanilate, 4,5-dihydroxy-2,7-naphthalene–disulfonic acid disodium salt, potassium phosphate monobasic, potassium pyrosulfate and *trans*-1,2-diaminocyclohexanetetra acetic acid trisodium salt. The authors are not aware of a field method for RDX in soil based on the reaction sequence shown in Fig. 1.

Procedure

For these soil methods[20–22] about 20 g of wet soil is shaken with 100 ml of acetone to extract the munition residues, and the extract is filtered with a disposable syringe filter. The methods then depend on the production of colored reaction products (Fig. 3) when three aliquots of these extracts are subjected to two simple reaction sequences. For TNT and 2,4-DNT, portions of the extract are reacted with a strong base and sodium sulfite (Fig. 1). The main difference between the two procedures is the contact time with the reactants before filtration; 3 min for TNT and 30 min for 2,4-DNT. For extracts containing only TNT, a reddish colored Janowsky complex is produced. For those containing only 2,4-DNT (or 2,4- and 2,6-DNT), a bluish–purple complex is produced. If 2,4-DNT is present as a minor component and TNT is present at much higher concentration, DNT will not be detectable with this procedure. The DNT procedure is, however, capable of detecting the presence of DNT in soils contaminated with several types of single-based propellants in which 2,4-DNT is a major component. Several other polynitroaromatics also produce colored complexes and hence are potential interferences.[9] For RDX another portion of the extract is passed through a disposable anion exchange cartridge to remove any nitrate or nitrite. Then the extract is acidified and reacted with powdered zinc. This converts RDX to nitrous acid, which is detected by adding a Hach NitriVer3 powder pillow (Fig. 3) and distilled water. The development of a pink color is indicative of the presence of RDX or one of several other military explosives which are potential interferences (HMX, nitroglycerine, PETN or nitrocellulose).

The intensities of the colors produced by these reactions can be measured with a battery-operated spectrophotometer. The absorbances at 540 nm for TNT and 507 nm for RDX are

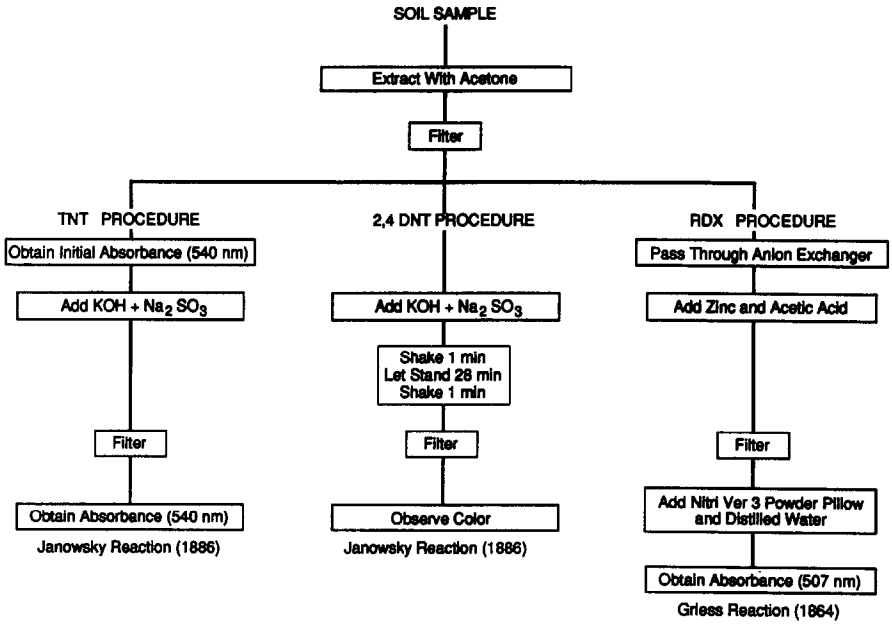

Fig. 3. Flow diagram for colorimetric field methods for 2,4,6-TNT, 2,4-DNT and RDX.

linearly related to concentration. Daily calibration is obtained with a single standard at 2 mg/l. Detection limits are about 1 μg/g for both TNT and RDX.[20,21] The linear range extends to 50 μg/g for TNT and 20 μg/g for RDX, respectively, for undiluted extracts. The absorbance for the 2,4-DNT complex (570 nm) is dependent on the water content of the extract, thus the method is only semiquantitative. The detection limit was 2 μg/g for a standard soil over a moisture content range of 10–50% (wet weight basis).[22]

EXPERIMENTAL

Analytical standards

Analytical standards for TNT and RDX were prepared from Standard Analytical Reference Material (SARM) obtained from the US Army Toxic and Hazardous Materials Agency (USATHAMA), Aberdeen Proving Ground, Maryland. Test solutions of 2,4-DNT were prepared from reagent grade 2,4-DNT (Eastman Organic Chemicals). Standard materials were dried to constant weight in a vacuum desiccator in the dark and standard solutions were prepared in HPLC grade acetone.

Soils

Soils used for laboratory extraction studies included field-contaminated and uncontaminated soils from a number of present and former military installations in ten different states. Interference tests utilized a humus-rich commercial potting soil obtained locally and uncontaminated soils obtained from a variety of military installations.

Soil extraction

Munition residues were extracted by manually shaking a 20-g soil subsample for 3 min with 100 ml of acetone and filtering the extracts with Millex-SR disposable syringe filters.

Generation of the Janowsky complexes for TNT and 2,4-DNT tests

For the TNT test, a pellet of potassium hydroxide and about 0.2 g of sodium sulfite were added to 25 ml of acetone soil extracts. Samples were manually shaken for 3 min, then filtered through a Millex-SR filter unit into a cuvette. The absorbance was measured at 540 nm. Unless the extracts contain a large amount of water, the solid reactants do not completely dissolve.

A similar procedure is used for the 2,4-DNT test except that two pellets of potassium hydroxide and about 0.75 g of sodium sulfite were added, the samples were shaken for one minute, allowed to stand for 28 min, and then shaken again for one minute prior to filtration. Absorbance was read at 570 nm.

Production of an azo dye from RDX

Acetone soil extracts were passed through an Alumina-A strong anion exchange cartridge

Table 1. Absorbance maxima and molar absorptivities for colored products from TNT, 2,4-DNT and RDX field screening tests

Analyte	Absorbance maxima (λ_{max})	Concentration of standard, *mg/l.*	Molar absorptivity $\times 10^{-4}$, *l. mole*$^{-1}$. *cm*$^{-1}$	Color
2,4,6-TNT	462	2.1	2.7	Red
	540		1.77	
2,4-DNT	570	2.9	1.12	Blue→purple
RDX	507	4.0	1.67	Pink

(Supelco, Inc) at 5 ml/min to remove any nitrate and nitrite which could be present. A 5-ml aliquot was acidified with 0.5 ml of glacial acetic acid and reacted with 0.3 g of zinc dust in the barrel of a syringe fitted with a disposable filter unit. This solution was rapidly filtered into a vial containing 20 ml of distilled water. The contents of a Hach NitriVer3 powder pillow were added. The sample is shaken briefly and allowed to stand for 10–15 min. Absorbance is read at 507 nm.

Spectrophotometers

Spectrophotometers were used to measure absorbance at various wavelengths in the visible region of the spectrum. A Coleman Junior II (Model 6/20) (bandpass 20 nm) was used for laboratory tests and either a Hach DR/2 or DR/2000 (bandpass 12 nm) was used in the field. Path length for the cuvettes was either 19 or 25 mm.

RESULTS AND DISCUSSION

Absorbance spectra and molar absorptivities

The visible absorbance spectra of the colored products produced from standards of TNT, 2,4-DNT and RDX (Figs 1 and 2) were obtained from 400–700 nm.[20–22] The absorbance maxima and molar absorptivities are given in Table 1.

The color-forming reactions used for these field screening methods are not specific for TNT, 2,4-DNT and RDX. Other polynitroaromatics such as 1,3-dinitrobenzene (DNB) and 1,3,5-trinitrobenzene (TNB) and polynitrophenols such as picric acid also give colored anions when reacted with strong base. During site clean-up activities, however, the ability to detect these other compounds as well as TNT and 2,4-DNT would be quite useful. Similarly, the same azo dye produced from the RDX test is also produced when other nitramines such as HMX (octahydro-1,3,5,7-tetranitro-1,3,5,7-tetrazocine) and tetryl (2,4,6-trinitrophenylnitramine) or nitrate esters such as NG (nitroglycerine), PETN (pentaerythritol tetranitrate) and NC (nitrocellulose) are treated under similar conditions. Table 2 lists munition-related compounds detected by these screening procedures.

Effects of variable concentrations of water in acetone extracts

In the field, soil extracts will be obtained by manually shaking 20 g of soil with 100 ml of

Table 2. Colors and λ_{max} obtained for acetone solutions of munition related compounds treated with (a) KOH and sodium sulfite or (b) zinc and acetic acid followed by Griess reagent

Compound	KOH and Na_2SO_3		Zinc and acetic acid, Griess reagent	
	Color observed	λ_{max} (400–600 nm)	Color observed	λ_{max} (400–600 nm)
1,3-Dinitrobenzene	Purple[7,17]	570	None	—
2,4-Dinitrotoluene	Blue[7,17]	570	None	—
2,6-Dinitrotoluene	Pinkish-purple[17]	550	None	—
1,3,5-Trinitrobenzene	Red[7,17]	460, 560	None	—
Tetryl	Orange[17]	460, 550	Pink	507
2-Amino-DNT	Pale yellow[17]	400	None	—
4-Amino-DNT	None[17]	—	None	—
Nitroglycerine	None[17]	—	Pink	507
PETN	None[17]	—	Pink	507
RDX	None[17]	—	Pink	507
HMX	None[17]	—	Pink	507
Picric Acid	Reddish-orange[7]	420	None	—
2,4-Dinitrophenol	Yellowish-orange[7]	430	None	—
TNT	Red[7,17]	462, 540	None	—

acetone. Since the soil will be moist in most cases, water will be a component of the soil extracts. In addition to a small amount of dilution, the presence of water may affect the kinetics of these reactions. To investigate this effect, standard solutions of TNT, 2,4-DNT and RDX were prepared with water added to simulate the extracts that would be obtained from soils with moisture contents ranging from 0–100% (wet weight basis). For all three analytes, little or no color formed when no water was present (Fig. 4). Over the range of moisture contents (10–75%) that should include the large majority of surface soils from potentially contaminated sites, absorbance varied little for the TNT and RDX solutions. However, absorbance for the 2,4-DNT standard significantly declined for water contents greater than 10%. Based on this variability, determinations for 2,4-DNT will be semi-quantitative while the corresponding procedures for TNT and RDX may be used quantitatively.

Reagent contact time

Experiments were conducted to determine if reagent contact time had an effect on measured absorbance. Contact time with potassium hydroxide and sodium sulfite was varied from 1 to 18 min for TNT and from 1.5 to 60 min for 2,4-DNT, after which solutions were filtered and absorbances measured. All experiments were conducted at laboratory temperature ($22 \pm 2°$).

Maximum absorbance for TNT was obtained after 3 min of continuous shaking.[20] Exposure to the reagents for periods longer than 8 min resulted in reduced absorbance at 540 nm. Thus a 3-min reaction time was selected.

For 2,4-DNT solutions, the time at which maximum absorbance was obtained depended on the water content of the solutions. In general, the absorbance obtained after 30 min of intermittent shaking was at least 90% of the maximum.[22] An additional experiment was performed to compare various shaking protocols. We found that if the solution was shaken initially for one minute, allowed to stand for 28 min, then shaken again for one minute just prior to filtration, the absorbance obtained was not significantly different from protocols that required more shaking.[22]

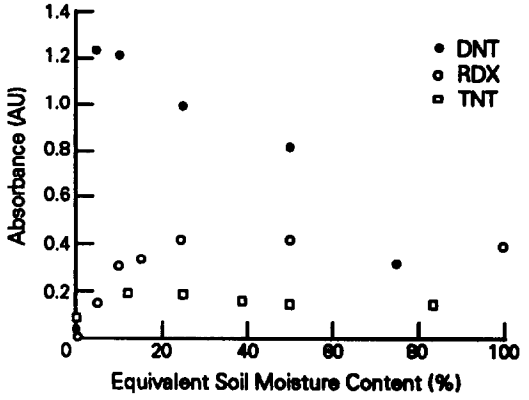

Fig. 4. Dependence of measured absorbance on water content of soil extracts.

Development of the azo dye from RDX is a two-step procedure. First, the RDX is reacted with zinc dust and acetic acid to produce nitrous acid. The nitrous acid then reacts with a Griess color reagent to produce the azo dye. The length of time the RDX is allowed to react with the zinc dust and acetic acid was found to be critical.[21] Reaction kinetics are fast when water is present in the acetone extract.[21] Contact times exceeding 30 sec resulted in less nitrous acid production, presumably because the nitrous acid was further reduced. Once the nitrous acid is produced, the solution must be filtered to remove the zinc dust. Because of the fast kinetics, this filtration is conveniently performed by reducing the RDX in the barrel of a syringe fitted with a disposable filter unit. Once the filtered solution is added to the color developing solution, full color development takes about 15 min.

For all three tests, the colors of the final solutions were stable for at least one hour.[20–22]

Potential interferences (other than munitions-related compounds)

Experiments with a variety of blank soils indicated that the color of acetone extracts will vary from colorless to yellow depending on the amount of humic matter present. Background absorbances for the yellow extracts is greatest over the range 400–500 nm,[20] and for this reason TNT determinations are made at 540 nm rather than at 462 nm, despite the lower molar absorptivity at 540 nm (Table 1). After soil extracts are reacted with potassium hydroxide and sodium sulfite for 3 min, the absorbance at 540 nm approximately doubles; thus an initial absorbance measurement must be made on aliquots of acetone extracts subjected to the TNT screening procedure and the DNT procedure as well, if used quantitatively. The initial absorbance is doubled and subtracted from the final absorbance to estimate TNT concentration.

As will be discussed later, heavy metal cations such as copper were found to interfere with 2,4-DNT determinations. These cations could form complexes with either the unreacted DNT[23] or the Janowsky complexes (Fig. 5).

For the RDX test, background absorbance from humic material is not a problem. Once the acetone extract is acidified and mixed with the color-forming reagent, the humic material precipitates and may be removed by filtration. Experiments with a wide variety of blank soils showed that background was negligible in all cases.[21]

Since the RDX test measures nitrous acid concentration, soil samples containing nitrite or nitrate would give a false positive if the nitrite and nitrate are not removed prior to reaction of RDX with zinc. This is accomplished by passing the extract through a disposable 3-ml strong anion exchanger (Supelco Alumina A). Experiments indicate that over 98% of the nitrate in a 9.8-mg/l. test solution was removed with this procedure.[21]

Extraction efficiency of field procedure

For a field method to provide accurate estimates of analyte concentration in the soil, the extraction step must be rapid. Previous extraction studies indicated that long extraction times were required when acetonitrile or methanol were used as the extraction solvent for nitroaromatics and nitramines.[24]

In order to determine how rapidly acetone will extract TNT, 2,4-DNT and RDX from soil,

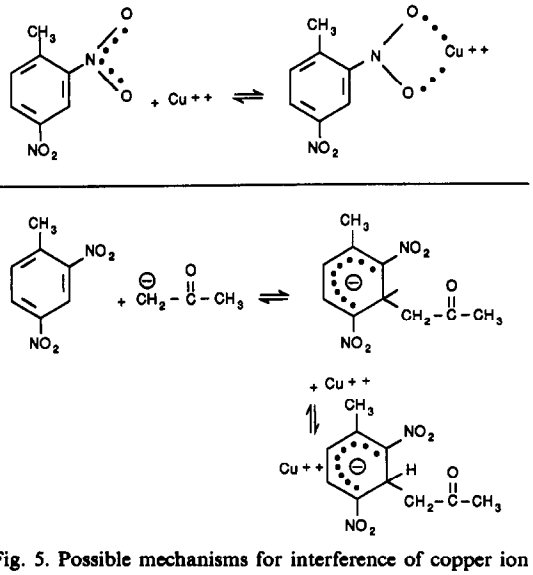

Fig. 5. Possible mechanisms for interference of copper ion with the 2,4-DNT method.

field-contaminated soil samples from 14 different sites were extracted with acetone, with 3 min of manual shaking. An aliquot of the extract was removed and the remaining soil/acetone slurries placed in an ultrasonic bath for 18 hr. Both sets of extracts (3 min and 18 hr) were analyzed by RP–HPLC as described elsewhere.[3,20] The results are presented in Table 3. The average recovery after 3 min of manual shaking with acetone for TNT was 96% and for RDX was 98% of that obtained with the more exhaustive procedure, indicating that acetone is an excellent extraction solvent with respect to its extraction kinetics for these two analytes over a wide concentration range.[20,21] The average recovery for 2,4-DNT was only 80.5%, with one low recovery (40.1%) for the soil with highest 2,4-DNT concentration.[22] Overall, the extraction efficiencies for all three analytes are sufficient for a field screening method.

Comparison of analyte concentration estimates

The field screening procedures were first tested in the laboratory with previously air-dried field-contaminated soils. Prior to extraction, the soils were wetted to simulate the moisture that would normally be present under field conditions. Estimates of analyte concentrations obtained by the colorimetric field procedure were correlated against those obtained by the standard RP–HPLC method. The colorimetric results for TNT were correlated with both the TNT estimate by HPLC and the sum of TNT and TNB. The best correlation was found with the sum of TNT plus TNB and resulted in a slope of 1.15 and an R^2 of 0.985 (Fig. 6). A paired t-test indicated that the concentration estimates for TNT from the colorimetric method and the sum of TNT and TNB by the HPLC procedure were not different at any level of significance.[20] Thus it appears that the colorimetric results are best represented as the sum of TNT plus TNB. The slope of 1.15 indicates that, in general, the colorimetric procedure gives a slightly greater estimate for TNT than can be accounted for by TNT and TNB (Fig. 6). One interpretation of these results is that other TNT degradation products such as trinitrobenzoic acid, trinitrobenzyl alcohol, and trinitrobenzaldehyde,[25] which are not identifiable by RP–HPLC analysis of the extracts, also form colored Janowsky complexes, thereby producing positive interference.

While we do not believe that the 2,4-DNT procedure can be used quantitatively in the field

Table 3. Comparison of extraction efficiency of field procedure and standard laboratory procedure

Sample origin		Analyte	Concentration, μg/g Field procedure*	Lab procedure†	Recovery, % by field procedure‡
Nebraska Ordnance Plant	A	TNT	0.065	0.071	91.5
	B	TNT	340	349	97.4
	C	TNT	63.5	67.9	93.5
	D	TNT	0.32	0.32	122
Hawthorne AAP (Nev.)	A	TNT	4.53	4.75	95.4
	B	TNT	5.79	5.65	102
	C	TNT	0.79	0.90	87.3
Weldon Springs (Mo.)	A	TNT	0.96	1.26	76.2
	B	TNT	163	176	92.6
	C	TNT	0.075	0.077	97.4
Vigo Chem. Plant (Ind.)		TNT	11.7	13.4	87.3
Hastings East Ind Park (Neb.)		TNT	67.6	68.8	98.3
Sangamon Ordnance Pt. (Il.)		TNT	21.5	23.2	98.2
Raritan Arsenal (NJ)		TNT	71.7	80.6	98.0
Lexington-Bluegrass Depot (Ky)		TNT	5.90	7.11	83.0
Chicksaw Ordnance Works (Ind.)		TNT	0.21	0.16	131
Nebraska Ordnance Plant	A	RDX	13.6	14.1	98.3
	B	RDX	60.2	65.9	95.5
	C	RDX	1073	1080	99.7
	D	RDX	9001	10,455	92.6
Hawthorne AAP (Nev.)	A	RDX	1.97	2.01	99.0
	B	RDX	3.32	2.96	105
Lexington Bluegrass Depot (Ky)		RDX	9.10	9.37	98.5
Camp Shelby (Ms.)	A	2,4-DNT	3.4	4.2	80.9
	B	2,4-DNT	226	563	40.1
	C	2,4-DNT	6.7	7.3	91.8
Eagle River Flats (Ak.)	A	2,4-DNT	12.7	13.6	93.4
	B	2,4-DNT	7.4	7.7	96.1

*20 g soil shaken with acetone for 3 min.
†20 g soil extracted with acetone for 18 hours in sonic bath.
‡Relative to laboratory procedure.

since calibration depends on water content, we tested the method in the lab with air-dried soils wetted such that the moisture content was 10%. This moisture content was chosen since absorbance would be close to maximum, based on the previous experiment on the effect of water content. Only five soils were available that were contaminated primarily with 2,4-DNT. These soils were collected from explosive ordnance disposal sites. Results are given in Table 4. The field procedure severely underestimated the concentration of 2,4-DNT in one sample from Eagle River Flats, Alaska. This particular sample was also contaminated with copper (347 μg/g). As discussed previously, copper is a potential interferant since it may complex with 2,4-DNT or the Janowsky complex. Correlation between estimates for the remaining four samples was excellent (>0.999); however, the field procedure underestimated 2,4-DNT concentration by 15–25%.

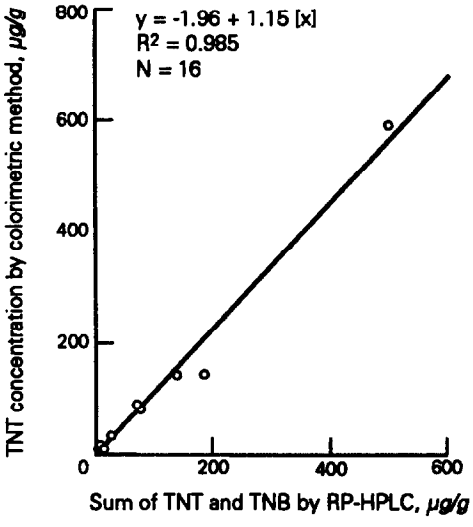

Fig. 6. Correlation of concentration estimates for TNT, using the field method with the sum of TNT and TNB by RP-HPLC.

To further explore the potential for false negatives, a series of soils from a number of Army installations that had been previously determined to be free of munitions residues were spiked with 2,4-DNT and analyzed by the field screening procedure. In all cases 2,4-DNT was easily detected, but as observed earlier, the measured concentrations were consistently lower than anticipated by up to 30%.[22] The magnitude of interference observed for the

Table 4. Comparison of colorimetric and RP–HPLC analysis of soil extracts

Sample origin	Colorimetric method, μg/g	RP–HPLC method, 2,4-DNT μg/g	RP–HPLC method, 2,6-DNT μg/g
Camp Shelby (Ms.)—A	3.3	3.4	0.6
Camp Shelby (Ms.)—B	203	226	12.1
Camp Shelby (Ms.)—C	5.0	6.7	0.2
Eagle River Flats (Ak.)—A	11.4	12.7	0.9
Eagle River Flats (Ak.)—B	0.8	7.4	0.5

Eagle River Flats sediment was not observed in any of these soils.

Eleven field-contaminated soils were used to compare the RDX concentrations estimated by the field method with those obtained by RP–HPLC analysis. The results from the field method were correlated with those obtained by the HPLC method for both RDX alone and the sum of RDX and HMX. The best correlation was obtained with RDX plus HMX and resulted in a slope of 0.9 and an R^2 of 0.995 (Fig. 7). Paired t-tests indicated that the estimates of RDX concentration obtained by the field procedure were not significantly different (0.05 significance level) from those obtained by the HPLC procedure for RDX alone or for the sum of RDX and HMX.

Estimation of detection capability

The reporting limits of TNT and RDX concentrations with these field procedures were established with the method of Hubaux and Vos[26] as adapted by the US Army Toxic and Hazardous Materials Agency.[27] The calculated certified reporting limits were 0.72 and 1.4 μg/g for TNT and RDX, respectively.

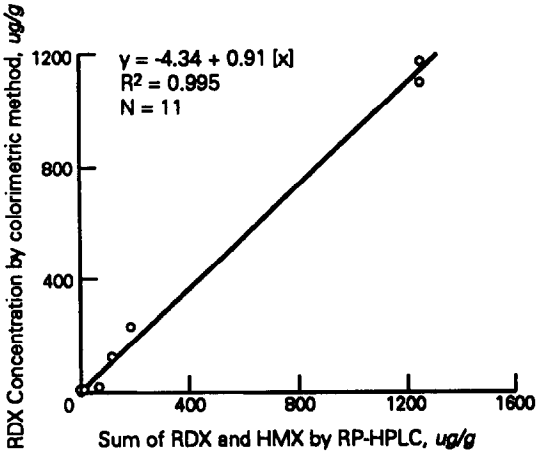

Fig. 7. Correlation of concentration estimates for RDX, using the field method with the sum of RDX and HMX by RP–HPLC.

The reporting limit for 2,4-DNT was 2 μg/g based on a certification procedure for methods that simply screen for contamination.[27] For the certification procedure four soils were spiked at a chosen concentration, in this case 2 μg/g. These soils, along with four soil blanks, were processed according to the method. After color development, four individuals were asked to distinguish the soil spikes from the blanks. Certification was performed three times, each at a different soil moisture content (10, 25 and 50% wet weight basis). In all cases, the soil spikes could be distinguished from blanks with 100% accuracy at 2 μg/g.

Field testing

Both the TNT and RDX procedures have been field tested and the concentration estimates obtained in the field compared with those obtained on separate subsamples processed by the standard RP–HPLC procedure.[3] Results are presented in Table 5.

The TNT procedure was initially tested at Umatilla Army Depot, Oregon. Since TNT concentrations were expected to be very high, a smaller subsample of soil was used and the extracts diluted before reaction with potassium hydroxide and sodium sulfite. This field test was conducted before the importance of reagent contact time was understood. Contact times of 10 min were used. Except for one sample, the results of laboratory analysis were higher than those obtained with the field method. This sample had a TNT concentration an order of magnitude higher than any of the other samples and was not included in this correlation. Correlation analysis was conducted comparing the field and laboratory results on the remaining 10 samples. This analysis resulted in an R^2 value of 0.865 which was significant at the 99% confidence level. The slope of the best fit relationship was 0.627, indicating the field procedure, on the average, gave results only about 63% as high as the laboratory results.

Table 5. Comparison of field estimates to lab estimates of concentration. Determinations made on separate subsamples

Site	Concentration, μg/g TNT Field*	TNT Lab	RDX Field*	RDX Lab
Umatilla Depot, Oregon	1060	2250	NT†	NT
	3560	7430	NT	NT
	704	1180	NT	NT
	3180	4030	NT	NT
	4490	8590	NT	NT
	2530	3990	NT	NT
	84	131	NT	NT
	102,000	38,600	NT	NT
	6610	7690	NT	NT
	109	183	NT	NT
	716	1300		
Newport, Indiana	NT	NT	<*d*	0.05
	NT	NT	1.0	1.31
	NT	NT	1.7	3.15
	NT	NT	6.0	15.5
	NT	NT	6.8	8.4
	NT	NT	160	299
	NT	NT	38	38.6
	NT	NT	48	258
	NT	NT	660	1800
	NT	NT	2100	3170
	NT	NT	4300	12,200

*Not corrected for moisture.
†NT = not tested.

Two factors may have contributed to the low results for the field method. First, an excessively long reagent contact time prior to filtration was used for the samples. Thus the absorbance would have been reduced relative to its maximum value. Second, the TNT concentrations in the Umatilla soil were much higher than those in the other field-contaminated soils tested, and the percentage extracted in the short extraction time used by the field method could have been reduced compared to the 18-hr extraction with acetonitrile used in the laboratory procedure. Nevertheless, the field results were encouraging for a first test.

The RDX method was field tested in Newport, Indiana. Correlation between estimates for all 11 samples yields a correlation coefficient of 0.95. However, the slope of the best fit relationship is only 0.36. This low value for the slope is strongly influenced by the last data point, where the estimates of RDX concentration were 4300 and 12,000 μg/g for the field and laboratory procedures, respectively. If the comparison is made with only those soils that had absorbances for the field procedure within the linear range (less than 0.7 absorbance unit) without dilution of the acetone extract, the R^2 value is 0.94 and the slope is 0.95. We feel this comparison is justified since for a field screening test we wish to distinguish the boundary between uncontaminated and contaminated soil, making accuracy at the lowest concentrations most important.

The TNT and RDX methods were also field tested at Eagle River Flats, Alaska, and Camp Shelby, Mississippi. Forty samples were screened at Eagle River Flats; all gave negative tests. The samples were subsequently analyzed by RP–HPLC and no explosive residues were detected in any sample. Some practical information was gained from this field test. Both potassium hydroxide and sodium sulfite are hygroscopic and should be protected from moisture under humid conditions by keeping reagent bottles tightly closed. Low ambient temperatures caused two problems. First, glacial acetic acid freezes at 16.6°. Second, reagent contact times for the TNT procedure had to be extended. The optimum time which depends on temperature was determined by observing the color development in a spiked sample.

At Camp Shelby, 22 samples were screened. Three samples gave positive indications for the presence of TNT, but no TNT was observed in these three samples by RP–HPLC. All three contained 2,4-DNT, as did some of the other samples, one of which was observed to give a purple color in the field TNT test. Nineteen of the soils gave a positive field screening response

for the RDX test. RDX was only detected by RP-HPLC in one of these soils. However, the RDX tests will also give a positive response for NC. NC is the primary component of single, double and triple base propellants. 2,4-DNT is an additive of single base propellant and its widespread presence at this site probably indicates the NC is present as well at even higher concentrations. In fact, propellant grains were observed scattered about the area. However, the soils were not analyzed for NC, since there is no reliable analytical technique to determine this compound in soil. So the explanation for false positives for the Camp Shelby samples must remain speculation. It should be pointed out that soils from this site were taken from areas which served as both an explosive ordnance disposal area and an artillery impact area and could have traces of a wide variety of munition compounds.

CONCLUSIONS

Simple field screening methods were developed for detecting 2,4,6-TNT, 2,4-DNT and RDX in soil. The procedure involves the extraction of munition residues from a soil subsample with acetone. Three portions of the extract are then reacted to two sets of reagents that form colors in the presence of nitroaromatics or nitramines. Concentration estimates obtained by this colorimetric procedure compared favorably with those obtained by the standard laboratory procedure. Field tests were conducted and the methods were found to be suitable for use under field conditions.

Acknowledgements—The authors would like to acknowledge the financial support and encouragement provided by the US Army Toxic and Hazardous Materials Agency (USATHAMA), Aberdeen Proving Ground, Maryland (M. H. Stutz and K. T. Lang, project monitors). They also acknowledge Dr C. L. Grant, Professor Emeritus, University of New Hampshire, and Daniel Leggett, CRREL, for useful comments on this manuscript. In addition, the following individuals are acknowledged for assistance in conducting field validation: Capt. Craig Myler and Jim Arnold of USATHAMA; Dr Richard Williams of Weston Corporation; Dr Richard Coghlan, Dames and Moore; Dr Charles Racine and Charles Collins of CRREL; Dr Murray Brown of the US Army Environmental Hygiene Agency; and Robbin Blackman and Terry Williams of the Mobile District, Corps of Engineers. Mr Steve Schnitker of the Missouri River Division Laboratory, Corps of Engineers, provided laboratory results for the Camp Shelby samples.

This publication reflects the personal views of the authors and does not suggest or reflect the policy, practices, programs, or doctrine of the US Army or Government of the United States.

REFERENCES

1. D. C. Leggett, T. F. Jenkins and R. P. Murrmann, *U.S. Army Cold Regions Research and Engineering Laboratory*, Special Report 77-16, Hanover, NH, 1977.
2. R. F. Spalding and J. W. Fulton, *J. Contaminant Hydrology*, 1988, **2**, 139.
3. T. F. Jenkins, M. E. Walsh, P. W. Schumacher, P. H. Miyares, C. F. Bauer and C. L. Grant, *J. Assoc. Off. Anal. Chem.*, 1989, **72**, 890.
4. T. F. Jenkins, P. H. Miyares and M. E. Walsh, *U.S. Army Cold Regions Research and Engineering Laboratory*, Special Report 88-23, Hanover, NH, 1988.
5. M. Hable, C. Stern, C. Asowata and K. Williams, *J. Chrom. Sci.*, 1991, **29**, 131.
6. J. V. Janowsky, *Berichte*, 1891, **24**, 971.
7. J. von Meisenheimer, *Leibig's Annalen der Chemie*, 1902, **323**, 205.
8. C. L. Jackson and R. B. Earle, *Am. Chem. J.*, 1903, **29**, 89.
9. R. W. Bost and F. Nicholson, *Ind. Eng. Chem., Anal. Ed.*, 1935, **7**, 180.
10. F. Terrier, *Chemical Reviews*, 1982, **82**, 77.
11. C. C. Ruchhoft and W. G. Meckkr, *Ind. Eng. Chem.*, 1945, **17**, 430.
12. K. Kay, *Can. J. Res.*, 1941, **19**, 86.
13. T. N. Hall and C. F. Poranski, in H. Feuer, *The Chemistry of the Nitro and Nitroso Groups*, Interscience Publishers, New York, 1970.
14. J. Yinon and S. Zitrin, *The Analysis of Explosives*, Pergamon Press, Oxford, 1981.
15. C. A. Heller, S. R. Greni and E. D. Erickson, *Anal. Chem.*, 1982, **54**, 286.
16. E. D. Erickson, D. J. Knight, D. J. Burdick and S. R. Greni, *Report NWC TP-6569*, Naval Weapons Center, China Lake, CA, 1984.
17. T. F. Jenkins and P. W. Schumacher, *U.S. Army Cold Regions Research and Engineering Laboratory*, Special Report 90-20, Hanover, NH, 1990.
18. J. B. Fox, *Anal. Chem.*, 1979, **51**, 1493.
19. R. E. Wyant, *Technical Report TR-185*, Naval Explosive Ordnance Disposal Facility, Indian Head, MD, 1977.
20. T. F. Jenkins, *U.S. Army Cold Regions Research and Engineering Laboratory*, Special Report 90-38, Hanover, NH, 1990.
21. M. E. Walsh and T. F. Jenkins, *ibid.*, Special Report 91-7, Hanover, NH, 1991.
22. *Idem*, *ibid.*, Special Report, Hanover, NH, in the press.
23. D. C. Leggett, *ibid.*, Special Report, Hanover, NH, in the press.
24. T. F. Jenkins and C. L. Grant, *Anal. Chem.*, 1987, **59**, 1326.
25. M. E. Walsh, *U.S. Army Cold Regions Research and Engineering Laboratory*, Special Report 90-2, Hanover, NH, 1990.
26. A. Hubaux and G. Vos, *Anal. Chem.*, 1970, **42**, 840.
27. *USATHAMA, USATHAMA QA Program*, January 1990, *U.S. Army Toxic and Hazardous Materials Agency*, Aberdeen Proving Ground, MD.

Talanta, Vol. 39, No. 4, pp. 429–441, 1992
Printed in Great Britain.

0039-9140/92 $5.00 + 0.00

FIBER-OPTIC FLUOROMETER SIGNAL ENHANCEMENT AND APPLICATION TO BIOSENSOR DESIGN

CLAIRE KOMIVES and JEROME S. SCHULTZ*
Center for Biotechnology and Bioengineering, University of Pittsburgh, Pittsburgh, PA, U.S.A.

(*Received* 3 *March* 1991. *Revised* 13 *June* 1991. *Accepted* 16 *June* 1991)

Summary—Fiber-optic fluorescence spectroscopy is currently the focus of active research because of the high sensitivity of fluorimetry and capacity for remote analysis with optical fibers. It is shown here that a further increase in sensitivity can be achieved by placing a mirror within a few fiber diameters of the distal end of the optical fiber in a solution of flourophore. A potentially four-fold signal enhancement results which is due to an increase in the excitation intensity as well as the reflection of the collected emitted light. The enhancement is shown to be dependent on the pathlength and concentration of the fluorophore, as well as the numerical aperture and core diameter of the optical fiber. The limit of detection of the fluorometer, which incorporates a mirror, is nanomolar dye concentrations, with the maximum response in path lengths of dye that are in the order of 6 fiber diameters. This principle can be applied to the design of optical sensors for continuously monitoring the concentration of specific biochemicals, and a conceptual design for such a sensor is described. A mathematical model is presented which describes the fluorescence output signal of a fiber-optic flourometer which incorporates a mirror.

Fluorescence spectroscopic methods are well known as highly sensitive, specific techniques for chemical analysis. The coupling of fluorescence to fiber-optic technology offers the possibility of remote analysis. While fiber-optic fluorometers have only recently become commercially available, they seem to have a bright future as an analytical tool with a broad range of applications.

An obvious use of fluorescence for concentration measurements is that of fluorescently labeled compounds. A number of reviews have shown the versatility of this method for chemical sensing.[1-3] These have principally described sensors utilizing excitation or emission wavelength selectivity. Betts *et al.*[4] have demonstrated the multi-dimensional capacity of fiber-optic fluorescence analysis with the measurement of fluorescence lifetimes and other parameters. Their results showed a 10-fold loss in sensitivity due to the use of optical fibers over direct laser excitation.

An additional loss in sensitivity can result from certain sample configurations with which signal capture must be compromised for the benefit of other parameters, such as response time. Deaton[5] has shown that the effective pathlength (L_E) for a fiber-optic fluorometer with distal light collection is a function of the fiber radius (a) and numerical aperture (NA), and the refractive index of the external fluid (n_{ext}):

$$L_E = 1.303a \cot \Theta \tag{1}$$

where

$$\Theta = \sin^{-1} \frac{NA}{n_{ext}} \tag{2}$$

This presents a constraint on the sample configuration. The use of a graded-index lens at the distal end can provide a means of controlling the collection efficiency of the fiber.[1,6]

Our work has involved a method of increasing the signal with reduced sample volume, by placing a mirror at the distal end of the optical fiber in the solution of the fluorophore. White[7] demonstrated that using *two* concave mirrors in a fluorescence spectrophotometer can increase the sensitivity by a factor of 3.8. One mirror reflects the excitation light, effecting a double pass of light through the sample cuvette, and the second mirror reflects the emitted light, which is collected at 90° from the excitation light source. The use of a single optical fiber for both collection and transmission obviates the complex structure required by two such mirrors, and we will show that a *single* mirror can serve both purposes. A plane mirror was used in these studies to provide for ease of fabrication. We will show that the signal enhancement is

*Author for correspondence.

dependent on the distance of the mirror from the optical fiber, because of dispersion of the light rays.

Also, as a way of achieving a greater understanding of the enhancement, we developed mathematical models of the signal intensity as a function of distance of the optical fiber from a mirror or from a non-reflecting surface. A similar analysis for a fiber optic lever displacement transducer was developed by Cook and Hamm.[8] Their model is for the case of separate fibers for excitation and collection and is not for fluorescence based sensors. A preliminary and simplified model of the fraction of fluorescence collection which is a function only of the core diameter, w, and the pathlength of the solution of fluorophore, l, was done by Schultz.[9] This model only accounts for the centerline rays.

$$1 - \frac{l/w}{\sqrt{1 + (l/w)^2}} \qquad (3)$$

A similar approach to the analysis presented here was taken by Deaton.[5] His work, which did not include a mirror in the distal cuvette, involved an analytical solution of the power flux at the fiber face as a function of pathlength of fluorophore solution, fiber numerical aperture and core radius. A more complete analysis of the transfer function between the optical fiber and a fluorophore solution has recently been published by Modlin and Milanovich.[10] Figure 1 shows a comparison of the model described here as well as those of Schultz[1] and Deaton.[2] The principle difference between our model and that of Deaton is that ours can accomodate loss of light transmission due to absorption of light. At the low concentration used in Fig. 1(a), the light absorption is not significant.

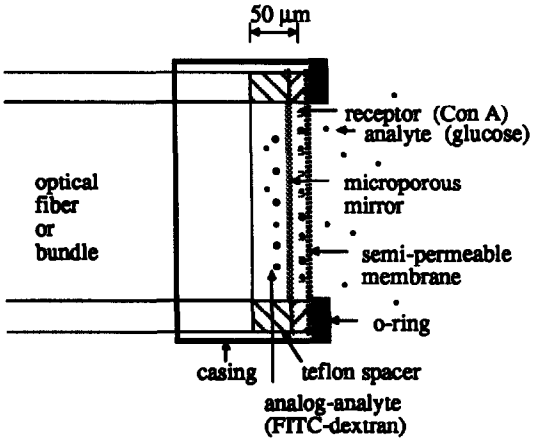

Fig. 2. Conceptual design competitive binding optical sensor with a porous mirror. Con A bioreceptor is immobilized in Region I. Bound fluorescently-labeled dextran in this region is shielded from the excitation beam by a porous opaque mirror. Displaced fluorescently-labeled dextran in Region II provides a fluorescence signal which increases with increasing glucose concentration.

In previous communications we have discussed the application of the concepts presented here to the construction of a sensor which utilizes a reflective surface to enhance the signal of a fluorescence-based sensor.[11,12] Previously, reflective surfaces to enhance response had only been reported for absorbance-based sensors.[13,14] Our concept for a distal cuvette sensor which functions analogously to that reported earlier (Mansouri *et al.*[15]) is illustrated in Fig. 2.

In this new configuration, the excitation light emanates from the optical fiber in the direction of the oncoming analyte, and therefore a means

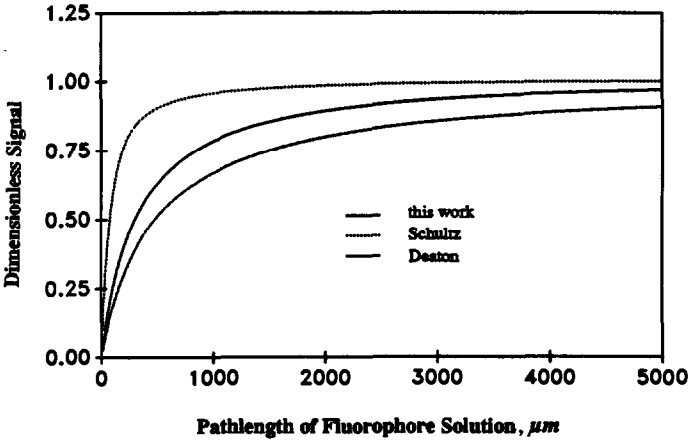

Fig. 1. Comparison of models of fluorescence signal with pathlength. Calculation for 100 μm core fiber, NA.2, Dye concentration $10^{-6}M$. (*a*) Schultz ···· [1], (*b*) Deaton ———, (*c*) This work ———

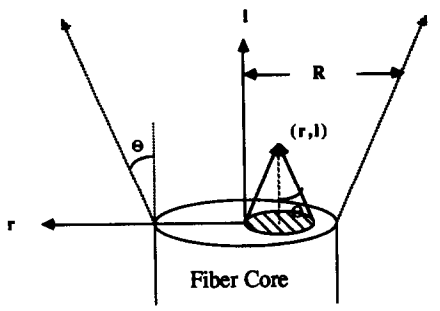

Fig. 3. Excitation from an optical fiber. Illumination from a point (r, l) is from light emanating from shaded region and at angles 0 to Θ as seen by the point (r, l).

of blocking its view of the dye bound to the receptor proteins is necessary. This is accomplished by placing a reflective porous barrier between the dye-bound layer and the optical fiber. This spacer permits the passage of analyte analog, while blocking the light. When the sensor is not in contact with the analyte, the fluorescent labeled analyte analog is bound to the immobilized receptors and the reflective membrane will return most of the excitation light to the optical fiber. When the sensor is placed in a solution of analyte, a competitive reaction takes place between the analyte and the analyte analog for the receptor sites. The free analyte analog is able to diffuse through the reflective membrane into the view of the optical fiber.

THEORY

The signal output of fluorescence-based optical sensors is due to emission photons which are captured and transmitted by the optical fiber to a detector and converted to an electrical signal. The intensity of the fluorescence is dependent upon the excitation intensity, which is not radially uniform in the case of an optical fiber. The rays emitted from a multimode optical fiber disperse in a cone of light. The intensity over

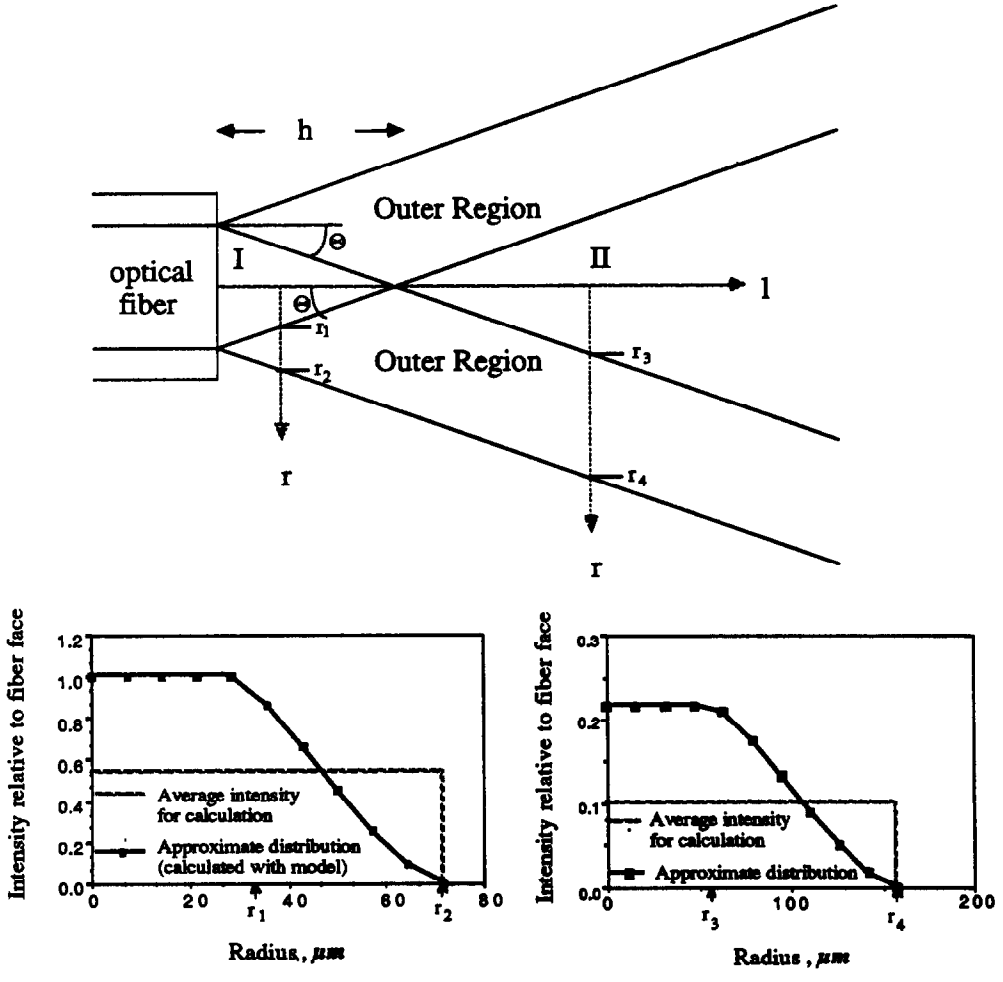

Fig. 4. Regions of different efficiency and excitation intensity.

any cross section of the light cone is assumed to be uniform. It is also assumed that the light intensity across the core of the optical fiber is uniform and any fluctuations in the refractive index are ignored. This assumption is fine for the model, because these fluctuations are irregular, and do not significantly affect the regional distribution.[16]

The amount of fluorescent light from any point (r, l) within the light cone which contributes to the fluorescence signal must be determined. A dye molecule at any point (r, l) can be excited by rays within a cone determined by the NA of an ideal optical fiber, as described in Fig. 3. Although the fluorescence emission is at 360 steradians from the molecule, only those within the same cone will contribute to the signal. Figure 4, adapted from the work of Deaton,[5] shows the regions of collection efficiency in the light cone. Within region I, the emission cone is complete, that is, the entire base overlaps the core of the optical fiber. Outside region I, only a portion of the base of the cone overlaps the fiber core. This simple concept is the basis for modeling the fluoresence signal with and without the mirror.

The same diagram that shows the regions of collection efficiency in the light cone can also be used to describe the actual light distribution in the cone, as described by Hirschfeld.[17] Region I has a uniform light distribution, with the intensity equal to that at the core of the optical fiber. The light is uniform across the cross section of region II, and it decreases in intensity with distance from the core, proportionate to the ratio of areas of the core circle and the emission cone base. Outside regions I and II, the intensity decreases radially to zero at the radius of the light cone; as shown in Figs. 4(a) and 4(b). These curves (solid lines) can be used to represent both the excitation intensity and the collection fraction distributions.

The collection efficiency of any point within the distal cone can be described by two overlapping circles, which is illustrated in Fig. 5. The shaded region is the overlap of the core face and the emission cone base. The core circle has a constant radius of a, and the emission circle has a variable radius of ρ. The distance between the centers of the circles is r. The angle, Θ, is assumed to be the same for the excitation and emission light cones for simplicity in the model. This is an approximation because the He–Ne laser light source is highly collimated while the fluorescence emission light is not. As a result,

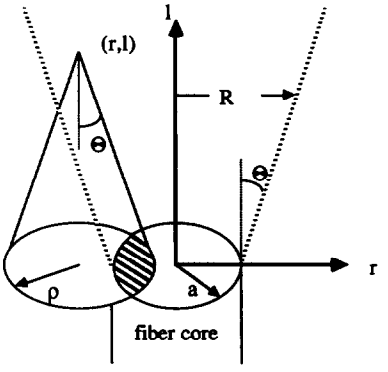

Fig. 5. Overlap of emission cone and fiber endface.

the emission cone is somewhat wider than the excitation cone, which has been described by Glass *et al.*[18]

By simple geometry, the following can be described:

$$\rho = l \tan \Theta \tag{4}$$

$$R = \rho + a \tag{5}$$

where R is the radius of the excitation cone at point 1, also defining ρ by equation (4). The length of the Region I cone, h is

$$h = \frac{a}{\tan \Theta} \tag{6}$$

The fraction of fluorescence energy returning to the fiber core which contributes to the output signal can be described by one of five sets of equations, depending on the point location which is illustrated in Fig. 6. The physical significance of regions III–V is the same, but the geometry for computation varies slightly. Regions III and IV are similar in that at least

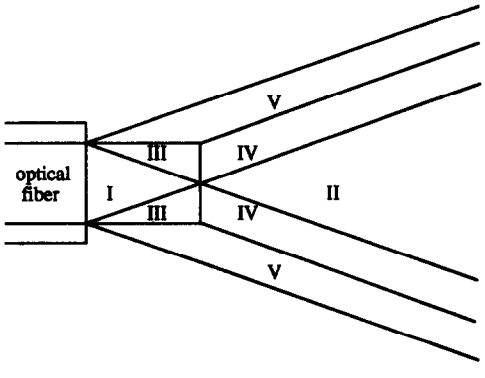

Fig. 6. Five regions for calculating collection fraction. The calculational algorithm used in the model is partitioned into five elements, one for each of these five regions.

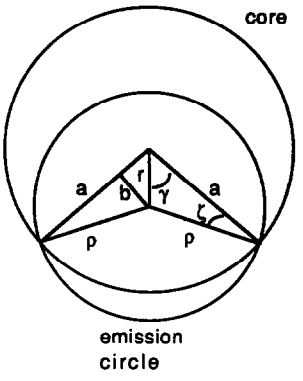

Fig. 7. Overlap region for calculation of region III collection fraction.

one of the centers of the circles are within the overlapped area. The equations are identical in format, with an exchange of a and ρ.

Figure 7 illustrates the overlapping circles. The fractional overlap in region III is calculated as,

$$\text{area}_{\text{region III}} = \frac{a^2\zeta + \rho^2(\pi - \gamma - \zeta) - ab}{\pi\rho^2} \quad (7)$$

where b is the perpendicular height of $\Delta a\rho p$. The angles, γ and ζ can be calculated from the law of cosines

$$\zeta = \cos^{-1}\left(\frac{a^2 + r^2 - \rho^2}{2ar}\right) \quad (8)$$

then,

$$b = r \sin\zeta \quad (9)$$

and

$$\gamma = \sin^{-1}(b/\rho) \quad (10)$$

Region V is similar in computation and is shown in Fig. 8. The same equations apply whether $a > \rho$ or $\rho > a$. The fractional area is calculated by

$$\text{area}_{\text{region V}} = \frac{a^2\gamma + \rho^2\zeta - rb}{\pi\rho^2} \quad (11)$$

Once again with the law of cosines,

$$\zeta = a\cos^{-1}\left(\frac{\rho^2 + r^2 - a^2}{2r\rho}\right) \quad (12)$$

Within region I, since the entire emission cone overlaps the fiber core, the fractional area is taken as unity for any increment which falls within the boundaries. In region II, as the entire core circle overlaps a portion of the emission cone, the area value is related to the ratio of areas of the two circles:

$$\text{area}_{\text{region II}} = a^2/\rho^2 \quad (13)$$

In each region, the collection fraction is a ratio of the overlap area to the area of the emission cone base.

The program is designed to calculate the fluorescence intensity as a function of distance of the fiber from the absorbing or reflective surface, based upon experimental values. The input values are NA, a, power (P), n_{ext}, molar absorptivity (ϵ), fluorescence quantum efficiency (ϕ_f), and dye concentration (c). Aside from ϵ and ϕ_f, which are provided with the dye, the others are measured experimentally.

A trapezoidal type algorithm is used with cyclindrical coordinates. Figure 9 illustrates a finite incremental segment for summation. Differential distance increments Δl are used as 10 μm, which is not greater than one tenth of the core diameter of the fibers used. The radius is divided into ten sections, the size of which increases with distance from the core because the total radius, R, over the cross section of the light cone increases with distance. For simplicity, the model curve for an absorbing surface will be referred to as the incident curve, because the

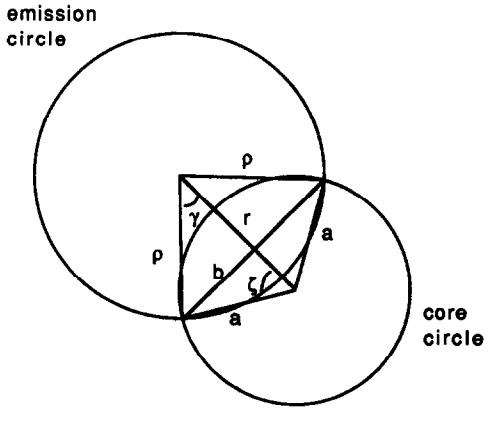

Fig. 8. Overlap region for calculation of region V collection fraction.

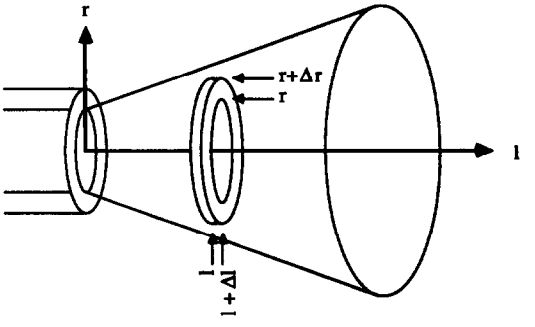

Fig. 9. Finite volume segment for summation in the model.

signal is due only to the light that is incident on the mirror or absorbing surface. The model curve for the case with a mirror will be referred to as the enhanced curve.

The entire incident curve, from $l = 0$ to the mirror, at a distance, D, is calculated each time D is incremented. When D is at the final distance, the values are stored in an array for output. The initial calculations are of constants dependent on the input variables.

$$\text{initial intensity } I_0 = P/\pi a^2 \tag{14}$$

$$\text{cone half angle } \Theta = a \sin(\mathrm{NA}/n_{\text{ext}}) \tag{15}$$

Because the model integrates by stepping through increments of 1, the reduction in light intensity at each increment can be determined by the light transmitted. The factor, α, is defined for a given dye and concentration, using the distance increment, Δl, as the pathlength:

$$\alpha = 10^{-\epsilon c \Delta l} \tag{16}$$

The length of region I cone, h, is found from equation (6).

The outermost loop is for setting D, which is initialized at 10 microns. For each value of D, the initial intensity of the incident ($I_{0,\mathrm{f}}$) and reflected ($I_{0,\mathrm{F}}$) cones is set.

$$I_{0,\mathrm{f}} = I_0 \tag{17}$$

$$I_{0,\mathrm{F}} = I_0 \alpha^{(2D-10)/\Delta D} \tag{18}$$

At each pathlength, the excitation intensity is found from the power at the fiber face divided by the area of the cross section of the light cone.

$$I_0(l) = P/\pi R^2 \tag{19}$$

In the case of the incident cone, the light intensity begins at I_0 and decreases with distance from the fiber core by the factor, α. The reflected intensity increases with distance from the core, by the same factor, α, with each increment. The intensity of the reflected cone at the core is less than the initial incident intensity by a factor of α raised to the power of twice the number of increments between the core and the mirror, as expressed by equation (18). The summations of the fluorescence signal contributions Δf and ΔF, of the incident and reflected cones, respectively, are set to 0.

At each distance, $1 + \Delta l$, the calculation begins with the incident cone, by determining $\rho(1)$ and R(1), with equations 4 and 5. The size of the radial increment is one tenth of the total radius of the cone.

$$\Delta R(l) = R(l)/10 \tag{20}$$

and the radius of the region I, II cone

$$r_{\text{regionI,II}}(l) = |a - \rho(l)| \tag{21}$$

Beginning with $r = \Delta R$, the program determines which of the 5 regions the point is in, considering first the incident cone. The program tests for region I as

$$a - \rho \leqslant 0 \tag{22}$$

and for region II as

$$a - \rho > 0 \tag{23}$$

The boundaries for the other regions

$$\text{region III } l < h \text{ and } r \leqslant a \tag{24}$$

$$\text{region IV } l \geqslant h \text{ and } r \leqslant \rho \tag{25}$$

$$\text{region V } l \leqslant h \text{ and } r > a$$

$$\text{or } l > h \text{ and } r > \rho \tag{26}$$

At each radius an incremental radial area, ΔA, is calculated

$$\Delta A = 2r\Delta R - \Delta R^2 \tag{27}$$

and both the excitation intensity and collection fraction are considered uniform in this area, with the excitation intensity being

$$\Delta I(l) = I_0 \frac{a^2}{R^2} \tag{28}$$

The fluorescence intensity is calculated with equation (29)

$$\Delta L_f = [1 - \alpha]\phi_f \Delta I(l) \text{area}_{\text{region}x} \tag{29}$$

and the contribution to the power at the fiber face which is transmitted to the detector,

$$\Delta f = \Delta I_f \Delta A \Delta l \tag{30}$$

The value is stored in an array, as well as the collection fraction for each of the 10 radial increments.

Placing a mirror in the field of view of an optical fiber results in a double pass of the excitation light as well as the reflection of the fluorescence emission light. The reflected cone is shown in Fig. 10. The additional signal produced by reflecting the light can be modeled by considering the contributions of a second, virtual molecule at a point $(r, 2D - l)$. In fact, by evaluating a parameter,

$$L = 2D - l \tag{31}$$

the equations used to calculate the light distribution without the mirror are repeated,

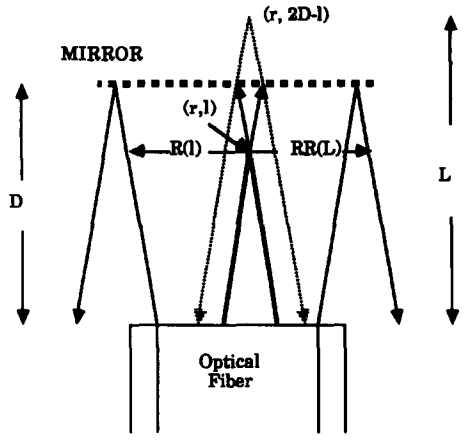

Fig. 10. Distal light distribution with a mirror.

substituting L for l. The only other difference is the number of intervals for calculation. In order to sum the contributions generated with and without the mirror, the corresponding areas to which the values refer must be identical. Since the radius of the reflected cone is larger than the radius of the incident cone, more intervals are needed in the former case

$$\Delta RR(L) = \Delta R(l) = \frac{R(l)}{10} \tag{32}$$

so the number of increments,

$$\text{index} = \frac{RR(L)}{\Delta RR(L)} \tag{33}$$

The other parameters are determined analogously to equations (4), (5) and (21) as follows:

$$\rho(L) = L \tan \Theta \tag{34}$$

$$RR(L) = \rho(L) + a \tag{35}$$

$$r_{\text{region I,II}}(L) = |a - \rho(L)| \tag{36}$$

The total enhanced signal curve is a sum of four contributing sources, as outlined in Fig. 11. The four curves represent the (a) direct excitation (top curve), and (b) the three components which are a result of the mirror. The lowest curve shows the additional fluorescence collected directly by the optical fiber due to the increased intensity of the excitation light reflected from the mirror. The middle two curves are nearly identical. One represents a contribution of the reflected excitation light and the fluorescence which is reflected back off the mirror before being collected by the optical fiber, and the other is due to fluorescence reflected off the mirror which is a result of direct excitation light. The three lower curves show a peak value which demonstrates the optimum of the dispersion of the excitation light and the increase in intensity due to the mirror.

This summation is accounted for in the model by using the sum of the incident and reflected light as the total excitation intensity:

$$\Delta I_{\text{total}} = \Delta I(l) + \Delta I(L) \tag{37}$$

and the sum of the two fractions of collection as the total contribution to the signal:

$$\text{area}_{\text{total}} = \text{area}_{\text{region } x}(l) + \text{area}_{\text{region } x}(L) \tag{38}$$

The enhanced fluorescence signal is then found

$$\Delta F = [1 - \alpha]\phi_f \Delta I_{\text{total}} \text{area}_{\text{total}} \Delta A \tag{39}$$

With the enhanced curve, moving the mirror affects the intensity distribution at each cross section. Therefore, it is necessary to sum both

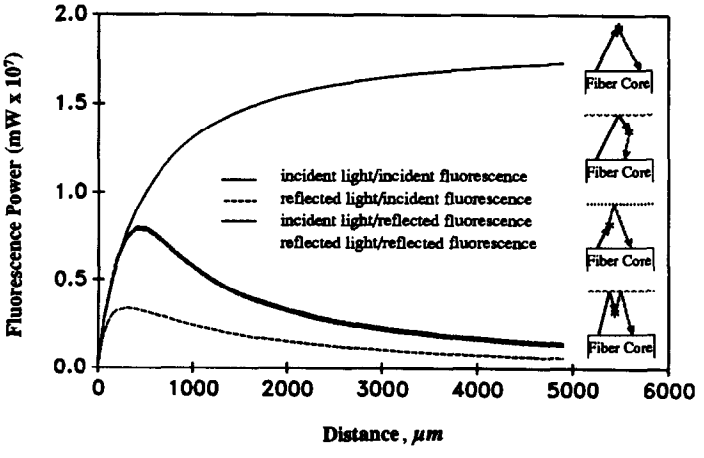

Fig. 11. Calculation of four sources of emitted light contributing to the enhanced signal.

across the radius and through the entire distance of fluorophore for each point of the curve.

$$F_{\text{enhanced curve}} = \sum_{l=0}^{D} \sum_{r=0}^{RR} \Delta F \qquad (40)$$

In the case of the incident curve, the values are summed as the calculation progresses away from the fiber core, because moving the fiber away from the black surface does not change the light distribution. The source code is a C program available from the authors.

EXPERIMENTAL

Reagents

The dye is cyanine based Cy5-18 acid obtained from Dr. Alan Wagonner at Carnegie Mellon University. The molar absorptivity is reported to be approximately 200,000 $1 \cdot \text{mole}^{-1} \cdot \text{cm}^{-1}$ at 648 nm, which was used as the basis for concentration measurements. The fluorescence quantum efficiency of the dye is 0.25. The dye was chosen because of its long excitation wavelength which results in very low ambient light interference, as well as reduced contributions to background from glass optical components. In addition, the excitation wavelength is in a range that permits the use of light emitting diodes (LED's) and other low cost light sources. The dye is completely water soluble, to make it particularly appropriate for use as a label for bioassay. Four concentrations of dye were used in the experiments which were 10^{-3}, 10^{-4}, 10^{-5} and $10^{-6}M$.

Apparatus

The schematic of the experimental set-up is shown in Fig. 12. The light source used was a Uniphase Model 1303p helium neon laser with a 2.0 milliwatt output. Filters were obtained from Omega Optical (Brattleboro, VT). Only one focusing lens, with a numerical aperture of 0.4 was used as part of the coupler which is a Newport F-915T multimode coupler. The detector was an Oriel 70680 photomultiplier tube (PMT) with an accompanying Model 7070 power supply/current amplifier. The signal was monitored with a Standford SR510 lock-in amplifier. Optical fibers were obtained from General Fiber Optics.

Procedure

Three fibers were tested and the apparent NA of each fiber was determined by measuring with a micrometer the diameter (dia) of the circle of light at a given distance (l) from the fiber endface aimed at a smooth surface in air. The diameter and distance translates into the fiber NA:

$$\text{dia} = 2(l \tan \Theta + a) \qquad (41)$$

and

$$\sin \Theta = NA/n_{\text{ext}} \qquad (42)$$

where a is the core radius of the optical fiber and n_{ext} is that of air which is 1.0. In all cases the apparent NA was less than the manufacturer specifications. An attempt at mode scrambling was made by subjecting the fiber to

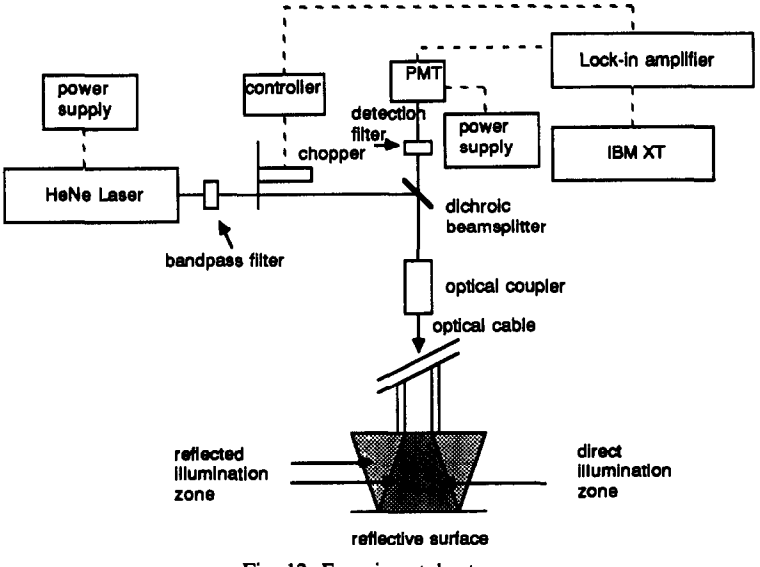

Fig. 12. Experimental set-up.

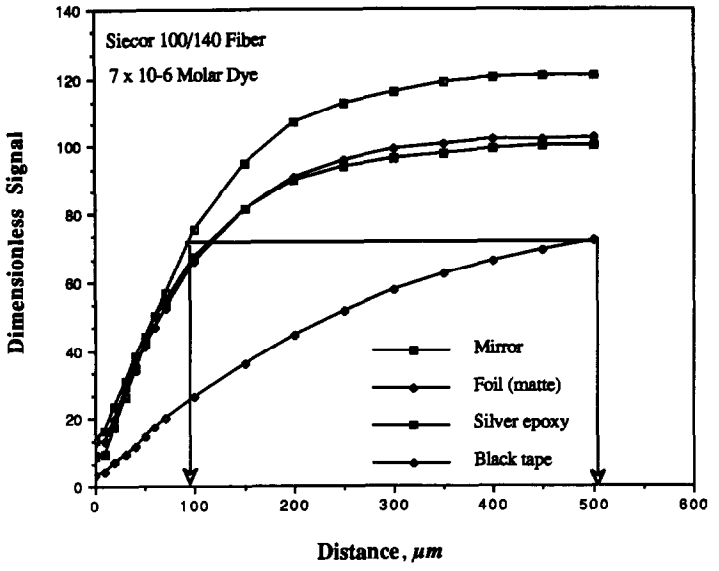

Fig. 13. Comparison of signal enhancement with various reflective surfaces and a black surface. Siecor 100/140 silica fiber, dye concentration $-7 \times 10^{-6} M$.

microbending, but the result was an unsteady power throughput.

The intensity *vs.* distance curves were acquired by measuring the PMT output with the fiber first placed in contact with the non-reflecting surface or mirror, which was then moved away from the fiber in defined increments by using a translation stage (Newport Model 416-B metric stage). In order to assure that the fiber initially was exactly at the surface, the fiber end was viewed through the side of the container of dye, using a horizontal 50× microscope. At each position the signal intensity was measured in milliwatts, but in order to compare the behavior of the system for different concentration levels, relative signal intensities are reported in most figures. The relative intensity is obtained by normalizing each intensity by the asymptotic leveling off intensity obtained when the surface was at very large distances from the fiber. These final intensities are given in millivolt units in each of the figures. A front surface silver mirror was used for reflecting the light, and black plastic electrical tape was used as the non-reflecting surface.

To determine the effect of the optical quality of the mirror on the signal enhancement, one experiment with dull aluminum foil and another with a silver epoxy coated surface was performed. The results as shown in Fig. 13 indicate that for distances less than about 60 μm, the quality of the reflector is not important. For each fiber tested, the signal as a function of distance in plain water was measured to estimate the contribution to background by the optical fiber. A comparision of the background values can be found in Fig. 14. In spite of the increase in background at very short pathlengths with the mirror in place, the limit of detection for the fluorometer was in the order of nanomolar concentrations of the dye.

RESULTS AND DISCUSSION

The experiments were performed to evaluate the effect of optical fiber numerical aperture and diameter on the signal enhancement. The goal was to reach a qualitative understanding of these factors to guide the selection of fibers for specific applications such as the use in

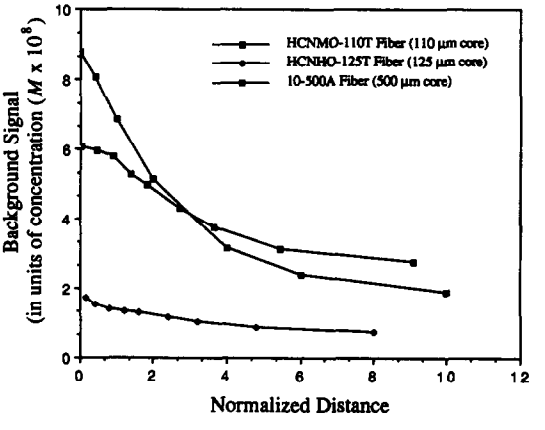

Fig. 14. Comparison of background signal values for various optical fibers. Dimensionless distance = actual distance/fiber diameter.

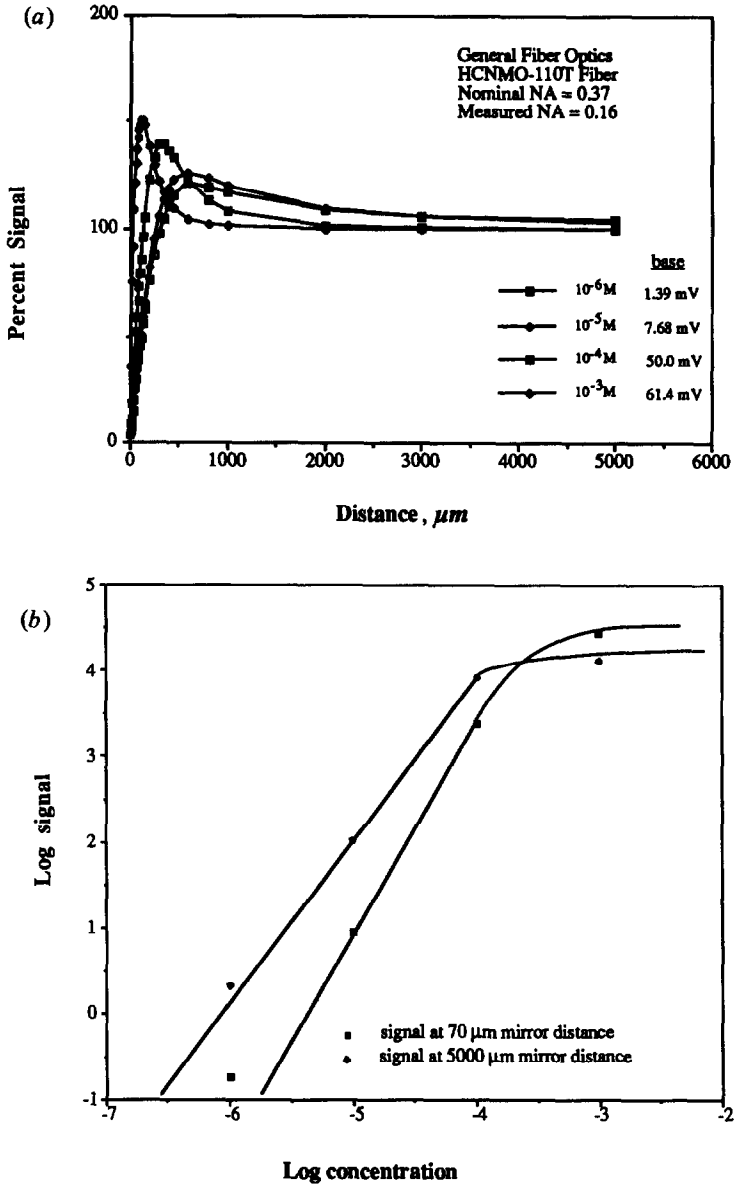

Fig. 15. (*a*) Percent signal as a function of fiber/mirror separation. "Base" signal is the actual PMT output when the mirror is placed 1 cm from fiber surface. (*b*) Log signal *vs.* log concentration.

new sensor configurations. Nominal numerical apertures chosen were 0.37 and 0.48, based on the manufacturers specifications. A silica core fiber with a numerical aperture higher than 0.48 was not available in 100 μ core diameter, so for a 0.58 NA, a 500 μm-plastic core fiber was tested. The actual measured cone half angle was used to calculate an apparent numerical aperture for the fiber with equation (41). The low measured apparent numerical apertures (0.16, 0.08, and 0.11, respectively) were likely to be a result of the highly collimated He–Ne laser light source, in addition to the short lengths of fibers that were tested (<10 meters).

Experimental results

Figure 15 shows the normalized signal plotted as a function of distance of the fiber from the mirror, for the Fiberguide Industries HCNMO-110T hard plastic clad silica fiber. The base signal values listed in the index of the figure are the actual PMT readings when the mirror is placed 1 cm from the fiber surface. Also in this figure is a plot of the log of the base signal values and of the signal values at 70-μm distance as a function of the log of the concentration. This shows the increase of the nonlinearity as the pathlength of the dye increases, which is due to the high extinction coefficient of the dye

(200,000). The response for all the fibers described similar curves, as the apparent NA's were similar. The exception was the response for the 500-μm fiber for which the response did not level off until about 20-mm separation distance between the fiber and mirror because the effective pathlength of a fiber-optic fluorometer increases proportionately with core diameter as described in equation (1).

The degree of absorption of incident light and self absorption of the fluorescent light is most visible at the high concentrations of dye. The base signal values can be compared for the different concentrations with the same fiber, but cannot be compared from fiber to fiber, as the output power and signal attenuation varies from fiber to fiber. The use of relative values for comparing the experimental results is necessary for several reasons. Physical factors such as variations in power loss across the filters, the fiber transmission efficiency and light coupling efficiency at the proximal end of the fiber are factored out of the relative responses.

Employing a mirror for enhancing a signal with a fiber-optic fluorometer will be the most advantageous for applications which require a small sample volume. From the model curves (Fig. 11), it can be seen that a potentially 4 × enhancement can be achieved at very short distances (<2 fiber diameters) and better than 3 × enhancement expected until about 4 fiber diameters. At high numerical apertures, the curves would level off and the degree of enhancement would reduce at smaller mirror displacements, because of higher dispersion of the light rays.

Signal enhancement with the mirror in place is dependent on concentration. Because the illumination and collection efficiency are the greatest closest to the fiber endface, the steepest response curves were obtained with higher solution concentrations showing the highest absorbance. Distances of the peak enhancement are shorter in high concentrations because of the reduced pathlengths due to higher light absorption. As a result, the degree of enhancement due to the mirror is indirectly related to the dye concentration.

Comparison of experimental results with mathematical model

Figure 16 shows a comparison of experimental results with model calculations (solid line) for the General Fiber Optics HCNHO-125T fiber. The dotted line represents the model calculations at a higher assumed numerical aperture of 0.12, which shows a closer resemblance to the experimental results. Figure 17 shows a similar comparison for the General Fiber Optics 10–500A fiber.

The use of the measured apparent numerical aperture in the model gives a much closer prediction of the experimental data than is obtained with the manufacturers rated numerical aperture for the fiber. The same approach was used by Deaton.[5] The measured numerical aperture is only valid for the excitation light cone, but is used in the model for the collection solid angles as well. The discrepancy between the experimental and model fit numerical apertures is probably due to this assumption.

Figure 18 shows a comparison of the experimental results with the model prediction with the General Fiber Optics HCNHO-110T fiber at dye concentrations of $10^{-4}M$ 100× greater

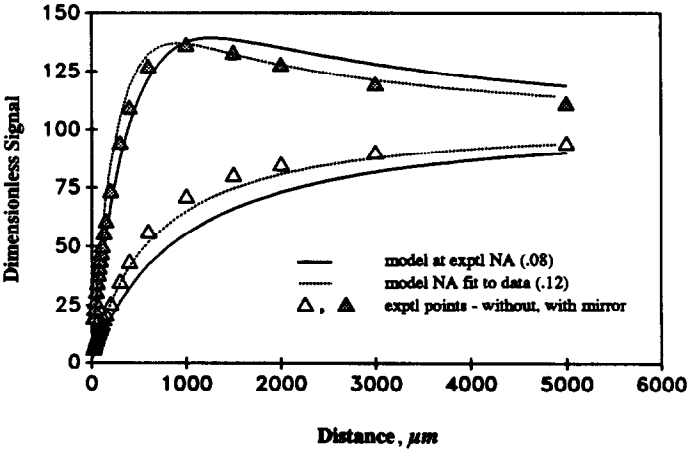

Fig. 16. Percent signal *vs.* distance from optical fiber. General Fiber Optics HCNHO-125T fiber dye concentration $10^{-6}M$, nominal NA 0.48.

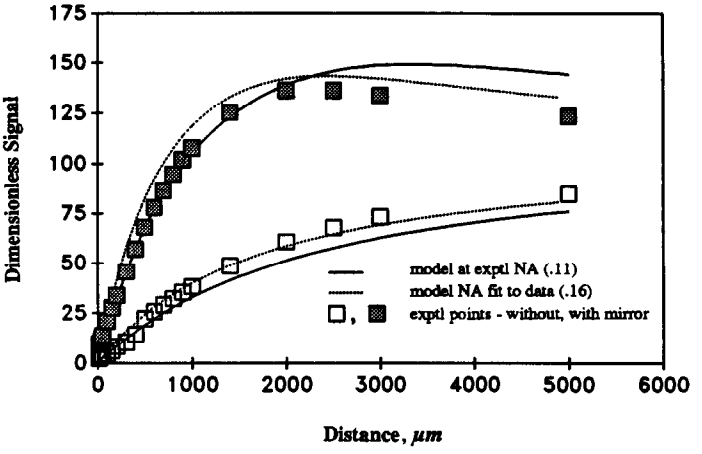

Fig. 17. Percent signal *vs.* distance from optical fiber. General Fiber Optics 10–500A fiber, dye concentration $10^{-6}M$, nominal NA 0.58.

than the previous two examples. The model curve was calculated with the measured numerical aperture of 0.16, rather than the manufacturer's nominal rated NA of 0.37. This example shows that the model is the poorest at high dye concentrations, as is expected considering that self-absorption is not accounted for in the calculations. Self-absorption is particularly significant with this dye, because of the overlap of the excitation and emission curves,[19] which at high dye concentrations affects the effectiveness of the mirror to reflect light back into the fiber.

CONCLUSION

Placing a mirror at the distal end of an optical fiber, which is used for excitation and collection of fluorescent light, results in an enhancement in the detected signal. This enhancement is potentially four-fold because of the increased excitation light as well as the reflection of the fluorescence emission light. Experimentally, a better than three-fold enhancement was achieved. The enhancement is higher for low concentrations of fluorophore, where the reduction of light transmission due to absorption is less significant. The principle can be used for constructing a continuous, reversible affinity sensor which may show some improvements over other designs.

A mathematical model was developed that successfully described the fluorescence signal as a function of distance of a mirror and non-reflecting surface from the optical fiber. A general, qualitative agreement with the data is achieved. While the model cannot be used *a priori*, it can provide a reliable estimate of trends once some fluorescence measurements are

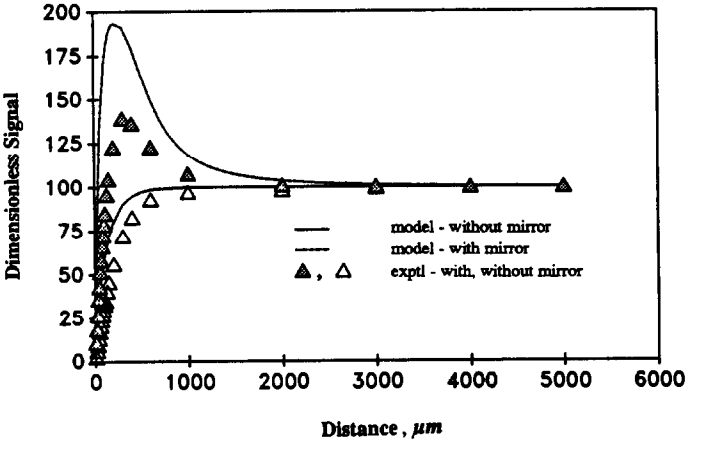

Fig. 18. Percent signal *vs.* distance from optical fiber. General Fiber Optics HCNMO-110T fiber, dye concentration $10^{-4}M$ nominal NA 0.37.

made with a specific fiber-dye combination and an apparent numerical aperture can be measured. The model accounts for the dependence of the enhancement on the diameter and numerical aperture of the fiber, as well as the concentration, fluorescence quantum efficiency, and molar absorptivity of the dye.

REFERENCES

1. S. M. Angel, *Spectroscopy*, 1987, **2**, 38.
2. W. R. Seitz, *Anal. Chem.*, 1984, **56**, 16A.
3. M. Aizawa, in *Biosensors International Workshop 1987*, R. Schmid (ed.), GBF Monographs Vol. 10, VCH Verlagsgesellschaft, Weinheim.
4. T. A. Betts, F. V. Bright, G. Catena, J. C. Huang, K. S. Litwiler, and D. P. Paterniti, in *Laser Techniques in Luminescence Spectroscopy*, T. Vo-Dinh and D. Eastwood (eds.), pp. 88–95. Philadelphia: American Society for Testing Materials, 1990.
5. T. K. Deaton, *Instrumentation and Methodology for Remote Fiber Fluorimetry*, Ph. D. Dissertation, University of California at Berkeley, 1982.
6. R. B. Thompson and F. S. Ligler, *Fiber Optic Biosensor Technology*, Naval Research Laboratory Memorandum Report 6182, May 12, 1988.
7. J. G. White, *Anal. Chem.*, 1976, **48**, 2089.
8. R. O. Cook and C. W. Hamm, *Appl. Opt.*, 1979, **18**, 3230.
9. J. S. Schultz, in *Biosensors: Fundamentals and Applications*, A. P. F. Turner, I. Karube and G. S. Wilson (eds.), pp. 638–654. Oxford University Press, Oxford, 1987.
10. D. N. Modlin and F. P. Milanovich, in *Fiber Optic Chemical Sensors and Biosensors*, O. S. Wolfbeis (ed.), pp. 237–302. CRC Press, Boca Raton, 1991.
11. C. Komives and J. S. Schultz, *12th Annual Int'l Conf. of the IEEE Engineering in Medicine and Biology Soc.*, proc. 12(2), pp. 478–479. Philadelphia, PA, Nov. 1–4, 1990.
12. *Idem*, *Medical Design and Material*, 1991, **1**, 24.
13. F. L. Dickert, S. H. Schreiner, G. R. Mages and H. Kimmel, *Anal. Chem.*, 1989, **61**, 633.
14. Jerome S. Schultz, US Patent 4,344,438, 1982.
15. S. Mansouri and J. S. Schultz, *BIO/TECHNOLOGY*, 1984, **2**, 885.
16. I. Masaaki, *Trans. IECE Jap.*, 1990, **E-63**, 16.
17. T. B. Hirschfeld, U.S. Patent 4577109, 1986.
18. T. R. Glass, S. Lackie and T. Hirschfeld, *Appl. Opt.*, 1987, **26**, 2181.
19. M. Wagner, L. Ernst, R. Mujamdar, S. Mujumdar, J. Chao and A. Waggoner, *Applications of New Cyanine Labeling Reagents in Flow Cytometry*, XIV International Meeting of the Society for Analytical Cytology, Asheville, NC, March 18–23, 1990.

NOMENCLATURE

Symbol	*Explanation*
a	fiber radius (cm)
$\text{area}_{\text{region } x}$	collection fraction based on the ratio of the overlap area of emission cone base and fiber core divided by the area of the emission cone base
ΔA	incremental area for summation in sample volume (cm^2)
c	concentration (moles/liter)
D	fiber/mirror separation (cm)
F	power of fluorescence at fiber face (milliwatts)
Δf	incremental power at fiber face (milliwatts)
F_T	flux of fluorescence power at fiber face (milliwatts)
I	intensity in light cone (milliwatts/cm^2)
ΔI	incremental intensity (milliwatts/cm^2)
l	axial distance from optical fiber (cm)
L	distance of virtual molecule from fiber (cm)
L_E	effective pathlength (cm)
NA	numerical aperture
n_{ext}	refractive index of external fluid
P	light power emanating from optical fiber (mW)
r	radial variable of light cone
$r_{\text{region,I,II}}$	radius of region I,II
R	radius of light cone (cm)
RR	radius of reflected light cone (cm)
ΔR	finite radial increment
x	variable to denote one of region I–V
V	sample volume
w	fiber diameter (cm)
α	fraction of light transmitted
ϵ	molar absorptivity (liters/mole/cm)
ϕ_f	fluorescence quantum efficienty (dimensionless)
γ	angle of triangle $\Delta a\rho r$
ρ	radius of emission cone base (cm)
Θ	half angle of light cone
$\omega(r, l)$	collection efficiency from a point (r, l)
ζ	angle of triangle $\Delta a\rho r$

Talanta, Vol. 39, No. 4, pp. 443–447, 1992
Printed in Great Britain.

0039-9140/92 $5.00 + 0.00

DETERMINATION OF NITRITE BASED ON MEDIATED OXIDATION AT A CARBON PASTE ELECTRODE MODIFIED WITH A RUTHENIUM POLYMER

THOMAS J. O'SHEA, DÓNAL LEECH, MALCOLM R. SMYTH* and JOHANNES G. VOS
School of Chemical Sciences, Dublin City University, Dublin 9, Ireland

(*Received* 13 *February* 1991. *Accepted* 26 *March* 1991)

Summary—The use of carbon paste electrodes modified with $[Ru(bpy)_2(PVP)_{10}Cl]Cl$ for the mediated detection of nitrite is described. This surface modifier substantially lowers the overpotential for nitrite oxidation, hence permitting its determination at a lower potential. Various electrode characteristics were optimized, including the modifier loading and the monitoring potential, using batch amperometry. Standard calibration curves yielded slopes of 0.30 $\mu A/\mu M$ over the linear range 5×10^{-8}–$5 \times 10^{-4} M$ nitrite with a detection limit of $3 \times 10^{-8} M$ (1.38 ppb) nitrite. The modified electrode response was shown to be relatively stable over a period of 5 days with a signal diminution of 8%. Electrode-to-electrode precision was measured as 11.4%. Flow-injection studies indicated the suitability of this electrode as a detector in flowing streams.

The design of chemically modified electrodes (CMEs) for electroanalysis has been the subject of increasing research since their inception over 15 years ago,[1] and it was the objective of this work to develop a CME for the determination of nitrite.

In recent years there has been growing concern about the role of the nitrite ion as an important precursor in the formation of N-nitrosamines, many of which have been shown to be carcinogens.[2] The occurrence of nitrite salts in the environment and their use as food preservatives is widespread; therefore it is important that sensitive and accurate methods be available for the determination of the nitrite ion.

A large number of analytical methods have been developed for the determination of this ion based principally on spectrophotometric methods,[3–5] but these have limited sensitivity and dynamic range, frequently depend on unstable colours, and involve long reaction times. Cox and Kulesza[6] reported a voltammetric procedure with a platinum electrode modified with iodine, but this method was limited by poor sensitivity. A more sensitive CME for the detection of nitrite was described by Kalcher[7] who used a carbon paste electrode modified with an anion exchanger, but this electrode suffered from long analysis times. More recently, several sensitive polarographic methods have been reported in the literature[8,9] for the detection of *nM* levels of nitrite. Methods based on solid electrodes are more desirable, however, for sensing and flow applications.

Redox polymers containing ruthenium sites have been studied extensively in recent years.[10–13] These studies showed that various metallopolymers of ruthenium act as redox catalysts for a number of substrates. The mediation by the Ru(II/III) couple has been shown to enhance the sensitivity of oxidation processes, and recently a glassy-carbon electrode coated with a Ru-containing polymer has been shown to be effective for the mediated oxidation of nitrite.[14] However, it was reported that in a flowing system, the response from this CME was not found to be stable due to the slow removal of the polymer film from the electrode surface, making their practical application difficult. This instability was alleviated to some extent by treatment with UV light or by coating with other polymer layers.[15]

The purpose of the present study was to investigate the application of carbon paste electrodes modified with the same ruthenium polymer, *i.e.*, $[Ru(bpy)_2(PVP)_{10}Cl]Cl$ where bpy = 2,2′-bipyridiyl and PVP = poly(4-vinylpyridine), for the amperometric detection of nitrite.

*To whom correspondence should be addressed.

EXPERIMENTAL

Chemicals and Reagents

Throughout this work analytical grade chemicals and demineralized water (obtained by passing distilled water through a Millipore water purification system) were used. Standard solutions of sodium nitrite were prepared daily in 0.1*M* sodium nitrate electrolyte and carrier solution. The preparation of $[Ru(bpy)_2(PVP)_{10}Cl]CL$ has been reported elsewhere.[16]

Apparatus

Cyclic voltammetry was performed with an EG & G Model 362 scanning potentiostat in conjunction with a Linseis LY17100 X-Y plotter to record the voltamperograms. A 10-ml homemade three-electrode cell was employed incorporating the modified electrode in addition to a Ag/AgCl reference electrode and a platinum wire auxilliary electrode. For batch amperometry, the detection system used was a Metrohm 641 VA detector. To achieve mass transfer, a 1-cm stirring bar was placed in the cell and rotated with an IKAMAG RET-G magnetic stirrer. A stirring rate of 600 rpm was used for all studies.

Flow-injection analysis was performed with a Waters 501 HPLC pump with an EG & G Model 400 electrochemical detector equipped with a homemade thin layer carbon paste cell (3-mm diameter), a Ag/AgCl reference electrode and a stainless steel auxilliary electrode. Sample injections were made through a Rheodyne injection valve (20 μl loop).

Procedures

The modified carbon paste (usually Nujol: graphite powder: Ru-polymer in a 40:55:5 ratio) was prepared by thoroughly mixing the required amounts for at least 30 min. Portions of the resulting mixture were then packed into either a glass tube (4 mm i.d.) or into the flow-injection cell base. The surface was smoothed on filter paper. Electrical contact in the glass tube electrodes was established via a copper wire which was inserted into the back of the carbon paste mixture.

Saliva was collected by expectoration into small vials. At least 1 ml was collected from each subject. No sample pretreatment was carried out on the samples which were diluted with 0.1*M* sodium nitrate supporting electrolyte.

RESULTS AND DISCUSSION

Cyclic voltammetry

Preliminary experiments to investigate the nature of the Ru-polymer in the carbon paste matrix and to confirm the retention of its ability to mediate nitrite oxidation were performed by cyclic voltammetry. Well defined oxidation and reduction responses associated with the surface bound Ru(II/III) couple were observed in 0.1*M* sodium nitrate (Fig. 1, curve A). This supporting electrolyte was used as it had been found to be optimum in a previously reported study with this polymer.[14] A linear dependence of the cathodic and anodic peak currents on scan rate was obtained up to 40 mV/sec, indicating the essential surface behaviour of the electrodes, as in the case of certain polymer modified electrodes.[17]

The addition of nitrite to the solution resulted in an electrocatalytic oxidation at the same potential as that observed for the Ru(II/III) system (Fig. 1, curve B). Using an unmodified carbon paste electrode, the oxidation of nitrite results in a broad response at 1.05 V (Fig. 1, curve C). The corresponding response on the modified electrode occurred at 0.78 V indicating a significant reduction in the overpotential of the nitrite oxidation.

As the Ru(II/III) couple is always present, the analytical signal for nitrite must be recorded on top of a substantial background current. Detection with conventional voltammetric techniques

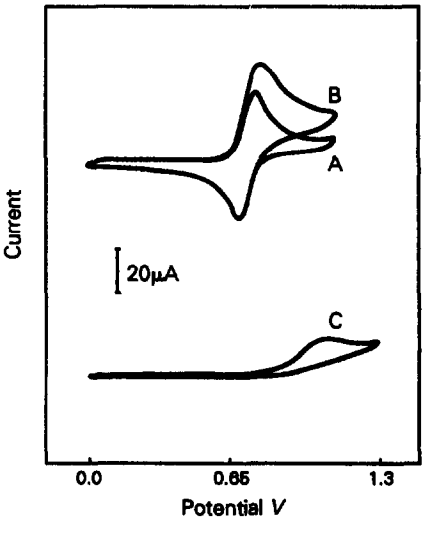

Fig. 1. Cyclic voltamperograms for (A) 5% (w/w) Ru-polymer CME; (B) same as (A) with the addition of $2 \times 10^{-4}M$ nitrite. Curve (C) is the response at an unmodified electrode for $2 \times 10^{-4}M$ nitrite. Scan rate: 100 mV/sec; electrolyte: 0.1*M* $NaNO_3$.

are therefore not recommended. Optimization of the analytical parameters for the mediated reaction were therefore performed with either constant potential batch amperometry or flow-injection analysis.

Batch amperometry in stirred solution

The effect of Ru-polymer loading in the carbon paste was investigated by constant potential batch additions (at 0.8 V) to determine the optimum composition. Calibration curves were constructed in the range 5×10^{-6}–$5 \times 10^{-4}M$ nitrite. Slopes of 0.2, 0.3, 0.3 and 0.25 $\mu A/\mu M$ and correlation coefficients of 0.9995, 0.9996, 0.9997 and 0.9991 were obtained for loadings of 2.5, 5, 10, 20% (w/v) modified electrodes, respectively. A loading of 5% (w/w) Ru-polymer was chosen as increased loadings did not result in an increased response. The decrease in sensitivity at the 20% loaded electrode may be attributed to a decrease in the conductivity of the electrode matrix caused by the high loading of the polymer. Furthermore, as the mediation was assumed to be a surface phenomenon, any Ru-polymer in the electrode not situated on the surface would not contribute to the measured current.

Hydrodynamic voltammetry was then attempted with a 5% (w/w) loaded modified electrode for batch additions of $1 \times 10^{-4}M$ nitrite. The potential of the electrode was increased in 50-mV steps and a two-plateau shaped response was observed (Fig. 2, curve A). The first wave is a result of the mediated current for the oxidation of nitrite at the Ru-polymer at the surface of the modified electrode. The second wave presumably arises due to the response of nitrite at the bare sections of carbon paste at the surface of the modified electrode. This wave is therefore lower in current due to the reduced surface area of carbon particles in the modified

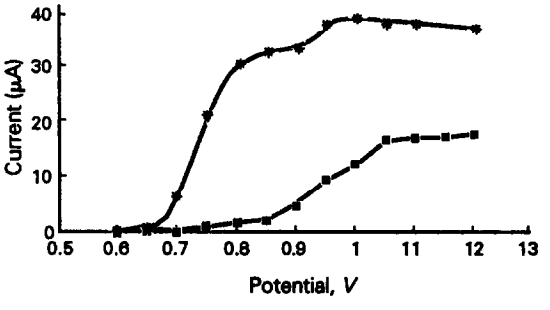

Fig. 2. Hydrodynamic voltamperograms obtained at (A) modified, and (B) unmodified electrode for $1 \times 10^{-4}M$ nitrite. Electrolyte: $0.1M$ $NaNO_3$; stirring rate: 600 rpm.

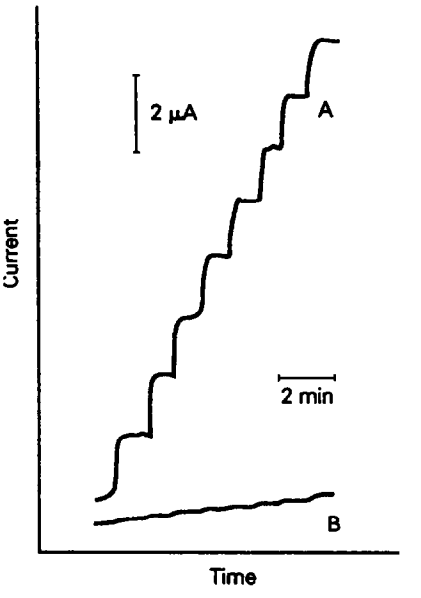

Fig. 3. Batch additions of $5 \times 10^{-6}M$ nitrite (final cell concentration) at (A) modified, and (B) unmodified electrode with constant potential detection at 0.8 V. Other conditions as in Fig. 2.

versus the unmodified electrode (Fig. 2, curve B). A potential of 0.8 V was selected for subsequent investigations in order to maximize the analytical response and minimize interferences obtained at higher potentials.

The response of the modified and unmodified electrodes to batch additions of $5 \times 10^{-6}M$ nitrite are shown in Fig. 3. From this one can see the fast response times needed to achieve a steady state current for the modified electrode. In addition, one can see the large increases in signal obtained for the modified electrode in comparison to the unmodified electrode at the monitoring potential of 0.8 V. The increase in sensitivity of the modified over the unmodified electrode was nearly 20-fold. A calibration curve constructed in the range 5×10^{-8}–$5 \times 10^{-4}M$ nitrite displayed excellent linearity with a slope of 0.30 $\mu A/\mu M$ and a correlation coefficient of 0.9999 ($n = 12$). The signal-to-noise characteristics (S/N = 3) resulted in a detection limit of $3 \times 10^{-8}M$ nitrite. To determine the surface to surface precision, 10 independently prepared electrodes were constructed and they yielded calibration curves with slopes of *ca.* 0.30 $\mu A/\mu M$ with a standard deviation of $\pm 11.4\%$.

The long-term stability of the modified electrode to the oxidation of nitrite was investigated over a 5-day period. The electrode exhibited a current diminution of only 8% during this

period, in contrast to that reported by Barisci *et al.*[14] who reported a 50% response reduction after only 8 hr for the same polymer chemisorbed on the surface of a glassy-carbon electrode. Obviously the carbon paste matrix provides a more stable fixture for the polymer.

Flow-injection analysis

When these Ru-polymer modified electrodes are used in a stationary cell with complex samples, their practical application is hampered by responses for easily oxidized species at the monitoring potential of 0.8 V. Consequently, this approach suffers from lack of selectivity. This drawback can be alleviated by using the modified electrode in a flowing system with a view to employing ion chromatographic separation with electrochemical detection.

For flow studies, 0.1M sodium nitrate was again used as the supporting electrolyte. The effect of flow-rate on the magnitude of response was investigated over the range 0.3 to 1.5 ml/min. Appreciable peak broadening was observed at low flow-rates *i.e.*, peak widths of 22 and 6 sec were obtained at 0.3 and 1.5 ml/min, respectively. A flow-rate of 1 ml/min was selected as the optimum rate as the compromise between sensitivity and sample throughput.

Typical flow-injection responses for nitrite at both the modified and unmodified surfaces are shown in Fig. 4. The linear range was found to be 2×10^{-7}–$1 \times 10^{-3}M$ nitrite. Calibration curves constructed yielded a slope of 0.032 $\mu A/\mu M$ with a correlation coefficient of 0.9998 ($n = 12$). A detection limit (S/N = 3) of $8 \times 10^{-8}M$ nitrite was calculated. These results indicate an attractive detection system for ion chromatographic determination of nitrite.

The short-term stability was ascertained by monitoring the current response for a series of 100 replicate injections of $2 \times 10^{-4}M$ nitrite over a 90-min period. The RSD of these 100 injections was 2.9%, demonstrating the short term stability of the modified electrode in flowing streams.

Determination of nitrite in saliva

The application of the Ru-polymer CME to the determination of nitrite in saliva was then investigated. Using flow-injection analysis, levels in samples taken from two volunteers were determined to be $2.05 \times 10^{-5}M$ (0.94 ppm) and $4.45 \times 10^{-5}M$ (2.05 ppm) nitrite. For both samples, known amounts of nitrite were added to check recovery which was estimated as

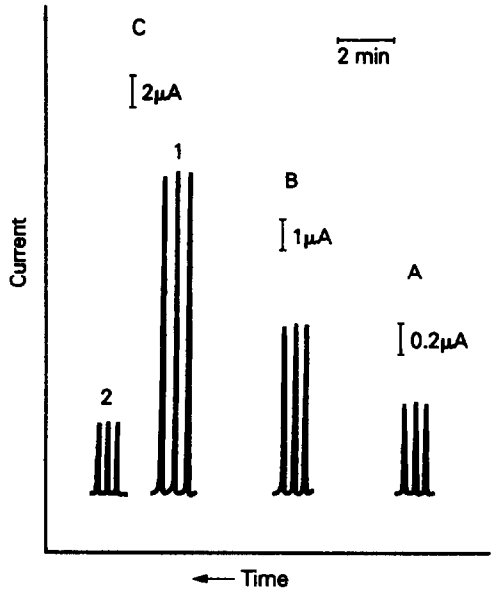

Fig. 4. Flow-injection response at the Ru-polymer modified electrode of (A) $3 \times 10^{-5}M$, and (B) $2 \times 10^{-4}M$ nitrite. (C) is the response for $8 \times 10^{-4}M$ at (1) modified, and (2) unmodified electrode. Constant potential operation at 0.8 V; electrolyte: 0.1M $NaNO_3$; flow rate: 1 ml/min.

$98 \pm 3\%$. The nitrite levels found in each sample were within the range previously reported for human saliva.[18]

CONCLUSIONS

In conclusion, the Ru-polymer modified carbon paste electrodes have been demonstrated to be both sensitive and stable for the determination of nitrite, offering a substantial decrease in overpotential for nitrite oxidation. The detection limit and dynamic linear range are only bettered by polarographic methods.[8,9] As previously mentioned, however, techniques based on mercury are generally undesirable for many practical applications, including flow analysis.

Acknowledgement—The authors would like to acknowledge a generous gift of $RuCl_3$ from Johnson Matthey.

REFERENCES

1. R. W. Murray, A G. Ewing and R. A. Durst, *Anal. Chem.*, 1987, **59**, 379A.
2. W. Lijinsky and S. S. Epstein, *Nature*, 1970 **223**, 21.
3. E. Szekely, *Talanta*, 1968, **15**, 795.
4. A. Chaube, A. K. Baveja and V. K. Gupta, *ibid.*, 1984, **31**, 391.
5. S. Flamerez and W. A. Bashir, *Analyst*, 1985, **110**, 1513.
6. J. A. Cox and P. J. Kulesza, *Anal. Chim. Acta*, 1984, **158**, 335.

7. K. Kalcher, *Talanta*, 1986, **33**, 489.
8. C. M. G. Van den Berg and H. Li, *Anal. Chim. Acta*, 1988, **212**, 31.
9. Z. Gao, G. Wang and Z. Zhao, *ibid.*, 1990, **230**, 1.
10. S. M. Geraty, D. W. M. Arrigan and J. G. Vos in *Electrochemistry, Sensors and Analysis*, M. R. Smyth and J. G. Vos (eds.), p. 303, Elsevier, Amsterdam, 1986.
11. N. Oyama and F. C. Anson, *Anal. Chem.*, 1980, **52**, 1192.
12. O. Haas and J. G. Vos, *J. Electroanal. Chem.*, 1980, **113**, 139.
13. O. Haas, H. R. Zumbrunnen and J. G. Vos, *Electrochim. Acta*, 1985, **30**, 1551.
14. J. N. Barisci, G. G. Wallace, E. A. Wilke, M. Meaney, M. R. Smyth and J. G. Vos, *Electroanalysis*, 1989, **1**, 245.
15. G. G. Wallace, M. Meaney, M. R. Smyth and J. G. Vos, *ibid.*, 1989, **1**, 357.
16. J. M. Clear, J. M. Kelly, C. M. O'Connell and J. G. Vos, *J. Chem. Res.*, 1981, **3**, 3039.
17. R. W. Murray, *Electroanalytical Chemistry*, A. J. Bard (ed.), Vol. 13, Marcel Dekker, New York, 1984.
18. S. R. Tannenbaum, A. J. Sinskey, M. Weisman and W. Bishop, *J. Natl. Cancer Inst.*, 1974, **53**, 79.

Talanta, Vol. 39, No. 4, pp. 449–456, 1992
Printed in Great Britain.

0039-9140/92 $5.00 + 0.00

CHARACTERIZATION OF THE POLYPYRROLE FILM–PIEZOELECTRIC SENSOR COMBINATION

STEPHEN J. VIGMOND, KRISHNA M. R. KALLURY, VIDA GHAEMMAGHAMI and MICHAEL THOMPSON*

Department of Chemistry, University of Toronto, 80 St. George Street, Toronto, Ontario, M5S 1A1, Canada

(*Received* 27 *February* 1991. *Revised* 14 *May* 1991. *Accepted* 16 *May* 1991)

Summary—Polymerization of pyrrole onto the electrode surfaces of thickness-shear-mode acoustic wave sensors at various levels of oxidation has been performed with electrochemical methods. The resulting films of polypyrrole have been characterized by scanning electron microscopy and X-ray photoelectron spectroscopy. Frequency decreases for the polypyrrole—coated sensors exposed to methanol, toluene and ammonia have been evaluated in terms of the various interactions occurring at the polymer surface.

Conducting films produced from polypyrrole have found extensive application in chemical sensor,[1–3] battery,[4] protective coating[5] and electrochromic device[6] technologies. The polymer is usually synthesized by electrochemical procedures which allow facile conversion between conductive and neutral insulating forms.[7] Preparation conditions such as concentration of reactants, nature of the solvent, reaction temperature, type of anion and applied potential are known to affect the conductivity of the polymer[8,9] which is derived from positively charged sites present along the backbone chain. These charges are compensated by the incorporation of one anionic species per three or four pyrrole units. Increase of the degree of oxidation tends to result in the pairing up of positively charged sites forming bipolarons which are thought to be responsible for conduction by an electron hopping mechanism. Transition between the oxidized and neutral forms of polypyrrole can be effected by application of an appropriate potential which results in incorporation or removal of counteranions by diffusion.

Changes in conductivity of the polymer caused by adsorption of various species from the gas phase have been employed to develop a chemical sensory strategy. For example, Bartlett and Ling-Chung[1] monitored reversible changes in the presence of a number of different saturated vapors. In the case of methanol, transient responses were interpreted in terms of a sorption model rather than a diffusion-limited mechanism.[10] The interaction of polypyrrole with several alcohols was studied by Josowicz *et al.*[11] who detected measurable changes in the electron work function of polymer-coated suspended gate field effect transistor devices.

Gustafsson *et al.*[12] studied the interaction of oxidized polypyrrole with ammonia. While low concentrations of ammonia produced a reversible increase in the resistance (approx. 15% change in the presence of 27 ppm ammonia in argon), concentrations of ammonia greater than 1 atm or the presence of water led to a permanent increase in resistance. The irreversible increase in resistance was attributed to nucleophilic attack by ammonia or hydroxide on the polymer leading to loss of conjugation and ring opening. Other gas phase studies indicate that the neutral polymer shows selectivity towards electron-accepting species through an oxidative incorporation of the gaseous molecule.[13]

Analogous experiments to the above have been performed in the solution phase. For example, Ikariyama and Heineman[14] monitored electro-inactive anions in a flow-injection system by cycling the polymer between its neutral and oxidized states. Other studies have involved the use of polypyrrole as an overlayer to simply entrap selective reagents such as enzymes near an electrode surface.[15]

In order to ascertain the applicability of polypyrrole films in chemical sensor configurations, the current work examines the nature of interactions of the basic polymer in its various oxidation states with organic species.

*Author for correspondence.

Scanning electron microscopy can be used to detect macroscopic changes in the polymer and x-ray photoelectron spectroscopy is sensitive to changes in the chemical environment of the material. While quartz microbalances have previously been used to study the mechanism of polypyrrole formation,[16] their ability to indicate the relative degree of interaction with certain chemical probes are being utilized in this study to determine the nature of these interactions. A major advantage in employing the thickness-shear-mode (TSM) acoustic wave sensor as the transduction device is that responses can be obtained from both the neutral and oxidized forms of polypyrrole. The chemical sensors described thus far monitor the resistance change of the oxidized form in the presence of the analyte; the polypyrrole films have no appreciable sensitivity in the neutral form. However, as the TSM sensor responds to changes of mass at the surface, the state of the polymer will not limit its use. Chemical changes may then be correlated to mass changes which will enable monitoring the flux of the counterions and solvent into and out of the polymer film.

EXPERIMENTAL

Reagents

Pyrrole (Aldrich) was distilled under vacuum before use while tetrabutylammonium perchlorate (Fluka) and ACS grade acetonitrile, methanol and toluene (BDH) were used as supplied. Helium and 4% ammonia were obtained from Matheson. 9 MHz gold-coated piezoelectric crystals from Oklahoma Crystal Manufacturing Co. were utilized as working electrodes in the polymerization of pyrrole with a combined platinum and Ag/AgCl electrode from Metrohm as the counter and reference electrode, respectively.

Apparatus

Scanning Electron Microscopy (SEM) was performed with a Hitachi S-570 SEM. Electrical contact from the sample holder to the underlying gold electrode was made with graphite paste. The crystals were cleaved for introduction into the SEM by scoring them with a diamond tip and then mounting them onto the holders with the scored side down.

All X-ray photoelectron spectra (XPS) were acquired with a Leybold Max 200 XPS system employing an unmonochromatized Mg X-ray source with an analysis area of 2 mm by 4 mm. The survey spectra and quantitative atomic measurements were obtained with a pass energy of 192 eV. The relative elemental surface compositions were calculated from satellite-subtracted spectra with sensitivity factors derived from Scofield Factors [C(ls) = 1.00, N(ls) = 1.66, O(ls) = 2.32, Cl(2p) = 2.50]. The high resolution spectra were acquired with a pass energy of 48 eV and then deconvoluted with software provided with the spectrometer. Oxidation of pyrrole solutions was achieved with a polarographic analyzer (model 473) from ECO Instruments.

Probing of the polypyrrole films by interacting with gas species was performed with the gas flow-through train described previously.[17] Frequency measurements were made with a universal frequency counter (Hewlett-Packard Model 5334B).

Procedures

Polymerization of pyrrole and deposition on sensors was performed by mounting piezoelectric crystals in the cell depicted in Fig. 1. Although only the contact to the upper electrode is required to apply a potential for coating, the cell was designed to allow the measurement of resonance frequency without removal of the device from the cell. A solution consisting of 0.1*M* pyrrole and 0.1*M* tetrabutylammonium perchlorate in acetonitrile was deoxygenated by nitrogen gas bubbling before use in the electrochemical deposition. The latter was performed for one minute per side at 1.0 V. Oxidation or reduction of the resulting polymer films was achieved with the same equipment with the exception that the solution was 0.1*M* tetrabutylammonium perchlorate in acetonitrile. All potentials reported are with respect to the Ag/AgCl electrode.

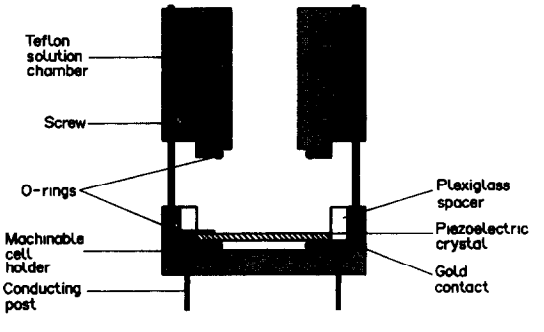

Fig. 1. Schematic of cell employed for polymerization of pyrrole.

In gas phase probe experiments a frequency reading was obtained for the polymer-coated crystal in a helium flow of 30 ml/min. Methanol and toluene were introduced into the flow-through train by diverting the helium flow over a 50-ml reservoir of the appropriate solvent contained in a solvent trap. A frequency decrease was observed which stabilized in about five minutes. The concentration of these analytes in the gas phase was determined by collecting the vapors in a liquid nitrogen-cooled trap for several hours. Ammonia was supplied as a 4% mixture in helium so the pure helium flow was interrupted before the ammonia was introduced into the system at the same flow rate. After the frequency readings had stabilized in the presence of the probe molecule for about two minutes, the pure helium flow was restored and the frequency reading would return to the initial value.

RESULTS AND DISCUSSION

Polypyrrole deposition

With a view to making meaningful comparisons between different sets of experiments, the same coating procedure was followed throughout. The crystals were coated one side at a time in order to produce a visually even coating; dipping both sides at once into the polymerization solution resulted in a non-uniform potential distribution over the electrode surface causing preferential polymerization at the electrode edges and at the solution-atmosphere interface. For the probe experiments, ensuring that the polymer coating occurred in the center of the piezoelectric crystal was necessary for maximum sensitivity. Although the perchlorate ion is the desired counteranion, some chloride ion from the reference electrode was also incorporated into the polymer occasionally.

The coating procedure, in general, lowered the frequency of the crystal by about 25,000 Hz which, for a 9 MHz crystal, roughly corresponds to 25 μg of coating. The initial and final measurements were made in air. The electrochemical deposition normally yields the polymer in its oxidized, doped state which is reported to incorporate about one perchlorate anion per three pyrrole rings. Using the modified Scofield parameters to correct area measurements derived from the XPS spectra, the as-prepared polymer was found to exhibit a lower value for this ratio than expected; the chlorine intensity is 27% that of the nitrogen signal and appears at a binding energy of 208 eV which is consistent with the perchlorate structure. Measurement of the potential of a circuit involving this polymer-coated crystal (with respect to a silver/silver chloride reference electrode) in 0.1*M* TBAP in acetonitrile yields a value of $+0.50 \pm 0.05$ V.

Upon reduction of the polymer at -1.5 V for 10 min, the frequency change (which is proportional to the mass added to a crystal) increases by 10–15%. Low resolution XPS analysis indicates complete chlorine elimination from the surface. However, if the initial polymer contains 27 mole per cent perchlorate anions (with respect to the number of pyrrole rings), removal of all the chlorine from the polymer should result in a frequency rise of about 30%. The much lower value recorded must be due to the diffusion of the perchlorate anion only from the upper layers of the surface (XPS signals arise only from the top 60 Å of the surface) or some exchange between anions and solvent to moderate the mass loss. The potential of the circuit involving this polymer ranges from about 0.0 to $+0.2$ V.

The polymer can also be reduced by chemical means. Treatment with zinc dust in a 1:1 acetic acid: water solution or simply extracting the polymer in a Soxhlet apparatus for six hours with acentonitrile was found to remove all observable chlorine from the XPS spectra. The resulting surfaces show potentials between -0.15 and $+0.15$ V. However, the frequency enhancement of the chemically-modified surfaces now ranges between 15 and 20%, which is significantly greater than that seen by electrochemical reduction. This additional mass loss may constitute evidence for the removal of some smaller oligomers from the polymer during the reaction in aqueous acetic acid or in the heated acetonitrile of the Soxhlet extraction.

While the electropolymerization produces a polymer in the oxidized state, subsequent application of a potential of $+1.0$ V to the polymer in 0.1*M* TBAP in acetonitrile appears to further enhance this state. This process is found to typically decrease the frequency by $\sim$5–10%. Its XPS spectrum shows the atomic composition of chlorine to be 60% that of the nitrogen but the total chlorine intensity is approximately equally divided between peaks at 208 and 200 eV. This lower binding energy signal is in the range of the chloride Cl(2p) binding energy peak. A recent paper has reported the incorporation of 45 mole percent of perchlorate and up to 55 mole percent of chloride as determined by

elemental analysis.[18] As in the reduction case discussed earlier, the frequency decrease is much smaller than expected for a corresponding mass increase of about 30%. The measured potential for this surface is found to increase to between +0.55 and +0.65 V.

Scanning electron microscopy

The macroscopic structure of the polymer on the crystal surface was studied by SEM. No obvious differences could be detected between the as-prepared polymer and those that had been either oxidized at +1.0 V or reduced at −1.5 V. A respresentative micrograph is shown in Fig. 2. The upper two pictures show the surface of an as-prepared polypyrrole film at two different magnifications. The films appeared rough and cracked, very similar to the underlying gold electrode (not shown), although the cracks seen in the gold surface become some-

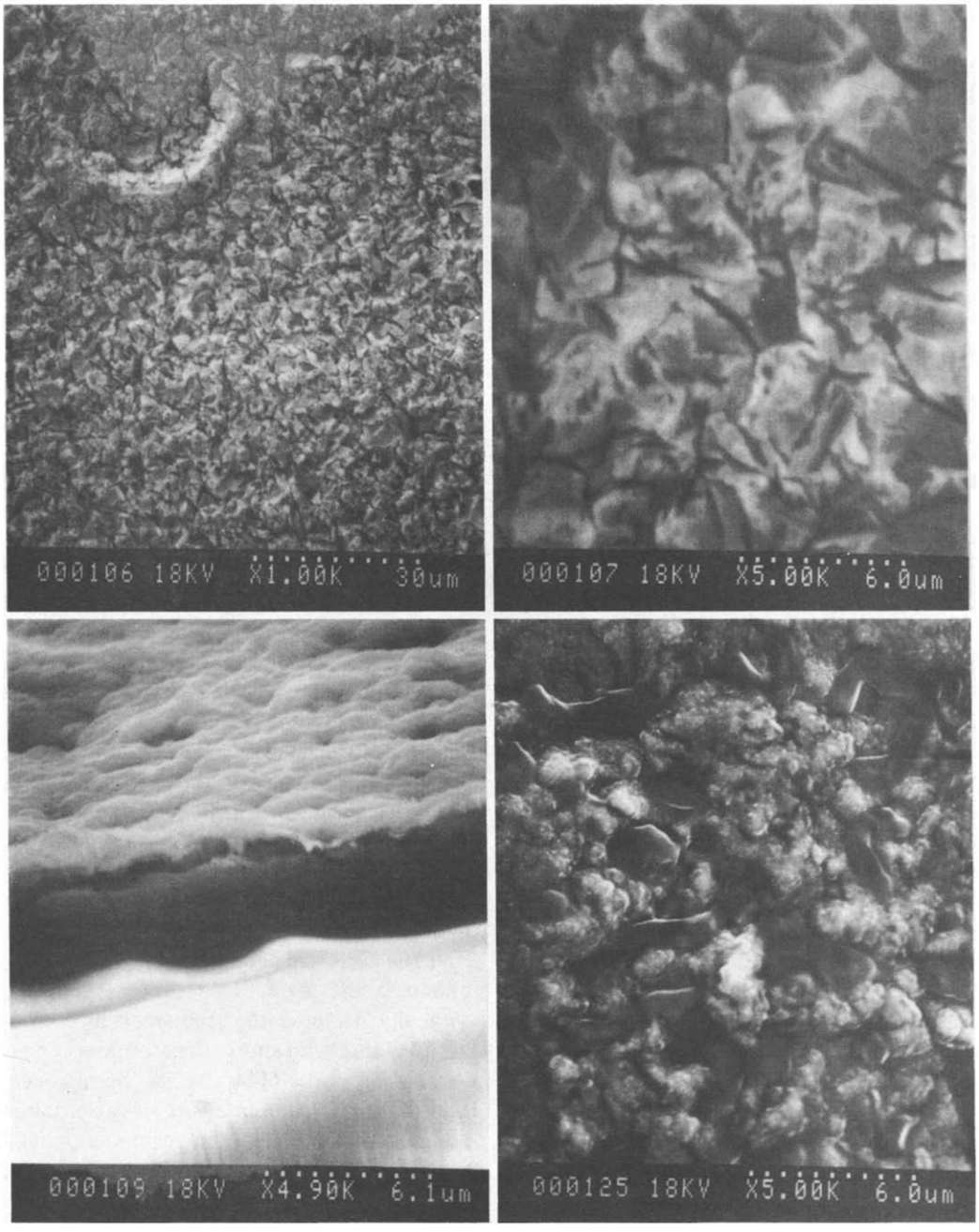

Fig. 2. Scanning electron micrographs of polypyrrole. Upper two micrographs are from the same surface, and the lower left constitutes a corresponding side view. The picture at the bottom right is from a polymer surface which has been lightly coated with gold.

what filled in. A view of the edge of the crystals indicated that the coatings are about one-half of a micrometer thick and variations in surface topology are predominantly the result of the gold layer underneath (lower left in Fig. 2). The polymer is the light coloured layer seen on top of the dark gold band.

Although literature reports indicate that the texture of the film is affected appreciably by factors such as thickness and presence of counteranion,[18,19] the micrographs of this work depict a much more angular surface than hitherto reported for polypyrrole. Most of the documented SEM show globular structures on the surface which are attributed to the polymer building up from localized sites, the accepted growth mechanism. However, we are able to observe similar structures only after vapor deposition of a thin film of gold onto the surface (20 mA current, 60 sec) which fills in the cracks and forms islands on the surface (lower right in Fig. 2). The gold deposited onto a polypyrrole surface seems to preferentially self-adhere causing the formation of globules.

XPS of the surface of polypyrrole films

The N(ls) spectra of the as-prepared, oxidized and neutral forms of the polymer are shown in Fig. 3. The spectrum of the former is in agreement with that published in previous work.[20,21] A major N(ls) signal occurs at a binding energy of 399.5 eV, together with significant enhancement on the high binding energy side of the peak. The higher binding energy peaks have been ascribed to nitrogen atoms present in the vicinity of the charged site on the polymer. Accordingly, positive charge delocalization over several atoms can result in increased charge on nitrogen atoms which have been postulated to range from one-sixth to a single charge. No significant peak is observed on the low binding energy side.

Further oxidation of the polymer in 0.1*M* TBAP causes a two-fold increase in the relative intensity of the higher binding energy nitrogen peak. This observation agrees well with the increased amount of chlorine that becomes incorporated into the polymer as discussed earlier. A small peak (about 5%) can now be detected on the low binding energy side of the main signal.

Reduction of polypyrrole at −1.5 V produces a material for which the XPS spectrum exhibits larger (~15%) and symmetrical enhancements on both sides of the main N(ls) photoline. Such

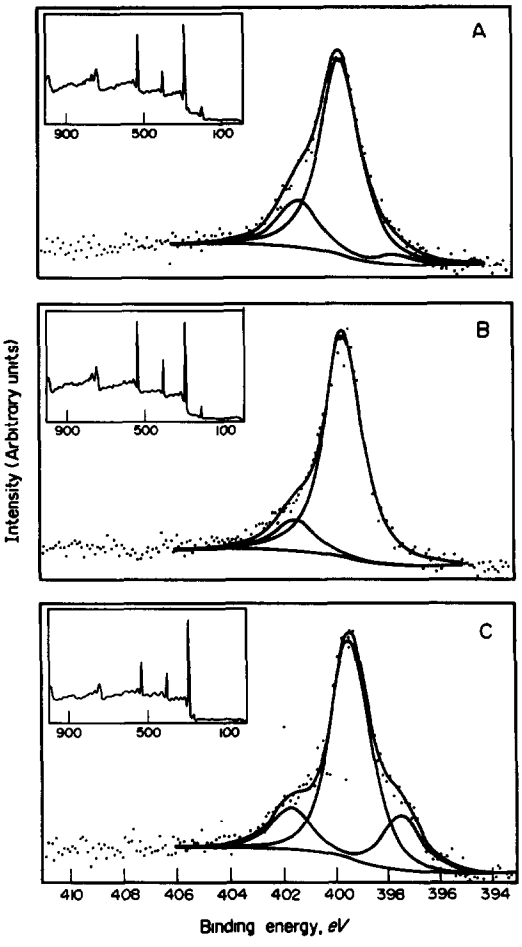

Fig. 3. Nitrogen (1s) region of XPS spectra of polypyrrole in oxidized (A), as-prepared (B) and neutral forms (C).

a spectrum can be attributed to a structure wherein a large proportion of the pyrrole units are involved in a hydrogen-bonded network, the shifts being a result of electron donation from one nitrogen to another. This interpretation derives support from a recent scanning tunneling microscopic study of polypyrrole in which the results were believed to arise from a helical structure for the oxidized polymer with the counteranions being held like spacers between the coils.[22] If the same model is extended to the current investigation, the loss of the anions would allow the nitrogen moieties of the pyrrole rings to interact and thereby produce the two smaller peaks that are observed. Application of a subsequent oxidizing potential reverts the material back to the oxidized form indicating a reversible redox system. While a similar nitrogen spectrum may be obtained by the application of potentials down to 0.0 V. (against a silver/silver chloride electrode), reductions of the oxidized polymer with either zinc or sodium

dithionite do not produce these enhancements. These conditions produce a polymer displaying a smaller enhancement on the high binding energy side in the N(ls) region of the spectrum along with the loss of the chlorine signal.

Interaction with gas phase probes

An alternative approach for the analyses of polypyrrole in different surface states involves adsorption of chemical probes from the gas phase. The analytes were chosen in the present work to demonstrate the effect of different types of interaction; *viz.* methanol for its capacity to hydrogen-bond, ammonia for its Lewis base behaviour and toluene as an aromatic representative. It should be noted that while most previous studies have focussed on an examination of the effect that various species have on the conductivity of the oxidized polymer, our protocol allows the monitoring of the degree of interaction of the chosen analytes with polypyrrole prepared at various levels of oxidation.

The magnitude of the frequency decrease occurring upon the introduction of the probes will be subject to several experimental parameters. The first is the amount of polymer present on the piezoelectric crystal; due to the porosity of the material and its thickness, the analyte is able to permeate the polymer and interact with the entire material. If only a surface interaction were to take place, simple approximations lead to an estimated frequency of about 20 Hz for these probes, which is very close to the change observed when an uncoated, gold piezoelectric crystal is employed. Yet another obvious factor is the concentration of the probe available to the polypyrrole. With the experimental configuration used, the concentrations of toluene and methanol are functions of their vapor pressure and the flow rate used while the ammonia concentration is fixed at the level at which it is supplied. By collecting the toluene and methanol vapors in a liquid nitrogen trap, their respective concentrations were determined to be 10 ± 5 ppm and 95 ± 10 ppm. However, our criterion is the change in the degree of interaction for the films as their states are altered.

Values from a typical run for each of the chemical probes are recorded in Table 1 and presented graphically in Fig. 4. The three sets of data have been normalized in the graph with respect to the frequency decrease observed for the interaction of polypyrrole after being held at a potential of 0.0 V. (versus the Ag/AgCl electrode) since this may be assumed to be an intermediate oxidation state. Therefore, changes arising from the extreme oxidizing and reducing potentials should become more pronounced with either an increased or decreased degree of interaction. The order of the potentials listed in Table 1 and recorded along the x-axis of the graph is the order that was followed experimentally. While the same qualitative results are obtained if the cycle is reversed, *i.e.*, applying a positive potential to the polymer before negative potentials, differences may be observed. These differences may arise from the polymer adopting different conformations upon reduction and oxidation which then relax either at a different rate or through an alternate mechanism upon reversing the potential so different structures may be possible for the polymer after being held at the same potential. A similar hypothesis has been put forth to explain differences in cyclic voltammetry and conductivity measurements of thin conducting polymers in forward and reverse directions.[23]

Table 1. Frequency decreases for piezoelectric sensors as a function of gas phase probe and oxidation state of polypyrrole overlayer, ± 3 Hz

Polymer appl. potential, *V*	Probe		
	NH_3	$C_6H_5CH_3$	CH_3OH
As prepared	830	1453	1425
−1.0	513	1411	1460
−1.5	439	1413	1568
0.0	400	1354	1343
+1.0	625	1178	1302
+1.4	1006	1091	1548

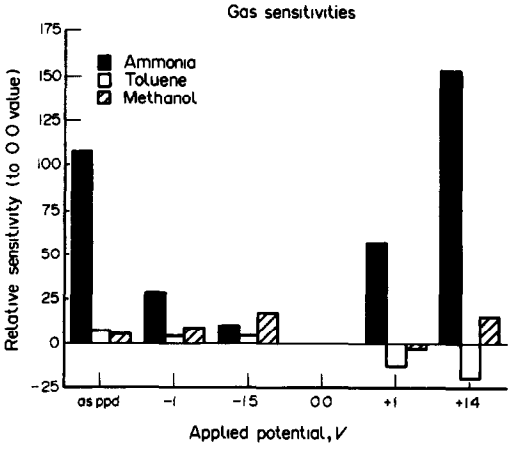

Fig. 4. Relative frequency decreases following the introduction of methanol, toluene and ammonia. Decreases after 0.0 V potential is the standard for each run. Actual frequency shifts are recorded in Table 1.

It can be seen that the polymer behaves quite differently towards the three analytes as its oxidation state is cycled from as-prepared to neutral and finally back to an oxidized state. The potentials measured with the polymer in the electrochemical circuit after the as-prepared, −1.0, −1.5, 0.0, +1.0 and +1.4 V, potentials are applied, usually correspond to about +0.5, +0.05, −0.05, 0.0, +0.5 and +0.6 V respectively. The least predictable values correspond to the surfaces subjected to the least extreme potentials.

The largest difference occurs in the presence of ammonia. The interaction of the oxidized polymer is about twice that observed with the neutral form. Gustafsson *et al.*[12] believed that the interaction is a result of either electron donation to the polymer or proton abstraction by the ammonia. In agreement with the results of these authors, the ammonia interaction was found to be reversible and was stable over tens of minutes.

The variations between the oxidized and neutral forms of polypyrrole with toluene and methanol are only in the range of about 10 to 20%. The preferred oxidation state for interaction with toluene is the neutral state. This effect was found to steadily diminish over a period of tens of minutes, in agreement with the conductivity results of Bartlett and Ling-Chung.[1] Similar experiments with methane indicate analogous behaviour; although there is a smaller preference seen with the neutral state for methane, the interaction must be weak as the frequency is seen to rise almost immediately after its initial decrease on exposure to the gas. The interaction with methanol is found to be the strongest at the most extreme oxidation states, usually after applying potentials of +1.4 and −1.5 V. The methanol-polypyrrole interaction is stable over periods of at least 300 min.

The mass responses of polypyrrole with the probe molecules show that several types of interactions are possible. The strongly basic ammonia shows a strong preference for the oxidized polymer while the neutral, aromatic toluene interacts most strongly with the neutral form, possibly through weak π-overlap. With the removal of the perchlorate anion between the polymer coils the rigid toluene structure may gain a parallel access to the neutral pyrrole rings. Methanol, being both a hydrogen bond acceptor and donor, shows enhancement after applying the extreme oxidizing and reducing potentials. Therefore, controlling the characteristics of this polymer may eventually lead to a minor degree of selectivity with polypyrrole-based sensors, which are generally nondiscriminating in the devices described in the literature so far.

The mass responses observed are also a function of other factors. Although no differences can be detected between the oxidized and neutral states of the polymer on the SEM scale, changes in the density of the film are possible, as has been observed with other polymers. While polyazulene is reported to shrink in going from the oxidized to the neutral form,[24] due to loss of counterions, polythiophene films expand upon reduction,[25] indicating a complex solvation pattern for this polymer. Besides the influence of solvent molecules known to be present, the hydrogen bonding network produced by electrochemical reduction indicates that intramolecular interactions may limit the accessibility of functionalities being presented to the analyte molecules.

CONCLUSIONS

Our studies demonstrate a complex behaviour for polypyrrole which needs to be rationalized to enable the optimization of prepared polymers for specific applications. The varying interactions of the probe molecules with respect to the oxidation state of polypyrrole indicate factors such as nature of the interaction and accessibility to the functional group control the behaviour of the polymer. The piezoelectric mass balance monitored the degree of solvation of polypyrrole as the state of the polymer was altered. The strong retention of acetonitrile seen here supports the observation of Vork and Janssen that polypyrrole retains acetonitrile even in vacuum conditions.[26] The presence of solvent molecules is certain to moderate the possible intra- and intermolecular interactions the material may experience, as has been stated by Blackwood and Josowicz.[27] The difference in the products obtained by chemical and electrochemical reductions of polypyrrole may arise from the reaction solvents used. The strongly hydrogen bonding aqueous acetic acid may not allow an intramolecular hydrogen bonding network to form as observed for the electrochemically reduced product in acetonitrile by XPS.

The results presented here from the SEM, XPS and chemical probe experiments are an attempt to obtain a fundamental understanding of the interactions polypyrrole may experience

in an effort to gain greater control of the physical characteristics of the polymer. The knowledge may then be more directly applied to specific applications in chemical sensor technology in order to generate more sensitive and selective films. While polypyrrole is now being used to entrap selective reagents in voltammetry-based sensors, studies on the stability and dynamics of this material will expand its applicability to a wide range of devices.

Acknowledgements—We are grateful to the Natural Sciences and Engineering Research Council of Canada and the Department of National Defence, Canada for support of this work. We also thank D. C. Stone for performing the SEM experiments.

REFERENCES

1. P. N. Bartlett and S. K. Ling-Chung, *Sens. Actuators*, 1989, **20**, 287.
2. C. Nylander, M. Armgarth and I. Lundström, *Proc. Int. Meet. Chem. Sensors, Japan*, 1983, 203.
3. N. M. Ratcliffe, *Anal. Chim. Acta*. 1990, **239**, 257.
4. T. Shimidzu, A. Ohtani, T. Iyoda and K. Honda, *J. Chem. Soc., Chem. Commun.*, 1987, 327.
5. R. S. Potember, R. C. Hoffman, H. S. Hu, J. E. Cocchiaro, C. A. Viands, R. A. Murphy and T. O. Poehler, *Polymer*, 1987, **28**, 574.
6. M. A. DePaoli, S. Ponero, P. Properi and B. Scrosati, *Electrochimica Acta*, 1990, **35**, 1145.
7. A. F. Diaz, K. K. Kanazawa and G. P. Gardini, *J. Chem. Soc., Chem. Commun.*, 1979, 635.
8. L. J. Buckley, D. K. Roylance and G. E. Wnek, *J. Polym. Sci.: Part B: Polym. Phys.*, 1987, **25**, 2179.
9. L. Olmedo, I. Chanteloube, A. Germain, M. Petit and E. M. Geniès, *Synth. Met.*, 1989, **30**, 159.
10. P. N. Bartlett and S. K. Ling-Chung, *Sens. Actuators.*, 1989, **19**, 141.
11. M. Josowicz, J. Janata, K. Ashley and S. Pons, *Anal. Chem.*, 1987, **59**, 253.
12. G. Gustafsson, I. Lundström, B. Liedberg, C. R. Wu, O. Inganas and O. Wennerström, *Synth. Met.*, 1989, **31**, 1989.
13. T. Hanawa and H. Yoneyama, *Bull. Chem. Soc. Jpn.*, 1989, **62**, 1710.
14. Y. Ikariyama and W. R. Heineman, *Anal. Chem.*, 1986, **58**, 1803.
15. G. Fortier, E. Brassard and D. Bélanger, *Biosens. and Bioelectr.*, 1990, **5**, 473.
16. C. K. Baker and J. R. Reynolds, *J. Electroanal. Chem.*, 1988, **251**, 307.
17. L. Rajaković, V. Ghaemmaghami and M. Thompson, *Anal. Chim. Acta.*, 1989, **217**, 111.
18. F. T. A. Vork, B. C. A. M. Schuermans and E. Barendrecht, *Electrochimica Acta.*, 1990, **35**, 567.
19. T. F. Otero, E. de Larreta and R. Tejada, *Makromol. Chem., Macromol. Symp.*, 1988, **20/21**, 615.
20. J. G. Eaves, H. S. Munro and D. Parker, *Polym. Commun.*, 1987, **28**, 38.
21. P. Pfluger and G. B. Street, *J. Chem. Phys.*, 1984, **80**, 544.
22. R. Yang, D. F. Evans, L. Christensen and W. A. Hendrickson, *ibid.*, 1990, **94**, 6117.
23. D. Ofer, R. M. Crooks and M. S. Wrighton, *J. Am. Chem. Soc.*, 1990, **112**, 7869.
24. X. Huang, M. T. Zhao, L. Janiszewska and P. N. Prasad, *Synth. Met.*, 1988, **24**, 245.
25. A. Hamnett and A. R. Hillman, *Ber. Bunsenges. Phys. Chem.*, 1987, **91**, 329.
26. F. T. A. Vork and L. J. J. Janssen, *Electrochimica Acta.*, 1988, **33**, 1513.
27. D. Blackwood and M. Josowicz, *J. Phys. Chem.*, 1991, **95**, 493.

Talanta, Vol. 39, No. 4, p. 457, 1992
Printed in Great Britain

0039-9140/92 $5.00 + 0.00
Pergamon Press plc

BOOK REVIEWS

Basic Measurement Techniques for Light Microscopy: S. BRADBURY, Oxford University Press, Oxford, 1991. Pages viii + 97. £9.95 (softback).

This, the latest (no. 23) in a series of excellent little handbooks from the Royal Microscopical Society, satisfactorily fulfils the author's intention to guide light microscopists to the various available techniques for the measurement of the size of microscopic objects. The emphasis is on simpler methods but there are also brief references to more recent digital and image analyser techniques.

The first chapter includes a very readable history of the origins and development of techniques and accessories; the final chapter provides a very short introduction to automated and electronic methods of linear measurement. In between there is a remarkably thorough coverage of a wide range of techniques. Chapters on approximation or comparison methods and on linear measurements by use of projection and drawing equipment precede the largest section, on linear measurement by using scales in the microscope. In general this chapter is clear in its treatment of its topics and its final section on sources of error in measurements is particularly valuable but there are disappointments also. First, figures spread over two or three pages have components that are large and clear but the legends and related text are then awkwardly remote. Secondly, in the section on the calibration and use of the graticule-containing eyepiece, the text paragraph immediately after the description of the determination of the micrometer value is alarmingly incomprehensible. However, these are small blemishes and perhaps negligible in the context of the wealth of information provided and the lucid manner of presentation in the whole. A short chapter on angular and depth measurements introduces interferometer systems but the larger topic of interference microscopy is scheduled to be the subject of another monograph.

This handbook, which includes over 90 literature references, given by chapter, will be an asset to those who wish to use the light microscope to measure biological materials, soil or smoke particles, droplets, crystals, etched surfaces, microcircuits and other microscopic objects.

J. A. HODGSON

Chromatographic Analysis of Pharmaceuticals: J. A. ADAMOVICS (editor), Dekker, New York, 1990. Pages vii + 661. $125.00 (U.S. and Canada), $150.00 (elsewhere).

Chromatographic Analysis of Pharmaceuticals is volume 49 in the chromatographic science series of monographs published by Marcel Dekker.

The first section of the book, which occupies about one third of the total, is divided into three parts—regulatory considerations, sample treatment (pretreatment and robotics), and chromatographic techniques (TLC, GC, headspace analysis and HPLC). These topics are dealt with in a precise and competent manner and the deliberate omission of theory (only a small number of very basic equations are included) makes for easy, as well as interesting, reading.

The final two thirds of the book is devoted to applications and this section establishes the volume as a handy reference source. Here the text is dominated by a single table which extends, without a break, over 319 pages. This table is a listing of the chromatographic methods that have been used to test over 1300 pharmaceuticals, their excipients and impurities. The table headings are: compound formulation (e.g., bulk, tablets, solution etc.), mode (e.g., TLC, GC, HPLC) sample pretreatment, sorbent and temperature, mobile phase, detection method, comments and reference source. In total the book contains about 2000 literature references up to the year 1988.

The book is an important addition to the literature because chromatographic analysis is the main technique used for the analysis of pharmaceutical substances in bulk and in formulations. The numerous applications quoted make this text a necessity for all those involved in the analysis of pharmaceuticals.

P. J. Cox

Talanta, Vol. 39, No. 5, pp. 459–467, 1992
Printed in Great Britain

0039-9140/92 $5.00 + 0.00
Pergamon Press plc

ION MOBILITY SPECTROMETRY AS FLOW-INJECTION DETECTOR AND CONTINUOUS FLOW MONITOR FOR ANILINE IN HEXANE AND WATER

GARY A. EICEMAN,* LIZBETH GARCIA-GONZALEZ, YUAN-FENG WANG and BOBBY PITTMAN
Department of Chemistry, New Mexico State University, Las Cruces, NM 88003, U.S.A.

G. EDWARD BURROUGHS
Division of Physical Sciences and Engineering, National Institute of Occupational Safety and Health, Cincinnati, OH 45226, U.S.A.

(*Received* 22 *August* 1991. *Revised* 22 *October* 1991. *Accepted* 14 *November* 1991)

Summary—Ion mobility spectrometry (IMS) was used as a flow-injection detector to quantitatively examine the ionization chemistry of aniline in hexane. A 5-μl sample was vaporized at 15–90-sec intervals in a flowing air stream and analyzed with an IMS equipped with acetone reactant ion chemistry, ambient temperature drift tube and membrane-based inlet. Precision was 3–11% relative standard deviation for 1–100 ppm aniline in hexane with 90-sec injection intervals and detection limits were *ca.* 0.5 ppm with 5-μl injections. Matrix effects with amine and organic solvent mixtures were observed and corrected for low and medium proton affinity interferences with standard addition methods. Pronounced fouling of the IMS occurred when a continuous water flow was introduced for aqueous flow injection–IMS. Continuous water monitoring without degraded IMS performance was possible by sampling air flow through a Silastic tube immersed in an aqueous sample.

Aromatic amines are substances which exhibit toxicity toward aquatic life[1] including fish,[2,3] *Daphnia magna*[4,5] and microbes in estuary water.[6] Consequently, aniline and certain aniline derivatives are classified as priority organic pollutants and the discharge of waste effluents containing aniline is regulated. Effective techniques for determining aniline and like compounds are gas or liquid chromatography which exhibit low detection limits and high specificity.[7] Other methods of identification or low level detection for these compounds include flow-injection analysis (FIA) with chemiluminescence detection,[8] electrochemical thermospray mass spectrometry[9] and ion mobility spectrometry (IMS).[10] The principal concern of the present work is instrumentation suited for continuous monitoring of aqueous effluents that are simple mixtures. The high proton affinities of aniline and other aromatic amines suggest that IMS may be suited to monitoring these compounds in aqueous industrial effluents. In positive polarity and with acetone reagent ion source chemistry, IMS exhibits little interference from common solvents making this analyzer attractive for routine applications.[11] Previously, aromatic amines were examined with both IMS and IMS/mass spectrometry[10] and mobility spectra were comprised principally of MH^+ ions. Such minor fragmentation favored possible application of IMS to effluent wastes when comprised of simple chemical mixtures. A last aspect of IMS, required for full assessment of potential usefulness, is that of quantitative response characteristics for IMS toward aniline alone and in moderately complex matrices.

In IMS, vapors are drawn into a reaction region where analyte is ionized through proton or electron transfers from a reservoir of charge, the reactant ions.[12] Ionization is based on competitive charge exchange and unequivocal response occurs when the target analyte has a proton affinity larger than that for any component in the sample matrix. Otherwise, response can become confusing even for simple mixtures.[13] Matrix effects in IMS can be alleviated somewhat though alternate reagent ion chemistry causing insensitivity to potential interferences and adding selectivity to response.[11] Ion separations in an ion drift region provide a second dimension of selectivity in IMS. Product ions are injected into a weak electric field where ions acquire constant velocities due to cross-

*Author for correspondence.

sectional areas of collision. Nonetheless, response in IMS is fundamentally governed by the original ion creation step which is limited by competitive ionizations; thus, if a product ion is not formed in the ion source, regardless of cause, a peak corresponding to that substance will not be observed in the mobility spectrum.

In the present work, IMS was used as a FIA detector with a chemically benign solvent (hexane) to evaluate the response characteristic and quantitative behavior of IMS configured for operation in harsh field environments.[12] A second portion of effort involved assessment and circumvention of water fouling in this instrument for continuous monitoring of aqueous stream as would be expected in industrial applications.

EXPERIMENTAL

Instrumentation

A flow injection–IMS set-up was assembled from a heated injector of a gas chromatograph and a hand-held IMS device, an Airborne Vapor Monitor (Graseby Ionics, Ltd, Watford, UK). Parameters of the IMS set-up were: reaction region, 12 mm; drift region, 39 mm; diameter of drift tube, 12 mm; field strength, 244 V/cm; ion source, 10 mCi ^{63}Ni; drift gas flow, air *ca.* 200 ml/min; drift tube temperature, ambient at 22–25°; drift tube pressure, ambient at 660–670 mm Hg; and nozzle air flow for sampling, 0.5 l./min. Air flow through the injector was *ca.* 5 ml/min and the injector temperature was 100°. Mobility spectra were acquired through digital signal averaging with an AT-compatible computer equipped with an interface board and software, the Advanced Signal Processor (Graseby Ionics, Ltd). Voltage from a portion of the mobility spectrum was taken from the signal processing board to a Hewlett–Packard model 3390A recording integrator to allow continuous monitoring and integration of aniline product ion intensities. The observation window for drift times for the aniline peak was *ca.* 0.1–0.2 msec wide and was centered on the drift time for aniline, 8.74 msec. Other parameters for signal collection were: number of waveforms, 32; points per spectrum, 512 and scale expansion factor, 0.25. The integrator parameters were: attenuation and threshold, both 9; chart speed, 1 cm/min; area reject, 10,000; and peak width, 0.5.

Preliminary studies of IMS as a flow-injection detector for aqueous streams were made by using a minipump (Milton Roy Co.) connected to the injector through *ca.* 1 m of 1-mm ID stainless steel tubing. A needle at the end of this tubing was inserted into the injector through a septum. For continuous monitoring of water, an inlet was constructed with 2 m of Silastic brand (0.012″ ID × 0.025″ OD) medical-grade tubing (Dow Corning Corp., Midland, MI). This tubing was wrapped in a 4-cm wide band around a 1-cm OD test tube and inserted into a 3-cm ID test tube. Aqueous solution was placed into the space between the test tubes and the Silastic tubing was loosely inserted into the IMS nozzle. Bottled air was passed through the Silastic tubing at 50 ml/min and into the IMS nozzle. This inlet attachment was kept at constant temperature in a model 1220 water bath (VWR Scientific).

Reagents and materials

The following solvents were obtained in high commercial purity and used without further treatment: hexane and acetone (Chromopure, Burdick & Jackson Co., Muskegon, MI), benzene (B&J Brand, Burdick & Jackson Co.), and ethyl acetate and methylene chloride (Fisher Scientific, Pittsburgh, PA). Aromatic amines included aniline, *m*-toluidine and *o*-toluidine (Aldrich Chemical Co., Milwaukee, WI, >99.5%) and benzylamine and *N*,*N*-dimethylaniline (Sigma Chemical Co., St. Louis, MO).

Procedures

General. A 5-μl liquid sample was delivered with a 10-μl syringe (Hamilton Co., Reno, NV) to the injector during continuous signal processing with the IMS. Intervals between analyses were 15–90 sec for restoration of inlet and IMS cleanliness. Several parameters were examined to determine optimum operating conditions and to access the reliability of IMS as a flow-injection detector. The first three studies involved ion chemistry with aniline in hexane. The last three studies were directed toward practical monitoring of effluents for which aqueous solutions were used.

The particular details of each of these studies are given below.

Clearance study and response curve. Five microliters of aniline in hexane at concentrations from 0 to 100 ppm were delivered ($n = 5$) at intervals in the range 15–90 sec. A response curve was prepared from peak areas. Later, a sleeve of borosilicate glass tubing, 25 mm long by 20 mm OD and 1–2 mm wall thickness was placed over the injector-nozzle region to diminish cross flows and turbulence.

Chemical interferences. Effects from common organic solvents were measured with 3 μl of 5 ppm aniline in selected solvents. The solvents were acetone, methylene chloride, benzene and ethylacetate in ratios (v/v) with hexane from 0.5 to 50%. Injections were made in triplicate at 90-sec intervals.

Three microliters of 5 ppm aniline and 3 μl of other aromatic amines in hexane were co-injected. These amines were *N,N*-dimethylamine, benzylamine, *m*-toluidine and *o*-toluidine at concentrations of 1, 10, 25, 50 and 100 ppm. Triplicate determinations were made at 60-sec injection intervals.

Standard addition methods. Three solutions were prepared with aniline in hexane at 10 ppm with matrices comprised of three potential interferences. The matrices included compounds with low to strong proton affinities at concentrations below the saturation level for the IMS ion source. The constituents were: low interfering solution—acetone, benzene, and methanol at 3% (v/v) each; medium interfering solution—ethylacetate, ethylether, and n-propanal at 1% (v/v) each; and strong interfering solution—pyridine, *N,N*-dimethylaniline and diethylamine at 30 ppm each. Five-point standard addition curves were made with each matrix and the experimental value for aniline compared to the actual value. In replicate determinations, the upper value for the highest addition was increased from 1 to 100 ppm aniline.

Effect of water on IMS performance. A calibration curve for 5 μl of aniline at 0–200 ppm in water was prepared with IMS with heated injector. Subsequently, demineralized water was introduced continuously at flows of 10–300 μl/min into the injector and the IMS was recalibrated.

Continuous monitoring of water. Solutions of aniline from 1 to 200 ppm in water were introduced into the Silastic tubing-inlet attachment and the temperature was controlled over the range 25–75°. The aniline peak height was monitored on the recording integrator for 15–25 min. At intervals of 0–96 hr, stability of response in the IMS was determined by analysis of 5 μl of 1 ppm aniline in hexane with the heated injector.

RESULTS AND DISCUSSION

Mobility spectra for aromatic amines

Mobility spectra for the reactant ion peak (RIP) and aniline with acetone (Ac) reagent ion chemistry in the hand-held IMS device are shown in Fig. 1. The RIP is a protonated dimer,

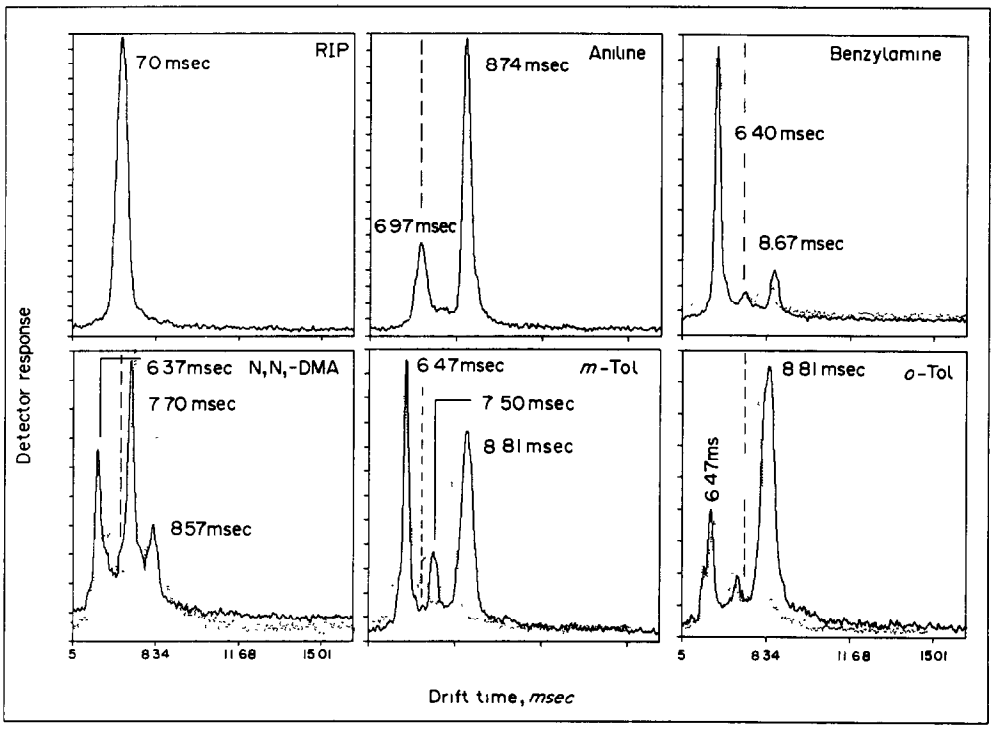

Fig. 1. Ion mobility spectra for aniline and aromatic amines in hexane with acetone ionization chemistry. Spectra were obtained in positive polarity with vapors from individual amines. The spectra made with dotted lines are for equal mixtures of aniline and the corresponding amine.

Ac_2H^+,[14] with a drift time of 7.0 ± 0.1 msec or a reduced mobility, K_o, of 1.83 $cm^2\ V^{-1}\ sec^{-1}$. The mobility spectrum for aniline contained a single symmetrical peak at a drift time of 8.74 msec, largely consistent with previous findings of a MH^+ product ion from water-based ionization chemistry. However, the K_o value was 1.32 $cm^2\ V^{-1}\ sec^{-1}$ versus 1.93 $cm^2\ V^{-1}\ sec^{-1}$ reported previously.[10] This difference is consistent with the formation of cluster ions such as MH^+*Ac arising from the Ac_2H^+ reactant ion.[14] Mobility spectra are also shown in Fig. 1 for other aromatic amines which may be considered environmental pollutants individually, or as matrix components, may be potential interferences in monitoring aniline. Reduced mobilities (in $cm^2\ V^{-1}\ sec^{-1}$) of 1.48, 1.49, 1.45 and 1.45 for benzylamine, *N,N*-DMA, *m*-toluidine, and *o*-toluidine, respectively were also lower than reported values of 1.78 for benzylamine and 1.81 for *N,N*-DMA. Such values are suggestive again of solvated ions of the kind MH^+*Ac seen earlier.[14] While ion identities are not known exactly, the results demonstrated the usefulness of this IMS as a FIA detector for aniline and portend possible chemical interferences for aniline determination (see above).

Clearance, reproducibility and response curve

The membrane-equipped inlet, ambient temperature drift tube and recirculated drift gas flows were expected to contribute to slow response for polar molecules like aniline and to memory effects lasting minutes after an exposure. These concerns were addressed in studies summarized in Table 1 where peak areas and percent relative standard deviations (%RSD) from repetitive determinations are listed for injection intervals of 15–90 sec. The %RSD ranged from 13 to 125 with a median of 21%, much greater than the expected 8–10% RSD.[11] This was associated with 13 m/min air flow in the fume hood causing turbulence at the injector-IMS nozzle region. A leak-tight connection was not employed initially to join injector and IMS nozzle due to concerns over membrane rupture in the IMS inlet from uncertain pressure gradients. A loose fitting sleeve was placed over the injector-nozzle to serve as a wind baffle and the deviations were reduced to 11% RSD or less (Table 1).

Memory effects in this IMS were visible in the mobility spectrum as a persistent product ion, seen as elevated peak areas at low injection intervals in Table 1, and as a rising offset or baseline voltage in the continuously monitored signal (not shown). The time for complete restoration to original reactant ion intensity was dependent upon concentration and ranged from *ca.* 5 sec at low levels to *ca.* 60 sec at 100 ppm. Concentrations below 20 ppm allowed injection intervals of 30 sec without serious memory effects (Table 1). An injection interval of 90 sec provided ample time for restoration of RIP intensity at concentrations from 1 to 100 ppm and was used in further studies.

Table 1. Peak areas from plots of aniline product ion intensity versus time in flow-injection ion mobility spectrometry

Aniline concentration, *ppm*	Peak area ($\times 10^6$) (% RSD) Interval for injection, *sec* 15	30	60	90	90[1]
0	0.83 (13)	1.6 (104)	0.84 (13)	1.1 (34)	*
0.4	2.8 (23)	5.4 (49)	2.5 (20)	2.0 (29)	*
1	6.8 (19)	5.2 (23)	4.6 (27)	3.6 (8.0)	26 (9.1)
5	19.6 (21)	14.9 (16)	16.0 (19)	10.9 (22)	83.3 (11.4)
10	32.6 (29)	32.9 (21)	30.4 (20)	26.1 (13)	151 (7.6)
20	*	35 (21)	41.9 (16)	46.6 (13)	240 (9.1)
40	*	49 (33)	40.4 (15)	37.6 (21)	356 (5.7)
100	*	95 (45)	62.7 (31)	42.5 (125)	649 (3.1)

*Baseline drift due to residual aniline was too severe for integration or recognition of a peak in flow injection IMS.

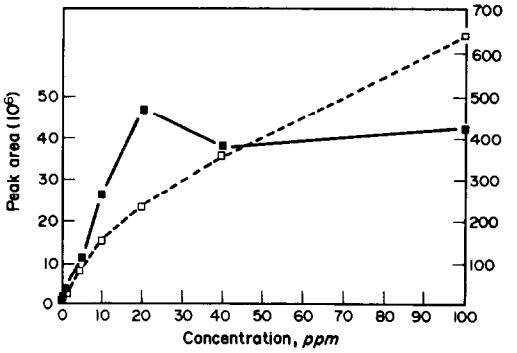

Fig. 2. Response curves for quantitative determination of aniline in hexane with IMS as detector for FIA. The curves are for interface configurations without (solid line) and with the injector-IMS nozzle sleeve to damp turbulence and cross flows.

Calibration curves, from values in Table 1, are shown in Fig. 2 for the 90-sec intervals and resembled previous response curves in IMS.[15] Such curves are comprised of a narrow linear range and a flat response at concentrations above the linear region. The narrow linear range with a saturated region originates with the comparatively slow kinetics of reactant ion formation from the beta-emitting ion source. This causes an effective limited reservoir of charge available for ionization of neutral analyte vapors.[16] The cause for differences between calibration curves with and without the sleeve (Fig. 2) are outside experimental error. The additional area is reasonable since mass transfer should be improved with a sleeve that reduces dilution from air flow in the fume hood. The sleeve-equipped interface eventually became flat at 200 ppm and the reason for this large working range is unknown.

Organic solvent interferences

The presence of various organic solvents in industrial effluents may degrade both the qualitative and quantitative response in IMS. Interfering vapors may either compete for charge hence masking the presence of the aniline, or overlap drift times hence confusing spectral interpretations. Alternatively, solvents in an ambient temperature cell can form ion-solvent clusters which lead to ambiguity through shifts in drift times for product ions.[14] These reactions will cause a decline in the certainty of a positive response or a false negative if no product ion is created or if the peak falls outside an observation window in the signal processing software. The magnitude of such effects should be governed by either proton affinities or polarities of prospective interferences.

Mobility spectra for four common organic solvents with low or medium proton affinities are shown in Fig. 3. Methylene chloride, with

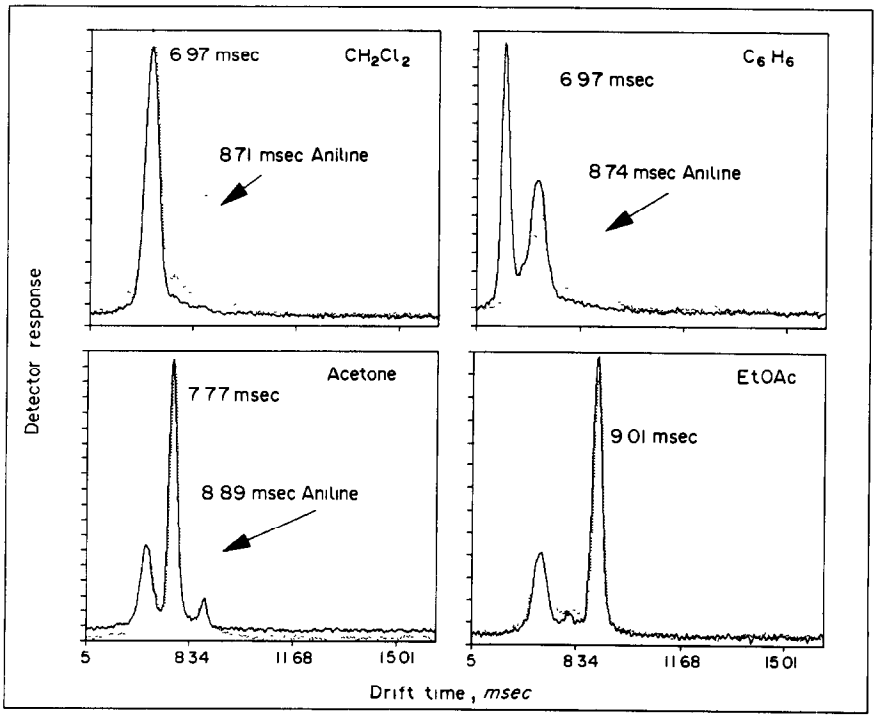

Fig. 3. Ion mobility spectra for organic solvents expected to be encountered in analysis of non-aqueous streams for aniline. Mobility spectra were obtained in positive polarity. Mobility spectra shown as dotted line spectra were for mixtures of 5 ppm aniline in an equal mixture of solvent with hexane.

low proton affinity, exhibited no product ions in positive polarity. Benzene, with weak proton affinity ($G^{\circ}_{300} = 19$ kcal/mole),[17] showed a weak response with an acetone reactant ion chemistry where the proton affinity of acetone is $G^{\circ}_{300} = 7.2$ kcal/mole. Acetone formed a cluster ion with drift times longer than that for the RIP through ion-molecule equilibria in the IMS drift region.[18] Only ethyl acetate (EtOAc) with a moderate proton affinity, *i.e.*, $G^{\circ}_{300} = 3.4$ kcal/mole, showed significant ionization from the RIP. Of these solvents, only benzene has been mass identified[18] as M^+, though acetates are known to form MH^+ and M_2H^+ product ions.[19]

Solvents in equal mixtures with hexane affected IMS spectra for 5 ppm injections of aniline as shown in Fig. 3 (dotted lines). Additionally, solvents influenced quantitative response at levels below 50% (v/v) as suggested in Fig. 4 though effects arose through different chemical events, not all of which are well described. Ethylacetate dominated aniline in the ionization step by virtue of concentration, even though proton affinities favored aniline ($G^{\circ}_{300} = -6.7$ kcal/mole) over ethylacetate. This occurred at 0.5% ethylacetate in hexane and virtually saturated the source so trends in response beyond 5% (v/v) were within experimental error. Benzene exhibited comparable interference even though the proton affinity for benzene is comparatively low. Evidently, benzene vapors were at levels sufficient to compete for protons through collisional ionizations. At low levels for acetone, no effect was obvious, at 25% and greater for acetone in hexane the signal associated with the mobility spectrum region for aniline increased. This was caused not

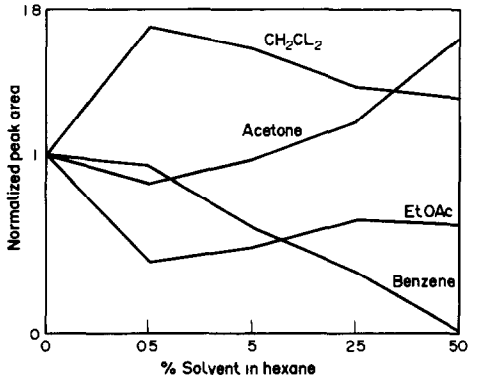

Fig. 4. Influence of organic solvents on FIA–IMS response to aniline. The normalized axis is peak area for aniline with the solvent divided by peak area for aniline at 5 ppm in hexane.

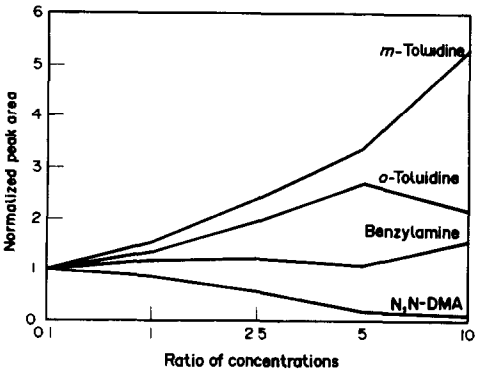

Fig. 5. Influence of aromatic amines on FIA–IMS response to aniline. The normalized axis is peak area for aniline with the solvent divided by peak area for aniline at 5 ppm in hexane.

by an aniline product ion but by the migration of an acetone product ion[14] into the mobility window used for aniline monitoring. In such a situation, only inspection of the mobility spectrum could avert an error in monitoring or analyses. The interference from methylene chloride was unexpected and the cause is unknown. These results suggest that solvent interferences can occur with this IMS configuration and matrix effects must be considered in quantitative monitoring. Previously,[20] Dam showed that similar complications in air monitoring by IMS could be corrected partially with standard addition methods (see above).

Aromatic amine interferences

Aromatic amines, with proton affinities larger than those for common organic solvents, should present serious interferences with aniline determinations by FIA or in continuous flow monitoring. The effects of concentratioon for four aromatic amines on the peak area of aniline are shown in Fig. 1 as dotted lines. The four aromatic amine compounds showed drift times near aniline and had proton affinities comparable to or greater than that for aniline. Toluidines were not well-resolved from aniline in the mobility spectra and were within the monitoring window. Appropriated charge combined with that for aniline to give enhanced apparent aniline product ion intensity. All of the aromatic amines, except *N,N*-DMA, yielded product ions at drift times different from aniline but close enough to enter the monitoring window and give false positives. In contrast, *N,N*-DMA ($G^{\circ}_{300} = 12.4$ kcal/mole) competed for charge in the ion source and caused a slight decrease in peak area for aniline (Fig. 5). Benzylamine was

not an interferent at ratios of 10:1 and below. Clearly, compounds with strong proton affinities if present in samples for FIA–IMS will cause substantial errors in aniline determinations.

Standard addition methods

Standard addition in IMS monitoring of flowing streams with variable matrices was demonstrated for airborne toxic vapors at an industrial site[20] and was deemed successful for improving accuracy in quantitative determinations. Issues here include both the type of matrix, *i.e.*, proton affinities of components and the concentration range of additions. Results from standard addition experiments are shown in Table 2 and provide clues into the general suitability of this IMS configuration for FIA measurements or for effluent stream monitoring. A total of 10% (v/v) of low proton affinity solvents, benzene ($G^{\circ}_{300} = 19.0$ kcal/mole), methanol (G°_{300} 19.3 kcal/mole) and acetone caused appreciable errors in direct measurements of aniline at 10 ppm. Standard addition methods resulted in low errors so long as a suitable range of additions was employed. Small increments should be expected to cause large uncertainty in the slope of the extrapolation. Large concentrations where source saturation occurs should extend the IMS into non-linear response also causing error. When the ion source is not saturated (10 ppm addition for a total of 20 ppm aniline) the error was low. A matrix which contains strong proton affinity interferences represents a debilitating condition (Table 2) for an IMS without a pre-separation inlet and no useful information was gleaned from the error figures. Medium interfering mixtures with moderate proton affinities, EtOAc, ethylether ($G^{\circ}_{300} = 3.7$ kcal/mole), n-propanal ($G^{\circ}_{300} = 10.9$ kcal/mole) were expected to provide an illustration of the strength of standard addition methods. Results were suggestive of source overload since the lowest concentration range (1 ppm total addition) gave a reasonable error of 23%. These results are considered only preliminary and it is encouraging that the quantitative IMS response is possible in low and possibly medium strength interferences given suitable concentrations of interferences.

Table 2. Errors from determination of aniline at 10 ppm in interfering matrices

Range of addition	Low interference	Percent error between measured versus known Medium interference	Strong interference
0–1 ppm	3.4×10^{2}	23	37
0–10 ppm	7×10^{-1}	1.9×10^{2}	8.8×10^{3}
0–50 ppm	52	1.8×10^{2}	3.0×10^{3}
0–100 ppm	1.3×10^{2}	3.5×10^{2}	1.6×10^{3}

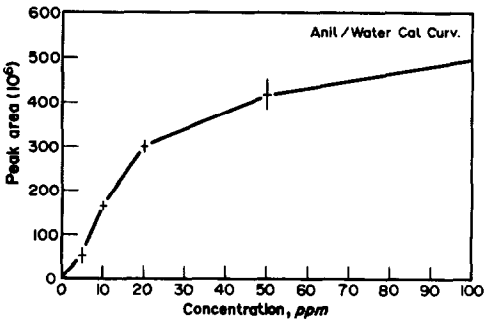

Fig. 6. Calibration curve for aniline in water by FIA–IMS.

Ion mobility spectrometry of aniline in aqueous solutions

When injections of aniline in water were made in the IMS with small volumes at intervals of *ca.* 90 sec, the performance of the IMS did not change perceptibly illustrating that water provided no dramatic interference in ionizaton and suggesting that the membrane inlet was functional. Mobility spectra were good quality and the linear range extended to 100 ppm (Fig. 6). This expanded linear range may originate with a water layer on the membrane of the inlet lowering membrane efficiency for aniline. This effect was also expected from the increased memory effect with water injections as shown in Fig. 7 where even low concentrations required long restoration times of clean ion source conditions. The effects of continuous water flow on

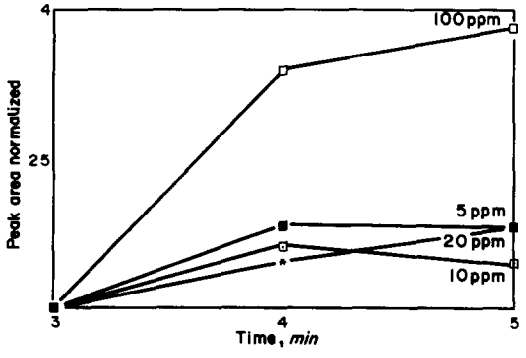

Fig. 7. Memory effect for injections of aniline during delivery of water continuously to the injector-IMS. Various flow-rates of water are given in the figure. The top bar is for aniline peak heights from FIA–IMS analysis taken intermittently during the time of the Silastic tube studies.

hand-held IMS were catastrophic (Fig. 8) for chemical measurements regardless of flow-rates from 10 to 300 μl/min. Clearly, the technology for this membrane based inlet as configured for military applications was not directly transferable to monitoring aqueous streams following volatilization of sample in a heated zone.

Two solvent-free approaches to isolating volatile organic compounds (VOCs) from water have been described and involve either removing water from a wet volatilized flow[21,22] or extracting VOCs from water into a gas flow.[23–25] Water was successfully removed from a wet nitrogen stream containing sample through the use of a Nafion drying tube.[21,22] However, aniline was not detected in the dried effluent from the Nafion and this approach was regarded as unpromising for polar compounds. The alternate approach of isolating VOCs from water via a permeable tube had previously been used with mass spectrometry[23–25] and concern existed that such behavior might be related to the mass spectrometer vacuum. A Silastic tube swept with air was effective in continuously detecting aniline in water from 1 to 200 ppm as shown in Fig. 9. The response was somewhat sluggish but certainly proportional to aqueous compositions and extraction efficiency was very sensitive to water temperature necessitating a temperature-controlled unit for future designs. A positive benefit of this attachment was the absence of water fouling of the IMS (Fig. 8) during the course of these experiments. Terminal studies are needed to establish the duty cycle for sieve packs used for recirculated IMS drift although three years of experience suggest an upper time limit of 90 days is the best condition.

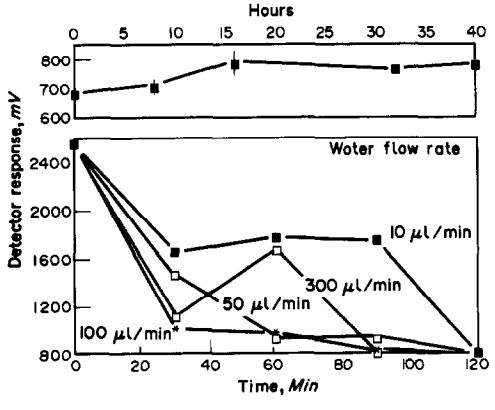

Fig. 8. IMS response to aniline during exposure to continuous flow of water. Top frame shows IMS response to aniline during studies with Silastic.

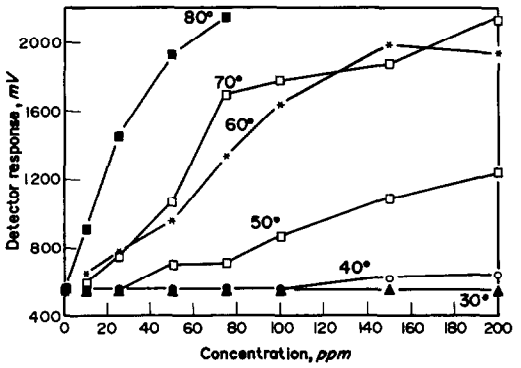

Fig. 9. Response of IMS as continuous flow monitor of water with Silastic tube inlet. Limit of detection (not shown) was *ca.* 0.1 ppm for upper temperatures.

CONCLUSIONS

Flow-injection studies showed that an ion mobility spectrometer was a quantitative detector for aniline with a precision of *ca.* 10%, a linear range of 1–100 ppm, and replicate analysis times of 90 sec or less. The susceptibility of response to potential solvent or chemical interferences suggests that use of IMS must be limited to chemical mixtures where competitive charge exchange does not alter response characteristics. Interest in IMS as a fixed aqueous waste stream monitor developed from the low cost, small size and field configurations. However, possible adaptation of a hand-held IMS for direct sampling of an aqueous stream was thwarted by water permeation of the inlet membrane which caused fouling of ion source chemistry. This can be circumvented by the use of Silastic membranes and preliminary findings supported further development of IMS as an effluent waste stream monitor.

Acknowledgements—Although the information in this paper has been funded wholly or in part by the US Environmental Protection Agency under award no. R-815991-01-0 to New Mexico State University, it does not necessarily reflect the view of the Agency and no official endorsement should be inferred. Mention of trade names or commercial products does not constitute endorsement or recommendation for use. We gratefully acknowledge the gift of Silastic from Dow Chemical Co.

REFERENCES

1. National Research Council, *Aromatic Amines: An Assessment of the Biological and Environmental Effects*, No. PB83-133058, Washington, DC, 1981.
2. S. P. Bradbury, T. R. Henry, G. J. Niemi, R. W. Carlson and V. M. Snarski, *Environ. Toxicol. Chem.*, 1989, **8**, 247.
3. L. D. Newsome, D. E. Johnson, D. J. Cannon and R. L. Lipnick, *QSAR Environ. Toxicol., Proc. Int. Workshop*, K. L. Kaiser (ed.), pp. 231–250. Reidel, Dordrecht, Netherlands, 1987.

4. R. Kuehn, M. Pattard, K. D. Pernak and A. Winter, *Water Res.*, 1989, **23,** 495.
5. R. M. Gersich and D. P. Milazzo, *Bull. Environ. Contam. Toxicol.*, 1988, **40,** 1.
6. H. M. Hwang, R. E. Hodson and R. F. Lee, *Water Res.*, 1987, **21,** 309.
7. R. M. Riggins, T. F. Cole and S. Billets, *Anal. Chem.*, 1983, **55,** 1862.
8. P. Van Zoones, D. A. Kamminga, C. Gooijer, N. H. Velthorst, R. W. Frei and G. Gubitz, *ibid.*, 1986, **58,** 1245.
9. G. Hambitzer and J. Heitbaum, *ibid.*, 1986, **58,** 1067.
10. Z. Karpas, *ibid.*, 1989, **61,** 684.
11. G. A. Eiceman, A. P. Snyder and D. A. Blyth, *Intl. J. Environ. Anal. Chem.*, 1990, **38,** 415.
12. G. A. Eiceman, *Crit. Rev. in Anal. Chem.*, 1991, **22,** 471.
13. G. A. Eiceman, D. B. Shoff and A. P. Snyder, *Anal. Chem.*, 1990, **62,** 1374.
14. J. M. Preston and L. Rajadhyax, *ibid.*, 1988, **60,** 31.
15. C. S. Leasure and G. A. Eiceman, *ibid.*, 1985, **57,** 1890.
16. E. Siegel, in *Plasma Chromatography*, T. W. Carr (ed.), 1984, Plenum Press, New York.
17. C. S. Harden, Personal communication from Army files.
18. S. H. Kim, K. R. Betty and F. W. Karasek, *Anal. Chem.*, 1978, **50,** 1754.
19. G. A. Eiceman, D. B. Shoff, C. S. Harden and A. P. Snyder, *Intl. J. Mass Spec. Ion Processes*, 1988, **85,** 265.
20. R. Dam, in *Plasma Chromatography* (ed.), T. W. Carr, 1984, Plenum Press, New York.
21. R. W. Coutant and G. W. Keigley, *Anal. Chem.*, 1988, **60,** 2536.
22. W. A. McClenny, J. D. Pleil, M. W. Holdren and R. N. Smith, *ibid.*, 1984, **56,** 2947.
23. M. A. LaPack, J. C. Tou and C. G. Enke, *ibid.*, 1990, **62,** 1265.
24. F. R. Lauritsen, *Intl. J. Mass Spec. Ion Processes*, 1990, **95,** 259.
25. R. G. Melcher and P. L. Morabito, *Anal. Chem.*, 1990, **62,** 2183.

Talanta, Vol. 39, No. 5, pp. 469–474, 1992
Printed in Great Britain

0039-9140/92 $5.00 + 0.00
Pergamon Press plc

ESTIMATION OF THE METHOD EVALUATION FUNCTION FOR THE DETERMINATION OF HYDRIDE-GENERATING ARSENIC COMPOUNDS IN URINE BY FLOW-INJECTION ATOMIC-ABSORPTION SPECTROMETRY

ANN J. L. MÜRER,* ANNE ABILDTRUP, OTTO M. POULSEN and JYTTE MOLIN CHRISTENSEN
Danish National Institute of Occupational Health, Department of Chemistry and Biochemistry, Lersø Parkalle' 105, DK-2100 Copenhagen, Denmark

(*Received* 11 *July* 1991. *Revised* 27 *September* 1991. *Accepted* 22 *October* 1991)

Summary—A direct flow-injection atomic-absorption spectrometric (FIA–AAS) method for the assessment of inorganic arsenic compounds and their metabolites was developed and statistically evaluated by the estimation of the method evaluation function (MEF), which provides detailed information on the analytical performance of the method, *i.e.*, the average combined uncertainty and the magnitude of potential systematic errors. The method evaluation study demonstrated that the use of standard addition was a necessity to obtain an acceptable method performance at low concentrations typical for low dose exposure. In contrast the use of calibration curves resulted in a method with reduced sensitivity and high systematic error. The developed method, using standard addition, had a limit of detection (2.9 μg/l.) sufficiently low for the determination of hydride-generating arsenic species in urine from non-exposed and low exposed persons. Organoarsenicals such as arsenobetaine and arsenocholine are not detected by this method. Hence, the contribution of these compounds derived from a diet containing seafood does not affect the monitoring of inorganic arsenic compounds after occupational or environmental exposure. The high capacity of the FIA–AAS system (three minutes per sample measured by standard addition) together with the low limit of detection makes this method suitable for biological monitoring of inorganic arsenic exposure even though standard addition is required.

As inorganic arsenic compounds are well known carcinogens,[1] assessment of environmental and occupational exposure is of medical and political importance. Occupational exposure to inorganic arsenic compounds occurs in industries involved in such things as wood preservation, glass production and manufacturing of lead accumulators. In 1985 arsenic pentoxide was among the 15 most widely used compounds in Danish industry.[2] Environmental exposure occurs in relation to either an ongoing industrial pollution[3] or a previous pollution of waste sites for example.[4]

During the last five years, assessment of airborne exposure has been supplemented by biological monitoring.[3-5] The good correlation between airborne concentrations of inorganic arsenic and the urinary excretion of inorganic arsenic and its metabolites monomethylarsonic acid (MMA) and dimethylarsinic acid (DMA), together with the convenience of collecting urine samples, makes urine the preferred biological material in biological monitoring.[4] The short half-life of the hydride-generating arsenic compounds means that only the exposure of the last few days is reflected in the urinary concentration measured.[6]

So far hydride-generating atomic-absorption spectrometry, using a MHS-10 system has been used for biological monitoring of the sum of inorganic arsenic and its metabolites.[7] However, the analytical capacity of this method is high only when calibration curves are used, assuming that no systematic error is introduced when different urine samples are analysed.

Whenever analytical results are associated with large consequences, *i.e.*, evaluation of health risk in relation to occupational or environmental exposure, documentation of the quality of the method should be mandatory. The method evaluation design developed at our institute[8-11] validates the analytical method by estimating the method evaluation function (MEF) resulting in a simultaneous estimation of the total errors of the analytical method, includ-

*Author for correspondence.

ing the within and between run uncertainties, and the systematic errors.

In order to enable the assessment of low dose occupational and environmental exposure of inorganic arsenic compounds, the aim of the present study was to develop a fast, automatic and direct flow-injection hydride-generation atomic-absorption (FIA–AAS) method for the measurement of inorganic arsenic compounds and their metabolites in urine. The experimental design mentioned above for method evaluation was modified to evaluate the method.

EXPERIMENTAL

Reagents

Demineralized water (18 mΩ) purified through a Millipore Purification System S.A. (Millipore Waters, Taastrup, A.B. Denmark) was used for all aqueous solutions. Unless otherwise stated all chemicals were of analytical reagent grade.

A 1000-μg/ml dimethylarsenic acid (DMA) stock solution was prepared by dissolving $(CH_3)_2AsO(OH)\cdot 3H_2O$ (Sigma no. C-0250, Dorset, United Kingdom) in water. This stock solution was used to prepare both the five different standards for standard addition and the method evaluation function (MEF) samples.

Pure samples of arsenite, arsenate, monomethylarsonic acid, dimethylarsenic acid, arsenocholine and arsenobetaine (all 1.00 g of the compound per litre) were from the ongoing intercomparison study on arsenic species organized by BCR.[12]

The reagents for flow-injection analysis and hydride-generation were: antifoaming agent tri-n-butylphosphate (BDH no. 30488, United Kingdom), argon used as carrier gas, sodium borohydride 0.5% (Fluka no. 71320, Buchs, Switzerland) in 0.04% sodium hydroxide (Merck no. 6498, Damstadt, Germany) used as a reductant and 2% hydrochloric acid (Merck no. 937, Damstadt, Germany) as an acidic carrier solution for the hydride generation.

Sample preparation for method evaluation

Three different urine pools were collected, two pools from unexposed persons (pool A and pool B) and one pool (C) from a slightly exposed person resident in a polluted area (9.3 μg/l. As in urine). All persons were requested to abstain from consuming seafood for three days before sampling.

For each of the three urine pools ten different method evaluation function (MEF) samples were prepared by spiking with a defined volume of the DMA stock solution to obtain concentrations in the linear range of the method (0–45 μg/l. As in urine). The samples were stored at −5°. The order of analysis of the MEF samples was randomly selected. Only two concentration levels from each urine pool were determined each day. Each MEF sample was determined twice on different days. A total of 57 MEF samples were measured.

Apparatus

The employed apparatus was a Perkin–Elmer 1100 B AAS equipped with an EDL Power Supply, autosampler AS 90, Flow-Injection Analysis FIAS 200 (all from Perkin–Elmer, Germany). The arsines were determined at 197.3 nm in a heated (900°) quartz cell.

The following modifications of the equipment were made in order to optimize the method:

(1) An enlarged gas/liquid separator with an inner cubic content of 8.29 cm^3 instead of the standard separator of inner cubic content 3.29 cm^3. This modification was necessary as proteins present in the urine samples produced large amounts of foam in the system disturbing the measurements in the AAS when using the standard separator.

(2) Three metres of mixing tube (inner diameter of 0.8 mm) with 20 knots giving coils with a diameter of 35 mm was used to improve the mixing resulting in a more optimal signal as compared with the signal obtained when no knots were used.

(3) A sample loop (inner diameter approximately 0.9 mm) containing 80 μl. This size is big enough to produce a signal with a low detection limit, and in combination with the previous described modifications, it is small enough to avoid problems with the foam producing proteins in the urine.

Procedure

Figure 1 outlines the basic design of the optimized FIA–AAS system.

It is of importance that the pH of the reaction mixture has reached a constant low pH (pH < 1) before reaching the gas/liquid separator to obtain optimum hydride generation. A final adjustment of the concentrations of reagents, the number of knots on the mixing tube and the flow-rates of the FIA-system was done by

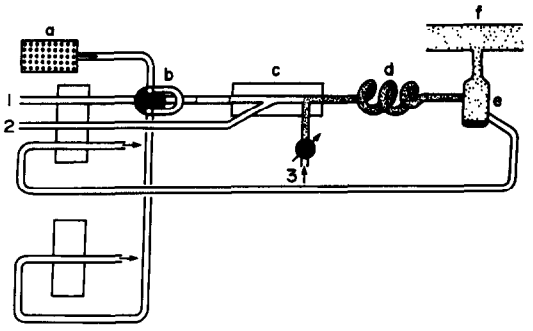

Fig. 1. The prediluted samples (a) were injected through the injection valve (b) into the carrier stream (1). $NaBH_4$ (2) was added in the chemifold (c) and the mixture was passed through the knotted mixing tube (d). Argon (3) was admitted (85 ml/min) to carry the developed arsines from the gas/liquid separator (e) to the heated quartz cell (f).

running a pH-indicator solution through the tubes and observing the colour change throughout the transparent system.

The concentration of hydride-generating arsenic compounds (arsenite, arsenate, MMA and DMA)[7] in urine was determined by using standard addition with five different concentrations of As (as DMA) ($x + 0$ μg/l., $x + 10$ μg/l., $x + 20$ μg/l., $x + 30$ μg/l. and $x + 40$ μg/l.) and weight regression analysis (3, 2, 1, 1 and 1) of the standard addition curves. In addition calibration curves with the same concentrations of DMA in urine were prepared for estimation of the arsenic concentration of the MEF samples. New samples for calibration were prepared each day with different batches of urine. Hence only two MEF samples from each urine pool (A, B and C) were measured on each calibration curve. This design includes matrix differences of the urine in the method evaluation.

Peak areas were recorded in all cases as recommended by Norin and Vahter.[7]

Statistics

Method evaluation was carried out as described previously.[8–11] The principles of the method evaluation design are as follows:

Any chemical method can be characterized by its method evaluating function (MEF) which is the estimated result of the chemical analysis, $E(Y|\mu)$, as a function of the true value of the analyte, μ. The equation of MEF is:

$$\text{MEF}(\mu) = E(Y|\mu) = \alpha + \beta\mu$$

The method evaluation is performed by statistical analysis of the MEF. The underlying theory is based on the assumption that the analytical method is in statistical control, *i.e.*, the distribution of Y given μ can be approximated by a normal distribution. Test for normal distribution is performed as described by Miller and Miller.[13] When the assumption is correct the standard deviation (SD) of Y given μ is an expression of the combined uncertainty of the method.

Linearity of the MEF plot is tested with the pure error lack of fit test.[14] The systematic error (the accuracy) is then the combination of the so-called zero point error (α) and the proportional error ($\beta - 1$). Ideally, an analytical method should be without any systematic error (*i.e.*, $\alpha = 0$ and $\beta = 1$). In practice it is, however, not possible to assure $\alpha = 0$ and $\beta = 1$ for all values of μ. When a least square regression analysis of the MEF is performed and the standard deviation of α and β is calculated, the accuracy of the measurements is validated by testing if $\alpha = 0$ and $\beta = 1$ using a T-test.[15] If the uncertainty of the method increases profoundly with increasing true value (μ) (*i.e.*, the relative standard deviation increases more than 50% over a 15-fold range of concentration[16]) weight regression analysis should be used to estimate the value and standard deviation of α and β, respectively.

RESULTS AND DISCUSSION

The method evaluation design originally developed for analytical methods, using calibration curves was used with the following modifications:

The concentration of hydride-generating arsenic compounds in the 57 MEF samples were determined using both calibration curves (C) and standard addition (S), respectively. For each of the three urine pools the average endogenous background values were estimated. These endogenous background values were subtracted from the spiked values of the 57 MEF samples prior to the final statistical treatment of MEF.

Plots of the MEF of S(ABC) (MEF plot of values obtained by standard addition on all samples from pool A, B and C) and the MEF of C(ABC) (MEF plot of values obtained by the use of calibration curves on all samples) is presented in Fig. 2. The results of the method evaluation are presented in Table 1.

The n-score test of all MEF presented in Table 1 revealed that in no case did the distribution of the MEF points around the line of

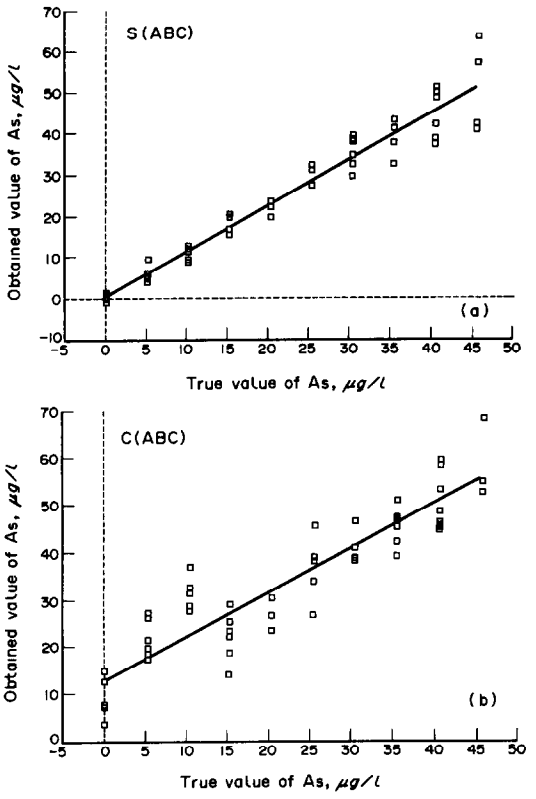

Fig. 2. The obtained values of the MEF samples are plotted against the true values. S(ABC) values are obtained using standard addition on all samples from pool A, B and C. C(ABC) values are obtained using calibration curves on all samples from pool A, B and C.

regression deviate from the normal distribution. The pure error lack of fit test for linearity showed that the use of standard addition results in a linear MEF [P = 0.980 for S(ABC)]. In contrast, the MEF obtained by using calibration curves significantly deviated from linearity [P = 0.0003 for C(ABC)]. In principle, it is not valid to perform the test for systematic errors in the case of C(ABC) since the MEF is non-linear. For the sake of comparison the values of α and β are, however, included in Table 1 and validated for both C(ABC) and S(ABC). The tests for systematic errors (α and β) revealed that MEFs using standard addition had no zero point error (*i.e.*, α was not significantly different from zero), whereas the MEF based on calibration curves had a profound zero point error. The reversed pattern was seen with respect to the proportional error, where standard addition resulted in a significant proportional error (*i.e.*, β was significantly different from one), whereas the use of calibration curves produced no significant proportional error. Weight regression analysis of S(ABC) did not result in estimates of α and β significantly different from the estimates obtained with unweighted regression analysis (Table 1). The employed weights were the inverse of the squared true values multiplied with 25 ($25/\mu^2$), hence the weight at $\mu = 5$ μg/l. was one. The same weight was used at $\mu = 0$ μg/l.

Table 1. Method evaluation parameters

MEF	α	SD_α	β	SD_β	$SD(Y\|\mu)$
S(A)	0.45	1.82	1.076	0.070	3.91
S(B)	1.21	1.44	1.093	0.060	3.88
S(C)	−0.14	1.82	1.194	0.070	4.73
S(ABC)	0.40	0.92	1.123	0.036	3.99
S_w(ABC)	0.14	0.27	1.145	0.032	0.99*
C(ABC)	12.8	1.4	0.949	0.056	6.12

*The SD $(Y|\mu)$ at weight = 1.

The FIA–AAS method using standard addition (S) was statistically evaluated for each of the three batches of urine alone [S(A), S(B) and S(C)] and in combination [S(ABC)]. S_w(ABC) denotes the MEF parameters obtained by weight regression analysis of the MEF plot. In addition the method using calibration curves was evaluated for all three batches in combination [C(ABC)]. $SD(Y|\mu)$ is the combined uncertainty of the method. SD_α and SD_β are the standard deviation of the estimated intercept (α) and slope (β) of the regression line.

The limit of detection, 2.9 μg/l., of the method was determined as three times the standard deviation of ten measurements of samples at a concentration level of 3.7 μg/l. This value is in accordance with the limit of detection obtained by estimating the MEF, using weight regression analysis (3 × 0.99 μg/l. ≈ 3.0 μg/l.).

Using the described method a single determination is done in 40 sec, meaning that a complete determination of a sample, using five standard additions lasts 3.3 min in total.

No certified reference urine materials is available with concentrations of hydride generating arsenic compounds in a range relevant for low dose exposure. In order to study both accuracy and the molar sensitivity of the developed FIA–AAS method, different arsenic species samples were prepared by spiking water and a pool of urine with 40 μg/l. of either arsenite, arsenate, MMA, DMA, arsenobetaine or arsenocholine, all from the ongoing BCR programme.[12] The arsenic concentration was measured by using standard addition with the DMA stock solution. The recovery of arsenite, MMA and DMA was not significantly different from 100%. By contrast, the sensitivity to arsenate was reduced by approximately 20%, and no signal was obtained for the organic compounds, arsenobetaine and arsenocholine.

Biological monitoring of environmental and occupational exposure to inorganic arsenic compounds often requires an analytical method with high capacity.[4] So far hydride-generating AAS, using a MHS-10 system has been used for monitoring the sum of inorganic arsenic and its metabolites.[7] However, the analytical capacity of this method is high only when calibration curves are used. The present MEF study demonstrated that the use of calibration curves may result in a method with a non-linear MEF. As indicated in Fig. 2 the non linearity originates from the three lowest concentrations of the MEF samples, which appears to be outside the linear range of the method. A possible contamination of these samples can be excluded since the same samples showed no bias in the method evaluation using standard addition. The bias may partly be explained by the fact that hydride-generating systems in general have a tendency to produce non-linear standard curves,[4] which produce overestimated values at the low concentrations when linear regression analysis is used to estimate the calibration equation. Consequently, non-linear regression analysis may reduce this bias. When the MEF is estimated for the MEF samples with As concentrations above 10 μg/l. a linear MEF is obtained. However, this MEF has both a zero point error ($\alpha = 4.75$) and a significant proportional error ($\beta = 1.18$) in addition to a fairly high uncertainty [$SD(Y|\mu) = 5.26$]. Consequently, the use of calibration curves resulted in an inferior FIA–AAS method as compared with the method based on standard addition. Only the latter is suited to the assessment of low dose arsenic exposure with an acceptable performance. The use of standard addition in combination with FIA–AAS gives a sufficient high capacity and the developed FIA–AAS method has been used at our department for biological monitoring of environmental and occupational exposure.[17]

The standard deviations of Y given μ in Table 1 represent the average uncertainty of the method with respect to the linear range studied. Since the uncertainty increases with increasing concentration of the arsenic compound (see Fig. 2) the average uncertainty is well above the uncertainty used for the calculation of the limit of detection (*i.e.*, three times the standard deviation at a very low concentration close to the expected limit of detection). When weight regression analysis was used to estimate MEF, the estimated standard deviation of Y given μ (at weight = 1) was in accordance with the uncertainty used for calculation of the limit of detection. These results add further weight to the usefulness of the method evaluation function design.[8–11]

The method evaluation study demonstrated a significant systematic proportional error ($\beta = 1.12$) of the FIA–AAS method using standard addition. The DMA concentration of the stock solution used for preparation of both the method evaluation samples and for the standard addition solutions was confirmed by using the BCR DMA standard solution. Consequently, it is not likely that the proportional error is due to a calibration error, so the proportional error must be considered an expression of the recovery of the method. The above mentioned explanation may still apply, *i.e.*, the standard addition curves of the FIA–AAS method tend to be non-linear, *i.e.*, the standard addition point at the highest concentration of the standard added is nearly always situated below the line of regression (data not shown). When least square regression analysis is used on this type of non-linear standard addition curves the concentration of the hydride-generating arsenic compounds will be overestimated. Part compensation for this tendency is obtained by the use of weight regression analysis on the standard addition curves. When the developed FIA–AAS method is used for measurements on urine samples the remaining systematic error is corrected by dividing the measured values by 1.12. An identical correction (measured conc/1.12) has been described by others.[4]

Recently, Larsen[12] published an optimized Zeeman–AAS method for determination of arsenite, arsenate, MMA, DMA, arsenobetaine and arsenocholine in aquatic solutions with the same molar sensitivity. Since this method measures both arsenocholine, arsenobetaine and the hydride-generating arsenic compounds it may be attractive to use this in combination with our FIA–AAS method in order to estimate the contribution of the organoarsenic compounds in urine. It should, however, be emphasized that the applicability of the Zeeman–AAS method has not yet been documented on biological samples.

The developed FIA–AAS method had a recovery of arsenite, MMA and DMA in urine not significantly different from 100%, whereas a reduced sensitivty to arsenate was observed. This result is in accordance with Buratti *et al.*[18] but in disagreement with Norin and Vahter,[7]

who showed the same sensitivity for MMA, DMA and arsenate. The reduced sensitivity to arsenate may be considered acceptable since this inorganic species represents only approximately 1% of the total urinary excretion of arsenic compounds.[6]

The developed FIA–AAS method does not measure the two organoarsenic compounds, arsenobetaine and arsenocholine. Consequently, a contribution of these compounds originating from a diet containing seafood is not likely to be measured. However, since seafood on some occasions does contain substantial amounts of hydride-generating arsenic compounds a restricted diet is requested by routine prior to assessment of occupational and environmental inorganic arsenic exposures.

REFERENCES

1. I. A. R. C. Monographs: Evaluation of carcinogenic risks to humans. Overall evaluations of carcinogenicity: An updating of IARC Monographs Volumes 1 to 42. *International Agency for Research on Cancer*, 1987, supplement 7, 100.
2. J. Hansen, *Kræftfremkaldende stoffer og materialer*, Komp. I, Del A, Arbejdstilsynet, 1989, 29.
3. L. Pollisar, K. Lowry-Coble, D. A. Kalman, J. P. Hughes, van G. Belle, D. S. Covert, T. M. Burbacher, D. Bolgiano and N. K. Mottet, *Environ. Res.*, 1990, **53**, 29.
4. M. Vahter, L. Friberg, B. Rahnster, Å. Nygren and P. Nolinder, *Int. Arch. Occup. Environ. Health.*, 1986, **57**, 79.
5. D. A. Kalman, J. Hughes, G. van Belle, T. Burbacher, D. Bolgiano, K. Coble, N. K. Mottet and L. Pollisar, *Environ. Health Perspect.*, 1990, **88**, 145.
6. V. Foà, A. Colombi, M. Maroni and M. Buratti. *Biological Indicators for the Assessment of Human Exposure to Industrial Chemicals.* Eds Alessio L., Berlin A., Bori M., Roi R. CEC, *ISPRA*, 1987, 25.
7. H. Norin and M. Vahter, *Scand. J. Work. Environ. Health*, 1981, **7**, 38.
8. I. B. Olsen and E. Holst, *Analyst*, in the press.
9. Å. M. Hansen, I. B. Olsen, E. Holst and O. M. Poulsen, *Ann. Occup. Hyg.*, 1991, **6**, 603.
10. J. M. Christensen, O. M. Poulsen and T. Anglov, *J. Anal. Atom. Spectrom.*, in the press.
11. O. M. Poulsen, E. Holst, T. Anglov and J. M. Christensen, *Proceedings of the Fourth International Symposium on the Harmonization of Quality Assurance Systems in Chemical Analysis*, Geneva, 2–3 May, 1991.
12. E. H. Larsen, *J. Anal. Atom. Spectrom.* 1991, **6**, 375.
13. J. C. Miller and J. N. Miller, *Statistics for Analytical Chemistry*, Wiley, New York, 1989.
14. P. Armitage, *Statistical Methods in Medical Research*, Blackwells, Oxford, 1971.
15. I. Miller and J. E. Freund, *Probability and Statistics for Engineers*, Englewood Cliffs, New Jersey, 1977.
16. W. Horwitz, *Anal. Chem.*, 1982, **54**, 67A.
17. J. M. Christensen, K. Rasmussen and N. J. Kjeldsen, *Ugeskr. Læger*, 1991, **153**, 2564.
18. M. Buratti, G. Calzaferri, G. Caravelli, A. Colombi, M. Maroni and V. Foa, *Intern. J. Environ. Anal. Chem.*, 1984, **17**, 25.

Talanta, Vol. 39, No. 5, pp. 475–480, 1992
Printed in Great Britain.

0039-9140/92 $5.00 + 0.00

POTENTIOMETRIC STUDY OF COMPLEX FORMATION EQUILIBRIA OF α-OXOOXIMES WITH COPPER(II) AND NICKEL(II) IONS

A. IZQUIERDO,* M. GRANADOS and J. L. BELTRAN
Departament de Química Analitica, Universitat de Barcelona, 08028 Barcelona, Spain

(*Received* 29 *March* 1991. *Revised* 8 *July* 1991. *Accepted* 26 *July* 1991)

Summary—Complex formation equilibria between copper(II) and nickel(II) with phenylglyoxal 2-oxime (HPGO) and 1-phenyl-1,2-propanedione 2-oxime (HPPO) have been studied in 50% (v/v) ethanol–water solution containing 0.5*M* sodium nitrate as constant ionic medium at 25°, using glass electrode potentiometry. The emf data obtained have been analysed with MINIGLASS and SUPERQUAD programs. Formation constants for the $Cu(PGO)^+$, $Cu_2(PGO)(OH)^{2+}$, $Cu_2(PGO)_2(OH)^+$, $Ni(PGO)^+$, $Ni_2(PGO)_3^+$, $Ni_2(PGO)_4$, $Ni_2(PGO)_2(OH)_2$, $Cu_2(PPO)(OH)^{2+}$ and $Cu_2(PPO)_2(OH)^+$ complexes are reported.

α-Oxooximes are analytical reagents widely used in spectrophotometry for metal ion determination,[1] but little attention has been paid to the complexation and distribution equilibria related to these systems.[2–6] Most of the literature about α-oxooxime metal complexes deals with the composition and structure of solid complexes.[7–11] These studies point out that α-oxooximes act as bidentate ligands, via carbonyl and oximic groups, forming five or six-membered chelate rings.

Complexation between Cr(III), Mn(II), Fe(III), Co(II), Ni(II) and Cu(II) and some α-oxooximes were studied by Bhargava and Tyagi[2] in 75% methanol–water mixtures and they identified only monomeric species (ML, ML_2 or ML_3). In the study about complexation between lanthanum(III) ions and α-oxooximes, Manku[3] also reports the formation of monomeric species. Nevertheless, in previous studies on solvent extraction of divalent ions with α-oxooximes,[5,6] we have found that polynuclear complexes can be formed. Moreover, some studies on solid complexes of these systems have also pointed out the existence of polynuclear species.[7,8]

In order to ascertain the possible formation of polynuclear complexes between α-oxooximes and divalent metal ions, we have studied the complexation equilibria between copper(II) and nickel(II) with phenylglyoxal 2-oxime (HPGO) and 1-phenyl-1,2-propanedione 2-oxime (HPPO). This work was carried out by means of glass electrode potentiometry at 25° and 0.5*M* sodium nitrate ionic strength. Because of the low solubility of the ligands in water, 50% (v/v) ethanol–water mixtures were used. The acid–base equilibria of the ligands in these conditions had been determined previously[12] and the dissociation constants are: $pK_{HPGO} = 8.77 \pm 0.02$ and $pK_{HPPO} = 10.07 \pm 0.02$.

*Author for correspondence.

EXPERIMENTAL

Reagents and solutions

Phenylglyoxal 2-oxime (Aldrich), 1-phenyl-1,2-propanedione 2-oxime (Aldrich), nitric acid (Merck AR), copper nitrate (Merck AR) and nickel nitrate (Merck AR) were used without further purification. Sodium nitrate (Probus AR) was purified by recrystallization in water. Sodium hydroxide solutions free from carbon dioxide were prepared by dilution of a concentrated solution of sodium hydroxide (Merck AR) according to Kolthoff *et al.*[13] These solutions were kept under a CO_2-free atmosphere and standardized by titration with potassium hydrogenphthalate. Nitric acid solutions were standardized volumetrically with tris(hydroxymethyl)aminomethane, copper(II) stock solution was standardized iodimetrically and nickel(II) stock solution was standardized as bis(dimethylglyoximate)nickel.[14] All these solutions were made 50% (v/v) ethanol–water by mixing doubly distilled freshly boiled water and ethanol (Merck AR). The ionic strength was kept at 0.5*M* with sodium nitrate. A flow of nitrogen (previously

Table 1. Experimental conditions of potentiometric titrations. (Ethanol–water 50% [v/v], I = 0.5*M* in $NaNO_3$ and T = 25°)

Titration number	[HPGO], *m*M	[HPPO], *m*M	[Cu^{2+}], *m*M	[Ni^{2+}], *m*M	Ligand–metal ratio	Range of $-\log[H^+]$
1	1.285		1.266		1.0	3.2–5.1
2	2.51		2.41		1.0	3.2–5.1
3	10.88		3.61		3.0	2.0–5.1
4	22.83		4.38		5.2	2.7–5.0
5	24.06		3.47		6.9	2.8–5.1
6	24.30		2.43		10.0	2.8–5.1
8		20.02	5.03		4.0	3.5–4.3
9		36.8	7.61		4.8	3.4–4.2
7		13.47	2.78		4.9	3.8–4.6
13		27.24	2.79		9.1	3.7–4.6
10		48.8	5.04		9.7	3.4–4.2
14		27.35	2.79		9.8	3.6–4.6
11		46.7	2.38		15.4	3.5–4.5
12		54.5	2.80		19.5	3.5–4.5
15	20.38			4.91	4.1	3.6–5.6
16	13.42			2.69	5.0	3.9–6.0
17	37.02			7.37	5.0	3.3–5.2
18	46.4			2.33	19.9	3.4–6.3
19	55.2			2.72	20.3	3.3–5.2
20	27.11			1.320	20.5	3.6–6.2

purified with vanadous perchlorate and barium hydroxide) was bubbled continuously through the solution in the potentiometric cell.

Apparatus

A Radiometer PHM64 pH meter equipped with a combined Ross pH-electrode (Orion 81-02) was used. The titrand (sodium hydroxide solution) was added with a Metrohm 655 Multi-Dosimat automatic burette with a 10.0-ml exchanging unit. Sample solutions were titrated in a double-walled vessel maintained at 25 ± 0.1° by circulating water and were stirred magnetically under a continuous flow of nitrogen. The potentiometric assembly was controlled by an HP 9816 microcomputer via an HP 3421A data acquisition control unit.[15]

Infra-red spectra (potassium bromide pellets) were recorded on a Perkin–Elmer 1330 spectrophotometer.

Procedure

The electrode system was calibrated in terms of hydrogen ion concentration from strong acid–strong base titrations by the Gran method.[16] The value of the ionic product of the medium is $-\log K_w = 14.165 \pm 0.015$. In this medium, the liquid junction potential, $E_j = j_{OH}[OH^-]$, must be taken into account in basic solutions: $j_{OH} = 282 \pm 5$ mV/*M*. In acidic medium, the liquid junction potential is negligible in the working range.

Complexation equilibria have been studied at several metal concentrations and different ligand-to-metal ion concentration ratios. The experimental conditions of the titrations performed are listed in Table 1. Taking into account the errors in the preparation of solutions (from glassware, weighing of ligands and the standardization of metal ion stock solutions), the errors in the concentrations listed are within 0.2–0.3% of its value. In all the systems studied the titrations were performed up to pH values at which the formation of precipitates began and unstable emf measurements were obtained.

The numerical analysis of all the experimental emf data was carried out with the computer programs MINIGLASS[15] and SUPERQUAD.[17] When SUPERQUAD was used, the errors in the titrant volume added and the measured emf value, were taken as 0.02 ml and 0.2 mV, respectively, according to the specifications of automatic burette and potentiometer used.

RESULTS AND DISCUSSION

Copper(II) complexation equilibria

The results obtained in the complexation study between copper(II) ions and HPGO or HPPO are given in Table 2. In the calculation of the confidence range of the logarithms of these formation constants, as well as those corresponding to the nickel(II) complexes, we

Table 2. Formation constants of copper(II)–HPGO and copper(II)–HPPO complexes at 25°, in ethanol-water (50% v/v) and 0.5*M* $NaNO_3$ ionic strength. The confidence intervals of log β are equal to three times the estimated standard deviation

Ligand	Species (mlh)*	MINIGLASS log β_{mlh}	MINIGLASS s†	SUPERQUAD log β_{mlh}	SUPERQUAD σ‡	SUPERQUAD χ^2§
HPGO	110	5.53 ± 0.06	0.0151	5.53 ± 0.09	1.02	17.85
	21–1	4.87 ± 0.03		4.87 ± 0.03		
	22–1	10.18 ± 0.03		10.18 ± 0.03		
HPPO	21–1	4.57 ± 0.03	0.0193	4.57 ± 0.03	1.58	25.91
	22–1	10.50 ± 0.09		10.57 ± 0.15		

*Stoichiometric coefficients for metal ion, deprotonated ligand and hydrogen ion, respectively.
†Standard deviations of the residuals with respect to added volumes.
‡Ratio of the root mean square of the weighted residuals to the estimated error in the working conditions.
§Chi-squared test based on weighted residuals on emf readings.

have taken into account the standard deviations in the constants given by the computer programs, and the standard error deviation from the error propagation law, on the basis of the errors in concentration of reactants and in the measured emfs.

From the values of the constants obtained, the distribution of species which contain copper(II) as a function of pH was evaluated for both systems (Figs. 1 and 2). In the copper(II)–HPGO system titrations can only be performed up to pH values around 5, because above this value precipitates are formed in the solutions. In the copper(II)–HPPO system precipitation takes place around pH 4.5. The formation curves are not superimposed in either system (Figs. 3 and 4), which points to the existence of protonated or polynuclear species or hydroxocomplexes.

In the copper(II)–HPGO system the best fit of the experimental data has been found with the model containing the monomeric 110 and the dimeric 21-1 and 22-1 species, expressed as mlh, where m, l and h are the stoichiometric coefficients for metal ion, deprotonated ligand and hydrogen ion, respectively. Although the 110 species is formed only to a maximum of 10%, its inclusion in the postulated model gives an improvement of the fitting.

In the copper(II)–HPPO system the proposed model is very similar and it is composed by the species 21-1 and 22-1. The 110 species is rejected by the programs. The 22-1 species is formed to a slight extent (less than 10% and not in all the titrations performed) before precipitation occurs, but its inclusion in the model improves the fitting significantly.

Elemental analysis of precipitates obtained from different ligand:metal ratios gives, in both systems, results that are between the theoretical values corresponding to the neutral species $[CuL_2]_x$ and $[CuL(OH)]_y$ (Table 3). As the ligand:metal ratio increases the results approach the values corresponding to $[CuL_2]_x$ species.

A comparison of the IR absorption spectra of the insoluble complexes and those of the pure ligands shows variations of some IR bands due to complexation. The most characteristic are the

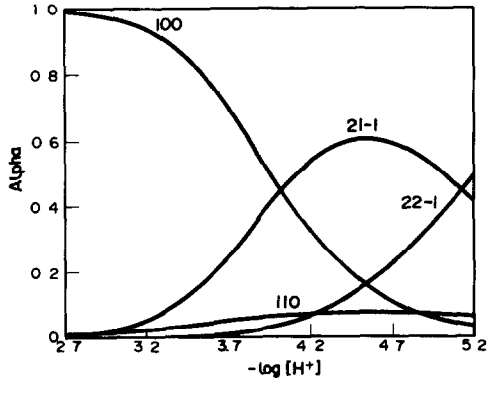

Fig. 1. Species distribution diagram for Cu(II)–HPGO complexes. $[Cu^{2+}] = 3.5mM$, $[HPGO] = 24.1mM$.

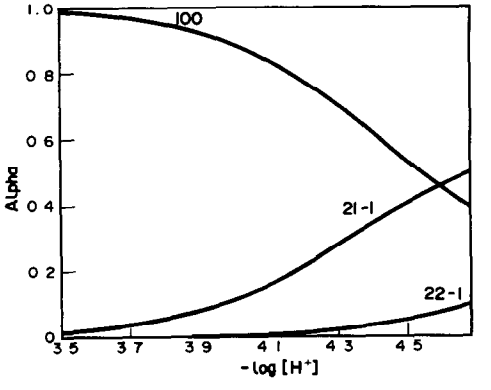

Fig. 2. Species distribution diagram for Cu(II)–HPPO complexes. $[Cu^{2+}] = 2.3mM$, $[HPPO] = 21.0mM$.

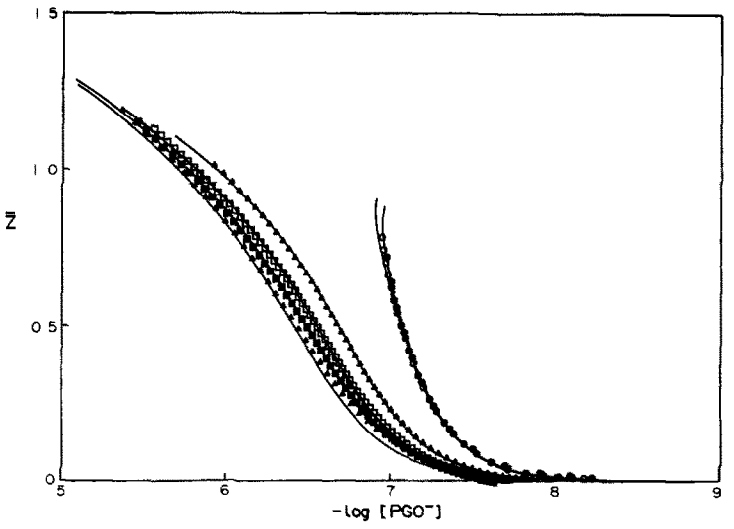

Fig. 3. Experimental formation curves for the Cu(II)–HPGO system. Symbols are: (●) titr. 1, (○) titr. 2, (△) titr. 3, (□) titr. 4, (■) titr. 5 and (▲) titr. 6. Solid lines are the theoretical curves obtained with the constants given in Table 2.

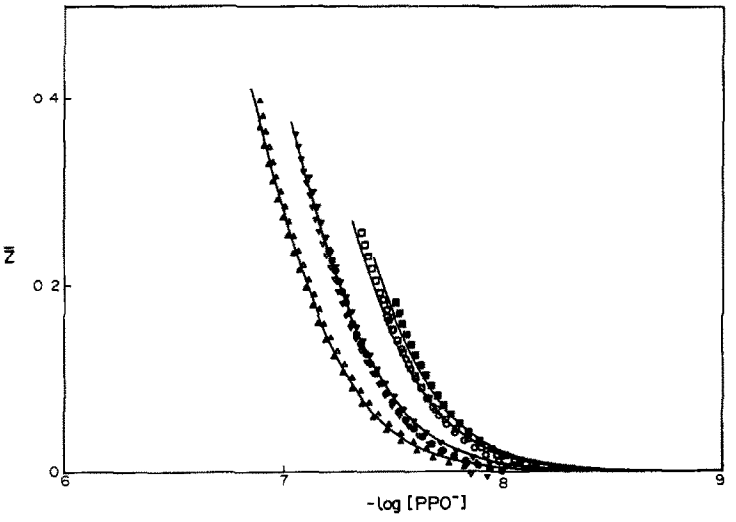

Fig. 4. Experimental formation curves for the Cu(II)–HPPO system. Symbols are: (■) titr. 7, (○) titr. 8, (□) titr. 9, (▽) titr. 10, (●) titr. 11, (▼) titr. 12, (△) titr. 13 and (▲) titr. 14. Solid lines are the theoretical curves obtained with the constants given in Table 2.

Table 3. Elemental analysis of the insoluble copper(II) complexes

Ligand	Ligand:metal ratio	%Cu*	%C†	%H†	%N†
HPGO	2	24.13	43.57	3.13	6.45
	5	20.81	45.35	3.22	6.95
	10	19.20	48.06	3.28	7.10
	$[Cu(PGO)_2]_x$	17.65	53.40	3.33	7.78
	$[Cu(PGO)(OH)]_y$	27.78	41.99	3.06	6.12
HPPO	2	24.98	45.35	3.82	5.75
	5	21.75	45.74	3.84	5.47
	10	19.23	47.75	4.00	6.12
	$[Cu(PPO)_2]_x$	16.37	55.68	4.12	7.22
	$[Cu(PPO)(OH)]_y$	26.16	44.50	3.71	5.27

*Iodometrically determined after mineralization of the precipitate with sulphuric acid.

†Analysed by automated microanalytical techniques.

Table 4. Formation constants of nickel(II)–HPGO complexes at 25°, in ethanol–water (50% v/v) and 0.5*M* $NaNO_3$ ionic strength (confidence intervals as in Table 2)

Species (mlh)*	MINIGLASS		SUPERQUAD		
	$\log \beta_{mlh}$	s†	$\log \beta_{mlh}$	σ‡	χ^2§
110	4.48 ± 0.04	0.0174	4.47 ± 0.04	1.37	30.29
230	16.52 ± 0.04		16.50 ± 0.07		
240	21.41 ± 0.04		21.41 ± 0.04		
22–2	0.50 ± 0.03		0.50 ± 0.03		

*, †, ‡ and § As in Table 2.

lowering of νC=O and the shifting of νN—O to higher frequencies, indicating coordination through these groups.[3,8–10] A strong broad band appears around 3300 cm^{-1}, corresponding to νO—H. This band was described by Danilewicz *et al.*[7] in the IR spectra of a complex of copper(II) and HPPO obtained from a ligand:metal ratio of 1:1. The stochiometry of this complex is Cu(PPO)(OH); it has been proposed that this compound is a dimer or indeed a polymer of higher order.

Some of the species detected in the potentiometric study appear to be previous steps to the formation of this kind of complex. $[CuL(OH)]_x$, but the neutral species have not been detected, probably because of their low solubility in common solvents.[7]

The complexing behaviour of HPGO and HPPO is very similar, both ligands showing a trend towards dimeric species, which is in accordance with the fact that they have the same active coordination centres against metal ions. On the other hand, in the copper(II)–HPGO system complexation begins at a pH lower than

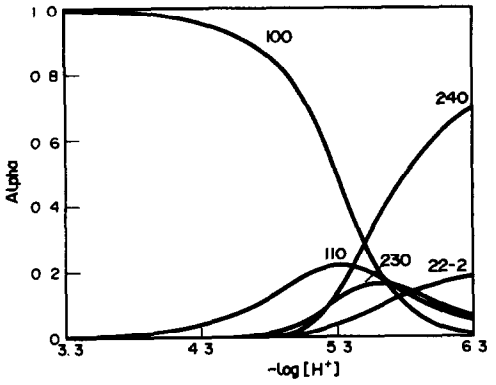

Fig. 5. Species distribution diagram for Ni(II)–HPGO complexes. $[Ni^{2+}] = 2.4mM$, $[HPGO] = 47.5mM$.

that in the copper(II)–HPPO system, as can be expected from the pK_a values of these reagents.

Nickel(II) complexation equilibria

It was not possible to carry out the complexation study betwen nickel(II) and HPPO because in the experimental conditions (ligand:metal ratio between 5 and 25) stable emf readings were only obtained at pH < 6, where complexation

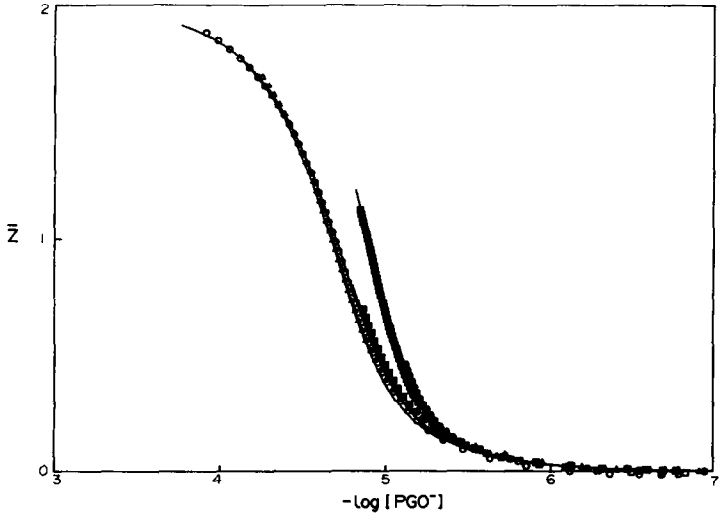

Fig. 6. Experimental formation curves for the Ni(II)–HPGO system. Symbols are: (▲) titr. 15, (□) titr. 16, (●) titr. 17, (○) titr. 18, (■) titr. 19 and (△) titr. 20. Solid lines are the theoretical curves after the constants given in Table 4.

does not take place; at pH values higher than 6 precipitation occurs and emf values become unstable.

The results obtained in the complexation study between nickel(II) and HPGO are shown in Table 4. The species distribution as a function of pH for this system, calculated from the values of the constants obtained, is shown in Fig. 5. In this system titrations can be performed up to pH values around 6, before precipitation takes place. The formation curves (Fig. 6), like those of the copper(II) systems, are not superimposed. The best fit of experimental data was found with the model containing the species 110, 230, 240 and 22-2.

While in some α-oxooximes–copper(II) systems hydroxocomplexes have been described[7,18] no references exist about hydroxocomplexes of nickel(II) and this class of ligands, but the inclusion of the 22-2 species in the model proposed is necessary in order to attain good fit with the experimental data in the higher pH range. Furthermore the existence of other polynuclear species (230 and 240) must be taken into account. Species 230 seems to be a previous step leading to the formation of the neutral species 240, which has been previously described by Thakkar and Haldar.[8] The inclusion of the species 120 resulted in a very slight improvement of the fitting, but this species was found to be formed only to a maximum of 5% in some titrations and therefore was not considered further. Because the model includes basically dimeric species, the 220 complex was also considered, but was rejected by the programs. Furthermore, an attempt was made to replace 110 by 220 in the model but the fitting was found to be less acceptable.

Elemental analysis of precipitates obtained from different ligand:metal ratios gives undefined stoichiometries, similar to that reported by Taylor and Ewbank for this system.[19] The results obtained (Table 5) are between the corresponding values of $[NiL_2]_x$ and $[NiL(OH)]_y$ complexes. As in the copper(II) systems, when the ligand:metal ratio increases, the results approach that of $[NiL_2]_x$ complexes. By means of the potentiometric studies two neutral species (240 and 22-2) have been identified. Thus the solids obtained must be mixtures of $[NiL_2]_x$ and $[NiL(OH)]_y$, with x and y equal to or higher than 2.

Table 5. Elemental analysis of the insoluble nickel(II)–HPGO complexes

Ligand:metal ratio	%Ni*	%C†	%H†	%N†
2	25.3	44.41	3.37	6.42
5	24.3	44.90	3.26	6.73
10	23.3	45.16	3.51	6.88
$[Ni(PGO)_2]_x$	16.55	54.13	3.38	7.89
$[Ni(PGO)(OH)]_y$	26.24	42.91	3.13	6.26

*Determined by titration with EDTA after mineralization of the precipitate with sulphuric acid.
†Analysed by automated microanalytical techniques.

The IR absorption spectra of the insoluble complexes, compared with the spectra of the pure ligand, show the same main features as those reported for the copper(II) systems—shifting to lower frequencies of νC=O, shifting to higher frequencies of νN—O and a broad band in the region of 3300 cm^{-1} corresponding to νO—H.

Complexation between nickel(II) and HPGO shows similar behaviour to that observed in the copper–α-oxooximes systems studied: a trend towards formation of dimeric species and hydroxocomplexes, although the latter are formed in smaller proportions.

REFERENCES

1. R. B. Singh, B. S. Garg and R. P. Singh, *Talanta*, 1979, **26**, 425.
2. P. P. Bhargava and M. Tyagi, *Indian J. Chem.*, 1986, **25A**, 193.
3. G. C. S. Manku, *Z. Anorg. Allg. Chem.*, 1971, **382**, 202.
4. V. M. Peshkova, Yu. A. Barbalat, T. V. Polenova and N. A. Plekhanov, *Zh. Anal. Khim.*, 1973, **28**, 902.
5. A. Izquierdo, R. Compañó, M. Granados and X. Duarri, *Polyhedron*, 1989, **8**, 1957.
6. A. Izquierdo, R. Compañó and M. Granados, *ibid.*, 1991, **10**, 919.
7. J. C. Danilewicz, R. D. Guillard and R. Wootton, *Inorg. Chim. Acta*, 1975, **15**, L5.
8. N. V. Thakkar and B. C. Haldar, *J. Inorg. Nucl. Chem.*, 1980, **42**, 843.
9. C. Natarajan and A. N. Hussain, *Indian J. Chem.*, 1981, **20A**, 307.
10. *Idem, Transition Met. Chem.*, 1982, **7**, 252.
11. S. V. Salvi, P. H. Umadikar, M. R. Patil and P. M. Dhadke, *Spectrochim. Acta*, 1984, **39B**, 965.
12. A. Izquierdo, J. L. Beltrán, J. Guiteras and M. Granados, *Mikrochim. Acta*, 1990 **III**, 129.
13. I. M. Kolthoff, E. B. Sandell, E. J. Meehan and S. Bruckentenstein, *Quantitative Chemical Analysis*, p. 781. Collier–Macmillan Canada, Toronto, Ontario, 1969.
14. A. I. Vogel, *Textbook of Quantitative Inorganic Analysis*, Longman, London, 1978.
15. A. Izquierdo and J. L. Beltrán, *Anal. Chim. Acta*, 1986, **181**, 87.
16. G. Gran, *Analyst*, 1952, **77**, 661.
17. P. Gans, A. Sabatini and A. Vacca, *J. Chem. Soc., Dalton Trans*, 1985, 1195.
18. T. W. J. Taylor and D. C. V. Roberts, *J. Chem. Soc.*, 1933, 1439.
19. T. W. J. Taylor and E. Ewbank, *ibid.*, 1926, 2818.

Talanta, Vol. 39, No. 5, pp. 481–486, 1992
Printed in Great Britain.

0039-9140/92 $5.00 + 0.00

PREPARATION OF A POLYPYRROLE–LEAD DIOXIDE COMPOSITE ELECTRODE FOR ELECTROANALYTICAL APPLICATIONS

D. VELAYUTHAM* and M. NOEL
Central Electrochemical Research Institute, Karaikudi, India 623 006

(*Received* 22 *April* 1991. *Revised* 12 *August* 1991. *Accepted* 13 *August* 1991)

Summary—A constant potential electrolytic method for the preparation of a new polypyrrole–lead dioxide composite electrode on glassy-carbon substrate is described. The method involves constant potential electrolysis (CPE) of 1*M* potassium nitrate containing 2m*M* lead acetate at +1.100 V *vs.* SCE for about 10 min, followed by addition of 25m*M* pyrrole and subsequent CPE at +0.800 V for about 2–3 min. The choice of experimental conditions for the preparation and mechanical stability, open circuit potential (ocp) response, background current levels and typical voltammetric response of Mn^{2+} in 1*M* sulphuric acid are also presented and discussed.

In spite of the fact that lead dioxide electrodes find wide application in electrochemical synthesis and electrochemical energy conversion,[1] basic studies on these electrodes are mainly confined to the nucleation growth process of lead dioxide crystallites.[2] Very few results concerning electroanalytical applications have been reported. Lead dioxide coated platinum electrodes have been used for the estimation of EDTA,[3,4] Ca^{2+}, Mg^{2+} and Zn^{2+} ions,[5,6] hydrogen peroxide,[7] polyphosphates[8] and sulphite anions.[9] In addition lead dioxide coated on Au and graphite,[10] wax bound carbon,[6] carbon paste,[11] and glassy-carbon (GC) substrates[12,13] have also been recommended for analytical applications. A recent report also recommends direct electrochemical oxidation of a solid lead electrode.[14] However, none of these electrodes have found wide spread application in electro analysis. A careful review of all the literature cited above and also some preliminary investigations in this laboratory have indicated that the electrodes prepared by such conventional means lack longterm stability, leading to mechanical peel off, as well as gassing through edges[9] and cracks.[13]

Recently, a slightly modified procedure involving constant potential electrolysis (CPE) with very low concentrations of Pb^{2+} ions ($<5mM$) have been proposed for preparing very thin lead dioxide films on gold substrates.[15–19] When efforts were made to adapt a similar procedure on GC substrates, the same type of stability problems mentioned above were encountered. Hence a novel method of preparing a stable lead dioxide electrode by codepositing lead dioxide along with a comparatively small proportion of polypyrrole (PP) was considered. Some of the preliminary results obtained in the fabrication and characterization of such a composite electrode are presented here.

EXPERIMENTAL

A 5-mm diameter GCE (Tokai Electrode Mfg. Co., Japan) fixed into a glass tube with epoxy resin was polished, cleaned and activated by electrochemical cycling as described earlier.[20] Care was taken to clean the GCE coated with lead dioxide after every experiment in 1:1 H_2O_2/HOAc mixture and 1:1 HCl/H_2O mixture[21] before usual surface pretreatments.

A typical H-type electrochemical cell with a Pt counter electrode and a luggin capillary connected SCE reference electrode was used. Nitrogen gas was used for deaeration. The experiments were carried out at 25 ± 1°. All AR chemicals and triply distilled water were used throughout.

A BAS 100 A electrochemical analyser was employed for CPE as well as CV measurements. A Jeol (Model 35 CF) scanning-electron microscope was used for surface characterization.

*Author for correspondence.

Preparation of polypyrrole–lead dioxide composite film

The main technical difficulty towards achieving the desired composite film lies in selecting the right experimental conditions in which simultaneous deposition of both lead dioxide and polypyrrole can occur at the same electrode potential. It is already well established that polypyrrole formation in aqueous solution will lead to an electronically insulating layer if the deposition potential exceeds +0.850 V *vs.* SCE.[22] In perchloric acid and nitric acid media electrodeposition of lead dioxide can begin only beyond +1.6 V *vs.* SCE.[2,23] On the other hand, in alkaline potassium hydroxide media, the electrodeposition of lead dioxide begins much earlier, *i.e.*, +0.400 V *vs.* SCE. Hence, a fairly neutral pH range alone seems to be suitable for further consideration towards development of a polypyrrole–lead dioxide composite electrode.

Another important requirement is the necessity of selecting the proper counter ion for maintaining good electronic conductivity of the polymer film. Since acetate anion does not belong to the established group of counter ions for conducting polymer films, nitrate ion as additive was chosen to serve this purpose.

With the two choices mentioned above it was indeed found that a reasonably close electrodeposition potential could be achieved for both polypyrrole and lead dioxide in the pH range close to 7.0. A typical cyclic voltamperogram of lead dioxide deposition on GC under these experimental conditions is presented in Fig. 1. In the first sweep lead dioxide deposition begins as low as +1.1 V due to nucleation overvoltage requirements. But in the subsequent sweeps where lead dioxide nuclei already exist on the surface, the electrodeposition process occurs as low as +0.8 V (Fig. 1). In this voltammetric experiment the potential was never allowed to decrease below zero voltage and move to the

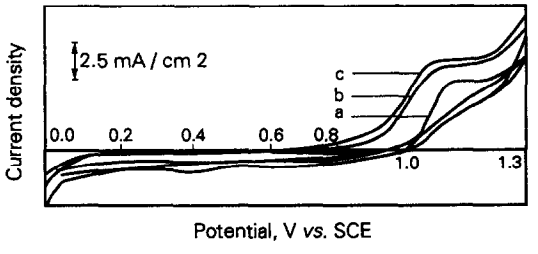

Fig. 1. Typical multisweep CV curves of deposition of PbO_2 on the glassy-carbon electrode in 1*M* KNO_3/0.1*M* $Pb(OAc)_2$; (a), (b) and (c) represent 1st, 5th and 11th cycles. pH = 6.9. V = 5 mV/sec.

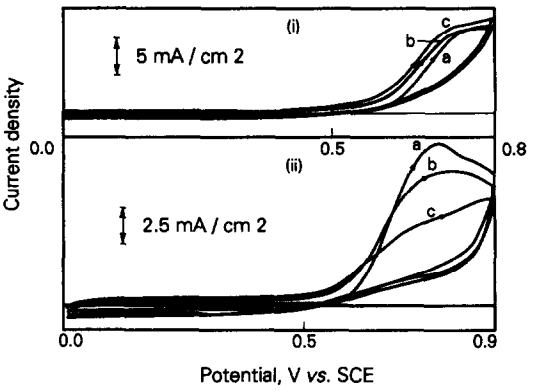

Fig. 2. The effect of the anodic potential limit on multisweep CV curves of pyrrole on the glassy-carbon electrode in 1*M* KNO_3/50m*M* pyrrole. V = 5 mV/sec; (a), (b) and (c) represents 1st, 2nd and 3rd cycles.

negative region, to ensure that the electrodeposited lead dioxide does not become reduced to Pb^{2+} and hence get stripped.

Under the same solvent-supporting electrolyte system (1*M* potassium nitrate) pyrrole also undergoes electrochemical oxidation in the usual potential range (Fig. 2). It may also be noted that during multisweep cyclic voltammetry if the anodic limit is held below +0.8 V, the polypyrrole formed remained conductive and in all subsequent sweeps the anodic current increased slightly [Fig. 2(i)]. On the other hand if the anodic limit exceeds +0.8 V, the polypyrrole film passivates and hence the anodic current decreases with increasing numbers of sweeps in multi-sweep voltammetry [Fig. 2(ii)]. This observation agrees very well with the earlier report on polypyrrole formation[22] from aqueous solutions. The passivation at more positive potentials is probably connected with overoxidation of the polypyrrole conjugated system and the resultant decreasing electronic conductivity.

In consideration of the above facts, a number of CPE experiments were carried out to optimize the conditions for preparing a polypyrrole–PbO_2 composite, parameters such as the concentration of Pb^{2+} ions and pyrrole, the relative proportions of these constituents, the anodic potential, the deposition time and the total charge passed for the deposition of composite were optimized to obtain a mechanically stable and electrochemically active composite electrode.

Some typical optimization experimental conditions and results obtained in the deposition processes are presented in Table 1. Pb^{2+} (2m*M*) and a 10-min deposition time was found to give

Table 1. Typical results of the constant potential electrolysis of Pb^{2+} and pyrrole (PY) showing the stability of the PbO_2, polypyrrole (PP) and PP–PbO_2 composite film electrode

Expt No.	$C_{Pb^{2+}}$, mM	C_{py} mM	Deposition time, min		Deposition charge, mC		Nature of deposit
			PbO_2	PP + PbO_2	PbO_2	PP + PbO_2	
1	5	—	4	—	85–90	—	PbO_2 deposit non uniform and unstable
2	2	—	10	—	85–90	—	PbO_2 deposit uniform but peels off during polarisation
3	1	—	30	—	15–20	—	PbO_2 deposit too low
4	—	5	—	15	—	10–12	PP deposit non-uniform and peels off during polarisation
5	—	25	—	7	—	110–120	PP deposit porous but peels off during polarisation
6	2	5	10	20	85–90	2–3	PP–PbO_2 composite film unstable during polarisation
7	2	5	10	30	85–90	4–5	PP–PbO_2 composite film unstable
8	2	15	10	20	85–90	5–7	PP–PbO_2 composite film unstable
9*	2	25	10	3	85–90	10–12	PP–PbO_2 composite film uniform, adherent and stable
10	2	25	10	5	85–90	45–50	PP–PbO_2 composite film peels off during polarisation

*Optimized condition for the preparation of PP–PbO_2 composite film electrode.

Note: (1) In all the experiments studied above PbO_2 deposition carried out at +1.1 V followed by addition of pyrrole and further deposition at +0.8 V *vs.* SCE.

(2) Polarisation study was carried out in 1.0*M* H_2SO_4 from 1.4 V to 1.8 V *vs.* SCE.

uniform deposits at an optimum deposition rate (experiments 1–3). For polypyrrole deposition, 25m*M* pyrrole solution and a deposition time of 10 min were found to be optimum. At lower concentrations of pyrrole, the deposition is non-uniform and at higher concentrations it becomes highly porous and unstable (experiments 4 and 5). Comparison of experiments 4 and 6 would indicate that, in the presence of 2m*M* Pb^{2+}, charge due to PP–PbO_2 composite deposition decreases substantially, even with increasing deposition time. This requires further optimization of concentration of pyrrole as well as composite deposition time. From these studies, conditions described in experiment 9 are selected to be the optimum for a mechanically stable as well as electrochemically active composite electrode. The experimental procedure for this process may be described in detail as follows.

Potassium nitrate (1*M*) containing 2m*M* $Pb(OAc)_2$ is taken in the working electrode compartment, deaerated with nitrogen for 15–20 min. The activated GC was then inserted and CPE was carried out at +1.1 V for about 10 min to achieve an overall deposition charge of 80–90 millicoulombs. The electrode is then taken out and washed with distilled water. Then 25m*M* pyrrole is added and the electrolyte stirred for 2–3 min taking care to keep the electrolyte under nitrogen atmosphere. The electrode is then inserted and CPE at +0.800 V is further carried out for a period of 2–3 min. During this period simultaneous deposition of polypyrrole as well as lead dioxide takes place and an overall electrodeposition charge of 10 mC is passed (a considerably larger concentration of pyrrole compared to Pb^{2+} always seems to be required; there appears to be some blocking effect for polypyrrole formation on lead dioxide crystallites especially when Pb^{2+} is simultaneously present in the solution). The electrode is then taken out, washed with triply distilled water, allowed to dry in the open air and then stored in a desiccator.

Characterization of polypyrrole–lead dioxide composite electrode

The electrodeposition of lead dioxide and polypyrrole–lead dioxide composite could be easily distinguished by using a metallurgical microscope of ×100 and ×450 magnification. This method was conveniently employed during the preparation and characterization studies. A typical set of SEM photographs containing these two deposits are shown in Fig. 3(a) and (b), respectively. It may be noticed that the lead dioxide layer before addition of pyrrole contains distinct spherical particles without any covering film. The overall deposit also has a bright appearance [Fig. 3(a)]. After polypyrrole–lead dioxide composite deposition the individual lead dioxide particles are submerged on a

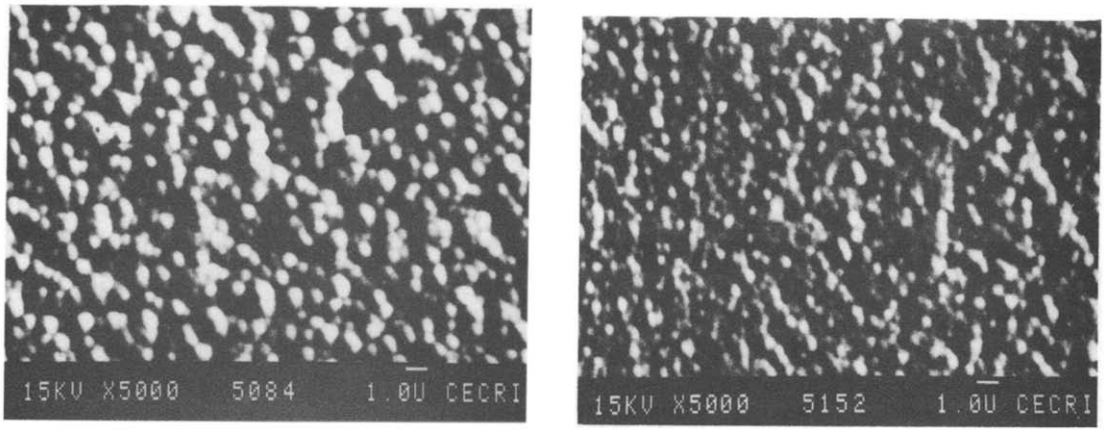

Fig. 3. Scanning electron micrographs of PbO_2 deposited on the glassy-carbon electrode. (a) GCE/PbO_2 (1*M* KNO_3/2m*M* $Pb(OAc)_2$, CPE at +1.100 V for 10 min). (b) GCE/PbO_2/polypyrrole (CPE of electrode from Fig. 3(a) after adding 25m*M* pyrrole at +0.800 V for 3 min).

continuous polypyrrole layer [Fig. 3(b)]. The composite also loses its brightness and shiny nature.

The rest potential of the lead dioxide electrode, as well as the polypyrrole–lead dioxide composite electrode, were also continuously monitored in 1*M* sulphuric acid at 24-hr intervals. During the first measurement, both the electrodes give rest potential values of $+1.4 \pm 0.02$ V, suggesting that both electrodes behave essentially like lead dioxide electrodes. However, the pure lead dioxide electrode does not remain stable to give a reproducible rest potential response for one day. The electrode slowly decomposes and the glassy-carbon surface is exposed. On the other hand the polypyrrole–lead dioxide composite remains stable and gives reproducible responses for about 10 days.

The anodic background currents from the rest potential region for lead dioxide as well as polypyrrole–lead dioxide composite electrode in 1*M* sulphuric acid at different sweep rates are presented in Fig. 4(a) and (b) respectively. As may be noticed from the figure, the background current values are very similar. Once again however pure lead dioxide electrode breaks down mechanically after a few cycles whereas the composite electrode shows remarkable stability. Although mechanical instability of pure lead dioxide material has also been reported earlier[24] the exact cause of this property is not known. Non-adherence of lead dioxide crystallites with the substrate, weak interactions between lead dioxide crystallite grain boundaries, effect of occluded oxygen gas bubbles and mechanical break down during oxygen evolution are some of the likely causes for the breakdown. However, in the PP–lead dioxide composite, lead dioxide particles are held in between.

The voltammetric responses of 5m*M* Mn^{2+} in 1*M* sulphuric acid at different sweep rates are presented in Fig. 5(a). It can be seen that the peak current increases with sweep rate (V). However, quantitative evaluation of peak current values becomes impossible because of the

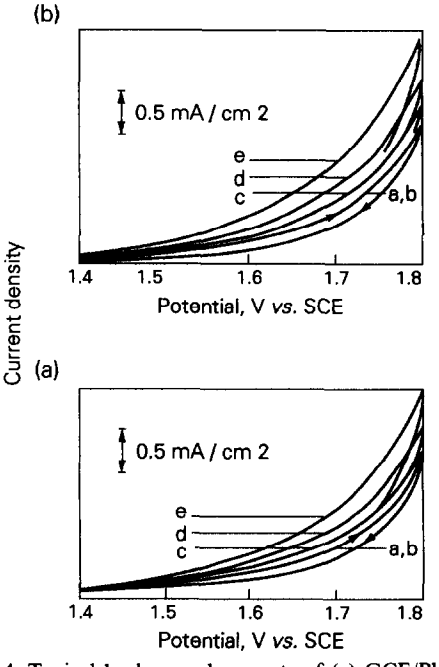

Fig. 4. Typical background currents of (a) GCE/PbO_2 (b) GCE/PbO_2/polypyrrole composite electrode in 1*M* H_2SO_4 V = 10, 20, 40, 80 and 160 mV/sec from (a)–(e) respectively.

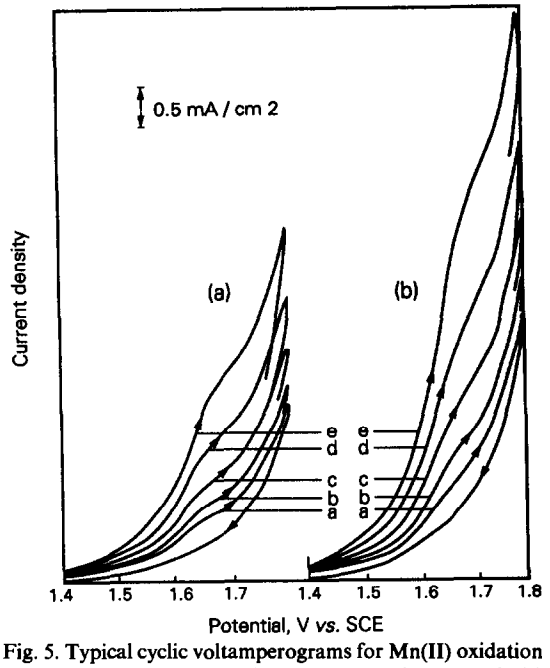

Fig. 5. Typical cyclic voltamperograms for Mn(II) oxidation in 1M H_2SO_4 on polypyrrole–PbO_2 composite electrode (a) 5mM Mn^{2+} (b) 10mM Mn^{2+}, V = 10, 20, 40, 80 and 160 mV/sec from (a)–(e) respectively.

closeness of the peak current to the continuously increasing background current. One may however notice that the peak currents are actually concentration dependent by comparing Figs. 5(a) and 5(b) for 5mM and 10mM Mn^{2+}, respectively, under identical sweep rate conditions. In this figure the I – E curves for the negative scan direction are not shown, except for the slow sweep rate for the sake of clarity. A pure lead dioxide electrode also showed quite similar responses, at least for a few voltammetric cycles, but once again mechanical break down prevents checking the reproducibility of the results. Some voltammetric responses for the same redox system for pure lead dioxide electrodes on Au[17] and stainless steel substrates[19] have been reported. At least on GCEs such reproducible responses on pure lead dioxide electrodes over long periods (say 10 days or more) could not be obtained in the present study.

Voltammetric responses of 25mM dimethyl sulphoxide (DMSO) at different sweep rates on PP–lead dioxide composite electrode are presented in Fig. 6. The peak current (i_p) and peak potential (E_p) responses for this system could be quantitatively evaluated; i_p is directly proportional to $V^{1/2}$ indicating diffusion controlled nature of the process. As indicated in the inset of Fig. 6, the peak current is also found to increase linearly with concentration of DMSO. From the $E_p - E_{p/2}$ values the transfer coefficient αn_a was calculated to be equal to 0.69. Using Nicholson and Shain's expression for irreversible charge transfer[25] and the diffusion coefficient value of the closely related molecule 2-mercapto ethanol to DMSO ($D = 1.3 \times 10^{-5}$ cm^2 sec^{-1}) from the literature,[26] the number of electrons (n) involved in the oxidation of DMSO was calculated to be 2.0 ± 0.1. This suggests that DMSO is oxidized to dimethyl sulphone[18] in an irreversible diffusion controlled charge transfer process. Hence in this case PP–lead dioxide composite electrode can be used effectively for quantitative estimation of DMSO in millimolar concentration range. More detailed work on this as well as a number of other redox systems which can be analysed using this electrode is in progress in this laboratory.

CONCLUSION

The present experimental results clearly indicate that a stable and electrochemically active polypyrrole–lead dioxide composite electrode can be easily prepared in aqueous solution

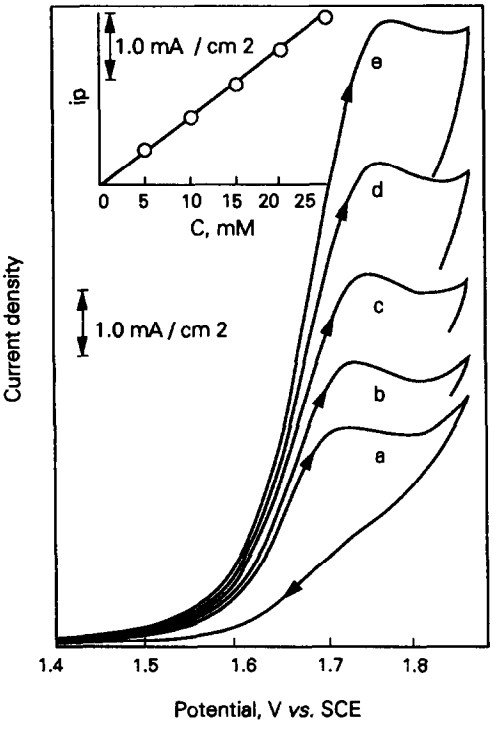

Fig. 6. Typical cyclic voltamperograms for DMSO oxidation in 1M H_2SO_4 on polypyrrole–PbO_2 composite electrode: C_{DMSO} = 25mM, V = 10, 20, 40, 80 and 160 mV/sec from (a)–(e) respectively.

under potentiostatic conditions, in 1*M* potassium nitrate solution with millimolar concentration of $Pb(OAc)_2$ and pyrrole. The porous and electronically conducting polypyrrole matrix containing electrochemically active lead dioxide particles serves as a mechanically stable electrode system without any decreasing electrochemical activity. Further investigations to establish the long-term stability and electrocatalytic properties of this electrode are in progress. The most important and interesting conclusion from this work however is the fact that one can actually think of a variety of polymer–oxide composite electrodes for catalytic effects and analytical applications.

Acknowledgements—The authors thank Prof. S. K. Rangarajan for his keen interest in the publication of this paper. They also thank Sri S. Chidambaram and Sri C. Chakkaravarthy, for their encouragements, discussion and provision of experimental facilities.

REFERENCES

1. *The Electrochemistry of Lead*, A. T. Kuhn (ed.), Academic Press, London, 1979.
2. D. Velayutham and M. Noel, *Electrochim. Acta*, 1991, **36**, 2031.
3. D. R. Tallant and C. O. Huber, *J. Electroanal. Chem.*, 1968, **18**, 413.
4. C. O. Huber and D. R. Tallant, *ibid.*, 1968, **18**, 421.
5. C. O. Huber, K. Dahnke and F. Hinz, *Anal. Chem.*, 1971, **43**, 152.
6. C. N. Wang, P. J. Kinlen, D. A. Schoeller and C. O. Huber, *ibid.*, 1972, **44**, 1152.
7. K. G. Schick, V. G. Magearu, N. L. Field and C. O. Huber, *ibid.*, 1976, **48**, 2186.
8. D. H. Karweik and C. O. Huber, *ibid.*, 1978, **50**, 1209.
9. F. Strafelda and J. Krofta, *Collec. Czech. Chem. Commun.*, 1971, **36**, 1634.
10. G. Belanger, *Anal. Chem.*, 1974, **46**, 1576.
11. C. Efron and M. Ariel, *Anal. Chim. Acta*, 1979, **108**, 395.
12. R. G. Barradas and A. Q. Contractor, *J. Electroanal. Chem.*, 1981, **129**, 327.
13. A. C. Ramamurthy and T. Kuwana, *ibid.*, 1982, **135**, 243.
14. F. Beck and W. Gabrie, *ibid.*, 1985, **182**, 355.
15. I. H. Yeo and D. C. Johnson, *J. Electrochem. Soc.*, 1987, **134**, 1973.
16. W. R. Lacourse, Y. L. Hsiao, D. C. Johnson and W. H. Weber, *ibid.*, 1989, **136**, 3714.
17. J. Feng and D. C. Johnson, *J. Electrochem. Soc.*, 1990, **137**, 507.
18. H. Chang and D. C. Johnson, *ibid.*, 1990, **137**, 2452.
19. J. Feng and D. C. Johnson, *J. Appl. Electrochem.*, 1990, **20**, 116.
20. M. Noel and P. N. Anantharaman, *Analyst*, 1985, **110**, 1095.
21. L. J. Li, M. Felishman and L. M. Peter, *Electrochim. Acta*, 1989, **34**, 459.
22. S. Asavapiriyanont, G. K. Chandler, G. A. Gunavardena and D. Pletcher, *J. Electroanal Chem.*, 1984, **177**, 229.
23. H. Chang and D. C. Johnson, *J. Electrochem. Soc.*, 1989, **136**, 17.
24. K. C. Narasimham, *B. Electrochem.*, 1991, **21**, 276.
25. R. S. Nicholson and I. Shain, *Anal. Chem.*, 1964, **36**, 706.
26. W. Stricks, J. K. Frischman and R. G. Mueller, *J. Electrochem. Soc.*, 1962, **109**, 518.

Talanta, Vol. 39, No. 5, pp. 487–492, 1992
Printed in Great Britain

0039-9140/92 $5.00 + 0.00
Pergamon Press plc

SALTING-OUT SURFACTANT EXTRACTION OF PORPHYRINS AND METALLOPORPHYRIN FROM AQUEOUS NON-IONIC SURFACTANT SOLUTIONS

WILLIAM J. HORVATH and CARMEN W. HUIE*
Department of Chemistry, State University of New York at Binghamton, Binghamton, New York 13902-6000, U.S.A.

(*Received* 4 *September* 1991. *Revised* 8 *November* 1991. *Accepted* 8 *November* 1991)

Summary—A number of cloud point temperature-depressing electrolytes have been investigated for the separation of a non-ionic surfactant (Triton X-100) from aqueous solutions and the corresponding extraction of the organic solutes into the smaller volume surfactant-rich phase using the salting-out method. High extraction efficiencies and preconcentration factors were obtained at room temperature for the extraction of several hydrophilic and hydrophobic metal-free porphyrins (uroporphyrin, coproporphyrin, protoporphyrin and hematoporphyrin) and one metalloporphyrin (iron-protoporphyrin) that were dissolved in the aqueous non-ionic surfactant solutions. Possible mechanisms responsible for the efficient extraction of these important biological molecules into the surfactant-rich layer are discussed.

Non-ionic surfactants containing polyoxyethylene functional groups are known to form neutral adducts with a variety of reagents such as sodium picrate[1] and ammonium tetrathiocyanato-cobaltate(II).[2] It has been postulated[3] that the metal cations within these adducts are coordinated to the polyoxyethylene groups via the unpaired electrons of the regularly spaced oxygen atoms; subsequent interaction of these cationic complexes with the anions form net neutral adducts, which can then be concentrated by extraction into organic solvents. This extraction process has been exploited as a sensitive method for the determination of non-ionic surfactants at low levels.[4] Recently, it has been shown[5] that aurocyanide ion-pairs with alkali metal ions can be extracted efficiently into organic solvents with the aid of a common long-chain polyoxyethylene non-ionic surfactant (Triton X-100) and interestingly, the experimental results agree favorably with those obtained from molecular mechanics calculations.

It is known[6] that many aqueous non-ionic surfactant solutions will separate into two liquid phases upon heating above a characteristic temperature (*Tc*) referred to as the cloud point. Watanabe and Tanake[7] have applied this unique property of non-ionic surfactants for the efficient extraction of metal chelates without the use of any conventional organic solvents. Advantages include experimental conveniences, lower cost, ease of waste disposal, and perhaps more importantly, enhanced analytical sensitivity due to the fact that the metal chelates can be easily extracted from the bulk aqueous medium into a much smaller solution phase mostly containing the surfactant. In their experiment it was necessary to use an uncommon non-ionic surfactant (PONPE-7.5) with cloud point temperature near that of room temperature in order to obtain high extraction efficiencies. When a common non-ionic surfactant (Triton X-100) with a *Tc* of $\sim 70°$ was used instead, leakage of surfactant and metal chelates back into the aqueous medium occurred when the temperature of the solution gradually fell towards room temperature, resulting in loss of extraction efficiency.

A large number of salting-out agents have been investigated by Matkovich and Christian[8] for the separation of acetone from aqueous solutions and its use for extraction of metal chelates. More recently, Jenkins *et al.*[9,10] have demonstrated the use of a salting-out solvent extraction method for preconcentration of organic solute from water into a smaller volume of organic phase. Schott and Royce[11] have shown that electrolytes can either cause salting out or salting in of non-ionic surfactants, resulting in the lowering or increasing of the magnitude of *Tc*, respectively. Several mechanisms

*Author for correspondence.

have been proposed for the effects of electrolytes on *Tc* of aqueous non-ionic surfactant solutions. For example, some electrolytes can depress *Tc* by the process of dehydration, while others can decrease *Tc* by enhancing self-association of water molecules. A large number of electrolytes have been classified as having either salting-out or salting-in properties and are ranked according to their salting strength.[11–13] However, to the best of our knowledge, surfactant extraction and preconcentration of organic solutes by the salting-out method has not been reported.

In this paper separation of aqueous non-ionic surfactant (Triton X-100) solutions into two liquid phases by the addition of relatively large amounts of cloud point-depressing electrolytes and the corresponding extraction of the organic analytes (porphyrins and metalloporphyrin) into the smaller volume phase rich in surfactant was performed. High extraction efficiencies and preconcentration factors were obtained at room temperature. Possible mechanisms responsible for the efficient extraction of the analytes into the surfactant-rich phase are mentioned.

EXPERIMENTAL

Reagent

Analytical grade Triton X-100 (a branched *p*-octylphenol with an average of 9–10 ethylene oxide units) and research grade bovine hemin were obtained from Sigma (St Louis, MO, U.S.A.). Sodium and potassium hydroxide, sodium and potassium sulfate, and ammonium sulfate were all of analytical grade and obtained from Fisher (Pittsburgh, PA, U.S.A.). Hematoporphyrin(IX), uroporphyrin(I), coproporphyrin(III) and protoporphyrin(IX) were all purchased from Porphyrin Products (Logan, UT, U.S.A.).

Apparatus

Measurements of porphyrin fluorescence spectra for the determination of extraction efficiency were takien with a SLM 800 photon-counting spectrofluorometer (Amico, Urbana, IL, USA). The bandwidths of the excitation and emission monochromators were set at 16 nm. The excitation wavelength of all the measurements was set at the Soret band at ~400 nm. Emission spectra were obtained by scanning the monochromator from 550 to 700 nm and the intensity of the fluorescence peak maxima of the various porphyrins situated between 610 and 630 nm were recorded. The sample solution was placed in a 1-cm pathlength quartz cell. Measurements of the non-fluorescent bovine hemin (iron–protoporphyrin) samples for determining extraction efficiency were performed with a Spectraspan 7 direct current plasma instrument (Applied Research Laboratories, Valencia, CA, USA, Model 112100). The emission monochromator was set at the iron line of 2599.4 Å for all measurements.

Procedure

To prepare the sample solutions, appropriate amounts of porphyrins were first dissolved in doubly distilled demineralized water (DDDW), and then an appropriate volume of Triton X-100 was added to the aqueous sample solution and stirred until completely dissolved. Each aqueous Triton X-100 solution was portioned into 20-ml aliquots and poured into a 60-ml separating funnel. To initiate the extraction process, an appropriate amount of a particular salting-out electrolyte was added to the separating funnel and the solution was thoroughly shaken to accelerate the dissolution of the electrolyte. At this point, separation of the aqueous Triton X-100 solution into two distinct phases can be effected in one of two ways. The fastest way is to place the sample solutions in a high-speed centrifuge and separation of the two phases will take about 10 min with the centrifuge set at 4000 rpm. If a high-speed centrifuge is not available, separation of the two phases can be effected by simply letting the solution stand in the dark at room temperature for a couple of hours. Heating the solution can speed up the separation; however, we avoided heating the sample solution because thermally labile solutes such as porphyrins can decompose under high temperature. Once the separation of the two phases was completed, the bottom layer (aqueous phase) was drained from the separating funnel into a standard flask and then filled with DDW up to 20 ml. The top layer (surfactant phase) remaining in the separating funnel was also diluted back up to 20 ml with DDW. It should be noted that extra care should be taken in draining the bottom layer from the funnel since the top layer is relatively thin compared to the bottom layer. In our experiment this process was facilitated by illuminating the sample solution with a hand-held ultraviolet lamp. The top layer appeared as a brightly-colored ring above the bottom layer,

Table 1. Degrees of extraction of hematoporphyrin (200 μg/l.) as a function of concentration and various salting-out electrolytes by Triton X-100 dissolved in aqueous solution (1% v/v)

Electrolytes	Concentration of electrolytes, *M*			
	1	5	10	15
			E%	
KOH	IS*	99.1 ± 2.1†/99.4 ± 1.9‡	99.3 ± 1.6/99.8 ± 3.7	98.9 ± 2.8/99.7 ± 1.8
NaOH	IS	99.3 ± 2.3/99.3 ± 0.8	99.4 ± 1.9/99.7 ± 3.2	99.6 ± 1.1/99.5 ± 1.7
	1	1.5	3.5	5.0
K_3PO_4	IS	98.9 ± 4.1/97.4 ± 2.1	99.5 ± 1.2/98.9 ± 2.1	97.3 ± 3.3/97.6 ± 1.9

*IS = incomplete separation of the aqueous Triton X-100 solutions into two distinct phases.
†E% calculated from determining porphyrin concentration in the top layer (surfactant phase).
‡E% calculated from determining porphyrin concentration in the bottom layer (aqueous phase).

thus making it easier to physically separate the two layers. Extraction efficiency for each sample solution was obtained by determining the concentration of the porphyrin present in both the top and bottom layers using the fluorescence technique. Since fluorescence spectra of porphyrins are dependent on the pH, ionic strength and surfactant concentration,[14] fluorescence calibration curves for both top and bottom layers were obtained by using a series of standards prepared by adding appropriate amounts of porphyrins into blank surfactant and aqueous phases. These blanks (top and bottom layers) were prepared in the same manner as the sample solutions except that porphyrin was not present in the DDDW prior to extraction but was added to the surfactant and aqueous phases after the two phases were separated. The procedures for the extraction of bovine hemin (iron-protophyrin) and preparation of the standards were identical to that of the metal-free porphyrins. However, extraction efficiencies were determined by using a plasma emission method. In calculating the extraction efficiencies for iron-protoporphyrin it was assumed that all the iron present in the extract was associated with the iron-protoporphyrin spiked into the blanks and sample solutions. Average extraction efficiencies and precision (standard deviation) of the measurements calculated from five repeated extractions for each sample solution are presented in Tables 1–3.

RESULTS AND DISCUSSION

Porphyrins and metalloporphyrins are highly significant biological molecules. Their unique chemical and physical properties have been harnessed by nature for carrying out important processes such as photosynthesis and transportation of oxygen in living systems. Interestingly, these molecules have found significant application in medicine; of particular importance is the use of hematoporphyrin derivatives and other porphyrin-related molecules in the detection and photodynamic therapy of tumors.[15] Table 1 shows the extraction efficiencies (*E*%) of hematoporphyrin (a mixture of dicarboxylic acid porphyrins) as a function of concentration and the type of electrolyte. The hydroxide anion has been determined to be one of the most effective *Tc* depressing electrolytes. It salts out aqueous non-ionic surfactant by promoting self-association among water molecules via hydrogen bonding, thereby tightening the structure of water and lowering its solvating power. On the other hand, phosphate anion salts out the non-ionic surfactant by competing with the surfactant for water of hydration,

Table 2. Degrees of extraction of hydrophilic and hydrophobic porphyrin (200 μg/l. each) by Triton X-100 dissolved in aqueous solution (1% v/v) as a function of various salting-out electrolytes

Electrolytes	Porphyrins			
	Proto-	Hemin	Copro-	Uro-
		E%*		
10*M* KOH	99.5 ± 1.7	96.4 ± 3.7	99.6 ± 2.2	1.6 ± 3.3
3.5*M* K_3PO_4	98.7 ± 2.3	NP†	97.5 ± 1.8	2.1 ± 3.1
2.5*M* Na_2SO_4	97.9 ± 1.9	NP	99.2 ± 0.8	98.5 ± 2.1
5.0*M* $(NH_4)_2SO_4$	99.3 ± 0.8	99.4 ± 2.1	98.7 ± 1.1	98.7 ± 1.9

*E% calculated from determining porphyrin concentration in the top layer.
†NP = Analysis was not performed with this particular electrolyte.

Table 3. Degrees of extraction of (A) hematoporphyrin (200 μg/l.) as a function of Triton X-100 concentration in aqueous solution and (B) various concentrations of hematoporphyrin by Triton X-100 dissolved in aqueous solution (1% v/v) with the addition of 5*M* $(NH_4)_2SO_4$ as the salting-out electrolyte

(A) Triton X-100 concentration, % by volume	*E*%*	(B) Preconcentration factor†	Hematoporphyrin concentration, μg/l.	*E*%‡
10	88.4 ± 4.3	9.8 ± 0.4	2	99.9 ± 1.8
1	99.2 ± 1.1	94.3 ± 3.8	2×10^2	99.3 ± 0.7
0.2	97.4 ± 2.9	>100	2×10^4	98.2 ± 2.1

**E*% calculated from determining porphyrin concentration in the top layer.

†Average preconcentration factors and standard deviations calculated from determining the volumes of the top and bottom layers based on five repeated determinations.

‡*E*% calculated from determining porphyrin concentration in the bottom layer due to the high concentration of porphyrin in the top layer.

thereby reducing the amount of water available for the hydration of the polyoxyethylene functional groups of the non-ionic surfactant and lowering the *Tc*.[11-13] Table 1 indicates that both the hydroxide and phosphate anions are very effective in causing separation of the Triton X-100 from aqueous solution once a certain threshold concentration of the electrolyte was added to the aqueous non-ionic surfactant solution. It can be seen that high *E*% values of hematoporphyrin from the aqueous medium into the surfactant phase were obtained when an electrolyte containing more than 5*M* hydroxide or 1.5*M* phosphate anion as the salting-out agent was added to the solutions. Also, it is interesting to note that the *E*% calculated from determining the hematoporphyrin concentrations in the top layer were slightly higher when using sodium hydroxide as the salting-out electrolyte as compared to potassium hydroxide; however, the corresponding *E*% values calculated with the bottom layer were very similar. From these data it is not clear whether or not different cations have an effect on the *E*% of hematoporphyrin. The role of cations in the formation of complexes and in the salting-out processes needs more detailed investigation in future experiments.

Figure 1(a) and (b) compare the *E*% of hematoporphyrin obtained with and without the addition of *Tc*-depressing electrolyte, respectively, as a function of time that the surfactant and aqueous phase sit together after separation of the two phases. It can be seen from Fig. 1(a) that with the addition of 10*M* potassium hydroxide, high *E*% was obtained for hematoporphyrin at room temperature immediately after the solution was separated into two phases (time = 0) and the *E*% stayed relatively constant when the two phases were allowed to sit together over a time period of 48 hr in the dark. Without the addition of any electrolytes, phase separation was performed by simply heating the surfactant solution above its *Tc* at ~70°. As shown in Fig. 1(b), the initial *E*% at time = 0 was significantly lower (~85%) and this value dropped exponentially as a function of time, suggesting that an appreciable fraction of the surfactant phase redissolved into the aqueous phase as the temperature of the solution approached room temperature. It should be noted that when compared to the solution in which no *Tc*-depressing electrolyte was added, a phase inversion occurred with the addition of large amounts of electrolytes, *i.e.*, the surfactant-rich phase was the top layer and the aqueous phase, which was the denser medium, became the bottom layer.

Table 2 shows the *E*% of hydrophobic and hydrophilic porphyrins with the addition of various salting-out electrolytes. As expected, protoporphyrin—having similar structure as hematoporphyrin in which two carboxylic acid groups are present in the periphery of the porphyrin ring—was also found to be extracted efficiently into the surfactant phase with

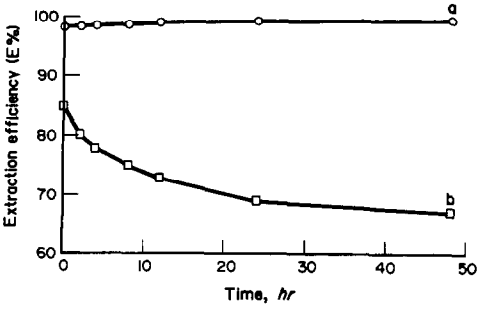

Fig. 1. Extraction efficiencies of hematoporphyrin (200 μg/l.) by Triton X-100 dissolved in aqueous solutions (1% v/v) as a function of time that the surfactant and aqueous phases sit together after separation (a) with the addition of 10*M* KOH and (b) without the addition of any electrolytes.

either hydroxide or phosphate added as the *Tc*-depressing electrolyte. It should be noted that protoporphyrin is an essential precursor of heme, the prosthetic group of hemoglobin. To investigate the $E\%$ of the present method for the extraction of metalloporphyrin, bovine hemin (iron-protoporphyrin) was spiked into the aqueous non-ionic surfactant solution and extracted by the same procedures as for metal-free porphyrin. As shown in Table 2, it was found that an average $E\%$ of ~96 and 99% were obtained with hydroxide and sulfate as the salting-out electrolyte, respectively.

Coproporphyrin and uroporphyrin—having four and eight carboxylic acid groups in the porphyrin ring, respectively—are also biologically important molecules since they are major components of total urinary porphyrin contents. In clinical laboratories porphyrins present in urine are usually measured after employing extraction procedures designed to separate out the "uroporphyrin" and "coproporphyrin" fractions.[16] Urine samples are considered abnormal when the total urinary porphyrin concentrations are greater than the threshold level between 100 and 200 μg/l. As in the case of hematoporphyrin and protoporphyrin it can be seen from Table 2 that the coproporphyrin also shows high $E\%$ with the addition of various electrolytes; however, the $E\%$ was found to be dramatically lower for the extraction of uroporphyrin with the addition of hydroxide or phosphate anion as the salting-out agent. This is not surprising since the eight carboxylic acid groups of uroporphyrin were likely to be ionized completely under the high basic environment of concentrated hydroxide and phosphate solutions, resulting in a significant increase in the aqueous solubility of uroporphyrin as compared to hydrophobic porphyrins such as proto- and coproporphyrins. It is interesting to see from Table 2 that the $E\%$ of uroporphyrin was significantly increased when using sulfate anion as the *Tc*-depressing electrolyte. This may be explained partly by the fact that since sulfate is less basic than either hydroxide or phosphate anion, ionization of the eight carboxylic groups would be less complete. This could result in the lowering of the aqueous solubility of uroporphyrin and in more effective complexation of uroporphyrin by the non-ionic Triton X-100; furthermore, sulfate anion is known to be a more effective *Tc*-depressing electrolyte when compared to phosphate in salting out non-ionic surfactant since it is more efficient in competing with the surfactant for hydration with water molecules.[11]

Table 3 shows the $E\%$ of hematoporphyrin as a function of the concentration of Triton X-100 and hematoporphyrin. Firstly, it can be seen that high recovery of hematoporphyrin is possible for a surfactant concentration of 1%; however, at a surfactant concentration of 10%, a significant drop in $E\%$ was found. It is possible that at higher surfactant concentrations, appreciable fractions of surfactant remain dissolved in the aqueous phase, leading to lower $E\%$. On the other hand, at a surfactant concentration of 0.2%, only a slight drop in $E\%$ was observed. Surfactant concentrations lower than 0.2% were not investigated in our experiment because the volume of the surfactant-rich phase at these concentrations were so small that it was experimentally difficult to separate the surfactant and aqueous phases. Secondly, it can also be seen from Table 3 that a preconcentration factor as high as 94.3 can be achieved with high $E\%$ at a surfactant concentration of 1%. Preconcentration factors higher than 100 can also be achieved with high $E\%$ at a surfactant concentration of 0.2%; however, it was difficult to determine the degree of preconcentration since the volume of the surfactant-rich phase was too small to be measured accurately. Lastly, Table 3 also shows that high $E\%$ can be obtained for a large concentration range of hematoporphyrin from 2 to 2×10^4 μg/l., which could be an important advantage for the extraction of porphyrin present in a variety of biological materials containing a wide range of porphyrin concentrations.

It has been known for a long time that strong interactions exist between surfactants and porphyrins.[17] For porphyrins dissolved in an aqueous surfactant solution above its critical micelle concentration, it has been postulated[18] that the porphyrin species is solubilized by the surfactant in such a manner that a doughnut-like structure is formed. In this porphyrin-micelle complex the pyrrole rings are embedded in the interior of the doughnut (hydrocarbon region of the micelle), with the porphyrin nitrogen situated in the inner ring of the doughnut coming into contact with the aqueous phase; the outer surface of the doughnut is covered with the surfactant head groups. Such a structure has been shown[18] to possibly favor the rate of formation of various metalloporphyrin complexes by attracting ions to the vicinity of the central pyrrole nitrogen atoms according

to the charge of the surfactant head groups. Complexes with a number of monovalent cations are known,[17] *e.g.*, Na_2, K_2, Li_2 complexes, in which one of the cations is likely to be situated slightly above and the other slightly below the plane of the porphyrin nucleus. In our experiment it is possible that a similar doughnut-like complex may form between the porphyrins and Triton X-100 surfactant in which the porphyrin species is immersed in the hydrophobic region (long-chain hydrogen and phenyl component) of this non-ionic surfactant; the long-chain polyoxyethylene functional groups lie in the outer surface of the doughnut. Furthermore, for the extraction of ions by extractants containing the polyoxyethylene functional groups, it has been postulated[3] that the so-called "cation-chelation" mechanism prevails in which the cation is coordinated to the oxygen within a helical structure formed by the polyoxyethylene chain and the co-extracted anion lies outside the helix. It is therefore also possible that the doughnut-like porphyrin-micelle complex in our experiment may be further stabilized by the chelation of the cations from the electrolytes, *e.g.*, Na^+, K^+, with the polyoxyethylene functional groups and resulting in concomitant interaction of this moiety with the porphyrin nucleus.

In summary, this work has shown that excellent extraction efficiencies and high preconcentration factors can be obtained for a large concentration range of porphyrins and metalloporphyrin dissolved in aqueous non-ionic surfactant solutions by effecting separation between the surfactant and aqueous medium, and taking the solubilized analytes into the surfactant phase upon the addition of cloud point-depressing electrolytes. A logical extension of this work might involve the use of the present method for the extraction of other important porphyrins or porphyrin-related molecules such as chlorophylls or the application of similar extraction procedures for the determination of trace amounts of clinically important porphyrins such as coproporphyrin and uroporphyrins. For example, the present salting-out extraction method could potentially be used as a simple and convenient approach for the preconcentraton and separation of urinary or serum coproporphyrin from uroporphyrin into a much smaller volume surfactant-rich phase for the differential diagnosis of diseases associated with impaired heme synthesis or metabolism without the use of any conventional organic solvents. Current extraction methods employed for the separation of coproporphyrin and uroporphyrin present in urine or serum are usually too time-consuming and inconvenient for routine use in the clinical laboratory.[16,19] Furthermore, it is important to gain some insights into the fundamental mechanisms responsible for the efficient extraction of porphyrins and metalloporphyrin by using non-ionic surfactant such as Triton X-100 and into the effects of electrolytes (both cations and anions) on the formation of complexes and salting-out processes. Work is in process in our laboratory to pursue these goals.

REFERENCES

1. L. Favretto and F. Tunis, *Analyst*, 1976, **101**, 198.
2. R. A. Greff, E. A. Stezkorn and W. D. Leslie, *J. Am. Oil Chem. Soc.*, 1965, **42**, 180.
3. R. F. Harmon, A. S. Khan and A. Chow, *Talanta*, 1982, **29**, 313.
4. P. T. Crisp, J. M. Eckert and N. A. Gibson, *Anal. Chim. Acta*, 1976, **104**, 93.
5. M. D. Adams, P. W. Wade and R. D. Hancock, *Talanta*, 1990, **37**, 875.
6. T. Nakagawa, in M. J. Schick, *Non-ionic Surfactants*, Vol. 1, pp. 481, 571, 843. Dekker, New York, 1967.
7. H. Watanabe and H. Tanaka, *Talanta*, 1978, **25**, 585.
8. C. E. Matkovich and G. D. Christian, *Anal. Chem.*, 1973, **45**, 1915.
9. D. C. Leggett, T. F. Jenkins and P. H. Migares, *ibid.*, 1990, **62**, 1355.
10. T. F. Jenkins and P. H. Migares, *ibid.*, 1991, **63**, 1341.
11. H. Schott and A. E. Royce, *J. Pharm. Sci.*, 1984, **73**, 793.
12. A. J. I. Ward, *J. Pharm. Pharmacol.*, 1982, **45**, 612.
13. Th. van den Boomgaard, Sh. M. Zourab and J. Lykbema, *Progr. Colloid. & Polymer Sci.*, 1983, **68**, 25.
14. C. F. Polo, A. L. Frisardi, E. R. Resnik, A. E. M. Schoua and A. M. del C. Batle, *Clin. Chem.* 1988, **34**, 757.
15. D. Kessel, in T. Dougherty, *Porphyrin Photosensitization, Advances in Experimental Medicine and Biology*, Vol. 160; Plenum, New York, 1983.
16. M. O. Doss, in H. Ch. Curtius and M. Roth, *Clinical Biochemistry—Principles and Methods*, Vol. 2, p. 1323. De Gruyter, New York, 1974.
17. J. E. Falk, in *Porphrins and Metalloporphyrins*, p. 37. Elsevier, New York, 1964.
18. M. B. Lowe and J. N. Philips, *Nature*, 1961, **190**, 262.
19. T. K. With, *Clin. Biochem.*, 1968, **2**, 97.

Talanta, Vol. 39, No. 5, pp. 493–496, 1992
Printed in Great Britain.

0039-9140/92 $5.00 + 0.00

EXTRACTION OF ACTINIDES AND FISSION PRODUCTS BY OCTYL(PHENYL)-*N*,*N*-DIISOBUTYLCARBAMOYLMETHYL-PHOSPHINE OXIDE FROM NITRIC ACID MEDIA

J. N. MATHUR, M. S. MURALI and P. R. NATARAJAN
Radiochemistry Division, Babha Atomic Research Centre, Bombay-400085, India

L. P. BADHEKA and A. BANERJI
Bio-organic Division, Bhabha Atomic Research Centre, Bombay-400085, India

(*Received* 22 *August* 1991. *Accepted* 21 *September* 1991)

Summary—Extraction of promethium(III), uranium(VI), plutonium(IV), americium(III), zirconium(IV), ruthenium(III), iron(III) and palladium(II) has been carried out with a mixture of octyl(phenyl)-*N*,*N*-diisobutylcarbamoylmethylphosphine oxide (CMPO) and tributyl phosphate (TBP) in dodecane. The effects of nitric acid, TBP and CMPO concentrations on the extraction of these metal ions have been studied. The nature of the species of the above metal ions extracted into the organic phase has been suggested.

Bidentate organophosphorous reagents, as a class, are most important for the extraction, separation and recovery of trivalent actinides and lanthanides from high level waste (HLW) solutions of the PUREX process. Encouraged from the early work of Siddall[1,2] on the extraction of americium(III) from acidic solutions by dialkyl-*N*,*N*-dialkylcarbamoylmethylphosphonate, various bidentate compounds have been prepared. Of these dihexyl-*N*,*N*-diethylcarbamoylmethylphosphonate (CMP) and octyl(phenyl)-*N*,*N*-diisobutylcarbamoylmethylphosphine oxide (CMPO) are the most promising reagents for extraction of trivalent actinides and lanthanides from nitric acid solutions and their easy and efficient stripping. Using CMPO as the extractant, the main emphasis has been on the extraction and recovery of americium(III) from nitric or hydrochloric acid solutions employing diethyl benzene, carbon tetrachloride, tetrachloroethylene or normal paraffinic hydrocarbons as the diluents.[3–7] Also, the extraction behaviour of neptunium and plutonium from nitric acid solutions with a mixture of CMPO and tributyl phosphate (TBP) in dodecane has been reported.[8,9] In a recent communication, extraction of europium(III) from nitric and hydrochloric acid solutions with CMPO alone or a mixture of CMPO and TBP in mesitylene or dodecane diluents has been reported.[10] No reports are available on the extraction of promethium(III) from nitric acid solutions with bidentate organophosphorous reagents. Since ^{147}Pm, a low energy β emitter, can be recovered in large quantities from HLW solutions of the PUREX process, a programme has been initiated to deploy different potential extracting agents for the extraction, removal and recovery of promethium(III) from nitric acid solutions. In this connection, in a recent communication we have reported the extraction of promethium(III) by CMP alone as well as its mixture with TBP in benzene.[11] In the present study, besides the extraction of promethium(III), we have undertaken studies on uranium(VI), plutonium(IV), americium(III), zirconium(IV), iron(III), ruthenium(III) and palladium(II) from nitric acid solutions by a mixture of CMPO and TBP in dodecane.

EXPERIMENTAL

Materials

CMPO was prepared by a modified three step procedure suggested by Horwitz and coworkers.[12] It was purified by successive treatments with macroporous cation (H^+) and anion (OH^-) forms of ion exchange resins.[12] The purity of CMPO was checked by IR and ^{1}H, ^{13}C and ^{31}P NMR spectroscopy. To confirm that the CMPO prepared is the solvent extraction (SX) grade (contains $\leqslant$0.02 wt% of acidic

impurities), D_{Am} at pH 2.0 (HNO_3) with 0.2*M* CMPO + 1.2*M* TBP in dodecane was determined and found to be very low (0.016).[13]

Tributyl phosphate (Bharat Vijay Chem., India) was purified by contact with a dilute solution of sodium hydroxide, washing with water and drying over anhydrous sodium sulphate. Dodecane (~93% C-12, sp. gr. 0.751, refractive index 1.42 and aromatics (<0.1%, distillation range 160–210°) was obtained from Transware Chemia Handelsgeselschaft, Hamburg, Germany and was used as such. All other chemicals used were of A.R. grade.

Radioactive tracers

The radioactive tracers ^{241}Am, ^{233}U, Pu (mainly 239) and ^{147}Pm were purified and prepared by standard procedures.[14–16] The tracers ^{95}Zr, ^{59}Fe and ^{103}Ru were procured from the Board of Radiation and Isotope Technology, Department of Atomic Energy (India) and their radiochemical purity was checked by taking γ-spectra. A ^{109}Pd stock solution was prepared by irradiating ammonium tetrachloro palladate in the Apsara research reactor of Bhabha Atomic Research Centre and dissolving it in 6*M* hydrochloric acid. A 25-μl portion of this solution was added to 1 ml of the aqueous phase for the extraction studies. The radioactive tracer solutions of ^{233}U, Pu (mainly 239) and ^{147}Pm were assayed by liquid scintillation counting and ^{95}Zr, ^{59}Fe, ^{103}Ru, ^{241}Am and ^{109}Pd (as ^{109}Ag, which is in secular equilibrium with ^{109}Pd) were counted with a well-type γ-scintillation counter, using a sodium iodide (Tl) detector.

Extraction of the metal ions by CMPO + TBP at various nitric acid concentrations

A 1-ml aliquot of aqueous phase (varying nitric acid concentrations from 0.01 to 6.0*M*) containing one of the radioactive tracers ^{233}U, Pu (mainly 239), ^{241}Am, ^{147}Pm, ^{95}Zr, ^{59}Fe, ^{103}Ru or ^{109}Pd was mixed with an equal volume of 0.2*M* CMPO + 1.2*M* TBP in dodecane (earlier pre-equilibrated with respective nitric acid solutions). The solutions were shaken for 1 hr by slow rotation in a temperature controlled bath at 25 ± 0.1°. This time was more than sufficient for attaining the equilibrium. The solutions were allowed to settle, centrifuged and pipetted for radioassay. In cases where the *D* (distribution ratio) values were very high or very low, at least three cycles of removing the phases and centrifuging was done before taking the samples for counting.

Extraction of metal ions at a fixed concentration of CMPO and varying TBP concentrations

A 1-ml aliquot of the aqueous phase (3.0*M* nitric acid) containing one of the above mentioned tracers was mixed with an equal volume of organic solution containing a fixed 0.2*M* concentration of CMPO and varying concentrations of TBP(0.6–1.4*M*) in dodecane. After shaking, the solutions were allowed to settle, centrifuged and aliquots were taken for radioassay as mentioned above.

Extraction of metal ions at a fixed concentration of TBP and varying CMPO concentrations

A 1-ml aliquot of the aqueous phase (3.0*M* nitric acid) containing one of the above-mentioned radioactive tracers was mixed with an equal volume of the organic phase containing a fixed 1.2*M* TBP concentration and a varying (0.01–0.2*M*) concentration of CMPO in dodecane. After settling, the solutions were processed as above for radioassay.

RESULTS AND DISCUSSION

Figure 1 gives the plots of log *D vs.* nitric acid concentration at 0.2*M* CMPO + 1.2*M* TBP in dodecane for the extraction of Am(III), Pm(III), U(VI), Pu(IV), Zr(IV), Fe(III), Ru(III) and

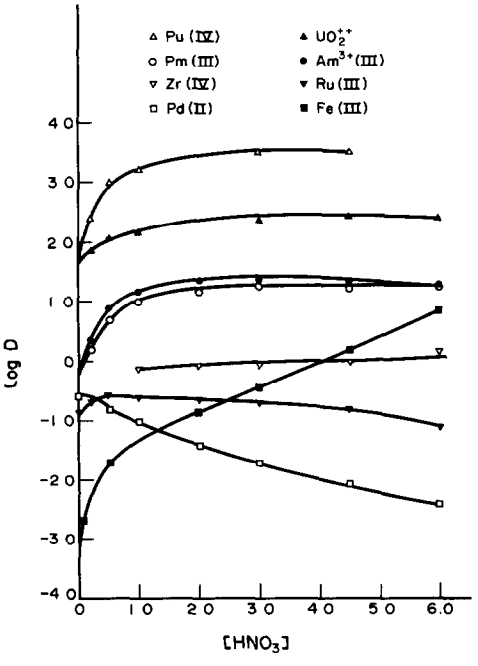

Fig. 1. Acid dependency on the extraction of Pm(III), Am(III), Pu(IV), U(VI), Zr(IV), Ru(III), Fe(III) and Pd(II) with 0.2*M* CMPO + 1.2*M* TBP in dodecane at 25°.

Pd(II). The results show that there is practically no difference in D values for americium(III) and promethium(III). Further, the D values do not show much variation for 2–6M nitric acid. This could be explained by the "intramolecular buffering effect".[7] Similar extraction behaviour was observed in the case of U(VI) and Pu(IV) as well. The order of extraction of promethium(III), americium(III), uranium(VI) and plutonium(IV) was found to be Pm(3.0) ~ Am(3.0) ≪ U(3.2) ≪ Pu(4.0). This could be explained on the basis of effective ionic charge for these metal ions (given in parentheses). The extraction of fission products such as zirconium(IV), ruthenium(III) and palladium(II) are much lower as compared to the actinides and promethium(III) reported in this study. Amongst these three, the order of extraction Pd < Ru < Zr could be explained on the basis of the ionic charge of these metal ions. In the case of zirconium(IV) the D values remain almost constant in the acidity range 1–6M nitric acid. In the case of ruthenium(III), the D values initially increase between the acidity range of 0.01–0.5M and then they start decreasing between 0.5 and 6.0M nitric acid, while in the case of palladium(II) there is a continuous decrease in the D value from 0.01 to 6.0M nitric acid. The decrease in the D values of palladium(II) and ruthenium(III) is possibly due to the formation of unextractable species. In the case of iron(III) the D value increases with increasing nitric acid concentration. Here, with increasing acidity, less iron(III) is in the hydrolysed form, and the formation of the extractable iron(III) nitrate species increases. It is clear that in the acidity range of about 2M (likely to be encountered in the HLW solutions) the extraction of plutonium(IV), uranium(VI), americium(III) and promethium(III) are much higher as compared to those of fission products and iron(III). From these studies it could be concluded that promethium(III) along with the actinides americium(III), uranium(VI) and plutonium(IV) could efficiently be extracted from HLW solutions of PUREX origin by 0.2M CMPO + 1.2M TBP in dodecane leaving behind most of the fission products present therein.

Figure 2 shows the plot of log D *vs.* log[TBP] at a fixed concentration of CMPO (0.2M) and 3.0M nitric acid for the metal ions studied here. In the case of plutonium(IV), uranium(VI), americium(III), promethium(III) and zirconium(IV), the straight lines are almost parallel to the x-axis indicating thereby that

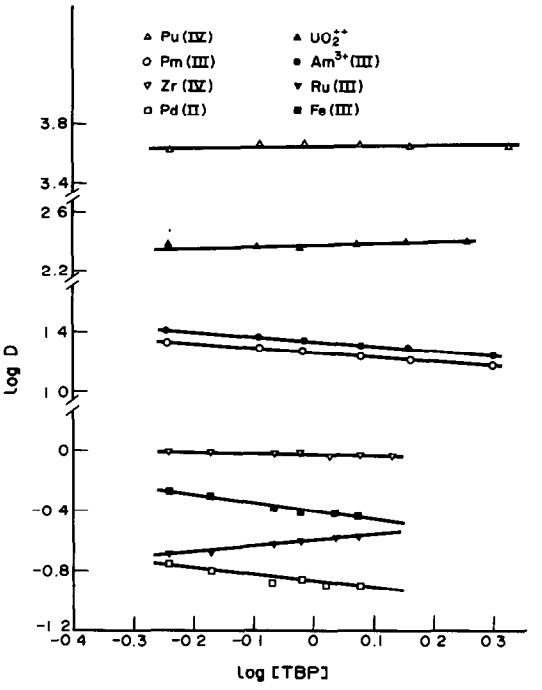

Fig. 2. Plots of log D *vs.* log [TBP] for Pm(III), Am(III), Pu(VI), U(VI), Zr(IV), Ru(III), Fe(III) and Pd(II) at 0.2M CMPO and 3.0M HNO_3, at 25°.

TBP is not one of the moieties in the species extracted in the organic phase. However, in the case of iron(III) and palladium(II), the D values were found to decrease with increasing TBP concentration, a negative slope of ~0.5 was obtained for both these metal ions. In the case of ruthenium(III), the D values slightly increased with increasing TBP concentration. The straight line in Fig. 2 shows a positive slope of 0.5. Further detailed study is needed in the case of iron(III), ruthenium(III) and palladium(II).

Figure 3 gives the plots of log D *vs.* log[CMPO] at fixed TBP (1.2M) and nitric acid (3.0M) concentrations. The concentration of CMPO was varied between 0.1 and 0.2M for the metal ions promethium(III), americium(III) and iron(III). The straight lines are obtained with a slope of 2.5. Similar lower slopes than the expected value of 3.0 have been reported in the case of americium(III) and europium(III) at CMPO concentrations higher than 0.1M in diethyl benzene or xylene when extracted from 0.5M nitric acid.[4] The non-ideality of the organic phase has been suggested as the reason for the lower stoichiometry of the extracted species by the slope analysis method at high concentrations of CMPO.[6] Under our experimental conditions the equilibria for the uptake of

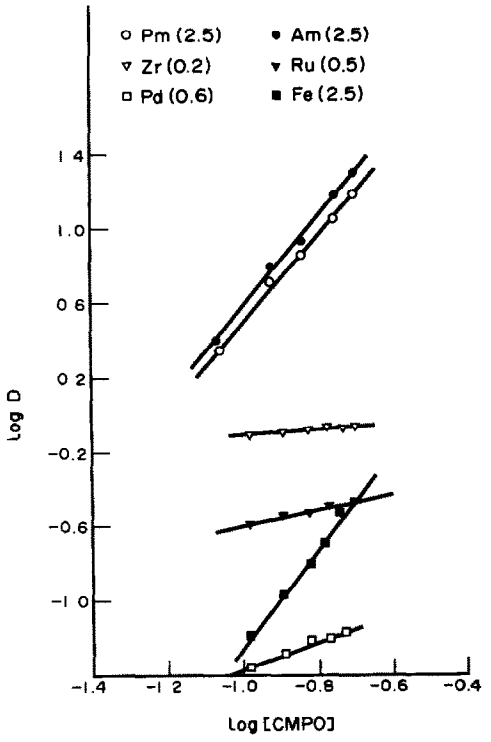

Fig. 3. Plots of log *D vs.* log [CMPO] for Pm(III), Am(III), Fe(III), Ru(III), Zr(IV) and Pd(II) at 1.2*M* TBP and 3.0*M* HNO_3, at 25°.

M(III) ions (M = Am, Pm and Fe) by CMPO may be written as:

$$M^{3+}(a) + 3NO_3^- (a) + 3CMPO \cdot (HNO_3)_{n(o)} \rightleftharpoons M(NO_3)_3(CMPO)_3 \cdot (HNO_3)_{m(o)} + (3n - m)\ HNO_{3(a)} \quad (1)$$

where (a) and (o) represent the aqueous and organic phases, respectively.

Under similar experimental conditions to the above, the plots of log *D vs.* log[CMPO] gave straight lines with a slope of 0.6 for palladium(II), 0.5 for ruthenium(III) and 0.2 for zirconium(IV). In these cases, the species formed is most probably $M(NO_3)_x \cdot (CMPO).(HNO_3)_m$ (where $x = 2$ for Pd, 3 for Ru and 4 for Zr).

It can be seen from Fig. 4 that in the CMPO concentration range 0.14–0.2*M* for uranium(VI) and 0.04–0.06*M* for plutonium(IV) the straight lines are obtained with slopes of 1.4. Here it may be suggested that the species formed are $M(NO_3)_x \cdot (CMPO)_2 \cdot (HNO_3)_m$ [where $x = 2$ for

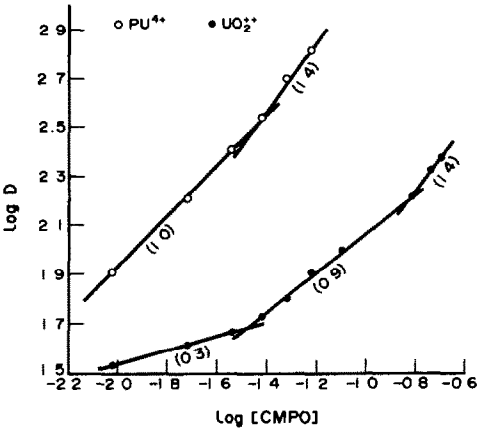

Fig. 4. Plots of log *D vs.* log [CMPO] for U(VI) and Pu(IV) at 1.2*M* TBP and 3.0*M* HNO_3, at 25°.

uranium(VI) and 4 for plutonium(IV)]. However, in the lower concentration ranges of CMPO, where slopes lower than 1.4 are obtained for both the ions, formation of species containing less than two CMPO moieties may be suggested.

REFERENCES

1. T. H. Siddall, *J. Inorg. Nucl. Chem.*, 1963, **25**, 883.
2. *Idem*, *ibid.*, 1964, **26**, 1991.
3. D. G. Kalina, E. P. Horwitz, L. Kaplan and A. C. Muscatello, *Sep. Sci. Technol.*, 1981, **16**, 1127.
4. E. P. Horwitz, D. G. Kalina, L. Kaplan, W. G. Mason and H. Diamond, *ibid.*, 1982, **17**, 1261.
5. E. P. Horwitz, H. Diamond and D. G. Kalina, *ACS Symposium Series No. 216, Plutonium Chemistry*, W. T. Carnall and G. R. Choppin (eds.), p. 433. 1983.
6. E. P. Horwitz and D. G. Kalina, *Solvent Extr. Ion. Exch.*, 1984, **2**, 179.
7. E. P. Horwitz, K. A. Martin, H. Diamond and L. Kaplan, *ibid.*, 1986, **4**, 449.
8. Z. J. Kolarik and E. P. Horwitz, *ibid.*, 1988, **6**, 247.
9. B. J. Mincher, *ibid.*, 1989, **7**, 645.
10. W. Liansheng, M. Casarci and G. M. Gasparini, *ibid.*, 1990, **8**, 49.
11. J. N. Mathur, M. S. Murali and P. R. Natarajan, *J. Radioanal. Nucl. Chem. Letters*, 1991, **155**, 195.
12. R. C. Gatrone, L. Kaplan and E. P. Horwitz, *Solvent Extr. Ion Exch.*, 1987, **5**, 1075.
13. W. W. Schulz and E. P. Horwitz, *Inst. of Chem. Engineers Symp. Series 103, Extraction-87*, EFEC Publ. Series No. 56, p. 245. 1987.
14. P. K. Khopkar and J. N. Mathur, *J. Inorg. Nucl. Chem.*, 1974, **36**, 3819.
15. *Idem*, *ibid.*, 1977, **39**, 2063.
16. J. N. Mathur, *Polyhedron*, 1991, **10**, 47.

Talanta, Vol. 39, No. 5, pp. 497–503, 1992
Printed in Great Britain.

0039-9140/92 $5.00 + 0.00

EXTRACTION OF AROMATIC ACIDS AND PHENOLS BY POLYURETHANE FOAM

P. FONG and A. CHOW
Department of Chemistry, University of Manitoba, Winnipeg, Manitoba, Canada R3T 2N2

(*Received* 9 *April* 1991. *Revised* 16 *August* 1991. *Accepted* 26 *August* 1991)

Summary—The extraction of several aromatic acids and phenols including salicylic acid, 8-hydroxyquinoline, 1-amino-2-naphthol-4-sulphonic acid and cinnamic acid in the presence of various protonated alkylamines, ammonia and alkali metal cations from aqueous solution by polyurethane foam has been investigated. These compounds are extracted only in the neutral form by a solvent extraction mechanism. The mechanism has been confirmed by the salting-out effect and pH studies. With the exception of 8-hydroxyquinoline, the compounds are more extractable by polyether foam than by polyester foam, suggesting that hydrogen bonding is stronger with the polyether foam.

Considerable progress has been made in recent years in the use of polyurethane foam for separation and preconcentration purposes. Both inorganic and organic substances can be extracted from different media. Several reviews[1–7] dealing with the extraction by polyurethane foam have appeared.

Considerable work has been done on the extraction of inorganic compounds by the foam, but only a few papers have discussed the extraction mechanism. Bowen[8] concluded that the extraction is not due to surface adsorption because of the relatively high capacity measurement (0.5–1.8 mole/kg) for species on the foam. A solvent extraction mechanism was suggested since the compounds extractable by the foam are also extractable by diethyl ether. Gesser and co-workers[9,10] extended this idea to describe the foam as a polymeric analogue of diethyl ether. This mechanism has been widely accepted by many workers to describe the extraction of various species, *e.g.*, $GaCl_4^-$,[9] $FeCl_4^-$,[10] $SnCl_5^-$,[11] $SbCl_4^-$[12] and $Rb(SCN)_6^{3-}$.[13,14]

Hamon *et al.*[15] proposed the cation chelation mechanism to account for the extraction of anionic metal complexes. According to this mechanism, the extraction of anionic metal complexes is facilitated by the efficient complexation of the cation with the crown-ether type of configuration in the foam. Polyether- and polyester-type polyurethane foams are referred to as polyether and polyester foams, respectively. The poly(ethylene oxide) portion of polyether foam which adopts a helical structure with inwardly-directed oxygen atoms is considered to be responsible for the specific interaction between the cation and the foam. It was observed that polyether foam demonstrates similar cation selectivity to 18-crown-6. Polyester foam does not readily assume such a helical structure, and hence the interaction with the cation is not as strong in comparison to polyether foam. As a result of this, polyether foam is a better extractor than polyester foam. Many extraction systems[16–21] involving inorganic compounds have been explained by this mechanism.

Polyurethane foam has been successfully applied to concentrate various organic contaminants from water such as chlorinated organic compounds and aromatic hydrocarbons (PAH). In 1971, Gesser *et al.*[22] used polyurethane foam packed in a column for the concentration of polychlorinated biphenyls. Foams were used as an alternative to activated carbon for the determination of trace organic contaminants in water by Gesser *et al.*[23] Musty and Nickless[24] reported the quantitative extraction of chlorinated insecticides by foam at pHs between 6 and 9, and they noted that the foam was superior to activated carbon since the material recovered from activated charcoal is often different from the original form due to catalytic effects. Afghan *et al.*[25] demonstrated that polyurethane foam is capable of concentrating PAH at parts per trillion levels in natural waters and has a concentrating ability similar to other sorbents such as XAD-2 and C18-bonded phase packing. Gough and Gesser[26] reported the retention and recovery of phthalate esters by the foam.

Table 1. Effect of salts on the extraction of salicylic acid from aqueous solution by polyurethane foam

Salt	Concentration ($\times 10^{-3}M$)	Distribution coefficient, *l./kg*		Equilibrium pH	
		Polyester	Polyether	Polyester	Polyether
None	0.00	96.9 ± 3.2	218 ± 4	3.20	3.25
sec-Butylamine	0.50	83.9 ± 1.2	185 ± 1	3.30	3.40
sec-Butylamine	0.99	65.6 ± 2.6	139 ± 4	3.50	3.60
iso Butylamine	0.99	67.3 ± 3.8	149 ± 2	3.45	3.55
sec-Butylamine	1.98	31.9 ± 0.8	51.9 ± 0.8	3.90	4.05
Ethylamine	1.06				
iso Propylamine	1.16	0	0	9.60	9.60
iso Butylamine	0.99				
LiCl	2.0	150 ± 2	321 ± 6	2.65	2.75
NaCl	2.0	150 ± 4	332 ± 8	2.80	2.85
KCl	2.0	125 ± 3	284 ± 8	3.05	3.10
$MgCl_2$	1.0	137 ± 3	256 ± 5	2.50	2.55
$BaCl_2$	1.0	111 ± 3	234 ± 7	2.65	2.75

Conditions: $2.9 \times 10^{-3}M$ salicylic acid, 0.300 g of foam, 100-ml solution, 24 hr extraction time.

Recent work by Schumack and Chow[27] studied the mechanism of the extraction of simple aromatic compounds by polyurethane foam. Comparison with identical extractions into diethyl ether and the salting-out effect observed suggest that the basic extraction mechanism is an ether-like solvent extraction mechanism. It was noted that compounds containing a phenolic or carboxylic group have larger distribution coefficients due to hydrogen bonding with the foam. The hydrogen bonding is prevented by the presence of a strong electron-donor group *ortho* to the hydrogen bonding group as in *o*-nitrophenol or salicylaldehyde where intramolecular hydrogen bonding can take place. It was concluded that hydrogen bonding is stronger with polyether foam relative to polyester foam.

Chow *et al.*[28] investigated the extraction of many organic dyes by polyurethane foam from aqueous and 50% aqueous methanol solutions. It was found that the extraction of neutral dyes can be explained by a simple solvent extraction mechanism, but the extraction of anionic dyes is consistent with the cation chelation mechanism.

It appears that many organic compounds are extracted by an ether-like solvent extraction mechanism, however, other extraction systems involving inorganic complex anions can be explained by the cation chelation mechanism. The extraction of salicylic acid, 8-hydroxyquinoline, 1-amino-2-naphthol-4-sulphonic acid and cinnamic acid was studied in this work. These compounds were chosen because they are quite hydrophobic and are likely to be extracted by the foam. Furthermore, they contain carboxylic acid and phenol groups which can dissociate to form the anions at appropriate pH. The extraction of these anions in the presence of some chelatable cations proposed in the cation chelation mechanism can then be investigated. The objective of the present study was to determine whether the extraction takes place by solvent extraction, cation chelation or by other mechanisms.

EXPERIMENTAL

Apparatus

UV absorbance measurements for the determination of the organic compounds were obtained with a Varian 634S spectrophotometer. A Fisher Accumet Model 520 pH-meter was used. The alkylamine concentration was determined by using a Hewlett-Packard 5710A gas chromatograph with a flame ionization detector and a 6-ft × 2-mm ID column packed with GP Carbopack B/4% Carbowax 20*M*/0.8% KOH.

Reagents

All chemicals were of reagent grade and water was purified by reverse osmosis and a Barnsted Nanopure II® system before use. The polyether foam (# 1338M) was obtained from G. N. Jackson Ltd (Winnipeg, Manitoba). The polyester foam (DiSPo) was obtained from Canlab (Winnipeg, Manitoba).

Procedure

Foam plugs of approximately 0.4 g each were cut from a polyurethane sheet. These plugs were soaked in 1*M* hydrochloric acid for 24 hr with occasional squeezing to remove any possible inorganic contaminants and washed with water

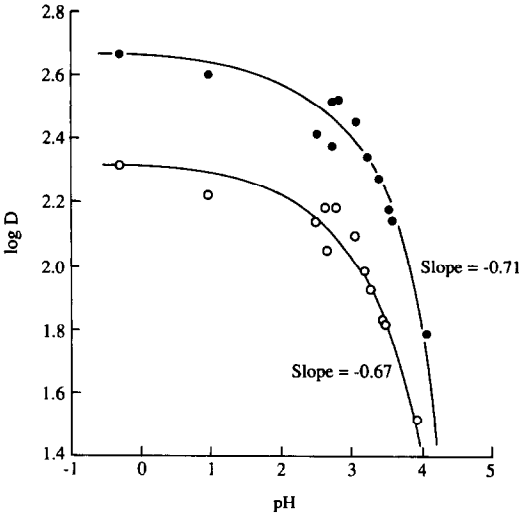

Fig. 1. Plot of log D *vs.* pH for the distribution of salicylic acid between foams and aqueous solution. Conditions: $2.9 \times 10^{-3}M$ salicylic acid, 0.300 g of foam, 100-ml solution, 24-hr extraction time, (●) polyether foam, (○) polyester foam.

until they were acid free. They were then extracted with acetone in a Soxhlet apparatus for 6 hr to remove organic contaminants and finally air dried in a 60° oven.

The sample solution (100 ml) and the foam plug (0.300 ± 0.005 g) were placed in a Pyrex glass cell. The foam was squeezed by means of a glass plunger operated by an automatic squeezer[29] in order to bring fresh solution into contact.

The % extraction and distribution coefficient (D) were calculated with:

$$\% \text{ extraction} = (1 - C'/C_0) \times 100$$

C_0 = concentration in solution before extraction
C' = concentration in solution after extraction

$$D = \frac{\% \text{ extraction}}{(100 - \% \text{ extraction})} \times \frac{\text{volume of solution (l)}}{\text{weight of foam (kg)}} \quad (1)$$

RESULTS AND DISCUSSION

To determine whether the alkylamines are extractable by polyurethane foam, the extraction of various amines including methylamine, ethylamine, isopropylamine, isobutylamine, n-butylamine, sec-butylamine and t-butylamine in $0.1M$ sulphuric acid was studied. No detectable amounts of the amines were extracted by either polyether or polyester foam after 24 hr extraction. These results suggest that the sulphate ions are too hydrophilic to form ion-pairs with these amines. Thus, the effect of the protonated amines on the extraction of various organic compounds which are more hydrophobic than sulphate was examined. It was expected that any ion-pair formation of the organic compounds with the protonated amines should result in the extraction of the amines as well as in the increase of the extraction of the organic compounds.

Extraction of salicylic acid

To determine the extractability of salicylic acid, solutions (100 ml) containing $2.9 \times 10^{-3}M$ of this acid were extracted with polyether and polyester foams (0.300 g). The initial pH of the solution was 3.15. Extraction equilibrium was reached within 1 hr. The distribution coefficients were 96.9 and 218 l./kg for polyester and polyether foams respectively (Table 1).

The extraction of salicylic acid in the presence of the amines was studied and the results are given in Table 1. Although salicylic acid is extractable, no extraction of the amines was observed. This result indicates that no ion-pair formation between salicylate and the protonated amines occurs. Salicylic acid extraction decreases with increasing amounts of added amine. In the presence of the same amount of amine, the extraction coefficients for salicylic acid are about the same for both sec-butylamine and *iso*butylamine. As the total amount of amine becomes greater than the amount of salicylic acid present, the pH increases markedly to 9.6 and no salicylic acid extraction was obtained. This observation suggests that the amount of amine added rather than the nature of the amines is important in the extraction of salicylic acid.

An increase in the amount of amine added increases the pH of salicylic acid solution and decreases the distribution coefficient of salicylic acid (Table 1). It is likely that the decrease of salicylic acid extraction is due to pH change. Therefore, the extraction of solutions of $2.9 \times 10^{-3}M$ salicylic acid in 0.1 and $2M$ hydrochloric acid solution with 0.300 g of foam was also studied. Figure 1 shows the relationship between log D and pH, and it includes the results of the extraction in the presence of various amines, alkali and alkali earth metal chlorides from Table 1. Two regions are apparent from the graph. These are the plateau of

Table 2. Effect of salts on salicylic acid extraction at pH 1

Salt	Concentration *M*	Distribution coefficient, *l./kg* Polyester	Polyether
None	0.0	164 ± 6	398 ± 14
LiCl	2.0	341 ± 9	818 ± 41
NaCl	2.0	312 ± 3	791 ± 29
KCl	2.0	260 ± 1	626 ± 23
$MgCl_2$	1.0	325 ± 8	780 ± 20
$BaCl_2$	1.0	275 ± 2	658 ± 18

Conditions: $2.9 \times 10^{-3}M$ salicylic acid, $0.1M$ HCl, 0.300 g of foam, 100-ml solution, 24-hr extraction time.

approximately zero slope below pH 2 and the linear segment with respective slopes of −0.71 and −0.67 for polyether and polyester foams. For the extraction of an acid of which the molecular species is extractable, slopes of 0 and −1 below and above the pK_a of the acid, respectively, would be expected. The pK_a value for salicylic acid is 2.75.[30] The slopes of the straight lines are approximately equal to 0 and −1 for pH values below 2 and above 3, respectively. The deviation of the values of the slopes from the theoretical values probably occurs because the pH of the data points is close to the pK_a value of salicylic acid. The results suggest that salicylic acid is extracted by a simple solvent extraction mechanism in which only the neutral molecular species is extractable.

According to the cation chelation mechanism, the presence of the potassium ion should facilitate the extraction of the anion more than the other alkali metal ions because of the better fit of this ion into the central cavity of the oxygen-rich helix in the polyether foam. Therefore, the effect of various alkali metal chlorides ($2M$) and alkaline earth metal chlorides ($1M$) on salicylic acid extraction was studied. Table 1 demonstrates significant increases in salicylic acid extraction in the presence of LiCl, NaCl, KCl, $MgCl_2$ and $BaCl_2$ by both polyester and polyether foams. The following order of extraction: $Li^+ \approx Na^+ > K^+$, $Mg^{2+} > Ba^{2+}$ was observed. The extraction of salicylic acid increases with increasing charge density on the cation. This order is different from that for a cation chelation extraction system where K^+ produces a greater increase for anion extraction than Na^+ and Li^+. This effect is consistent with a solvent extraction mechanism with the salts acting as salting-out agents. Added ions increase the extraction of an organic compound into the organic phase by reducing the number of water molecules available to solvate the organic compound because some water molecules are used to solvate the ions. Ions with higher charge density are expected to exert a greater effect. The charge density for the cations studied is $Li^+ > Na^+ > K^+$ and $Mg^{2+} > Ba^{2+}$. Thus the influence of the salts can be explained by the salting-out effect on a solvent extraction system.

To confirm the salting-out effect of the salts, an extraction was carried out in $2.9 \times 10^{-3}M$ salicylic acid solution containing $0.1M$ hydrochloric acid. At pH 1, 99% of the salicylic acid is in the neutral form as opposed to 50% at pH 2.75. Comparing the results of Tables 1 and 2, the added salts increase the extraction of salicylic acid more in a solution of pH 1 than at high pH owing to the increased amount of neutral salicylic acid. The effect of the salts remains the same for the sequence $Li^+ > Na^+ > K^+$ and $Mg^{2+} > Ba^{2+}$.

It can be concluded that salicylic acid is only extractable in the neutral form. The protonated alkylamine cations are too hydrophilic to affect the extraction of salicylate anions from aqueous solution by either polyester or polyether foam.

Extraction of 8-hydroxyquinoline

8-Hydroxyquinoline is more hydrophobic than salicylic acid. To evaluate the extractability of 8-hydroxyquinoline, solutions (100 ml) of $1.0 \times 10^{-3}M$ 8-hydroxyquinoline were extracted with 0.300 g of foam for 1 hr. In addition, extractions of 8-hydroxyquinoline in the presence of $1.0 \times 10^{-3}M$ methylamine and n-butylamine were also studied to determine whether the amines are extractable. Table 3 shows the amines have no effect on the extraction of 8-hydroxyquinoline. Both methylamine and n-butylamine were found to be non-extractable. The pK_a values for 8-hydroxyquinoline are 5.02 and 9.81.[30] At pH 6.4, the major species is the molecular form, therefore, no extraction of the amines was found. To ionize the (—OH) group of 8-hydroxyquinoline, a pH above 11 is required; however, at pH 11 undissociated amine is predominant. These difficulties prevent a proper investigation and no further studies on this compound were carried out.

Extraction of 1-amino-2-naphthol-4-sulphonic acid (ANS)

Solutions (100 ml) of $1.0 \times 10^{-3}M$ ANS containing methylamine or butylamine ($1.0 \times 10^{-3}M$) were extracted with 0.300 g of foam for 6 hr. Table 3 shows that methylamine and butylamine have no effect on the distribution coefficient (D) of ANS.

Table 3. Effect of amines on the extraction of 8-hydroxyquinoline and 1-amino-2-naphthol-4-sulphonic acid (ANS) extraction

Compound	Amine	Concentration, *M*	Distribution coefficient, *l./kg*	
			Polyester	Polyether
8-Hydroxyquinoline	None	0.0	173 ± 3	165 ± 3
	Methylamine hydrochloride	1.0×10^{-3}	170 ± 4	164 ± 3
	n-Butylamine	1.0×10^{-3}	156 ± 4	158 ± 2
	Hydrochloric acid	1.0×10^{-3}		
1-Amino-2-naphthol-4-sulphonic acid	None	0.0	9.3	30.8
	Methylamine hydrochloride	1.0×10^{-3}	8.1	28.2
	n-Butylamine	1.0×10^{-3}	11.1	32.1
	Hydrochloric acid	1.0×10^{-3}		

Conditions: (i) $1.0 \times 10^{-3}M$ 8-hydroxyquinoline, 0.300 g of foam, 100-ml solution, 1-hr extraction time, pH = 6.4. (ii) $1.0 \times 10^{-3}M$ ANS, 0.300 g of foam, 100-ml solution, 6-hr extraction time, pH = 3.5.

The pK_a values for ANS shown as (1) in Fig. 2, could not be found in the literature, however the (—SO_3H) group is expected to be completely ionized. The pK_a for 1-naphthylamine, (2) in Fig. 2 is 3.92.[30] In the presence of the (—SO_3H) group, the pK_a for the (—NH_2) group would be lowered. Thus at pH 3.5, the forms of ANS (3) and (4) may be present in comparable amounts. Since there is no change of *D* with the addition to the amines, it is clear that the extraction of the possible ion-pair between the amine cation and (4) does not occur. Thus, the neutral molecule (3) must be the extractable species.

The effect of potassium chloride and ammonium chloride on the extraction of ANS was studied. To verify that (3) is the extractable species, the extraction of ANS in $0.1M$ hydrochloric acid was also carried out. Table 4 demonstrates that there is no significant change of *D* for ANS with the addition of ammonium chloride and potassium chloride up to $0.1M$. Thus, ANS is too hydrophilic to extract K^+ and NH_4^+ from aqueous solution. However, *D* increases in $0.1M$ hydrochloric acid which can be the result of the increased formation of the neutral species (3) at pH 1. This result is consistent with a solvent extraction mechanism.

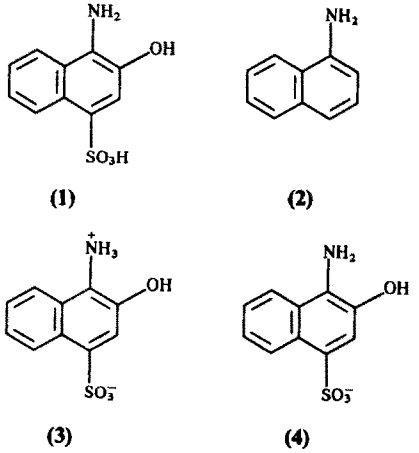

Fig. 2. Various forms of 1-amino-2-naphthol-4-sulphonic acid and 1-naphthylamine.

Extraction of cinnamic acid

Solutions (100 ml) of $1.0 \times 10^{-3}M$ cinnamic acid at pH 3.9 were extracted with 0.300 g of foam for 24 hr. Distribution coefficients of 195 and 343 for polyester and polyether foams respectively were obtained. Extraction of cinnamic acid in $1.0 \times 10^{-2}M$ potassium hydroxide was also carried out. The pH of the solution was above 12 and no detectable amount of cinnamic acid was extracted. The pK_a value for cinnamic acid is 4.44,[30] and therefore at pH 12, cinnamic acid is fully ionized. Therefore, the results indicated that dissociated cinnamic acid is not extractable. At pH 3.9, 77.6% of cinnamic acid is in the neutral form. Thus, only the undissociated cinnamic acid is extractable.

Table 4. Effect of salt and pH on 1-amino-2-naphthol-4-sulphonic acid (ANS) extraction

Salt	pH	Concentration, *M*	Distribution coefficient, *l./kg*	
			Polyester	Polyether
NH_4Cl	3.5	1.0×10^{-3}	9.0	29.2
NH_4Cl	3.5	0.1	4.7	25.3
KCl	3.5	1.0×10^{-3}	7.7	30.3
KCl	3.5	0.1	8.6	29.5
HCl	1.0	0.1	30.8	66.9

Conditions: $1.0 \times 10^{-3}M$ ANS, 0.300 g of foam, 100-ml solution, 6-hr extraction time.

Table 5. Comparison of the distribution coefficients of various organic compounds extracted by polyester and polyether foams

Compound	Distribution coefficient, *l./kg*		
	Polyester	Polyether	$D_{Polyether}/D_{Polyester}$
Salicylic acid	96.9 ± 3.2	218 ± 4	2.2
8-Hydroxyquinoline	173 ± 3	165 ± 3	1.0
Cinnamic acid	195 ± 3	343 ± 4	1.8
1-Amino-2-naphthol-4-sulphonic acid	9.3	30.8	3.3

Conditions: (1) salicylic acid: $2.9 \times 10^{-3}M$ salicylic acid, 0.300 g of foam, 100-ml solution, 24-hr extraction, pH = 3.2. (2) 8-hydroxyquinoline: $1.0 \times 10^{-3}M$ 8-hydroxyquinoline, 0.300 g of foam, 100-ml solution, 1-hr extraction time, pH = 6.4. (3) cinnamic acid: $1.0 \times 10^{-3}M$ cinnamic acid, 0.300 g of foam, 100-ml solution, 24-hr extraction time, pH = 3.9. (4) 1-amino-2-naphthol-4-sulphonic acid (ANS): $1.0 \times 10^{-3}M$ ANS, 0.300 g of foam, 100-ml solution, 6-hr extraction time, pH = 3.5.

Water is a solvent with a high dielectric constant. Ions in aqueous solution are well solvated and so it is difficult for ions to form ion-pairs in aqueous solution. Ion-pair formation is facilitated in solvents with low dielectric constant. To determine whether ionized cinnamic acid is extractable in a low dielectric constant solvent, extractions of $1.0 \times 10^{-3}M$ cinnamic acid with $1.0 \times 10^{-2}M$ sodium hydroxide and potassium hydroxide in 50% v/v dioxane solution at pH 10.4 were carried out. No extraction of the cinnamic acid was observed. It is apparent that cinnamic acid is too hydrophilic to form ion-pairs with Na^+ or K^+ even in 50% dioxane solution.

Hydrogen bonding

Schumack and Chow[27] examined the extraction of a wide variety of organic compounds by polyether and polyester foams. It was concluded that a solvent extraction mechanism is responsible for the extraction of these organic compounds. It was also found that compounds containing a (—OH) hydroxyl group are generally more extractable by polyether foam than by polyester foam. Hydrogen bonding between the (—OH) group on the organic compound and polyurethane foam can account for this observation because polyether foam is able to form stronger hydrogen bonds than polyester foam. In addition, when hydrogen bonding is prevented by placing a strongly intramolecular hydrogen bonding group adjacent to the (—OH) group as in the case of *o*-nitrophenol, salicylaldehyde or *o*-methoxyphenol, the extraction by polyester and polyether foams is about the same.

The various organic compounds used in this study all contain the (—OH) group. The distribution coefficients (*D*) for these compounds under different conditions with polyester and polyether foams are summarized in Table 5. With the exception of 8-hydroxyquinoline, the compounds are more extractable by polyether foam. It is possible that intramolecular hydrogen bonding takes place in 8-hydroxyquinoline which prevents hydrogen bonding between it and the foam. For salicylic acid, there are two groups per molecule able to form hydrogen bonds as opposed to one group for cinnamic acid. The higher $D_{polyether}/D_{polyester}$ ratio for salicylic acid could be ascribed to greater hydrogen bonding between the compound and the foam. Although there are two groups per molecule capable of hydrogen bonding for salicylic acid and ANS, the $D_{polyether}/D_{polyester}$ ratio for ANS is somewhat higher than the salicylic acid. it is possible that the ($—NH_3^+$) group can have an ion–dipole interaction with the foam in addition to hydrogen bonding, resulting in higher extraction for ANS. Considering the lower *D* values for ANS compared with those for salicylic acid, the relatively higher error of *D* for ANS may result in the higher $D_{polyether}/D_{polyester}$ ratio. Overall, the results obtained in this work are consistent with those previously reported.[27]

CONCLUSION

The study of the extraction of salicylic acid, 8-hydroxyquinoline, 1-amino-2-naphthol-4-sulphonic acid and cinnamic acid shows that these compounds are extracted in their neutral form by a simple solvent extraction mechanism. This conclusion is supported by the salting-out

phenomenon and the pH effect. The anionic species are too hydrophilic to facilitate the extraction of alkylamine and alkali metal cations from aqueous solution. Although a simple solvent extraction mechanism is involved, these compounds, except 8-hydroxyquinoline, are more extractable by polyether foam than polyester foam. This result can be attributed to the stronger hydrogen bonding of the organic compound with polyether foam since all these compounds contain a (—OH) group which is capable of forming hydrogen bonds with the foam. For 8-hydroxyquinoline, it is possible that intramolecular hydrogen bonding in the compound prevents the intermolecular hydrogen bonding with the foam resulting in about the same extraction for both types of foam.

Acknowledgement—This work was supported by the Natural Sciences and Engineering Research Council of Canada.

REFERENCES

1. T. Braun and A. B. Farag, *Anal. Chim. Acta*, 1978, **99**, 1.
2. G. J. Moody and J. D. R. Thomas, *Analyst*, 1979, **104**, 1.
3. T. Braun, *Z. Anal. Chem.*, 1983, **314**, 652.
4. *Idem*, *Cellular Polymers*, 1984, **3**, 81.
5. *Idem*, *Z. Anal. Chem.*, 1989, **333**, 785.
6. G. J. Moody and J. D. R. Thomas, *Chromatographic Separation and Extraction with Foamed Plastics and Rubbers*, Marcel Dekker Inc., New York and Basel, 1982.
7. T. Braun, J. D. Navratil and A. B. Farag, *Polyurethane Foam Sorbents in Separation Science*, CRC Press, Boca Raton, 1985.
8. H. J. M. Bowen, *J. Chem. Soc. A*, 1970, 1082.
9. H. D. Gesser, E. Bock, W. G. Baldwin, A. Chow, D. W. McBride and W. Lipinsky, *Sep. Sci.*, 1976, **11**, 315.
10. J. J. Oren, K. M. Gough and H. D. Gesser, *Can. J. Chem.*, 1979, **57**, 2032.
11. V. S. K. Lo and A. Chow, *Talanta*, 1981, **28**, 157.
12. *Idem*, *Anal. Chim. Acta*, 1979, **106**, 161.
13. S. Al-Bazi and A. Chow, *Anal. Chem.*, 1981, **53**, 1073.
14. *Idem*, *Talanta*, 1984, **31**, 431.
15. R. F. Hamon, A. S. Khan and A. Chow, *ibid.*, 1982, **29**, 313.
16. S. Al-Bazi and A. Chow, *ibid.*, 1982, **29**, 507.
17. *Idem*, *ibid.*, 1983, **30**, 487.
18. *Idem*, *ibid.*, 1984, **31**, 189.
19. *Idem*, *Anal. Chim. Acta*, 1984, **157**, 83.
20. R. Caletka, R. Hausbeck and V. Krivan, *Talanta*, 1986, **33**, 315.
21. A. S. Khan and A. Chow, *ibid.*, 1983, **30**, 173.
22. H. D. Gesser, A. Chow, F. C. Davis, J. F. Uthe and J. Reinke, *Anal. Lett.*, 1971, **4**, 883.
23. H. D. Gesser, A. B. Sparling, A. Chow and C. W. Turner, *J. Am. Water Works Assoc.*, 1973, **65**, 220.
24. P. R. Musty and G. Nickless, *J. Chromatog.*, 1974, **100**, 83.
25. B. K. Afghan, R. J. Wilkinson, A. Chow, T. W. Findley, H. D. Gesser and K. I. Srikameswaran, *Water Res.*, 1984, **18**, 9.
26. K. M. Gough and H. D. Gesser, *J. Chromatog.*, 1975, **115**, 383.
27. L. Schumack and A. Chow, *Talanta*, 1987, **34**, 957.
28. A. Chow, W. Branagh and J. Chance, *ibid.*, 1990, **37**, 407.
29. R. F. Hamon, *Ph.D. Thesis*, University of Manitoba, 1981.
30. Z. Rappoport, *Handbook of Tables for Organic Compound Identification*, 3rd Ed., The Chemical Rubber Co., Cleveland, 1967.

Talanta, Vol. 39, No. 5, pp. 505–510, 1992
Printed in Great Britain

0039-9140/92 $5.00 + 0.00
Pergamon Press plc

SPECTROSCOPIC STUDIES OF A NEAR-INFRARED ABSORBING pH SENSITIVE CARBOCYANINE DYE

ANNE E. BOYER, SRINIVASAN DEVANATHAN, DAVID HAMILTON and GABOR PATONAY*
Department of Chemistry, Georgia State University, Atlanta, GA 30303, U.S.A.

(*Received* 11 *June* 1991. *Revised* 29 *August* 1991. *Accepted* 29 *August* 1991)

Summary—Near-infrared dyes can be derivatized with appropriate functional groups for use as analytical probes for numerous applications. A dye derivatized with pH-sensitive functional groups may show spectral changes when the pH of its environment is changed. These dyes are valuable to the researcher since they absorb and fluoresce at long wavelengths where interference is minimal and their absorption maxima permit the use of semiconductor lasers. In this paper we have evaluated the sensitivity to pH of a *bis*-carboxylic acid derivative of a near infrared dye to illustrate its potential as a probe for determining pH. The dye has an absorption maximum at 795 nm in aqueous solution, a region where several commercially available laser diodes have their output maximum. The analytical utility of near-infrared laser diodes for pH determination has also been evaluated.

The pH determination of aqueous solutions is an important aspect of analytical chemistry.[1] In the past many dyes have been evaluated as potential acid/base indicators for the determination of solution pH.[2–4] The analytical detection method preferred for this purpose is fluorescence, which offers enhanced selectivity and sensitivity. An appropriate pH indicator must therefore fluoresce in either its molecular or ionized state, or exhibit fluorescence differences between these forms.

Fluorescent indicators are particularly useful in determining the pH of biological samples which have significant absorbance.[5,6] In particular, the near-infrared (NIR) region of the spectrum has proven useful in the study of biological samples because their absorbance in this region is minimal and does not interfere with the absorbance or fluorescence of an NIR chromophore.[7,8] Indeed, the analytical applications of NIR chromophores have increased dramatically over the last few years. Their advantages include a strong absorption band in the NIR spectral region (600–1000 nm) and large molar absorptivities which facilitate low detection limits. Additionally, due to the relatively low interference in this spectral region, considerable selectivity can be achieved. When semiconductor lasers are used as the excitation source, the advantages of the NIR region are further enhanced.[8,9]

Spectrophotometry is a convenient and rapid analytical tool for pH determination and many studies have attempted to develop and characterize suitable dyes for pH determination using spectrophotometry.[10,11] Although many pH indicator dyes have been evaluated, few NIR absorbing dyes have been investigated for this purpose. The polymethine cyanine dyes are excellent candidates for pH determination. Their absorption and fluorescence maxima generally fall in the 600–1000 nm region, determined by the length of the polymethine chain. Additionally, laser diodes may be used for the NIR dye excitation since their output wavelengths closely match the dye absorption and fluorescence maxima. The output wavelength of the 680-nm laser diode is very close to that of the dicarbocyanine dyes and the tri-carbocyanine dyes can be used with laser diodes of 780-nm output wavelength.[12] Once a dye with the appropriate absorbance and fluorescence characteristics is chosen, it can be easily modified to fit the analytical application. By combining the use of laser diodes with the analytical possibilities afforded by NIR pH-sensitive chromophores, the development of a multitude of analytical techniques is possible.

The absorption and fluorescence properties of many NIR chromophores have been evaluated in the past; including their use as laser dyes,[13] potential sensitive probes,[14] and covalent and non-covalent labels.[15] However, their use as pH indicators has not yet been evaluated, primarily

*Author for correspondence.

because suitable dyes were not available. An appropriate pH indicator dye must have pH sensitive functional groups that can change from the ionized to the non-ionized form as the concentration of the hydrogen ions changes. A change in the ionization of the functional group may influence the conjugation of the π system of the indicator molecule resulting in spectral changes which can be used for determining pH. To date, there are no commercially available NIR dyes that contain these functional groups. However, routine synthetic steps can be followed to introduce pH sensitive functional groups, carboxyl, amino, or phenol(-OH), into NIR dyes.[12]

We report here the pH dependence of the absorption and fluorescence characteristics of a new NIR pH sensitive dye, a *bis*-carboxylic acid derivative of 2-{4′-chloro-7′[2″-(1″-ethyl-3″,3″-dimethyl indolenine)]-3′,5′-(1′″,3′″-propanediyl)-1′,3′,5′-heptatrien-1′-yl]-1-ethyl-3,3-dimethyl indolenine bromide (Fig. 1). These studies may serve as a framework for the development of a new class of NIR dyes that can be used as pH probes utilizing laser diode excitation.

EXPERIMENTAL

Reagents and chemicals

The chemical structure of the pH sensitive dye used in this study is depicted in Fig. 1. It is a *bis*-carboxylic acid derivative of 2-{4′-chloro-7′-[2″-(1″-ethyl-3″,3″-dimethyl indolenine)]-3′,5′-(1′″,3′″-propanediyl)-1′,3′,5′-heptatrien-1′-yl]-1-ethyl-3,3-dimethyl indolenine bromide which has been prepared in our laboratory as follows: 4.65 g of *p*-hydrazinobenzoic acid and 9 ml of 3-methyl-2-butanone were refluxed in ethanol for 45 min. Workup of this reaction mixture included cooling to 0° to give the hydrazone. The hydrazone was refluxed in glacial acetic acid under a nitrogen atmosphere for 4 hr. The reaction mixture was then cooled and poured into ice cold water followed by ether extraction. Acetic acid was removed by washing with water several times. The analytically pure 2,3,3-trimethyl-5-carboxy-3-H-indole has a mp of 210–211°. Reaction of the 3-H indole with 2 g of ethyl bromide in 15 ml of acetonitrile under pressure gave the quaternary salt. Subsequent transformation of this bromide into the final dye was conducted according to cyanine dye synthesis procedures.[16,17] Crude dye was crystallized twice from ethanol, and the product was heated at 60° under reduced pressure of 0.1 mm Hg for 12 hr producing the analytically pure dye sample that is shown in Fig. 1. The dye structure is fully consistent with the proton NMR spectrum ($CDCl_3$).

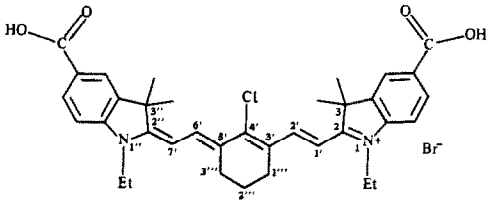

Fig. 1. Chemical structure of the pH sensitive NIR dye used in this study.

Chemicals used in the dye synthesis were obtained from Aldrich Chemical Company (Milwaukee, WI). Spectrophotometric grade methanol was also obtained from Aldrich. Hydrochloric acid, sodium hydroxide and buffer components were obtained from Fisher Scientific (Pittsburgh, PA).

Method

Stock solutions ($10^{-3}M$) of the pH sensitive NIR dye were prepared in spectrophotometric grade methanol. For the pH studies solutions were prepared by pipetting the required amount of dye stock solution dissolved in methanol into a 50-ml standard flask. The standard flask was then filled with demineralized water or 0.05M Tris buffer and briefly sonicated. The final solutions contained less than 0.05% v/v methanol which had no effect on the dye spectra or pH. The dye preparation is simplified by diluting from a stock solution in methanol, compared to removing methanol from the stock solution with dry nitrogen gas. The concentration of the final dye solution was $4 \times 10^{-6}M$ unless otherwise stated.

Solution pH was varied for two separate sets of dye solutions in order to evaluate dye behaviour at different ionic strengths. The low ionic strength solutions were prepared by slowly adding appropriately diluted hydrochloric acid or sodium hydroxide to the dye solutions. Minute quantities of acid or base were used to avoid spectral changes caused by dilution. The high ionic strength solutions were prepared in 0.05M buffers. For both sets of solutions, the pH was monitored continuously with glass pH electrodes.

Instrumentation

Absorbance spectra were obtained on a Perkin–Elmer Lambda 2 UV/VIS/NIR spectrophotometer, interfaced to a Zenith 286 computer

to store spectra and control the spectrophotometer. Each spectrum was recorded with a PECSS program. All data were obtained at room temperature, using solutions in equilibrium with air. Solution pH was measured with an Orion Research Model 701A Digital Ionanalyzer. Fluorescence spectra were recorded on an SLM 8000 spectrofluorometer interfaced to an IBM PS/2. The instrument was modified to accommodate an NIR laser diode excitation source.[18] A 30-mW laser diode was used with a 782-nm output wavelength; the optical and electronic design of this modification has been discussed previously.[18] Dye pK_a values were obtained with the Schott Model 250 autotitrator and Model T90/10 autoburet interfaced to a 286 computer.

RESULTS AND DISCUSSION

Representative absorption spectra of the pH sensitive NIR dye in methanol is shown in Fig. 2. The dye maximum is at 795 nm, comparable to the output wavelength of the commercially available laser diodes. Dye spectra were similar in both aqueous and methanol solutions except for a minor spectral shift of the NIR absorption maxima. The dye molar absorptivities in methanol and in water at different wavelengths are summarized in Table 1 indicating values typical of most cyanine dyes. The relatively high molar absorptivities typical of most cyanine dyes, enhances their detection limits. In the case of spectrophotometric pH probes, a high molar absorptivitiy allows the use of lower dye concentrations which minimizes interference resulting from dye acid/base equilibria.

Several indicator dyes work on the premise of ionization of pH sensitive groups, amino, phenol, hydroxyl or carboxyl. Changes in these groups may influence the π system of the indicator

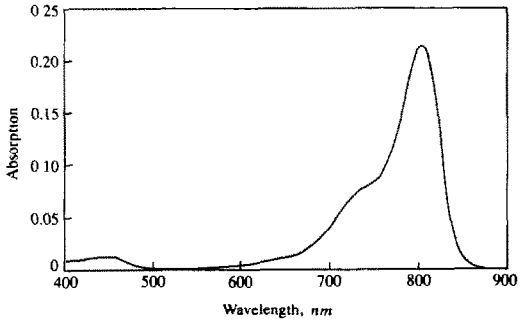

Fig. 2. Typical absorption spectra of the pH sensitive NIR dye in methanol.

Table 1. Molar absorptivity values for the NIR pH sensitive dye

Solvent	$\epsilon_{298\,nm}$	ϵ_{NIR}
Water	13,050	150,000 (795 nm)
Methanol	11,200	166,000 (803 nm)

molecule resulting in changes in the absorption and fluorescence spectra. Since the carboxylic groups are directly attached to the aromatic nuclei of the NIR dye described in this study, we presume that the conjugation and the charge distribution in the molecule is dependent on the ionization of these carboxylic groups. We chose to prepare a *bis*-carboxylic acid derivative of the NIR dye 2-{4′-chloro-7′-[2″-(1″-ethyl-3″,3″-dimethyl indolenine)]-3′,5′-(1‴,3‴-propanediyl)-1′,3′,5′-heptatrien-1′-yl]-1-ethyl-3,3-dimethyl indolenine bromide (Fig. 1) rather than the monosubstituted analogue, for two reasons. First, it is much easier to prepare a symmetrical cyanine dye and second, due to the presence of two carboxylic groups, a much larger perturbation of the π system of the molecule is expected upon ionization of the carboxylic groups. Two distinct pK_a values were also expected for the NIR dye acid. The presence of two carboxylic groups in the dye molecule should widen the pH range where changes in the spectral properties are expected. This should also increase the emission or excitation spectral shift upon ionization of the carboxylic groups.

The pK_a values of the dye acid were determined with automated titrators using $0.039M$ sodium hydroxide. Titration curves showed pK_a values of 4.90 and 6.80, respectively, for the two carboxylic groups. These values are in good agreement with pK_a values for carboxylic acid derivatives of other heterocyclic compounds.[12] The non-ionized form of the indicator dye depicted in Fig. 1 is cationic. The relatively low pK_a value of the first carboxylic group can be explained by the positive charge of the dye molecule. Since the molecule is symmetrical, including the positive charge distribution between the quaternary nitrogens, either carboxylic group may be ionized first. Once the first carboxylic group is fully ionized, the neutral zwitterionic form will predominate. Ionization of the second carboxylic group is more difficult because of the lack of a net positive charge.

We expect that the ionization steps result in changes of the π system of the NIR dye molecule. The relative influence of the two ionization steps on absorption spectra of the NIR indicator dye may be estimated by the

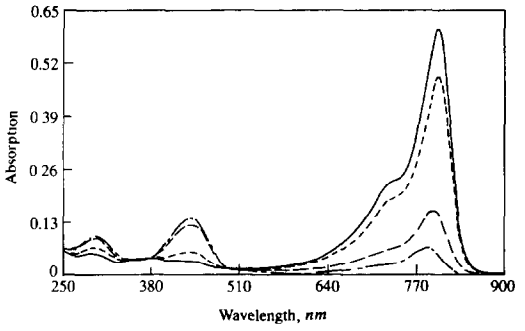

Fig. 3. Typical absorption spectra of the NIR dye in pH 7 (——), 8 (– – –), 9 (—·—) and 9.7 (———) solutions.

Henderson–Hasselbach equation if we compare the dye spectra at different pHs.

Typical absorption spectra of the NIR dye acid in the low ionic strength solution (water) at different pHs are shown in Fig. 3. These changes in the absorption spectra were repeatedly observed when the pH of the same solution was varied by addition of acid or base, indicating the hydrogen ion concentration was the primary determining factor. These experiments showed spectral reproducibility and stability of the NIR dye in its aqueous environment as the pH was increased and decreased repeatedly. Photostability of this NIR dye has been evaluated. The dye solution was continuously illuminated at its absorption maximum for about two hours. No change in absorption or fluorescence was observed during this period.

Spectral changes with pH of the dye in the higher ionic strength buffer solutions (0.05*M* Tris) resulted in almost identical spectra and therefore are not shown here. As can be seen from Fig. 3, at higher pH values, an absorption peak at 435 nm appears and increases with increasing pH. At corresponding pH values, the NIR peak at 795 nm decreases with increasing pH. According to the Henderson–Hasselbach equation, the first carboxylic group will be approximately 90% ionized at $pH = pK_{a1} + 1$ and the second carboxylic group will be 90% ionized at $pH = pK_{a2} + 1$.

Figure 4(a) shows a plot of NIR dye absorbance at 435 nm and 4(b) at 795 nm for each pH value from 2 to 12. Both Figs. 4(a) and 4(b) show that at pH 6, where the first carboxylic group is about 90% ionized, very little spectral change is observed, indicating that the first ionization step probably has little influence on the distribution of positive charge between the quaternary nitrogens. This positive charge distribution usually has a large influence on the spectral properties of polymethine cyanine dyes.[12]

The second ionization step results in much more pronounced changes in the dye absorption spectra. At pHs above 8.5 we expect most of the dye molecules to be fully ionized. Figure 3 shows that significant NIR absorption is still present at pH 8.5, indicative of other possible factors influencing the molar absorptivities of the dye molecule at the second ionization. This phenomena is interesting when you consider that the molar absorptivity of the dye remains unchanged when the first carboxylic group is ionized. This difference in molar absorptivities between the mono- and di-ionized form of the NIR indicator dye further emphasizes the extent of perturbation in the π system upon the second ionization step. This also indicates that the quaternary nitrogens probably have much less influence on these spectral changes since they are very basic.[12]

Both the 435-nm or NIR peaks can be used for determining the pH of the environment around the dye molecule. Figure 4(a) can be used as a calibration curve for determining the pH, using the 435 nm absorption peak. Figure 4(a) indicates that this peak is not present in the dye spectra in acidic solutions. In basic solutions

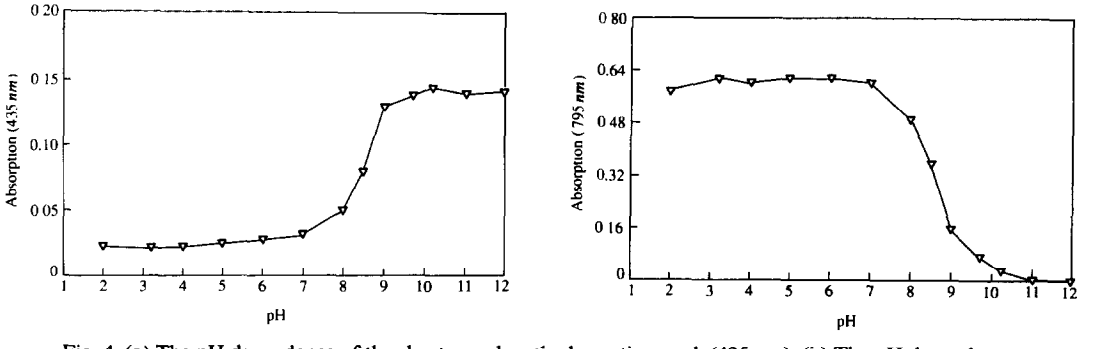

Fig. 4. (a) The pH dependence of the short wavelength absorption peak (435 nm). (b) The pH dependence of the NIR absorption peak (795 nm).

however, the 435-nm absorption peak appears and the intensity of the peak increases with increasing basicity of the solution and levels off at pH 10. The appearance of this short wavelength absorption peak corresponds to a decrease in the NIR peak [Fig. 4(b)], clearly indicating that the presence of negatively charged carboxylate groups disrupts the delocalization of the positive charge between the quaternary nitrogen atoms. Although this phenomenon may be used for pH determination, the 435-nm peak is in the region of higher interference and therefore, may be less useful for this purpose.

The NIR peak at 795 nm, however, may be more useful for pH determination. This dye could be suitable for measuring the pH, using laser diodes or other NIR light sources. Although the intensity of the NIR absorption peak remains unchanged in acidic solutions, at pH 7 and higher the intensity of this peak decreases due to ionization of the carboxyl groups. The NIR peak intensity gradually decreases as the solution pH increases and becomes insignificant above pH 10.

Since the chromophore is fluorescent in both aqueous and non-aqueous media, the NIR fluorescence of this dye may also be used for determining the pH of solutions. The absorption maximum of the NIR dye acid is in the region where inexpensive consumer laser diodes have their output maximum (785–795 nm). As indicated by several earlier studies,[9,18] laser diodes are excellent excitation sources for fluorescence measurements. The fluorescence of this dye has also been evaluated with a laser diode modified SLM 8000 fluorometer which has been described earlier.[18] A representative fluorescence spectrum for the dye is shown in Fig. 5. The NIR fluorescence intensity of the NIR dye acid was determined using a laser diode excitation source of 782 nm, 30 mW in aqueous solutions of different

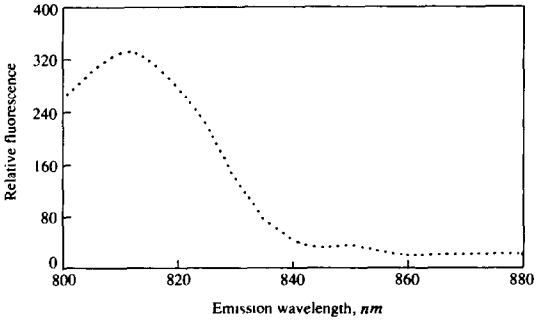

Fig. 5. Fluorescence spectra of the NIR pH sensitive dye at pH = 4.1 (Excitation: 795 nm).

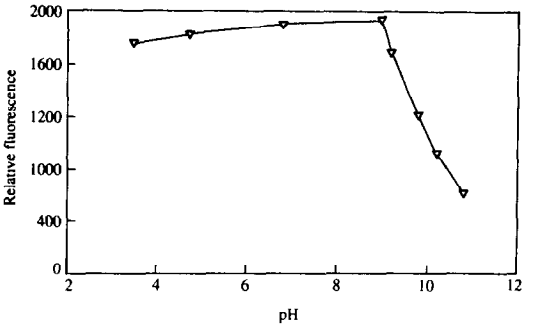

Fig. 6. Solution pH determination with NIR laser diode excitation (λ_{ex} = 782 nm, λ_{em} = 820 nm).

pHs. Fluorescence intensity was measured at 820 nm, using a 10-nm band width interference filter. The calibration curve obtained (Fig. 6) indicates that NIR laser diode induced fluorescence may be used for determining pH in solutions. A comparison between Figs. 4(b) and 6 reveals that the NIR absorbance or fluorescence changes occur at different pH values; the NIR absorbance begins to decrease at pH 7 and the fluorescence begins to decrease at pH 9. This difference is expected since fluorescence is characteristic of the excited state of the molecule while absorption is characteristic of the ground state of the molecule. The fluorescence enhancement above pH 4 may be attributed to the first ionization step. Although the absorption spectra do not show significant changes until the second ionization step occurs, fluorescence properties of the dye may be influenced by changing charge distribution.

CONCLUSIONS

A new NIR cyanine dye has been shown to be sensitive to changes in pH. The NIR absorption and fluorescence characteristics of this dye could be useful in actual samples since interference is negligible in near-infrared fluorometry. The laser diode used in these studies has an output wavelength of 782 nm, at room temperature and as mentioned, laser diodes with different output wavelengths may be used to match the varying spectral characteristics of different dye structures. The dicarbocyanine dyes which have an absorption band that closely matches the output maxima of 680-nm laser diodes, may also be useful for this purpose. Their heterocyclic nuclei may influence the absorption maxima of the dye. However, the heterocyclic nuclei have a greater influence on the pK_a values and therefore on the useful pH range. It is clear

that additional studies are required for determining the exact role of the heterocyclic nuclei on the useful pH range. Numerous other possibilities for designing appropriate dye structures exist. Other functional groups may be used in the NIR dye molecule to achieve pH sensitivity. For example, NIR dyes with aromatic amino groups are expected to be indicators in the acidic pH region, while phenolic groups may be used to extend the useful pH range to more basic pHs. The introduction of additional charge into the dye molecule may also be used to fine-tune the pH range desired.

Although the use of NIR dye solutions and laser diodes for determining pH may be useful when low interference is desired, immobilized dye attached to the end of fiber optic should give greater versatility for the method. Using different dyes with different absorption maxima and pK_a values, a large pH range may be achieved if multi-laser diode excitation is utilized. Other NIR dyes that have spectral pH dependence closer to their pK_a values may be developed for physico-chemical applications, for example in the determination of pK_a.

Acknowledgements—This work was supported in part by a grant from the National Science Foundation (CHE-890456). Acknowledgement is also made to the donors of the Petroleum Research Fund, administered by the American Chemical Society, for partial support of this research.

REFERENCES

1. G. G. Guilbault, *Practical Fluorescence*, Marcel Dekker, New York, 1973.
2. E. Bosch, E. Casassas, A. Izquierdo and M. Roses, *Anal. Chem.*, 1984, **56**, 1422.
3. B. A. Woods, J. Růžička, G. D. Chrisitian and R. J. Charlson, *ibid.*, 1986, **58**, 2496.
4. Y. Israel, *Anal. Chim. Acta*, 1988, **206**, 313.
5. T. Mashimo, H. Kamaya and I. Udea, *Mol. Pharmacol.*, 1986, **29**, 149.
6. J. C. LaManna and K. A. McCracken, *Anal. Biochem.*, 1984, **142**, 117.
7. G. Patonay and M. D. Antoine, *Anal. Chem.*, 1991, **63**, 321A.
8. T. Imasaka and N. Ishibashi, *ibid.*, 1990, **62**, 363A.
9. J. Hicks and G. Patonay, *Anal. Instrum.*, 1989, **18**, 213.
10. C. Reilley and E. Smith, *Anal. Chem.*, 1960, **32**, 1233.
11. R. Narayanaswamy and F. Sevilla, *Anal. Chim. Acta*, 1986, **189**, 365.
12. D. J. Fry, in *Rodd's Chemistry of Carbon Compounds*, S. Coffey (ed.), 2nd Ed., pp. 369–423. Elsevier, New York, 1977.
13. E. G. Arthurs, D. J. Bradley and A. G. Roddie, *Appl. Phys. Lett.*, 1972, **20**, 125.
14. J. C. Smith, *Biochem. Biophys. Acta*, 1990, **1016**, 1.
15. K. Sauda, T. Imasaka and N. Ishibashi, *Anal. Chem.*, 1986, **58**, 2649.
16. S. M. Makin, I. I. Boiko and O. A. Shavrygina, *Z. Org. Khim.*, 1977, **3**, 1189.
17. *Idem*, *ibid.*, 1977, **13**, 2440.
18. J. Hicks, D. Andrews-Wilberforce and G. Patonay, *Anal. Instrum.*, 1990, **19**, 29.

Talanta, Vol. 39, No. 5, pp. 511–515, 1992
Printed in Great Britain.

0039-9140/92 $5.00 + 0.00

TITRIMETRIC DETERMINATION OF FLUORIDE IN SOME PHARMACEUTICAL PRODUCTS USED FOR FLUORIDATION

BILJANA F. ABRAMOVIĆ* and FERENC F. GAÁL
Institute of Chemistry, Faculty of Sciences, University of Novi Sad, Trg Dositeja Obradovića 3, 21000 Novi Sad, Yugoslavia

SRETEN D. CVETKOVIĆ
Military Medical Centre, Herceg Novi, Yugoslavia

(*Received* 9 *September* 1991. *Revised* 28 *October* 1991. *Accepted* 31 *October* 1991)

Summary—Two titrimetric methods were developed for the determination of fluoride contents in some pharmaceutical preparations used for fluoridation. One of the methods is catalytic controlled-current potentiometry involving two identical platinum indicator electrodes and thorium nitrate as titrant. The reaction between hydrogen peroxide and potassium iodide in the presence of acetate buffer (pH 3.6), which is catalysed by the excess of thorium nitrate, served for the end-point indication. The other method is the automatic potentiometric titration involving a fluoride-selective electrode and lanthanum nitrate as titrating agent. In both procedures, special attention was paid to sample pretreatment and to determination of optimal experimental conditions. Fluoride contents in the range 16–32 μg/ml are determined with a relative standard deviation less than 1.34%. The results are compared to those obtained by standard methods described in the United States Pharmacopeia XXI and recommended by the manufacturer of the preparations.

Fluorine compounds, both organic and inorganic, have their specific use in modern medical practice. The most important of these compounds are synthetic fluorinated corticosteroids, neuroleptics, anaesthetics, uroanesthetics, cytostatics and antirheumatics. Besides, fluorine compounds are used in the prevention of caries.

Although fluorine preparations for caries prevention have been in use in Yugoslavia for a long time they have not been treated in Farmakopeja SFRJ, Ph. Jug. IV.[1] The only reference is concerned with pure sodium fluoride, but the titrimetric method recommended therein is not suitable for the determination of fluoride in these preparations because of the necessity to use a relatively large amount of sodium fluoride (50 mg/probe). A similar situation applies to the British Pharmacopoeia 1980.[2] However, the United States Pharmacopeia XXI[3] contains several monographs on fluoride preparations used in caries prevention. The recommended method for fluoride determination is direct potentiometry with a fluoride-selective electrode. The application of this method,[4,5] together with spectrophotometry[6] and isotachophoresis[7] for determination of fluoride content in pharmaceutical preparations have also been described in the literature.

As a continuation of our studies on the determination of pharmacologically active components in pharmaceutical preparations,[8–10] the present article describes the development of a simple, relatively fast and sufficiently accurate analytical method for the determination of fluoride content in fluoridation preparations which could be performed even in a modestly-equipped laboratory. For this purpose a catalytic titrimetric method with thorium nitrate as titrant was employed with the use of controlled-current potentiometry to follow the course of the titration.[11] Besides, for the same purpose we used the potentiometric titration with lanthanum nitrate as titrating agent.

EXPERIMENTAL

Chemicals and solutions

All chemicals used were of analytical purity. Solutions were prepared with doubly distilled water.

*Author for correspondence.

The fluoride content was determined in the following pharmaceutical preparations: Fluonatril tablets (Belupo 1, Ludberg), 0.55 and 2.21 mg of sodium fluoride per tablet; NAF tablets (Bosnalijek, Sarajevo) 0.55 and 2.21 mg of sodium fluoride per tablet; Aminfluorid solution (Belupo 2, Koprivnica) 12.140% of *N,N,N'*-tri-(2 - hydroxyethyl) - *N'* - octadecyl - 1,3 - diaminopropane-dihydrofluoride (I) and 1.135% of 1-amino-9-octadecen hydrofluoride (II) (which corresponds to a total fluoride content of 1.000%), and Aminfluorid gel (Belupo 2, Koprivnica) 3.032% of I, 0.287% of II, and 2.210% of sodium fluoride (total fluoride content 1.250%).

Standard thorium nitrate and lanthanum nitrate solutions (0.01*M*) were standardized against a known amount of fluoride by potentiometric titration with the fluoride-selective electrode.

Potassium iodide solution, $1.8 \times 10^{-2}M$, hydrogen peroxide solution, $5.5 \times 10^{-2}M$ and acetate buffer, pH 3.6, were prepared as described previously.[11]

Solutions for direct potentiometric measurements were prepared according to the US Pharmacopeia XXI.[3]

Apparatus

The course of catalytic titrations was monitored by a controlled-current potentiometric ($I = 2\ \mu A$) method with two identical indicator electrodes. The laboratory-constructed indicator electrodes[12] used in fluoride determination in the model solution were made of platinum (Pt), graphite (C) and glassy carbon (GC). To determine fluoride contents in the investigated preparations, use was made of a platinum indicator electrode couple. Titration curves were recorded on a chart recorder (Goerz-Electro Servogor 2S RE-571) at a rate of 30 mm/min.

For automatic potentiometric titrations with the electrode couple fluoride-selective electrode (Radiometer F-1052F) and SCE (Radiometer K-401), a Radiometer pHM 26 coupled to a Radiometer TTT 60, was used.

The titrant was added continuously by means of a Radiometer ABU 12 piston burette (volumes of 2.50 and 25.00 ml). The rate of titrant addition was 0.282 ml/min in catalytic titrations and 0.035 and 0.35 ml/min, respectively, in automatic titrations.

The comparative direct potentiometric method was performed with a Radiometer pHM 62 Standard pH meter and the above fluoride-selective electrode in combination with a saturated calomel electrode.

Analysis of tablets

After homogenization of 250 of the tablets to be analysed by grinding in a mortar, the procedure used in catalytic potentiometric ($I = 2\ \mu A$) titration was as follows. A 50-mg amount (for a sodium fluoride content of 2.21 mg/tablet which corresponded to the mass of one tablet), or 100 mg (if sodium fluoride content was 0.55 mg/tablet, which corresponded to the mass of two tablets) of the homogenized powder was placed in a 70-ml plastic reaction vessel and 10.0 ml of water were added. After heating the mixture on a water bath for 30 min and cooling to room temperature, the following solutions were added: 16.0 ml of ethanol, 4.0 ml of acetate buffer, 0.5 ml of hydrogen peroxide and 0.5 ml of sodium iodide. The solution was titrated with the standard thorium nitrate solution.

In automatic potentiometric titrations the following procedure was used. The homogenized powder was weighed as in the previous case and placed into a 70-ml reaction vessel. Then, 10.0 ml of water and 25.0 ml of ethanol were added and the solution titrated with the standard lanthanum nitrate solution. Before starting the titration, the "proportional band" on the titrator was set at the value 1 and the appropriate end-point potential.

The procedure in comparative direct potentiometric determination was the one described in the US Pharmacopeia XXI.[3]

Analysis of Aminfluorid solution and Aminfluorid gel

In both catalytic and automatic potentiometric titrations, the following procedure was used. To 100 mg of the sample placed in a 70-ml reaction vessel 10.00 ml of water was added and the reaction mixture homogenized by stirring with a magnetic stirrer. Further procedure was identical to that used in fluoride determination in tablets.

The procedure in comparative direct potentiometric determinations was similar to that in the analysis of tablets.

In the neutralization titrations the following procedure was used. About 3.00 g of Aminfluorid solution (*i.e.*, about 5.00 g of Aminfluorid gel), was dissolved in 40 ml of ethanol in a 70-ml plastic vessel. After adding several drops of phenolphthalein solution, the solution was titrated with the 0.1*M* standard ethanolic

potassium hydroxide solution to a light-rose colour.

The end-point of the catalytic titration in all cases was determined graphically from the intersection of straight-line interpolations before and after the equivalence point. The results were corrected for the blank.

RESULTS AND DISCUSSION

Optimization of conditions

As already mentioned, the most suitable method for titrimetric determination of fluoride content in model solutions was the controlled-current ($I = 2$ μA) potentiometry, using two identical platinum indicator electrodes.[11] However, it was interesting to examine the effect of the nature of indicator electrodes on the shape of titration curves and on the results of these determinations. For this purpose we compared the performance of three electrode pairs made of platinum, spectral graphite and glassy carbon (Fig. 1). As can be seen, the largest change in the potential is observed in the case of glassy-carbon electrodes (curve 2). However, the pair of platinum electrodes was chosen because the corresponding titration curve (curve 1) is characterized by the most pronounced potential change around the equivalence point.

As the fluoride content in the analysed tablets was 2–4 times lower than in the model solution,[11] it was necessary to examine the possibility of using catalytic titrations for the determination of these lower quantities of fluoride. It was found that for the investigated range of quantities of sodium fluoride (Table 1) the resulting titration curves were suitable for the end-point determination, but the results thus obtained were not satisfactory.

An analysis of these results showed that in all cases, irrespective of the quantity determined, the same absolute error was observed, which was in agreement with our earlier observations.[11] A probable explanation of this could be the difference in experimental conditions in recording a catalytic titration curve for the sample and the corresponding curve for the blank. Because of that we have investigated the possibility of employing the standard addition method in which, instead of titrating the blank, a probe containing a certain amount of sodium fluoride was titrated both alone and in combination with the probe of the sample. The content of fluoride in the analysis was obtained from the difference between the results of the two titrations. The recoveries thus obtained agreed well with the expected ones.

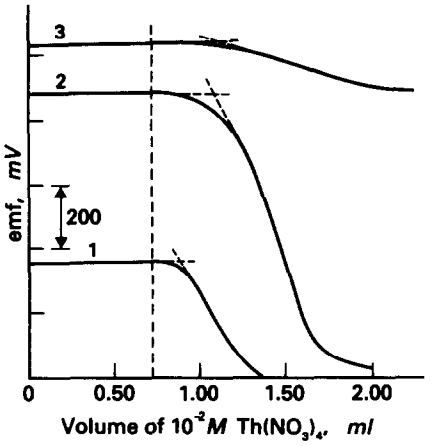

Fig. 1. Effect of nature of indicator electrode on the shape of catalytic constant-current potentiometric titration curve of 1.202 mg of sodium fluoride: (1) [Pt(+)/Pt(−)]; (2) [GC(+)/GC(−)]; (3) [C(+)/C(−)]. The dotted line indicates the equivalence point.

The possibility of employing the calibration graph method has also been investigated. The obtained plot was linear in the investigated range of concentrations, so that it could be represented by the following equation:

$$y = 64.09x + 9.98 \qquad r = 0.99999$$

where y is the length of the titration curve to the equivalence point (mm) (the blank subtracted)

Table 1. Results of catalytic titrimetric determination of sodium fluoride in model solutions ($n = 6$)

	Procedure			
	Direct		Standard addition	Calibration curve
NaF taken, *mg*	Found, %	RSD, %	Found, %	Found, %
0.600	127.6	1.61	101.2	100.2
0.900	119.0	1.75	101.6	100.3
1.202	114.0	0.55	99.2	99.8
1.801	109.8	0.61	100.8	99.8
2.404	107.8	0.31	100.2	100.1

and x is the amount of sodium fluoride (mg) under the given experimental conditions.

It comes out from the above equation that only amounts of sodium fluoride higher than 16 mg can be determined by the direct method with a relative error less than 1%. On the other hand, the results obtained by the calibration graph method are also satisfactory (Table 1). Because of that, this method was employed to determine fluoride contents in the investigated preparations.

In the course of establishing optimal experimental conditions for determination of fluoride by automatic potentiometric titration it was found that the amounts of 1.20–12.00 mg of sodium fluoride could be determined without any difficulty as to the accuracy of the results.

In view of the slow attainment of a steady potential at the fluoride-selective electrode in the solutions with low fluoride concentrations it was necessary to find an optimal rate of titrant addition. For this purpose, the accuracy and precision of determination were tested for the titrant addition rate in the range 35–282 μl/min. It appeared, however, that this effect was rather small provided the standardization of the lanthanum nitrate solution was carried out under the same conditions as the sample analysis, which is understandable. In view of the highest precision obtained, all further determinations were carried out at the lowest rate of titrant addition, although such titrations lasted a relatively long time (60 min).

Because of the presence of certain amounts of fillers in the analysed tablets, which are not completely soluble in the water–ethanol mixture used in the titration, it was also necessary to optimize the procedure of sample (tablets) pretreatment. For this purpose, several pretreatment procedures of Fluonatril tablets were employed (Table 2). As can be seen, according

Table 2. Effect of mode of preparation of Fluonatril tablets on the results of catalytic titration of fluoride. Declared content of F^-: 1.00 mg/tablet ($n = 6$)

Method of sample preparation	F^- found, *mg*	RSD, %	F-ratio†
A	1.006	0.66	4.10
B	1.007	1.27	
C	1.001	0.92	
D	0.991	0.57	

After adding water, ethanol and buffer, the sample was stirred on a magnetic stirrer for 5 min (A), 30 min (B) and 60 min (C). For D, 10.0 ml of water were added to the sample and the mixture was heated for 30 min in a water bath; †$F_{0.05,3,20} = 3.10$; $F_{0\,01;3;20} = 4.94$.

Table 3. Determination of fluoride content in some pharmaceutical products for fluoridation ($n = 6$)

Preparation	Certified fluorid value	Method								
		Catalytic titration		Automatic potentiometric titration		Direct potentiometric titration		Neutralization titration		
		Found	RSD*	Found	RSD	Found	RSD	Found	RSD	*F*-value
Fluonatril tablets	1.00 mg/tbl	0.991 mg/tbl	0.54	0.993 mg/tbl	0.58	0.990 mg/tbl†	0.72	—	—	0.46‡
	0.25 mg/tbl	0.266 mg/tbl	0.89	0.269 mg/tbl	1.09	0.252 mg/tbl†	0.92	—	—	89.00‡
NAF tablets	1.00 mg/tbl	0.975 mg/tbl	1.34	0.978 mg/tbl	0.23	0.978 mg/tbl†	0.76	—	—	0.28‡
	0.25 mg/tbl	0.280 mg/tbl	1.34	0.270 mg/tbl	0.47	0.249 mg/tbl†	0.92	—	—	253.48‡
Aminfluorid gel	1.250%	1.290%	0.99	1.261%	0.87	1.238%	0.40	0.236%	1.79	40.19§
Aminfluorid solution	1.000%	1.091%	0.48	1.042%	0.78	1.089%	0.87	1.046%	0.59	75.89‖

*RSD relative standard deviation (%).
†USP method[3].
‡$F_{0\,05,2,15} = 3.68$.
$F_{0.01,2,15} = 6.36$.
§$F_{0\,01,2,15} = 6.36$.
‖$F_{0\,01,3,20} = 4.94$.

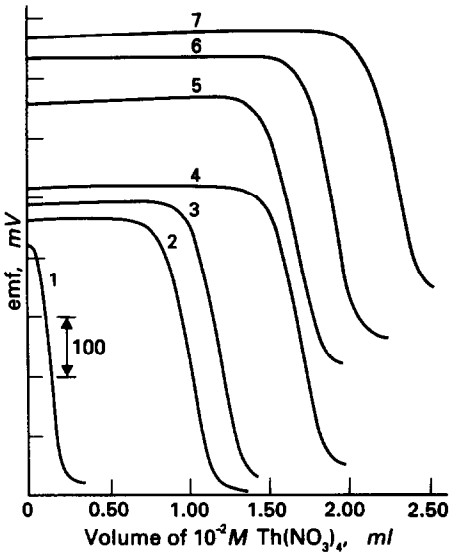

Fig. 2. Catalytic potentiometric [Pt(+)/Pt(−)] ($I = 2$ μA) titration curves obtained in determination of fluoride in: (1) blank; (2) 0.09916 g of Fluonatril tablets with 0.25 mg F^-/tablet; (3) 0.10035 g NAF tablets with 0.25 mg F^-/tablet; (4) 0.05047 g NAF tablets with 1.00 mg F^-/tablet; (5) 0.04940 g of Fluonatril tablets with 1.00 mg F^-/tablet; (6) 0.09184 g of Aminfluorid gel; (7) 0.13368 g of Aminfluorid solution.

to one-way analysis of variance there was a significant difference between all the mentioned methods. On comparing these results with those obtained by the other two methods (Table 3), Procedure D was chosen as the optimal one.

Applicability of methods

Typical catalytic titration curves of the analysed samples are presented in Fig. 2.

Some of the results of determination of fluoride content in the analysed preparations are given in Table 3. As none of the above pharmacopoeias[1-3] contains the monograph for the determination of fluoride content in Aminfluorid solution and gel, the neutralization titration (the procedure recommended by the manufacturer) and the direct potentiometry (as in the determination of fluoride in tablets[3]) were used as comparative methods. A relatively low fluoride content found by the neutralization titration of Aminfluorid gel is understandable if it is borne in mind that only 0.25% of fluoride is present in the form of hydrofluoride.

As can be seen from Table 3, if the fluoride content in the product is higher (1 mg F^-/tablet) then, the application of all the above procedures yields a satisfactory agreement of the results. However, if the fluoride content is lower, as in the case of Aminfluorid solution and gel, and especially with tablets containing 0.25 mg F^-/tablet, such an analysis shows a highly significant difference between all the mentioned methods. This is probably a consequence of a higher content and different nature of the filler because it can also react in some way with the titrant. For this reason, the titrant standardization should be performed in the presence of an appropriate amount of the filler in the solution.

On the basis of all the above, it can be concluded that catalytic controlled-current and automatic potentiometric titrations are equally suitable for the determination of fluoride content in the preparations used for fluoridation. However, a certain advantage can be given to catalytic titrations because no strict reproducibility of the potential changes is required, as is the case with the automatic titrations. Similarly, on comparing the titrimetric methods with the direct potentiometric method, it can be concluded that the former ones have a certain advantage because of a somewhat simpler preparation procedure.

Acknowledgement—The authors thank the Research Fund of Vojvodina for partial financial support of this work.

REFERENCES

1. *Farmakopeja SFRJ, Ph. Jug. IV*, Vol. II, p. 690. Federal Health Protection Institute, Beograd, 1984.
2. *British Pharmacopoeia*, p. 412. HM Stationery Office, London, 1980.
3. *The United States Pharmacopeia XXI*, pp. 969–974. Mack, Easton, PA, 1985.
4. R. Marzilli, *J. Assoc. Off. Anal. Chem.*, 1984, **67**, 682.
5. A. Kaniewski, A. Rydzewska and M. Chmielnik, *Czas. Stomatol.*, 1987, **40**, 779.
6. P. Topolewski and S. Zommer-Urbanska, *Microchem. J.*, 1987, **35**, 145.
7. H. Klein and R. Teichmann, *Pharm. Ztg.*, 1987, **132**, 2986.
8. F. F. Gaál and B. F. Abramović, *Mikrochim. Acta*, 1982, **I**, 465.
9. B. F. Abramović, M. M. Marinković and F. F. Gaál, *Acta Pharm. Jugosl.*, 1989, **39**, 733.
10. B. F. Abramović, M. M. Marinković and F. F. Gaál, *Analyst*, 1990, **115**, 79.
11. F. F. Gaál, B. F. Abramović and V. D. Canić, *Talanta*, 1978, **25**, 113.
12. F. F. Gaál and B. F. Abramović, *ibid.*, 1980, **27**, 733.

Talanta, Vol. 39, No. 5, pp. 517–522, 1992
Printed in Great Britain.

0039-9140/92 $5.00 + 0.00

COMPUTER EVALUATION OF WATER SORPTION ON ION EXCHANGERS

JOSEF HAVEL
Department of Analytical Chemistry, Masaryk University, Kotlářská 2, 611 37, Brno, Czechoslovakia

ERIK HÖGFELDT
Department of Inorganic Chemistry, The Royal Institute of Technology, S-100 44, Stockholm, Sweden

(*Received* 21 *May* 1991. *Revised* 25 *July* 1991. *Accepted* 23 *September* 1991)

Summary—Water sorption on an ion exchanger can be described by formation of several hydrates. The general least squares program WSLET based on the "pit-mapping" approach has been written for evaluating such equilibria. It is written in FORTRAN 77 for use on personal computers. Besides finding the best values for the equilibrium constants of the various hydrates the program also searches for best values of the stoichiometric indices by using the so-called ESI-method. The program is provided with least-squares procedures and blocks for statistical analysis of the residuals as well as for data simulation. It has been tested with data on the strong base resin Dowex 1 as well as on simulated data. In the present paper an illustrative example is given together with data simulation. It is found that in most cases WSLET helps to find a better fit than earlier models quite efficiently, showing the advantage of the ESI method in combination with least-squares methods.

Ion exchangers are part of the basic arsenal in analytical chemistry. The water content related to the crosslinking of resins has a profound influence on their properties. Knowledge of the water uptake is thus of practical interest.

Recently, Kellomäki[1,2] tried to fit water sorption data onto resins with the BET isotherm. He found that only the beginning of the isotherm could be fitted to this equation. Similar results were found by Soldatov *et al.*[3] They compared four isotherm equations and found that only the model described below gave an acceptable fit over the whole range of the isotherm.

It has been shown elsewhere[4] that water uptake can be described by a chemical model, where water molecules are added stepwise to an ion exchanger similar to ordinary complex formation. The method has been applied to water sorption on salts of the liquid ion exchanger dinonylnaphthalene sulphonic acid (HD)[5,6] as well as the solid anion exchanger Dowex 1.[7]

However, not all possible species are formed and the search for the "best model" is tedious. For that reason the program WSLET has been constructed permitting a more efficient search for the species formed. In the evaluation of the data pocket calculators and computer programs, such as LETAGROP, have been used. Recently, a new method for treating such data was suggested by Zargarov.[8] This method is rather tedious, however, in its present form. It was felt that a computer program containing the ESI block might considerably speed up the calculations. In the ESI method the stoichiometric indices are also estimated together with the equilibrium constants in order to get a faster appreciation of the possible species present, using non-linear regression. This is done in the WSLET program described in this paper together with some examples of both experimental and simulated data. The program also contains a block for statistical analysis of the residuals, which is lacking in LETAGROP. A preliminary report of the program with examples has been reported elsewhere.[9]

THEORETICAL

The model

Consider the reaction

$$RX(s) + mH_2O(g) \rightleftharpoons RX(H_2O)_m(s) \quad (1)$$

Here RX stands for the ion exchanger in a certain salt form. The number of water molecules per ion exchanging group, W, is defined by

$$W_{exp} = [H_2O]_{iex}/s_0 \quad (2)$$

$[H_2O]_{iex}$ = Water sorbed by the ion exchanger.
s_0 = Ion exchange capacity of sample on the same concentration scale as $[H_2O]_{iex}$.

From equilibrium analysis

$$W_{calc} = \sum_1^n mk_m\alpha^m \Big/ \left(1 + \sum_1^n k_m\alpha^m\right) \quad (3)$$

n = number of species present.
k_m = equilibrium constant of reaction (1) for formation of $RX(H_2O)_m$.
$\alpha = \{H_2O\}$ = water activity.

Besides comparing W_{exp} with W_{calc} on a plot $W = f(\alpha)$ the distribution of the various hydrates is of interest.

Three different distribution functions can be recognized. The fraction of resin present in each hydrate, α_m, is defined by

$$\alpha_m = [RX(H_2O)_m]/s_0$$
$$= k_m\alpha^m \Big/ \left(1 + \sum_1^n k_m\alpha^m\right) = k_m\alpha^m/S \quad (4)$$

The fraction of unhydrated exchanger is given by $1/S$. The contribution of each hydrate to the maximal water uptake β_m (*i.e.*, for $\alpha = 1$ or the highest water activity reached) is given by

$$\beta_m = m\alpha_m \Big/ \sum m\alpha_m \quad (\alpha \to 1) \quad (5)$$

The contribution of each hydrate to the total water uptake at a given water activity, γ_m, is given by

$$\gamma_m = m\alpha_m \Big/ \sum m\alpha_m \quad (6)$$

The fractions α_m and γ_m are those used in equilibrium analysis.

The program

The program WSLET (Water Sorption data evaluation program using ABLET[13] searches for the combination of m- and k-values giving the best possible fit to the experimental isotherm

$$W = f(\alpha)$$

by searching for the minimum in the residual squares sum, U, defined by

$$U = \sum_1^n (W_{exp} - W_{calc})_i^2 \quad (7)$$

W_{calc} is computed from equation (3) with current m- and k-values.

The program is written in FORTRAN 77 for use on personal computers. From the many minimizing procedures available[10] the well-known pit-mapping approach[11] in the ABLET form[12] is used. This approach is described in detail elsewhere.[13] It has been modified for use on PCs. The structure of the program is similar to POLET[14] and other programs of the ABLET family.[13]

The simultaneous estimation of stoichiometric indices and equilibrium constants (ESI) was suggested earlier[14,15] and quite successfully applied in potentiometry,[11] spectrophotometry[16] and kinetics.[17] The parameters to be determined are k_1, m_1, k_2, m_2, *etc.*, and estimates of these quantities must be given in this order in the input. The minimization procedure can either be controlled by the operator or automatically by the program. Input data should be prepared as described in the manual.[18] The organization of data is similar to other programs of the ABLET family. (The manual and the program can be purchased from E.H. in Stockholm for 20 US dollars.)

Some statistical criteria

Before the program is applied to experimental and simulated data the criteria for the goodness of fit will be given. These criteria use statistical analysis of the residuals. Besides the residual squares sum, U, defined by equation (7) above they are:

$$\text{Residual mean} \quad |r| = \sum |r_i|/n \quad (8)$$

$$\text{Mean residual} \quad r_m = \sum r_i/n \quad (9)$$

$$\text{Variance} \quad m_{r,2} = \left(\sum r_i^2\right)\Big/n - \left[\left(\sum r_i\right)\Big/n\right]^2 \quad (10)$$

$$\text{Standard deviation} \quad s(W) = \sqrt{m_{r,2}} \quad (11)$$

The Hamilton R-factor in per cent, $R(\%)$, is defined by

$$R(\%) = 100\sqrt{\sum r_i^2 \Big/ \sum y_{exp}^2} \quad (12)$$

The summations in equations (8)–(12) are taken from $1 \to n$ as in equation (7). The weighting factors are set to unity.

In the following equations (7), (11) and (12) are used to illustrate the fit. Also other statistical parameters for a more detailed fitness test are available in the program: chi-square, kurtosis, skewness, *etc.*

EXAMPLES

Water sorption by Dowex 1 in fluoride form

Sosinovich *et al.*[7] studied among other systems the water uptake by Dowex 1 with 4% DVB in fluoride form. In Table 1 the results of the calculations are given. Run 1 gives the

Table 1. Results of the calculations with the data given in reference [7]

Run	k-values	Fitness test	Reference
1	$k_2 = 393$ $k_5 = 6960$ $k_{10} = 23200$ $k_{22} = 40000$ $k_{50} = 8000$	$U = 0.505$ $s(W) = \mp 0.205$ $R(\%) = 2.20$	7
2	$k_2 = 394 \mp 40$ $k_3 = 6084 \mp 303$ $k_{10} = (2.43 \mp 0.8)10^4$ $k_{22} = (3.29 \mp 0.14)10^4$ $k_{50} = 8517 \mp 316$	$U = 0.259$ $s(W) = \mp 0.147$ $R(\%) = 1.57$	This work
3	Species 2, 5, 10, 22, 59.1	$U = 0.187$	This work
4	$k_2 = 377 \mp 9$ $k_3 = 7063 \mp 67$ $k_{11} = (2.55 \mp 0.02)10^4$ $k_{22} = (3.29 \mp 0.03)10^4$ $k_{64} = 6134 \mp 51$	$U = 0.013$ $s(W) = \mp 0.032$ $R(\%) = 0.35$	This work

results orginally found. Run 2 shows that with the same species the fit can be improved. In an attempt to improve the model further the m-value of the highest hydrate, $m = 50$, was allowed to vary. The value found $m = 59.01 \mp 3.72$ again improved the fit as seen for run 3 in Table 1. Finally, all ten parameters were allowed to vary at the same time giving the m-values: 2.01, 5.11, 10.83, 21.57 and 63.54. These values were rounded off to 2, 5, 11, 22 and

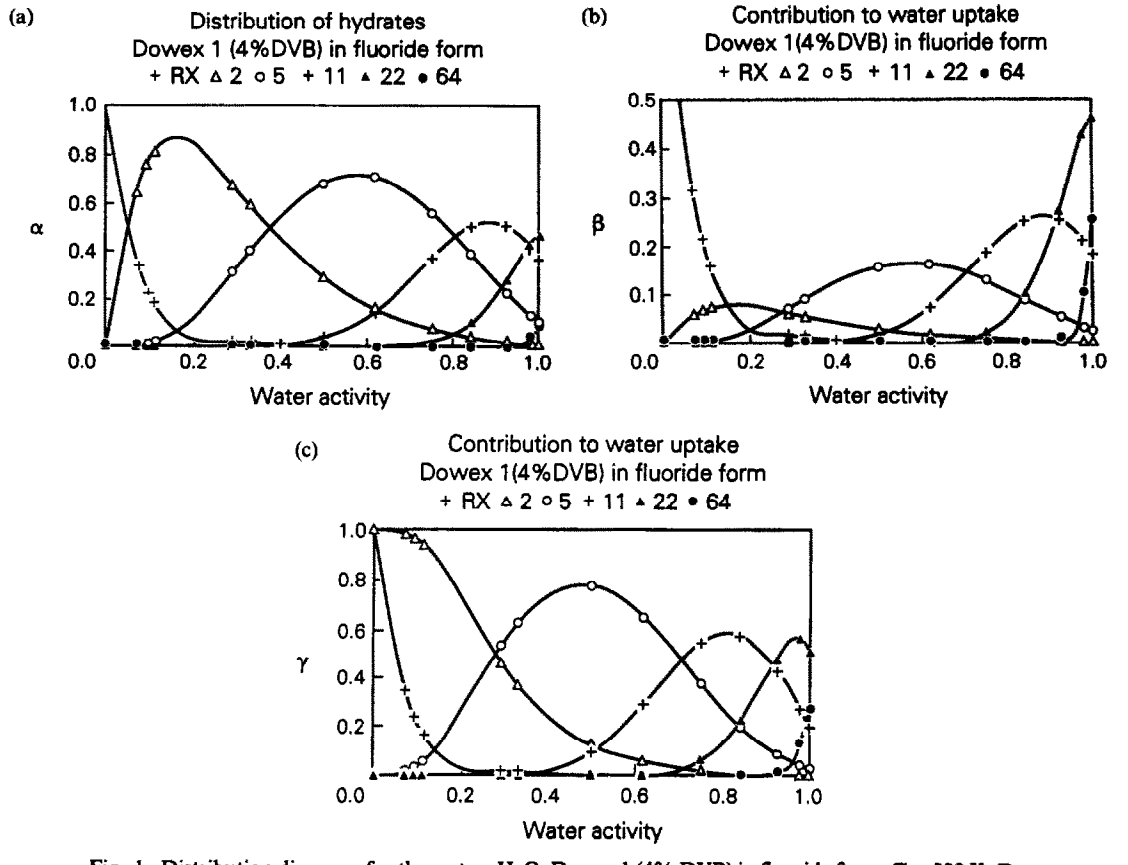

Fig. 1. Distribution diagrams for the system H_2O–Dowex 1 (4% DVB) in fluoride form, $T = 298$ K. Data from reference 7. (a) Distribution of the various hydrates in the resin: + $m = 0$, △ $m = 2$, ○ $m = 5$, + $m = 11$, ▲ $m = 22$, ● $m = 64$. (b) Contribution of hydrates to total water uptake: + $m = 0$, △ $m = 2$, ○ $m = 5$, + $m = 11$, ▲ $m = 22$, ● $m = 64$. (c) Contribution of hydrates to temporary water uptake: + $m = 0$, △ $m = 2$, ○ $m = 5$, + $m = 11$, ▲ $m = 22$, ● $m = 64$.

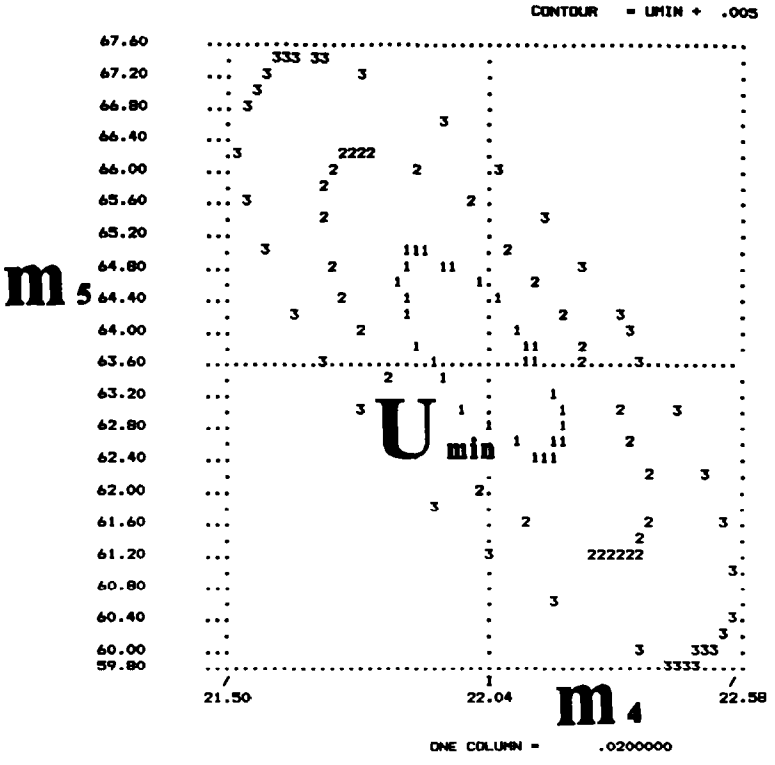

Fig. 2. Contour map for $U = f(m_4, m_5)$ and the system in Fig. 1, *i.e.*, for species with $m = 22$ and $m = 64$.

64 and the data recalculated giving the results for run 4 in Table 1. From this table it is evident that the standard deviation found is close to the experimental uncertainty ($\simeq \mp 0.03$). The three distribution diagrams corresponding to this model are shown in Figs. 1(a)–(c).

In Fig. 2 the contour map is given for U with variation of m-values around 22 and

Table 2. Results of calculations on the system RSO_4–H_2O resin Dowex 1 with 4% DVB. Data from reference 7

Run	k-values		Fitness test	Reference
1	$k_2 = 634$		$U = 0.237$	7
	$k_5 = 12100$		$s(W) = 0.140$	
	$k_{12} = 26600$		$R(\%) = 1.83$	
	$k_{30} = 16000$			
2	$k_2 = 642 \mp 60$		$U = 0.207$	This work
	$k_5 = (1.31 \mp 0.39)10^4$		$s(W) = 0.131$	
	$k_{12} = (2.68 \mp 0.13)10^4$		$R(\%) = 1.71$	
	$k_{30} = (1.69 \mp 0.13)10^4$			
3	$m_1 = 1.97 \mp 0.03$	$kn_1 = 739 \mp 33$	$U = 0.0503$	This work
	$m_2 = 5.41 \mp 0.04$	$kn_2 = (1.81 \mp 0.04)10^4$	$s(W) = 0.065$	
	$m_3 = 12.2 \mp 0.1$	$kn_3 = (2.28 \mp 0.07)10^4$	$R(\%) = 0.845$	
	$m_4 = 26.9 \mp 0.2$	$kn_4 = (2.34 \mp 0.03)10^4$		
4	$m_1 = 1.96 \mp 0.03$	$kn_1 = 736 \mp 35$	$U = 0.0531$	This work
	$m_2 = 5.00 \mp 0.06$	$kn_2 = 8706 \mp 231$		
	$m_3 = 5.95 \mp 0.09$	$kn_3 = (1.03 \mp 0.03)10^4$		
	$m_4 = 12.07 \mp 0.11$	$kn_4 = (2.27 \mp 0.08)10^4$		
	$m_5 = 26.85 \mp 0.16$	$kn_5 = (2.43 \mp 0.03)10^4$		
5	$k_2 = 775 \mp 50$		$U = 0.060$	This work
	$k_5 = 8654 \mp 1343$		$s(W) = 0.070$	
	$k_6 = (1.04 \mp 0.17)10^4$		$R(\%) = 0.919$	
	$k_{12} = (2.26 \mp 0.09)10^4$			
	$k_{27} = (2.43 \mp 0.03)10^4$			

64. The minimum is observed close to the integers.

Water sorption by Dowex 1 in sulphate form

Sosinovich *et al.*[7] also studied that the water sorption on Dowex 1 with 4% DVB in sulphate form. The results of these calculations are shown in Table 2. First in run no. 1 the model from ref. 7 is given. Run 2 gives the same model computed with WSLET. A better fit is found. In run 3 the same model is used but here also the m-values are allowed to vary. Values close to integers are found with the exception of $m = 5$, where the exact value is $m = 5.41 \mp 0.4$. The highest m changes from 30 to a value close to 27. The value $m = 5.4$ may be due to the presence of two hydrates. For that reason the model with m-values of 2, 5, 6, 12 and 27 was tried in run 4.

Table 3. Simulated data for formation of $RX(H_2O)_m$ with $k_2 = 393$, $k_5 = 6960$ and $k_{10} = 23200$; s (inst = ∓ 0.100)

i	$\alpha = \{H_2O\}$	W (accurate)	$\mp$Error	$= W$ (loaded)
1	0.070300	1.335132	−0.092452	1.242680
2	0.092000	1.574044	−0.000982	1.573062
3	0.110500	1.719960	+0.212395	1.932355
4	0.290000	2.859235	+0.007843	2.867078
5	0.330000	3.156407	−0.081685	3.074722
6	0.499700	4.448176	+0.033953	4.482129
7	0.618300	5.506893	+0.030009	5.536902
8	0.752800	6.871953	+0.054076	6.926029
9	0.842600	7.706212	−0.055153	7.651059
10	0.924800	8.324565	−0.071267	8.253298
11	0.980000	8.654253	+0.005594	8.659847
12	1.000000	8.757802	+0.118354	8.876156

Here also the m-values were allowed to vary giving values close to integers. The final model with m-values of 2, 5, 6, 12 and 27 is given in run 5. A considerable improvement from run 1 is obtained.

Table 4. Results of computation on simulated data

Run	s (inst)	Species and constants	U	$s(W)$	R, %
1	0.00001	$k_2 = 393.01 \mp 0.02$ $k_5 = 6960.17 \mp 0.25$ $k_{10} = 23200.76 \mp 0.75$	7.71×10^{-8}	8.45×10^{-5}	0.015
2	0.0001	$k_2 = 393.17 \mp 0.23$ $k_5 = 6962.2 \mp 2.6$ $k_{10} = 23210.1 + 7.5$	7.73×10^{-6}	8.4×10^{-4}	0.015
3	0.005	$k_2 = 393.9 \mp 1.2$ $k_5 = 6971 \mp 13$ $k_{10} = 23251 \mp 38$	1.93×10^{-4}	0.0042	0.073
4	0.010	$k_2 = 394.7 \mp 2.4$ $k_5 = 6982 \mp 26$ $k_{10} = 23303 \mp 76$	7.73×10^{-4}	0.0085	1.46
5	0.100	$k_2 = 411 \mp 25$ $k_5 = 7193 \mp 266$ $k_{10} = 24262 \mp 768$	0.0774	0.0829	1.46
6	0.100	$k_2 = 452 \mp 221$ $k_5 = (4.5 \mp 2.5)10^3$ $k_9 = (2.6 \mp 1.1)10^4$	0.9047	0.2746	4.73
7	0.100	$k_1 = (8.2 \mp 8.3)10^3$ $k_5 = (7.8 \mp 6.4)10^5$ $k_{10} = (2.2 \mp 1.6)10^6$	1.3895	0.3403	5.86
8	0.100	$k_2 = 244 \mp 108$ $k_4 = (4.5 \mp 1.8)10^3$ $k_{10} = (2.5 \mp 0.9)10^4$	0.7971	0.2577	4.44
9	0.100	$k_2 = 438 \mp 59$ $k_5 = (7.9) \mp 1.0)10^3$ $k_{10} = (2.6 \mp 0.3)10^4$ $k_{12} = (7.5 \mp 8.3)10^2$	0.09448	0.0887	1.53
10	0.100	$k_2 = 408 \mp 58$ $k_5 = (7.2 \mp 1.1)10^3$ $k_{10} = (2.4 \mp 0.4)10^4$ $k_{13} = 219 \mp 937$	0.08812	0.0857	1.48
11	0.100	$kn_1 = 501 \mp 23$ $m_1 = 2.18 \mp 0.03$ $kn_2 = (6.8 \mp 0.2)^3$ $m_2 = 5.20 \mp 0.05$ $kn_3 = (2.13 \mp 0.06)10^4$ $m_3 = 10.05 \mp 0.06$	0.0518	0.069	1.19

Search for model on simulated data

Water sorption data were simulated for a system with $m = 2$, 5 and 10 and constants $k = 393$, 6960 and 23,200. These values are close to those for the fluoride system discussed above. The theoretical values were loaded with noise, having the standard deviation s(inst), on various levels. Data for $s(\text{inst}) = \mp 0.01$ are given in Table 3.

Table 4 gives the results of the computation. First, in runs no. 1–5 the effect of experiment uncertainty is shown. The standard deviations of the k-values increase with increasing s(inst), but even for $s(\text{inst}) = \mp 0.10$ values close to the theoretical ones are obtained. For $s(\text{inst}) = \mp 0.10$, which is slightly higher than the experiment uncertainty in W, it is shown in runs 6–10 that false models give a poorer fit than the correct one for the same s(inst).

In runs 9 and 10 one additional false species with $m = 12$ and 13 have been added. As might have been expected the standard deviation for that species is much larger than the constant itself and should thus be excluded in an ordinary search. In run 11 the advantage of the direct search is demonstrated. The initial values for m were 1, 2, 3 or 2, 5, 15. After some cycles both gave m-values 2.2, 5.2 and 10.1, *i.e.*, the correct model after rounding off to the nearest integers. Thus, the correct model can be found rather direct. After rounding off to nearest integers the equilibrium constants of the model are computed.

CONCLUSIONS

The WSLET program makes it easy to search for the best possible model to a certain set of data. The calculations on simulated data show that false species are likely to be eliminated as long as the experiment uncertainty is not too high.

It is advisable to try m-values around those found by the ESI method in order to make certain the model arrived at is the best possible one under the circumstances. The model finds primary hydration species ($m < 10$) and secondary species ($m > 10$). That not all possible hydration numbers are to be expected is obviously due to the restrictions imposed by the three-dimensional network of the ion exchanger. Since a limited number of experimental points are available, the model arrived at can only be said to be the best possible with the experimental material available, using the fitness criteria mentioned above.

Acknowledgement—The financial support of the Swedish Technical Development Board, STU, is gratefully acknowledged.

REFERENCES

1. A. Kellomäki, *Acta Chem. Scand.* 1978, **A32**, 747.
2. *Idem., ibid.*, 1980, **A34**, 43.
3. V. S. Soldatov, V. I. Tsygankov, I. S. Elinson, A. A. Shunkevich and E. Högfeldt, to be published.
4. E. Högfeldt, *Nature* 1966, **210**, 941.
5. E. Högfeldt and F. Fredlund, *Arkiv Kemi*, 1971, **32**, 377.
6. E. Högfeldt, V. S. Soldatov and Z. I. Kuvaeva, *Chemica Scripta*, 1976, **10**, 210.
7. Z. I. Sosinovich, L. V. Novitskaya, V. S. Soldatov and E. Högfeldt, *Progress in Ion Exchange and Solvent Extraction*, Vol. 9, Chap. 5, pp. 303–338. Dekker, New York, 1985.
8. T. Zargarov, *Private communication*, Minsk, 1990.
9. J. Havel and E. Högfeldt, *Proc. CHEMOMETRICS II Conf.*, Brno, Czechoslovakia, September 3–6, 1990.
10. M. Meloun, J. Havel and E. Högfeldt, *Computation of Solution Equilibria, A Guide to Methods in Potentiometry, Extraction and Spectrophotometry*. Horwood, Chichester, 1988.
11. D. Dyrssen, N. Ingri and L. G. Sillén, *Acta Chem. Scand.*, 1961, **15**, 694.
12. M. Meloun and J. Čermák, *Talanta*, 1984, **31**, 947.
13. J. Havel and M. Meloun, *Computational Methods for the Calculation of Formation Constants*, D. J. Legget (ed.), pp. 221–290. Plenum Press, New York, 1985.
14. J. Havel and M. Meloun, *Talanta*, 1986, **33**, 525.
15. J. Havel and M. Vrchlabský, *EUROANALYSIS V*, Paper XVIII–20, 465. Cracow, Poland, Aug. 26–31, 1984.
16. M. Meloun, M. Javůrek and J. Havel, *Talanta*, 1986, **33**, 513.
17. J. Havel and J. L. González, *Kinet. Catal. Lett.*, 1989, **39**, 141.
18. J. Havel, *WSLET*, Program manual, KTH, Stockholm, 1990.

Talanta, Vol. 39, No. 5, pp. 523–527, 1992
Printed in Great Britain

0039-9140/92 $5.00 + 0.00
Pergamon Press plc

DETERMINATION OF URANIUM(VI) IN SEAWATER BY ION-EXCHANGER PHASE ABSORPTIOMETRY WITH ARSENAZO III

TOSHIO NAKASHIMA*
Department of Chemistry, Faculty of Education, Oita University, Dan-noharu 700, Oita 870-11, Japan

KAZUHISA YOSHIMURA
Chemistry Laboratory, College of General Education, Kyushu University, Ropponmatsu, Chuo-ku, Fukuoka 810, Japan

TOMITSUGU TAKETATSU
Kurume Institute of Technology, Kamitsu, Kurume 830, Japan

(*Received* 16 *July* 1991. *Revised* 1 *October* 1991. *Accepted* 2 *October* 1991)

Summary—An ion-exchange phase absorptiometric method with Arsenazo III has been developed for the determination of uranium(VI). A flow cell with 0.1 ml of anion exchange resin was employed to achieve a detection limit for uranium of 0.16 μg/l. in 100 ml of a seawater sample. The sensitivity is about 300 times higher than for corresponding solution spectrophotometry.

For the determination of uranium in seawater, it is usually necessary to separate and/or concentrate uranium from a solution containing large amounts of background electrolytes. Among a number of preconcentration techniques reported, methods using ion-exchange or chelating resins[1–8] have sometimes proven to be more effective. However, the uranium species sorbed on the solid phase has usually been eluted for succeeding measurement, leading to an undesirable dilution of the uranium.

Ion-exchanger phase absorptiometry,[9–12] based on the direct absorptiometric measurements of adsorbed analytes on ion exchange resins, has been conveniently used for the determination of trace amounts of components present in natural waters: this method does not need any such preconcentration and/or undesirable dilution by elution. Neodymium[11] and cobalt(II)[12] have been successfully determined recently by this method, the sensitivities being 260 and 1000 times higher than conventional solution spectrophotometries, respectively. In this study ion-exchanger phase absorptiometry has been applied to uranium determination using Arsenazo III as a colouring agent.[13] The present method is highly sensitive and directly applicable to uranium analysis of sea-water without any other means of preconcentration.

EXPERIMENTAL

Reagents

Analytical grade Bio-Rad AG 1-X2 anion exchange resin (100–200 mesh, Cl^- form) was used in the original wet state. EDTA solution ($2 \times 10^{-3} M$) was prepared by dissolving an appropriate amount of disodium salt of EDTA (Dojindo, Japan). Arsenazo III was purchased from Dojindo, Japan. All chemicals were of analytical grade.

Apparatus

The attenuances† of the ion exchanger were measured with a double-beam Nippon Bunko spectrophotometer, Model UVIDEC-320 and a perforated metal disc with an attenuance of 2.0 was used to balance the light intensities.

A small-volume flow cell was supplied by Nippon Quartz Glass Co. This cell was black-sided with a 0.5-cm path length and 0.035-ml

*Author for correspondence.

†In ion-exchanger phase absorptiometry, the contribution of light scattering in a measurement is considerable, so the term "attenuance" is preferable to "absorbance", although attenuance has essentially the same meaning as absorbance.

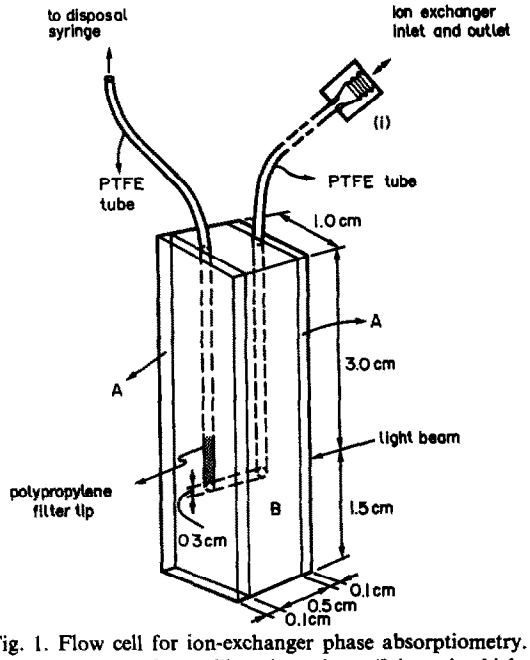

Fig. 1. Flow cell for ion-exchanger phase absorptiometry. Two transparent fused silica glass plates (0.1 cm in thickness), A, are pasted on both sides of black cell glass, B, of 0.5-cm thickness.

cell volume. The cell was fitted with a polypropylene filter tip, as shown in Fig. 1, to retain the ion exchange resin.

Procedure for the determination of uranium(VI) in seawater

To 100 ml of seawater sample, 1 ml of 0.5*M* formate buffer solution (pH 3.2), 2 ml of 0.002% Arsenazo III, 1 ml of $2 \times 10^{-3}M$ EDTA were added. Then, 0.10 ml of anion exchanger slurry was collected with suction in a fused-silica tube (0.15 cm i.d., 6.0 cm in length), fitted on one side with a polypropylene filter tip and connected with a disposable syringe [Fig. 2(A)], and then poured into the solution with a small amount of water. The mixture was stirred for 60 min at room temperature. After settling, the resin beads were collected in the fused-silica tube mentioned above and transferred to a flow cell with a syringe [Fig. 2(B)]. The attenuances at 665 and 800 nm were measured against air as reference. The difference in attenuances (ΔA) at 665 nm and 800 nm, was used for the determination of uranium by means of a calibration graph.

Distribution measurement

The pH of about 230 ml of a water sample containing 1.05×10^{-6} moles of uranium(VI), C_1, and 0.13 moles of sodium chloride was adjusted to 3.3 with formate. Then 5×10^{-6} moles of Arsenazo III and 2×10^{-6} moles of EDTA were added and the total solution volume was adjusted to 250 ml. After a short mixing period, 0.81 ml of Bio-Rad AG 1-X2 was added. After one hour equilibration, the solution and the ion-exchanger were separated and the attenuance, ΔA_1, of the ion-exchanger phase was measured. To the filtrate a further 0.81 ml of Bio-Rad AG 1-X2 was added and the solution was stirred for one hour. The exchanger attenuance, ΔA_2, was again measured and the distribution ratio, D, was calculated from

$$D = \frac{\text{mmoles of uranium sorbed per ml of exchanger}}{\text{mmoles of uranium per ml of solution}}$$

$$= \frac{(C_1 - C_1 \cdot \Delta A_2/\Delta A_1)/0.81}{(C_1 \cdot \Delta A_2/\Delta A_1)/250}$$

$$= 309(\Delta A_1/\Delta A_2 - 1) \qquad (1)$$

ΔA_1 and ΔA_2 were found to be 0.87 and 0.024, respectively, giving 1.1×10^4 as the value of the distribution ratio.

RESULTS AND DISCUSSION

Enhancement of sensitivity with a flow cell of small volume

For an ion-exchanger layer prepared with V ml of ion exchanger which was previously equilibrated with V' ml of solution containing a sample component at $C_o M$, the net absorbance, A, of the ion exchanger phase due to the sorbed coloured complex can be expressed as:

$$A = \varepsilon C_o \, l \, \frac{V'}{V} \, \frac{1}{1 + 1/VD} \qquad (2)$$

where ε and l are the molar absorptivity of the complex and the light path length in cm in the ion exchanger phase, respectively. The distribution ratio of the complex between the solid and solution phase is represented by D. This equation means that, if D is sufficiently large as in the case of the present system, higher sensitivity can be attained by using a large amount of sample volume and/or a small amount of ion exchanger within the limits of the resin capacity: the resin capacity measured by acid–base titration was 0.0554 ± 0.0003 meq for 0.1 ml of the ion exchanger aliquoted with the device mentioned below. Therefore, a small amount of ion exchanger slurry could increase

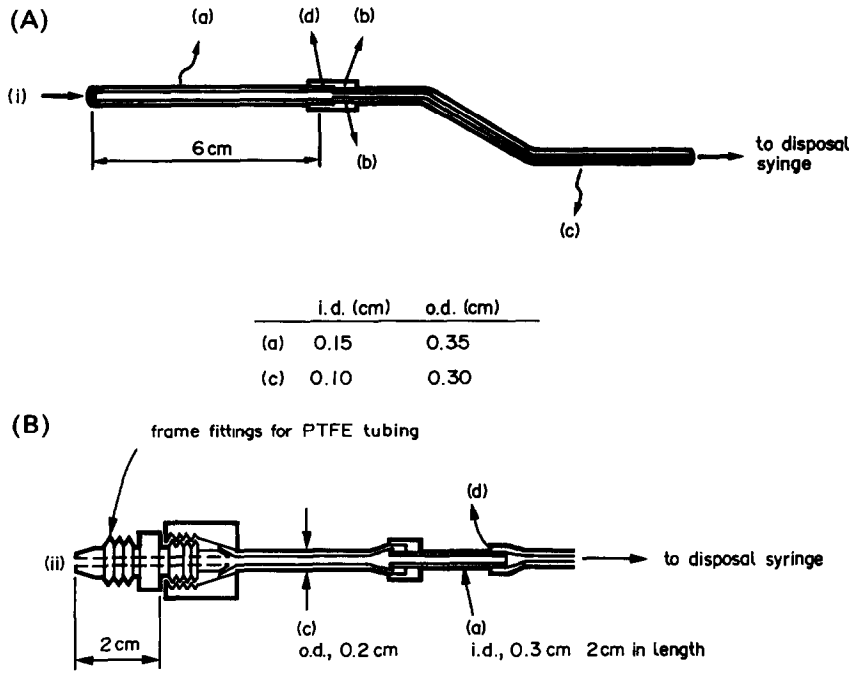

Fig. 2. Capillary fused silica tube; (A) for measuring a constant amount of ion-exchanger slurry; (B) for collecting colour-developed ion-exchanger beads; (a): fused silica tube; (b): silicone rubber tube; (c): PTFE tube; (d): polypropylene filter tip

the sensitivity if it could be handled reproducibly. To achieve this reproducibility, the fused-silica tube apparatus shown in Fig. 2(A) was designed. Ion exchanger was collected into the tube from the left (i) and water was discarded with a disposal syringe. The ion exchange resin could then be added to a sample with a small amount of water. After equilibration, the ion exchanger was collected from the inlet (ii) and then introduced into the flow cell by connecting the frame fitting [Fig. 2(B)] to nut (i) of the flow cell. The relative standard deviation of the resin amounts collected by using this resin aliquoting method was 0.5% for 6 repeated measurements.

Optimization of conditions

Absorption spectra in the anion exchanger. Arsenazo III forms a 1:1 complex with uranyl ion in the pH range 1.5–2.0 in an aqueous solution. The purplish red colour complex has a maximum absorption at about 650 nm with a molar absorptivity of 4.4×10^4 $l.mole^{-1}.cm^{-1}$ in the presence of a large excess of Arsenazo III.[13] This complex is easily sorbed on an anion exchanger, together with free Arsenazo III, because of its high anionic charge. Absorption spectra of the complex in an anion exchanger and solution are shown in Fig. 3. In order to make the contribution of free Arsenazo III low, the attenuance measurements of the complex in anion exchanger phase should be done at the longest wavelength possible. Therefore 665 nm was selected as the wavelength for the determination of uranium(VI).

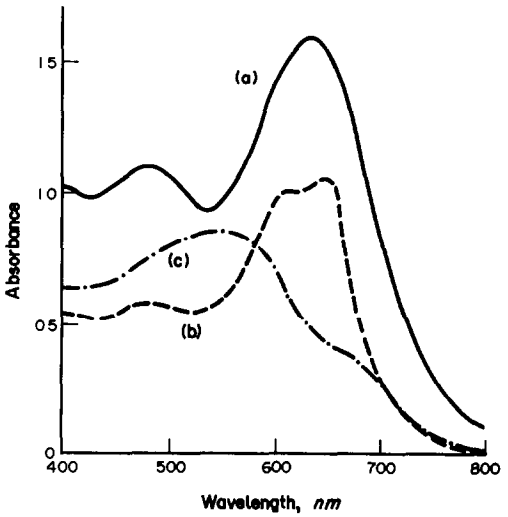

Fig. 3. Absorption spectra of uranium(VI)–Arsenazo III complex in anion exchanger and aqueous solution. (a) Spectrum in anion exchanger phase: U(VI): $5.25 \times 10^{-3}M$; Arsenazo III: $1 \times 10^{-3}M$; resin: 0.80 g; solution volume: 250 ml, pH 3.3. (b) Spectrum in solution: U(VI): 5.25×10^{-5}mM; Arsenazo III: 1.0×10^{-5} mM; pH 3.3. (c) Spectrum in anion exchanger phase (Arsenazo III in excess): U(VI): 5 μg; Arsenazo III: 1.3×10^{-4} mmoles; resin: 0.10 g; solution volume: 250 ml; pH 3.3.

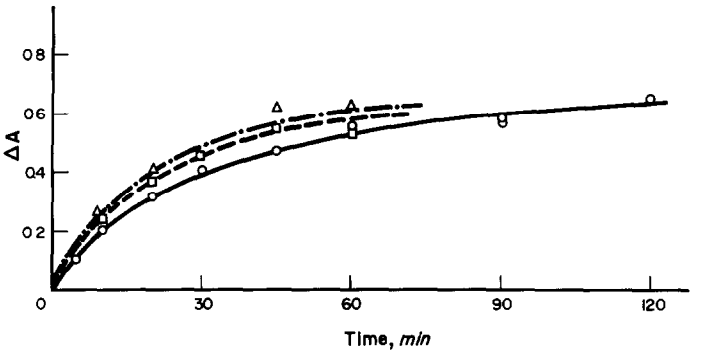

Fig. 4. Effect of colour development on stirring time. Sample: 100 ml, pH 3.2, 0.25 μg U(VI), 0.05 moles of NaCl; resin: 0.10 ml; cell length: 0.5 cm. —○—○— 20°; --□--□-- 40°; —-△—-△—- 56°.

Stirring time and temperature dependence. The dependence of colour development on stirring time at different temperatures is shown in Fig. 4. Attenuance reached a constant value within one hour of stirring and colour development did not accelerate appreciably at higher temperatures. Accordingly, the solution-ion exchanger mixture was stirred for one hour at room temperature. The distribution ratio of the complex was 1.1×10^4, and 92% of the uranium in the sample solution could be recovered.

pH Dependence of colour development in anion exchanger. The UO_2–Arsenazo III complex is strongly sorbed on an anion-exchanger in the pH range 2.5–5.0. Free Arsenazo III is also sorbed in this pH range but the reagent has a low constant absorption at 655 nm, as shown in Fig. 5. Therefore the pH of the sample solution was adjusted to 3–4.

Dependence on sodium chloride concentration. The effect of sodium chloride concentration on colour development is shown in Fig. 6. ΔA gradually increased with sodium chloride concentration up to 0.4*M* and reached a constant value at 0.6*M*, while ΔA for the reagent blank is almost constant at 0.25. The apparent ΔA increase may be due to contraction of the ion-exchanger and the same phenomenon was

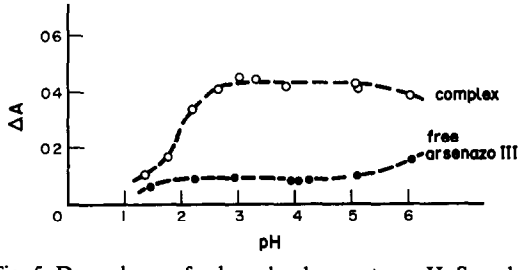

Fig. 5. Dependence of colour development on pH. Sample: 40 ml, pH 3.2, 0.8 μg U(VI), 2.1×10^{-8} moles of Arsenazo III; resin: 0.10 ml; stirring time: 30 min; cell length: 0.5 cm.

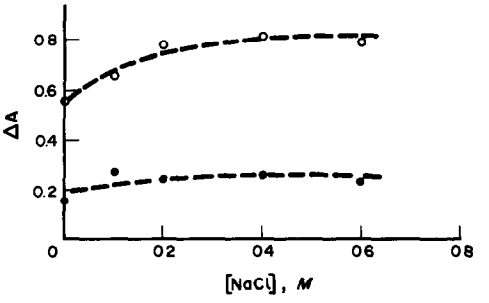

Fig. 6. Effect of sodium chloride concentration. Sample: 40 ml, pH 3.2, 0.4 μg U(VI), 2.1×10^{-8} moles of Arsenazo III; resin: 0.10 ml; stirring time: 60 min; cell length: 0.5 cm. ○---○; ΔA for sample. ●---●; ΔA for reagent blank.

observed in the determination of cobalt by ion-exchanger phase absorptiometry.[12] Consequently, uranium in seawater may be conveniently analysed without dilution of the salt matrix because sensitivity at 0.6*M* sodium chloride concentration is 40% higher than that in the absence of sodium chloride.

Table 1. Effects of foreign ions on the determination of uranium(VI)

Type	Foreign ion amount, *mg/l.*	A*	U found, *μg/l.*	Relative error, %
Mg	1300	0.556	10.2	+2
Ca	1100	0.535	9.8	−2
Fe(III)	1	0.536	9.8	−2
	10	0.029	0.5	−95
La(III)	0.01	0.467	6.7	−33
Th(IV)	0.01	0.562	10.3	+3
EDTA	7.5×10^{-5}†	0.544	10.0	0
	5.0×10^{-4}†	0.551	10.0	0
	1.0×10^{-3}†	0.575	10.5	+5

Solution: 100 ml, 1 μg U(VI), pH 3.2 (formate, 5.2×10^{-8} moles of Arsenazo III, 0.055 moles of NaCl; Resin, Bio-Rad AG 1-X2 (Cl^- form, 100–200 mesh), 0.1 ml; Stirring time, 60 min.

*$A = \Delta A - \Delta A$ (for the blank). †*M*.

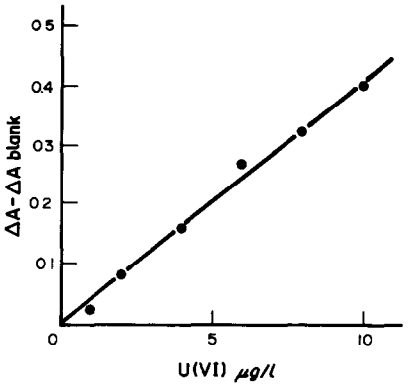

Fig. 7. Calibration curve for the determination of U(VI). Sample: 100 ml, pH 3.2, 0.05 moles of NaCl, 2.1×10^{-8} moles of Arsenazo III; resin: 0.10 ml; stirring time: 60 min; cell length: 0.5 cm.

Effect of foreign ions

Table 1 shows the effect of foreign ions on the determination of uranium. Below the concentration levels present in the seawater no heavy metals except uranium(VI) can complex with Arsenazo III in these experimental conditions, therefore no coexisting ions interfered. All the sample solutions contained $2 \times 10^{-5}M$ EDTA in order to mask foreign ions such as iron(III) present in seawater. Further increase in EDTA concentration at least up to $5.0 \times 10^{-4}M$ did not interfere with the uranium determination. Therefore this procedure may also be applied to other solution systems which contain foreign ions up to $5 \times 10^{-4}M$.

Calibration curve

A calibration curve for uranium(VI) is shown in Fig. 7. The linearity holds up to 10 μg/l. of uranium, but the curve became convex at more than 10 μg/l. of uranium(VI).

Sensitivity and detection limit

The uranium concentrations giving a final absorbance of 0.1 were $7.7 \times 10^{-9}M$ for the present method and $2.3 \times 10^{-6}M$ for conventional solution absorptiometry,[13] corresponding to about 300 times enhancement by the present method.

The detection limit was measured in a matrix of a 100-ml blank solution containing 0.055 moles of sodium chloride. For 6 determinations, ΔA was 0.315 ± 0.004. The detection limit (the concentration corresponding to an attenuance equal to twice the magnitude of the error) was 0.29 μg/l.

Table 2. The standard addition method for determination of uranium(VI) in sea water

U(VI) added, μg	0	0	0.63	1.25	1.88
A*	0.185	0.160	0.302	0.410	0.565
U(VI) found, μg	0.96	0.75	1.44	2.10	2.80

Sample volume: 100 ml. Resin: 0.10 ml.
*$A = \Delta A - \Delta A$ (for the blank).

Determination of uranium(VI) in seawater

Seawater samples were analysed by the standard-addition method in order to check the recovery of added uranium. As shown in Table 2, the recovery of the spiked uranium was quantitative. In coastal seawater from Mitoma, Fukuoka (open sea), the uranium content was found to be 3.5 ± 0.3 μg/l. The content was in accord with those reported previously.[3,4]

Recently, ion-exchanger phase absorptiometry has been extended to flow analysis.[14,15] Using this method, trace levels of a target element can be determined in water only in fairly small volumes. However, the present system could not be applied to flow analysis, because the uranium–Arsenazo III complex is difficult to be desorbed from the ion exchanger.

REFERENCES

1. J. Korkisch and I. Steffan, *Anal. Chim. Acta*, 1975, **77**, 312.
2. R. J. N. Brits and M. C. B. Smit, *Anal. Chem.*, 1977, **49**, 67.
3. R. Kuroda, K. Oguma, N. Mukai and M. Iwamoto, *Talanta*, 1987, **34**, 433.
4. R. Kuroda, Y. Hayashibe, K. Oguma and K. Kurosu, *Z. Anal. Chem.*, 1989, **335**, 404.
5. E. S. Gladney, R. J. Peters and D. R. Perrin, *Anal. Chem.*, 1983, **55**, 976.
6. A. A. Prange, A. Knochel and W. Michaelis, *Anal. Chim. Acta*, 1985, **172**, 79.
7. K. H. Lieser and B. Gleitsmann, *Z. Anal. Chem.*, 1982, **313**, 289.
8. M. Ochsenkuhn-Petropulu and G. Parissakis, *ibid.*, 1985, **321**, 581.
9. K. Yoshimura, H. Waki and S. Ohashi, *Talanta*, 1976, **23**, 449.
10. K. Yoshimura and H. Waki, *ibid.*, 1985, **32**, 345.
11. K. Yoshimura and T. Teketatsu, *Z. Anal. Chem.*, 1987, **328**, 553.
12. T. Nakashima, K. Yoshimura and H. Waki, *Talanta*, 1990, **37**, 735.
13. H. Onishi and Y. Toita, *Bunseki Kagaku*, 1969, **18**, 592.
14. K. Yoshimura, *Anal. Chem.*, 1987, **59**, 2922.
15. K. Yoshimura, S. Nawata and G. Kura, *Analyst*, 1990, **115**, 843.

Talanta, Vol. 39, No. 5, pp. 529–534, 1992
Printed in Great Britain.

0039-9140/92 $5.00 + 0.00

ON THE STABILIZATION OF NIOBIUM(V) SOLUTIONS BY ZIRCONIUM(IV) AND HAFNIUM(IV)

E. SØRENSEN and A. B. BJERRE
Risø National Laboratory, DK-4000 Roskilde, Denmark

(*Received* 12 *November* 1990. *Revised* 27 *September* 1991. *Accepted* 2 *October* 1991)

Summary—Niobium cannot be separated from zirconium or hafnium when these elements occur together in solution with common anions such as chloride and sulphate. This is ascribed to the co-polymerization of niobium(V) and the hydrolysed ionic species of zirconium(IV) and hafnium(IV) to form colloidal particles. In hydrochloric acid the particles are positively charged, whereas in sulphate solution the Zr- and Hf-sulphate complexes confer a negative charge. The two cases are considered separately.

During some work on recovery of zirconium and niobium from a complex zirconium ore, a crucial point was the separation of these elements. This was accomplished by means of solvent extraction,[1] but only after we had studied the classical precipitation method based on hydrolysis of the niobium. Weiss and Landecker[2] stated that the precipitation is complete from perchloric acid solution, and Silverman[3] used this principle for determining niobium in steel. However, we have found that in the presence of certain elements such as titanium and zirconium, the expected reaction does not take place at all.

Marignac[4] has shown that on hydrolysis of a solution containing niobium and titanium, some niobium remains in solution and some titanium is precipitated. This effect has been termed "loss of individuality".

Schoeller[5] mentions that zirconium may prevent the precipitation of Nb_2O_5.aq, and Chekmarev *et al.*[6] conclude from extraction data that niobium and hydrolysed zirconium probably form mixed-metal compounds in solution.

As the information available seems rather vague we have investigated the relationship between zirconium and niobium in solution. The chemical similarity between zirconium and hafnium made it natural to include the latter in the investigation, and it was then possible to use radioactive ^{181}Hf as a tracer (zirconium has no radioactive isotopes convenient for the purpose). During the work we found a marked difference in behaviour between the systems in chloride and sulphate media. Consequently the two cases were examined separately.

Since the above-mentioned Zr–Nb ore also contained tantalum, which is even more inclined than niobium to hydrolyse, the behaviour of tantalum was also considered.

EXPERIMENTAL

Preparation of solutions

Nb in hydrochloric acid. $KNbO_3$ (1 g) was dissolved in 10 ml of water, and the solution was poured slowly, with vigorous stirring, into a beaker containing 20 ml of concentrated hydrochloric acid. The mixture was heated to boiling, then water was added until the solution was completely clear (about 30 ml was needed). This solution was transferred to a Visking dialysis tube and allowed to dialyse against a large volume of 0.2*M* hydrochloric acid. After 24 hr, a clear solution of $(Nb_2O_5.nH_2O)_x$ remained in the tube.

Nb in sodium hydrogen sulphate solution. Nb_2O_5 (0.2 g) was fused with 20 g of sodium hydrogen sulphate in a silica crucible. After the crucible had cooled to about 50°, a few ml of saturated sodium hydrogen sulphate solution were added, followed by small additions of water with stirring and heating until all was dissolved. The resulting solution was clear and nearly saturated with sodium hydrogen sulphate.

Turbidimetry

The absorbance of the solutions gave a reproducible measure of their stage of polymerization. With a Zeiss spectrophotometer, the absorbance was measured in 1-cm cells at 400 nm.

Methods of separation

Dialysis. The Visking dialysis tube (Union Carbide) is made from cellulose. A 1/2-in. bore tube with 24-Å pores was used. A practically stationary state of dialysis was reached after 3 days. The 24-Å pores retain particles with M.W. larger than $\sim 10^4$.

Precipitation. Hydrosols are often coagulated by addition of organic solvents such as alcohol or acetone. This applies to the solution of Nb_2O_5 in hydrochloric acid. $ZrOCl_2$ and $HfOCl_2$, in the concentration range used, are still fully soluble after addition of acetone in 2:1 v/v ratio to the aqueous solution, so this offers a method for their separation from the polymers. The sulphates of zirconium and hafnium are only slightly soluble in acetone–water mixture, so for the sulphate system this method is of no avail.

Analysis

Tagging with the radioactive isotopes ^{95}Nb and ^{181}Hf allowed us to determine the distribution of these elements by gamma-counting with a well-type NaI crystal. The precipitates were ignited and weighed, and with knowledge of the amount of starting material, it was possible to calculate the composition of the products obtained.

RESULTS AND DISCUSSION

Behaviour of niobium in hydrochloric acid

Measurement of stability by turbidimetry. First the stability of pure niobium solutions in dilute acid was established. The experimental solution, which at room temperature remains clear for weeks, was heated at 95° with various concentrations of hydrochloric acid. The degree of stability was measured by the time elapsed before turbidity just became visible. The results shown in Table 1 agree reasonably well with the finding by Nabivanets[7] that $Nb_2O_4^{2+}$ ions tend to polymerize at hydrogen-ion concentrations below 2*M*.

Table 1. Time elapsed before turbidity is just visible in 0.03 *M* Nb_2O_5 solutions at 95°

[HC], *M*	Min
0.5	5
1.0	15
1.5	90
2.5	200

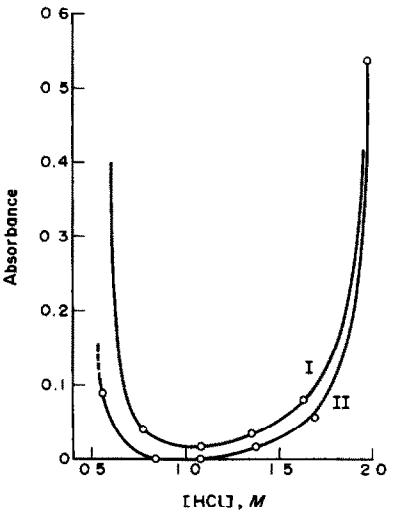

Fig. 1. Absorbance of solutions of Nb(V) and Zr(IV), 0.028*M* in Nb, in varying concentrations of hydrochloric acid after heating at 95° for 6 hr. The respective unheated solutions were used for reference. Curve I corresponds to the atomic ratio Zr/Nb = 0.50. Curve II corresponds to the atomic ratio Zr/Nb = 0.62.

If $ZrOCl_2$ or $HfOCl_2$ was added to the niobium solution before this was heated, the stability was greatly changed. Solutions were prepared with various acidities and two different ratios of [Zr] or [Hf] to [Nb]. The solutions were heated for 6 hr at 95°, then the absorbances were measured. The results seen in Figs. 1 and 2 show that the solutions stay clear over an acidity range which becomes wider the greater the [Zr]/[Nb] ratio. The effect is similar with hafnium, but the stability range is somewhat narrower.

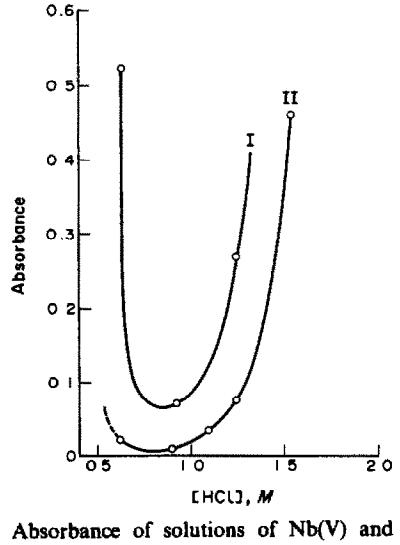

Fig. 2. Absorbance of solutions of Nb(V) and Hf(IV), 0.0275*M* in Nb, in conditions similar to those for Fig. 1. Curve I, Hf/Nb = 0.50. Curve II, Hf/Nb = 0.62.

At the upper acidity limit the solutions are turbid but fairly stable; at the lower limit the colloidal particles coagulate. The precipitate contains Zr or Hf ions even though these are normally completely soluble at the relevant acid concentration.

The hypothesis that hydrolysed species of Zr(IV) and Hf(IV) co-polymerize with Nb(V) is supported by the following experiments.

Separation of the polymers by dialysis. Some $HfOCl_2$ containing radioactive ^{181}Hf was mixed with Nb_2O_5 solution to give an atomic Hf/Nb ratio of 0.35 (6.5 g/l. HfO_2, 11.7 g/l. Nb_2O_5). This low ratio was chosen in order to make the effect of co-polymerization more perceptible. The hydrochloric acid concentration was 1.7*M*. Portions were subjected to four different treatments.

(1) No heating.
(2) Heating to 95° within 3 min, then cooling to 25° in 1 min.
(3) Rapid heating to 95° and keeping at 95° for 36 min followed by fast cooling.
(4) Like (3) but keeping at 95° for 60 min.

The samples were then placed in Visking tubes and dialysed for 3 days against an equal volume of pure 1.7*M* hydrochloric acid. The ratio of [Hf] inside the tube to that outside ($[Hf]_{in}$:$[Hf]_{out}$) was then determined for each sample, by gamma counting (see Table 2).

Hafnium ions pass freely through the Visking membrane, as shown by the 1:1 distribution ratio found for the unheated sample. After heating at 95° the hafnium is more or less retained within the dialysis tube, depending on the duration of heating. This retention is ascribed to an association with the colloidal particles of Nb_2O_5.aq. Assuming the concentration of free hafnium ions on both sides of the membrane will be the same, and remembering that the volumes are equal, we find that the fraction of hafnium associated with the colloidal particles is given by

$$\frac{[Hf]_{in} - [Hf]_{out}}{[Hf]_{in} + [Hf]_{out}}$$

(see right-hand column, Table 2).

Table 2. Equilibrium ratio of [Hf] in the inner and outer liquid after dialysis of differently treated mixtures with Nb_2O_5 in hydrochloric acid solution

Treatment	$[Hf]_{in}/[Hf]_{out}$	Per cent of Hf trapped
No heating	1.0	0
Heating to 95° within 3 min, followed by cooling to 25° in 1 min	1.3	13
Heating at 95° for 36 min	2.9	49
Heating at 95° for 60 min	5.0	67

Precipitation of the polymer by addition of acetone. Some $HfOCl_2$ containing ^{181}Hf was mixed with Nb_2O_5 solution to give an atomic ratio of Hf to Nb of 0.4 (4.2 g/l. HfO_2, 6.6 g/l. Nb_2O_5). The hydrochloric acid concentration was 0.85*M*. The mixture was heated to 95° and samples were taken after 10, 34 and 60 min. Each sample was added to twice its volume of acetone; the precipitates were collected and analysed, with the results shown in Table 3.

In an analogous experiment, solutions with the same Nb_2O_5 content but different Hf/Nb ratios were all heated to 95° for 60 min before precipitation by addition of the acetone. The compositions of the precipitates are shown in Table 4.

There is indication that for a given time of heating the Hf/Nb ratio in the precipitate approaches that of the solution when the Hf-level is diminished, as seen also from Table 3, but the absolute amount of precipitate decreases with increasing initial ratio of Hf to Nb.

General properties of the polymer. Both the silky residue left by gentle evaporation of a dilute hydrochloric acid solution containing Nb(V) and Zr(IV), and the coagulated solid obtained by addition of acetone, can be redissolved in water. When ammonia is added

Table 3. Compositions of acetone precipitates from Hf-containing Nb_2O_5 solutions in hydrochloric acid which have been heated for different periods

Time of heating at 95°, *min*	Nb and Hf in acetone precipitate: Weight, *mg*		Per cent of initial amount in solution		Atomic ratio Hf/Nb in ppte.
	Nb_2O_5	HfO_2	Nb_2O_5	HfO_2	
10	6.87	1.13	50	13	0.104
34	10.92	4.68	80	54	0.271
60	11.94	7.36	87	85	0.391

Table 4. Compositions of acetone precipitates from Hf-containing Nb_2O_5 solutions of varying Hf/Nb ratio, all heated to 95° for 60 min

Nb and Hf in initial solution			Nb and Hf in acetone precipitate				
			Weight, *mg*		Per cent of initial amount in solution		
Nb_2O_5, *mg*	HfO_2, *mg*	Atomic ratio Hf/Nb	Nb_2O_5	HfO_2	Nb_2O_5	HfO_2	Atomic ratio Hf/Nb in ppte.
48	39	0.51	38.8	23.4	81	60	0.38
48	52	0.68	31.5	22.4	66	43	0.45
47	65	0.87	18.4	17.5	39	27	0.60

to the solution a "hydroxide" is formed, which can be redissolved with hydrochloric acid. Electromigration experiments confirmed that the niobium was contained in positively charged particles.

Discussion. It has been demonstrated that in niobium solutions with hydrochloric acid concentrations of less than 2*M*, hydrolytic polymerization proceeds until turbidity or eventually a precipitate is produced. The inhibitory effect of ZrO^{2+} or HfO^{2+}* is assumed to be due to a reaction of the type

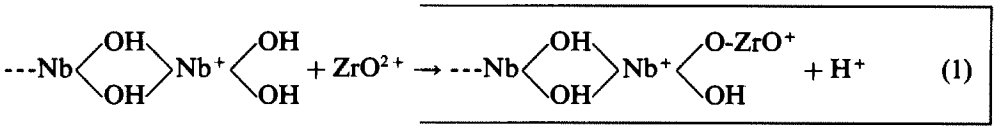

(1)

by which the colloidal particles are studded with ZrO^+ or HfO^+. The resulting increase in charge density leads to stabilization of the sol.

The precipitate formed by addition of excess of ammonia is soluble in hydrochloric acid, indicating that most of the bonds are similar to those occurring in the zirconium or hafnium hydroxides.

The upper and the lower acidity limits of the stability interval in Figs. 1 and 2 are set by decreasing charge on the colloidal particles, but for different reasons. High $[H^+]$ leads to a gradual rupture of the —O— bridges, whereby ZrO^{2+} or HfO^{2+} is split off.

The solution becomes more and more turbid, but remains fairly stable. At low $[H^+]$ the positive charges are neutralized by hydrolysis, and coagulation occurs within a narrow range of $[H^+]$. Since the coagulated material cannot be redissolved in acids, it is assumed to be a polymer of Nb_2O_5.aq. The co-precipitated Zr and Hf are trapped in the structure by occlusion and are thus also made insoluble. Comparison of Figs. 1 and 2 shows that the stability interval of the Hf compounds is shifted towards lower $[H^+]$, in accordance with the slightly more electropositive character of Hf.

The results of the dialysis experiment, shown in Table 2, confirm that the HfO^{2+} ions are caught by the colloidal particles, and further show that the process continues for more than 60 min at 95°. This is confirmed by the precipitation experiment (Table 3). Here the sorting of particles by size is brought about by the acetone–water solvent. The amount of Nb precipitated is seen to increase with heating time, which suggests that the particles grow during the heating period. Table 4 shows that a higher Hf/Nb ratio leads to a smaller amount of Nb being precipitated. This indicates more efficient coverage of the larger surface area presented by the smaller particles.

Behaviour of niobium in sodium hydrogen sulphate solution

Stabilization of niobium solution by precipitation of hydroxide and redissolution. If the $NaHSO_4$-saturated solution of Nb is diluted, it polymerizes immediately. Simple addition of zirconium or hafnium salts will not prevent this polymerization. If, however, $ZrOCl_2$ or $HfOCl_2$ is mixed with the $NaHSO_4$-saturated Nb solution and the mixture is poured into an excess of ammonia solution, then the precipitate formed can be dissolved in sulphuric acid to form a stable solution. The same behaviour is obtained if Nb_2O_5 and ZrO_2 are fused with sodium hydrogen sulphate and the cooled melt is dissolved.

The solution of Nb_2O_5 in sodium hydrogen sulphate was divided into eight equal samples to which were added varied amounts of $ZrOCl_2$ or $HfOCl_2$. After homogenization of the mixtures, ammonia solution was added to each, and the

*The symbols ZrO^{2+} and HfO^{2+} are used for convenience to designate the more complex positive ions that actually occur.

resulting precipitates were collected, washed, and redissolved in 2 ml of 2*M* sulphuric acid. Finally 2 ml of 2*M* sodium sulphate were added, and water to give a final volume of 8 ml.

After heating of these mixtures at 95° for 6 hr it appeared that stabilization was obtained for Zr/Nb > 3 and Hf/Nb > 2. Figure 3 shows the plot of absorbance *vs.* Zr/Nb and Hf/Nb.

Separation of the polymer by dialysis. Excess of sulphate, (Hf, Zr)O^{2+} and H^+ can be removed by dialysis. If this is done stepwise, alternated with heating periods, stable solutions are obtained up to approximately pH 1.8, the highest value at which a solution of zirconium sulphate remains clear.[8]

These solutions of pure colloidal Nb and Zr or Nb and Hf sulphate will coagulate on addition of only a slight amount of free H^+ unless the sulphate concentration is simultaneously increased. It appears that in the case of Zr the ratio $[H^+]/[SO_4^{2-}]$ must be less than 1.2, and in the case of Hf less than 1.0 if the solutions are to stay clear for 6 hr at 95°.

General properties of the polymer. Evaporation at room temperature leaves a clear glass that breaks into scales with a conchoidal fracture. The glass redissolves easily in water, from which it may again be precipitated by addition of acetone. This property is not as useful as in the chloride case, since zirconium sulphate, and sulphates in general, are also precipitated from aqueous solutions by acetone. Electromigration shows that the colloidal particles are negatively charged.

Discussion. The positively charged $[Nb_mZr_n(OH)_x(H_2O)_y]^{5m+4n-x}$ particles will, on addition of sulphate, form negatively charged sulphate complexes, and the presence at the same time of positively charged particles leads to coagulation. Therefore a particular method of preparation must be employed.

In the concentrated sodium hydrogen sulphate solution, Nb and Zr or Hf ions are prevented from coming into close contact by the complexing sulphate ligands. On dilution, Nb will hydrolyse first and polymerize without being protected by Zr or Hf. When excess of ammonia is added, co-polymerization becomes possible. When the redissolved precipitate is aged at suitable concentrations of H^+ and SO_4^{2-} a co-polymerized Zr or Hf sulphate is formed, which presumably surrounds the Nb_2O_5 particles.

Since aggregation is prevented by maintaining a negative charge on the particles, it is evident that sulphate ions act as a stabilizer, whereas hydrogen ions have the reverse effect.

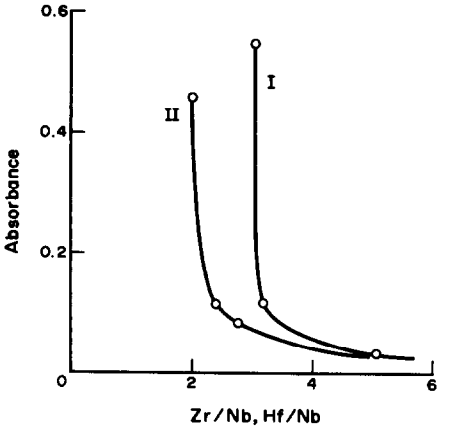

Fig. 3. I, Absorbance of sulphate solutions of Nb(V) and Zr(IV), 0.0235*M* in Nb, at pH = 1.8, at varying values of the atomic ratio of Zr to Nb. II, Absorbance of solutions of the corresponding Hf compound.

A higher sulphate concentration is required in the case of Hf, probably because the stability constant of hafnium sulphate is lower than that of zirconium sulphate. On the other hand, there seems to be no obvious reason for the marked difference between the atomic ratios Zr/Nb and Hf/Nb that are just sufficient to stabilize the respective solutions (Fig. 3).

Behaviour of niobium in carbonate solutions

It is well known that ZrO^{2+} forms soluble carbonate complexes. This is also true for the Zr–Nb compounds, although they are less stable and can be prepared only with a limited yield.

Samples (20 ml) from the chloride and sulphate solutions, each containing 10 mg of Nb_2O_5 and 100 mg of ZrO_2, were added to 20 ml of 1*M* sodium carbonate. In the chloride solution, a precipitate was seen immediately, and in the sulphate solution, after a few seconds. The same experiments with 20 ml of ammonium bicarbonate solution yielded a precipitate from the chloride solution after 1 hr, but not before 24 hr from the sulphate system. Tagging with radioactive ^{95}Nb made it simple to determine the niobium distribution after precipitation. Table 5 shows that in all cases a considerable fraction of the niobium remained in the solution.

Table 5. Percentage of Nb left in solution after precipitation with the reagents quoted, and standing for 24 hr

	Fraction of original Nb in solution, %	
Anion	Sodium carbonate	Ammonium bicarbonate
Cl^-	15	32
SO_4^{2-}	36	50

Discussion. The failure to precipitate Nb by carbonate, a reaction which is otherwise complete even in the presence of complexing agents, appears to give strong evidence for a masking effect exerted by ZrO^{2+} on colloidal Nb_2O_5.

The transformation into the carbonate form takes place more completely when the particles are negatively charged beforehand, as in the sulphate solution. Further, the solubility is higher in ammonium bicarbonate solution than in sodium carbonate solution because of the lower hydroxide concentration.

Tantalum compounds

An attempt was made to prepare solutions of Ta stabilized with Zr analogously to those of Nb, but they always appeared to be turbid, probably because Ta has a greater tendency to hydrolyse than Nb. However, with Ta, Nb and Zr in atomic ratio 0.2:1:5 clear stable solutions can be obtained both in dilute hydrochloric acid and sulphate media.

The oxides are fused with sodium hydrogen sulphate and the cooled melt is dissolved as described above for the preparation of solutions in sodium hydrogen sulphate. Conversion into the chloride form is accomplished by precipitation with ammonia solution, collection, and then addition of just enough hydrochloric acid to dissolve the precipitate.

It has been known for a long time[5] that in mixtures of Nb and Ta a certain amount of one of these elements can be masked by the other. Lassner and Püschel[9] indicate the following scheme for formation of a heteropolymer:

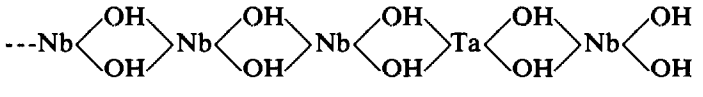

An increase in the proportion of Ta leads to turbid solutions. It may be expected that colloidal particles of the composition shown require a higher ZrO^{2+} concentration to prevent more extensive polymerization than do those of pure Nb_2O_5.aq.

CONCLUSIONS

In solutions containing weakly complexing anions, Nb_2O_5.aq adsorbs ionic species of Zr(IV) and Hf(IV). As a result, the niobium species are stabilized and to a certain extent assume the behaviour of Zr and Hf compounds in an $[H^+]$-domain where they would otherwise undergo hydrolytic precipitation. In the presence of sulphate, complex formation causes a negative charge on the particles; for this reason the solution is sensitive to H^+ unless it is stabilized by an excess of SO_4^{2-}.

The higher the Zr/Nb ratio, the more Nb loses its chemical individuality; thus it becomes able to behave like Zr in carbonate solution and in phase distribution equilibria (solvent extraction).

Tantalum, when masked by niobium, behaves in a similar manner.

Acknowledgements—The authors thank S. A. Markland for valuable discussions during the work and Karen Nilsson for her comments on the manuscript of this paper.

REFERENCES

1. S. A. Markland, *Dansk Patent*, 128288, 1974.
2. L. Weiss and M. Landecker, *Z. Anorg. Chem.*, 1909, **64**, 65.
3. L. Silverman, *Ind. Eng. Chem., Anal. Ed.*, 1934, **6**, 287.
4. M. C. Marignac, *Ann. Chim. Phys.*, 1868, **13**, 5.
5. W. R. Schoeller, *The Analytical Chemistry of Tantalum and Niobium*, Chapman & Hall, London, 1937.
6. A. M. Chekmarev, O. A. Sinegribova and G. A. Yagodin, *J. Radioanal. Chem.*, 1974, **21**, 129.
7. B. I. Nabivanets, *Zh. Neorgan. Khim.*, 1964, **9**, 1079.
8. E. S. Pilkington and W. Wilson, *Anal. Chim. Acta*, 1965, **33**, 577.
9. E. Lassner and R. Püschel, *J. Less-Common Metals*, 1967, **12**, 146.

Talanta, Vol. 39, No. 5, pp. 535–539, 1992
Printed in Great Britain.

0039-9140/92 $5.00 + 0.00

IMPROVED SPECTROPHOTOMETRIC DETERMINATION OF OSMIUM(VIII) WITH 4-(2-PYRIDYLAZO) RESORCINOL IN MIXED SURFACTANTS

ITSUO MORI,* YOSHIKAZU FUJITA, MINAKO TOYODA and YUKI HASEGAWA
Osaka University of Pharmaceutical Sciences, 2-10-65, Kawai, Matsubara-city, Osaka 580, Japan

(*Received* 26 *November* 1990. *Revised* 10 *September* 1991. *Accepted* 21 *September* 1991)

Summary—The colour development between 4-(2-pyridylazo)-resorcinol(PAR) and osmium(VIII) in the presence of cationic and nonionic surfactants in a weakly acidic medium was more stable and reproducible than in the absence of surfactant (PAR-alone method). An improved spectrophotometric determination of osmium(VIII) with PAR was investigated in the presence of mixed surfactants of *N*-hexadecyltrimethylammonium chloride (HTAC) and Brij 58 [poly(oxyethylene)lauryl ether] as cationic and nonionic surfactants at pH 6.0–7.2. The calibration graph was linear in the range 0–110 μg/10 ml osmium(VIII), and the apparent molar absorptivity was 2.4×10^4 l.mole^{-1}.cm^{-1} with a Sandell sensitivity of 0.0079 μg/cm^2 osmium(VIII).

Although the spectrophotometric determination of osmium with 4-(2-pyridylazo)resorcinol (PAR) as a water-soluble agent has been reported,[1–3] the PAR–osmium(VIII) complex in the absence of surfactant was unstable and poor in sensitivity. The effectiveness of various coexisting surfactants in improving the stability or sensitivity has been recognized in a number of spectrophotometric or fluorophotometric methods.[4–10] In this paper, the colour formation reactions between PAR and osmium(VIII) in the presence of various surfactants (simple or mixed micellar media) were systematically investigated with a view to obtaining more reproducible and sensitive spectrophotometric measurement of osmium(VIII).

EXPERIMENTAL

Reagents and apparatus

Standard osmium(VIII) solution ($5.0 \times 10^{-4}M$) was prepared by dilution of $1.0 \times 10^{-3}M$ stock osmium(VIII) solution (prepared by dissolving osmium tetraoxide in $5.0 \times 10^{-1}M$ sodium hydroxide solution). A $1.0 \times 10^{-3}M$ PAR solution was prepared according to a previous report,[10] and a 1.0–5.0% HTAC (*N*-hexadecyltrimethylammonium chloride) or Brij 58 [poly(oxyethylene)lauryl ether] solution was prepared by dissolving HTAC or Brij 58 in water. A Sörensen phosphate buffer solution (M/15 Na_2HPO_4–KH_2PO_4, pH 6.0–7.2) was used for the pH adjustments. All other reagents were of analytical grade without further purification.

Shimadzu Model UV-260 and 240 recording spectrophotometers with 1.0-cm quartz cells were used for recording absorption spectra and absorbance measurements.

Standard procedure

A sample solution containing up to 110 μg of osmium(VIII) was placed in a 10-ml standard flask. A 1.0-ml portion of 5.0% Brij 58 solution, 1.0 ml of 1.0% HTAC solution, 2.5 ml of phosphate buffer solution (pH 6.5) and 1.5 ml of $1.0 \times 10^{-3}M$ PAR solution were added (Solution A). The solution was diluted to the mark with water, mixed well, kept at 50° for 30 min, and then cooled in water for 5 min. The absorbance of Solution A was measured at 540 nm against the reagent blank (Solution B) treated in the same way.

RESULTS AND DISCUSSION

Colour reaction between PAR and osmium(VIII), and absorption spectra

The colour reaction systems between PAR and osmium(VIII) in the presence (single

*Author for correspondence.

surfactant or combinations) or absence of surfactants were respectively investigated in aqueous solution at room temperature or 50°. The colour developments in the presence of small amounts of surfactant (less than the CMC values) or absence of surfactant were generally unstable, and less sensitive in comparison with those in the micellar media with large amounts of surfactants. In particular, the colour development in a combination of cationic and nonionic surfactants (mixed micellar media) was very stable and more reproducible than that in the absence of surfactants (PAR alone method) or presence of a single surfactant.

Figure 1 shows the absorption spectra of the PAR–osmium(VIII) complex solution (Solution A) and PAR solution (Solution B) in the presence or absence of a HTAC–Brij 85 mixture.

A slight bathochromic shift based on the coexistence of large amounts of cationic surfactant was observed, and the maximum difference of absorbances between Solutions A and B was obtained at 540 nm, with an increase of about 20% in the presence of the mixed surfactants (micellar of cationic and nonionic surfactants).

Figure 2 shows the stability of the PAR–osmium(VIII) complex solution in the presence of HTAC alone and HTAC–Brij 58 mixture.

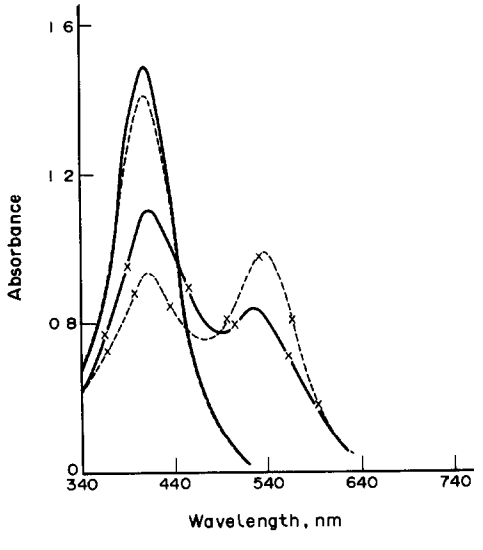

Fig. 1. Absorption spectra of PAR and PAR–osmium(VIII) solutions in the presence or absence of HTAC and Brij 58. Osmium(VIII), PAR, $5.0 \times 10^{-5}M$; pH, 6.5; HTAC, 0.1%; Brij 58, 0.5%; Reference: water. ——: PAR soln.; —x—: PAR-osmium(VIII) soln.; – – – –: PAR–HTAC–Brij 58 soln.; ---x---: PAR–HTAC–Brij 58-osmium(VIII) soln.

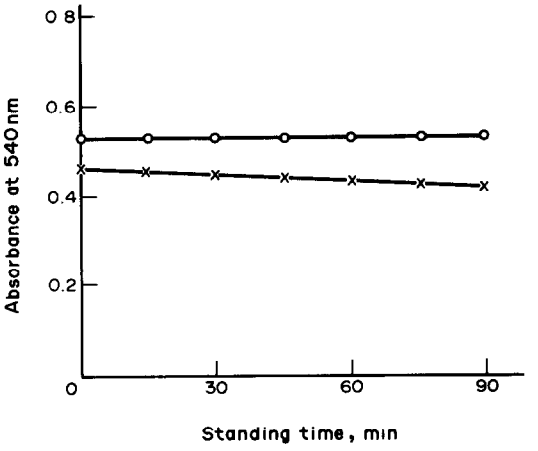

Fig. 2. Stability of Os(III)–PAR complex soln. Os(III), $2.5 \times 10^{-5}M$; PAR, $1.5 \times 10^{-4}M$; Brij 58, 0.5%; HTAC, 0.1%; pH, 6.5; Reference, reagent blank. —x—: Os(III)–PAR–HTAC soln.; —○—: Os(III)–PAR–HTAC–Brij 58 soln.

Effects of pH and surfactants

For the colour development between PAR and osmium(VIII), a maximum and constant absorbance at 540 nm was obtained at pH 6.0–7.2 with a Sörensen phosphate buffer solution, and the optimum amount of buffer solution was 1.5–3.0 ml per 10 ml.

The effects of surfactants, single or surfactant combinations, were examined in terms of stability and sensitivity of the colour reaction. Nonionic surfactants {Brij 35 [poly(oxyethylene)hexadecylether], Brij 58, Triton × 100, Tween 20 [poly(oxyethylene)-sorbitanmonolaurate], PVA [poly(vinyl)alcohol, $n = 200$]}, cationic surfactants [HTAC, HPC (hexadecylpyridinium chloride), Zephiramine [Zp, benzyldimethyltetradecylammonium chloride], anionic surfactants [SDS(sodium dodecylsulphate)] and an amphoteric surfactant [LS(sodium *N*-lauroylsarcosine)] were studied. As shown in Table 1 and Fig. 2, the use of the surfactant-combination of HTAC as cationic surfactant and Brij 58 as nonionic surfactant was most effective, and the colour development was stable and reproducible. The optimum amounts of surfactants were $\geqslant$0.5 ml of 5.0% Brij 58 solution and $\geqslant$0.5 ml of 1.0% HTAC solution in a final volume of 10 ml, *i.e.*, 0.25% Brij 58 and 0.05% HTAC, as shown in Fig. 3. Accordingly, further investigation was carried out on the mixed micellar media of final 0.5% Brij 58 and 0.1% HTAC.

Table 1. Effects of surfactants alone or in combination

Surfactants				λ max	Absorbance
Cationic	Anionic	Amphoteric	Nonionic		
—	—	—	—	533	0.448
HTAC*	—	—	—	545	0.462
—	SDS*	—	—	533	0.459
—	—	LS*	—	533	0.448
—	—	—	Tween 20*	533	0.455
—	—	—	Brij 58*	533	0.460
—	—	—	Brij 35*	533	0.450
—	—	—	PVA*	533	0.448
—	—	—	Triton X100*	533	0.450
HTAC*	—	—	Tween 20†	540	0.540
—	SLS*	—	Tween 20†	533	0.465
HTAC*	—	—	Brij 58†	544	0.550
HTAC*	—	—	Brij 35†	544	0.375
HTAC*	—	—	Triton X100†	543	0.472
HTAC*	—	—	PVA**	535	0.484
HPC*	—	—	Brij 58†	541	0.475
Zp*	—	—	Brij 58†	559	0.499

Osmium(VIII), $2.5 \times 10^{-5}M$; PAR, $1.5 \times 10^{-4}M$; pH: 6.5.
*0.1%.
†0.5%.
Reference, reagent blank.

Effect of PAR concentration

The recommended amount of PAR was a final concentration in the range $1.0–2.0 \times 10^{-4}M$; 1.5 ml of $1.0 \times 10^{-3}M$ PAR solution in 10 ml was used for further investigation.

Effect of temperature

The relationship between reaction temperature and reaction time was examined at the following conditions: room temperature, 40°, 50° and 60° for 10–40 min. Maximum and constant absorbance was obtained by standing at 50° for 30 min, and cooling to room temperature (10–25°) in water for 5 min.

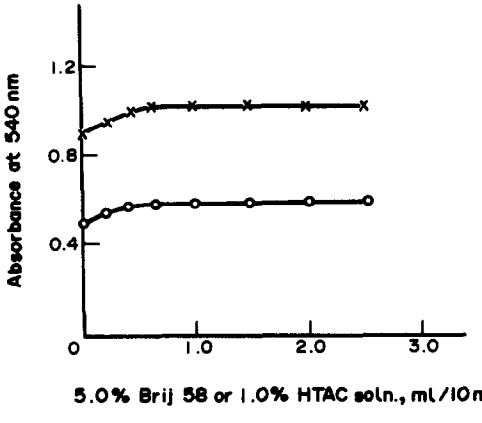

Fig. 3. Effect of Brij 58 and HTAC concentrations PAR, $1.5 \times 10^{-4}M$; pH, 6.5; —×—: effect of Brij 58 in the presence of 0.1% HTAC; Os(III), $5.0 \times 10^{-5}M$; —○—: effect of HTAC in the presence of 0.5% Brij 58; Os(III), $2.5 \times 10^{-5}M$; Reference, reagent blank

Calibration graph and reproducibility

The calibration graph was linear in the range 0–110 μg of osmium(VIII) in a final volume of 10.0 ml. The relative standard deviation (R.S.D.) for 50 μg of osmium(VIII)/10 ml was 0.9% ($n = 5$). Table 2 shows the apparent molar absorptivities (ε) and Sandell's sensitivities in the presence or absence of surfactant No. 1 (proposed method—stable and reproducible) and Nos. 2–6 (single surfactant or non-micellar media—unstable and irreproducible).

Effect of foreign ions

As shown in Table 3, the coexistence of such elements as copper(II), cobalt(II), iron(III), palladium(II) and mercury(II) showed positive error owing to reaction with PAR, but aluminium(III) and zirconium(IV) up to 10-fold excess over osmium(VIII) were permitted. Anions such as sulphate, bromide, nitrate, fluoride and chloride did not interfere, but oxalate ion caused a slight interference at high concentrations. On the other hand, cyanide ion gave a negative error at a 1/10 molar ratio to osmium(VIII). The interferences of iron(III), cobalt(II) or aluminium(III) at high concentrations could be masked by addition of large amounts of ethylenediaminetetraacetic acid (EDTA), nitrilotriacetic acid (NTA) or sodium fluoride. In the second case, large amounts of

Table 2. Apparent molar absorptivities (ε) and Sandell sensitivities with PAR in the presence or absence of surfactants

Method No.	Surfactants				Sensitivity		
	Cationic	Anionic	Amphoteric	Non ionic	ε, *l. mole. cm*$^{-1}$	Sandell, $\mu g/cm^2$	R.S.D., %
1	HTAC*	—	—	Brij 58†	2.4×10^4	0.0078	0.9
2	—	SLS*	—	—	1.8×10^4	0.0103	7.4
3	—	—	LS*	—	1.8×10^4	0.0103	6.8
4	—	—	—	Brij 58*	1.8×10^4	0.0103	6.5
5	HTAC*	—	—	—	1.9×10^4	0.0096	7.1
6	—	—	—	—	1.8×10^4	0.0103	9.3

*0.1%.
†0.5%.
Methods No. 2–6 were unstable and irreproducible.

NTA gave a negative error, but its interference could be compensated by preparing a calibration graph in the presence of NTA. Therefore, the assay of osmium(VIII) together with foreign ions such as iron(III) was investigated. Firstly, the amount of osmium(VIII) was found by measuring the absorbance at 540 nm of Solution A in the presence of NTA [PAR–osmium(VIII)–iron(III)–NTA complex] and using the osmium(VIII) calibration graph in the presence of NTA. Secondly, the amount of iron(III) was calculated by measuring the absorbance at 540 nm of Solution A [PAR–osmium(VIII)–iron(III) complex], and by using the iron(III) calibration graph prepared with iron in the presence of the determined amount of osmium(VIII). [Note that it should be possible also to determine the iron from the increase in absorbance in the absence of NTA and comparison against an iron(III) calibration curve in the absence of osmium.]

Composition of the complex

The molar ratio of PAR to osmium(VIII) in the presence of HTAC and Brij 58 mixed micellar media was estimated to be 1:1 by the molar ratio and Job's continuous variation methods. The molar ratio was identical to that in the absence or presence of HTAC or Brij 58 alone.

CONCLUSION

The colour reaction between PAR and osmium(VIII) in the presence (single or combinations of surfactants) or absence of surfactants was systematically investigated, and the mixture

Table 3. Effect of foreign ions

Foreign ion	Added			Masking agent	Absorbance at 540 nm	Recovery, %
	as	μg	molar ratio			
—	—	—	—	—	0.532	100.0
Cu(II)	sulphate	0.3	1/50	—	0.552	103.7
		15.8	1	—	1.446	251.1
		15.8	1	EDTA	0.517	97.1
Co(II)	nitrate	0.7	1/20	—	0.502	94.3
		14.7	1	—	1.438	270.3
		14.7	1	EDTA	0.521	97.9
Fe(III)	alum	0.6	1/20	—	0.557	104.6
		13.9	1	—	1.012	190.2
		13.9	1	NTA	0.523	98.3
Al(III)	chloride	67.4	10	—	0.532	100.0
		134.8	20	NTA	0.523	98.3
Hg(II)	nitrate	5.0	1/10	—	0.552	103.7
		50.2	1	NTA	0.525	98.7
Zr(IV)	chloride	45.6	2	—	0.502	94.3
Mg(II)	nitrate	60.7	10	—	0.537	100.9
Pd(II)	chloride	1.0	1/25	—	0.553	103.9
F^-	sodium	2374.8	500	—	0.532	100.0
CN^-	potassium	0.6	1/10	—	0.494	92.8
$C_2O_4^{2-}$	sodium	440.1	20	—	0.505	94.8

Osmium(VIII) taken: 45.0 μg/10 ml; PAR: $1.5 \times 10^{-4}M$; Brij 58: 0.5%; HTAC: 0.1%; NTA, EDTA: $5.0 \times 10^{-4}M$; pH: 6.5; Reference: reagent blank.

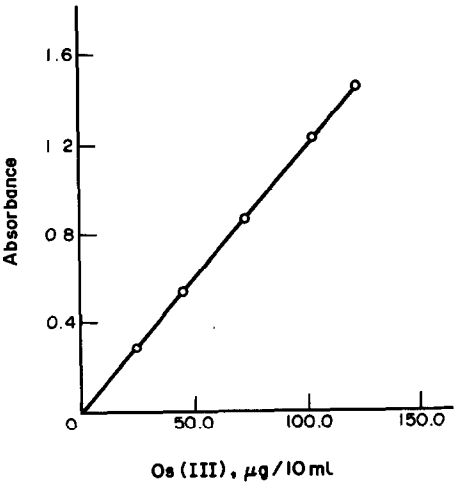

Fig. 4. Calibration graph of osmium(VIII) in the presence of iron(III) and NTA. PAR, $1.5 \times 10^{-4}M$; Brij 58, 0.5%; HTAC, 0.1%; NTA, $5.0 \times 10^{-3}M$; pH, 6.5; iron(III), $2.5 \times 10^{-5}M$; Reference, PAR–NTA soln.

of HTAC and Brij 58, the mixed micellar cationic and nonionic surfactant combination, was most effective in terms of sensitivity, stability and reproducibility. Therefore, an improved, simple spectrophotometric method for the determination of osmium(VIII) with PAR is proposed. The method is more sensitive and reproducible than the PAR-alone method.[1,3]

REFERENCES

1. N. T. Yatshomskaya and V. M. Ivanov, *Zhur. Anal. Khim.*, 1986, **40**, 1754.
2. M. Sivoki and M. Koren, *Mikrochim. Acta*, 1973, 75.
3. W. Quianfong, *Talanta*, 1985, **32**, 507.
4. J. Li and H. Shi, *Fenxi Huaxue*, 1985, **13**, 418; *Anal. Abstr.*, 1986, **48**, 3B143.
5. H. Nishida, *Bunseki*, 1977, 271.
6. V. P. Antonovich, M. M. Novoselova and V. A. Nazarenko, *Zhur. Anal. Khim.*, 1984, **39**, 1157.
7. K. Ueno, *Bunseki Kagaku*, 1971, **20**, 736.
8. M. E. D. Garcia and A. Sanz-Medel, *Talanta*, 1986, **33**, 255.
9. I. Mori, Y. Fujita, K. Fujita, S. Kitano and T. Kotake, *Bunseki Kagaku*, 1986, **35**, 136.
10. I. Mori, Y. Fujita, K. Fujita, Y. Nakahashi, K. Kato and T. Nakamura, *Anal. Lett.*, 1988, **21**, 2359.

Talanta, Vol. 39, No. 5, pp. 541–545, 1992
Printed in Great Britain.

0039-9140/92 $5.00 + 0.00

A RAPID SPECTROPHOTOMETRIC METHOD FOR DETERMINATION OF FLUORIDE IN SILICATES WITH THE ZIRCONYL–XYLENOL ORANGE COMPLEX

P. SAHU,* J. D. PANDA and B. C. SINHA†
Dalmia Institute of Scientific and Industrial Research, Rajgangpur-770017 Orissa, India

(*Received* 15 *April* 1989. *Revised* 12 *September* 1991. *Accepted* 20 *September* 1991)

Summary—A critical study has been made of the effect of acid concentration and of polymerized and depolymerized zirconyl ions on the formation of ZrO–XO complexes and their stabilities. At an optimum acidity of 0.5–0.6*M* hydrochloric acid, most of the common cations occurring in silicates do not interfere. Maximum colour development is almost instantaneous for the depolymerized ZrO–XO complex, but takes a few hours for the polymerized complex; the colour is stable for several hours. The absorbance is highest for the depolymerized ZrO–XO complex and decreases with an increase in polymerization of the zirconyl ions. Dissolved oxides of nitrogen affect the stability of the ZrO–XO complex but can be eliminated with urea. A simple, rapid and sensitive spectrophotometric method has been worked out for use of this complex in determination of fluoride in silicates, without separation, after fusion of the sample with sodium hydroxide at 450–550°.

Among the available methods for determination of small amounts of fluoride, the spectrophotometric and ion-selective electrode methods are most widely used. In silicate analyses, the sample is usually decomposed by fusion with sodium carbonate[1–6] or sodium carbonate plus zinc oxide at 900°,[7] and fluoride is then separated by distillation, pyrohydrolysis or ion-exchange before its determination. It has been reported[8] that there is some loss of fluoride during fusion of samples at 900°. Low-temperature fusion with sodium hydroxide has been recommended for use in the determination of fluoride by the ion-selective electrode method.[9] It has been reported that with alkaline fusion the same results are obtained with or without separation of the fluoride.[10–12] However, there are practically no studies on spectrophotometric determination of fluoride after alkaline fusion at low temperature, without a separation step.

Several reagents[2,4,7,13–27] have been used for direct and indirect spectrophometric determination of fluoride. Xylenol Orange (XO) which forms an intensely coloured complex with zirconium even in 1*M* nitric or hydrochloric acid[28] has been successfully utilized for determination of zirconium.[29–33] The bleaching of the ZrO–XO complex by fluoride has been used for determination of fluoride in mineral water,[33] wastewater,[27] bone and teeth[20] and uranium oxide.[22] However, at pH $\geqslant$ 2 cations such as Al^{3+}, Fe^{3+}, TiO^{2+}, which are invariably present in significant amounts in silicates or ceramic materials, interfere seriously by forming stable complexes with fluoride and with XO. In the spectrophotometric methods based on the ZrO–XO complex and its bleaching, the effect of polymerization of zirconyl ions has seldom been studied or discussed. Sinha and Das Gupta[28] reported the polymerization of zirconyl ions on aging or boiling in $<1M$ hydrochloric or nitric acid, and suggested quantitative depolymerization by boiling in 2–3*M* hydrochloric or nitric acid (preferably the latter) for accurate direct titration with EDTA. Sinha[34] later reported that depolymerization of zirconyl ions is also essential in the indirect determination with EDTA. It is very likely that quantitative depolymerization of zirconyl species is essential in any spectrophotometric method based on the ZrO–XO complex or its bleaching, since the characteristics of the two systems will be different. Cabello-Tomas and West[35] reported that the reaction between slightly aged $ZrOCl_2$ solution and XO is catalysed by substoichiometric amounts of F^-, SO_4^{2-}, PO_4^{3-}, AsO_4^{3-}, citrate or oxalate, and this was used for spectrophotometric determination (at 15°) of 0.005–0.05 ppm fluoride. They also reported that maximum colour took 90 min to develop and it remained constant for 60 min.

*Author for correspondence.
†Consultant and retired scientist from Central Glass and Ceramics Research Institute (CSIR) Calcutta, India.

The present investigation concerned the effect of polymerization of zirconyl ions on the quantitative formation of ZrO–XO complexes and their stabilities, and application of the results to derive a rapid, sensitive and accurate method for direct spectrophotometric determination of fluoride in silicates and other ceramic raw materials and products, after low-temperature alkaline fusion of samples.

EXPERIMENTAL

Apparatus

A Systronic type 103 spectrocolorimeter was used.

Reagents

All reagents used were of analytical grade.

Zirconium nitrate stock solution (0.9 mg/ml Zr). Dissolve 0.66 g of $ZrO(NO_3)_2 \cdot 2H_2O$ in 35 ml of 8*M* nitric acid. Boil for 5 min to depolymerize the zirconyl ions[28] and dilute to 250 ml. Standardize by EDTA titration in 1*M* nitric acid with XO as indicator.[28]

Working depolymerized zirconyl solution (0.036 mg/ml Zr). Boil 10 ml of stock solution with 60 ml of 4*M* nitric acid for 5 min, cool, and dilute to 250 ml.

Partly polymerized zirconyl solution (0.036 mg/ml Zr). Bring a mixture of 10 ml of stock solution and 50 ml of water just to the boil, cool, and dilute to 250 ml.

Highly polymerized zirconyl solution (0.036 mg/ml Zr). Boil 10 ml of stock solution with 50 ml of water for 10 min, cool, and dilute to 250 ml.

Stock fluoride solution (1 mg/ml F^-). Dissolve 2.211 g of sodium fluoride (dried at 110° for 3 hr) in water and dilute to 1 litre. Dilute 5 ml to 500 ml to obtain a 10 μg/ml fluoride working solution.

Xylenol Orange indicator. Dissolve 0.5 g of XO in water, add one drop of hydrochloric acid (1 + 1), dilute to 250 ml with water and filter.

Procedure

Fuse 4–5 g of sodium hydroxide in a nickel crucible and cool. Weigh 0.2–0.5 g of sample (containing up to 2 mg of fluoride) into the crucible and fuse the mixture for about 20 min at 450–550°. Cool the melt, extract it with 50 ml of hot water, then rinse the crucible and remove it. Add 20–30 ml of concentrated hydrochloric acid and boil the solution at 200–300° for 5–10 min. Add 20 ml of 50-mg/ml zinc nitrate solution, with stirring, add a few drops of phenalphthalein indicator and then 5*M* sodium hydroxide dropwise until a faint pink colour is obtained, transfer into a 250-ml standard flask and dilute to the mark. Filter a portion of the solution through a dry filter paper and pipette 5–10 ml of the filtrate (containing 10–40 μg of fluoride) into a 100-ml standard flask. Add 10 ml of hydrochloric acid (1 + 1), then exactly 3 ml of dilute zirconium solution (0.036 mg/ml Zr), with shaking, and let the solution stand for about 10 min. Dilute the solution to about 70 ml, add 5 ml of 100-mg/ml urea solution and exactly 2 ml of Xylenol Orange indicator, and make up to volume. Measure the absorbance at 535 nm against a blank prepared by diluting 10 ml of hydrochloric acid (1 + 1), 5 ml of the urea solution and exactly 2 ml of Xylenol Orange indicator to volume in a 100-ml standard flask. Prepare a calibration curve in the same way with 0, 1, 2, 3 and 4 ml of 10-μg/ml fluoride solution.

RESULTS AND DISCUSSION

Effect of acid concentration

Figure 1 shows that the absorbance of the depolymerized ZrO–XO complex increases with increase in hydrochloric acid concentration to a constant maximum at 0.3–0.6*M* acid, then decreases sharply with further increase in acidity. In this optimum range of acid concentration, particularly at 0.5–0.6*M*, most other cations (including Al^{3+} and TiO^{2+}) form hardly any coloured complex with the protonated XO. The fluoride complexes of these cations also do not form (owing to practically complete protonation of the fluoride). However, because of the large difference in the relative strengths of

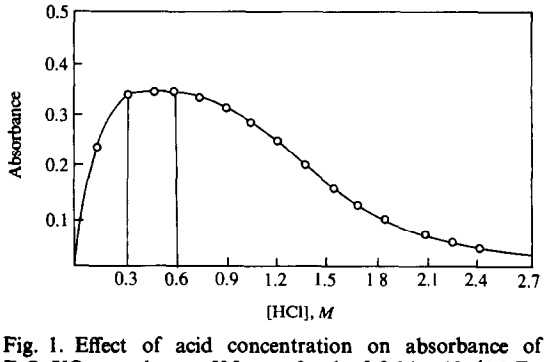

Fig. 1. Effect of acid concentration on absorbance of ZrO–XO complex at 535 nm: 3 ml of $3.94 \times 10^{-4}M$ Zr, 2 ml of $2.97 \times 10^{-3}M$ XO and appropriate volumes of hydrochloric acid (1 + 1), diluted to 100 ml.

Table 1. Tolerance limits for various ions in determination of 10 μg of fluoride

Ion	Ion:F molar ratio	Ion	Ion:F molar ratio
Al(III)	30	Zn(II)	200
Cr(VI)	1	Ba(II)	1000
Cr(III)	200	Sulphate	390
Fe(III)	2.5	Phosphate	4
Ti(IV)	2.5		
Th(IV)	3	Oxalate	trace amount bleaches
Ca(II)	360	Peroxide	trace amount bleaches
Mg(II)	240	Nitrite	5
Ni(II)	255	Acetate	1500
Cu(II)	237	Borate	2000
La(III)	5	Silicate	200

HF and XO, at this high acidity fluoride can decompose the ZrO–XO complex.

The tolerance limits for a number of ions in the method are given in Table 1. It shows that several elements will interfere at the levels present in the type of sample for which the method was designed, and must therefore be eliminated, or reduced in concentration to below the tolerance level. This can be done by the treatment with zinc nitrate and sodium hydroxide, as discussed below.

Effect of polymerization of zirconyl ions

Figure 2 shows that depolymerized zirconyl ions form the ZrO–XO complex instantaneously

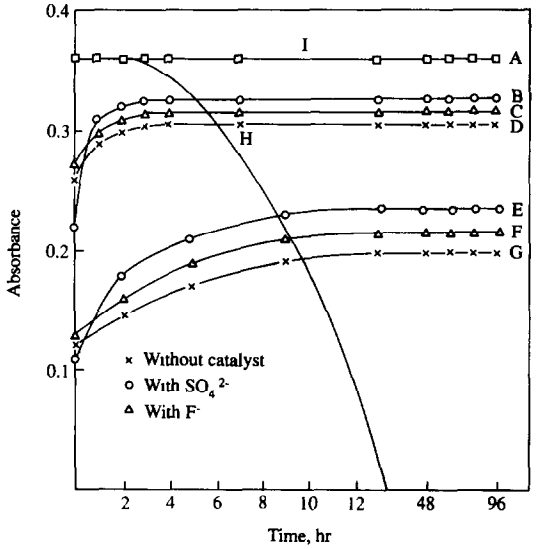

Fig. 2. Effect of depolymerized and polymerized zirconyl ions on formation and stability of the XO complex in 0.5–0.6*M* hydrochloric acid at room temperature (30 ± 2°). A, in absence of oxides of nitrogen or after their removal with urea; B, C and D, less polymerized ZrO–XO complexes; E. F and G, highly polymerized ZrO–XO complexes; H, depolymerized ZrO–XO complex in presence of oxides of nitrogen.

and the colour is stable for some days (curve A). However, if the solution contains a little dissolved oxides of nitrogen the absorbance decreases sharply after about 3 hr (curve H). This adverse effect of oxides of nitrogen can be removed with urea (curve A is again obtained).

The absorbance of the XO complexes with polymerized zirconyl ions increases with time to a constant value, the rate and the final absorbance being dependent on the degree of polymerization. Substoichiometric amounts of sulphate or fluoride slightly increase the rate of reaction as well as increasing the absorbance (curves B, C, E and F), in accordance with the observations by Cabella-Tomas and West.[35] However, the maximum absorbance is much lower than that of the depolymerized ZrO–XO complex. It has been reported that zirconyl ions form complexes in which Zr:XO is 1:1,[30] 1:2,[31] 2:1,[36] and it is possible that the 1:1 complex may actually be a 2:2 complex. Since the molar absorptivity will be essentially a function of the XO moiety in the complex, that of the 1 : 1 and 2 : 2 complexes should be similar but those for species such as

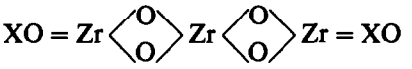

and

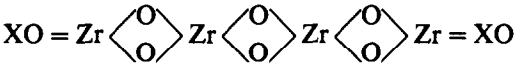

and higher polymers will be progressively lower, as indicated by the curves in Fig. 2.

Xylenol Orange

To test the quality of XO available in the market, six samples, three each from BDH and Merck, with different batch numbers, were obtained. Their molar absorptivities were found to range from 4.2×10^4 to 1.4×10^5 $l.mole^{-1}.cm^{-1}$, indicating the variation in purity of the reagents. However, a linear relationship was found between zirconium concentration and the absorbance of the XO complex, and between fluoride concentration and decrease in absorbance of the ZrO–XO complex, with different sensitivities. The purest of these reagents was used in the present study.

Decomposition of silicate samples

A preliminary study to eliminate the separation of fluoride by distillation was made by precipitating silica along with the R_2O_3 group

Table 2. Analysis of filtrate after separation of silica and the R_2O_3 group

Species	Found, *mg**	Removal, %
Al^{3+}	1.63	98.8
Fe^{3+}	0.17	99.3
Ti^{4+}	0.15	99.0
Zn^{2+}	0.28	99.1
SiO_2	0.25	98.7

*Average of 3 analyses

Table 3. Determination of fluoride in simulated samples

Composition, *mg*						F found, *mg*	
Al	Fe	Ti	CaO	Na_2SiO_3	F	Present method	Distillation method
10	10	10	200	200	5.00	4.95	4.80
20	10	10	400	400	5.00	5.05	4.82
30	10	10	500	500	5.00	4.96	4.75
30	5	10	400	400	4.00	4.03	3.90
30	10	10	400	400	4.00	3.92	3.82
30	20	10	400	400	4.00	3.95	3.85
30	10	5	400	400	2.00	2.00	1.90
30	10	10	400	400	2.00	2.03	1.85
30	10	20	400	400	2.00	1.98	1.80

Table 4. Determination of fluoride in cement, ceramic raw materials, and products

Description	Found, %	Certified value, %
O.P. Cement (BCS No. 372)	0.071, 0.068, 0.066	0.060
O.P. Cement (BCS-CRM No. 372/1)	0.043, 0.042, 0.045	0.040
Slag (CECA-878-1)	0.152, 0.155, 0.146	0.149
Limestone	0.098, 0.102, 0.095	0.08
Clinker	0.140, 0.142, 0.135	0.132
Clay	0.050, 0.048, 0.045	0.043
NCBM Cement	0.068, 0.070, 0.067	0.063
Bauxite	0.025, 0.032, 0.028	0.023

elements, according to the method of Huang and Johns[7] for decomposition of the sample by fusion with sodium carbonate and zinc oxide at 900°, but did not yield satisfactory results. Besides loss of fluoride during the decomposition, as reported by Troll and Farzaneh,[8] it was found that the filtrate often became turbid on acidification, owing to formation of colloidal silicic acid. Fusion with sodium hydroxide and zinc oxide also failed to yield satisfactory results, owing to incomplete separation of silica. The difficulty has been overcome by fusion of the samples with sodium hydroxide at 450–550°, extraction with water and hydrochloric acid, addition of zinc nitrate solution, and precipitation of silica and the R_2O_3 group at pH ~ 8. On acidification the filtrate gave a clear solution, analysis of which (Table 2), clearly showed satisfactory removal of most of the other constitutents.

Applications

The method has been applied to a variety of simulated and natural samples. The results (Tables 3 and 4) clearly show that the fluoride found, though slightly higher than that obtained by the distillation method, compared very favourably with the actual amounts of fluoride taken or the standard values, indicating better accuracy of the method. The slightly lower values obtained by the distillation method are attributed to incomplete recovery of the fluoride.

The method is simple, accurate and reasonably rapid, since it does not involve a distillation. The determination of fluoride in cement and other silicates can easily be completed within 2 hr.

REFERENCES

1. A. Hall and J. N. Walsh, *Anal. Chim. Acta*, 1969, **45**, 341.
2. C. R. Edmond, *AMDEL Bull.*, 1969, **7**, 1.
3. B. L. Ingram, *Anal. Chem.*, 1970, **42**, 1825.
4. J. Debras-Guedon, *Bull. Soc. Fr. Ceram.*, 1978, April–June, 39.
5. S. J. Haynes, *Talanta*, 1978, **25**, 85.
6. I. Szucs, *Magy. Kem. Foly.*, 1979, **85**, 481.
7. W. H. Huang and W. D. Johns, *Anal. Chim. Acta*, 1967, **37**, 508.
8. G. Troll and A. Farzaneh, *Interceram (Lübeck)*, 1978, **27**, 400.
9. B. Fabbri and F. Donati, *Analyst*, 1981, **106**, 1338.
10. M. A. Peters and D. M. Ladd, *Talanta*, 1971, **18**, 655.
11. D. S. Russell, H. B. Macpherson and V. P. Clancy, *ibid.*, 1980, **27**, 403.
12. R. T. Oliver and A. G. Clayton, *Anal. Chim. Acta*, 1970, **51**, 409.
13. C. A. Horton, in I. M. Kolthoff and P. J. Elving (eds.), *Treatise on Analytical Chemistry*, Part II, Vol. 7, pp. 207–334. Interscience, New York, 1961.
14. P. L. Sarma, *Anal. Chem.*, 1964, **36**, 1684.
15. E. J. Dixon, *Analyst*, 1970, **95**, 272.
16. W. H. Evans and G. A. Sergeant, *ibid.*, 1967, **92**, 690.
17. R. R. Rickard, F. L. Ball and W. W. Harris, *Anal. Chem.*, 1951, **23**, 919.
18. R. N. Rogers and S. K. Yasuda, *ibid.*, 1959, **31**, 616.
19. L. C. Peck and V. C. Smith, *Talanta*, 1964, **11**, 1343,
20. J. A. Růžička, H. Jakschová and L. Mrklas, *ibid.* 1966, **13**, 1341.
21. L. Dobiasová, N. Hlasivcová and J. Novák, *Chem. Listy*, 1967, **61**, 1658.
22. T. N. Kukisheva, E. S. Sinitsyna and N. S. Efimova, *Zh. Analit. Khim.*, 1971, **26**, 953.
23. J. A. Růžička, *Collection Czech. Chem. Commun.*, 1965, **30**, 2717.
24. J. M. Icken and B. M. Blank, *Anal. Chem.*, 1953, **25**, 1741.
25. J. Mayer and E. Hlucháň, *Chem. Zvesti*, 1958, **12**, 143.

26. N. I. Larina and N. E. Gelman, *Zh. Analit. Khim.*, 1967, **22**, 582.
27. I. A. Shevchuk, Yu. K. Borodai, V. I. Manshilin, Yu. G. Dubchenko and V. F. Galat, *Ukr. Khim. Zh.*, 1979, **45**, 659.
28. B. C. Sinha and S. Das Gupta, *Analyst*, 1967, **92**, 558.
29. K. L. Cheng, *Talanta*, 1959, **2**, 61, 186, 226; 1959, **3**, 81.
30. A. K. Babko and M. I. Shtokalo, *Ukr. Khim. Zh.*, 1961, **27**, 566.
31. P. M. Champion, P. Crowther and D. M. Kemp, *Anal. Chim. Acta*, 1966, **36**, 413.
32. K. F. Karlysheva, A. V. Koshel and L. F. Vashun, *Ukr. Khim Zh.*, 1972, **38**, 493.
33. R. Valach, *Talanta*, 1961, **8**, 443.
34. B. C. Sinha, *Ind. J. Chem.*, 1971, **9**, 178.
35. L. Cabello-Tomas and T. S. West, *Talanta*, 1969, **16**, 781.
36. B. Buděšínský, *Collection Czech. Chem. Commun.*, 1963, **28**, 1858.

Talanta, Vol. 39, No. 5, pp. 547–553, 1992
Printed in Great Britain.

0039-9140/92 $5.00 + 0.00

SPECTROPHOTOMETRIC RESOLUTION OF TERNARY MIXTURES OF SALICYLALDEHYDE, 3-HYDROXYBENZALDEHYDE AND 4-HYDROXYBENZALDEHYDE BY THE DERIVATIVE RATIO SPECTRUM-ZERO CROSSING METHOD

J. J. BERZAS NEVADO and C. GUIBERTEAU CABANILLAS
Department of Analytical Chemistry and Foods Technology, University of Castilla-La Mancha, 13071 Ciudad Real, Spain

F. SALINAS
Department of Analytical Chemistry, University of Extremadura, 06071 Badajoz, Spain

(*Received* 21 *May* 1991. *Revised* 25 *July* 1991. *Accepted* 6 *September* 1991)

Summary—A new spectrophotometric method for resolving ternary mixtures is proposed. The method is based on the simultaneous use of the first derivative of ratio spectra and measurements of zero-crossing wavelengths. The ratio spectrum is obtained by dividing the amplitudes of the absorption spectrum of the mixture by a standard spectrum of one of the components giving the first derivative of the ratio spectrum. The concentrations of the other components is then determined from their respective calibration graphs established by measuring the ratio derivative analytical signal at the selected zero-crossing points. The method has been applied to resolving ternary mixtures of the isomers salicylaldehyde, 3-hydroxybenzaldehyde and 4-hydroxybenzaldehyde. Previously, we also resolved the binary mixture of salicylaldehyde and 3-hydroxybenzaldehyde. The method compares favourably with other spectrophotometric methods.

One of the classic analytical problems is the simultaneous determination of two or more compounds in the same sample, without previous chemical separation. In this way, derivative spectrophotometry is an analytical technique of great utility and offers greater selectivity than normal spectrophotometry.[1,2] Also mixtures have been resolved by using a multicomponent analysis program.[3,4] Blanco and co-workers[5,6] reported a method called multi-wavelength linear regression analysis (MLRA).

The resolution of binary mixtures of compounds with overlapped spectra by derivative spectrophotometry is frequently made on the basis of zero-crossing measurements.[1,7] In general, this technique is not suitable for ternary mixtures of compounds with overlapped spectra and in the case of binary mixtures it is often necessary to use a wavelength with low sensitivity in the measurements. Recently, Salinas *et al.*[8] developed a new spectrophotometric method for resolving binary mixtures. The method is based on the use of the first derivative of the ratio spectra. The absorption spectrum of the mixture is obtained and divided (amplitudes at each wavelength) by the absorption spectrum of a standard solution of one of the components, and the first derivative of the ratio spectrum is obtained. The concentration of another component is then determined from a calibration graph. This method permits the use of the wavelength of greatest sensitivity as the signal of measurement, a maximum or a minimum.

However, this method shows some limitation because in the wavelength range where the absorbance of the standard solution used as divisor is zero (or below the baseline) the noise is strongly exalted. In consequence, the useful wavelength range must be selected and, if noise is now slightly exalted, a smoothing function (prior to derivation) can be used as in classical derivative spectrophotometry. In experimental practice, we have observed that there are some mixtures which cannot be treated by this method.

The approach taken has now been extended to resolving ternary mixtures by simultaneous use of the zero-crossing method and Salina's method.

With the aim of testing this method, it has now been applied to the simultaneous determination of three isomer compounds with overlapped spectra, salicylaldehyde (SA), 3-hydroxybenzaldehyde (3HBA) and 4-hydroxybenzaldehyde (4HBA).

At first, it is necessary to resolve the different binary mixtures. In previous papers,[9,10] we have studied the SA and 4HBA, and 3HBA and 4HBA binary mixtures, and new methods for resolving their mixtures were described.

In this paper, the last binary mixture (SA and 3HBA) is studied and chemical and instrumental parameters are optimized. On the other hand, the SA, 3HBA and 4HBA ternary mixture is studied and several mixtures are resolved by using the proposed method for ternary mixtures. The results obtained were compared with those obtained by derivative spectrophotometry, and, in the case of binary mixtures, also by the method of Blanco and co-workers.[5,6]

THEORY

Consider a mixture of three compounds, M, N and P. If Beer's Law is obeyed for all compounds over the whole wavelength range used and the path-length is 1 cm, the absorption spectrum of the mixture is defined by the equation:

$$A_{m,\lambda_i} = \epsilon_{M,\lambda_i} C_M + \epsilon_{N,\lambda_i} C_N + \epsilon_{P,\lambda_i} C_P \qquad (1)$$

where A_{m,λ_i} is the absorbance of the mixture at wavelength λ_i, ϵ_{M,λ_i}, ϵ_{N,λ_i} and ϵ_{P,λ_i} are the molar absorptivities of M, N and P at wavelength λ_i and C_M, C_N, and C_P are the molar concentration of M, N and P, respectively.

If equation (1) is divided by the corresponding equation for the spectrum of a standard solution of one of the components (*e.g.*, M of concentration C_M°) and the first derivative of the result is obtained, the following equation can be written:

$$\frac{d}{d\lambda}\left[\frac{A_{m,\lambda_i}}{\epsilon_{M,\lambda_i} C_M^\circ}\right] = \frac{C_N}{C_M^\circ}\frac{d}{d\lambda}\left[\frac{\epsilon_{N,\lambda_i}}{\epsilon_{M,\lambda_i}}\right] + \frac{C_P}{C_M^\circ}\frac{d}{d\lambda}\left[\frac{\epsilon_{P,\lambda_i}}{\epsilon_{M,\lambda_i}}\right] \qquad (2)$$

If $C_N = 0$, we have the binary mixture of M and P, and the equation in this case is:

$$\frac{d}{d\lambda}\left[\frac{A_{m,\lambda_i}}{\epsilon_{M,\lambda_i} C_M^\circ}\right] = \frac{C_P}{C_M^\circ}\frac{d}{d\lambda}\left[\frac{\epsilon_{P,\lambda_i}}{\epsilon_{M,\lambda_i}}\right] \qquad (3)$$

Equation (3) indicates that the "derivative ratio spectrum" of the binary mixtures is dependent only on the values of C_P and C_M° and is independent of the value of C_M in the binary mixture.

A calibration graph is obtained by recording and storing the spectra of the solution of pure P at different concentrations, and the spectrum of a standard of pure M of concentration C_M°.

The stored spectra of the solutions of pure P are divided by the standard spectrum of M of concentration C_M° by use of "Data Leader Software".

The ratio spectra thus obtained are then differentiated with respect to wavelength and the derivative values for a given wavelength are plotted against C_P for a given calibration graph. M can be determined by an analogous procedure. This is the basis of the method of Salinas *et al.*[8] A new method can be developed from this for resolving ternary mixtures, by simultaneous use of the zero-crossing method and Salinas's method.

Equation (2) indicates that the derivative ratio spectrum of the ternary mixture is independent of the value of C_M and dependent of the value of C_N, C_P and C_M° in the ternary mixtures.

The content of N and P can be resolved by the zero-crossing method by measuring at adequate wavelengths and by use of calibration graphs.

Two calibration graphs are obtained by recording and storing the spectra of solution of pure N and pure P at different concentrations and the spectrum of a solution of pure M of concentration C_M°. The amplitudes of the spectra of N and P are then divided, wavelength by wavelength, by the corresponding amplitudes for M°. The "ratio spectra" thus obtained are then differentiated with respect to wavelength. The derivative values

$$\frac{C_N}{C_M^\circ}\frac{d}{d\lambda}\left[\frac{\epsilon_{N,\lambda_i}}{\epsilon_{M,\lambda_i}}\right]$$

are plotted against C_N for a given wavelength corresponding to zero crossing of the ratio spectrum of P (in this wavelength

$$\frac{d}{d\lambda}\left[\frac{\epsilon_{p,\lambda_i} C_P}{\epsilon_{M,\lambda_i} C_M^\circ}\right] = 0)$$

to give a calibration graph. The calibration graph for P is obtained by plotting derivative values

$$\frac{C_P}{C_M^\circ}\frac{d}{d\lambda}\frac{\epsilon_{P,\lambda_i}}{\epsilon_{M,\lambda_i}}$$

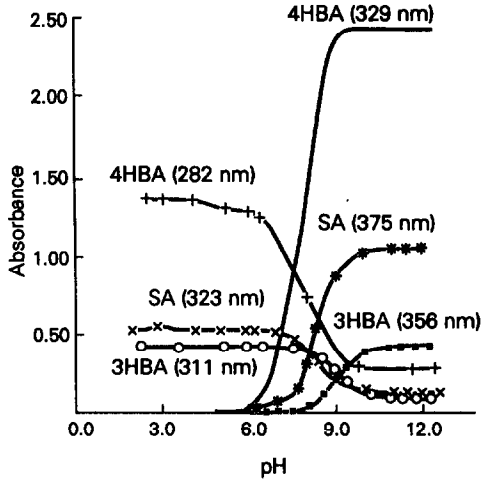

Fig. 1. Influence of pH value SA (20 ppm); 3HBA (20 ppm); 4HBA (10 ppm).

against C_P at λ_i corresponding to zero crossing of the ratio spectrum of N (at this wavelength

$$\frac{d}{d\lambda}\left[\frac{\epsilon_{N,\lambda_i} C_N}{\epsilon_{M,\lambda_i} C_M^\circ}\right] = 0).$$

Application of the method to the sample containing M, N and P and use of the calibration graphs, will then give the values of C_N and C_P in the ternary mixtures.

M can be determined by an analogous procedure. If we use a spectrum of standard solution of N or P of concentration C_N° or C_P° we can determine M and P in the presence of N, or M and N in the presence of P.

EXPERIMENTAL

Apparatus

A Beckmann Instrument DU-50 spectrophotometer connected to an IBM PC-286-XT fitted with Beckmann Data Leader Software and an Olivetti DM-282 printer was used for all the measurements and treatment of data.

Solutions

All solvents and reagents were of analytical reagent-grade. Salicylaldehyde, 3-hydroxybenzaldehyde and 4-hydroxybenzaldehyde ethanol –water 1:1 solutions were prepared from the Merck products. Sodium hydroxide solution 0.2*M* was prepared by dissolving 8.0 g of sodium hydroxide (Merck) and diluting to one litre.

Procedure

Samples were prepared in 25-ml calibrated flasks containing 2–20 ppm salicylaldehyde and/or 2–30 ppm 3-hydroxybenzaldehyde and/or 1–10 ppm 4-hydroxybenzaldehyde, plus 2 ml of 0.2*M* sodium hydroxide. They were diluted with water and ethanol to the mark (the resulting final solution is 10% in ethanol). The absorption spectra were recorded with 1-nm resolution against water and stored in the IBM PC 286-XT.

The stored spectra of the binary mixtures, salicylaldehyde and 3-hydroxybenzaldehyde and of the ternary mixtures were divided by a standard spectrum of salicylaldehyde of 10 ppm. The ratio spectra were smoothed through the use of 15 experimental points and the first derivates calculated with $\Delta\lambda = 4$ nm.

In the binary mixtures we can determine 3-hydroxybenzaldehyde by measuring at $^1DD_{290}$ (derivative divided spectrum at 290 nm).

In the ternary mixtures we can determine 3-hydroxybenzaldehyde by measuring at 304 nm ($^1DD_{304}$) and 4-hydroxybenzaldehyde at 295 nm ($^1DD_{295}$). The concentration of 3-hydroxybenzaldehyde was proportional to the amplitude of the minimum at 240 nm and to the amplitude at 304 nm, and 4-hydroxybenzaldehyde to the amplitude at 295 nm.

On the other hand, stored spectra of binary as well as ternary mixtures were divided by a standard spectrum of 3-hydroxybenzaldehyde of 15 ppm concentration. In the same way as we have previously described we obtained the first derivatives from smoothed ratio spectra. Now, we can determine salicylaldehyde by measuring at 394 nm ($^1DD_{394}$) in binary mixtures and by measuring at 398 nm ($^1DD_{398}$) in ternary mixtures. The concentration of salicylaldehyde was

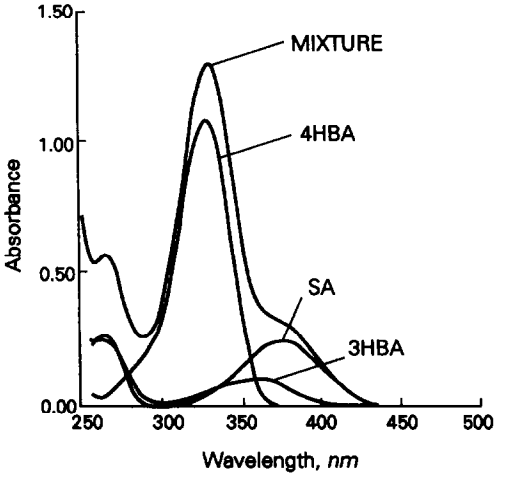

Fig. 2. Absorption spectra of SA (5 ppm), 3HBA (7 ppm), 4HBA (5 ppm) and their mixture.

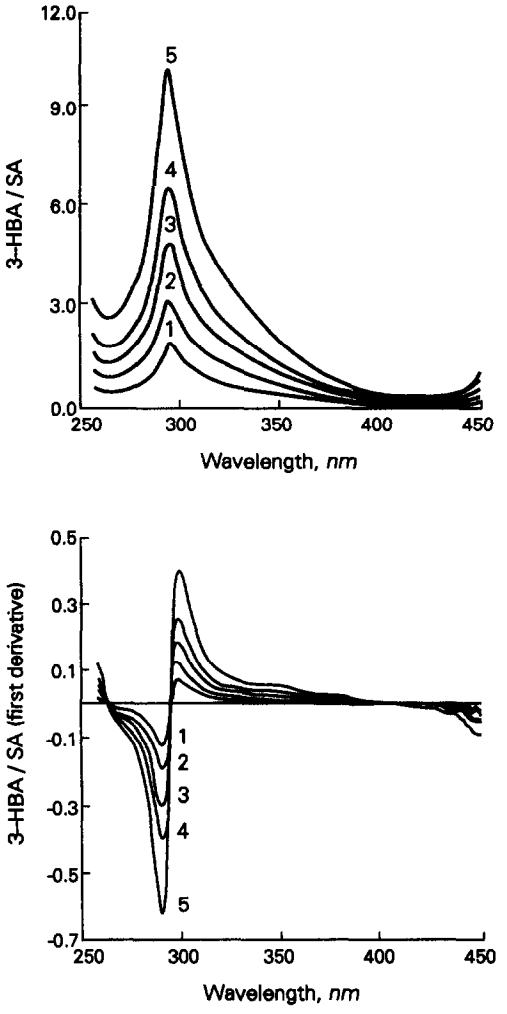

Fig. 3. Ratio spectra and first derivatives for different concentrations of 3HBA when SA was 10 ppm 1 (5 ppm), 2 (10 ppm), 3 (15 ppm), 4 (20 ppm), 5 (30 ppm).

proportional to the amplitudes at 394 nm and 398 nm.

RESULTS AND DISCUSSION

With the aim of testing theoretical considerations in an experimental system, we have chosen three isomer compounds which have overlapped spectra. The ternary mixture selected was salicylaldehyde (SA) and its 3-hydroxybenzaldehyde (3HBA) and 4-hydroxybenzaldehyde (4HBA) isomers. We emphasize that this mixture has been selected exclusively and with the sole purpose of testing the method described.

The UV spectra of SA, 4HBA and 3HBA, showed two absorption maxima for all pH values studied (2–13). In order to establish suitable pH values for use throughout, a range of values were examined between pH 2 and 13 (Fig. 1). Only small changes were experienced between pH 2 and 5 and between pH 11 and 13. Therefore pH values of 12 and 4.5 must be considered suitable for use throughout. However, for the pH value of 4.5 the results obtained were not acceptable and the method is only developed at pH = 12.

These compounds are soluble in ethanol –water. The ethanol content of the medium slightly affects the absorbances of the three compounds; 10% was selected as optimum. Under these conditions, SA, 3HBA and 4HBA solutions were stable for 2 hr at least.

Figure 2 shows the absorption spectra of SA, 3HBA, 4HBA and their mixture in basic medium (pH = 12). The spectra of three compounds overlap sufficiently to demonstrate the resolving power of the proposed method for the ternary mixture and for the binary mixture of SA and 3HBA.

Binary mixture of SA and 3HBA

Figure 3 shows the ratio spectra of different 3HBA standards (spectra divided by the spectrum of a 10-ppm SA solution) and their first derivatives were calculated. The first derivative amplitudes at a given wavelength are proportional to the 3HBA concentration.

Table 1. Results obtained for different binary mixtures of SA and 3HBA by use of the proposed method

Composition mixture		15 ppm 3HBA (divisor)		10 ppm SA (divisor)	
		$^1DD_{394}$		$^1DD_{299}$	
SA, *ppm*	3HBA, *ppm*	SA, Found *ppm*	Recovery, %	3HBA, Found, *ppm*	Recovery, %
5.00	5.00	4.80	96.0	4.65	93.0
5.00	15.00	4.93	98.6	14.56	97.1
2.00	12.00	2.03	101.5	11.63	96.9
2.00	20.00	2.03	101.5	19.70	98.5
15.00	5.00	15.01	100.1	5.50	110.0
12.00	2.00	11.81	98.4	2.09	104.5
20.00	2.00	19.98	99.9	2.68	134.0

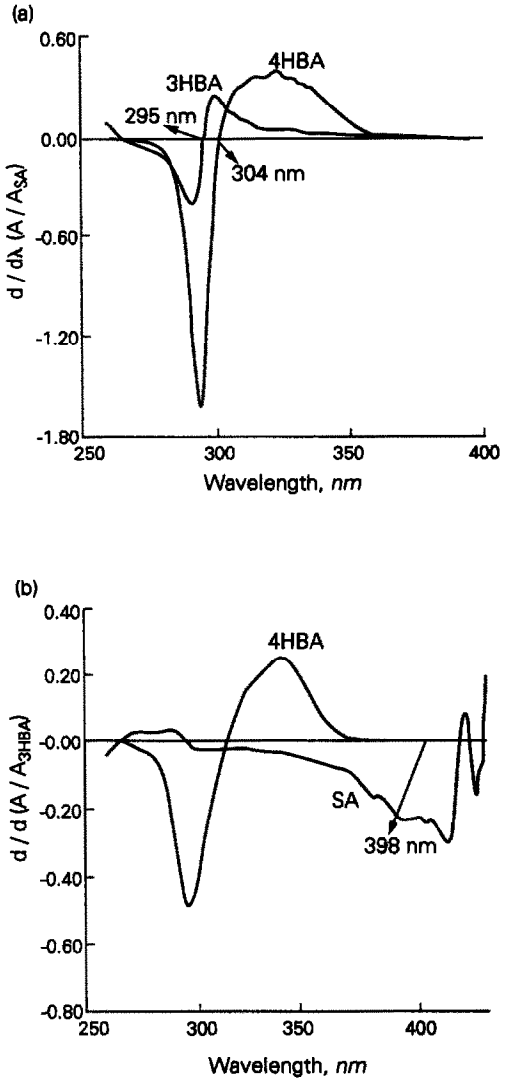

Fig. 4. First derivative of the ratio spectra of (a) 3HBA and 4HBA (10 ppm) of SA as divisor) (b) 4HBA and SA (15 ppm 3HBA as divisor).

Due to the extent of the noise levels on the ratio spectra, a smoothing function was used on the basis of the Savitzky and Golay method[11,12] and 15 experimental points were considered as optimum.

The influence of $\Delta\lambda$ for obtaining the first derivative was tested; $\Delta\lambda = 4$ nm was considered as suitable. The concentration of divisor (SA in this case) can be modified, and different calibration graphs are then obtained. We selected an SA concentration of 10 ppm. The calibration graph was established by measuring at 290 nm corresponding to a minimum ($^1DD_{290}$) and it gave a straight line up to 30 ppm SA.

For determining the other component (SA) an analogous procedure was followed. We obtained the ratio spectra of different SA standards (spectra divided by the spectrum of a 15 ppm 3HBA solution) and their first-derivatives were calculated. The ratio spectra were smoothed with experimental points and the first derivatives were calculated with $\Delta\lambda = 4$ nm. The concentration of the divisor (3HBA) was 15 ppm.

The calibration graph was obtained by measuring at 394 nm ($^1DD_{394}$) and it gave straight lines up to 20 ppm SA.

Several mixtures of SA and 3HBA were prepared and resolved by the proposed method. The results are summarized in Table 1. In all cases recovery between 96.0 and 101.0% were obtained for determining SA. The determination of 3HBA is possible when the ratio SA/3HBA $\leqslant 6$, with recovery between 93.0 and 110.0%.

Ternary mixtures of SA, 3HBA and 4HBA

After developing the methods for resolving SA, 3HBA and 4HBA in their possible binary mixtures, SA and 3HBA are described in this paper while SA–4HBA and 3HBA–4HBA have been described previously.[9,10] We developed the new method for resolving the ternary mixture.

We did not have to establish the experimental optimum conditions because it was made in binary mixtures. We only needed to select the adequate wavelength to determine each component.

Table 2. Results obtained for differents ternary mixtures of SA, 3HBA and 4HBA by using the proposed method

Composition mixture			15 ppm 3HBA (divisor)		10 ppm SA (divisor)			
			$^1DD_{394}$		$^1DD_{299}$		$^1DD_{295}$	
SA	3HBA	4HBA	SA, Found *ppm*	Recovery, %	3HBA, Found *ppm*	Recovery, %	4HBA, Found *ppm*	Recovery %
5.00	5.00	5.00	5.00	100.0	5.50	110.0	5.05	101.0
10.00	10.00	10.00	10.07	100.7	9.80	98.0	9.97	99.7
10.00	5.00	10.00	9.92	99.2	5.60	112.0	9.94	99.4
5.00	10.00	5.00	4.90	98.0	9.71	97.1	5.07	101.4
5.00	10.00	10.00	5.06	101.2	9.90	99.0	10.02	100.2
10.00	10.00	5.00	10.04	100.4	11.00	110.0	5.14	102.8

Table 3. Results obtained for different binary mixtures by others methods

Mixture composition, ppm		Method of Blanco et al.							
		3HBA, divisor (350–420 nm)		SA, divisor (270–330 nm)		First derivative		Second derivative	
		Recovery %		Recovery, %		Recovery, %		Recovery, %	
SA	3HBA	SA	3HBA	SA	3HBA	SA	3HBA	SA	3HBA
5.00	5.00	96.0	109.8	107.2	92.8	98.2	92.6	98.6	106.8
5.00	15.00	100.6	100.4	67.6	115.8	90.0	87.3	94.8	98.3
2.00	12.00	102.0	98.6	67.0	106.2	93.0	91.8	85.0	101.0
2.00	20.00	104.5	99.2	22.5	108.4	89.0	99.0	75.0	102.5
15.00	5.00	103.9	93.0	90.1	132.2	100.1	65.6	99.9	96.4
12.00	2.00	101.8	80.5	98.2	119.5	100.5	29.0	99.4	81.0
20.00	2.00	103.1	17.0	93.2	168.5	99.6	39.0	99.9	79.0

Figure 4 shows the first derivative of the ratio spectra of (a) 3HBA and 4HBA (10 ppm SA as divisor) and (b) 4HBA and SA (15 ppm 3HBA as divisor).

Taking into account the zero crossing method, 4HBA can be determined by measuring at 295 nm (zero-crossing of 3HBA/SA) and 3HBA can be determined at 304 nm (zero crossing of 4HBA/SA), with SA as divisor [Fig. 4(a)]. SA can be determined by measuring at 398 nm in the first derivative of the ratio spectra with 3HBA as divisor [Fig. 4(b)].

The calibration graphs were obtained at wavelengths selected previously and gave straight lines up to 20 ppm SA, up to 30 ppm 3HBA and up to 10 ppm 4HBA.

Several mixtures of SA, 3HBA and 4HBA were prepared and resolved by the proposed method. The results obtained are summarized in Table 2. In all cases good recovery values were obtained.

Comparative study

The binary mixtures were also resolved by using the method of Blanco and co-workers,[5,6] and classical derivative spectrophotometry (first and second orders). SA can be determined by measuring at 345 nm in the first derivative mode ($^1D_{356}$) and at 381 nm in the second derivative mode ($^2D_{381}$). 3HBA can be determined by measuring at 375 nm in the first derivative mode ($^1D_{375}$) and at 350 nm in the second derivative mode ($^2D_{350}$).

Various values of the experimental points were tested for smoothing the absorption spectra and 15 points were selected as optimum. We also optimized the value of $\Delta\lambda$ to obtain the first and second derivative smoothed spectra and 4 nm and 28 nm were selected as optimum respectively.

Table 3 shows the results obtained for the mixtures of SA and 3HBA by the first and second derivative mode and by the method of Blanco and co-workers[5,6] (by using 10 ppm SA and 15 ppm 3HBA as divisors).

We also tested the derivative spectrophotometry method (first to fourth orders) for resolving the ternary mixtures. We couldn't

Table 4. Statistical data for calibration graphs

Range, ppm	Equation	r	S_m	S_b
Binary mixture				
2–20	$^1D_{356} = 0.0000 + 0.0012\ C_{SA}$	1.0000	5×10^{-6}	7×10^{-5}
2–20	$^2D_{381} = 0.0001 + 0.0005\ C_{SA}$	1.0000	3×10^{-6}	6×10^{-5}
2–20	$^1DD_{394} = -0.0024 + 0.0150\ C_{SA}$	0.9999	1×10^{-4}	2×10^{-3}
2–30	$^1D_{375} = 0.0005 + 0.0021\ C_{3HBA}$	0.9982	2×10^{-5}	3×10^{-4}
2–30	$^2D_{350} = 0.0000 + 0.0002\ C_{3HBA}$	0.9997	2×10^{-6}	4×10^{-5}
2–30	$^1DD_{290} = -0.0065 + 0.0206\ C_{3HBA}$	0.9968	9×10^{-4}	2×10^{-2}
Ternary mixture				
2–20	$^1DD_{398} = 0.0004 + 0.0152\ C_{SA}$	0.9999	1×10^{-6}	2×10^{-3}
2–30	$^1DD_{304} = 0.0046 + 0.0073\ C_{3HBA}$	0.9990	2×10^{-5}	1×10^{-3}
1–10	$^1DD_{295} = 0.0013 + 0.3662\ C_{4HBA}$	0.9999	9×10^{-4}	6×10^{-4}

C_{SA} = SA concentration (ppm)
C_{3HBA} = 3HBA concentration (ppm)
C_{4HBA} = 4HBA concentration (ppm)
r = Regression coefficient
S_m = Standard deviation of slope
S_b = Standard deviation of intercept

Table 5. Statistical parameters for SA, 3HBA and 4HBA determination

	Signal measured	Standard deviation, *ppm*	Relative standard deviation	Determination limit, *ppm*
Binary mixture				
SA	$^1D_{356}$	0.0292	±0.66	0.46
	$^2D_{381}$	0.0304	±0.68	0.00
	$^1DD_{394}$	0.0311	±0.74	0.11
3HBA	$^1D_{375}$	0.1577	±0.77	2.40
	$^2D_{350}$	0.1574	±0.67	0.00
	$^1DD_{290}$	0.8460	±3.74	1.70
Ternary mixture				
SA	$^1DD_{398}$	0.1140	±0.94	0.48
3HBA	$^1DD_{304}$	0.2440	±1.25	1.99
4HBA	$^1DD_{295}$	0.0293	±0.45	0.04

find, in the same order of derivative spectra, the appropriate wavelengths for the simultaneous determination of the three compounds. Therefore 4HBA can be determined by measuring at 299 nm in the first derivative order, SA can be determined at 396 nm in the third derivative order ($^3D_{396}$) and 3HBA can't be determined by this method.

Table 4 summarizes the different calibration graphs of SA and 3HBA in binary mixtures and SA, 3HBA and 4HBA in ternary mixtures, and their linear regression coefficients which are very good.

To check the precision of the methods, replicated samples were measured ($n = 10$) containing SA (10 ppm), 3HBA (10 ppm) and 4HBA (5 ppm) individually (Table 5); in addition determination limits were calculated for each of the compounds.[13,14]

CONCLUSION

The proposed method permits the resolution of ternary mixtures of compounds which have overlapping spectra, as in the case of isomers studied, SA, 3HBA and 4HBA while derivative spectrophotometry for resolving the same mixtures does not provide good results.

Acknowledgement—The authors gratefully acknowledge financial support from the DGCICYT project PB88-0431.

REFERENCES

1. T. C. O'Haver and G. L. Green, *Anal. Chem.*, 1976, **48**, 312.
2. P. Levillain and D. Fompeydie, *Analusis*, 1986, **14**, 1.
3. Y. R. Tahboud and H. L. Pardue, *Anal. Chem.*, 1985, **57**, 38.
4. D. T. Rossi and H. L. Pardue, *Anal. Chim. Acta*, 1985, **175**, 153.
5. M. Blanco, J. Gene, H. Iturriaga, S. Maspoch and J. Riba, *Talanta*, 1987, **34**, 987.
6. M. Blanco, J. Coello, H. Iturriaga and S. Maspoch, *Técnicas de Laboratorio*, 1988, **XII**, 198.
7. T. C. O'Haver, *Clin. Chem.*, 1979, **25**, 1548.
8. F. Salinas, J. J. Berzas Nevado and A. Espinosa Mansilla, *Talanta*, 1990, **37**, 347.
9. J. J. Berzas Nevado, C. Guiberteau Cabanillas and F. Salinas, *Anal. Lett.*, 1990, **23**, 2077.
10. *Idem.*, *Bull. Soc. Chim. Belg.*, 1991, **100**, 79.
11. A. Savitzky and M. J. E. Golay, *Anal. Chem.*, 1964, **36**, 1627.
12. J. Steiner, Y. Termonia and J. Deltour, *ibid.*, 1972, **44**, 1906.
13. I.U.P.A.C. Nomenclature, Symbols, Units and Their Usage in Spectrochemical Analysis, *Pure Appl. Chem.*, 1976, **45**, 105.
14. A.C.S. Committee on Environmental Improvement, *Anal. Chem.*, 1980, **52**, 2242.

Talanta, Vol. 39, No. 5, pp. 555–561, 1992
Printed in Great Britain.

0039-9140/92 $5.00 + 0.00

A CHEMICAL ENHANCEMENT METHOD FOR THE SPECTROPHOTOMETRIC DETERMINATION OF TRACE AMOUNTS OF ARSENIC

K. PALANIVELU, N. BALASUBRAMANIAN and T. V. RAMAKRISHNA*
Department of Chemistry, Indian Institute of Technology, Madras-600 036, India

(*Received* 3 *May* 1991. *Revised* 1 *August* 1991. *Accepted* 1 *August* 1991)

Summary—A highly sensitive spectrophotometric method for the determination of 0.03–1.0 μg of arsenic is described. After extraction as AsI_3 into benzene, it is selectively stripped into water. Both the arsenic(III) and iodide present in the aqueous phase are made to react with iodate in acidic medium in the presence of chloride to form the anionic chloro complex, ICl_2^-. The determination is completed after extraction of ICl_2^- species as an ion-pair with Rhodamine 6G into benzene and measuring the absorption of the extract at 535 nm. The coefficient of variation is 1.5% for 10 determinations of 0.5 μg of arsenic. The method has been applied to the determination of arsenic content in plant materials, high purity iron, copper base alloys and inorganic arsenic levels of natural waters.

The widely used methods for the spectrophotometric determination of trace amounts of arsenic are based on the formation of molybdenum blue[1] and the reaction of arsine with silver diethyldithiocarbamate.[2] Methods based on the formation of an ion-pair between arsenomolybdate and a large dye cation have been described to improve the sensitivity and selectivity of the determination.[3–5] None of these methods, however, are sufficiently sensitive to establish the arsenic levels of natural waters without resorting to a preconcentration step.

The ability of arsenic(III) to react with potassium iodate in the presence of chloride in an acidic medium to form the anionic chlorocomplex is well known[6] and has been applied to the spectrofluorimetric determination of 0.3–1.5 μg of arsenic(III) after extraction of the anionic complex as an ion-pair with Rhodamine B into benzene.[7] The presence of ions that are oxidized by iodate however interferes seriously in the determination. Since iodide can also react with potassium iodate to form the anionic chlorocomplex[6] similar to arsenic(III), it seemed worthwhile to examine whether the formation of the anionic complex and its interaction with a cationic dye could be put to advantage for the spectrophotometric determination of both arsenic(III) and arsenic(V) after extractive separation as arsenic triiodide into benzene. Such an approach, besides improving the selectivity (since relatively few ions extract into benzene from iodide media), would also provide considerable enhancement in sensitivity arising due to reaction of iodide, in addition to arsenic(III) present in arsenic triiodide with potassium iodate to form the anionic chloro-complex. Detailed examination disclosed that the reaction with potassium iodate in acidic chloride containing medium after selectively stripping the arsenic triiodide into water and subsequent interaction of the anionic iodine complex with Rhodamine 6G can form the basis for the spectrophotometric determination of arsenic. The resulting ion-pair, after extraction into benzene, had maximum absorption at 535 nm, and arsenic concentration as low as 0.03 μg in a final volume of 25 ml can be determined with this procedure. The method was found suitable for the rapid determination of arsenic concentration of natural waters and applicable to the determination of arsenic in plant materials, high purity iron and copper base alloys without prior separation of arsine.

*Author for correspondence.

EXPERIMENTAL

Apparatus

Absorbances were measured with a Carl Zeiss PMQ II spectrophotometer with 10-mm quartz cells.

Reagents

Standard arsenic(III) solution, 1.0 mg/ml. Prepared by dissolving 0.1321 g of arsenious oxide in 10 ml of 1*M* sodium hydroxide, adding 7.5 ml of 1*M* sulphuric acid and diluting to volume with water in a 100-ml standard flask. A suitable volume of this solution was diluted to obtain working standards.

The following solutions were prepared by dissolving appropriate amounts of the reagents in distilled water.

Potassium iodate solution, 0.01%.

Rhodamine 6G solution, 0.02%.

Sodium chloride solution, 15%.

*Saturated sodium chloride solution, ~5*M.

*Potassium iodide solution, 2*M.

*Sodium hypophosphite, monohydrate solution, 2*M.

*Sulphuric acid, 2.5 and 12.5*M.

Benzene (thiophene free[8]). Used for extraction.

*Di-*isopropyl *ether solvent.* Di-*iso*propyl ether containing 0.015 weight per cent peroxide was prepared by equilibrating 50 ml of the solvent rendered free from peroxide[9] with 50 ml of 0.5*M* sulphuric acid containing 0.3 weight per cent of hydrogen peroxide for 5 min. It was prepared fresh every week, stored in a brown bottle and kept in a refrigerator.

Procedure

Separation of arsenic. Transfer a portion of the sample solution into a 125-ml separating funnel. Add enough sulphuric acid and sodium chloride to make their concentration 3*M* (4*M* for sample volumes greater than 30 ml) and 2*M* respectively. Add 1 ml of 2*M* sodium hypophosphite solution followed by sufficient potassium iodide to provide an overall concentration of 0.3*M*. Shake the solution for 2 min with 10 ml of benzene (separate the aqueous layer and repeat the extraction with 10 ml of benzene if the initial sample volume used is >30 ml).

Collect the organic phase(s) in a 60-ml separating funnel, treat with 2 ml of di-*iso*propyl ether solvent (4 ml if the extraction is performed twice) containing 0.015% peroxide, mix well and allow to stand for 15 min. Then extract with 10 ml of water for one minute and discard the organic layer.

Determination

Transfer an aliquot of the stripping agent containing not more than 1.0 μg of arsenic into a 25-ml standard flask. Add 2 ml each of 2.5*M* sulphuric acid, 0.01% potassium iodate solution and 0.02% Rhodamine 6G solution followed by 4 ml of 15% sodium chloride solution. Dilute to volume with water and allow to stand for 5 min. Transfer the made up solution into a 60-ml separating funnel and extract with 5 ml of benzene for one minute. Separate the organic layer into a dry test tube and add about 1 g of anhydrous sodium sulphate. Measure the absorbance of the extract at 535 nm in 10-mm cells against a reagent blank run through the entire procedure. Establish the concentration of arsenic by reference to a calibration graph prepared with 0.03–1.0 μg of arsenic, following the above procedure.

RESULTS AND DISCUSSION

Extractive separation of arsenic as arsenic triiodide

Although arsenic can be extracted from an iodide medium into a variety of solvents, the extraction into hydrocarbon solvents as arsenic triiodide from a highly acidic medium (>8*N*) has been shown to be highly selective.[10–13] It was found that from solutions of lower acidity, extraction becomes quantitative in the presence of sodium chloride as a salting-out agent. Using simplex optimization,[14] it was established that for quantitative extraction the overall concentration with respect to sulphuric acid, potassium iodide and sodium chloride should be 3, 0.3 and 2*M* respectively.

A single equilibration for two minutes with 10 ml of benzene was adequate for quantitative extraction which remained unaffected up to an aqueous phase volume of 30 ml. Beyond this volume, the extraction was incomplete and repetition of the extraction on the aqueous phase was not effective. Increasing the concentration of potassium iodide up to 0.6*M* showed no marked improvement in the recovery of arsenic. For quantitative extraction of arsenic from aqueous volume up to 100 ml, it was found necessary to equilibrate the solution twice with 10 ml of benzene each time, after raising the acidity to >4*M* with respect to sulphuric acid. A single equilibration for one minute with 10 ml of water was found adequate for stripping the arsenic from the organic layer.

Determination with Rhodamine 6G

Preliminary studies under conditions found optimal (hydrochloric acid—1.5*M*, IO_3^-—

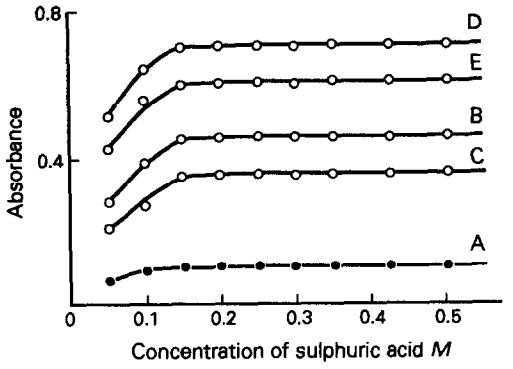

Fig. 1. *Effect of acidity.* A. 2 ml of 0.01% KIO_3, 5 ml each of 0.01% Rhodamine 6G and 15% NaCl, "x" ml of 2.5*M* H_2SO_4, diluted to 25 ml, extracted with 5 ml of benzene measured against benzene at 535 nm in 10-mm cells. B. As in (A) with 5 μg of As(III). C. As in (B) but measured against (A). D. As in (A) with 5 μg of I^-. E. As in (D) but measured against (A).

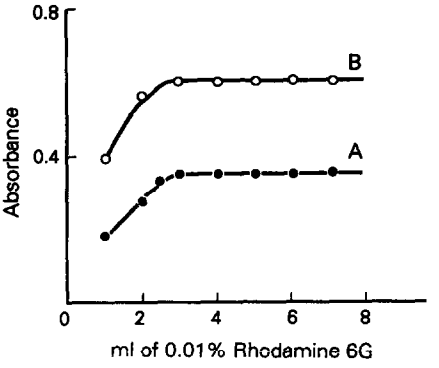

Fig. 3. *Effect of Rhodamine 6G concentration.* A. 5 μg of As(III) with "x" ml of 0.01% Rhodamine 6G, 2 ml each of 2.5*M* H_2SO_4 and 0.01% KIO_3, 5 ml of 15% NaCl, total volume 25 ml, extracted with 5 ml of benzene, measured against respective reagent blank. B. As in (A) with 5 μg of I^- instead of As(III).

0.025m*M* and Rhodamine B—0.025m*M*) for the spectrofluorimetric determination of arsenic[7] showed that the colour when extracted into benzene gradually faded on standing. This was overcome by using Rhodamine 6G instead of Rhodamine B, the use of which stabilized the colour of the extract that absorbed maximally at 535 nm for 75 min. Acidification with sulphuric acid in the presence of sodium chloride was preferred to hydrochloric acid because in the former the blank was low and reproducible, due to lower levels of impurities.

Variation of the acidity of the reaction medium as shown in Fig. 1, revealed that the ion-pair extraction remained maximal and constant when the overall acidity was greater than 0.15*M* for both arsenic(III) and iodide. The influence of potassium iodate, Rhodamine 6G and sodium chloride on the extraction of the ion-pair into benzene are shown in Figs. 2, 3 and 4, respectively. Based on these experiments an overall concentration of 0.2*M* sulphuric acid, 0.04m*M* (0.0008%) potassium iodate, 0.035m*M* (0.0016%) Rhodamine 6G and 0.04*M* (2.4%) sodium chloride were chosen as optimum for the determination of both arsenic(III) and iodide. Although the presence of sodium chloride and Rhodamine 6G in excess of the recommended concentration caused a slight increase in blank value, the net absorbance due to reaction with arsenic(III) and iodide remained unaffected.

The formation of the ion-pair in both instances was found to be almost instantaneous and mixing the phases for about 30 sec was found to be sufficient for its quantitative extraction into benzene. Benzene, toluene,

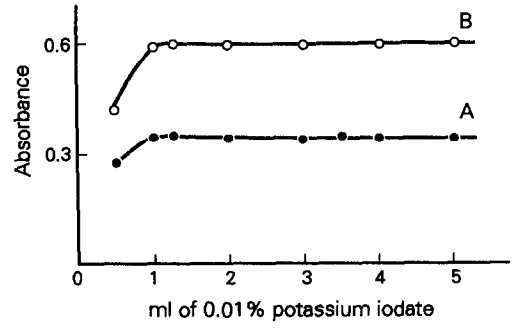

Fig. 2. *Effect of potassium iodate concentration.* A. 5 μg as As(III) with "x" ml of 0.01% KIO_3, 2 ml of 2.5*M* H_2SO_4, 5 ml each of 0.01% Rhodamine 6G and 15% NaCl solution, total volume 25 ml, extracted with 5 ml of benzene measured against respective reagent blank. B. As in (A) with 5 μg of I^- instead of As(III).

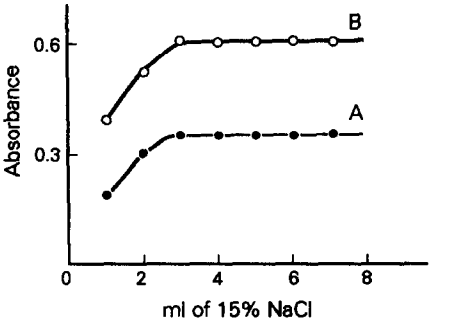

Fig. 4. *Effect of sodium chloride concentration.* A. 5 μg of As(III) with "x" ml of 15% NaCl, 2 ml each of 2.5*M* H_2SO_4, 0.01% KIO_3 and 0.02% of Rhodamine 6G, total volume 25 ml, extracted with 5 ml of benzene, measured against respective reagent blank. B. As in (A) with 5 μg of I^- instead of As(III).

xylene, hexane, cyclohexane, carbon tetrachloride, chloroform, and *iso*amyl acetate were investigated as extraction solvents. However, only benzene proved to be satisfactory, as the extraction of the ion-pair was found to be maximum in this solvent.

When independently checked, linear calibration curves passing through the origin were obtained for arsenic(III) and iodide in the range 0.15–11.0 μg and 0.1–6.0 μg, respectively. The molar absorptivities were found to be 2.6×10^4 $l.mole^{-1}.cm^{-1}$ for arsenic(III) and 7.6×10^4 $l.mole^{-1}.cm^{-1}$ for iodide.

Extractive separation and determination of arsenic

As the optimal conditions for the determination of arsenic(III) and iodide were found to be identical, it was decided to apply the method for the determination of arsenic, after its extraction as arsenic triiodide into benzene and stripping into water. Difficulties were encountered because the blank was intensely coloured, evidently due to co-extraction of hydroiodic acid. As washing the benzene layer with acid solution was found to be ineffective in removing the hydroiodic acid, the use of a dilute solution of hydrogen peroxide was considered for washing purposes. The use of a 0.3 weight per cent solution of hydrogen peroxide in 5*M* sulphuric acid was effective in minimizing the blank value, but the results were not reproducible. Blank values comparable to the normal blank resulted only when the hydrogen peroxide concentration in the wash liquid was increased above 1.0%, but this resulted in a considerable decrease in the sample absorbance also. In this instance the absorbance of the sample extract corresponded to that of arsenic alone, indicating the oxidative loss of the iodide that remained associated with arsenic.

Addition of organic solvents containing peroxide to the benzene layer after the separation of the aqueous layer was examined next. The solvents examined included, *iso*amyl acetate, cyclohexanone, di-*iso*propyl ether, *iso*butyl methyl ketone and mesityl oxide. After adding 1 ml of the solvent, the benzene layer was mixed and allowed to stand for 15 min before stripping with water. In all instances, there was a considerable reduction in the blank. As the addition of di-*iso*propyl ether containing 0.022 weight per cent peroxide was found to be most effective among the solvents examined it was used, with an optimal amount of peroxide, for destroying the co-extracted hydroiodic acid.

In order to establish the optimal range of peroxide in di-*iso*propyl ether that would be effective for produding low and reproducible blanks, the solvent was first rendered free from peroxide[9] and then varying amounts of peroxide were introduced by equilibrating for five min with an equal volume of 0.5*M* sulphuric acid containing 0.1–1.0 weight per cent hydrogen peroxide. After equilibration the solvent was found to contain peroxide in the range 0.005–0.035 weight per cent.

The effect of the addition of 2 ml of each peroxide containing ether to the benzene extract was examined separately. After the addition of ether, the extracts were allowed to stand for 15 min before stripping into water for completing the determination. The results, shown in Fig. 5, clearly indicate that the addition of 2 ml of ether containing peroxide in the range 0.012–0.026 weight per cent effectively reduces the blank value without affecting the sample. When the recommended procedure was followed for the preparation of peroxide containing ether, it was found to contain 0.015 weight per cent. After the addition of 2 ml of this solvent to the benzene extract, a standing time of 10 min was found to be adequate (Fig. 6) to destroy the co-extracted hydroiodic acid, and the recovery

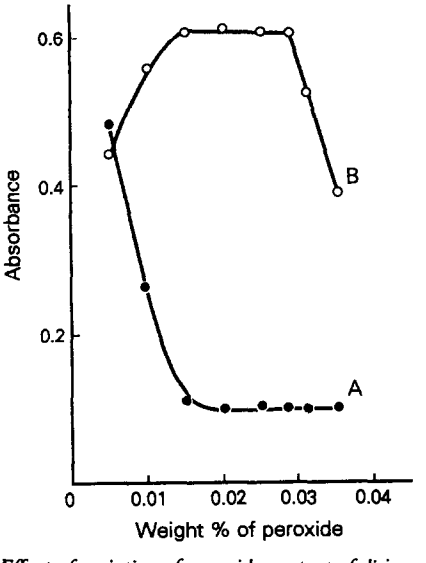

Fig. 5. *Effect of variation of peroxide content of di-*iso*-propyl ether.* A. 10 ml of benzene extract, 2 ml of di-*iso*-propyl ether solvent, standing time 15 min, before stripping and colour development. Measured against benzene. B. As in (A) using benzene extracts obtained with 1 μg of arsenic, measured against (A).

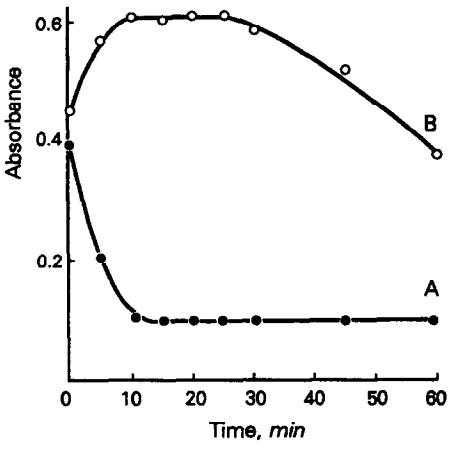

Fig. 6. *Influence of standing time after the addition of di-*iso*-propyl ether solvent on the stability of AsI_3 in the benzene extract.* A. 10 ml of benzene extract, 2 ml of di-*iso*-propyl ether solvent (0.015%), standing time × min before stripping and colour development. Measured against benzene. B. As in (A) with benzene extracts obtained with 1 μg of arsenic, measured against (A).

of arsenic remained unaffected up to a standing time of 25 min before stripping into water.

When the procedure described in the Experimental section was followed, 1.0 μg of arsenic(III) gave an absorbance of 0.62 ± 0.02 compared to the expected value of 0.66 [0.07 for 1 μg of arsenic(III) and 0.59 for 5.0 μg of associated iodide]. The calibration graph was linear over the range 0.03–1.0 μg of arsenic. From the slope of the calibration plot the molar absorptivity was established to be 2.37×10^5 $l.mole^{-1}.cm^{-1}$. The Sandell sensitivity was found to be 8×10^{-5} $\mu g/cm^2$.

The precision of the proposed procedure was checked by establishing the concentration of 10 samples containing 0.50 μg of arsenic. The mean recovery was found to be 0.497 μg with a coefficient of variation of 1.5%.

Nature of the extracted species

The equilibrium shift method[15] was employed to establish the ratio of arsenic to iodide. The slope of the straight line obtained by plotting log *D vs.* log $[I^-]$ was found to be 2.98, indicating that arsenic was extracted into the benzene layer as arsenic(III) triiodide, which conforms to the findings reported in the literature.[13]

When the benzene layer was equilibrated with water, both arsenic(III) and the associated iodide were readily stripped into water. The stripping, when reacted with iodate in acidic medium, leads to the formation of iodine as shown in the following equations:

$$5AsO_3^{3-} + 2IO_3^- + 2H^+ \rightleftharpoons I_2 + 5AsO_4^{3-} + H_2O \quad (1)$$

$$5I^- + IO_3^- + 6H^+ \rightleftharpoons 3I_2 + 3H_2O \quad (2)$$

In the presence of chloride, the excess iodate[6] present in the solution can further oxidize the generated iodine and stabilize it as ICl_2^- species in accordance with

$$2I_2 + IO_3^- + 6H^+ + 5Cl^- \rightleftharpoons 5ICl + 3H_2O \quad (3)$$

$$ICl + Cl^- \rightleftharpoons ICl_2^- \quad (4)$$

The overall reaction for the formation of ICl_2^- from AsO_3^{3-} and iodide can be represented as

$$2AsO_3^{3-} + IO_3^- + 2H^+ + 2Cl^- \rightleftharpoons 2AsO_4^{3-} + ICl_2^- + H_2O \quad (5)$$

$$2I^- + IO_3^- + 6H^+ + 6Cl^- \rightleftharpoons 3ICl_2^- + 3H_2O \quad (6)$$

While the reaction with iodide can give rise to only ICl_2^-, the possibility of the formation of ICl_4^-, due to the reduction of the iodate to I^{3+} state and stabilization as ICl_4^- can also be expected in the case of arsenic(III) in accordance with

$$AsO_3^{3-} + IO_3^- + 4H^+ + 4Cl^- \rightleftharpoons AsO_4^{3-} + ICl_4^- + 2H_2O \quad (7)$$

As both ICl_2^- and ICl_4^- can form ion-pairs with Rhodamine 6G and extract into benzene, investigations were carried out to establish the nature of species responsible for the extraction of the ion-pair in the determination of arsenic(III) with iodine solution in benzene and completing the determination under conditions optimal for the determination of arsenic(III). Though this experiment would not give direct evidence for the formation of ICl_4^-, it would provide indirect evidence of whether the formation of ICl_2^- was responsible for the observed colour.

Experiments with iodine solution in benzene showed a linear relationship with an increasing amount of iodine and the absorbance of 0.20 produced by 2.0 μg of iodine was identical to that produced by 2.94 μg of arsenic(III). Since, 2.0 μg of iodine would result from 2.94 μg of arsenic(III) [equation (1)], it was felt reasonable to conclude that the ICl_2^- species was responsible for the observed absorbance with arsenic(III). Had ICl_4^- been the species, as evident from equation (7), 1.47 μg of arsenic(III) would have been adequate to produce the observed absorbance.

Table 1. Determination of arsenic in various materials

S. No.	Sample	Arsenic present	Arsenic added, μg	Arsenic found,† (Mean value ± σ), μg	%	Recovery, %
1	Brass	0.0057%*	—	27.0 ± 0.57	0.0054	
	(0.5 g/50 ml)		2.50	51.5		98.0
2	BCS No. 207/2					
	Gun metal (Cu-base)	0.006%	—	64.5 ± 0.87	0.64	
	(0.1 g/50 ml)		2.50	88.7		96.8
3	BCS No. 260/3					
	High purity iron	0.026%	—	12.0 ± 0.10	0.024	
	(0.05 g/25 ml)		10.0	22.2		102.0
4	Plant materials					
	(1 g/25 ml)					
	a. Grass	2.5 μg/g	—	2.6 ± 0.10		
			5.0	7.5		98.0
	b. Mango leaf	2.0 μg/g*	—	1.8 ± 0.05		
			5.0	6.8		100.0
	c. Plantain leaf	4.0 μg/g*	—	4.0 ± 0.17		
			5.0	8.9		98.0
5	Water (50 ml)					
	a. Tap water	2.3 μg/l*	—	0.125 ± 0.005 (2.5 μg/l)		
			0.5	0.620		99.0
	b. Sea water (Bay of Bengal, Madras)	2.8 μg/l*	—	0.145 ± 0.003 (2.9 μg/l)		
			0.5	0.65		101.0

*Molybdenum blue method.
†Average value of three determinations.

Another evidence in support of the formation of ICl_2^- species in the case of arsenic(III) was obtained by establishing the stoichiometry of the species extracted as an ion-pair into benzene. The combined ratio of the anionic chloro-complex and the dye cation was established by determining the ratio of arsenic(III) to Rhodamine 6G by the continuous variation and mole ratio methods. Both methods showed that for maximum extraction of the ion-pair, the medium should contain 2 moles of arsenic(III) and 1 mole of Rhodamine 6G. Since 2 moles of arsenic(III) would yield 1 mole of ICl_2^- species [equation (5)] and 2 moles of ICl_4^- species [equation (7)], it was concluded that ICl_2^- species and the monovalent Rhodamine 6G cation interact in a 1:1 ratio for the formation of the ion-pair. If ICl_4^- were to be the species, the arsenic(III) and Rhodamine 6G would have reacted in a 1:1 ratio.

Effect of interfering metal ions

The presence of one milligram amounts of various ions which are known to react with iodide were examined in the determination of 0.5 μg of arsenic by the proposed procedure. The ions examined included Ag^+, Bi^{3+}, Cd^{2+}, Cu^{2+}, Fe^{3+}, Ge^{4+}, In^{3+}, MoO_4^{2-}, Tl^+, TeO_2^{2-}, Sb^{3+}, SeO_3^{2-}, Sn^{4+} and Zn^{2+}. The determinations were carried out in the presence of sodium hypophosphite solution to prevent the liberation of iodine. Although 1 ml of 2*M* sodium hypophosphite was adequate, the addition of larger volumes would be necessary in the presence of excessive amounts of iron(III) and copper(II). The excess hypophosphite had no effect on the recovery of arsenic.

Only antimony(III) at all concentration levels and germanium(IV) in excess of 100 μg were found to cause positive interference in the determination of arsenic. The influence of antimony(III) could be overcome by extracting off as antimony(III) triiodide into a 1:1 mixture of cyclohexanone–isobutyl methyl ketone from 0.5*M* sulphuric acid and 0.25*M* potassium iodide. The inclusion of this step also eliminated the difficulties arising due to dispersion of copper(I) iodide in the organic layer when copper(II) in excess of 1 mg was present with arsenic.

Application of the method to real samples

Table 1 presents the results of the analysis of several arsenic containing samples with and without added standard by the proposed procedure. The water samples were filtered immediately after collection and acidified with sulphuric acid to ~pH 1. The solid samples were brought into solution with 1:1 sulphuric acid and hydrogen peroxide.[16,17] After evaporating almost to dryness to decompose excess

peroxide, the residue was dissolved in 10 ml of water, filtered if necessary, and made up to known volume with water. Suitable aliquots were subjected to determination following the procedure given under 'Experimental'. As no standard samples were available, the arsenic content of brass,[17] plant materials[18] and water[19] was also established following the standard molybdenum blue method after separation of arsenic. The results summarized in Table 1 clearly show that the method developed works satisfactorily for the analysis of traces of arsenic in various materials.

CONCLUSION

The method described provides a simple and reliable means of determining trace amounts of arsenic by spectrophotometry. It is more sensitive ($\epsilon = 2.37 \times 10^5$ $1.mole^{-1}.cm^{-1}$) than those based on the formation of Molybdenum Blue ($\epsilon = 2.5 \times 10^4$ $1.mole^{-1}.cm^{-1}$) and reaction with silver diethyldithiocarbamate ($\epsilon = 1.4 \times 10^4$ $1.mole^{-1}.cm^{-1}$). It is superior to the fluoresence method based on the use of Rhodamine B in that the colour system is quite stable and can find use for the determination of both arsenic(III) and arsenic(V) in the range 0.03–1.0 μg. The method also has the advantage of virtual freedom from interferences from extraneous ions and can therefore find use for the rapid and precise determination of trace amounts of arsenic in natural and synthetic samples.

Acknowledgement—One of us (KP) is grateful to CSIR, New Delhi for the award of a Research fellowship.

REFERENCES

1. K. Sugawara, M. Tanaka and S. Manamori, *Bull. Chem. Soc.* Japan, 1956, **29**, 670.
2. G. Stratton and H. C. Whitehead, *J. Am. Wat. Wks. Ass.*, 1962, **54**, 172.
3. C. Matsubara, Y. Yamamoto and K. Takamura, *Analyst*, 1987, **112**, 1257.
4. T. Nasu and K. Kan, *ibid.*, 1988, **113**, 1683.
5. T. V. Ramakrishna and K. Palanivelu, *Indian J. Environ. Protection*, 1989, **9**, 265.
6. *Vogel's Quantitative Inorganic Analysis Including Elementary Instrumental Analysis* (revised by J. Bassett, R. C. Denney, G. H. Jefferey and J. Mendnan), 4th Ed., p. 386. ELBS, Longman, London, 1978.
7. D. Yamamoto and K. I. Kisu, *Japan Analyst*, 1974, **23**, 638; *Anal. Abstr.*, 1975, **29**, 1B134.
8. *Volgel's Text book of Practical Organic Chemistry including Qualitative Organic Analysis* (B. S. Furniss, A. J. Hannford, V. Rogers, P. W. G. Smith and A. R. Tatchell), 4th Ed., p. 266. ELBS and Longman, London, 1978.
9. *Ibid.*, B. S. Furniss, A. J. Hannford, V. Rogers, P. W. G. Smith and A. R. Tatchell), 4th Ed., p. 272. ELBS and Longman, London, 1978.
10. A. R. Byrne and D. Gorenc, *Anal. Chim. Acta*, 1972, **59**, 81.
11. E. M. Donaldson and M. Want, *Talanta*, 1986, **33**, 35.
12. K. Tanaka, *Japan Analyst*, 1960, **9**, 700, *Anal. Abstr.*, 1961, **9**, 3714.
13. N. Suzuki, K. Satoh, H. Shoji and H. Imura, *Anal. Chim. Acta*, 1986, **185**, 239.
14. D. E. Long, *ibid.*, 1969, **46**, 193.
15. S. Motomizu and K. Toei, *ibid.*, 1977, **89**, 167.
16. *Report of the analytical methods committee on oxidation of organic matter*, *Analyst*, 1967, **92**, 403.
17. F. D. Snell, *Photometric and Fluorimetric Methods of Analysis of Metals*, Part I, p. 354. Wiley-Interscience, New York, 1978.
18. *Idem*, *ibid.*, Part I, p. 343. Wiley-Interscience, New York, 1978.
19. F. J. Welcher, *Standard Method of Chemical Analysis*, Vol. 2, Part B, 6th Ed., p. 2402. D. Van Nostrand Co., 1963.

Talanta, Vol. 39, No. 5, pp. 563–566, 1992
Printed in Great Britain.

0039-9140/92 $5.00 + 0.00

TECHNICAL NOTE

ELEMENTAL ANALYSIS OF BOVINE LIVER BY INDUCTIVELY COUPLED PLASMA ATOMIC EMISSION SPECTROMETRY BY USING A SIMPLE DISSOLUTION PROCEDURE

T. N. Asp and W. Lund
Department of Chemistry, University of Oslo, Box 1033, N-0315 Oslo, Norway

(*Received* 31 *May* 1991. *Revised* 5 *September* 1991. *Accepted* 23 *October* 1991)

Summary—A simple digestion with nitric acid followed by filtration of the undigested lipids was found to be suitable for the decomposition of bovine liver, prior to multielement determination by inductively coupled plasma atomic emission spectrometry. Using reference materials, accurate results were obtained for cadmium, copper, iron, manganese, molybdenum and zinc.

The determination of metals in bovine liver by inductively coupled plasma atomic emission spectrometry (ICP–AES) requires dissolution of the sample. Many different decomposition methods can be used for this purpose.[1] Decomposition with a single acid or acid mixtures is performed either on a hot plate, in a microwave oven or under pressure in Teflon-lined steel bombs. Dry ashing is done either in a temperature-programmed muffle furnace, or by low temperature ashing in a low pressure oxygen plasma. Also solubilization with tetramethyl ammonium hydroxide may be used. De Boer and Maessen[2] compared all of these methods for the decomposition of bovine liver prior to ICP–AES analysis, and showed that in skilled hands, most of the methods gave accurate results for at least some elements. Dahlquist and Knoll[3] have compared wet and dry ashing of bovine liver for ICP–AES analysis, and found that wet ashing gave poorer detection limits because of the dilution, whereas dry ashing gave rise to element losses. Other workers have also used dry ashing[4] or low temperature ashing[5] for multielement analysis of bovine liver and other biological tissues by ICP–AES.

Apparently, there is not one decomposition method that stands out as the method of choice. However, the methods differ much with respect to the reagents used and the equipment and time needed for the digestion. An acid mixture which includes perchloric acid will normally ensure a complete mineralization of the biological material, but the use of perchloric acid should be avoided whenever possible, for safety reasons. Dry ashing in a muffle furnace usually requires heating for 10–30 hr, and the choice of a suitable crucible material and temperature programming is often essential. In addition, the use of an ashing aid such as magnesium nitrate is not to be recommended for dry ashing in combination with ICP–AES, because a high concentration of magnesium gives rise to an enhanced background and a depression of the emission signals.[6–8] The use of a microwave oven, high pressure bombs and low temperature ashing all require special equipment.

For routine analysis, an attractive decomposition procedure would be one that utilizes standard equipment, has a short digestion time, low reagent consumption and a low dilution factor. The last point is important because of the moderate detection limits of ICP–AES.

The suitability of a simple procedure based on heating with nitric acid was investigated in this work. A low dilution factor was considered essential, in order to determine trace metals like cadmium. Bovine liver is not a difficult matrix to dissolve, but some fat usually remains after treatment with nitric acid. Low values have been reported for copper and iron in bovine liver, using extraction with cold nitric acid.[2]

EXPERIMENTAL

Apparatus

A Perkin–Elmer ICP 5500B sequential inductively coupled argon plasma atomic emission spectrometer was used. The plasma generator, operating at 27.12 MHz, and the torch box was identical with those of the Perkin–Elmer ICP 6500, but the data system was a Model 3600 computer with a PR-100 printer. An all-quartz torch was used instead of the demountable torch. A peristaltic pump and a cross-flow nebulizer were used for sample introduction.

Materials

All reagents were of analytical-reagent grade. Multielement standard solutions were prepared from 1000 ± 0.5 ppm single-element standards (Spectrascan, Oslo). The bovine liver materials analysed were SRM 1577a from the National Institute of Standards and Technology (NIST; Gaithersburg, USA) and NSC-2 from Czechoslovakia.[9]

Digestion procedures

Procedure A (recommended). To a 0.5-g sample, add 10 ml of 65% nitric acid in a beaker and boil on a hot plate until *ca.* 1 ml of acid remains (1–2 hr). Transfer to a 10-ml standard flask and dilute to volume with water. Filter through a filter paper (Black Ribbon) before the ICP analysis.

Procedure B. Same as procedure A, except that the solution, including the water used for washing the beaker is filtered, before dilution to 10 ml in a standard flask.

Procedure C. To a 0.8–1.0-g sample, add 7 ml of nitric acid and 7 ml of water in a beaker and let it stand for 24 hr at room temperature. Filter the solution (and the washings) through a filter paper into a 25-ml standard flask and dilute to volume.

Procedure D. Same as procedure A, except that the remaining solution (*ca.* 1.5 ml) is finally diluted to 10 ml with methanol instead of water, and the filtration is omitted.

Procedure E. To a 1-g sample, add 16 ml of an acid mixture consisting of 9 ml of nitric acid, 6 ml of perchloric acid (70%) and 1 ml of sulphuric acid (95.5%). Heat on a water bath by slowly increasing the bath temperature to 100°, then continue the digestion on a hot plate until *ca.* 1 ml of acid remains. Cool, transfer to a 25-ml standard flask and dilute to volume with water.

Measurements

The plasma conditions used in this work were: plasma power 1.0 kW, plasma gas flow-rate 15 l./min, nebuliser gas flow-rate 1 l./min and viewing height 18 mm. The wavelengths used for the emission measurements were (in nm): Cd: 228.80, Cu: 324.75, Fe: 261.19, Mn: 257.61, Mo: 281.62, Zn: 213.85. Background correction was used for cadmium, manganese and molybdenum. The instrument was standardized with two multielement standard solutions. For each digestion procedure, the standards were matrix-matched with the samples, with respect to the concentration of acids. Also, three blank digestions were carried out for each procedure. Of the resulting solutions, one was run as a blank, while the other two were run as unknowns (control). The blank values were usually less than 10% of the sample concentrations.

RESULTS AND DISCUSSION

The two bovine liver materials SRM 1577a and NSC-2 were analysed. NSC-2 was obtained from Czechoslovakia and had a certified value only for cadmium.[9] The results obtained, using the digestion procedures A, B, C and E (see Experimental) are given in Tables 1–3. The two sets of results reported for procedure A in Tables 1 and 3 refer to digestions carried out at different dates. Each value given represents

Table 1. Results (μg/g; $n = 3$) for cadmium, copper and iron in SRM 1577a (NIST) bovine liver

	Cadmium		Copper		Iron	
Procedure	Mean	S.D.	Mean	S.D.	Mean	S.D.
Certified value	0.44	0.06*	158	7*	194	20*
A	0.48	0.06	160	5	188	9
A	0.40	0.02	167	3	206	12
B	0.30	0.03	125	6	154	5
C	0.27	0.03	125	2	115	5

*95% confidence limit.

Table 2. Results (μg/g; $n = 3$) for manganese, molybdenum and zinc in SRM 1577a (NIST) bovine liver

	Manganese		Molybdenum		Zinc	
	Mean	S.D.	Mean	S.D.	Mean	S.D.
Certified value	9.9	0.8*	3.5	0.5*	123	8*
Procedure A	10.7	0.3	3.5	0.2	123	3

*95% confidence limit.

the mean of the results from three parallel digestions. The corresponding standard deviations are also given. The standard deviations for repeated ICP-analyses of each sample solution are not shown, but these were generally lower than the standard deviations for parallel digestions.

From the Tables it can be seen that only procedure A gave results in agreement with the certified values for all metals and both samples studied. For copper and iron in NSC-2, the results should be compared with those obtained by procedure E, due to the absence of certified values.

The concentration of cadmium (Tables 1 and 3) was close to the detection limit. When the detection limit was determined experimentally,[10] a value of 4 μg/l. was obtained, based on three times the standard deviation of the background signal. This corresponds to 0.08 μg/g dry liver, when procedure A is used. For the other elements, the detection limits were of little interest, because these were at least a factor of 0.002 lower than the actual concentrations in the liver material, except for molybdenum, where the factor was *ca.* 0.05.

All samples were apparently dissolved completely, after being boiled with nitric acid for 1–2 hr (procedure A). However, when the digest was cooled, some fat appeared on the surface, and some was also formed when the digest was diluted with demineralized water. For this reason, the solution was filtered before the ICP analysis. From Tables 1 and 3 it can be seen that the filtration must be done after the sample has been diluted to volume (procedure A). If the digest is filtered before the final dilution to 10 ml (procedure B), low results are obtained, because of adsorption losses during the filtration. It was found that the adsorption losses could be minimized by a more thorough washing of the filter paper, but the resulting larger dilution factor prevented the quantitative determination of cadmium in this case.

Low results were also obtained with procedure C, indicating that treatment with diluted nitric acid at room temperature for 24 hr does not release all metal. The method is similar to the extraction procedure used by De Boer and Maessen,[2] who also obtained low results for copper and iron. Obviously a high temperature is more efficient than a long time for releasing these metals. Somewhat better results were obtained when concentrated nitric acid was used instead of the 1 + 1 diluted acid in procedure C, but the values were still low.

To avoid the formation of fat, attempts were made to dilute the solution to volume with methanol instead of water (procedure D). It was found that the resulting solution (85% methanol) could be handled by the ICP-instrument, provided a more narrow injection tube (0.85 mm), a higher power (1.3 kW), and an auxiliary gas flow (1 l./min) were used. However, the methanol depressed the emission signals, and caused a high and structured background around the three most useful

Table 3. Results (μg/g; $n = 3$) for cadmium, copper and iron in NSC-2 (Czechoslovakia) bovine liver

	Cadmium		Copper		Iron	
Procedure	Mean	S.D.	Mean	S.D.	Mean	S.D.
Certified value	0.43	0.03*				
A	0.49	0.03	52	1	301	8
A	0.43	0.07	49	2	303	16
B	0.30	0.06	40	4	246	26
C	0.29	0.04	41	1	220	4
E	0.48	0.05	49	2	297	13

*95% confidence limit.

cadmium lines (214.44, 226.50 and 228.80 nm). Therefore, cadmium could not be determined in the samples diluted with methanol. In addition, the plasma was unstable and carbon was deposited in the injection tube. Therefore, the use of a methanol–water mixture as solvent appears to be unattractive for the determination of trace metals in biological material by ICP–AES.

REFERENCES

1. F. J. M. J. Maessen, in P. W. J. M. Boumans (ed.), *Inductively Coupled Plasma Emission Spectroscopy*, Part 2, p. 100. John Wiley, New York, 1987.
2. J. L. M. De Boer and F. J. M. J. Maessen, *Spectrochim. Acta*, 1983, **38B**, 739.
3. R. L. Dahlquist and J. W. Knoll, *Appl. Spectrosc.*, 1978, **32**, 1.
4. K. A. Wolnik, J. I. Rader, C. M. Gaston and F. L. Fricke, *Spectrochim. Acta*, 1985, **40B**, 245.
5. K. Shiraishi, G. Tanaka and H. Kawamura, *Talanta*, 1986, **33**, 861.
6. T. N. Asp and W. Lund, unpublished results.
7. G. F. Larson and V. A. Fassel, *Appl. Spectrosc.*, 1979, **33**, 592.
8. M. Thompson and M. H. Ramsey, *Analyst*, 1985, **110**, 1413.
9. P. Mader, J. Kucera, J. Cibulka and D. Miholova, *Chem. Listy*, 1989, **83**, 765.
10. G. F. Wallace and P. Barrett, *Analytical Methods Development for Inductively Coupled Plasma Spectrometry*, p. 3–3. Perkin–Elmer, Norwalk, 1981.

Talanta, Vol. 39, No. 5, p. 567, 1992
Printed in Great Britain

0039-9140/92 $5.00 + 0.00
Pergamon Press plc

BOOK REVIEW

Principles and Practice of Chromatography: B. RAVINDRANATH, Ellis Horwood, Chichester, 1989. Pages 502. £67.70.

This book is divided into four unequal parts. The first part—Basic Principles—is 62 pages long and consists of an overview and some theoretical concepts. The second part—Gas Chromatography—is a little longer (100 pages) and deals with basic instrumentation, separation and detection systems. The third part—Liquid Chromatography—is the longest (200 pages) and is broken up into three sections. The first section—Principles and Methods—includes work on size-exclusion chromatography (SEC), hydrodynamic chromatography (HDC), field-flow fractionation (FFF), counter-current chromatography (CCC), ion-exchange chromatography (IEC), suppressor ion chromatography (SIC), and hydrophobic (interaction) chromatography (HIC). The second section is on HPLC and the third section is headed "Planar Chromatography" and includes some work on HPTLC. Part 4—Applications—is 80 pages long and is divided into chemical, biological and biomedical, industrial, and miscellaneous subsections. The last includes some environmental applications. The references cover the period up to 1987.

The book is well written and the diagrams are good. It is quite comprehensive and is to be recommended.

W. BRYCE

Talanta, Vol. 39, No. 6, pp. 569–572, 1992
Printed in Great Britain.

0039-9140/92 $5.00 + 0.00

SURFACE ENHANCED RAMAN SPECTROSCOPY ON COPPER HYDROSOLS

MARTIN J. ANGEBRANNDT and JAMES D. WINEFORDNER*
University of Florida, Gainesville, Florida 32611, U.S.A.

(*Received* 1 *August* 1991. *Revised* 7 *November* 1991. *Accepted* 14 *November* 1991)

Summary—Surface enhanced Raman spectroscopy (SERS) allows the detection of trace quantities of molecular species adsorbed onto a surface. The potential use of silver colloids as substrates for analytical SERS measurements is demonstrated. Detection limits and other analytical figures of merit for pyridine, *p*-aminobenzoic acid and *p*-nitrobenzoic acid are presented.

It has been established that the Raman scattering cross section can be increased by up to six orders of magnitude by bringing the molecule close to a surface.[1,2] Copper, gold and silver surfaces have generated the largest enhancements.[3,4] Because of this enhancement, Raman spectrometry can compete more effectively as a trace analysis technique with other molecular spectroscopies, such as fluorescence and phosphorescence. The advantage of surface enhanced Raman spectrometry (SERS) over these techniques is two-fold. First, not all molecules fluoresce or phosphoresce, whereas all molecules have vibrational modes accessible to SERS. Secondly, a SERS spectrum provides a wealth of information, allowing one to identify the molecule and/or differentiate it from a similar molecule. These provide the impetus for the development of SERS as a trace analytical technique. Reviews by Garrell[5] and Campion and Woodruff[6] have focussed on the application of Raman techniques to analytical problems.

Silver and gold colloids were first used as SERS substrates in 1979 by Creighton *et al.*[7] Most research on SERS has involved silver colloids as the substrate. Silver colloids are easily produced, provide fresh surfaces for adsorption of analyte molecules, and are easily excited by the 514.5 nm line of an argon ion laser. Silver hydrosols have been used for the quantitative analysis of drugs[8–10] and nitrogen containing heterocycles.[11,12]

Silver hydrosols have also been adapted for use with flow-injection analysis[13–15] and HPLC[16,17] systems; on line measurements increase reproducibility, thus lowering limits of detection. SERS has also been adapted to both paper[17,18] and thin layer chromatography[19] in an effort to further increase the detection power as well as the identification power of these separation techniques.

Copper colloids were first evaluated[20] for SERS in 1983; other studies[21–23] have also shown useful SERS spectra could be obtained with copper colloids. In this study, the SERS enhancement of pyridine by a citrate stabilized copper hydrosol was investigated. A later study found there was competitive adsorption between pyridine and citrate onto the silver colloid surface.[24] To minimize this interference, an unprotected copper colloid was used in the present study. The chemical enhancement mechanism should play a larger role with copper colloids than with silver colloids. However, the strength of the SERS signal also depends upon the number of analyte molecules in contact with the surface. The present work involves the investigation of copper colloids for use as an analytical SERS substrate. The colloidal surface is prepared by a simple borohydride reduction of cupric nitrate. These results illustrate the future of SERS on copper colloids for qualitative and quantitative analytical use.

EXPERIMENTAL

Apparatus

The instrumental set-up involved conventional 90° excitation–observation measurements. A Spectra Physics 2040 argon ion laser was used to pump a Spectra-Physics model

*Author for correspondence.

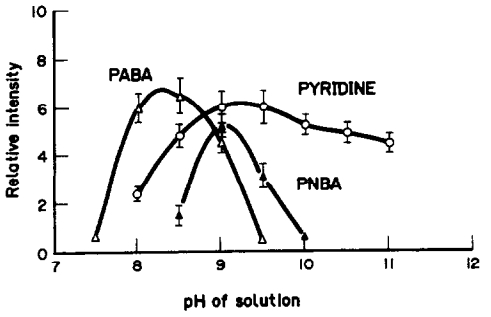

Fig. 1. The relative SERS intensity of the most intense band of the analytes as a function of pH. A 10 μg/ml solution and the 1010 cm^{-1} band were used for the pyridine curve. A 50 μg/ml solution was used for the evaluation of the 1397 cm^{-1} band of PABA and the 1387 cm^{-1} band of PNBA. Excitation is at 660 nm (150 mW).

375 dye laser (Spectra-Physics, Mountain View, CA). DCM (Exciton, Dayton, OH) was used to produce the necessary wavelengths. All measurements were made relative to the 200 mW of 660-nm exciting radiation. The stability of the output power and lasing frequency were continuously monitored with both a power meter and a 0.3-m McPhereson model 218 monochromator (McPhereson, Acton, OH) with a R928 Hamamatsu photomultiplier tube. The laser beam was directed through the sample twice and the scattered radiation collected at 90°. A 0.22-m Spex model 1680B double monochromator (Spex, Edison, NJ) with slits set for 6 cm^{-1} resolution was used for wavelength discrimination. The Raman scatter was detected with a thermoelectrically cooled (R636 Hamamatsu) photomultiplier tube. The photoelectron pulses were amplified and counted with a Stanford model 440 photon counter with a 1-sec acquisition time. The data was collected on an IBM PC. The Raman bands used for quantitative measurements were 1010, 1397 and 1387 cm^{-1} for pyridine, *p*-aminobenzoic acid, and *p*-nitrobenzoic acid respectively.

Chemicals and procedure

A 30-ml volume of a $2 \times 10^{-3} M$ cupric nitrate solution was added dropwise to 70 ml of a fresh $1.4 \times 10^{-2} M$ sodium borohydride solution at room temperature with stirring. Volumes (50 μl–200 ml) of analyte (1–200 μg/ml) were added to 100 ml of the above colloidal solution. The pH of the solution was then adjusted to maximize the SERS signal as shown in Fig. 1, using a small amount of nitric acid. The pyridine solutions were prepared in Barnstead distilled water. The PABA and PNBA solutions were prepared in 50:50 methanol:water solutions, using sonication if necessary. A portion of this pH adjusted solution was then placed in a standard 1×1 cm^2 cuvette. Measurements began 2.0 min after the first two reagents were completely combined. All glassware had been cleaned thoroughly with concentrated nitric acid and then rinsed repeatedly with Barnstead water. Pyridine, *p*-nitrobenzoic acid (PNBA), methanol and sodium borohydride were obtained from Kodak (Rochester, NY). Cupric nitrate and *p*-aminobenzoic acid (PABA) were obtained from Fisher Scientific (Pittsburgh, PA). The solutions of PABA and PNBA were prepared in 20% (v/v) methanol. All chemicals were analytical reagent grade or equivalent and were used without further purification.

RESULTS AND DISCUSSION

Pyridine (the major SERS peaks are given in Table 1) was chosen as the test compound for the initial optimization because it is soluble in water, has a large Raman cross section, adsorbs strongly to colloidal surfaces and SERS from pyridine has been observed previously on copper colloids. The enhancement factor for the pyridine 1010 cm^{-1} band, corrected for prefilter and post filter effects was calculated to be 1.8×10^5, which is in good agreement with previous results.[20] Pyridine proved a good choice, because of the relatively small effect that pH had upon its SERS signal relative to those of the other analytes (Fig. 1). The pH (~8.5) for the observation of the maximum SERS signal from pyridine differed from the pH previously observed for the copper electrode[25] and the copper colloid[20] studies. The pH for peak SERS signals for our system is 1.5 units higher than the study with the copper electrode,[25] where a

Table 1. Major SERS Peaks for Pyridine, PABA and PNBA

Molecule	Solution	SERS
Pyridine	715	705
	1006	1010
	1020	
	1362	1359
	1635	1630
PABA		1211
		1278
		1397
		1506
		1606
PNBA		1387
		1487
		1595

pH of 7.0 was used; the copper colloids undergo dissolution at approximately pH 7.0. The surface potential of the colloid in our case was controlled by the adsorbed species and the ionic strength, rather than with a potentiostat. The largest difference between these colloidal systems is the use of citrate as a protecting agent; citrate covers the colloid surface changing both the surface charge of the colloid and the partitioning of the pyridine between the bulk phase and the surface. In addition, there is competition between citrate and pyridine for the colloidal surface. PABA and PNBA exhibit a rather narrow pH range (optimum pH ~ 8.0 for PABA and pH ~ 9.5 for PNBA) over which appreciable SERS signals were obtained. The major SERS peaks (550–1900 cm^{-1}) for PABA and PNBA are given in Table 1; peaks agree well with those measured by other workers[26–29] obtained at silver electrodes and with silver-colloids.

Absorption spectra taken over a time period of about 15 min indicated colloidal particle sizes between ~20 and 100 nm and indicated considerable temporal instability of the copper colloids. As a result of the poor colloid stability, it was difficult to obtain reliable Raman spectra with wavelength scanning. Others[20,22–24] have obtained greater stabilities; however, in these cases, citrate was used to stabilize the colloids. Unfortunately, citrate competes with the analytes for the available surface sites and thus smaller enhancement factors should result with the previous citrate method. In addition, the time required for the citrate stabilized copper colloids[20,22–24] to reach maximum enhancement was 2–4 times as long as for our colloids (~13 min in our case). The present copper colloids protocol should therefore find more analytical use in flow-injection systems where timing and flow rates can be carefully controlled.[13,14] Nevertheless, we have evaluated the copper colloid system for *para*-aminobenzoic acid (PABA) and *para*-nitrobenzoic acid (PNBA) as well as pyridine (PY). The time-dependent SERS signals (1606 and 1397 cm^{-1}) for PABA are shown in Fig. 2.

The copper colloid system has a much lower background from Mie scatter than that observed with silver colloidal system because of the longer wavelength used for the former. Unfortunately, the SERS signals are also smaller, so that the signal to background ratio is not improved. An additional problem as stated above is that our copper colloid solutions

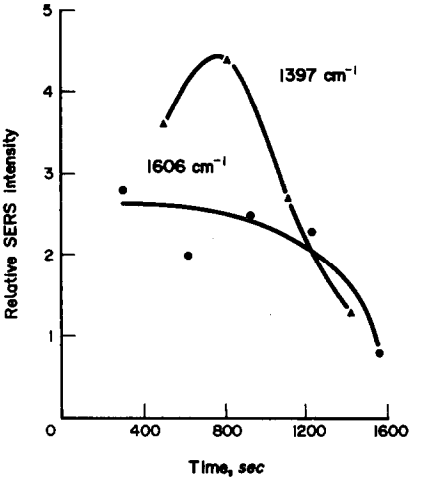

Fig. 2. Intensities of the 1606 cm^{-1} (filled triangle) and 1397 cm^{-1} (filled circle) SERS bands of PABA as a function of time. Conditions are the same as those in Fig. 1.

cannot be prepared more than 15 min ahead of time, whereas the silver colloid can be made stable for weeks.[7,16]

The colloidal copper surface has a linear dynamic range of 1–1.5 orders of magnitude (see Fig. 3) with an RSD of 15%. This limited dynamic range (LDR) is common with colloidal systems, since the signal is dependent on the adsorption isotherm. The limited LDR is the greatest disadvantage of colloidal based SERS. The limits of detection for PY, PABA, and PNBA are estimated to be 1.5 μg/ml ($1.9 \times 10^{-5} M$), 2.5 μg/ml ($1.8 \times 10^{-5} M$), and 13 μg/ml ($7.8 \times 10^{-5} M$), respectively. These results represent the first reported detection limits for SERS with copper colloids.

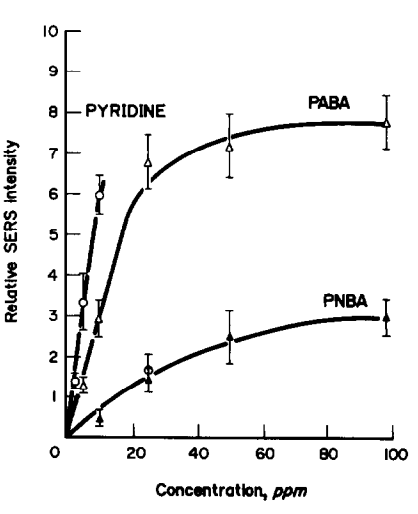

Fig. 3. Calibration curves for pyridine, PABA and PNBA. Conditions are as stated in Fig. 1 (excitation wavelength, laser region, peak pH values and Raman peaks).

REFERENCES

1. M. Fleishmann, P. J. Hendra and A. J. McQuillan, *Chem. Phys. Lett.*, 1974, **26**, 123.
2. D. L. Jeanmaire, R. P. Van Duyne, *J. Electroanal. Chem.*, 1977, **84**, 1.
3. H. Seki, *J. Electron Spec. Relat. Phenom.*, 1986, **39**, 289.
4. D. A. Weitz, M. Moskovits and J. A. Creighton, in *Chemistry & Structure at Interfaces: New Laser & Optical Techniques*, R. B. Hall and A. B. Ellis (eds.), p. 197. VCH Publishers, New York, 1986.
5. R. L. Garrell, *Anal. Chem.*, 1989, **61**, 401A.
6. A. Campion and W. H. Woodruff, *ibid.*, 1987, **59**, 1299A.
7. J. A. Creighton, C. G. Blatchford and M. G. Albrecht, *J. Chem. Soc. Faraday Trans. II*, 1979, **75**, 790.
8. W. S. Sutherland, J. J. Laserna, M. J. Anbebranndt and J. D. Winefordner, *Anal. Chem.*, 1990, **62**, 689.
9. E. L. Torres and J. D. Winefordner, *ibid.*, 1987, **59**, 1626.
10. J. J. Laserna, E. L. Torres and J. D. Winefordner, *Anal. Chim. Acta*, 1987, **200**, 469.
11. T. Vo-Dinh, in *Chemical Analysis of Polycyclic Aromatic Compounds*, T. Vo-Dinh (ed.), p. 451. Wiley, New York, 1989.
12. J. J. Laserna, A. D. Campiglia and J. D. Winefordner, *Anal. Chem.*, 1989, **61**, 1697.
13. J. J. Laserna, A. Berthod and J. D. Winefordner, *Microchem. J.*, 1988, **38**, 125.
14. *ibid.*, *Appl. Spectrosc.*, 1987, **41**, 1137.
15. R. D. Freeman, R. M. Hammaker, C. E. McLean and W. G. Fateley, *Appl. Spectrosc.*, 1988, **42**, 456.
16. R. Sheng, R. Ni and T. M. Cotton, *Anal. Chem.*, 1991, **63**, 437.
17. A. Berthod, J. J. Laserna and J. D. Winefordner, *J. Pharm. Biomed. Anal.*, 1988, **6**, 599.
18. J. M. Sequaris and E. Koglin, *Z. Anal. Chem.*, 1985, **321**, 758.
19. J. M. Sequaris and E. Koglin, *Anal. Chem.*, 1987, **59**, 527.
20. J. A. Creighton, M. S. Alvarez, D. A. Weitz, S. Garoff and M. W. Kim, *J. Phys. Chem.*, 1983, **87**, 4793.
21. L. A. Lipscomb, S. Nie, S. Feng and N. T. Yu, *Chem. Phys. Lett.*, 1990, **170**, 457.
22. S. Sanchez-Cortes and J. V. Garcia-Ramos, *J. Raman Spectrosc.*, 1990, **21**, 679.
23. S. M. Angel, L. F. Katz, D. P. Archibald and D. E. Honig, *Appl. Spectrosc.*, 1989, **43**, 367.
24. S. M. Heard, F. Grieser, C. G. Barraclough and J. V. Sanders, *J. Phys. Chem.*, 1985, **89**, 389.
25. T. P. Mernagh and R. P. Cooney, *J. Raman Spectrosc.*, 1985, **16**, 62.
26. P. G. Roth, R. S. Venkatachalam and F. J. Doeno, *J. Chem. Phys.*, 1986, **85**, 1150.
27. S. San, R. L. Birke, J. R. Lombardi, K. G. Leung and A. Z. Genach, *J. Phys. Chem.*, 1988, **92**, 5965.
28. H. Parks, S. Bok, K. Kim and M. S. Kim, *J. Phys. Chem.*, 1990, **94**, 7576.
29. R. S. Venkatachalam, F. J. Boernig and P. G. Roth, *J. Raman Spectrosc.*, 1988, **19**, 281.
30. P. B. Johnson and R. W. Christy, *Phys. Rev. B.*, 1972, **6**, 4370.

Talanta, Vol. 39, No. 6, pp. 573–580, 1992
Printed in Great Britain.

0039-9140/92 $5.00 + 0.00

DETECTION OF LOW MOLECULAR WEIGHT ALDEHYDES IN AQUEOUS SOLUTION BY MEMBRANE INTRODUCTION MASS SPECTROMETRY

TARUN K. CHOUDHURY, TAPIO KOTIAHO* and R. GRAHAM COOKS†
Department of Chemistry, Purdue University, West Lafayette, IN 47907, U.S.A.

(*Received* 25 *September* 1991. *Revised* 5 *November* 1991. *Accepted* 6 *November* 1991)

Summary—Membrane introduction mass spectrometry (MIMS) is used to detect low molecular weight aldehydes in aqueous solutions. The best sensitivity was obtained by aqueous phase derivatization of aldehydes with *O*-(2,3,4,5,6-pentafluorobenzyl)-hydroxylamine (PFBOA) and electron capture detection. This negative chemical ionization mass spectrometry procedure allowed the measurement of C_1–C_6 aldehydes at low concentrations in mixtures. The characteristic ion signals in the mass spectrum of the mixture were verified by examining the full mass spectra and product ion MS/MS spectra of the derivatives of individual aldehydes. A reaction scheme is proposed to explain the fragmentation pattern of the molecular anions ($M^{-\cdot}$) of the derivatives. The processes observed include loss of HF to form $(M–HF)^{-\cdot}$ ions which then competitively fragment by elimination of H(R)CN and NO$^{\cdot}$ to produce ions of *m/z* 178 and $(M–50)^{-\cdot}$, respectively. Multiple reaction monitoring was applied to establish the lower limits of detection. Formaldehyde could be detected without preconcentration at 1 ppb with S/N = 3/1. The detection limits of acetaldehyde, propanal and butanal were found to be 10 ppb and that of pentanal and hexanal were found to be 20 ppb. Response curves *vs.* concentration are linear in the ppb range. This method is not as readily applicable to the corresponding ketones.

Low molecular weight carbonyl compounds are often present in drinking water,[1] where one of the major sources is the ozonation process used during water purification.[1] In addition to its use as a disinfectant, ozone is used to control odor, color and to reduce the iron and manganese content of water.[2] Carbonyl compounds are also formed naturally by the photodissociation of dissolved organic compounds in water.[3] In addition, industrial effluents can be a direct source of carbonyl compounds which are major by-products of some industrial processes and of such materials as industrial surfactants.[4] Of the low molecular weight carbonyl compounds, formaldehyde is of special interest because of its toxicity. Formaldehyde is mutagenic for some bacteria, fungi and yeasts[5] and has also been proven to be carcinogenic to rats and mice during long term inhalation exposure, even at low concentrations (2 ppm).[5] Due to these facts, safety levels of 0.11 mg/l. for adults[6] and 0.030 mg/l. for children[7] have been proposed for formaldehyde in drinking water. The high reactivity of carbonyl compounds with nucleophiles is an additional factor which makes the qualitative and quantitative analysis of these compounds in drinking water desirable.

Various analytical techniques have been applied for the detection of carbonyl compounds in ozonated water. Sievers *et al.*[8] used gas chromatography (GC) and gas chromatography/mass spectrometry (GC/MS) to study the products of secondary treated domestic waste water. They concentrated their samples with a polymeric sorbent (Tenax) prior to gas chromatographic analysis with a flame ionization detector or mass spectrometric detection. They were able to measure sub ppb levels of low molecular weight aldehydes. Kobayashi *et al.*[9] used GC with a flame ionization detector to quantify the low molecular weight carbonyl compounds in aqueous solutions as their pentafluorophenyl hydrazone derivatives at 200 ppb–8 ppm levels. Yamada and Somiya[10] used *O*-(2,3,4,5,6-pentafluorobenzyl)-hydroxylamine (PFBOA) to derivatize carbonyl compounds and GC with electron capture detection (ECD) to measure low ppb levels of the PFBOA derivatives. Glaze *et al.*[1] modified the aqueous-phase derivatization method for the detection of carbonyl compounds by using a high resolution

*On leave from Technical Research Center of Finland, Chemical Laboratory, Biologinkuja 7, 02150 Espoo, Finland.
†Author for correspondence.

capillary GC together with electron capture detection (ECD) or mass spectrometric detection (MS) with electron impact ionization. The reported detection limits were in the low ppb range for both detection modes.

PFBOA is an excellent derivatizing agent for carbonyl compounds since it reacts with them in aqueous solution to form the corresponding oximes (reaction 1).

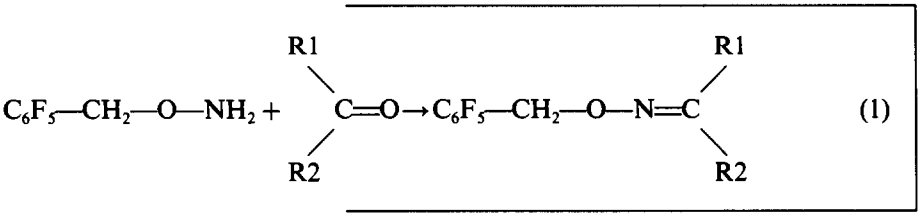

Also the high fluorine atom content of PFBOA derivatives of carbonyl compounds suggests that very low detection limits might be achieved if electron capture detection is used with negative chemical ionization mass spectrometry. The first results of this type are presented here. Another advantage of electron capture negative ion chemical ionization mass spectrometry is the improvement in selectivity and sensitivity.[11-13] Moreover, the stability and volatility of the PFBOA derivatives suggest that membrane introduction mass spectrometry could be an excellent analytical method to analyze these compounds directly from aqueous samples.

Membrane introduction mass spectrometry (MIMS) is a successful analytical technique for the introducton of volatile non-polar organic molecules from aqueous solution.[14] The use of semipermeable membranes as a selective barrier which allows permeation of dissolved gases, but not the liquid phase, was first introduced by Hoch and Kok[15] to monitor dissolved gases produced by photosynthesis. Since then, MIMS has been used increasingly for the detection of trace organic compounds and for monitoring reaction products.[16-26] In most of these experiments, the membrane was placed externally to the mass spectrometer. This kind of experimental arrangement can suffer from poor response time, memory effects and analyte dilution because of condensation along the transfer line between the membrane and the ion source of the mass spectrometer. These problems can be reduced by sweeping the permeate into the mass spectrometer with an inert gas.[18] Alternatively, they are eliminated by the flow-through method which uses a direct insertion membrane probe (DIMP).[27-29] The DIMP places the membrane within the ion source of the mass spectrometer and allows the sample to be transported directly into the heated ion source. These probes have been successfully used for detection of a variety of organic compounds in water at parts-per-billion levels[29,30] and for on-line monitoring or organic reactions and fermentation products of bioreactors.[31-35]

This paper reports the application of membrane sample introduction, in combination with negative ion mass spectrometry, to measure quantitatively low molecular weight aldehydes in aqueous solutions. The PFBOA derivatives of the aldehydes were introduced into the mass spectrometer, using the membrane introducton probe and characterized by their negative ion electron capture spectra. Detection limits were also of interest and were measured with multiple reaction monitoring.

EXPERIMENTAL

The experimental arrangement used is shown in Fig. 1. A tandem mass spectrometer with a sheet membrane mounted in a direct insertion membrane probe (S-DIMP), already described in previous publications,[29-32] was used for this study. The membrane chosen was a dimethyl vinyl silicone polymer (ASTM: VMQ Dow Corning) with a thickness of 0.25 cm. The membrane probe used is provided with a programmable temperature control system which was used to maintain the membrane at a tem-

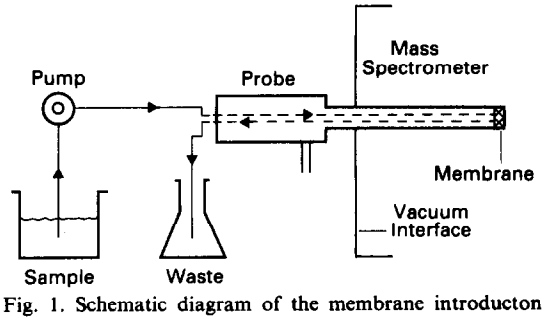

Fig. 1. Schematic diagram of the membrane introducton apparatus used in this study.

perature of 70° as read by a thermocouple located within the probe. A methanol–water (1:1) mixture was continuously pumped through the membrane interface at a rate of 1 ml/min with a peristaltic pump (Ismatec, Switzerland: model 7618-30). Methanol was used in the mixture in order to keep the sample introduction system clean. Sample plugs of 0.2-ml volume were injected into the methanol–water flow stream with a six-port liquid injector. The mass spectrometer used (Finnigan Corporation, San Jose, California, Model TSQ 4500) was operated with an INCOS data system. Negative ion chemical ionization was performed with isobutane as chemical ionization (CI) reagent to moderate electron energies and facilitate electron capture. The reagent gas pressure was 0.4 torr. Tandem mass spectrometry (MS/MS) product spectra were recorded in order to confirm the identity of the ions present in the mass spectra. In order to record the product spectra, a 20-eV collision energy and 1 mtorr of argon collision gas (*i.e.*, multiple collision conditions, approximately 80% beam attenuation) was chosen.

A stock solution containing 100 ppm each of C_1–C_7 aldehydes was made by dissolving the appropriate quantity of the compounds in methanol and diluting with distilled water. The stock solution was diluted successively with distilled water in order to make a series of solutions in the concentration range of 1 ppb–10 ppm for the measurement of detection limits. A 100-ppm solution of each of the compounds was prepared separately in order to study the mass spectra and MS/MS product ion spectra of individual aldehydes. *O*-(2,3,4,5,6-Pentafluorobenzyl)-hydroxylamine hydrochloride (PFBOA), supplied by Aldrich Chemical Company, Milwaukee, Wisconsin, was 99% pure. It was dissolved in distilled water in order to make a 1-mg/ml solution. The PFBOA derivatives were prepared by the method of Glaze *et al.*[1] To 5 ml of the aqueous sample was added 2 drops of 0.1*M* sodium thiosulphate and 0.5 ml of PFBOA solution. The mixture was shaken and allowed to react for a few minutes. Finally 1 drop of concentrated sulphuric acid was added before injection of the derivatized solution into the methanol–water flow stream.

RESULTS AND DISCUSSION

Electron impact (EI) spectra of the underivatized aldehydes examined in methanol at 100 ppm, were first recorded by MIMS. In the EI mass spectrum of formaldehyde, the molecular ion peak (*m/z* 30) was not readily observed because of the strong signals due to oxygen gas (*m/z* 32) and nitrogen gas (*m/z* 28). Similarly, in the EI mass spectrum of acetaldehyde, the signal due to carbon dioxide made it difficult to identify the molecular ion peak (*m/z* 44). For propanal a distinct molecular ion peak was observed at *m/z* 58 in the EI mass spectrum, but, it was not possible to detect sub ppm levels. For the other aldehydes (C_4–C_7), only fragment ions and no molecular ion peaks were observed. Since much better signal intensity and characteristic peaks for each of the aldehydes were observed by negative ion chemical ionization mass spectrometry of the PFBOA derivatives, this method was used to develop an analytical procedure for direct analysis of aldehydes in water samples.

Figure 2 shows the negative ion chemical ionization mass spectrum of a mixture of PFBOA derivatives of the C_1–C_7 aldehydes. The base peak at *m/z* 181 and the peak at *m/z* 197 both arise from the derivatizing group and are due to the pentafluorobenzyl anion $C_6F_5CH_2^-$ and the pentafluorobenzyloxy anion $C_6F_5CH_2O^-$, respectively. The second most intense peak at *m/z* 178 is due to successive loss of the neutral molecules HF and HCN (or RCN) *i.e.* ($M^{-\cdot}$–HF–H(R)CN). The loss of HF must involve a fluorine atom from the aromatic ring and is proposed to involve the cyclization shown in scheme 1. Further loss of HCN (or RCN) yields the quinoid anion radical shown.

The intact molecular ions of the PFBOA derivatives are of very low abundance compared to the base peak, *e.g.*, that for formaldehyde (*m/z* 225) is ~4% of the base peak. The peaks for the molecular anions are at *m/z* 239, 253, 267, 281 and 295 for the derivatives of acetaldehyde, propanal, butanal, pentanal and hexanal have less than 1% of the base peak abundance. The molecular ion peak for hepatanal (*m/z* 309) is of negligible intensity. Different ion source temperatures in the range 60–200° were used in order to check the effect of ion source temperature on the ion abundance. But, there was no noticeable change of signal intensity with the change of temperature indicating that the reactions shown in scheme 1 are ionic processes without contributions from thermal dissociation of the neutral PFBOA derivative. The $(M–HF)^{-\cdot}$ peaks at *m/z* 205, 219, 233, 247, 261, 275 and 289 for formaldehyde, acet-

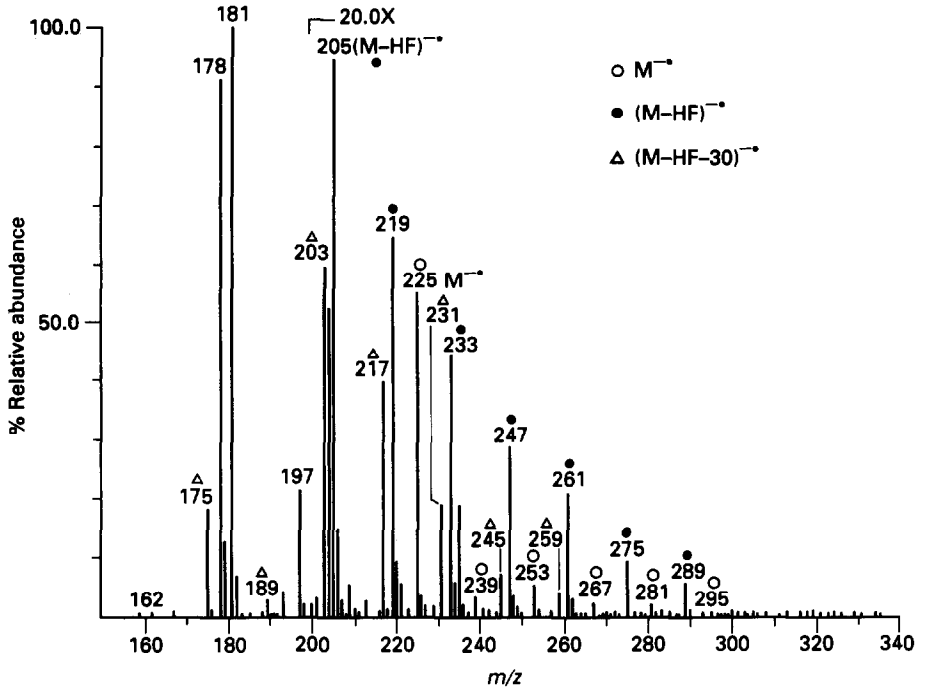

Fig. 2. Negative ion chemical ionization mass spectrum of PFBOA derivatives of a mixture containing 100 ppm of C_1–C_7 aldehydes.

aldehyde, propanal, butanal, pentanal, hexanal and heptanal, respectively, are significantly more abundant than the corresponding molecular ion peaks. As we go from m/z 205 towards m/z 289, the peak intensity decreases, indicating that as the size of the molecule increases the rate of permeation through the membrane decreases.

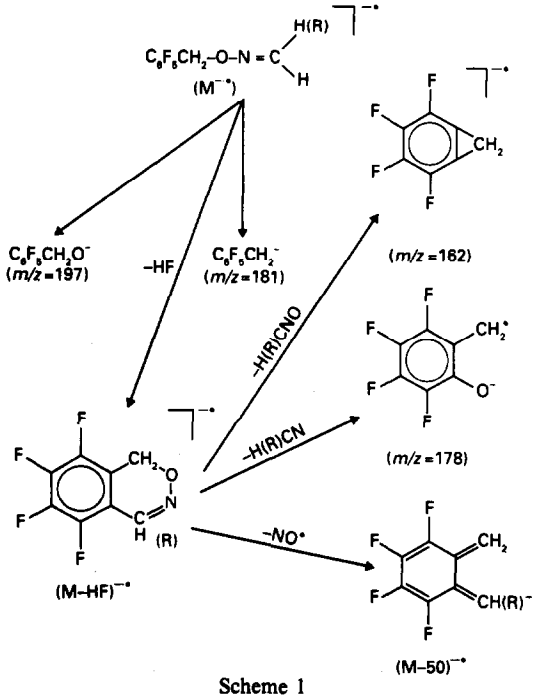

Scheme 1

Another factor that may be partly responsible for this observation is the higher reactivity of the smaller aldehydes towards the derivatizing agent. Similar results were observed by Glaze *et al.*[1]

In order to confirm the identity of the characteristic peaks in the mixture, mass spectra and product MS/MS spectra for each of the compounds were examined individually. The product MS/MS spectra of the molecular anion radicals for formaldehyde, acetaldehyde and propanal derivatives are shown in Fig. 3(a), (b) and (c), respectively. The product MS/MS spectra for the other aldehydes (C_4–C_7) are similar to these three. Each of the product ion spectra displays $(M–HF)^{-\cdot}$, m/z 181 ($C_6F_5CH_2^-$) and m/z 178 [$M^{-\cdot}$–HF–H(R)CN] peaks, in addition to their molecular ion peaks. A minor peak in the MS/MS spectra which is of considerable intensity in the mass spectra is ($M^{-\cdot}$–HF–30) occurs at m/z 175 for formaldehyde, 189 for acetaldehyde, 203 for propanal, 217 for butanal, 231 for pentanal, 245 for hexanal and 259 for heptanal. The origin of these peaks was confirmed by examining the product MS/MS spectra of ($M^{-\cdot}$–HF) for each of the compounds. As an example, the product MS/MS spectra of the ($M^{-\cdot}$–HF) ions of butanal, pentanal and hexanal derivatives are shown in Fig. 4(a), (b) and (c), respectively, and they are seen

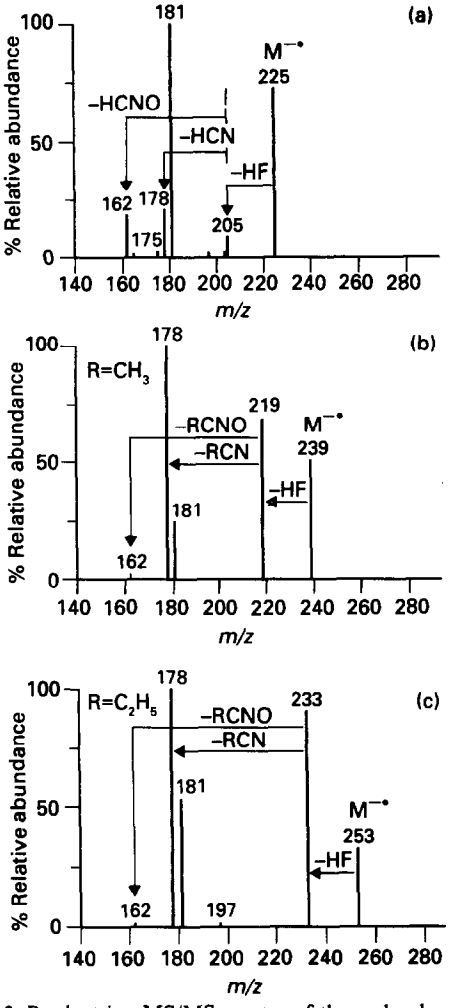

Fig. 3. Product ion MS/MS spectra of the molecular anion radicals of (a) formaldehyde, (b) acetaldehyde and (c) propanal; collision energy 20 eV and collision gas (argon) pressure 1 mtorr.

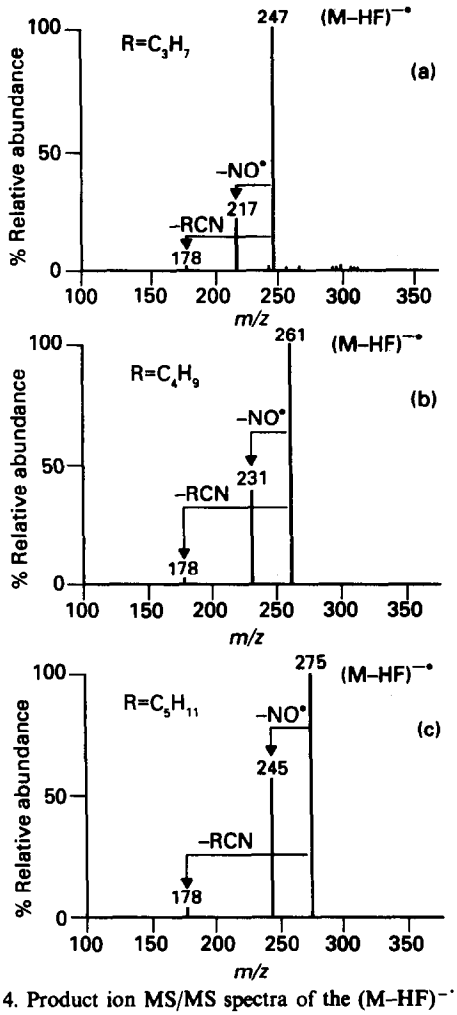

Fig. 4. Product ion MS/MS spectra of the $(M-HF)^{-\cdot}$ ions for (a) n-butanal, (b) n-pentanal and (c) n-hexanal; collision energy 20 eV and collision gas (argon) pressure 1 mtorr.

to be dominated by an ion due to loss of 30 daltons. These peaks are assigned to the loss of NO from ($M^{-\cdot}$–HF) ions and yield closed shell quinoid anions as shown in Scheme 1. The alternative possibility, that 30 corresponds to CH_2O loss, is consistent only with the data for the PFBOA derivative of formaldehyde itself but not with that for the higher aldehydes. The ($M^{+\cdot}$–30) ion peaks observed by Glaze *et al.*[1] for the PFBOA derivatives of formaldehyde, acetaldehyde and propanal were assumed to be due to the loss of NO from the molecular ions. In our negative ion electron capture mass spectra and MS/MS spectra no ($M^{-\cdot}$–NO) ion peak was observed. The characteristic ion peaks for each of the aldehydes are shown in Table 1.

Table 1. Characteristic ions for PFBOA derivatives of aldehydes

	$M^{-\cdot}$	($M^{-\cdot}$–HF)	($M^{-\cdot}$–HF–30)	Peaks from derivatizing reagent
Formaldehyde	225	205	175	197, 181, 178
Acetaldehyde	239	219	189	197, 181, 178
Propanal	253	233	203	197, 181, 178
n-Butanal	267	247	217	197, 181, 178
n-Pentanal	281	261	231	197, 181, 178
n-Hexanal	295	275	245	197, 181, 178
n-Heptanal	309*	289	259	197, 181, 178

*Observed in the mass spectrum of the individual compound but not observed in the mass spectrum of the mixture.

Table 2. Detection limits measured by multiple reaction monitoring

	Ion selected with first quadrupole	Ions monitored	Detection limit
Formaldehyde	225	225, 205, 178, 181	1 ppb
Acetaldehyde	239	239, 219, 178, 181	10 ppb
Propanal	253	253, 233, 178, 181	10 ppb
n-Butanal	267	267, 247, 178, 181	10 ppb
n-Pentanal	281	281, 261, 178, 181	20 ppb
n-Hexanal	275	275, 178, 181	20 ppb
n-Heptanal	289	289, 178, 181	1 ppm

Another characteristic feature of the fragmentation patterns is the appearance of a significant amount of ion m/z 162 in the product MS/MS spectra of the molecular ion of the derivatives, especially in the case of formaldehyde, whereas in the full mass spectra, the intensity of the signal for m/z 162 is very small. Due to the addition of internal energy supplied to the parent ion in the collision region during the MS/MS experiment an additional fragmentation route opens up leading to the production of m/z 162 ions. This reaction channel dominates over the direct decomposition channel of the molecular ion to produce m/z 197 which appears as quite an intense signal in the mass spectra.

In order to test the capability of the method to distinguish between isomers, mass spectra and product MS/MS spectra of n-butanal and isobutanal were compared. Some differences were observed but they were sufficiently small to make it difficult to distinguish the isomers in mixtures.

In order to measure detection limits for the aldehydes, multiple reaction monitoring was used. For formaldehyde, $M^{-\cdot}$ (m/z 225) of the PFBOA derivative was selected by using the first quadrupole, and the characteristic product ions m/z 205, 178 and 181 were monitored to establish the detection limit. The detection limit of formaldehyde was found to be 1 ppb with S/N = 3/1. The detection limits for other aldehydes were established in a similar way. The molecular ions selected with the first quadrupole and the product ions monitored during an MS/MS experiment to measure the lower limits of detection of the aldehydes are listed in Table 2. Table 2 also lists the detection limit for each of the aldehydes. The detection limit for acetaldehyde, propanal and butanal was found to be 10 ppb and that of pentanal and hexanal was 20 ppb. Linearity up to 100 ppb was observed for the C_1–C_6 aldehydes. Figure 5 shows the range of linearity for each of the aldehydes. For heptanal, it was possible to detect below 1 ppm but, it was hard to establish the linear dynamic range. As the size of the aldehyde molecule increases, the reactivity towards the derivatizing agent decreases and at the same time the ease of passage of the derivative through the membrane decreases. This is also evident from Fig. 2 which shows that the intensity of the characteristic peaks of the derivatized aldehydes decreases with the increase in molecular weight.

An alternative method of achieving low detection limits is to employ $(M–HF)^{-\cdot}$ ions as precursors for aldehydes in multiple reaction monitoring. Some experiments, in which $(M–HF)^{-\cdot}$ ions on C_2, C_5 and C_6 aldehydes were selected as precursor ions in multiple reaction monitoring, were therefore done and comparable detection limits were observed. The greater abundance of the parent ions is offset by the slightly higher noise level observed in $(M–HF)^{-\cdot}$ ions than $M^{-\cdot}$ ions.

An attempt was made to use the tandem mass spectrometer equipped with the DIMP to detect the PFBOA derivatives of ketones in a mixture of aldehyde and ketone derivatives. When examined independently, the derivatives of acetone, 2-butanone and 2-pentanone passed through the membrane. The mass spectra of the ketones showed peaks for $(M^{-\cdot}–HF)$ ions in addition to the characteristic ions due to the

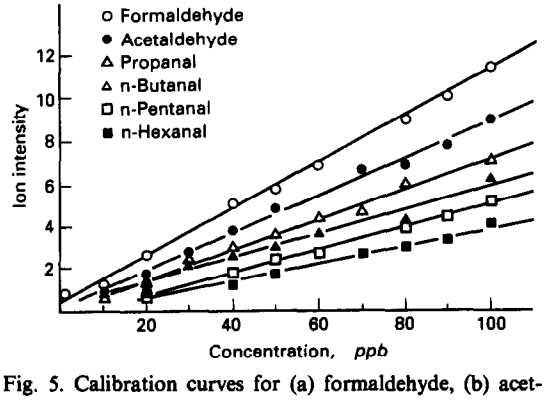

Fig. 5. Calibration curves for (a) formaldehyde, (b) acetaldehyde, (c) propanal, (d) n-butanal, (e) n-pentanal and (f) n-hexanal. The data were collected by multiple reaction monitoring.

derivatizing agent at m/z 181 and 197. Ketones generally took longer to undergo derivatization and, their detection limit was about 1 ppm. However when a mixture of derivatives of aldehydes and ketones was examined, the mass spectrum showed only the peaks for aldehydes. For example, in an experiment on a mixture of formaldehyde ($M^{-\cdot}$, m/z 225), acetaldehyde ($M^{-\cdot}$, m/z 239), acetone ($M^{-\cdot}$, m/z 253), 2-butanone ($M^{-\cdot}$, m/z 267) and 2-pentanone ($M^{-\cdot}$, m/z 281), the negative ion spectrum showed only the characteristic signals for formaldehyde and acetaldehyde and no signals for the ketones. This is not because of a failure to derivatize the ketones but due to preferential membrane transport of the aldehyde derivatives over the ketone derivatives in the presence of each other.

CONCLUSIONS

Sample introducton via a direct insertion membrane probe was used to detect low molecular weight aldehydes directly from an aqueous solution containing a mixture of C_1–C_7 aldehydes. Electron impact ionization of the underivatized aldehydes is unable to detect sub ppm levels of these compounds. Derivatization with PFBOA and ionization by electron capture allows the measurement of much lower concentrations of the aldehydes. A fragmentation scheme is proposed to explain the identity of the ion signals observed in the mass spectra and MS/MS product spectra of the derivatives. The molecular ions ($M^{-\cdot}$) produced via electron capture in the ion source of the mass spectrometer lose HF to produce $(M–HF)^{-\cdot}$ ions which, in the mass spectra, show significantly more intense signals than do the corresponding molecular ions. The $(M–HF)^{-\cdot}$ ions undergo further dissociation to produce ions m/z 178 and $(M–HF–30)^{-\cdot}$ which also appear as intense signals in the mass spectra. The use of multiple reaction monitoring helps to measure the detection limits of each of the aldehydes to the low ppb level. Calibration curves were linear up to 100 ppb. The method is less satisfactory for the corresponding ketones when a silicone membrane is used as an interface.

Acknowledgements—The authors acknowledge the support of the US Environmental Protection Agency (EPA CR-815749-01-0). The support provided by the Emil Aaltonen Foundation and Suomen Kulttuurirahasto is greatly appreciated (T.K.). The assistance of T. K. Majumdar and A. Ranashinghe is acknowledged.

REFERENCES

1. W. H. Glaze, M. Koga and D. Cancilla, *Environ. Sci. Technol.*, 1989, **23**, 838.
2. W. H. Glaze, *ibid.*, 1987, **21**, 224.
3. D. J. Kieber, J. McDaniel and K. Mopper, *Nature*, 1989, **341**, 637.
4. R. J. Kieber and K. Mopper, *Environ. Sci. Technol.*, 1990, **24**, 1477.
5. C. Auerbach and M. Moutschen, *Mutat. Res.*, 1977, **39**, 317.
6. NAS/NRC, Committee on Aldehydes, *Formaldehyde and Other Aldehydes*, p. 267. Board of Toxicology and Environmental Health Hazards, Assembly of Life Sciences, National Academy Press, Washington, DC, 1981.
7. U.S. Environmental Protection Agency, *Draft Informal Guidance Document*, Washington, DC, Office of Drinking Water, 1981.
8. R. E. Sievers, R. M. Barkley, G. A. Eiceman, R. H. Shapiro, H. F. Walton, K. J. Kolonko and L. R. Field, *J. Chromatog.*, 1977, **142**, 745.
9. Kobayashi, M. Tanaka, S. Kawai and T. Ohno, *ibid.*, 1979, **176**, 118.
10. H. Yamada and I. Somiya, *Ozone. Sci. Eng.*, 1989, **11**, 127.
11. D. F. Hunt and F. W. Crow, *Anal. Chem.*, 1978, **50**, 1781.
12. R. C. Dougherty, *ibid.*, 1981, **53**, 625A.
13. H. Budzikiewicz, *Mass Spectrom. Rev.*, 1983, **2**, 515.
14. T. Kotiaho, F. R. Lauritsen, T. K. Choudhury, R. G. Cooks and G. T. Tsao, *Anal. Chem.*, 1991, **63**, 875A.
15. G. Hoch and B. Kok, *Arch. Biochem. Biophys.*, 1963, **101**, 160.
16. L. B. Westover, J. C. Tou and J. H. Mark, *Anal. Chem.*, 1974, **46**, 568.
17. J. C. Weaver and J. H. Abrams, *Rev. Sci. Instrum.*, 1979, **50**, 478.
18. L. E. Slivon, M. R. Bauer, J. S. Ho and W. L. Budde, *Anal. Chem.*, 1991, **63**, 1335.
19. D. Wenhu, C. Kuangnan, L. Jiliani and D. Zhenying, *Mass Spectros. (Tokyo)*, 1987, **35**, 122.
20. J. C. Tou and G. J. Kallos, *Anal. Chem.*, 1974, **46**, 1866.
21. J. E. Evans and T. J. Arnold, *Environ. Sci. Technol.*, 1975, **9**, 1134.
22. J. C. Weaver, M. K. Mason, J. A. Jarrel and J. W. Peterson, *Biochim. Biophys. Acta.*, 1976, **438**, 296.
23. J. S. Brodbelt and R. G. Cooks, *Anal. Chem.*, 1985, **57**, 1153.
24. W. J. Pinnick, B. K. Lavine, C. R. Weisenberger and L. B. Anderson, *ibid.*, 1980, **52**, 1102.
25. F. R. Lauritsen, *Int. J. Mass Spectrom. Ion. Proc.*, 1990, **95**, 259.
26. F. R. Lauritsen, S. Bohatka and H. Degn, *Rapid Comm. Mass Spectrom.*, 1990, **4**, 401.
27. M. E. Bier, R. G. Cooks, J. S. Brodbelt, J. C. Tou and L. G. Westover, *U.S. Pat.*, 1989, 4791292.
28. M. E. Bier and R. G. Cooks, *Anal. Chem.*, 1987, **59**, 597.
29. M. E. Bier, T. Kotiaho and R. G. Cooks, *Anal. Chim. Acta*, 1990, **231**, 175.
30. A. K. Lister, K. V. Wood, R. G. Cooks and K. R. Noon, *Biomed. Environ. Mass Spectrom.*, 1989, **18**, 1063.
31. T. Kotiaho, M. J. Hayward and R. G. Cooks, *Anal. Chem.*, 1991, **63**, 1794.

32. M. J. Hayward, T. Kotiaho, A. K. Lister, R. G. Cooks, G.D.Austin,R.Narayan,andG.Tsao,*ibid.*,1990,**62**,1798.
33. M. J. Hayward, A. K. Lister, R. G. Cooks, G. D. Austin, R. Narayan and G. T. Tsao, *Biotechnol. Tech.*, 1989, **3**, 361.
34. G. D. Austin, G. T. Tsao, M. J. Hayward, T. Kotiaho, A. K. Lister and R. G. Cooks, *Process Control & Quality*, 1991, **1**, 117.
35. M. J. Hayward, D. E. Reiderer, T. Kotiaho, R. G. Cooks and G. T. Tsao, *ibid.*, 1991, **1**, 105.

Talanta, Vol. 39, No. 6, pp. 581–587, 1992
Printed in Great Britain.

0039-9140/92 $5.00 + 0.00

APPLICATION OF THE SLOTTED QUARTZ TUBE IN FLOW-INJECTION FLAME ATOMIC-ABSORPTION SPECTROMETRY

SHUKUN XU, LIJING SUN and ZHAOLUN FANG*

Flow-Injection Analysis Research Centre, Institute of Applied Ecology, Academia Sinica, Box 417, 110015 Shenyang, China

(*Received* 25 *July* 1991. *Revised* 19 *November* 1991. *Accepted* 19 *November* 1991)

Summary—The slotted quartz tube has been applied to flow-injection flame atomic-absorption spectrometry (FI–FAAS) showing several important advantages. The tube life was improved by a factor of 5–6 compared to conventional continuous aspiration. Flow impact systems were found not to be necessary in the applications so that larger enhancement factors may be achieved without sacrifice in precision. For 1.0 mg/l. copper, 1.0 mg/l. lead, 0.1 mg/l. cadmium and 1.0 mg/l. gold sensitivity enhancement factors of 3.1, 5.5, 5.3 and 4.0 were obtained with precisions of 1.3%, 1.1%, 1.6% and 1.7% RSD ($n = 11$) respectively. Application of the slotted quartz tube FI–FAAS method to the determination of heavy metals in urine has shown improved tolerance to interfering matrices. Recoveries obtained by spiking undiluted urine samples with 0.1 mg/l. copper and lead, and 0.01 mg/l. cadmium were in the range 100–102%.

In 1977, Watling first reported the application of a slotted quartz tube to improve the sensitivity of flame atomic-absorption spectrometry (FAAS) for a number of volatile elements.[1] In most applications sensitivity may be enhanced by a factor of 3–5 due to an increase in the residence time of the analyte atoms in the light path of the atomic-absorption spectrometer. Despite the simplicity of the approach, the application of the technique has been rather limited. One of the principle reasons for this seems to be the relatively short life time of the quartz tube, particularly when the samples contain substantial amounts of alkaline metals. It has been reported that the lifetime of the quartz tube may be prolonged by coating the tube with aluminium oxide.[2] This may be easily achieved by conventionally nebulizing an aluminium nitrate solution on the heated quartz tube for 10–15 min.[2] Later, Brown *et al.* conducted a critical comparison of the lifetimes of uncoated tubes and tubes coated with aluminium oxide, aluminium metal and lanthanum oxide.[2] The study revealed that the coating procedure prolonged the tube lifetime for more than one-fold. However, even with the coating treatment, the tubes lasted for only 240–360 samples containing 1% sodium chloride (w/v) using conventional continuous sample introduction. In order to further extend the tube lifetime, Brown and Taylor suggested discrete sampling (100-μl aliquots) of urine samples,[3] which increased the lifetime of an uncoated tube more than one-fold. However, deterioration of the sensitivity and precision were also observed, and hence could not always be recommended.

The flow-injection (FI) technique has been used successfully for the introduction of micro-samples in FAAS. It was shown recently that under optimized conditions of carrier flow-rate, nebulization rate and with careful control of sample dispersion in the sample loop and transport conduit, as low as 70-μl sample volumes may be introduced, giving almost the same sensitivity and precision as conventional continuous sample introduction.[4] As smaller sample volumes may shorten the exposure of the quartz tube to detrimental effects, flow-injection sample introduction appears to be a reasonable approach for further increasing the lifetime of the slotted quartz tube without sacrificing sensitivity and precision. The feasibility and performance of such a combination are studied in this work.

EXPERIMENTAL

A Perkin–Elmer Model 2100 atomic-absorption spectrophotometer was used with deuterium arc background correction. Copper,

*Author for correspondence.

cadmium, lead and gold lamps were operated at 15, 6, 10, and 10 mA with wavelengths set at 324.8, 228.8, 283.3, and 242.8 nm, respectively. The spectral bandpass was 0.7 nm for all the elements studied. The instrument was operated either with a flow spoiler or impact bead system, or without any impact system, as specified separately for the individual experiments. Results were evaluated in the peak height mode with a time constant of 0.5 sec. Flame conditions were as recommended by the instrument manufacturer. Three different designs of slotted quartz tubes were used in this study. The dimensions of the narrower slotted quartz tubes were mainly those given by Taylor and Brown,[5] which were 8 mm i.d., 10 mm o.d. and 130 mm long, with either a single slot along the axis measuring 50 mm long (tube A), or two slots on opposite sides of the tube, with the lower slot measuring 50 and the upper slot measuring 40 mm long (tube B). The slot widths were not given in reference 5; a slot of 0.7 mm was used in this study as recommended by Liu *et al.*[6] The dimensions of the wider slotted tube (tube C) were those following a design of Burns *et al.*[7] The tube was 15 mm i.d., 18 mm o.d. and 130 mm long, with a lower slot measuring 3 mm wide and 110 mm long. Six holes, of 6 mm diameter and 9 mm apart were made on the tube 180° opposite the slot. The tubes were fixed directly above the burner, using a holder made of 3-mm diameter aluminium wire which was clamped on the back wall of the burner compartment. The arrangement was made to facilitate the ignition of the burner. The burner head could then be moved out of the light beam, in which the slotted tube was positioned, and cleared out a space for the ignitor to function without disturbing the tube position. Fine adjustments were made so that the tube slot (or slots) were aligned exactly over, and in the central section of the burner slot. Experiments were conducted to optimize the gap width for the three tube designs in respect to sensitivity and precision. The optimum gap width between the tube and the burner was 4 mm for the tubes A and B, and 10 mm for tube C, and these were used for further experiments.

A Perkin–Elmer FIAS-200 FI system was used for sample introduction. The FI manifold was as described previously.[8] The transport conduit was a 20-cm long, 0.35-mm i.d. Tygon tubing, and the sample loops were 0.5-mm i.d. Micro-line tubing (Thermoplastic Scientifics, Sterling, NY, U.S.A.), knotted into a 3-dimensionally disoriented configuration to limit the dispersion.[4] The instrument was programmed to operate with a sample loading period of 10 sec and an injection period of 5 sec. The demineralized water carrier stream had a flow rate of 6.0 ml/min, and the nebulizer free uptake rate was 8.0 ml/min.

The aluminium coatings were applied by conventionally nebulizing an aluminium sulphate solution containing 0.5% (w/v) aluminium for 15 min with the quartz tube in the operation position. Experiments were conducted to compare the lifetimes of coated and uncoated quartz tubes under FI conditions by repeatedly introducing samples in batches of 99 at a time, the tubes were cooled down to room temperature between batches. The tests were carried on until complete breakdown of the quartz tubes occurred.

All reagents were of analytical reagent grade, and demineralized water was used throughout. The test solutions were prepared from 2-step dilutions of 1000 mg/l. stock solutions of the analyte elements. An aqueous solution containing 0.5% Al (w/v) in the form of aluminium sulphate was used for coating the quartz tubes. Urine samples were acidified with 10% hydrochloric acid (v/v) to contain 0.1% hydrochloric acid (v/v) immediately after collection; no further dilutions were made for the AAS determinations.

RESULTS AND DISCUSSIONS

Studies on various experimental parameters

The impact systems in the spray chamber of an atomic-absorption spectrometer are considered mandatory for good precision in conventional FAAS. Although some impact systems, such as the flow spoiler, produces significantly lower sensitivity than using an impact bead or without impact systems, the detection limits do not become poorer due to the better precision. This is because of the more favourable droplet size distribution of the aerosol, after excluding a bigger fraction of the larger droplets. The situation might be somewhat different when a slotted quartz tube is used in the flame, or when FI sample introduction is used with carrier flow-rates lower than the free nebulizer uptake rate. In the former case, the longer residence time of the dried aerosol particles in the heated quartz tubes, and additional collision of the particles on the heated tube walls may provide a better opportunity for any

Table 1. Effect of spectrometer impact system on the sensitivity and precision of 0.100 mg/l. cadmium with conventional FAAS, FI–AAS and slotted quartz tube FI-AAS

Method	Performance	Impact system		
		Flow spoiler	Impact bead	None
Conventional	Characteristic concentration (*mg/l.*)	0.041	0.032	0.027
	RSD, % ($n = 11$)	1.8	2.3	3.5
FI–AAS	Characteristic concentration (*mg/l.*)	0.043	0.033	0.028
	RSD, % ($n = 11$)	1.5	1.3	1.6
Conventional introduction and slotted tube	Characteristic concentration (*mg/l.*)	0.012	0.008	0.006
	RSD, % ($n = 11$)	1.4	2.0	2.8
Slotted tube FI–AAS	Characteristic concentration (*mg/l.*)	0.012	0.009	0.007
	RSD, % ($n = 11$)	1.5	1.4	1.5

undissociated larger particles to atomize; the tube may also act as a damping system to lower the short term flickering noise of the flame. In the latter case, nebulization efficiency is enhanced with lower carrier flows, which was also assumed to produce more favourable droplet size distributions. In both cases improvements in precision have been reported.[1,8] The improvement in droplet size distribution may also obviate the need for impact systems in the spray chamber, as has been shown previously.[8] Therefore, a comparison was made in this work to assess the function of the flow spoiler and impact bead systems with FI sample introducton, and with a slotted quartz tube flame atomizer, using cadmium as a model element. The results shown in Table 1 again demonstrate the favourable precision of flow-injection sample introduction without using impact systems, whereas the improvement in precision by applying slotted tubes were less pronounced. Although an improvement in precision could be observed with the slotted tube with or without impact systems using conventional sample introduction, the effect was no more noticeable in the FI mode. It seems that the impact system could not be dispensed with when samples are introduced conventionally, even using the slotted tube. In the FI mode, however, the impact systems only produced deteriorating effects on the sensitivity, with no improvement in the precision, regardless of the presence or absence of the slotted tube, at least under the experimental conditions adopted in this work. Thus, the best performance may be expected when the slotted tube is used in the FI mode without any impact systems, and the latter was removed from the spray chamber for all further studies.

The gap width between the slotted quartz tube and the burner seems to be an important parameter affecting the enhancement factor, particularly for copper. In this work, a preliminary study was made with FI sample introduction, using the narrow bored slotted tubes (A and B). The results in Table 2 show a significant decrease in enhancement factors with an increase in the gap width between the tube and burner, even from 2 to 4 mm, using a single slotted tube (tube A). The dual slotted narrow tube (tube B) behaved similarly. In fact, the

Table 2. Effect of gap width between burner and slotted tube on sensitivity enhancement factors and reproducibility, using FI sample introduction without impact system

Analyte element	Enhancement factor*			RSD, % ($n = 11$)		
	Tube A		Tube C	Tube A		Tube C
	2 mm gap	4 mm gap	10 mm gap	2 mm gap	4 mm gap	10 mm gap
Cu	3.2	2.1	3.1	1.3	1.5	1.3
Pb	6.6	5.2	5.5	1.7	1.8	1.1
Cd	6.0	5.3	5.3	1.5	1.6	1.6
Au	6.0	5.0	4.0	1.5	1.5	1.7

Concentration of test solutions Cu, 1.00; Pb, 1.00; Cd, 0.100; Au, 1.00 mg/l. Sample volume, 200 μl for Cu and 100 μl for all other elements.

*Enhancement factors derived from comparison of the slopes of the calibration curves obtained by FI introduction using the slotted tube without impact system and that obtained in the conventional mode using a spoiler impact system and without the slotted tube.

enhancement effect for copper was completely lost with a 4-mm gap; the enhancement factor would have been unity if compared to peak height obtained by flow-injection without impact systems. However, despite the higher enhancement factors of the smaller gaps, distances closer than 4 mm cannot be recommended, at least when the burner system used in this study was allowed to heat the tube continuously, owing to danger of overheating the burner head. The sensitivity enhancement effect for some elements, such as copper, can only be fully exploited, using more efficiently cooled burners. However, studies using the wide bored slotted tube (tube C) with a large gap of 10 mm between the tube and burner produced sensitivities and precisions which were almost identical to those of the narrow bored tube with a 2-mm gap. Therefore this latter design is recommended to prevent overheating of the burner head.

Previous studies on FI micro-sample introduction in FAAS showed that with careful control of sample dispersion, the steady state signal obtained by conventional nebulization may be approached with about 70 μl of sample.[4] With the slotted tube, however, a longer time (*i.e.*, a larger sample volume) is necessary to reach the steady state signal (see Fig. 1), the length of time depending on the analyte element. Therefore larger sample volumes had to be used to achieve a near steady state peak height signal. As larger samples containing substantial amounts of alkaline metals will inevitably shorten the lifetime of the tube (see later section), a compromise was made by using a sample volume of 100 μl for cadmium, lead and gold, achieving more than 90% of the steady state signal. For copper, however a larger sample volume of 200 μl was necessary to reach the same percentage.

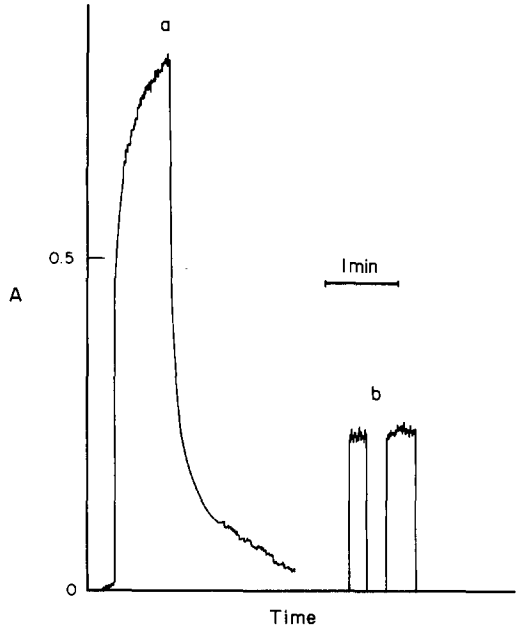

Fig. 1. Graphic recordings of 5 μg/ml Cu solution introduced in conventional FAAS mode (a) with slotted quartz tube and (b) without slotted quartz tube.

The model 2100 atomic-absorption spectrometer used in this study is an instrument with a single beam optical system, but capable of performing background offset correction in the double beam mode by automatically moving the burner in and out of the beam for each measurement as a standard mode of operation. Preliminarily, this feature was thought to be advantageous for increasing the lifetime of the quartz tube, as the heating period was shortened by moving the flame out of the tube during the sample loading period. This was not completely verified in the later experiments presumably because of the harmful effects created by frequently heating and cooling the quartz tubes and because the increase in lifetime of the quartz tube was not significant. Unexpectedly, however, when the burner was moved below the tube 2 sec before the injection of the sample, the enhancement factors for cadmium and copper were improved by 46, and 53%, respectively. Although the phenomenon still requires explaining, the beneficial effect may well be exploited when higher sensitivities are desired for these elements. However, to facilitate comparison, all data presented in this work were collected in the single beam mode, *i.e.*, without moving the burner.

Performance of aluminium oxide coated slotted quartz tubes with FI sample introduction

The sensitivity enhancement factors and the precisions of the aluminium oxide coated slotted quartz tube for copper, lead, cadmium and gold, using FI sample introduction are shown in Table 2 and are compared to those obtained under conventional slotted tube FAAS conditions. The enhancement factors for copper, lead, cadmium and gold with FI sample introducton with slotted tube C were 50, 20, 20 and 60% higher than those for conventional sample introduction, respectively, while precisions were marginally better in the FI mode. The reason for the better performance in the FI mode is that a flow spoiler was used in the conventional mode to ensure acceptable

precision, whereas no impact systems were necessary in the FI approach. The enhancement factors would have been similar if the comparisons were made against conventional sample introduction without an impact system; however, the precision in the conventional mode would have been significantly worse.

The small sample volumes injected (less than one-tenth of that consumed in conventional mode) allowed high sampling frequencies of over 360 samples/hr. Figure 2 shows the recordings from the graphic screen for the determination of cadmium in 1% sodium chloride matrix with and without the slotted tube. Besides the higher sensitivity for the slotted tube, it is also interesting to note a suppression of the background from the matrix. The phenomenon does not seem to have been reported previously, and may be associated with a more complete dissociation of molecular species in the sample matrix, but a closer study may be necessary to explain it fully.

Lifetime of the slotted quartz tube using FI sample introduction

The lifetimes of coated and uncoated slotted quartz tubes with FI sample introduction of samples containing 1% sodium chloride are shown in Table 3. Uncoated quartz tubes were reported to be quickly devitrified by sodium atoms in the flame, presumably through migration of the atoms into the hot quartz, forming sodium silicates, which on cooling, contracted and eventually destroyed the tube.[9] Coating of the tubes with a refractory oxide film by conventionally aspirating 0.5% lanthanum (as nitrate), aluminium (as nitrate), or vanadium (as ammonium vanadate) on the heated tube substantially increased the lifetime of the tubes.[2,9] In this work a comparison was made between aluminium oxide coated tubes and uncoated tubes. A comparison was also made between tubes coated by continuously nebulizing aluminium sulphate solution for 10–15 min, as recommended by other workers[2] and using a more dilute coating solution (0.1% Al) as a carrier stream after the preliminary coating. The latter procedure was expected to provide a steady regeneration of the film when it was gradually consumed with extended use. The difference in lifetime of the two alternatives was, however, not significant, and the carrier stream approach was discontinued due to an accumulation of aluminium oxide on the burner slot, which then required frequent cleaning. It has been reported that the tube lifetime could also be prolonged by using discrete micro-volume sampling (pulsed nebulization) instead of conventional continuous nebulization.[2,3] Although specific data on the effect were not given, it may be drawn from the related data that about 800 samples containing 1% sodium chloride may be

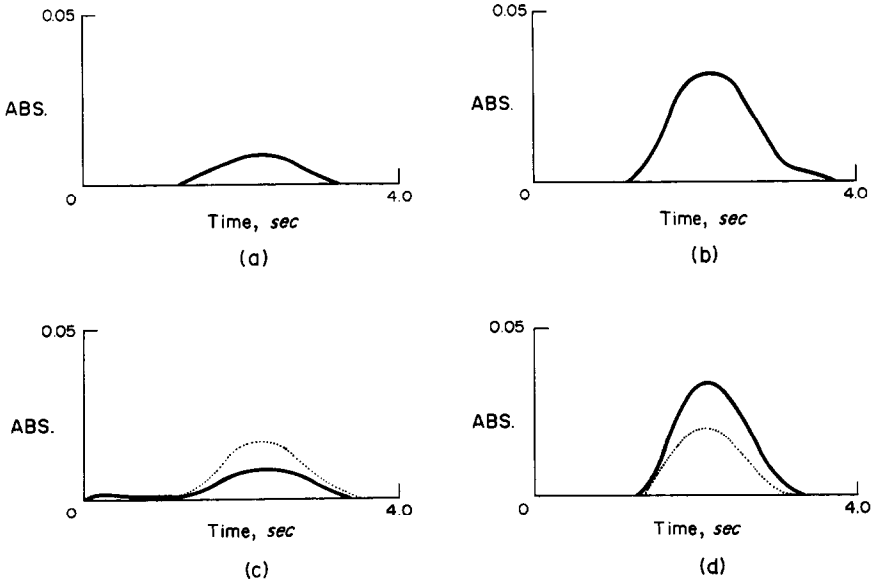

Fig. 2. Graphic recordings of FI–FAAS. Determination of 50 μg/l. Cd in (a) and (b), simple aqueous solutions; and (c) and (d), 1% NaCl solution; (a), (c), without slotted quartz tube; and (b), (d), with slotted quartz tube. No impact system was used. Carrier flow-rate, 6 ml/min; nebulizer free uptake, 8 ml/min. Sample volume, 100 μl. Solid lines, analyte absorption signals; dotted lines, background absorption signals.

Table 3. The lifetime of slotted quartz tubes in the analysis of samples containing 1% sodium chloride, in number of samples analysed

Tube coating	Continuous nebulization	Pulsed nebulization	FI
Aluminium oxide	240 (ref. 3)	(~800)	1900–2100
Uncoated	140 (ref. 3)	320 (ref. 3)	910

analysed by using coated quartz tubes with discrete introduction of 100 μl-samples. However, pulsed nebulization was found to degrade both the sensitivity and precision of the results,[3] the benefits gained by using the slotted quartz tube were therefore at least partially lost.

As shown in Table 3, the improvement in the lifetime of the slotted tube using FI sample introduction is quite significant, even when compared to conventional pulsed nebulization. Approximately 2000 samples containing 1% sodium chloride analysed with a single aluminium oxide coated quartz tube appears to be the longest lifetime reported thus far for slotted quartz tubes. The reason for the improvement is presumably the stronger washing action of the carrier stream which has previously been shown to be very effective in decreasing the accumulation of salts on the burner slot.[10] This would in turn decrease the exposure of the quartz tube to the corrosive matrix salts.

In contrast to conventional pulsed nebulization, FI sample introduction did not produce deteriorating effects on the sensitivity and precision of the determinations for the elements studied in comparsion to conventional continuous sample introduction. In fact, a slightly higher sensitivity may even be achieved in some cases, a phenomenon which has been observed and discussed previously.[8] The increase in the tube lifetime, which was reported to be 240 samples with aluminium oxide coated tubes (1% sodium chloride sample) with conventional sample introduction[2] is thus much more meaningful than using conventional discrete sampling.

Application of the slotted quartz tube to the determination of copper, cadmium, and lead in urine samples by FI–FAAS

The determination of heavy metals in serum and urine has been a main field of application of the slotted quartz tube technique in recent years.[2,3,5,6,9] While simple aqueous standards may be used for the analysis of diluted serum samples, the determination of lead, cadmium and copper in urine samples required the use of "urine equivalent" standards to achieve good recoveries.[2] The observed matrix effect in urine samples was thought to be at least in part due to changes in the aspiration rate. With FI sample introduction, such effects may be minimized by using a pump-propelled steady carrier flow. With this in mind, we attempted to use simple aqueous standards for the FI analysis of original urine samples. The recoveries obtained by spiking the urine samples with 0.1 mg/l. copper and lead, and 0.01 mg/l. cadmium were 100, 102 and 101% respectively, which demonstrate yet another advantage of the FI approach.

CONCLUSIONS

FI sample introduction significantly improves the lifetime of the slotted quartz tube atomizer used for FAAS by a factor of 5–6, compared to conventional continuous aspiration, without loss in sensitivity and precision, thus overcoming one of the main disadvantages of the slotted quartz tube technique. Impact systems were not found to produce better precision with FI sample introduction either with or without the slotted quartz tube, but higher sensitivities may be achieved without impact systems. Application of the FI method to the determination of heavy metals in urine has shown improved tolerance of interfering matrix effects and significantly higher sample throughputs.

The sensitivity enhancement effects of the slotted quartz tube technique may not be as impressive as FI on-line column preconcentration procedures for FAAS where 20–30 fold enhancements could be achieved under normal FAAS sampling frequencies and sample consumption levels.[11] However, preliminary studies on applying the two techniques simultaneously have shown that the enhancement effects of the two techniques are completely multiplicative. It is therefore reasonable to anticipate the achievement of enhancement factors of 100 or more with sampling frequencies of 120 samples/hr in the near future. Work on the above is now under development.

Acknowledgements—The authors express their thanks to Bodenseewerk Perkin–Elmer for financial support and loan of instrument.

REFERENCES

1. R. J. Watling, *Anal. Chim. Acta*, 1977, **94**, 181.
2. A. A. Brown, B. A. Milner and A. Taylor, *Analyst*, 1985, **110**, 501.

3. A. A. Brown and A. Taylor, *ibid.*, 1984, **109,** 1455.
4. Z.-L. Fang, B. Welz and M. Sperling, *J. Anal. At. Spectrom.*, 1991, **6,** 179.
5. A. Taylor and A. A. Brown, *Analyst*, 1983, **108,** 1159.
6. Y.-M. Liu, B.-L. Gong, C.-H. Li and J.-D. Wang, *Fenxi Huaxue*, 1988, **16,** 55.
7. D. T. Burns, G. D. Atkinson, N. Chimpalee and M. Harriot, *Z. Anal. Chem.*, 1988, **331,** 814.
8. Z.-L. Fang and B. Welz, *J. Anal. At. Spectrom.*, 1989, **4,** 83.
9. A. A. Brown, D. J. Roberts and K. V. Kahokola, *ibid.*, 1987, **2,** 201.
10. Z.-L. Fang, B. Welz and G. Schlemmer, *J. Anal. At. Spectrom.*, 1989, **4,** 91.
11. Z.-L. Fang and B. Welz, *ibid.*, 1989, **4,** 543.

Talanta, Vol. 39, No. 6, pp. 589–592, 1992
Printed in Great Britain.

0039-9140/92 $5.00 + 0.00

A DUAL-WAVELENGTH LIGHT-EMITTING DIODE BASED DETECTOR FOR FLOW-INJECTION ANALYSIS PROCESS ANALYSERS

JIALIN HUANG, HANGHUI LIU, AIMIN TAN, JINHUA XU and XINNA ZHAO

Centre for Process Analytical Chemistry, Department of Chemistry, Central South University of Technology, Changsha, Hunan 410083, People's Republic of China

(*Received* 5 *August* 1991. *Revised* 1 *November* 1991. *Accepted* 1 *November* 1991)

Summary—In this paper, a small dual-wavelength light-emitting diode (LED) based detector for FIA process analysers is designed. The detector's optical parts include a flow cell, a dual-wavelength LED and a photodiode. Neither mirrors nor lenses are used. The optical paths for the different light beams are almost the same, distinguishing it from previously reported LED based detectors. The detector's electronic components, including a signal amplifier, an A/D and D/A converter, and an Intel 8031 single-chip microcomputer, are integrated on one small board. In order to obtain response signals of approximate intensity for the two colours, the D/A converter and a multiplexer are used to adjust the emission intensity of the two colours respectively. Under microcomputer control, light beams are rapidly electronically modulated. Therefore, dark current and intensity of the two light beams are measured almost simultaneously; as a result, the effect of drift is negligible. While a solution of absorbance 0.875 was measured repeatedly, an RSD (relative standard deviation) of 0.24% could be reached. Furthermore, such a detector with a red/yellow LED has been coupled with the FIA technique for the determination of $10^{-6}M$ levels of cobalt.

In industrial process analysis the use of dual-wavelength spectrophotometric methods for the analysis of samples with turbidity, for simultaneous multicomponent determination and for high concentration analytes, offers obvious advantages;[1–3] and also increases the sensitivity and accuracy of the analysis.

Conventional dual-wavelength spectrophotometers used in the laboratory consist of two monochromators to obtain two paths of monochromatic light of different wavelengths and is equipped with modulator and demodulator. Both the optical system and the electric circuit are complicated. Lenses, mirrors and many mechanical moving parts are needed. Recent use of a photodiode array[4–6] is a practical instrumental improvement. Such spectrophotometers have good properties but the cost is high.

For industrial on-line process analysis, the environment is severe and the task is usually specific and not very complicated. A reliable and inexpensive dual- (or multi-) wavelength spectrophotometer of rugged simple construction is desirable.

Since commercially available light-emitting diodes (LED) emit visible radiation over a narrow wavelength range with high light intensity, short response time and a very long life time, its use as a light source for spectrophotometers is increasing.[4] The application of LEDs for photometric detection in FIA has recently been reported and reviewed.[7,8] When monochromatic light of different wavelengths is needed, LEDs of different colours may be selected. Sometimes, a combination of LEDs may be used.[8]

The purpose of this work is to employ a multi-colour LED as the light source in conjunction with a single photodiode as detector,[9] thus a compact rugged dual-wavelength spectrophotometer is designed and constructed, which can be used in connection with a flow-injection analysis system as a process analyser for industrial purposes.

EXPERIMENTAL

Apparatus

Dual-wavelength LED based photometer. A block diagram of the dual-wavelength LED based detector is shown in Fig. 1.

A dual-wavelength LED is employed as the light source. Light beams of different wavelengths emitted from the LED use the same optical path and share a common photodiode detector. This configuration greatly simplifies

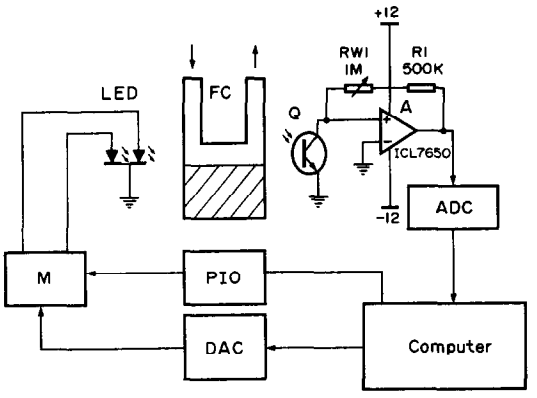

Fig. 1. A block diagram of the dual-wavelength LED based detector: FC is a common Hellma flow-cell with 10 mm of optical length and 1.5 mm of diameter; Q is the photo-transistor, 3DU80A; A is the amplifier, ICL7650; ADC is a 12-bit analogue to digital converter, AD574; DAC is an 8-bit digital to analogue converter, DAC0832; M is an analogue multiplexer, CD4051; computer is an Intel 8031 single-chip microcomputer.

the instrumentation and enhances the detector's stability.

The detector's electronic control system consists of current/voltage converter, A/D converter, D/A converter, electronic analogue multiplexers and a microcomputer. Under the control of the microcomputer, the electronic analogue multiplexers change the colour of the LED with very high speed, giving forth alternate light beams with different wavelengths, which falls onto the photodiode detector after being absorbed by the solution in the flow cell. The current generated is then converted into voltage which is digitized by the A/D converter at the rate of 1000 times per second. Then, the computer proceeds to process the data and display the results on the recorder. Under the control of the computer, the change of wavelengths of the light beam can be accomplished with extremely high speed (in milliseconds) so that the absorbance of the sample solution at different wavelength can be simultaneously or almost simultaneously obtained, which can be applied either for the elimination of the disturbances of background turbidity or for the simultaneous determination of multiple components.

Owing to the fact that the light intensities of different colour from the multi-colour LED may be different, and considering that the sensitivity of the detector towards light with different wavelengths may be different, for each wavelength, the 100% transmittance must be calibrated. Usually a double-beam instrument is used, of which one optical path is for calibration and the other path is for determination. Such a double-beam instrument is far more complicated than the single-beam instrument. In our work, we calibrate and compensate the difference electronically and automatically with the aid of the computer.

The detector's electronic part, including a signal amplifier, an A/D converter, a D/A converter, and an Intel 8031 8-bit single-chip microcomputer, is integrated on one small board. Prisms or gratings, lenses and mirrors *etc.*, are not needed. The detector thus constructed is compact, simple, inexpensive, robust and suitable for use with a FIA system. Different multi-colour LEDs can be easily incorporated in different applications.

The flow-injection system used was a FIA-21A instrument (Xin Tong Co., China) which has two 4-channel peristaltic pumps and one six-port rotary valve.

Reagents and solutions

The solutions employed include 1.6×10^{-5} g/ml bromothymol blue + 0.01*M* Borax,[10] 1% NaAc + 0.01% 5-Cl-PADAB,[11] 4% sulphuric acid, and 100 μg/ml cobalt stock solution. All the reagents employed are of analytical grade.

RESULTS AND DISCUSSION

Absorbance measurement and precision

While in operation, the LED diodes are switched on and off sequentially and as a result the signal observed (Fig. 2) is pulse like. Absorbance at the two wavelengths are calculated according to the following equation:

$$A = \log [(I_o - I_d)/(I - I_d)] \qquad (1)$$

where A is the absorbance, I_d is the dark current, I_o and I are the light intensities observed before and after being absorbed by the sample.

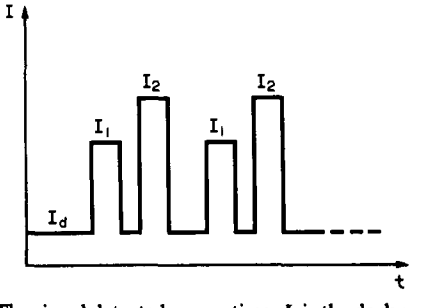

Fig. 2. The signal detected versus time. I_d is the dark current; I_1 and I_2 are the currents observed when different LEDs are switched on.

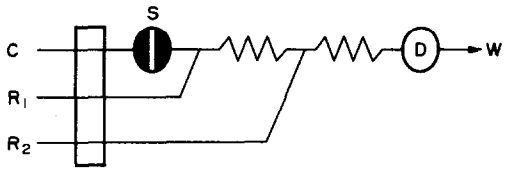

Fig. 3. FIA manifold for the determination of cobalt: C is H_2O; R_1 and R_2 are 1% NaAc + 0.01% 5-Cl-PADAB and 4% H_2SO_4 respectively; D is the LED-based photometer; W is the waste; S is the injection port.

The absorbances measured for a series of bromothymol blue solutions by using a red/green dual-wavelength LED with the emission maxima at 630 nm and 565 nm are summarized in equations (2) and (3).

$$A = 0.0194 + 4.909 \times 10^4\ C \text{ (for 630 nm)} \quad (2)$$

$$A = 0.0016 + 5.475 \times 10^4\ C \text{ (for 565 nm)} \quad (3)$$

where A is the absorbance and C is the concentration of bromothymol in g/ml. The regression coefficients of equations (2) and (3) are 0.9994 and 0.9999, respectively. In order to demonstrate the precision, a blank and a dye solution of absorbance 0.794 at 630 nm and 0.875 at 565 nm were measured 11 times. For the blank, the standard deviation of absorbance at 630 nm and 565 nm was 0.0009 and 0.0007, respectively; for the dye solution, the standard deviation of absorbance was 0.0020 at 630 nm and 0.0021 at 565 nm, with a resulting RSD of 0.25% and 0.24% for red and green colours, respectively.

Coupling with FIA for the determination of 10^{-6}M levels of cobalt

A red/yellow dual-wavelength LED (with the emission maxima at 665 and 585 nm) was selected as the light source for the determination of cobalt by the spectrophotometric method with 5-Cl-PADAB as the complexing reagent.[11] The FIA system designed for sample handling is shown in Fig. 3.

A series of standard cobalt solutions were prepared and measured with the above mentioned instrument. The results are shown in Table 1.

Effect of solution turbidity on the determination of cobalt. Solutions of cobalt ($3.224 \times 10^{-5}M$) with a different degree of turbidity were measured under the same conditions as mentioned above. The results are shown in Table 2. The peak heights at 665 nm show the absorbance caused by solution turbidity; the peak heights at 585 nm show the absorbance of the coloured sample and the turbidity.

Table 2 shows that although the turbidity is different for the above three samples, the difference in peak heights between the two wavelengths remains basically the same, which means that the disturbance of turbidity on the determination of cobalt in this case can be overcome.

CONCLUSION

A dual-colour LED based photometer has been designed and constructed. The experimental test shows that it has the following advantages:

The instrument is simple, compact and rugged; it is composed mainly of electronic devices, with no lenses, no mirrors, no sophisticated optical parts and no mechanical moving parts; in connection with a FIA system, it provides a cost-effective, robust process analyser for industrial purposes.

The study of the simultaneous determination of two components in turbid samples for on-line analysis for industrial purposes with this instrumentation is under progress in our laboratory.

Table 1. Absorbance of cobalt solutions

Conc. of Co M	8.484×10^{-4}	1.697×10^{-5}	2.543×10^{-5}	3.394×10^{-5}
Difference of peak heights between 665 and 585 nm	0.0554	0.1046	0.1526	0.1958
Relative standard deviation	2.0%	1.0%	1.2%	1.1%
Regression coefficient		0.9996		

Table 2. Effect of sample turbidity ([Co] = $3.224 \times 10^{-5}M$)

Sample No.	1 (no turbidity)		2		3	
Peak height (585 nm)	0.185	0.187	0.213	0.213	0.258	0.260
Peak height (665 nm)	0.016	0.016	0.046	0.047	0.088	0.091
Difference of the two peak heights	0.169	0.171	0.167	0.166	0.170	0.169

REFERENCES

1. Galen W. Ewing, *Instrumental Methods of Chemical Analysis*, 4th Ed., pp. 88–90. McGraw-Hill, 1975.
2. *Modern Instrumental Analysis*, pp. 149–152. Anal. Chem. Division, Qinghua University, Qinghua University Press, 1983.
3. D. A. Skoog and D. M. West, *Principles of Instrumental Analysis*, 2nd Ed., p. 108. Saunders College, 1980.
4. Y. Talmi, *Appl. Spectrosc.*, 1982, **36**, 1.
5. R. B. Bilhorn, J. V. Sweedler, P. M. Epperson and M. B. Denton, *ibid.*, 1987, **41**, 1114.
6. J. Sedlmair, S. G. Ballard and D. C. Mauzerall, *Rev. Sci. Instrum.*, 1986, **57**, 2995.
7. M. Trojanowicz, P. J. Worsfold and J. R. Clinch, *TrAc*, 1988, **7**, 301.
8. M. Trojanwicz and S. Szpunar, *Anal. Chim. Acta*, 1990, **230**, 125.
9. Jialin Huang, Hanghui Liu, Aimin Tan, Jinhua Xu and Xinna Zhao, Pittsburgh Conference on Analytical Chemistry and Applied Spectroscopy, Chicago, 1991.
10. J. Růžička and E. H. Hansen, *Flow Injection Analysis*, p. 131. Wiley, 1981.
11. Wanchun Li, Bin Fu, *Fenxi Shiyanshi*, 1990, **9**, 5.

Talanta, Vol. 39, No. 6, pp. 593–598, 1992
Printed in Great Britain.

0039-9140/92 $5.00 + 0.00

DETERMINATION OF AQUEOUS OZONE FOR POTABLE WATER TREATMENT APPLICATIONS BY CHEMILUMINESCENCE FLOW-INJECTION ANALYSIS. A FEASIBILITY STUDY

HYUNG-KEUN CHUNG, HARVEY S. BELLAMY and PURNENDU K. DASGUPTA*
Department of Chemistry and Biochemistry, Texas Tech University, Lubbock, TX 79409-1061, U.S.A.

(*Received* 15 *August* 1991. *Revised* 15 *September* 1991. *Accepted* 20 *September* 1991)

Summary—The feasibility of determining aqueous ozone by chemiluminescence flow-injection analysis (CL–FIA) was studied for applications in potable water treatment. The ozonated water sample is injected into a pure water carrier and mixed with a dye reagent in front of a photodetector. Many reagents undergo fast CL reactions with aqueous ozone. Most of these reactions display considerable selectivity for ozone over other oxidants of importance in water treatment. Even when there is steady-state response to another oxidant, significant discrimination against the interferents is possible by taking advantage of the much faster kinetics of the CL reaction with ozone. A simple design of a Siemens-type ozone generator and preparation of standard ozone solutions are also described.

A large number of organic compounds have been reported to exhibit chemiluminescence (CL) when they react with high concentrations of gaseous ozone.[1] The CL reaction between gaseous ozone and ethylene[2] constitutes the reference method for ambient ozone measurements.[3] CL occurs when O_3(g) reacts with Rhodamine B/gallic acid in solution;[4] Rhodamine B has also been utilized for the development of solid phase reagent systems.[5,6] The CL resulting from passing O_3(g) over a fiber pad saturated by a continuously flowing solution of Eosin Y, Rhodamine B, or fluorescein permits detection of very low [O_3] levels.[7] CL analysis based on direct mixing of aqueous indigo-5,5′disulfonate and O_3(g) reportedly provides a limit of detection (LOD) of 0.4 ppbv.[8]

Aqueous O_3 has also been determined by CL reactions albeit less frequently than O_3(g). The CL reaction between O_3(aq) and luminol[9] was the basis of an early instrument. Despite refinements,[10] this reaction is not specific for ozone. Takeuchi and Ibusuki used Rhodamine B/gallic acid[11] and more recently indigo disulfonate[12] for the determination of aqueous ozone. With photon counting equipment, an LOD of 6 ng/l., suitable for direct measurement of O_3(aq) in cloudwater, was reportedly possible with the latter reagent.

Because of health concerns regarding the formation of halogenated organic compounds from the use of chlorine and related oxidants, ozone is increasingly being used as the primary oxidant in potable water treatment.[13–15] In the US, there are approximately 40 water treatment plants currently utilizing ozone with another 20 under design or construction.[15] The levels to be measured are higher than those in atmospheric applications but it is necessary to discriminate the O_3 from secondary oxidants resulting from O_3 (notably H_2O_2 and MnO_4^-) and other added oxidants (*e.g.*, Cl_2). We report here an inexpensive means of generating aqueous ozone at concentrations involved in drinking water treatment and on a feasibility evaluation of selective measurement of ozone by CL–FIA.

EXPERIMENTAL

Instrumentation

All measurements were performed with a programmable timer controller FIA system consisting of a multichannel peristaltic pump (Minipuls 2, Gilson Medical Electronics, Middleton, WI), an electropneumatically actuated dual loop sample injection valve (loop volumes 1 and 0.2 ml, Dionex Corp., Sunnyvale, CA), and a homemade flow-through reaction cell installed in front of an end-on type 4283B photomultiplier tube (PMT) typically operated at 1200 V. One pump channel was used to

*Author for correspondence.

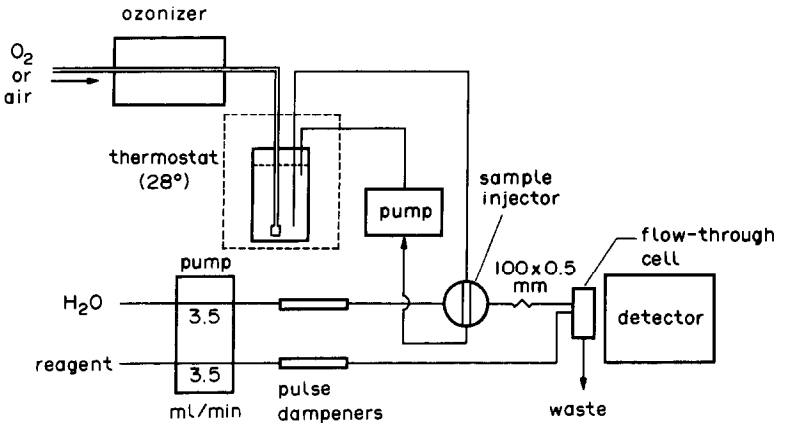

Fig. 1. Schematic diagram of the CL–FIA system.

aspirate aqueous ozone solutions into the sample loop from the sample reservoir. All tubing in the analytical conduit was polytetrafluoroethylene (PTFE), 0.5 mm in bore. Ozone solutions are unstable; the length of tubing between the aqueous ozone generator/reservoir and the valve was minimized and a high pumping rate (10 ml/min) with a ceramic/fluorocarbon pump (Fluid Metering Inc., Oyster Bay, NY) was used to avoid decomposition. Figure 1 shows a schematic diagram of the measurement system.

A Siemens-type ozone generator was constructed from a neon sign transformer (9 kV, 30 mA). A snugly fitting stainless steel tube was inserted in a 30 cm × 8 mm i.d. glass tube which was in turn inserted into a 25 cm × 16 mm i.d. glass tube wrapped in aluminium foil. Polypropylene tees at each end (9.5 mm i.d.) allow the inner tube to pass through via seals made by PTFE sleeves. Feed gas (air or O_2) was metered in (FC-280, Tylan General, Torrance, CA) and the product O_3 exited through the T-ports. The electrical field applied across the steel tube and the aluminum foil results in silent discharge in the annular space between the two concentric glass tubes. The O_3 output, controlled by a variable input voltage from a variable voltage transformer, was monitored with a photometer (1003 AH, Dasibi Corp., Glendale, CA; factory-modified with a 0.75-mm pathlength flow cell).

Solutions

Aqueous O_3 was prepared by continuously bubbling ozone in high purity water contained in a temperature-controlled vessel. The absorbance due to O_3(aq) at 258 nm was continuously monitored by circulating the solution through an absorbance detector (model 757, ABI, Ramsey, NJ; modified with a flow cell made from 3-mm square quartz tubing to avoid frequent problems with trapped bubbles) via PTFE lines.

Water used in the preparation of reagent solutions and the carrier stream of distilled demineralized water were determined to be free from ozone demand. All test reagents (Aldrich chemical or J. T. Baker) were used without further purification; the reagents were typically used at a concentration of $1 \times 10^{-4}M$.

RESULTS AND DISCUSSION

Preparation of aqueous ozone standards and gaseous ozone generation

Since O_3(aq) is readily decomposed, preparation of standards for calibration are non-trivial; the toxic nature of O_3(g) at high concentrations also mandate that experiments be conducted in a well ventilated hood. The best approach is to continuously equilibrate pure water (acidification can be used to increase the stability of the dissolved O_3)[16] with a stable concentration of O_3(g). To determine the concentration of O_3(aq), a value of 3100 $l.mole^{-1}.cm^{-1}$ was used for ϵ_{258}; a critical survey of literature data has indicated that this value is subject to a maximum error of $\pm 5\%$.[17] In potable water treatment, concentrations up to 5 mg/l. (*ca.* $100\mu M$) O_3(aq) need to be determined in the gas contact chambers. Based on a Henry's law constant of $0.015M$ atm^{-1} at 293 K,[18] the O_3(g) concentration necessary to make such a solution approaches the per cent level. Necessary generators are commercially available but the design reported here is simply constructed at a fraction of the cost. The generator provides a

stable O_3(g) output; the performance characteristics are summarized below.

The i-V relationship in the primary coil of the high voltage transformer is shown in Fig. 2. The point of departure from the initial linear relationship also indicates the experimentally observed onset of significant O_3 production. The relationship between the discharge energy, which we assume to be the product of the voltage and the difference between the total current and the linearly voltage dependent inductive current in the transformer (extrapolated straight line in Fig. 2), and the O_3 output is shown in Fig. 3. Two separate regions clearly exist regarding the efficiency of O_3 production. It is noteworthy that the slope (efficiency of O_3 production) in the higher current regime is five times larger for O_2 than for air suggesting that the efficiency is linearly related to pO_2. The mass of O_3 generated is essentially independent of the flow rate; Fig. 4 shows that the concentration of ozone generated is inversely proportional to feed gas flow rate with a near-zero intercept (the gas phase O_3 photometer is known to suffer from negative errors at very high concentrations; the departure of the highest concentration point from the lower linear portion is likely an artifact).

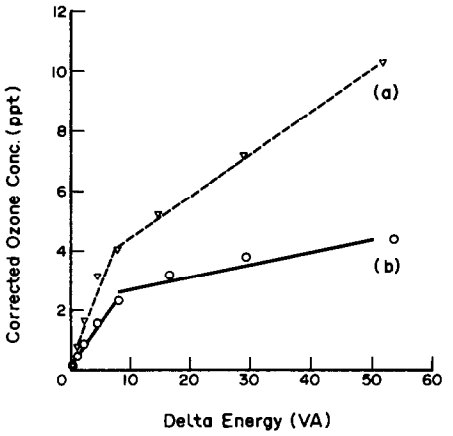

Fig. 3. Dependence of ozone output on discharge energy. Feed gas was (a) O_2(g) and (b) air at 200 standard cm^3/min.

Design of the chemiluminescence cell

The CL reaction of O_3 with most test reagents occurs on a time scale faster than it is commonly possible to achieve complete mixing in a FIA system; the half-life for the O_3-indigodisulfonate CL reaction, for example, is <1 msec.[12] It is therefore necessary to initiate the CL reaction directly in front of the PMT and in a controlled manner to obtain good signal reproducibility. Three types of reaction cells (Fig. 5) were studied for the reaction between O_3(aq) and indigotrisulfonate (ITS). In cell 5(a), the analyte and the reagent enter at the center of the cell via separate opaque tubes. The entrance bore is 0.3 mm and the streams are mixed at a right angle to achieve as rapid a mixing as possible. The stream then travels through the maze-like channel (V-shaped groove 0.3 mm deep, 0.5 mm wide, 21 cm total length, volume 16 μl) while CL occurs and is registered by the PMT through the Plexiglas window. A similar entrance geometry is used for cell 5(b) except that a much larger inner volume (100 μl) was used and the geometry was not constrained to facilitate hydrodynamic mixing. In cell 5(c), analyte enters into a relatively low velocity stream of the reagent and the total view volume in front of the PMT is large (800 μl). In all cases, the mixer windows are directly positioned in front of the end-on PMT and the same flow-rates were used for both the carrier stream and the reagent. Interestingly, all the tested cells produced

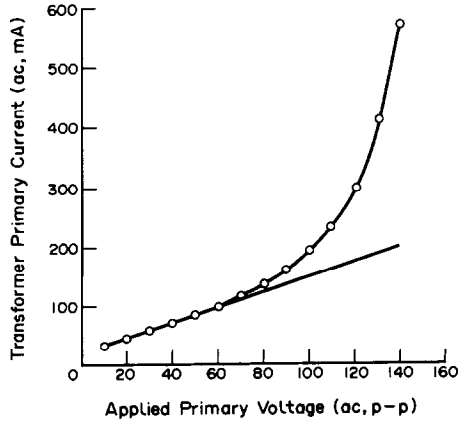

Fig. 2. Dependence of transformer primary current on applied primary voltage.

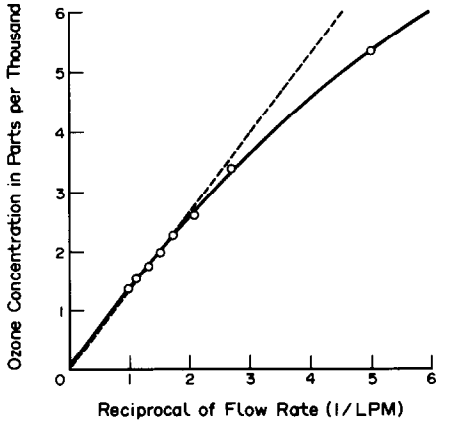

Fig. 4. Dependence of generated O_3(g) concentration on the reciprocal of O_2(g) flow-rate.

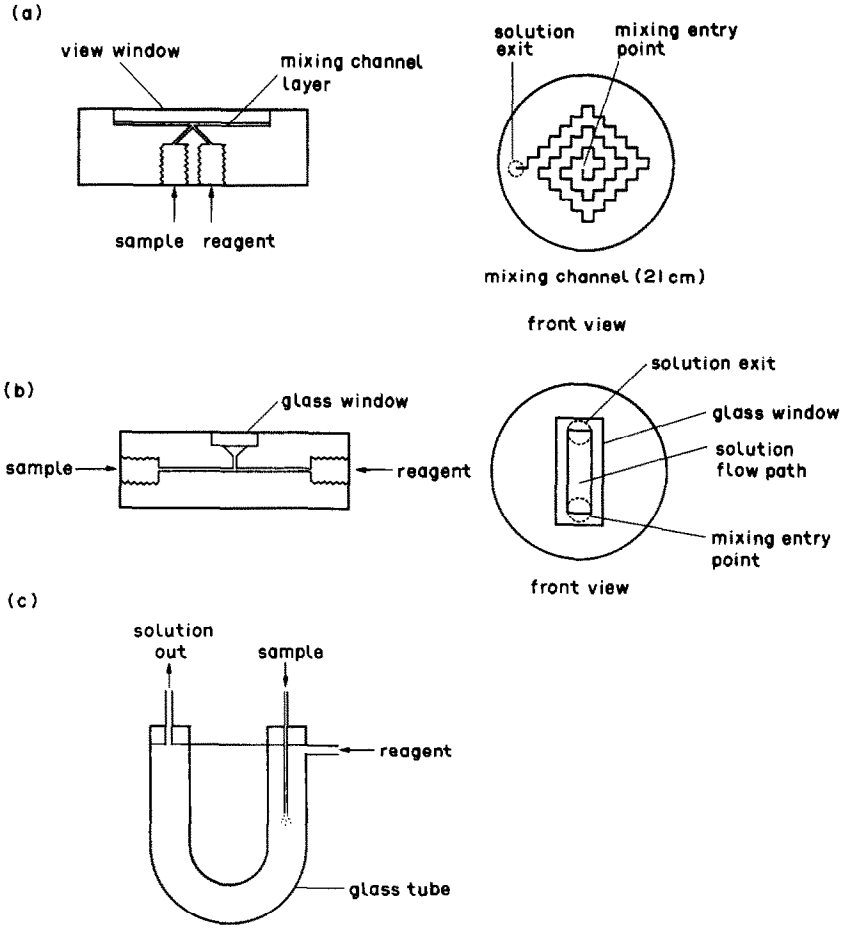

Fig. 5. Flow-through reaction cells. The test cells are constructed with (a) Plexiglas, (b) Kel-F (chlorofluorocarbon), and (c) glass tube.

essentially the same CL signal height, indicating that the CL reaction is being controlled by diffusional mixing. However, the best RSD (<1.5%) was observed with cell 5(a); typical RSD values were 2–3% for cell B and >4% for cell C. Additionally, cell 5(a) is preferred because a lower residence volume is desirable for kinetic discrimination against slower

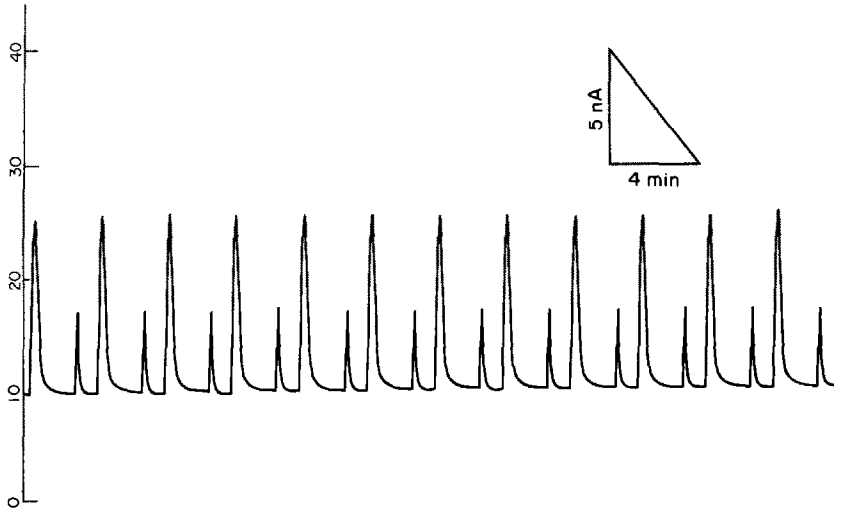

Fig. 6. Typical system output shown for the indigotrisulfonate–O_3(aq) reaction system at an O_3(aq) concentration of 1.8 mg/l.

Table 1. Relative intensity of chemiluminescence of ozone with various substrates

Reagent	Relative CL signal
Quinine sulfate	0.4
Benzoflavin	4.8
Acridine Yellow	9.8
Indigotrisulfonate	20
Fluorescein	22
Eosin Y	35
Rhodamine B	55
Chromotropic acid	90

reacting interferents. A typical system output at the 1.8-mg/l.O_3(aq) level is shown in Fig. 6. The dual loop arrangement can effectively provide two independent calibration ranges without changing the instrument gain.

Effectiveness of different test reagents

In order to generate CL, the excited intermediate produced by the ozone–substrate reaction must luminesce itself or transfer its energy to another molecule that can. The situation is simplified if the substrate is itself fluorescent. Therefore a number of organic compounds that fluoresce in dilute aqueous solutions were evaluated for the determination of aqueous ozone by CL–FIA. Table 1 shows the relative CL signals obtained with different reagents. For our experimental arrangement, the calculated LOD (based on the S/N = 3 criterion) for the most thoroughly studied ITS reaction system was 2 μg/l.; this is acceptable for the determination of residual ozone in water treatment applications. Chromotropic acid, Rhodamine B and Eosin Y, all of which produced more intense CL than ITS, may yield more sensitive determination systems. However, when Rhodamine B and Eosin Y solutions were used in the system for a continued period, adsorption of the reagent on the view window occurred, resulting in a gradual decrease in sensitivity and deterioration of the run-to-run reproducibility. For the Rhodamine B system, the addition of a surfactant (Triton-X-100, 0.1% w/v) was studied. It increased the CL signal by *ca.* 30% but did not solve the adsorption problem.

Effect of pH and salinity

The effects of varying pH and salinity in a real water sample on the system response are important. Using 0.1*M* phosphate and acetate buffers at pH 2 and 4.7 respectively for the ITS reagent, the CL signal increased by 60% at the higher pH. With 0.1*M* sodium chloride to add salinity, the CL signal for this system was higher by a factor of *ca.* 5 at pH 7 compared to pH 2. Interestingly, the colorimetric response (bleaching of indigo) determined by a parallel system[17] was independent of the reagent pH. The salinity did not affect the magnitude of the signal as much as it affected the precision of replicate injections—whether it is due to any real chemical reasons or Schlieren effects from imperfect mixing needs to be investigated. The importance of appropriately buffering the reagent was, however, evident.

Effect of potential interferents

While further studies and field validation will be necessary before a CL–FIA method can be recommended for the determination of O_3(aq), a major incentive to pursue this route is the fact that for many of the reagents, on a short time measurement scale (*e.g.*, <1 sec), the effect of potential slower reacting interferents are either nonexistent or can be minimized. For chromotropic acid, Rhodamine B, and Eosin Y as reagents, H_2O_2, Cl_2 (as OCl^-) at concentrations <10 mg/l. and MnO_4^- at a concentration <1 mg/l. showed no measurable response in the present measurement system with cell 5(a).

With ITS, significant response was found only with MnO_4^-; based on a colorimetric FIA study,[17] the decolorization reaction of ITS by MnO_4^- is 20% complete in 1.6 sec while the reaction with ozone is 100% complete. However, the CL reaction for the ITS–MnO_4^- system appears to be faster, CL presumably precedes decolorization. On an oxidant equivalents basis (note that ozone is a 4-electron oxidant for indigo), MnO_4^- produced $\geq 65\%$ of the ozone response in a reaction cell with a calculated residence time <150 msec. Therefore significant interference from MnO_4^- may result from waters with significant Mn content (albeit such Mn concentrations do not occur frequently) if ITS is chosen as the reagent. However, the other three reagents mentioned above produce negligible CL with MnO_4^- and may more conveniently form the basis for sensitive analytical methods immune to interferences from oxidants other than ozone.

Acknowledgements—This work was supported in part by funds from the American Water Works Association Research Foundation (AWWA-RF). We are grateful to the Project Advisory Committee (PAC) for constructive criticism. However, endorsement of this work by the AWWA-RF or the PAC should not be inferred. We thank our co-workers, Daniel P. Y. Chang and Jeannie L. Darby at the University of California, Davis, for their moral support. We gratefully acknowledge the machining assistance of Kavin Morris.

REFERENCES

1. R. L. Bowman and N. Alexander, *Science*, 1966, **154**, 1454.
2. G. W. Nederbragt, A. van der Horst and J. van Duijn, *Nature*, 1965, **206**, 87.
3. Ambient Air Monitoring Reference and Equivalent Methods, *Federal Register*, 1975, 40:33, Part 2, February 18, 7042.
4. D. Bersis and E. Vassiliou, *Analyst*, 1966, **91**, 499.
5. V. H. Regner, *J. Geophys. Res.*, 1964, **69**, 3795.
6. J. A. Hodgeson, K. J. Krost, A. E. O'Keeffe and R. K. Stevens, *Anal. Chem.*, 1970, **42**, 1795.
7. J. D. Day, D. H. Stedman and G. J. Wendel, *ibid.*, 1986, **58**, 598.
8. K. Takeuchi, S. Kutsuna and T. Ibusuki, *Anal. Chim. Acta*, 1990, **230**, 183.
9. I. V. Ardzhanov, V. S. Gritsenko, N. G. Domostroeva, G. P. Konopleva and L. B. Shaginyan, *Izmer. Tekh.*, 1976, **5**, 70.
10. M. A. Karabegov, S. A. Khurshudyan, I. V. Ardzhanov and V. S. Gritsenko, *Prib. Sist. Upr.*, 1977, **4**, 25.
11. K. Takeuchi and T. Ibusuki, *Bunseki Kagaku*, 1987, **36**, 311.
12. *Idem*, *Anal. Chem.*, 1989, **61**, 619.
13. J. Hoigne and H. Bader, *Ozone: Sci. Eng.*, 1979, **1**, 357.
14. J. Merritt, *Waterworld News*, May/June, 1987.
15. B. R. Langlais, D. A. Rekhow and D. R. Brink (eds.), *Ozone in Water Treatment: Application and Engineering*, Lewis Publishers, Inc., Chelsea, MI, 1991.
16. G. Gordon and G. E. Pacey, *Assessment of Disinfectant Residual Measurement Methods*, AWWA Research Foundation Comprehensive Assessment, American Water Works Association Research Foundation, 1988.
17. P. K. Dasgupta, J. L. Darby and D. P. Y. Chang, *Automated Measurement of Aqueous Ozone Concentration*, Final Report, American Water Works Association Research Foundation, 1991.
18. J. A. Roth and D. E. Sullivan, *Ind. Eng. Chem. Fundam.*, 1981, **20**, 137.

Talanta, Vol. 39, No. 6, pp. 599–607, 1992
Printed in Great Britain.

0039-9140/92 $5.00 + 0.00

QUANTITATIVE COMPARISONS USING LIQUID CHROMATOGRAPHY WITH DUAL-LABEL RADIOACTIVITY MEASUREMENTS FOR EVALUATION OF ISOTOPE AND IMPURITY EFFECTS

LAWRENCE C. THOMAS
Department of Chemistry, Seattle University, Seattle, Washington 98122, U.S.A.

(*Received* 1 *July* 1991. *Revised* 1 *November* 1991. *Accepted* 15 *November* 1991)

Summary—Dual-label methods with radiometric measurements with liquid chromatography are evaluated for assessing effects of impurities and isotopic composition in reaction experiments. The procedure is suitably sensitive to detect interferences caused by effects of impurities in reactants, isotope exchange during reaction and effects of kinetic differences due to differing masses of the differently labeled forms. The methods show marked improvements in data quality for comparisons of product formations and relative product abundances in multiple-pathway reaction systems. The results from computer simulations for the procedures are shown to be relatively unaffected by large variations in uncertainties in pretreatment steps and volume measurements. Moreover, these methods yield much better quantitative results than do commonly used corresponding conventional comparisons, and the benefits are corroborated by results from experiments with microsomal reactions.

Radioactivity measurements for chromatography can be used to obtain quantitative information in experiments involving multiple reaction pathways. Radiochemical detection of reaction products separated by chromatography can provide good selectivity, low limits of detection and freedom from many interferences.[1] However, several factors plague radiometric chromatography procedures for reaction product evaluations and can cause large uncertainties in data and results.[2–5] Typically, those procedures require both availability and careful characterization of appropriate reference materials for every measured component. Unfortunately, for complex systems such as metabolism studies, several reaction product analytes may be measured for each sample and appropriate pure standards may not be available for them all. Moreover, identities of the products are not always known, which precludes use of either conventional internal- or external-standard methods.

In related work,[2,5] compounds labeled with two different radioactive isotopes were separated by HPLC for special dual-label procedures which mimic internal-standard methods. In those studies biologically generated radiolabeled reference solutions were used and their components separated along with differently labeled respective coeluting metabolites from samples from biological experiments. The dual-label approaches allow for compensation for variations in extraction efficiencies, variable losses during concentration of extracts, imprecisions of volume measurements and uncertainties in specific activities of dosage compounds. Moreover, the procedures greatly obviate difficulties caused by unavailability of pure reference compounds and do not necessarily require eluate identifications.

Similarly, as done herein for characterizing isotope effects and impurity interferences, one may use a combined solution of differently labeled forms of the same compound, with concurrent exposure of the two forms in the same reaction system via addition of an aliquot of the mixed reactant solution.[3] The two forms thereby concurrently react under identical conditions. The respective reaction products may then serve as mutual internal standards in dual-label HPLC procedures for quantitative comparisons to evaluate: (a) effects of impurities on reaction product formation experiments, (b) effects of isotope exchange upon those experiments, and (c) effects of kinetic differences between the forms which may be caused by their different respective masses.

Improvements from the dual-label method for assessing isotope or impurity interferences in reaction experiments have been estimated for a

few selected circumstances,[3] but no detailed evaluations of data-quality enhancements offered by the dual-label techniques have been done. In this work, computer simulations are used for detailed theoretical studies of improvements provided by use of the dual-label quantitative comparisons for evaluating isotope effects and impurity interferences, and the results from simulations are corroborated by laboratory experiments.

THEORY

A main advantage of the dual-label procedure for assessing interferences is that selected special ratios, described below, yield well-defined theoretically predictable results which may be tested statistically.[2,3,5] One may concurrently react in the same solution both an X-labeled test compound and the same compound which is labeled differently, *e.g.*, Y-labeled, perhaps one or both of unknown concentration. If the two differently labeled reactant compounds are chemically identical their respective reaction products will typically also be identical, except for their respective radioactivities; this equivalence is a reasonable assumption unless isotope exchange occurs during reaction, or if kinetics are affected as a result of differences in isotopic masses. Moreover, if the reaction products are pretreated together in the same solution prior to measurement, the pretreatments will typically have equivalent extraction/concentration/dilution efficiencies, E, for the two forms of each reaction product i, *i.e.*, $E_{X,i} = E_{Y,i}$. Thus, if V_t is the volume of the sample solution from the reaction mixture, V_{ss} is the volume of the prepared subsample used for chromatographic separation, and M is the mass of specified analyte in the original sample, then

$$M_{X,i} = (A_{X,i} V_t)(E_{X,i} V_{ss} S_{X,i})^{-1}$$

and

$$M_{Y,i} = (A_{Y,i} V_t)(E_{Y,i} V_{ss} S_{Y,i})^{-1}$$

where $A_{X,i}$ and $A_{Y,i}$ are corrected measured radioactivities, respectively, for the X-labeled and Y-labeled forms of eluate component i from volume V_{ss}, and $S_{X,i}$ and $S_{Y,i}$ are respective specific activities for the labeled component i.

Intrasample comparisons

To evaluate isotope or impurity effects for reaction systems, special intrasample ratios can be defined for X- *vs.* Y-labeled reaction products. For this, V_t is identical for both labeled forms of each reaction product taken together from the same sample solution. Similarly, V_{ss} is the same or both forms of each product. Accordingly, a ratio of respective masses can be calculated and $M_{X,i} M_{Y,i}^{-1} = (A_{X,i} S_{Y,i})(A_{Y,i} S_{X,i})^{-1}$ for any component i. Furthermore, separated reaction products, i *vs.* j, derived from the same reaction experiment can then be compared,

$$Q_{i,j} = (M_{X,i} M_{Y,i}^{-1})(M_{X,j} M_{Y,j}^{-1})^{-1} = (A_{X,i} A_{Y,j}) \times (A_{Y,i} A_{X,j})^{-1} (S_{Y,i} S_{X,j})(S_{X,i} S_{Y,j})^{-1}$$

If relative specific activities for components i *vs.* j are known, then Q_{ij} may be calculated from radioactivity data in combination with those appropriate $S_{Y,i}/S_{Y,j}$ and $S_{X,i}/S_{X,j}$ ratios. Moreover, if there is no isotope exchange during reaction $S_{Y,i} = S_{Y,j}$ and $S_{X,i} = S_{X,j}$, and so, $Q_{ij} = (A_{X,i} A_{Y,j})(A_{Y,i} A_{X,j})^{-1}$. Thus, Q_{ij} may be computed from corrected measured radioactivity data of the dual-label chromatogram only, without knowing specific activities.

If there has been neither isotope exchange nor differences in kinetics, nor contributions to the specified components due to impurities, then $Q_{ij} = 1$; that is, the relative isotopic composition for all components is the same. If isotope effects or impurities cause interferences, then Q_{ij} may be significantly different than unity, and one may test Q_{ij} statistically for each i,j pair via replications and a null hypothesis that the measured reaction products are unaffected by impurities or isotope effects.

Intersample comparisons

Similarly, one could compare intersample Q-ratios to ascertain intersample differences due to impurities or isotope effects; for compound i, $Q_{12,i} = (M_{X,i,1} M_{Y,i,1}^{-1})(M_{X,i,2} M_{Y,i,2}^{-1})^{-1}$ for comparisons for samples 1 *vs.* 2, both resulting from reactions of identical aliquots of the same test solution containing both X- and Y-labelled reactant. Conveniently, $S_{X,i,1} = S_{X,i,2}$ and $S_{Y,i,1} = S_{Y,i,2}$ for those intersample comparisons, thus $Q_{12,i} = (A_{X,i,1} A_{Y,i,2})(A_{X,i,2} A_{Y,i,1})^{-1}$, which can be readily calculated from radioactivity data only and can be tested statistically for $Q_{12,i} = 1$, as above, and does not require specific activity data.

Likewise, intrasample comparisons can be extended to comparisons of two or more component concentration ratios relative to the same

components in intersample sets of measurements, *e.g.*, $Q_{ij,1}/Q_{ij,2} = Q_{ij,12}$. This might correspond to comparing products of two reaction pathways and, of course, $Q_{ij,12} = 1$ if the reaction product profiles are unaffected by impurities or isotope effects. Again, the Q-ratio can be calculated from radioactivity data only without knowing specific activities, and can be tested statistically.

EXPERIMENTAL

Reagents

All organic solvents used were Mallinckrodt ChomAR. Radiolabeled compounds were purchased from Amersham Corporation. Water used was distilled in all-glass apparatus and other chemicals were reagent grade quality.

Apparatus

An Altex HPLC system with two Model 110 pumps, a Model 420 control module and a Beckman Model 171 dual-channel flow-through radioactivity counter with a 150-μl flow cell volume, interfaced to an Equity I+ computer and an Epson Model 800 printer was used. Separations were done at 1 ml/min eluant flow through an Altex 4 mm i.d. × 25 cm length stainless column packed with 5 μm octadecylsilyl reverse phase column material. Eluted fractions were collected every 30 sec in scintillation vials by a Pharmacia FRAC-100 fraction collector after automatic mixing with Beckman Ready-Flow II scintillation cocktail, added at 4.0 ml/min, in the Model 171. Collected fractions were counted on a Beckman Model 5000 liquid scintillation counter (LSC) and corrected for energy overlaps according to conventional procedures. Labware used was treated with dimethyldichlorosilane in hexane, and washed with water and acetone prior to use.

Computer simulations. An Epson Equity II+ computer with EGA graphics, a 20-Mbyte hard disk, an Intel 80287 mathematics co-processor and an Epson LX 810 printer were used for mathematical modeling of dual-label chromatography separations and measurements. Computer programs were written in Microsoft's Quickbasic 4.0 (listings available from author upon request).

Procedure for computer simulations

Chromatograms from the simulations were generated for specified enzymatic reaction rates of aryl hydrocarbon hydroxylases (AHH), using relative metabolite concentrations from others' data compilations.[6] For rats metabolizing benzo(a)pyrene (BaP), relative concentrations in Table 1 were used, with other minor reaction products[6] ignored.

Efficiencies of component recoveries from extractions, reduction of extract volumes and dilutions to appropriate volume were taken from other work with reasonable standard deviations[2,6] (see Table 1). No differences in these efficiencies were assumed for the differently labeled forms, consistent with their nearly identical chemical properties.[2,3] Random variations in these efficiencies were generated by an accepted procedure.[7] Variations in volume measurements for the diluted extract, the added reference solution and the subsample taken for HPLC were generated with reasonable standard deviations for volume measurements[8] and random gaussian deviations.[7]

Masses for each respective reaction product in subsamples taken for HPLC were calculated from assumed but varied AHH activities in the respective reaction systems, uncertainties in pretreatment recoveries, uncertainties in volumes and the volumes used. Mass *vs.* time relations for components separated by HPLC were calculated from respective injected masses, assumed

Table 1. Metabolite retentions, percentage of metabolites and uncertainties due to pretreatments used for simulations

Metabolite	Retention, *min*	% Met*	E/C/D Eff† ± (SD × *n*) (%; *n* = 1, 2 or 3)
9,10 BaP Dihydrodiol	16	8%	0.4 ± 0.05 n
7,8 BaP Dihydrodiol	24	6%	0.4 ± 0.05 n
1,6 BaP Dione	31	7%	0.5 ± 0.05 n
3,6 BaP Dione	34	8%	0.5 ± 0.10 n
6,12 BaP Dione	38	7%	0.8 ± 0.10 n
9-Hydroxy BaP	45	11%	0.8 ± 0.10 n
3-Hydroxy BaP	54	40%	0.9 ± 0.05 n
BaP	65		0.9 ± 0.05 n

*Percentage of total metabolites.
†Extraction/Concentration/Dilution efficiency.

HPLC peak widths at half-maximum of 1.0 min and presumed gaussian peak shapes. The radioactivities of the two labeled forms eluting from the column were calculated over all 1-sec intervals throughout the separation duration. These interval radioactivities were then summed into consecutive 30-sec intervals to simulate contents of collected fractions (see Fig. 1).

Radioactivities were assumed to be for ^{3}H- and ^{14}C-labeled compounds for these calculations. The simulated measured radioactivity for each fraction was calculated from the contained masses, specific activities, appropriate counting efficiencies for the relative amounts of solvents and mixed scintillation cocktail, and imposed random variations in counting according to accepted procedures, with appropriate compensation for energy overlaps.[7,9] Histograms simulating counted elution fractions were generated and integrated measured radioactivities for each labeled form of each separated metabolite were calculated by conventional methods.[9] Those data were saved for later computations and statistical analyses.

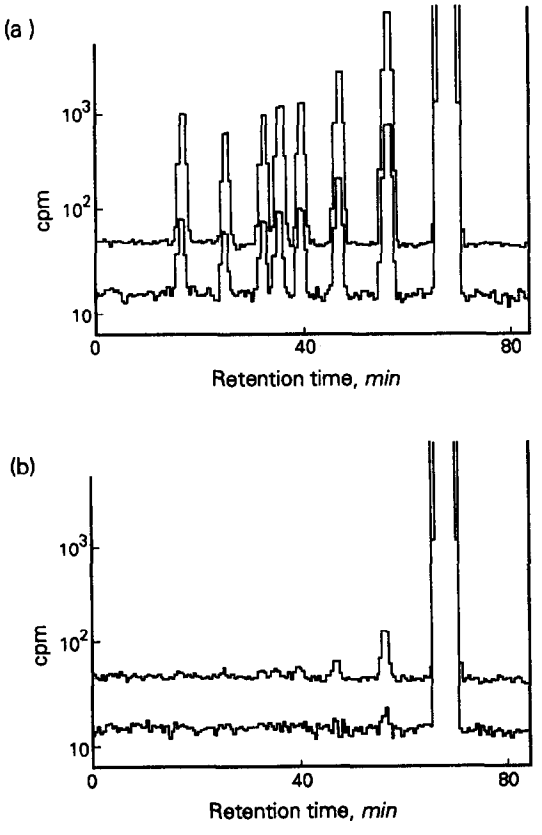

Fig. 1. Histograms of simulated measured radioactivity *vs.* time for 30-sec eluted fractions. Upper chromatograms with approximately 49 cps background are for ^{3}H BaP reaction product eluates and lower chromatograms with approximately 16 cps background represent corresponding ^{14}C BaP components from samples. AHH enzymatic activities for the incubations of the combined ^{3}H BaP and ^{14}C BaP mixtures with initial concentrations such that [^{3}H-BaP] = 10[^{14}C-BaP]: (a) 10^{-3} I.U./l. and (b) 10^{-5} I.U./l.

Fifteen replicates were done for each simulated variation in combinations of: (a) nine combinations of reactant concentrations, with ^{3}H BaP concentrations of 10^{-2}, 10^{-3} and $10^{-4}M$ and ^{14}C BaP concentrations varied in factors of 10 between 10^{-3} and $10^{-7}M$, but always lower than the ^{3}H BaP concentration, *i.e.*, providing relative (^{3}H BaP/^{14}C BaP) concentrations ranging between 10^{-1} and 10^{-4}, (b) 20 values for AHH reaction rates for the sample solution varying between 10^{-2} I.U./l. to 2×10^{-8} I.U./l., and (c) three values for uncertainties in extraction/concentration/dilution efficiencies ($\pm$s, $\pm$2s, and $\pm$3s; see Table 1 for values). Other values were held constant: (a) 10-min counting times were used, (b) 60-min enzymatic incubations were assumed, (c) specific activities of 500 and 325 mCi/mmole for ^{3}H-labeled and ^{14}C-labeled BaP, respectively, (d) 100 ml for the sample incubation volume, 1.00 ml for the combined ^{3}H and ^{14}C mixture's resulting concentrate, and 0.100 ml used for separation by HPLC, and (e) background count rates of 49 cpm for ^{3}H and 16 cpm for ^{14}C.

Simulated measured radioactivities for each labeled form of each metabolite were saved and those data were later used to calculate Q-ratios for metabolite-label pairs and corresponding conventional ^{14}C-ratio results. Means (x) and standard deviations (s) were computed and data quality was estimated as x/s for each compared set. Confidence ranges ($x \pm s$) were calculated for Q-ratio results and for conventional results for various replicate sets and were plotted *vs.* AHH enzymatic activities for sample solutions under otherwise identical conditions.

Procedure for laboratory studies: test organisms

S-10 fraction microsomes were collected as 60-min $\times$ 60,000 $\times$ **g** centrifugate, obtained from 20-min $\times$ 20,000 $\times$ **g** supernatant of liver tissue homogenized in 1% potassium chloride. Livers were excised from Sprague–Dawley rats (approximately 200 g) and treated immediately for microsomal collection. Microsomes were stored at $-80°$ for future use if not used immediately after preparation.

Microsomes were incubated with NADPH, glucose-6-phosphate and glucose-6-phosphate dehydrogenase in oxygen-saturated 0.1M phosphate buffer at pH 7.5 and radiolabeled BaP

dosage commpounds at 37.5°. After a two-hour incubation, the metabolism was halted by the addition of acetone. The incubates were then saturated with sodium chloride and extracted four times with ethyl acetate. Descriptions of reagent volumes and concentrations may be found elsewhere.[2,3] The extracts were evaporated to dryness at 25° under a $N_{2(g)}$ stream and the residue partially dissolved into 1.0 ml of methanol. A 50-μl aliquot of each methanolic concentrate was taken for separation by HPLC with the effluent being mixed with scintillation cocktail just prior to flow-through counting. The outflow from the Model 171 counter was collected as one-minute fractions in glass scintillation vials and each was counted for 20 min on a multichannel LSC.

Data were plotted as histograms and net activities calculated for the eluted components. Eluate radioactivities were then used for Q-ratio computations, for conventional comparisons using ^{14}C-ratios and for statistical calculations.

RESULTS AND DISCUSSION

Computer simulations

Dual-label chromatograms from simulations were developed to generate histograms representing collected fraction radioactivities *vs.* time (Fig. 1) that mimic chromatograms expected from corresponding biological experiments.[2,6] The simulated chromatograms represented a wide range of variations in peak areas, including those for which all metabolite peaks' radioactivities were easily calculated [Fig. 1(a)] and others for which many eluates were below the limits of reliable measurement [Fig. 1(b)], with some circumstances allowing easy measurement of one labeled form but difficult-to-unfeasible measurements for the other.

Intrasample Q-ratio comparisons show Q_{ij} values which closely approximate unity, as predicted by theory (Figs. 2 and 3). The relative uncertainties, *e.g.*, relative standard deviations for Q_{ij} values within a replicate set, are often slightly worse than relative uncertainties for ratios of corresponding single-label ^{14}C-ratios; however, results found for single-label ratios vary considerably, with no theoretically predicted value achieved. Also, the Q_{ij} ratios are only slightly affected by large variations in extraction/concentration/dilution efficacies (see Fig. 2). As expected, lower measured activities yield less precise results (Fig. 3), but the Q-ratio results maintain their tendency toward unity, unless the uncertainties of measured activities are overwhelming. Consequently, testing of the null hypothesis, that the measured reaction products are unaffected by impurities or isotope effects, is dramatically more powerful if Q-ratio comparisons are used instead of conventional approaches with ^{14}C-ratios.

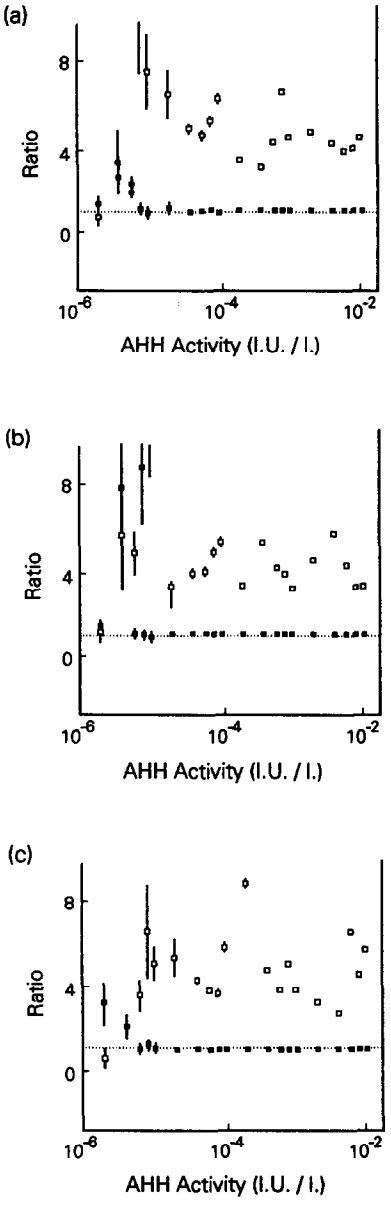

Fig. 2. Simulated sample AHH enzymatic rate (I.U./l.) *vs.* intrasample Q-ratios (■) or corresponding ratios using only the C-label data (□): These figures show results for three levels of extraction/concentration/dilution uncertainties: (a) ±10% and ±5% (RSD), (b) ±20% and ±10% (RSD), and (c) ±30% and ±15% (RSD) for 9-hydroxy BaP and 3-hydroxy BaP, respectively. These data were attained with intrasample comparisons between 9-hydroxy BaP and 3-hydroxy BaP.

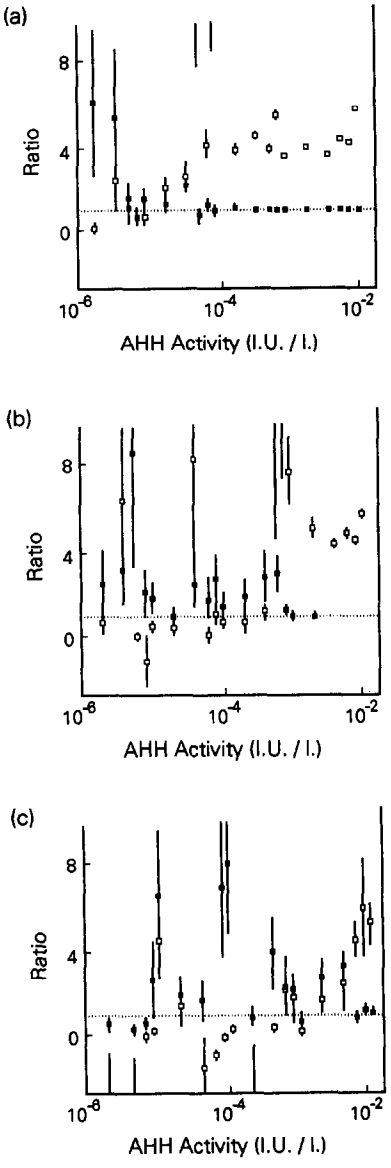

Fig. 3. Simulated sample AHH enzymatic rate (I.U./l.) *vs.* intrasample Q_{ij} ratios (■) or corresponding ratios with only the C-label data (□): these figures show results for three levels of components radioactivities resulting from initial incubation concentrations such that (a) $[^3\text{HBaP}] = 10^2[^{14}\text{CBaP}]$, (b) $[^3\text{HBaP}] = 10^3[^{14}\text{CBaP}]$ and (c) $[^3\text{BaP}] = 10^4[^{14}\text{CBaP}]$. Data are for intrasample comparisons between 9-hydroxy BaP and 3-hydroxy BaP metabolism products, with extraction/concentration/dilution uncertainties of ±10% (RSD) for 9-hydroxy BaP and ±5% (RSD) for 3-hydroxy BaP.

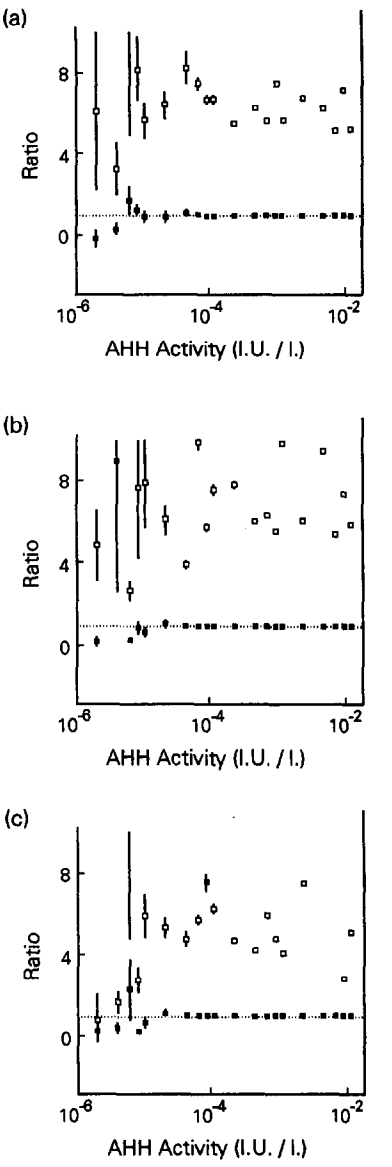

Fig. 4. Simulated sample AHH enzymatic rate (I.U./l.) *vs.* intersample $Q_{12,i}$-ratios (■) and corresponding ratios with only C-label data (□). These figures show results for three levels of extraction/concentration/dilution uncertainties: (a) ±10% (RSD), (b) ±20% (RSD) and (c) ±30% (RSD). These data are for intersample comparisons *vs.* a reference set of 15 replicate incubations with AHH enzymatic rates of 10^{-3} I.U./l., with each individual datum for 6,12 BaP dione being compared to averaged 6,12 BaP dione data of the reference set.

Intersample comparisons, relative to a specified component from a specified replicate sample set, show dramatic benefits for Q-ratios. The advantage of using Q-ratios, rather than corresponding conventional comparisons via singly labeled reaction products, is distinct. The conventional methods' results are typically somewhat more precise for individual selected comparisons among replicates, partly because fewer radioactivity measurements are used. However, conventional comparisons yield results which vary widely between such comparisons (see Fig. 4). More importantly, the Q-ratio results yield theoretically predictable values, *i.e.*,

$Q_{12,i} = 1$ for the null hypothesis, while conventional comparisons results are disparate and reveal no such predicted value.

Intersample comparisons for selected pairs of products, relative to corresponding pairs from a specified replicate sample set also yield theoretically predictable results via Q-ratios, *i.e.*, $Q_{ij,12} = 1$ for the null hypothesis (see Fig. 5). Conventional comparisons' results among replicate sets are somewhat more precise, in general, but their results vary widely between such comparisons and do not yield theoretically predictable values.

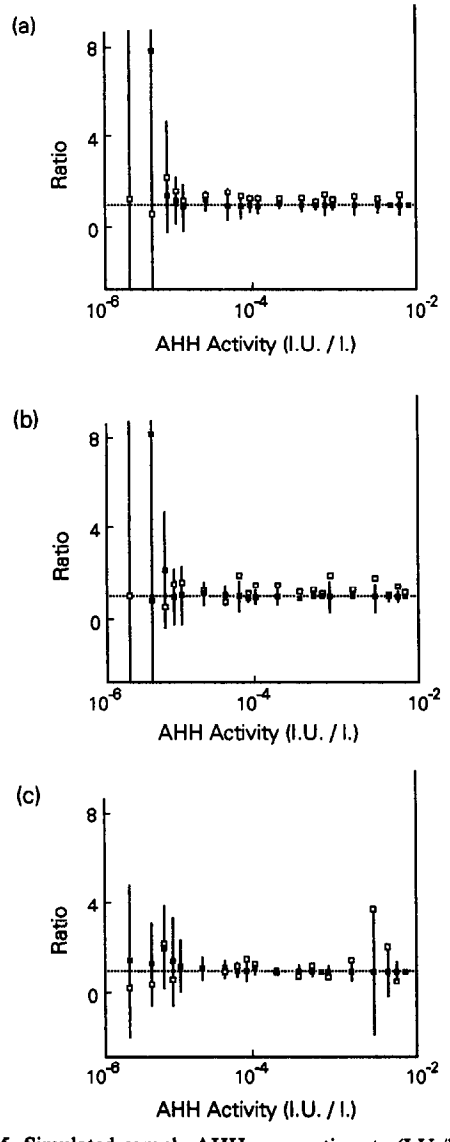

Fig. 5. Simulated sample AHH enzymatic rate (I.U./l.) *vs.* intersample $Q_{ij,12}$-ratios (■) and corresponding ratios with only C-label data (□). These figures show results for 6,12 BaP dione at three levels of extraction/concentration/dilution uncertainties: (a) ±10% (RSD), (b) ±20% (RSD) and (c) ±30% (RSD). These data are for intersample comparisons *vs.* a reference set of 15 replicate incubations with AHH enzymatic rates of 10^{-3} I.U./l., with individual data for intrasample ratios between 6,12 BaP dione and 3-hydroxy BaP being compared to corresponding averaged 6,12 BaP dione *vs.* 3-hydroxy BaP ratios of the reference set, with extraction/concentration/dilution uncertainties of ±15% (RSD), ±10% (RSD) and ±5% (RSD), respectively, for the 3-hydroxy BaP data of the reference set.

As extraction/concentration/dilution imprecisions increase greatly, corresponding Q-ratios become a little less precise, but are relatively insensitive to great changes in pretreatment effectiveness. Moreover, the predictability, *i.e.*, the uncertainty for unity in the null hypothesis, changes only slightly due to those somewhat larger standard deviations in the Q-ratios (see Figs. 2, 4 and 5). Thus, use of the Q-ratios substantially reduces difficulties encountered due to large variations in recovery efficiencies and other pretreatment variables.

As the AHH enzymatic activity increases, the Q-ratios become relatively more precise, but are not dramatically better above a certain threshold region for AHH enzymatic activity (see Figs. 2–5) and depend upon the concentrations of selected metabolites formed (see Figs. 3, 6 and 7). This is apparent for intrasample Q-ratios as shown in Fig. 2, and for intersample Q-ratios depicted in Figs. 4–7. However, low component concentrations, typical of very low initial concentrations of reactant or of very low AHH activity, *e.g.*, $< 10^{-5}$ I.U./l., result in either large s/x ratios with wide confidence ranges or immeasurable values which are shown in the figures as zero values.

Increased numbers of replicates enhance data quality for Q-ratios. As expected, improvements are significant for low numbers of replications, *e.g.*, 2 *vs.* 3, but the added relative advantage for high numbers of trials is much less dramatic. Thus, one may select a number of replicates which allows for appropriate statistical comparisons, *e.g.*, 3–5, and save the expense of using many repetitions of the corresponding experiments; when using conventional single-label comparisons, even very high numbers of replications do not result in the excellent predictability offered by only a few replicates with the Q-ratios.

Use of the dual-label procedure discussed above has the potential for dramatically improving statistical evaluations of interferences in reaction product formation experiments. This is mainly due to the theoretically valid predictability for the Q-ratios, *i.e.*, $Q = 1$ for the null hypothesis. Also, because the components are

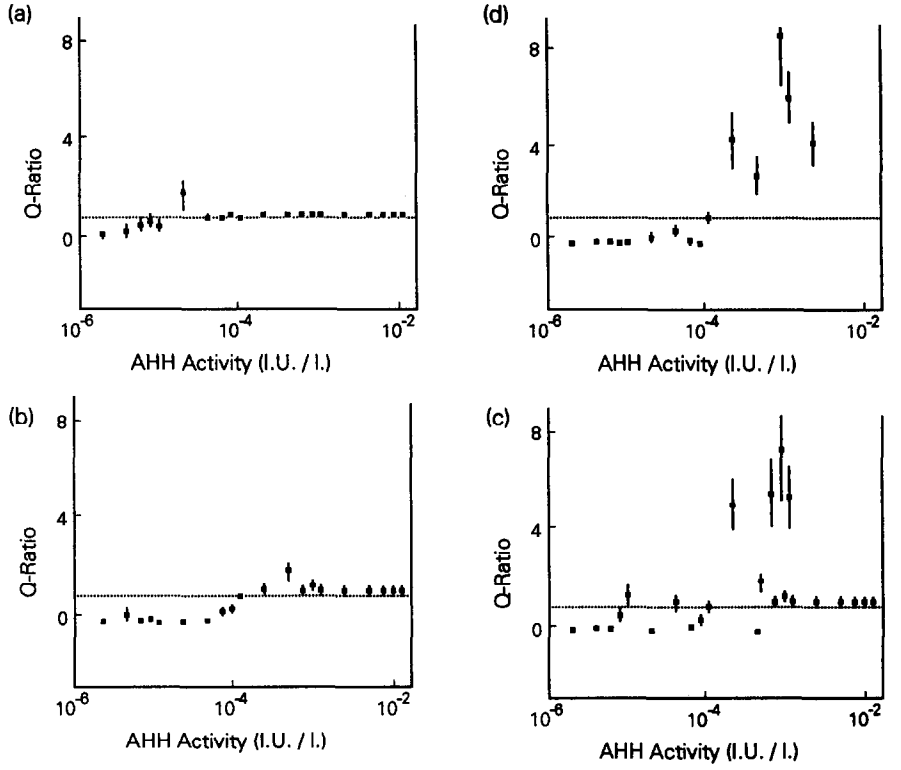

Fig. 6. Simulated sample AHH enzymatic rate (I.U./l.) *vs.* intersample $Q_{12,i}$-ratios for four levels of components' radioactivities resulting from initial concentrations such that (a) [^{3}HBaP] = 10 [^{14}CBaP], (b) [^{3}HBaP] = 10^2[^{14}CBaP], (c) [^{3}HBaP] = 10^3[^{14}CBaP] and (d) [^{3}HBaP] = 10^4[^{14}CBaP]. Data are for intersample comparisons *vs.* a reference set of 15 replicate incubations with AHH enzymatic rate of 10^{-4} I.U./l, with individual data for 3,6 BaP dione being compared to averaged 3,6 BaP dione data of the reference set, with extraction/concentration/dilution uncertainties of ±10% (RSD) for the 3,6 BaP dione.

chemically alike and treated identically, contributions due to uncertainties in recoveries, volume measurements, *etc.* are reduced appreciably, resulting in small standard deviations for corresponding Q-ratios. Moreover, because of the mathematical form of these ratios, requirements for identifying all eluates, obtaining pure analyte reference compounds, and carefully defining specific activities and some other variables may be obviated.

Experimental measurements

Results of laboratory tests with microsomes are consistent with the simulated results discussed above. For replicates obtained by splitting individual samples after incubation but prior to pretreatments and separations, Q-ratios were typically 1.0 ± 0.06 (RSD; $n = 5$) for comparisons relative to 3-OH-BaP. Corresponding values for conventional ratios for the same radioactivity data, based upon comparisons of ^{14}C data only, varied dramatically with percent RSD values between 50 and 300%, with no discernible tendency toward unity. All these results were somewhat worse than predicted by theory, perhaps due to interferences from other components and drifting chromatogram baselines. However, the marked advantages predicted for the Q-ratio, as discussed above, were corroborated by the experimental results.

These dual-label techniques are powerful for assessing problems due to isotope effects or impurities in reaction studies and should be adaptable to isotope-selective measurements such as emission spectrometry, mass spectrometry and resonance spectroscopic methods, which would allow for use of nonradioactive compounds. Additionally, they could be easily used for both biological and nonbiological reaction systems such as photodegradations or pyrolyses.

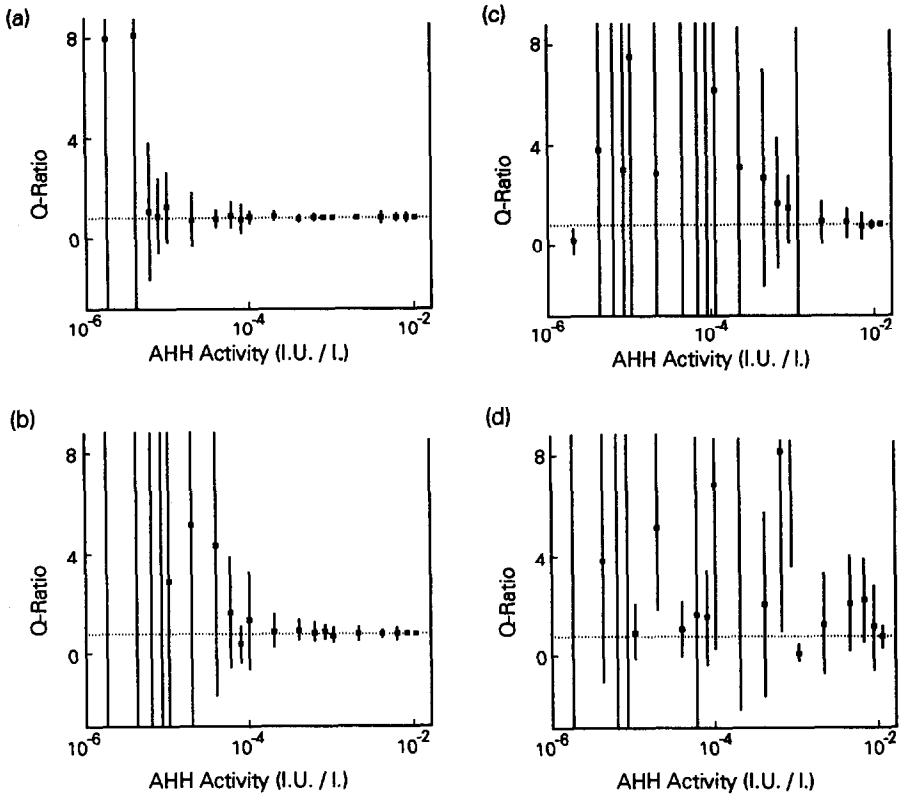

Fig. 7. Simulated sample AHH enzymatic rate (I.U./l.) *vs.* intersample $Q_{ij,12}$-ratios for four levels of components' radioactivities resulting from initial concentrations such that (a) $[^3HBaP] = 10[^{14}CBaP]$, (b) $[^3HBaP] = 10^2[^{14}CBaP]$, (c) $[^3HBaP] = 10^3[^{14}CBaP]$ and (d) $[^3HBaP] = 10^4[^{14}CBaP]$. Data are for intersample comparisons *vs.* a reference set of 15 replicate incubations with AHH enzymatic rate of 10^{-4} I.U./l., with each individual data for intrasample ratio between 1,6 BaP dione and 3-hydroxy BaP being compared to averaged 1,6 BaP dione *vs.* 3-hydroxy BaP data of the reference set, with extraction/concentration/dilution uncertainties of $\pm 5\%$ (RSD) for both components.

Acknowledgement—We thank the National Institutes of Health for their support of this and earlier work via grant number 1R15 GM36273-01A1.

REFERENCES

1. H. C. Barth, W. E. Barber, C. H. Lochmuller, R. E. Majors and F. E. Regnier, *Anal. Chem.*, 1988, **60**, 387R.
2. L. C. Thomas and T. L. Ramus, *Anal. Chim. Acta*, 1983, **154**, 143.
3. L. C. Thomas and T. L. Ramus, *Anal. Lett.*, 1984, **17**, 2001.
4. L. C. Thomas, W. D. MacLeod, Jr and D. C. Malins, in *Natl. Bur. Stand. Spec. Publ. No. 519*, National Bureau of Standards, Gaithersburg, MD, 1979.
5. L. C. Thomas and C. L. Wood, *J. Chromatog.*, 1990, **522**, 117.
6. R. I. Freudenthal, S. G. Hundley and S. M. Cattaneo, in *Carcinogenesis. Vol. 3, Polynuclear Aromatic Hydrocarbons*, P. W. Jones and R. I. Freudenthal (eds.), pp. 313–323. Raven Press, New York, 1978.
7. P. R. Bevington, *Data Reduction and Error Analysis for the Physical Sciences*, McGraw-Hill, New York, 1969.
8. G. D. Christian, in *Analytical Chemistry*, 4th Ed., Wiley, New York, 1986.
9. T. R. Roberts, *Radiochromatography*, Elsevier, Amsterdam, 1978.

Talanta, Vol. 39, No. 6, pp. 609–612, 1992
Printed in Great Britain.

0039-9140/92 $5.00 + 0.00

HIGH PERFORMANCE LIQUID CHROMATOGRAPHIC DETERMINATION OF COPPER(II) AND NICKEL(II) BY USING SOLVENT EXTRACTION AND BIS-(ACETYLPIVALYLMETHANE)ETHYLENEDIIMINE AS COMPLEXING REAGENT

M. Y. KHUHAWAR and ALTAF I. SOOMRO
Institute of Chemistry, University of Sindh, Jamshoro, Sindh, Pakistan

(*Received* 20 *June* 1991. *Revised* 2 *October* 1991. *Accepted* 2 *October* 1991)

Summary—The reagent bis(acetylpivalylmethane)ethylenediimine has been examined for the HPLC separation of copper(II), nickel(II), palladium(II) and oxovanadium(IV) chelates on reversed phase HPLC columns (250 × 4 mm) packed with Hypersil ODS, 5 μ and (150 × 3.9 mm) Nova Pak C_{18} with guard column. The complexes are eluted with a binary mixture of methanol and water or methanol, acetonitrile and water. Detection is achieved with a UV detector. The solvent extraction procedure is used for the determination of copper and nickel simultaneously at microgram levels, corresponding to ng levels and pg levels respectively, per injection. The method has been applied to the determination of copper and nickel in a coin, nickel–aluminum alloy and water samples.

The use of high performance liquid chromatography (HPLC) for the separation and determination of organic compounds is extensive, but a number of reports on the corresponding use of HPLC for inorganic determinations have also appeared.[1–3] The tetradentate ketoamine Schiff bases are interesting, because they form neutral and highly stable copper(II), nickel(II), palladium(II) and oxovanadium(IV) chelates and involve fewer interferences.[4,5]

Belcher *et al.*[6] have used bis(acetylpivalylmethane)ethylenediimine (H_2APM_2en) for the solvent extraction and gas chromatographic (GC) determination of copper and nickel in alloy samples and copper in drinking water. Dilli and Patsalides[7] have applied H_2APM_2en as derivatizing reagent for the determination of vanadium in petroleum crudes and fuel oils by gas chromatography. In the present work, a similar procedure has been used for the solvent extraction of copper and nickel, for determination by HPLC.

EXPERIMENTAL

The reagent bis(acetylpivalylmethane)ethylenediimine (H_2APM_2en) and its copper and nickel complexes were prepared as reported by Belcher *et al.*[6]

A column (250 × 4 mm) packed in the laboratory with Hypersil ODS, 5 μm, diameter particles, or a Nova Pak C_{18} (150 × 3.9 mm) with ODS guard column (Waters) was used.

Procedures

Solvent extraction. An aliquot of sample (1–2 ml) containing copper and nickel (2–120 μg) separately or in a mixture was transferred to a well-stoppered test tube (10 ml) to which was added 1 ml of sodium acetate (1*M*) to adjust the pH within 7–8. Reagent H_2APM_2en (1.5 ml) [0.2*M* in ethanol:water (2:1)] was added and the contents were warmed on a water bath at 70–80° for 15 min. After cooling, cyclohexane (2 ml) was added and copper and nickel were extracted by shaking with a mechanical shaker for 30 min. The organic layer was separated and one-half (1 ml) transferred to another test tube and evaporated to dryness. Methanol (1 ml) was then added and the methanolic solution (1 μl) was injected on the Nova Pak C_{18} reversed phase column with ODS guard column. The complexes were eluted with methanol:water (87:13) at a flow-rate of (0.7 ml/min). The detection was carried out with a UV detector at 260 nm.

Dissolution method. To a solution (1–2 ml) containing 2–20 μg of copper and nickel was added 1 ml of sodium acetate (1*M*) to adjust the pH within 7–8, followed by 2 ml reagent

solution (0.02*M*) in methanol. The contents were warmed on a water bath at 70–80° for 15 min. After cooling the mixture, 2 ml of methanol were added and the contents were mixed thoroughly by shaking on a mechanical shaker for 30 min. Finally, the volume was adjusted to 10 ml with methanol. The solution (1–5 μl) was injected on the HPLC column as described in solvent extraction.

Analysis of copper in a coin

To the copper coin (3.004 g) was added 20 ml of *aqua regia* [hydrochloric acid:nitric acid (3:1)] and the mixture was heated gently to near dryness. Hydrochloric acid (10 ml) was added and the mixture was again heated to dryness. To the residue was added water and the volume was adjusted to 100 ml. A 1-ml aliquot of the solution was further diluted to 100 ml. The solution (0.4 ml) was transferred to a well-stoppered test tube and 0.3 ml of ammonium fluoride (1*M*) were added and the procedure followed as for solvent extraction.

Analysis of nickel in nickel–aluminum alloy

Nickel–aluminum alloy (0.2 g) was dissolved in *aqua regia* as for the copper coin. After necessary dilution extractions were carried out, using the procedure described in solvent extraction.

The amount of copper and nickel in the samples was evaluated from standard calibration curves prepared from known amounts of copper and nickel.

Analysis of copper in water samples

Distilled water (10 ml) from a copper still and collected in a copper tank, and 10 ml of domestic water from a stainless steel tank collected after allowing water to flow for 5 min were analysed with the solvent extraction procedure, except that 3 ml of reagent was used and 5 μl of the final solution was injected.

The calibration curve was prepared from doubly distilled water containing 5–70 μg of copper per 10 ml, using the same procedure as for the analysis of samples.

RESULTS AND DISCUSSION

The separation of copper(II) and nickel(II) complexes was investigated on a Hypersil ODS column. Complete separation between reagent, nickel and copper was obtained, when the complexes were eluted with a ternary mixture of methanol:acetonitrile:water (68:13:19) with retention volumes of 4.84 and 5.33 ml for nickel and copper complexes, respectively, using a flow-rate of 0.7 ml/min (Fig. 1). We should note that separation from the oxovanadium and palladium complexes was also complete (retention volumes of 2.62 and 3.69 ml, respectively (see Fig. 1).

In order to use the separation for the quantitative determination of copper and nickel by using solvent extraction procedures, the optimum conditions for the extraction of copper and nickel were confirmed. The effects of variation in pH, solvent, reagent concentration, heating and shaking time were investigated for the extraction of 50 μg of copper and nickel. It was observed that sodium acetate (1*M*, 1–2 ml), covered the pH range between 7–8 (adjusted to 7.5) satisfactorily for the maximum extraction of copper and nickel. The solvents n-hexane, cyclohexane, benzene and toluene were tested for the extraction of copper and nickel. Cyclohexane gave more reproducible results and was therefore used for the extraction of copper and nickel. The reagent concentration (0.02*M*, 1.5 ml) proved adequate for the extraction of

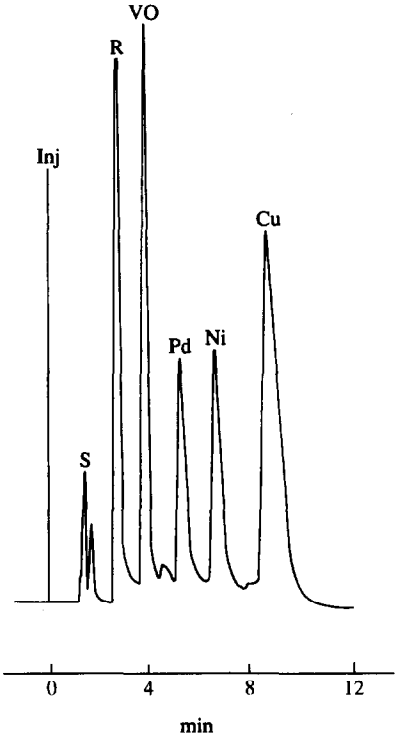

Fig. 1. HPLC separation of reagent, oxovanadium, palladium nickel and copper chelates of H_2APM_2en on column (250 × 4 mm) packed with Hypersil ODS, 5 μ. Elution: Methanol:acetonitrile:water (68:13:19). Flow-rate: 0.7 ml/min; UV detection at 300 nm.

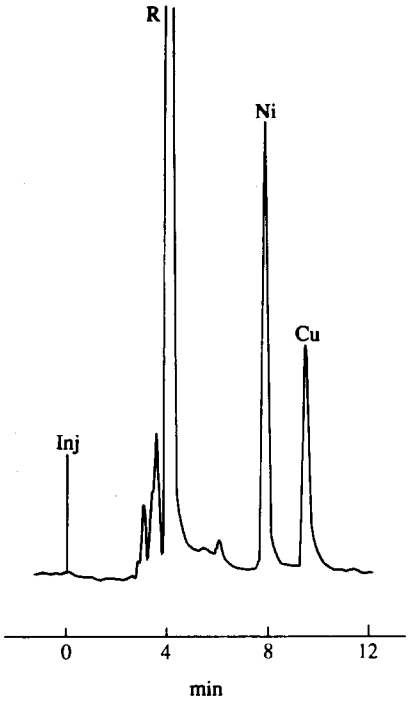

Fig. 2. HPLC separation of copper and nickel chelates extracted with H_2APM_2en on Nova Pak C_{18} column with guard ODS column. Elution: Methanol:water (87:13). Flow-rate 0.7 ml/min; UV detection at 260 nm.

10–120 μg of metal ions. The heating time of 15 min at 70–80° and a shaking time of 30 min enable the extraction of copper and nickel quantitatively and reproducibly.

The reversed phase HPLC column, Nova Pak C_{18} with guard ODS column, was used because of the ease of separation of copper and nickel from each other and from the excess of the reagent with a binary mixture of methanol:water (87:13) (Fig. 2). However, it required evaporation of the extracting solvent and redissolution in methanol before HPLC determination. We therefore considered dissolving the copper and nickel complexes in methanol or a mixture of methanol and acetonitrile, after complexation in the aqueous phase to obviate the need for the extraction of complexes in cyclohexane. This would also enable one to inject directly the complexes on the reversed phase HPLC column. The dissolution method was therefore investigated for the preparation of solutions. It was observed that the method provided similar results to those obtained with the solvent extraction procedure when the solution contained 2–20 μg of copper and nickel. However, when the amount of copper and nickel in the solution increased, some difficulties were encountered in the preparation of clear solutions. Reproducible results were thus not obtained. In the place of methanol, a mixture of methanol:acetonitrile (1:1) was also tried, but no improvement in the results was obtained. The solvent extraction, procedure was therefore used for the quantitative determination of copper and nickel.

In order to assess the reagent for the HPLC determination of copper and nickel simultaneously, using the solvent extraction procedure different amounts of copper and nickel in 10 ml of water were taken and after complexation and extraction in cyclohexane, 1 ml of extract was evaporated and redissolved in 1 ml of methanol. A 1-μl aliquot of the solution was injected on the HPLC column. The average peak height of at least two injections was measured and linear calibration curves were found in the range 10–120 μg and 10–80 μg of copper and nickel, respectively, in the original solution. The relative standard deviation of six replicates was found to be within $\pm 2.6\%$. The detection limits were found to be 20 ng (copper) and 40 ng (nickel) in an aliquot, when the complexes were extracted in 1 ml of cyclohexane and 0.5 ml of the extract was evaporated, the complexes were redissolved in 0.5 ml of methanol, and 4 μl of solution was injected at the optimized conditions of the HPLC determination.

Finally, in order to examine the use of the reagent for the determination of copper and nickel in samples, a coin, a nickel–aluminum

Table 1. Results of analysis of copper and nickel by RP-HPLC

Sample	Metal ion	Amount found by HPLC	Amount found by AA	Expected values
Copper coin	Copper	$54.1\% \pm 1.5\%$	$57.2 \pm 1\%$	—
Nickel–aluminum alloy	Nickel	$48.0\% \pm 1.0\%$	—	50%
Water sample from copper still	Copper	360 ± 12 μg/l	—	—
Water sample from metallic tank	Copper	182 ± 10 μg/l	—	—

alloy and water samples were analysed. The results in Table 1 are within the reasonable range of the expected values or those obtained by atomic absorption.

REFERENCES

1. H. Veening and B. R. Willeford, *Rev. Inorg. Chem.*, 1979, **3**, 281.
2. G. Nickless, *J. Chromatog.*, 1984, **313**, 129.
3. Y. Nagaosa and H. Kawabe, *Anal. Chem.*, 1991, **63**, 281.
4. P. C. Uden and D. E. Henderson, *Analyst*, 1977, **102**, 889.
5. P. C. Uden, *J. Chromatog.*, 1984, **313**, 3.
6. R. Belcher, A. Khalique and W. I. Stephen, *Anal. Chim. Acta*, 1978, **100**, 503.
7. S. Dilli and E. Patsalides, *ibid.*, 1981, **128**, 109.

Talanta, Vol. 39, No. 6, pp. 613–616, 1992
Printed in Great Britain.

0039-9140/92 $5.00 + 0.00

POLAROGRAPHIC ANALYSIS OF THE MIXED-LIGAND SYSTEM Cu(II)–GLYCINE–GLYCINATE

J. C. RODRIGUEZ PLACERES,* T. BORGES MIQUEL, G. RUIZ CABRERA and M. T. SANZ ALAEJOS

Departments of Physical Chemistry and Analytical Chemistry, University of La Laguna, Tenerife, Canary Islands, Spain

(*Received* 3 *April* 1989. *Revised* 31 *July* 1991. *Accepted* 27 *September* 1991)

Summary—The polarographic method has been applied to the study of the mixed-ligand system Cu(II)–glycine–glycinate, in aqueous medium, at $I = 1.0M$ ($NaClO_4$) and $25 \pm 0.1°$. The stabilization of the mixed complex $[CuG(G^-)]^+$ has been made clear and its stability constant ($\beta_{11} = 1 \times 10^9$) has been determined. The stability constants of the complexes $[CuG]^{2+}$ ($\beta_{10} = 17$), $[CuG_2]^{2+}$ ($\beta_{20} = 230$), $[Cu(G^-)]^+$ ($\beta_{01} = 2.1 \times 10^8$) and $[Cu(G^-)_2]$ ($\beta_{02} = 1.7 \times 10^{15}$) have also been calculated.

The general interest in the study of mixed complexes and metal ion–amino-acid complexes has been made clear.[1,2]

Earlier, we undertook determination of the stability constants of the complexes of Cu(II) with glycine (G) and glycinate (G^-),[3] and clearly showed the increased stabilization by co-ordination of two ligands: $[CuG]^{2+}$ ($\beta_{10} = 59$), $[CuG_2]^{2+}$ ($\beta_{20} = 510$) and $[Cu(G^-)_2]$ ($\beta_{02} = 1.7 \times 10^{15}$).

In that paper,[3] studying the system Cu(II)–glycinate ion, the value for β_{01} obtained from the ordinate by extrapolation of $B' = \beta_{01} + \beta_{11} G_T$ was of the order of 10^{12}, much greater than the mean value reported in the literature, 1.8×10^8, and leading to an abnormally high value many orders of magnitude greater than the value predicted from the equations due to Watters and DeWitt[4] which would be 10^9. This surprising discrepancy required, on the one hand, ratification with further complementary studies, and on the other, determination of the stability constant of the mixed-ligand complex $[CuG(G^-)]^+$ under different experimental conditions.

Morever, our work on determination of the free concentration of ligands[5,6] induced a critical review of the proposed values for the stability constants of the complexes formed with the undissociated amino-acids.

The object of this work was to throw more light on these aspects of the equilibria in the Cu(II)–glycine–glycinate system.

*Author for correspondence.

EXPERIMENTAL

A Metrohm E506 polarograph and E505 polarographic stand were used in recording i–E curves. A saturated calomel electrode and a platinum electrode were employed as the reference and auxiliary electrodes, respectively. The temperature was always $25 \pm 0.1°$ and the drop time was set at 3 sec. The ionic strength was maintained constant at $1.0M$ by addition of sodium perchlorate. The pH measurements were made with a Radiometer pHM84 digital pH-meter and a GK2401C combination electrode. For five studies at variable pH the metal concentration was $1 \times 10^{-5}M$; for the three studies at constant pH, it was $1 \times 10^{-4}M$.

The cupric perchlorate was prepared beginning from cupric oxide and perchloric acid, both Merck p.a., and was standardized complexometrically; the glycine and sodium perchlorate were also Merck p.a.

The values taken for the acidity constants[7] were $pK_{a1} = 2.36$ and $pK_{a2} = 9.56$.

THEORY

If the molecule of neutral glycine (G) and the glycinate ion (G^-) are considered to be possible ligands of Cu(II), the Schaap and McMasters[8] F_{00} function will be developed as follows:

$$F_{00} = \{1 + \beta_{10}[G] + \beta_{20}[G]^2\} + \{\beta_{01} + \beta_{11}[G]\}[G^-] + \{\beta_{02}\}[G^-]^2 \quad (1)$$

Since the Cu(II)–glycinate system was studied by varying the pH of the initial solution in a range where $G_T = [G] + [G^-]$ is fulfilled

(G_T = total glycine concentration), then by substitution in (1) and rearranging, we obtain

$$F_{00} = \{1 + \beta_{10}G_T + \beta_{20}G_T^2\} + \{-\beta_{01} - 2\beta_{20}G_T + \beta_{01} + \beta_{11}G_T\}[G^-] + \{\beta_{20} - \beta_{11} + \beta_{02}\}[G^-]^2 \quad (2)$$

and if we bear in mind that β_{10} and β_{20} are negligible relative to both β_{01} and β_{02}, and that all the other constants are also negligible relative to β_{02}, then

$$F_{00} = \{1 + \beta_{10}G_T + \beta_{20}G_T^2\} + \{\beta_{01} + \beta_{11}G_T\}[G^-] + \{\beta_{02}\}[G^-]^2 \quad (3)$$

Therefore:

$$F_{00} = A' + B'[G^-] + C'[G^-]^2 \quad (4)$$

and A′, B′ and C′ can be calculated in the usual way.

The C' values will be those of β_{02}, and those of B' will enable the stability constants of the complexes $[Cu(G^-)]^+$ and $[CuG(G^-)]^+$ to be determined.

Certain studies were made at constant pH but with modification of the total concentration of amino-acid so that [G] and [G⁻] vary with G_T. At these low values of pH it is to be expected that the high concentration of the undissociated amino-acid relative to that of the glycinate ion largely compensates for the much lower stability constants of its copper complexes and that these can be determined. Bearing in mind the expression for K_{a2}, equation (1) can be transformed into:

$$F_{00} = 1 + \{\beta_{01}(K_{a2}/[H^+] + \beta_{10}\}[G] + \{\beta_{02}(K_{a2}/[H^+])^2 + \beta_{11}(K_{a2}/[H^+]) + \beta_{20}\}[G]^2 \quad (5)$$

Table 1. Cu(II)–glycinate–$NaClO_4$ system: range of concentrations of the different species

Study	pH limits	G_T, 10^{-2}M	[G⁻], 10^{-3}M	[G] 10^{-2}M
I	7.01_5/7.87	9.98/9.86	0.283/1.974	9.96/9.67
II	7.05/9.10	9.97/9.42	0.307/24.25	9.93/6.99
III	7.10_5/8.23	49.7/47.6	1.737/21.26	49.5/45.5
IV	6.65_5/7.43	74.8/73.2	1.031/5.386	74.7/72.7
V	6.65/7.71	99.5/96.6	1.223/13.45	99.4/95.2

and, since pH = constant, we can write

$$F_{00} = 1 + B''[G] + C''[G]^2 \quad (6)$$

where B'' and C'' can be calculated in the usual way and will enable all the constants of the complexes to be determined, if the different values of pH are known.

On the other hand if the pH required is very low, the concentration of the glycinium ion, HG^+, may be high and even modify the ionic strength. This effect can be minimized by decreasing G_T as required.

RESULTS AND DISCUSSION

Cu(II)–glycinate system

The five studies were made with variation of the pH of an initial solution, and thus the concentration of the different forms of glycine between the limits indicated in Table 1.

For every solution studied, the polarograms showed good symmetry and a regular outline, and reduction by a reversible two-electron process was indicated by the plots of $\log[(\bar{i}_d - \bar{i})/\bar{i}]$ *vs.* $-E$. The plot of F_{01} *vs.* [G⁻] was a straight line, Fig. 1, which ratifies the theoretical approach and allows B' and C' to be obtained, by a least-squares method; the values are presented in Table 2.

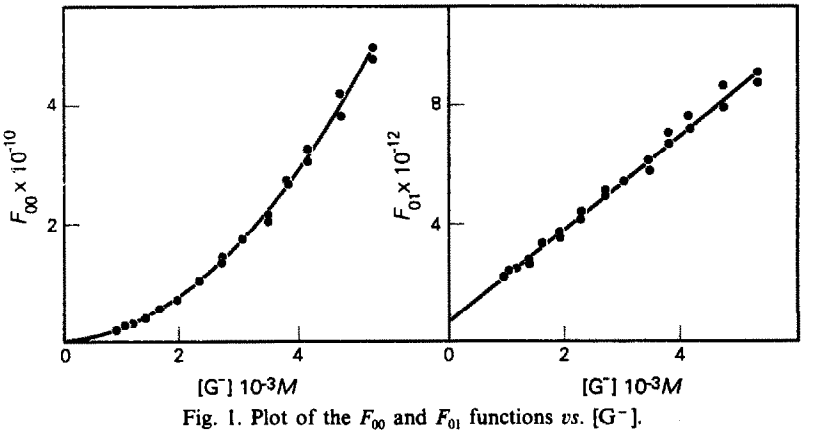

Fig. 1. Plot of the F_{00} and F_{01} functions *vs.* [G⁻].

Table 2. Cu(II)–glycinate–$NaClO_4$ system: values of B' and C'

Study	B'	C'
I	1.77×10^{11}	1.93×10^{15}
II	4.23×10^{11}	1.96×10^{15}
III	5.36×10^{11}	1.55×10^{15}
IV	6.93×10^{11}	1.57×10^{15}
V	10.25×10^{11}	1.67×10^{15}

The good concordance between the values of C' indicates the goodness of the determinations and of the stability constant calculated therefrom: $\beta_{02} = 1.7 \times 10^{15}$. This value is in good agreement with those obtained potentiometrically by Mercier and Pâris[9] ($\beta_{02} = 1.6 \times 10^{15}$) and spectrophotometrically by Mercier *et al.*[10] ($\beta_{02} = 1.9 \times 10^{15}$) under the same conditions of ionic medium and temperature.

The B' values of the order 10^{11}–10^{12}, much higher than β_{01}, ratified our preceding results and observations, and indicated the suitability of examining the mixed-ligand complex $[CuG(G^-)]^+$ under different experimental conditions, *viz.* at low pH.

Mixed-ligand Cu(II)–glycine–glycinate system

Three studies of this system, at constant pH and variation of the total concentration of glycine between the limits indicated in Table 3, were made.

The polarograms showed good symmetry and regular outline, for all the solutions studied, and the logarithmic plots revealed that a two-electron reduction was involved. Beginning from the reversible asymptote, the reversible half-wave potentials were determined.

Table 3. Cu(II)–glycine–glycinate–$NaClO_4$ system: range of concentrations of the different species

Study	pH	G_T, M	$[G^-]$, 10^{-8}M	[G], 10^{-2}M
VI	$3.23_5/3.21$	0.1/1.0	4.10/38.42	8.67/86.03
VII	3.29/3.27	0.1/1.0	4.79/39.57	8.92/86.33
VIII	3.30/3.29	0.2/1.0	9.80/46.53	17.84/86.44

Table 4. Cu(II)–glycine–glycinate–$NaClO_4$ system: values of B'' and C''

Study	Mean pH	B''	C''
Ref. 3	2.87	58.7	—
Ref. 3	2.87	59.2	498
Ref. 3	2.87	59.1	526
VI	3.22	115.1	965
VII	3.26	110.1	1209
VIII	3.29	133.5	1266

The plots of F_{00} and F_{10} *vs.* concentration of glycine are shown in Fig. 2. The values of B'' and C'' were obtained by least-squares, and are shown in Table 4 together with those of our earlier[3] paper.

From the plot of B'' *vs.* $K_{a2}/[H^+]$ in Fig. 3, $\beta_{10} = 17$ and $\beta_{01} = 2.1 \times 10^9$ were obtained by least-squares. The good concordance between these and the values reported in the literature[3,11,12] is noteworthy.

From equation (5) it can be proved that the plot of $C'' - \beta_{02}\,(K_{a2}/[H^+])^2$ *vs.* $K_{a2}/[H^+]$ must be a straight line, with intercept β_{20} and slope β_{11}. Least-squares treatment of this dependence, Fig. 4, gives $\beta_{20} = 230$ and $\beta_{11} = 1 \times 10^9$. The value of β_{11} is in acceptable agreement with the only two literature values:[13,14] 7.6×10^8 and $(0.92\text{–}2.5) \times 10^9$.

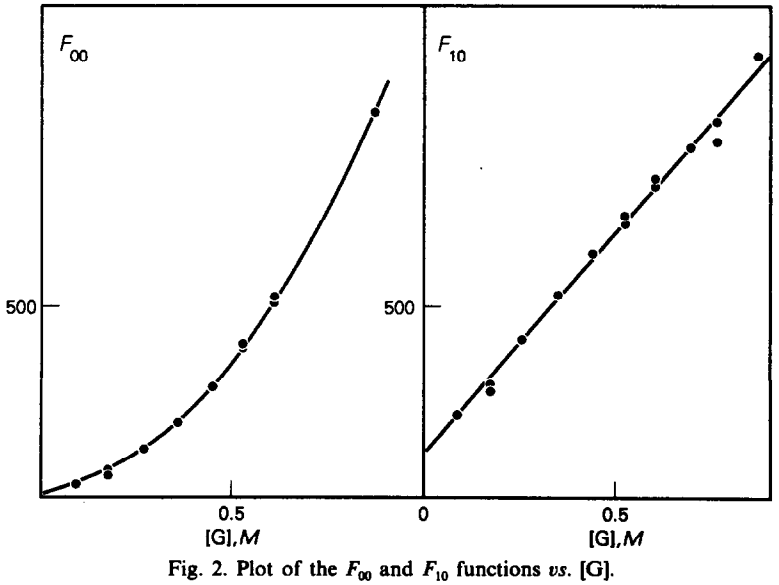

Fig. 2. Plot of the F_{00} and F_{10} functions *vs.* [G].

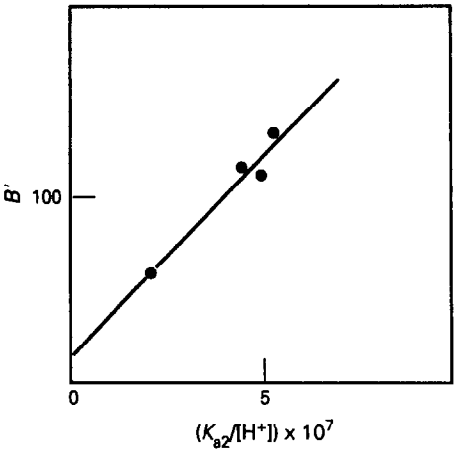

Fig. 3. Plot of B″ *vs.* $(K_{a2}/[H^+])$.

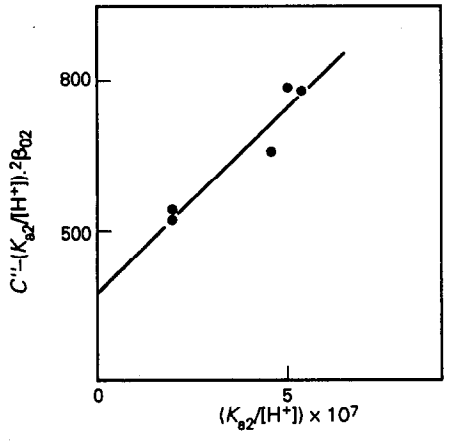

Fig. 4. Plot of $C'' - (K_{a2}/[H^+])^2\beta_{02}$ *vs.* $(K_{a2}/[H^+])$.

The value determined for β_{11}, and its concordance with the reported data in the literature and with that statistically predictable from the Watters and DeWitt's equation[4] ($\beta_{11} = 1.3 \times 10^9$), cast doubt on the abnormally high value obtained from the B' data[3] at high pH, $\beta_{11} \simeq 10^{12}$.

The resolution of these unexpected discrepancies is being further investigated.

REFERENCES

1. J. C. Rodriguez Placeres, M. Barrera, C. Carreño and A. Arevalo, *An. Quim.*, 1981, **77,** 199.
2. G. Ruiz Cabrera, C. Quintana Perera, J. C. Rodriguez Placeres and A. Arevalo, *Polyhedron*, 1986, **5,** 933.
3. J. C. Rodriguez Placeres, M. T. Sanz Alaejos and F. Garcia Montelongo, *An. Quim.*, 1985, **81,** 348.
4. J. I. Watters and R. DeWitt, *J. Am. Chem. Soc.*, 1960, **82,** 1333.
5. M. T. Sanz Alaejos, *Thesis*, Universidad de La Laguna, 1987.
6. J. C. Rodriguez Placeres, M. T. Sanz Alaejos and F. Garcia Montelongo, *Talanta*, 1992, **39,** 649
7. M. Molina, C. V. Melios, M. Jafelicci, Jr. and L. C. Luchiaru, *Ecletica. Quim.*, 1977, **2,** 103.
8. W. B. Schaap and D. L. McMasters, *J. Am. Chem. Soc.*, 1961, **83,** 4699.
9. R. P. Martin and R. A. Pâris, *Bull. Soc. Chim. France*, 1963, **570,** 1600; 1964, 80.
10. R. C. Mercier, M. Bonnet and M. R. Pâris, *ibid.*, 1965, 2926.
11. D. D. Perrin, *Stability Constants of Metal-Ion Complexes*, Part B, *Organic Ligands*. Pergamon Press, Oxford, 1987.
12. R. M. Smith and A. E. Martell, *Critical Stability Constants*, Plenum Press, New York, Vol. 1, 1974.
13. J. K. Beattie, D. J. Fensom and H. C. Freeman, *J. Am. Chem. Soc.*, 1976, **98,** 500.
14. C. W. Childs and D. D. Perrin, *J. Chem. Soc. A*, 1969, 1039.

Talanta, Vol. 39, No. 6, pp. 617–620, 1992
Printed in Great Britain.

0039-9140/92 $5.00 + 0.00

ANIONIC RESPONSES OF ELECTROCHEMICALLY SYNTHESIZED POLYPYRROLE FILMS

AODHMAR CADOGAN,* ANDRZEJ LEWENSTAM and ARI IVASKA†
Laboratory of Analytical Chemistry, Åbo Akademi University, SF-20500 Turku-Åbo, Finland

(*Received* 23 *September* 1991. *Revised* 13 *November* 1991. *Accepted* 14 *November* 1991)

Summary—Conducting polypyrrole films with thickness of about 8 μm were prepared on platinum by continuous scanning in 0.1*M* pyrrole and 0.1*M* electrolyte (LiCl, $LiBF_4$ or $NaBF_4$). Scan-rates of 10, 20 and 50 mV/sec with scan-times of 30, 45 and 60 min were used. The potentiometric response of the films was tested over a range of anions. Films were found to be anion-sensitive but very non-selective. The influence of the doping cation was also investigated.

Progress continues into the development and investigation of electrodes incorporating modified membranes capable of sensing ions, molecules and large biomolecules. These sensing devices and in particular those sensitive to small ions (Ion–Selective Electrodes) have found wide applications in the industrial, clinical, environmental and pharmaceutical areas. Since the introduction of organic conducting polymers and in particular electrochemically synthesized polymers such as polypyrrole and polyphenylene, first reported by Diaz and coworkers,[1] numerous publications have appeared on the subject.[2–6] While the primary interest has been in the use of these polymers as charge storage materials[7] and electrochromic devices,[8] they can also function as organic electrode materials[9] and protecting films on semiconductor devices to prevent photocorrosion.[10]

Several papers have emerged describing the use of modified conducting polymers as gas sensors,[11–13] for immobilization of enzymes[14,15] or even as a method of pH control.[16] Ikarijama *et al.*[17] reported the use of polypyrrole as a detector for anions in a FIA system based on the doping effect of anions in the flowing stream on a polypyrrole film held at its doping potential. Dong *et al.* have reported chloride and perchlorate sensors also based on polypyrrole.[18,19]

Even though the practical process in performing electrochemical polymerization is straightforward and simple, the chemical processes leading to film formation are complicated and therefore the nature of the resulting film and its response are ultimately affected by many factors such as solvent, impurities in the solvent, temperature, applied potential, electrode substrate and the type and concentration of the doping salt. We describe here the electrochemical preparation of thick polypyrrole layers on platinum with three commonly used doping salts and we report the performance of the various films as potentiometric anion sensors.

EXPERIMENTAL

Reagents

Pyrrole (Py) obtained from Merck was purified by double distillation and stored at low temperature protected from light. Analytical grade reagent salts obtained from Merck and Fluka were used without further purification and dissolved in distilled, demineralized water.

Apparatus

A Princeton Applied Research Corporation model 273 Potentiostat/Galvanostat with software version 2.00 was used for the electrochemical polymerizations and cyclic voltammetry. The potentiometric measurements of the polypyrrole films were performed with an Orion Research Expandable Ion Analyser EA 940 in conjunction with an Orion Ag/AgCl reference electrode. A Perkin–Elmer 56 pen recorder was used for the traces. The electrochemical cell was a conventional three electrode system. The working electrode was a platinum 3-mm diameter disc electrode. The counter electrode was a glassy-carbon rod and the reference electrode

*Permanent address: School of Chemical Sciences, Dublin City University, Dublin 9, Ireland.
†Author for correspondence.

was aqueous Ag/AgCl satd. KCl. All electrodes were from Metrohm. The platinum surface was polished to a mirror finish with 1-μm diamond paste followed by 0.3 μm aluminium oxide paste. All solutions were degassed by bubbling with high purity nitrogen and all electropolymerizations were performed under nitrogen. The scanning electron microscope (SEM) measurements were done with a Cambridge Instruments Stereoscan 360.

Polypyrrole film preparation

Polypyrrole (PPy) films were prepared by continuous scanning in 0.1M pyrrole and 0.1M electrolyte aqueous solutions from 0.0 to 1.0 V. Three different salts (LiCl, $LiBF_4$ and $NaBF_4$) were used as the doping electrolytes. PPy films were synthesized with scan-rates of 10, 20 and 50 mV/sec and scanning times of 30, 45 and 60 min were used. The films were activated by soaking in 0.1M solutions of the doping salt for at least three hours after preparation to allow the films to reach a stable rest potential. The potentiometric response of each electrode was recorded after 6 min. In some cases the potential of the electrode continued to drift beyond that period and when they showed no indications of stabilizing a reading, no stable potentiometric response (npr) was recorded. Scanning electron microscope (SEM) measurements of films formed at 20 mV/sec for 45 min with 0.1M $NaBF_4$ as the doping salt showed an average film thickness of 7–8 μm with a slight thickening of the film at the outer edges 10–11 μm.

RESULTS AND DISCUSSION

Table 1 shows the slopes of the potentiometric responses of the PPy film electrodes to the small Cl^- anion and the larger BF_4^- anion recorded in the concentration range of 0.1–0.001M. In each case the cation is the same as the one used in the electropolymerization. The error in the slopes given in Table 1 varies in the range of 0.1–4.0 S.D. units. This error can be regarded to be very high and is a direct reflection of the difficulty in making reproducible films. The linear range for electrodes incorporating the BF_4^- doping anion was 10^{-1}–$10^{-3}M$ and somewhat better for elec-

Table 1. Response slopes of polypyrrole film electrodes in solutions of chloride and tetrafluoroborate, 0.001–0.1M, in each case the potentials were recorded with the same cation as used in the synthesis. Equilibration time in each solution was 6 min

Electrode #	Scan-rate, mV/sec	Scan-time, *min*	Slope, *mV/decade* Cl^-	BF_4^-
LiCl as doping salt*				
1	20	30	−48.9	npr†
2		45	−52.7	−19.8
3		60	−52.1	−36.2
4	50	30	−46.2	−28.2
5		45	−50.9	−37.5
6		60	−53.5	−38.5
$LiBF_4$ as doping salt*				
7	10	30	−38.9	npr
8		45	−50.1	−33.2
9		60	−46.6	−44.7
10	20	30	−41.6	npr
11		45	−47.3	−37.4
12		60	−49.6	−42.9
13	50	30	−33.0	−31.6
14		45	−49.7	−35.1
15		60	−53.0	−46.9
$NaBF_4$ as doping salt*				
16	10	30	−50.0	npr
17		45	−47.3	−28.1
18		60	−46.1	−45.3
19	20	30	−48.1	−42.2
20		45	−48.5	−41.8
21		60	−51.1	−45.6
22	50	30	−39.4	npr
23		45	−52.5	−42.4
24		60	−52.7	−43.8

*The doping salt used in the electrochemical polymerization.
†npr = no stable potentiometric response.

trodes containing Cl^- as the anion, typically 10^{-1}–$10^{-4}M$. Membranes incorporating $NaBF_4$ tended to lose their potentiometric properties after 24–48 hr of continuous contact with the aqueous electrolyte but electrodes incorporating LiCl and $LiBF_4$ salts showed better stability with time.

The results in Table 1 indicate clearly that better slopes were observed for the smaller Cl^- than for the bigger BF_4^- anion. This is especially pronounced in the cases where Cl^- was used as the doping anion in preparing the film. It is obviously easier for the smaller Cl^- anion to be intercalated in the polymer film and to show an anionic potentiometric response when the film is in contact with the electrolyte solution.

Effect of scanning time/film thickness

The thicker films, formed at 45 and 60 min, showed stable responses to both chloride and tetrafluoroborate anions. With thinner films (<30 min scanning time) a Nernstian response was observed for a few minutes. This was then followed by drift of the potential at all concentration levels stabilizing at the rest potential of the PPy in the supporting electrolyte used. If scanning periods longer than 60 min were used, the polymer growth went beyond the platinum over the Teflon surround and the film became very brittle and difficult to remove intact from the platinum. If membranes were made too thick, they tended to lift off the platinum surface following long periods of soaking in aqueous solutions. This behaviour is obviously due to overoxidation of the polymer material which is an unavoidable result of long polymerization times in electrochemical synthesis of conducting polymers.

Effect of scan rate

As can be seen in Table 1, rather good responses to the anions studied were obtained with 20 mV/sec and 50 mV/sec scan-rates for the electropolymerization. The response was somewhat poorer when a 10-mV/sec scan-rate was used with having the same scan time.

Selectivity towards other anions

Figure 1 shows the absolute potentials of the response of electrode #21 in Table 1, prepared in $NaBF_4$, to other electrolyte solutions across the concentration range 10^{-1}–$10^{-4}M$. The electrode was soaked in a $0.01M$ solution of each interfering ion for 20 min before measuring the response. There is virtually no selectivity

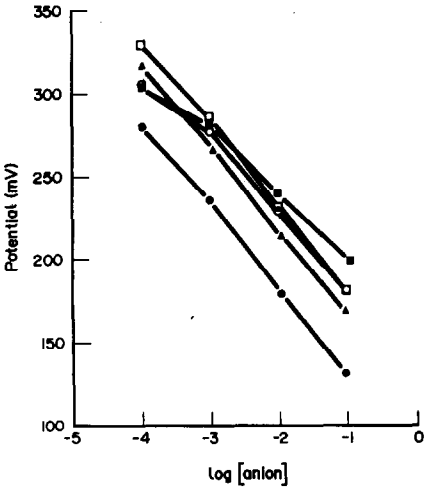

Fig. 1. Calibration curves for a PPy film electrode prepared in $0.1M$ pyrrole and $0.1M$ $NaBF_4$ with a 20-mV/sec scan-rate and a 60-min scan-time over the potential range 0.0–1.0 V. Response to sodium salts of —□— Cl^-, —○— ClO_4^-, —▲— NO_3^-, —■— BF_4^- and —●— SCN^- are shown. The equilibration time is 6 min for each solution. The electrode is soaked for 20 min in each new electrolyte before calibration.

between the various anions. The electrode responded well to Cl^-, ClO_4^-, NO_3^- and had a slightly poorer response to BF_4^- with some selectivity over SCN^-. Similar plots were obtained for PPy electrodes based on the LiCl and $LiBF_4$ doping salts.

Effect of doping anion and counter cation

Although many papers on the subject of conducting PPy films deal with the effect of the electrolyte on the morphology and the conductivity of the polymers very little attention has been given to the effect of the electrolyte on the potentiometric response of a polymer membrane. Table 2 shows a comparison of the responses in terms of slope for the three doping electrolytes (LiCl, $LiBF_4$ and $NaBF_4$) to various solutions of sodium and lithium salts. The errors in the values of the slopes are in the same range as the errors in Table 1. It should be emphasized that no thorough error analysis was done either for the values given in Table 1 or in Table 2. Due to the high errors involved it is more appropriate to follow the general trends shown by the films rather than the absolute values of the slopes. In practically all cases the PPy films responded better in the electrolyte containing the same cation as that used for the electrochemical synthesis. The size of the intercalating anion used in the electrochemical polymerization is known to affect

Table 2. Slopes (mV/decade) of polypyrrole electrodes formed by constant scanning in 0.1*M* pyrrole and 0.1*M* aqueous electrolyte solutions. Electrodes as in Table 1

Doping electrolyte		LiCl	$LiBF_4$	$NaBF_4$
Electrode #		3	11	21
		Slope, *mV/decade*		
Anion	Cation			
Cl^-	Li^+	−52.1	−47.3	−49.1
	Na^+	−49.4	−41.2	−51.1
NO_3^-	Li^+	−54.2	−53.1	−48.9
	Na^+	−49.6	−48.5	−51.2
ClO_4^-	Li^+	−53.6	−53.5	−50.7
	Na^+	−49.6	−49.0	−48.3
BF_4^-	Li^+	−36.2	−37.4	−34.1
	Na^+	−39.7	−29.3	−41.8
SCN^-	Na^+	−52.5	−57.1	−53.1

the structure of the resulting polymer, but the cation seems to have some effect on the doping/undoping, in our study of the potentiometric, behaviour of the polymer film. No clear and definite explanation of this behaviour of the PPy film can be given at this stage. The same type of cation behaviour was also noted by Marque *et al.*[20] in their studies on the electrolyte effects of poly (3-methylthiophene) films.

CONCLUSIONS

Thick PPy films electropolymerized in LiCl, $LiBF_4$ and $NaBF_4$ display a potentiometric response to anions. In all cases the films responded better to the smaller chloride anion than the larger tetrafluoroborate anion. Of the three doping anion systems investigated, the best sensitivity to the BF_4^- anion was obtained with $NaBF_4$ as the doping salt. The thickness of the PPy film was found to be very important. In order to obtain stable potentiometric responses thicker films are required but at the same time overoxidation of the polymer material should be avoided. All the PPy membranes display a sensitivity to anions but from the selectivity data it can be seen that there is not much discrimination between the different anions. Although the responses of the films investigated were not exactly Nernstian nor selective enough to be used as individual "ions" sensors, the anionic responses of polypyrrole films may be exploited in other ways. The observed cationic sensitivity of the potentiometric response will make it even more difficult to make PPy membranes selective to individual anions due to the presence of cations in the sample solutions. Nevertheless success in preparing anion selective PPy membranes has been claimed earlier by one research group.[18,19]

One of the main advantages of conducting polymer membranes is that the conductivity/redox state at the bulk polymer can be externally controlled. They also possess other advantages such as insolubility in organic and inorganic solvents and low resistance and may find further use in the area of all solid state electrodes.

Acknowledgements—A.C. thanks the Ministry of Education of Finland for her scholarship and the authors are grateful to the referee for his comments in reviewing the manuscript.

REFERENCES

1. A. F. Diaz, K. K. Kanazawa and G. P. Gardini, *J. Chem. Soc., Chem. Comm.*, 1979, 635.
2. T. A. Skotheim (ed.), *Handbook of Conducting Polymers*, Vols. I and II. Marcel Dekker, New York, 1986.
3. S. Roth, H. Bleier and W. Pukacki, *Faraday Discuss. Chem. Soc.*, 1989, **88**, 223.
4. E. M. Genies, G. Bidan and A. F. Diaz, *J. Electroanal. Chem.*, 1983, **149**, 101.
5. S. Asavapiriyanont, G. K. Chandler, G. A. Gunawardena and D. Pletcher, *ibid.*, 1984, **177**, 229.
6. H. Mao, J. Ochmanska, C. D. Paulse and P. E. Pickup, *Faraday Discuss. Chem. Soc.*, 1989, **88**, 165.
7. L. W. Shacklette, J. E. Toth, N. S. Murthy and R. H. Baughman, *J. Electrochem. Soc.*, 1985, **132**, 1529.
8. F. Garnier, G. Tourillon, M. Gazard and J. C. Dubois, *J. Electroanal. Chem.*, 1983, **148**, 299.
9. R. A. Bull, F.-R. F. Fan and A. J. Bard, *J. Electrochem. Soc.*, 1982, **129**, 1009.
10. G. Horowitz and F. Garnier, *ibid.*, 1985, **132**, 634.
11. A. Boyle, E. M. Genies and M. Lapkowski, *Synth. Met.*, 1989, **28**, C769.
12. M. Josowicz, J. Janata, K. Ashley and S. Pons, *Anal. Chem.*, 1987, **59**, 253.
13. P. N. Bartlett and S. K. Ling-Chung, *Sensors and Actuators*, 1989, **20**, 287.
14. P. N. Barlett and R. G. Whitaker, *J. Electroanal. Chem.*, 1987, **224**, 27.
15. M. Umaña and J. Waller, *Anal. Chem.*, 1986, **58**, 2979.
16. M. Okano, A. Fujishima and K. Honda, *J. Electroanal. Chem.*, 1985, **185**, 393.
17. Y. Ikariyama, C. Galiatsatos, W. R. Heineman and S. Yamauchi, *Sensors and Actuators*, 1987, **12**, 455.
18. S. Dong, Z. Sun and Z. Lu, *Analyst*, 1988, **113**, 1525.
19. Z. Lu, Z. Sun and S. Dong, *Electroanalysis*, 1989, **1**, 271.
20. P. Marque, J. Roncali and F. Garnier, *J. Electroanal. Chem.*, 1987, **218**, 107.

Talanta, Vol. 39, No. 6, pp. 621–629, 1992
Printed in Great Britain.

0039-9140/92 $5.00 + 0.00

ELECTROCHEMICAL REDUCTION OF GALLIUM(III) IN NON-AQUEOUS SOLVENTS, ASSISTED BY 2,2′-BIPYRIDINE

PABLO COFRE,* GASTON EAST† and CLAUDIA AGUIRRE
Facultad de Química, Pontificia Universidad Católica de Chile, Vicuña Mackenna 4860, Santiago, Chile

(*Received* 20 *August* 1991. *Revised* 28 *October* 1991. *Accepted* 29 *October* 1991)

Summary—The electrochemistry of gallium(III) perchlorate in dimethylsulfoxide (DMSO) and acetonitrile (MeCN) at a mercury drop electrode is described and compared to that in water. The reduction of 2,2′-bipyridine (DIPY) and its interaction with free protons in the solvents mentioned is also surveyed. The electrochemistry of tris-(2,2′-bipyridine) gallium(III) perchlorate was studied in DMSO and MeCN. A gallium metal deposit is obtained by reduction of the complex compound in the first solvent, whereas lower valence gallium–DIPY species are obtained in the second. The existence of different catalytic prepeaks in DMSO is described. The first catalytic peak, which renders a metal deposit, is studied in detail, together with the possible interference of oxygen and free protons. These studies serve the basis of future development of an analytical procedure for the determination of trace concentrations of gallium.

The electrochemical reduction of gallium(III) in acidic aqueous media is a highly irreversible process[1] which has challenged many authors in the past to seek conditions to lower its overpotential. Different supporting electrolyte compositions have been tried in polarographic studies[2] to obtain a reversible process. Of special interest are thiocyanate or salicylic acid-based electrolytes.[3]

A sodium thiocyanate electrolyte together with high sodium perchlorate concentration has proved to be effective in achieving a reversible reduction[4,5] and has been used in thorough studies of phase-selective anodic stripping analysis (PSAS) of trace concentrations of gallium.[6,7] The concurrent effects of SCN^-, high ionic strength and temperature indicate[2] the existence of a highly solvated (possibly polynuclear) ionic structure of aquo gallium(III) in acidic media which would be responsible for the irreversibility observed. The role of SCN^- could be considered in the light of ligand catalysis,[8] whereas the beneficial effect of sodium perchlorate has been attributed to sodium ion,[9] which has a role in determining the double layer structure and potential difference profile or favours the formation of ion pairs, which would facilitate the reduction of gallium(III). However, the high salt concentration required (4–6*M* sodium perchlorate) is a clear disadvantage when determining trace concentrations of gallium due to metal impurities introduced by the reagents. This effect is especially important in anodic stripping voltammetry where zinc can form an intermetallic compound[10] which precludes the detection of gallium below $2 \times 10^{-7}M$.

In the present work we explore the possibility of using non-aqueous media (DMSO and MeCN) and organic ligands in lower concentration to obtain electrocatalytic reduction of gallium(III). The exclusion of water, the adsorption of the ligand on the mercury electrode surface and its ability to act as a charge transfer bridge should contribute to a more facile and reversible process.

2,2′-Bipyridine fulfils all the ligand requirements and is therefore our first choice. Its electrochemistry and metal complex compounds in water have been reviewed[11] and it has been used in the determination of cobalt by a.c. polarography, based on catalytic reduction in acetate–ammonia buffer.[12] It is also known to form a stable gallium(III) complex.[13]

Our results in DMSO show the existence of a catalytic process which could be the basis for developing analytical procedures to determine

*Author for correspondence.
†On sabbatical leave from Departamento de Química, Universidade de Brasilia, Brasil.

gallium, using either the cathodic or the anodic process.

EXPERIMENTAL

Instrumentation

The cyclic voltamperograms were obtained with an EG & G Princeton Applied Research polarographic analyzer model 384B provided with a 303A static mercury drop electrode (HMDE), a Houston Instrument model DMP-40 plotter, glass cells and a silver/silver chloride reference electrode filled with an aqueous tetramethyl ammonium chloride (TMACl) solution. The TMACl concentration was adjusted so that the reference electrode potential was that of a saturated calomel electrode (SCE). Ring-disc electrode voltamperograms were obtained with a Pine Instruments Company ASRE rotator provided with a GC ring–GC disc (GC: glassy carbon) electrode tip (disc radius, $r_1 = 0.382$ cm, inner ring radius, $r_2 = 0.416$ cm, outer ring radius, $r_3 = 0.556$ cm, collection efficiency $N = 0.418$) controlled by an ASR speed control. Potential control was provided by a model RDE 3 bipotentiostat. Voltamperograms were recorded on a Hewlett Packard measurement plotting system model HP 7090 A.

Chemicals

Acetonitrile (MeCN, >99% purity) and dimethylsulfoxide (DMSO, >99% purity) were from Aldrich. Tetraethyl ammonium perchlorate (TEAP) used as supporting electrolyte was made by neutralization of 20% (w/w) aqueous solution of tetraethyl ammonium hydroxide (Aldrich) with 70% perchloric acid ("Baker Analyzed", J. T. Baker Chemical Company) and recrystalization from absolute ethanol (Merck, *p.a.*). Gallium(III) perchlorate [$Ga(ClO_4)_3.6H_2O$] was prepared by dissolving 6*N* gallium metal (Strem chemicals) in 70% perchloric acid ("Suprapur" Merck) following a known procedure.[14] The tris-(2,2′-bipyridine) gallium(III) perchlorate [$Ga(DIPY)_3(ClO_4)_3$] was synthesized by reaction of $Ga(ClO_4)_3$-$6H_2O$ with 2,2′-bipyridine (DIPY) (Aldrich) in absolute ethanol following a known procedure.[13] Solutions were degassed with high purity argon (INDURA). High purity distilled water[15] was used when required.

All stock solution volumes were delivered with Gilson Pipetman micropipettes (models P20 and P200).

Procedure

The required amount of TEAP, $Ga(ClO_4)_3$-$6H_2O$, $Ga(DIPY)_3(ClO_4)_3$, and DIPY were weighed out directly into the cell, and 10 ml of the appropriate solvent were added, before each cyclic voltammetry experiment. When studying the [DIPY]:[Ga] ratio, a 0.1*M* DIPY stock solution in MeCN was used. Calibration plots were obtained by adding increasing amounts of a 1×10^{-2} or $4 \times 10^{-2}M$ $Ga(DIPY)_3(ClO_4)_3$ stock solution in DMSO. When studying the effect of free protons, a tritrated 0.48*M* perchloric acid stock solution in 50% MeCN + 50% DMSO was used. (Warning: concentrated perchloric acid and DMSO form an explosive mixture, therefore it is advisable to dilute perchloric acid with MeCN first, and then complete to the final volume with DMSO).

RESULTS AND DISCUSSION

Electrochemistry of gallium(III); solvent effect

The irreversible reduction of gallium perchlorate in aqueous sodium perchlorate solution is illustrated by the cyclic voltamperogram in Fig. 1(a). A single three-electron cathodic peak is observed at −1.6 V, which can overlap with two less distinct cathodic peaks (not shown) at less negative potentials, if gallium(III) has hydrolyzed to any extent before the experiment. The relative heights of these cathodic peaks are

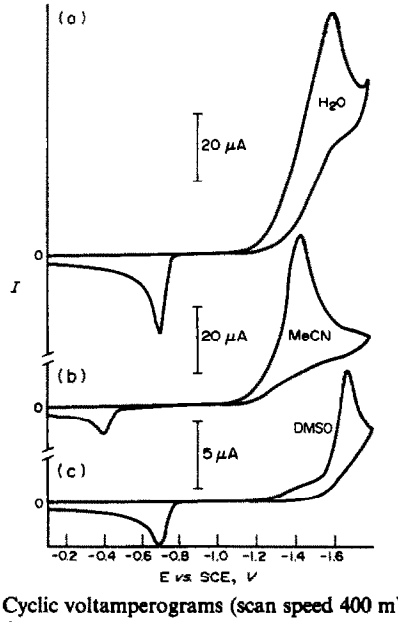

Fig. 1. Cyclic voltamperograms (scan speed 400 mV/sec) of $2 \times 10^{-3}M$ $Ga(ClO_4)_3.6H_2O$ at a HMDE in different solvents: 0.6*M* aqueous $NaClO_4$ pH 2.2 (a); 0.1*M* TEAP, MeCN (b); 0.1*M* TEAP, DMSO (c).

pH dependent and are attributed to the presence of different polynuclear hydroxylated gallium(III) species.[2] A single anodic peak is observed at −0.7 V on the reverse scan, which is due to the stripping of gallium deposit to produce gallium(III), as one can infer from its shape, peak potential and anodic stripping experiments (its height increases linearly with deposition time).

The ratio of anodic/cathodic peak currents increases when decreasing the scan speed, as would be expected for a metal deposit, but the ratio of anodic/cathodic charge (measured at 10 mV/sec) is unity. This is consistent with an overall electrode reaction

$$Ga(III) + 3e^- \xrightarrow{(Hg)} Ga(Hg)_x$$

The cathodic peak current has a linear dependence on $v^{1/2}$, and $\Delta E_p = E_{p,a} - E_{p,c}$ is a function of scan speed v.

If the sodium perchlorate supporting electrolyte is replaced by TEAP, no gallium(III) reduction is observed before the solvent cathodic limit. The addition of sodium perchlorate after adding TEAP produces a well-defined cathodic peak at a more negative potential than with pure sodium perchlorate. Sodium ion has been suggested[9] to have an important role by determining the structure of the double layer and potential difference profile or by favouring the formation of ion pairs. This would facilitate the reduction of gallium(III) in water.

The behaviour of gallium(III) in MeCN is shown in Fig. 1(b). The cathodic peak is shifted to −1.4 V, whereas the anodic peak is observed at −0.4 V. The cathodic peak current increases linearly with v rather than $v^{1/2}$. The ratio of anodic/cathodic charges is less than one, even at low scan speed. This, together with changes in peak shape (at 1000 mV/sec), splitting (at 50 mV/sec) and formation of small bumps on the reverse scan, suggests a change in the reaction mechanism which may involve stabilization and adsorption of lower oxidation state gallium species.

The shift of peak potentials observed is attributed to the lower solvating power of this solvent as compared to water. Labilization of the polynuclear hydroxylated gallium(III) species would facilitate its reduction while on the reverse process, dissolution of gallium metal would be less favoured in a less-solvating media.

Figure 1(c) shows the redox behaviour of gallium(III) in DMSO. The cathodic peak potential is only slightly negative to that in water while the anodic peak potential is coincident. The cathodic peak current increases linearly with $v^{1/2}$ at lower scan speed while it increases linearly with v at higher scan speed. The ratio of anodic/cathodic charge is close to unity at low scan speed whereas the magnitude of the cathodic peak current is significantly lower than in the two previous solvents. DMSO is closer to water in solvating power than MeCN. This explains the small or nil potential shifts observed. However, its viscosity is clearly higher than that of the other two solvents, what accounts for the smaller currents observed. The effect of voltage scan-rate on the cathodic peak is indicative of a reaction mechanism more similar to that in aqueous media.

The presence of sodium ion is not essential to facilitate the gallium(III) reduction in both aprotic solvents.

One can conclude from these experiments that changing from aqueous to non-aqueous solvents is not sufficient to obtain a reversible reduction. Also small amounts of water, either present in the solvents or incorporated as hydration water by the $Ga(ClO_4)_3 \cdot 6H_2O$, may still remain strongly bound to the gallium(III) so that the energy barriers for metal reduction are still very high.

Electrochemistry of DIPY; solvent effect and catalytic proton reduction

The electrochemical activity of the ligand DIPY is also influenced by the solvent. Figure 2(a) shows the cyclic voltamperogram of DIPY in DMSO. The first cathodic peak at −2.14 V is a reversible process. Its peak current increases linearly with $v^{1/2}$ and a corresponding anodic peak is observed on the reverse scan. This is a one-electron process that involves the reduction of the aromatic ring.

$$DIPY + e \rightleftharpoons DIPY^-$$

The second cathodic peak at −2.57 V has no anodic peak associated on the reverse scan. Its height is twice that of the first peak and increases linearly with $v^{1/2}$ only at very low scan speeds. The peak potential becomes more negative when increasing the scan-rate.

This suggests a two-electron process followed by a chemical step:

$$DIPY + 2e \rightarrow DIPY^{2-}$$

$$DIPY^{2-} + 2H^+ \rightarrow DIPYH_2$$

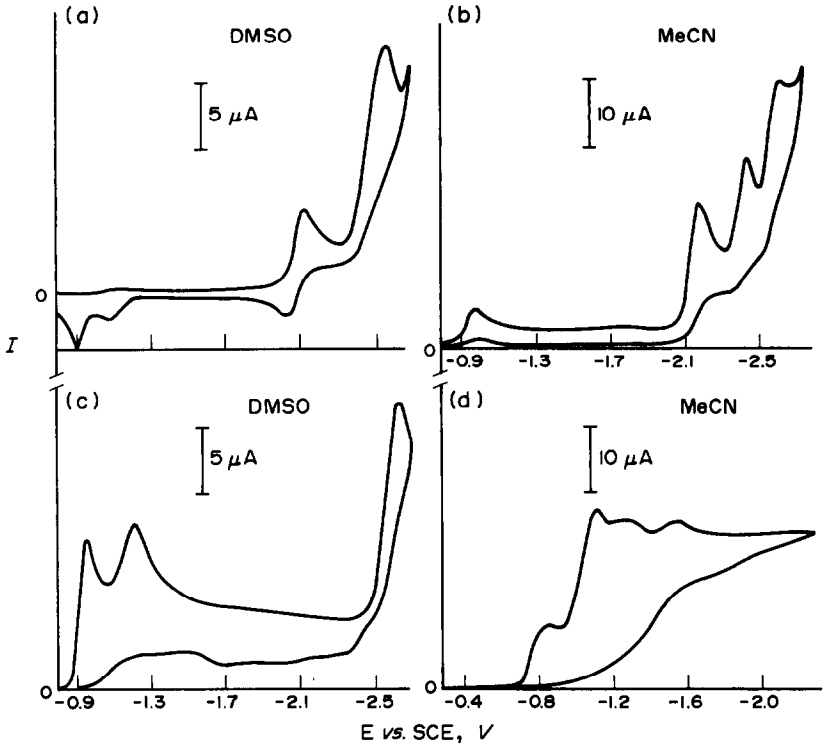

Fig. 2. Cyclic voltamperograms (scan speed 200 mV/sec) of $2 \times 10^{-3}M$ DIPY ($0.1M$ TEAP) at a HMDE in DMSO (a) and MeCN (b). Effect of protons (added as $HClO_4$) is shown for $2 \times 10^{-3}M$ DIPY, $8.4 \times 10^{-3}M$ $HClO_4$ (c) and $5 \times 10^{-3}M$ DIPY, $4.8 \times 10^{-3}M$ $HClO_4$ (d).

The highly reactive dianion reacts with protons from traces of water present in the solvent.[10]

A different behaviour is observed in the less solvating MeCN. Figure 2(b) shows the cyclic voltamperogram, with three equal height cathodic peaks at -2.17, -2.43 and -2.62 V. None of them shows an associated anodic peak on the reverse scan. Their heights increase linearly with $v^{1/2}$ only in a limited scan speed range in the lower end, and their potentials shift negatively with increasing scan-rate. The lower stability of anion radicals in this solvent as compared to DMSO suggests a different reaction mechanism involving three one-electron reduction steps which produce non-oxidizable species that cannot be detected on the reverse scan:

$$\text{DIPY} + \text{H}^+ + e \rightarrow \text{DIPYH} \qquad Ep = -2.17\ \text{V}$$

$$\left.\begin{array}{l}\text{DIPYH} + e \rightarrow \text{DIPY}^- + \text{H}^\cdot \\ (2\text{H}^\cdot \rightarrow \text{H}_2)\end{array}\right\} \qquad Ep = -2.43\ \text{V}$$

$$\left.\begin{array}{l}(\text{DIPY}^- + \text{H}^+ \rightarrow \text{DIPYH}) \\ \text{DIPYH} + \text{H}^+ + e \rightarrow \text{DIPYH}_2\end{array}\right\} \qquad Ep = -2.62\ \text{V}$$

The proton source is the residual water present in the solvent.

The anodic peaks at -1.1 and -0.9 V observed in DMSO are not observed in MeCN and can be attributed to the stepwise (one electron each) oxidation of the final product $DIPYH_2$. The higher solvating power of DMSO would favour those processes, by better solvation of the resulting protons, while in MeCN these oxidations are out of the potential span available with the 384B.

The addition of free protons (as perchloric acid) has a different effect on the electrochemistry of DIPY in both solvents. Figure 2(c) shows the observed behaviour in DMSO. The two initial cathodic peaks at -2.14 and -2.57 V are replaced by a single irreversible peak at a slightly more negative potential (-2.64 V) with a height corresponding to a two-electron process. At the same time, two new cathodic peaks with no associated anodic peaks on the reverse scan emerge at -0.96 and -1.21 V. The more negative peak increases with proton concentration, and its peak potential is coincident with that of the reduction of free protons in this solvent. The less negative peak increases with

DIPY concentration. These peaks are associated with the processes:

$$2H^+ + 2e \rightarrow H_2 \qquad Ep = -1.21\ V$$

$$\left.\begin{array}{l} H^+ + e \rightarrow H^{\cdot} \\ H^{\cdot} + DIPY \rightarrow DIPYH \end{array}\right\} Ep = -0.96\ V$$

Figure 2(d) shows the observed behaviour in MeCN. The three initial cathodic peaks are completely suppressed by excess protons. New cathodic peaks are observed at −0.84, −1.12, −1.27 and −1.56 V with no associated anodic peaks on the reverse scan.

The −0.84 V peak increases with DIPY concentration while the −1.12 V peak increases with proton concentration. These two are associated with the reduction of free protons, which is now observed at less negative potentials because of the lower solvating power of MeCN as compared to DMSO.

$$2H^+ + 2e \rightarrow H_2 \qquad Ep = -1.12\ V$$

$$\left.\begin{array}{l} H^+ + e \rightarrow H^{\cdot} \\ H^{\cdot} + DIPY \rightarrow DIPYH \end{array}\right\} Ep = -0.84\ V$$

The other two cathodic peaks observed in MeCN, but not in DMSO, are attributed to the reduction of protonated DIPY species which can exist in MeCN but not in DMSO due to the higher solvating power of the latter on the protons present.

$$DIPYH_2^{2+} + e \rightarrow DIPYH_2^{+} \qquad Ep = -1.27\ V$$

$$DIPYH_2^{+} + e \rightarrow DIPYH_2 \qquad Ep = -1.56\ V$$

Electrochemistry of $Ga(DIPY)_3(ClO_4)_3$ and solvent effect

A cyclic voltamperogram obtained in DMSO is shown in Fig. 3(a). Cathodic peaks at −1.16, −1.30, −1.50, −1.69 and −1.85 V are observed on the forward scan. When solid $Ga(DIPY)_3(ClO_4)_3$ is added directly into DMSO, a gradual increase of the −1.69 V peak is observed during the first few scans. This peak potential is coincident with that observed for $Ga(ClO_4)_3 \cdot 6H_2O$ in this solvent as shown in Fig. 1(c) and is less pronounced in a dryer DMSO, which suggests that some degree of ligand substitution by solvent or residual water has occurred upon dissolution. The other cathodic peaks are of equal height at this scan speed (200 mV/sec). When increasing the $Ga(DIPY)_3(ClO_4)_3$ concentration, the first reduction peak at −1.16 V increases and shifts

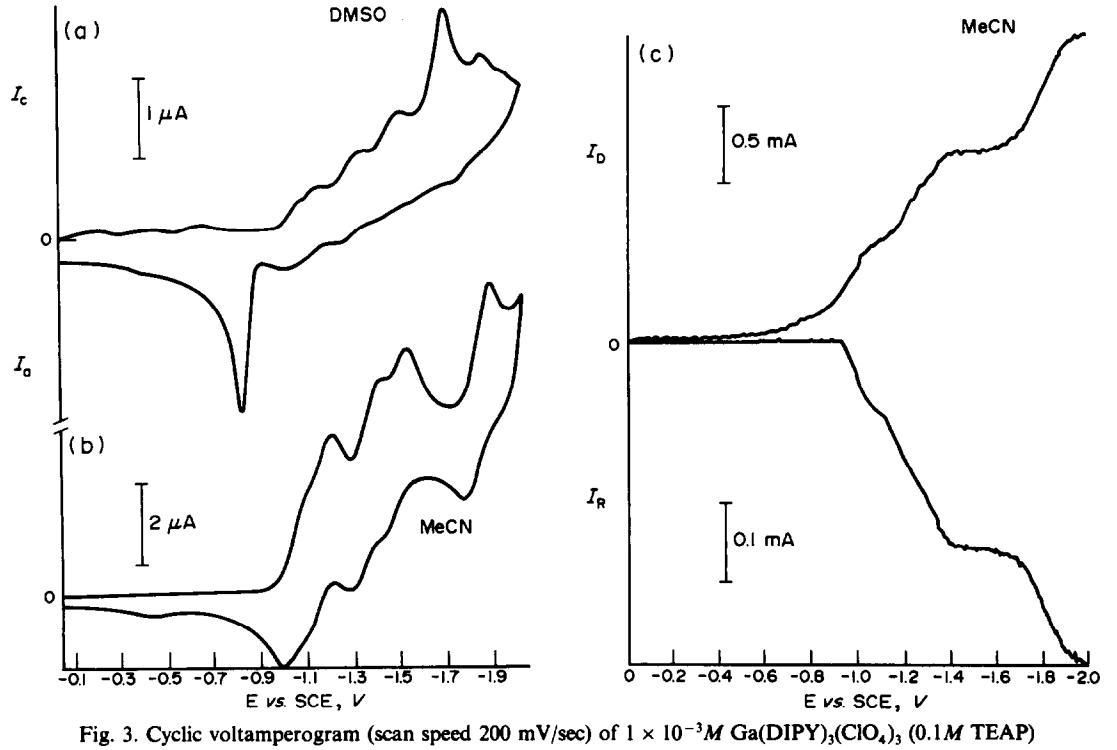

Fig. 3. Cyclic voltamperogram (scan speed 200 mV/sec) of $1 \times 10^{-3} M$ $Ga(DIPY)_3(ClO_4)_3$ (0.1 M TEAP) at a HMDE in DMSO (a) and MeCN (b). Rotating(GC)ring–(GC)disc electrode voltamperogram (2000 rpm; $E_R = 0.000$ V) of the same solution in MeCN; upper curve, reduction at the disc electrode; lower curve, oxidation at the ring electrode (c).

negatively, but it is gradually replaced by a more positive reduction peak. The relative heights of all the reduction peaks change with concentration, as if different species in equilibrium were involved; they become more distinct and their peak potentials gradually shift negatively.

While these peaks become more important, the -1.69 V peak decreases as the scan speed decreases. This is consistent with the existence of different Ga–DIPY species being reduced at different electrode potentials and the rather slow equilibrium displacement between the Ga–DIPY species as they are consumed by the electrode reaction.

On the reverse scan, a single important anodic peak is observed at -0.82 V which is about 0.12 V more negative than the gallium stripping peak observed for $Ga(ClO_4)_3 \cdot 6H_2O$ in DMSO as shown in Fig. 1(c). The -0.82 V peak corresponds to the dissolution of the gallium deposit facilitated by DIPY complexing of the resultant soluble species.

Different scan reversal potentials were tested, coming immediately after each of the cathodic peaks described. A clear gallium stripping peak was obtained for all the cases.

The electrochemical behaviour in MeCN shown in Fig. 3(b) is completely different. Comparatively higher currents are obtained as a result of higher diffusion coefficients in this less viscous solvent. All the cathodic peaks but that at -1.69 V obtained in DMSO are also observed in MeCN. This is an indication that ligand substitution has not occurred upon dissolution of the solid $Ga(DIPY)_3(ClO_4)_3$ in this solvent.

On the reverse scan, clear distinct anodic peaks associated with each of the corresponding cathodic peaks described are observed, but, except for a small bump at -0.4 V, no gallium deposit stripping peak is obtained.

This is consistent with the generation of a lower oxidation state gallium–DIPY species of different metal:ligand ratios at each cathodic peak, which are stable in this solvent to the point of being detected on the reverse scan and to hinder further reduction to gallium metal.

The generation of soluble species was confirmed from rotating ring-disc collection efficiency experiments carried out on a GC–GC electrode since the voltammetric behaviour was the same as at a mercury electrode in this solvent. Figure 3(c) shows different species that are detected at the ring (held at $E_d = 0.000$ V) while the disc is scanned negatively. For each reduction wave at the disc, a corresponding oxidation wave is obtained at the ring. The reduction at -0.75 V, which shows no oxidation current at the ring, is due to residual oxygen. The corresponding superoxide ion is not detected because of its reaction with the gallium species, which also explains the collection efficiencies observed below the theoretical value.

From these experiments, one can conclude that a ligand catalysed reduction of gallium(III) to gallium metal can be obtained with DIPY in DMSO but not in MeCN. The role of solvent can be understood by the ability of DMSO to displace DIPY from the coordination sphere, producing species with less steric hindrance, which can better approach the electrode surface either to be adsorbed or coordinate with adsorbed DIPY. Electron bridging through adsorbed DIPY would facilitate the gallium(III) reduction to gallium metal.

The electrochemical activity of this ligand is observed at more negative potentials, as shown in Fig. 2, but the presence of protons can interfere.

First cathodic peak of $Ga(DIPY)_3^{3+}$ in DMSO

The overall reaction for this peak produces a gallium deposit which is clearly observed on the reverse scan of a cyclic voltamperogram. When increasing scan speed, a negative shift of the cathodic peak potential and a gradual distortion are obtained, whereas the anodic peak does not shift. The reaction rate requires a rather slow scan speed to get a well shaped cathodic peak. Great benefit is obtained from increasing the DIPY concentration well over the stoichiometric ratio. Figure 4(a) shows a typical cyclic voltamperogram for a solution containing DIPY:Ga = 300:1, and Fig. 4(b) shows the effect of increasing DIPY:Ga ratios on both cathodic and anodic peak currents. When the ratio is increased from the stoichiometric value to 150, both peaks are nearly doubled. A further increase in the ligand:metal ratio has little effect on the cathodic peak and a negative effect on the anodic peak. The anodic peak potential is not affected by increasing the DIPY:Ga ratio, whereas the cathodic peak potential shifts positively. The magnitude of this potential shift is proportional to log [DIPY]. These results are an indication that shifting of complex species equilibria and adsorption of DIPY on the electrode surface play an important role on the reaction mechanism in this solvent.

With a $10^{-3}M$ $Ga(DIPY)_3(ClO_4)_3$ solution with excess DIPY in DMSO (DIPY:Ga = 100), the effect of scan speed was explored over the range 20–2000 mV/sec. The cathodic peak currents ($I_{p,c}/\mu A$) fit the equation $I_{p,c} = 0.1333\ v^{1/2} + 9.0 \times 10^{-2}$, ($r = 0.9991$), which is indicative of a diffusion-controlled current.

Calibration plots were obtained by starting with $0.015M$ (for the range 10^{-5}–$10^{-4}M$ gallium) and $0.15M$ (for the range 10^{-4}–$10^{-3}M$ gallium) DIPY concentrations and adding increasing amounts of $Ga(DIPY)_3(ClO_4)_3$. Cathodic peak currents ($I_{p,c}/\mu A$) obtained at 40 mV/sec give linear plots which fit the equations $I_{p,c} = 1294.0\ [Ga] + 1.04 \times 10^{-3}$, ($r = 0.9999$) for the 10^{-5}–$10^{-4}M$ range and $I_{p,c} = 1061.3\ [Ga] - 1.7 \times 10^{-3}$, ($r = 0.9992$) for the 10^{-4}–$9 \times 10^{-4}M$ range. Higher concentrations give a negative deviation.

Oxygen and free proton interference

The possible interference of oxygen was studied by cyclic voltammetry at an HMDE and by rotating GC ring–GC disc electrode voltammetry.

Oxygen is reversibly reduced to superoxide ion in DMSO[16] at a less negative potential than $Ga(DIPY)_3^{3+}$. The −0.80 V cathodic peak of oxygen is preceded by a less negative potential peak (−0.58 V) and the superoxide oxidation peak is not observed when $Ga(DIPY)_3^{3+}$ is added into solution, as shown in Fig. 5(b). The cathodic peaks of $Ga(DIPY)_3^{3+}$ in the presence of excess DIPY [Fig. 5(a)] are hindered by dissolved oxygen, while the gallium stripping peak is completely suppressed [Fig. 5(b)].

A collection efficiency experiment is shown in Fig. 5(c) and (d). Superoxide generated by reduction of oxygen on the disc electrode is clearly detected by oxidation on the ring electrode [Fig. 5(c)] but when $Ga(DIPY)_3^{3+}$ plus excess DIPY are added, superoxide is not detected at all [Fig. 5(d)]. DIPY itself has no effect.

All of these results are an indication of a chemical reaction between superoxide ion and the gallium–DIPY species, which interferes with the DIPY catalyzed reduction of gallium(III). The −0.58 V peak is due to the oxygen reduction facilitated by the following chemical reaction, while the absence of a gallium stripping peak shows that the species resulting from this reaction cannot be reduced to gallium

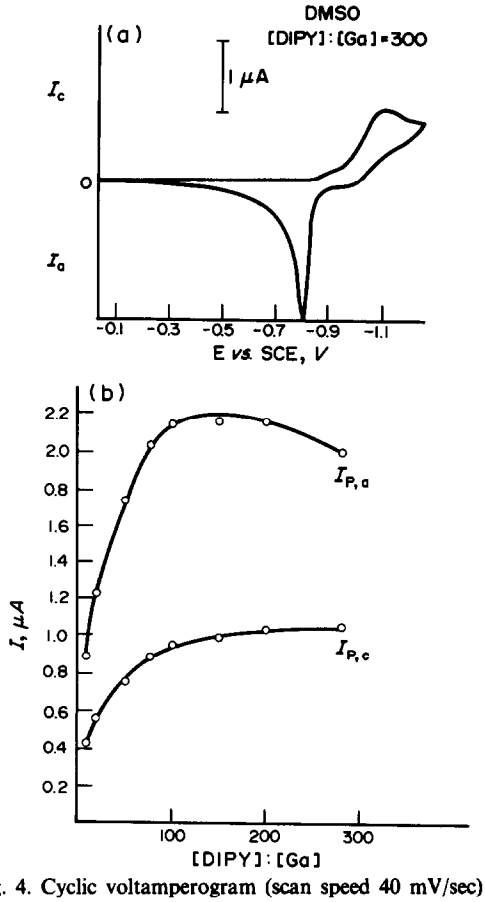

Fig. 4. Cyclic voltamperogram (scan speed 40 mV/sec) of $1 \times 10^{-3}M$ $Ga(DIPY)_3(ClO_4)_3$ ($0.1M$ TEAP) at a HMDE in DMSO in the presence of excess ligand; [DIPY]:[Ga] = 300 (a). Effect of other [DIPY]:[Ga] ratios on the cathodic ($I_{p,c}$) and anodic ($I_{p,a}$) peak currents are shown in (b).

metal. Interactions between superoxide ion and transition metal ions have been described elsewhere,[17] but to our knowledge no reference to a gallium(III)—superoxide interaction has been given.

The effect of free protons added as perchloric acid was studied by cyclic voltammetry. The cathodic peak corresponding to the catalyzed reduction of gallium(III) is enhanced by the acid but it overlaps with the catalyzed reduction of free protons which is observed at a less negative potential.

The cyclic voltamperogram prior to [Fig. 6(a)] and after [Fig. 6(b)] the addition of perchloric acid shows this interference, which has to be considered when designing an analytical procedure based on this catalytic process. However, the presence of a controlled concentration of protons could be beneficial in the case of the anodic peak. Figure 6(c) shows a plot of gallium stripping peak currents *vs.* acid

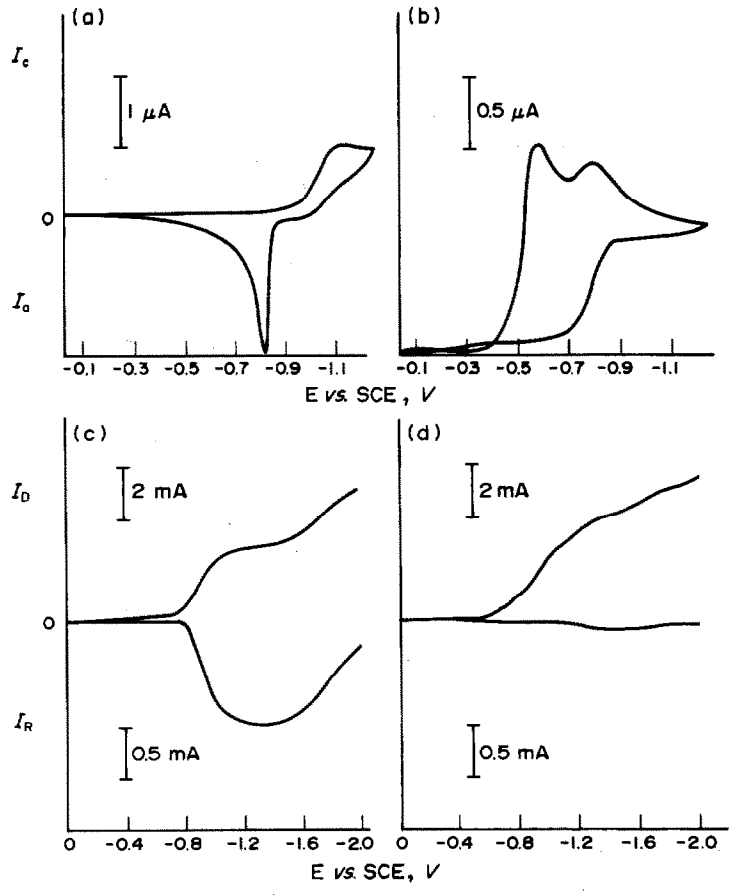

Fig. 5. Cyclic voltamperogram (scan speed 40 mV/sec) of $1 \times 10^{-3}M$ $Ga(DIPY)_3(ClO_4)_3 + 0.15M$ DIPY ($0.1M$ TEAP) at a HMDE in DMSO, after argon (a) and air (b) saturation. Rotating (GC) ring–(GC) disc electrode voltamperogram (2000 rpm; $E_R = 0.000$ V) of an air-saturated $0.1M$ TEAP solution in MeCN, before (c) and after (d) addition of $1 \times 10^{-3}M$ $Ga(DIPY)_3(ClO_4)_3 + 0.1M$ DIPY; upper curve, reduction at the disc electrode; lower curve, oxidation at the ring electrode.

concentration. Current enhancement is obtained with $1 \times 10^{-3}M$ acid concentration. Higher concentrations produce a gradual current decrease.

This positive effect could be useful in an analytical procedure based upon the anodic stripping of gallium.

One can understand this effect by considering that DIPY is a bidentate ligand with two basic nitrogens. The protonation of one of the nitrogens on a coordinated DIPY would labilize to some extent the electroactive Ga–DIPY species, facilitating and accelerating its reduction to gallium metal.

CONCLUSIONS

A catalytic cathodic peak is observed for the reduction of gallium(III) to gallium metal in DMSO with an excess of 2,2′-bipyridine. While free protons can interfere with this process due to the catalytic action of the ligand on the proton reduction, the anodic peak corresponding to gallium stripping is enhanced by their presence. The oxygen interference observed is due to a direct interaction between the superoxide generated by oxygen reduction and the metal ion, which precludes the metal deposition, making solution degassing a stringent requirement. The ligand electrochemistry does not interfere with the gallium reduction and the characteristics of both cathodic and anodic peaks make them attractive for the development of analytical procedures to determine traces of gallium(III). The direct use of the cathodic process may prove to be restricted by the interference of free protons, however the characteristics of the anodic peak are appropriate for anodic stripping analysis. One possible way to separate gallium(III) from its mineral matrix, and incorporate it into a non-aqeuous medium, is via solvent extraction[18] as gallium chloride.

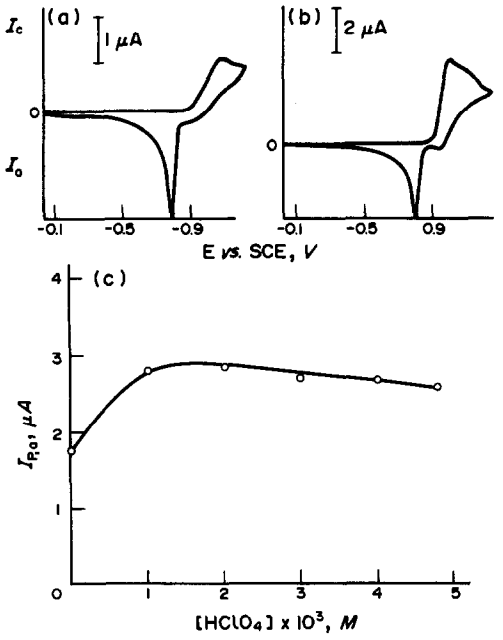

Fig. 6. Cyclic voltamperogram (scan speed 40 mV/sec) of $1 \times 10^{-3}M$ $Ga(DIPY)_3(ClO_4)_3 + 0.15M$ DIPY ($0.1M$ TEAP) at a HMDE in DMSO prior to (a) and after (b) the addition of $2 \times 10^{-3}M$ $HClO_4$. The effect of $HClO_4$ concentration on the anodic peak current for the same solution as in (a) is illustrated in (c).

REFERENCES

1. K. Asada, P. Delahay and A. K. Sundaram, *J. Am. Chem. Soc.*, 1961, **83**, 3396.
2. T. I. Popova, I. A. Bagotskaya and E. D. Moorhead, *Encycl. Electrochem. Elem.*, A. J. Bard (ed.), Vol. 8, pp. 207–262. Dekker, New York, 1978.
3. F. Vidra, K. Stulik and E. Julakova, *Electrochemical Stripping Analysis*, pp. 197–199. Ellis Horwood, Chichester, 1976.
4. E. D. Moorhead and P. H. Davis, *Anal. Lett.*, 1974, **7**, 781.
5. E. D. Moorhead and G. A. Forsberg, *Anal. Chem.*, 1975, **47**, 231.
6. E. D. Moorhead and P. H. Davis, *ibid.*, 1975, **47**, 622.
7. E. D. Moorhead and G. A. Forsberg, *ibid.*, 1976, **48**, 751.
8. O. E. Ruvinskii and Ya I. Tur'yan, *Zh. Anal. Khim.*, 1976, **31**, 543.
9. E. D. Moorhead and G. M. Frame II, *Anal. Chem.*, 1968, **40**, 280.
10. P. Cofré and K. Brinck, *Talanta*, 1992, **39**, 000.
11. G. V. Prokhorova, E. A. Osipova, P. K. Agasyan and V. I. Fadeeva, *Zh. Anal. Khim*, 1987, **42**, 787.
12. E. A. Osipova, G. V. Prokhorova, P. K. Agasyan and S. V. Rudometkin, *ibid.*, 1983, **38**, 689.
13. T. N. Srivastava and G. Mohan, *Z. Anorg. Allg. Chemie*, 1970, **379**, 79.
14. L. S. Foster, *J. Am. Chem. Soc.*, 1939, **61**, 3122.
15. E. Bishop and J. R. B. Sutton, *Anal. Chim. Acta*, 1960, **22**, 590.
16. D. T. Sawyer and J. L. Roberts, Jr., *J. Electroanal Chem.*, 1966, **12**, 90.
17. D. T. Sawyer and J. S. Valentine, *Acc. Chem. Res.*, 1981, **14**, 393.
18. P. H. Davis and E. D. Moorhead, *Anal. Lett.*, 1975, **8**, 387.

Talanta, Vol. 39, No. 6, pp. 631–635, 1992
Printed in Great Britain.

0039-9140/92 $5.00 + 0.00
Pergamon Press Ltd

ELECTROANALYTICAL STUDY OF SULPHAMERAZINE AT A GLASSY-CARBON ELECTRODE AND ITS DETERMINATION IN PHARMACEUTICAL PREPARATIONS BY HPLC WITH AMPEROMETRIC DETECTION

J. M. PINGARRON CARRAZON, A. DOMINGUEZ RECIO and L. M. POLO DIEZ*
Department of Analytical Chemistry, Faculty of Chemistry, Complutense University of Madrid, 28040-Madrid, Spain

(*Received* 11 *April* 1990. *Revised* 29 *July* 1991. *Accepted* 2 *August* 1991)

Summary—An electroanalytical study of the oxidation of sulphamerazine at a glassy-carbon electrode has been made by use of different voltammetric techniques. The limiting current is diffusion-controlled, at pH 7.0, for sulphamerazine in the concentration range 2.0×10^{-5}–$1.0 \times 10^{-4}M$. The limits of determination found for differential pulse voltammetry at a stationary electrode and at a rotating electrode were 5.9×10^{-6} and $3.3 \times 10^{-6}M$ respectively. A reversed-phase HPLC method with amperometric detection for the analysis of sulphamerazine, sulphadiazine and phthalylsulphathiazole mixtures has been developed, and applied to a commercial pharmaceutical preparation.

Sulphamerazine (**I**) and other sulphonamides are extensively used for the treatment of bacterial infections of the gastrointestinal tract. Analytical techniques used to determine sulphamerazine include liquid chromatography,[1,2] gas chromatography,[3] thin-layer chromatography,[4,5] spectrophotometry,[6] mass spectrometry,[7] thermal analysis,[8] potentiometric titration,[9] photometric titration[10] and a.c. polarography.[11] Here we describe an electroanalytical study of the oxidation of sulphamerazine at a glassy-carbon electrode and its use for determination of sulphamerazine by anodic voltammetry at low concentrations.

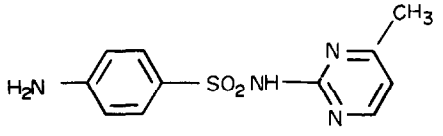

I

Sulphamerazine pharmaceutical preparations usually also contain other sulphonamides, such as sulphadiazine and phthalylsulphathiazole, so its direct voltammetric determination in these formulations is not possible. In earlier papers we described electroanalytical studies of the oxidation of sulphadiazine,[12] and of succinylsulphathiazole and phthalylsulphathiazole[13] at a glassy-carbon electrode (GCE), by different voltammetric techniques, and applied differential pulse voltammetry to determine these sulpha drugs in pharmaceutical preparations. This work is now extended to develop an HPLC method with amperometric detection for the analysis of a mixture of sulphamerazine, sulphadiazane and phthalylsulphathiazole.

EXPERIMENTAL

Apparatus

A multifunctional electroanalytical system consisting of an Amel 551 potentiostat, an Amel 560 interface, an Amel 566 function generator, and a Hewlett-Packard 7035 B X–Y recorder was used. A Metrohm E 506 Polarecord equipped with an E 505 polarographic stand, and Metrohm E 510 pH-meter were also used.

Chromatographic separation of sulphadiazine, sulphamerazine and phthalylsulphathiazole was achieved with a Waters Liquid Chromatograph consisting of a WISP 710 B automatic injector, a model 590 solvent-delivery pump and an electrochemical detection system comprised of a Metrohm 641 VA-Detector in conjunction with a Metrohm 656 Electrochemical Detector. The analytical column was a 150 × 4 mm i.d. Nucleosil 5 C_{18} column (Technorama).

*Author for correspondence.

Electrodes and electrochemical cell

A Metrohm 6.1204.000 GC rotating disc electrode, also used as a stationary electrode, served as the working electrode for the electroanalytical study of sulphamerazine. An Ingold 10 303 3000 saturated calomel reference electrode and a platinum wire counter-electrode were used. A double-wall Metrohm EA 867-20 polarographic cell was employed.

A Metrohm 6.0805.010 GCE as working electrode, a Metrohm 6.0727.000 Ag/AgCl/KCl 3*M* reference electrode and a gold auxiliary electrode built into the detector cell were used in the electrochemical detection system.

Reagents

Stock solutions (0.010*M*) of sulphamerazine, sulphadiazine and phthalylsulphathiazole (Sigma) were prepared in 0.020*M* sodium hydroxide. A Britton–Robinson buffer solution, containing each component acid at 0.2*M* concentration, was used as supporting electrolyte. All chemicals used were of analytical grade. Water was obtained from a Milli-Q (Millipore) purification system.

The mobile phase used for the HPLC was a 70:30 v/v mixture of 30 m*M* acetate buffer (pH 5.0) and methanol (HPLC grade, Mallinckrodt).

The method was validated by analysis of "Bio Hubber simple" tablets (Hubber, S.A.), prescribed for treatment of infections of the gastrointestinal tract. Each tablet has the following nominal composition: streptomycin (hydrochloride), 25 mg; phthalylsulphacetamide, 100 mg; sulphadiazine, 75 mg; sulphamerazine, 75 mg; phthalylsulphathiazole, 100 mg; saccharin (sodium salt), 10 mg.

Pretreatment of the indicator electrodes

For the electroanalytical study of sulphamerazine, before each scan the GCE was immersed in 95% ethanol for 1 min with continuous stirring, and then similarly in chloroform. The electrode was then cleaned carefully with non-abrasive tissue paper soaked in chloroform, and dried with a dry tissue.[14] Next, the GCE was immersed in 2*M* sodium hydroxide for 1 min with continuous stirring, and finally rinsed with distilled water and dried.

The GCE used in the electrochemical detection system was pretreated as above, every day. Finally, the electrode was kept in the mobile phase used, at 1.30 V *vs.* the reference electrode, for 20 min.

Procedure

Several "Hubber" tablets were finely ground and homogenized. A weight of powder equivalent to the average weight of a tablet was stirred with 50 ml of methanol for about 5 min, and then diluted with water to about 100 ml with continuous stirring. Any insoluble matter was filtered off on a medium porosity acid-washed paper, and washed with two 10-ml portions of water. The filtrate and washings were accurately diluted to 1 litre with water, and 10 ml of this solution were transferred into a 50-ml standard flask and diluted to volume in order to obtain sulpha drug concentrations close to $5.0 \times 10^{-5}M$. A 10-μl portion of this solution was injected into the HPLC column, and chromatographed at 1 ml/min flow-rate. The potential applied to the indicator electrode was 1.15 V *vs.* the reference electrode. A single calibration point was used for each drug, with a 10-μl injection of a $5.0 \times 10^{-5}M$ standard solution.

RESULTS AND DISCUSSION

Electroanalytical study of sulphamerazine

Sulphamerazine exhibits one well-defined oxidation wave (or peak) at the GCE for all the voltammetric techniques used. Deaeration of the test solution was shown to be unnecessary under the recommended working conditions.

Voltammetry at a rotating disc electrode. The effect of pH on $E_{1/2}$ and the limiting current (i_L) is shown in Fig. 1. The $E_{1/2}$ *vs.* pH plot shows four regions of linearity, the intersection points indicating the pK_a values of the reduced and oxidized forms of the electroactive species.[15] The shape of this plot agrees quite well with that of the corresponding plots for sulphadiazine[12] and

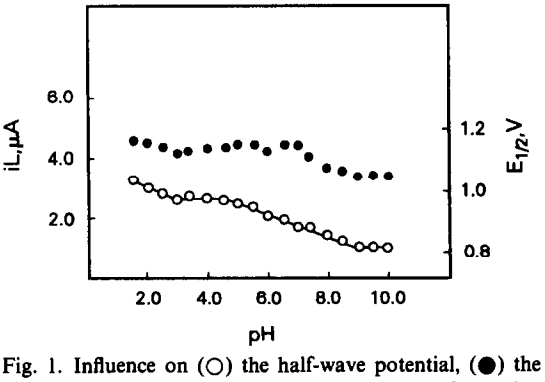

Fig. 1. Influence on (○) the half-wave potential, (●) the limiting current for anodic voltammetry at a GC rotating disc electrode. Sulphamerazine $6.0 \times 10^{-5}M$; ω 1500 rpm; scan rate 50 mV/sec.

Table 1. Analytical characteristics of the methods for the determination of sulphamerazine: pH 7.0 Britton–Robinson buffer

Voltammetric technique	RSD, %	Determination limit, M	Detection limit, M
Linear sweep/ rotating GCE	1.9	2.2×10^{-5}	6.6×10^{-6}
Linear sweep/ stationary GCE	3.7	1.5×10^{-5}	4.5×10^{-6}
Differential pulse/ stationary GCE	1.7	5.9×10^{-6}	1.9×10^{-6}
Differential pulse/ rotating GCE	2.4	3.3×10^{-6}	1.0×10^{-6}

phthalylsulphathiazole.[13] The intersection points found at pH 3.0 and 9.0 correspond to deprotonation of the amine and the amide groups of sulphamerazine respectively. Likewise, the pK_a value of the sulphamerazine oxidation product was 4.5. For pH values higher than 10.0, the wave is poorly defined, which prevents accurate measurements of $E_{1/2}$ values. The limiting current remains practically constant up to pH 7.0; at pH values higher than 7.0 i_L begins to decrease; pH 7.0 was chosen for the further electroanalytical studies.

Fick's law is obeyed in the concentration range 2.0×10^{-5}–$1.0 \times 10^{-4}M$ sulphamerazine for different rotation rates in the range 1000–2500 rpm, suggesting that the limiting current is probably diffusion-controlled in this concentration range.

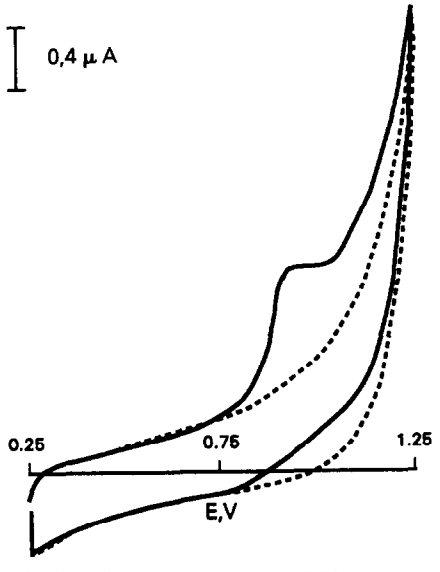

Fig. 2. Cyclic voltamperograms at a GCE: (----) $0.1M$ pH 7.0 Britton–Robinson buffer; (——) $6.0 \times 10^{-5}M$ sulphamerazine and $0.1M$ pH 7.0 Britton–Robinson buffer.

Levich's law is also obeyed for rotation rates of 500–3000 rpm within the concentration range 2.0×10^{-5}–$1.0 \times 10^{-4}M$ (as an example, the i_L *vs.* $\omega^{1/2}$ plot for $6.0 \times 10^{-5}M$ sulphamerazine yields an r value of 0.9996), confirming that the limiting current is diffusion-controlled at the concentration levels studied.

These results allow a method to be developed for the determination of sulphamerazine by use of a calibration graph. The analytical characteristics of the method for a rotation rate of 1500 rpm are summarized in Table 1. The relative standard deviation was calculated for a concentration level of $6.0 \times 10^{-5}M$ sulphamerazine. The limit of determination was calculated according to the $10s$ criterion,[16] and the detection limit was defined as $3s/m$,[17] where s is the standard deviation ($n = 10$) of the signal for $3.0 \times 10^{-5}M$ sulphamerazine aliquots and m is the slope of the calibration graph.

Linear sweep voltammetry at a stationary electrode. Voltamperograms obtained at pH 7.0 showed a well developed oxidation peak at a potential of 1.20 V.

The plots of i_p against sulphamerazine concentration for potential-scan rates (v) of 20, 50 and 100 mV/sec were linear ($r = 0.9995$, 0.9996 and 0.9987 respectively) over the concentration range 2.0×10^{-5}–$1.0 \times 10^{-4}M$.

The linearity ($r = 0.9990$) of the i_p *vs.* $v^{1/2}$ plot for $8.0 \times 10^{-5}M$ sulphamerazine in the range 10–200 mV/sec for v shows that the oxidation current is diffusion-controlled.[18]

The analytical characteristics of the method based on the linear i_p *vs.* concentration plot, for $v = 50$ mV/sec, with the criteria mentioned above, are also summarized in Table 1. The relative standard deviation was calculated for a concentration of $6.0 \times 10^{-5}M$ ($n = 10$), and the limits of determination and detection were

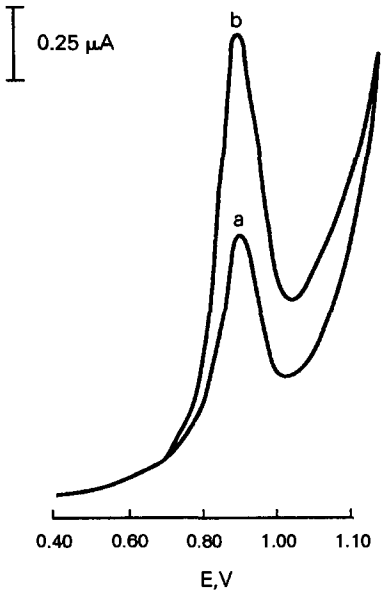

Fig. 3. Differential pulse voltammetry of $6.0 \times 10^{-5}M$ sulphamerazine, scan rate 10 mV/sec; ΔE 50 mV. (a) stationary GC electrode; (b) rotating GC disc electrode, $\omega = 1500$ rpm.

calculated from the standard deviation ($n = 10$) for $3.0 \times 10^{-5}M$ sulphamerazine.

In a reverse scan to cathodic potentials at $v = 50$ mV/sec, no reduction peak appeared in the potential range studied (Fig. 2), which indicates non-reversibility of the electrode process. However, a small shoulder appears in the sweep toward negative potentials, which probably indicates that a further reaction takes place after the initial anodic reaction.

Differential pulse voltammetry at a stationary electrode. From the E_p–pH plot for $5.0 \times 10^{-5}M$ sulphamerazine, with $\Delta E = 50$ mV, the pK_a values of the protonated amine and of the amide groups of sulphamerazine were found to be 3.0 and 8.8 respectively, while the pK_a value of the sulphamerazine oxidation product was 4.6. These results are very similar to those obtained by using the rotating disc electrode. The i_p–pH plot indicated that the highest sensitivity was reached at pH 7.0.

The i_p *vs.* pulse amplitude plot for $4.0 \times 10^{-5}M$ sulphamerazine shows good linearity over the ΔE range 5–50 mV, but deviates from linearity at higher values of ΔE. The upper value of the linear range was chosen for the further electroanalytical study.

The ranges of linearity obtained for the i_p *vs.* sulphamerazine concentration plots were $1.0 \times 10^{-5} - 1.0 \times 10^{-4}M$ ($r = 0.9999$), with slope and intercept of 1.9×10^4 μA.l.mole^{-1} and -0.04 μA, and 7.0×10^{-6}–$1.0 \times 10^{-5}M$ ($r = 0.9990$), with slope and intercept of 2.4×10^4 μA.l.mole^{-1} and -0.11 μA.

The analytical characteristics of the method based on these calibration graphs are summarized in Table 1. The relative standard deviation was calculated for $4.0 \times 10^{-5}M$ sulphamerazine ($n = 10$). The limits of determination and detection were calculated from 10 replicate measurements of $9.0 \times 10^{-6}M$ sulphamerazine.

Differential pulse voltammetry (dpv) at a rotating disc electrode. This technique gave a significantly greater peak current than that for dpv at a stationary electrode (Fig. 3). The i_p increases with rotation rate of the electrode, the i_p *vs.* $\omega^{1/2}$ plot for $6.0 \times 10^{-5}M$ sulphamerazine being linear ($r = 0.998$) over the range 500–3000 rpm. The plot of i_p *vs.* sulphamerazine concentration at pH 7.0, $\Delta E = 50$ mV and 1500 rpm, was linear between 4.0×10^{-6} and $1.0 \times 10^{-5}M$.

The analytical characteristics of the method based on this calibration graph are given in Table 1. The relative standard deviation was calculated for a concentration level of $7.0 \times 10^{-6}M$ ($n = 10$). The limits of determination and detection were calculated from the standard deviation ($n = 10$) for $5.0 \times 10^{-6}M$ sulphamerazine. These results show that the sensitivity is about twice as great as that for dpv at a stationary electrode.

An additional conclusion from Table 1 is that the precision obtained by voltammetry at a rotating disc electrode and by differential pulse voltammetry at a stationary electrode allows their use for quality control work.

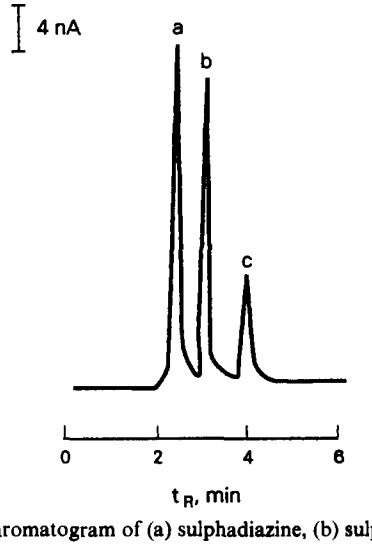

Fig. 4. Chromatogram of (a) sulphadiazine, (b) sulphamerazine and (c) phthalylsulphathiazole, with amperometric detection. Concentration of each compound $5.9 \times 10^{-5}M$. Injection volume 10 μl.

Determination of sulphamerazine, sulphadiazine and phthalylsulphathiazole in pharmaceutical preparations by HPLC with amperometric detection

The results reported above for sulphamerazine, together with knowledge of the oxidative voltammetric behaviour of sulphadiazine and phthalylsulphathiazole at the GCE,[12,13] allowed amperometric detection of a mixture of these three sulpha drugs after their separation by reverse-phase HPLC.

The potential applied to the GCE was 1.15 V. Because our main interest was the determination of sulphamerazine, this value was chosen after studying the effect on the peak height obtained for $5.0 \times 10^{-5}M$ sulphamerazine when the potential applied to the electrode was varied from 1.00 to 1.30 V. This potential was also enough to provide detection of the other two sulpha drugs.

Figure 4 shows a chromatogram obtained from a mixture containing each sulpha drug at $5.0 \times 10^{-5}M$ level as described in the procedure. The capacity factors were 0.8, 1.3 and 2.8 for sulphadiazine, sulphamerazine and phthalylsulphathiazole respectively, and good resolution was obtained. The analysis time was 4.5 min, and the response factors were 1.0, 1.1. and 0.3 for sulphamerazine, sulphadiazine and phthalylsulphathiazole respectively.

Linear calibration graphs were obtained for all three drugs within the range 1.0×10^{-5}–$9.0 \times 10^{-5}M$.

"Bio Hubber simple" tablets were then analysed, with one-point calibrations, as specified in the procedure. Results obtained from 5 determinations yielded sulphadiazine, sulphamerazine and phthalylsulphathiazole contents of 70.5 ± 0.9, 70.6 ± 1.8 and 94.6 ± 1.5 mg respectively, the confidence interval being calculated for a significance level of 0.05 (RSD values were 1.0%, 2.1% and 1.3% respectively). The accuracy of the proposed method was evaluated by recovery studies after adding 150 μl of each sulpha drug stock solution to the analytical solution of the pharmaceutical product. Results from five determinations yielded mean recoveries of 97% for sulphadiazine and 98% for sulphamerazine and phthalylsulphathiazole, the relative standard deviations being 2.0, 2.4 and 2.2% respectively (the confidence intervals of the mean recoveries were ± 2.5, ± 3.0 and ± 2.7% respectively).

Acknowledgement—The authors thank Dr. B. Cañas Montalvo for this help in the HPCL experiments.

REFERENCES

1. S. D. Revett and M. E. Tenneson, *Anal. Proc.*, 1984, **21**, 248.
2. P. H. Cobb and G. T. Hill, *J. Chromatog.*, 1976, **123**, 444.
3. E. Pawelczyk and M. Opielewicz, *Acta Pol. Pharm.*, 1981, **38**, 75.
4. T. Okumura and T. Nagaoka, *J. Liq. Chromatog.*, 1980, **3**, 1947.
5. J. Jarzebinski, S. Tonska and K. Gryz, *Acta Pol. Pharm.*, 1982, **39**, 135.
6. C. S. P. Sastry, T. M. K. Reddy and B. G. Rao, *Indian Drugs*, 1984, **21**, 145.
7. W. C. Brumley, Z. Min, J. E. Matusik, J. A. G. Roach, C. J. Barnes, J. A. Sphon and T. Fazio, *Anal. Chem.*, 1983, **55**, 1405.
8. F. I. Khattab, N. Y. M. Hassan and M. M. Amer, *J. Therm. Anal.*, 1981, **22**, 41.
9. K. K. Verma and A. K. Gupta, *Anal. Chem.*, 1982, **54**, 249.
10. E. Pelizzetti and E. Pramauro, *Anal. Chim. Acta*, 1981, **128**, 273.
11. G. Grossi, C. Mondi and R. Tanini, *G. Med. Mil.*, 1981, **131**, 263.
12. J. M. Pingarrón Carrazón, P. Corona Corona and L. M. Polo Díez, *Electrochim. Acta*, 1987, **32**, 1573.
13. J. M. Pingarrón Carrazón, A. Domínguez Recio and L. M. Polo Díez, *Electroanalysis*, 1989, **1**, 317.
14. M. K. Chan and A. G. Fogg, *Anal. Chim. Acta*, 1979, **109**, 341.
15. J. D. Voorhies and R. N. Adams, *Anal. Chem.*, 1958, **30**, 346.
16. ACS Committee on Environmental Improvement, *ibid.*, 1983, **55**, 2210.
17. K. Hasebe and J. Osteryoung, *ibid.*, 1975, **47**, 2412.
18. R. N. Adams, *Electrochemistry at Solid Electrodes*, Chap. 8 and p. 126. Dekker, New York, 1969.

Talanta, Vol. 39, No. 6, pp. 637–641, 1992
Printed in Great Britain.

0039-9140/92 $5.00 + 0.00
Pergamon Press Ltd

STUDY OF THE REACTION OF COMPLEXATION OF PENICILLIN V WITH COBALT(II) IN METHANOLIC MEDIUM

JUAN HERNANDEZ MARTINEZ, PEDRO J. MARTINEZ, PILAR GUTIERREZ and MA ISABEL MARTINEZ
Department of Physical Chemistry, Faculty of Pharmacy, University of Granada, Granada, Spain

(*Received* 25 *July* 1991. *Revised* 18 *November* 1991. *Accepted* 21 *November* 1991)

Summary—As shown by spectrophotometry, two specific complexes with stoichiometry 1:1 and 2:1 are formed when penicillin V reacts with cobalt(II) in a methanolic medium. Stability constants are determined at 20°, as well as the molar absorptivities at 510 nm. The results obtained are: $\log \beta_{1:1} = 1.67 \pm 0.01$ $l \cdot mole^{-1}$ and $\log \beta_{2:1} = 5.76 \pm 1.01$ $l^2 \cdot mole^{-2}$, $\epsilon_{1:1} = 13.62 \pm 0.73$ and $\epsilon_{2:1} = 12.95 \pm 0.61$ $l \cdot mole^{-1} \cdot cm^{-1}$.

Penicillin and ampicillins interact with metallic ions forming complexes.[1–6] To study the chelation sites we took an aminopenicillin which has two sites of chelation, one formed for the aminic group of the lateral chain and the C=O group in the β-lactam ring and the other formed by the carboxylate group and the tertiary nitrogen of the said ring.[7] Pivampicillin has been used, which, once the carboxylate group has been esterificated, has only one site of chelation, the one formed by the aminic group of the lateral chain and the C=O of the β-lactam ring.[8] In this work we have used penicillin V without the aminic group in the lateral chain as a ligand and therefore only one chelation site is present, formed by the carboxylate group and the tertiary nitrogen of the β-lactam ring.

The union from this nitrogen has greater access to the lone pair of electrons on the nitrogen compared with that in normal amides, due to the spatial structure of the β-lactam ring. The stability constants and molar absorptivities at 20° of the penicillin V complexes with cobalt(II) were calculated in methanolic medium.

EXPERIMENTAL

Materials

All chemicals used in this study were reagent grade. Potassium penicillin V (purer than 99%) was from Sigma. Cobalt(II) nitrate hexahydrate and methanol were purchased from Merck and used as provided without further purification.

Instruments

A Bausch & Lomb Spectronic 2000 spectrophotometer, a Selecta thermostat (±0.1°), an Amstrad PC-1512 computer equipped with a plotter sekonic spl-410 and 1-cm thick spectrophotometric cells were used.

Spectra

To prove the formation of the complexes we recorded spectra (between 850 and 400 nm) of methanolic solutions which contained penicillin V ($2.66 \times 10^{-2} M$); cobalt(II) nitrate ($1.33 \times 10^{-2} M$) and also a mixture of these solutions. The spectra obtained are shown in Fig. 1.

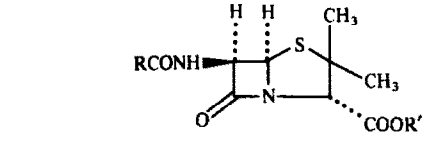

R	R'	
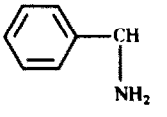	H	Ampicillin
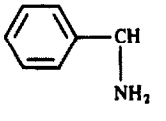	$CH_2OCOC(CH_3)_3$	Pivampicillin
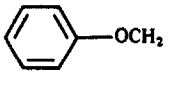	H	Penicillin V

Scheme 1

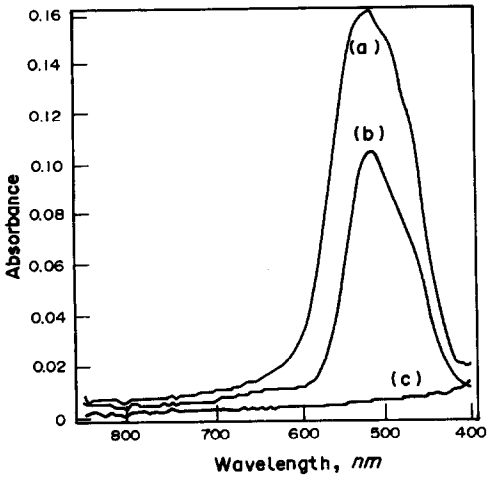

Fig. 1. Absorption curves of methanolic solutions: (a) cobalt(II) $1.33 \times 10^{-2}M$ (b) penicillin V $2.66 \times 10^{-2}M$ (c) penicillin V–cobalt(II) at the same concentrations. $T_a = 20°$.

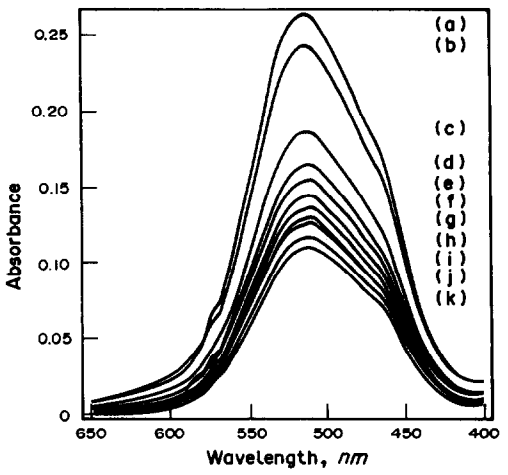

Fig. 2. Absorption curves of methanolic solutions [series (b)] of potassium penicillin V 2.72, 2.50, 2.00, 1.76, 1.67, 1.58, 1.50, 1.43, 1.36, 1.30, $1.25 \times 10^{-2}M$ and cobalt(II) nitrate at the same concentrations respectively at 20°.

In order to characterize the influence of concentration of the reagents and determine the number of absorbant species, the visible absorption spectra of methanol solutions of potassium penicillin V and cobalt(II) nitrate hexahydrate were studied in four different series, where the concentration of the metal remained constant ($1.2 \times 10^{-2}M$) and that of penicillin V was varied to obtain different molar ratios.

Solutions with an excess of metal. We registered the spectra of methanolic solutions which contained a constant cobalt(II) concentration ($1.2 \times 10^{-2}M$) while that of penicillin V was variable (4.8×10^{-3}–$1.2 \times 10^{-2}M$). The solutions thus prepared had molar ratios between 0.4:1 and 1:1.

Solutions with a constant molar ratio of reactives of 1:1. In this case the stoichiometric relation was kept constant and we varied the concentrations of penicillin V and metal.

Solutions with a molar ratio of reactives between 1:1 and 2:1. In this series the ligand concentrations were between 1.44×10^{-2} and $2.64 \times 10^{-2}M$.

Solutions with a constant molar ratio of reactives of 2:1. We varied the concentration of penicillin V and metal but always maintained the 2:1 stoichiometric relation.

All these experiments have been realized in a methanolic medium with a temperature of 20°.

Figures 2 and 3 show some spectra obtained.

Number of absorbant species and stoichiometry of complexes

Coleman's matrix method[10] was applied in graphic form to the absorbance data obtained in the previous section in order to find the number of absorbant species. Job's method[11] was employed to determine the stoichiometric balance of the complexes.

Stability constants and molar absorptivity coefficients of complexes

These values were calculated from the absorbance data of the various methanolic solutions at different concentrations of ligand and metal with the MINISPEF program.[12] This program can calculate the optimum values of the overall stability constants and molar absorptivities of a maximum of 8 species formed by the reaction which can be expressed as:

$$qM + pL + rH^+ \rightleftharpoons M_qL_pH_r^+ \qquad (1)$$

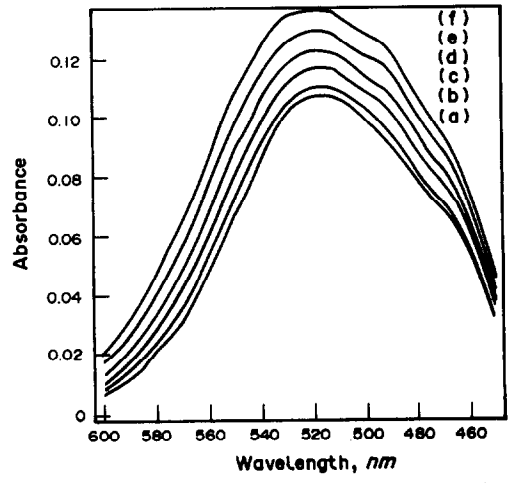

Fig. 3. Absorption curves of methanolic solutions (series c) of cobalt(II) nitrate $1.2 \times 10^{-2}M$ and potassium penicillin V 1.44, 1.68, 1.92, 2.16, 2.40, $2.64 \times 10^{-2}M$ at 20°.

where q or r can be zero. The stability constants are defined as:

$$B = [M_qL_pH_r]/[M]^q[L]^p[H^+]^r \quad (2)$$

The logarithms of the overall stability constants and the molar absorptivities are treated as unknown parameters. The MINISPEF program calculates those values which yield the minimum sum of the squares of the residuals (U) of the measured (A_{meas}) and calculated (A_{cal}) absorbances, together with the probable errors.

$$U = \sum_i (A_{meas,i} - A_{cal,i})^2 \quad (3)$$

RESULTS AND DISCUSSION

Figure 1 shows how the absorbance at 510 nm for penicillin V–cobalt(II) in a 2:1 ratio does not correspond to the sum of the absorbances of the separated reactives, which shows the formation of one or more complexes.

To study the number of species present in solutions, Coleman's test was applied to the four series of solutions previously described.

Application of Coleman's test to absorption data of methanolic solutions shows the existence of two absorbant species. This can be deduced by the groups of straight lines obtained representing A_{ij}/A_{580j} *vs.* A_{510j}/A_{580j} (Fig. 4). These two species can be attributed to cobalt(II) which is found in equilibrium with a 1:1 stoichiometric complex.

In a second series of solutions, Coleman's test was applied to the absorbance data obtained in the experimental section. Graphic representation leads to a group of straight lines radiating from the origin (Fig. 5), which demonstrates the existence of only one absorbant species in solution that can be assigned to a stoichiometric complex of 1:1.

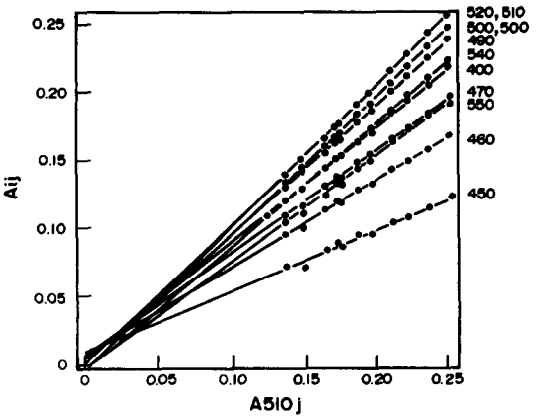

Fig. 5. Coleman's test for one species applied to the data of series (d).

The application of Coleman's test on the third series of solutions led to a group of straight lines similar to those described in Fig. 4, which confirms the existence of two absorbant species which could correspond to stoichiometric complexes 1:1 and 2:1 which are found in equilibrium.

For the fourth series of solutions Coleman's test was applied. The result is a group of straight lines coinciding at the origin very similar to those described in Fig. 5, which confirm the existence of only one absorbant species that can be assigned to the stoichiometric complex 2:1.

To determine the stoichiometry and in accordance with Job's method, the absorbance, once corrected due to the absorbance of cobalt(II), was graphically represented *vs.* the molar fraction of penicillin (Fig. 6). A maximum molar fraction of 0.66 can be seen, which

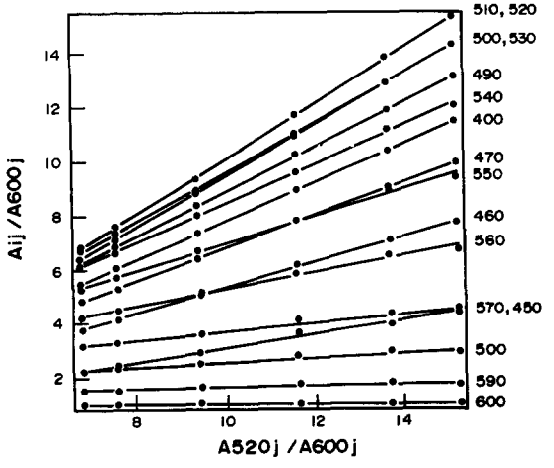

Fig. 4. Coleman's test for two species applied to the data of series (c).

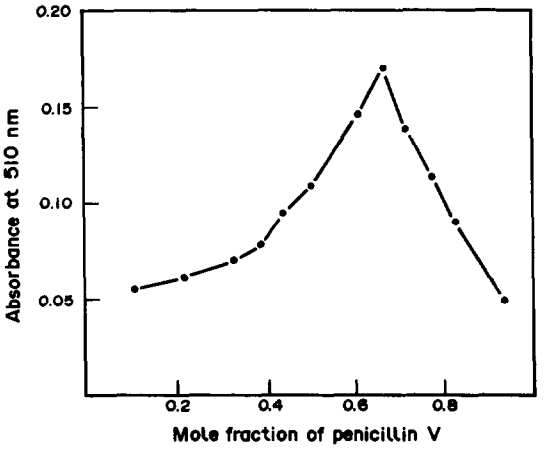

Fig. 6. Job's plot. The sum of concentration of reactants, penicillin and cobalt(II) was 0.06M.

Table 1. Absorption values at 510 nm, A_{510}, of methanolic solutions of penicillin V and cobalt(II) nitrate of different concentrations. $T_a = 20°$

2:1			1:1		
[Pen V] ($\times 10^2$)	[Co(II)] ($\times 10^2$)	A_{510}	[Pen V] ($\times 10^2$)	[Co(II)] ($\times 10^2$)	A_{510}
4.00	2.00	0.247	3.00	3.00	0.293
3.75	1.88	0.230	2.14	2.14	0.203
3.53	1.76	0.217	2.00	2.00	0.183
3.33	1.67	0.204	1.87	1.87	0.170
3.16	1.58	0.193	1.76	1.76	0.162
3.00	1.50	0.185	1.67	1.67	0.152
2.86	1.43	0.172	1.58	1.58	0.141
2.73	1.36	0.170	1.50	1.50	0.134
2.61	1.30	0.161	1.43	1.43	0.127
2.50	1.25	0.146	1.36	1.36	0.124
2.40	1.20	0.145	1.30	1.30	0.115
2.31	1.15	0.133	1.25	1.25	0.108

Table 2. Stability constants (20°) and molar absorptivity at 510 nm with its probable errors and the squares of residuals (U), for the Co(II)–penicillin V complexes

Complex	log β	ϵ_{max}, $l \cdot mole^{-1} \cdot cm^{-1}$	ϵ_M	U
1:1	1.67 ± 0.01	13.62 ± 0.73	6.74	3.88×10^{-5}
2:1	5.76 ± 1.01	12.95 ± 0.61	6.74	1.33×10^{-4}

ϵ_M = Absorption coefficients of the metal at the wavelength of the absorption maximum of the complexes.

indicates the existence of a stoichiometric complex of 2:1. Variation in the slope for a molar fraction of around 0.5 can be observed, confirming the existence of a stoichiometric complex of 1:1.

All of this permits us to conclude the following reaction scheme:

$$\text{Pen V} + \text{Co(II)} \xleftrightarrow{K_1} \text{Pen V Co}$$

$$\text{Pen V Co} + \text{Pen V} \xleftrightarrow{K_2} (\text{Pen V})_2\,\text{Co}$$

We used the MINISPEF program[12] to calculate the absorbance data of 510-nm solutions of reactives in molar ratios of 2:1 and 1:1 (Table 1) to calculate the stability constants, log $\beta_{1:1}$ and log $\beta_{2:1}$, and the molar absorptivities to 510 nm, $\epsilon_{1:1}$ and $\epsilon_{2:1}$ of the formed complexes.

In both cases and in accordance with previous results we consider that only one complex is respectively formed for each, 2:1 and 1:1.

The global stability constants and the molar absorption coefficients are represented in Table 2 as is the square of the residuals (U).

The U values obtained (Table 2) show the difference between the absorbance data measured and the calculated absorbance to be less than ± 0.005, which falls within the margin of spectrophotometric error. Furthermore, the values of molar absorption coefficients of the metallic ion, ϵ_M, found by applying the calculation program, agree with those experimentally determined. These facts constitute a validity test to the finding about the number of complexes formed in each case, as in their stoichiometry.

The stability constants of the compounds of penicillin V–cobalt(II) are very high. This can

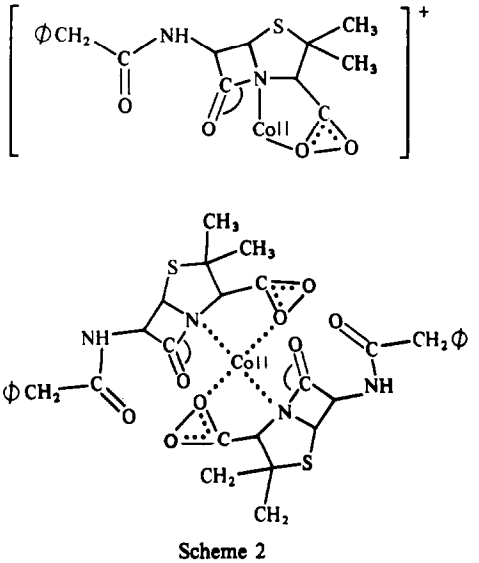

Scheme 2

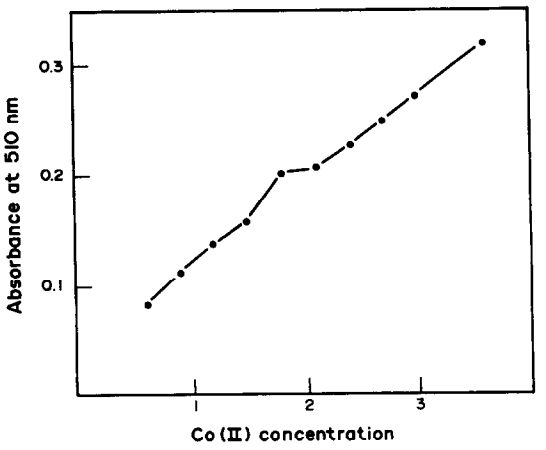

Fig. 7. Curve of spectrophotometric valoration of penicillin V with cobalt(II) in methanolic medium at 510 nm.

indicate that the compounds formed are chelates and therefore penicillin V acts as a bidentate ligand.

As penicillin V is not an aminopenicillin it does not have an amino group in the lateral chain; it can be considered that the coordination is done by the carboxylate group and the tertiary nitrogen of the β-lactam ring, which can be drawn for both stoichiometries.

The high stability values found can be attributed therefore to the methanolic medium, where the reaction occurs easier than in water.

The formation of the complexes, of a high formation constant (Table 2), could be used as a base for the spectrophotometric analysis of penicillin V with a solution of cobalt(II) at 510 nm. The end-point of the analysis (maximum light absorption) takes place at a 1.3:1 molar ratio of the reactants according to Fig. 7. With this method concentrations of penicillin V between 2×10^{-2} (absorbance 0.1) and $6 \times 10^{-2} M$ (highest solubility concentration) could be analysed.

REFERENCES

1. P. J. Niebergall, D. A. Hussar, W. A. Cressman, E. T. Sugita and J. T. Doluisio, *J. Pharm. Pharm.*, 1966, **18**, 729.
2. W. A. Cressman, E. T. Sugita, J. T. Doluisio and P. J. Niebergall, *ibid.*, 1969, **58**, 1471.
3. K. Karemi, H. Sezaki, K. Iwamoto, H. Kobayashi and K. Inui, *Chem. Pharm. Bull.*, 1971, **19**, 730.
4. G. V. Fazakerley and G. E. Jackson, *J. Pharm. Sci.*, 1977, **66**, 553.
5. M. G. Abd el Wahed and M. Ayad, *Anal. Lett.*, 1984, **17**, 205.
6. D. S. Veselinovic and W. P. Kapetanovic, *J. Serb. Chem. Soc.*, **50**, 401.
7. P. Martínez, P. Gutiérrez, M. I. Martínez and A. Cordoba, *Ann. Quim.*, 1989, **85**, 122.
8. P. Gutiérrez, P. Martínez, L. Mayo and A. Márquez, *Afinidad*, 1991, **48**, 431.
9. D. Crowfoot, C. W. Bunn, B. W. Rogers-Low and A. Turner-Jones, *The Chemistry of Penicillin*. Princeton University Press, Princeton, 1949, 443.
10. J. S. Coleman, L. P. Varga and S. H. Mastin, *Inorg. Chem.*, 1970, **9**, 1015.
11. P. Job, *Ann. Chim.*, 1928, **9**, 113.
12. F. Gaizer and A. Puskas, *Talanta*, 1981, **28**, 925.

Talanta, Vol. 39, No. 6, pp. 643–647, 1992
Printed in Great Britain.

0039-9140/92 $5.00 + 0.00

CHARACTERIZATION AND ANALYTICAL APPLICATION OF THE ION-ASSOCIATION COMPLEX CRYSTAL VIOLET–CADMIUM BROMOPYROGALLOL RED

ZHI-QIANG ZHAO*
Department of Chemistry, Hebei Normal University, Shijiazhuang city, Hebei Province, People's Republic of China

RUO-MEI GAO
Department of Public Health, Hebei Medical College, Shijiazhuang city, Hebei Province, People's Republic of China

LIANG-CHENG ZHAO
Center of Analysis and Testing of Geological Bureau of Hebei Province, Baoding city, People's Republic of China

(*Received* 6 *February* 1991. *Revised* 24 *September* 1991. *Accepted* 25 *September* 1991)

Summary—In the presence of polyvinylalcohol (PVA-124) and polyethylene glycol monooctylphenyl ether (emulsifier OP), cadmium ions(II) can form a colour ion-association complex with both Bromopyrogallol Red (BPR) and Crystal Violet (CV). In the NH_3–NH_4Cl medium, the ion-association complex has a composition of Cd:BPR:CV = 1:1:2, and its corresponding molecular formula is $[CV]_2[Cd(BPR)]$. The maximum absorption of the colour complex is located at 654 nm with an apparent molar absorptivity of 1.79×10^5 l.mole^{-1}.cm^{-1}. Beer's law is obeyed for cadmium over the range 0–10 μg/25 ml. A highly sensitive spectrophotometric method for trace cadmium in water and zinc was developed with good precision and accuracy. The mechanism of the reaction is also discussed.

It is well known that many cadmium compounds are very toxic to the environment and humans. Therefore, the determination of cadmium is important.

Bromopyragallol Red (BPR) has been widely used as a reagent in spectrophotometry, but is little used for the determination of cadmium. Xu *et al.* have studied the formation of the cadmium complex with both BPR and cetyltrimethyl ammonium bromide (CTAB), and have observed a molar absorptivity of 4.2×10^4 l.mole^{-1}.cm^{-1}.[1]

In recent years, several spectrophotometric methods based on coloured ternary complex systems have been recommended for the determination of cadmium(II).[2–4] Some of these are ion-association complexes,[5,6] in which the cadmium complex anion is a simple inorganic complex (*e.g.* $[CdI_4^{2-}]$). Synergistic chromophoric reactions by double chromogenic reagents for the determination of cadmium have not been reported.

In the work presented here, the complex formation of the double chromogenic reagents, Bromopyrogallol Red (BPR) and Crystal Violet (CV), with cadmium(II) was studied. In an NH_3–NH_4Cl medium (pH 8.5), cadmium ions form an ion-association complex with a composition of Cd:BPR:CV = 1:1:2. In the presence of polyvinylalcohol (PVA-124) and polyethylene glycol monooctylphenyl ether (emulsifier OP), the stability and sensitivity are enhanced. The maximum absorption of the complex was located at 654 nm with an apparent molar absorptivity of 1.79×10^5 l.mole^{-1}.cm^{-1}, which is much higher than those reported earlier for the cadmium complex with BPR (8.0×10^3 l.mole^{-1}.cm^{-1}), and BPR–CTAB (4.2×10^4 l.mole^{-1}.cm^{-1}). Beer's law is obeyed for cadmium over the concentration range 0–10 μg/25 ml. This method has been applied to the determination of cadmium in water and zinc with good precision and accuracy.

*Author for correspondence.

EXPERIMENTAL

Apparatus

A Perkin–Elmer Model Lambda-17 UV-Vis spectrophotometer was used.

Reagents

All the reagents used were of analytical reagent grade. Distilled water was used throughout.

BPR and OP were obtained from Shanghai Chemical Reagent Works, CV from (Germany) and PVA-124 from (Japan).

Stock standard solution of cadmium(II), 1 mg/ml. A 1.6308-g sample of cadmium(II) chloride (oven-dried at 105° for 4 hr) was dissolved in water and made up to 1000 ml. Working solutions were prepared by suitable dilution.

NH_3–NH_4Cl buffer solution, pH = 8.5. Prepared by dissolving 40.0 g of ammonium chloride and 8.80 ml of concentrated ammonium hydroxide in water and diluting to 500 ml with water.

BPR, 1.00×10^{-3}M in 50% ethanol.
CV, 1.00×10^{-3}M in water.
PVA-124, 2.0% (w/v) in water.
Emulsifier OP, 1.0% (v/v) in water.

Procedures

NH_3–NH_4Cl buffer solution (pH = 8.5) 3.50 ml, 5.00 μg of cadmium standard, 0.80 ml BPR ($1.00 \times 10^{-3}M$), 1.00 ml CV ($1.00 \times 10^{-3}M$), 2.00 ml PVA-124 (2.0%) and 0.40 ml of emulsifier OP (1.0%) were added to a 25-ml calibrated flask (whilst mixing thoroughly), then diluted to the mark with water and mixed well. The resulting mixture was allowed to stand for 5 min, and then the absorbance was measured at 654 nm with a 1-cm cell against a reagent blank.

RESULTS AND DISCUSSION

Absorption spectra

The absorption spectra of the reagents and their cadmium(II) complex were measured over the range of 600–800 nm (see Fig. 1). The absorption maximum of the complex occurred at 654 nm.

Effect of pH

The method was examined in various pH buffer solutions, *e.g.* NH_3–NH_4Cl buffer solution (pH = 8.0, 8.5, 9.0, 9.5, 10.0), CH_3COOH–CH_3COONa buffer solution (pH = 4.7), NaH_2PO_4–Na_2HPO_4 (pH = 7.2). In all systems, pH = 8.5 seems optimal. The absorbance of the complex was maximal and constant when adding at least 2.00 ml of NH_3–NH_4Cl buffer solution (pH = 8.5) and was unstable below 2.00 ml, (the other reagent amounts were the same as described in Procedures), therefore 3.50 ml was selected as optimal.

Effect of amount of BPR and CV

When $1.00 \times 10^{-3}M$ BPR and CV were varied respectively from 0.40 to 1.00 ml and from 0.80 to 1.50 ml (the other reagent amounts were the same as in Procedures), the absorbance of the complex was maximal and constant, so use of 0.80 ml of BPR and 1.00 ml of CV were recommended for the determination.

Effect of PVA-124 and emulsifier OP

It has been reported[7] that an increase in detection sensitivity and stability results from the addition of some micromolecular compounds (PVA, arabic gum, *etc.*) and non-ionic surfactants (OP, Tween, *etc.*) to coloured ion-association complex systems. In the work presented here, the absorbance remains stable for 4 hr with PVA-124 and OP, but only 40 min without them. Also, a higher sensitivity system can be obtained by the addition of PVA-124 and OP (see Fig. 2). When PVA-124 (2.0%) and OP (1.0%) were varied respectively from 1.00 to 3.00 ml and from 0.20 to 0.50 ml, the absorbance of the complex was maximal and constant, so that the use of 2.00 ml of PVA-124 and 0.40 ml of OP was recommended.

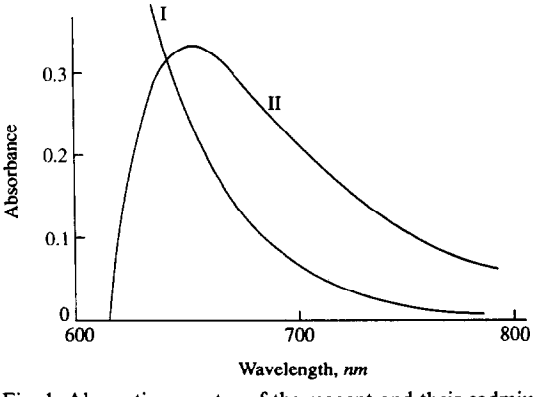

Fig. 1. Absorption spectra of the reagent and their cadmium(II) complexes, for 5 μg/25 ml Cd(II). Curve I: BPR–CV (agains water as reference). Curve II: Cd(II)–BPR–CV (against reagent as reference).

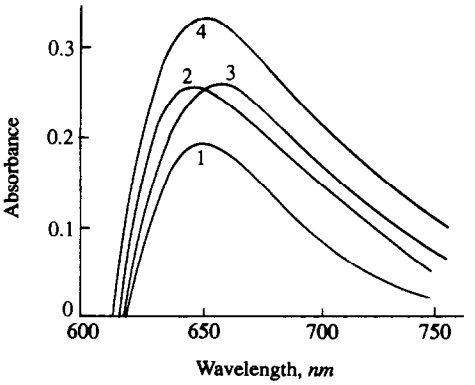

Fig. 2. Effect of PVA-124 and emulsifier OP on absorbance of the complex for 5 μg/25 ml Cd(II). Curve I: Cd–BPR–CV complex. Curve II: Cd–BPR–CV complex with PVA-124. Curve III: Cd–BPR–CV complex with OP. Curve IV: Cd–BPR–CV complex with both PVA-124 and OP.

Calibration curves

Beer's law was obeyed over the cadmium concentration range 0–10 μg/25 ml. The simple linear regression calibration equation can be represented by:

$$A = 0.064C + 0.0052 \ (C = \mu g/25 \text{ ml})$$

with a correlation coefficient of 0.9988. The apparent molar absorptivity obtained from the calibration equation was 1.79×10^5 $l.mole^{-1}.cm^{-1}$.

Detection limits

The detection limits, C_L, were determined by repeatedly measuring the absorbance of the blank solutions. The value of standard deviations of the blank measurements for a water sample was estimated by extrapolation after analysis of suitable samples containing low (less than 10 C_L) concentrations of cadmium, and for a high purity zinc sample not containing cadmium (less than C_L). From the standard deviations of the blank measurements, the detection limit (3 times the standard deviation of the blank) was 0.017 μg/ml for the water sample and 0.026 μg/ml for the zinc sample.

Interferences

The selectivity of the proposed method was investigated by determining 5.00 μg of cadmium in the presence of various other ions. The results indicated that K^+, Na^+, NH_4^+, NO_3^-, Cl^- and SO_4^{2-} do not interfere, even when present in large excess. The tolerable amounts of other diverse ions giving a maximum error of $\pm 4\%$ in the determination are summarized in Table 1.

The reaction mechanism and the composition of the complex

An increase in the absorption intensity of the cadmium complex results from synergistic chromophoric reactions by the double chromogenic reagents.[8] The apparent molar absorptivity of the Cd(II)–BPR–CV system was about twenty times that of the binary system [8.0×10^3 $l.mole^{-1}.cm^{-1}$ for the Cd(II)–BPR system].

The composition of the complex was studied by the molar-ratio,[9] slope-ratio[10] and logarithmic equilibrium shift methods.[11] A molar-ratio of Cd to BPR of 1:1 was found by both the molar-ratio and slope-ratio methods. The stoichiometry of the Cd and CV was studied by the logarithmic method of equilibrium shift. A 1:2 stoichiometric ratio of Cd to CV was observed. So the molar ratio of Cd to BPR and CV was Cd:BPR:CV = 1:1:2. From the composition of the complex and the reagent properties, it follows that the reaction may be presented by:

$$Cd^{2+} + BPR + 4OH^- = [Cd(BPR)]^{2-} + 4H_2O$$

$$[Cd(BPR)]^{2-} + 2CV^+ = [CV]_2[Cd(BPR)]$$

The structures of BPR and CV are as follows:

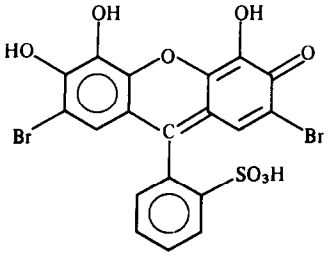

BPR

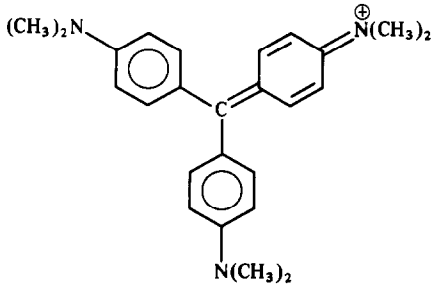

CV

Table 1. Influence of the diverse ions on the determination of cadmium(II), (5.0 μg/25 ml)

Tolerated ratio to Cd (w/w)	Ions	Tolerated ratio to Cd (w/w)	Ions
6	Hg^{2+}	60	Cu^{2+}*, Co^{2+}*, Fe^{3+}*
10	Mn^{2+}, Cr^{3+}, Cr^{6+}	100	As^{3+}, Ca^{2+}*, Mg^{2+}*
12	Mo^{6+}, Bi^{3+}*	180	PO_4^{3-}
20	Zn^{2+}, Ni^{2+}	200	Pb^{2+}, F^-
30	Sn^{2+}, Al^{3+}	2000†	Tartaric acid

*2.00 ml of 0.2*M* tartaric acid added.
†Maximum ratio tested.

Table 2. Results for determination of cadmium in water and zinc ($n = 5$)

Sample	Certified value, μg/ml	Determined value, μg/ml	Standard deviation
Synthetic water*	5.00	5.10	0.18
Waste water		1.13	0.083
Zinc	0.0160%†	0.0162%	0.054

*There were 5.00 μg of Cd and Hg(II), 10 μg of Fe(III), Cr(III), Pb(II), Mn(II), Cu(II), Zn(II), Co(II) and Ni(II) in 1 ml of synthetic water.
†Determined by AAS.

Table 3. Recovery of added cadmium

Sample	Cd taken, μg/25 ml	Cd added, μg/25 ml	Cd determined, μg/25 ml	Recovery, % Total	Added Cd
Synthetic water	5.00	1.00	5.90	98	90
		2.00	7.14	102	107
		3.00	8.47	106	116
		4.00	8.83	98	96
Zinc	1.62	1.00	2.83	108	121
		3.00	4.48	97	95
		5.00	6.88	103	105
		7.00	8.12	94	93

The coloured ion-association complex is a neutral complex with the following possible structure:

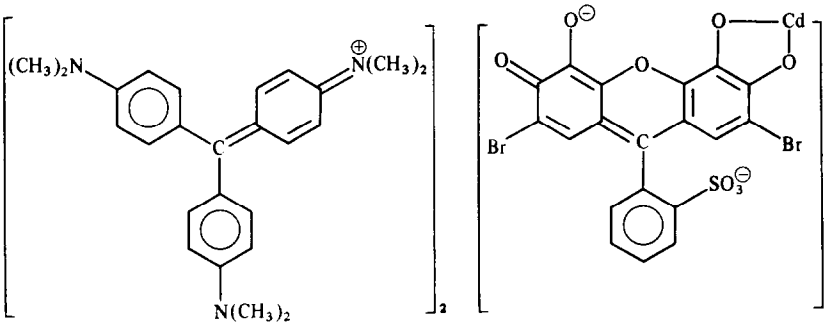

Application to water and zinc samples

The method was tested on water and zinc samples. The results are given in Table 2 and recovery of added cadmium is presented in Table 3.

The determination of trace cadmium in water

A volume of water sample (containing up to 10 μg of cadmium) was added to a 25-ml calibrated flask, and the pH was adjusted to 7 with ammonium hydroxide and hydrochloric acid (if necessary 2.00 ml of 0.02*M* tartaric acid was added). The remaining procedures were the same as that stated above.

The determination of trace cadmium in zinc

Sample solution of zinc: a 0.2000-g zinc sample was placed in a 50-ml beaker; and then 3 ml of hydrochloric acid (1:1) and 3 drops of hydrogen peroxide (30%) were added successively to the beaker. The resulting mixture was boiled for a few minutes, and then cooled and

transferred to a 100-ml standard flask, diluted to the mark with water and mixed.

Reagent blank solution of high purity zinc (Cd < 0.08 μg/g) The procedure was the same as for the sample solution, except that high purity zinc was used.

By pipette, a 10.00 ml portion of the zinc sample solution was added to a 25-ml calibrated flask (if necessary, 2.00 ml of 0.02*M* tartaric acid was added). The remaining procedures were the same as above.

CONCLUSION

The method is simple and convenient for the determination of cadmium in water and zinc samples. The results obtained show that the precision and accuracy are satisfactory.

REFERENCES

1. Q. H. Xu and Z. W. Zhou, *YunNan Metallurgy (Chinese)*, 1984, **3**, 57.
2. S. Yi, *Microchem. J.*, 1987, **36**, 386.
3. C. F. Ishak and R. T. Pflaum, *Analyst*, 1988, **113**, 941.
4. X. Ch. Qui, Y. Q. Zhu and J. P. Yan, *ibid.*, 1988, **113**, 1329.
5. S. J. Xu and L. P. Wan, *Analytical Laboratory (Chinese)*, 1989, **8**, 1.
6. W. Lu and X. W. Wu, *Environmental Chemistry (Chinese)*, 1987, **6**, 22.
7. W. B. Qi and H. SH. Luo, *Chemical Journal of Chinese Universities*, 1989, **10**, 197.
8. H. X. Shen and Y. Liu, *ibid.*, 1988, **9**, 897.
9. J. H. Yoe and A. L. Jones, *Ind. Eng. Chem., Anal. Ed.*, 1944, **16**, 111.
10. J. H. Yoe and A. E. Harvey, *J. Am. Chem. Soc.*, 1950, **17**, 648.
11. H. P. Tarasiewicz, A. Grudmiewska and M. Tarasiewicz, *Anal. Chim. Acta*, 1977, **94**, 435.

Talanta, Vol. 39, No. 6, pp. 649–652, 1992
Printed in Great Britain.

0039-9140/92 $5.00 + 0.00

ON THE DETERMINATION OF THE FREE CONCENTRATION OF LIGANDS

J. C. RODRIGUEZ PLACERES,* M. T. SANZ ALAEJOS and F. J. GARCIA MONTELONGO

Departments of Analytical Chemistry and Physical Chemistry, University of La Laguna, 38204-La Laguna, Tenerife, Canary Islands, Spain

(*Received* 27 *March* 1989. *Revised* 25 *October* 1991. *Accepted* 10 *November* 1991)

Summary—Working with a sufficient excess of any of the protonated forms of a ligand is shown to guarantee the validity of the determination of its free concentration when calculated by disregarding complexing effect. This result significantly extends the possibilities of studying the stability constants of co-ordination systems.

Many methods for determination of the stability constants of metal ion–ligand systems require previous knowledge of the concentration of the free ligand. Thus, it is necessary to work with a large excess of the ligand with respect to the metal ion in order that the free ligand concentration can be considered to be approximated by its total concentration. This requirement has greatly limited the analysis of many complexation equilibria, for which it was not feasible to work under such conditions.

An approach permitting this difficulty to be overcome is presented in this work.

THEORY

The presence of a ligand in solution with a metal ion will cause establishment of the corresponding complexation equilibria, together with those of protolytic reactions of the ligand. The equations which permit the calculation of the free concentration of the ligand must be determined.

The first case to be considered is the simplest, that of a monoprotic complexing species, X, capable of forming a single complex species, MX, with a metal ion, M. The equilibria to be considered are:

$$HX \rightleftharpoons H + X \quad K_a = \frac{[H][X]}{[HX]}$$

$$M + X \rightleftharpoons MX \quad \beta = \frac{[MX]}{[M][X]}$$

For simplicity, charges on species are omitted throughout.

The total concentration of ligand will be given by:

$$X_T = [X] + [HX] + [MX]$$

$$= [X] \times \left\{ \frac{K_a + [H] + K_a \dfrac{[MX]}{[X]}}{K_a} \right\}$$

which can be rearranged to:

$$X_T = [X] \left\{ \frac{[H] + K_a \left(1 + \dfrac{[MX]}{[X]} \right)}{K_a} \right\} \qquad (1)$$

from which the fractions of each ligand species can readily be determined, as a function of the total concentration of ligand:

$$\psi_0 = \frac{[HX]}{X_T} = \frac{[H]}{[H] + K_a \left(1 + \dfrac{[MX]}{[X]} \right)} \qquad (2)$$

$$\psi_1 = \frac{[X]}{X_T} = \frac{K_a}{[H] + K_a \left(1 + \dfrac{[MX]}{[X]} \right)} \qquad (3)$$

These equations allow the calculation of the free concentration of the ligand species in solution. However, their use for this purpose requires prior knowledge of the stability constants, the values of which are the object of the research requiring the knowledge of [X]. If no complexa-

*Author for correspondence.

Table 1

Values of $\frac{[X]'}{[X]} = \frac{[H] + K_a\left(1 + \frac{[MX]}{[X]}\right)}{[H] + K_a}$ for $\frac{[MX]}{[X]} = 100$

K_a \ [H]	10^0	10^{-2}	10^{-4}	10^{-6}	10^{-8}	10^{-10}
10^0	51	100	101	101	101	101
10^{-2}	1.990	51	100	101	101	101
10^{-4}	1.010	1.990	51	100	101	101
10^{-6}	1.000	1.010	1.990	51	100	101
10^{-8}	1.000	1.000	1.010	1.990	51	100
10^{-10}	1.000	1.000	1.000	1.010	1.990	51

Table 3

Values of $\frac{[X]'}{[X]} = \frac{[H] + K_a\left(1 + \frac{[MX]}{[X]}\right)}{[H] + K_a}$ for $\frac{[MX]}{[X]} = 1$

K_a \ [H]	10^0	10^{-2}	10^{-4}	10^{-6}	10^{-8}	10^{-10}
10^0	1.5	2	2	2	2	2
10^{-2}	1.010	1.5	2	2	2	2
10^{-4}	1.000	1.010	1.5	2	2	2
10^{-6}	1.000	1.000	1.010	1.5	2	2
10^{-8}	1.000	1.000	1.000	1.010	1.5	2
10^{-10}	1.000	1.000	1.000	1.000	1.010	1.5

tion is taken into account, equations (2) and (3) would reduce to:

$$\psi'_0 = \frac{[HX]'}{X_T} = \frac{[H]}{[H] + K_a} \tag{4}$$

$$\psi'_1 = \frac{[X]'}{X_T} = \frac{K_a}{[H] + K_a} \tag{5}$$

and utilization of these equations for calculation of the concentration of the ligand species does not require any knowledge about the formation constant of the complex. The conditions under which the simplest equations (4) and (5) can be applied to study of complexation constants without any significant error must be found, however.

Equating equations (3) and (5) for a given value of X_T gives

$$\frac{[X]'}{[X]} = \frac{[H] + K_a\left(1 + \frac{[MX]}{[X]}\right)}{[H] + K_a} \tag{6}$$

which relates the two concentrations [X] and [X]′. These two values will become closer as the quotient [MX]/[X] decreases. In the limit, where this quotient is zero (non-existence of complex), these concentrations would be equal. [X] and [X]′ will be closer, the greater the concentration of ligand with respect to that of the metal ion M.

However, the acidity constants of the ligand and of the pH of the medium will also have great influence on the final result. In order to visualize this triple dependence, values of [X]′/[X] for various values of each of these factors are shown in Tables 1–5, where the [X]′/[X] values have been rounded off from the computed values (*e.g.*, 1.00999900 to 1.010).

It can be seen that, for a marked excess of ligand, *i.e.*, [MX]/[X] = 0.01, the ratio [X]′/[X] is practically unity for any value of the acidity constant and the pH. When [MX]/[X] > 0.01, the deviation of [X]′/[X] from unity increases as [MX]/[X] increases.

For the particular case studied, working with excess of ligand ensures the validity of calculations of its free concentration from the simple equation (5), disregarding the complexing effect.

For the HX species, and from equations (2) and (4), the quotient between the "apparent" and "true" concentrations will be:

$$\frac{[HX]'}{[HX]} = \frac{[H] + K_a\left(1 + \frac{[MX]}{[X]}\right)}{[H] + K_a} \tag{7}$$

which is identical with equation (6), indicating that the relative error of the determination of the concentration of both these ligand species is

Table 2

Values of $\frac{[X]'}{[X]} = \frac{[H] + K_a\left(1 + \frac{[MX]}{[X]}\right)}{[H] + K_a}$ for $\frac{[MX]}{[X]} = 10$

K_a \ [H]	10^0	10^{-2}	10^{-4}	10^{-6}	10^{-8}	10^{-10}
10^0	6	10.9	11	11	11	11
10^{-2}	1.100	6	10.9	11	11	11
10^{-4}	1.001	1.100	6	10.9	11	11
10^{-6}	1.000	1.001	1.100	6	10.9	11
10^{-8}	1.000	1.000	1.001	1.100	6	10.9
10^{-10}	1.000	1.000	1.000	1.001	1.100	6

Table 4

Values of $\frac{[X]'}{[X]} = \frac{[H] + K_a\left(1 + \frac{[MX]}{[X]}\right)}{[H] + K_a}$ for $\frac{[MX]}{[X]} = 0.1$

K_a \ [H]	10^0	10^{-2}	10^{-4}	10^{-6}	10^{-8}	10^{-10}
10^0	1.05	1.100	1.100	1.100	1.100	1.100
10^{-2}	1.001	1.05	1.100	1.100	1.100	1.100
10^{-4}	1.000	1.001	1.05	1.100	1.100	1.100
10^{-6}	1.000	1.000	1.001	1.05	1.100	1.100
10^{-8}	1.000	1.000	1.000	1.001	1.05	1.100
10^{-10}	1.000	1.000	1.000	1.000	1.001	1.05

Table 5.

Values of $\frac{[X]'}{[X]} = \frac{[H] + K_a\left(1 + \frac{[MX]}{[X]}\right)}{[H] + K_a}$ for $\frac{[MX]}{[X]} = 0.01$

K_a \ [H]	10^0	10^{-2}	10^{-4}	10^{-6}	10^{-8}	10^{-10}
10^0	1.005	1.010	1.010	1.010	1.010	1.010
10^{-2}	1.000	1.005	1.010	1.010	1.010	1.010
10^{-4}	1.000	1.000	1.005	1.010	1.010	1.010
10^{-6}	1.000	1.000	1.000	1.005	1.010	1.010
10^{-8}	1.000	1.000	1.000	1.000	1.005	1.010
10^{-10}	1.000	1.000	1.000	1.000	1.000	1.005

the same. This result could be expected since [X] and [HX] are related by the acidity constant, K_a.

An excess of X relative to M allows [HX] to be calculated by the simplified equation (4) irrespective of its actual value; this is surprising, since it would be intuitively expected that if no excess of the HX species exists with respect to M, the complexation equilibrium in which X is involved could significantly affect [HX]′. The reason, of course, is that the M–X–H system behaves as a buffer system over a certain range of concentration ratios.

A similar conclusion may be reached by expressing equations (2) and (3) as a function of [HX] instead of [X], by using the expression for K_a, thus:

$$\psi_0 = \frac{[HX]}{X_T} = \frac{[H]}{[H] + K_a + K_a\frac{[MX][H]}{K_a[HX]}} = \frac{[H]}{[H]\left(1 + \frac{[MX]}{[HX]}\right) + K_a} \tag{8}$$

$$\psi_1 = \frac{[X]}{X_T} = \frac{K_a}{[H] + K_a + K_a\frac{[MX][H]}{K_a[HX]}} = \frac{K_a}{[H]\left(1 + \frac{[MX]}{[HX]}\right) + K_a} \tag{9}$$

These equations yield

$$\frac{[HX]'}{[HX]} = \frac{[H]\left(1 + \frac{[MX]}{[HX]}\right) + K_a}{[H] + K_a} \tag{10}$$

and

$$\frac{[X]'}{[X]} = \frac{[H]\left(1 + \frac{[MX]}{[HX]}\right) + K_a}{[H] + K_a} \tag{11}$$

from which the same considerations as before can be established, when a sufficient excess of [HX] is present relative to the concentration of metal ion.

That is, it is sufficient to work with an excess, relative to M, of the protonated ligand form, HX, in order to determine accurately the true free concentration of X, by way of the simplified equation [5], which does not take into account the complexation equilibrium.

Therefore, an excess of the free ligand under study, [X], with respect to the metal ion M, is unnecessary, for the true concentration [X] to be calculable by means of the simplified equation (5), irrespective of its value. Even if [X] is much smaller than the total concentration of the metal ion, $[X] \ll [M]_{total}$, the true value of [X] can be calculated, provided that the concentration of HX, which itself does not complex M, is in sufficient excess relative to $[M]_{total}$.

The equations for more complex systems are presented in Tables 6–9. In all these cases it can be proved that the considerations shown above for the simplest system are valid. Thus a simple method is established for calculating the free concentrations of all the possible species of a substance susceptible to multiple protonation, and hence for studying co-ordination systems without the need to work with excess of the complexing ligand form. To this end, it is sufficient that the concentration of any one of the ligand species or, in general, the total concentration, X_T, is much greater than that of the metal ion.

It is evident that this result has many applications in the study of metal-ion complexes and would allow study of systems which have not been analysed until now because of the limitations imposed by the impossibility of working with excess of free ligand. It also opens up the possibility of more readily studying mixed-ligand complexes with different complexing species present in the protonation equilibria.

Table 6. Monoprotic system, with species HX and X, and formation of the complexes MX and MX_2

$$\frac{[X]'}{[X]} = \frac{[HX]'}{[HX]} = \frac{[H] + K_a\left(1 + \frac{[MX]}{[X]} + 2\frac{[MX_2]}{[X]}\right)}{[H] + K_a}$$

$$\frac{[X]'}{[X]} = \frac{[HX]'}{[HX]} = \frac{K_a + [H]\left(1 + \frac{[MX]}{[HX]} + 2\frac{[MX_2]}{[HX]}\right)}{K_a + [H]}$$

Table 7. Diprotic system, with species H_2X, HX and X, and formation of the complexes MX and MHX

$$\frac{[X]'}{[X]}=\frac{[HX]'}{[HX]}=\frac{[H_2X]'}{[H_2X]}=\frac{[H]^2+K_{a1}[H]+K_{a1}K_{a2}\left(1+\frac{[MX]}{[X]}+\frac{[MHX]}{[X]}\right)}{[H]^2+K_{a1}[H]+K_{a1}K_{a2}}$$

$$\frac{[X]'}{[X]}=\frac{[HX]'}{[HX]}=\frac{[H_2X]'}{[H_2X]}=\frac{[H]^2+K_{a1}K_{a2}+K_{a1}[H]\left(1+\frac{[MX]}{[HX]}+\frac{[MHX]}{[HX]}\right)}{[H]^2+K_{a1}K_{a2}+K_{a1}[H]}$$

$$\frac{[X]'}{[X]}=\frac{[HX]'}{[HX]}=\frac{[H_2X]'}{[H_2X]}=\frac{K_{a1}K_{a2}+K_{a1}[H]+[H]^2\left(1+\frac{[MX]}{[H_2X]}+\frac{[MHX]}{[H_2X]}\right)}{K_{a1}K_{a2}+K_{a1}[H]+[H']^2}$$

Table 8. Diprotic system, with species H_2X, HX and X, and formation of the complexes MX, MX_2, MHX, $M(HX)_2$ and M(HX)X

$$\frac{[X]'}{[X]}=\frac{[HX]'}{[HX]}=\frac{[H_2X]'}{[H_2X]}=\frac{[H]^2+K_{a1}[H]+K_{a1}K_{a2}\left(1+\frac{[MX]}{[X]}+2\frac{[MX_2]}{[X]}+\frac{[MHX]}{[X]}+2\frac{[M(HX)_2]}{[X]}+2\frac{[M(HX)X]}{[X]}\right)}{[H]^2+K_{a1}[H]+K_{a1}K_{a2}}$$

$$\frac{[X]'}{[X]}=\frac{[HX]'}{[HX]}=\frac{[H_2X]'}{[H_2X]}=\frac{K_{a1}K_{a2}+[H]^2+K_{a1}[H]\left(1+\frac{[MX]}{[HX]}+2\frac{[MX_2]}{[HX]}+\frac{[MHX]}{[HX]}+2\frac{[M(HX)_2]}{[HX]}+2\frac{[M(HX)X]}{[HX]}\right)}{K_{a1}K_{a2}+[H]^2+K_{a1}[H]}$$

$$\frac{[X]'}{[X]}=\frac{[HX]'}{[HX]}=\frac{[H_2X]'}{[H_2X]}=\frac{K_{a1}K_{a2}+K_{a1}[H]+[H]^2\left(1+\frac{[MX]}{[H_2X]}+2\frac{[MX_2]}{[H_2X]}+\frac{[MHX]}{[H_2X]}+2\frac{[M(HX)_2]}{[H_2X]}+2\frac{[M(HX)X]}{[H_2X]}\right)}{K_{a1}K_{a2}+K_{a1}[H]+[H]^2}$$

Table 9. General equation

$$\frac{[X]'}{[X]}=\frac{[HX]'}{[HX]}=\cdots=\frac{[H_NX]'}{[H_NX]}=\frac{[H]^N+K_{a1}[H]^{N-1}+K_{a1}K_{a2}[H]^{N-2}+\cdots+K_{a1}K_{a2}\cdots K_{a(N-1)}[H]+K_{a1}K_{a2}\cdots K_{aN}(1+C)}{[H]^N+K_{a1}[H]^{N-1}+K_{a1}K_{a2}[H]^{N-2}+\cdots+K_{a1}K_{a2}\cdots K_{a(N-1)}[H]+K_{a1}K_{a2}K_{a3}\cdots K_{aN}}$$

where

$$C=\left\{\frac{[MX]}{[X]}+2\frac{[MX_2]}{[X]}+3\frac{[MX_3]}{[X]}+\cdots\right\}+\left\{\frac{[M(HX)]}{[X]}+2\frac{[M(HX)_2]}{[X]}+3\frac{[M(HX)_3]}{[X]}+\cdots\right\}$$
$$+\left\{2\frac{[MX(HX)]}{[X]}+3\frac{[MX(HX)_2]}{[X]}+4\frac{[MX(HX)_3]}{[X]}+\cdots\right\}+\left\{3\frac{[MX_2(HX)]}{[X]}+4\frac{[MX_2(HX)_2]}{[X]}+5\frac{[MX_2(HX)_3]}{[X]}+\cdots\right\}$$
$$+\left\{\frac{[M(H_2X)]}{[X]}+2\frac{[M(H_2X)_2]}{[X]}+3\frac{[M(H_2X)_3]}{[X]}+\cdots\right\}+\cdots$$

Finally, a general equation is presented for the case of polyprotic systems, with formation of complexes with each of the possible complexing species X, HX . . . , and their corresponding mixed complexes.

Acknowledgements—The authors acknowledge financial support of this work by CAICYT (Spain), grant no. 0663/82. One of them (M.T.S.A) would like to thank the Cabildo Insular de Tenerife for a Scholarship.

Talanta, Vol. 39, No. 6, pp. 653–657, 1992
Printed in Great Britain

0039-9140/92 $5.00 + 0.00
Pergamon Press Ltd

ION EXCHANGE BEHAVIOUR OF HYDROUS TIN OXIDE: KINETICS OF ANION EXCHANGE

I. M. EL-NAGGAR,* E. I. SHABANA and M. I. EL-DESSOUKY
Nuclear Chemistry Department, Nuclear Research Centre, Atomic Energy Authority, Atomic Energy Post Office 13759, Cairo, Egypt

(*Received* 18 *February* 1991. *Revised* 11 *July* 1991. *Accepted* 30 *August* 1991)

Summary—The kinetic behaviour of Cl^-, Br^- and SCN^- exchanges on hydrous tin oxide have been investigated under conditions of particle diffusion and the limited bath technique. Values for the diffusion coefficients, energy of activation and entropy of activation have been calculated. The data obtained have been compared with those reported for other organic and inorganic exchangers.

Hydrous oxides exhibit a high selectivity to some elements and their exchanging properties are often connected with a fairly good stability towards high temperature and ionizing radiations. The factors underlying the behaviour of hydrous oxides as ion exchangers are not clearly understood and contradictory data are often obtained.[1,2] Various works have been carried out to clarify different aspects of the ion exchange behaviour of hydrous oxides. Towards this goal, several studies have been carried out on the ion exchange properties of hydrous tin(IV) oxide,[3–14] for which various composition and ion exchange characteristics have been reported by different investigators, whereas hydrous tin(IV) oxide has been shown to have anionic and cationic ion exchange properties in acidic and alkaline media, respectively.[5–15] Though some kinetic studies have been performed in this laboratory on hydrous oxides;[16–18] such studies on inorganic ion exchangers are generally lackadaisical.[2]

In the present paper, the kinetics of exchange of Cl^-, Br^- and SCN^- with OH^- on hydrous tin oxide are described, and the thermodynamic parameters for the exchange are calculated. The data obtained for this material are compared with those for organic resins and other inorganic exchangers.

EXPERIMENTAL

Reagents

Boiled distilled water and analytical grade chemicals were used.

Hydrous tin oxide. Hydrous tin oxide was prepared by acidification of a sodium stannate solution with nitric acid, followed by treatment of the obtained precipitate with 0.1*M* nitric acid and finally by a prolonged washing with distilled water. After washing, the sample was dried at 50°, immersed in hot water to remove the trapped air, redried at 50°, and stored in a nitrogen atmosphere over saturated ammonium chloride solution.

Kinetic measurements

The radius of the particle of the sieved fractions was determined by measuring the diameter of 100 particles with an optical microscope. The particles were assumed to be spherical and the mean equivalent radius was calculated.

Rates of exchange were determined by the "limited bath technique". A certain weight of the OH^--form of the exchanger was shaken in a thermostatic bath at the desired temperature with a certain volume of (NaX + HX) solution (X = Cl^- or Br^-) of 0.11*M* total halide molarity and 0.01*M* acid concentration. Experiments with SCN were performed at nitric acid and sodium thiocyanate concentrations of 0.01 and 0.1*M*, respectively. The experiments were conducted at a volume of 25 ml/g of solid. After measured time intervals, samples of the supernatant solution were removed for analysis to determine the extent of exchange. The experiments were conducted at 30, 45 and 60° (±1°). In kinetic experiments the results agreed to ±6% for reaction times ≤one minute. At higher reaction times, a better agreement of ±3% was obtained.

*Author for correspondence.

Analysis

The concentration of Cl^-, Br^- and SCN^- ions was determined by volumetric analysis with a standard solution of silver nitrate.[19] Duplicates of the experiments have shown that the results are reproducible to $\pm 3\%$.

RESULTS AND DISCUSSION

Under the conditions of particle diffusion control, a relatively large particle size of the exchanger and vigorous shaking, the following equation applied, provided that the particle diffusion is the rate controlling mechanism.[20]

$$F(t) = 1 - \frac{6}{\pi^2} \sum_{n=1}^{\infty} \frac{1}{n^2} \exp(-n^2 Bt). \qquad (1)$$

where $F(t)$ is the fractional attainment of equilibrium, n is an integer, $B = \pi^2 D_i / r^2$, in which D_i is the effective diffusion coefficient of the exchanging ion inside the exchanger and r is the radius of the particle. When $F(t)$ is less than about 0.4, equation (1) can be approximated to a simpler form.[21]

$$F(t) = \frac{6}{r} (D_i t/\pi)^{1/2} \qquad (2)$$

which hold to a fairly good approximation. Therefore, a plot of $F(t)$ against the square root of the contact time must give a straight line passing through the origin in the region in which $F(t)$ is less than 0.4.

The study of the effect of concentration on the rate of exchange for Cl^-/OH^- at 30° showed that at concentrations higher than $0.05M$, the rate was independent of the concentration of solutions; the straight lines between $F(t)$ and $t^{1/2}$ had the same slope within the experimental errors. When the chloride ion concentration was $0.01M$, however, the rate was much slower than that obtained for the solutions $\geqslant 0.05M$. In addition, linearity between $F(t)$ and $t^{1/2}$ did not hold. These facts show that at $0.11M$ concentration (generally used in this work) of Cl^-, particle diffusion is the controlling mechanism and film diffusion can be excluded.[20]

The plots *Bt vs. t* for the exchange of Cl^-, Br^- and SCN^- on hydrous stannic oxide at different conditions are given in Figs. 1–4. These figures show that straight lines passing through the origin are obtained, which is further proof of a particle diffusion mechanism. The *Bt–t* plots were used instead of equation (2), because the fast rate of the exchange reaction causes a decrease in the number of experimental points falling within the limit of the validity of the equation [$F(t) \leqslant 0.4$]; due to a technical difficulty.

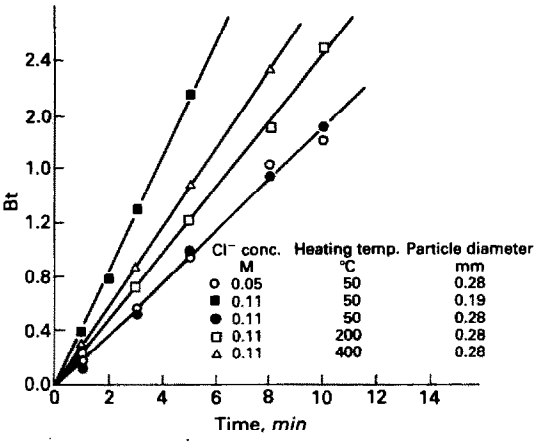

Fig. 1. *Bt vs. t* plots for exchange of Cl^- at 30° on hydrous tin oxide at different conditions.

The effect of the particle size on the rate of exchange for $0.11M$ Cl^- concentration is shown in Fig. 1. Here, *Bt* values were calculated from the measured values of $F(t)$ by using the equation derived by Reichenberg:[22]

$$Bt = 2\pi - \pi^2 3F(t) - 2\pi[1 - \frac{\pi}{3} F(t)]^{1/2} \qquad (3)$$

This equation gives a fairly good approximation in the region where $F(t)$ is less than 0.85.[22] Figure 1 shows that the rate of exchange of Cl^- ion on hydrous tin oxide increases with the decrease of particle diameter, although the effective diffusion coefficients are approximately

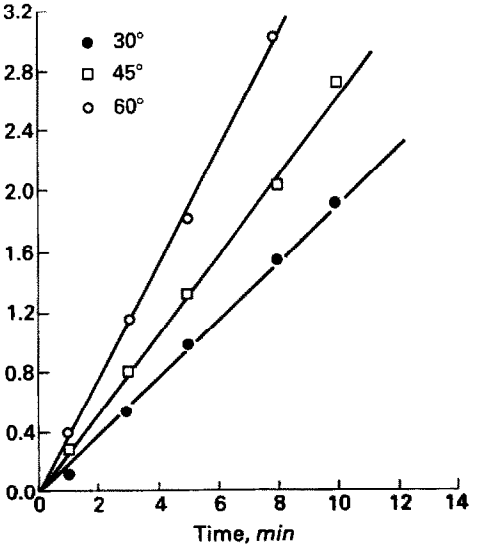

Fig. 2. *Bt vs. t* plots for exchange of Cl^- at different temperatures on hydrous tin oxide.

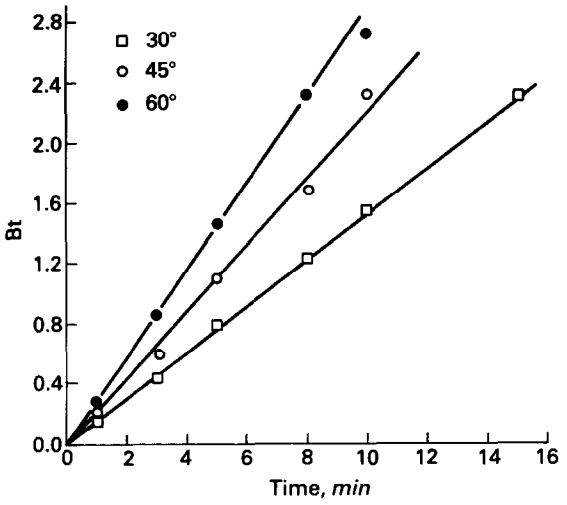

Fig. 3. *Bt vs. t* plots for exchange of Br^- at different temperatures on hydrous tin oxide.

constant (Table 1). This indicates that under these conditions, the rate-determining step is diffusion through the particles.

Figure 1 and Table 1 show an appreciable increase of D_i with an increase in the heating temperature from 50 to 400°. The heating of the same sample of hydrous tin oxide[13,23] increases the porosity and pore size, crystallinity and the pK value of the base behaviour of the remained active sites, due to condensation of the surface OH groups, but decreases the surface area and the pK value of the acid behaviour of these sites (OH groups), in addition to the reduction or elimination of water molecules inside the matrix. The increase of the pK value of the base behaviour decreases the mobility inside the

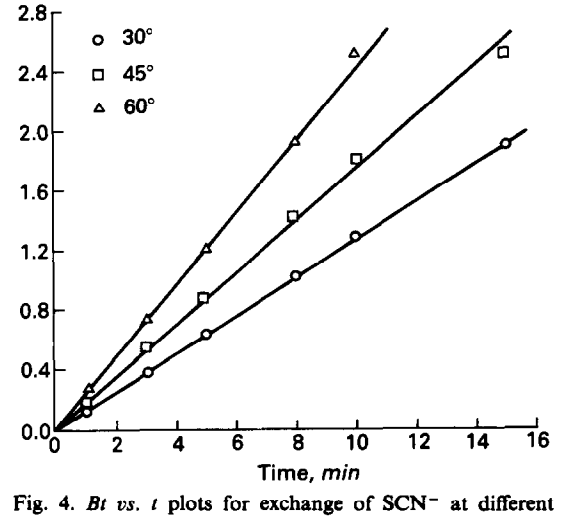

Fig. 4. *Bt vs. t* plots for exchange of SCN^- at different temperatures on hydrous tin oxide.

Table 1. Effective diffusion coefficients at 30° of Cl^- exchange system in hydrous tin oxide at different conditions

Initial Cl^- conc., M	Heating temp. of solid, °C	Particle diameter, *mm*	D_i ($\times 10^{12}$), m^2/sec
0.11	50	0.28 ± 0.025	6.63
0.06	50	0.28 ± 0.025	6.63
0.11	50	0.19 ± 0.03	6.41
0.11	200	0.28 ± 0.025	8.28
0.11	400	0.28 ± 0.025	8.84

particles due to the increase of electrostatic interaction between the anion and the exchange sites.[13] This is not the case and this effect is minor compared to effects of porosity, pore size and crystallinity. Higher porosity means more free water inside the structure which facilitates ion diffusion.[24] The results of the porous texture[13] showed that the most probable hydraulic pore radius, r_h, for the sample dried at 50° is about 0.5 nm, while some widening of the pores occurs at 100–200°, where r_h is around 0.7 nm. This means, the increase of the exchanger rate for the sample heated at 200° may be partly due to the increase of r_h from about 0.5 to 0.7 nm. The further increase of the exchange rate for a sample heated at 400° may be partly due to the further increase of the diffusion coefficient produced by the increase of r_h to about 2.5 nm. Also, the X-ray diffraction patterns of the same sample[13] showed that the crystallinity increases with an increase in heating temperature which may be due to the gradual growth of particles. If the retarding effect of pore walls on the diffusion of ions is small in a well-ordered exchanger matrix, the effective diffusion coefficient of ions may be increased by crystallization of the material. As an example, Nancollas reported that the effective diffusion coefficient of sodium ions in hydrous thorium(IV) oxide was increased by the crystallization of the matrix.[25] Therefore, it may be stated that the porous texture together with the crystallinity have the more important roles of determining the ion mobility inside the matrix.

The initial pH of the solution changes with time during the ion exchange process; this is due to the anion uptake by the solid being accompanied by the release of OH^- in solution. At equilibrium, the pH has a constant value (final pH) which gives an indication about the ion exchange process and the ion uptake in the solid. The percent uptake of Cl^- at 30° on hydrous tin oxide at different

Table 2. Sorption and pH variation at 30° for uptake of Cl^- by hydrous tin oxide under various conditions at liquid: solid ratio (V/m) 25 ml/g

Initial Cl^- conc., M	Initial pH	Heating temp. of solid, °C	Final pH	% Uptake
0.11	2.02	50	2.23	3.37
0.06	2.01	50	2.20	5.96
0.11	2.02	200	2.18	2.73
0.11	2.02	400	2.12	1.88

conditions is given in Table 2. This table shows an increase in pH values due to the release of OH^- ions in solution, since hydrous tin oxide behaves as an anion exchanger in acidic solutions.[5,6,15,23]

The plots of Bt *vs.* t for the exchange of Cl^-, Br^- and SCN^- on hydrous tin oxide dried at 50° are given in Figs. 2, 3 and 4, respectively, for the particle diameter 0.28 ± 0.02 mm at the reaction temperatures 30, 40 and 60°. It is seen from these figures that straight lines passing through the origin are obtained in all cases. The values of D_i obtained under the different conditions are given in Table 3.

The values of the diffusion coefficient obtained (Table 3) for Cl^- and Br^- on hydrous tin oxide are less than that obtained for a strongly anionic resin,[26] but much higher than those for hydrous ceria.[27] On polystyrene resin, D_i for Cl^- and Br^- are reported to be 4.89×10^{-7} and 3.92×10^{-7} cm²/sec, respectively.[26] For hydrous ceria, however, the values of the effective diffusion coefficients are much smaller and are reported to be 42×10^{-10} and 94×10^{-10} cm²/sec for Cl^- and Br^-, respectively.[27] The D_i value of Cl^- at 30° on zirconia, given by Misak *et al.*[28], is 7.8×10^{-8} cm²/sec. Thus, the comparison of the values of the diffusion coefficient reported herein with those of organic resins and other inorganic exchangers indicates that hydrous tin oxide gives rates of exchange less than those of strongly anionic resins but nearly equal to those for some inorganic exchangers.

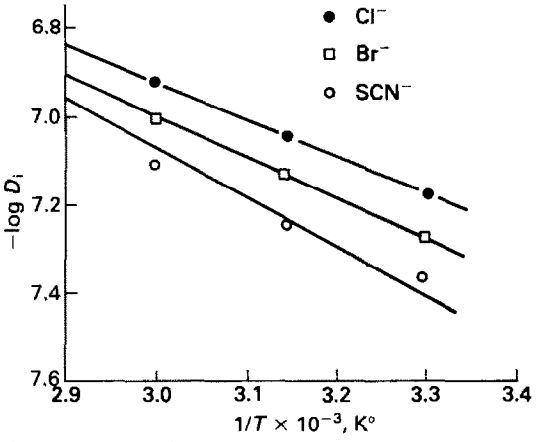

Fig. 5. Arrhenius plots for exchange of Cl^-, Br^- and SCN^- on hydrous tin oxide.

When log D_i is plotted against $1/T$ (Fig. 5), straight lines are obtained, enabling the energy of activation (E_a) and the pre-exponential constant (D_o) to be estimated from an Arrhenius equation

$$D_i = D_o \exp(-E_a/RT)$$

The entropy of activation ($\Delta\overset{*}{S}$) can then be calculated from D_o by substituting in the equation proposed by Barrer *et al.*[29]

$$D_o = 2.72\,(KTd^2/h) \exp(\Delta\overset{*}{S}/R),$$

where K is the Boltzmann constant, T is 273K, d is the average distance between two successive positions in the process of diffusion which was taken as 0.5 mm and h is Planck's constant.

Comparing the diffusion coefficient values (Table 3) at any given temperature it is seen that these are always in the order, $SCN^- < Br^- < Cl^-$. Activation energy values are in the order $SCN^- > Br^- > Cl^-$. It is to be noted that electron affinity follows the reverse of the latter trend; the respective values for the above ions being 209, 329 and 348 kJ/mole. The negative values for the entropy of activation given in Table 3, suggest that upon exchange of these anions no significant structural change occurs in hydrous tin oxide.

Table 3. Diffusion coefficients and other thermodynamic parameters calculated for the exchange of some anions on hydrous tin oxide dried at 50°

System	Diffusion coefficients D_i (× 10^{12}), m^2/sec 30°	45°	60°	D_o (× 10^9), m^2/sec	E_a, $kJ/mole$	ΔS^*, $J\,°C^{-1}\,mole^{-1}$
Cl^-/OH^-	6.63	8.84	12.00	4.11	16.20	−56.94
Br^-/OH^-	5.30	7.36	9.47	5.29	17.40	−54.84
SCN^-/OH^-	4.28	5.68	7.80	32.70	22.53	−39.69

REFERENCES

1. V. Vesely, V. Pekonek, *Talanta*, 1972, **19**, 219.
2. A. Clearfield, *Inorganic Ion Exchange Materials*, CRC Press, Boca Raton, Florida, 1982.
3. K. A. Kraus, H. V. Philips, T. A. Carlson and J. S. Johnson, *Prog. Int. Conf. on Peaceful Use of Atomic Energy*, 1958, **28**, 3.
4. E. Merz, *Z. Electrochem.*, 1959, **63**, 288.
5. J. D. Donaldson, and M. J. Fuller, *J. Inorg. Nucl. Chem.*, 1968, **30**, 1083, 2841.
6. *Idem*, *ibid.*, 1970, **32**, 1703.
7. P. C. Ho, F. Nelson and K. A. Kraus, *J. Chromatog.*, 1976, **147**, 263.
8. Y. Inoue and H. Yamazaki, *Bull. Chem. Soc. Jpn.*, 1982, **55**, 3782.
9. N. Z. Misak, H. N. Salama and I. M. El-Naggar, *Chemica Scripta*, 1983, **22**, 74.
10. *Idem*, *ibid.*, 1984, **23**, 34.
11. N. Z. Misak and I. M. El-Naggar, *Reactive Polymers*, 1988, **8**, 161.
12. I. M. El-Naggar, H. B. Maghrawy, N. Z. Misak and N. Sh. Petro, *Materials Science*, 1988, **XIV**, 3.
13. N. Sh. Petro, I. M. El-Naggar, E. I. Shabana and N. Z. Misak, *Colloids and Surfaces*, 1990, **49**, 219.
14. I. M. El-Naggar and E. I. Shabana, *ibid.*, 1991, in the press.
15. M. Abe and T. Ito, *Nippon Kagaku Zasshi*, 1965, **86**, 1259.
16. I. M. El-Naggar and H. B. Maghrawy, *J. Radio. Anal. Nucl. Chem., Articles*, 1987, **116**, 325.
17. N. Z. Misak and I. M. El-Naggar, *Reactive Polymers*, 1989, **10**, 67.
18. N. Z. Misak, I. M. El-Naggar, H. B. Maghrawy, H. F. Ghomeimy and N. Sh. Petro *(IAEA-TECDOC-350) IAEA*, Vienna, 1985.
19. A. I. Vogel, *A Text-Book for Quant. Inorg. Analysis*, Longmans, London, 1961.
20. F. Helfferich, *Ion Exchange*. McGraw–Hill, New York, 1962.
21. G. E. Boyd, A. W. Adamson and L. S. Myers, *J. Am. Chem. Soc.*, 1947, **69**, 2836.
22. D. Reichenberg, *ibid.*, 1953, **75**, 589.
23. E. I. Shabana, *Ion Exchange Characteristics of Hydrous Tin Oxide*, Ph.D. Thesis, Ain Shams University, Cairo, 1987.
24. H. O. Sharma, R. E. Servis and L. W. McMillen, *J. Phys. Chem.*, 1970, **74**, 969.
25. G. H. Nancollas and R. Paterson, *J. Inorg. Nucl. Chem.*, 1961, **22**, 259.
26. V. G. Dedgaonker and C. M. Bhavsar, *Int. J. Appl. Rad. Isotopes*, 1981, **12**, 895.
27. N. Z. Misak and E. M. Mikhail, *J. Appl. Chem. Biotechnol.*, 1978, **28**, 499.
28. N. Z. Misak and H. F. Ghoneimy, *J. Chem. Tech. Biotechnol.*, 1982, **32**, 709.
29. R. M. Barrer, R. F. Barthalomew and L. V. C. Rees, *J. Phys. Chem. Solids*, 1961, **12**, 12.

Talanta, Vol. 39, No. 6, pp. 659–663, 1992
Printed in Great Britain.

0039-9140/92 $5.00 + 0.00

ORGANOPHOSPHORUS REAGENTS AS EXTRACTANTS—PART 3. SYNERGIC EFFECT OF TRIPHENYL PHOSPHINE OXIDE AND BIS(DIPHENYL PHOSPHINYL) ALKANES ON EXTRACTION OF IRON(III) FROM THIOCYANATE MEDIUM WITH 2,4-PENTDIONE

TARLOK S. LOBANA* and PUSHVINDER K. BHATIA
Department of Chemistry, Guru Nanak Dev University, Amritsar-143005, India

(*Received* 8 *March* 1991. *Revised* 20 *June* 1991. *Accepted* 26 *August* 1991)

Summary—The extraction of iron(III) from thiocyanate medium was carried out with a synergic combination of 2,4-pentdione (Hacac) and either triphenyl phosphine oxide (Ph_3PO) or *bis* (diphenylphosphinyl) alkanes, $Ph_2P(O)(CH_2)_n \cdot P(O)Ph_2$ [ligand abbreviation, n: $dpeO_2$, 2; $dpbO_2$, 4]. Iron(III) was quantitatively separated from its binary mixture with chromium(III), manganese(III), cobalt(II), nickel(II), zinc(II), cadmium(II), mercury(II), lead(II), magnesium(II) and from steel samples. Copper(II) and silver(I) however, interfered. The percentage extraction was 99.0%. The respective extraction constants, K_{HA}, K_L or K_{syn}, for the extracted species, $[Fe(NCS)(acac)_2(H_2O)]$ (HA = Hacac), $Fe(NCS)_3L_2$ [L = Ph_3PO, $dpeO_2$ or $dpbO_2$], or $Fe(NCS)(acac)_2L$ were found to be: K_{HA}, 1.48×10^3, K_L, 1.80×10^2 (L = Ph_3PO), 2.02×10^2 (L = $dpeO_2$ or $dpbO_2$) and K_{syn} 1.87×10^6 (L = Ph_3PO), 2.56×10^6 [L = $dpeO_2$ or $dpbO_2$].

Trioctyl phosphine oxide (TOPO) acts as a synergist in the extraction of iron(III), using 1-phenyl-3-methyl-4-(trifluoroacetyl) pyrazole-5-one from aqueous solution (pH 1.5–2.8).[1] Similarly, TOPO–Hacac extracts iron(III) in the presence of perchlorate ions.[2,3] However, no efforts have been made for the separation of iron(III) from various binary, ternary mixtures or steel samples with these reagents. Organophosphorus reagents with aryl substituents on phosphorus are believed to be better extractants than those with alkyl groups.[4]

Recently, we have reported the extraction of silver(I) with Ph_3PO[5] and also used Ph_3PO as a synergist in the extraction of cobalt(II)/zinc(II) with 8-hydroxyquinoline.[6] This paper reports a new and novel method for separating iron(III) from a series of binary mixtures and steel samples, using a simple and readily available combination of Ph_3PO with Hacac. The extraction ability of Ph_3PO is compared with those of its bis (tertiary phosphine oxide) analogues, $Ph_2P(O)(CH_2)_nP(O)Ph_2$ (n = 2,4). The synergic potential of thiocyanate induced extraction of iron(III) with mixed-reagents was demonstrated recently.[7]

*Author for correspondence.

EXPERIMENTAL

Reagents and apparatus

Ammonium ferrous sulphate (Mohr salt) and potassium thiocyanate (KSCN) were of analytical grade and were purchased from Glaxo, Bombay. 2,4-Pentdione (Hacac) and triphenyl phosphine (Ph_3P) were purchased from Sisco-Chem-Industry, Bombay and used as received. 1,2-Ethylene bis(diphenylphosphine) (dpe) and 1,4-butylenebis (diphenyl phosphine) (dpb) were prepared and purified by the literature procedure.[8] All the metal salts were of laboratory reagent grade and were standardized before use. The phosphine oxides, Ph_3PO, $dpeO_2$ and $dpbO_2$, were prepared by oxidation of the corresponding phosphines with potassium permanganate in acetone.[9] Spectrophotometric measurements were made with a Shimadzu UV–visible (UV-240) recording spectrophotometer.

Stock solutions

A stock solution of iron(III) for extraction/calibration containing 10 mg of Fe per 100 ml was prepared from ferrous ammonium sulphate (0.070 g, $1.79 \times 10^{-3}M$) by treating it with 5 ml of concentrated nitric acid followed by the addition of 3.884 g of potassium thiocyanate

(0.4M after removal of the acid) and dilution to 100 ml. The pH of the solution was 2.77–2.80. Alternatively, the stock solution of iron(III) can be made by treating 0.070 g of Mohr salt with 5 ml of 30% hydrogen peroxide. Evaporate to dryness, add 0.5 ml of concentrated hydrochloric acid and 10 ml of distilled water. Then add potassium thiocyanate as above and make up to 100 ml. Similarly, stock solutions of Hacac, Ph_3PO, $dpeO_2$ and $dpbO_2$ of molarities 0.1M each were prepared in $CHCl_3$. The stock solutions of metal ions of different molarities tested for their interference, if any, were prepared and standardized with EDTA (Xylenol Orange as indicator).[10]

For estimation of extracted iron, the thiocyanate method was employed,[7] measuring the absorbance of the red solution at a λmax of 460 nm with a recording UV–Vis spectrophotometer. (The manually operated spectrophotometer VSU2-P instrument gave λmax at 510 nm for the thiocyanate complex.[7])

Procedure for thiocyanate extraction

An aqueous phase containing 2 ml of iron(III) solution with thiocyanate and 3 ml of distilled water was equilibrated with 5 ml of Hacac in $CHCl_3$ (range 0.01–0.10M, see Fig. 1) in a round-bottomed flask with a magnetic stirrer. The equilibrium time was found to be 30 min. After allowing the contents to stand for a further 10–15 min, the two layers were separated and iron(III) from the organic layer was transferred to an aqueous layer by stripping it with a solution of 1 ml of concentrated nitric acid and 4–5 ml of distilled water. After this, evaporate the aqueous solution to dryness to remove excess nitric acid and then add a few ml of distilled water and 5 ml of 0.01M potassium thiocyanate solution. Make the volume to 10 ml and measure the absorbance at 460 nm as before. Determine iron from a calibration curve. Similarly, iron left in the original aqueous layer after extraction was determined with 0.01M potassium thiocyanate. (If 1 ml of concentrated hydrochloric acid is used for stripping, its removal is not necessary.) The procedure for extraction of iron(III) with Ph_3PO, $dpeO_2$ or $dpbO_2$ was similar, in which Hacac in $CHCl_3$ was replaced with a phosphine oxide [range 0.01–0.10M, see Fig. 1 (b–d)].

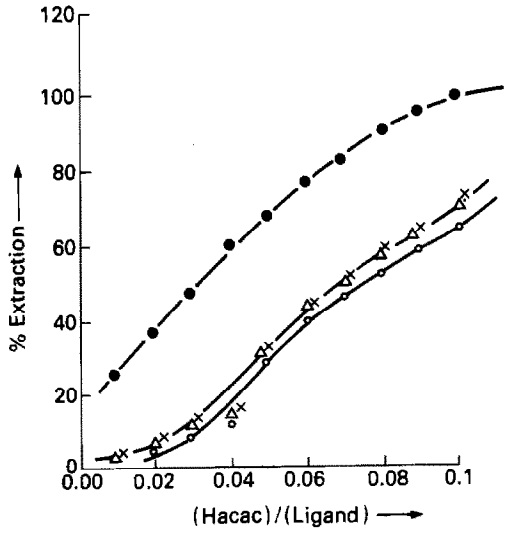

Fig. 1. Plot of % extraction *vs.* (a) ● [Hacac] (b) ○ [Ph_3PO] (c) △ [$dpeO_2$] (d) * [$dpbO_2$]

Synergic extraction

Three synergic systems were developed for enhanced extraction of iron(III) from the thiocyanate medium. One synergic system involves the equilibration of 2 ml of iron(III) solution ($1.79 \times 10^{-3}M$) with 5 ml of 0.05M Hacac and 5 ml of 0.01M Ph_3PO solutions in $CHCl_3$ and 8 ml of distilled water (for keeping the volumes of the two phases the same). For other systems, 2 ml of iron(III) solution was equilibrated with 5 ml of 0.04M Hacac and 5 ml of 0.01M $dpeO_2$ or $dpbO_2$ solutions in $CHCl_3$ and 8 ml of distilled water. The equilibrium time was 15 min instead of 30 min with Hacac alone. The rest of the procedure was similar to above.

Separation of iron(III) from binary mixtures and steel samples

Varying amounts of a metal salt (0.01M) were added to the above synergic combinations for testing their interference. The metals added were estimated by EDTA titration in order to check any possible transfer of the metal to the organic layer.[10] Various metal salts used were: $CrCl_3$ (hydrated), $MnSO_4H_2O$, $CoCl_2 \cdot 6H_2O$, $Co(NO_3)_2 \cdot 6H_2O$, $CoSO_4 \cdot H_2O$, $Co(CH_3CO_2)_2 \cdot 4H_2O$, $NiCl_2 \cdot 6H_2O$, $Ni(NO_3)_26H_2O$, $Ni(CH_3CO_2)_2 \cdot 4H_2O$, $Cu(CH_3CO_2)_2 \cdot H_2O$, $CuCl_2 \cdot 2H_2O$, $Cu(NO_3)_2$, $CuSO_4 \cdot 5H_2O$, $ZnSO_4 \cdot 7H_2O$, $ZnCl_2$, $Zn(CH_3CO_2)_2 \cdot 2H_2O$, $Zn(NO_3)_2 \cdot 6H_2O$, $CdCl_2$, $HgCl_2$, $AgNO_3$, $MgCl_2 \cdot 6H_2O$, $Mg(NO_3)_2 \cdot 6H_2O$, $MgSO_4 \cdot 7H_2O$ and $Pb(CH_3CO_2)_2$.

By using the synergic combination Hacac–Ph_3PO, a new method was developed to separate iron(III) from steel samples. The method is as follows: weigh 0.100 g of the steel sample (blade) and treat it with 5 ml of concen-

trated hydrochloric acid to dissolve the sample and then add 5–10 ml of concentrated nitric acid. Evaporate the solution to dryness, repeat the process with another 5 ml of nitric acid, add a few milliliters of water and 3.88 g of potassium thiocyanate and make up volume to 100 ml with distilled water. Take 0.2 ml of this solution and equilibrate for 15 min with 5 ml of 0.05*M* Hacac in $CHCl_3$ and 5 ml of 0.01*M* Ph_3PO in $CHCl_3$ and 9 ml of distilled water. Separate the two layers and estimate iron from each layer as described earlier to determine extraction efficiency. In order to check whether iron was quantitatively extracted from the steel sample, iron was also determined from a steel sample with the thiocyanate method or the 1,10-phenanthroline method.[11]

RESULTS AND DISCUSSION

The extraction of iron(III) from 0.4*M* potassium thiocyanate with Hacac in $CHCl_3$ can be represented by the equation:

$$Fe^{3+} + mSCN^- + nHacac \overset{K_{HA}}{\rightleftharpoons} Fe(acac)_n(SCN)_{m-n} + nHSCN \quad (1)$$

The extraction of iron increases with an increase in concentration of Hacac and becomes quantitative at about 0.1*M* Hacac [Fig. 1(a)]. From Fig. 2(a), which is a plot of log *D vs.* log [Hacac], it can be seen that for 0.01–0.07*M* Hacac concentration, the slope of the line is 2, suggesting $Fe(SCN)(acac)_2$(hydrated) as the extracted species and for 0.075–0.10*M* Hacac concentration, the slope was 3, suggesting $Fe(acac)_3$ as the extracted species.

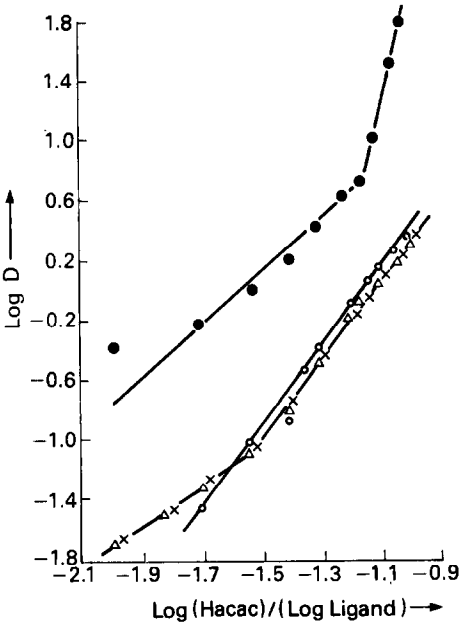

Fig. 2. Plot of log *D vs.* (a) ● Log [Hacac] (b) ○ Log [Ph_3PO] (c) △ Log [$dpeO_2$] (d) * Log [$dpbO_2$]

In order to develop a synergic system, consisting of Hacac and tertiary phosphine oxides, the extraction of iron(III) with Ph_3PO, $dpeO_2$ or $dpbO_2$ was also carried out separately. The extraction of iron(III) in the presence of SCN^- with Ph_3PO, $dpeO_2$ or $dpbO_2$ can be written as shown in equation (2):

$$Fe^{3+} + 3SCN^- + nL \overset{K_L}{\rightleftharpoons} Fe(SCN)_3L_n \quad (2)$$

(L = Ph_3PO, $dpeO_2$ or $dpbO_2$).

Again from the log *D vs.* log [Ph_3PO] plot [Fig. 2(b)], the slope of the line is 2.2, suggesting that iron(III) was extracted as $Fe(NCS)_3(OPPh_3)_2$. The extraction with Ph_3PO increases with an increase in its concentration from 0.01–0.10*M* [Fig. 1(b)], but the maximum extraction was 65.4% at 0.10*M* Ph_3PO. The extraction with $dpeO_2$ or $dpbO_2$ was slightly better, but even here no quantitative extraction could be achieved at 0.1*M* $dpeO_2$ or $dpbO_2$ concentration [Fig. 1(c) and 1(d)]. From log *D vs.* log [L] plots [Fig. 2(c) and 2(d)], the species were found to be $Fe(SCN)_3L_{1.5-2}$ (L = $dpeO_2$ or $dpbO_2$).

The synergic extraction of iron(III) with Hacac and the phosphine oxide ligands may be represented as shown in equation (3).

$$Fe^{3+} + mSCN^- + nHacac + pL \overset{K_{syn}}{\rightleftharpoons} [Fe(SCN)_{m-n}(acac)_nL_p] + nHSCN \quad (3)$$

(L = Ph_3PO, $dpeO_2$ or $dpbO_2$).

Again, for a linear plot of log *D vs.* log [Hacac] at fixed Ph_3PO concentration, the slope of the line was 2, indicating that only two Hacac molecules are attached to iron(III) in the synergic species. Similarly, from the plot of log *D vs.* log [Ph_3PO] at fixed Hacac concentration [Fig. 3(a)], the slope of one indicates the attachment of only one Ph_3PO molecule. Thus, iron(III) was extracted as $Fe(SCN)(acac)_2(OPPh_3)$. Hence, the enhanced Hacac extraction is attributed to the replacement of water by Ph_3PO from $Fe(SCN)(acac)_2(H_2O)$, the species when Hacac alone is the extractant.

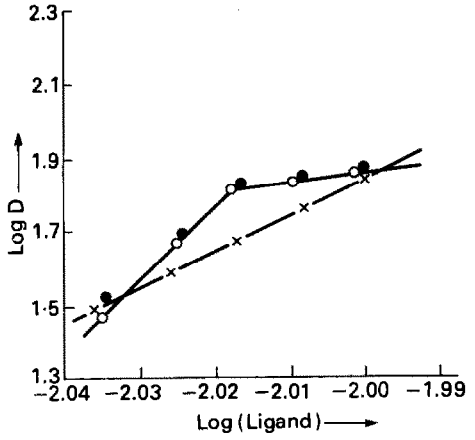

Fig. 3. Plot of log D *vs.* (a) * Log [Ph_3PO] (b) ○ Log [$dpeO_2$] (c) ● Log [$dpbO_2$] (Constant [Hacac])

Similarly, from the linear plot of log D *vs.* log [Hacac] at constant $dpeO_2$ or $dpbO_2$ concentration, the slope of the line was 2. And the plot of log D *vs.* log [L] (L = $dpeO_2$ or $dpbO_2$) at fixed Hacac concentration, showed slopes of one in each case [Fig. 3(b) or 3(c)]. From these studies, the extracted species was identified as $Fe(SCN)(acac)_2L$ (L = $dpeO_2$ or $dpbO_2$).

A 0.05M Hacac solution shows 68.5% extraction of iron(III) while 0.01M Ph_3PO shows no measurable extraction; however, the combination of the two gives 98.5% extraction indicating synergism enhancement of 30%. Similarly, using 0.04M Hacac shows 61.0% extraction while 0.01M $dpeO_2$ or $dpbO_2$ shows no extraction and the combination of the two again shows 99.0% extraction with a synergism of 37%. The increase in chain length from $n = 2$ to 4 made no impact. Since only one coordination site is undergoing replacement of water by a phosphine oxide, the possibility of a chelate effect is remote. A plausible explanation for the higher synergism shown by bisphosphine oxides is the enhanced hydrophobic environments generated by the bulky diphosphine oxides *vs.* Ph_3PO.

By following the procedure as described in the literature[12,13] the expressions for D can be written as:

$D = K_{HA}$ [Hacac]^2
[from equation (1), 0.01–0.07M Hacac range].

$D = K_L$ [L]^2 [from equation (2)].

$D = K_{syn}$ [Hacac]^2 [L] [from equation (3)].
(L = Ph_3PO, $dpeO_2$ or $dpbO_2$).

Using linear regression analysis,[14,15] the values of K_{HA}, K_L and K_{syn} were calculated (Table 1). This table shows that K_L and K_{syn} for bidentate ligands ($dpeO_2$ or $dpbO_2$) are somewhat higher than for Ph_3PO.

The stability constant ($\beta = K_{syn}/K_{HA}$) for the synergic reaction:

$$Fe(SCN)(acac)_2(H_2O) + L \overset{\beta}{\rightleftharpoons} Fe(SCN)(acac)_2L + H_2O \quad (4)$$

(L = Ph_3PO, $dpeO_2$ or $dpbO_2$).

was $1.26 \times 10^3 M^{-1}$ for $Fe(NCS)(acac)_2(Ph_3PO)$ and $1.73 \times 10^3 M^{-1}$ for $Fe(NCS)(acac)_2(L)$ (L = $dpeO_2$ or $dbbO_2$). This shows that the stability of the synergic species was similar for all three types of ligands.

Separation of iron(III) from different metal ions and steel samples

The separation of iron(III) from the binary mixtures of different metal ions was carried out with synergic combination (Hacac and Ph_3PO). Iron(III) was separated from chromium(III), manganese(II), cobalt(II), nickel(II), zinc(II), cadmium(II), mercury(II), lead(II) and magnesium(II); however copper(II) and silver(I) interfered. There was no effect of Cl^-, NO_3^-, CH_3COO^- or SO_4^{2-} ions tested (added as sodium salts) on extraction of iron(III). In the case of chromium(III), it was initially noted that multiple extraction was needed for extraction when chloride was the anion. But later the effect was traced to the presence of hydrochloric acid possibly associated with chromium chloride [obtained from treatment of $Cr(CH_3CO_2)_3$ with concentrated hydrochloric acid] and formation of Fe–SCN ... $HCrCl_4$ species appears likely. The addition of concentrated hydrochloric, nitric, ethanoic or sulphuric acids interfered in the extraction. Thus, from the above, thiocyanate induced extraction of iron(III) is highly specific

Table 1. The extraction constant data

Species	K values	σ*
$[Fe(SCN)(acac)_2(H_2O)]$	1.48×10^3 (K_{HA})	11.5
$[Fe(SCN)_3L_2]$		0.129
L = Ph_3PO	1.80×10^2 (K_L)	
L = $dpeO_2$ or $dpbO_2$	2.02×10^2 (K_L)	0.143
$[Fe(SCN)]acac)_2(L)]$		
L = Ph_3PO	1.87×10^6 (K_{syn})	19.8
L = $dpeO_2$, $dpbO_2$	2.56×10^6 (K_{syn})	20.2

*The standard deviation (σ) was calculated by using the equation: $\sigma = \sqrt{\Sigma(D_{cal} - D_{exp})^2/n_p - 1}$ where D_{exp} is the experimental value of the distribution coefficient and D_{cal} is the corresponding value calculated from K by a computer program and n_p is the number of experimental points.

in the presence of other ions and quantitative. Iron(III) present up to 10^{-6} g per ml could be readily extracted.

A new method of separation of iron(III) from a number of steel samples (*i.e.*, from blades of different quality) is reported by using the synergic combination Hacac–Ph_3PO. The percentage of iron(III) from steel samples selected for extraction was found to be $72.00 \pm 0.10\%$. The percentage of iron(III) in the steel sample was $71.00 \pm 0.02\%$ as checked by the 1,10-phenanthroline or thiocyanate method.[11] Thus, it is demonstrated that the Hacac–Ph_3PO (or Hacac–$dpeO_2$ or –$dpbO_2$) combination is a simple and novel method of quantitative separation of iron(III) present in different samples.

Effect of different solvents

Finally, the same percentage extraction was obtained when chloroform was replaced by benzene or toluene in the synergic system, Hacac–Ph_3PO–SCN^-. However, Ph_3PO was poorly soluble in carbon tetrachloride, n-hexane, or cyclohexane and thus they could not be studied.

Acknowledgements—Financial assistance from CSIR, New Delhi [Scheme No. 1 (1095)/87-EMR II] and laboratory facilities (PVKB) by the Guru Nanak Dev University, Amritsar are gratefully acknowledged.

REFERENCES

1. S. Umetani, M. Matsui, T. Kuzunishi and Y. Nishikawa, *Bull. Inst. Chem. Res. Kyoto Univ.*, 1982, **60**, 254; *Chem. Abstr.*, 1983, **98**, 129940j.
2. J. Aggette, *Chem. Ind. (London)*, 1966, 27.
3. *Idem*, *J. Inorg. Nucl. Chem.*, 1970, **32**, 2767.
4. T. S. Lobana and S. S. Sandhu, *Coord. Chem. Rev.*, 1982, **47**, 283.
5. T. S. Lobana and P. V. K. Bhatia, *Indian J. Chem.*, Sect A, 1990, **29**, 93.
6. *Idem*, *Indian J. Chem.*, Sect. A, 1990, **29**, 933.
7. T. S. Lobana and A. Sharma, *Indian J. Environ. Prot.*, 1989, **6**, 447.
8. L. Maier, in *Organic Phosphorus Compounds*, G. M. Kosolapoff and L. Maier (eds.), Chap. 1, p. 4. Wiley Interscience, New York, 1972.
9. T. S. Lobana, *Nat. Acad. Sci. Letter* (Allahabad), 1985, **8**, 271; *Chem. Abstr.*, 1987, **106**, 196510r.
10. J. Bassette, R. C. Denny, G. H. Jeffery and J. Mendham, *Vogel's Textbook of Quantitative Inorganic Analysis*, p. 265. ELBS and Longman, London, 1978.
11. E. B. Sandell and H. Onishi, *Photometric Determination of Metals*, Vol. 3, 4th Ed. Wiley Interscience, New York, 1978.
12. J. N. Mathur, S. A. Pai and M. S. Subramania, *J. Inorg. Nucl. Chem.*, 1977, **19**, 653.
13. V. Salvado, X. Ribas and A. Masana, *Polyhedron*, 1989, **8**, 2099.
14. D. A. Skoog and X. E. West, *Principles of Instrumental Analysis*, 3rd Ed., New York, 1985.
15. F. Daniels, *Mathematical Preparation for Physical Chemistry*, p. 238. McGraw-Hill, New York, 1956.

Talanta, Vol. 39, No. 6, pp. 665–670, 1992
Printed in Great Britain.

0039-9140/92 $5.00 + 0.00

ACID–BASE EQUILIBRIA IN SUBSTITUTED 4-QUINOLONE CARBOXYLIC ACID SOLUTIONS

MILENA JELIKIĆ
Faculty of Pharmacy, University of Beograd, P.O. Box 146, 11000 Beograd, Yugoslavia

DRAGAN VESELINOVIĆ
Faculty of Science, Physical Chemistry Department, University of Beograd, P.O. Box 550, 11000 Beograd, Yugoslavia

PREDRAG DJURDJEVIĆ*
Faculty of Science, "Svetozar Markovic" University, P.O. Box 60, 34000 Kragujevac, Yugoslavia

(*Received* 27 *September* 1991. *Revised* 8 *November* 1991. *Accepted* 14 *November* 1991)

Summary—The protonation constants of some substituted 4-quinolone carboxylic acid anions (ofloxacin, pefloxacin and ciprofloxacin) were determined in lithium chloride solution of various concentrations at 293, 303 and 313 K using the pH-metric and spectrophotometric methods. The values of thermodynamic parameters (ΔG, ΔH and ΔS) for the first protonation step of these anions in 0.1*M* lithium chloride at 293 K, are reported. The formation of intramolecular hydrogen bonds is discussed.

Ofloxacin (**I**), pefloxacin (**II**) and ciprofloxacin (**III**) are broad spectrum antibiotics developed during the last decade.[1] They all possess a carbonyl group in position "4" thus, they are often referred to as 4-quinolones. These quinolone carboxylic acids are active against many gram-positive and gram-negative bacteria.[2–4] Increase in their antibacterial activity is greatly influenced by substituent groups at positions 6, 7 and 8.[5] The antibacterial activity of 4-quinolones is pH-dependent since they act by inhibition of bacterial DNA gyrase, a process which depends upon both the pH and concentration of the acid.[1] Therefore, the examination of protonation equilibria in 4-quinolone acid solutions is essential in understanding their antibacterial activity. Furthermore, the investigation of the complexing ability of these ligands towards some essential bio-elements and $Al^{(III)}$ and $Mg^{(II)}$ ions is of interest since they may interact with other drugs, during the parallel therapy [especially with antacids containing $Al^{(III)}$ and $Mg^{(II)}$ ions in drug formulation] as well as with the essential metal ions in the serum [$Fe^{(III)}$, $Cu^{(II)}$ *etc.*]. For such investigations the determination of their thermodynamic parameters is needed in order to quantitatively characterize these interactions.

Protonation constants of anionic forms of (**I**)–(**III**) 4-quinolones have not been reported in the literature so far, hence present work is aimed at the determination of protonation constants of these compounds at various temperatures and ionic strengths of the lithium chloride medium using the pH and spectrophotometric measurements.

EXPERIMENTAL

Reagents

Ofloxacin [abbreviated as H(ofl)] was from Hoechst (Frankfurt am Main, F.R.G.), purity 100%, pefloxacin-methanesulphonate dihydrate (H_2pef 2 H_2O), Rhone (Pulenc, France) purity 99.6% and ciprofloxacin hydrochloride monohydrate (H_2cip H_2O), Bayer (Leverkusen, F.R.G.) purity 99.5%. Standardization was performed by potentiometric titration, showing the high purity of the acids. The lithium chloride p.a. Merck (Darmstadt, F.R.G.) was used as ionic medium. Carbonate-free sodium hydroxide solution, standardized with potassium hydrogenphthalate, was used as titration agent. Hydrochloric acid solution was prepared from "Suprapure" hydrochloric acid (Merck) and standardized against tris(hydroxymethyl) aminomethane. The pH-meter was adjusted with the phosphate buffer, pH = 7.00 ± 0.02

*Author for correspondence.

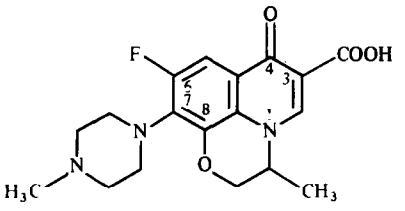

I

Ofloxacin

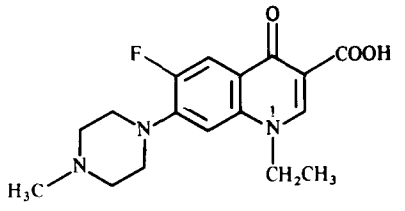

II

Pefloxacin

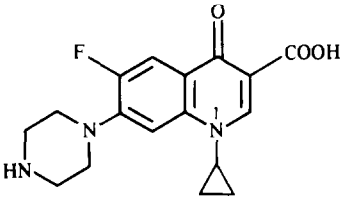

III

Ciprofloxacin

Scheme 1.

and phthalate buffer, pH = 4.01 ± 0.01, at 293 K (products of Radiometer). The stock solution of acids (nominally $5.00 \times 10^{-3} M$) were prepared by dissolution of a weighed amount of solid substances, at room temperature. The working solutions were made by dilution of stock solutions and addition of lithium chloride and water until the volume reached 25.00 ml. For preparation of the solutions doubly distilled water, degassed with purified nitrogen gas, was used.

Instrumentation and procedure

The following equipment was used: a PHM-62 Radiometer (Denmark) pH-meter with combined GK 2401C electrode, a TTT-60 titrator with ABU-12 burette (Radiometer), a UV–Vis Shimadzu (Japan) model 2100 spectrophotometer with 1-cm quartz cells, an IR Perkin–Elmer (U.S.A.) Model 137 spectrophotometer and an NMR Bruker (F.R.G.) Model WM-250 spectrometer operating at 200 MHz. The calculations were performed on a PC AT 386/25 compatible computer equipped with an i387 coprocessor.

The electrochemical cell, filled with working solution, was immersed in a paraffin-oil thermostat and a constant temperature was maintained within ±0.02 K. Titrations were performed at 293, 303 and 313 K. The nitrogen gas, purified by passing through the series of washing bottles (10% sulphuric acid, 10% sodium hydroxide, Fieser's solution, water and lithium chloride solution, same as used for the medium in working solutions) was bubbled through the cell. Sodium hydroxide ($0.0874 M$) was added stepwise, every 20 min and pH readings were recorded every minute until stable values within ±0.01 pH units were obtained. The electrode system was calibrated, in terms of hydrogen ion concentration according to Irving *et al.*[6] Dilute hydrochloric acid solutions (2.5 and $5.0 \text{m}M$) were titrated with standard alkali under the same medium and temperature conditions as the test solutions. The value of p[H] (−log[HCl]) was calculated at various points on the titration curves and subtracted from the pH values read from the pH-meter. In this way, the calculated values of the correction factor, A, according to the equation:

$$\text{pH} = \text{p[H]} + A \qquad (1)$$

were used in the conversion of the pH readings (obtained in test solution titrations) into p[H]. The final volume of solution, at the end of titration, did not exceed 26.0 ml, so that it may be assumed that the total concentration of acid was kept constant during the titration (change in concentration less than 4%).

UV spectra were taken in the 200–400-nm wavelength range in water, methanol and ethanol as solvents. IR spectra were obtained with the potassium bromide pellet technique. ^{1}H-NMR spectra of ciprofloxacin were taken in d_6-DMSO at pH ~ 3.5 and in D_2O at pD ~ 10.0. Chemical shifts are reported relative to DDS in ppm.

RESULTS AND DISCUSSION

Potentiometric measurements

The protonation constants of ofloxacin, pefloxacin and ciprofloxacin were determined in 0.10, 0.05 and 0.02*M* lithium chloride medium at 293 K as well as in 0.1*M* lithium chloride at 293, 303 and 313 K. Owing to low concentrations of the acids used, the ionic strength of the solutions was assumed to be equal to the concentration of the ionic medium.

In each medium concentration at least two titrations were carried out with various acid concentrations (2.5 and 4.0m*M*) in the pH range 4.0–10.5. Approximately 60–70 pH-volume readings were taken.

The protonation constants, defined according to the equilibrium:

$$iH + L \leftrightharpoons H_iL; \quad K_i = \frac{[H_iL]}{[H][H_{i-1}L]} \qquad (2)$$

L = ofl, pef or cip

were estimated by use of the general equation:

$$\log K_i = \log \frac{(1-a+n-i)C_{H_nL} - [H] + [OH]}{(a-n+i)C_{H_nL} + [H] - [OH]} + p[H] \qquad (3)$$

where K_i is the ith protonation constant of L and a is the degree of titration.* Obtained values of protonation constants were further refined with the aid of the general least-squares program SUPERQUAD.[7,8] The constants were calculated by minimizing the error-square sum, U of potentials:

$$U = \sum w_i (E_{obs} - E_{calc})^2 \qquad (4)$$

where E_{obs} is a potential obtained from the measured value of p[H] according to the formula:[7]

$$E_{obs} = 10 + RT/F \times p[H] \qquad (5)$$

and E_{calc} refers to the potential calculated from the trial values of protonation constants. The weighting factor, w_i, is defined as the reciprocal of the estimated variance of measurement:

$$w_i = 1/\sigma^2 = 1\Big/\left[\sigma_E^2 + \left(\frac{\partial E}{\partial V}\right)\sigma_V^2\right] \qquad (6)$$

where σ_E^2 and σ_V^2 are the estimated variances of the potential (*i.e.*, due to pH) and volume readings, respectively. The quality of fit was judged by the values of sample standard deviation, s, and the goodness of fit, χ^2 (Pearson's test). At $\sigma_E = 0.01$ pH and $\sigma_V = 0.003$ ml, the values of s, in different sets of titrations were between 1.4 and 1.8 and χ^2 was between 1.4 and 12.9, thus indicating a good fit of experimental data. In some titrations the resultant statistics were unacceptable ($s > 3.0$ and $\Delta \log K > 0.15$). It was thought that this may be caused by the errors in alkali and total proton concentrations. Therefore, these quantities were refined together with $\log K$. The alkali concentration changed from the initial value of 0.0874 to 0.0862*M* and total proton concentration changed by 0.8%. These changes resulted in much better statistics ($s < 2.0$, $\Delta \log K < 0.02$) and improved scatter of residuals. In cases where no better statistics were obtained the titration was discarded.

The calculated values of protonation constants are presented in Table 1 together with calculated standard deviations given in parenthesis.

The calculated standard deviations in protonation constants reflect only the random errors, inherent to experiments. In order to calculate total absolute errors in protonation constants, other sources of errors, such as standardization and dilution of reagents, calibration of pH-meter, *etc.*, were considered. The error-propagation law gives the absolute error in $\log K$ as:

$$\Delta \log K = \sum \frac{\partial \log K}{\partial X_i} \Delta X_i \qquad (7)$$

where pH, volume of base added, V and equivalence volume, V_{eq} (which accounts for errors in reagents standardization) where taken as independent variables, X_i. Absolute errors in these values were: $\Delta pH = 0.01$, $\Delta V = 0.003$ ml and $\Delta V_{eq} = 0.01$ ml. Partial derivatives were calculated according to Still.[9] It was found that total absolute errors in all protonation constants are less than 0.04 log units.

Table 1. Protonation constants of 4-quinolone acids, H_iL in lithium chloride medium. Calculated standard deviations are given in parenthesis

		log K_i				
		Ofloxacin	Pefloxacin		Ciprofloxacin	
μ	$T(K)$	$i=1$	$i=1$	$i=2$	$i=1$	$i=2$
	293	8.45 (1)	7.50 (1)	6.34 (2)	8.72 (1)	6.00 (1)
0.1	303	8.12 (2)	7.47 (1)	6.32 (2)	8.50 (1)	6.11 (1)
	313	8.00 (2)	7.33 (2)	6.26 (1)	8.30 (2)	6.00 (1)
0.05	293	8.42 (1)	7.51 (1)	6.48 (2)	8.71 (2)	6.13 (1)
0.02	293	8.32 (2)	7.50 (2)	6.40 (2)	8.66 (1)	6.18 (1)
0	293	8.22 (2)	7.40 (2)	6.49 (2)	8.62 (2)	6.34 (1)

*Charges are omitted for simplicity.

Table 2. Thermodynamic parameters of the first dissociation step of 4-quinolone acids at a temperature 293 K and ionic strength $\mu = 0M$, ΔG, kJ/mole, ΔH, kJ/mole, ΔS, J mole^{-1} K^{-1}

	Ofloxacin	Pefloxacin	Ciprofloxacin
ΔG	−46.1	−41.5	−48.4
ΔH	−17.3	−10.5	−16.1
ΔS	98	106	110

Thermodynamic protonation constants at zero ionic strength, at 293 K have been determined by extrapolation of the straight line log K_i *vs.* $\sqrt{\mu}$ and they are also given in Table 1. Changes in thermodynamic functions, ΔG, ΔH and ΔS, related to the first protonation step of ligands, at 293 K, were calculated by use of the equation:[10]

$$\log K_1 = -\frac{\Delta H}{RT} + \frac{\Delta C_p}{R} \ln T + \frac{\Delta S - \Delta C_p}{R} \quad (8)$$

$$\Delta G = \Delta H - T\Delta S$$

by plotting log K_1 *vs.* $1/T$ and assuming $\Delta C_p = 0$ over the temperature range investigated. The values obtained are presented in Table 2.

There are two available protonation sites in ofloxacin, *i.e.*, nitrogen at position 4′ in piperazinyl substituent and the carboxylate group. The protonation constant for $i = 1$, in Table 1 refers to protonation of the carboxyl group at position 3 since ofloxacin was originally in the base form with respect to piperazinyl nitrogen, and no free strong acid was added prior to titration. It may be concluded, judging by the value of the obtained constant, that the protonation constant K_1 of pefloxacin and ciprofloxacin also refers to protonation of the carboxyl group. The second protonation constant of pefloxacin, K_2 refers to protonation of the methylsulphonic group ($CH_3SO_3^-$) since pefloxacin was originally in the form of methanesulphonate, while in ciprofloxacin the K_2 refers to protonation of the nitrogen in the piperazinyl substituent. The log K_2 value for ciprofloxacin is 6.34 and for piperazine[11] 5.68, thus the basic character of piperazinyl nitrogen in ciprofloxacin is more pronounced than in piperazine.

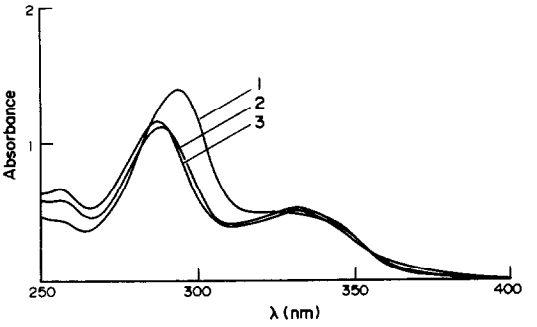

Fig. 1. Spectra of ofloxacin: (1) 0.1M HCl, (2) pH = 5.94, (3) 0.1M NaOH.

Spectrophotometric measurements

The spectra of ofloxacin, pefloxacin and ciprofloxacin solutions ($4.00 \times 10^{-5}M$) at pH values between 4.0 and 10.0, and in 0.1M sodium hydroxide as well as in 0.1M hydrochloric acid were recorded in the wavelength range 200–400 nm at 293 K. The pH of the solutions was adjusted by the buffers prepared according to Perrin.[12] Part of the spectra obtained are shown in Fig. 1 (ofloxacin), Fig. 2 (pefloxacin) and Fig. 3 (ciprofloxacin).

Spectra exhibit two well defined bands; the higher energy band is symmetric, while the lower energy band is asymmetric with a shoulder for ofloxacin. For pefloxacin and ciprofloxacin this band is split at pH values higher than 7.3 into two close bands. A higher energy band, centred at 280 nm may be attributed to the $\pi \rightarrow \pi^*$ transition in the

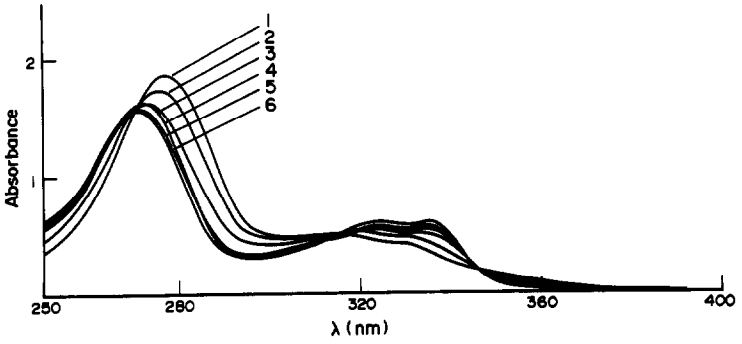

Fig. 2. Spectra of pefloxacin: (1) 0.1M HCl, (2) pH = 5.90, (3) pH = 6.55, (4) pH = 7.27, (5) pH = 8.33, (6) 0.1M NaOH.

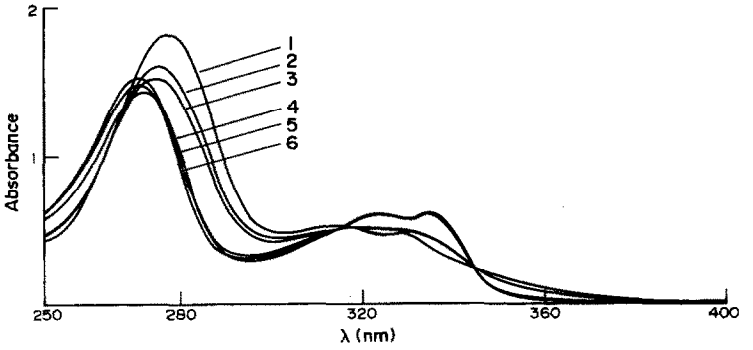

Fig. 3. Spectra of ciprofloxacin: (1) 0.1*M* HCl, (2) pH = 5.77, (3) pH = 5.90, (4) pH = 7.27, (5) pH = 8.33, (6) 0.1*M* NaOH.

quinolone nucleus whilst the broad, lower energy band, situated at 310–350 nm may partly arise from the piperazinyl substituent. The position and intensity of all bands are pH-dependent. The values of protonation constants and molar absorptivities of each species in solution were calculated with the aid of SQUAD[13] and SPECFIT[14] programs. Both programs were compiled with MicroWay's NDP386 v. 3.1 Fortran compiler. The performance of both programs was nearly equal though SPECFIT ran a bit faster and needed less iterations to achieve convergence. The data used for calculation comprised 10 spectra for each acid, between pH 5.0–9.0 in the 250–360-nm wavelength interval; absorbance readings were taken every 5 nm. Both programs gave nearly the same results (the differences in calculated constants and molar absorptivities were less than 1%). The calculated values of protonation constants, molar absorptivities and wavelengths of maximum absorption, are presented in Table 3.

The standard deviation of absorbance data was less than 1.5×10^{-3} and standard deviations of protonation constants were in the range 0.03–0.05 log K units, indicating a good fit of the data. The log K_1 values obtained are within 0.2 log K units of potentiometrically determined values, whilst the values determined for log K_2 show better agreement with potentiometric data.

Comparison of the acid strength shows that the pefloxacin is stronger than the other two acids (dissociation of the carboxyl group). The strength of the acids studied here, with respect to dissociation of the carboxyl group at position 3 is primarily determined by two effects: (a) the resonant acid-weakening effect in the quinolone nucleus and (b) the hydrogen bond between carbonyl oxygen (at position 4) and hydrogen from the carboxyl group. The strength of the resonant effect depends upon the mobility of the free electron pair located on nitrogen at position 1. This in turn, depends on the nature of the substituent on that nitrogen. As can be seen from formulae **I–III**, all the substituents on nitrogen at position 1 exhibit a positive inductive effect but the ethyl substituent in pefloxacin is in this respect stronger than the other two. It should lead to a slight decrease in negative charge located on the carbon at position 3 (*meta* with respect to nitrogen) thus giving rise to an increase in acidity. It would be of interest to compare the strength of the acids **I–III** with unsubstituted 4-quinolone-3-carboxylic acid. However, to the best of our knowledge there is presently no available data in the literature. It

Table 3. Spectral characteristics and log K values determined for 4-quinolone acids at 293 K

Species	λ_{max}/nm ($10^{-4}\epsilon_{max}$/dm^3 mole^{-1} cm^{-1})	log K_1	log K_2
ofl	292.9 (3.86); 335.0 (1.15)		
Hofl	290.5 (2.26); 330.0 (1.58)	8.16	
pef	271.9 (4.04); 325.0 (1.45)		
Hpef	270.9 (3.87); 322.0 (1.40)	7.78	
H_2pef	276.6 (4.54); 315.5 (1.30)		6.45
cip	271.5 (3.56); 335.0 (1.51)		
Hcip	269.9 (3.89); 325.0 (1.56)	8.47	
H_2cip	276.8 (4.12); 315.0 (1.28)		6.32

has been reported that structurally similar nalidixic acid,[16] which has a naphthyridine nucleus, possesses a dissociation constant $pK_a = 6.0$. Such an increase in acidity, in comparison with quinolone acids, may be explained in terms of a negative resonant effect from the pyridine part of the naphthyridine nucleus.

The second effect playing an important role in the acid strength of 4-quinolone acids is the formation of hydrogen bonds. As can be seen from formulae **I–III** the formation of *intra*molecular hydrogen bonds is accompanied by closing the six membered ring leading to an increase in the stability of the bond. The PMR spectrum of ciprofloxacin in D_2O, at pD ~ 10.0 consists of two well-resolved resonances at 1.1 and 1.3 ppm arising from cyclopropan hydrogens (CH_2) and a singlet at 3.6 ppm (CH), two sharp multiplet resonances at 3.1 and 3.3 ppm from piperazinyl hydrogens, two doublets centred at 7.5 and 7.9 ppm from hydrogens belonging to the quinolone nucleus and a singlet sharp resonance at 8.46 ppm belonging to hydrogen in piperazine substituent bonded to nitrogen. In d_6-DMSO the position of resonances are only slightly changed, however at 9.30 ppm a broad low-intense resonance appears, arising from the hydrogen of the carboxyl group. The shape and position of this resonance indicate that the hydrogen of the carboxyl group is involved in the hydrogen bond. The position and shape of this resonance was virtually unchanged upon dilution. The formation of an *intra*-molecular hydrogen bond is supported by UV spectral data obtained in methanol and ethanol solvents. The position of the higher energy peak was almost unchanged with respect to water. The peak intensity slightly increased when changing from ethanol to methanol and water. Ciprofloxacin was practically insoluble in n-hexane, dioxane and $CHCl_3$, so that the spectra in these solvents could not be obtained. The IR spectrum shows a band at 3550 cm^{-1} of medium intensity and a weak band at 3400 cm^{-1}; both are attributed to the stretching vibrations of the associated OH^- group.[17] In the carboxylate stretching region two sharp intensive bands occur at 1720 and 1650 cm^{-1}, indicating the presence of a hydrogen bond.[17]

REFERENCES

1. M. Neuman, *Clinical Pharmacokinetics*, 1988, **14**, 96.
2. B. Joos, B. Ledergerber, M. Flepp, S. D. Bettex, R. Luthy and W. Siegenthaler, *Antimicrob. Agents Chemother.*, 1985, **27**, 353.
3. J. Smith, *Pharm. J.*, 1984, **233**, 299.
4. K. Sato, Y. Inoue, T. Fujii, H. Aoyama and M. Inoue, *Antimicrob. Agents Chemother.*, 1986, **30**, 777.
5. A. Bryskier and J. F. Chantot, *International Congress of Chemotherapy*, Abstract WS-9-4, Kyoto, 1985.
6. H. M. Irving, M. G. Miles and L. D. Pettit, *Anal. Chim. Acta*, 1967, **38**, 475.
7. P. Gans, A. Sabatini and A. Vacca, *J. Chem. Soc. Dalton Trans.*, 1985, 1195.
8. L. D. Pettit, Private communication.
9. E. R. Still, *Talanta*, 1980, **27**, 573.
10. R. P. Bell, *The Proton in Chemistry*, 2nd Ed., p. 72. Chapman & Hall, London, 1973.
11. A. Albert and E. P. Serjeant, *The Determination of Ionization Constants*, Chapman & Hall, London, 1971.
12. D. D. Perrin and B. Dempsey, *Buffers for pH and Metal Ion Control*, Chapman & Hall, London, 1974.
13. D. J. Leggett (ed.), *Computational Methods for the Determination of Formation Constants*, Plenum Press, New York, 1985.
14. H. Gampp, M. Maeder, C. J. Meyer and A. D. Zuberbuhler, *Talanta*, 1985, **32**, 95.
15. H. Gampp, M. Maeder, C. J. Meyer and A. D. Zuberbuhler, *ibid.*, 1985, **32**, 257.
16. A. C. Moffat (ed.), *Clarke's Isolation and Identification of Drugs*, p. 795. The Pharmaceutical Press, London, 1986.
17. E. Pretsch, J. Seibl and W. Simon, *Tabellen zur Strukturaufklarung Organischer Verbindungen mit Spektroskopischen Methoden*, Springer Verlag, Berlin Heidelberg, 1981.

Talanta, Vol. 39, No. 6, pp. 671–674, 1992
Printed in Great Britain.

0039-9140/92 $5.00 + 0.00

PRECONCENTRATION OF TRACE AMOUNTS OF MANGANESE FROM NATURAL WATERS BY MEANS OF A MACRORETICULAR POLY(DITHIOCARBAMATE) RESIN

M. C. YEBRA-BIURRUN,* M. C. GARCÍA-DOPAZO, A. BERMEJO-BARRERA and M. P. BERMEJO-BARRERA

Department of Analytical Chemistry, Nutrition and Bromatology, Chemistry Faculty, University of Santiago de Compostela, 15706-Santiago de Compostela, Spain

(*Received* 2 *September* 1991. *Revised* 15 *October* 1991. *Accepted* 24 *October* 1991)

Summary—A chelating poly(dithiocarbamate) resin (PDTC) with macroreticular support is characterized as effective collector for traces of manganese from natural waters. Using small PDTC columns preconcentration of manganese can be achieved even at high flow-rates (5–6 ml/min) and sample volumes (1500 ml). Accordingly, PDTC resin is used for the preconcentration of manganese from water samples prior to its determination by flame atomic-absorption spectrometry. A series of ions abundant in natural waters do not interfere. The sensitivity and detection limit were 2.5 and 0.5 μg/l., respectively. The relative standard deviations of the results for a manganese concentration of 40–400 μg/l. are in the range 1.1–6.2%. In mineral and tap waters analysed, the manganese concentration range was between 2.9 and 30.8 μg/l.

Manganese is an important element from the environmental perspective, being essential for organisms and plants. However, excessive intake can cause lesions.[1]

In general, concentrations of manganese in fresh waters[2] are in the range 0.02–130 μg/l. Therefore the determination of this metal ion often requires atomic spectrometric methods offering low detection limits, for instance AAS combined with preconcentration techniques.[3] An important technique used for the collection of manganese from water samples is ion-exchange. The iminodiacetate-containing resin Chelex-100 is the most commonly employed chelating resin for the removal and preconcentration of trace heavy metals from waters.[4–7] However, that technique is rather time-consuming (sample flow-rates of 1–2 ml/min) and suffers from the fact that removal of calcium and magnesium from the resin prior to elution of trace metals requires careful washing procedures.[6,7] Some work has been done to synthesize and use the preconcentration chelating collectors containing the dithiocarbamate group which forms chelates with a relatively wide variety of metal ions. Horváth and Barnes[8] evaluated the alteration of chelating efficiency of a poly(dithiocarbamate) resin caused by thiocyanate contamination for copper, cobalt and iron(III). Van Berkel and Maesson[9] described a method for the determination of traces of transition elements in seawater and biological materials with sample enrichment by a PDTC resin, but at the pH used (pH 5) the sequestration of manganese is poor. Leyden and Luttrell[10] used a chelating collector containing dithiocarbamate groups with a matrix of silica gel. Manganese reaches a 90% extraction level with this sorbent at pH 9.5. Imai *et al.*[11] synthesized dithiocarbamate celluloses and investigated the pH dependency of the adsorption of various metal ions by four DTC celluloses: the adsorption of manganese increased sharply in the alkaline region.

The application of a poly(dithiocarbamate) resin (PDTC) with macroreticular support to the determination of manganese in natural waters is reported here. The synthesis and characterization of this resin have been described elsewhere.[12] According to Yebra-Biurrun *et al.*[12] the PDTC resin revealed no affinity for alkali and alkaline earth elements. Moreover, very high preconcentration factors could be achieved at high flow-rates using flame atomic absorption spectrometry (FAAS) for the determination of analytes, *e.g.*, manganese.

EXPERIMENTAL

Apparatus

Glass chromatography columns (10 mm inner diameter, 200 mm long) were used.

*Author for correspondence.

A Crison standard pH-meter with electrode INGOLD U 455 and a Perkin–Elmer 5000 atomic absorption spectrophotometer were also used. An oxidizing air-acetylene flame was used under the conditions recommended by the instrument manufacturer for manganese (279.5 nm).

All chemical appliances, such as bottles, columns, flasks and tubes were prepurified before use with 10% nitric acid (12 hr) and rinsed with ultrapure water twice.

Reagents and solutions

All chemicals were of analytical reagent grade. Ultrapure water of 18.3M Ω cm specific resistivity was obtained from a Milli-Q water system (Millipore Corp.) and was used throughout.

Poly(dithiocarbamate) resin with macroreticular support (20–30 mesh) was synthesized as described in a preceding work.[12] The resin synthesis was carried out in three steps:

(1) Chloromethylation of Amberlite XAD-4 resin.
(2) Amination of chloromethylated resin.
(3) Introduction of dithiocarbamate group. After 6 days of reaction sulphur content is 15% (≈2.35 mmoles of dithiocarbamate/g of resin).

Stock metal ion solutions (1000 μg/ml) were prepared in 1M nitric acid from high-purity metal salts. Nitric acid (8M aqueous solution), and ammonia solution (25%) (d = 0.91 kg/l.) were used.

Certified Reference Material Simulated Fresh Water IAEA/W-4 was obtained from the International Atomic Energy Agency (Vienna, Austria).

Standards and samples were stored in precleaned polypropylene bottles.

Procedure for preliminary studies

The sorption of manganese was studied by a dynamic method, passing a solution of the metal through a column filled with PDTC resin. Firstly, 25 ml of ultrapure water and then the metal standard solution at pH 10 were passed through the resin (the effect of pH on degree of sorption has been studied previously[12]). Subsequently, the trace metals were eluted with 8M nitric acid. Manganese was determined by FAAS.

Blanks of ultrapure water were processed with the same procedure as the metal standards.

Recommended procedure for natural waters

Resin preconditioning. Prior to passage of a sample for preconcentration, the analytical column filled with the resin (0.5 g) was conditioned with about 25 ml of ultrapure water at pH 10.

Water samples (100 ml) were adjusted at pH 10 with ammonia and passed at 4 ml/min through the column. The sorbed metals were eluted with 5 ml of 8M nitric acid. The concentration of manganese was determined by FAAS.

For calibration, standard solutions containing between 0–400 μg/l. of manganese were used. Standards were treated in the same way as the samples. Calibration is linear in the eluates by as much as 2 μg/ml manganese.

The equation obtained for calibration curve was:

$$A = 2.7 \times 10^{-4} + 4.2 \times 10^{-4} \times \text{concentration of Mn } (\mu g/l.)$$

$r = 0.9999$ where A = absorbance.

RESULTS AND DISCUSSION

Procedure optimization

Effect of flow rate. The effect of flow rate on the sorption of manganese was studied in the range 0.7–10 ml/min. The volume of sample passed through the columns was 100 ml and sample concentration was 100 μg/l. manganese. The resin capacity was 9.1 μmoles/g for manganese.[12] Table 1 shows that quantitative manganese recoveries can be attained at a flow rate ≤5 ml/min. Thus, for further separation experiments a flow rate of 4 ml/min was chosen.

Effect of sample volume. The influence of the solution volume on manganese sorption was studied by passing 100, 300, 500, 1000 and 1500-ml sample volumes through the column at a constant flow rate of 4 ml/min.

According to Table 2, the manganese recovery (*e.g.*, 10 μg/l.) is practically independent of

Table 1. Effect of flow rate in the retention of manganese*

Flow-rate, *ml/min*	% Retention
0.7	100.3
2	97.5
4	97.5
8	86.0
10	80.2

*Mn concentration in standards was 100 μg/l.

Table 2. Effect of sample volume on sorption of manganese* (five replicates)

Sample volume, *ml*	[Mn] found, *μg/l.*	RSD, %
100	10.00	3.0
300	9.83	1.2
500	9.70	1.0
1000	9.75	0.7
1500	9.73	0.7

*Amount of poly(dithiocarbamate) resin: 0.5 g. Mn concentration in standards was 10 μg/l.

Table 4. Effect of pH on retention of manganese* (five replicates)

pH	% Retention (mean)	RSD, %
4	58.8	1.2
6	94.1	0.7
8	94.1	0.5
10	97.1	0.4
12	97.1	0.5

*Manganese concentration was 1 μg/ml.

the chosen sample volume, which is important for applications in water analysis.

Effect of eluent volume. A significant preconcentration of metals from natural waters can only be effected if the volume of the eluate is small relative to the initial sample volume. For this reason 3, 5, 10, 15, 20 and 25-ml volumes of 8*M* nitric acid were studied for manganese elution. As can be seen in Table 3, a volume of 5 ml of 8*M* nitric acid is sufficient for quantitative elution of manganese.

Effect of pH on degree of sorption. The effect of pH on the degree of sorption was studied for 1 μg/ml manganese (25 ml sample). The pH interval studied was 4–12, and a pH of 10 was chosen for optimal preconcentration of manganese (Table 4).

Effect of other ions. Since the main constituents of natural waters (calcium, magnesium and the alkali metals) are not retained on poly(dithiocarbamate) resin, the effect of other ions on the separation of manganese was studied. A series of important ions (*e.g.*, Al^{3+}, Cu^{2+}, Zn^{2+}, Fe^{3+}, Si(IV), Cl^-, SO_4^{2-} and NO_3^-) present in natural waters (mineral and tap water) were studied. Their concentration range was chosen according to average concentration values calculated for natural waters.[2]

The analytical signal from solutions containing only manganese was compared with that from solutions containing the interfering element and manganese.

Table 3. Effect of eluent volume (8*M* nitric acid) on recovery of manganese* (five replicates)

Eluent volume, *ml*	% Recovery (mean)	RSD, %
3	89.8	0.6
5	97.7	0.7
10	97.4	1.7
15	97.6	2.5
20	97.7	2.3
25	98.5	0.8

*Mn amount was 5 μg.

Results expressed in % relative absorption are shown in Table 5. 100 ± 5% relative absorption were considered as negligible interference. According to the above findings none of these elements interfere on the separation and determination of manganese.

Reproducibility and recovery from the ion-exchange column

The recovery and reproducibility of the combined procedure were studied by carrying out five determinations of solutions containing 0, 40, 100, 200 and 400 μg/l. Mn.

Manganese assays were carried out as described above, both with and without preconcentration by the ion-exchange process. The recovery experiments with the above solutions prove that manganese in the solution can quantitatively be extracted by the PDTC resin (Table 6). The average manganese retention was 97.2%. The relative standard deviations (s_r) in the range 1.1–6.2% obviously depending on the manganese concentration.

Hence the resin provides a reliable way for manganese preconcentration.

Table 5. Effect of foreign cations and anions on the separation and determination of manganese*

Added element	Amount, *mg/l.*	% Relative absorption†
Al(III)	0.3	97.2
Cu(II)	3	97.2
Zn(II)	2	95.9
Fe(III)	0.5	98.5
Pb(II)	0.03	98.5
Si(IV)	25	97.2
Cl^-	25	97.2
SO_4^{2-}	25	97.2
NO_3^-	25	97.2
NH_4^+	0.5	98.5

*Manganese concentration was 200 μg/l.

†Calculated from % Relative absorption = *A*(standard Mn plus element)/*A*(standard alone) × 100, where *A* is absorbance.

Table 6. Reproducibility of the combined procedure

Mn, μg/l.	Recovery*, %	RSD, %
40	97.3	6.2
100	97.0	4.0
200	97.8	2.5
400	97.5	1.1

*Calculated from Recovery (%) = [A(with resin)/[A (without resin)] × 100, where A is absorbance.

Detection limit and sensitivity

The detection limit was 0.5 μg/l. manganese (based on 3 times the standard deviation of the blank) for 100 ml of samples and the sensitivity of the method (related to $A = 0.0044$) was 2.5 μg/l. manganese. The quantitation limit, defined as 10 times the standard deviation of the blank was 1.7 μg/l. manganese.

The detection limit, sensitivity and quantitation limit can be decreased by one order of magnitude by increasing the sample volume (*e.g.*, 1000 ml).

Accuracy of the method

To study the accuracy of the method, certified reference material simulated fresh water IAEA/W-4 of IAEA with a manganese content of 23–27 μg/l. was analysed. The manganese content obtained was 23.5 μg/l.

Application to natural waters

The method outlined here was applied to samples of water from different sources in order to determine their manganese content (Table 7).

Table 7. Results for determination of manganese in water samples

Water	Sample	Mn, μg/l.
Tap water*	1 (La Coruña)	4.7
	2 (La Coruña)	5.2
	3 (Lugo)	3.5
	4 (Lugo)	6.7
	5 (Lugo)	5.2
	6 (Lugo)	6.7
	7 (Orense)	2.9
	8 (Orense)	3.7
	9 (Orense)	3.5
	10 (Orense)	5.2
	11 (Pontevedra)	6.7
	12 (Pontevedra)	5.5
Mineral water†	13 (Orense)	17.0
	14 (Orense)	9.0
	15 (Pontevedra)	30.8
	16 (Pontevedra)	21.3
	17 (Lugo)	9.1

*After 0.45 μm filtration. Water samples preserved by acid.
†Bottle material: plastic.

Water samples were taken from the municipal water supply of several townships of Galicia (Spain) and various brands of bottled Galician mineral waters.

CONCLUSIONS

The capabilities of macroreticular PDTC resin to collect quantitatively manganese in trace concentrations from natural waters with little pretreatment has been demonstrated. This resin is an effective means for separation and concentration of manganese (and other trace metals, *e.g.*, lead(II), cadmium(II), copper(II), iron(III), zinc(II), *etc.*) from complex matrices prior to quantitation by FAAS, owing to its low affinity to alkali and alkaline earth elements. Chelex-100, similarly applicable for manganese collection, has a potentially serious disadvantage since the resin has a considerable affinity for alkali and alkaline earth metals.[13] Since the ion-exchange separation described in the present paper can be performed more or less automatically and a little sample volume and a high flow-rate can be used to shorten the analysis time, many samples can be analysed within a short period. Thus, the combined procedure is suitable for the routine determination of manganese in natural water even in the μg/l. range.

REFERENCES

1. E. Merian, *Metals and Their Compounds in the Environment*, p. 1035. VCH, Weinheim, 1991.
2. H. J. M. Bowen, *Environmental Chemistry of the Elements*, p. 15. Academic Press, London, 1979.
3. A. Mizuike, *Enrichment Techniques for Inorganic Trace Analysis*. Springer-Verlag, Berlin, 1983.
4. J. P. Riley and D. Taylor, *Anal. Chim. Acta*, 1968, **41**, 175.
5. T. M. Florence and G. E. Batley, *Talanta*, 1976, **23**, 179.
6. H. M. Kingston, I. L. Barnes, T. J. Brady, T. C. Rains and M. A. Champ, *Anal. Chem.*, 1978, **50**, 2064.
7. R. E. Sturgeon, S. S. Berman, A. Desaulniers and D. S. Russell, *Talanta*, 1980, **27**, 85.
8. Zs. Horváth and R. M. Barnes, *Anal. Chem.*, 1986, **58**, 725.
9. W. W. Van Berkel and F. J. M. Maessen, *Spectrochim. Acta*, 1988, **43B**, 1337.
10. D. E. Leyden and G. H. Luttrell, *Anal. Chem.*, 1975, **47**, 1612.
11. S. Imai, M. Muroi, A. Hamaguchi, R. Matsushita and M. Koyama, *Anal. Chim. Acta*, 1980, **113**, 139.
12. M. C. Yebra-Biurrun, A. Bermejo-Barrera and M. P. Bermejo-Barrera, *Analysis*, in the press.
13. R. E. Van Grieken, C. M. Bresseleers and B. M. Vanderbolght, *Anal. Chem.*, 1977, **49**, 1326.

Talanta, Vol. 39, No. 6, pp. 675–679, 1992
Printed in Great Britain.

0039-9140/92 $5.00 + 0.00

A RAPID COMPLEXOMETRIC SCHEME FOR ANALYSIS OF IRON, ALUMINIUM, CALCIUM AND MAGNESIUM IN SLAGS

K. C. GHOSH, B. C. MUKHERJEE, N. N. GANGULY, M. YUSUF and V. N. CHOUDHURY
National Metallurgical Laboratory, Jamshedpur 831007, India

(*Received* 3 *May* 1991. *Revised* 17 *October* 1991. *Accepted* 17 *October* 1991)

Summary—A simple and rapid complexometric method has been developed for the simultaneous determination of iron, aluminium, calcium and magnesium in a single solution in slags. Phosphorous and small amounts of chromium (1.5 mg) and vanadium (1 mg) do not interfere in the titration. Titanium and manganese are suitably masked with lactic acid and tetra sodium pyrophosphate, respectively. In a suitable aliquot, iron is titrated at pH 2 with EDTA, using sulphosalicylic acid as indicator. To this solution, excess disodium 1,2-cyclohexane diamine tetra acetic acid (DCTA) is added and aluminium is titrated by titrating the excess DCTA with standard copper sulphate solution at pH 3.5, using 1-(2-pyridylazo)-2-naphthol (PAN) as an indicator. A known excess of EDTA is added, the pH is raised to 10 and calcium and magnesium are jointly titrated by titrating the excess EDTA with copper sulphate solution, using PAN indicator. The Ca–EDTA complex is demasked with ammonium oxalate at pH 5 and the released EDTA equivalent to calcium is titrated with copper sulphate solution at pH 10 with PAN indicator. Results of analysis compare favourably with certified values and values obtained by standard methods for BCS and other slags. A set of five samples can be analysed for iron, aluminium, calcium and magnesium in four hours as compared to three days by the classical conventional method.

The chemical composition of slag depends on the raw materials used and the production conditions. Since the composition of the slag varies from lot to lot, a rapid and accurate evaluation of a slag composition by chemical analysis is essential for quality control of the raw materials and the finished products.

The classical methods[1] for determination of alumina, calcium and magnesium in slags are the well-known oxinate, oxalate and pyrophosphate methods, respectively, which are tedious and time consuming. In most of the complexometric methods of determination, calcium and magnesium are usually titrated together with EDTA at pH 10 in an ammoniacal buffer and then calcium alone in another aliquot at pH 12 when magnesium precipitates as hydroxide.[2-6] Manganese, if present in slags, interferes seriously with the EDTA titration of calcium and magnesium by precipitating out as brown manganese hydroxide which absorbs metallochromic indicator to yield an unsatisfactory end point. Therefore, it is essential to separate manganese by the lengthy process of sulphide precipitation[1] or mercury cathode electrolysis[7] prior to the titration of calcium and magnesium with EDTA. Solvent extraction procedures for removal of manganese with diethyl dithiocarbamate[8] and oxine[9] have also been reported. Titanium,[10,11] chromium[2] and vanadium[12] seriously interfere with aluminium as they form stable complexes with EDTA at pH 3.5–5.5. The interference of phosphate[13] in the titration of calcium and magnesium at pH 10 has also been reported. However, no attempt has yet been made to develop a rapid complexometric method for the simultaneous determination of iron, aluminium, calcium and magnesium in a single solution in slags in the presence of titanium and manganese.

As iron, aluminium, calcium and magnesium form stable complexes with EDTA at different pH values, a simple and rapid complexometric scheme has been developed based on this property for the simultaneous determination of these elements in slags in a single solution, using lactic acid[11] and tetra sodium pyro-phosphate[14] as masking agents for titanium and manganese respectively.

EXPERIMENTAL

Reagents

Unless otherwise stated, all reagents were of analytical reagent grade and all solutions were prepared in a one-litre calibrated flask with redistilled water.

EDTA solution. Two solutions (0.025 and 0.01*M*) were prepared by dissolving 9.306 and 3.7225 g, respectively, of disodium ethylene diamine tetra acetate dihydrate in water and diluting to volume.

DCTA solution. Two solutions (0.025 and 0.01*M*) were prepared by dissolving 8.659 and 3.4636 g, respectively, of 1,2-diaminocyclohexane tetra acetic acid in 100 ml of 1*M* sodium hydroxide solution and 200 ml of water, and diluting to volume.

Standard copper sulphate solution. Two solutions (0.025 and 0.01*M*) were prepared by dissolving 6.25 and 2.5 g, respectively, of $CuSO_4.5H_2O$ in water and diluting to volume.

Aluminium solution. A 0.025*M* solution was prepared by dissolving 0.675 g of aluminium foil (99.99%) in hydrochloric acid (1 + 1) and diluting to the mark.

Calcium chloride solution. A 0.025*M* solution was prepared by dissolving 2.5 g of dried (150°) calcium carbonate in 5 ml of 12*M* hydrochloric acid and 25 ml of water. The solution was boiled, cooled and diluted up to the mark.

Magnesium chloride solution. A 0.01*M* solution was prepared by dissolving 2.03 g of $MgCl_2.6H_2O$ in water and diluting to volume.

Iron solution. A 0.01*M* solution was prepared by dissolving 0.56 g of pure iron wire in 10 ml of concentrated hydrochloric acid and diluting to volume.

Ammonia–ammonium chloride buffer (pH 10). Prepared by dissolving 67.5 g of ammonium chloride in 250 ml of water and 570 ml of liquid ammonia and diluting to volume.

Ammonium acetate, 25%. Prepared by dissolving 25 g of ammonium acetate in 100 ml of water.

Ammonium oxalate, 5%. Prepared by dissolving 5 g of ammonium oxalate in 100 ml of water.

Lactic acid, 10%. Prepared by diluting 10 ml of lactic acid to 100 ml with water.

Tetra sodium pyrophosphate, 10%. Prepared by dissolving 10 g of tetra sodium pyrophosphate in 100 ml of water.

1-(2-Pyridylazo)-2-naphthol (PAN), 0.05%. Prepared by dissolving 50 mg of the indicator in 100 ml of methanol.

Sulphosalicylic acid (solid).

Foreign ion solution. All solutions were prepared in a 250-ml calibrated flask.

Titanium (1 mg/ml). A 0.416-g sample of ignited titanium dioxide was fused with 4 g of potassium bisulphate. After cooling the fused mass was dissolved in 50 ml of 10% sulphuric acid and diluted to volume with water.

Chromium (1 mg/ml). A 0.707-g sample of dried (180°) potassium dichromate was dissolved in water and heated with 5 ml of concentrated hydrochloric acid and 15 ml of ethyl alcohol. The solution was cooled and diluted to volume with water.

Phosphorous (1 mg/ml). A 1.258-g sample of sodium dihydrogen orthophosphate was dissolved in water and diluted to volume.

Manganese (1 mg/ml). A 0.687-g sample of anhydrous manganese sulphate was dissolved in water containing 1 ml of concentrated sulphuric acid and diluted to volume.

Vanadium (1 mg/ml). A 0.574-g sample of ammonium metavanadate was dissolved in water and diluted to volume.

Procedure

Preliminary tests. A series of tests on synthetic solutions were carried out to ascertain the recovery of known amounts of iron, aluminium, calcium and magnesium in the presence of potential interferents like titanium, manganese, chromium, phosphorous and vanadium that would be encountered in the analyses of slags. Based on these experiments, a procedure was developed for the analyses of slags which is given below.

Dissolution. The sample (0.5 g) was treated with 20 ml of 12*M* hydrochloric acid and 5 ml of 16*M* nitric acid in a beaker and the mixture was carefully evaporated to dryness. A few ml of hydrochloric acid and 100 ml of water were then added and the solution was boiled. The solution was cooled and filtered through Whatman No. 40 filter paper with pulps. The residue was washed with dilute hydrochloric acid (1 + 9) 5–6 times with hot water. After removing the silica with hydrofluoric acid, the residue was fused with 2–3 g of potassium bisulphate and the cooled melt was dissolved in 5% hydrochloric acid on heating, and added to the main filtrate. The solution was transferred to a 250-ml calibrated flask and diluted to volume.

Titration of iron. A 50-ml portion of the sample solution was taken in a beaker and diluted with 50 ml of water. Ammonium hydroxide (1 + 1) was added until the solution became turbid. The turbidity cleared with a minimum quantity of dilute hydrochloric acid (1 + 3). A few drops were added in excess to adjust the pH to *ca.* 2. Then 50 mg of sulphosalicylic acid indicator were added and the solution

was warmed. This solution was titrated with standard 0.01*M* EDTA solution with constant stirring to a sharp colour change from violet to a colourless or pale yellow solution.

Titration of aluminium. After titration of iron, a known aliquot of 0.025 or 0.01*M* DCTA was added depending upon the alumina content of the sample. Then 10 ml of 10% lactic acid were added to mask titanium. The pH of the solution was adjusted to 3.5 with 25% ammonium acetate solution. The solution was just warmed and titrated the excess DCTA with 0.025 or 0.01*M* copper sulphate solution, using ten drops of PAN indicator to a sharp colour change from yellow to violet.

Titration of calcium plus magnesium. A 50-ml portion of 0.025*M* excess EDTA was added to the titrated solution after aluminium determination and 5 ml of 10% tetra sodium pyrophosphate were added to mask manganese. The pH of the solution was adjusted to 10 with ammonia buffer. The solution was warmed and the excess of EDTA was titrated with 0.025*M* copper sulphate solution with ten drops of PAN indicator to a sharp colour change from yellow to violet. This titre value corresponds to the sum of calcium and magnesium.

Titration of calcium. After the titration of calcium plus magnesium, the pH of the solution was reduced to 5 with dilute hydrochloric acid (1 + 3). Then 20 ml of 5% hot ammonium oxalate solution were added to precipitate calcium as calcium oxalate. The solution was digested for 20 min, cooled and transferred along with the precipitate to a 250-ml standard flask. The solution was diluted to the mark with the washings.

A 100-ml portion of the solution was filtered dry and then 10 ml of the ammonia buffer (pH 10) were added. The solution was warmed and the liberated EDTA equivalent to calcium was titrated with 0.025*M* copper sulphate solution with ten drops of PAN indicator until the colour turned violet, which lasted for 15–30 sec. The volume of EDTA was subtracted from the sum of calcium and magnesium titre value. The difference is the volume of EDTA required to titrate the magnesium.

A blank was also run but showed no significant amounts of iron, aluminium, calcium and magnesium.

RESULTS AND DISCUSSION

Table 1 shows the results of determination of iron, aluminium, calcium and magnesium in the presence of potential interferents like phosphorus, chromium, vanadium, titanium and manganese in synthetic solutions. Chromium[2] and vanadium[12] seriously interfere with aluminium as they form stable complexes with EDTA at pH 3.5–5.5. In the present method DCTA was preferred to EDTA in the titration of aluminium at pH 3.5, for its better selectivity in the presence of chromium[15] and vanadium.[16] It was found that chromium and vanadium up to 1.5 and 1 mg, respectively, did not interfere in the titration of aluminium at pH 3.5. More than 1.5 mg of chromium seriously interfered in the titration of aluminium due to the formation of a purple complex of Cr–DCTA. Vanadium more than 1 mg could not be tolerated as the transition of colour change of the indicator was not sharp. However, the chromium and vanadium content in slags is not usually more than 1% of each.

Phosphate[13] interferes in the titration of calcium and magnesium at pH 10. In the present method the phosphate interference was obviated by back titration of excess EDTA with copper sulphate so that all calcium present combined with EDTA. There is no evidence of the complexation of copper with phosphate and as expected phosphorus up to 16 mg did not

Table 1. Titration of Fe, Al, Ca and Mg in the presence of various potential interferents

Element added, *mg*		Taken, *mg* Standard method				Found, *mg* Proposed method			
		Fe	Al	Ca	Mg	Fe	Al	Ca	Mg
P	16.0	2.8	13.5	20.0	3.6	2.78	13.52	20.08	3.58
Cr	1.5	2.8	13.5	20.0	3.6	2.78	13.53	20.10	3.57
V	1.0	2.8	13.5	20.0	3.6	2.82	13.56	20.05	3.58
Ti*	3.0	2.8	13.5	20.0	3.6	2.82	15.60	20.10	3.57
Mn†	12.0	2.8	13.5	20.0	3.6	2.82	13.48	20.08	9.53

*Interferes with Al.
†Interferes with Mg.

Table 2. Titration of Fe, Al, Ca and Mg in the presence of Ti (masking agent for Ti: 10 ml of 10% lactic acid)

Ti added, mg	Taken, mg Standard method				Found, mg Proposed method			
	Fe	Al	Ca	Mg	Fe	Al	Ca	Mg
3.0	2.8	13.5	20.0	3.6	2.78	13.52	20.04	3.58
5.0	2.8	13.5	20.0	3.6	2.82	13.54	20.08	3.58
7.0	2.8	13.5	20.0	3.6	2.80	13.54	20.10	3.56

Table 3. Titration of Fe, Al, Ca and Mg in the presence of Mn (masking agent for Mn: 5 ml of 10% tetra sodium pyrophosphate)

Mn added, mg	Taken, mg Standard method				Found, mg Proposed method			
	Fe	Al	Ca	Mg	Fe	Al	Ca	Mg
8.0	2.8	13.5	20.0	3.6	2.82	13.50	19.97	3.62
10.0	2.8	13.5	20.0	3.6	2.80	13.54	20.04	3.58
12.0	2.8	13.5	20.0	3.6	2.80	13.56	19.97	3.62

interfere (Table 1). Actually in synthetic solution phosphorus was added in excess of that normally found in slags.

Titanium and manganese seriously interfere with the determination of aluminium and magnesium, respectively, as they form stable complexes at pH 3.5 and 10 (Table 1). In the present method lactic acid[11] was used to mask titanium and addition of 10 ml of 10% lactic acid was found to mask up to 7 mg of titanium as shown in Table 2. However, for more than 7 mg of titanium, the end point was sluggish. Fog[17] used potassium cyanide for masking manganese in EDTA titration of magnesium. In the present method cyanide cannot be used as a masking agent because copper sulphate is used as back titrant. The interference due to manganese was eliminated by complexing it with tetra sodium pyrophosphate.[14] The stability constant of the manganese–pyrophosphate complex is not known. However, it was observed that in the presence of tetra sodium pyrophosphate, manganese does not react with EDTA. This shows that the manganese–pyrophosphate complex must be more stable than the manganese–EDTA complex. In the present method it was observed that 5 ml of 10% tetrasodium pyrophosphate were able to mask up to 12 mg of manganese (Table 3). The concentration of masked manganese is well above the concentration of manganese found in slags.

Table 4 shows the results of analysis of iron, aluminium, calcium and magnesium in some slags by the proposed method. The results of

Table 4. Determination of Fe, Al_2O_3, CaO and MgO in slags

Slags		Certified value, %	Found by proposed method,* %	Deviation
BCS No. 381	Fe	13.30	13.20	−0.1
Basic slag	Al_2O_3	0.67	0.63	−0.04
	CaO	49.00	49.30	+0.3
	MgO	1.03	0.97	−0.06
BCS No. 382/1	Fe	19.90	19.70	−0.2
Basic slag	Al_2O_3	3.79	3.86	+0.07
	CaO	40.10	40.30	+0.2
	MgO	3.73	3.68	−0.05
BCS No. 367	Fe	0.78	0.73	−0.05
Blast furnace slag	Al_2O_3	20.00	20.10	+0.1
	CaO	32.40	32.60	+0.2
	MgO	7.10	6.97	−0.13
Submerged arc	Fe	4.48†	4.43	−0.05
furnace slag	Al_2O_3	14.33†	14.36	+0.03
	CaO	38.30†	38.60	+0.3
	MgO	2.49†	2.45	−0.04

*Average of three determinations.
†Standard conventional method.

analysis are in very good agreement with the certified values and the values obtained by the standard conventional method. Though the value of calcium oxide reported by the proposed method is higher than the certified value, the deviations reported in the Table are within the precision of the method.

The proposed method is simple, rapid and accurate, and avoids multi-separation steps that are often involved in the standard conventional methods. A set of five samples can be analysed for iron, aluminium, calcium and magnesium in four hours as compared to three days by standard conventional methods.

Acknowledgement—The authors thank Prof. S. Banerjee, Director, National Metallurgical Laboratory, Jamshedpur for his kind permission to publish this paper.

REFERENCES

1. W. W. Scott, *Standard Methods of Chemical Analysis*, 5th Ed., Vol. I, p. 208. Technical Press, London, 1939.
2. G. Schwarzenbach and H. Flaschka, *Complexometric Titrations*, 2nd Ed., Trans. H.M.N.H. Irving, Methuen, London, 1969.
3. V. Williams, *Iron Steel (London)*, 1955, **28**, 525.
4. I. N. Basilevskaya, *Zavod. Lab.*, 1956, **22**, 166.
5. P. Szarvas, J. Korondan and I. Raisz, *Magy. Kem. Lab.*, 1967, **3**, 149.
6. A. Hitchen and G. Zechanowitsch, *Talanta*, 1980, **27**, 269.
7. W. Westwood and R. Presser, *Analyst*, 1951, **76**, 191.
8. V. Rett, *Hutn. Listy*, 1965, **20**, 134.
9. N. N. Lapin, A. T. Slyusarev and N. S. Prilutskaya, *Sb. Nauch, Trud. Zhdanovsk. Metallurgy, Inst.*, 1960, 393.
10. E. Vanninen and A. Ringbom, *Anal. Chim. Acta*, 1955, **12**, 308.
11. Y. C. Chen and H. Y. Li, *Acta Chim. Sin.*, 1965, **31**, 391.
12. D. Filipov and N. Kirtscheva, *Compt. Rend. Acad. Bulg. Sci.*, 1964, **17**, 467.
13. C. Cimerman, A. Alon and J. Mashall, *Anal. Chim. Acta*, 1958, **19**, 461.
14. J. C. Bailar Jr., H. J. Emeleus, Sir R. Nyholm and A. F. Trotman Dickenson, *Comprehensive Inorganic Chemistry*, 1st Ed., 1973, 830.
15. R. Pribil and V. Vesely, *Talanta*, 1962, **9**, 23.
16. E. Lassner and R. Puschel, *Mikrochim. Ichnoanal. Acta*, 1963, 950.
17. H. M. Fog, *Acta Chem. Scand.*, 1968, **22**, 791.

Talanta, Vol. 39, No. 6, pp. 681–685, 1992
Printed in Great Britain

0039-9140/92 $5.00 + 0.00
Pergamon Press Ltd

WASTE WATER ANALYSIS BY PURGE AND TRAP CAPILLARY GC–FTIR SPECTROMETRY

J. PHILIPPAERTS, C. VANHOOF and E. F. VANSANT
University of Antwerp, Universiteitsplein 1, 2610 Wilrijk, Belgium

(*Received* 9 *February* 1991. *Revised* 29 *July* 1991. *Accepted* 4 *September* 1991)

Summary—Gas chromatography with Fourier transform infra-red spectroscopic detection (GC–FTIR) is used for the analysis of waste water samples. Compared to GC–MS, this technique offers a more complete identification of organic compounds. Lower concentrations of organic volatiles however require preconcentration techniques such as a Purge and Trap (P&T) preconcentrator. Using this combination, concentrations of organic volatiles in the ppb range can be detected and positively identified.

The analysis of waste water containing volatile organic compounds is often carried out by gas chromatography with mass spectrometric detection (GC–MS). Due to the high sensitivity of the detector it is even possible to sample the vapor phase above the water surface (head space analysis). In this way, detection problems which are caused by the water are avoided. However, using the mass spectrometer as a detector, a lot of compounds can only be partially identified.[1] The compound functionality can be recognized in this way, but useful information is obtained about the aliphatic portion of the molecules. Here IR-spectra can give additional (or complementary) information.[2,3] The IR spectra clearly show the functional groups of a compound and allow an accurate identification. The possibility of GC–FTIR to distinguish isomeric forms, contrary to GC–MS, makes it an interesting analytical tool to determine and identify volatiles. Conventional gas chromatography–Fourier transform infra red (GC–FTIR) measurements, however, also deal with problems when waste water is injected "as such". Concentrations are limited to the parts per thousand and ppm ranges since the injected volumes are only microlitres and the IR-detection requires several nanograms of the products. Water can damage the potassium bromide lightpipe windows and disturb the measurements. Since the IR detection limits are much higher than MS,[4] the head space analysis technique is not suitable here. When the concentration of volatile compounds is very low (ppm to ppb range), extraction or preconcentration procedures are necessary.

The IR detection problem can be solved by the use of Purge and Trap (P&T) preconcentrators.[5] This method is already widely used in combination with gas chromatography and GC–MS. One might expect that, when coupled with GC–FTIR, the suitability of this method will be enhanced. Indeed, the analysis of volatiles in water or solids (*e.g.*, soils) using this technique allows for detection of very small amounts of compounds (down to the ppb-range). This paper demonstrates the performance in the case of waste water samples.

EXPERIMENTAL

Different types of aqueous mixtures and waste water samples were analysed with the Purge and Trap capillary GC–FTIR system.

Synthetic aqueous mixtures were prepared by adding compounds to water so that for each component a final concentration of 0.5 ppm was obtained. The 50 ppb and 10 ppb samples were prepared by diluting the original 0.5 ppm sample. The organic compounds given in Table 1 are the components of the mixture which is described further in this paper.

An unknown waste water sample, obtained from a petrochemical company was also analysed. Furthermore, the performance of a substrate to efficiently remove the organic compounds or pollutants from water is shown. The substrate used for the removal of organic compounds was a synthetic zeolite, silicalite, obtained from Union Carbide.

For each analysis a sample of 5 or 25 ml was taken in a 5- or 25-ml fritted sparge tube of a

Table 1. Components of the synthetic aqueous mixture

Methanol	Chlorobenzene
Isopropanol	Toluene
1-Butanol	*o*-Xylene
Ethoxyethanol	Benzene
Diethylether	Ethylacetate
Propylacetate	Thiophene
4-Methyl-2-pentanone	α-Chloro-*p*-xylene
1,1,2,2-Tetrachloroethane	1,2,4-Trichlorobenzene
2-Chlorotoluene	Dimethylamine
N,N-Dimethylaniline	

Tekmar LSC 2000 Purge and Trap Concentrator. The purge conditions depended on the type of sample used (see Table 2).

The volatiles are trapped on a Tenax column which is then desorbed at room temperature for the removal of adsorbed water (dry purge). After desorption at 200°, the effluents are transferred through a heated glass-lined transfer line (180°) to a trap at −120° of a capillary interface. After the transfer, the interface is heated very quickly to 200° so that an "on column" injection can take place (injection over 2 min). A HP 5890 GC is used, which communicates with the Nicolet computer of the FTIR-spectrometer (Model 20SX). The Tekmar concentrator automatically gives the start signal when the injection begins.

A wall-coated open tubular (WCOT) fused silica (25 m × 0.32 mm I.D., 0.4 μm CP-Sil-5 CB) column was used with a He flow of 0.8 ml/min. Before the entrance of the light pipe, an additional He flow of 0.4 ml/min (make up gas) was added in order to obtain a good transport of the column output. This also reduces tailing effects.[6]

The temperature program for all the analyses was a constant temperature at 30° for three minutes, then a gradual increase of 10°/min to 200°, which is then held until all compounds are eluted.

The medium band MCT (mercurium–cadmium–tellurium)-detector takes 7 scans/sec at 8 cm^{-1} resolution. For analysis of the compounds the GC elutes past the light pipe and the IR spectra are measured in real time using a gold coated 1.0 mm × 15.0 cm proprietary light pipe (at 220°). The GC column is connected directly to the light pipe inlet in order to reduce the dead volume. The outlet of the light pipe is connected to the FID detector of the GC.

The spectral search was carried out with the Aldrich Vapor Phase library containing the spectra of about 5000 compounds.

RESULTS AND DISCUSSION

Synthetic mixtures

The 640–1200 cm^{-1} reconstruction chromatograms obtained from the analysis of the 0.5 ppm, 50 ppb and 10 ppb synthetic aqueous samples are plotted in Fig. 1. From the 19 compounds in the mixture, 14 could be detected and completely identified in the 0.5 ppm sample (in one experiment α chloro-*p*-xylene was also detected). In the 50 ppb and the 10 ppb mixture, respectively 13 and 11 compounds were still detectable with complete identification (Table 3).

Of the 5 undetectable compounds in the 0.5 ppm sample, 3 were alcohols and one was an amine. These types of compound are known to possess a low purge efficiency due to their high aqueous solubility. Therefore their detection limit is higher than 0.5 ppm.

From these results it can be concluded that the detection limits for several compounds are in the low ppb range. Indeed, note that neither the GC-program, nor the column was optimized for the analysed compounds.

Waste water

The waste water sample contained rather high concentrations of volatile organic compounds, so that a "fingerprint" of the major organic compounds was obtained by purging for only two minutes at 45 ml/min. The upper curve in Fig. 2 shows the Gram–Schmidt reconstruction

Table 2. Purge conditions for aqueous samples

Sample	Sparger, *ml*	Temp, *°C*	Time, *min*	Flow-rate, *ml/min*	Dry purge, *min*
0.5 ppm Mixture	5	25	11	45	2
50 ppb Mixture	25	40	10	45	12
10 ppb Mixture	25	40	20	45	12
Unknown waste water	5	25	2	45	5
Treated sample B	5	25	2	45	5
Treated sample C	5	25	2	45	5
Treated sample C	5	25	6	45	12

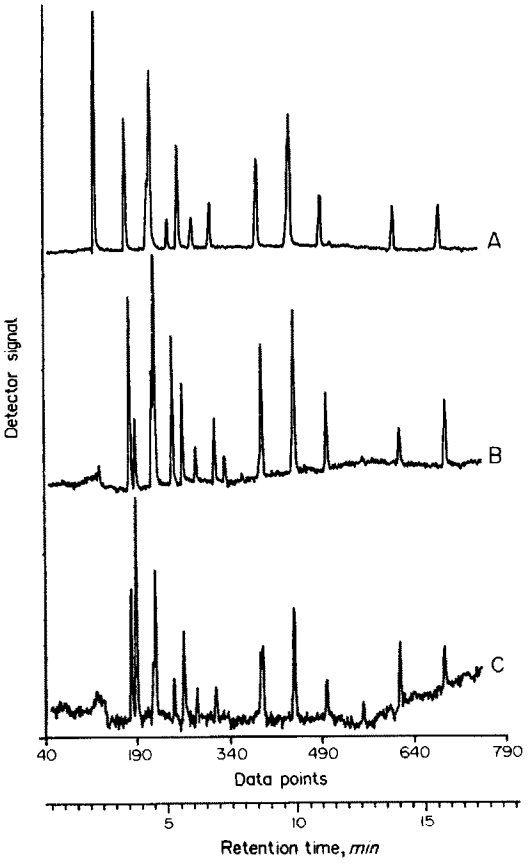

Fig. 1. 640–1200 cm^{-1} reconstruction chromatogram of A: the 0.5 ppm aqueous sample. B: the 50 ppb aqueous sample. C: the 10 ppb aqueous sample.

chromatogram from this measurement. The lower curve shows a 640–1200 cm^{-1} reconstruction chromatogram which clearly demonstrates fingerprint patterns since water had no contribution to the signal in this region. Table 4 lists

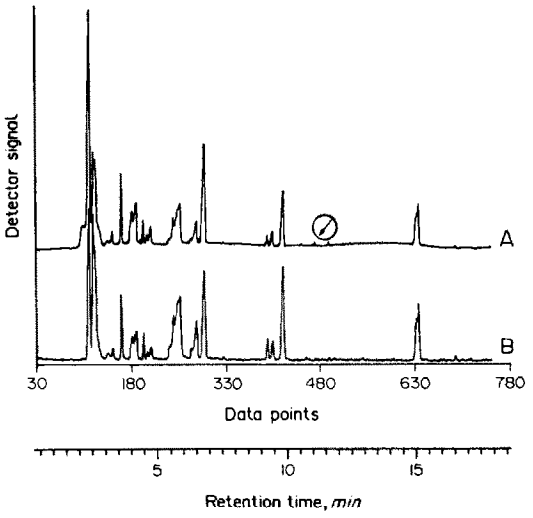

Fig. 2. A: Gram–Schmidt reconstruction chromatogram. B: 640–1200 cm^{-1} reconstruction chromatogram of waste water.

the major compounds detected in this waste water with the complete (+) or partial (≈) identification as obtained by the library search. Figure 3 shows the spectral quality of a low-intensity peak in the chromatogram (indicated by an arrow) and the best library search result from the Aldrich Vapor Phase library.

Note that isopropanol and 2-ethoxyethanol are detectable in this waste water mixture while they are not observed in the synthetic mixtures. These observations indicate that the concentrations of these compounds are significantly higher than 0.5 ppm.

The P&T–GC–FTIR analysis method was also used to analyse various waste water samples and to study the selective adsorption

Table 3. Detectable compounds in the aqueous 0.5 ppm, 50 ppb and 10 ppb mixtures

Compounds	Retention time, *min*	Mixture 0.5 ppm	50 ppb	10 ppb
Diethylether	2.66	+	+	−
Ethylacetate	3.88	+	+	+
Benzene	4.80	+	+	+
Thiophene	4.95	+	+	+
1-Butanol	5.13	+	−	−
Propylacetate	6.03	+	+	+
4-Methyl-2-pentanone	6.59	+	+	+
Toluene	7.35	+	+	+
Chlorobenzene	9.29	+	+	+
o-Xylene	10.60	+	+	+
1,1,2,2-Tetrachloroethane	10.80	+	+	−
2-Chlorotoluene	11.98	+	+	+
N,N-Dimethylaniline	14.98	+	+	+
1,2,4-Trichlorobenzene	16.93	+	+	+

+: detected; −: not detected.
Detected once in the 0.5 ppm mixture: α chloro-*p*-xylene.
Not detected: methanol, isopropanol, ethoxyethanol, dimethylamine.

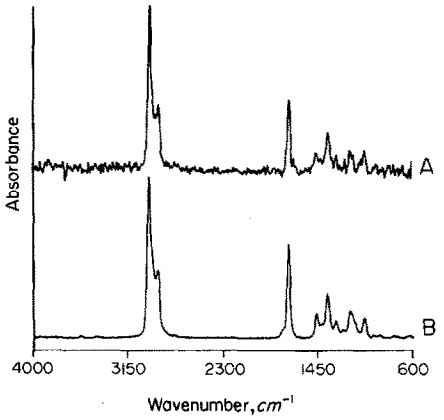

Fig. 3. A: I.R. spectrum of the GC peak at time 10.97 min (indicated by the arrow in Fig. 2). B: best library search result (Aldrich Vapor Phase) is 2-methyl-4-heptanone.

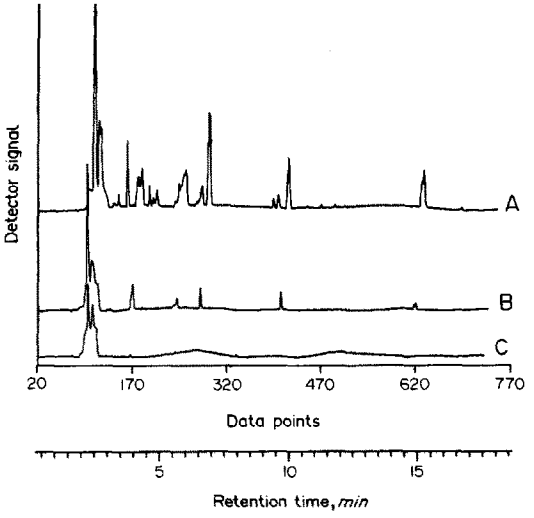

Fig. 4. Gram–Schmidt reconstruction chromatograms of A: waste water (pure). B: waste water in contact for 5 min with silicalite. C: after a second contact with fresh silicalite.

of the organic compounds on different sorbents effective in the removal of the organic pollutants. This is demonstrated in Fig. 4, which shows the Gram–Schmidt reconstruction chromatogram of the waste water (sample A) and, using the same purge conditions, of the waste water after a 5-min contact time between 100 ml of waste water and 1 gram of a highly siliceous aluminosilicate (silicalite) (treated sample B). The selectivity depends upon the nature of the organic compounds as can be seen with this technique for each type of waste water.

A second contact (again for 5 min) between the former water sample and one gram of fresh silicalite (treated sample C) resulted in an almost "clean" water as shown by the reconstruction chromatogram in Fig. 4C. Compounds with a low boiling point (*e.g.*, acetone) are still present in rather high concentrations, indicating the lower capacity of the silicalite for these compounds. This phenomenon might be explained by break through effects.

Table 4. Major compounds detected in the waste water sample

Peak number	Retention time, *min*	Compound identification	Best library search result
1	2.33	+	Acetone
2	2.48	≈	Ester of formic acid
3	2.58	+	Isopropanol
4	3.07	+	Propanol
5	3.30	+	2-Butanone
6	3.60	+	Ethylacetate
7	3.99	+	2-Methyl-1-propanol
8	4.52	+	Isopropylacetate
9	4.65	+	1-Butanol
10	5.55	+	Propylacetate
11	5.62	+	2-Ethoxyethanol
12	5.75	+	Formic acid butyl ester
13	5.93	+	2-Butoxyethanol
14	6.42	≈	Ethyleneglycoldiethylether
15	6.88	+	Isobutylacetate
16	7.77	+	Amylacetate
17	9.56	+	2-Butoxyethylacetate
18	9.71	+	2-Butoxyethanol
19	10.12	≈	Ester of acetic acid
20	10.97	+	2-Methyl-4-heptanone
21	11.53	+	2,6-Dimethyl-4-heptanol
22	12.07	+	2-Ethyl-1-hexanol
23	15.62	+	1,2-Butoxyethoxy-2-propanol
24	17.20	+	2-Butoxyethylacetate

+: complete identification.
≈: partial identification.

Table 5. Compounds detected in treated waste water C

Peak number	Retention time, *min*	Compound identification	Best library search result
1	2.33	+	Acetone
2	2.48	+	Isopropylacetate
3	3.12	+	1-Propanol
4	4.06	+	2-Methyl-1-propanol
5	5.91	+	2-Ethoxyethanol
6	8.33	≈	Dichloroethylene
7	11.20	+	Phenol
8	12.55	≈	2-Tert.butyl-5-methyl-cyclohexanol

+: complete identification.
≈: partial identification.

In order to identify the compounds in this last water sample, the purge conditions were changed (6 min purge at room temperature, 12 min dry purge) so that the detection of these compounds (Table 5) could be enhanced.

Many organic alcohols are observed, indicating the relationship between group functionality and adsorption phenomena in the waste water treatment with silicalite under conditions as described above.

CONCLUSION

The Purge and Trap preconcentration technique was used in combination with GC–FTIR. It displays several advantages over GC–MS. The detection of low concentrations of organic volatiles is combined with superior identification power.

Applications to waste water prove sensitive, reproducible and less time-consuming than extraction techniques. Various types of volatiles can be identified completely by this analysis method and the purification by adsorbers can be directly assessed. By selecting a suitable substrate organics are very efficiently removed from the waste water.

REFERENCES

1. K. H. Shafer, T. L. Hayes, J. W. Brasch and R. J. Jacobsen, *Anal. Chem.*, 1984, **56**, 237.
2. D. F. Gurka, M. Hiatt and R. Titus, *ibid.*, 1984, **56**, 1102.
3. D. F. Gurka, *Appl. Spectr.*, 1985, **39**, 827.
4. P. E. Kester, Tekmar Application Notes.
5. D. F. Gurka, R. Titus, D. Henry and A. Giorgetti, *Anal. Chem.*, 1987, **59**, 2362.
6. E. S. Olson and J. W. Diehl, *ibid.*, 1987, **59**, 443.

Talanta, Vol. 39, No. 6, pp. 687–691, 1992
Printed in Great Britain

0039-9140/92 $5.00 + 0.00
Pergamon Press Ltd

APPLICATION OF REDOX REACTIONS IN SPECTROPHOTOMETRY—I

THE IRON(III)/1,10-PHENANTHROLINE COMPLEX AS A REAGENT FOR THE DETERMINATION OF SOME ANIONS AND ORGANIC COMPOUNDS

S. KOCH and G. ACKERMANN
Bergakademie Freiberg, Fachbereich Chemie, 0-9200 Freiberg, Germany

(*Received* 12 *February* 1990. *Revised* 5 *November* 1991. *Accepted* 20 *November* 1991)

Summary—It is shown that the complex of iron(III) with 1,10-phenanthroline(phen) is suitable as a reagent for determination of some anions and organic compounds. By a redox reaction with the analytes the reagent forms the intensely coloured chelate $[Fe(phen)_3]^{2+}$, which is extractable as an ion-association complex with a suitable counter-ion and allows the development of sensitive spectrophotometric methods of determination. Besides the fundamentals, some remarks on analytical applications are given.

There are comparatively few spectrophotometric methods for the determination of anions. Many of them are indirect methods based on the effect of side-reactions in methods for determination of cations. Another possibility is the use of redox reactions giving products which are suitable for photometric determination.[1,2]

Redox reactions can be described by the generalized formula

$$m\mathrm{Ox}_r + n\mathrm{Red}_s \rightleftharpoons p\mathrm{Red}_t + q\mathrm{Ox}_w \qquad (1)$$

which allows for the participation of polynuclear species. Ox_r and Red_t may be complexes of a metal (in two oxidation states M and M′) with a ligand, and equation (1) can be rewritten as

$$m\mathrm{M}_r\mathrm{L}_x + n\mathrm{Red}_s \rightleftharpoons p\mathrm{M}'_t\mathrm{L}_y + q\mathrm{Ox}_w \qquad (2)$$

where x and y may or may not be equal, depending on the nature of the metal ion and the ligand. One or both of these complexes may be coloured, which would make the system useful for spectrophotometric analysis. A further possibility is extraction of one of the species involved, which can increase the selectivity and sensitivity. The sensitivity will depend on several factors, such as the completeness of the redox and/or complexation reactions, the distribution coefficient if an extractable species is formed, and any solvent or other effects on the molar absorptivity of the species selected for measurement.

The iron(III)/phenanthroline system[3–6] is particularly useful, since the reduction product obtained from it is always ferroin, $[Fe(phen)_3]^{2+}$, which has a fairly high molar absorptivity, is stable, and can be extracted as an ion-association complex with perchlorate, iodide *etc.* as counter-ion.

EXPERIMENTAL

The spectrophotometric measurements were performed with a Beckman DU spectrophotometer and a Zeiss Specord M 40 instrument. The pH adjustments were made with dilute acid or ammonia solutions and controlled by use of an MV 870 pH-meter (VEB Präcitronic, Dresden). For measurement of electrode potentials a platinum-electrode/SCE combination and the MV 870 were used at 25°. All potentials became stable after 15 min.

Aqueous solutions of ionic strength 0.3 (Na_2SO_4) were used at room temperature for all measurements. The components were mixed in the following order: Fe(III), phen, sodium sulphate, pH adjuster, reductant. The solutions must be protected by an atmosphere of nitrogen.

Reagents

The parent 1*M* iron(III) solution was prepared by dissolving $Fe_2(SO_4)_3 \cdot x H_2O$ (*p.a.*, Riedel de Haën) in 0.1*M* sulphuric acid and

standardized by titration with 0.1*M* EDTA (tiron as indicator).

Fe^{2+} solutions were always freshly prepared from $(NH_4)_2Fe(SO_4)_2 \cdot 6H_2O$ (*p.a.*, UCB). The 0.01*M* 1,10-phenanthroline solution was made by dissolving the solid (*z.A.*, Chemapol) in 0.05*M* sulphuric acid. The degree of purity of the phen was checked by potentiometric titration of an aqueous solution with 0.1*M* hydrochloric acid (glass electrode). All the organic compounds tested were commercial products, the purity of which was checked by determination of the melting point or refractive index.

The system Fe^{3+}/phen

1,10-Phenanthroline is almost completely insensitive to oxidizing agents. Both its nitrogen atoms can be protonated, resulting in the following protolytic equilibria:[7]

$$H_2phen^{2+} \rightleftharpoons Hphen^+ + H^+ (pK_{a1} = 1.9)$$

$$Hphen^+ \rightleftharpoons phen + H^+ (pK_{a2} = 4.96)$$

In aqueous solutions Fe^{3+} and phen can form different chelates. Oxidation of the red iron(II) chelate results in the blue complex $[Fe(phen)_3]^{3+}$ ($\log \beta_3 = 14.1$).[8] The direct reaction of iron(III) and phen leads to a binuclear yellow-brown compound. The blue chelate slowly changes into the yellow-brown form, probably because steric repulsion takes place in the trichelate.[9]

According to Anderegg[10] the yellow-brown solution contains different species, with the ratio Fe:phen = 2:4. Other work[11] with dilute solutions ($c_{Fe} = 10^{-3}M$) has shown that formation of the complex is complete at pH 3–4 in presence of excess of the ligand ($c_{phen}/c_{Fe} \geq 3$). The species $[Fe_2(OH)_2(phen)_4]^{4+}$, $[Fe_2(OH)O(phen)_4]^{3+}$ and $[Fe_2O_2(phen)_4]^{2+}$ were identified, and have hydroxo or oxo bridges between the metal ions.

It is scarcely necessary to emphasize that the blue chelate is not suitable for photometric determination, because of its low kinetic stability. However, the yellow-brown dimer shows good stability at room temperature. When higher temperatures, which may be needed in the application of redox reactions, are used, the system Fe^{3+}/phen in the pH range 2–9 ($c_{Fe} = 10^{-3}M$, heated for 1 hr at 60°) shows the following behaviour after cooling to room temperature.

In the interval from pH 3.2 to 4.2 a precipitate is formed in the clear solutions, which is soluble in methanol or hydrochloric acid to give a yellow solution containing iron(III) and phenanthroline. It is supposed that a polymeric Fe^{3+}–phen product is formed. This effect does not occur in more dilute solutions, with $c_{Fe} = 10^{-4}M$. Therefore use of lower reagent concentrations is more suitable in practical applications.

The system Fe^{2+}/phen

The very stable covalent chelate $[Fe(phen)_3]^{2+}$ ($\log \beta_3 = 21.3$)[8] exists in the system Fe^{2+}/phen. As spectrophotometric and electrophoretic examinations have shown, the orange-red complex (ferroin) is stable in water in the pH range 2–9 and also in water–methanol (1:1 v/v) mixtures. Ferroin exhibits typical charge-transfer absorption by intramolecular electron-exchange:

$$[Fe(II)(phen)_3]^{2+} \rightleftharpoons [Fe(III)(phen)_2(phen)^-]^{2+}$$

The effect is based on electron transfer from an occupied level of Fe(II) to the unoccupied orbital of the ligand. As a result there are maxima at 450 and 490 nm and a main band at $\lambda_{max} = 510$ nm. From repeated measurements the molar absorptivity at 510 nm is found to be $\epsilon = (1.119 \pm 0.009) \times 10^4$ $l \cdot mole^{-1} \cdot cm^{-1}$ (*P* 0.95; 100 replicates).

For its practical application it is advantageous that the complex gives not only high sensitivity, but also has very good kinetic stability, its solutions being stable for some months and not affected by heating.

There is also the possibility of extracting the chelate as an ion-association complex, into an appropriate organic solvent:[12]

$$[Fe(phen)_3]^{2+}_{aq} + 2R^-_{aq} \rightleftharpoons \{[Fe(phen)_3]^{2+} \cdot 2R^-\}_{org}$$

where R^- is a colourless counter-ion such as ClO_4^-, I^-, CN^-. In this way the sensitivity can be further increased. Extended research work[13] has shown that perchlorate in combination with EDTA as a sequestering agent and nitrobenzene as the solvent is very suitable, because the interference of excess of iron(III) can be eliminated.

Electrode potentials in the Fe^{3+}/Fe^{2+}/phen system

The orange-red Fe^{2+} complex, when used as a redox indicator (ferroin), is oxidized to the blue Fe^{3+} chelate:

$$[Fe(phen)_3]^{2+} \rightleftharpoons [Fe(phen)_3]^{3+} + e^- \qquad E^0 \sim 1.0 \text{ V}$$

Because of the instability of the blue product, this reaction is of no importance for photometric determination. On the other hand, the electrode potentials for the brown-yellow forms $[Fe_2O_2(phen)_4]^{i+2+}$ $(i = 0, 1, 2)$ have not been known up to now. Therefore these potentials and their dependence on pH were determined. The results are shown in Fig. 1. As can be seen, the system Fe^{3+}/Fe^{2+}/phen acts as an oxidizing agent, and the higher potential of 0.85 V (compared with that of 0.77 V for the system Fe^{3+}/Fe^{2+}) has its cause in the high stability of the iron(II) chelate $[Fe(phen)_3]^{2+}$. It can also be seen that the redox potential can be influenced by the pH over a wide range. The following iron(III) species are mainly involved in this behaviour:

pH 2.0 $[Fe_2(OH)_2(phen)_4]^{4+}$; Fe^{3+}

pH 3.0 $[Fe_2O(OH)(phen)_4]^{3+}$; $Fe(OH)_2^+$

pH 4.0 $[Fe_2O(OH)(phen)_4]^{3+}$; $Fe(OH)_2^+$

pH 5.0 $[Fe_2O(OH)(phen)_4]^{3+}$; $Fe(OH)_2^+$

pH 6.0 $[Fe_2O_2(phen)_4]^{2+}$; $Fe(OH)_2^+$

With increasing pH more and more protolytic (and also polynuclear) forms of iron(III) appear in addition to the iron chelates, so the real potential decreases with increasing pH. At pH 4 only one species of the iron(III) complex exists and the redox equilibrium can be written as

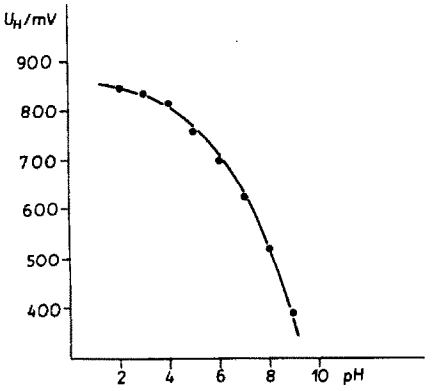

Fig. 1. Conditional potentials (U_H) of the system Fe^{3+}/Fe^{2+}/phen as a function of pH. $[Fe^{3+}] = [Fe^{2+}] = 10^{-3}M$; $c_{phen}/c_{Fe} = 5$; temperature = 25°; (Na_2SO_4).

Reactions with the Fe^{3+}/phen system

For reactions with this system the analyte A must be a reducing agent.

$$[Fe_2(OH)_2(phen)_4]^{4+} + 2phen + A \rightleftharpoons 2[Fe(phen)_3]^{2+} + 2OH^- + A^*$$

(A* = oxidation product of A)

The identification of the type of reaction results from the experimental examination of the colour reaction by measuring λ_{max} after reaching the equilibrium of system S and comparison with a solution of known composition (system C).

Starting system, S	System for comparison, C	
(Fe^{3+}, phen, A)	(Fe^{2+}, phen)	$\lambda_{max}(S) = \lambda_{max}(C)$ redox reaction
(Fe^{3+}, phen, A)	(Fe^{2+}, phen)	$\lambda_{max}(S) \neq \lambda_{max}(C)$ complex formation
(Fe^{3+}, phen, A)	(Fe^{2+}, A/phen)	$\lambda_{max}(S) = \lambda_{max}(C)$ formation of a binary complex
(Fe^{3+}, phen, A)	(Fe^{2+}, A/phen)	$\lambda_{max}(S) \neq \lambda_{max}(C)$ formation of a ternary complex

$$2[Fe(phen)_3]^{2+} + 2H_2O \rightleftharpoons [Fe_2O(OH)(phen)_4]^{3+} + 2Hphen^+ + H^+ + 2e^- \qquad (E = 0.82\ V)$$

This shows that the Fe^{3+}/phen reagent system is suitable for photometric determination and that some selectivity will arise because of the medium oxidation potential.

For practical application is was necessary to find out which experimental factors significantly affect the reaction. With the aid of the multifactor design due to Plackett and Burman[14] and pyrocatechol as a model, the absorbance was used as an output (2 parameter levels, 4 variables and 3 dummy variables). Table 1 gives the corresponding formalism, and the parameter

Table 1. Variables of the design matrix[14] for reaction of iron(III), 1,10-phenanthroline and pyrocatechol

Influencing factor	Variables	Low level (−)	High level (+)
pH	x_A	3.0	7.0
$[Na_2SO_4]$, M	x_B	0.01	0.1
Time, hr	x_C	1	3
[phen], M	x_D	5×10^{-4}	1×10^{-3}

levels. The measured absorbances between 0.134 and 0.220 resulting from the individual experiments (λ 510 nm; 1-cm cells; $c_{Fe} = 10^{-4}M$; $c_{Pyr} = 5 \times 10^{-6}M$) gave the following values for the estimated extent, W_i, of the influence[15] of the factors examined:

$$|W_A| = 0.035 > W^*$$

$$|W_B| = 0.003 < W^*$$

$$|W_C| = 0.045 > W^*$$

$$|W_D| = 0.014 < W^*$$

$$W^* = 0.016$$

The calculated values W_i are significant only if they are greater than the standard deviation, and a factor has a valid influence if $W_i \geqslant W^* = t_{(0.99,f)}s$.[15] The values of W_i and W^* shown above indicate that only pH (x_A) and time (x_C) significantly influence the system. The concentration of phen is without influence if at least a 5-fold excess relative to iron(III) is used. Likewise the concentration of sodium sulphate up to an ionic strength of 0.3 is without effect.

Further experiments made it plain that these reactions generally need some hours to reach equilibrium. We suppose that the reactions run by an inner-sphere mechanism, since it has been reported that iron(III) complexes with 1,10-phenanthroline and oxalate[16] occur as a typical transition state. These compounds are destroyed by the action of light or heat by an intramolecular redox reaction, forming carbon dioxide and $[Fe(phen)_3]^{2+}$. With pyrocatechol (H_2R) a mixed-ligand complex also exists in weakly alkaline solution (pH_{max} 9.3):[17]

$$Fe^{3+} + 2HR^- + \text{phen} \rightleftharpoons [Fe(phen)R_2]^- + 2H^+.$$

Because many organic compounds are reducing agents, we tested a selection of them. As the reaction is kinetically hindered, the reaction rate must be increased by use of a higher temperature. The conditions used were $c_{Fe} = 10^{-4}M$; $c_{phen}:c_{Fe} = 10$; $c_A:c_{Fe} = 0.1$; pH = 2–9; temperature 60°.

As expected, hydrocarbons (n-heptane, cyclohexane, benzene), alcohols (ethanol, benzyl alcohol, glycerol), carboxylic acids (acetic, oxalic, benzoic), ethers (diethyl, dioxan) and aliphatic amines (ethylenediamine, triethanolamine, triethylamine) do not react with Fe^{3+}/phen. It is unexpected, however, that aldehydes (formaldehyde, acetaldehyde, benzaldehyde) and ketones (acetone, isobutyl methyl ketone) also give no colour reaction. Phenols react only if their OH-groups are free; their esters or ethers (anisole) do not react. The reaction behaviour of monophenolic compounds is strongly dependent on the nature of any substituents. Phenols, cresols, xylenols and methoxyphenols undergo colour reactions, but nitro- (4-nitrophenol, 2,4-dinitrophenol, picric acid) and halogen-substituted compounds (2-chlorophenol, 4-chlorophenol) as well as other phenols substituted with groups with a $-I$ effect (salicylic acid, salicylaldehyde, methyl p-hydroxybenzoate) do not react. In the case of polyphenols the reactions are positive for all types of compounds (diphenols, triphenols, substituted compounds). This is also valid for dyes (Eriochrome Black T, Bromopyrogallol Red, PAR) with aromatic OH-groups. However, these reactions do not have better sensitivity. It is of interest that compounds with quasi-aromatic OH-groups (kojic acid, meconic acid) do not react. Naphthols (1-naphthol, 2-naphthol, 2,3-dihydroxynaphthalene, chromotropic acid) form intensely coloured products.

Aliphatic enols (acetylacetone, acetoacetic ester) can act as reducing agents, because of the keto–enol tautomerism. Acetylacetone gives only a weak colour reaction, as a result of the low concentration of the enol form. Acetoacetic ester hardly reacts at all because the equilibrium is even more in favour of the ketone. Ascorbic acid, as an enediol, shows an intense colour reaction, which occurs even at room temperature. Aromatic amines exhibit reactions similar to those of the phenols, but pyridine and quinoline do not react. Reactions can be observed with phenylenediamine, aminophenols and also monoamines (aniline, 1-naphthylamine) and their derivatives, such as diphenylamine or benzidine. There is no reaction with aminobenzoic acids, again showing the strong influence of substituents with a $-I$ effect. Compounds containing thiol groups

(thioethanol, thiophenol, toluene-3,4-dithiol) give orange-red reaction products, without heating. Moreover, kinetically hindered reactions are observed with many inorganic reductants and these reactions are also activated by increasing the temperature.

The following inorganic species react: SO_3^{2-}, $S_2O_5^{2-}$, $S_2O_3^{2-}$, $S_2O_4^{2-}$, S^{2-}, $Fe(CN)_6^{4-}$, I^-, NO_2^-, NH_2OH, N_2H_4. In this connection it must be mentioned that anions which are not reducing agents will not react.

Another possibility for the application of the redox system Fe^{3+}/Fe^{2+}/phen is based on the reaction of Fe^{2+}/phen with an oxidative analyte. Unlike the reactions discussed above, here the iron(II) complex reacts with the analyte and the intensity of its colour decreases. As the reactions with Ce(IV) or ClO^- show, the blue complex $[Fe(phen)_3]^{3+}$ appears as an intermediate compound, and then changes to the yellow-brown chelate of iron(III). These reactions likewise depend on pH and time. This type of reaction makes it possible to determine H_2O_2, $S_2O_8^{2-}$, Cl_2, ClO^-, Br_2, BrO_3^-, IO_4^-. However, NO_3^-, NO_2^- and ClO_4^- and (remarkably) also ClO_3^- and IO_3^- do not react in this way. Note, however, that NO_2^- gives the reduction reaction as noted above.

REFERENCES

1. Z. J. Vejdělek and B. Kakáč, *Farbreaktionen in der spektralphotometrischen Analyse organischer Verbindungen*, Vol. II, Fischer-Verlag, Jena, 1973.
2. G. Charlot, *Colorimetric Determination of Elements*, Elsevier, Amsterdam, 1964.
3. R. Bailey and D. F. Boltz, *Anal. Chem.*, 1959, **31**, 117.
4. D. R. Erickson and W. L. Dunkley, *ibid.*, 1964, **36**, 1055.
5. T. J. Bydalek, J. E. Poldoski and D. B. John, *ibid.*, 1970, **42**, 929.
6. F. Buhl and M. Chwistek, *Chem. Anal. (Warsaw)*, 1984, **29**, 581.
7. D. D. Perrin, *Stability Constants of Metal-Ion Complexes*, Part B, *Organic Ligands*, p. 879. Pergamon Press, Oxford, 1983.
8. T. S. Lee, I. M. Kolthoff and D. L. Leussing, *J. Am. Chem. Soc.*, 1948, **70**, 2348.
9. D. L. Manning and A. E. Harvey, *ibid.*, 1952, **74**, 4744.
10. G. Anderegg, *Helv. Chim. Acta*, 1962, **45**, 1643.
11. S. Koch and G. Ackermann, *Z. Chem.*, 1989, **29**, 73.
12. D. W. Margerum and C. V. Banks, *Anal. Chem.*, 1954, **26**, 200.
13. S. Koch, G. Ackermann and S. Uhlig, *Z. Chem.*, 1989, **29**, 298.
14. R. L. Plackett and J. P. Burman, *Biometrika*, 1946, **33**, 305.
15. K. Doerffel and K. Eckschlager, *Optimale Strategien in der Analytik*, p. 115. Deutscher Verlag für Grundstoffindustrie, Leipzig, 1981.
16. P. Thomas, M. Benedix and H. Henning, *Z. Anorg. Allgem. Chem.*, 1980, **468**, 213.
17. S. Koch and G. Ackermann, *Z. Chem.*, 1989, **29**, 297.

Talanta, Vol. 39, No. 6, pp. 693–696, 1992
Printed in Great Britain

0039-9140/92 $5.00 + 0.00
Pergamon Press Ltd

APPLICATION OF REDOX REACTIONS IN SPECTROPHOTOMETRY—II*

DETECTION AND SPECTROPHOTOMETRIC DETERMINATION OF PHENOLIC COMPOUNDS WITH THE IRON(III)/1,10-PHENANTHROLINE COMPLEX

S. KOCH, G. ACKERMANN and P. LINDNER
Bergakademie Freiberg, Fachbereich Chemie, 0-9200 Freiberg, Germany

(*Received* 6 *March* 1990. *Revised* 5 *November* 1991. *Accepted* 20 *November* 1991)

Summary—To test the utility of the iron(III)/1,10-phenanthroline reagent system for the determination of organic compounds, its reaction with phenolic compounds has been characterized. By a redox reaction the reagent forms the chelate $[Fe(phen)_3]^{2+}$, which is extractable as ion-association complexes. Determinations based on these complexes are very sensitive.

Redox reactions are frequently used in spectrophotometric determinations,[1] particularly those in which coloured reaction products are formed. The Fe^{3+}/1,10-phenanthroline (Fe^{3+}/phen) system is a valuable reagent for analytes with reducing properties, because the final product is the intensely coloured and extractable chelate $[Fe(phen)_3]^{2+}$.[2]

Because phenols are more or less strong reducing agents, they give deeply coloured compounds with this reagent system, but only a few publications deal with this type of reaction.[3–5]

The aim of this paper is to report the detection and spectrophotometric determination of a variety of phenols with Fe^{3+}/phen.

EXPERIMENTAL

Apparatus

A Beckman DU spectrophotometer and Zeiss M 40 and UR 20 spectrophotometers were used.

To increase the reaction rate, samples were kept for 1 hr in a thermostat at 60°. The pH was adjusted with dilute sulphuric acid or ammonia solution and checked with an MV 870 pH-meter (VEB Präcitronic, Dresden).

Reagents

All solutions were prepared on the day of use. A 1*M* iron(III) solution in 0.1*M* sulphuric acid was prepared from $Fe_2(SO_4)_3 \cdot xH_2O$ (*p.a.*, Riedel de Haën) and standardized by EDTA titration with tiron as indicator. 1,10-Phenanthroline (*z.A.*, Chemapol) was used for preparation of a 0.01*M* solution in 0.1*M* sulphuric acid. The purity of the phen was checked by potentiometric titration of an aqueous solution with 0.1*M* hydrochloric acid. All phenols were obtained commercially. Demineralized water was additionally purified by dissolving potassium permanganate in it and distilling.

RESULTS AND DISCUSSION

Reactions in the system iron(III)/1,10-phenanthroline/analyte

The system Fe^{3+}/Fe^{2+}/phen has pH-dependent positive electrode potentials. With a reducing agent A as an analyte, the reaction scheme is:[2]

$$[Fe_2(OH)_2(phyen)_4]^{4+} + 2phen + A \rightleftharpoons 2[Fe(phen)_3]^{2+} + 2OH^- + A_{ox},$$

where A_{ox} is the oxidized form of the analyte A.

Other forms of the binuclear Fe^{3+}/phen complex can also appear, depending on the reaction conditions, *e.g.*, $[Fe_2O_2H_i(phen)_4]^{i+2}$ ($i = 0, 1$). The orange-red chelate $[Fe(phen)_3]^{2+}$ (λ_{max} 510 nm, $\epsilon_{510} = 1.12 \times 10^4$ $l.mole^{-1}.cm^{-1}$ is well known as a very stable complex cation.

Phenols can react with the system Fe^{3+}/phen, especially in a weakly acidic medium. These reactions are influenced by various parameters. Examination by a multifactor design[2] has shown

*Part I—*Talanta*, 1992, **39**, 687.

there is a significant influence of the pH value and reaction time, but not of the concentration of 1,10-phenanthroline provided that there is a 5-fold excess relative to iron(III). At room temperature the final state is reached only after several hours because of kinetic hindrance. An inner-sphere mechanism is assumed, because ternary iron(III) complexes could be detected in systems containing excess of the ligand. In an earlier work[6] the following blue species were detected:

$$[Fe(phen)(catechol)_2]^-$$

$$[Fe(phen)(tiron)_2]^{5-}$$

$$[Fe(phen)(gallic\ acid)_2]^{3-}$$

The oxidation products A_{ox} are quinonoid compounds that have not yet been fully characterized. According to textbooks of organic chemistry the oxidation of phenols leads to reaction products which are very seldom of uniform composition. Radicals arise as intermediates, and can react to form ring compounds by different ways of dimerization.

In the present work the Fe^{3+}/phen system was used to oxidize phenols at pH 4.0 and 60° and the oxidation products were extracted with diethyl ether. After evaporation of the ether the residue was dried under reduced pressure over anhydrous calcium chloride and then examined by infrared spectroscopy.

The following products could be identified: *p*-benzoquinone from phenol or hydroquinone; *o*-benzoquinone from pyrocatechol; *o*- and *p*-benzoquinone from pyrogallol and phloroglucinol. Condensed aromatic ring systems could also be detected, besides the benzoquinones.

Extraction of the $[Fe(phen)_3]^{2+}$ chelate

The sensitivity of the basic reaction can be increased by extraction of the coloured complex ion. With perchlorate as a counter-ion we have:

$$[Fe(phen)_3]^{2+}_{(aq)} + 2ClO^-_{4(aq)} \rightleftharpoons [Fe(phen)_3]^{2+}\cdot(ClO^-_4)_{2(org)}$$

As shown earlier,[7] extraction of this with nitrobenzene in the presence of EDTA is possible in the pH range 3–9. The EDTA (H_2Y^{2-}) is used to suppress the reaction of the excess of iron(III) with 1,10-phenanthroline and perchlorate to form a yellow-brown product that would also be extractable:

$$[Fe_2O(OH)(phen)_4]^{3+} + 2H_2Y^{2-} + 3H^+ \rightleftharpoons 2FeY^- + 4Hphen^+ + 2H_2O$$

The ion-pair of the iron(II) complex with perchlorate has maximum absorbance at 515 nm and a molar absorptivity in nitrobenzene of 1.25×10^4 l.mole^{-1}.cm^{-1} at that wavelength.

The redox systems were characterized by the mole-ratio method.[8] For the system

$$m\,Fe^{3+} + n\,Red \rightleftharpoons p\,Fe^{2+} + q\,Ox$$

the absorbance (A) was determined with c_{Fe}, pH, ionic strength and λ constant, and increasing concentrations of Red. From the breakpoint of the function $A = f(c_{Red}/c_{Fe})$ the ratio n/m was obtained and from this value the smallest values of the coefficients. The number of electrons z_A exchanged during the reaction can be derived simply as $z_A = mz_{Fe}$, and since $z_{Fe} = 1$, it follows that $z_A = m$.

Statistical characterization

The apparent molar absorptivities were calculated in the normal way and the relative standard deviation was obtained from 16 measurements of solutions with medium concentration ($A \sim 0.7$). The calibration function $A = bc + a$, where c is the analyte concentration, was calculated by linear regression with 6 degrees of freedom, and the detection limit according to Kaiser and Specker,[9] as the concentration corresponding to a signal equal to $a + 3s_a$, where s_a is the standard deviation of the intercept. Because the sensitivity of photometric measurements is best in the interval $0.1 < A < 1.5$, the range of application was defined as $(a + 0.1) < A < (a + 1.5)$.

Detection reactions were characterized by the dilution limit D, defined as

$$D = \frac{\text{limit of perceptibility } (\mu g)}{\text{volume of test sample (ml)} \times 10^6}$$

Determination without extraction

In a 50-ml standard flask place 10 ml of Fe^{3+}/phen reagent ($10^{-3}M$ Fe^{3+}, $10^{-2}M$ phen, pH 4.0) followed by 5 ml of $1M$ acetate buffer (pH 4) and up to 25 ml of analyte solution, and dilute to the mark with water. Heat the closed flask for 1 hr in a thermostat at 60°, cool to room temperature, and measure the absorbance at 510 nm in 1-cm cells, against water.

Table 1. Spectrophotometric determination of phenols with Fe^{3+}/phen as reagent ($\lambda = 510$ nm)

Analyte	z_A	ϵ, 10^4 l.mole^{-1}.cm^{-1}	s_{rel}, %	Range of application, μg	Detection limit, μg	Calibration function*	pD
Pyrogallol	12.2	9.00	0.9	7–103	1.0	$A = 0.0145c + 0.100$	8.3
Gallic acid	7.8	9.49	0.8	9–131	0.8	$A = 0.0114c + 0.099$	7.1
Phloroglucinol	5.0	6.49	0.6	10–146	1.7	$A = 0.0103c + 0.114$	6.9
Catechol	8.3	12.46	1.3	4–64	0.9	$A = 0.0235c + 0.072$	7.2
4-Nitrocatechol	6.2	10.85	0.6	7–107	2.0	$A = 0.0140c + 0.110$	7.2
Tiron	4.1	5.55	0.8	28–428	5.7	$A = 0.0035c + 0.089$	6.5
Hydroquinone	1.6	2.22	0.5	23–351	2.4	$A = 0.0043c + 0.094$	6.9
3,4-Xylenol	3.8	3.75	0.5	16–241	4.2	$A = 0.0062c + 0.110$	6.4
2,5-Xylenol	2.3	2.48	0.7	25–374	3.9	$A = 0.0040c + 0.105$	6.5
2,3-Dihydroxynaphthalene	5.6	7.49	1.3	11–166	1.4	$A = 0.0090c + 0.074$	7.5
Chromotropic acid	6.0	7.16	1.1	26–388	2.7	$A = 0.0039c + 0.080$	7.5
1-Naphthol	2.9	3.78	0.6	19–286	1.4	$A = 0.0052c + 0.057$	5.8
2-Naphthol	2.3	2.82	0.2	28–424	6.6	$A = 0.0035c + 0.108$	6.4
1,2-Aminophenol	4.5	6.70	1.7	8–127	3.5	$A = 0.0118c + 0.160$	6.9
1,3-Aminophenol	4.0	5.50	0.5	10–151	5.8	$A = 0.0099c + 0.152$	6.4
1,4-Aminophenol	2.0	2.68	1.1	21–319	2.2	$A = 0.0047c + 0.047$	6.3

*c expressed as μg/50 ml.

Determination with extraction

Prepare the samples as given above, but with only 1 ml of Fe^{3+}/phen reagent. After cooling, transfer the solution to a 100-ml separatory funnel, add 1 ml of 0.05M EDTA and 1 ml of 1M sodium perchlorate and immediately extract with 5.0 ml of nitrobenzene, shaking the mixture for 30 sec. Separate the extract, dry it with 2 g of anhydrous sodium sulphate, and measure the absorbance at 515 nm in 1-cm cells, against nitrobenzene.

Detection

In a semimicro test-tube place 1 ml of Fe^{3+}/phen reagent ($10^{-4}M$ Fe^{3+}, $10^{-3}M$ phen, pH 4.0) followed by 5 drops of 1M acetate buffer (pH 4) and some drops of sample solution. Heat the test-tube for about 30 sec in a boiling water-bath and compare with a reagent blank. For use of the extraction method, add to the cooled solution 3 drops of 0.05M EDTA, 3 drops of 1M sodium perchlorate and 5 drops of nitrobenzene, and shake the tube. Compare the colour of the organic phase with that of a reagent blank.

CONCLUSIONS

As shown in Tables 1 and 2, the Fe^{3+}/phen system is a valuable reagent for the detection and determination of phenolic compounds,

Table 2. Extraction-photometric determination of phenols with Fe^{3+}/phen as a reagent ($\lambda = 515$ nm)

Analyte	ϵ'* 10^4 l.mole^{-1}.cm^{-1}	s_{rel}, %	Range of application, μg	Detection limit, μg	Calibration function†	pD
Pyrogallol	8.29	1.4	0.7–10.8	0.5	$A = 0.1387c + 0.088$	8.8
Gallic acid	8.04	3.5	1.1–15.8	0.3	$A = 0.0948c + 0.071$	8.3
Phloroglucinol	5.49	2.2	1.2–17.9	0.6	$A = 0.0839c + 0.143$	8.1
Catechol	11.59	1.1	0.5–7.1	0.2	$A = 0.2105c + 0.039$	8.2
4-Nitrocatechol	9.94	1.8	0.8–12.3	0.2	$A = 0.1221c + 0.130$	8.1
Tiron	5.66	1.5	2.8–41.3	0.8	$A = 0.0363c + 0.114$	7.8
Hydroquinone	2.45	3.0	2.3–34.0	0.5	$A = 0.0441c + 0.099$	7.8
3,4-Xylenol	4.08	1.1	1.6–23.4	0.5	$A = 0.0640c + 0.101$	7.1
2,5-Xylenol	2.39	0.8	2.5–37.8	1.6	$A = 0.0397c + 0.228$	7.8
2,3-Dihydroxynaphthalene	7.90	2.4	1.0–15.8	0.6	$A = 0.0951c + 0.074$	8.5
Chromotropic acid	7.20	2.0	2.6–38.9	0.4	$A = 0.0386c + 0.104$	8.3
1-Naphthol	4.27	2.7	1.7–25.8	0.5	$A = 0.0580c + 0.087$	6.8
2-Naphthol	3.48	2.1	2.1–31.3	0.7	$A = 0.0480c + 0.179$	7.1
1,2-Aminophenol	9.04	1.1	0.6–9.1	0.1	$A = 0.1650c + 0.137$	7.9
1,3-Aminophenol	5.11	1.1	1.1–16.0	0.1	$A = 0.0940c + 0.177$	7.0
1,4-Aminophenol	2.67	0.8	2.0–30.7	0.2	$A = 0.0489c + 0.114$	7.4

*Conditional molar absorptivity in nitrobenzene, assuming that the extraction coefficient is 1.00.

†c expressed as μg/50 ml.

especially by the extraction method. Only aromatic amines, enediols and aliphatic or aromatic thiol groups will react similarly and can interfere with the detection or determination of phenols.[2] However, there is practically no selectivity for phenols themselves. Only nitrophenols, halogen-substituted phenols and other phenols containing substituents with a negative induction effect do not react with the reagent. Polyhydroxy phenols and naphthols give positive reactions.

It is possible to detect (with and without extraction) phenol (p*D* 7.0; 6.3), *o*-cresol (p*D* 6.8; 5.9), *m*-cresol (p*D* 6.4; 5.8) and *p*-cresol (6.4; 5.7), but determination of these compounds is not possible, because of non-linearity of the function $A = f(c)$.

The following conditional molar absorptivities ($l.mole^{-1}.cm^{-1}$) (two-fold excess of reagent, $c_A = 5 \times 10^{-5} M$) were calculated: phenol, 4.8×10^4; *o*-cresol, 1.6×10^4; *m*-cresol 5.2×10^4; *p*-cresol 1.8×10^4.

The results demonstrate that the procedures are very sensitive for the detection and determination of single species. The small selectivity within the groups makes it possible to determine the sum of compounds giving similar molar absorptivities, because λ_{max} and pH are the same for all the compounds discussed here. As a standard substance, phloroglucinol (which gives a medium number of exchanged electrons) can be recommended.

The semiquantitative determination of a mixture of compounds is possible and is based on the additivity of the absorbances. A test with phloroglucinol, pyrocatechol, hydroquinone, 2,3-dihydroxynaphthalene and 1,2-aminophenol at levels giving $A \sim 0.1$ per compound showed the following total absorbances (measured; calculated):

without extraction	0.63; 0.62
with extraction	0.62; 0.62

Acknowledgments—The authors express their gratitude to Dr. Rentrop, FB Chemie, Bergakademie Frieberg, for his assistance with the infrared spectroscopy, and also thank Dr. Chalmers for his valuable help in preparing the English text.

REFERENCES

1. Z. J. Vejdělek and B. Kakáč, *Farbreaktionen in der spektralphotometrischen Analyse organischer Verbindungen*, Vol. II, Fischer Verlag, Jena, 1973.
2. S. Koch and G. Ackermann, Talanta 1992, **39**, 687.
3. Z. K. Vejdělek and B. Kakáč, *Farbreaktionen in der spektralphotometrischen Analyse organischer Verbindungen*, Supplement II, p. 217. Fischer Verlag, Jena, 1982.
4. F. Buhl and M. Chwistek, *Chem. Anal. (Warsaw)*, 1984, **29**, 581.
5. A. Besada, *Talanta*, 1987, **34**, 731.
6. S. Koch and G. Ackermann, *Z. Chem.*, 1989, **29**, 297.
7. S. Koch, G. Ackermann and S. Uhlig, *ibid.*, 1989, **29**, 298.
8. S. Koch and G. Ackermann, *ibid.*, 1988, **28**, 376.
9. H. Kaiser and H. Specker, *Z. Anal. Chem.*, 1956, **149**, 46.

Talanta, Vol. 39, No. 6, pp. 697–701, 1992
Printed in Great Britain

0039-9140/92 $5.00 + 0.00
Pergamon Press Ltd

o-HYDROXYACETOPHENONE THIOSEMICARBAZONE AS A REAGENT FOR THE RAPID SPECTROPHOTOMETRIC DETERMINATION OF PALLADIUM

G. V. RAMANA MURTHY* and T. SREENIVASULU REDDY
Department of Chemistry, Sri Krishnadevaraya University, Anantapur 515003, India

(*Received* 22 *August* 1989. *Revised* 25 *September* 1991. *Accepted* 28 *October* 1991)

Summary—*o*-Hydroxyacetophenone thiosemicarbazone has been synthesized and employed as a new reagent for the spectrophotometric determination of palladium(II), which forms two complex species with it in aqueous dimethylformamide at pH 6.0, these having 1:1 and 1:2 metal–ligand ratios. The Job and molar-ratio plots have an unusual shape that is due to the stepwise conversion of the 1:1 complex into the 1:2 species. The molar absorptivity at 370 nm is 9×10^3 l.mole^{-1}.cm^{-1}. Beer's law is obeyed over the range 0.42–10.6 μg/ml palladium.

Derivatives of hydroxyacetophenone have been extensively developed as analytical reagents.[1–8] Earlier we reported the use of *o*-hydroxyacetophenone thiosemicarbazone (HAPT) as a spectrophotometric reagent for the determination of copper,[9] cobalt[10] and nickel,[11] and now report its application to determination of palladium. Most of the spectrophotometric methods using thiosemicarbazones suffer from low sensitivity, the need for heating or extraction, and poor selectivity.[12–20] The proposed method based on HPAT is free from these drawbacks.

Although the proposed method does not provide any significant improvement in sensitivity over existing methods, a very interesting feature is the unusual shape of the Job and molar-ratio plots used to characterize the complexation reaction. In both cases there is a minimum in the absorbance between the maxima corresponding to 1:1 and 1:2 metal:ligand ratios. Similar behaviour in Job plots has been reported by others.[21–24]

EXPERIMENTAL

Apparatus

A Beckmann DU-2 spectrophotometer and an Elico LI-120 pH-meter were employed.

Reagents

Analytical-reagent grade chemicals and doubly distilled water were used.

A stock solution of palladium(II) was prepared by dissolving 1.773 g of palladous chloride in distilled water and diluting to volume in a 100-ml standard flask, standardized,[25] and further diluted as required.

A 0.2*M* acetic acid–sodium acetate buffer (pH 6.0) was used.

Preparation of the reagent

Thiosemicarbazide and a few drops of glacial acetic acid were dissolved in the minimum amount of water and an equimolar amount of *o*-hydroxyacetophenone was dissolved in the minimum of ethanol, then the solutions were mixed. The mixture was refluxed for 3 hr on a boiling water-bath. The hot solution was filtered under suction and cooled. Yellow crystals of HAPT were obtained and were recrystallized from ethanol (yield 65%, m.p. 183–186°). A stock solution (0.05*M*) was prepared by dissolving 0.5352 g of the reagent in 50 ml of dimethylformamide (DMF). It was stable for a day.

Elemental analysis and spectral characteristics of the reagent

Analysis gave C 51.0%, H 5.2%, N 20.0%; $C_9H_{11}N_3OS$ requires C 51.65%, H 5.24%, N 20.08%.

The infrared spectrum was obtained (KBr discs) and bands were assigned to the stretching vibrations of NH–NH_2 at 3330–2950 cm^{-1}, >C=N at 1630 cm^{-1} and >C=S at 1050, 850 cm^{-1}.

The proton NMR spectrum was obtained in d_6-DMSO with tetramethylsilane as reference.

*Present address: 17/84-A, T.V. Street, Nellore 524001, India.

The peaks were assigned as follows: (δ) 2.5, (3H, singlet —CH_3), 3.59 (2H, singlet —NH_2), 5.74 (1 H, singlet —NH); 7.8 (multiplet, C_6H_6).

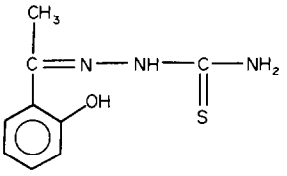

HAPT

HAPT is soluble in dimethylformamide (20 g/l.) and dimethylsulphoxide (12 g/l.) and sparingly soluble in methanol, water, chloroform, carbon tetrachloride and cyclohexanone.

Reactions with metal ions

No visible colour reactions were observed with 25 cations tested, except for palladium, copper, iron, cobalt, nickel, vanadium, silver, gold and platinum. The photometric characteristics of the complexes of these metal ions in solution are given in Table 1.

Recommended procedure

For calibration, to each of a set of 25-ml standard flasks containing 12.5 ml of pH 6.0 buffer, 3 ml of DMF and 2 ml of 0.05*M* reagent, add appropriate volumes of $5 \times 10^{-4}M$ palladium(II) solution to cover the range up to 10 μg/ml palladium, and dilute to the mark with distilled water. Read the absorbance at 370 nm against a reagent blank. Analyse samples in the same way.

RESULTS AND DISCUSSION

Absorption spectra and effect of pH

The complex formed between Pd(II) and HAPT has maximum absorbance at 370 nm (Fig. 1) and a plot of absorbance *vs.* pH shows that the absorbance remains constant in the pH range 5.0–9.0. Use of pH 6.0 is recommended. The absorbance of the complex remains stable for one day. The system obeys Beer's law over the range 0.4–10.6 μg/ml palladium, and the optimum range (Ringbom plot) is 1.1–9.5 μg/ml. The molar absorptivity is 9.0×10^3 l.mole^{-1}.cm^{-1}.

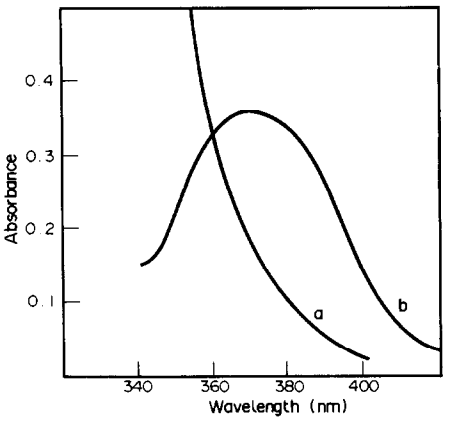

Fig. 1. Absorption spectra (a) HAPT *vs.* buffer blank; (b) Pd-HAPT system *vs.* reagent blank. [Pd(II)] $4 \times 10^{-5}M$; [HAPT] $1 \times 10^{-3}M$; pH 6.0.

Effect of DMF concentration

The Pd(II)–HAPT complex is soluble in DMF, and 14% v/v DMF in water is required to keep the complex in solution. At lower DMF concentration the solution is turbid.

Effect of reagent concentration

The molar-ratio plot showed that a fivefold ratio of HAPT to palladium is sufficient for full colour development, but a tenfold molar ratio is recommended.

In addition to this, the molar-ratio plot indicated that 1:1 and 1:2 metal:ligand complexes were formed successively, but there was a marked decrease in absorbance between the corresponding intersections on the plot (Fig. 2).

Table 1. Characteristics of metal ion–HAPT complexes

Cation	pH	λ_{max}, *nm*	Molar absorptivity, 10^3 *l.mole*$^{-1}$*.cm*$^{-1}$	M:L	Beer's law range, *ppm*	Optimum range (Ringbom plot), *ppm*	Stability constant
Gold(III)	7.0	350	10.3	1:2	—	—	1.96×10^{11}
Cobalt(II)	5.5	360	10.0	1:2	0.47–5.30	0.71–5.30	1.80×10^{8}
Copper(II)	5.5	360	9.5	2:3	0.40–6.60	0.67–3.94	6.60×10^{12}
Silver(I)	4.0	360	9.5	1:2	0.92–4.30	0.87–4.20	8.95×10^{4}
Nickel(II)	7.5	355	9.1	1:1	0.23–6.50	0.71–5.30	4.36×10^{4}
Palladium(II)	6.0	370	9.0	1:2	0.40–10.60	1.12–9.54	7.67×10^{10}
				1:1			4.05×10^{5}
Vanadium(IV)	5.0	360	8.5	1:1	1.02–4.59	1.53–4.59	2.40×10^{4}
Vanadium(V)	5.0	360	8.3	1:1	0.20–4.60	0.61–4.60	6.05×10^{5}
Platinum(IV)	3.0	335	7.2	1:2	—	—	8.61×10^{10}
Iron(III)	6.0	360	6.2	1:2	0.24–5.20	0.71–5.20	1.53×10^{4}

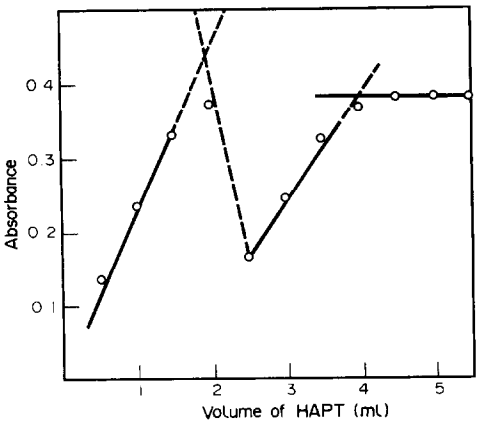

Fig. 2. Molar ratio plot. [Pd(II)] = [HAPT] = $5 \times 10^{-4}M$; pH 6.0. Pd(II) solution 2 ml; total volume 25 ml; blank 12.5 ml of buffer + 2.5 ml of DMF.

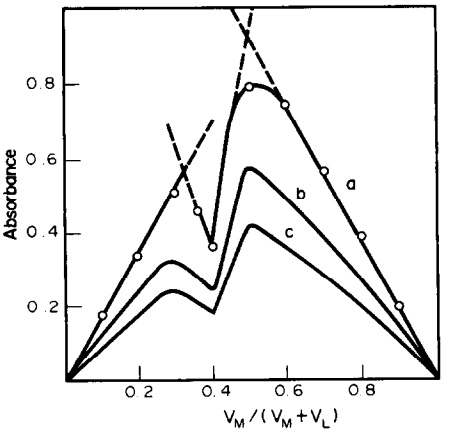

Fig. 3. Job plots: (a) at 370 nm, $5 \times 10^{-4}M$ reactants; (b) at 370 nm, $4 \times 10^{-4}M$ reactants; (c) at 380 nm, $3 \times 10^{-4}M$ reactants; blank 12.5 ml of buffer + 2.5 ml of DMF.

Formation of more than one complex was confirmed by the Vosburgh and Cooper method.[26]

A Job plot was also anomalous, having two maxima corresponding to Pd:HAPT ratios of 1:1 and 1:2, with a sharp decrease in absorbance between them (Fig. 3). The position of the maxima and minima did not change with variation of either the wavelength or the concentration used.

It is interesting (and unusual) that the molar absorptivity of both complexes is almost the same. From this behaviour it is evident that a drastic reorganization of the structure of the complex takes place in conversion of the 1:1 into the 1:2 (metal:ligand) complex. A possibility for this was proposed by Rao *et al.*[24] for the Pd(II) complexes with 5,6-dimethyl-1,3-indanedione-2-oxime.

The shape of the molar-ratio plot and Job curves presented in Figs 2 and 3 suggests that two complexes with compositions corresponding to 1:1 and 1:2 metal:ligand are formed under the experimental conditions. The minimum between the two maxima in the Job curve not only indicates that considerable reorganization is involved as the ligand:metal ratio is increased, but also that this reorganization does not take place smoothly and immediately. By analogy with the work of Campbell and Grzeskowiak on the copper complexes of some thiosemicarbazides,[27] we consider that our results could be accounted for by postulating formation of a polymeric 1:1 type complex with both an anionic bridge and a thiosemicarbazone bridge between neighbouring palladium ions (structure Ia, below), and depolymerization of this in presence of excess of HAPT, to form a 1:2 square coplanar complex with two loosely attached anions (structure Ib, below).

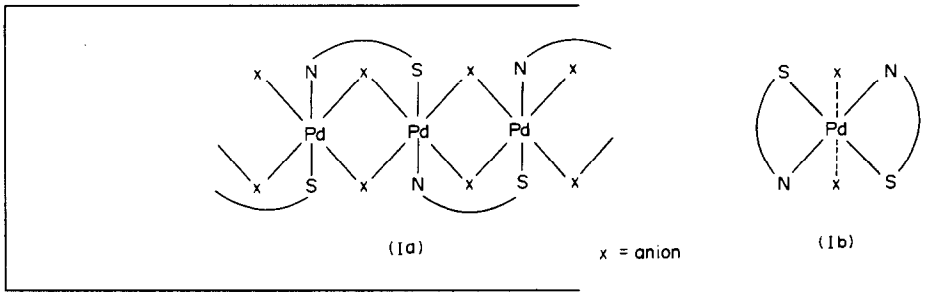

Infrared spectral data

The infrared spectral data in Table 2 allow some conclusions to be drawn about the bonding sites in the Pd–HAPT complex. The band at 1630 cm^{-1} is shifted to lower frequency (1585 cm^{-1}), indicating the participation of the azomethine nitrogen atom in co-ordination.[29,30] A sharp band at 1050 cm^{-1} due to the >C=S band in the ligand shifts to lower frequency in the complex, suggesting co-ordination of the sulphur atom of the ligand.[28,31] Absence of the band due to the S—H stretching mode at 2570 cm^{-1} suggests that in the solid state the

Table 2. Physicochemical data for the solid Pd–HAPT complex

Ligand		Complex	Assignment
3300–2950 cm^{-1}		330/2950 cm^{-1}	NH and NH_2[28]
1630(bd) cm^{-1}		1585(ms) cm^{-1}	>C = N[29,30]
1050(S) cm^{-1}		1030(ms) cm^{-1}	>C = S[28,31]
850(S) cm^{-1}		855 (ms) cm^{-1}	>C = S[30,32]
	Molar conductance (in DMF), $ohm^{-1}.cm^{-2}.mole^{-2}$	17.35	Non-ionic
	Magnetic susceptibility (B.M)		Diamagnetic
	Elemental analysis: Pd 16.2%, C 40.7%, H 4.2%, N 12.8%; $ML_2(OAc)_2$ requires Pd 16.54%, C 41.08%, H 4.38%, N 13.08%		

Table 3. Determination of palladium in synthetic mixtures corresponding to alloys

Alloy	Synthetic mixture composition, %	Pd, μg Taken	Pd, μg Found*
Au–Pd alloy	Au 50.0; Pd 50.0	31.8	31.5
		42.4	42.9
		53.0	53.9
Alloy for electrical contacts	Pd 35.0; Ag 30.0	42.0	42.4
	Pt 10.0; Cu 14.0	56.0	56.7
	Au 10.0; Zn 1.0	70.0	70.9
Low melting dental alloy	Pd 34.0; Ni 34.0	34.0	34.0
	Co 22.0; Au 10.0	40.8	40.8
		47.6	47.6
OAKAY alloy (Pd–Ni)	Pd 10.5; Ni 60.0	27.0	26.5
	Pt 20.0; V 9.5	36.0	35.8
		54.0	53.3

*Average of three determinations.

ligand remains in thioketo form.[33] Based on the infrared spectral investigations, the structure of the solid Pd–HAPT complex is assumed to be that shown as Ib above.

Effect of foreign ions

Various amounts of foreign ions were added to a fixed amount of palladium(II) (80 μg) and the recommended procedure for the spectrophotometric determination was followed. The amounts (mg) at which various ions did not cause more than $\pm 2\%$ change in the absorbance are given below.

Ascorbic acid (53); tartrate (44); nitrate (37); phosphate (29); citrate (28), iodide (19), perchlorate (15), sulphate (14), oxalate (13), bromide (12), EDTA (11), chloride (11), thiocyanate (8.7), thiourea (7.6), fluoride (5.7), U(VI) (3.6), Th(IV) (3.5), W(VI) (2.8), Pb(II) (2.1), Cd(II) (1.7), Mn (0.83), Ce(IV) (0.70), Mo(VI) (0.30), Al(III) (0.27), Zn(II) (0.20), Os(VIII) (0.010). Cu(II), Co(II), Ni(II), Cr(III), V(V), V(IV), Pt(IV), Au(III) (0.95, 0.88, 0.88, 0.78, 0.76, 0.76, 0.33, 0.22 mg respectively) could be masked with 11 mg of EDTA. Fe(III) (0.11 mg) was masked with 19 mg of phosphate. Ag(I) and Sn(II) interfere, forming a turbidity.

Application to synthetic mixtures

The method was applied to the determination of Pd(II) in certain synthetic mixtures corresponding to its alloys. Phosphate and EDTA were added to mask iron and copper, cobalt, nickel, vanadium, platinum and gold. Ag(I) was separated by precipitation as silver chloride. The complete data are presented in Table 3.

Acknowledgements—Thanks are due to Prof. S. Brahmaji Rao, Professor of Chemistry (Academic), Andhra Pradesh Open University, Hyderabad, India for his interest in this work and to Dr. R. A. Chalmers for helpful advice.

REFERENCES

1. A. Aydin and F. Baykut, *Chim. Acta Turcica*, 1975, **3**, 51.
2. K. H. Reddy, K. G. Reddy, K. M. M. S. Prakash and D. V. Reddy, *Indian J. Chem.*, 1984, **23A**, 535.
3. A. V. Reddy and Y. K. Reddy, *Talanta*, 1986, **33**, 617.
4. A. V. Reddy, G. S. Reddy and Y. K. Reddy, *J. Radioanal. Nucl. Chem.*, 1986, **103**, 167.
5. *Idem, ibid.*, 1985, **93**, 279.
6. A. V. Reddy, Y. K. Reddy and M. L. P. Reddy, *ibid.*, 1984, **86**, 391.
7. J. R. Shah and R. P. Patel, *J. Indian Chem. Soc.*, 1973, **50**, 157.
8. M. C. Patel and J. R. Shah, *ibid.*, 1973, **50**, 560.

9. G. V. R. Murthy and T. S. Reddy, *Current Science*, 1989, **58**, 1024.
10. *Idem*, *Chim. Acta Turcica*, 1989, **17**, 189.
11. *Idem*, *J. Indian Council Chemists*, in the press.
12. K. Shravah, P. P. Sinha and S. K. Sindhwani, *Analyst*, 1986, **111**, 1339.
13. J. M. Lopez Fernandez, M. Valcárcel and F. Pino Peréz, *Quim. Anal.*, 1976, **30**, 8.
14. D. V. Khasnis and V. M. Shinde, *Talanta*, 1979, **26**, 593.
15. *Idem*, *J. Indian Chem. Soc.*, 1982, **59**, 93.
16. M. González Balairon, J. M. Cano Pavón and F. Pino Peréz, *Quim. Anal.*, 1976, **30**, 411.
17. J. M. Cano Pavón, M. T. Martínez Aguilar and A. García de Torres, *An. Quim.*, 1978, **74**, 915.
18. L. I. Mas'ko, V. P. Kerentseva and M. D. Lipanova, *Zh. Analit. Khim.*, 1975, **30**, 315.
19. S. Hoshi, J. Yotsuyanagi and K. Aomura, *Bunseki Kagaku*, 1977, **26**, 592.
20. A. Asuero, A. M. Jiménez and M. A. Herrador, *Analyst*, 1986, **111**, 747.
21. D. P. Dave and B. C. Halder, *J. Indian Chem. Soc.*, 1978, **55**, 781.
22. U. B. Talwar and B. C. Haldar, *Anal. Chem.*, 1966, **38**, 1929.
23. *Idem*, *Anal. Chim. Acta*, 1967, **39**, 264.
24. D. M. Rao, K. H. Reddy and D. V. Reddy, *Talanta*, 1991, **38**, 1047.
25. A. I. Vogel, *Textbook of Quantitative Inorganic Analysis*, 4th Ed., ELBS, Longmans, 1978.
26. W. C. Vosburgh and G. R. Cooper, *J. Am. Chem. Soc.*, 1941, **63**, 437.
27. M. J. Campbell and R. Grzeskowiak, *J. Chem. Soc. A*, 1967, 396.
28. L. Bhal, R. V. Singh and J. P. Tandon, *Indian J. Chem.*, 1983, **22A**, 951.
29. K. H. Reddy, K. M. M. S. Prakash, K. G. Reddy and D. V. Reddy, *J. Indian Inst. Sci.*, 1984, **65(B)**, 119.
30. K. H. Reddy and D. V. Reddy, *Indian J. Chem.*, 1985, **24A**, 154.
31. M. C. Jain and P. C. Jain, *J. Inorg. Nucl. Chem.*, 1977, **39**, 2183.
32. K. K. Aravindakshan and C. G. R. Nair, *Indian J. Chem.*, 1981, **20A**, 684.
33. K. M. M. S. Prakash, L. D. Prabhakar and D. V. Reddy, *Analyst*, 1986, **111**, 1301.

Talanta, Vol. 39, No. 6, pp. 703–707, 1992
Printed in Great Britain.

0039-9140/92 $5.00 + 0.00

SPECTROPHOTOMETRIC DETERMINATION OF CEPHALEXIN IN DOSAGE FORMS WITH IMIDAZOLE REAGENT

A. A. ALWARTHAN, S. ABDEL FATTAH and N. M. ZAHRAN
Chemistry Department, College of Science, King Saud University, P.O. Box 2455, Riyadh-11451, Saudi Arabia

(*Received* 18 *March* 1991. *Revised* 1 *August* 1991. *Accepted* 16 *September* 1991)

Summary—A simple spectrophotometric method is proposed for the determination of cephalexin. The method involves acetylation of cephalexin with acetic anhydride in aqueous solution at pH 11.5 to yield α-acetamidocephalexin and subsequent measurement at 335 nm of α-acetamidocephalexin mercuric mercaptide. The method characterizes a newly developed, sensitive procedure for the determination of cephalexin in different pharmaceutical preparations. The effect of several reaction conditions were investigated. Beer's law was obeyed over the concentration range 30–340 μg/ml. The results compare favourably with those obtained by the official B.P. 1980 method.

Cephalosporins are a series of antibiotics containing a β-lactam ring fused to a six-membered ring with a sulphur atom.

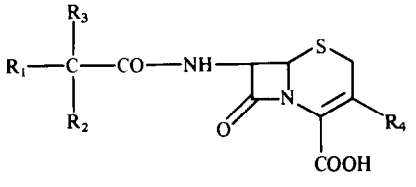

They have antibacterial action against Gram-positive and Gram-negative bacteria. Cephalexin, a potent cephalosporin, exhibits a broad spectrum of antibiotic activity.[1] Several analytical procedures are available in the literature for the analysis of cephaloxin, *viz.* spectrophotometric,[2–6] titrimetric with potassium iodate,[7,8] fluorimetric,[9] polarographic,[10] chromatographic,[11] and iodometric methods.[12]

The aim of this paper was to develop a simple and reproducible spectrophotometric procedure for determining cephalexin monohydrate in alkaline aqueous solution, using imidazole reagent containing mercuric chloride.

EXPERIMENTAL

Apparatus

A Varian Model DMS 100 spectrophotometer interfaced with a Varian Model DS 15 Data station and a Hewlett–Packard Model 82905 B Printer was used for all absorbance measurements. Matched sets of 10-mm silica cells were used throughout.

Materials

Pure drug sample was kindly provided by Chemical Industries Development, Giza, Egypt. Dosage forms were obtained from local sources. Several formulations were used:

(A) Cephalexid, 250 mg of cephalexin per capsule (Chemical Industries Development, Giza, Egypt).
(B) Ibilex, 250 mg of cephalexin per capsule (Ibi Instituto Biochemico Italiano Giovanni Lorenzini S.P.A., Milano, Italy).
(C) Keflex, 250 mg of cephalexin per capsule (Eli Lilly and Company Ltd., Basingstoke, England).
(D) Keflex, 500 mg of cephalexin per tablet (Eli Lilly and Company Ltd., Basingstoke, England).
(E) Keflex granules, 250 mg of cephalexin per packet (Eli Lilly and Company Ltd., Basingstoke, England).
(F) Ospexin, cephalexin suspension, 250 mg of cephalexin per 5 ml (Biochemie GmbH, Vienna, Austria).

Reagents

The reagents used were all of analytical or pharmaceutical grade. Distilled demineralized water was used throughout.

Cephalexin solution. A stock solution of $9.18 \times 10^{-4} M$ was prepared by dissolving 0.3354 g in 2 ml of 0.1*M* sodium hydroxide and then diluting one litre with water.

Imidazole reagent. A 1.2*M* aqueous imidazole solution containing $10^{-3}M$ mercuric chloride with pH adjusted to 6.8.

*Acetic anhydride solution, 0.2*M. Acetic anhydride (1.0 ml) diluted to 50 ml with acetonitrile.

*Borate buffer, 0.1*M. Boric acid (1.24 g) dissolved in 10.6 ml of 1*M* sodium hydroxide and diluted to 200 ml with distilled water to give a solution with pH 11.5.

Analysis of authentic samples

An aliquot of cephalexin (34 μg/ml–350 μg/ml) was transferred to a 25-ml standard flask. Then 0.5 ml of the borate buffer, 0.03 ml of acetic anhydride solution and 2 ml of imidazole reagent were added and the volume was completed to the mark. The mixture of the solutions was heated at 60° for 55 min. Then the solution was cooled to room temperature and the absorbance was measured at 335 nm against a blank prepared with all the reagents but no cephalexin. The calibration curve was obtained by applying the same procedure, using standard cephalexin solutions.

Analysis of dosage forms

Capsules and granules. The contents of ten capsules or three granule packets were weighed and powdered. An amount of powder equivalent to 20 mg of the active constituent was weighed accurately and transferred into a 100-ml calibrated flask. It was shaken with 50 ml of distilled water and then diluted to volume with distilled water. An aliquot of this solution giving an analyte concentration of 200 μg/ml was transferred into a 50-ml calibrated flask and analysed as for authentic samples.

Tablets. Ten tablets were weighed and powdered. An amount of powder equivalent to 20 mg of the active constituent was weighed accurately and transferred into a 100-ml calibrated flask. It was dissolved in 50 ml of distilled water and then diluted to volume with distilled water. The solution was filtered through a Whatman No. 1 filter paper. The first 15 ml of filtrate was discarded. An aliquot of this solution to give an analyte concentration of 200 μg/ml was transferred into a 50-ml calibrated flask and analysed as for authentic samples.

Suspension. The contents of a well mixed suspension were filtered through dry filter paper. An aliquot of this suspension equivalent to 200 μg/ml was pipetted into a 100-ml calibrated flask and analysed as for authentic samples.

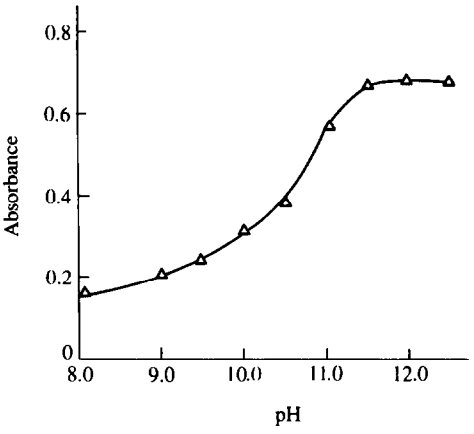

Fig. 1. Effect of pH on the absorbance of the drug complex.

RESULTS AND DISCUSSION

Several parameters such as pH, acetic anhydride concentration, temperature, heating time and the volume of imidazole reagent were optimized to achieve high sensitivity, low blank reading and high stability.

Effect of pH

Cephalexin has a similar chemical structure to ampicillin. Bundgaard found that ampicillin undergoes an imidazole-catalysed rearrangement into the corresponding penicillenic acid which yields the corresponding stable mercuric mercaptides in the presence of mercuric chloride at pH 6.8.[13] Therefore, in order to get the best medium for the quantitative determination of cephalexin in aqueous solution, different borate buffer solutions, with different pHs were prepared. The absorbance readings were maximum at pH 11.0–12.5 as shown in Fig. 1. A solution of boric acid adjusted to pH 11.5 with sodium hydroxide was used in the calibration measurements.

Effect of acetic anhydride concentration

Different amounts of acetic anhydride were added keeping other conditions constant. As shown in Table 1, 30 μl of 0.2*M* acetic anhydride is sufficient for complete acetylation of the cephalexin amino group.

Effect of imidazole concentration

The effect of imidazole was similarly investigated by taking various amounts of imidazole. It was observed that 2 ml of imidazole gave maximum absorbance in its reaction with cephalexin, as shown in Table 2.

Table 1. Effect of acetic anhydride concentration

Cephalexin	1 ml of 31 μg/ml solution
Borate buffer	0.5 ml
Acetic anhydride	x ml
Imidazole reagent	2 ml
λ_{max}	335 ml
Acetic anhydride added, *ml*	Absorbance
0.01	0.75
0.02	0.87
0.03	1.25
0.04	1.25
0.05	1.25

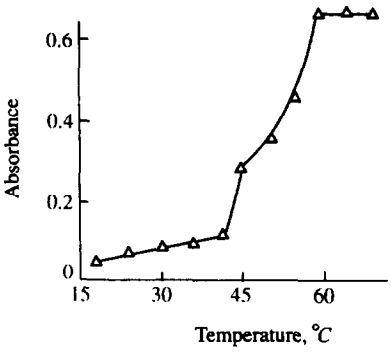

Fig. 2. Effect of temperature on the absorbance of the drug complex.

Effect of temperature

The reaction between cephalexin and the aqueous imidazole solution to form a product with a measurable absorbance is temperature dependent. Therefore, the effect of temperature on the formation of the product was studied in the range 18–70°. It was found that the absorbance increased slowly during heating up to 55°. However, a significant increase was observed at 60° above which the absorbance remained constant as shown in Fig. 2.

Effect of heating time

The effect of heating time on the formation of the product was studied at the optimal temperature (60°). The absorbance was found to increase with time reaching its maximal value after 55 min as shown in Fig. 3.

The proposed method exposes the β-lactam compound (cephalexin) to rather harsh conditions before derivatization with imidazole/$HgCl_2$ reagent. Therefore, to study how much of the cephalexin originally present was eventually used for quantification, the imidazole/$HgCl_2$ reagent was added to the solution of cephalexin together with the other reagents required, at 5-min intervals from 0–60 min. The results obtained are shown in Fig. 4. They indicate that if such harsh conditions have destroyed the β-lactam (cephalexin), the imidazole/$HgCl_2$ reagent would not couple with the degraded cephalexin and the absorbance would be zero.

Table 2. Effect of imidazole concentration

Cephalexin	1 ml of 31 μg/ml solution
Borate buffer	0.5 ml
Acetic anhydride	0.03 ml
Imidazole reagent	x ml
λ_{max}	335 ml
Imidazole added, *ml*	Absorbance
0.5	0.75
1.0	1.15
1.5	1.25
2.0	1.50
2.5	1.50
3.0	1.50

Using the above described optimum parameters, a calibration graph correlating the absorbance versus concentrations was found to be linear with slope 0.19 and correlation coefficient 0.999. Beer's law was obeyed over the range 30–340 μg/ml. The regression equation, calculated from the calibration graph, was $A = 0.009 + 0.19C$ where A = absorbance and C = concentration (μg/ml). To test its validity, the method was applied to authentic samples of cephalexin. The results given in Table 3 show that the method is accurate and precise.

The method was applied to some dosage forms containing cephalexin. The performance of the recommended method was assessed by calculation of the t-values. A mean value of $t = 0.877$ was obtained in a student's t-test,[13] showing the absence of any systematic error in the method; the corresponding tabulated t-value for five degrees of freedom and for a 95% confidence level is 2.571. Therefore, it can be

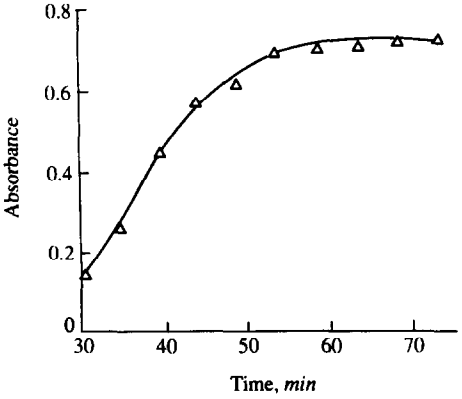

Fig. 3. Effect of heating time on colour formation of the drug product.

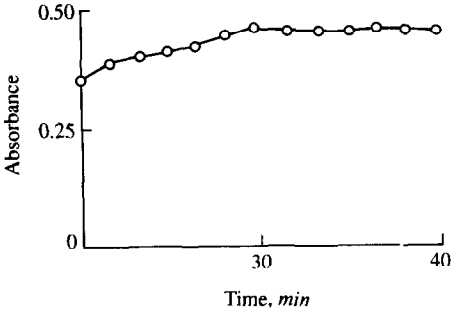

Fig. 4. The effect of cephalexin derivatization by the imidazole/$HgCl_2$ reagent (at pH 11.5 and 60°) on its quantitative determination.

concluded that there is no significant difference between the proposed method and the official one. Table 4 gives the results of these applications. However, the present method has the advantage of ease of operation, convenience, small sample/reagent consumption, and can be used as a stability indicating method.

Preliminary studies have shown that the present method can be automated with an Autoanalyzer system or flow-injection analysis, which may have useful application in routine or research laboratories. This procedure will be reported later when more results are available.

The method of the imidazole and mercury(II) reaction for determination of cephalosporines and penicillins is favoured currently in many laboratories,[14] because imidazole reacts with the intact β-lactam compound and hence can be used as a stability indicating method. However, it has the disadvantage of using mercury(II) which is a potential chemical hazard. This method is general for all cephalosporins containing the β-lactam ring fused to a six-membered ring with sulphur atom. But the method dose differentiate between the intact molecule and the degraded one.

The quantitative determination of cephalexin, using the procedure mentioned previously, is similar to that for penicillin.[15] Therefore, the reaction of cephalexin can be represented by the proposed mechanism as shown in the following scheme:

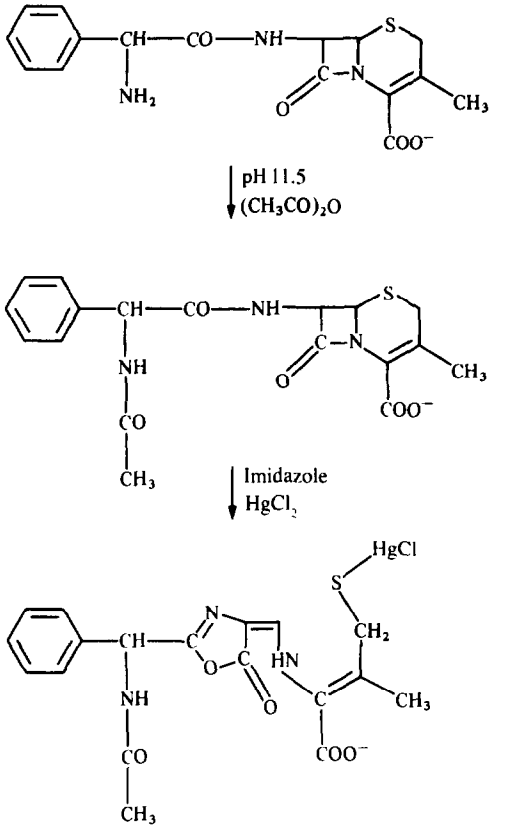

Proposed mechanism of the reaction between cephalexin and imidazole reagent.

Table 3. Analysis of authentic sample of cephalexin by the proposed and official method*

Taken, *mg/ml*	Found, *mg/ml*	Recovery	Official method[12]
0.3	0.300	100	99.7
0.7	0.699	99.9	99.4
0.9	0.900	100	100
1.3	1.28	98.5	101.2
2.0	2.010	100.5	98.7
2.4	2.395	99.8	99.5

*Each result is the average of 4 determinations.

Table 4. Analysis of some dosage forms containing cephalexin by the proposed and official method

	Proposed method	Official method	
Preparation	Recovery ± SD, %*	Recovery ± SD, %*	*t*†
Cephalexid-capsules	100.1 ± 0.25	99.5 ± 0.80	0.644
Keflex-tablets	100 ± 0.38	99.5 ± 0.31	0.875
Keflex-granules	100.0 ± 0.04	100.0 ± 0.07	0.000
Ospexin-suspension	99.6 ± 0.52	98.3 ± 0.26	1.990

*Average of five determinations.
†*t* = Calculated *t*-value (the theoretical value is 2.571 at 95%).

Acknowledgement—This research (Chem/1409/34) was supported by the Research Center, College of Science, King Saud University, Riyadh, Saudi Arabia.

REFERENCES

1. J. E. F. Reynolds and A. B. Prasad, *Martindale, The Extra Pharmacopoeia*, 28th Ed., The Pharmaceutical Press, London, 1982.
2. M. A. Abdalla and A. G. Fogg, *Analyst*, 1983, **108**, 53.
3. A. G. Fogg and M. A. Abdalla, *J. Pharm. Biomed. Anal.*, 1985, **3**, 315.
4. M. A. Korany, A. H. El-Sayed and S. M. Galal, *Anal. Lett.*, 1989, **22**, 141.
5. *Idem*, *ibid.*, 1989, **22**, 159.
6. J. A. Murillo, J. Rodriguez, J. M. Lemus and A. Alanon, *Analyst*, 1990, **115**, 117.
7. L. P. Marrelli, *J. Pharm. Sci.*, 1972, **61**, 1547.
8. J. K. Grime and B. Tan, *Anal. Chim. Acta*, 1979, **105**, 369.
9. R. H. Barbhaiya and P. Turner, *J. Pharm. Pharmac.*, 1976, **28**, 791.
10. J. A. Squella, L. J. Vergara and E. M. Gonzalez, *J. Pharm. Sci.*, 1978, **67**, 1466.
11. H. Fabre, M. D. Blanchin, D. Lerner and B. Mandrous, *Analyst*, 1985, **110**, 775.
12. *British Pharmacopoeia 1980*, H.M. Stationary Office, London, 1980.
13. J. C. Miller and J. N. Miller, *Statistics for Analytical Chemistry*, Ellis Horwood, Chichester, 2nd Ed., 1988.
14. R. Mendez, T. Alemany, A. Negro and J. Martin, Villacorta, *Anal. Lett.*, 1990, **23**, 1335.
15. H. Bundgaard, *J. Pharm. Sci.*, 1974, **26**, 385.

Talanta, Vol. 39, No. 6, pp. 709–713, 1992
Printed in Great Britain.

0039-9140/92 $5.00 + 0.00

THREE SIMPLE SPECTROPHOTOMETRIC METHODS FOR THE DETERMINATION OF SULPHINPYRAZONE

C. S. P. SASTRY,* A. SAILAJA, T. THIRUPATHI RAO and D. MURALI KRISHNA

Foods and Drugs Laboratories, School of Chemistry, Andhra University, Visakhapatnam 530 003, India

(*Received* 24 *June* 1991. *Accepted* 29 *August* 1991)

Summary—Three simple and sensitive spectrophotometric methods for the determination of sulphinpyrazone (SP) in bulk samples and pharmaceutical formulations are described. They are based on the oxidation of sulphinpyrazone with excess *N*-bromosuccinimide (NBS) and determination of the unconsumed NBS with metol–isonicotinic acid hydrazide (method A, λ_{max}: 620 nm); by the reduction of Folin–Ciocalteu reagent (method B, λ_{max} 770 nm); or by the formation of a chloroform-soluble, coloured ion-association complex between the drug and Methylene Violet (MV) at pH 7.0 (method C, λ_{max} 545 nm).

Sulphinpyrazone is chemically known as 3,5-pyrazolidine dione, 1,2-diphenyl-4-[2-(phenyl sulphinyl) ethyl]. Its structure is given in Scheme 1. It is widely used as a uricosuric agent and reduces elevated concentrations of uric acid in the blood and causes the slow depletion of urate deposits in tissues. It is used in the treatment of recurrent and chronic gout and is official in U.S.P.[1] and B.P.[2] Reported methods include a single titrimetric[3] and two visible spectrophotometric[4,5] methods besides a few GLC[6,7] and HPLC[8,9] methods. The first visible spectrophotometric method with *p*-dimethylaminocinnamaldehyde as the chromogenic agent requires a preliminary treatment of the drug with acetic acid and hydrochloric acid. The second method with 2,2′-diphenyl-1-picrylhydrazyl is not satisfactory for microgram quantities.

Sulphinpyrazone exhibits acidic character and reducing properties due to the presence of sulphoxide and enolic hydroxyl groups. These have not been exploited so far for its estimation. Three sensitive visible spectrophotometric methods have been developed based on

*Author for correspondence.

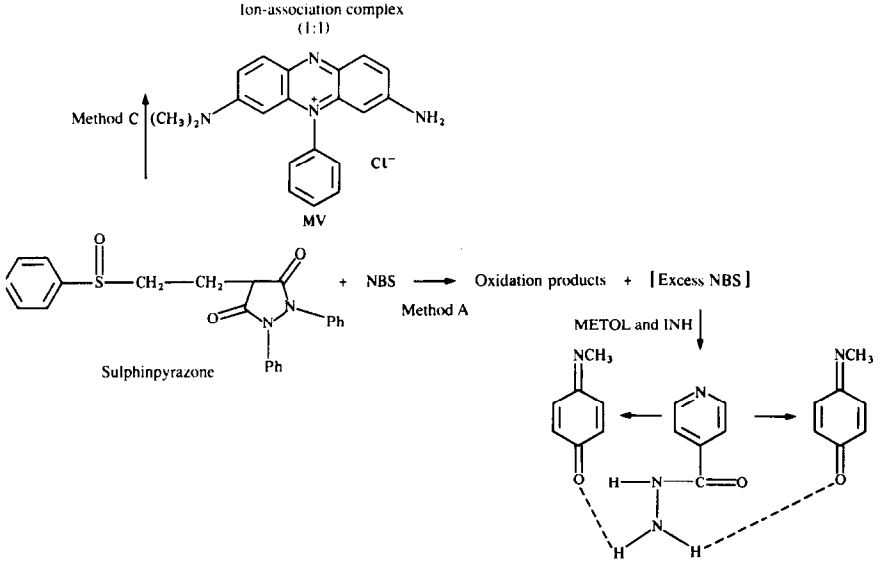

Scheme 1

these properties. *N*-Bromosuccinimide (NBS) contains unstably bound bromine and is used for brominations and dehydrogenations in organic compounds. Sastry *et al.*[10] suggested a procedure for determining isonicotinic acid hydrazide (INH) by treatment with *p*-*N*-methyl aminophenol sulphate (MAP, metol) and oxidant. In method A of the present study, SP was treated with standard NBS in excess. The consumed NBS corresponding to SP was obtained by estimating excess NBS spectrophotometrically with metol and INH and deducting it from the NBS initially taken (*i.e.*, blank). Folin–Ciocalteu reagent in the presence of alkali has been utilized as a chromogenic agent for the determination of a number of drugs.[11] The basic dye, methylene violet, has been used for the determination of drugs which are acidic in nature.[12] This basic dye was used for the determination of SP. All three methods have been applied to bulk samples and pharmaceutical preparations.

EXPERIMENTAL

Apparatus

A Systronics model 106 spectrophotometer with 1-cm matched glass cells was used for all the absorbance measurements. An Elico-digital model LI-120 pH meter was used for pH measurements.

Reagents

All solutions were prepared in doubly distilled water. Freshly prepared aqueous solutions of 0.8% metol (*p*-*N*-methyl aminophenol, Loba-Chemie), 0.045% NBS (*N*-Bromosuccinimide, Loba-Chemie, standardized iodometrically), 0.1% INH (isonicotinic acid hydrazide, Wilson Labs) and 1% acetic acid (BDH) were prepared.

A 10% (w/v) sodium carbonate (BDH) aqueous solution and commercially available 2*N* Folin–Ciocalteu (Loba-Chemie) reagent were used.

A 0.068% (w/v) aqueous methylene violet solution (Gurr, MV; C.I. No. 50210) was prepared. A buffer solution (pH 7.0) was obtained by mixing 390 ml of 0.067*M* potassium hydrogen phosphate (Merck) and 610 ml of 0.067*M* disodium hydrogen phosphate (Merck).

Standard drug solution. A 1-mg/ml solution of sulphinpyrazone was prepared in 0.01*N* sodium hydroxide. The working solutions (methods A, 100 μg/ml; B, 50 μg/ml; C, 10 μg/ml) were obtained by further dilution of the stock solution with distilled water.

All chemicals used were of analytical or pharmacopoeial grade.

Analysis of bulk samples

Method A. Aliquots of the standard drug solution (0.75–4.0 ml, 100 μg/ml) were transferred into a series of 25-ml graduated test tubes and the total volume in each tube was brought to 4 ml with distilled water. Then 2 ml of NBS was added to each and the test tubes were kept aside for 15 min at room temperature (25–30°). Next 15 ml of acetic acid and 1 ml of metol were added and the solutions were mixed thoroughly. After 2 min, 1 ml of INH was added. The solutions were made up to the mark with methanol. The absorbances were measured at 620 nm after 15 min and before 25 min against distilled water. A blank experiment was also carried out, omitting the drug. The decrease in the absorbance corresponding to sulphinpyrazone was obtained by subtracting the absorbance of the drug solution from the blank. The amount of sulphinpyrazone was computed from the standard calibration curve.

Method B. Aliquots of the drug solution (0.75–5.0 ml, 50 μg/ml) were transferred into a series of 25-ml graduated test tubes. The total volume in each test tube was brought to 5.0 ml with distilled water. A 2.5-ml portion of Folin–Ciocalteu reagent and 7 ml of sodium carbonate were added and the mixture kept aside for 40 min. Then the solutions were made up to 25 ml with distilled water and the absorbances measured at 770 nm immediately against a reagent blank prepared in a similar manner. The coloured species was stable for eight hours. The amount of drug was computed from the calibration graph.

Method C. Aliquots of the standard drug solution (1.0–5.0 ml, 10 μg/ml) were placed in a series of 125-ml separating funnels. Then 10 ml of buffer (pH 7.0) and 1 ml of MV solution were added to each separating funnel. The total volume of aqueous layer in each separating funnel was brought to 16 ml with distilled water. A 10-ml portion of chloroform was added to each and the contents were shaken for 1 min. The absorbance of the separated chloroform layer was measured at 545 nm against a reagent blank within the stability period (1 min–1 hr). The amount of drug was calculated from its calibration graph.

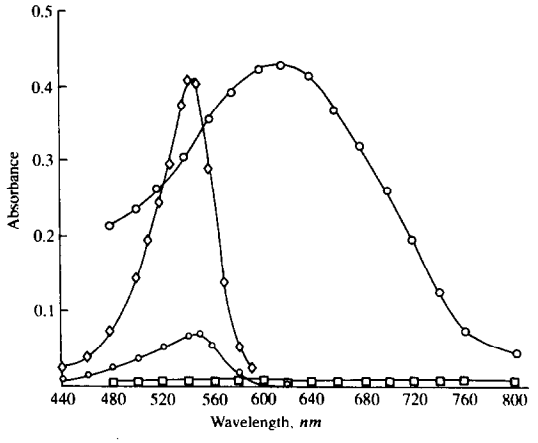

Fig. 1. Absorption spectra of ○——○ NBS–metol–INH system. □——□ Metol–INH *vs.* distilled water. △——△ Sulphinpyrazone–Methylene Violet system. ●——● Blank *vs.* chloroform. NBS: $1.52 \times 10^{-4}M$, Metol: $9.3 \times 10^{-4}M$, INH: $2.92 \times 10^{-4}M$; Sulphinpyrazone: $7.42 \times 10^{-4}M$, MV: $2.32 \times 10^{-3}M$.

Analysis of pharmaceutical preparations

As the tablets and capsules were not available in the local market, we prepared our own according to the literature method.[13,14] An amount of the powdered tablet or capsule content equivalent to 100 mg was treated with 100 ml of $0.01N$ sodium hydroxide and the insoluble residue was filtered to obtain a stock solution of 1 mg/ml. The stock solutions were further diluted with distilled water to provide working solutions as in the case of standard drug solutions and were analysed by the three different procedures.

RESULTS AND DISCUSSION

The absorption spectra of the reaction products in methods A, B and C show characteristic λ_{max} values (Figs. 1 and 2). The reaction conditions were established by variation of one parameter at a time. Method A involves two stages:—oxidation of SP by NBS (first stage) and estimation of unconsumed NBS with metol–INH reagent (second stage). In the first stage for the oxidation of sulphinpyrazone, use of 1.5–2.5 ml of NBS and a waiting period of 10–30 min were found necessary. In the second stage, 12–18 ml of acetic acid, 0.5–1.5 ml of metol solution and 0.5–1.5 ml of INH solution were found optimal. The intermittent waiting period prior to the addition of INH was 1–3 min.

In method B, 2.20–2.80 ml of Folin–Ciocalteu reagent and 6–8 ml of sodium carbonate were found to give maximum colour intensity. The order of addition however was found not to have a significant effect. Sodium hydroxide instead of sodium carbonate did not give a positive test.

In method C, in order to establish the optimum pH range, sulphinpyrazone was allowed to react with MV in aqueous solutions buffered to pH 4.0–7.5 and the complex formed was extracted into chloroform for measurement. Constant absorbances were obtained over the pH range 6.8–7.2 in phosphate buffer. Hence a pH of 7.0 was used. A 0.75–1.20 ml-portion of MV solution was found to be optimal. Shaking times of 0.5–4.0 min produced constant absorbance, hence a shaking time of 1.0 min was selected for use. A ratio of 1.6:1 of aqueous to chloroform phases was required for efficient extraction of the coloured species.

Analytical data

The Beer's law limits, molar absorptivity, regression equation, and correlation coefficient obtained by linear least squares treatment of the results are given in Table 1. The precision and accuracy were found by analysis of six separate samples containing known amounts of the drug (300 μg in method A, 200 μg in method B, 30 μg in method C) and the results are summarized in Table 1. The relative standard deviation, and % range of error at 95% confidence level are also given in Table 1.

The values obtained by the proposed and reference methods for pharmaceutical prep-

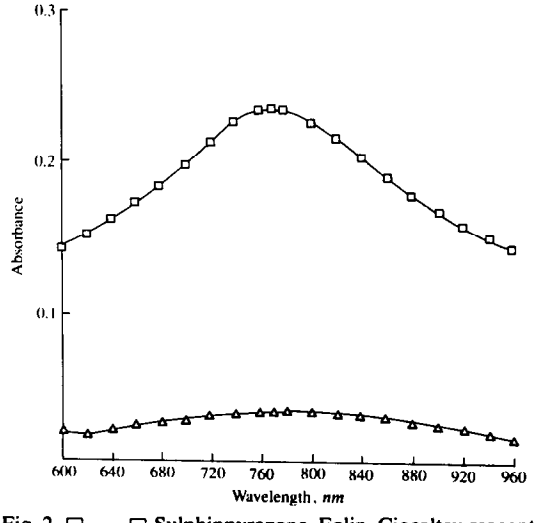

Fig. 2. □——□ Sulphinpyrazone–Folin–Ciocalteu reagent. △——△ Reagent blank *vs.* distilled water. Sulphinpyrazone: $1.97 \times 10^{-5}M$, F–C: $0.2M$.

Table 1. Optical characteristics, precision and accuracy

Parameters	Method A	Method B	Method C
Beer's law limits (μg/ml)	2–16	1.4–10	0.4–5
Molar absorptivity (l.mole^{-1}.cm^{-1})	1.08×10^4	1.17×10^4	5.48×10^4
Sandell's sensitivity (μg/cm^2/0.001 absorbance unit)	0.037	0.034	0.007
Regression equation (Y)*			
Slope (n)	2.66×10^{-2}	2.88×10^{-2}	13.64×10^{-2}
Intercept (m)	0.095×10^{-2}	0.111×10^{-2}	0.149×10^{-2}
Correlation coefficient (r)	0.9999	0.9999	0.9998
Relative standard deviation† (%)	0.54	0.51	0.50
Range of error† (%, 95% confidence limit)	0.56	0.54	0.53

*$Y = m + nC$ where C is the concentration (μg/ml).
†Six replicate samples.

arations are compared in Table 2 and are in good agreement. These results were compared statistically by the F-test and found not to differ significantly. The results of the recovery experiments by the proposed methods are also listed in Table 2. The commonly used excipients and additives in the formulations of sulphinpyrazone such as starch, lactose, talc, stearic acid, boric acid, gelatin, magnesium carbonate and sodium lauryl sulphate were found not to interfere in the analysis.

The proposed methods are simple and sensitive and can be used for the routine determination of sulphinpyrazone.

Chemistry of the coloured species

Method A is based on the oxidation of sulphinpyrazone by excess NBS to form oxidation products (probably a mixture, but reproducible under the proposed experimental conditions, each mole of drug consuming 3.83 moles of NBS), and the unreacted NBS was determined with metol–INH. The coloured complex may be regarded as a charge-transfer type shown in scheme 1, presumed to be taking place involving electron transfer from the highest occupied molecular orbital of INH to the lowest empty molecular orbital (π^*) of the two adjacent *p-N*-methylbenzoquinonemonoimine (formed *in situ* from metol and NBS) molecules as in the metol, iodine and INH reaction.[10]

The colour formation by the F–C reagent in the presence of sulphinpyrazone may be explained based on analogy with the literature.[15] The mixed acids in the FC preparation are the final chromogens and involve the following chemical species:

$$3H_2O.P_2O_5.13WO_3.5MoO_3.10H_2O$$

and

$$3H_2O.P_2O_5.14WO_3.4MoO_3.10H_2O.$$

Sulphinpyrazone probably affects the reduction of 1, 2 or 3 oxygen atoms from tungstate and/or molybdate thereby producing one or more of several possible reduced species which have a characteristic blue colour (770 nm).

Table 2. Assay of sulphinpyrazone in pharmaceutical preparations

Pharmaceutical preparations	Nominal amount, mg	Found,* % Proposed methods A	B	C	Reference† method	% Recovery by proposed methods‡ A	B	C
Capsules								
I	200	98.9 ± 0.4 $F = 1.15$	99.4 ± 0.6 $F = 1.60$	99.6 ± 0.4 $F = 1.05$	99.9 ± 0.4	99.6 ± 0.4	99.6 ± 0.6	99.8 ± 0.4
II	200	99.1 ± 0.3 $F = 1.20$	99.6 ± 0.6 $F = 1.25$	99.8 ± 0.6 $F = 1.70$	99.8 ± 0.5	98.9 ± 0.3	99.0 ± 0.6	99.4 ± 0.5
Tablets								
I	200	99.6 ± 0.5 $F = 1.30$	99.0 ± 0.7 $F = 1.15$	99.8 ± 0.4 $F = 1.20$	99.4 ± 0.6	99.2 ± 0.5	99.0 ± 0.6	100.1 ± 0.3
II	100	99.4 ± 0.4 $F = 1.35$	98.8 ± 0.6 $F = 1.30$	98.8 ± 0.5 $F = 1.10$	99.2 ± 0.5	99.8 ± 0.3	99.3 ± 0.4	99.5 ± 0.4

*Average ± standard deviation of 6 determinations; F-values refer to comparison of the proposed method with the reference method. Theoretical values at 95% confidence limit $F = 5.05$.
†U.S.P. Method.
‡Recovery of 50 mg added to the pharmaceutical preparation.

Sulphinpyrazone—being acidic—forms an ion-association complex with the basic dye Methylene Violet (MV C.I. No. 50210) which is extractable into chloroform from the aqueous phase. The stoichiometric ratio of the drug to MV was determined with the slope-ratio method[16] and found to be 1:1 (ion-pair).

REFERENCES

1. *United States Pharmacopoeia*, 18th Ed., p. 698. Mack Publishing Co., Easton, PA, 1970.
2. *British Pharmacopoeia*, Vol. II, p. 1007. Her Majesty's Stationery Office, London, 1988.
3. A. M. Taha, B. A. El-Zeany, M. M. Amer and O. A. El-Sawy, *Egypt. J. Pharm. Sci.*, 1981, **22**, 47.
4. El-Kommos and E. Michael, *Analyst*, 1983, **108**, 1144.
5. M. Kamla Emara, El-Kommos and E. Michael, *Alexandria, J. Pharm. Sci.*, 1990, **4**, 69.
6. J. Rosenfeld, M. Buchanan, P. Powers, J. Hirsh, H. J. M. Barnett and R. K. Stuart, *Thromb. Res.*, 1978, **12**, 247.
7. P. Jakobsen, A. and A. Kirstein Pedersen, *J. Chromatog.*, 1979, **163**, 259.
8. E. G. W. M. Lentjes, Y. Tan and C. A. M. Van Ginneken, *Pharm. Weekbl. Sci. Ed.*, 1986, **7**, 252.
9. L. Nagy and Z. Klatsmanyi Siklosi, *Gyogyszereszet*, 1987, **31**, 95; *Chem. Abstr.* 107, 17119w.
10. C. S. P. Sastry, B. S. Reddy and B. G. Rao, *Indian J. Pharm. Sci.*, 1981, **43**, 118.
11. C. S. P. Sastry, T. N. V. Prasad, A. Rama Mohana Rao and E. Venkata Rao, *Indian Drugs*, 1988, **5**, 206.
12. C. S. P. Sastry, Tipirneni A. S. R. Prasad and M. V. Suryanarayana, *Analyst*, 1989, **114**, 513.
13. H. A. Liberman and L. Lachman (Eds.), *Pharmaceutical Dosage Forms: Tablets*, Vol. I, Dekker, New York, 1980.
14. L. Lachman, H. A. Lieberman, and J. L. Kanig (eds.), *The Theory and Practice of Industrial Pharmacy*, 2nd Ed., Henry Kimpton Publishers, London, 1976.
15. G. L. Peterson, *Anal. Biochem.*, 1979, **100**, 201.
16. H. Irving, F. J. C. Rossovathi and R. J. P. Williams, *J. Chem. Soc.*, **1955**, 1906.

Talanta, Vol 39, No 7, pp 857–862, 1992
Printed in Great Britain

0039-9140/92 $5.00 + 0.00

INFLUENCE OF MEDIUM POLARITY UPON SELECTIVITY AND EFFICIENCY OF ALKALI METAL CATION SORPTION BY POLYETHER CARBOXYLIC ACID RESINS

TAKASHI HAYASHITA, JOUNG HAE LEE,* JONG CHAN LEE, JAN KRZYKAWSKI and RICHARD A BARTSCH†

Department of Chemistry and Biochemistry, Texas Tech University, Lubbock, Texas 79409-1061, U S A

(*Received* 23 *July* 1991 *Revised* 12 *September* 1991 *Accepted* 20 *September* 1991)

Summary—The influence of medium polarity upon competitive sorption of alkali–metal cations from aqueous and aqueous methanolic solutions by the polymethacrylic acid resin Amberlite CG-50, two acyclic polyether carboxylic acid resins, and six *sym*-(alkyl)dibenzo-16-crown-5-oxyacetic acid resins has been investigated Addition of methanol was found to strongly depress the selective Li^+ sorption of CG-50 and one of the acyclic polyether carboxylic acid resins Enhancement of metal ion-crown ether interactions as the percentage of methanol in the medium was increased accentuates the Na^+ sorption selectivity for the lariat ether carboxylic acid resins The highest Na^+ sorption selectivity was obtained for *sym*-(alkyl)-dibenzo-16-crown-5-oxyacetic acid resins with ethyl and propyl groups in 80% methanol–20% water

Macrocyclic polyethers (crown ethers) are superior ligands for complexation of alkali–metal cations.[1] Attachment of a side arm with one or more potential coordination sites to a crown ether gives a lariat ether for which the efficiency and selectivity of alkali–metal cation complexation may be altered.[2] Incorporation of crown and lariat ether units into resin matrices should provide chelating resins which can be used for selective separation of alkali–metal cations from solution.

Recently we prepared acyclic polyether carboxylic acid resin **2** and lariat ether carboxylic acid resins **3–8** (Fig. 1) which are a new type of ion-exchange resin with both ion-exchange and polyether binding sites for metal ions.[3,4] For competitive sorption of alkali metal cations from aqueous solutions by these resins, the sorption efficiency and selectivity were influenced by: (1) the pH of the aqueous sample solution; (2) whether the polyether unit was acyclic or cyclic; (3) conformational positioning of the carboxylic acid group with respect to the cyclic polyether unit in resins **3–8**; and (4) the length of the alkyl group chain in resins **4–8**.[3–5] The highest sorption efficiencies and Na^+ selectivities were noted for *sym*-(alkyl)-dibenzo-16-crown-5-oxyacetic acid resins **4–6** which have methyl, ethyl, and propyl alkyl groups, respectively. For the lariat ether units in **4–6**, the carboxylic acid group of the side arm is positioned over the polyether cavity when the alkyl group points away from the polar polyether ring. Such preorganization of the binding site[6] produces high loading of the resins and enhanced Na^+ sorption selectivity. The presence of longer alkyl groups makes the resins more hydrophobic which decreases the effective ion-exchange capacity.[4] Thus not only the steric configuration of the binding site but also the micro-environment of the resin was found to play an important role in metal ion sorption.

The polarity of the sample medium should also affect the micro-environment of the resin. Metal ion-crown ether interactions generally increase as the polarity of the solution is diminished,[7] which might increase the sorption selectivity and efficiency of a polyether carboxylic acid resin. To investigate this possibility, the competitive alkali metal cation sorption behavior of Amberlite CG-50, a commercial polymethacrylic acid resin, the previously reported and new acyclic polyether carboxylic acid resins **2** and **1**, respectively, and lariat ether carboxylic acid resins **3–8** in aqueous and aqueous methanolic solutions, are now compared.

*Permanent address Korea Standards Research Institute, Taedok Science Town, Taejon 305-606, Republic of Korea.

†Author for correspondence

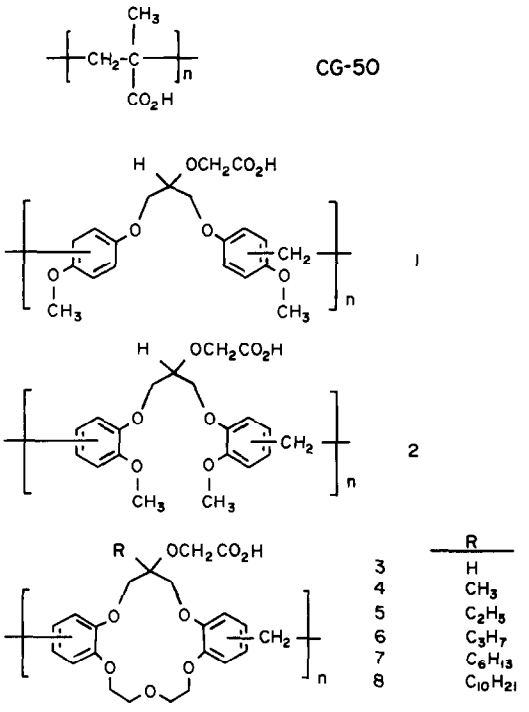

Fig 1 Structures of carboxylic acid resins that were utilized in this study

EXPERIMENTAL

Apparatus

The apparatus was the same as that utilized in the previous study.[3] To prevent metal contamination, all glassware was soaked in 5% nitric acid solution for 24 hr then rinsed with distilled, demineralized water before use.

Reagents

Resin **2** from 1,3-di(*o*-methoxyphenoxy)-2-(oxyacetoxy)propane, resin **3** from *sym*-dibenzo-16-crown-5-oxyacetic acid, and resins **4–8** from *sym*-(alkyl)dibenzo-16-crown-5-oxyacetic acids were prepared by condensation polymerization of the dibenzo polyether carboxylic acid monomers with formaldehyde in formic acid as described previously in detail.[3,5] Unless specified otherwise, reagent grade compounds and solvents were obtained from chemical suppliers and used as receivers. Stock aqueous solutions of alkali metal chlorides and hydroxides (1.00*M* and 0.50*M* each of lithium hydroxide, sodium chloride, potassium chloride, rubidium chloride and cesium chloride) were stored in polyethylene bottles. Sample solutions were prepared by diluting these solutions with water and methanol. Purified water was prepared by passing distilled water through three Barnstead D8922 combination cartridges in series.

*Preparation of 1,3-di(*p*-methoxyphenoxy)-2-propanol*

By the procedure reported for the synthesis of 1,3-di(*o*-methoxyphenoxy)-2-propanol[3] but replacing *o*-methoxyphenol by *p*-methoxyphenol, the title compound (mp 99–101°) was synthesized in 54% yield. IR (deposit on sodium chloride plate from $CDCl_3$ solution) 3417 (OH), 1233, 1107 (CO) cm^{-1}. ^1H NMR ($CDCl_3$) δ 2.83 (s, 1), 3.95 (s, 6), 3.94–4.08 (m, 4), 4.24–4.36 (pen, 1), 6.82–6.89 (m, 8). Analysis calculated for $C_{17}H_{20}O_5$: C, 67.09; H, 6.62. Found: C, 67.28; H, 6.70.

*Preparation of 1,3-di(*p*-methoxyphenoxy)-2-(oxyacetoxy)propane*

With the procedure reported for the synthesis of 1,3-di(*o*-methoxyphenoxy)-2-(oxyacetoxy)-propane,[3] but replacing 1,3-di(*o*-methoxyphenoxy)-2-propanol with 1,3-di(*p*-methoxyphenoxy)-2-propanol, the title compound was prepared in 84% yield as a yellow liquid. IR (neat) 3213 (OH), 1760 (C=O), 1226, 1038 (CO) cm^{-1}. ^1H NMR ($CDCl_3$) δ 3.68 (s, 6), 4.06 (s, 5), 4.34 (s, 2), 6.76–6.77 (m, 8). Analysis calculated for $C_{19}H_{22}O_7$: C, 62.97; H, 6.12. Found: C, 62.87; H, 6.15.

*Preparation of 1,3-di(*p*-methoxyphenoxy)-2-(oxyacetoxy)propane resin* **1**

Resin **1** was synthesized by condensation polymerization of 1,3-di(*p*-methoxyphenoxy)-2-(oxyacetoxy)propane with formaldehyde in formic acid by the reported general method[3] in 61% yield. IR (KBr) 3448 (COOH), 1740 (C=O), 1207, 1028 cm^{-1}. Analysis calculated for a hydrate of the partially crosslinked general structure given in reference 3: C, 63.84; H, 5.93. Found: C, 63.74; H, 5.72.

Procedure

A resin (0.050 g) and 5.00 ml of an aqueous or aqueous methanolic solution containing 0.10*M* (each) lithium hydroxide, sodium chloride, potassium chloride, rubidium chloride and cesium chloride was shaken for 3.0 hr in a 30-ml separating funnel at room temperature (21–23°) with a Burrell Model 25 wrist-action shaker. The aqueous phase was filtered with a sintered glass funnel (15 ml, medium porosity). The measured equilibrium pH of the aqueous phase was in the range 12.5–12.9. The resin was washed with 100 ml of distilled, demineralized water and dried. Of the dried resin, a 0.020 g

sample was shaken with 5.0 ml of 0.10*M* hydrochloric acid for 1.0 hour to strip the alkali–metal cations from the resin into an aqueous solution for analysis with a Dionex Model 2000i ion chromatograph.

RESULTS AND DISCUSSION

Competitive sorption of alkali–metal cations by Amberlite CG-50 and acyclic polyether carboxylic acid resins 1 and 2

In earlier work, Amberlite CG-50, a commercially available polymethacrylic acid, and acyclic polyether carboxylic acid resin **2** were used as model systems for interpreting the competitive sorption of alkali–metal cations from aqueous solutions by lariat ether carboxylic acid resins **3**–**8**.[3–5] The acyclic polyether carboxylic acid resin **1** has now been prepared to serve as an additional model compound. Resin **1** is a structural isomer of resin **2** in which the *para*-positioned methoxy groups can no longer form the pseudo-cyclic arrangement of the four alkyl aryl ether polyether oxygens that is possible in resin **2**.

To probe the effect of medium polarity upon alkali–metal cation sorption by Amberlite CG-50 and acyclic polyether carboxylic acid resins **1** and **2**, each resin was shaken with an aqueous or aqueous methanolic solution (10, 20, 40, 60 and 80 volume percent of methanol) which was 0.10*M* in each of the five alkali–metal cations as the chlorides and hydroxides. The mixture was filtered and the equilibrium pH of the filtrate was measured and found to be in the range 12.5–12.9. For these weakly acidic ion exchange resins, maximum alkali–metal cation sorption would be expected under such alkaline conditions.[3] The filtered resin was thoroughly washed with distilled demineralized water and dried. A portion of the dried resin was shaken with 0.10*M* hydrochloric acid to strip the metal ion species from the resin for analysis by ion chromatography.

Although the general sorption selectivity ordering for cation-exchange resins is $Cs^+ > Rb^+ > K^+ > Na^+ > Li^+$,[8] carboxylic acid resins exhibit a reversed ordering under alkaline conditions due to strong ion-associative interaction of carboxylate groups with alkali–metal cations of smaller ionic dimensions.[9,10] Data for the competitive sorption of alkali–metal cations by CG-50 and acyclic polyether carboxylic acid resins **1** and **2** are presented in Figs. 2 and 3(a) and (b), respectively.

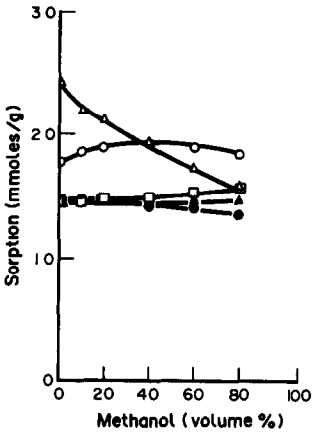

Fig. 2. Competitive sorption of alkali–metal cations by Amberlite CG-50 *vs.* the methanol percentage in the aqueous methanolic solvent at pH 12.5–12.9. (△) Li^+ (○) Na^+ (□) K^+ (▲) Rb^+ (●) Cs^+.

For CG-50, Li^+ sorption decreases linearly as the volume percentage of methanol increases (Fig. 2). On the other hand, only minor changes in sorption for the other four alkali–metal cations are noted as the medium is systematically varied from water to 80% methanol–20% water. Thus the pronounced Li^+ sorption selectivity for CG-50 in water changes to equal sorption propensity for Li^+ and Na^+ in 40% methanol–60% water. When the methanol content of the medium is increased even further, CG-50 exhibits modest sorption selectivity for Na^+.

A similar competitive sorption profile is observed for acyclic polyether carboxylic acid resin **1** [Fig. 3(a)] and the resin exhibits Li^+ sorption selectivity from aqueous solution. However, the diminution of Li^+ sorption with increasing methanol content of the medium is not as severe for **1** as that for CG-50 and the decrease in Li^+

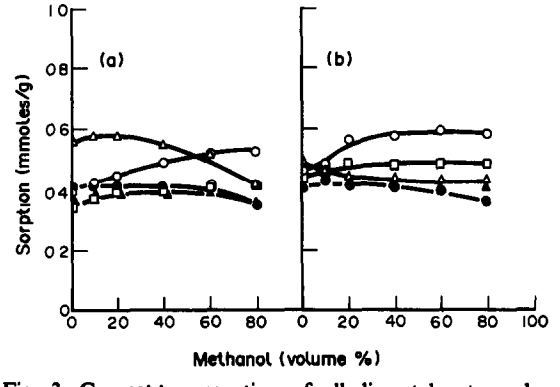

Fig. 3 Competitive sorption of alkali–metal cations by acyclic polyether carboxylic acid resins (a) **1** and (b) **2** *vs.* the methanol percentage in the aqueous methanolic solvent at pH 12.5–12.9. (△) Li^+ (○) Na^+ (□) K^+ (▲) Rb^+ (●) Cs^+

sorption is offset by an enhancement of Na^+ sorption.

For acyclic polyether carboxylic acid resin **2**, the sorption selectivity for Li^+ from water is slight and the decrease in Li^+ sorption with enhanced methanol content in the medium is much smaller than that observed for CG-50 or resin **1**. Resin **2** becomes Na^+ selective for alkali–metal cation sorption from 20% methanol–80% water.

Diminution of Li^+ sorption upon addition of methanol to the medium is in the order CG-50 > resin **1** > resin **2** which suggests that Li^+ solvation at the binding site is an important factor. For CG-50 the binding site is only the carboxylate ion so highly hydrated Li^+ is probably involved and association of the cation and anion may occur through one of the solvating water molecules.[9] In resin **1**, the binding site, which contains three ether oxygens and the carboxylate ion, is much more hydrophilic and interactions of Li^+ with one or more ether oxygens replace some of the solvating water molecules. This trend continues on going to resin **2** for which the binding site possesses five ether oxygens (if the polyether framework adopts a pseudo-cyclic conformation) and the carboxylate anion. Thus the binding site in resin **2** becomes even more hydrophilic which further diminished the need for solvating water molecules and reduces the sensitivity of Li^+ sorption to added methanol in the medium. The similar sorption profiles for acyclic polyether carboxylic acid resin **2** and lariat ether carboxylic acid resin **3** [Fig. 4(a)] suggests that the four alkyl aryl oxygens in the former do indeed adopt a pseudo-cyclic arrangement.

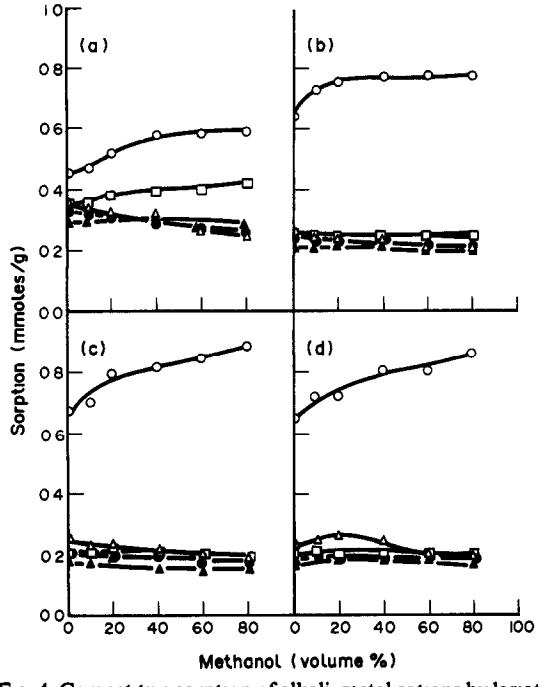

Fig. 4. Competitive sorption of alkali–metal cations by lariat ether carboxylic acid resins (a) **3**, (b) **4**, (c) **5**, and (d) **6** *vs.* the methanol percentage in the aqueous methanolic solvent at pH 12.5–12.9: (△) Li^+ (○) Na^+ (□) K^+ (▲) Rb^+ (●) Cs^+.

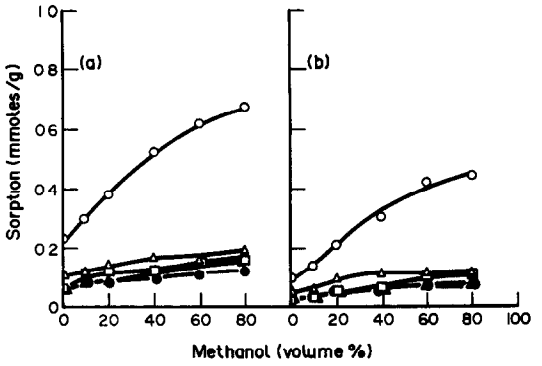

Fig 5 Competitive sorption of alkali–metal cations by lariat ether carboxylic acid resins (a) **7** and (b) **8** *vs.* the methanol percentage in the aqueous methanolic solvent at pH 12 5–12 9· (△) Li^+ (○) Na^+ (□) K^+ (▲) Rb^+ (●) Cs^+.

Competitive sorption of alkali–metal cations by cyclic polyether carboxylic acid resins 3–8

The influence of methanol concentration in the medium upon competitive sorption of alkali–metal cations by lariat ether carboxylic acid resins **3–6** is shown in Figs. 4(a)–(d), respectively. Sorption selectivity for Na^+ would be predicted for the 16-crown-5 ring size and is observed for all four resins. Also for all four resins, the Na^+ sorption selectivity increases when the medium is changed from water to aqueous methanol. Such enhancements in Na^+ sorption selectivity are reasonable in view of the two-to-three log unit increases in stability constants for metal ion–crown ether interactions when the solvent is changed from water to methanol.[7]

Compared with lariat ether carboxylic acid resin **3** (Fig. 4(a)] attachment of methyl, ethyl and propyl groups to the polyether ring carbons that bear the sidearms in resins **4–6** [Figs. 4(b)–(d)], respectively, substantially enhances the Na^+ sorption selectivity in water. As proposed earlier, this is attributed to conformational positioning of the pendent carboxylic acid function over the cyclic polyether ring when an alkyl group is introduced.[3] Such preorganization of the bind site[6] enhances sorption

Table 1 Alkali-metal cation loadings for polyether carboxylic acid resins 1–8

Resin	Alkyl chain	Ion-exchange capacity,* *mmoles/g*	Percent metal ion loading for different methanol contents of the medium, % 0†	40†	80†
1	None‡	2 66	80	86	84
2	None‡	2 66	83	87	86
3	None	2 39	77	79	76
4	Methyl	2 31	65	75	72
5	Ethyl	2 23	64	70	72
6	Propyl	2 17	65	74	73
7	Hexyl	1 93	25	53	67
8	Decyl	1 79	12	32	44

*Calculated from elemental analysis data
†Volume percentage of methanol in the medium
‡An acyclic polyether carboxylic acid resin

selectivity. The increased Na^+ sorption selectivity of resins **4–6** over that of resin **3** in water is further accentuated in aqueous methanol. This is consistent with enhanced metal ion–cyclic polyether interactions in aqueous methanol. The highest Na^+ sorption selectivity was observed in 80% methanol–20% water for resins **5** and **6** in which the positioning alkyl groups are ethyl and propyl.

For lariat ether carboxylic acid resins **7** and **8** which have much longer alkyl groups, the sorption profiles are considerably different than those for resins **4–6**. Compared with the sorption of alkali–metal cations from aqueous solutions by lariat ether carboxylic acid resins **4–6** [Figs. 4(b)–(d)], the sorption efficiencies for resins **7** and **8** are much lower [Figs. 5(a), (b)]. This is attributed to the longer alkyl groups of resins **7** and **8** which enhance the hydrophobicity of the resins and hinder penetration of the aqueous solution into the resins and also diminishes effective interactions between the metal cations and the binding sites.[4] For resins **7** and **8**, the addition of methanol to the medium produces a much larger enhancement in Na^+ sorption selectivity and efficiency than was observed with resins **4–6**. The markedly enhanced Na^+ sorption for **7** and **8** is consistent with better penetration of the alkali–metal cation solution into the resins for the aqueous methanolic solvent.

The total alkali–metal cation loadings for polyether carboxylic acid resins **1–8** for water, 40% methanol–60% water, and 80% methanol–20% water are compared in Table 1. The loading is defined as the total sorption, as calculated from total alkali–metal cation concentration in the stripping solution, divided by the ion-exchange capacity for the resin, as calculated from the elemental analysis data.[3,4] For acyclic and cyclic polyether carboxylic acid resins **1–6**, the percent loading observed for aqueous solutions increases by 4–10% in the aqueous methanolic media. In contrast, resins **7** and **8** exhibit 2.7 and 3.7-fold increases in loading percentages for a change of medium from water to 80% methanol–20% water. Thus the reduced efficiency for alkali–metal cation sorption from water which results from the presence of long alkyl groups in *sym*-(alkyl)dibenzo-16-crown-5-oxyacetic acid resins may be partially overcome by decreasing the polarity of the medium to improve penetration of the alkali–metal cation solution into the resin matrix.

CONCLUSIONS

This study demonstrates that competitive sorption of alkali–metal cations by polyether carboxylic acids **1–8** is influenced by the polarity of the medium from which the alkali–metal cations are sorbed. Similarity of alkali–metal cation sorption behavior for acyclic polyether carboxylic acid resin **2** and lariat ether carboxylic acid resin **3** suggests a pseudo-cyclic conformation for the former. The enhanced Na^+ sorption selectivity of *sym*-(alkyl)dibenzo-16-crown-5-oxyacetic acid resins **4–6** over resin **3**, which does not possess a side arm-positioning alkyl group, is further increased as the medium polarity is diminished to promote greater metal ion–crown ether interactions. The low alkali–metal cation sorption from water by hydrophobic lariat ether resins **7** and **8** is markedly improved when the polarity of the medium is lowered.

Acknowledgements—This research was supported by the Division of Chemical Sciences of the Office of Basic Energy Sciences of the US Department of Energy (Grant DE-FG05-88ER13832) and the Advanced Technology Program of the Texas Higher Education Coordinating Board. Joung Hae Lee received a postdoctoral fellowship from the Korea Science and Engineering Foundation

REFERENCES

1 C J. Pedersen, *J. Am Chem. Soc*, 1967, **89**, 7017.
2 G. W Gokel and J E. Trafton, *Cation Binding by Macrocycles. Complexation of Cationic Species by Crown Ethers*, Y Inoue and G W Gokel (eds), pp 253–310 Marcel Dekker, New York, 1990
3. T. Hayashita, M -J Goo, J. S. Kim and R. A. Bartsch, *Anal Chem*, 1990, **62**, 2283
4 *Idem, Talanta*, 1991, **38**, 1453.
5. T. Hayashita, J H. Lee, S Chen and R. A Bartsch, *Anal Chem*, 1991, **63**, 1844
6 D. J. Cram, *Angew Chem. Int. Ed Engl.*, 1986, **25**, 1039.
7 R. M. Izatt, J S. Bradshaw, S A Nielsen, J. D Lamb and D Sen, *Chem. Rev*, 1985, **85**, 271
8 F. Helfferich, *Ion Exchange*, pp. 95–249. McGraw–Hill, New York, 1962.
9 H R Gregor, J. J Hamilton, R. J Oza and F. Bernstein, *J. Phys Chem.*, 1956, **60**, 263
10. D Reichenberg, *Ion Exchange*, J. A. Marinsky (ed.), pp 227–276. Marcel Dekker, New York, 1966.

Talanta, Vol 39, No 7, pp 863–868, 1992
Printed in Great Britain

0039-9140/92 $5 00 + 0 00
Pergamon Press Ltd

KINETIC AND MECHANISTIC STUDY OF THE REACTION OF 2,6-DICHLOROPHENOL–INDOPHENOL AND CYSTEINE

C. N. KONIDARI, S. M. TZOUWARA-KARAYANNI, L. E. BOWMAN* and M. I. KARAYANNIS†

Chemistry Department, University of Ioannina, 451 10 Ioannina, Greece

(*Received* 4 *November* 1991 *Revised* 20 *December* 1991. *Accepted* 20 *December* 1991)

Summary—In this work the reaction of cysteine (H_2Q) with 2,6-dichlorophenolindophenol (D) is studied kinetically in the pH range 2 5–9.0. Taking into consideration the distribution diagrams for the species H_3Q^+, H_2Q, HQ^-, Q^{2-} for cysteine and DH_2^+, DH, D^- for 2,6-dichlorophenolindophenol the reaction rate constants k_i for all possible combinations of the reacting species were determined. The maximum reactivity appears at pH 6 88 with an overall reaction constant $k = 306$ l.mole^{-1}.sec^{-1} at 22° The effect of the concentrations of the reagents and the ionic strength on the reaction rate is also given. From Arrhenius plots an activation energy $E_a = 8.1$ kcal/mole was calculated. Working curves for the determination of cysteine in aqueous solutions are also presented applying the reaction rate method Finally the paper includes important analytical information for the calculation of the errors due to interference of cysteine by the kinetic determination of ascorbic acid, using its reaction with 2,6-dichlorophenolindophenol

The reaction of ascorbic acid with 2,6-dichlorophenol–indophenol (DCPI) has been used in a series of analytical methods, both equilibrium and kinetic, for the determination of ascorbic acid in several food and biological samples.[1–4]

An important source of error in the determination of ascorbic acid, especially in equilibrium methods, is the reaction of DCPI with concomitant reducing species such as sulphites (common preservatives in fruit juices), reducing amino acids (*e.g.*, cysteine) and metal ions of lower oxidation state (*e.g.*, Fe^{2+} and Sn^{2+}). Because these species generally react with DCPI more slowly than ascorbic acid, they pose a more serious interference to equilibrium methods than to kinetic methods. However, under certain conditions the rate of reaction with DCPI can be comparable to that for ascorbic acid, causing a serious interference with kinetic methods also.[5]

Cysteine was chosen for this study because of its use in the preparation of tissue extracts for the determination of ascorbic acid. Cysteine is added to reduce concomitant dehydroascorbic acid to ascorbic acid. Samples treated in this manner contain more ascorbic acid than untreated samples as determined by titration with DCPI. Some investigators disagree as to the actual basis for the measured increase as excess cysteine can also react with DCPI. Further complicating the determination of ascorbic acid, cysteine is similar to ascorbic acid with respect to reduction of DCPI.

In addition to its use in sample treatment, cysteine is important as it often coexists with ascorbic acid in natural products.

Previous investigators found that cysteine at any equimolar concentration with ascorbic acid increased the result by 7–9%, and at a 10:1 molar concentration by 40–50%. The interference of cysteine in the determination of ascorbic acid depends on the pH of the reaction mixture.[6] Although slow, the reaction of cysteine with DCPI may also interfere with the determination of ascorbic acid by kinetic methods.[1,7] This is due to changes in first- or pseudo-first-order rate constants of both reactions because of variations in experimental conditions, such as pH, ionic strength, *etc.* Therefore for both equilibrium-based analyses and reaction rate methods for ascorbic acid, it is important to have a complete understanding of the reaction of 2,6-dichlorophenolindophenol with cysteine.

*Present address: Department of Chemistry, University of British Columbia, 2036 Main Mall, Vancouver, BC V6T 1V6, Canada.
†Author for correspondence

EXPERIMENTAL

Apparatus

The experimental apparatus consists of a single beam stopped-flow spectrophotometer (SFS), equipped with a logarithmic photometric unit and a storage oscilloscope. Data acquisition was accomplished with an IBM Data Acquisition and Control Adapter (IBM corporation, Boca Raton, FL) and an IBM-compatible personal computer. Data acquisition software was written in Microscoft QuickBASIC and Macroassembler (Microsoft, Redmond, WA), and uses the computer's interrupt system for rapid data acquisition.[8] The software allows the collection of 2500 points from the reaction curve, the measurements of the slopes at any point of the curve and the constant k_{ob}, applying the infinite time method, *e.g.*, graphical presentation of $\ln(A_t - A_\infty) = f(t)$.[9] The system is also connected with a printer and a plotter.

A pHM83 Autocal pHmeter (Radiometer, Denmark) was used for pH measurements.

Reagents

Buffer solutions. The buffer solutions used were based on 0.1*M* potassium hydrogenphthalate and either 0.1*M* hydrochloric acid or 0.1*M* sodium hydroxide for the pH-range 2.5–6.0, on 0.1*M* potassium dihydrogenphosphate and 0.1*M* sodium hydroxide for the pH-range 6.0–8.0 and on 0.025*M* borax and either 0.1*M* hydrochloric acid or 0.1*M* sodium hydroxide for the pH-range 8.0–10.0. For the entire pH-range the ionic strength was kept almost constant, $I = 0.05$, by carefully adjusting the ratio as well as the absolute concentrations of the buffer reagents. As it is state in the paragraph "Effect of Ionic Strength", there is a small effect on the reaction rate.

2,6-Dichlorophenolindophenol (DCPI). A stock solution, $7.5 \times 10^{-4}M$ in DCPI (Sigma, U.S.A.), containing 210 mg/l. $NaHCO_3$, was prepared. This solution was standarized by titration with freshly prepared ascorbic acid solution and stored in a refrigerator. Working solutions of different concentrations in DCPI were prepared from this stock solution daily by diluting with a $NaHCO_3$ solution of the above concentration. The concentration of the DCPI-solution was spectrophotometrically verified at 522 nm (isosbestic point of DCPI), where the molar absorptivity is 8600 $l.mole^{-1}\ cm^{-1}$.[10]

Cysteine. Working solutions of cysteine (Sigma, U.S.A.), were prepared daily by diluting an aqueous stock solution ($5.0 \times 10^{-2}M$ in cysteine) with the working buffer solution. The stock solution kept refrigerated in amber bottles was stable for at least one week.

Procedure

The stopped-flow spectrophotometer was calibrated for zero and 100% transmittance with the solution of cysteine in the observation cell. The concentration of the reactants was adjusted to create pseudo first-order conditions in respect to DCPI. The stopped-flow apparatus was flushed several times to remove bubbles from the system and the observation cell. The reaction was repeated until the trace observed on the oscilloscope was reproducible. Data from the next run were collected and evaluated with the computer. The number of the collected points and the interval between them was adjusted according to the total reaction time. The software allows the probing of a maximum of 2500 points on the reaction curve, which was observed on the monitor's screen as absorbance *vs.* time. The software, except the initial rate, $(dA/dt)_{in}$, also allows the measurement of the reaction rate $(dA/dt)_t$ at any point of the curve and also the calculation of the observed reaction rate constant, k_{ob}.

In all the experiments the concentrations given in the figures and the tables are the initial concentrations of the reagents in the observation cell.

All solutions and the cell compartment were kept at $22.0 \pm 0.1°$ via a circulating thermostat.

RESULTS AND DISCUSSION

Effect of pH

Figure 1 shows the dependence of the second-order reaction rate constant k on pH.

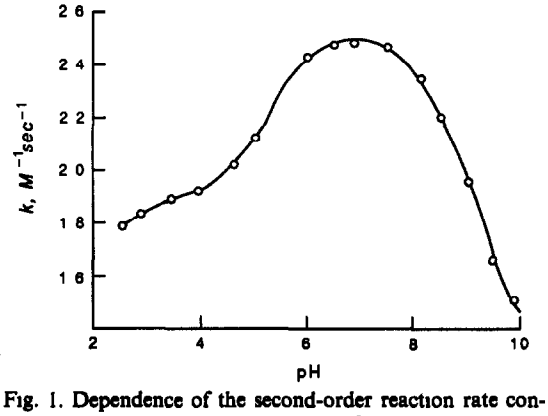

Fig. 1. Dependence of the second-order reaction rate constant on pH. $[DCPI]_o = 2.95 \times 10^{-5}M$, $[Cys]_o = 5.00 \times 10^{-4}M$, $t = 22.0 \pm 0.1°$.

Table 1. Effect of concentrations of the reacting reagents in k_{ob} pH = 6.88, $t = 22.0 \pm 0.1°$. The parameters k and k_j are means calculated from individual experiments and from regression analysis, respectively

$[DCPI]_o$, M	(1) 9.83×10^{-6}		(2) 1.97×10^{-5}		(3) 2.95×10^{-5}		Mean value	
$[Q]_o$, M	k_{ob}, sec^{-1}	k, $l.mole^{-1}\ sec^{-1}$	k_{ob}, sec^{-1}	k, $l.mole^{-1}\ sec^{-1}$	k_{ob}, sec^{-1}	k, $l.mole^{-1}\ sec^{-1}$	$k \pm s_k$, $l.mole^{-1}.sec^{-1}$	
4.0×10^{-4}	0.115	288	0.115	288	0.115	288	288	A
6.0×10^{-4}	0.178	297	0.170	283	0.171	285	288 ± 19	B
8.0×10^{-4}	0.236	295	0.233	291	0.229	286	291 ± 11	C
10.0×10^{-4}	0.288	288	0.287	287	0.285	285	287 ± 4	D
Mean value, $\bar{k} \pm s_{\bar{k}}$, $l.mole^{-1}\ sec^{-1}$		292 ± 7		287 ± 5		286 ± 2		
$k_j \pm s_b$, $l.mole^{-1}.sec^{-1}$		289 ± 37		290 ± 7		284 ± 6		

The second order reaction rate constant was calculated by dividing the value of the observed reaction rate constant k_{ob} by the concentration of the reductant.

Effect of concentration of the reacting substances

The effect of the concentration of the reacting substances on k_{ob} is shown in Table 1. In this table k_j denotes the value of the second-order reaction rate constant calculated by regression analysis of the equation $k_{ob} = kC_q$, where C_q is the initial (analytical) concentration of cysteine.

From Table 1 it is evident that:
(1) The values of k_{ob} show a linear dependence on the initial concentration of cysteine by constant concentration of DCPI (columns 1, 2, 3)
(2) At constant concentrations of cysteine the k_{ob} values remain constant within the limits of the experimental error (lines A, B, C and D).

The evaluation of the experimental data, shown in Table 1, proves that the reduction of DCPI by cysteine is a first order reaction with respect to each of the reagents and second order in all.

Effect of ionic strength

The ionic strength was varied with different concentrations of sodium sulphate. The increase of k seems to be about 6% for the range of ionic strength from 0.05 to 0.55 ionic strength.

For pH 6.88, the dependence of ln k on the ionic strength is linear in the range 0.05–3.00 ionic strength and the regression equation is: $\ln k = 5.68 + 0.121\ [I]$ with a correlation coefficient of 0.9997. This behaviour of the system is consistent with the fact that at this pH the reaction takes place mainly between H_2Q and D^- species which are already at their maximum concentrations. There are also some minor contributions to the reaction from the couples HQ^-/D^- and H_2Q/DH with rate constants $k_9 = 45.3$ $l.mole^{-1}.sec^{-1}$ and $k_5 = 78.5$ $l.mole^{-1}.sec^{-1}$, respectively. An increase in the dissociation constants with increasing ionic strength might also be responsible for the increase of the reaction rate. Such an effect of the ionic strength is more significant on the k_{Q3}.

Effect of temperature

The effect of the temperature on k_{ob} of the reaction was studied under the following experimental conditions: $[DCPI]_o = 1.97 \times 10^{-5} M$, $[Cysteine]_o = 6.00 \times 10^{-4} M$, pH = 6.88 and temperature 21.0–46.0°.

Treatment and evaluation of the experimental data plotting the logarithmic form of the Arrhenius equation gave a straight line with slope $(= -E_a/2.303R)$ of -1762.75 and an activation energy $E_a = 8.1$ kcal/mole.

The dependence of the reaction rate constant k on pH can be explained, at least qualitatively, by assuming the following mechanism:

In aqueous solutions, cysteine exists as a mixture of four species: H_3Q^+, H_2Q, HQ^- and Q^{2-} with ionization constants:[11] $K_{Q1} = 0.011$, $K_{Q2} = 4.365 \times 10^{-9}$ and $K_{Q3} = 5.248 \times 10^{-11}$. The oxidant DCPI exists in three forms: DH_2^+, DH and D^- with ionization constants:[12] $K_{D1} = 0.3$ and $K_{D2} = 2.69 \times 10^{-6}$.

From the distribution diagrams of DCPI and cysteine, shown in Fig. 2 and the fact that decolourization of DCPI occurs over a wide range of pH values, it is logical to conclude that the total reaction is a summation of partial reactions between the various forms of the two reagents in all possible combinations. Table 2 shows the probable partial reactions between the forms of the reducing and the oxidizing agents.

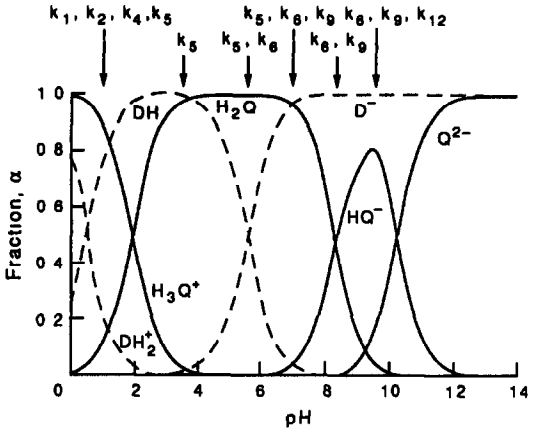

Fig. 2. Distribution diagrams for mixtures of species resulting from DCPI (DH_2^+, DH, D^-) and cysteine (H_3Q^+, H_2Q, HQ^-, Q^{2-}) *vs* pH

The reaction between DCPI (D) and cyteine (Q) has the general form:

$$D_{ox} + Q_r \xrightarrow{k} D_r + Q_{ox} \quad (3)$$

where the subscripts ox and r denote the oxidized and the reduced forms of the DCPI and cysteine respectively. The reduced form of DCPI is the leuco-compound of the dye and the oxidized form of cysteine is cystine.

The rate constant of the entire reaction is calculated, considering the partial parallel reactions, which take place at any pH. For instance at pH = 5 only two reactions take place:

$$DH + H_2Q \xrightarrow{k_5} \text{Products} \quad (4)$$

$$D^- + H_2Q \xrightarrow{k_6} \text{Products} \quad (5)$$

For these parallel reactions, rate equation (6) is valid:

$$-\left(\frac{dC_d}{dt}\right) = k_5[DH][H_2Q] + k_6[D^-][H_2Q] \quad (6)$$

The concentration [DH], [H_2Q] and [D^-] can be calculated with equations (7), (8) and (9):

$$\alpha_1' = \frac{[DH]}{C_d} = \frac{K_{D1}[H^+]}{[H^+]^2 + K_{D1}[H^+] + K_{D1}K_{D2}} \quad (7)$$

$$\alpha_2' = \frac{[D^-]}{C_d} = \frac{K_{D1}K_{D2}}{[H^+]^2 + K_{D1}[H^+] + K_{D1}K_{D2}} \quad (8)$$

$$\alpha_1 = \frac{[H_2Q]}{C_q} = \frac{K_{Q1}[H^+]^2}{[H^+]^3 + K_{Q1}[H^+]^2 + K_{Q1}K_{Q2}[H^+] + K_{Q1}K_{Q2}K_{Q3}} \quad (9)$$

Table 2. Possible combinations of reactions between species of cysteine and DCPI with the corresponding reaction rate constant

D\Q	H_3Q^+	H_2Q	HQ^-	Q^{2-}
DH_2^+	k_1	k_4	–	–
DH	k_2	k_5	–	–
D^-	–	k_5	k_9	k_{12}

where α_1', α_2' and α_1 are the distribution coefficients for DH, D^- and H_2Q respectively. C_d and C_q are the initial (analytical) concentrations of DCPI and cysteine, respectively.

Substitution of equations (7)–(9) to equation (6) gives equation (10):

$$-\left(\frac{dC_d}{dt}\right) = (k_5\alpha_1'\alpha_1 + k_6\alpha_2'\alpha_1)C_d.C_q \quad (10)$$

Since $C_q \gg C_d$, the equation (10) gives:

$$-\left(\frac{dC_d}{dt}\right) = k_{ob}c_d \quad (11)$$

where: $k_{ob} = (k_5\alpha_1'\alpha_1 + k_6\alpha_2'\alpha_1)C_q$

Dividing the k_{ob} values by C_q the reaction rate constant k is given by equation (12):

$$k = \frac{k_{ob}}{C_q} = k_5\alpha_1'\alpha_1 + k_6\alpha_2'\alpha_1 \quad (12)$$

Substitution of equations (7)–(9) into equation (12) yields:

$$k = \frac{k_5 + k_6\dfrac{K_{D2}}{[H^+]}}{\left(1 + \dfrac{[H^+]}{K_{Q1}} + \dfrac{K_{Q2}}{[H^+]} + \dfrac{K_{Q2}K_{Q3}}{[H^+]^2}\right)\left(1 + \dfrac{[H^+]}{K_{D1}} + \dfrac{K_{D2}}{[H^+]}\right)} \quad (13)$$

Applying similar arguments and considering all possible parallel reactions between the forms of the reducing and the oxidizing agent, equation (14) is produced whose graphical presentation is the solid line of Fig. 1.

Table 3 Second-order reaction rate constants k for different combinations of reacting species of the DCPI and cysteine $t = 22.0 \pm 0.1°$

k_1	k_2	k_5	k_6	k_9	k_{12}
k_1, $l.mole^{-1}.sec^{-1}$	4.9	78.5	336.0	45.3	1.4

$$k = \frac{k_1\frac{[H^+]^2}{K_{Q1}K_{D1}} + k_2\frac{[H^+]}{K_{Q1}} + k_4\frac{[H^+]}{K_{D1}} + k_5 + k_6\frac{K_{D2}}{[H^+]} + k_9\frac{K_{Q2}K_{D2}}{[H^+]^2} + k_{12}\frac{K_{Q2}K_{Q3}K_{D2}}{[H^+]^3}}{\left(1+\frac{[H^+]}{K_{Q1}}+\frac{K_{Q2}}{[H^+]}+\frac{K_{Q2}K_{Q3}}{[H^+]^2}\right)\left(1+\frac{[H^+]}{K_{D1}}+\frac{K_{D2}}{[H^+]}\right)} \quad (14)$$

The values of k_i ($i = 1, 2, \ldots$), calculated on the basis of equation (14), are presented in Table 3.

An attempt was made to differentiate equation (14) and calculate the pH at the maximum value of the reaction rate constant, k_{max}. In order to simplify equation (14), all the terms which include the partial constants k_1, k_2, k_4 and k_{12} are eliminated because their contribution in the reaction is negligible in the pH range 6–8. This is evident if one refers to the distribution diagrams of Fig. 2 and Table 3. As a second approximation the terms $[H^+]/K_{Q1}$, $K_{Q2}K_{Q3}/[H^+]^2$ and $[H^+]/K_{D1}$ from the denominator of equation (14) can also be eliminated as very small compared to 1 for pH's 6–8. After these approximations equation (14) becomes:

$$k = \frac{k_5[H^+]^2 + k_6K_{D2}[H^+] + k_9K_{Q2}K_{D2}}{[H^+]^2 + [H^+](K_{Q2}+K_{D2}) + K_{Q2}K_{D2}} \quad (15)$$

The derivative of equation (15) is given by equation (16). The denominator of equation (16) is always positive. Getting the numerator equal to zero, $[H^+]_{max}$ and k_{max} can be calculated. The results are $[H^+]_{max} = 1.16 \times 10^{-7}$ or pH = 6.94 and $k_{max} = 315$ l.mole^{-1}.sec^{-1}.

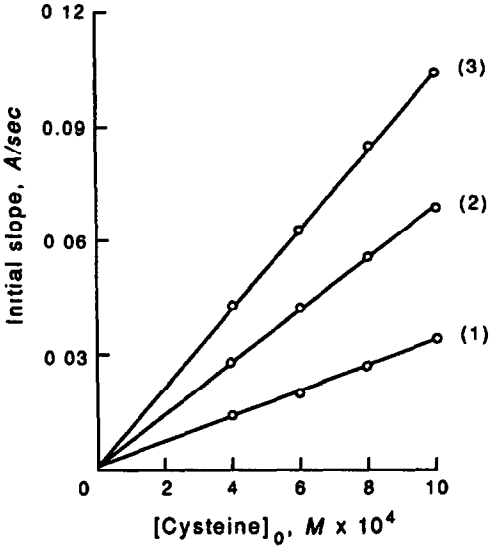

Fig 3. Working curves for the determination of cysteine pH = 6 88, $t = 22.0 \pm 0\,1°$. (1) [DCPI] = $9.83 \times 10^{-6}M$, $y = 3 \times 10^{-4} + (34 \pm 4).x$, $r = 0.9993$. (2) [DCPI] = $1\,97 \times 10^{-5}M$, $y = 1 \times 10^{-3} + (68 \pm 7).x$, $r = 0.9994$. (3) [DCPI] = $2.95 \times 10^{-5}M$, $y = 2 \times 10^{-3} + (103 \pm 8)$ x, $r = 0.9996$

$R_A = (dA/dt)_{in}$ are very reproducible as one can conclude from the quality and the statistics of the regression equations given in Fig. 3.

$$k = \frac{\{k_5K_{Q2} + k_5K_{D2} - k_6K_{D2}\}[H^+]^2 + \{2k_5K_{Q2}K_{D2} - 2k_9K_{Q2}K_{D2}\}[H^+] - K_{Q2}K_{D2}\{k_6K_{D2} - k_9K_{Q2} - k_9K_{D2}\}}{\{[H^+]^2 + (K_{Q2}+K_{D2})[H^+] + K_{Q2}K_{D2}\}^2} \quad (16)$$

Analytical application

The procedure described above can be applied to the kinetic determination of cysteine in aqueous solutions. The measurements were taken at pH = 6.88, which is the pH of maximum reaction rate constant according to the findings already presented.

The reaction rate measured as initial slope of the reaction curve is proportional to the concentration of cysteine. The working curves are linear for the range 1.0×10^{-4}–$1.0 \times 10^{-3}M$ for the concentration of DCPI 1.0×10^{-5} to $3.0 \times 10^{-5}M$. This range can be lowered to $10^{-5}M$ of cysteine if the concentration of DCPI is accordingly adjusted. The slopes

Although many equilibrium methods exist for the determination of cysteine, the kinetic method[13] in some cases offers additional advantages: (i) it is fast, (ii) it provides the possibility to differentiate intereferences which, depending on pH, react either faster or slower with DCPI, (iii) it can avoid intereferences due to turbidity and background absorbances of coloured solutions containing substances not reacting with DCPI.

Table 4 demonstrates the effect of cysteine on the kinetic determination of ascorbic acid (AA). The error introduced by the determination of ascorbic acid in samples containing cysteine in different ratios might be very serious depending on the working pH-range. By pH's in the range

Table 4. Error introduced because of intereference of cysteine by the kinetic determination of ascorbic acid [Cysteine]$_0 = 1.00 \times 10^{-3} M$. Temperature 22.0 ± 0.1°

pH	Ascorbic acid C_{AA}, M taken	Ascorbic acid C_{AA}, M calculated*	$(k_{obAA} + k_{obQ})$†, sec^{-1}	Error, %
2 50	$1\,00 \times 10^{-5}$	$1\,12 \times 10^{-5}$	0.537 + 0 062	12 0
2.50	$1\,00 \times 10^{-4}$	1.01×10^{-5}	5 369 + 0.062	1 0
4.50	$1\,00 \times 10^{-5}$	$1\,60 \times 10^{-5}$	0.163 ± 0 098	60 0
4 50	$1\,00 \times 10^{-4}$	$1\,06 \times 10^{-5}$	1 632 ± 0 098	6 0
6.00	$1\,00 \times 10^{-4}$	$2\,80 \times 10^{-4}$	0 146 ± 0.263	>100
6 00	$1\,00 \times 10^{-4}$	$6\,81 \times 10^{-4}$	0 730 ± 0 263	36 2
6.00	$1\,00 \times 10^{-3}$	$1\,18 \times 10^{-3}$	1 459 ± 0 363	18.0
6 00	$2\,00 \times 10^{-3}$	$2\,18 \times 10^{-3}$	2 918 ± 0.263	9.0
7 00	$1\,00 \times 10^{-4}$	$7\,96 \times 10^{-4}$	0 046 ± 0 316	>100
7.00	$1\,00 \times 10^{-3}$	1.69×10^{-3}	0 455 ± 0.316	69 0
7 00	5.00×10^{-3}	$5\,69 \times 10^{-3}$	2 275 ± 0 316	13 8
7.00	$1\,00 \times 10^{-2}$	1.07×10^{-2}	4 550 ± 0 316	7.0

*Calculated considering cysteine interference
†k_{obAA} taken from reference,[7] k_{obQ} from this work

6–7 the error is significantly high, while for pH < 4 it is relatively small. This can be explained by considering the curve of Fig. 1 and the known dependence of the reaction of ascorbic acid and DCPI on the pH, published in our previous work.[7]

From the experimental results of this work and also data given in previous publications,[7] it is possible to determine simultaneously the concentrations of both reductants in mixtures. It can be done by measuring either the initial rates (R_A, R'_A) or by calculating the observed reaction rate constants (k_{ob}, k'_{ob}) from the reaction curves of two experiments performed at two pH's (pH, pH'). This can be done applying equations [17(a)] and [17(b)] or the couple [18(a)] and [18(b)].

$$k_{ob} = k_{AA} C_{AA} + k_c C_q \qquad [17(a)]$$

$$k'_{ob} = k'_{AA} C_{AA} + k'_c C_q \qquad [17(b)]$$

$$R_A = (k_{AA} C_{AA} + k_c C_q) C_d \qquad [18(a)]$$

$$R'_A = (k'_{AA} C_{AA} + k'_c C_q) C_d \qquad [18(b)]$$

In these equations k_{AA}, k'_{AA} are the values of the second order reaction rate constants, for DCPI + ascorbic acid reaction[7] and k_c, k'_c are the values of the second order reaction rate constants for the DCPI + cysteine reaction, given in this work, for the two pH's.

The parameters k_{ob}, k'_{ob}, R_A, R'_A are experimentally available. C_d is the concentration of 2,6-dichlorophenolindophenol and C_{AA}, C_q are the unknown concentrations of ascorbic acid and the cysteine, respectively.

The validity of this technique was verified experimentally in our laboratory with artificial mixtures of ascorbic acid and cysteine.

Acknowledgements—The authors wish to thank Peter Wentzell and Mark Victor for their help with the graphics and acquisition portion of the software.

REFERENCES

1 M. I Karayannis and D I. Farasoglou, *Analyst*, 1987, **112**, 767.
2 J Z. Tilmans, *Lebensm—Unters Forsch*, 1927, **54**, 33.
3 R. Strohecker and R Vaubel, *Angew. Chem*, 1936, **49**, 666
4 R Strohecker and H M. Henning, *Vitamin Assay—Tested Methods*, pp. 227–253. Verlag Chemie, 1966.
5 C N. Konidari and M I. Karayannis, *Talanta*, 1991, **38**, 1019
6. L W Mapson and L. J. Harris, *Brit. J. Nutr*, 1947, **1**, 7.
7 M I Karayannis, *Talanta*, 1976, **23**, 27.
8. L. E. Bowman, M. A Victor and S. R. Crouch, *Trends. Anal Chem.*, 1990, **9**, 111.
9. M G Fleck, *Chemical Reaction Mechanisms*, pp. 36 Holt, Rinehart and Winston, New York, 1971.
10. J McD. Armstrong, *Biochim. Biophys. Acta*, 1964, **86**, 194.
11. J. A Dean (Ed), *Lange's Handbook of Chemistry*, 12th Ed, pp 5–24. McGraw Hill, Inc., New York, 1979.
12. B. Tonomura, H. Nakatani, M Ohnishi, J Yamaguchi-Ito and K Hiromi, *Anal Biochem.*, 1978, **84**, 370.
13. A. Cardoso, M. Silva and D. Perez-Bendito, *Talanta*, 1989, **36**, 963.

Talanta, Vol 39, No 7, pp 869–873, 1992
Printed in Great Britain

0039-9140/92 $5 00 + 0.00

CONTINUOUS AUTOMATIC DETERMINATION OF AMMONIA BY USING AN INTEGRATED SEPARATION/DETECTION UNIT

MIGUEL DE LA TORRE, M. D. LUQUE DE CASTRO and MIGUEL VALCARCEL
Department of Analytical Chemistry, Faculty of Sciences, University of Córdoba, 14004 Córdoba, Spain

(*Received* 31 *July* 1991 *Revised* 2 *December* 1991 *Accepted* 16 *December* 1991)

Summary—An automatic continuous-flow photometric method for the determination of ammonia is proposed It is based on the Berthelot reaction, the product of which is temporarily immobilized on a suitable support (Sephadex QAE) located in the flow-cell The retained product is eluted after measurement by a cationic surfactant contained in the carrier solution. The method allows the determination of the analyte between 0 4 and 20 0 μg/ml, with an RSD of 0 8%, at a sampling frequency of 13/hr The determination limit can be reduced by a factor of ten by using a flow-cell with a two-fold longer path length, but the sampling frequency is also reduced as a result The method was applied to the determination of this analyte in agricultural samples (plants and soils) and compared with standard methods for these types of samples

Ammonia (or ammonium ion) is commonly determined in areas of social interest (clinical, environmental, industrial, *etc.*), hence the large number of methods developed for its determination, which rely on a variety of principles.

There are a number of papers describing the flow injection determination of ammonia with or without use of gas-diffusion units.[1-3] Recently, several flow systems in which reaction, retention and detection are integrated have been described.[4,5] They can be considered as an alternative to conventional probe-type sensors.

Sensor design and characterization is an area of great current interest.[6,7] Several types of sensor based on the basic nature of this ammonia have also been described for the determination of this analyte; photometric and fluorimetric acid–base indicators have been most often used for this purpose.

Probe-type sensors making use of optical fibres and a colorimetric indicator (*p*-nitrophenol) were used by Arnold and Osteer[8] to build a photometric sensor from disposable pipette tips. A similar principle (in this case bromothymol blue immobilized on a hydrophylic matrix) but with reflectance measurements, was used by Caglar and Narayanaswamy to build another sensor for this analyte.[9] A fluorimetric indicator and optical fibre as transmitter have also been employed by Smock *et al.*[10] to construct a probe for the determination of ammonia in blood, and by Wolfbeis and Posch,[11] who designed a similar device which they gave no practical application.

The continuous-type sensors for ammonia designed so far have been used for the determination of urea; all of them entail the use of an enzyme (urease) and the quantitation of ammonia as a product of the catalysed reaction. All these devices are optosensors involving measurements based on the presence of a colorimetric indicator.[12-14] The selectivity of the determinations was improved by using a gas-diffusion unit to ensure the exclusive presence of compounds occurring in the sample, which were converted into gases in the acceptor stream in contact with the indicator. In all cases, the use of integrated microconduits allowed sample and reagent consumption to be dramatically decreased. Units such as timers or active interfaces to a microcomputer were coupled to the configuration to implement the stopped-flow mode for the calculation of kinetic parameters and equilibrium constants.[12] An enzymatic sensor for this analyte based on a different principle was reported by Shiono *et al.*,[15] who used a field-effect transistor onto whose gates the enzyme (urease) was immobilized. It provided quite satisfactory results in flow systems.

Some few ammonia sensors based on non-reversible (ninhydrin reagent),[16,17] and reversible (oxazyne dye)[18] derivatizing reactions have so far been reported. The flow-through sensor system proposed herein is based on the reaction

between the analyte and the phenol/hypochlorite mixture (Berthelot reaction). The product is retained (transient retention) on a suitable support located in the flow-cell and is rapidly eluted after the measurements. Its functioning was optimized by using a flow injection system, which allowed the development of a method for the determination of ammonia that was applied to agricultural samples (plants and soils) with excellent results.

EXPERIMENTAL

Instruments and apparatus

A Philips PU 8620 UV/Vis–NIR spectrophotometer equipped with a Radiometer REC 80 recorder and 138 OS, 178.52QS, 178.12QS and 137 OS Hellma flow-cells[19] was used. A Gilson Minipuls-2 peristaltic pump, a Tecator TM III chemifold and a Selecta S-380 thermostat were also used.

Reagents

Phenol solution. A 50-g amount of phenol with 120 g of sodium hydroxide and 100 ml of ethanol were diluted up to one litre with distilled water.

Hypochlorite solution. A 400-ml volume of ClO^-, as sodium salt, of 60 g/l + 20 g of borax + 20 g of sodium hydroxide diluted up to one litre with distilled water.

Carrier/eluent solution. A 7.7075-g amount of dodecyltrimethylammonium bromide diluted up to 250 ml with distilled water. Standard aqueous solution of ammonia (1 g/l.) prepared from $(NH_4)_2SO_4$.

All reagents were of analytical grade.

Sample pretreatment

Plant samples (Kjeldahl distillation). Dried sample (1 g) was introduced into a digestor tube and 1 g of catalyst (potassium sulphate and metal selenium 20:1) + 15 ml of concentrated sulphuric acid were added to digest the sample at 420° for one hour. After cooling, distilled water was added to two-thirds of the tube digestor height and together with some pieces of Zn dust. Then, the tube was fitted to the distillation device and 50 ml of 40% sodium hydroxide was added. The distillation process was continued up to consumption of about 150 ml. The distillate was collected into 50 ml of 2% boric acid, after which the sample was ready for introduction into the FIA system.

Soil samples (solid–liquid extraction). Sample (20 g) was introduced into an Erlenmeyer flask and mixed with 100 ml of 2*M* potassium chloride. After stirring for one hour, the mixture was filtered and the filtrate was stored at 4° until the determination.

Standard methods

Plant samples. Acid–base titration with bromocresol green/methyl red as indicator.

Soil samples. A 5-ml portion of the filtrate was mixed with 1 ml of 10^{-2} *M* EDTA in a 25-ml standard flask, then 2 ml of phenol–nitroprusside and 4 ml of buffer hypochlorite were added and the flask was made up to volume and immersed in a water bath kept at 40°, for 30 min. After allowing it to cool to room temperature for 40 min the absorbance was measured at 636 nm.

Calibration curves run with standards treated like samples were obtained.

Flow-cell packing

The outlet of the flow cell was packed with glass-wool and a small fragment of the Technicon filter to retain the support in the flow cell. The cell itself was packed with support up to 8 mm from the bottom, so that the light beam passed through the upper part of the packed material, which required a period of 5 min with solution flowing through the cell for proper packing. Otherwise, the baseline absorbance increased slightly with time, probably because the solid support became increasingly compacted.

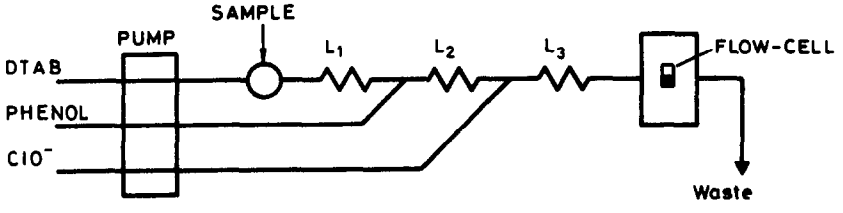

Fig. 1 Scheme of the FIA configuration used for the development of a flow-through sensor for the determination of ammonia (for details see text).

Manifold and procedure

Figure 1 depicts the FIA manifold used. A 0.1*M* solution of surfactant acted as carrier, into which 300 μl of sample was injected and then merged successively with streams of phenol (50 g/l) and hypochlorite (24 g/l); the dye developed along reactor L_3. On passage through the flow-cell, the reaction product was retained on the support and concentrated during the interval over which the sample was passed through it. Elution was effected while the surfactant/carrier solution was circulated again through the flow-cell. A FIA peak was obtained, its height was used to calculate the concentration of the analyte by comparing it with the calibration curve obtained under the same working conditions. A blank was also processed under the same working conditions. The difference between the FIA peak of the sample and that of the blank gave the analytical signal.

RESULTS AND DISCUSSION

Preliminary studies

The conventional absorption spectra of the reaction product were recorded at different times from sample/reagent mixing. A small bathochromic shift of the maxima at 360 and 625 nm was observed during the time period. FIA absorption spectra of the product obtained by using the manifold described in the Experimental section were recorded successively and compared with the blank (injection of distilled water with an ionic strength similar to that of the sample). A slight bathochromic shift of the maxima relating to the above values at an identical time was observed when the product was retained in the flow-cell. This phenomenon has also been observed in other flow-through systems of the same type.[19] A wavelength of 644 nm was selected for measurements in studying variables. This value was modified when the variables determining the residence time (reactor length and flow-rate) were optimized. The injection of a blank yielded a positive signal reflecting a change in the support compactness; hence this value must be subtracted from the sample peak to obtain the net value of the analytical signal. Other FIA configurations such as merging zones with simultaneous injection of the sample and phenol, hypochlorite or both, and a two-channel configuration, were tested with the aim of decreasing the elution time. However, both provided worse results than the original.

Study of variables

The univariate method was followed to optimize variables characteristic of the retention/detection unit, chemical, FIA variables and temperature.

Hellma 138 OS, 178.52QS, 178.12QS and 137 OS model cells were assayed. The first provided the best results because of its small inner cavity and hence smaller amount of non-irradiated resin and higher analyte concentration in the light path. The path of the cell (1.0 mm) provided good sensitivity with not too high a background absorbance from the support. Its inner volume was 20 μl. Special cells made by Hellma, similar to the 138 OS model but with longer path-lengths allowed the sensitivity to be doubled by increasing the slope of the calibration curve and decreasing the determination limit, but to the detriment of the sampling frequency, which was dramatically decreased.

After assaying different types of Sephadex supports, Sephadex QAE was found to be most suitable because of its non-polar aromatic nature. The anionic character of the product to be retained avoided the use of cationic exchangers (Sephadex SP and CM). Strong (Sephadex QAE) and weak (Sephadex DEAE) basic exchangers provide good analytical signals and elution times (twice longer for Sephadex DEAE than that of QAE type). Other exchangers assayed (XAD type: XAD 2, XAD 4 and XAD 8) in which the absence of charged groups allowed the derivatized product to be weakly retained and rapidly eluted, were highly absorbant, approaching the detector saturation.

The level of the support in the flow-cell was a key variable to the sensitivity of the method. This level must always be above the light path (the higher the level, the lower the sensitivity because the maximum retention occurred at the solid–liquid interface). The most appropriate height was 8 mm.

The chemical variables to be optimized were phenol and hypochlorite concentration, ethanol content, ionic strength, pH, eluent and presence of catalysts.

Increasing hypochlorite concentrations resulted in increasing the analytical signal; nevertheless, concentrations above 24 g/l. degraded the resin, which lost some retention capacity and increased in compactness. Phenol concentrations above 50 g/l. posed the same problems.

The presence of ethanol up to 10% improved the analytical signal by stabilizing the reaction product; above this content the signal decreased again.

The influence of the ionic strength, a key to the resin compactness, was eliminated by the high reagent concentrations and confluence points used, which ensured a constant and homogeneous ionic strength in the stream reaching the detector.

The optimum pH values of the different solutions were 12.4 and 12.2 for phenol and hypochlorite, respectively, and were adjusted with sodium hydroxide and borax/sodium hydroxide buffer. The presence of the buffer in the hypochlorite solution made the sample pH insensitive.

Of the different ways assayed to elute the product retained in the flow-cell, namely use of bulky counterions, pH changes, use of organic solvents and surfactants, the last was the most effective because very acidic media and high organic solvent contents resulted in resin degradation, while bulky counterions had appreciable effect. The best results were obtained with cationic surfactants; the three assayed (cetylpyridine chloride CPC-, cetyltrimethylammonium bromide -CTAB- and dodecyltrimethylammonium bromide -DTAB-) resulted in no appreciable differences. The last was chosen and used at an optimum concentration of 0.1*M*.

The influence on the derivatizing reaction of several catalysts described in the literature (acetone,[20] manganese,[21] nitroprusside and ferrocyanide[22]) was studied. Samples containing these compounds were measured and compared with others in the absence of catalyst. Positive results were obtained only in the presence of nitroprusside, but the values of the analytical signal were of the same order as those obtained in the presence of ethanol under the working conditions, thus, the last was preferred.

Increasing temperatures resulted in slightly increasing signals up to 35°, above which the signals decreased. This last, which contradicts literature reports,[23] must be a result of the effect of this variable on the retention equilibrium.

The variables characteristic of the FIA system were the reactor lengths, flow-rate and injected volume.

The evolution of the reaction depended on the order of sample/reagent mixing and was contradictory to the behaviour of the conventional method.[23] Reactor L_1 had no influence on the reaction. The first step took place at reactor L_2, but a length of 100 cm was enough because this step was very fast. The slow rate of the second step called for an optimum length of 450 cm for L_3. The resulting dispersion did not affect the analytical signal thanks to the features of the sensor (*in situ* concentration).[19]

The signal increased as the flow-rate decreased, but the dependence of the sampling frequency on the flow-rate led us to choose 0.8 ml/min as a compromise. At the residence time obtained under these conditions, the absorption maximum also appeared at 640 nm.

Large sample volumes saturated the support with the reaction product, while small volumes resulted in poor sensitivity. A volume of 300 μl was found to be optimum.

Features of the method

The calibration curve was linear between 0.4 and 20.0 μg/ml and conformed to the equation $y = 0\,032 + 3.82 \times 10^{-3}x$, where y is the peak height after subtracting the blank and x is the ammonia concentration in μg/ml. The regression coefficient was 0.998.

The reproducibility ($\pm 0.8\%$) of the method was studied on 11 samples containing 6 μg/ml and injected in triplicate.

The sampling frequency achieved under the working conditions was 13/hr.

The sensitivity of the method was increased by over one order of magnitude by using a flow-cell similar to the Hellma 138 OS, but with a path length of 2 mm; this involved a longer elution time as a result of the larger amount of support in the flow-cell, so the sampling frequency was roughly halved.

Application of the sensor to the determination of ammonia in agricultural samples

The applicability of the proposed method was tested by assaying two types of agricultural sample (plants and soils) requiring different pretreatments. These, and the conventional method required to compare the analyte concentration found by the proposed method were commented on in the Experimental section. Different calibration curves were run for each type of sample because of the different media required in the pretreatment step; these resulted in slightly different slopes.

The results found for the plant samples by the proposed and conventional methods, the dilution required and the study of the analyte recovery are summarized in Table 1, while Table 2 lists the concentrations found for soil

Table 1. Determination of ammonia in plants

Sample No	Concentration, μg/ml: Conventional method	Concentration, μg/ml: Proposed method	Dilution: Proposed method	Recovery, %: Added, μg/ml 2	Recovery, %: Added, μg/ml 4
1	47 30	47.01	1·10	99	99
2	152 60	151 91	1 10	98	98
3	311 30	310 50	1 20	105	102
4	122 60	122 00	1 10	110	107
5	137 00	136 23	1 10	98	99
6	302 67	302 57	1 20	100	100

Table 2 Determination of ammonia in soils

Sample No	Concentration, μg/ml: Conventional method	Concentration, μg/ml: Proposed method
1	3 70	3 39
2	3 19	2 99
3	3 48	3 36
4	3 82	3 69
5	3 55	3 26
6	3 18	3 07

samples by the proposed and conventional methods. From these data the suitability of the proposed method for the analysis of agricultural samples is apparent.

Acknowledgements—Dirección General de Investigación Científica y Técnica, DGICyT, is thanked for financial support (Grant No PB90-0925)

REFERENCES

1 J Slanina, F Bakker, A Bruyn-Hes and J J Mols, *Anal Chim Acta*, 1980, **113**, 331
2 F J. Krug, B F Reis, M F Gine, E A G Zagatto, J. R Ferreira and A O Jacintho, *ibid*, 1983, **151**, 39
3. G. Schulze, C Y Liu, M Brodowski and O Elsholz, *ibid.*, 1988, **214**, 121
4. M Valcárcel and M. D Luque de Castro, *Analyst*, 1990, **115**, 699.
5 M D. Luque de Castro and M Valcárcel, *Trends Anal Chem*, 1991, **10**, 114
6. W Gopel, J Hesse and J. N. Zemel (eds.), *Sensors. Fundamental and General Aspects*, VCH, Weinheim, 1989
7 J Janata, *Principles of Chemical Sensors*, Plenum Press, New York, 1989.
8 M A Arnold and T J Osteer, *Anal Chem*, 1986, **58**, 1137
9 P Caglar and R Narayanaswamy, *Analyst*, 1987, **112**, 1285
10 P L Smock, T A Orofino, G W Wooten and W S. Spencer, *Anal Chem*, 1979, **51**, 505
11 O S Wolfbeis and H E Posch, *Anal Chim Acta*, 1986, **185**, 321
12 J Růžička and E H Hansen, *ibid*, 1985, **173**, 3
13 B A Petersson, H B Andersen and E H. Hansen, *Anal Lett*, 1987, **20**, 1977
14 T D Yerian, G D Christian and J Růžička, *Anal. Chim Acta*, 1988, **204**, 7
15 S Shiono, Y Hanazato, M Nakako and M Maeda, *ibid*, 1987, **202**, 131
16 D David, M C Wilson and D S. Ruffin, *Anal. Lett*, 1976, **9**, 389
17 P L Smock, T A. Orofino, G W. Wooten and W S Spencer, *Anal Chem*, 1979, **51**, 505
18 J F Giuliani, H Wohltjen and N L Jarvis, *Opt Lett*, 1983, **8**, 54
19 F Lázaro, M D Luque de Castro and M. Valcárcel, *Anal Chim Acta*, 1988, **214**, 217
20 J A Russell, *J. Bio Chem.*, 1944, **156**, 457
21 A B. Crowther and R S. Large, *Analyst*, 1956, **64**, 81
22 R. L Searcy, G S. Gough, J. L Korotzer and L. M Bergqist, *Am. J Technol.*, 1961, **27**, 255.
23. W T Boleyer, C J. Bushman and P. W Tidwell, *Anal Chem.*, 1961, **33**, 592.

Talanta, Vol 39, No 7, pp 875–878, 1992
Printed in Great Britain

0039-9140/92 $5.00 + 0.00

STUDY ON SELECTIVE QUANTITATIVE DETERMINATION OF BARIUM BY SULPHONAZO III IN COMPLEX MATRICES

F MANNA, F CHIMENTI, A. BOLASCO and A. FULVI
Department of Chemical and Technological Studies of Biologically Active Substances, University of Rome "La Sapienza", 00185 Rome, Italy

(*Received* 5 *September* 1991 *Revised* 24 *October* 1991 *Accepted* 25 *October* 1991)

Summary—Selective quantitative determination of barium by commercially available Sulphonazo III was studied in complex matrices The application of two more promising methods was tried, but interferences derived from cations and anions present in natural waters and waste waters made them unuseful

Many authors studied the stability of some complexes of alkaline-earth metals and their application to the colorimetric determination of barium and strontium.[1-6] The most promising of complexing agents for their analysis was the 2,7-bis-(2′-sulphophenylazo)-1,8-dihydroxy-3,6-naphthalenedisulphonic acid (Sulphonazo III).

Budesinsky and Vrzalova[1] first reported conditions under which barium might be determined colorimetrically by Sulphonazo III although no analytical data were given. Later, since Sulphonazo III had become commercially available, Kemp and Williams[4] attempted to use this in direct simultaneous method for barium and strontium determination in the presence of other cations masked by chelons EGTA [ethylen glicol bis(amino-ethyl ether)-*N*,*N*′-tetracetic acid] and CDTA (trans-1,2-diamino-cycloexane-*N*,*N*′-tetracetic acid). They gave analytical data relative only to synthetic matrices.

Since a simple direct colorimetric method for detection of barium and strontium is not available, we decided to study the application of previous methods to the analysis of natural and waste waters, utilizing the commercially available Sulphonazo III, without further purification.

EXPERIMENTAL

Apparatus

A Perkin–Elmer spectrophotometer model 552 with 1-cm quartz cells was used for UV spectra; IR spectra were registered on a Perkin–Elmer spectrophotometer model 297, and NMR spectra on a Varian EM-390 instrument, using TMS as internal standard. The pH control was carried out by a Metrohm apparatus model E512.

Sulphonazo III

The IR and NMR spectra of the synthetic product and of commercial Sulphonazo III were identical and confirmed their structures:

IR, KBr (cm^{-1}): 1580 (C—N=); 3400–3500 (OH).
NMR ($CDCl_3$) ppm: 17.20 (s, 2 H, 2 OH); 8.20 (d, 2 H, H6′); 7.90 (d, 2 H, H3′); 7.80–7.30 (m, 6 H, H4, H5, H4′, H5′).

Hexamine/nitric acid buffer was prepared in accordance with Budesinsky.[1]

Effect of pH on Sulphonazo III and its complexes

Desired values of pH (2.5, 7.5, 9.1, 10.7, 11.3) potentiometrically controlled were obtained by dilution of 0.1*M* nitric acid and 0.1*M* potassium hydroxide.

Solutions for spectrophotometric measurements were prepared by mixing 5 ml of nitric acid or potassium hydroxide, 5 ml of $10^{-3}M$ Sulphonazo III and 5 ml of $3.2 \times 10^{-4}M$ barium or interfering ions [calcium(II), magnesium(II) and strontium(II)] solutions; nitrates were used.

Variations of Sulphonazo III concentrations

Volumes of 5 ml of nitric acid (pH 6.8 or 2.4) and 5 ml of 10^{-6}, 10^{-5}, 10^{-4}, 10^{-3},

$10^{-2}M$ Sulphonazo III solutions were added to 5 ml of $3.2 \times 10^{-4}M$ barium stock solution [$Ba(NO_3)_2$].

Calibration curve

A 1-ml volume of $0.1M$ nitric acid and 10 ml of $10^{-4}M$ Sulphonazo III were added to 10 ml of barium solutions containing 1, 2, 3, 4 and 5 mg/l. barium nitrate [0.7, 1.4, 2.1, 2.9 and 3.6×10^{-2}mM]. Absorbance values were measured at 641 nm and were respectively 0.075, 0.146, 0.225, 0.285, 0.353.

Effect of chloride and acetate

Mixtures of barium and interfering ions were prepared by dilution of a barium nitrate stock solution (Ba^{2+} 50 mg/l.) with sodium acetate and sodium chloride solutions at a suitable concentration. Nitric acid ($0.1M$, 1 ml) and 10 ml of $10^{-4}M$ Sulphonazo III were added to 10 ml of barium/chloride or barium/acetate mixtures.

Interfering cations

First tests were carried out using solutions containing 5 mg/l. barium and interfering cation, obtained by dilution of 50 mg/l. cation nitrate stock solution; 1 ml of $0.1M$ nitric acid and 10 ml of $10^{-4}M$ Sulphonazo III were added to 10 ml of barium/interfering ions solutions. Another test was carried out on equimolar $3.6 \times 10^{-5}M$ solutions of barium and interfering cations obtained by dilution of $3.6 \times 10^{-3}M$ standard solutions.

Effect of EDTA

A 1-ml volume of $0.1M$ nitric acid and 10 ml of $10^{-4}M$ Sulphonazo III were added to 10 ml of $3.6 \times 10^{-5}M$ cation and EDTA solution.

Internal standard

A calibration curve was prepared by adding different amounts of barium nitrate to natural waters and waste waters in order to have final solution concentrations from 1 to 5 mg/l. ($0.7–3.6 \times 10^{-2}$mM) of barium ion. A 1-ml volume of $0.1M$ nitric acid and 10 ml of $10^{-4}M$ Sulphonazo III were added to 10 ml of barium solution.

The EGTA–CDTA method was performed in accordance with Kemp[4] and the same procedure was used to the internal standard method. A blank solution was constituted of drinking water containing appropriate amounts of barium and strontium.

RESULTS AND DISCUSSION

The control of experimental conditions reported by Budesinsky at pH 2.4 showed a shift of the maximum absorption value of the commercial Sulphonazo III we used from 550 nm to 580 nm, in agreement with Kemp and Williams.[4] Thus Sulphonazo III was synthesized according to the method reported by Budesinsky and Vrzalova[1] and compared with a commercially available product, the compounds were identical and showed a maximum absorption value at 580 nm.

Furthermore the pH 2.4 hexamine/nitric acid buffer showed a slow and continuous variation of pH during the time derived from dissociation of hexamine, together with a decrease of complex absorbance; therefore a solution of nitric acid of suitable concentration was used in order to obtain the desired pH value.

The absorption spectrum of Sulphonazo III did not vary with pH, while its complex with barium had a maximum absorption value at 640 nm in alkaline medium. The shift could have been useful for increasing the sensitivity of the method, but interferences of calcium also increased at pH 9–10.

A $10^{-3}M$ concentration of Sulphonazo III determined a shift of the maximum absorption of the barium complex to 659 nm accompanied by rapid variations of absorbances (few hours), while a $10^{-4}M$ solution was the most suitable for its stability and sensitivity.

Unlike Budesinsky's statement, some cations and anions commonly present in superficial and waste waters interfered; strontium(II), lead(II) and copper(II) caused an increase of absorbance while sodium(I), potassium(I) and calcium(II) its decrease. Cadmium(II), iron(III), zinc(II), chromium(III) and magnesium(II) did not interfere up to 40 mg/l. Chlorides decreased the absorbance of the barium/Sulphonazo III complex at concentrations of 25 mg/l., while nitrates and acetates didn't interfere.

Addition of EDTA, suggested by Budesinsky to eliminate interferences at pH 2.4, binded only lead(II) and calcium(II), leaving other interactions practically unchanged (Fig. 1).

The internal standard method applied, using drinking and waste water, gave an increase in

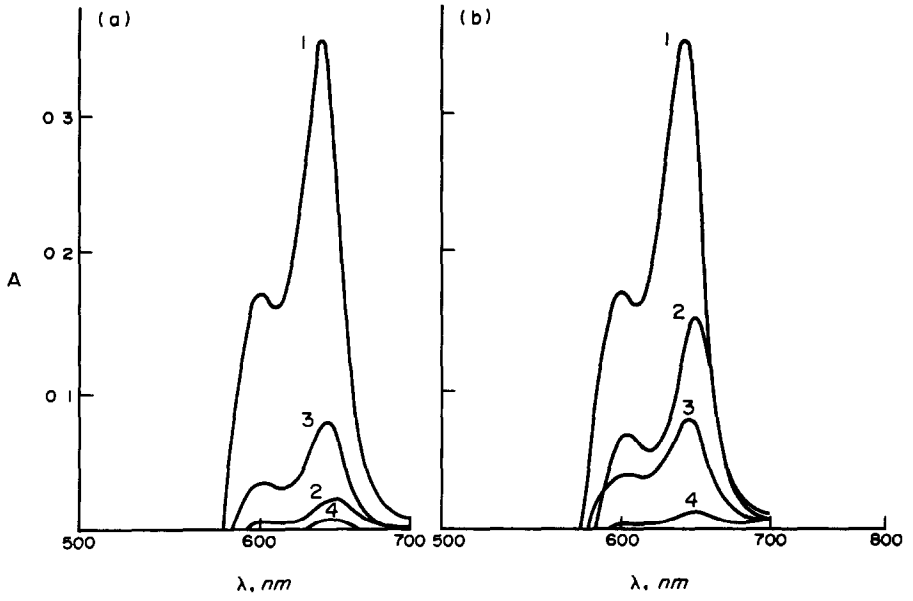

Fig 1 Effect of EDTA on Sulphonazo III complex formation with Ba(II), Sr(II), Ca(II), Pb(II) (a) = with EDTA $3\,6 \times 10^{-5}M$ $C_{Me} = 3\,6 \times 10^{-5}M$, $C_R = 1 \times 10^{-4}M$, $l = 1$ cm (1) Ba(II), (2) Pb(II), (3) Sr(II), (4) Ca(II), (b) = without EDTA

absorbances relative to lower barium concentrations producing a levelling of values between 0.38 and 0.50 units which made this method useless. It was therefore impossible to apply Budesinsky's method to the analysis of complex matrices (Fig. 2).

The more promising method of Kemp and Williams[4] was therefore tested, using commercially available Sulphonazo III without further purification, that didn't show any difference with that used by Kemp.

We noted that concentrations of barium and strontium standards ($0.5–10 \times 10^{-5}M$) were in contrast with values used for experimental measurements. They were required to be in the range $0.5–10 \times 10^{-4}M$ to give final concentrations after dilution of $0.5–10 \times 10^{-5}M$.

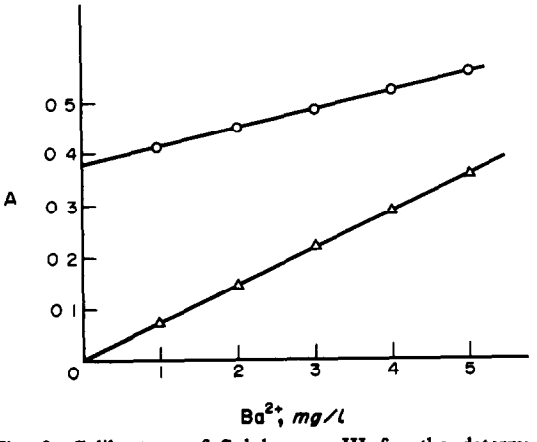

Fig. 2. Calibration of Sulphonazo III for the determination of barium. $C_R = 1 \times 10^{-4}M$; $l = 1$ cm, △ = water; ○ = internal standard by using drinking water

CONCLUSIONS

The determination of barium and strontium in drinking water showed continuous and rapid variations of absorbances, and a positive interference of other cations. The internal standard method was also used but the Beer–Lambert Law was not obeyed (Fig. 3) so a calibration curve could not be constructed Low sensitivity and interferences also made this method unsuitable for use.

The best method of determination of barium, found by Kragten,[7] is direct photo-

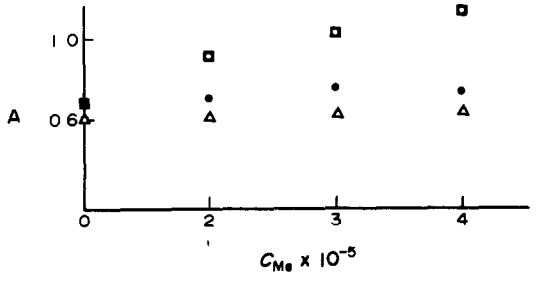

Fig 3 Calibration of Sulphonazo III for determination of barium and strontium by the internal standard method (drinking water). $C_{Ba} = (0–4) \times 10^{-5}M$ and $C_{Sr} = 1 \times 10^{-5}M$; $C_{Sr} = (0–4) \times 10^{-5}M$ and $C_{Ba} = 1 \times 10^{-5}M$; $C_R = 1 \times 10^{-4}M$; $l = 1$ cm. ○ = Ba(CDTA); □ = Ba(EGTA); △ = Sr(CDTA); ● = Sr(EGTA).

metric titration with sulphate with an automatic titrator (which ensures reproducibility) after adding propylalcohol 3-fold, to lower the solubility product of barium sulphate. The precipitate deviates from the stoichiometry for about 2–3%, but the results are even so reproducible. The titration takes about 15 min to perform.

There are hardly any interfering ions at pH 3.5 where the titration is performed. Sulphonazo III is the best indicator in these cases.

REFERENCES

1 B Budesinsky and D Vrzalova, *Z Analyt Chem.*, 1955, **210**, 161
2 *Idem*, *Talanta*, 1965, **13**, 1217.
3 Z Slovac, J Fischer and J Borak, *ibid*, 1968, **15**, 831
4 P J Kemp and M B Williams, *Anal Chem*, 1973, **45**, 124
5 V Michaylova and N Konleva, *Talanta*, 1974, **21**, 523
6 S. Umetani, K Sasayama and M Matsui, *Anal. Chim Acta*, 1982, **134**, 327
7 J Kragten, University of Amsterdam, unpublished results

Talanta, Vol 39, No 7, pp 879–881, 1992
Printed in Great Britain

0039-9140/92 $5 00 + 0 00

BOOK REVIEWS

Non-Chromatographic Continuous Separation Techniques: M. VALCÁRCEL and M D. LUQUE DE CASTRO, The Royal Society of Chemistry, Cambridge, 1991. Pages xii + 290. £42 50.

As the authors proclaim on page 8 of their book, "analytical separation techniques play a transcendental role in today's analytical chemistry" According to the philosopher Kant, transcendental refers to what is beyond experience, or cannot be experienced, and what is a perogative for having experience. It is quite clearly the aim of the authors to provide the reader with the necessary experience to exploit analytical separations intelligently and diligently. While these techniques can be classified according to a number of criteria, "they can basically be divided into two broad groups according to whether or not a flow of one of the two phases is used to facilitate the differential displacement of the mixture (sample) components", *i.e*, Static Separation Techniques (discrete or batch types) and Dynamic Separation Techniques It is the latter of these· *i e*, "continuous non-chromatographic separation techniques using a detector—usually optical or electrochemical—connected on-line to the separation system", that is covered in this text

The book is divided into five Chapters, and Chapter 1 introduces the reader to the subject matter The next three chapters describe non-chromatographic continuous separation techniques grouped, as the authors have opted, according to the type of interface across which mass transfer takes place Thus, Chapter 2 deals with gas–liquid systems (direct introduction of gas samples, gas diffusion, hydride generation, vaporization), while Chapter 3 discusses the two most commonly used liquid–liquid systems, namely dialysis and extraction. Chapter 4 is devoted to the wide variety of non-chromatographic separations involving solid–liquid interfaces (sorption, precipitation, electrochemical stripping and leaching) Finally, Chapter 5 provides an overall evaluation of the techniques dealt with in the preceding three Chapters and a brief description of two recent techniques of increasing interest, *i e*, field flow fractionation and capillary electrophoresis

The book might equally well have been called the execution of non-chromatographic continuous separation techniques by flow injection analysis (FIA), because the examples given are overwhelmingly dominated by FIA (although this term has not managed to find its way into the subject index). This should not be considered as a negative remark On the contrary, this reviewer was pleasantly surprised to observe the ramifications that FIA has had on modern analytical chemistry It is at the same time a distinct asset for the book because the authors are well known experts in FIA They are prolific writers of scientific papers on FIA—in particular on its use in various separation techniques—and they are the authors of one of the early FIA monographs Hence the book contains many FIA references (notably to the authors' own publications). However, it is also characterized by much recycling from previous FIA monographs and has obviously presented Valcárcel and Luque de Castro with a golden opportunity to update their earlier FIA monograph in a new wrapping.

In the first Chapter of their book, the authors have made a very good dissection of the anatomy of the Analytical Process, pointing out, that although it comprises several links (preliminary operations such as sampling, sample preservation and appropriate treatment, signal measurement and transducing; and data handling and treatment), there is, nevertheless, a widespread tendency to underestimate the preliminary operations, which although often trivial, time consuming, complex and requiring dedication from the operator, in fact, might be the potential sources of major errors in the analytical chain. Therefore, the first stage of the analytical process decisively influences its precision, accuracy, sensitivity, selectivity, rapidity and cost The authors have succeeded very well in emphasising these points in the many practical examples in their book, and if only for this reason the book is well worth consulting It is commendedly very detailed in its many descriptions, and should therefore also serve as a useful handbook for practical chemists. In this context, it is interesting to consult the Preface where the authors write, that the intent with their book "is neither for use as a monograph nor as a textbook, but as something in between" Obviously they have succeeded in reaching that goal. If I should point to a negative aspect of the book, then it is to the language (as in the opening phrase of this review). It is obvious that the authors have written their manuscript in their mother tongue (Spanish) and then used a translation editor to produce the English version It is somewhat doubtful if that person was a trained analytical chemist, because in addition to making the general language somewhat bombastic, he has at places construed some rather startling expressions. Yet it does make the reading entertaining.

E. H. HANSEN

Advances in Steroid Analysis '90: S GÖRÖG and E HEFTMANN (editors), Akadémiai Kiadó, Budapest, 1991 Pages xiii + 493. £36.00.

This book presents the proceedings of the 4th symposium on the analysis of steroids held at Pécs, Hungary, 24–26 April, 1990 and a total of 62 papers from authors in 16 different countries is included. The quality of binding and the variation in print size and intensity of the multi-authored compilation do not do justice to the high quality of a number of contributions.

The papers are arranged under five headings receptor binding studies, immunoassays, chromatography, spectroscopy, clinical studies and finally, miscellaneous. The link between all these is provided by the subject index but only the names of the various steroids are listed. The papers are compact, normally about seven pages long, and contain references.

Talanta, Vol 39, No 7, pp 879–881, 1992
Printed in Great Britain

0039-9140/92 $5 00 + 0 00

BOOK REVIEWS

Non-Chromatographic Continuous Separation Techniques: M. VALCÁRCEL and M D. LUQUE DE CASTRO, The Royal Society of Chemistry, Cambridge, 1991. Pages xii + 290. £42 50.

As the authors proclaim on page 8 of their book, "analytical separation techniques play a transcendental role in today's analytical chemistry" According to the philosopher Kant, transcendental refers to what is beyond experience, or cannot be experienced, and what is a perogative for having experience. It is quite clearly the aim of the authors to provide the reader with the necessary experience to exploit analytical separations intelligently and diligently. While these techniques can be classified according to a number of criteria, "they can basically be divided into two broad groups according to whether or not a flow of one of the two phases is used to facilitate the differential displacement of the mixture (sample) components", *i.e*, Static Separation Techniques (discrete or batch types) and Dynamic Separation Techniques It is the latter of these· *i e*, "continuous non-chromatographic separation techniques using a detector—usually optical or electrochemical—connected on-line to the separation system", that is covered in this text

The book is divided into five Chapters, and Chapter 1 introduces the reader to the subject matter The next three chapters describe non-chromatographic continuous separation techniques grouped, as the authors have opted, according to the type of interface across which mass transfer takes place Thus, Chapter 2 deals with gas–liquid systems (direct introduction of gas samples, gas diffusion, hydride generation, vaporization), while Chapter 3 discusses the two most commonly used liquid–liquid systems, namely dialysis and extraction. Chapter 4 is devoted to the wide variety of non-chromatographic separations involving solid–liquid interfaces (sorption, precipitation, electrochemical stripping and leaching) Finally, Chapter 5 provides an overall evaluation of the techniques dealt with in the preceding three Chapters and a brief description of two recent techniques of increasing interest, *i e*, field flow fractionation and capillary electrophoresis

The book might equally well have been called the execution of non-chromatographic continuous separation techniques by flow injection analysis (FIA), because the examples given are overwhelmingly dominated by FIA (although this term has not managed to find its way into the subject index). This should not be considered as a negative remark On the contrary, this reviewer was pleasantly surprised to observe the ramifications that FIA has had on modern analytical chemistry It is at the same time a distinct asset for the book because the authors are well known experts in FIA They are prolific writers of scientific papers on FIA—in particular on its use in various separation techniques—and they are the authors of one of the early FIA monographs Hence the book contains many FIA references (notably to the authors' own publications). However, it is also characterized by much recycling from previous FIA monographs and has obviously presented Valcárcel and Luque de Castro with a golden opportunity to update their earlier FIA monograph in a new wrapping.

In the first Chapter of their book, the authors have made a very good dissection of the anatomy of the Analytical Process, pointing out, that although it comprises several links (preliminary operations such as sampling, sample preservation and appropriate treatment, signal measurement and transducing; and data handling and treatment), there is, nevertheless, a widespread tendency to underestimate the preliminary operations, which although often trivial, time consuming, complex and requiring dedication from the operator, in fact, might be the potential sources of major errors in the analytical chain. Therefore, the first stage of the analytical process decisively influences its precision, accuracy, sensitivity, selectivity, rapidity and cost The authors have succeeded very well in emphasising these points in the many practical examples in their book, and if only for this reason the book is well worth consulting It is commendedly very detailed in its many descriptions, and should therefore also serve as a useful handbook for practical chemists. In this context, it is interesting to consult the Preface where the authors write, that the intent with their book "is neither for use as a monograph nor as a textbook, but as something in between" Obviously they have succeeded in reaching that goal. If I should point to a negative aspect of the book, then it is to the language (as in the opening phrase of this review). It is obvious that the authors have written their manuscript in their mother tongue (Spanish) and then used a translation editor to produce the English version It is somewhat doubtful if that person was a trained analytical chemist, because in addition to making the general language somewhat bombastic, he has at places construed some rather startling expressions. Yet it does make the reading entertaining.

E. H. HANSEN

Advances in Steroid Analysis '90: S GÖRÖG and E HEFTMANN (editors), Akadémiai Kiadó, Budapest, 1991 Pages xiii + 493. £36.00.

This book presents the proceedings of the 4th symposium on the analysis of steroids held at Pécs, Hungary, 24–26 April, 1990 and a total of 62 papers from authors in 16 different countries is included. The quality of binding and the variation in print size and intensity of the multi-authored compilation do not do justice to the high quality of a number of contributions.

The papers are arranged under five headings receptor binding studies, immunoassays, chromatography, spectroscopy, clinical studies and finally, miscellaneous. The link between all these is provided by the subject index but only the names of the various steroids are listed. The papers are compact, normally about seven pages long, and contain references.

The contribution by Duax and Griffin on the stereochemical aspects of receptor binding of steroids provides a good introduction to the receptor binding section (66 pages) The immunoassay section (49 pages) is subdivided into radioimmunoassay, enzyme immunoassay and other immunoassays and an interesting paper by Meyer on the combination of HPLC and EIA for multi-residue screening of anabolic steroids and stilbenes is included in this section The chromatography section (152 pages) contains 18 papers covering the techniques of GC, HPLC, GC–MS, HPLC–MS, and TLC. The paper by Shackleton on GC–MS and HPLC–MS in clinical steroid analysis is the largest single contribution in the book Some of the contributions span two or more of the section headings such that their location in the book is a little arbitrary The spectroscopy section (53 pages) is subdivided into mass spectroscopy, other spectroscopic methods (NMR, optical rotation, colorimetry), and complex application of spectroscopic techniques The latter part includes a contribution from the main editor (Görög) and others on the analysis of impurities in ethynodiol acetate. Clinical studies occupies a large section of the book (138 pages) and covers biosynthesis and metabolism, diagnosis, and other studies. Many analytical methods mentioned in previous papers are again included in this section The final miscellaneous section contains just two papers, one concerns thermal methods and the other is a polarographic study Practising steroid chemists will no doubt add this book to the previous work on steroid analysis by Gorog.

P J Cox

Electroanalytical Chemistry, Volume 17: A J Bard (editor), Dekker, New York 1991 Pages xii + 393 $145 00 (US and Canada), $174 00 (elsewhere)

This collection of reviews is concerned not with the analytical capability of electrochemistry, but with applications of analytical techniques to electrochemical problems. *Applications of the Quartz Crystal Microbalance to Electrochemistry* by D. A Buttry (85 pages) has many interesting things to say on electro-deposition and should be useful to those contemplating the use of piezoelectric detectors in the liquid phase Figure 13, however, purports to show a shift in frequency decreasing with time, t, but increasing with $t^{1/2}$, while values at $t = 1$ are unequal. *Optical Second Harmonic Generation as an* in situ *Probe of Electrochemical Interfaces* by G. L Richmond (94 pages) describes the applications to monolayer films on metals and makes it clear that the technique is still in its early stages. I certainly would have needed a longer and more basic introduction to SHG itself before I derived much from this review. The title *New Developments in Electrochemical Mass Spectroscopy* by B Bittins-Cattaneo, E Cattaneo, P Konigshoven and W Vielstich (40 pages) involves a misnomer. This application examines the MS of gases evolved at electrodes, which yields insights into absorptive as well as redox processes Although applications so far are not numerous, this is an interesting chapter *Carbon Electrodes: Structural Effects on Electron Transfer Kinetics* by R L McCreery (152 pages) summarizes a great deal of background structural information for users of carbon electrodes in voltammetry and should be a favourite with graduate students Overall, this is a source-book for researchers in electrochemistry rather than a text for analysts It is worth its place on the library shelf, but will not attract many individual purchasers

D Midgley

Mass Spectrometry: E Constantin and A Schnell, Ellis Horwood, Chichester, 1990 Pages 184 £39 95.

This book is an English translation of the book originally published in French in 1986 As can be judged from a few references, some updating has been carried out.

It is a concise book containing information on the principles of mass spectrometry, practical aspects and a limited number of applications Several chapters contain selected lists of references and collected together at the end of the book there are additional lists of references and a general bibliography as well as a subject index There are many figures, some more relevant and informative than others

There are times when the book appears to be too concise, almost appearing like a catalogue It probably attempts to cover too many features in too few pages For many readers, further information will be required and other sources will have to be consulted For an organic/analytical chemist, for example, too little information is given on fragmentation pathways, there are already various spectroscopy books which cover this aspect really well and these will be preferentially consulted

As a general book, it has value but it is difficult to see it having many personal buyers However, it should have a place in many institutional libraries

J L Wardell

Modern NMR Techniques and Their Application in Chemistry: A I Popov and K Hallenga (editors), Dekker, New York, 1991. Pages x + 665. $135.00 (US and Canada), $162.00 (elsewhere)

This book contains ten chapters written by nine scientists from Europe and North America. The chapters are on (1) NMR properties of Nuclei, (2) Fourier-Transform NMR: Theoretical and Practical Aspects, (3) Solid State NMR of Spin-$\frac{1}{2}$ Nuclei, (4) Solid State NMR of Quadrupolar Nuclei, (5) Quantitative Chemical Analysis by NMR, (6) Structural Determination of Organic Compounds, (7) Structural Determination of Inorganic Compounds, (8) Equilibria Studies in Solutions, (9) Reaction Kinetics and Exchange and (10) Two-Dimensional NMR Studies.

The contribution by Duax and Griffin on the stereochemical aspects of receptor binding of steroids provides a good introduction to the receptor binding section (66 pages) The immunoassay section (49 pages) is subdivided into radioimmunoassay, enzyme immunoassay and other immunoassays and an interesting paper by Meyer on the combination of HPLC and EIA for multi-residue screening of anabolic steroids and stilbenes is included in this section The chromatography section (152 pages) contains 18 papers covering the techniques of GC, HPLC, GC–MS, HPLC–MS, and TLC. The paper by Shackleton on GC–MS and HPLC–MS in clinical steroid analysis is the largest single contribution in the book Some of the contributions span two or more of the section headings such that their location in the book is a little arbitrary The spectroscopy section (53 pages) is subdivided into mass spectroscopy, other spectroscopic methods (NMR, optical rotation, colorimetry), and complex application of spectroscopic techniques The latter part includes a contribution from the main editor (Görög) and others on the analysis of impurities in ethynodiol acetate. Clinical studies occupies a large section of the book (138 pages) and covers biosynthesis and metabolism, diagnosis, and other studies. Many analytical methods mentioned in previous papers are again included in this section The final miscellaneous section contains just two papers, one concerns thermal methods and the other is a polarographic study Practising steroid chemists will no doubt add this book to the previous work on steroid analysis by Gorog.

P J Cox

Electroanalytical Chemistry, Volume 17: A J Bard (editor), Dekker, New York 1991 Pages xii + 393 $145 00 (US and Canada), $174 00 (elsewhere)

This collection of reviews is concerned not with the analytical capability of electrochemistry, but with applications of analytical techniques to electrochemical problems. *Applications of the Quartz Crystal Microbalance to Electrochemistry* by D. A Buttry (85 pages) has many interesting things to say on electro-deposition and should be useful to those contemplating the use of piezoelectric detectors in the liquid phase Figure 13, however, purports to show a shift in frequency decreasing with time, t, but increasing with $t^{1/2}$, while values at $t = 1$ are unequal. *Optical Second Harmonic Generation as an* in situ *Probe of Electrochemical Interfaces* by G. L Richmond (94 pages) describes the applications to monolayer films on metals and makes it clear that the technique is still in its early stages. I certainly would have needed a longer and more basic introduction to SHG itself before I derived much from this review. The title *New Developments in Electrochemical Mass Spectroscopy* by B Bittins-Cattaneo, E Cattaneo, P Konigshoven and W Vielstich (40 pages) involves a misnomer. This application examines the MS of gases evolved at electrodes, which yields insights into absorptive as well as redox processes Although applications so far are not numerous, this is an interesting chapter *Carbon Electrodes: Structural Effects on Electron Transfer Kinetics* by R L McCreery (152 pages) summarizes a great deal of background structural information for users of carbon electrodes in voltammetry and should be a favourite with graduate students Overall, this is a source-book for researchers in electrochemistry rather than a text for analysts It is worth its place on the library shelf, but will not attract many individual purchasers

D Midgley

Mass Spectrometry: E Constantin and A Schnell, Ellis Horwood, Chichester, 1990 Pages 184 £39 95.

This book is an English translation of the book originally published in French in 1986 As can be judged from a few references, some updating has been carried out.

It is a concise book containing information on the principles of mass spectrometry, practical aspects and a limited number of applications Several chapters contain selected lists of references and collected together at the end of the book there are additional lists of references and a general bibliography as well as a subject index There are many figures, some more relevant and informative than others

There are times when the book appears to be too concise, almost appearing like a catalogue It probably attempts to cover too many features in too few pages For many readers, further information will be required and other sources will have to be consulted For an organic/analytical chemist, for example, too little information is given on fragmentation pathways, there are already various spectroscopy books which cover this aspect really well and these will be preferentially consulted

As a general book, it has value but it is difficult to see it having many personal buyers However, it should have a place in many institutional libraries

J L Wardell

Modern NMR Techniques and Their Application in Chemistry: A I Popov and K Hallenga (editors), Dekker, New York, 1991. Pages x + 665. $135.00 (US and Canada), $162.00 (elsewhere)

This book contains ten chapters written by nine scientists from Europe and North America. The chapters are on (1) NMR properties of Nuclei, (2) Fourier-Transform NMR: Theoretical and Practical Aspects, (3) Solid State NMR of Spin-$\frac{1}{2}$ Nuclei, (4) Solid State NMR of Quadrupolar Nuclei, (5) Quantitative Chemical Analysis by NMR, (6) Structural Determination of Organic Compounds, (7) Structural Determination of Inorganic Compounds, (8) Equilibria Studies in Solutions, (9) Reaction Kinetics and Exchange and (10) Two-Dimensional NMR Studies.

The contribution by Duax and Griffin on the stereochemical aspects of receptor binding of steroids provides a good introduction to the receptor binding section (66 pages) The immunoassay section (49 pages) is subdivided into radioimmunoassay, enzyme immunoassay and other immunoassays and an interesting paper by Meyer on the combination of HPLC and EIA for multi-residue screening of anabolic steroids and stilbenes is included in this section The chromatography section (152 pages) contains 18 papers covering the techniques of GC, HPLC, GC–MS, HPLC–MS, and TLC. The paper by Shackleton on GC–MS and HPLC–MS in clinical steroid analysis is the largest single contribution in the book Some of the contributions span two or more of the section headings such that their location in the book is a little arbitrary The spectroscopy section (53 pages) is subdivided into mass spectroscopy, other spectroscopic methods (NMR, optical rotation, colorimetry), and complex application of spectroscopic techniques The latter part includes a contribution from the main editor (Görög) and others on the analysis of impurities in ethynodiol acetate. Clinical studies occupies a large section of the book (138 pages) and covers biosynthesis and metabolism, diagnosis, and other studies. Many analytical methods mentioned in previous papers are again included in this section The final miscellaneous section contains just two papers, one concerns thermal methods and the other is a polarographic study Practising steroid chemists will no doubt add this book to the previous work on steroid analysis by Gorog.

P J Cox

Electroanalytical Chemistry, Volume 17: A J Bard (editor), Dekker, New York 1991 Pages xii + 393 $145 00 (US and Canada), $174 00 (elsewhere)

This collection of reviews is concerned not with the analytical capability of electrochemistry, but with applications of analytical techniques to electrochemical problems. *Applications of the Quartz Crystal Microbalance to Electrochemistry* by D. A Buttry (85 pages) has many interesting things to say on electro-deposition and should be useful to those contemplating the use of piezoelectric detectors in the liquid phase Figure 13, however, purports to show a shift in frequency decreasing with time, t, but increasing with $t^{1/2}$, while values at $t = 1$ are unequal. *Optical Second Harmonic Generation as an* in situ *Probe of Electrochemical Interfaces* by G. L Richmond (94 pages) describes the applications to monolayer films on metals and makes it clear that the technique is still in its early stages. I certainly would have needed a longer and more basic introduction to SHG itself before I derived much from this review. The title *New Developments in Electrochemical Mass Spectroscopy* by B Bittins-Cattaneo, E Cattaneo, P Konigshoven and W Vielstich (40 pages) involves a misnomer. This application examines the MS of gases evolved at electrodes, which yields insights into absorptive as well as redox processes Although applications so far are not numerous, this is an interesting chapter *Carbon Electrodes: Structural Effects on Electron Transfer Kinetics* by R L McCreery (152 pages) summarizes a great deal of background structural information for users of carbon electrodes in voltammetry and should be a favourite with graduate students Overall, this is a source-book for researchers in electrochemistry rather than a text for analysts It is worth its place on the library shelf, but will not attract many individual purchasers

D Midgley

Mass Spectrometry: E Constantin and A Schnell, Ellis Horwood, Chichester, 1990 Pages 184 £39 95.

This book is an English translation of the book originally published in French in 1986 As can be judged from a few references, some updating has been carried out.

It is a concise book containing information on the principles of mass spectrometry, practical aspects and a limited number of applications Several chapters contain selected lists of references and collected together at the end of the book there are additional lists of references and a general bibliography as well as a subject index There are many figures, some more relevant and informative than others

There are times when the book appears to be too concise, almost appearing like a catalogue It probably attempts to cover too many features in too few pages For many readers, further information will be required and other sources will have to be consulted For an organic/analytical chemist, for example, too little information is given on fragmentation pathways, there are already various spectroscopy books which cover this aspect really well and these will be preferentially consulted

As a general book, it has value but it is difficult to see it having many personal buyers However, it should have a place in many institutional libraries

J L Wardell

Modern NMR Techniques and Their Application in Chemistry: A I Popov and K Hallenga (editors), Dekker, New York, 1991. Pages x + 665. $135.00 (US and Canada), $162.00 (elsewhere)

This book contains ten chapters written by nine scientists from Europe and North America. The chapters are on (1) NMR properties of Nuclei, (2) Fourier-Transform NMR: Theoretical and Practical Aspects, (3) Solid State NMR of Spin-$\frac{1}{2}$ Nuclei, (4) Solid State NMR of Quadrupolar Nuclei, (5) Quantitative Chemical Analysis by NMR, (6) Structural Determination of Organic Compounds, (7) Structural Determination of Inorganic Compounds, (8) Equilibria Studies in Solutions, (9) Reaction Kinetics and Exchange and (10) Two-Dimensional NMR Studies.

Thus all aspects of NMR spectroscopy are covered. solution and solid state, theory and practice, 1D and 2D, *etc.*

The preface indicates that the book is intended to complement existing books written by specialists for specialists and it is for those chemists who require NMR as a tool and who need to discover what advances have been made in the last decade This reviewer is just that target. However, my clear impressions of this book are that the book was written by experts and it surely needs a specialist to find it an easy and joyful read Everything is there. all the maths, for example, for Fourier transform NMR and for solid state NMR of quadrupolar nuclei, is remorselessly presented with no concessions at all for the non-mathematically inclined. To follow such detail is probably too much for the average chemist who just wants to use the NMR technique

There is clearly much useful information in the book and to persevere with it will be rewarding. However, the difficulties many readers may experience in attempting to follow the great detail classifies the book as somewhat reader-unfriendly. The book as a whole, and not just the contents, was not attractive to this reviewer. Some of the Figures are badly reproduced (*e.g*, Figure 3 on page 576)

The book has a place in a chemistry library due to the importance of NMR but scope remains for a book more sympathetic to the average chemist

J L. WARDELL

Wood and Cellulose Chemistry: D N-N HON and N SHIRAISHI (editors), Dekker, New York, 1991. Pages viii + 1020 $195 00 (US and Canada) $234.00 (elsewhere).

There are many books on wood and cellulose chemistry but this massive one is a very welcome and worthy newcomer. It has the features one would wish but also incorporates much work of Japanese origin. This is quickly recognized to rectify imbalances of reportage in other texts Japan is at the forefront of investigations of the chemistry of wood and its utilization The majority of the contributors are Japanese but there are also several Americans

The text is divided into three substantial sections, namely, I, Structure and Chemistry, II, Degradation, and III, Modification and Utilization In the first section after an introductory chapter on chemical composition and distribution there are others on cellulose, hemicelluloses, extractives and lignin, and others on the chemistry of bark and the characterization of wood and its components. The second section deals with colour and discoloration of woods, before dealing in separate chapters with various factors affecting the degradation of wood and its components including chemical, photochemical and pyrolytic degradations and enzymatic, microbial and biomimetic degradation of lignin and biodegradation of cellulosic materials. The last section has chapters on chemical modification of wood, chemical modification of cellulose, characterization of chemically modified cellulose, wood plasticization, wood–polymer composites, adhesion and adhesives and utilization of wood and cellulose for chemicals and energy

The text is comprehensive, highly detailed, up-to-date, well-written, and supported by extensive, and attractively presented and clear, tables and figures Future authors will be indebted to the ease of access the volume provides to work (and workers) they might easily have overlooked Japanese reportage is not at the expense of reportage of other work which is incorporated seamlessly into a splendid text The editors and contributors are to be congratulated on providing a stimulating and desirable addition to the works already available.

K. C B WILKIE

Factor Analysis in Chemistry, 2nd Ed.: E R MALINOWSKI, Wiley, Chichester, 1991 Pages xii + 350. £43 70.

The ideas of principal component and factor analysis were first proposed by the great statistician Pearson as early as 1901, but it was not until sixty years later that it was introduced into analytical chemistry by Malinowski as part of his doctorate The first edition of this book followed in 1980, and it proved to be a milestone in the acceptance of the method by the chemical community It was a timely publication coinciding as it did with the advent of the personal computer, and the increasing sophistication of analytical instruments under computer control producing large amounts of data that needed factor analysis to extract and interpet the underlying physical chemistry

Since the book is an established classic, it is the additions and amendments to the second edition that will be of interest to many people. Much of the text remains the same, especially chapters 7–10 which deal with chemical applications, there are, for example, only 19 references post 1980 out of a total of 157 in these chapters which is something of a disappointment. However, the earlier sections do include a considerable number of new techniques with practical examples in a later chapter. The new methods include autocorrelation techniques, statistical methods for target testing, and errors in the factor loadings, *etc* These are listed in full in the Preface, so anyone who has the first edition can easily decide for themselves whether to invest over £43 on a new copy

The approach remains clear and readable, with mathematics limited, in general, to matrix methods in a way that never becomes indigestible, there is always adequate discussion and illustration of what the underlying mathematics means. Couple this with a host of chemical examples and you have a book that remains indispensable for those working with factor analysis

C. J. GILMORE

Thus all aspects of NMR spectroscopy are covered. solution and solid state, theory and practice, 1D and 2D, *etc.*

The preface indicates that the book is intended to complement existing books written by specialists for specialists and it is for those chemists who require NMR as a tool and who need to discover what advances have been made in the last decade This reviewer is just that target. However, my clear impressions of this book are that the book was written by experts and it surely needs a specialist to find it an easy and joyful read Everything is there. all the maths, for example, for Fourier transform NMR and for solid state NMR of quadrupolar nuclei, is remorselessly presented with no concessions at all for the non-mathematically inclined. To follow such detail is probably too much for the average chemist who just wants to use the NMR technique

There is clearly much useful information in the book and to persevere with it will be rewarding. However, the difficulties many readers may experience in attempting to follow the great detail classifies the book as somewhat reader-unfriendly. The book as a whole, and not just the contents, was not attractive to this reviewer. Some of the Figures are badly reproduced (*e.g*, Figure 3 on page 576)

The book has a place in a chemistry library due to the importance of NMR but scope remains for a book more sympathetic to the average chemist

J L. WARDELL

Wood and Cellulose Chemistry: D N-N HON and N SHIRAISHI (editors), Dekker, New York, 1991. Pages viii + 1020 $195 00 (US and Canada) $234.00 (elsewhere).

There are many books on wood and cellulose chemistry but this massive one is a very welcome and worthy newcomer. It has the features one would wish but also incorporates much work of Japanese origin. This is quickly recognized to rectify imbalances of reportage in other texts Japan is at the forefront of investigations of the chemistry of wood and its utilization The majority of the contributors are Japanese but there are also several Americans

The text is divided into three substantial sections, namely, I, Structure and Chemistry, II, Degradation, and III, Modification and Utilization In the first section after an introductory chapter on chemical composition and distribution there are others on cellulose, hemicelluloses, extractives and lignin, and others on the chemistry of bark and the characterization of wood and its components. The second section deals with colour and discoloration of woods, before dealing in separate chapters with various factors affecting the degradation of wood and its components including chemical, photochemical and pyrolytic degradations and enzymatic, microbial and biomimetic degradation of lignin and biodegradation of cellulosic materials. The last section has chapters on chemical modification of wood, chemical modification of cellulose, characterization of chemically modified cellulose, wood plasticization, wood–polymer composites, adhesion and adhesives and utilization of wood and cellulose for chemicals and energy

The text is comprehensive, highly detailed, up-to-date, well-written, and supported by extensive, and attractively presented and clear, tables and figures Future authors will be indebted to the ease of access the volume provides to work (and workers) they might easily have overlooked Japanese reportage is not at the expense of reportage of other work which is incorporated seamlessly into a splendid text The editors and contributors are to be congratulated on providing a stimulating and desirable addition to the works already available.

K. C B WILKIE

Factor Analysis in Chemistry, 2nd Ed.: E R MALINOWSKI, Wiley, Chichester, 1991 Pages xii + 350. £43 70.

The ideas of principal component and factor analysis were first proposed by the great statistician Pearson as early as 1901, but it was not until sixty years later that it was introduced into analytical chemistry by Malinowski as part of his doctorate The first edition of this book followed in 1980, and it proved to be a milestone in the acceptance of the method by the chemical community It was a timely publication coinciding as it did with the advent of the personal computer, and the increasing sophistication of analytical instruments under computer control producing large amounts of data that needed factor analysis to extract and interpet the underlying physical chemistry

Since the book is an established classic, it is the additions and amendments to the second edition that will be of interest to many people. Much of the text remains the same, especially chapters 7–10 which deal with chemical applications, there are, for example, only 19 references post 1980 out of a total of 157 in these chapters which is something of a disappointment. However, the earlier sections do include a considerable number of new techniques with practical examples in a later chapter. The new methods include autocorrelation techniques, statistical methods for target testing, and errors in the factor loadings, *etc* These are listed in full in the Preface, so anyone who has the first edition can easily decide for themselves whether to invest over £43 on a new copy

The approach remains clear and readable, with mathematics limited, in general, to matrix methods in a way that never becomes indigestible, there is always adequate discussion and illustration of what the underlying mathematics means. Couple this with a host of chemical examples and you have a book that remains indispensable for those working with factor analysis

C. J. GILMORE

Talanta, Vol. 39, No. 8, pp. 883–886, 1992
Printed in Great Britain.

0039-9140/92 $5.00 + 0.00

TWO-COLOR LASER DESORPTION MASS SPECTROMETRY USING A SINGLE LASER

JEFFREY R. APPLING* and D. DANELLE BLAND
Department of Chemistry, University of Kentucky, Lexington, KY 40506, U.S.A.

(*Received* 17 *October* 1991. *Revised* 19 *November* 1991. *Accepted* 19 *November* 1991)

Summary—A Nd:YAG laser has been used to perform IR desorption of analytes followed by UV ionization, all within the same laser pulse. At moderate laser powers, mass spectra recorded using this method are dominated by molecular ions.

In recent years there have been important advances in mass spectrometric techniques,[1,2] many of which were largely motivated by the need for analysis of non-volatile and high molecular weight compounds. These methods include[2] SIMS, field desorption, fast atom[3] and ion bombardment,[4,5] plasma desorption,[6] and laser desorption.[1,7] Laser desorption mass spectrometry (LDMS) has proven itself to be one of the most powerful methods, especially when used in the matrix-assisted format.[7–10] Another LDMS strategy[1,11,12] relies on the use of two lasers for separate desorption and ionization. A distinct advantage is gained by desorbing intact neutral molecules (with infrared radiation for example) for subsequent ionization and detection. The present work was prompted by the desire to simplify this two-color desorption/ionization approach through the use of a single laser. Employing a Nd:YAG laser, we have successfully performed IR desorption of analytes detected with UV ionization within the same laser pulse.

Use of a single laser wavelength for sample vaporization and ionization often leads to indiscriminant destruction of analytes due to the power densities necessary to bring about the ionization process. Ion intensities depend greatly on the matrix,[9] which can make relative and absolute quantitation difficult. This is especially true for organic species that tend to fragment easily under conditions that promote ionization. In addition, substrate materials can contribute ions which may cause a serious interference problem. Infrared laser pulses are useful for desorption due to their ability to remove surface molecules with less fragmentation[13] than shorter wavelengths. Conditions which do not generate surface ions will still produce large amounts of neutral molecules.[14,15] This can be put to advantage by using a separate ionization scheme to detect ejected species. UV laser pulses can provide a convenient "soft" ionizaton for these molecules.

To accomplish this two-color desorption/ionizaton with a single laser we use a frequency-quadrupled Nd:YAG laser which has a fundamental IR output at 1064 nm. Coincident pulses of 1064 nm, frequency-doubled 532 nm, and frequency-quadrupled 266 nm light are filtered to eliminate the visible radiation. The remaining IR and UV pulses are passed through a short focal length lens prior to interaction with a sample target inside a time-of-flight mass spectrometer. Since focal length depends upon wavelength, this lens causes a spatial separation of the IR and UV laser beams. Thus we are able to position the UV focus above the target surface to intercept analyte molecules desorbed from the substrate by the IR laser pulse.

EXPERIMENTAL

The schematic diagram presented in Fig. 1 shows the arrangement of our home-built linear time-of-flight (TOF) mass spectrometer, detection electronics, and laser source. The spectrometer is composed of modular 40-mm Kwik Flange (KF-40) vacuum fittings (MDC) pumped by a 110 l./sec turbomolecular pump (Balzers). The detector is a single 18-mm microchannel plate (Varian VUW-8960) mounted

*Author for correspondence.

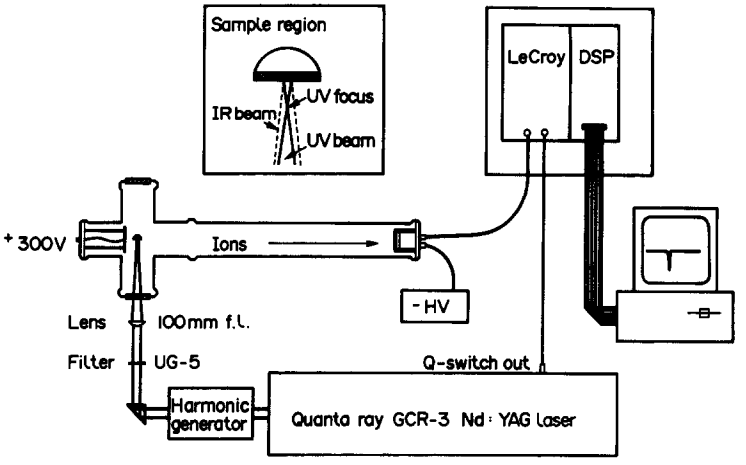

Fig. 1. Schematic of laser desorption time-of-flight system.

on a KF-40 flange outfitted with Safety High Voltage (SHV) feedthroughs (Insulator Seal, Inc.). A repeller plate biased at +300 V is used to push ions into the flight tube. Ions created above the target surface travel approximately 50 cm before they strike the detector.

The laser used for these preliminary experiments was a Quanta-Ray GCR-3 Nd:YAG laser equipped with a harmonic generator to produce doubled and guadrupled laser frequencies. The visible 532-nm (doubled) light was rejected with a UG-5 Schott glass filter, which also attenuates the IR (about 70%) and UV (about 20%) beams. The IR and UV pulses, with a temporal width of 9 nsec, are focused through the same 100-mm focal length fused silica lens mounted on a positioning stage outside the vacuum chamber. The IR and UV focal points are approximately 1 cm apart under these conditions. The inset of Fig. 1 shows the relative positions of the IR and UV focii as they would be during a surface analysis. In practice, the UV focus is first positioned directly on the surface creating large signals from substrate ions, then the lens is backed away from the target until these substrate ions disappear. The lens is then moved laterally to probe a fresh part of the target surface.

Ion signals were preamplified (SRS model SR445) before input into a 200-MHz transient digitizer (LeCroy TR8828C) for time characterization. The digitizer is contained in a CAMAC crate (Kinetic Systems) interfaced to a personal computer via a DSP 6001 crate controller. Data acquisition is accomplished with custom software. The Q-switch output of the laser is used to trigger the digitizer, and spectra can be collected from single or multiple laser shots.

RESULTS AND DISCUSSION

Figure 2 shows the sequential removal of glutamic acid from a target one laser shot at a time, with a constant lens position. Each trace corresponds to the mass spectrum (near the molecular ion) acquired from individual laser shots. The laser was fired manually about every 45 sec. The target substrate is a 5 mm × 5 mm × 2 mm section of a flat natural pyrite crystal face (origin unknown), which is known to be pure iron(II) sulfide from analysis by Rutherford Backscattering. This target is identical to those used in our current study[16] of adsorption of organic molecules to metal sulfide surfaces. In this case, the glutamic acid was simply deposited on the target by evaporation of one droplet of 20m*M* aqueous solution. We estimate a coverage of approximately 500 ng/cm^2 on the surface. A single shot mass spectrum shows the molecular ion only, as depicted in Fig. 3. These results indicate that the IR pulse desorbs glutamic acid molecules intact for ionization by the UV pulse.

Unfortunately, the spectra in Fig. 2 corresponding to the first three laser shots are just outside the dynamic range of the digitizer, so they appear to have the same ion intensity. But subsequent laser shots clearly show a decreasing surface concentration until no analyte is left (the twelfth laser shot yielded no ions). The glutamic acid was localized to a very small area on the surface, as expected for a dried droplet of solution. Preliminary work[16] with pyrite exposed to solutions of cysteine and serine show uniform coverage indicative of surface adsorption.

Mass spectra collected in this fashion are dependent on laser power. The laser was

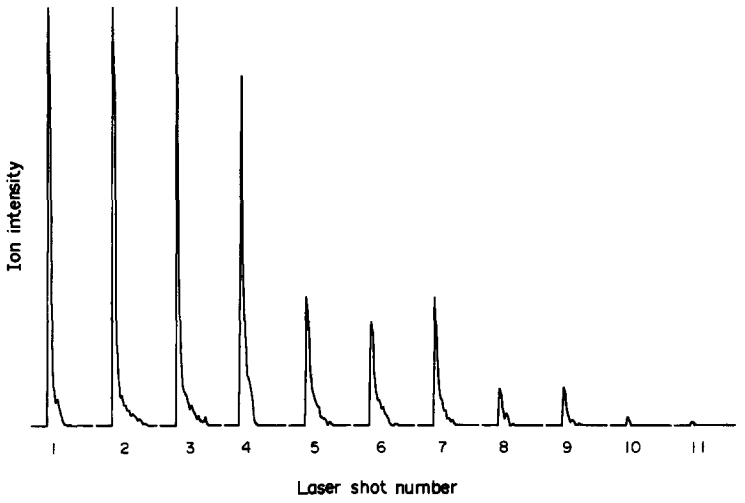

Fig. 2. Sequential removal of glutamic acid from a natural pyrite target. Each spectrum is collected after a single laser shot.

operated with the oscillator flashlamps only. For the spectra in Figs. 2 and 3, the pulse energies for the IR and UV pulses were about 50 and 1 mJ, respectively, before passing through the filter. After attenuation by the filter the energy ratio was reduced to about 20:1. Significantly higher laser powers remove material at a given target position in a few laser shots, and mass spectra are dominated by fragment ions. To obtain spectra of molecular ions, the laser energy was adjusted just above a lower threshold for ion production.

Under the conditions outlined above, only absorbed analyte molecules are observed to ionize; no surface substrate ions are detected. This leads to the conclusion that the IR pulse desorbs analytes under conditions of low irradiance[17] ($\approx 10^5$–10^6 W/cm^2). High heating rates at the surface[18] cause the release of intact molecules[17] in a plume that can be intercepted by the focused UV pulse. Thus molecular ions dominate the mass spectrum generated by the IR/UV pulse combination.

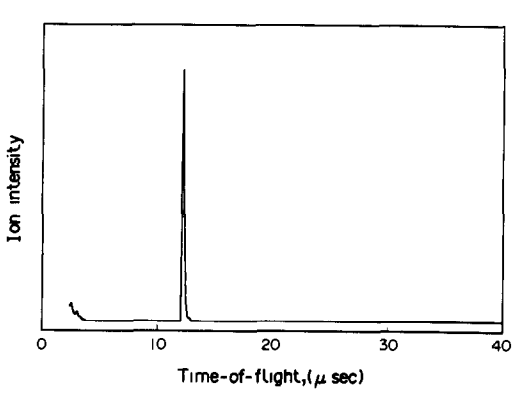

Fig. 3. Time-of-flight mass spectrum of glutamic acid absorbed to pyrite substrate. The feature at early time is the tail of an intense peak created when scattered laser light reaches the detector. This tail obscures ion signals for masses less than 10 amu.

The UV beam expands enough before it strikes the surface so that it does not generate surface ions or destroy analyte molecules to a great extent. When the "focal point" is pulled back from the surface to eliminate surface ionization, the focal volume is positioned about 1 mm above the target. Success of this method requires that analytes desorbed by the head of the IR pulse have enough time to move into the UV ionization region. This feature will limit the maximum mass of analyte which can be detected, since massive molecules will take too long to move away from the surface to be ionized within the 9 nsec laser pulse. We intend to explore these upper mass limit capabilities for our system.

CONCLUSIONS

A single Nd:YAG laser with a pulse duration of 9 nsec can be used to desorb and ionize surface-deposited molecules with little or no fragmentation. This is accomplished by positioning the spatially separated focii of the IR and UV laser beams so that the UV focus is just above a target surface, and the IR beam strikes the target under conditions of low irradiance. The main advantages of this method lie in the simplicity of the laser and optical system needed to perform two-color laser surface analyses. It seems possible that low-cost modifications

could allow incorporation of this technique into current commercial laser microprobe mass analyzers which use Nd:YAG laser sources.

Acknowledgements—DDB gratefully acknowledges support from NSF as a 1991 Research Experiences for Undergraduates (REU) participant. The authors thank Vahid Majidi for his valuable assistance and many helpful discussions.

REFERENCES

1. D. M. Lubman, *Anal. Chem.*, 1987, **59**, 31A.
2. E. R. Grant and R. G. Cooks, *Science*, 1990, **250**, 61.
3. H. Egge, J. P. Katalinic, M. Karas and B. Stahl, *Pure Appl. Chem.*, 1991, **63**, 491.
4. F. M. Kimock, J. P. Baxter, D. L. Pappas, P. H. Kobrin and N. Winograd, *Anal. Chem.*, 1984, **56**, 2782.
5. J. B. Pallix, U. Schuhle, C. H. Becker and D. L. Huestis, *ibid.*, 1989, **61**, 805.
6. G. Allmaier, E. R. Schmid, K. Hagspiel, C. P. Kubicek, M. Karas and F. Hillenkamp, *Anal. Chim. Acta*, 1990, **241**, 321.
7. M. Karas, U. Bahr, A. Ingendoh, E. Nordhoff, B. Stahl, K. Strupat and F. Hillenkamp, *ibid.*, 1990, **241**, 175.
8. S. Zhao, K. V. Somayajula, A. G. Sharkey, D. M. Hercules, F. Hillenkamp, M. Karas and A. Ingendoh, *Anal. Chem.*, 1991, **63**, 450.
9. M. Karas, U. Bahr and F. Hillenkamp, *Int. J. Mass Spectrom. Ion Processes*, 1989, **92**, 231.
10. R. C. Beavis and B. T. Chait, *Chem. Phys. Lett.*, 1991, **181**, 479.
11. C. H. Becker, L. E. Jusinski and L. Moro, *Int. J. Mass Spectrom. Ion Processes*, 1990, **95**, R1.
12. F. Engelke, J. H. Hahn, W. Henke and R. N. Zare, *Anal. Chem.*, 1987, **59**, 909.
13. A. Overberg, M. Karas, U. Bahr, R. Kaufmann and F. Hillenkamp, *Rapid Commun. Mass Spectrom.*, 1990, **4**, 293.
14. R. B. Van Breeman, M. Snow and R. J. Cotter, *Int. J. Mass Spectrom. Ion Phys.*, 1983, **49**, 35.
15. U. Boesl, J. Grotemeyer, K. Walter and E. W. Schlag, *Anal. Instrum.*, 1987, **16**, 151.
16. J. R. Appling and D. D. Bland, unpublished results.
17. A. Vertes, P. Juhasz, L. Balazs and R. Gijbels, *Microbeam Analysis—1989*, p. 273. San Francisco Press, San Francisco, 1989.
18. A. Dereux, A. Peremans, J.-P. Vigneron, J. Darville and J.-M. Gilles, *J. Electron Spectros. Relat Phenom.*, 1987, **45**, 261.

Talanta, Vol. 39, No. 8, pp. 887–891, 1992
Printed in Great Britain.

0039-9140/92 $5.00 + 0.00

NEW COMPUTATIONAL APPROACH FOR THE SIMULTANEOUS PHOTOMETRIC DETERMINATION OF CATALYSTS AND ACTIVATORS

ANDREU CLADERA, ARTURO CARO, ENRIQUE GÓMEZ, JOSÉ MANUEL ESTELA and VÍCTOR CERDÀ*
Departamento de Química, Facultad de Ciencias, Universidad de las Islas Baleares, E-07071 Palma de Mallorca, Spain

(*Received* 2 *September* 1991. *Revised* 28 *October* 1991. *Accepted* 5 *November* 1991)

Summary—A new method for the simultaneous kinetic determination of catalysts and activators was developed on the basis of a mathematical model. The parameters and variables are optimized from experimental data obtained by application of a multiple standard-addition method and use of the Gauss–Newton and Simplex method, both of which provide identical results. The proposed method was applied to the simultaneous photometric determination of Mn(II) and Pb(II) on the basis of their catalytic and activating effects, respectively, on the oxidation of Tiron by hydrogen peroxide. Data were both acquired and processed with the aid of software developed by the authors. The linear determination range achieved was 1.00–5.00 ng/ml Mn(II) and 200–800 ng/ml Pb(II). Experimental readings were made at 450 nm with a fibre optics detector. The most serious interference with the method was posed by Cr(III).

Catalytic reactions can be accelerated by using a variety of substances known as "activators". These are usually organic compounds[1,2] and, less often, metal ions.[3,4] As a rule, activators, which enhance the effect of the catalysts, are determined with lower sensitivity than catalysts.[5]

Despite the wide use of kinetic spectrophotometric methods for the catalytic determination of metals on account of their high sensitivity, few of them rely on activating effects for determination purposes.[6] Thus, activating effects have so far only been used in general to increase the sensitivity—and, occasionally, the selectivity—of catalyst determinations. No simultaneous determination of both types of substance, however, appears to have been attempted to date.

In previous work involving the kinetic thermometric determination of Mn(II) based on its catalytic effect on the oxidation of Tiron by hydrogen peroxide[7] we found Pb(II) to exert an activating effect on the analytical reaction. This led us to develop a simultaneous kinetic photometric determination taking advantage of both effects.

The problem was addressed by developing a new mathematical model based on a multiple standard-addition method. Thus, a general mathematical expression accounting for the potential non-catalytic effect, the Mn(II)-catalysed reaction and the activating effect of Pb(II) was used as starting point. The different parameters and variables included in the equation were calculated from experimental data that were processed by two different optimization methods (Gauss-Newton and Simplex) in order to compare the results obtained.

Both the acquisition of kinetic data, which was effected by using the initial-rate method, and the calculation of the parameters and variables in the starting mathematical expression were performed with the aid of software developed by the authors.[8,9]

The results obtained showed that the proposed simultaneous determination is an alternative to, for example, thermometric determinations on account of its higher sample throughput—the slope of the kinetic curve can be obtained in less than 30sec.

THEORY

The catalytic effect and the activating action of chemical substances can be exploited for the simultaneous determination of catalysts and activators. This requires the use of a mathematical equation relating the rates of the two reactions with the concentrations of the two analytes. The parameters involved in such an equation can be optimized by several

*Author for correspondence.

mathematical methods, for instance the Gauss–Newton or Simplex method.

The starting equation for development of the mathematical method was as follows:

$$v = A + (B + C[Y])[X]$$

where parameter A represents the contribution of the potential uncatalysed reaction, coefficient B is related to the exclusively catalytic process of X, and C denotes the activating effect of Y.

Therefore, by applying the multiple standard addition method, the above equation can be written as:

$$v = A + (B + C\{[X]_i + [X]_x\})([Y]_i + [Y]_x)$$

where subscript i denotes the known concentrations of each substance added to the sample or the determinations, and subscript x denotes the unknown concentrations in the sample to be determined.

The optimization will thus be made via a function U dependent on the three parameters and the two variables such that the expression

$$U(A, B, C, [Y]_x, [X]_x) = \Sigma(v_{exp} - v_{calc})^2$$

takes a minimum value.

We addressed the problem by first calculating the three parameters A, B and C from solutions of known catalyst and activator concentrations and then optimizing the two variables that yielded the analyte concentrations by a method resembling that of standard additions but involving two components rather than one. The determination could in principle also be performed by simultaneously calculating all five unknowns; however, this procedure yielded poor results.

The problem was resolved mathematically by using two different algorithms in order to compare the results obtained, namely:

—the Gauss–Newton method, which is based on the development of the partial derivative matrix of the function until a minimum condition is met.

—the Simplex method, which requires no prior knowledge of the function relating the different variables to be optimized, so it involves a much larger number of iterations than do differential methods. This is a result of the foundation of the smoothing procedure, yet poses no hindrance thanks to the high computational power of current computers. On the other hand, inasmuch as the optimization procedure is based on a mathematical model, it calls for no additional experimental work, but only for the parameters to be fitted to the model. The Simplex method was applied in its simple unidirectional advance variant, with contraction and no quadratic interpolation.

A more detailed description of the most common optimization procedures is provided elsewhere.[10]

EXPERIMENTAL

*Apparatus and software**

The measuring set-up used consisted of a Metrohm 662 fibre optics photometric detector connected via an RS232C interface to a PC computer for data acquisition and processing by means of the program FIBER, a magnetic stirrer, a reaction cell that was thermostated by means of a cryostat, and a Crison microBur 2031 autoburette furnished with an RS232C interface and controlled by the computer for addition of reagents to the cell.

Kinetic data were acquired by using the program FIBER.[8] Once the solution was homogenized, the program plotted the measured absorbances against time and then calculated the slope of the resulting kinetic curve. The reaction rates obtained on addition of different amounts of Mn(II) or Pb(II) were processed in order to optimize the parameters of the mathematical equation and determine the concentration of the two analytes by using the following programs:[9]

—GKCAL.EXE and GKAD.EXE to optimize parameters and variables, respectively, by the Gauss–Newton method.

—SIMKINCA.EXE and SIMKINAD.EXE to optimize parameters and variables, respectively, by the Simplex method.

Reagents

All reagents used were pro-analysis reagent-grade chemicals and distilled water was employed throughout. The solutions used were as follows:

0.1M Tiron (sodium pyrocatechol-3,5-disulphonate), prepared from the corresponding monohydrate salt (Merck).

0.05M 1,10-phenanthroline, made from its hydrochloride (BDH Chemicals Ltd).

*The software used can be obtianed on request from SCIWARE, Banco de Programas, Departamento de Química, Universidad de las Islas Baleares, E-07071 Palma de Mallorca, Spain.

0.1*M* borax buffer of pH 9.7, made from $Na_2B_4O_7 \cdot 10H_2O$ (Merck).

1000 mg/l. Mn(II) standard, prepared from $MnSO_4 \cdot H_2O$ (Merck).

1000 mg/l. Pb(II) standard, prepared from $Pb(NO_3)_2$ (Panreac).

1.5*M* H_2O_2, made from a 30% solution (Probus) titrated with $KMnO_4$.

Procedure

In a 50-ml standard flask place in the following order: 1 ml of 0.1*M* Tiron, 1 ml of 0.05*M* 1,10-phenanthroline, 10 ml of 0.1*M* borax buffer of pH 9.7, *x* ml of sample containing Mn(II) and Pb(II) in amounts providing concentrations in the ranges 1–5 ng/ml Mn(II) and 200–800 ng/ml Pb(II) on dilution to the mark. Next, pour the solution into a thermostated cell at 20 ± 0.1°. Once the temperature has stabilized, have the autoburette inject 1 ml of 1.5*M* hydrogen peroxide and obtain the corresponding kinetic curve by monitoring the absorbance at 450 nm, which yields the initial slope. The data thus obtained are subsequently processed by the optimization software in order to calculate the concentrations of the two metal ions.

RESULTS AND DISCUSSION

To demonstrate the capacity of the proposed method we have used the catalytic and activating effects of Mn(II) and Pb(II), respectively, on the oxidation of Tiron by hydrogen peroxide.[7] The simultaneous determination of both ions will be addressed by photometric monitoring at 450 nm.

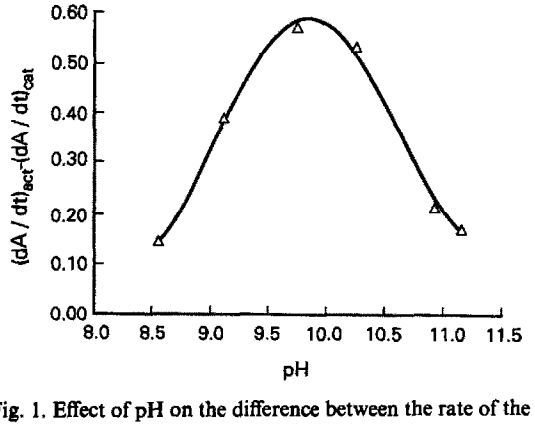

Fig. 1. Effect of pH on the difference between the rate of the activated and catalysed reaction. T = 20°. [Mn(II)] = 10 ng/ml, [Pb(II)] = 1 μg/ml, [1,10-phen] = $10^{-3}M$, [Tiron] = $2 \times 10^{-3}M$, $[H_2O_2] = 0.09M$, λ = 450 nm.

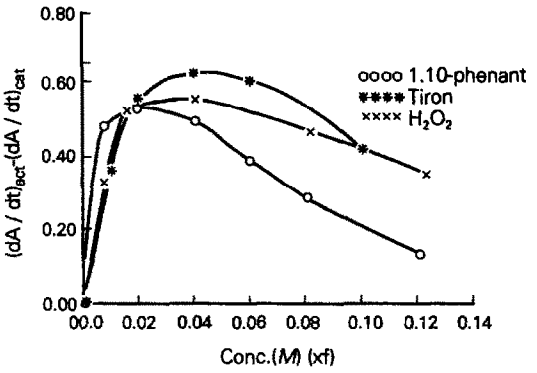

Fig. 2. Effect of the concentrations of 1,10-phenanthroline (f = 40, [Tiron] = $2 \times 10^{-3}M$; $[H_2O_2] = 0.09M$), Tiron (f = 10, [1,10-phen] = $10^{-3}M$; $[H_2O_2] = 0.09M$) and H_2O_2 (f = 1, [1,10-phen] = $10^{-3}M$; [Tiron] = $2 \times 10^{-3}M$) on the difference between the rate of the activated and catalysed reaction. T = 20°, [Mn(II) = 10 ng/ml, [Pb(II)] = 1 μg/ml, pH 9.7, λ = 450 nm.

Optimization of experimental variables

The variation of the rates of the catalysed and activated reaction (dA/dt) as a function of the temperature has been studied over the range 10–30°. Both rates increase with increasing temperature throughout the range studied; however, the increase is more gradual between 10 and 20°, the latter of which was chosen for subsequent experiments on account of its ready achievement in the laboratory environment.

Reactant concentrations and the reaction medium were optimized for the greatest difference in absorbance between the catalysed and activated reaction. Thus, the influence of pH was studied by using borax buffers of pH between 8.5 and 11.2. As can be seen in Fig. 1, the maximum difference between the two signals was obtained at pH 9.7.

Figure 2 shows the differences between the rates of the catalysed and activated reaction obtained at various 1,10-phenanthroline, Tiron and hydrogen peroxide concentrations, the optimal values of which were found to be 10^{-3}, 2×10^{-3} and 0.03*M*, respectively.

Once the optimal working conditions had been established, the linear determination range for each element in the presence of the other was calculated. The results obtained showed the slope of the kinetic curves to be linearly related to the catalyst concentration over the range 1–5 ng/ml Mn(II) in the presence of activator concentrations between 200–800 ng/ml Pb(II). Over these linear ranges, the theoretical equation can be applied.

Table 1. Results obtained in the simultaneous determination of Mn(II) and Pb(II) by the proposed method in synthetic mixtures

Sample	Added, ng/ml Mn(II)	Added, ng/ml Pb(II)	Gauss–Newton, ng/ml Mn(II)	Gauss–Newton, ng/ml Pb(II)	Simplex, ng/ml Mn(II)	Simplex, ng/ml Pb(II)
1	1.0	400	1.00	397	1.00	398
2	3.0	500	2.97	500	2.98	498
3	2.5	300	2.55	294	2.51	307

Simultaneous determination of Mn(II) and Pb(II)

The proposed method was applied to the determination of the two metal ions in several synthetic mixtures containing Mn(II) and Pb(II) concentrations in the linear ranges. The results obtained are summarized in Table 1. As can be seen, the results obtained are quite consistent with the reference concentrations.

Next, as an example, we develop the mathematical treatment for the first mixture.

Gauss–Newton method

Table 2 lists the contents of the results file used for the calculation of the parameters relating the rates of reaction involved in the photometric method with the concentrations of catalyst and activator by using standard mixtures.

Once A, B and C (-0.268, 0.900 and 0.136) were determined, the data file was used to obtain the Mn(II) and Pb(II) concentrations in the first mixture of Table 1. From this in turn the result file was obtained (Table 3). Then, by using the same parameter values, the second and third mixtures of Table 1 were resolved in the same way.

Table 2. Results file used for the obtainment of the parameters of the calibration curve for the simultaneous determination of the catalyst and activator by the Gauss–Newton and Simplex methods

[Mn(II)], ng/ml	[Pb(II)], μg/ml (×10)	$(\tan\alpha)_{exp}$ (×100)	$(\tan\alpha)_{calc}$ (×100)	Difference
1.000	8.000	1.700	1.717	−0.017
2.000	8.000	3.800	3.702	0.098
3.000	8.000	5.600	5.687	−0.087
4.000	8.000	7.800	7.672	0.128
5.000	8.000	9.500	9.657	−0.157
1.000	4.000	1.140	1.175	−0.035
3.000	4.000	4.000	4.060	−0.060
4.000	4.000	5.400	5.503	−0.103
5.000	4.000	7.000	6.945	0.055
2.000	6.000	3.100	3.160	−0.060
3.000	6.000	5.000	4.874	0.126
4.000	6.000	6.700	6.587	0.113

	Gauss–Newton method	Simplex method
A	−0.26756	−0.26756
B	0.90034	0.90034
C	0.13557	0.13557
Error	2.6865×10^{-8}	0.10908
No. of iterations	2	200
RMS	9.5342×10^{-2}	9.5342×10^{-2}

Number of parameters, variables and points = 3, 2 and 12.

Table 3. Results file used for the simultaneous determination of the catalyst activator concentrations by the Gauss–Newton and Simplex methods

Experiment	$(\tan\alpha)_{exp}$ (×100)	$(\tan\alpha)_{calc}$ (×100) Gauss	$(\tan\alpha)_{calc}$ (×100) Simplex	Difference Gauss	Difference Simplex
1	1.140	1.177	1.179	−0.037	−0.039
2	4.000	4.058	4.060	−0.058	−0.060
3	5.400	5.498	5.501	−0.098	−0.101
4	7.000	6.938	6.941	0.062	0.059
5	3.100	3.162	3.163	−0.062	−0.063
6	5.000	4.875	4.875	0.125	0.125
7	6.700	6.587	6.587	0.113	0.113
8	1.700	1.723	1.724	−0.023	−0.024
9	3.800	3.707	3.707	0.093	0.093
10	5.600	5.691	5.690	−0.091	−0.090
11	7.800	7.676	7.672	0.124	0.128
12	9.500	9.660	9.655	−0.160	−0.155

	Gauss–Newton method	Simplex method
No. iterations	4	200
Error	9.6259×10^{-4}	0.1089
RMS	9.5241×10^{-2}	9.52845×10^{-2}
[Mn(II)](ng/ml)	1.003	1.004
[Pb(II)](μg/ml × 10)	3.972	3.984

Number of parameters, variables and points = 2, 2 and 12.
A, B and $C = -0.268$, 0.900 and 0.136.

Simplex method

Table 2 lists the content of the results file used for the determination of parameters *A*, *B* and *C*, which were found to be −0.268, 0.900 and 0.136, respectively, *i.e.*, identical to those obtained by the Gauss–Newton method.

These values were subsequently used to construct the data entry file for calculation of the Mn(II) and Pb(II) concentrations. After a smoothing process the results given in Table 3 were obtained. As can be seen, the catalyst and activator concentrations found were virtually identical to those provided by the Gauss–Newton method.

Selectivity

A study of potential interferents revealed Cr(III) to pose the most serious problems; in fact, this ion resulted in an increase in the reaction rate at concentrations above 10 ng/ml in the presence of 3 ng/ml Mn(II) and 800 ng/ml Pb(II). Iron(III) was found to interfere at concentrations above 200 ng/ml, while the effect of Mg(II), Zn(II) and Co(II) was only felt above 400 ng/ml. On the other hand, such metals as Cu(II), Ca(II), Al(III), Ni(II) and Cd(II) only interfered at concentrations over 600 times higher that of Mn(II). None of the commoner anions (chloride, nitrate, sulphate and phosphate) had any appreciable effect on the reaction rate at concentrations up to 100 μg/ml.

CONCLUSIONS

The proposed kinetic method based on experimental data obtained by multiple standard–additions proved to be a useful alternative for the simultaneous determination of catalysts and activators.

The approach is potentially applicable to other chemical systems for the determination of catalyst–activator and catalyst–inhibitor pairs on the basis of a virtually identical theoretical foundation.

Acknowledgement—The authors are grateful to the DGICyT (Spanish Council for Research in Science and Technology) for financial support granted through Project PB 90-0359.

REFERENCES

1. H. A. Mottola and G. L. Heath, *Anal. Chem.*, 1972, **44**, 2322.
2. K. B. Yatsimirskii, E. E. Kriss and G. T. Kurbatova, *Zh. Analit. Khim.*, 1976, **31**, 598.
3. A. Moreno, M. Silva, D. Pérez-Bendito and M. Valcárcel, *Analyst*, 1983, **108**, 85.
4. A. Marín, M. Silva and D. Pérez-Bendito, *Anal. Chim. Acta*, 1987, **197**, 77.
5. D. Pérez-Bendito and M. Silva, *Kinetic Methods in Analytical Chemistry*, Ch. 3, Ellis Horwood, Chichester, 1988.
6. S. P. Klochkovskii and G. D. Klochkovskaya, *Zh. Analit. Khim.*, 1978, **33**, 1749.
7. E. Gómez, J. M. Estela and V. Cerdà, *J. Thermal Anal.*, 1991, **37**, 195.
8. A. Cladera, A. Caro, E. Gómez, J. M. Estela and V. Cerdà, *J. Anal. Chem.*, 1992, **342**, 322.
9. E. Gómez, J. M. Estela and V. Cerdà, *Anal. Chim. Acta*, 1991, **251**, 305.
10. J. Cerdà and V. Cerdà, *Quimiometría*, M. Blanco and V. Cerdà (eds.), Barcelona, 1988.

Talanta, Vol. 39, No. 8, pp. 893–898, 1992
Printed in Great Britain.

0039-9140/92 $5.00 + 0.00

ADSORPTION MECHANISM OF POLYLYSINE ON HYDROXYAPATITE AND ITS EFFECT ON DISSOLUTION PROPERTIES OF HYDROXYAPATITE

HIDEJI TANAKA,* YOUKO NUNO, SHINOBU IRIE and SHIGERU SHIMOMURA

Laboratory of Pharmaceutical Analytical Chemistry, Faculty of Pharmaceutical Sciences, The University of Tokushima, Sho-machi 1-78-1, Tokushima 770, Japan

(*Received* 20 *September* 1991. *Revised* 13 *December* 1991. *Accepted* 14 *December* 1991)

Summary—Adsorbed amounts of poly-L-lysine (pLys) and bromide ion on hydroxyapatite (HAp) from aqueous solutions of poly-L-lysine hydrobromide, and amounts of calcium and phosphate ions liberated concurrently from HAp during the adsorption of pLys were determined at 25°. The pLys was adsorbed on HAp by the mechanism of ion-exchange between its amino groups and calcium ions of HAp. The released amount of calcium ion increased, therefore, with the adsorbed amount of pLys. On the other hand, the released amount of phosphate ion first decreased and then increased after attaining a minimum with the equilibrium concentration of pLys. The analysis using an equilibrium dialysis method revealed that the released phosphate ions were mainly in the bound state to the amino groups of pLys remaining in the solution, and that the concentrations of calcium and phosphate ions free from both HAp and pLys were restricted by each other under the law of the solubility product of HAp. The first decrease in the released amount of phosphate ion was concluded to be attributed primarily to the increase in the released amount of calcium ion because pLys remaining in the solution was little in this region. When sodium hydroxide was added to the solution, the adsorbed amount of pLys increased and then slightly decreased with the equilibrium pH of the solution due to the increase or decrease of the electrostatic attractive force between the adsorbate and the adsorbent. However, conformational change in pLys around pH 10 seemed to have little effect on the adsorption.

Hydroxyapatite (HAp), a basic calcium phosphate which has the chemical formula $Ca_{10}(PO_4)_6(OH)_2$, is the most stable phase of calcium phosphates under ordinary conditions.[1,2] This has been widely used for chromatographic separations of proteins, nucleic acids, enzymes, and so on, since Tiselius *et al.* introduced it as a packing material for liquid chromatography in 1950's.[3] Today, many commercial HAp-columns for high performance liquid chromatography are on the market.

In the studies on HAp-column chromatography, the factors governing interactions between proteins and HAp have been investigated, and some mechanisms, such as specific or non-specific complex formation between functional groups of protein and calcium or phosphate ions of HAp and as ion-exchange between the groups and the ions, were proposed.[4–7] However, detailed mechanism of the adsorption is still unknown because complexity of conformation and diversity of side chains of proteins make the elucidation of the mechanism difficult.

On the other hand, HAp is known to dissolve slightly in aqueous media. This behaviour is complicated and, in spite of many studies,[8–12] not elucidated entirely, mainly because HAp exists in the form of very small crystallites and its physicochemical properties depend on the surface state.[13] The dissolution properties of HAp seem important in connection with the durability of HAp-columns.

Poly-L-lysine (pLys) is a typical homopolypeptide, the molecular structure of which has been studied extensively. In the present study, the interactions between pLys and HAp are investigated by using an equilibrium dialysis technique. The adsorbed amount of pLys on HAp and the amounts of calcium and phosphate ions liberated from HAp are determined, and the results are discussed taking into account ion-exchange between calcium ions of HAp and amino groups of adsorbed pLys, binding of phosphate ions to the groups of pLys in solution, and the solubility product of HAp.

*Author for correspondence.

EXPERIMENTAL

Reagents

Hydroxyapatite was synthesized according to the method of Avnimelech *et al.*[14] The calcium/phosphorus ratio was 10.38/6, and the point of zero charge (PZC) determined by pH titration was 6.70. The specific surface area determined by the BET procedure at 77 K with nitrogen gas as an adsorbate was 29.0 m^2/g. Poly-L-lysine hydrobromide (pLysHBr) was purchased from Sigma Chemical Co., and its viscosity average molecular weight assessed by the supplier was 21,500. The standardization of a stock solution of the pLysHBr was performed by the colloidal titration method[15] for amino group of pLys, using a standard solution of potassium polyvinyl sulphate (Wako Pure Chemical Industries, Ltd.) with Toluidine Blue indicator, and by the mercuric thiocyanate method[16,17] for bromide ion. Water was demineralized with a Milli-QSP water purification system (Millipore Co.).

Apparatus

A Nippon Jarrel-Ash ICAP-750N multichannel inductively coupled plasma atomic emission spectrometer was used. The nebulizer used was a conventional cross-flow type and argon gas flow-rates were 0.5 (carrier), 0.6 (auxiliary) and 16 (coolant) l l./min. A Hitachi 330 spectrophotometer, Hitachi 650 spectrofluorometer, Jasco J-600 spectropolarimeter and Horiba F-11 pH meter were also used for the analyses described below.

Procedure

The adsorption experiment was carried out by suspending HAp (1 g) to aqueous solutions of pLysHBr (50 ml) at 25° for 5 days. After filtration with a Millipore filter with a pore size of 0.1 μm, the filtrates were analysed.

The dialysis experiment was carried out as follows: HAp (0.6 g) was suspended in pLysHBr solutions (30 ml). A dialysis bag (Visking Company, type 36/32) containing water (20 ml) was immersed in each suspension. After 5 days, the dialysis bags were taken out and the concentrations of the ions in the inner solutions were determined. The suspensions remaining in the vessels were filtered through the Millipore filters, and the filtrates were analysed.

The concentration of pLys was determined by fluorometry at 475 nm with excitation at 335 nm, using *o*-phthalaldehyde and 2-mercaptoethanol according to the method of Roch.[18] The reaction was performed at pH 9.0 by using sodium dihydrogen phosphate–potassium hydroxide buffer. Hereafter, the concentration of pLys is given in terms of molarity of the lysine residue of pLys. The concentration of bromide ion was determined by spectrophotometry at 458 nm, using mercuric thiocyanate and ferric nitrate.[16,17]

The concentrations of calcium and phosphate species in solution were determined by inductively coupled plasma atomic emission spectrometry (ICP–AES) at 393.4 and 214.9 nm, respectively. Working standards were prepared from 1,000 mg/l. standards (Kanto Chemical Co.) by mixing and diluting them with 1% nitric acid. It was confirmed that pLys up to 5m*M* does not interfere with the determination. For the determination of phosphate in the solutions inside the dialysis bags, where the phosphate level was very low (around 0.01m*M*) and pLys was absent, spectrometry at 720 nm using ammonium molybdate and stannous chloride[19] was adopted instead of ICP–AES.

Circular dichroism (CD) spectra of the pLys solutions in the range of 200–250 nm were measured at various pH values on the spectropolarimeter. Solutions of pLys in the three forms (*i.e.*, random coil, α-helix and β-sheet) were prepared according to the method of Greenfield *et al.*[20,21]

RESULTS AND DISCUSSION

Adsorption of pLys on HAp and concurrent release of calcium and phosphate ions from HAp

The adsorbed amounts of pLys and bromide ion (X_{pLys} and X_{Br}) on HAp from aqueous solutions of pLysHBr are shown in Fig. 1 as a function of the equilibrium concentration of pLys (C_{pLys}), where both amounts increased with C_{pLys}, and X_{pLys} was larger than X_{Br}.

It was found that calcium and phosphate ions were released from HAp incongruently (non-constant in the calcium/phosphorus ratio) during the adsorption of pLys on HAp. The equilibrium concentrations of calcium and phosphate ions in the solutions were plotted against C_{pLys} in Fig. 2(a). The equilibrium concentration of calcium ion (C_{Ca}) increased and that of phosphate ion (C_{Pi}) decreased with C_{pLys}. However, the latter increased after attaining a minimum when C_{pLys} became high. Figure 2(b) shows the relationship between the

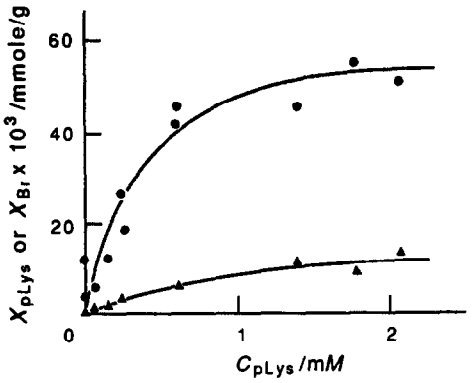

Fig. 1. Adsorbed amounts of pLys and bromide ion on HAp from aqueous solutions of pLysHBr as a function of equilibrium concentration of pLys. No buffering solutions were used in order to avoid the effect of buffering agents on the properties of the adsorbate and the adsorbent. The closed circles and closed triangles correspond to X_{pLys} and X_{Br}, respectively.

Table 1. Equilibrium values (solution volume, concentrations and pH) in adsorption and dissolution experiment with an equilibrium dialysis technique [mean ($n = 4$) ± S.D.]. Initial concentrations: (A) pLys 2.31, Br^- 1.98 m*M*; (B) pLys 3.08, Br^- 2.64 m*M*

	Inside	Outside
(A)		
Equilibrium volume, *ml*	18.7 ± 0.6	31.3 ± 0.6
C_{pLys}		0.155 ± 0.046
C_{Br}	1.01 ± 0.08	1.18 ± 0.02
C_{Ca}	0.354 ± 0.010	0.268 ± 0.120
C_{Pi}	0.0196 ± 0.0099	0.101 ± 0.033
(pH)	6.21 ± 0.05	6.43 ± 0.11
(B)		
Equilibrium volume, *ml*	17.9 ± 1.7	32.1 ± 1.7
C_{pLys}		0.522 ± 0.111
C_{Br}	1.27 ± 0.23	1.62 ± 0.20
C_{Ca}	0.398 ± 0.009	0.301 ± 0.017
C_{Pi}	0.0111 ± 0.0034	0.119 ± 0.006
(pH)	6.44 ± 0.16	6.48 ± 0.05

Concentrations in m*M*.

equilibrium pH of the solutions and C_{pLys}, where the pH had the similar tendency to C_{Pi}.

Migration of released ions through dialyzing membrane

From the outer suspension in contact with the dialysis bag containing water, some of the bromide ions (added as pLysHBr) and some of the calcium and phosphate ions (released from HAp) migrated into the inside of the bag to reach membrane equilibrium. The equilibrium values of the dialysis experiment are listed in Table 1; initial concentration of pLys was 2.31 (A) or 3.08 m*M* (B). The concentrations of anionic species in the outer solution were higher than those in the inner solution, whereas the concentration of calcium ion in the outer solution were lower than that in the inner solution. Equilibrium pH of the outer solution was higher than that of the inner solution.

Effect of pH on adsorption of pLys on HAp

Figure 3(A) shows the adsorbed amounts of pLys and bromide ion on HAp as a function of the equilibrium pH. Initial concentration of pLys was kept constant at 2.89 m*M* and pH was adjusted by addition of sodium hydroxide. The X_{pLys} (closed circles) increased with the pH and then decreased slightly after attaining a

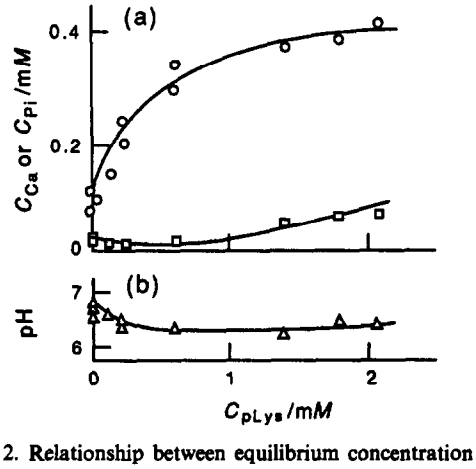

Fig. 2. Relationship between equilibrium concentration of pLys and concentrations of calcium and phosphate ions released from HAp (a), and equilibrium pH of solution (b). The experimental condition was the same as that in Fig. 1. The open circles and open squares correspond to C_{Ca} and C_{Pi}, respectively.

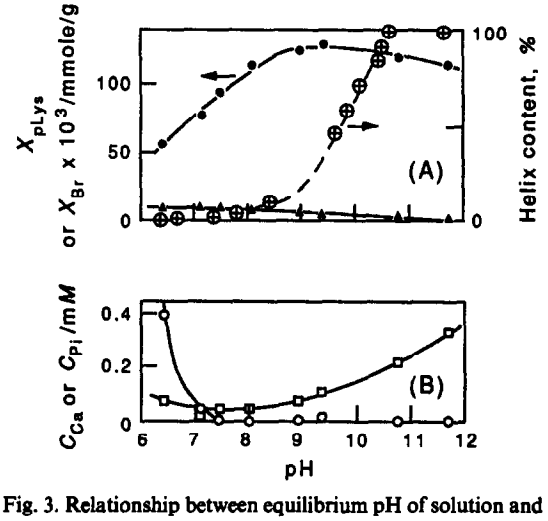

Fig. 3. Relationship between equilibrium pH of solution and adsorbed amounts of pLys and bromide ion on HAp (A), and equilibrium concentrations of calcium and phosphate ions released from HAp (B). All the symbols are the same as those in Figs. 1 and 2. The dotted line on ⊕ in Fig. 3(A) shows the helix content (%) in pLys.

maximum around pH 9.5. On the other hand, X_{Br} (closed triangles) was low and decreased monotonously with the pH. Figure 3(B) shows the equilibrium concentrations of calcium and phosphate ions (C_{Ca} and C_{Pi}) as a function of the equilibrium pH. It shows that C_{Ca} decreased monotonously, and C_{Pi} increased after attaining a minimum with the pH. This dissolution property of HAp in basic media was discussed before.[22]

In aqueous solution of calcium phosphates, the chemical species of Ca^{2+}, PO_4^{3-}, HPO_4^{2-}, $H_2PO_4^-$, H_3PO_4, $CaHPO_4$ and $CaH_2PO_4^+$ are formed through protonation of phosphate ion and through complex formation between calcium and phosphate ions.[23] Moreover, in the presence of pLys, a part of anionic species of phosphate is considered to be bound to amino groups of pLys. The concentration of calcium species determined by the ICP–AES is, therefore, the sum of the concentrations of Ca^{2+}, $CaHPO_4$ and $CaH_2PO_4^+$; the concentration of phosphate species determined simultaneously is the sum of the concentrations of PO_4^{3-}, HPO_4^{2-}, $H_2PO_4^-$, H_3PO_4, $CaHPO_4$, $CaH_2PO_4^+$ and phosphate which is bound to pLys in solution.

The concentrations and activities of chemical species in the solutions inside the dialysis bags can be calculated from the data shown in Table 1 using the first, second and third dissociation constants of phosphoric acid (K_1, K_2 and K_3, respectively) and the formation constants of $CaHPO_4$ and $CaH_2PO_4^+$ (K_x and K_y, respectively).[24] The obtained values were listed in the middle part of Table 2, where brackets and parentheses mean concentration and activity, respectively. The numerical values used were as follows: K_1 7.08×10^{-3}, K_2 6.31×10^{-8}, K_3 4.17×10^{-13},[25] K_x 244 and K_y 8.20.[24] The activity coefficient for each ion (γ) was calculated through the Debye–Hückel equation;

$$\log\gamma = -Az^2I^{\frac{1}{2}}/(1 + Ba^\circ I^{\frac{1}{2}}) \qquad (1)$$

where z is the valency of the ion, I is the ionic strength of the medium, A and B are constants ($A = 0.515$ and $B = 0.329$ at 25° for aqueous solution),[26] and a° is an ion size parameter (H^+ 9, OH^- 3.5, $H_2PO_4^-$ 4.25, HPO_4^{2-} 4, PO_4^{3-} 4, Ca^{2+} 6, Br^- 3 and $CaH_2PO_4^+$ 4.25).[27] The values of $-\log(Ca^{2+})^{10}(PO_4^{3-})^6(OH^-)^2$ were found to be 122.1 and 120.1 for initial concentrations of pLys of 2.31 and 3.08 mM, respectively. These values were in agreement with the literature values of the solubility product (K_{sp}) of HAp (108–125).[28] This result means that the concentrations of calcium and phosphate ions in the inner solutions were limited by each other under the law of the K_{sp} of HAp.

Table 2. Equilibrium values in solutions inside and outside dialysis bag calculated from data listed in Table 1. The symbol Y means the amount of phosphate or bromide ion which is bound to pLys in the solution per lysine residue of pLys: $Y_{Pi} = [Pi]_b^\circ/C_{pLys}$, $Y_{Br} = [Br^-]_b^\circ/C_{pLys}$. Initial concentrations: (A) pLys 2.31, Br^- 1.98 mM; (B) pLys 3.08, Br^- 2.64 mM

	(A)	(B)
$X_{pLys} \times 10^3$, mmole/g	108	126
$X_{Br} \times 10^3$, mmole/g	6.32	7.64
$[H_3PO_4]^i$	1.46×10^{-6}	4.48×10^{-7}
$[H_2PO_4^-]^i$	1.74×10^{-2}	9.13×10^{-2}
$[HPO_4^{2-}]^i$	2.02×10^{-3}	1.82×10^{-3}
$[PO_4^{3-}]^i$	1.68×10^{-9}	2.62×10^{-9}
$[Ca^{2+}]^i$	3.54×10^{-1}	3.98×10^{-1}
$[CaHPO_4]^i$	1.25×10^{-4}	1.23×10^{-4}
$[CaH_2PO_4^+]^i$	4.28×10^{-5}	2.49×10^{-5}
$[H^+]^i$	6.43×10^{-4}	3.80×10^{-4}
$[OH^-]^i$	2.48×10^{-5}	4.23×10^{-5}
$-\log(Ca^{2+})^{10}(PO_4^{3-})^6(OH^-)^2$	122.1	120.1
$[Pi]_f^\circ$	0.0228	0.0130
$[Pi]_b^\circ$	0.0782	0.106
$[Br^-]_f^\circ$	1.16	1.46
$[Br^-]_b^\circ$	0.02	0.16
Y_{Pi}	0.505	0.203
Y_{Br}	0.129	0.307

Concentrations in mM.

When membrane equilibrium is attained, the K_{sp} of HAp are equal on both sides of the membrane, under the assumption that the standard chemical potential of HAp on both sides of the membrane are the same. Therefore, even in the outer solutions containing pLys, the activities of calcium and phosphate ions were mutually restricted under the law of the K_{sp} of HAp. It was concluded that the released phosphate ions in the outer solution exist mainly in the bound state to the amino groups of pLys in the solution. On the other hand, adsorbed pLys expels calcium ion from HAp through the ion-exchange between positively charged amino groups of pLys and calcium ions of HAp to keep electroneutrality of the surface phase. The concomitant increase of C_{Ca} and C_{Pi} shown in Fig. 2(A) were attributed to these facts. The tendency of C_{Pi} to decrease with an increase in C_{Ca} was observed only in the region of low C_{pLys}, where the amount of phosphate ions which were bound to pLys in the solution phase was little.

Taking the Donnan's membrane equilibrium into account, the concentrations of anions, *i.e.*, phosphate and bromide ions, free from both pLys and HAp in the outer solution ($[Pi]_f^\circ$ and $[Br^-]_f^\circ$) can be evaluated from the

following equations;

$$[Pi]_f^o = [H_3PO_4]_f^o + [H_2PO_4^-]_f^o + [HPO_4^{2-}]_f^o + [PO_4^{3-}]_f^o + [CaHPO_4]_f^o + [CaH_2PO_4^+]_f^o \quad (2)$$

$$= [H_3PO_4]^i + [([H_2PO_4^-]^i)^2[Ca^{2+}]^i/[Ca^{2+}]^o]^{\frac{1}{2}} + [HPO_4^{2-}]^i[Ca^{2+}]^i/[Ca^{2+}]^o + [([PO_4^{3-}]^i)^2([Ca^{2+}]^i)^3/([Ca^{2+}]^o)^3]^{\frac{1}{2}} + [CaHPO_4]^i + [CaH_2PO_4^+]^i[H^+]^o/[H^+]^i \quad (2')$$

and

$$[Br^-]_f^o = [([Br^-]^i)^2[Ca^{2+}]^i/[Ca^{2+}]^o]^{\frac{1}{2}} \quad (3)$$

where the subscript "f" means "free", and the superscripts "i" and "o" mean "inside" and "outside", respectively. It was assumed that the activity coefficients for uni- and bivalent ions and the concentrations of neutral species, *i.e.*, H_3PO_4 and $CaHPO_4$, were equal on both sides of the dialysis membrane, and that the cationic species did not interact with pLys. Accordingly, the concentrations of phosphate and bromide ions which were bound to pLys in the outer solution are obtained;

$$[Pi]_b^o = C_{Pi}^o - [Pi]_f^o \quad (4)$$

and

$$[Br^-]_b^o = C_{Br}^o - [Br^-]_f^o \quad (5)$$

The calculated values were listed in the bottom part of Table 2. It shows that phosphate ions in the outer solution exist mostly in the bound state as presumed above.

When the solution pH becomes higher than the PZC of HAp (6.7), the electrostatic attraction between the cationic pLys and the negatively charged HAp surface increases. Thus, X_{pLys} increased with the pH. However, when the pH further increases, pLys comes to lose its positive charges and the conformational change between random coil (at lower pH) and α-helix (at higher pH) occurs in pLys. The dotted line in Fig. 3(A) shows the helix content, estimated from the CD-spectra of the pLys solutions according to the procedure of Greenfield *et al.*[21] It shows that the helix content increased sharply in the range of pH 9–11. However, no pronounced change in X_{pLys} was observed in this region. It was concluded, therefore, that the conformational change of pLys in this region does not give a significant effect on the adsorption of pLys.

In general, as for the adsorption of highly solvated polymers on an impenetrable surface, a fraction of the molecules is actually attached to the sorbent surface, and the remainder dangles in solution.[29] Therefore, the following model explaining the phenomena found in the present study was considered as shown in Fig. 4. A fraction of adsorbed pLys which was actually attached to HAp (c) released calcium ions from HAp (d) by the mechanism of ion-exchange. Co-adsorbed bromide ions were captured by the amino groups of the remaining fraction of adsorbed pLys (b), because the affinity of bromide ion to HAp is very low.[30] In addition to the ion-exchange mechanism, calcium ions were released from HAp through the dissolution of HAp (e). On the other hand, phosphate ions were released only through the dissolution (e). Most of these phosphate ions protonated (g) and/or were bound to pLys in the solution phase (i). Some released phosphate ions formed complexes with calcium ions (h). The dissolution of HAp and the protonation of phosphate ions (g) increased the concentration of hydroxide ion in solution (e) and (f). The similar tendency between the shape of curves of C_{Pi} and (pH) in

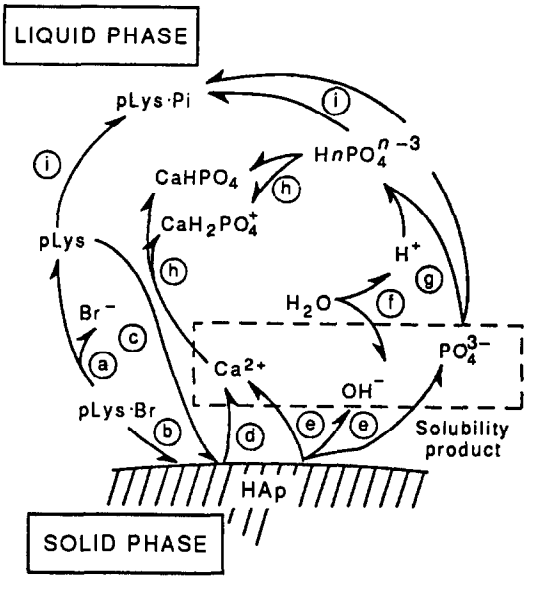

Fig. 4. Scheme of interactions occurring between pLysHBr and HAp. (a) Liberation of bromide ion from pLys, (b) co-adsorption of pLys and bromide ion on HAp, (c) ion-exchange adsorption of pLys on HAp, (d) release of calcium ion through ion-exchange with adsorbed pLys, (e) dissolution of HAp, (f) dissociation of water, (g) protonation of phosphate ion, (h) complex formation between calcium and phosphate ions, (i) counterion binding of phosphate to pLys. For simplicity, arrows are expressed only for the direction of mass transfer or reaction mainly occurs in the course of adsorption of pLys on HAp.

Fig. 2 is attributed to this fact. The concentrations of Ca^{2+}, OH^- and PO_4^{3-} were limited by each other under the restriction of the K_{sp} of HAp (enclosed with the dotted line). Therefore, the release of phosphate ions through the dissolution of HAp (e) was suppressed by the excess release of calcium ions through the ion-exchange (d) when the equilibrium concentration of pLys in solution was low. These facts were responsible for the marked incongruent dissolution properties of HAp in the presence of pLys.

It is known that the constituent ions of HAp having the same sign of electric charge as that of the adsorbed polymeric ions are released from HAp during their adsorption.[31,32] On the other hand, little attention is paid to the behaviour of the constituent ions having a counter-charge to the adsorbate. One of the exceptions is a report of Juriaanse *et al.*[33] They found that not only calcium ions but also phosphate ions were released from HAp in the presence of pLys and poly-L-ornithine; not only phosphate ions but also calcium ions were released in the presence of poly-L-asparaginate. Although they did not refer to it, initial decrease in the released amount of the counter-charge ions, such as that shown in Fig. 2(a), was seen in their reported data. These facts suggest that the dissolution tendency of HAp found in the present study is not specific for the case of adsorption of pLys but is common to those of other cationic peptides, and that the behaviour of phosphate and calcium ions changed place with each other according to the sign of the electric charge of the adsorbed polymeric ions. The results obtained in the present study are, therefore, important as a basis for understanding the interaction between charged polymers and HAp.

REFERENCES

1. T. P. Feenstra and P. L. de Bruyn, *J. Phys. Chem.*, 1979, **83**, 475.
2. M. J. J. M. van Kemenade and P. L. de Bruyn, *J. Colloid Interface Sci.*, 1987, **118**, 564.
3. A. Tiselius, S. Hjertén and Ö. Levin, *Arch. Biochem. Biophys.*, 1956, **65**, 132.
4. M. J. Gorbunoff, *Anal. Biochem.*, 1986, **136**, 425.
5. *Idem, ibid.*, 1986, **136**, 433.
6. *Idem, ibid.*, 1986, **136**, 440.
7. K. Makino and B. H. Kim, *J. Chromatographic Sci.*, 1989, **27**, 659.
8. G. J. Levinskas and W. F. Neuman, *J. Phys. Chem.*, 1955, **59**, 164.
9. H. M. Rootare, V. R. Deitz and F. G. Carpenter, *J. Colloid Sci.*, 1964, **17**, 179.
10. V. R. Deitz, H. M. Rootare and F. G. Carpenter, *ibid.*, 1964, **19**, 87.
11. A. N. Smith, A. M. Posner and J. P. Quirk, *J. Colloid Interface Sci.*, 1974, **48**, 442.
12. W. F. Kaufman and I. Kleinberg, *Calcif. Tissue Int.*, 1979, **27**, 143.
13. S. Chander and D. W. Fuerstenau, *J. Colloid Interface Sci.*, 1979, **70**, 506.
14. Y. Avnimelech, E. C. Moreno and W. E. Brown, *J. Res. Nat. Bur. Stand., Sect. A*, 1973, **77**, 149.
15. R. Senju, *Koroido Tekitei-hou (Colloidal Titration Method)*, Nankodo, Tokyo, 1976.
16. The Chemical Society of Japan (ed.), *Shin Jikken Kagaku Koza*, Vol. 9, p. 250. Maruzen, Tokyo, 1976.
17. A. Tomonari, *Nippon Kagaku Zasshi*, 1952, **83**, 693.
18. M. Roch, *Anal. Chem.*, 1973, **43**, 149.
19. A. Gee, L. P. Domingues and V. R. Deitz, *ibid.*, 1954, **26**, 1487.
20. N. Greenfield, B. Davidson and G. D. Fasman, *Biochemistry*, 1967, **6**, 1630.
21. N. Greenfield and G. D. Fasman, *ibid.*, 1969, **8**, 4108.
22. H. Tanaka, K. Miyajima, M. Nakagaki and S. Shimabayashi, *Chem. Pharm. Bull.*, 1989, **37**, 2897.
23. A. Chugtai, R. Marshall and G. H. Nancollas, *J. Phys. Chem.*, 1968, **72**, 208.
24. E. C. Moreno, T. M. Gregory and W. E. Brown, *J. Res. Nat. Bur. Stand., Sect A*, 1968, **72**, 773.
25. The Chemical Society of Japan (ed.), *Kagaku Binran Kiso-hen*, 2nd ed., p. 994. Maruzen, Tokyo, 1975.
26. R. A. Robinson and R. H. Stokes, *Electrolyte Solutions*, p. 458. Butterworths, London, 1968.
27. J. Kielland, *J. Am. Chem. Soc.*, 1937, **59**, 1675.
28. S. Chander and D. W. Fuerstenau, *Adsorption on and Surface Chemistry of Hydroxyapatite*, D. W. Misra (ed.), p. 31. Plenum Press, New York, 1984.
29. W. Norde, *Adv. Colloid Interface Sci.*, 1986, **25**, 267.
30. S. Shimabayashi, H. Tanaka and M. Nakagaki, *Chem. Pharm. Bull.*, 1987, **35**, 4687.
31. J. V. Garbacia-Ramos, P. Carmona and A. Hidalgo, *J. Colloid Interface Sci.*, 1981, **83**, 479.
32. H. R. Rawls and I. Cabasso, *Adsorption on and Surface Chemistry of Hydroxyapatite*, D. W. Misra (ed.), p. 115. Plenum Press, New York, 1984.
33. A. C. Juriaanse, J. Arends and J. J. T. Bosch, *J. Colloid Interface Sci.*, 1980, **76**, 220.

Talanta, Vol. 39, No. 8, pp. 899–906, 1992
Printed in Great Britain.

0039-9140/92 $5.00 + 0.00

DIFFERENTIAL PULSE POLAROGRAPHIC STUDY OF THE HYDROLYSIS OF ENDOSULFAN AND ENDOSULFAN SULPHATE IN EMULSIFIED MEDIUM. APPLICATION TO THE DETERMINATION OF BINARY MIXTURES OF ORGANOCHLORINE PESTICIDES

A. J. Reviejo, J. M. Pingarron* and L. M. Polo

Department of Analytical Chemistry, Faculty of Chemistry, Complutense University of Madrid, 28040 Madrid, Spain

(*Received* 4 *November* 1991. *Revised* 19 *December* 1991. *Accepted* 3 *January* 1992)

Summary—Hydrolysis reactions of endosulfan and endosulfan sulphate in the emulsified medium formed with ethyl acetate and a mixture of the two surfactants Hyamine 2389 and Triton X-405 are studied by differential pulse polarography. Besides the heptachlor–endosulfan sulphate pair, whose peak potentials are sufficiently different at pH 8.0 to allow their simultaneous determination, the organochlorine pesticide binary mixtures endosulfan–endosulfan sulphate, dieldrin–endosulfan and dieldrin–endosulfan sulphate can be determined based on their hydrolysis reactions in basic medium and on their different reaction rates. The endosulfan–endosulfan sulphate pair can be determined by allowing the mixture to hydrolyse at pH 11.0 and measuring the endosulfandiol peak for the determination of endosulfan. The analysis of the mixture dieldrin–endosulfan is based on endosulfan hydrolysis at pH 12.0 in which dieldrin is not hydrolysed. Dieldrin and endosulfan sulphate can also be determined simultaneously in a 0.5*M* sodium hydroxide medium. When determining one pesticide in binary mixtures containing a $5.0 \times 10^{-6}M$ concentration of the other pesticide, the lower limits of the calibrations obtained were: endosulfan–endosulfan sulphate mixture, 4.0×10^{-6} and $1.0 \times 10^{-6}M$ respectively; heptachlor–endosulfan sulphate mixture, $2.0 \times 10^{-6}M$ for endosulfan sulphate; all other cases, $3.0 \times 10^{-6}M$.

The importance of organochlorine pesticides from a toxicological point of view is well established due to their bioaccumulative ability. These pesticides as well as their degradation products have been detected in foodstuffs, waters and soils.[1]

Further, electroanalysis in oil/water emulsified media has proved to be a useful technique because of the predominantly aqueous nature of these media, which offers some practical advantages.[2–5] Recently, we performed[6] a polarographic study of the cyclodiene organochlorine pesticides dieldrin (I), heptachlor (II), endosulfan (III) and endosulfan sulphate (IV) (all included in the E.P.A. list of priority pollutants) in the emulsified medium formed with ethyl acetate and a mixture of two surfactants, Hyamine 2389 and Triton X-405, as emulsifying agent. Our investigation of how the i_p and E_p values of each of the four pesticides were affected by the others showed that all except heptachlor and endosulfan sulphate interfere with each other. Therefore, the direct simultaneous determination of the components of binary mixtures, other than the mixture containing heptachlor and endosulfan sulphate, was not possible at the working pH used for their individual determination. Nevertheless, the possibility of using hydrolysis processes of endosulfan and endosulfan sulphate in basic medium was envisaged as a means of introducing differences which allow simultaneous determination of the components of binary mixtures containing endosulfan and/or endosulfan sulphate. In this paper, hydrolysis reactions of endosulfan and endosulfan sulphate in the above-mentioned emulsified medium are studied. Based on these reactions, the simultaneous determination of the components of some binary mixtures of these organochlorine pesticides is proposed. These mixtures could appear in samples of fruits and vegetables treated directly with commercial pesticide formulations.

EXPERIMENTAL

Apparatus

A Metrohm E626 Polarecord equipped with a Metrohm 663 VA polarographic stand was

*Author for correspondence.

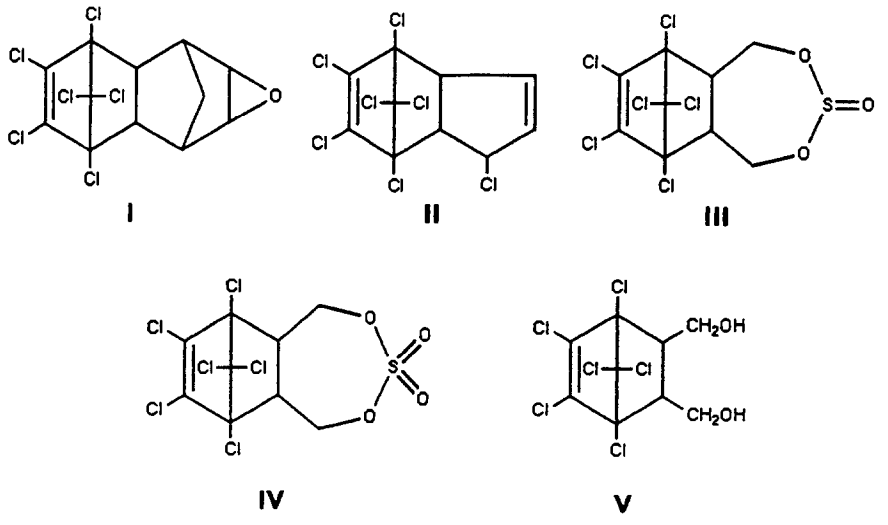

Scheme 1.

used. A P-Selecta Ultrasons ultrasonic bath was also used.

Electrodes and electrochemical cell

A Metrohm 6.1246.020 multimode mercury electrode equipped with a Metrohm 6.1226.030 capillary tube, a Metrohm 6.0728.000 Ag/AgCl/KCl 3*M* reference electrode, a Metrohm 6.1247.000 glassy-carbon electrode (as counter electrode), and a double-walled Metrohm EA 876-20 cell were used.

Reagents and solutions

Heptachlor, endosulfan ($\alpha + \beta$) and endosulfan sulphate (Riedel de Haën), and dieldrin (Sigma) were used. Triton X-405 and Hyamine 2389 (Serva) were the surfactants used as emulsifying agents. The organic solvent was ethyl acetate (Carlo Erba). All chemicals used were of analytical-reagent grade and the water used was obtained from a Milli-Q (Millipore) system.

Stock solutions of each of the pesticides ($2.5 \times 10^{-3}M$) in ethyl acetate were prepared by weighing. More dilute standards were prepared by suitable dilution with the same organic solvent. Stock solutions of surfactants were 10% v/v and 5% v/v in aqueous solution for Triton X-405 and Hyamine 2389 respectively. Buffer solutions, used as supporting electrolyte, were a Britton–Robinson solution containing each component acid at 0.2*M*, a HPO_4^{2-}/NaOH solution 0.50*M* in monoacid phosphate and a 1.0*M* sodium hydroxide solution.

Procedure

To a 50-ml flask were added a suitable volume of the pesticide stock solution in ethyl acetate, sufficient ethyl acetate to obtain a final organic phase volume of 2.0 ml, 1.0 ml of the 10% Triton X-405 solution, 2.0 ml of the Hyamine 2389 solution, and 25.0 ml of the appropriate buffer solution in that order; the solution was diluted to the mark with water. After shaking for a few seconds, the flask was placed in the ultrasonic bath for 3 min.

The emulsion obtained was transferred to the electrochemical cell and deaerated by passing an argon stream through it for 20 min (or longer times). Differential pulse polarograms were registered at $20 \pm 1°$ while keeping an inert atmosphere in the cell. Experimental conditions were : scan rate, 10 mV/sec; pulse amplitude, -50 mV, and $t = 0.5$ sec.

RESULTS AND DISCUSSION

Hydrolysis of endosulfan and endosulfan sulphate in basic medium

Some knowledge is now available about the hydrolysis of endosulfan and endosulfan sulphate in basic medium to form endosulfandiol (V).[7,8] We have found that this compound is electroactive in the emulsified medium used, giving rise to a well defined reduction peak at potential values between -1.16 and -1.18 V.

The hydrolysis reaction of both pesticides, at a concentration of $5.0 \times 10^{-5}M$, was studied in the pH range 9.0–13.0 by measuring i_p values of endosulfan, endosulfan sulphate and endosulfandiol for hydrolysis times between 20 and 80 min. Figure 1(a) summarizes data for pH 9.0 and 10.0, whereas in Fig. 1(b) peak current values are plotted as a function of time for pH 11.0 and 12.0. At pH 9.0, endosulfan is slowly

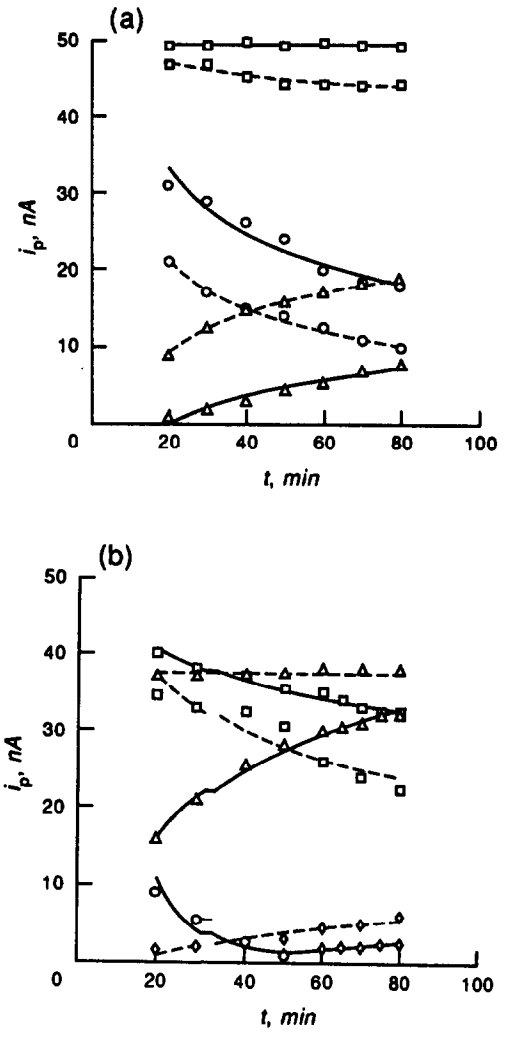

Fig. 1. Peak current as a function of time for $5.0 \times 10^{-5}M$ endosulfan and endosulfan sulphate in emulsified medium. (a) (——) pH 9.0; (-----) pH 10.0. (b) (———) pH 11.0; (– – – –) pH 12.0. (○) endosulfan; (□) endosulfan sulphate; (△) endosulfandiol (hydrolysis product of endosulfan); (◇) endosulfandiol (hydrolysis product of endosulfan sulphate). $\Delta E = -50$ mV; $v = 10$ mV/sec; $t = 0.5$ sec; 2.0 ml of ethyl acetate, 0.2% Triton X-405 + 0.2% Hyamine 2389.

hydrolysed (deaeration of the emulsion for 60 min gives an i_p value 35% lower than that obtained after 20 min deaeration) while endosulfan sulphate is practically unhydrolysed. At pH 10.0, the endosulfan hydrolysis rate is only slightly higher (i_p drop between 20 and 60 min is now 40%), and a very small decrease over time of the endosulfan sulphate peak current is observed (only 5% between 20 and 80 min), although it is not possible to yet see the endosulfandiol reduction peak [Fig. 2(A)]. At pH 11.0, the endosulfan peak [peak a of Fig. 2(B)] decreases sharply with time and practically disappears after 60 min, whereas the peak

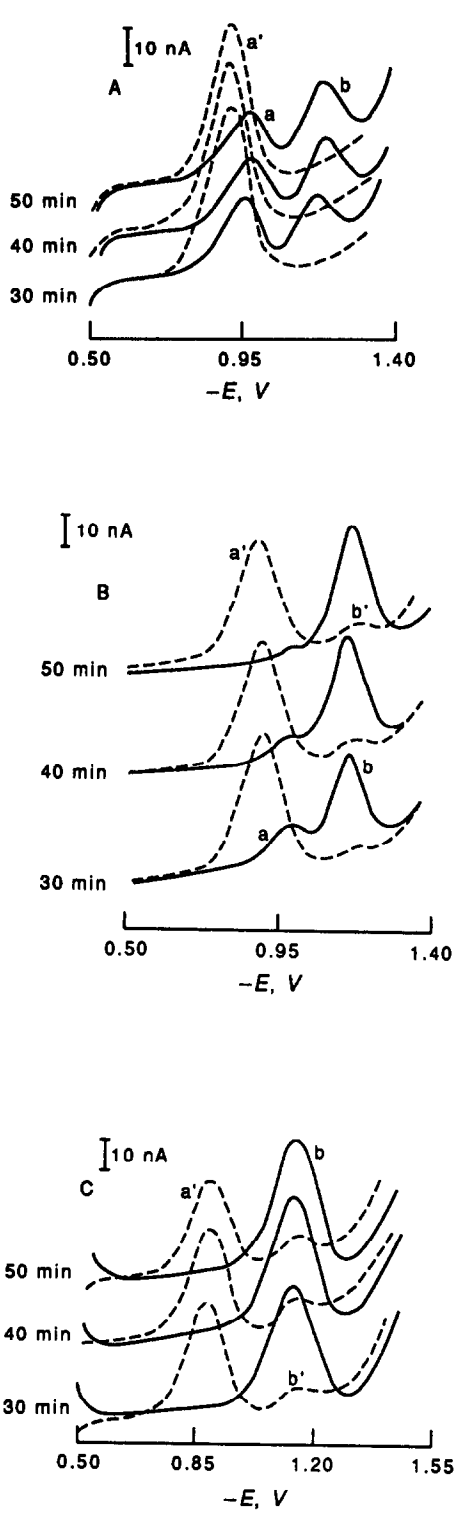

Fig. 2. Differential pulse polarograms of $5.0 \times 10^{-5}M$ endosulfan (solid line) and endosulfan sulphate (dashed line) in emulsified medium. (A) pH 10.0, (a) endosulfan, (b) endosulfandiol, (a′) endosulfan sulphate; (B) pH 11.0, (a) endosulfan, (b) endosulfandiol, (a′) endosulfan sulphate, (b′) endosulfandiol; (C) pH 12.0, (b) endosulfandiol, (a′) endosulfan sulphate, (b′) endosulfandiol; 2.0 ml of ethyl acetate, 0.2% Triton X-405 + 0.2% Hyamine 2389. $\Delta E = -50$ mV; $v = 10$ mV/sec; $t = 0.5$ sec.

corresponding to endosulfandiol [peak b of Fig. 2(B)] increases with time until reaching a practically constant value at 80 min. However, hydrolysis of endosulfan sulphate is still rather slow.

At pH 12.0, endosulfan is completely hydrolysed, even at 20 min, and only the endosulfandiol reduction peak is observed in the polarograms [Fig. 2(C)]. On the other hand, endosulfan sulphate is more quickly hydrolysed than at pH 11.0, and the polarograms show peaks of both endosulfan sulphate and endosulfandiol [Fig. 2(C)]. Finally, at pH 13.0, obtained in 0.1*M* sodium hydroxide, both pesticides are completely hydrolysed, although a hydrolysis time of at least 40 min is necessary to suppress the endosulfan sulphate peak.

Based on the above results, pH 11.0 was chosen to study the endosulfan–endosulfan sulphate mixture, as a compromise between a sufficiently rapid endosulfan hydrolysis and a sufficiently slow endosulfan sulphate hydrolysis; so a more detailed study of the hydrolysis reactions of these two pesticides at this pH value was carried out. Figure 3 shows ln $(i_p - i_{p\infty})$ versus time plots at 20° for endosulfan and endosulfan sulphate. Linear relationships were observed, indicating that the hydrolysis processes can be described by pseudo-first-order reactions. Apparent reaction rate constants obtained from the slopes of these plots were 7.4×10^{-2} and 8.5×10^{-3} sec^{-1} for endosulfan and endosulfan sulphate respectively.

The hydrolysis reactions of endosulfan and endosulfan sulphate were also studied at this pH value for a concentration level of $5.0 \times 10^{-6}M$

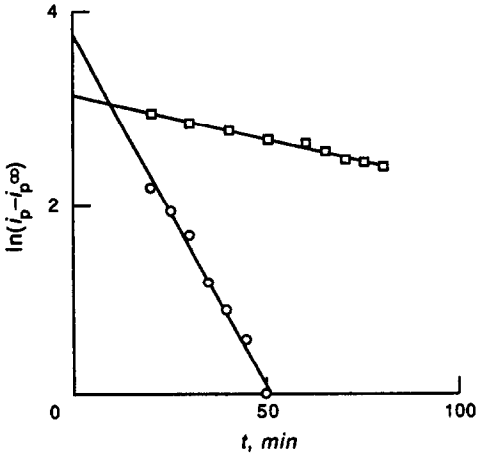

Fig. 3. Plots of $\ln(i_p - i_{p\infty})$ *vs.* time for the hydrolysis of endosulfan and endosulfan sulphate at pH 11.0 in emulsified medium. $5.0 \times 10^{-5}M$ (○) endosulfan; (□) endosulfan sulphate.

of both pesticides. Endosulfan hydrolysis is practically complete after 30 min, whereas the peak currents of endosulfandiol, coming from endosulfan, and of endosulfan sulphate (it is not possible to observe any endosulfandiol peak in this instance) remain practically constant between 30 and 80 min.

Kinetic curves of the hydrolysis of endosulfan and endosulfan sulphate mixtures at pH 11.0. The hydrolysis of endosulfan and endosulfan sulphate mixtures at pH 11.0 in the emulsified medium was studied. Figure 4 shows i_p values of the peaks of non-hydrolysed endosulfan and endosulfan sulphate and of endosulfandiol, formed as a hydrolysis product of both pesticides as a function of time for a fixed $5.0 \times 10^{-5}M$ endosulfan (*a*, *d*) or endosulfan sulphate (*c*, *b*) concentration when the endosulfan sulphate (*a*, *d*) or endosulfan (*b*, *c*) concentration is varied in the range 1.0×10^{-5}–$9.0 \times 10^{-5}M$. The curves obtained are fitted to equations of the type $i_p = -a + b \ln t$ (*b*, *d*) or $i_p = a\,t^{-b}$ (*a*, *c*). As can be observed, the decrease of the current with time for peak 1 is very similar for all the endosulfan sulphate concentrations studied [Fig. 4(a)], while peak currents are approximately the same after 80 min and practically coincident at 100 min when the endosulfan concentration is changed [Fig. 4(c)]. Furthermore, the endosulfandiol peak current is very similar for all endosulfan concentrations at short hydrolysis times, rising progressively faster with time as the endosulfan concentration increases [Fig. 4(b)]; when the endosulfan sulphate concentration is varied, i_p values tend to become the same at long hydrolysis times (100 min) [Fig. 4(d)].

All the above results led us to study the possibility of simultaneously determining the components of binary mixtures containing endosulfan and/or endosulfan sulphate. In order to accomplish this, calibration graphs for these components in the ranges 1.0×10^{-5}–$1.0 \times 10^{-4}M$ and 1.0×10^{-6}–$1.0 \times 10^{-5}M$ were prepared in the presence of the other mixture component at a constant concentration of $5.0 \times 10^{-5}M$ or $5.0 \times 10^{-6}M$ respectively.

Endosulfan–endosulfan sulphate mixture

Figure 4 suggests that both pesticides could probably be determined simultaneously at pH 11.0 by allowing the mixture to hydrolyse for 80–100 min, and then measuring the endosulfan sulphate peak for the determination of endosulfan sulphate and the endosulfandiol peak for the

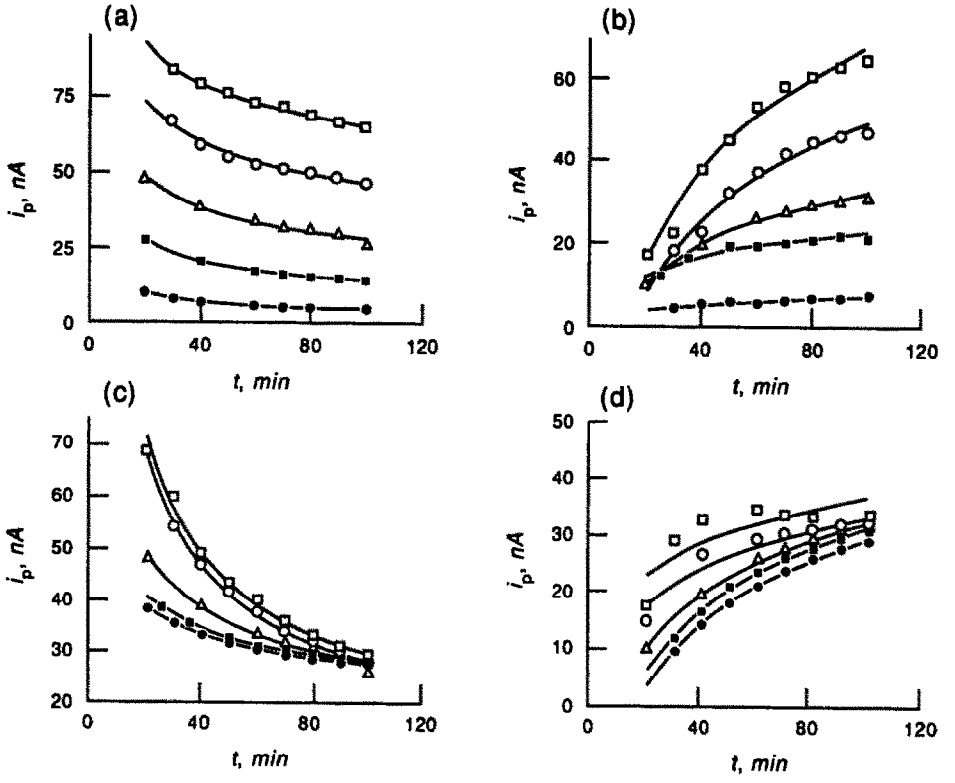

Fig. 4. Peak current as function of time of endosulfan and endosulfan sulphate mixtures at pH 11.0 in emulsified medium. (a) and (c), non-hydrolysed endosulfan and endosulfan sulphate peak current; (b) and (d) endosulfandiol peak current. (a, d), $5.0 \times 10^{-5}M$ endosulfan; (b, c), $5.0 \times 10^{-5}M$ endosulfan sulphate. (●) 1.0×10^{-5}, (■) 3.0×10^{-5}, (△) 5.0×10^{-5}, (○) 7.0×10^{-5} and (□) $9.0 \times 10^{-5}M$ endosulfan sulphate (a, d) or endosulfan (b, c).

determination of endosulfan. To confirm this, calibration graphs for endosulfan (via endosulfandiol) were obtained at 80 and 100 min keeping the endosulfan sulphate concentration constant. Linear calibrations were obtained for both hydrolysis times; the slopes and intercepts were quite similar (Table 1). Analogously, linear calibration graphs for endosulfan sulphate were obtained for the same hydrolysis times and keeping a constant endosulfan concentration; once more the slopes and intercepts were similar.

To obtain calibration graphs for both pesticides in the lower concentration range, keeping a constant concentration of the other pesticide of $5.0 \times 10^{-6}M$, it was enough to allow the mixture to hydrolyse for 30 min, as stated above. A linear calibration graph was obtained for endosulfan (via endosulfandiol) in the concentration range 4.0×10^{-6}–$1.0 \times 10^{-5}M$ (the

Table 1. Characteristics of the i_p *vs.* concentration plots obtained by dpp in emulsified medium for endosulfan (via endosulfandiol) in the presence of endosulfan sulphate, and vice versa [2.0 ml of ethyl acetate, 0.2% Triton X-405 + 0.2% Hyamine 2389 and 0.1*M* Britton–Robinson buffer (pH 11.0)]

Concentration range, *M*	Hydrolysis time, *min*	Pesticide present, *M*	*r*	Intercept, *nA*	Slope, *nA* l./mol ($\times 10^5$)
		Endosulfan sulphate			
Endosulfan					
1.0×10^{-5}–1.0×10^{-4}	80	5.0×10^{-5}	0.998	-1 ± 5	6.6 ± 0.8
	100		0.997	-1 ± 5	7.0 ± 0.8
4.0×10^{-6}–1.0×10^{-5}	30	5.0×10^{-6}	0.998	-0.6 ± 0.3	4.5 ± 0.5
		Endosulfan			
Endosulfan sulfate					
1.0×10^{-5}–1.0×10^{-4}	80	5.0×10^{-5}	0.997	-6 ± 6	8.1 ± 1
	100		0.997	-7 ± 6	7.6 ± 1
1.0×10^{-6}–1.0×10^{-5}	30	5.0×10^{-6}	0.998	0.4 ± 0.4	6.4 ± 0.7

The confidence intervals of intercepts and slopes were calculated for a significance level of 0.05.

lower concentration is imposed by the proximity of the endosulfandiol peak to the medium reduction barrier), while the range of linearity for endosulfan sulphate was between 1.0×10^{-6} and $1.0 \times 10^{-5}M$; the characteristics of these calibration graphs are summarized in Table 1. In order to verify these results, the pesticides were simultaneously determined in mixtures containing 5.0×10^{-5} or $5.0 \times 10^{-6}M$ each of endosulfan and endosulfan sulphate. The results obtained from three determinations of each mixture yielded endosulfan sulphate contents of $(5.3 \pm 0.2) \times 10^{-5}M$ for a hydrolysis time of 80 min, and $(5.4 \pm 0.6) \times 10^{-6}M$ for a hydrolysis time of 30 min, while endosulfan concentrations were $(4.6 \pm 0.4) \times 10^{-5}M$ and $(4.7 \pm 0.6) \times 10^{-6}M$ respectively, the confidence intervals being calculated for a significance level of 0.05.

Dieldrin–endosulfan mixture

The analysis of this mixture is based on the observation that endosulfan, but not dieldrin, hydrolyses at pH 12.0. Indeed, at this pH value, endosulfan is practically completely hydrolysed after 20 min; however, dieldrin does not hydrolyse at all. Under these conditions, at pesticide concentrations of $5.0 \times 10^{-5}M$ the peak potential of the endosulfandiol formed (-1.18 V) is sufficiently different from the dieldrin peak potential (-0.98 V) to permit the simultaneous determination of the components of this mixture. A HPO_4^{2-}/NaOH mixture, $0.25M$ in monoacid phosphate, was used as buffer solution.

Calibration graphs for dieldrin and endosulfan (measuring the endosulfandiol peak current) at pH 12.0 were prepared in the presence of a constant concentration of endosulfan and dieldrin respectively, and were compared with those obtained in the absence of the latter. In the lower concentration range studied, the $5.0 \times 10^{-6}M$ endosulfan or dieldrin reduction peak prevents the accurate measurement of the dieldrin or endosulfan peak respectively for concentrations lower than $3.0 \times 10^{-6}M$.

The characteristics of the linear calibration graphs obtained are summarized in Table 2. These data show that the presence of endosulfan (actually endosulfandiol because endosulfan is completely hydrolysed at this pH value) affects the slope of the dieldrin calibration curves in both concentration ranges studied, and therefore the use of the standard additions method is necessary to determine dieldrin in the presence of endosulfan. However, the presence of dieldrin does not seem to significantly affect the slope in either concentration range when endosulfan (via endosulfandiol) is determined.

Dieldrin–endosulfan sulphate mixture

In order to carry out the simultaneous analysis of the components of this mixture it would be necessary to hydrolyse completely endosulfan sulphate to endosulfandiol in a sufficiently alkaline medium, without dieldrin undergoing hydrolysis in such a medium. As stated above, endosulfan sulphate hydrolysis is practically complete from pH 13.0, and therefore the analysis of this mixture was accomplished in $0.5M$ sodium hydroxide medium after deaerating the mixture for 30 min. Dieldrin peak potential and current values are the same as those obtained at pH 6.0,[6] thus confirming that this pesticide does not hydrolyse in that medium.

The possibility of obtaining calibrations for dieldrin and endosulfan sulphate (measuring the endosulfandiol peak) under the above-mentioned conditions was evaluated in the presence of either endosulfan sulphate or dieldrin. The characteristics of the calibration graphs obtained are summarized in Table 2, which also shows calibrations in this medium in the absence of endosulfan sulphate or dieldrin. The lowest concentration that can be accurately measured is $3.0 \times 10^{-6}M$ for both pesticides. The slopes of the dieldrin calibrations in the presence and absence of endosulfan sulphate suggest that the standard additions method must be used to determine dieldrin in the presence of endosulfan sulphate. Moreover, calibration graphs for dieldrin in the absence of endosulfan sulphate, in this $0.5M$ sodium hydroxide medium, have slopes very similar to those obtained at pH 6.0, which confirms that dieldrin does not undergo hydrolysis in the alkaline medium used. However, the slopes of the endosulfan sulphate calibration graphs (via endosulfandiol) in the presence and absence of dieldrin are not very different, which seems to indicate that dieldrin does not significantly influence the endosulfan sulphate calibrations.

Heptachlor-endosulfan sulphate mixture

As mentioned in the introduction, the direct simultaneous determination of the components of the heptachlor–endosulfan sulphate mixture should be possible. Indeed, the difference between the E_p values of the two pesticides at

Table 2. Characteristics of the i_p *vs.* concentration plots obtained by dpp in emulsified medium for organochlorine pesticides in the absence and in the presence of the other component of some binary mixtures (2.0 ml of ethyl acetate, 0.2% Triton X-405 + 0.2% Hyamine 2389 and 0.2*M* HPO_4^{2-}/NaOH buffer (pH 12.0) for the dieldrin/endosulfan pair, 0.5*M* NaOH for the dieldrin/endosulfan sulphate pair and 0.1*M* Britton–Robinson buffer (pH 8.0) for the heptachlor/endosulfan sulphate pair)

Concentration range, *M*	Pesticide present, *M*	*r*	Intercept, *nA*	Slope, *nA l./mole* ($\times 10^5$)
Dieldrin	Endosulfan			
1.0×10^{-5}–1.0×10^{-4}	5.0×10^{-5}	0.998	1 ± 4	6.1 ± 0.6
	—	0.998	5 ± 3	7.7 ± 0.5
3.0×10^{-6}–1.0×10^{-5}	5.0×10^{-6}	0.997	-0.7 ± 0.6	4.7 ± 0.9
	—	0.998	-0.2 ± 0.4	7.8 ± 0.6
Endosulfan	Dieldrin			
1.0×10^{-5}–1.0×10^{-4}	5.0×10^{-5}	0.998	1 ± 4	7.1 ± 0.6
	—	0.998	1 ± 4	6.9 ± 0.5
3.0×10^{-6}–1.0×10^{-5}	5.0×10^{-6}	0.998	-0.7 ± 0.3	5.3 ± 0.9
	—	0.998	-0.4 ± 0.3	5.7 ± 0.6
Dieldrin	Endosulfan sulphate			
1.0×10^{-5}–1.0×10^{-4}	5.0×10^{-5}	0.997	-2 ± 4	6.7 ± 0.6
	—	0.998	6 ± 4	7.6 ± 0.5
3.0×10^{-6}–1.0×10^{-5}	5.0×10^{-6}	0.998	-0.9 ± 0.5	4.7 ± 0.7
	—	0.998	-0.2 ± 0.4	7.4 ± 0.6
Endosulfan sulphate	Dieldrin			
1.0×10^{-5}–1.0×10^{-4}	5.0×10^{-5}	0.998	0.2 ± 4	6.8 ± 0.7
	—	0.998	-3 ± 3	7.5 ± 0.4
3.0×10^{-6}–1.0×10^{-5}	5.0×10^{-6}	0.998	-0.7 ± 0.3	5.3 ± 0.3
	—	0.998	-0.4 ± 0.3	5.8 ± 0.4
Heptachlor	Endosulfan sulphate			
1.0×10^{-5}–1.0×10^{-4}	5.0×10^{-5}	0.999	2 ± 2	7.8 ± 0.4
	—	0.999	1 ± 4	10.7 ± 0.6
3.0×10^{-6}–1.0×10^{-5}	5.0×10^{-6}	0.999	-0.4 ± 0.3	7.8 ± 0.3
	—	0.999	-0.3 ± 0.1	9.7 ± 0.2
Endosulfan sulphate	Heptachlor			
1.0×10^{-5}–1.0×10^{-4}	5.0×10^{-5}	0.999	3 ± 3	8.6 ± 0.4
	—	0.999	2 ± 3	10.5 ± 0.5
2.0×10^{-6}–1.0×10^{-5}	5.0×10^{-6}	0.998	-0.2 ± 0.3	8.5 ± 0.5
	—	0.999	0.5 ± 0.3	10.1 ± 0.5

pH 8.0 in this emulsified medium is about 140 mV and polarograms of mixtures of these two pesticides showed two well-separated reduction peaks. In order to verify this simultaneous determination, heptachlor and endosulfan sulphate calibration graphs at pH 8.0 were prepared in the presence of the other pesticide, and were compared with those obtained in its absence.

In the lower concentration range studied, the endosulfan sulphate reduction peak prevents the accurate measurement of the heptachlor peak for concentrations lower than $3.0 \times 10^{-6}M$, and similarly, the $5.0 \times 10^{-6}M$ heptachlor reduction peak prevents the measurement of the endosulfan sulphate reduction peak at concentrations lower than $2.0 \times 10^{-6}M$.

Linear calibration graphs were obtained in all instances; their characteristics are summarized in Table 2. From these data it can be deduced that the simultaneous determination of heptachlor and endosulfan sulphate is possible, but the comparison of the calibration slopes obtained in the absence and in the presence of the other pesticide, in both concentration ranges studied, suggests the necessity of using the standard additions method to carry out the analysis of heptachlor in the presence of endosulfan sulphate and vice versa.

Other mixtures

Direct simultaneous determination of the components in the binary mixtures heptachlor–dieldrin and heptachlor–endosulfan is not possible. Separation methods need to be applied before polarographic determination. Similarly, mixtures of three of the pesticides studied and a mixture of all four cannot be

resolved directly, and separation methods also need to be applied before polarographic determination, as will be reported in a further paper. Nevertheless, from the above results it can be deduced that the determination of dieldrin is possible in the presence of endosulfan and endosulfan sulphate if a sufficiently basic working medium (0.5*M* sodium hydroxide) is used to achieve a complete hydrolysis of the last two pesticides. Likewise, the determination of endosulfan sulphate in the presence of heptachlor and endosulfan will be possible at pH 11.0, after allowing the practically complete hydrolysis of endosulfan.

CONCLUSIONS

Based on the hydrolysis of endosulfan and endosulfan sulphate in basic medium, and on their different hydrolysis rates, the simultaneous determination of the components of the organochlorine pesticide binary mixtures endosulfan–endosulfan sulphate, dieldrin–endosulfan and dieldrin–endosulfan sulphate is possible by dpp in emulsified medium. Endosulfan and endosulfan sulphate can be determined simultaneously at pH 11.0 by allowing the mixture to stand for 80–100 min, if concentration levels of both pesticides of about $10^{-5}M$ are involved, or for 30 min, if concentrations of about $10^{-6}M$ are involved, and then measuring the endosulfan sulphate peak to determine endosulfan sulphate and the endosulfandiol peak to determine endosulfan. The analysis of the mixture dieldrin–endosulfan can be achieved at pH 12.0 by allowing the endosulfan to hydrolyse completely (20 min) and then measuring the dieldrin and endosulfandiol peaks. Dieldrin and endosulfan sulphate can also be determined simultaneously in a 0.5*M* sodium hydroxide medium by allowing the endosulfan sulphate to hydrolyse completely (30 min) and measuring the dieldrin and endosulfandiol peaks. Also, the components of the mixture heptachlor–endosulfan sulphate can be determined directly at pH 8.0 in a Britton–Robinson buffer solution. The use of the standard additions method has been shown to be necessary in many cases to carry out analysis. Although this methodology does not attempt to be an alternative to gas chromatography for complex samples, it could be useful in some particular applications. Moreover, it is particularly interesting when the analytes can be extracted from the sample into organic solvents that are able to form emulsions.

Acknowledgement—Financial support from the Spanish CICYT (project ALI 89-0055) is gratefully acknowledged.

REFERENCES

1. M. A. Luke, H. T. Masumoto, T. Cairns and H. K. Hundley, *J. Assoc. Off. Anal. Chem.*, 1988, **71**, 415.
2. J. M. Pingarrón Carrazón, A. J. Reviejo García and L. M. Polo Díez, *J. Electroanal. Chem.*, 1987, **234**, 175.
3. J. M. Pingarrón Carrazón, A. Gordón Vergara, A. J. Reviejo Carcía and L. M. Polo Díez, *Anal. Chim. Acta*, 1989, **216**, 231.
4. J. M. Pingarrón Carrazón, A. J. Reviejo García and L. M. Polo Díez, *Analyst*, 1990, **115**, 869.
5. A. González Cortés, J. M. Pingarrón Carrazón and L. M. Polo Díez, *Electrochim. Acta*, 1991, **36**, 1573.
6. A. J. Reviejo García, A. Samprón Pérez, J. M. Pingarrón Carrazón and L. M. Polo Díez, *Electroanalysis*, 1992, **4**, 111.
7. N. M. Chopra and A. M. Mahfouz, *J. Agric. Food Chem.*, 1977, **25**, 32.
8. S. E. Forman, A. J. Durbetaki, M. V. Cohen and R. A. Olofson, *J. Org. Chem.*, 1965, **30**, 165.

Talanta, Vol. 39, No. 8, pp. 907–911, 1992
Printed in Great Britain

0039-9140/92 $5.00 + 0.00
Pergamon Press Ltd

FLOW INJECTION FLUORIMETRIC DETERMINATION OF THIAMINE AND COPPER BASED ON THE FORMATION OF THIOCHROME

T. PEREZ-RUIZ,* C. MARTINEZ-LOZANO, V. TOMAS and I. IBARRA
Department of Analytical Chemistry, Faculty of Sciences, University of Murcia, Murcia, Spain

(*Received* 14 *November* 1991. *Accepted* 2 *December* 1991)

Summary—The reaction, involving the oxidation of thiamine by copper(II) in basic solutions to fluorescent thiochrome, has been adapted to the determination of thiamine by flow-injection analysis. Linear calibration graphs are obtained between 0.30 and 6.02 μg/ml with a sampling rate of 50 samples/hr and a relative standard deviation of 0.53%. This reaction has also been adapted to the determination of copper(II) over the range 0.5–5.0 μg/ml. The applicability of both methods for determination of thiamine and copper is demonstrated by investigating the effect of potential interferences and by the analysis of real samples (pharmaceuticals for thiamine and ores and alloys for copper).

The thiamine (vitamin B_1) is a natural nutrient present in many foods and is also added as an essential nutrient. It has been used for the prevention and treatment of beriberi, neuralgia, *etc.* in medical doses or vitamin B_1 enriched foods or drinks. Since its discovery and isolation, several methods have been reported for determining this important compound, including microbiological methods, chromatography, direct molecular absorption spectroscopy, spectrofluorimetry, polarography, reaction-rate method and electrodes sensitive to vitamin B_1.[1–6]

The chemical methods most widely used involve the reaction between the vitamin and potassium hexacyanoferrate(III) in alkaline solution to form thiochrome (TC), which is then measured fluorimetrically;[2,7] this procedure is the official U.S.P. method[8] and has been automated by flow injection with fluorimetric[9] and chemiluminiscence detection.[10]

The oxidation of thiamine to fluorescent TC is always accompanied by the simultaneous formation of thiamine disulphide (TDS) a condensation product of two thiamine molecules. Oxidizing agents such as potassium permanganate, hydrogen peroxide and iodine favour the production of nonfluorescent TDS.[11]

However, the use of hexacyanoferrate(III) as oxidant in the thiochrome method suffers disadvantages since the yield of the reaction is about 67% and the extraction of TC is necessary in order to separate it from potassium hexacyanoferrate(III) which quenches the TC fluorescence.[12–13]

Apart from potassium hexacyanoferrate(III) other oxidizing agents have been used to oxidize thiamine such as cyanogen bromide,[14] copper(II),[15] mercury(II)[13,16,17] with a higher yield in thiochrome.

This paper describes a sensitive procedure for the determination of thiamine involving a simple FIA technique based on the oxidation of the vitamin to TC by Cu(II). The results of an extensive interference study and the application of the method to the determination of thiamine in multivitamin-mineral preparations are reported.

On the other hand, the reaction has also been applied to flow injection determination of copper. Many methods suitable for the determination of copper have been reported and some of these are based on flow injection analysis with the aim of developing fast, reliable and simple methods for routine analysis,[18] although the FIA methods with fluorimetric detection are scarce.[19–21] This paper reports a new fluorimetric flow injection method for the determination of copper with a reverse FIA mode (rFIA) based in the formation of thiochrome.

EXPERIMENTAL

Apparatus

A Perkin–Elmer model 3000 spectrofluorimeter connected to a Linseis 6512 recorder was

*Author for correspondence.

used as a detector with a Hellma 176.052 QS flow cell (inner volume 25 μl).

A Gilson Minipuls HP4 peristaltic pump, and an Omnifit injection valve were used. PTFE tubing of 0.5 mm i.d. was used for the mixing coil and for all connections.

Reagents

All chemicals used were analytical-reagent grade and doubly distilled water was used throughout.

Thiamine stock solution $10^{-3}M$ was prepared dissolving the solid (Sigma), previously dried, in water and adjust to pH 4 with hydrochloric acid. This solution was stable for months if kept refrigerated. Working solutions of vitamin B_1 were prepared daily and protected from light.

A stock solution of copper $10^{-2}M$ was prepared by dissolving copper nitrate (Merck) in distilled water and standardized by titration with EDTA. Working standard solutions were prepared from the stock solution by appropriate dilution with water.

Phosphate buffers prepared from $0.2M$ disodium or dipotassium hydrogen phosphate and sufficient $5M$ potassium hydroxide to give the desired pH. These buffers also contain NH_3 ($0.1M$) in order to hinder the Cu(II) precipitation.

Manifold

The manifold employed is shown in Fig. 1. The thiamine solution is introduced with the aid of an injection valve. The Cu(II) and the thiamine solution are mixed with the phosphate buffer solution in R_1. The reaction coil, R_2, is submerged in a water-bath, the temperature of which is adjustable. A timer, synchronized to the injection system allows the flow to be stopped for a given period of time.

Recommended procedure

Thiamine determination. The Cu(II) solution and the buffer solution were pumped at a rate of 2.8 and 0.9 ml/min respectively. A 185-μl sample, containing between 0.30 and 6.02 μg/ml of thiamine, was injected into the FIA manifold. The timer was programmed so that after 10 sec the flow stops for one minute and then the pump starts again. The TC fluorescence ($\lambda_{ex} = 370$ nm, $\lambda_{em} = 465$ nm) was measured and recorded.

Copper(II) determination. For copper(II) determination, good results were obtained between 0.5 and 5 μg/ml with the reverse FIA, using the same manifold shown in Fig. 1. The volume of thiamine injected was 185 μl.

Preparation of assay solutions

Tablets. Ten tablets are powered and an amount equivalent to one milligram of thiamine was weighed accurately and dissolved in *ca.* 100 ml of water. The solution was filtered through Whatman No. 1 filter-paper and the filtrate and two washings, each of 20 ml, were collected in a 1000-ml calibrated flask and diluted to volume with water.

Injections. An injection vial solution was shaken thoroughly and a volume equivalent to one milligram of thiamine is transferred into a 1000-ml calibrated flask and diluted to the mark with distilled water.

Ores and alloys. For analysis of copper in ores and alloys the sample (0.5–1.0 g) was digested with nitric acid and sulphuric acid. The residue was filtered off and washed filtrate and washing were combined, evaporated nearly to dryness, diluted with doubly distilled water and evaporated again to low volume to reduce the acidity. The solution is transferred into a 50-ml standard flask and diluted to volume with doubly distilled water.

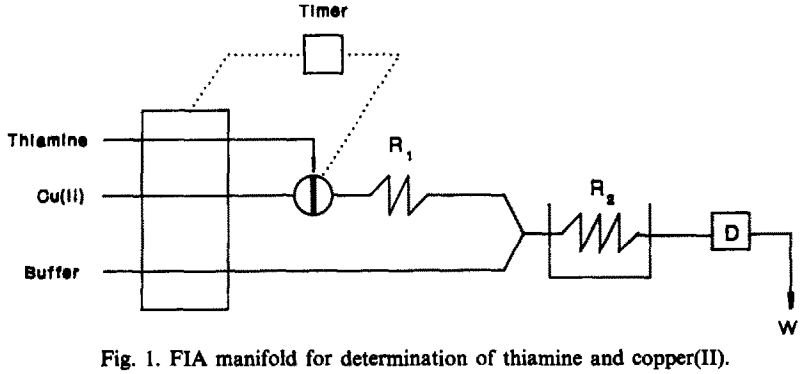

Fig. 1. FIA manifold for determination of thiamine and copper(II).

RESULTS AND DISCUSSION

When thiamine is oxidized by Cu(II) in a FIA system the largest yield of TC is obtained at a high Cu(II) concentration and in an alkaline medium. The time taken to reach equilibrium decreases with increasing Cu(II) and OH^- concentrations.

Optimization of variables

The investigation of the effect of the chemical and FIA variables on the fluorescence intensity were performed by altering each variable in turn, while keeping the others constant.

As the reaction rate is pH dependent (Fig. 2) the reaction mixture must be well buffered. The buffer solution selected was 0.2*M* in phosphate and 0.1*M* in ammonia because it provides a good buffering capacity at pH 12, precision in the measurements and avoided the precipitation of copper.

On the other hand, the order of addition of the reagents is critical. The thiamine must be mixed with Cu(II) before the addition of the buffer, in order to achieve that thiamine be stabilized by the formation of a complex with Cu(II), which can be easily oxidized to TC when the base is added.

The effect of copper(II) concentration was investigated (Fig. 3) and $5 \times 10^{-4}M$ was selected.

The influence of the temperature exerts the opposite effect, both on the reaction development (positive effect) and on the fluorescence emission (negative effect). The net effect is a decrease of the fluorescence intensity with increasing temperature. A temperature of 30° was selected to obtain an appropriate peak height.

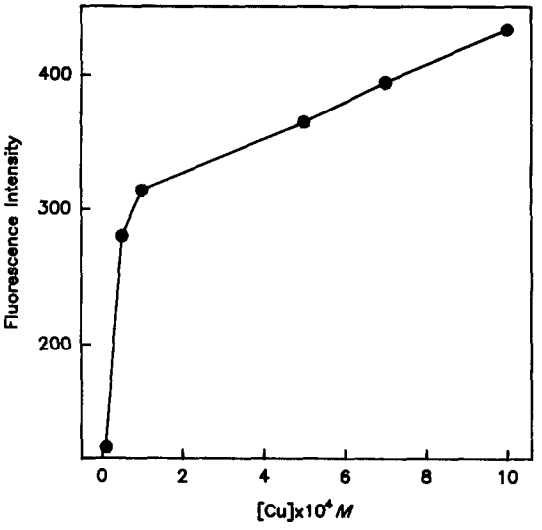

Fig. 3. Influence of pH on peak height other conditions as Fig. 2.

The influence of the flow-rate of each channel on the analytical signal was studied. Maximum peak height was obtained at flow-rates of 2.9 ml/min for the copper(II) line and 0.8 ml/min for the buffer line.

The effect of loop size and length of the coil R_2 is shown in Fig. 4. The optimum values for these variables are sample injection volume = 185 μl and reactor length $R_2 = 100$ cm. A 100-cm reaction coil R_1 was selected in order to ensure the formation of the complex thiamine–Cu(II) before merging with the buffer line.

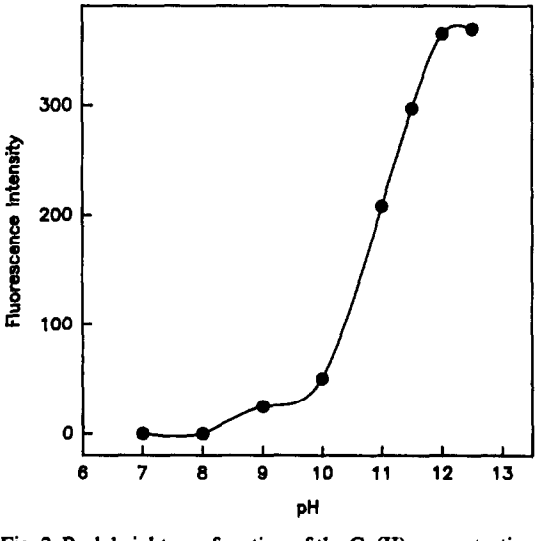

Fig. 2. Peak height as a function of the Cu(II) concentration. Sample volume 185 μl, $10^{-5}M$ thiamine, 0.2*M* phosphate buffer pH 12, flow-rate 2.8 ml/min and stop-time 1 min.

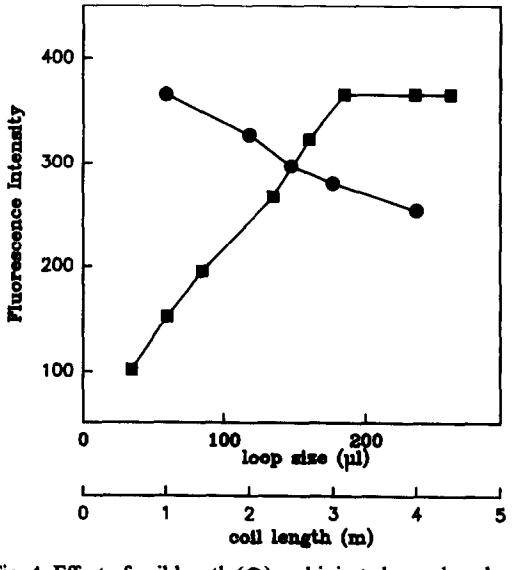

Fig. 4. Effect of coil length (●) and injected sample volume (■) on the peak height.

The peak height increased with increasing residence time because the oxidation of the thiamine to TC by Cu(II) is not very fast. The best results were obtained if the pump was stopped when the plug was located in the reaction coil R_2. After a given period of time the pump was triggered by a timer and the reaction zone was directed toward the detector. The timer was programmed so that after 10 sec the flow stops for one minute as a compromise between analytical signal and sampling rate.

Determination of thiamine

A series of standard solutions were injected in triplicate to test the linearity of the calibration graphs. The calibration graph was found to be linear from 0.30 to 6.02 μg/ml. The least-squares calibration equation was $I_F = 4.29 + 118C$ ($r = 0.9996$) where the concentration (C) was measured in μg/ml and the fluorescence intensity I_F in arbitrary units. The sampling rate is about 40 samples/hr. The statistical study performed on two series of 10 samples of 0.75 and 3.01 μg/ml of thiamine yielded a RSD of 0.54 and 0.52% respectively. The limit of detection was 0.17 μg/ml and the quantification limit was 0.23 μg/ml.

Interferences

An extensive interference study aimed at the determination of thiamine in vitamin-mineral preparations was performed. Samples containing a fixed concentration of thiamine (3 μg/ml) and various concentrations of the foreign substances were injected into the FIA system. A substance was considered not to interfere if the variation in the peak height of thiamine was less than $\pm 3\%$ in its presence. The results are shown in Table 1.

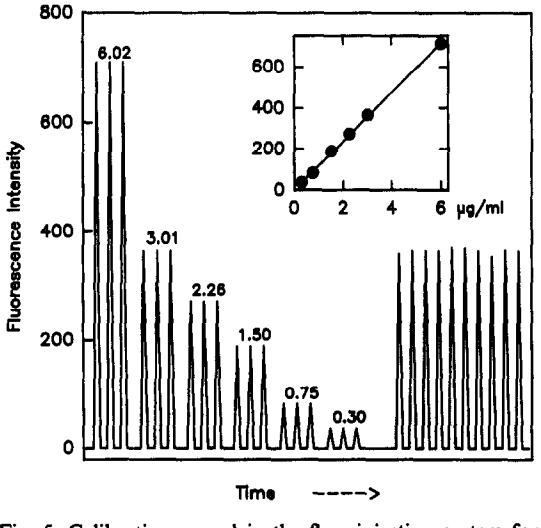

Fig. 5. Calibration record in the flow injection system for triplicate injections of 185 μl of thiamine standard solutions. Values on the peaks represent concentrations in μg/ml.

Table 1. Tolerance of other substance in the proposed procedure for thiamine

Substance	Tolerable mole ratio (substance/thiamine)
Nitrate, chloride	1000*
Sulphate, acetate, molybdate	500
Lactose, fructose, perchlorate, starch,† Ba(II), Ca(II), Fe(III)	200
Bromide, pyridoxine (vitamine B_6), Zn(II), Ni(II), Mg(II), Co(II)	100
Vanadate, calcium pantothenate, cyanocobalamine (vitamin B_{12})	10
Iodide, sucrose, Mn(II)	1
Ascorbic acid (vitamin C), Biotin (vitamin H), Fe(II), Hg(II)	0.1
Riboflavine (vitamin B_2)	0.01

*Maximum tested.
†Tolerable w/w ratio.

Analysis of pharmaceutical dosage forms

The proposed method was applied to the determination of thiamine in pharmaceutical dosage forms. Commercially available formulations were analysed and the results obtained are summarized in Table 2.

As can be seen for all the formulations, the assay results were in good agreement with the declared content.

Determination of copper

The oxidation of the thiamine to thiochrome by Cu(II) was also applied to the fluorimetric determination of copper using a reverse FIA mode.

Optimization of the flow system

Of all the FIA techniques tested the best results were obtained with the reverse mode

Table 2. Determination of thiamine in pharmaceutical preparations

Sample*	Source	Thiamine content, *mg*	Thiamine found, *mg*†	% Error
Benerva	Roche	100	103.8	3.3
Betabion	Merck	100	98.5	1.5
Nervobion	Merck	100	99.8	0.2

*Composition of samples. Benerva: thiamine, 100 mg; water, 1 g. Betabion: thiamine 100 mg; water 2 g. Nervobion: thiamine, 100 mg; pyridoxine, 100 mg; cyanocobalamine 1000 γ.
†Average of four determinations.

shown in Fig. 1, because it resulted in an increase in sensitivity and a decrease in the number and level of interferences. The optimum values for the variables are flow-rates of the buffer line of 0.5 ml/min and the sample line of 1 ml/min, injection volume of thiamine ($2 \times 10^{-5}M$) of 185 μl, and length of the first coil (R_1) of 100 cm and the second coil (R_2) of 200 cm.

The timer was programmed so that after 10 sec, when the sample zone was in the reactor R_2, the flow was stopped for 60 sec and the pump started again.

Calibration graph

Under the recommended conditions the peak height *vs.* copper concentration was linear in the range 0.5–5 μg/ml. The least-squares calibration equation was $I_F = 3 + 81.3C$ ($r = 0.9994$) where the concentration (C) is measured in μg/ml. The sampling rate is 35 samples/hr. The repeatability of the method is good; two standard solutions containing 2.54 and 1.27 μg/ml were injected 10 times and relative standard deviations of 0.644 and 0.371% were obtained respectively.

Interferences

An interference study aimed at the determination of copper in alloys and ores was performed. Samples containing a fixed concentration of Cu(II) (0.64 ppm) and various concentrations of foreign substances were analysed in the flow system. The results are shown in Table 3.

Copper determination in real samples

In order to check the validity of the proposed method, it has been applied satisfactorily to the determination of copper in real samples, alloys and ores certified by Gebr. Hoepfner of Hamburg. The results obtained are summarized in Table 4 and showed a good agreement with the certified values.

Table 3. Tolerance of other substance in the proposed procedure for copper(II)

Substance	Tolerable mole ratio [substance/copper(II)]
Nitrate	1000*
Acetate	500
Sulphate, perchlorate	100
Tartrate, chloride, vanadate, molybdate, Zn^{II}, Mg^{II}, Pb^{II}, Cd^{II}	10
Ca^{II}	5
Fe^{II}	2
Bromide, Co^{II}, Ag^{I}	1
Mn^{II}	0.5
Iodide, oxalate, Ni^{II}	0.1

*Maximum tested.

Table 4. Determination of copper in ores and alloys

Sample*	Copper content (%)†	Copper found (%)‡	% Error
Bronze III	86.21	86.55	0.40
Lead tin bronze I	83.53	88.63	0.35
Copper ore	11.83	11.86	0.44

*Composition of sample. *Bronze III*: copper, 86.21%; lead, 1.09%; tin, 12.41%; nickel 0.23%; iron, 0.08%; zinc remainder. *Lead tin bronze*: copper, 83.53%; lead, 4.56%; tin, 4.83%; nickel 0.37%; iron, 0.21%; zinc remainder. *Copper ore*: copper, 11.83%; iron, 11.94%; silica 54.34%; sulphur, 3.7%.

†Certificate value.

‡Average of three determinations.

Acknowledgement—The authors acknowledge the financial support given by DGICYT, project PB90-0008.

REFERENCES

1. R. Strochecker and H. M. Henning, *Vitamin Assay Tested Methods*, Verlag Chemie, Weinhein, 1965.
2. *Methods of Vitamin Assay*, Association of Vitamin Chemist, Interscience, New York, 1966.
3. I. E. Davidson, in W. F. Smyth (ed.), *Polarography of Molecules of Biological Significance*, Academic Press, London, 1979.
4. R. B. Roy, J. K. Foreman and P. B. Stockwell, *Topics in Automatic Chemical Analysis*, Horwood, Chichester, 1979.
5. N. Ishibashi, K. Kina and N. Maekawa, *Chem. Lett.*, 1973, 119–120.
6. G. H. Zhang, T. Imato, Y. Asano, T. Sonda, H. Kobayashi and N. Ishibashi, *Anal. Chem.*, 1990, **62**, 1644.
7. D. J. Hennesy and L. R. Cerecedo, *J. Am. Chem. Soc.*, 1939, **61**, 179.
8. United States Pharmacopeial Convention, *U. S. Pharmacopeia*, XXI Ed., Mack, Easton P.A., 1985.
9. B. Karlberg and S. Thelander, *Anal. Chim. Acta*, 1980, **114**, 129.
10. N. Grekas and A. C. Calokerinos, *Talanta*, 1990, **37**, 1043.
11. P. Syke and A. R. Todd, *J. Chem. Soc.*, 1951, 534.
12. P. Ellinger and M. Holden, *Biochem. J.*, 1944, **38**, 147.
13. M. A. Ryan and J. D. Ingle, *Anal. Chem.*, 1980, **52**, 2177.
14. M. Fujimara and K. Matsui, *ibid.*, 1953, **25**, 810.
15. W. Cui, L. Mi and H. Shi, *Fenxi Huaxue*, 1988, **16**, 657.
16. V. Gonzalez, S. Rubio, A. Gomez-Hens and D. Perez Bendito, *Anal. Lett.*, 1988, **21**, 993.
17. C. Martinez-Lozano, T. Perez-Ruiz, V. Tomas and C. Abellan, *Analyst*, 1990, **115**, 217.
18. J. Růžička and E. H. Hansen, *Flow-Injection Analysis*, 2nd Ed., Wiley, New York, 1988
19. F. Lazaro, M. D. Luque de Castro and M. Valcarcel, *Anal. Chim. Acta*, 1984, **165**, 177.
20. *Idem*, *Z. Anal. Chem.*, 1985, **320**, 128.
21. *Idem*, *Analyst*, 1984, **109**, 333.

Talanta, Vol. 39, No. 8, pp. 913–917, 1992
Printed in Great Britain.

0039-9140/92 $5.00 + 0.00

STUDIES ON THE EQUILIBRIA OF *o*-PHTHALIC AND PHOSPHORIC ACIDS IN MIXED DIMETHYL SULPHOXIDE–WATER MIXTURE

H. A. AZAB

Chemistry Department, Faculty of Science, Assiut University, Assiut, Egypt

(*Received* 8 *July* 1991. *Revised* 18 *November* 1991. *Accepted* 29 *November* 1991)

Summary—The secondary dissociation constants of *o*-phthalic and phosphoric acids have been determined in 50% w/w dimethyl sulphoxide–water from reversible emf measurements of the cell of the type: Pt, H_2 (1 atm), M_2A (m), MHA (m), MCl, AgCl; Ag at different temperatures (288.15–308.15 K) and at different ionic strengths. To minimize the unsteadiness in potential measurements palladium-coated platinum electrodes have been used. The large set of such emf values has been analysed in terms of a multi-linear regression method recommended in recent IUPAC documents. The thermodynamic values $\Delta G°$, $\Delta H°$, $\Delta S°$ for the respective equilibria were estimated. The possibility of using these acids as a basis for some buffer solutions in 50% dimethyl sulphoxide (Me_2SO)-water mixture is discussed.

Many potentiometric equilibrium measurements have nevertheless, been made in mixed solvents on the basis of calibration with aqueous buffers.[1–5] The meter reading, pH(R), obtained in a partially aqueous or non-aqueous medium differs by an amount, δ, from the reading, pH*, obtained when the meter is standardized with appropriate standard pH* buffers. This method is not a procedure of high accuracy as the asymmetry potential of the glass electrode is likely to vary when the electrode is removed from the aqueous standardizing medium and then immersed in the solvent system in which measurement is to be made.[6] The study of the dissociation equilibria of phosphoric and *o*-phthalic acids in water[7–10] has permitted the combination of a series of standard aqueous buffer solutions. The standardization of pH* measurements in mixed solvents, needs similar studies regarding the dissociation equilibria of certain adequate electrolytes in these solvents.[11–17] In the present work the second-stage dissociation constants of phosphoric and *o*-phthalic acid in 50% w/w dimethyl sulphoxide (Me_2SO)–water mixture have been determined in continuation to work in the field of preparing standard buffer solutions.[10,18,19]

EXPERIMENTAL

All reagents used were of AnalaR(BDH) grade. All stock solutions were prepared in doubly-distilled air free conductivity water. 50% Dimethyl sulphoxide-water mixtures were prepared by mixing appropriate weights of analytical grade dimethyl sulphoxide, fractionally distilled before use, with conductivity water. Owing to the low solubility of dipotassium hydrogen phosphate in the given solvent, disodium hydrogen phosphate was used. *o*-Phthalic acid, potassium chloride, certified ULTREX Baker potassium hydrogen phthalate, before use, were dried at 110°. The potentiometric equilibrium measurements, using the electrochemical cell provided with a hydrogen electrode were carried out with an OP-208 Radelkis digital millivolt meter–pH meter accurate to $\pm 1 \times 10^{-4}$ V. To minimize the instability in potential measurements palladium-coated platinum electrodes have been used.[20]

The silver–silver chloride electrode was of the thermoelectrolytic type and was prepared in the laboratory.[21] It was immersed for 24 hr in a solution of pure hydrochloric acid (0.05*M*) and tested in a cell of the type:

$$(Pt)H_2/HCl(0.1M)/AgCl;\ Ag$$

whose emf must equal 0.3523 V; this corresponds to a standard potential of 0.2223 V of the Ag; AgCl, Cl^- ($a = 1$) electrode. Several electrodes were prepared and those were used whose potential did not differ by more than ± 0.0001 V from the standard value. The values of the standard potential of the Ag/AgCl electrode, ${}_sE°_{AgCl}$, in 50% dimethyl sulphoxide–

Table 1. Values of ${}_sE^\circ_{AgCl}$ in 50% dimethyl sulphoxide–water mixture at different temperatures

T, K	${}_sE^\circ_{AgCl}$, V
288.15	0.2247
293.15	0.2206
298.15	0.2164
303.15	0.2121
308.15	0.2073

H_2O mixture at different temperatures (288.15–308.15 K) have been determined and are given in Table 1. Each measured emf value was corrected to 1 atm (101325 Pa) pressure of hydrogen from the barometic pressure and the vapor pressure of the solution, the latter being taken as the same as the vapor pressure of the solvent.[22–24] An average of about four independent cells were measured at each electrolyte molality and at each temperature. The large set of such emf values has been analysed in terms of a multilinear regression method recommended in recent IUPAC documents.[25]

RESULTS AND DISCUSSION

Electrochemical cell without liquid junction potential of the type:

$$\text{Pt; } H_2 \text{ (1 atm), } M_2A(m), \text{ MHA}(m), \text{ MCl}(m), \text{ AgCl; Ag} \quad (1)$$

has been used in the determination of pK_{a_2} values of *o*-phthalic and phosphoric acids in 50% w/w dimethyl sulphoxide–water mixture at different temperatures (288.15–308.15 K), where A^{2-}, represents the $C_6H_4(COO)_2^{2-}$ and HPO_4^{2-} anions and M^+ the Na^+ or K^+ cations.

The emf of cell (1) is given by:

$$E = {}_sE^\circ_{AgCl} - \frac{RT}{F}\ln a_{H^+} \cdot a_{Cl^-} \quad (2)$$

$$= {}_sE^\circ_{AgCl} - \frac{RT}{F}\ln a_{H^+} \cdot m_{Cl^-} \cdot \gamma_{Cl^-} \quad (3)$$

For the equilibrium under study

$$HA^- \rightleftharpoons A^{2-} + H^+$$

one can write

$$K_2 = \frac{a_{H^+} \cdot m_{A^{2-}} \cdot \gamma_{A^{2-}}}{m_{HA^-} \cdot \gamma_{HA^-}} \quad (4)$$

from equations (3) and (4):

$$E - {}_sE^\circ_{AgCl} = -\frac{RT}{F}\ln \times \left[K_2 \frac{m_{Cl^-} \cdot m_{HA^-}}{m_{A^{2-}}}\left(\frac{\gamma_{HA^-} \cdot \gamma_{Cl^-}}{\gamma_{A^{2-}}}\right)\right] \quad (5)$$

Taking the salt concentrations so that $m_{Cl^-} = m_{HA^-} = m_{A^{2-}} = m$, the relationship (5) takes the following form:

$$pK_{a2} - \log\left(\frac{\gamma_{Cl^-} \cdot \gamma_{HA^-}}{\gamma_{A^{2-}}}\right) = \frac{F(E - {}_sE^\circ_{AgCl})}{2.303RT} + \log m \quad (6)$$

The term containing the activity coefficients can be approximated at ionic strengths smaller than 0.1 by means of the Debye–Hückel equation:

$$\log\left(\frac{\gamma_{Cl^-} \cdot \gamma_{HA^-}}{\gamma_{A^{2-}}}\right) = \frac{2AI^{1/2}}{1 + Ba^\circ I^{1/2}} - \beta I \quad (7)$$

where A and B are the constants of the Debye–Hückel equation for the respective solvents which were derived for 50% w/w dimethylsulphoxide from the expressions given by Robinson and Stokes:[26]

$$A = (1.825 \times 10^6)/(\epsilon T)^{1/2} \text{ mole}^{-1/2} \text{ L}^{1/2} K^{1/2}, \quad (8)$$

$$B = 50.29/(\epsilon T)^{1/2} \text{ mole}^{-\frac{1}{2}} \text{ L}^{1/2} K^{1/2} \quad (9)$$

β is the salting out parameter and a° the "ion-size" parameter which has been assigned the widely used value of 4.4 A° in the present calculation. Electric permittivities (ϵ), necessary for the calculation of Debye–Hückel constants, for solvents containing Me_2SO were not available in the literature for temperatures other than 25°.[27–29] However, it was observed from the data of Akerlof[30] that the relationship between the log of the electric permittivity and temperature is linear and that the gradients of the lines for various organic solvents and their aqueous mixtures are essentially parallel. This provided an acceptable method of extrapolating the measured electric permittivities for Me_2SO–H_2O mixtures at 25°.[27–29] An equation for the least-squares regression line for the relationship between $\log \epsilon_{H_2O}$ and temperature was derived from the data given by Hamer.[31]

$$\log \epsilon = -0.00197t + 1.9431 \quad (10)$$

The Debye–Hückel constants for 50% w/w Me_2SO–H_2O mixtures at temperatures other

than 25° were calculated with electric permittivities estimated from the known difference between ϵ_{H_2O} and the electric permittivity for the mixed solvent at 25° by extrapolating the difference to different temperatures. Combination of equation (6) and (7) results:

$$pKa_2 + \beta I = \frac{(E - {}_sE^\circ_{AgCl})F}{2.303RT} + \log m + \frac{2AI^{1/2}}{1 + Ba^\circ I^{1/2}} \quad (11)$$

Representing graphically the right hand side of equation (11) versus concentration (m) one obtains a straight line intersecting the ordinates at pKa_2.

Seven cell solutions containing hydrochloric acid at molalities ranging from 0.05 to 0.005 m were tested for the emf measurements leading to the standard potential of the silver–silver chloride electrode. The standard potential E_m, on the molality scale was obtained by extrapolation of the function ($E^{\circ\prime}$) of the emf, E, to $m = 0$:

$$E^{\circ\prime} \equiv E^\circ_m - bm = E + 2k \log m - \frac{2kAm^{1/2}}{1 + Ba^\circ m^{1/2}} \quad (12)$$

This function is derived from the Nernst equation, where a Debye–Hückel expression has been included to approximate the mean activity coefficient of hydrochloric acid. The term k is written for $RT \ln 10/F$ and the Debye–Hückel constant A and B were calculated as mentioned above.

By using ${}_sE^\circ_{AgCl}$, we obtain the acidity function $P_s(a_H \cdot \gamma_{Cl})$ from the emf of the hydrogen–silver chloride cell (1) containing the standard solutions (with added chloride) in dimethyl sulphoxide–water medium.[32]

$$P_s(a_H \cdot \gamma_{Cl}) = \frac{(E - {}_sE^\circ_{AgCl})F}{2.303RT} + \log m_{Cl} \quad (13)$$

and then pa_{H^*} by the nonthermodynamic step

$$pa_{H^*} = P_s(a_H \cdot \gamma_{Cl}) + \log \gamma_s Cl \quad (14)$$

Data for the experimental measurements of the emf of cell (1) at different temperatures (288.15 – 308.15 K) and different ionic strengths are given in Tables 2 and 3 for both *o*-phthalic and phosphoric acid in 50% w/w dimethyl sulphoxide–water medium. As the concentration of the supporting electrolyte increased, the salting out effect is observed. This is because the activity coefficient of the

Table 2. Experimental data obtained by electrochemical cell (1) for $C_6H_4(COOK)_2(m) + HKC_6H_4(COO)_2(m) + KCl(m)$ in dimethyl sulphoxide–water mixture 50% w/w

T, K	m	I	E, V	$P_s(a_H \cdot \gamma_{Cl^-})$	$-\log \gamma_{Cl^-}$	paH^*
	0.002	0.01	0.7582	6.6306	0.0526	6.578 ± 0.001
	0.004	0.02	0.7362	6.5469	0.0704	6.476 ± 0.001
288.15	0.006	0.03	0.7212	6.4607	0.0830	6.377 ± 0.001
	0.008	0.04	0.7062	6.3233	0.0928	6.230 ± 0.001
	0.010	0.05	0.6912	6.1579	0.1010	6.057 ± 0.002
	0.002	0.01	0.7670	6.6227	0.0527	6.570 ± 0.002
	0.004	0.02	0.7463	6.5680	0.0706	6.497 ± 0.001
293.15	0.006	0.03	0.7323	6.5034	0.0832	6.420 ± 0.002
	0.008	0.04	0.7213	6.4392	0.0930	6.346 ± 0.001
	0.010	0.05	0.7103	6.3471	0.1012	6.245 ± 0.002
	0.002	0.01	0.7743	6.5898	0.0532	6.537 ± 0.001
	0.004	0.02	0.7492	6.4666	0.0712	6.395 ± 0.002
298.15	0.006	0.03	0.7340	6.3858	0.0839	6.302 ± 0.002
	0.008	0.04	0.7220	6.3079	0.0938	6.214 ± 0.001
	0.010	0.05	0.7132	6.2561	0.1021	6.154 ± 0.002
	0.002	0.01	0.7813	6.5529	0.0536	6.499 ± 0.002
	0.004	0.02	0.7603	6.5049	0.0719	6.433 ± 0.002
303.15	0.006	0.03	0.7453	6.4317	0.0847	6.347 ± 0.002
	0.008	0.04	0.7303	6.3073	0.0947	6.213 ± 0.001
	0.010	0.05	0.7153	6.1548	0.1030	6.052 ± 0.002
	0.002	0.01	0.7900	6.5451	0.0542	6.491 ± 0.002
	0.004	0.02	0.7680	6.4864	0.0727	6.414 ± 0.002
308.15	0.006	0.03	0.7495	6.3600	0.0855	6.274 ± 0.002
	0.008	0.04	0.7350	6.2478	0.0957	6.152 ± 0.002
	0.010	0.05	0.7205	6.1057	0.1041	6.003 ± 0.001

Table 3. Experimental data obtained by electrochemical cell (I) for $KH_2PO_4(m) + Na_2HPO_4(m) + NaCl(m)$ in dimethyl sulphoxide–water mixture 50% w/w

T, K	m	I	E, V	$P_s(a_H \cdot \gamma_{Cl^-})$	$-\log \gamma_{Cl^-}$	paH*
	0.001	0.005	0.8202	7.4138	0.0386	7.375 ± 0.001
	0.002	0.010	0.8002	7.3651	0.0526	7.312 ± 0.001
288.15	0.003	0.015	0.7862	7.2963	0.0625	7.234 ± 0.002
	0.004	0.020	0.7730	7.1905	0.0705	7.120 ± 0.001
	0.005	0.025	0.7652	7.1509	0.0772	7.074 ± 0.002
	0.001	0.005	0.8262	7.3270	0.0388	7.288 ± 0.002
	0.002	0.010	0.8052	7.2794	0.0527	7.226 ± 0.002
293.15	0.003	0.015	0.7912	7.2148	0.0627	7.152 ± 0.002
	0.004	0.020	0.7812	7.1678	0.0706	7.097 ± 0.001
	0.005	0.025	0.7742	7.1444	0.0774	7.067 ± 0.002
	0.001	0.005	0.8322	7.2673	0.0391	7.228 ± 0.002
	0.002	0.010	0.8102	7.1965	0.0532	7.143 ± 0.002
298.15	0.003	0.015	0.7950	7.1157	0.0632	7.052 ± 0.002
	0.004	0.020	0.7852	7.0751	0.0712	7.004 ± 0.002
	0.005	0.025	0.7750	6.9996	0.0780	6.922 ± 0.002
	0.001	0.005	0.8372	7.1811	0.0395	7.142 ± 0.002
	0.002	0.010	0.8172	7.1497	0.0537	7.096 ± 0.002
303.15	0.003	0.015	0.8032	7.0897	0.0638	7.025 ± 0.002
	0.004	0.020	0.7942	7.0684	0.0719	6.996 ± 0.002
	0.005	0.025	0.7862	7.0323	0.0790	6.953 ± 0.002
	0.001	0.005	0.8432	7.1140	0.0399	7.074 ± 0.002
	0.002	0.010	0.8232	7.0880	0.0542	7.034 ± 0.002
308.15	0.003	0.015	0.8092	7.0352	0.0645	6.971 ± 0.002
	0.004	0.020	0.7992	6.9965	0.0727	6.924 ± 0.002
	0.005	0.025	0.7912	6.9626	0.0796	6.883 ± 0.002

uncharged particles present in solution is changed on increasing the concentration of the dissolved salt.

The secondary dissociation constants of *o*-phthalic and phosphoric acids in a 50% w/w Me_2SO–H_2O mixture at different temperatures (288.15–308.15 K) and at different ionic strengths are given in Tables 4 and 5. Values of pK_{a2} at different ionic strengths have been calculated with a convenient form of the Debye–Hückel equation, such as that due to Davies.[33] Values of the thermodynamic parameters $\Delta G°$, $\Delta H°$ and $\Delta S°$ for the second dissociation stage of *o*-phthalic and phosphoric

Table 4. pka_2 values of *o*-phthalic acid in DMSO–H_2O mixture (50% w/w) at different temperatures and ionic strengths

288.15 K		293.15 K		298.15 K		303.15 K		308.15 K	
I	pka_2	I	pka_2	I	pka_2	I	pka_2	I	pka_2
0	6.932 ± 0.003	0	6.920 ± 0.002	0	6.907 ± 0.004	0	6.887 ± 0.003	0	6.881 ± 0.004
0.01	6.888 ± 0.004	0.01	6.876 ± 0.002	0.01	6.863 ± 0.003	0.01	6.843 ± 0.002	0.01	6.837 ± 0.002
0.02	6.752 ± 0.003	0.02	6.740 ± 0.003	0.02	6.727 ± 0.002	0.02	6.708 ± 0.002	0.02	6.701 ± 0.002
0.03	6.719 ± 0.004	0.03	6.707 ± 0.002	0.03	6.695 ± 0.004	0.03	6.674 ± 0.003	0.03	6.668 ± 0.003
0.04	6.694 ± 0.003	0.04	6.682 ± 0.004	0.04	6.669 ± 0.003	0.04	6.649 ± 0.004	0.04	6.643 ± 0.004
0.05	6.673 ± 0.003	0.05	6.661 ± 0.003	0.05	6.648 ± 0.004	0.05	6.628 ± 0.003	0.05	6.622 ± 0.003

Table 5. pka_2 values of phosphoric acid in DMSO–H_2O mixture (50% w/w) at different temperatures and ionic strengths

288.15 K		293.15 K		298.15 K		303.15 K		308.15 K	
I	pka_2	I	pka_2	I	pka_2	I	pka_2	I	pka_2
0	7.565 ± 0.002	0	7.553 ± 0.003	0	7.540 ± 0.002	0	7.520 ± 0.002	0	7.514 ± 0.003
0.01	7.521 ± 0.003	0.01	7.509 ± 0.002	0.01	7.496 ± 0.003	0.01	7.493 ± 0.004	0.01	7.470 ± 0.002
0.02	7.385 ± 0.002	0.02	7.489 ± 0.003	0.02	7.360 ± 0.002	0.02	7.358 ± 0.003	0.02	7.334 ± 0.002
0.03	7.352 ± 0.004	0.03	7.456 ± 0.002	0.03	7.328 ± 0.003	0.03	7.324 ± 0.002	0.03	7.301 ± 0.002
0.04	7.327 ± 0.002	0.04	7.431 ± 0.002	0.04	7.302 ± 0.002	0.04	7.299 ± 0.002	0.04	7.276 ± 0.002
0.05	7.306 ± 0.002	0.05	7.410 ± 0.003	0.05	7.281 ± 0.003	0.05	7.278 ± 0.003	0.05	7.255 ± 0.003

Table 6. Thermodynamic parameters for the secondary dissociation stage of *o*-phthalic and phosphoric acids in 50% w/w dimethyl sulphoxide–water mixture

Acid	*T*, K	$\Delta G°$, *kJ/mole*	$\Delta H°$, *kJ/mole*	$-\Delta S°$, JK^{-1} *mole*$^{-1}$
	288.15	38.24 ± 0.03	3.81 ± 0.02	119.48 ± 0.05
	293.15	38.84 ± 0.02	3.95 ± 0.01	119.01 ± 0.04
o-phthalic	298.15	39.43 ± 0.04	4.08 ± 0.01	118.56 ± 0.06
	303.15	39.98 ± 0.03	4.22 ± 0.02	117.96 ± 0.04
	308.15	40.60 ± 0.02	4.36 ± 0.02	117.60 ± 0.03
	288.15	41.74 ± 0.04	4.76 ± 0.01	128.33 ± 0.03
	293.15	42.40 ± 0.02	4.93 ± 0.02	127.81 ± 0.04
Phosphoric	298.15	43.04 ± 0.03	5.10 ± 0.01	127.25 ± 0.03
	303.15	43.65 ± 0.02	5.28 ± 0.02	126.57 ± 0.04
	308.15	44.33 ± 0.03	5.45 ± 0.01	126.17 ± 0.03

acids have been calculated and are given in Table 6.

The need for reliable pH measurements at different temperatures in mixed solvents such as dimethyl sulphoxide (Me_2SO) and water has become increasingly apparent in the studies of the preservation of biological cells, tissues, and organs.[34,35] The data obtained in the present report can be used for preparing standard buffer solutions for p*a*H* measurements in 50% DMSO–water mixture at different temperatures (288.15–308.15 K) as shown in Tables 2 and 3.

REFERENCES

1. W. Simon, *Angew. Chem.*, Internat. Edn., Engl., 1964, **2**, 661.
2. G. Douheret, *Bull. Soc. Chim. France* 1967, 1412.
3. *Idem, ibid.*, 1968, 3122.
4. R. Reynaud, *Compt. Rend.*, 1969, **269**, 777.
5. Lesquibe and R. Reynaud, *Compt. Rend.*, 1970, **271**, 1193.
6. D. D. Perrin, and B. Dempsey, *Buffers for pH and Metal Ion Control*, Chapman and Hall, London 1974.
7. W. J. Hamer and S. F. Acree, *J. Res. Nat. Bur. Stand.*, 1944, **32**, 215; 1945, **35**, 381.
8. G. G. Manov, N. Delollis, P. W. Lindwal and S. F. Acree, *ibid.*, 1946, **36**, 543.
9. R. G. Bates, V. E. Bower, R. G. Miller and E. R. Smith, *ibid.*, 1951, **47**, 433.
10. H. A. Azab, *Bull. Soc. Chim. France*, 1987, 265.
11. M. Paabo, R. A. Robinson and R. G. Bates, *J. Am. Chem. Soc.*, 1965, **87**, 415.
12. R. N. Roy, J. J. Gibbons, B. Kennan and F. Steven, *J. Chem. Soc., Faraday Trans.*, 1984, **80**, 3167.
13. R. N. Roy, J. J. Gibbons and G. E. Baker, *Cryobiology*, 1985, **22**, 589.
14. R. N. Roy, J. J. Gibbons, B. Kennan and F. Steven, *J. Chem. Thermodyn.*, 1982, **14**, 1011.
15. C. A. Vega and J. C. Halle, *Bull. Soc. Chim. France*, 1979, **3–4**, Pt. 1, 124.
16. R. L. Parks, H. D. Crockfard and S. B. Knight, *J. Elisha. Mitchell. Sci. Soc.*, 1957, **73**, 289.
17. C. L. Deligny, P. F. M. Luykx, M. Rehbach and A. A. Wieneke, *Rec. Trav. Chim.*, 1960, **79**, 699.
18. H. A. Azab, R. M. Hassan and S. A. Ibrahim, *Ann. Chim. (Rome)*, 1986, **76**, 221.
19. H. A. Azab and Ahmed Hassan, *J. Chin. Chem. Soc.*, 1989, **36**, 413.
20. R. G. Bates, *J. Soln. Chem.*, 1986, **15**, 891.
21. G. J. Janz, *Reference Electrodes*, D. J. G. Ives and G. J. Janz (ed.), Chap. 4, Academic Press, New York, N.Y., 1961.
22. R. G. Bates, *Determination of pH*, p. 282, Wiley, New York, 1973.
23. M. Sankar, J. B. Macaskill and R. G. Bates, *J. Sol. Chem.*, 1979, **8**, 887.
24. A. Patterson and W. A. Felsin, *J. Am. Chem. Soc.*, 1942, **64**, 1478.
25. S. Rondinini, P. R. Mussini and T. Mussini, *Pure Appl. Chem.*, 1987, **59**, 1549.
26. R. A. Robinson and R. H. Stokes, *Electrolyte Solutions*, 2nd Ed., Butterworths, London, 1968.
27. K. H. Khoo, *J. Chem. Soc. A*, 1971, 1177.
28. *Idem, ibid.*, 1971, 2932.
29. J. J. Lindberg and J. Kenttamaa, *Suom. Kemistil. B*, 1960, **33**, 104.
30. G. Akerlof, *J. Am. Chem. Soc.*, 1932, **54**, 4125.
31. W. J. Hamer, in *Handbook of Chemistry and Physics* 52nd Ed., R. S. Weast (ed.), Chemical Rubber Co., Cleveland, Ohio, 1971.
32. R. G. Bates, *Determination of pH Theory and Practice*, p. 225. Wiley, New York, 1964.
33. C. W. Davies, *J. Chem. Soc.*, 1983, 2093.
34. D. E. Pegg, *J. Clin. Pathol.*, 1976, **29**, 271.
35. M. J. Taylor, C. A. Walter and B. C. Elford, *Cryobiology*, 1978, **15**, 452.

Talanta, Vol. 39, No. 8, pp. 919–922, 1992
Printed in Great Britain.

0039-9140/92 $5.00 + 0.00

ELECTROCHEMICAL STUDY OF SOLVENT EXTRACTION WITH 8-QUINOLINOLS AS COMPLEXING AGENT— I. DISTRIBUTION BEHAVIOR OF 8-QUINOLINOLS

SINRU LIN

Shanghai Institute of Metallurgy, Chinese Academy of Sciences, Shanghai 200050, China

HENRY FREISER

Strategic Metals Recovery Research Facility, University of Arizona, Tucson, AZ 85721, U.S.A.

(*Received* 31 *May* 1991. *Revised* 27 *November* 1991. *Accepted* 30 *November* 1991)

Summary—The distribution behavior of 8-quinolinols (HQ) in organic and acidic aqueous solutions (or alkaline solutions) was electrochemically examined by current scan polarography and chronopotentiometry. It follows from the results that the half wave potential of the observed polarographic waves, corresponding to the Faradaic transfer of quinolinolium ions (or oxinate ions) formed in the aqueous solution after distribution of quinolinols is dependent on the dissociation constant of H_2Q^+ (or HQ) and the pH of the aqueous solution, but independent of the distribution constant of 8-quinolinols.

Previous work on tervalent lanthanide ions extracted by 1,2-dichloroethane with 4-acyl-5-pyrazolones as chelating agent[1] demonstrated that powerful insights into the mechanisms of ion transfer processes in a solvent extraction system can be gained by electrochemical study of ITIES (interface of two immiscible electrolyte solutions). 8-Quinolinol has a hydrogen atom which can be replaced by a metal ion and a heterocyclic nitrogen which form a five-membered chelate ring with this metal ion, so it is one of the most useful and versatile chelating agents in metal ion extraction. This report is aimed at learning more about the distribution behavior of 8-quinolinol and some of its derivatives.

EXPERIMENTAL

Apparatus

Current scan polarography at the ascending water electrode (AWE), constant current chronopotentiometry and current reversal chronopotentiometry at the stationary water electrode (SWE) were employed. The electrolytic cell, apparatus and experimental procedures were described previously.[1–5]

Materials

The organic phase solvents used were nitrobenzene (NB) and 1,2-dichloroethane (DCE). Tetraheptylammonium tetraphenylborate (THA^+, TPB^-) was used as the supporting electrolyte in the organic phase.

8-Quinolinol (Eastman Kodak Co.) and its 2-methyl-, 5-chloro-, 5-nitro- and 5,7-dibromo-derivatives (Aldrich Chemical Company, Inc.) were used without further purification.

RESULTS AND DISCUSSION

A well-defined anodic wave at the AWE was obtained when 8-quinolinol (HQ) in NB was in contact with 1*M* magnesium sulphate solution with pH <4 (Fig. 1). The wave has the following characteristics:

(a) The limiting current (i_l) is proportional to the initial concentration of 8-quinolinol in NB and is essentially independent of the pH of the aqueous phase.

(b) The half-wave potential ($\Delta_0^a E_{1/2}$) is linearly dependent on the pH of the aqueous solution with a slope of 56 mV/pH (the experimental error for the half-wave potential is ± 4 mV).

(c) The variation of $\log[i/(i_l - i)]$ with $\Delta_0^a E$ is linear with a slope of 53 mV.

Hence, it can be seen from the characteristics that the limiting current is controlled by diffusion of 8-quinolinol in NB and that the cationic species, whose Faradaic transfer from the aqueous into the organic phase results in the wave, is singly charged. Constant current chronopotentiometry at the SWE was carried out to further test this interpretation (Fig. 2).

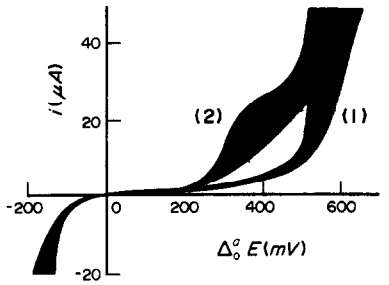

Fig. 1. Current scan polarograms of 8-quinolinol in nitrobenzene. Aqueous phase: 1*M* $MgSO_4$, pH 2.5. NB phase: (1) 20m*M* THA^+, TPB^-; (2) 20m*M* THA^+, TPB^- + 0.3m*M* 8-quinolinol.

It was found that the product of the applied current and the square root of transition time ($i\tau^{1/2}$) is independent of the applied current. The diffusion coefficient of 8-quinolinol in NB, evaluated from the data according to the Sand equation, was found to be $8.1(\pm 0.3) \times 10^{-6}$ cm^2/sec. Figure 3 shows the effect of the standing time (t_s) of the SWE on τ of the anodic chronopotentiometry (*i.e.*, before the electrolysis system is subjected to a controlled current, the SWE is allowed to stand in contact with the organic phase for a time t_s). It is seen that $\tau^{1/2}$ increases linearly with $t_s^{1/2}$, indicating that the singly charged cation accumulates in the aqueous phase during t_s. Inasmuch as the amount of the proton in the aqueous electrolyte remains constant, the cation transferring across the interface must be the 8-quinolinolium ion (H_2Q^+), which forms in the aqueous phase after HQ distributes there. When AWE and SWE experiments were repeated with HQ initially in the aqueous phase, waves with identical half-wave potentials to those of the previous experiments were obtained at the AWE, but with the

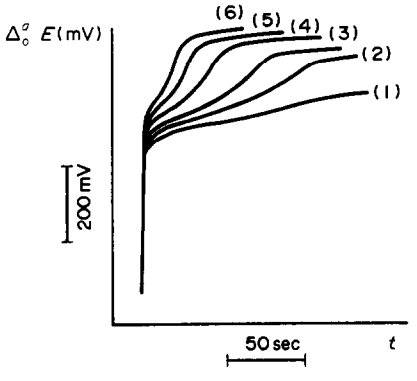

Fig. 2. Constant current chronopotentiograms at SWE. Aqueous phase: 1*M* $MgSO_4$, pH 2.5. NB phase: 20m*M* THA^+, TPB^- + 0.3m*M* 8-quinolinol. Current (μA): (1) 3, (2) 3.5, (3) 4, (4) 5, (5) 6, (6) 7. Surface area of SWE: 0.41 cm^2.

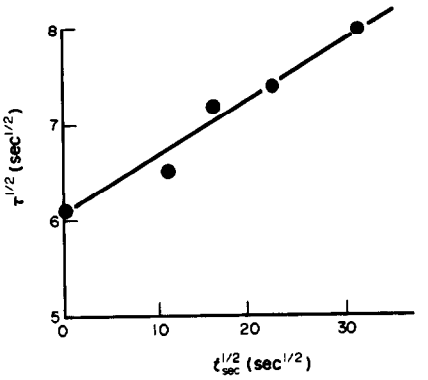

Fig. 3. Effect of standing time on transition time at SWE. Aqueous phase: 1*M* $MgSO_4$, pH 2.5. NB phase: 20m*M* THA^+, TPB^- + 0.3m*M* 8-quinolinol. Current: 5 μA. Surface area of SWE: 0.41 cm^2.

SWE no variation of τ with t_s was observed, entirely in keeping with the explanation of the transfer process given above.

Well-defined anodic waves were also observed when NB contained 2-methyl-8-quinolinol or 5-chloro-8-quinolinol, but no wave appeared when the organic phase contained 5-nitro- or 5,7-dibromo-quinolinol. The characteristics of the waves observed are the same as those of the 8-quinolinol wave, whereas the 2-methyl-8-quinolinolium wave appears at 40 mV less positive $\Delta_0^a E_{1/2}$ while the 5-chloro-8-quinolinolium wave is 75 mV more positive. The following discussion will give the explanation for the difference in $\Delta_0^a E_{1/2}$ among quinolinols.

As shown previously,[2,4] the half wave potential of the protonated wave can be expressed as follows:

$$\Delta_0^a E_{1/2,H_2Q^+} = \Delta_0^a E^0_{H_2Q^+} + \frac{RT}{2nF} \ln \frac{D_{HQ,O}}{D_{H_2Q^+,O}} + \frac{RT}{nF} \ln(K_{D,HQ} K_{a,H_2Q^+}) - \frac{RT}{nF} \ln H^+ \quad (1)$$

where $\Delta_0^a E^0$ is the standard potential difference, D the diffusion coefficient, $n = 1$, subscript 0 stands for the organic phase (none is used for aqueous phase),

$$K_{D,HQ} = \frac{[HQ]_0}{[HQ]} \quad (2)$$

$$K_{a,H_2Q^+} = \frac{[H^+][HQ]}{[H_2Q^+]} \quad (3)$$

As is known,

$$\Delta_0^a E^0_{H_2Q^+} = \frac{\Delta G^{0,a\to 0}_{tr,H_2Q^+}}{F} = -\frac{RT}{F} \ln K_{D,H_2Q^+} \quad (4)$$

Table 1. Comparison of observed and reported pK_a values

	I			II		
	$H_2Q^+ \overset{K_{a,H_2Q^+}}{\rightleftharpoons} H^+ + HQ$			$HQ \overset{K_{a,HQ}}{\rightleftharpoons} H^+ + Q^-$		
	$\Delta\Delta_0^a E_{1/2}$, mV	pK_a		$\Delta\Delta_0^a E_{1/2}$, mV	pK_a	
	Observed	Calculated*	Reported	Observed	Calculated*	Reported
8-Quinolinol			4.99[6]			9.66[6]
2-Methyl-8-quinolinol	−40	5.67	5.77[7]	37.5	9.02	10.04[7]
5-Chloro-8-quinolinol	76	3.72	3.68[8]	75	8.39	10.45[8]
5,7-Dibromo-8-quinolinol	/	/	2.6[9]	176	6.69	7.3[9]

*Calculated value with observed $\Delta\Delta_0^a E_{1/2}$ and equation (8).

$\Delta G_{tr,H_2Q^+}^{0,a\to 0}$ in equation (4) is the standard Gibbs energy of transfer of protonated quinolinols from the aqueous to the organic phase and

$$K_{D,H_2Q^+} = \frac{[H_2Q^+]_0}{[H_2Q^+]} \quad (5)$$

In the Yoshida and Freiser's report,[2] a comparison of a series of phenanthrolines indicates that the difference between $\ln K_D$ of neutral and protonated species is a constant factor, *i.e.*,

$$\ln K_{D,H_2Q^+} = \ln K_{D,HQ} - C \quad (6)$$

where C is a constant.

From equations (1), (4) and (6) we have the expression,

$$\Delta_0^a E_{1/2,H_2Q^+} = \frac{RT}{2F} \ln \frac{D_{HQ,O}}{D_{H_2Q^+,O}} + \frac{RT}{F} \ln K_{a,H_2Q^+} - \frac{RT}{F} \ln H^+ + \frac{RT}{F} C \quad (7)$$

The above equation indicates that if the difference between D_{HQ} and $D_{H_2Q^+}$ in the organic phase is negligible, $\Delta_0^a E_{1/2}$ of the wave for transfer of protonated 8-quinolinols is independent of their K_D values. It follows from equation (7) that if the organic solutions of 8-quinolinol and its derivatives are in contact with the aqueous solutions with the same pH, the difference in $\Delta_0^a E_{1/2}$ arises from the difference of their K_a values:

$$pK_{a,H_2Q^+}^d = pK_{a,H_2Q^+}^p - \frac{\Delta\Delta_0^a E_{1/2}}{59} \quad \text{(at 25°)} \quad (8)$$

where $\Delta\Delta_0^a E_{1/2}$ (in mV) $= \Delta_0^a E_{1/2}^d - \Delta_0^a E_{1/2}^p$, superscript d and p stand for derivative and parent, respectively. It can be seen from part I in Table 1 that the results observed coincide with those reported. Obviously, no protonated wave will be observed in 8-quinolinol systems under conditions in this work if the pK_{a,H_2Q^+} is smaller than about 3, because the wave shifts to such a positive value that it would be overlapped by the background current. 5-Nitro- and 5,7-dibromo-derivatives are such cases.

8-Quinolinols have an amphoteric nature. They form 8-quinolinolium ions with protons in acidic solutions and oxinate ions (Q^-) by deprotonation in alkaline solutions. Cathodic waves, which correspond to the Faradaic transfer of oxinate ions from the alkaline aqueous phase into the DCE phase, were observed (Fig. 4). For 8-quinolinol and its 2-methyl derivative, the well-defined cathodic wave can be observed when their DCE solutions are in contact with sodium hydroxide solution $\geqslant 0.1M$. For 5-chloro-8-quinolinol, the wave can be observed with sodium hydroxide solution $\geqslant 0.01M$ and for 5,7-dibromo-8-quinolinol with sodium hydroxide solution $\geqslant 10^{-4}M$ ($0.5M$ sodium sulphate as supporting electrolyte). The heights of these waves are proportional to the amount of 8-quinolinols in the DCE phase and independent of the sodium hydroxide amount in the aqueous phase. The half wave potentials of the waves shift by about 52 mV more positive with one decade increase in the sodium hydroxide concentration. The difference in $\Delta_0^a E_{1/2}$ between 8-quinolinol and its derivatives observed is

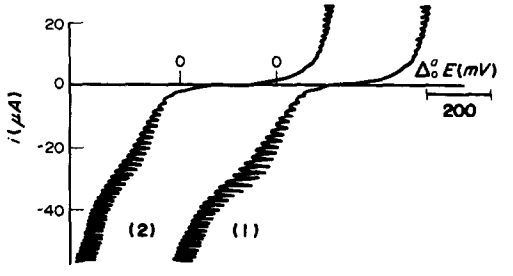

Fig. 4. Current scan polarograms of 5,7-dibromo- and 5-chloro-8-quinolinol in 1,2-dichloro-ethane. Aqueous phase: $1M$ NaOH. DCE phase: 10mM THA^+, TPB^- + (1) 0.3mM 5,7-dibromo-8-quinolinol; (2) 0.3mM 5-chloro-8-quinolinol.

listed in part II of Table 1. If the neutral and the deprotonated 8-quinolinols have the relationship expressed by equation (6) the $pK_{a,HQ}$ values of 8-quinolinols should decrease in the order from the parent to 2-methyl, 5-chloro and 5,7-dibromo derivatives according to their $\Delta_0^a E_{1/2}$ with equation (8), whereas the values reported in the references are not in keeping with the order. For the case of 5,7-dibromo-8-quinolinol, the $pK_{a,HQ}$ value elucidated from the difference in $\Delta_0^a E_{1/2}$ between it and its parent is in reasonable agreement with the value reported.[9] For the case of 5-chloro-8-quinolinol, the $pK_{a,HQ}$ value should be smaller than its parents, not greater as reported.[8] Because Cl is an electrophilic functional group, deprotonation becomes easier. Its illustration can be found in phenol and its chloro derivative. The negative logarithm dissociation constant reported for phenol is 9.10,[10] that for chloro-phenol is 8.78.[11] Obviously, the value 8.39 elucidated from the experimental $\Delta_0^a E_{1/2}$ for 5-chloro-8-quinolinol in this work and 7.47 reported[12] for 5,7-dichloro-8-quinolinol is reasonable. But, for the case of 2-methyl-8-quinolinol, the $pK_{a,HQ}$ value should be greater, not smaller, than that of its parent because of the methyl group being an electrophobic functional group. Alternatively, the $\Delta_0^a E_{1/2}$ for the 2-methyl case should be less positive than that for the 8-quinolinol case. Further work will be needed to investigate the cause of the unreasonable experimental value in the case of 2-methyl-8-quinolinol.

Acknowledgements—Most of the laboratory work was carried out in the laboratory of H. F. This research was partly supported by a grant from the Nature Science Foundation of China (No. 2880239).

REFERENCES

1. S. Lin and H. Freiser, *Anal. Chem.*, 1987, **59**, 2834.
2. Z. Yoshida and H. Freiser, *J. Electroanal. Chem.*, 1984, **162**, 307.
3. S. Lin and H. Freiser, *ibid.*, 1985, **191**, 437.
4. S. Lin, Z. Zhao and H. Freiser, *ibid.*, 1986, **210**, 137.
5. F. Wang and S. Lin, *Huaxue Xuebao*, 1991, **49**, 468.
6. D. Dyrssen, *Svensk Kem. Tidskr.*, 1952, **64**, 213.
7. *Idem, ibid.*, 1956, **68**, 212.
8. A. Ermakov, V. Voronin and V. Nelyubin, *Khim. Farm. Zh.*, 1985, **19**, 199.
9. J. Stary and H. Freiser, *Equilibrium Constants of Liquid–Liquid Distribution Reactions, Part IV: Chelating Extractions*, p. 85, 86, Pergamon Press, New York, 1979.
10. K. Jabalpurwala and R. Milburn, *J. Am. Chem. Soc.*, 1966, **88**, 3224.
11. C. Postmus, Jr., L. Magnusson and C. Craig, *Inorg. Chem.*, 1966, **5**, 1154.
12. D. Dyrssen, M. Dyrssen and E. Johansson, *Acta Chem. Scand.*, 1956, **10**, 341.

Talanta, Vol. 39, No. 8, pp. 923–930, 1992
Printed in Great Britain.

0039-9140/92 $5.00 + 0.00

A COMPARISON OF GRADIENT CAPACITY ANION CHROMATOGRAPHY USING MACROCYCLES D-2.2.2 AND D-2.2.1 IN CONSTANT OR VARIABLE TEMPERATURE MODE

JOHN D. LAMB* and ROBERT G. SMITH
Department of Chemistry, Brigham Young University, Provo, UT 84602, U.S.A.

(*Received* 29 *October* 1991. *Revised* 9 *December* 1991. *Accepted* 9 *December* 1991)

Summary—The ability of macrocyclic ligands to complex alkali metal cations has been exploited to perform chromatographic separations of anions. Macrocycles adsorbed to reversed phase columns can complex eluent cations, thus generating anion exchange sites. Gradient separations of anions can be performed by changing the column capacity during the course of the separation, either by changing the eluent cation or by changing the column temperature. Gradient anion separations are performed by changing the eluent from sodium hydroxide to lithium hydroxide with the cryptand D-2.2.2, while similar anion separations are achieved with D-2.2.1 by a KOH–LiOH gradient. Since the complexation of cations by macrocycles is exothermic, increasing the column temperature decreases the anion column capacity, allowing temperature gradient separations. The experimentally measured ΔH values for D-2.2.1 are higher than for D-2.2.2, leading to steeper gradients and thus better separations with D-2.2.1.

Macrocyclic ligands, such as crown ethers and cryptands, have been noted for their ability to selectively complex cations. This unique complexing ability has been exploited in ion chromatography. The ability of the macrocycle to complex a given cation is related to the ability of the cation to fit into the central cavity of the macrocycle.[1] Those cations that fit most closely into the macrocyclic cavity are often most strongly bound, while those cations that are either too large or too small to fit well into the cavity are less strongly bound. Thus retention in macrocycle-based chromatographic columns is determined, in general, by the size of the cation, with those that most closely match the macrocyclic cavity being retained longer than those cations that do not fit as closely.[2,3]

Macrocycle-based columns have also been used to separate anions. The cation bound to the macrocycle must be closely associated with an anion in order to maintain electrical neutrality, since most macrocycles are uncharged. Anions that are more hydrophobic in nature allow stronger interaction in low dielectric media since the macrocycle is also generally hydrophobic. Therefore not only can cations in the presence of a common anion be separated, but also anions in the presence of a common cation.[4–8] While macrocycles are noted for their cation selectivity, anion separations have been achieved which are at least as interesting, if not more so, than separations of cations.

We have performed anion separations with macrocycle-based columns in an ion exchange mode rather than a ligand exchange mode by using an alkali metal hydroxide as eluent.[9] The alkali metal cation forms a positively charged complex with the macrocycle, creating the anion exchange site, while the OH^- serves to elute anions. We have performed gradient separations by decreasing the column anion exchange capacity during the course of the separation by two different methods. In the first, the identity of the cation in the eluent is changed from one with a high affinity for the macrocycle to one of a lower affinity, and thereby decreasing the number of cation-macrocycle complexes, reducing the column anion exchange capacity.[10] A second method of decreasing the column capacity is to raise the column temperature. Since most cation-macrocycle complexation reactions are exothermic, increasing the column temperature results in fewer cation-macrocycle complexes, with a decrease in ion exchange capacity.[11] These capacity gradient separations show advantages over conventional ion exchange gradient separations which are carried out by increasing the eluent strength. With

*Author for correspondence.

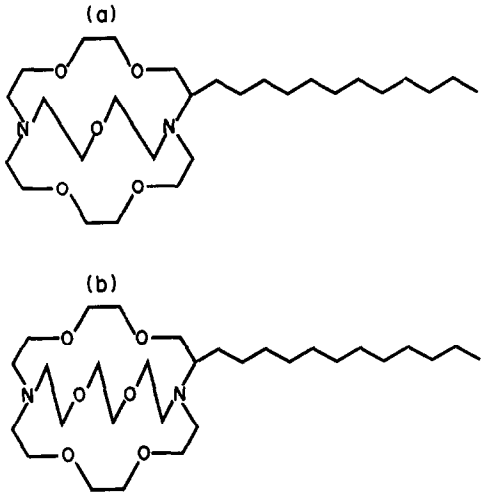

Fig. 1. Structures of the cryptands (a) n-decyl-2.2.1 (D-2.2.1) and (b) n-decyl-2.2.2 (D-2.2.2).

capacity gradients the eluent ionic strength is unchanged or changed very little, resulting in much greater baseline stability.

In this work, we compare anion separations in these two modes with two different macrocycles, the cryptands decyl-2.2.2 (D-2.2.2) and decyl-2.2.1/(D-2.2.1). Advantages of separations performed with each of these macrocycles are discussed.

EXPERIMENTAL

Materials

Reagent grade cryptands *n*-decyl-2.2.2 (D-2.2.2) and *n*-decyl-2.2.1 (D-2.2.1) whose structures are shown in Fig. 1, were obtained from EM Science (Gibbstown, NJ., U.S.A.). Reagent grade compounds were used in making standards and eluents. All water used in making eluents and standards was purified to 18 mΩ resistivity with a Milli-Q water purification system (Millipore) and eluents were degassed by sparging with helium.

Apparatus

All chromatography was performed on a Dionex 4000i Series ion chromatograph. Dionex anion micro membrane (AMMS) suppressors were used for eluent suppression prior to conductometric detection with a Dionex conductivity detector. Suppressant was 12.5m*M* sulphuric acid flowing at 3–5 ml/min. Columns used were Dionex MPIC NS-1 reversed phase columns. Temperature was controlled by either coiling one metre of tubing just prior to the column and placing the coiled tubing and column in a water jacket connected to a constant temperature bath circulating a 50:50 water:ethylene glycol mixture or by placing the coiled tubing in a Dionex column heater. The chromatograph was controlled and data collected on a personal computer with Dionex AI400 software.

Column preparation

The macrocycle-based columns were prepared in the manner previously described[9] by circulating a solution of the appropriate cryptand in a 60:40 methanol:water solution through the MPIC column for 12 hr.

RESULTS AND DISCUSSION

Macrocycle-based separation system

Macrocycles have been explored for use in separating both anions and cations in a ligand exchange mode at other laboratories. In our studies, however, we have focused on a method to separate anions on macrocycle-based columns by ion exchange rather than ligand exchange. This method has the advantages that anion retention is not a function of anion concentration or sample cation, drawbacks manifested when anions are separated in the ligand exchange mode. Anion exchange sites are formed by the complexation of cations with the neutral macrocycle. The resulting positively charged complex forms an anion exchange site, and the hydroxide counterion elutes the anions from the column.

Effect of eluent cation on column capacity

The number of exchange sites formed, and hence column capacity, is determined by the amount of ligand adsorbed on the column and the type and concentration of the cation in the

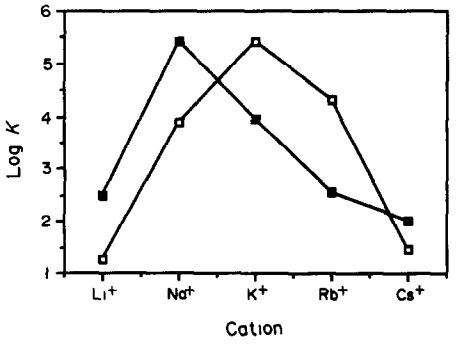

Fig. 2. Variation in log *K*, the formation constant for alkali metal complexes, in water for the cryptands 2.2.1 (■) and 2.2.2 (□) at 25° (from ref. 1).

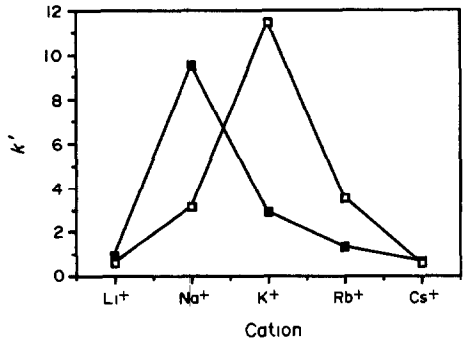

Fig. 3. Variation in Cl^- capacity factor, k', with eluent alkali metal cation (20mM), on D-2.2.2 (□) and D-2.2.1 (■) columns. The points for Cs^+ coincide.

eluent. Those cations that form the strongest complexes with the macrocycle, as measured by the binding constant, will generate more exchange sites than those cations that do not bind as strongly to the macrocycle. Column capacity is therefore a function of the binding constant for the reaction of the cation in the eluent with the macrocycle loaded on the column. Figure 2 plots the log of the binding constants for the cryptands 2.2.2 and 2.2.1 with the alkali metal cations. The cryptand 2.2.2 shows the highest binding with K^+, followed by Rb^+, Na^+, Cs^+ and Li^+. On the other hand 2.2.1, which has a smaller central cavity, shows the selectivity for Na^+, followed by K^+, Rb^+, Li^+ and Cs^+.

The dependence of anion retention on the eluent cation is illustrated by measuring the anion retention on the same column with different cations in the eluent. The retention of Cl^- on identical columns loaded with the same amount of D-2.2.2 and D-2.2.1 with different alkali metal cations in the eluent is demonstrated in Fig. 3. The eluent in each case was a 20mM alkali metal hydroxide. It is clear that the amount of retention is strongly related to the binding constant of the metal ion with the

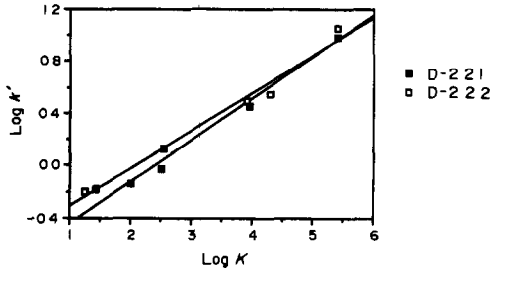

Fig. 4. Variation in log of the capacity factor (log k') for Cl^- versus log of the eluent cation binding constant in water (log K) for D-2.2.1 and D-2.2.2.

cryptand. The retention for the D-2.2.2 column follows the same order as the binding constants, with the K^+ eluent showing the most retention, followed by Rb^+, Na^+, Cs^+ and Li^+. The D-2.2.1 column retains anions most strongly with the Na^+ eluent, followed by K^+, Rb^+, Li^+ and Cs^+, respectively, in direct agreement with the order of the binding constants of these cations with 2.2.1. The relationship between the degree of anion retention and the strength of eluent cation binding to the column is shown in Fig. 4, in which the logarithm of the capacity factor of Cl^-, k', and the log of the cation-macrocycle binding constant are linearly related. This dependence of retention on eluent cation is most graphically demonstrated by Fig. 5, which shows the separation of a seven anion standard on the D-2.2.1 column with eluents composed of the different alkali metal hydroxides.

Cation capacity gradients

Gradient separations can be performed by changing the eluent cation from a cation with a higher affinity for the macrocycle to one with a lower affinity during the course of the

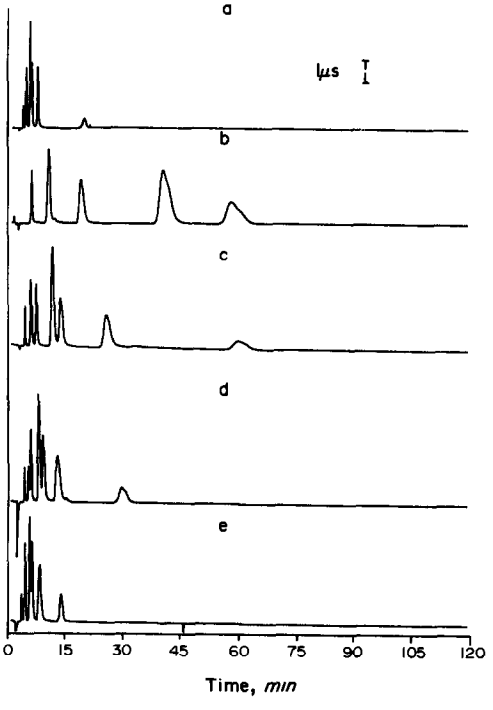

Fig. 5. Separation of 7 common anions on D-2.2.1 column in order of elution from left to right: 1 = F^-, 1.5 ppm; 2 = acetate, 10 ppm, 3 = Cl^-, 2.5 ppm; 4 = NO_2^-, 10 ppm; 5 = Br^-, 10 ppm; 6 = NO_3^-, 10 ppm; 7 = SO_4^{2-}, 10 ppm with different 20mM alkali metal hydroxide eluents: (a) Li^+ (b) Na^+ (c) K^+ (d) Rb^+ (e) Cs^+.

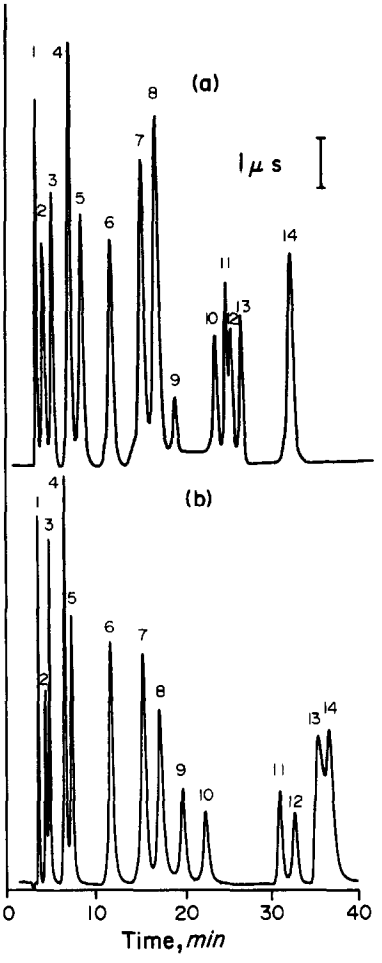

Fig. 6. Capacity gradient separation of 14 anions: 1 = F^-, 1.5 ppm; 2 = acetate, 10 ppm; 3 = Cl^-, 2.5 ppm; 4 = NO_2^-, 10 ppm; 5 = Br^-, 10 ppm; 6 = NO_3^-, 10 ppm; 7 = SO_4^{2-}, 10 ppm; 8 = oxalate, 10 ppm; 9 = CrO_4^{2-}, 10 ppm; 10 = I^-, 10 ppm; 11 = PO_4^{3-}, 10 ppm; 12 = phthalate, 10 ppm; 13 = citrate, 10 ppm; 14 = SCN^-, 10 ppm; on (a) D-2.2.2 column, with 30m*M* NaOH/30m*M* LiOH linear gradient for 20 min; (b) D-2.2.1 column, with 30m*M* KOH/30m*M* LiOH linear gradient for 20 min.

separation. The number of exchange sites decreases during the chromatogram as the higher binding cation is replaced by the cation with lower affinity and bleeds off the column. The resulting column has fewer exchange sites, and thus shows lower retention of anions.

The choice of cation combinations useful for capacity gradients is determined by the binding constants of the metal ions with the macrocycle, the rate at which the cations bleed from the column (*i.e.*, the cation complexation–decomplexation rate), and the background conductivity of the cation. For the D-2.2.2 column a successful gradient is achieved by changing the eluent from sodium hydroxide to lithium hydroxide as shown in Fig. 6(a). We are able to separate 14 anions in less than 40 min with a gradient from 30m*M* sodium hydroxide to 30m*M* lithium hydroxide. The potassium hydroxide eluent shows too much retention and bleeds from the column too slowly to make a good gradient. Rubidium and cesium cannot be used in the eluent as either the first or last cation because the background conductivity of these eluents is too high, resulting in unacceptable baseline drift. With D-2.2.1 column, a successful gradient is achieved with a potassium hydroxide to lithium hydroxide gradient. A gradient from 30m*M* potassium hydroxide to 30m*M* lithium hydroxide separates the 14 anion standard in just over 40 min, shown in Fig. 6(b). Sodium cannot be used as the first cation because it bleeds too slowly from the column, with the column capacity decreasing too slowly to be useful.

Both D-2.2.2 and D-2.2.1 columns can be used with gradients from one cation to another to separate a wide variety of anions. The resulting separations are similar, with the same elution order for all anions. However in comparing the two separations, we can see that the D-2.2.2 column is better suited for this type of gradient. In particular, the separation is achieved faster with the D-2.2.2 column. The binding constant of D-2.2.2 with Na^+ is close to that of D-2.2.1 with K^+, resulting in the same column capacity for the D-2.2.2 column with a sodium hydroxide eluent and the D-2.2.1 column with the potassium hydroxide eluent. The difference lies in the fact that the D-2.2.1 binds Li^+ better than D-2.2.2, resulting in higher column capacity at the end of the gradient, and thus more retention of longer retained peaks and a slower separation.

Effect of temperature on column capacity

Another method to change the column capacity during the course of a separation with a macrocycle-based column is to slowly increase the column temperature under isocratic eluent conditions. In conventional ion chromatography of both anions and cations the ion exchange reaction can be either exothermic or endothermic, depending on the ions involved. The ion exchange equilibrium can be shifted in either direction, resulting in either more or less retention, as the temperature is increased.

The complexation reaction of cations with macrocycles is generally exothermic. As the temperature is increased the equilibrium is shifted to form fewer cation–macrocycle complexes. The degree to which the equilibrium is

shifted, and hence the number of complexes formed, depends on the magnitude of the change in enthalpy for the complexation reaction. Since the retention of cations in macrocycle-based ion chromatography is based on the complexation–decomplexation reaction there should be less retention of cations at higher temperatures. For the separation of anions the situation is a little more complex. The column capacity is expected to be lower at elevated temperatures due to the decreased complexation and concomitantly fewer exchange sites. But since we are separating the anions by an ion exchange mechanism the retention behavior should also display the effect of temperature on conventional ion exchange.

The variation of capacity factors as a function of temperature is described by the equation:

$$\ln k' = -\frac{\Delta H}{RT} + \frac{\Delta S}{R} + \ln \varphi$$

where k' is the capacity factor, ΔH the enthalpy change for the reaction, R the molar gas constant, T the temperature at which the separation is carried out, ΔS the entropy change for the reaction, and φ the phase ratio for the column, a constant for a given column. Thus if we plot the capacity factor versus $1/T$ we should obtain a straight line with the slope $-\Delta H/R$, allowing us to obtain an estimate of ΔH for the reaction.

We measured the retention of both cations and anions on both D-2.2.2 and D-2.2.1 columns at varying temperatures. The columns were placed in a water jacket connected to a constant temperature bath to carefully regulate the temperature. For the cation separations a pure water eluent was used and the appropriate cation was injected while the column was maintained at the desired temperature by the constant temperature bath. Figure 6 shows the plot of the log of the capacity factor versus the reciprocal of the temperature, showing that the retention of all the alkali metal cations decreases significantly as the temperature is raised. From these plots we are able to calculate the ΔH for the cation retention reaction from the slopes of the lines obtained, the results of which are tabulated in Table 1. We see that the values are of the same order of magnitude for both the D-2.2.2 and D-2.2.1 columns. The significant difference between ΔH values measured for the macrocycle on the column and those for the parent compound in water is a clear indication that the cation reaction with column-bound macrocycle does not occur with the macrocycle portion floating free in the eluent, but must be involved in the extraction process.[11]

The anions were separated in a similar system, with a 20mM sodium hydroxide eluent used for the D-2.2.2 column and a 20mM potassium hydroxide eluent used for the D-2.2.1 column. The resulting plot of ln k' *vs.* $1/T$ in Fig. 7 shows that retention of all of the anions on both the D-2.2.2 and D-2.2.1 columns decreases with increasing temperature. The slopes of the lines obtained have a slightly higher value for the D-2.2.1 column than the D-2.2.2 column, indicating a larger negative value of ΔH for the retention reaction. This is demonstrated by the values for the enthalpy change tabulated in Table 1. The values for the ΔH's obtained under chromatographic conditions are lower than the reported values for the homogeneous solution complexation reactions.[1] The thermodynamic behaviour of these systems will be the subject of a future paper.

The separation of anions on the macrocycle column takes place mainly through an ion exchange mechanism. However if this were the only effect the temperature dependence of retention should be the same as for conventional ion exchange, with the retention of some anions increasing and others decreasing, as we have previously shown.[11] As demonstrated in Fig. 8 we see that the retention of all anions decreases. This decrease in retention for all anions can be

Table 1. Measured ΔH values for D-2.2.1 and D-2.2.2 macrocycle-based columns for various cations and anions compared to literature values for parent compound–cation reaction in water

	ΔH, kcal/mole		ΔH, kcal/mole	
Ion	D-2.2.1 on column*	2.2.1 in H_2O†	D-2.2.2 on column*	2.2.2 in H_2O†
Li^+	+0.29	0	−12.14	−1.40
Na^+	−3.64	−5.35	−6.86	−7.40
K^+	−4.63	−6.81	−5.43	−11.46
Rb^+	−4.15	−5.40	−9.21	−11.80
Cs^+	−0.74	—	—	−5.19
F^-	−3.72		−3.81	
Acetate	−4.66		−3.75	
Cl^-	−5.63		−3.73	
NO_2^-	−6.62		−4.45	
Br^-	−7.90		5.17	
NO_3^-	−8.37		−5.39	
SO_4^{2-}	6.41		−3.59	

*ΔH for the cation–macrocycle complexation on the stationary phase, for cations. For anions, ΔH of the exchange reaction between analyte anions and hydroxide ions.

†ΔH for the homogeneous solution cation–macrocycle complexation in water at 25° (from ref. 1).

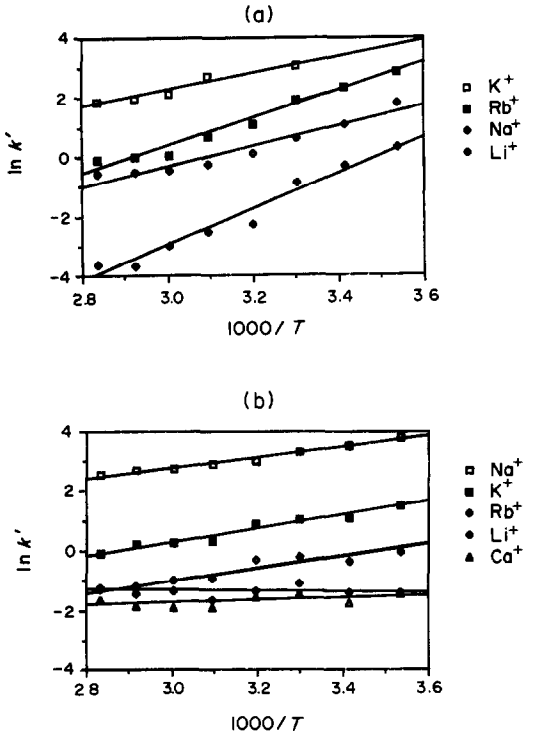

Fig. 7. Variation in ln k' versus $1/T$ for alkali metal cations on (a) D-2.2.2 column and (b) D-2.2.1 column, with a pure water eluent.

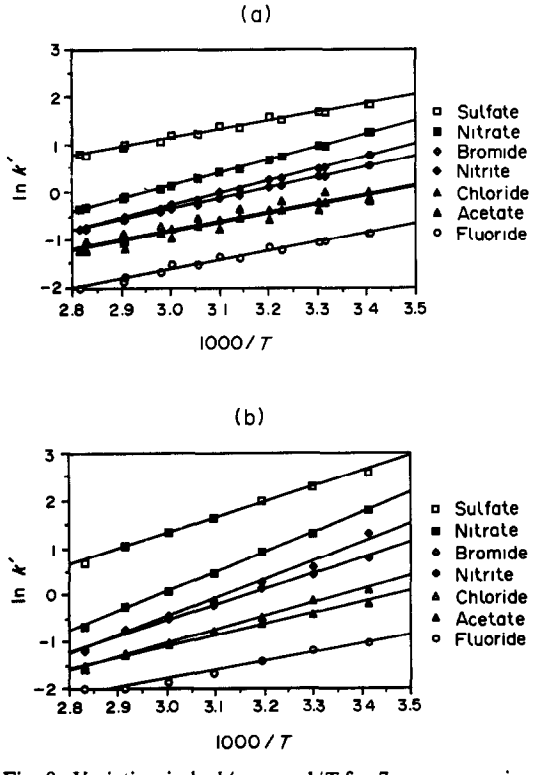

Fig. 8. Variation in ln k' versus $1/T$ for 7 common anions on (a) D-2.2.2 column with 20mM NaOH eluent and (b) D-2.2.1 column with 20mM KOH eluent.

explained by measuring the column capacity as a function of temperature.

The column capacity was measured for the macrocycle columns at different temperatures by the following method. The column was equilibrated with the eluent, a 20mM sodium hydroxide eluent for the D-2.2.2 column and a 20mM potassium hydroxide eluent for the D-2.2.1 column. The column was switched out of line and the connecting tubing rinsed free of eluent by pure water. The column was switched back in line and the cations eluted from the column by 0.1M nitric acid and the column effluent was collected. The concentration of the eluent cation in the effluent was determined, and by knowing the original eluent concentration, the uptake of eluent cation by the column was calculated, taking into account the column dead volume and original eluent cation concentration to correct for the amount of cation in the column dead volume. This was done at temperatures ranging from 20–80° for both the D-2.2.2 and D-2.2.1 columns. By plotting the amount of eluent cation taken up by the column, and hence the column anion exchange capacity, versus the column temperature, shows that for both columns the exchange capacity decreases significantly with increasing temperature (Fig. 9). This effect outweighs the effect of the anion exchange reaction, explaining the decrease of retention for all anions with increasing temperature.

Temperature gradient separations

Temperature gradient separations on both cryptand columns were carried out by placing one metre of tubing immediately ahead of the column in a Dionex column heater. The temperature was then controlled by the Dionex

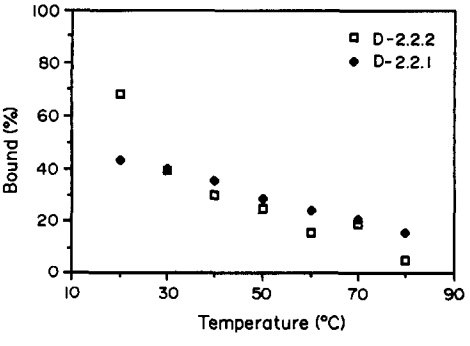

Fig. 9. Variation in column anion exchange capacity of D-2.2.2 and D-2.2.1 columns versus temperature expressed as percent of macrocycle sites containing bound sodium cations for D-2.2.2 column and potassium cations for D-2.2.1 column.

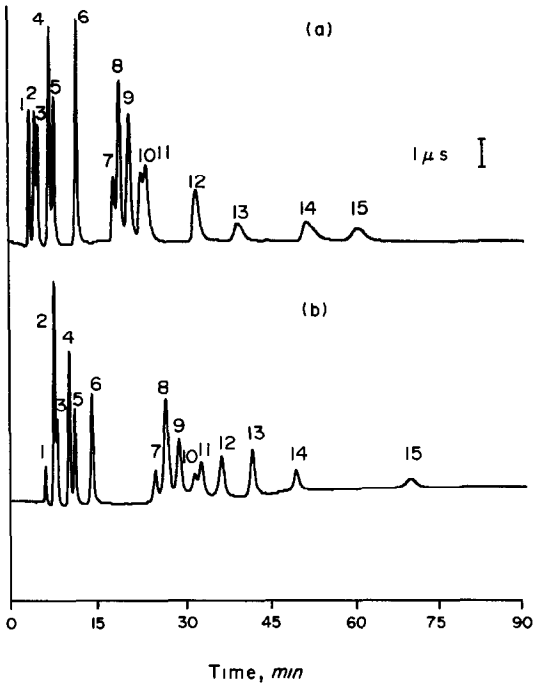

Fig. 10. Temperature gradient separation of 15 common anions: 1 = F^-, 1.5 ppm; 2 = acetate, 10 ppm; 3 = Cl^-, 2.5 ppm; 4 = NO_2^-, 10 ppm; 5 = Br^-, 10 ppm; 6 = NO_3^-, 10 ppm; 7 = I^-, 10 ppm; 8 = SO_4^{2-}, 10 ppm; 9 = oxalate, 10 ppm; 10 = CrO_4^{2-}, 10 ppm; 11 = MoO_4^-, 10 ppm; 12 = SCN^-, 10 ppm; 13 = ClO_4^-, 10 ppm; 14 = PO_4^{3-}, 10 ppm; 15 = phthalate, 10 ppm; with temperature gradient program starting at 30° and increasing to reach 80°, beginning at 5 min and ending at 30 min on (a) D-2.2.1 column with 20m*M* KOH eluent and (b) D-2.2.2 column with 20m*M* NaOH eluent.

AI400 software. The eluent for the D-2.2.2 column was 20m*M* sodium hydroxide and 20m*M* potassium hydroxide for the D-2.2.1 column, each at 1.0 ml/min. These cations were chosen for the respective eluents because they showed enough retention of anions to separate the early eluting peaks, yet would bleed off the column rapidly enough to allow a gradient separation. The temperature gradient program began at 30° and increased to 80°, beginning at five minutes and ending at 30 min. The resulting separations are shown in Fig. 10. The resulting chromatograms show good resolution of the earlier eluting peaks, while eluting strongly retained species in a reasonable time. It is interesting to note several changes in the elution order compared to the cation gradient system. With temperature gradient separations some late eluting species switch elution order, with strongly retained monovalent anions such as perchlorate and thiocyanate elution before polyvalent phosphate and phthalate. In temperature programming the baseline may be affected by the increase in mobile phase temperature since conductivity is a strong function of temperature. With suppressed conductivity detection the temperature of the eluent reaching the detector cell is kept constant by the cooling of the eluent in the suppressor by the room temperature regenerant, flowing 3–5 times faster than the eluent. The resulting baseline shows little perturbation due to the increase in the eluent temperature during temperature programmed elution.

Since the experimentally measured values for the enthalpy change for the retention of anions on the D-2.2.1 column are generally larger for the corresponding values for the D-2.2.2 column, we would expect to see a larger change in retention for the D-2.2.1 column. The separation of an anion standard does indeed show that for the D-2.2.1 column the separation is carried out slightly faster, with little or no loss of resolution, than for the D-2.2.2 column.

CONCLUSION

The ability to perform gradient separations of anions by dynamically altering the column capacity during the course of the separation has been demonstrated. Two different methods can be used to change the column capacity: changing the cation in the eluent and raising the column temperature. The macrocycle that is most effective is dependent on the method used. The capacity gradient by changing cation is more effective with D-2.2.2 than D-2.2.1 because D-2.2.2 binds lithium less strongly than D-2.2.1, allowing lower column capacity. Temperature gradients are more effective with D-2.2.1 because of the higher change in enthalpy, resulting in a greater shift in the complexation equilibrium to less cation-complex formation. Overall, cation gradient separations result in faster separations than temperature programmed separations. However temperature gradient separations show a more stable baseline and a different selectivity for some anions.

Acknowledgements—The authors express appreciation to Chad Jorgensen for his assistance and to Dionex Corporation, which provided funding for this research.

REFERENCES

1. R. M. Izatt, J. S. Bradshaw, S. A. Nielsen, J. D. Lamb and J. J. Christensen, *Chem. Rev.*, 1985, **85**, 271.
2. E. Blasius and K. P. Janzen, *Top. Curr. Chem.*, 1981, **98**, 163.

3. K. Kimura, H. Harino, E. Hayata and T. Shono, *Anal. Chem.*, 1986, **58**, 2233.
4. E. Blasius, K. P. Janzen, W. Klein, H. Klotz, V. B. Nguyen, T. Ngyen-Tien, R. Pfieffer, G. Scholten, H. Simon, H. Stockemer and A. Toussaint, *J. Chromatog.*, 1980, **201**, 147.
5. M. Nakajima, K. Kimura and T. Shono, *Bull. Chem. Soc. Jpn.*, 1983, **56**, 3052.
6. M. Takagi and H. Nakamura, *J. Coord. Chem.*, 1986, **15**, 53.
7. T. Iwachido, H. Naito, F. Samukawa, K. Ishimaru and K. Toei, *Bull. Chem. Soc. Jpn.*, 1986, **59**, 1475.
8. M. Lauth and P. Gramain, *J. Chromatog.*, 1987, **395**, 107.
9. J. D. Lamb and P. A. Drake, *ibid.*, 1989, **482**, 367.
10. J. D. Lamb, P. A. Drake and K. Wooley, in *Advances in Ion Chromatography*, P. Jandik and R. M. Cassidy (eds.), Vol. 2, p. 197. Century International, Medfield, MA, 1990.
11. R. G. Smith, P. A. Drake and J. D. Lamb, *J. Chromatog.*, 1991, **546**, 139.

Talanta, Vol. 39, No. 8, pp. 931–935, 1992
Printed in Great Britain.

0039-9140/92 $5.00 + 0.00

LIQUID FILM PERTRACTION—A LIQUID MEMBRANE PRECONCENTRATION TECHNIQUE

Z. LAZAROVA and L. BOYADZHIEV
Institute of Chemical Engineering, Bulgarian Academy of Sciences, Sofia 1113, Bulgaria

(*Received* 11 *November* 1991. *Revised* 2 *January* 1992. *Accepted* 2 *January* 1992)

Summary—A new liquid membrane technique for preconcentration of trace components from aqueous solutions is proposed. This technique, known as liquid film pertraction (LFP), provides simple and stable continuous operation and high enrichment factors. Experiments are carried out with two types of model systems, preconcentrating copper(II) ions and aromatic amines (*m*-toluidine). In the first case the liquid membrane of C_{11}–C_{13} normal paraffins, contained commercial chelating extractant LIX 65N, but in the second one the membrane of liquid paraffins with no additives was used. The influence of flow-rates of donor and acceptor solutions were studied as well as the effect of the membrane circulation and the initial solute concentration in the treated donor solution. Applying the new LFP technique enrichment factors in the order of 10 were obtained.

Contemporary ecological problems cannot be solved, unless effective waste-free technologies are developed or novel effective techniques for trace analysis of various substances are established. To prepare suitable samples of industrial waste waters, physiological fluids, natural waters, *etc.*, generally selective extraction of a particular component from these solutions is required, combined with component enrichment in an appropriate liquid medium for subsequent analysis. Therefore, the use of a liquid membrane method for simultaneous selective extraction and preconcentration of various species, presents an attractive research problem. Compared to the classical solvent extraction, the liquid membrane separation ensures higher extent of recovery of the solutes from the initial dilute solutions. In particular, this feature becomes essential in cases where the distribution coefficient of the solute between the organic solvent and the aqueous phase, is in order of one or even less.[1]

The early results published confirmed the idea that the liquid membranes might be used as a suitable method for preconcentration of metal ions or organic compounds dissolved in aqueous effluents. A number of such studies have been employed and so called emulsion liquid membranes (ELM) for preconcentration of metals, as uranium, cerium, cobalt, manganese, strontium, *etc.*[2–4] Other authors preferred to use the supported liquid membranes (SLM) technique.[5–7] For example, Audunsson[8,9] used a *n*-undecane-impregnated PTFE membrane of 70% porosity for preconcentration of various amines from urine. Amines have been the subject also of other studies, focused on the mathematical modelling of the transfer processes in the above-mentioned ELM systems.[10–13] An attempt was also made to separate enantiomers and other isomers by means of aqueous membranes, supported on thin cellulose sheets.[14]

Our studies were directed towards selective recovery and preconcentration of metal ions as well as of organic compounds from their diluted aqueous solutions by means of another liquid membrane technique, namely liquid film pertraction (LFP).[15] Copper(II) ions and the aromatic amine *m*-toluidine were subject to preconcentration.

EXPERIMENTAL

Apparatus

Figure 1 represents the principle diagram of the LFP method. Both aqueous solutions—the donor solution F, initially containing the analyte, and the acceptor or the receiving one, R, where the extracted solute is concentrated, flew down along the hydrophilic surfaces of the solid supports 4 and 5 in the form of thin liquid films. The organic liquid, S, acting as a membrane, occupied the free space of the apparatus and was continuously recirculated in counter current with respect to both aqueous solutions F and R as shown in the figure.

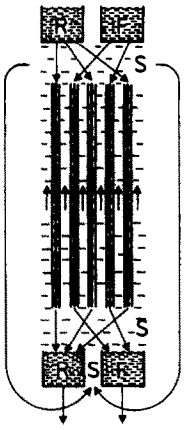

Fig. 1. Principal flow diagram of the LFP technique.

The experiments were carried out in a simple laboratory pertractor shown in Fig. 2. The device made of organic glass contained three vertical hydrophilic supports, the central one for the treated solution F and the other two supporting the acceptor liquid. These supports, intended for the aqueous solutions were made of regenerated porous cellulose sheets. The operational height of supports was 50 cm, the thickness—0.4 and 0.05 cm, respectively, and the distance in between—0.5 cm. The latter represents the real thickness of the membrane liquid layer.

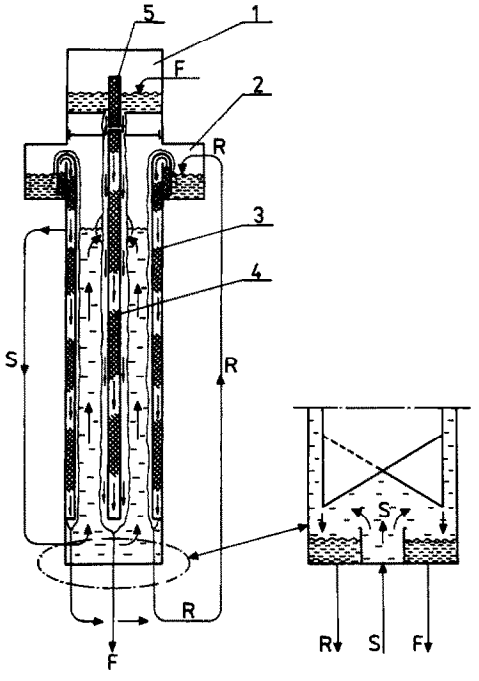

Fig. 2. Scheme of laboratory apparatus used in the experiments: 1. donor solution (F) compartment. 2. Acceptor solution (R) compartment. 3. Lateral hydrophylic supports for recirculating acceptor solution (R). 4. Central hydrophylic support for donor solution (F). 5. Disposable filter-distributor of donor liquid (F). Right: side view of bottom collectors for both aqueous solutions, explains the way the two liquids are separated.

The initial aqueous solutions F_0 and R_0 were fed into the appropriate feeding pertractor chambers by means of two peristaltic pumps, operated independently by means of timers in order for both solutions to be supplied periodically. This mode of liquid supply provides uniform horizontal distribution of the solutions and garantees their plug flow down the supports, especially when very low flow-rates, are used. When high concentration degree is needed, the acceptor solution R was recirculated in a close loop, too. The membrane liquid was set into motion by a magnetically-driven centrifugal pump, and its velocity in the device was measured and controlled.

Reagents and analytical methods

Copper ion preconcentration was carried out using a solution of the copper-selective chelating extractant LIX 65N (Henkel Corp.) in normal paraffins, as a liquid membrane. The active carrier in this commercial extractant is 2-hydroxy-5-nonyl benzophenone oxime. The oxime was used without special purification in concentrations of 5–20% (vol.) in a regular boiling point range of normal paraffins NORPAR 10/13 containing 0.1% *n*-nonane, 3.4% *n*-decane, 17.3% *n*-undecane, 45.7% *n*-dodecane, 33.2% *n*-tridecane and 0.4% *n*-tetradecane and higher *n*-paraffins. The paraffins were washed at least five times with large amounts of distilled water to remove any traces of ammonia or other water soluble impurities.

Regarding the preconcentration of *m*-toluidine, the organic membrane used was the above-mentioned hydrocarbon mixture without additives.

Model donor aqueous solutions were prepared by dissolving $CuSO_4.5H_2O$ (p.a. from KZ Co) or *m*-toluidine (pro synth., Merck) in distilled water. The donor solutions were not buffered. The acceptor solutions contained 1.5 or 1 *M* sulphuric acid (p.a. from KZ Co.).

The copper concentrations in the aqueous solutions were measured complexometrically by using EDTA.[16]

The amine concentration in the aqueous solution was measured by a UV–Vis spectrophotometer SPECORD(Carl Zeiss) at $\lambda = 287$ nm.[17] The pH-values were monitored with a LP-17 digital pH-meter. The experiments were carried out at 20°.

All concentrations in the sections to follow, are in ppm (w/v), and each point presents an average value obtained on the basis of three independent concentration measurements.

RESULTS AND DISCUSSION

The experimental studies were intended to evaluate the effects of the major concentration and flow variables upon the so-called enrichment factor EF, which was considered as a preconcentration efficient parameter. This parameter was defined as a ratio of final analyte concentration in the receiving solution R, to its initial concentration in the treated solution F, at steady state conditions. The steady state conditions were reached within 30 min–2 hr continuous operation, depending on the flow-rate (Q_F) of the donor solution and on the organic membrane circulation velocity Q_S.

The preconcentration of copper

The following three-liquid phase system was employed in the studies: aqueous solution of copper sulphate—solution of LIX 65N in the above-mentioned normal paraffins—3N sulphuric acid. The flow-rates of both solutions, F and R, were maintained constant, *i.e.*, $Q_F = 0.05$ cm^3/sec and $Q_R = 0.005$ cm^3/sec. The initial pH value of the donor liquid was 2.3. As well as the initial copper concentration which was varied between 50 and 1000 ppm, the other parameters relevant to the process were the concentration of LIX 65N in the paraffins [5 or 20% (vol.)] and the recirculation flow-rate of the membrane liquid, Q_S (0 to 3 cm^3/sec).

The effect of membrane recirculation intensity upon the EF value at 5 and 20% (vol.)

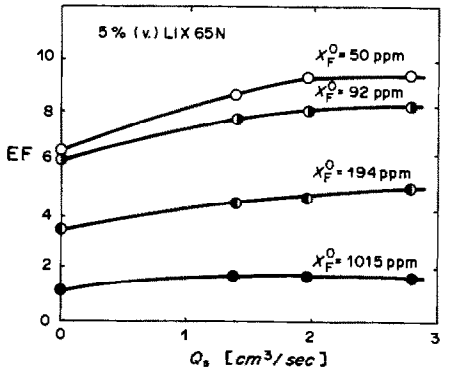

Fig. 3. Effect of recirculation flow-rate (Q_S) of the membrane liquid containing 5% (vol.) LIX 65N on the enrichment factor (EF) at various initial copper(II) concentrations in the donor solution (X_F^0).

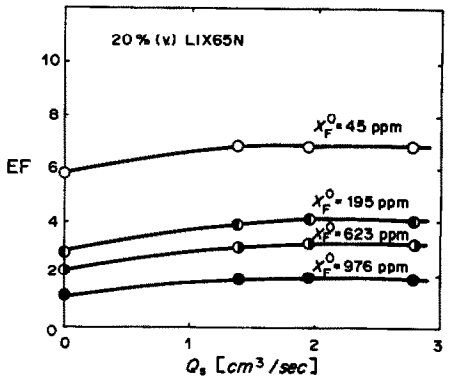

Fig. 4. Effect of recirculation flow-rate (Q_S) of the membrane liquid, containing 20% (vol.) of LIX 65N on enrichment factor (EF) at various initial copper(II) concentrations in the donor solution (X_F^0).

of LIX 65N in the membrane liquid, is shown in Figs. 3 and 4. Evidently, the rise of flow-rate Q_S, which increases the membrane mobility, resulted in a positive effect, particularly at the lowest copper concentrations. When the initial copper content in the treated solution exceeded 500 ppm, is only slightly affected by Q_S. By the donor solutions with relatively high copper concentration, copper transfer was hindered, which was likely to occur, due to the limited loading capacity of the carrier in the membrane liquid. The effect of copper content in the treated solution at mobile membrane phase, is illustrated in Fig. 5. As seen from the figure in the region exceeding 700 ppm, EF remained constant, regardless of oxime concentration in the membrane liquid, *i.e.*, there was no difference between the runs carrier with the membrane containing 5 and 20% active carrier. In contrast, at concentrations below 300 ppm, the lower the LIX 65N concentration was, the better the results were at constant initial copper

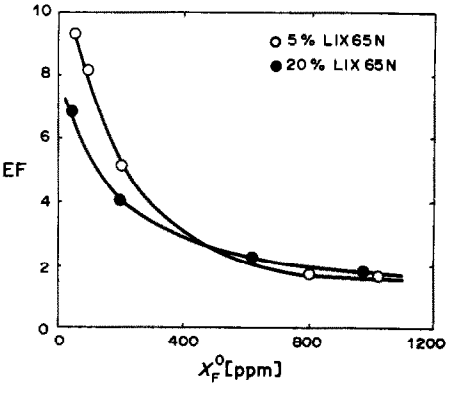

Fig. 5. Effect of initial copper(II) concentration in the donor solution on the enrichment factor (EF). $Q_S = 2.77$ cm^3/sec; $Q_F = 0.12$ cm^3/sec.

concentrations. As supported by the results obtained, the higher concentrations of the oxime in the paraffins results in a significant increase of membrane viscosity which slow down the rate of the mass transfer across the membrane layer.

From these results, it was concluded that the recirculation of the membrane liquid, applied for donor solutions with low initial copper concentrations, results in higher rates of extraction and more efficient preconcentration of the analyte in the receiving solution, R. For example, starting at 50 ppm by using a 5% LIX 65N solution in the membrane liquid, the EF rises, as shown in Fig. 3, from 6.46 (for immobile membrane) to 9.3 (for membrane circulation flow-rate of 2.77 cm^3/sec). The time required to reach a steady state in this case was 30 min. The enrichment factor obtained is close to the value reported by Cox *et al.*,[7] using LIX 64N as carrier.

It should be noted that, besides the enhancement of membrane phase circulation, two more variables facilitate achievement of higher EF. The first one is the change in the coefficient of copper distribution between membrane and donor liquids. Our previous experiments[18] as well as the results of other authors[19,20] have shown that this coefficient strongly depends on the donor solution pH value. Due to the equimolar counter diffusion of hydrogen ions from the receiving acidic solution R, the pH value of the donor liquid fell from 2.3 to 2. The higher the pH-value of solution F, the higher the copper distribution coefficient, and hence the higher the rate of copper transfer obtained. The second factor enhancing the enrichment factor is the recirculation of the receiving solution R which facilitates the transmembrane copper transport.

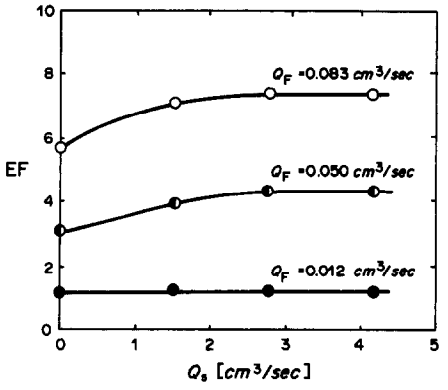

Fig. 7. Effect of membrane liquid circulation (Q_S) on the enrichment factor (EF) at various donor solution flow-rates (Q_F). $X_F^0 = 10$ ppm.

The preconcentration of m-*toluidine*

The second three-liquid-phase system used to study the LFP preconcentration technique was an aqueous solution of *m*-toluidine—NORPAR 10/13—2*N* sulphuric acid. The results obtained in the preconcentration of this aromatic amine are shown in Figs. 6–8. Figure 6 illustrates the effect of donor solution flow-rate (Q_F) on the enrichment factor at an initial *m*-toluidine concentration of 105 ppm. As seen from the figure, the increase of Q_F which also means a decrease of the mean residence time of the solution in the apparatus, also resulted in a rise of EF. However, this relationship was not linear, *e.g.*, the EF rise was accompanied by a fall in the efficiency of amine recovery. This fact has to be accounted for, since this is a major factor in the calculations of analyte preconcentration. Thus, at $Q_F = 0.012$ cm^3/sec, $Q_S = 1.76$ cm^3/sec the extraction efficiency was 95.3%, while a ten-fold increase of flow-rate Q_F shows EF = 8.97, but the efficiency falls to

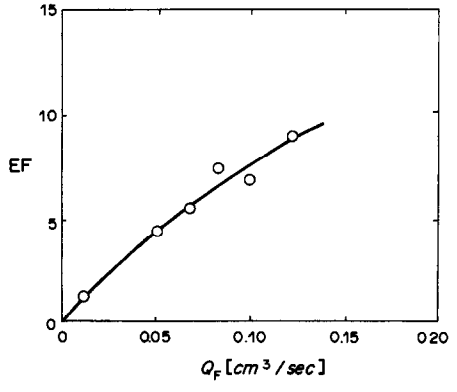

Fig. 6. Effect of donor solution flow-rate (Q_F) on the enrichment factor (EF). $X_F^0 = 105$ ppm; $Q_S = 1.76$ cm^3/sec.

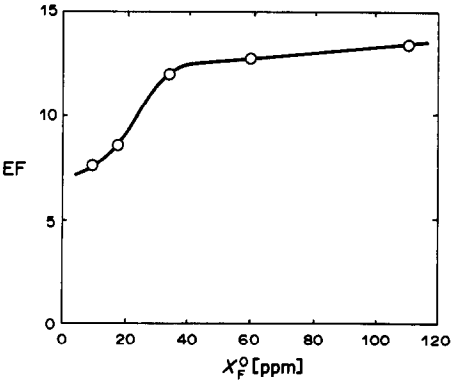

Fig. 8. Effect of initial concentration of *m*-toluidine in the treated (donor) solution (X_F^0) on the enrichment factor (EF). $Q_F = 0.083$ cm^3/sec; $Q_S = 1.76$ cm^3/sec.

71.4%. Obviously, an appropriate relationship between the flow-rate Q_F and the values of EF and E, has to be established.

Figure 7 shows the influence of the membrane flow-rate, Q_S on the value of EF at three donor solution flow-rates, Q_F. At the higher Q_F which, as already mentioned, leads to an increase in the EF the membrane circulation intensity exhibits some influence. At $Q_F = 0.083$, EF increased from 5.6, which corresponded to a quasistagnant membrane, to 7.4 at membrane circulation velocities exceeding 2.7 cm^3/sec. The circulation of membrane liquid showed no effect on the EF value at the lowest flow-rate level, *i.e.*, when $Q_F = 0.012$ cm^3/sec, it is likely that at this liquid film velocity the mass transfer resistance was located entirely in the donor solution F and any changes in membrane hydrodynamics did not influence the over-all mass transfer rate.

The effect of initial amine concentration on the enrichment factor EF, is shown in Fig. 8. It can be seen that for concentrations under 40 ppm, EF is affected significantly by the initial amount of amine in the donor solution: EF increased from 7.5, at an initial concentration of 10 ppm, to about 13.0, by the concentrations exceeding 35–40 ppm. The peculiar form of the curve is difficult to explain, but is very likely related to the dissociation of amine molecules in the donor solution and/or the amine solubility in the organic membrane.

CONCLUSION

The experiments carried out showed that the liquid film pertraction is an efficient liquid membrane technique for selective preconcentration of various solutes from their dilute aqueous solutions. Enrichment factors in the range of 5–15 were obtained. Additions of appropriate selective extractants to a neutral membrane of liquid paraffins provide good results in the case of copper preconcentration. For preconcentration of aromatic amines a membrane of liquid paraffins is quite suitable. In this case the enrichment factor depends strongly on amine solubility and dissociation in the treated aqueous solution.

Acknowledgement—This project has been supported financially by the Ministry of Science and Education under Research Contract No. 0155.

REFERENCES

1. L. Boyadzhiev, *Sep. Sci. and Technol.*, 1990, **25**, 187.
2. F. Macàsek, *Proc. SIS '85*, Smolenice, Czechoslovakia, 1985, 44.
3. F. Macàsek, Pajec, V. Reháček, A. Vu Ngoc and T. J. Popovnàkovà, *J. Radioanal. Nucl. Chem.*, 1985, **5**, 529.
4. M. R. Izatt, R. L. Bruening, Wu Geng, M. H. Cho and J. J. Christensen, *Anal. Chem.*, 1987, **59**, 2405.
5. K. Akiba and H. Hashimoto, *Talanta*, 1985, **32**, 824.
6. H. Sakamoto, K. Kimura and T. Shono, *Anal. Chem.*, 1987, **59**, 1513.
7. J. A. Cox, A. Bhatnagar and R. W. Francis, *Talanta*, 1986, **33**, 713.
8. G. Audunsson, *Anal. Chem.*, 1988, **60**, 1340.
9. *Idem, ibid.*, 1986, **58**, 2714.
10. M. Teramoto, H. Takihama, M. Shibutani, T. Yuasa, Y. Miyake and H. Teranishi, *J. Chem. Eng. Japan*, 1981, **14**, 122.
11. H. S. Park, J. H. Yoo, I. S. Suh, P. S. Han, W. K. Kang, M. Burgard and M. J. F. Leroy, *Proc. ISEC '83*, Denver, II-87, 1983.
12. R. Baird, D. Reed and A. Bunge, *NATO ASI SER. E*, 1986, **107**, 585.
13. R. S. Baird, A. L. Bunge and R. D. Noble, *AIChE Journal*, 1987, **33**, 43.
14. D. W. Armstrong and H. L. Jin, *Anal. Chem.* 1987, **59**, 2237.
15. L. Boyadzhiev, E. Bezenshek, Z. Lazarova, *J. Membr. Sci.*, 1984, **21**, 137.
16. G. Schwarzenbach and H. Flaschke, *Die komplexometrische Titration* p. 203. Ferdinand Enke Publ., Stuttgart, 1965.
17. *Handbook of Ultraviolet and Visible Absorption Spectra of Organic Compounds*, p. 322. Plenum Press Data Division, New York, 1967.
18. M. Jin, Z. Lazarova and L. Boyadzhiev, *Water Treatment*, 1991, **6**, 219.
19. K. Fujinawa, T. Komatsu, M. Hozawa, N. Imashi and H. Ino, *Kagaku Kogaku Ronbunshu*, 1984, **10**, 75.
20. M. Goto, K. Kondo and F. Nakashio, *J. Chem. Eng. Jap.*, 1989, **22**, 79.

Talanta, Vol. 39, No. 8, pp. 937–941, 1992
Printed in Great Britain

0039-9140/92 $5.00 + 0.00
Pergamon Press Ltd

SYNTHESIS AND CHARACTERIZATION OF A MACROPOROUS POLY(VINYL-AMINOACETONE) CHELATING RESIN FOR THE PRECONCENTRATION AND SEPARATION OF TRACES OF GOLD, PALLADIUM, RHODIUM AND RUTHENIUM

XIJUN CHANG,* XINGYIN LUO,* GUANGYAO ZHAN and ZHIXING SU
Department of Chemistry, Lanzhou University, Lanzhou 730000, Gansu, People's Republic of China

(*Received* 13 *August* 1991. *Revised* 20 *November* 1991. *Accepted* 20 *November* 1991)

Summary—An inductively coupled plasma atomic-emission spectrometry (ICP–AES) procedure is established with a new macroporous poly(vinyl-aminoacetone) chelating resin (PVAA) for preconcentration and separation of traces of Au(III), Pd(IV), Rh(III) and Ru(III) from sample solutions. The conditions of quantitative enrichment and desorption of these analytes from PVAA columns, including investigations of the stability, the regeneration capabilities and the adsorption capacities of that collector, are discussed. Moreover, interferences of foreign ions on the analytes are not observed and analysis of a real sample is performed with reliable results. Recoveries of these elements added to non-ferrous matrices are above 95% with relative standard deviations (RSD) between 2.0 and 4.0%.

A series of papers reported that polystyrene-based chelating resins are useful for preconcentration of trace elements.[1–7] Difficult syntheses of such resins, however, often lower their analytical value. Chang and co-workers have reported the syntheses of macroporous poly(vinyl-ethylenediamine), poly(vinyl-diethylenetriamine), poly(vinyl-propionamide oxime), and poly(vinyl-amidine thiocyanate-thiourea) chelating resins,[8–11] which were used to enrich different trace elements from various matrices with better effects than earlier resins.

In this paper, the synthesis of a macroporous resin with immobilized poly(vinyl-aminoacetone) chelating groups (PVAA) and its application for enrichment of noble metal ions is described. An ICP–AES procedure is established for the determination of traces of Au, Pd, Rh and Ru in real samples after preconcentration on PVAA. The acidity, the flow-rates, the performance, the adsorption capacity, and interferences of foreign ions on the separation of the analytes, as well as the conditions of desorbing these ions from the collector, are characterized. Moreover, the precision and the accuracy of the analytical procedure using this resin investigated by analysis of a real sample, with satisfactory results.

*Authors for correspondence.

EXPERIMENTAL

Instrumentation and conditions

A Perkin–Elmer ICP/6500 inductively coupled plasma system equipped with a PE 7300 computer and RF power supply was operated according to standardized conditions (forward power 1100 W, viewing height 17 mm, Ar plasma gas flow 14 l./min, Ar auxiliary gas flow 0.4 l./min, Ar nebulizer gas flow 1.0 l./min, solution uptake rate 1.0 ml/min, wavelengths: Au 201.200 nm, Pd 229.651 nm, Rh 233.477 nm, and Ru 240.272 nm). Wavelengths were scanned in ascending order to determine Au, Pd, Rh and Ru with the ICP/6500 (integration time 10 sec, each). A Perkin–Elmer 577 Crafting Infra-red spectrometer was used to determine the structure of the PVAA resin.

To prepare the column, 0.3 g of chelating resin, soaked in high-purity water overnight, was loaded into a glass tube (15 cm long, inner diameter 0.4 cm, 0.15 cm at the lower end) enclosed with small cotton wads.

Reagents and standards

Reagents of high or analytical purity were used for all experiments. Stock solutions of 1 g/l. Au, Pd, Rh, Ru each were prepared by dissolving spectroscopically pure $HAuCl_4 \cdot 4H_2O$, $(NH_4)_2PdCl_6$, $(NH_4)_2RuCl_5$ and $Rh_2O_3 \cdot 5H_2O$ (Shanghai Reagent Station) in

diluted hydrochloric acid. They were diluted and mixed in 0.5*M* hydrochloric acid to 16 μg/ml Au and Ru and 12 μg/ml Pd and Rh to give standard stock solution.

Synthesis of chelating resin

A 10-g amount of spherical poly(vinyl chloride) particles of 0.32–1.3 mm diameter, 30 g of ethylenediamine and 1.5 g of sodium carbonate were mixed in a three-necked flask. After refluxing for 4 hr at 113°, the resin was washed with 400 ml of water until the resin was neutral and dried under an IR lamp. An aminated resin was obtained. Then 10 g of the aminated resin and 30 g of (1 + 1) acetone and formaldehyde were added to another three-necked flask and refluxed for 6 hr at 65°, and washed with water and dried as above. Synthesis of a new aminoacetone chelating resin was thus achieved. The aminoacetone functional group in the resin was verified through the IR spectrum shown in Fig. 1.

According to the Mannich reaction principle,[12] the synthesis reaction of PVAA chelating resin can be briefly expressed as follows:

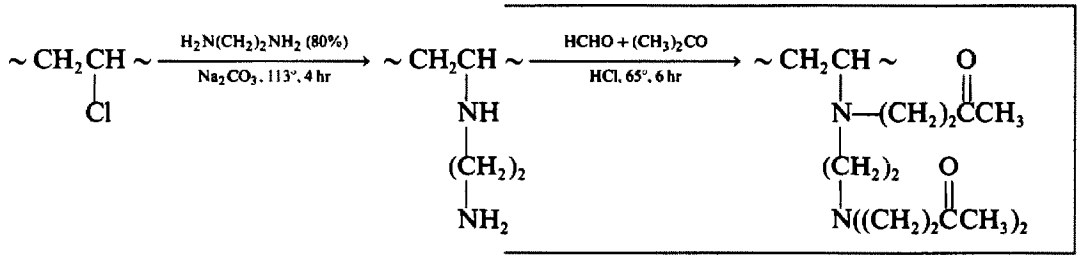

The average pore diameter and pore volume of the synthesized resin determined by the mercury intrusion method[13] was 6500 Å and 0.51 cm^3/g, respectively. Its specific surface area measured by the Brunner Emmett Teller method[13] was 5.9 m^2/g. The nitrogen content of this resin determined by an elemental analyser (ARLO ERBR 1106) was 9.21%. Because cross linkage reactions of the resin occur simultaneously with the above reaction,[14] conjugated bonds were formed, so that the N-content of the resin cannot be further increased.[14]

Analytical procedures

Standard solutions of Au, Pd, Rh and Ru were prepared in high-purity vessels (200–500 ml samples). Subsequently, the pH was adjusted to an appropriate value with a Clark–Lubs buffer solution and the solution passed through the column under a controlled flow-rate (*e.g.*, 1.5 ml/min). After elution of the analytes from the column by 10 ml of mixed 6*M* hydrochloric acid and 3% $CS(NH_2)_2$ solution, traces of Au, Pd, Rh and Ru in the 10 ml of eluate were determined by ICP–AES.

Procedure for non-ferrous metal analysis

A 0.1000-g portion of a ferrous sample with Cu, Ni and Fe matrix from a smelter was weighed into a Ni-crucible and 0.8 g of (1 + 12) sodium nitrite and sodium hydroxide were added. The crucible was heated in a furnace for an hour at 600° and then cooled. The melted sample in the crucible was leached with 50 ml of boiling distilled water into a beaker and neutralized with 6*M* hydrochloric acid, and then the Clark–Lubs buffer solution of pH 6 was added. Thus, the sample solution was passed through the chelation column according to the above analytical procedures.

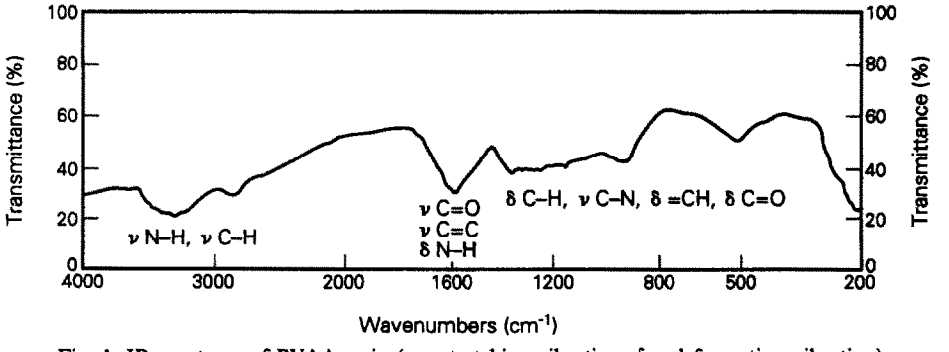

Fig. 1. IR spectrum of PVAA resin (ν = stretching vibration, δ = deformation vibration).

RESULTS AND DISCUSSION

Influence of pH value on quantitative enrichment

Appropriate solutions of Au, Pd, Rh and Ru (60–80 ng/ml each) were enriched by means of the column procedures described in the pH range 2–9. Traces of Au, Pd, Rh and Ru can be adsorbed quantitatively by the resin between pH 5–9 with recoveries in the range 92–100% (Fig. 2). A pH of 6 was selected as the optimum value for preconcentration.

On the basis of the column procedure, Pt(IV) and Ir(IV) (60–80 ng/ml each) in the pH range 5–9, Cr(III), Pb(II), Cu(II), V(V), and Y(III) (40–100 ng/ml each) in the pH range 7–9, and Ti(IV) (50 ng/ml) in the pH range 8–9 can also be adsorbed by the resin with recoveries of over 90%, while recoveries of Fe(III), In(III), Sn(IV) and Bi(III) (100–500 ng/ml each) adsorbed by the resin at pH 7 below can only reach 10–40%. The above ions do not interfere with the Au, Pd, Rh and Ru preconcentrations at pH 6. In addition, Na, K, Be, Mg, Ca, Ba, Ga(III), Tl(I), As(III), Cd(II), Co(II), B(III) and Ge (IV) (100–500 ng/ml each) are not adsorbed by the resin at pH <7. Accordingly, the resin separation of trace Au, Pd, Rh and Ru at pH 6 is not interfered with by these other ions.

Because Ag(I) can combine with chlorine ion in the solution to form a precipitate and Os(VIII) volatilizes easily at ordinary temperatures, these ions were not tested. When the above noble metal ions are in high acidity solution, their adsorption by the PVAA resin is not satisfactory.

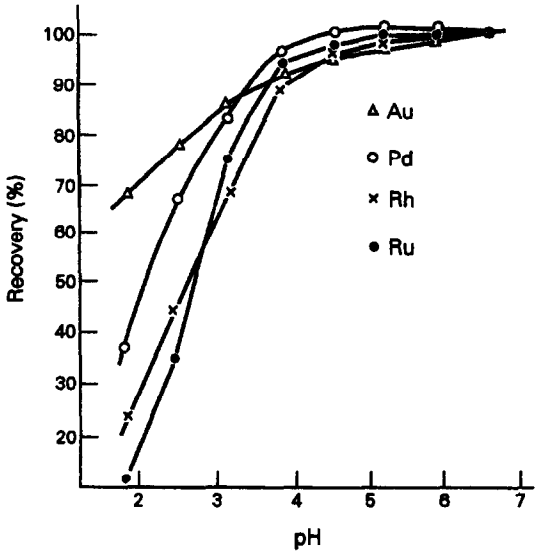

Fig. 2. Separation of Au, Pd, Rh and Ru by PVAA resin as a function of pH.

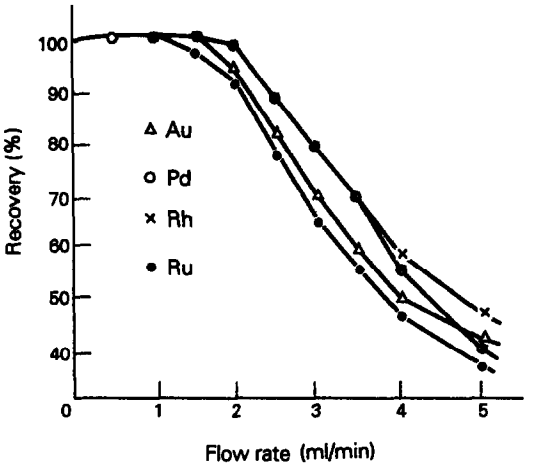

Fig. 3. Effect of collection on flow-rate on the recovery of Au, Pd, Rh and Ru by PVAA columns.

Flow-rates of separation

With the column procedure, the influence of the flow rate (0.5 to 6 ml/min) on the separation of Au, Pd, Rh, and Ru ions was investigated. As Fig. 3 shows these ions can be adsorbed quantitatively by the resin at flow-rates ≤ 2 ml/min. Based on this finding, the flow-rate during the following separation experiments was kept at 1.5 ml/min.

Conditions for quantitative desorption

Subsequent to their separation, Au, Pd, Rh and Ru ions were eluted from the columns by means of 10-ml mixture solutions (hydrochloric acid and thiourea) of different concentrations. The desorption flow-rate was kept at 3 ml/min. The results of this determination, presented in Figs. 4 and 5, reveal that Rh and Ru can be desorbed with $4M$ HCl + 3% $CS(NH_2)_2$ or $6M$ HCl + 1% $CS(NH_2)_2$ solution; Au can be desorbed with $6M$ HCl + 2% $CS(NH_2)_2$ solution; but desorption of Pd requires $6M$ HCl + 3%

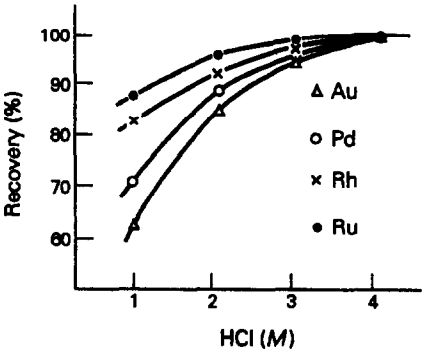

Fig. 4. Elution curves of Au, Pd, Rh and Ru as a function of HCl concentration [in 3% $CS(NH_2)_2$].

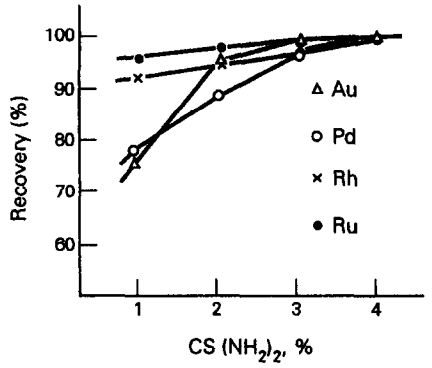

Fig. 5. Elution curves of Au, Pd, Rh and Ru as a function of $CS(NH_2)_2$ concentration (in 6*M* HCl).

$CS(NH_2)_2$ solution. The desorption recoveries were above 93%. Thus, 10 ml of 6*M* HCl + 3% $CS(NH_2)_2$ solution was selected for elution of analytes.

In separation experiments, we found that the elution of Pt ion from the resin requires 8*M* HCl + 8% $CS(NH_2)_2$ solution, while the elution of Ir ion requires 4% (1 + 1) $NaNO_2 + NH_4Cl$ solution (recoveries $\geq$90%). However, the quantitative elutions of Cr, Pb, Cu, V, Y and Ti ions from the resin require only 2–4*M* hydrochloric acid solution. Because the conditions of Pt and Ir ions eluted from the resin were different from Au, Pd, Rh and Ru ions, both ions were not investigated further in following experiments.

Resin stability, regeneration and capacity

After the chelating resin was treated with strong acids or concentrated bases, the adsorptions of Au, Pd, Rh and Ru ions were over 92%. The swelling rate of the resin was 28.3% (in 0.1*M* hydrochloric acid, 270 min).

When the resin was used repeatedly as described for the determination of Au, Pd, Rh and Ru ions up to seven times [after Au, Pd, Rh and Ru were desorbed from the resin each time with 6*M* HCl + 3% $CS(NH_2)_2$ solution, the resin column was washed with 1*M* sodium hydroxide solution and distilled water to neutrality, thus, a regeneration of the resin was reached], the adsorption efficiency was still above 95%. The saturated adsorption capacities of the PVAA resin for these elements were 124 mg/g for Au, 66.8 mg/g for Pd, 67.0 mg/g for Rh, and 45.5 mg/g for Ru.

Interferences of foreign ions

Standard solutions of 200 ml of Au, Pd, Rh and Ru ions (60–80 ng/ml each) containing different metal (Cu, Ni, Zn, Mn, Fe, Al, Ca, Mg) ions as interferents were analysed according to the combined ICP procedure. The results (recovery rates) summarized in Table 1 show that hundred-fold excesses of these foreign ions do not affect the recovery of the above analytes.

Precision and accuracy

The precision and accuracy of the combined ICP procedure were characterized by the analysis of standard solutions containing 64 ng/ml Au and Ru, each and 48 ng/ml Pd and Rh, each. Accordingly, the average values of 7 determinations were 62 ng/ml Au, 64 ng/ml Ru and 48 ng/ml Pd, Rh each, and the relative standard deviations (RSD) were 3.6% for Au, 2.0% for Ru, 2.7% for Pd and 3.3% for Rh. When the lowest analyte concentrations were 32 ng/ml Au, Ru each and 24 ng/ml Pd, Rh each, the RSD of these ions determined in accordance with the above analytical procedure were still between 2.0 and 4.0%.

Moreover, the accuracy of the combined procedure was checked by the analysis of an aqueous sample solution from a smelter nonferrous sample with about 0.5 mg/ml of Ni and Co metal matrix, using the standard addition method for calibration. The results listed in Table 2 reveal >95% recoveries for traces of Au, Pd, Rh and Ru, and show the analyte concentrations in the sample solution detected by the ICP procedure were 44 ng/ml for Au, 58 ng/ml for Pd, 33 ng/ml for Rh, and 20 ng/ml for Ru. When the analytical procedures were applied to the analysis of a ferrous sample solution with Cu, Ni and Fe metal matrix, the contents of Au, Pd, Rh and Ru determined by the proposed procedure in the real matrix were in

Table 1. Influence of foreign ions on the Au, Pd, Rh and Ru recovery

Interfering ions		Ca^{2+}	Mg^{2+}	Zn^{2+}	Ni^{2+}	Cu^{2+}	Mn^{2+}	Fe^{3+}	Al^{3+}
Conc. (10^3 ng/ml)		40	40	20	20	20	15	15	10
Recovery* (%)	Au	98.5	103	90.1	90.0	90.6	93.0	94.0	93.4
	Pd	95.8	104	91.7	104	108	98.8	100	97.0
	Rh	92.5	95.8	106	102	108	100	104	91.8
	Ru	106	106	98.5	103	92.0	95.6	100	100

*The concentration of Au and Ru was 80 ng/ml each, the concentration of Pd and Rh was 60 ng/ml each.

Table 2. Analytical results of real samples with non-ferrous matrix

	Solution sample				Control sample	
Elements	Conc. found *ng/ml*	Added, *ng/ml*	Sum found *ng/ml*	Recovery, %	Conc. found *ng/ml*	Expected (ETAAS) *ng/ml*
Au	44 ± 2	80	120 ± 4	95.0	163 ± 6	163
Pd	58 ± 2	60	120 ± 3	103	161 ± 4	161
Rh	33 ± 1	60	93 ± 3	100	50.5 ± 1.6	50.4
Ru	20 ± 1	80	98 ± 2	97.5	21.2 ± 0.4	21.1

good agreement with the analytical results measured by a ETAAS method (Table 2).

The above results demonstrate the reliability and feasibility of the proposed analytical procedure for the chelating adsorption for traces of Au, Pd, Rh and Ru in real sample solutions.

CONCLUSION

The macroporous PVAA chelating resin can be synthesized readily. It shows good chemical and mechanical stability. Separations of traces of Au, Pd, Rh and Ru from matrix elements by the new collector can be carried out applying a reliable column procedure. When combined with ICP–AES, the procedure offers considerable advantages in convenient operation, low interference, good precision and accuracy for the analytes Au, Pd, Rh and Ru.

Acknowledgement—The authors thank Peifen Ma and Xun Lu for their help with the experimental work.

REFERENCES

1. G. Koster and G. Schmuckler, *Anal. Chim. Acta*, 1967, **38**, 179.
2. H. F. Walton, *Anal. Chem.*, 1980, **52**, 15R.
3. P. K. Pttrie and J. W. Morgan, *J. Radioanal. Chem.*, 1982, **74**, 15.
4. K. Brajter and K. Slonawska, *Talanta*, 1983, **30**, 7.
5. Yiyong Chen, Fang Hua and Xiaobin Wu, *High Molecular News Report*, 1985, **5**, 355.
6. Lanxiang Meng, Yingmei Liu and Ainan Feng, *Fenxi Huaxue*, 1985, **9**, 682.
7. Shouting Wan, Weizhu Chen and Binglin He, *Chem. J. Chinese Universities*, 1987, **8**, 81.
8. Xijun Chang, Zhixing Su, Guangyao Zhan and Xingyin Luo, *Acta Chim. Sinica*, 1990, **48**, 166.
9. Xijun Chang, Yanfeng Li, Xingyin Luo, Guangyao Zhan and Zhixing Su, *Anal. Chim. Acta*, 1991, **245**, 13.
10. Xijun Chang, Xingyin Luo and Zhixing Su, *Chem. J. Chinese Universities*, 1988, **9**, 574.
11. Zhixing Su, Xijun Chang, Guangyao Zhan and Xingyin Luo, *Microchem. J.*, 1991, **44**, 78.
12. Daozheng Wan, *Mannich Reaction and Mannich Base's Chemistry*, p. 85. Publishing House of Science, Beijing, 1986.
13. Binglin He and Zuoqing Shi, *Ion Exchange and Adsorption*, 1987, **3**, 44.
14. K. S. Minsgel and G. T. Fitosheeva, *Degradation and Stability of Polyvinyl Chloride* (U.S.S.R.), pp. 25, 56, 97, 118. Translated by Wenje Ma and Zizheng Huang, Publishing House of Light Industry, Beijing, 1985.

Talanta, Vol. 39, No. 8, pp. 943–951, 1992
Printed in Great Britain.

0039-9140/92 $5.00 + 0.00

BATCHWISE SEPARATION OF GALLIUM BY AN ANION EXCHANGE RESIN LOADED WITH A SULPHONATED AZO DYE

MARIA PESAVENTO, TERESA SOLDI and ANTONELLA PROFUMO
Dipartimento di Chimica Generale, Università di Pavia, V. Taramelli 12, 27100 Pavia, Italy

(*Received* 8 *July* 1991. *Revised* 21 *October* 1991. *Accepted* 21 *October* 1991)

Summary—Gallium(III) is sorbed by a strong base anion exchange resin loaded with a sulphonated azo-dye, T-azo-R [1-(tetrazolylazo)-2-hydroxynaphthalene-3,6-disulphonic acid], which is able to complex it in aqueous solution. As sorption takes place at acidities at which the hydrolysis of gallium is not negligible, it must be considered as concomitant equilibrium. The distribution equilibria depend on the amount of ligand sorbed, and on the volume, acidity and ionic composition of the aqueous solution, according to the Gibbs–Donnan model. The thermodynamic complexation constant in the resin phase can be calculated from the experimental distribution coefficients; the value of $\log K = -1.24(0.20)$ is in acceptable agreement with that in aqueous solution [$\log K = -0.75(0.33)$] which was also determined in the present investigation. Two equations deriving from the Gibbs–Donnan model are used for predicting the conditions for sorption and elution of gallium by a batch procedure, and for separating it from aluminium.

The possibility of predicting the distribution of heavy metal ions between aqueous solution and strong base anion exchange resin containing chelating sulphonated azo dyes has been shown in some previous papers.[1,2] To this purpose it is convenient to accept the model proposed by Boyd,[3] Gregor,[4] Helfferich[5,6] and more recently by Marinsky.[7] In that case, if the same standard and reference state are assumed for the solution and the resin phase, the activities of proton and metal ion inside the resin depend on the activities in aqueous solution, according to the Gibbs–Donnan equilibrium.

Let's suppose that the ion exchange takes place by the following reaction

$$\mathrm{M} + \overline{\mathrm{H}_x\mathrm{L}} \rightleftharpoons \overline{\mathrm{MH}_r\mathrm{L}} + q\mathrm{H} \qquad (1)$$

$$K_{ex} = \frac{\overline{[\mathrm{MH}_r\mathrm{L}]}[\mathrm{H}]^q}{[\mathrm{M}]\overline{[\mathrm{H}_x\mathrm{L}]}} \qquad (2)$$

where barred symbols indicate the species in the resin.

The fraction of the sorbed metal ion to the total ion (f) is given by the following equation

$$f = \frac{\overline{[\mathrm{MH}_r\mathrm{L}]}g}{[\mathrm{M}]_t V + \overline{[\mathrm{MH}_r\mathrm{L}]}g} = \frac{1}{1 + \dfrac{[\mathrm{H}]^q V Z_{\mathrm{M}} Z_{\mathrm{HxL}}}{K_{ex}\bar{c}_{\mathrm{L}} g}} \qquad (3)$$

where $Z_{\mathrm{M}} = [\mathrm{M}]_t/[\mathrm{M}]$ and $Z_{\mathrm{HxL}} = \bar{c}_{\mathrm{L}}/\overline{[\mathrm{H}_x\mathrm{L}]}$.

$[\mathrm{M}]_t$ indicates the total concentration of metal ion in the solution phase and $\bar{c}_{\mathrm{L}}$ the total concentration of the ligand not complexed in the resin. V is the volume of the aqueous solution (in cm^3) and g are the grams of water sorbed on the resin. All quantities in equation (3) are experimentally accessible by independent determination, or are evaluable. The exchange coefficients can also be evaluated on the basis of the model, as previously suggested,[3–7] and by estimating the activity coefficients of the ionic species involved by the Specific Interaction Theory (SIT).[8] The following equation is used:

$$\log K_{ex} = \log K\gamma_{\overline{\mathrm{HxL}}}/\gamma_{\overline{\mathrm{MHrL}}}\{\overline{\mathrm{Y}}\}^{(z-q)} + (z-q)\log[\mathrm{Y}] - \frac{0.51I^{1/2}}{1+1.5I^{1/2}} \times [z^2 + (z-q)z_{\mathrm{Y}}^2 - qz_{\mathrm{H}}^2] + [b(\mathrm{M},\mathrm{Y}) + (z-q)b(\mathrm{N},\mathrm{Y}) - qb(\mathrm{H},\mathrm{Y})]I \qquad (4)$$

where NY is the salt of the ionic medium, z is the charge of the metal ion and K is the thermodynamic complexation constant in aqueous solution. I is the ionic strength of the solution. Symbols between { } indicate activities, γ the activity coefficients and b the specific interaction coefficients defined by SIT.

In the case of chelating resins consisting of a strong base anion exchange resin containing a

sulphonated azo-dye at low concentration, predictions on sorption and elution of metal ions are easily done. First of all the chelating groups are introduced on the resin under very mild conditions, simply by ion exchange. Thus they keep the same molecular structure and chelating properties as in aqueous solution, where they are known in many cases, or can be determined by the usual equilibrium analysis methods. Moreover the activity of the counter ion Y in the resin phase is constant, since the number of counter ion moles substituted for the ligand is low, and the resin is rigid enough to have a constant water content. The activity of the counter ion in the resin phase has been evaluated in some previous work.[9]

The complexing properties of some azo-dyes with two metals of the Group IIIB, indium and aluminium, in aqueous solution have been previously investigated.[10,11] A very peculiar behaviour of the two metal ions has been observed. One of the ligands previously considered, which derives from R salt, T-azo-R [1-(tetrazolylazo)-2-hydroxynaphthalene-3,6-disulphonic acid], is a good ligand for indium,[10] while it does not complex aluminium[11] at all. On the contrary a ligand with similar structure, derived from Chromotropic acid, T-azo-C [2-(tetrazolylazo)-1,8-dihydroxynaphthalene-3,6-disulphonic acid], reacts only slightly with indium,[10] but is a good complexing agent for aluminium.[11] The same was observed also when comparing other derivatives of R salt and Chromotropic acid, and was to be expected since a peri-di-hydroxylic structure is required to form stable complexes with aluminium.

Nothing is known about the behaviour of these ligands with gallium, so this point had to be investigated before making any prediction. However some preliminary observations showed that gallium forms steady complexes with both the sulphonated azo dyes T-azo-R and T-azo-C in aqueous solution at pH values higher than about 2. It is expected that the same happens when the dyes are sorbed on AG MP-1.

The aim of the present investigation is to check the possibility of using the loaded resin for sorbing gallium from aqueous solution, and for separating it from aluminium.

As a matter of fact gallium is often obtained as a by-product in the aluminium metallurgical industries, since it is present in aluminium minerals as an impurity at different concentration levels, from 0.01 to 0.1%. Thus it is important to separate it for determination in the presence of large amounts of aluminium.

The hydrolysis of gallium had also to be studied because it is a concomitant equilibrium at the acidity at which the complexation in aqueous solution and the sorption on the loaded resin take place.

EXPERIMENTAL

Materials and apparatus

The sulphonated azo dyes T-azo-R [1-(tetrazolylazo)-2-hydroxynaphthalene-3,6-disulphonic acid] and T-azo-C [2-(tetrazolylazo)-1,8-dihydroxynaphthalene-3,6-disulphonic acid] were prepared and characterized by the previously reported methods.[12,13] Their standard solutions were prepared directly by weighing the solid.

The strong base resin AG MP-1 was obtained from Bio-Rad and converted to the nitrate form as previously described.[9] Its capacity for anions was 4.2 meq per g of dry resin and the water content was 1.42 g of water per g of dry resin, in agreement with that declared. It was then loaded with the sulphonated azo-dye according to the usual procedure.[2]

Gallium nitrate stock solution was prepared by dissolving the 99.999% pure metal obtained from Aldrich in a small excess of nitric acid diluted 1 to 1, by gentle heating and refluxing. The gallium concentration in the stock solution was determined both gravimetrically by precipitating the hydroxide with ammonia and weighing the oxide, and volumetrically with EDTA.[14] The acidity of the stock solution was determined by passing a known volume on a strong cation exchange resin (Dowex 50) in the hydrogen form, and titrating potentiometrically the protons in the solution. The protons exchanged for gallium were subtracted from the total acidity titrated. The excess acidity in the final solution was 0.12*M*. All other reagents were of analytical grade and triply distilled water was used.

Spectrophotometric determinations were made with a Varian Cary 3 UV–Vis spectrophotometer.

The acidity (pH) was measured potentiometrically by a Ross combined glass electrode (Orion 8102-SC). The potentiometric cell was standardized daily in proton concentration by the previously described standard addition method.[13] All measurements were made under a

small nitrogen overpressure in a temperature-controlled cell. The same was used for the potentiometric titrations.

Voltammetric determination of gallium

Gallium concentration was determined in the test solution and the amount of sorbed metal was estimated by difference from the total amount added; f was then calculated.

The determination of gallium in the test solution was done by analysing a known volume of clear solution. A very sensitive technique (anodic stripping voltammetry, D.P.) should be used to allow volumes of test solution as small as possible to be used. A polarograph AMEL Analyzer 433 was used, with Hg as indicator electrode, Ag/AgCl, saturated KCl as reference electrode and Pt wire as counter electrode. The supporting electrolyte was $0.1M$ sodium chloride and $8 \times 10^{-3}M$ hydrochloric acid. Other conditions were: pulse amplitude, 50 mV; scanning speed, 20 mV/sec; pre-electrolysis time, 60 sec; drop, a.u. = 20; stirring rate, 300 r.p.m. At these conditions E_p was -0.6 V, and the sensitivity was 0.04 μA/10 ppb Ga.

Separation of gallium traces from an aluminium solution

To 50 ml of sample containing aluminium and less than 0.01 mmole of gallium(III), 5 g of dry resin loaded with 1 mmole of T-azo-R were added. After one hour of stirring, the resin was separated by filtration on porous glass, washed with water, transferred to a beaker and stirred for one hour with 20 ml of $0.2M$ nitric acid to elute gallium(III).

RESULTS AND DISCUSSION

Hydrolysis of gallium

In order to correctly interpret the equilibria of gallium with the ligands considered here, both in aqueous solution and in the resin, its hydrolysis reactions must be exactly known. While a number of investigations on this subject have been reported,[15] it has never been studied at the conditions considered in the present study (sodium nitrate aqueous solutions, 25° and gallium concentrations lower than $1 \times 10^{-3}M$). The investigation was made by titrating solutions containing fixed concentrations of sodium nitrate, gallium and nitric acid, with standard sodium hydroxide. The mean number of hydroxyl ions bound per mole of gallium (n) was then calculated according to the following relationship, obtained from the mass equilibria

$$n = \frac{[H] - H}{c_{Ga}} \quad (5)$$

where H is the analytical concentration of protons, and c_{Ga} is the total concentration of gallium.

Some results obtained in $0.1M$ sodium nitrate aqueous solutions are reported in Fig. 1 as a function of pH. The curves obtained at different gallium concentrations coincide at low pH, but differ in less acidic solutions. This indicates that a mononuclear complex is first formed, which then reacts further to give one or more polynuclear hydroxo derivatives.

The final results were obtained by the program SUPERQUAD,[16] by considering all together the titrations at different gallium concentrations. Two hydroxo derivatives were detected, one with molar composition 1 to 1 (GaOH) and the other 5 to 15 [$Ga_5(OH)_{15}$]. Their formation constants are reported in Table 1, together with those obtained at other sodium nitrate concentrations.

The variations of the conditional hydrolysis constants with ionic strength were interpreted on the basis of the Specific Interaction Theory (SIT).[17] According to this the conditional constant of the hydrolysis equilibrium

$$m\mathrm{Ga} + n\mathrm{H_2O} \rightleftharpoons \mathrm{Ga}_m(\mathrm{OH})_n + n\mathrm{H} \quad (6)$$

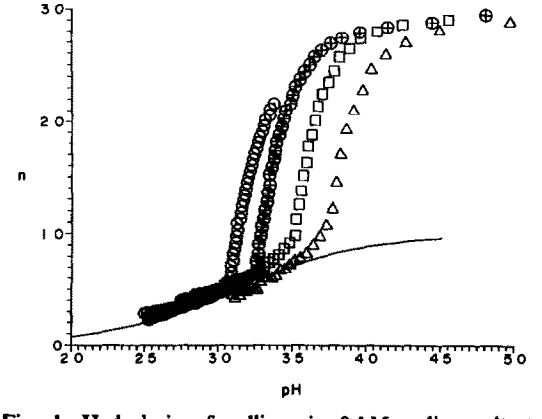

Fig. 1. Hydrolysis of gallium in $0.1M$ sodium nitrate T = 25°. Ordinates: mean number of hydroxyl ions bound per mole of gallium (n) ○ $c_{Ga} = 2.89 \times 10^{-3}M$; ⊕ $c_{Ga} = 9.84 \times 10^{-4}M$; □ $c_{Ga} = 2.45 \times 10^{-4}M$; △ $c_{Ga} = 7.44 \times 10^{-5}M$. The continuous line has been calculated for GaOH, with $\log K_{1,1} = -2.94$.

Table 1. Hydrolysis of gallium(III) in sodium nitrate and in sodium perchlorate at different concentrations. T = 25°; $c_{Ga} = 2.998 \times 10^{-4} M$

		$NaNO_3$		
I(M)	$\log K_{1,1}$	$\log K_{T1,1}$	$\log K_{5,15}$	$\log K_{T5,15}$
0.01	−3.02	−2.84	−35.35	−34.02
0.05	−2.97	−2.63	−35.26	−32.70
0.1*	−2.94	−2.50	−35.51	−32.23
0.5	−3.08	−2.38	−36.82	−31.57
1.0	−3.32	−2.50	−37.92	−31.80
		$NaClO_4$		
	$\log K_{1,1}$	$\log K_{T1,1}$	$\log K_{5,15}$	$\log K_{T5,15}$
0.01	−3.06	−2.88	−34.76	−33.43
0.05	−3.16	−2.82	−35.69	−33.13
0.1†	−3.11	−2.67	−35.83	−32.55
0.5	−3.59	−2.89	−37.86	−32.61
1.0	−3.89	−3.07	−38.60	−32.48

*Values obtained with SUPERQUAD, considering four titrations at the same time, respectively with $c_{Ga} = 7.44 \times 10^{-5}$, 2.45×10^{-4}, 9.84×10^{-4}, $2.89 \times 10^{-3} M$.

†Values obtained with SUPERQUAD, considering two titrations at the same time, one with $c_{Ga} = 2.998 \times 10^{-4} M$ and the other with $c_{Ga} = 2.099 \times 10^{-4} M$.

depends on the ionic strength of the solution as shown by the following relationship

$$\log K_{m,n} = \log K_{Tm,n} - \frac{0.51 I^{0.5}}{1 + 1.5 I^{0.5}} \times [m z_{Ga}^2 - z_{Gam(OH)_n^q}^2 - n z_H^2] + \{mb(Ga, Y) - b[Ga_m(OH)_n, Y] - nb(H, Y)\} I \quad (7)$$

$Z = m z_{Ga}^2 - z_{Gam(OH)_n}^2 - n z_H^2$ has a value of 4 and 30 respectively for the formation of GaOH and $Ga_5(OH)_{15}$.

The parameters $\log K_{Tm,n}$ and $B = mb(Ga, Y) - b[Ga_m(OH)_n, Y] - nb(H, Y)$ are evaluated by a least-squares method, assuming I as the independent variable and $\log K_{m,n} + 0.51 I^{0.5}(m z_{Ga}^2 - z_{Gam(OH)_n^q}^2 - n z_H^2)/(1 + 1.5 I^{0.5})$ as dependent variable. The following results were obtained (standard deviations are reported in brackets): $\log K_{T1,1} = -2.64(0.17)$; $\log K_{T5,15} = -32.99(0.82)$; B is not significantly different from 0. The values of $\log K_{Tm,n}$ calculated from the conditional constants at each ionic strength on the basis of equation 7, and $B = 0$, are shown in Table 1.

In order to verify that nitrate does not complex gallium, the hydrolysis was also studied in sodium perchlorate. The conditional hydrolysis constants of gallium in sodium perchlorate are: $\log K_{T1,1} = -2.78(0.10)$ and $\log K_{T5,15} = -33.06(0.35)$, and B is again not significantly different from 0. The agreement between the results obtained in sodium nitrate and in sodium perchlorate indicates that gallium is not complexed by the anions of the ionic media considered here.

Complexation of gallium in aqueous solution by T-azo-R and T-azo-C

The complex formation in sodium perchlorate aqueous solution was studied by molecular absorption spectrophotometry. The spectral characteristics of the complexes of gallium with the azo-dyes T-azo-R and T-azo-C are reported in Table 2. The complexation equilibrium and constant are

$$m\mathrm{Ga} + p\mathrm{H}_x\mathrm{L} \rightleftharpoons \mathrm{Ga}_m\mathrm{H}_r\mathrm{L}_p + q\mathrm{H}$$

$$K_{cm,p} = \frac{[\mathrm{Ga}_m\mathrm{H}_r\mathrm{L}_p][\mathrm{H}]^q}{[\mathrm{Ga}]^m[\mathrm{H}_x\mathrm{L}]^p} = K_{cTm,p} \frac{\gamma_{Ga}^m \gamma_{HxL}^p}{\gamma_{GamHrLp} \gamma_H^q} \quad (8)$$

Table 2. Spectral characteristics of T-azo-R, T-azo-C and of their complexes with gallium in aqueous solution

	T-azo-R	T-azo-C
Protonation of ligands:[18]	$\log K_{T2} = 3.60$ $B = 0.46$	$\log K_{T2} = 4.09$ $B = 0.37$
Absorbance maximum of H_2L:	400 nm	468 nm
Absorbance maximum of HL:	465 nm	480 nm
Isosbestic point H_2L-HL:	426 nm	453 nm
Wavelength of maximum absorbance of the complex with gallium (metal ion excess):	485 and 510 nm	580 nm
Molar absorbance of the complex at the calculation wavelength:	1.83×10^4 (510 nm)	7.6×10^3 (580 nm, metal ion excess) 8.4×10^3 (580 nm, ligand excess)
Molar absorbance of the free ligand at maximum wavelength of complex:	ϵ_{H_2L}: 5.2×10^2 ϵ_{HL}: 5.1×10^4	ϵ_{H_2L}: 0 ϵ_{HL}: 75
Isosbestic point free ligand-complex:	450 nm	495 nm

$B = b(H_{x-1}L, Na) + b(H, ClO_4) - b(H_xL, Na)$.
Molar absorbances ϵ in $l.mole^{-1}.cm^{-1}$.

$K_{cTm,p}$ is the thermodynamic complexation constant:

$$K_{cTm,p} = \frac{\{Ga_mH_rL_p\}\{H\}^q}{\{Ga\}^m\{H_xL\}^p} \quad (9)$$

The composition of the complex and the formation constants were determined by the spectrophotometric method previously described,[13] based on the following absorbance and mass balances:

$$A = \epsilon_{HxL}[H_xL] + \epsilon_{H_{x-1}L}[H_{x-1}L] + \epsilon_{GamHrLp}[Ga_mH_rL_p]$$

$$c_{Ga} = [Ga] + [GaOH] + [Ga_5(OH)_{15}] + [Ga_mH_rL_p]$$

$$c_L = [H_xL] + [H_{x-1}L] + [Ga_mH_rL_p] \quad (10)$$

It is important to take into account the formation of the hydroxo derivatives, considering that the complexes are formed at pH higher than about 2 (that with T-azo-R) and 3 (that with T-azo-C), at which hydrolysis is not negligible.

To set the value of p and m, two groups of experiments were performed at constant composition of the ionic medium (0.1M sodium perchlorate). In one of them the metal ion concentration was much higher than that of the ligand ($c_{Ga} \gg c_L$), and in the other the concentration of ligand was higher than that of metal ion ($c_L \gg c_{Ga}$). The calculations were performed at fixed wavelengths, corresponding to the maximum absorbance of the complexes, *i.e.*, 510 nm for T-azo-R and 580 nm for T-azo-C. In each case the diprotonated form of the ligand H_2L was considered to react.

The values $m = 1$, $p = 1$ and $q = 2$ were obtained in 0.1M sodium perchlorate for the complexation of gallium with T-azo-R both in excess of metal ion and of ligand. The formation constants $K_{cm,p}$ of the complex obtained in some independent experiments are reported in Table 3. The formation constants $K_{cm,p}$ obtained at other sodium perchlorate concentrations are reported in Table 4. They depend on the ionic strength I of the solution according to the following relation, derived from the Specific Interaction Theory[8]

$$K_{cm,p} = K_{cTm,p} - \frac{0.51I^{1/2}}{1 + 1.5I^{1/2}} \times (mz_M^2 + pz_{HxL}^2 - z_{MmHrL_p}^2 - qz_H^2) + [mb(M, Y) + pb(H_xL, N) - b(M_mH_rL_p, Y, N) - qb(H, Y)]I \quad (11)$$

The parameters of equation 11, $\log K_{cTm,p}$, $(mz_M^2 + pz_{HxL}^2 - z_{MmHrL_p}^2 - qz_H^2) = Z$, and $[mb(M, Y) + pb(H_xL, N) - b(M_mH_rL_p, Y, N) - qb(H, Y)] = B$, can be evaluated by a multiple linear regression procedure. Their values are reported in Table 4.

The complexation with T-azo-C takes place at an acidity only slightly lower than that with T-azo-R. This indicates that gallium has a behaviour intermediate between indium[10] and aluminium.[11] Also a polynuclear complex is

Table 3. Complexation constants of gallium with T-azo-R and T-azo-C at different ligand/metal ion ratios in 0.1M sodium perchlorate, T = 25.0°

T-azo-R:	$Ga + H_2L \rightleftharpoons GaL + 2H$ (510 nm)		
$c_{Ga}(M)$	$c_L(M)$	$\log K_{c1,1}$	No. of points
1.994×10^{-4}	1.630×10^{-5}	−1.83(0.21)	7
2.990×10^{-4}	1.630×10^{-5}	−1.80(0.12)	8
4.984×10^{-4}	1.630×10^{-5}	−1.91(0.14)	6
3.984×10^{-5}	1.532×10^{-4}	−1.82(0.13)	4
3.984×10^{-5}	2.998×10^{-4}	−1.98(.17)	7
3.984×10^{-5}	2.001×10^{-5}	−1.92(.28)	6
T-azo-C:	Excess of gallium $2Ga + H_3L \rightleftharpoons Ga_2(OH)L + 4H$ (580 nm)		
$c_{Ga}(M)$	$c_L(M)$	$\log K_{c2,1}$	No. of points
1.994×10^{-4}	1.554×10^{-5}	−6.50(0.15)	8
2.990×10^{-4}	1.554×10^{-5}	−6.24(0.12)	10
3.987×10^{-4}	1.554×10^{-5}	−6.21(0.22)	8
	Excess of ligand $Ga + H_3L \rightleftharpoons GaL + 3H$ (580 nm)		
$c_{Ga}(M)$	$c_L(M)$	$\log K_{c1,1}$	No. of points
1.994×10^{-5}	1.554×10^{-4}	−7.16(0.25)	7
1.994×10^{-5}	3.109×10^{-4}	−7.37(.14)	6
1.994×10^{-5}	4.663×10^{-4}	−7.41(.15)	5

Table 4. Complexation of gallium with T-azo-R and T-azo-C in sodium perchlorate solutions at different ionic strength at T = 25°

T-azo-R

$c_{Ga} = 2.990 \times 10^{-4}M$; $c_{T\text{-azo-R}} = 1.661 \times 10^{-5}M$
pH = 2.097
$Ga + H_2L \rightleftharpoons GaL + 2H$

Conc. $NaClO_4$	A(510 nm)	$\log K_{c1,1}$
0.008	0.063	−1.24
0.094	0.036	−1.72
0.221	0.029	−2.04
0.443	0.030	−2.07
0.646	0.036	−1.84
1.034	0.039	−1.73
1.374	0.036	−1.77
1.922	0.024	−2.12
2.415	0.023	−2.08

$c_{Ga} = 3.98 \times 10^{-5}M$; $c_{T\text{-azo-R}} = 2.215 \times 10^{-4}M$
pH = 2.097
$Ga + H_2L \rightleftharpoons GaL + 2H$

Conc. $NaClO_4$	A(510 nm)	$\log K_{c1,1}$
0.008	0.233	−1.12
0.102	0.198	−1.70
0.227	0.204	−2.10
0.455	0.208	−3.09
0.653	0.209	−2.92
1.029	0.197	−2.55
1.309	0.192	−2.08
1.911	0.172	−1.82
2.445	0.162	−1.66

$\log K_{cT1,1} = -0.75(0.33)$ $Z = 10.54(2.69)$ $B = 0.62(0.20)$

T-azo-C

$c_{Ga} = 2.990 \times 10^{-4}M$; $c_{T\text{-azo-R}} = 1.554 \times 10^{-5}M$
pH = 3.520
$2Ga + H_3L \rightleftharpoons Ga_2(OH)L + 4H$

Conc. $NaClO_4$	A(580 nm)	$\log K_{c2,1}$
0.085	0.092	−4.87
0.219	0.073	−5.30
0.427	0.063	−5.63
0.623	0.053	−5.90
0.926	0.046	−6.11
1.282	0.041	−6.30
1.779	0.040	−6.44
2.318	0.036	−6.44

$c_{Ga} = 1.994 \times 10^{-5}M$; $c_{T\text{-azo-R}} = 3.109 \times 10^{-4}M$
pH = 3.520
$Ga + H_3L \rightleftharpoons GaL + 3H$

Conc. $NaClO_4$	A(580 nm)	$\log K_{c1,1}$
0.062	0.085	−6.64
0.182	0.071	−7.05
0.416	0.063	−7.54
0.616	0.061	−7.82
0.986	0.059	−8.06
1.370	0.062	−7.64
1.884	0.059	−7.68
2.409	0.053	−7.82

$\log K_{cT2,1} = -3.48(0.05)$ $Z = 13.10(0.27)$ $B = -0.05(0.03)$;
$\log K_{cT1,1} = -6.06(0.35)$ $Z = 8.02(1.58)$ $B = 0.46(0.18)$.

formed with T-azo-C in a large excess of metal ion. The equilibrium reactions and constants in 0.1M sodium perchlorate are reported in Table 3, and those at other ionic strengths in Table 4. In this case too the thermodynamic complexation constant, and Z and B were estimated by equation (11). Their values are reported in Table 4.

The expected[18] values of Z are 6 for the complexation of gallium with T-azo-R and T-azo-C (1 to 1 complexes) and 12 for the complexation with T-azo-C (2 to 1 complex) which are inside the found confidence limits (95%).

Sorption of gallium on AG MP-1 loaded with T-azo-R

If the sorption of a metal ion on a strong base anion exchange resin containing a chelating group H_xL takes place by equilibrium (1), the fraction of sorbed ion at the given condition can be estimated by means of equation (3), where K_{ex} can be estimated according to the Gibbs–Donnan model (equation 4), and considering that $\log \gamma_{\overline{H_xL}}/\gamma_{\overline{MHrL}} = 1$[1] and $\log\{\overline{NO_3}\}^{z-q} = -(z-q)0.71$.[9]

For instance the estimated value of $\log K_{ex}$ in a 0.5M sodium nitrate aqueous solution is −1.39 for a resin loaded with T-azo-R and −6.40 for a resin loaded with T-azo-C. The fraction f of metal ion sorbed at pH = 3, on a resin containing 0.1 mmoles of dye, from 25 ml of solution, which are typical conditions for a batch experiment, should be respectively 0.98 and 0.50. The hydrolysis constants are those in 0.5M aqueous solution, and are either experimentally found, or evaluated by equation (7). K_{a2} is the apparent protonation coefficient of the ligand in the resin, and can be evaluated from

$$\log K_{ax} = \log K_{axi}\gamma_{\overline{Hx-1L}}/\gamma_{\overline{HxL}}\{\overline{NO_3}\} + \log[NO_3] - \frac{0.51I^{1/2}}{1+1.5I^{1/2}}(z_{NO_3^-}^2 + z_H^2) + [b(NO_3, Na) + b(NO_3, H)]I \quad (12)$$

where again $\log \gamma_{\overline{Hx-1L}}/\gamma_{\overline{HxL}} = 1$ and $\log\{\overline{NO_3}\} = -0.71$,[9] and K_{axi} is the thermodynamic

Table 5. Sorption of gallium on AG MP-1 not containing ligand. $V = 25.0$ ml; 2.5 g of dry resin; $0.06M$ $NaNO_3$

pH	f
2.92	0
3.02	0.22
3.28	0.51
3.71	0.80
4.61	1.00

protonation constant. The values of the apparent protonation coefficients in $0.5M$ solution are $\log K_{a2} = 2.95$ for T-azo-R and $\log K_{a2} = 4.15$ for T-azo-C.[18]

From the estimated values of f it seems preferable to investigate the sorption by the resin containing T-azo-R, because of its ability to quantitatively sorb the metal at pH lower than 3, at least under selected conditions. As a matter of fact at pH higher than about 3 gallium is sorbed not only through equilibrium 1, but also directly by the resin, as demonstrated by the data reported in Table 5, where the sorption of gallium on AG MP-1 not containing ligand is shown. The sorption of a cation on a strong base anion exchange resin is quite surprising, because cations are usually excluded from such resins, due to the existence of a potential difference (Donnan potential) between the resin and the solution phase.[7] However a similar behaviour was observed for aluminium.[2] An interpretation of the sorption by the resin AG MP-1 not containing anionic ligand will be given below. Moreover, the sorption of gallium by a resin containing T-azo-R is probably useful for separating gallium from aluminium because T-azo-R doesn't complex aluminium in aqueous solution. Thus the sorption properties of AG MP-1 loaded with T-azo-R have been extensively investigated. Some results are reported in Table 6, where the fraction f of gallium sorbed on AG MP-1 loaded with T-azo-R under different conditions is shown. Each experiment was performed at fixed volume and ionic strength of aqueous solution, with fixed amount of resin, sorbed ligand and total metal ion, and by changing the acidity which was then measured potentiometrically.

Table 6. Extraction of gallium(III) from sodium nitrate aqueous solution by AG MP-1 (2.5 g) loaded with T-azo-R

$I = 0.025M(NaNO_3)$; $c_{Ga} = 4.45 \times 10^{-4}M$; $V = 32.0$ ml; mmol T-azo-R = 0.1040; $\log K_{a2} = 1.62$; $\log K_{1,1} = -3.22$; $\log K_{5,15} = -35.4$

pH	f	Z_{Ga}	Z_{H_2L}			
2.38	0.04	1.15	6.86	$q = 2.56(.58)$	$\log K_{ex} = -2.62(.59)$	$\log K = -1.21$
2.52	0.09	1.20	9.09			
2.69	0.11	1.30	13.0			

$I = 0.06M(NaNO_3)$; $c_{Ga} = 4.57 \times 10^{-4}M$; $V = 25.0$ ml; mmol T-azo-R = 0.096; $\log K_{a2} = 1.84$; $\log K_{1,1} = -3.33$; $\log K_{5,15} = -36.2$

pH	f	Z_{Ga}	Z_{H_2L}			
2.59	0.14	1.18	6.61	$q = 2.72(.12)$	$\log K_{ex} = -2.71(.12)$	$\log K = -1.46$
2.71	0.18	1.24	8.39			
2.84	0.28	1.33	11.0			
3.01	0.42	1.48	15.7			

$I = 0.100M(NaNO_3)$; $c_{Ga} = 4.45 \times 10^{-4}M$; $V = 25.0$ ml; mmol T-azo-R = 0.1910; $\log K_{a2} = 1.95$; $\log K_{1,1} = -3.40$; $\log K_{5,15} = -36.7$

pH	f	Z_{Ga}	Z_{H_2L}			
2.21	0.24	1.07	2.81	$q = 2.45(.41)$	$\log K_{ex} = -2.32(.42)$	$\log K = -1.15$
2.37	0.32	1.09	3.61			
2.42	0.49	1.11	3.93			
2.60	0.56	1.16	5.44			

$I = 0.500M(NaNO_3)$; $c_{Ga} = 4.45 \times 10^{-4}M$; $V = 35.0$ ml; mmol T-azo-R = 0.1040; $\log K_{a2} = 2.26$; $\log K_{1,1} = -3.66$; $\log K_{5,15} = -38.7$

pH	f	Z_{Ga}	Z_{H_2L}			
2.22	0.25	1.04	1.92	$q = 1.89(.34)$	$\log K_{ex} = -2.14(.40)$	$\log K = -1.15$
2.51	0.33	1.07	2.80			
2.76	0.70	1.13	4.21			
3.06	0.68	1.25	7.40			

The value of f was determined at each pH as previously described.

The value of q was experimentally found by plotting $\log(1/f-1)/Z_M Z_{H_2L}$ *vs.* pH. Only the points at pH lower than 3 were taken into account, in order to consider only the sorption which takes place according to equation (1). Straight lines with slopes of about -2 were obtained in each case, so bearing out that the sorption reaction is the same as the complexation reaction in aqueous solution, as expected from the Gibbs–Donnan model. The values of $\log K_{ex}$ calculated at different ionic strengths are reported in Table 6, together with $\log K$ evaluated from equation (4) with $b(M,Y)+(z-q)b(N,Y)-qb(H,Y)=0$. The average value obtained is $-1.24(0.20)$, in acceptable agreement with the value $-0.75(0.33)$ found in aqueous solution. Thus also in the case of gallium, the convenience of the Gibbs–Donnan model for the prediction of sorption and elution from chelating resin is confirmed.

Sorption of gallium on AG MP-1 not loaded

The sorption of gallium on an unmodified anion exchange resin (see data in Table 5) can be explained as follows. It is known[1] that a small amount of weak acid groups are present in strong base anion exchange resins AG-1 and Dowex 1. It has been found by potentiometric titration that the resin AG MP-1 considered here is able to exchange 0.02 protons per g. This should also be the maximum capacity for metal ions. So 2.5 g of dry resin should be able to sorb 0.05 meq of metal ion. This is demonstrated by some saturation experiments of AG MP-1 anion exchange resin not loaded reported in Table 7.

The sorption mechanism could be

$$Ga + 3\overline{HX} \rightleftharpoons \overline{GaX_3} + 3H \qquad (13)$$

$$K_{exGa} = \frac{\overline{[GaX_3]}[H]^3}{[Ga]\overline{[HX]}^3} \qquad (14)$$

where X indicates the weak cation exchanging groups on the resin. In this case the fraction of gallium sorbed by the resin not loaded is given by

$$f = \frac{\overline{[GaX_3]}g}{[Ga]_t V + \overline{[GaX_3]}g} = \frac{1}{1+\dfrac{[H]^3 V Z_{Ga} Z_{HX^3}}{K_{exGa}\bar{c}_x^3 g}} \qquad (15)$$

By plotting $\log(1/f-1)/Z_{Ga}Z_{HX}$ *vs.* pH it is expected that a straight line with slope -3 is obtained. In practice from the data reported in Table 5 a straight line with slope $-2.33(0.10)$ was obtained, in acceptable agreement with the expected one.

Sorption and separation of gallium(III) traces from an aluminium solution

It is known[10] that in aqueous solution T-azo-R is not able to complex aluminium, which requires a peri-di-hydroxylic structure to form stable chelates with this kind of ligand. According to the Gibbs–Donnan model, the same would be valid when the ligand is sorbed on a strong base anion exchange resin. Thus it is to be expected that the separation of gallium from aluminium by using a resin loaded with T-azo-R is possible. This prediction was checked by considering a synthetic sample containing $0.1M$ $Al(NO_3)_3$ and gallium $1\times10^{-5}M$ (sample *l*). Reasonable conditions for a batch separation are those reported in the experimental section: 50 ml of sample treated with 5 g of dry resin AG MP-1 loaded with 1 mmole of T-azo-R. Higher concentrations of ligand can't be permanently held on the resin. Thus, to have a quantitative sorption of gallium by a unique batch treatment, a pH as high as 3 is required. At these conditions 98% gallium should be sorbed through equation (1), as calculated with $\log K\gamma_{\overline{HxL}}/\gamma_{\overline{MHrL}}\{NO_3\} = -1.24$, *i.e.*, the value actually found. Probably the sorption yield is even better because at this acidity gallium is also partly sorbed by equation (13). On the contrary aluminium is expected not to be sorbed at all. Another problem is the determination of the best conditions for elution, which can also be predicted by equations (3) and (4). A well-suited

Table 7. Sorption of gallium on the strong base anion exchange resin AG MP-1 from $0.06M$ $NaNO_3$. $V=25$ ml; pH = 4.20; 2.5 g of dry resin in nitrate form

Total concentration of gallium (M)	Conc. in solution (M)	mmoles of Ga sorbed per g of dry resin
4.57×10^{-4}	1.09×10^{-4}	3.48×10^{-3}
9.14×10^{-4}	1.28×10^{-4}	7.86×10^{-3}
12.19×10^{-4}	5.10×10^{-4}	7.09×10^{-3}

solution for eluting gallium is 0.2*M* nitric acid. Solutions at higher acidity can't be used, because nitrate at higher concentration can release the sulphonated azo-dye from the resin. The volume of eluting solution which must be used for a quantitative (99.3%) recovery of gallium by one batch treatment was 25 ml as calculated from equations (3) and (4). Based on the above considerations, the separation of gallium was performed as suggested in the experimental section. The concentration of gallium and aluminium were then determined in the eluting solution. Gallium was quantitatively recovered (99%), while the concentration of aluminium was below the limits of the spectrophotometric method employed.[2] The concentration of aluminium in sample *l* after treatment with the loaded resin was also determined spectrophotometrically and found to be unchanged. This demonstrates that gallium is completely separated from aluminium solution, as predicted on the basis of the Gibbs–Donnan model. However gallium cannot be preconcentrated by this method, because relatively large volumes of eluting solution are required for a quantitative recovery. The same loaded resin can be used many times without any loss of reagent.

Acknowledgement—This research was financially supported by Italian MURST (Ministry of University and Scientific and Technological Research).

REFERENCES

1. M. Pesavento, A. Profumo and R. Biesuz, *Talanta*, 1988, **35**, 431.
2. M. Pesavento, A. Profumo, C. Riolo and T. Soldi, *Analyst*, 1989, **114**, 623.
3. G. E. Boyd, J. Schubert and A. W. Adamson, *J. Am. Chem. Soc.*, 1947, **69**, 2818.
4. H. P. Gregor, *ibid.*, 1948, **70**, 1293.
5. F. Helfferich, *Ion Exchange*, McGraw-Hill, New York, 1962.
6. *Idem*, *ibid.*, p. 135. McGraw-Hill, New York, 1962.
7. J. A. Marinsky, *J. Phys. Chem.*, 1982, **86**, 3318.
8. M. Pesavento, A. Profumo and R. Biesuz, *Ann. Chim. (Rome)*, 1991, **81**, 131.
9. M. Pesavento and R. Biesuz, *Reactive Polymers*, 1991, **14**, 239.
10. M. Pesavento, T. Soldi, C. Riolo and P. Garrone, *Ann. Chim. (Rome)*, 1981, **71**, 371.
11. M. Pesavento, C. Riolo, T. Soldi and R. Garzia, *ibid.*, 1982, **72**, 217.
12. T. Fulle Soldi, C. Bertoglio Riolo, G. Gallotti and M. Pesavento, *Gazz. Chim. Ital.*, 1977, **107**, 347.
13. M. Pesavento, C. Riolo Bertoglio, T. Soldi Fulle and G. Cervio, *Ann. Chim. (Rome)*, 1979, **69**, 649.
14. G. Charlot, *Les Methodes de la Chimie Analytique*, p. 753. Masson, Paris, 1961.
15. L. G. Sillen, *Stability Constants of Metal Ion Complexes*, Chem. Soc. Spec. Publication No. 17, 1968, and 25, 1971.
16. P. Gans, A. Sabatini and A. Vacca, *J. Chem. Soc., Dalton Trans.*, 1985, **11**, 95.
17. G. Biedermann, *Dahlem Workshop on the Nature of Seawater*, p. 339. Dahlem Konferenzen, Berlin, 1975.
18. M. Pesavento, A. Profumo, R. Biesuz and L. Cucca, *IX Congresso Nazionale Divisione di Chimica Analitica*, p. 44. Ferrara, Italy, October 28, November 1, 1990.

Talanta, Vol. 39, No. 8, pp. 953–958, 1992
Printed in Great Britain.

0039-9140/92 $5.00 + 0.00

THIN-LAYER CHROMATOGRAPHY OF LASER DYES AND DYE ANALOGS WITH CYCLODEXTRINS IN THE MOBILE PHASE

IEVA R. POLITZER,* KATHLEEN T. CRAGO, KEITH AMOS, KYRAN MITCHELL and TIFFANY HOLLIN
Department of Chemistry, Xavier University, New Orleans, Louisiana 70125, U.S.A.

(*Received* 19 *September* 1991. *Revised* 14 *November* 1991. *Accepted* 15 *November* 1991)

Summary—The addition of β-cyclodextrin and substituted hydroxyethyl and hydroxypropyl-β-cyclodextrins to aqueous urea-containing mobile phases, can be used to enhance the migration of various laser dyes on thin layer chromatography. Selected laser dyes from the coumarin, rhodamine and bimane families were examined, as well as a number of dye analogs. Silica gel, polyamide and C18 reverse phase plates were utilized. Overall, the substituted hydroxypropyl-β-cyclodextrins appeared to be the most effective for increasing dye migration.

Cyclodextrins (CDs) are cycloamylases which are known for their ability to form inclusion complexes with a wide range of guest molecules.[1] They are extensively used as stationary phase components in gas chromatography as well as stationary or mobile phase additives in liquid chromatography.[2–5] In contrast, there has been relatively little utilization of CDs in thin layer chromatography (TLC). The recent introduction of urea as a solubilizing agent for aqueous CD solutions, has opened the way for more extensive TLC applications.[6,7] Our earlier work has indicated probable inclusion complexation between certain laser dyes and CDs.[8–10] Thus, it seemed likely that the TLC characteristics of these laser dyes would also be affected by CDs in the mobile phase.

In this investigation, urea solubilized β-CD and the substituted hydroxyethyl and hydroxypropyl-β-CDs were used as aqueous mobile phase additives. Their effects were examined on the separation of selected laser dyes and dye analogs. Stationary phases for this TLC study included silica gel plates as well as polyamide and C18 reverse phase plates.

EXPERIMENTAL

Materials

Beta-cyclodextrin (Advanced Separation Technologies, Whippany, NJ), hydroxyethyl-β-cyclodextrins, hydroxypropyl-β-cyclodextrins, urea, 2,5-diphenyl oxazole, fluorescein, indole (Aldrich Chemical Co., Milwaukee, WI), ethanol, acetone, tert-butyl alcohol (Fisher Scientific Co., Raleigh, NC), coumarin laser dyes and rhodamine laser dyes (Eastman Kodak, Rochester, NY) were used as received without further purification. The bimanes were synthesized and purified as reported previously.[11] In-house demineralized water was used to prepare all aqueous solutions.

The thin layer chromatography plates employed included Whatman KC18F reverse phase (10 × 10 cm, 200 μ), Baker-flex polyamide 6-F (5 × 20 cm) and Baker-flex silica gel 1B-F (20 × 20 cm) plates. These plates were used as received.

Methods

The mobile phase solutions were patterned after those described by Hinze *et al.* and were prepared as follows. First, aqueous solutions of 4.0*M* urea were made. Next, appropriate amounts of various cyclodextrins were dissolved in the urea solutions to make the final solutions 0.1*M* for the respective cyclodextrin to be studied. Each mobile phase to be used with reverse phase C18 plates was also made 0.5*M* in sodium chloride and 5% v/v with tert-butyl alcohol. When necessary, the solutions were warmed gently (~50°) to dissolve the cyclodextrins and then allowed to cool to room temperature prior to use. Stock solutions of the different test solutes were generally prepared by dissolving 2.0 mg of the solid in 1.0 ml of methanol. A few microliters of these solute stock solutions were applied 2 cm from the lower edge of the plates.

*Author for correspondence.

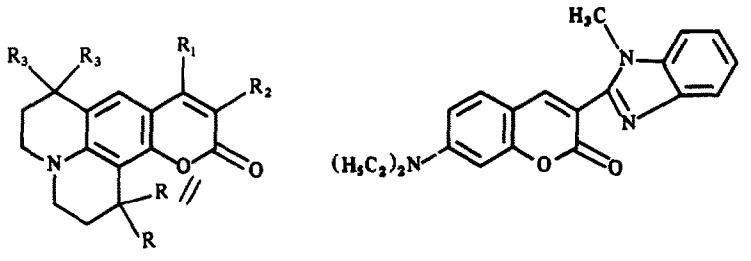

Coumarin laser dyes: Coumarin 30

Coumarin 102 : $R_1 = CH_3$ $R_2 = R_3 = H$
Coumarin 153 : $R_1 = CF_3$ $R_2 = R_3 = H$
Coumarin 314 : $R = R_3 = H$ $R_2 = CO_2C_2H_5$
Coumarin 314T: $R_1 = H$ $R_2 = CO_2C_2H_5$ $R_3 = CH_3$

Fig. 1. Structures of selected coumarin laser dyes.

Ascending thin layer chromatography was performed in 27 × 8 × 25 cm rectangular chambers which were lined with mobile phase-soaked filter paper. The final positions of the solutes were located under UV-Vis light (Mineralight UVSL-58). Most of these compounds moved as distinct spots thus facilitating determination of retardation factors.

RESULTS AND DISCUSSION

The ability of cyclodextrins (CDs) to modify the characteristics of selected laser dyes on thin layer chromatography (TLC) was examined. The β-cyclodextrin (β-CD) as well as hydroxyethyl and hydroxypropyl substituted cyclodextrins were individually added to the aqueous urea mobile phases. Commercially available polyamide, silica gel and reverse phase C18 plates served as solid supports. The retardation factor (R_f) values were obtained and compared for selected laser dyes from the coumarin, rhodamine and bimane families as well as for a number of other heterocycles. (R_f = Distance compound travels/distance solvent travels.) Corresponding capacity factor (k') values were calculated[12] by using the relationship $k' = (1 - R_f)/R_f$.

Coumarin laser dyes

Five coumarin laser dyes (C30, C314, C314T, C102 and C153) were examined (see Fig. 1). Using polyamide TLC plates, an aqueous solution of 4.0*M* urea was compared to aqueous solutions of urea with various added cyclodextrins in the mobile phase. In all cases, when β-CD, the substituted hydroxyethyl, or hydroxypropyl CDs were in the mobile phase, the R_f values of the dyes increased. As shown in Table 1, for the selected coumarins, the hydroxypropyl-β-CDs were overall the most effective agents for increasing R_f values on

Table 1. R_f and capacity factor (k') values of coumarin laser dyes on polyamide TLC plates with aqueous 4.0*M* urea mobile phases containing $10^{-1}M$ substituted and unsubstituted betacyclodextrins*

Coumarin dye		β-CD	HE*MS = 1	HE*MS = 1.6	HP*MS = 0.6	HP*MS = 0.9	Urea only
C30	R_f	0.96	0.76	0.65	1	0.76	0.05
	k'	0.04	0.32	0.54	0	0.32	19.0
C314	R_f	0.43	0.39	0.42	0.45	0.46	0.05
	k'	1.33	1.56	1.38	1.22	1.17	19.0
C314T	R_f	0.23	0.34	0.37	0.42	0.42	NM
	k'	3.35	1.94	1.70	1.38	1.38	—
C102	R_f	0.08	0.17	0.24	0.21	0.25	NM
	k'	11.5	4.88	3.17	3.76	3.00	—
C153	R_f	0.02	0.06	0.06	0.07	0.10	NM
	k'	49.0	15.7	15.7	13.3	9.00	—

*β-CD: Betacyclodextrin.
HE*MS = 1 and HE*MS = 1.6: hydroxyethyl betacyclodextrin with average molecular substitution of 1 and 1.6, respectively.
HP*MS = 0.6 and HP*MS = 0.9: hydroxypropyl betacyclodextrin with average molecular substitution of 0.6 and 0.9, respectively.
NM: no movement.

Table 2. R_f and capacity factor (k') values of coumarin laser dyes on silica gel TLC plates with aqueous 4.0M urea mobile phases containing $10^{-1}M$ substituted and unsubstituted betacyclodextrins*

Coumarin dye		β-CD	HE*MS = 1	HE*MS = 1.6	HP*MS = 0.6	HP*MS = 0.9	Urea	Ethanol
C30	R_f	0.80	0.65	0.56	0.70	0.51	0.02	0.63
	k'	0.25	0.54	0.79	0.43	0.96	49.0	0.59
C314	R_f	0.71	0.66	0.64	0.70	0.64	0.06	0.58
	k'	0.41	0.52	0.56	0.43	0.56	15.7	0.72
C314T	R_f	0.27	0.44	0.44	0.51	0.47	NM	0.62
	k'	2.70	1.27	1.27	0.96	1.13	—	0.61
C102	R_f	0.24	0.49	0.51	0.48	0.54	0.03	0.61
	k'	3.17	1.04	0.96	1.08	0.85	32.3	0.64
C153	R_f	0.01	0.05	0.08	0.05	0.12	NM	0.62
	k'	99.0	19.0	11.5	19.0	7.33	—	0.61

*β-CD: Betacyclodextrin.

HE*MS = 1 and HE*MS = 1.6: hydroxyethyl betacyclodextrin with average molecular substitution of 1 and 1.6, respectively.

HP*MS = 0.6 and HP*MS = 0.9: hydroxypropyl betacyclodextrin with average molecular substitution of 0.6 and 0.9, respectively.

NM: no movement.

polyamide plates. These coumarins have very similar R_f and k' values on silica gel TLC plates with ethanol as the mobile phase. Substitution of aqueous 4.0M urea as the mobile phase on the other hand, resulted in uniformly low R_f values. Aqueous solutions of urea and added CDs, however, led to a wide range of R_f and k' values and facilitated identification of the coumarins on silica gel plates. These results are summarized in Table 2.

The coumarins listed above did not move at all on reverse phase C18 plates with a mobile phase consisting of aqueous 4.0M urea, 5% v/v t-butyl alcohol, 0.5M sodium chloride and 0.1M CD. The CDs examined here as mobile phase additives were β-CD and hydroxypropyl-β-CD (molecular substitution, MS = 0.9).

Bimane laser dyes

Five bimane dyes [syn- and anti-(Me,Me), syn and anti (Me,Cl), and syn-(Ph, Cl) bimane] were studied. Their structures are shown in Fig. 2. TLC was carried out on polyamide and reverse phase C18 plates as described above. The presence of β-CD or the substituted hydroxyethyl and hydroxypropyl CDs in the mobile phases did not make any significant difference in the R_f values obtained for these bimanes. All of the bimanes examined gave R_f values above 0.50 and k' values below 1 on silica gel plates with ethanol as the mobile phase. The R_f values were markedly decreased when aqueous 4.0M urea was substituted as the mobile phase. Addition of CDs, particularly hydroxypropyl-β-CD, to the urea mobile phase again elevated the R_f values, but not to the same levels as found with ethanol. The results with silica gel plates are shown in Table 3. As can be seen, using the urea-CD mobile phase may be useful in the separation of certain bimanes on silica gel plates.

Rhodamine laser dyes

The rhodamine laser dyes, Rh6G and RhB as well as sulforhodamine B and sulforhodamine 101 (see Fig. 3) were examined on polyamide TLC plates as described earlier. In all cases, except for sulforhodamine 101, the addition of CDs to the urea mobile phase increased the R_f values of the rhodamines. These results (R_f and k' values) are shown in Table 4. In contrast,

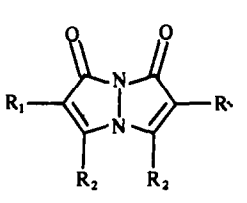

syn-(R_2, R_1) bimanes:

syn-(CH_3, Cl) bimane: R_1 = Cl R_2 = CH_3

syn-(CH_3, CH_3) bimane: R_1 = CH_3 R_2 = CH_3

syn-(C_6H_5, Cl) bimane: R_1 = Cl R_2 = C_6H_5

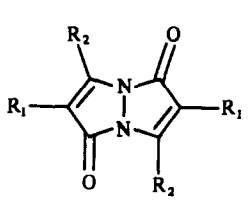

anti-(R_2, R_1) bimanes:

anti-(CH_3, Cl) bimane: R_1 = Cl R_2 = CH_3

anti-(CH_3, CH_3) bimane: R_1 = CH_3 R_2 = CH_3

Fig. 2. Structures of selected bimanes.

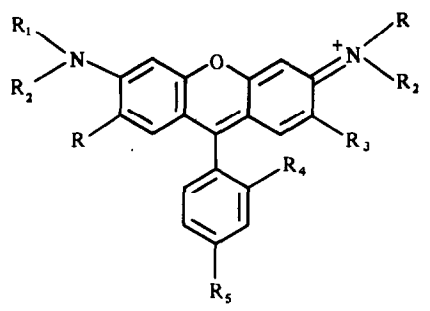

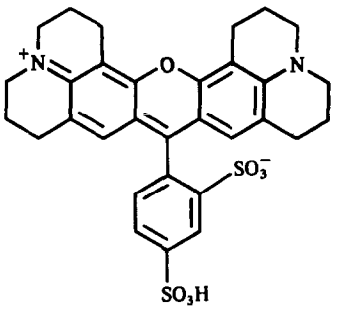

Rhodamine laser dyes:

Rhodamine 6G: $R_1 = R_5 = H$ $R_2 = C_2H_5$ $R_3 = CH_3$ $R_4 = CO_2C_2H_5$ Cl^-

Rhodamine B: $R_1 = R_2 = C_2H_5$ $R_3 = R_5 = H$ $R_4 = CO_2H$ Cl^-

Sulforhodamine B: $R_1 = R_2 = C_2H_5$ $R_3 = H$ $R_4 = SO_3^-$ $R_5 = SO_3H$

Sulforhodamine 101

Fig. 3. Structures of selected rhodamine laser dyes.

when reverse phase C18 plates were used, the introduction of β-CD or hydroxypropyl-β-CD (MS = 0.9) had very little effect on the R_f values.

When silica plates were used, the advantages of CDs in the mobile phase became particularly striking. The rhodamines examined exhibited very little migration on the silica gel plates with either acetone or aqueous urea as the mobile phase. However, upon addition of CDs, considerable elevation of the R_f values was obtained (see Table 5 for R_f and k' values). This could prove quite useful in the identification and/or separation of the rhodamine family members.

Fluorescein, a laser dye akin in structure to the rhodamines, qualitatively has similar TLC characteristics. Aqueous urea mobile phases did not promote any migration of this compound on the solid supports examined here. Upon addition of CDs however, fluorescein R_f values were increased. This was most pronounced with hydroxypropyl-β-CD (MS = 0.9), whereupon fluorescein R_f values of 0.19, 0.22 and 0.72 were obtained on polyamide, C18 and silica gel plates respectively. Hydroxypropyl-β-CDs were also the most effective aqueous mobile phase additives for the aromatic heterocycle, indole. Whereas no migration of indole was obtained in aqueous urea, R_f values of 0.42, 0.18 and 0.51 can be obtained (polyamide, C18 and silica gel plates respectively) upon addition of hydroxypropyl-β-CD (MS = 0.9) to the mobile phase.

As seen from the above, the addition of CDs and urea to aqueous mobile phases can be used to increase the migration of various laser dyes and dye analogs on TLC. Often, better separation or better selectivity is facilitated. Selectivity refers to the capability of a chromatographic system to distinguish between two compounds. The separation or selectivity factor, α, for two

Table 3. R_f and capacity factor (k') values of bimane laser dyes on silica gel TLC plates with aqueous 4.0M urea mobile phases containing $10^{-1}M$ substituted and unsubstituted betacyclodextrins*

Bimane dye		β-CD	HE*MS = 1	HE*MS = 1.6	HP*MS = 0.6	HP*MS = 0.9	Urea	Ethanol
syn (Me,Me)	R_f	0.39	0.45	0.47	0.47	0.54	0.35	0.58
	k'	1.56	1.22	1.13	1.13	0.85	1.86	0.72
anti (Me,Me)	R_f	0.64	0.65	0.65	0.63	0.68	0.55	0.72
	k'	0.56	0.54	0.54	0.59	0.47	0.82	0.39
syn (Me,Cl)	R_f	0.39	0.43	0.49	0.48	0.52	0.35	0.65
	k'	1.56	1.33	1.04	1.08	0.92	1.86	0.54
anti (Me,Cl)	R_f	0.42	0.44	0.43	0.48	0.46	0.33	0.72
	k'	1.38	1.27	1.33	1.08	1.17	2.03	0.39
syn (Ph,Cl)	R_f	0.02	0.03	0.03	0.04	0.04	NM	0.68
	k'	49.0	32.3	32.3	24.0	24.0	—	0.47

*β-CD: Betacyclodextrin.

HE*MS = 1 and HE*MS = 1.6: hydroxyethyl betacyclodextrin with average molecular substitution of 1 and 1.6, respectively.

HP*MS = 0.6 and HP*MS = 0.9: hydroxypropyl betacyclodextrin with average molecular substitution of 0.6 and 0.9, respectively.

NM: no movement.

Table 4. R_f and capacity factor (k') values of rhodamine laser dyes on polyamide TLC plates with aqueous 4.0M urea mobile phases containing $10^{-1}M$ substituted and unsubstituted betacyclodextrins*

Rhodamine dye		β-CD	HE*MS = 1	HE*MS = 1.6	HP*MS = 0.6	HP*MS = 0.9	Urea only
RhB	R_f	0.97	0.91	0.92	0.92	0.96	0.37
	k'	0.03	0.10	0.09	0.09	0.04	1.70
Rh6G	R_f	0.64	0.58	0.52	0.52	0.68	0.43
	k'	0.56	0.72	0.92	0.92	0.47	1.33
Sulfo RhB	R_f	0.35	0.24	0.25	0.33	0.27	0.07
	k'	1.86	3.17	3.00	2.03	2.70	13.3
Sulfo Rh101	R_f	0.03	0.03	0.05	0.03	0.04	0.04
	k'	32.3	32.3	19.0	32.3	24.0	24.0

*β-CD: Betacyclodextrin.
HE*MS = 1 and HE*MS = 1.6: hydroxyethyl betacyclodextrin with average molecular substitution of 1 and 1.6, respectively.
HP*MS = 0.6 and HP*MS = 0.9: hydroxypropyl betacyclodextrin with average molecular substitution of 0.6 and 0.9, respectively.
NM: no movement.

Table 5. R_f and capacity factor (k') values of rhodamine laser dyes on silica gel TLC plates with aqueous 4.0M urea mobile phases containing $10^{-1}M$ substituted and unsubstituted betacyclodextrins*

Rhodamine dye		β-CD	HE*MS = 1	HE*MS = 1.6	HP*MS = 0.6	HP*MS = 0.9	Urea	Acetone
Sulfo RhB	R_f	0.79	0.67	0.64	0.68	0.72	0.28	0.02
	k'	0.27	0.49	0.56	0.47	0.39	2.57	49.0
RhB	R_f	0.57	0.51	0.40	0.45	0.46	0.08	0.26
	k'	0.75	0.96	1.50	1.22	1.17	11.5	2.85
Rh6G	R_f	0.33	0.24	0.25	0.28	0.25	0.10	0.06
	k'	2.03	3.17	3.00	2.57	3.00	9.00	15.7
Sulfo Rh101	R_f	0.25	0.34	0.38	0.36	0.47	0.22	NM
	k'	3.00	1.94	1.63	1.78	1.13	3.55	—

*β-CD: Betacyclodextrin.
HE*MS = 1 and HE*MS = 1.6: hydroxyethyl betacyclodextrin with average molecular substitution of 1 and 1.6, respectively.
HP*MS = 0.6 and HP*MS = 0.9: hydroxypropyl betacyclodextrin with average molecular substitution of 0.6 and 0.9, respectively.
NM: no movement.

Table 6. Capacity factor (k') and selectivity factor (α) values for coumarin laser dyes with β-CD or hydroxypropyl-β-CD in the mobile phase

Coumarin dye	β-CD k'	α	HP*MS = 0.6 k'	α	HP*MS = 0.9 k'	α
			Polyamide TLC plates			
C30	0.04	33.0	0	—	0.32	3.66
C314	1.33	2.52	1.22	1.13	1.17	1.18
C314T	3.35	3.42	1.38	2.72	1.38	2.17
C102	11.5	4.26	3.76	3.53	3.00	3.00
C153	49.0		13.3		9.00	
			Silica gel TLC plates			
C30	0.25	1.64	0.43	1.00	0.96	1.71
C314	0.41	6.59	0.43	2.23	0.56	2.02
C314T	2.70	1.17	0.96	1.13	1.13	1.32
C102	3.17	31.2	1.08	17.6	0.85	8.62
C153	99.0		19.0		7.33	

β-CD: Betacyclodextrin.
HP*MS = 0.6 and HP*MS = 0.9: hydroxypropyl betacyclodextrin with average molecular substitution of 0.6 and 0.9, respectively.

solutes A and B, can be related to their capacity factor by the equation

$$\alpha = k'_B/k'_A$$

where B is the more strongly retained species and A is the less strongly held species. By this definition, α is always greater than unity. As α approaches 1, separation becomes difficult.[13,14] Tables 6 and 7 show capacity factors and selectivity factors for the various coumarin and rhodamine laser dyes when β-CD or the hydroxypropyl-β-CDs are added to the mobile

Table 7. Capacity factor (k') and selectivity factor (α) values for rhodamine laser dyes with β-CD or hydroxypropyl-β-CD in the mobile phase

Rhodamine dye	β-CD k'	α	HP*MS = 0.6 k'	α	HP*MS = 0.9 k'	α
			Polyamide TLC plates			
RhB	0.03	18.7	0.09	10.2	0.04	11.8
Rh6G	0.56	3.32	0.92	2.21	0.47	5.74
Sulfo RhB	1.86	17.4	2.03	15.9	2.70	8.89
Sulfo Rh101	32.3		32.3		24.0	
			Silica gel TLC plates			
Sulfo RhB	0.27	2.78	0.47	2.60	0.39	3.00
RhB	0.75	2.71	1.22	2.11	1.17	2.56
Rh6G	2.03	1.48	2.57	1.44	3.00	2.65
Sulfo Rh101	3.00		1.78		1.13	

β-CD: Betacyclodextrin.
HP*MS = 0.6 and HP*MS = 0.9: hydroxypropyl betacyclodextrin with average molecular substitution of 0.6 and 0.9, respectively.

Table 8. Capacity factor (k') and selectivity factor (α) values for bimane isomers on silica gel TLC plates with β-CD or hydroxypropyl-β-CD in the mobile phase

Bimane isomers	β-CD k'	α	HP*MS = 0.6 k'	α	HP*MS = 0.9 k'	α
Syn (Me,Me)	1.56	2.79	1.14	1.92	0.85	1.81
Anti (Me,Me)	0.56		0.59		0.47	
Syn (Me,Cl)	1.56	1.13	1.08	1.00	0.92	1.27
Anti (Me,Cl)	1.38		1.08		1.17	

β-CD: Betacyclodextrin.
HP*MS = 0.6 and HP*MS = 0.9: hydroxypropyl betacyclodextrin with average molecular substitution of 0.6 and 0.9, respectively.

phase. In most cases, α is greater than 1. Capacity factors and selectivity factors are also shown for two sets of isomeric bimanes in Table 8. The selectivity factors reflect the better separation of the syn- and anti- (Me,Me) bimane isomers as contrasted to the syn- and anti- (Me, Cl) bimane isomers. Overall, the substituted hydroxypropyl-β-CDs appear to be the most effective in increasing the migration of coumarin, rhodamine and bimane laser dyes, especially on polyamide or silica gel plates. This achievement of good TLC separations on the commonly used silica gel plates by introduction of CDs in the mobile phase, may prove to be particularly useful.

Acknowledgement—We gratefully acknowledge an unrestricted grant from the Monsanto Company for support of this research.

REFERENCES

1. J. Szejtli, *Cyclodextrin Technology*, Kluwer Academic Publishers, Dordrecht, 1988.
2. W. L. Hinze, *Sep. Purif. Methods*, 1981, **10**, 159.
3. D. W. Armstrong, *Anal. Chem.*, 1987, **59**, 84A.
4. D. Sybilska and E. Smolkova-Keulemansova in J. L. Atwood, J. E. D. Davies and D. D. MacNicol (eds.), *Inclusion Compounds*, Vol. 3, p. 173. Academic Press, New York, 1984.
5. A. M. Pena, T. T. Ndou, V. C. Anigbogu and I. M. Warner, *Anal. Chem.*, 1991, **63**, 1018.
6. W. L. Hinze, D. Y. Pharr, Z. S. Fu and W. G. Burkert, *ibid.*, 1989, **61**, 422.
7. D. Y. Pharr, Z. S. Fu, T. K. Smith and W. L. Hinze, *ibid.*, 1989, **61**, 275.
8. I. R. Politzer, K. T. Crago, D. L. Kiel and T. Hampton, *Anal. Lett.*, 1989, **22**, 1567.
9. I. R. Politzer, K. T. Crago, T. Hampton, J. Joseph, J. H. Boyer and M. Shah, *Phys. Chem. Lett.*, 1989, **159**, 258.
10. I. R. Politzer, K. T. Crago, S. Garner, J. Joseph, J. H. Boyer and M. Shah, in *Proceedings of the International Conference on Lasers '89*, D. G. Harris and T. M. Shay (eds.), p. 434. STS Press, McLean, Virginia, 1990.
11. E. M. Kosower and B. Pazhenchevsky, *J. Am. Chem. Soc.*, 1980, **102**, 4983.
12. D. W. Armstrong, F. Nome, L. A. Spino and T. D. Golden, *J. Am. Chem. Soc.*, 1986, **108**, 1418.
13. D. A. Skoog, D. M. West and F. J. Holler, *Fundamentals of Analytical Chemistry*, 5th Ed., pp. 604, 605. Saunders College Publishing, New York, 1988.
14. R. E. Majors in G. D. Christian and J. E. O'Reilly (eds.), *Instrumental Analysis*, 2nd Ed., pp. 670, 671. Allyn and Bacon Inc., Boston, 1986.

Talanta, Vol. 39, No. 8, pp. 959–965, 1992
Printed in Great Britain.

0039-9140/92 $5.00 + 0.00

THERMODYNAMIC STUDY IN AQUEOUS SOLUTIONS OF WEAKLY SOLUBLE IONIC COMPOUNDS

JEAN-CLAUDE BOLLINGER

Laboratoire de Chimie Générale et Analytique, Faculté des Sciences, 123 avenue Albert-Thomas, 87060 Limoges Cédex, France

BERNARD BOURG, JEAN-YVES GAL* and PHILIPPE ROUYER

Laboratoire de Chimie Analytique, Université de Montpellier II, Place Eugène-Bataillon, 34095 Montpellier Cédex 5, France

(*Received* 28 *January* 1991. *Revised* 2 *July* 1991. *Accepted* 30 *August* 1991)

Summary—Any investigation for a better knowledge of precipitation/dissolution problems necessitates the availability of all the β formation constants of the uncharged soluble species (ion-pair). Several difficulties dealing with solubility measurements are briefly reviewed, especially related to phase structure variations, time-lag or supersaturation phenomena. Thanks to some thermodynamic considerations, the evolution of the uncharged soluble species with hydration and solid phase modifications can give a new explanation about the observed dispersion in literature values for some weakly soluble ionic compounds. When not given elsewhere, the evaluation of thermodynamic data of interest (formation constants, solubility product, *etc.*) is made possible according to given methods.

The application of conditional calculations, as introduced by Ringböm,[1] has permitted the development of rational use of computers to study the thermodynamics of electrolytic solutions. Two of us have shown, mainly as a pedagogical tool,[2] that computers easily allow all the equilibria between the ions in the solution to be taken into consideration, thus avoiding any approximation.

Hereafter, our intensive practical insights into industrial (*e.g.*, waste management, plating, *etc.*) and environmental (*e.g.*, geology, ecotoxicity, *etc.*) processes lead us to study the behaviour of weakly soluble compounds, for which the solubility product is a classical approach.

In this work, we want to study the solution equilibria of a weakly soluble compound ML in water:

$$\underset{\text{Saturated solution of } ML_{aq}}{ML_S} \Leftrightarrow \underset{}{ML^0_{aq}} \Leftrightarrow \underset{\text{Dissociation of } ML_{aq} \text{ in solution}}{M^+_{aq} + L^-_{aq}}$$

Most frequently, we only know the solubility product:

$$K_S = |M^+_{aq}||L^-_{aq}|$$

either from Gibbs energy calculations, or from solubility measurements. In both cases, the determination of K_S currently neglects the presence of the molecular form ML^0 in solution, so we can explain, in part, the apparent variability observed in the literature.

The first equilibrium is markedly dependent on the crystalline form of the solid ML; this is well known, and can also lead to some spread in the solubility data. An amorphous precipitate evolving to a crystalline form strongly diminishes the solubility, as is the case for numerous hydroxides or for calcium orthophosphate (with its apatite form). Much work on saturation time-lag gives evidence of a large body for new studies taking the nature of the intermediate form ML^0_{aq} into account.

Saturation

When we consider a solution of ML at a concentration below saturation, the second equilibrium can be characterized by the classical thermodynamic constant β,

$$\beta = |ML^0_{aq}|/|M^+_{aq}||L^-_{aq}|$$

(where $||$ stands for activities), depending only on temperature, pressure and ionic strength. If we progressively raise the ML concentration in water, the limiting solubility is obtained for a given value S of this concentration.

Therefore $\beta \Rightarrow S/|M^+_{aq}||L^-_{aq}|$ and with the solubility product: $\beta = S/K_S$.

*Author for correspondence.

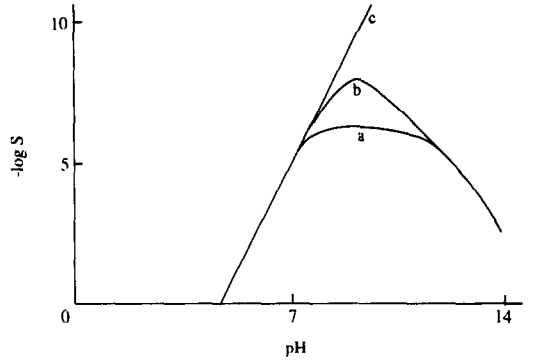

Fig. 1. Solubility in the Cu^{2+}–OH^- system; influence of the knowledge of various β formation constants (curves a, b, c: see text).

So, while β is a constant, every variation in the limiting solubility for the molecular form leads experimentally to a variation in the solubility product. Knowing β precisely is a very useful topic, as this allows us to calculate the ML^0 activity in a given solution from the measured values for M^+ and L^-

$$|ML^0| = \beta\,|M^+_{aq}|\,|L^-_{aq}|$$

As long as the solution maintains limpidity, we have either under-saturation if $|ML^0| < S$, or over-saturation if $|ML^0| > S$.

The importance of knowing both β and S becomes evident in the study of diluted solutions, or when dealing with the environmental hazards of toxic metallic salts. In these cases, we cannot systematically neglect the solubility of the molecular form in comparison with the very low concentrations in free ions.

As an example, we want to present here the results for the solubility calculations in a Cu^{2+}/OH^- solution, at an ionic strength $I = 0.15M$. In Fig. 1, curve (a) is the solubility of all metal species, taking into account the $\beta_{2,OH}$ formation constant of the weakly soluble hydroxide $Cu(OH)^0_2$:

$$S = [Cu^{2+}] + [CuOH^+] + [Cu(OH)^0_2] + [Cu(OH)^-_3] + [Cu(OH)^{2-}_4]$$

$$S = |Cu^{2+}|/\gamma_{2+} + |CuOH^+|/\gamma_+ + |Cu(OH)^0_2| + |Cu(OH)^-_3|/\gamma_- + |Cu(OH)^{2-}_4|/\gamma_{2-}$$

$$S = |Cu^{2+}|/\gamma_{2+} \times \{1 + \beta_{1,OH}|OH^-|/\gamma_+ + \beta_{2,OH}|OH^-|^2 + \beta_{3,OH}|OH^-|^3/\gamma_- + \beta_{4,OH}|OH^-|^4/\gamma_{2-}\}$$

[where [] stands for concentrations, || for activities, and γ_i for activity coefficients]. In such cases, for concentrations Ringböm introduces the conditional solubility product K'_S and the α coefficient, *i.e.*:

$$K'_S = [Cu^{2+}]_T[OH^-]^2 = \alpha_{Cu(OH)} \cdot K_S$$

(see ref. 1, p. 67).

However, in order to obtain the correct curve (a) for the total metal solubility from the conditional solubility product, it is important to take into account the presence of the $Cu(OH)^0_2$ species in the $\alpha_{Cu(OH)}$ term;[2] but the pertinent data were not available at the time of the publication by Ringböm.[1]

When we ignore the $\beta_{2,OH}$ value (which is most frequent for compounds other than hydroxides) we write only

$$S = [Cu^{2+}] + [CuOH^+] + [Cu(OH)^-_3] + [Cu(OH)^{2-}_4]$$

and the calculated solubility at pH = 9.5, for example, is 100 times smaller than the correct value [compare curves (a) and (b), Fig. 1].

In order to obtain a straightforward calculation, some authors consider the presence of free metallic ions only, obtaining:

$$S = [Cu^{2+}] = K_{S,Cu(OH)_2}/(|OH^-|^2\gamma_{Cu^{2+}})$$

which is presented as curve (c) in Fig. 1. The importance of such approximations is evident, and their consequences may be dramatic, particularly when dealing with a compound of ecotoxicological importance.

For two weakly soluble compounds under competition, one implicitly supposes that the more insoluble compound is also the more stable; this is not always true however. If we write for the two competing ligands L^- and X^- with the cation M^+:

$$ML_S + X^- \underset{(a)}{\Leftrightarrow} ML^0 + X^- \underset{(b)}{\Leftrightarrow} MX^0 + L^- \underset{(c)}{\Leftrightarrow} MX_S + L^-$$

the formation of the precipitate MX_S, even more insoluble than ML_S, depends on the evolution of the solution equilibrium (*b*), *i.e.*, on the β formation constants for ML^0 and MX^0, and of the dissolution/precipitation kinetics for equilibria (*a*) and (*c*).

This is the reason why we review, in the present article, some secondary phenomena and some thermodynamic considerations related to

the precipitate formation and to the use of β formation constants.

Supersaturation and difficulties in the determination of solubilities

In spite of an apparent facility, solubility determinations are not easy to obtain with sufficient precision,[3] as one has to successively prepare a saturated solution, separate it from the solid in excess and finally analyse this solution. All steps can lead to many uncertainties,[4] and only careful checking of the system gives useful data. Here we want to focus on the various phenomena leading to a spread in solubility data.

When the solute concentration is increased, the solution progressively goes from an unsaturated state to an oversaturated one (where the precipitate forms spontaneously), but an intermediate metastable step arises frequently. The current way studying a solid/solution equilibrium is to introduce the supersaturation ratio

$$\Omega = |M^+||X^-|/K_{S,MX}$$

The driving force for the formation of the precipitate is given by the Gibbs free energy on going from the supersaturated solution to equilibrium

$$\Delta G = -(RT/2)\ln \Omega$$

But the nucleation of crystals from aqueous solutions is not a straightforward process; it may be heterogeneous (crystallization is induced by foreign ions or by the reactor wall) or homogeneous, which requires high supersaturation ratios.[5] This nucleation phenomenon may be dependent on particle size; moreover, its time delay is generally inversely proportional to the concentration.[5-7] Afterwards, a diffusion process in the solution is necessary, in order to assure the growth of crystals; this heterogeneous equilibrium is also associated with some time-lag.

Analytical chemists are well aware of the different behaviour between fresh and aged precipitates,[8] when a very fine crystalline solid progressively converts to a more ordered phase. The particle size may also play a significant role in the conversion from one polymorphous form to another, such as in the case with the various hydrated forms; and due to the time-lag for the solid-state interconversion, it is not necessarily the most stable hydrate that is present, as shown later in this article.

The coexistence of different phases in equilibrium is also a frequent situation, especially in natural waters (and geological compounds therein),[4,9,10] and this can lead to solid solutions, either homogeneous or heterogeneous, where the activity of the solid phase under study is decreased.

Finally, the presence of other ions in the solution gives rise to several effects. First, an ionic strength effect, modifying the values of all thermodynamic constants (see hereafter); secondly, some complexes can be formed, either soluble or insoluble, whose formation constants have to be taken into consideration; thirdly, foreign ions frequently have a kinetic effect, either catalytic or inhibiting, on the precipitation rate.

According to the preceding considerations, it will not be astonishing to reach solubility product values in great variation, and it is not uncommon to have a 10-fold dispersion for K_S. In such a case, the classical treatment infers a $\sqrt{10}$ multiplication for the ion solubility (*i.e.*, $\times 3.16$); but when we are dealing with the ion pair, its concentration is multiplied by 10, which is very different.

It should be noted that when dissolution of a weakly soluble compound in excess of precipitant does not take place, this does not mean that complex formation is impossible: the value of β depends on the S/K_S ratio and even if S and K_S are very small, β may be high.

Solvation of ions

The solubility product can be obtained by a combination of tabulated Gibbs free energy data, according to the well-known relationship:

$$MS_S \Leftrightarrow M_h^+ + X_h^- \quad K_S = |M^+||X^-|/|MX|$$

$$\Delta G^0 = -RT \ln K_S$$

$$= \Delta G_f^0(M_h^+) + \Delta G_f^0(X_h^-) - \Delta G_f^0(MX_S)$$

where S is the solid form, and h the hydrated one.

In fact, the free energy for this reaction is the sum of two terms related to the separation of ions from the crystal (dissolution) and to their hydration:

$$\Delta G^0 = \Delta G_d^0 + \Delta G_h^0$$

Any modification into the solid (nature of the crystal lattice or of the amorphous form, particle dimension, *etc.*) leads to variations of these two terms and also of the solubility product.[11-13]

In such a model, we can write when various solid forms α, β, *etc.* are available:

$$M_h^+ + X_h^- \Leftrightarrow (MX_S)_\alpha \quad \Delta G_\alpha ; K_{S\alpha}$$

$$M_h^+ + X_h^- \Leftrightarrow (MX_S)_\beta \quad \Delta G_\beta ; K_{S\beta}$$

where

$$\Delta G_\alpha = \Delta G_d + \Delta G_{h(\alpha)}$$

$$\Delta G_\beta = \Delta G_d + \Delta G_{h(\beta)}$$

and the variations in K_S are related to modifications in the solid form.[11–13]

Free energies of formation ΔG_f^0 for the solid salts MX are sometimes difficult to obtain, due to the possibility of various crystalline or amorphous phases being present (see preceding paragraph). But the obtention of thermodynamic data for the formation of ions in solution is somewhat cumbersome, as we are concerned by (hypothetic) individual ions where solvation state is unknown; this can be resolved, in part, from a Born–Haber type formulation and some arbitrary partition.[14]

Two different conventions are used in thermochemical data compilations for ions in solution, each referring to the hydrated proton H_h^+; they concern either its standard formation

$$1/2H_{2g} \rightarrow H_h^+ \quad \Delta H_f^0(H_h^+) = \Delta G_f^0(H_h^+) = 0$$

or the hydration of the gaseous proton

$$H_g^+ \rightarrow H_h^+ \quad \Delta H_f^0(H_g^+) = \Delta G_f^0(H_g^+) = 0$$

In fact, solvent shells can be built up by the stepwise attachment of molecules to gas-phase ions. So, measurements of the thermochemistry of clustering reactions (in the gas phase) such as

$$M^+ \cdot (n-1)H_2O + H_2O \rightleftharpoons M^+ \cdot nH_2O$$

or

$$X^- \cdot (n'-1)H_2O + H_2O \rightleftharpoons X^- \cdot n'H_2O$$

allow an insight into ion-solvent interactions in the inner solvation shells, and constitute a useful step towards elucidation of the ion solvation in the condensed liquid phase. Such studies have been conducted recently, thanks to high-pressure or pulsed electron-beam mass spectrometry techniques.[15,16] Other determinations by emf measurements and calculations[17–19] lead to the admitted experimental values (in good accordance with the hypothesis of equality between these values):

$$\left.\begin{aligned} \Delta H_h^0(H_g^+) &= (-1100 \pm 10)\ \text{kJ/mole} \\ \Delta G_h^0(H_g^+) &= (-1060 \pm 10)\ \text{kJ/mole} \end{aligned}\right\} \text{ for } H_g^+ \rightarrow H_h^+$$

Although the conventional value is eliminated by subtraction during the calculation of ΔG^0, tabulated values should be examined with care before any discussion and use. On the other hand, some corrections or re-evaluations for the free energy of formation of any ion in solution can lead to solubility products with differences in several orders of magnitude from previous values: this is the case for metal sulphides, as recently detailed by Licht.[20]

Another complicating factor is the solvation of the ion-pair, while for the overall solubilization process of a weakly soluble ionic compound

$$MX_S \Leftrightarrow MX_h^0 \Leftrightarrow M_h^+ + X_h^-$$

we have to take into account the different behaviour of the solid MX (in its crystalline or amorphous form) and of MX in solution, *i.e.*, of the ion-pair MX^0 somewhat hydrated. When referring to the usual model for the solvation of an ionogen,[21] we propose to write here a series of equilibria such as

$$\underset{\text{ionic solid}}{M^+X_S^-} \Leftrightarrow \underset{\text{contact ion-pair}}{(M^+X^-)_h^0} \Leftrightarrow \underset{\text{solvent-separated ion-pair}}{(M^+//X^-)_h^0} \Leftrightarrow \underset{\text{free solvated ions}}{M_h^+ + X_h^-}$$

According to the analytical technique, the measured equilibrium constant (or any thermodynamic data) will refer to any combination of the intermediate data. Contact ion-pair and solvent-separated ion-pair are separated by an energy barrier corresponding to the formation of a hole between the ions, with a dimension compatible with the size of a solvent molecule to be introduced in between.

The ion-pair model is most understandable when introduced starting from a saturated solution; here we have to write a formation constant for the soluble species

$$M_h^+ + X_h^- \Leftrightarrow (M^+X^-)_h^0$$

$$\beta = \frac{|(M^+X^-)_h^0|}{|M_h^+||X_h^-|} = S/K_S$$

valid also after the beginning of precipitation. It implies that the solubility S for the (solvated) ion-pair depends on the K_S value, *i.e.*, on the final state of the solid form.

So they are limiting solubilities related to each form of ion-pair solvation; these species determine the nucleation type. The unsolvated (*i.e.*, totally dehydrated) ion-pair MX^0 will be the less soluble species. A dehydration

reaction is endothermal,[22] and the formation of an amorphous solid can be facilitated during the precipitation, as corresponding to a minimum in free energy.

It is possible that in solution the evolution of a hydrated species to another (such as various aggregates or various solvation steps) should be relatively small in comparison with the differences between the solid forms. With this hypothesis, we maintain a unique value for β which is in fact a conditional formation constant for all the MX species in the solution:

$$\beta' = |(M^+X^-)^0_h|_T / |M^+_h|\,|X^-_h|$$

$$\Delta G' = -RT \ln \beta'$$

The solution model becomes:

$$M^+_h + X^-_h \Leftrightarrow (M^+_h)_a(X^-_h)_a + (M^+_h)_b(X^-_h)_b + \cdots$$

$$\begin{array}{ccc} & \overset{\Delta G_a}{\updownarrow} & \left(\begin{array}{c}\\ \end{array}\right) \overset{\Delta G_b}{\updownarrow} \\ (MX_S)_\alpha & & (MX_S)_\beta \end{array}$$

and

$$\Delta G_\alpha = \Delta G_d + \Delta G_{h(\alpha)} = \Delta G' + \Delta G_a$$

$$\Delta G_\beta = \Delta G_d + \Delta G_{h(\beta)} = \Delta G' + \Delta G_b$$

With such a model, we can better understand the supersaturation phenomenon or the preferential formation of a given solid species, as the repartition of the species $(M^+_h)_a$, $(X^-_h)_a$, $(M^+_h)_b$, $(X^-_h)_b$, *etc.*, depends on the solution composition. Such polymorphic transformations due to successive dissolution/recrystallization processes have been characterized (with a time-lag of only some hours) in highly supersaturated calcium carbonate solutions at 50°.[23,24] When several morphological or crystalline forms of a solid co-exist, the form with the highest energy will dissolve first, and the measured solubility will correspond to the solubility of the most energetic form still undissolved. We can also explain how a solid form is transformed into another, in humid conditions[8,11] (dashed arrow in the preceding diagram): the authorized transformation is only $\alpha \Rightarrow \beta$ due to the ΔG criterion, but also with a solubility criterion. Starting from the β solid species, we can only solubilize $S_\beta < S_\alpha$ while $(M^+_h)_b$, $(X^-_h)_b$ and $(MX_S)_b$ are in equilibrium, and the system is not in saturation condition according to the α species. Bearing in mind this model of a series of equilibria between hydrated uncharged ion-pairs in solution, we can better explain some apparent contradictions, for example concerning the high phosphate content in waste waters *vs.* lake waters:[25–27] with a slow circulation flow, there is sufficient time for the precipitate to give a more stable species (see also the evolution of calcium carbonate[8,23,24] or calcium phosphate[11] crystalline forms in solution).

Moreover, according to the experimental techniques used for precipitation/dissolution studies, it becomes less easy to obtain $K_{S\alpha}$ with precision, as the transformation kinetics can interfere, and also the supersaturation ratio related to the species of interest.[6] Studying the dissolution on solid compound (of known structure) gives rise to K_S measured in good accordance from one study to another; this is not always the case when the corresponding solid is obtained through a precipitation reaction, while the operating conditions are not exactly the same, and while the solid structure may differ. Such a problem can explain some discrepancies between K_S or β values for calcium carbonate, for example;[10,28–31] this will be developed in a forthcoming article.

Choice/estimation of thermodynamic constants

The preceding discussion has focused on the importance of the knowledge of the β formation constant for a MX^0 uncharged soluble complex, in order to calculate the total solubility of a given metal in a given solution system.

Due to various IUPAC compilations,[32–35] we have a lot of critical data for inorganic (and also organic) ligands, with complex stability constants, solubility product, and other thermodynamic values. Other data are available, for many metal/ligand systems in the book by Kragten[35] and for hydroxide compounds in the book by Baes and Mesmer,[37] for example. Thanks to the recent developments of microinformatic treatment of electrochemical data concerning solubility equilibria, many teams are actually beginning to establish new β values for a lot of compounds, mainly of environmental interest.

However many data are missing or are sometimes contradictory; this is especially the case when dealing with weakly soluble compounds, for which the β formation constant is rarely known. In order to avoid any dubiousness in the speciation studies, we have to estimate this β value, which can be obtained from the solubility data and the $\beta = S/K_S$ relationship.

A method given by Clifford[38,39] can be used to extimate the unknown β or K_S value for a given compound: he observed a linear variation of

Table 1. Estimation of solubilities and formation constants for insoluble divalent metal sulphides, from the values for corresponding insoluble carbonates (as described in the text)

		Cd^{2+}	Cu^{2+}	Pb^{2+}	Zn^{2+}	Fe^{2+}
MCO_3	$\log \beta_1$ (lit.)	4.4	6.8	6.2	4.8	5.3
	pK_S (lit.)	12.5	9.6	12.8	10.7	10.2
MS	pK_S (lit.)	26.6	35.1	26.1	22.8	18.1
	$-\log S$ (lit.)	15.1	15.6	13.2	11.9	8.8
	$\log \beta_1$ (est.)	11.5	19.5	12.9	10.9	9.3

$-\log \beta$ or pK_S against the metal electronegativity (after some corrections). This author was consequently able to correct some inadequate data, and merely to predict the values when not yet determined, as applied to a lot of sulphides, hydroxides, carbonates, sulphates, *etc.* On the other hand, in a recent study concerning the simultaneous complexation of divalent heavy metallic cations by carbonate and sulphide ions,[40] we have proposed the hypothesis that for each precipitate of a given cation, the ratio of the solubility over the M^{2+} concentration is constant. That is

$$S_{MCO_3}/[M^{2+}] = F \quad (MCO_3 \text{ precipitate})$$

$$S_{MS}/[M^{2+}] = F \quad (MS \text{ precipitate})$$

As β formation constants for heavy metal carbonates are well known, this hypothesis allows us to estimate a value for the β formation constant of the corresponding sulphide.

From the tabulated values of β_1 and K_S for MCO_3, we can write

$$F = S_{MCO_3}/[M^{2+}] - \beta_{1,MCO_3}[K_{S,MCO_3}]^{1/2}$$

and hereafter

$$S_{MS} = F[K_{S,MS}]^{1/2}$$

and

$$\beta_{1,MS} = \beta_{1,MCO_3}[K_{S,MCO_3}]^{1/2}/[K_{S,MS}]^{1/2}$$

The estimated values (Table 1) are well in the range of the literature data, when available. If in error, they give a first approximation, and they have allowed us a good accordance between a speciation calculation and the substrate analysis.[40]

Another point of importance, in the use of the β constants within a speciation calculation, lies in the ionic strength correction. In fact, many compiled data are given for infinitely diluted solution ($I = 0$) or for some finite values (such as $I = 0.1$; 0.5 or $1M$); but the system under study can be at any other value, such as $0.04M$ for a given soil, $0.7M$ for seawater, *etc.*

The classical way for estimating the β value at a given ionic strength is from the activity coefficient correction, as given by the Debye–Hückel equation or any modification.[41,42] At low ionic strength, Linder and Murray have proposed[43] a useful approach, in order to estimate the value from only one or two data points, and their results are no more dispersed than other literature values.

In multicomponent systems with a speciation study, we frequently have to use an algorithmic method[40,42] in which a first estimated value of ionic strength (and of thermodynamic equilibrium constants) gives rise to a more precise value of any concentration for all the species in the system, and so a novel estimate for the ionic strength.

Another way to estimate the activity coefficients in a multicomponent system with an ionic strength up to $2M$ is the Pitzer equation,[44,45] which takes into account pairwise interactions between ions of opposite charge sign. Activity coefficients in salt mixtures can be estimated, in Pitzer's ion interaction treatment, through computer programs.[46] Due to a considerable effort in the determination and compilation of the empirical parameters, we are able to describe any system under study, even when somewhat cumbersome.[47]

Other models can be used in order to obtain ionic activity coefficients; this is the case of the mean spherical approximation, whose results in aqueous electrolyte mixtures[48] are also satisfactory when compared to experimental data.

REFERENCES

1. A. Ringböm, *Complexation in Analytical Chemistry*, Wiley, New York, 1963.
2. J. Y. Gal, J. Gal and B. Bourg, *Etude Analytique des Réactions Chimiques dans l'Eau*, Lavoisier, Paris, 1989.
3. K. C. James, *Solubility and Related Properties*, M. Dekker, New York, 1986.
4. W. Stumm and J. J. Morgan, *Aquatic Chemistry*, 2nd Ed., Wiley, New York, 1981.

5. M. D. Cohen, R. C. Flagan and J. H. Seinfeld, *J. Phys. Chem.*, 1987, **91**, 4583.
6. E. Koumanakos, E. Dalas and P. G. Koutsoukos, *J. Chem. Soc. Faraday Trans.*, 1990, **86**, 973.
7. E. Dalas, J. Kallitsis, S. Sakkopoulos, E. Vitoratos and P. G. Koutsoukos, *J. Colloid Interface Sci.*, 1991, **141**, 137.
8. J. Kragten, *Talanta*, 1977, **24**, 483.
9. C. Tarits, P. Leroy, R. Letolle and P. Blanc, *C. R. Acad. Sci. Paris (Ser. II)*, 1990, **311**, 1297.
10. E. Königsberger and H. Gamsjäger, *Marine Chem.*, 1991, **30**, 317.
11. R. M. Garrels, M. E. Thompson and R. Siever, *Amer. J. Sci.*, 1960, **258**, 402.
12. J. Christoffersen, M. R. Christoffersen, W. Kibalczyc and F. A. Andersen, *J. Cryst. Growth*, 1989, **94**, 767.
13. M. R. Christoffersen, J. Christoffersen and W. Kibalczyc, *ibid.*, 1990, **106**, 349.
14. B. E. Conway, *J. Solution Chem.*, 1978, **7**, 721.
15. M. Meot-Ner (Mautner) and V. C. Speller, *J. Phys. Chem.*, 1986, **90**, 6616.
16. K. Hiraoka, *Bull. Chem. Soc. Jpn.*, 1987, **60**, 2555.
17. R. Gomer and G. Tryson, *J. Chem. Phys.*, 1977, **66**, 4413.
18. S. Trassati, *ibid.*, 1978, **69**, 2938.
19. R. Gomer and G. Tryson, *ibid.*, 1978, **69**, 2939.
20. S. Licht, *J. Electrochem. Soc.*, 1988, **135**, 2971.
21. C. Reichardt, *Solvent Effects in Organic Chemistry*, pp. 30, 34. Verlag Chemie, Weinheim, 1979.
22. W. Kibalczyc. A. Zielenkiewicz and W. Zielenkiewicz, *Thermochim. Acta*, 1988, **131**, 47.
23. T. Ogino, T. Susuki and K. Sawada, *Geochim. Cosmochim. Acta*, 1987, **51**, 2757.
24. *Idem*, *J. Cryst. Growth*, 1990, **100**, 159.
25. T. Moutin, J. Y. Gal, H. El Halouani, B. Picot and J. Bontoux, *Water Res.*, in the press.
26. J. Kleiner, *ibid*, 1988, **22**, 1259.
27. Th. Menanteau, *L'eau, l'industrie, les nuisances*, 1990, **135**, 37.
28. F. S. Nakayama, *Soil Sci.*, 1968, **106**, 429.
29. G. M. Lafon, *Geochim. Cosmochim. Acta*, 1970, **34**, 935.
30. R. L. Jacobson and D. Langmuir, *ibid.*, 1974, **38**, 301.
31. G. Dorange, A. Marchand and M. Le Guyader, *Rev. Sci. Eau*, 1990, **3**, 261.
32. L. G. Sillen and A. E. Martell, *Stability Constants of Metal-Ion Complexes*, The Chemical Society, London, 1964.
33. L. G. Sillen and E. Högfeldt, *ibid.*, The Chemical Society, London, 1971.
34. E. Högfeldt, *Stability Constants of Metal-Ion Complexes, Part A—Inorganic Ligands*, Pergamon Press, Oxford, 1982.
35. R. M. Smith and A. E. Martell, *Critical Stability Constants*, 5 Vols. Plenum Press, New York, 1976–1982.
36. J. Kragten, *Atlas of Metal-Ligand Equilibria in Aqueous Solution*, Ellis Horwood, Chichester, 1978.
37. C. F. Baes and R. E. Mesmer, *The Hydrolysis of Cations*, Wiley, New York, 1976.
38. A. F. Clifford, *J. Am. Chem. Soc.*, 1957, **79**, 5404.
39. *Idem*, *J. Phys. Chem.*, 1959, **63**, 1227.
40. P. Rouyer, *Thesis*, University of Montpellier-2, November 1990.
41. C. W. Davies, *Ion Association*, Butterworths, London, 1962.
42. G. Sposito, *Soil Sci. Soc. Am. J.*, 1984, **48**, 531.
43. P. W. Linder and K. Murray, *Talanta*, 1982, **29**, 377.
44. K. S. Pitzer, in R. M. Pytkowicz (ed.), *Activity Coefficients in Electrolyte Solutions*, Vol. I, p. 157. C.R.C. Press, Boca Raton FL, 1979.
45. K. S. Pitzer, *Pure Appl. Chem.*, 1986, **58**, 1599.
46. R. Andreu, J. A. Cejudo and E. S. Marcos, *Comput. Chem.*, 1985, **9**, 185.
47. C. E. Harvie, N. Moeller and J. H. Weare, *Geochim. Cosmochim. Acta*, 1984, **48**, 723.
48. H. R. Corti, *J. Phys. Chem.*, 1987, **91**, 686.

Talanta, Vol. 39, No. 8, pp. 967–970, 1992
Printed in Great Britain.

0039-9140/92 $5.00 + 0.00

TRACE DETERMINATION OF SULPHIDE AND SULPHUR DIOXIDE BY VAPOR MOLECULAR ABSORPTION SPECTROMETRY USING MAGNESIUM AND TELLURIUM HOLLOW CATHODE LAMPS

QINHAN JIN,* HANQI ZHANG, YIXIANG DUAN, AIMIN YU, XINWEI LIU and LISHUANG WANG
Department of Chemistry, Jilin University, Changchun, 130023, People's Republic of China

(*Received* 21 *August* 1991. *Revised* 22 *November* 1991. *Accepted* 23 *November* 1991)

Summary—A new method has been developed in this paper for determining sulphide and sulphur dioxide simultaneously. Two emission lines, 202.6 nm and 214.3 nm which are emitted from hollow cathode lamps (HCL) of magnesium and tellurium, respectively, were used as radiation sources for measurement of absorbances of H_2S at 202.6 nm and SO_2 at 214.3 nm or 202.6 nm. The detection limit for S^{2-} was shown to be 0.01 μg/ml and the detection limits for SO_2 with 202.6 nm and 214.3 nm lines were 0.05 and 0.2 μg/ml, respectively. The method has been employed to satisfactorily analyse practical samples.

Atomic absorption spectrometry (AAS) has been very successful for determining most metallic elements, but its use is limited for the determination of nonmetallic elements. This disadvantage arises from the following reasons:

(1) The most sensitive resonance lines of the nonmetallic elements are situated in the vacuum ultraviolet region (below 190 nm) and, therefore, they cannot be directly determined with the usual instruments covering the spectral range from 190 to 700 nm.

(2) There is a lack of appropriate hollow cathode lamps for the nonmetallic elements. Molecular absorption spectrometry (MAS) for determining sulphur-containing compounds has been reviewed.[1-2] Vapour molecular absorption spectrometry (VMAS) is one of the simplest methods in MAS. Winkler and Syty[3-5] used VMAS to determine sulphur dioxide and sulphide. They used a hydrogen hollow cathode lamp as a continuum source to determine SO_2 at 210 nm and the detection limit was 2 μg/ml. For sulphide, a deuterium arc lamp was used as the source and the detection limit was shown to be 1.2 μg/ml S^{2-} at 200 nm. In this paper, two emission lines, 202.6 nm and 214.3 nm, from hollow cathode lamps of magnesium and tellurium, respectively, were used as radiation sources to measure absorbance of H_2S at 202.6 nm and SO_2 at 214.3 nm or 202.6 nm. The detection limit for S^{2-} at 202.6 nm was shown to be 0.01 μg/ml. The detection limits for SO_2 were 0.05 μg/ml at 202.6 nm and 0.2 μg/ml at 214.3 nm, respectively. Thus detection limits are improved by 1–2 orders of magnitude.

*Author for correspondence.

EXPERIMENTAL

Apparatus

Absorption measurements were made with a Model WF5 atomic absorption spectrophotometer (Xintian Optical Fine Instrument Factory, P.R. China). The instrument was modified for cold vapour analysis by replacing the burner with a 15-cm long, 0.7-cm i.d. flow through glass absorption cell (Fig. 1). The SO_2 and H_2S evolution vessel (reaction cell) used is also shown in Fig. 1. The spectrophotometer was equipped with a recorder readout accessory and a strip-chart recorder. The hollow cathode lamps of magnesium and tellurium were used as sources of radiation. The lamps were operated at a current of 6 mA and the wavelengths selected were 202.6 nm for Mg HCL and 214.3 nm for Te HCL.

Reagents

Standard S^{2-} stock solution (1000 μg/ml). A 7.5-g amount of sodium sulphide $Na_2S.9H_2O$ was dissolved in dilute sodium hydroxide solution and diluted to 1000 ml with water.

Standard SO_2 stock solution (1000 μg/ml). A 1.97-g amount of sodium sulphite was dissolved in dilute sodium hydroxide solution and diluted to 1000 ml with water.

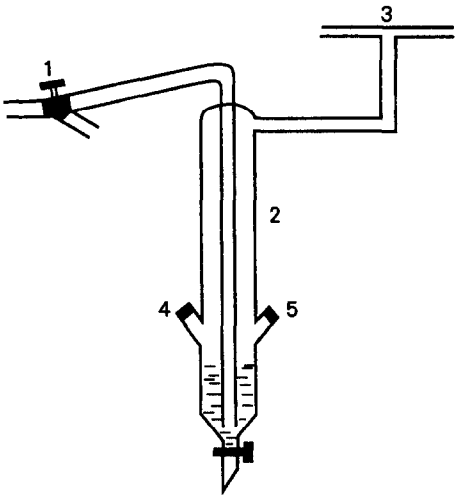

Fig. 1. Apparatus for SO_2 and H_2S evolution. 1. 3-way stopcock, 2. reaction cell, 3. absorption cell, 4. sample injection port, 5. reaction solution injection port.

The accurate concentrations of S^{2-}, and SO_2 were standardized by iodometry just before use. All reagents used were of superpure or analytical grade. Solutions were prepared with demineralized water.

Procedure

About 2 ml of 2*M* sulphuric acid was placed into the reaction cell. Either nitrogen or compressed air may serve as the carrier gas and generally the former was preferred to minimize the possibility of oxidation of SO_2 in the presence of moist air. The 3-way stopcock was adjusted to let the carrier gas flow into the air. The recorder was turned on and a base line was recorded. With the gas flow and the strip-chart recorder on, sample solution was injected into the side-arm of the reaction cell through the rubber septum with a syringe. After reaction for a certain time (defined as the reaction time) the 3-way stopcock was turned to let the carrier gas flow into the reaction cell and the absorption signal was recorded.

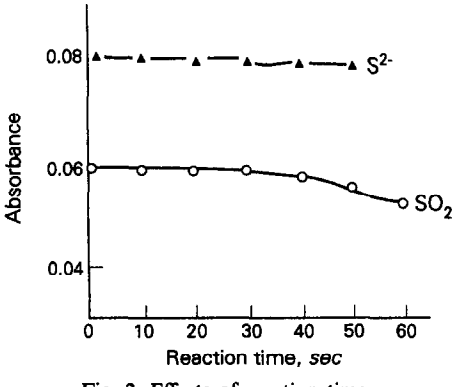

Fig. 2. Effects of reaction time.

RESULTS AND DISCUSSION

Optimization of operating conditions

Wavelength. The SO_2 and H_2S absorption spectra have been reported in the literature[4,5]. The absorption maximum of SO_2 and H_2S occurs at 210–220 nm and 194–200 nm, respectively. In this work, the absorption spectra of SO_2 and H_2S were obtained by using hollow cathode lamps of different elements as the radiation sources. The experimental results indicate that the absorption maxima of SO_2 and H_2S are all at about 200 nm.

In this paper, the hollow cathode lamps of magnesium and tellurium were used as radiation sources to measure the absorbance of H_2S at 202.6 nm and SO_2 at 202.6 nm or 214.3 nm.

Reaction conditions. The signal depends on a number of variables such as volume of solution, acid concentration, volume of sample solution and carrier gas flow rate. These parameters were investigated, and the results generally confirmed those of Syty.[4,5]

The successive injections of sample solutions into the same aliquot of reaction solution were proved to be unacceptable because of a decreasing trend in the resulting absorbance. It took about a few minutes per injection for the evolved gas to be flushed out of the reaction vessel and for the pen to return to the baseline. The lack of signal reproducibility and the time consumed per injection indicate also that successive injections of sample into the same aliquot of acid is not a desirable approach.

The time interval from the sample injection into the reaction cell to the carrier gas flow into the reaction cell was defined as the reaction time. The effect of reaction time on absorbance is shown in Fig. 2. It is evident that with an increase in the reaction time the absorbance remains constant when the reaction time is less than 30 sec, and decreases slightly above 30 sec. In our experiment, the carrier gas flows into the

Table 1. Operating condition

Mg-HCL	202.6 nm (for S^{2-} or SO_2)
Te-HCL	214.3 nm (for SO_2)
Current of HCL	6 mA
Reaction solution	2*M* H_2SO_4
Volume of reaction solution	2 ml
Volume of sample solution	3 ml
Reaction time	A few seconds
Carrier gas flow rate	200 ml/min

Table 2. Comparison of detection limits and linear ranges

Species	Radiation source	Wavelength, *nm*	Detection limit, *μg/ml*	Linear range, *μg/ml*	Reference
SO_2	Mg-HCl	202.6	0.05	0.2–80	This work
SO_2	Te-HCl	214.3	0.2	1–80	This work
SO_2	H_2-HCl	215.0	2	10–5000	4
SO_2	H_2-HCl	210.0	2	2.0–200	3
S^{2-}	Mg-HCl	202.6	0.01	0.05–6.0	This work
S^{2-}	D_2 arc lamp	200.0	1.2	1.2–400	5

Table 3. Measurement of absorptivity values for S^{2-} and SO_2

Species	Concentration, *μg/ml*	A_{203}	A_{214}	$a_{203}^{S^{2-}}$	$a_{214}^{S^{2-}}$	$a_{203}^{SO_2}$	$a_{214}^{SO_2}$
S^{2-}	0.72	0.048	0.015	0.067	0.021	—	—
SO_2	9.91	0.116	0.059	—	—	0.012	0.006

reaction cell immediately after sample injection into the reaction cell.

Based on these experimental results and those of Syty,[4,5] the optimum conditions selected for the method are summarized in Table 1.

Detection limits and linear range

The detection limits which are defined as the concentration of analyte which gives a signal twice the standard deviation of the blank signal, and linear ranges for S^{2-} and SO_2 are shown in Table 2. For comparison, the results obtained in the literature are also included. The method appears particularly attractive in view of its lower detection limits.

Interferences

The effects of eight diverse anions on the determination of S^{2-} (concentration of S^{2-} remains 0.93 μg/ml) at 202.6 nm were investigated. Cl^- (100-fold), Br^- (100), I^- (100), CO_3^{2-} (100), SCN^- (100), NO_3^- (100), NO_2^- (10) and CN^- (10), did not affect the determination of sulphide. When the SO_2 concentration remains at 9.9 μg/ml, the effect of concomitant anions on the determination of SO_2 at 214.3 nm were as follows: Cl^- (100-fold), Br^- (100), I^- (100) and NO_3^- (100) did not effect the determination of sulphur dioxide.

Simultaneous determination of S^{2-} and SO_2

The simultaneous determination of S^{2-} and SO_2 in the gas phase can be accomplished from measurements at two different wavelengths. In analogy to simultaneous spectrophotometric methods, two simultaneous equations may be written:

$$a_{203}^{S^{2-}} C_{S^{2-}} + a_{203}^{SO_2} C_{SO_2} = A_{203}$$

$$a_{214}^{S^{2-}} C_{S^{2-}} + a_{214}^{SO_2} C_{SO_2} = A_{214}$$

where a is the absorptivity of the component to be determined and C is its concentration in solution. To obtain the value of a the absorbances at 202.6 and 214.2 nm were measured when the sample solution only contained S^{2-} or SO_3. The results are listed in Table 3.

To examine the reliability of the method, certain amounts of standard S^{2-} and SO_2 were simultaneously added to a water sample and analysed according to the procedure described above. Results obtained are shown in Table 4. It is obvious from the results that the method can be satisfactorily employed for the simultaneous determination of sulphide and sulphur dioxide and for determination of either single component.

Table 4. Analytical results of spiked samples

	Quantity added, *μg/ml*		Absorbance		Quantity found, *μg/ml*	
Sample	SO_2	S^{2-}	202.6 nm	214.3 nm	SO_2	S^{2-}
1	9.91	0.72	0.163	0.073	9.8	0.68
2	9.91	1.44	0.210	0.088	9.9	1.4
3	7.69	2.65	0.259	0.098	7.5	2.5
4	3.85	1.59	0.148	0.054	3.4	1.6

CONCLUSIONS

By using two emission lines at 202.6 nm and 214.3 nm emitted from Mg and Te HCLs, respectively as radiation sources, the simultaneous determination of trace sulphide and sulphur dioxide is possible by vapour molecular absorption spectrometry. However, from the point of view of sensitivity the measurement of sulphide at 202.6 nm is not ideal because the maximum of the absorption spectrum of H_2S lies between 194.0 and 200,0 nm. It is therefore predictable that if a line source in this wavelength range, such as an Se electrodeless discharge lamp (196.0 nm), is available, the detection of sulphide will be improved. Since two line sources instead of a continuum radiation source were used in this method, it is also probable that a nondispersion absorption spectrometer would be suitable in this kind of cold vapour molecular absorption spectrometry.

REFERENCES

1. M. Garcia-Vargas, M. Milla and J. A. Perez-Bustamante, *Analyst*, 1983, **108**, 1417.
2. K. Dittrich, *CRC Crit. Rev. Anal. Chem.*, 1986, **16**, 223.
3. H. E. Winkler and A. Syty, *Environ. Sci. Technol.*, 1976, **10**, 913.
4. A. Syty, *Anal. Chem.*, 1973, **45**, 1744.
5. *Idem, ibid.*, 1979, **51**, 911.

Talanta, Vol. 39, No. 8, pp. 971–975, 1992
Printed in Great Britain.

0039-9140/92 $5.00 + 0.00

SPECTROFLUORIMETRIC DETERMINATION OF MOLYBDENUM IN SOME REAL AND ENVIRONMENTAL SAMPLES

BIJOLI KANTI PAL,* K. ANAND SINGH and KHANA DUTTA
Analytical Chemistry Division, Jadavpur University, Calcutta-700 032, India

(*Received* 30 *August* 1991. *Accepted* 22 *October* 1991)

Summary—A very simple, highly-sensitive and selective quenchofluorimetric method for the rapid determination of molybdenum(VI) in aqueous media is described. The method is based on the instantaneous quenching action by the metal-ion upon the native fluorescence of bathophenanthrolinedisulphonate (4,7-diphenyl-1,10-phenanthrolinedisulphonate) solution [λ_{ex} (max) 288 nm; λ_{em} (max) 444.8 nm] in the optimum pH-range of 3.0–3.7 at room temperature (25 ± 5°). The fluorescence quenching is co-linear in the range of 0.01–1.0 ppm molybdenum. Large excesses of over 50 cations, anions and some common complexing agents were found to have no interference. Cu, Ni, Co, Fe and V can be tolerated only up to the corresponding amount of molybdenum. Interference from greater amounts can however be removed by a one-step ion-exchange separation process. The developed method was successfully tested over several standard alloys, synthetic mixtures of various compositions, factory effluents and in spiked environmental waters.

The industrial importance of molybdenum, its impact on the environment, its microessentiality, its adverse effects on living systems, and the assessment of existing fluorimetric methods for molybdenum(VI) have been discussed and reviewed recently by the authors.[1] We have previously described the bathophenanthroline method[1] in which an alcoholic solution of bathophenanthroline (4,7-diphenyl-1,10-phenanthroline) was used as the quenchofluorimetric reagent for trace analysis of molybdenum(VI) and which overcame many of the limitations of earlier methods.[2–5] The present method is a further improvement over the previous one prescribed from this laboratory.[1] Here emphasis has been given to the introducton of a sulphonate group to the bathophenanthroline ring to remove the water insolubility problem experienced with bathophenanthroline. The method has achieved two distinct advantages over the previous one by (i) using a new fairly water soluble fluorimetric reagent, bathophenanthrolinedisulphonate (4,7-diphenyl-1,10-phenanthrolinedisulphonate) and (ii) using buffer solution (sodium acetate-acetic acid buffer) for pH maintenance that makes the method much simpler and yields higher accuracy and reproducibility of results. The method is based on the instantaneous, virtually specific quenching action of molybdenum(VI) on the native fluorescence of bathophenanthrolinedisulphonate in slightly acidic media (pH 3–3.7) under the optimum experimental conditions. The standard deviation and relative standard deviation for 11 replicate determinations of 0.1 ppm molybdenum(VI) were found to be ±0.009 and 0.76%, respectively.

*Author for correspondence.

EXPERIMENTAL

Apparatus

A Shimadzu spectrofluorophotometer (Model RF-5000) fitted with a video accessory was used to record the uncorrected spectra and to measure the fluorescence intensity. A pH meter, Model pH 5651 (Electronic Corporation of India Ltd), was used to measure pH. A Hanovia U.V. lamp set was used for the qualitative visual study of fluorescence intensity changes.

Reagents

A $10^{-3}M$ solution of the reagent, bathophenanthrolinedisulphonate (4,7-diphenyl-1,10-phenanthrolinedisulphonate) (Loba-Chemie, Wien-Fischamend) was prepared by dissolving the requisite amount in demineralized water. From this stock solution, more dilute solutions

were prepared as and when needed. The reagent solution is very stable. A stock solution of 1000 ppm molybdenum(VI) was prepared by dissolving 0.1840 g of ammonium molybdate, $(NH_4)_6Mo_7O_{24}\cdot 4H_2O$ (J. T. Baker), in 100 ml of demineralized water and subsequently standardized by EDTA titration.[6] More dilute solutions were prepared by appropriate dilution of aliquots from the stock solution with demineralized water. A 100-ml buffer solution of pH 3.5 was prepared by mixing 5 ml of 0.2*M* sodium acetate (Merck) and 95 ml of 0.2*M* acetic acid (Merck).

A large number of solutions of inorganic ions and complexing agents were prepared from their Analar grade or equivalent grade water soluble salts. In case of insoluble substances, special dissolution methods were adopted.[7] Doubly distilled demineralized water was used throughout the study.

General procedure

To a 10-ml standard flask containing 0.1–1 μg or 1–10 μg of molybdenum(VI) were added 0.5 ml or 1.5 ml of $10^{-4}M$ reagent bathophenanthrolinedisulphonate reagent, respectively, and 2 ml of sodium acetate–acetic acid buffer of pH 3.5. The volume was then made up with demineralized water, and the fluorescence intensity was measured against a reagent blank at 444.8 nm, using excitation at 288 nm. The fluorescence quenching due to molybdenum(VI) is achieved by subtracting the relative fluorescence intensity of the molybdenum–reagent system from that of the corresponding reagent blank solution.

RESULTS AND DISCUSSION

Spectral characteristics

The uncorrected excitation and emission spectra of the bathophenanthrolinedisulphonate solution are shown in Fig. 1. The wavelength maxima of excitation and of emission were found to occur at 288 nm and 444.8 nm, respectively.

Effect of pH

The effect of pH studies showed that the maximum and constant quenching occurred over the pH range 3.0–3.7.

Effect of buffer

Citric acid–disodium hydrogen phosphate buffer (pH 3.4) masked the quenching action

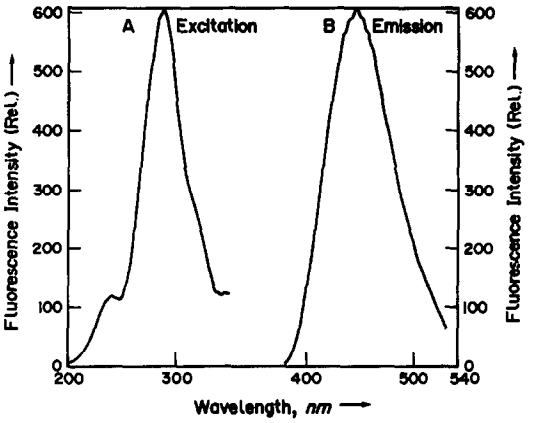

Fig. 1. Uncorrected excitation (A) and emission (B) spectra of bathophenanthrolinedisulphonate.

of molybdenum(VI) while potassium hydrogen phthalate–hydrochloric acid buffer (pH 3.18) quenched the fluorescence of the reagent solution. Up to 5 ml of sodium acetate–acetic acid buffer (pH 3.5) was added to the total 10-ml solution containing molybdenum(VI) and had no effect on the quenching intensity. Consequently, 2 ml of this buffer solution was added throughout the experiment.

Effect of time

The maximum quenching was reached immediately after making up the volume, and remained constant for 24 hr. Longer time periods were not studied.

Effect of metal concentration (calibration graph)

The fluorescence quenching intensity exhibited a linear dependance on the molybdenum(VI) concentrations over a wide range (10 ppb–1.0 ppm) distributed over two different molybdenum concentration ranges (10 ppb–0.10 ppm and 0.10–1.0 ppm) for convenience of fluorescence intensity measurement.

Interferences

Over 50 cations, anions and common complexing agents, in the presence of 0.10 ppm molybdenum(VI) were found to have no interference at all. Five thousand-fold excess each of oxalate, perchlorate, phosphate, sulphate, acetate, thiosulphate, thiocyanate, halides, H_2O_2, alkali and alkaline earth metals, Zr^{4+}, Hf^{4+}, Zn^{2+}, La^{3+}, Th^{4+} and Se^{4+} ions do not interfere. The amount mentioned is not the tolerance limit but the actual amount studied. However, for those ions whose tolerance limits have been studied, their tolerance ratios are mentioned in Table 1.

Table 1. Table of tolerance limits of foreign ions.* Tolerance ratio, [species (x)]/Mo (w/w)

Species, x	Tolerance ratio, x/Mo
NO_3^-	500
NO_2^-	500
As(III)	500
Be	200
CN^-	100
Bi(III)	100
Al	100
Ga	100
U(VI)	100
Ascorbic acid	100
Tartarate	100
Mn(II)	50
Mg	50
Pb(II)	50
Tl(III)	50
Sb(III)	50
Thiourea	50
Rh	20
Citrate	20
EDTA	20
Ce(III)	20
Cr(III)	10
Cr(VI)	10
Hg(II)	50*
Cd	50†
W(VI)	50‡

*Tolerance limit defined as ratio that causes less than 5 percent interference.
†With thiosulphate.
‡With tartarate.
§With fluoride.

Cu^{2+}, Co^{2+}, Ni^{2+}, $Fe^{2+,3+}$ and V^{5+} interfere when present in amounts in excess of the molybdenum(VI). Interferences from these metal ions have been effectively removed by a short single-step ion-exchange separation process, using AG1-X8 (sulphate form, 100–200 mesh) anion exchanger as mentioned below.

Separation of interfering ions through anion exchanger

One gram of a strong base anion exchange resin, AG1-X8 (chloride form 100–200 mesh) resin was placed in a beaker and washed repeatedly with demineralized water to remove the fine particles. It was then immersed in demineralized water and kept overnight. Later, a small column (5 cm × 1 cm) was made with the resin supported over quartz wool in an all-glass column. The packed resin bed was washed with sufficient volume of 3M sulphuric acid to convert it into the sulphate form. The washing was discontinued when the eluate did not contain chloride (silver nitrate test solution). The resin was then washed with demineralized water to completely free it from sulphate ions (barium chloride test solution). A solution containing known amounts of molybdenum(VI) and other interfering ions was mixed with 1 ml of 30% hydrogen peroxide and diluted to 50 ml with demineralized water. It was then quantitatively passed through the conditioned resin column at a flow-rate of 1–2 ml/min. The resin bed was then washed with 50 ml of 1M ammonium sulphate–0.02M sulphuric acid. Molybdenum(VI) was finally eluted with 25 ml of 0.5M sodium chloride–0.5M sodium hydroxide at a flow-rate of 0.5 ml/min. The eluate was boiled for few minutes, cooled, neutralized with dilute sulphuric acid and finally diluted to 50 ml with demineralized water. From suitable aliquots, the molybdenum content was then determined fluorimetrically with bathophenanthrolinedisulphonate as described earlier, with the calibration graph being prepared from standard molybdenum(VI) solutions, also adsorbed on the resin bed and eluted identically. The results were very satisfactory. It is worth mentioning that the concentration of hydrogen peroxide is necessary to retain molybdenum(VI) on the column and there should be at least 0.3–6% peroxide in the final solution, particularly if iron(III) is present that acts as catalyst[8] for deterioration of the resin activity.

Table 2. Molybdenum(VI) determination in synthetic mixture

Sample no.	Composition of the mixture, *ppm*	Mo(VI) content, *ppm*	Mo(VI) found*		
			Spiked, *ppm*	Unspiked, *ppm*	Recovery, %
A	Mo^{6+} (0.1), Ni^{2+} (0.5), Cu^{2+} (0.5), Fe^{2+} (0.5), Fe^{2+} (0.5), V^{5+} (0.4), Co^{2+} (0.4), Zn^{2+} (1)	0.1	0.102	0.00	102
B	As in A, Cr^{3+} (0.2), As^{3+} (0.4), Pb^{2+} (0.3), Mn^{2+} (0.3), Tartarate (10), Cd^{2+} (1)	0.1	0.102	0.00	102
C	As in B, Mg (0.2), $S_2O_3^{2-}$ (100), Hg^{2+} (4)	0.1	0.100	0.00	100
D	As in C, Al^{3+} (1), Tl^{3+} (2), Sb^{3+} (2), F^- (100), W^{5+} (0.4)	0.1	0.101	0.00	101

*Average of 5 replicate determinations.

Table 3. Mo(VI) determination in certified reference materials

Sample reference and certified composition, %	Mo(VI) content in C.R.M. sample, %	Mo(VI) spiked, *ppm*	Mo(VI) found*	R.S.D., %
NBS (33b) Alloy Cast Iron Mn = 0.64, Cr = 0.061 Mo = 0.04, Ni = 2.24 Si = 2.74, P = 0.11	0.04		0.043† ± 0.007§	2.69
BAS (32a) Aluminium Bronze Cu = 85.9, Zn = 0.94 Mn = 0.27, Fe = 2.67 Ni = 1.16, Al = 8.8	—	0.10	0.107‡ ± 0.002§	1.87
BAS (5f) Brass Cu = 70.8, Zn = 24.2 Sn = 1.85, Pb = 2.52 Fe = 0.31, P = 0.06 Mn = 0.12, Ni = 0.17	—	0.10	0.106‡ ± 0.002§	1.76

*Mean value of 5 determinations.
†Value in percentage.
‡Value in ppm.
§The measure of precision in the standard deviation.

Table 4. Mo(VI) determination in environmental waters

Sample	Composition,* *ppm*	Mo(VI) spiked			Mo(VI) unspiked found, *ppm*
		Added, *ppm*	Found,† *ppm*	Recovery, %	
Pond water	—	0.10	0.106	106 ± 0.0016‡	0.00
		0.15	0.154	102.6 ± 0.0019‡	0.00
Laboratory tap water	—	0.10	0.103	103 ± 0.0014‡	0.00
		0.15	0.149	99.33 ± 0.0019‡	0.00
Behala Tap		0.10	0.103	103 ± 0.0014‡	0.00
		0.15	0.149	99.33 ± 0.0024‡	0.00
Drain water (Ordinance Factory)					
Collection Site A	As^{3+} <0.01, Hg^{2+} <0.01 Pb^{2+} <0.01, Cr^{3+} = 0.09, Ni^{2+} = 0.20, Ag^{+} = 0.02, Zn^{2+} = 0.19, Na^{+} = 56.0 Cu^{2+} = 0.03, Cl^{-} = 108 SO_4^{2-} = 25	0.10	0.10	100 ± 0.002‡	0.00
		0.15	0.150	100 ± 0.0026‡	0.00
Collection Site B	As^{3+} = 0.01, Hg^{2+} = 0.01 Pb^{2+} = 0.01, Cr^{3+} = 0.04, Ni^{2+} = 0.18, Ag^{+} = 0.008, Zn^{2+} = 0.19, Na^{+} = 52.0 Cu^{2+} = 0.02, Cl^{-} = 105, SO_4^{2-} = 23	0.10	0.110	99 ± 0.0022‡	0.011
		0.15	0.163	101.3 ± 0.0024‡	0.011
Collection Site C	As^{3+} = 0.01, Hg^{2+} = 0.01 Pb^{2+} = 0.01, Cr^{3+} = 0.01 Ni^{2+} = 0.15, Ag^{+} = 0.005 Zn^{2+} = 0.32, Na^{+} = 54.0 Cu^{2+} = 0.01, Cl^{-} = 106 SO_4^{2-} = 24	0.10	0.11	110 ± 0.016‡	0.00
		0.15	0.149	99.33 ± 0.0021‡	0.00
Collection Site D	As^{3+} = 0.01, Hg^{2+} = 0.01, Pb^{2+} = 0.01, Cr^{3+} = 0.005 Ni^{2+} = 0.10 Na^{+} = 53.0, Cu^{2+} = 0.01 Cl^{-} = 105, SO_4^{2-} = 23	0.10	0.13	110 ± 0.014‡	0.02
		0.15	0.169	99.32 ± 0.003‡	0.02

*Composition by AAS.
†Averages given are the average of 5 replicate determinations.
‡The measure of precision is the standard deviation.

Applications

Molybdenum(VI) determination in synthetic mixture. Synthetic inorganic mixtures of different compositions were prepared. These were subjected to the ion-exchange separation process, eluted and diluted to a known volume as described earlier. From suitable aliquots, the molybdenum(VI) content was then determined fluorimetrically with bathophenanthroline-disulphonate as above. Results are shown in Table 2. Accurate recoveries were achieved in all solutions.

Molybdenum(VI) determination in certified reference materials

An accurately weighed 0.1-g portion of the sample was dissolved in 4 ml of a mixture (1:1) of concentrated HCl–HNO_3 with heating and was then diluted to 100 ml with demineralized water. Suitable aliquots of this sample solution with and without molybdenum(VI) spiking were processed through the anion exchange resin AG1-X8, eluted and diluted to a known volume as described earlier. Then, from suitable aliquots of the eluate, the molybdenum(VI) content was fluorimetrically determined as described before. The results are shown in Table 3. The certified molybdenum value in the alloy cast iron was obtained. Added molybdenum was accurately recovered from the other metals.

Molybdenum(VI) determination in environmental waters

Aliquots (50 ml) of filtered environmental water samples were mixed with 1 ml of concentrated sulphuric acid and 2 ml of concentrated nitric acid. The mixture was heated until SO_3 fumes were evolved and then cooled. The solution was treated with 2 ml of perchloric acid and again heated until SO_3 fumes were evolved. The resulting solution was cooled again and filtered (if necessary). The filtrate was neutralized with dilute ammonium hydroxide solution and made up to the mark with demineralized water in a 50-ml standard flask. Suitable aliquots of this solution with and without molybdenum(VI) spiking were subjected to the anion exchange AG1-X8, eluted and diluted to a known volume according to the earlier procedure. Then, from suitable aliquots, the molybdenum(VI) content was fluorimetrically determined. The results are shown in Table 4. The spiked quantities of molybdenum were accurately recovered.

Acknowledgements—The authors are grateful to Professor A. K. Majumdar for his keen interest and constant encouragement. One of us (K.A.S.) expresses his gratitude to the authorities of Jadavpur University for providing laboratory facilites, to the Manipur State Government for extending financial support and to Moriang College Authority for sanctioning study leave for conducting Ph.D. research here. The use of the COSIST instrument spectrofluorophotometer of this department is also acknowledged.

REFERENCES

1. B. K. Pal and S. Banerjee, *Indian J. Environ. Protect.*, 1989, **9**, 453.
2. G. F. Kirkbright, T. S. West and C. Woodward, *Talanta*, 1966, **13**, 1637.
3. *Idem*, *ibid.*, 1966, **13**, 1645.
4. K. Masamitsu, H. Hirotoshi and K. Tomihito, *Bull. Chem. Soc. Japan*, 1984, **57**, 1083.
5. Yu. B. Titkov, *Ukr. Khim. Zh.*, 1970, **36**, 613.
6. A. I. Busev, V. G. Tiptsova and V. M. Ivanov, *Analytical Chemistry of Rare Elements*, p. 229. Mir Publishers, Moscow, 1981.
7. B. K. Pal and B. Choudhury, *Mikrochim. Acta*, 1984 **II**, 121.
8. A. I. Busev, V. G. Tiptsova and V. M. Ivanov, *Analytical Chemistry of Rare Elements*, p. 250. Mir Publishers, Moscow, 1981.

Talanta, Vol. 39, No. 8, pp. 977–979, 1992
Printed in Great Britain

0039-9140/92 $5.00 + 0.00
Pergamon Press Ltd

SIMULTANEOUS DETERMINATION OF ACETAMINOPHEN AND CAFFEINE IN TABLET PREPARATIONS BY PARTIAL LEAST-SQUARES MULTIVARIATE SPECTROPHOTOMETRIC CALIBRATION

ABDÜRREZZAK BOZDOĞAN, ALPER MERT ACAR and GÖNÜL KANDEMIR KUNT
Yildiz University, Department of Chemistry, Şişli, Istanbul, Turkey

(*Received* 25 *July* 1991. *Revised* 9 *December* 1991. *Accepted* 20 *December* 1991)

Summary—The use of partial least-squares spectrophotometric calibration for the simultaneous determination of analgesic tablets in a multicomponent formulation is presented. This method is applied to the determination of acetaminophen and caffeine in tablet preparations. The results show that these components in a molar ratio of about 21:1 in tablets have been determined simultaneously with high precision.

Ultraviolet visible spectrophotometry is an instrumental technique in wide use in pharmaceutical analysis on account of its rapidity, simplicity and applicability to the pharmacologically active species and their derivatives absorbing in that spectral zone. The quantitation methods traditionally used involve measuring the analyte absorbance at a given wavelength. However, the analyte of interest is often accompanied by other compounds absorbing in the same spectral region. In such cases, spectral overlap is often a serious limitation and requires resolution by using sample clean-up and separation procedures.[1,2] Thus, HPLC has become one of the analytical techniques most frequently used in pharmaceutical analysis.[3,4] But, these methods are expensive and time-consuming. In order to avoid these procedures, the simultaneous determination of active components in analgesic formulations has been performed by using instrumental approaches[2,5] or various numerical methods based on multiple regression and SIMPLEX.[6] However, the mathematical programs used for spectrophotometric multicomponent analysis are based on an ordinary multiple regression method.[7,8] The important limitations of these analyses based on multiple regression are due to deviations from linearity, interaction between components and severe overlap of spectral bands. To solve these problems, a partial least-squares (PLS) method has been developed and found that PLS methods are also better suited to calibration problems than multiple regression is.[7–9]

The interest in PLS calibration has been increased in recent years.[7,8] However, the potential of this method for the assay of active components in tablet preparations has not been studied in detail. Therefore, the present paper describes the use of the PLS method in the simultaneous spectrophotometric analysis of acetaminophen (AAP) and caffeine (CAF) in tablet preparations.

Partial least squares

The theory of the PLS method has been thoroughly discussed elsewhere.[7,10] Therefore, this presentation will be restricted to its application to the present work.

In this study, the absorbances measured in the selected wavelengths were used as X-variables. The corresponding acetaminophen and caffeine concentrations were used as Y-variables. Thus, for n samples, two matrices are formed, and their inter-relationship must be calculated. The model can then be used to analyse samples of unknown composition.

Calibration with use of the PLS method is done by decomposition of both the concentration and absorbance matrices into latent variables

$$Y = F_y L_y + E_y \quad (1)$$

$$X = F_x L_x + E_x \quad (2)$$

where F_y is the latent concentration matrix with n rows (mixtures) and d columns (number of dimensions), L_y represents the concentration

loading matrix with d rows and m columns (number of components), F_x is the nxd latent absorbance matrix, L_x is the dxp absorbance loading matrix (where p is the wavelength), and E_y and E_x are error matrices that have the same dimensions as the original concentration matrix (nxm) and absorbance matrix (nxp), respectively. Relating the latent variable matrix from equation (1) to that in equation (2), one obtains a diagonal regression matrix V according to

$$F_y = F_x \cdot V + E_e \quad (3)$$

where E_e is an error matrix. The matrix V is used in the prediction step for estimation of the unknown concentrations from the absorbance spectrum x_0 of the sample as follows,

$$y_0 = x_0(F_y'X)' \; VL_y \quad (4)$$

Here the matrices F_y,L_y and X are known from calibration.

EXPERIMENTAL

Apparatus and computations

A Philips Model PU 8740 UV–Vis scanning spectrophotometer was used for obtaining digitized absorbance. Computations were run on an IBM PC/2/30 computer. A computer program for PLS was written according to previous work.[7]

Reagents

The AAP, CAF and Vermidon tablets were supplied from İLTAS Tic. San. A.Ş. Redistilled water was used throughout the work.

Procedure

The calibration set was generated by a 5-level full factorial design[11,12] and thus 25 samples were used to construct the model. The levels selected for AAP are 11, 13, 15, 17, 19 μg/ml, and for CAF 0.3, 0.6, 0.9, 1.2, 1.5 μg/ml in this design. By this choice of design, possible interactions and non-linearities can be accounted for.

Calibration solutions were prepared by dissolving AAP and CAF in water. The absorbances were recorded in 1-cm cuvettes between 190 and 300 nm every 5 nm. In this way a signal concentration matrix which could be subjected to data analysis was obtained. The calibration samples were measured in random order so that experimental errors due to drift were not introduced. In analyzing the active components of Vermidon, 20 tablets were ground and mixed. The amount of the tablet mass equivalent to one tablet was dissolved in one litre of water. This solution was stirred for 30 min and then filtered.

RESULTS AND DISCUSSION

For this investigation, two substances found in analgesic pharmaceutical formulations were chosen, namely acetaminophen and caffein. In such formulations, if all components contribute similarly to the mixture absorbance, the results obtained by any procedure are usually satisfactory. However, significant errors occur when components contributing to a much lesser extent than the others are determined. This is a rather common situation in the analysis of pharmaceutical formulations.

As the above situation described, CAF was present at a much lower concentration than AAP in our formulation. The molar ratio of these components is about 1:21. Thus, the strongest absorbance was obtained from AAP in this mixture. In such cases, since the conventional calibration procedures cannot provide good quantitative determinations, a reliable computational method is required. Therefore, PLS method was applied to the resolution of mixtures of two components AAP and CAF in this study.

The correlation coefficients between the true and predicted concentrations found by two-factor PLS solution are 0.9992 and 0.9993 for calibration of AAP and CAF, respectively.

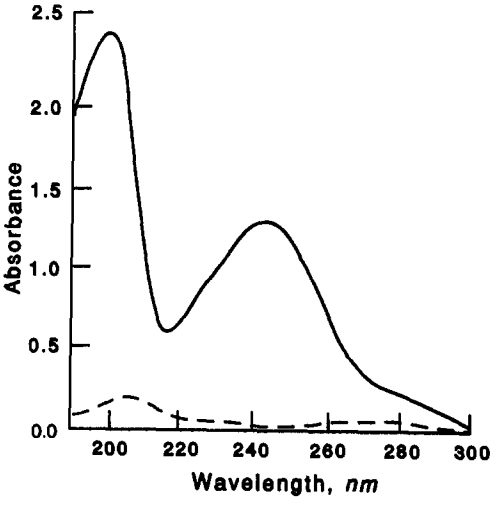

Fig. 1. Spectra of AAP (——) and CAF (– – –) at their nominal analytical concentrations.

Table 1. Determination of active components in Vermidon

Sample	% AAP	% CAF
1	98.5	100.2
2	100.2	100.5
3	99.6	100.3
4	100.2	100.6
5	100.1	100.5
6	100.5	100.6
7	100.1	100.6
8	99.9	100.5
9	98.0	99.6
10	99.8	100.5
Mean value	99.7	100.4
Standard deviation	0.8	0.3

Tablet analysis

Vermidon is available in tablets with nominal contents of 500 mg of AAP and 30 mg of CAF. The spectra of these active components at their nominal analytical concentrations are shown in Fig. 1. The results obtained by two-factor PLS solution in Vermidon analysis are listed in Table 1. In this table, values are reported as percentages of label contents.

CONCLUSION

As seen from the results, all two components AAP and CAF in analgesic formulations have been determined highly accurately by using the PLS method. This method demands calibration for developing the model to determine unknown concentrations of the components. For accurate resolution of the mixture, the calibration set must contain the same components and the same interferences as in the actual samples. Compared with other approaches, the PLS calibration has several advantages. In this method, the information from the calibration set is better used and the unidentified species in the mixture can be compensated. The method also has a much shorter computation time and gives lower prediction errors than other methods.

In order to investigate further the potential of the method, our work has been directed to analysing more complex pharmaceutical mixtures.

REFERENCES

1. T. Higuchi and E. Brochmann-Hanssan (eds.), *Pharmaceutical Analysis*, pp. 313–543. Interscience, New York, 1961.
2. M. A. Korany, A. M. Wahbi, S. Mandour and M. A. Elsayed, *Anal. Lett.*, 1985, **18**, 21.
3. W. Poethke and H. Köhne, *Pharmazeutische Zentralhalle*, 1965, **104**, 630.
4. P. R. Cockaerts and J. Hoomartens, *J. Pharm. Biomed. Anal.*, 1986, **4**, 367.
5. F. Onur and N. Acar, *FABAD Farm. Bil. Der.*, 1989, **14**, 1.
6. G. Sala, S. Maspoch, H. Iturriaga, M. Blanco and V. Cerda, *J. Pharma. Biomed. Anal.*, 1988, **6**, 765.
7. H. Martens and T. Naes, *Multivariate Calibration*, pp. 77–354. Wiley, Chichester, 1989.
8. W. Wegscheider, *Multivariate calibration in spectroscopy*, 6th COMETT Chemometrics School, Bruges, Belgium, 1990.
9. M. Otto and W. Wegscheider, *Anal. Chem.*, 1985, **57**, 63.
10. B. R. Kowalski (ed.), *Chemometrics: Mathematics and Statistics in Chemistry*, pp. 18–95. Reidel, Dordrecht, The Netherlands, 1984.
11. G. E. P. Box, W. G. Hunter and J. S. Hunter, *Statistics for Experimenters. An Introduction to Design, Data Analysis and Model Building*, pp. 306–322. Wiley, New York, 1978.
12. S. N. Deming and S. L. Morgan, *Experimental Design: A Chemometric Approach*, pp. 181–218. Elsevier, New York, 1987.

Talanta, Vol. 39, No. 8, pp. 981–986, 1992
Printed in Great Britain.

0039-9140/92 $5.00 + 0.00

SPECTROPHOTOMETRIC STUDY OF THE COMPLEX FORMATION OF 3-(2-HYDROXYPHENYL)-2-MERCAPTOPROPENOIC ACID WITH Ni(II) AND Zn(II)

J. L. BELTRAN, G. CENTENO, A. IZQUIERDO and M. D. PRAT
Department of Analytical Chemistry, University of Barcelona, Diagonal 647, 08028 Barcelona, Spain

(*Received* 13 *May* 1991. *Revised* 9 *December* 1991. *Accepted* 9 *December* 1991)

Summary—The dissociation and complex formation equilibria between Ni(II) and Zn(II) with 3-(2-hydroxyphenyl)-2-mercaptopropenoic acid, at 25° in aqueous 0.1 and 1.0*M* sodium perchlorate solutions, containing about 1% ethanol, have been studied spectrophotometrically. The data were connected directly from the spectrophotometer to an IBM-PC via a serial interface, using the DUMOD program (written in BASIC), described in the paper. The obtained spectra were treated by the factor analysis program NIPALS in order to determine the number of absorbing species and the experimental error. Dissociation constants of ligand (H_3L), and formation constants for the complexes Ni(HL), $Ni(HL)_2$, Zn(HL) and $Zn(HL)_2$ at 0.1 and 1.0*M* ionic strengths, refined by the SQUAD program, are reported.

The chelating ability of α-mercaptoacids is well known. Their reactivity and the structural arrangement of the oxygen and sulphur donor atoms lead to the formation of highly stable chelates with most of the common metal ions.

The coordination chemistry of these ligands with metal ions, mainly zinc(II) and nickel(II) has been widely investigated. A comparison of different α-mercaptoacids shows that the presence of an aryl group confers greater stability on the complexes formed,[1] and that 3-aryl-2-mercaptopropenoate complexes, with a conjugated double bond in the ligand molecule, are more stable than the corresponding 3-aryl-2-mercaptopropanoates.[2,3] Furthermore, whereas the complex formation between nickel(II) and 3-phenyl-2-mercaptopropanoic acid, and other α-mercaptoacids, leads to polynuclear complexes,[1,3–8] only monomeric species, ML and ML_2, are formed between 3-aryl-2-mercaptopropenoic acids and the divalent metal ions nickel, zinc, iron and cobalt.[2,3,9]

The metal complexing ability of these ligands makes them useful not only in analytical chemistry (as spectrophotometric reagents and masking agents), but also in biology. The interaction of heavy metals with biological systems frequently involves their bonding to mercapto groups of enzymes. Chelating agents that themselves contain mercapto groups can compete for metal ions with the biological binding sites and reverse the action of the metal ion. Thus, it was shown that 3-phenyl-2-mercaptopropenoic acid inhibits the metal-dependent enzymes, like alkaline phosphatase and carboxypeptidase,[10] and 3-(2-furyl)-2-mercaptopropenoic acid increases the serum zinc concentration may times.[11]

In previous potentiometric studies on the complex equilibria between some 3-aryl-2-mercaptopropenoic acids and metal ions, the formation constants with nickel(II) and zinc(II) ions have been reported;[2,3,9] however, the poor solubility of these ligands and their complexes in water requires the use of mixed solvents, such as ethanol–water of dioxane–water. In some cases, the formation constants of the systems studied have been applied to simulate their effect in the distribution of metal ions in biological systems,[12] despite the fact that the constants were determined in mixed solvents media.

In the present work, the complexes formed between 3-(2-hydroxyphenyl)-2-mercaptopropenoic acid (H_3L) with nickel(II) and zinc(II) ions have been studied by UV-Vis spectrophotometry, at two ionic strengths, 0.1 and 1.0*M* in sodium perchlorate, at 25°. Spectrophotometric measurements can be done at concentration levels at which the ligand and the complexes formed are soluble in water.

The determination of the number of absorbing species in solution was carried out by the NIPALS program,[13] based on the principal

component regression (PCR) algorithm NIPALS.[14] The protonation constants of ligand and the complex formation constants were determined using the SQUAD program.[15]

EXPERIMENTAL

Apparatus

The pH values were measured with a Radiometer PHM 84 pH-meter, with a G 202 B glass electrode and a K 801 Ag/AgCl reference electrode, the latter filled with saturated sodium chloride solution instead of saturated potassium chloride solution to prevent clogging of the electrode frit by precipitation of potassium perchlorate. Calibration of the electrode system at 0.1*M* ionic strength was done with buffer solutions at pH 4.008, 6.863 and 9.185 (at 25°) according to DIN 19266. The hydrogen ion concentration is calculated from the activity coefficient given by the Davies equation[16] (0.771 at 0.1*M* ionic strength and T = 25°). Hydrogen ion concentrations at $I = 1.0M$ were measured by calibrating the electrode system with standard perchloric acid solutions, with pCH = 2.000, 3.000 and 4.000, with ionic strength adjusted to 1.0*M* by addition of sodium perchlorate. The nernstian response of the electrode was also checked by Gran titrations.[17]

The temperature of the solutions was kept constant at 25 ± 0.2° with a Selecta model Tectron thermostatic bath.

Absorbance data were recorded on a Beckman DU-7 single beam spectrophotometer, with a 10-mm path length cell, connected to an IBM PC via a serial interface (RS-232-C). The program used for this purpose is commented on later.

Reagents

3-(2-Hydroxyphenyl)-2-mercaptopropenoic acid was synthesized as described previously,[18] and recrystallized from benzene. Its purity was periodically tested by iodometric titrations.[19] In all experiments freshly prepared aqueous solutions, containing less than 1% ethanol, were used.

Standard stock solutions of metals (about 0.05*M*) were prepared as their perchlorate salts. They were obtained by dissolving nickel carbonate and zinc oxide in perchloric acid (1:1), followed by evaporation and recrystallization from water. The nickel(II) and zinc(II) solutions were standardized gravimetrically with dimethylglyoxime, and volumetrically with EDTA, respectively.

The ionic strength of solutions (0.1 and 1.0*M*) was adjusted by the addition of sodium perchlorate solution (0.5 and 5.0*M*).

All reagents were of analytical grade.

Procedures

Aqueous solutions containing ligand, metal ion (when required), buffer solution, and sodium perchlorate to adjust the ionic strength to 0.1–1.0*M* were prepared as above. The solutions were thermostated in a waterbath at 25°. The absorbance was recorded at 5-nm intervals over the spectral range required (see Table 1), and the pH or pCH value was measured.

The residual absorbance error of the spectrophotometer [$S_{inst(A)}$] was 0.0023 absorbance units, as evaluated by the Werimont's procedure.[20]

In the determination of the protonation constants of ligand, buffer solutions covering the pH ranges given in Table 1 were prepared according to Perrin.[16] In the complex formation equilibria, the solutions of Ni(II) and Zn(II) were buffered with formic acid/sodium formiate and acetic acid/sodium acetate, respectively, with total concentration of formic or acetic acids about 0.002*M*, because of their low complex formation constants with Ni(II) and Zn(II).[21]

The upper limit of ligand and metal concentrations was set by the solubility of the ligand and metal complexes, as well as by the absorbance readings.

Spectral data acquisition: DUMOD program

To acquire the absorbance data from the Beckman DU-7 spectrophotometer on an IBM-PC computer, a BASIC program named DUMOD was developed. The program has been compiled with Microsoft Quick-Basic 4.0, and runs on an IBM-PC or compatible computer with an RS-232 serial interface, 256 Kbytes of memory, one diskette unit (360 or 720 Kbytes), and a CGA or Hercules graphics screen. The operating system must be MS-DOS 3.1 or later.

Table 1. Experimental conditions ($T = 25°$)

Equilibria	Spectral range (nm)	−log H range	C_L(μM)	C_M(μM)
Acid–base	250–450	1–12	100	—
Ni complexes	350–500	3.7–5.3	20–460	70–99
Zn complexes	250–450	3.2–5.7	10–170	25–70

The possible options of this program are:

(1) Recording of the data from the spectrophotometer. After this, the data are saved in an ASCII file.

(2) Draw the stored spectra on a HP-GL compatible plotter.

(3) Draw the spectra on the computer screen.

(4) List the directory of the disk.

Data treatment

The equilibria studied can be generalized as:

$$pL + qM + rH \rightleftharpoons L_pM_qH_r$$

and the overall formation constants are defined by:

$$\beta_{pqr} = [L_pM_qH_r]/[L]^p[M]^q[H]^r$$

where M, L and H are the free concentrations of metal ion, ligand and hydrogen ion. Charges are omitted for simplicity.

The experimental data were prior processed by using the NIPALS program[13] in order to determine the number of absorbing species in solution by factor analysis of absorbance matrices, as described by Kankare.[22] The program calculates the eigenvalues and the eigenvectors corresponding to an absorbance matrix, and recalculates the data array corresponding to k eigenvalues and eigenvectors, the values of k changing from 1 to 20. For each value of k, the standard deviation of absorbance values obtained in the reconstruction of the original data array as a function of the number of eigenvectors [$s_{k(A)}$] is calculated. The determination of the number of absorbing species is done by plotting $s_{k(A)}$ versus k.

Figure 1 shows the $s_{k(A)}$ values obtained in the protonation and complex equilibria, from the data corresponding to 1.0M ionic strength. As expected, four species are detected in the ligand protonation data, as it has three dissociation constants. In this case, $s_{4(A)} = 0.0016$, slightly under the instrumental error.

The treatment of data corresponding to Zn(II) complexes shows that at least three species are needed to explain the experimental data [$s_{3(A)} = 0.0018$, $s_{4(A)} = 0.0011$]. Taking into account that in the pH range studied, the ligand species H_3L and H_2L are predominant (less than 5% of the ligand is in the HL form), we conclude that two zinc complexes are formed.

The case of Ni(II) complexes is very different, as in the wavelength range studied the ligand absorption is low, and the absorption band in this range corresponds to the formation of nickel complexes. The values of $s_{2(A)} = 0.0021$ and $s_{3(A)} = 0.0009$ indicate that there are two principal species, and a third less important. From this, we can deduce that the two former species correspond to two Ni(II) complexes.

All the experimental data (protonation and complex equilibria) were processed later by the

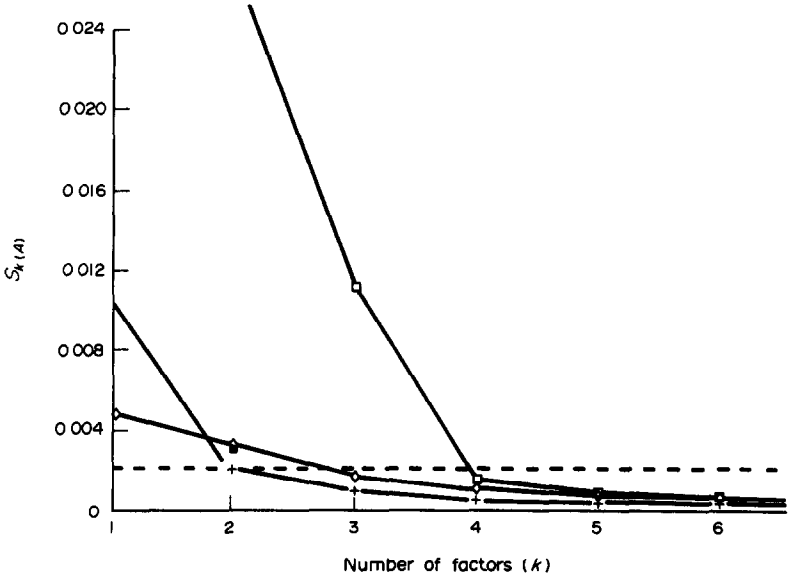

Fig. 1. Graphical determination of the number of absorbing species. Plot of the calculated standard deviation of absorbance matrix [$s_{k(A)}$] as estimated by factor analysis of the absorbance data matrix versus the number of factors (k) (from the data obtained at $I = 1.0M$). Dashed line indicates the instrumental error. Symbols are: (□): dissociation equilibra; (+): Ni(II) complexes; (◇): Zn(II) complexes.

Table 2. Calculated formation constants (at 25°, ionic strength adjusted with sodium perchlorate)

Equilibrium	$I = 0.1M$ log β ($\sigma_{\log\beta}$)	sdr*	$I = 1.0M$ log β ($\sigma_{\log\beta}$)	sdr*
$H^+ + L^{3-} \rightleftharpoons HL^{2-}$	11.54 (0.02)	0.0064	10.88 (0.01)	0.0048
$2H^+ + L^{3-} \rightleftharpoons H_2L^-$	18.45 (0.02)		17.74 (0.02)	
$3H^+ + L^{3-} \rightleftharpoons H_3L$	21.70 (0.02)		21.03 (0.02)	
$Ni^{2+} + HL^{2-} \rightleftharpoons Ni(HL)$	6.73 (0.01)	0.0058	6.97 (0.01)	0.0066
$Ni^{2+} + 2\,HL^{2-} \rightleftharpoons Ni(HL)_2$	13.91 (0.01)		14.41 (0.01)	
$Zn^{2+} + HL^{2} \rightleftharpoons Zn(HL)$	7.23 (0.02)	0.0057	7.43 (0.03)	0.0062
$Zn^{2+} + 2\,HL^{2-} \rightleftharpoons Zn(HL)_2$	13.63 (0.02)		13.81 (0.03)	

*sdr means the standard deviation of residuals, in absorbance units.

least-squares program SQUAD.[15] This program refines the equilibrium constants and calculates the unknown molar absorbances at the working wavelengths. The function minimized (U) is based on the residuals of absorbance values of the solutions:

$$U = \sum_{i=1}^{ns} \left[\sum_{j=1}^{nw} (A_{i,j,\text{exp}} - A_{i,j,\text{calc}})^2 \right]$$

Where ns and nw are the number of solutions and wavelengths, respectively. The results of the dissociation and complex formation constants are shown in Table 2.

RESULTS AND DISCUSSION

3-(2-Hydroxyphenyl)-2-mercaptopropenoic acid (H_3L) has three dissociation constants which can be assigned to the carboxylate, thiol and phenol groups. The spectral differences between the different species allow the determination of the three pK_a values. The protonation constants obtained, together with the standard deviations of the absorbance residuals are presented in Table 2.

In the complex formation studies we postulated that the hydroxyl group does not coordinate with the metal ions, because its high pK value, compared with those of mercapto and carboxylic groups. Moreover, since β-aryl-α-mercaptopropenoic acids do not form polynuclear complexes, we assumed that the predominant metal complexes were M(HL) and $M(HL)_2$. Figures 2 and 3 show some of the spectra obtained in the determination of complexation constants of the ligand with Ni(II) and Zn(II), and Table 2 summarizes the formation constants obtained. The greater standard deviation obtained in the formation constants of the zinc complexes could be due to the smaller spectral differences between the zinc complex and the ligand when we compare the nickel complexes.

The values of the ligand acidity constants show that the difference in the first dissociation (carboxylic group) at 0.1 and $1.0M$ ionic strength is negligible (within the experimental error). However, the dissociation of the mercapto group is favoured at the higher ionic strength (0.2 pK units lower), and the differences in the pK values of the hydroxyl group are still larger (0.7 units lower at $1.0M$ ionic strength).

As shown in Table 2, the Ni(II) complexes are more stable at higher ionic strength. The magnitude of the increments [0.25 units in log β for the Ni(HL) complex, and 0.5 units for the $Ni(HL)_2$ complex] correspond to the higher acidity of the mercapto group of the ligand at 1.0 ionic strength. The Zn(II) complexes are also more stable at the higher ionic strength, but the difference in the $Zn(HL)_2$ complex is less important.

The acquisition of spectral data by the DUMOD program proved to be reliable, simple and easy to use. Although the data can be collected from the spectrophotometer with the Beckman Data capture software (DC, also used in this work) or Beckman Data Leader package, the program DUMOD has several features that make it very useful when the absorbance data must be treated numerically after their acquisition.

For example, when the Beckman DC program is used to acquire the spectral data, it saves all the absorbance values (in our conditions, at 600 nm/min scanning speed, corresponding to an absorbance reading after every 0.5 nm) in a file in binary format (BSF: Beckman Standard Format). A file is needed for each recorded spectrum. However, if these data are used as input data for the least-squares SQUAD program, we have two more tasks: to translate the BSF files to ASCII files, and to take the absorbance values at the desired wavelength interval (*e.g.*, each 2, 5 or 10 nm). A BASIC program, also supplied by Beckman, was

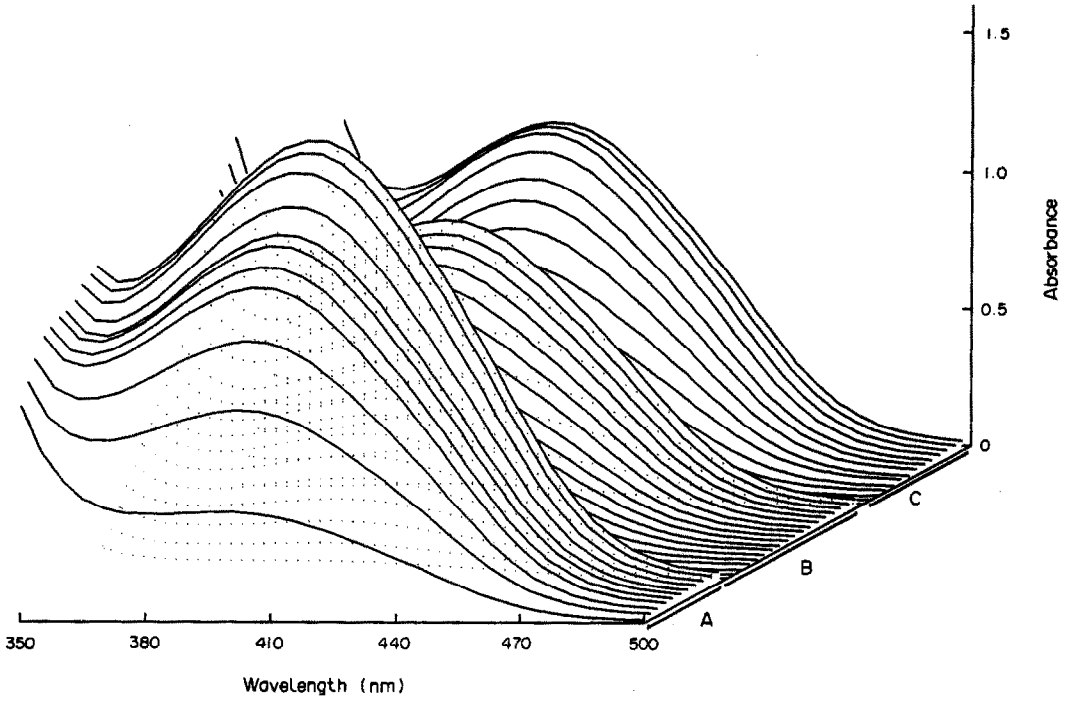

Fig. 2. Absorption spectra of the system Ni(II)–H_3L at $I = 1.0M$ in $NaClO_4$. The experimental conditions for these series are: (A) $C_M = 0.99 \times 10^{-4}M$, $C_L = 2.65 \times 10^{-4}M$; pH changed from 3.2 to 5.3. (B) $C_M = 7.07 \times 10^{-5}M$. The C_L/C_M ratio changes from 0.25/1 to 6.1/1; pH is maintained about 3.7. (C) $C_M = 7.07 \times 10^{-5}M$. The C_l/C_M ratio changes from 0.5/1 to 6.5/1. pH is maintained at about 4.7.

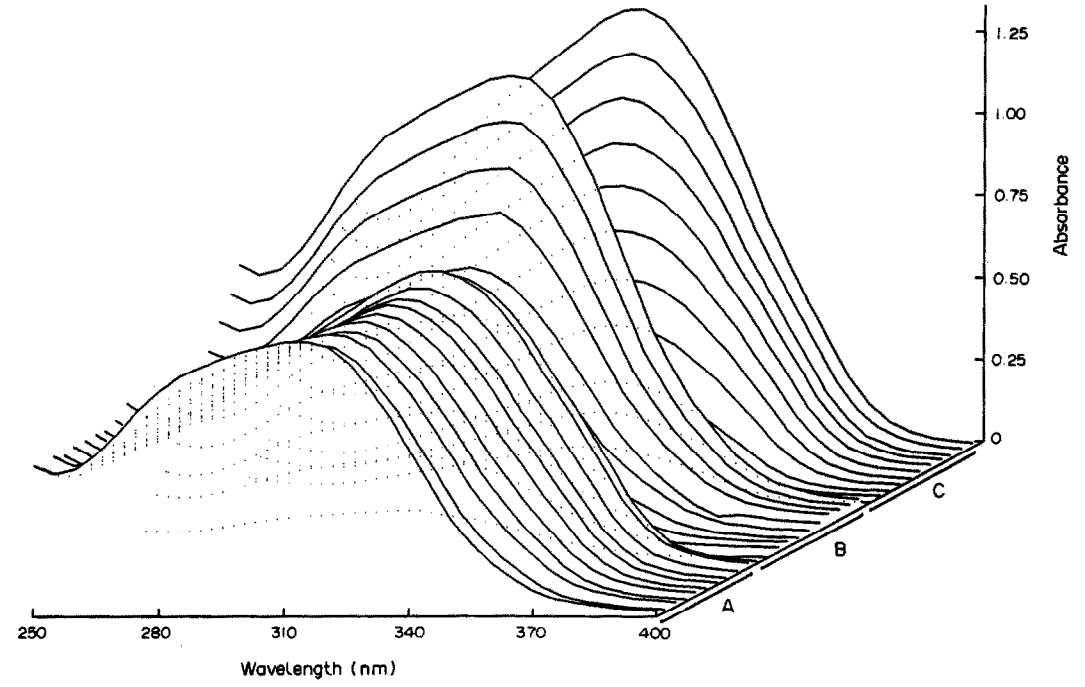

Fig. 3. Absorption spectra of the system Zn(II)–H_3L at $I = 1.0M$ in $NaClO_4$. The experimental conditions for these series are: (A) $C_M = 2.58 \times 10^{-5}M$, $C_L = 1.06 \times 10^{-4}M$; pH changed from 3.9 to 5.3. (B) $C_M = 2.58 \times 10^{-5}M$. The C_L/C_M ratio changes from 0.65/1 to 6.5/1; pH is maintained about 4.2. (C) $C_M = 2.58 \times 10^{-5}M$. The C_L/C_M ratio changes from 0.65/1 to 6.5/1; pH is maintained about 5.2.

adapted to do this work, but it is a tedious task when we need to transform 30–50 spectra for each system studied. More recently, the new Beckman Data Leader software can transform the BSF files to ASCII files directly, but the selection of the absorbances at the desired wavelengths remains an "a posteriori" task.

In the DUMOD program, these difficulties are overcome when the spectra are acquired in real time: they are stored directly in ASCII format, taking the absorbance values at wavelength intervals selected by the user, and all the spectra can be located in only one file. The number of the spectra in the file is limited only by the disk capacity. The arrangement of absorbance values in the data files obtained corresponds to the input data for the SQUAD program.

The task that remains for the user when the data are used as input for the program SQUAD is just the preparation of the head of the input (description of the system and the equilibria involved) and the typing of the concentrations of reactants, pH and pathlength in each spectrum. These tasks can be carried out directly with a PC text editor.

REFERENCES

1. E. Casassas, M. Filella, A. Izquierdo, M. D. Prat and R. Rodriguez, *Polyhedron*, 1985, **4**, 1951.
2. A. Izquierdo, L. Garcia-Puignou and J. Guasch, *ibid.*, 1986, **5**, 1253.
3. M. Filella, N. Garriga and A. Izquierdo, *J. Chim. Phys.*, 1987, **84**, 93.
4. D. L. Leussing, R. E. Laramy and G. S. Alberts, *J. Am. Chem. Soc.*, 1960, **82**, 4862.
5. D. D. Perrin and I. G. Sayce, *J. Chem. Soc.*, 1967, 82.
6. H. F. De Brabander, L. C. van Poucke and Z. Eeckhaut, *Anal. Chim. Acta*, 1974, **70**, 401.
7. H. F. Brabander, A. M. Goemmine and L. C. van Poucke, *J. Inorg. Nucl. Chem.*, 1975, **37**, 799.
8. M. Filella, N. Garriga and A. Izquierdo, *Talanta*, 1987, **34**, 971.
9. A. Izquierdo and J. L. Beltrán, *Polyhedron*, 1987, **6**, 613.
10. J. Wagner, P. Vitali, J. Schaun and E. Giroux, *Can. J. Chem.*, 1977, **55**, 4028.
11. N. J. Prakash, P. J. Schechter, E. Giroux and A. Sjoerdsma, *Clin. Exp. Pharmacol. Physiol.*, 1977, **4**, 17.
12. M. Filella, N. Garriga, A. Izquierdo and D. R. Williams, *Plzen. lek.Sborn.*, 1988, **56**, 33.
13. R. Tauler, A. Izquierdo-Ridorsa and E. Casassas, *An. Quim.*, in the press.
14. H. Martens and T. Naes, *Multivariate Calibration*, Wiley, Chichester 1989.
15. D. J. Leggett, S. L. Kelly, L. R. Shiue, Y. T. Wu, D. Chang and K. M. Kadish, *Talanta*, 1985, **30**, 579.
16. D. D. Perrin and B. Dempsey, *Buffers for pH and Metal Ion Control*, Chapman & Hall, London, 1974.
17. G. Gran, *Analyst*, 1952, **77**, 661.
18. A. Izquierdo and M. Giné, *An. Quim.*, 1978, **74**, 53.
19. Y. Okuda, *Biochem J.*, 1925, **5**, 201.
20. G. Wernimont, *Anal. Chem.*, 1967, **39**, 554.
21. S. Kotrly and L. Sucha, *Handbook of Chemical Equilibria in Analytical Chemistry*, Ellis Horwood, Chichester, 1985.
22. J. J. Kankare, *Anal. Chem.*, 1970, **42**, 1322.

Talanta, Vol. 39, No. 8, pp. 987–991, 1992
Printed in Great Britain

0039-9140/92 $5.00 + 0.00
Pergamon Press Ltd

SPECTROPHOTOMETRIC DETERMINATION OF THE TOTAL AMOUNT OF RARE-EARTH ELEMENTS IN AGRICULTURAL SAMPLES WITH *p*-CHLORO-CHLOROPHOSPHONAZO*

SHIHE LI, SHENGQUAN LI† and YUEJUN ZHANG
Department of Basic Sciences, Shanxi Agricultural University, Taigu, People's Republic of China

(*Received* 3 *January* 1991. *Revised* 30 *May* 1991. *Accepted* 5 *June* 1991)

Summary—A simple, sensitive and accurate spectrophotometric method for determination of the total amount of rare-earth elements in agricultural samples with *p*-chloro-chlorophosphonazo [*p*CCPA, *i.e.*, 2-(4′-chloro-2′-phosphon-benzylazo)-7-(4″-chlorophenyl)-1,8-dihydroxynaphthalene-3,6-disulphonic acid] in sulphuric acid medium has been developed. The apparent molar absorptivity of RE*x*O*y* (the general formula of rare-earth oxides)–*p*CCPA complex is 8.17×10^4 l.mole^{-1}.cm^{-1} at 676 nm, and Beer's law is obeyed for the mixture of RE*x*O*y* in the range 0–12 μg/25 ml. The proposed method has been successfully applied to the determination of the total amount of rare-earth elements in soils, herbs, vegetables, dried stems of maize, water samples and rare-earth microelement fertilizer samples with satisfactory results.

Spectrophotometric methods for determination of the total amount of rare-earth elements in steels,[1-3] alloys,[3,4] rocks and minerals,[1,5] human hair[6] and water samples[1,7,8] have been reported. *p*-Chloro-chlorophosphonazo (*p*CCPA) has been shown to be a reliable colorimetric reagent for yttrium[9] and scandium.[10] To our knowledge no systematic spectrophotometric investigations concerning the determination of the total amount of rare-earth elements in agricultural samples with *p*CCPA in aqueous solutions have been published previously. Recently, more and more applications of rare-earths (mainly nitrate) in agriculture are being investigated.[11] Applications of the rare-earths in agriculture have been reported to increase crop yield by 10–20% over controls. For example, oil-bearing crops have increased by 11–15%, cottons by 2.6–23.6%, vegetables by 11%, water melons by 15–23%, grapes by 10–25%, *etc.*[11] The contents of rare-earth elements in soil range from 200 to 1500 μg/g (cerium being the richest element) and the amounts of rare-earth elements in plants depend on their type and on the relative amounts of rare-earths in the soil in which the plants grow. Obviously, it is important for convenient methods to be available for determining the amounts of rare earths in soils. In this paper, the proposed method for the determination of total amounts of rare-earths in agricultural samples is shown to be simple and accurate. In the presence of proper masking agents, the determination is free of interferences from major elements and other microelements in agricultural samples, without the need for preliminary separation steps.

*Project supported by the Natural Sciences Foundation of Shanxi Province, China.
†Author for correspondence.

EXPERIMENTAL

Reagents

All chemicals used were of analytical-reagent grade unless otherwise indicated. Demineralized water was used throughout.

*Standard solution of a single RE*xOy, *1 mg/ml.* Dissolve 0.1000 g of RE*x*O*y* (purity, 99.999%, Yue Long Chemical Plant, Shanghai) in 2 ml of hot hydrochloric acid (6*M*) with dropwise addition of hydrogen peroxide. Cool, add 0.5 ml of concentrated sulphuric acid, heat and evaporate until acid fumes appear, cool, then add 2 ml of water and 1–2 drops of hydrogen peroxide. Boil to remove residual hydrogen peroxide, cool and dilute to 100 ml with water.

*Standard solution of mixed RE*x*O*y, 1 mg/ml. Prepared by mixing 40 ml of 1 mg/ml CeO_2 solution, 30 ml of 1 mg/ml Y_2O_3 solution, 15 ml of 1 mg/ml La_2O_3 solution and 15 ml of 1 mg/ml

Nd_2O_3 solution. The stock solution is further diluted to 10 μg/ml as working solution.

p-Chloro-chlorophosphonazo (pCCPA) aqueous solution, 0.05% (w/v).

*Sulphuric acid, 1*M.

Masking agent solution. Prepared by mixing 40 ml of 0.1*M* EDTA, 20 ml of 0.5*M* NaF, 5 ml of 0.1*M* citric acid and 5 ml of 0.1*M* oxalic acid.

Apparatus

Absorption spectra were measured with a Hitachi Model 220 double beam UV-Vis spectrophotometer (Japan) and the absorbance measurements were performed on a Model 721 spectrophotometer (Shanghai). A Fei-Yue-Pai Model WL-5001 Microwave oven (Radio Plant 18 of Shanghai) and polytetrafluoroethylene pot (Plant 9759 of PLA, Wuxi, P. R. China) were used for treatment of samples.

Procedure

General. To an aliquot of standard solution or sample solution containing 0–12 μg of REx*O*y in a 25-ml calibrated flask, add 0.5–1.6 ml of masking agent (not needed for standard solution), 3 ml of 1*M* sulphuric acid, and 3 ml of 0.05% *p*CCPA solution, dilute to the mark with water and shake thoroughly. Leave at room temperature for 30 min. Measure the absorbance in a 2-cm cell at 676 nm against a reagent blank prepared similarly.

Treatment of sample. For the control mineral specimen, fuse 0.1000 g of specimen with 2 g of sodium hydroxide and 2 g of sodium peroxide at a temperature of 700° for 15 min, cool and add 100 ml of boiling water, 10 ml of triethanolamine-water (1:1 v/v) solution, 1 g of EGTA, and 2 ml of 5% (w/v) $MgCl_2$ solution, boil and filter. The precipitate is dissolved in 15 ml of concentrated hydrochloric acid, followed by 100 ml of hot water and 20 ml of concentrated ammonia. The mixture was filtered after cooling to room temperature, and the precipitate was dissolved with 15 ml of hydrochloric acid (6*M*, 80°) and washed with 25 ml of 1.2*M* hydrochloric acid (about 80°). The solution was made up to 100 ml after cooling.

For the agricultural samples (except water samples), weigh accurately 0.2000 g of sample that has been treated preliminarily (dried, crushed, ground and sifted). Transfer the sample to a polytetrafluoroethylene pot, add 2.0 ml of concentrated sulphuric acid, and 1 ml of 30% hydrogen peroxide. Screw the lid on the pot, then place the pot in a microwave oven, and digest the sample for 3 min (6 min for soil samples). The pot is cooled for 20 min after being taken out of the oven. Unscrew the lid and transfer the solution to a 25-ml standard flask, and dilute to the mark with water. Samples are also digested by weighing 0.5000–2.000 g (determined by the total amount of rare-earths in the sample) of sample treated preliminarily and placed in a Kjeldahl flask. Add 5–10 ml of concentrated sulphuric acid and leave at room temperature for about 12 hr. Boil for 5–10 min, cool a moment and add several drops of hydrogen peroxide, continue to boil for about 5 min, and follow the same process until the solution appears clear. Boil to remove residual hydrogen peroxide, cool, filter (if necessary), transfer the solution to a 100-ml standard flask and dilute to the mark with water.

Water samples were prepared by concentrating via evaporation (the final volume depended on the total amount of rare-earths).

RESULTS AND DISCUSSION

Absorption spectra

Figure 1 shows the absorption spectra of the REx*O*y–*p*CCPA complexes and the mixed REx*O*y–*p*CCPA complex. There are two strong absorption bands in the wavelength range of 560–760 nm. Maximum absorption of

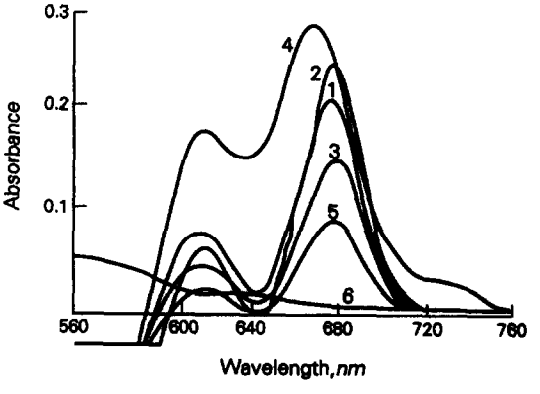

Fig. 1. Absorption spectra of complexes: 1, 10 μg La_2O_3/25 ml + *p*CCPA complex against reagent blank; 2, 12 μg CeO_2/25 ml + *p*CCPA complex against reagent blank; 3, 8 μg Nd_2O_3/25 ml + *p*CCPA complex against reagent blank; 4, 10 μg Y_2O_3/25 ml + *p*CCPA complex against reagent blank; 5, mixed REx*O*y (5 μg/25 ml) + *p*CCPA complex against reagent blank; 6, *p*CCPA against demineralized water.

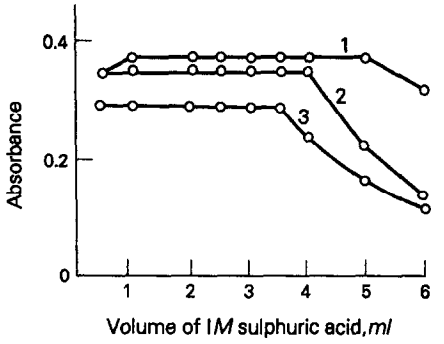

Fig. 2. Effect of acidity: 1, 10 μg CeO_2/25 ml; 10 μg La_2O_3/25 ml; 10 μg mixed REx*O*y/25 ml. Wavelength is 676 nm. 2, 10 μg Nd_2O_3/25 ml, 676 nm. 3, 5 μg Y_2O_3/25 ml (but at 667 nm).

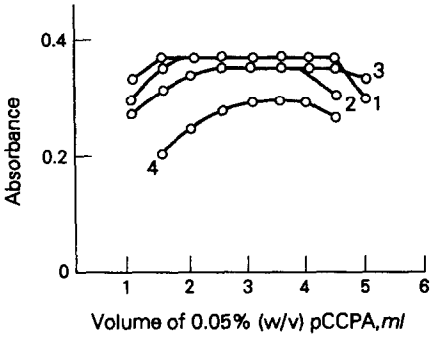

Fig. 3. Effect of *p*CCPA concentration: 1, 10 μg CeO_2/25 ml; 10 μg mixed REx*O*y/25 ml; 676 nm. 2, 10 μg La_2O_3/25 ml; 676 nm. 3, 10 μg Nd_2O_3/25 ml; 676 nm. 4, 5 μg Y_2O_3/25 ml, 667 nm.

the complexes of La, Ce, Pr, Nd, Sm and Eu with *p*CCPA and the mixed REx*O*y–*p*CCPA omplex is at 676 nm, but that of Gd, Tb, Dy, Er, Tm and Y with *p*CCPA is at 667 nm, measured against a reagent blank. Because the amounts of light rare-earths in agricultural samples are greater than those of heavy rare-earths, 676 nm was chosen as the measurement wavelength.

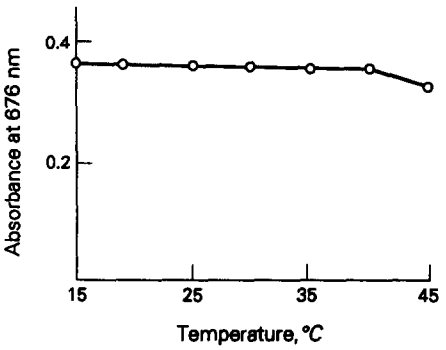

Fig. 4. Effect of temperature.

Effect of acidity

The effect of acidity on the absorbance of the complexes was studied with 1*M* sulphuric acid. The results obtained are shown in Fig. 2. The recommended amount of acid is 3 ml.

Effect of p*CCPA concentration*

The effect of *p*CCPA concentration on the absorbance of complexes was studied. The usable ranges are shown in Fig. 3. The recommended amount is 3.0 ml.

Effect of temperature

The influence of the temperature on the reaction of REx*O*y–*p*CCPA was studied by holding samples at different temperatures between 15 and 45°. The absorbance is not appreciably affected by changes in the temperature between 15 and 40° (Fig. 4).

Characteristics of the system

Table 1 shows some of the calibration and precision characteristics of the measurement system for different rare-earths. Table 2 gives the apparent molar absorptivities of REx*O*y–*p*CCPA complexes.

Table 1. Calibration and precision characteristics of the system

REx*O*y	L.R.E.*	*R*†	R.B.L.O.‡	S.D.	RSD, %
Mixed REx*O*y	$A = 0.005 + 0.042C$	0.9998	0–12	3.83×10^{-3}	1.0
CeO_2	$A = 0.009 + 0.037C$	0.9999	0–12	4.06×10^{-3}	1.4
La_2O_3	$A = 0.005 + 0.037C$	0.9998	0–10	4.18×10^{-3}	1.4
Nd_2O	$A = 0.007 + 0.039C$	0.9827	0–9	8.51×10^{-3}	2.7
Y_2O_3	$A = 0.009 + 0.047C$	0.9998	0–8	7.68×10^{-3}	1.8

*Linear regression equation.
†Correlation coefficient.
‡Range of Beer's law obeyed (μg/25 ml).
A, absorbance; *C*, μg/25 ml REx*O*y.

Table 2. The apparent molar absorptivities of REx*O*y–*p*CCPA complexes at 676 nm

Element	Mixed RE	LA	Ce	Pr	Nd	Sm	Eu	Gd	Tb	Dy	Er	Tm	Y
$\varepsilon(\times 10^4)$	8.17	7.97	8.42	8.22	7.83	8.36	7.78	8.50	8.18	8.34	8.46	7.84	7.34

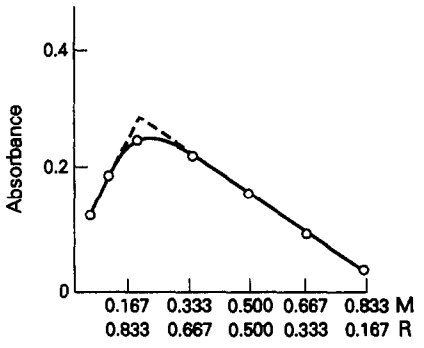

Fig. 5. Method of continuous variations. M: Mole fraction of RE; R: Mole fraction of *p*CCPA.

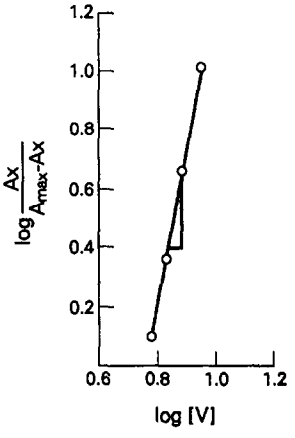

Fig. 6. Method of equilibrium shift. V: Volume of *p*CCPA; A: Absorbance.

Job's method of continuous variation and the method of equilibrium shift shows that the reaction ratio of RE (rare-earths) to *p*CCPA is 1:5 (Figs. 5 and 6).

Effect of reaction time

The reactions of La, Ce, and Nd with *p*CCPA are very rapid. The absorbance reached a maximum immediately after the solutions were made up to final volume. But the absorbance of the Y_2O_3–*p*CCPA complex reached its maximum 30 min after the solution was made up to final volume. The absorbances of all RE*x*O*y*–*p*CCPA complexes are stable for up to 3 hr.

Table 3. Effect of foreign species

Foreign species	Tolerance limit, *mg*
NO_3^-	200
NH_4^+	100
ClO_4^-	80
Na^+, Cl^-	50
Hg^{2+}, CH_3COO^-	40
F^-, B(III)	25
P(V), Si(IV)*	15
K^+, As(V)	10
Cs^+, Mn^{2+}	8.0
Li^+, Mg^{2+}, Sr^{2+}, Zn^{2+}	5.0
Co^{2+}, Cr^{3+}, Al^{3+}†	2.5
Ge(IV)	1.5
Fe^{2+}‡, Fe^{3+}‡, Ti(IV), Se(IV)	1.0
Cd^{2+}	0.5
Cu^{2+}	0.4
V(V)	0.25
Ca^{2+}§, Ni^{2+}, Mo(VI), W(VI)	0.2
Ba^{2+}	0.1
Ag^+	50 μg
Rh(III)	40 μg
Pb^{2+}	10 μg
Pd^{2+}	6 μg

*Masked with 0.1*M* (0.5 ml) oxalic acid solution.
†Masked with 0.5*M* (1.5 ml) NaF solution.
‡Masked with 0.1*M* (1.5 ml) EDTA solution.
§Masked with 0.1*M* (1.0 ml) citric acid solution.

Table 4. The comparison between the highest limits of the amounts of elements in soils and the tolerance limits of diverse ions

Element	Amounts in soils, *mg*	Tolerance limit, *mg*
Si	3.3	15
Al	0.71	2.5
Fe	0.38	10
Ca	0.17	0.2
K	0.136	10
Na	0.063	50
Mg	0.06	5.0
Ti	0.046	1.0
P	0.008	15
Cl	0.001	50
B	0.001	25
Zn	0.003	5.0
Mn	0.05	8.0
Mo	9×10^{-5}	0.2
Cu	1.3×10^{-3}	0.4
Co	5.9×10^{-4}	2.5

Selectivity

The selectivity was investigated by the measurement of 10 μg of mixed RE*x*O*y* (in 25 ml) in the presence of a series of other ions.

Table 5. Results of determination of total rare-earths in control mineral specimens

Control specimen	Certified amount of RE*x*O*y*, %	RE*x*O*y* found*, %	Relative error, %
No. 28	0.0190	0.0191	0.526
No. 29	0.0690	0.0683	−1.01

*Average of five separate determinations.

Table 6. Results of determination and recovery of total rare-earths in agricultural samples*

Sample and source	Amount determined: Before adding REExOy, μg†	Added, μg	After adding REExOy, μg	Recovery, %	Amount found in sample, μg/g‡
Soil from Yuncheng	4.18	4.00	8.15	99.5	837
Soil from Ruicheng	4.97	4.00	9.09	103.0	995
Alfalfa from Taiyuan Zoogarden	1.05	3.00	4.02	99.0	66.0
Vetch from Wu Tai-shan Mountain	1.29	4.00	5.32	100.1	80.6
Plains crazy-weed from Qinyuan	1.35	6.00	7.32	99.5	84.2
Skin of mung bean from Taigu	1.14	2.00	3.14	100.0	55.3
Stems of maize from Taigu	0.55	1.00	1.52	97.0	25.3
Celery from Taigu	4.90	2.00	6.88	99.0	48.6
Water sample I					3.28 (μg/l.)
Water sample II					35.01 (μg/l.)
RE-bearing microelement-fertilizer from Henan Province					39.8%

*All determined values given in Table 6 are averages of three separate determinations.

†The REExOy amount in a sample in 25 ml (*i.e.*, the value determined by the procedure described, but consideration must be given to both the range of Beer's law and the range of permissible acidity of the proposed method when the volume of a sample solution is decided).

‡The amount of rare-earths in the sample was obtained by converting the determined value to weight per gram of a given sample.

The stated levels of the species shown in Table 3 did not cause an error exceeding 5%.

The amounts of major elements and microelements in soils have a range of values. In order to show the selectivity of the proposed method for soil analysis, a comparison between the highest limits of the amounts of major elements and microelements in soils (statistical averages)[12] and the tolerance limits of diverse ions is given in Table 4.

It can be seen from Table 4 that the tolerance limits of diverse ions are by far, larger than the highest limits in soils. Therefore, the selectivity of the proposed method for soil analysis is satisfactory.

Accuracy and validity

In order to check the accuracy and the validity of the proposed method, control mineral specimens and various agricultural samples were analysed. The results are shown in Tables 5 and 6.

Acknowledgements—The authors are indebted to Professor Changsong Liu (the Department of Chemistry, Shanxi University, Taiyuan) and Professor Dingcheng Guo (the Department of Basic Sciences, Shanxi Agricultural University) for their help. We thank the Laboratory of the Geology Department of Shanxi Province for supplying the control mineral specimens.

REFERENCES

1. X. Wang and G. Zhao, *Fenxi Huaxue*, 1988, **16**, 49.
2. H. Dai, *Lihua Jianyan (Huaxue Fence), 1988*, **24**, 25.
3. Q. Wang and C. Ouyang, *Fenxi Huaxue*, 1986, **14**, 67.
4. Z. Zhou and Y. Chen, *ibid.*, 1985, **13**, 289.
5. D. B. Gladilovich, V. Kuban and L. Sommer, *Talanta*, 1988, **356**, 259.
6. R. Cai, L. Wang, L. Cheng and X. Yu, *Lihua Jianyan (Huaxue Fence)*, 1988, **24**, 2.
7. G. Chen, Q. Yang, Z. Zhang, J. Chen and C. Wang, *Fenxi Huaxue*, 1985, **13**, 840.
8. Q. Yang, G. Chen, Z. Zhang, X. Deng and H. He, *ibid.*, 1985, **13**, 864.
9. W. Chen, J. Pan and Z. Wu, *Huaxue Shiji*, 1986, **8**, 238.
10. W. Chen, J. Pan, Z. Xu and S. Ge, *Mikrochim. Acta*, 1985, **3**, 417.
11. J. Yang and S. Zhang, *Shanxi Nongye Daxue Xuebao*, 1989, 1.
12. Department of Soil Science and Agricultural Chemistry, Shanxi Agricultural Institute, P. R. China, *Soil Science*, p. 192. Renmin Jiaoyu Chubanshe, Beijing, 1975.

Talanta, Vol. 39, No. 8, pp. 993–996, 1992
Printed in Great Britain.

0039-9140/92 $5.00 + 0.00

SPECTROPHOTOMETRIC DETERMINATION OF TRACE AMOUNTS OF SELENIUM WITH CATALYTIC REDUCTION OF BROMATE BY HYDRAZINE IN HYDROCHLORIC ACID MEDIA

A. AFKHAMI, A. SAFAVI* and A. MASSOUMI
Department of Chemistry, College of Sciences, Shiraz University, Shiraz, Iran

(*Received* 7 *June* 1991. *Revised* 24 *September* 1991. *Accepted* 26 *September* 1991)

Summary—A method is presented for the determination of selenium, based on the catalytic effect of selenium(IV) on the reduction reaction of BrO_3^- by $N_2H_4 \cdot 2HCl$. The decolourization of Methyl Orange by the reaction products was used to monitor the reaction spectrophotometrically at 525 nm. This method is precise, highly sensitive, simple, rapid, widely applicable and selective for the determination of selenium(IV) and total selenium. The variables which affected the reaction rate were fully investigated and the optimum conditions were established. Selenium, as low as 1 ng/ml, can be determined by this method. The relative standard deviation of 20 ng of selenium was 0.94% ($N = 10$). The method was applied to the determination of Se(IV) in a health-care product.

Selenium is becoming increasingly important from a toxicological and physiological point of view.[1] Selenium is an essential micro-nutrient for animals although excesses have been known to cause toxicity. On the other hand selenium deficiency syndromes have also been reported. It has been reported that selenium acts as an antidote for mercury, cadmium, arsenic and other elements.[2]

On the basis of this background, the determination of micro amounts of selenium is becoming increasingly important. Determination of selenium as hydrogen selenide by atomic-absorption spectrometry is subject to many interferences[3] such as Ag, Cu, Ni, Pd, Pt, Rh, Ru and Sn, and it is necessary to ensure that the matrix being analysed does not interfere. An alternative method for determination of traces of selenium is based on the spectrophotometric or fluorimetric measurement of piazselenol formed by the reaction of selenium(IV) with diaminonaphthalene.[4–6] These methods are tedious, time consuming and the reagents used are toxic and relatively unstable.

Catalytic kinetic methods, which are simple, sensitive and selective for many elements,[7] have also been applied to the determination of this element, and some of them are described below. Selenium(IV) has been determined by using its catalytic effect on the reduction of methylene blue by sodium sulphide;[8] this method had a detection limit of 0.05 μg. Another catalytic method for the determination of selenium is based on the reduction of 1,4,6,11-tetraazanaphthacene by glyoxal and hypophosphorous acid and has a detection limit of 0.03 μg of Se.[9] This method suffers from a non-linear calibration and has the drawback of requiring a reagent that is not commercially available. A third method is based on the catalytic effect of selenium on the reduction of tetranitro blue tetrazolium by dithiothreitol.[10]

Recently, we reported a highly sensitive and selective method for the determination of selenium based on its catalytic effect on the reduction reaction of resazurin by sulphide.[11] This paper describes the development of a new method for the determination of selenium(IV) based on its catalytic effect on the reduction reaction of bromate by hydrazine dihydrochloride. This method which is very rapid, simple, highly selective and sensitive, uses only readily available reagents.

EXPERIMENTAL

Reagents

Demineralized triply-distilled water was used throughout. Selenite standard solutions were prepared by dissolving 1.40 g of selenium dioxide (Merck) in water and diluting to the

*Author for correspondence.

mark in a one-litre standard flask. This solution was standardized iodimetrically.[12] Working solutions were prepared by diluting the stock solution with water.

A 0.5*M* solution of hydrazine dihydrochloride was prepared by dissolving 13.12 g of $N_2H_4 \cdot 2HCl$ (BDH) in water and diluting to the mark in a 250-ml standard flask. Bromate (0.24*M*) was prepared by dissolving 10.02 g of potassium bromate (Merck) in water and diluting to the mark in a 250-ml standard flask.

Methyl Orange, 0.1% was prepared by dissolving 0.1 g of Methyl Orange (Merck) in water and diluting to the mark in a 100-ml standard flask.

A pH = 1 buffer solution (Merck) of glycine–hydrochloric acid was used.

Apparatus

A Perkin–Elmer model 35-spectrophotometer with a 1-cm glass cell was used for absorbance measurements.

Procedure

All the measurements were performed at 25.0 ± 0.1°.

Into a 10-ml standard flask introduce a suitable aliquot of the sample solution containing 0.05–8.0 μg of selenium(IV) and 1.5 ml of buffer solution. Add 2 ml of 0.5*M* hydrazine dihydrochloride followed by 0.2 ml of 0.1% methyl orange solution and 1 ml of 0.24*M* bromate, then dilute the solution to the mark with water and mix well. Transfer a portion of the solution to a glass cell within 30 sec and measure the absorbance at 525 nm. Find the initial reaction rate ($\Delta A/\Delta T$) during the first three minutes after starting the reaction.

RESULTS AND DISCUSSION

Selenium(IV) has a catalytic effect on the reduction reaction of bromate by hydrazine dihydrochloride. The steps involved in this reaction are:

$$2BrO_3^- + 10Cl^- + 12H^+ \rightleftharpoons Br_2 + 5Cl_2 + 6H_2O \text{ (slow)} \quad (1)$$

$$2Cl_2 + (N_2H_6)^{2+} \rightleftharpoons N_2 + 4Cl^- + 6H^+ \text{ (fast)} \quad (2)$$

$$2Br_2 + (N_2H_6)^{2+} \rightleftharpoons N_2 + 4Br^- + 6H^+ \text{ (fast)} \quad (3)$$

The first step of the reaction is slow and the second and third are fast. Selenium(IV) acts as a catalyst for the first step. The presence of hydrazine in the medium slows down step (1) which is fairly fast in its absence or when the medium is very acidic.[13] Methyl Orange reacts with the products of the reaction (bromine and chlorine) and is decolourized.

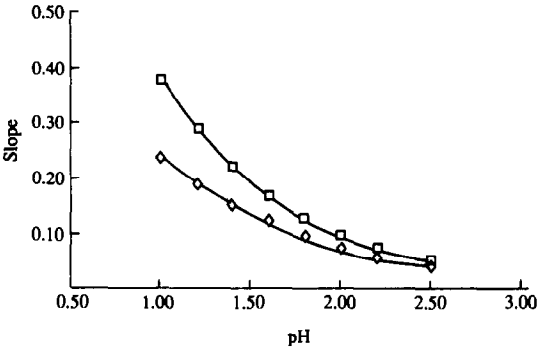

Fig. 1. Effect of pH on the rate of (■) catalysed and (●) uncatalysed reaction.

This reaction can be monitored spectrophotometrically by measuring the decrease in absorbance versus time for the first three minutes of the reaction.

Effects of variables

The graph of the decrease in absorbance versus time at 525 nm was linear during the first three minutes and the slope (tan α = dA/dt) was used as a measure of the initial reaction rate.

The reaction rate of both catalyzed and uncatalyzed reactions increased with decreasing pH. Figure 1 shows the influence on the catalyzed and uncatalyzed reaction of pH in the range 1.0–2.5.

Samples with pH lower than 1 were not tested because the rate of the uncatalyzed reaction is too fast at these pH values. Therefore, pH 1 was selected for routine works.

The influence of the concentrations of bromate and hydrazine dihydrochloride on the reaction rate was also studied. The reaction rate increases as the concentration of these two reagents is increased. On the other hand a high increase in the reaction rate causes perturbation in the absorbance reading by the appearance

Table 1. Accuracy and precision of the recommended procedure

Amount of Se(IV) taken, *ng/ml*	Relative error, %	Relative standard deviation, % ($n = 10$)
20	1.4	0.94
50	1.8	0.83
300	2.3	0.53
500	0.95	0.10

Table 2. Effect of diverse species on the determination of 0.5 μg/ml Se(IV)

Ion	Tolerance limit μg/ml
Th(IV), Se(VI), Pd(II), La(III),* Os(VIII), Co(II), Mn(II), Hg(II), Ce(IV),* Mo(VI), W(VI), Ce(III), K(I), Na(I), Tl(I), UO_2^{2+}, Zn(II), Ni(II), Fe(III),* Ca(II), Mg(II), As(V), Te(VI), As(III), Cd(II), Co(III), Al(III), PO_4^{3-}, CH_3OO^-, F^-, SO_4^{2-}, NO_3^-	100
I^-, IO_3^-, Br^-	30
Hg_2^{2+}, Cu^{2+}*	10
V^{3+}, Pd(II)†	2
EDTA	0.05*M*

*After addition of 0.5 ml of 0.1*M* EDTA.
†After addition of 1 ml of saturated dimethyl-glyoxime solution.

of nitrogen bubbles. Therefore the optimum concentration of these two reagents is the concentration at which the reaction has a high reaction rate and N_2 bubbling does not perturb the absorbance reading. These concentrations were found to be 0.10 and 0.024*M* for $N_2H_4 \cdot 2HCl$ and BrO_3^-, respectively.

Increasing temperature increased the reaction rate of both the catalyzed and uncatalyzed reactions, but at high temperatures N_2 gas bubbles are formed. For this reason and also for simplicity $25° \pm 0.1$ was selected for routine work.

Ionic strength up to 0.81*M* had no effect on the reaction rate.

Analytical parameters

The calibration graph was obtained under the experimental conditions chosen. A plot of initial reaction rates as a function of selenium(IV) concentration is linear in the range 5–800 ng/ml, with the equation:

$$\tan \alpha = 1.482 \times 10^{-4} C + 0.0806$$

with $r = 0.9994$, where C is the concentration of selenium(IV) in ng/ml.

The limit of detection, defined as the average of the blank value plus three times its standard deviation, was 1 ng/ml. Table 1 shows the accuracy and precision of the recommended procedure.

Effects of foreign species

The effects of various cations and anions on the determination of 0.5 μg/ml selenium(IV) were studied. The results are summarized in Table 2. The tolerance limit was defined as the concentration of added ion causing less than 3% relative error. Most ions did not interfere with the determination even when they are present at concentrations 200 times as great as that of selenium(IV).

Positive interferences were observed from lanthanum(III), copper(II), palladium(II), vanadium(III), tellerium(IV) and bromide because they could also catalyse the reaction. Negative interferences were observed from iodate and iodide, because they inhibit the indicator reaction. Hg_2^{2+} interferes by precipitation with the reagents. Iron(III) and cerium(IV) interfere by changing the colour of the solution probably by complexation with Methyl Orange. The interfering effect of copper(II) in concentrations less than 2 μg/ml and palladium(II) in concentrations less than 2 μg/ml can be removed by the addition of EDTA and dimethylglyoxime, respectively. However, higher concentrations of copper(II) can be removed by extracting its complex with dimethylglyoxime into chloroform, and higher concentrations of palladium(II) can be removed by extracting its complex with oxine into chloroform. The interfering effect of vanadium(III) can also be removed by extracting its complex with oxine into chloroform.

Determination of selenium in a health-care product

In order to test the described method, selenium was determined in a health-care product (a shampoo for the treatment of dandruff). Sample dissolution was carried out by the procedure described by Belarra *et al.*[14] Approximately 1 g of sample was weighed into a 100-ml Kjeldahl flask. Concentrated sulphuric acid (1 ml) was added and the mixture was heated to fuming for 15 min. The solution was allowed to cool and 5 ml of 30% w/v hydrogen peroxide was added. The mixture was boiled vigorously to eliminate excess of hydrogen peroxide and the flask was allowed to cool. The mixture was diluted to 1.0 litre with triply distilled water. A 0.5-ml volume of this solution was taken for determination of selenium(IV) as in the recommended procedure.

The results showed the presence of 13.45 ± 0.42 g/l. selenium ($n = 7$). (Manufacturer's value is given as 13.81 g/l. selenium as selenium sulfide.)

CONCLUSIONS

This method can be used to determine selenium as low as 1.0 ng/ml without the need for any preconcentration step. The method is very simple and more selective than the other kinetic methods reported previously or hydride generation atomic-absorption spectrometry which is subject to many interferences. Also, the limit of detection obtained by the proposed method (1.0 ng/ml) is lower than that obtained by hydride generation atomic-absorption spectroscopy (5 ng/ml).[3]

Since the method only responds to selenium(IV) species, the determination of selenium(IV) in the presence of selenium(VI) is possible.

Acknowledgement—The authors wish to express their gratitude to Shiraz University Research Council for their support of this work.

REFERENCES

1. H. Robberecht and R. Van Grieken, *Talanta*, 1982, **29**, 823.
2. K. Toei and Y. Shimoishi, *ibid.*, 1981, **28**, 867.
3. A. E. Smith, *Analyst*, 1975, **100**, 300.
4. M. W. Brown and J. H. Watkinson, *Anal. Chim. Acta*, 1977, **89**, 35.
5. Y. Shimoishi and K. Toei, *ibid.*, 1978, **100**, 65.
6. N. D. Michie, E. J. Dixon and N. G. Bunton, *J. Assoc. Anal. Chem.*, 1978, **61**, 48.
7. K. B. Yatsimirskii, *Kinetic Methods of Analysis*, Pergamon Press, Oxford, 1966.
8. P. W. West and T. V. Ramakrishna, *Anal. Chem.*, 1968, **40**, 966.
9. T. Kawashima and M. Tanaka, *Anal. Chim. Acta*, 1968, **40**, 143.
10. W. C. Hawkes, *ibid.*, 1986, **183**, 197.
11. A. Safavi, A. Afkhami and A. Massoumi, *ibid.*, 1990, **232**, 351.
12. A. I. Vogel, *A Text Book of Quantitative Inorganic Analysis*, 3rd Ed., Longman, London, 1961.
13. P. Linares, M. D. Luque de Castro and M. Valcarcel, *Analyst*, 1986, **111**, 1405.
14. M. A. Belarra, F. Gallarta, J. M. Anzano and J. R. Castillo, *J. Anal. At. Spect.*, 1986, **1**, 141.

Talanta, Vol. 39, No. 8, pp. 997–1000, 1992
Printed in Great Britain.

0039-9140/92 $5.00 + 0.00

TRIPHENYLTETRAZOLIUM CHLORIDE FOR DETERMINATION OF IODATE AND PERIODATE

M. KAMBUROVA
Department of Chemistry, Higher Institute of Agriculture, 4000 Plovdiv, Bulgaria

(*Received* 11 *February* 1991. *Revised* 11 *June* 1991. *Accepted* 14 *June* 1991)

Summary—Optimum conditions for complexation in the systems triphenyl-tetrazolium chloride-iodate-iodide-dichlorethane and triphenyltetrazolium chloride-periodate-iodide-dichlorethane were found. The molar absorptivity of the complex was 7.48×10^4 l. mole^{-1}. cm^{-1} for the iodate, and 9.09×10^4 l. mole^{-1}. cm^{-1} for the periodate. Beer's law is adhered to in the range of 0.04–0.7 μg/ml for iodate and 0.02–0.35 μg/ml for periodate. The influence of foreign ions was studied. Cr(VI), Hg(II) and $S_2O_3^{2-}$ interfere. The proposed method has been applied to analysis of iodate and periodate in fresh water.

There are a few methods for determination of iodates and periodate described in the literature.[1–5] The existing methods for spectrophotometric determination of these ions are, to some degree, unsatisfactory as the procedures require strict maintenance of the experimental conditions (*e.g.*, a strictly fixed pH, standing of the samples before the determination of the iodate or periodate and low stability of the compounds formed).

During our investigations we found that triphenyltetrazolium chloride (TTC), in acidic medium, reacted with iodate or periodate. The good solubility of the compounds obtained in organic solvents can be used in a determination of iodate or periodate and also in their isolation from other ions. This led to the development of an extraction spectrophotometric method for determination of iodate and periodate. The method we suggest is superior to some of the reported methods, in sensitivity,[1] stability of the complex obtained[2,3] and rapidity.[3]

EXPERIMENTAL

Apparatus

A Carl Zeiss VSU 2-P spectrophotometer (Jena, DDR) was used with 1-cm cuvettes, and measurement at 255 and 295 nm.

Reagents

2,3,5-Triphenyltetrazolium chloride (TTC), (Renal), $5 \times 10^{-4}M$ potassium iodate, *p.a.* $1 \times 10^{-5}M$, potassium periodate, *p.a.* $1 \times 10^{-5}M$, potassium iodide, *p.a.* $1 \times 10^{-3}M$ sulphuric acid, *p.a.* $-2M$ phosphoric acid, *p.a.* $-2M$ 1,2 dichlorethane, Merck.

Procedure

Determination of iodate. Aqueous solutions of the sample containing 0.4–7 μg of iodate are introduced into separating funnels. Portions of 3 ml of phopshoric acid $2M$, 0.4 ml of potassium codate $1 \times 10^{-3}M$ and 0.5 ml of $5 \times 10^{-4}M$ TTC are added. The volumes are brought up to 10 ml with distilled water and the solutions are extracted with 3 ml of $C_2H_4Cl_2$ for 15 sec. After phase separation, the organic phase is measured at 255 nm in a 1-cm cuvette. A blank containing no codate is run in parallel.

Determination of periodate. Aqueous solutions of the sample containing 0.2–3.5 μg of periodate are introduced into separating funnels. Portions of 0.5 ml of $2M$ sulphuric acid, 0.6 ml of $1 \times 10^{-3}M$ potassium iodate and 0.2 ml of $5.10^{-4}M$ TTC are added. The volumes are brought up to 10 ml with distilled water and the solutions extracted with 3 ml of $C_2H_4Cl_2$ for 15 sec. After phase separation, the organic phase is measured at 295 nm in a 1-cm cuvette. A blank is run in parallel as above.

RESULTS AND DISCUSSION

Optimization of conditions

The technique suggested for determination of iodate and periodate is based on their interaction, in acidic medium, with an excess of iodide ions which are oxidized to iodine. The complex anion obtained, I_3^-, is extracted as an

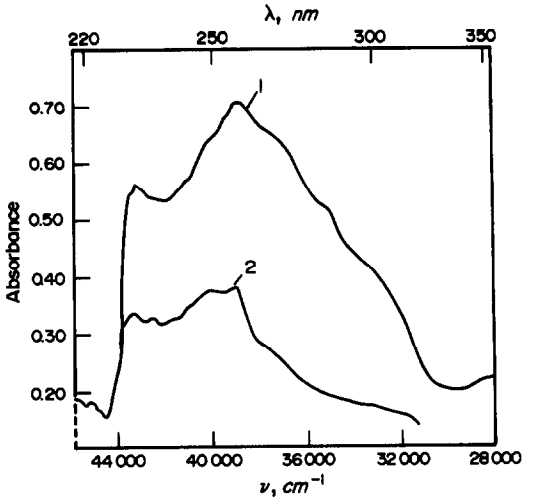

Fig. 1. Absorption spectra in $C_2H_4Cl_2$ of: 1-ion-association complex of TTC with IO_3^-, 2-TTC in phosphoric acid solutions; $C_{IO_3^-} = 8 \times 10^{-6}M$, $C_{TTC} = 2.5 \times 10^{-5}M$.

ion association complex with triphenyltetrazolium chloride. The solubility of the associates in the following organic solvents was investigated: chloroform, dichlorethane, benzene, nitrobenzene, tetrachloromethane. The associates showed highest solubility in dichlorethane. The absorption spectra of the ion-pair in dichlorethane which triphenyltetrazolium chloride formed with iodate and periodate are shown in Figs. 1 and 2. The associate formed from TTC and iodate has a maximum absorption at $\lambda = 255$ nm and the associate from TTC and periodate has two maxima, at $\lambda = 255$ nm and 295 nm. The determination of the periodate was carried out at 295 nm because the absorption of TTC is lower.

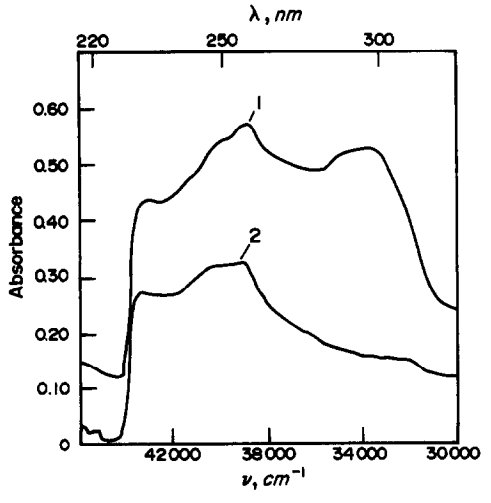

Fig. 2. Absorption spectra in $C_2H_4Cl_2$ of: 1-ion-association complex of TTC with IO_4^-, 2-TTC in sulphuric acid solutions; $C_{IO_4^-} = 8 \times 10^{-6}M$, $C_{TTC} = 2.5 \times 10^{-5}M$.

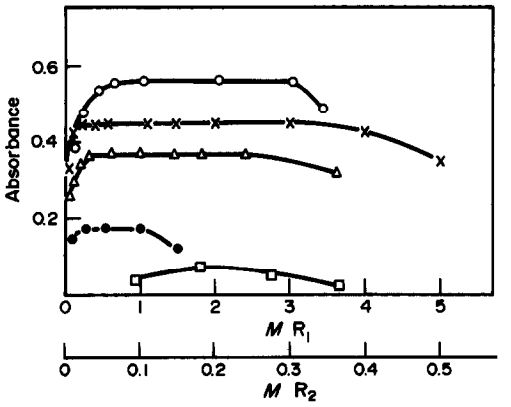

Fig. 3. Investigation of the acidity influence on the extraction of IO_3^- with TTC; R_1: (○) H_3PO_4, (×) H_2SO_4, (△) HCl, (●) HNO_3; R_2: (□) $HClO_4$; $C_{IO_3^-} = 3 \times 10^{-6}M$, $C_{TTC} = 1 \times 10^{-5}M$.

To optimize the reaction conditions we studied the effect of the type of the mineral acid and its concentration upon the interaction of TTC and iodate or periodate. The effect of the phosphoric, sulphuric, hydrochloric, nitric and perchloric acids upon the extraction equilibrium was studied. The experimental data (Fig. 3) showed that the maximum absorption for the iodate was obtained with the phosphoric acid in the range of 0.6–3M. Maximum extraction of periodate was reached in sulphuric acid medium (Fig. 4), with the maximum absorption in the range 1×10^{-1}–0.1M sulphuric acid. In both cases the experimental data showed that it is possible to work in a rather wide range of pH values.

The effect of triphenyltetrazolium chloride concentration upon the determination of iodates and periodates was studied. The absorbance increased with an increase in the TTC concentration. At an aqueous phase acidity of 0.6M phosphoric acid, the maximum extraction

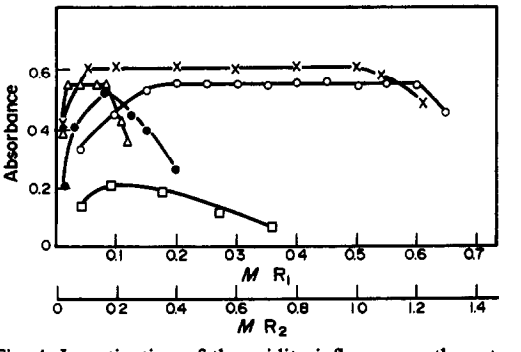

Fig. 4. Investigation of the acidity influence on the extraction of IO_4^- with TTC; R_1: (□) $HClO_4$, (●) HNO_3, (△) HCl; R_2: (○) H_3PO_4, (×) H_2SO_4; $C_{IO_4^-} = 1 \times 10^{-6}M$, $C_{TTC} = 1 \times 10^{-5}M$.

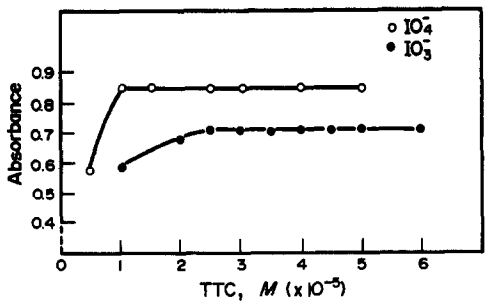

Fig. 5. Dependence of the light absorption change on the concentration of TTC; $C_{IO_3^-} = 0.7\ \mu g/ml$, $C_{IO_4^-} = 0.35\ \mu g/ml$.

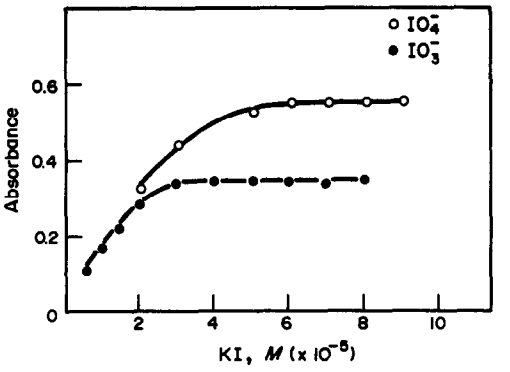

Fig. 6. Dependence of the light absorption change on the concentration of KI; $C_{IO_3^-} = 3 \times 10^{-6}M$, $C_{IO_4^-} = 1 \times 10^{-6}M$, $C_{TTC} = 1.10^{-5}M$.

of the iodate was reached at a concentration of TTC $\geqslant 2.5 \times 10^{-5}M$ (Fig. 5). At an acidity of the aqueous phase of $0.1M$ sulphuric acid, the maximum extraction of periodate was reached at a concentration of TTC $\geqslant 1 \times 10^{-5}M$.

The formation of ion-pairs between TTC and iodate or periodate largely depends on the concentration of potassium iodide. In order to shift the equilibrium towards formation of the ion-pairs, the concentration of iodide ions should be high. For the extraction of $3 \times 10^{-6}M$ iodate, the concentration of KI should be $\geqslant 3 \times 10^{-5}M$, and for the extraction of $1 \times 10^{-6}M$ periodate, the concentration of KI should be $\geqslant 6 \times 10^{-5}M$ (Fig. 6).

Photometric characteristics

In the presence of phosphoric acid, Beer's law is adhered to in the range 0.04–0.7 μg/ml iodate. The molar absorptivity at 255 nm is 7.84×10^4 $l.mole^{-1}.cm^{-1}$. The relative standard deviation

Table 1. Effect of foreign ions $C_{IO_3^-} = 0.2\ \mu g$; $C_{H_3PO_4} = 0.6M$ $C_{TTC} = 2 \times 10^{-5}M$; $C_{IO_4^-} = 0.2\ \mu g$; $C_{H_2SO_4} = 0.1M$ $C_{TTC} = 2 \times 10^{-5}M$

		Limiting ratio		Limiting conc. of foreign ion, *mg*	
N	Foreign Ion	$C_x/C_{IO_3^-}$, *mg*	$C_x/C_{IO_4^-}$, *mg*	IO_3^-	IO_4^-
1	SO_4^{2-}	8000:1	10,000:1	16	20
2	CO_3^{2-}	5000:1	10,000:1	10	20
3	PO_4^{3-}	2500:1	10,000:1	5	20
4	Br^-	2500:1	2500:1	5	5
5	NO_3^-	50:1	3000:1	0.1	6
6	Cl^-	8000:1	10,000:1	16	20
7	$C_2O_4^{2-}$	6000:1	250:1	12	0.5
8	BO_3^{3-}	5000:1	500:1	10	1
9	SCN^-	1.5:1	15:1	0.003	0.03
10	$S_2O_3^{2-}$	interfere			
11	BrO_3^-	5:1	1:1	0.01	0.002
12	Cu(II)	250:1	500:1	0.5	1
13	W(VI)	25:1	500:1	0.05	1
14	Hg(II)	interfere			
15	V/V	1000:1	1000:1	2	2
16	Cr(VI)	interfere			
17	K(I)	70,000:1	100,000:1	140	200
18	Bi(III)	1000:1	500:1	2	1
19	Mg(II)	2500:1	2500:1	5	5
20	Ni(II)	20,000:1	37,500:	40	75
21	Sr(II)	2500:1	2500:	5	5
22	Mo(VI)	1500:1	3000:1	3	6
23	Na(I)	1000:1	1000:1	2	2
24	Ag(I)	5:1	50:1	0.01	0.1
25	Co(II)	150:1	500:1	0.3	1
26	Mn(II)	5:1	150:1	0.01	0.3
27	Al(III)	50:1	500:1	0.1	1
28	EDTA	1000:1	500:1	2	1
29	Zn(II)	5000:1	2500:1	10	5
30	Fe(III)	40:1	5:1	0.08	0.01
31	Pb(II)	1000:1	750:1	2	1.5

Table 2. Accuracy and precision of the methods

Anion	Amount taken μg/ml	Accuracy E_r %	Precision RSD, %
Iodate	0.06	−1.2	0.7
	0.18	+0.9	0.5
Periodate	0.02	+1.3	0.7
	0.15	−1.1	0.4

*Relative error.
†Relative standard deviation.

(10 determinations with 0.5 μg of iodate, 95% confidence level) of the method is +0.35%. The Sandell sensitivity index[6] is 2.22×10^{-3} μg/cm². The absorbance of the organic phase is maximum and stable for seven days.

Beer's law is obeyed between 0.02 and 0.35 μg/ml periodate in sulphuric acid medium. The molar absorptivity at 295 nm is 9.09×10^4 l.mole^{-1}.cm^{-1}. The relative standard deviation (10 determinations with 0.5 μg of periodate, 95% confidence level) of the method is ±0.27%. The Sandell sensitivity index is 2.10×10^{-3} μg/cm². The ion-pair is stable for seven days.

Effects of foreign ions

The effect of some ions upon the extraction equilibrium in the determination of 0.2 μg of iodate and periodate was studied. The concentration limit of the foreign ions as well as the top ratio with iodate and periodate is given in Table 1. Most of the ions studied do not interfere even when in high concentration. No masking reagents were used. Only Cr(VI), Hg(II) and $S_2O_3^{2-}$ showed interfering action. The results in Table 1 show that the formation reaction of the ion-pair of TTC with periodate is more selective than the reaction between TTC and iodate.

Determination of iodate-iodine and periodate-iodine in fresh waters

Methods for determination of iodate and periodate based on the experimental data were developed. The experiment was carried out using artificial fresh water containing 10 mg/l. sodium, calcium, chloride, sulphate and bicarbonate, together with 200 μg/l. of iodate and periodate.

Add 3 ml of 2*M* phosphonic acid, 0.4 ml of 1×10^{-3} potassium iodate 0.5 ml of $5.10^{-4}M$ for determination of iodide–iodine, and 0.5 ml of 2*M* sulphuric acid, 0.6 ml of $1 \times 10^{-3}M$ potassium iodide, 0.2 ml of $5 \times 10^{-4}M$ TTC for determination of periodate–iodine in the sample of fresh water. Then dilute to 50 ml with distilled water. Extract with 3 ml of $C_2H_4Cl_2$ for 15 sec. Measure at $\lambda = 255$ nm and 295 nm. A blank is run likewise.

The concentrations of iodate and periodate are determined by preconstructed standard curves. The results are given in Table 2.

Advantages of these methods is the good accuracy and the wide range of pH that can be used. Besides, no standing is needed before determining the ions. The associates obtained are very stable.

REFERENCES

1. A. Fernandez-Gutierrez, A. Munoz and J. Murillo, *Anal. Lett.* 1983, **A16,** 759.
2. Roman Ceba M., J. Sánchez, and T. Diaz, *Microchem. J.*, 1985, **31, 256.**
3. A. Hareez and W. Bashir, *ibid.*, 1985, 375 **31.**
4. M. Callejon and J. Munoz, *ibid.*, 1986, 83. **34.**
5. M. Sapragonene, E. Ramanauskas and V. Ukonite, *Nauch. Tr.VUZ LitSSR, Chimiya i chim. technol.*, N 14, 37, 1972.
6. E. Sandell, *Colorimetric Determination of Traces of Metals*, Interscience, New York, 1959.

Talanta, Vol. 39, No. 8, pp. 1001–1006, 1992
Printed in Great Britain

0039-9140/92 $5.00 + 0.00
Pergamon Press Ltd

NEW BF_4^-- AND ClO_4^--SELECTIVE MEMBRANE ELECTRODES AND THEIR PHARMACEUTICAL APPLICATIONS

A. A. BUNACIU, MARIANA S. IONESCU, NIRVANA BUDIŞTEANU, A. DINULESCU and V. V. COŞOFREŢ

Institute of Chemical and Pharmaceutical Research Bucharest 74351, Şos. Vitan 112, Bucharest-3, Romania

(*Received* 29 *April* 1991. *Revised* 6 *January* 1992. *Accepted* 8 *January* 1992)

Summary—The construction and general performance characteristics of ion-selective membrane electrodes sensitive to BF_4^- and ClO_4^- anions, respectively, are described. All electrodes show near-Nernstian responses in the range 10^{-2}–$10^{-5}M$. The selectivity of the electrodes to a number of organic and inorganic anions are reported. The electrodes are useful in the potentiometric determination of a few pharmaceutical preparations. The method is simple, rapid and does not require prior sample pre-treatment.

Drug control quality is a branch of analytical chemistry that has a wide impact on public health, and so development of reliable quick and accurate methods for the active ingredient determination is welcomed.

Ion-selective membrane electrodes (ISMEs) development has seen spectacular achievements in the last few years, and, theoretically, it should be possible to construct such electrodes for any ionic species.

ISMEs are used extensively for quality control of various drugs and became a useful tool for solving analytical problems connected with complex pharmaceutical formulations.[1–7] Much effort is required in the development of a rapid, simple and sensitive method for the determination of a certain drug, as it may be found also in complex pharmaceutical preparations or in human fluids,[8] not only in pure form.

The paper describes the preparation and the characterization of two types of BF_4^--selective membrane electrodes and a ClO_4^--selective membrane electrode among those existing in the literature.[9–11] The electrodes use tricaprylmethylammonium cation as the counter-ion in the electroactive material of the membrane. One of the BF_4^--selective electrodes is based on the ion-pair complex dissolved in nitrobenzene ($5 \times 10^{-3}M$), (Electrode A), and the other on the same ion-pair complex embedded in a PVC matrix, (Electrode B). The ClO_4^--selective electrode is based on the ion-pair complex embedded in a PVC matrix (Electrode C). The electrodes exhibit useful analytical characteristics for the determination of some compounds of pharmaceutical interest, such as colidinium,[12] trimethylpyrylium and trimethylpyrydinium salts[13] and potassium perchlorate.

EXPERIMENTAL

Apparatus

A Präcitronic digital pH/mV-meter, model 870 MV (±0.01 mV precision) was used for all direct potentiometric measurements. The electrodes proposed were used in direct potentiometry in conjunction with an Orion 91-01 double junction reference electrode with saturated $Na_2B_4O_7$ solution in the outer compartment. The potentiometric titrations were performed with an automatic assembly, consisting of ABU 12 Autoburette, TTT 2 Titrator and SBR 2 c Recorder (Radiometer). The pH measurements were performed with a Radiometer G202 B glass electrode in combination with a Radiometer K401 calomel electrode.

Reagents and materials

All reagents were of analytical reagent grade. $NaBF_4$ and $KClO_4$ were supplied by Reactivul, while *n*-dodecanol was from Sigma. Other materials were: tricaprylmethylammonium chloride (Aliquat 336S), (General Mills Chemical Inc.); 2-nitrophenyloctylether (2-NPOE) (Fluka), and poly(vinylcholoride) (PVC) of high molecular mass (Aldrich). The pharmaceutical preparations were synthesized in our laboratory by one of us.[12,13] Standard solutions of sodium

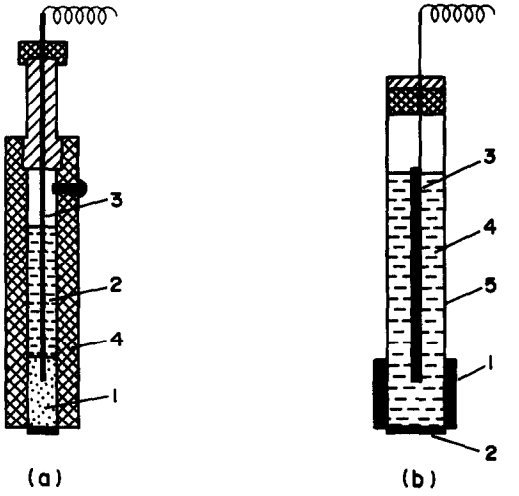

Fig. 1. The electrode design: (a) liquid membrane electrode. 1—graphite rod; 2—internal filling solution; 3—internal reference electrode; 4-electrode body. (b) PVC membrane electrode. 1—Tygon tube; 2—electroactive material; 3—internal reference electrode; 4—internal filling solution; 5—glass tube (electrode body).

tetrafluoroborate were prepared by serial dilution while keeping the pH constant at 2.7 (acetic acid/sodium hydroxide). Standard solutions of potassium perchlorate were prepared by serial dilution while keeping pH at a constant value of 6.4 with borax–KH_2PO_4 buffer.

Standard solution of sodium tetraphenylborate (NaTPB) ($5 \times 10^{-2}M$). An amount of 17.112 g of sodium tetraphenylboron was dissolved in distilled water and diluted to one litre. Potentiometric titration with $5 \times 10^{-2}M$ silver nitrate standard solution using an Ag_2S electrode as indicator was used to determine the solutions titre.

Procedures

Direct potentiometry. Standard solutions of 10^{-3}, 10^{-4}, 10^{-5} and $10^{-6}M$ concentrations were prepared by serial dilution of a $10^{-2}M$ potassium perchlorate solution. The electrodes were placed in the stirred standard solution in the order 10^{-6}–$10^{-2}M$. A plot of E (mV) against log[concentration] was recorded and the unknown concentration was determined from the calibration graph.

Potentiometric titration. The electrodes were placed in a sample solution (30–40 ml, concentration *ca.* $10^{-2}M$), then the sample was titrated with the $5 \times 10^{-2}M$ sodium tetraphenylborate standard solution. The end-point corresponds to the maximum slope on the E(mV) *vs.* volume titrant curve (1 ml of $5 \times 10^{-2}M$ tetraphenylborate solution is equivalent to 10.5 mg of 2,4,6-trimethylpyrylium tetrafluoroborate, 16.8 mg of colidinium tetrafluoroborate, 15.37 mg of 2,4,6-trimethylpyrydinium-*N*(acetoxiethyl) perchlorate and 17.04 mg of 2,4,6-trimethylpyrydinium-*N*(stearylamino) tetrafluoroborate, respectively).

Content uniformity assay of $KClO_4$ tablets. Ten individual tablets were placed in separate 100-ml standard flasks and dissolved by shaking with distilled water. The pH was kept constant at 6.4 with borax–KH_2PO_4 buffer and then the concentration was determined with a direct potentiometric method, as described above.

Electroactive materials

The quaternary ammonium cation, tricaprylmethylammonium (Aliquat 336S), is a well-known extracting agent and was used to obtain the ion-pair association complexes with the tetrafluoroborate and perchlorate anions respectively. Five grams of Aliquat 336S was mixed with 5.0 g of *n*-dodecanol and equilibrated with ten separate 10–15 ml aliquots of $0.1M$ $NaBF_4$ or $0.1M$ potassium chlorate, respectively. The organic phases were washed twice with distilled water until the reaction of chloride ion was negative, and then centrifugated until clear solutions were obtained.

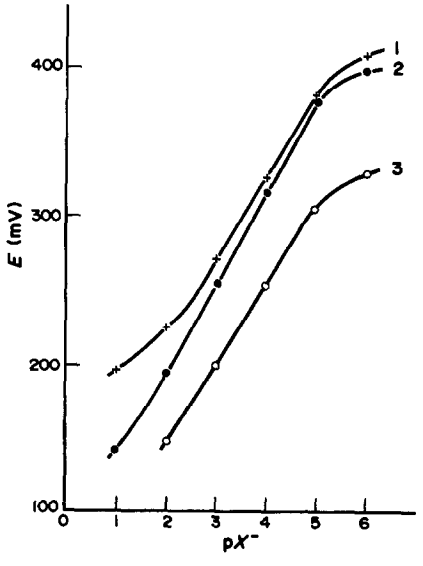

Fig. 2. The electrode functions of the X^--selective membrane electrodes ($X^- = BF_4^-$ and ClO_4^-). 1—Electrode A (BF_4-Aliquat 336S in nitrobenzene); 2—Electrode B (BF_4-Aliquat 336S in PVC matrix); 3—Electrode C (ClO_4-Aliquat 336S in PVC matrix).

Table 1. Response characteristics for X^--selective membrane electrodes ($X^- = BF_4^-$ and ClO_4^-)

Parameter	BF_4^--electrodes Electrode A	BF_4^--electrodes Electrode B	ClO_4^--electrode Electrode C
Slope* (*mV/decade*)	55 ± 1	61 ± 0.5	52 ± 0.5
Intercept, E_0' (*mV*)	107 ± 1.5†	74 ± 0.9†	38 ± 1.0†
Linear range (*M*)	5×10^{-3}–10^{-5}	$3 \times 10^{-2} - 10^{-5}$	$10^{-2} - 2 \times 10^{-5}$
Detection limit (*M*)	5.7×10^{-6}	6.0×10^{-6}	7.5×10^{-6}
(*μg/ml*)	0.75	0.78	1.04

*Standard deviation of average slope values in the linear range.
†Standard deviation of values recorded during one month ($n = 45$).

Preparation of the electrodes

The BF_4^--selective membrane electrode (Electrode A), was prepared as described elsewhere[14,15] by impregnating the support material [a graphite rod 15 mm long, 6.5 mm diameter (6) attached to the end of a PTFE tube (1)], with a solution of ion-pair complex in nitrobenzene (2). The electrode was stored in the same electroactive material solution as the inner filling solution and was washed with distilled water after use. The BF_4^--selective membrane electrode (Electrode B) and the ClO_4^--selective membrane electrode (Electrode C) were prepared as described elsewhere.[16–18] The ion-pair complexes were embedded in a PVC matrix containing 2-NPOE as plasticizer. The membrane composition, selected to be one of the best among those studied, was 4% w/w electroactive material 64% w/w 2-NPOE and 32% w/w PVC. A disc (0.9 cm diameter) was cut from the membrane and fixed to the end of a 10-mm Tygon tube using a PVC–tetrahydrofuran solution as adhesive. The other end of the Tygon tube was fitted on to a glass tube to form the electrode body. A Ag/AgCl wire was then inserted and the electrode body was filled with a $10^{-3}M$ standard solution of $NaBF_4$ and $KClO_4$, respectively. The electrodes were stored in the air between the measurements and washed with distilled water after use. Figure 1 shows the electrode design for both types used in the present investigation.

RESULTS AND DISCUSSION

Electrode responses

The emf measurements were made with electrochemical cells of type (I):

X^--selective membrane electrode | X^- (C_{X^-}) pH constant | Ag/AgCl (I)

where $X^- = BF_4^-$ and ClO_4^- respectively, C_{X^-} is the anion concentration ranging from 10^{-1} to $10^{-6}M$ for the BF_4^--selective membrane electrodes and respectively from 10^{-2} to $10^{-6}M$ for the ClO_4^--selective membrane electrode. The emf of the cells of type (I) are given by:

$$E_{(A)} = E'_{o(A)} - 0.055 \log[BF_4^-] \quad \text{for electrode A} \qquad (1)$$

$$E_{(B)} = E'_{o(B)} - 0.061 \log[BF_4^-] \quad \text{for electrode B} \qquad (2)$$

$$E_{(C)} = E'_{o(C)} - 0.052 \log[ClO_4^-] \quad \text{for electrode C} \qquad (3)$$

where E_0' represents the conditional standard potentials for the electrodes A, B and C, respectively, under the conditions of use of cell (I) and 0.055, 0.061 and 0.052 represent the $dE/d[\log X^-]$, respectively. Figure 2 shows the electrode functions for the three electrodes.

The critical response characteristics for the electrodes are shown in Table 1. The calibration curves for the individual electrodes were found to be reproducible from day to day.

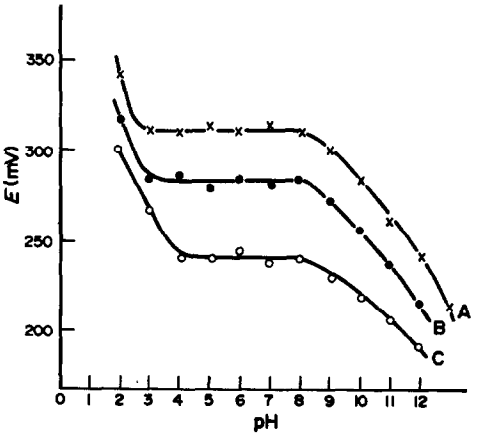

Fig. 3. The influence of pH on the response of the X^--selective membrane electrodes (A, B and C) in $10^{-3}M$ solutions.

Table 2. Selectivity coefficients for various anions with X^--selective membrane electrodes*
($X^- = A = BF_4^-$ and ClO_4^-)

Interfering species (B)	Selectivity coefficient, BF_4^--electrodes Electrode A	Electrode B	$K^{pot}_{A,B}$ ClO_4^--electrode Electrode C
Tetrafluoroborate	—	—	1.3×10^{-2}
Perchylorate	2.1	4.2	—
Acetate	$<10^{-4}$	$<10^{-4}$	$<10^{-4}$
Bromide	$<10^{-4}$	$<10^{-4}$	$<10^{-4}$
Chloride	2.3×10^{-3}	7.7×10^{-3}	1.4×10^{-3}
Citrate	$<10^{-4}$	$<10^{-4}$	$<10^{-4}$
Iodide	$<10^{-4}$	2.5×10^{-3}	2.3×10^{-3}
Nitrate	$<10^{-4}$	$<10^{-4}$	1.3×10^{-3}
Phosphate ($H_2PO_4^-$	$<10^{-4}$	$<10^{-4}$	$<10^{-4}$
Sulphate	$<10^{-4}$	$<10^{-4}$	$<10^{-4}$

*Except potassium perchlorate, all the other salts used were those containing Na^+ cation.

Influence of pH

The effect of pH on the potentials of the electrodes was examined by measuring the emf of the cell (I), in which the pH was varied by adding appropriate amounts of acetic acid/sodium hydroxide solution. At pH values between 3 and 8 no significant change in the membrane potential was observed for the BF_4^--selective membrane electrodes (A, B), while for the ClO_4^--selective membrane electrode the pH range was 4–8. At pH values higher than 8.0–8.5 the potential decreased slowly because of hydroxide anion interference (Fig. 3).

Response time

The response time of the electrodes was tested over the range used, the sequence of measurements was from low concentrations to high concentrations. The PVC matrix electrodes provide a stable emf reading, and the response time is a few seconds at higher concentrations (10^{-1}–$10^{-3}M$) and about 2–3 min in diluted solutions. The liquid membrane electrode also provides a stable emf reading, but the response time is 1–2 min even in concentrated solutions, and about 5 min in low concentration solutions.

The selectivity of the electrodes

Potentiometric selectivity coefficients for all the electrodes were evaluated by the mixed solution method and calculated as previously described.[19]

The results presented in Table 2 show that the tetrafluoroborate selective membrane electrode potentials are affected by the presence of perchlorate anions. If the BF_4^--selective membrane electrodes are exposed, even for a short period of time to perchlorate solution, these will displace BF_4^- ions from the ion-pair complex and become selective to ClO_4^-.

The data presented show good selectivity of the X-selective membrane ($X^- = BF_4^-$, ClO_4^-) over a number of potentially interfering ionic species.

Analytical applications

The electrodes proved useful for the assay of some compounds of pharmaceutical interest. The BF_4^--selective membrane electrodes were used for the potentiometric titration of some pharmacologically active compounds, such as 2,4,6-trimethylpyrylium tetrafluoroborate, colidinium tetrafluoroborate, 2,4,6-trimethylpyrydinium-*N*-(2-acetoxiethyl)perchlorate and

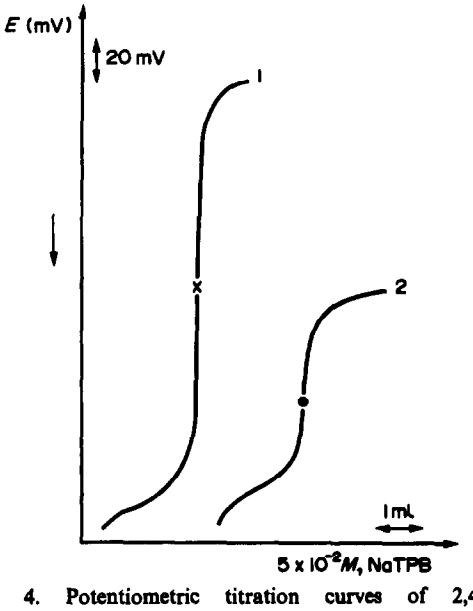

Fig. 4. Potentiometric titration curves of 2,4,6-trimethylpyrylium tetrafluoroborate using BF_4^--selective electrodes. 1—liquid membrane electrode (Electrode A); 2—PVC membrane electrode (Electrode B).

Table 3. Potentiometric determination of some pharmaceutical compounds used X^--selective membrane electrodes ($X^- = BF_4^-$ and ClO_4^-)

Pharmaceutical compound	Formula	Found (%) (standard deviation for Liquid-membrane electrode	Found (%) (standard deviation for PVC matrix membrane electrode
Potassium perchlorate	Drug-substance	—	98.4 (SD = 1.4; $n = 5$
	Tablets 0.05 g $KClO_4$	—	99.6 (SD = 1.3; $n = 5$
2,4,6-Trimethylpyrylium tetrafluoroborate	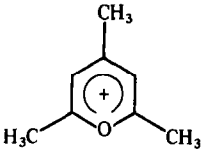	100.4 (SD = 1.1; $n = 5$)	100.8 (SD − 2.0; $n = 5$)
Colidinium tetrafluoroborate	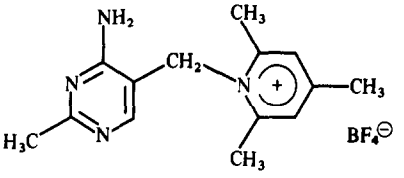	103.1 (SD = 3.8; $n = 5$)	98.5 (SD = 1.0; $n = 3$)
2,4,6-Trimethylpyrydinium N(2-acetoxiethyl) perchlorate	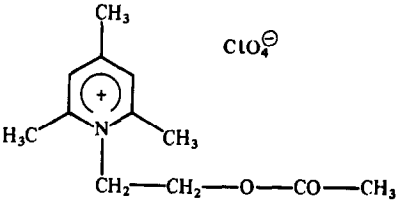	98.6 (SD = 2.3; $n = 5$)	98.1 (SD = 1.9; $n = 3$)
2,4,6-Trimethypyrydinium N(stearylamino) tetrafluoroborate	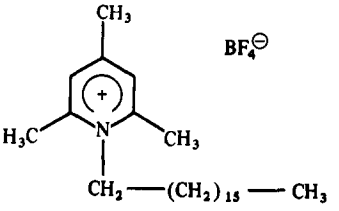	97.6 (SD = 2.5; $n = 3$)	98.4 (SD = 1.5; $n = 3$)

2,4,6-trimethylpyrydinium-*N*(stearylamino) tetrafluoroborate, respectively, using NaTPB as titrant. The reaction is based on the property of tetraphenylborate ion to form more insoluble products with the above mentioned organic cations, the potential jumps around the equivalence point are high enough for accurate evaluation of the equivalence volumes. Two potentiometric titration curves for the quantitative determination of 2,4,6-trimethylpyrylium tetrafluoroborate are presented in Fig. 4 (curve 2 is displaced for clarity).

The ClO_4^--selective membrane electrode was used for the quantitative determination of potassium perchlorate both as raw material for drug formulations and tablets.

The Table 3 presents the results obtained by using X^--selective membrane electrodes for the analytical determination of the mentioned products of pharmaceutical interest.

CONCLUSIONS

The X^--selective membrane electrodes prepared and characterized present a linear response in the range 10^{-2}–$10^{-5}M$ with a near-Nernstian response slope and good reproducibility. They can be applied with good results for the potentiometric determination of some pharmaceutical compounds and formulations.

REFERENCES

1. V. V. Coşofreţ, *Ion-Sel. Electrode Rev.*, 1980, **2**, 159.
2. *Idem*, *Membrane Electrodes in Drug-Substances Analysis*, Pergamon Press, Oxford, 1982.
3. T. C. Pinkerton and B. L. Lawson, *Clin. Chem.*, 1982, **28**, 1946.
4. E. Pungor, Z. Fehér, G. Nagy and K. Tóth, *Anal. Proc.*, 1982, **19**, 79.
5. V. V. Coşofreţ and R. P. Buck, *Ion-Sel. Electrode Rev.*, 1984, **6**, 59.
6. Zhang Zong-Rang and V. V. Coşofreţ, *Sel. Electrode Rev.*, 1990, **12**, 35.
7. L. Campagnella and M. Tomassetti, *ibid.*, 1989, **11**, 69.
8. C. R. Martin and H. Freiser, *Anal. Chem.*, 1980, **52**, 1772.
9. E. Hopârtean and E. Ştefaniga, *Rev. Roum. Chim.*, 1977, **22**, 653.
10. Kazuo Miiro, Kawahara Akinori and Tanaka Takashi, *Anal. Chim. Acta*, 1979, **110**, 321.
11. T. Ya. Bart, M. Meterova and V. Izmailova, *Kuban Gos. Univ.*, 1977, **232**, 58.
12. A. Dinculescu and A. T. Balaban, *Rev. Roum. Chim.*, 1980, **25**, 1505.
13. *Idem*, *Org. Prep. Proced. Int.*, 1982, **14**, 39.
14. V. V. Coşofreţ, *Rev. Roum. Chim.*, 1978, **23**, 1489.
15. V. V. Coşofreţ, G. E. Baiulescu and C. Cristescu, *Rev. Chim.*, 1975, **26**, 429.
16. G. J. Moody and J. D. R. Thomas, in H. Freiser (ed.) *Ion-Selective Electrodes in Analytical Chemistry*, p. 287. Plenum Press, 1978.
17. G. J. Moody, J. D. R. Thomas and R. B. Oke, *Analyst*, 1970, **95**, 910.
18. V. V. Coşofreţ and R. P. Buck, *J. Pharm. & Biomed. Anal.*, 1986, **1**, 4.
19. *Idem*, *Anal. Chim. Acta*, 1984, **162**, 357.

Talanta, Vol. 39, No. 8, pp. 1007–1011, 1992
Printed in Great Britain

0039-9140/92 $5.00 + 0.00
Pergamon Press Ltd

DETERMINATION OF SULFIDE WITH CHLORANILIC ACID BY BIAMPEROMETRIC AND AUTOMATIC POTENTIOMETRIC END-POINT DETECTION WITH A LEAD CHLORANILATE SELECTIVE ELECTRODE

J. RABA, M. A. MALLEA, S. QUINTAR and V. A. CORTINEZ
Department of Analytical Chemistry, Faculty of Chemistry, Biochemistry and Pharmacy, National University of San Luis, San Luis 5700, Argentina

(*Received* 30 *March* 1990. *Revised* 9 *December* 1991. *Accepted* 18 *December* 1991)

Summary—A titrimetric method for determination of sulfide and of sulphur in steels with chloranilic acid by biamperometric and automatic potentiometric end-point detection is described. The construction of the sensor for potentiometric indication is also described. The results obtained agree with those of the iodine–thiosulfate method and with the certified values for the steels.

Determination of sulfide in various natural and manufactured materials is important. As the critical quantities of sulfide are generally small (trace level), sufficiently sensitive methods must be used. Classical titrimetry uses iodine or potassium hexacyanoferrate(III) as the titrant.[1] The Methylene Blue method[2] is most often used for spectrophotometric determination.

The instrumental techniques for rapid determination of sulfur in steels and alloys involve oxidation to sulfur dioxide in a current of oxygen and determination of this product by gas chromatography, spectrophotometry, coulometry or conductimetry.[3]

Sulfide has also been determined by an automatic potentiometric procedure[4] and in MnS and FeS inclusions in steels by absorbing in alkali the hydrogen sulfide evolved on acidification, followed by voltammetric analysis of the solution.[5]

Recently, potentiometric titration, with ion-selective indicator electrodes, has been used for sulfur determination in air and steel samples[6] and in sulfur, polysulfide and thiosulfate mixtures.[7]

Chloranilic acid (2,5-dichloro-3,6-dihydroxy-*p*-benzoquinone) forms sparingly soluble complexes with metal ions such as Pb(II), Bi(III), Hg(II) and Hg(I), and has been used in precipitation titrations with biamperometric indication for the determination of these ions and for phosphate determination.[8–12]

This paper describes an indirect method for determining sulfide in sulfide solutions and sulfur in steels. It is based on the classical evolution procedure,[13] with absorption of hydrogen sulfide in excess of standard hydroxoplumbate(II) solution, the surplus Pb(II) being determined by titration with chloranilic acid. Biamperometric and automatic potentiometric indication is used for end-point detection, the first giving high accuracy, and the second considerably shortening the determination time. The detector is a solid-state ion-selective electrode, constructed by impregnating graphite with lead chloranilate by a procedure similar to that described by Hassan and Habib.[14]

EXPERIMENTAL

Apparatus

Biamperometric measurements were made by use of a conventional polarization source, with a digital voltmeter and microammeter. A potential difference of 1.00 V was applied across the electrodes. A twin Metrohm (60308000) electrode was used as current sensor. The titrant was added from a 10-ml Metrohm E 485 buret. The sample solution was stirred with a Metrohm G 1514-220 magnetic stirrer.

The potentiometric measurements were made with an Orion ionalyzer Model 701 and Orion Automatic Titrator (Automatic System 960), by using the graphite–lead chloranilate electrode in conjunction with a double-junction reference electrode (Orion 90-02). When the Orion Ionalyzer was used, the reagent was added with a Metrohm EA485 multiburet.

In the determination of sulfur in steels, the basic equipment for the evolution method[13] was used, modified by replacing the absorption flask with a long glass tube (400 mm × 7 mm) with delivery tube penetrating far enough into the absorption solution to avoid loss of hydrogen sulfide (Fig. 1).

Reagents

All reagents used were of analytical grade. Doubly distilled water was used throughout.

No differences in behavior were found between commercially available chloranilic acid and a product purified by recrystallization or sublimation.[15,16]

Chloranilic acid solutions in distilled water were standardized by amperometric titration with standard lead(II) solution.[17] The stock solution was stored in a darkened container at 1–5°. Periodic checks showed that the solutions could be preserved in this way for a long period of time.

Lead chloranilate was prepared by modification of a method for the preparation of barium chloranilate,[18] 1000 ml of 0.1*M* lead nitrate were placed in a 2000-ml beaker and 0.01*M* chloranilic acid was added from a separating funnel at a rate of 40–60 drops/min, with continual magnetic stirring. The precipitate was left in contact with the supernatant liquid overnight, then centrifuged and washed with water until the purple-red color of the chloranilic acid had disappeared. The product was dried in a vacuum oven at 120° for 12 hr.

Preparation of the lead chloranilate electrode

Two spectrographic graphite rods (30 mm × 50 mm) were treated as follows: (*a*) a suspension of lead chloranilate in glacial acetic acid was drawn into one of the rods by suction (Electrode I). (*b*) 0.01*M* lead nitrate solution was first drawn into the other rod by suction, followed by 0.01*M* chloranilic acid to form a precipitate inside the pores and channels of the graphite. Both rods were then dried in a vacuum oven at 120° overnight.

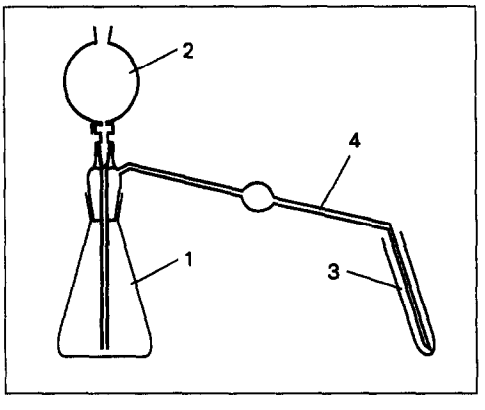

Fig. 1. Apparatus for determination of sulfur by a modification of the evolution method. (1) 250-ml Erlenmeyer flask; (2) 100-ml separatory funnel; (3) 50-ml collector tube; (4) delivery tube.

The rods were inserted into glass tubes, with 20 mm of the rod exposed to constitute the active surface. The ends of the rods within the tubes were connected to a copper wire (1 mm o.d.) for external contact. The surface between the glass and the graphite was insulated with a waterproof material (SILOC®).

Procedures

Determination of sulfide. Fifty milliliters of ~0.001*M* sodium sulfide solution were added to a mixture of 10 ml of 0.01*M* lead nitrate treated with enough 2*M* sodium hydroxide to turn all the Pb(II) into hydroxoplumbate(II) (pH 13), and the mixture was stirred magnetically for 15 min. The precipitate was filtered off on a medium texture paper, and washed 3 or 4 times with small quantities of 0.3*M* sodium hydroxide. The filtrate and washings were evaporated to ~30 ml, cooled, adjusted to 0.1*M* acidity with 4*M* nitric acid, and titrated with 0.01*M* chloranilic acid.

Since aqueous sulfide solutions are unstable, all the samples were treated with the hydroxoplumbate(II) solution at the same time.

Sulfur in steels. A sample (between 1 and 2.5 g in weight, depending on the sulfur content) was placed in the Erlenmeyer flask and 100 ml of 6*M* hydrochloric acid (3*M* acid for the higher sample weights) were added from a separating funnel. The absorption tube was loaded with 5–10 ml (depending on the amount of sulfur) of 0.01*M* lead nitrate, distilled water, and enough 2*M* sodium hydroxide to give pH 13 (total volume ~30 ml).

The Erlenmeyer flask was heated gently and the hydrogen sulfide evolved was absorbed in the hydroxoplumbate(II) solution. When dissolution of the steel was complete, the delivery tube was disconnected and rinsed with 2 or 3 small volumes of 0.3*M* sodium hydroxide. The sulphide was then titrated as described above.

RESULTS AND DISCUSSION

Lead chloranilate electrodes

Potential drift and response time. It was observed that in manual titrations the electrode

attained a stable potential in 5–10 min. Reagents were added every 30 sec throughout the titration, except near the end-point, where additions were made every 2 min since stable potential values were attained in this time. The total time for each titration was 20 min. The behavior of the electrode in a standard titration is shown in Fig. 2. Both electrodes tested gave a large potential break at the end-point, but electrode I gave the larger and therefore was used for further tests.

Effect of acidity. The optimum acidity range was 0.01*M* nitric acid, in agreement with that observed in titrations with biamperometric indication.[8] At acid concentrations higher than 0.1*M* the solubility of lead chloranilate increases considerably, but when the acid concentration is lower than 0.01*M* the electrochemical reaction of chloranilate is inhibited by the poor buffer capacity at the electrode–solution interface.[19] The sensitivity of the electrode to changes in acid concentration is shown in Fig. 3.

Range of determinable concentrations. The sensor gave a good response in the range from $3 \times 10^{-3}M$ to $1 \times 10^{-4}M$ lead (II). For concentrations lower than $1 \times 10^{-4}M$ the end-point potential break is much reduced, and the solubility of chloranilic acid becomes the limiting factor for determining lead concentrations higher than $3 \times 10^{-3}M$.

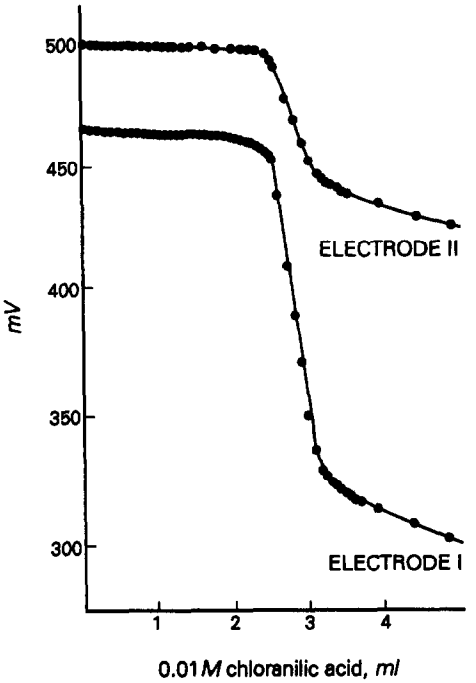

Fig. 2. Response of electrodes I and II in the titration of 25 ml of ~0.0010*M* lead(II) with chloranilic acid at pH = 1.0.

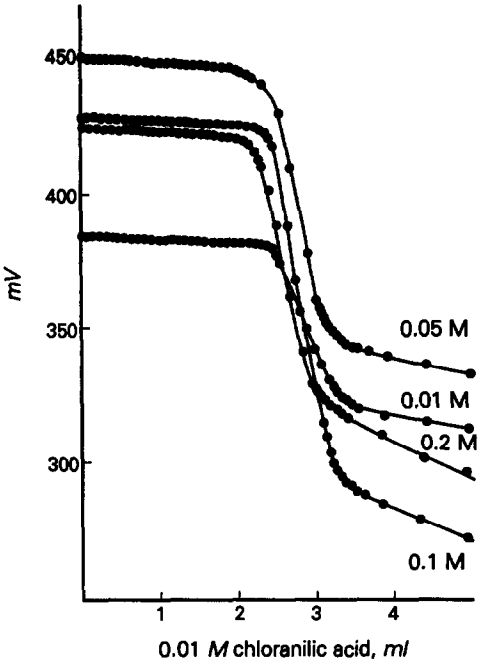

Fig. 3. Titrations of 25 ml of ~0.0010*M* lead(II) with chloranilic acid at various nitric acid concentrations, with use of electrode I.

Accuracy and precision. Twelve titrations of ~0.001*M* lead nitrate in 0.1*M* nitric acid with 0.01*M* chloranilic acid gave a mean of 0.207 g/l. lead, with a standard deviation of 0.0007 g/l. The relative error was estimated by comparison of the values obtained by potentiometric indication with those corresponding to the average of three titrations performed with biamperometric indication, and was about 2%.

The behavior of the sensor in automatic titrations was checked with nine repetitive analyses of another lead nitrate solution; the mean found was 0.223 g/l.lead, standard deviation 0.008 g/l. Titration with biamperometric indication gave 0.219 g/l. (mean of three titrations).

Analysis of sulfide solutions. Table 1 shows the results of six replicate biamperometric and automatic potentiometric titrations of 25 ml of nominally 0.030 g/l. sodium sulfide solution with 0.01*M* chloranilic acid and of titrations by the iodine–thiosulfate method recommended by Budd and Bewick[2] for standardization of sodium sulfide solutions in the Methylene Blue method.

The displacement reaction between mercury chloranilate and sulfide, used by Hoffmann for absorptiometric sulfide determination,[20] were found not to be suitable for titrations.

The pH of the Pb(II) solution was chosen as ~13 because at a pH lower than 7 sulfide was

Table 1. Comparison of results obtained in the analysis of 25 ml of 0.030 g/l. sulfide solution by different methods ($n = 6$)

	Iodine–thiosulfate method	Biamperometric method	Potentiometric method
Mean, *g/l.*	0.0296	0.0297	0.0298
St. devn., *g/l.*	0.0009	0.0015	0.0010

Table 2. Comparison of results obtained in the determination of sulphur in three certified steels samples by the biamperometric and potentiometric methods ($n = 6$)

	IPT 14A	IPT 43	IPT 37
Sample weight, *g*	2.000	1.000	2.500
Certified S value, %	0.036	0.112	0.082
S found ± std. devn., %			
Biamperometric method	0.0357 ± 0.0016	0.112 ± 0.007	0.0813 ± 0.0020
Potentiometric method	0.0356 ± 0.0016	0.111 ± 0.00	0.0817 ± 0.0012

only partially retained, and between pH 7 and 12.5 lead hydroxide is precipitated.

Steel analyses

Three certified samples from the "Instituto de Pesquisas Tecnologicas" (IPT), San Pablo, Brazil: IPT No. 43 (AISI 1132), IPT No. 14A (AISI 1040) and IPT No. 37 grey iron were analyzed for sulfur content. The results are shown in Table 2.

It was verified that the optimum weight of sample for steels containing about 0.1% of sulfur was about 1 g. With higher weights of sample (*e.g.*, 2.5 g), the evolution of hydrogen sulfide was very fast, causing considerable losses. Also, prolonged heating was necessary to complete the dissolution, and some hydrochloric acid distilled into the absorption tube. Lower weights of sample allowed more dilute acid (3*M*) to be used, which considerably reduced this risk.

When the sulfur content is lower, as in the IPT standards 14A and 37, it is more convenient to use higher weights of sample (2–2.5 g) in order to decrease the amount of lead chloranilate precipitate, which disturbs the end-point location by either detection mode.

The procedure proposed shows several advantages over the classical evolution method. (*a*) It is more exact and precise since it diminishes the risk of hydrochloric acid distilling into the absorption solution (because it requires a lower weight of sample, which also reduces the dissolution time). (*b*) The electrochemical behavior of chloranilic acid at $E = 1.00$ V allows amperometric curves to be obtained with a great number of points in both branches (Fig. 4). This means that the determination of the end-point can be made more accurate by applying the least-squares method. (*c*) When automatic potentiometric titration is used, the time required for the determination is mainly that consumed in the dissolution of the sample and conditioning of the solution for the titration. (*d*) The potentiometric sensor developed is strong, very low in cost, easily manufactured, long-lasting and very easily reactivated. Its optimum acidity range allows it to be used in solutions where the use of other sensors, such as the Orion 94-82-00 lead electrode,[21] is impossible.

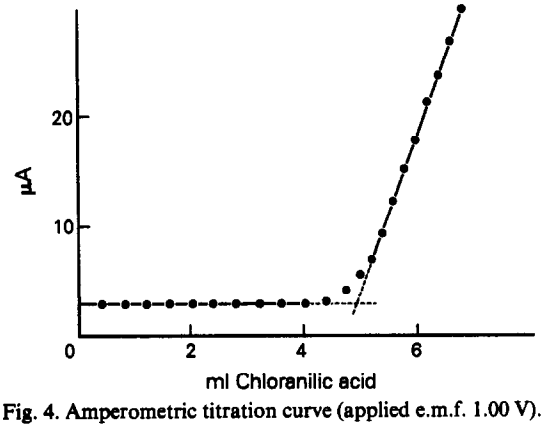

Fig. 4. Amperometric titration curve (applied e.m.f. 1.00 V).

Acknowledgements—The authors wish to thank the Consejo Nacional de Investigaciones Cientificas y Técnicas (CONICET) for financial support of this research, and Lic. Maria Estela López for linguistic advice.

REFERENCES

1. L. A. Haddock, in C. L. Wilson and D. W. Wilson (eds.), *Comprehensive Analytical Chemistry*, Vol. Ic, p. 282. Elsevier, Amsterdam. 1962.
2. M. Budd and H. A. Bewick, *Anal. Chem.*, 1952, **24**, 158.
3. B. Nebesar, *J. Chem. Educ.*, 1971, **48**, A751.
4. B. A. Furmanov, L. N. Strebkova and O. L. Cherkasskaya, *Bum. Prom-st.*, 1985, No.1, 18; *Chem. Abstr.*, 1985, **102**, 115385w.

5. I. Zezula, *Hutn. Listy*, 1985, **40**, 197; *Chem. Abstr.*, 1985, **102**, 170476b.
6. A. C. Calokerinos, M. Timotheou-Potamia, E. Sarantonis and T. P. Hadjiioannou, *Anal. Chim. Acta*, 1983, **151**, 85.
7. T. D. Gornostaeva, V. A. Pronin and V. Ya. Semenov, *Zavodsk Lab.*, 1983, **49**, No.7, 14; *Chem. Abstr.*, 1983, **99**, 132949v.
8. V. A. Cortinez and C. B. Marone, *Quim. Anal.*, 1976, **30**, 33; *Chem. Abstr.*, 1977, **86**, 164752y.
9. V. A. Cortinez, O. Baudino and C. B. Marone, *Afinidad*, 1979, **36**, 495; *Chem. Abstr.*, 1980, **93**, 60421t.
10. O. M. Baudino, V. A. Cortinez and C. B. Marone, *Rev. Asoc. Bioquim. Argent.*, 1976, **41**, 212; *Chem. Abstr.*, 1978, **88**, 197744s.
11. M. A. Mallea, H. Marini, V. A. Cortinez and C. B. Marone, *Cron. Chim.*, 1981, **66**, 14.
12. M. A. Mallea, S. Quintar de Guzman and V. A. Cortinez, *Talanta*, 1989, **36**, 792.
13. F. Welcher (ed.), *Standard Methods of Chemical Analysis*, 6th Ed., Vol. IIA, p. 677. Van Nostrand, Princeton, 1963.
14. S. S. M. Hassan and M. M. Habib, *Anal. Chem.*, 1981, **53**, 508.
15. B. J. Thamer and A. F. Voight, *J. Phys. Chem.*, 1952, **56**, 225.
16. D. K. Cabbiness, E. S. Amis and K. C. Jackson, *J. Chem. Eng. Data*, 1967, **12**, 90.
17. H. A. Flaschka, *Titrations*, 2nd Ed., p. 80. Pergamon Press, Oxford, 1964.
18. R. J. Bertolacini and J. E. Barney II, *Anal. Chem.*, 1957, **29**, 281.
19. O. H. Müller, *Polarography*, in A. Weissberger (ed.), *Physical Methods of Organic Chemistry*, 4th Ed., Vol. I, Part. IV, P. 3155. Interscience, New York, 1060.
20. E. Hoffmann, *Z. Anal. Chem.*, 1962, **185**, 372.
21. Orion Research, *Analytical Method Guide*, 1978.

Talanta, Vol. 39, No. 8, pp. 1013–1018, 1992
Printed in Great Britain.

0039-9140/92 $5.00 + 0.00

ION-EXCHANGER PHASE PHOTOACOUSTIC SPECTROMETRY FOR TRACE ANALYSIS OF METAL IONS

SUNAO YAMADA and KAZUHISA YOSHIMURA

Chemistry Laboratory, College of General Education, Kyushu University, Ropponmatsu, Chuo-ku, Fukuoka 810, Japan

(*Received* 1 *July* 1991. *Revised* 16 *December* 1991. *Accepted* 17 *December* 1991)

Summary—Laser-induced photoacoustic spectroscopy has been applied to the determination of chromate, uranyl, and Cr(VI) and Fe(II) ions as coloured complexes that were sorbed on ion-exchanger beads. A simple photoacoustic cell has been constructed; it consisted of a fused silica glass tube and an attached cylindrical piezoelectric transducer. A pulsed laser light at 532 or 355 nm irradiated the ion-exchanger beads that had been collected in the glass tube of the cell. Since a sample material was effectively concentrated on the ion exchanger, the sensitivity was much higher than that in the corresponding photoacoustic spectrometry in a solution state. The lowest detection limit was 0.21 ng/ml Fe for Fe(II)–DPPS (4,7-diphenyl-1,10-phenanthrolinedisulphonate) complex sorbed on QAE-Sephadex gel. Analytical characteristics of the present method are described.

Although photoacoustic spectroscopy (PAS) is a well characterized quantitative spectroscopic technique for homogeneous samples, its real utility must appear in applications to heterogeneous samples such as opaque solids and powders. The use of lasers as excitation light sources has greatly improved the sensitivity[1] and expanded the applicability such as for the study of a single microparticle,[2,3] because of their high photon flux, monochromaticity, and excellent spatial and temporal coherence.

Ion-exchanger phase absorptiometry[4] is very sensitive and practical for the determination of trace amounts of various kinds of inorganic analytes;[5,6] this technique is based on the direct measurement of light absorption by metal complexes pre-concentrated on an ion exchanger. Since PAS is based on light absorption, it must be possible to detect such metal complexes sorbed on an ion exchanger. In fact, PAS has been recently applied to the determination of some metal ions complexed on modified silica gel[7] and phosphate as molybdenum blue adsorbed on anion-exchanger beads,[8] but the sensitivities were at most μg/ml levels and analytical procedures seemed to be somewhat complicated and time-consuming.

From these viewpoints, we have first applied laser-induced PAS (LIPAS) for the determination of some metal ion species sorbed on ion exchangers. A simple photoacoustic cell with a fused silica glass tube and an attached cylindrical piezoelectric transducer was constructed, and a pulsed laser light was used. Basic characteristics of the present system and its analytical applications are presented.

EXPERIMENTAL

Apparatus

The block diagram of the experimental apparatus is shown in Fig. 1. A Nd:YAG laser (Continuum YG660B-10S; pulse duration, 4–6 nsec; repetition rate, 5 Hz) was used as an excitation light source; a 532-nm (second harmonic) or 355-nm (third harmonic) laser light passed through an aperture (4 mm in diameter) and irradiated the cell. Pulse-to-pulse intensity fluctuations of the 532-nm and the 355-nm light are nominally 3.5 and 4%, respectively. The laser pulse energy was varied with the use of appropriate neutral density filters (Sigma Koki MANY-25-5—50) and glass filters. It was monitored and measured with a photodiode (Hamamatsu S1722 or S1336) and an oscilloscope (Iwatsu SS-6122); the photodiode output was calibrated with a calorimeter (Photon Control Model 25V-Vis). The resultant pulsed photoacoustic signal was amplified with an amplifier (NF P61, 100 kHz, gain 100) and then averaged over 16 laser pulses with a digital storage oscilloscope (Iwatsu DS-6411).

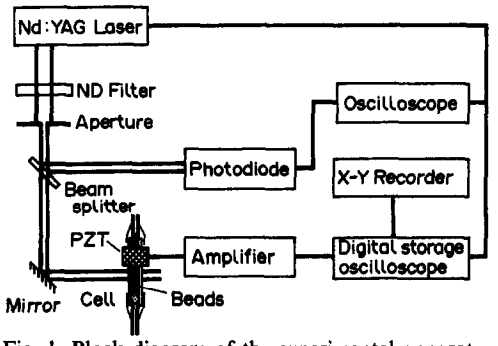

Fig. 1. Block diagram of the experimental apparatus.

Its output was recorded with an X–Y recorder (Graphtec WX1100).

Photoacoustic cell

Figure 2(a) shows the photoacoustic cell compartment. The pulsed photoacoustic signal was detected with a cylindrical piezoelectric transducer (PZT) (Tokin NPM, NR; 7 mm o.d., 5 mm i.d., 7 mm in length); it was attached to a fused silica glass tube (4 mm o.d., 1.5 mm i.d., 38 mm in length) via a brass cylinder. A silver paste (Dojindo) was used to fix the brass cylinder with the glass tube and to electrically grind the inside of the PZT through the brass cylinder and an aluminium body which provided electrical shielding. The outside terminal of the PZT detected the signal. A washer was used to fit the PZT tightly in the aluminium body. A poly(tetrafluoroethylene) (PTFE) sheet (0.1 mm in thickness) was inserted between the bottom of the PZT and the washer for electrical insulation [Fig. 2(a)]. A PTFE tube (2 mm o.d., 1 mm i.d.) was connected in each end of the glass tube with a thermally shrinkable PTFE tube. A polypropylene filter tip (1.5 mm in diameter, 3 mm in length) was placed at the bottom of the glass tube. The glass tube and PTFE tubes were also fixed inside the aluminium body with an epoxy adhesive. Then, the cell was attached on a micrometer-driven translation stage in order to adjust the distance between the laser beam and the PZT.

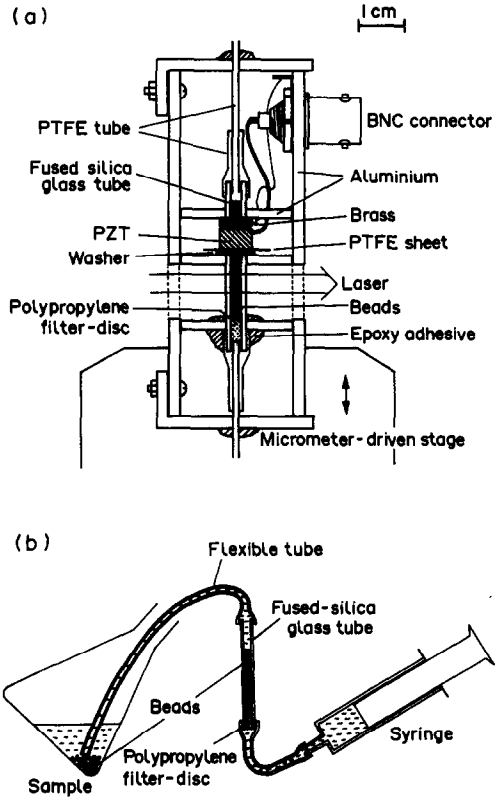

Fig. 2. Schematic diagram of the photoacoustic cell (a) and sample introduction (b): PZT, piezoelectric transducer.

Chemicals

All chemicals used were of analytical grade. Water, purified with a Milli-Q SP reagent water system (Millipore), was used for the dilution of samples and reagents.

Ion exchangers of analytical grade were purchased from Bio-Rad, and crosslinked dextran-type ion exchangers from Pharmacia.

Sample preparation

For chromate (CrO_4^{2-}), to a 20-ml solution containing 0.4–40 μg of chromium (as chromate) was added 0.104 ml of QAE-Sephadex A-25 gel (in the chloride form).

For the chromium(VI)–1,5-diphenylcarbazide [Cr(VI)–DPC] system, to a 20-ml solution containing 0.04–2 μg of chromium (as chromate) were added 1 ml of 0.5*M* sulphuric acid, 1 ml of 0.01% (w/v) acetone solution of DPC (Kishida Chemicals), and then 0.104 ml of AG 50W-X2 (100–200 mesh) in the hydrogen form.

For the iron(II)–1,10-phenanthroline [Fe(II)-PHEN] complex, to a 20- ml solution containing 0.1—5 μg of iron were added 2 ml of a solution containing hydroxylammonium chloride [2.5% (w/v)], acetate (0.2*M*, pH 4.8) and PHEN [0.1% (w/v), Wako Pure Chemicals], and then 0.104 ml of AG 50W-X2 or SP-Sephadex C-25 (40-120 μm, in the hydrogen form).

For iron(II)–4,7-diphenyl-1,10-phenanthroline–disulphonate [Fe(II)-DPPS] complex, to a 20-ml solution containing 0.05–5 μg of iron were added 2 ml of a solution containing hydroxylammonium chloride [2.5% (w/v)], acetate (0.2 *M*, pH 4.8) and DPPS [0.1% (w/v), Dojindo], and then 0.104 ml of AG 1-X2

(100–200 mesh, in the chloride form) or QAE-Sephadex A-25.

For uranyl (UO_2^{2+}), to a 20-ml solution containing 10–200 μg of uranium (as uranyl chloride) was added 0.104 ml of SP-Sephadex C-25.

Procedure for signal measurements

The mixture of a sample solution and an ion exchanger was stirred for 20 min in a flask. In order to evaluate the amount (height) of the collected beads in the glass tube of the cell, we have prepared another fused-silica glass tube (1.5 mm i.d., 60 mm in length); its one end had a polypropylene filter tip, and a disposable syringe was connected to this end via a flexible tube, while the other end had a flexible tube to collect the beads. The beads were once collected in this glass tube using the syringe, and the height of the collected beads was measured. Then, the beads were transferred into the glass tube of the cell by connecting the flexible tube with the PTFE tube of the cell [Fig. 2(b)]. The cell was filled with water in all measurements.

In the presence of air bubbles in the cell, both intensity and waveform of the signal varied drastically and irregularly, probably because of complicated travel routes of sound; in other words, the presence or absence of air bubbles could be confirmed from signal waveform. In the absence of air bubbles, the signal was stable and reproducible.

For analytical studies, the height of the collected beads was 20 mm, and the distance (L) between the center of the laser beam and that of the PZT was maintained constant at 10.5 mm. One of the largest peak-to-peak heights (Δh) of positive and negative excursions that were observed in the $\sim$19–$\sim$23 μsec region of the photoacoustic signal waveform was used for calibration (*vide infra*).

RESULTS AND DISCUSSION

Characterization of the cell

Shida *et al.*[8] applied PAS to the determination of phosphate as molybdenum blue species sorbed on an anion exchanger. They measured the photoacoustic signal of 10 mg of beads that were placed in a PAS cell for each sample. However, there seems to be considerable room to improve more conveniently and sensitively for practical use of ion-exchanger phase spectrometry with photoacoustic detection.

In ion-exchanger phase absorptiometry, the volume ratio, V/v, defined as the ratio of the volume of the sample solution (V) to that of the ion exchanger (v), profoundly affects the detection sensitivity, since the sample is effectively concentrated on ion-exchanger beads;[4,5] the larger the volume ratio, the higher the sensitivity. Therefore, the cell volume should be as small as possible. In addition, it is desirable that the ion-exchanger beads can be collected easily in the cell and removed easily from it. From these viewpoints, we have designed the cell as shown in Fig. 2(a).

In order to investigate the characteristics of the photoacoustic cell, Fe(II)–DPPS complex sorbed on QAE-Sephadex gel was used as a test sample. The pulsed photoacoustic signal is obtained at various distances of the laser beam from the PZT along the glass tube, as shown in Fig. 3; the beads were collected for about 20 mm in height (*vide infra*). Similar photoacoustic cells consisting of glass tubes and PZTs have been

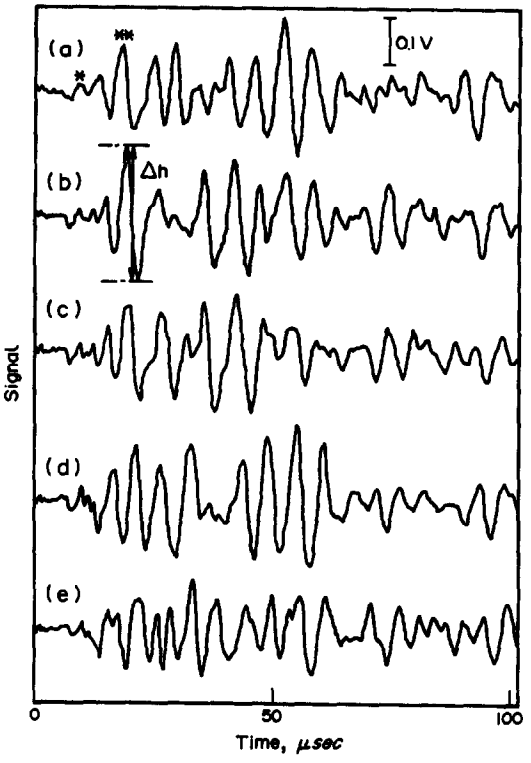

Fig. 3. Typical waveforms of the photoacoustic signals for Fe(II)–DPPS complex, when the height of the beads was about 20 mm. Distance L between the center of the laser beam and that of the PZT: (a) 8.5; (b) 10.5; (c) 11.5; (d) 13.5; (e) 15.5 mm (see Fig. 4). Sample solution: 20 ml, 0.2 μg/ml Fe; ion exchanger: QAE-Sephadex A-25, 0.104 ml. The first and the third positive excursions are marked by * and ** in the waveform (a). The peak-to-peak height of the large excursion shown by Δh in the waveform (b) was used for evaluating the signal intensity. The laser pulse energy at 532 nm is 5.5 mJ.

reported.[9-11] Rowlen *et al.*[11] carefully investigated and analysed the waveform of the photoacoustic signal, with the cell consisting of a fused silica glass tube (6 mm o.d., 1 mm i.d., 19.3 or 26.7 cm in length) and a cylindrical PZT attached on it; the signal was very complicated due to electrical and mechanical ringing, damping, acoustic reflections in the cell, and so on. This must also be the case in this study. However, detailed assignments of the signal waveform is not the aim in this study.

Although the signal waveform was affected by the distance L, the amplitude of the largest excursions did not differ substantially (Figs. 3 and 4). The first weak positive excursion [marked by * in the waveform (a)] was observed even in the absence of the beads and its delay time from the laser flash did not change; it was not observed when the laser did not irradiate the cell. Thus, it may arise from some mechanical vibration of the cell due to laser irradiation. On the other hand, the delay time of the third positive excursion [marked by ** in the waveform (a)] clearly changed with L; the relationship between L and the delay time was linear with a slope of 1.45×10^3 m/sec. The corresponding value for Fe(II)–DPPS complex in 95% ethanol solution was 1.11×10^3 m/sec; it agreed well with the literature value of 1.24×10^3 m/sec for the velocity of sound in ethanol at 18°.[12] The velocity of sound in distilled water at 18° is 1.52×10^3 m/sec.[12] These facts strongly suggest that the third positive excursion is due to the sound which is produced from the sample and arrives at the PZT via transport through the solvent, water.

A set (positive and negative) of large excursions was observed around 20 μsec after the laser flash when the distance L was about 10 mm, as was seen in Fig. 3(b) (L = 10.5 mm). The peak-to-peak height, Δh shown in Fig. 3(b), was used for evaluating the intensity of the photoacoustic signal.

Figure 4 shows the relationship between the packed amount (height) of the beads in the tube of the cell and the signal intensity Δh. The signal waveform was insensitive but the signal intensity was sensitive to the packed amount of beads. The Δh value was large when the height of the beads lay between the laser irradiation position and the PZT; it became ~20% smaller when the beads were collected over the position of the PZT, but it was roughly constant even when the beads were collected further. For practical convenience, therefore, all analytical measurements were carried out with the height of the collected beads at about 20 mm, slightly above the position of the PZT.

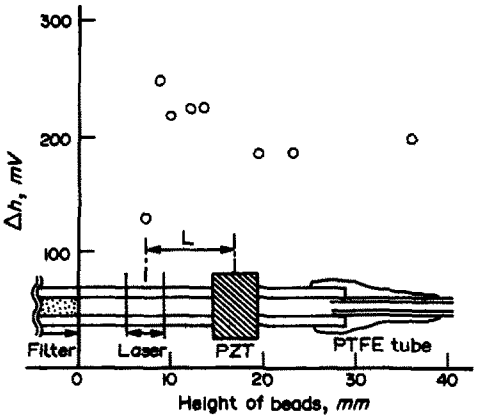

Fig. 4. Effect of the packed amount (height) of beads in the glass tube of the cell on Δh for Fe(II)–PHEN complex. Sample solution: 25 ml, 0.2 μg/ml Fe; ion exchanger: QAE-Sephadex A-25, 0.104 ml. L: 10 mm. The laser pulse energy at 532 nm is 2.5 mJ, and other conditions are identical to those of Fig. 3. The abscissa shows the height of the beads collected in the tube from the top of the filter. Positions of the laser beam and the PZT are shown schematically, and the distance L is also shown.

Sensitivity and detection limit

For low light absorption conditions where the absorbed power is small, the intensity of photoacoustic signal, I_{PAS}, can be approximately expressed as:[13]

$$I_{PAS} = kI_0\epsilon Cl.\beta, \quad (1)$$

where I_0 is the excitation intensity, ϵ the absorptivity of a sample, l. the light path, C the sample concentration, β a measure of the conversion efficiency of absorbed power to heat by radiationless processes, and k an instrumental proportionality constant. In the measurement of the photoacoustic signal for the ion-exchanger phase that is prepared with v ml of ion-exchanger beads and V ml of solution containing C_0 M of a sample, equation (1) can be rewritten as:

$$I_{PAS} = kI_0C_0\bar{\epsilon}\bar{l}\bar{\beta}(V/v)\{1 + V/(vD)\}^{-1}, \quad (2)$$

where D is the distribution ratio of the sample between the ion exchanger and the solution, and $\bar{\epsilon}$, $\bar{l}$. and $\bar{\beta}$ stand for the corresponding terms for the ion-exchanger phase.[14] Under the condition of $V \ll vD$, equation (2) can be simplified to:

$$I_{PAS} = kI_0C_0(V/v)\bar{\epsilon}\bar{l}.\bar{\beta}. \quad (3)$$

In this study, the signal intensity was linear to the laser pulse energy (~0.5–~5 mJ). Thus, the signal obtained under the identical condition should be proportional to C_0 and the volume ratio V/v.

For each system examined, a calibration graph was obtained by plotting the Δh value versus the concentration of the analyte, giving a straight line at least within the concentration range studied. The sensitivity, defined as the concentration giving 100 mV of Δh, and the detection limit, defined as the concentration giving the photoacoustic signal equal to three times the standard deviation of the blank signal, were summarized in Table 1.

The sensitivities of Fe(II)–PHEN and Fe(II)–DPPS for the ion-exchanger phase were compared with those for the solution state (Table 1). The D values for these species exceeded 10^4. As the sample species in 20 ml of a solution was concentrated on 0.104 ml of the ion exchanger, the volume ratio was 190. Thus, the sensitivity in the ion-exchanger phase can be expected to be 190 times greater than that in the solution state. Table 1 shows that the expected sensitivities could be obtained by using ion exchangers for both complexes.

For the Fe(II)–PHEN complex, variation of the volume of the sample solution from 10 to 200 ml resulted in a proportional increase in the signal. Thus, much higher sensitivities will be achieved by employing larger volumes of sample solution, that is, larger volume ratios.

The molar absorptivity for each sample species at the excitation wavelength is also shown in Table 1. The larger the molar absorptivity, the higher the sensitivity, as can be expected from equation (3).

The polystyrene-type ion exchanger has a larger D value than the dextran-type one; but the former has considerable absorptivity at 355 nm and causes a high background in the absorptiometry.[15] It was also the case in this study. In addition, laser irradiation at 532 nm caused some unexpected cracking in the resin beads. The dextran-type ion exchanger, on the other hand, showed no such problems at 532 nm.

In the previous ion-exchanger phase absorptiometry where $V/v = 1200$, the detection limits were 0.11 ng/ml Cr for the Cr(VI)–DPC system[16] and 0.9 ng/ml of Fe for Fe(II)–PHEN complex.[17] In the present study where the V/v value was 190, the corresponding detection limits with AG 50W-X2 ion exchanger were 0.58 and 4.7 ng/ml, respectively. Thus, the present method is as sensitive as the absorptiometry.

In the Cr(VI)–DPC system, the Cr(III)–diphenylcarbazone complex mainly forms by redox reaction and this complex is sorbed on the cation-exchanger beads. As shown in Fig. 5, the photoacoustic signal of this complex sorbed on AG 50W-X2 decreased with proceeding laser irradiation, indicating decomposition by light absorption. In the present method, however, the signal could be obtained very quickly (within 3 sec), and the signal obtained by the first run was linear with respect to the concentration of Cr(VI). Thus, the present method can also be useful for such an unstable analyte.

In this paper, we have demonstrated that LIPAS was very useful for highly sensitive

Table 1. Sensitivity and detection limit*

System	Medium	Wavelength, *nm*	Molar absorptivity, $l.mole^{-1}.cm^{-1}$	Sensitivity† *ng/ml* of metal	Detection limit,‡ *ng/ml* of metal
CrO_4^{2-}	Solution	355	4200	—	—
	QAE-Sephadex	355	—	1200§	19§
Cr(VI)–DPC	Solution	532	30 000	—	—
	AG 50W-X2	532	—	13	0.58
Fe(II)–PHEN	Solution	532	7600	9100	550
	AG 50W-X2	532	—	43	4.7
	SP-Sephadex	532	—	64	1.4
Fe(II)–DPPS	Solution	532	24 000	3700	95
	AG 1-X2	532	—	18	1.0
	QAE-Sephadex	532	—	17	0.21
UO_2^{2+}	Solution	355	3	—	—
	SP-Sephadex	355	—	8600	120

*Laser pulse energies at 355 and 532 nm were 0.5–0.7 and 5–6 mJ, respectively. Sample solution: 20 ml; ion exchanger: 0.104 ml.

†The concentration giving the intensity of $\Delta h = 100$ mV.

‡The concentration giving the intensity equal to three times the standard deviation of the background intensity.

§The calibration curve was not linear.

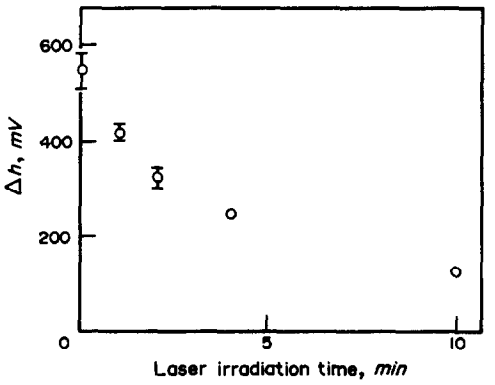

Fig. 5. Effect of laser irradiation time on the signal of the Cr(VI)–DPC system. Sample solution: 20 ml, 50 ng/ml chromium as chromate; ion exchanger: AG 50W-X2, 0.104 ml.

ion–exchanger phase spectrometry; direct measurement of the ion exchanger by LIPAS enabled detection sensitivity at ng/ml levels or lower. Application of the present system to flow analysis is quite attractive and will appears in our companion paper.[18]

REFERENCES

1. C. K. N. Patel and A. C. Tam, *Rev. Mod. Phys.*, 1981, **53**, 517.
2. A. Yoshinaga, Y. M. Hsueh, T. Sawada and Y. Gohshi, *Anal. Sci.*, 1989, **5**, 147.
3. Y. M. Hsueh, A. Harata, T. Kitamori and T. Sawada, *ibid.*, 1990, **6**, 67.
4. K. Yoshimura, H. Waki and S. Ohashi, *Talanta*, 1976, **23**, 449.
5. K. Yoshimura and H. Waki, *ibid.*, 1985, **32**, 345.
6. T. Nakashima, K. Yoshimura and H. Waki, *ibid.*, 1990, **37**, 735.
7. R. S. Field, D. E. Leyden and R. S. S. Murthy, *Anal. Chim. Acta*, 1986, **186**, 123.
8. J. Shida, K. Kasama, H. Honda and K. Oikawa, *ibid.*, 1990, **233**, 135.
9. E. P. C. Lai, S. Y. Su, E. Voigtman and J. D. Winefordner, *Chromatographia*, 1982, **15**, 645.
10. E. P. C. Lai, B. L. Chan and L. L. Chan, *Anal. Chem.*, 1983, **55**, 2441.
11. K. L. Rowlen, J. W. Birks, K. A. Duell and J. P. Avery, *ibid.*, 1988, **60**, 311.
12. *Handbook of Chemistry and Physics*, 50th Ed. The Chemical Rubber Co., Cleveland, Ohio, 1969.
13. M. J. Adams, A. A. King and G. F. Kirkbright, *Analyst*, 1976, **101**, 73.
14. H. Waki, S. Noda and M. Yamashita, *Reaction Polymers*, 1988, **7**, 227.
15. H. Waki and J. Korkisch, *Talanta*, 1983, **30**, 95.
16. K. Yoshimura and S. Ohashi, *ibid.*, 1978, **25**, 103.
17. S. Nigo, K. Yoshimura and T. Tarutani, *ibid.*, 1981, **28**, 669.
18. K. Yoshimura and S. Yamada, *ibid.*, 1992, **39**, 1019.

Talanta, Vol. 39, No. 8, pp. 1019–1024, 1992
Printed in Great Britain.

0039-9140/92 $5.00 + 0.00

APPLICATION OF ION-EXCHANGER PHASE PHOTOACOUSTIC SPECTROSCOPY TO FLOW ANALYSIS OF TRACE AMOUNTS OF IRON IN WATER

KAZUHISA YOSHIMURA and SUNAO YAMADA

Chemistry Laboratory, College of General Education, Kyushu University, Ropponmatsu, Chuo-ku, Fukuoka 810, Japan

(*Received* 1 *July* 1991. *Revised* 16 *December* 1991. *Accepted* 17 *December* 1991)

Summary—Ion-exchanger phase photoacoustic spectroscopy has been applied to the flow analysis of trace amounts of iron in water. The reaction product of iron(II) with 4,7-diphenyl-1,10-phenanthroline-disulphonate, introduced into a carrier solution stream in the flow system, was concentrated on a small amount of QAE-Sephadex gel settled in a fused silica glass tube (1.5 mm i.d.) of a photoacoustic cell. The photoacoustic signal produced by pulsed laser irradiation of the gel beads at 532 nm was detected by a cylindrical piezoelectric transducer which was attached outside the glass tube. When 3.7 ml of a sample solution was introduced into the flow system, the sensitivity of this method was 590 times higher than that of the corresponding solution photoacoustic spectrometry and the detection limit of iron was 0.33 ng/ml. Because the coloured complex was desorbed from the cell with a desorbing agent solution, the present method could afford repeated analyses of natural water samples containing iron at ng/ml levels without any preconcentration procedures.

Photoacoustic spectroscopy (PAS) is one of the most useful spectroscopic techniques for quantitative analysis in a condensed phase. Laser-induced PAS (LIPAS) has been especially sensitive and useful for the detection in a small volume, because of high photon flux and excellent spatial coherence of the laser light. Thus, LIPAS has been employed as a detection method for liquid chromatography.[1–5]

On the other hand, ion-exchanger phase absorptiometry, a method based on the direct measurement of the absorption of light by metal complexes pre-concentrated on an ion-exchanger, is sensitive and practical for the determination of inorganic analytes in water,[6,7] and has been applied to flow analysis.[8,9] In this flow analysis method, a target element is exclusively concentrated in the ion-exchanger phase as coloured complex during absorptiometric measurement. Thus, it is not affected by the sample-zone colour dispersion (the dilution effect), which is unavoidable in conventional flow injection analysis. In addition, higher sensitivity can easily be attained by using a larger amount of water sample.

PAS (LIPAS) is also effective for the study of heterogeneous and/or opaque samples. Recently, PAS has been applied to the determination of metal ions complexed on modified silica gel[10] and of phosphate as molybdenum blue sorbed on anion-exchanger beads,[11] but the sensitivities were at most μg/ml levels and analytical procedures were somewhat complicated and time-consuming. As has been shown in our companion paper,[12] we have successfully applied LIPAS to the determination of some metal ions as their coloured complexes sorbed on ion-exchanger beads; a typical detection limit was 0.58 ng/ml of chromium(VI).

In this paper, we have extended the LIPAS measurements in ion-exchanger phase to flow analysis of iron in water. 4,7-Diphenyl-1,10-phenanthrolinedisulphonate (DPPS) was used as a colour forming agent.[13]

EXPERIMENTAL

Chemicals

All chemicals used were of analytical grade. Water was purified with a Milli-Q SP reagent water system (Millipore) and was used for the dilution of samples and reagents.

The standard iron(III) solution (1000 μg/ml) was supplied from Wako Pure Chemicals.

A buffer solution (pH 5.3) was prepared by dissolving 15.4 g of ammonium acetate with water, mixing it with 12.6 ml of acetic acid, and

then diluting the mixture with water to the total volume of 100 ml.

A hydroxylamine solution was prepared by dissolving 10 g of hydroxylammonium chloride with water, adjusting pH of the solution to 4.8 with ammonia, and diluting it to 100 ml with water. These two solutions were filtered through a 0.45-μm membrane filter-paper (Millipore).

A colouring reagent solution was prepared by dissolving 0.1 g of sodium salt of DPPS, supplied by Dojindo Laboratories, and 2.3 g of ammonium acetate in a mixture of 0.63 ml of acetic acid and 10 ml of the hydroxylamine solution, and then diluting it to 100 ml with water.

A carrier solution was prepared by diluting the mixture of 10 ml of the acetate buffer and 10 ml of the hydroxylamine solution to one litre with water and dissolving 1 mg of DPPS in the solution.

A desorbing agent solution was prepared by dissolving 80 g of ammonium nitrate into 250 ml of water, filtering the solution through a 0.45-μm membrane filter paper, and mixing the solution with 250 ml of ethyl alcohol. Dissolved gases were expelled from the solution for 3 hr with an ultrasonic bath.

QAE-Sephadex A-25, crosslinked dextran-type ion-exchanger gel, was purchased from Pharmacia.

Apparatus

The experimental apparatus is almost identical to that reported in our companion paper.[12] One of intense excursions in the photoacoustic signal waveform could be simultaneously integrated with a boxcar integrator (NF BX530-A) for evaluating its intensity. It was recorded on a strip-chart recorder (RDK R-02) set at 5 V in full scale.

The photoacoustic cell used for the batch colour development method was also employed for the present method. The QAE-Sephadex gel beads were settled in a fused silica glass tube (4 mm o.d., 1.5 mm i.d., 38 mm in length), with its height 5 mm from the top of the polypropylene filter tip. The upper and large parts of the beads were irradiated with the laser beam (4 mm in diameter) [Fig. 1(a)], since the analyte was preferentially concentrated from the top of the packed beads.

Flow diagram

Figure 1(b) shows the schematic diagram of the flow analysis system. The carrier solution was pumped by a Sanuki pump, Model DMX-2000. A sample solution (3.7 ml) and a desorbing agent (1 ml of the alcoholic solution of ammonium acetate) were introduced into the flow system by means of respective six-way valves with PTFE [poly(tetrafluoroethylene)] tube loops. All tubings were made of PTFE (2 mm o.d., 1 mm i.d.). The flow rate was maintained constant at 1.3 ml/min. The solution flowed into the flow-through cell from its top.

Iron present in the carrier solution as an impurity should be eliminated. Thus, the carrier solution was on-line purified: the carrier solution containing a small amount of DPPS was passed through a PTFE tube (3 mm in diameter, 10 cm in length) packed with AG 1-X2 (100–200 mesh) in the acetate form.[14]

Procedure for determination of water-soluble (total) iron in fresh water

When a natural water was sampled, 0.1 ml of concentrated hydrochloric acid was added per 50 ml of sample immediately after filtration through a 0.45-μm cellulose nitrate membrane filter by using a disposable polyethylene syringe and a filter unit (Advantec Dismic-25). The sample solutions were stored in polyethylene containers.

To a 5-ml sample solution containing 5–500 ng of iron, 1 ml of the colouring agent solution was added and then the solution was diluted to 10 ml with water. A 3.7-ml aliquot of the solution was introduced into the flow system. The photoacoustic signal was continuously monitored; the signal waveform was measured if necessary, while the signal intensity was monitored with time to obtain a signal development profile. After the signal development was completed, about 1 ml of the desorbing solution was introduced into the stream by means of the other six-way rotary valve to regenerate the ion exchanger in the cell. A calibration graph was obtained by plotting the signal intensity increase from the background level at 4.5 min after sample introduction versus the concentration of iron, and the iron concentrations of water samples were determined by means of this graph.

RESULTS AND DISCUSSION

Selection of colouring agent for iron

DPPS is soluble in water and forms a water-soluble 3:1 complex with iron(II) in the pH range 3–7.[13] We chose DPPS as a colouring

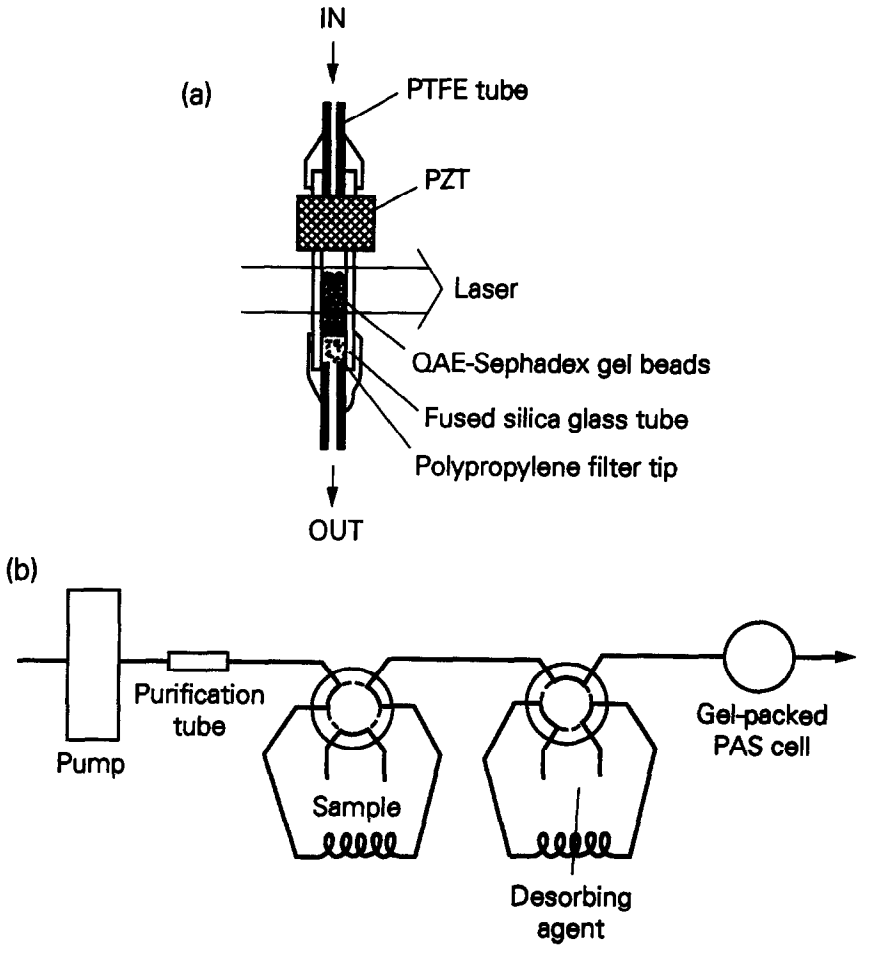

Fig. 1. (a) Schematic diagram of the ion-exchanger phase photoacoustic cell for flow analysis, showing the positions of the laser beam and the beads. (b) Schematic diagram of the flow analysis system. Flow-rate: 1.3 ml/min.

agent for iron, because its molar absorptivity at 532 nm was 2.4×10^4 l. mole^{-1}. cm^{-1}, much higher than that of 1,10-phenanthroline (7.6×10^3 l. mole^{-1}. cm^{-1}). In addition, the coloured complex can be easily sorbed on a dextran-type anion exchanger due to its highly negative charge (−4).

Photoacoustic signal

A typical waveform of the photoacoustic signal for Fe(II)–DPPS complex is shown in Fig. 2. The signal is complicated due to electrical and mechanical fluctuations, acoustic reflections in the cell, and so on, as in the case of similar PAS studies[2,5] but the analysis of the waveform is not the aim of the present study. Some negative drift of baseline of the waveform was observed only when the solution flowed through the cell, lasting for about 60 μsec after the laser flash. This baseline drift was almost unchanged at a constant flow-rate and caused no significant problems for the measurements.

Signal development profiles were investigated for several excursions, and the detection at the largest positive excursion showed the best result;

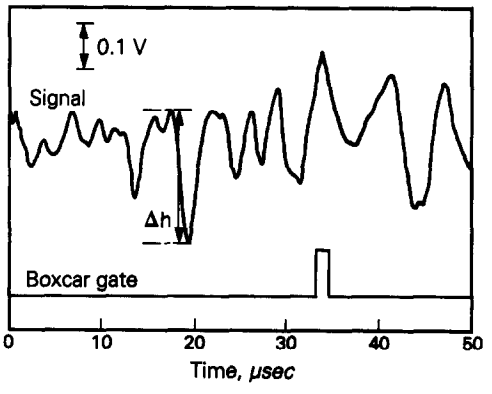

Fig. 2. A typical photoacoustic signal waveform for 7.5 ng/ml of Fe. Sample volume, 3.7 ml. The position and the duration of the boxcar gate is also shown.

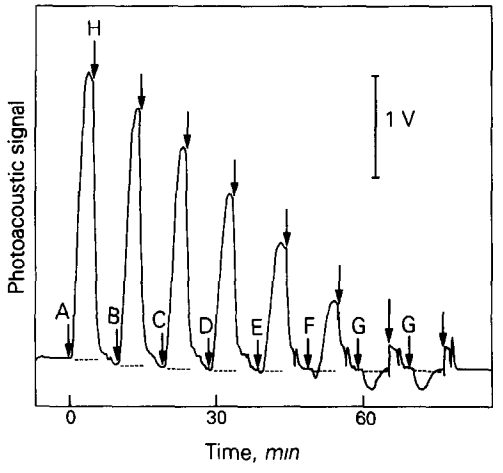

Fig. 3. Development profiles of the photoacoustic signals for Fe(II)–DPPS complex. Sample volume, 3.7 ml: A, 15.0; B, 12.5; C, 10.0; D, 7.5; E, 5.0; F, 2.5 ng/ml Fe; G, blank; H, desorbing agent. The solution was introduced at a position shown by an arrow. Dashed lines are assumed baselines.

thus, the boxcar gate was adjusted at this excursion, as shown in Fig. 2.

Chemical and flow variables

Concentration of reagents. In ion-exchanger phase absorptiometry, the present reagent system has already been employed and successfully applied to iron analysis of highly purified water for electronic industries.[14] The final concentrations of reagents employed were similar to those in the previous work: 0.01% DPPS, 0.1% hydroxylammonium chloride, 0.02*M* acetic acid, and 0.02*M* ammonium acetate.

Standing time of colour development. At least 5 min after mixing the reagents, colour development was completed and a constant signal was obtained.

Flow rate. Lower flow-rates required a longer measurement time, while higher flow-rates increased in the inner pressure of the flow system. The flow-rate should, therefore, be compromised and maintained constant in the range 1.0–1.5 ml/min.

Flow analysis

Figure 3 shows typical signal development profiles for iron(II)–DPPS complex sorbed on QAE-Sephadex gel. By introducing 15 ng/ml Fe for the Fe–DPPS complex at the position A, the signal developed with time because Fe(II)–DPPS complex was continuously concentrated on the beads. In the case of the reagent blank, which was introduced at the position G in Fig. 3, the signal showed some negative baseline drift probably due to the composition difference between the carrier solution and a sample solution. After the development was completed, the desorbing agent was introduced at the position H. Then, the signal dropped rather steeply; the sample could be completely desorbed within a few minutes.

The calibration graph for iron was obtained by plotting the signal height from the baseline in Fig. 3 versus the corresponding iron concentration. The graph was slightly convex. The detection limit, defined as the concentration giving the signal height equal to three times the standard deviation of the blank height, was 0.33 ng/ml (Table 1). The detection limit for the corresponding ion-exchanger phase absorptiometry was 0.2 ng/ml (the sample volume introduced into the flow system was 4.8 ml).[14] The sensitivity of the present method is almost comparable to the absorptiometry.

Enhancement of sensitivity

As discussed in our companion paper,[12] for a system with large distribution ratio of coloured species between ion-exchanger and solution, the sensitivity of ion-exchanger phase spectrometry is proportional to the volume ratio, V/v, where v is the volume of the ion-exchanger in ml and V is the sample volume in ml.

Table 1. Comparison of sensitivity and detection limit of PAS for iron in some media*

Method	Medium	Sample volume *ml*	Sensitivity† *ng/ml*	Amounts of Fe detected‡ *ng*	Detection limit§ *ng/ml*
Batch	Solution	—	3700	26	95
Batch‖	QAE-Sephadex	20	17	23	0.21
Flow‖	QAE-Sephadex	3.7	6.3	23	0.33

*The laser pulse energy: batch, 5–6 mJ;[12] flow, 4.5–5 mJ.

†The concentration giving the intensity of $\Delta h = 100$ mV.

‡The amount of iron virtually detected in the laser irradiated region.

§The concentration giving an intensity equal to three times the standard deviation of the background intensity (95% confidence).

‖The amount of ion exchanger collected in the cell: batch, 0.104 ml; flow, 0.009 ml.

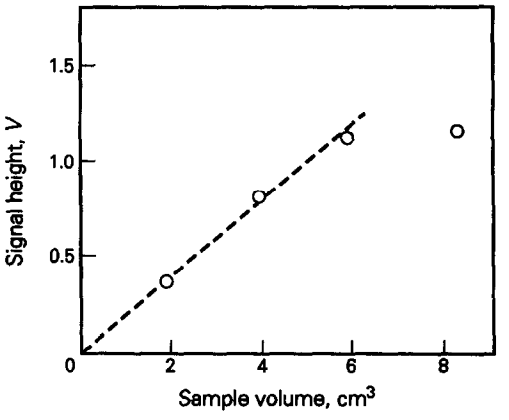

Fig. 4. Effect of sample volume on the signal intensity. Fe concentration: 5 ng/ml.

The sensitivity, defined as the concentration giving 100 mV of Δh (the peak-to-peak height of the signal waveform in the 17–20 μsec region as shown in Fig. 2) was compared with those for the corresponding batch systems; the results are summarized in Table 1.

In our batch system,[12] the iron–DPPS complex in 20 ml of the solution is completely sorbed on 0.104 ml of the ion-exchanger, and therefore the sensitivity was expected to be improved 190 times over that of the corresponding solution PAS because $V/v = 190$.

In the present flow method, the laser beam (4 mm in diameter) is expected to strike less than 0.007 ml of the ion exchanger beads and almost all of the analyte introduced into the flow system was used for measurements. On the other hand, the batch system required 0.104 ml of the ion-exchanger beads for collecting the beads from the equilibrated solution and packing them into the tube in the cell,[12] and the laser beam irradiated only 1/15 of the beads added in the sample solution. Therefore, the flow system improves the sensitivity by about 15-fold over the batch system, provided that other measurement conditions are identical. The observed sensitivity was enhanced by a factor of about three, because the sample volumes used were 3.7 ml for the flow system and 20 ml for the batch system. Above all, the amounts of iron giving the same signal intensity were almost identical in all cases, as shown in Table 1.

The sensitivity can also be improved by increasing the volume of sample solution. The effect of sample volume on the photoacoustic signal is shown in Fig. 4. The signal developed proportionally to the sample volume up to about 5 ml.

Effect of foreign ions

Although some transition metals react with DPPS, giving coloured (*e.g.*, nickel, cobalt and copper) or colourless (*e.g.*, zinc) complexes, at least the comparable amounts of these metal ions with that of iron do not interfere with the determination.[13] The concentration levels found in river waters are 200–400, 0.3–2.5, 1.5–7 and 4–20 ng/ml for iron, nickel, copper and zinc, respectively:[15] in general, iron is most abundant among transition metal ions in natural water. Therefore, the presence of these metals that occur in river water are generally tolerable, and the present method can be applied to the analysis of iron in river water without any pre-treatments for those metals.

The validity of the present method for the determination of trace amounts of iron in river waters has been examined; the recovery test for a river water sample was performed by adding known amounts of iron(III) (Table 2). The recovery of iron was almost quantitative. Another examination has also been done; the analytical value obtained by the present method was compared with that by atomic-absorption spectroscopy. The sample solution (No. 4 in Table 3) was carefully concentrated up to 1/20 in volume by evaporation of water in a PTFE vessel. The concentration of iron in the solution was determined by using a calibration curve prepared at similar electrolyte concentrations to those in the sample solution. The analytical value (13.7 ng/ml) for the sample water determined by atomic-absorption spectrometry was in fairly good agreement with that (12.6 ng/ml) determined by the present method.

The presence of a large amount of a background electrolyte such as sodium chloride resulted in both a volume contraction of the ion-exchanger beads and a decrease in the

Table 2. Recovery test*

Iron added,† *ng*	Iron found,† *ng*	Net recovery, *ng*	% Recovery
0	18.9	—	—
12.5	30.5	11.6	93
25.0	40.9	22.0	88
37.5	59.0	40.1	107
50.0	70.0	51.1	102

*Sample: gorge water of Shintate River (Kasuya, Fukuoka), site number 2 (see Table 3); sample volume: 5 ml. The bulk composition of the sample was as follows: Na^+, 6.9; K^+, 0.4; Mg^{2+}, 9.1; Ca^{2+}, 11.6; Cl^-, 9.5; HCO_3^-, 62.8; NO_3^-, 4.4; SO_4^{2-}, 13.1; SiO_2, 20.1 (in μg/ml).

†Amount of iron in a 10-ml calibrated flask. The volume introduced into the system was 3.7 ml.

Table 3. Determination of water-soluble (total) iron in gorge water of Shintate River (Kyushu University Forest, Kasuya, Fukuoka)

Sampling site number	1	2	3	4	5	6	7	8
Concentration, *ng/ml*	3.3	3.8	2.2	12.6*	7.7	4.1	7.3	5.6

*13.7 ng/ml by atomic-absorption spectrometry.

distribution ratio of the iron complex. In such cases, the iron concentration should be evaluated by means of a calibration graph prepared at electrolyte concentrations similar to those in the sample solution.

Determination of water-soluble (total) iron in river water

The present method was applied to the determination of the total amounts of water-soluble iron species in river waters. After filtration of water samples through a 0.45-μm membrane filter, pH values of filtered samples were adjusted to 1.5 by adding concentrated hydrochloric acid, and the samples were stored in polyethylene vessels; under this condition the loss of iron is negligible.[16] Analytical values of iron at eight sites of Shintate River (Kasuya, Fukuoka) are summarized in Table 3. The contents of the water-soluble (total) iron were in the range of 2.2–12.6 ng/ml. The contents in two tributary streams (Nos 4 and 5), where trees were cut down over the catchment basins, were somewhat high.

The precision was investigated with a sample solution (No. 1 in Table 3). For three determinations, the analytical value was 3.34 ± 0.32 ng/ml (90% confidence).

By using the present method, six water samples containing water-soluble (total) iron [iron(II) and (III)] at concentrations of ng/ml levels could be analyzed within one hour; such a highly sensitive detection was impossible in conventional flow-injection analysis without any preconcentration procedure. It may be possible to determine the contents of iron in different oxidation states with the use of citrate as a masking agent for iron(III).[17]

CONCLUSION

We have demonstrated in these two back-to-back papers that LIPAS is quite applicable either for the batch or flow method of ion-exchanger phase spectrometry. A smart combination of ion-exchange concentration and direct measurement of the ion exchanger by LIPAS enabled the detection sensitivity at ng/ml levels or lower.

Compared with ion-exchanger phase absorptiometry, the present cell compartment is very simple. A fused silica tube packed with a small amount of ion-exchanger beads is combined only with a piezoelectric transducer attached on it. In addition, room light and scattered light do not affect the sensitivity and reproducibility in this method. A system with higher molar absorptivity at an excitation wavelength and larger distribution ratio will certainly improve the analytical sensitivity even for smaller sample volumes.

REFERENCES

1. S. Oda and T. Sawada, *Anal. Chem.*, 1981, **53**, 471.
2. E. P. C. Lai, S. Y. Su, E. Voigtman and J. D. Winefordner, *Chromatographia*, 1982, **15**, 645.
3. E. Voigtman and J. D. Winefordner, *J. Liq. Chromatogr.*, 1982, **5**, 2113.
4. E. Voigtman and J. D. Winefordner, *ibid.*, 1983, **6**, 1275.
5. K. L. Rowlen, J. W. Birks, K. A. Duell and J. P. Avery, *Anal. Chem.*, 1988, **60**, 311.
6. K. Yoshimura, H. Waki and S. Ohashi, *Talanta*, 1976, **23**, 449.
7. K. Yoshimura and H. Waki, *ibid.*, 1985, **32**, 345.
8. K. Yoshimura, *Anal. Chem.*, 1987, **59**, 2922.
9. K. Yoshimura and U. Hase, *Analyst*, 1991, **116**, 835.
10. R. S. Field, D. E. Leyden and R. S. S. Murthy, *Anal. Chim. Acta*, 1986, **186**, 123.
11. J. Shida, K. Kasama, H. Honda and K. Oikawa, *ibid.*, 1990, **233**, 135.
12. S. Yamada and K. Yoshimura, *Talanta*, 1992, **39**, 1013.
13. H. Onishi, "Photometric Determination of Traces of Metals", John-Wiley, New York (1986).
14. U. Hase and K. Yoshimura, *Analyst*, in the press.
15. Y. Kitano, "Environmental Chemistry of the Earth", Syokabo, Tokyo (1984).
16. K. S. Subramanian, C. L. Chakrabarti, J. E. Sueiras and I. S. Maines, *Anal. Chem.*, 1978, **50**, 444.
17. S. Nigo, K. Yoshimura and T. Tarutani, *Talanta*, 1981, **28**, 669.

Talanta, Vol. 39, No. 8, pp. 1025–1030, 1992
Printed in Great Britain.

0039-9140/92 $5.00 + 0.00

PNEUMATOAMPEROMETRIC DETERMINATION OF CHLORINE IN WATER

KAREL ŠKÁCHA
District Hygienic Station, Prachatice, Czechoslovakia

PŘEMYSL BERAN*
Department of Analytical Chemistry, Charles University, Albertov 2030, 128 40, Prague 2, Czechoslovakia

STANLEY BRUCKENSTEIN*
Department of Chemistry, State University of New York at Buffalo, Buffalo, NY 14214, U.S.A.

(*Received* 9 *November* 1990. *Revised* 23 *December* 1991. *Accepted* 5 *January* 1992)

Summary—Free chlorine in water can be determined by acidifying the water sample, purging it with nitrogen and determining the chlorine present in the nitrogen stream with a gold porous electrode. The current response of gold porous electrode is related to the concentration of free chlorine by using a calibration curve. This pneumatoamperometric method gives results fully comparable to the standard *o*-toluidine photometric method used for water supplies. It is uninfluenced by the presence of other dissolved oxidants and requires only one milliliter of sample.

Our previous paper[1] dealt with the possibility of the pneumatoamperometric determination of trace amounts of oxidants and the total dissolved chlorine in water. The method involved the reaction of various oxidants with iodine. A stream of nitrogen transported the iodine vapors to a gold porous electrode, AuGPE. The current at the AuGPE corresponded to the total amount of the test oxidants.

Pneumatoamperometry is also suitable for the determination of free chlorine (hydrochlorite) because chlorine can be purged rapidly from an acidified solution. The equilibrium,

$$HClO + H^+ + Cl^- = Cl_2 + H_2O \qquad (1)$$

shifts to the right on acidification and on purging with nitrogen, molecular chlorine enters the gas phase. The chlorine/nitrogen mixture impinges on the AuGPE which is held at a potential where chlorine reduces to chloride ion. This reduction causes a cathodic current at potentials between +0.2 to −0.2 V. The results we report below show that this chlorine determination is rapid, sufficiently sensitive, and simple to perform. The method's analytical accuracy for determination of chlorine in waters is comparable to presently used standard methods.[2,3] The pneumatoamperometric method satisfies the analytical requirements of water supply establishments and possesses certain advantages over the standard methods which are discussed below.

EXPERIMENTAL

Reagents

All the reagents we used were of p.a. purity. The water used for the preparation of standard solutions and synthetic chlorine-containing water samples was distilled twice from a glass apparatus. The chlorine demand was compensated by adding 200–250 μg of Cl_2 per liter of water and then exposing the water to sunlight for 4–5 days. Nitrogen (99.5%) purged this water for at least two hours prior to use. The water then exhibited no reaction with *o*-toluidine reagent. A pressure cylinder supplied the 99.5% nitrogen which was not further purified. The chlorine stock solution (*ca.* $10^{-2}M$) was prepared by saturating the distilled water with gaseous chlorine of the kind used for water supply purposes.[4] The stock solution was stored in a dark glass bottle at laboratory temperature and standardized by iodometric titration.

Apparatus

The AuGPE was prepared by stretching a porous Teflon membrane, vacuum-coated

*Authors for correspondence.

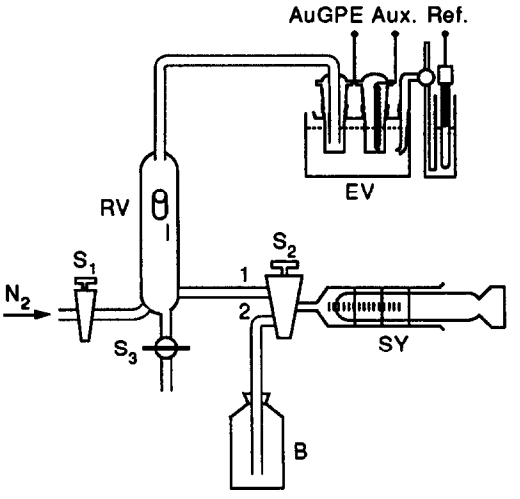

Fig. 1. Diagram of the pneumatoamperometric apparatus for determination of chlorine in water. S1 and S3 are on–off stopcocks, S2 is a two-way stopcock with positions 1 and 2, B is a vessel containing $5M$ H_2SO_4, SY is a syringe, RV is the reaction vessel, I is the port for sample injection and is sealed with a rubber septum, EV is the electrolysis vessel, Aux is the auxiliary electrode, Ref is reference electrode, AuGPE is the gold porous electrode.

with gold (thickness, 650 $\mu g/cm^2$) over the glass portion of a gas electrode. Electrical contact to the porous gold was made by the method of Gifford and Bruckenstein.[5] The electrolysis vessel contained $1M$ sulfuric acid as the supporting electrolyte. Either an operational amplifier potentiostat,[1,4] or a PA 3 polarographic analyzer was used with a TZ 4100 line recorder (all from Laboratorní Přístroje, Czechoslovakia). A saturated calomel electrode (SCE) was used as the reference electrode and all potentials are reported with respect to it.

Figure 1 depicts the pneumatoamperometric apparatus used. Chlorine is liberated in the reaction vessel, RV, which has an inlet, I, sealed by a rubber septum. Stopcock S1 introduces nitrogen into the vessel. Stopcock S3 serves as the solution outlet. If stopcock S2 is in position 2, the acid solution can be aspirated from vessel B into syringe SY. In position 1 of stopcock 2, acid can be injected into RV to shift reaction (1) to the right. The evolved chlorine reaches the AuGPE placed in electrolysis vessel EV, which also contains a reference SCE electrode and a counter electrode.

Procedure

Step 1. Open stopcock S1 and introduce nitrogen into the apparatus at a flow-rate of 0.5 l./min.

Step 2. Turn the potentiostat on and set the working electrode potential to 0 V. Wait until the rate of the residual current decrease becomes 10 nA/min. Then prepolarize the AuGPE by a step potential change to +1.25 V and scan the AuGPE between +1.25 V and 0 V at a rate of 100 mV/sec three times, stopping at 0 V.

Step 3. Set stopcock S2 to position 2. Aspirate 1 ml of $5M$ sulfuric acid into syringe SY. Turn S2 to position 1 to transfer the acid to the empty RV and close S2. Wait for the residual current to stabilize (*ca.* 5 min).

Step 4. Inject 0.1 ml of a solution containing 1.0 to 1.5 mg Cl_2/l. through the septum sealing opening I using a syringe. This is to preoxidize any reducing impurities in the sulfuric acid. Wait until the residual current stabilizes (*ca.* 2 min) and then inject a one-ml water sample to be analyzed for Cl_2 content through the septum using a syringe. Record the peak current response.

Step 5. Wait until the electrode current reattains a stable residual value and then drain the solution out of RV through stopcock S3.

The AuGPE should be stored dry if intervals between the measurements are greater than one day. The electrode activity and response stability of a new AuGPE, or of one that has been stored dry for a long period, should be determined by making three to five measurements with a standard chlorine solution.

RESULTS AND DISCUSSION

Effect of the electrode potential

Voltammograms obtained with a gold ring disk electrode (AuRDE) show that the limiting reduction current for chlorine (or hypochlorous acid) starts at *ca.* +0.2 V.

Currents for chlorine reduction at the AuGPE are poorly reproducible at potentials more negative than −0.2 V, and so the potential, 0 V, was used for all pneumatoamperometric measurements.

Effect of cyclic prepolarization

The AuGPE current response for chlorine reduction is poorly reproducible under conditions of long term constant applied potential within the region, +0.2 to −0.2 V. When the time between the determinations was longer than one hour, the next determination yielded *ca.* 20% lower current peak as compared to the peak found for an immediately performed replicate determination. Reproducible, 20% higher

values were reattained by performing four replicate determinations in rapid succession. This undesirable behavior can be eliminated by cyclic prepolarizaton before each measurement.

We tested the effect of varying the polarization interval from 0 to +1.5 to 0 to +0.7 V, varying the polarization rate from 5 to 500 mV/sec and using step potential changes. The reproducibility of the results is poorer for polarization intervals narrower than 0 to +0.9 or wider than 0 to +1.3 V. Cyclic prepolarization at a uniform scan rate leads to a gradual increase in the current peak height. Stepping the potential to a positive value and scanning back to 0 V produced the best reproducibility. Higher potential scan rates causes the residual current to stabilize faster. Three potential step/scan cycles produced optimal results.

The prepolarization procedure we finally used consisted of three repetitions of stepping the potential from 0 to +1.25 V and scanning it back to 0 V at a rate of 100 mV/sec. This procedure stabilized the residual current within 4–5 min and the current remains stable (±5%) for at least 15 min. Then the procedure must be repeated.

Effect of sulfuric acid concentration in the reaction vessel

One-milliliter water samples containing 0.41 μg of Cl_2 were injected into one milliliter of sulfuric acid whose initial concentration was varied from 0.1 to 5*M*. Figure 2 shows that the current peak height increases with the concentration of the acid. Acid concentrations higher than 5*M* (final 2.5*M*) were impractical.

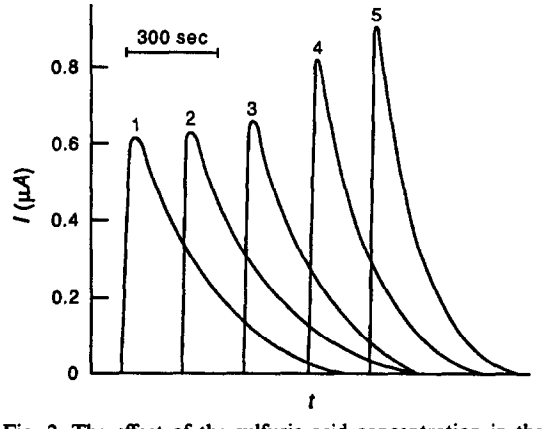

Fig. 2. The effect of the sulfuric acid concentration in the reaction vessel on the AuGPE current response. $E_{AuGPE} = 0$ V, flow-rate of $N_2 = 0.5$ l./min., $[Cl_2] = 0.41$ mg/l., 1 ml of $H_2SO_4 + 1$ ml of sample, H_2SO_4 concentration: 1—0.1, 2—0.5, 3—1, 4—2.5, 5—5*M*.

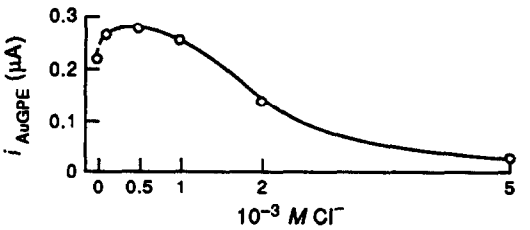

Fig. 3. The effect of the chloride concentration in the sample on the AuGPE current response. $E_{AuGPE} = 0$ V, flow-rate of $N_2 = 0.5$ l./min., $[Cl_2] = 0.28$ mg/l., 1 ml of 5*M* $H_2SO_4 + 1$ ml of sample.

The effect of chloride in the reaction vessel

Figure 3 illustrates the effect of changing the chloride ion concentration. The current peak height increases by *ca.* 20% on adding a small amount of chloride. The maximum current response occurs at *ca.* $5 \times 10^{-4}M$ Cl^- and the current peak height is nearly one-tenth of the maximum value at a concentration of $5 \times 10^{-3}M$ Cl^-. The time required to purge chlorine from the sample decreases substantially at higher chloride ion concentrations.

Most water standards permit concentrations of 100 mg Cl^-/l. (*i.e.*, *ca.* $3 \times 10^{-3}M$). Hence we adapted our method to a chloride concentration of $1.5 \times 10^{-3}M$ (52 mg Cl^-/l.) in our samples to minimize the influence of chloride that might be present initially, and obtained a calibration curve. A new calibration curve would have to be determined for samples with higher chloride contents. As the concentration of chloride is often routinely determined in water samples, a

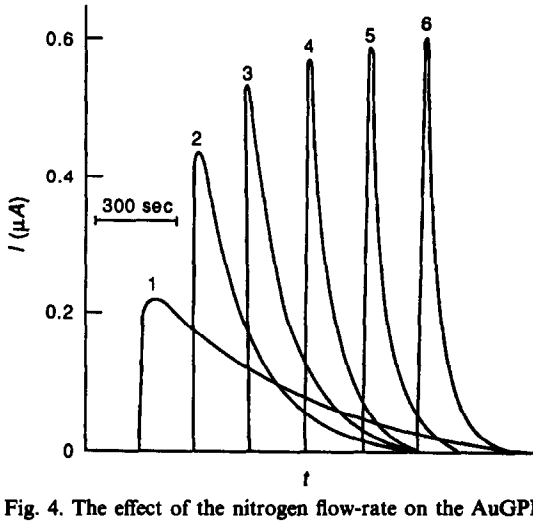

Fig. 4. The effect of the nitrogen flow-rate on the AuGPE current response. $E_{AuGPE} = 0$ V, $[Cl_2] = 0.45$ mg/l., 1 ml of 5*M* $H_2SO_4 + 1$ ml of sample, $[Cl^-] = 1.5 \times 10^{-3}M$. N_2 flow-rate (l./min): 1—0.1, 2—0.3, 3—0.5, 4—0.8, 5—1.0, 6—1.5.

correction factor could be incorporated in the procedure or the chloride content of calibration standards adjusted accordingly. A standard additions calibration would also eliminate the influence of chloride.

The influence of nitrogen flow rate

Figure 4 shows how the purging gas flow-rate affects the current peak height. The shape of the current–time response is the expected one, but the peak current value is higher. We selected a nitrogen flow-rate of 0.5 l. N_2/min for practical analyses.

The concentration dependence

We determined the dependence of peak current height on chlorine concentration in the range 0.06–0.90 mg Cl_2/l. All these test samples contained $1.5 \times 10^{-3}M$ chloride ion. Two procedures were employed. First, a one-milliliter water sample was added to one milliliter of $5M$ sulfuric acid and the peak current accompanying gas purging was recorded (Fig. 5, lower curve). Secondly, to eliminate the effect of trace reductants that might be present in the sulfuric acid, 0.1 ml of a solution containing 1.0–1.5 mg Cl_2/l. was added to 1 ml of $5M$ sulfuric acid. The mixture was bubbled with nitrogen to attain a constant residual current (*ca.* 2 min). Only then did we add a 1.0-ml water sample and record the peak current (Fig. 5, upper curve).

The peak current height–chlorine concentration responses were not linear. The character of the curvature is the same in both the above procedures and is qualitatively identical with the shape of the voltammetric response reported by Pungor *et al.*[7]

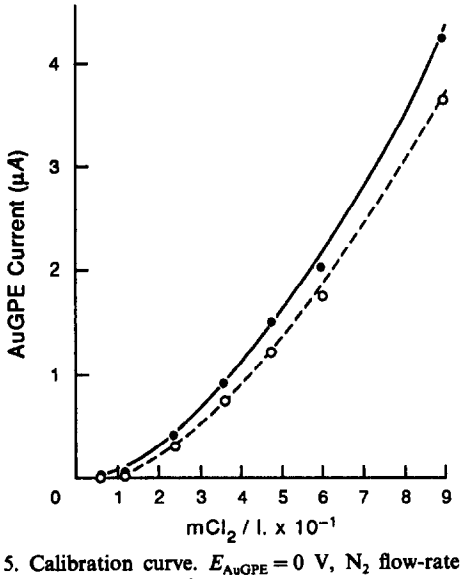

Fig. 5. Calibration curve. $E_{AuGPE} = 0$ V, N_2 flow-rate 0.5 l./min., $[Cl^-] = 1.5 \times 10^{-3}M$. (○) 1 ml of $5M$ H_2SO_4 + 1 ml of sample; (●) 1 ml of $5M$ H_2SO_4 + 0.1 ml of a solution containing 1 mg Cl_2 per liter, 1-ml sample after 2 min.

The effect of any formation of chloramines, of the matrix, and of organic impurities can be excluded, as the same curve shape was obtained for water treated by standing with chlorine, followed by bubbling out the chlorine and then distilling in a quartz apparatus.

Adding chlorine to the sulfuric acid before adding the water sample (the second procedure) is advantageous in the determination of very low chlorine concentrations. The second procedure yields higher peak currents than the first one. For a chlorine concentration of 0.06 mg/l. the peak current is higher by 275% and for a concentration of 0.120 mg/l. it is higher by *ca.* 100% (the lowest two points in Fig. 5). The differences in the results obtained by the two procedures can be attributed to the presence of traces of reductants in the sulfuric acid equivalent to *ca.* 0.12 mg/l. chlorine. Reducing impurities have the greatest relative influence when determining low chlorine concentrations.

The curvature in the current–concentration response at low chlorine concentrations may be due to kinetics. The ratio $(Cl_2)/(HClO)$ during purging is constant and independent of total dissolved Cl_2 because both the hydronium and chloride ion concentrations are constant ($2.5M$ $H_2SO_4 + 1.5 \times 10^{-3}M$ Cl^{-1}). The instantaneous equilibrium concentration of Cl_2 in the flowing N_2 would be proportional to the dissolved Cl_2 concentration if equilibrium existed, and no curvature in the current concentration response would occur. This is not the case however. The curvature of the concentration plot suggests, as one possibility, that the partitioning of $(Cl_2)_{aqueous}$ to the gas phase becomes rate-determining.

The effect of the electrolyte composition

The gold porous, reference and auxiliary electrodes are immersed in $1M$ sulphuric acid supporting electrolyte. The sulfuric acid concentration has no significant effect on the peak current response for the reduction of chlorine. The current only increases slightly with the concentration of the acid. The presence of chloride ions in the sulfuric acid supporting electrolyte significantly increases the peak currents for chlorine reduction. We observed as much as a 20-fold increase, but this sensitivity increase was accompanied by poorer reproducibility. Also,

the sensitivity decreases and the AuGPE residual current increases with time. The electrode lifetime in chloride-containing solutions is limited to a few weeks after which time the current response suddenly drops to zero.

Effect of oxidizing agents

While strong oxidants are not likely to be present, we tested our procedure in the presence of MnO_4^- (1.0 and 2.0 × $10^{-5}M$), Fe^{3+} (1.0 and 2.0 × $10^{-5}M$) and NO_3^- (1.0 and 2.0 × $10^{-3}M$) in solutions containing 0.30 mg Cl^-/l. and 0.28 mg Cl_2/l., and noted no effect on the pneumatoamperometric response. The photometric response, on the other hand, was nearly doubled and tripled in the presence of the MnO_4^-.

Reproducibility

Figure 6 illustrates the reproducibility of the measurements on the same water sample. Replicate measurements on two different water samples gave the following results: for a water sample containing 0.275 mg Cl_2/l., the estimate of the standard deviation was 0.003 mg Cl_2/l. (7 measurements); the corresponding value for the sample containing 0.520 mg Cl_2/l. was 0.007 mg Cl_2/l. (7 measurements).

Practical water samples

Chlorine was determined in water samples using the pneumatoamperometric method (described in the Procedure) and the results were compared with those obtained by the *o*-toluidine photometric method.[3] The sensitivity of the pneumatoamperometric method does not differ appreciably from the *o*-toluidine photometric method. As can be seen from Table 1, our pneumatoamperometric method yields higher values than the photometric technique. One possible explanation for the difference may lie in the observation that the literature does not contain any evidence that the reaction between *o*-toluidine and chlorine is stoichiometric. The Czechoslovak standard[3] merely recommends that this reaction be carried out at a pH of 1.2, and that the *o*-toluidine: chlorine ratio be at least 3:1. Lower ratios lead to decomposition of the oxidized form of *o*-toluidine. American standards recommend that the *o*-toluidine reagent: chlorine ratio be 8:1 in the analysis of potable waters. Thus complete agreement about the chemical reagent conditions for the photometric method does not exist. The *o*-toluidine method has, in fact, been replaced in more recent

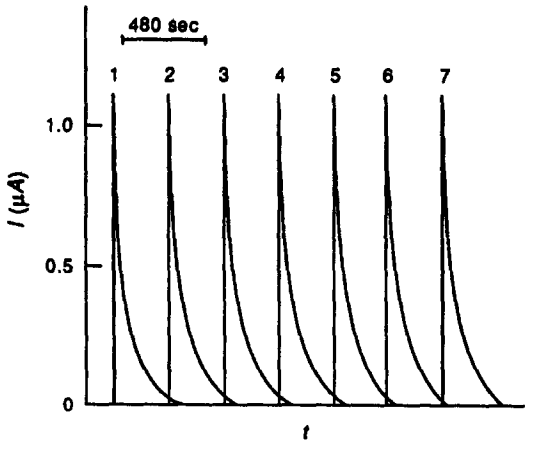

Fig. 6. Measuring reproducibility with the AuGPE. $E_{AuGPE} = 0$ V, N_2 flow-rate = 0.5 l./min., $[Cl^-] = 1.5 \times 10^{-3}M$, 1 ml $5M$ H_2SO_4 + 0.1 ml of solution containing 1 mg Cl_2 per litre, followed by 1 ml sample after 2 min. $[Cl_2] = 0.63$ mg/l., $s_x = 0.0035$ mg Cl_2/l. at the 95% confidence level.

Table 1. Determination of chlorine in various water samples

Sample	Found, mg Cl_2/l. Photometry	Pneumatoamperometry	Notes (concentrations are in mg/l.)
1*	0.075	0.120	MnO_4^- demand—0.9; NH_4^+—0.05; NO_2^-—0.0 Fe—0.0; color 5
2†	0.225	0.275	
2‡	0.225	0.275	The content of Fe in sample 2 was artificially increased to 1.1.
2†	0.230	0.275	The content of NO_3^- in sample 2 was artificially increased to 140
3*	0.180	0.330	MnO_4^- demand—3.1; NH_4^+—0.20; Fe—0.30; NO_2^-—0.05; color—15
4†	0.230	0.380	
5‡	0.560	0.700	
6*	0.090	0.110	MnO_4^- demand—6.7; NH_4^+—0.20; NO_2^-—0.08 Fe—0.20; color—20
7†	0.180	0.240	
8‡	0.510	0.530	

*Sampling at the farthest location in the water supply system.
†Sampling in the middle of the water supply system.
‡Sampling at the beginning of the water supply system.

editions of Standard Methods, although it is still the standard in Czechoslovakia for the moment. We, unfortunately, do not have access to the reagents needed to carry out the supposedly more accurate DPD or FACB methods. Because of the known limitations of the *o*-toluidine method, the comparisons in Table 1 at least demonstrate reasonable agreement.

A second reason for discrepancies between the two methods may be that the photometric determination is performed in open vessels at pH = 1.3 while stirring the sample. The distribution diagram for the various forms of dissolved chlorine shows that molecular chlorine exists in water under these conditions. Some of this molecular chloride could volatilize and lead to less than quantitative recovery of dissolved chlorine. Finally, it is not clear how the presence of dissolved organic substances will affect the photometric procedure.

We believe that the pneumatoamperometric method is free of these type of problems. We use a closed system and inject samples into it. The chlorine in the sample is purged with a flowing gas stream and the chlorine is detected by electroreduction to chloride ion. This procedure is inherently less subject to complications arising from the presence of other species in the water sample.

We found that the time of analysis is similar for the two methods. A simple, dedicated analyzer for free chlorine in water based on this pneumatoamperometric method is being designed.

CONCLUSIONS

The pneumatoamperometric method for determination of free chlorine in water supplies gives precision and, we believe, accuracy fully comparable to the standard *o*-toluidine photometric method. The pneumatoamperometric method has two advantages as compared to the *o*-toluidine method. First, smaller samples suffice and secondly, dissolved oxidants do not interfere as they do in the optical method. A standard additions procedure would alleviate chloride dependence. While we have been unable to compare these preliminary results against a more accurate method, our method can certainly serve as a simple screening procedure requiring no sample treatment/reactions, and for monitoring threshold levels of Cl_2 (to establish if Cl_2 is above a minimum level).

REFERENCES

1. P. Beran, F. Opekar and S. Bruckenstein, *Anal. Chim. Acta*, 1982, **136**, 389.
2. American Public Health Association, American Water Works Association, and Water Pollution Control Federation, *Standard Methods for the Examination of Water and Wastewater*, 14th Ed., American Health Assoc., Washington, D.C. 1976.
3. Czechoslovak Standard 83 0520, Prague, 1978.
4. Czechoslovak Standard 65 4356, Prague, 1566.
5. P. R. Gifford and S. Bruckenstein, *Anal. Chem.*, 1988, **52**, 1024.
6. P. Beran, K. Micka and Vu Thi Gai, *Collection Czechoslovak Chem. Commun.* 1988, **53**, 487.
7. E. Pungor, E. Szepesvary and P. Szepesvary, *Talanta*, 1978, **17**, 334.

Talanta, Vol. 39, No. 8, pp. 1031–1037, 1992
Printed in Great Britain.

0039-9140/92 $5.00 + 0.00

STUDY OF THE TRANSPORT OF SILVER ACROSS A SUPPORTED LIQUID MEMBRANE CONTAINING SULPHIDE PODAND

ELWIRA LACHOWICZ

Department of Analytical Chemistry, Warsaw University of Technology, Noakowskiego 3, 00-664 Warsaw, Poland

(*Received* 26 *August* 1991. *Revised* 4 *December* 1991. *Accepted* 4 *December* 1991)

Summary—The transport of silver through a supported liquid membrane saturated with a polydentate neutral ionophore 1,12-di-thienyl-2,5,8,11-tetrathiadodecane in *m*-chlorotoluene has been studied. Thiosulphate was used as the stripping solution. The influence of the feed solution composition, the type of a microporous polypropylene Celgard support, the ratio of feed/receiving solution volume, and the initial Ag concentration on the rate of transport of silver was examined. Transport of Ag is selective towards Cu(II), Pb and Zn, but these cations affected the rate of the Ag flux.

Supported liquid membranes (SLMs) are the subject of widespread investigation[1–16] as a potential method of separation and preconcentration for both technical and analytical purposes.

A micro-porous polymer support with immobilized organic solution of ionophore is interposed between sample (feed) solution and receiving solution. A continuous transport of ions across that membrane occurs due to simultaneously arising processes of extraction and back-extraction.

A complexing reagent incorporated into the organic phase acts as the carrier for metal ions and first of all its selectivity towards the desired ions determines the overall selectivity of the process. A very small volume of reagent solution enables the use of ionophores of higher cost. A driving force for active "up-hill" transport of ions (against their concentration gradient) is provided by (1) a gradient of H^+ concentration or (2) by complexing or redox reaction of target ions in a receiving phase.

Danesi *et al.*[10] listed the factors favourable to forming stable SLMs: a low solubility of organic liquid in water, a low difference of the ionic strength between feed and stripping solutions, a high organic/water interfacial tension, small pore radii and low hydrophobicity of a polymer support. The latter three points were also stressed by Takeuchi *et al.*[11]

Izatt and co-workers[4,5] confirmed that the time stability of SLM depends on the boiling point and solubility of the solvent in water.

Among recently published papers on SLMs were studies on the transport of Li,[14] K,[13] alkali metal and alkaline earth cations[4] across a membrane that contained crown ethers, Cu(I)[15] or Cu(II)[9] across a membrane with a thioeter or a mixture of oximes respectively, Zn(II) ions through SLM with incorporated dithizone[8] or bis-(2,4,4-trimethylpentyl)phosphinic acid,[7] rare earth cations[12] with use of some β-diketones as carriers, and uranium(VI) with TOPO.[16]

The present paper is a continuation of our studies on a solvent extraction of metal ions with the sulphide podand (open-chain analog of thiocrown) 1,12-di-2-thienyl-2,5,8,11-tetrathiadodecane (TTD).

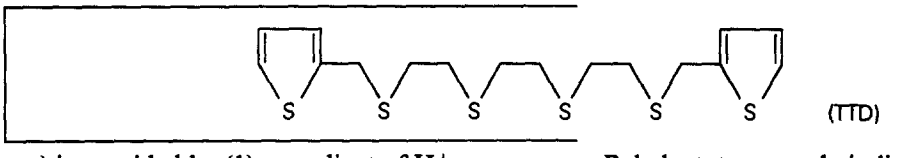

(TTD)

Polydentate open-chain ligands, so-called podands according to the Weber and Vögtle classification,[17] form similar crown ethers and cryptands, the host-guest complexes. TTD, being a neutral all-sulphur ligand reacts selectively with metal ions classified as "soft" in Pearson's HSAB approach.[18] Studies on extraction of Ag,[19,20] Pd and Au[21] by TTD solution in 1,2-dichloroethane, 4-methylpentanone

(MIBK) or chloroform were presented previously. Recently it was found by Chayama and Sekido[22] that the acyclic tetrathio ethers show a higher extractability than the corresponding cyclic tetrathio ethers.

In the present study the transport of Ag ions across a liquid membrane with immobilized TTD will be presented. The effect of a composition of a sample solution, a type of polymeric membrane and other conditions of process on a rate of up-hill transport, as well as a selectivity problem will be discussed.

EXPERIMENTAL

Reagents

1,12-Di-2-thienyl-2,5,8,11-tetrathiadodecane (TTD) was synthesized as described previously[19] and used as 0.1M solution in m-chlorotoluene. A stock $10^{-2}M$ solution of silver was prepared from silver nitrate dissolved in water with nitric acid. Other reagents used were all of analytical purity.

Apparatus

A Thermo Jarrell-Ash S11 atomic-absorption spectrometer was used for determination of Ag (328.1 nm), Cu (324.7 nm), Zn (213.8 nm) and Pb (217.0 nm).

Membrane cell

The apparatus used followed the device described by Cox and Bhatnagar.[8] Experiments were carried out in the device including a glass container for a feed solution, a Teflon tube (i.d. 40 mm) closed at one end with microporous membrane fixed with a Teflon screw-nut (Fig. 1). The feed solution (500 ml) was stirred with a magnetic stirring bar. A volume of receiving solution (0.1M thisulphate) was 50 ml unless otherwise stated. In some experiments with 50 ml of receiving solution, this solution was stirred by a second (paddle) stirrer.

The 0.1M (unless otherwise stated) solution of TTD in m-chlorotoluene was pipetted onto a membrane. A volume of 2–3 drops was sufficient to saturate the membrane.

Samples of 2 ml from the feed phase or 1 ml from the receiving solution were transferred to calibration flasks of appropriate volume and diluted with water to the mark. Concentration of Ag as well as Cu, Zn and Pb ions was determined by AAS method.

Results are expressed as the enrichment coefficient $c_{r,t}/c_{f,0}$ *i.e.*, the ratio of the concentration of silver in the receiving phase at the time t, $c_{r,t}$ to the initial concentration of silver in the feed solution, $c_{f,0}$.

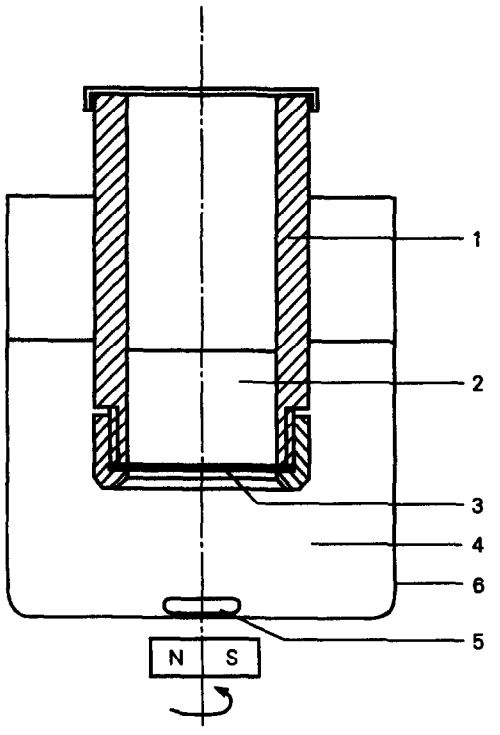

Fig. 1. Diagram of membrane cell. 1—Teflon tube; 2—receiving phase; 3—SLM; 4—feed phase; 5—stirring bar; 6—glass container.

A value of flux of ion J (in M cm^{-2} hr^{-1}) calculated as the amount of moles transferred across the 1-cm^2 area of SLM during one (first) hour of experiment will also be used, mainly for comparison of transport of various cations.

Membranes

Four hydrophobic polypropylene Celgard membranes (kindly supplied by the Hoechst Celanese Corporation) were tested: the Celgard 2400 and 2500 membranes as well as their laminates on a polypropylene nonwoven web: Celgard 4410 and 4510 respectively. The laminate variants exhibit an improved strength, toughness and tear-resistance, but also an increased thickness over a basic membrane. The properties of membranes are shown in Table 1.

The area of contact of membrane and solution was 12.5 cm^2.

RESULTS AND DISCUSSION

Dependence of Ag flux on composition of feed solution

Silver ions were extracted[19] with a high selectivity and efficiency from solutions of pH 1–6 in

Table 1. Celgard microporous polypropylene membranes

Type	Porosity, %	Effective pore size, μm	Average thickness, μm
2400	38	0.05	25 ± 2.5
2500	45	0.075	25 ± 2.5
4410	38	0.05	175 ± 75
4510	45	0.075	175 ± 75

the presence of ClO_4^-, and from HNO_3, $HClO_4$ or $HNO_3 + HClO_4$ solutions by TTD in 1,2-dichloroethane or MIBK. The value of log D (log of the distribution coefficient of Ag between the organic and water phases) ranged from 1.8 to 2.2. The complex cation Ag–TTD$^+$ was transferred into an organic phase as an ion pair with ClO_4^- or NO_3^- acting as the counter ion.

Here, the transport of Ag from various media into 0.1M thiosulphate, used as the stripping solution, was examined. Thiosulphate medium was chosen (log $K = 8.82$ for complexation with Ag[23]) to facilitate the release of silver in the receiver and eliminate an overall rate controlling stage from the stripping process. Experiments were carried out with the Celgard 4410 membrane. Results are shown in Fig. 2.

The transport of silver occurs in acetic buffer (with the presence of ClO_4^-) and in acidic media. As follows from experiments at pH 4.7, the increase in sodium perchlorate concentration and the increase in the concentration of TTD was profitable for Ag transport. Using a concentration much higher than 0.1M TTD was not feasible because 0.2M TTD solution is close to saturation. The flux of Ag from 0.1M perchloric acid is higher than that from 0.1M nitric acid. Similarly, the extraction of Ag from perchloric acid solution has been characterized by higher D values[19] than in the case of nitric acid. The effect of an anion on the rate of transport of a cation complex of a metal ion with a neutral crown ether as an ionophore was discussed by Lamb *et al.*[24] on the basis of anion hydration reaction. They showed that anions with small Gibbs free energies of hydration (ClO_4^- has the smallest among the presented group) allowed faster transport of metal cation.

The medium 0.1M $HNO_3 + 0.05M$ $HClO_4$ has been chosen in this study because of a better balance (in comparison to 0.1M $HClO_4$) of Ag in both aqueous phases during long-time experiments.

Comparison of microporous membranes

The experiments carried out for the four polypropylene supports point out the differences among them. The curves in Fig. 3 present the mean values of two transport experiments for each of the membranes. Range is ±10%. The mean values of Ag transport expressed in $10^{-8}M$ cm^{-2} hr^{-1} are as follows: 35.6 and 12.4 for Celgard 2500 and Celgard 2400 and 18.6 and 13.0 for their laminates respectively.

As follows from this comparison the addition of a polypropylene web diminishes the rate of transport for a membrane of higher porosity, but, in the range of error, has no influence on lower porosity support. In the case of Celgard 4510—laminated membrane of higher porosity—the silver flux is still better than for Celgard

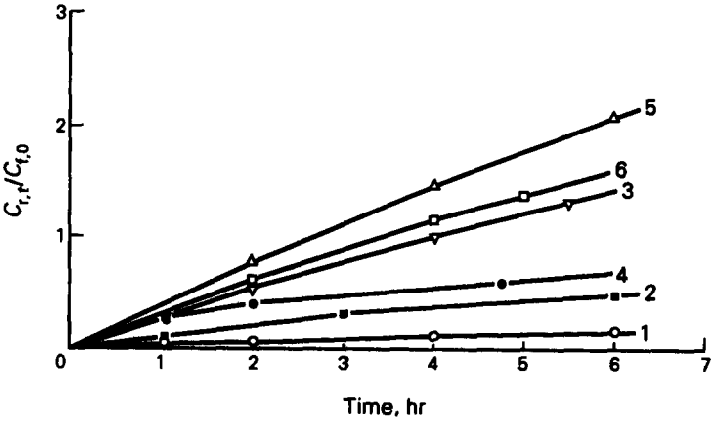

Fig. 2. Effect of the composition of feed solution on transport of silver through the liquid membrane supported on Celgard 4410. Composition of feed solution and TTD concentration in *m*-chlorotoluene: 1—pH 4.7, 0.002M $NaClO_4$; 0.01M TTD; 2—pH 4.7, 0.02M $NaClO_4$; 0.01M TTD; 3—pH 4.7, 0.05M $NaClO_4$; 0.1M TTD; 4—0.1M HNO_3; 0.1M TTD; 5—0.1M $HClO_4$; 0.1M TTD; 6—0.1M $HNO_3 + 0.05M$ $HClO_4$; 0.1M TTD. Feed solution: 500 ml, $10^{-4}M$ Ag. Receiving solution: 50 ml 0.1M $Na_2S_2O_3$, both phases stirred.

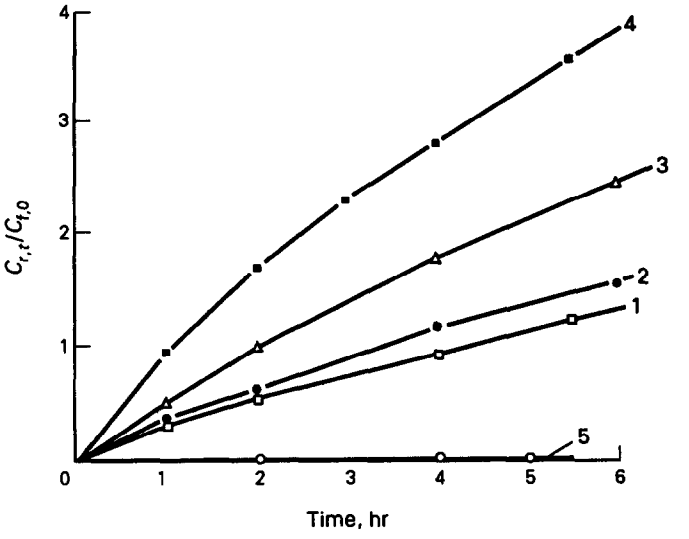

Fig. 3. Transport of silver ions from 0.1*M* HNO_3 + 0.05*M* $HClO_4$ solution across various Celgard membranes saturated with 0.1*M* TTD in *m*-chlorotoluene. 1—Celgard 2400; 2—Celgard 4410; 3—Celgard 4510; 4—Celgard 2500; 5—Celgard 2500 saturated with *m*-chlorotoluene (without TTD). Other conditions as for Fig. 2.

2400. Further investigations will be carried out for Celgard 2500 membranes. A blank experiment carried out for Celgard 2500 support saturated with *m*-chlorotoluene only (without ionophore) demonstrated no Ag transport (Fig. 3, curve 5).

Effect of stirring

In preliminary tests it was noticed that the rate of transport of Ag during a rest time (without stirring) was only *ca.* 5-fold lower than when both aqueous phases were stirred. Therefore the stirring in the receiver was abandoned. Next, the influence of the rate of stirring of the feed solution was investigated. For given compositions of both solutions the over-all transport rate seems to be limited by diffusion in the very thin organic layer and therefore increase in beyond gentle stirring contributes to the damage of the liquid membrane, as observed by partial loss of transparency and a diminishing of the Ag flux.

Transport of silver from solutions containing zinc, copper(II) and lead ions

It has been demonstrated previously[19,21] that TTD does not extract Cu(II), Pb or Zn, but besides silver, it forms extractable complexes also with mercury(II), palladium, gold and copper(I).

Transport of silver in the presence of another cation [Cu(II), Pb or Zn] or the mixture of four cations was examined. Results are presented in Table 2. Experiments were carried out for five hours. After that time a concentration of interfering cations in the stripping solution was negligible. It indicates that the "up-hill" transport of Ag is very selective relative to Cu(II), Pb and Zn ions.

The flux of silver is greater in a single cation system than in a binary or multi-cation system. This diminishing effect is more distinct for Zn and Pb than for Cu(II) ions. The flux of silver in the presence of 10-fold higher concentration of Cu(II), Zn or Pb equals respectively 83, 73, and 70% of that value for Ag transport in similar conditions, but without interferents.

In the literature, the opposing effects of a second cation in the bulk membrane[25,26] and the up-hill SLM[7-9] transport are reported. In the

Table 2. Transport of silver from a mixture with Cu, Zn and Pb

	Ions in source solutions				
Flux $J \times 10^8$ ($M cm^{-2} hr^{-1}$)	Ag	Ag +Cu(II)	Ag +Zn	Ag +Pb	Ag +Cu(II) +Zn + Pb*
Flux of silver	35.6	29.6	26.0	24.8	29.6
Flux of interfering ion	—	<0.05	<0.05	<0.05	<0.01 for each interferent

Source solution: 500 ml, 0.01*M* HNO_3 + 0.05*M* $HClO_4$, $10^{-4}M$ Ag, $10^{-3}M$ Cu(II) or Zn or Pb, optimum rate of stirring.

Receiving solution: 50 ml of 0.1*M* $Na_2S_2O_3$, unstirred.

Celgard 2500 membrane with 0.1*M* TTD in *m*-chlorotoluene.

*$10^{-4}M$ Cu(II), Zn, Pb.

case of an ionophore reacting with both cations, the flux of the target cation in the presence of a second cation was unchanged[7] or lower[8] than in a single-cation system. For ligands selective towards the first cation, the diminishing effect of the second cation was reported [Cd influence on Pd transport[25] with sulphur substituted macrocycles, Fe(III) effect on Cu(II) transport[9] with LIX 64], but small increasing effects[25] were also found. The reduction of Ag flux noticed in this study is difficult to explain because the copper(II), zinc(II) and lead(II) ions are not extracted or complexed by TTD, and their concentration is too low to produce a considerable change in the redox potential of the feed phase or in an ion strength. Therefore, surface phenomena rather than competition in complexation with the ionophore are probably responsible for the effect.

Dependence of silver accumulation on time and feed/receiving volume ratio

The time-dependence of Ag transport from Ag + Cu(II) + Zn + Pb mixture at 10:1 (curve 1) and 100:1 (curve 2) feed/receiving volume ratios is shown in Fig. 4. The shapes of both curves are very similar despite *ca.* 10-fold higher concentration of Ag in the 5-ml receiving solution (Fig. 4, curve 2). It indicates that the back-extraction reaction in the receiver does not control the overall rate of transport. After 24 hr equilibrium was not reached but the membrane was still working. The majority of Ag was removed selectively and concentrated in the receiver.

The dependence of silver accumulation in a receiving solution after a 24-hr experiment on the volume of the receiving phase is presented in Fig. 5. The enrichment coefficient of silver (curve 1 in Fig. 5) is almost inversely proportional to the volume of the stripping solution, so the amount of Ag (Fig. 5, curve 2) is, over a wide range, independent of the feed/receiving volume relation. For the highest volume ratio (500 ml:3 ml), the ratio of concentrations between the receiving and the feed solutions after a 24-hr process is 1.4 mg/ml to 1.4 μg/ml, *i.e.*, 10^3. The amount of silver selectively transferred during a 24-hr period into receivers of 3–50 ml volume ranges from 85 to 95% of the initial Ag. The highest enrichment coefficient obtained was equal to about 140 (for a 3-ml receiver).

Effect of initial silver concentration

The relation between an initial concentration of an analyte in a feed solution and its concentration response, after a fixed time of preconcentration, in a compartment separated by a liquid membrane, was investigated experimentally for uranium[16] and zinc[7] as well as being considered theoretically.[13]

The effect of the initial concentration on the value of the enrichment coefficient obtained

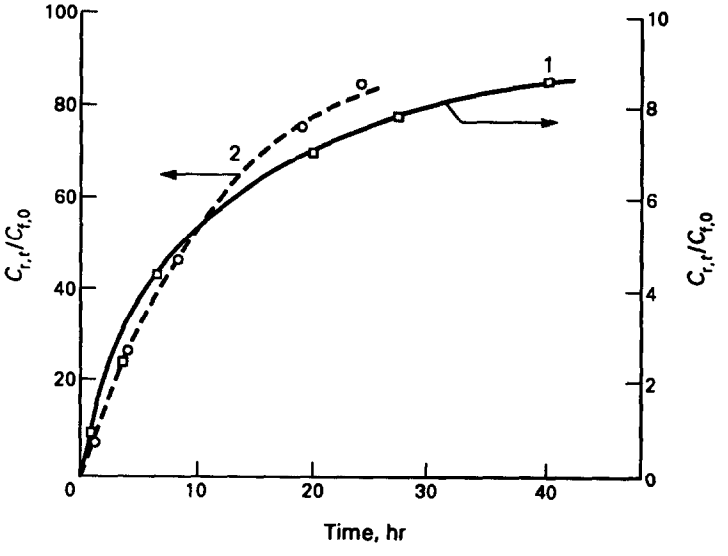

Fig. 4. Enrichment coefficient for Ag transport from Ag + Cu(II) + Zn + Pb mixture *vs.* time at two feed/receiving volume ratios. Feed solution: 500 ml, 0.1*M* HNO_3 + 0.05*M* $HClO_4$, 10^{-4}*M* Ag, stirred with optimum rate. Celgard 2500, 0.1*M* TTD in *m*-chlorotoluene. Curve 1—10^{-4}*M* Cu(II), Zn, Pb, in feed phase; 50 ml receiving phase (unstirred). Curve 2—10^{-3}*M* Cu(II), Zn, Pb in feed phase; 5 ml receiving phase (unstirred).

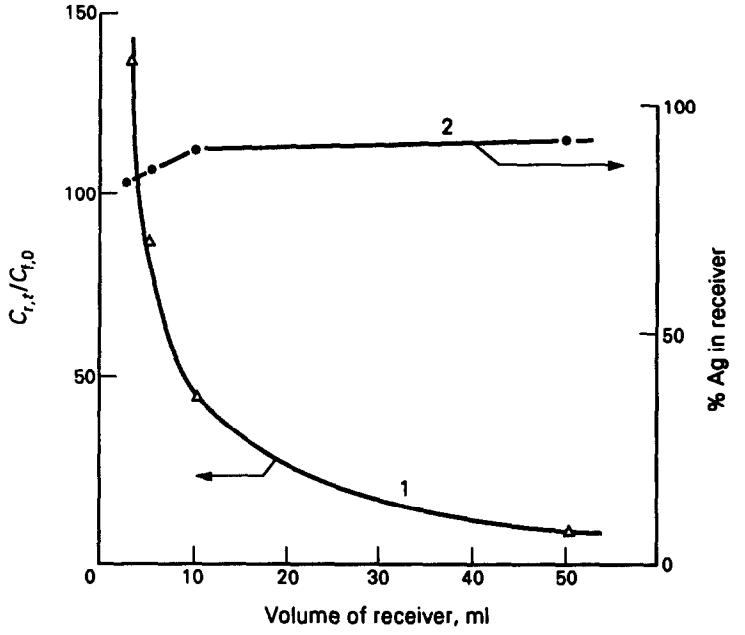

Fig. 5. Enrichment coefficient (curve 1) and amount of silver (curve 2) transferred to the receiver as a function of volume of receiving phase, 24 hours experiment. Feed solution: 500 ml, 0.1*M* HNO_3 + 0.05*M* $HClO_4$, 10^{-4}*M* Ag, 10^{-3}*M* Cu(II), Zn, Pb, stirred with optimum rate. Receiving solution: 0.1*M* $Na_2S_2O_3$ (unstirred), Celgard 2500, 0.1*M* TTD in *m*-chlorotoluene.

after a one-hour experiment is presented in Table 3. The ratio of sample to receiver volumes equals 100:1. In the range 10^{-6}–10^{-4}*M* Ag, the enrichment coefficient remains practically constant. A similar conclusion was drawn in the study of transport of zinc[7] and uranium[16] in the same concentration range.

CONCLUSION

The flux of silver through the SLM containing sulphide podand (1) depends on the composition of feed solution in a similar way to the distribution coefficient does in solvent extraction,[19] (2) increases in the sequence of membranes: Celgard 2400, Celgard 4410 < Celgard 4510 < Celgard 2500 and the rise of flux between Celgard 2400 and 2500 is higher than the ratio of their porosity, (3) is proportional to the initial Ag concentration, (4) is, over a wide range, independent of the stripping solution volume, (5) is selective towards Cu(II), Zn and Pb ions in 10-fold higher concentrations but (6) is diminished in their presence.

The highest observed concentration gradient between receiving and exhausted source phase was 1000, and the best enrichment factor equaled 140. The membrane with podand in *m*-chlorotoluene is stable for *ca.* 4 days.

Acknowledgement—The support for this research by the Ministry of Education through Grant No. T/09/195/90-2 is gratefully acknowledged.

Table 3. Effect of the initial silver concentration on the value of its enrichment coefficient after a one-hour process ($c_{r,1}/c_{f,0}$)

Ag concentration, *M*	$c_{r,1}/c_{f,0}$	*n*	R.S.D., %
10^{-4}	6.7	3	3.8
10^{-5}	6.5	4	2.9
10^{-6}	7.1	3	5.3

Source phase: 500 ml, 0.1*M* HNO_3 + 0.05*M* $HClO_4$, optimum stirring rate.
Receiving phase: 5 ml of 0.1*M* $Na_2S_2O_3$, unstirred.
2500 Celgard, 0.1*M* TTD in *m*-chlorotoluene.

REFERENCES

1. R. M. Izatt, G. C. Lind, R. L. Bruening, J. S. Bradshaw, J. D. Lamb and J. J. Christensen, *Pure and Appl. Chem.*, 1986, **58**, 1453.
2. R. D. Noble, J. D. Way, in *Liquid Membranes: Theory and Applications*, R. D. Noble, J. D. Way (eds.), pp. 1–26, 111–122. American Chemical Society, Washington DC, 1987.
3. E. Weber, *Kontakte (Darmstadt)*, 1984, 26.
4. J. D. Lamb, R. L. Bruening, R. M. Izatt, Y. Hirashima, P.-K. Tse and J. J. Christensen, *J. Membr. Sci*, 1988, **37**, 13.
5. R. M. Izatt, J. D. Lamb and R. L. Bruening, *Sep. Sci. Technol.*, 1988, **23**, 1645.

6. K. B. Yatsimirskii and G. G. Talanova, *Zh. Analit. Khim.*, 1990, **45**, 1686.
7. J. A. Cox and A. Bhatnagar, *Talanta*, 1990, **37**, 1037.
8. *Idem*, *Anal. Chem.*, 1988, **60**, 986.
9. J. A. Cox, A. Bhatnagar and R. W. Francis, Jr, *Talanta*, 1986, **33**, 713.
10. P. R. Danesi, L. Reichly-Yinger and P. G. Rickert, *J. Membr. Sci.*, 1987, **31**, 117.
11. H. Takeuchi, K. Takahashi and W. Goto, *ibid.*, 1987, **34**, 19.
12. M. Sugiura, M. Kikkawa, S. Urita and A. Ueyama, *Sep. Sci. Technol.*, 1989, **24**, 685.
13. M. Sugawara, H. Yoshida, A. Henmi and Y. Umezawa, *Anal. Sci.*, 1991, **7**, 141.
14. H. Sakamoto, K. Kimura and T. Shono, *Anal. Chem.*, 1987, **59**, 1513.
15. A. Ohki, T. Takeda, M. Takagi and K. Ueno, *J. Membr. Sci.*, 1983, **15**, 231.
16. K. Akiba and H. Hashimoto, *Anal. Sci.*, 1986, **2**, 541.
17. E. Weber and F. Vögtle, in F. L. Boschke (ed.), *Host-Guest Complex Chemistry*, Vol. I, p. 1. Akademie Verlag, 1982.
18. R. G. Pearson, *J. Am. Chem. Soc.*, 1963, **85**, 3533.
19. E. Lachowicz, A. Krajewski and M. Goliński, *Anal. Chim. Acta*, 1986, **188**, 239.
20. E. Lachowicz, *Analyst*, 1987, **112**, 1623.
21. E. Lachowicz and M. Czapiuk, *Talanta*, 1990, **10**, 1011.
22. K. Chayama and E. Sekido, *Anal. Sci.*, 1990, **6**, 883.
23. A. E. Martell and R. M. Smith, *Critical Stability Constants*, Vol. 3, Plenum Press, New York, 1977.
24. J. D. Lamb, J. J. Christensen, S. R. Izatt, K. Bedke, M. S. Astin and R. M. Izatt, *J. Amer. Chem. Soc.*, 1980, **102**, 3399.
25. R. M. Izatt, L. Eblerhardt, G. A. Clark, R. L. Bruening, J. S. Bradshow, M. H. Cho and J. J. Christensen, *Sep. Sci. Technol.*, 1987, **22**, 701.
26. R. M. Izatt, D. W. McBride, Jr, P. R. Brown, J. D. Lamb and J. J. Christensen, *J. Membr. Sci.*, 1986, **28**, 69.

Talanta, Vol. 39, No. 8, pp. 1039–1044, 1992
Printed in Great Britain.

0039-9140/92 $5.00 + 0.00

SUBCUTANEOUS MICRODIALYSIS PROBE COUPLED WITH GLUCOSE BIOSENSOR FOR *IN VIVO* CONTINUOUS MONITORING

D. MOSCONE and M. PASINI
Dipartimento di Scienze e Tecnologie Chimiche, Universitá di Roma Tor Vergata, 00173 Roma, Italy

M. MASCINI*
Dipartimento di Sanitá Pubblica, Epidemiologia e Chimica, Analitica Ambientale, Universitá di Firenze, Via Gino Capponi 9, 50121 Firenze, Italy

(*Received* 3 *June* 1991. *Revised* 2 *December* 1991. *Accepted* 4 *December* 1991)

Summary—Microdialysis probes have been tested to evaluate the influence of flow-rate, probe dimensions and temperature when used as sampling systems inserted subcutaneously for *in vivo* monitoring of glucose. The probe was coupled with a glucose biosensor obtained from a thin layer electrochemical cell generally used as detector for liquid chromatography. Glucose oxidase was immobilized on a nylon net membrane and it was placed over an acetate cellulose membrane into the cell in contact with the platinum anode.

Microdialysis is a new sampling technique for *in vivo* analysis and continuous monitoring.[1–3] The technique has been mainly developed for measurement of neurotransmitters in the brain and coupled to liquid chromatography to identify specific compounds.[4–6]

The *in vivo* continuous measurement of glucose is a challenge for developing a wearable artificial pancreas.

Needle shaped glucose biosensors have been developed for *in vivo* analysis and have been inserted subcutaneously or in the bloodstream of anaesthetized animals. The technique has been developed in a few laboratories[7–13] and several problems have arisen.

The production of useful biosensors is low (only 20–50% of sensors produced are useful); the biosensors have only been inserted in anaesthetized animals because any movement affects the output signal; the biosensors should be sterilized which impairs the enzyme activity; there is a marked variation in the sensitivity when biosensors are implanted *in vivo*;[8–10] this can only be controlled with an *in vivo* calibration of the device, which can only be done indirectly.[12]

There is also a potential health hazard. To leave a needle in the human body is considered a low risk if the site is subcutaneous, medium risk if intraperitoneal and high risk if it is placed directly into the blood stream.

However diabetics need a continuous glucose control and the dream of a closed loop artificial pancreas where the continuous output of a glucose biosensor drives the insulin infusion into a diabetic patient is a challenge for many research teams.

In this paper we show a complete apparatus suitable for *in vivo* glucose monitoring obtained by coupling a microdialysis probe and a glucose biosensor in a thin layer flow cell configuration. The system could be easily miniaturized for the development of a wearable glucose monitor.

The principle is outlined as follows: a physiological buffer is pumped at constant flow (10–30 μl/min) into a thin dialysis fiber with diameter of 200 μm (the microdialysis probe) placed subcutaneously (or in the bloodstream); the buffer equilibrates with the subcutaneous liquid (or with blood), then flows into a thin layer cell provided with a glucose biosensor which continuously monitors the glucose value. As microdialysis probe we compared *in vitro* a commercial probe and a single sterilized thin dialysis hollow fiber.

The system has several advantages over the insertion of a bioprobe-needle into the body; the sensitivity of the biosensor can be checked regularly, the hollow fiber used as microdialysis probe can be easily sterilized, it can be inserted

*Author for correspondence.

in animals and humans while awake; the overall process of the *in vivo* implantation can be controlled much more and processes such as inflammation and clotting (when inserted in bloodstream) can easily be followed and eliminated.

Preliminary experiments with a hollow fiber sterilized on animals and humans are discussed.

EXPERIMENTAL

Materials and apparatus

Glucose oxidase (GOD, E.C.1.1.3.4, from Aspergillus Niger, type VII, 132,000 U/g) was obtained from Sigma.

A GOD immobilized-nylon net membrane was prepared as previously reported.[14]

The glucose solution was prepared with β-$D(+)$glucose from Farmitalia Carlo Erba (Milano, Italy), allowed to equilibrate overnight and suitably diluted.

The buffer solution, Dulbecco's physiological buffer (pH = 7.4), was prepared in doubly distilled water.

All chemicals were analytical grade.

Cellulose acetate (53% acetyl) and polyvinyl acetate of high molecular weight were obtained from Farmitalia Carlo Erba (Milano, Italy). For casting the cellulose membrane a precision gauge tool (from Precision Gage and Tool Co., Dayton, OH, U.S.A.) was used. This membrane, with about 100 Dalton MWCO, was prepared as previously reported.[15-17]

Peristaltic pump, Minipuls 3, for flow analysis was from Gilson (France). Thermostat model F3 was from Haake.

Rheodyne valve (U.S.A.) Model 7125 was used as injection valve.

A complete thin-layer transducer cell for LCEC (liquid chromatography/electrochemistry) was obtained from BAS (BioAnalytical Systems, IN, U.S.A.). A LC-4B Amperometric detector from BAS was connected to an Amel Model 868 recorder.

The CMA/10 Microdialysis probe (fitted with a polycarbonate–polyether co-polymeric membrane, i.d. 400 μm, wall thickness 60 μm and molecular cut-off approximately 20,000 Dalton) was obtained from Carnegie Medicine (Stockholm, Sweden).

The hollow fiber Filtral 12 AN 69 HF polyacrylonitril sodium metalil sulphonate (i.d. 200 μm and molecular cut-off approximately 35,000 Daltons) was obtained from Hospal Industie (Meyziev, France).

Silicone tubing (i.d. 0.300 mm, o.d. 0.630 mm, wall thickness 0.165 mm) from A-M Systems and Teflon tubing (i.d. 0.330 mm, o.d. 0.482 mm, wall thickness 0.152 mm) from Firie (Genova, Italy) were used to connect hollow fibers to the flow-system.

Assembling of the sensor

A complete thin-layer transducer cell includes three separate electrodes: the working electrode (platinum disk with diameter of 3 mm), the reference (Ag/AgCl) and the auxiliary electrode (stainless steel). Figure 1 shows the assembly of the sensor.

A thin (20 μm) membrane of cellulose acetate was stretched over the entire plastic block where the electrode area was located; it removes the electrochemical interferences (uric acid, ascorbate, *etc.*) with its nominal MWCO of 100;[15-17] this figure is obtained as a rough number and mainly means that ascorbic and uric acids do not reach the electrode surface while hydrogen peroxide passes through easily. A dialysis membrane with a nominal claimed MWCO of 100

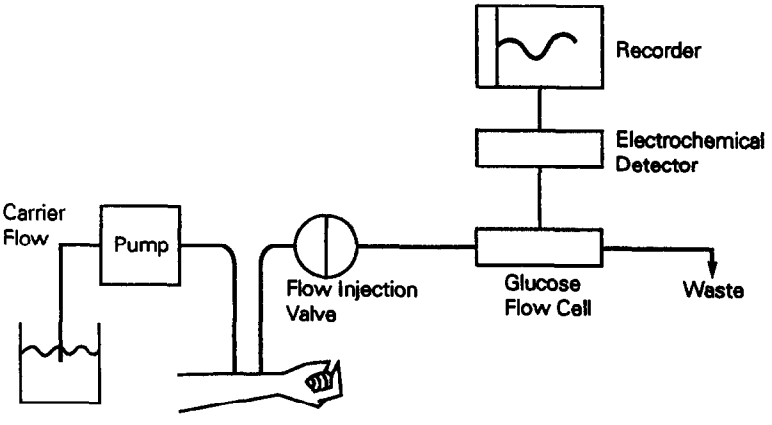

Fig. 1. Schematic diagram of the thin layer cell.

recently became commercially available from Spectrum Med. Ind. (CA, U.S.A.). Unfortunately this last membrane cannot be used, because it shows high interferences from uric and ascorbic acids, common substances in blood and subcutaneous liquid.

A nylon net (thickness 100 μm, with diameter of 6 mm) with the immobilized glucose oxidase enzyme was placed over the electrode area. Then a gasket is put on the half cell before assembling the cell. The upper half of the cell contains two ports to insert the inlet and outlet tubing.

The microdialysis probe is connected to the inlet tubing, the outlet is connected to the reference electrode and then to waste.

Procedures

The flow system for *in vitro* experiments is shown in Fig. 2. The peristaltic pump drives carrier solution through the microdialysis probe immersed in glucose standard solutions at constant rate. A steady-state current is obtained.

The standard solutions where the microdialysis probe was immersed were manually changed.

The CMA/10 probe was used as received. The hollow fiber probe (200 μm) was connected to the Teflon tubes of the flow system. *In vivo* experiments have been performed only with a sterilized hollow fiber.

To place the microdialysis hollow fiber subcutaneously a sterilized needle was inserted transcutaneously through the skin for about one centimeter and the needle tip was pulled out. Then the sterilized fiber was inserted from the needle tip and the needle taken out leaving the hollow fiber under the skin. The fiber was connected to Teflon tubes and fixed with epoxy glue.

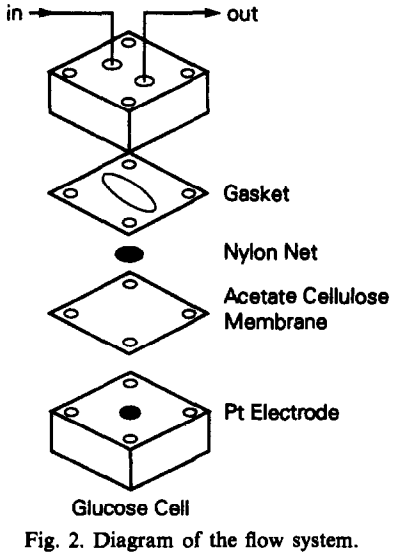

Fig. 2. Diagram of the flow system.

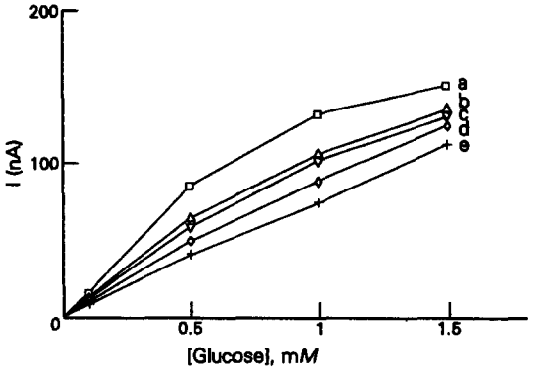

Fig. 3. Calibration curves of glucose biosensor at different flow-rates (without the microdialysis probe). (a) = 10 μl/min, (b) = 20 μl/min, (c) = 30 μl/min, (d) = 40 μl/min, (e) = 50 μl/min. Room temperature.

For checking variations in sensitivity during the experiments, a flow injection system was used. A Rheodyne injection valve with a 20-μl sample loop was introduced into the flow system just after the microdialysis probe. A glucose standard buffered solution filled the loop of the injection valve and flowed through the glucose biosensor.

Then we obtained a current profile similar to a peak. The dispersion coefficient of the apparatus was 1.1.

These peaks demonstrate the high reproducibility in "*in vitro*" experiments.

RESULTS AND DISCUSSION

In vitro *experiments*

Typical calibration curves for the glucose flow cell, without the microdialysis probe, at different flow-rates are shown in Fig. 3.

When the flow-rate is increased the linear range of the calibration curve increases and the current values decrease. This is a common experience with a glucose biosensor with hydrogen peroxide detection in a flow cell. The logical explanation is that hydrogen peroxide reaching the electrode surface decreases by increasing the flow-rate. This is due partly to a lower conversion of glucose and partly to a lower fraction of hydrogen peroxide reaching the electrode surface. Calibration curves obtained with hydrogen peroxide standards show a parallel variation with the flow-rate.

The non-linearity of the calibration curve at a concentration higher than about 1mM is

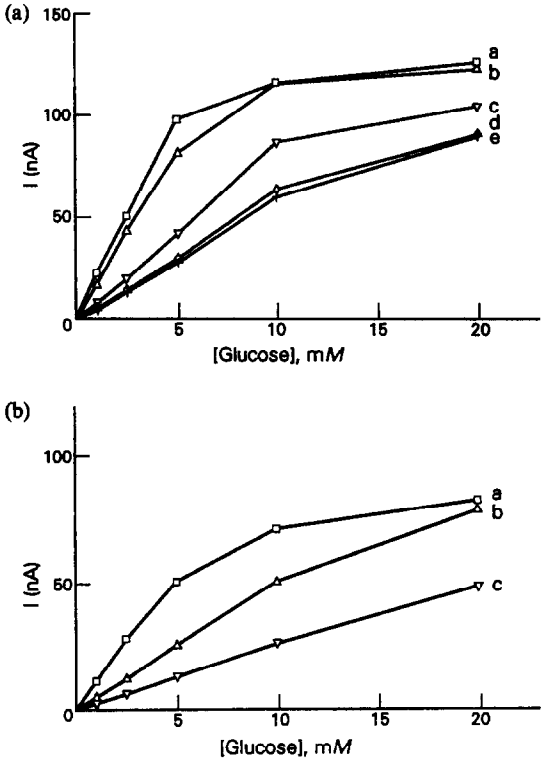

Fig. 4. Calibration curves of glucose with the microdialysis probe at different flow-rates. (a) CMA/10, length = 10 mm, $T = 37°$; (a) = 10 μl/min, (b) = 20 μl/min, (c) = 30 μl/min, (d) = 40 μl/min, (e) = 50 μl/min; (b) Hollow fiber, length = 20 mm, $T = 37°$; (a) = 10 μl/min, (b) = 30 μl/min, (c) = 50 μl/min.

mainly due to depletion of molecular oxygen, a cofactor in the glucose oxidase reaction.[18]

In Fig. 4(a) and 4(b) calibration curves are shown where the glucose biosensor is coupled with a microdialysis probe (CMA/10 and hollow fiber).

The upper limit of concentration attained in this case (20mM) is much higher and due to the limited diffusion of glucose through the microdialysis probe and reaching the glucose biosensor.

Besides this effect we observe a flow-rate influence as in Fig. 3, but in this case the diffusion rate through the microdialysis probe also affects the results.

It is interesting to notice how the two microdialysis probes show similar results in spite of the different materials and the different geometries (Carnegie length 10 mm and diameter of 400 μm, hollow fiber length 20 mm and diameter of 200 μm).

In Fig. 5 the length of the microdialysis probe (hollow fiber) was varied and the linearity range and the current values are greatly affected by this parameter. This is shown for the hollow fiber microdialysis probe, but similar results were obtained with the commercial probe.

To obtain a linear calibration curve up to 20mM (the high value for glucose in blood for diabetes) we chose a hollow fiber one centimeter long and a flow-rate of 30 μl/min. This flow is feasible for a wearable instrument, since it corresponds to less than 50 ml/day which can be stored easily.

In Fig. 6 dynamic curves are reported for the hollow fiber. The system, microdialysis and biosensor, shows such a fast response and recovery that it was difficult to forecast; only a few seconds are necessary to reach a stable current value corresponding to a defined concentration. The reproducibility of the current is very high, it was evaluated in several experiments as less than 5% over 10 consecutive assays.

Delay time was greatly reduced by using narrow bore tubing (Teflon tube 0.3 mm) between the microdialysis probe and the glucose biosensor (under 50 μl of volume).

The influence of temperature on the dialysis probe was evaluated. At 37° the current is about 30% higher and the linearity range is slightly reduced; this reflects the variation of the diffusion coefficient of the glucose through the microdialysis probe.

The stability of the signal with a hollow fiber during a ten-hour period was followed *in vitro*. Fluctuations smaller than 15% were generally obtained due to random variations in the experimental parameters.

Glucose biosensor is known to be stable during such interval of time, so it is not the primary source of fluctuation.

In vivo *experiments*

Fast response and recovery, simple apparatus and procedures have allowed the proposed

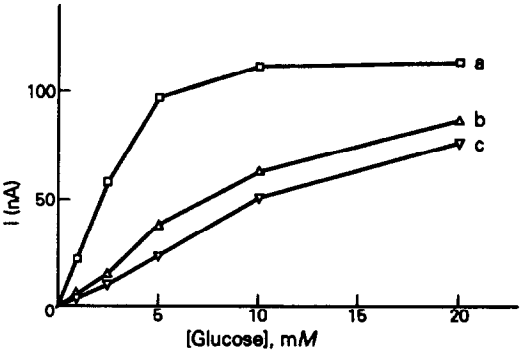

Fig. 5. Calibration curves of glucose with different membrane length microdialysis probes. Flow-rate = 30 μl/min, $T = 37°$, (a) = 40 mm, (b) = 20 mm, (c) = 10 mm.

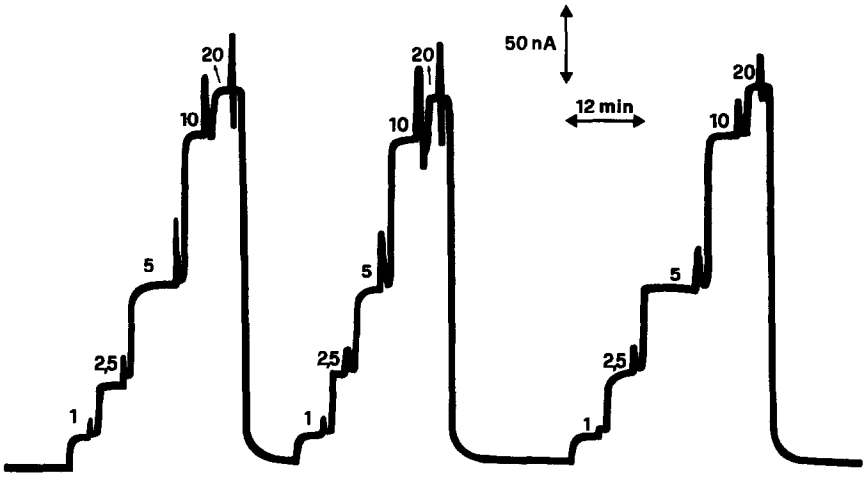

Fig. 6. Response time of the hollow fiber as microdialysis probe. Flow-rate = 30 μl/min, room temperature, membrane length = 20 mm.

method to be directly applied in *in vivo* experiments.

The fiber can be sterilized, it is rugged and easily handled and the material is reported to be highly biocompatible.[19]

Figure 7(a) shows preliminary results obtained monitoring glucose by sampling with a hollow fiber inserted subcutaneously in a rabbit [Fig. 7(a)] and in a human volunteer [Fig. 7(b)] during a glucose load experiment.

The stability of the signal before the glucose load shows how the removal of glucose by the probe does not disturb the physiological process. After a glucose load the current increases and then decreases following normal behavior. The variation of sensitivity was checked

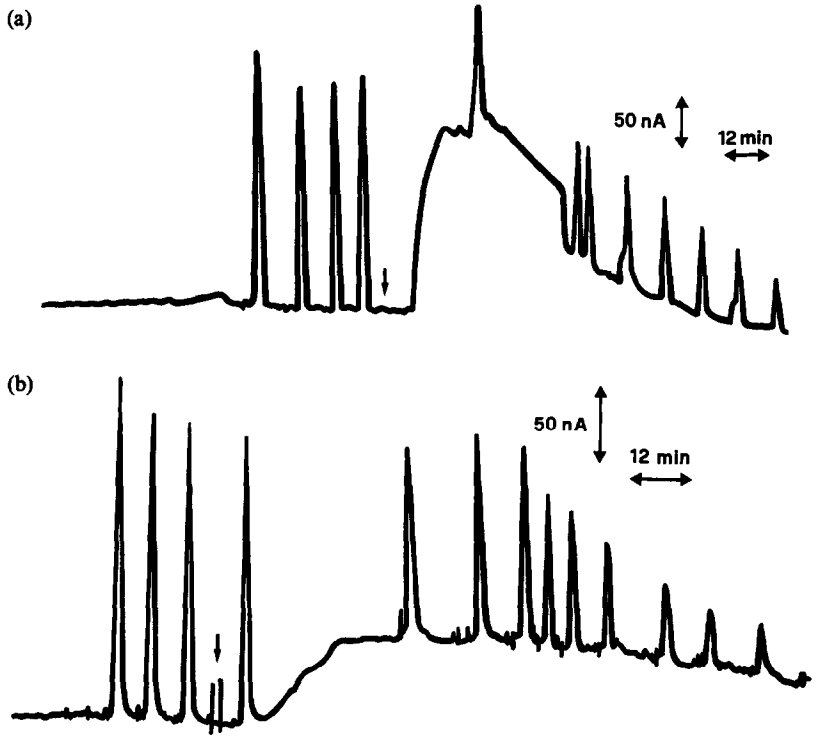

Fig. 7. *In vivo* experiments during glucose loading. Hollow fiber as microdialysis probe, flow-rate = 30 μl/min, membrane length = 10 mm; (a) rabbit weight 2.5 kg, fasting, unanesthetized (intravenous glucose loading = 3.5 g glucose). (b) On a human volunteer (oral loading = 70 g). The arrow shows the glucose administration. The peaks show the monitoring of sensitivity variation. The glucose standard solution was 1m*M*.

regularly by the flow injection apparatus described. A sharp decrease of the sensitivity is evident after about two hours in both experiments [Fig. 7(a) and (b)]. This effect was not previously detected.[20] If the microdialysis probe was disconnected and buffer as carrier was pumped through the cell, the glucose biosensor recovered the initial sensitivity in 15–30 min. We think an unknown substance is produced in the physiological liquid, probably in response to the fiber introduction. We believe it is released as a consequence of an inflammatory reaction and is able to diffuse through the hollow fiber and interfere with the enzyme or the electrode reaction.

This sensitivity variation can explain why the attempts to measure glucose *in vivo* by directly inserting needle glucose biosensors in blood or inserting subcutaneously fail more or less rapidly and it may explain the variations in sensitivity (slope of response *i vs.* concentration of glucose) reported in literature.[8–10] It is the first time that this phenomenon was followed during an *in vivo* experiment.

The problem of tissue reaction was reported recently in a few cases[10] to explain the high failure of subcutaneous glucose monitoring.

We are trying now to identify this compound and to use a suitable microdialysis fiber to overcome this problem.

However we did not notice this effect when the probe was inserted into the bloodstream; in this case normal behaviour was obtained and the output was related to the glucose concentration. Other experiments are now planned with clinicians for inserting the probes *in vivo* to obtain more data on this interesting effect.

CONCLUSIONS

The system shown is suitable for measuring glucose *in vivo* by coupling microdialysis with a glucose biosensor in the form of a thin layer cell. The system follows rapidly the variations of glucose concentration at the site where the "probe" is inserted. Preliminary results obtained placing the probe subcutaneously revealed the formation of an interferent species for the glucose oxidase enzyme or for the electrode. Such species are considered the result of an inflammatory reaction and it can explain the failure of experiments reported so far with the subcutaneous insertion of needle glucose biosensors.[8–10]

However, the same effect was not detected when the probe was placed in the bloodstream. We can explain it with the vascularized nature of the bloodstream but more *in vivo* experiments will clarify the nature of this effect.

Acknowledgement—This work has been supported by the C.N.R. Target Project Biotechnology and Bioinstrumentation, which is gratefully acknowledged.

REFERENCES

1. International Symposium on Microdialysis, Indianapolis, U.S.A., May 17–19, 1989.
2. C. F. Mandenius, *Anal. Letters*, 1988, **21**, 1817.
3. Bibliography on Microdialysis, by A. Eliasson, Carnegie Medicine, Stockholm, 1989.
4. P. K. Kissinger, *J. Chromatog.*, 1989, **488**, 31.
5. Y. L. Hurd, J. Kehr and U. Ungerstedt, *J. Neurochemistry*, 1988, **51**, 1314.
6. C. Speciale, U. Ungerstedt and R. Schwarcz, *Life Sci.*, 1988, **43**, 777.
7. M. Shichiri, N. Asakawa, Y. Yamasaki, R. Kawamori and H. Abe, *Diabetes Care*, 1986, **9**, 298.
8. R. Sternberg, M. B. Barrau, L. Gangiotti, D. Thevenot, D. Bindra, G. Wilson, G. Velho, P. Froguel and G. Reach, *Biosensors*, 1988, **4**, 27.
9. J. Pickup, G. Shaw, D. Claremont, *Diabetologia*, 1989, **32**, 213.
10. K. Rebrin, U. Fisher, T. Woedtke, P. Abel and E. Brunstein, *ibid.*, 1989, **32**, 573.
11. D. Matthews, E. Bown, T. Beck, E. Plotkin, L. Lock, E. Gosden and M. Wickham, *Diabet. Med.*, 1988, **5**, 248.
12. M. Koudelka, F. Rohner-Jeanrenaud, J. Terrettaz, E. Bobbioni-Harsch, N. de Rooij and B. Jeanrenaud, *Biosens. Bioelect.*, 1991, **6**, 31.
13. S. Churchouse, C. Battersby, W. Mullen and P. Vadgama, *Biosens.*, 1986, **2**, 325.
14. M. Mascini, G. Palleschi and M. Iannello, *Anal. Chim. Acta*, 1983, **156**, 135.
15. M. Mascini and F. Mazzei, *ibid.*, 1987, **192**, 9.
16. P. J. Taylor, E. Kmetec and J. M. Johnson, *Anal. Chem.*, 1977, **49**, 789.
17. G. Palleschi, M. A. Nabi Rahni, G. J. Lubrano, J. N. Ngwainbi and G. G. Guilbault, *Anal. Biochem.*, 1986, **159**, 114.
18. A. D. Gough, J. Y. Lucisano, P. H. S. Tse, *Anal. Chem.*, 1985, **57**, 2351.
19. Informations obtained by Hospal Industie.
20. T. Huang and P. Kissinger, *Current Separations*, 1989, **9**, (No. 1/2), 9.

Talanta, Vol. 39, No. 8, pp. 1045–1049, 1992
Printed in Great Britain.

0039-9140/92 $5.00 + 0.00

RELIABLE AND FACILE METHOD FOR PREPARATION OF SOLVENTLESS BILAYER LIPID MEMBRANES FOR ELECTROANALYTICAL INVESTIGATIONS

DIMITRIOS P. NIKOLELIS* and ULRICH J. KRULL†

Chemical Sensors Group, Department of Chemistry, Erindale Campus, University of Toronto, 3359 Mississauga Road North, Mississauga, Ontario, Canada L5L 1C6

(*Received* 25 *October* 1991. *Revised* 2 *December* 1991. *Accepted* 4 *December* 1991)

Summary—Bilayer lipid membranes continue to be of interest as elements for development and investigation of chemically-modified electrodes and biosensors, yet also continue to be difficult to prepare and replicate with precision. A simplified and reliable technique for the rapid formation of solventless bilayer lipid membranes is described, and the method has been shown to produce membranes which nominally vary by only 5–10% with respect to ion conductivity. Methods for rapid physical and chemical characterization of these membranes for establishment of reproducibility and quality are given.

Perturbation of the structure and electrostatic fields of artificial bilayer lipid membranes (BLMs) caused by a selective binding event of a "receptor" with a ligand (analyte) can be monitored electrochemically as changes in transmembrane conductivity. This strategy for the development of chemically-selective sensors has as the main advantage an increased sensitivity which is derived from an intrinsic amplification process.[1] Other favorable features of these membranes are fast response times, small size, a wide range of concentration level determination, flexibility for application of a wide variety of selective "receptors", and reversibility for continuous signal generation.

The perpetual problem faced by the sensor specialists has been the difficulty of preparation of BLMs with a lifetime that is sufficient for completion of electrochemical experiments. Planar BLMs are formed by the "brush" technique and the folding method. The former systems which retain the hydrocarbon solvent are referred to as "black lipid films" and the latter as "solventless" or "solvent-free" bilayers because they do not contain significant quantities of residual solvent. Retention of solvent reduces precision in electroanalytical experimentation and makes the use of solventless BLMs preferable. This technical note describes a method for the formation of solventless BLMs, which in our experience can provide BLMs suitable for experimentation in a period of minutes with a 90% success rate. Methods for physicochemical characterization of these membranes are also presented and a comparison of electrochemical properties with black lipid films and natural membranes are made.

EXPERIMENTAL

Reagents and apparatus

A number of different lipids can be used for the formation of stable BLMs.[2,3] The common feature among these lipids is that they usually have a head group of high polarity and two hydrophobic acyl chains. Egg phosphatidylcholine (PC) is commonly employed to form BLMs, and stearic acid, dipalmitoylphosphatidic acid (DPPA) and dipalmitoylphosphatidylserine (DPPS) can be used in a mixture with egg PC to prepare negatively charged membranes. Control of ion transport across BLMs can be made by chemical modification of interfacial regions between phase domains[4] or by adjustment of the amount of the negatively charged lipid in a membrane.[5]

Planar BLMs separate two aqueous phases and each side of the BLM must be in contact with an electrolyte solution (*e.g.*, 0.1*M* potassium chloride). Such a solution provides the inorganic ions desired for electrochemical studies and assists electrostatic stabilization of the structure of a membrane.

*University of Athens, Laboratory of Analytical Chemistry, Panepistimiopolis, Kouponia, GR 157 71, Athens, Greece.
†Author for correspondence.

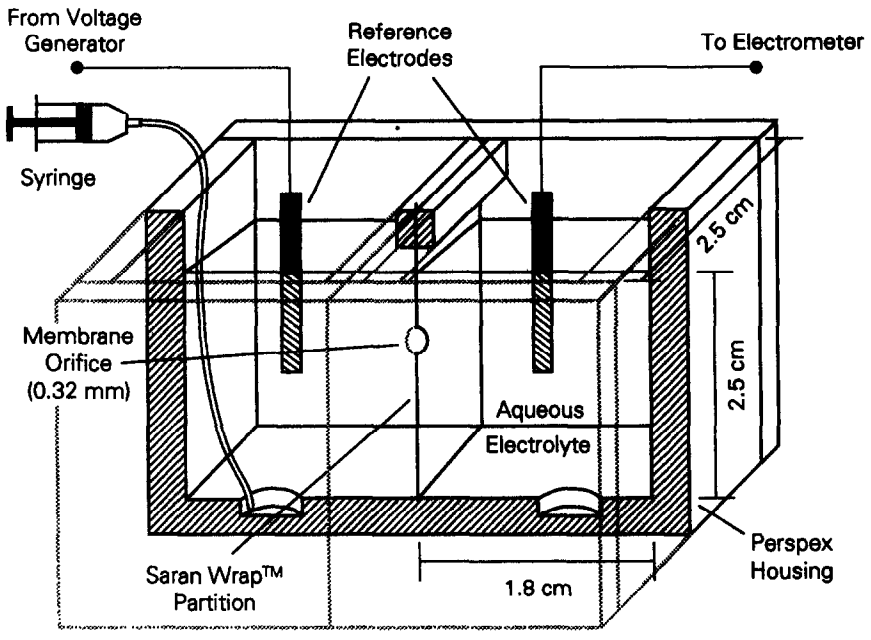

Fig. 1. Basic electrochemical cell used for the study of BLM. Gentle stirring (2.5 rpsec) can be done by a magnetic flea in the small well(s) (0.9 cm diameter) at the bottom of each chamber.

Simple apparatus for the formation of membranes consists of two chambers separated by a thin plastic sheet. Before the chambers are used, they should be hydrated and rinsed several times with purified water. The plastic sheet contains a small aperture in which the membrane is formed (Fig. 1). We have found that Saran Wrap® about 10 μm thick provides excellent results, and that a thicker partition results in membrane instability (although partitions of 25-μm thickness have been reported in the literature[2]). A paper cutter is used to shape the Saran Wrap® partition to the desired size, and care should be exercised to avoid contamination of the plastic partition with residue from one's fingers. The plastic sheet should extend beyond the limits of the edges of the chambers so that no ion current leakage can occur around this barrier. For the same reason the chambers should be clamped tightly together, but must not pinch or stretch the plastic sheet at points where the corners of the chambers meet. The aperture in the film can be made by punching with a perforation tool similar to the one described previously[6] (Fig. 2). The size of the aperture is critical for preparation of stable membranes. The protocol required for the formation of solvent-free bilayers is that such membranes should not have areas larger than 0.1 mm^2 otherwise they are unstable.[7] We have found that circular apertures of 0.32 mm diameter give BLMs with excellent stability over 4 hr, with lifetimes extending up to 24 hr, while BLMs formed in holes with diameters of about 0.6 mm last only about 1–5 min. The hole should be inspected visually with a microscope to measure the diameter and to ensure that the aperture is circular, and free of edge defects and irregularities.

A simple circuit that is commonly used for the measurement of the ion current through a BLM consists of a voltage reference source (VRS) and an electrometer with an input resistance much higher ($>10^{14}$ Ω) than the membrane resistance ($\sim 10^{10}$ Ω). An external DC potential of about 25 mV is applied across the BLM between a pair of reference electrodes (*e.g.*, Ag/AgCl or calomel) from the power supply to provide the driving force for ion transport across the membrane. The applied DC potential is small to restrict any substantial electrochemical reaction from occurring in the electrodes and also to avoid electroconstriction and membrane bulging. The electrochemical cell and electrometer should be shielded from external electromagnetic interference in a grounded copper screen Faraday cage.

Procedures

The formation of BLMs by the folding method was introduced by Takagi[8] and refined by Montal and Mueller.[9] The technique was based on the transfer of two opposing

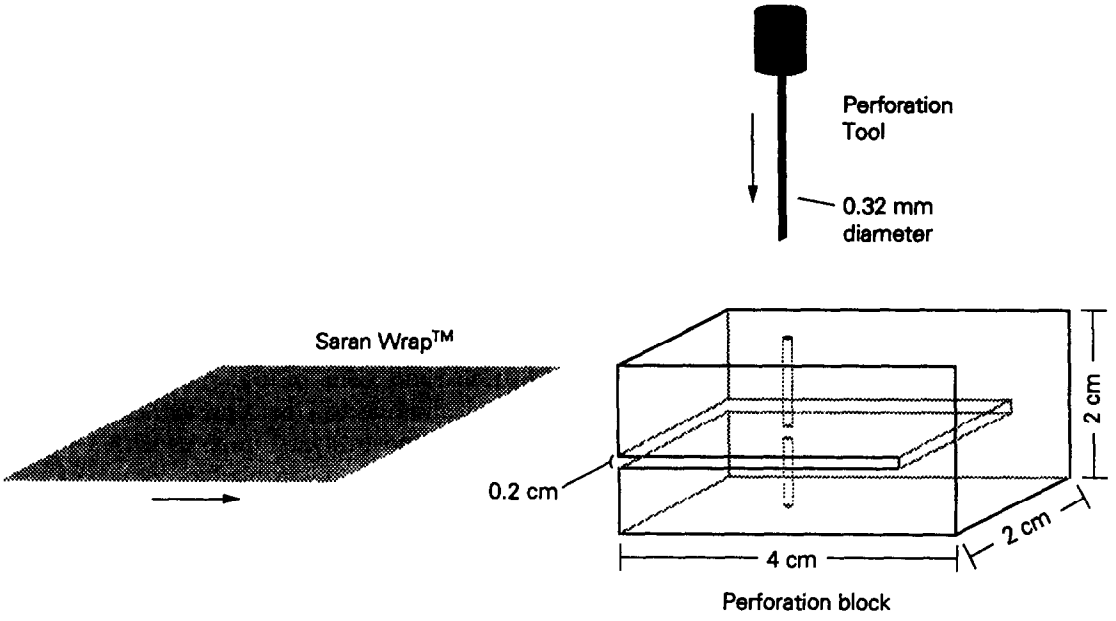

Fig. 2. The perforation tool used to punch an aperture in the Saran Wrap® sheet in which the bilayer is formed. Two stainless-steel plates were fixed at a common joint, and a hole (0.32 mm) was drilled through the plates. The punch was a steel rod which was sharpened. The Saran Wrap® sheet was clamped between the plates and a firm and fast movement was used to push the punch through the film so that the plastic did not warp or pinch.

monolayers at an air–water interface of a Teflon trough into a Teflon sheet by using the Langmuir–Blodgett dip casting technique. A simplified version of this method was later described for the formation of solventless bilayers.[2,10] Two Teflon chambers with a volume of about 2 ml each, an air–water interface of about 1 cm^2 each, and separated by a plastic septum were used instead of the Langmuir–Blodgett trough. The amount of the lipid used was in excess of the quantity to form a monolayer (5–10 μl of 0.1–1% w/v of lipid solution in *n*-hexane in each compartment), but the multilayer that was formed thinned to a bilayer structure. We have found that polymethylmethacrylate blocks with a volume of about 10 ml and an air–water interface of about 3 cm^2 for each cell can be used instead of the Teflon chambers. The lipid concentration can be less than that described previously to form stable membranes (0.02% w/v) with a substantially reduced torus volume.

For the formation of a membrane, the lipid solution (5–10 μl) is added dropwise to the water surface in one cell compartment. The drops are applied to the water surface near the partition and surface impurities are swept away from the partition as the lipid solution spreads at the air–water interface. Over a period of a few seconds the electrolyte level in one solution compartment is manually adjusted and is brought below the aperture level and then raised again with a 10-ml disposable syringe (with plastic tubing at the end). An amount of about

Table 1. Comparison of electrochemical properties of artificial BLMs and natural cell membranes

Property	Black lipid films	Solventless BLMs	Cell membranes
Membrane specific resistance (Ω cm^2)	10^6–10^8	10^6–10^8	$<10^6$
Membrane specific capacity ($\mu F/cm^{-2}$)	0.45 ± 0.05	0.9 ± 0.1	1.0 ± 0.2
Thickness of hydrocarbon region obtained from			
(a) Capacitance data	42 Å	22 Å	16–24 Å
(b) X-ray data	—	29 Å	28–35 Å
Increase of membrane conductance caused by the addition of 0.1 μM levels of Gramicidin	10^3	10^3	$<10^3$

2 ml of electrolyte solution is taken out from the cell compartment with the syringe. A flow-rate of about 3 ml/sec is used when the electrolyte solution is injected back to the chamber.

The formation of the membrane can be checked by monitoring the ion current through the aperture. In the unusual event that the first attempt for formation of a membrane is not successful, then an additional 5 to 10 μl of *n*-hexane can be spread across the air–water interface and the procedure for membrane formation can be repeated. The formation of a membrane takes only a few seconds, and many membranes can be formed by this technique in a short period of time, although each membrane requires about 5–10 min to fully stabilize before quantitative measurements can begin. This arrangement for membrane formation provides stable BLMs which last for periods of more than 4 hr, and in most cases the formation of BLMs is immediately successful. Pretreatment of the aperture with petroleum jelly or squalene is unnecessary and does not facilitate the formation of BLMs.[10]

The electrical capacitance of a membrane can be measured by applying a voltage step of 25 mV through the reference electrodes across the membrane. The time constant, τ, of current versus time is measured and the membrane capacitance, C_m, is calculated from the equation:

$$C_m = \tau J_0 / V \qquad (1)$$

where J_0 is the current extrapolated at zero time, and V the applied voltage. The capacitance of a membrane can also be measured directly with a lock-in amplifier by applying a sinusoidal waveform to the reference electrodes and observing the out-of-phase component of charge flow.

RESULTS AND DISCUSSION

Any BLMs used for electroanalytical experimentation must first be characterized to demonstrate the existence of the BLM structure, and to establish reproducibility. Specific capacitance is often used as the primary criterion mainly for characterization of membranes. In fact a few studies have been reported that involve capacitance measurements to detect selective binding interactions.[11] The specific capacitance of these solventless BLMs is almost twice the magnitude observed for black lipid films (0.9 ± 0.1 $\mu F/cm^2$) and approaches the corresponding value for natural cell membranes (Table 1). The values of specific capacitance can be used to estimate the hydrocarbon thickness, d, of a membrane using the equation:

$$C_m = \epsilon_0 \epsilon / d \qquad (2)$$

(ϵ_0, the permittivity of free space is 8.85×10^{-2} F/cm^2, and ϵ the dielectric constant of the hydrocarbon core of the membrane is 2.1). The membrane can be represented as a large capacitor (polar layers) in series with a smaller capacitor (the hydrophobic core of the membrane), and d is therefore almost equal to the thickness of the hydrocarbon layer of the membrane. The values of specific capacitance and apparent thickness for solvent-free membranes as compared with black lipid films indicate a decrease of the membrane thickness for the hydrocarbon region of the solventless BLMs and exclusion of the hydrocarbon solvent. Using PC as a lipid the apparent thickness for solventless BLMs was found to be about 25 Å.[4]

The specific resistance of the solventless BLMs and the black lipid films is similar ($\sim 10^8$ Ω/cm^2) and cannot be used to differentiate between the two structures. The membrane resistance can be calculated from the inverse of the slope of current–voltage recordings obtained when applying a linear ramp of voltage with time. The sweep-rate should be such that there is no substantial contribution of the capacitive current. Resistance can also be calculated from the steady-state values of current when applying voltage increments of about 20 mV. The linearity between current and voltage extends to about 400 mV (dielectric breakdown of these membranes).

Chemical characterization of the bimolecular thickness of solventless BLMs can be derived from addition of gramicidin (A, B or C) at concentration levels of about 0.1μM. This peptide transports cations through the membrane by formation of ion-channels and the conductance increases many fold as shown in Table 1. Gramicidin does not induce conductance changes if the membrane is thicker than one bilayer.[9]

Acknowledgement—We are grateful to the Natural Sciences and Engineering Research Council of Canada for financial support for this work.

REFERENCES

1. U. J. Krull and M. Thompson, *Trends Anal. Chem.*, 1985, **4**, 90.
2. M. Montal, in *Methods in Enzymology*, S. P. Colowick and N. O. Kaplan (eds.), Vol. 32, pp. 545–554. Academic Press, New York, 1974.
3. U. J. Krull and M. Thompson, *Anal. Chim. Acta*, 1983, **147**, 1.
4. D. P. Nikolelis, J. D. Brennan, R. S. Brown, G. McGibbon and U. J. Krull, *Analyst*, 1991, **116**, 1221.
5. D. P. Nikolelis, J. D. Brennan, R. S. Brown and U. J. Krull, *Anal. Chim. Acta*, 1992, **257**, 49.
6. P. Tancrède, P. Paquin, A. Houle and R. M. Leblanc, *J. Biochem. Biophys. Methods*, 1983, **7**, 299.
7. V. Vodyanoy and R. B. Murphy, *Biochim. Biophys. Acta*, 1982, **687**, 189.
8. M. Takagi, in *Experimental Techniques in Biomembrane Research*, T. Ohnishi (ed.), pp. 385–392. Nankodo Publ. Co., Tokyo, 1967.
9. M. Montal and P. Mueller, *Proc. Natl. Acad. Sci. USA*, 1972, **69**, 3561.
10. R. Benz, O. Fröhlich, P. Läuger and M. Montal, *Biochim. Biophys. Acta*, 1975, **394**, 323.
11. D. A. Haydon, J. R. Elliot, B. M. Henry and B. W. Urban, in *Molecular and Cellular Mechanism of Anasthesia*, S. H. Roth and K. W. Miller (eds.), pp. 267–277. Plenum Press, New York, 1986.

Talanta, Vol. 39, No. 8, pp. 1051–1055, 1992
Printed in Great Britain.

0039-9140/92 $5.00 + 0.00

CONSTRUCTION AND PERFORMANCE OF PROBE-TYPE CELLS CONNECTED IN A SERIES ASSEMBLY

MA WANLI

Research Institute for Material Protection, Wuhan Institute of Technology, Wuhan 430070, People's Republic of China

(*Received* 5 *February* 1991. *Revised* 24 *July* 1991. *Accepted* 26 *July* 1991)

Summary—Construction of a newly improved cells connected in series (CCS) assembly is introduced. The random error model presented by previous investigators has been revised. The assembly was so designed that it can be used in conventional ion-selective electrode measurements, but resulted in multiplied response thus enhancing the precision and accuracy of potentiometric analyses.

The CCS (cells connected in series) assemblies, proposed by Stepak[1,2] and Suzuki,[3] show promise in significantly enhancing the precision and accuracy of potentiometric analyses. Yet, their practical application is limited owing to the fact that they require rather large volumes of sample solution and are inconvenient to use. Although a microsized container may be used for each cell, filling each container with sample still remains a time-consuming and troublesome process. The resistance of the electrode membrane is far greater than that of the sample solution, so any attempt to test with all indicating and reference electrodes inserted in one beaker will prove futile. Therefore, separate cells must be employed. To make further improvements, other routes were tried. The construction of a CCS assembly which can be used like a conventional single electrode is described in this paper.

EXPERIMENTAL

Reagents

Demineralized doubly distilled water and A. R. grade chemicals were used throughout unless otherwise stated. Quinine hydrochloride was Chinese pharmacopoeia quality (>99%). Mono- and di-protonated quinine–tetraphenylborate (TPB) ion-pair complexes were prepared by mixing quinine hydrochloride and tetraphenylborate sodium solutions at pH = 2.0 and 6.0, respectively, in stoichiometric ratios.

Construction of the CCS assembly

The assembly mold was constructed as shown in Fig. 1.

The bottom cylinder, on which five square holes were uniformly bored, was actually made of two 5-mm diameter perspex plates. In each hole, a pair of indicating and reference electrodes were oppositely arranged to construct an independent unit. Together with a ready made perspex rod, the three parts were affixed with 10% perspex–acetone solution. The mold surface was coated with a thin layer of wax (melting point 90°) with an area left for the heads of the indicating and reference electrodes. The usual electrode membranes were then prepared separately by applying electroactive material dropwise[4] onto each silver disc. The membrane contained 30% (w/w) poly(vinyl chloride) (PVC) and 70% dibutyl-*o*-phthalate (DOP, in which about 5m*M* mono- or di-protonated quinine-TPB ion-pair complex was dissolved). A 0.1 potassium chloride solution was used for filling all Ag/AgCl reference electrodes; the loss of solution from the exits of their conduits can be compensated with an injector. When in use, the outlet wires of the required number of cells were connected in series. In case any unit had a defect, it was left out and a new one used instead. When the electrode membranes needed to be restored, the old membranes were scraped off and new ones were prepared by the same procedure.

EMF measurement

The sensing part of the assembly was immersed in the sample solution with stirring. After 20 sec, it was lifted above the water surface, and the samples in the different cells were separated due to the hydrophobicity of the wax. The output potential was monitored with

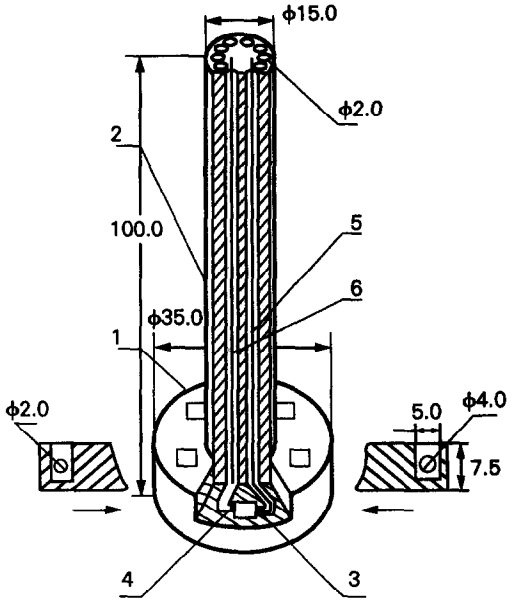

Fig. 1. The CCS assembly mold (units in mm). 1—perspex plate; 2—perspex rod; 3—silver disc, on which the electrode membrane was supported; 4—porous material, obtained from damaged Model 217 saturated calomel electrode (Shanghai, China); 5—shielded copper wire, bent to contact the silver disc; 6—Ag/AgCl wire, 0.5 mm in diameter.

an Orion 980 Digital Ion Analyser. After testing, the sample solutions can be easily cleaned by inserting a piece of rolled-up filter paper to each cell. The assembly was then ready for the next sample. The testing process of the proposed CCS assembly, as described, is almost the same as that of a conventional single electrode, except the recording of the potential was performed after the assembly had been lifted out of the solution. The assembly can also be applied for microsample testing. The sample could be added with a dropper; no more than two drops were needed for each cell. Calibration graphs for the assembly were obtained for

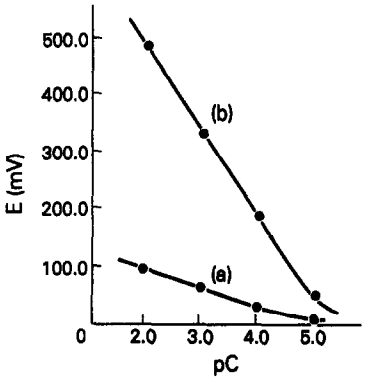

Fig. 2. Calibration curves for the CCS assembly with (a) $n = 1$ and (b) $n = 5$ at pH = 2.0.

Table 1. Experimental results: response slope (S_n), membrane resistance (R_n) and detection limit (pC_{lim})

pH	n	1	2	3	4	5
2.0	S_n	29.3	58.0	88.2	115.4	146.2
	R_n	15.1	31.6	44.5	62.0	78.3
	pC_{lim}	5.1	5.0	4.9	5.1	4.8
6.0	S_n	58.1	117.1	173.8	232.6	
	R_n	19.4	36.5	56.4	76.2	
	pC_{lim}	4.3	4.3	4.5	4.4	

ionic strength $I = 0.5$, pH = 2.0 and 6.0 buffered[5] solutions containing quinine in concentrations ranging from 10^{-5} to $10^{-2}M$, respectively.

RESULTS AND DISCUSSION

Performance of the CCS assembly

The calibration curves obtained with $n = 1$ and 5 at pH = 2.0 are demonstrated in Fig. 2, where n is the number of cells. The response slope, membrane resistance and detection limit are summarized in Table 1. The proposed CCS assembly resulted in an increased response slope, indicating that the output signal for a given concentration variation (sensitivity) can be amplified. The detection limit and selectivity coefficient (Table 2) remained the same as for the conventional electrode. When as many as five cells were connected in series, the multiplication of membrane resistance had no obvious influence on electrode behaviour.

Random error model

The measurement of potential is the major source of random error in potentiometry. Each connected unit contributes its potential (E_i) independently of the whole circuit (E), and each unit is also an independent source of random error. If one assumes that E_i is normally distributed around its true value (μ_i) with variance

Table 2. Selectivity coefficients obtained by both the CCS assembly ($n = 4$) and conventional PVC membrane electrode ($n = 1$). pH = 6.0, mixed solution method

Interference	pK_{ij}	
	Conventional	CCS
NaCl	4.06	4.13
KCl	3.38	3.29
$CaCl_2$	4.87	4.90
$MgSO_4$	4.77	4.73
Diethylamine	1.08	1.05
Tetramethyl ammonium bromide	1.30	1.31
Vitamin B_6	1.74	1.73

Table 3. Deviation analysis for the experimental results. pC = 3.0, degrees of freedom = 10 − 1

pH	n	1	2	3	4	5
	$S_E^{(n)}$	0.95	1.21	1.52	1.56	1.73
2.0	$S_{pC}^{(n)} \times 10^2$	1.91	1.22	1.01	0.79	0.69
	F	1.00	0.41	0.28	0.17	0.13
	$S_E^{(n)}$	1.06	1.50	1.34	1.89	
6.0	$S_{pC}^{(n)} \times 10^2$	1.66	1.61	0.70	0.67	
	F	1.00	0.49	0.18	0.16	

*$F_{(0.025)9,9} = 0.248$[6].
$S_E^{(n)}$—standard deviation of measured potential.
$S_{pC}^{(n)}$—standard deviation of pC determination.
F—F-analysis, comparing the precisions of pC determination results obtained by the CCS assembly with $n = 1$ and $n = n$, respectively.

(d_i), $N(\mu_i, d_i)$, then upon the convolution principle of normal distribution,[6]

$$E = \sum_{i=1}^{n} E_i = N\left[\sum_{i=1}^{n} \mu_i, \left(\sum_{i=1}^{n} d_i^2\right)^{1/2}\right] \quad (1)$$

For all units made under the same conditions, assume $d_1 = d_2 = \cdots = d_n$, then

$$\frac{S_E^{(n)}}{S_E^{(1)}} = \frac{\left(\sum_{i=1}^{n} d_i^2\right)^{1/2}}{d_i} = \sqrt{n} \quad (2)$$

The standard deviations of determination (S_x) and of the measured potential (S_E) are related by

$$\frac{S_x^{(1)}}{S_x^{(n)}} = n\frac{S_E^{(1)}}{S_E^{(n)}} \quad (3)$$

Comparing with equation (2) yields

$$\frac{S_x^{(1)}}{S_x^{(n)}} = \sqrt{n} \quad (4)$$

Note that the assumption made by Parczewski and Stepak,[2] that $S_E^{(n)}$ does not depend on n, is invalid.

For $S_E^{(n)}[=\sqrt{n}S_E^{(1)}] > S_E^{(1)}$, it was demonstrated experimentally that, unlike a conventional single electrode whose potential can usually stabilize to within 1.0 mV, the data fluctuated on the digital frame in a certain range (about 4 mV for $n = 5$ in our experiment). The potential finally recorded was the value which appeared most often, this usually occurred at the centre of the potential fluctuation range, and

Table 4. Deviation analysis for simulated samples ($N = 1000$)

n	1	2	3	4	5
$S_E^{(n)}$	1.00	1.42	1.73	1.96	2.23
ΔE(max, min)	5.92	8.52	11.07	12.73	14.70

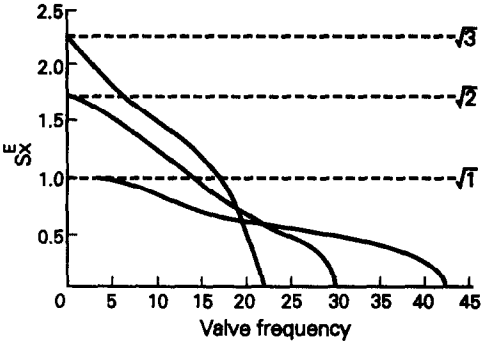

Fig. 3. Filtering tendencies for $n = 1$, 3 and 5.

is where the true value in a normal distribution exists. Therefore, a filtering process occurred when the data were recorded. With more cells connected in series, the resulting wider potential fluctuation range allowed easier estimation of the midpoint range (true value). The improved precision was actually better than when calculated with equation (4).

Model verifications

Experimental results. The experimental result obtained by Parczewski and Stepak[2] [$S_x^{(1)}/S_x^{(n)}$ approaches $\sqrt{n}$] has already proved the validity of equation (4). It largely originates from the cumulative effect of random errors and not by the appearance of new error sources.

Here we offer another example for further verification. Summarized in Table 3 is the deviation analysis result for replicate determinations on the sample pC = 3.0 at pH = 2.0 and 6.0, respectively. All the tested ratios of $S_E^{(n)}$ to $S_E^{(1)}$ are found to be approximately equal to or less than $\sqrt{n}$, indicating that the determination precision has been enhanced $\sqrt{n}$ times or more. According to the density function of normal distribution, the dispersion degree of the random errors will be reduced with improved precision. Thus the accuracy of a single determination will also be statistically enhanced. F-Analysis demonstrates that, when $n \geqslant 3$ for

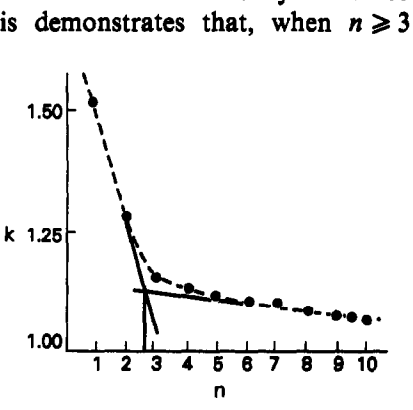

Fig. 4. Standard deviation decrease (k) *vs.* no. of cells (n).

Table 5. Recovery of quinine hydrochloride tested both with the CCS assembly (pH = 2.0, $n = 4$; pH = 6.0, $n = 3$) and with the conventional single electrode

	pH = 2.0 Found and % Recovery				pH = 6.0 Found and % Recovery			
Added *mg/ml*	CCS		Conv.		CCS		Conv.	
3.970	3.969	100.0	3.962	99.8	3.970	100.0	3.954	99.5
1.191	1.189	99.8	1.211	101.7	1.190	99.9	1.210	101.6
0.397	0.395	99.5	0.388	97.7	0.394	99.2	0.395	99.5
0.119	0.120	100.8	0.123	103.4	0.120	100.8	0.122	94.1
0.0397	0.0398	100.3	0.0389	98.0	0.0392	98.7	0.0403	101.5
0.0119	0.0119	100.0	0.0122	102.5	0.0120	100.8	0.0122	102.5

pH = 6.0 or $n \geqslant 4$ for pH = 2.0, this kind of enhancement is significant at $\alpha = 0.05$.

To achieve a full appreciation of what this means, more samples are needed which should be obtained under ideal conditions.

Monte Carlo simulation. The random errors of a definite cell are assumed normally distributed with a standard deviation of 1.0 around its mathematical expectation 0.0, $N(0.0, 1.0)$. At a given moment, this equals $(E_i - \mu_i)_t$. The momentary potential deviation of the assembly can be calculated by summing up the errors generated by all the cells connected at the moment.

$$\Delta E_t = \sum_{i=1}^{n} (E_i - \mu_i)_t \qquad (5)$$

Table 4 shows the computer simulation results with 1000 samples for $n = 1, 2, \ldots, 5$, respectively.

Obviously, the $S_E^{(n)}/S_E^{(1)}$ approaches $\sqrt{n}$ as expected, and also, the potential variation range grows wider with increasing n.

To observe the filtering effect, all the generated samples have been accurate to 0.1 mV and their frequencies counted. By increasing the valve frequency in steps, the samples whose frequencies are less than the valve value will be gradually filtered off. The random errors of the samples left are then analysed and the results are shown in Fig. 3.

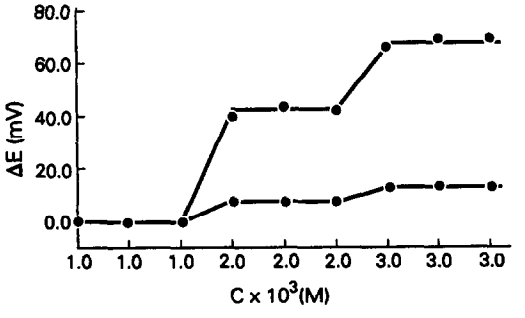

Fig. 5. Step potential signal monitored by both the CCS ($n = 5$) assembly and the conventional single electrode when the concentration of quinine changes stepwise from $1.0 \times 10^{-3}M$ to $2.0 \times 10^{-3}M$ to $3.0 \times 10^{-3}M$, pH = 2.0.

Higher precision is obtained as more lower-frequency samples are filtered off. The efficiency of this kind of improvement increases with the number of cells connected. However, the cells cannot be added infinitely. Apart from the consideration that connecting too many cells may generate a potential exceeding the maximum determination range of the employed instrument, the standard deviation reduction (k) with one extra cell

$$k = \frac{S_x^{(n)}}{S_x^{(n+1)}} = \sqrt{\frac{n+1}{n}} \qquad (6)$$

becomes negligible when n reaches a certain level. As shown in Fig. 4 the improvement becomes small at $n > 2$–3, *i.e.*, 3 or 4 cells would be appropriate.

Application

Shown in Table 5 are the results for the determination of quinine hydrochloride obtained by both the CCS assembly and a corresponding conventional PVC membrane electrode through repetitive measurements (three repetitions). It is obvious that those obtained with the proposed CCS assembly show improved precision and accuracy. It cannot be denied that, through repetitive measurements, conventional single electrodes can also provide accurate data. However, single electrode measurements may have deviations up to 5%. For the proposed CCS assembly, the deviation is scarcely more than 1%, which is the result of the significant enhancement of the precision of determination. From Table 5, $F_{(\text{CCS, Conventional})} = 0.061$ $(F_{0.025,11,11} = 0.288)$[6] can be calculated.

The assembly can also be used for process monitoring. A slight potential change which might be missed when testing with a conventional single electrode can be expanded when testing with the proposed CCS assembly. Figure 5 illustrates the relative response changes.

The system is particularly useful for multivalent ions, for which the response slope is small for corresponding single electrodes.

REFERENCES

1. R. Stepak, *Z. Anal. Chem.*, 1983, **315**, 629.
2. A. Parczewski and R. Stepak, *ibid.*, 1983, **316**, 29.
3. K. Suzuki, *Anal. Lett.*, 1987, **20**, 1773.
4. S. Z. Yao, J. Shiao and L. H. Nie, *Talanta*, 1987, **34**, 977.
5. P. J. Elving, J. M. Markowitz and I. Rosenthal, *Anal. Chem.*, 1956, **28**, 1179.
6. D. A. S. Fraser, *Probability and Statistics*, Theory and Application, Wadsworth Publishing Co., Belmont, California, U.S.A., 1976.

Talanta, Vol. 39, No. 8, pp. 1057–1059, 1992
Printed in Great Britain

0039-9140/92 $5.00 + 0.00
Pergamon Press Ltd

LETTER TO THE EDITORS

SIRS,

It has been drawn to our attention that in our paper on further developments of the RAMESES algorithm,[1] after commenting on the potential for error from the representation of species such as $Al(OH)_3$ by "AlH_{-3}", ironically we ourselves failed to realize the consequences of this notation when we were using the log β values given in the literature for the test systems[2,3] selected, primarily because no explanation was given there. In particular, we failed to recognize that the values reported corresponded to what in IUPAC nomenclature[4,5] would be log $^*\beta$ values, and hence should have been corrected by the addition of $-n \log K_w$ (where K_w is the ion product for water) to convert log $^*\beta$ for a species designated MLH_{-n} into log β for the corresponding species $ML(OH)_n$. For example, the log β value we used for $[Cu_2(cit)_2OH^{3-}]$ in System II should have been 25.87 instead of 11.90. The result was that the log β values reported for System II,[2,3] and program ES4EC,[2] were mistakenly criticized by us, and we unreservedly apologize to Professor Sammartano and his co-workers for any trouble or embarrassment caused them in consequence. We take this opportunity to say that a similar error arose in our computation[6] for other systems tested where such a notational difficulty was present, but we should add that there were no previous results published which might have alerted us to the problem.

However, after making the necessary corrections to the log β values and recalculating for System II with RAMESES, we still found discrepancies between our results and those reported by De Robertis *et al.*[2] The reason for these differences was eventually traced to a printer's error in that paper, where the list of constants for System II, on p. 391, included the species $[CuNi(cit)H_{-2}]$, and this was the species we had used in our calculation. However, this species *should* have been $[CuNi(cit)_2H_{-2}]$, as is shown by examination of the footnotes to Table 4 in that paper and correction of a further printer's error for species (18), where Cu had been omitted from the formula. It may also be noted that species (12) should have been $[Cu_2(cit)H_{-1}]$, not $[Cu(cit)H_{-1}]$; we made a similar error in proof-reading ourselves in our own paper,[1] where a species was given as (10) $[Ca_2(cit)_2OH_2^{4-}]$ instead of $[Cu_2(cit)_2(OH)_2^{4-}]$. Recalculation for System II with the correct formula gives good agreement with the results reported by De Robertis *et al.*[2] and excellent agreement with an independent calculation with program EQCAL.[7] Figure 1 shows the extraordinarily and unexpectedly large effect of this apparently trivial error, on the proper distribution of the species concerned.

We believe that confusion may have arisen in the past because of the nature of the various computer programs developed for such calculations, most of which use $[H^+]$ as a variable but exclude $[OH^-]$, though some allow use of $[OH^-]$ instead. It may be noted that RAMESES handles $[H^+]$ and $[OH^-]$ together directly, because the dissociation of water is used as an explicit equilibrium, essential for proper accounting and charge balance. If, as appears to be the case, the notation under discussion has arisen from program limitations, it is seen to be entirely unnecessary. Whether these other programs may be modified is unknown. Even so, RAMESES handles negative stoichiometry coefficients without difficulty, and we have rerun each of the relevant systems in that style and obtained results identical to those achieved with what we regard as the more realistic convention.

The definition of $^*\beta$ was given in the first[4] and subsequent editions of "Stability Constants of Metal Ion Complexes" and again in the IUPAC Information Bulletin.[5] A clear explanation is given by Sillén in a review[8] and an illustration has been given by Dyrssen *et al.*[9] The notion of treating addition of OH^- as equivalent to abstraction of H^+ from H_2O dates back to about 1954, when it appeared in a footnote to a paper by Sillén,[10] and was used in a paper by Hietanen and Sillén.[11] The first use of the H_{-n} notation seems to be about 1961, though with β instead of $^*\beta$.[12] Its use is implied in the Appendix to the description of MINIQUAD (example 3, where $^*\beta$ is called β'),[13]

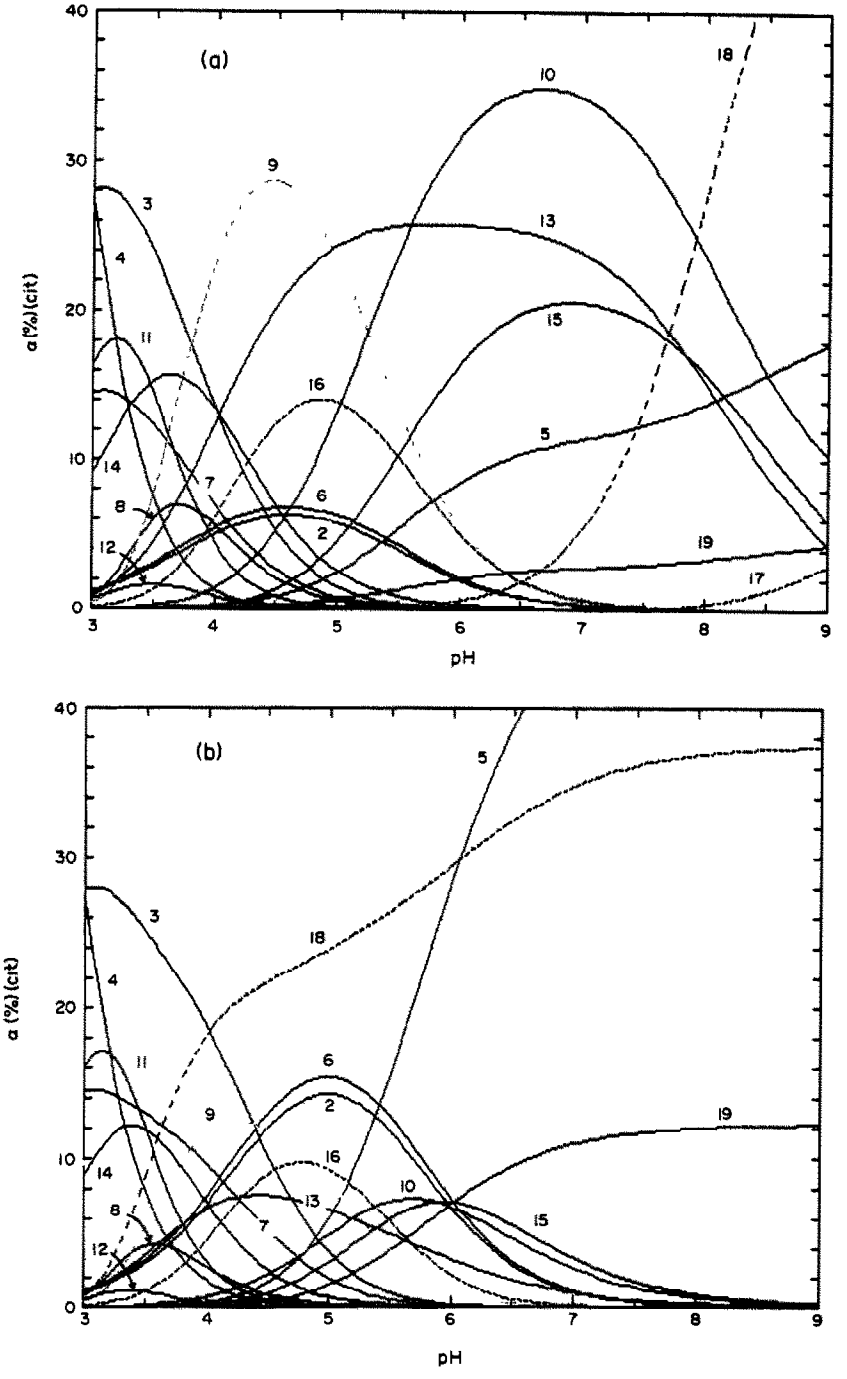

Fig. 1. The species distribution for System II, calculated by RAMESES with (a) species (18) taken correctly as $CuNi(cit)_2H_{-2}$; (b) species (18) taken incorrectly, as $CuNi(cit)H_{-2}$. The correctly calculated distribution is in good agreement with that reported by de Robertis *et al.*[2] The species are (2) [H(cit)]; (3) [H_2(cit)]; (4) [H_3(cit)]; (5) [K(cit)]; (6) [K(cit)H]; (7) [K(cit)H_2]; (8) [$Cu_2(cit)_2$]; (9) [$Cu_2(cit)_2H_{-1}$]; (10) [$Cu_2(cit)_2H_{-2}$]; (11) [Cu(cit)H]; (12) [$Cu_2(cit)H_{-1}$]; (13) [Ni(cit)]; (14) [Ni(cit)H]; (15) [$Ni(cit)_2$]; (16) [$Ni(cit)_2H$]; (17) [$Ni(cit)_2H_{-2}$]; (18) [$CuNi(cit)_2H_{-2}$]; (19) [cit] (this species was not shown in Fig. 2 in reference 2). α (%) (cit) indicates the citrate content of a species, calculated as a percentage of total citrate.

and an explicit use can be found in 1979 (with β instead of $^*\beta$).[14] A further trap for the unwary is that in the case of polynuclear hydroxo complexes, such as $Fe_3(OH)_4^{5+}$, the subscript used to identify β in tabular material generally has the number of hydroxide ions (or number of hydrogen ions "released") given *first*, *e.g.*, β_{43} in the example quoted.

We hope that this letter will help to prevent confusion and error in the future, and make amends for any in the past. Nevertheless, the fact of the existence of such an error and the large number of programs for computation of species distribution leads us to wonder whether a suite of validation examples should be assembled and a "Round Robin" conducted to compare results. We would be happy to act as convenors for such an exercise, which should ultimately be to everyone's benefit. Potential participants are invited to write to us to express an interest in the first instance.

We should like to thank Dr R. A. Chalmers and Dr M. R. Masson of the University of Aberdeen for help with the historical aspect of this letter and the EQCAL calculation, respectively.

REFERENCES

1. B. W. Darvell and V. W.-H. Leung, *Talanta*, 1990, **37**, 413.
2. A. De Robertis, C. de Stefano and S. Sammartano, *Anal. Chim. Acta*, 1986, **191**, 385.
3. C. de Stefano, P. Princi, G. Rigano and S. Sammartano, *Comput. Chem.*, 1988, **12**, 305.
4. J. Bjerrum, G. Schwarzenbach and L. G. Sillén (eds.), *Stability Constants of Metal Ion Complexes*, Part II, *Inorganic Ligands*, p. xiii. Chemical Society, London, 1958.
5. *IUPAC Information Bulletin*, 1966, No. 26, p. 25.
6. B. W. Darvell and V. W.-H. Leung, *Talanta*, 1991, **38**, 875.
7. L. Backman, *EQCAL*, Biosoft, Cambridge, 1988.
8. L. G. Sillén, *Quart. Rev.*, 1959, **13**, 146.
9. D. Dyrssen, D. Jagner and F. Wengelin, *Computer Calculation of Ionic Equilibria and Titration Procedures*, p. 40. Almqvist & Wiksell, Stockholm; Wiley, London, 1968.
10. L. G. Sillén, *Acta Chem. Scand.*, 1954, **8**, 299.
11. S. Hietanen and L. G. Sillén, *ibid.*, 1954, **8**, 1607.
12. L. G. Sillén, *ibid.*, 1961, **15**, 1981.
13. A. Sabatini, A. Vacca and P. Gans, *Talanta*, 1974, **21**, 53.
14. P. Amico, P. G. Daniele, V. Cucinotta, E. Rizzarelli and S. Sammartano, *Inorg. Chim. Acta*, 1979, **36**, 1.

B. W. Darvell
V. W.-H. Leung

Dental Materials Science Unit
The Prince Philip Dental Hospital
34 Hospital Road
Hong Kong

23 *January* 1992

Talanta, Vol. 39, No. 8, pp. 1061–1064, 1992
Printed in Great Britain.

0039-9140/92 $5.00 + 0.00

BOOK REVIEWS

Analysis of Substances in the Gaseous Phase: E. SMOLKOVA-KEULEMANSOVA and L. FELTL, in Comprehensive Analytical Chemistry, Volume XXVIII, G. Svehla (editor), Elsevier, Amsterdam, 1991. Dfl 400.00.

This book has been a great disappointment to me. Books on gas analysis are few and far between, and the subject is rarely dealt with in modern analytical textbooks, yet it is a field of analytical chemistry which occupies many workers, both in plant control and in environmental monitoring. A glance at the glossy trade journals shows how many manufacturers are vying for their share of the market for dedicated gas analysers as well as for gas chromatographs, infrared spectrometers and mass spectrometers. And yet, in spite of the publisher's claim that this volume "provides a comprehensive description of the state of the art," I find it distinctly weak on the modern instrumental techniques.

A short chapter on "Qualitative and semi-quantitative methods" deals only with chemical detector tubes. This would be a very slow and expensive way of dealing with an unknown gas. I would first record the infrared absorption spectrum, surely the most powerful technique for identification, and would then measure the gas density to get the molecular weight. Gas density is mentioned briefly (later on) only as the basis of certain on-line gas analysers.

Infrared spectrometry is dismissed, along with UV and visible techniques, in a brief 12 pages, most of it is taken up with a general account of dispersive spectrometers and general spectrophotometry. Bolometers and pneumatic detectors are listed as components for IR instruments, but none of the modern semiconductor detectors, nor the pyro-electric capacitative detectors, ideal for small portable instruments with modulated light sources, are mentioned. FT-IR has apparently not been discovered yet, which is a pity when it is capable of giving good quantitative performance over several orders of magnitude down to ppm concentrations when used with a variable long-path cell.

A discussion of mass spectrometry for gas analysis need not dwell on the theory of deflection of ions, but should give help on the type of inlet system to be purchased for gas analysis. To dismiss the possibilities as "cold" (relevant), "hot" (irrelevant for gases) and chromatographic (very rare for gas analysis) is to demonstrate a lack of appreciation of the real problems. The choice between membrane, ceramic and jet inlet systems is rather important, and depends on the type of sample, the analyte, and the type of pumping system used. Sample flow systems with membranes are excellent for trace organic vapours in air but are, for example, useless for trace permanent gases such as O_2 in high-purity argon.

The authors are clearly more at home when dealing with gas chromatography, though here again the introductory section could have been shortened to advantage. The merits of flow control versus pressure control for carrier gas are compared, but the authors do not point out that one cannot combine flow control with a gas sampling valve, which is the usual sample introduction device for gas samples, because it takes too long for the loop to be filled up with carrier gas, resulting in severe peak broadening. Later, in a section on columns, PLOT columns are mentioned, but nowhere are we told what types are now available, and what impressive separations can be achieved (such as the argon–oxygen separation at room temperature, or light hydrocarbon analysis for many isomers). Mention is made of graphitised carbon black, which is useful for polar organic molecules, but it is not clear to me what steroid analysis (Fig. 10.45) has to do with gas analysis. Under detectors we are given a wrong cross reference to 9.3.4 for the flame photometric detector, and there (in 9.3.3) we find a statement that the response is *linear* to sulphur compounds, when it is well documented that the relationship is a square law one due to the emission originating from the S_2 molecule.

So, do we perhaps get a good account of the widely used chemical methods of gas analysis, based on pumping through selective absorbents followed by selective colour chemistry? I am afraid the answer is no. This section is a mere four pages long and does not even give a comparison of the performance of different methods for the determination of SO_2, surely the most widely determined air pollutant.

The topic of standards for the calibration of gas analysers is an important one, and also a difficult one. It is therefore a pity that we are told that gases "cannot be weighed simply. . ." because this *is* the only way to make accurate gas mixtures of non-reactive gases. And we are neither told about making mixtures by pressure nor the problems of non-ideality.

So, what does fill these pages? There are twenty pages on classical volumetric methods including drawings of the apparatus of Orsat, Hempel and Gooderham, and a great many pages of background material to the instrumental techniques. What a pity to waste this opportunity to produce a book for which there is a real need. There are plenty of people struggling with the real problems of gas analysis who would welcome a book with a good account of the modern methods and solutions to some of their difficulties. This book will probably be of little assistance to them and they will have to look elsewhere or wait patiently.

I. L. MARR

Wilson and Wilson's Comprehensive Analytical Chemistry Volume XXIV—Energy dispersive X-ray Fluorescence Analysis: B. DZUNIKOWSKI, Elsevier, Amsterdam, 1989. Pages xx + 431. Dfl 420.00.

The aim of this book is to "present in a concise manner the physical principles and some technical aspects of EDXRFA and to survey its various applications". In this aim the book seems to succeed, with a very practical vein running throughits entire length.

Talanta, Vol. 39, No. 8, pp. 1061–1064, 1992
Printed in Great Britain.

0039-9140/92 $5.00 + 0.00

BOOK REVIEWS

Analysis of Substances in the Gaseous Phase: E. SMOLKOVA-KEULEMANSOVA and L. FELTL, in Comprehensive Analytical Chemistry, Volume XXVIII, G. Svehla (editor), Elsevier, Amsterdam, 1991. Dfl 400.00.

This book has been a great disappointment to me. Books on gas analysis are few and far between, and the subject is rarely dealt with in modern analytical textbooks, yet it is a field of analytical chemistry which occupies many workers, both in plant control and in environmental monitoring. A glance at the glossy trade journals shows how many manufacturers are vying for their share of the market for dedicated gas analysers as well as for gas chromatographs, infrared spectrometers and mass spectrometers. And yet, in spite of the publisher's claim that this volume "provides a comprehensive description of the state of the art," I find it distinctly weak on the modern instrumental techniques.

A short chapter on "Qualitative and semi-quantitative methods" deals only with chemical detector tubes. This would be a very slow and expensive way of dealing with an unknown gas. I would first record the infrared absorption spectrum, surely the most powerful technique for identification, and would then measure the gas density to get the molecular weight. Gas density is mentioned briefly (later on) only as the basis of certain on-line gas analysers.

Infrared spectrometry is dismissed, along with UV and visible techniques, in a brief 12 pages, most of it is taken up with a general account of dispersive spectrometers and general spectrophotometry. Bolometers and pneumatic detectors are listed as components for IR instruments, but none of the modern semiconductor detectors, nor the pyro-electric capacitative detectors, ideal for small portable instruments with modulated light sources, are mentioned. FT-IR has apparently not been discovered yet, which is a pity when it is capable of giving good quantitative performance over several orders of magnitude down to ppm concentrations when used with a variable long-path cell.

A discussion of mass spectrometry for gas analysis need not dwell on the theory of deflection of ions, but should give help on the type of inlet system to be purchased for gas analysis. To dismiss the possibilities as "cold" (relevant), "hot" (irrelevant for gases) and chromatographic (very rare for gas analysis) is to demonstrate a lack of appreciation of the real problems. The choice between membrane, ceramic and jet inlet systems is rather important, and depends on the type of sample, the analyte, and the type of pumping system used. Sample flow systems with membranes are excellent for trace organic vapours in air but are, for example, useless for trace permanent gases such as O_2 in high-purity argon.

The authors are clearly more at home when dealing with gas chromatography, though here again the introductory section could have been shortened to advantage. The merits of flow control versus pressure control for carrier gas are compared, but the authors do not point out that one cannot combine flow control with a gas sampling valve, which is the usual sample introduction device for gas samples, because it takes too long for the loop to be filled up with carrier gas, resulting in severe peak broadening. Later, in a section on columns, PLOT columns are mentioned, but nowhere are we told what types are now available, and what impressive separations can be achieved (such as the argon–oxygen separation at room temperature, or light hydrocarbon analysis for many isomers). Mention is made of graphitised carbon black, which is useful for polar organic molecules, but it is not clear to me what steroid analysis (Fig. 10.45) has to do with gas analysis. Under detectors we are given a wrong cross reference to 9.3.4 for the flame photometric detector, and there (in 9.3.3) we find a statement that the response is *linear* to sulphur compounds, when it is well documented that the relationship is a square law one due to the emission originating from the S_2 molecule.

So, do we perhaps get a good account of the widely used chemical methods of gas analysis, based on pumping through selective absorbents followed by selective colour chemistry? I am afraid the answer is no. This section is a mere four pages long and does not even give a comparison of the performance of different methods for the determination of SO_2, surely the most widely determined air pollutant.

The topic of standards for the calibration of gas analysers is an important one, and also a difficult one. It is therefore a pity that we are told that gases "cannot be weighed simply. . ." because this *is* the only way to make accurate gas mixtures of non-reactive gases. And we are neither told about making mixtures by pressure nor the problems of non-ideality.

So, what does fill these pages? There are twenty pages on classical volumetric methods including drawings of the apparatus of Orsat, Hempel and Gooderham, and a great many pages of background material to the instrumental techniques. What a pity to waste this opportunity to produce a book for which there is a real need. There are plenty of people struggling with the real problems of gas analysis who would welcome a book with a good account of the modern methods and solutions to some of their difficulties. This book will probably be of little assistance to them and they will have to look elsewhere or wait patiently.

I. L. MARR

Wilson and Wilson's Comprehensive Analytical Chemistry Volume XXIV—Energy dispersive X-ray Fluorescence Analysis: B. DZUNIKOWSKI, Elsevier, Amsterdam, 1989. Pages xx + 431. Dfl 420.00.

The aim of this book is to "present in a concise manner the physical principles and some technical aspects of EDXRFA and to survey its various applications". In this aim the book seems to succeed, with a very practical vein running throughits entire length.

The physical principles underlying the technique are covered first, with treatments of the basic ideas of atomic spectroscopy and the generation of primary (incident) and secondary (sample) radiation. I found the references in these early chapters to experimental evidence, supporting the assertions made, somewhat sketchy and they could possibly have been augmented with more diagrams relating to the examples cited to prove the postulated ideas.

The practical basics concerned with production and detection of the relevant radiations continued with descriptions of X-ray sources and typical EDXRFA spectrometers. At this stage a significant amount of theoretical background was hinted at, but I found this section contained too much unsubstantiated theory—merely quoting equations without derivation can be confusing. Doubtless reference to the bibliography would fill in these gaps but I did find it rather disconcerting. While one appreciates the scope of the work as a practical guide, some derivations, in an Appendix say, would have been welcome. One further point regarding this—I found the free flow of interchange between computational/theoretical discussion and extremely practical considerations of techniques somewhat off-putting. This tended to interrupt the flow for the systematic reader.

After the introduction of the basics, a further comprehensive series of techniques used in actual measurements are discussed, eventually evolving into a discussion of the computational techniques used in modern analysis.

It was slightly disconcerting to read the book and find that the precise definition of what constitutes the energy-dispersive technique and the consequent distinction between wavelength ($d\theta/d\lambda$) and energy (dV/dE) dispersive techniques does not emerge explicitly until Chapter 5. More seriously, having covered almost half of the book I found myself wondering about questions of sensitivity of the technique, and how precise in absolute terms these measurements are, since there is no account of these given early in the work.

The last 1/3 of the book is devoted to an account of some practical applications, including at last an indication of the vital facts regarding the sensitivity of the technique (in fact typically 10^{-3}% in careful quantitative analyses). The examples given rounded off the discussion, indicating the highly practical nature of EDXRFA in geology, processing control and in trace analysis, including the important field of air pollutants, among others. In the latter section (Chapter 13) there is finally a justification given for EDXRFA, when it is said that it is advantageous because of its "rapidity, possibility of simultaneous detection of several elements and satisfactory detection and determination limits"; again a point it would have been good to know at an earlier stage.

In general, I found the layout of the book not terribly clear, but as a 'dip-in' reference and bibliographic text, the information is clearly all there. It is a practical book, leaning heavily away from detailed, in depth discussions of theory, as opposed to discussions of basics, which are well covered. My main criticism of the book is the lack of an introductory chapter to capture the imagination, define the problem, give a short account of the achievements and limitations of the technique and put the succeeding discussions rather more into context. This would certainly induce more enthusiasm in the reader for finding out what EDXRFA can do and how it does it.

C. C. WILSON

Standardization Within Analytical Chemistry: P. KIVALO, Akadémiai Kiadó, Budapest, 1989. Pages 155 + appendices. US$36.00.

As a scientific discipline, analytical chemistry is a branch of metrology. As Lord Kelvin pointed out, "... when you can measure what you are speaking about and express it in numbers, you know something about it." The expression of analytical information in numbers unfortunately cannot always be referred uniquely to the basic physical constants. For this reason it is often necessary to specify in detail how the measurement is to be performed. Uniform procedures are essential if the highest reliability and repeatability are to be attained. The requisite definitions, procedures, and calculations are collectively embodied in the standardization for each particular measurement.

This book discusses in detail the several aspects of standardization and the steps in their development. Standard methods or techniques are based on sound scientific principles. Nevertheless, standardized or test methods for specific purposes or commercial products must often take into account the individual characteristics of the material to be analysed in order to ensure quality control and fitness for the intended purpose. In these instances, "pure" analytical chemistry becomes "applied" analytical chemistry in the development of protocols and certified reference materials. This process, the domain of numerous national and international standardizing bodies, is traced with logic and clarity in the seven chapters of the book.

Following an introduction, the history of analytical chemistry and the development of metrology are reviewed briefly. In chapters 3 and 4, the reader is introduced to early international standardization efforts, especially through ISO and IEC (of which Lord Kelvin was the first president), and the International Union of Pure and Applied Chemistry (IUPAC). Chapter 5, at 53 pages the longest of the book, is devoted to such matters as terminology, sampling and quality assurance, collaborative studies, and standard reference materials. The latter subject may merit more attention than it receives in the few pages allotted to it. Reference standards are currently available in a variety of forms, and they may be certified for composition or for many different properties critical to special analytical problems. The short final chapters discuss legal aspects and future trends in standardization.

Especially commendable is the inclusion, among the appendices, of the 49-page ISO Guide 2-1986, "General terms and their definitions concerning standardization and related activities." Terms relating to all aspects of standardization are defined in English, French, and Russian, while the equivalent terms in German, Spanish, Italian, Dutch and Swedish are listed.

This book is recommended to all who are concerned with the development, nature, and application of analytical standards.

R. G. BATES

The physical principles underlying the technique are covered first, with treatments of the basic ideas of atomic spectroscopy and the generation of primary (incident) and secondary (sample) radiation. I found the references in these early chapters to experimental evidence, supporting the assertions made, somewhat sketchy and they could possibly have been augmented with more diagrams relating to the examples cited to prove the postulated ideas.

The practical basics concerned with production and detection of the relevant radiations continued with descriptions of X-ray sources and typical EDXRFA spectrometers. At this stage a significant amount of theoretical background was hinted at, but I found this section contained too much unsubstantiated theory—merely quoting equations without derivation can be confusing. Doubtless reference to the bibliography would fill in these gaps but I did find it rather disconcerting. While one appreciates the scope of the work as a practical guide, some derivations, in an Appendix say, would have been welcome. One further point regarding this—I found the free flow of interchange between computational/theoretical discussion and extremely practical considerations of techniques somewhat off-putting. This tended to interrupt the flow for the systematic reader.

After the introduction of the basics, a further comprehensive series of techniques used in actual measurements are discussed, eventually evolving into a discussion of the computational techniques used in modern analysis.

It was slightly disconcerting to read the book and find that the precise definition of what constitutes the energy-dispersive technique and the consequent distinction between wavelength ($d\theta/d\lambda$) and energy (dV/dE) dispersive techniques does not emerge explicitly until Chapter 5. More seriously, having covered almost half of the book I found myself wondering about questions of sensitivity of the technique, and how precise in absolute terms these measurements are, since there is no account of these given early in the work.

The last 1/3 of the book is devoted to an account of some practical applications, including at last an indication of the vital facts regarding the sensitivity of the technique (in fact typically 10^{-3}% in careful quantitative analyses). The examples given rounded off the discussion, indicating the highly practical nature of EDXRFA in geology, processing control and in trace analysis, including the important field of air pollutants, among others. In the latter section (Chapter 13) there is finally a justification given for EDXRFA, when it is said that it is advantageous because of its "rapidity, possibility of simultaneous detection of several elements and satisfactory detection and determination limits"; again a point it would have been good to know at an earlier stage.

In general, I found the layout of the book not terribly clear, but as a 'dip-in' reference and bibliographic text, the information is clearly all there. It is a practical book, leaning heavily away from detailed, in depth discussions of theory, as opposed to discussions of basics, which are well covered. My main criticism of the book is the lack of an introductory chapter to capture the imagination, define the problem, give a short account of the achievements and limitations of the technique and put the succeeding discussions rather more into context. This would certainly induce more enthusiasm in the reader for finding out what EDXRFA can do and how it does it.

C. C. WILSON

Standardization Within Analytical Chemistry: P. KIVALO, Akadémiai Kiadó, Budapest, 1989. Pages 155 + appendices. US$36.00.

As a scientific discipline, analytical chemistry is a branch of metrology. As Lord Kelvin pointed out, "... when you can measure what you are speaking about and express it in numbers, you know something about it." The expression of analytical information in numbers unfortunately cannot always be referred uniquely to the basic physical constants. For this reason it is often necessary to specify in detail how the measurement is to be performed. Uniform procedures are essential if the highest reliability and repeatability are to be attained. The requisite definitions, procedures, and calculations are collectively embodied in the standardization for each particular measurement.

This book discusses in detail the several aspects of standardization and the steps in their development. Standard methods or techniques are based on sound scientific principles. Nevertheless, standardized or test methods for specific purposes or commercial products must often take into account the individual characteristics of the material to be analysed in order to ensure quality control and fitness for the intended purpose. In these instances, "pure" analytical chemistry becomes "applied" analytical chemistry in the development of protocols and certified reference materials. This process, the domain of numerous national and international standardizing bodies, is traced with logic and clarity in the seven chapters of the book.

Following an introduction, the history of analytical chemistry and the development of metrology are reviewed briefly. In chapters 3 and 4, the reader is introduced to early international standardization efforts, especially through ISO and IEC (of which Lord Kelvin was the first president), and the International Union of Pure and Applied Chemistry (IUPAC). Chapter 5, at 53 pages the longest of the book, is devoted to such matters as terminology, sampling and quality assurance, collaborative studies, and standard reference materials. The latter subject may merit more attention than it receives in the few pages allotted to it. Reference standards are currently available in a variety of forms, and they may be certified for composition or for many different properties critical to special analytical problems. The short final chapters discuss legal aspects and future trends in standardization.

Especially commendable is the inclusion, among the appendices, of the 49-page ISO Guide 2-1986, "General terms and their definitions concerning standardization and related activities." Terms relating to all aspects of standardization are defined in English, French, and Russian, while the equivalent terms in German, Spanish, Italian, Dutch and Swedish are listed.

This book is recommended to all who are concerned with the development, nature, and application of analytical standards.

R. G. BATES

The Kirk-Othmer Encyclopedia of Chemical Technology: Volume 1, Fourth Edition. A to Alkaloids. J. I. KROSCHWITS, M. HOWE-GRANT, M. BICKFORD and L. GRAY (editors), Wiley-Interscience, Chichester, 1991. Pages xxxii + 1087. £135.00.

Volume one of the fourth edition of this *Encyclopedia* covers topics in alphabetical order ranging from ablative materials to alkaloids. The volumes in the previous third edition were published between the years 1978 to 1984 and hence I expect it will be some considerable time before all volumes in this new edition appear. All the articles in the new work are reported to have been rewritten and updated with many new subjects added.

Contributions to the first volume have been made by 65 authors (nearly all from the U.S.A.) and 33 topics have been covered. The more dominant topics include (1) acrylamide, acrylic ester and acrylonitrile polymers, (2) adsorption (gas and liquid), (3) air conditioning and pollution and (4) alcohols. In this volume and those planned for future publication about one-half of all the articles are concerned with chemical substances. Many cross references for these substances are given and CAS registry numbers together with formula follow the names of compounds. The preamble to this volume also mentions an index for many common names, for some systematic names and for trade names. Presumably this index will appear at a later date. Substances described in volume one include acetaldehyde, acetic acid, acetone, acetylene, adipic acid, aldehydes and alkali and chlorine products. Related compounds are also mentioned, in particular, acetic acid derivatives such as acetamide, acetic anhydride, acetyl chloride, dimethylacetamide and halogenated derivatives.

The industrial significance of chemical substances is emphasized and there are numerous flow diagrams of industrial processes and tables of physical properties. The headings for topics that might be expected to appear between two existing articles are quoted, e.g., as follows: ACACIA. See DIURETICS; GUMS. This implies, intriguingly, that articles such as ACACIA are dealt with in volumes not yet published.

An encyclopaedia should be comprehensive, informative and easy to read and I certainly found that to be true of this volume. The articles are well written and numerous up-to-date references are quoted. Much information such as annual production figures and government regulations are specific to the U.S.A. Although emphasis is on technology there are also examples of some slightly more theoretical concepts such as the electronic configurations of the actinides and reaction paths to adipic acid. There is a scarcity of spectroscopic data in this first volume. I enjoyed reading about the current use of alcohol fuels (especially in Brazil), the concise but competent section on aerosols, the various types and use of abrasive materials and the final section on alkaloids which contains much structural chemistry. Other important articles are concerned with absorption, adhesives and aeration.

This volume certainly whets the appetite for what is to follow. The *Encyclopaedia* should prove to be a major work and should be well received. Volume one is refreshingly up-to-date and well produced. I eagerly await future volumes.

P. J. COX

pH Measurement: H. GALSTER, Verlag Chemie, Weinheim, 1991. Pages xvii + 356. £58.00.

One of the most commonly measured parameters in the chemical laboratory must surely be pH, and yet it is generally true that the simpler a procedure the less one thinks about it. Interlaboratory comparisons of pH measurement on river waters have revealed how great the discrepancies can be, and anyone running teaching experiments will be well aware of the difficulties of obtaining compatible data sets from groups of students using different pH meters. As more laboratories introduce quality assurance procedures and are obliged to think about the quality of their pH measurements, there will be an increasing demand for a reference source which answers the many questions to which disagreeing results give rise.

This very thorough treatise will provide a great many answers, not just for the inexperienced, but for those who think they already know a little about pH measurement. Perhaps, you will argue, most of the 350 pages will be only for the specialist. Perhaps you will be proved wrong, for I found the greater part of this volume to be of very practical relevance, combining the accounts of the troublesome phenomena associated with glass electrodes and the discussions of the underlying theory which can explain the effects. "The existence of two pH scales (the BS and the NBS/IEC/DIN) with definitions that are fundamentally different is not only unnecessary, it also adds to the difficulty of understanding the already complex basis of pH values..." For peace of mind stemming from a lack of conflicting data, use the single-standard BS pH scale and have faith in your pH electrode and meter. For peace of mind stemming from confidence in the quality of your results, however, read this book and be prepared to get involved in a lot of checking of your buffers, electrodes and even the meter itself.

The eight chapters deal with Fundamentals, pH scales, pH measurement cells, (including detailed discussions of glass electrodes, theory, use and care in handling) pH meters, Other pH measurement methods, Experimental procedures, (including pH measurement in aqueous solutions, non-aqueous solutions, and titrations), Process pH measurement and pH control. The book has a large number of clear illustrations, a substantial bibliography and a detailed index. However, I must disagree with the claim of the publishers on the back cover: "A book written by an expert for experts..." It is certainly written by an expert, and has been translated into very easily readable English, but it is a book for every laboratory where pH is measured, and that must mean, for a very wide readership indeed. I have enjoyed reading this book, and recommend it strongly.

I. L. MARR

Applications of Fluorescence in Immunoassays: I. A. HEMMILÄ, Wiley-Interscience, New York, 1991. Pages xi + 343. £67.00.

This is another book in the Wiley Chemical Analysis Series. It is an ideal reference text for those beginning or already involved in this area.

The first seven chapters give essential up-to-date background information on such assay methods. Particularly commendable are the chapters on instrumentation and photoluminescent probes—these cover every currently used instrument and probe together with their applications.

The Kirk-Othmer Encyclopedia of Chemical Technology: Volume 1, Fourth Edition. A to Alkaloids. J. I. KROSCHWITS, M. HOWE-GRANT, M. BICKFORD and L. GRAY (editors), Wiley-Interscience, Chichester, 1991. Pages xxxii + 1087. £135.00.

Volume one of the fourth edition of this *Encyclopedia* covers topics in alphabetical order ranging from ablative materials to alkaloids. The volumes in the previous third edition were published between the years 1978 to 1984 and hence I expect it will be some considerable time before all volumes in this new edition appear. All the articles in the new work are reported to have been rewritten and updated with many new subjects added.

Contributions to the first volume have been made by 65 authors (nearly all from the U.S.A.) and 33 topics have been covered. The more dominant topics include (1) acrylamide, acrylic ester and acrylonitrile polymers, (2) adsorption (gas and liquid), (3) air conditioning and pollution and (4) alcohols. In this volume and those planned for future publication about one-half of all the articles are concerned with chemical substances. Many cross references for these substances are given and CAS registry numbers together with formula follow the names of compounds. The preamble to this volume also mentions an index for many common names, for some systematic names and for trade names. Presumably this index will appear at a later date. Substances described in volume one include acetaldehyde, acetic acid, acetone, acetylene, adipic acid, aldehydes and alkali and chlorine products. Related compounds are also mentioned, in particular, acetic acid derivatives such as acetamide, acetic anhydride, acetyl chloride, dimethylacetamide and halogenated derivatives.

The industrial significance of chemical substances is emphasized and there are numerous flow diagrams of industrial processes and tables of physical properties. The headings for topics that might be expected to appear between two existing articles are quoted, e.g., as follows: ACACIA. See DIURETICS; GUMS. This implies, intriguingly, that articles such as ACACIA are dealt with in volumes not yet published.

An encyclopaedia should be comprehensive, informative and easy to read and I certainly found that to be true of this volume. The articles are well written and numerous up-to-date references are quoted. Much information such as annual production figures and government regulations are specific to the U.S.A. Although emphasis is on technology there are also examples of some slightly more theoretical concepts such as the electronic configurations of the actinides and reaction paths to adipic acid. There is a scarcity of spectroscopic data in this first volume. I enjoyed reading about the current use of alcohol fuels (especially in Brazil), the concise but competent section on aerosols, the various types and use of abrasive materials and the final section on alkaloids which contains much structural chemistry. Other important articles are concerned with absorption, adhesives and aeration.

This volume certainly whets the appetite for what is to follow. The *Encyclopaedia* should prove to be a major work and should be well received. Volume one is refreshingly up-to-date and well produced. I eagerly await future volumes.

P. J. COX

pH Measurement: H. GALSTER, Verlag Chemie, Weinheim, 1991. Pages xvii + 356. £58.00.

One of the most commonly measured parameters in the chemical laboratory must surely be pH, and yet it is generally true that the simpler a procedure the less one thinks about it. Interlaboratory comparisons of pH measurement on river waters have revealed how great the discrepancies can be, and anyone running teaching experiments will be well aware of the difficulties of obtaining compatible data sets from groups of students using different pH meters. As more laboratories introduce quality assurance procedures and are obliged to think about the quality of their pH measurements, there will be an increasing demand for a reference source which answers the many questions to which disagreeing results give rise.

This very thorough treatise will provide a great many answers, not just for the inexperienced, but for those who think they already know a little about pH measurement. Perhaps, you will argue, most of the 350 pages will be only for the specialist. Perhaps you will be proved wrong, for I found the greater part of this volume to be of very practical relevance, combining the accounts of the troublesome phenomena associated with glass electrodes and the discussions of the underlying theory which can explain the effects. "The existence of two pH scales (the BS and the NBS/IEC/DIN) with definitions that are fundamentally different is not only unnecessary, it also adds to the difficulty of understanding the already complex basis of pH values..." For peace of mind stemming from a lack of conflicting data, use the single-standard BS pH scale and have faith in your pH electrode and meter. For peace of mind stemming from confidence in the quality of your results, however, read this book and be prepared to get involved in a lot of checking of your buffers, electrodes and even the meter itself.

The eight chapters deal with Fundamentals, pH scales, pH measurement cells, (including detailed discussions of glass electrodes, theory, use and care in handling) pH meters, Other pH measurement methods, Experimental procedures, (including pH measurement in aqueous solutions, non-aqueous solutions, and titrations), Process pH measurement and pH control. The book has a large number of clear illustrations, a substantial bibliography and a detailed index. However, I must disagree with the claim of the publishers on the back cover: "A book written by an expert for experts..." It is certainly written by an expert, and has been translated into very easily readable English, but it is a book for every laboratory where pH is measured, and that must mean, for a very wide readership indeed. I have enjoyed reading this book, and recommend it strongly.

I. L. MARR

Applications of Fluorescence in Immunoassays: I. A. HEMMILÄ, Wiley-Interscience, New York, 1991. Pages xi + 343. £67.00.

This is another book in the Wiley Chemical Analysis Series. It is an ideal reference text for those beginning or already involved in this area.

The first seven chapters give essential up-to-date background information on such assay methods. Particularly commendable are the chapters on instrumentation and photoluminescent probes—these cover every currently used instrument and probe together with their applications.

The high standard of information is maintained in the subsequent chapters on FIA and ELFIA. Possible future developments are reviewed and make for thought-provoking reading.

Presentation is of a high standard throughout. The liberal use of tables to augment the information given in the text makes for ease of reference, *e.g.*, the requirement for an immunoassay kit based on a particular method. The text is also well referenced (over 1900 references are given) and current to 1990.

This unique book represents a fund of information for those who have an interest in fluorescence and immunoassaays.

R. R. MOODY

Chromatography Today: C. F. POOLE and S. K. POOLE, Elsevier, Amsterdam. 1991. Pages ix + 1026. Dfl. 295.00 (Hardback), Dfl. 150.00 (Paperback).

Those with a little knowledge of chromatography will find this book an ideal source of information for both updating and expanding their understanding of modern chromatographic systems.

The frequent use of tables to summarize or extend the information given in the text and the very extensive list of references given at the end of every Chapter makes the book a very useful reference source for any chromatographer. The book covers in some detail the fundamental relationships of chromatography, GC, HPLC, TLC and Supercritical Fluid Chromatography.

The authors succeed in showing that an understanding of the theory of the separation procedures involved and the apparatus used will aid in the selection of a chromatographic system and its optimization for a particular separation. The book also contains a valuable Chapter detailing the many methods available for sample preparation prior to chromatography (860 references). Identification of separated components may require the use of "hyphenated systems", *e.g.*, GC–Mass spectrometry.

The final Chapter clearly shows how such systems work, the options available and the difficulties that will be encountered. The quality of the presentation and the accuracy of the text is of uniformly high standard throughout. This up-to-date textbook will be a welcome addition to the chromatography section of any library.

R. R. MOODY

Cation Binding by Macrocycles: Y. INOUE and G. W. GOKEL (editors), Dekker, New York, 1990. Pages x + 761. $150.00 (US and Canada), $180.00 (elsewhere).

This book's eighteen chapters by a total of 20 authors give a comprehensive review of the chemistry of the interactions of cationic species with crown ethers and related compounds. The aspects covered include thermodynamics, equilibrium constants, kinetics and mechanism, crystallography, ion-selective electrodes, chromoionophores, and the reactions of various types of macrocycles (natural and synthetic) with various different groups of metal ions; and methods for studying all of these. The book is nicely produced, amply illustrated, and well referenced. I am sure that it will become compulsory reading for workers in the field, and will be particularly useful for those starting research in this area.

M. MASSON

The high standard of information is maintained in the subsequent chapters on FIA and ELFIA. Possible future developments are reviewed and make for thought-provoking reading.

Presentation is of a high standard throughout. The liberal use of tables to augment the information given in the text makes for ease of reference, *e.g.*, the requirement for an immunoassay kit based on a particular method. The text is also well referenced (over 1900 references are given) and current to 1990.

This unique book represents a fund of information for those who have an interest in fluorescence and immunoassaays.

R. R. MOODY

Chromatography Today: C. F. POOLE and S. K. POOLE, Elsevier, Amsterdam. 1991. Pages ix + 1026. Dfl. 295.00 (Hardback), Dfl. 150.00 (Paperback).

Those with a little knowledge of chromatography will find this book an ideal source of information for both updating and expanding their understanding of modern chromatographic systems.

The frequent use of tables to summarize or extend the information given in the text and the very extensive list of references given at the end of every Chapter makes the book a very useful reference source for any chromatographer. The book covers in some detail the fundamental relationships of chromatography, GC, HPLC, TLC and Supercritical Fluid Chromatography.

The authors succeed in showing that an understanding of the theory of the separation procedures involved and the apparatus used will aid in the selection of a chromatographic system and its optimization for a particular separation. The book also contains a valuable Chapter detailing the many methods available for sample preparation prior to chromatography (860 references). Identification of separated components may require the use of "hyphenated systems", *e.g.*, GC–Mass spectrometry.

The final Chapter clearly shows how such systems work, the options available and the difficulties that will be encountered. The quality of the presentation and the accuracy of the text is of uniformly high standard throughout. This up-to-date textbook will be a welcome addition to the chromatography section of any library.

R. R. MOODY

Cation Binding by Macrocycles: Y. INOUE and G. W. GOKEL (editors), Dekker, New York, 1990. Pages x + 761. $150.00 (US and Canada), $180.00 (elsewhere).

This book's eighteen chapters by a total of 20 authors give a comprehensive review of the chemistry of the interactions of cationic species with crown ethers and related compounds. The aspects covered include thermodynamics, equilibrium constants, kinetics and mechanism, crystallography, ion-selective electrodes, chromoionophores, and the reactions of various types of macrocycles (natural and synthetic) with various different groups of metal ions; and methods for studying all of these. The book is nicely produced, amply illustrated, and well referenced. I am sure that it will become compulsory reading for workers in the field, and will be particularly useful for those starting research in this area.

M. MASSON

Talanta, Vol. 39, No. 9, pp. 1065–1072, 1992
Printed in Great Britain.

0039-9140/92 $5.00 + 0.00

ANALYTICAL AND MECHANISTIC ASPECTS OF THE ROOM-TEMPERATURE FLUORESCENCE AND PHOSPHORESCENCE OF BENZO(*f*)QUINOLINE ADSORBED ON SILICA GEL CHROMATOPLATES WITH HUMIDIFIED GASES

LINDA A. CITTA and ROBERT J. HURTUBISE*
Chemistry Department, University of Wyoming, Laramie, Wyoming 82071, U.S.A.

(*Received* 24 *September* 1991. *Accepted* 19 *December* 1991)

Summary—The solid-matrix room-temperature fluorescence and room-temperature phosphorescence properties of benzo(*f*)quinoline adsorbed on silica gel chromatoplates were investigated over a wide range of humidities in N_2, air and O_2. Both neutral and acidic conditions were used and even at the highest relative humidity used, 93% relative humidity, the room-temperature fluorescence and phosphorescence intensities from benzo(*f*)quinoline were not totally quenched. However, in all experiments, the room-temperature phosphorescence was much more sensitive to humidity quenching than the room-temperature fluorescence. The results gave rather detailed information on quenching of the room-temperature fluorescence and phosphorescence in the different gases at a variety of humidities. It was possible to calculate the contribution to the percent decrease in luminescence due to moisture or a quenching gas. Thus, a more detailed assessment could be made about the quenching of moisture and individual quenching gases on the solid-matrix fluorescence and phosphorescence.

Room-temperature phosphorescence (RTP) and room-temperature fluorescence (RTF) from compounds adsorbed on solid matrices are important analytical techniques.[1–4] In most cases, the RTP intensity can be greatly reduced by the presence of moisture,[5–13] and it is usually necessary to dry the sample to observe appreciable RTP emission. Schulman and Parker[13] investigated the effects of dry and humidified argon and oxygen on the RTP of sodium 4-biphenylcarboxylate adsorbed on filter paper. This study involved a detailed investigation of the effects of moisture and oxygen on RTP with a silica gel chromatoplate as the solid matrix. The RTP of *p*-aminobenzoic acid adsorbed on sodium acetate was noted by von Wandruszka and Hurtubise[14] to be quite insensitive to moisture in the atmosphere. Limited studies have been reported on the effects of different gases on phosphorescence[7,15,16] and fluorescence.[16–19] Ramasamy *et al.*[20] have noted that higher quantum yields for RTF and RTP were obtained for *p*-aminobenzoic acid adsorbed on sodium acetate and 4-phenylphenol adsorbed on poly(acrylic acid)–sodium bromide with nitrogen present compared to the samples in the presence of air. McAleese *et al.*[21] reported that for relative humidities of 60% or less, samples adsorbed on sodium citrate impregnated filter paper appeared to be insensitive to immediate moisture and oxygen quenching as compared to similar samples adsorbed on filter paper and then spotted with water in place of sodium citrate. For relative humidities greater than 60%, the insensitivity to oxygen and moisture was not observed. Contrary to the usual results of optimal RTP with the presence of little or no moisture, Dalterio and Hurtubise[22] found enhanced RTP for 4-phenylphenol when a sizeable amount of water was present in the poly(acrylic acid)–salt matrix. They also noted that α-naphthoflavone adsorbed on a 1% poly(acrylic acid)–sodium bromide mixture gave the same RTP intensity as the initial intensity after seven days of exposure to atmospheric humidity. Recently, Citta and Hurtubise[23] have reported the effects of moisture, N_2, air and O_2 on the RTF and RTP of several compounds adsorbed on filter paper. In earlier work silica gel chromatoplates with a polyacrylate binder were shown to induce strong RTF and RTP signals from several compounds, and the chromatoplates were very easy to manipulate.[1,4,16] However, there have been no

*Author for correspondence.

reports on the influence of moisture and gases on the RTF and RTP signals of the compounds adsorbed on chromatoplates. This paper reports the effects of humidified N_2, air and O_2 on the RTF of benzo(f)quinoline and the RTF and RTP of B(f)QH$^+$ (B = benzo, Q = quinoline) adsorbed on silica gel chromatoplates which contained a polyacrylate binder. Also, a system designed to measure RTP and RTF intensities under humidified conditions is described.

EXPERIMENTAL

Apparatus

A Schoeffel spectrodensitometer was used to obtain the RTP and RTF intensity measurements. Details of the instrument have been described previously.[16] A polyethylene glove bag was fitted and secured to enclose the sample compartment of the densitometer. The polyethylene glove bag was used to provide a controlled environmental chamber to contain an atmosphere of the dry or the humidified gas. A digital hygrometer (Model 3309-50, Cole-Parmer) was used to measure the percent relative humidity (% RH) and the temperature inside the glove bag chamber. Several precautions were taken for the control of temperature inside the glove bag chamber. The lamp housing and illumination tube of the densitometer were wrapped with insulation material. A polystyrene foam cup with a vacuum line attachment was fitted over the monochromator to draw heat away, and a container of dry ice was placed in the sample compartment of the densitometer but outside the glove bag chamber to prevent the stage of the densitometer from warming up.

For dry air, compressed gas was allowed to flow through an activated charcoal purifier and through Drierite. Air was humidified by passing the air at 820 ml/min through three gas wash bottles each containing 500 ml of an aqueous sulfuric acid solution. A glass U-tube packed with glass wool was used to trap any sulfuric acid aerosol. To obtain a desired humidity inside the glove bag chamber, appropriate concentrations of aqueous sulfuric acid solutions had to be used.[24,25]

Reagents

Ethanol was purified by distillation. Prior to use, aluminum backed silica gel chromatoplates (EM Science, Cherry Hill, NJ) were developed in ethanol three times to collect impurities at one end. Benzo(f)quinoline (Aldrich) was used as received.

Procedures

Humidity experiments. Silica gel chromatoplates were dried at 190° for 30 min before use. Afterwards, the silica gel chromatoplate was placed inside a desiccator and transferred to a polyethylene glove bag which contained an atmosphere of dry nitrogen. Dry nitrogen was passed through an oxygen trap, activated charcoal, and Drierite before the gas filled the polyethylene glove bag. Inside the polyethylene glove bag, the sample solutions were spotted (1 μl) in duplicate on the silica gel chromatoplates. Benzo(f)quinoline (100 ng) was adsorbed on the silica gel chromatoplate either from ethanol, 0.1M hydrobromic acid–ethanol, or 0.1M hydrochloric acid–ethanol solutions. After spotting, the chromatoplate was allowed to dry inside the polyethylene glove bag for 5 min, and it was then transferred to an oven to dry for 15 min at 105°. The silica gel chromatoplate was removed from the oven and placed on the stage of the densitometer which was enclosed by the glove bag chamber and allowed to cool under an atmosphere of dry gas (0% RH).

Intensity measurements for the samples under the atmosphere of the dry gas were obtained after the samples had been inside the glove bag chamber for at least 10 min. After the measurements were obtained in the dry gas, the humidified gas was allowed to flow into the glove bag chamber, and the atmosphere with the desired humidity was reached after approximately 90 min. For each humidity investigated, measurements were obtained at 10-min intervals over a 70–120-min time span of exposure of the sample to humidified gas. There was little or no change in the emission intensities over this length of time. The emission intensities reported in this work were obtained after the 90-min exposure time, and the reproducibility from run to run was very good. For example, for the RTF of B(f)QH$^+$ the average intensity ratio for three runs gave 0.72 ± 0.17 at the 95% confidence level.

The system developed was a dynamic one in that the gas was allowed to continuously flow into the glove bag chamber, and the gas was not directly passed over the face of the sample. Thus, the sample was exposed to a surrounding atmosphere of the dry or humidified gas.

Excitation and emission wavelengths. The following excitation and emission wavelengths were used: RTP of B(*f*)Q with 0.1*M* hydrochloric acid–ethanol and 0.1*M* hydrobromic acid–ethanol, 370 nm, 510 nm; RTF of B(*f*)Q with 0.1*M* hydrochloric acid–ethanol and 0.1*M* hydrobromic acid–ethanol, 370 nm, 430 nm; RTF of B(*f*)Q with ethanol, 360 nm, 430 nm.

RESULTS AND DISCUSSION

Experimental considerations

It is known that silica gel absorbs moisture in varying degrees.[26] Ford and Hurtubise[27] found enhanced phosphorescence when samples adsorbed on silica gel were reheated. The increase in RTP was attributed to the loss of water adsorbed on the silica gel surface. In this work, to ensure each chromatoplate contained very small amounts of moisture, the silica gel chromatoplates were dried for 30 min at 190°.

With a flow-rate of 820 ml/min, the relative humidity inside the glove bag chamber did not reach the static humidity expected for the aqueous sulfuric acid solutions used in the gas wash bottles.[24,25] Lassen[28] found that a flow-rate of no more than 400 ml/min passing through the gas wash bottles would yield the same humidity as the static humidity associated with the concentration of sulfuric acid inside the wash bottles. The glove bag chamber enclosed a large area of the sample compartment due to the size of the chopper accessory.[16] Thus, a flow-rate of 350 ml/min into the glove bag chamber took about three hours for the system to come close to the desired humidity. However, a flow-rate of 820 ml/min required 90 min to reach a stable humidity inside the glove bag chamber. By experimentation, aqueous solutions with the appropriate concentration of sulfuric acid were found which gave the desired humidities inside the glove bag chamber. With this system, it was not possible to reach a relative humidity of 100% inside the chamber. The maximum relative humidity possible inside the glove bag chamber with air was 93%. To reach this humidity, the gas wash bottles which contained the aqueous sulfuric acid solution had to be heated in a water bath to 45°.

The phosphoroscope assembly was used when both RTP and RTF intensities were obtained. For RTP measurements, the chopper was in the position as described by Ford and Hurtubise.[16] The assembly had to be moved to a different position for RTF measurements so the chopper did not block the source radiation to the sample or the emission from the sample to the detector. The rotating chopper was needed for proper mixing of the humidified atmosphere inside the glove bag chamber. RTF measurements obtained without the mixing of the atmosphere by the chopper resulted in very nonreproducible data, whereas with the chopper turned on, quite reproducible results were obtained. Since the chopper was turned on for RTP measurements, there was no difficulty with the reproducibility of the results.

Effects of humidity on RTP and RTF in air

The RTP properties of several aromatic nitrogen heterocycles adsorbed on silica gel have been investigated.[29–31] Ford and Hurtubise[29] and Ramasamy and Hurtubise[32,33] have explored the various interactions responsible for the RTP of nitrogen heterocycles adsorbed on solid surfaces. Therefore, for analytical purposes, it was considered important to study the effects of humidified air on the RTP and RTF of B(*f*)Q as a model compound adsorbed on silica gel chromatoplates.

For the RTP of B(*f*)QH$^+$ in air, the average relative intensity ratios decreased as % RH increased. The average RTP ratio values of B(*f*)QH$^+$ adsorbed as a hydrobromic acid solution at a given humidity were much smaller than the average ratio values for RTP of B(*f*)QH$^+$ adsorbed as a hydrochloric acid solution (Fig. 1). Also, the RTP of B(*f*)Q with hydrobromic acid was more sensitive to humidified air than the RTP of B(*f*)Q with hydrochloric acid. In Fig. 1 for B(*f*)Q with hydrobromic acid, there was a dramatic

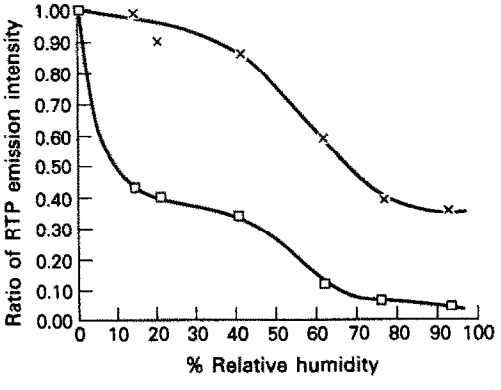

Fig. 1. Ratio of the RTP emission intensity in air at a given humidity to the RTP emission intensity in dry air for 100 ng of B(*f*)QH$^+$ adsorbed on EM silica gel chromatoplates from ethanol/0.1*M* HCl (×) and ethanol/0.1*M* HBr (□) solutions as a function of % relative humidity.

reduction in RTP over the humidity range 0–93% RH; however, the RTP signal was not totally quenched. The decrease in RTP was largest between 0 and 20% RH. From 20 to 40% RH there was a small change in the RTP ratio values for B(f)Q with hydrobromic acid. As shown in Fig. 1, another significant decrease in the RTP ratio values was observed between 40 and 60% RH. Between 60 and 93% RH, the decrease in RTP for B(f)Q with hydrobromic acid was relatively small. For B(f)Q with hydrochloric acid, there was a more gradual decrease in RTP (Fig. 1). A rapid decrease in RTP for B(f)Q with hydrochloric acid was observed between 40 and 75% RH. The change in the RTP intensity ratio values for B(f)Q with hydrochloric acid between 75 and 93% RH was small. Again it was observed that the RTP signal remained quite evident in air at 93% RH. For the RTP of B(f)Q with hydrochloric and hydrobromic acids, there was a relatively slow change in the ratio of RTP values from 20 to 40% RH.

Figure 2 gives the average ratio of the RTF peak height in air at a given humidity to the RTF peak height in dry air versus relative humidity at 90 min. The average ratio values for RTF of B(f)Q with hydrochloric acid followed a linear relationship over the humidity range of 0–93% RH (correlation coefficient = −0.973). After the initial drop in the RTF ratio values for B(f)Q adsorbed with ethanol from 0 to 20% RH in Fig. 2, the RTF values remained relatively constant over the humidity range of 20–60% RH. The RTF ratio values for B(f)Q from 40 to 93% can be fitted to a linear relationship with a correlation coefficient of −0.974. The RTF for B(f)Q with hydrobromic acid gave unusual results in that the ratio values at 20, 40 and 93% RH were greater than the ratio value of 1.00 for dry air.

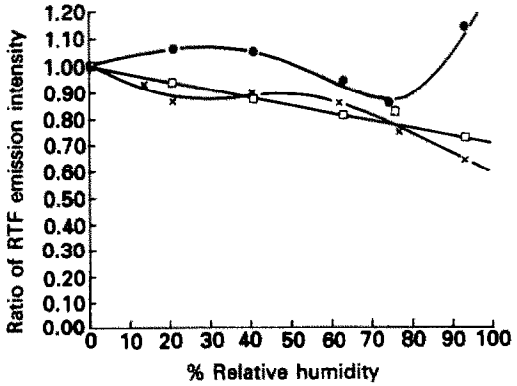

Fig. 2. Ratio of the RTF emission intensity in air at a given humidity to the RTF emission intensity in dry air for 100 ng of B(f)Q adsorbed on EM silica gel chromatoplates from ethanol (×), and 100 ng B(f)QH$^+$ from HBr (●) and from ethanol/0.1M HCl (□) solutions as a function of % relative humidity.

As discussed, the RTF of B(f)Q was not affected by the humidified air as much as the RTP of B(f)Q. This is most likely related to the shorter lifetime of RTF as compared to RTP. For B(f)Q with hydrochloric acid, the relative decrease in the RTF and RTP ratio values from 0 to 40% RH was almost the same. Thus, it appears that humidified air has a similar effect on RTF and RTP over this humidity range. After 40% RH, the reduction in the relative intensity ratio values was more dramatic for RTP of B(f)Q with hydrochloric acid than for RTF of B(f)Q with hydrochloric acid (see Figs. 1 and 2).

For the RTP of B(f)QH$^+$ adsorbed with hydrochloric acid under an atmosphere of air, a range of 0–20% RH would be most useful analytically. Due to the dramatic decrease in RTP intensity for B(f)Q with hydrobromic acid in the 0–20% RH region, it would be important to keep the chromatoplate very dry during the measurement step. However, the emission intensity in the humidity range 20–40% RH offers a relatively constant RTP signal for analytical work. For the RTF of B(f)Q with hydrochloric acid, there was a relatively constant rate of decrease in emission intensity over the humidity range 0–93% RH. The RTF signal was still quite strong even with air at 93% RH. However, the optimum humidity range for intense signals appears to be from 0 to 40% RH.

RTF and RTP intensities relative to dry nitrogen at different humidities in different gases

The RTF intensities relative to dry nitrogen for B(f)Q adsorbed with hydrochloric acid were obtained in nitrogen and oxygen at different humidities. The RTP intensities relative to dry N_2 were obtained in N_2, air and O_2. By comparing the data in this fashion, direct comparisons could be made between the effects of humidity and different gases on the RTF and RTP signals for B(f)QH$^+$ adsorbed on the chromatoplate. Figure 3 gives graphs for the effects of nitrogen and oxygen on the RTF of B(f)QH$^+$ at different humidities. It was assumed that N_2 had no effect on the RTF signals. As indicated in Fig. 3, the RTF signals decreased by about 22% from 0 to 20% RH and

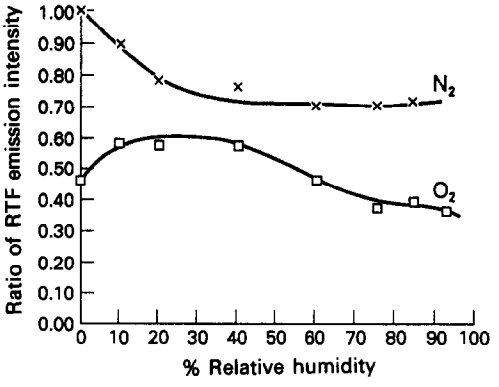

Fig. 3. Ratio of the RTF emission intensity relative to dry N_2 for 100 ng of B(*f*)QH$^+$ adsorbed on EM silica gel chromatoplates from ethanol/0.1*M* HCl as a function of % relative humidity. N_2(×), O_2(□).

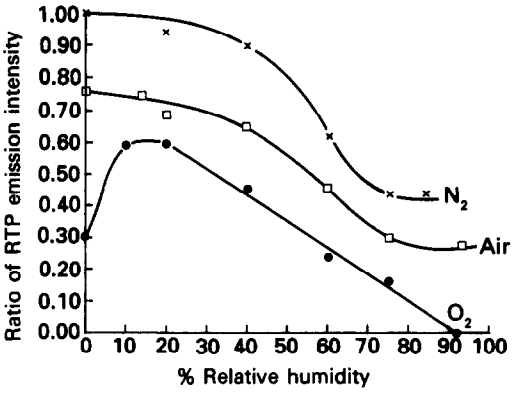

Fig. 4. Ratio of the RTP emission intensity relative to dry N_2 for 100 ng of B(*f*)QH$^+$ adsorbed on EM silica gel chromatoplates from ethanol/0.1*M* HCl as a function of % relative humidity. N_2(×), air (□), O_2(●).

then level off after a 30% decrease in RTF. With O_2 under dry conditions, the RTF signal was less than half the signal obtained under dry conditions with N_2 (Fig. 3). As shown in Fig. 3, the RTF signals increase from 10 to 40% relative humidity in the presence of O_2, decrease from 40 to 75% relative humidity and finally level off from 75 to 92% relative humidity. The type of graph obtained with O_2 indicated a somewhat complicated interaction of the gas and moisture with the fluorophor. The graph obtained with N_2 implies that fluorophor molecules near the surface are quenched by moisture in the approximate range of 0–20% relative humidity and the solid matrix provides considerable protection of B(*f*)QH$^+$ molecules buried in the three dimensional matrix of the chromatoplate.

Figure 4 shows the RTP intensities in three different gases as a function of % RH for B(*f*)QH$^+$ adsorbed from a hydrochloric acid solution. In N_2 the RTP signals were the strongest and in air the general shape of the curve is the same as that obtained for N_2, but there is a global shift to lower RTP intensities. This shift to lower intensities is due to the presence of O_2 in the air. In Fig. 4, the RTP intensities in the presence of O_2 increased from 0 to 20% relative humidity and then showed a linear decrease in RTP intensities from 20 to 92% relative humidity. At 92% relative humidity the RTP signal was zero. Because the RTP signals remained in the presence of N_2 at 84% relative humidity and in the presence of air at 92% relative humidity, then a fraction of the phosphor molecules were very well protected by the solid matrix under these conditions. In order to sort out the contributions from moisture and the quenching gases, it was necessary to determine the percentage contributions from moisture and a quenching gas. These aspects are discussed in the next section.

Percentage contribution to luminescence quenching from moisture and quenching gases

In earlier work, Schulman and Parker[13] discussed equations that are useful in determining the various quenching contributions of moisture and gases to the RTP of model compounds adsorbed on filter paper. Recently, Citta and Hurtubise[23] reported a somewhat modified version of the Schulman and Parker equations for use with filter paper. These equations were used in this work and are listed in Table 1. The equations give the percent decrease in luminescence signals and permit a more quantitative evaluation of the effects of moisture and gases

Table 1. Equations used to distinguish the contribution to quenching due to moisture and the gases

% Decrease due to H_2O:	$\frac{I^0_{N_2} - I_{N_2}}{I^0_{N_2}} \times 100$
% Decrease due to H_2O + air:	$\frac{I^0_{N_2} - I_{Air}}{I^0_{N_2}} \times 100$
% Decrease due to air:	$\frac{I_{N_2} - I_{Air}}{I^0_{N_2}} \times 100$
% Decrease due to $H_2O + O_2$:	$\frac{I^0_{N_2} - I_{O_2}}{I^0_{N_2}} \times 100$
% Decrease due to O_2:	$\frac{I_{N_2} - I_{O_2}}{I^0_{N_2}} \times 100$

$I^0_{N_2}$ Intensity in dry N_2.
I_{N_2} Intensity in N_2 at a given humidity.
I_{Air} Intensity in air at a given humidity.
I_{O_2} Intesnity in O_2 at a given humidity.

on the solid-matrix luminescence intensity. Figure 5 shows the % decrease in RTF for B(f)QH$^+$ in the presence of both H_2O and O_2 and two graphs that represent individual contributions from H_2O and O_2. With both H_2O and O_2 present, the % decrease in RTF is between 42 and 64% over the entire range of humidity investigated. For O_2 from 0 to 20% relative humidity, the percent decrease in RTF actually becomes less than with dry O_2, whereas the RTF decrease becomes greater compared to dry N_2. At relative humidities greater than 20%, the contributions to the percent decrease in RTF for H_2O and O_2 are about the same.

Figure 6 gives several graphs for the % decrease in RTP versus % RH for B(f)QH$^+$ adsorbed on a silica gel chromatoplate. The graph for % RTP decreases with H_2O and O_2 shows a drop in the % RTP decrease from 0 to 20% relative humidity. The graph becomes linear from 20 to 94% relative humidity. A similar graph for the same model compound on filter paper gave a linear relationship over the entire range of humidity investigated.[23] In Fig. 6, the plot for % RTP decrease with water shows that the % decrease is linear from 0 to 40% relative humidity, but with only an overall % decrease in RTP of 10%. Then from 40 to 75% relative humidity, the slope of the curve is much greater and a maximum of 56% decrease in RTP occurs. Finally the curve levels off at 75% relative humidity and remains constant to the maximum % relative humidity (84%). In similar relative humidity work by Citta and Hurtubise[23] with B(f)QH$^+$ adsorbed on filter paper, the shape of the H_2O curve gave a dramatic rise in %RTP decrease to about 40% relative humidity

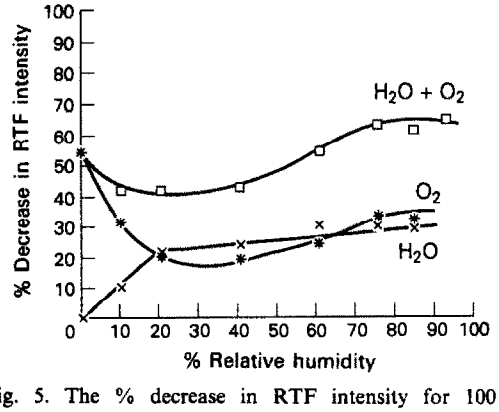

Fig. 5. The % decrease in RTF intensity for 100 ng B(f)QH$^+$ adsorbed on EM silica gel chromatoplates from ethanol/0.1M HCl due to moisture and O_2. □ = % Decrease due to H_2O and O_2; ● = Calculated % decrease due to O_2; × = Calculated % decrease due to H_2O.

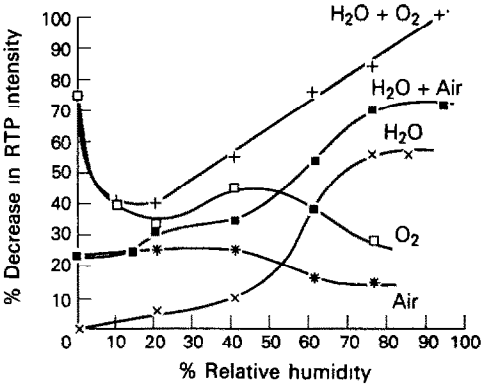

Fig. 6. The percent decrease in RTP intensity for 100 ng of B(f)QH$^+$ adsorbed on EM silica gel chromatoplates from ethanol/0.1M HCl due to moisture and gases. + = % Decrease due to H_2O and O_2; ■ = % decrease due to H_2O and air; × = % decrease due to H_2O; □ = calculated % decrease due to O_2; ● = calculated % decrease due to air.

and then the curve showed a gradual rise as the humidity increased beyond 40% relative humidity.

In Fig. 6, the % decrease in RTP due to O_2 shows that the quenching effects from O_2 decrease with increasing % relative humidity, and the quenching effects are roughly constant from 20% relative humidity and beyond. Interestingly, with filter paper and B(f)QH$^+$ a similar graph was obtained for O_2.[23] Finally in Fig. 6, the % decrease in RTP due to air remained essentially constant from 0 to 40% relative humidity and then decreased somewhat beyond 40% humidity. B(f)QH$^+$ adsorbed on filter showed a similar trend.[23]

Analytical and mechanistic aspects related to the decrease in RTF and RTP signals

It is clear from the results presented that RTF is much less affected by moisture and gas quenching than is RTP. This is most likely related to the much shorter lifetime of the excited singlet state relative to the lifetime of the excited triplet state. Because a substantial amount of RTF signal remained at high humidity and in the presence of pure oxygen (Figs. 3 and 5), then the matrix offered considerable protection of the fluorophor. Also, in the presence of air and high moisture content (Fig. 2), and nitrogen and high moisture (Fig. 3), a substantial amount of the fluorescence remained. The mechanistic aspects of the RTF of B(f)QH$^+$ obtained on dry EM silica gel chromatoplates were discussed by Ford and Hurtubise.[29] Because the chromatoplates contain a polyacrylate binder, the acid solution

deposited on the chromatoplate converts the polyacrylate salt to the acid form of the polymer. Thus, both silanol groups and carboxyl groups would interact with B(*f*)QH$^+$.[29] Because B(*f*)QH$^+$ in the singlet state would interact with both silanol groups and carboxyl groups, it is not possible to give a detailed interaction mechanism for the fluorophor in the presence of moisture and quenching gases without carrying out additional experiments such as fluorescence lifetime measurements.

The RTP signals were much more sensitive to environmental conditions than were the RTF signals (Figs. 1, 4 and 6). As considered earlier by Ford and Hurtubise,[29] the polymer binder in the chromatoplates was essential for RTP, and silica gel without the polyacrylate binder was an inefficient matrix for obtaining RTP. In fact, the acid form of the polymer binder was primarily responsible for inducing RTP from B(*f*)QH$^+$ adsorbed on the chromatoplate, and the silanol groups in the silica gel were not highly important in obtaining strong RTP signals. However, if one assumes that the binder is homogeneously dispersed in the silica gel matrix then the changes in the RTP signals should be a function of the adsorption of moisture by the matrix. Rassi *et al.*[34] have reported a detailed water adsorption isotherm for LiChrosorb SI 60 (Merck) from 0 to 100% relative humidity. Their isotherm has the same shape and characteristics as the water adsorption isotherm for silica gel 60 provided in the technical bulletin by Merck for the silica gel 60 chromatoplates. The isotherm given by Rassi *et al.*[34] shows that from 0 to 40% relative humidity there is a relatively flat region and the weight percent increase in water is less than 10%. In Fig. 6, the % decrease in RTP as a function of relative humidity in N_2 or in air shows the same trend over this humidity range. Namely, there is very little decrease in RTP as the humidity changes from 0 to 40% relative humidity. Rassi *et al.*[34] showed that beyond 50% relative humidity there was a dramatic increase in the moisture uptake by silica gel. In Fig. 6, the % decrease in RTP shows the same trend for B(*f*)QH$^+$ in N_2. The only major difference between the % decrease RTP curve in Fig. 6 and the water isotherm reported by Rassi *et al.*[34] is that in Fig. 6 the % decrease in RTP reaches an approximate plateau near 75% relative humidity in N_2 and air. Unger[35] has explained the large increase in moisture uptake in silica beyond 50% relative humidity to capillary condensation of water vapor in the pores of the silica. Based on our RTP results and the results reported by Rassi *et al.*,[34] it appears that the phosphor molecules near the surface of silica are quenched in the range of approximately 0–40% relative humidity and then from 50% relative humidity to about 75% relative humidity, where capillary condensation occurs, the phosphor molecules in the pores are quenched. Because a fraction of the phosphor molecules are not quenched beyond 75% relative humidity, then they are most likely in pores that are not available to water. The previous description for the RTP change with % relative humidity is obviously an over simplification because polyacrylic acid is dispersed throughout the silica gel and plays a very important role in obtaining RTP. Based on the RTP results obtained in this work, it would seem that the polyacrylic acid is not only homogeneously distributed in the silica gel matrix but the carboxyl functionality can penetrate into the pores of the silica gel and interact with B(*f*)QH$^+$ which is one of the main factors in permitting RTP to be observed from B(*f*)QH$^+$ adsorbed on silica gel.

CONCLUSIONS

The effects of moisture and quenching gases on solid-matrix luminescence are very important.[1,2,5] The silica gel chromatoplates used in this work were shown previously to give very good reproducibility and low limits of detection for RTF and RTP.[16,27,29] The results from this work will permit analysts to determine, in general, the conditions needed for optimal RTF and RTP with the silica gel chromatoplates. An important conclusion is that RTF was not affected much by quenching gases and moisture. In addition, the RTP signals were obtained in some cases even in very high humidity in N_2 and air. The same conclusions were reached by similar experiments with filter paper.[23] The results are also important mechanistically in solid-matrix luminescence because so little work has been done in the area of the effects of quenching gases and moisture in solid-matrix luminescence. For example, the particular correlation found between the water adsorption isotherm for silica gel and the decrease in RTP in N_2 for B(*f*)QH$^+$ with humidity would be important in mechanistic studies and in practical applications.

Acknowledgement—Financial support for this project was provided by the Department of Energy, Division of Basic Energy Sciences, Contract No. DE-AC02-80ER10624 and Grant No. DE-FG02-86ER13547.

REFERENCES

1. R. J. Hurtubise, *Solid Surface Luminescence Analysis: Theory, Instrumentation, Applications*, Marcel Dekker, New York, 1981.
2. T. Vo-Dinh, *Room Temperature Phosphorimetry for Chemical Analysis*, Wiley-Interscience, New York, 1984.
3. J. N. Miller, *Pure & Appl. Chem.*, 1985, **57**, 515.
4. R. J. Hurtubise, *Phosphorimetry: Theory, Instrumentation, and Applications*, VCH Publishers, New York, 1990.
5. E. M. Schulman and C. Walling, *Science*, 1972, **178**, 53.
6. T. Vo-Dinh, E. Lue Yen and J. D. Winefordner, *Anal. Chem.*, 1976, **48**, 1186.
7. T. Vo-Dinh, G. L. Walden and J. D. Winefordner, *ibid.*, 1977, **49**, 1126.
8. E. M. Schulman and C. Walling, *J. Phys. Chem.*, 1973, **77**, 902.
9. E. Lue Yen Bower and J. D. Winefordner, *Anal. Chim. Acta*, 1978, **101**, 319.
10. S. L. Wellons, R. A. Paynter and J. D. Winefordner, *Spectrochim. Acta, Part A*, 1974, **30**, 2133.
11. R. A. Paynter, S. L. Wellons and J. D. Winefordner, *Anal. Chem.*, 1974, **46**, 736.
12. R. T. Parker, R. S. Freedlander, E. M. Schulman and R. B. Dunlap, *Anal. Chem.*, 1979, **51**, 1921.
13. E. M. Schulman and R. T. Parker, *J. Phys. Chem.*, 1977, **81**, 1932.
14. R. M. A. von Wandruszka and R. J. Hurtubise, *Anal. Chem.*, 1976, **48**, 1784.
15. E. Lue Yen Bower and J. D. Winefordner, *Anal. Chim. Acta*, 1978, **102**, 1.
16. C. D. Ford and R. J. Hurtubise, *Anal. Chem.*, 1979, **51**, 659.
17. A. A. Boulton, *J. Chromatogr.*, 1971, **63**, 141.
18. F. De Croo, G. A. Bens and P. De Moerloose, *J. HRC & CC*, 1980, **3**, 423.
19. C.-H. Wu, I. Salmeen and H. Niki, *Environ. Sci. Technol.*, 1984, **18**, 603.
20. S. M. Ramasamy, V. P. Senthilnathan and R. J. Hurtubise, *Anal. Chem.*, 1986, **58**, 612.
21. D. L. McAleese, R. S. Freedlander and R. B. Dunlap, *ibid.*, 1980, **52**, 2443.
22. R. A. Dalterio and R. J. Hurtubise, *ibid.*, 1983, **55**, 1084.
23. L. A. Citta and R. J. Hurtubise, *Appl. Spectrosc.*, 1991, **45**, 1547.
24. R. C. Weast (ed.), *CRC Handbook of Chemistry and Physics*, 59th Ed., p. E-46. CRC Press, Boca Raton, Florida, 1978.
25. M. Lapinski, K. Kostyrko and W. Wtopdarski, *Modern Methods for the Control and Measurement of Humidity and Moisture*, p. 89. Foreign Scientific Publications Department of the National Center for Scientific, Technical and Economic Information, Warsaw, Poland, 1976.
26. J. C. Touchstone and M. F. Dobbins, *Practice of Thin Layer Chromatography*, pp. 302–303. Wiley-Interscience, New York, 1978.
27. C. C. Ford and R. J. Hurtubise, *Anal. Chem.*, 1978, **50**, 610.
28. S. V. H. Lassen, *A Study in Hygrometry*, pp. 12–17. The University of Southern California Press, Los Angeles, 1937.
29. C. D. Ford and R. J. Hurtubise, *Anal. Chem.*, 1980, **52**, 656.
30. S. M. Ramasamy and R. J. Hurtubise, *ibid.*, 1982, **54**, 1642.
31. V. P. Senthilnathan and R. J. Hurtubise, *ibid.*, 1984, **56**, 913.
32. S. M. Ramasamy and R. J. Hurtubise, *ibid.*, 1982, **54**, 2477.
33. *Idem, Anal. Chim. Acta*, 1983, **152**, 83.
34. Z. El Rassi, C. Gonnet and J. L. Rocca, *J. Chromatogr.*, 1976, **125**, 179.
35. K. K. Unger, *Porous Silica*, pp. 195–197. Elsevier Scientific Publishing Co., New York, 1979.

Talanta, Vol. 39, No. 9, pp. 1073–1079, 1992
Printed in Great Britain.

0039-9140/92 $5.00 + 0.00

AN EVALUATION OF THE HPLC–GEL CHROMATOGRAPHIC METHOD FOR ANALYZING METALLOTHIONEINS IN AQUATIC ORGANISMS

STEFAN MICALLEF,* YVES COUILLARD, PETER G. C. CAMPBELL and ANDRE TESSIER
Université du Québec, INRS-Eau, C.P. 7500, Sainte-Foy, Québec, Canada G1V 4C7

(*Received* 8 *October* 1991. *Revised* 17 *February* 1992. *Accepted* 17 *February* 1992)

Summary—The use of high-performance liquid chromatography to determine the concentrations of metal-binding proteins (MBP) in freshwater mussels has been evaluated. Initial use of dilute buffers (*e.g.*, 10m*M* TRIS, pH 7 or 8), to minimize competition between the buffer and the metal-cytosolic ligand complexes, proved unacceptable; high losses of low molecular weight marker proteins occurred during chromatographic separation, presumably as a result of adsorption to the gel-permeation column packing. Losses were more dependent on salt than pH; satisfactory recoveries were obtained in the pH range 6–8 with 10m*M* buffer solutions and 100m*M* added electrolyte (NaCl; KCl). Competition experiments performed with commercial metallothionein (pre-labelled with ^{109}Cd) and fresh mussel cytosol extract demonstrated that no appreciable metal exchange occurred during the 20-min pre-equilibration or the subsequent chromatographic separation step. With ^{203}Hg-labelled metallothionein occasional losses were noted, however, appreciable loss of the radioisotope ranging from 50 to 58% did occur with ^{65}Zn-labelled metallothionein during the chromatographic separation step. These results, particularly for Zn indicate that the recovery of metals after separation using this chromatographic method may vary, even for metals sharing similar chemical properties.

Freshwater and marine mussels have been proposed as biomonitors for metal pollution in the aquatic environment.[1,2] In addition to their documented ability to bioaccumulate metals from the environment, these organisms are also able to carry out the *de novo* synthesis of low molecular weight, heat stable proteins containing a high cysteine content. Often referred to as metallothioneins, or more generally as metal-binding proteins (MBP), these molecules have a high affinity for certain "soft" cations. The presence of MBP is not restricted to bivalves and their occurrence has been reported in mammals,[3] fish,[4] echinoderms,[5] crustaceans,[6] insects[7] and phytoplankton.[8]

Several reports propose the use of MBP as a specific biochemical indicator of sublethal metal exposure and suggest that from an ecotoxicological point of view, an elevated MBP level in an organism may indicate chronic metal exposure long before any deleterious effects occur.[9,10] It should be noted, however, that basal levels of MBP may well be present in organisms that have not been exposed to excessive metal levels, given that MBP have been implicated in normal metal metabolism.[11]

In recent years, different methodologies have evolved to estimate the concentration of MBP in the different tissues of aquatic invertebrates. Techniques such as polarography,[12] immunoassays[13,14] and metal saturation assays[15,16] have found support for the quantification of MBP in aquatic invertebrates, particularly in marine species. The use of gel-filtration chromatography, coupled with post-column metal detection by such means as inductively coupled plasma atomic emission spectroscopy (ICP–AES)[17,18] or 4-(2-pyridylazo)-resorcinol (PAR) derivatization,[19] has also been advocated as a sensitive, quick technique for the separation and detection of MBP and their respective bound metals.[20] This technique has the advantage that chromatographic separation of a cytosol extract produces the whole protein profile. This approach, together with metal analyses of the different eluate fractions collected after chromatographic separation, has been used by many investigators to determine the distribution of metals among the different cytosolic ligands (ML′, ML″, *etc.*) and thus to detect metal "spillover" from the low molecular weight MBP to the high molecular weight (presumably

*Present address: Regional Marine Pollution Emergency Response Centre for the Mediterranean Sea, Manoel Island, Malta.

enzymatic) sites. However, as pointed out in the review by Winge and Brouwer,[21] potential problems do exist with this approach, notably with respect to possible dissociation of ML metal–ligand complexes during the chromatographic step and possible metal ion or ML interactions with column walls and/or packing; the potential influence of these reactions on HPLC results does not seem to be widely appreciated.

The objectives of the present study were thus to investigate the use of gel-permeation HPLC to determine MBP concentrations in freshwater invertebrates; we identify possible problems that may arise when using this method and suggest suitable conditions for the separation and detection of cytosolic proteins.

EXPERIMENTAL

To evaluate the extent of protein–column interactions, and to identify a suitable eluant that would minimize their importance, a range of the molecular weight standards was used: dextran (2×10^6), bovine albumin (66,000), egg albumin (45,000), carbonic anhydrase (29,000), chymotrypsinogen (25,000), myoglobin (17,000), ribonuclease a (13,700), cytochrome c (12,400), aprotinin (6500), vitamin B_{12} (1355) and trytophan (204). All standards were obtained from Sigma Chemical Co., St. Louis, MO, U.S.A. and were used at a concentration of 1 mg/ml. Each standard was first scanned for its UV absorption in the wavelength range 200–300 nm (Varian DMS 2000 spectrophotometer); to calibrate the high performance liquid chromatography (Waters 600 HPLC), the absorption was then measured in the HPLC detector at two predetermined wavelengths (254 and 280 nm) without the analytical column attached. Following this calibration procedure, the entire chromatographic set-up was reassembled with a gel-permeation column (TSK gel SW2000, 30×0.75 cm) and pre-column (TSK 7.5×0.75 cm) and used for elution of the marker molecules.

To determine the optimum buffer conditions, various eluant solutions were tested (all solutions contained 0.03% NaN_3): 10m*M* TRIS–HCl, pH 8.0; 10m*M* TRIS–HCl, pH 7.0; 100m*M* TRIS–HCl, pH 7.0; 200m*M* TRIS–HCl, pH 7.0; 10m*M* TRIS–HCl, 100m*M* NaCl, pH 7.0; 10m*M* MES, pH 6.0; 10m*M* MES, 100m*M* NaCl, pH 6.0; 100m*M* K_2HPO_4, 100m*M* KCl, pH 7.0. [TRIS = tris(hydroxymethyloamino)methane; MES = 2-(*N*-morpholino)-ethane sulphonic acid.] In all these cases the HPLC was operated in an isocratic mode with a flow-rate of 0.5 ml/min, at room temperature (22°) and with a pressure cut-off of 2075 kPa. In addition, each eluant was degassed with helium before use and periodically degassed during HPLC operation.

In a second investigation ligand competition experiments were performed in triplicate to determine if interaction and exchange can occur between metal bound to MBP and other proteins during the chromatographic separation step. A degassed solution of commercially available horse kidney or rabbit liver metallothionein (Sigma Chemical Co., St. Louis, MO, U.S.A.) was spiked with ^{203}Hg (NEN DuPont Canada Ltd., Toronto; initial specific activity 12 mCi/mg Hg) and left to stand for 15–20 min at room temperature under a nitrogen atmosphere. Unbound mercury was removed by the addition of hemolysed blood.[22] The resulting mixture was heated in a boiling water bath for 3–4 min, cooled and centrifuged at 10,000 *g* for 10 min. The supernatant was filtered by positive pressure through a 0.4-μm polycarbonate filter (Nucleopore). The hemolysate addition, heating, centrifugation and filtration steps yielded a clear mercury-radiolabelled metallothionein solution (final concentration 1 mg/ml), from which an aliquot was taken and the amount of radioactivity determined (LKB Wallac model 1282 gamma counter). An equivalent aliquot was injected into the HPLC system using a 10m*M* TRIS–HCl, 100m*M* NaCl, 0.03% NaN_3, pH 7.0 solution as the eluant buffer. Eluate fractions were collected and the radioactivity in each was determined by gamma counting. Additional radiolabelled metallothionein aliquots were taken and incubated separately with a solution of bovine albumin, egg albumin or vitamin B_{12} for 20 min at room temperature. These calibration markers were used to simulate the metal stripping properties of a high molecular cytosol fraction (egg/bovine albumin) and a low molecular cytosol fraction (vitamin B_{12}) respectively. In this context it should be noted that egg albumin has been used as a scavenger of unbound metal during the quantification of MBP by metal saturation methods.[23] To avoid the procedural artifacts of metal redistribution shown to take place when chemical agents are used to maintain buffers under reducing conditions,[24,25] the competition experiments were

performed under a nitrogen atmosphere in a glove bag. After the 20-min equilibration period, aliquots of these mixtures were taken for counting and an equivalent volume was injected into the HPLC; fractions were collected and counted as before.

A similar competition experiment was performed, also in triplicate, with cytosol mussel extract instead of the model cytosol components. To prepare the cytosolic extract, adult freshwater mussels, *Anodonta grandis*, of uniform size (7 to 8 cm) were collected from Lac St. Joseph, Quebec, Canada. Prior to dissection, the animals were kept in chlorine-free tap-water for 24 hr to depurate. The excised soft tissue was stored at −40° until use. The soluble fraction of the tissue was prepared by mechanical homogenization of the soft-tissue (Brinkman tissue grinder, model CH-6010) in an equal volume of ice-cold TRIS–HCl buffer (25m*M*, pH 7.2) under a nitrogen atmosphere. The homogenate was centrifuged at 170,000 *g* for 60 min at 2°. The supernatant (*ca.* 75 mg of organic matter/ml) was then incubated for 20 min at room temperature with an equivalent volume of the solution of ^{203}Hg-labelled metallothionein under a nitrogen atmosphere. A 100-μl aliquot was counted whilst an equivalent volume was injected into the HPLC and, as above, fractions were collected and counted for radioactivity. Similar combination experiments were performed with metallothionein that had been radiolabelled with ^{65}Zn or ^{109}Cd. Each set of competition or exchange experiments was performed with the same mussel cytosol extract.

RESULTS AND DISCUSSION

Results for the elution experiments designed to test the ability of the different buffers to elute the molecular weight markers from the analytical column are presented in Table 1. All markers exhibited UV absorption in the range 200–300 nm and thus, if eluted, would be readily detected by the HPLC 254/280 nm dual wavelength detector. All markers with molecular weights higher than the upper molecular weight cut-off of the analytical column (30,000) were quantitatively eluted, irrespective of the concentration or type of buffer used for elution, implying that no interaction of these proteins with the column lining took place. The results in Table 1 also show that the highest concentration of TRIS–HCl (200m*M*) was as efficient in eluting the protein markers as was the phosphate buffer or a low concentration (10m*M*) of TRIS–HCl or MES with the addition of salt (NaCl, 100m*M*). Difficulties in the elution of some proteins in the molecular working range of the column arose when low buffer concentrations were used with no added electrolyte. Thus, for example, whereas myoglobin was eluted with the lowest TRIS–HCl concentration, only the highest concentration of TRIS–HCl or a low concentration of TRIS–HCl with the addition of sodium chloride (100m*M*) was successful in eluting cytochrome c. Successful elution of molecular markers such as chymotrypsinogen, ribonuclease a and aprotinin also required high concentrations of either the eluant buffer or an added electrolyte.

The results in Table 1 would suggest that adsorption of the marker molecules to the column is more salt- than pH-dependent, since the introduction of 100m*M* sodium chloride to 10m*M* solutions of either TRIS–HCl or MES buffers in the pH range 6–8 was sufficient to ensure successful elution. The only marker to exhibit appreciable pH sensitivity was myoglobin, the elution of which at pH 6 was slower than at pH 7 or 8, possibly as a result of changes in the hydrodynamic radius of the myoglobin molecule at the lower pH.

The retention of certain molecular weight markers on the column in the presence of low ionic strength eluants is probably the result of interactions between highly charged marker molecules and silanol groups remaining on the surface of the gel-permeation support.[26] The high salt concentration effectively suppressed the residual silanol activity of the column packing, thereby limiting protein-column interaction. The original choice of a low concentration of TRIS–HCl, as utilized in the work of Suzuki and his co-workers,[27–29] was designed to limit the metal-complexing ability of the TRIS–HCl eluant since it has been demonstrated that at high concentrations this buffer may remove metals from proteins.[30] To minimize such re-equilibration is critical for a true study of the *in vivo* distribution of metals bound to different cytosolic ligands. Furthermore, the utilization of a mobile phase of relatively low ionic strength reduces the corrosion of internal metallic surfaces within the stainless steel components of commercially available chromatography systems.[31] On the other hand, as has been shown here, the use of a low concentration of TRIS–HCl can lead to a low recovery or no recovery at all of certain proteins. Clearly, as a

Table 1. Elution of different molecular weight markers on TSK gel SW2000 columns using different eluant buffer systems

		Elution buffers							
		TRIS–HCl					PO_4/KCl	MES	
Marker Name	Mol. Wt.	10m*M* pH 8	10m*M* pH 7	100m*M* pH 7	200m*M* pH 7	10m*M*, pH 7 100m*M* NaCl	100m*M* pH 7	10m*M* pH 6	10m*M*, pH 6 100m*M* NaCl
Dextran	2×10^6	+	+	N.D.	+	+	+	+	+
Bovine Albumin	66,000	+	+	N.D.	N.D.	N.D.	+	N.D.	N.D.
Egg Albumin	45,000	+	+	N.D.	N.D.	+	+	+	N.D.
Carbonic Anhydrase	29,000	+	+	N.D.	N.D.	N.D.	N.D.	+	N.D.
Chymotrypsinogen	25,000	−	−	+	+	+	+	−	+
Myoglobin	17,000	+	+	N.D.	N.D.	N.D.	+	+*	N.D.
Ribonuclease a	13,700	−	−	+	+	+	+	−	+
Cytochrome c	12,400	−	−	−	+	+	+	−	+
Aprotinin	6,500	−	−	N.D.	N.D.	N.D.	+	−	+
Vitamin B_{12}	1,355	+	+	N.D.	N.D.	+	+	+	N.D.
Tryptophan	204	+	+	N.D.	+	N.D.	+	+	N.D.

+ = Eluted.

− = Not eluted.

N.D. = Not determined.

* = Myoglobin eluted after trytophan.

result of an inappropriate choice of eluant, key information regarding the presence of certain proteins with their associated metals might be lost during the chromatographic step, due to the retention of the metal–protein complex on the column. In all subsequent runs we used an eluate composition (10m*M* TRIS–HCl, 100m*M* NaCl, 0.03% NaN_3, pH 7) designed to minimize competition between the buffer and the cytosolic ligands in solution, and to reduce chemical interactions between the ligands and the chromatographic gel.

A typical HPLC elution profile following a competition experiment involving mussel cytosol and radiolabelled metal bound to commercial metallothionein is shown in Fig. 1, while results for the recoveries of radiolabelled metal bound to metallothionein are presented in Table 2. In excess of 96% of the ^{109}Cd was recovered with the metallothionein fraction

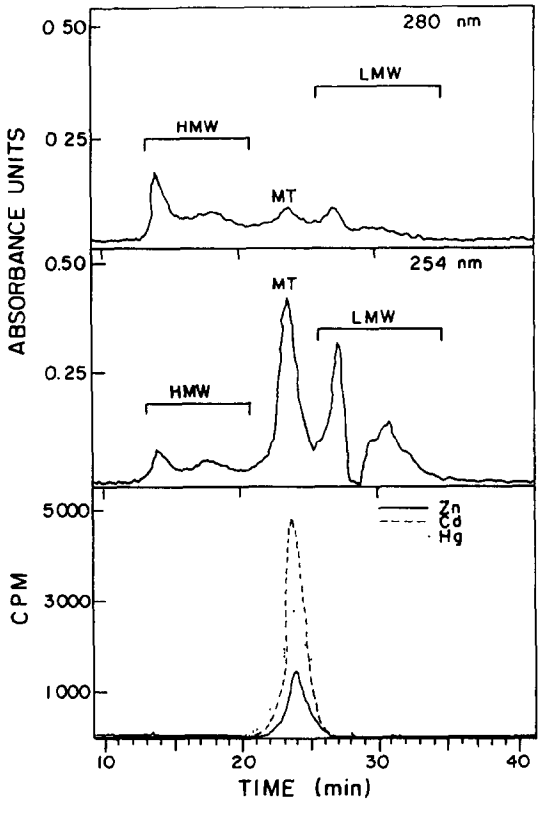

Fig. 1. Representation of an elution profile obtained by gel-permeation HPLC after a competition experiment involving mussel cytosol extract and radiolabelled metal initially bound to commercial metallothionein. Upper graphs—UV absorbance at 280 nm and 254 nm (HMW = high molecular weight fraction; MT = metallothionein fraction; LMW = low molecular weight fraction). Lower graph—typical ^{109}Cd, ^{203}Hg and ^{65}Zn profiles (cpm) with peaks corresponding to metallothionein.

after chromatographic separation, either when radiolabelled cadmium metallothionein was chromatographed on its own or when incubation with a mussel cystosol extract took place prior to chromatographic separation. Recovery of ^{203}Hg-labelled metallothionein was also quantitative when it was chromatographed alone. However, occasional recovery problems did arise when the radiolabelled mercury metallothionein preparation included other ligands. The results indicate very little exchange of the ^{203}Hg between the metallothionein and the other ligands, *i.e.*, the relative distribution of ^{203}Hg among the three molecular weight fractions remains unchanged in the eluate. Note that as expected a control injection of inorganic $^{203}HgCl_2$ gave 0% recovery.

The results for the recovery of radiolabelled zinc bound to metallothionein also show that very little ^{65}Zn exchange took place between the metallothionein and the other cytosolic ligands, *i.e.*, the relative distribution of ^{65}Zn among the three molecular weight fractions remains unchanged. However, in this case recovery of the metal was consistently low, ranging from 52 to 58% of the total zinc activity injected. Another subtle difference between these results and those obtained for mercury was that problems of recovery of radiolabelled zinc bound to metallothionein were evident even when such a preparation was injected in absence of other cytosolic ligands.

It should be noted that the loss of radioisotope (^{203}Hg, ^{65}Zn) during the HPLC separation does not necessarily imply that the metallothionein itself was lost to the column; metal exchange between the radiolabelled metallothionein and cold metal present in the HPLC system would yield the same results. Such a mechanism for loss of radiolabel seems unlikely for Hg, but may have occurred with Zn (an omnipresent metal). However, even if such exchange did occur, it does not weaken our argument. In fact, our central thesis is that metal-metallothionein complexes originally present in cytosol extracts may be labile during HPLC separation; loss of radiolabel by exchange with cold metal demonstrates just such lability.

In conclusion, these results show that problems may arise in the separation of metal-binding proteins by HPLC, as suggested by Winge and Brouwer.[21] In recent years, numerous studies have been undertaken to isolate MBP by HPLC. In many instances, 4 to 5 molecular

Table 2. Competition experiments between radiolabelled metallothionein and mussel cytosol extract: recovery (cpm) of ^{203}Hg, ^{109}Cd and ^{65}Zn in eluate fractions after chromatographic separation

	Hg						Cd				Zn			
Exp. 1 MT-Hg (only)		Exp. 2 MT-Hg + Albumin		Exp. 3 MT-Hg + Vit. B_{12}		Exp. 4 MT-Hg + cytosol		Exp. 5 MT-Cd (only)		Exp. 6 MT-Cd + cytosol		Exp. 7 MT-Zn (only)		Exp. 8 MT-Zn + cytosol	
Added	11,539	Added	10,989	Added	8615	Added	7396	Added	22,931	Added	10,630	Added	11,691	Added	5,777
HMW	0 (0)	HMW	279 (2.5)	HMW	5 (0.1)	HMW	85 (1.2)	HMW	3 (0.0)	HMW	25 (0.2)	HMW	6 (0.1)	HMW	15 (0.3)
MT	12,756 (110)	MT	10,638 (96.8)	MT	9545 (111)	MT	5963 (80.6)	MT	22,485 (98.1)	MT	10,829 (102)	MT	6071 (51.9)	MT	2867 (49.6)
LMW	0 (0)	LMW	35 (0.3)	LMW	20(0.2)	LMW	80 (1.1)	LMW	53 (0.2)	LMW	66 (0.6)	LMW	9 (0.1)	LMW	23 (0.4)
Σ	12,756 (110)	Σ	10,952 (100)	Σ	9570 (111)	Σ	6128 (83)	Σ	22,485 (98)	Σ	10,920 (102)	Σ	6086 (52)	Σ	2905 (50)
Added	11,539	Added	11,115	Added	7989	Added	5054	Added	22,931	Added	10,294	Added	11,691	Added	5474
HMW	0 (0)	HMW	33 (0.3)	HMW	0 (0)	HMW	64 (1.3)	HMW	0 (0.0)	HMW	33 (0.3)	HMW	15 (0.1)	HMW	47 (0.9)
MT	10,736 (93)	MT	10,923 (98.3)	MT	8412 (105.3)	MT	2384 (47.1)	MT	22,137 (96.5)	MT	10,973 (106.6)	MT	6765 (57.9)	MT	3258 (59.9)
LMW	0 (0)	LMW	119 (1.1)	LMW	207 (2.6)	LMW	30 (0.6)	LMW	40 (0.2)	LMW	104 (1.0)	LMW	19 (0.2)	LMW	32 (0.5)
Σ	10,736 (93)	Σ	11,075 (100)	Σ	8619 (108)	Σ	2478 (49)	Σ	22,177 (97)	Σ	11,110 (108)	Σ	6799 (58)	Σ	3358 (61)
		Added	11,223	Added	7377	Added	5054			Added	8035			Added	5799
		HMW	13 (0.1)	HMW	6 (0.1)	HMW	181 (3.6)			HMW	5 (0.1)			HMW	47 (0.8)
		MT	5229 (46.6)	MT	4912 (67.0)	MT	4497 (89.0)			MT	8488 (104.5)			MT	3305 (57.0)
		LMW	79 (0.7)	LMW	58 (0.8)	LMW	27 (0.5)			LMW	73 (0.9)			LMW	21 (0.4)
		Σ	5321 (47)	Σ	4976 (68)	Σ	4705 (93)			Σ	8566 (105)			Σ	3373 (58)
Range % Recovery	93–110		47–100		68–111		49–93		97–98		103–107		52–58		50–58

HMW = High molecular weight fraction.
MT = Metallothionein fraction.
LMW = Low molecular weight fraction.

markers have been used for calibration of the steric exclusion gel-permeation column. In view of the results of this study, it would seem more appropriate to use a whole range of (protein) markers for calibration to ensure that minimal protein–column interaction takes place during chromatographic separation. It is also recommended that the justification for a particular eluant buffer be included in future research communications so as to help in the standardization of the HPLC method by research laboratories, if this approach is to be used for determining metallothionein concentrations and/or metal spillover as indices of sublethal metal stress. Furthermore, researchers should be aware that metal complexes originally present in cytosol extracts may be labile during HPLC separation; in the present study, such lability has been clearly demonstrated for one of the metals (Zn). If the distribution of a metal among various cytosolic ligands is to be used as an indication of metal spillover, it is strongly recommended that the stability of the cytosolic metal complexes during the HPLC separation step be tested.

Acknowledgements—Thanks are due to Simone Micallef for typing all manuscript drafts. Financial support from the Natural Sciences and Engineering Research Council of Canada (NSERC strategic grant; NSERC postgraduate award to YC) and from the Quebec Fonds pour la Formation de Chercheurs et Aide à la Recherche (FCAR team grant; NSERC post-doctoral fellowship to SM) is gratefully acknowledged.

REFERENCES

1. D. J. H. Phillips, *Quantitative Aquatic Biological Indicators*, 1980, Appl. Sci. Publishers Ltd., London, UK.
2. S. Micallef and P. A. Tyler, *Bull. Environ. Contam. Toxicol.*, 1989, **42,** 344.
3. K. L. Wong and C. D. Klaasen, *J. Biol. Chem.*, 1979, **254,** 12399.
4. R. Dallinger, E. Carpene, G. J. Dalla Via and P. Cortesi, *Arch. Environ. Contam. Toxicol.*, 1989, **18,** 554.
5. H. Ohtake, T. Suyemitsu and M. Koga, *Biochem. J.*, 1983, **211,** 109.
6. K. Lerch, D. Ammer and R. W. Olafson, *J. Biol. Chem.*, 1982, **257,** 2420.
7. Y. Aoki, S. Hatakeyama, E. Kobayashi, Y. Sumi, T. Suzuki and K. T. Suzuki, *Comp. Biochem. Physiol.*, 1989, **93C,** 345.
8. Y. Maita and S. Kawaguchi, *Bull. Environ. Contam. Toxicol.*, 1989, **43,** 394.
9. D. W. Engel and G. Roesijadi, in W. B. Vernberg, A. Calabrese, F. P. Thurberg and F. J. Vernberg [eds.], *Pollution Physiology of Estuarine Organisms*, Univ. South Carolina Press, 1987, 421.
10. P. V. Hudson, *Aquat. Toxicol.*, 1988, **11,** 3.
11. D. W. Engel and M. Brouwer, *Biol. Bull.*, 1987, **173,** 239.
12. R. W. Olafson and R. G. Sim, *Anal. Biochem.*, 1979, **100,** 343.
13. K. M. Chan, W. S. Davidson, C. L. Hew and G. L. Fletcher, *Can. J. Zool.*, 1989, **67,** 2520.
14. G. Roesijadi, M. E. Unger and J. E. Morris, *Can. J. Fish. Aquat. Sci.*, 1988, **45,** 1257.
15. P. B. Lobel and J. F. Payne, *Comp. Biochem. Physiol.*, 1987, **86C,** 37.
16. A. E. Funk, F. A. Day and F. O. Brady, *Comp. Biochem. Physiol.*, 1987, **86C,** 1.
17. H. Sunaga, E. Kobayashi, N. Shimojo and K. T. Suzuki, *Anal. Biochem.*, 1987, **160,** 160.
18. A. Viarengo, G. Mancinelli, G. Martino, M. Pertica, L. Canesi and A. Mazzucotelli, *Mar. Ecol. Prog. Ser.*, 1988, **46,** 65.
19. A. Mazzucotelli, R. Fache, A. Viarengo and G. Martino, *Talanta*, 1988, **35,** 693.
20. K. T. Suzuki, *Experientia Suppl.*, 1987, **52,** 265.
21. D. R. Winge and M. Brouwer, *Environ. Health Persp.*, 1986, **65,** 211.
22. A. M. Scheuhammer and M. G. Cherian, *Toxicol. Appl. Pharmacol.*, 1986, **82,** 417.
23. M. D. Dutton, M. Stephenson and J. F. Klaverkamp, *Environ. Toxicol. Chem.*, submitted for publication.
24. P. B. Lobel, *Comp. Biochem. Physiol.*, 1989, **92C,** 189.
25. G. Roesijadi and A. S. Drum, *Comp. Biochem. Physiol.*, 1982, **71B,** 455.
26. W. S. Hacock (ed.), *CRC Handbook of HPLC for the Separation of Amino-acids, Peptides and Proteins*, CRC Press Inc., Boca Raton, Florida, 1984.
27. K. T. Suzuki, H. Sunaga and T. Yajima, *J. Chromatogr.*, 1984, **303,** 131.
28. Y. Mochizuki, K. T. Suzuki, H. Sunaga, E. Kobayashi and R. Doi, *Comp. Biochem. Physiol.*, 1985, **82C,** 249.
29. K. T. Suzuki, H. Sunaga, E. Kobayashi and N. Sugihira, *J. Chromatogr.*, 1987, **400,** 233.
30. D. B. McPhail and B. A. Goodman, *Biochem. J.*, 1984, **221,** 559.
31. A. Z. Mason, *Chromatogram*, 1989, **10,** 7.

Talanta, Vol. 39, No. 9, pp. 1081–1087, 1992
Printed in Great Britain

0039-9140/92 $5.00 + 0.00
Pergamon Press Ltd

DETERMINATION OF ABSORPTION EFFICIENCIES OF CARBON DIOXIDE ABSORBENTS BY GAS CHROMATOGRAPHY

WU LIXIN* and HE HUANNAN
Shanghai Institute of Metallurgy, Academia Sinica, Shanghai, 200050, P.R. China

(*Received* 7 *May* 1991. *Revised* 2 *April* 1992. *Accepted* 4 *April* 1992)

Summary—An HP-5880A gas chromatograph equipped with FID has been used to determine the efficiency of various CO_2 absorbents and some molecular sieves. Temperature, the CO_2 concentration in the absorbed gas mixture and space velocity of the gas mixture have effects on the absorption efficiency to different degrees, but temperature is a controlling factor. It has been established that in gas analysis the systematic errors arising from CO_2 impurities in the carrier gas are negligible when CO_2 is absorbed by carbon dioxide absorbents. Three methods for eliminating blank error are presented. The differential volume method through preconcentrating at the same time but at different flow-rates (DVMST) is proposed as the best method in preconcentration analysis. With the preconcentration technique, the minimum detectable level for CO_2 in a 10-litre sample is around 0.3 ppb(v/v).

Carbon dioxide absorbents are extensively used not only in analysis and purification of gases but also in the chemical and food industries, clinics, spacecraft and submarines, *etc.* There have been many reports about the absorption mechanism and absorption efficiencies of carbon dioxide absorbents.[1–7] Gootjes and Lagerweij[8] have investigated the dust content, flow resistance, colourshift and CO_2 absorption capacity of six brands of CO_2 absorbents under the same clinical conditions. However, a detailed report on the CO_2 residues that pass through carbon dioxide absorbents and effects on the absorption efficiencies has not been recorded yet, as far as we know. Herein, the CO_2 residue represents the residual (unabsorbed) carbon dioxide amount (ppb, v/v) of a gas mixture that passed through the carbon dioxide absorbent. Although gas chromatography with TCD has been generally used to determine residual carbon dioxide, unsatisfactory sensitivity means that the amount of CO_2 which passes through CO_2 absorbents (especially for those used in gas analysis) cannot be determined. The residues were therefore mostly reported as being no larger than a fixed value (*e.g.*, 0.01%, 5 ppm,[9] *etc.*). In order to demonstrate the main performances of the CO_2 absorbent prepared in our laboratory and other commercial products, to find out whether the residues will produce systematic errors in gas analysis, it is necessary to study the residues and effects on the residues of factors such as temperature, velocity, *etc.* Since zeolite molecular sieves have good adsorption to carbon dioxide, the CO_2 residues of gas mixtures adsorbed by zeolite molecular sieves are also determined in this paper.

Gas chromatography is the most effective method for trace gas analysis. To determine trace amounts of carbon dioxide, the gas is generally transformed to methane and then detected by a flame ionization detector (FID). If a preconcentration technique is used, the detection limit can be reduced to 10^{-10}–10^{-11} v/v.[10] In this work, an HP-5880A GC equipped with FID and combined with a preconcentration technique is used to determine the CO_2 residues that pass through CO_2 absorbents and zeolite molecular sieves.

It is well known that the accuracy of trace gas analysis is affected if a blank is too large or uncertain. The blank is mainly from impurities of carrier gas and gas penetration from the atmosphere. In preconcentration analysis, the blank will become more serious because of its accumulation. In order to minimize the analytical error, we aim to improve the preconcentration method and propose three calculation methods which make the results more accurate.

*Author for correspondence.

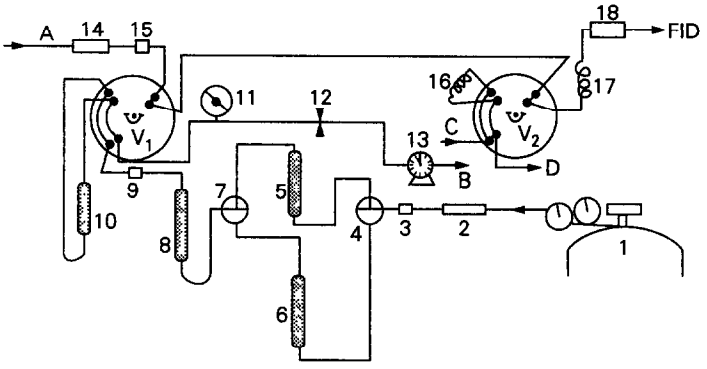

Fig. 1. Schematic diagram of experimental system 1, gas mixture cylinder; 2, mass flowmeter/controller; 3,9,15, injection ports; 4,7, 3-way valves; 5,6, CO_2 absorbing tubes (packed with different absorbents); 8, drying tube; 10, pre-concentration column (packed with porous polymer beads, GDX) 11, pressure gauge; 12, needle valve; 13, wet test meter; 14, carrier gas purification system; 16, sample loop; 17, chromatographic column; 18, reduced nickel catalyst tube; A, carrier gas inlet; B, sample gas outlet; C, standard gas inlet; D, standard gas outlet; V_1,V_2, 6-port valves (both off).

EXPERIMENTAL

Apparatus and chromatographic conditions

The experimental system is shown in Fig. 1. A gas mixture containing CO_2 passes through CO_2 absorbent and desiccant. After absorption by the CO_2 absorbent, the gas mixture is preconcentrated in the preconcentration column.

An HP-5880A GC (Hewlett Packard Co., U.S.A.) equipped with FID is used. The chromatographic conditions are as follows: stainless steel chromatographic column ($\frac{1}{8}$ inch × 800 mm) packed with carbon molecular sieve "601" (Shanghai Reagent Factory), 40–60 mesh; oven temperature 60°; injection temperature 150°; detector temperature 200°; carrier gas, hydrogen 56 ml/min; air 440 ml/min; nitrogen 24 ml/min; reduced nickel catalyst tube, $\phi 3 \times 150$ mm, 380–400°.

Recovery efficiency of CO_2 preconcentration

As shown in Fig. 1, the reference gases are injected in two ways. One is injected directly from injection port 15, the other is injected from injection port 9 and transported to the preconcentration column (−196°) by ultra pure hydrogen at different flow-rates. The ultra pure hydrogen was released from a hydrogen storage cylinder. Its CO_2 impurities are so little that CO_2 cannot be detected even if two litres of hydrogen are concentrated. Therefore, the peak areas in Table 1 do not require deduction of contributions from CO_2 impurities of ultra pure hydrogen. It can be seen from Table 1 that the preconcentration of carbon dioxide is complete when the flow-rate of the preconcentrated gases ranges from 400 to 800 ml/min. The recovery efficiency can reach 96.9% even when the flow-rate is 1000 ml/min.

Calibration curve

The standard reference gas (0.957% CO_2 in hydrogen) is injected in different amounts by micro syringe. The volume injected is plotted *vs.* CO_2 peak area (Fig. 2). The calibration curve is a straight line passing through the origin.

Table 1. The recovery efficiency of CO_2 preconcentration

Method of injection	Flow-rate of ultra pure hydrogen, *ml/min*	CO_2 Peak area	Recovery efficiency of preconcentration %
Direct injection*		2211.32	
2 litre†	400	Undetectable	
Preconcentration injection*	400	2210.82	99.98
	600	2210.14	99.94
	800	2167.05	98.00
	1000	2142.74	96.90

*40 μl of reference gas (0.957% CO_2) is injected by micro syringe.
†The preconcentration volume of ultra pure hydrogen, no extra gases are injected.

Analysis process

As shown in Fig. 1, the sample gas is concentrated at a constant flow-rate. When a given amount of sample is concentrated, the sampling valve V_1 is turned to the "ON" position and the Dewar vessel containing liquid nitrogen is removed. After 10 sec a hot water bath at 80° is put around the preconcentration column and the "START RUN" key is pressed. The chromatograph then runs automatically.

Minimum detectable level

According to the minimum peak area detected by the integrator, the minimum detectable level for CO_2 with a 10-litre sample is around 0.3 ppb (v/v).

RESULTS AND DISCUSSION

Absorption efficiencies of various CO_2 absorbents under different conditions

Carbon dioxide residues which passed through some CO_2 absorbents and molecular sieves. Some brands of CO_2 absorbents and zeolite molecular sieves are packed in an absorbing tube (15 mm i.d. × 100 mm) respectively. A gas mixture (4.2% CO_2 in hydrogen) is passed through the tube at a rate of 400 ml/min at a temperature of 25°. After CO_2 in the gas mixture is absorbed by the absorbent, the residual CO_2 portion is determined by chromatographic detection. The results are summarized in Table 2.

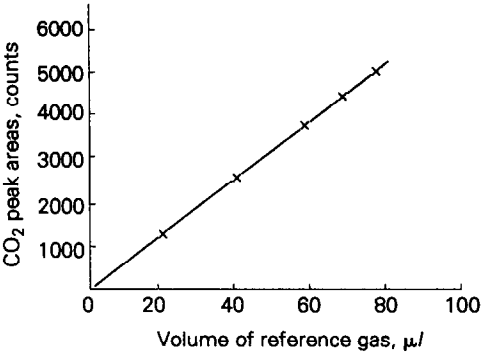

Fig. 2. Calibration curve for measurement of CO_2.

It can be seen from Table 2 that the residues that passed through HP-1 CO_2 Absorbent and Soda Asbestos are the lowest. All of the absorbents used for gas analysis (HP-1 Absorbent, Soda Asbestos, Ascarite II and Carbosorb AS) can absorb CO_2 completely. The residual CO_2 can be lower to ppb levels. Molecular sieves also have very good adsorption for CO_2, but their adsorptions are closely related to their degrees of activation. Due to their poor selectivity, molecular sieves are not widely used as CO_2 absorbents in gas analysis.

Effect of temperature on the residues. The CO_2 residues that passed through some absorbents and molecular sieves at different temperatures are listed in Table 3. The experimental conditions are as follows: gas mixture, 4.2% CO_2 in hydrogen; flow-rate, 400 ml/min; absorbing tube, 15 mm i.d. × 100 mm.

Table 2. CO_2 residues which passed through some CO_2 absorbents and molecular sieves

Absorbents	Number of determinations	Average of CO_2 residues, *ppb(v/v)*	Relative standard deviation, %
HP-1 CO_2 absorbent (our laboratory)	6	3.3	3.0
Soda asbestos (E. Merck Co., Germany)	3	3.5	4.4
Ascarite II (LECO Co., USA)	4	11.9	4.4
Carbosorb AS (B.D.H. Co., England)	4	7.2	3.3
Soda lime (Shanghai Reagent Factory, China)	4	365	3.1
5A Molecular sieve* (Linde Co., Germany)	3	240	4.8
10x Molecular sieve* (Karlsruhe Co., Germany)	3	123	4.6
13x Molecular sieve* (Schuchardt Co., Germany)	4	63.9	3.1

*Molecular sieves are activated at 500–550° in a furnace for 15 hr. Pure hydrogen is passed through the activated molecular sieves at 150 ml/min for 1–2 hr before analysing.

Table 3. Effect of temperature on the residues [units of ppb(v/v)]

Temperature, °C	0	25	50	75	95
HP-1 CO_2 absorbent	2.3	3.3	7.1	16.1	25.8
Soda asbestos	2.6	3.5	6.8	14.2	24.2
Ascarite II	5.7	11.9	—	31.8	—
Carbosorb AS	3.1	7.2	15.3	—	—
5A Molecular sieve	54.0	240	1400	—	—
10x Molecular sieve	42.7	123	—	—	—
13x Molecular sieve	12.8	63.9	—	—	—

Table 3 shows that CO_2 residues passing through CO_2 absorbents and molecular sieves will increase when the temperature increases because it is a thermopositive process. However, compared with CO_2 absorbents, molecular sieves are more sensitive to temperature change due to its characteristics of physical adsorption. They can make CO_2 residues as low as those of CO_2 chemical absorption at low temperature, which is very useful in gas separation and purification.

Effect of space velocity on the residues. When a gas mixture (4.2% CO_2 in hydrogen) is passed through the absorbents at different space velocities, their results are listed in Table 4. Herein, the space velocity means the number of volumes of gases that pass through one unit volume of the absorbent in unit time. The calculation method is: flow-rate of gas (ml/hr) divided by volume of the absorbent (ml).

In Table 4 the residues are lower at the space velocity of 18000 hr^{-1} because of incomplete preconcentration, since the flow-rate of the preconcentrated gas is over 1000 ml/min at that time. It can be concluded that the residues do not increase when the space velocity of the absorbed gas mixture ranges from 1500 to 18000 hr^{-1}. This demonstrates that the absorbents absorb CO_2 completely and rapidly.

Effect of CO_2 concentration of absorbed gases on the residues. In Table 5 it can be seen that the residues will increase slightly if the CO_2 concentration of the absorbed gas mixture is higher. As we know, when the absorbed gas containing high-concentration CO_2 passes through the absorbent, particularly at high space velocity, large amounts of heat may be released in very

Table 4. Effect of space velocity on the residues [units of ppb(v/v)]

Space velocity, hr^{-1}	1500	5200	13000	18000
HP-1 CO_2 absorbent	4.3	4.5	4.3	4.2
Soda asbestos	4.1	4.3	—	4.2

Table 5. Effect of CO_2 concentration of absorbed gas mixture on the residues [units of ppb(v/v)]

CO_2 concentration of absorbed gases (%)	4.2	10	16
HP-1 CO_2 absorbent	4.5	4.9	5.7
Soda asbestos	4.2	4.4	5.5

short time periods owing to intense reaction. The heat will be carried to the upside of the absorbing tube with gas flow and the temperature of the absorbent rises. Hence, the absorption efficiency of the absorbent will be decreased.

The residues absorbed by CO_2 absorbents in analogous gas analysis experiment. In practical gas analysis (*e.g.*, determination of carbon and oxygen in metals) carbon and oxygen are generally released in the form of CO_2. Since carbon/oxygen reacts with oxygen/carbon rapidly, the concentration distribution of released carbon dioxide is peak-like. The concentration of carbon dioxide may be very high at the top of the peak. The question arises as to whether such large amounts of carbon dioxide passing through the absorbent give a breakthrough of CO_2. In order to imitate the above situation, pure carbon dioxide is injected from injection port 3 (see Fig. 1) when gas mixture passes through the absorbent (gas mixture, 4.2% CO_2 in hydrogen; flow-rate, 400 ml/min; temperature, 25°).

It can be seen from Table 6 that a small amount of gas mixture containing high-concentration CO_2 does not cause the residues to increase. Compared with the amounts of released carbon dioxide, the residues are very slight. Accordingly, it can be concluded that the systematic error from the residual CO_2 in gases are negligible if they are absorbed by the absorbent in gas analysis. However, when the reagent only remains 2 cm in height, a breakthrough of CO_2 will occur.

Residues absorbed by CO_2 absorbents in gas purification. In order to investigate the absorbent's efficiency in absorbing micro amounts of carbon dioxide, pure hydrogen containing 2.3 ppm CO_2 impurities is used as absorbed gas.

Table 6. The CO_2 residues absorbed by CO_2 absorbents in analogous gas analysis [units of ppb(v/v)]

Height of unabsorbed absorbent (*cm*)		7–9		2
Amounts of pure CO_2 injected (*ml*)	0	30	50	30
Ascarite II	11.9	11.8	12.1	51
HP-1 CO_2 absorbent	3.5	—	4.0	63

When the pure hydrogen is purified by HP-1 CO_2 Absorbent, its CO_2 impurities can be reduced to 3.8 ppb (temperature, 28°; flow-rate, 800 ml/min).

Comparison of preconcentration methods for eliminating blank error

Preconcentration sampling is one of the most important means for measuring trace impurities in gases by GC. Compared with direct sampling, however, preconcentration sampling will naturally introduce a problem from the blank. The impurities of carrier gas, sample gas and penetration from outside will become obvious in trace gas analysis because of time accumulation and violent temperature changes in preconcentrating processes. The blank cannot generally be neglected and may sometimes lead to the wrong conclusion. Previously, eliminating blank error has been mainly done by deducting the measured blank value. In our view however, the method has at least two disadvantages: (1) In the blank test, an ultra pure gas which is assumed as absolutely pure is usually used in place of the sample gas in order to determine the blank value, but because the ultra pure gas will not be absolutely pure, the calculated blank must contain a new blank which comes from the impurities of the absolutely pure gas. (2) Since the experimental conditions in practical analysis are not always the same as those used in the blank test, the practical blank may change during long experimental processes. Considering the above situation, we present three methods for improving preconcentration sampling:

(1) Differential Volume Method through preconcentrating at the same flow-rate but different times (DVMSF);

(2) Differential Time Method through preconcentrating the same volume at different flow-rates (DTMSV) and

(3) Differential Volume Method through preconcentrating at the same time but different flow-rates (DVMST).

DVMSF can eliminate the blank error which comes from the impurities of carrier gas and sample gas, while DTMSV can eliminate the blank error which comes from CO_2 penetration from the atmosphere. DVMST which actually combines DVMSF with DTMSV can eliminate the above two errors.

As we know, at the very beginning of preconcentration, parts of the sample gas will be trapped in the preconcentration column with dramatic fall in temperature, but these parts cannot be included in the preconcentration volume because their volume is not known exactly, which will give a "sample gas blank". After preconcentration, there are a few seconds before desorbing the trapped gas with hot water in order to get good quality peaks. But during this time the impurities of carrier gas are trapped due to the very low temperature column, which will bring a "carrier gas blank". But, if sample gas flow-rate and release time are the same, the above two blanks are unchangeable whenever the preconcentration volumes are different. So we can use the DVMSF method to deduct the blank. The calculation formulae are as follows:

$$C_x = \frac{V_s \cdot C_s}{A_s} \cdot \frac{(A_2 - A_1)}{(V_2 - V_1)} \times 10^3$$

where C_x is the concentration of sample gas (ppb); V_s, C_s, A_s are the volume (ml), concentration (%) and peak areas of standard reference gas; V_2, V_1, A_2, A_1 are the preconcentration volume (litre) and corresponding peak areas at the same flow-rate but different preconcentration time.

Another blank, the "penetration blank", is more influential in trace gas analysis. It is very difficult to prevent air from penetrating into the analytical system completely. Although the amounts of air are very small, the amounts of CO_2 in air intruded are very large in comparison with the analysed gas in the trace analysis. If those parts penetrated from atmosphere are not deduced in experiment a large error will be produced, and a wrong conclusion may sometimes result. Since the penetration blank is equal at the same preconcentration time, we can use DVMST method to eliminate this blank error. The calculation formulae are as follows:

$$k = \frac{A_2 - A_1}{t_2 - t_1} \quad A_1' = A_1 - kt_1 \quad A_2' = A_2 - kt_2$$

where k is the correction factor; t_2, t_1, A_2, A_1 are the preconcentration time ($t_2 > t_1$) and corresponding peak areas at the same preconcentration volume but different flow-rate; A_1', A_2' are the corrected peak areas of A_1, A_2 respectively. Then the results can be calculated according to the routine peak area method (PAM), *i.e.*,

$$C_x = \frac{V_s \cdot C_s}{A_s} \cdot \frac{A_1'}{V_1} \quad \text{or} \quad C_x = \frac{V_s \cdot C_s}{A_s} \cdot \frac{A_2'}{V_2}$$

In order to obtain a convenient and effective method for eliminating the blank error, the DVMST method is proposed to be the best.

Table 7. Comparison of some preconcentration methods

Group	No. of experiment	Preconcentration: Time, *min*	Flow, *ml/min*	Volume, *litres*	Peak areas: CO_2	Corrected by DTMSV	CO_2 residues, ppb: PAM	DVMSF	DTMSV + PAM	DTMSV + DVMSF	DVMST
1	1	24.2	200	5.0	381.88	109.18	12.4		3.6	3.1	3.0
	2	24.1	400	10.0	473.52	202.40	7.7	7.2	3.3	(2–1)	(2–1)
	3	11.4	400	5.0	237.60	110.17	7.7	(4–2)	3.6	3.2	
	4	34.3	400	15.0	689.40	303.98	7.5	7.4 (4–3)*	3.3	3.1 (4–3)	
2	5	6.6	400	3.0	74.00	69.70	3.3	3.2	3.1	3.0	
	6	16.9	400	7.6	182.25	171.24	3.2	(6–5)	3.0	(6–5)	
	7	5.4	400	2.5	60.46	56.88	3.3	3.2	3.1	3.0	
	8	11.4	200	2.5	64.31	56.88	3.5	(6–7)	3.1	(6–7)	

*(4–3) means that the result is calculated from the difference of volumes and peak areas of Experiments No. 4 and No. 3 according to DVMSF method. Others are on the analogy of this.

The method has taken both sides of gas blank and penetration blank into consideration. Its calculation formula is identical with DVMSF's except some used symbols have different meaning, where V_2, V_1, A_2, A_1 are the preconcentration volumes (litre) and corresponding peak areas at the same preconcentration time but different flow-rate.

Table 7 summarizes the calculation results of some preconcentration methods. In Table 7, both Group 1 and 2 are the results of determining CO_2 residue that passed through HP-1 CO_2 Absorbent. In order to illustrate the superiority of the proposed methods, we let air penetrate into the analytical system in Group 1 quite seriously on purpose. It can be seen that the results calculated by DVMSF are a bit lower than those calculated by PAM as a result of deducting sample gas blank and carrier gas blank. When the penetration of CO_2 is serious, the results should be calculated by DTMSV or DVMST, otherwise, its accuracy will be very poor although its precision is satisfactory. It can also be seen that the results of DVMST are nearly equal to those of DTMSV + DVMSF; the results of DVMST and DTMSV in Group 1 are also identical with those of Group 2 where the penetration of CO_2 is slight. This proves our proposed methods to be correct and efficient.

Compared to the deduction method for blanks measured in the blank test, DVMST and DTMSV have the following advantages: (1) they can deduct the blank error without doing a blank test; (2) the analytical precision is better because only the flow-rate of the sample gas changes during the entire process; (3) the blank correction is dynamic, independent, and the corrected results are not affected by changes in the blank during experiments; (4) the blank change can be seen clearly and timely, which allows the measures to reduce the system blank to be taken purposefully. These methods will become more efficient in determining trace amounts of oxygen or nitrogen.

CONCLUSION

An HP-5880A gas chromatograph equipped with FID has been used to determine the CO_2 residues that passed through CO_2 absorbents produced by our laboratory, E. Merck Co., B.D.H. Co., LECO Co. and molecular sieves, such as 5A, 10x, 13x. In combination with preconcentration technique, the minimum detectable level for CO_2 with a 10-litre sample is around 0.3 ppb (v/v).

The results demonstrate that the CO_2 residue that passed through HP-1 CO_2 Absorbent (prepared in our laboratory) and Soda Asbestos (produced by E. Merck Co.) is the lowest (3–4 ppb at room temperature). Temperature, CO_2 concentration of absorbed gas mixture, space velocity have effects on the residues in different degrees, but temperature is a controlling factor. The residues will increase with rising temperature. The systematic errors coming from the residual CO_2 in gases are negligible when they are absorbed by CO_2 absorbents in gas analysis.

Blank problems in preconcentration techniques are discussed. Three methods for eliminating blank error are presented: differential volume method through preconcentrating at the same flow-rate but different times (DVMSF), differential time method through preconcentrating the same volume at different flow-rates (DTMSV), and differential volume method

through preconcentrating at the same time but different flowrates (DVMST). DVMST is proposed to be the best method in preconcentration analysis for its convenience and accuracy.

REFERENCES

1. C. Alvarez-Fuster, N. Midoux, A. Caurent and J. C. Charpentier, *Chem. Eng. Sci.*, 1981, **36**, 1513.
2. D. W. Savage, G. Astarita and S. Joshi, *ibid.*, 1980, **35**, 1513.
3. P. C. Tseng, W. S. Ho and D. W. Savage, *AIChE J.*, 1988, **34**, 922.
4. T. Inui, Y. Okugawa and M. Yasuda, *Ind. Eng. Chem. Res.*, 1988, **27**, 1103.
5. H. Foerster and N. Schunann, *J. Chem. Soc. Faraday Trans. 1*, 1989, **85**, 1149.
6. A. Purer, G. A. Deason and M. L. Nuckols, AD-A122290, 1983.
7. W. Spaur, E. D. Thalman and R. C. Maulbeck, AD-065549, 1978.
8. P. Gootjes and E. Lagerweij, *Anaestesist*, 1987, **30**, 261.
9. L. H. Slaugh and C. L. Willis, *US Patent 4433981*, 1984.
10. X. Li, H. He, J. Zhu, B. Yu and P. Mao, *Z. Anal. Chem.*, 1988, **331**, 520.

Talanta, Vol. 39, No. 9, pp. 1089–1096, 1992
Printed in Great Britain.

0039-9140/92 $5.00 + 0.00

DETERMINATION OF TOTAL SELENIUM IN WATER BY ATOMIC-ABSORPTION SPECTROMETRY AFTER HYDRIDE GENERATION AND PRECONCENTRATION IN A COLD TRAP SYSTEM

ULF ÖRNEMARK,* JEAN PETTERSSON and ÅKE OLIN
University of Uppsala, Department of Analytical Chemistry, P.O. Box 531, S-751 21 Uppsala, Sweden

(*Received* 28 *October* 1991. *Revised* 4 *February* 1992. *Accepted* 4 *February* 1992)

Summary—A cold trap system for the determination of selenium by hydride generation–atomic absorption spectrometry (HG–AAS) is described. For a 30-ml sample the limit of detection is <2 ng/l. and the precision is better than 4% at the 30 ng/l. level. A number of digestion procedures for the destruction of organic matter prior to the determination of total dissolved selenium in water has been tested and compared. Concordant results were obtained except for oxidation by peroxodisulphate in strongly acidic solutions with a high content of organic material. The selenium concentrations found were in agreement with those obtained by HG–AAS after preconcentration by evaporation and dry ashing with the magnesium nitrate–nitric acid–hydrochloric acid method.

Hydride generation, followed by collection of the hydride in a cold trap, is used as a preconcentration step in the determination of several elements occurring in the low ng/l. range in natural waters. Since the work by Holak[1] in 1969 more than 80 papers have described trap systems for the determination of antimony, arsenic, bismuth, germanium, lead, selenium,[2–8] tellurium and tin. Selective hydride generation is possible since optimum conditions for hydride formation vary between the elements and between oxidation states of the same element. In addition to the usual information on speciation provided by the different reactivity of oxidation states, further information can be obtained by the cold trap technique by subjecting the contents of the trap to selective vaporization[9,10] or separation on a chromatographic column.[10]

There are difficulties connected with the cold trap technique due to the limited stability of the hydrides. Proper choice and pretreatment of the materials in the apparatus are essential. Volatile concomitants already present in the sample or formed during the hydride generation will also collect in the trap, and the amounts may reach levels that interfere with the determination of the analyte. Removal of such interferents by chemical sorbents[1,9] in the gas stream is not always possible due to decomposition of the hydride on the sorbent. It is therefore not surprising that the technique has been most frequently applied to the determination of arsenic, selenium, tin, antimony and germanium, which form the most stable hydrides.

In the present work a cold trap system assembled for the determination of selenium will be described. This element is present as selenite, selenate or organic selenium in natural waters. Great variations have been reported for the relative amounts of the three fractions.[11–13] The concentrations are low and for most Swedish surface and ground waters the total selenium concentration is <200 ng/l.[14] This concentration is close to the detection limit of the hydride generation–atomic absorption spectrometric (HG–AAS) method without preconcentration.[15] Thus the addition of a preconcentration step is needed for a study of these waters. A determination of total selenium requires that organic forms are transformed to inorganic selenium. Wet digestion with nitric acid or mixtures of this acid with other oxidizing agents,[16–18] permanganate,[19] peroxodisulphate,[20] and ultraviolet irradiation[21] have been used for this purpose. We here report the results from a comparative study of destruction methods for dissolved organics in water for use in the determination of total selenium by HG–AAS combined with a cold trap. The efficiency of the method to transform various forms of organic selenium to inorganic forms was also studied.

*Author for correspondence.

EXPERIMENTAL

Apparatus

The hydride generation and cold trap system shown in Fig. 1 consisted of a peristaltic pump (Minipuls 2, Gilson Medical Electronics, France) with PVC-tubings and four U-tubes in series. Solutions were transported through 0.5-mm PTFE-tubing and T-connections (Kabi-Pharmacia, Sweden) were used for mixing solutions and introduction of the carrier gas (N_2). The U-tubes were made of borosilicate glass (length 300 mm, inner diameter 16 mm, wall thickness 1 mm), silanized, connected by latex tubing and closed with silicone stoppers. The first tube served as a gas–liquid separator and the next two as water vapour traps. The latter were immersed in a cooling bath (Model D8-GH, Haake, Germany) containing ethanol at $-15°$. The selenium hydride was trapped at liquid nitrogen temperature by a plug of silanized quartz wool (50 mg) on the outlet side of the fourth U-tube. The flow of carrier gas was 550 ml/min and the flow of tetrahydroborate solution and sample were 5.6 and 12 ml/min, respectively.

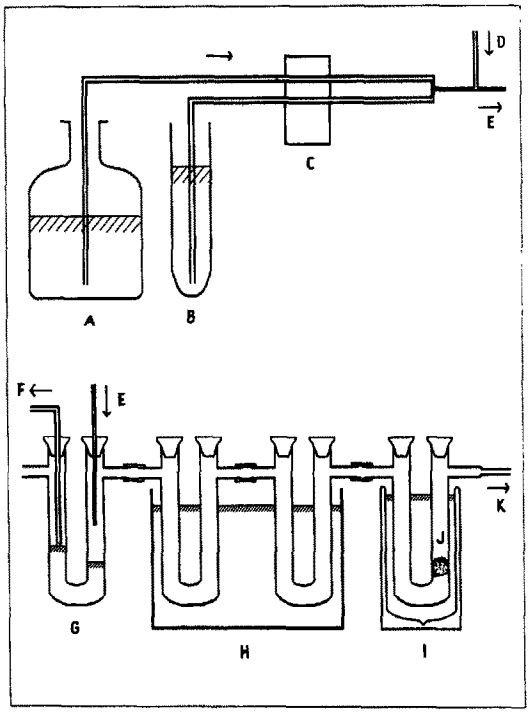

Fig. 1. Apparatus to generate, dry and collect hydrogen selenide. (A) Sodium tetrahydroborate, (B) acidified sample, (C) peristaltic pump, (D) carrier gas inlet, (E) to gas–liquid separator, (F) to waste, (G) gas–liquid separator, (H) water vapour traps, (I) hydride trap, (J) silanized quartz wool, (K) to quartz furnace.

The atomic-absorption measurements were made with a Perkin–Elmer 3100 double beam spectrometer. It was modified to hold the Perkin–Elmer MHS-20 oven with the quartz cuvette kept at 800°. The electrodeless discharge lamp (Perkin–Elmer) was operated at 7.6 W. The wavelength was 196.0 nm and the spectral band-width 0.7 nm. The deuterium background corrector of the instrument could not be used with our EDL power supply.

Determinations in the 1–10 ng Se/ml range were carried out on the flow-injection instrumentation described by Pettersson *et al.*[22]

Digestions and reductions of selenate to selenite were carried out in test tubes of borosilicate glass placed in a temperature controlled aluminium block[22] or in beakers on a hot plate. UV-irradiation was performed in 60-ml closed quartz tubes with the equipment described by Gustavsson *et al.*[23]

Chemicals

All chemicals were of analytical grade from Merck unless otherwise stated. Demineralized distilled water passed through a Millipore 3 filter cartridge system was used throughout.

A stock solution of selenium(IV), 1 g/l., was prepared from an ampoule of selenium dioxide in dilute nitric acid and its concentration was checked by an amperometric titration with thiosulphate after addition of a large excess of iodide (T. A. Bengtsson, unpublished method). The stock solution of selenium(VI), 1 g/l., was prepared by dissolving sodium selenate decahydrate (BDH) in water containing 2 ml/l. of concentrated nitric acid. Its concentration was checked against a selenium(IV) standard solution. Standard solutions of selenium(IV) and (VI) were prepared by dilution of stock solutions and contained 2 ml/l. of concentrated hydrochloric acid.

The organoselenium compounds studied were:

(A) 4,4-bis-(hydroxymethyl)-1,2-diselenolane[24]
(B) Se-benzyl-*N*-acetylselenocysteine methyl ester[25]
(C) 1,2-diselenane-3,6-dicarboxylic acid[24]
(D) seleno-DL-methionine, 99% (Sigma)
(E) seleno-DL-cystine, 90% (Sigma)
(F) trimethylselenonium iodide, 99.999% (TRI Chemical Lab., Kanagawa, Japan)

Compounds (A)–(E) were analyzed for selenium after wet digestion according to a variation of Gould's method[26] using a 10:1 (v/v)

mixture of concentrated sulphuric acid and fuming nitric acid and the amperometric titration method mentioned above. Test solutions in 0.01*M* hydrochloric acid of the organoselenium compounds, corresponding to 15 μg Se/l., were used in the experiments.

Tetrahydroborate solution, (0.5% w/v), was prepared by adding 2.5 g of sodium tetrahydroborate, 0.5 g of sodium hydroxide and 0.5 g of barium hydroxide octahydrate to 500 ml of water. After agitation, the solution was filtered through a membrane filter (0.45 μm, Millipore).

Solutions of sodium hydroxide, 5% (w/v), potassium peroxodisulphate, 2%, and potassium permanganate, 1%, were all prepared by dissolution in water.

Nitrogen used as carrier gas in the cold trap system was passed through a stainless steel column (300 × 23 nm) containing soda lime pellets to remove traces of carbon dioxide.

Water samples

The drinking water is a mixture of ground water and infiltrated surface water. At most 0.5 mg/l. of sodium hypochlorite is added at the water works. The lake water, which contained 24 mg C/l., was collected as surface water from lake Lafssjön, north of Uppsala. Both waters were filtered through a membrane filter (0.45 μm, Millipore), acidified to pH 2 with hydrochloric acid and stored in polyethylene bottles in a refrigerator.

Cleaning procedures

When first used, glassware was soaked for 12 hr in a 2% alkaline detergent (RBS-25, LabKemi, Sweden), rinsed with water, then leached for 24 hr in 4*M* nitric acid and finally rinsed with water. Glassware used in the cold trap system was, in addition, leached in 0.1*M* hydrochloric acid. Between uses utensils were soaked for a few hours in 4*M* nitric acid. The latex tubing was cleaned with the same acid and PVC tubing with 1*M* hydrochloric acid for a few hours and then rinsed with water and dried.

Conditioning of the glass used in the cold trap system involved cleaning and deactivation of the surface by silanization. The cleaned U-tubes were dried at 110° for 1 hr, soaked in a 5% dimethyldichlorosilane (Macherey-Nagel, Germany) solution in toluene for 2 hr, rinsed with small portions of toluene followed by methanol and dried at 100° for 1 hr. The U-tubes were then assembled and subjected to a continuous flow of 2–3 ml/min of nitrogen when not in use.

Pretreatment of water samples

In each of the following procedures (a)–(d), 150 ml of water were digested in a 250-ml glass beaker covered with a watch glass. In the reduction step 60 ml of concentrated hydrochloric acid were added in (b)–(e) and in (a) from the beginning. After digestion and reduction the sample was transferred to a 250-ml standard flask and diluted to volume with water.

(a) Peroxodisulphate in 3*M* hydrochloric acid; mix water, hydrochloric acid and peroxodisulphate solution (10 ml for lake water and 1.5 ml for tap water) and boil gently for 1 hr.

(b) Peroxodisulphate at pH 2; mix water and peroxodisulphate solution (10 ml for lake water and 1.5 ml for tap water) and boil gently for 0.5 hr. Add hydrochloric acid and continue boiling for 1 hr.

(c) Peroxodisulphate in alkaline medium; mix water, peroxodisulphate and sodium hydroxide solution (10 and 12 ml, respectively, for lake water and 1.5 and 7 ml for tap water) and boil gently for 0.5 hr. Add hydrochloric acid and continue boiling for 1 hr.

(d) Permanganate at pH 2; mix water and 5 ml of permanganate solution and boil gently for 0.5 hr. Add hydrochloric acid and continue boiling for 1 hr.

(e) UV-irradiation; to three quartz tubes add 50 ml of water, 50 μl of hydrogen peroxide and 1 ml of 6*M* hydrochloric acid. Irradiate for 3 hr at 600 W. Transfer to a 250-ml glass beaker, add hydrochloric acid and boil gently for 1 hr.

(f) Magnesium nitrate–nitric acid–hydrochloric acid; mix 200 ml of water, 1 ml of 6*M* hydrochloric acid, 5 ml of concentrated nitric acid and 2 g of magnesium nitrate hexahydrate in a 250-ml glass beaker. Evaporate to about 10 ml. Transfer to a 50-ml digestion tube, dilute to 20 ml and apply the following temperature programme to the aluminium block: 135°—3 hr, 175°—3 hr, 225°—2 hr, 300°—1 hr and 500°—5 hr. Cool and dissolve the residue in 10 ml of 6*M* hydrochloric acid. Heat at boiling temperature for 1 hr, cool and dilute to 25 ml.

Pretreatment of organoselenium compounds

Each of the organoselenium compounds (A)–(F) were subjected to the decomposition–reduction pretreatments (a)–(f) above. Digestions and reductions were carried out on 10-ml samples in open 50-ml digestion tubes placed in an aluminium block and in (e) as described for water samples. The samples contained 150 ng of selenium. The following reagent volumes were added: (a) 5 ml of concentrated hydrochloric acid and 0.3 ml of peroxodisulphate, (b) 0.3 ml of peroxodisulphate, (c) 0.7 ml of sodium hydroxide and 0.3 ml of peroxodisulphate, (d) 0.5 ml of permanganate, (e) 20 μl of hydrogen peroxide and 1 ml of 1*M* hydrochloric acid, (f) as for water samples. After addition of the reagents the samples were diluted to 20 ml. In the reduction step in (b)–(e) 5 ml of concentrated hydrochloric acid was added. The reaction times stated above were used.

The reduced samples were diluted to 50 ml corresponding to a selenium concentration of 3 μg/l. Selenium was determined by the flow-injection apparatus.[22]

Selenium determination

Adjust the acidity of a 30-ml sample containing not more than 5 ng of selenium to 1*M* with hydrochloric acid. Immerse the hydride trap into the liquid nitrogen. After 30 sec turn on the peristaltic pump. When the sample has been consumed, rinse the sample container and tubing with 1*M* hydrochloric acid. Turn off the pump 3 min after the start, wait for 10 sec and replace the liquid nitrogen with cold ethanol (−15°). Initiate the reading cycle of the spectrometer. Don't remove the ethanol bath until the whole selenium peak has been measured.

Prior to the next determination, remove the water vapour in the hydride trap by heating the trap with a heat gun.

RESULTS AND DISCUSSION

Cold trap system

The cold trap system was composed of silanized,[27] open-ended U-tubes with silicon rubber stoppers. They were connected by short lengths of latex rubber, which made our system flexible and easy to handle. When the traps were connected by teflon joints with viton rubber seals high blanks were observed, which disappeared when these connections were replaced by latex rubber. An all-glass system, except for the connection to the quartz furnace, failed to give acceptable precision. We believe that this was due to lack of oxygen, since oxygen is necessary for the atomization process in the heated cuvette.[5] With latex tubings enough oxygen was added to the carrier gas by diffusion through the walls. In order to protect silanized surfaces from moisture when the apparatus was not in use, the system was continuously flushed with a few ml of nitrogen per minute. The silanization of the gas–liquid separator deteriorated somewhat after a few weeks in use but the shape of the absorbance peak, precision and sensitivity were unaffected. However, as a precaution the equipment was resilanized after about 300 determinations.

Silanized quartz wool in the hydride trap proved satisfactory and a small plug, about 50 mg, placed on the outlet side of the trap was sufficient to collect all hydrogen selenide. A bigger piece of wool resulted in broader peaks.

Ambient air or water of room temperature was used initially to warm the trap and desorb the hydride. The peak height precision obtained with water was better than with air. However, a drift in baseline occurred during desorption. This observation was suspected to be caused by small amounts of water, which had escaped the water trap, collected in the hydride trap and subsequently been released in the desorption step. This problem disappeared when desorption was made with ethanol at −15°, which apparently held back any water present in the trap.

About 10 mg of water were transferred per minute from the gas–liquid separator to the cold trap system during the hydride generation. With two water traps about 95% of the water was removed. The remaining 5% of water, which condensed in the hydride trap, could easily be removed by heating the hydride trap for 15 sec with a heat gun between determinations. A layer of ice was gradually built up at the inlet of the first water trap. It was removed by raising the trap from the cooling bath for a short time. This was done 2 or 3 times a day. It was not necessary to empty the trap until the end of a day's measurements because of the big volume of the water trap. The second water trap needed no attention.

Several variations of the hydride trap were tried mainly to minimize the dead volume between the trapping zone and the quartz furnace. A V-shaped trap,[28] where only the knee was

filled with quartz wool and cooled, resulted in sharper peaks and the sensitivity almost doubled. However, peak height precision was poor. Peak splitting often occurred and the peak shape depended on the way the quartz wool was placed in the trap indicating that the desorption of the hydride from the trap was non-uniform. An obvious way to reduce the dead volume is to diminish the dimensions of the equipment following the plug of quartz wool. However, in the flow system there is a fairly delicate balance between the pressures built up in the various parts. If the dimensions of the outlet are made smaller, pressures must be increased on the inlet side. The increase in inlet pressure, when the diameter of the outlet was reduced, caused malfunction of the gas–liquid separator. Hence an equipment with fairly large inner diameters was chosen as a compromise between sensitivity and precision on one hand and ease of handling on the other.

Hydride generation, interferences and analytical performance

A sample input of 12 ml/min was used, which represented the maximum capacity of the peristaltic pump. The optimal concentration of sodium tetrahydroborate was found to be 0.5% (w/v) and the solution was stabilized by addition of sodium hydroxide. This solution contained carbonate which was released in the acid hydride generation step. The carbon dioxide was transported along with the hydrogen selenide and interfered with the selenium determination. Several experiments were performed in which test solutions with and without additions of carbonate were processed in the apparatus. The absorbance signal increased in all cases where carbonate had been deliberately added. Furthermore, the ratio between peak height and peak area changed from the value obtained with carbonate-free solutions. Addition of barium hydroxide to the tetrahydroborate solution followed by filtration through a membrane filter,[3] reduced the blank to about 75 pg of selenium. We believe that most of the reduction in the blank was due to removal of carbonate. No selenium could be detected in the precipitated barium carbonate.

The sensitivity increased with the hydrochloric acid concentration in the range 1–4*M*. Since the increase was only about 20%, 1*M* acid was chosen in order to prolong the life-time of the silanization and reduce corrosion.

The measured absorbance diminished with the time elapsed between hydride generation and desorption due to depletion of hydrogen in the carrier gas.[5] The decrease was about 40% during the first minute. It is therefore necessary to desorb the hydride at a short and fixed time after the hydride generation has ended.

In the determination of selenium by hydride generation the severe interference from nitrite[29] and the potential interference from nitrate[7] are well-known. Since both ions are present in natural waters, their influence on the performance of our system was investigated. The interferences increased with the concentration of hydrochloric acid in the sample. For samples containing 1*M* acid, as used here, normal nitrate concentrations in natural waters[30] do not interfere, but preservation of water samples by addition of nitric acid to pH 2 could not be used. Nitrite was found to interfere in 1*M* hydrochloric acid when the concentration exceeded 5μM, which leaves some margin to natural concentration levels.[31] At least part of the interference could be caused by nitrogen oxides. Trapped selenium was exposed for 1 min to the gases from hydride generation of blank solutions containing nitrate or nitrite in 4*M* hydrochloric acid. The absorbance signal decreased by 50% for 5μM nitrite and 20% for 0.2*M* nitrate.

Hypochlorite was found not to interfere at the concentrations added to potable water, <0.5 mg/l.

The calibration graph was linear below 5 ng of selenium or 0.17 μg/l. for the standard sample volume of 30 ml. The correlation coefficient was 0.999 or better. Absorbance was proportional to the sample volume at least up to 250 ml at 10 ng/l. Some loss in recovery was indicated for lower concentrations. Thus the recovery of 1 ng of selenium started to drop when the sample volume exceeded 100 ml and was about 75% at 200 ml. The shapes of the absorbance signals for various amounts of selenium are shown in Fig. 2. A frequency of 10 samples/hour could be analysed.

The sensitivity (average and standard deviation) calculated from calibration curves obtained during a period of three months ($n = 24$) was $26.7(1.4)10^{-3}$/ng Se for peak height and $99.2(5.3)10^{-3}$ s/ng Se for peak area. For repetitive measurements ($n = 3$) the precision was better than 4% for 1 ng of selenium. The limit of detection (3σ) estimated from the

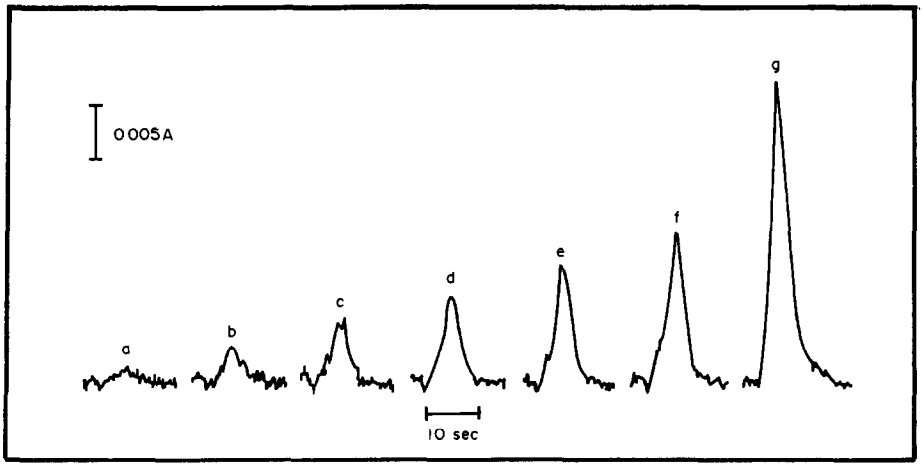

Fig. 2. Traces of selenium recorded after preconcentration from a sample volume of 30 ml in the cold trap system. (a) blank, (b) 100 pg Se, (c) 200 pg Se, (d) 300 pg Se, (e) 400 pg Se, (f) 500 pg Se, (g) 1000 pg Se.

standard deviation of the blank was 50 pg or <2 ng/l. selenium for a 30-ml sample.

Decomposition methods

In most methods for the determination of total selenium, organic selenium must be transformed to selenite. This transformation starts with a decomposition of the organoselenium compounds. The decomposition will also destroy organic matter that may interfere with the hydride generation[6,32] or the reduction of selenium(VI) to selenium(IV).[33] As discussed in the introductory part, a number of oxidizing agents have been used for destruction of organic material in water. Comparisons between the efficiencies of various destruction methods in conjunction with determination of selenium have been rather few,[16,34] and this work reports for the first time a comparative study of a range of methods. Wet digestion methods involving nitric acid were excluded. Although such methods[35] have been demonstrated to completely decompose selenium compounds they require addition of perchloric acid and evaporation of the sample. The interference caused by nitrogen oxides in our apparatus further detracted from the use of nitric acid.

The destruction methods (a)–(f) described in the experimental part were applied to the organic selenium compounds (A)–(F) and two water samples, one with high and one with a low organic matter content. The organic compounds represent the following bonding arrangements around the selenium atom: -C-Se-C- (B), (D); -C-Se-Se-C- (A), (C), (E); C_3-Se (F). The organic selenium in water may be present in proteins and peptides as selenoamino acids, notably selenomethionine, bound to humic substances, alkylselenides, alkyldiselenides and selenonium ions.[4,13] The various forms of organoselenium are thus represented in our selection of test compounds.

The results for the organoselenium compounds are presented in Table 1. The recoveries were quantitative for most compounds and destruction methods with the notable exception of the trimethylselenonium ion, which is known to be difficult to destruct.[35] The low result obtained with methods (a), (d) and (e) were not due to loss of selenium, since treatment by method (c)

Table 1. Recovery (%) of 150 ng selenium from organoselenium compounds (A)–(F) after pretreatment with digestion procedures (a)–(f). Signals recorded with the flow injection system and evaluated with the method of standard additions

	Organoselenium compound											
	A		B		C		D		E		F	
Digestion procedure	Range, %	*n*	Range, %	*n*	Range, %	*n*	Range, %	*n*	Range, %	*n*	Range, %	*n*
a	45–61	4	99–105	3	101–103	2	100–101	3	98–99	3	0	3
b	99–101	2	92–96	2	103–104	3	98–102	3	99–101	3	102–105	3
c	99–101	2	91–98	2	97–103	2	92–98	3	97–99	3	104–106	3
d	98–102	2	96–100	2	100–106	3	102–104	2	100–103	3	0	3
e	103–105	2	97–98	2	102–103	2	96–104	3	97–99	3	5–6	3
f	97–104	2	95–101	3	98–102	3	101–103	3	99–103	3	97–99	3

Table 2. Total selenium concentrations found in lake water and drinking water. Triplicate digests for all decomposition methods. Signals recorded with the cold trap system (a)–(e) and with the flow injection system after preconcentration by evaporation (f). Concentrations evaluated with the method of standard additions

	Lake water				Drinking water			
	Peak area		Peak height		Peak area		Peak height	
Digestion Procedure	Mean, *ng/l.*	RSD, %	Mean, *ng/l.*	RSD, %	Mean, *ng/l.*	RSD, %	Mean, *ng/l.*	RSD, %
a	103	1.6	106	1.0	214	9.2	219	4.9
b	143	2.6	138	0.5	208	11.7	209	5.2
c	118	7.9	126	5.2	211	5.4	218	3.6
d	126	5.3	130	5.0	228	0.5	222	1.2
e	118	6.3	127	1.6	207	2.2	203	3.5
f	—	—	135	1.4	—	—	222	3.8

of aliquots of the digests from these methods resulted in quantitative recovery of selenium. The low figure obtained for (A) treated with peroxodisulphate in 3*M* hydrochloric acid is significant.

The analytical results were evaluated with the method of standard additions. The slopes of the graphs did not differ from the slope of the calibration graph obtained with standards, which indicated that interferences from the chemicals used were absent.

The results from the water samples are collected in Table 2. For drinking water no difference was observed between the digestion methods, whereas for the lake water the results with method (a) were low. Apparently the rate of decomposition of peroxodisulphate increases faster with acidity than the rate of oxidation of organic material.[36] The sample remained slightly yellow in method (a), whereas the yellow colour of the humic substances disappeared in methods (b) and (c). A better recovery could probably have been achieved by increasing the peroxodisulphate concentration, but then the blank would also increase. The concentration of hydrochloric acid in (a) has been chosen so that the decomposition of the organic material and the reduction of selenium(VI) to selenium(IV) should proceed concurrently. The method is thus attractive but our results indicate that it should be used with caution.

It is gratifying that the preconcentration by evaporation used in method (f) yielded the same result as the cold trap system. We also tried to use the magnesium nitrate–nitric acid–hydrochloric acid method without preconcentration. However, it did not work in conjunction with the cold trap system. The reason for this could not be definitely established, but the interferences were similar to those found in the presence of nitrate indicating that some undecomposed nitrate remained.

CONCLUSIONS

The results indicate that methods (b) and (c), which use peroxodisulphate at pH 2 or higher, are the most efficient of the methods studied here for the destruction of organic selenium compounds in water. They decomposed all test objects including the very resistant trimethylselenonium ion. This substance was not decomposed by permanganate or oxidative UV-irradition, although they both decomposed the other test objects. Hence methods (b) and (c) can be recommended for water samples. Excess peroxodisulphate does not interfere in the reduction of Se(VI) to Se(IV) since it is rapidly decomposed in boiling 3*M* hydrochloric acid and the blank is low. The recommendation does not imply that methods (b) and (c) can cope with all types of water samples. As a check, evaporation and destruction with a mixture of nitric, perchloric and sulphuric acid or the magnesium nitrate–nitric acid–hydrochloric acid method can be used. Of these methods the latter is recommended since it does not involve perchloric acid.

Acknowledgements—Thanks are due to Professor B. Nygård and Dr. G. Zdansky for providing us with some of the organoselenium compounds.

REFERENCES

1. W. Holak, *Anal. Chem.*, 1969, **41**, 1712.
2. G. A. Cutter, *Anal. Chim. Acta*, 1978, **98**, 59.
3. J. Piwonka, G. Kaiser and G. Tölg, *Z. Anal. Chem.*, 1985, **321**, 225.
4. T. D. Cooke and K. W. Bruland, *Environ. Sci. Technol.*, 1987, **21**, 1214.
5. J. Dědina, *Prog. Analyt. Spectrosc.* 1988, **11**, 251.

6. D. R. Roden and D. E. Tallman, *Anal. Chem.*, 1982, **54,** 307.
7. R. M. Brown Jr, R. C. Fry, J. L. Moyers, S. J. Northway, M. B. Denton and G. S. Wilson, *ibid.*, 1981, **53,** 1560.
8. S. C. Apte and A. G. Howard, *J. Anal. At. Spectrom.*, 1986, **1,** 379.
9. S. D. W. Comber and A. G. Howard, *Anal. Proc.*, 1989, **26,** 20.
10. O. F. X. Donard, S. Rapsomanikis and J. H. Weber, *Anal. Chem.*, 1988, **58,** 772.
11. Y. Sugimura, Y. Suzuki and Y. Miyake, *J. Oceanogr. Soc. Japan*, 1978, **34,** 93.
12. K. Takayanagi and G. T. F. Wong, *Mar. Chem.*, 1984, **14,** 141.
13. D. Tanzer and K. G. Heumann, *Anal. Chem.*, 1991, **63,** 1984.
14. M. Remberger, Institutet för vatten- och luftvårds-forskning, Report B-564, Stockholm, 1980.
15. B. Welz and M. Schubert-Jacobs, *At. Spectrosc.* 1991, **12,** 91.
16. D. D. Nygaard and J. H. Lowry, *Anal. Chem.*, 1982, **54,** 803.
17. E. L. Henn, *ibid.*, 1975, **47,** 428.
18. F. J. Schmidt and J. L. Royer, *Anal. Lett.*, 1973, **6,** 17.
19. J. R. Rossum and P. A. Villarruz, *J. Am. Water Works Assoc.*, 1962, **54,** 746.
20. P. D. Goulden and P. Brooksbank, *Anal. Chem.*, 1974, **46,** 1431.
21. G. E. Batley, *Anal. Chim. Acta*, 1986, **187,** 109.
22. J. Pettersson, L. Hansson and Å. Olin, *Talanta*, 1986, **33,** 249.
23. I. Gustavsson and L. Hansson, *Int. J. Environ. Anal. Chem.*, 1984, **17,** 57.
24. B. Nygård, Thesis, Almqvist & Wiksell, Uppsala, 1967.
25. G. Zdansky, Thesis, Almqvist & Wiksell, Uppsala, 1968.
26. E. S. Gould, *Anal. Chem.*, 1951, **23,** 1502.
27. D. C. Reamer, C. Veillon and P. T. Tokousbalides, *ibid.*, 1981, **53,** 245.
28. V. F. Hodge, S. L. Seidel and E. G. Goldberg, *ibid.*, 1979, **51,** 1256.
29. G. A. Cutter, *Anal. Chim. Acta*, 1983, **149,** 391.
30. J. Buffle, Complexation reactions in aquatic systems, p. 44. Ellis Horwood Ltd., Chichester, 1988.
31. A. Wilander, Personal communication.
32. S. M. Workman and P. N. Soltanpour, *Soil Sci. Soc. Am. J.*, 1980, **44,** 1331.
33. K. Itoh, M. Chikuma, M. Nishimura, T. Tanaka, M. Tanaka, M. Nakayama and H. Tanaka, *Z. Anal. Chem.*, 1989, **333,** 102.
34. G. Pyen and M. Fishman, *At. Absorpt. Newsl.*, 1978, **17,** 47.
35. J. Nève, M. Hanocq, L. Molle and G. Lefebvre, *Analyst*, 1982, **107,** 934.
36. P. D. Goulden and D. H. J. Anthony, *Anal. Chem.*, 1978, **50,** 953.

Talanta, Vol. 39, No. 9, pp. 1097–1105, 1992
Printed in Great Britain

0039-9140/92 $5.00 + 0.00
Pergamon Press Ltd

INVESTIGATIONS FOR THE DETERMINATION OF TIN BY FLOW INJECTION HYDRIDE GENERATION ATOMIC-ABSORPTION SPECTROMETRY

BERNHARD WELZ,* MARIANNE SCHUBERT-JACOBS and TIEZHENG GUO†
Department of Applied Research, Bodenseewerk Perkin-Elmer GmbH, D-7770 Überlingen, Germany

(*Received* 26 *September* 1991. *Revised* 17 *January* 1992. *Accepted* 19 *January* 1992)

Summary—It could be shown that the pre- or double peaks which are frequently observed in the determination of tin by hydride generation atomic-absorption spectrometry are not due to reagent contamination or memory effects. Rather they originate from the silica material used to make the quartz tube atomizer. At elevated temperatures the tin diffuses to the surface and it can be volatilized and atomized only in the presence of hydrogen. The height of the pre-peak depends, among other things, on the time for which the quartz tube atomizer has been at a high temperature without hydrogen. The pre-peaks disappear when argon with 10% (v/v) hydrogen is used as the purge gas. In flow injection the pre-peaks can be separated in time from the analytical signal by using a program in which hydrogen is generated by reaction of sodium tetrahydroborate reductant solution with the acid carrier prior to the injection of the sample. Also investigated was the influence of the acid and sodium tetrahydroborate concentration on sensitivity and freedom from interferences. Best results were obtained when a saturated boric acid solution containing 0.1*M* hydrochloric acid was used for standards, samples and carrier solution, and a 0.4% (m/v) sodium tetrahydroborate solution with 0.05% (m/v) sodium hydroxide as the reductant. Under these conditions tin could be determined accurately in the range 0.008–0.1% in low alloy steel standard reference materials, with matrix-free standard solutions for calibration.

A sometimes confusing diversity of design approaches has been described in the literature for hydride generation (HG) and atomization systems since the introducton of this technique by Holak[1] in 1969 for use in atomic absorption spectrometry (AAS). Batch systems were used more frequently for HG AAS, but continuous flow and more recently also flow injection (FI) systems have been described as well. In addition to the various designs of HG systems, a number of methods with different reagents and reagent concentrations are reported in the literature. These details have to be considered very carefully in comparing published data because they could significantly influence not only sensitivity and peak shapes but also interferences in HG AAS.[2–5]

Tin is among those elements which are not too frequently determined by HG AAS. One of the reasons for that might be that the above-described variabilities have a particularly strong influence on this element. Among the difficulties described repeatedly in the literature are high blank values,[6–10] memory effects[8,10] and particularly the strong dependence of the sensitivity of tin from the acid content of the solution.[2,8,10–13] Åström[14] was the first to use FI for HG AAS in 1982, the number of publications in this field, however, remained scarce over the following years, and no application of this technique to the determination of tin has been reported until only recently. In an evaluation of the first commercially available accessory for FI HG AAS[15] we have investigated the influence of acid, sodium tetrahydroborate and sodium hydroxide concentration on the sensitivity for tin, however, the procedure was not optimized for this element. Fang *et al.*[16] found it very difficult to control the acid concentration to the extent which was necessary for a reliable determination of tin in canned food. They therefore used an on-line ion-exchange separation to modify the sample matrix and achieve optimized and reproducible conditions for HG.

The scope of this work was to optimize the parameters for the determination of tin in a way that an automatic and reliable determination of this element could be carried out with FI HG AAS. In order to achieve this goal we firstly investigated the reasons for the sporadic

*Author for correspondence.
†On leave from Institute of Rock and Mineral Analysis, Chinese Academy of Geological Sciences, Beijing, China.

Table 1. Recommended conditions for the determination of tin using the FIAS–200 flow-injection accessory

Carrier solution:	0.1*M* HCl in saturated H_3BO_3 solution
Reductant solution:	0.4% (m/v) $NaBH_4$ + 0.05% (m/v) NaOH
Carrier gas:	100 ml/min (Ar or 99% Ar + 1% O_2)
QTA temperature:	900°

Step	Time, *sec*	Pump 1, *rev/min*	Pump 2, *rev/min*	Valve position
1	10	100	120	FILL
2	15	—	120	INJECT

pre-peaks and searched for methods for their elimination. Secondly we wanted to optimize the analytical parameters such as acid and reductant concentration and composition in order to obtain a reproducible sensitivity and a high freedom from interferences. The determination of tin in low alloy steel standard reference materials was chosen in order to test the ruggedness of the proposed procedure.

EXPERIMENTAL

Instrumentation

Most of the investigations were carried out with Perkin–Elmer Models 4000 and 2100 atomic-absorption spectrometers, equipped with a Perkin–Elmer FIAS-200 flow injection accessory and an AS-90 autosampler. A hollow cathode lamp, operated at 30 mA, was used as the light source, the wavelength was set to 224.6 nm and the slit width was 0.7 nm. The signals obtained with the Model 2100 were printed with an Epson EX-800 printer, whereas a recorder Model 56 was used with the Model 4000. For some of the measurements a Perkin–Elmer Model MHS-20 batch hydride system was used and the Model 4000 was equipped with a Perkin–Elmer data station 3600, an electrodeless discharge lamp for tin, operated at 8 W, and the wavelength at 286.3 nm was used. The signals obtained with this system were plotted with a Hewlett–Packard data plotter Model 7225 A.

The FIAS-200 flow injection accessory has been described in detail elsewhere.[15] The operating parameters are summarized in Table 1. Somewhat different conditions were used for some of the experiments and will be described in the Results and Discussion section. For investigating the origin of the pre-peaks the set-up shown in Fig. 1 was used which allowed the controlled addition of a second gas to the purge gas for the quartz tube atomizer (QTA). In this case hydrogen was added with a flow-rate of 34 ml/min to the argon carrier gas which was flowing at 230 ml/min.

The data reported in this work have been collected in part over a period of several years with different instruments and particularly with several different QTAs. It has been found that the sensitivity for tin may change significantly (up to a factor of 2) for different QTAs, possibly

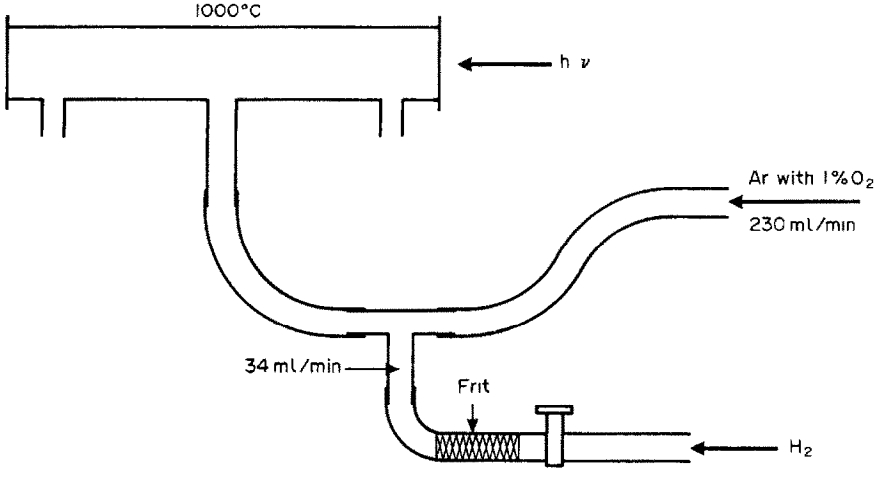

Fig. 1. Experimental set-up for the controlled addition of a second gas (hydrogen) to the purge gas (argon) of the QTA.

depending on the content of trace transition metals, such as copper and nickel, in the silica material. Concentrations in the order of 1 μg/g of these elements could be detected with ICP–MS. Differences in sensitivity for tin in the various figures should therefore not be over-interpreted. However, because we were aware of this problem, care was taken that all data within one set of experiments were obtained with the same QTA so that results remained comparable.

Reagents

All reagents, except for sodium tetrahydroborate (for which no purity was given) were of analytical reagent grade and obtained from Merck (Darmstadt, Germany).

Carrier solution. Saturated boric acid solution containing 0.1*M* hydrochloric acid. Standard and sample solutions were diluted with the same acid mixture.

Reduction solution. Prepared by dissolving 0.4 g of sodium tetrahydroborate (Riedel-de Haen, Seelze, Germany) in 100 ml of water and adding 0.05 g of sodium hydroxide.

Carrier gas. Argon 5.0 (99.9990%) was obtained from Sauerstoffwerk Friedrichshafen (Germany). Argon Sl (99% Ar + 1% O_2) was obtained from Linde (Germany). The mixtures 98% Ar + 1% H_2 + 1% O_2 and 89% Ar + 10% H_2 + 1% O_2 were custom-made by Sauerstoffwerk Friedrichshafen.

Samples and sample preparation

NBS standard reference materials Nos. 361, 362, 363 and 364 (low alloy steel) from the National Institute of Standards and Technology (Gaithersburg, MD, U.S.A). The steel sample (0.5 g) was placed in a 250-ml standard flask, 12 ml *aqua regia* was added, heated slowly to 90° and held at this temperature for 2–3 hr. After cooling to room temperature the digest was diluted to the mark with demineralized water. A 500-μl portion of this solution was transferred to a 50-ml standard flask and diluted to volume with the saturated boric acid–0.1*M* hydrochloric acid mixture. For higher concentrations of tin (*ca.* 0.1%) this solution was further diluted with the acid mixture.

RESULTS AND DISCUSSION

In batch systems for HG AAS, pre-peaks could be observed quite frequently, but their size and height was very variable and unpredictable. Nothing has been done until now to investigate the source of these pre-peaks. An additional problem, which confused the situation, was that these pre-peaks typically disappeared in the analyte signal when, as usual, a recorder was used for signal evaluation. It is quite likely that the high and variable blank values, the memory and carry-over effects frequently reported in the literature for this element were, at least in part, such pre-peaks. Only with the high time resolution and distortion-free registration of the signal shown in Fig. 2, could the pre-peak clearly be distinguished from the actual analytical signal. With this high time resolution it also became obvious that the pre-peak and the analytical signal reached their maxima at distinctly different points in time. However, when an ordinary recorder was used, these differences became less apparent, and the risk for a misinterpretation increased. This could eventually lead to errors, particularly if an automatic peak height readout was used for signal evaluation.

In FI HG AAS these pre-peaks could be observed as well as is shown in Fig. 3, and these peaks could also be very much different in height. With this technique, however, the pre-peaks appeared only before the first signal of a sequence of measurements, provided that hydrogen was generated continuously, *i.e.*, the acid carrier and the tetrahydroborate solution were pumped permanently. Because of this

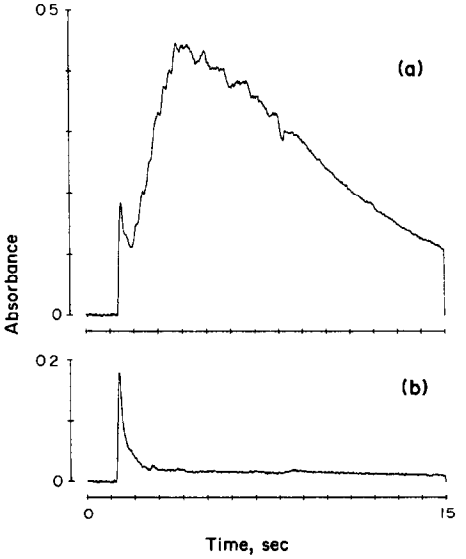

Fig. 2. Determination of tin using a batch HG AA system with high time resolution of the signal. *A.* 100 ng of Sn with pre-peak. *B.* Pre-peak which was misinterpreted as a blank.

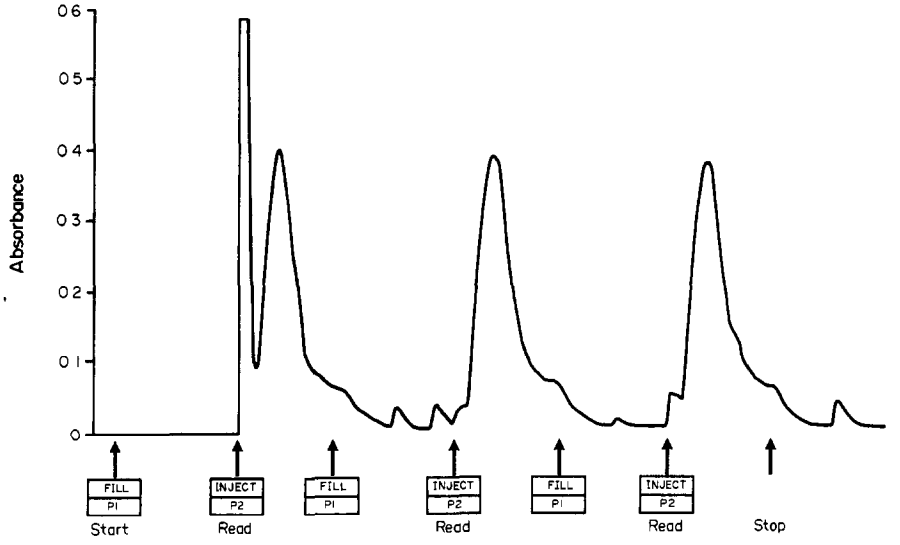

Fig. 3. Determination of 5 ng of Sn using FI HG AAS. Reductant flow and sample injection are initiated at the same time.

interconnection between the generation of hydrogen, which became apparent in all the experiments, it proved very easy to separate the pre-peak in time from the analytical peak in FI HG AAS. The pre-peak appeared right in front of the analytical signal only if the pump for sodium tetrahydroborate was activated together with the rotation of the valve, *i.e.*, introducton of the sample into the carrier stream. This was done in Fig. 3, and this is also the situation in all batch systems where the generation of hydrogen and reduction of the analyte element to the gaseous hydride are initiated at the same time by adding the tetrahydroborate to the acid sample solution. The pre-peak could be shifted at will in FI HG AAS simply by activating the pump for sodium tetrahydroborate prior to the injection of the sample or standard into the carrier stream as is shown in Fig. 4. This way the pre-peak could easily be generated early enough so that it would not appear in the time frame for signal recording. While this was an elegant means to circumvent the source of error inherent in these pre-peaks, it did not answer the question for their origin, except that they were associated with the generation of hydrogen.

This question was, however, of particular interest because, with the knowledge of their origin, it might have been possible to find better ways to avoid or eliminate the pre-peaks rather than to shift them only in time. First of all we found that these signals were generated when, after turning on the FI accessory, carrier and sodium tetrahydroborate solution were mixed and the hydrogen reached the heated QTA. As can be seen in Fig. 5 using continuous registration, a sharp signal was generated at the

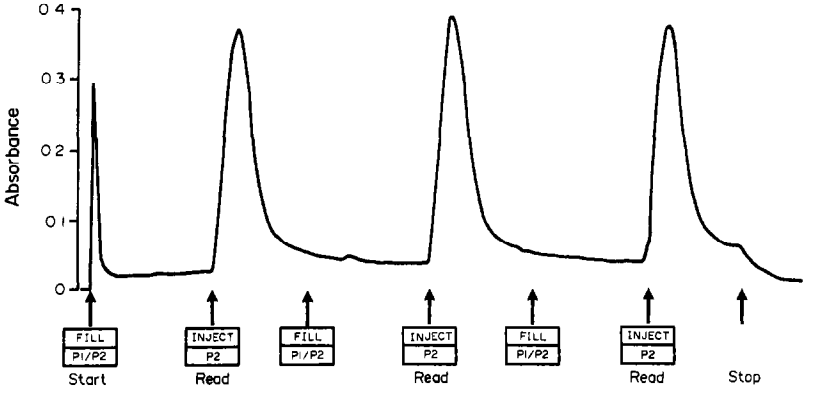

Fig. 4. Determination of 5 ng of Sn using FI HG AAS. Reductant flow is started 10 sec prior to sample injection (program in Table 1).

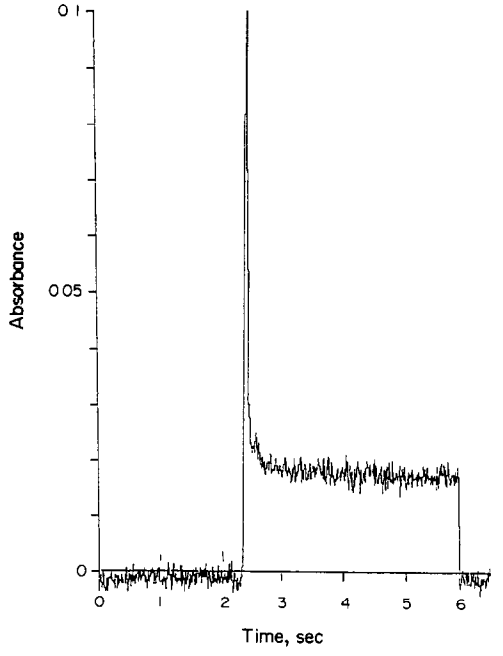

Fig. 5. Pre-peak and "blank" signal for tin recorded upon initiation of carrier and reductant flow and, hence, the generation of hydrogen. (AA spectrometer model 2100).

moment when hydrogen entered the QTA, which decreased at a slightly slower rate and finally reached a stable value. Similar to a "blank", this signal persisted at its elevated level until the reagent pump was turned off and hydrogen generation ceased. The absorbance of this continuous signal depended on the QTA temperature. In addition it was characteristic for a given QTA, but could be significantly different for different QTAs. The height of this continuous signal could not be influenced by the use of a background corrector, and the same was actually true for the sharp early peak which was generated at the appearance of hydrogen in the QTA. The height of this signal, however, depended also from the length of time for which the QTA was at a high temperature but without hydrogen flowing through.

The fact that neither the pre-peak nor the following continuous signal were influenced by background correction indicated already that these signals were due to tin atomic absorption. This was further supported by measurements at three resonance lines of different sensitivity for tin at 224.6 nm, 286.3 nm and 270.7 nm. At the same time we investigated systematically the previously mentioned influence of the length of time for which the QTA was left without hydrogen. For that purpose we used the modified set-up which was shown in Fig. 1 and which permitted the controlled addition of hydrogen to the purge gas. With this arrangement the experiment also became independent of any chemical reaction for hydrogen generation and hence from any possible side-effects caused by the reagents.

The QTA was heated to 900° and flushed continuously with argon. After various time periods of flushing with argon, hydrogen was admixed to the purge gas and the absorbance of the resulting pre-peak recorded. Figure 6 shows the dependence of the peak absorbance from the time without hydrogen for the three analytical lines for tin. The ratio of the reciprocal sensitivities of 1:1.9:2.4 obtained for the three lines corresponded quite reasonably with the characteristic concentration reported for these lines.[17] In addition the relation between the peak absorbance and the time without hydrogen was linear for times between 1 and 4 min.

All this essentially confirmed that the pre-peak and the following continuous absorbance were real absorbance signals caused by tin atoms. The experiments with pure gases with no chemical reaction going on in parallel have shown in addition that these peaks could not be caused by any contamination in the reagents. Finally, a memory-effect or carry-over could be excluded as a possible explanation because the signals were equally observed in "virgin" QTAs which have never come into contact with tin, and all efforts to clean the QTAs with various acids, including 40% (m/v) hydrofluoric acid, did not influence the height of the observed signals substantially. The only

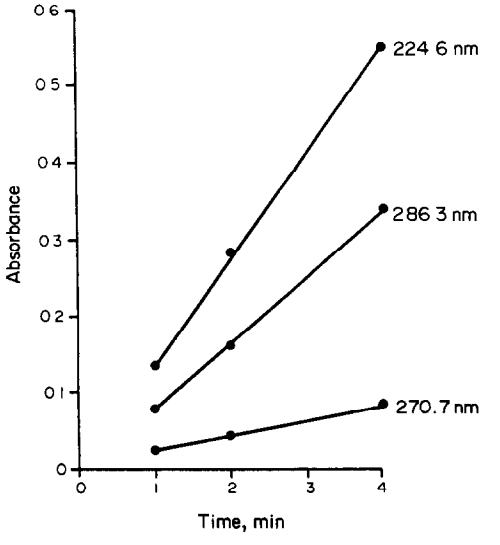

Fig. 6. Influence of the time without hydrogen on the absorbance of the pre-peak for tin at three different wavelengths.

significant influence, as already mentioned, came from the QTA itself, *i.e.*, the magnitude of the signals was different for different QTAs and was somehow typical for each QTA investigated.

In order to gain more information on that phenomenon we broke two quartz tube atomizers, dissolved some pieces in hydrofluoric acid and analysed them with ICP–MS. Among a few other elements we also found tin in a concentration around 0.5–1 μg/g in the solid silica material. If we assume a weight of approximately 20 g for the heated portion of the quartz tube, this means that some 10 μg of Sn was contained in that part of the atomizer. This was a mass of tin which was at least four orders of magnitude higher than that necessary to generate an analytical signal of about 0.1 absorbance units.

This leads to the assumption that the signals were caused by "endogenous" tin, *i.e.*, an impurity which was present in the silica material and which was continuously diffusing to the surface at temperatures typically used for HG AAS. In the absence of hydrogen the tin species remained at the surface of the QTA and accumulated with time. As soon as hydrogen was introduced, however, tin was volatilized and atomized readily. This process of diffusion of tin out of the silica material and its volatilization and atomization was going on continuously in the presence of a flow of hydrogen, producing the steady-state signal observed in these experiments (see Fig. 5). It is not very likely that this volatilization and atomization of tin was the work of molecular hydrogen, and it appears much more plausible that hydrogen radicals take part in the mechanism. Similar volatilization and atomization from the condensed phase has been observed earlier for arsenic, antimony and other volatile hydride forming elements[18–21] and has been associated with a mechanism in which hydrogen radicals were involved as the active species.

The dependence of the height of the pre-peaks from the temperature of the QTA is shown in Fig. 7. The highest signals were obtained between 800° and 900° with the sensitivity falling off to lower and to higher temperatures. The latter was in contrast to experiments with stannane where the sensitivity for tin increased with increasing temperature up to 1000° when argon was the purge gas, and the signal was independent of the temperature between 700° and 1000° when argon with 1% oxygen was used. No

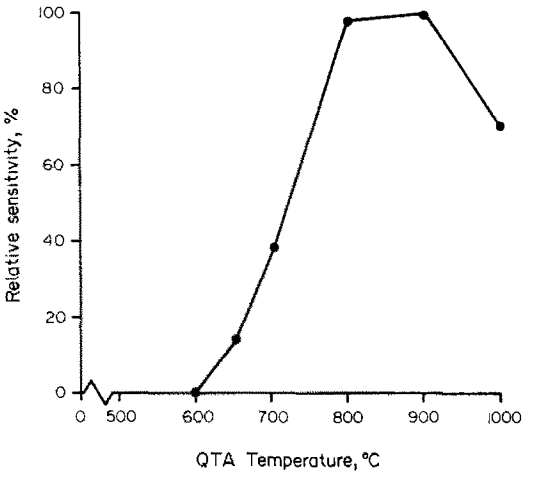

Fig. 7. Influence of QTA temperature on the relative height of the pre-peak for tin.

explanation can be given for this different behaviour at this point in time, it could be assumed, however, that it resulted from the different tin species under consideration and/or the differences in the atomization mechanisms. The diffusion of the tin species, most probably an oxide, out of the silica material, the rate of which is undoubtedly temperature dependent, must certainly also be taken into account.

As contamination of the silica material has been shown to be the source of the pre-peaks and the "blank" signals for tin, the question arises if and how these signals could be removed or avoided. The most obvious way would undoubtedly be to produce the QTAs from "tin-free" silica. However, no such material could be obtained until now. It has been mentioned earlier that all attempts to clean the QTAs with various acids, including 40% (m/v) hydrofluoric acid, had no long-term effect on the pre-peaks or blank signals. This confirmed that the tin species was diffusing from the depth of the material to the surface, *i.e.*, from parts which were not reached by acid cleaning. Experiments in which the QTAs were heated for extended periods of time in the presence of hydrogen were equally unsuccessful for the same reason.

Finally we investigated the use of various gas mixtures as carrier gases to see if at least the pre-peaks could be eliminated this way. The results of these experiments are shown in Fig. 8. When argon containing 1% (v/v) oxygen was used as the carrier gas, the sensitivity for tin was increased by about 35% over that in pure argon at a QTA temperature of 900°. This was in agreement with earlier experiments.[18] The

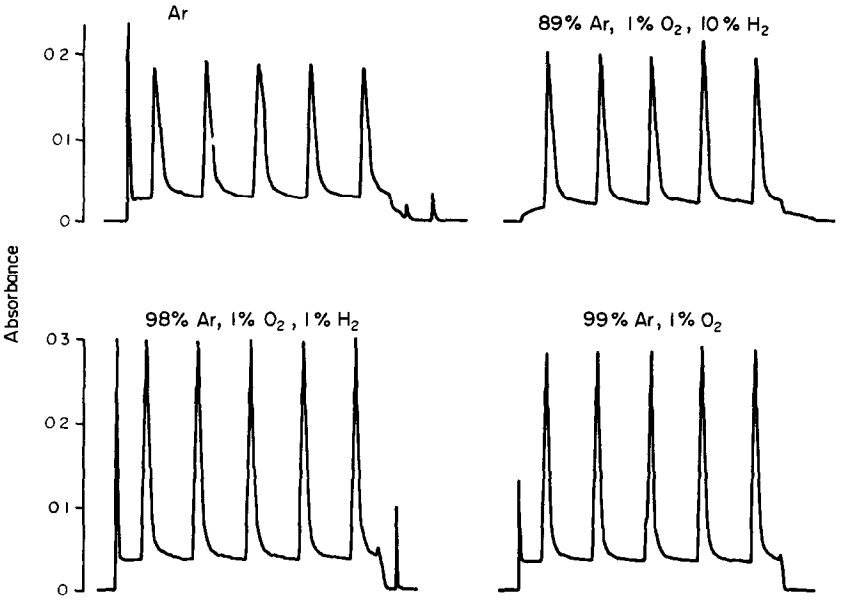

Fig. 8. Influence of oxygen and hydrogen concentration in argon purge gas on pre-peaks and signals for 5 ng of tin.

presence of oxygen, however, had no influence on the pre-peaks which was as expected because tin could only be atomized in the presence of hydrogen radicals. When a mixture of 98% Ar, 1% O_2 and 1% H_2 was used as the purge gas, the sensitivity for tin was highest, but the pre-peaks could not be eliminated. This only succeeded with a mixture of 89% Ar, 1% O_2 and as much as 10% H_2. With this carrier gas, however, the sensitivity for tin was reduced again approximately to the level obtained in pure argon. This means that the enhancing effect of oxygen was apparently offset by the excess of hydrogen.

It is obvious that these investigations were more of academic than of practical use because a mixture of 89% Ar, 1% O_2 and 10% H_2 is not likely to be used in any routine application. It is interesting, however, to realize that a fairly high concentration of 10% H_2 was required in the purge gas to avoid the pre-peaks, *i.e.*, to remove the tin which is continuously diffusing out of the silica material. As expected, the blank signal *i.e.*, the continously elevated level of tin, could not be avoided by any of the gas mixtures. Tin diffuses out of the silica material continuously and is hence atomized permanently in the presence of hydrogen which develops in the reaction of sodium tetrahydroborate with the acid carrier. For routine purposes the simplest approach to avoid errors due to the pre-peaks appears to be the separation in time by an early generation of hydrogen prior to sample injection. This can obviously be only used in FI HG AAS but not in batch systems. If highest sensitivity is to be obtained the use of argon containing 1% of oxygen may be of advantage and was used for most of our investigations.

Finally, in order to apply the determination of tin by FI HG AAS routinely, it was necessary to optimize carrier and reagent composition and concentration, and it is well documented in the literature that the acid concentration is most critical in the determination of tin. Fang *et al.*[16] have actually found that the effects of acidity were further enhanced in the FI mode, compared to batch HG AAS. The situation seemed to be particularly hopeless for hydrochloric and sulphuric acids for which virtually no stable region of influence on sensitivity could be found. The use of boric acid together with the strong acids which was successfully applied in the batch mode,[2] produced no improvement in the performance of FI HG AAS. This was somewhat in contrast to preliminary results obtained in our laboratory,[15] in which a stable signal for tin was obtained in 0.05–0.2*M* nitric and hydrochloric acids, added to saturated boric acid solution. It has to be kept in mind, however, that the influence of acids on the tin signal also depends on the concentration of the sodium tetrahydroborate solution and on the amount of sodium hydroxide in that solution.[15] Hence it was not really surprising that our results were different from those of Fang *et al.*[16]

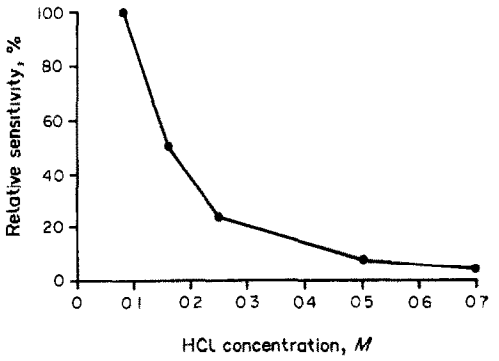

Fig. 9. Influence of hydrochloric acid concentrations in saturated boric acid solution on the sensitivity for tin.

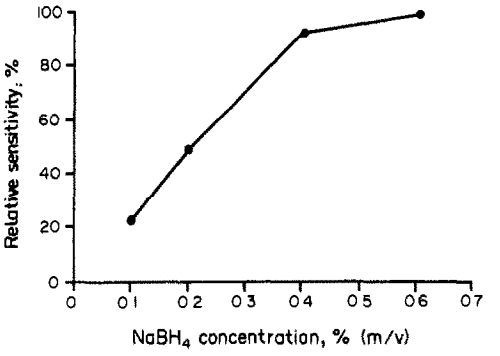

Fig. 10. Influence of sodium tetrahydroborate concentration on the sensitivity for tin.

as they were using a 0.2% (m/v) sodium tetrahydroborate solution containing 0.01*M* (0.03% m/v) sodium hydroxide whereas we used 1% (m/v) sodium tetrahydroborate with 0.5% (m/v) sodium hydroxide. As the influence of the acids was obviously correlated to the concentration of the other reagents, we decided to carry out the optimization procedure one more time.

In agreement with previous results obtained with batch systems[2] as well as with FI HG AAS[15] we could confirm that a saturated boric acid solution had a releasing effect on the influence of strong acids, such as hydrochloric acid, on the tin signal. The sensitivity for tin increased very significantly with decreasing hydrochloric acid concentration, as can be seen in Fig. 9. For concentrations lower than 0.1*M* hydrochloric acid, however, the sensitivity increase was marginal and the signals were no longer reliable, *i.e.*, we observed occasionally a sudden drop in sensitivity and a significant decrease in precision. As hydrolysis of tin(IV) has been reported to be rapid in solutions of low acidity, producing insoluble hydrolysis products which polymerize and are difficult to redissolve,[22] the highest tolerable acid concentration resulting in good sensitivity and a reliable signal for tin, *i.e.*, 0.1*M* was used throughout.

The influence of the tetrahydroborate concentration on the tin signal in 0.1*M* hydrochloric acid/saturated boric acid solution is shown in Fig. 10. The sensitivity clearly increased up to a sodium tetrahydroborate concentraton of 0.4% (m/v). The sodium hydroxide concentration was found to have only a very minor effect on the tin signal in the range between 0.05 and 1% (m/v) as long as the hydrochloric acid concentration did not exceed 0.1*M*. It was therefore kept at its lowest level of 0.05% (m/v).

The tetrahydroborate concentration did not only have an influence on the sensitivity of tin but also on the freedom from interferences when tin was determined in low alloy steel. It can be seen in Fig. 11 that the slope of the curve for tin added to a steel sample was different from that

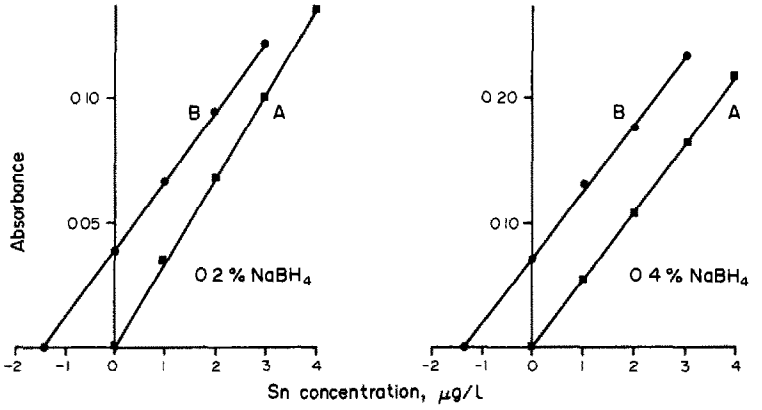

Fig. 11. Influence of sodium tetrahydroborate concentration on matrix interferences in the determination of tin in steel. *A*. Calibration curve established with matrix-free reference solutions. *B*. Tin added to acid steel digests.

Table 2. Determination of tin in NIST standard reference materials low alloy steels

	Concentration of tin (% in steel)	
SRM	Certified	Found ($n = 5$)
NIST 361	0.010 ± 0.001	0.009 ± 0.0001
NIST 362	0.016 ± 0.001	0.017 ± 0.001
NIST 363	0.104 ± 0.005	0.101 ± 0.004
NIST 364	0.008 ± 0.001	0.007 ± 0.0002

for matrix-free standards when 0.2% (m/v) sodium tetrahydroborate was used as the reductant, whereas the slopes were essentially identical with 0.4% (m/v) sodium tetrahydroborate. The results for the determination of tin in four low alloy steel Standard Reference Materials using 0.1*M* hydrochloric acid in saturated boric acid as the carrier and the diluent for standards and samples, and 0.4% (m/v) sodium tetrahydroborate with 0.05% (m/v) sodium hydroxide as the reductant are summarized in Table 2. The agreement of the results in the range of 0.008–0.1% tin in steel, obtained by direct calibration against matrix-free reference solutions, with the certified values is good, indicating an interference-free determination.

CONCLUSION

The pre-peaks in the determination of tin, which have previously been confused with blank values, memory effects and carry-over, originate from volatilization and atomization of tin from the silica material in the presence of hydrogen, most probably via hydrogen radicals. In batch systems these pre-peaks are difficult to separate from the analytical signal and may well cause errors in signal evaluation. In FI HG AAS these pre-peaks can be separated very easily in time and hence be removed from the time frame used for signal evaluation. The results of this study further support the hydrogen radical theory of atomization in heated quartz tube atomizers.

REFERENCES

1. W. Holak, *Anal. Chem.*, 1969, **41**, 1712.
2. B. Welz and M. Melcher, *Spectrochim. Acta*, 1981, **36B**, 439.
3. *Idem*, *Analyst*, 1984, **109**, 569.
4. *Idem*, *ibid.*, 1984, **109**, 577.
5. B. Welz and M. Schubert-Jacobs, *J. Anal. At. Spectrom.*, 1986, **1**, 23.
6. R. S. Braman and M. A. Tompkins, *Anal. Chem.*, 1979, **51**, 12.
7. O. Lindsjö, in *Atomspektrometrische Spurenanalytik*, B. Welz (ed.), p. 437. Verlag Chemie, Weinheim 1982.
8. K. de Donker, R. Dumarey, R. Dams and J. Hoste, *Anal. Chim. Acta*, 1986, **187**, 163.
9. J. R. Castillo, C. Martinez, R. Tomas and J. M. Mir, *J. Anal. At. Spectrom.*, 1988, **3**, 595.
10. A. Rakotz, F. Schlegmilch, H. Grygiel, K. Lohau, M. Mittelstädt and H. Bosch, in *CAS, 5. Colloquium Atomspektrometrische Spurenanalytik*, B. Welz (ed.), p. 101. Bodenseewerk Perkin–Elmer, Überlingen 1989.
11. F. J. Fernandez, *At. Absorpt. Newslett.*, 1973, **12**, 93.
12. M. Legret and L. Divet, *Anal. Chim. Acta*, 1986, **189**, 313.
13. G. H. Alvarez and S. G. Capar, *Anal. Chem.*, 1987, **59**, 530.
14. O. Åström, *ibid.*, 1982, **54**, 90.
15. B. Welz and M. Schubert-Jacobs, *At. Spectrosc.*, 1991, **12**, 91.
16. Z. Fang, E. H. Hansen, L. Sun, J. E. Olesen and L. M. Henriksen, *Talanta*, 1992, **39**, 383.
17. L. Capacho-Delgado and D. C. Manning, *Spectrochim. Acta*, 1966, **22**, 1505.
18. B. Welz and M. Melcher, *Analyst*, 1983, **108**, 213.
19. B. Welz and M. Schubert-Jacobs, *Z. Anal. Chem.*, 1986, **324**, 832.
20. B. Welz, M. Schubert-Jacobs, M. Sperling, D. L. Styris and D. A. Redfield, *Spectrochim. Acta*, 1990, **45B**, 1235.
21. B. Welz and T. Guo, *ibid.*, 1992, **47B**, in the press.
22. J. D. Smith, *Anal. Chim. Acta*, 1971, **57**, 371.

Talanta, Vol. 39, No. 9, pp. 1107–1111, 1992
Printed in Great Britain.

0039-9140/92 $5.00 + 0.00

STUDIES ON SOME CADMIUM MIXED LIGAND COMPLEXES USING DIFFERENTIAL PULSE POLAROGRAPHY

M. I. ISMAIL

Department of Chemistry, Faculty of Science, University of Ain Shams, Cairo, Egypt

(*Received* 5 *November* 1991. *Revised* 15 *January* 1992. *Accepted* 27 *January* 1992)

Summary—Differential pulse polarography was used to study the mixed ligand complexes of imidazole and some dicarboxylate anions namely, oxalate, tartrate and malonate with Cd(II) at constant ionic strength ($\mu = 1$, $NaNO_3$) at $25 \pm 0.1°$. It has been found that the reduction of complexes is reversible and diffusion-controlled. Three mixed complexes are formed with malonate (or oxalate) whereas four mixed complexes are formed with tartrate. The overall stability constants for each system were calculated and discussed.

Mixed ligand complexes of metal ions, especially those playing an important role in various biological processes, have been studied extensively in recent years.[1–3] The physico-chemical properties of one of the important nitrogen containing heterocyclic compounds, namely, imidazole and its metal complexes have attracted increasing attention. It has been reported that a large number of imidazole derivatives possess diverse pharmacological effects, including anti-inflammatory, antimicrobial, antimalarial and antitumor activities.[4–6] The presence of imidazole in the histidyl residue of proteins provides a potential binding site for metal ions.[6]

The overall formation constants of Cd(II)–imidazole complexes have been the subject of several investigations. For instance, Li *et al.*[7] have studied polarographically the compositions and stability constants of simple complexes of Cd(II) with imidazole in aqueous and alcoholic media. The results revealed the formation of three complexes with stability constants; $\log \beta_2 = 5.0$, $\log \beta_3 = 6.3$ and $\log \beta_4 = 7.5$. However, the method employed by these authors was reported to be inaccurate.[8] Tanford and Wagner[9] have studied the same system potentiometrically, where the formation of four successive complexes was indicated with stability constants: $\log \beta_1 = 2.8$, $\log \beta_2 = 2.1$, $\log \beta_3 = 1.6$ and $\log \beta_4 = 1.1$. In this work, it was stated that the site of binding in the imidazole molecule is the pyridine nitrogen rather than the pyrrole nitrogen. On the other hand, the polarographic study of the Cd(II)–imidazole system provided by Shivhare and Singh[10,11] also revealed the formation of four complexes with stability constants $\log \beta_1 = 2.7$, $\log \beta_2 = 4.0$, $\log \beta_3 = 5.3$ and $\log \beta_4 = 7.0$ these differ considerably from those reported by Tanford and Wagner.[9]

In other work of Shivhare *et al.*,[12] concerning the stability constants of the Cd(II)-imidazole–malonate system from dc-polarography, the formation of three mixed complexes was observed with overall stability constants $\log \beta_{11} = 4.0$, $\log \beta_{12} = 4.4$ and $\log \beta_{21} = 5.9$. The recent polarographic study of the Cd(II)–1-methylimidazole–oxalate system by Gamal *et al.*[13] indicated the formation of three mixed complexes. Although the ligands used in the latter two systems were quite different, the stability constants of the three mixed complexes recorded by Gamal *et al.*[13] were identical to those given by Shivhare *et al.*,[12] *viz.*, $\log \beta_{11} = 4.0$, $\log \beta_{12} = 4.4$ and $\log \beta_{21} = 5.9$. In our opinion, these data,[13] seem to be unreliable. The uncertainty originates from the values reported for the stability constants in the simple Cd(II)–oxalate system (namely, $\log \beta_1 = 1.0$, $\log \beta_2 = 2.6$ and $\log \beta_3 = 3.6$), which are markedly different from those recommended earlier[14–16] for this system under the same experimental conditions: $\log \beta_1 = 2.7 \pm 0.2$, $\log \beta_2 = 4.2 \pm 0.1$ and $\log \beta_3 = 5.1 \pm 0.1$.

Accordingly, in view of the conflicting results reported in the literature regarding the number of complexes formed and the values of their stability constants, it became of special importance to undertake further study using differential pulse-(dp-) polarography on simple

complexes of Cd(II) with imidazole as well as on mixed complexes in the presence of some dicarboxylate anions (namely oxalate, tartrate and malonate). This technique offers a considerable advantage as compared to dc-polarography.[17] The dp-polarography gives more accurate measurements of $\Delta E_{1/2}$-values, leading most probably to proper calculation of the stability constants of the complexes under study.

EXPERIMENTAL

Chemicals and solutions

All chemicals used were analytical grade (BDH) and their solutions were prepared in demineralized water. Imidazole (Im), potassium malonate (Mal), potassium tartrate (Tart) and potassium oxalate (Ox) were used as ligands. A surfactant was not used as maximum suppressor.

Apparatus and working procedure

A polarographic analyser PAR Model 174A with PAR/GE Model 303A static mercury drop electrode as working electrode, saturated Ag/AgCl as reference electrode and platinum as counter electrode were used for dp-polarography. The polarograms were recorded on a Houston Omingraphic Model RE0089 X–Y recorder. A potential pulse of 50 mV was used throughout the dp-polarographic measurements. The dc-polarograms were recorded with a Sargent Welch polarograph Model XVI. The characteristics of the capillary in 0.1M potassium chloride at open-circuit was $m = 1.68$ mg/sec, $t = 4.76$ sec at $h = 45$ cm. All measurements were made at $25 \pm 0.1°$ and an ionic strength was maintained constant using 1M sodium nitrate as supporting electrolyte. The concentration of Cd^{2+} ions throughout the study was $1 \times 10^{-4}M$. Purified nitrogen gas was used for removing the dissolved oxygen.

Theoretical considerations

The stability constants of polarographically reversible systems may be determined through dp-polarography by using the Deford–Hume equation[18] as modified by Heath and Hefter.[17] This equation can be expressed as,

$$F_0(X) = \text{antilog}\left[\frac{0.4343nF}{RT}\Delta E_p + \log\frac{(I_p)_s}{(I_p)_c}\right]. \quad (1)$$

where, $F_0(X)$ represents the experimentally measured right-hand side of the equation, ΔE_p $[=(E_p)_s - (E_p)_c]$ is the shift in the peak potential due to complexation, I_p is the peak current of the dp-wave and the subscripts s and c refer to the free and complex ions, respectively.

Schaap and McMasters[14] developed a logical extension of the Deford–Hume method by applying the latter to cases where metal ions coordinate simultaneously with two different ligand species (X, Y) in the solution. Thus, the $F_0(X)$ function in equation (1) may be extended to give a new function, $F_{00}(X, Y)$ expressed in the following form,

$$F_{00}(X, Y) = \text{antilog}\left[\frac{0.4343nF}{RT}\Delta E_p + \log\frac{(I_p)_s}{(I_p)_c}\right]. \quad (2)$$

It has been reported[17] that for a reversible diffusion-controlled process, the peak potential (E_p) obtained from dp-polarography is related to the half-wave potential ($E_{1/2}$) of dc-polarography as follows:

$$E_p = E_{1/2} - \frac{\Delta E}{2}$$

where, ΔE is the magnitude of the pulse amplitude.

From Leden's approach,[19]

$$F_{00}(X, Y) = A + B[X] + C[X]^2 + D[X]^3. \quad (3)$$

The original graphical method[18] may be applied to F_{00} if the activity of one of the ligands (Y) is held constant while that of the other one (X) is varied. The intercept of the F_{00} axis in the plot of F_{00} *vs.* [X] gives A. Consequently,

$$F_{10} = \frac{F_{00} - A}{[X]} = B + C[X] + D[X]^2$$

By a similar plotting of F_{10} *vs.* [X], B is obtained and then C and D are obtained by iteration.

From the knowledge of C, the mixed stability constants β_{21} may be calculated. In order to determine β_{11} and β_{12}, B must be evaluated at two different concentrations of Y.

RESULTS AND DISCUSSION

The dp-polarography of imidazole does not show any reduction peaks within the normally available potential range. This lack of redox activity is not likely associated with the aromatic nature of the five-membered system of imidazole ring existing in a large number of

Table 1. Stability constants of simple complexes at 25 ± 0.1°

1. Cd(II)–imidazole system
   $[Cd(Im)]^{2+}$; $\log \beta_{10} = 2.82$
   $[Cd(Im)_2]^{2+}$; $\log \beta_{20} = 4.32$
   $[Cd(Im_3]^{2+}$; $\log \beta_{30} = 5.29$
   $[Cd(Im)_4]^{2+}$; $\log \beta_{40} = 6.89$
2. Cd(II)–oxalate system
   [Cd(Ox)]; $\log \beta_{01} = 2.68$
   $[Cd(Ox)_2]^{2-}$; $\log \beta_{02} = 4.21$
   $[Cd(Ox)_3]^{3-}$; $\log \beta_{03} = 5.01$
3. Cd(II)–malonate system
   [Cd(mal)]; $\log \beta_{01} = 1.24$
   $[Cd(Mal)_2]^{2-}$; $\log \beta_{02} = 2.84$
   $[Cd(Mal)_3]^{4-}$; $\log \beta_{03} = 3.58$
4. Cd(II)–tartrate system
   $[Cd(Tart)_2]^{2-}$; $\log \beta_{02} = 3.68$

resonance forms[20] as confirmed by their stability towards chemical reduction.[21] On the other hand, Cd(II) exhibits one reduction peak (E_p) at −0.511 V representing the uptake of two electrons.

The stability constants of simple complexes of Cd(II) with imidazole (Im), oxalate (Ox), tartrate (Tart) and malonate (Mal) were determined separately prior to the study of the mixed ligand systems. Identical conditions were maintained for both the simple and the mixed systems. The Deford–Hume equation[18] as modified by Heath and Hefter[17] (equation 1) was applied to determine the stability constant of the simple complexes using dp-polarography. Table 1 includes the values of the stability constants of the simple complexes, and they are in good agreement with the previously reported values,[10,12,14,15]

Table 2. Stability constants of mixed complexes at 25 ± 0.1°

1. Cd(II)–imidazole–oxalate system
   [Cd(Im)(Ox)]; $\log \beta_{11} = 4.68$
   $[Cd(Im)(Ox)_2]^{2-}$; $\log \beta_{12} = 5.04$
   $[Cd(Im)_2(Ox)]$; $\log \beta_{21} = 6.08$
   $\log K_M = 0.415$; $\log K_S = 0.114$
2. Cd(II)–imidazole–tartrate system
   [Cd(Im)(Tart)]; $\log \beta_{11} = 4.56$
   $[Cd(Im)(Tart)_2]^{2-}$; $\log \beta_{12} = 4.48$
   $[Cd(Im)_3(Tart)]$; $\log \beta_{31} = 5.87$
   $[Cd(Im)_2(Tart)_2]^{2-}$; $\log \beta_{22} = 6.13$
   $\log K_M = 0.56$, $\log K'_S = 0.259$
3. Cd(II)–imidazole–monalate system
   [Cd(Im)(Mal)]; $\log \beta_{11} = 3.98$
   $[Cd(Im)(Mal)_2]^{2-}$; $\log \beta_{12} = 4.43$
   $[Cd(Im)_2(Mal)]$; $\log \beta_{21} = 6.03$
   $\log K_M = 0.40$, $\log K_S = 0.099$

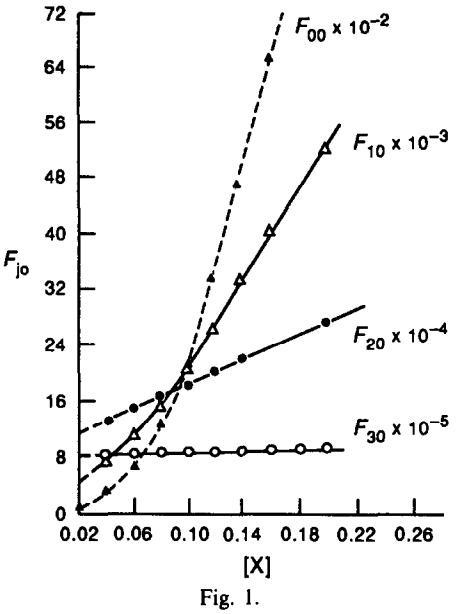

Fig. 1.

taking into consideration the differences in experimental conditions. As shown in Table 1, Cd(II) forms four successive complexes with (Im), three complexes with each of (Ox) and (Mal), and only one with (Tart).

As reported by several researchers,[22,23] a value of 62 mV is assigned for the half-peak width of the dp-polarographic reversible two-electron reduction step with a pulse of 50 mV. In the present work, the dp-polarograms of Cd(II) in nitrate medium showed half-peak widths of 62 ± 1 mV for both simple and mixed complexes, indicating the reversibility of the reduction process. Further confirmation was provided by using dc-polarography under the same conditions as the dp-polarography. The slopes of the linear plots of $\log i/i_l - i$ *vs.* E were 31 ± 1 mV, indicating a high degree of reversibility. Moreover, the plots of the limiting current (i_l) of the dc-waves against $h^{1/2}$ of the mercury column were linear, supporting the conclusion that reduction of the simple and mixed complexes is diffusion-controlled.

For mixed ligand systems, the concentration of imidazole was varied between 0.02 and 0.2*M*, keeping the concentration of dicarboxylate ions constant at either 0.1 or 0.2*M*. The stability constants of the mixed ligand complexes (Table 2), were evaluated using the Schaap and McMasters method[14] [equation (2)]. Figures 1 and 2 represent the plotting of F_{jo} function *vs.* [X] for the Cd(II)–imidazole–malonate system as a representative example for the studied systems. It is evident that three mixed complexes

Table 3. Equilibria involved in Cd(II)–imidazole–malonate system and equilibrium constant log(K) values

Equilibrium			log K at 25°
1. $Cd^{2+} + Im + Mal^{2-}$	$\rightleftharpoons$	$[Cd(Im)(Mal)]$	3.98
2. $Cd^{2+} + Im + 2Mal^{2-}$	$\rightleftharpoons$	$[Cd(Im)(Mal)_2]^{2-}$	4.63
3. $Cd^{2+} + 2Im + Mal^{2-}$	$\rightleftharpoons$	$[Cd(Im)_2(Mal)]$	6.03
4. $[Cd(Im)(Mal)] + Im$	$\rightleftharpoons$	$[Cd(Im)_2(Mal)]$	2.05
5. $[Cd(Im)(Mal)_2)^{2-} + Im$	$\rightleftharpoons$	$[Cd(Im)_2(Mal)] + Mal^{2-}$	1.4
6. $[Cd(Im)]^{2+} + Mal^{2-}$	$\rightleftharpoons$	$[Cd(Im)(Mal)]$	1.16
7. $[Cd(Im)_2]^{2+} Mal^{2-}$	$\rightleftharpoons$	$[Cd(Im)_2(Mal)]$	1.71
8. $[Cd(Im)]^{2+} + 2Mal^{2-}$	$\rightleftharpoons$	$[Cd(Im)(Mal)_2]^{2-}$	1.81
9. $[Cd(Mal)] + Im$	$\rightleftharpoons$	$[Cd(Im)(Mal)]$	2.74
10. $[Cd(Mal)_2]^{2-} + Im$	$\rightleftharpoons$	$[Cd(Im)(Mal)_2]^{2-}$	1.79
11. $[Cd(Mal)] + 2Im$	$\rightleftharpoons$	$[Cd(Im)_2(Mal)]$	4.79
12. $[Cd(Mal)_2] + 2Im$	$\rightleftharpoons$	$[Cd(Im)_2(Mal)] + Mal^{2-}$	3.19
13. $[Cd(Mal)_3]^{4-} + Im$	$\rightleftharpoons$	$[Cd(Im)(Mal)_2]^{2-} + Mal^{2-}$	0.85

are formed with imidazole and malonate (or oxalate), whereas four mixed complexes are formed with tartrate. Theoretical estimation of the stability constants of the mixed complexes under study was performed, using the Watters and DeWitt method.[24] The theoretical values seem to be less than those observed by about $10^{0.6 \pm 0.07}$. The higher experimental values may be derived from the cooperative effects of the electrostatic forces and steric effects[14,25,26] between the different kinds of ligands.

From the values of the stability constants for the simple and mixed complexes (*cf.* Tables 1 and 2), the affinity of Cd^{2+} ions toward the dicarboxylate ligands follow the order: Ox (5.2) >Tart (6.8) >Mal (8.0). The values given in parentheses are the overall basicity constants of the ligands.[27] Apparently, the observed stability constants do not necessarily follow the order of basicity for the ligands. The enhanced stabilization of the tartrate complexes as compared to those of malonate is probably due to the fact that one of the hydroxo groups of tartrate is coordinating the metal ion, whereas the stabilization of oxalate complexes over those of malonate (or tartrate) is mainly attributed to the differences in the chlelate ring size. The mixing constants,[28] namely $\log K_M = \log \beta_{11}^{-1/2} (\log \beta_{02} + \log \beta_{20})$ and the stabilization constants[29] namely, $\log K_s = \log K_M - \log 2$, for each system were also evaluated. The obtained positive values of $\log K_M$ and $\log K_S$ suggests that the ternary complexes are more stable than the binary ones. Moreover, the equilibrium constants were calculated for the Cd(II)–imidazole–malonate system as a representative example (Table 3). Inspection of these values confirms that the tendency of the imidazole ligand to add to the complexes is stronger than that of the dicarboxylate ions; this may be linked with the weaker nature of the dicarboxylate ligands.

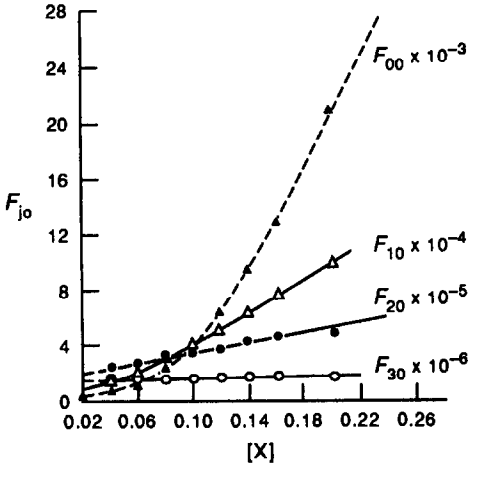

Fig. 2.

REFERENCES

1. H. Siegerman, *Differential Pulse Polarography of Antibiotics*, J. Hase (Ed.), Vol. 43, Academic Press, New York, 1975.
2. D. L. Kloyman, J. P. Scovill, J. F. Bartosvich and J. Bruch, *J. Med. Chem.*, 1985, **26**, 35.
3. K. Wegner, *Arch. Pharm.*, 1985 **318**, 377.
4. W. J. Eilbeck, F. Holmes and A. E. Underhill, *J. Chem. Soc.*, 1967, 757.
5. K. C. Mahapatra and K. C. Dash, *J. Inorg. Nucl. Chem.*, 1977, **39**, 1252.
6. S. J. Yan, W. H. Burton, P. L. Chien and C. C. Cheng, *J. Heterocyclic Chem.*, 1978, **15**, 297.
7. N. C. Li, J. M. White and E. Doody, *J. Am. Chem. Soc.*, 1954, **76**, 6219.
8. D. R. Crow, *Polarography of Metal Complexes*, p. 62. Academic Press, New York, 1969.
9. C. Tanford and M. L. Wagner, *J. Am. Chem. Soc.*, 1953, **75**, 434.

10. M. Shivhare and M. Singh, *J. Inorg. Nucl. Chem.*, 1981, **43,** 1599.
11. *Idem, J. Indian Chem. Soc.*, 1981, **58,** 647.
12. M. Shivhare, Krishna, N. Jain and M. Singh, *J. Inorg. Nucl. Chem.*, 1981 **43,** 2885.
13. Gamal B. Mohamed and A. M. Ahmed, *Portugaliae Electrochem. Acta*, 1988, **6,** 105.
14. W. B. Schaap and D. L. McMasters, *J. Am. Chem. Soc.*, 1961, **83,** 4699.
15. H. M. Killa, M. G. Abdel-Wahed and H. A. Dessouki, *Polyhedron*, 1985, **4,** 1219.
16. S. C. Khurana, J. K. Gupta and C. M. Gupta, *Electrochim. Acta*, 1973, **18,** 59.
17. G. A. Heath and G. Hefter, *J. Electroanal. Chem.*, 1977, **84,** 295.
18. D. D. Deford and D. N. Hume, *J. Am. Chem. Soc.*, 1951, **73,** 5321.
19. I. Leden, *Z. Phys. Chem.*, 1941, **188,** 160.
20. D. J. Gram and G. S. Hammond, *Organic Chemistry*, McGraw-Hill, New York, 1959.
21. A. Albert, *Heterocyclic Chemistry*, 2nd Ed., Oxford University Press, New York, 1968.
22. J. W. Dillard and K. W. Hanck, *Anal. Chem.*, 1976, **48,** 218.
23. J. W. Dillard, J. A. Turner and R. A. Osteryoung, *ibid.*, 1977, **49,** 1246.
24. J. I. Watters and DeWitt, *J. Am. Chem. Soc.*, 1960, **82,** 1333.
25. A. R. Aggarwal, H. K. Arora, K. B. Pandeya and R. P. Singh, *J. Inorg. Nucl. Chem.*, 1981, **43,** 601.
26. E. D. Hughes, C. K. Ingold, S. Patai and Y. Pocker, *J. Chem. Soc.*, 1957, 1206.
27. L. G. Sillen and A. E. Martell, *Stability Constants of Metal Ions Complexes*, Suppl. 1, Royal Society of Chemistry, London, 1968.
28. S. L. Jain, J. Kishan and R. C. Kapoor, *Indian J. Chem.*, 1979, **18A,** 133.
29. A. R. Aggarwal, K. B. Pandeya and R. P. Singh, *ibid*, 1981, **20,** 752.

Talanta, Vol. 39, No. 9, pp. 1113–1120, 1992
Printed in Great Britain.

0039-9140/92 $5.00 + 0.00

ANALYSIS OF ACROLEIN AND ACRYLONITRILE IN AQUEOUS SOLUTION BY MEMBRANE INTRODUCTION MASS SPECTROMETRY

TARUN K. CHOUDHURY, TAPIO KOTIAHO* and R. GRAHAM COOKS†
Department of Chemistry, Purdue University, West Lafayette, Indiana 47907, U.S.A.

(*Received* 2 *December* 1991. *Revised* 16 *January* 1992. *Accepted* 23 *January* 1992)

Summary—Acrolein and acrylonitrile can be quantified directly at low levels in aqueous solution using membrane introduction mass spectrometry. Electron impact was used to generate positively charged ions and electron capture of the O-(2,3,4,5,6-pentafluorobenzyl)hydroxyl amine (PFBOA) derivative was used to generate negatively charged ions of acrolein in aqueous solutions. The origins of all ions in the mass spectra and product MS/MS spectra recorded using both ionization methods were assigned and a reaction scheme is given which accounts for the fragmentation of the PFBOA derivative. Detection limits were measured using multiple reaction monitoring in both the methods. With electron capture detection, acrolein could be detected without preconcentration at 10 ppb levels. Electron impact ionization and multiple reaction monitoring both allowed the measurement of acrylonitrile at levels as low as 10 ppb.

Acrolein and acrylonitrile are on the US EPA priority list of pollutants because of their toxicity. Acrolein has been reported to have severe biological effects on humans and other mammals. Short term (1–5 min) inhalation exposure to low concentrations (low ppm) of acrolein causes moderate to severe nasal and eye irritation as well as lacrymation, and exposure to higher concentrations (~150 ppm) for 10 min or longer can be fatal.[1] Acrylonitrile is reported to be carcinogenic.[1] Inhalation exposure to ppm levels of this compound for a few hours causes effects which range from slight transitory to fatal effects in animals.[1] There is therefore an obvious need to make correct qualitative and quantitative measurements of these compounds in water. This task is made difficult by the fact that the compounds are water soluble so that the usual procedure of extraction into an organic solvent is not applicable.

The methods generally used for the determination of acrolein are spectrophotometry,[2] fluorometry,[3,4] liquid chromatography,[5,6] gas chromatography with electron capture detection,[7,8] and HPLC with fluorescence detection.[9] Cohen and Altshuller[2] derivatized acrolein with 4-hexylresorcinol in ethyl alcohol prior to spectrophotometric determination at the low ppm levels. The fluorometric method of Suzuki and Imai[3] and that of Alarcon[4] allows the measurement of acrolein at low ppb levels but suffers from a lack of specificity. Similar detection limits were observed with liquid chromatography when used with appropriate methods of detection.[5,6] For example, application of HPLC in combination with fluorescence detection, allowed the low ppb level measurement of acrolein.[9] Detection limits of acrolein at and even below the ppb level were obtained by Nishikawa *et al.*[7,8] by bromination of the O-methyloxime derivative followed by electron capture detection.

Most of the methods[10–15] used for the detection of acrylonitrile involve purge and trap preconcentration, followed by detection with gas chromatography (GC) or gas-chromatography–mass spectrometry (GC–MS). Ramstad and Nicholson[10] used a combination of steam distillation, elevated temperature purge and trap of the distillate and detection by gas chromatography/flame ionization in order to detect sub ppb levels of acrylonitrile in aqueous solutions. In EPA priority pollutant method 603,[11] which was developed for the measurement of acrolein and acrylonitrile, an inert gas bubbled through the water sample in a heated purge cell transfers the analyte into the vapor phase where it is swept through a sorbent and trapped. The trap is subsequently heated and

*On leave from Technical Research Center of Finland, Chemical Laboratory, Biologinkuja 7, 02150 Espoo, Finland.
†Author for correspondence.

flushed with helium in order to desorb and carry the analyte to the GC for separation and detection with a flame ionization detector. This method can be applied to detect acrolein and acrylonitrile in the sub ppb to low ppb range, depending upon the interference of the sample matrix. The EPA method 624[12] uses an ambient temperature purge cell, a packed column, and a quadrupole mass spectrometer as a detector. This method suffers from the fact that purging at room temperature is not highly efficient. The "modified 624" method,[15] using a purge and trap capillary GC–MS, allows identification and quantification of acrylonitrile to low ppb levels. Trussell *et al.*[14] isolated acrolein and acrylonitrile by purging with helium and cryotrapping in a capillary column. The analytes were then desorbed from the trap by heating before they were injected into the mass spectrometer where they were analyzed by electron ionization down to sub ppb levels. Though there are many methods for the measurement of acrolein and acrylonitrile, there is still a need for a direct, simple and more reliable analytical method for the analysis of these compounds in drinking water.

Membrane introduction mass spectrometry (MIMS), which eliminates the solvent reduction or analyte preconcentration step, might provide the basis for such a method. MIMS is a technique for the introduction of volatile organic compounds from an aqueous solution into the ion source of a mass spectrometer, and is currently undergoing rapid development.[16] The selective permeation of low molecular weight volatile compounds makes possible the qualitative and quantitative detection of these compounds at very low levels and a wide variety of applications has been reported.[16–39] The development of the flow-through technique,[30–33] which allows the sample to flow through the membrane within the ion source of the mass spectrometer, is particularly valuable for continuous on-line monitoring. This technique has proved to be valuable in detecting trace amounts of volatile compounds in aqueous solutions[33,34] and in monitoring organic and biochemical reactions.[35–39] The "flow-over" method, which uses a helium-purged hollow fiber membrane in which aqueous sample flows continuously over the surface of the membrane and the flow of helium through the interior sweeps analytes into the ion source of the mass spectrometer, has also shown low detection limits.[29]

The present study reports the application of MIMS for the detection of acrolein and acrylonitrile in aqueous solution. Since acrolein contains a carbonyl group, it can be derivatized with O-(2,3,4,5,6-pentafluorobenzyl)hydroxylamine (PFBOA) to the corresponding oxime according to equation (1). This reaction can be performed in aqueous solution and since the derivative contains 5 fluorine atoms, it can be readily detected by electron capture using negative ion chemical ionization mass spectrometry.

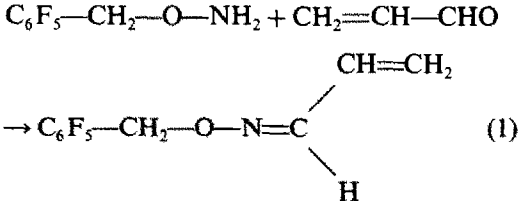

Ionization by electron capture facilitates qualitative and quantitative detection of many organic molecules compared to their ionization by positive ion EI or CI methods[40] because of the remarkable improvements in selectivity and sensitivity achieved by examining negative ions.[40–42] For example, this technique has been successfully applied to the analysis of drugs and drug metabolites in biological samples.[42,43] PFBOA derivatization followed by electron capture has previously been applied to the detection of low ppb levels of C_1–C_7 aldehydes.[44] This paper also reports the application of MIMS for sample introduction and subsequent electron impact mass spectrometry for qualitative and quantitative measurements of low concentrations of acrylonitrile in aqueous solution.

EXPERIMENTAL

An experimental arrangement reported previously,[33–36] which allows the introduction of sample into the mass spectrometer using a membrane introduction probe is shown in Fig. 1. The

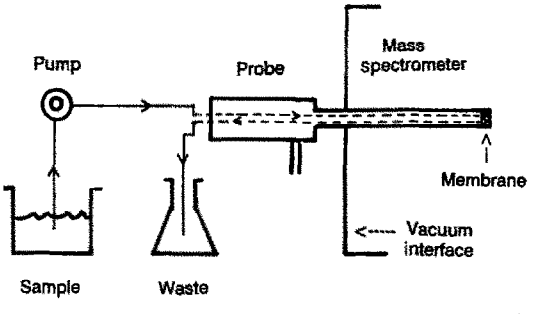

Fig. 1. Schematic diagram of the membrane introduction apparatus used in this study (taken from ref. 44).

dimethylvinyl silicone polymer membrane (ASTM: VMQ Dow Corning, Midland, MI) used for these experiments was 0.01 inches thick. In order to control the temperature of the membrane independently of the ion source, the probe is provided with a programmable temperature control device which was used to set the membrane temperature at 70° throughout the experiment. A stream of methanol and water in the ratio of 1:1 was continuously supplied to the membrane with a peristaltic pump (model 7618-30: Ismatic, Switzerland) and sample plugs of 0.2-ml volume were injected into the stream at intervals via a six-port liquid injector. The only purpose of using methanol in the mixture was to keep the sample introduction system clean. A Finnigan 4500 TSQ mass spectrometer (Finnigan Corporation, San Jose, CA) operated with an INCOS data system was used for all the measurements. The mass spectrometer was operated under both electron impact (EI) and chemical ionization (CI) conditions using an electron energy of 70 eV. The source pressure was 0.5 Torr for the CI experiments. The ion source was maintained at a temperature of 190°. Both full mass spectra and MS/MS product spectra were recorded. In order to record the MS/MS product ion spectra, a 20-eV collision energy was chosen and argon, typically at 1 m Torr was used as a collision gas in the second quadrupole. In order to establish detection limits, multiple reaction monitoring experiments were performed.

Acrolein (97% pure) and acrylonitrile (<99% pure) were supplied by Aldrich Chemical Company, Milwaukee, Wisconsin. Stock solutions (100 ppm) of acrolein and acrylonitrile were prepared by dissolving the appropriate quantity of the compounds in water. A series of dilutions was made to yield solutions with concentrations in the range of 1 ppb–10 ppm. PFBOA, supplied by Aldrich Chemical Company (Milwaukee, WI) was 99% pure. A solution (1 mg/ml) of O-(2,3,4,5,6-pentafluorobenzyl)hydroxylamine hydrochloride was prepared by dissolving the appropriate quantity of the compound in water. The PFBOA derivative of acrolein was prepared following the method of Glaze *et al.*[45] To 5 ml of acrolein solution, 2 drops of 0.1*M* $Na_2S_2O_3$ solution and 0.5 ml of the PFBOA solution were added and the mixture was allowed to stand for a few minutes. The product was liberated by addition of a drop of concentrated sulphuric acid before the sample was injected into the membrane introduction probe via a six-port liquid injection system. Mass spectra for acrylonitrile were recorded by using elecron ionization. For acrolein, mass spectra were collected using electron ionization or negative ion chemical ionization for the PFBOA derivative using isobutane as the reagent gas.

RESULTS AND DISCUSSION

The electron ionization (EI) mass spectrum of an aqueous solution (100 ppm) of acrolein, recorded using the membrane introduction probe, is presented in Fig. 2(a). For comparison, an EI spectrum of pure acrolein, is presented in Fig. 2(b). Though there are differences in relative abundances of ions m/z 25–29 due to the transmission of air through the membrane, the presence of the characteristic ion signals for acrolein in Fig. 2(b) confirms that membrane introduction mass spectrometry can be used for the detection of acrolein in aqueous solutions. The spectrum shows a discernible molecular ion signal at m/z 56. The peak $(M + 1)^+$ at m/z 57 must be the result of an ion-molecule reaction occurring in the ion source and is presumed to be due to the protonated molecule $CH_2{=}CHCHOH^+$. The $(M - 1)^+$ ion at m/z 55 could be due to H_2 loss from protonated acrolein[46] and/or to the formation of

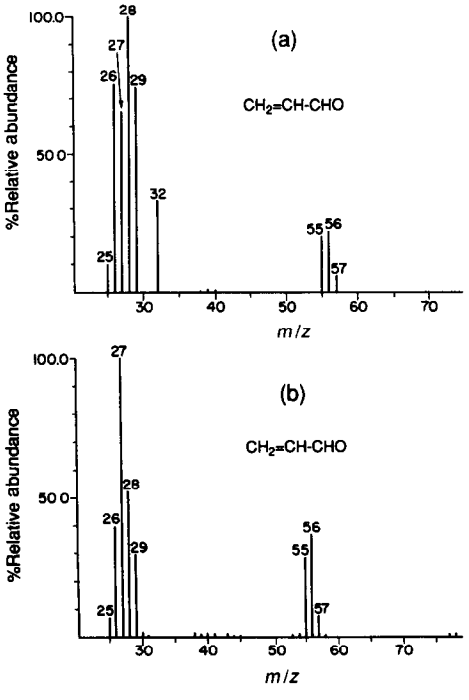

Fig. 2. (a) EI mass spectrum of a solution containing 100 ppm of acrolein recorded using membrane introduction probe, (b) EI mass spectrum of pure acrylonitrile.

CH_2=$CHCO^+$ as a result of fragmentation of the radical cation.[47] The presence of this ion in the MS/MS spectrum of $M^{+\cdot}$ (see below) favors at least some contribution from the latter mechanism. The large abundance of $(M-1)^+$ relative to $M^{+\cdot}$ is characteristic of aliphatic aldehydes.[48] The relative abundances of ions m/z 26, 27, 28 and 29 are much higher than that of the molecular ion. The origin of the peaks at m/z 26, 27, 28 and 29 were also confirmed by the MS/MS product spectrum of the acrolein molecular ion. The spectrum, which is shown in Fig. 3, is very simple indeed. The product ion peak at m/z 28 is assigned to the formation of the $C_2H_4^+$ ion according to equation (2) since thermochemical data[49] show this set of products to be favored over the complementary pair. The production of HCO^+ according to

$$CH_2{=}CHCHO^+ \rightarrow C_2H_4^+ + CO \qquad (2)$$

$$CH_2{=}CHCHO^+ \rightarrow C_2H_3 + HCO^+ \qquad (3)$$

equation (3), accounts for the appearance of the peak at m/z 29. The peak $(M—CHO)^+$ produced by the cleavage of the C—C bond adjacent to the C=O group is also unique in the fragmentation of low molecular weight aliphatic aldehydes.[48] In the present mass spectrum, this ion occurs in low abundance at m/z 27. The ion signals at m/z 26 and 25 in the mass spectrum (Fig. 2) are due to the formation of $C_2H_2^+$ and C_2H^+ respectively.

The detection limit of acrolein, studied by electron ionization and multiple reaction monitoring, was measured to be 50 ppb (S/N = 2). In this multiple reaction monitoring experiment, the ion at m/z 56 was selected in the first quadrupole and the products m/z 28, 29 and 56 were monitored. Since earlier results on C_1–C_7 aldehydes proved that significantly lower detection limits can be obtained by using negative ion chemical ionization for PFBOA derivatives of aldehydes,[44] this method was also applied for acrolein. Figure 4 shows the negative ion chemical ionization mass spectrum of the PFBOA derivative of acrolein. The mass spectrum is similar to those of C_1–C_7 aldehydes reported earlier.[44] The intensity of the molecular ion peak (M^-) of the derivative at m/z 251 is very low compared to the fragment at m/z 231 which is due to the elimination of HF from the molecular anion. Such an elimination of a ring fluorine probably leads to the formation of a cyclic product. The origin of the ion m/z 231 is confirmed by examining the product MS/MS spectrum of m/z 251 shown in Fig. 5. The peak at m/z 201 is proposed to be due to the elimination of NO· from $(M—HF)^-$ and the origin of this peak was confirmed by recording the product MS/MS spectrum of m/z 231. In addition to these peaks, the electron capture mass spectrum of the PFBOA derivative of acrolein contains the peaks m/z 178, 181 and 197. The peaks at m/z 181 and 197 are due to the formation of pentafluorobenzyl anion $(C_6F_5CH_2^-)$ and pentafluorobenzyloxy anion $(C_6F_5CH_2O^-)$ respectively, both originating from the derivatizing agent. The ion at m/z 178

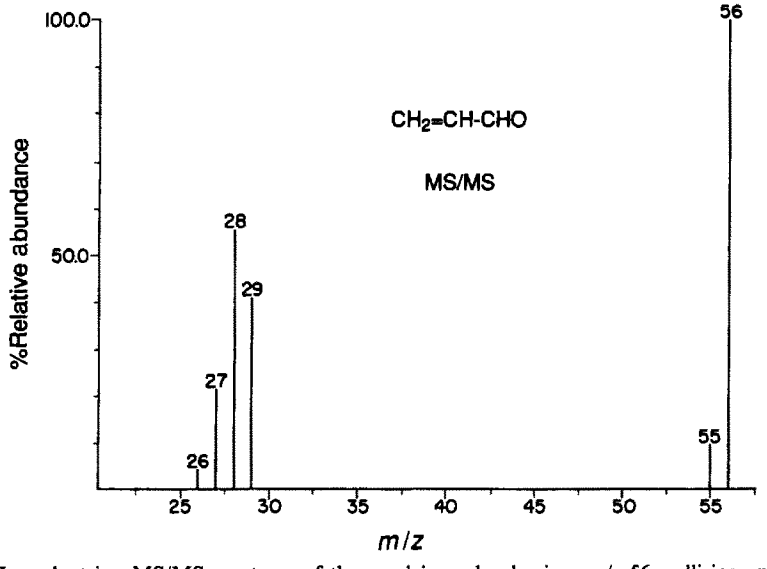

Fig. 3. EI product ion MS/MS spectrum of the acrolein molecular ion, m/z 56; collision energy 20 eV and collision gas (argon) pressure 0.5 mTorr.

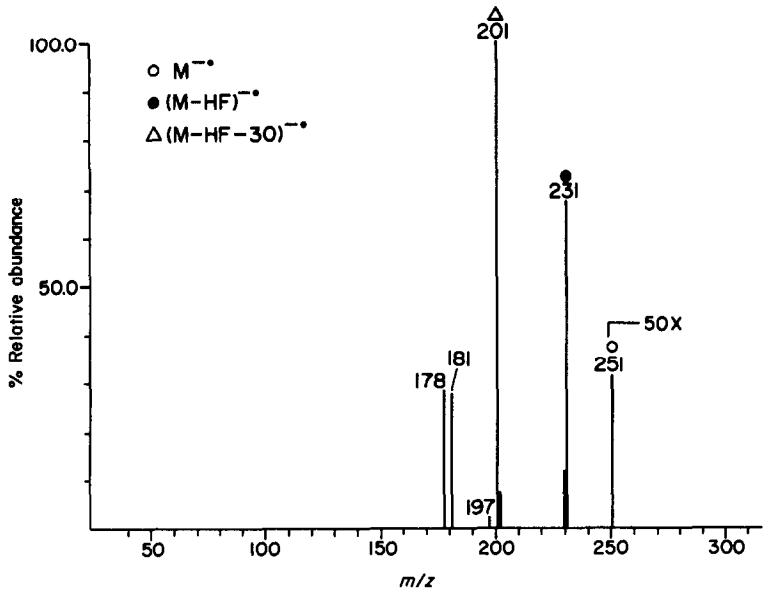

Fig. 4. Negative ion chemical ionization mass spectrum of the PFBOA derivative of acrolein (100 ppm solution).

is due to successive loss of HF and CH_2=CH—CN from the molecular ion. The appearance of the signal at m/z 162 in the product MS/MS spectrum (Fig. 5) can be rationalized as being due to the elimination of CH_2=CHCNO from the cyclic species formed by elimination of HF from the molecular ion $M^{-\cdot}$. In summary, the fragmentation pattern of the PFBOA derivative of acrolein is similar to that of other aldehydes studied earlier,[44] and can be explained with the help of reaction scheme 1.

The mass spectrometer was operated in the multiple reaction monitoring mode to measure the lowest level at which the PFBOA derivative of acrolein could be detected by electron capture negative ion chemical ionization. To do this the ion at m/z 231 was selected using the first quadrupole and the ions at m/z 231 and 201 were monitored. The detection limit for acrolein by derivatization followed by electron capture detection was found to be 10 ppb with S/N = 3/1 and the calibration curve was found to be linear from the detection limit up to at least 100 ppb.

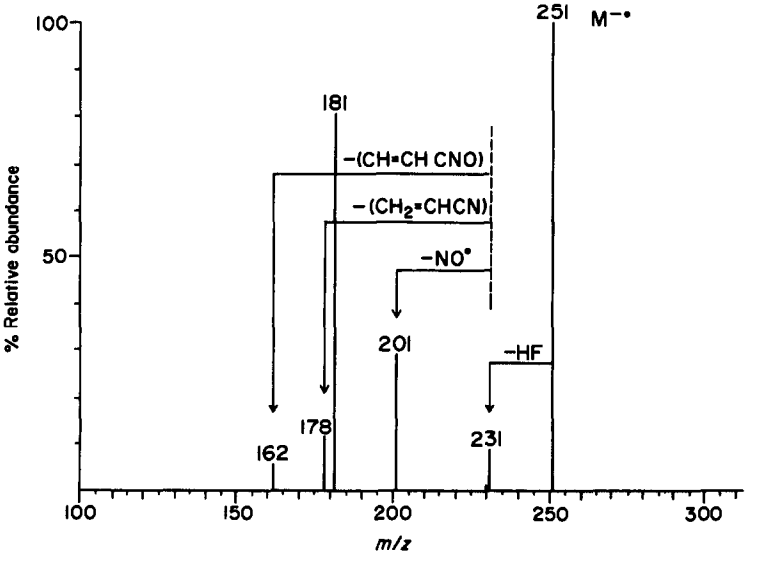

Fig. 5. Product ion MS/MS spectrum of the molecular anion of PFBOA derivative of acrolein; collision energy 20 eV and collision gas (argon) pressure 1 mTorr.

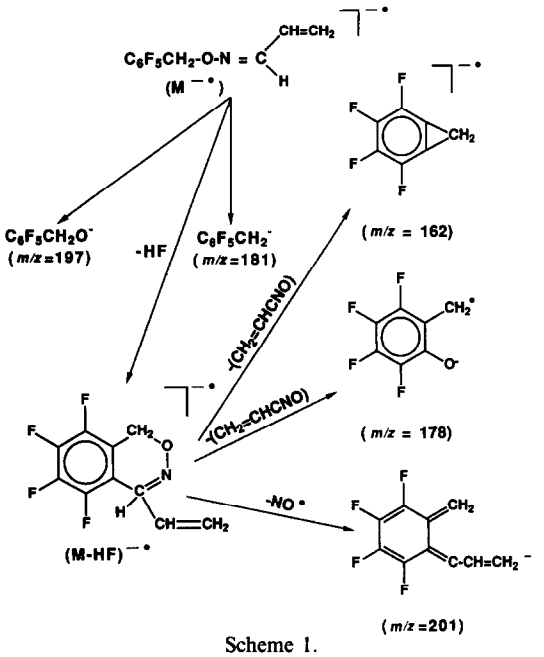

Scheme 1.

The EI mass spectrum of acrylonitrile is shown in Fig. 6. Comparison with the mass spectrum available in the literature[50] shows the presence of characteristic fragment ions. In addition, signals are observed at m/z 32 due to oxygen and, (at least in part) at m/z 28 due to nitrogen. The molecular ion shows a strong signal at m/z 53. The $(M+1)^+$ ion at m/z 54 under EI conditions is characteristic of aliphatic nitriles and is due to the formation of $CH_2{=}CHCNH^+$ as a result of an ion-molecule reaction involving abstraction of a hydrogen atom.[48] The $(M-1)^+$ peak at m/z 52, which may be in part the result of an ion/molecule reaction, is also diagnostic of aliphatic nitriles.[48] The $(M-2)^+$ peak at m/z 51 is due to formation of $HC{\equiv}CCN^+$. The EI MS/MS product spectrum of acrylonitrile is shown in Fig. 7. The product ion at m/z 52 is due to the loss of the alpha hydrogen atom from the molecular ion. The signal at m/z 27 is due to the formation of $C_2H_3^+$ and/or HCN, m/z 26 to CN^+ and $C_2H_2^+$ and m/z 25 to C_2H^+.

Multiple reaction monitoring was applied in order to establish the detection limit of acrylonitrile in aqueous solution. The molecular ion, m/z 53, was selected in the first quadrupole and the ions m/z 25, 26, 27, 52 and 53 were monitored. The detection limit for acrylonitrile was found to be 10 ppb with a S/N ratio of 2/1 and the calibration curve was found to be linear from the detection limit up to 100 ppb. The dynamic range over which detection of acrolein and acrylonitrile is linear is evident from the calibration curves shown in Fig. 8.

CONCLUSIONS

The present work demonstrates the capability of membrane introduction mass spectrometry to allow qualitative and quantitative measurements to be made on acrolein and acrylonitrile present in low concentrations in aqueous solution. Both electron ionization of underivatized acrolein and electron capture of the PFBOA derivative of acrolein were applied to measure the detection limits. Electron capture detection

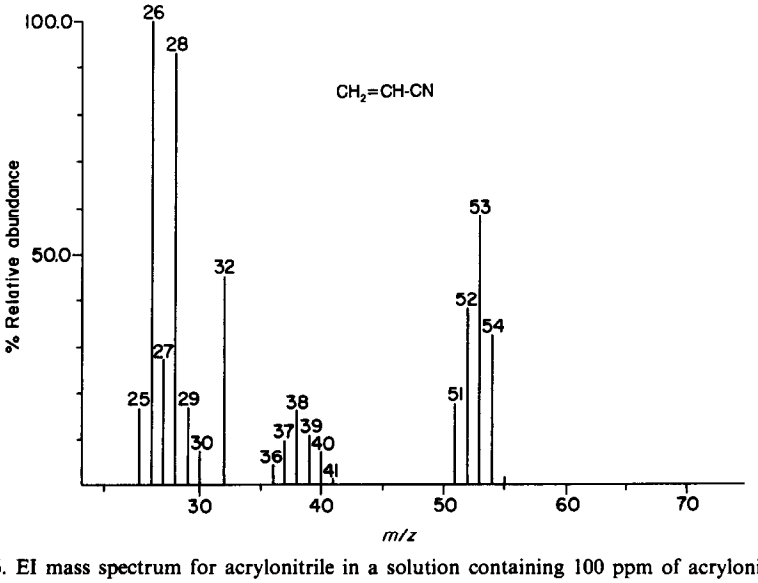

Fig. 6. EI mass spectrum for acrylonitrile in a solution containing 100 ppm of acrylonitrile.

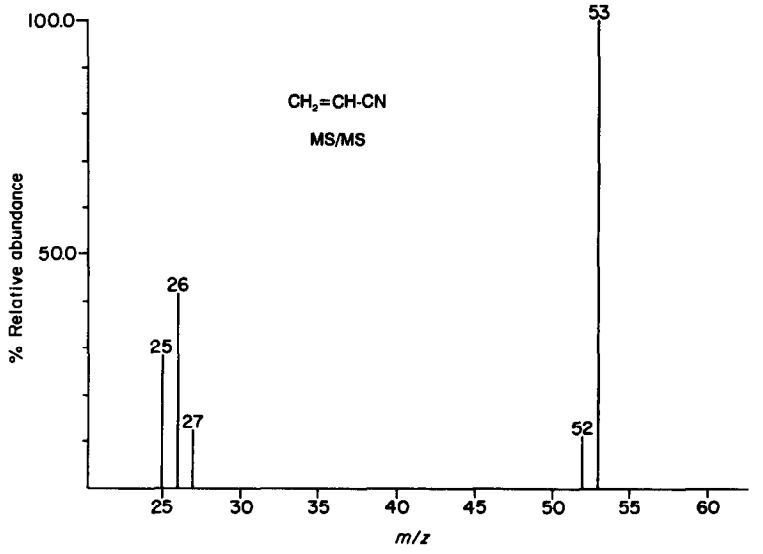

Fig. 7. EI product ion MS/MS spectrum of acrylonitrile; collision energy 20 eV and collision gas pressure 1 mTorr.

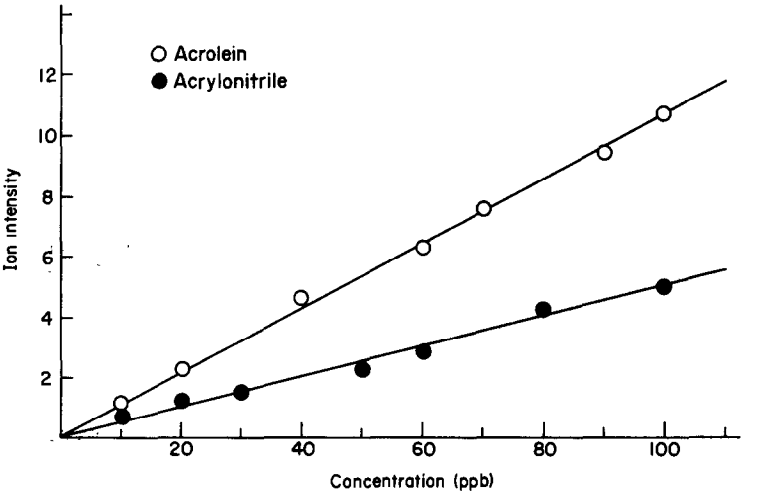

Fig. 8. Calibration curves for acrolein (○) using negative ions formed by electron capture detection of the PFBOA derivative and acrylonitrile (●) using positive ions formed by electron ionization. The data were collected using multiple reaction monitoring.

of the derivatized acrolein gave better signal intensity and a lower detection limit than did electron impact. The most intense ion signal in the negative ion chemical ionization spectrum was due to the ion m/z 231 which is generated by the elimination of HF from the molecular ion $M^{-\cdot}$. The fragmentation pattern of the molecular ion of the PFBOA derivative of acrolein is analogous to that of aliphatic aldehydes examined previously. For acrylonitrile, electron ionization experiments were conducted in order to determine the lowest level of detection. For both acrolein and acrylonitrile, detection limits were measured by using the mass spectrometer in the multiple reaction monitoring mode. The calibration curves were found to be linear up to 100 ppb.

Acknowledgement—The authors acknowledge the support of the US Environmental Protection Agency (EPA CR-815749-01-0). The support of the Emil Aaltonen Foundation is acknowledged (T.K.)

REFERENCES

1. K. Verschueren, *Handbook of Environmental Data on Organic Chemicals*, Van Nostrand Reinhold Company, New York, 1983.
2. I. R. Cohen and A. P. Altshuller, *Anal. Chem.*, 1961, **33**, 726.
3. Y. Suzuki and S. Imai, *Anal. Chim. Acta* 1982, **136**, 155.
4. R. A. Alarcon, *Anal. Chem.*, 1968, **40**, 1704.

5. K. Kuwata, M. Uebori, H. Yamasaki, Y. Kuge and Y. Kiso, *ibid.*, 1983, **55,** 2013.
6. S. J. Swarin and F. Kipari, *J. Liq. Chromatogr.*, 1983, **6,** 425.
7. H. Nishikawa, T. Hayakawa and S. Ikeda, *J. Chromatog.*, 1986, **351,** 566.
8. H. Nishikawa, T. Hayakawa and T. Sakai, *Analyst*, 1987, **112,** 45.
9. Y. Osaki, M. Nagase and T. Matsueda, *Bunseki Kagaku*, 1989, **38,** 239.
10. T. Ramstad and L. W. Nicholson, *Anal. Chem.*, 1982, **54,** 1191.
11. *Fed. Regist.*, 1984, October 26, Vol. 49, No. 209, p. 43281.
12. *Fed. Regist.*, 1984, October 26, Vol. 49, No. 209, p. 43373.
13. F. A. Dreisch and T. O. Munson, *J. Chromatogr. Sci.*, 1983, **21,** 111.
14. A. R. Trussell, J. G. Moncur, F. Y. Lieu and L. Y. C. Leong, *J. High Resolut. Chromatog. Chromatogr. Commun.*, 1981, **4,** 156.
15. D. L. Vassilaros and T. J. Bzik, *Environ. Sci. Technol.*, 1991, **25,** 878.
16. T. Kotiaho, R. R. Lauritsen, T. K. Choudhury, R. G. Cooks and G. T. Tsao, *Anal. Chem.*, 1991, **63,** 875A.
17. G. Hoch and B. Kok, *Arch. Biochem. Biophys.* 1963, **101,** 160.
18. L. B. Westover, J. C. Tou and J. H. Mark, *Anal. Chem.*, 1974, **46,** 568.
19. J. C. Weaver and J. H. Abrams, *Rev. Sci. Instrum.*, 1979, **50,** 478.
20. S. Dhendhanoo and J. Dulak, *Rapid Commun. Mass Spectrom.*, 1989, **3,** 175.
21. D. Wenhu, C. Kuangnan, L. Jianli and D. Zhenying, *Mass Spectros. (Tokyo)*, 1987, **35,** 122.
22. J. C. Tou and G. J. Kallos, *Anal. Chem.*, 1974, **46,** 1866.
23. J. E. Evans and J. T. Arnold, *Environ. Sci. Technol.*, 1975, **9,** 1134.
24. J. C. Weaver, M. K. Mason, J. A. Jarrell and J. W. Peterson, *Biochim. Biophys. Acta*, 1976, **438,** 296.
25. J. S. Brodbelt and R. G. Cooks, *Anal. Chem.*, 1985, **57,** 1153.
26. F. R. Lauritsen, *Int. J. Mass Spectrom. Ion. Proc.*, 1990, **95,** 259.
27. F. R. Lauritsen, S. Bohatka and H. Degn, *Rapid Comm. Mass Spectrom.*, 1990, **4,** 401.
28. W. J. Pinnick, B. K. Lavine, C. R. Weisenberger and L. B. Anderson, *Anal. Chem.*, 1980, **52,** 1102.
29. L. E. Silvon, M. R. Bauer, J. S. Ho and W. L. Budde, *ibid.*, 1991, **63,** 1335.
30. M. E. Bier, R. G. Cooks, J. S. Brodbelt, J. C. Tou and L. G. Westover, *U.S. Patent*, 1989, 4791292.
31. M. E. Bier and R. G. Cooks, *Anal. Chem.*, 1987, **59,** 597.
32. M. E. Bier, T. Kotiaho and R. G. Cooks, *Anal. Chim. Acta*, 1990, **231,** 175.
33. A. K. Lister, K. V. Wood, R. G. Cooks and K. R. Noon, *Biomed. Environ. Mass Spectrom.*, 1989, **18,** 1063.
34. T. Kotiaho, M. J. Hayward and R. G. Cooks, *Anal. Chem.*, 1991, **63,** 1794.
35. M. J. Hayward, T. Kotiaho, A. K. Lister, R. G. Cooks, G. D. Austin, R. Narayan and G. T. Taso, *ibid.*, 1990, **62,** 1798.
36. M. J. Hayward, A. K. Lister, R. G. Cooks, G. D. Austin, R. Narayan and G. T. Taso, *Biotechnol. Tech.*, 1989, **3,** 361.
37. G. D. Austin, G. T. Tsao, M. J. Hayward, T. Kotiaho, A. K. Lister and R. G. Cooks, *Process Control & Quality*, 1991, **1,** 117.
38. M. J. Hayward, D. E. Riederer, T. Kotiaho, R. G. Cooks and G. T. Tsao, *ibib.*, 1991, **1,** 105.
39. T. Kotiaho, A. K. Lister, M. J. Hayward and R. G. Cooks, *Talanta*, 1991, **38,** 195.
40. D. F. Hunt and F. W. Crow, *Anal. Chem.*, 1978, **50,** 1781.
41. R. C. Dougherty, *ibid.*, 1981, **53,** 625A.
42. H. Budzikiewicz, *Mass Spectrom. Rev.*, 1983, **2,** 515.
43. J. R. Hass, M. D. Friesen, D. J. Harvan and C. E. Parker, *Anal. Chem.*, 1978, **50,** 1474.
44. T. K. Choudhury, T. Kotiaho and R. G. Cooks, *Talanta*, 1992, **39,**
45. W. H. Glaze, M. Koga and D. Cancilla, *Environ. Sci. Technol.*, 1989, **23,** 838.
46. F. Turecek in *The Chemistry of Enones*, S. Patai and Z. Rappoport (ed.) Ch. 6, Wiley, New York, 1989.
47. F. Turecek, D. E. Drinkwater and F. W. McLafferty, *J. Am. Chem. Soc.*, 1991, **113,** 5950.
48. F. W. McLafferty, *Interpretation of Mass Spectra*, 3rd Ed., University science Books, California, 1980.
49. *J. Phys. & Chem. Ref. Data*, Vol. 6, 1977.
50. *EPA/NIH data base Mass Spectral Data Base*, Vol. 1, NSRDS-NBS 63, U.S. Government Printing Office, Washington, 1978.

Talanta, Vol. 39, No. 9, pp. 1121–1126, 1992
Printed in Great Britain.

0039-9140/92 $5.00 + 0.00

A SIMPLE DIFFERENTIAL TITRATOR FOR AUTOMATIC POTENTIOMETRIC TITRATION AT ZERO CURRENT, WITH TWO IDENTICAL INDICATOR ELECTRODES

A. ARREBOLA RAMIREZ and C. JIMENEZ LINARES
Department of Analytical Chemistry, Faculty of Sciences, University of Granada, 18071 Granada, Spain

(*Received* 21 *March* 1990. *Revised* 23 *December* 1991. *Accepted* 31 *January* 1992)

Summary—A simple differential titrator for automatic potentiometric titration at zero current, with two identical indicator electrodes, is described. The autoburette is a normal microburette connected to one tube of a peristaltic pump, and the differentiating system is a closed-flow circuit in a second tube of the pump, this tube containing two electrodes 5 cm apart. The apparatus has been applied to the determination of halides and sulphide–disulphide mixtures, with electrodes coated with an appropriate silver salt.

Most commercially available automatic titrators are differential, that is to say, they record the slope of the titration curve, $E = f(V)$, directly. MacInnes *et al.*[1-4] were the first to develop a simple experimental device for differential titrations using two identical indicator electrodes, but the measurements were not continuous and the differential curve could not be obtained automatically. Baker and Müller[5] showed that an electronic pulse amplifier can be used for the purposes of differential titration and can also be easily adapted to obtain automatic results. Later, Malmstadt and Fett[6] extended Baker and Müller's principle to develop an automatic differential titrator that responds to the second derivative of the titration curve and stops the flow of titrant when this second derivative is zero. Nowadays, titrators incorporate a microprocessor to store the experimental data and calculate the results by whatever method is required, *e.g.*, differential titration, Gran titration,[7,8] addition techniques, and so on.

Here we describe a differential titration method which can be put into practice with a simple instrument, the components of which are readily available in any analytical laboratory.

EXPERIMENTAL

Reagents

All chemicals used were of analytical reagent grade. Silver nitrate was dried at 110° and an appropriate amount was dissolved in demineralized water to give a 0.1*M* solution. Solutions of sodium chloride, potassium bromide and potassium iodide in demineralized water were standardized by potentiometric titration with the silver nitrate solution, and their concentrations were found to be 0.0996, 0.1000 and 0.0996*M*, respectively. A solution of hydrogen sulphide in demineralized water was standardized iodimetrically; its concentration was $4.86 \times 10^{-3}M$. Sulphuric acid (5*N*) and 1*M* potassium nitrate were prepared.

Apparatus

Two silver wires (2.5 cm long and 0.8 mm in diameter) were inserted into a silicone-rubber tube (2 mm in diameter) with a distance of 5 cm between them. They were then electro-oxidized in 0.1*M* solutions of potassium chloride, potassium bromide, potassium iodide or ammonium hydrogen sulphide (as appropriate) to form a precipitate layer.

The difference in potential between the two electrodes was measured with a Metrohm E 536 potentiometer, incorporating a graphic recorder.

An Eyela MP3 peristaltic pump with two tubes, and a 5-ml microburette were used.

Experimental device

The components of the experimental device are shown in Fig. 1. A microburette, connected to the pump by a silicone-rubber tube (1 mm internal diameter), supplies a constant flow of titrant, measured by observing the volume released over a given time. The differentiating system is a closed-flow circuit made up of the titration vessel and a silicone-rubber tube with

the two electrodes inserted close to the junction with the titration vessel.

Recommended procedure

Twenty ml of 5*N* sulphuric acid or 5 ml of 1*M* potassium nitrate solution are added to a measured volume of the solution to be titrated and the mixture is diluted accurately to 80 ml with demineralized water. This solution is then stirred at a high enough speed to ensure rapid and efficient mixing in the titration vessel. The closed-flow circuit is connected to the pump and the pump is switched on for about a minute. The tube connected to the microburette is introduced into the titration vessel and the titration begun, the pump and the recorder being switched on simultaneously. The titrant flow (ϕ) must be determined either before or after the titration. Alternatively, the titrant flow need not be measured if the pump and recorder are stopped simultaneously and a reading is taken of the volume of titrant added. When the titration is complete, the titration vessel is emptied and rinsed and the closed-flow loop is emptied by starting the pump, and then rinsed by pumping water through it for 2–3 min, and again emptied. The system is then ready for the next sample.

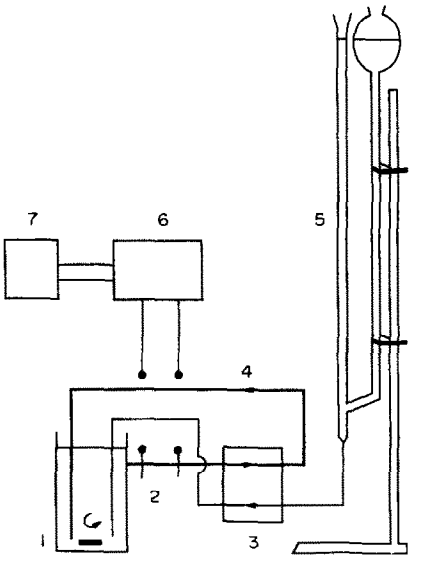

Fig. 1. Differential potentiometric titrator: 1, titration vessel; 2, electrodes; 3, peristaltic pump; 4, closed-flow circuit; 5, microburette; 6, potentiometer; 7, graphic recorder.

THEORY

The normal way of finding the end-point of a potentiometric titration is to measure the e.m.f. (E) as a function of the volume (V) of titrant added, and to take the end-point as the value of V at which $\Delta E/\Delta V = f(V)$ [or $\Delta E = f(V)$ since ΔV is small and constant]. With the experimental device described here, the potentials of the two electrodes represent two consecutive points on the titration curve, corresponding to addition of an increment ΔV of titrant, ΔV being the volume of titrant added in the time it takes for the solution to traverse the distance between the electrodes. Thus a linear concentration gradient is established in the closed-flow circuit tube, and the recorder will continuously give the function $\Delta E = f(V)$; the constant value for ΔV can be altered by changing the distance between the electrodes. A similar effect can be obtained by changing the concentration of the titrant. The speed of the pump does not influence the value of ΔV, but it does affect the time needed to carry out the titration, and also the probability that the potential of the electrodes will be a stable equilibrium potential. It should be emphasized here that, as no reference electrode is used, there is no liquid-junction potential. The end-point is indicated by the sharp maximum or minimum that appears on the derivative curve when the "front" of the fully titrated solution reaches the mid-point between the electrodes.

This experimental system involves two determinate errors, both of which can be easily evaluated and corrected for. The first is the time (t_0) which the solution to be titrated takes to cover the distance (l_0) between the beginning of the closed-flow circuit and the mid-point between the electrodes; t_0 can be measured and subtracted from the time (t_2) taken to reach the maximum (or minimum) on the titration curve. The second error is due to the volume of solution (V_1) contained in the length of tubing (l_1) between the mid-point between the electrodes and the end of the circuit, which still contains some unreacted titrand and will need a certain volume of titrant (ϕt_1) to reach the end-point.

At time t_2 (corresponding to the apparent end-point) there is a slight overtitration of the solution in the titration vessel and length l_0 of the circuit loop, and an undertitration of the solution in the rest of the loop. If the length of the loop is adjusted so that these two effects just cancel, t_2 will be the true titration time.

If V_0 is the initial total volume in the titration vessel before the loop has been filled and f is the

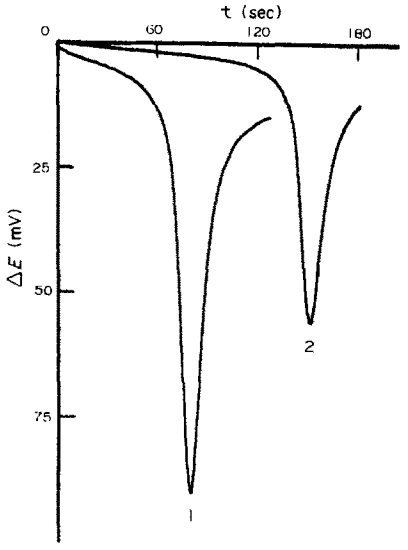

Fig. 2. Titration of 2 ml of 0.1*M* chloride with 0.1*M* silver nitrate (curve 1) or 0.05*M* silver nitrate (curve 2).

fraction of V_1 that is still untitrated, it can be shown that

$$t_1 = \frac{fV_1(t_2 - t_0)}{V_0 + \phi t_2 - fV_1} \quad (1)$$

If we operate so that $V_0 \gg \phi t_2 - fV_1$, this expression may be simplified to

$$t_1 = fV_1(t_2 - t_0)/V_0 \quad (2)$$

It can also be shown that if $t_2 - t_0$ is equal to $nl_1 t_0/l_0$, the value of f at the exit end of the loop is $1/n$. Since $f = 0$ at the mid-point between the electrodes at time t_2, and there is a linear titrand concentration gradient along the loop, the mean value of f is $1/2n$.

By combination of these equations we obtain

$$t_1 = l_1 V_1 t_0 / 2l_0 V_0 \quad (3)$$

and t_2 will be the true titration time if the circuit is designed so that $l_1 V_1 = 2l_0 V_0$ or

$$l_1 = \sqrt{2V_0 l_0/\pi r^2} \quad (4)$$

where r is the inner radius of the circuit tubing. For example, if $l_0 = 3.5$ cm, $V_0 = 80.0$ ml and $r = 0.1$ cm, l_1 must be 133.5 cm.

As this is an approximation, based on equation (3), the error of the titration will not be strictly zero, but nonetheless will be very small. Equation (3) can be made more exact by substituting $V_0 + \phi t_2 - fV_1$, yielding

$$t_1 = \frac{l_1 V_1 t_0}{2l_0(V_0 + \phi t_2 - fV_1)} = \frac{V_0 t_0}{V_0 + \phi t_2 - fV_1} \quad (5)$$

which allows calculation of the difference $t_1 - t_0$ and the relative error, on the basis of the equations

$$t_1 - t_0 = -\frac{(\phi t_2 - fV_1)t_0}{V_0 + \phi t_2 - fV_1} \quad (6)$$

$$\text{Error (\%)} = \frac{100(\phi t_2 - fV_1)t_0}{t_2(V_0 + \phi t_2 - fV_1)} \simeq \frac{100\phi t_0}{V_0} \quad (7)$$

For $V_0 = 80.0$ ml, $\phi = 30$ μl/sec and $t_0 = 1.4$ sec, the error will not exceed 0.05%.

An alternative development of the theory is given in the Appendix.

RESULTS AND DISCUSSION

Titration curves

The curves obtained on titrating, by the recommended procedure, 2 ml of 0.1*M* chloride with standard silver solutions are shown in Fig. 2. Both curves show a minimum corresponding to the end-point of the titration. Analogous curves are obtained in titrations of bromide, iodide and sulphide with silver.

Figure 3 shows the curve obtained on titrating a mixture of sulphide and disulphide with silver. This curve has two minima, the first due

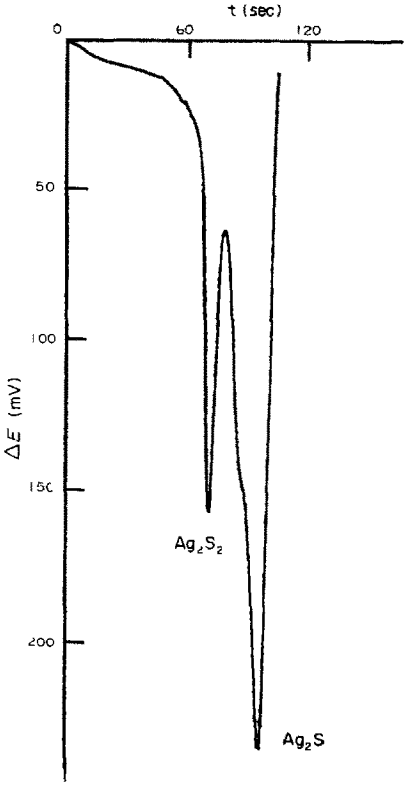

Fig. 3. Titration of a sulphide and disulphide mixture with 0.1*M* silver nitrate.

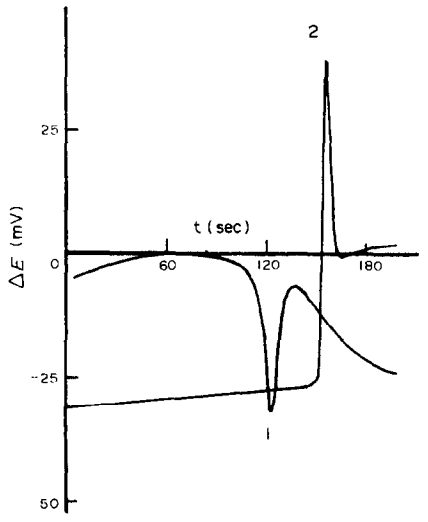

Fig. 4. Titration of ferrous iron with dichromate, using two platinum electrodes (curve 1), and the inverse titration (curve 2).

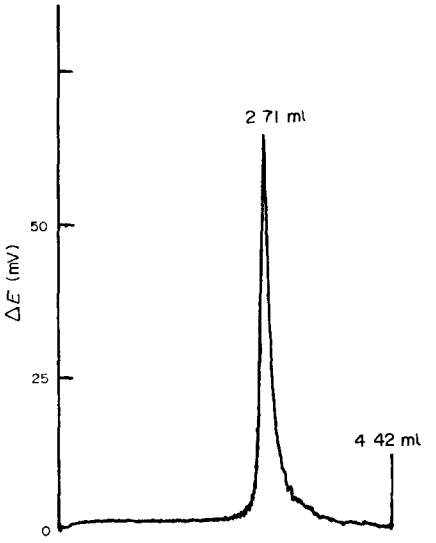

Fig. 5. Titration curve of 2 ml of 0.1*N* sulphuric acid with 0.075*N* sodium hydroxide, using two platinum electrodes.

to precipitation of Ag_2S_2 and the second to precipitation of Ag_2S, since the second peak is displaced when an H_2S solution is added to the sample.

The proposed method can be applied to other types of potentiometric titrations, such as acid–base, oxidation–reduction, *etc.*, by use of the appropriate electrodes. Thus, Fig. 4 shows the curves obtained on titrating 5 ml of 0.04*N* ferrous solution with 0.05*N* dichromate solution (curve 1), and 4 ml of 0.05*N* dichromate with approximately 0.04*N* ferrous solution (curve 2). The curve corresponding to the titration of 2 ml of 0.1*N* sulphuric acid with 0.075*N* sodium hydroxide is represented in Fig. 5. In this last titration, the pump and recorder were stopped simultaneously and the titrant volume added was read.

Precision of the method

We checked the precision of the method by titrating several Cl^-, Br^-, I^- and S^{2-} solutions with 0.1*M* Ag^+ solution. The results obtained (averages of ten determinations) are given in Table 1.

The precision obtainable with this simple titration device is comparable to that with conventional titrators. Thus, titration of 2 ml of a 0.1*M* chloride solution, with use of the Metrohm E 536 automatic titrator, gave a precision of 1.2%, whereas with our device we obtained a value of 1.4%.

Precision of flow measurement

Flow-measurement precision was determined from ten experiments, in which the volumes released by the microburette (between 2000 and 4000 μl) and the corresponding times were measured. The mean $\pm$ standard deviation was 26.36 ± 0.07 μl/sec.

Applications

The proposed method has been applied to determination of the chloride content of drinking water (200 ml) and two samples of wine

Table 1. Precision of the method

Ion titrated	Titrand (0.1*M*), μl	ϕ μl/sec	t,* sec	$\bar{V}$ titrant (0.1*M*),† μl	Error %
Cl^-	2000	24.83	80.1	1989 ± 27	−1.4
Br^-	1000	20.31	50.3	1021 ± 32	+3.1
Br^-	4000	25.86	153.4	3967 ± 28	−0.7
I^-	2000	25.53	77.0	1966 ± 28	−1.4
S^{2-}	730	27.44	53.9	1479 ± 36	+2.4
Ag^+	3000	25.37	119.9	3042 ± 35	+1.1

*Average time.

†Average volume $\pm$ standard deviation.

Table 2. Applications

Sample	Ion	Titrated, *meq*	Found, *mg/l.*	Error, %	Found by other methods, *mg/l.*
Drinking water	Cl^-	0.05	9.5	5.6	10.2[a]
Table wine	Cl^-	0.04	27.4	5.2	29.8[b]
Sherry	Cl^-	0.04	21.4	3.5	23.9[b]
NH_4HS solution	S^{2-}	0.05	384	12.9	370[c]
	S_2^{2-}	0.15	2464	2.1	2410[c]
$Na_2HPO_4 \cdot 12H_2O$	PO_4^{3-}	0.15	967	0.7	950[d]

[a]Mohr method; [b]potentiometric titration; [c]iodimetric method and gravimetric determination as $BaSO_4$; [d]gravimetric determination as $(NH_4)_3PO_4 \cdot 12MoO_3$.

(50 ml), and to determination of the sulphide and disulphide concentrations of an ammonium hydrogen sulphide solution. The phosphate content of a sample of $Na_2HPO_4 \cdot 12H_2O$ was determined according to the following procedure: a measured volume of sample, containing less than 0.4 meq of phosphate, was transferred to the titration vessel, 4.00 ml of 0.1*M* silver nitrate solution and 5 ml of 1*M* potassium nitrate solution were added and the mixture was diluted accurately to 80 ml with demineralized water and neutralized. The excess of silver was titrated with 0.1*M* sodium chloride.

The results obtained (averages of six determinations) are given in Table 2.

Conclusions

This automatic differential titrator is a simple instrument with components (a potentiometer, a graphic recorder, a peristaltic pump with two tubes and a microburette) which are readily available in any analytical laboratory. Its cost is approximately a fifth of that of a commercial automatic differential titrator. In addition, the development of cheap and easily manufactured new coated wire[9] and tubular[10] microelectrodes considerably extends the field of application of the proposed method.

Acknowledgement—The authors are grateful to Dr. R. A. Chalmers for his contribution to improvement of this paper.

REFERENCES

1. D. A. MacInnes and P. T. Jones, *J. Am. Chem. Soc.*, 1926, **48**, 2831.
2. D. A. MacInnes, *Z. Phys. Chem. (Leipzig)*, 1927, **130A**, 217.
3. D. A. MacInnes and M. Dole, *J. Am. Chem. Soc.*, 1929, **51**, 1119.
4. D. A. MacInnes and I. A. Cowperthwaite, *ibid.*, 1931, **53**, 555.
5. H. H. Baker and R. H. Müller, *Trans. Electrochem. Soc.*, 1939, **76**, 75.
6. H. B. Malmstadt and E. R. Fett, *Anal. Chem.*, 1954, **26**, 1348; 1955, **27**, 1757.
7. G. Gran, *Acta Chem. Scand.*, 1950, **4**, 559.
8. *Idem*, *Analyst*, 1952, **77**, 661.
9. R. W. Cattrall and H. Freiser, *Anal. Chem.*, 1971, **43**, 1905.
10. S. Alegret, J. Alonso, J. Bartoli, J. M. Paulis, J. L. F. C. Lima and A. A. S. C. Machado, *Anal. Chim. Acta*, 1984, **164**, 147.

APPENDIX

At time $t_2 - t_0$ all the solution in the titration vessel has been titrated and the solution in the circuit loop has a titrand concentration gradient from zero at the entrance, to the titration vessel concentration at time $t_2 - t_0 - t_l$, at the exit, where t_l is the time taken for liquid to traverse the whole loop. During the time between $t_2 - t_0 - t_l$ and $t_2 - t_0$, $t_l \phi C$ μeq of titrant (concentration C μeq/μl) will have been added to the system, and divided between the titration vessel and the loop. To a first approximation, the fraction added to the titration vessel will be

$$t_l \phi C[V_0 - \tfrac{1}{2}V_l + (t_2 - t_0 - t_l)\phi]/[V_0 + (t_2 - t_0 - t_l)\phi]$$

where V_l is the *total* volume of the loop, and this fraction must have been equal to the amount of untitrated titrand present in the titration vesel at time $t_2 - t_0 - t_l$. Hence the titration vessel concentration of free titrand at that time was

$$t_l \phi C[V_0 - \tfrac{1}{2}V_l + (t_2 - t_0 - t_l)\phi]/$$
$$[V_0 + (t_2 - t_0 - t_l)\phi][V_0 - V_l + (t_2 - t_0 - t_l)\phi]$$

and this will therefore be the concentration at the exit of the loop at time $t_2 - t_0$. The loop therefore contains

$$V_l t_l \phi C[V_0 - \tfrac{1}{2}V_l + (t_2 - t_0 - t_l)\phi]/$$
$$2[V_0 + (t_2 - t_0 - t_l)\phi][V_0 - V_l + (t_2 - t_0 - t_l)\phi]$$

μeq of titrand still untitrated, and if t_2 is to be the true titration time, this must be equal to the $t_0 \phi C$ μeq of titrant to be added in time t_0. We therefore have

$$V_l t_l[V_0 - \tfrac{1}{2}V_l + (t_2 - t_0 - t_l)\phi]$$
$$= 2t_0[V_0 + (t_2 - t_0 - t_l)\phi][V_0 - V_l + (t_2 - t_0 - t_l)\phi]$$

Expanding, putting $V_l = (l_o + l_1)\pi = \pi x$, and $t_l = x/v$ wehre v is the linear velocity of the liquid in the loop, gives, after rearrangement:

$$\left(\frac{\pi^2}{2} + \frac{\phi\pi}{v}\right)x^3 - \left[\pi V_0 + (t_2 - t_0)\phi\pi - 2t_0\phi\left(\pi + \frac{\phi}{v}\right)\right]x^2$$
$$-2t_0(\pi v + 2\phi)[V_0 + (t_2 - t_0)\phi]x$$
$$+2t_0[V_0^2 v + 2V_0(t_2 - t_0)\phi v + (t_2 - t_0)^2\phi^2 v] = 0$$

This cubic equation contains one variable besides x, namely t_2, but that is to be expected because t_2 depends on the origial sample concentration, and determines the degree of dilution during the titration.

Substitution of $V_0 = 8.0 \times 10^4$ μl, $l_0 = 35$ mm, $t_0 = 1.4$ sec, $v = 25$ mm/sec and $t_2 - t_0 = 100$ sec gives

$$8.704713x^3 - 2.603875 \times 10^5 x^2$$
$$-3.219685 \times 10^7 x + 5.22430 \times 10^{11} = 0$$

which yields

$$x = l_0 + l_1 = 1387 \text{ mm, or } l_1 = 135.2 \text{ cm.}$$

For $t_2 - t_0 = 50$ sec, the equation is

$$8.704713x^3 - 2.556751x^2$$
$$-3.161479 \times 10^7 x + 5.050575 \times 10^{11} = 0$$

which yields

$$x = l_0 + l_1 = 1381 \text{ mm, or } l_1 = 134.6 \text{ cm.}$$

These values are in good agreement with the value of 133.5 cm for l_1, as deduced from the approximate equation (4). It is obvious from the terms in the cubic equation that V_0 is the most critical factor, and the initial dilution to this volume should be as accurate as possible. A tall and narrow titration vessel (marked accurately to indicate capacity V_0) is to be preferred, provided that its dimensions are also suitable for ensuring the fastest possible mixing.

Talanta, Vol. 39, No. 9, pp. 1127–1137, 1992
Printed in Great Britain

0039-9140/92 $5.00 + 0.00
Pergamon Press Ltd

SOME NEW ALGORITHMS APPLICABLE TO POTENTIOMETRIC TITRATION IN ACID–BASE SYSTEMS

TADEUSZ MICHAŁOWSKI

Department of Analytical Chemistry, Faculty of Chemistry, Jagiellonian University, 30-060 Kraków, Poland

(*Received* 6 *January* 1988. *Revised* 7 *January* 1992. *Accepted* 28 *January* 1992)

Summary—The paper describes some regression equations adaptable for determination of parameters such as concentrations, equilibrium constants and hydrogen-ion activity coefficients in systems comprising hydrolysable salts of type MeB_u and monoprotic and polyprotic acids or their salts. These equations are based on the charge and mass balances. Two unconventional types of regression equations are applied: (*i*) Padé functions $W = G_1(h)/G_2(h)$ relating the sum (W) of V_0 ml of titrand and V ml of titrant, $W = V_0 + V$, to polynomial functions $G_1(h)$ and $G_2(h)$ of the hydrogen-ion activity, h, and (*ii*) functions of the type $1/W = \phi(h)$, based on the Simms titration constants involved. The latter functions are notable for determination of acids and/or their salts in mixtures. The regression equations are developed for systems at constant ionic strength. The parameters of the system can be calculated by means of the computer program MINUITS. Other possibilities of the method, *e.g.*, application to mixed complexes and extraction systems, are also presented.

Potentiometric acid–base titration is the most common and straightforward method for the determination of acids. The mathematical methods used for interpretation of the titration data have been reviewed, *e.g.*, by Anfält and Jagner[1] and by Michałowski.[2] The methods are applied for acids (or bases) that are readily soluble over a wide pH range. Much less attention has been paid to theoretical considerations of mixtures of salts of MeB_u type formed by a hydrolysable cation Me^{+u} and the anion of a strong acid HB. Owing to formation of hydroxo-complexes, the Me^{+u} ions can be treated as acids. On the other hand, the hydroxide $Me(OH)_u$ which is insoluble in water over a defined pH range, can be treated as an analogue, from the opposite side of the pH scale, of a slightly soluble acid (*e.g.*, H_2SiO_3).

An aqueous solution of pure MeB_u contains protons originating from hydrolysis or dismutation.[3] Solutions of the commercial salt, however, may contain free strong acid (HB) or base (MOH) resulting from the preparation procedure. Neglect of the free acid or base leads to very dubious values for any equilibrium constants determined with such a solution. A detailed discussion concerning free acid/base has been made by von Barsewisch and Hasty[4] and Michałowski.[5]

A method described below has been developed to distinguish between the hydrolytic effect of the Me ions and the protolytic effect(s) caused by the presence of acids, bases or salts. It provides both analytical and physicochemical data, namely concentrations, equilibrium constants and the hydrogen-ion activity coefficient. The concentrations and physicochemical data form a set of internal parameters for a non-linear regression equation. The method can also be applied for determination of equilibrium constants in liquid–liquid extraction systems or in mixed or non-aqueous solvent systems.

The method presented here is based on semi-empirical regression equations obtained from the charge and concentration balances for unconventionally prepared titrand + titrant systems in which the sample solution is present in both the titrand and the titrant.[6,7] It is assumed that the titrand and titrant form a single phase (which may also be in equilibrium with an immiscible liquid phase) throughout the titration. The values of the internal parameters of the system are obtained by fitting an appropriate regression equation to the experimental points (V_j, pH_j) of a pH-titration performed according to a well-established optimization program run on a computer. The method has the following advantages.[8–11]

(1) Precise definition of the free acid or base terms and the possibility of distinguishing their effects from those resulting from hydrolysis and complexation reactions.

(2) The regression equations are relatively simple and have similar forms for all

applications; these features are very convenient for programming.

(3) It is easy to keep the ionic strength constant during the titration without prior knowledge of the composition of the sample.

(4) The similarity in composition of titrand and titrant practically eliminates any effect of change in dielectric constant during the titration.[12]

(5) Precipitation of basic salts or hydroxides can be avoided.

Such advantages are not offered by other systems based on use of computer programs;[13–20] in particular, TITRA[18] and TITAN[19,20] cannot be recommended for systems containing hydrolysable salts; the algorithms applied there are related to direct titration of mixture of acids with NaOH as titrant. Moreover, the form of the regression functions based on mass and charge balances is not convenient for computation because the response function in the regression equations contains unknown parameters, namely the hydrogen-ion activity coefficient and the ionic product for water (K_w). This makes the optimization procedure complex in its form and length; *e.g.*, TITAN[20] has about 1400 statements. In contrast, the optimization procedure in the method described here has only about 70 statements (not including the number of statements for entering the MINUITS optimization procedure[21] applied).

GENERAL ASSUMPTIONS

Composition of the sample

The following general composition is assumed:

$$Me^{(s)}B_{u_s}(s = 1, \ldots, P_{Me}) + HB + M_{m_t}H_{n_t - m_t}L^{(t)} \quad (t = 1, \ldots, P_L) \quad (1)$$

or

$$Me^{(s)}B_{u_s}(s = 1, \ldots, P_{Me}) + MOH + M_{m_t}H_{n_t - m_t}L^{(t)} \quad (t = 1, \ldots, P_L) \quad (2)$$

where $Me^{(s)}$, with charge $+u_s$, is a hydrolysable cation of the s-th kind, B^- the anion of a strong acid HB, M^+ a non-hydrolysable cation of a strong base MOH, $H_{n_t}L^{(t)}$ a weak acid of the t-th kind ($t = 1, \ldots, P_L$; $m_t = 0, \ldots, n_t$) forming the species $H_jL^{(t)}$ with charge $-n_t + j$ in solution ($j = 0, \ldots, q_t$; $q_t \geq n_t$). The molar concentrations of $Me^{(s)}B_{u_s}$, $M_{m_t}H_{n_t - m_t}L^{(t)}$, HB and MOH are denoted by $C_{0(s)}$, $C_{L(t)}$, C_a and C_b, respectively.

Titrand and titrant composition (example)

The titrand and titrant are prepared in standard flasks, of volume V_f. To do this, equal volumes (V^*) of the sample are placed in both flasks, then one of them is treated with volume V_B ml of C mole/l. HB solution or with V_M ml of C mole/l. MOH solution. Then, after addition of volumes V_{MB} and V'_{MB} of a solution (concentration C_1) of the non-hydrolysable salt MB, both solutions are made up to the mark with distilled water, see Table 1, system 4.

The presence of HB (C mole/l.) or MOH (C mole/l.) in the titrand or titrant ensures an appreciable pH change during the titration and this will be greater when the buffer capacity of the titrant is much greater than that of the titrand.

The isomolarity condition

The condition for constant ionic strength during the titration is expressed by the equation

$$C_1 V_{MB} = C_1 V'_{MB} + CV_B \quad (3)$$

for systems where HB is added, or

$$C_1 V_{MB} = C_1 V'_{MB} + CV_M \quad (4)$$

for systems where MOH is added; *e.g.*, equation (4) is the isomolarity condition for the system discussed in the example of titrand and titrant composition, see above. The presence of strong acid or strong base in one of the solutions is compensated by the corresponding surplus of MB in the other. This surplus can easily be calculated from $V_{MB} - V'_{MB} = CV_B/C_1$ or $V_{MB} - V'_{MB} = CV_M/C_1$.

Admissible complexes

In the mathematical models for the titrand + titrant systems containing the sample, represented by equations (1) or (2), the following types of soluble complexes are assumed:

Type 1:

$$[Me_{i_s}^{(s)}]M_\alpha H_\eta B_\beta L^{(t)} + [Me_{i_s}^{(s)}]M_\alpha B_\beta \quad (5)$$

Type 2:

$$[Me_{i_s}^{(s)}]M_\alpha H_\eta (OH)_\lambda B_\beta L^{(t)} + [Me_{i_s}^{(s)}]M_\alpha (OH)_\lambda B_\beta \quad (6)$$

where

$$[Me_{i_s}^{(s)}] = Me_{i_1}^{(1)} \ldots Me_{i_{P_{Me}}}^{(P_{Me})} \quad (7)$$

Complexes containing more than one $L^{(t)}$ ligand are not allowed in the model, nor are mixed

ligand complexes, *e.g.*, those containing two different ligands $L^{(t_1)}$, $L^{(t_2)}$. In the case of type 1 complexes, soluble hydroxo-complexes are neglected in the defined pH-interval.

As can be seen from literature data,[22,23] the exclusion of mixed-ligand complexes is justifiable for systems containing mixtures of chelating agents such as EDTA and citric or tartaric acid.

Relative contents of components of the system

Let us consider a titrand + titrant system containing a sample, as represented by equation (1) or (2). If the analytical concentrations $c_{Me(s)}$, c_M and c_B of $Me^{(s)}$, M and B in these solutions are much greater than the analytical concentrations $c_{L(t)}$ of the species containing $L^{(t)}$, *i.e.*,

$$c_{Me(s)} \gg c_{L(t)}, \quad c_M \gg c_{L(t)}, \quad c_B \gg c_{L(t)} \tag{8}$$

then, writing

$$\rho = \eta - \lambda \tag{9}$$

we can assume that the quantities [see equations (32), (36), (37)]:

$$P_{\eta t} = \sum_{t,\alpha,\beta} K^{(t)}_{(i_s)\alpha\eta\beta} \prod_s [Me^{(s)}]^{i_s}[M]^{\alpha}[B]^{\beta} \tag{10}$$

$$Q_{\rho t} = \sum_{t,\alpha,\beta} K^{(t)}_{(i_s)\alpha\eta,\beta} \prod_s [Me^{(s)}]^{i_s}[M]^{\alpha}[B]^{\beta} \tag{11}$$

$$R_{\lambda} = \sum_{t,\alpha,\beta} K_{(i_s)\alpha\lambda\beta} \prod_s [Me^{(s)}]^{i_s}[M]^{\alpha}[B]^{\beta} \tag{12}$$

remain constant during the titration.

Constancy of dielectric constant

This condition is ensured by the similar composition of the titrand and titrant. The quantity of HB or MOH, *i.e.*, $C_a V_B$ or $C_b V_M$, is small in comparison with that of the salt MB.

pH-titration

The total volume after addition of V_j ml ($j = 1, 2, \ldots, N$) of titrant to V_0 ml of titrant is

$$W_j = V_0 + V_j \tag{13}$$

Let pH_j be the pH measured after addition of V_j ml of titrant. The pair (V_j,pH_j) defines this experimental point. The pH is defined as the negative logarithm of the hydrogen-ion activity (h)

$$pH = -\log h \tag{14}$$

so

$$h = f[H] \tag{15}$$

where f is the hydrogen-ion activity coefficient.

PROTON BALANCES AND THEIR TRANSFORMATIONS

Let us assume the existence of soluble complexes as given in equation (5). Defining the concentrations of the corresponding complexes by

$$c^{(t)}_{(i_s)\alpha\eta\beta} \ (t = 1, \ldots, P_L) \text{ and } c_{(i_s)\alpha\beta}$$

respectively and assuming the sample composition given by equation (1), we can write the balances related to the titrand + titrant system 4 in Table 1 as follows:

$$\sum_{t,s,i,\alpha,\eta,\beta} (i_s u_s + \alpha + \eta - \beta - n_t) c^{(t)}_{(i_s)\alpha\eta\beta} + \sum_{s,i,\alpha,\beta} (i_s u_s + \alpha - \beta) c_{(i_s)\alpha\beta} + [H] - [OH] = 0 \tag{16}$$

$$\sum_{t,i,\alpha,\eta,\beta} i_s c^{(t)}_{(i_s)\alpha\eta\beta} + \sum_{i,\alpha,\beta} i_s c_{(i_s)\alpha\beta} = dC_{0(s)} \tag{17}$$

$$\sum_{s,i,\alpha,\eta,\beta} c^{(t)}_{(i_s)\alpha\eta\beta} = dC_{L(t)} \tag{18}$$

$$\sum_{t,s,i,\alpha,\eta,\beta} \beta c^{(t)}_{(i_s)\alpha\eta\beta} + \sum_{s,i,\alpha,\beta} \beta c_{(i_s)\alpha\beta} = d \sum_s u_s c_{0(s)} + dC_a + C_i V_{MB}/V_f - b_M/W \tag{19}$$

$$\sum_{t,s,i,\alpha,\eta,\beta} \alpha c^{(t)}_{(i_s)\alpha\eta\beta} + \sum_{s,i,\alpha,\beta} \alpha c_{(i_s)\alpha\beta} = d \sum_t m_t C_{L(t)} + C_i V_{MB}/V_f \tag{20}$$

where:

$$(i_s) = i_1 \ldots i_{pMe} \tag{21}$$

$$d = V^*/V_f \tag{22}$$

$$b_M = CV_M V_0/V_f \tag{23}$$

$$W = V_0 + V \tag{13(a)}$$

(some of the parameters i_s can be equal to zero). The concentrations of the corresponding complexes can be expressed by the equations:

$$c^{(t)}_{(i_s)\alpha\eta\beta} = K^{(t)}_{(i_s)\alpha\eta\beta} \prod_s [Me^{(s)}]^{i_s}[M]^{\alpha}[H]^{\eta}[B]^{\beta}[L^{(t)}] \tag{24}$$

$$c_{(i_s)\alpha\beta} = K_{(i_s)\alpha\beta} \prod_s [Me^{(s)}]^{i_s}[M]^{\alpha}[B]^{\beta} \tag{25}$$

If a complex characterized by a given set of parameters

$$(i_1, \ldots, i_{pMe}, \alpha, \eta, \beta) \text{ or } (i_1, \ldots, i_{pMe}, \alpha, \beta)$$

does not exist, the corresponding equilibrium constants

$$K^{(t)}_{(i_s)\alpha\eta\beta} \text{ or } K_{(i_s)\alpha\beta}$$

will be equal to zero.

Linear combination of equations (16)–(20) gives the proton balance

$$\sum_{t,s,i,\alpha,\eta,\beta} \eta c^{(t)}_{(i_s)\alpha\eta\beta} + [H] - [OH] = d\left[\sum_t (n_t - m_t)C_{L(t)} + C_a\right] - b_M/W \quad (26)$$

Under analogous conditions, but with hydroxo-complexes present as in equation (6), at concentrations denoted by

$$c^{(t)}_{(i_s)\alpha\eta\lambda\beta} \quad \text{and} \quad c_{(i_s)\alpha\lambda\beta}$$

respectively, the proton balance is

$$\sum_{t,s,i,\alpha,\eta,\lambda,\beta} \rho c^{(t)}_{(i_s)\alpha\eta\lambda\beta} - \sum_{s,i,\alpha,\lambda,\beta} \lambda c_{(i_s)\alpha\lambda\beta} + [H] - [OH] = d\left[\sum_t (n_t - m_t)C_{L(t)} + C_a\right] - b_M/W \quad (27)$$

The concentrations of the corresponding complexes are given by [see equation (9)]:

$$c^{(t)}_{(i_s)\alpha\eta\lambda\beta} = K^{(t)}_{(i_s)\alpha\eta\lambda\beta} \prod_s [Me^{(s)}]^{i_s}[M]^{\alpha}[H]^{\rho}[B]^{\beta} \quad (28)$$

$$c_{(i_s)\alpha\lambda\beta} = K_{(i_s)\alpha\lambda\beta} \prod_s [Me^{(s)}]^{i_s}[M]^{\alpha}[H]^{-\lambda}[B]^{\beta} \quad (29)$$

In systems with polyprotic acids $H_{n_t}L^{(t)}$ or their salts $M_{m_t}H_{n_t-m_t}L^{(t)}$ it is often the case that some species are present at such low concentrations that they can be omitted in the corresponding balances, which makes the regression equation simpler. For example, in aqueous solutions of orthophosphoric acid at pH < 4, the concentrations of PO_4^{-3} and HPO_4^{-2} can be omitted from the charge and concentration balances and the η values in the summations will be $\eta_1 = 2$ (the number of protons in $H_2PO_4^-$) and $\eta_2 = 3$ (the number of protons in H_3PO_4). Analogously, we can denote by $\eta_1 t$ and $\eta_2 t$ the lower (infimum, abbr. inf) and upper (supremum, sup) values of η for complexes containing a ligand form $L^{(t)}$:

$$\eta_1 t = \inf_t \{\eta\} \quad \text{and} \quad \eta_2 t = \sup_t \{\eta\} \quad (30)$$

The Bjerrum function then has the form

$$\bar{n}_t = \sum_{s,i,\alpha,\eta,\beta} \eta c^{(t)}_{(i_s)\alpha\eta\beta} \Big/ \sum_{s,i,\alpha,\eta,\beta} c^{(t)}_{(i_s)\alpha\eta\beta} = \sum_{s,i,\alpha,\eta,\beta} \eta c^{(t)}_{(i_s)\alpha\eta\beta}/dC_{L(t)} \quad (31)$$

$$= \sum_{\eta=\eta_1 t}^{\eta_2 t} \eta x_{\eta t}[H]^{\eta} \Big/ \sum_{\eta=\eta_1 t}^{\eta_2 t} x_{\eta t}[H]^{\eta} \quad [31(a)]$$

where

$$x_{\eta t} = P_{\eta t}/P_{\eta_2 t} \quad (32)$$

and $P_{\eta_2 t}$ is the $P_{\eta t}$ value [see equation (9)] related to $\eta t = \eta_2 t$.

Putting (31) into (26) gives, after transformation,

$$1/W = -\left[\sum_{t=1}^{P_L} (m_t + q_t - n_t)C_{L(t)} - C_a\right]\Big/a_M - (h/f - K_w f/h)b_M + \sum_{t=1}^{P_L} (q_t - \bar{n}_t)C_{L(t)}/a_M \quad (33)$$

where f and h are defined in equation (15), q_t is the maximal number of protons co-ordinated to the form $L^{(t)}$, and

$$a_M = b_M/d \quad (34)$$

$$k_w = [H][OH] \quad (35)$$

The proton balance for hydroxo-complexes [(27)] can be transformed into

$$1/W = -\left[\sum_{t=1}^{P_L} (m_t + q_t - n_t)C_{L(t)} - C_L\right]\Big/a_M - (h/f - K_w f/h)b_M + \sum_{\lambda=1}^{\Lambda} \lambda R_\lambda (h/f)^{-\lambda}/b_M + \sum_{t=1}^{P_L} (q_t - \bar{n}'_t)C_{L(t)}/a_M \quad (36)$$

where:

$$\bar{n}'_t = \sum_{s,i,\alpha,\eta,\lambda,\beta} \rho c^{(t)}_{(i_s)\alpha\eta\lambda\beta}/dC_{L(t)} = \sum_{\rho=\rho_1 t}^{\rho_2 t} \rho Q_{\rho t}[H]^{\rho} \Big/ \sum_{\rho=\rho_1 t}^{\rho_2 t} Q_{\rho t}[H]^{\rho} \quad (37)$$

$$= \sum_{\rho=\rho_1 t}^{\rho_2 t} \rho y_{\rho t}[H]^{\rho} \Big/ \sum_{\rho=\rho_1 t}^{\rho_2 t} y_{\rho t}[H]^{\rho} \quad [37(a)]$$

$$\rho_1 t = \inf_t \{\rho\}, \ \rho_2 t = \sup_t \{\rho\} \quad (38)$$

$$\Lambda = \sup \{\lambda\} \quad (39)$$

$$y_{\rho t} = Q_{\rho t}/Q_{\rho_2 t} \quad (40)$$

Here $Q_{\rho_2 t}$ is the $Q_{\rho t}$ value [see equation (11)] corresponding to $\rho t = \rho_2 t$ and Λ is related to the number of OH-groups in the complexes of $Me^{(s)}_{i_s}M_\alpha(OH)_\lambda B_\beta$ type, [see equation (6)].

The proton balance related to titrand + titrant systems can be presented in the general forms:

$$d\sum_{t=1}^{P_L} \bar{n}_t C_{L(t)} + [H] - [OH] = F \quad (41)$$

$$d\sum_{t=1}^{P_L}\bar{n}_t' C_{L(t)} - \sum_{\lambda=1}^{A}\lambda R_\lambda [H]^{-\lambda} + [H] - [OH] = F \quad (42)$$

In Table 1, the samples corresponding to equations (1) and (2) are called Sample I and Sample II, respectively. The expressions for J_a and J_b are:

$$J_a = \sum_{t=1}^{P_L}(n_t - m_t)C_{L(t)} + C_a \quad (43)$$

$$J_b = \sum_{t=1}^{P_L}(n_t - m_t)C_{L(t)} - C_b \quad (44)$$

Note that the corresponding expressions for F become identical on substitution of $-b_M$ for b_B and/or $-C_b$ for C_a. Moreover, the form of the F-expressions for the systems containing HB or MOH in the titrand differ from those for the systems with these species in the titrant.

With $F = dJ_a - b_M/V_0 + b_M/W$ (system 3 in Table 1) and rearrangement, equation (41) becomes

$$1/W = 1/V_0 + \left[\sum_{t=1}^{P_L}(m_t + q_t - n_t)C_{L(t)} - C_a\right]\Big/a_M - (h/f - K_w f/h)/b_M - \sum_{t=1}^{P_L}(q_t - \bar{n}_t)C_{L(t)}/a_M \quad (45)$$

The substitutions $-b_B$ for b_M, $-a_B$ for a_M, $-C_b$ for C_a in (45), where $a_B = b_B/d$, lead to the equation

$$1/W = 1/V_0 - \left[\sum_{t=1}^{P_L}(m_t + q_t - n_t)C_{L(t)} + C_b\right]\Big/a_B + (h/f - K_w f/h)/b_B + \sum_{t=1}^{P_L}(q_t - \bar{n}_t)C_{L(t)}/a_B \quad (46)$$

for system 5 in Table 1.

Making the same substitutions in (33) leads to

$$1/W = \left[\sum_{t=1}^{P_L}(m_t + q_t - n_t)C_{L(t)} + C_b\right]\Big/a_B + (h/f - K_w f/h)/b_B - \sum_{t=1}^{P_L}(q_t - \bar{n}_t)C_{L(t)}/a_B \quad (47)$$

for system 6 in Table 1.

For systems with $P_{Me} \geqslant 1$, the experimental points (V_j,pH_j) are chosen, as a rule, such that $[H] \gg [OH]$. This enables [OH] to be omitted from the proton balances; the same effect is attained by putting $K_w = 0$ in the regression equations.

REGRESSION EQUATIONS

Padé type

Regression equations of the Padé type will be applied, in this paper, to titrand and titrant systems where $P_L = 1$ and $P_{Me} \geqslant 0$ in the sample. In this case, the notation may be simplified by omitting qualifying index t in equations (9), (10), (30), (38) and (40) and replacing $L^{(t)}$ by L. Then:

$$x_\eta = \begin{cases} P_\eta/P_{\eta_2} \text{ for } \eta = \eta_1, \ldots, \eta_2 - 1 \\ 1 \text{ for } \eta = \eta_2 \\ 0 \text{ for other } \eta \text{ values} \end{cases} \quad (48)$$

$$y_\rho = \begin{cases} Q_\rho/Q_{\rho_2} \text{ for } \rho = \rho_1, \ldots, \rho_2 - 1 \\ 1 \text{ for } \rho = \rho_2 \\ 0 \text{ for other } \rho \text{ values} \end{cases} \quad (49)$$

$$J_a = (n - m)C_L + C_a \quad (50)$$

$$J_b = (n - m)C_L - C_b \quad (51)$$

Equations (31a), (41), (37a) and (42) then become, respectively:

$$\bar{n} = \sum_{\eta=\eta_1}^{\eta_2}\eta x_\eta [H]^\eta \Big/ \sum_{\eta=\eta_1}^{\eta_2} x_\eta [H]^\eta \quad (52)$$

$$dC_L\bar{n} + [H] - [OH] = F \quad (53)$$

Table 1. Composition of titrand (D) and titrant (T) for different isomolar systems and the corresponding expressions for F [equations (41), (42)]: $b_B = CV_0V_B/V_f$, $b_M = CV_0V_M/V_f$, $d = V^*/V_f$

	Sample I		Sample II		HB, C		MOH, C		MB, C_t		
System	D	T	D	T	D	T	D	T	D	T	F
1	V^*	V^*	—	—	—	V_B	—	—	V_{MB}	V'_{MB}	$dJ_a + b_B/V_0 - b_B/W$
2	V^*	V^*	—	—	V_B	—	—	—	V'_{MB}	V_{MB}	$dJ_a + b_B/W$
3	V^*	V^*	—	—	—	—	—	V_M	V_{MB}	V'_{MB}	$dJ_a - b_M/V_0 + b_M/W$
4	V^*	V^*	—	—	—	—	V_M	—	V'_{MB}	V_{MB}	$dJ_a - b_M/W$
5	—	—	V^*	V^*	—	V_B	—	—	V_{MB}	V'_{MB}	$dJ_b + b_B/V_0 - b_B/W$
6	—	—	V^*	V^*	V_B	—	—	—	V'_{MB}	V_{MB}	$dJ_b + b_B/W$
7	—	—	V^*	V^*	—	—	—	V_M	V_{MB}	V'_{MB}	$dJ_b - b_M/V_0 + b_M/W$
8	—	—	V^*	V^*	—	—	V_M	—	V'_{MB}	V_{MB}	$dJ_b - b_M/W$

$$\bar{n}' = \sum_{\rho=\rho_1}^{\rho_2} \rho y_\rho [\mathrm{H}]^\rho \Big/ \sum_{\rho=\rho_1}^{\rho_2} y_\rho [\mathrm{H}]^\rho \tag{54}$$

$$dC_\mathrm{L}\bar{n}' - \sum_{\lambda=1}^{\Lambda} \lambda \mathrm{R}_\lambda [\mathrm{H}]^{-\lambda} + [\mathrm{H}] - [\mathrm{OH}] = F \tag{55}$$

The expressions for F are those presented in Table 1, but $\mathrm{J_a}$ and $\mathrm{J_b}$ are defined by equations (50) and (51).

Example 1. Let us take system 1 in Table 1 as an example. From equations (52) and (53):

$$b_\mathrm{B}/W \sum_{\eta=\eta_1}^{\eta_2} x_\eta [\mathrm{H}]^{\eta+1} = K_\mathrm{w} \sum_{\eta=\eta_1}^{\eta_2} x_\eta [\mathrm{H}]^\eta + \sum_{\eta=\eta_1}^{\eta_2} (d\mathrm{J_a} + b_\mathrm{B}/V_0 - \eta dC_\mathrm{L}) x_\eta [\mathrm{H}]^{\eta+1} - \sum_{\eta=\eta_1}^{\eta_2} x_\eta [\mathrm{H}]^{\eta+2} \tag{56}$$

Multiplying both sides of (56) by f^{η_2+2}/h^{η_1} and setting

$$\eta_2 - \eta_1 = \mathrm{p} \quad \text{and} \quad \eta = \eta_1 + \mathrm{i} \tag{57}$$

we have $\mathrm{i} = 0$ for $\eta = \eta_1$ and $\mathrm{i} = \mathrm{p}$ for $\eta = \eta_2$, so

$$b_\mathrm{B}/W \sum_{\mathrm{i}=0}^{\mathrm{p}} x_{\eta_1+\mathrm{i}} f^{\mathrm{p}+1-\mathrm{i}} h^{\mathrm{i}+1} = K_\mathrm{w} \sum_{\mathrm{i}=0}^{\mathrm{p}} x_{\eta_1+\mathrm{i}} f^{\mathrm{p}+2-\mathrm{i}} h^{\mathrm{i}} + \sum_{\mathrm{i}=0}^{\mathrm{p}} [d\mathrm{J_a} + b_\mathrm{B}/V_0 - (\eta_1 + \mathrm{i})dC_\mathrm{L}] \times x_{\eta_1+\mathrm{i}} f^{\mathrm{p}+1-\mathrm{i}} h^{\mathrm{i}+1} - \sum_{\mathrm{i}=0}^{\mathrm{p}} x_{\eta_1+\mathrm{i}} f^{\mathrm{p}-\mathrm{i}} h^{\mathrm{i}+2} \tag{58}$$

From (48), $x_{\eta_2+1} = x_{\eta_1-1} = x_{\eta_1-2} = 0$, and finally

$$W = \sum_{\mathrm{i}=0}^{\mathrm{p}} A_\mathrm{i} h^{\mathrm{i}+1} \Big/ \left[\sum_{\mathrm{i}=0}^{\mathrm{p}+1} B_\mathrm{i} h^\mathrm{i} - h^{\mathrm{p}+2} \right] \tag{59}$$

where:

$$A_\mathrm{i} = b_\mathrm{B} x_{\eta_1+\mathrm{i}} f^{\mathrm{p}+1-\mathrm{i}} \tag{60}$$

$$B_\mathrm{i} = \{K_\mathrm{w} x_{\eta_1+\mathrm{i}} + d[(\mathrm{n} - \mathrm{m} - \eta_1 + 1 - \mathrm{i})C_\mathrm{L} + C_\mathrm{a} + a_\mathrm{B}/V_0] x_{\eta_1-1+\mathrm{i}} - x_{\eta_1-2+\mathrm{i}}\} f^{\mathrm{p}+2-\mathrm{i}} \tag{61}$$

Substituting $-b_\mathrm{M}$ for b_B, and $-a_\mathrm{M}$ for a_B, in equations (60) and (61), we obtain the expressions for A_i and B_i for system 3 in Table 1. Particular cases of the expressions have been published elsewhere.[9,10]

Example 2. For system 4 in Table 1, at $[\mathrm{H}] \gg [\mathrm{OH}]$, from equations (52) and (53) we have

$$b_\mathrm{M}/W \sum_{\eta=\eta_1}^{\eta_2} x_\eta [\mathrm{H}]^\eta = \sum_{\eta=\eta_1}^{\eta_2} d(\mathrm{J_a} - \eta C_\mathrm{L}) x_\eta [\mathrm{H}]^\eta - \sum_{\eta=\eta_1}^{\eta_2} x_\eta [\mathrm{H}]^{\eta+1} \tag{62}$$

Multiplying both sides of equation (62) by f^{η_2+1}/h^{η_1} and rearranging gives

$$W = \sum_{\mathrm{i}=0}^{\mathrm{p}} A_\mathrm{i} h^\mathrm{i} \Big/ \left[\sum_{\mathrm{i}=0}^{\mathrm{p}} B_\mathrm{i} h^\mathrm{i} - h^{\mathrm{p}+1} \right] \tag{63}$$

where:

$$A_\mathrm{i} = b_\mathrm{M} x_{\eta_1+\mathrm{i}} f^{\mathrm{p}+1-\mathrm{i}} \tag{64}$$

$$B_\mathrm{i} = \{d[(\mathrm{n} - \mathrm{m} - \eta_1 - \mathrm{i})C_\mathrm{L} + C_\mathrm{a}] x_{\eta_1+\mathrm{i}} - x_{\eta_1-1+\mathrm{i}}\} f^{\mathrm{p}+1-\mathrm{i}} \tag{65}$$

Particular cases of equations (63)–(65) have been discussed elsewhere.[8,11]

Example 3. For system 4 in Table 1, from equations (54) and (55) we obtain, at $[\mathrm{H}] \gg [\mathrm{OH}]$,

$$b_\mathrm{M}/W \sum_{\rho=\rho_1}^{\rho_2} y_\rho [\mathrm{H}]^{\rho+\Lambda} = \sum_{\rho=\rho_1}^{\rho_2} d(\mathrm{J_a} - \rho C_\mathrm{L}) y_\rho [\mathrm{H}]^{\rho+\Lambda} + \sum_{\lambda=1}^{\Lambda} \lambda \mathrm{R}_\lambda [\mathrm{H}]^{\Lambda-\lambda} \sum_{\rho=\rho_1}^{\rho_2} y_\rho [\mathrm{H}]^\rho - \sum_{\rho=\rho_1}^{\rho_2} y_\rho [\mathrm{H}]^{\rho+\Lambda+1} \tag{66}$$

Multiplication of both sides of (66) by $f^{\eta_2+\Lambda+1}/h^{\rho_1}$ and further rearrangement leads to

$$W = \sum_{\mathrm{i}=\Lambda}^{\omega+\Lambda} A_\mathrm{i} h^\mathrm{i} / g(h) \tag{67}$$

where $\omega = \rho_2 - \rho_1$ and

$$A_\mathrm{i} = b_\mathrm{M} y_{\rho_1-\Lambda+\mathrm{i}} f^{\omega+\Lambda+1-\mathrm{i}} \tag{68}$$

$$g(h) = \sum_{\mathrm{i}=\Lambda}^{\omega+\Lambda} d[(\mathrm{n} - \mathrm{m} - \rho_1 + \Lambda - \mathrm{i})C_\mathrm{L} + C_\mathrm{a}] \times y_{\rho_1-\Lambda+\mathrm{i}} f^{\omega+\Lambda+1-\mathrm{i}} h^\mathrm{i} + \sum_{\lambda=1}^{\Lambda} \lambda \mathrm{R}_\lambda \sum_{\mathrm{i}=\Lambda-\lambda}^{\omega+\Lambda-\lambda} + y_{\rho_1-\Lambda+\lambda+\mathrm{i}} f^{\omega+\Lambda+1-\mathrm{i}} h^\mathrm{i} - \sum_{\mathrm{i}=\Lambda+1}^{\omega+\Lambda} y_{\rho_1-\Lambda-1+\mathrm{i}} f^{\omega+\Lambda+1-\mathrm{i}} h^\mathrm{i} - h^{\omega+\Lambda+1} \tag{69}$$

The regression equations presented above [equations (59), (63), (67)] are examples of functions of the Padé type (also called Padé approximants[24] or PADE W functions[9]). These functions can be presented in the general form

$$W = G_1(h)/G_2(h) \tag{70}$$

where $G_1(h)$ and $G_2(h)$ are polynomials of the hydrogen-ion activity, and the degree of

polynomial $G_2(h)$ is higher than that of polynomial $G_1(h)$. It should be noted that all components of $G_1(h)$ are of the same sign. Then the reciprocal

$$1/W = G_2(h)/G_1(h) \qquad (71)$$

has no singular points for positive values of f and x_η (or y_ρ). Equation (71) expresses the PADE $1/W$ function.[9]

The class of Padé functions is a subset of the set of rational functions.

Equations with Simms constants[25]

The differences $q_t - \bar{n}_t$ [equation (33)] and $q_t - \bar{n}'_t$ [equation (36)] can be expressed by means of the Simms titration constants[2,18–20,25–28] g_{tv} and g'_{tv} according to

$$q_t - \bar{n}_t = q_t - p_t - \eta_1 t + \sum_{v=1}^{p_t} g_{tv}/(h/f + g_{tv}) \qquad (72)$$

$$q_t - \bar{n}'_t = q_t - \omega_t - \rho_1 t + \sum_{v=1}^{\omega_t} g'_{tv}/(h/f + g'_{tv}) \qquad (73)$$

where

$$p_t = \eta_2 t - \eta_1 t \quad \text{and} \quad \omega_t = \rho_2 t - \rho_1 t \qquad (74)$$

{*cf.* equations [31(a)] and [37(a)]}. Substituting (72) into (33) or (73) into (36), we obtain examples of the SIMMS $1/W$ functions.[9]

In particular, if $\eta_1 t = 0, \eta_2 t = q_t$, *i.e.*, $p_t = q_t$, then from (72)

$$q_t - \bar{n}_t = \sum_{v=1}^{q_t} g_{tv}/(h/f + g_{tv}) \qquad (75)$$

If equations (52) and (57) are applied

$$q - \bar{n} = q - p - \eta_1 + \sum_{v=1}^{p} g_v/(h/f + g_v) \qquad (76)$$

At $\eta_1 = 0, \eta_2 = q$, *i.e.*, $p = q$, equation (76) leads to

$$q - \bar{n} = \sum_{v=1}^{q} g_v/(h/f + g_v) \qquad (77)$$

The Simms constants g_v [equation (76)] are involved with x_η [equation (52)] in a set of p symmetrical equations, similar to ones quoted elsewhere:[9]

$$\begin{aligned}
x_{k_1+p-1} &= g_1 + g_2 + \ldots + g_p \\
x_{k_1+p-2} &= \sum_{i=1}^{p-1} \sum_{j=i+1}^{p} g_i g_j \\
x_{k_1+p-3} &= \sum_{i=1}^{p-2} \sum_{j=i+1}^{p-1} \sum_{k=j+1}^{p} g_i g_j g_k \\
&\ldots\ldots\ldots\ldots\ldots\ldots\ldots \\
x_{k_1} &= g_1 g_2 \ldots g_p
\end{aligned} \qquad (78)$$

APPLICATIONS

Determination of free acid (or base) and hydrolysable cation in the mixture

The titrand + titrant systems presented above are characterized by a high concentration of Me-ions [equation(8)] in comparison with a weak acid H_nL or its salt, acting as buffering agent there.

This section discusses titrand + titrant systems containing a hydrolysable salt, MeB_u, and a strong acid, HB, or strong base, MOH, in the sample tested, at comparable and rather low concentrations: $c_0 = dC_0$, $c_a = dC_a$ or $c_b = dC_b$, respectively, where d is expressed by equation (22). Such systems, prepared according to system 1 in Table 1, have already been examined by Gordienko and Sidorenko,[6] who used a graphical method based on an equation obtained on the assumption that only one hydroxo-complex, $MeOH^{+u-1}$, is formed in the solution.

In comparison with the system described by the conditions in (8), the system discussed here has the requirements:

$$c_L = 0, c_M \gg c_{Me}, c_B \gg c_{Me} \qquad (79)$$

The forms of the regression equations become relatively simple if the hydroxo-complexes formed are only of $MeM_\alpha(OH)_\lambda B_\beta$ type, *i.e.*, mononuclear with respect to Me. This restriction can sometimes apply to dilute solutions of certain metal ions.

Let us consider system 1 in Table 1, containing MeB_u and HB at concentrations C_0 and C_a, respectively. At [H] ≫ [OH], the PADE W function then has the form

$$W = \sum_{i=0}^{\Lambda} A_i h^i \Big/ \left[\sum_{i=0}^{\Lambda} B_i h^i - h^{\Lambda+1} \right] \qquad (80)$$

where Λ is defined by equation (39), and

$$A_i = b_B x_{\Lambda-i} f^{\Lambda+1-i} \qquad (81)$$

$$B = \{d[C_a + (\Lambda - i)C_0 + a_B/V_0] \times x_{\Lambda-i} - x_{\Lambda+1-i}\} f^{\Lambda+1-i} \qquad (82)$$

$$x_\lambda = \begin{cases} 1 \text{ for } \lambda = 0 \\ R_\lambda/R_0 \text{ for } \lambda = 1, \ldots, \Lambda \\ 0 \text{ for other } \lambda \text{ values} \end{cases} \qquad (83)$$

$$R_\lambda = \sum_{\alpha,\beta} K_{\alpha\lambda\beta}[M]^\alpha[B]^\beta \qquad (84)$$

$$[MeM_\alpha(OH)_\lambda B_\beta] = K_{\alpha\lambda\beta}[Me][M]^\alpha[H]^{-\lambda}[B]^\beta \qquad (85)$$

For a sample consisting of a salt $MeO_m(OH)_v B_{u-2m-v}$ and a strong acid HB, the regression function and A_i are defined by equations (80) and (81), and

$$B_i = \{d[(A - 2m - v - i)C_0 + C_a + a_B/V_0]x_{A+1-i} - x_{A+1-i}\} f^{A+1-i}$$

Determination of equilibrium constants

The method can be applied to determination of the stability constants of mixed metal complexes of $M_\mu M'_\nu H_\eta L$ type in aqueous media and the equilibrium constants of complexes of H_2LB type in extraction systems.

Stability constants of $M_\mu M'_\nu H_\eta L$ *complexes.* Let us assume that (*a*) $M_\mu M'_\nu H_\eta L$ complexes are formed by anionic forms of the weak acid H_nL and non-hydrolysable singly-charged cations M and M′; (*b*) q = n, *i.e.*, H_nL is the most highly protonated form of L; (*c*) H_nL forms no complexes in the system; (*d*) the pH interval covered by the experimental points (V_j,pH_j) comprises the predominance ranges of all species with different degree of protonation. The last assumption requires some supplementary experimental conditions, *e.g.*, addition of the proper quantities of strong acid, HB, particularly when a salt $M_mH_{n-m}L$ of the weak acid is used.

The titrand and titrant compositions are the same as for system 3 in Table 1, with the addition of $V_{M'B}$ ml of a solution of M′B (concentration C_2). The isomolarity condition is still expressed by equation (4).

The system is then described by the regression equation

$$W = \sum_{i=0}^{n} A_i h^{i+1} \Big/ \left[\sum_{i=0}^{n+1} B_i h^i - h^{n+2}\right] \quad (86)$$

where

$$A_i = -b_M x_i f^{n+1-i} \quad (87)$$

$$B_i = \{K_w x_i + d[(n - m + 1 - i)C_L + C_a - a_M/V_0]x_{i-1} - x_{i-2}\} f^{n+2-i} \quad (88)$$

[*cf.* equations (59)–(61)] and

$$x_\eta = \begin{cases} P_\eta/P_n \text{ for } \eta = 0, \ldots, n-1 \\ 1 \text{ for } \eta = n \\ 0 \text{ for other } \eta \text{ values} \end{cases} \quad (89)$$

$$P_\eta = \sum_{\mu,\nu} K_{\mu\nu\eta}[M]^\mu[M']^\nu \quad (90)$$

$$[M_\mu M'_\nu H_\eta L] = K_{\mu\nu\eta}[M]^\mu[M']^\nu[H]^\eta[L]$$

and, on the basis of assumption (*b*),

$$P_n = K_{00n} \quad (91)$$

From (89)–(91) we have

$$x_\eta = \sum_{\mu,\nu} \frac{K_{\mu\nu\eta}}{K_{00n}}[M]^\mu[M']^\nu = \frac{K_{00\eta}}{K_{00n}} + \frac{K_{10\eta}}{K_{00n}}[M] + \frac{K_{01\eta}}{K_{00n}}[M'] + \cdots \quad (92)$$

where $\eta = 0, \ldots, n-1$, $K_{000} = 1$. Determination of $K_{\mu\nu\eta}/K_{00n}$ for N^* different values of the fraction $n_M/n_{M'}$ with $n_M + n_{M'}$ constant (n_X = number of mmoles of component X) leads to determination of the stability constants $K_{\mu\nu\eta}$. For

$$\mu + \nu + \eta \leqslant n \quad (93)$$

it is required that

$$N^* \geqslant \binom{n+2}{2} + 1$$

The equilibrium constant given by $K_{\mu\nu\eta}/K_{00n}$ corresponds to the reaction

$$\mu M + \nu M' + H_nL = M_\mu M'_\nu H_\eta L + (n - \eta)H$$

Determination of equilibrium constants in extraction system. The literature[29,30] gives some data indicating the existence of neutral complexes of H_2LB type in solvents such as isoamyl alcohol, methyl isobutyl ketone, butyl acetate, *etc.*, which suggests that they are also present in the aqueous phase in an extraction system.

Let $W = V_0 + V$ and W_{org} denote, respectively, the volumes of the aqueous and organic phases in the system obtained by addition of V ml of titrant to volume V_0 of titrand, in equilibrium with W_{org} ml of an organic solvent immiscible with water. Let HL be a weak acid forming ionic species H_2L^+ and L^- in solution (*e.g.*, 8-hydroxyquinoline). Let H_2L^+ and L^- form the ion-association complexes H_2LY and ML with anion Y^- of a strong acid HY or a cation M^+, respectively. In acidic media, with $[H] \gg [OH]$, the method implies the following equilibria in the system in question:

$$HL + H^+ \rightleftharpoons H_2L^+$$

$$H_2L^+ + Y^- \rightleftharpoons H_2LY$$

$$H_2LY \rightleftharpoons H_2LY_{org}$$

$$HL \rightleftharpoons HL_{org}$$

expressed by the equilibrium constants:

$$k_1 = [H_2L]/([H][HL]) \quad (94)$$

$$K_Y = [H_2LY]/([H_2L][Y]) \quad (95)$$

$$P_Y = [H_2LY]_{org}/[H_2LY] \quad (96)$$

$$P_{HL} = [HL]_{org}/[HL] \quad (97)$$

where changes are omitted for simplicity.

The compositions and preparation of the titrand and titrant are as follows.

	Titrand	Titrant
$HL(C_L) + HB(C_a)$	V^*	V^*
$HB(C)$	—	V_B
$MB(C_1)$	V_{MB}	V'_{MB}
$MD(C_2)$	V_{MD}	V_{MD}
H_2O	$V_f - V^* - V_{MB} - V_{MD}$	$V_f - V^* - V_B - V'_{MB} - V_{MD}$

V_{MB} and V'_{MB} fulfil equation (3). Because the pH measurements are made at different concentrations of species B, it is necessary to add a second salt of a strong acid in sufficient amount to make the number of mmoles of Y (where Y = B or D) constant, so that the ionic strength also remains constant.

The balances related to the systems are expressed by the equations

$$[H_2L] + [HL] + [L] + [H_2LB] + [L_2LD] + [ML] + ([H_2LB]_{org} + [H_2LD]_{org} + [HL]_{org} + [ML]_{org})W_{org}/W = dC_L \quad (98)$$

$$[B] + [H_2LB] + [H_2LB]_{org} W_{org}/W = dC_a + C_1 V_{MB}/V_f \quad (99)$$

$$[D] + [H_2LD] + [H_2LD]_{org} W_{org}/W = C_2 V_{MD}/V_f \quad (100)$$

$$[M] + [ML] + [ML]_{org} W_{org}/W = C_1 V_{MB}/V_f + C_2 V_{MD}/V_f - b_B/V_0 + b_B/W \quad (101)$$

$$[H_2L] + [M] + [H] = [OH] + [B] + [D] + [L] \quad (102)$$

Combination of equations (98)–(102) yields

$$[H] - [OH] = d(C_a - C_L) + b_B/V_0 - b_B/W + [HL] + [HL]_{org} W_{org}/W + 2([L] + [ML] + [ML]_{org} W_{org}/W) \quad (103)$$

In acidic media, the concentrations [OH], [L], [ML], $[ML]_{org}$ can be omitted in equations (98) and (103). Then equation (103) simplifies to

$$W[H] = \theta W - b_B + [HL](P + W) \quad (104)$$

where

$$\theta = d(C_a - C_L) + b_B/V_0$$

$$P = P_{HL} W_{org} \quad (105)$$

From equations (94)–(96), with Y = B and D,

$$[H_2L] = k_1[H][HL] \quad (106)$$

$$[H_2LY] = k_1 K_Y [Y][H][HL] \quad (107)$$

$$[H_2LY]_{org} = k_1 K_Y P_Y [Y][H][HL] \quad (108)$$

Substitution of (97) and (105)–(108) into the simplified form of (98) gives

$$[HL] = \frac{dC_L W}{P + W + Q[H] + RW[H]} \quad (109)$$

where

$$Q = k_1 W_{org}(K_B P_B[B] + K_D P_D[D]) \quad (110)$$

$$R = k_1(1 + K_B[B] + K_D[D]) \quad (111)$$

Combining (104) and (109) and the hydrogen-ion activity (h) leads to

$$W^2h^2 = A_1 + A_2h + A_3W + A_4Wh + A_5W^2 + A_6W^2h + A_7Wh^2 \quad (112)$$

where

$$A_1 = -b_B x_2 f^2$$

$$A_2 = -b_B x_3 f$$

$$A_3 = [(\theta + dC_L)x_2 - b_B x_1]f^2$$

$$A_4 = (\theta x_3 - x_2 - b_B)f$$

$$A_5 = (\theta + dC_L)x_1 f^2$$

$$A_6 = (\theta - x_1)f$$

$$A_7 = -x_3$$

in which $x_1 = 1/R$, $x_2 = P/R$, $x_3 = Q/R$.

Equations (110) and (111) can then be presented in the forms

$$Q = d_1[B] + d_2[D] \quad (113)$$

$$R = b_0 + b_1[B] + b_2[D] \quad (114)$$

where $b_0 = k_1$; $b_1 = k_1K_B$; $b_2 = k_1k_D$; $d_1 = k_1K_BP_B$; $d_2 = k_1K_DP_D$.

Equation (112) can be converted into

$$T_2W^2 + T_1W + T_0 = 0 \quad (115)$$

where

$$T_0 = A_1 + A_2h$$

$$T_1 = A_3 + A_4h + A_7h^2$$

$$T_2 = A_5 + A_6h - h^2$$

From equation (115) we obtain two equivalent functions

$$W = [(T_1^2 - 4T_0T_2)^{1/2} - T_1]/(2T_2) \quad (116)$$

$$1/W = -[(T_1^2 - 4T_0T_2)^{1/2} + T_1]/(2T_0) \quad (117)$$

$1/W$ is always positive, because T_0 is always < 0.

The method proposed enables finding of all the equilibrium constants related to the extraction system. In particular, it is possible to determine the partition constants P_Y [equation (96)] of complexes of H_2LY type between the organic and aqueous phases. This possibility is not offered by the method presented by Kuz'min *et al.*[29] Moreover, that method needs use of several other (pH-metric, spectrophotometric, titrimetric) techniques. As a result, only the fraction $P'_B = [H_2LB]_{org}/[H_2L]$, corresponding to incomplete reaction, was obtained there. The P'_B value thus obtained depends on the concentration of B^- ions, according to the formula $P'_B = K_B P_B[B]$ [see equations (95) and (96)].

The solubility of the neutral form (HL) of the weak acids discussed above is rather low. Higher concentrations of HL in such titrand + titrant systems are ensured by dissolution of the corresponding organic acid in an organic phase. If the concentrations of HL in the titrant and in the organic phase are identical and equal to c_L, then the sum $c_L V + c_L W_{org} = c_L W + c_L(W_{org} - V_0)$, expressing the total content (in mmole) of L in the system, will be equal to $c_L W$ for $W_{org} = V_0$ [compare with equation (98)].

To avoid any volume changes resulting from mutual solubility of the organic phase and electrolyte solution, the phases should be mutually saturated before addition of HL in preparation of the titrand and titrant. The titrand, titrant and their mixtures (at any stage of titration) should all be at the same temperature.

FURTHER DETAILS

Definitions of free acid and free base

The free acid can be defined as the concentration of hydrogen ions resulting from the presence of a strong acid HB and a weak acid, base or salt in the sample. The free base can be defined as the proton deficiency resulting from the presence of a strong base MOH.[9]

As examples, let us consider any titrand + titrant system, *e.g.*, system 3 in Table 1, with (*a*) $M_mH_{n-m}L$ (concentration C_L) + HB (concentration C_a), and (*b*) $M_mH_{n-m}L(C_L)$ + MOH(C_b). The corresponding proton balances are

$$(a) \quad [H] - [OH] = d[(n - \bar{n} - m)C_L + C_a] - b_M/V_0 + b_M/W \quad (118)$$

$$(b) \quad [H] - [OH] = d[(n - \bar{n} - m)C_L - C_b] - b_M/V_0 + b_M/W \quad (119)$$

The proton balances relating to the systems containing two-component mixtures: (*c*) $M_mH_{n-m}L$ $[C_L(1)] + M_{m-1}H_{n-m+1}L$ $[C_L(2)]$ and (*d*) $M_mH_{n-m}L$ $[C_L(1)] + M_{m+1}H_{n-m-1}L$ $[C_L(3)]$ are

$$(c) \quad [H] - [OH] = d[(n - \bar{n} - m)C_L(1) + (n - \bar{n} - m + 1)C_L(2)] - b_M/V_0 + b_M/W \quad (120)$$

$$(d) \quad [H] - [OH] = d[(n - \bar{n} - m)C_L(1) + (n - \bar{n} - m - 1)C_L(3)] - b_M/V_0 + b_M/W \quad (121)$$

From comparison of equations (118) with (120), and of (119) with (121) we have

$$C_a = C_L(2) \quad \text{when } C_L(1) + C_L(2) = C_L$$

$$C_b = C_L(3) \quad \text{when } C_L(1) + C_L(3) = C_L$$

respectively. Thus a system composed of $M_mH_{n-m}L$ ($m \leqslant n - 1$) and MOH as contamination ($C_b < C_L$) is equivalent to the mixture composed of $M_mH_{n-m}L$ and $M_{m+1}H_{n-m-1}L$.

Contamination with carbon dioxide

Solutions stored in badly sealed flasks, or exposed to the atmosphere, will contain some carbon dioxide.[31,32] The presence of this species can be taken into account in the corresponding regression equations presented in the sections on proton balances and their transformations.

Standardization

The method has already been applied for standardization of sodium hydroxide solution against commercial potassium hydrogen phthalate.[9]

Optimization procedure

Determination of the internal parameters of the non-linear regression equations is based on multiparametric curve-fitting. The degree of approximation of the Padé W function to the

titration data (V_j, pH_j) can be expressed as the sum of the squares of the residuals

$$SS = \sum_{j=1}^{N} (W_j - W_{j,calc})^2 = \sum_{j=1}^{N} (V_j - V_{j,calc})^2 \quad (122)$$

where $W_{j,calc}$ is the W-value calculated from the corresponding regression equation at pH_j, and $V_{j,calc} = W_{j,calc} - V_0$ [see equation (13)].

If the Padé $1/W$ function is used, the criterion of fit will be

$$SS1 = V_0^4 \sum_{j=1}^{N} (1/W_j - 1/W_{j,calc})^2 \quad (123)$$

The aim is to find the set of internal parameters corresponding to minimal values of SS or SS1. The factor V_0^4 in equation (123) makes these minimal values comparable in magnitude.

The optimized values of the internal parameters are sometimes the basis for further calculations, *e.g.*, in the determination of equilibrium constants in extraction systems. From the algorithms presented in that section, the following search procedure may be used for determining the equilibrium constants.

(1) Determination of parameters $(x_1, x_2, x_3) = (x_{1i}, x_{2i}, x_{3i})$ for the i-th ratio $n_D^{(i)}/n_B^{(i)}$ at constant $n_B^{(i)} + n_B^{(i)}$; $i = 1, \ldots, T$; $T \geqslant 4$, according to the curve-fitting method applied. The (x_{1i}, x_{2i}, x_{3i}) values are the basis for calculation of $(P, Q, R) = (P_i, Q_i, R_i)$, from $P = x_2/x_1$; $Q = x_3/x_1$; $R = 1/x_1$.

(2) d_1 and d_2 in equation (113) (at $T-2$ degrees of freedom) and b_0, b_1 and b_2 in equation (114) (at $T-3$ degrees of freedom) can be evaluated according to the least-squares method and then k_1, K_B, K_D, P_B and P_D are calculated [see definitions after equation (114)].

(3) The parameters $P_{HL}[=x_2/(x_1 W_{org})]$, C_L, C_a and f can be found from the results of one titration, at a given value of the fraction $n_D^{(i)}/n_B^{(i)}$. The C_a value can be treated as resulting from contamination of HL by a strong acid HB. If HL is contaminated with a strong base, MOH (C_b), then C_a is negative and $C_b = -C_a$.

Note that the equilibrium constants of complexes of ML type, predominating in alkaline media, can be found from titrations performed in isomolar systems containing two different non-hydrolysable salts, MB and M′B.

Acknowledgement—The investigations were supported financially within the scope of problem CPBP No. 10.17.

REFERENCES

1. T. Anfält and D. Jagner, *Anal. Chim. Acta.* 1971, **57,** 165.
2. T. Michałowski, *Zesz. Nauk. Univ. Jagiellon., Pr. Chem.*, 1989, **32,** 15.
3. N. Damien and P. Cauchetier, *Anal. Chim. Acta*, 1968, **41,** 483.
4. E. H. R. von Barsewisch and R. A. Hasty, *Report MINTEK*, 1985.
5. T. Michałowski, *Chem. Anal. (Warsaw)*, 1990, **35,** 375.
6. V. I. Gordienko and V. I. Sidorenko, *Zh. Anal. Khim.*, 1982, **37,** 216, 1715.
7. T. Michałowski, *Euroanalysis V*, Cracow, 1984, Abstracts, p. 498.
8. T. Michałowski, A. Rokosz and A. Tomsia, *Analyst*, 1987, **112,** 1739.
9. T. Michałowski, *ibid.*, 1988, **113,** 833.
10. T. Michałowski, A. Rokosz and E. Negrusz-Szczęsna, *ibid.*, 1988, **113,** 969.
11. T. Michałowski, A. Rokosz, P. Kościelniak, J. M. Łagan and J. Mrozek, *ibid.*, 1989, **114,** 1689.
12. B. E. Conway, *Electrochemical Data*, pp. 46–47. Elsevier, Amsterdam, 1952.
13. D. M. Barry and L. Meites, *Anal. Chim. Acta*, 1974, **68,** 435.
14. D. M. Barry, L. Meites and B. Campbell, *ibid.*, 1974, **69,** 143.
15. T. Meites and L. Meites, *Talanta*, 1972, **19,** 1131.
16. T. N. Briggs and J. E. Stuehr, *Anal. Chem.*, 1974, **46,** 1517.
17. B. M. Maryanov, *Zh. Analit. Khim.*, 1979, **34,** 655.
18. A. Johansson and S. Johansson, *Analyst*, 1979, **104,** 601.
19. W. E. Gordon, *J. Phys. Chem.*, 1979, **83,** 1365.
20. *Idem, Anal. Chem.*, 1982, **54,** 1595.
21. F. Jones and M. Ross, *CERN Program Library*, D 506, Kraków, 1984.
22. J. Inczédy, *Analytical Applications of Complex Equilibria*, Horwood, Chichester, 1976.
23. L. G. Sillén and A. E. Martell, *Stability Constants of Metal-Ion Complexes*, The Chemical Society, London, 1964; Suppl. No. 1, 1971.
24. G. A. Baker, Jr. and J. L. Gammel, *The Padé Approximant in Theoretical Physics*, Academic Press, New York, 1970.
25. H. S. Simms, *J. Am. Chem. Soc.*, 1926, **48,** 1239.
26. J. Klas, *Anal. Chim. Acta*, 1968, **41,** 549.
27. L. Pehrsson, F. Ingman and S. Johansson, *Talanta*, 1976, **23,** 781.
28. S. Johansson, *Analyst*, 1979, **104,** 593.
29. N. N. Kuz'min, L. S. Khorkina, A. I. Lebedev and Yu. A. Zolotov, *Zh. Analit. Khim.*, 1979 **25,** 1257.
30. J. Starý and Yu. A. Zolotov, *Critical Evaluation of Equilibrium Constants Involving 8-Hydroxyquinoline and Its Metal Chelates*, Pergamon Press, Oxford, 1979.
31. M. Wozniak and G. Nowogrocki, *Talanta*, 1979, **26,** 581.
32. T. Michałowski, *J. Chem. Educ.*, 1988, **65,** 181.

Talanta, Vol. 39, No. 9, pp. 1139–1147, 1992
Printed in Great Britain.

0039-9140/92 $5.00 + 0.00

FACTORS INFLUENCING PERFORMANCE IN THE RAPID SEPARATION OF AFLATOXINS BY MICELLAR ELECTROKINETIC CAPILLARY CHROMATOGRAPHY

RODERIC O. COLE, RICKY D. HOLLAND and MICHAEL J. SEPANIAK*
Department of Chemistry, The University of Tennessee, Knoxville, TN 37996-1600, U.S.A.

(*Received* 23 *January* 1992. *Accepted* 28 *January* 1992)

Summary—Micellar electrokinetic capillary chromatography (MECC) is applied to the high-speed analysis of aflatoxins. Baseline separation of the four common aflatoxins G_1, G_2, B_1 and B_2, is accomplished in less than 30 sec. Small (25 μm) internal diameter capillaries are found to be critical in maintaining high efficiency under rapid MECC separation conditions. Van Deemter-like plots are generated in order to study the effects of capillary diameter and organic solvent on efficiency under high electric field conditions. Other experimental parameters affecting efficiency are investigated, including buffer concentration, surfactant concentration, and detector time constant. Simple on-column laser-based fluorescence detection, employing helium-cadmium laser radiation at 325 nm for excitation, allows for limits of detection in the range of 0.05–0.9 femtomoles injected for underivatized aflatoxins. Considerations important in the analysis of aflatoxins in real matrices are presented.

It is well established that capillary electrokinetic separation techniques such as capillary zone electrophoresis (CZE) and micellar electrokinetic capillary chromatography (MECC) are capable of highly efficient separations of minute amounts of many classes of compounds.[1-3] The MECC technique addresses the separation of neutral molecules and offers additional selectivity, relative to CZE, for charged analytes via analyte-specific interactions with the micellar phase. In principle, experimental conditions can be adjusted to facilitate rapid capillary electrokinetic separations. In a unique recent report, extremely rapid (2 second) separations of fluorescently derivatized amino acids were demonstrated.[4,5] Very small capillary columns (*ca.* 10 μm i.d.) and a unique photoinjection system were employed. This system, while permitting rapid separations, is thus far limited to molecules labeled with fluorescein isothiocyanate (FITC). Rapid (<one minute) separations are demonstrated herein using capillary electrokinetic methods with conventional injection and detection instrumentation.

Rapid separations are particularly desirable in situations where large numbers of samples are to be analyzed. As applications for MECC and CZE increase, analyses requiring high sample throughput are inevitable. Rapid separations require top performance from the chromatographic system employed. Conventional HPLC approaches generally employ short (~3 cm) columns packed with small (~3 μm) particles. The combination of high flow-rate and short column provides for short elution times, while the small particle diameters provide relatively efficient mass transfer, even for moderately high flow-rates. Adversely, extremely high flow-rates can degrade efficiency resulting in loss of resolution and, due to the use of very small column packing material, produce very high column pressure drops that often result in settling of the packing bed.

In situations where highly efficient liquid phase separations of neutral molecules are required, MECC can be very effective.[6,7] Unlike hydrostatically-pumped open tubular systems, MECC is not limited by mobile phase resistance to mass transfer.[8] High efficiency in the former separation technique is only achieved if solutes rapidly diffuse radially across the parabolic flow profile of the mobile phase, thereby averaging the velocity differences encountered. The large flow-rates needed for rapid separations exacerbate the mass transfer problem. Electroosmotic pumping produces a relatively flat ("plug-like") flow profile,[8] minimizing the need for rapid radial diffusion in CZE and MECC. Moreover, the micelles in MECC are somewhat analogous to conventional packed column particles. The

*Author for correspondence.

small size of micelles (~40 Å in diameter for sodium dodecyl sulfate) and close, uniform (electrostatic) packing produces an ideal packing bed and further contributes to the high separation performance of MECC. MECC has been used to separate a variety of compounds including vitamins,[9] amino acids,[10] polyaromatic hydrocarbons,[11] and pharmaceutical compounds.[12-16]

One potentially important application of high speed separations is the analysis of mycotoxins, particularly aflatoxins. Aflatoxins are extremely toxic metabolites of fungi such as *Aspergillus Flavus*. These fungi occur in a variety of foodstuffs intended for both livestock and human consumption. Peanuts, corn, grain, rice, soybeans, and oats have all been found to support aflatoxin production.[17] Aflatoxins pose significant health risk even at low concentrations (ppb) and are generally found to target the liver.[18] Thus, analyses of aflatoxins are of utmost importance in assuring safe food supplies, but are challenging due to the presence of the toxins at trace levels in complex matrices. Moreover, the nonuniform distribution of aflatoxin in contaminated unprocessed commodities can result in a need for very high sample throughput (see ref. 17, p. 104). Conventional methods for aflatoxin analysis are numerous and include thin layer chromatography, HPLC, and immunochemical methods.[19]

The focus of the work reported herein is the optimization of rapid, sensitive separations in MECC as applied to aflatoxin separations. Experimental factors which maximize efficiency and minimize analysis time are investigated. Under the constraint of rapid separation, new experimental considerations for attaining high efficiency are revealed. Laser-based fluorescence detection is employed and exhibits injected concentration detection limits in the 20–100 ppb range. Illustrations involving the analysis of aflatoxins in corn samples are presented.

EXPERIMENTAL

Apparatus

Two laser-based fluorescence detection schemes were employed in this work. The instrumentation used for studies of analysis speed and efficiency has been recently described in detail,[20] and employs a monochromator/filter combination to isolate the desired emission wavelength (450 nm, FWHM = 6 nm). An alternate system was used for the determination of detection limits in an attempt to collect a wider portion of the emission spectrum and to increase transmission of signal to the photomultiplier tube. This was particularly important in this work due to the poor condition of the laser that was employed (see below). Fluorescence emission was collected at 90° with an f/2 lens and focused onto a 2-mm slit, placed in the center of a light-tight 2 inch cube that contained inlet and outlet apertures. The desired wavelength range was isolated with a bandpass filter (452 nm, FWHM = 20 nm) that is placed in the inlet aperture of the spatial filter cube (Oriel Corp., Stratford, CT, U.S.A.). Fluorescence excitation was provided by a helium–cadmium laser (Liconix Model 4230 NB, Sunnyvale, CA, U.S.A.) at 325 nm. Laser power ranged from 3–5 mW. Chromatograms were recorded with Varian Models 4270 and 4400 integrators (Palo Alto, CA, U.S.A.). Capillaries of 50 and 25 μm internal diameter (i.d.) were purchased from Polymicro Technologies (Phoenix, AZ, U.S.A.). Fluorescence spectra were obtained with a Spectrovision DA-10 spectrofluorimeter. Specific spectral acquisition conditions are given where appropriate.

Chemicals

Aflatoxin standards, sodium dodecyl sulfate (SDS), and Bile Salts were purchased from Sigma Chemical Co. (St. Louis, MO, U.S.A.). All water and solvents used were of HPLC grade and were obtained from Baxter Healthcare Corp. (Stone Mountain, GA, U.S.A.). *Aspergillus Favus* spores were obtained from Northern Regional Research Laboratories (Peoria, IL, U.S.A.). Corn meal was obtained from a middle Indiana dairy farm.

Procedures

Chromatography. Capillary columns were rinsed with 0.01*M* sodium hydroxide for approximately 10 min before filling with mobile phase. The system was allowed to equilibrate for 10–15 min using an applied voltage of 20 kV prior to injection of sample. Applied voltages during chromatographic runs ranged from 8 to 36 kV. Efficiency studies were performed using hydrostatic injection, 7 seconds at a height differential of 10 cm. Chromatograms for standard solutions and corn meal extracts were obtained using electroinjection, 2 kV for 30 sec. Capillaries used in the work were 40 cm in length, and 35 cm to detection window, unless otherwise noted.

Efficiency calculations. Plate numbers were calculated by using the relationship

$$N = 2\pi\left(\frac{t_R h}{A}\right)^2$$

where N is number of theoretical plates, h is peak height counts, A is peak area counts and t_R is retention time.[7] It is essential to note that for some integrators area and height count response factors may not be equivalent and appropriate conversion factors need to be included in the equation. Plate height, H, is calculated as the capillary length to the detection zone divided by N.

Sample preparation. Standards were prepared by adding one milliliter of HPLC grade acetonitrile to one milligram solid aflatoxin and making appropriate dilutions with mobile phase. Stock acetonitrile solutions were stored in the dark at approximately 0°. Corn inoculated with *Aspergillus Flavus* spores were extracted with two 100-ml portions of chloroform as previously described,[21] with the exception that the dry residue was dissolved in HPLC grade acetonitrile. Further clean-up of this solution was provided by the solid phase extraction (SPE) procedure described below.

Corn meal samples (approximately 50 g) were extracted with 100 ml of an 80/20 (v/v) methanol/water solution. One ml of this solution was diluted to 5.0 ml with 0.5% (v/v) aqueous acetic acid and subjected to the following SPE sample clean-up procedures: 3.0-ml SPE tubes containing 40 μm of LC-CN (Supelco, Bellefonte, PA) bonded phase were preconditioned with 2.0 ml 0.5% (v/v) aqueous acetic acid followed by a one-minute drying time with air passing through the tube via aspiration. The 5.0 ml of diluted extracted sample was placed on the column. The sample was washed by passing 0.5 ml of 20% (v/v) tetrahydrofuran in 0.5% (v/v) aqueous acetic acid followed by 2.0 ml of HPLC grade hexane. After a drying period of 2 min, the SPE tube was washed with 3.0 ml of 25% (v/v) tetrahydrofuran in hexane followed by a one-minute wash. The aflatoxins were eluted from the SPE tube with two 2.0-ml portions of CH_2Cl_2/tetrahydrofuran (99:1). The elution solvent was evaporated and the remaining residue dissolved in 200 μL acetonitrile. 50 μL of this solution was diluted with 200 μL mobile phase prior to injection. Further details concerning this SPE procedure can be found in product literature available from Supelco.

Safety precautions

The extremely toxic nature of aflatoxin demands the utmost in attention to safety precautions. Gloves were worn at all times when preparing or handling solutions. Standards were dissolved in an appropriate solvent and transferred via syringe. All working areas and equipment were wiped down with a 5% solution of NaOCl (bleach) to form considerably less toxic derivatives, and all waste solutions were made approximately 5% in NaOCl.

RESULTS AND DISCUSSION

Optimization of analysis time and efficiency

Several experimental parameters influence efficiency and analysis time in MECC. Most directly, the voltage applied across the capillary is the primary factor in determining the velocity of the mobile phase and, consequently, separation time. Figure 1 illustrates the inverse relationship between capillary void time, t_0, (*i.e.*, length of capillary to the detection zone divided by electroosmotic flow velocity), and the elution time of aflatoxin B_1, (*i.e.*, total aflatoxin separation time) on applied field. When this data is used to plot applied voltage versus flow-rate, positive deviations from the normal linear relationship are observed at high fields. This is not surprising, because decreases in mobile phase viscosity (hence increases in electrophoretic mobilities) are expected at large applied voltages, as

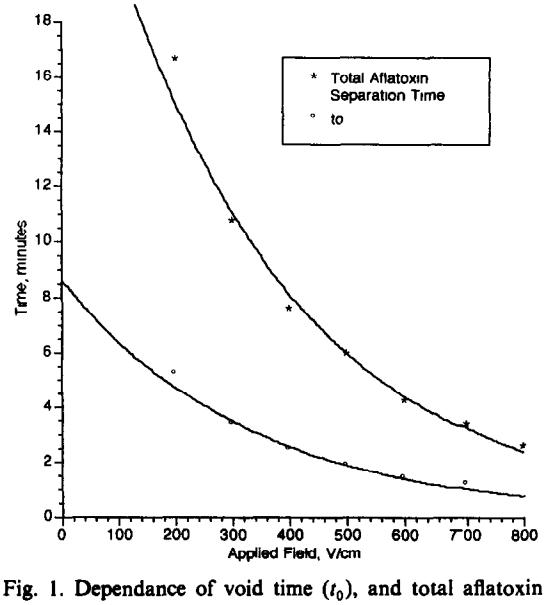

Fig. 1. Dependance of void time (t_0), and total aflatoxin separation time on applied field. Mobile phase composition: 0.05*M* SDS, 0.01*M* Na_2HPO_4, 0.006*M* $Na_2B_4O_7$. t_0 marked by methanol system peak.

the ability of the capillary to dissipate Joule heat is exceeded and its temperature increases.[1] However, the practical ramifications of this behavior in rapid MECC separations are interesting. In our laboratory, we have often observed that several minutes into separations performed at the highest fields expressed in Fig. 1, the system breaks down due to degassing or boiling of the mobile phase. The rapid separations of aflatoxins shown later in this work occur before the onset of this problem and, in fact, analysis times are even shorter than predicted based on extrapolations from low field separations. Presumably in the most common CZE/MECC arrangement (capillary in air), several minutes may be required to reach complete thermal equilibrium, following the initial application of voltage. It is possible that the temperature of the mobile phase increases during the course of the rapid separations presented herein. Thus, thermostated CZE/MECC systems and measures to correct for temperature related changes in retention time,[22] may be especially important in obtaining reproducible rapid separations with these techniques.

Efficiency in MECC is also dependant on mobile phase velocity, as well as factors such as buffer and surfactant concentration, column diameter, and detector time constant. An experimental parameter that is key to achieving rapid separations in MECC is the i.d. of the capillaries employed. The use of small diameter capillaries (i.d. <50 μm) permits the application of high field strengths while maintaining high efficiency. This is illustrated, along with the effects of other parameters, in Table 1. Note that the efficiency data in the table is reported in number of theoretical plates/minute to give a better idea of the temporal performance of the technique. Retention times for aflatoxin G_1 are less than 5 min. The "standard conditions" used in this work for the table were as follows: buffer composed of 0.01M Na_2HPO_4 and 0.006M $Na_2B_4O_7$, surfactant concentration of 0.05M SDS or sodium deoxycholate (NaDC), capillary 25 μm i.d. by 50 cm long (40 cm to detection zone), field strength of 600 V/cm, and a detector time constant that was limited by the 60 Hz acquisition rate of the integrator employed. Narrowbore capillaries effectively dissipate heat, resulting in less distortion of the flat flow profile and better efficiency (see below). In our studies, the use of 50 μm i.d. capillaries limited maximum applied fields to roughly 300–400 V/cm due to higher conductivity and poorer heat dissipation than the 25-μm i.d. capillaries. Application of fields exceeding this value to capillaries with i.d. ≥ 50 μm generally resulted in degradation of efficiency or complete breakdown of the system.

Figure 2 contains plots of applied field *vs.* efficiency (plate height) using both 50- and 25-μm i.d. capillaries. The plots are computer generated best fits to data obtained from single injections of aflatoxin G_1. Van Deemter-like plots such as these can be helpful in studying band broadening mechanisms in MECC.[6] At lower fields, efficiency is degraded due to the onset of problems with longitudinal diffusion. Long capillary residence times provide the solute bands with significant opportunity to disperse along the axis of the capillary due to molecular diffusion. As field strength is increased, residence time in the capillary decreases, and an optimum value of field strength is observed (see Fig. 2). Efficiency begins to degrade at higher fields due to increased resistance to mass transfer[6] and, more importantly, increased thermal load. This not only produces a general increase in temperature as discussed above, but can also result in radial temperature gradients in the capillary. The temperature gradient can cause band dispersion due to a distortion of the flat flow profile of electroosmotic flow.[23] Radial variances in phase ratio, due to the temperature dependence of critical micelle concentration (CMC), and partition coefficient can also lead to band dispersion. Since

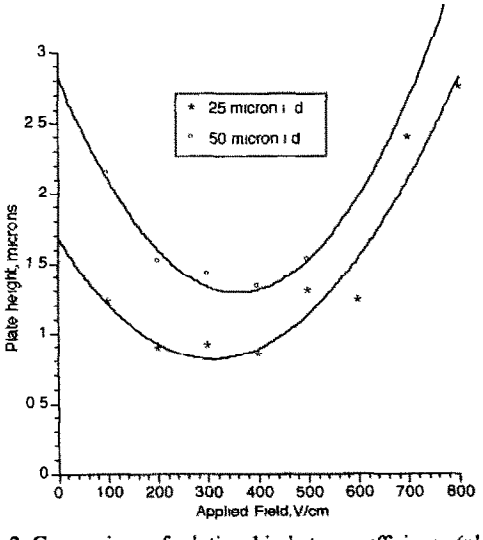

Fig. 2. Comparison of relationship between efficiency (plate height) and applied field for 50 and 25 μm i.d. capillaries. Mobile phase composition: 0.05M SDS, 0.01M Na_2HPO_4, 0.006M $Na_2B_4O_7$. Data for aflatoxin G_1.

temperatures may be changing rapidly during the early stages of electrophoretic runs (see discussion above), these problems may be more severe for rapid separations. Use of smaller diameter capillaries allows greater potentials to be applied without critical losses in efficiency. As illustrated in Fig. 2, the optimized plate height is significantly lower and the working range of applied field is much wider for the 25-μm i.d. capillary. The optimum value of applied field is roughly the same for the two capillaries. However, since different silica surface composition and different thermal properties may be involved, it should not be inferred that the two capillaries have similar optimums in terms of linear flow velocities. The use of smaller i.d. capillaries is clearly very important when performing high-speed MECC separations.

Further evidence of the importance of Joule heating as a source of band dispersion is given by the buffer concentration data in Table 1. At higher salt concentrations, current passing through the capillary is greater, and the resulting large thermal load results in band dispersion. Dramatic losses in efficiency are observed for both surfactant systems when the buffer concentration is increased above the standard conditions case. Working at a relatively low buffer concentration is thus essential for maximizing efficiency.

Surfactant concentration is perhaps the most fundamental adjustable mobile phase parameter in MECC. The working range of surfactant concentration in MECC is bounded at the lower end by the surfactant CMC and at the upper end by the creation of the thermal problems cited above. At the low end of this concentration range micelle-monomer exchange kinetics are such that the adverse effects of micelle polydispersity are generally observed.[3,6,7] Increasing the surfactant concentration counteracts this effect and efficiency improves as indicated in the table.[24] Reducing the standard conditions surfactant concentration by half reduces the efficiency with NaDC by nearly 70%, while SDS shows a 20% reduction. The difference in the magnitude of the reduction of efficiency between the two surfactants may be attributed to the fact that the bile salt has a higher CMC than the SDS. In all of our work, efficiency in MECC degrades dramatically when the surfactant concentration is reduced to values near the CMC.

Efficiency may also be affected by injection and detection conditions and instrumentation.[7,25] Efficient, rapid separations necessarily have very small temporal peak variances that require rapid data acquisition and fast detector time constants. Table 1 also shows the effect of time constant on efficiency for aflatoxin G_1. As a consequence of the short time constants that are needed to maintain efficiency in high-speed MECC, baseline noise and limits of detection are increased. Trade-offs between efficiency and detection time constant, as well as injection plug length, must thus be reached.

Retention control also plays an important role in achieving high-speed separations. Optimizing capacity factors in terms of resolution and analysis time can be critical. Poorly retained solutes elute quickly but may not be well-separated and strongly retained solutes tend to coelute at the micelle migration time. The optimum capacity factor, k', in MECC falls in the range of 1–5.[2] In our laboratory, two approaches are commonly used to control and optimize separations. First, organic modifiers

Table 1. Factors influencing efficiency in rapid MECC separations

Experimental parameter	*Sodium Deoxycholate (NaDC)* Plates/min*	*Sodium Dodecyl Sulfate SDS* Plates/min*
Standard conditions†	129,000	104,000
Column diameter‡		
50 μm	16,000	16,000
Buffer concentration		
0.005M Na_2HPO_4 0.003 M $Na_2B_4O_7$	202,000	154,000
0.02M Na_2HPO_4 0.012 M $Na_2B_4O_7$	81,000	67,000
Surfactant concentration		
0.025M	49,000	83,000
Detector time constant		
0.1 second	110,000	99,000

*All data for Aflatoxin G_1.

†Standard conditions: applied field 600 V/cm, detector time constant in "out" position, integrator data acquisition rate 60 Hz, 0.05M surfactant, 0.01M Na_2HPO_4, 0.006M $Na_2B_4O_7$, column: 25 μm i.d. × 50 cm total length, 40 cm to detector window.

‡Applied field 300 V/cm.

such as methanol, acetonitrile, and 2-propanol are added to the mobile phase. These solvents have the effects of decreasing mobile phase polarity and extending the elution range.[6,26,27] In some cases, k' is reduced to more optimal values. In addition to reducing mobile phase polarity, organic solvents generally reduce conductivity, which can improve efficiency at high fields.[26,27] Figure 3 contains plots of applied field *vs.* plate height for SDS mobile phases containing 0 and 10% (v/v) acetonitrile. The minimum values of plate height are approximately equal, but plate height does not increase at high fields as sharply for the mixed aqueous–organic mobile phase. Under these conditions, a wider range of (higher) fields can be applied without significant loss of efficiency. This effect is the result of a decrease in dielectric constant of the mobile phase upon addition of the acetonitrile to the mobile phase, which reduces the conductivity of the mobile phase and, hence, the current that is passed at a given voltage. Decreases in mobile phase polarity with the addition of organic solvents generally reduce k' values, causing solutes to spend more time in the faster moving mobile phase. While reduction of electroosmotic flow and a concomitant extension of elution range is often observed upon addition of organic solvent to the mobile phase, the reduction of solute k' often dominates and solutes elute more quickly.[28] However, it should be noted that, depending on the nature and concentration of the organic solvent, electroosmotic flow may be reduced to a point where analysis time is increased, sometimes dramatically.[26]

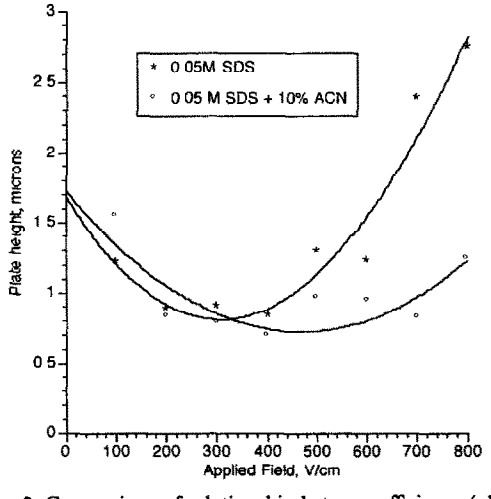

Fig. 3. Comparison of relationship between efficiency (plate height) and applied field for 25 μm i.d. capillary using mobile phases containing 0% and 10% acetonitrile. Other conditions as in Fig. 2.

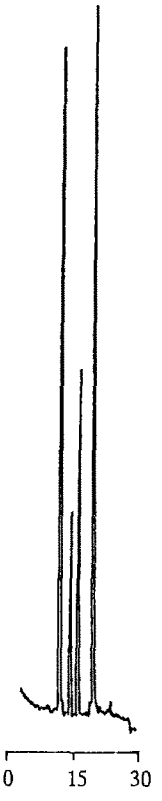

Fig. 4. High-speed separation of aflatoxin standards. Mobile phase composition: 0.05*M* NaDC, 0.01*M* Na_2HPO_4, 0.006*M* $Na_2B_4O_7$, 5% Acetonitrile. Applied voltage 36 kV. Elution order is G_2, G_1, B_2, B_1.

The second approach to control capacity involves the use of bile salt surfactants.[11,24] These naturally-occurring surfactants are based on a hydroxy-substituted steroidal backbone and are more polar in nature than the conventional *n*-alkyl variety.[11,24] Hence, they retain moderately to highly hydrophobic solutes less (k' values are generally closer to the optimum range). They have found use in MECC for chiral separations,[14,16,24,29,30] and for the separation of hydrophobic molecules.[11,31] Figure 4 shows the separation of the four common aflatoxins with a bile salt micellar phase, using conditions that have been optimized in terms of overall resolution and analysis time.

Detection

The very small i.d. capillaries that are essential for rapid MECC separations exacerbate problems with attaining adequate detection sensitivity. In order to preserve the integrity of the narrow solute bands, on-column detection is generally employed. Absorbance detection is

Table 2. Fluorescence properties for aflatoxins in various solvents

	Fluorescence emission maximum (nm)*				Relative intensity at λ_{max}†			
Solvent	G_2	G_1	B_2	B_1	G_2	G_1	B_2	B_1
EtOH	445	448	433	429	68.6	100	6.03	91.4
Water	463	452	440	441	77.4	31.5	100	57.1
SDS‡	456	454	440	434	100	52.9	69.8	76.2
NaDC‡	460	452	438	437	89.2	46.9	88.6	100

*Wavelength data acquired at 10 nm/min, 1 sec time constant.
†Intensity data acquired at 50 nm/min, 2 sec time constant.
‡Surfactant concentrations 0.05*M* in water.

limited in small i.d. capillaries due to very short optical pathlengths, low throughput, and large levels of stray light.[32] Laser-based fluorescence detection schemes offer high sensitivity as well as compatibility with capillaries of diminutive dimensions.[3,9,20,33] Aflatoxins readily absorb the 325-nm output of helium–cadmium lasers and exhibit native fluorescence, allowing sensitive laser-based detection to be employed.[34] Fluorescence detection in MECC can be influenced by the type of pseudostationary phase employed, since emission wavelengths and intensities are often affected.[28] Association of solute with micelles often enhances fluorescence emission.[35] The spectroscopic behavior of the aflatoxins in different solvents or micelle solutions is shown in Table 2. This data illustrates the importance of considering both the spectroscopic characteristics and the chromatographic properties of the micellar phase in MECC. The varied spectroscopic nature of each individual aflatoxin indicates that multichannel detection might be advantageous, both in terms of identification and increased sensitivity.[33]

The absence of inner filter related curvature of calibration plots for laser fluorometric detection in narrow-bore capillaries is well established.[28] Thus, linearity was not evaluated in this work. However, short response plots were constructed from single injections of three standard solutions that all yielded S/N (peak height/baseline noise) of less than 25. Extrapolation of the plots to a S/N of 3 yielded the limits of detection (LODs) shown in Table 3. The electroinjection procedure used to obtain this data (see Experimental section) resulted in an injection volume of approximately 2 nl. An internal standard was added to correct for variations in detector response. While these concentration LODs are not as low as previous reports,[34] the weakly fluorescent G_1 and B_1 were quantitated without prior conversion to more fluorescent derivatives. The use of chemical derivitization techniques can result in the formation of highly fluorescent derivatives, leading to improved limits of detection.[36] Moreover, the laser used in this work, due to an ageing plasma tube, suffered from low output power and sporadic changes in both power and mode structure. Relatively large amounts of baseline drift and noise were observed, adversely affecting detectability and reproducibility.

In general, optical detection in capillary separations exhibits somewhat higher concentration LODs than when applied to conventional analytical scale separation techniques. Conversely, because of the very small volumes involved with capillary separations, absolute LODs can be extremely low and far superior. Although sophisticated signal acquisition and processing was required, recent reports of "zeptomole" absolute LODs for laser fluorometric detection in CZE illustrate this capability.[37,38]

Analysis of corn samples

Aflatoxins are sometimes present in foodstuffs at ppb levels, requiring extraction and concentration. Figure 5(a) shows the chromatogram resulting from the solid-phase extraction of an Indiana corn meal sample that was spiked at the 16 ppm (w/w) level. Since ultimate speed was not sought in this separation, a SDS micelle system was used. No detectable levels of aflatoxins were found in the unspiked sample. Based on the procedure used and the S/N of the spiked sample, the LOD in the corn meal is estimated to be about one ppm. However, it is

Table 3. Limits of detection for aflatoxins in MECC*

Aflatoxin	Injected concentration, *M*	Amount injected, femtomoles
G_2	2.85×10^{-8}	0.06
G_1	4.36×10^{-7}	0.9
B_2	2.64×10^{-8}	0.05
B_1	1.26×10^{-7}	0.2

*Limits of Detection based on S/N = 3; SDS mobile phase used.

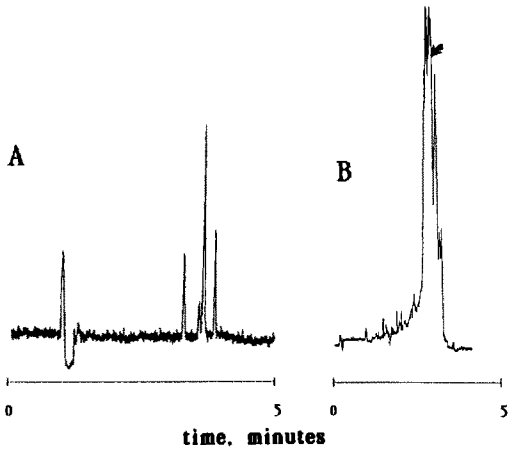

Fig. 5. Chromatograms of spiked (16 ppm w/w) corn meal extract (A) and artificially innoculated corn extract (B). Mobile phase composition: 0.05*M* SDS, 0.01*M* Na_2HPO_4, 0.006*M* $Na_2B_4O_7$, 10% v/v Acetonitrile. Applied voltage 20 kV. Arrow denotes expected retention of B_1.

expected that the LOD could be lowered by orders of magnitude via simple modifications of the sample work-up procedure. For example, only 1% of the initial extract was subjected to the SPE procedure and the sample was ultimately taken-up in 200 μl of solvent, while multiple injections from solutions with volumes of less than 10 μl can be routinely accomplished with this technique.

Considering the cooler climate from which it was obtained, it was not expected that the corn meal would contain aflatoxins. Aflatoxin production is most favored under conditions of high humidity and temperature;[17,18] contamination is thus more of a problem in southern climates. To assure the presence of aflatoxins in a complex sample matrix, *Aspergillus Flavus* spores were introduced onto a sample of moist corn kernels and allowed to grow for two weeks at 28°. Figure 5(b) shows the chromatogram of an extract of this sample obtained as described previously. The more complex sample matrix clearly illustrates the need for thorough sample clean-up, as aflatoxin peaks (see arrow for approximate retention time of B_1) are not clearly resolved from extraneous fluorescent compounds in the sample. However, if a more selective detection scheme was employed, it might be possible to discern individual aflatoxin peaks in such a mixture. Possible detection schemes include multichannel or time resolved detection.[32,39] Although not pursued in this work, it should be possible to reoptimize the separation to accommodate the more complex sample. The use of longer capillaries to increase plate numbers and/or the incorporation of alcoholic solvents in the mobile phase to significantly increase the elution range could provide the necessary resolution (albeit at the expense of analysis time).

CONCLUSIONS

MECC offers a viable method of rapid aflatoxin analysis, and for other compounds requiring routine monitoring. Separation times in the order of tens of seconds are readily achieved if experimental parameters are optimized, and provide the opportunity for large sample throughput via the simultaneous work-up of numerous samples. Significant samples include foodstuff extracts and pharmaceutical formulations. In addition, separations involving enantiomers may well lend themselves to high-speed MECC separation using bile salt surfactant systems. Detection still remains a limiting factor in applications of rapid MECC and CZE methods, but improvements in laser sources and the development of sensitive alternate schemes will increase the applicability of these techniques.

Acknowledgements—This work was sponsored by The Division of Chemical Sciences, Office of Basic Energy Sciences, United States Department of Energy, under grant DE-FG05-86ER13613 with The University of Tennessee, Knoxville. The authors wish to thank Professor F. A. Draughon of the Food Science and Technology Department, The University of Tennessee, Knoxville, for providing the inoculated corn sample and helpful advice. We also wish to thank Supelco, Inc. for providing the SPE apparatus.

REFERENCES

1. J. W. Jorgenson and K. D. Lukacs, *Anal. Chem.*, 1981, **53**, 1298.
2. S. Terabe, K. Otsuka and T. Ando, *ibid.*, 1985, **57**, 834.
3. M. J. Sepaniak, A. C. Powell, D. F. Swaile and R. O. Cole, in *Handbook of Capillary Electrophoresis*, J. C. Colburn, P. D. Grossman (eds), Chap. 6., Academic Press, New York, 1992.
4. J. W. Jorgenson and M. M. Bushey, *Anal. Chem.*, 1990, **62**, 978.
5. J. W. Jorgenson and C. A. Monnig, *ibid.*, 1991, **63**, 802.
6. M. J. Sepaniak and R. O. Cole, *ibid.*, 1987, **59**, 472.
7. S. Terabe, K. Otsuka and T. Ando, *ibid.*, 1989, **61**, 251.
8. J. H. Knox and I. H. Grant, *Chromatographia*, 1987, **24**, 135.
9. D. E. Burton, M. J. Sepaniak and M. P. Maskarinec, *J. Chromatogr. Sci.*, 1986, **24**, 347.
10. S. Terabe, H. K. O. Ozaki and T. Ando, *J. Chromatogr.*, 1985, **332**, 211.
11. R. O. Cole, M. J. Sepaniak, W. L. Hinze, K. Oldiges and J. Gorse, *ibid.*, 1991, **557**, 113.

12. S. Fujiwara, S. Iwase and S. Honda, *ibid.*, 1988, **1988,** 133.
13. T. Nakagawa, Y. Oda, A. Shibukawa and H. Tanaka, *Chemical & Pharmaceutical Bulletin*, 1988, **36,** 1622.
14. H. Nishi, T. Fukuyama, M. Matsuo and S. Terabe, *J. Chromatogr.*, 1990, **515,** 233.
15. D. F. Swaile, D. E. Burton, A. T. Balchunas and M. J. Sepaniak, *J. Chromatogr. Sci.*, 1988, **26,** 406.
16. S. Terabe, H. Nishi, R. Fukuyama and M. Matsuo, *J. Microcol. Sep.*, 1989, **1,** 234.
17. J. E. Smith and M. O. Moss, *Mycotoxin Formation, Analysis, and Significance*, John Wiley and Sons, New York, 1985.
18. D. J. Smith, Thesis, The University of Tennessee, 1989.
19. D. M. Wilson, *Arch. Environ. Contam. Toxicol.*, 1989, **18,** 308.
20. D. F. Swaile and M. J. Sepaniak, *Anal. Chem.*, 1991, **63,** 179.
21. F. A. Draughon, M. E. Elahi and D. R. West, *J. Agric. Food Chem.*, 1983, **31,** 692.
22. T. T. Lee and E. S. Yeung, *Anal. Chem.*, 1992, **63,** 2842.
23. E. Grushka, R. M. McCormick and J. J. Kirkland, *ibid.*, **61,** 241.
24. R. O. Cole, M. J. Sepaniak and W. L. Hinze, *J. High Res. Chrom.*, 1990, **13,** 579.
25. D. E. Burton, M. J. Sepaniak and M. P. Maskarinec, *Chromatographia* 1986, **21,** 583.
26. A. T. Balchunas and M. J. Sepaniak, *J. Anal. Chem.*, 1987, **59,** 1466.
27. *Idem, ibid.*, 1988, **60,** 617.
28. A. T. Balchunas, D. F. Swaile, A. C. Powell and M. J. Sepaniak, *Sep. Sci. Technol.*, 1988, **23,** 1891.
29. S. Terabe, M. Shibata and Y. Miyashita, *J. Chromatogr.*, 1989, **480,** 403.
30. H. Nishi, T. Fukuyama, M. Matsuo and S. Terabe, *Anal. Chim. Acta*, 1990, **236,** 281.
31. *Idem, J. Chromatogr.*, 1990, **513,** 279.
32. M. J. Sepaniak, D. F. Swaile and A. C. Powell, *ibid.*, 1989, **480,** 185.
33. M. J. Sepaniak and D. F. Swaile, *J. Microcol. Sep.*, 1989, **1,** 155.
34. R. D. Zare and G. J. Diebold, *Science*, 1977, **196,** 1439.
35. L. J. Cline Love, J. G. Habarta and J. G. Dorsey, *Anal. Chem.*, 1984, **56,** 1132.
36. R. W. Beaver, *Arch. Environ. Contam. Toxicol.*, 1989, **18,** 315.
37. J. V. Sweedler, J. B. Shear, H. A. Fishman, R. N. Zare and R. H. Scheller, *Anal. Chem.*, 1991, **63,** 496.
38. H. Swerdlow, J. Zhang, D. Chen, H. R. Harke, R. Grey, S. Wu, N. J. Dovichi and C. Fuller, *Anal. Chem.*, 1991, **63,** 2835.
39. L. B. McGown and W. T. Cobb, *ibid.*, 1990, **62,** 186.

Talanta, Vol. 39, No. 9, pp. 1149–1154, 1992
Printed in Great Britain.

0039-9140/92 $5.00 + 0.00

ELECTROCHEMICAL REDUCTION OF NICERGOLINE AND ITS ANALYTICAL DETERMINATION IN DOSAGE FORMS

J. C. STURM

Instrumental Analysis Laboratory, Faculty of Chemical and Pharmaceutical Sciences, University of Chile, PO Box 233, Santiago, Chile

LUIS J. NUNEZ-VERGARA and J. A. SQUELLA

Pharmacology and Electrochemistry Laboratory, Faculty of Chemical and Pharmaceutical Sciences, University of Chile, PO Box 233, Santiago, Chile

(*Received* 20 *November* 1991. *Accepted* 25 *January* 1992)

Summary—Electrochemical reduction of nicergoline was studied at different pH and concentrations using differential pulse polarography and linear sweep voltammetry. Both techniques reveal that the reduction process occurs with strong adsorption of the product. Nicergoline is an excellent model for the previously developed theory related to the effects of strong adsorption of electroactive species in voltammetry. At concentrations below 0.1m*M*, the adsorption prepeak is linearly dependent on nicergoline concentration. This peak was used to develop a new differential pulse polarographic method for the determination of the drug in pharmaceutical dosage forms. The method is simple and not time-consuming because nitrogen purging of samples and previous separation of the excipients were not needed. A comparative UV spectrophotometric assay was applied. Recovery data and composite and uniformity content studies for both methods are reported.

Nicergoline[8β]-10-methoxy-1,6-dimethylergoline-8-methanol-5-bromo-3-pyridine carboxylate (ester) (Fig. 1), is a drug with vasoactive properties due to its alpha-adrenergic blocking activity, which causes peripheral and central vasodilation. In different tests, the drug has proved to have cerebral-anti-ischemic action, also exhibiting platelet antiaggregating and disaggregating actions.[1,2]

Several clinical studies[3,4] have demonstrated that nicergoline was effective in lowering total peripheral resistance and normalized blood pressure without producing reflex tachycardia and concluded that the drug was useful in the early phases of acute myocardial infarction, due to its lowering of myocardial oxygen consumption.

Biotransformation of nicergoline both in man and animals demonstrated extensive metabolism in all species tested, the main metabolites being 1,6-dimethyl-8β-hydroxymethyl-10-alpha-methoxyergoline and 8β-hydroxymethyl-10-alpha-methoxy-6-methylergoline, as well as their glucuronides, all of which were excreted by the kidneys.[5,6] Therefore, the most important routes of chemical transformation in man appear to be hydrolysis of the ester linkage and *N*-demethylation.

To our knowledge, no analytical assays for nicergoline have appeared in the literature. Electrochemical methods have become very competitive from the analytical point of view because of sophisticated developments in electronics, three-electrodes systems, pulse voltammetry, *etc.* Modern polarography and voltammetry show important advantages in pharmaceutical analyses. Several reviews and papers related to the electrochemical determination of drugs in pharmaceutical forms have been published recently.[7,8]

This paper reports the electrochemical behaviour of nicergoline and the development of a novel method to determine the drug in dosage forms (injectable and tablets). For comparative purposes, a UV spectrophotometric assay was also used.

EXPERIMENTAL

Reagents and materials

Drug. Nicergoline was obtained from Chile Laboratories, Santiago, Chile (100% chromatographically pure, 99.8% activity).

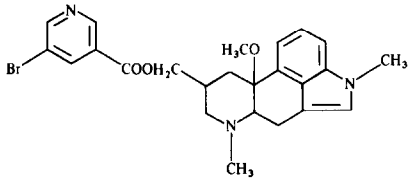

Fig. 1. Chemical structure of nicergoline.

Buffer solutions. To study the effect of pH on the electrochemical behaviour of the drug, 0.04*M* Britton Robinson buffer with a pH range between pH 2.0 and 9.0 was used. The ionic strength was kept constant at 0.3*M* with potassium chloride. For analytical determinations, 0.1*M* hydrochloric acid was selected as the supporting electrolyte. All other reagents were analytical grade.

Drug solutions. (a) Standard stock solutions were prepared by weighing Nicergoline and dissolving in 0.1*M* hydrochloric acid to obtain a concentration of $1 \times 10^{-3}M$. Solutions for the calibration curves were individually prepared by diluting the standard solution with 0.1*M* hydrochloric acid to obtain solutions which varied from 2×10^{-5} to $1 \times 10^{-4}M$. The narrow range is due to the adsorption nature of the polarographic peaks.

(b) Sample solutions. Samples were dissolved in 0.1*M* hydrochloric acid to give solutions about $8 \times 10^{-5}M$ nicergoline.

(c) Synthetic samples for recovery studies were prepared according to the manufacturer's batch formulas for 10 mg of nicergoline tablets. The solutions were directly assayed by polarography. However, for UV spectrophotometric determinations, they were previously filtered.

(d) Composite studies. Eleven tablets were finely ground and aliquots equivalent to a tablet average weight (0.1038 g) were dissolved and diluted to 250 ml with 0.1*M* hydrochloric acid to obtain final concentrations about $8 \times 10^{-5}M$. For the spectrophotometric studies, the above solutions were filtered.

Apparatus

Differential pulse polarography (DPP) was performed with a PARC 174 A polarographic analyzer equipped with a Metrohm polarographic stand, model E 554, containing a 5-ml constant-temperature cell with a three electrode system. The working electrode was a dropping mercury electrode, the reference electrode a saturated calomel electrode (SCE) and the auxiliary electrode a platinum foil.

The following polarographic conditions were used for measurements: potential range, −0.5–1.2 V; current range, 2–10 μA full scale; scan rate, 2 mV/sec; pulse modulation, 100 mV p.p.; drop time, 1 sec. The temperature of the experiments was kept constant at 25 ± 1° and samples were purged with pure nitrogen for 10 min, unless otherwise stated. Polarograms were recorded on a Hewlett–Packard 7004 B X–Y recorder.

Linear sweep and cyclic voltammetry experiments were carried out in a Inelecsa assembly similar to that previously described.[9] The working electrode was a hanging mercury drop electrode (hmde), Metrohm model EA-290, with a saturated calomel electrode as the reference electrode and a platinum wire as the auxiliary electrode. Controlled potential coulometric measurements and large scale electrolysis were performed with the same equipment and electrodes as was previously reported.[10]

Spectrophotometric measurements were carried out with a Perkin–Elmer model 550 spectrophotometer in 1-cm quartz cells. Spectra were run between 200 and 400 nm, and quantitative sample measurements were made at 275 nm using 0.1*M* hydrochloric acid as a blank.

RESULTS AND DISCUSSION

Preliminary experiments showed that the polarographic behaviour of nicergoline markedly depends on the concentration of the solutions at constant drop time. At concentrations below 0.1m*M*, we observe only one peak with a peak potential at approximately −700 mV in 0.1*M* hydrochloric acid.

The behaviour of this peak with the nicergoline concentration is illustrated in Fig. 2. As can be seen, its height is linearly dependent on concentration up to 0.1m*M*. Above 0.1m*M*, the height of this peak remains unchanged, but a second peak with a peak potential at approximately −1000 mV appears. The height of this second peak also increases with the increasing of nicergoline concentration [Fig. 3].

The above behaviour is essentially the same as described by Laviron[11] for the case of strong adsorption of the product by classical polarography. In our case, the first peak is an adsorption prepeak corresponding to the general process:

$$Ox + ne \rightarrow [Red]_{ads} \quad (1)$$

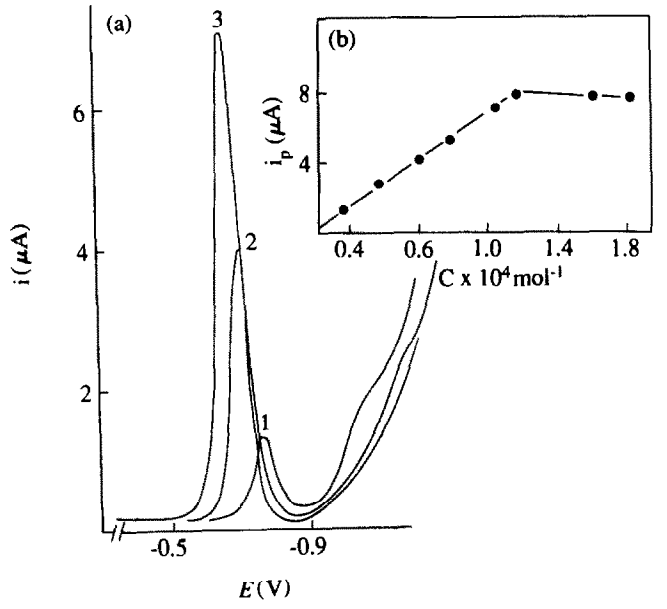

Fig. 2. (a) Some differential pulse polarograms of nicergoline at low concentrations (1) 0.02mM (2) 0.062mM; (3) 0.1mM. (b) Relationship between peak current and concentration for the prepeak.

At sufficiently high nicergoline concentrations [>0.1mM], a compact film of adsorbed product is formed and the reduction of nicergoline will occur now through the film, originating a second peak (diffusion peak) at more negative potentials due to the general process:

$$\mathrm{Ox} + ne \rightarrow \mathrm{Red} \qquad (2)$$

Linear sweep voltammetry (LSV) was also used to confirm the above described behaviour. Linear sweep voltamperograms of nicergoline exhibit two peaks: an adsorption peak (I) and a normal diffusion peak (II) (Figs. 4 and 5). The former appears at less negative potentials than the latter.

The dependence of voltamperograms on scan rate and on nicergoline concentrations was studied. As the scan rate increases, the ratio of the adsorption peak to the diffusion peak increases (Fig. 4). As the bulk concentration of nicergoline is increased, a relative decrease in the height of the adsorption peak and an anodic shift in its

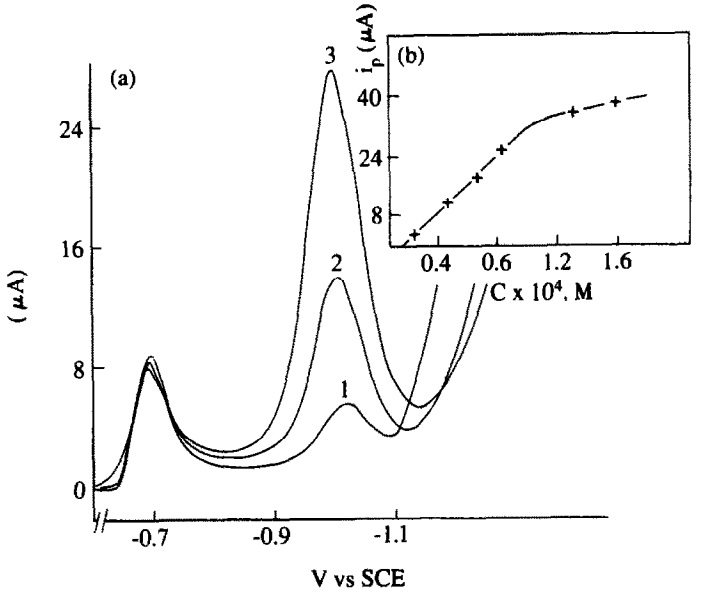

Fig. 3. (a) Differential pulse polarograms of nicergoline solutions at high concentrations: (1) 0.24mM; (2) 0.45mM; (3) 0.65mM.

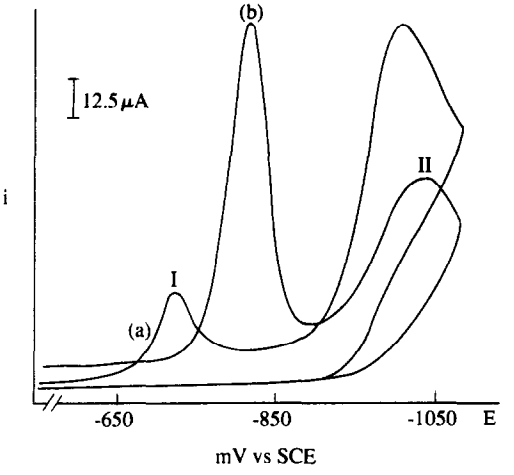

Fig. 4. Linear sweep cyclic voltamperograms of 1.0m*M* nicergoline at two different sweep rates: (a) 0.5 V/sec; (b) 25 V/sec.

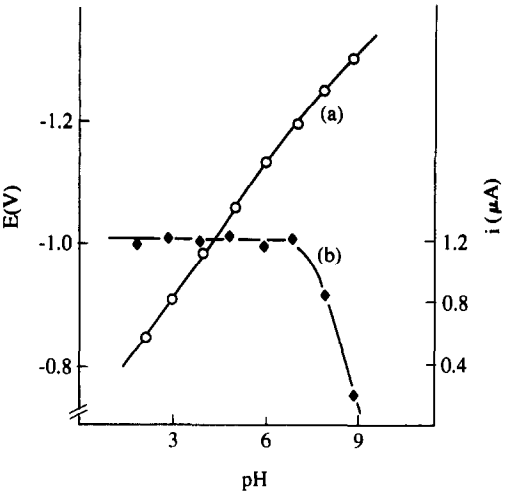

Fig. 6. D.p. polarographic variation with the pH of: (a) potential (*E*p) and (b) peak current.

potential is observed. The behaviour is shown in Fig. 5 (all other parameters were kept constant).

The above voltammetric response is completely consistent with a process where the electrode reaction involves the strong adsorption of the product. Nicergoline is shown to be an excellent model for the previously developed theory related to the effects of adsorption of electroactive species in voltammetry.[12]

Since the first pulse polarographic peak of nicergoline at concentrations below 0.1m*M* is limited by diffusion and is governed by the Ilkovic equation, we preferred it for a more thorough study and for quantitative analysis. For higher concentrations, the second peak

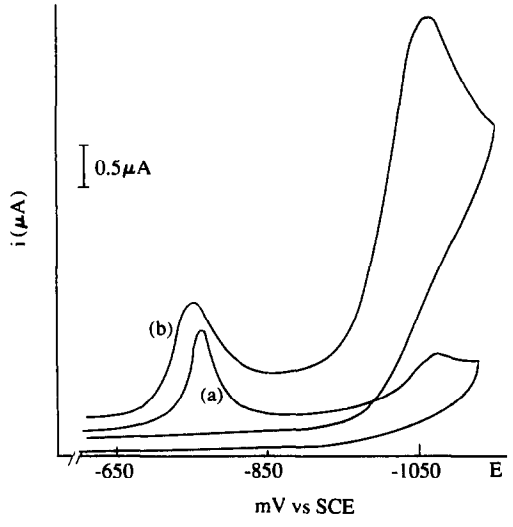

Fig. 5. Linear sweep cyclic voltamperograms of nicergoline at two different concentrations: (a) 0.1m*M*; (b) 0.5m*M*. Sweep rate: 0.5 V/sec.

may be used, although its intercept is not at the origin; the sum of the two peak currents should actually give a curve through the origin.

The peak potential of the first peak was strongly dependent on pH solutions. Between pH 1.0 and 6.5, a linear dependence was obtained with a slope of 0.071 V/pH. A second linear dependence was also found above pH 7.0, with a slope of 0.057 V/pH. This behaviour is shown in Fig. 6. The peak currents are nearly constant in the pH range between pH 1.0 and 7.0. However, above pH 7.0 a sharp decrease is observed, and the peak practically disappears at pH values higher than 9.0.

From the *E*p/pH plot, we have obtained a polarographic pK_a of 6.4. The dependence of the *i*p/pH curve shows a behaviour in accord with a process in which a proton transfer precedes the electroreduction of the acidic form, *e.g.*, the protonation of the pyridine nitrogen to form the electroactive species. At pH values higher than pK_a, the proton transfer is slow and the process appears to be kinetic controlled.

UV spectrophotometric studies at different pH values also permit us to obtain a pK_a value [pK_{UV} = 4.9]. A comparison of polarographic and spectrophotometric pK's shows a higher value of the former. This apparent discrepancy may be due to the kinetic character of the polarographic system, in which the equilibrium is established in a period comparable to that of a drop-life, resulting in a pK_a greater than the equilibrium pK.[13]

Considering the above dependences on nicergoline concentration and pH, we postulate the

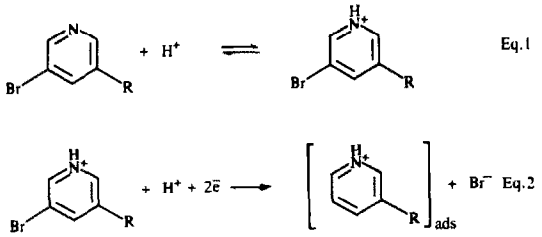

mechanism summarized in Scheme 1 for nicergoline concentrations below which a compact film of product is formed (approximately <0.1 mM).

The first step is the chemical proton transfer reaction in order to form the electroactive protonated nicergoline, being the non-protonated electroinactive nicergoline. This step proceeds fast at pH values less than pK values, producing an independence between the limiting current and pH. At more alkaline pH values than pK, this step proceeds slowly, with a decrease in the limiting current with increasing pH values. In order to verify the occurrence of the second step, we have carried out controlled potential electrolysis and Br- was identified in the electrolyzed solution.[14] Furthermore, previous works related to halogenopyridines agree with this proposed mechanism.[15-19]

Nicergoline exhibits a well-defined polarogram in 0.1M hydrochloric acid with a peak potential between -700 and -650 mV *vs.* SCE, which was used for analytical determination of the drug in pharmaceutical dosage forms.

This peak was diffusion-controlled and the peak current exhibited a linear dependence in the concentration range between 4×10^{-6} and $1 \times 10^{-4}M$. However, for the analytical assay of nicergoline, a working range between 2×10^{-5} and $1 \times 10^{-4}M$ was chosen. The calibration curve is described by the following regression equation:

$$ip\ (\mu A) = 69{,}774\ C(M) - 0.268$$

with a correlation coefficient of 0.9995 for $n = 10$, where ip is the peak current and C is the molar concentration of nicergoline. The detection limit was $1 \times 10^{-6}M$. With the purpose of developing a rapid analytical method, we have studied the effect of not purging the nicergoline solutions with nitrogen prior to polarographic measurements. Our results indicate that previous purging was not essential because calibration curves without purging were similar

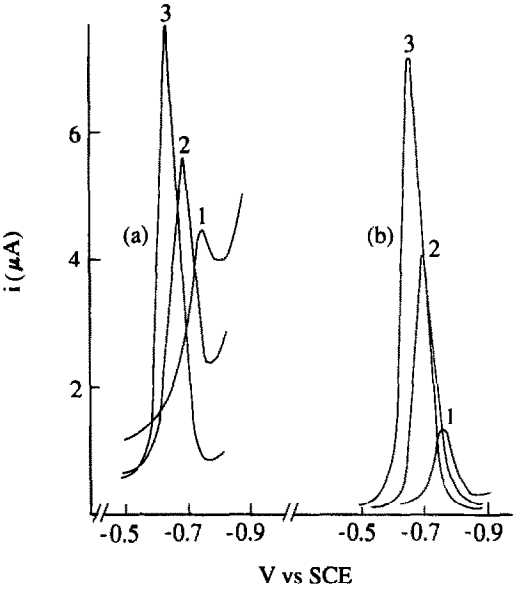

Fig. 7. Comparison of some differential pulse polarograms of nicergoline (b) with nitrogen purging (a) and without purging, at three different concentrations (1) 0.02mM; (2) 0.062mM; (3) 0.1mM.

(slope comparisons through a Student t-test were not significantly different, $p > 0.01$). However, the detection limit in the case with no-purging was about $9 \times 10^{-6}M$ (Fig. 7). The presence of oxygen produces a sloping baseline, but this effect is reduced as the concentration of nicergoline is increased. This fact can be interpreted as an inhibition of the reduction wave of the oxygen due to strong adsorption of the product on the mercury electrode. In conclusion, the purging of the nicergoline solutions with nitrogen is not needed for the quantitative determination of either the pure drug or dosage

Table 1. Recovery of nicergoline* from synthetic samples

Polarographic method			Spectrophotometric assay	
Added, *mg*	Found, *mg*	Rec, %	Found, *mg*	Rec, %
10.0	9.9	99.0	10.2	102.0
10.1	10.0	99.0	10.0	99.0
9.9	9.8	98.9	10.0	101.0
10.0	9.9	99.0	10.1	101.0
9.9	10.0	101.0	9.9	100.0
10.0	9.9	99.0	10.1	101.0
10.1	9.9	98.0	10.0	99.0
10.0	10.0	100.0	10.0	100.0
10.0	10.2	102.0	10.1	101.0
9.8	10.0	102.0	9.9	101.0
Average		99.7		100.5
SD_{n-1}		1.4		0.97
CV, %		1.4		0.96

*Synthetic mix prepared containing 10 mg of nicergoline standard and excipients.

Table 2. Composite studies of commercial nicergoline tablet samples*

Polarographic method		Spectrophotometric assay
Sample	Found, *mg*	Found, *mg*
1	9.57	10.49
2	9.65	10.61
3	9.63	10.61
4	9.65	10.65
5	9.48	10.61
6	9.57	10.65
7	9.57	10.53
8	9.65	10.61
9	9.48	10.65
10	9.57	10.72
Av.	9.58	10.61
SD	0.06	0.07
CV, %	0.67	0.61

*Nicergoline tablets, Chile Laboratories, Santiago, Chile. Declared amount: 10 mg of nicergoline.

forms, reducing the analysis time approximately 10–15 min per run. For recovery studies on synthetic samples containing 10 mg of nicergoline, we have obtained an average recovery of 9.97 mg with a SD of 1.4, indicating adequate accuracy and precision for the developed assay (Table 1).

As a comparative method, a UV spectrophotometric assay was used. Samples were measured at 287 nm and filtration was necessary prior to the determination, with an average recovery of 100.5 and an SD of 0.97%.

Table 3. Individual assays for nicergoline dosage forms

	Polarographic determination		Spectrophotometric determination	
	Tablet*	Injectable†	Tablet	Injectable
	Found, *mg*		Found, *mg*	
	9.75	3.93	9.70	3.86
	10.12	3.91	10.30	3.92
	9.62	4.01	10.10	3.98
	9.88	3.89	10.40	3.90
	9.90	3.96	10.40	3.92
	10.25	3.98	10.50	4.05
	9.38	4.00	9.80	3.97
	10.25	3.95	10.50	4.10
	10.50	3.97	10.60	3.93
	10.62	4.02	10.60	3.95
	9.38	3.98	10.00	3.99
Av.	9.97	3.96	10.26	3.96
SD	0.42	0.04	0.32	0.07
CV, %	4.20	1.00	3.12	1.77

*Nicergoline tablets, Chile Laboratories, Santiago, Chile. Declared amount: 10 mg of nicergoline.

†Sermion, Carlo Erba Laboratories, Santiago, Chile. Lyophilyzed injectable powder, declared 4 mg of nicergoline.

Composite analyses of tablets containing declared amounts of 10 mg of nicergoline show mean values of 9.58 and 10.61 mg for the polarographic and spectrophotometric determinations ($n = 10$), with a SD of 0.064 and 0.065, respectively (Table 2).

Individual dosage form assays of both tablets and injectables are shown in Table 3. It can be concluded that the polarographic determination developed here represents a good analytical alternative, because sample preparation is easy and the method is rapid. The present method is recommended for the quantitative determination of nicergoline in dosage forms and uniformity content tests.

Acknowledgements—This research was supported by Grants Q-3121-9013 and 1120-92 from DTI University of Chile and FONDECYT, respectively.

REFERENCES

1. D. Goo, E. Palosi and L. Szporny, *Drug Dev. Res.*, 1988, **15**, 75.
2. O. Pastoris, L. Vercesi, F. Allorio and M. Dossena, *Il Farmaco. Ed. Sci.*, 1988, **43**, 627.
3. E. Triulzi, S. Devizzi and A. Margonato, *Il Farmaco. Ed. Prat.*, 1981, **36**, 449.
4. M. Truchand, *Ann. Pharm. Fr.*, 1983, **41**, 321.
5. F. Arcamone, A. H. Glasser, J. Grafnetterova, A. Minghetti and V. Nicolella, *Biochem. Pharmacol.*, 1972, **21**, 2205.
6. F. Arcamone, A. H. Glasser, A. Minghetti, V. Nicolella, *Bull. Chim. Farm.*, 1971, **110**, 704.
7. P. M. Bersier and J. Bersier, *The Analyst*, 1989, **114**, 1531.
8. G. J. Patriarche and H. Zhang, *Electroanalysis*, 1990, **2**, 573.
9. L. N. Núñez-Vergara, J. A. Squella, M. Domínguez and M. Blázquez, *J. Electroanal. Chem.*, 1988, **243**, 133.
10. J. A. Squella, Y. Borges, C. Celedón, P. Peredo and L. J. Núñez-Vergara, *Electroanalysis*, 1991, **3**, 221.
11. E. Laviron, *J. Electroanal. Chem.*, 1974, **52**, 355.
12. R. H. Wopschall and I. Shain, *Anal. Chem.*, 1967, **39**, 1514.
13. P. Zuman, in *Advances in Physical Organic Chemistry*, V. Golg (ed.), Vol. 5, p. 34. Academic Press, London, 1967.
14. A. I. Vogel, *Química Analítica Cualitativa*, p. 281. Buenos Aires, 1959.
15. J. Holubek and J. Volke, *Collect. Czech. Chem. Comm.*, 1962, **27**, 680.
16. R. F. Evilia and A. J. Diefander, *J. Electroanal. Chem.*, 1969, **22**, 407.
17. G. Dryhurst, in *Electrochemistry of Biological Molecules*, p. 513. Academic Press, London, 1977.
18. C. L. Perrin, in *Progress in Physical Organic Chemistry*. S. Cohen, A. Streitweisser and R. Taft (eds.), Vol. 3, p. 268. Interscience, New York, 1965.
19. J. Tirouflet, *Advan. Polarog.*, 1960, **2**, 740.

Talanta, Vol. 39, No. 9, pp. 1155–1161, 1992
Printed in Great Britain

0039-9140/92 $5.00 + 0.00
Pergamon Press Ltd

ELECTROCHEMICAL STUDY OF METHYLCOBALAMIN

DETERMINATION OF THE REDUCTION POTENTIAL FOR A QUASIREVERSIBLE SYSTEM WITH A FAST FOLLOWING REACTION

QINGDONG HUANG and DAVID K. GOSSER, JR*

Department of Chemistry, City College of the City University of New York, New York, NY 10031, U.S.A.

(*Received* 2 *December* 1991. *Accepted* 9 *January* 1992)

Summary—The reductive electrochemistry of methylocobalamin in nonaqueous solution is typical of many electrochemical mechanisms in that the initial electron transfer at the electrode is followed by a fast chemical reaction. The rate constant of the following chemical step, methyl radical cleavage, was measured by double potential step chronoamperometry to be 590 sec^{-1} in a solvent mixture (DMF 40%, methanol 60%, at −30°). The cyclic voltammetric response in the slow scan-rate regime was analyzed by the simulation-fitting program CVFIT to extract the remaining parameters of the electrode reaction–chemical reaction mechanism: the formal reduction potential ($E^{0\prime} = -1.529 \pm 0.004$ V), the standard heterogeneous rate-constant ($k^0 = 0.012 \pm 0.002$ cm/sec), and the transfer coefficient ($\alpha = 0.78 \pm 0.02$). This method of analysis allows for the rigorous determination of reduction potentials under conditions where the cyclic voltammetric response appears irreversible (no reverse peak is observed). A detailed analysis of the actual reversibility of the system and its effect on the apparent transfer coefficient is presented.

Vitamin B_{12}, the antipernicious-anemia factor, is a group of organometallic compounds which are among the most complex of the naturally occurring compounds.[1] Methylcobalamin, an important member in the B_{12} family, is involved in the methyl group transfer reaction as a coenzyme.[2] In general, the involvement of vitamin B_{12} compounds in a variety of metabolic neurological diseases is a major reason for the thorough understanding of their chemistry and biochemistry, particularly of their redox chemistry. The nature of the cobalt-carbon bond is a fundamental concern, both from the point of view of basic chemistry and as an aid in understanding the function of the coenzyme in protein substrates. The electrochemistry of vitamin B_{12} species has been reviewed by Lexa and Saveant.[3] Since it is a cobalt coordination compound where the cobalt ion can have three different formal oxidation states, redox chemistry is expected to play an important role in their enzymatic reactions.

The reduction of methylcobalamin is typical of many electrochemical reactions in that the electron transfer is followed by a fast and irreversible chemical reaction. In such systems the determination of the formal reduction potential $E^{0\prime}$ by cyclic voltammetry (CV) is problematical. No reverse wave is obtained at slow scan-rates. At a fast scan-rate[4] data are distorted by iR drop (the error in potential control due to the uncompensated solution resistance) and capacitive current that prevents a precise analysis of the CV wave shape. Also for the case of slow electron transfer, the range of scan-rate will be limited. We present here a detailed cyclic voltammetric study in the slow scan-rate regime. Analysis by CV simulation and simplex curve fitting, combined with double potential step chronoamperometry (DPSC), allows for the determination of $E^{0\prime}$ within a few millivolts. Even with the combination of sluggish charge transfer and fast following chemical reaction for this mechanism, which results in apparently irreversible cyclic voltamperograms, the thermodynamic and kinetic parameters can be determined by careful data analysis.

The mechanism of the reductive electrochemistry of methylcobalamin was suggested by Lexa and Saveant using rapid sweep CV in 50 : 50% ratio of DMF and 1-propanol.[4] They were able to show the existence of one electron adduct and estimated the rate constant for the following chemical reaction k_{chem} as 1200 sec^{-1}

*Author for correspondence.

at $-30°$ and the formal reduction potential to be $E^{0'} = -1.6$ V. Spectroelectrochemical experiments have confirmed that the product formed by exhaustive reduction is [Co(I)]cobalamin,[5-7] the vitamin B_{12s}. The electrode process has been shown one electron overall because of the results of controlled potential coulometry. Gas chromatography–mass spectrometry has indicated that ethane is greater than 97% of the cleavage product of the methylcobalamin reduction.[7] Based on these results, the mechanism in Scheme 1 was put forward. Such a mechanism where a chemical reaction follows electron transfer near the electrode is termed as an EC (electrode reaction–chemical reaction) mechanism. This mechanism was further studied through a combination of CV and potential step experiments by Kim and Birke.[8] It is apparent that this mechanism might actually be understood as a sequence of steps more complicated than that shown in Scheme 1. For instance, the timing of the base-on to base-off transition is not resolved. However, our present analysis considers only the rate of the overall reaction.

Our goal in pursuing this work was to fully characterize this EC mechanism by CV simulation analysis using the program CVFIT.[9] A complete characterization of the EC mechanism requires the determination of E^0, k^0, α and k_{chem}, where $E^{0'}$, k^0 and α are the kinetic parameters of the Butler–Volmer equation and k_{chem} influences the concentration of the reducing products in the same equation.[10]

In order to characterize the electrochemical properties of a system by simulation and fitting analysis, a working electrode that gives facile charge transfer is essential. Methylcobalamin usually shows adsorption on common electrode materials. When a mercury electrode was used in DMF with ethanol or 1-propanol solvent mixture, some interfacial adsorption was noticeable even though the results were better than that obtained with a gold or vitreous carbon disk electrode.[4] Reduction of alkylcobalamins on mercury in the presence of ethanol leads to the formation of the corresponding alkylmercury compounds.[11] We examined the electrode responses of methylcobalamin at a number of electrodes in order to find a system which would be amenable to a rigorous simulation analysis. Platinum and silver electrodes had poor characteristics. Glassy carbon was better, but the performance deteriorated quickly with time. A silver amalgam electrode was found to have the best electrode response. It is very stable and its surface does not need to be repolished during the experimental period. This electrode is suitable for the present experiments with methylcobalamin and other alkylcobalamins utilizing a low temperature cell where frequent electrode treatment is inconvenient.

EXPERIMENTAL

The reference electrode was an Ag/AgCl electrode with ethanol solvent saturated by lithium chloride (ultrapure grade, Alfa) at $-85°$, the lowest temperature the temperature control system could reach. The cell temperature was controlled by a Multicool temperature bath controller (FTS Systems). The temperature was monitored near the working electrode with an Omega temperature probe. The solvent was a mixture of DMF (Burdick Jackson Laboratories, Inc.) and methanol (Fisher Scientific) in the ratio 40 : 60%. The DMF was dried over type 3A molecular sieves (Alfa). The supporting electrolyte was TBAF (tetrabutylammonium fluoroborate, Fisher Scientific) in 0.30M and the concentration of methylcobalamin (Sigma) was 2.0mM for CV. Experiments were performed by a BAS-100A electrochemical analyzer. The experimental results were transferred to a PC-XT computer, then converted and analyzed.

The working electrodes were silver amalgam electrodes with diameters of 0.25 and 1.60 mm, which were made from silver wire. The original silver electrode was polished with fine aluminum oxide powders (0.05 μm) and put into an electrochemical cell in which there was a drop of liquid mercury on the bottle immersed by nitric

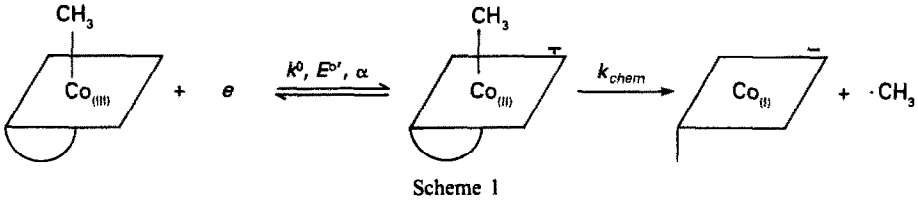

Scheme 1

acid solution at pH 1.5. Using an aqueous Ag/AgCl electrode as reference electrode and a platinum wire as auxiliary electrode, a potential of -1.0 V was applied. This potential reduced hydrogen ions in solution and produced hydrogen gas at the silver working electrode where the surface was activated. After 3 min, the silver electrode was contacted with the mercury in the cell while still holding the same potential. A film of mercury was formed on the surface of the silver electrode. This electrode was rinsed with demineralized distilled water several times and then was immersed in the same type of water for 50 min. The electrode was polished with aluminum oxide powder again and finally washed with demineralized distilled water followed by DMF–methanol solvent.

Several solvent mixtures with different ratios of DMF and methanol were tested. Since there is limited solubility for methylcobalamin in DMF and a higher freezing point compared with methanol, we avoided using a high ratio of DMF. On the other hand, methanol has lower dielectric constant compared with DMF, which causes higher resistance particularly at low temperatures. Experiments showed no significant difference in CV for the reduction of methylcobalamin from ratio 25 : 75% to 75 : 25% for DMF with methanol, ethanol and 1-propanol and so on, except that the rate of the following chemical reaction was sensitive to the exact solvent mixture.[12] These solvent mixtures were not frozen as low as $-85°$. The nitrogen, which was saturated by the same ratio of components and pre-cooled through a U-tube immersed in the cooling system, was used to purge solvent until the initial background current was minimized. CV results of methylcobalamin, by a silver amalgam electrode of 1.6 mm diameter, were background subtracted with data taken under the same experimental conditions but only using solvent and electrolyte. The DPSC experiments for the chemical reaction rate k_{chem} were carried out with time resolution (100 μsec) by a silver amalgam electrode of 0.25 mm diameter.

The CVFIT program includes the correction of iR drop in CV. For this iR correction, uncompensated resistance was analyzed by potential step chronoamperometry. The initial potential was set to the same as the initial potential in CV experiments, and then a step of -50 mV to the initial potential was applied. This step potential was applied for 1 or 2 msec. Since the procedure did not involve faradaic current, the current response follows the relationship

$$i_t = \frac{\Delta E}{R} \exp\left(\frac{-t}{RC_{dl}}\right) \tag{1}$$

where i_t is the response current, ΔE is the potential step applied, R is resistance, C_{dl} is the capacitance of the double layer and t is the time. A plot of t *vs.* $\ln(i_t)$ extrapolated to zero time was used to find the resistance from the intercept.[13]

RESULTS AND DISCUSSION

The rate constant of the following chemical reaction was determined by DPSC and later used as a fixed parameter in the simulation and fitting analysis. The DPSC results were fitted by the theoretical curve developed by Schwarz and Shain.[14] The first few points of data due to double layer charging current were ignored. The usable time window was confirmed by the Cottrell equation[10] where constancy of $it^{1/2}$ was observed. The cathodic current was fitted first within time $0 < t \leqslant \tau$, where τ is the period of pulse applied. It follows the relation

$$i_c = nFAC_0^* \sqrt{\frac{D_0}{\pi t}} \tag{2}$$

where n is the number of electrons involved in the charge transfer, F is the Faraday constant, A is the area of the electrode, C_0^* is the bulk concentration of methylcobalamin and D_0 is the diffusion coefficient. Then k_{chem} was adjusted when the same parameters (n, A, C_0^* and D_0) were kept within time $\tau < t \leqslant 2\tau$ until the anodic current could be fitted by the relation

$$i_a = nFAC_0^* D_0^{1/2} \left[\frac{\phi}{\sqrt{\pi(t-\tau)}} - \frac{1}{\sqrt{\pi t}}\right] \tag{3}$$

where

$$\phi = e^{-k_{chem}\tau/2} I_0\left(\frac{k_{chem}\tau}{2}\right) + 2\, e^{-k_{chem}\tau/2} \times e^{-k_{chem}(t-\tau)} \sum_{n=1}^{\infty} I_n\left(\frac{k_{chem}\tau}{2}\right) \times \frac{\int_0^{k_{chem}(t-\tau)} \cdots \int_0^{\lambda_2} \lambda_1^n e^{\lambda_1} d\lambda_1 \cdots d\lambda_n}{[k_{chem}(t-\tau)]^n} \tag{4}$$

and $I_n(k_{chem}\tau/2)$ represents the modified Bessel functions. Three terms of the infinite series

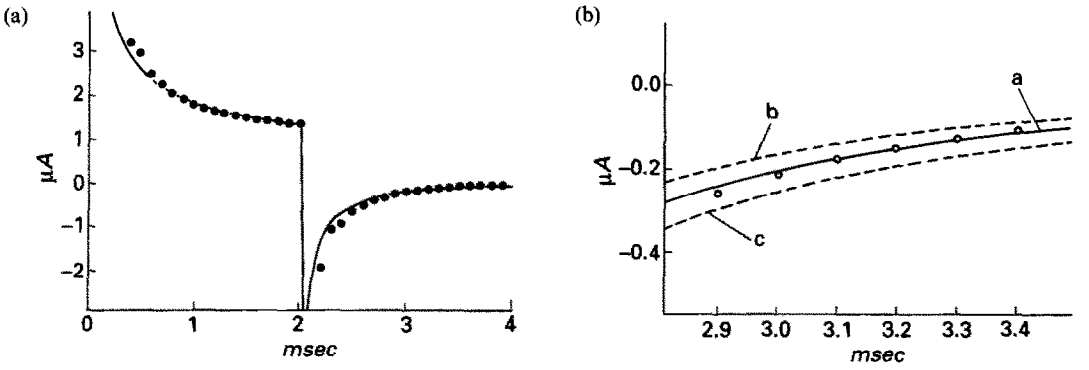

Fig. 1. Double potential step chronoamperometry experiment and fitting result of methylcobalamin in solvent mixture DMF (40%) and methanol (60%) at −30°. Silver amalgam electrode (0.25 mm in diameter), methylcobalamin = 1mM, TBAF = 0.30M. The initial potential was −1.35V, the step potential −1.60V and the final potential back to −1.35V. (a) Result fitted by $k_{chem} = 590$ sec^{-1}, the solid points are experimental results. (b) Detail of the fitting with an error range, where the data close to noise background (at the end of the time period) are ignored. The hollow points are experimental results. Curves a with $k_{chem} = 590$ sec^{-1}, b with 690 sec^{-1} and c with 490 sec^{-1}.

were used. The results are shown in Fig. 1 in which (a) is a general experimental and fitting result and (b) is a detail with the error range indicated. The k_{chem} results were also checked by the measured current ratios $-i_a/i_c$ with the working curve data.[14] All results fall within 5–15% of an average value.

CV with a resolution of one millivolt per point was carried out at −30° with the silver amalgam working electrode. The cyclic voltamperograms at scan-rates 50, 100 and 300 mV/sec are shown in Fig. 2. These voltamperograms are characterized by a cathodic wave showing a well-defined current maximum but no anodic

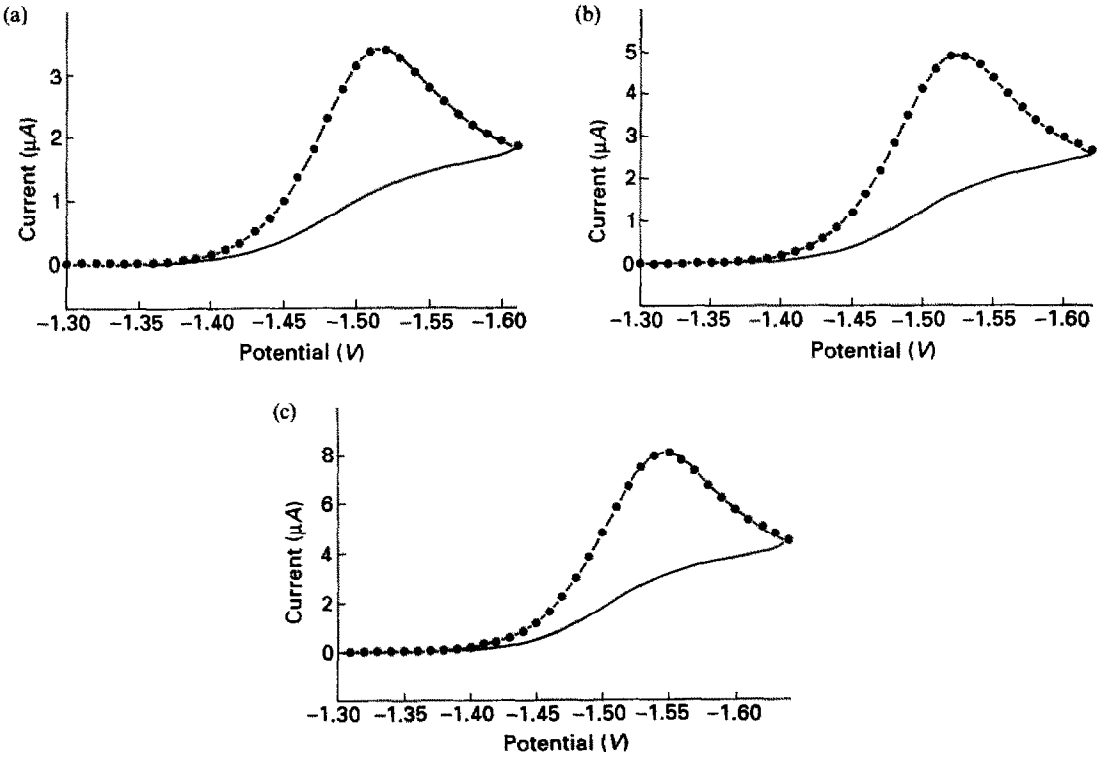

Fig. 2. Cyclic voltamperograms of 2.0mM methylcobalamin in a solvent mixture of DMF (40%) and methanol (60%) at −30°. The supporting electrolyte is TBAF in 0.30M and the working electrode is a silver amalgam electrode in diameter 1.6 mm. The simulation-fitting results of parameter are shown in Table 1. Solid lines are experimental data and solid dots are the simulation-fitting results. Scan rates: (a) 50 mV/sec; (b) 100 mV/sec and (c) 300 mV/sec.

wave on the reserve scan. The digital simulation and fitting results from CVFIT program are also shown on the same voltamperograms. The input parameters of the program included diffusion coefficient D_0, the rate of the following chemical reaction k_{chem}, the resistance R, and experimental condition including scan-range and scan-rate. First guess parameters were provided for the formal reduction potential $E^{0'}$, the standard heterogeneous charge transfer constant k^0, the transfer coefficient α, and a proportionality constant that includes small errors in concentration of methylcobalamin and the electrode area. The program CVFIT utilized Nelder and Mead's modified simplex minimizing procedure to find the best fit between the experimental and simulation results by adjusting these guesses in the simulation process.[9,15,16] (The diffusion coefficient used at $-30°$ was measured by DPSC in the time window of constancy $it^{1/2}$ and checked by CV.) The iR drop was corrected by adding each experimental point of current multiplied with the measured solution resistance to the applied potential, then the calibrated potential (E) was used through equation (5) in simulation:[17]

$$E = E_{applied} + iR \tag{5}$$

The errors are estimated by summation of the square of the difference between experiment and simulation-fitting current for corresponding potentials:

$$\chi^2 = \sum_{j=1}^{n} W_j[\text{current}_j(\text{measured}) - \text{current}_j(\text{theory})]^2 \tag{6}$$

where the weighting factor W_j is set to one in the case of constant variance.

The formal reduction potentials, the heterogeneous rate constants and the transfer coefficients obtained through simulation-fitting are listed in Table 1. The constancy of the reduction potential and other fitted parameters for repeat experiments and the experiments at three different scan-rates provides strong evidence that the values obtained are not spurious or the result of the location of fortuitous local minimum in the fitting procedure. In addition, the $E^{0'}$ value is in agreement with the less precise value (-1.6 V *vs.* SCE) obtained by Lexa and Saveant in the similar experimental condition with fast scan-rate.[4]

In order to estimate the error of the $E^{0'}$ measurement which is caused by the error in the measurement of the following chemical reaction k_{chem}, a series of CV simulations with different scan-rates and k_{chem} were performed. It was found that the deviation in k_{chem} would not affect $E^{0'}$ measurement in our electrochemical system. At a scan-rate of 300 mv/sec, the peak potential shift is less than one millivolt as k_{chem} changes from 490 to 690 sec^{-1}; and the shift is 1 mV in the same k_{chem} change range at the scan-rate 50 mV/sec.

It has been suggested that the reduction potential can be estimated at slow scan-rates by assuming electron transfer reversibility and applying the formula for the kinetic shift due to the following chemical reaction under such circumstances:[10,18]

$$E^{0'} = E_p + 0.780\frac{RT}{nF} - \frac{RT}{2nF}\ln\left(\frac{RT}{nF}\frac{k_{chem}}{v}\right) \tag{7}$$

where E_p is the peak potential in CV and v is the scan-rate. Application of this formula to our system even at the slowest scan-rate (50 mV/sec) leads to an error in the reduction potential of 30 mV compared to that obtained by the more rigorous method presented here (± 4 mV).

From the simulation and fitting results, we obtained α equal to 0.78. A value of $\alpha > 0.5$ indicates that the structure of the transition state for reduction is close to the reactant.[10] Our results ($\alpha = 0.78$) support the mechanism in Scheme 1 where the transition state $[B^{\bullet}_{12a}]^-$ is

Table 1. Simulation-fitting results for methylcobalamin electrochemical parameters at $-30°$. The iteration indicates the simplex iteration times. The resistance measured and used in CVFIT program is 1650 Ω

Rate, *mV/sec*	$E^{0'}$, *V*	k^0, *cm/sec*	α	A, 10^{-2} *cm*^{2}	χ^2, 10^{-13} *ampere*^{2}	Iteration
50	-1.529	0.012	0.79	1.9	1.0	125
50	-1.533	0.014	0.75	1.9	1.1	72
100	-1.524	0.010	0.80	2.0	2.2	102
100	-1.523	0.010	0.80	2.0	2.1	95
300	-1.530	0.012	0.77	1.9	7.9	100
300	-1.532	0.013	0.75	1.9	7.0	120
	-1.529 ± 0.004	0.012 ± 0.002	0.78 ± 0.02	1.9 ± 0.006		

expected to have a similar structure to the reactant B_{12a}.

Although the cyclic voltamperograms appear irreversible, analysis of the data showed this is not entirely the case (otherwise we could not expect to obtain a reliable $E^{0\prime}$).* In order to understand this more fully we carried out a study of the reversibility of the system. The electrochemical current corresponds to the difference between the rate of the forward electron transfer $k_f[B_{12a}]$ and its rate $k_b[B^{\bullet}_{12a}]^-$ for the reverse process. However, with a following chemical reaction, the reversibility of the system will be influenced. If the following chemical reaction-rate is much faster than the rate of the reverse electron transfer, the rate of the forward electron transfer will become rate limiting. Under these circumstances, the electrochemical process is totally irreversible. If the rate of the forward electron transfer is not completely rate limiting, the system is described as quasi-reversible. In general the reversibility of an EC mechanism depends on the heterogeneous kinetics, the homogeneous kinetics and the scan-rate. The reversibility factor f_r, introduced by Klingler and Kochi,[19] describes the reversibility of the system. It is a continuous function of the electrode kinetics varying smoothly from $f_r = 1$ for Nernstian behavior to $f_r = 0$ for total irreversibility. It can also be applied to estimate the error range for the transfer coefficient α. The reversibility factor f_r for the methylcobalamin system is described as

$$f_r \frac{[B_{12a}]_0}{[B^{\bullet}_{12a}]_0^-} = \exp\left[\frac{nF}{RT}(E - E^{0\prime})\right] \qquad (8)$$

where $[B_{12a}]_0$ and $[B^{\bullet}_{12a}]_0^-$ are the corresponding concentrations on the electrode surface in Scheme 1. These concentrations can be obtained from the digital simulation by extrapolating the concentrations in the first few spatial grid points of the simulation to the electrode surface. The variation of the reversibility factor f_r as the function of the heterogeneous charge transfer constant is shown in Fig. 3. The reversibility factors f_r were evaluated at the corresponding peak potential. The results demonstrate that electrode reversibility is actually a continuum, with total irreversibility merely being one limiting extreme. For the value of the chemical rate constant in our system ($k_{chem} = 590$ sec^{-1}), the reversibility factors have a maximum value of $f_r = 0.73$ as the heterogenous rate increases. We are particularly interested in the reversibility under the conditions of our experiments. The CV simulations for methylcobalamin at $-30°$ result in reversibility factors $f_r = 0.18$ at scan-rate 300 mV/sec and $f_r = 0.21$ at 50 mV/sec. Both of them are close to the root of the curve, but they are not completely irreversible even though the cyclic voltamperograms appear "irreversible".

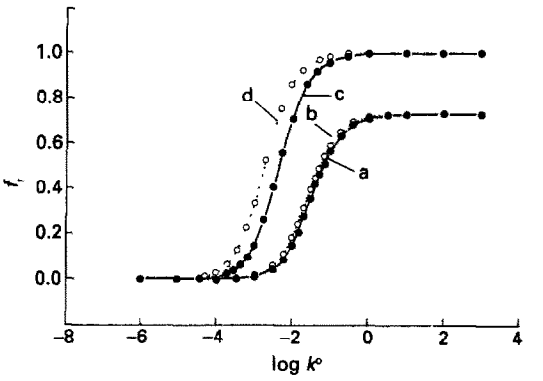

Fig. 3. The relationship of the reversibility factor f_r and the heterogeneous charge transfer constant k^0. The concentrations of the electroactive species in the electrode surface were evaluated at the peaks of cyclic voltamperogram by digital simulation with $E^0 = -1.529$ V, $\alpha = 0.78$, $D_0 = 1.8 \times 10^{-6}$ cm^2/sec at $-30°$. The reversibility factor f_r was calculated through equation (8). (a) 300 mV/sec and $k_{chem} = 590$ sec^{-1}, (b) 50 mV/sec and $k_{chem} = 590$ sec^{-1}, (c) 300 mV/sec and $k_{chem} = 0$ sec^{-1}, (d) 50 mV/sec and $k_{chem} = 0$ sec^{-1}.

The charge transfer coefficient α is an important electrochemical parameter. For a totally irreversible system, α is given by [10,19]

$$\alpha = \frac{1.857RT}{nF}\frac{1}{|E_p - E_{p/2}|} \qquad (9)$$

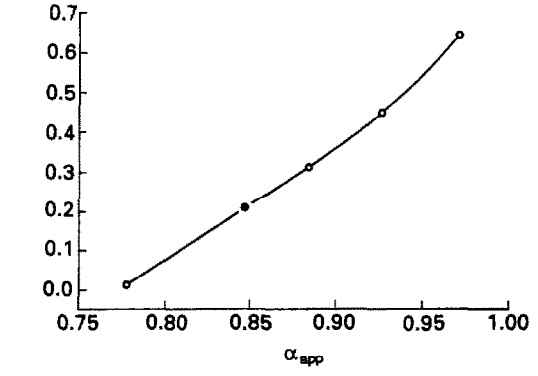

Fig. 4. The relationship of the reversibility factor f_r and the apparent transfer coefficient α_{app}. The solid point represents the simulation and fitting result of Fig. 2(a), estimated through equation (9).

*An examination of the Butler–Volmer equation suggests that both forward and reverse processes must be occurring in order to separate the three terms $E^{0\prime}$, k^0 and α.

Table 2. Various measurements of α. The values of α_{app} are measured from experimental results through equation (9). The values of $\alpha_{app,corr}$ are the experimental results measured through equation (9) and corrected through equation (10). The values of α_{fit} are measured from simulation-fitting of the cyclic voltamperograms with input $E^{0\prime} = -1.529$ V, $k^0 = 0.012$ cm/sec, $D_0 = 1.8 \times 10^{-6}$ cm^2/sec and $k_{chem} = 590$ sec^{-1} at $-30°$

Rate, mV/sec	α_{app}	$\alpha_{app,corr}$	α_{fit}	f_r
300	0.72	0.80	0.76	0.18
	0.71	0.80		
	0.71	0.80		
	0.71	0.80		
100	0.76	0.83	0.80	0.20
	0.78	0.84		
	0.78	0.84		
	0.78	0.84		
50	0.81	0.85	0.77	0.21
	0.81	0.86		
	0.81	0.86		
	0.81	0.86		

where $E_{p/2}$ is the potential of half peak. We expect that α_{app} obtained in this manner will be a reasonable value even though the system is not totally irreversible. Klingler and Kochi's results[19] and our digital simulation data also show the influence of f_r to α_{app} values by equation (9); the larger α_{app} value will have the smaller error if a system has similar irreversibility. Since $\alpha = 0.78$ in this system, we expect a small error estimating α_{app} through equation (9) if f_r is in the foot area of the curves *a* and *b* in Fig. 3. The small error in potentials used in equation (9) due to *iR* drop also results in errors of α_{app} values. We introduce *iR* correction into equation (9) in the following way:

$$E_p - E_p/2 = (E_p - i_p R)_{exp} - (E_{p/2} - i_{p/2} R)_{exp}$$
$$= (E_p - E_{p/2} - \tfrac{1}{2} i_p R)_{exp} \quad (10)$$

where i_p is the peak current and $i_{p/2}$ is the half wave height peak current. The values of $\alpha_{app,corr}$ from measurements after *iR* correction through equation (10) in cyclic voltamperograms are listed in Table 2. These results are consistent with the α values obtained by simulation. Figure 4 shows the influence of f_r to α values by estimation calculated from simulation and through equation (10). The error is also consistent with the experimental measurements. The reason for slightly larger values in $\alpha_{app,corr}$ than that in α_{fit} is that the system is not completely irreversible or f_r is not small enough.

Acknowledgements—The research project was supported in part by grant number 661325 from the PSC-CUNY research Award Program of the City University of New York. We thank Professor Ronald L. Birke and Mr. Feng Zhang for helpful discussions.

REFERENCES

1. D. O'Sullivan, *Chem. & Engineering News*, Feb. 4. p. 30, 1991.
2. H. P. C. Hogenkamp and S. Holmes, *Biochemistry*, 1970, **9**, 1886.
3. D. Lexa and J. M. Saveant, *Acc. Chem Res.*, 1983, **16**, 235.
4. Idem, *J. Am. Chem. Soc.*, 1978, **100**, 3220.
5. T. M. Kenyhercz, T. P. DeAngelis, B. J. Norris, W. R. Heineman and H. B. Mark, *ibid.*, 1976, **98**, 2469.
6. D. Lexa, J. M. Saveant and J. Zickler, *ibid.*, 1977, **99**, 2786.
7. K. A. Rubinson, E. Itabashi and H. B. Mark, *Inorg. Chem.*, 1982, **21**, 3571.
8. M. H. Kim and R. L. Birke, *J. Electroanal. Chem.*, 1983, **144**, 331.
9. D. K. Gosser and F. Zhang, *Talanta*, 1991, **38**, 715.9.
10. A. Bard and L. Faulkner, *Electrochemical Methods, Fundamentals and Applications*, Wiley, New York, 1980.
11. H. A. O. Hill, J. M. Pratt, M. P. O'Riordan, F. R. Williams and R. P. J. Williams, *Chem. Soc.*, 1971, **A**, 1859.
12. Unpublished results.
13. P. He and L. R. Faulkner, *Anal. Chem.*, 1986, **58**, 517.
14. W. M. Schwarz and I. Shain, *J. Phys. Chem.*, 1965, **69**, 30.
15. D. K. Gosser and P. H. Reiger, *Anal. Chem.*, 1988, **60**, 1159.
16. F. H. Walters, L. R. Parker, Jr., S. L. Morgan and S. N. Deming, *Sequential Simplex Optimization*, CRC Press, Boca Raton, Florida, 1991.
17. W. J. Bowyer, E. E. Engelman and D. H. Evans, *J. Electroanal. Chem.*, 1989, **262**, 67.
18. V. D. Parker, K. L. Handoo, F. Roness and M. Tilset, *J. Am. Chem. Soc.*, 1991, **113**, 7493.
19. R. J. Klingler and J. K. Kochi, *J. Phys. Chem.*, 1981, **85**, 1731.

Talanta, Vol. 39, No. 9, pp. 1163–1173, 1992
Printed in Great Britain.

0039-9140/92 $5.00 + 0.00

MICELLAR CATALYSIS IN KINETIC METHODS OF ANALYSIS: IMPROVEMENT OF SPECTROPHOTOMETRIC CATALYTIC DETERMINATION OF COPPER

Mª Loreto Lunar, Soledad Rubio and Dolores Perez-Bendito
Department of Analytical Chemistry, Faculty of Sciences, University of Córdoba, Córdoba, Spain

(*Received* 7 *October* 1991. *Revised* 20 *January* 1992. *Accepted* 10 *February* 1992)

Summary—The combined effects of micellar and chemical catalysis were studied with a view to improving the features of catalytic kinetic determinations. For this purpose we chose the reaction between *N,N*-dimethyl-*p*-phenylenediamine (DPD) and *N,N*-dimethylaniline (DA) to form Bindschedler's Green leuco base, which is oxidized by hydrogen peroxide in a reaction catalysed by Cu(II). This reaction was found to be accelerated by anionic sodium dodecylsulphate (SDS) and cationic dodecyltrimethylammonium bromide (DTAB) micelles. Several advantages were gained in relation to the analytical features of the kinetic photometric determination of Cu(II) when the reaction was developed in the presence of micelles compared to that occurring in an aqueous medium. Such advantages include a lower detection limit, higher sensitivity, precision and solubility of DPD and DA, and substantially increased selectivity in some cases. A detailed study of the parameters which influence both reactions is reported. Some observations on the effect of SDS and DTAB on the reaction are also commented on.

The fact that micelles accelerate chemical reactions is being increasingly frequently exploited to improve determinations of substrates[1–3] and catalysts[4–6] by using kinetic methods. Micellar catalysis has been rationalized in terms of favourable reagent distribution and/or changes in the apparent dissociation constants of ionizable functional groups. Various quantitative kinetic treatments have been developed to assess the intrinsic reactivity of substances in micelles.[7–12]

The analytical features of kinetic methods can be enhanced by confining the chemical reaction in micelles. Thus, sensitivity can be greatly augmented as a direct result of the increased effective concentration of reactants on the micellar surface. Enhanced selectivity with respect to some interferent ions has also been reported.[2,6] It is very difficult however to predict the potential advantages that micelles can provide in relation to this analytical feature because of a number of factors affecting the behaviour of foreign ions in micellar media. The use of micelles as catalysts can also shorten analysis times, increase sample throughputs and make assays more convenient and less expensive. In this context, there are some examples in the literature in which the reaction time of photometric[13] and fluorimetric[14] methods has been reduced from 90–120 min to only 1–5 min.

The greater experimental convenience that can be achieved if kinetic measurements are made in an appropriate micellar medium is particularly desirable for those methods permitting the analyte to be determined with a high sensitivity but suffering from drawbacks such as the involvement of different consecutive reactions that must occur under different experimental conditions and/or long reaction times. This paper reports an example of this type of application of micelles. A previously reported[15] sensitive catalytic method for the spectrophotometric determination of Cu(II) was selected. It is based on the reaction between *N,N*-dimethyl-*p*-phenylenediamine (DPD) and *N,N*-dimethylaniline (DA) to yield Bindschedler's Green leuco base (BGL), which is oxidized by hydrogen peroxide to a colored compound ($\lambda = 730$ nm). Copper(II) catalyses this oxidation, which allows its determination between 0.2 and 2 ng/ml with good selectivity. However, the working curve is not linear and preparation of the samples involves two steps, each of which takes about ten minutes. Also, it is necessary to quench the reaction by placing the vessel in ice cold water and measure the absorbance within 20 min. In addition, solubility problems must be considered when DPD and DA concentrations in the reaction medium are increased above 1×10^{-4} and $1.5 \times 10^{-2} M$, re-

spectively. As shown below, implementation of this method in the presence of micelles is much more convenient.

EXPERIMENTAL

Apparatus

Kinetic measurements were made on a Hewlett–Packard 8452 A diode array spectrophotometer furnished with 1-cm quartz and glass cells. The temperature of the cell compartment was kept at constant temperature by circulating water through it. Kinetic data were collected and processed by a Hewlett–Packard Vectra E/S 12 computer interfaced to a ThinkJet printer.

Reagents

All reagents used were of analytical grade and were employed as supplied. Doubly distilled water was used throughout. A stock Cu(II) solution was prepared by dissolving 1.000 g of Cu metal (Merck) in 15 ml of concentrated nitric acid and diluting up to one litre with 1:1 nitric acid. Working solutions ($1.57 \times 10^{-5}M$) were prepared daily by dilution with doubly distilled water. A $3.39 \times 10^{-3}M$ solution of *N,N*-dimethyl-*p*-phenylendiamine (DPD) (Aldrich) was prepared daily in 1:1 ethanol water. A $0.28M$ *N,N*-dimethylaniline (DA) (Aldrich) solution in ethanol was also prepared. Hydrogen peroxide solution ($2.0\,M$) was prepared daily. Buffer solutions of pH 6.0, 7.0 and 7.8 were made by mixing disodium hydrogen phosphate dihydrate and ammonia (final concentrations in the mixture 0.1 and $1.07M$) with the appropriate volume of $2M$ hydrochloric acid. Aqueous dodecyltrimethylammonium bromide (DTAB) (Sigma) ($1.62 \times 10^{-1}M$) and sodium dodecylsulphate (SDS) (Aldrich) ($6.94 \times 10^{-2}M$) solutions were also prepared. Solutions of the other surfactants tested, *viz.* cetylpyridinium chloride (CPC) (Serva), sodium dioctyl sulphosuccinate (Aerosol OT) (Aldrich), Triton X-100 (Serva), cetyltrimethylammonium bromide (CTAB) (Serva) and *N*-dodecyl-*N,N*-dimethylammonium-3-propanesulphonate (SB-12, sulphobetaine) (Serva) were prepared in a similar way. Less readily soluble surfactants were dissolved with warming.

Procedures for the kinetic photometric determination of copper(II)

In the presence of SDS. To a 10-ml standard flask are added, in sequence, 0.30 ml of $3.39 \times 10^{-3}M$ DPD, 0.50 ml of $0.28M$ DA, 1.5 ml of ammonia–phosphate buffer (pH 7.8), 2 ml of $6.94 \times 10^{-2}M$ SDS, 1.0 ml of $2M$ hydrogen peroxide and appropriate volumes of Cu(II) standard solution ($1.57 \times 10^{-5}M$) to obtain a final concentration between 1.5 and 5 ng/ml. The stopclock is then started and the solution is diluted to the mark with water. An aliquot of the reaction mixture is transferred to a cell kept at $50 \pm 0.1°$ and the absorbance at 730 nm is recorded as a function of time. Measurements are performed exactly 45 sec after the stopclock is started. Absorbance–time data are collected over an interval of *ca.* 1 min. The reaction rate is calculated by a linear least-squares fit of the data using the kinetics module of the HP 89531 A UV/Vis operating software. A blank solution containing no Cu(II) and prepared similarly is also measured and the resulting reaction rate subtracted from that yielded by the samples.

In the presence of DTAB. The procedure and reactant concentrations used to prepare the sample and blank solutions used in the presence of DTAB are identical with those given above, except that 0.35 ml of $3.39 \times 10^{-3}M$ DPD, 1.5 ml of $1.62 \times 10^{-1}M$ DTAB and 1.5 ml of ammonia–phosphate buffer (pH 7) solutions are added instead of the DPD, SDS and buffer solutions, respectively. The final concentration of Cu(II) must be between 1 and 6 ng/ml.

RESULTS AND DISCUSSION

Copper(II) ion catalyses the oxidation of the Bindschedler's Green leuco base (BGL) by hydrogen peroxide. The reagent is formed *in situ* by reaction of DPD and DA. According to Kawashima *et al.*,[15] *in situ* formation is compulsory since high reagent blank readings are obtained if commercially available BGL is used, probably because of the oxidation and/or decomposition products of BGL formed during its storage. Since the proposed experimental procedure requires about 25 min to obtain each measurement, with time control at 10 and 20 min we tested the possibility of making the assay more convenient and reducing the analysis time by carrying out the reaction in an appropriate micellar medium.

Selection of the micellar system

In order to choose an appropriate micellar system to increase the rate of this reaction, one must take into account the type of charge the reactants bear since the accelerating effect of

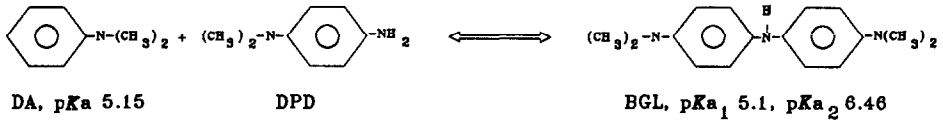

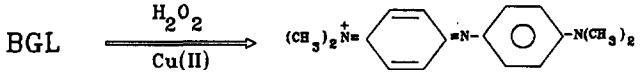

BG, pKa 3.27

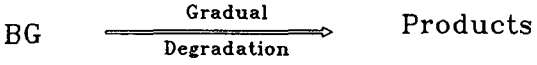

Scheme 1.

micelles arises essentially from electrostatic and hydrophobic interactions between the reactants and the micellar surface. The simplified scheme of the overall reaction and the dissociation constant of hydrogen ions at the dimethylamino groups as reported in the literature are shown in scheme 1.

No data were found for the dissociation constants of DPD. Because of the different reactions involved and the changes that the micelles can induce in the acid constants of the reactants it was quite difficult to predict which type of micelle would increase the rate of the overall reaction at the pH values (6–8) tested. Thus, surfactants of different nature [cationic (DTAB, CPC, CTAB), anionic (SDS, Aerosol OT), nonionic (Triton X-100) and zwitterionic (SB-12)] were tested. Since it is rather difficult to determine the exact critical micelle concentration (cmc) of surfactants in dynamic systems where species are consumed and produced as a function of time hence the cmc value may change throughout the reaction, we assayed surfactant concentrations over a wide range encompassing their cmc in water in order to ensure that micelles of each tested surfactant were obtained under the experimental conditions used. The assays were carried out by mixing all ingredients involved in the reaction according to the procedure described in the Experimental section and monitoring the overall reaction by measuring the rate of formation of BG at 730 nm. The cationic surfactants DTAB, CPC and CTAB, and the anionic surfactant SDS increased both the rate and the final absorbance of the recorded kinetic curves. Aerosol OT and Triton X-100 had no influence on the reaction and SB-12 decreased its rate. The most significant catalytic effect was exerted by DTAB and SDS, so, they were chosen for subsequent experiments. Figure 1 shows the kinetic curves obtained for both surfactants compared to that obtained in an aqueous medium. Although the acceleration of the reaction rate induced by both surfactants was similar, the shape of the resulting kinetic curves was rather different (BG is more stable in SDS than it is in DTAB micelles) and it seems logical to think that both surfactants act on the reaction in a different way. As shown in Fig. 1, the reaction also developed in an aqueous medium, but the sensitivity for the determination of Cu(II) was smaller compared to that obtained in the above described procedure[15] in which reagents are mixed in two steps.

The influence of the concentration of SDS and DTAB on the reaction rate is shown in Fig. 2 for the uncatalysed and Cu(II)-catalysed reaction. Both surfactants enhance the accelerating

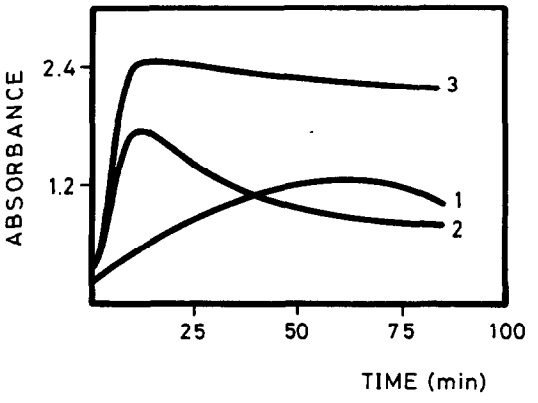

Fig. 1. Absorbance-time kinetic curves for the reaction in an aqueous (1), DTAB (2) and SDS (3) medium. $[DA]=6\times10^{-3}M$, $[DPD]=5\times10^{-5}M$, $[H_2O_2]=0.2M$, [Cu(II)]=4 ng/ml, pH = 6, T = 30°. Procedure as described under Experimental.

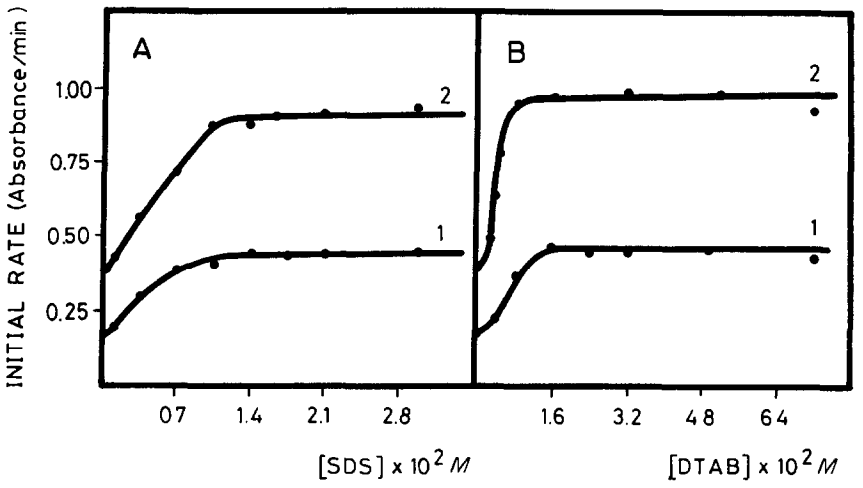

Fig. 2. Influence of the concentration of SDS (curves A) and DTAB (curves B) on the rate of the uncatalysed (curves 1) and Cu(II)-catalysed (curves 2, 4 ng/ml) BGL oxidation reaction. Solutions were prepared as described under Experimental.

effect of the catalyst, as can be inferred from the Fig. 2 by comparing the reaction rate increments of curves 1 and 2 at the SDS concentrations 0 and $1.4 \times 10^{-2}M$ and at the DTAB concentrations 0 and $2.5 \times 10^{-2}M$. Therefore, the kinetic determination of Cu(II) in the presence of these surfactants will be more sensitive compared to that developed in the aqueous medium.

Effect of DTAB and SDS on the reaction

In order to study the action of DTAB and SDS on the Cu(II)-catalysed DPD–DA–hydrogen peroxide reaction we must first consider the net changes that these surfactants induce on the reaction features. The observed alterations were as follows (Fig. 1):

Acceleration of the formation of the oxidation product, which is monitored at 730 nm.
Modification of the maximal absorbance obtained from the kinetic curves recorded.
Variation of the rate of degradation of BG.

Since the overall reaction includes at least three consecutive reactions (see Scheme 1) and, on the other hand, BG and BGL were not commercially available from major chemical manufacturers, it was very difficult to establish the real action of each surfactant on the studied reaction. However, several experiments (described below) permitted us to shed some light on the observed alterations to the reaction features caused by the presence of SDS and DTAB.

DA and DPD-micelles interaction. Reagent–micelle interactions can often be made evident by shifts in the absorption spectrum of the reagent when this is dissolved in the micelle. If no spectral shifts are observed, then other methods such as solubilization, separation, cmc depressions induced by the solute, *etc*, can be used. To determine whether there is any interaction between DA, DPD with SDS or DTAB several experiments were done.

DA–micelle interaction was shown to occur by recording the spectra of $6 \times 10^{-3}M$ DA at pH 7 and 7.8 in aqueous and in DTAB- and SDS-micellar media. The pH values used did not influence the spectral features of DA. SDS and DTAB modified the DA spectrum by introducing a shoulder at about 310 nm (Fig. 3). Because cationic (DTAB) and anionic (SDS) micelles had the same effect, and taking into account the p*K*a value of DA in the aqueous medium (5.15), it is logical to think that DA is uncharged in the reaction medium and that hydrophobic interactions are determinant for the DA–DTAB and DA–SDS association. The identical behaviour of both surfactants is not difficult to understand if one considers that SDS and DTAB are made up of the same hydrophobic chain.

DPD–micelle interaction was difficult to evidence spectrophotometrically at the DPD concentrations used in the reaction medium (about 100-fold lower than that of DA) since DPD only absorbs in the UV region where SDS and DTAB also absorb. In order to study this interaction we used solubilization methods

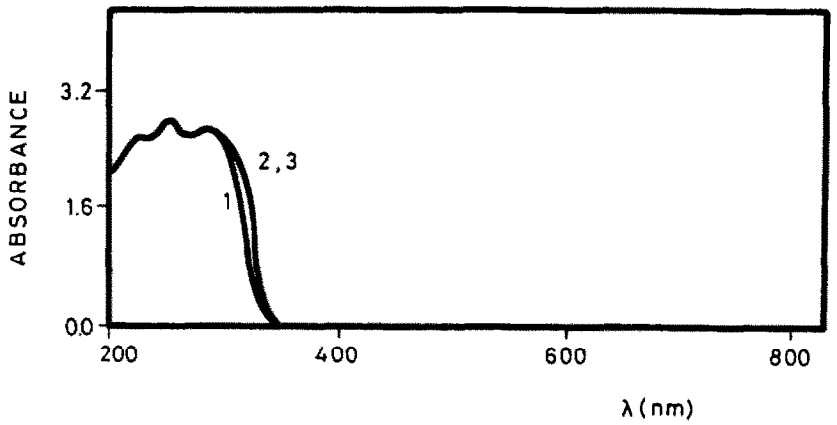

Fig. 3. Absorption spectra of $6 \times 10^{-3}M$ DA in an aqueous medium (1) and in DTAB (2) and SDS (3) micelles.

based on the enhancement of the solubility of some solutes by the presence of micelles. Qualitative experiments were carried out by assaying the solubilization of DPD $5.87 \times 10^{-4}M$ in the three media, namely: water, DTAB and SDS micelles. The reagent was only completely dissolved in SDS micelles. Saturated solutions were obtained in water and DTAB, although more reagent was dissolved in DTAB micelles. Since all solutions obtained were coloured we used the spectrophotometric technique to compare the amount of reagent dissolved after separation of no solubilized reagent. Figure 4 shows the results obtained. DTAB (curve 2) does not substantially alter the spectral features of DPD in the aqueous medium (curve 1), although a greater absorbance is obtained as a result of the greater solubilization of DPD in the micellar medium. In addition to significantly increased solubility of DPD, SDS causes a long shift in the spectral features of this reagent (curve 3). This experiment was also done at pH 7 and 7.8 and identical results were obtained. The divergent behaviour in the presence of SDS and DTAB seems to indicate a different mechanism for the solubilization of DPD in both micelles. Thus, the dimethylamino group is likely to be uncharged at the working pH used and DPD can associate to DTAB through it. The amino group, however, may bear a positive charge through which SDS can bond strongly to DPD.

Since both DA and DPD were concentrated on or within SDS and DTAB, real micellar catalysis occurred. This explains why the order of addition of reactants in determining Cu(II) must be such that the surfactant is added with DA and DPD to obtain the maximum possible signal.

Bindschedler's Green-micelles interaction. The interaction of BG with SDS and DTAB can shed some light on the alteration of the maximal absorbance in the kinetic curves obtained and/or the rate of degradation of BG in both micellar media (Fig. 1).

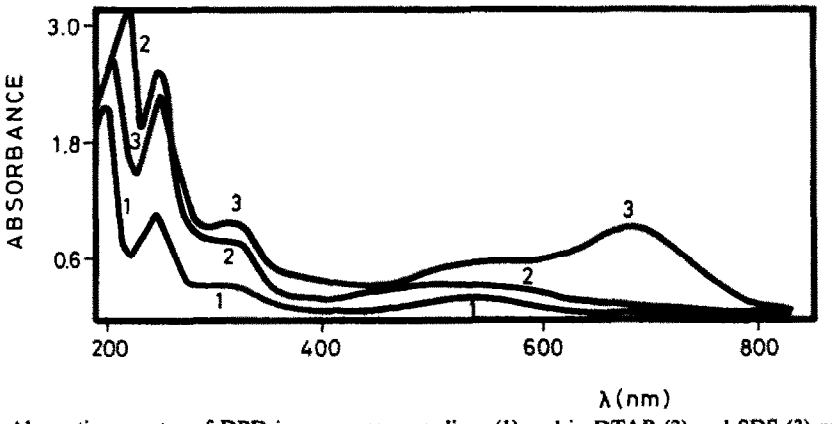

Fig. 4. Absorption spectra of DPD in an aqueous medium (1) and in DTAB (2) and SDS (3) micelles. For the DPD concentrations used, see text.

Micelles are known to increase the molar absorptivity of compounds, which result in increased final absorbances and apparently increased reaction rates if reaction development is monitored via the formation or disappearance of the compound. In order to clarify this point several experiments were done in which the potential sensitization of BG by SDS and DTAB was investigated. The experiments were carried out by mixing all reaction ingredients according to the procedure described in the Experimental section, but adding no SDS or DTAB. Once the reaction was complete, SDS or DTAB was added and both the absorbance obtained after the addition of surfactant and its evolution with time for about one hour was observed. This evolution was compared with that obtained in the absence of surfactant and is shown in Fig. 5, from which some important conclusions can be drawn. The absorbance of BG is not altered when SDS or DTAB is added (compare the absorbance at time zero in Fig. 5), so no sensitization of BG by these micelles occurs.

SDS substantially increases the stability of BG (curve 3, Fig. 5) with respect to the aqueous medium (curve 1, Fig. 5). DTAB does not influence the rate of degradation of BG (curve 2), so the apparently greater instability in this micellar medium (Fig. 1) is probably a direct result of the greater rate of formation of BG. Other variables such as temperature, reagent concentrations, *etc.*, also influence the rate of degradation of BG, probably because of similar causes. This instability is not improved by addition of non ionic surfactants such as Brij 35 or Triton X-100.

The stabilization of BG in the SDS micellar medium is logical if one considers that this reaction product is positively charged (see scheme 1), so it can bond tightly to anionic micelles. The BG–SDS micelles interaction does not modify the spectral features of BG.

Study of the optimum reaction conditions

The effect of the different variables affecting the reaction rate was studied in the presence and absence of SDS or DTAB. Blank reactions involving no Cu(II) were also examined. The optimum conditions resulted in a maximum initial rate, which corresponded to pseudo-zero-order concentrations. Hence, the initial reaction rate was not affected by small variations in the concentrations.

Figure 6(A) shows the variation in the initial rate as a function of pH for the Cu(II) (curve 1), DTAB–Cu(II) (curve 2) and SDS–Cu(II)-catalysed (curve 3) reactions. The initial rates yielded by the blanks [without Cu(II)] were subtracted prior to plotting. Since the reaction practically does not occur in the absence of ammonia, the net effect of the pH could not be determined. This variable was studied by keeping the buffer concentration constant and changing the pH by adding sodium hydroxide or hydrochloric acid. As shown in Fig. 6(A), the surfactants studied shift the optimum pH range at which the reaction takes place. The shift is not directly related to changes in the ionization constant of the reactants as both the anionic and the cationic surfactant resulted in an effect of the same sign. The pH was adjusted with an ammonia–phosphate buffer. The reaction rate increased with the ammonia concentration, at

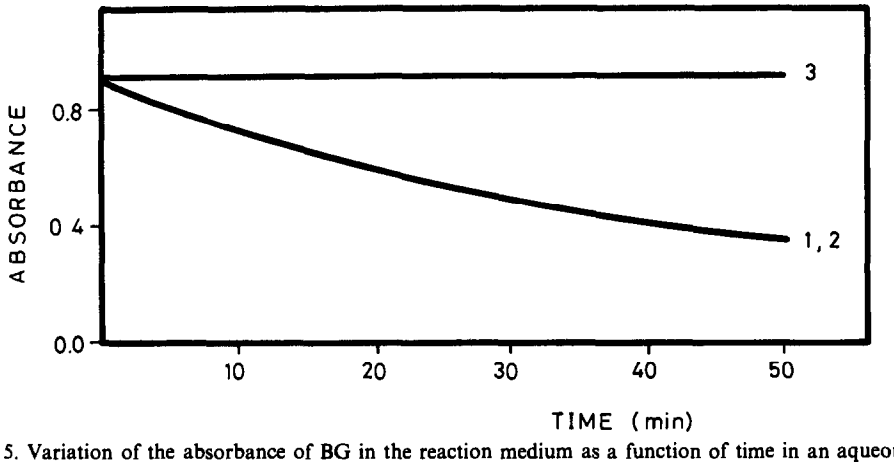

Fig. 5. Variation of the absorbance of BG in the reaction medium as a function of time in an aqueous medium (1) and in DTAB (2) and SDS (3) micelles.

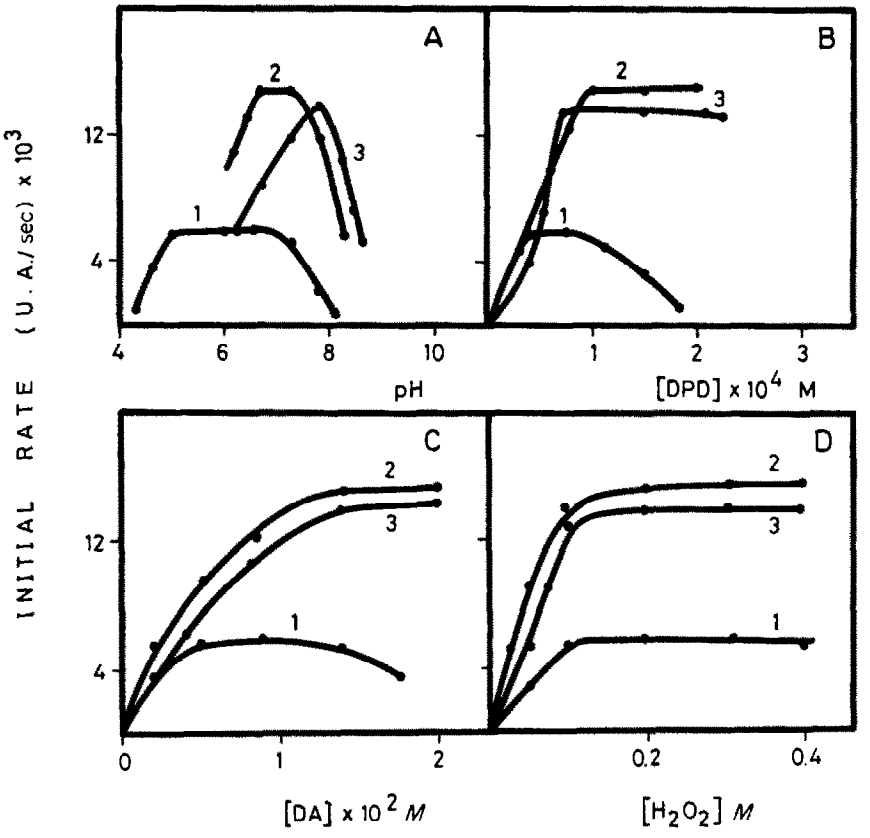

Fig. 6. Influence of (A) pH and the concentration of (B) DPD, (C) DA and (D) hydrogen peroxidse on the rate of the Cu(II) (curve 1), Cu(II)–DTAB (curve 2) and Cu(II)–SDS-catalysed (curve 3) DPD–DA–H_2O_2 reaction. Temperature = 50°.

least up to 0.65*M*. However, buffer concentrations higher than 0.2*M* resulted in irreproducible kinetic curves, so 0.16*M* was selected as optimal. The influence of the phosphate concentration on the different systems was studied over the 1×10^{-3}–$1 \times 10^{-1}M$ range. The reaction rate remained virtually constant and maximum between 1×10^{-2} and $2 \times 10^{-2}M$ phosphate.

The dependence of Cu(II)-catalysed reactions [curve 1, Figure 3(B)] on the DPD concentration is rather different from that shown by the Cu(II)–DTAB and Cu(II)–SDS-catalysed reactions [Fig. 6(B), curves 2 and 3, respectively] at DPD concentrations higher than about $8 \times 10^{-5}M$. This is probably due to the insolubilization of the reagent in the aqueous reaction medium above this concentration. Something similar occurs at DA concentrations above $1.5 \times 10^{-2}M$ [Fig. 6(C)]. Micelles solubilize both reagents.

Figure 6(D) shows the variation in the initial rate with the hydrogen peroxide concentration for the different reactions. This initial rate was found to depend linearly on the hydrogen peroxide concentration up to about 0.1*M*, above which it rapidly dropped to zero order. A 0.2*M* hydrogen peroxide concentration was selected in order to ensure maximum sensitivity.

The temperature influenced both the rate of formation and that of degradation of BG. The instability of this oxidation product increased with the temperature as shown in Fig. 7 [(A), (B) and (C)] in some kinetic curves recorded for the three studied systems. The dependence of the initial rate of Cu(II)-[Fig. 7(A′)] and Cu(II)–SDS-catalysed [Fig. 7(B′)] reactions on the temperature was similar. The optimum interval was between 40 and 60°. This dependence was more critical for the Cu(II)–DTAB-catalysed reaction [Fig. 7(C′)].

Increasing ionic strengths, which were adjusted with sodium chloride and potassium nitrate, resulted in slightly increased rates for all the systems studied up to 1*M*. Since the presence of an electrolyte in an aqueous solution decreases the cmc of anionic and cationic surfactants,[16] the reaction medium contained enough micelles when the effect of the electrolytes on the

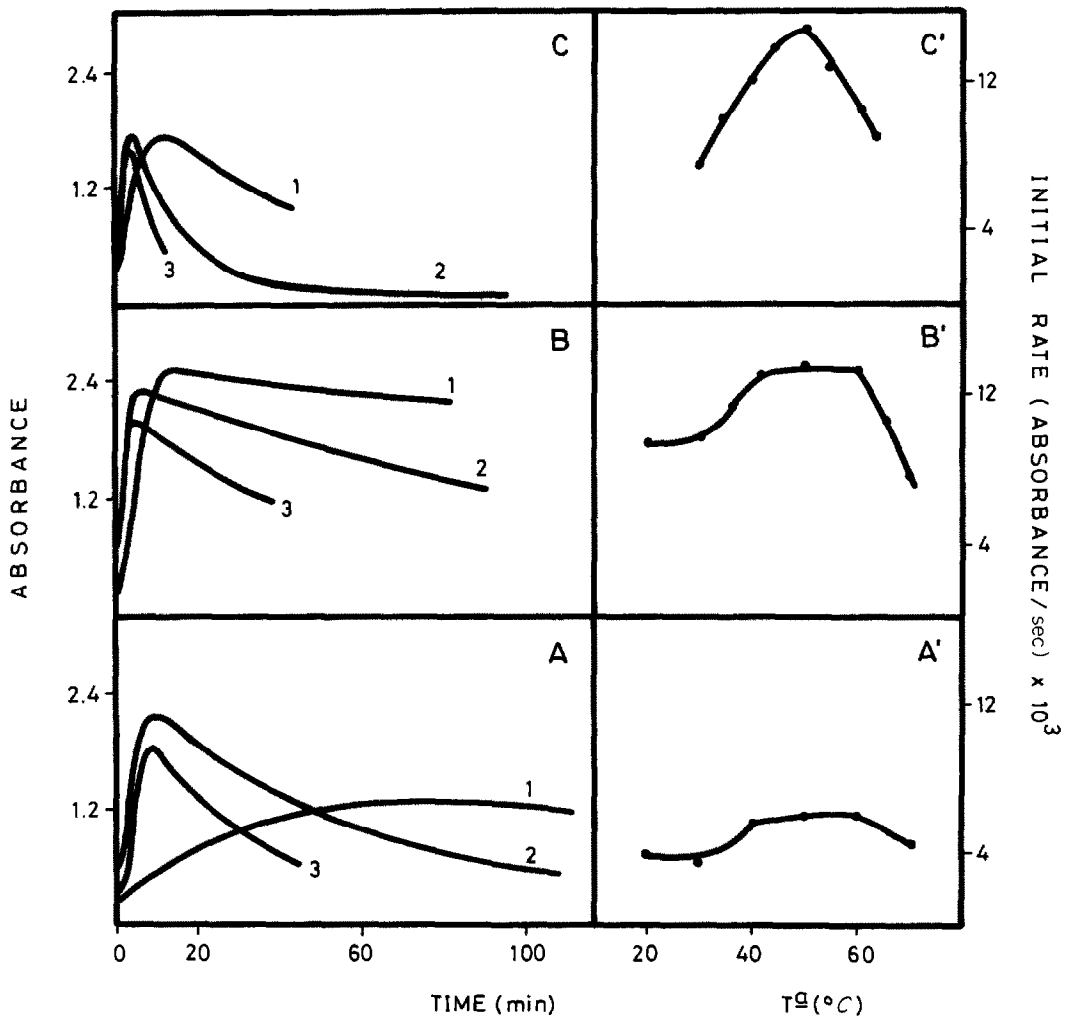

Fig. 7. Influence of the temperature on the profile of the kinetic curves (A, B, C) and initial rate (A', B', C') of the Cu(II) (A, A'), Cu(II)–SDS (B, B') and Cu(II)–DTAB-catalysed (C, C') BGL oxidation reactions. Temperature: curve 1, 30°; curve 2, 50° and curve 3, 60°.

initial rate was tested. Such an effect was similar for all the systems studied (with and without surfactants), so it cannot be attributed to changes in the cmc of the surfactants.

The ethanol concentration had hardly any effect on the reaction rate up to 20%. Higher contents of this solvent decreased the initial rate of all the reactions, particularly that of the Cu(II)–SDS-catalysed reaction. This behaviour is consistent with the common effect of short-chain polar compounds such as ethanol on the cmc of ionic surfactants. Low bulk phase concentrations of these compounds slightly depress the cmc,[17] so the fact that ethanol does not influence the initial rate of the reactions considered up to a concentration of 20% is quite logical. However, at high bulk phase concentrations, ethanol may increase the cmc, probably by decreasing the cohesive energy density of the water, thus increasing the solubility of the monomeric form of the surfactant,[18] or by reducing the dielectric constant of the aqueous phase, thereby increasing mutual repulsion of the ionic heads in the micelle.[19] This increase in the cmc value may diminish the initial rate of the reaction (Fig. 2).

Several orders of addition of reactants were assayed. The order in which Cu(II) and the surfactant were added to the solution was crucial. Optimum results were obtained when the surfactant was mixed with DPD, DA and the buffer and then hydrogen peroxide and Cu(II) were added to the mixture. If Cu(II) was added at the beginning or the surfactant was added at the end, the reaction rate was dramatically decreased.

Analytical features

Calibration graphs for the determination of Cu(II) in the SDS and DTAB micellar media were run under the optimal conditions given in the Experimental section. Their figures of merit are summarized in Table 1, which also includes such analytical features as the detection limit and precision. The same analytical features for the kinetic method, using no surfactant, are also included for contrast. All determined parameters are quite similar for both micellar media. Some advantages over the kinetic method, using no surfactant, include higher sensitivity and precision, and a lower detection limit. The standard errors of the estimates and the correlation coefficients suggest very good linearity, which is quite an advantage over the equilibrium method,[15] in which the calibration graph is not linear.

Since the proposed procedures involve taking measurements when the reaction has hardly developed, the calibration graphs obtained did not allow the determination of Cu(II) concentrations lower than 0.8 ng/ml. The equilibrium method,[15] in which the reaction is allowed to go to completion permits the determination of Cu(II) between 0.2 and 2 ng/ml.

The kinetic procedure is simpler than the equilibrium procedure since it features a shorter analysis time (3 min *vs.* about 25 min) and makes the assay more convenient (the equilibrium procedure involve two steps, each of which takes 10 min, and requires immersing the sample in an ice water bath).

In order to determine whether the micellar media resulted in increased selectivity towards Cu(II), the effect of various ions on the BGL-hydrogen peroxide system in the presence of DTAB and SDS was studied. Table 2 summarizes the results obtained including the type of error (negative, positive, precipitation, *etc.*) caused by the various ions. The maximal tested ion concentration was 100 and 400 μg/ml, respectively, for typical cations and anions, *i.e.*, 50.000 and 200.000 times the concentration of Cu(II). The tolerated concentrations of these ions in the equilibrium method[15] are also included for contrast. No data for the type of error were reported in this reference. Since kinetic methods are often more selective than equilibrium methods, we also studied the tolerated concentrations of the same ions by the kinetic method using no surfactant in order to determine whether increased or decreased selectivity resulted from the kinetic methodology or the micelles used. The results obtained are also included in Table 2. A substantial increase in the selectivity was achieved by the kinetic method compared to the equilibrium method. Micelles provide a further improvement over the kinetic method in the absence of surfactant for ions such as Mn(II), Cd(II), Hg(II), Pb(II), Ni(II), Zn(II), Cr(VI), Mo(VI) and Co(II). Two ions [V(V) and ClO_4^-] and five ions [Ca(II), W(V), Fe(III), Br^- and I^-] are tolerated at lower

Table 1. Analytical features of the kinetic determination of Cu(II) by its catalytic effect on the oxidation of the Bindschedler's Green leuco base by hydrogen peroxide

Parameter	With DTAB	With SDS	Without surfactant
Linear range (ng/ml)	0.8–6	1–5	3.5–8
Slope ± SD (absorbance sec^{-1} ng^{-1} ml)	$(1.82 \pm 0.05) \times 10^{-3}$	$(1.58 \pm 0.03) \times 10^{-3}$	$(0.41 \pm 0.03) \times 10^{-3}$
Intercept ± SD (absorbance sec^{-1})	$(-2.5 \pm 1.7) \times 10^{-4}$	$(-1.03 \pm 1.32) \times 10^{-4}$	$(1.08 \pm 1.88) \times 10^{-4}$
r	0.998	0.999	0.998
Standard error of the estimate (absorbance sec^{-1})	2.92×10^{-4}	1.51×10^{-4}	3.88×10^{-4}
Initial rate for blank measurements (absorbance min^{-1})	7.1×10^{-3}	7.2×10^{-3}	3.2×10^{-3}
*Detection limit (ng/ml)	0.5	0.7	2.5
†RSD (%)	3.4	3.6	5.8

*3 σ.

†$n = 11$, for 3 ng/ml Cu(II) in the presence of DTAB and SDS, and for 6 ng/ml Cu(II) without surfactant.

Table 2. Effect of foreign ions on the determination of 2 ng/ml Cu(II)

	Tolerated concentration of ion (μg/ml)			
		Kinetic methods		
Ion tested	Equilibrium method*	Without surfactant	With SDS	With DTAB
†Mg(II)	2	100	100	100
†Ca(II)	2	↓20	↓10	↓20
†Mn(II)	2	+5	+20	+50
†Cd(II)	0.2	↓50	100	100
†Hg(II)	0.2	+2.5	100	100
†Pb(II)	0.2	↓20	↓30	↓30
†Al(III)	0.2	−1	−1	−1
†Ni(II)	0.02	+0.1	+1	+1
†Zn(II)	0.02	↓10	↓75	↓30
†Co(II)	0.01	+0.2	+0.5	+0.5
†Fe(III)	0.02	+1	+0.1	−1
†VO_3^-	0.2	+40	+50	+10
†$WO_4^=$	0.2	100	−10	100
†AsO_4^{3-}	2	100	100	100
†$CrO_4^=$	0.02	+0.05	−1	−1
†$MoO_4^=$	0.02	+1	−5	100
‡F^-	200	400	400	400
‡ClO_4^-	200	400	400	↓100
‡Br^-	20	400	−100	400
‡I^-	0.2	+2	−1	+2
‡Cl^-	120	400	400	400
‡NO_3^-	145	400	400	400
‡$SO_4^=$	135	400	400	400

*From reference 15. Maximum tested ion concentration: †100 μg ml^{-1}, ‡400 μg ml^{-1}.

concentrations when DTAB or SDS are added, respectively, to the reaction medium compared to the kinetic method using no surfactant. The only instance of lower selectivity in a kinetic method is that of ClO_4^- in the presence of DTAB, and is a result of the precipitation of a quaternary ammonium perchlorate salt that is scarcely soluble in water.[20] There is no clear correlation between the ionic charge of the micelles and the type of error caused by the various ions. On the other hand, since the exact effect of DTAB and SDS on the reaction studied could not be determined accurately as noted earlier, the enhanced or decreased selectivity resulting from the presence of the various ions cannot be accounted for plausibly.

CONCLUSIONS

The features of some analytical kinetic methods can be improved by developing the reactions involved in micellar media. Thus, we have shown the determination of Cu(II) based on its catalytic effect on the BG-hydrogen peroxide reaction to be more sensitive, precise and somewhat more selective in this type of medium. Further research is required in order to establish the advantages with which micellar media can endow kinetic methods of analysis, but previously reported results[4,6] show that real advantages are to be expected for some reactions.

Acknowledgement—The authors are grateful to the CICyT for financial support (Project No. PB87-0821).

REFERENCES

1. E. Athanasiou-Malaki and M. K. Koupparis, *Anal. Chim. Acta*, 1989, **219**, 295.
2. S. Rubio and D. Pérez-Bendito, *ibid.*, 1989, **224**, 185.
3. H. A. Archontaki, M. A. Koupparis and C. E. Efstathiou, *Analyst*, 1989, **114**, 591.
4. M. L. Lunar, S. Rubio and D. Pérez-Bendito, *Anal. Chim. Acta*, 1990, **237**, 207.
5. D. Sicilia, S. Rubio and D. Pérez-Bendito, *Analyst*, 1990, **115**, 1613.
6. *Idem*, Talanta, 1991, **38**, 1147.
7. C. A. Bunton, *Pure Appl. Chem.*, 1977, **49**, 969.
8. E. H. Cordes, *ibid.*, 1978, **50**, 617.
9. F. M. Menger, *ibid.*, 1979, **51**, 999.
10. I. V. Berezin, K. Martinek, A. K. Yatsimirskii, *Russ. Chem. Rev.*, 1973, **42**, 787.
11. L. S. Romsted, Ph. D. Thesis, Indiana University, 1975.
12. F. H. Quina and H. J. Chaimovich, *J. Phys. Chem.*, 1979, **83**, 1844.
13. S. Spurlin, W. L. Hinze and D. W. Armstrong, *Anal. Lett.*, 1977, **10**, 997.
14. S. A. Chang, S. R. Spurlin and W. L. Hinze, *Science-Ciencia*, 1978, **6**, 54.

15. S. Nakano, M. Sakai, M. Tanaka and T. Kawashima, *Chem. Lett.*, 1979, 473.
16. M. J. Rosen, *Surfactants and Interfacial Phenomena*, p. 104. Wiley, New York, 1978.
17. *Idem, ibid.*, p. 106. Wiley, New York, 1978.
18. M. S. Shick and A. H. Gilbert, *J. Colloid Sci.*, 1965, **20**, 464.
19. S. H. Herzfeld, M. L. Corrin and W. D. Harkins, *J. Phys. Chem.*, 1950, **54**, 271.
20. C. A. Bunton, *Catal. Rev. Sci. Eng.*, 1979, **20**, 1.

Talanta, Vol 39, No. 9, pp. 1175–1180, 1992
Printed in Great Britain.

0039-9140/92 $5.00 + 0.00

AUTOMATIC KINETIC DETERMINATION OF OXAZEPAM BY THE CONTINUOUS ADDITION OF REAGENT TECHNIQUE

MANUEL CARMONA, MANUEL SILVA and DOLORES PEREZ-BENDITO
Department of Analytical Chemistry, Faculty of Sciences, University of Córdoba, 14004 Córdoba, Spain

(*Received* 22 *October* 1991. *Revised* 27 *January* 1992. *Accepted* 27 *January* 1992)

Summary—An automatic continuous-addition-of-reagent method for the routine determination of oxazepam based on the formation of a coupling product between diazotized 2-amine-5-chlorobenzophenone (the hydrolysis product of oxazepam) and 1-naphthol in a basic medium is proposed. The reaction is developed by continuously adding basic 1-naphthol to a reaction vessel containing the other ingredients and is monitored spectrophotometrically at 530 nm. The results obtained show the proposed kinetic method to surpass the performance of its conventional equilibrium counterpart as it permits distinguishing the intact drug from its hydrolytic degradation product and is suitable for the determination of oxazepam in dosage forms and urine samples.

Benzodiazepines make a major class of sedative-hypnotic drugs of wide use in the treatment of anxiety and insomnia. They are also the most frequently encountered in cases of drug overdose.[1] The detection and rapid determination of benzodiazepines in various biological and non-biological specimens is therefore of paramount importance in a number of clinical, forensic and pharmaceutical applications. Oxazepam, a 1,4-benzodiazepine derivative of this type, is widely employed as an antidepressant.

Analytical methods currently available for the determination of benzodiazepines in various matrices include gas chromatography[2] and high-performance liquid chromatography procedures[3] that take just a few minutes to complete. In addition, the thermal instability of some of these drugs—particularly oxazepam—complicates their gas chromatography and HPLC analyses for this compound often require careful selection of the mobile phase. As far as the determination of oxazepam is concerned, official pharmacopeias[4,5] recommended a spectrophotometric assay for assaying this drug in dosage form. The spectrophotometric methods used for this purpose are generally based on the acid hydrolysis of this compound, which is followed by ring opening, and the subsequent determination of the benzophenone thus obtained. In fact, oxazepam and other benzodiazepines have been determined in binary mixtures by UV-Vis spectrophotometry using micellar media[6] or by fourth-derivative spectrophotometric techniques after separation by HPLC.[7] In other methods, benzophenone is diazotized with nitrous acid and then coupled with a chromogenic reagent such as *N*-(1-naphthyl)ethylenediamine, Bratton–Marshall reaction,[8,9] or 1-naphthol.[10,11]

A new method for the kinetic determination of oxazepam is presented in this paper. It is based on the rate of coupling between 1-naphthol and diazotized benzophenone obtained from the acid hydrolysis of this drug. This automatic kinetic method is substantially simpler, faster and more sensitive than its equilibrium counterpart and relies on the continuous-addition-of-reagent (CAR) technique.[12] It is quite inexpensive to implement and lends itself readily to routine analyses for benzodiazepines. It has been previously used in various application fields with good results.[13]

EXPERIMENTAL

Reagents

The reagents used were of analytical-reagent grade and distilled water and ethanol were used to prepare the solutions. The oxazepam solution (200 μg/ml) was prepared by dissolving 200.0 mg of the drug (Sigma Chemical Co.) in one litre of ethanol. More dilute solutions were prepared as needed. The coupling reagent solution for the CAR procedure was prepared by mixing 5.0 ml of $3.47 \times 10^{-2}M$ 1-naphthol in 2:3 v/v ethanol/water and 20 ml of $7.5M$

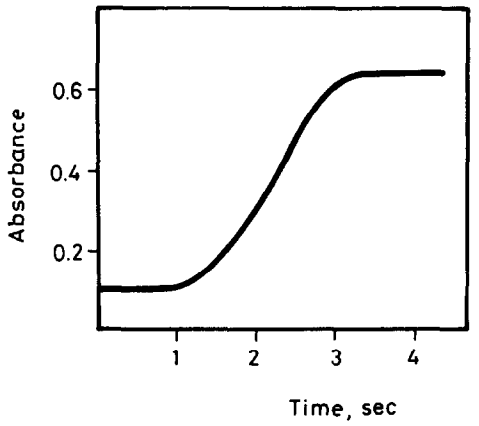

Fig. 1. Typical response curve obtained in the CAR determination of 1.5 μg/ml oxazepam by using the proposed reaction. (For experimental conditions, see Procedure.)

sodium hydroxide in a 50-ml standard flask and diluting to the mark with 2:3 v/v ethanol/water. A $1.45 \times 10^{-2}M$ sodium nitrite solution was also used.

Apparatus

All measurements were made by using a CAR system described elsewhere,[12] which consists essentially of an automatic burette (Mettler DL40), a fan stirrer, a photometric detector (Mettler DK18), an immersion probe (Mettler DK181) for measuring the absorbance in the visible region and a data acquisition and processing unit consisting of a Hewlett–Packard 98561AE computer and a 16-bit Hewlett–Packard analog-to-digital converter provided with a program for the determination of the reaction rate written by the authors. A Radiometer PHM62 pH-meter was also used.

Procedures

Kinetic determination of oxazepam. A volume of standard oxazepam solution (9–220 μg) of up to 10 ml was mixed with the same volume of 6*M* hydrochloric acid in a 100-ml reaction vessel and allowed to stand in a boiling water-bath for one hour. Once the solution was cool, 0.6 ml of $1.45 \times 10^{-2}M$ sodium nitrite solution was added and the mixture was accurately diluted to 60 ml with distilled water. The reaction was developed by continuously adding the coupling reagent solution at a rate of 35 ml/min with stirring at 200 rpm. The reaction was monitored at 530 nm and kinetic data (absorbance *vs.* time) were collected at a rate of 30 msec per point and subsequently processed by the computer. The reaction rate was measured in about 1.0 sec and each sample was assayed in triplicate.

Preparation and analysis of pharmaceutical and clinical samples

Pharmaceutical samples. To prepare the commercial pharmaceutical samples for analyses, a given number of tablets or capsules was ground to a fine powder. The accurately weighed sample was then stirred with 50 ml of ethanol (one portion of 20 ml and two portions of 15 ml) until dissolution was complete. If a residue was formed, it was filtered off and washed with portions of ethanol, and the filtrate and washings were hydrolysed as described above, the final solution being diluted to 100-ml in a standard flask containing ethanol. In all cases appropriate aliquots of these solutions were analysed for oxazepam by the above-described procedure.

Extraction of human urine samples. After collection, the human urine samples (approximate volume 25 ml) were spiked with various known amounts of oxazepam (50 to 450 μg) from the stock solution, pH adjusted to *ca.* 10 with sodium hydroxide and filtered. Next, each filtrate was shaken with 25 ml of methylene chloride in a 100-ml separating funnel for 5 min. The resulting organic extract was evaporated to almost dryness and the resulting residue was dissolved in 30 ml of ethanol and hydrolysed as described above. The remaining solution was diluted with distilled water in a 50-ml standard flask and 20-ml aliquots were used to analyse for oxazepam by using the above-described procedure.

RESULTS AND DISCUSSION

Acidic solutions of diazotized 2-amine-5-chlorobenzophenone (the hydrolysis product of oxazepam) react with basic 1-naphthol added from the autoburette of the CAR system to yield a red coupling product. Since this reaction is time-dependent and very fast, oxazepam must be determined by the continuous-addition-of-reagent technique by monitoring the reaction rate spectrophotometrically at 530 nm (absorption maximum of the coupling product formed). A typical absorbance *vs.* time plot for an oxazepam concentration of 1.5 μg/ml is shown in Fig. 1.

As stated in the literature, the acid hydrolysis of benzodiazepines to benzophenones is carried

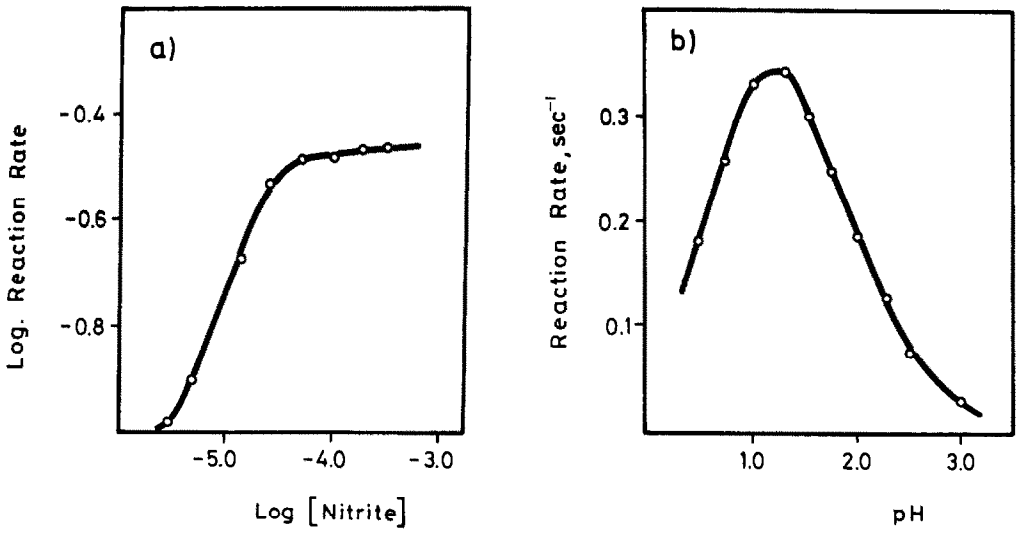

Fig. 2. Effect of (a) the sodium nitrite concentration and (b) pH on the kinetic determination of 1.5 μg/ml oxazepam. (For experimental conditions, see Procedure.)

out with hydrochloric acid at high temperatures.[6,14–19] In our method, oxazepam is quantitatively (99.5%) hydrolysed to 2-amine-5-chlorobenzophenone with 6*M* hydrochloric acid at 100° in a boiling water-bath for 1 hr. Thus, a kinetic study of the influence on the rate of the coupling reaction was performed in order to develop a kinetic method for the determination of the drug.

Optimization of experimental variables

Chemical and instrumental variables were optimized in order to maximize the sensitivity and precision of the proposed kinetic method. In short, stock 2-amine-5-chlorobenzophenone solutions were used and each variable was changed in turn while keeping all other constant. In this case, a 1.0-μg/ml benzophenone solution was equivalent to one containing 1.24 μg/ml oxazepam.

The influence of the sodium nitrite concentration was assessed over a wide range (2.42×10^{-6}–$2.90 \times 10^{-4}M$). The absorbance *vs.* time curves obtained show an increase in the reaction rate with increase in the diazotizing agent concentration up to $4.84 \times 10^{-5}M$, above which it remains virtually constant. This dependency shown in Fig. 2(a) (a log–log plot) arises from the wide concentration range studied. A concentration of $1.45 \times 10^{-4}M$ (0.6 ml of a $1.45 \times 10^{-2}M$ solution), which lay on the plateau, was selected. The influence of pH is closely related to the former variable since the true diazotizing agent for benzophenone is

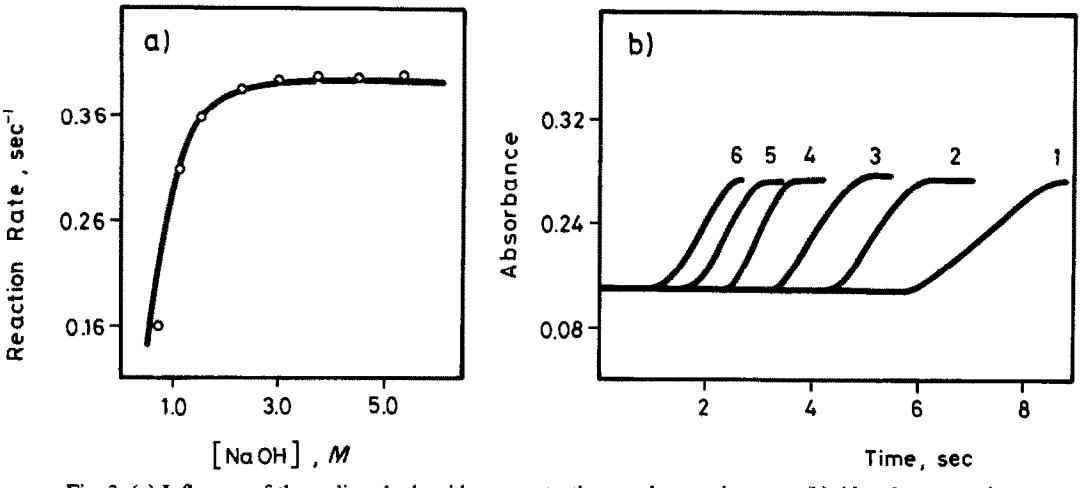

Fig. 3. (a) Influence of the sodium hydroxide concentration on the reaction rate. (b) Absorbance *vs.* time curves recorded at different NaOH concentrations: 1, 0.75; 2, 1.125; 3, 1.50; 4, 2.25; 5, 3.0 and 6, 3.75–5.25*M*. Oxazepam concentration, 1.5 μg/ml. (For experimental conditions, see Procedure.)

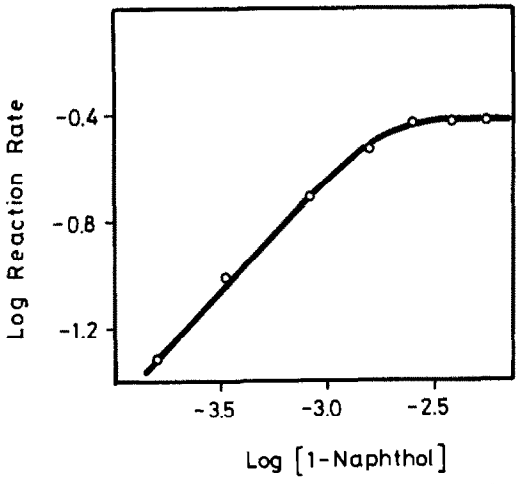

Fig. 4. Variation of the reaction rate as a function of the 1-naphthol concentration. Oxazepam concentration, 1.5 μg/ml. (For experimental conditions, see Procedure.)

nitrous acid. Thus, the effect of pH was studied between 0.5 and 3.0 [Fig. 2(b)]. The plot of the reaction rate *vs.* pH shows maximum dependency at about pH 1.25, above which it decreases. Taking into account this dependency, a pH of 1.30 (nitrous acid is not dissociated) was selected for use in the kinetic determination of oxazepam. At this pH, not only the reaction rate, but also the final absorbance was maximal.

The effect of the sodium hydroxide concentration in the reagent solution added from the autoburette was also tested in the range 0.75–5.25*M*; as shown in Fig. 3(a), the reaction rate increases sharply with an increase in this variable up to 1.5*M*, above which it remains virtually constant. Continuous addition of this chemical to the reaction vessel has two distinct effects: first, it neutralizes the acid present in the reaction vessel, which is required for the diazotizing reaction to develop; then it provides the basic medium needed for the coupling reaction with 1-naphthol. Therefore, the kinetic curves obtained in this study show a pseudo-induction period which is proportional to the sodium hydroxide concentration added from the autoburette, as shown in Fig. 3(b). Taking into account this behaviour, a concentration of 3.0*M* (20 ml of 7.5*M* sodium hydroxide in a final volume of 50 ml) was chosen for subsequent experiments. The concentration of 1-naphthol was varied over the range 1.38×10^{-4}–$5.52 \times 10^{-3}M$ in order to investigate its effect on the reaction rate (Fig. 4), which increased with increase in the concentration of this reagent up to about $2.08 \times 10^{-3}M$, above which it remained constant. A concentration of $3.47 \times 10^{-3}M$ (5 ml of $3.47 \times 10^{-2}M$ 1-naphthol in a final volume of 50 ml), which resulted in a maximal reproducibility and sensitivity, was selected.

Table 1. Influence of other benzodiazepines on the kinetic determination of 0.8 μg/ml oxazepam

Benzodiazepine added	Tolerance ratio
Flurazepam, chlotiazepam, loprazolam, lormetazepam, alprazolam	100
Diazepam*	50
Nitrazepam, chlordiazepoxide, lorazepam, bromazepam	<1

*Maximum ratio assayed owing to its solubility.

The rate of addition of the coupling reagent, the initial volume of the sample solution and the stirring speed are the three instrumental variables which exert an appreciable effect on the kinetic curves. The rate of addition of the alkaline 1-naphthol solution was studied in the range 5–35 ml/min. The reaction rate remained virtually constant throughout this interval, although as with the effect of sodium hydroxide, a pseudo-induction period (the length of which was inversely proportional to the rate of addition) was also observed. Thus, a rate of 35 ml/min was selected for further experiments. The influence of the initial sample volume (between 60–100 ml) and the stirring speed (50–300 rpm) on the reaction rate was also examined. The values advocated under Procedure were chosen as optimal.

Kinetic determination of oxazepam

Quantification of the drug was achieved by plotting the reaction rate against its concentration. Linear correlation ($r = 0.9995$, $n = 8$) over the concentration range 0.15–3.65 μg/ml was obtained. A representative calibration graph for oxazepam provided the following linear regression equation:

$$\text{Reaction rate} = 0.023 + 0.216\ [\text{Oxazepam}]$$

where the drug concentration is expressed in μg/ml. The detection limit of the proposed kinetic procedure was determined by calculating the minimum concentration of drug that could be detected. A concentration of 40 ng/ml oxazepam gave rise to a response (reaction rate) that was three times the standard deviation of the reaction rate for 20 determintions on a sample containing a low analyte concentration.[20] The precision (RSD = 1.26%) was confirmed by analysing 11 replicate samples each containing 1.0 μg/ml of oxazepam in the

Table 2. Analysis of synthetic mixtures of oxazepam and its hydrolysis product

Taken, μg/ml		Oxazepam		Benzophenone	
Oxazepam	Benzophenone	Found, μg/ml	Error, %	Found, μg/ml	Error, %
0.40	3.20	0.38	5.0	3.20	0.0
0.70	2.80	0.71	−1.4	2.78	0.7
1.00	2.00	0.96	4.0	2.03	1.5
1.50	1.50	1.46	2.6	1.50	0.0
2.00	1.00	2.02	−1.0	0.99	1.0
2.80	0.70	2.81	−0.3	0.68	2.8
3.20	0.40	3.15	1.6	0.40	0.0

reaction vessel. The sampling rate, as determined for triplicate runs on the same sample, was about 60 samples/hr.

A study of interferences was made in order to determine the tolerance to other benzodiazepines in the kinetic determination of 0.8 μg/ml of oxazepam. The tolerated limits for the foreign compounds were taken as the largest amounts yielding an error less than ±3% in the reaction rate measurements. As can be seen in Table 1, the proposed method is quite selective. The most serious interferences arise from other benzodiazepines or hydrolysis products of these including a primary amine group in their structures.

The acid-induced degradation product of oxazepam, 2-amine-5-chlorobenzophenone, is obviously a major interferent for the proposed method; however, its perturbation can be avoided by simultaneously determining oxazepam and its hydrolysis product using one hydrolysed and another unhydrolysed sample aliquot. Laboratory-prepared mixtures of oxazepam and its degradation product were thus assayed. Table 2 lists the results obtained; the analysis of oxazepam/benzophenone mixtures was feasible over the weight ratio range from 1:8 to 8:1 (maximum relative error, ±5%). These results are quite satisfactory and confirm that the proposed method allows the resolution of this mixture at lower degrees of hydrolysis of oxazepam in the sample (about to 10%). The average of the results from 11 samples each containing 1.0 μg/ml oxazepam and hydrolysis product yielded an overall relative standard deviation of 1.5% for the method.

Applications

In order to check the applicability of the proposed method we used it to analyse for oxazepam in pharmaceutical and urine samples. The pharmaceutical samples were treated as described above, and in order to detect potential matrix effects from other components, the recoveries of oxazepam added to these samples were also determined. Table 3 shows the results obtained in the determination of oxazepam in such samples, which are consistent with the nominal values of this drug given by the manufacturers (the recoveries ranged from 93.1 to 100.7%, with an average of 96.5%). These results show the good performance of the proposed method for the kinetic determination of oxazepam.

The analysis for oxazepam in urine samples is of great clinical significance since this drug is the main urinary metabolite of several benzodiazepines such as chlordiazepoxide, diazepam, halazepam, medazepam, *etc.*[21] Therefore, its determination in this type of sample can be used

Table 3. Kinetic determination of oxazepam in dosage forms by the CAR technique

Sample	Oxazepam, mg: Stated by manufacturer	Found by proposed method*	Mean recovery, %
Adumbram	10	9.2 ± 0.1	100.7
Aplakil	20	18.9 ± 0.6	94.7
Buscopax†	10	9.7 ± 0.1	93.1
Suxidina‡	5.0	4.86 ± 0.07	98.2
Novo-aerofil§	5.0	4.75 ± 0.08	95.9

*Average of four determinations. Co-occurring substances include †butilescopolamine bromide (10 mg); ‡oxazepam as succinate acid, aspergillus oryzae (4200 units), metochlopramide hydrochloride (5 mg) and dimeticone (10 mg); §metochlopramide hyrochloride (5 mg) and dimeticone (10 mg).

Table 4. Recovery of oxazepam added to urine samples

Added, μg/ml	Found, μg/ml	Mean recovery, %
2.00	2.05, 1.85	97.5
5.00	4.83, 4.97	98.0
10.00	9.35, 9.86	96.0
15.00	14.45, 14.15	95.3
18.00	17.05, 17.45	95.8

as a bulk analysis of these drugs or for the quantitative analysis of a given drug when only one benzodiazepine is present. Different urine samples were analysed by pretreating them as described under Experimental. The samples were spiked with 2–18 μg/ml oxazepam (Table 4) and the average recovery found, 96.5 ± 1.2%, shows the reliability of the proposed kinetic method for the determination of this drug in this type of sample. Finally, it is worth noting that this method can be used to determine smaller amounts of oxazepam in urine samples if these are used entirely for this analysis after the pretreatment. Thus, if 50 ml of urine are treated and then diluted to 60 ml in the reaction vessel to determine its oxazepam content by the proposed CAR method, the minimum amount of oxazepam that can be determined in this case is about 50 ng/ml, taking into account the detection limit of the proposed kinetic method.

CONCLUSIONS

Oxazepam was assayed in dosage forms and urine samples by using the continuous-addition-of-reagent technique. The method used for this purpose is simple, rapid, precise and more sensitive than the corresponding equilibrium approach in which the determination is feasible over the range 2–160 μg/ml.[10,11] The present method can be applied to quality control testing and drug stability monitoring as a good alternative to other methods available for the determination of this drug.

Acknowledgement—The authors are grateful to the CYCIT (Project PB87-0821) for financial support granted for the realization of this work.

REFERENCES

1. A. A. Nanji, A. H. Lawrence and N. Z. Mikhael, *J. Toxicol. Clin. Toxicol.*, 1987, **25**, 501.
2. J. M. F. Douse, *J. Chromatogr.*, 1984, **301**, 137.
3. R. Jochemsen and D. D. Breimer, *ibid.*, 1982, **227**, 199.
4. British Pharmacopeia 1980, p. 758. HM Stationery Office, London, 1980.
5. United States Pharmacopeia XXII, p. 982. United Stated Pharmacopeial Convention, Rockville, MD, 1989.
6. M. de la Guardia, M. V. Galdú, J. Monzó and A. Salvador, *Analyst*, 1989, **114**, 509.
7. M. E. Abdel-Hamid and M. A. Abuirjeie, *ibid.*, 1988, **113**, 1443.
8. S. F. Palermo and A. Poklis, *Can. Soc. Forensic. Sci. J.*, 1977, **10**, 77.
9. A. Poklis, *J. Anal. Toxicol.*, 1981, **5**, 174.
10. A. F. Fartushnii, E. B. Muzhanovs'kii, A. P. Sukhin, A. I. Sedov and E. V. Kvasov, *Farm. Zh. (Kiev)*, 1985, **4**, 45.
11. *Idem*, *ibid.*, 1986, **5**, 47.
12. M. Márquez, M. Silva and D. Pérez-Bendito, *Analyst*, 1988, **113**, 1733.
13. D. Pérez-Bendito, M. Silva and A. Gómez-Hens, *Trends Anal. Chem.*, 1989, **8**, 302.
14. J. A. F. de Silva, M. A. Schartz, V. Stefanovic, J. Japlan and L. d'Arconte, *Anal. Chem.*, 1964, **36**, 2099.
15. P. Lafargue, J. Meunier and Y. Lemontey, *J. Chromatogr.*, 1971, **62**, 423.
16. K. Florey *Analytical Profiles of Drug Substances*, Volumes 1 and 3. Academic Press, New York, San Francisco, London, 1972.
17. W. W. Han, J. G. Yakatan and D. D. Maness, *J. Pharm. Sci.*, 1976, **65**, 1198.
18. *Idem*, *ibid.*, 1977, **66**, 573.
19. H. Schutz, *Benzodiazepines*. Springer, New York, 1982.
20. J. A. Glaser, D. L. Foerst, G. D. McKee, S. A. Quave and W. L. Budde, *Environ. Sci. Technol.*, 1981, **15**, 1426.
21. G. R. Jones *Benzodiazepines* in *Abused Drugs Monograph Series*, R. C. Baselt Editor, Abbot Laboratories, Diagnostic Division, Irving, Texas, 1988.

Talanta, Vol. 39, No. 8, pp. 1181–1188, 1992
Printed in Great Britain.

0039-9140/92 $5.00 + 0.00

STUDIES ON COMPLEXATION EQUILIBRIA BETWEEN WATER-SOLUBLE HYDRAZONES WHICH CONSIST OF 5-NITRO-2-PYRIDYLHYDRAZINE AND HETEROCYCLIC KETONES AND DIVALENT METAL IONS

HAJIME ISHII,* MITSURU YAMAGUCHI† and TSUGIKATSU ODASHIMA
Institute for Chemical Reaction Science, Tohoku University, Katahira, Aoba-ku, Sendai, 980 Japan

(*Received* 14 *October* 1991. *Revised* 31 *December* 1991. *Accepted* 2 *January* 1992)

Summary—Complexation equilibria between five water-soluble hydrazones which consist of 5-nitro-2-pyridylhydrazine and heterocyclic ketones and divalent metal ions have been studied spectrophotometrically. Equilibrium constants of the complexation reactions and overall formation constants of the resultant complexes have been determined and species of the complexes clarified.

In earlier works[1–3] various water-soluble hydrazones which consist of 5-nitro-2-pyridylhydrazine and various heterocyclic ketones having one or two sulpho groups in their molecules were synthesized in order to develop highly sensitive and/or selective reagents for metals. Among them α-(5-nitro-2-pyridyl)-hydrazono-α-(2-pyridyl)-3-toluenesulphonic acid (NPHPTS),[1] α-(5-nitro-2-pyridyl)hydrazono-α-(2-quinolyl)-3-toluenesulphonic acid (NPHQTS),[2] α-(2-benzothiazolyl)-α-(5-nitro-2-pyridyl)hydrazono-3-toluenesulphonic acid (BTNPHTS),[2] α-(2-benzimidazolyl)-α-(5-nitro-2-pyridyl)hydrazono-3-toluene-sulphonic acid (BINPHTS)[2] and disulphonated (2-benzimidazolyl) (phenyl)methanone 5-nitro-2-pyridylhydrazone (DSBINPH)[3] were found to be very useful as highly sensitive spectrophotometric reagents for metals, some of them being applied to the determination of traces of cobalt[1,4] and nickel.[3,5] In this work complexation equilibria between the above-mentioned five hydrazones and metal ions including cadmium(II), cobalt(II), copper(II), iron(II), palladium(II) and zinc(II) have been investigated spectrophotometrically in detail in order to more fully understand these complexation reactions.

*Author for correspondence.
†Present address: Center for Analytical Chemistry, Central Research Laboratories, Nippon Mining Co., Ltd., 3-17-35, Niizo-minami, Toda-shi, Saitama, 335 Japan.

EXPERIMENTAL

Reagents

All reagents were of analytical-reagent grade and all solutions were prepared with distilled, demineralized water, unless stated otherwise.

Standard solutions of cadmium(II), cobalt(II), copper(II), iron(II), palladium(II) and zinc(II) (about 0.5 mg/ml) were prepared by first dissolving their nitrates salts in 0.01*M* perchloric acid and then standardizing by EDTA titration. Working solutions were prepared by dilution of these solutions with water.

Hydrazone solutions, 5.0×10^{-4} or $1.0 \times 10^{-3}M$ were prepared by dissolving each hydrazone synthesized as in earlier works[1–3] in water or 0.01*M* sodium hydroxide solution. These solutions were further diluted with water if necessary.

Buffer solutions were the same as described in a previous paper.[3]

RESULTS AND DISCUSSION

Acid dissociation constants of hydrazones

As is apparent from their structures, the five hydrazones studied in this work exist in solution in any of the following forms, depending upon the acidity or pH:

$$H_{b-i+4}L^{(i-4)-} \overset{K_{ai}}{\rightleftharpoons} H_{b-i+3}L^{(i-3)-} + H^+ \quad (1)$$

$$K_{ai} = \frac{[H_{b-i+3}L^{(i-3)-}][H^+]}{[H_{b-i+4}L^{(i-4)-}]} \quad (i = 1, 2, \ldots, 7) \quad (2)$$

Table 1. Acid dissociation constants of hydrazones

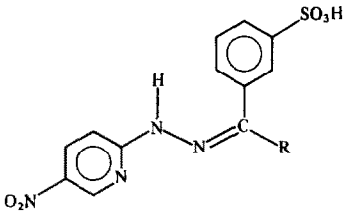

Hydrazone	R	pK_{a3}	pK_{a4}	pK_{a5}	pK_{a6}	pK_{a7}	Reference
NPHPTS	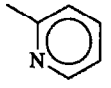	0.72	4.37	11.49			1
NPHQTS	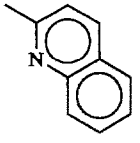	0.70	4.38	11.54			2
BTNPHTS	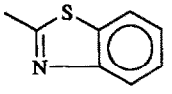	<0.80	1.32	10.74			2
BINPHTS	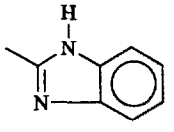	0.70	3.58	10.61	12.61		2
DSBINPH	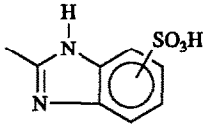		0.70	3.37	10.20	12.72	3

Here H_bL represents the neutral species of the hydrazones, b denotes the number of their dissociable protons ($b = 2$ for NPHPTS, NPHQTS and BTNPHTS, $b = 3$ for BINPHTS and $b = 4$ for DSBINPH) and K_{ai} is the acid dissociation constant. The pK_{ai} values of the hydrazones, which were already determined in earlier works,[1-3] are necessary for the calculation of the formation constants and are summarized in Table 1. Here K_{a3}, K_{a4}, K_{a5} and K_{a6} of the four hydrazones except DSBINPH may be assigned to the deprotonations from the protonated pyridine–nitrogens in the hydrazine and aldehyde moieties, the secondary amino group and the imino group in the benzimidazole moiety, respectively. In the case of DSBINPH, K_{a4}, K_{a5}, K_{a6} and K_{a7} correspond with the above-mentioned assignment, respectively. The values of pK_{a1}, pK_{a2} and pK_{a3} of DSBINPH and those of pK_{a1} and pK_{a2} of the other four hydrazones, which correspond to the deprotonations from the sulpho group and C = N nitrogen, were not determined because these deprotonations are complete in less acidic solutions than those studied.

Effect of pH on complexation and absorption spectra of complexes

The effect of pH on the formation of divalent-metal complexes of the hydrazones was investigated, with absorption spectra of the complexes formed under the optimum conditions. The results are summarized in Table 2 along with the complex compositions determined by the continuous variation method.

Complexation equilibria

In the analysis of complexation equilibria the method of Sommer and Langova[6] was referred to.

In general, the complexation equilibrium between the specified hydrazone and the divalent-metal ion, M^{2+}, may be expressed as

Table 2. Optimal pH ranges for complexation and characteristics of complexes

Complex	Optimal pH range	Absorption maximum, *nm*	Apparent molar absorptivity, $M^{-1}\,cm^{-1}$	Composition (M:L)
Cd(II)-NPHPTS	8.8–10.0	477	8.00×10^4	1:2
Cd(II)–NPHQTS	8.4–10.0	505	8.65×10^4	1:2
Cd(II)–BTNPHTS	9.5	509	7.83×10^4	1:2
Cd(II)-BINPHTS	9.5	495	6.80×10^4	1:2
Cd(II)-DSBINPH[a]	8.9–10.0	495	6.65×10^4	1:2
Co(III)-NPHPTS[b]	2.3–9.5	497	5.90×10^4	1:2
Co(III)-NPHQTS[b]	4.0–9.5	530	4.70×10^4	1:2
Co(III)-BTNPHTS[b]	4.2–7.5	538	5.75×10^4	1:2
Co(III)-BTNPHTS[b]	2.7–4.7	517	6.65×10^4	1:2
	6.5–9.4	513	6.24×10^4	1:2
Co(III)-DSBINPH[a]	3.8–4.1	518	6.40×10^4	1:2
	6.0–6.9	518	5.96×10^4	1:2
Cu(II)-NPHPTS	4.5–5.4	487	4.00×10^4	1:1
	8.4–10.0	483	7.55×10^4	1:2
Cu(II)-NPHQTS	4.1–4.9	518	3.80×10^4	1:1
	7.9–9.7	507	7.30×10^4	1:2
Cu(II)-BTNPHTS	3.4–6.4	530	4.30×10^4	1:1
Cu(II)-BINPHTS	3.5–7.5	509	4.10×10^4	1:1
Cu(II)-DSBINPH[a]	4.5–7.3	510	4.40×10^4	1:1
Fe(II)-NPHPTS	6.0–10.0	474	5.60×10^4	1:2
Fe(II)-NPHQTS	4.0–9.1	505	4.80×10^4	1:2
Fe(II)-BTNPHTS	4.0–8.0	509	4.90×10^4	1:2
Fe(II)-BINPHTS	4.7–9.5	496	5.40×10^4	1:2
Fe(II)-DSBINPH[a]	5.5–7.9	493	5.40×10^4	1:2
Ni(II)-NPHPTS[c]	7.5–10.0	480	8.20×10^4	1:2
Ni(II)-NPHQTS[c]	6.5–9.5	510	8.10×10^4	1:2
Ni(II)-BTNPHTS[c]	5.5–8.2	517	8.80×10^4	1:2
Ni(II)-BINPHTS[c]	6.5–8.9	498	8.70×10^4	1:2
Ni(II)-DSBINPH[a]	7.2–8.5	501	8.80×10^4	1:2
Pd(II)-NPHPTS	1.9–7.8	531	2.40×10^4	1:1
Pd(II)-NPHQTS	0.0–3.2	564	1.55×10^4	1:1
Pd(II)-BTNPHTS	−0.3–0.3	595	2.60×10^4	1:1
Pd(II)-BINPHTS	0.3–4.0	562	2.75×10^4	1:1
Pd(II)-DSBINPH[a]	3.3–4.5	565	3.36×10^4	1:1
Zn(II)-NPHPTS	7.8–10.0	476	8.20×10^4	1:2
Zn(II)-NPHQTS	7.6–10.0	506	8.35×10^4	1:2
Zn(II)-BTNPHTS	8.9–9.5	509	8.50×10^4	1:2
Zn(II)-BINPHTS	8.3–9.3	493	7.75×10^4	1:2
Zn(II)-DSBINPH[a]	9.1	494	7.72×10^4	1:2

[a, b, c] Measured in earlier works.[3–5]

$$M^{2+} + nH_{b-i+4}L^{(i-4)-} \underset{}{\overset{K_{eq}}{\rightleftharpoons}} M(H_{b-i+4}L)_{n-m}(H_{b-i+3}L)_m^{Z-} + mH^+ \quad (3)$$

$$K_{eq} = \frac{[M(H_{b-i+4}L)_{n-m}(H_{b-i+3}L)_m^{Z-}][H^+]^m}{[M^{2+}][H_{b-i+4}L^{(i-4)-}]^n} \quad (4)$$

where $Z = n(i-4) + m - 2$ and K_{eq} is the equilibrium constant. If the initial concentration of the ligand, C_L, is much higher than that of the metal ion, C_M, and the acid dissociation of the ligand is taken into consideration, equation (4) can be approximated as

$$K_{eq} = \frac{x[H^+]^m}{(C_M - x)\left(\frac{C_L[H^+]}{K_{ai} + [H^+]}\right)^n} \quad (5)$$

where x is the equilibrium concentration of the complex formed. On the other hand, as the system obeys Beer's law additively over the wavelength range of interest, equation (6) can be deduced

$$A = \epsilon_L(C_L - nx) + \epsilon_C x \quad (6)$$

where ϵ_L and ϵ_C are apparent molar absorptivities of the ligand and the complex at a specified wavelength, respectively, and A is the absorbance of the solution containing the metal

ion and the ligand. When the absorbance of the solution is measured against a reagent blank, from equations (5) and (6), equation (7) can finally be obtained:

$$\frac{C_M}{A} = \frac{1}{\epsilon_C - n\epsilon_L} + \frac{[H^+]^m}{(\epsilon_C - n\epsilon_L)C_L^n K_{eq}} \times \left(1 + \frac{K_{ai}}{[H^+]}\right)^n \quad (7)$$

Equation (7) means that either the plot of C_M/A *versus* $1/C_L^n$ at constant values of C_M and $[H^+]$ or the plot of C_M/A *versus* $[H^+]^m\{1 + (K_{ai}/[H^+])\}^n$ at constant values of C_M and C_L should give a straight line, provided that the values of n and/or m were correctly assumed. The value of K_{eq} can be calculated from the intercept and the slope of either line.

When the hydrazone exists as one species under experimental conditions, the pH value of the solution is much smaller than the pK_{ai} value of the hydrazone. So the value of $K_{ai}/[H^+]$ becomes negligibly small. Therefore, equation (7) can be simplified to give equation (8):

$$\frac{C_M}{A} = \frac{1}{\epsilon_C - n\epsilon_L} + \frac{[H^+]^m}{(\epsilon_C - n\epsilon_L)C_L^n K_{eq}} \quad (8)$$

Also in this case the value of K_{eq} can be calculated from the intercept and the slope of either a plot of C_M/A *versus* $1/C_L^n$ or C_M/A *versus* $[H^+]^m$ in the same way as in the case of equation (7).

The overall formation constant, β_n, of the complex formed by

$$M^{2+} + (n-m)H_{b-i+4}L^{(i-4)-} + mH_{b-i+3}L^{(i-3)-} \rightleftharpoons M(H_{b-i+4}L)_{n-m}(H_{b-i+3}L)^{Z-} \quad (9)$$

is given by

$$\beta_n = \frac{[M(H_{b-i+4}L)_{n-m}(H_{b-i+3}L)_m^{Z-}]}{[M^{2+}][H_{b-i+4}L^{(i-4)-}]^{n-m}[H_{b-i+3}L^{(i-3)-}]^m} \quad (10)$$

and can be calculated from the values of K_{eq} and K_{ai} as follows:

$$\beta_n = K_{eq}/K_{ai}^m \quad (11)$$

In the case of palladium(II), the metal ion forms a 1:1 complex with each hydrazone and in the presence of a large excess of chloride ion over palladium(II) it forms a mixed ligand complex with each hydrazone and chloride ion, so the complexation equilibrium may be expressed as

$$Pd^{2+} + H_{b-i+4}L^{(i-4)-} + qCl^- \overset{K_{eq}}{\rightleftharpoons} Pd(H_{b-i+4-m}L)Cl_q^{Z-} + mH^+ \quad (12)$$

$$K_{eq} = \frac{[Pd(H_{b-i+4-m}L)Cl_q^{Z-}][H^+]^m}{[Pd^{2+}][H_{b-i+4}L^{(i-4)-}][Cl^-]^q} \quad (13)$$

Here $Z = i + m + q - 6$. In analogy with the derivation of equation (7), equation (14) can finally be obtained:

$$\frac{C_{Pd}}{A} = \frac{1}{\epsilon_C - \epsilon_L} + \frac{[H^+]^m}{(\epsilon_C - \epsilon_L)C_L K_{eq} C_{Cl}^q} \times \left(1 + \frac{K_{ai}}{[H^+]}\right) \quad (14)$$

where C_{Cl} is the initial concentration of chloride ion. The values of m and q can be determined by closely examining the linearity of plots of C_{Pd}/A *versus* $[H^+]^m\{1 + (K_{ai}/[H^+])\}$ and C_{Pd}/A *versus* $1/C_{Cl}^q$, respectively, the value of K_{eq} being calculated from the intercept and the slope of either line.

The overall formation constant, β, of the complex can be calculated from equation (15):

$$\beta = \frac{[Pd(H_{b-i+4-m}L)Cl_q^{Z-}]}{[Pd^{2+}][H_{b-i+4-m}L^{(i-4+m)-}][Cl^-]^q} = \frac{K_{eq}}{K_{ai}K_{a(i+1)}\cdots K_{a(i+m-1)}} \quad (15)$$

Cadmium(II) complexes

Cadmium(II) forms 1:2 (metal:ligand) complexes with all the hydrazones in weakly alkaline solutions as described already. Since each hydrazone exists as one species under the experimental conditions adopted, plots of C_{Cd}/A *vs.* $1/C_L^n$ and C_{Cd}/A *vs.* $[H^+]^m$ based on equation (8) were prepared for each cadmium(II)–hydrazone system. Both plots gave straight lines when it was assumed $n = 2$ and $m = 1$ in every system. An example of each plot is shown in Figs. 1 and 2. These results indicate that the complexation reactions proceed according to equations (16)–(18). With NPHPTS, NPHQTS and BTNPHTS:

$$Cd^{2+} + 2HL^- \rightleftharpoons Cd(HL)L^- + H^+ \quad (16)$$

with BINPHTS:

$$Cd^{2+} + 2H_2L^- \rightleftharpoons Cd(H_2L)(HL)^- + H^+ \quad (17)$$

and with DSBINPH:

$$Cd^{2+} + 2H_2L^{2-} \rightleftharpoons Cd(H_2L)(HL)^{3-} + H^+ \quad (18)$$

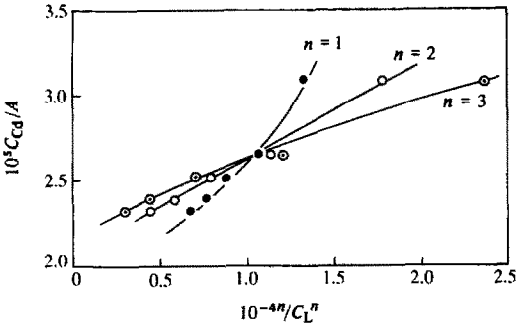

Fig. 1. Plots of C_{Cd}/A *versus* $1/C_L^n$ for the formation of the cadmium(II)–BINPHTS complex. C_{Cd}, $3.58 \times 10^{-6}M$; pH, 7.4; ionic strength, 0.2 ($NaClO_4$); wavelength, 495 nm; temperature, $25 \pm 0.1°$; standing time, 30 min.

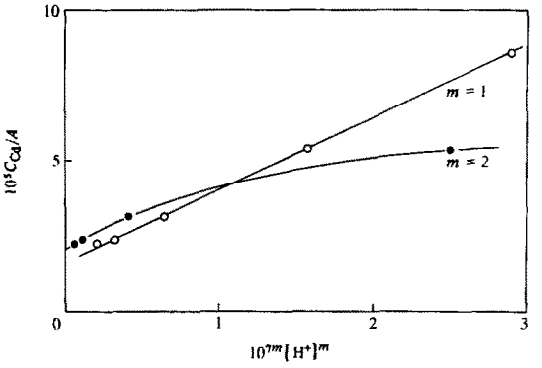

Fig. 2. Plots of C_{Cd}/A *versus* $[H^+]^m$ for the formation of the cadmium(II)–BINPHTS complex. C_{Cd}, $3.58 \times 10^{-6}M$; C_L, $1.74 \times 10^{-4}M$. Other conditions are the same as for Fig. 1.

The log K_{eq} value calculated from the intercept and the slope of each plot and the log β_2 value for each complex calculated by equation (11) are given in Table 3.

Copper(II) complexes

Copper (II) forms 1:1 complexes with all the hydrazones in weakly acidic solutions and, in addition, 1:2 complexes with NPHPTS and NPHQTS in weakly alkaline solutions. As two species of each hydrazone exist in acidic solutions where the 1:1 complex is formed, plots of C_{Cu}/A *vs.* $1/C_L^n$ and C_{Cu}/A *vs.* $[H^+]^m\{1+(K_{ai}/[H^+])\}^n$ based on equation (7) were prepared for each copper(II)–hydrazone system in the study of the formation equilibrium of the 1:1 complex. These plots gave straight lines when it was assumed $n = 1$ and $m = 1$ in every system. An example is shown in Fig. 3. These results indicate that the complexation reactions proceed according to equations (19)–(22).

With NPHPTS and NPHQTS:

$$Cu^{2+} + H_2L \rightleftharpoons Cu(HL)^+ + H^+ \quad (19)$$

and with BTNPHTS, BINPHTS and DSBINPH:

$$Cu^{2+} + HL^- \rightleftharpoons CuL + H^+ \quad (20)$$

$$Cu^{2+} + H_3L \rightleftharpoons Cu(H_2L)^+ + H^+ \quad (21)$$

and

$$Cu^{2+} + H_3L^- \rightleftharpoons Cu(H_2L) + H^+ \quad (22)$$

respectively. In the study of the formation equilibria of the 1:2 complexes formed with NPHPTS and NPHQTS in weakly alkaline solutions, plots of C_{Cu}/A *vs.* $1/C_L^n$ and C_{Cu}/A *vs.* $[H^+]^m$ gave straight lines when it was assumed $n = 2$ and $m = 1$ similarly to the case of the formation equilibria of cadmium(II) complexes described above. These results indicate that the complexation reactions with both hydrazones proceed according to equation (23):

$$Cu^{2+} + 2HL^- \rightleftharpoons Cu(HL)L^- + H^+ \quad (23)$$

Calculated values of log K_{eq}, log β_1 and log β_2 in each system are given in Table 3. The β_1 value of the BTNPHTS complex is remarkably larger than those of the other hydrazone complexes. The reason is as follows: as is clear from the pK_{a4} value of BTNPHTS, the species of BTNPHTS which reacts with copper(II) around pH 3 where the experiment was performed is HL^- but not H_2L, which is different from the species in the cases of NPHPTS and NPHQTS, and is as shown in equation (20). So, the K_{a5} value was used for the calculation of the β_1 value of the BTNPHTS complex, which makes the log β_1 value of the BTNPHTS complex remarkably large.

Palladium(II) complexes

Palladium(II) forms 1:1 complexes with all the hydrazones in acidic solutions. In the presence of a large excess of chloride ion, it forms a mixed ligand complex with each hydrazone and chloride ion. So, plots of C_{Pd}/A *vs.* $1/C_{Cl}^q$ and C_{Pd}/A *vs.* $[H^+]^m\{1+(K_{ai}/[H^+])\}$ based on equation (14) were prepared for each system except for the Pd(II)–NPHQTS–Cl system, their linearity being closely examined. In the Pd(II)–NPHQTS–Cl system, the complex was precipitated because of its low solubility, so its complexation equilibrium was not studied. The results revealed that $m = 2$ and $q = 1$ in every system except for the Pd(II)–BTNPHTS-Cl system in which $m = 1$ and $q = 2$, indicating that the complexation reactions with NPHPTS,

Table 3. Equilibrium constants, overall formation constants and species of complexes

System	Species of complex	log K_{eq}	log β_1	log β_2
Cd(II)-NPHPTS	$Cd(HL)L^-$	0.64 ± 0.02		12.12 ± 0.05
Cd(II)-NPHQTS[a]	$Cd(HL)L^-$	1.56 ± 0.04		13.10 ± 0.07
Cd(II)-BTNPHTS	$Cd(HL)L^-$	0.27 ± 0.10		11.00 ± 0.13
Cd(II)-BINPHTS	$Cd(H_2L)(HL)^-$	0.32 ± 0.04		10.94 ± 0.07
Cd(II)-DSBINPH	$Cd(H_2L)(HL)^{3-}$	0.41 ± 0.02		10.61 ± 0.05
Cu(II)-NPHPTS	$Cu(HL)^+$	0.73 ± 0.04	5.09 ± 0.07	
Cu(II)-NPHPTS	$Cu(HL)L^-$	1.24 ± 0.04		12.72 ± 0.06
Cu(II)-NPHQTS[a]	$Cu(HL)^+$	1.02 ± 0.03	5.40 ± 0.07	
Cu(II)-NPHQTS[a]	$Cu(HL)L^-$	2.89 ± 0.05		14.43 ± 0.08
Cu(II)-BTNPHTS	CuL	1.95 ± 0.03	12.69 ± 0.06	
Cu(II)-BINPHTS[a]	$Cu(H_2L)^+$	1.33 ± 0.02	4.91 ± 0.05	
Cu(II)-DSBINPH	$Cu(H_2L)$	1.36 ± 0.03	4.73 ± 0.08	
Fe(II)-NPHPTS				
Fe(II)-NPHQTS[a]	$Fe(HL)L^-$	8.73 ± 0.05		20.27 ± 0.08
Fe(II)-BTNPHTS	$Fe(HL)L^-$	5.04 ± 0.10		15.78 ± 0.14
Fe(II)-BINPHTS				
Fe(II)-DSBINPH	$Fe(H_2L)(HL)^{3-}$	8.73 ± 0.05		15.25 ± 0.08
Ni(II)-NPHPTS[b]	NiL_2^{2-}	-2.36 ± 0.03		20.60 ± 0.09
Ni(II)-NPHQTS[b]	NiL_2^{2-}	-1.59 ± 0.04		21.49 ± 0.11
Ni(II)-BTNPHTS[b]	NiL_2^{2-}	-0.33 ± 0.03		21.15 ± 0.09
Ni(II)-BINPHTS[b]	$Ni(HL)_2^{2-}$	-2.71 ± 0.04		18.51 ± 0.12
Ni(II)-DSBINPH[c]	$Ni(HL)_2^{4-}$	-1.02 ± 0.08		19.38 ± 0.08
Pd(II)-NPHPTS	$Pd(HL)^+$	4.92 ± 0.05	10.01 ± 0.08	
Pd(II)-NPHQTS	$Pd(HL)^+$	4.83 ± 0.06	9.91 ± 0.09	
Pd(II)-BTNPHTS	$Pd(HL)^+$	4.90 ± 0.02	6.92 ± 0.06	
Pd(II)-BINPHTS	$Pd(H_2L)^+$	4.91 ± 0.03	9.18 ± 0.07	
Pd(II)-DSBINPH	$Pd(H_2L)$	5.06 ± 0.04	9.13 ± 0.08	
Pd(II)-NPHPTS-Cl	Pd(HL)Cl	8.03 ± 0.02	13.16 ± 0.05[d]	
Pd(II)-NPHQTS-Cl				
Pd(II)-BTNPHTS-Cl	$Pd(H_2L)Cl_2$	12.51 ± 0.03	13.21 ± 0.06[d]	
Pd(II)-BINPHTS-Cl	$Pd(H_2L)Cl$	8.44 ± 0.03	12.72 ± 0.05[d]	
Pd(II)-DSBINPH-Cl	$Pd(H_2L)Cl^-$	8.56 ± 0.02	12.63 ± 0.05[d]	
Zn(II)-NPHPTS	$Zn(HL)L^-$	1.51 ± 0.03		12.99 ± 0.05
Zn(II)-NPHQTS[a]	$Zn(HL)L^-$	2.85 ± 0.03		14.39 ± 0.07
Zn(II)-BTNPHTS	$Zn(HL)L^-$	0.67 ± 0.04		11.40 ± 0.08
Zn(II)-BINPHTS	$Zn(H_2L)(HL)^-$	1.11 ± 0.05		11.72 ± 0.08
Zn(II)-DSBINPH	$Zn(H_2L)(HL)^{3-}$	1.04 ± 0.03		11.24 ± 0.06

Temperature: $25 \pm 0.1°$, Ionic strength: 0.2 ($NaClO_4$).

[a] Measured in aqueous 10% v/v 1,4-dioxane solutions.

[b,c] Determined in earlier works.[3,5]

[d] Shows the overall formation constant, β, of the mixed ligand complex.

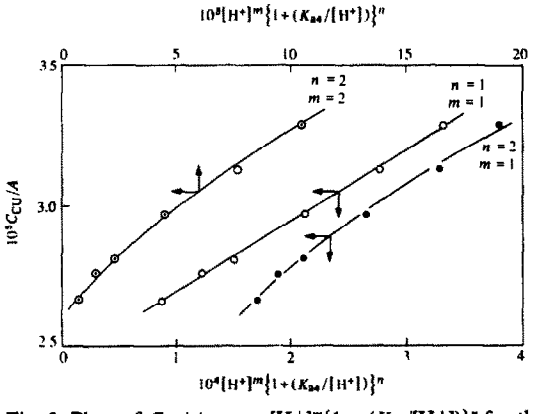

Fig. 3. Plots of C_{Cu}/A *versus* $[H^+]^m\{1+(K_{a4}/[H^+])\}^n$ for the formation of the copper(II)–NPHPTS complex. C_{Cu}, $6.33 \times 10^{-6}M$; C_L, $1.92 \times 10^{-4}M$; wavelength, 487 nm. Other conditions are the same as for Fig. 1.

BTNPHTS, BINPHTS and DSBINPH proceed according to equations (24)–(27), respectively:

$$Pd^{2+} + H_3L^+ + Cl^- \rightleftharpoons Pd(HL)Cl + 2H^+ \quad (24)$$

$$Pd^{2+} + H_3L^+ + 2Cl^- \rightleftharpoons Pd(H_2L)Cl_2 + H^+ \quad (25)$$

$$Pd^{2+} + H_4L^+ + Cl^- \rightleftharpoons Pd(H_2L)Cl + 2H^+ \quad (26)$$

$$Pd^{2+} + H_4L + Cl^- \rightleftharpoons Pd(H_2L)Cl^- + 2H^+ \quad (27)$$

Calculated values of $\log K_{eq}$ and $\log \beta$ for each system are given in Table 3.

In the absence of chloride ions, the investigation of the complexation equilibria by the above-mentioned equilibrium-shift method could not be applied because the spectral change due to the complexation was very small. So, Hildebrand–Reilley's method[3,7] was applied here, in which the complexation equilibria were investigated in the presence of a large excess of palladium(II) over the ligand and chloride ion, the linearity of the plot of the left hand side of equation (28) *vs.* $\log[H^+]$ for each system having closely been examined.

$$\log \frac{A}{A_\infty - A} + \log\left(1 + \frac{K_{ai}}{[H^+]}\right) - \log C_{Pd} = \log K_{eq} - m \log[H^+] \quad (28)$$

Here A_∞ is the limiting absorbance when all of the ligand is complexed quantitatively with the metal ion at higher pH. This plot for each system gave a straight line with a slope of about -2. An example is shown in Fig. 4. These results indicate that the complexation reactions proceed according to equations (29)–(31):

With NPHPTS, NPHQTS and BTNPHTS

$$Pd^{2+} + H_3L^+ \rightleftharpoons Pd(HL)^+ + 2H^+ \quad (29)$$

with BINPHTS and DSBINPH

$$Pd^{2+} + H_4L^+ \rightleftharpoons Pd(H_2L)^+ + 2H^+ \quad (30)$$

and

$$Pd^{2+} + H_4L \rightleftharpoons Pd(H_2L) + 2H^+ \quad (31)$$

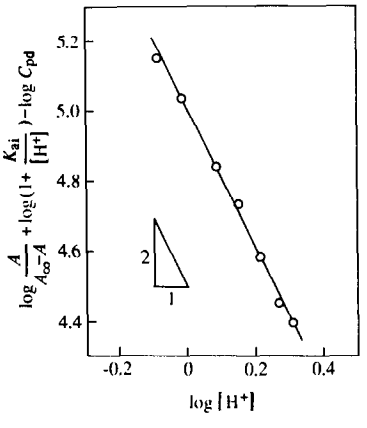

Fig. 4. Plot of $\log\{A/(A_\infty - A)\} + \log\{1 + (K_{ai}/[H^+])\} - \log C_{Pd}$ *versus* $\log[H^+]$ for the formation of the Pd(II)–DSBINPH complex. C_{Pd}, $6.43 \times 10^{-4} M$; C_L, $1.62 \times 10^{-5} M$; ionic strength, 2.0 ($NaClO_4$); wavelength, 520 nm. Other conditions are the same as for Fig. 1.

respectively. The value of $\log K_{eq}$ calculated from the intercept of each plot and that of $\log \beta_1$ of each complex obtained from equation (15) (in this case $q = 0$) are given in Table 3. The β_1 value of the BTNPHTS complex is considerably smaller than those of the other hydrazone complexes. The reason may be attributed to the large K_{a4} value of BTNPHTS, in other words, the weak basicity of the benzothiazole-nitrogen of BTNPHTS.

As is clear from the above results, the formation constant, β, of the Pd(II)–hydrazone–Cl complexes are larger than those, β_1, of the corresponding Pd(II)–hydrazone complexes. Incidentally, the formation constant of the Pd(II)–hydrazone–Cl complex when it was assumed to be formed by the reaction of the Pd(II)–hydrazone complex with chloride ion, β', is defined as equation (32) and is rewritten as equation (33) by using β_1 given by equation (34) and β already defined by equation (15) (in this case $m = 2$ and $q = 1$).

$$\beta' = \frac{[Pd(H_{b-t+2}L)Cl^{(t-3)-}]}{[Pd(H_{b-t+2}L)^{(t-4)-}][Cl^-]} \quad (32)$$

$$\beta' = \beta/\beta_1 \quad (33)$$

$$\beta_1 = \frac{[Pd(H_{b-t+2}L)^{(t-4)-}]}{[Pd^{2+}][H_{b-t+2}L^{(t-2)-}]} \quad (34)$$

The magnitude of the contribution of chloride ion to the Pd(II)–hydrazone–Cl complex may be estimated by using the value of β'. Calculated values of $\log \beta'$ for the complexes of NPHPTS, BINPHTS and DSBINPH were 3.15, 3.54 and 3.50, respectively, indicating that the β' value is independent of the kind of the hydrazone ligand.

Other metal complexes

Cobalt(II) forms 1:2 complexes with all the hydrazones in weakly acidic to alkaline solutions, the resultant cobalt(II) complexes being rapidly oxidized to the corresponding stable cobalt(III) complexes by dissolved oxygen. Both the formation of the cobalt(II) complexes and their oxidation to the tervalent complexes were very rapid and it was difficult to control the concentration of dissolved oxygen in solution, so the complexation equilibria of cobalt(II) with the hydrazones were not studied here.

Iron(II) forms 1:2 complexes with all the hydrazones in weakly acidic to neutral and/or alkaline solutions. Under experimental conditions for the study of formation equilibria of iron(II) complexes, two kinds of species must be

taken into consideration for each hydrazone, so plots of C_M/A *vs.* $1/C_L^n$ and C_M/A *vs.* $[H^+]^m\{1+(K_{ai}/[H^+])\}^n$ were investigated for each iron(II)–hydrazone system. Both plots gave straight lines when it was assumed $n=2$ and $m=1$ in every system except for the iron(II)–NPHPTS and iron(II)–BINPHTS systems. Calculated values of $\log K_{eq}$ and $\log \beta_2$ are summarized in Table 3 along with the species of the complex formed in each system. In the case of the iron(II)–NPHPTS and iron(II)–BINPHTS systems, mixtures of a 1:1 and a 1:2 complex are formed around pH 3 where the experiments were carried out (although stable 1:2 complexes were formed at higher pH), so values of K_{eq} and β_n of the NPHPTS and BINPHTS complexes could not be determined.

As for the formation equilibria between zinc(II) and the hydrazones, plots of C_M/A *vs.* $1/C_L^n$ and C_M/A *vs.* $[H^+]^m$ based on equation (8) were prepared for each system. Every plot gave a straight line when it was assumed $n=2$ and $m=1$. Calculated values of $\log K_{eq}$ and $\log \beta_2$ are summarized in Table 3 along with those for each nickel(II)–hydrazone complexes determined in earlier works.[3,5]

REFERENCES

1. T. Odashima, T. Kikuchi, W. Ohtani and H. Ishii, *Analyst*, 1986, **111**, 1383.
2. K. Kohata, Y. Kawamonzen, T. Odashima and H. Ishii, *Bull. Chem. Soc. Jpn.*, 1990, **63**, 3398.
3. T. Odashima, M. Yamaguchi and H. Ishii, *Mikrochim. Acta*, 1991 **I**, 267.
4. H. Ishii, T. Odashima and Y. Kawamonzen, *Anal. Chim. Acta*, 1991, **244**, 223.
5. *Idem*, *Bull. Chem. Soc. Jpn.*, 1990, **63**, 3405.
6. L. Sommer and M. Langova, *CRC Crit. Rev. Anal. Chem.*, 1988, **19**, 225.
7. G. P. Hildebrand and C. N. Reilley, *Anal. Chem.*, 1957, **29**, 258.

Talanta, Vol. 39, No. 9, pp. 1189–1194, 1992
Printed in Great Britain

0039-9140/92 $5.00 + 0.00
Pergamon Press Ltd

RAPID CHELATOMETRIC DETERMINATION OF BISMUTH, TITANIUM AND ALUMINIUM USING SEMI-XYLENOL ORANGE WITH VISUAL END-POINT INDICATION

MEDHAT ABD EL-HAMIED HAFEZ
Chemistry Department, Faculty of Science, Mansoura University, El-Mansoura, Egypt

(*Received* 13 *September* 1991. *Revised* 5 *March* 1992. *Accepted* 6 *March* 1992)

Summary—A rapid and simple general complexometric method was presented for the determination of bismuth, titanium and aluminium in laboratory synthesized alloys similar to those of some bauxites, clay, ilmenite, Portland cements and ceramic products. The precision and accuracy attainable in successive titrations of Bi^{3+}, Ti^{4+} and Al^{3+} with 0.01 and/or 0.001*M* solutions of disodium ethylenediaminetetraacetate (Na_2EDTA) and standard $ZnCl_2$ of the same concentration, using Semi-Xylenol Orange (SXO) as a metallochromic indicator with visual end-point indication were studied. For one aliquot Bi^{3+} was at first directly titrated at pH 1–2 (HNO_3) with Na_2EDTA using SXO as indicator in the presence of *L*-ascorbic acid to reduce Fe^{3+} to Fe^{2+}. At the bismuth end-point, an excess of Na_2EDTA was added, the pH was adjusted with hexamine buffer (pH 5) and the excess of Na_2EDTA was back-titrated with solution of standard zinc(II) chloride for both the simultaneous and consecutive titrations in the presence of (SXO) as indicator. For the simultaneous titration, fluoride was added to release the Na_2EDTA combined with both Al^{3+} and Ti^{4+}. For the consecutive titration, phosphate was added to release the Na_2EDTA combined with Ti^{4+} and then fluoride to release the Na_2EDTA combined with Al^{3+}. The interference of various anions and cations in the determination of Bi^{3+}, Ti^{4+} and Al^{3+} was studied. A comparison of the accuracy of both the simultaneous and consecutive titration was also carried out. The proposed methods were applied successfully to some real samples of bauxites, clay, ilmenite, Portland cements and ceramic products and the results were satisfactory.

Although Ti^{4+}, Al^{3+} and/or Bi^{3+} are common components of some clays, minerals, Portland cement and ceramic products, rapid and simple general methods for their analysis have encountered difficulties. The standard gravimetric methods are tedious and more time consuming. A comparatively small number of papers have dealt with the quantitative approach to the determination of $Ti^{4+} + Al^{3+}$ or $Ti^{4+} + Bi^{3+}$ or $Al^{3+} + Bi^{3+}$ ions.[1–7] It has been previously shown that the spectrophotometric indication of complexometric titrations using Semi-Xylenol Orange (SXO) as indicator gives very accurate and precise results at the microgram level.[8–11]

The aim of this work is to present a rapid and simple general complexometric method for the determination of Bi^{3+}, Ti^{4+} and Al^{3+} if present together by either two sample solutions (simultaneous titration) or a single aliquot solution (consecutive titration) with high precision and accuracy. At first artificial mixtures similar to those of some bauxites, clay, ilmenite, Portland cements and ceramic products were determined by visual end-point indication using SXO as a metallochromic indicator followed by an application of the proposed methods for real naturally occurring samples containing some of such metals. The problem of Ti^{4+} hydrolysis was avoided by using the very weak hexamine base solution to adjust the pH of the solution before the back-titration of Ti^{4+}. For the simultaneous titration, Ti^{4+} was separated as the hydroxide from Al^{3+} which was back-titrated with Na_2EDTA in one aliquot and then both Al^{3+} and Ti^{4+} were simultaneously determined in another sample, where Ti^{4+} was found by difference. For the consecutive titration no separation was required and both Ti^{4+} and Al^{3+} could be simply determined individually by firstly demasking quantitatively the Na_2EDTA equivalent to Ti^{4+} using $H_2PO_4^-$ ion[12] followed by the release of Na_2EDTA corresponding to Al^{3+} using F^- ion.[13,14]

EXPERIMENTAL

Reagents and solutions

A 0.01*M* solution of disodium ethylenediaminetetraacetate (Na_2EDTA) was prepared by dissolving the required mass of Na_2EDTA

(analytical-reagent grade, BDH, Poole, Dorset, UK) in bidistilled water and diluting to the necessary volume. Standard bismuth(III), titanium(IV) and aluminium(III) chloride solutions were prepared by dissolving high-purity (99.99%) bismuth, titanium and aluminium powdered metals (BDH) in boiling concentrated hydrochloric acid and diluting to the necessary volume with 0.3*M* hydrochloric acid. The Na_2EDTA solution ($\simeq 0.01M$) was standardized by the spectrophotometric titration of 0.001*M* Bi(III) chloride using Xylenol Orange as indicator in nitric acid solution (pH 1–1.5, 530 nm). All other salts were prepared by dissolving the calculated mass of each salt (BDH) in the required volume of bidistilled water. Zinc(II) solution was standardized by titration against standard Na_2EDTA solution using Xylenol Orange as indicator in hexamine buffer. The hexamine-HNO_3 buffer solution (1*M*) was prepared from analytical-reagent grade chemicals (BDH) by pH metric titration of 125 ml (2*M*) solution of hexamine against nitric acid (2*M*) until a pH of 5 was obtained and then the whole solution was completed to a total volume of 250 ml in a measuring flask using potassium nitrate solution (2*M*). Purified sample of indicator obtained by solvent-counter current separation[15,16] was used for preparing 0.01*M* solution of SXO (ammonium salt) in doubly distilled water.

Apparatus

A Beckman (Fullerton, CA, U.S.A.) digital pH meter with glass and saturated calomel electrodes calibrated on the operational pH scale with standard buffer solutions was used.

Decomposition of samples

The processes of crushing, grinding (200 mesh), decomposition by different fusion mixtures and dissolution of various real samples were carried out as described in literature.[17,18] For each sample $\simeq 0.5$ g was usually taken and dissolved after the described pretreatment into a 250-ml measuring flask. Silica must be completely separated in each case in the customary manner.[17,18]

RESULTS AND DISCUSSION

Simultaneous titration of Al^{3+} and Ti^{4+} with Bi^{3+} by visual end-point indication using SXO

Because of the importance of some of the three studied ions in many bauxites, clays, ilmenite, Portland cements and ceramic products, a rapid and simple complexometric method for the determination of the three ions with high precision and accuracy by visual titration using SXO as indicator would be helpful. Different series containing various proportions of Bi^{3+}, Ti^{4+} and Al^{3+} ions with constant concentraton of Fe^{3+} and Ca^{2+} ions were determined. The same procedure was applied for real naturally occurring samples. In one of such series (Series I), 5 ml of 0.01*M* of each of Bi^{3+}, Ti^{4+} and Al^{3+} solution were transferred into a conical flask containing 2 ml of Fe^{3+} solution (0.01*M*) and 8 ml of Ca^{2+} solution of the same concentration. A 2.5-ml volume of nitric acid (1*M*), 1 ml of *L*-ascorbic acid (1*M*) to reduce Fe^{3+} to Fe^{2+} and a few drops of SXO indicator to allow the end-point to be easily detected by the human eye were added to the ions to be determined. The whole solution was diluted by 80–100 ml of bidistilled water. The mixture was directly titrated against 0.01*M* Na_2EDTA until the colour changed from red to yellow; this step produces the Bi^{3+} ion. At the bismuth end-point an excess of 30 ml of Na_2EDTA was added, followed by 1*M* hexamine solution to a pH of $\simeq 5$ (pH test paper), and finally 2.5 ml of hexamine–HNO_3 buffer of pH 5 were added. The whole solution was boiled for 2–3 min, cooled to room temperature and then diluted to about 160–180 ml. A few drops of SXO solution were added, stirred and the excess of Na_2EDTA was back titrated against 0.01*M* standard zinc chloride solution until the colour changed from yellow to bright red.

For the simultaneous titration of both Al^{3+} and Ti^{4+}, 2 ml of 1*M* sodium fluoride were added to the latter end-point solution, boiled for 2–3 min, cooled and a few drops of SXO and 2.5 ml of hexamine–HNO_3 buffer (pH 5) were added. The whole solution was titrated again with 0.01*M* Zn(II) solution (this step gives $Al^{3+} + Ti^{4+}$). Another aliquot containing the same concentration of the studied cations was taken and Ti^{4+} was completely quantitatively precipitated together with Bi^{3+}, Fe^{3+} and most of Ca^{2+} as the corresponding hydroxides by the dropwise addition of sodium hydroxide solution (1*M*) until a pH of $\simeq 13.5$ (pH test paper) was approached where Al^{3+} exists in solution as AlO_2^-. The latter solution was boiled for 5 min, cooled and the precipitate was separated by filtration, washed several times with bidistilled water. The precipitate was neglected. The pH of the filtrate was lowered to a value of 2 by nitric

acid (1*M*) where aluminium exists in solution as simple Al^{3+} ion, then raised to a value of $\simeq 5$ by hexamine solution (pH test paper) and then hexamine–HNO_3 buffer (pH 5) was added. Aluminium(III) was determined in the filtrate by adding an excess known volume of standard Na_2EDTA followed by back-titration with standard Zn^{2+} solution of the same concentration as Na_2EDTA using SXO as indicator and titanium was found by difference. Calcium does not react with Na_2EDTA at a pH of 5, so any traces of such ion present in the filtrate will not interfere with aluminium.[11]

The feasibility of the simultaneous titration of Al^{3+} and Ti^{4+} with Bi^{3+} was studied for different ratios of them with Fe^{3+} and Ca^{2+}. Eight series of simultaneous titrations were performed with molar ratios of $Bi^{3+}:Ti^{4+}:Al^{3+}$ ranging from 10:4:1 to 1:10:4 to 4:1:10, respectively. For each series constant concentration of both Fe^{3+} and Ca^{2+} was added. No difficulties were encountered in the end-point detection for all the three metals studied. The results of parallel determinations of the three ions using the simultaneous titration method of Ti^{4+} and Al^{3+} with Bi^{3+} are given in Table 1. The calculated results show that the determination of Bi^{3+} is more accurate than the determination of both of Ti^{4+} and Al^{3+}.

Consecutive titration of Al^{3+} and Ti^{4+} with Bi^{3+} by visual end-point indication using SXO

The same experimental procedures described for the determination of Bi^{3+} and of the back-titration of excess Na_2EDTA in the simultaneous titration of one of such series were also exactly adopted in the consecutive titration. A 2-ml volume of sodium dihydrogen phosphate 1*M* were added to the latter solution. The whole mixture was boiled for 2–3 min, cooled and then few drops of SXO and 2.5 ml of hexamine–HNO_3 buffer were added. The analyte solution mixture was titrated against standard zinc(II) chloride solution, until a yellow colour changed to bright red (this step gives Ti^{4+}). For the determination of Al^{3+}, 2 ml of 1*M* sodium fluoride were added to the Ti^{4+} end point solution. The latter solution was boiled for 3–5 min then few drops of SXO and hexamine buffer (2.5 ml) were added and the whole solution was titrated while hot versus standard zinc(II) chloride solution (this titration gives Al^{3+}).

Table 1. Statistical evaluation of eight series of simultaneous titrations of Ti^{4+} and Al^{3+} with Bi^{3+} by visual detection of the end-point using SXO as indicator (pH 1–2 for Bi^{3+} and 5 for Ti^{4+} and Al^{3+}) for all series $c_{Fe^{3+}} = 0.02mM$, $c_{Ca^{2+}} = 0.08mM$, $c_{Na_2EDTA} = c_{Zn^{2+}} = 0.01$ and/or $0.001M$

Series	Metal ion	Titrated concentration of metal, *m*M	Metal taken, *mg*	Mean, *mg*
1	Bi^{3+}	0.050	10.45	10.4*
	Ti^{4+}	0.050	2.40	2.4†
	Al^{3+}	0.050	1.35	1.3
2	Bi^{3+}	0.100	20.90	20.9
	Ti^{4+}	0.025	1.20	1.2
	Al^{3+}	0.025	0.68	0.7
3	Bi^{3+}	0.025	5.23	5.2
	Ti^{4+}	0.025	1.20	1.2
	Al^{3+}	0.100	2.70	2.7
4	Bi^{3+}	0.025	5.23	5.2
	Ti^{4+}	0.100	4.79	4.8
	Al^{3+}	0.025	0.68	0.7
5	Bi^{3+}	0.100	20.90	20.9
	Ti^{4+}	0.040	1.92	1.9
	Al^{3+}	0.010	0.27	0.3
6	Bi^{3+}	0.010	2.09	2.1
	Ti^{4+}	0.100	4.79	4.8
	Al^{3+}	0.040	1.08	1.1
7	Bi^{3+}	0.040	8.36	8.3
	Ti^{4+}	0.010	0.48	0.5
	Al^{3+}	0.100	2.70	2.7
8	Bi^{3+}	0.070	14.63	14.7
	Ti^{4+}	0.025	1.20	1.2
	Al^{3+}	0.055	1.49	1.5

*End-point from red to yellow.
†Ti^{4+} was determined by difference in a 2nd sample.
End-point from yellow to bright red.

Table 2. Statistical evaluation of eight series of consecutive titrations of Ti^{4+} and Al^{3+} with Bi^{3+} by visual detection of the end-point using SXO as indicator. Conditions as in Table 1

Series	Metal ion	Titrated concentration of metal, *m*M	Metal taken, *mg*	Mean, *mg*
1	Bi^{3+}	0.050	10.45	10.4*
	Ti^{4+}	0.050	2.40	2.4†
	Al^{3+}	0.050	1.35	1.3†
2	Bi^{3+}	0.100	20.90	20.8
	Ti^{4+}	0.025	1.20	1.2
	Al^{3+}	0.025	0.68	0.7
3	Bi^{3+}	0.025	5.23	5.2
	Ti^{4+}	0.025	1.20	1.2
	Al^{3+}	0.100	2.70	2.7
4	Bi^{3+}	0.025	5.23	5.2
	Ti^{4+}	0.100	4.79	4.8
	Al^{3+}	0.025	0.68	0.7
5	Bi^{3+}	0.100	20.90	20.9
	Ti^{4+}	0.040	1.92	1.9
	Al^{3+}	0.010	0.27	0.3
6	Bi^{3+}	0.010	2.09	2.1
	Ti^{4+}	0.100	4.79	4.8
	Al^{3+}	0.040	1.08	1.1
7	Bi^{3+}	0.040	8.36	8.4
	Ti^{4+}	0.010	0.48	0.5
	Al^{3+}	0.100	2.70	2.7
8	Bi^{3+}	0.070	14.63	14.7
	Ti^{4+}	0.025	1.20	1.2
	Al^{3+}	0.055	1.49	1.50

*End-point from red to yellow.
†End-point from yellow to bright red.

The same series used in the simultaneous titration method was investigated by the consecutive titration procedure for a meaningful comparison of the accuracy between the two methods.

The results of eight series of parallel determination of the three ions with constant concentration of Fe^{3+} and Ca^{2+} ions are given in Table 2. The obtained results show that the determination of Bi^{3+} is more accurate than the determination of both Ti^{4+} and Al^{3+}. Comparisons of the accuracy between the simultaneous and consecutive titration for the determination of Ti^{4+} and Al^{3+} (Tables 1 and 2) show that the simultaneous method gives more accurate results for Ti^{4+} than the consecutive one specially for the lower concentration of Ti^{4+}. For higher Ti^{4+} concentration the accuracy of the two methods are approximately the same. The accuracy of Al^{3+} determination is almost the same for both methods.

Interference of foreign species

The interference of different anions was studied. It was found that 50-fold excess of Cl^-, Br^-, I^-, NO_3^-, SO_4^{2-} and ClO_4^- slightly interfered. Even equal concentrations of F^-, PO_4^{3-} and tartarate ions interfered. It was found that Fe^{3+}, Ni^{2+}, Th^{4+}, Zr^{4+}, Zn^{2+}, Cd^{2+}, Pb^{2+}, Mn^{2+}, Sn^{2+}, Cu^{2+} and lanthanides interfered seriously when present at 1 or 2 fold excess of the titrated metals. The interfering effect of Fe^{3+} on Bi^{3+} determination could be removed by *L*-ascorbic acid. Fortunately all other interfering cations are rarely found in ceramic products and both Al^{3+} and Ti^{4+} minerals.

The success of the present methods depends on the fact that Ti^{4+} is not hydrolysed when the pH is controlled. The results obtained (Tables 1 and 2) show that those cations can be kept in solution at pH $\simeq$ 5. However, hydrolysis often occurs unless the pH is controlled by dropwise addition of a weak base such as hexamine. It was found that the use of strong base, without respect to its careful addition to the solution, causes the precipitation of titanium after the determination of Bi^{3+}. When solid hexamine was added, it was also found that it causes slight precipitation of Ti^{4+}. Once hydrolysis occurs, an irreversible precipitation of Ti^{4+} happens immediately. In all our previous work, it was found that hexamine solution was preferable to any other weak base and gives a sharper end-point with Semi-Xylenol Orange.[9-11] In the

Table 3. Results of determination of aluminium and titanium in ores by classical and proposed rapid chelatometric method (simultaneous titration, ST)

Sample	Methods, Al_2O_3 (%)		Methods, TiO_2 (%)†	
	Classical	(ST)*	Classical	(ST)*
Bauxite (France)	55.5	56.4	2.6	2.6
Bauxite (India)	56.5	56.5	6.3	6.3
Bauxite (Brazil)	58.4	58.3	1.1	1.7
Bauxite (Greece)	60.2	60.1	3.0	2.9
Bauxite (Ireland)	41.6	41.5	4.3	4.3
Bauxite (Jamaica)	49.4	49.3	2.7	2.7
Bauxite (Yugoslavia)	53.2	53.0	3.4	3.4
Bauxite—brown (Sinai, Egypt)	50.0	50.1	2.9	2.8
Bauxite—greenish white (Sinai, Egypt)	60.1	59.9	2.7	2.6
Cement—Fondu	39.0	39.1	1.6	1.6
Portland cement, ordinary	7.1	7.1	—	—
Kaoline, T. Plateau (Sinai, Egypt)	36.6	36.5	1.8	1.8
Kaoline, Hasber Mountain, (Sinai, Egypt)	37.8	37.9	1.8	1.8
Burnt Egyptian referactory	68.5	68.4	2.6	2.6

*Average of three weighed samples (≃0.5 g/250 ml).
†Titanium is found by difference in a second titration.

consecutive titration, sodium dihydrogen phosphate was used to release Na_2EDTA and determine selectively large amounts of Ti^{4+} in the presence of Al^{3+}. The other advantage of using this salt was that it didn't alter the pH of the solution (≃5). The white precipitate of titanium phosphate formed did not affect the colour change at the end-point. Because of the determination of Al^{3+} and Ti^{4+} combined or alone after Bi^{3+} is based on two titrations, the first being unrecorded ($Ti^{4+} + Al^{3+}$ + blank). The detection limit[19,20] of the two applied methods was 20.9 ppm for Bi^{3+}, 4.79 ppm for Ti^{4+} and 2.7 ppm for Al^{3+}.

Application of the proposed methods

The results of the determination of Bi^{3+}, Ti^{4+} and Al^{3+} in a series of naturally occurring samples containing some of these ions are shown in Tables 3 and 4. These results (average of ten determinations for three weighed samples) are in good agreement with the values obtained by the standard classical methods. The relative standard deviation as calculated from the range method[9] was found to be (0.15–1.95%) and (0.25–0.85%) for both simultaneous and consecutive titration respectively. From the obtained results, it is clear that the analytical determination of the three metal ions in different real samples is simple, reliable and can be applied with good reproducibility. It has been previously shown that SXO is preferable to Xylenol Orange (XO) for both visual and spectrophotometric titrations because of its high precision and accuracy, sensitivity, sharp end-point and formation

Table 4. Results of determination of aluminium, titanium and bismuth in ores by classical and proposed rapid chelatometric method (consecutive titration, CT)

Sample	Methods, Al_2O_3 (%)		Methods, TiO_2 (%)		Methods, Bi_2O_3 (%)	
	Classical	(CT)*	Classical	(CT)*	Classical	(CT)*
Ilmenite Concentrate (Western Coast, Egypt)	2.8	2.8	25.7	25.6	—	—
Ilmenite Concentrate (Black Sand, Rosetta, Egypt)	—	—	34.4	34.3	—	—
Standard Ilmenite	—	—	52.7	52.5	—	—
Bismatite (Arizona, USA)†	—	—	—	—	86.2	86.1
Bismuth Concentrate (Czechoslovakia)†	—	—	—	—	11.8	11.7
Bismuth Concentrate (San Gregoria, Peru)†	—	—	—	—	22.3	22.2
Bauxite (India)	56.5	56.4	6.3	6.3	—	—
Bauxite (Ireland)	41.6	41.5	4.3	4.3	—	—
Aluminium–Bismuth Alloy (laboratory synthesized by fusion)	94.2	94.0	—	—	5.8	5.7

*Average of three weighed samples (≃0.5 g/250 ml).
†Samples does not contain Al_2O_3 or TiO_2.

of (1:1) ratio complex with all of the earlier studied metal ions.[9-11]

Acknowledgements—I would like to express my sincere gratitude to Dr Omar Hegab Abd El-Rahman, Professor of Sedimentology, Geology Department, Faculty of Science, Mansoura University and Mr Mohamed Salah El Din (M.Sc.) the Chief of Geological Museum in the same University for providing me with all of the real samples under investigation.

REFERENCES

1. R. Přibil, *Talanta*, 1965, **12**, 925.
2. *Idem*, *Applied Complexometry*, Pergamon Press, Oxford, 1982.
3. S. L. Culp, *Chemist-Analyst*, 1967, **56**, 29.
4. R. Přibil and P. Schneider, *Coll. Czech. Chem. Commun.*, 1950, **15**, 886.
5. R. Přibil and V. Veselý, *Talanta*, 1963, **10**, 383.
6. *Idem*, *Chemist-Analyst*, 1963, **52**, 43.
7. G. Morar and C. G. Macarovici, *Rev. Roum. Chem.*, 1972, **17**, 1061.
8. M. A. H. Hafez, I. M. M. Kenawy and M. A. Kabil, *Anal. Lett.*, 1985, **18**, 2043.
9. M. A. H. Hafez and M. E. M. Emam, *Analyst*, 1986, **111**, 1435.
10. M. A. H. Hafez, A. M. A. Abdallah and N. E. S. Abd El-Grany, *ibid.*, 1990, **115**, 221.
11. M. A. H. Hafez, A. M. A. Abdallah and T. M. A. Wahdan, *ibid.*, 1991, **116**, 663.
12. I. Sajo, *Mag. Kem. Foly.*, 1954, **60**, 331.
13. J. Kinnunen and B. Merikanto, *Chemist-Analyst*, 1955, **44**, 75.
14. T. S. West, *Complexometry with EDTA and Related Reagents*, 3rd Ed., p. 106. Broglia Press, Bournemouth, U.K., 1969.
15. M. A. H. Hafez, Ph.D. Thesis, University of Chemical Technology, Pardubice, Czechoslovakia, 1980.
16. Unpublished work, Dr Pijpers, Laboratory of Analytical Chemistry, University of Amsterdam, Holland.
17. A. Richard, *Sample Pretreatment and Separation*, p. 60. Wiley, New York, 1987.
18. A. I. Vogel, *Text Book of Quantitative Inorganic Analysis*, 3rd Ed., Longman, London, 1972.
19. H. Kaiser, *Z. Anal. Chem.*, 1965, **209**, 1.
20. H. Kaiser and H. Specker, *ibid.*, 1956, **149**, 46.

Talanta, Vol. 39, No. 9, pp. 1195–1198, 1992
Printed in Great Britain.

0039-9140/92 $5.00 + 0.00

DETERMINATION OF CARBAMATE HERBICIDE ASULAM IN PEACHES FOLLOWING FLUORESCAMINE FLUORIGENIC LABELLING

F. GARCIA SANCHEZ, A. AGUILAR GALLARDO and C. CRUCES BLANCO
Department of Analytical Chemistry, Faculty of Sciences, The University, 29071-Málaga, Spain

(*Received* 18 *October* 1991. *Revised* 23 *January* 1992. *Accepted* 23 *January* 1992)

Summary—Because of the primary aminic character of asulam, it is readily labelled with fluorescamine. A study of the variables affecting the derivatization reaction has been made. Two analytical approaches, that is, direct, synchronous spectrofluorimetry have been tested, and they both show good analytical performances. The linear dynamic range of the synchronous approach is 0.043–0.214 μg/ml and the relative standard deviation is 1.6%. The methods have been applied to the determination of asulam residues in peaches with recoveries of 85–106%.

Asulam (methyl 4-aminobenzenesulphonylcarbamate) is a translocation herbicide, absorbed by leaves and roots causing slow chlorosis in susceptible plants. It interferes with cell division and expansion and is used to control the growth of grasses.[1]

The original method for asulam residues quantification[2] was based on a colorimetric reaction.[3] Analysis for asulam using HPLC in wheat flour was reported,[4] but the metabolites were not examined. Using HPLC reverse phase column,[5] asulam was determined in peaches fortified at the 0.1 μg/ml, together with its metabolites, sulphanilamide and acetylasulam. GLC was used for determination of asulam and acetylasulam after hydrolysis to sulphanilamide.[6] Similarly asulam is analysed in forage crops and animal tissue by HPLC after derivatization.[7] Determination of asulam in soils by isotachophoresis and liquid chromatography,[8] using UV and conductivity detection has also been reported. Thin-layer chromatography using fluorescamine as labelling reagent has been used to analyse soil samples for the herbicide.[9]

Because Asulam does not show native fluorescence, the technique of spectrofluorimetry has not been previously applied to its determination.

Udenfriend *et al.*,[10] introduce fluorescamine as a labelling reagent to determine primary amines; this is superior to dansyl chloride because both the reagent and its hydrolysis products are nonfluorescent and permit homogeneous fluorogenic labelling. Such an approach has proved its usefulness in numerous analytical applications for some 30 years.

This paper describes the use of the synchronous derivative technique to determine the fluorescent derivative of asulam herbicide. This method may be used for the quantitative analysis of asulam residues in peaches fortified at levels of ng/ml.

EXPERIMENTAL

Apparatus

Emission measurements were done with a luminescence spectrometer, Perkin–Elmer LS-5, (Perkin–Elmer, Beaconsfield, Buckinghamshire, U.K.), equipped with a xenon discharge lamp (9.9 W) pulsed at line frequency, monochromators F/3 Monk-Gillieson type, and 1 × 1-cm quartz cells. The spectrofluorometer was operated in the computer-controlled mode via the RS232C serial interface by a Perkin–Elmer Model 3600 data station microcomputer. Instrumental control and data collection were achieved by using the commercially available Perkin–Elmer computerized luminescence software (PECLSII). For graphical recording, an Epson FX-85 printer–plotter was connected to the spectrofluorometer. All fluorescence spectra are uncorrected because no significant wavelength shifts are observed when comparing with corrected spectra.

UV absorption spectra were recorded with a Shimadzu UV-240 Graphicord recording spectrophotometer. A rotary vacuum evaporator.

Reagents

Stock solutions of asulam (99% pure, Dr. S. Ehrenstofer), were prepared in ethanol at concentrations of 1.0 mg/ml. Working solutions at 100 μg/ml were prepared in ethanol.

The analytical-reagent-grade Fluorescamine (4-phenylspiro[furan-2(3H),1′-phtalan]-3,3′-dione) was obtained from Aldrich and was dissolved in acetone (1 mg/ml).

All solvents used were of analytical reagent grade (Merck) and only demineralized water was used in this work.

Procedures

General procedure. To a 10-ml standard flask add the volume of stock solution needed to obtain a final concentration of asulam between 0.042 and 2.14 μg/ml. Add 0.5 or 2.5 ml (low or high concentration range) of fluorescamine ($3.59 \times 10^{-3}M$) and 2 ml of buffer solution (phthalate/HCl, pH 3) and dilute to the mark with demineralized water. For normal spectrofluorimetry, measure fluorescence intensity at 498 nm, with excitation at 402 nm, against a reagent blank.

For synchronous spectrofluorimetry, prepare the samples exactly as above, record the spectrum at $\Delta\lambda = 96$ nm (corresponding to the Stokes shift) at a time constant of 2 sec and scan speed of 240 nm/min.

Extraction procedure. To chopped peaches (50 g), add 60 μl of standard ethanolic solution of asulam 1170 μg/ml, and blend at high speed for 5 min in 50 ml of acetone. The blended sample was filtered through a fritted glass Büchner (coarse porosity) under reduced pressure. Add to the filtrate 25 ml of saturated sodium chloride and 50 ml of methylene chloride, make up to 250 ml with demineralized water and transfer to a 500-ml separating funnel. The organic phase was concentrated just to dryness by using a rotary evaporator and the residue diluted with demineralized water to a final volume of 25 ml. Aliquots of this solution were then analysed according to the proposed analytical procedure.

RESULTS AND DISCUSSION

Optimization of the derivatization reaction

Fluorescamine (FC), itself non-fluorescent, reacts rapidly with primary aliphatic or aromatic amines to give highly fluorescent pyrrolinone derivatives and non-fluorescent hydrolysis products.[11]

The fluorescence spectra obtained when the reaction takes place in an aqueous solution of 2 μg/ml at pH 3 exhibit two excitation maxima at 325 and 402 nm and an emission band at 498 nm. In order to check that the excess of fluorescamine is hydrolysed and gives no fluorescence signal, a blank test was performed without asulam. No significant blank signal was found.

We examined the effect of the pH on derivative formation in the media and the relative fluorescence intensity of the asulam derivative. In the range pH 2.8–3.1, the variations were minimum, and pH values greater than 10 produce very little fluorescence. To maintain the pH, a set of buffers was assayed and significant differences were found. Figure 1 shows the results obtained from a 10-ml solution containing $3.6 \times 10^{-4}M$ of FC and 2 μg/ml of asulam. Two sets of data points are shown, one obtained by adjusting the pH by little additions of diluted solutions of sodium hydroxide or hydrochloric acid to the phthalate buffer of pH 3, and the other by using 2-ml aliquots of different buffer solutions.

To keep the optimum pH selected to carry out the derivatization reaction constant, several buffers of different composition may be possible. Experiments to test the influence of the nature of buffer in fluorescence signal show that it is a critical variable, since phthalate based

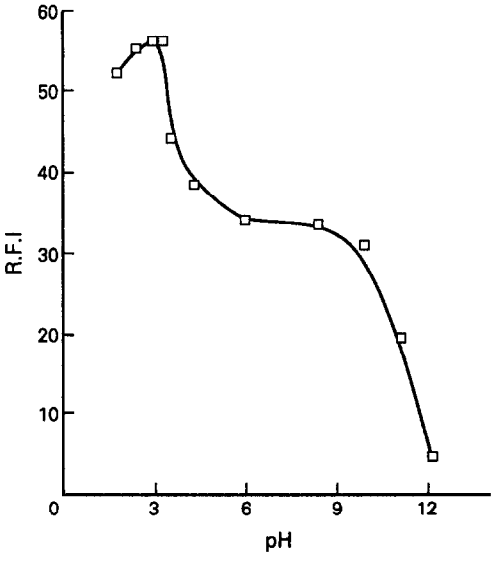

Fig. 1. Influence of pH on the fluorescence intensity of fluorescamine derivative of asulam. [Asulam] = $8.7 \times 10^{-8}M$; [FC] = $3.6 \times 10^{-4}M$. $\lambda_{exc} = 402$ nm, $\lambda_{em} = 498$ nm.

buffer gives twice the signal of glycine or citrate based buffer.

Also, buffer concentration affects the relative fluorescence intensity. A 1-ml portion of 0.05*M* phthalate buffer in an over-all volume of 10 ml produces a constant and maximum signal; higher concentrations of buffer depress the signal. This effect is due, probably, to changes in ionic strength and in the thermodynamic hydrolysis constant of FC. No changes have been found in the derivatization reaction on changing the addition order of the reactants, if we kept in mind that Asulam must be in the flask when buffer and FC are added.

The amount of FC used was found to influence the results. Approximately a 20-fold reagent excess is required to complete derivative formation.

The possibility of enhancing the sensitivity of the FC derivative by using different organic solvents to extract or dissolve the fluorophor was investigated. Derivative fluoresence was found to be strongest in the aqueous medium.

Synchronous derivative spectrofluorimetry

The most appropriate parameters to register synchronous derivative spectra for the procedure were selected. The contribution of this approach to the analytical methodology when the problem is the determination of an isolated compound, not a multicomponent fluorescent compound sample, is the improved sensitivity that may be attained. In this case, the limiting factor in the estimation of the detection limit is the blank signal and the associated standard deviation, and this figure can be significantly reduced since less contribution of the blank signals are observed, especially when the broad band blank spectra are obtained. In addition, the band narrowing effect that synchronous spectrofluorimetry applies, together with the sensitivity of the first derivative to narrowest spectral profiles, gives a gain in analytical sensitivity of the method. Also, in general, in the synchronous scanning the signal is stabilized and is less affected by random fluctuations, thus better precision in measurements can be obtained.

For simple analysis, the recommended scanning interval is the one that provides the highest intensity and the minimum peak half-width, which often corresponds to the Stokes shift. The derivative amplitude is normally taken as the vertical distance from peak to trough.

In this work, the best results were $\Delta\lambda = 96$ nm. The reduction of the peak half-width and the position of the synchronous maxima were calculated.[12] A reduction of $\Delta\lambda$ from 72 to 45 nm was observed. It is important to note that the effectiveness of derivative spectroscopy is a function of the bandwidth of the normal spectrum.

Analytical parameters

The calibration curves were recorded for both the direct and synchronous techniques. The linear dynamic ranges were from 0.043 to 2.14 μg/ml, were identical, that is while the correlation coefficients were 0.996 and 0.999, respectively ($n = 5$).

The precision of the methods determined by analyzing seven replicate of 64.2 ng/ml, was 6.2 and 1.6%, respectively.

Residue analysis of asulam in peaches

To check the usefulness and to compare two fluorimetric procedures proposed in the present work, known amounts of asulam were added to peach extracts and the samples were analysed as indicated under the general procedure.

Fruits were bought from the local market and their origin and previous treatment were unknown. The fruits were spiked with the herbicide at 0.14 μg/ml.

The results obtained for the analysis of the herbicide in peaches using direct and synchronous spectrofluorimetry are given in Table 1.

Recoveries obtained show that the synchronous technique fits the results with almost 100% efficiency with better precision than the direct approach. Because of its simplicity, the

Table 1. Recovery assay of Asulam in fortified peaches

[Asulam] Added, $\mu g/ml$	Synchronous Found, $\mu g/ml$	Synchronous Recovery, %	Direct Found, $\mu g/ml$	Direct Recovery, %
0.140	0.120	85.6	0.169	120.0
0.140	0.141	100.4	0.137	97.5
0.140	0.149	106.0	0.162	115.5
$\bar{X}$	0.137 ± 0.015	97.4 ± 10.5	0.156 ± 0.017	111 ± 11.9

method might find use as a rapid screening technique for pesticides.

REFERENCES

1. C. de Liñan y Vicente, *Vademecum de Productos Fitosanitarios*, 85–86, Madrid, 1985.
2. C. H. Brockelsby and D. F. Mubbleton, in *Analytical Methods for Pesticides and Plant Growth Regulators*, G. Zweig and J. Sherma (eds.), Vol. 7, p. 497. 1974. Academic Press: New York.
3. A. C. Bratton and E. K. Jr. Marshall, *J. of Biol. Chem.*, 1939, **128,** 537.
4. J. F. Lawrence, L. G. Panopio and H. A. McLeool, *J. Agric. Food Chem.*, 980 **28,** 1323.
5. R. T. Kon, L. Geissel and R. A. Leavitt, *Food Addit. Contam.*, 1984, **1,** 67.
6. P. C. Bardalaye, N. P. Thompson and D. A. Carlson, *J. Ass. Off. Anal. Chem.*, 1980, **63,** 511.
7. A. Guardigli, C. Guyton, N. Somma and M. Piznik, in *Asulam* (with updated analytical methodology), *Analytical Methods for Pesticides and Plant Growth Regulators*, G. Zweig and J. Sherma (eds.), Vol. 8, Academic Press: New York, 1985.
8. D. Kaniansky, V. Madajova, M. Hutta and I. Zilkova, *J. Chromatogr.*, 1984, **286,** 395.
9. A. E. Smith and L. J. Milward, *ibid.*, 1983, **265,** 378.
10. S. Udefriend, S. Stein, P. Bohlem, W. Dairman, W. Leimgruber and M. Weigele, *Science*, (Washington DC, 1803), 1972, **178,** 871.
11. K. Samejima, W. Dairman and S. Undefriend, *Anal. Biochem.*, 1971, **42,** 222.
12. F. García Sánchez, A. Navas and M. Santiago, *Anal. Chim. Acta*, 1985, **167,** 217.

Talanta, Vol. 39, No. 9, pp. 1199–1203, 1992
Printed in Great Britain.

0039-9140/92 $5.00 + 0.00

THE DETERMINATION OF LEACHABLE URANIUM IN MARINE AND LACUSTRINE SEDIMENTS BY STEAM DIGESTION

DARRIN K. MANN,* THOMAS J. OATTS* and GEORGE T. F. WONG†
Dept. of Oceanography, Old Dominion University , Norfolk, VA 23529-0276, U.S.A.

(*Received* 31 *October* 1991. *Revised* 30 *January* 1992. *Accepted* 30 *January* 1992)

Summary—Uranium can be leached with a mixture of nitric and perchloric acids from 1 g of marine or lacustrine sediment in an autoclave at 275° and 2 atm in 4 hr. The leachate resulted from this steam digestion may then be analyzed for uranium by isotope dilution alpha spectrometry with a precision of about ±7%. In comparison to the conventional leaching scheme by wet digestion in an open beaker, this method is less time consuming, less labor intensive, requires the use of smaller amounts of acids while it yields data with comparable accuracy and precision. In the analysis of a set of samples collected from a variety of depositional environments, this method yielded results that were indistinguishable from those obtained by the conventional method.

The sedimentary geochemistry of uranium in aquatic environments has been studied extensively because it is a rather abundant and ubiquitous trace element with interesting geochemical properties and its longest-lived isotopes are also the ultimate parents of two decay series whose members have been used widely as tools for describing and quantifying the sedimentary processes.[1,2] The initial step in the determination of uranium in marine and lacustrine sediments usually involves a wet digestion of the sample in the presence of a yield tracer with some combination of nitric, hydrochloric, perchloric and/or hydrofluoric acids in an open beaker in order to solubilize the uranium from the solid phase for subsequent quantification.[3–8] The choice of the combination of acids used is determined by the expected phase association of the uranium in the sample.[4,8–11] The total amount of acid needed is relatively large, ranging from 50 to 200 ml.[3,9,10] The time for digestion is relatively long, ranging mostly between 24 and 48 hr. Frequent replenishment of the acids lost by evaporation during the process is often needed. As a result, more or less continuous attention must be given to this digestion step. Once the leaching process is complete, the leachate must be separated from the residual particulate material by filtration or centrifugation before it can be further processed.[1,12] The filtration of this highly acidic leachate-sediment slurry is somewhat cumbersome, potentially hazardous and thus must be handled with great care.

Recently, Nielsen and Hrudey[13] reported that trace metals in sewage and sludge may be determined by leaching them from the samples by steam digestion instead of wet digestion. We have adopted a modified version of this method for solubilizing uranium from lacustrine and marine sediments. The resulting method is simpler, less time consuming and less labor intensive and it yields results that are indistinguishable from those obtained by using the conventional method.

EXPERIMENTAL

Reagents and apparatus

All reagents used were of analytical grade.

A solution containing ^{236}U, with a specific acitivity of 11.27 dpm/ml, was prepared from $^{236}U_3O_8$ provided by the Oak Ridge National Laboratory (Batch 201DR2). This solution was standardized against a ^{238}U solution prepared from natural U_3O_8 supplied by the National Bureau of Standards (NBS SRM 950b).

An alpha counting system consisting of two Ortec Model 576 dual-detector alpha spectrometers, a Tracor Northern Model TN-1247 four

*Present Address: Martin Marietta Energy Systems, P.O. Box 2003, Oak Ridge, TN 37831-7458, U.S.A.
†Author for correspondence.

input multiplexor-router and a Model TN-7200 multichannel analyzer was used for alpha spectrometry.

Electroplating was carried out in teflon plating cells with platinum anodes similar to the one designed by Herada and Tsunogai[14] and modified by Anderson and Fleer.[4]

Procedures

Sample preparation for steam digestion. Transfer about 1 g of the dried, powdered and weighed sediment, 20 ml of 8*M* nitric acid, 1 ml of concentrated perchloric acid and 0.5 ml of the standardized ^{236}U solution into a 30-ml polysulfone centrifuge tube. Seal the centrifuge tube with a sealing cap. (Centrifuge tubes supplied by Nalgene are durable and relatively inexpensive. However, the caps that come with them may leak during centrifugation and they must be replaced with sealing caps.) Agitate the content in the tube with a vortex mixer for two minutes. Then, transfer the tube to an autoclave and incubate it for 4 hr at 275° and 2 atm. (Up to 60 samples may be digested simultaneously in a 12-l. autoclave.) Centrifuge it at 3000 rpm for 20 min and decant off the supernatant leachate. Wash the sediment twice with 10 ml of 2*M* hydrochloric acid and twice with 10 ml of demineralized water by resuspending the sediment in each washing with a vortex mixer for 2 min. Separate the sediment from the washings by centrifugation and combine the washings with the leachate.

Sample preparation for wet digestion. The method of Roe and Burnett[8] is followed. Transfer about 2–3 g of the dried, powdered and weighed sediment to a beaker together with 50 ml of concentrated nitric acid, 2 ml of concentrated perchloric acid and 0.5 ml of the standardized ^{236}U solution. Digest the mixture at about 80° for 24 hr. Separate the leachate from the sediments by filtration through a glass fiber filter. Wash the sediment 3 times with 15 ml of 2*M* hydrochloric acid and add the washings to the filtrate.

Purifying and electroplating uranium. The general scheme of Ku[3] and Anderson and Fleer[4] is used for the separation and determination of uranium in the leachate. Remove most of the iron from the solution by extracting it with diethyl ether. Convert the solution to 9.6*M* hydrochloric acid by evaporating it to near dryness and then diluting it with 9.6*M* hydrochloric acid. Separate uranium from most of the other matrix elements by passing the sample through an AG1 × 8 anion exchange resin column in the chloride form, equilibrated with 9.6*M* hydrochloric acid and with a bed volume of about 11 ml (1 cm diameter × 14 cm height), and then eluting the column by a serial gradient elution with 9.6*M* hydrochloric acid and then 0.1*M* hydrochloric acid in succession. Evaporate the fraction in 0.1*M* hydrochloric acid to near dryness and then dilute it with 8*N* nitric acid. Further separate uranium from other elements by passing the sample through an AG1 × 8 anion exchange resin column in the nitrate form, equilibrated with 8*N* nitric acid and with a bed volume of 6 ml (0.6-ml diameter × 20-cm height), and then eluting the column successively with 8*M* nitric acid, 9.6*M* hydrochloric acid and then 0.1*M* hydrochloric acid. Evaporate the fraction in 0.1*M* hydrochloric acid to near dryness. Dilute it with 1*M* nitric acid. Evaporate it to near dryness again and then dilute it with 0.1*M* nitric acid. Transfer the solution to the electroplating cell with washings of 2*M* ammonium chloride which has been adjusted to pH 2 with hydrochloric acid. Electroplate the uranium onto a silver disk for 3.5 hr at 0.8 amps and analyze for uranium by alpha spectrometry.

RESULTS AND DISCUSSION

Sub-samples of a single sample of marine sediment were digested by steam digestion for various amounts of time varying from 2 to 5 hr and then analyzed for the concentrations of ^{238}U and ^{234}U. Two to four sub-samples were analyzed at each time for digestion. Another four sub-samples were digested also by the conventional wet-digestion method in an open beaker and then analyzed for the uranium isotopes. The results are shown in Fig. 1 and Table 1.

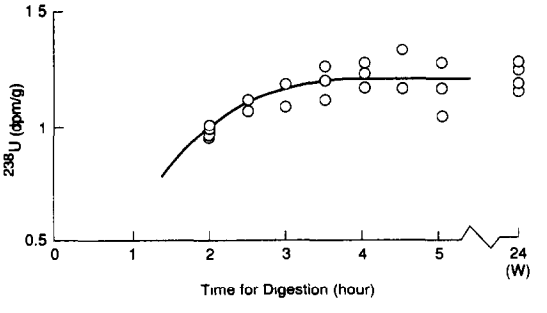

Fig. 1. The effect of the time for steam digestion on the recovery of ^{238}U in sediments from Tom's Cove, Virginia. (W) denotes the concentrations of ^{238}U determined by using the conventional wet digestion.

Table 1. Effect of time for digestion on the determination of uranium by steam digestion

Digestion method	Time for digestion, hr	Conc. in sub-samples 1	2	3	4	Avg.	S.D.,* %
I. ^{238}U (Concentration in dpm/g)							
Wet	24	1.22	1.13	1.25	1.15	1.18	5
Steam	2.0	0.97	0.95	0.94	0.99	0.96	2
Steam	2.5	1.05	1.10			1.08	4
Steam	3.0	1.16	1.07			1.12	5
Steam	3.5	1.17	1.10	1.23		1.17	6
Steam	4.0	1.25	1.15	1.20		1.20	4
Steam	4.5	1.30	1.14			1.22	9
Steam	5.0	1.25	1.02	1.14		1.14	10
Average (3.5 to 5 hr for digestion) = 1.18 dpm/g ± 7%							
II. ^{234}U (Concentration in dpm/g)							
Wet	24	1.51	1.44	1.41	1.54	1.48	4
Steam	2.0	1.29	1.22	1.23	1.21	1.24	3
Steam	2.5	1.35	1.24			1.30	6
Steam	3.0	1.25	1.38			1.32	7
Steam	3.5	1.21	1.37	1.37		1.32	7
Steam	4.0	1.32	1.36	1.34		1.34	2
Steam	4.5	1.36	1.20			1.28	9
Steam	5.0	1.37	1.27	1.28		1.31	5
Average (3.5 to 5 hr for digestion) = 1.31 dpm/g ± 5%							
III. $^{234}U/^{238}U$ (Activity ratio)							
Wet	24	1.23	1.27	1.13	1.34	1.24	7
Steam	2.0	1.34	1.29	1.31	1.22	1.29	4
Steam	2.5	1.28	1.12			1.20	9
Steam	3.0	1.08	1.30			1.19	13
Steam	3.5	1.04	1.25	1.12		1.14	10
Steam	4.0	1.05	1.18	1.11		1.11	6
Steam	4.5	1.05	1.05			1.05	0
Steam	5.0	1.10	1.24	1.12		1.15	7
Average (3.5 to 5 hr for digestion) = 1.12 ± 7%							

*Standard Deviation—1 sigma in %.

For a given time for digestion, steam digestion yielded highly precise results with precision ranging from ±2 to ±10% (1 standard deviation) for ^{238}U and ±2 to ±9% (1 standard deviation) for ^{234}U. (The uncertainty in the concentration of the ^{236}U yield tracer is not included in the calculation of the precision of the method. Any error from this source should have stayed constant throughout this study since the same tracer solution was used in all the analyses.) In most cases, the precision was better than ±5%. Between 2 and 3.5 hours of time for digestion, the concentration of ^{238}U increased with increasing time from 0.96 to 1.17 dpm/g. The concentration of ^{234}U followed a similar trend. Eleven sub-samples were digested for 3.5 to 5 hours. In this group of samples, the concentration of ^{238}U did not increase systematically with increasing time for digestion. The concentration ranged between 1.02 and 1.30 dpm/g with an average of 1.18 dpm/g ± 7% (1 standard deviation). These concentrations should be considered indistinguishable from each other within the analytical uncertainty of the analysis and the possible compositional variability among the sub-samples. We have adopted a time for digestion of 4 hours in order to insure that a constant recovery is reached. The concentration of ^{234}U and the activity ratio of $^{234}U/^{238}U$ in these samples ranged from 1.2 to 1.37 dpm/g with an average of 1.31 dpm/g ± 5%, and 1.04 to 1.25 with an average of 1.12 ± 7%, respectively. In comparison, by using the conventional wet digestion method, the concentration of ^{238}U, ^{234}U and the activity ratio of $^{234}U/^{238}U$ were 1.18 dpm/g ± 5%, 1.48 dpm/g ± 4% and 1.24 ± 7% respectively. The exact correspondence in the concentration of ^{238}U is probably fortuitous. However, the data do demonstrate clearly that the steam digestion can produce

Table 2. Steam and wet digestion for the determination of uranium in different types of sediments

LOI* %	Digestion method	^{238}U, dpm/g	^{234}U, dpm/g	$^{234}U/^{238}U$
Oyster Point, fringing marsh, intertidal zone				
2.8	Wet	1.03	1.37	1.32
	Steam	1.04	1.30	1.25
	Difference†	+0.01	−0.07	−0.07
Oyster Bay, open lagoon, high productivity				
5.2	Wet	1.21	1.49	1.24
	Steam	1.14	1.45	1.28
	Difference†	−0.07	−0.04	+0.04
Back Bay, brackish lagoon				
5.6	Wet	0.74	1.04	1.42
	Steam	0.84	1.12	1.33
	Difference†	+0.10	+0.08	−0.09
Tom's Cove, coastal bay, high productivity				
10.4	Wet	1.99	2.50	1.26
	Steam	2.09	2.30	1.10
	Difference†	+0.10	−0.20	−0.16
Lake Drummond, blackwater lake				
57.8	Wet	0.44	0.74	1.67
	Steam	0.61	0.83	1.37
	Difference†	+0.17	+0.09	−0.30

*LOI—Weight loss on ignition at 550°.
†Difference = (Result from Steam Digestion − Result from Wet Digestion).

data indistinguishable from those obtained by the conventional method.

The concentration of uranium in sediments collected from five different depositional environments was determined by using steam digestion and the conventional method of digestion. (Standard reference sediments that have been analyzed for leachable uranium are not yet available commercially for an intercalibration study.) These samples ranged from a fine grained sediment with a low organic content (<3% of weight loss on ignition at 550° or LOI) collected from a brackish environment to a highly organic sediment (>50% of LOI) collected from a fresh, black water lake. The results are shown in Table 2. The concentration of ^{238}U and ^{234}U ranged from 0.44 to 1.99 dpm/g and 0.74 to 2.5 dpm/g respectively. Although the chemical characteristics and the concentrations of ^{238}U and ^{234}U in these five samples of sediments varied considerably, both methods of digestion yielded results that are indistinguishable from each other when the analytical uncertainty of each method and the possibility of inhomogeneity among the sub-samples are taken into account. The differences in the concentrations of ^{238}U and ^{234}U as determined by these two methods were mostly less than 0.1 dpm/g. It is interesting to note that the largest percent difference in concentration was found in the most organic-rich sediment collected from Lake Drummond, where the LOI was about 58%, and steam digestion yielded the higher concentrations of ^{238}U and ^{234}U. This suggests that, with this type of sediment, the leaching of uranium with wet digestion may be less complete than with steam digestion. However, sediments with such a high organic content are not commonly found in the marine and lacustrine environments. The concentrations of ^{238}U are related to each other as follows:

$$U_s = (0.96 \pm 0.09)\quad U_w + (0.11 \pm 0.11)$$

$$\text{and}\quad r^2 = 0.98$$

where U_s and U_w are the concentrations of ^{238}U as measured by steam digestion and by the conventional digestion method respectively and r is the correlation coefficient (Fig. 2). The intercept of the line is indistinguishable from zero and the slope of the line is indistinguishable from unity suggesting that both methods yield identical results within analytical uncertainties.

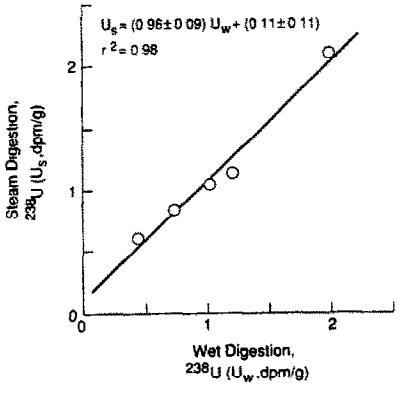

Fig. 2. The relationship between the concentration of ^{238}U determined by using steam digestion, U_s, and the conventional wet digestion, U_w. The best fit line and its equation are shown.

CONCLUSION

Steam digestion can greatly simplify the determination of uranium in lacustrine and marine sediments while yielding data with similar accuracy and precision as the conventional wet digestion method. The time for digestion is reduced from 24 to 4 hr. The amount of acid required can be reduced by up to a factor of ten. No special attention to the samples is required during the digestion. The

entire sample preparation may be carried out in a single centrifuge tube. Filtration may be circumvented. The resulting method is less time consuming and less labor intensive.

Acknowledgements—This work was supported in part by the National Oceanic and Atmospheric Administration under grant number R/CBT-2 529816. It also constitutes part of the doctoral dissertation research of D. Mann.

REFERENCES

1. M. Ivanovich, in M. Ivanovich and R. S. Harmon, *Uranium Series Disequilibrium: Applications to Environmental Problems*, pp. 56–76. Clarendon, Oxford, 1982.
2. C. Barnes and J. K. Cochran, In J. C. Guary, P. Guengueniat and R. J. Pentreath, *Radionuclides: A Tool for Oceanography*, pp. 162–171. Elsevier, London, 1988.
3. T. L. Ku, "*Uranium Series Disequilibrium in Deep-sea Sediments*", Ph.D. Thesis, Columbia University, New York, 1966.
4. R. F. Anderson and A. P. Fleer, *Anal. Chem.*, 1982, **54**, 1142.
5. A. E. Lally, in M. Ivanovich and R. S. Harmon, *Uranium Series Disequilibrium: Applications to Environmental Problems*, pp. 79–106. Clarendon, Oxford, 1982.
6. J. Mitchel, *Geochim. Cosmochim. Acta*, 1984, **48**, 1249.
7. W. S. Moore, *ibid.*, 1984, **48**, 987.
8. K. K. Roe and W. C. Burnett, *ibid*, 1985, **49**, 1581.
9. K. Krishnaswami, D. Lal and B. L. K. Somayajulu, *Earth Plant. Sci. Lett.*, 1976, **32**, 403.
10. M. Yamada and S. Tsunogai, *Mar. Chem.*, 1983, **54**, 263.
11. J. K. Cochran, A. E. Carey, E. R. Sholkovitz and L. D. Surprenant, *Geochim. Cosmochim. Acta*, 1986, **50**, 663.
12. J. K. Katz and G. T. Seaborg, *The Chemistry of the Actinides Elements*, pp. 94–194. Wiley, New York, 1957.
13. J. S. Nielsen and S. E. Hrudey, *Environ. Sci. Technol.*, 1984, **18**, 130.
14. K. Herada and S. Tsunogai, *J. Oceanogr. Soc. Japan*, 1988, **41**, 98.

Talanta, Vol. 39, No. 9, pp. 1205–1208, 1992
Printed in Great Britain.

0039-9140/92 $5.00 + 0.00

SPECTROPHOTOMETRIC AND VOLUMETRIC MOLYBDENUM DETERMINATION WITH 2,2′-BIQUINOXALYL

IRENA BARANOWSKA and KATARZYNA BARSZCZEWSKA
Department of Analytical and General Chemistry, Silesian Technical University 44-100 Gliwice, Poland

(*Received* 7 *June* 1991. *Revised* 12 *February* 1992. *Accepted* 12 *February* 1992)

Summary—Volumetric and spectrophotometric methods for molybdenum determination based on reaction with 2,2′-biquinoxalyl (2,2′-BQx) in concentrated hydrochloric acid media have been developed. Absorption spectra of the 1,1′-dihydro 2,2′-biquinoxalylene complex shows the most intensive absorption band at 685 nm with molar absorptivity $\epsilon = 3.3 \times 10^4$ l.mole^{-1}.cm^{-1}. The compound is characterized by good durability to high temperatures and concentrated acid media. The mentioned indicator gives distinct colour changes at the titration end-point. The spectrophotometric method for molybdenum determination is based on the use of the difference in absorbance between the oxidized and reduced forms of 2,2′-BQx. The indicator is reduced with Sn(II) and then part of it is reoxided as a result of addition of Mo(VI). The difference in absorbance between the blank determination and molybdenum sample increases linearily in the concentration range 0.2–2.0 μg Mo/cm^3. 2,2′-Biquinoxalyl was used as an indicator in the volumetric method for the determination of molybdenum concentrations in steel alloy. The interfering ions Fe(III) and Cr(III) are easily eliminated as the precipitate of hydroxides. The mineral acids, hydrochloric sulphuric and perchloric acids, have been tested as reaction media.

Raw-materials used for the preparation of molybdenum are characterized by large variations in their quantitative compositions. Amounts of molybdenum are in the range of: 20–90% in molybdenum ores; 50–80% in ferromolybden and 0.005–0.1% in copper ores. Such wide concentration ranges require large ranges of applicability when considering methods.

The aim of this work was to examine the usefulness of 2,2′-biquinoxalyl (2,2′-BQx) for the spectrophotometric and volumetric (stannometric) determination of molybdenum, and to verify this method on real samples.

The "Analysen Testprobe" Nr 4.4/7 (Head Office of Measures DDR Prüfdienstelle 301 Magdeburg) containing 2.28% of molybdenum was used as the standard sample. Previous works[1–6] show, that the 2,2′-BQx is a useful spectrophotometric reagent for the determination of strong reducing and oxidizing agents. It has also been applied as the redox indicator in volumetric methods.

On the basis of previous investigations with other metals it was assumed that optimum conditions were: a medium of 6*M* hydrocholoric acid, 3*M* sulphuric acid and a temperature of 80°.

The redox potential of the 2,2′-BQx$_{OX}$/2,2′-BQx$_{RED}$ system, which is equal to 0.4 V,[1] shows that separation of preliminary chromium, iron and other oxidants is necessary during stannometric molybdenum determination when 2,2′-BQx is used as indicator.

In this work, separation of heavy metals in the form of precipitates of their hydroxides, as recommended by Polish Standard PN-82/H-04207, was applied.

EXPERIMENTAL

Reagents and apparatus

*Molybdenum standard solution, 0.1*M *in 6*M *hydrochloric acid.* Dissolve 12.3556 g of $(NH_4)_6Mo_7O_{24}.4H_2O$ in 50 ml of concentrated hydrochloric acid and dilute to 100 ml with water. From this solution prepare the $2 \times 10^{-5}M$ concentrated solution by appropriate dilution.

*Stannous chloride standard solution, 0.5*M. Dissolve 112.8150 g of $SnCl_2.2H_2O$ in one litre of 6*M* hydrochloric acid. Less concentrated solutions (8×10^{-4} and $2.5 \times 10^{-4}M$) were made by appropriate dilution of the standard solution with deoxidized hydrochloric acid just before measurement.

2,2′-BQx (own synthesis by ref. 7). Appropriate weighed amounts of 2,2′-BQx were dissolved in concentrated hydrochloric acid.

Table 1. The results of molybdenum determination by the volumetric method

Mo taken, *mg*	$V_{Sn/Mo}$, *ml*	V_{KBrO_3}, *ml*	Mo found, *mg*	
	2.70	6.70	34.71	
33.56	2.70	6.10	31.60	$\bar{m}_{Mo} = 32.94$
	2.75	6.16	32.50	$s = 1.60$
	5.65	6.18	67.01	
	5.75	6.38	70.40	
	5.60	6.20	66.63	
67.12	5.60	6.30	67.70	$\bar{m}_{Mo} = 67.28$
	5.75	5.94	65.54	
	5.75	5.94	65.54	$s = 1.69$
	5.35	6.64	68.17	
	11.35	6.24	135.91	
	11.50	5.94	131.09	
134.24	11.49	5.90	130.09	$\bar{m}_{Mo} = 133.92$
	10.50	6.80	137.02	
	9.70	7.28	135.51	$s = 3.11$

The results were calculated by the equation

$$m_{Mo} = 1.919 . V_{Sn/Mo} . V_{KBrO_3} \text{ (mg)}$$

*Potassium bromate standard solution (1/6 $KBrO_3$) = 0.1*M. A weighed amount of $KBrO_3$ was dissolved in one litre of water. A Specol spectrophotometer (Zeiss Jena) with 10-mm cells was used for all measurements.

Volumetric molybdenum determination in the alloy

A known volume of molybdenum standard solution (5, 10 or 20 ml) was transferred into a 300-ml conical flask. Then 150 ml of 3*M* sulphuric acid was added. The sample prepared in this way was heated to 80°.

The sample was titrated with *ca.* 0.1*M* Sn(II) solution until it changed from yellow to dark-green. The end-point of the titration was indicated by the unchanging dark-green colour of the sample. Volume of 0.2 ml of 0.1% indicator solution was added to each sample. The concentration of stannous chloride was determined bromometrically immediately.

In order to check the reproducibility of the method three series of samples with known amounts of molybdenum were analysed. The average and standard deviation were calculated and the results are shown in Table 1.

Sample preparation. The alloy was ground in a boron carbide mortar and sieve. The powder ($\phi = 0.15$ mm) was solubilized.

Sample solubilization. About 2.5 g of the powdered sample was put into a quartz crucible. A 20-ml amount of a mixture of concentrated nitric and sulphuric acids (1 : 1) was added and the content was heated to obtain a moist residue. The procedure was repeated until the sample was completely solubilized. Then 5 ml of concentrated sulphuric acid was added to completely remove nitric oxides.

Separation of interfering ions. The contents of the crucible were cooled and 75 ml of water were added. The mixture was then boiled and the hot solution containing precipitated silica was filtered. Chromic and ferric hydroxides were precipitated from the filtrate with 30% sodium hydrochloride. The solution was decanted and the precipitated hydroxides were vacuum filtered. The precipitate was washed twice with 25 ml of sodium hydroxide. If the solution has just been prepared no coprecipitation will be observed. The clear filtrate (pH 10) was neutralized with sulphuric acid to pH 7. Sulphuric acid was then added to a final concentration of 3*M*. Then 0.2 ml of 0.1% 2,2′-BQx solution was added to the (80°) sample and titrated with Sn(II) solution. The concentration of the tin(II) chloride solution was determined bromometrically immediately. Results are shown in Table 2.

Spectrophotometric molybdenum determination

Ordinary method. Hydrochloric acid (30 ml, 6*M*) and 10 ml of 1×10^{-4}*M* 2,2′-BQx solution were added to each of six 50-ml measuring flasks. Samples were deoxidized with nitrogen, after which, 1 ml of 8×10^{-4} stannous chloride was added.

The reaction of Sn(II) with 2,2′-BQx leads to formation of 1,1′-dihydro 2,2′-biquinoxalylene. The molar absorptivity of this compound equals 3.3×10^4 l.mole^{-1}.cm^{-1} at the most intensive absorption band, with λ_{max} at 685 nm.

Maximum absorbance was attained after one hour, and 2, 4, 5, 6 and 7 ml of ammonium molybdate were then added. Samples were diluted to 50 ml with 1 : 1 hydrochloric acid. The difference in absorbance between the reagent blank and samples containing molybdenum was measured after 10 min. The results are given in Table 3. The analytical curve was given by the equation

$$\Delta A = 0.17c + 6.9 \times 10^{-3}$$

Table 2. Determination of molybdenum in the alloy sample with the volumetric method

Sample, *g*	Mo content, *mg*	%	Mo found, *mg*	%	
2.6047	59.40		56.40	2.16	
2.3289	53.10		54.08	2.37	
2.3962	54.63	2.28	55.79	2.33	$\bar{m}_{Mo} = 2.28\%$
2.4172	54.95		54.55	2.26	
2.2678	51.71		52.08	2.30	

Table 3. Absorbance variation according to the range of molybdenum sample taken (ordinary method)

	1	2	3	4	5	6
2,2′-BQx ml $1 \times 10^{-4}M$	10	10	10	10	10	10
Sn(II) (ml) $8 \times 10^{-4}M$	1	1	1	1	1	1
Mo $2 \times 10^{-5}M$ (ml)	—	2	4	5	6	7
Mo (μg)	—	26.86	53.72	67.16	80.59	94.02
Mo (μg/ml)	—	0.53	1.07	1.34	1.61	1.88
Absorbance	0.53	0.43	0.33	0.30	0.25	0.19
$\Delta A(1-n)$	—	0.10	0.20	0.23	0.28	0.34

where ΔA is the difference in absorbance and c is the concentration of molybdenum (μg/ml).

Ultimate precision method. Volumes of 30 ml of $6M$ hydrochloric acid were transferred to seven 50-ml measuring flasks. Then 10 ml of $1.5 \times 10^{-4}M$ 2,2′-BQx solution was added to six of them while 3 ml of the same solution was added into the remaining flask. In order to secure complete reduction of 2,2′-BQx, an excess of Sn(II) was added to the first and second flasks and 5 ml of $2.5 \times 10^{-4}M$ Sn(II) was added to the other five flasks. When the solutions obtained maximum absorbance, 1, 2, 4 and 5 ml portions of $2 \times 10^{-5}M$ ammonium molybdate were added to each flask. Samples, where the excess Sn(II) in relation to 2,2′-BQx had been added, were used as the standard solutions for 0 and 100% transmittance adjustment. In this way, an extended (T_r) scale of transmittance was obtained. In this manner tranmittances of the other samples were measured. The transmittances of standard solutions were measured on the ordinary scale (T_z). Transmittances on the extended scale (T_r) were reduced to transmittances on the ordinary scale (T_z) and then to absorbance. Differences in absorbance between the reagent blank and samples with molybdenum were calculated and the results are presented in Table 4.

The analytical curve was given by the equation

$$\Delta A = 0.15c + 0.025$$

where ΔA is the difference in absorbance and c is the concentraton of molybdenum (μg/ml).

RESULTS AND DISCUSSION

Stannometric molybdenum determination with 2,2′-BQx as the indicator was verified for amounts of 30–140 mg in $3M$ sulphuric acid. Solutions of hydrochloric and perchloric acids are inferior media in which to carry out the reaction.

The distinctive feature of an efficient indicator is a colour change that can be visible after adding the first excessive drop of titrant at the end-point of titration, carried on in 80°, 2,2′-BQx reacts with strong reducers in concentrated mineral acid medium. The product of reaction is blue 1,1′-dihydro 2,2′-biquinoxalylene, the molar absorptivity of this compound is 3.3×10^4 l.mole^{-1}.cm^{-1} (λ_{max} at 685 nm). Introduction of molybdenum is connected with reoxidation of biquinoxalyl and discharge of them.

The described spectrophotometric method was studied for molybdenum determination in the range 0.2–2.0 μg Mo/ml. This method is an alternative to coulometric titration[8] which enables determination of an amount of molybdenum not lower than 70 μg/ml. It is also competitive to the catalytic method.[9] The latter method is based on the observation of the

Table 4. Absorbance variation according to the range of molybdenum sample taken (ultimate precision method)

	Standard solutions 1	2	3	4	5	6	7
2,2′-BQx (ml) $1.5 \times 10^{-4}M$	10	3	10	10	10	10	10
Sn(II) (ml) $2.5 \times 10^{-5}M$	10	10	5	5	5	5	5
Mo (ml) $2.0 \times 10^{-5}M$	—	—	—	1	2	4	5
Mo (μg)	—	—	—	13.4	26.9	53.7	67.2
Mo (μg/ml)	—	—	—	0.27	0.54	1.07	1.34
	Measured			Calculated			
A_z	1.0	0.30	0.83	0.77	0.71	0.68	0.59
T_z, %	10	50	14.8	17.0	19.6	20.8	26.0
T_r,%	0.0	100	12	17.5	24	27	40
$\Delta A_z[n-(n+1)]$				0.06	0.12	0.15	0.24

influence of molybdenum on the reaction between hydrogen peroxide and potassium iodate, and makes possible the determination of molybdenum in the range 10–100 μg/ml.

REFERENCES

1. I. Baranowska, *Zesz. Nauk. Pol. Sl. (Chemia)* 1988, 117.
2. R. Baranowski, I. Baranowska, W. Karmiński and Z. Gregorowicz *Z. Anal. Chem.*, 1974, **269**, 122.
3. I. Baranowska, R. Baranowski and Z. Gregorowicz, *Chem. Anal.*, 1986, **31**, 245.
4. *Idem, Microchem. J.*, 1979 **24**, 367.
5 1. Baranowska, *ibid.*, 1981, **26**, 55.
6. *Idem, Chem. Anal.*, 1986, **31**, 245.
7. H. S. Broadbent and R. C. Anderson, *J. Org. Chem.*, 1962, **27**, 2676.
8. P. Agasian and K. Tarienowa, *Z. Anal. Chim.* 1967, **33**, 547.
9. G. Svehla and L. Erdey, *Microchem. J.*, 1963, **7**, 206.

Talanta, Vol. 39, No. 9, pp. 1209–1212, 1992
Printed in Great Britain

0039-9140/92 $5.00 + 0.00
Pergamon Press Ltd

SPECTROPHOTOMETRIC STUDY OF COBALT, NICKEL, COPPER, ZINC, CADMIUM AND LEAD COMPLEXES WITH MUREXIDE IN DIMETHYLSULPHOXIDE SOLUTION

MOJTABA SHAMSIPUR*
Department of Chemistry, Shiraz University, Shiraz, Iran

NAADER ALIZADEH
Department of Chemistry, Tarbiat Modarres University, Tehran, Iran

(*Received* 4 *November* 1991. *Revised* 9 *January* 1992. *Accepted* 9 *January* 1992)

Summary—The complexation reactions between murexide and Co^{2+}, Ni^{2+}, Cu^{2+}, Zn^{2+}, Cd^{2+} and Pb^{2+} ions have been studied spectrophotometrically in dimethylsulphoxide solution at 25°. The stoichiometry of the complexes was found to be 1:1. The stability constants of the complexes were determined, and found to follow the Irving–Williams rule for the cations of the first transition series. In dimethylsulphoxide solution, the complexes are much more stable than those in aqueous solution.

Murexide, the ammonium salt of purpuric acid (**I**), is frequently used as a complexing agent for a large number of metal ions, including the divalent ions of the first transition series, in aqueous solution over a wide range of experimental conditions.[1–5] It is known as a convenient ligand for the quantitative determination of metal ion concentrations in aqueous solution with visible spectrophotometry.[6,7] The equilibrium between various metal ions and metallochromic indicator murexide has been used to determine the stability constants of metal–ligand equilibria by monitoring spectrophotometrically the displacement of metal–murexide equilibrium due to metal–ligand binding.[8–11] Some of the metal–ligand equilibria involve biologically important macromolecules as ligands.[11]

However, the stability constants of murexide complexes with most metal ions are not very large in aqueous solutions[2–5] which possibly cause some limitations in the use of murexide as a chromogenic indicator. Since, in the complexation reactions, the ligand must compete with solvent molecules for cations, use of solvents of lower dielectric constant and solvating ability than water[12] is expected to lead to greater stability of the corresponding murexide complexes.

It was of interest to us to study the effect of solvent properties on the thermodynamics of the metal ion–murexide complexes. We have already reported some results obtained from the study of murexide complexes with a number of metal ions in non-aqueous[13,14] and mixed solvent.[15] In this paper we report a spectrophotometric study of the murexide complexes with Co^{2+}, Ni^{2+}, Cu^{2+}, Zn^{2+}, Cd^{2+} and Pb^{2+} ions in dimethylsulphoxide solution at 25°.

EXPERIMENTAL

Reagent grade $CoCl_2.6H_2O$, $NiCl_2.6H_2O$, $CuCl_2.2H_2O$ and $Cd(NO_3)_2.4H_2O$ (all from Merck) were completely dehydrated by heating in an oven of proper temperature[16] until a predetermined weight was reached. The resulting water free solid salts were stored over phosphorus pentoxide under vacuum before use. Reagent grade zinc chloride, lead nitrate (both

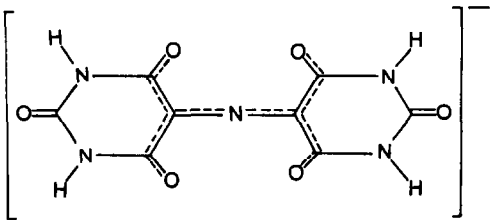

I

*Author for correspondence.

from Merck), tetraethylammonium perchlorate (TEAP, Fluka) and murexide (Merck) were of the highest purity available and used without further purification except for vacuum drying over phosphorus pentoxide for 72 hr. Spectroscopic grade dimethylsulphoxide (DMSO, Merck) was used as received. All spectra were obtained with a Model 2100 Shimadzu UV–Vis spectrophotometer at $25 \pm 1°$.

The formation constants of 1:1 complexes between murexide and the metal ions used were determined by the absorbance measurements, at λ_{max} of each complex, of solutions in which varying concentration of metal ions (2.0×10^{-4}–$1.0 \times 10^{-3} M$) were added to a fixed concentration of murexide ($2.0 \times 10^{-5} M$) in DMSO. The ionic strength of all solutions was kept constant at $0.1 M$ with TEAP. All solutions were neutral and, hence, the ligand existed in its monovalent form, Mu^-, throughout.[2,13,14,17] Attainment of equilibrium was checked by the observation of no further change in the spectra after several hours.

When a metal ion, M^{2+}, reacts with murexide, Mu^-, to form a 1:1 complex, the formation constant is given as

$$K_f = \frac{[MMu]}{[M][Mu]} \quad (1)$$

(the charges are omitted for simplicity). The total concentration of Mu, C_{Mu}, and the absorbance at λ_{max} of the complex, A, are expressed as

$$C_{Mu} = [MMu] + [Mu] \quad (2)$$

$$A = \epsilon_{MMu}[MMu] + \epsilon_{Mu}[Mu] \quad (3)$$

where ϵ_{MMu} and ϵ_{Mu} are the molar absorptivities of complexed and free murexide, respectively.

By substitution of equation (1) into equations (2) and (3) we obtain

$$C_{Mu} = (K_f[M] + 1)[Mu] \quad (4)$$

$$A = (\epsilon_{MMu} K_f[M] + \epsilon_{Mu})[Mu] \quad (5)$$

Dividing equation (5) by (4) gives

$$\frac{A}{C_{Mu}} = \frac{\epsilon_{MMu} K_f[M] + \epsilon_{Mu}}{K_f[M] + 1} \quad (6)$$

By considering $[M] = C_M - [MMu] \approx C_M$ (since $C_M \gg C_{Mu}$) and $A_o = \epsilon_{Mu} C_{Mu}$ and rearrangement of equation (6) we have

$$AK_f C_M + A = \epsilon_{MMu} K_f C_M + A_o \quad (7)$$

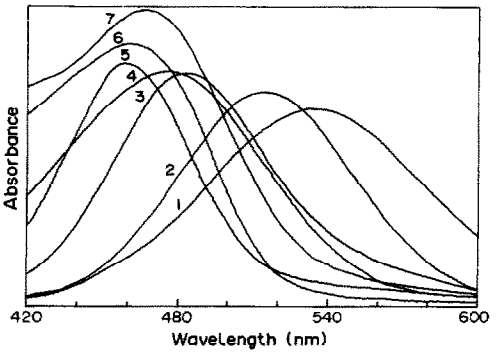

Fig. 1. Visible region spectra of murexide and its metal complexes in DMSO: 1, murexide; 2, Pb^{2+}; 3, Cd^{2+}; 4, Cu^{2+}; 5, Zn^{2+}; 6, Ni^{2+}; 7, Co^{2+}.

Dividing equation (7) by A_o and its rearrangement gives

$$(A/A_o - 1)/C_M = \epsilon_{MMu}/\epsilon_{Mu} K_f - K_f A/A_o \quad (8)$$

According to equation (8), there is a linear relation between $(A/A_o - 1)/C_m$ and A_o/A (Fig. 3). From the intercept of the line, the formation constant of the murexide complex could be obtained.

RESULTS AND DISCUSSION

The visible spectra of murexide and its complexes with the metal ions used in DMSO solution are shown in Fig. 1. All the complexes are distinguished by a strong and ion specific blue-shift, the reasons for which are discussed elsewhere.[13,14] The stoichiometry of the complexes was examined by the mole ratio method,[18,19] and found to be 1:1 in all cases. Some of the resulting absorbance–mole ratio plots are shown in Fig. 2. As can be seen, each plot consists of two straight lines, the intersections of which determines the stoichiometry of the complex (Table 1).

The complexation equilibria between murexide and the metal ions were studied

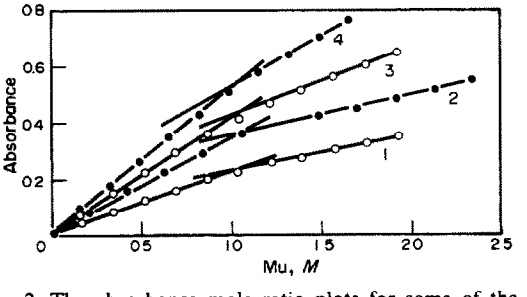

Fig. 2. The absorbance–mole ratio plots for some of the metal ions used: 1, Cd^{2+}; 2, Cu^{2+}; 3, Co^{2+}; 4, Ni^{2+}.

Table 1. Log K_f of different metal ion–murexide complexes in DMSO and water

Solvent	Cation	λ_{max} nm	Stoichiometry, (Mu^-/M^{2+})	log K_f
DMSO	Murexide	533	—	—
	Co^{2+}	475	1.02	4.56 ± 0.03
	Ni^{2+}	461	1.01	5.45 ± 0.05
	Cu^{2+}	477	0.96	5.65 ± 0.03
	Zn^{2+}	460	0.97	4.27 ± 0.04
	Cd^{2+}	483	1.02	4.63 ± 0.03
	Pb^{2+}	515	1.11	4.52 ± 0.03
H_2O	Murexide	522	—	—
	Co^{2+}	470	1	2.48
	Ni^{2+}	460	1	3.38
	Cu^{2+}	478	1	4.36
	Zn^{2+}	452	1	3.00
	Cd^{2+}	483	1	4.15
	Pb^{2+}	502	1	4.40

spectrophotometrically, by using solutions containing the ligand and the metals of the concentrations, $C_M \gg C_{Mu}$. The absorbance at the peak of each murexide complex (Table 1) was observed to increase with increasing concentration of each cation. The experimental results obtained showed the linear relations between $(A/A_o - 1)/C_m$ and A/A_o, according to equation (8), for all the metal ions used which were independent of C_{Mu}. The corresponding plot for Zn^{2+} ion is shown in Fig. 3. From the slopes of the lines, the formation constants of the murexide complexes were obtained. All calculated formation constants of the resulting 1:1 complexes along with the corresponding λ_{max} values and their stoichiometries are presented in Table 1. The corresponding reported values in aqueous solution[2] are also included for comparison.

From Table 1, it is immediately obvious that the solvent plays an important role in the complexation reactions. The resulting complexes in DMSO are much more stable (up to about 2 orders of magnitude for cobalt, nickel and copper complexes) than those in aqueous solution. There is actually an inverse relationship between the solvating ability of the solvent, as expressed by the Gutmann donicity number,[12] and the stability of the complexes. Water is a solvent of higher solvating ability (DN = 33)[20] than DMSO (DN = 29.8)[12] and, hence, can compete more effectively with murexide for the cations. Thus, it is reasonable to expect an increase in the formation constants when changing the reaction medium from water to DMSO. A similar solvent effect has already been reported.[9,10,13,14,21]

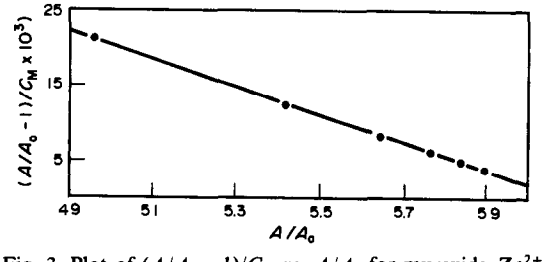

Fig. 3. Plot of $(A/A_o - 1)/C_M$ *vs.* A/A_o for murexide–Zn^{2+} system in DMSO.

Moreover, the lower dielectric constant of DMSO (46.7) in comparison with that of water (78.5) would also cause the electrostatic contributions to the bond formation between the two charged partners (*i.e.*, M^{2+} and Mu^-) to increase in DMSO solution.

The data in Table 1 show that the sequence of stability of the murexide complexes with the cations of the first transition series (*i.e.*, $Co^{2+} < Ni^{2+} < Cu^{2+} < Zn^{2+}$) follows the Irving–Williams order,[22] which generally holds for the equilibrium constants of transition metals. However, among cations Zn^{2+}, Cd^{2+} and Pb^{2+}, cadmium–murexide complex in DMSO solution shows the highest stability, this is probably due to the proper size of Cd^{2+} ion which could favour a suitable spatial fit with flexible donating atoms of the ligand (bridging nitrogen atom and neighbouring oxygen atoms).[14] Cadmium ion has about the same ionic size as Na^+ and Ca^{2+} ions[16] which has been shown to form the most stable murexide complexes among alkali and alkaline earth ions, respectively.[2,13,14]

Acknowledgement—We gratefully acknowledge the support of this work by the Shiraz University Research Council.

REFERENCES

1. G. Shwarzenback and H. Gysling, *Helv. Chim. Acta*, 1949, **32**, 1314.
2. G. Geier, *ibid.*, 1967, **50**, 1879.
3. K. S. Balaji, S. Dinesh Kumar and P. Gupta-Bhaya, *Anal. Chem.*, 1978, **50**, 1972.
4. M. Fischer, W. Knoche, B. H. Robinson and J. H. Maclagan Wedderburn, *J. Chem. Soc., Faraday I*, 1979, **75**, 119.
5. C. O'Mara, J. Walsh and M. J. Hynes, *Inorg. Chim. Acta*, 1984, **92**, L1.
6. A. Scarpa, *Methods Enzymol.*, 1972, **24B**, 343.
7. M. B. Williams and J. H. Moser, *Anal. Chem.*, 1953, **25**, 1414.
8. V. M. Loyola, R. Pizer and R. G. Wilkins, *J. Am. Chem. Soc.*, 1977, **99**, 7185.
9. M. B. Gholivand, S. Kashanian and M. Shamsipur, *Polyhedron*, 1987, **6**, 535.
10. S. Kashanian and M. Shamsipur, *Inorg. Chim, Acta*, 1989, **155**, 203.
11. M. J. Hynes and H. Diebler, *Biophys. Chem.*, 1982, **16**, 79.
12. V. Gutmann, *Coordination Chemistry in Nonaqueous Solvents*, Springer-Verlag, Vienna, 1968.
13. S. Kashanian, M. B. Gholivand, S. Madaeni, A. Nikrahi and M. Shamsipur, *Polyhedron*, 1988, **7**, 1227.
14. M. Shamsipur, S. Madaeni and S. Kashanian, *Talanta*, 1989, **36**, 773.
15. M. Shamsipur, A. Esmaeili and M. K. Amini, *ibid.*, 1989, **36**, 1300.
16. R. C. Weast, Editor, CRC Handbook of Chemistry and Physics, 54th Ed., CRC Press, Cleveland, Ohio, 1973.
17. K. L. Cheng, K. Ueno and T. Imamura, *CRC Handbook of Organic Analytical Reagents*, p. 291. CRC Press, Boca Raton, Florida, 1982.
18. J. H. Yoe and A. L. Jones, *Ind. Eng. Chem. Anal. Ed.*, 1944, **16**, 11.
19. R. Jakubiec and D. F. Boltz, *Anal. Chem.*, 1969, **41**, 78.
20. R. H. Erlich and A. I. Popov, *J. Am. Chem. Soc.*, 1971, **93**, 5620.
21. M. K. Amini and M. Shamsipur, *Inorg. Chim. Acta*, 1991, **183**, 65.
22. H. Irving and R. J. P. Williams, *J. Chem. Soc.*, 1953, 3192.

Talanta, Vol. 39, No. 9, p. 1213, 1992
Printed in Great Britain

0039-9140/92 $5.00 + 0.00
Pergamon Press Ltd

BOOK REVIEW

Nucleotide Analogues as Antiviral Agents: J. C. MARTIN (ed.), American Chemical Society, Washington, DC, 1989. Pages viii + 190. $44.95 (US and Canada), $53.95 (elsewhere).

The introduction of acyclovir into clinical practice a decade ago revealed a tantalizing glimpse of a revolution in the treatment of viral diseases, which has yet to be realized. Largely as a result of the vast commitment to AIDS research and recent advances in molecular biology, the prospect of other selective antivirals, with low toxicity, becoming available seems closer, and the next few years promises some exciting developments.

The appearance of this book, in the ACS Symposium Series, is therefore welcome and timely, representing a useful reference source for all who are engaged in antiviral research. The twelve chapters, each by subject leaders, review latest developments in the synthesis of novel antiviral agents together with notes on structure-activity relationships, mode of action and host cell toxicity. Whilst there is an emphasis on activity against HIV and the herpes group of viruses, effects against some other viruses are also documented.

An earlier chapter discusses the substrate requirements of viral-encoded thymidine kinase responsible for the activation of certain nucleosides effective against the herpes simplex virus. Four chapters describe strategies for the development of acyclonucleoside phosphonates which are resistant to degradation by cellular phosphorylases and circumvent the need for activation by viral kinases. Some of these analogues are highly effective against herpes and some other DNA viruses which lack thymidine kinase activity, whilst retaining a low level of toxicity to mammalian cells. Other derivatives investigated are inhibitors of reverse transcriptase and may find application in the treatment of HIV.

Other sections in this book describe the development of viral thymidine kinase inhibitors, nucleotide dimers related to azidothymidine, simple pyrophosphate inhibitors of viral nucleic acid polymerases, and many more.

The final chapter explores the activity of nuclease-resistant short-chain oligonucleotides which, in principal, can interfere with viral genetic expression by hybridization with viral nucleic acids. The authors cite several modified oligomers with promising antiviral activity which are being evaluated. This general approach may allow specific viral nucleotide sequences to be targeted whilst minimizing host cell toxicity, and is undoubtedly an area for future development.

P. A. CAPPS

Talanta, Vol. 39, No. 10, pp. 1215–1218, 1992
Printed in Great Britain.

0039-9140/92 $5.00 + 0.00

INVESTIGATION OF FOLDING IN PROTAMINE BY FTIR

JOSEPH J. PESEK and FARIBA RAISI SHABARY
Department of Chemistry, San Jose State University, San Jose, CA 95192, U.S.A.

(*Received* 10 *February* 1992. *Revised* 19 *March* 1992. *Accepted* 22 *March* 1992)

Summary—The secondary structure of purified protamine, a non-specific DNA binding protein, was studied in solution at pH 4, 7 and 8 by FTIR. This permitted analysis of the folded form of the protein (acidic pH) as well as the folded conformers (neutral and basic pH). Hg^{2+} was utilized to probe the accessibility of the free thiol groups (cysteine residues). The SH groups form when disulfides, which play the major role in stabilizing the conformation of this protein, are broken. It was possible to observe different conformational states in protamine as a function of pH and the presence of Hg^{2+} via spectral changes primarily in the amide region. The results lead to the conclusion that protamine is not completely folded under conditions similar to those found *in vivo* (37°, neutral pH, phosphate buffer and high protein concentration).

Biochemical studies have revealed that DNA in most vertebrate sperm is associated with only one protein class, the protamines.[1] These proteins are small (approx. 5 kD) and extremely basic; 50% of the amino acids are arginine. Structural studies have shown that both the primary and secondary structure of protamine vary depending on the organism.[2] The secondary structure is controlled primarily by disulfide formation. The cysteine residues in mammalian species, initially present as free sulfhydryls when the proteins are deposited on DNA, are oxidized forming intra and intermolecular disulfide bonds that lock adjacent protamine molecules together around the DNA helix.

Previous results suggest that only the carboxyl and amino-terminal regions of protamine actually fold. This occurs in both the presence and absence of DNA. The central polyarginine sequence is believed to be the region of the molecule that binds to DNA. Kinetic pathways of unfolding and refolding are defined by the intermediate conformation states.[3] For a complex process like protein folding, there are often a large number of intermediate states.

FTIR is just beginning to develop as a powerful means of studying protein structure and function.[4] Early studies in solution[5–7] have generally involved high concentrations (> 100 mg/ml) and long path length cells (> 50 μm) using D_2O instead of H_2O as the solvent.[5,6,8] However, some of the earliest studies on proteins involved anhydrous films[9,10] in order to overcome the strong background absorbance of both H_2O and D_2O. A recent study[11] has shown that thin films in conjunction with ATR can be used to detect an enzyme–substrate intermediate at relatively low concentrations (2.5 mg/ml) in the original solution.

The vibrational spectra of proteins can be characterized by three amide bands:[12,13] Amide I between 1630–1680 cm^{-1}, Amide II near 1550 cm^{-1} and Amide III between 1230–1300 cm^{-1}. The positions of the Amide I and III bands can be used to estimate the relative populations of α-helix, β-sheet and random coil in a particular protein.[14–16] For cytochrome b_5 the FTIR data correlated well with other techniques[17] and for α-chymotrypsin the FTIR of the thin film was consistent with both the solution spectrum as well as crystallographic measurements.[11] Finally, it should be noted that other functional group vibrations can provide information about the structure of the protein. For protamine the thiol group is important since it controls the secondary structure as mentioned above. Several studies have focussed on the S–H stretch which usually occurs between 2400–2600 cm^{-1}. Reports concerning hemoglobin,[18–20] myosin[21] and chymopapain[22] among others have appeared in the literature. The object of this study was to determine if FTIR could monitor, through changes in the amide and/or the thiol regions, how both pH and the presence of a heavy metal, Hg^{2+}, affect the overall structure of protamine.

EXPERIMENTAL

Materials

Bull and hamster protamine were obtained from Dr. Rod Balhorn at Lawrence Livermore National Laboratory. The proteins were purified by HPLC and the purity was determined by gel electrophoresis. The proteins were obtained as lyophilized powders in the reduced form[1,2] and stored dry. All buffers and other chemicals used in the experiments were reagent grade or the highest purity available.

Instrumentation

FTIR spectra were obtained on a Perkin–Elmer Model 1800 spectrometer equipped with a DTGS detector. Data were collected and processed on a Perkin–Elmer 7000 computer using the CDS-5 applications program. Spectra were taken on the Perkin–Elmer Multiple Internal Reflectance Accessory using a germanium crystal. The Ge crystal was determined to be most impervious to etching and fogging by the protein/buffer solutions used in these experiments. In general 100 scans at 2 cm^{-1} resolution were used for most samples.

Sample preparation

Protamine was weighed on an analytical balance and dissolved in the appropriate 0.10*M* buffer solution (acetate for pH 4 and phosphate for pH 7 and 8). When used, $HgCl_2$ was added to the solution before additional buffer was added to make the final concentration of protamine 1m*M*. The solution was allowed to stand for 30 min before placing it in the ATR cell or before applying it to the Ge crystal for a thin film.

To make a thin film, a small aliquot of solution was placed on the crystal and gently dried with a stream of argon. Before the sample was completely dry, a second aliquot of sample was placed on the crystal and the drying process was continued. This process was repeated until a uniform layer was formed on the crystal surface. Development of such a protocol led to reproducible thin films and allowed for deposition of more sample than would be possible from higher concentration solutions due to protein aggregation. After the sample was prepared, the ATR accessory was placed in the sample chamber which was purged with dry nitrogen for 30 min before spectral acquisition.

RESULTS AND DISCUSSION

Initial experiments involved attempting to obtain spectra on typical solutions of protamine using the ATR accessory. It was determined that a concentration of at least 100 mg/ml was necessary in order to obtain a reasonable signal to noise ratio. At these concentrations aggregation and long term stability were a problem so that in general reproducible results were difficult to obtain. With these limitations in mind, it was decided to try the thin film method for studying the samples. Spectra obtained on thin film samples were essentially identical in spectral detail to those obtained in solution. This result is consistent with the data of an earlier study[11] in which the thin film and solution spectra were identical.

Figure 1 shows a partial spectrum of bull protamine in acetate buffer at pH 4. This portion of the spectrum has been examined because the sulfhydryl region is of interest for the protamines due to SH participation in the secondary structure. At pH 4 protamine should be completely unfolded with the thiol groups intact, *i.e.*, not oxidized to form disulfide linkages.[2] The frequencies of the absorbance are shifted to the low end of the normal range of the S–H stretching mode probably due to hydrogen bonding effects. However, eight separate bands can be identified at 2391, 2384, 2368, 2358, 2340, 2327, 2320 and 2312 cm^{-1}. This result is reasonable since previous studies have identified seven cysteine residues per bull protamine. Since these absorbances are not in the frequency range of water vapor, carbon dioxide or the buffer, they must be part of the protamine molecule. Careful spectral subtraction of both the background and the buffer also suggest that the peaks observed here are due to protamine vibrational absorption. Addition of Hg^{2+} to the original

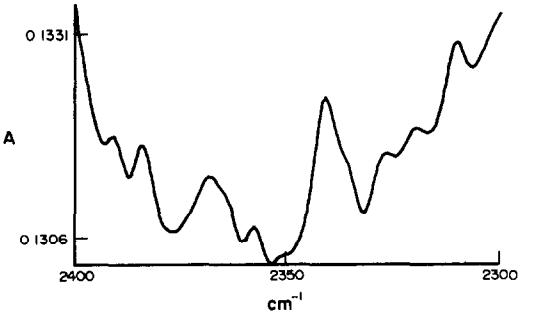

Fig. 1. Partial ATR FTIR difference spectrum (sulfhydryl region) of a thin film of protamine deposited on a germanium crystal from a pH 4 solution.

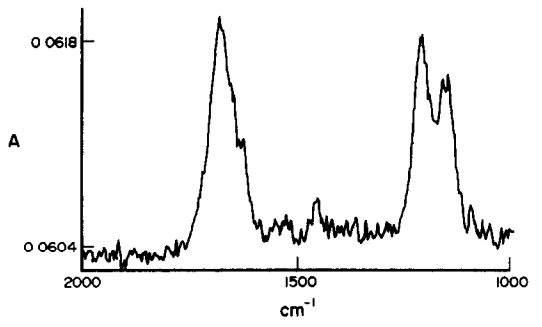

Fig. 2. Partial ATR FTIR difference spectrum (amide region) of a thin film of protamine deposited on a germanium crystal from a pH 4 solution.

protamine solution or raising the pH causes these bands to disappear. This is consistent with complexation of the thiols by Hg^{2+} and with formation of disulfide bridges in the folding process. The oxidant is thought to be oxygen but the mechanism is still under investigation. Lowering the pH will cause the protein to return to the unfolded state only if a reducing agent such as β-mercaptoethanol is present.

While the above data show that meaningful results can be obtained from the SH region of the spectrum, it is apparent from earlier studies that the amide region has the potential for providing more information about the overall structure of the molecule. Figure 2 shows a typical ATR thin film spectrum of protamine in the region encompassing the amide absorbances. These spectra can be used to determine the band positions shifts as a result of varying the pH or adding Hg^{2+}.

Table 1 is a summary of the data obtained from the various FTIR spectra. These results clearly show two readily identifiable trends. Both an increase in the pH and the addition of Hg^{2+} result in a shift of the Amide I from lower to higher frequency. The frequency range of various secondary structures for proteins has been assigned as follows: α-helix 1645–1660 cm^{-1}, β-sheet 1665–1680 cm^{-1} and disordered structure or random coil 1660–1670 cm^{-1}.[15,16] At pH 4, the Amide I peak is centered near 1655 cm^{-1} which is indicative of some α-helix component as well as perhaps a disordered or random coil contribution. This result is consistent with the reported nature of protamine which is thought to be completely unfolded at pH 4. Certainly a helical component in protamine would not be unusual since it has been shown to wrap around DNA in its initial state which mainly consists of free sulfhydryls. The existence of the free sulfhydryls at pH 4 has been confirmed by the data in the 2300–2400 cm^{-1} region. Addition of Hg^{2+} at pH 4 causes a substantial shift of the Amide I band to 1680 cm^{-1}. This indicates a major change in the secondary structure of protamine upon complexation with the metal ion. This could be a disruption of the helix component because hydrogen bonding is no longer available through the sulfhydryls, or it could involve some folding of the protein through sulfur–mercury–sulfur bridges. The β-sheet structure which might develop in the latter case can shift the Amide I band to 1680 cm^{-1} [15,16] but it can also have components as high as 1690 cm^{-1}.[17] Therefore, some combination of a random structure with a significant β-sheet component through S–Hg–S is the most likely configuration of protamine at pH 4 in the presence of mercury.

When the pH of the protamine solution is raised to 7, the Amide I band shifts to 1660 cm^{-1}. This is consistent with the known behavior of protamine which indicates increased folding of the molecule as free sulfhydryls are converted to disulfide linkages. This Amide I frequency is indicative of a greater β-sheet contribution to the structure which is expected when the two ends of the protein fold to form the disulfide bridges. Addition of Hg^{2+} causes a further shift in the Amide I band to 1675 cm^{-1}. This result is similar to that observed at lower pH indicating that additional changes in the secondary structure occur upon complexation with mercury. As mentioned above, these changes may involve the formation of S–Hg–S linkages or other types of interaction between mercury and another site (P–S–Hg···X–P) on the protein which results in a more β-sheet-like structure.

Raising the pH to 8 causes a further shift in the Amide I frequency to 1664 cm^{-1}. This result confirms that as the protein continues to undergo more folding the shift in the absorbance band will be to higher wave numbers. Addition of mercury shifts the Amide I to approximately the same value obtained at pH 7 indicating that the final structural state is somewhat similar at both pHs.

Table 1. Amide I frequencies of Protamine thin films

pH	Frequency (cm^{-1}) native	with Hg^{2+}
4	1655	1680
7	1660	1675
8	1664	1676

In summary, it appears that FTIR is a useful technique for studying the effects of both pH and external agents such as heavy metal ions on the secondary structure of proteins. In the case of protamine, the results obtained at various pH's can be correlated with those obtained from other techniques. This allows conclusions to be made about the structural effects when mercury is added to the system which have not been studied by other methods. In particular, protamine appears not to be completely folded under physiological conditions since further shifts in the Amide I band are observed when the pH is raised to 8.

REFERENCES

1. R. Balhorn, *J. Cell Biol.*, 1982, **93,** 298.
2. J. A. Mazrimas, M. Corzett, C. Campos and R. Balhorn, *Biochim. Biophys. Acta*, 1986, **872,** 11.
3. T. T. Herskovits and J. Brahms, *Biopolymers*, 1976, **15,** 687.
4. C. W. Wharton, *Biochem. J.*, 1986, **233,** 25.
5. J. G. Belasco and J. R. Knowles, *Biochemistry*, 1983, **22,** 122.
6. *Idem, ibid.*, 1980, **19,** 472.
7. J. Fischer, J. G. Belasco, S. Khosla and J. R. Knowles, *ibid.*, 1980, **19,** 2895.
8. P. J. Tonge and C. W. Wharton, *Biochem. Soc. Trans.*, 1985, **13,** 929.
9. P. L. Gordon, C. Huang, R. Lord and I. V. Yannas, *Macromolecules*, 1974, **7,** 954.
10. M. Ruegg and H. Hanni, *Biochim. Biophys. Acta*, 1975, **400,** 17.
11. S. A. Swedberg, J. J. Pesek and A. L. Fink, *Anal. Biochem.*, 1990, **186,** 153.
12. T. Miyazawa, T. Shimanouchi and S. Mizushina, *J. Chem. Phys.*, 1958, **29,** 611.
13. T. Miyazawa, *J. Chem. Phys.*, 1960, **32,** 1647.
14. M. C. Chen and R. C. Lord, *Biochemistry*, 1976, **15,** 1889.
15. J. L. Lippert, D. Tyminski and P. J. Desmeules, *J. Am. Chem. Soc.*, 1976, **98,** 7075.
16. J. S. Vincent, C. J. Steer and I. W. Levin, *Biochemistry*, 1984, **23,** 625.
17. P. W. Holloway and H. H. Mantsch, *ibid.*, 1989, **28** , 931.
18. J. O. Alben, G. H. Bare and P. A. Bromberg, *Nature*, 1974, **252,** 736.
19. G. H. Bare, J. O. Alben and P. A. Bromberg, *Biochemistry*, 1975, **14,** 1578.
20. J. A. Alben and G. H. Bare, *J. Biol. Chem.*, 1980, **255,** 3892.
21. M. Nakaishi, T. Yamada, H. Shimizu and M. Tsuboi, *Biochim. Biophys. Acta*, 1981, **671,** 99.
22. C. W. Wharton, *Eur. Spectrosc. News*, 1981, **54,** 311.

Talanta, Vol. 39, No. 10, pp. 1219–1228, 1992
Printed in Great Britain.

0039-9140/92 $5.00 + 0.00

ATOMIZATION EFFICIENCY OF A MASSMANN-TYPE GRAPHITE FURNACE

S. J. CATHUM

Centre for Analytical and Environmental Chemistry, Department of Chemistry, Carleton University, Ottawa, Ontario, Canada K1S 5B6

(*Received* 21 *January* 1992. *Revised* 7 *April* 1992. *Accepted* 9 *April* 1992)

Summary—The atomization efficiency of the Perkin–Elmer HGA-400 for the production and containment of atomic vapour has been determined for Al, Co, Au, Ni, Fe, Ag, Ga and Cu by a method developed under non-isothermal conditions. The method takes into account the residence time and the shape of the absorbance signal profile. It is based on the entire absorption signal profile rather than on any part of it. The uncertainty in the method arises from calculation of the rate constant of atom loss due to temperature gradient which has a pronounced effect on the "effective" length of the analysis path when the atomizer is operated under non-isothermal conditions. The average value of the atomization efficiency for the eight elements used for this study was found to be about 0.10.

The efficiency of the graphite furnace to produce and contain analyte atoms has been the subject of several studies.[1–5] Smets[5] has used a correction factor, β, given by the following equation,

$$\beta = \frac{\int_0^\infty R_{\text{form}}\,dt}{N_0} \qquad (1)$$

to account for the fraction of the total number of analyte atoms that enter the analysis volume during each stage of atomization, where R_{form} is the rate of atom formation, and N_0 is the total number of atoms introduced as sample. Note that $\int_0^\infty R_{\text{form}}\,dt$ is the number of vaporized atoms that enter the analysis volume during the time interval $0 \rightarrow \infty$, and N_0 is the total number of analyte atoms deposited in the graphite furnace assumed to be totally vaporized to the gas phase during the time interval $0 \rightarrow \infty$.

L'vov[6] has assumed a 100% atomization efficiency for the graphite furnace operated under STPF (stabilized temperature platform furnace) technique and deviations from this value include all the other factors which cause the theoretical and experimental values to differ. Sturgeon and Berman[2] have defined the efficiency of atomization, ϵ_a, for an electrothermal atomizer at the time the signal has attained its maximum value, as the ratio of the number of neutral analyte atoms, N_m, plus ionized analyte atoms, N_i, to the total number of analyte atoms introduced as sample, N_0, *i.e.*,

$$\epsilon_a = \left(\frac{N_m + N_i}{N_0}\right) \qquad (2)$$

This method requires existence of thermodynamic equilibria in the furnace during atomization. Falk and Tilch[3] have determined the atom number density within the atomizer using the following equation:

$$N_m = \left(\frac{(8.69 \times 10^7) A_m (T_m/M)^{0.5}}{l\gamma H(w, a) f \lambda_{21}}\right) \times \left(\frac{Z(T)}{\exp(-E_1/kT_m)}\right) \qquad (3)$$

where N_m is the atom number density within the atomizer, A_m is the peak-height absorbance, $Z(T)$ is the partition function at temperature T_m, the subscript m indicates that values of the subscripted terms are taken at the absorbance maximum, γ is a coefficient accounting for hyperfine splitting of the atomic line, $H(w, a)$ is the Voigt integral for the point of the absorption line contour at a distance of $w = 0.72a$ from the line center, f is the oscillator strength, λ_{21} is the wavelength of the absorption line, E_1 is the energy of the lower level involved, k is the Boltzmann constant and l and M are the atomizer tube length and the molar mass of the analyte atom, respectively. Determination of N_m

by using equation (3) introduces uncertainties in the terms used in the equation.[2] van den Broek and de Galan[1] have reported that the number of analyte atoms at the absorbance maximum, N_m, is given by:

$$N_m = N_0(\tau_R/\tau_s) \quad (4)$$

where N_0 is the total number of analyte atoms initially deposited and τ_R and τ_s are the overall time constants for the removal and the supply function, respectively. Chakrabarti *et al.*[7] have reported that for isothermal atomization in a graphite furnace the number of analyte atoms at the absorbance maximum, N_m, is given by equation (5),

$$N_m = N_0 \exp(-k_2 t_m) \quad (5)$$

where k_2 is a first-order rate constant for atom loss and t_m is the time at which the absorbance reaches its maximum value. L'vov *et al.*[8] has used fundamental constants to calculate the ratio of experimental to theoretical characteristic mass. In his 1990 paper,[6] L'vov revised his spectroscopic data published earlier in 1986[8] and he reported a value of 0.86 ± 0.10 for the ratio of experimental to theoretical characteristic mass using the STPF technique. The atomization efficiency by the method of L'vov is actually assumed 100% and deviations in the ratio must include all the factors which cause the theoretical and experimental values to differ.

Frech and Baxter[4] have defined the atomization efficiency as the ratio of the number of free analyte atoms present in the analysis volume to the number of atoms initially deposited in the graphite furnace. They have pointed out that it is not yet possible to count the number of free atoms produced directly, instead a measurable property of the atomic vapour must be related to this number using the necessary theoretical expression. The atomization efficiency by Frech and Baxter[4] is,

$$\epsilon_a = \frac{m_0(\text{calc})}{m_0(\text{exp})} \quad (6)$$

where m_0(calc) and m_0(exp) are the calculated and the experimental characteristic mass, respectively. To calculate, ϵ_a by equation (6) the graphite furnace must be operated under isothermal conditions (STPF). For the absolute analysis it was necessary to produce free analyte atoms in isothermal conditions and to measure integrated absorbance signals. To overcome the difficulty of obtaining isothermal atomization in the Massmann-type furnace L'vov[9] proposed the use of a platform to delay sample vaporization until the temperature of the graphite tube and the purging gas reaches a steady-state value. Slavin[10] has incorporated these suggestions together with a number of additional methodological and instrumental developments in the STPF technique. It would be useful to investigate the atomization efficiency of non-platform furnaces operated under non-isothermal conditions since tube wall atomization is still used in routine analysis and also in studying the mechanism of atomization. A low value of atomization efficiency, for instance, indicates formation of a non-absorbing species, which must be taken into account in proposing the mechanism of atomization.

The present work was undertaken in order to determine the atomization efficiency of the standard Perkin–Elmer HGA-400 operated under non-isothermal conditions.

THEORY

In the rapidly-heated graphite furnace used for this study, the number of analyte atoms present in the analysis volume at time t is determined by the release, and the transport of atoms into and their loss from the analysis volume.[11] The efficiency of the graphite furnace to produce and contain the analyte atomic vapour is governed by its ability to release neutral analyte atoms from the atomizer surface and to transport them into the analysis volume. Ideally, this process requires that the amount of analyte atoms released from the atomizer surface at any time of atomization should enter the analysis volume. In reality, however, some of the analyte atomic vapour formed may be lost during any stage of atomization by various atom loss processes, for example, loss by diffusion to the cooler ends of the atomizer and through the injection hole, by re-adsorption, by expulsion and by convection. It is also possible that analyte atoms are lost as non-absorbing molecular species, such as, oxides, carbides, chlorides *etc.*

The total number, $N(t)_g$, of analyte atoms including stable molecular species that have diffused to the gas phase at time t is given by the difference between the number of analyte atoms initially deposited in the graphite furnace, N_0, and that, $N(t)_w$, left unatomized on the graphite surface. Once atomization commences gaseous analyte atoms start to diffuse to the gas phase. It should be pointed out that not all of the

analyte atoms which are transported to the gas phase necessarily enter the analysis volume; a fraction of them may be lost. The loss of analyte atomic vapour from a Massmann-type atomizer (The Perkin–Elmer HGA-72), operated under non-isothermal conditions, has been estimated by van den Broek and de Galan[1] to be about 90% of the deposited atoms. Various authors have used a correction factor to account for the atom loss at each stage of the atom formation.[5,12–15] Note that, according to Smets,[5] $\beta N(t)_g$ represents the analyte atoms which are transported into the analysis volume at a given time t, and $N(t)_g$ is the total number of analyte atoms vaporized from the atomizer surface at time t, not necessarily as free atoms. Analyte vapour that diffuses to the atomizer cavity as a result of the increasing temperature of the graphite surface could be a mixture of free analyte atoms and molecular species. Existence of stable molecular species in the gas phase during atomization is acknowledged in the literature.[16] In the gas-interrupt mode of operation, diffusion out of the analysis volume is assumed to be the major loss process for atoms.[1,5,17,18] Under these conditions and taking the above definition for $N(t)_g$ into account, the number of analyte atoms, $N(t)_w$, which are left unatomized on the graphite surface is given by the following equation (see the Appendix):

$$N(t)_w = \frac{\langle k_2 \rangle}{Q\beta} \int_t^\infty A(t)\,dt \qquad (7)$$

where Q is a constant linking the number of gaseous analyte atoms in the atomizer with the measured absorbance signal, $A(t)$, *i.e.*, $A(t) = QN(t)_g$, and $\langle k_2 \rangle$ is the mean value of the rate constant of atom removal, k_2 taken over the indicated time interval, reported constant within 10%.[5] $\langle k_2 \rangle$ is assumed to be equal to k_2; hence, from now on k_2 will be used for $\langle k_2 \rangle$. Therefore, upon substituting equation (7) into the following equation for $N(t)_w$,

$$N(t)_w = N_0 - N(t)_g \qquad (8)$$

and rearranging terms one gets,

$$A(t) = QN_0 - \frac{k_2}{\beta} \int_t^\infty A(t)\,dt \qquad (9)$$

Equation (9) shows that a plot of $A(t)$ *vs.* $\int_t^\infty A(t)\,dt$ should be linear with a slope $-k_2/\beta$ and intercept QN_0 equals a hypothetical absorbance pulse when 100% atomization is achieved. The measurements of the peak-height absorbance and the integrated absorbance are

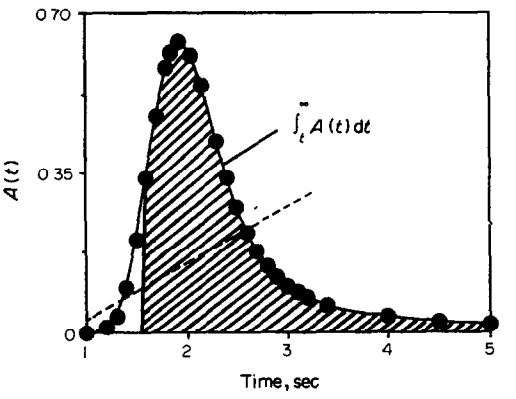

Fig. 1. Measurements of the peak-height absorbance, $A(t)$, against integrated absorbance, $\int_t^\infty A(t)\,dt$.

illustrated in Fig. 1. The shaded area represents the integrated absorbance over the indicated time interval. The temperature profile is also shown for reference. A peak-area program used to calculate the integrated absorbance was obtained from Nicolet Instrument Corporation, Madison, Wisconsin, U.S.A. At the leading edge, equation (9) shows that as $\int_t^\infty A(t)\,dt$ decreases $A(t)$ increases. This relationship between $A(t)$ and $\int_t^\infty A(t)\,dt$ as given by equation (9) should hold true starting from the initial time to t_m (defined as the time when the absorbance signal reaches its maximum). The value of k_2 can be obtained from an expression developed earlier by L'vov *et al.*,[8]

$$k_2 = \frac{8D}{l^2} \qquad (10)$$

where D is the concentration diffusion coefficient of the analyte element in Ar gas, which can be calculated by a formula given in the literature,[8,9] and l is the geometric length of the graphite tube (2.8 cm). The values of the parameters used for determining D can be found in the literature.[20] Since the length l used in equation (10) is greater than the "effective" length of the graphite tube because of the pronounced temperature gradient in the horizontal axis of the long tube (the Perkin–Elmer tube used in this study), the value of k_2 so obtained gives only an estimate of k_2.[21] The slope of the plot of $A(t)$ *vs.* $\int_t^\infty A(t)\,dt$ then yields $-k_2/\beta$ from which β is obtained after differentiation from equation (10).

Atomization efficiency is defined in this paper[1–3,7] as the ratio of the number of neutral analyte atoms present in the analysis volume at

the time when the absorbance reaches its maximum to the total number of analyte atoms deposited in the graphite furnace,

$$\epsilon_a = \frac{N_m}{N_0} \tag{11}$$

where ϵ_a is the atomization efficiency and N_m is the number of analyte atoms present in the analysis volume at the time when the absorbance reaches its maximum. This definition of ϵ_a has been used by various authors.[1-4,7] Using the relationship between A_m and N_m (*i.e.*, $A_m = QN_m$, where Q is a proportionality constant), equation (11) may be re-written as:

$$\epsilon_a = \frac{A_m}{QN_0} \tag{12}$$

When the graphite furnace is operated in the gas-interrupt mode, the denominator of equation (12), may be expressed as follows[1,5,12,15] (see also the Appendix):

$$QN_0 = \frac{k_2}{\beta}\int_0^\infty A(t)\,dt \tag{13}$$

where β is as defined earlier. Substituting equation (13) into equation (12) yields the following equation,

$$\epsilon_a = \frac{\beta A_m}{k_2\int_0^\infty A(t)\,dt} \tag{14}$$

Here ϵ_a is the overall atomization efficiency determined when the graphite furnace is operated under the gas-interrupt mode. Equation (14) shows a linear relationship between ϵ_a and β. Hence, ϵ_a will increase when β increases, *i.e.*, if all the analyte atoms released from the atomizer surface are transported completely into the analysis volume ($\beta = 1$) and remain there for a relatively long time. Equation (14) also shows that ϵ_a is inversely proportional to the rate constant of atom loss, k_2 (which is inversely proportional to the residence time of analyte for a first-order loss process). Note that as k_2 is increased, for instance by forced convection, a low absorbance peak will result because of appreciable decrease in the residence time, which will also mean that ϵ_a will decrease. In order to increase ϵ_a, the experiment should be conducted in the gas-interrupt mode and using long graphite tubes (such as the Perkin–Elmer tubes) since these two factors will increase the residence time of analyte atoms which will result in a high value of ϵ_a.

EXPERIMENTAL

Apparatus

The Perkin–Elmer atomic absorption spectrophotometer model 503, modified to allow recording of the absorbance signal with a 20-msec time constant and equipped with a D_2-arc background corrector and HGA-400 atomizer was used. The graphite furnace was heated slowly with a laboratory-made power supply to lowest atomization temperatures. The temperatures used are somewhat low, this is to broaden the absorbance signal profiles to ease the measurement of the peak-height and integrated absorbance at different times. The temperature of the atomizer surface was measured with two automatic optical pyrometers (Ircon Inc., Skokie, IL, U.S.A.); high temperatures with a 1100 series pyrometer and low temperatures with a 300 series pyrometer. The standard Perkin–Elmer pyrolytically-coated graphite tubes (part No. B0091-504) were used. Signals were recorded with a Nicolet digital oscilloscope model 4094 (Nicolet Instrument Corporation, Madison, Wisconsin, U.S.A). The values of the integrated absorbance were measured at different times using a software package by Nicolet Instrument Corporation. Figure 1 shows how the peak-height absorbance, $A(t)$, was measured against the integrated absorbance, $\int_t^\infty A(t)\,dt$. Hollow-cathode lamps of cobalt (Perkin–Elmer), aluminum (EEL), copper, silver, iron, gold, nickel and gallium (the last six by Westinghouse) were operated at the lowest lamp current level still sufficient for reliable measurement of the absorbance signal. The spectral band width was set to 0.7 nm.

Standard solutions

Chemically pure metals or their salts were used to prepare stock solutions of standards. The stock solution of silver nitrate was prepared by dissolving an appropriate mass of silver nitrate in ultrapure water and diluting the solution to make the concentration 100 μg/ml. Stock solutions of cobalt and iron were prepared separately by dissolving each metal in nitric acid (ULTREX) by heating and then diluting the solution with ultrapure water to make the concentration 1000 μg/ml. Stock solutions of gallium and copper were prepared separately by dissolving each metal in nitric acid (ULTREX) by heating and then diluting the solutions with ultrapure water to make the concentrations 1000 μg/ml. The stock solution

Table 1. Experimental and instrumental parameters*

Element	Wavelength, nm	m_o(exp) (pg/0.0044)	Charring temperature, K	Atomization temperature, K
Al	309.3	26	1050	2700
Co	240.7	21	1090	2600
Cu	324.8	9	1000	2600
Ga	287.4	45	900	2600
Ag	328.1	9	800	2000
Fe	248.3	10	1080	2600
Au	242.8	16	1000	2400
Ni	232.0	16	1100	2600

*Spectral band width = 0.7 nm.

of aluminum was prepared by dissolving the metal in 20% (v/v) nitric acid (ULTREX) with heating; the solution was then diluted to 1000 μg/ml with ultrapure water. The stock solution of gold was prepared by dissolving an appropriate mass of the metal in *aqua regia* and diluting the solution to 1000 μg/ml with ultrapure water.

All test solutions were prepared daily by serial dilution of the stock solutions with ultrapure water just prior to determinations. Ultrapure water of resistivity 18.3 megaohm-cm was obtained direct from a Milli-Q2 water purification system (Millipore Co., Mississauga, Ontario, Canada).

Standard and test solutions were prepared to contain 1% (v/v) nitric acid (Ultrex, J. T. Baker Chemical Co.).

Argon gas

Argon gas (99.995% pure) was used both as sheath gas and as purge gas for the graphite furnace.

Procedure

In order to reach the maximum possible sensitivity for each analyte element, the lamp current of the light source was varied. The lowest lamp current which still gives sensitive and reliable absorbance signal profile was chosen for the analysis. In all cases, 10 μl of the test solution was injected into the graphite furnace with an Eppendorf micropipet fitted with disposable plastic tips. The absorbance signal and temperature profiles were recorded with a digital oscilloscope and stored on a floppy disc for later evaluation. In each case the blank signal was subtracted from the absorbance signal.

Experimental and instrumental parameters

Table 1 summarizes the experimental and instrumental parameters used.

RESULTS AND DISCUSSION

Table 2 summarizes the values of β for eight elements, Al, Co, Au, Ni, Fe, Ag, Ga and Cu, determined using the gas-interrupt mode of operation of the graphite furnace. The values of β ranged from 0.04 for Ga to 0.77 for Cu and had a precision of about 3% relative standard deviation calculated for three replicate determinations. Figures 2–9 show the plots of $A(t)$ *vs.* $\int_t^\infty A(t)\,dt$ for Al, Co, Au, Ni, Fe, Ag, Ga and Cu. Slopes of the plots were calculated from linear regions using the least-squares method. As equation (9) predicts, β increases as the slope of the plot of $A(t)$ *vs.* $\int_t^\infty A(t)\,dt$ decreases. Since the value of the slope is determined by the shape of the absorbance signal profile, the latter plays an important role in determining the value of β, as reported by van den Broek and de Galan.[1] To illustrate how the shape of the absorbance signal profile affects the value of β, plots of $A(t)$ *vs.* $\int_t^\infty A(t)\,dt$ for Ga and Cu are shown in Figs. 8 and 9. The reason for taking these two plots of $A(t)$ *vs.* $\int_t^\infty A(t)\,dt$ as an example as that Ga and Cu have equal values of k_2 (Table 2). Thus, if the β values of Ga and Cu differ from each other the only factor that should account for this difference is the slopes of the plots of $A(t)$ *vs.* $\int_t^\infty A(t)\,dt$ (Figs. 8 and 9), which are significantly different

Table 2. Set of data used in calculation of the atomization efficiency, ϵ_a

Element	D* (cm^2 sec^{-1})	k_2 (sec^{-1})	slope $(-k_2/\beta)$	β
Al	8.7	8.0	−36.0	0.25
Co	6.4	6.5	−20.2	0.32
Cu	6.9	7.0	−9.1	0.77
Ga	6.9	7.0	−156.0	0.04
Ag	3.4	3.5	−17.8	0.20
Fe	6.5	6.6	−36.0	0.18
Au	4.5	4.6	−14.4	0.32
Ni	6.8	6.9	−10.2	0.68

*The values of the parameters used in the calclation of D have been taken from Ref. 20.

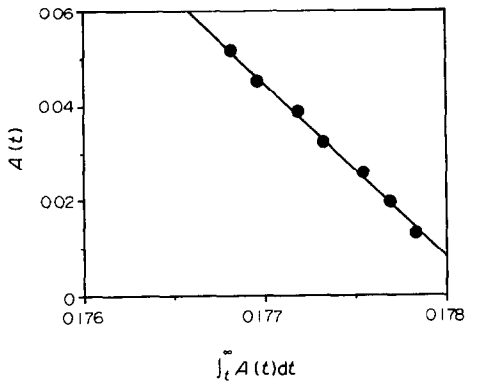

Fig. 2. Plot of peak-height absorbance, $A(t)$, *vs.* $\int_t^\infty A(t)\,dt$ for aluminum (taken as the nitrate).

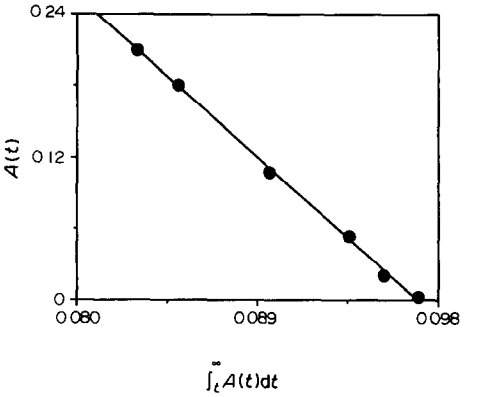

Fig. 4. Plot of peak-height absorbance, $A(t)$, *vs.* $\int_t^\infty A(t)\,dt$ for gold (taken as gold dissolved in *aqua regia*).

(9.1 for Cu and 156 for Ga), and hence give different values of β (for equal values of k_2). This difference in the slopes makes the value of β for Cu (0.77) differ from that of Ga (0.04) by a factor of 19. For identical absorbance signal profiles [giving identical slopes of the plots of $A(t)$ *vs.* $\int_t^\infty A(t)\,dt$], the values of β should be equal, provided that k_2 values are equal.

Table 3 summarizes the values of the overall atomization efficiency, ϵ_a, for Al, Co, Au, Ni, Fe, Ag, Ga and Cu determined by using equation (14). The precision, calculated for three replicate determinations, is about 3% relative standard deviation, which reflects the combined reproducibility of the furnace thermal program and that of atom formation and loss. Our results for β and ϵ_a are different from L'vov[6] and Frech and Baxter.[4] Probably, the main reason for this difference is attributed to experimental conditions used in determination of the atomization efficiency. They used the STPF technique to produce free analyte atoms under isothermal conditions, we used a Massmann-type furnace operated under non-isothermal conditions to generate data for determination of the atomization efficiency. Certainly, different modes of atomization will result in different atom release processes (*i.e.*, different reaction paths) which will appreciably influence the value of the atomization efficiency. Another reason could be the response time of the measuring system (having a time constant 20 msec) which may decrease the sensitivity of the analyte element thereby altering the efficiency of atomization.

Turning now to an important aspect of the atomization efficiency, ϵ_a. In GFAAS, research is conducted mainly to improve the sensitivity and limit of detection of the analysis method. Thus, it would be useful to know whether or not there is any room for such an improvement. The value of ϵ_a shows that only a small fraction roughly about 10% of the total number of the deposited atoms are actually atomized, the rest are lost as non-absorbing species. This indicates that there is still some more research to be done on the graphite furnace to

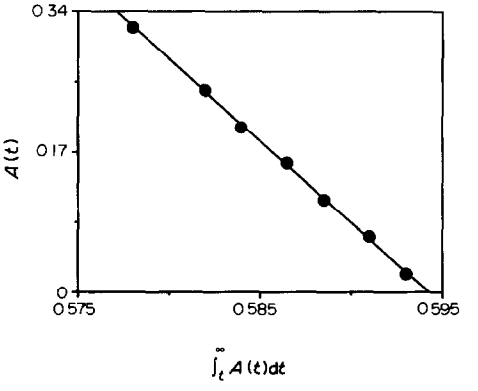

Fig. 3. Plot of peak-height absorbance, $A(t)$, *vs.* $\int_t^\infty A(t)\,dt$ for cobalt (taken as the nitrate).

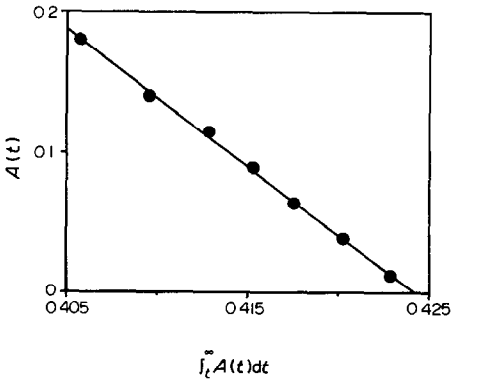

Fig. 5. Plot of peak-height absorbance, $A(t)$, *vs.* $\int_t^\infty A(t)\,dt$ for nickel (taken as the nitrate).

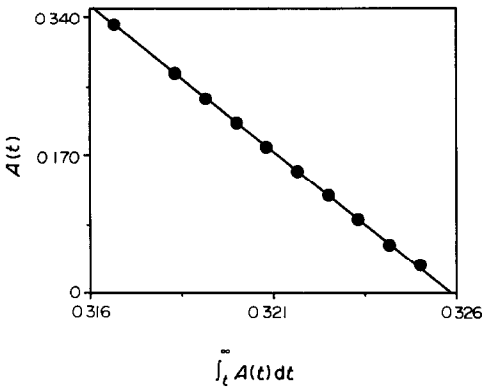

Fig. 6. Plot of peak-height absorbance, $A(t)$, *vs.* $\int_t^\infty A(t)\,dt$ for iron (taken as the nitrate).

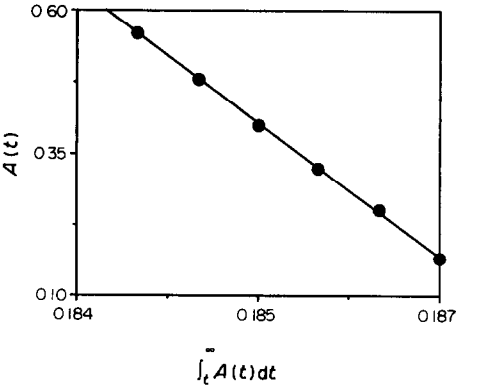

Fig. 8. Plot of peak-height absorbance, $A(t)$, *vs.* $\int_t^\infty A(t)\,dt$ for gallium (taken as the nitrate).

increase its efficiency. Most of the researchers[1-3,5,7] agree that a 100% efficient atomizer has not been yet achieved. As mentioned earlier, ϵ_a is inversely proportional to the rate constant of atom loss, k_2. Hence, ϵ_a can be increased by decreasing k_2, for example, by operating the atomizer in the gas-interrupt mode at low atomization temperatures. The effect of forced convection on the absorbance signal of most elements is obvious when the graphite furnace is operated in the gas-flow mode. The value of ϵ_a of a particular element should hold constant for a set of experimental conditions, such as, the inner gas flow rate and atomization temperature. The combination of these two factors and others play an important role in determining the residence time of the atomic vapour in the analysis volume, and ultimately the value of ϵ_a. Thus, in order to make the value of ϵ_a as a useful indicator for different atomizers all of experimental and instrumental parameters must be maintained unchanged. Another important experimental parameter which may have no effect on the calculation of the theoretical characteristic mass under isothermal conditions (*i.e.*, STPF conditions) but does have an effect on the shape of the absorbance signal recorded under non-isothermal conditions is the heating rate of the graphite furnace. This parameter must also be maintained constant if the atomization efficiency of different graphite furnaces needs to be compared. It is not difficult to fix the heating rate of the graphite furnace if the latter is heated slowly from a charring temperature to a predetermined atomization temperature.

From equation (14) the following observations on the values of β and ϵ_a are made. Since the $A_m/[k_2\int_0^\infty A(t)\,dt]$ values given in Table 3 are < 1 one would expect, according to equation (14), that the ϵ_a values to be less than the β values. As mentioned earlier, the β values have uncertainties originating from the use of equation (10) for calculating the first-order rate constant for atom dissipation, k_2. It is therefore reasonable to conclude that the ϵ_a values which are obtained by using β values have greater uncertainties than the β values. Hence, the ϵ_a

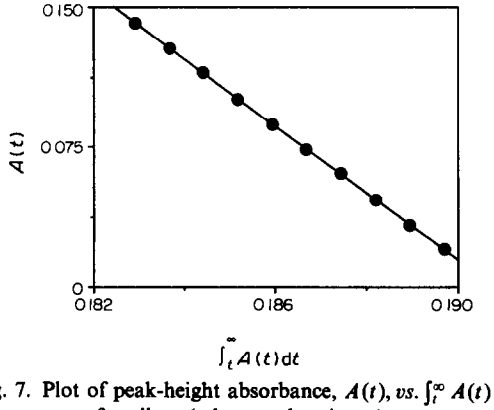

Fig. 7. Plot of peak-height absorbance, $A(t)$, *vs.* $\int_t^\infty A(t)\,dt$ for silver (taken as the nitrate).

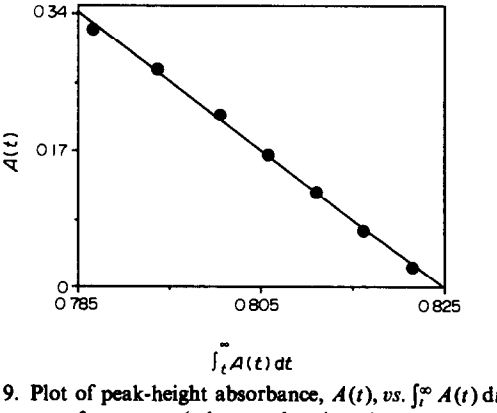

Fig. 9. Plot of peak-height absorbance, $A(t)$, *vs.* $\int_t^\infty A(t)\,dt$ for copper (taken as the nitrate).

Table 3. Atomization efficiency, ϵ_a, calculated under non-isothermal conditions

Element	A_m	$\int_0^\infty A(t)\,dt$	$A_m/k_2\int_0^\infty A(t)\,dt$	ϵ_a
Al	0.230	1.769×10^{-1}	0.146	0.04
Co	0.520	5.508×10^{-1}	0.143	0.05
Cu	0.716	9.379×10^{-1}	0.109	0.08
Ga	0.530	1.868×10^{-1}	0.405	0.02
Ag	0.338	1.980×10^{-1}	0.488	0.10
Fe	0.401	3.259×10^{-1}	0.186	0.03
Au	0.350	9.649×10^{-2}	0.789	0.25
Ni	0.317	4.258×10^{-1}	0.108	0.07

values given in Table 3 should be considered only as a reasonable estimate of ϵ_a.

On the basis of the definition of β as the fraction of the total number of analyte atoms that have gone into the analysis volume at a given instant of atom formation and that of ϵ_a which is the ratio of the neutral analyte atoms that exist in the analysis volume to the total number of atoms initially deposited in the graphite furnace one would expect that ϵ_a is always less than β. The value of β represents a fraction of the total number of analyte gaseous species which are released from the graphite surface to the gas phase. To illustrate the definition of β, suppose that the total number of analyte atoms which are vaporized from the graphite surface at time t_1 is 10, and suppose that $\beta = 0.50$. The number of free atoms that will enter the analysis volume will be 5 atoms, the other 5 atoms will be lost as non-absorbing species or they may not get a chance to diffuse into the analysis volume. As the atomization proceeds more gaseous atoms will be released. Let us assume that at time t_2 the total number of analyte atoms vaporized from the surface becomes 20 atoms, the number of analyte atoms that will enter the analysis volume, in this case, are 10 atoms, the rest will be lost as non-absorbing species, and so forth. Thus, β remains constant during the entire duration of the absorbance signal, *i.e.*, at each stage of atom formation. This characteristic property of β made it possible to determine the activation energy by Smets equation[5] and calculate its value from the slope of the plot of $A(t)$ *vs.* $\int_t^\infty A(t)\,dt$. On the other hand, ϵ_a represents analyte atom population when the absorbance reaches its maximum. Notice the difference between the two definitions of β and ϵ_a, the latter is directly proportional to the former only at the absorbance maximum. Both of β and ϵ_a depend appreciably on the shape of the absorbance signal profile. This is clear if one carefully examines the magnitude of the slope, $-k_2/\beta$, and ϵ_a. The slope and ϵ_a are very sensitive to the shape of the absorbance signal and they should not change appreciably if all experimental and instrumental parameters are kept constant during absorbance measurements. Their values will be a characteristic property of a particular analyte element. The value of ϵ_a will be of prime importance for research workers since it represents the overall atomization efficiency of the graphite furnace to produce and contain the analyte atomic vapour under non-isothermal conditions. A value of less than one, for instance, means that the graphite furnace is not 100% efficient suggesting that more research can be done in order to increase the atomizer efficiency to its maximum.

Because β and ϵ_a imply a greater sensitivity for peak area and peak-height absorbance it is of interest to compare the signal to noise ratio, $(S/N)_{ht}$, which arises from peak-height measurements with that obtained by peak area, $(S/N)_{area}$, and show how these two modes of measurement influence the precision of β and ϵ_a. But first, let us mention the sources for the uncertainty in the measurement of the absorbance signal. Generally, absorbance signal consists of two components: a desirable component, which is related to the free analyte atoms, and an undesirable component, which is termed noise. The noise in the absorbance signals results from two distinct types: fundamental noise which arises from the motion of discrete charges in electrical circuits and cannot be completely eliminated, and excess noise which arises from imperfect instrumentation or non-ideal component behaviour and can in principle be reduced to insignificant levels. Assuming the noise is stationary white noise and keeping with a recent publication by Voigtman[22] the comparison of the two types of signal-to-noise ratios, mentioned above, can be made in the following manner. The $(S/N)_{ht}$ is computed from the following relationship:

$$\left(\frac{S}{N}\right)_{ht} \equiv \frac{A_m}{\sigma_{ind}} \qquad (15)$$

where A_m is the average peak-height absorbance and σ_{ind} is the relative standard deviation of the measurement. The expression for the $(S/N)_{area}$ is as follows:

$$\left(\frac{S}{N}\right)_{area} \equiv \frac{\frac{1}{t_{ind}}\int_t^\infty A(t)\,dt}{\sigma_{sum}} \qquad (16)$$

where t_{ind} is the integration time constant used by Voigtman,[22] equal to the time constant of the instrument (0.02 sec), and σ_{sum} is the relative standard deviation of the integrated absorbances (or peak areas). The ratio of signal-to-noise is then,

$$\frac{\left(\frac{S}{N}\right)_{ht}}{\left(\frac{S}{N}\right)_{area}} = \frac{A_m/\sigma_{ind}}{\frac{1}{\sigma_{sum}t_{ind}}\int_t^\infty A(t)\,dt} \qquad (17)$$

which is slightly rearranged to

$$\frac{\left(\frac{S}{N}\right)_{ht}}{\left(\frac{S}{N}\right)_{area}} = \frac{\sigma_{sum}}{\sigma_{ind}}\frac{A_m t_{ind}}{\int_t^\infty A(t)\,dt} \qquad (18)$$

But the 'sigma ratio' factor is given by the following equation:

$$\sigma_{sum} = \sigma_{ind}\left(\frac{t_{sum}}{t_{ind}}\right)^{0.5} \qquad (19)$$

where t_{sum} is the time over which the area is integrated, so equation (18) becomes

$$\frac{\left(\frac{S}{N}\right)_{ht}}{\left(\frac{S}{N}\right)_{area}} = (t_{sum}t_{ind})^{0.5}\frac{A_m}{\int_t^\infty A(t)\,dt} \qquad (20)$$

For copper, $t_{sum} = 4$ sec, and $t_{ind} = 0.02$ sec, $A_m = = 0.716$ (A.U.) and peak area $= 9.379 \times 10^{-1}$ (A.sec). Thus, with these numerical values the $(S/N)_{ht}/(S/N)_{area}$ is 0.22 which is substantially less than unity as predicted by Voigtman,[22] which also means that peak-height measurements may cause greater uncertainty in β and ϵ_a calculation relative to peak-area measurements.

Acknowledgement—The author is grateful to Professor C. L. Chakrabarti and Professor E. G. Voigtman for helpful comments of this work.

REFERENCES

1. W. M. G. T. van den Broek and L. de Galan, *Anal. Chem.*, 1977, **49**, 2176.
2. R. E. Sturgeon and S. S. Berman, *Anal. Chem.*, 1983, **55**, 190.
3. H. Falk and J. Tilch, *J. Anal. At. Spectrom.*, 1987, **2**, 527.
4. W. Frech and D. Baster, *Spectrochim. Acta*, 1990, **45B**, 867.
5. B. Smets, *ibid.*, 1980, **35B**, 33.
6. B. V. L'vov, *ibid.*, 1990, **45B**, 633.
7. C. L. Chakrabarti, D. Ferrarotto, S. J. Cathum and C. J. Rademeyer, *Can. J. Chem.*, 1987, **65**, 1079.
8. B. V. L'vov, V. G. Nikolaev, E. A. Norman, L. K. Polzik and M. Mojica, *Spectrochim. Acta*, 1986, **41B**, 153.
9. B. V. L'vov, *ibid.*, 1978, 153.
10. W. Slavin, *Graphite Furnace AAS. A Source Book*, The Perkin-Elmer Corp., Norway, 1984.
11. G. Tessari and G. Torsi, *Anal. Chem.*, 1976, **48**, 1318.
12. W. Frech, N. G. Zhou and E. Lundberg, *Spectrochim. Acta*, 1982, **37B**, 691.
13. S. J. Cathum, C. L. Chakrabarti and J. C. Hutton, *ibid.*, 1991, **46B**, 35.
14. C. L. Chakrabarti and S. J. Cathum, *Talanta*, 1991, **38**, 157.
15. Yan Xiuping, Lin Tiezheng and Liu Zhijun, *ibid.*, 1990, **37**, 167.
16. D. L. Styris, *Anal. Chem.*, 1984, **56**, 1070.
17. B. V. L'vov, *Atomic Absorption Spectrochemical Analysis*, pp. 116–118. Adam Hilger, 1970.
18. R. E. Sturgeon and C. L. Chakrabarti, *Anal. Chem.*, 1977, **49**, 1100.
19. H. Falk, *CRC, Crit. Rev. Anal. Chem.*, 1988, **19**, 29.
20. B. V. L'vov and V. G. Nikolaev, *Zh. Prikl. Spektrosk.*, 1987, **46**, 7.
21. S. Wu, C. L. Chakrabarti and J. T. Rogers, *Prog. Anal. Spectrosc.*, 1987, **10**, 110.
22. E. G. Voigtman, *Appl. Spec.*, 1991, **45**, 237.
23. A. Guerrieri, L. Lampugnani and G. Tessari, *Spectrochim. Acta*, 1984, **39B**, 193.

APPENDIX

To show how equation (7) has been obtained the derivation of the Smets equation[5] has to be considered. To derive his equation Smets has used the following differential equations:

$$\frac{dN(t)_g}{dt} = R_{form} - R_{diss} \qquad (A1)$$

where $dN(t)_g/dt$ is the rate of change in the number of gaseous analyte atoms in the atomizer (assumed to be proportional to the rate of change of the number of atoms in the optical pathway), R_{form} is the rate of analyte atoms formation given by,

$$R_{form} = k_1 N(t)_w \qquad (A2)$$

where k_1 is a first-order rate constant and $N(t)_w$ is the number of analyte atoms left unatomized on the graphite surface; R_{diss} is the rate of atom dissipation given by[5]

$$R_{diss} = k_2 N(t)_g \qquad (A3)$$

Here k_2 is a first-order rate constant for atom dissipation.

Smets[5] has assumed that, for the strip heater (used by him), during all stages of atom formation, the rate of disappearance is approximately equal to the rate of atom formation [*i.e.*, $dN(t)_g/dt = 0$]. Other authors[23] have assumed that a local thermodynamic equilibrium between the analyte atomic vapour and the condensed phase prevails over the entire duration of the atom formation similar to

that prevailing during vaporization from a Langmuirian film. Under these conditions one gets for equation (A1),

$$R_{form} = R_{diss} \tag{A4}$$

At this stage one may address the following question: how can one account for the observed absorbance signal if an equilibrium is established during atom formation? To answer this question one has to fall back on the expression of the pressure equilibrium constant K_p which upon substituting equations (A2) and (A3) in equation (A4) yields,

$$K_p = p_{N_g} \tag{A5}$$

where K_p is equal to k_1/k_2 for elementary reactions. Since, K_p increases with temperature for endothermic reactions ($\ln K_p = -\Delta H°/RT + \Delta S°/R$), the pressure of the analyte atomic vapour will increase resulting in increased absorbance.

The integrated rate of atom formation, $\int_0^\infty R_{form}\,dt$, has been assumed[5] to be directly proportional to the number of analyte atoms, N_0, initially deposited in the graphite furnace as given by the following expression:

$$\int_0^\infty R_{form}\,dt = \beta N_0 \tag{A6}$$

Similarly,

$$\int_0^t R_{form}\,dt = \beta N(t)_g \tag{A7}$$

where β in equations (A6) and (A7) is the correction factor (constant) used by Smets to account for the analyte loss during all stages of atomization. According to equation (A7) the number of analyte atoms that will diffuse into the analysis volume during the indicated time interval is $\beta N(t)_g$ and that diffuses to the gas phase is $N(t)_g$. The next step in developing the above equation is to substitute equation (A4) into (A6) and (A7) for R_{form} and considering equation (A2) to get the following equations:

$$\langle k_2 \rangle \int_0^t N(t)_g\,dt = \beta N(t)_g \tag{A8}$$

$$\rangle k_2 \langle \int_0^t N(t)_g\,dt = \beta N_0 \tag{A9}$$

where $\langle k_2 \rangle$ and $\rangle k_2 \langle$ are the values of k_2 over the indicated time intervals (assumed to be constant within 10%[5]) as defined by the following two equations:[5]

$$\langle k_2 \rangle = \frac{\int_0^t k_2 N(t)_g\,dt}{\int_0^t N(t)_g\,dt} \tag{A10}$$

and

$$\rangle k_2 \langle = \frac{\int_0^\infty k_2 N(t)_g\,dt}{\int_0^\infty N(t)_g\,dt} \tag{A11}$$

Smelts[5] has further assumed that the number of analyte atoms, $N(t)_w$, left unatomized on the graphite surface is given by

$$N(t)_w = N_0 - N(t)_g \tag{A12}$$

where $N(t)_g$ is the total number of atoms in the gas phase and N_0 is the number of analyte atoms deposited in the graphite furnace. Therefore, upon substituting equations (A8) and (A9) in (A12) for N_0 and $N(t)_g$ one gets,

$$N(t)_w = \frac{1}{Q\beta}\left(\rangle k_2 \langle \int_0^\infty A(t)\,dt - \langle k_2 \rangle \int_0^t A(t)\,dt\right) \tag{A13}$$

where Q is a constant relating $A(t)$ to $N(t)g$. Setting $\langle k_2 \rangle = \rangle k_2 \langle = k_2$, yields,

$$N(t)_w = \frac{k_2}{Q\beta_1}\int_t^\infty A(t)\,dt \tag{A14}$$

which is equation (7) mentioned in Theory.

It is of interest to note that the Smets equation[5] is obtained as follows: Substituting equations (A2) and (A3) into (A4) and re-arranging terms one gets,

$$k_1 = k_2 \frac{N(t)}{N(t)_w} \tag{A15}$$

and then equation (A14) into (A15) to yield

$$k_1 = \frac{k_2 N(t)_g}{(k_2/\beta Q)\int_t^\infty A(t)\,dt} \tag{A16}$$

which, after setting $N(t)_g = A(t)/Q$ and cancellation of common term becomes

$$k_1 = \beta\left(\frac{A(t)}{\int_t^\infty A(t)\,dt}\right) \tag{A17}$$

Talanta, Vol. 39, No. 10, pp. 1229–1232, 1992
Printed in Great Britain

0039-9140/92 $5.00 + 0.00
Pergamon Press Ltd

SEQUENTIAL DETERMINATION OF IRON AND TITANIUM BY FLOW-INJECTION ANALYSIS

M. G. M. ANDRADE, S. L. C. FERREIRA, B. F. SANTOS and A. C. S. COSTA
Instituto de Química, Universidade Federal de Bahia Salvador, Bahia 40210, Brazil

(*Received* 8 *October* 1991. *Revised* 13 *February* 1992. *Accepted* 21 *February* 1992)

Summary—A flow-injection method has been developed for the sequential spectrophotometric determination of iron and titanium using 3,4 dihydroxybenzoic acid as chromogenic reagent. The system involves the sequential measurement of the absorbances of the complexes at 380 and 570 nm. The system is designed using a simultaneous injection of sample and reagent into separate carrier streams. The proposed method is characterized by a precision of about 2%, a sampling rate of about 50 samples per hour, and a reagent consumption of 200 μl (0.50% solution) per sample. It is relatively free of interferences and was used for the sequential determination of titanium and iron in rocks.

Flow-injection analysis (FIA) is a rapid and precise technique which has found wide application, especially in agricultural, environmental, geochemical, clinical and pharmaceutical analysis. The reaction between 3,4 dihydroxybenzoic acid (protocatechuic acid) or DHB with iron(III) and titanium(IV) allows the sequential determination of iron and titanium by flow injection, based on the additive property of the absorbances. Iron(III) reacts with this reagent, forming a complex with absorption maxima at 380 and 570 nm, and titanium(IV) forms a complex with an absorption peak at 380 nm. Considering these facts, a method is proposed in which the absorbances are measured at 380 and 570 nm. DHB is a good reagent for flow-injection analysis, because it is soluble in water (2 g/100 ml)[1] and does not absorb in the visible region of the spectrum. The reaction of iron(III) with DHB was studied by Hsieh and Liang[2] and of titanium(IV) with DHB by Sommer.[3] The 3,4 dihydroxybenzoic acid reagent has been used in the flow-injection analysis of manganese[4–6] and for conventional spectrophotometric determination of molybdenum,[7] vanadium,[8,9] cerium[10] and niobium.[11]

EXPERIMENTAL

Reagents

3,4 Dihydroxybenzoic acid solution. A 2.5-g amount was dissolved in 500 ml of water.

Standard iron(III) solution. Prepared from iron(III) sulfate heptahydrate and standardized gravimetrically.

Standard titanium(IV) solution.[12] Prepared by dissolving titanium(IV) oxide (0.20 g) in sulfuric acid (8 ml) and ammonium sulfate (3.2 g), heating and dilution with distilled water.

Buffer solution (pH 6.0). Prepared by dissolving 0.31 ml of acetic acid and 12.88 g of sodium acetate trihydrate in one litre of distilled water.

Apparatus

A Varian DMS 100 spectrophotometer equipped with an 8-μl flow cell, a Fisher 600 pH meter, a Micronal B332 peristaltic pump and an Intralab recorder were used.

Sample preparation

Weigh 0.2–0.3 g of dry material (110°), transfer to a Teflon beaker, and add a few mililiters of water so as to form a wet mixture. Add 1 ml of sulphuric acid (98%) and 10 ml of hydrofluoric acid (40%). Heat, on a hot plate, until almost dry.

Add an additional 1 ml of sulphuric acid and 10 ml of hydrofluoric acid and heat until white fumes. Add 5–10 ml of hydrochloric acid (37%) and transfer the contents of the beaker to a 250-ml glass beaker.

Boil to dissolve completely all the residue, cool to room temperature and transfer, with demineralized water, to a standard flask and dilute to volume.

Flow-injection analysis

Carrier solution C (buffer solution pH 6.0) is pumped into the analytical lines at a flow-rate of 3.50 ml/min with a peristaltic pump

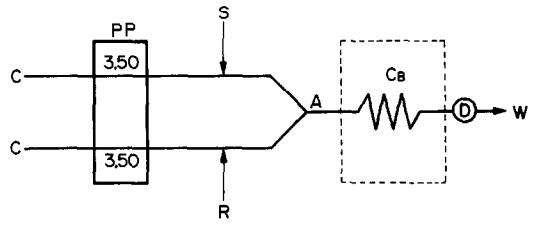

Fig. 1. Flow diagram: C carrier solution (buffer solution pH 6.0), PP peristaltic pump, S sample, R chromogenic reagent solution, A confluence point, CB mixing coil (0.5 mm i.d., 100 cm long), D detector—equipped with flow cell (volume 8 μl), W waste.

[Fig. 1]. The sample solution *S* (200 μl) and reagent solution *R* (200 μl) are introduced simultaneously into the carrier streams by a double proportional injector and the absorbance of the complex is monitored in the flow-through cell D at 380 nm for the titanium(IV)-complex and 380 and 570 nm for the iron(III)-complex, against the carrier solution as reference (baseline), separate injections are made for measurements at the two wavelengths. A narrow coil (100 cm long) is attached before the flow-through cell, as a back-pressure and mixing coil.

For calibration, similarly treated standard solutions are injected between the sample runs. The area or height of the absorbance peak can be used for calibration.

RESULTS AND DISCUSSION

The iron(III) reacts with DHB in the range pH 5.0–6.0 forming a complex with absorption maxima at 380 and 570 nm and molar absorptivities of 2.84×10^3 and 4.10×10^3 $l \cdot mole^{-1} \cdot cm^{-1}$, respectively. The titanium forms a complex with DHB in the pH range 4.0–6.0, with an absorption maximum at 380 and a molar absorptivity of 1.54×10^4 $l \cdot mole^{-1} \cdot cm^{-1}$ (Fig. 2). The DHB has an absorption peak at 280 nm and does not absorb in the visible spectrum. Considering these facts, the present method is proposed by measuring the absorbances at 380 and 570 nm, based on the additive property of the absorbances.

Optimization of flow system

Buffer concentration. The effect of the concentration of buffer solution was investigated from 0.100 to 1.000*M* acetate. Increasing the buffer to high concentrations increases the sensitivity but decreases the reproducibility. Concentrations below 0.100*M* are not recommended because the "buffering capacity" is low and the sample solutions are acid. The proposed system utilizes a dilute acetate solution, 0.100*M*, as the carrier stream.

Effect of pH. The effect of pH was investigated by using acetate buffer (0.100*M*) of various pH values as the carrier stream. Maximum absorbance is found between pH 5.5 and 6.0.

Flow rate. The effect of the flow-rate on the peak height was studied in the range of 2–4.5 ml/min, by injecting 200 μl each of iron standard and reagent solution. The maximum signal was obtained with a flow-rate of 3.50 ml/min for each stream.

Reagent and sample volume. The influence of the sample volume on the absorbance was investigated by injecting different volumes (50–300 μl) of iron and titanium standard solutions into the carrier stream at the recommended flow-rate and coil length, keeping the reagent volume at 200 μl. The injection volume has a significant effect, yielding increased peak height and reproducibility with increasing injection volume. However, increasing the injection volume widens the sample zone and lowers the sampling rate, so that 200 μl is taken as a compromise.

Length of coil. The effect of the length of the reaction coil was examined for various flow-rates. Coil lengths of 50, 100 and 150 cm were tested. Increasing the coil length lowered the peak height but improved the reproducibility. The optimum length was established as 100 cm.

Reagent concentration. The influence of the 3,4-dihidroxybenzoic acid concentration, ranging from 0.10 to 1.00%, was tested, using 200 μl of reagent and of sample. A calibration graph was obtained for each concentration of reagent with iron and titanium standards,

Table 1. Sequential determination of iron and titanium in synthetic samples

Proportion iron:titanium	Titanium (μg/ml) present	Titanium (μg/ml) found*	Iron (μg/ml) present	Iron (μg/ml) found*
1.1	11.06	10.68 ± 0.10	11.27	10.91 ± 0.10
2.8	8.05	8.33 ± 0.12	22.55	22.23 ± 0.12
4.5	8.05	8.12 ± 0.15	36.08	35.91 ± 0.15
9.0	4.02	4.09 ± 0.10	36.08	36.14 ± 0.11

*95% Confidence level.

Table 2. Sequential determination of iron and titanium in geological matrices

Standards rocks	Titanium (TiO_2) (%) certified	found*	Iron (Fe_2O_3) (%) certified	found*
Bauxite NBS-USA	2.78	2.86 ± 0.10	5.82	5.79 ± 0.15
Clay 1—IPT-SP	0.24	0.2 ± 0.07	1.93	1.88 ± 0.10
Clay 2—IPT-SP	1.04	0.96 ± 0.11	1.28	1.28 ± 0.09
Granite-CEPED-Ba	0.26	0.29 ± 0.09	1.62	1.63 ± 0.11
Bauxite-CEPED-Ba	1.19	1.24 ± 0.12	9.44	9.61 ± 0.13

*95% Confidence level.

Table 3. Compositions of standards analyzed

Standards	Al_2O_3 (%)	SiO_2 (%)	CaO (%)	MgO (%)	Na_2O (%)	K_2O (%)
Bauxite NBS-USA*	55.00	6.01	0.29	0.02	0.02	0.01
Clay 1—IPT-SP†	38.40	45.10	0.07	0.14	0.01	0.85
Clay 2—IPT-SP*	29.10	55.80	0.09	0.20	0.01	0.29
Granite-CEPED-BA*	15.06	71.80	1.21	0.50	3.79	4.78
Bauxite-CEPED-Ba*	61.47	—	0.04	0.05	0.06	0.03

*Source of the certified sample.

ranging from 10.0 to 30.0 μg/ml; all measurements were performed in triplicate. The maximum and constant slope of the calibration curve was obtained above 0.40% reagent concentration, so 0.50% concentration was selected as optimal. A study was made with 200 μl of the reagent solution.

Calibration graph

A calibration graph was obtained at the optimum working conditions: reaction coil = 100 cm, flow-rates 3.50 ml/min, reagent concentration = 0.50%, volume injected = 200 μl and carrier stream = acetate buffer pH 6.0. The calibration graph was linear over the range 2–10 μg/ml for titanium and 10–40 μg/ml for iron.

Effect of foreign ions

The interference due to several anions and cations was studied in detail. In the flow-injection spectrophotometric determination of 2 ppm of iron(III) and 1 ppm of titanium(IV), V(V), Mo(VI), Ce(III), Nb(V), phosphate and tartrate ions interfered seriously. The following ions [when present in the amounts (in ppm) shown in brackets] do not interfere: Mn^{2+} (20), Hg^{2+} (4), Cu^{2+} (10), Co^{2+} (40), Al^{3+} (50), Ni^{2+} (60), Ca^{2+} (75), Mg^{2+} (75), Pb^{2+} (40), La^{3+} (40), Bi^{3+} (40), Sr^{2+} (40), SO_4^{2-} (200), CO_3^{2-} (40), Cl^- (200) and NO_3^- (200).

However, the proposed method can be conveniently applied for the simultaneous determination of iron(III) and titanium(IV) in silicate rocks that do not contain interferents such as vanadium(V), molybdenum(IV), cerium(III) and niobium(V), as illustrated below.

Determination of iron and titanium in synthetic samples and standard samples of rocks by flow-injection analysis

The flow-system proposed was used for the simultaneous determination of iron and titanium in several samples. The results in Table 1 show that the method can be used for determination of iron and titanium in several proportions.

The analysis of rocks revealed (Table 2) that the proposed method has satisfactory precision and can be used for determination

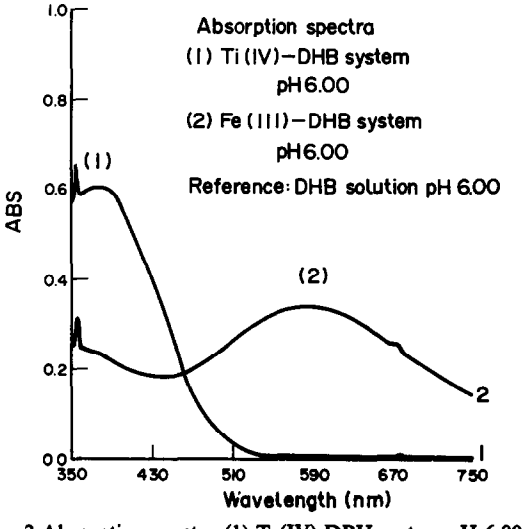

Fig. 2 Absorption spectra (1) T_i(IV)-DBH system pH 6.00 (2) Fe(III)-DHB system pH 6.00 reference: DHB solution pH 6.00.

of iron and titanium in rock samples with different composition (Table 3).

DHB does not show as high a sensitivity for iron as other reagents do but it is good for titanium. However, this presents a favorable situation for the sequential determination of these elements because, in large numbers of samples, the iron level is superior to that of titanium.

REFERENCES

1. *Lang's—Handbook of Chemistry* McGraw—Hill Book Company.
2. K. Hgieh and S. Liang, *Huaxue Xuebao*, 1981, 270; *Chem. Abstr.*, **98**, 171882.
3. L. Sommer, *Coll. Czech. Chem. Commun.*, 1963, **28**, 2102.
4. T. Yamane and Y. Nozawa, *Bunseki Kagaku*, 1984, **33**, 652; *Chem. Abstr.*, **102**, 142390a.
5. T. Yamane, *Anal. Sci.*, 1986, **2**, 191.
6. T. Kitamura and T. Yamane, *Bunseki Kagaku*, 1988, **37**, 360; *Chem. Abstr.*, **109**, 182661r.
7. P. Szarvas, Z. Jarabin and M. V. Braun, *Proc. Conf. Appl. Phys.-Chem. Methods Chem. Anal.*, 1966, **3**, 155; *Chem. Abstr.*, **69**, 15836a.
8. T. Matsumoto, M. Satake and T. Yonekubo, *Nippon Kagaku Zasshi*, 1968, **89**, 944; *Chem. Abstr.*, **70**, 16827f.
9. E. P. Klimenko, G. N. Prokof'eva and S. Ya. Shnaiderman, *Khim. Prom. Ukr.*, 1969, **2**, 41, *Chem. Abstr.*, **71**, 9408n.
10. J. Horak, *Scr. Fac. Sci. Nat. Univ. Purkynianae Brun*, 1974, **4**, 1; *Chem. Abstr.*, **84**, 25477h.
11. C. V. Rao, M. S. Rao and K. Srinivasulu, *Indian J. Chem.*,1980, **19A**, 931; *Chem. Abstr.*, **94**, 244465.
12. I. M. Kolthoff and P. J. Elving, *Treatise on Analytical Chemistry*, Part II, Vol. 5, p. 16. Interscience, New York, 1961.

Talanta, Vol. 39, No. 10, pp. 1233–1238, 1992
Printed in Great Britain.

0039-9140/92 $5.00 + 0.00

FLOW-INJECTION ANALYSIS OF SERUM UREA USING *o*-PHTHALALDEHYDE AND NAPHTHYLETHYLENEDIAMINE

D. NARINESINGH and A. POPE
Department of Chemistry, University of the West Indies, St Augustine, Trinidad, West Indies

T. T. NGO
BioProbe International, 14272 Franklin Ave., Tustin, California, CA 92680, U.S.A.

(*Received* 19 *September* 1991. *Revised* 17 *January* 1992. *Accepted* 24 *January* 1992)

Summary—An analytical procedure is developed for the determination of urea using flow injection analysis. The methodology is based on the color that develops (λ_{max}, 517 nm) when urea reacts with *o*-phthalaldehyde in the presence of naphthylethylenediamine under acidic conditions. Calibration curves are found to be linear up to 51 mg urea N/dl when the FIA manifold is operated at 42°, utilizing 90-μl samples and a flow-rate of 0.44 ml/min. By manual injection up to 40 samples can be analysed per hour. Recovery yields varied between 95–99%. The within day CV was 0.5–2.2% whereas the day to day CV was 2.1–3.9%. When applied to the analysis of urea in serum samples, excellent correlations (>0.998) are obtained when the FIA results are compared with those obtained for the same serum samples analysed by the free urease/Berthelot's and the hospital method (employing the Abbot Bichromatic Analyser). Interferences are observed with sulphur compounds such as sulphanilamide (>0.76 mg/dl) as well as with many amino acids but at relatively high concentrations (>21 mg/dl).

The quantitative determination of urea in biological fluids and soil samples are analyses that are routinely carried out in analytical laboratories. A wide variety of methodologies can and have been employed in such analyses. For example, there is the direct method in which the urea itself can be monitored by HPLC[1] or colorimetrically using diacetyl monoxime,[2,3] dimethylglyoxime,[4] *p*-dimethylaminobenzaldehyde[5] or *o*-phthalaldehyde in the presence of naphthylethylenediamine.[6–8] There are also enzyme based methods. These include the urease-glutamate dehydrogenase method[9] in which the nicotine adenine dinucleotide produced is monitored at λ_{340} and the urease hydrolysis method where the ammonia produced can be monitored either spectrophotometrically using Nessler's,[10] Berthelot's[11,12] or *o*-phthalaldehyde[13] reagents or potentiometrically using an ammonia gas sensing electrode.[14,15]

The diacetyl monoxime method is quite sensitive and very specific.[2,3] However, the color produced is unstable and a high incubation temperature (90°) is usually required. The methodologies based on urease hydrolysis are also highly specific and sensitive.[10–15]

However, these methods suffer from the disadvantages of urease inhibition, instability of reagents and possible contamination from environmental and/or endogenous ammonia.[10–15] Also some of these methods require sample pretreatment, expensive cofactors or relatively large reagent volumes.[9–11]

We now report on the development of a modified, improved method for the direct determination of urea in biological fluids employing *o*-phthalaldehyde (OPA) and naphthylethylenediamine (NED) as the colorimetric reagents for flow-injection analysis. This colorimetric method, using OPA and NED was first proposed by Jung *et al.*[16] and later modified by Lequang *et al.*[17] The reagents are stable and non-volatile and color development is very rapid (<3 min) at relatively low temperature (<40°), quite unlike diacetyl monoxime which requires an incubation temperature of about 90° for rapid color development.[2,3] These reaction characteristics make this method ideally suited for use in non-segmented continuous flow analyses such as FIA which is characterized by low reagent consumption, small sample volume requirement, high sample throughput (30–720 samples/hr) and high reproducibility.[18]

The coupling reactions which occur when urea reacts with OPA and NED are shown in Scheme 1. The chromogenic compound, **II**,

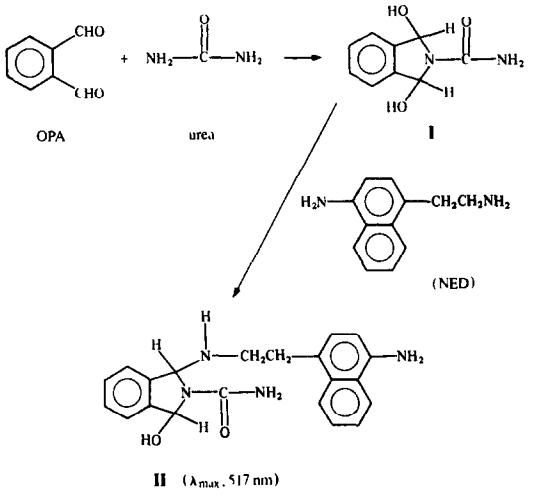

Scheme 1.

formed has a λ_{max} of around 517 nm but can be readily monitored over the wavelength range 480–520 nm. The extent of color development is directly proportional to the urea concentration.

EXPERIMENTAL

Materials

o-Phthalaldehyde (OPA) and Triton X-100 were purchased from Aldrich Chemical Company. Naphthylethylenediamine dihydrochloride (NED) and all other chemicals used were of analytical reagent grade and were obtained from BDH (Poole, U.K.). Serum samples were kindly provided by the Biochemistry Laboratory, Port of Spain General Hospital, Trinidad, West Indies.

Reagents

o-Phthalaldehyde reagent (OPA reagent). This reagent was prepared by first dissolving OPA (600 mg) in demineralized, distilled water (800 ml) containing concentrated sulphuric acid (1 ml) and Triton X-100 (7 g) and then making up to one litre with demineralized, distilled water.

Naphthylethylenediamine reagent (NED reagent). This reagent was prepared by first dissolving NED (600 mg) in demineralized, distilled water (600 ml) containing boric acid (5 g), concentrated sulphuric acid (224 ml) and Triton X-100 (7 g) and then making up to one litre with demineralized, distilled water.

These reagents when stored in amber colored bottles at 4° are stable for several years.[16]

The FIA manifold

The FIA manifold used in this study is shown in Fig. 1. Except for the pump tubing (polypropylene), PTFE tubing (0.50 mm, i.d.) was used throughout the manifold. The OPA and NED reagent streams were pumped through the FIA manifold via a peristaltic pump (Gilson Minipuls II, Surrey, U.K.). Samples of urea (90 μl) were injected into the OPA stream. Any urea–OPA–NED complex (II) formed was allowed to develop rapidly in a thermostated water bath maintained at 42° and monitored at 510 nm on a Pye-Unicam SP6-550 UV/VIS spectrophotometer equipped with a 10-μl flow cell and a strip chart recorder. The use of two separate reagent streams (Fig. 1) rather than one is recommended because of the instability of the mixed reagents upon standing.

RESULTS AND DISCUSSION

Optimization of the operating parameters

In the development of this FIA method as a viable alternative to the reported end point,[16] segmented continuous flow and kinetic methods for the direct determination of urea using NED and OPA as the colorimetric reagents several operating parameters had to be optimized in order to achieve high sensitivity, good repro-

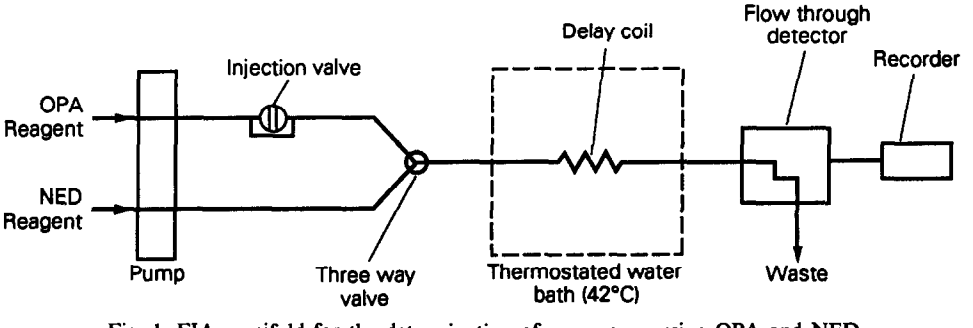

Fig. 1. FIA manifold for the determination of serum urea using OPA and NED.

ducibility, minimum interference and at the same time high sample throughput. The operating parameters that were optimized included temperature, flow-rate, sample injection volume and length of reaction coil. The effects of these various parameters on the sensitivity of the detection method are discussed below.

Temperature optimization

Jung *et al.*[16] reported in their studies that the rate of colored product formation is directly related to temperature only up to 40°, and that temperatures above 40° lead to color instability. However, in the present study it was observed that when a solution containing 3.8 mg urea N dl^{-1} was allowed to react with OPA and NED at various temperatures, the absorbance after any fixed reaction time interval (at least up to 10 min) was found to increase linearly up to 65° (Fig. 2). It was only at temperatures above 65° that product breakdown appears to take place. Also at such high temperatures (>65°) color development was observed when urea was added to OPA even in the absence of NED. Thus it should be possible to carry out analyses at temperatures below 65°. It should be noted that even if analyses were to be carried out at temperatures above 65°, then under FIA conditions this may prove not to be too critical as say in the endpoint or kinetic methods of Jung *et al.*[16] where precise timing would then be crucial. In FIA under any fixed set of operating conditions the time taken for the sample plug to travel from the point of injection to the point of detection is a constant. Thus it should be possible to obtain a high degree of precision even if there is product breakdown.

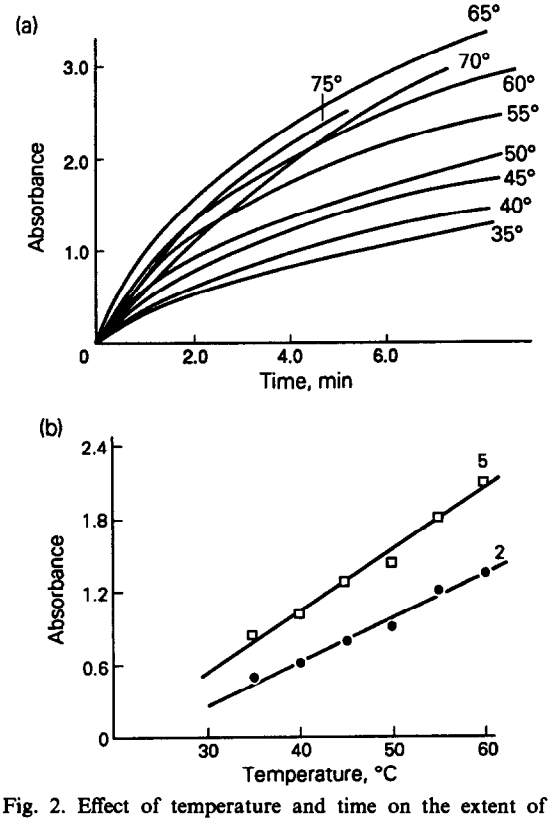

Fig. 2. Effect of temperature and time on the extent of color development of the urea–OPA–NED complex. Urea conc. = 3.8 mg N dl^{-1}. (a) Change in absorbance with time at various temperatures. (b) Absorbances at various fixed intervals and temperatures. The numbers on the graphs indicated the fixed time intervals (min) after which absorbances were measured at each temperature. Data taken from Fig. 2(a).

Typical calibration curves at selected temperatures gave the following linear regression equations ($r > 0.995$, $n = 7$):

$$29.5°\ \text{Abs} = 0.0041\ (\text{urea, mg N dl}^{-1}) + 0.0011$$
$$35.0°\ \text{Abs} = 0.0045\ (\text{urea, mg N dl}^{-1}) + 0.0028$$
$$42.0°\ \text{Abs} = 0.0080\ (\text{urea, mg N dl}^{-1}) + 0.0055$$

Flow-rate optimization

The flow-rates of both the OPA and NED reagent streams were varied by using pump tubings of varying internal diameters. It was found that maximum color development is achieved when a flow-rate ratio of 1:1 is used. Utilizing this optimized ratio and a reaction coil length of 59 cm, the overall effluent flow-rate was then varied over the range 0.26 to 0.88 ml/min. These results show that increasing effluent flow-rates results in decreased absorption intensities (peak heights). A flow-rate of 0.44 ml/min was eventually selected for use in all subsequent investigations since it provided a compromise between sample throughput and sensitivity.

Reaction coil length optimization

The effect of varying the reaction coil lengths (59, 119, 178 and 238 cm) were also investigated. The results show that with increasing reaction coil length (increased incubation time) there is a corresponding increase in absorption intensity. Use of longer reaction coils may lead to increased sensitivity but significantly increased reagent consumption and analysis time would be experienced. Also the dispersion coefficient was found to increase (1.72–1.85) as the total length of the tubing between the points of injection and detection increased. However, they

all fall into the dispersion category described as limited by Růžička and Hansen,[18] a condition which is desirable in the operation of any FIA system. A reaction coil length of 119 cm was eventually selected for urea serum analysis since it provided a compromise between sensitivity, dispersion and sample throughput rate.

Sample volume optimization

The influence of sample injection volume (90, 160 and 225 μl) was also investigated. The responses obtained for the 160 and 225-μl sample loop sizes were broad and large with sharp onset but relatively long peak decay times. With the 90-μl sample loop the peaks obtained were considerably narrower and sharper, with rapid onset and decay times and with peak heights being decreased only by about 14% (at 10 mg urea N dl^{-1} concentration) relative to the 225-μl injection volume. This increased sharpness of peaks coupled with an increase in sample throughput and a relatively small sample volume requirement led to the choice of the 90-μl loop size for all subsequent investigations.

Calibration graph, precision and detection limit

Utilizing the above compromised conditions for operating the FIA manifold (Fig. 1) calibration graphs were prepared and found to be linear over the concentration range up to 51 mg urea N dl^{-1}, curvature being observed at higher concentrations. More concentrated urea samples can be readily analysed by simply diluting so as to fall within the linear calibration range. A typical calibration curve is shown in Fig. 3.

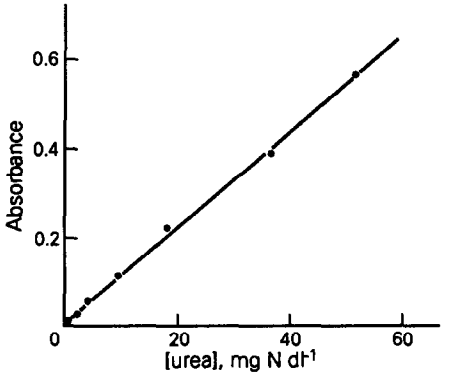

Fig. 3. Urea calibration graph under optimized compromise FIA conditions: T = 42°, flow-rate = 0.44 ml/min, sample volume = 90 μl; ratio of NED:OPA = 1:1; delay coil length = 119 cm.

The following least-squares regression equation ($r = 0.997$) was found to hold.

$$\text{Abs} = 0.107\ (\text{urea, mg N dl}^{-1}) + 0.0058$$

Urea concentrations as low as 1 mg urea N dl^{-1} can be detected at a flow-rate of 0.44 ml/min. Lower detection limits can be achieved at lower flow-rates.

The within-day coefficient of variations for the determination of a 3.0 and a 36.0 mg urea N dl^{-1} serum, obtained from 16 replicate analyses performed over a period of 6 hr were found to vary between 0.5 and 2.2%. The corresponding day to day coefficient of variation for the same 3.0 and 36.0 mg urea N dl^{-1} serum samples was found to vary between 2.1–3.9% indicating a high degree of precision of the method.

Interferences

There are many substances which are present in the blood stream and which will react with the OPA and NED reagents to produce a similar color to that obtained with urea. Comprehensive studies on the possible interferences by such substances have been reported.[16]

The present study shows that under the FIA conditions employed the amino acids, *L*-arginine, *L*-lysine, glycine and *D,L*-tryptophan and the serum protein albumin showed no interferences at least up to the concentrations specified in Table 1. These concentrations are higher than those normally found in the blood stream and hence should not interfere with urea analysis of samples. Similar non-interferences have been reported by Jung *et al.*[16] using the segmented continuous flow techniques of

Table 1. Concentration levels below which non-interference is observed for certain compounds in the reaction between urea, OPA and NED under FIA conditions

Substance	Non-interfering concentrations (mg/dl)*
L-Arginine	<3368.0
L-Lysine monohydrochloride	<228.0
Bovine albumin	<2510.0
Glycine	<656.0
Ammonium chloride	<210.0
Tryptophan (*D,L*)	<355.0
†Sulphanilamide	

*Concentrations below which no absorption is detected under FIA conditions.
†Interferences at levels as low as 0.76 mg/dl.

analysis. However, sulphanilamide was found to interfere significantly.

The latter gave the same amount of color per mole equivalent to about 25 moles of urea. This compares to the 15 and 9 mole equivalents observed by Jung *et al.*[16] using the segmented continuous flow and manual procedures respectively. These variations in urea color equivalents using the different analytical techniques can be accounted for as follows. The reaction between sulphur compounds and the OPA/ NED reagents is very fast and hence color development very rapid. However, the color fades rapidly with time. Hence the extent of interference will be dependent upon the time at which absorbance measurements are made. With the manual method reported by Jung *et al.*[16] absorbance measurements were made after an incubation time of 30 min. In contrast, in the present FIA system, the time taken for the sample plug to travel between the point of injection and the point of detection (incubation time) is only about 45 sec.

Analysis of urea in serum samples

In these analyses, triplicate samples of serum from hospitalized patients and containing both normal and abnormal urea levels (16–280 mg urea N dl^{-1}), appropriately diluted, were analysed for their urea content using the FIA manifold shown in Fig. 1. Simultaneously, independent analyses were carried out on these same serum samples for their urea content using free urease and Berthelot's reagent.[11,12]

The results were matched statistically and pair-data t-tests of the values indicate that there was a >99.9% probability that samples analysed for urea by the hospital (employing the Abbot Bichromatic Analyser) and FIA methods would yield similar results. This is reinforced by the plots of the values obtained for the same serum samples by these methods [Figs. 4(a) and (b)] and which give correlation coefficients >0.999.

Recovery studies

Samples of serum of known urea concentration were supplemented with urea to give final concentrations in the range 2–51 mg urea N dl^{-1} (normal range of urea nitrogen in blood). Analysis of these samples under FIA conditions, gave recoveries in the range 95–99% (Table 2).

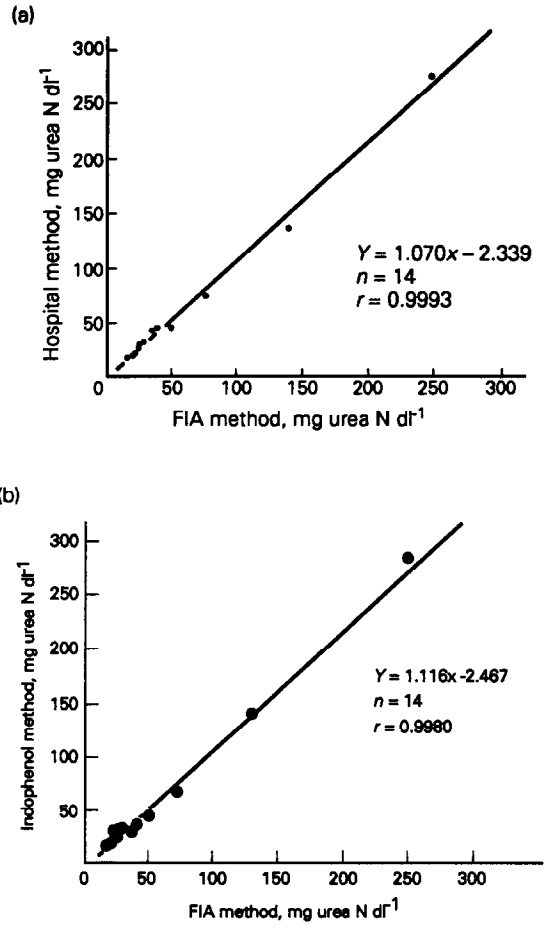

Fig. 4. Regression lines for the same serum urea samples analysed for by different methods. (a) The FIA method against the Hospital method. (b) The FIA method against the Test-Tube method.

Table 2. Analytical recovery of urea

Added urea, *mg N dl*$^{-1}$	Urea found,* *mg N dl*$^{-1}$	Recovery, %
0	2.20	—
12.35	14.27	98
24.70	26.53	99
37.05	37.87	96
49.40	49.20	95

*Average of triplicate analysis.

REFERENCES

1. H. Mueller, *Z. Anal. Chem.*, 1988, **332**, 464.
2. D. R. Wybenga, J. Di Giorogia and J. Vincent, *Clin. Chem.*, 1971, **17**, 891.
3. Z. Pan, Q. Di, B. Gao, H. Wang and P. Yen, *Zhnongguo Yike Daxue Xuebano*, 1988, **17**, 232.
4. V. Gutoranov, *Lab. Delo.*, 1982, **10**, 605.
5. H. Schulz, *Arch. Acker-Pflanzenban Bodenkd*, 1975, **19**, 397.

6. V. Chromy, H. Konecna, S. Hakzer and J. Voznicek, *Biochem. Clin. Bohemoslov*, 1983, **12**, 165.
7. T. Momose, *Talanta*, 1980, **27**, 605.
8. T. Momose and T. Momose, *Clin. Chim. Acta.*, 1981, **114**, 297.
9. C. J. Hallett and J. G. H. Cook, *ibid.*, 1971, **35**, 33.
10. C. L. Gentzkow and J. M. Masen, *J. Biol. Chem.*, 1942, **143**, 531.
11. I. Gutman and H. U. Bergmeyer, in *Methods of Enzymatic Analysis*, H. U. Bergmeyer (ed.), Vol. 4, pp. 1791–1794. Academic Press, New York, 1974.
12. J. C. Mathies, *Clin. Chem.*, 1964, **10**, 366.
13. S. S. Goyal, D. W. Rains and R. C. Huffaker, *Anal. Chem.*, 1988, **60**, 175.
14. M. Mascini and G. Palleschi, *Anal. Chim. Acta.*, 1983, **145**, 213.
15. F. Winquist, A. Spetz, I. Lundström and B. Danielsson, *ibid.*, 1984, **163**, 143.
16. D. Jung, H. Briggs, J. Erikson and P. U. Ledyard, *Clin. Chem.*, 1975, **21**, 1136.
17. N. T. Lequang, G. Migueres, D. Roche, M. L. Migueres and F. Labrousse, *Spectra Biol.*, 1987, **87-4**, 44.
18. J. Růžička and E. H. Hansen, *Flow Injection Analysis*, pp. 17 and 130. Wiley-Interscience, New York, 1981.

Talanta, Vol. 39, No. 10, pp. 1239–1244, 1992
Printed in Great Britain

0039-9140/92 $5.00 + 0.00
Pergamon Press Ltd

CATALYTIC KINETIC DETERMINATION OF ULTRATRACE AMOUNTS OF NITRITE WITH DETECTION BY LINEAR SCAN VOLTAMMETRY AT A DME

JIANG ZHI-LIANG, QIN HAI-CUO and WU DA-QIANG
Department of Chemistry, Guangxi Normal University, Guilin, People's Republic of China

(*Received* 24 *September* 1991. *Revised* 25 *March* 1992. *Accepted* 25 *March* 1992)

Summary—Nitrite has a very strong catalytic effect on the bromate oxidation of Methyl Orange in dilute sulphuric acid medium. The oxidation product of methyl orange exhibits a well derivative voltammetric wave at −0.41 V *vs.* SCE in sodium hydroxide medium. The linear scan voltammetric behaviour for the product at a DME has been studied, and it was selected as indicator component for the indicator reaction. Based on these studies, a novel and highly sensitive and selective catalytic reaction–voltammetric method for nitrite is proposed. A detection limit of $2 \times 10^{-9}M$ and calibration graph from 4×10^{-9} to $4 \times 10^{-7}M$ nitrite are obtained. Nitrite in water samples was determined by this method, with satisfactory results.

Nitrite ion can react with amines and amides, and form nitrosamino compounds that cause cancer.[1,2] Its analysis in water is also important.[3] So the development of sensitive, selective and facile analytical methods for nitrite has important significance.

Several polarographic methods for the determination of nitrite have been reported.[4–10] But their sensitivity and/or selectivity are generally unsatisfactory. Recently Wang and Li have developed a 2.5th order differential electroanalytical method to determine nitrite as low as 5 ng/ml based on the diazo-reaction.[11] Catalytic kinetic methods for nitrite are rare.[12–15] A sensitive kinetic spectrophotometric method for nitrite has been presented, based on the nitrite induced catalysis of the reaction system Fe(III)–SCN^-–I^-. However, the analysis time is relatively long (24 min).[12] Recently, Zhang has proposed a catalytic spectrophotometric method for nitrite with a detection limit of 4 ng/ml, using the new indicator reaction of bromate and Janus green.[14] Catalytic methods with oscillopolarographic (linear scan voltammetry at the DME) detection is a sensitive means of catalytic kinetic analysis.[16–25] Catalytic reaction–oscillopolarographic methods for several metals have been reported.[16–30] Catalytic reaction–oscillopolarographic methods for inorganic anions are rare.[31] And no method for nitrite has been reported.

Methyl Orange is a commonly used indicator for acid–base titrations. It has been applied for the catalytic spectrophotometric determination of As,[32] Br,[33] Cr,[34] Fe,[35] I[33] and Ru.[36] However, it does not seem to have been used for the catalytic determination of nitrite. In preliminary experiments, we have found that nitrite considerably catalyses bromate oxidation of Methyl Orange in sulphuric acid medium, and the reaction product of Methyl Orange exhibits an oscillopolarographic wave at −0.41 V. In the present work, we investigated the new indicator reaction for nitrite by linear-sweep oscillopolarography. A very sensitive and selective catalytic reaction–oscillopolarographic method for nitrite is proposed. This method is the most sensitive oscillopolarographic measurement and the most sensitive catalytic method for nitrite reported.

EXPERIMENTAL

Apparatus

A model JP-2 single-sweep oscillopolarograph (Chendu Instrumental Factory) with a three-electrode system (DME as working electrode, SCE as reference electrode, and platinum electrode as auxiliary electrode) was used. A thermostat was used to control the temperature.

Reagents

A standard solution of nitrite ($1.000 \times 10^{-2}M$) was prepared from sodium nitrate.

Working solutions were prepared by dilution of the standard solution shortly before use. Solutions of potassium bromate (0.10*M*), Methyl Orange (MO, $1.00 \times 10^{-4}M$), sulphuric acid (0.10*M*) and sodium hydroxide (1.0*M*) were used.

Procedure

Into a 25-ml graduated test tube fitted with a glass stopper, a known volume of solution containing between 5×10^{-11} and 5×10^{-9} mole of nitrite, 0.50 ml of $1.00 \times 10^{-4}M$ MO, 1.0 ml of 0.10*M* sulphuric acid and 0.30 ml of 0.10*M* potassium bromate were placed, followed by dilution to 10 ml with double distilled water. The tube was kept in a thermostat bath (at $60 \pm 0.1°$). After 15 min the reaction was quenched by tap water-cooling. Then 2.5 ml of 1.0*M* soidum hydroxide solution was added while the tube was shaken vigorously. A portion of the solution was transferred into a polarographic cell and the second derivative peak current, $(I''_p)_{t,cs}$, was measured with scanning from -0.20 V in the positive direction. $(I''_p)_{t,un}$ for the uncatalysed reaction was measured in a similar way. The $\Delta(I''_p)$ $[=(I''_p)_{t,cs} - (I''_p)_{t,un}]$ values for a range of nitrite concentrations were plotted as a function of nitrite concentration to prepare a calibration graph.

RESULTS AND DISCUSSION

Oscillopolarographic behaviour of the reaction product for MO

The polarographic character of azo-compounds has been studied extensively. Pittoni[37] reported the reduction potential for MO. However, the application of MO in inorganic oscillopolarographic analysis does not seem to have been reported. Our experiments indicated that MO and its oxidation product (MO_{ox}) exhibit oscillopolarographic waves at -0.50 and -0.41 V in sodium hydroxide medium, respectively (Fig. 1). Using the reaction product as the indicator component in catalytic kinetic analysis, provides simplicity, rapidity and high selectivity. In this work, MO_{ox} was chosen as the indicator component, and its oscillopolarographic behaviour was investigated. The I''_p is maximum and constant when the sodium hydroxide concentration is 0.15–0.40*M*, and so 0.20*M* sodium hydroxide was selected for use. The influence of bromate and bromide ions on the wave in sodium hydroxide medium was considered, and no effect was observed.

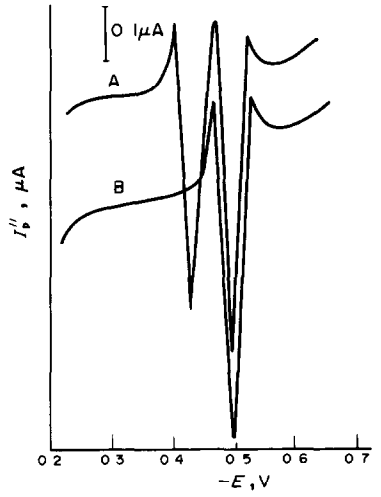

Fig. 1. The second derivative wave for MO and MO_{ox}. A: $4 \times 10^{-7}M$ NO_2^-; B: $0M$ NO_2^-. Other conditions as in procedure.

Under the conditions as in Fig. 2(A), the MO was completely oxidized to form MO_{ox} (that is, the solution is colourless). The electrocapillary curve is lower in the presence of MO_{ox} than in its absence, owing to adsorption of MO_{ox} on the surface of the DME, changing the surface tension of the mercury drop (Fig. 2). The anodic and cathodic waves are shown in Fig. 3, from which $-I_{pc}/I_{pa} = 1.82$ and $\Delta E = 30$ mV (under the conditions, the MO was completely oxidized to form MO_{ox}). The mean temperature coefficient is -1.05%/deg in the range of 15–35°. The I''_p decreases when Triton X-100, peregal O, polyvinyl alcohol and sodium dodecyl sulphonate are added. This confirms that the MO_{ox} has adsorption character.

The results demonstrate that the wave is an adsorption wave.

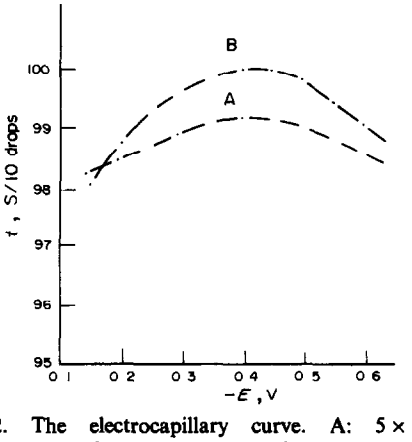

Fig. 2. The electrocapillary curve. A: $5 \times 10^{-6}M$ NO_2^-–$1.6 \times 10^{-6}M$ MO; B: $5 \times 10^{-6}M$ NO_2^-–$0M$ MO.

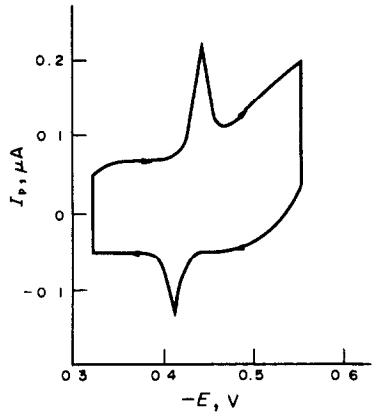

Fig. 3. Cathodic and anodic waves for the catalytic system containing $5 \times 10^{-6}M$ NO_2^- + $1.6 \times 10^{-6}M$ MO.

Principle for the catalytic determination of nitrite with oscillopolarographic detection

We first found that nitrite considerably catalysed the decolorization reaction between MO and bromate ion in dilute sulphuric acid medium at elevated temperature, and no catalytic action for nitrite occurs in sodium hydroxide media. MO_{ox} exhibits an oscillopolarographic wave at −0.41 V in sodium hydroxide medium. The reaction is very slow in sulphuric acid at room temperature. Hence, cooling by tap water or addition of sodium hydroxide can quench the reaction. The I_p'' remains constant for 120 min after quenching the reaction as in the procedure.

In the catalytic reaction solution, the catalysed and uncatalysed reactions occur simultaneously

$$MO + BrO_3^- \xrightarrow[\text{fast}]{H_2SO_4,\ 60°,\ \text{catalysed by } NO_2^-} MO_{ox} + Br^- \quad (1)$$

$$MO + BrO_3^- \xrightarrow[\text{slow}]{60°,\ H_2SO_4} MO_{ox} + Br^- \quad (2)$$

The rate equation for the catalytic reaction is

$$V_{cs} = [d(MO_{ox})/dt]_{cs} = k_c'(H_2SO_4)^a(BrO_3^-)^b(MO)^c(NO_2^-) + k_{un}'(H_2SO_4)^a(BrO_3^-)^b(MO)^c \quad (3)$$

where k_c' and k_{un}' are the rate constants of the catalytic and uncatalysed reactions respectively. And a, b and c are the reaction orders for H_2SO_4, BrO_3^- and MO respectively. Under the chosen conditions, the bromate, MO and sulphuric acid concentrations are greater than MO_{ox} concentration, and their concentrations held constant in the reaction process. Equation (3) can be expressed as

$$[d(MO_{ox})/dt]_{cs} = k_c(NO_2^-) + k_{un} \quad (4)$$

where k_c and k_{un} are the apparent rate constants of the catalytic and uncatalysed reactions, respectively. Integration of equation (4) gives

$$(MO_{ox})_{t,cs} = [k_c(NO_2^-) + k_{un}]t + B \quad (5)$$

where $B = (MO_{ox})_{0,cs}$, is the initial concentration of MO_{ox} in the catalytic reaction solution. When $(NO_2^-) = 0$, only the uncatalysed reaction takes place, and equation (5) has the form

$$(MO_{ox})_{t,un} = k_{un} \times t + B \quad (6)$$

where $(MO_{ox})_{t,un}$ is the concentration of MO_{ox} in the uncatalysed reaction solution at time t. Combining equations (5) and (6), we obtain

$$\Delta(MO_{ox}) = (MO_{ox})_{t,cs} - (MO_{ox})_{t,un} = k_c(NO_2^-)t \quad (7)$$

According to the Randel–Servick equation, $I_p'' = k'(MO_{ox})$, and equation (7) may be rewritten as

$$\Delta(I_p'') = (I_p'')_{t,cs} - (I_p'')_{t,un} = k(NO_2^-)t \quad (8)$$

where $k = k_c k'$. Equation (8) indicates that the $\Delta(I_p'')$ term is proportional to the NO_2^- concentration with the other variables and the reaction time and temperature held constant for the given system.

Effects of variables

The effects of the concentrations of sulphuric acid, potassium bromate and MO, reaction time

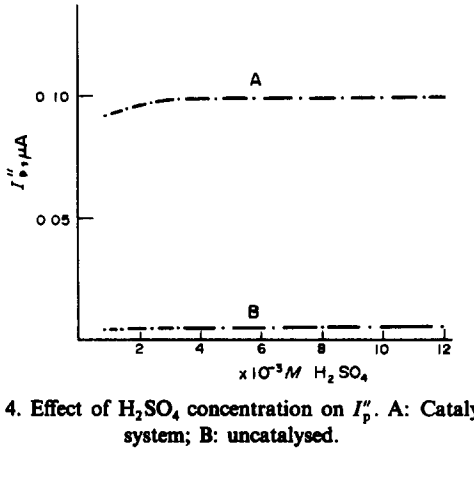

Fig. 4. Effect of H_2SO_4 concentration on I_p''. A: Catalytic system; B: uncatalysed.

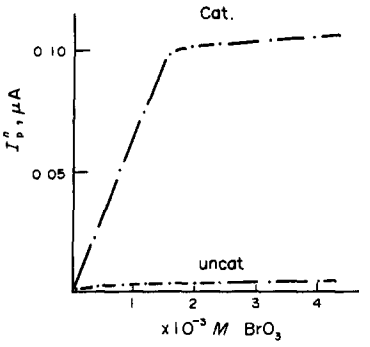

Fig. 5. Effect of BrO_3^- concentration on I_p''.

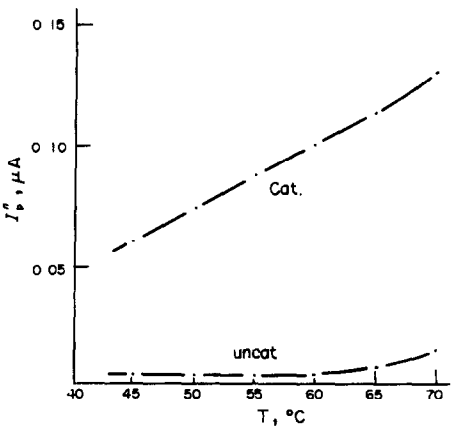

Fig. 7. Influence of temperature on I_p''.

and temperature on the $(I_p'')_{t,cs}$ and $(I_p'')_{t,un}$ were studied by the fixed-time procedure. A fixed-reaction time of 15 min was chosen, giving a good compromise between high sensitivity and analysis time. The relationship of I_p'' and sulphuric acid concentration is shown in Fig. 4. When the sulphuric acid concentration is 2.4×10^{-3}–$1.2 \times 10^{-2}M$, $(I_p'')_{t,cs}$ and $(I_p'')_{t,un}$ are constant, and $a = 0$. A concentration of $8.0 \times 10^{-3}M$ sulphuric acid was chosen. Figure 5 shows that the $(I_p'')_{t,cs}$ is proportional to bromate concentration at less than $1.6 \times 10^{-3}M$, and $b = 1$. And $(I_p'')_{t,cs}$ is stable when the concentration is more than $1.6 \times 10^{-3}M$, and $b = 0$. A $2.4 \times 10^{-3}M$ concentration of potassium bromate was selected for use. The effect of MO concentration on (I_p'') is indicated in Fig. 6, from which the order c is small and becomes zero at almost $2.5 \times 10^{-6}M$. A concentration of $4 \times 10^{-6}M$ was selected.

Under the selected conditions, $(I_p'')_{t,un}$ is very small, and can be considered negligible. Equation (8) may be rewritten as

$$k = (I_p'')_{t,cs}/(NO_2^-)t \ (A/M \cdot s) \qquad (9)$$

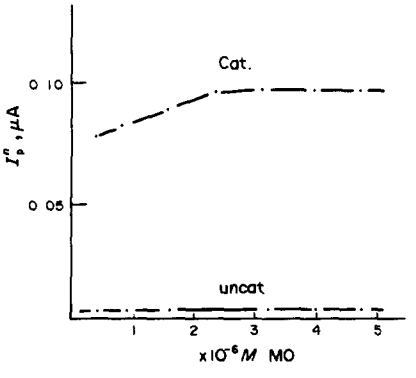

Fig. 6. Effect of MO concentration on I_p''.

The magnitude of $(I_p'')_{t,cs}$ increases with temperature (Fig. 7), and substituting the relevant data into (9), an apparent rate constant at different temperatures (45, 50, 55, and 60°) is obtained. Then according to the Arrhenius equation, an apparent activation energy $E_a = 51.7$ kJ/mole is obtained. The $(I_p'')_{t,cs}$ is very small when temperature is less than 30°. A temperature of 60° was chosen, giving a low blank value.

Effect of foreign ions

The effect of 38 foreign ions on the catalytic determination of $8 \times 10^{-8}M$ nitrite was examined. The results are shown in Table 1, and demonstrate that the catalytic method with oscillopolarographic detection has high selectivity. The tolerance limit is that multiple of the

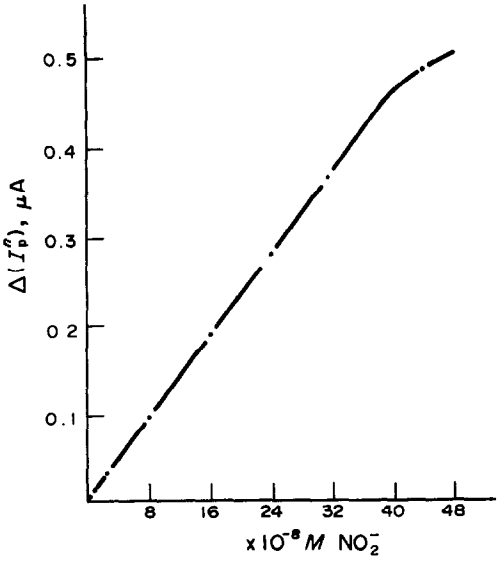

Fig. 8. Calibration graph for nitrite.

Table 1. Influence of foreign ions on determination of nitrite of $8 \times 10^{-8}M$

Tolerance limit (Ion)/(nitrite)	Ion added
1×10^4	PO_4^{3-}, SiO_3^{2-}, ClO_4^-, ClO_3^-, NH_4^+
2×10^3	NO_3^-, Cl^-, Al^{3+}, Ba^{2+}
1×10^3	CN^-, Zn^{2+}, Mg^{2+}, Ca^{2+}, Bi(III), Cd^{2+}
1×10^2	Ag^+, Hg^{2+}, Pb^{2+}, Se(IV), Co^{2+}, Ni^{2+}, Mo(VI), W(VI), Ce(III), As(III), Sb(III), Te(IV), F^-, SO_3^{2-}
80	V(V), Fe^{3+}, Cu^{2+}, Pt(IV), Cr(VI), Br^-, Os(IV)
50	I^-, Ru(III)

Table 2. Analysis results and recovery

Sample	NO_2^- added, *nmole*	NO_2^- found, *nmole*	Recovery, %	Content, $\mu g/l$. This method	Griess method[39]
Rain water	0	0.900	—	25.2	
	0	0.950	—	26.6	27.0
	0	0.960	—	26.9	
	0.5	1.40	92.6		
	1.0	1.90	96.3		
Well water	0	1.50	—	21.0	
	0	1.60	—	22.4	22.5
	0	1.60	—	22.4	
	1.0	2.50	93.0		
	2.0	3.50	96.5		
River water	0	1.90	—	53.2	
	0	1.90	—	53.2	55.0
	0	2.10	—	58.8	
	1.0	2.90	93.0		
	2.0	4.00	101		

interference concentration relative to nitrate giving not more than $\pm 6\%$ error.

Calibration graph

Under the conditions as in the procedure, $\Delta(I_p'')$ is proportional to the nitrite concentration in the range 4×10^{-9}–$4 \times 10^{-7}M$. The detection limit [defined as the concentration for which $(I_p'')_{t,cs}$ is equal to $(I_p'')_{t,un} + 2\sigma$][38] is $2 \times 10^{-9}M$. The relative standard deviation for 2×10^{-8}, 8×10^{-8} and $1 \times 10^{-7}M$ was 5.3, 3.0 and 2.4%, respectively (10 determinations).

Analysis of samples

The catalytic method was applied to the direct determination of nitrite in water samples, which were also analysed by the Griess spectrometric method.[39] Recovery of standard additions of nitrite to the sample was also determined. The results given in Table 2 illustrate good recovery and accurate analysis when compared with the spectrophotometric method.

REFERENCES

1. H. Egan, *Fd Cosemet. Toxic.*, 1971, **9**, 81.
2. I. A. Wolff and A. E. Wasserman, *Science*, 1972, **177**, 15.
3. J. Gabbay, Y. Almong, M. Davidson and A. E. Donagi, *Analyst*, 1977, **102**, 371.
4. Wang Ziyun and Huang Shenhui, *Kexue Tongbao*, 1976, **21**, 536.
5. S. K. Chang, R. Kozeniauskas and G. W. Harrington, *Anal. Chem.*, 1977, **49**, 2272.
6. S. T. Sulaiman, *Microchem. J.*, 1984, **29**, 201.
7. Cai Xiaohua, Li Peibiao and Chao Zhaofan, *Fenxi Huaxue*, 1987, **15**, 470.
8. Liu Changgan and Chen Guiyi, *ibid.*, 1987, **15**, 640.
9. G. Lu and S. Yao, *Anal. Lett.*, 1989, **227**, 1743.
10. S. T. Sulaiman, *Anal. Chem.*, 1984, **56**, 2405.
11. Wang Yaoguang and Li Ke, *Fenxi Huaxue*, 1990, **18**, 1.
12. S. Utsumi, T. Okutani, A. Sakuragawa and A. Kenmotsu, *Bull. Chem. Soc. Jpn.*, 1978, **51**, 3496.
13. Zhang Zhenui and Zhang Gailan, *Yankuan Ceshi*, 1988, **7**, 180.
14. Zhang Zhenhui, *Fenxi Huaxue*, 1989, **17**, 122.
15. Zhang Zhenhui and Zhang Gailan, *Fenxi Shiyanshi*, 1988, **4**, 341.
16. Jiang Zhiliang, *Fenxi Huaxue*, 1991, **19**, 339.
17. *Idem*, *Xiyou Jinshu*, 1988, **12**, 310.

18. Jiang Zhiliang and Liang Aihui, *Talanta*, 1990, **37**, 1077.
19. Jiang Zhiliang and Lu Ba, *Fenxi Huaxue*, 1991, **19**, 111.
20. Min Jing and Li Nanqiang, *ibid.*, 1991, **19**, 707.
21. Li Lixia, *Fenxi Cheshi Tongbao*, 1988, **7**, 16.
22. Jiang Zhiliang and Liang Xin, *Ganhan Huanjing Jianche*, 1989, **3**, 25.
23. Jiang Zhiliang, *Talanta*, 1991, **38**, 621.
24. Ma Zhichen, *Yejin Fenxi*, 1983, **3**, 220.
25. Jiang Zhiliang, *Electroanal.*, 1991, **3** 823.
26. *Idem*, *Gui-jin-shu*, 1991, **12**, 24.
27. *Idem*, *Huaxue Xuebao*, 1991, **50**, 484.
28. *Idem*, *Anal. Chim. Acta*, 1992, 260, 45.
29. Jiang Zhiliang and Li Changqun, *Yejin Fenxi*, in the press.
30. Qin Chenzhen, Li Xiaojin and Jiang Zhiliang, *Chinese Chemical Letters*, 1991, **2**, 641.
31. Jiang Zhiliang, *Dizhi Shiyanshi*, 1992, **8**, in the press.
32. A. E. Burgess and J. M. Ottaway, *Analyst*, 1972, **97**, 357.
33. Chen Shizhen, *Fenxi Huaxue*, 1978, **6**, 24.
34. E. I. Jasinskine and E. B. Bilidiene, *Zh. Analit. Khim.*, 1968, **23**, 143.
35. L. M. Tamarchenko, *Zh. Analit. Khim.*, 1975, **30**, 127.
36. P. V. Subba Rao, M. Vijayasyee, G. V. Saradamba and K. Ramakrisshna, *J. Indian. Chem. Soc.*, 1986, **63**, 743.
37. A. Pittoni, *Ricerca Sci. e. Ricostruz.*, 1947, **17**, 1396: *Chem. Abstr.* 1949, **43**, 7368.
38. Jiang Zhiliang, Liang Aihui and Dai Guaozhong, *Fenxi Huaxue*, 1989, **17**, 447.
39. W. J. Williams (ed.), *Qu Changlin Tran. Yinlizhi Ceding Shouce*, p. 199. Yejin Gongye, Beijing, 1987.

Talanta, Vol. 39, No. 10, pp. 1245–1253, 1992
Printed in Great Britain

0039-9140/92 $5.00 + 0.00
Pergamon Press Ltd

ADSORPTIVE STRIPPING VOLTAMMETRIC BEHAVIOUR OF COPPER COMPLEXES OF SOME HETEROCYCLIC AZO COMPOUNDS

PERCIO A. M. FARIAS,* SERGIO L. C. FERREIRA,† ANIY K. OHARA, MARGARIDA B. BASTOS and MAURICIO S. GOULART

Department of Chemistry, Pontifícia Universidade Católica, 22453 Rio de Janeiro, Brazil

(*Received* 27 *August* 1991. *Accepted* 25 *September* 1991)

Summary—Controlled adsorptive accumulation of copper complexed with TAN, TAC, TAR and TAM (heterocyclic azo-compounds) on a static mercury drop electrode provides the basis for the direct stripping measurement of this element in the nanomolar concentration level. The ligand TAN exhibited great sensitivity and better separation of the peak current of the ligand in relation to the complex. The reduction current of adsorbed complex ions of copper is measured by linear scan cathodic stripping voltammetry, preceded by a period of accumulation of a few minutes. The peak potential is at ~ -0.37 V vs. Ag/AgCl. Optimal experimental parameters were found to be a TAN concentration of $1 \times 10^{-5}M$, an accumulation potential of -0.22 V, and a solution pH of 3.7 (acetate buffer). The detection limit is $0.8nM$ after a 5-min accumulation with a stirred solution, and the response is linear up to 50 μg/l. Many common cations and anions do not interfere in the determination of copper. The interference of titanium is eliminated by addition of fluoride ion. Results are reported for a fresh water sample.

Heterocyclic azo-compounds are widely used in analytical chemistry for the spectrophotometric determination of many elements and as complexometric indicators.[1] Recently Farias and Ohara developed a sensitive method for the determination of uranium with the heterocyclic azo-compound 4-(2-pyridylazo)resorcinol (PAR) as the complexing agent, utilizing the cathodic adsorptive stripping voltammetry technique.[2] This new technique is a useful tool for measuring electroactive species that cannot be accumulated by electrolysis; for this purpose, a controlled adsorptive accumulation is used as an effective preconcentration step, prior to the voltammetric measurement of the surface species.[3,4]

Several methods have been reported in recent years for the determination of copper, using this new technique, with different reagents: catechol,[5–7] 8-hydroxyquinoline,[8] thiourea[9] and CSN^-.[10] These methods present advantages and disadvantages in relation to the sensitivity, selectivity and resolution of the adsorptive stripping current peak. For example, the disadvantage of using catechol to determine copper lies in its instability toward oxidation by dissolved oxygen; and lead and cadmium interfere when 8-hydroxyquinoline is used as the ligand.

The present paper describes preliminary experiments with various heterocyclic azo-compounds as complexing ligands in order to investigate their use for the determination of copper, using repetitive cyclic and adsorptive stripping voltammetry. The ligands studied were: 1-(2-thiazolylazo)-2-naphthol, TAN; 2-(2-thiazolylazo)-4-methylphenol, TAC; 4-(2-thiazolylazo)-resorcinol, TAR; and 2-(2-thiazolylazo)-5-dimethylaminophenol, TAM.

Similar adsorptive voltammetric behaviour of the copper complexes with these ligands was observed. Greater sensitivity and better separation of peak current of the complex from that of the ligand was obtained with TAN. The results of a detailed study into the optimal analytical conditions for the determination of copper using this ligand are also reported in this paper.

EXPERIMENTAL

Solutions and instrumentation

The EG&G Princeton Applied Research (PAR) model 303A static mercury drop electrode was employed with an Ag/AgCl (saturated potassium chloride reference electrode and a platinum wire auxiliary electrode and was

*Author for correspondence.
†Permanent address: Institute of Chemistry, Universidade Federal da Bahia, 40210 Salvador (BA), Brazil.

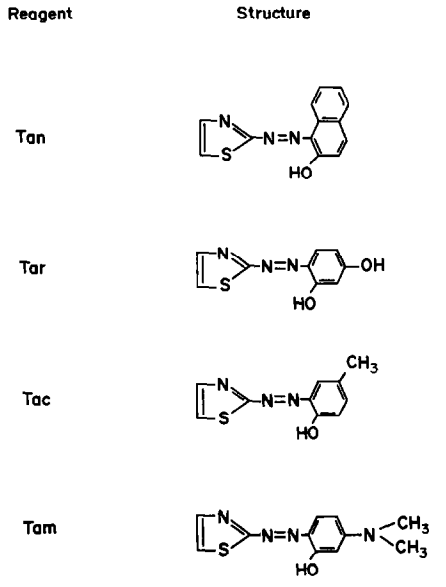

Fig. 1. Structural formula of the heterocyclic azo compounds used in the present study.

interfaced to the PAR 264 stripping analyzer, as recommended by the manufacturer. Instrument settings were as follows: medium drop size (surface area 0.016 cm^2); equilibrium time, 30 sec; potential scan rate, 100 mV/sec; filter 0.1 sec; DC stripping. Cyclic voltamperograms were obtained at 100 mV/sec. A PAR model RE 0089 X–Y recorder was used for the collection of experimental data. The sample cell was the PAR model 0057. Dissolved oxygen was removed from the test solutions by prepurified nitrogen. A magnetic stirrer (model 305) and a stirring bar (Nalgene cat no. 6600–0010) provided the convective transport during the accumulation step.

A 1000 mg/l. copper stock solution (Merck atomic-absorption standard) was used, and $2.0 \times 10^{-3}M$ TAN, TAC, TAR and TAM (Baker) stock solutions were prepared by dissolving the compounds in ethanol (Merck 99.5%). All solutions were prepared from water purified in a Milli-Q (Millipore) system, and analytical grade reagents.

Procedure

Ten milliliters of the supporting electrolyte solution [usually 2.0 ml of $0.25M$ acetate buffer (pH 3.7) + 8.0 ml of purified water] containing $1 \times 10^{-5}M$ of the heterocyclic azo compound was added to the cell and degassed with nitrogen for 8 min (and for 30 sec before each adsorptive stipping cycle). The preconcentration potential (usually 0.0 V) was applied to the electrode for a selected time (the length of the period of preconcentration depends on the copper concentration) while the solution was stirred. The stirring was then stopped, and after 30 sec the voltamperogram was recorded by applying a cathodic linear scan. The scan was terminated at −0.6 V, and the adsorptive stripping cycle was repeated using a new mercury drop. After the background stripping voltamperogram was obtained, aliquots of the copper standard were introduced. The entire procedure was automated, as controlled by the PAR 264 A

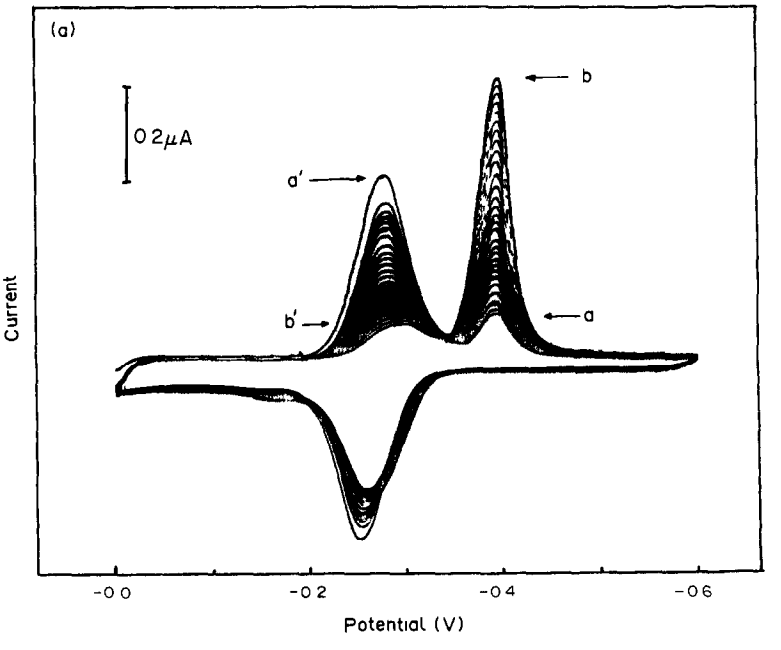

Fig. 2(a).

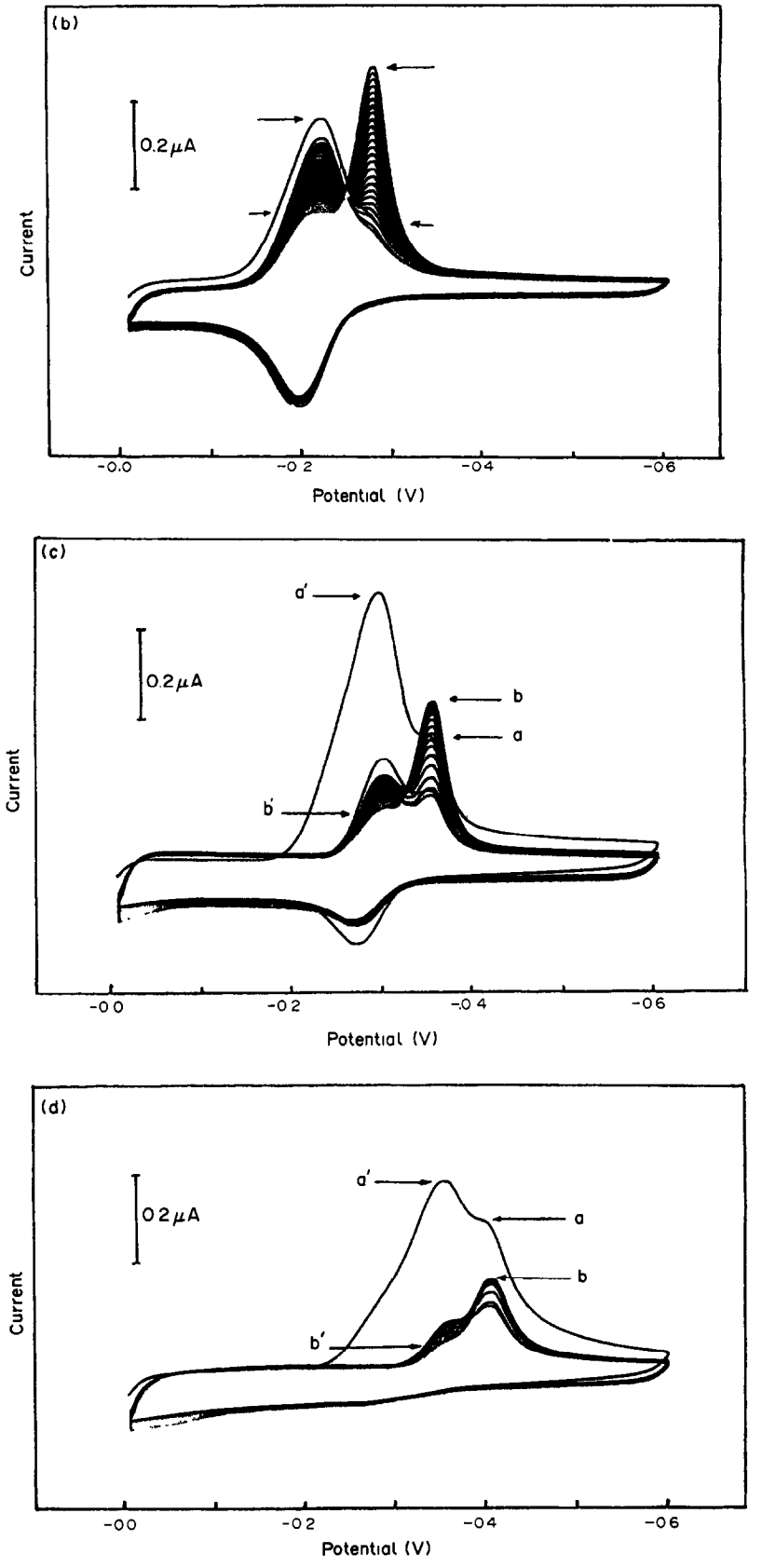

Fig. 2. Repetitive cyclic voltamperograms for $1 \times 10^{-5}M$ TAN (A), TAC (B), TAR (C) and TAM (D) complexed with 40 μg/l. of copper in an unstirred acetate buffer (pH 3.5) solution: scan rate, 100 mV/sec; first (a', a) and last (b', b) scan over approximately 4.5 min.

Table 1. Characteristics of the adsorptive stripping peak currents

Linear scan*

	E_{p1}	E_{p2}	i_{p1}	$b_{1/2}1$	$b_{1/2}2$	
	(V)		(nA)		(mV)	
(1) TAN	−0.26	−0.37	0.72	†	58.8	†
TAC	−0.21	‡ §	0.31	‡	90.2	‡
TAR	−0.28	‡	0.37	‡	98.0	‡
TAM	−0.27	0.35	0.29	0.33	86.0‡	54.9
(2) Cu-TAN	−0.26	−0.37	0.41	0.63	78.4	39.2
Cu-TAC	−0.18	−0.26	0.26	0.35	70.5	43.0
Cu-TAR	−0.28	−0.34	0.31	0.57	125.0	39.0
Cu-TAM	−0.27	−0.39	0.31	0.55	78.0‡	47.0

Differential pulse§

	E_{p1}	E_{p2}	i_{p1}	i_{p2}	$b_{1/2}1$	$b_{1/2}2$
	(V)		(nA)		(mV)	
(1) TAN	−0.23	−0.35	1.11	†	47.0	†
TAC	−0.15	‡	0.23	‡	70.0	‡
TAR	−0.24	‡	0.24	‡	94.0	‡
TAM	−0.23	−0.32	0.24	0.17	54.9	47.0
(2) Cu-TAN	−0.24	−0.35	0.54	0.26	54.9	35.2
Cu-TAC	0.15	−0.23	0.31	0.21	43.0	54.9
Cu-TAR	−0.22	−0.31	0.31	0.24	78.0	27.4
Cu-TAM	−0.24	−0.36	0.24	0.16	54.9‡	35.3

*Conditions: Values for the linear scan stripping voltamperograms for 20 μg/l. copper in 0.06M acetate buffer containing $1 \times 10^{-5}M$ thiazolylazo dye. Copper absent (1). Accumulation for one minute at 0.0 V with stirring; scan rate 50 mV/sec; other conditions as in Fig. 3(A).

†Negligible current.

‡b—Peaks overlapping.

§Conditions: Values of the differential pulse stripping voltamperograms. Scan rate 10 mV/sec, pulse amplitude 25 mV and 0.2 sec repetition time. Other conditions as in*.

stripping analyzer. Throughout this operation, nitrogen was passed over the solution surface. All data were obtained at room temperature. UV-irradiation of the sample is recommended if the presence of organic surfactants is suspected.

RESULTS AND DISCUSSION

The structures of the ligands used in this study are represented in Fig. 1. Figure 2 shows repetitive cyclic voltamperograms for $1 \times 10^{-5}M$ of the studied heterocylcic azo compounds complexed with 40 μg/l. copper in an unstirred acetate buffer (pH 3.5) solution. The TAN ligand ($E_{pc} \sim -0.28$ V and $E_{pa} \sim 0.25$ V) and its complex with copper ($E_{pc} \sim -0.40$ V and no peak in the anodic branch) is represented in Fig. 2(A), which was plotted using repetitive scans for approximately 4.5 min with a scan rate of 100 mV/sec. The cathodic current of the complex gradually increases upon repetitive scanning (a–first and b–last scan) while that of the free ligand decreases (a′–first and b′–last scan). The peak current with the adsorbed complex at saturation is several times greater than that of the solution species alone (estimated from the first scan). A small variation of the potential and peak current is observed in the reverse or anodic repetitive. A 120-mV separation of the cathodic peak potentials between the ligand and the complex is better in relation to other heterocyclic azo compounds studied. Progressive increases of the complex peak currents were observed in similar experiments using TAC [Fig. 2(B)], TAR [Fig. 2(C)] and TAM [Fig. 2(D)]. In the case of TAC, a 65-mV separation of the cathodic peak potential between the ligand and the complex, and a 30-mV separation between the cathodic and anodic current peaks of the ligand, were observed. The TAR cyclic voltamperograms were characterized by a large first peak (at −0.30 V) in the forward, cathodic scan and small peaks (at −0.28 V) in the anodic branch. The TAR–copper peak current is separated from the free ligand by 50-mV. TAM exhibited weak complexation with copper. This effect is probably due to the presence of the dimethylamine group in the structure of the ligand.

The spontaneous adsorption process can be utilized as an effective preconcentration step prior to the voltammetric measurement. In this

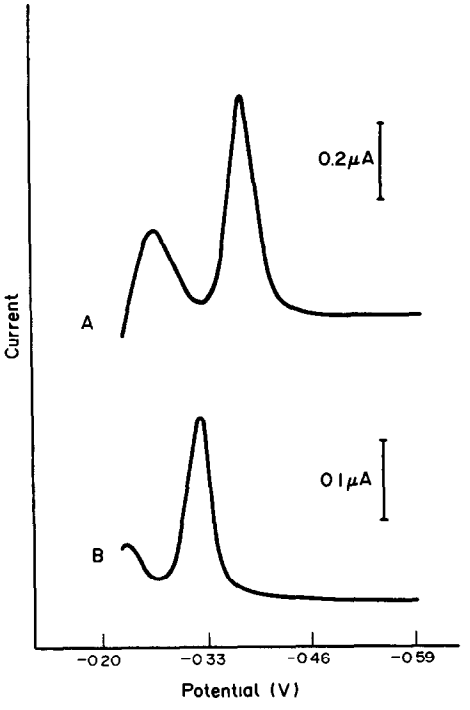

Fig. 3. Linear-scan (A) and differential-pulse (B) stripping voltamperograms for 20 μg/l. copper in a acetate buffer solution (2.0 ml of 0.25*M* acetate buffer (pH 3.4) + 8.0 ml of purified water) containing $1 \times 10^{-5}M$ TAN. Accumulation for one min at 0.22 V with stirring. Scan rate, 100 (A) and 10 (B) mV/sec; pulse amplitude (B), 25 mV; filter 0.15 (A); medium drop size and equil. time 30 sec.

way highly sensitive measurements of copper with heterocyclic azo compounds can be achieved by using the method of adsorptive stripping voltammetry.

Linear scan and differential pulse mode

Table 1 summarizes the characteristics of the stripping peaks of the heterocyclic azo compounds and their complexes with copper, in linear scan and differential pulse modes [potentials, E_{p1} (first peak), E_{p2} (second peak); currents, i_{p1}, i_{p2}; and half-widths, $b_{1/2}$ of 1, $b_{1/2}$ of 2). The TAN ligand exhibits the best efficiency in relation to sensitivity and resolution for development of a new and sensitive method to copper. Figure 3 compares linear-scan(A) and differential-pulse (B) stripping voltamperograms for 20 μg/l. copper, following 1-min accumulation. Both stripping modes exhibit significant peak current enhancements compared to direct voltammetric measurements. In particular, a considerable peak enhancement is obtained by the linear-scan mode. This mode offers good signal-to-background characteristics and greater speed, and thus is recommended for the determination of copper with the ligand TAN.

Effect of electrolyte

Among the various electrolytes (tartaric acid/sodium hydroxide, triethanolamine, citric acid/ammonium hydroxide and acetate buffer) examined for the adsorptive stripping study, best results were obtained in acetate buffer media. The effect of the electrolyte concentration on the adsorptive stripping response was evaluated and is represented in Fig. 4(A). The peak height of the complex Cu–TAN is constant when the concentration is increased from 0.050 to 0.090*M*.

Effect of pH

The peak potentials of the free ligand and of the Cu–TAN complex were also measured as a function of pH after an accumulation period of 60 sec at 0.0 V in acetate buffer (pH 3.0–5.0)

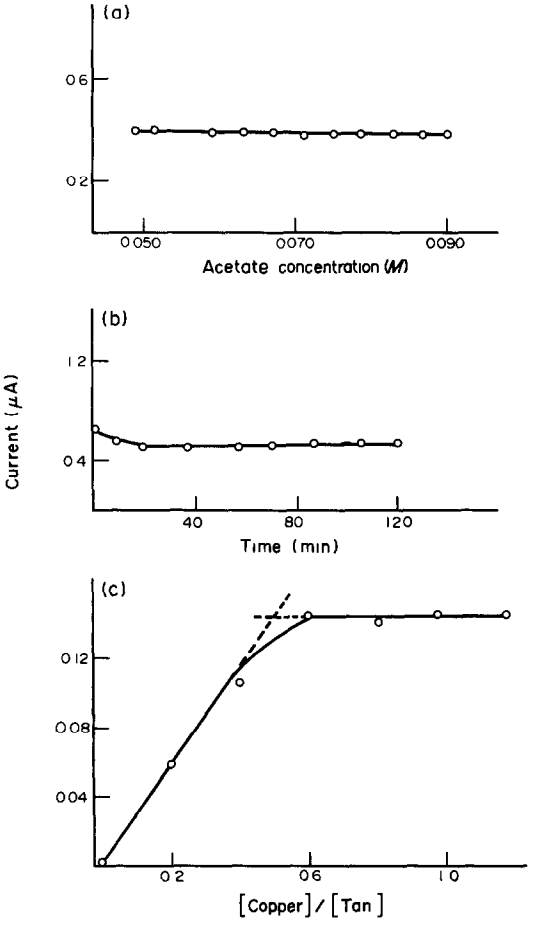

Fig. 4. Effects of acetate concentration (A), time study (B) and mole-ratio (C) on the stripping response for Cu–TAN complex. Conditions: electrolyte acetate buffer (1.0 ml of 0.50*M* [pH 3.5] + 9.0 ml of purified water) solution (B, C) containing copper and TAN; copper concentration 20 (A, B) and 1–12 (C) μg/l.; TAN concentration 1×10^{-5} (A, B) and 1.6×10^{-7} (C) *M*. Other conditions as Fig. 3(A).

Table 2. Effect of pH on the adsorptive stripping peak potential of TAN ligand and Cu–TAN complex

	Linear scan		Differential pulse	
	E_p(V)			
	Ligand*	Complex†	Ligand‡	Complex§
pH				
3.00	−0.22	−0.34	−0.18	−0.32
3.20	−0.24	−0.36	−0.20	−0.33
3.40	−0.24	−0.37	−0.21	−0.34
3.60	−0.25	−0.37	−0.22	−0.35
3.80	−0.26	−0.38	−0.24	−0.35
4.00	−0.28	−0.40	−0.26	−0.37
5.00	−0.37	−0.47	−0.34	−0.44

*Conditions: values for linear scan stripping voltammperograms in acetate buffer solution (2.0 ml of 0.25*M* acetate buffer [pH 3.00–5.00] + 8.0 ml of purified water), containing $1 \times 10^{-5}M$ TAN. Other conditions as in Table 1.

†20 μg/l. copper added. Other conditions as (*).

‡Conditions: Values for differential pulse stripping voltammperograms. Other conditions as in (*) and Table 1.

§20 μg/l. copper added. Other conditions as in (‡).

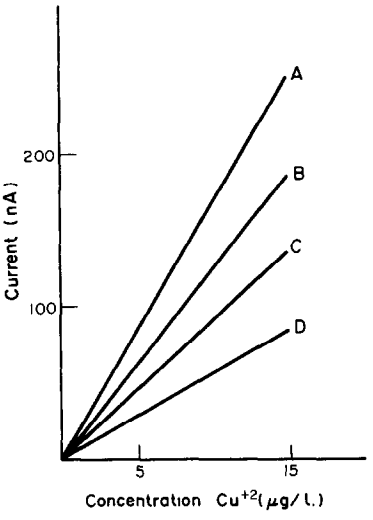

Fig. 6. Calibration plots of copper complexed with TAN (A), TAR (B), TAM (C) and TAC (D). Conditions: electrolyte acetate buffer [2.0 ml of 0.50*M* (pH 3.5) + 8.0 ml of purified water solution] containing $1 \times 10^{-5}M$ the thiazolylazo dye. Accumulation potential 0.00 V. Other conditions as in Fig. 3(A).

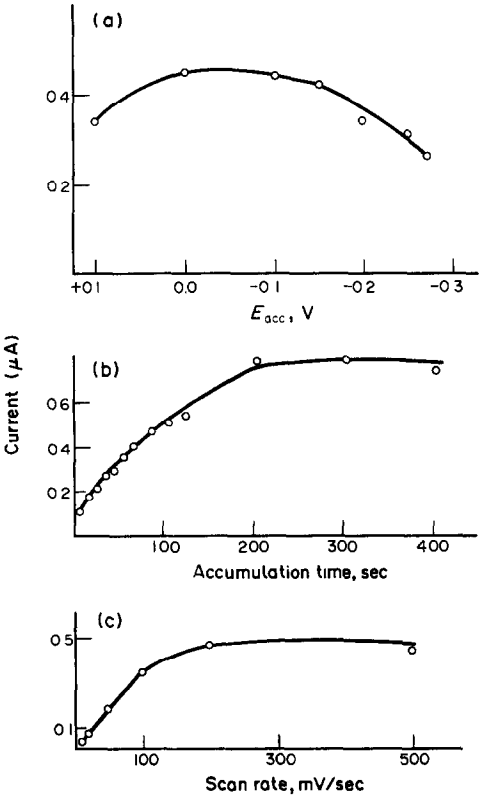

Fig. 5. Dependence of stripping peak current on the accumulation potential (A), accumulation time (B) and scan rate (C) for the Cu–TAN complex. Conditions: accumulation potential at −0.22 V (B, C) for one minute (A, C) with stirring; scan rate 50 mV/sec (A, B). Other conditions as Fig. 3(A).

containing $1 \times 10^{-5}M$ TAN and a 20 μg/l. addition of copper. It was found that the peak potentials shifted about 0.060 V/pH unit in the negative direction with increasing pH (Table 2).

Accumulation time and potential

The extent of preconcentration depends on the length of time over which the adsorption is allowed to proceed [Fig. 5(B)]. The longer the accumulation time, the more Cu-TAN complex is adsorbed and the larger the peak current. The peak increases almost linearly at first and then curves slightly toward the time axis. Such time-dependent profiles represent the corresponding adsorption isotherms because the peak current depends on the amount adsorbed. As in all types of stripping measurements, the choice of accumulation time requires a trade-off between sensitivity and speed. Forced convection during the accumulation period affects the resulting stripping response by increasing the rate of transport of Cu–TAN molecules to the surface. Such mass-transport control indicates a fast rate of adsorption.

The effect of the accumulation potential on the stripping peak current of the complex was examined over the +0.10 to −0.27 V range [20 μg/l. copper with one minute accumulation time, other conditions is in Fig. 5(A)]. The peak current remains essentially the same over the range from 0.0 to −0.15 V region; a small decrease in the peak is observed when the preconcentration

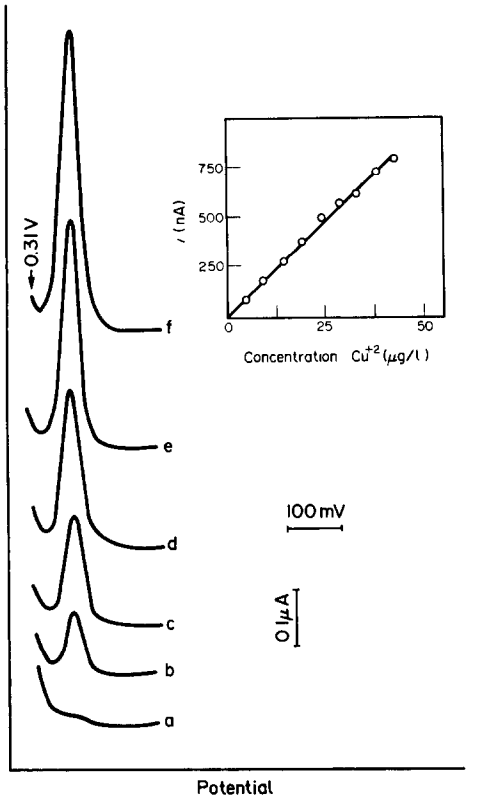

Fig. 7. Stripping voltammperogram obtained in the presence of TAN for increasing copper concentration, 5.0–29.0 μg/l. (b–f). Copper is absent in curve (a). Other conditions as 3A. Also shown is the resulting calibration plot (5.0–43.0 μg/l.).

potential varies from −0.0 to +0.10 V and from −0.20 to −0.27 V. For accumulation potentials less than −0.27 V, accentuated decrease in the complex stripping peak was also noted. The improved resolution obtained by a proper choice of the accumulation potential (at −0.22 V) reduces competition on the electrode surface by the free TAN.

Scan rate

Other conditions that affect the adsorptive response of the Cu–TAN complex are scan rate and stability. The effect of scan rate [Fig. 5(C)] on the stripping peak current of the complex was examined over the 10–500 mV/sec range; the peak increases linearly at first and then levels off. The half-width ($b_{1/2}$) of the peaks in this range varies from 29.1 to 100.8 mV. The complex is stable for at least 2 hr, as shown in Fig. 4(B), in which the solution was remeasured at time intervals. The composition of the complex was investigated by the adsorptive stripping voltammetry (Fig. 4C) technique. The TAN concentration ($1.6 \times 10^{-7}M$) was held constant and the concentration of copper was varied (0.16×10^{-7}–$1.89 \times 10^{-7}M$), and the current was plotted as a function of the molar ratio of ligand to metal ion in the solution. The ratio of ligand to metal ion at the "end point" ($0.8 \times 10^{-7}M$ copper $1.6 \times 10^{-7}M$ TAN) corresponds to the ratio in the complex, indicating that TAN/Cu in the complex is 2:1.

Analytical application

Figure 6 shows the relative slopes of calibration curves obtained for the linear adsorptive stripping voltammetry of copper with the heterocyclic azo compounds studied [correlation coefficients with corrected background: 0.9928 (A), 0.9974 (B), 0.9988 (C) and 0.9918 (D)]. The greatest advantage of the adsorptive stripping voltammetric measurements of copper complexed with TAN and other heterocyclic azo compounds is their inherent sensitivity. When TAN is used, the signal enhancement associated with the adsorptive preconcentration step results in significantly lower detection limits compared to those obtained by conventional voltammetric measurements. A detection limit of $8.3 \times 10^{-10}M$ was estimated from quantitiation of $3.2 \times 10^{-8}M$ copper after a 5-min accumulation (S/N = 2). Thus, 0.53 ng could be detected in the ten milliliters of solution used. Such detection limits compare favorably with those obtained in measurements of heavy metals by anodic stripping voltammetry.

In order for the adsorptive preconcentration step to possess significant analytical utility, it must exhibit a concentration dependence which is both well characterized and highly reproducible. Figure 7 shows linear scan voltammperograms obtained after successive standard additions of copper (5 to 29 μg/l.) in an electrolyte acetate buffer (pH 3.5) solution containing $1 \times 10^{-5}M$ of ligand TAN, after one minute of accumulation with stirring at −0.22 V. Well-defined stripping peaks were observed over this concentration range. The resulting calibration plot is also shown in Fig. 7. The stripping peak current increases linearly with the concentration. Least-squares analysis of this plot yielded a slope of 18.6 nA μg.$^{-1}$l.$^{-1}$ and 0.995 as correlation coefficient. In another experiment, solutions of increasing concentrations (0–12 μg/l.) also provided a linear response (same conditions as in Fig. 7). Deviations from linearity are expected at higher concentrations and/or when using longer preconcentration times. The high sensitivity of

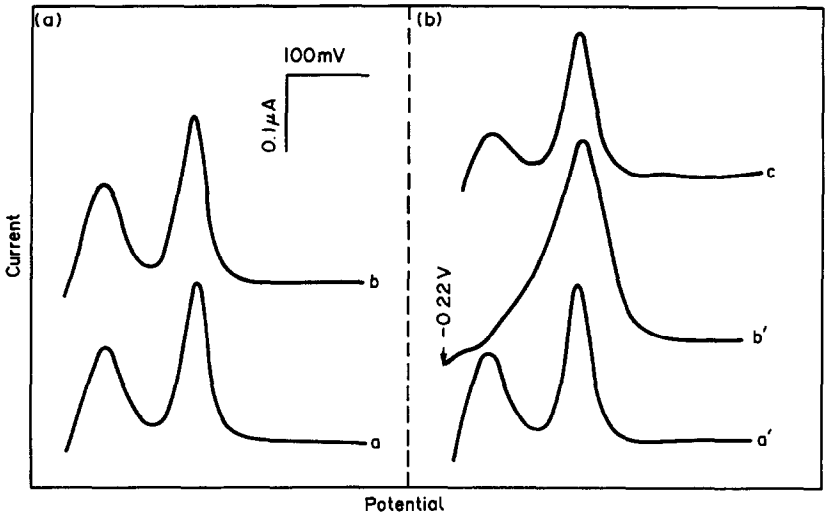

Fig. 8. Determination of copper (A) and copper with titanium (B) in the presence of fluoride: (a, a') acetate buffer (pH 3.5) solution containing $1 \times 10^{-5}M$ TAN with 20 μg/l. copper; (b) same as (a) after addition of 10 μg/ml F^-; (b') same as (a') after addition of 5 μg/ml titanium; (c) same as (b') after addition of 10 μg/ml F^-. Other conditions as in Fig. 3(A).

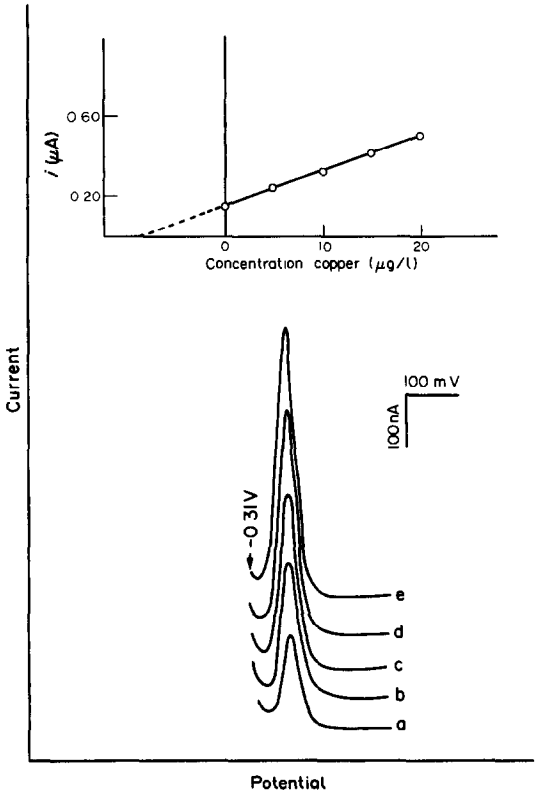

Fig. 9. Measurements of copper in fresh water from Carajás-Pará-Brazil (1.0 ml of fresh water + 2.0 ml of acetate buffer $0.5M$ + 7.0 ml of purified water + $1 \times 10^{-5}M$ TAN). (a) voltammperograms for the sample folowing 60 sec of preconcentration at −0.22 V; (b, c, d and e) same as (a) after addition of 5.0, 10.0, 15.0 and 20.0 μg/l. copper, respectively. Other conditions as in Fig. 3(A). Also shown is the resulting standard addition plot.

adsorptive stripping voltammetry is accompanied by good reproducibility of the results. This can be attributed to the reproducible area and self-cleaning control provided by the PAR 264 stripping analyzer (the use of a new drop of reproducible area in each run); as well as the stability of the formed complex Cu–TAN.

Interference studies

Interference from coexisting metal ions capable of forming complexes with TAN or depositing at the mercury electrode were evaluated. Ions tested at the 5 μg/ml level and found not to interfere in the determination of 20 μg/l. copper were Zn(II), Pb(II), Cd(II), Al(III), Ca(II), Mn(II), Sr(II), Ba(II), Co(II), Mg(II), Th(IV), In(III), Bi(III), U(VI), Cr(III), SO_4^{-2}, F^-, CO_3^{-2}, Br^-, $S_2O_3^{-2}$, NO_3^{-2} and Cl^-; CN^-, Fe(III) and Ni(II) do not interfere at the 2, 0.2 and 0.02 μg/ml respectively. The addition of 5 μg/ml V(V), Mo(II), Ti(IV), Fe(III) and Ni(II) resulted in drastic increase of the copper peak, and the appearance of new peaks for Fe(III) and Ni(II) at −0.41 V and ~ −0.39 V, respectively. The addition of $2 \times 10^{-6}M$ CDTA resulted in the dissapearence of the free ligand TAN. It was possible to eliminate the Ti(IV) interference by using F^- as masking agent. This effect is demonstrated in Fig. 8.

Determination of copper in environmental samples

The suitability of the method for the determination of copper in environmental samples is illustrated in Fig. 9. Four successive standard

additions to the "Carajás" fresh water (Pará, Brazil) samples result in well-defined adsorptive stripping peaks. The Cu–TAN peak in the original sample (Curve a) can thus be quantified based on the resulting standard addition plot (also shown in Fig. 9). These results were confirmed by differential pulse anodic stripping voltammetry (DPASV).

In conclusion, the present study describes an effective means for the determination of trace levels of copper. The use of TAN offers an attractive alternative to other ligands. It gives a similar detection limit but with reduced interference from several cations and anions, and a well-defined peak current shape. Each ligand may have an advantage over the others for certain applications. TAC, TAR and TAM present strong adsorption on the surface of the mercury electrode and potential complexation with adsorption of other important metals. We are also investigating the modification of the structure of heterocyclic azo compounds to further improve sensitivity and selectivity in the development of new analytical procedures.

Acknowledgements—The authors thank Dr. R. V. F. Bravo for critically reading this manuscript and Dr. A. L. R. Wagener for samples from Carajás (Pará, Brazil). Support of this research by SCT, CNPQ and CAPES of the Brazilian Government is gratefully acknowledged.

REFERENCES

1. V. M. Ivanov, *Heterocyclic Azo Compounds Containing Nitrogen*, pp. 229. Nauka, Moscow, 1982.
2. P. A. M. Farias and A. K. Ohara, *Electronalysis*, 1991, **3**, 985.
3. R. Kalvoda and M. Kopanica, *Pure & Appl. Chem.* 1989, **61**, 97.
4. J. Wang, *Voltammetry Following Non-Electrolytic Preconcentration, in Electroanalytical Chemistry*, A. J. Bard (ed.), Marcel Dekker, Vol. 16, New York, 1989.
5. N. K. Lam, R. Kalvoda and M. Kopanica, *Anal. Chim. Acta*, 1983, **154**, 79.
6. C. M. G. Van Den Berg, *Anal. Chim. Acta*, 1984, **164**, 195.
7. A. Nelson, *ibid.*, 1985, **169**, 273.
8. C. M. G. Van Den Berg, *J. Electroanal. Chem.*, 1986, **215**, 111.
9. Ch. Yarnitzky and R. Schreiber-Stanger, *ibid.*, 1986, **214**, 65.
10. R. Kalvoda, *Anal. Chim. Acta*, 1982, **138**, 11.

Talanta, Vol. 39, No. 10, pp. 1255–1258, 1992
Printed in Great Britain

0039-9140/92 $5.00 + 0.00
Pergamon Press Ltd

VOLTAMMETRIC STUDY OF THE BEHAVIOR OF AMARANTH AT A MERCURY THIN FILM ELECTRODE ON A SILVER SUBSTRATE

SHUCHENG MO,* JIANMIN NA and HUA MO
Department of Chemical Engineering, Beijing Institute of Light Industry, Beijing, 100037, China

XINHUA QU*
Department of Chemistry, Syracuse University, Syracuse, NY 13244, U.S.A.

(*Received* 14 *June* 1991. *Revised* 12 *September* 1991. *Accepted* 24 *September* 1991)

Summary—The voltammetric behavior of amaranth at a mercury thin film electrode on a silver substrate was studied in this paper. It was found that amaranth gave a sensitive reduction peak with the potential of −0.24 V at pH 4.0 in aqueous solution. The mercury thin film electrode on a silver substrate gave good reproducibility and useful life time. The peak currents depended linearly on the concentrations of amaranth from 0 to 100 ppb.

Amaranth, 1-(4′-sulfonyl-1′-azonaphthyl)-2-naphthanol-3,6-disulfonate, is one of the food colorants in widespread use in many countries. Some scientists have pointed out that amaranth might be causing abnormalities and toxicity for fetuses. Also, the carcinogenity cannot be ruled out. So the amounts of amaranth that can be added to foods are strictly limited by most countries using these colorants.

Most works on the determination of synthetic food colorants have usually involved thin-layer chromatographic methods, spectrophotometric methods,[1–6] high-performance liquid chromatographic methods,[6–11] although several other methods have also been described.[12–16]

Wang[17–18] and Luan[19] have determined the synthetic food colorants, tartrazine and ponceau 4R, at pH 9 by adsorptive stripping voltammetry on a hanging mercury drop electrode, respectively.

Using the hanging mercury drop electrode, Fogg and his co-workers[20–23] studied extensively the determination of a variety of synthetic food colorants by voltammetric methods and found that amaranth has a signal of detection at −620 mV (*vs.* SCE) at pH 10 buffer solution after accumulating 2 min at 400 mV. There was a linear relationship betweed the peak current and concentration of amaranth in the range 0–50 ppm. They suggested that amaranth can be determined directly at a hanging mercury drop electrode using the stripping voltammetric method in alkaline buffer solution. The sensitivity of determination should be much higher than HPLC and spectrophotometric methods.

In this paper, we studied the voltammetric behavior of amaranth on a mercury thin film electrode on a silver substrate under some different conditions. An advantage of this electrode relative to the hanging mercury drop electrode is that the mercury thin film electrode on a silver substrate is rigid and would not be deformed by a flowing fluid. It was found that amaranth has its most sensitive reducing signals at the mercury thin film electrode in buffer solutions at pH less than 7. The detection limits were in the ppb range. The mercury thin film electrode gave good reproducibility and usable life time. These cases showed that the mercury thin film electrode may be a convenient sensor combined with other instruments for monitoring synthetic food colorants.

EXPERIMENTAL

Equipment

A model AD-2 polarographic system was used for experiments with 3 electrodes consisting of the silver, platinum, and saturated calomel electrodes for experiments. The silver electrode was used as a substrate for coating a mercury thin film. The voltammetric signal was

*Author for correspondence.

recorded automatically by an autobalance chart recorder model XWX-1042. A model pH-S3 digital pH meter was used for measurement of pH. To ensure a high quality recording of the signal, a stabilized voltage source model WYJ-6C was used.

Reagents

Demineralized water was used throughout the study. Boric acid, phosphoric acid, glacial acetic acid, sodium hydroxide, sodium acetate, potassium chloride, nitric acid and mercury were all of reagent grade. Amaranth was biochemical reagent grade. A cylinder of highly purified nitrogen was used to remove the oxygen dissolved in sample solutions.

Procedure

Preparation of the Britton–Robinson buffer solution. A 2.7-g amount of boric acid, 2.3 ml of glacial acetic acid, and 2.7 ml of phosphoric acid were dissolved in demineralized water and diluted to one liter (pH of 1.90). The pH was then adjusted by 2*M* sodium hydroxide solution to values of 4.00, 6.00, 8.00 and 10.0, as required for study.

Preparation of stock solution of amaranth. A 0.0100-g amount of amaranth was weighed precisely and dissolved in a small amount of demineralized water, and then diluted to 100 ml. This stock solution (I) contained 100 ppm amaranth. A 5-ml solution of I was rediluted to 50 ml to obtain stock solution II containing 10 ppm amaranth. Both of these were kept in dark brown bottles at 4°.

Preparation of the mercury thin film electrode. A silver electrode (a silver rod of 1.0-cm length and 1.5 mm diameter) was de-oiled by acetone, the de-oiled electrode was treated with 10% nitric acid for 30 sec, and then washed thoroughly with demineralized water. The silver electrode was touched to a droplet of mercury weighing about 20–30 mg. The mercury spread on the surface of silver and formed a thin film of mercury.

The mercury thin film electrode was put into 0.5*M* potassium chloride solution. The solution was deaerated for 10 min by a stream of nitrogen.

Under the atmosphere of nitrogen, the potential was maintained at −1.80 V for 5 minutes, then swept to −1.0 V. This process was repeated for several times. The electrode was kept in demineralized water prior to use.

Experiment. An appropriate amount of stock solution (II) was injected with a microsyringe into a 2.5-ml Britton–Robinson buffer solution which had been adjusted to the required pH as mentioned. These solutions were diluted then to 25 ml.

In measurement, the compound was accumulated from a reproducibly stirred solution by adsorption at a mercury thin film electrode for a suitable fixed time before being determined in quiescent solution by means of a potential sweep. In this study, the order was: deoxygenation (for 10 min)—sample injection—accumulation (in a stirred solution)—solution quiescence—potential sweep.

Usually the quiescent time was 0.5 min, and the potential sweep was from 0.00 to −1.00 V.

RESULTS AND DISCUSSION

The effect of pH on peak potential and current

Figure 1 shows the curves of peak potential (V_p) and peak currents (i_p) versus pH at mercury thin film electrode in 100 ppb amaranth aqueous solution with one minute accumulation and 40 mV/sec of sweep rate.

Curve 1 shows that V_p shifted negatively as pH increased, and curve 2 indicates that i_p decreased with pH for pH > 4. The sensitivity at pH 8–10 was much less than at pH 2–4. Although the highest sensitivity occurred at pH 1.9 in these studies, it was not the optimum because the V_p (−0.10 V) at this pH was too close to the accumulation potential. The operating parameter in this work was selected as pH 4 ($V_p = -0.24$).

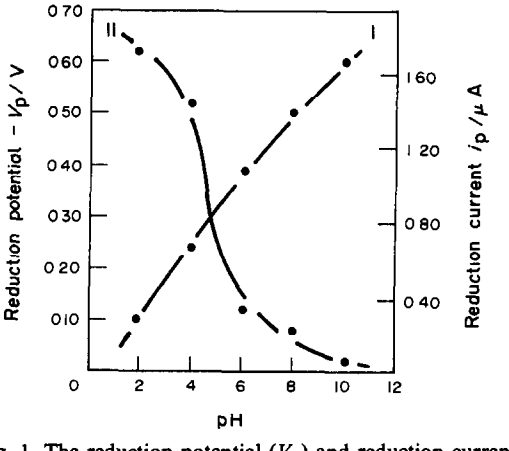

Fig. 1. The reduction potential (V_p) and reduction current (i_p) dependence on pH. Curve I: V_p *vs.* pH, Curve II: i_p *vs.* pH; Concentration of amaranth: 0.10 ppm; Accumulation potential: 0.0 V; Accumulation time: 1.0 min; Range of sweep: 0.1 → −1.0 V; Sweep rate: 40 mV/sec

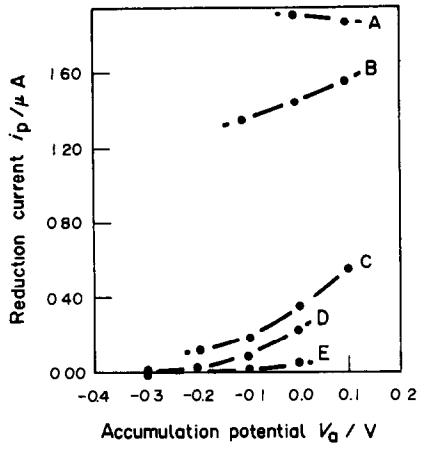

Fig. 2. The reduction current (i_p) dependence on accumulation potential (V_a) at different pH. Curve A: pH = 1.9 Curve B: pH = 4.0; Curve C: pH = 6.0 Curve D: pH = 8.0; Curve E: pH = 10.0 ; Concentration of amaranth: 0.10 ppm; Accumulation time: 1.0 min; Range of sweep: 0.0 → −1.0 V; Sweep rate: 40 mV/sec

The effect of accumulation potential on peak currents

Figure 2 shows the effect of accumulation potential on peak currents at different pH values. Obviously, the curves in Fig. 2 imply that the i_p increased with pH rather than accumulation potential. The accumulation potential has a relatively weak effect on i_p, also indicating that the process of accumulation was mainly the process of adsorption. To avoid occurrence of other reactions, 0.0 V was used as the accumulation potential.

The effect of accumulation time on the peak currents

The peak current dependence on the accumulation time (t_a) is shown in Fig. 3. It can be seen that peak currents increased linearly with t_a less than 2.5 min because amaranth adsorption

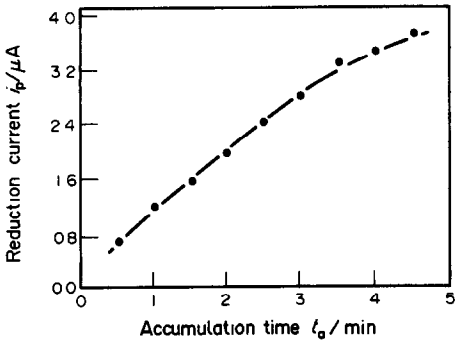

Fig. 3. The reduction current (i_p) dependence on accumulation time (t_a) at pH = 4.0. Concentration of amaranth: 0.10 ppm; Accumualtion time: 1.0 min; Range of sweep: 0.0 → −1.0 V; Sweep rate: 40 mV/sec

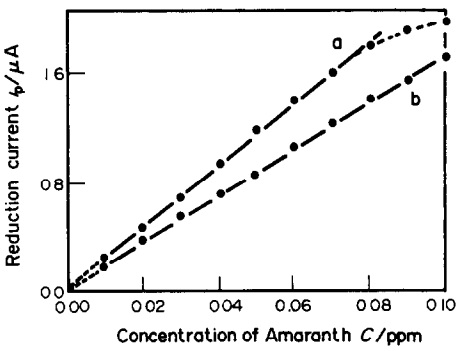

Fig. 4. The reduction current (i_p) dependence on concentration of amaranth (C) at pH = 1.9; Curve (a): Sweep rate: 40 Mv/sec, Accumulation time: 1.0 min. Curve (b): Sweep rate: 40 mV/sec, Accumulation time: 0.5 min. Range of sweep: 0.0 → −1.0 V; Sweep rate: 40 mV/sec.

was not saturated on the surface of the mercury thin film electrode. However, the adsorption tended to saturate when t_a was larger than 4 min, so it would not be available for increasing peak currents by prolonging accumulation time. Therefore, one minute t_a was adopted for this study.

The peak current dependence on concentration of amaranth

The sizes of peak currents obtained at various concentrations of amaranth at pH 1.9 are plotted in Fig. 4 for accumulation times of 1.0 and 0.5 min. Current was linearly proportional to concentration over the interval of 0–80 ppb for curve (a) as well as curve (b).

Figure 5 describes the peak current dependence on concentrations of amaranth at pH 4.0. The accumulation times of curve 1, 2 and 3 were 2.0, 1.0 and 1.0 min. Obviously, curves

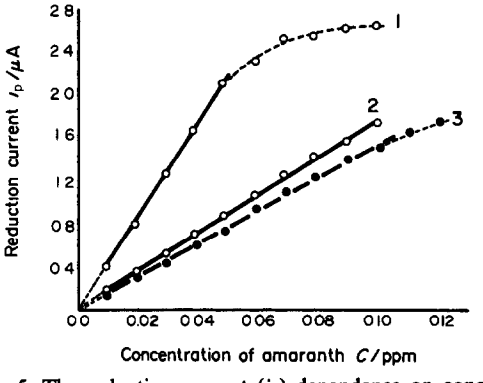

Fig. 5. The reduction current (i_p) dependence on concentration of amaranth (C) at pH = 4.0. Point ●: Data in Britton–Robinson buffer solution. Point ○: Data in HAc–NaAc buffer solution. Curve ①: Sweep rate 40 mV/sec, Accumulation time 2.0 min. Curve ②, ③: Sweep rate 40 mV/sec, Accumulation time 1.0 min. Accumulation potential: 0.0 V; Range of Sweep: 0.0 → −1.0 V.

2 and 3 exhibited linear dependence in the concentration interval 0–100 ppb. For curve 1, although the peak currents were higher in this interval, the linear region was limited to less than 50 ppb concentration. In this case, the sensitivity could be improved only by reducing the linear calibration range. This was one of the reasons for using an accumulation time of one minute in this study.

The useful life time of mercury thin film electrode and interferences

After fifty cycles of continuous potential sweeping, the peak currents still remained stable, with a coefficient of variation of 1% when the thin film electrode was used for 100 ppb amaranth solution at pH 4.0. This showed that the life time of this electrode was excellent.

No interferences were found in the presence of indigo carmine, tartrazine, or ponceau 4R at concentrations five times larger than that of amaranth. The determination was not interfered with by sugar, citric acid or benzoic acid.

CONCLUSION

Amaranth was detected with a sensitive voltammetric signal of amaranth at the mercury thin film electrode on silver substrate. The i_p at pH < 4 was much larger than that at pH > 4. Accumulation potential was a little effect on i_p. Appropriately prolonging the accumulation time is profitable for increasing the peak currents.

Suitable operating parameters are suggested as follows:

$$\text{pH} = 4.0 (V_p = -0.24\ \text{V}), \quad V_a = 0.0\ \text{V}$$

$$t_a = 1.0\ \text{min} \quad \text{sweep rate} = 40\ \text{MmV/sec}$$

Using these parameters, the peak currents increased linearly with the concentrations 0–100 ppb of amaranth. The mercury thin film electrode has good usable life time and reproducibility under these conditions.

REFERENCES

1. *Food and Drugs: Composition and Labelling: The Coloring Matter in Food Regulations 1973.* SI No. 1340, HM Stationery Office, London, 1973.
2. K. Macek, (ed.), *Pharmaceutical Applications of Thin-Layer and Paper Chromatography*, p. 618. Elsevier, Amsterdam, 1972.
3. D. Pearson, *The Chemical Analysis of Foods*, 7th Ed., p. 50. Churchill Livingstone, Edinburgh, 1976.
4. J. Vankataraman, *The Analytical Chemistry of Synthetic Dyes*, p. 465. Wiley, New York, 1977.
5. R. A. Meyer, F. Gruendig and R. Schaefer, *Nahrung*, 1989, **3**, 261.
6. Z. M. Zhang, D. X. Huang and H. Shui, *J. of Shandong University, Part I. (Chin)* 1989 **3**, 123.
7. D. P. Wittmer, N, O. Nuessle and W. G. Haney Jr., *Anal. Chem.*, 1975, **47**, 1422.
8. J. H. Knox and G. R. Laird, *J. Chromat.*, 1976, **122**, 17.
9. M. H. Salagoity-Auguste, A. Bertrand and P. Sudraud, *Sci. Ailments*, 1983, **1**, 127.
10. M. L. Young, *J. Assoc. Off. Anal. Chem.*, 1984, **5**, 1022.
11. S. L. Reynolds, M. J. Scotter and R. Wood., *J. Assoc. Public Anal.*, 1988. **1**, 7.
12. M. L. Young, *J. Assoc. Off. Anal. Chem.*, 1988, **3**, 458.
13. U. V. Prasad, P. L. Kumari and T. E. Divakar, *Acta Gienc. India (Ser) Chem.* 1985, **11**, 115.
14. M. I. Alberto Quinto, C. Sanchez-Pedreno, E. Martinez-Garcia, *Afinidad*, 1987, **410**, 305.
15. G. Xu, *Chem. Sensor.*, 1989, **1**, 26.
16. K. Tsunoda, N. Inoue and M. Aoyama, *J. Food Hygenics*, 1987, **6**, 473.
17. L. Z. Wang, N. Chen., G. L. Li, *J. Medical Analysis*, 1989, **6**, 327.
18. L. Z. Wang, Q. Li, S. Q. Wen and R. L. Chen, *Chinese Journal of Applied Chemistry*, 1989, **3**, 82.
19. X. K. Luan and S. G. Bai, *Anal. Chem.* 1987, **5**, 444.
20. A. G. Fogg, A. A. Barros and J. O. Cabral., *Analyst*, 1986, **11**, 831.
21. A. G. Fogg and D. Bhanot, *ibid.*, 1987, **112**, 1319.
22. A. A. Barros, J. O. Cabral and A. G. Fogg, *ibid.*, 1988, **113**, 853.
23. A. G. Fogg and A. M. Summan, *ibid.*, 1984, **109**, 743.

Talanta, Vol. 39, No. 10, pp. 1259–1267, 1992
Printed in Great Britain

0039-9140/92 $5.00 + 0.00
Pergamon Press Ltd

SIMULTANEOUS DETERMINATION OF Cl^-, Br^-, I^- AND F^- WITH FLOW-INJECTION/ION-SELECTIVE ELECTRODE SYSTEMS

FADHIL M. NAJIB* and SHIREEN OTHMAN
Department of Chemistry, University of Salahaddin, Arbil, Iraq

(*Received* 20 *February* 1989. *Revised* 23 *September* 1991. *Accepted* 8 *November* 1991)

Summary—Flow-through ion-selective electrodes were constructed from compressed pellets (8–10 mm thick, 13 mm diameter, 10 tons/cm^2 pressure) of Ag_2S/AgX (X = Cl^-, Br^- or I^-) drilled longitudinally (1.5 mm diameter hole) to be suitable for use in flow-injection analysis. A column of AgCl (5.5 cm long, 2–3 mm i.d.) was included in the Cl^--electrode manifold to remove interferences from $10^{-4}M$ Br^- and $3 \times 10^{-5}M$ I^- and S^{2-}. A column of amalgamated lead (2–3 cm long, 2–3 mm i.d.) was used in the Br^--electrode manifold to remove interference from $2 \times 10^{-5}M$ I^-, $3 \times 10^{-5}M$ S^{2-} and $7 \times 10^{-4}M$ Cl^-. These columns and the addition of ascorbic acid were not required when I^- was determined with the iodide electrode. The carrier stream was $0.1M$ sodium perchlorate (pH 4) at a flow-rate of 0.5 ml/min. The sample pH could be 4–7. Simultaneous determination of Cl^- and I^-, Cl^-, I^- and Br^- and Cl^-, I^-, Br^- and F^- ions was possible with combinations of the corresponding electrodes and columns in series and/or parallel in specially designed manifolds. Calibration plots were linear, with almost theoretical slopes, down to $10^{-6}M$ I^-, $5 \times 10^{-6}M$ Br^-, $10^{-4}M$ Cl^- and $5 \times 10^{-6}M$ F^-, with precision better than 1%. Sampling rates for single-ion determinations were 72, 102, 90 and 80 per hr for the one-, two-, three- and four-electrode systems respectively. Determinations of these ions in water samples by the recommended procedure and by established batch methods showed no significant difference at the 95% confidence limits in a paired comparison t-test.

Ion-selective electrodes (ISEs) have been widely used as detectors in flow-injection analysis (FIA).[1–13] This combination of techniques can be extended by use of several electrodes in the same manifold for determination of a number of ions in the same sample. Few such application have been reported,[2,7,14] and none concerning the halides.

In the present work, home-made $AgCl/Ag_2S$, $AgBr/Ag_2S$ and AgI/Ag_2S membranes and a commercial fluoride-selective electrode were used, and mutual interferences between the halides were eliminated automatically within the manifold.

EXPERIMENTAL

Apparatus

A Desaga STA pump and an Omnifit injection valve with a 60-μl sample loop were used. All connecting tubes used in the manifold were 0.8 mm i.d. The commercial electrodes used were an Ingold 157205 F for fluoride, a Radiometer F 1012 Cl for chloride, an Orion 94-53 for iodide, and Orion 90-01 single-junction and 90-02 double-junction Ag/AgCl as references. Potentials were measured with an Orion 811 Ionalyzer, a Radiometer pH M62, and a Wissenchaftlich-Technische Werkstatten (Weilheim) model 410, and recorded with Philips PM 825 and Servograph REC 61 single-pen recorders and a Servogor 220 double-pen recorder.

Reagents

All chemicals were of analytical grade and ordinary distilled water was used for all preparations. Silver and mercuric sulphides were prepared[15] by adding $0.5M$ silver or mercuric nitrate dropwise to excess of $0.1M$ sodium sulphide. The precipitates were collected, washed first with dilute nitric acid, then distilled water and finally ethanol, and were dried at 50° for 12 hr.

Preparation of flow-through pellets

A weight of 6.5 g of a 1:1 molar ratio mixture of AgCl or AgBr with Ag_2S or 3:1 molar ratio

*Author for correspondence. Present address: Chemistry Department, College of Science, Babylon University, Hilla, P.O. Box 4, Iraq.

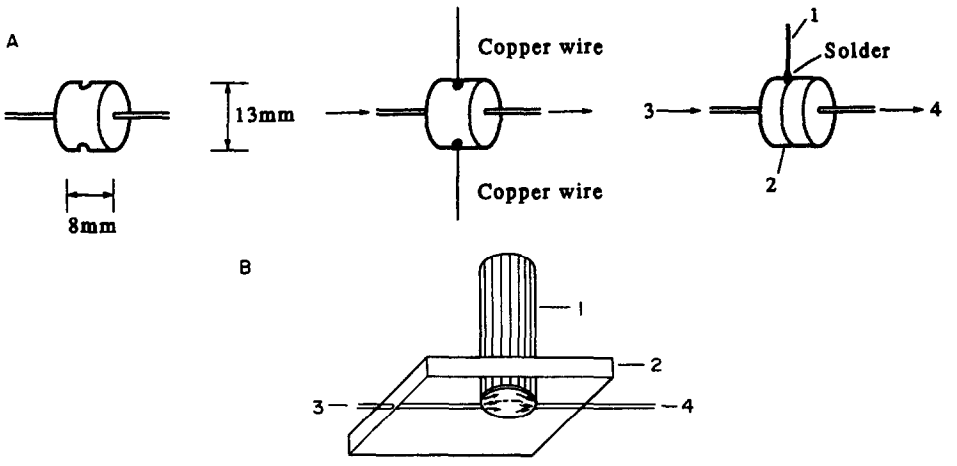

Fig. 1. Schematic diagram for A, flow-through pressed pellets of I^-, Br^- and Cl^- electrodes; 1, electrical conducting wire; 2, PVC tape; 3, inlet; 4 outlet; B, flow-through cell for F^--electrode; 1, commercial F^--electrode; 2, piece of Perspex; 3, inlet; 4, outlet.

mixture of AgI and Ag_2S was crushed to pass a 0.053-mm (300-mesh) sieve. The fine dry powder was pressed between two 13-mm diameter stainless-steel plates in a die-press under 10 tons/cm^2 pressure with continuous withdrawal of air before and during pressing, and left under pressure for 12 hr. The pellet thus obtained was about 8–10 mm long and 13 mm in diameter. It was drilled longitudinally to make a channel 1.5 mm in diameter. Electrical connection was made, as shown in Fig. 1A, by making another two holes of the same diameter and about 2–3 mm deep on opposite sides of the pellet. Two copper wire leads, 0.8 mm in diameter and about 5 cm long, were soldered into each hole. One wire was then bent round the pellet and soldered to the other, which was insulated and connected to the pH-meter by a properly screened wire lead. The electrode and wire lead were insulated with PVC tape, screened with thin aluminium foil and earthed. The flow-through cell for the fluoride electrode was made as follows. A piece of Perspex (2 × 2 cm, 6 mm thick) was drilled at the centre to accept a commercial fluoride electrode (Fig. 1B). The other surface of the plate was grooved on opposite sides of the central hole to accept two short Teflon tubes (0.8 mm i.d.). A piece of very thin nylon or PVC sheet was then glued over this surface and the electrode membrane surface was kept close to it to minimize the dead volume. A little flexibility in this cover helped to absorb any pulses produced during pressure build-up.

Preparation of interference suppressor columns

AgCl, AgBr and AgI columns. The salt was crushed to pass a 0.425-mm (36-mesh) sieve. The desired length of a 2-mm bore tube was filled with the salt and closed at both ends with glass wool. A silicone rubber tube was connected at each end with the aid of UHU-glue, and the tube was wrapped with black PVC tape to protect it from light. The column was placed in the manifold between the injection point and the chloride electrode.

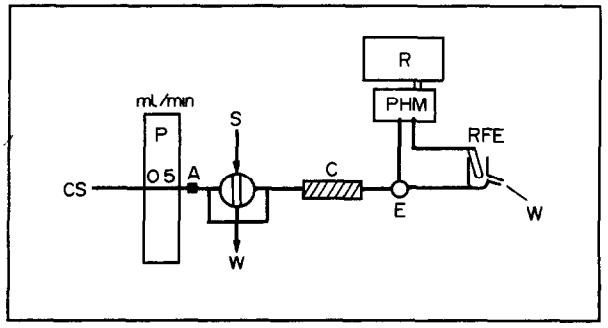

Fig. 2. Manifold for the determination of Br^- or Cl^-. CS, Carrier stream; P, pump; A; pulse suppressor; S, sample injection; C, interference suppressor column; E, flow-through detector; RFE, reference electrode; PHM, pH/mV-meter; R, chart recorder; W, waste.

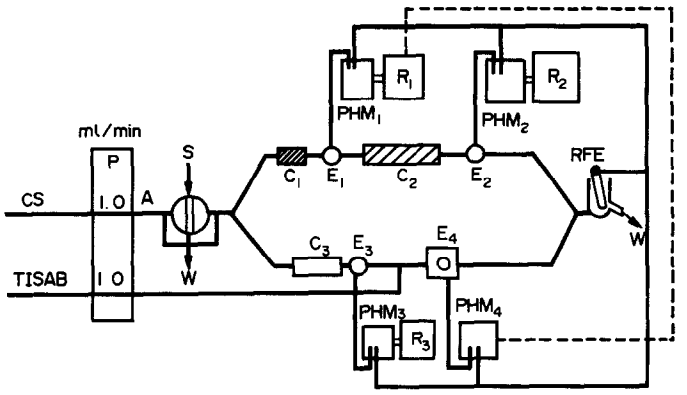

Fig. 3. Manifold used for simultaneous determination of I^-, Br^-, Cl^- F^-. E_1, E_2, E_3, E_4 are I^-, Cl^-, Br^- and F^- ISEs respectively; C_1, C_3, amalgamated-lead columns, 1.5 and 2.5 cm long, respectively; C_2, AgCl column; RFE, reference electrode; PHM, pH/mV-meter; S, sample injection; CS, carrier stream; P, pump; R, chart recorder; W, waste.

Lead or amalgamated lead columns. Granulated lead was passed through a 1-mm (16-mesh) sieve and treated with 1*M* hydrochloric acid in a small beaker for 1 min. The acid was then poured off and the lead was washed several times with water and packed into a short length of 2-mm bore glass tubing.

Lead that had been sieved and washed as above was amalgamated by stirring with 30 ml of 0.2*M* mercuric nitrate for 3 min. The liquid was poured off, and the lead was washed well with water, dried between two filter papers and packed in a glass tube (2 mm bore).

Manifolds

Figure 2 shows the manifold used for single measurements. The interference suppressor column (C) was used only with chloride and bromide electrodes, and was a column of AgCl (5.5 cm long, 2 mm diameter) when a Cl^--electrode was used, or an amalgamated lead column (2.5 cm long, 2 mm diameter) with a Br^--electrode. It was followed by the flow-through ISE (E) and a cell housing the Ag/AgCl single-junction reference electrode. The waste outlet of this cell was slightly higher than the inlet, to allow some carrier stream to remain in it for continuous electrical connection. The two electrodes were connected to the pH-meter and the electrode response was recorded.

Manifolds used for successive measurements

A manifold for consecutive Cl^- and I^- measurements was constructed with the two electrodes in series (line 1 in Fig. 3), the iodide electrode being placed first after the injection valve, followed by the AgCl interference-suppressor column, the chloride flow-through pellet, and the common reference electrode.

For successive determination of Cl^-, Br^- and I^-, or of Cl^-, Br^-, I and F^-, the bromide flow-through pellet and/or fluoride cell were added to this manifold (line 2 in Fig. 3) in parallel with the iodide and chloride detectors, the carrier stream being split by a Y-piece just after the injection point. The internal diameter of line 1 was 0.8 mm and that of line 2 was 0.5 mm; the angle between them was 90°. The two streams were recombined again by a Y-piece to pass through the common reference electrode. The bromide electrode was preceded by a lead-amalgam column, and the fluoride electrode, which followed it, needed an additional stream, connected by a T-piece just before the electrode, to carry TISAB III directly to the electrode.

Each electrode was connected to a separate pH-meter, each of which was connected to the common reference electrode. Each pH-meter was connected to a chart recorder, or a pair of pH-meters with the two channels of a double-pen chart recorder.

Obviously other electrode combinations can be used.

Procedure

A 0.1*M* sodium perchlorate solution (or sodium acetate if the Cl^--electrode is used alone) adjusted to pH 4 is used as the carrier stream and ionic strength adjuster (ISA). Its flow-rate at the waste outlet is adjusted to 0.5 ml/min. Standards containing from one to all four of the halides, as appropriate, in concentrations covering the sample ranges expected, are then injected after the samples.

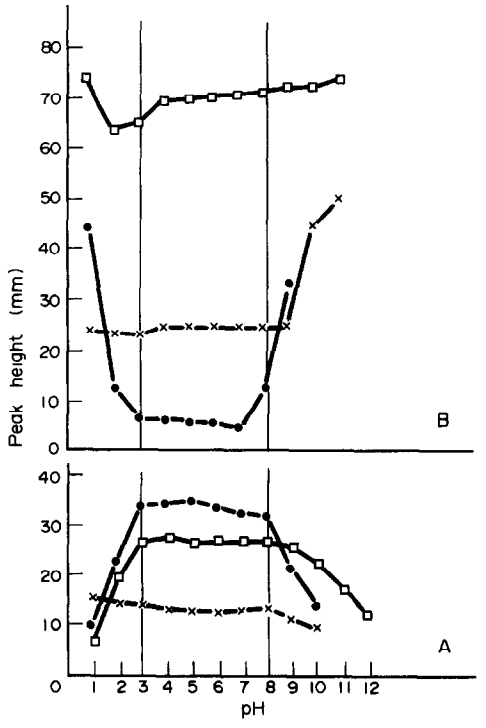

Fig. 4. Effect of pH on the response of the electrodes: A, pH of the carrier stream; B, pH of sample solutions with carrier stream at pH 4; ●, $10^{-5}M$ Cl^-; ×, $10^{-5}M$ Br^-; □, $10^{-5}M$ I^-.

The output of each electrode is recorded when the sample zone passes through the electrode. Average peak heights for the standards, measured from the base-line, are plotted *vs.* the logarithm of the analyte concentration to give the calibration graph. The concentration of each ion should not be less than $10^{-4}M$ for Cl^-, $5 \times 10^{-6}M$ for Br^-, $10^{-6}M$ for I^- and $5 \times 10^{-6}M$ for F^-.

RESULTS AND DISCUSSION

Optimization

The system was optimized for each electrode individually.

Carrier. The background electrolytes usually used in work with ISEs, such as KNO_3, $NaNO_3$, $NaClO_4$ and CH_3COONa, were examined at $0.1M$ concentration. They gave peak heights (mm) of 22, 33, 36 and 41 for $10^{-3}M$ Cl^-, 10, 16, 17 and 13 for $10^{-5}M$ Br^- and 20, 20, 20 and 15 for $10^{-6}M$ I^- respectively. Accordingly, sodium acetate solution was chosen as carrier for use with the chloride electrode, and sodium perchlorate solution for the bromide and iodide electrodes or for simultaneous use of all three electrodes.

pH. Figure 4 shows the effect of changing the pH of the carrier between 1 and 12, with constant sample pH, and of varying the sample pH from 1 to 12 with the carrier pH kept at 4, the optimum found from the first set of tests. The electrode response is practically constant when the sample pH is in the range 4–6 and the carrier pH is 4–6.

Flow-rate and response time. A flow-rate of 0.5 ml/min, measured at the outlet, gave the best sensitivity for all three electrodes. By using coloured solutions it was found that the sample zone remained in contact with the electrode for only 2.6 sec at this flow-rate, as shown in Table 1, which also shows that all three electrodes have practically Nernstian response at this flow-rate but not at 1 ml/min flow-rate.

When exposed to a continuous flow of sample solution, the electrodes gave the response times shown in Table 1, for reaching 50, 95 and 100% of the equilibrium signal (t_{50}, t_{95} and t_{eq}, respectively). The t_{95} values ranged between 9 and 30 sec, considerably longer than the contact time of 2.6 sec for a sample zone in the FIA system. This suggests that when FIA is used, it is not necessary for the electrode response to reach equilibrium, and a flow-rate of 0.5 ml/min would be optimal.

If the electrode response becomes sluggish and the slope decreases to about 50 mV/decade, the electrode can be reconditioned by passage of $10^{-3}M$ analyte solution for several hours, or in severe cases of contamination the channel can be redrilled to expose a new polished surface.

Table 1. Electrode characteristics

	Continuous flow of analyte as carrier stream				Injection of analyte into $NaClO_4$ carrier stream			
					Flow-rate 0.5 ml/min		Flow-rate 1 ml/min	
	Response time, *sec*			Mean response slope at t_{eq}, *mV/decade*	Contact time, *sec*	Response slope, *mV/decade*	Contact time, *sec*	Response slope, *mV/decade*
Electrode	t_{50}	t_{95}	t_{eq}					
Cl^-	13	30	65	57	2.6	55	1.1	49
Br^-	5	9	27	56	2.6	56	1.1	46
I^-	9	24	52	56	2.6	54	1.1	4.4

Table 2. Selectivity coefficients (K_{ij}^{pot}) of chloride, bromide, and iodide flow-through pellets measured by the mixed solution method and FIA, and comparison with published data obtained by using static methods

Interfering ion j	K_{ij}^{pot}								
	Cl^--electrode*			Br^--electrode*			I^--electrode*		
	This work	R_1	R_2	This work	R_1	R_2	This work	R_1	R_2
Cl^-	—	—	—	7.2×10^{-4}	6×10^{-3}	2.3×10^{-3}	6×10^{-5}	6.6×10^{-6}	6.6×10^{-6}
Br^-	2.5	1.2	2.1	—	—	—	8.1×10^{-3}	6.5×10^{-5}	—
I^-	1.1	88.3	86.5	2.6	20	10^2	—	—	—
S^{2-}	5.2	—	—	0.7	—	—	0.5	$>10^{10}$	—
CN^-	1.3	400	—	3.6	25	—	6×10^{-2}	0.34	—
SCN^-	2.5	—	—	6.5×10^{-2}	—	0.4	6×10^{-2}	—	—

*Composition of the electrodes: AgX/Ag_2S in this work; AgX for R_1 and R_2 (X = Cl, Br or I).
R_1 from J. Koryta, *Ion-Selective Electrodes*, Cambridge University Press, 1975, p. 89.
R_2 from W. E. Morf, *The Principles of Ion-Selective Electrodes and of Membrane Transport*, Elsevier, 1981, p. 197.

Interferences

The very short contact time with the electrode means that interference will be reduced if the electrode response to the interferent is slower than that to the analyte. This can be seen in Table 2 which gives values of the selectivity coefficient (K_{ij}) of chloride, bromide and iodide electrodes and compares these with published data obtained from static procedures. In general, better selectivities were obtained in the FIA method except with the iodide electrode, which gave about 10- and 100-fold better selectivity for I^- in the static procedure, in the presence of the interfering ions Cl^- and Br^- respectively. The reason for this may be kinetic, as mentioned above, or the difference in the membrane compositions.

However, since the K_{ij} values were large in most cases (generally >1) the removal of these interferences became necessary, especially at low concentrations of the analyte.

Among the methods available for removing interference with a halide electrode by the other halides under static conditions,[16-19] that of Hara and Wakizaka,[19] employing a silver chloride suspension, seemed suitable for adaptation to column use.

In addition to the silver chloride column used to remove interference by Br^-, I^- and S^{2-} with the chloride electrode in the manifold, columns of silver bromide and iodide were examined and the results are shown in Table 3. The silver chloride column was the most effective in eliminating the interference caused by a mixture of $10^{-4}M$ Br^-, I^- and S^{2-} in calibration for chloride. Table 3 shows that this column gave better accuracies than the other two columns in the determination of chloride ion in model solutions of chloride, with and without interfering ions

Table 3. Evaluation of the suppressor columns for removal of the interference of $10^{-4}M$ $Br^- + 3 \times 10^{-5}M$ $I^- + 3 \times 10^{-5}M$ S^{2-} with the Cl^--electrode, and of $7 \times 10^{-4}M$ $Cl^- + 2 \times 10^{-5}M$ $I^- + 3 \times 10^{-5}M$ S^{2-} with the Br^--electrode

Electrode	Test, solution	[Analyte], mM	Absolute measurement error, mM			
			No column	AgCl column	AgBr column	AgI column
Cl^-	Cl^-	0.2	−0.011	+0.009	+0.018	+0.026
		0.4	−0.021	+0.010	−0.010	+0.025
		0.6	−0.020	+0.003	−0.032	0.0
		0.8	−0.021	0.0	−0.021	+0.010
	Cl^- plus interferents	0.2	+0.150	+0.018	+0.032	+0.034
		0.4	+0.240	+0.022	+0.022	+0.026
		0.6	+0.342	−0.020	−0.020	+0.019
		0.8	+0.440	−0.021	−0.021	+0.024
			Absolute measurement error, mM			
			No column	Pb–Hg column	Pb column	
Br^-	Br^-	0.02	−0.0013	−0.0010	−0.0020	
		0.04	−0.0017	−0.0010	−0.0021	
		0.06	−0.0022	−0.0020	−0.0030	
	Br^- plus interferents	0.02	+0.0070	+0.0013	+0.0040	
		0.04	+0.0068	+0.0020	+0.0040	
		0.06	+0.0078	+0.0025	−0.0048	

present. The reproducibility with all three columns was better than 0.8%.

None of the columns was suitable for use with the Br^--electrode, however, since they all remove some bromide. Consideration of solubility products suggested that a column of lead might solve this problem, but a trial showed that there was still some loss (Table 3). It was then thought that use of amalgamated lead might improve matters, and the results in Table 3 show that this column was quite effective for eliminating the effect of $10^{-3}M$ chloride, $3 \times 10^{-5}M$ sulphide and $2 \times 10^{-5}M$ iodide in calibration for bromide and analysis of synthetic samples. It was found that the effect was not due to lead alone, since a column of pure lead was much less effective. The reproducibility in this case was better than 0.5% with both columns.

The calibration graph for the fluoride-electrode was not subject to interference either with or without use of the column of amalgamated lead.

When the efficiency of the silver halide columns decreased, it was restored by passage of 10 ml of $0.2M$ silver nitrate at a rate of 0.5 ml/min, followed by washing with water until the washings were free from Ag^+.

The amalgamated lead column was regenerated by passage of 2 ml of 1% mercuric nitrate solution.

The mechanism by which the columns remove the interferences is not clear and needs further investigation. Some suppositions may be made, however. Hara *et al.* suggested that the mechanism is related to solubility and specific adsorption effects,[19] but which is predominant and why AgCl is more effective than AgBr and AgI is yet to be explained. There is, however, an important difference between their method and ours in that Hara *et al.* used a freshly made surfactant-stabilized colloidal suspension of silver chloride whereas we employ a column of comparatively large particle-size silver halide, and the resulting difference in surface area (and degree of adsorption of silver or chloride ions) will cause a difference in the behaviour of the two systems.

If ion-exchange is the sole mechanism, then an equivalent amount of chloride should be liberated from the AgCl column and cause a positive error, unless the chloride liberated is itself adsorbed on the column. In order to explain the results obtained for chloride in the absence of interferents but with use of the AgCl column, it would then be necessary to postulate that the chloride in the sample also gives an exchange reaction on the column and that this continues along the column with final release of chloride into the sample stream, so that a steady state is set up in the column. These two postulates seem to be self-contradictory. It seems

Table 4. Effect of interfering ions on the Cl^--electrode without and with an AgCl column, in absence and presence of a constant concentration of Cl^-

		Without column		With AgCl column	
$[Cl^-]$	Interferent*	Peak height, *mV*	Error, %	Peak height, *mV*	Error, %
Zero	$10^{-6}M$ I^-	—	—	—	—
	$10^{-5}M$ I^-	9	—	—	—
	$5 \times 10^{-5}M$ I^-	34	—	0.4	—
	$10^{-4}M$ I^-	55	—	0.8	—
	$5 \times 10^{-4}M$ I^-	107	—	36	—
	$10^{-3}M$ I^-	117	—	55	—
Zero	a	—	—	—	—
	b	—	—	—	—
	c	4	—	—	—
	d	58	—	12	—
	e	131	—	51	—
		67	—	51	—
$10^{-3}M$	a	68	+1	52	+3
	b	68	+1	52	+3
	c	68	+1	52	+2
	d	86	+28	53	+3
	e	120	+78	71	+38

*a = $10^{-7}M$ Br^- + $10^{-8}M$ I^- + $10^{-8}M$ S^{2-}.
b = $10^{-6}M$ Br^- + $10^{-7}M$ I^- + $10^{-7}M$ S^{2-}.
c = $10^{-5}M$ Br^- + $10^{-6}M$ I^- + $10^{-6}M$ S^{2-}.
d = $10^{-4}M$ Br^- + $10^{-5}M$ I^- + $10^{-5}M$ S^{2-}.
e = $10^{-3}M$ Br^- + $5 \times 10^{-4}M$ I^- + $5 \times 10^{-4}M$ S^{2-}.

more likely that adsorption of the interferent takes place on the surface of the column material. Although it cannot be ruled out that both mechanisms may be involved, it seems most probable that the adsorption mechanism would predominate. This view seems to be supported by the absolute values shown in Table 3 for the errors in determination of chloride with and without use of the suppressor columns. The magnitude of these errors is practically independent of the chloride concentration, and of whether a column is used. With interferents present, however, the results obtained without use of the columns are difficult to explain, since the positive errors are greater than can be accounted for by ion-exchange of interferent for chloride on the electrode surface, but less than those calculated from the K_{ij}^{pot} values, and are not constant in value. Presumably there is a complicated combination of effects arising from the kinetics of ion-exchange and adsorption on the electrode surface, the response rates of the electrode to different ions, and the concentration ratios of the analyte and interferents.

Table 4 gives additional information on the problem. When no chloride is present and no column is used, the electrode response increases with iodide concentration above $10^{-5}M$, quantitatively at concentrations higher than $5 \times 10^{-5}M$. When the AgCl column is used, however, the electrode response does not start until the iodide concentration is at least $10^{-4}M$, a tenfold improvement in interference tolerance. Similar behaviour is observed with mixtures of bromide, iodide and sulphide. At the $10^{-3}M$ chloride level, there is again a tenfold improvement in the interference tolerance.

It also appears from Table 3 that the efficiency of the three silver halide columns as interference suppressors is in the order AgCl > AgBr > AgI, as might be expected from the solubility products (and hence adsorption characteristics) of these three species. At chloride concentrations above $2 \times 10^{-4}M$, however, all three give fairly comparable performance. It is believed that if these columns are suitable for removal of interference by halides and sulphide, they will also be suitable for removal of other anions which form sparingly soluble silver salts at the pH used in the system. These ions and other metal ions which form precipitates or complexes with halides or sulphide were not considered further in the present work, since they are not present at significant levels in waters,[19] analysis of which formed the main application of the work.

It is believed that the working mechanism of the amalgamated lead column is adsorption on the mercury surface. Use of this column did not affect the determination of fluoride or change the slope of the calibration graph. The column has another advantage, which was discovered by accident during the work. It was found that when the iodide electrode or the AgCl column was used in the manifold, negative peaks appeared in the recording for low concentrations of iodide or chloride, respectively, but when the lead-amalgam column was used, no negative peaks were obtained. Further investigation showed that this column should be kept short (preferably 1.0, but not more than 1.5 cm). The reason for appearance of the negative peaks was not clear; the presence of silver ions is a possibility, but the matter was not pursued. In any case, the negative peaks do not affect the results for iodide or chloride.

At $10^{-6}M$ iodide concentration, the iodide electrode response was not affected by up to $10^{-3}M$ bromide, $10^{-5}M$ sulphide or $0.1M$ chloride. Although dissolved oxygen has been reported to affect the electrode,[20–22] and ascorbic acid has been used to eliminate this effect, it was found that the iodide electrode was not affected at iodide levels down to $10^{-6}M$.

Table 5. Conditions recommended for determination of Cl^-, Br^- and I^- with the ISE–FIA system

Electrode	Carrier stream	Flow-rate, *ml/min*	Sampling rate, *samples/hr*	Lowest level determined	Interfering ion tolerance at lowest analyte concentration
Chloride	$0.1M$ $NaClO_4$, pH 4	0.5	72	$10^{-4}M$	$3 \times 10^{-5}M$ I^- $3 \times 10^{-5}M$ S^{2-} $10^{-4}M$ Br^-
Bromide	$0.1M$ $NaClO_4$, pH 4	0.5	72	$5 \times 10^{-6}M$	$2 \times 10^{-5}M$ I^- $3 \times 10^{-5}M$ S^{2-} $7 \times 10^{-4}M$ Cl^-
Iodide	$0.1M$ $NaClO_4$, pH 4	0.5	72	$3 \times 10^{-6}M$	$7 \times 10^{-1}M$ Cl^- $10^{-3}M$ Br^-

Table 6. Simultaneous determination of Cl^-, Br^-, I^- and F^- ($\mu g/ml$) in water samples by combination of 2-, 3- and 4-electrode systems

Sample	Chloride determination				Iodide determination				Bromide determination		Fluoride determination	
	Reference method[27]	2-electrode system	3-electrode system	4-electrode system	Reference method[25]	2-electrode system	3-electrode system	4-electrode system	3-electrode system	4-electrode system	Reference method[26]	4-electrode system
1	3.69	3.81	3.69	4.08	0.16	0.19	0.19	0.19	1.08	1.08	0.142	0.146
2	3.90	3.93	4.06	4.23	0.13	0.15	0.16	0.18	1.27	1.20	0.155	0.159
3	3.20	3.55	3.02	3.43	0.21	0.20	0.20	0.21	1.08	1.09	0.127	0.131
4	4.26	4.62	4.60	4.30	0.28	0.23	0.26	0.29	1.52	1.52	0.209	0.220
5	4.98	5.31	5.08	5.11	0.31	0.32	0.29	0.28	1.67	1.75	0.256	0.274
6	3.55	3.79	3.83	3.71	0.30	0.28	0.31	0.33	1.44	1.40	0.303	0.294
7	3.83	4.22	3.90	3.50	0.20	0.20	0.20	0.20	0.96	1.04	0.266	0.246
8	30.2	28.0	29.1	29.5	0.38	0.38	0.41	0.41	4.39	4.46	0.228	0.250

Because of the different circumstances for use of the fluoride electrode (pH, interferences, *etc.*) an additional line was added to the manifold, for introduction of TISAB III to adjust the pH and eliminate interferences by Al(III) and Fe(III).[23] The positioning of this line upstream of the fluoride electrode does not affect any of the other electrodes (Fig. 3). The iodide electrode must be placed before the AgCl column, since it is not affected by the other halides, and the AgCl would remove iodide if positioned before the iodide electrode. The fluoride electrode can be placed after the bromide electrode because its performance is not affected by the amalgamated lead column.

Table 5 gives the conditions for the determination of Cl^-, Br^- and I^- by the recomended procedure. Linear calibration plots were obtained for the ranges 10^{-4}–$10^{-2}M$ chloride, 5×10^{-6}–$10^{-3}M$ bromide and $10^{-6}M$–$10^{-4}M$ iodide.

Because of the delaying effects of the three- and four-electrode combinations in the manifolds, it is necessary to use different speeds of the pump to maintain a flow-rate of 0.5 ml/min at the output. Results obtained for simultaneous determination of the four halide ions in eight water samples, and comparisons with published values obtained by a batch method, are given in Table 6. Paired *t*-test comparison between each of the relevant methods showed no significant differences at the 95% confidence level. The reproducibility of the results was always better than 1%.

The excellent agreement shown in Table 6 indicates the efficiency of the procedure for analysis of water and similar samples. It also indicates the effectiveness of removal of interfering ions and that no other ions in the samples caused interference.

The sampling rates for single-ion determinations with one-, two-, three- and four-electrode combinations, were 72, 102, 90 and 80 samples/hr respectively. The highest sampling rate is obtained with the two-electrode combination, but in theory, could be increased even further by use of a parallel instead of a series arrangement.

Acknowledgement—The authors wish to thank Dr. R. A. Chalmers for his careful revision and giving useful suggestions during editing of this paper.

REFERENCES

1. J. Růžička, E. H. Hansen and E. A. Zagatto, *Anal. Chim. Acta*, 1977, **88**, 1.
2. E. H. Hansen, A. K. Ghose and J. Růžička, *Analyst*, 1977, **102**, 705.

3. E. H. Hansen, J. Růžička and A. K. Ghose, *Anal. Chim. Acta*, 1978, **100,** 151.
4. W. E. van der Linden and R. Oostervink, *ibid.*, 1978, **101,** 419.
5. D. S. Papastathopoulos, E. P. Diamandis and T. P. Hadjiioannou, *Anal. Chem.*, 1980, **52,** 2100.
6. E. H. Hansen, J. Růžička and A. K. Ghose, *Soil Nitrogen Fert. Poll., Proc. Rep. Res. Coord. Meet. 1978,* pp. 77–91. IAEA, Vienna, 1980.
7. R. Virtanen, in *Ion-Selective Electrodes, 3,* E. Pungor and I. Buzás (eds.), p. 375. Elsevier, Amsterdam, 1981.
8. G. B. Marshall and D. Midgley, *Analyst*, 1983, **108,** 701.
9. S. Alegret, J. Alonso, J. Bartrolí, J. M. Paulís, J. L. F. C. Lima and A. A. S. C. Machado, *Anal. Chim. Acta*, 1984, **164,** 147.
10. H. Muller, in *Modern Trends in Analytical Chemistry*, p. 353. Elsevier, Amsterdam, 1984.
11. M. G. Glaister, G. J. Moody and J. D. R. Thomas, *Analyst*, 1985, **110,** 113.
12. T. Greatorex and P. B. Smith, *J. Inst. Water Eng. Sci.*, 1985, **39,** 81.
13. J. F. van Staden, *Anal. Chim. Acta*, 1986, **179,** 407.
14. J. Slanina, W. A. Lingerak and F. Bakker, *ibid.*l, 1980, **117,** 91.
15. J. F. Lechner and I. Sekerka, *J. Electroanal. Chem.*, 1974, **57,** 317.
16. J. Havas, E. Papp and E. Pungor, *Acta. Chim. Hung.*, 1968, **58,** 9.
17. A. R. Selmer-Olsen and A. Øien, *Analyst*, 1973, **98,** 412.
18. M. T. Karim, F. M. Najib and M. S. Mohammad, *J. Food Technol.*, 1986, **21,** 559.
19. H. Hara, Y. Wakizaka and S. Okazaki, *Analyst*, 1985, **110,** 1087.
20. J. Kontoyannakos, G. J. Moody and J. D. R. Thomas, *Anal. Chim. Acta*, 1976, **85,** 47.
21. A. Hulanicki, A. Lewenstam and M. Maj-Żurawska, *ibid.*, 1979, **107,** 121.
22. V. A. Nikashina and A. N. Krachak, *Zh. Analit. Khim.*, 1979, **34,** 2236.
23. M. S. Frant and J. W. Ross, Jr., *Anal. Chem.*, 1968, **40,** 1169.
24. G. B. Marshall and D. Midgley, *Analyst*, 1978, **103,** 438.

Talanta, Vol. 39, No. 10, pp. 1269–1272, 1992
Printed in Great Britain.

0039-9140/92 $5.00 + 0.00

PREPARATION AND APPLICATION OF SELENITE ION SELECTIVE ELECTRODE

QIANTAO CAI,* YUELING JI, WENZHAO SHI and YAN LI
Department of Chemistry, Huazhong University of Science and Technology, Wuhan, 430074, People's Republic of China

(*Received* 1 *October* 1991. *Revised* 17 *January* 1992. *Accepted* 22 *January* 1992)

Summary—A new selenite ion selective electrode using 4,6-dibromopiaselenole as active material, PVC as membrane matrix and dibutyl phthalate as plasticizer has been developed. An analytically useful potential change occurs from about 10^{-6}–$10^{-1}M$ Se(IV), and the slope of the linear portion is −23.6 mV/10-fold change in Se(IV) concentration at a temperature of 21°. The electrode shows fairly good selectivity for selenite ion over other anions and has been used for the successful determination of total selenium in human hair.

The determination of selenium using ion selective electrodes has been reported, but most were indirect methods based on the catalytic effect of selenium on the reaction between picrate and sulphide, which is monitored with a picrate-selective electrode.[1–4] A selenium ion selective electrode used to determine trace Se(IV) directly has been described only by Malon and Christian,[5] in which the active ingredient in a liquid membrane consisting of a saturated solution of 3,3′-diaminobenzidine in hexane. Its linear response range is $\geqslant 10^{-4}M$ Se(IV) or above. Because the life-span of the electrode is shorter than one day and its potential readings as a function of Se(IV) concentration are easily affected by flowing pressure and mechanical stirring of the experimental solution, the application of the electrode to determining selenium is difficult.

Reaction of selenium(IV) with aromatic *o*-diamines to form corresponding derivatives of piaselenole is a special reaction and serves as the basis for the selective determination of small amounts of selenium by a variety of instrumental methodes,[6–8] such as spectrophotometry, fluorimetry, polarography, chromatography and voltammetry. The reaction is:

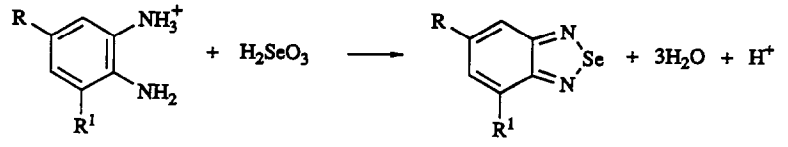

(R—R′–H⁺PD) (R—R′–PIS) (1)

where R and R′ represent the substituent groups, and the charge of the reactant species is dependent on the pH. The substance R—R′–PIS has the ability to enter into heterogeneous equilibrium with selenite ion, as described by equation (1), when dissolved in an organic solvent. When porous material such as poly(vinyl chloride) (PVC) is impregnated with suitable organic ionophore, it forms the basis of a membrane for an ion selective electrode. Ion selective electrodes offer certain advantages over other measurement techniques, such as their ability to measure activity non-destructively. After initial studies of the potential properties of the electrodes using several piaselenoles as active ingredients, such as 4,6-dibromopiaselenole (4,6-diBr–PIS),5-nitropiaselenole(5-NO_2–PIS) and 5,6-benzopiaselenole(5,6-B–PIS), the electrode using 4,6-diBr–PIS as active ingredients was selected for further investigation. We describe here an electrode for the measurement of selenium(IV) using 4,6-diBr-PIS as the active membrane constituent, PVC as the membrane matrix and dibutyl phthalate as the plasticizer or solvent, and its application.

*Author for correspondence.
Present address: Department of Chemistry, National University of Singapore, Lower Kent Road, Singapore 0511.

EXPERIMENTAL

Apparatus

Potentiometric measurements were made *vs.* a SCE with a Digital Ionanalyzer, Model PXD-12 (China). A double-walled 20-ml beaker was used as the measuring cell. Water was circulated continuously through the measuring cell jacket with a pump kept at constant temperature. All measurements were taken under constant stirring with a magnetic stirring bar.

Reagent

Unless otherwise stated, all reagents were of analytical-reagent grade or guaranteed-reagent. All solutions were prepared with tri-distilled water from a quartz still. A stock $0.100M$ solution of selenium(IV) was prepared by dissolving elemental selenium in a small amount of nitric acid and diluting to 250 ml with water. Formate buffer solution was prepared by adjusting 10% (v/v) formic acid to the desired pH value 2.5 with ammonia solution. 1,2-Diamino-3,5-dibromobenzene (DBDA) was synthesized and purified as described.[9] A stock solution containing 0.5% (w/v) DBDA was prepared in aqueous ethanol(1 + 1).

Preparation of electrode

In a 50-ml beaker, milligram quantities of selenium(IV) and millilitre quantities of complexing agent (0.5% DBDA) solution were added, and the mixture was then made up to about 40 ml with pH 2.5 formate buffer solution. The solution was heated at 50° in a water bath for 30 min, cooled to room temperature and then transferred into a 125-ml separating funnel. After millilitre quantities of cyclohexane or toluene were added, the solution was vigorously shaken for 2 min, and the 4,6-diBr–PIS which formed was extracted. The extract was washed twice with 15 ml of hydrochloric acid ($2M$) and transferred into a flat-bottommed beaker after the phase separation. The flat-bottommed beaker was placed in an infrared drier to evaporate the solvent gently and then the active material (4,6-diBr–PIS) was obtained. A 100-mg portion of poly(vinyl chloride) was added to a flat-bottommed beaker about 4.2 cm in internal diameter, and was dissolved in 5 ml of tetrahydrofuran, and then 0.3 ml of dibutyl phthalate and an appropriate amount of 4,6-diBr–PIS were added. After the 4,6-diBr–PIS was dissolved, the solution was placed in an infrared drier to evaporate the tetrahydrofuran gently and formed a 0.3-mm thick and 14-cm^2 area of PVC active membrane. A disk of the membrane corresponding to the external diameter of a PVC tube was cut and mounted with forceps on the polished end. A small amount of PVC was dissolved in tetrahydrofuran and the solution used as an adhesive to seal the outer edge of the circular membrane to the end of the PVC tube. After setting for 3 hr, the tube was filled with an internal reference solution consisting of $0.1M$ sodium chloride and $0.1M$ Na_2SeO_3. A silver/silver chloride internal reference electrode was immersed in this solution. The PVC membrane electrode was conditioned by soaking it in the $10^{-5}M$ standard Se(IV) solution for several hr and then was washed with tri-distilled water before use until the potential readings were stable. All test solution contained $0.1M$ sodium sulphate used to control ionic strength.

RESULTS AND DISCUSSION

Composition of electrode membrane

In order to obtain an electrode with optimal characteristics, it is important to investigate the individual membrane constituents, since the limit of detection, selectivity and long-term stability are a function of the composition of the electrode membrane. On the basis of our studies, dibutyl phthalate (DBP) is a better plasticizer than dioctyl phthalate or diisooctyl sebacate and the optimal membrane composition was about 27% PVC, 71% DBP and 2% 4,6-diBr–PIS (wt/wt).

Principal properties of membrane electrode

With moderate stirring, the response time of the electrode is less than 90 sec at $\geqslant 10^{-4}M$ Se(IV), two minutes at $< 10^{-4}M$ Se(IV) and is prolonged at a Se(IV) concentration near its detection limit. As the stirring rate or temperature is increased, the response time will shorten. The thinner the membrane, the shorter the response time.

The potential readings at 1.0×10^{-6} to $1.0 \times 10^{-1}M$ Se(IV) were recorded five times over a period of one day at 2-hr intervals, and the relative standard deviations of potential readings thus calculated were less than 2 mV except at $1.0 \times 10^{-6}M$ Se(IV) (Table 1). Only a small drift of 1.5 mV in potential reading at $1.0 \times 10^{-3}M$ Se(IV) was observed during continuous measurements over two hours.

Table 1. Results of potential stability of the electrode at various $C_{Se(IV)}$

$C_{Se(IV)}$ (M)	1.0×10^{-1}	1.0×10^{-2}	1.0×10^{-3}	1.0×10^{-4}	1.0×10^{-5}	1.0×10^{-6}
Standard deviation of potential (mV)*	1.6	1.3	1.1	1.5	1.9	4.8

*$n = 5$

Table 2. The selectivity coefficients $K_{I,J}^{pot}$ of the electrode*

J	SO_4^{2-}	NO_3^-	Cl^-	MoO_4^{2-}	HPO_4^{2-}	TeO_3^{2-}	AsO_2^-	ClO_4^-	I^-	$C_6H_5CO_2^-$	$C_6H_4(CO_2^-)_2$
$K_{I,J}^{pot}$	4.6×10^{-6}	5.6×10^{-6}	5.6×10^{-6}	4.1×10^{-6}	5.1×10^{-6}	2.3×10^{-3}	7.8×10^{-4}	1.1×10^{-5}	1.0×10^{-5}	6.1×10^{-6}	7.5×10^{-6}

*Determine by separate solution method, pH = 10, I and J stand for selenite ion and interfering ion, respectively, $C_I = C_J = 1.0 \times 10^{-3} M$.

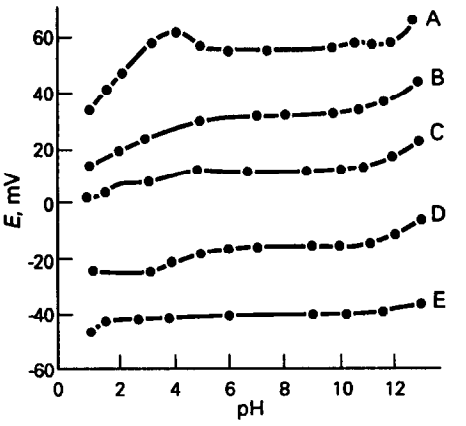

Fig. 1. Effect of pH on the potential readings at various Se(IV) concentrations (M): (A) 1.0×10^{-5}; (B) 1.0×10^{-4}; (C) 1.0×10^{-3}; (D) 1.0×10^{-2}; (E) 1.0×10^{-1}.

The life-span of the electrode is about one week if it is used for continuous measurements and can be extended to several months if stored dry.

The potential dependence on pH is summarized in Fig. 1. The potential reading remains unchanged within the pH range about 6–11 at various concentrations of Se(IV), the pH range becoming narrower as the concentration of Se(IV) decreases.

Potential readings as a function of selenium(IV) concentration are given in Fig. 2. An analytically useful change in the potential occurs from 3.2×10^{-6}–$1.0 \times 10^{-1} M$ Se(IV), and the slope of the linear portion is -23.6 mV/10-fold change of Se(IV) concentration at a temperature of 21°. The limit of detection for the electrode is $1.0 \times 10^{-6} M$ Se(IV).

The selectivity coefficient $K_{I,J}^{pot}$, where I and J stand for selenite ion and interfering ion, repectively, of the electrode for selenite ion with

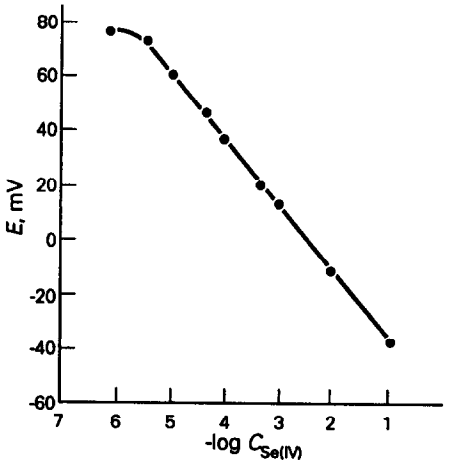

Fig. 2. Calibration curve for selenium(IV) pH = 10, $t = 21°$.

respect to more than ten anions have been determined using the separate solution method[10] at $C_I = C_J = 10^{-3}M$ and the same ionic strength (Table 2). All the value of $K_{I,J}^{pot}$ for most anions except AsO_2^- and TeO_3^{2-} are less than 1.0×10^{-5}, none of those ions interferes. As(II) or Te(IV), however, exerts slight interference if its concentration is sufficiently high, and the interference can be eliminated by means of extraction of these species, As(III) can be extracted with carbon tetrachloride from 8–12M hydrochloric acid solution, and Te(IV) can be extracted with methyl isobutylketone from 4–6M hydrochloric acid solution.[12]

In conclusion, the electrode exhibits fairly good selectivity for selenium(IV) over other ions, and practical long-term stability, response time, life-span and pH range, and can be used to determine trace Se(IV) directly.

Application of electrode to determining total selenium in hair

In this application, we use concentrated nitric acid (61%)–concentrated perchloric acid (70%) (5 + 1) to digest the sample, and hydrochloric acid as reductive and protective agent for Se(VI) and Se(IV), respectively, thus every species of Se in the sample can be converted into Se(IV).[11] In order to eliminate the effect of sample matrix on the response slope and give the same matrix concentration as for the sample solution, non-selenium hair sample solution was added to test standard solutions for the measurement of the calibration curve. Thus the experimental response slope (S) of the E *vs.* log $C_{Se(IV)}$ can be obtained from the calibration curve, and the S was used for the calculation of Se concentration in samples. The non-selenium hair sample solution was prepared by boiling the hair sample solution with hydrobromic acid.[13]

Table 3. The results for the determination of total selenium and recoveries in hair samples

Sample taken (g)	Selenium(IV) added (μg)	Selenium(IV) found (μg)	Recoveries (%)
0.500	0	0.150	
	2.00	2.15	100
	4.00	4.10	99

Table 4. Comparison of results obtained by this method and other methods

Method	This method	Fluorimetry[8]	Polarographic adsorption wave[7]
Se content of hair ($\mu g/g$)	0.300	0.348	0.330

After the extraction separation of Te(IV) with methyl isobutylketone, the total selenium in human hair and the recoveries of standard selenium added to human hair have been determined successfully by the standard addition method. Table 3 and Table 4 show that the recoveries of standard Se were fairly good and the result determined by this method is basically in agreement with the results obtained by either the fluorescence method[8] or polarographic adsorption wave method.[7] The Te was separated to assume no interference in unknown samples, since it exerts a slight interference at high concentrations (435 times greater than that of Se). This step can probably be avoided in many applications.

REFERENCES

1. E. P. Diamandis and T. P. Hadjiioannou, *Anal. Chim. Acta*, 1981, **123**, 143.
2. E. P. Diamandis, M. A. Koupparis and T. P. Hadjiioannou, *Microchem. J.*, 1977, **22**, 498.
3. Wanyi Li, Wenzhao Shi and Qiantao Cai, *Huaxue Chuanganqi* (China), 1985, **1**, 49.
4. Wanyi Li, Wenzhao Shi and Qiantao Cai, *J. of Huazhong University of Science and Technology (China)*, 1986, **2**, 269.
5. T. L. Malone and G. D. Christian, *Anal. Lett.*, 1974, **7**, 33.
6. J. Neve, H. Michel and M. Leopold, *Mikrochim. Acta*, 1980 **I**, 41.
7. Qiantao Cai and Wenzhao Shi, *Chemical J. of Chinese University*, 1988, **3**, 287.
8. Qiantao Cai and Wenzhao Shi, *Fenxi Shiyanshi (China)*, 1988, **3**, 287.
9. Y. Shimoishi, *J. Chromatogr*, 1977, **136**, 85.
10. G. A. Rechnitz and M. R. Kresz, *Anal. Chem.*, 1966, **38**, 1786.
11. Analytical Methods Committee, *Analyst*, 1979, **104**, 778.
12. Yu. A. Zolotov, V. A. Bodnya and A. N. Zagruzina, *CRC Crit. Rev. Anal. Chem.*, 1982, **14**, 93.
13. Zilan Yi, Wenzhao Shi, Ao Li and Huarong Hou, *J. of Huazhong University of Science and Technology (China)*, 1985, **3**, 127.

Talanta, Vol. 39, No. 10, pp. 1273–1276, 1992
Printed in Great Britain

0039-9140/92 $5.00 + 0.00
Pergamon Press Ltd

ADSORPTIVE–CATALYTIC STRIPPING MEASUREMENTS OF ULTRATRACE VANADIUM IN THE PRESENCE OF CUPFERRON AND BROMATE

JOSEPH WANG,* BAOMIN TIAN and JIANMIN LU
Department of Chemistry, New Mexico State University, Las Cruces, New Mexico 88003, U.S.A.

(*Received* 23 *January* 1992. *Accepted* 22 *February* 1992)

Summary—An extremely sensitive stripping voltammetric procedure for ultratrace measurements of vanadium is reported. The method is based on the interfacial accumulation of the vanadium–cupferron complex onto the hanging mercury drop electrode, followed by the catalytic reduction of the adsorbed complex in the presence of bromate. The dual amplification effect associated with these accumulation and catalytic processes results in a detection limit of $4.9 \times 10^{-12} M$ (0.25 ppt). The relative standard deviation (at 50 ppt) is 1.6%. The procedure is also very selective. Such coupling of catalytic and adsorptive collection processes holds great promise for the development of an ultrasensitive voltammetric procedure for other trace metals.

Because of the importance of vanadium and its extremely low levels in various matrices, an ultrasensitive method is required for its reliable quantitation. For example, atomic spectroscopic procedures for determining vanadium in seawater usually require laborious enrichment steps (coprecipitation, solvent extraction, *etc.*). Voltammetry has been shown useful for trace measurements of vanadium. Catalytic currents of vanadium complexes, in the presence of various oxidants, have permitted convenient polarographic determinations of nanomolar concentrations.[1,2] Adsorptive stripping procedures, based on the interfacial accumulation of vanadium complexes in catechol[3] or bromopyridylazo-diethylaminophenol,[4] have been exploited for measurements at the subnanomolar level.

This paper reports an extremely sensitive stripping voltammetric procedure for ultra-trace measurements of vanadium based on the coupling of catalytic and adsorption processes. The procedure relies on the catalytic response of the adsorbed vanadium–cupferron complex in the presence of bromate:

$$\mathrm{V(V)Cupf_{soln}} \xrightarrow{\text{accumulation}} \mathrm{V(V)Cupf_{surf}} \quad (1)$$

$$\mathrm{V(V)Cupf_{surf}} + e^- \rightarrow \mathrm{V(IV)Cupf_{surf}} \quad (2)$$

$$\mathrm{6V(IV)Cupf_{surf}} + \mathrm{BrO_3^-} + \mathrm{6H^+} \rightarrow \mathrm{6V(V)Cupf_{surf}} + \mathrm{Br^-} + \mathrm{3H_2O} \quad (3)$$

The dual current–magnifying effect associated with the adsorptive–catalytic stripping scheme offers remarkable sensitivity, with detection limit at the picomolar (sub–ppt) level, and high selectivity. Analogous procedures have been reported recently for measurements of picomolar levels of titanium,[5] molybdenum[6] and platinum.[7]

EXPERIMENTAL

Apparatus and reagents

An EG&G PAR voltammetric analyzer (Model 264A) was used in connection with the EG&G PAR Model 303 static mercury drop electrode. A medium-size hanging mercury drop electrode (HMDE), with an area of 0.016 cm^2, was employed. Data were displayed on an EG&G PAR Model 0073 X–Y recorder.

All solutions were prepared from doubly-distilled water. Stock solutions of vanadium [(1000 ppm) atomic adsorption standard, Aldrich] were diluted daily as required. The supporting electrolyte was $5 \times 10^{-3} M$ acetate buffer solution (of pH 4.8).

Procedures

The supporting electrolyte solution (10 ml), containing $2 \times 10^{-5} M$ cupferron and $6 \times 10^{-3} M$

*Author for correspondence.

sodium bromate, was pipetted into the cell, and purged with nitrogen for 8 min. The preconcentration potential (usually +0.1 V) was applied to a fresh mercury drop while the solution was stirred. Following the preconcentration period, the stirring was stopped, and after 15 sec the voltamperogram was recorded by applying a negative-going differential pulse scan (with 10 mV/sec scan rate and 25 mV amplitude). The scan was terminated at −0.5 V. Aliquots of the vanadium standards were introduced after recording the background voltamperograms. Throughout this operation, nitrogen was passed over the solution. All data were obtained at room temperature.

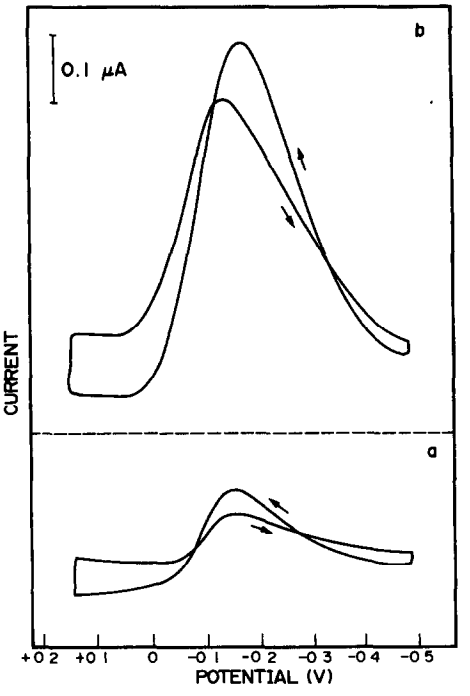

Fig. 1. Cyclic voltamperograms for 0.5 ppb vanadium following 0(a) and 120(b) sec stirring (400 rpm) at +0.15 V. Scan rate, 50 mV/sec; solution, acetate buffer (5m*M*, pH 4.8), containing $2 \times 10^{-5}M$ cupferron and $6 \times 10^{-3}M$ sodium bromate.

RESULTS AND DISCUSSION

Figure 1 shows cyclic voltamperograms for 0.5 ppb vanadium, in an acetate buffer solution containing $2 \times 10^{-5}M$ cupferron and $6 \times 10^{-3}M$ sodium bromate, after 0(a) and 120(b) sec accumulation at 0.15 V. One cathodic peak is observed at −0.14 V during the negative-going scan. Scanning in the reverse direction also exhibits a cathodic peak, indicative of a catalytic process. The response increases dramatically when an accumulation period precedes the potential scan [comparing (a) and (b)], indicating enhancement by adsorption. Subsequent scans resulted in a highly stable response, indicating that both forms of the complex remain adsorbed on the surface [equation (2)]. The fact that a defined and intense (μA) response is obtained in cyclic voltammetry for ppb concentrations indicates the remarkable sensitivity associated with the coupling of the catalytic and interfacial accumulation processes. Additional gains can be obtained in a differential pulse stripping operation, as illustrated below.

Figure 2 shows differential pulse voltamperograms for 50 ppt ($9.8 \times 10^{-10}M$) vanadium after different preconcentration times. A well-defined peak is observed at −0.09 V at this ultratrace level. The peak height increases with increasing

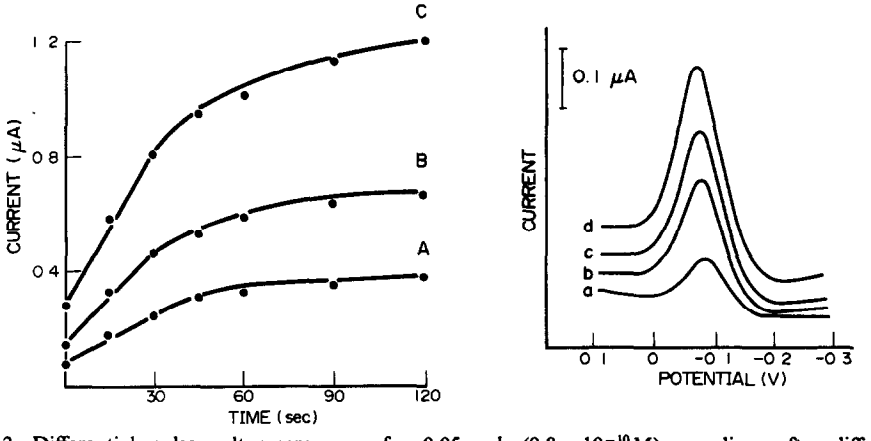

Fig. 2. Differential pulse voltamperograms for 0.05 ppb ($9.8 \times 10^{-10}M$) vanadium after different preconcentration times (a) 0 (b) 15, (c) 45, and (d) 90 sec, with 400 rpm stirring at +0.10 V. Also shown are current *vs.* preconcentration time plots for 0.05(A), 0.10(B) and 0.20(C) ppb vanadium. Differential pulse scan with 10 mV/sec rate 25 mV amplitude. Solution, as in Fig. 1.

preconcentration time, due to an enhancement of the vanadium–cupferron surface concentration. For example, with 90-sec preconcentration, there is a four-fold enhancement of the peak relative to that obtained without preconcentration [(*a*) *vs.* (d)]. Also shown in Fig. 2 are plots of peak current *vs.* preconcentration time for 50(A), 100(B) and 200(C) ppt. The current rises rapidly with time at first, and then more slowly.

The concentrations of the ligand and catalyst have a profound effect on the stripping current. For example, the stripping peak for 0.5 ppb vanadium increases rapidly with increasing cupferron concentration up to $1 \times 10^{-5}M$, and then more slowly [(Fig. (3)]. Similarly, as the bromate concentration increases, the vanadium response increases linearly at first and then more slowly [Fig. 3(B)]. The dependence of the stripping current on the preconcentration potential was examined over the range 0.0–0.2 V [Fig. 3(C)]. Only slight variations in the response are observed, with optimal accumulation around 0.05 V. The acetate buffer concentration also affects the response, with 5mM yielding the most favorable peak height and shape. The differential pulse waveform yielded significantly better signal-to-background characteristics than corresponding linear scan measurements, and was used throughout this work. Most subsequent work was thus performed in a 5mM acetate buffer solution (pH 4.8), containing $2 \times 10^{-5}M$ cupferron and $6 \times 10^{-3}M$ sodium bromate, using an accumulation potential of +0.10 V, and a differential pulse waveform.

Figure 4 shows stripping voltamperograms obtained for solutions of increasing vanadium concentrations (20–100 ppt) after a 15-sec preconcentration time. The very favorable signal-to-background characteristics permit convenient measurements of ppt concentrations. Calibration plots over a wide concentration range (10–200 ppt), obtained by using different preconcentration times, are also shown in Fig. 4.

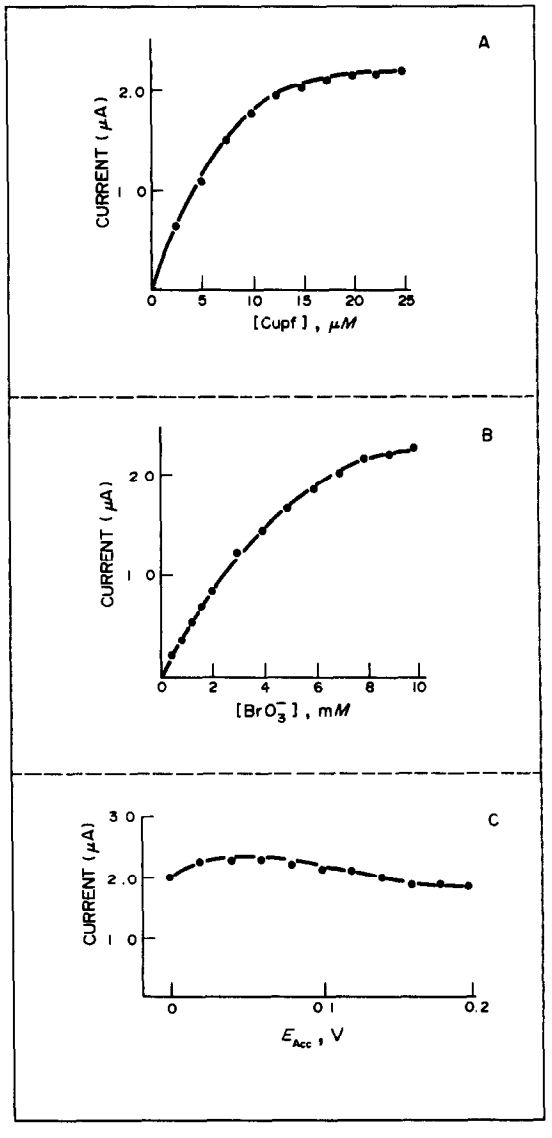

Fig. 3. Dependence of the stripping current for 0.5 ppb vanadium on the cupferron (A) and bromate (B) concentrations, as well as on the preconcentration potential (C). Preconcentration for 60 sec. Cupferron concentration: 5 × 10^{-5}(B) and 2 × 10^{-5}(C)M. Other conditions, as in Fig. 2.

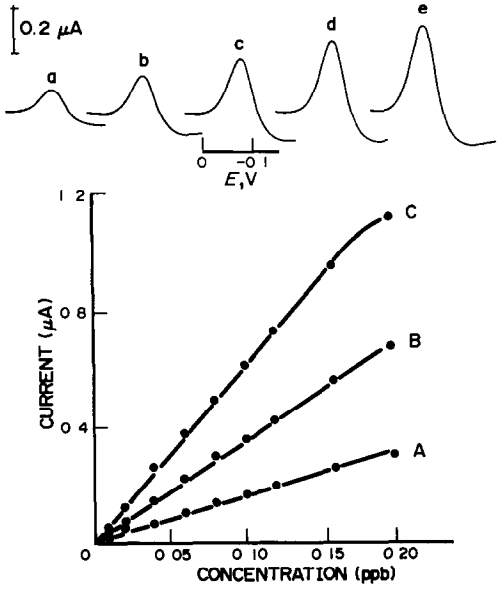

Fig. 4. Stripping voltamperograms obtained for solutions of increasing vanadium concentration over the range 20–100 ppt [(a)–(e)]. Preconcentration for 15 sec. Other conditions as for Fig. 2. Also shown are calibration plots for different preconcentration times: 0(A), 15(B), and 45(C) sec.

For 0- and 15-sec accumulation, the response is linear over the entire range [slope, 1.47(A) and 3.56(B) μA/ppt]. With 45-sec preconcentration, linearity prevails up to 150 ppt (slope of 5.99 μA/ppt). Such curvature is expected for a process that is limited by adsorption. The detection limit was estimated from measurements of 5 ppt ($9.8 \times 10^{-11} M$) vanadium following a 5-min accumulation [Fig. 5(a)]. The signal-to-noise characteristics of these data ($S/N = 3$) correspond to a detection limit of 0.25 ppt ($4.9 \times 10^{-12} M$). This value means that in the 10 ml of solution used, 2.5 pg can be detected. Such an extremely low value is attributed to the dual-amplification effect associated with the interfacial and catalytic processes. It is significantly lower than detection limits of previous polarographic and stripping schemes,[1-4] as well as of a recently reported[8] procedure using inductively coupled plasma atomic emission spectroscopy (0.25 ppb). Also, shown in Fig. 5(b) is the corresponding response using the catechol-based adsorptive stripping procedure.[3] Apparently, this scheme is not sensitive enough to allow convenient quantitation at the 5 ppt level. The precision was estimated from twenty repetitive measurements of 50 ppt vanadium (30-sec preconcentration). This series yielded a relative standard deviation of 1.6% (mean peak current of 54.0 nA, with a range of 53–55 nA). Hence, high precision is maintained despite the remarkably low concentration.

High selectivity is another attractive feature of the adsorptive–catalytic stripping procedure. The following metal ions were tested at the 5 ppb level and found not to interfere with the measurement of 50 ppt vanadium: Pb(II), Co(II), Mn(II), Bi(III), Cd(II), Cr(III), Ag(I), Hg(II), Zn(II), Ni(II), Ti(IV), Cu(II), Te(VI), As(III), Sb(III), Ga(III), Mo(VI), Sn(IV), U(VI), Fe(III), Pt(IV), TI(I), Zr(IV) and Ge(IV). Additional peaks were observed (at −0.60 V and −0.31 V) in the presence of titanium and copper, respectively, which did not affect the quantitation of vanadium. In contrast, surface-active organic materials, could compete for surface adsorption sites. For example, gelatin at 0.5 and 1.0 ppm resulted in 3 and 9% depressions, respectively, of the 0.5 ppb vanadium response (60 sec preconcentration). Depending on the nature of the sample, destruction of surfactants prior to the voltammetric analysis, *e.g.*, through u.v. irradiation, may be required. It is essential also to remove the dissolved oxygen due to a large overlapping peak.

In conclusion, this study demonstrates that the coupling of catalytic and adsorption processes can constitute the basis for an ultrasensitive voltammetric procedure for vanadium. The adsorptive-catalytic stripping procedure offers remarkably low (sub-ppt) detection limits and high selectivity, and should be suitable for *in situ* and on-line monitoring of vanadium. Compared to analogous catalytic–polarographic measurements,[1] the adsorptive accumulation results in a 2–3 orders of magnitude lowering of the detection limit. Such use of catalysis to greatly amplify the response of the accumulated complex should further expand the power and scope of stripping voltammetry.

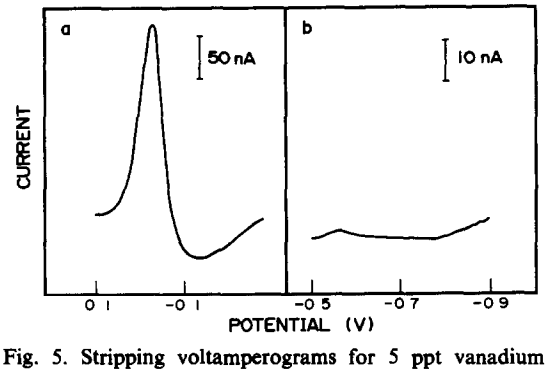

Fig. 5. Stripping voltamperograms for 5 ppt vanadium obtained in the presence of cupferron/bromate (a) and catechol (b). Preconcentration for 10 min (a) acetate buffer (2.5mM, pH 4.8) containing $1 \times 10^{-5} M$ cupferron and $2 \times 10^{-3} M$ sodium bromate, (b) $0.01 M$ Pipes buffer (pH 6.9), containing $2 \times 10^{-4} M$ catechol: preconcentration potential (b), −0.50 V. Other conditions, as in Fig. 2.

Acknowledgements—This work was supported by grants from Battelle Pacific Northwest Laboratory (subcontract No. 095895-A-P1) and Sandia National Laboratories (contract DE-AC04-76 DP 00789).

REFERENCES

1. E. Barrado, V. Alvarez, R. Pardo and P. S. Batanero, *Electroanalysis*, 1991, **3**, 715.
2. N. Kato and K. Aoki, *J. Electroanal. Chem.*, 1989, **261**, 309.
3. C. M. C. van den Berg and Z. Q. Huang, *Anal. Chem.*, 1984, **56**, 2383.
4. J. Lu, W. Jin and S. Wang, *Anal. Chim. Acta*, 1990, **238**, 375.
5. K. Yokoi and C. M. C. van den Berg, *ibid.*, 1991, **245**, 167.
6. J. Wang, J. Lu and Z. Taha, *Analyst*, 1992 **117**, 35.
7. J. Wang, J. Zadeii and M. S. Lin, *J. Electroanal. Chem.*, 1987, **237**, 281.
8. V. Dupont, Y. Auger, C. Jeandel and M. Wartel, *Anal. Chem.*, 1991, **63**, 520.

Talanta, Vol. 39, No. 10, pp. 1277–1280, 1992
Printed in Great Britain

0039-9140/92 $5.00 + 0.00
Pergamon Press Ltd

THE DETERMINATION OF TRACE LEVELS OF SELENIUM CONTAINED IN CHINESE HERBAL DRUGS BY DIFFERENTIAL PULSE POLAROGRAPHY

HANG TAIJUN* and ZHANG ZHENGXING
Department of Pharmaceutical Analysis, China Pharmaceutical University, Nanjing, 210009, People's Republic of China

DONG SHANSHI and ZHU YU
Modern Analytical Centre, China Pharmaceutical University, Nanjing, 210009, People's Republic of China

(*Received* 8 *August* 1991. *Revised* 13 *November* 1991. *Accepted* 16 *November* 1991)

Summary—A differential pulse polarographic method for the determination of trace amounts of selenium contained in Chinese herbal drugs is described. In the Na_2SO_3–KIO_3–NH_3–NH_4Cl medium (pH > 9) the selenium complex $Se(O)SO_3^{2-}$ gives a catalytic wave, the peak potential of the wave is −0.76 V *vs.* Ag/AgCl–KCl (1*M*), and the peak current is directly proportional to selenium in the range 0.01–1.0 μg per 0.5 g of sample (0.08–8 ng/ml). The recoveries of selenium added to the samples tested are between 95 and 105%. The method is simple, sensitive, accurate and rapid. The results are in good agreement with those found by a DAN (2,3-diamino-naphthalene) spectrofluorimetric method.

Selenium is one of the essential elements for humans and animals. In proper amounts, it can enhance our ability to protect against certain cancer and heart diseases. But too much selenium may cause neurosystem, skin and some other problems.[1] Increasing concerns about the significance and toxicity of selenium have led to extensive research in the biomedical realm and to the development of numerous analytical methods for its determination in various materials.[2,3] The selenium(IV)–Na_2SO_3–KIO_3 catalytic polarographic method provides a simple, sensitive and rapid approach to the determination of the element.[4] In this paper we propose a differential pulse polarographic method using this system and apply it to the determination of trace levels of selenium contained in Chinese herbal drugs. The results are compared with those measured by a spectrofluorimetric method.[5]

EXPERIMENTAL

Apparatus

The differential pulse polarograms were recorded with an F-78 type pulse polarograph (Fudan University, Shanghai, China), coupled with a YEW type 3066 chart recorder (Yokogawa Hokushin Electric, Tokyo, Japan), and with dropping mercury, platinum foil and Ag/AgCl–KCl (1*M*) electrode as working, counter and reference electrode, respectively. The fluorimetric data were measured by a MPF-4 spectrofluorimeter (Hitachi, Japan) with 10-mm quartz cells.

Reagents

All reagents used were of analytical grade and all aqueous solutions were prepared with quartz doubly distilled water.

Stock selenium solution (0.1000 mg/ml). Dissolve 10.00 mg of selenium powder (purity 99.99%) in 3 ml of concentrated nitric acid and 0.2 ml of concentrated perchloric acid. Place the solution in a boiling bath for 3 hours. Cool and then add 1.0 ml of concentrated hydrochloric acid, and again place the solution in the boiling bath for 5 min. Quantitatively transfer the solution to a 100-ml standard flask and dilute to the mark with water.

Selenium standard solution (0.1000 μg/ml). Pipette 1 ml of the stock solution to a one-litre standard flask and dilute to volume with 0.10*M* hydrochloric acid.

Digestion solution (H_2SO_4–$HClO_4$–Na_2MoO_4). Dissolve 2.5 g of $Na_2MoO_4 2H_2O$ in 50 ml of

*Author for correspondence.

water, then slowly add 67 ml of concentrated perchloric acid and 50 ml of concentrated sulphuric acid, and mix well.

Solutions for catalytic polarography. A 5.0% (w/v) solution of EDTA–2Na, a 1.3*M* solution of sodium sulphite (freshly prepared within two weeks), a NH_3–NH_4Cl buffer solution (dissolve 40.2 g of ammonium chloride in 50 ml of water and mix with 150 ml of ammonium hydroxide, pH 10.2), 0.20*M* potassium iodate and 0.10% (w/v) gelatin solution were used.

Analytical procedures

Sample treatment. The Chinese herbal drugs to be tested were first identified and then dried at 60° after which they were finely crushed and passed through 40 mesh sieves. The five kinds of Chinese herbal drugs tested are as follows:

Waterplantain	*Alisma orientalis* (Sam.) Juzep
Milkvetch	*Astraglus membranaceus* (Fisch.) Bge Var. mongholicus
Yam	*Dioscorea opposita* Thunb
Fig-tree	*Ficus carica* L.
Rehmannia	*Rehmannia glutinosa* Libosch

Sample digestion. Accurately weigh out about 0.5 g of sample and place in a 150-ml conical flask. Quantitatively add 5.00 ml of the digestion solution and put aside for about 12 hr. Then a small amount of water (2–5 ml) is added and it is placed on an electric burner (800 W) with an asbestos sheet or the equivalent for slow and even heating. Heat slowly until an intense reaction occurs in the solution and the perchloric acid starts to evaporate with white fumes, *i.e.*, the solution changes from muddy brown to colourless and then to greenish yellow; continue heating for a further minute. Let the solution cool and then add 5.0 ml of 6*M* hydrochloric acid and place in a boiling water bath for 15 min. Cool and quantitatively transfer the solution to a 50-ml standard flask and dilute with water to the mark.

Selenium determination. Pipette 10.00 ml of the prepared sample solution into a 25-ml standard flask and add 2.0 ml of 5.0% EDTA–2Na, 2.0 ml of 1.3*M* sodium sulphite, 5.0 ml of NH_3–NH_4Cl buffer, 2.00 ml of 0.20*M* potassium iodate and 2.00 ml of 0.10% gelatin solution in that order and mix thoroughly after each addition. Finally dilute with water to volume (pH 9.4). Purge oxygen from the solution with pure nitrogen. Record the cathodic sweeping differential pulse polarogram on the polarograph from −0.50 to −0.83 V [the catalytic wave P1 as shown in Fig. 1(a)]. The instrumental parameters are: sweep rate, $v = 2$ mV/sec, pulse period, $t = 0.5$ sec, pulse amplitude, $\Delta E = 20$ mV.

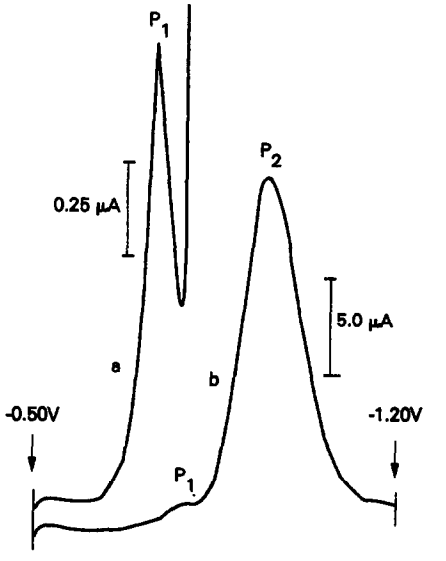

Fig. 1. Se(IV)–Na_2SO_3–KIO_3 cathodic sweeping differential pulse polarograms. Se concentration: 0.4 ng/ml, *i.e.*, 0.05 μg per sample. P1 catalytic wave, P2 reduction peak of IO_3^-.

RESULTS AND DISCUSSION

Catalytic wave mechanism

In acidic solution, selenium(IV) reacts with SO_3^{2-} to form the $Se(O)SO_3^{2-}$ complex, and then in the basic measurement solution (pH > 9) the reduction of the complex in a two-electron reversible mode at the dropping mercury electrode and the simultaneous reacting of the reduction product with the IO_3^- at the electrode surface produces a very sensitive polarographic catalytic wave P1. The peak potential of the wave is at −0.76 V versus Ag/AgCl–KCl (1*M*). The IO_3^- itself is reduced at a more negative potential, yielding a reduction peak P2 at −0.97 V [Fig. 1(b)]. The processes may be represented in the following equations:[4]

$$H_2SeO_3 + 3H_2SO_3 \xrightarrow{\{H^+\}} H_2Se(O)SO_3 + 2H_2SO_4 + H_2O$$

$$Se(O)SO_3^{2-} \xrightarrow[(+2e,\ \text{electrode process})]{\{OH^-\}} Se^{2-} + SO_3^{2-}$$

$$3SO_3^{2-} + 3Se^{2-} + IO^- + 3H_2O \xrightarrow[\text{(parallel chemical reaction)}]{\{OH^-\}} I^- + 6OH^- + 3Se(O)SO_3^{2-}$$

Thus the reagents must be added in accordance with the proposed procedures and the solution should be mixed well after each addition.

Experimental variables

The polarographic method measures selenium(IV), so a proper reductant should be added to the solution after the digestion to convert selenium(VI) to selenium(IV), while the selenium(IV) is not affected. Hydrochloric acid (6*M*) can quantitatively reduce selenium(VI) to selenium(IV) at 90°.[6] For this reason 5 ml of 6*M* hydrochloric acid was added to the digested sample solution, instead of hydroxylamine hydrochloride (NH_2OH-HCl) solution which has the ability to reduce selenium(IV) to elemental selenium.[7]

The peak current of the catalytic wave also has a linear relation with the concentration of potassium iodate. The presence of gelatin can strongly reduce the peak current of the catalytic wave, but in small amounts the gelatin makes the catalytic wave more stable and improves the linear range of the calibration curve while the effect on the limit of detection is negligible. Consequently, the potassium iodate and the gelatin solution must be quantitatively added to the system. Sodium sulphite in this system reacts with selenium(IV) and takes part in the electrode processes of the selenium. An excess of sodium sulphite has no obvious influence on the peak current of the catalytic wave. We found that 2.0 ml was an adequate amount for each of potassium iodate (0.2*M*), gelatin (0.10% w/v) and sodium sulphite (1.3*M*).

The instrumental parameters have great influence on the catalytic wave. The faster the sweep rate or the longer the pulse period, the smaller the catalytic wave peak current and the more asymmetric the wave. The larger the pulse amplitude, the larger the catalytic wave peak current and the more asymmetric the wave. Hence the sweep rate (v), pulse period (t) and pulse amplitude (ΔE) selected were 2 mV/sec, 0.5 sec and 20 mV, respectively.

Digestion solution selection

We tried HNO_3–$HClO_4$[8] and H_2SO_4–$HClO_4$–Na_2MoO_4[5] for the digestion of Chinese herbal drugs. The first method was very tedious and a severe selenium loss was observed, whereas the second one was very simple and easy to control with a sharp end-point of digestion. On approaching the end-point, the solution was a greenish yellow, and with further heating until the perchloric acid fumes diminished there was not significant selenium loss.

Interferences

Because the detection medium was an ammoniacal one with the presence of EDTA, the results of the interference tests showed that when the selenium level was 0.05 μg per sample, the presence of Cd, Co, Cr, Cu, Pb, Sn or Zn at 1,000 times as much as the selenium did not interfere with the determination. Therefore the selectivity of the method is very good.

Blank wave

Because the concentrated sulphuric acid contains a small amount of selenium and it is used

Table 1. Determination of selenium contained in five kinds of Chinese herbal drugs*

Drug		Waterplantain	Milkvetch	Yam	Fig-tree	Rehmannia
DPP	X ± SD (μg/g)	0.074 ± 0.006	0.048 ± 0.002	0.18 ± 0.02	0.21 ± 0.02	0.56 ± 0.01
	n	8	5	5	5	8
	RSD, %	8.4	4.2	8.5	7.2	2.5
	Rc% (*n*)	102 (4)[a]	103 (3)[b]	95.7 (3)[b]	95.2 (3)[b]	104 (4)[a]
	RSD, %	7.0	2.2	3.2	3.0	8.2
FL	X ± SD (μg/g)	0.092 ± 0.005	0.050 ± 0.006	0.18 ± 0.01	0.19 ± 0.02	0.53 ± 0.05
	n	6	4	5	4	7
	RSD, %	5.3	11.0	6.4	10.3	9.4
	RC% (*n*)				90.8 (4)[b]	
	RSD, %				9.8	
t(cal.)		−5.949	−0.800	1.038	2.067	1.520
t(*F*, *n*)		2.179	2.365	2.306	2.365	2.160

*Rc% (*n*) is the mean standard addition recovery of *n* tests.
t(cal.) is the calculated Significance test value.[9]
**t*(*F*, *n*) is the Student's *t*-Distribution value when *F* is 0.975 and the degree of freedom is *n*[9].
[a]0.10 μg of selenium added. [b]0.05 μg of selenium added.

as received, the blank solution also produces a small catalytic wave. However, when the digestion solution was quantitatively added and the blank determination was done in parallel, the blank wave did not appreciably influence the experimental results. The magnitude of the blank was equivalent to 0.08 μg of Se.

Calibration curve

We found that a linear current response was observed over the range from 0.01 to 1.0 μg of selenium with a limit of detection of 0.01 μg. The linear regression equation was:

$$i(\mu A) = 1.63 + 20.5 \times Se(\mu g),$$

$$r = 0.999 \ (n = 6).$$

The limit of detection was calculated from the following equation:

$$i(l) - i(m.b) > 2SD(b).$$

Where i(l) is the current response at the limit of detection, i(m.b) is the mean current response of the blank and SD(b) its standard deviation.

Application

The proposed differential pulse polarographic (DPP) method was used to determine trace levels of selenium contained in five kinds of Chinese herbal drugs. The results are shown in Table 1 (DPP). The good recoveries show that the method is accurate. From the significance test values included in Table 1, it can be seen that the results are in good agreement with those found by the DAN spectrofluorimetric method (FL) [Table 1 (FL)], except Waterplantain. But the DPP method is simpler and more rapid. It can be applied to selenium determination in a variety of samples.

REFERENCES

1. L. D. Koller and J. H. Exon, *Can. J. Vet. Res.*, 1986, **50**, 297.
2. L. Fishbein, *Int. J. Environ. Anal. Chem.*, 1984, **17**, 113.
3. H. J. Robberecht and H. A. Deelstra, *Talanta*, 1984, **31**, 497.
4. Jiao Kui, He Chengjie and Zhang Xiyu, *Acta Scientiarum Naturalium Universitatis Pekinensis*, 1984, **4**, 89.
5. Lin Shilan, Zhao Luhua, Dong Shanshi and An Dengkui, *J. of China Pharmaceutical University*, 1989, **20**, 46.
6. S. P. Brimmer, W. R. Fawcett and K. A. Kulhavy, *Anal. Chem.*, 1987, **59**, 1470.
7. Ragnar Bye, *ibid.*, 1988, **60**, 1631.
8. Chris C. Y. Chan, *Anal. Chim. Acta*, 1976, **82**, 213.
9. W. H. Beyer, *CRC Standard Mathematical Tables*, 28th Ed., pp. 538, 571. CRC Press, Florida, 1987.

Talanta, Vol. 39, No. 10, pp. 1281–1288, 1992
Printed in Great Britain.

0039-9140/92 $5.00 + 0.00

MULTI-PURPOSE CAPILLARY ELECTROPHORESIS SYSTEM WITH CONCENTRATION GRADIENT DETECTION

JIAQI WU and JANUSZ PAWLISZYN*
Department of Chemistry, University of Waterloo, Waterloo, Ontario, Canada N2L 3G1

(*Received* 26 *December* 1991. *Revised* 11 *March* 1992. *Accepted* 15 *March* 1992)

Summary—A robust, inexpensive and versatile capillary electrophoresis (CE) system for routine and rapid analysis is reported, which consists of a rugged cartridge holding a 20-μm i.d. 15-cm long capillary, and an inexpensive, universal and sensitive concentration gradient detector. The design of the cartridge simplifies the sample introduction process and makes it possible to perform many separation modes, including moving boundary capillary electrophoresis (MBCE), capillary zone electrophoresis (CZE), capillary isotachophoresis (CITP) and capillary isoelectric focusing (CIEF), on the same system. This arrangement provides more information about a sample's components since analytes can be separated by different modes performed on the same CE system. The detector only consists of a low-power He–Ne laser, or laser diode, and a photodiode position sensor. Amino acids and proteins of 10^{-6}–$10^{-3}M$ concentration can be separated by different capillary electrophoretic modes, and detected directly by the detector. The universal detector shows particularly good sensitivity when applied to CE separation modes having self-concentration and focusing effects. Femtomoles of proteins were separated and detected with CIEF. In addition, a short and narrow capillary allows use of high electrical fields which facilitate rapid separations. Four amino acids at millimolar concentrations were fully separated and detected in less than 80 sec by the MBCE mode when a high electric field was applied. The physical size of the whole system is much smaller than that of conventional CE instruments with UV absorbance or fluorescence detector.

Capillary electrophoresis (CE) has become a fundamentally important separation method in bioanalytical chemistry.[1,2] Separation and detection of components in very small amounts of biological samples, in the order of pl–nl volumes, can be achieved with CE which are not possible with more conventional methods such as HPLC. Capillary electrophoresis is also a rapid analytical technique which achieves high resolution of sample components in a few minutes. In CE, many separation modes have been developed based on traditional electrophoretic techniques for different kinds of samples, such as capillary zone electrophoresis (CZE),[3] capillary isotachophoresis (CITP),[4] capillary isoelectric focusing (CIEF)[5] and moving boundary capillary electrophoresis (MBCE).[1] One of the most promising applications of CE is for routine quality and process control in pharmaceutical and biotechnology industries and clinical analysis. Capillary electrophoresis instruments for these applications should be versatile so that all CE separation modes can be performed with them in order to deal with different kinds of samples. In many cases, rapid separation and detection of samples, for example, in about 1 min, is required, because the feedback of the analysis data is essential for observing the effectiveness of a therapy, or adjusting drug doses in treatment of patients in hospital, and controlling process conditions in industrial manufacturing. Although CE is a relatively rapid separation method (separation of a mixture usually requires between 5 and 30 min with present commercial CE instruments), the speed is still slow relative to many requirements of routine analysis, and for monitoring the dynamics of the chemical system.[6] Also, for typical commercial CE instruments, the operators cannot change one separation mode into another mode because of instrument structure and capillary cartridge design.

For routine analysis, the most desirable detector is a universal type. Although conventional absorption spectrophotometric detectors can be considered as universal, they are not sensitive enough for CE with capillaries narrower than 50 μm, and they require an expensive monochromator. Fluorometric detectors not only need an expensive laser and photomultiplier but also

*Author for correspondence.

require fluorescent derivatization for most analytes.[7,8] The commercial CE instruments with such detectors are usually expensive and large devices.

A concentration gradient detector based on Schlieren optics is one of the promising universal detectors.[9] Use of modern optical equipment, such as lasers and silicon photodiodes, dramatically improves the detector, making it a sensitive sensor with a pl–nl detection volume.[9] As shown in Fig. 1, when the detector is used for detection in CE, a collimated probe laser beam, from a low power He–Ne laser or a diode laser, is focused directly onto the capillary. The direction of the beam is deflected when it encounters a refractive index gradient produced by migrating sample zones, and the deflection can be detected by a light beam position sensor. This deflection signal can be generated by any substance which has a refractive index different from that of the buffer. The deflection signal θ of the probe beam can be given as:[9]

$$\theta = \frac{L}{n}\frac{dn}{dx} = \frac{L}{n}\frac{dn}{dC}\frac{dC}{dx}, \quad (1)$$

where n is the refractive index of the solution in the capillary, L is the inner diameter of the capillary, and C is the concentration of the sample. In this equation, dn/dC is approximately a constant for a given solute, independent of absolute concentration.[9] Therefore, equation (1) shows a linear relationship between the amplitude of the deflection signal and the first derivative of the analyte concentration spatial distribution. Because of the high separation efficiency of CE, narrow sample zones are produced, which generate high concentration gradients along the capillary, and thereby give the concentration gradient detector good sensitivity.[9] Besides the universality property and good sensitivity, the detector is also an inexpensive sensor, which consists only of a low power He–He laser or a laser diode and a photodiode position sensor.[9]

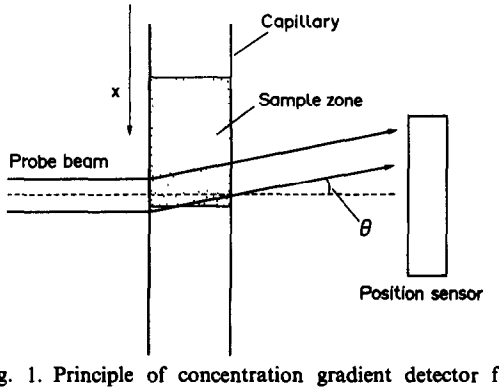

Fig. 1. Principle of concentration gradient detector for capillary electrophoresis.

In this report, the main focus is given to construction and performance of a rugged inexpensive and versatile capillary electrophoresis system consisting of a cartridge holding a short piece of capillary, which facilitates all modes of capillary electrophoretic separations with a single instrument.

EXPERIMENTAL

Chemicals

All chemicals were reagent grade, and solutions were prepared using deionized water. Buffers of 0.05*M*, 0.02*M* and 0.002*M* $H_2PO_3^-/H_3PO_4$ at pH 3 were used for amino acid and protein separations in CZE and MBCE modes. The samples were alanine, tryptophan, histidine and proline, which were dissolved in buffers. In the CITP mode, ammonium acetate (Aldrich) and tetraoctylammonium bromide were used as the leading electrolyte and tailing electrolyte, respectively. The samples used in CITP experiments were ethyltriphenylphosphonium bromide (Aldrich) and hexadecyl ammonium bromide (Sigma). For isoelectric focusing of proteins, 10m*M* phosphonic acid and 20m*M* sodium hydroxide were used as anolyte and catholyte, respectively.[10] Samples used in CIEF experiments included α-chymotrypsin (type II, Sigma), phosphorylase b (Sigma) and ovalbumin (grade V, Sigma). Samples for IEF were mixed with 2% ampholyte (Pharmalyte pH 3–10, Sigma) solution.[5] Solutions were filtered using 0.2-μm pore size cellulose acetate filters (Sartorius, Gottingen, Germany).

CE instrument and detector

A 20-μm i.d. and 350-μm o.d. fused silica capillary (Polymicro Technologies, Tucson, AZ) or a 25-μm i.d., 150-μm o.d. coated capillary (donated by Bio-Rad) was used for separations. For IEF and ITP separation modes, it is necessary that the capillary inner wall be coated with non-crosslinked acrylamide to eliminate electroosmosis.[11] The MBCE and CZE modes can be performed on either coated or uncoated capillaries. The total length of the capillary was about 15 cm. The cartridge which holds the capillary and the detection system are shown in Fig. 2. The capillary was fixed on the plexiglass

plate cartridge using epoxy glue, and its two ends were connected to two small buffer reservoirs made of polyethylene. The whole system was mounted on a vibration isolation table. The separations of samples were driven by a high voltage dc power supply (Spellman, Plainview, New York). The current passing through the capillary was monitored at the cathodic end of the capillary.

As shown in Fig. 2, the probe beam was a laser beam from a He–Ne laser (Uniphase, San Jose, CA, U.S.A.), and was focused by a 30-mm focal length lens directly into the capillary. The probe beam deflection was monitored by a position sensor consisting of a dual silicon photodiode with a differential amplifier.[9] The probe beam was arranged so that the far field intensity profile points to the centre between the two photodiodes placed close together in the position sensor. When irradiated uniformly, the photodiodes generate equal amounts of photocurrent. Upon encountering a concentration gradient inside the capillary, the probe beam is deflected by a refractive index gradient produced by the concentration gradient, and the amount of light reaching the two photodiodes is not equal. The difference in photocurrent associated with the two photodiodes corresponds to the magnitude of the deflection of the probe beam. The data were collected by an IBM DACA board, in a PC-AT personal computer, using the software ASYST™ (Asyst Software Technology Inc., Rochester, New York).

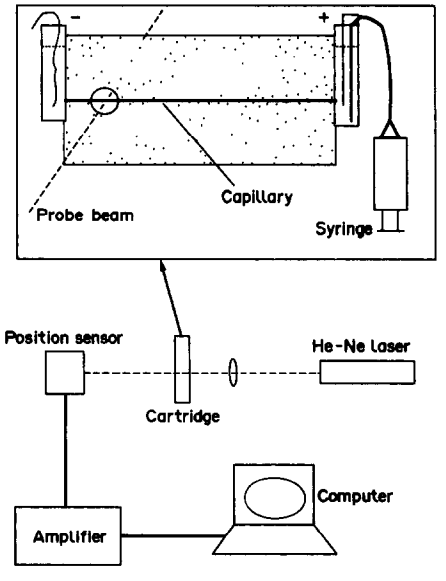

Fig. 2. Diagram of experimental set-up.

Operation of the CE system

In the MBCE mode, first, both reservoirs and the capillary were filled with buffer, and the high dc voltage was turned on. Then, as shown in Fig. 2, buffer in the reservoir of the anodic end was drawn off by a syringe and the reservoir was filled with sample solution. The separation began to occur immediately after the sample solution reached the separation capillary.[12]

In the CZE separation of amino acids, the capillary was filled with 0.05*M* phosphate buffer, and then a plug of sample was introduced into the capillary by the electrokinetic method, in which the reservoir at its anodic end was filled with sample solution, and the dc voltage was turned on. The plug length could be controlled by the introduction time and the voltage.[13] The introduction time was 3 sec. Then the reservoir was filled again with the buffer.

The field-amplified sample injection method[14] was also used in the CZE separation mode to increase the sensitivity of detection by the concentration gradient detector. In this injection method, first, the capillary was filled with 0.02*M* phosphate buffer. Then a plug of 0.002*M* phosphate buffer was hydrodynamically introduced into the anodic end of the capillary by filling the reservoir of this end with the 0.002*M* buffer. The plug length could be controlled by the introduction time and the height difference between solution levels in the two reservoirs.[13] After the introduction of a plug of low concentration buffer, the reservoir was filled with sample solution. The sample was introduced into the capillary by the electrokinetic method. The introduction time was typically 60–90 sec. Finally, the reservoir was filled with 0.02*M* phosphate buffer, and the dc voltage was applied again.

The hydrodynamic introduction method was also used in the CITP separation mode. The introduction time was 20 sec and the height difference between capillary ends was 10 cm. The IEF separation of proteins included two processes. In the focusing process, and 8 kV dc voltage was applied for 4–7 min, and current passing through the capillary was monitored to follow the focusing process. Then the focused proteins were removed from the capillary by a mobilization process. The mobilization process required exchanging catholyte with a solution containing 20m*M* sodium hydroxide and 80m*M* sodium chloride.[10] The dc voltage applied to the capillary during the mobilization was 10 kV. During the mobilization, the proteins moved

through the capillary in order of decreasing isoelectric point (pI). All experiments were repeated 2–3 times to assure reproducibility.

RESULTS AND DISCUSSION

CZE separations

When the CZE mode of separation is performed, three steps are required for the injection and separation of samples: filling the capillary with buffer; injecting the sample plug into one end of the capillary; and immersing the end again in the buffer. As described in the Experimental section, these steps can be completed on the CE cartridge by only operating the syringe which can be easily automated using a low pressure syringe pump. For the CE separation of the amino acid mixture in the CZE mode, for example, the four amino acids of proline, alanine, tryptophan and histidine, four zones are generated inside the capillary. These zones have a Gaussian concentration profile along the capillary, when the amino acids are fully separated.[2] When these zones migrate through the detection volume of the concentration gradient detector, beam deflection signals are produced. The shapes of the detected signals should be derivatives of Gaussian peaks for the separated amino acid zones since the signal magnitude is proportional to the first derivative of the concentration profile along the capillary as described by equation (1).[9] As expected, four derivative peaks are observed in the electropherogram shown in Fig. 3(a), which correspond to these four amino acids. Figure 3(b) shows the integral of the electropherogram in Fig. 3(a), which represents the actual refractive index trace along the capillary. The actual refractive index trace is subject to drift associated with temperature fluctuations inside the capillary. This low frequency noise can be effectively reduced by the derivative nature of the detector[9] as shown in Fig. 3(a), in which high signal peaks are generated only by narrow sample zones. The detection limit in Fig. 3(a) is estimated to be lower than 5m*M*, from the signal-to-noise ratio of Fig. 3(a). This low sensitivity is due to the widening of the sample zones and dilution effect during their migration in the capillary. The dilution factor is estimated to be about 2 in the separation shown in Fig. 3(a).[15] The concentration maximum of a peak decreases and its width increases with increasing retention time, because of the diffusion process. This results in a decrease of the concentration gradient at the zone boundaries.

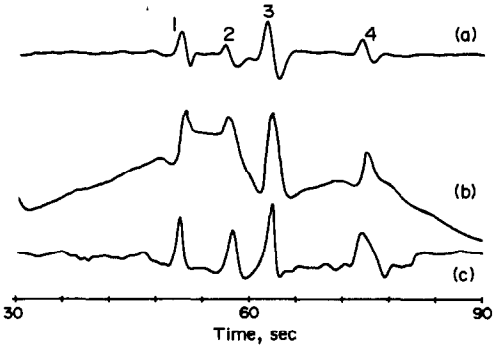

Fig. 3. (a) Electropherogram of four amino acids separated in the CZE mode: 10m*M* proline (peak 1), 10m*M* alanine (peak 2), 5m*M* tryptophan (peak 3) and 5m*M* histidine (peak 4); (b) Integral of electropherogram in (a); (c) electropherogram of four amino acids separated in the MBCE mode: 4m*M* proline (peak 1), 4m*M* alanine (peak 2), 2m*M* tryptophan (peak 3), and 2m*M* histidine (peak 4). Applied voltage is 12 kV.

MBCE separations

One method for reducing the dilution effect is by using the MBCE mode, in which the frontal injection method for the sample is employed. In the MBCE mode, sample components are not fully separated from one another to form discrete zones, rather they form boundaries since various sample components migrate with different velocities.[1] The concentration maximum in the capillary for each component is constant during the separation process. Concentration gradients are generated at the boundaries which can be detected by the concentration gradient detector.[12] Figure 3(c) shows the electropherogram of the four amino acids separated in the MBCE mode and detected by the concentration gradient detector. Four peaks are produced corresponding to the four amino acids in the injected sample. The results show high separation efficiency and high separation detection and speed because of the use of the narrow and short capillary. Four amino acids are fully separated in less than 80 sec. The number of theoretical plates for the tryptophan peak in Fig. 3(c) is estimated to be more than 2.5×10^4 for the 15-cm long capillary. High speed and high efficiency separation can be obtained by increasing the applied dc voltage, but overheating of the buffer solution inside the capillary is limiting.[6] These conditions can be achieved by using a narrow capillary which provides good heat dissipation.[2] In the above experiments, a 25-μm i.d., coated capillary was used, and the electric field applied to the capillary was 800

V/cm, which is higher than that typically employed with conventional CE, 200–400 V/cm. Under this applied voltage, the 25-μm i.d. capillary seems to provide enough heat dissipation.

The sample injection method is another factor affecting the separation efficiency. It is desirable to make an injection while the system is maintained at operating voltage, otherwise, the dispersion of the peak associated with diffusion of analytes during sample injection is unavoidable. The frontal injection method fulfills these requirements. The design of the cartridge facilitates use of the frontal injection method, in which the buffer in the reservoir at the anodic end of the capillary is removed and replaced by the sample by simply operating the syringe, while the high dc voltage is kept on. In this way, the dispersion of sample during injection is almost eliminated. The whole injection and separation process is simple and easily automated for the cartridge. For example, this can be accomplished by using two syringe pumps controlled by a PC computer.

The concentration gradient detection used is the best way for detecting moving boundaries in the MBCE mode[12] which are difficult to monitor by detectors based on concentration detection. Unlike most of the other separation modes, the concentration trace along the capillary in MBCE mode consists of "steps". In the above experiment, because of the lack of dilution of the sample during separation, and an efficient sample injection method, good sensitivity for the amino acid is obtained. The sensitivity is expected to be about two times higher than that of CZE mode which has a dilution factor of 2. Indeed the signal-to-noise ratio is about the same in Figs. 3(a) and 3(c), although the concentrations of analytes introduced to the system are about twice as high for CZE [Fig. 3(a)] compared to MBCE [Fig. 3(c)]. The detection limit is estimated to be about 1mM for these small molecular weight samples from the signal-to-noise level in Fig. 3(c). The design of the cartridge and use of the concentration gradient detector also allow for the use of a short capillary (for example, 3–15 cm long[9,12]), which provides high separation speed. The combination of MBCE operated with a narrow, short capillary, and the concentration gradient detector proved to be a good match, and MBCE performed on the proposed CE system was confirmed to be suitable for high speed separation and detection of biochemical samples, such as amino acids and sugars.[9,12]

Field-amplified injection

For detection of low concentration samples by the concentration gradient detector, on-column concentration and focusing techniques can be employed to achieve high sensitivity of detection without sacrificing resolution. These concentration and focusing techniques include field-amplified sample injection,[14] ITP,[4] and IEF.[5] Narrow sample zones or boundaries are created by these techniques. The sensitivity of the concentration gradient detector may be expressed as a function of the zone or boundary width, σ_x:[16]

$$\theta_{max} = \pm 0.24 \frac{L}{n} \frac{dn}{dC} \frac{C_0 l}{\sigma_x^2}, \qquad (2)$$

where σ_x is the standard deviation of the concentration distribution in the zone or boundary which is Gaussian, C_0 is the concentration of the injected sample and the l is the plug length of the injected sample. Equation (2) predicts that the sensitivity of the concentration gradient detector increases quickly with decreasing zone width, σ_x, and the concentration gradient detector is expected to have good sensitivity for the CE modes which have self-concentration and focusing properties.

The field-amplified sample injection process can be performed on the cartridge as described in the Experimental section. The four steps in the sample injection process can be completed by filling the reservoir at the anodic end of the capillary with different solutions with the syringe. Figure 4 shows the electropherogram of alanine and histidine separated in the CZE mode on a 20-μm i.d. capillary using the field-amplified injection technique. The wide band in the electropherogram behind the sample zones corresponds to the refractive index change caused by the plug of low concentration buffer injected before the injection of the sample. Since the sample is concentrated during the injection, amino acids of $10^{-4}M$ concentrations can be

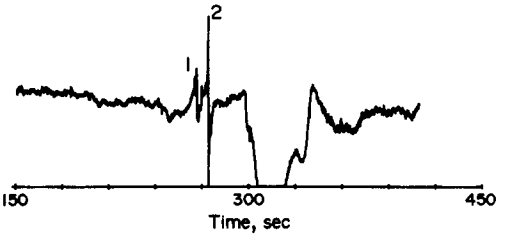

Fig. 4. Electropherogram of 0.5mM alanine (peak 1) and histidine (peak 2) introduced by zone injection with the field-amplified method. Applied voltage is 4 kV.

detected without any chemical derivatization. This sensitivity is about 10 times higher than that of the MBCE mode.

CITP separations

The CITP mode is another CE technique having self-concentration and focusing effects, which is suitable for detection of impurities in samples, such as pharmaceutical products.[17,18] In the ITP mode, the samples are injected as a plug between the leading and tailing electrolytes. During the course of the separation, each component of the sample becomes separated into a pure zone, stacked sequentially between the leading and tailing electrolytes, and migrates towards the detection end of the capillary. The zone width is proportional to the concentration of the component.[4] The zones remain narrow during the entire separation process because of self-sharpening and concentration effects.[4] Like the field-amplified injection, CITP can also be performed on the same CE cartridge. CITP separation of two small cations was performed on the CE system. For the separation of ethyltriphenylphosphonium and hexadecyl ammonium ions, three sharp boundaries should be formed between the leading electrolyte, samples and tailing electrolyte. Figure 5 shows three sharp peaks corresponding to the three boundaries. The injection concentration of the sample was 1m*M* in this experiment. The lengths of sample zones between the three peaks become shorter during the separation process because of the self-concentration effect.[4] The absolute amount of sample injected into the capillary can be estimated to be 10^2 fmoles from the sample volume, about 0.6 nl calculated from the 20-sec introduction time and the 10-cm height difference,[13] and the concentration of the sample

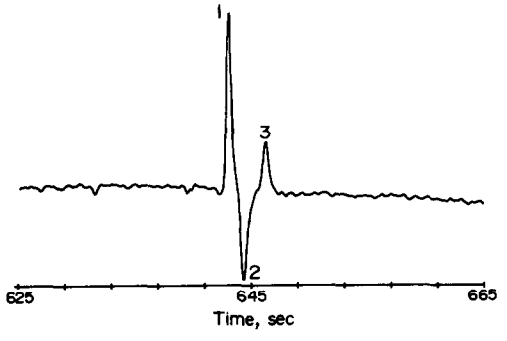

Fig. 5. Electropherogram of 1.0m*M* ethyltriphenylphosphonium ion (betweeen peaks 1 and 2) and 1.0m*M* hexadecyl ammonium ion (between peaks 2 and 3) separated in the ITP mode. The applied voltage is 7 kV.

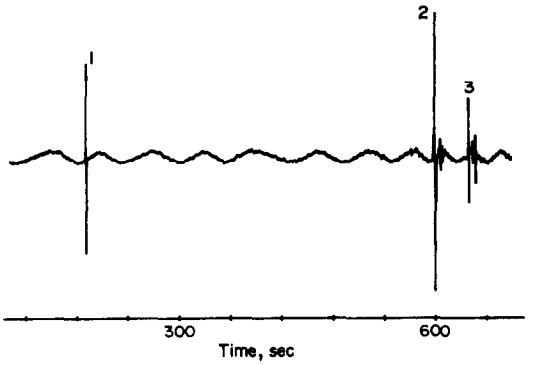

Fig. 6. Mobilization electropherogram of focused α-chymotrypsin (peak 1), phosphorylase b (peak 2) and ovalbumin (peak 3) in the CIEF mode with a 20-μm i.d. coated capillary. Concentrations of the samples are 0.3 mg/ml (0.1 mg/ml for ovalbumin), which correspond to 0.01m*M* α-chymotrypsin, 0.003m*M* phosphorylase b and 0.002m*M* ovalbumin. The focusing voltage is 8 kV, and focusing times is 4 min. The mobilization voltage is 10 kV.

1m*M*. More details about this application of the concentration gradient detector are given in Refs. 17 and 18.

CIEF separations

Capillary isoelectric focusing (CIEF) is a powerful technique for the separation of proteins, based on difference in isoelectric points. When a dc voltage is applied to two ends of a capillary filled with carrier ampholytes and protein samples, a pH gradient is established by isoelectric stacking of the ampholytes, arranged under the electric current in order of increasing pI from anode to cathode.[5] At the same time, proteins will also migrate to the point in the capillary where their pI values are equivalent to the pH, and migration ceases, creating discrete narrow zones. Zone broadening is eliminated in the CIEF, because of its focusing properties, which creates a high concentration gradient at the zone boundary. As predicted by equation (2), the concentration gradient detector is expected to be sensitive for CIEF. The configuration of the cartridge also makes the CE system a suitable instrument for performing CIEF. First, as shown in Fig. 2, the samples are placed in one of the reservoirs, and introduced into the capillary by pressure generated by a syringe. Then the two reservoirs are filled by syringe with anolyte and catholyte, respectively, and the high dc voltage was turned on.

Figure 6 shows a mobilization electropherogram of α-chymotrypsin, phosphorylase b and ovalbumin focused in a 20-μm i.d., coated

capillary. Sharp peaks are observed in the electropherogram, in which the zone width of ovalbumin is estimated to be 70 μm. This width already reaches the resolution limit of the detector, even when a focused laser beam is used as the probe beam. As predicted by equation (2), because of extremely narrow zones, the concentration gradient detector shows good sensitivity. The detection limit for the injected sample is at the $10^{-7}M$ level, which means that 1 fmole of absolute amounts of proteins inside the 20-μm i.d. capillary can be separated and detected by the system without chemical derivatization. It should be noted that the concentration gradient generated by the components of the carrier ampholytes can also be detected as broad variations in the baseline because of the universal nature of the detector as shown in Fig. 6. However, since these ampholytes only form wide bands in the capillary,[19,20] as mentioned above, the derivative nature of the detector makes the detector insensitive to these wide bands compared with narrow protein zones.

The above results illustrate that all four separation modes can be performed on the proposed CE cartridge. Highly efficient separation and sensitive, universal detection can be achieved by this system. It is straight forward to switch from one separation mode to another on the CE cartridge when analyzing an unknown sample. More information about the unknown sample can be obtained during this process since many electrophoretic techniques differ in their physical principles of operation. For example, the CZE separates samples based on differences in their mobilities, and the CIEF is based on isoelectric point differences. Figures 7 and 8 show electropherograms of ovalbumin separated by three separation modes. The ovalbumin was purified by the manufacturer with slab zone electrophoresis, which is based on mobility differences. As expected, when a pH 3 buffer is used, the electropherogram of the CZE in

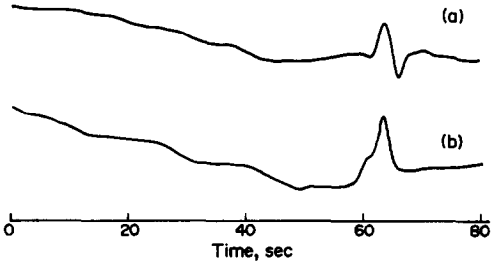

Fig. 7. (a) Electropherogram of ovalbumin (7 mg/ml) separated in the CZE mode; and (b) in the MBCE mode. Applied voltage is 12 kV.

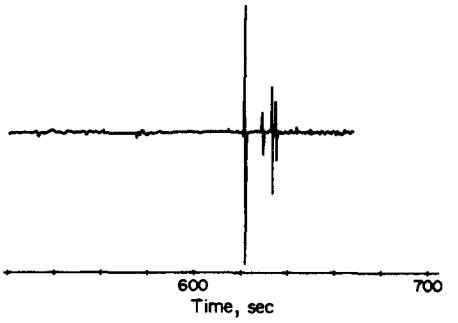

Fig. 8. Mobilization electropherogram of ovalbumin (1 mg/ml) separated in the CIEF mode. Conditions are the same as those of Fig. 6.

Fig. 7(a) only shows one peak. The electropherogram of the MBCE mode as shown in Fig. 7(b) also shows one peak since it is based on the same principle as that of the CZE. However, the electropherogram of the CIEF in Fig. 8 shows at least four peaks. The highest peak corresponds to ovalbumin, and other peaks can be attributed to impurities or minor components in the sample which have almost the same mobilities as that of ovalbumin, but different isoelectric points from ovalbumin. Separation of all those impurities or minor components may be achieved by the CZE or MBCE modes if the buffer's pH is adjusted so that it is in the range of pI's of the proteins. But for the unknown sample, it requires continuous adjustment of the buffer's pH value. By using the proposed CE system, the component information of the sample may be obtained by only switching between two separation modes.

This CE system is small and inexpensive, especially, when a diode laser is used as the probe beam source.[9] The design of the cartridge accommodates and allows for the convenient use of a short piece of capillary which results in rapid separations. The device can be constructed on a single substrate wafer since the majority of the components are silicone devices. In addition to industrial and clinical applications the system can be used as the pedagogical tool since it can built at a cost of just a few hundred dollars.

Acknowledgements—This work was supported by the Natural Sciences and Engineering Research Council of Canada. The high voltage power supply and the 25-μm i.d., coated capillary were donated by Beckman Instruments Inc., and Bio-Rad, respectively.

REFERENCES

1. J. W. Jorgenson, *Anal. Chem.*, 1986, **58**, 743A.
2. A. G. Ewing, R. A. Wallingford and T. M. Olefirowicz, *ibid.*, 1989, **61**, 292A.

3. J. W. Jorgenson and K. D. Lukacs, *ibid.*, 1981, **53,** 1298.
4. P. Bocek, M. Deml, P. Gebauer and D. Dolnik, *Analytical Isotachophoresis*, VCH Publishers, Weinheim, 1988.
5. T. Wehr, M. Zhu, R. Rodriguez, D. Burke and K. Duncan, *American Biotechnology Laboratory*, 1990, **8,** 22.
6. C. A. Monnig and J. W. Jorgenson, *Anal. Chem.*, 1991, **63,** 802.
7. T. J. Pang and M. D. Morris, *ibid.*, 1985, **57,** 2153.
8. M. J. Sepaniak, J. D. Kettler and M. P. Maskarinec, *ibid.*, 1984, **56,** 1252.
9. J. Pawliszyn, *Spectrochimica Acta Rev.*, 1990, **13,** 311.
10. M. Zhu, D. L. Hansen, S. Burd and F. Gannon, *J. Chromatogr.*, 1989, **480,** 311.
11. F. Kilar and S. Hjerten, *Electrophoresis*, 1989, **10,** 23.
12. J. Pawliszyn and J. Wu, *J. Chromatogr.*, 1991, **559,** 111.
13. D. J. Rose and J. W. Jorgenson, *Anal. Chem.*, 1988, **60,** 642.
14. R-L. Chien and D. S. Burgi, *J. Chromatogr.*, 1991, **559,** 141.
15. V. R. Meyer, *ibid.*, 1985, **334,** 197.
16. J. Pawliszyn, *Anal. Chem.*, 1986, **58,** 243.
17. T. McDonnell and J. Pawliszyn, *ibid.*, 1991, **63,** 1984.
18. *Idem*, *J. Chromatogr.*, 1991, **559,** 489.
19. P. G. Righetti, *Isoelectric Focusing: Theory, Methodology and Applications*, Elsevier Press, Amsterdam, 1983.
20. J. Wu and J. Pawliszyn, *Anal. Chem.*, 1992, **64,** 219.

Talanta, Vol. 39, No. 10, pp. 1289–1292, 1992
Printed in Great Britain.

0039-9140/92 $5.00 + 0.00

CHEMICALLY AMPLIFIED CURRENT RESPONSE OF VITAMIN C BASED ON THE CYCLIC REACTION BETWEEN L-ASCORBIC ACID AND DEHYDROASCORBIC ACID, USING DITHIOTHREITHOL AND ASCORBATE OXIDASE

SHUNICHI UCHIYAMA

Department of Environmental Engineering, Saitama Institute of Technology, 1690 Fusaiji, Okabe, Saitama 369-02 Japan

(*Received* 19 *November* 1991. *Revised* 4 *March* 1992. *Accepted* 4 *March* 1992)

Summary—A cyclic reaction between the reduced and the oxidized forms of vitamin C takes place by combining the ascorbate oxidase reaction and the reduction of L-ascorbic acid to dehydroascorbic acid by dithiothreithol. L-Ascorbic acid is oxidized by the dissolved oxygen and its consumption is not compensated by the chemical regeneration of L-ascorbic acid from dehydroascorbic acid. The dissolved oxygen then continues to decrease during the cyclic reaction, consequently, the decrease of the reduction current of oxygen is amplified. The amplification factor of $5 \times 10^{-5}M$ L-ascorbic acid at $5 \times 10^{-3}M$ dithiothreithol and pH 7.5 was found to be 10.6 when enzyme activity is 0.64 units/ml and the reaction time is 10 min.

The electrochemical measurements of the reduced form of vitamin C (L-ascorbic acid) with high selectivity have been carried out by amperometric biosensors[1–5] or a coulometric method using ascorbate oxidase.[6] In most of these methods, the consumption of dissolved oxygen takes place in an enzymatic reaction and is detected by an oxygen electrode or the decrease of L-ascorbic acid measured by an enzymatic reaction electrochemically.

On the other hand, the oxidized form of vitamin C (dehydroascorbic acid) is electroinactive and has to be chemically reduced to L-ascorbic acid before detection. Dithiothreithol has been found to be an effective reducing agent of dehydroascorbic acid.[7–9] Ascorbate oxidase catalyses the oxidation of L-ascorbic acid to dehydroascorbic acid (DAA) and can drive the reaction in the opposite direction to that of the chemical reduction of L-ascorbic acid. By comparing both reactions, we can recognize that the consumed oxygen in the enzymatic reaction is not compensated for by the chemical reduction. Therefore, if dithiothreithol does not affect the enzyme activity of ascorbate oxidase, the cyclic reaction should take place and the consumption of the dissolved oxygen should continue until its concentration becomes zero. This cyclic reaction can be described by the following cyclic reaction scheme:

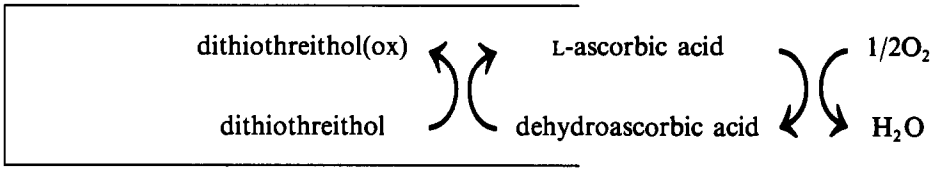

This scheme suggests that the enzymatic current response of L-ascorbic acid is amplified when L-ascorbic acid is added to the solution containing both ascorbate oxidase and dithiothreithol. The significant feature of this cycle is that dehydroascorbic acid is detected as well as L-ascorbic acid, although the response of dehydroascorbic acid begins later than that of L-ascorbic acid because of the reaction time needed to convert dehydroascorbic acid to L-ascorbic acid by dithiothreithol.

In this work, the amplification of the response current of vitamin C in this cycle has been evaluated and the effects of pH, concentration of dithiothreithol and enzyme activity on the amplification factors are described.

EXPERIMENTAL

Ascorbate oxidase (Toyo Jyozo Corp., 64.0 units/mg) solution (1 mg/ml) was prepared by dissolving ascorbate oxidase into 0.1*M* Tris buffer solution (pH 7.0) and this solution (100–500 μl) was added into the sample solutions before use. Dithiothreithol, L-ascorbic acid and dehydroascorbic acid used were all reagent grade chemicals. All experiments were done at room temperature.

Other agents for reducing dehydroascorbic acid to L-ascorbic acid exist, such as the reduced form of glutathione or homocysteine, but most of these compounds are not stable and are oxidized by oxygen. The stable compound, dithiothreithol, was then selected as a reducing agent for dehydroascorbic acid in the experiment.

The concentration of the dissolved oxygen in the sample solution was monitored by a Clark type oxygen electrode (Denki Kagaku Keiki Ltd) with a gold working electrode and a gas permeable membrane. The electrode potential of the working electrode was maintained by a potentiostat (Nikko Keisoku NPOT 2501) at −0.7 V *vs.* Ag–AgCl counter electrode and the reduction current of the oxygen was recorded by a pen recorder (Nippon Denshi Kagaku, Unicorder U-228).

The sample solutions (50 ml) were prepared by dissolving dithiothreithol and ascorbate oxidase into buffer solutions and were stirred by a magnetic stirrer throughout the experiment. If a small oxygen electrode is used, the sample solution volume can be reduced to several millilitres, and the large solution volume does not restrict the utility of the present method. After the background current of the dissolved oxygen in 0.1*M* Tris buffer solution reached a steady-state value (about 1.2 μA), vitamin C was added to this solution and the response current was recorded.

RESULTS AND DISCUSSION

The cyclic reaction of vitamin C results in a continuing decrease of the oxygen current, but the current response with L-ascorbic acid in the presence of enzyme without dithiothreithol reaches a limiting value as the L-ascorbic acid is depleted. The typical current responses (decreases) caused by L-ascorbic acid obtained in the presence of the enzyme solution with and without dithiothreithol are shown by lines (A) and (C), respectively, in Fig. 1. These results indicate that the current change in (A) is larger than 10 times at 10 min compared with that in (C), and support that the cyclic reaction of vitamin C takes place. A similar current response to (A) was obtained by $4.5 \times 10^{-5}M$ dehydroascorbic acid when dithiothreithol is contained in the enzyme solution as shown in (B) in Fig. 1. In this curve, a short time lag (T) was always observed because the change of current is begun after dehydroascorbic acid is reduced to L-ascorbic acid by dithiothreithol.

The current continues to increase up to almost zero because the cyclic reaction does not stop and the long reaction time required until the current reaches a steady state level after the sample addition. Measurement was carried out after 10 min and the RSD of 10 measurements after this time was 3.2%.

The response curves of $5 \times 10^{-5}M$ L-ascorbic acid, $3.4 \times 10^{-5}M$ DAA and a mixture of these solutions ($4.2 \times 10^{-5}M$ total vitamin C) indicated that the response curve of the mixture is between the other two curves and the total vitamin C can be detected when the sample solution contains both L-ascorbic acid and dehydroascorbic acid.

The amplified current response is pH dependent because the enzyme activity of ascorbate oxidase is decreased in acidic and alkaline media and the reduction rate of dehydroascorbic acid to L-ascorbic acid by dithiothreithol is decreased in acidic media. The effect of pH on the amplified current response of L-ascorbic acid is shown in Fig. 2. A significant variation was

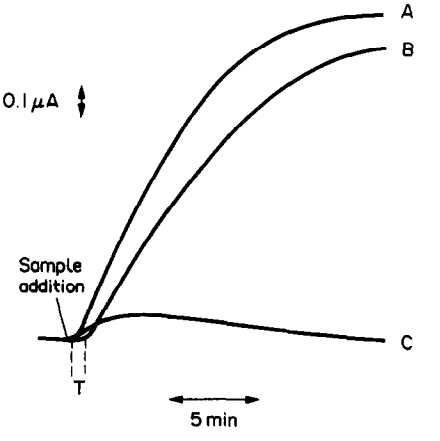

Fig. 1. Typical current responses of $5 \times 10^{-5}M$ L-ascorbic acid (*A*) and $4.5 \times 10^{-5}M$ dehydroascorbic acid (*B*) obtained by the enzyme solutions (pH 7.5) with $5 \times 10^{-3}M$ dithiothreithol and the current response of $5 \times 10^{-5}M$ L-ascorbic acid (*C*) obtained by the enzyme solution without dithiothreithol. Enzyme activity: 0.64 unit/ml.

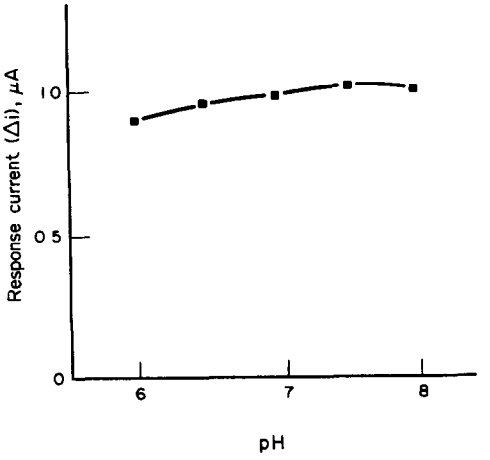

Fig. 2. Effect of pH on the current response of $5 \times 10^{-5}M$ L-ascorbic acid at reaction time 10 min.

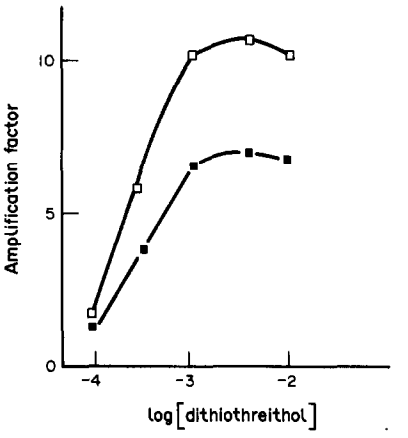

Fig. 4. Effect of the concentration of dithiothreithol on the amplification factor for $5 \times 10^{-5}M$ L-ascorbic acid at reaction times 5 min (■) and 10 min (□).

not observed in the pH range from 6 to 8, pH 7.5 was chosen throughout the experiment for maximum response.

The amplified current response is also dependent on the activity of enzyme and the effect is shown in Fig. 3. The amplified current was increased with increase in the amount of enzyme and 500 μl of enzyme (enzyme activity of the sample solution is 0.64 units/ml) was chosen for the remainder of the experiments.

The effect of the concentration of dithiothreithol on the amplified response of L-ascorbic acid at reaction times of 5 and 10 min are shown in Fig. 4. The current responses were increased by increasing the concentration of dithiothreithol but decreased slightly when the concentration was greater than $7 \times 10^{-3}M$. The decrease is because the consumption of the dissolved oxygen by the oxidation of dithiothreithol becomes important and the background current of the reduction of the dissolved oxygen is decreased. Then, the measurable current range becomes narrower, resulting in the reduction of the current response value. From the results described above, the measurement of L-ascorbic acid and dehydroascorbic acid were carried out under the conditions of pH 7.5, enzyme activity 0.64 units/ml and dithiothreithol $5 \times 10^{-3}M$.

When $5 \times 10^{-3}M$ L-ascorbic acid was added into the enzyme solution containing $5 \times 10^{-3}M$ dithiothreithol, the amplification factor obtained was 10.6 at 10 min reaction time. The relative standard deviation of this amplification factor ($n = 6$) was found to be 3.5%.

The amplified and non-amplified calibration curves of L-ascorbic acid are shown in Fig. 5. The latter was obtained from the peak current response values of each L-ascorbic acid concentration and in the case of the amplified calibration curve, while the former was obtained after a 10-min reaction time. These results indicate that a dynamic range is moved in

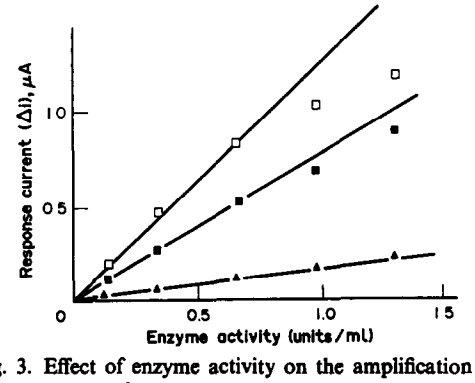

Fig. 3. Effect of enzyme activity on the amplification factors for $5 \times 10^{-5}M$ L-ascorbic acid at each reaction time: (▲) 1 min (■) 5 min (□) 10 min.

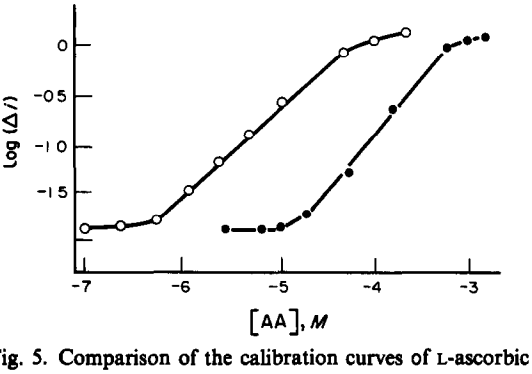

Fig. 5. Comparison of the calibration curves of L-ascorbic acid at reaction time 5 min obtained in the pH 7.5 buffer solution with (○) and without (●) $5 \times 10^{-3}M$ dithiothreithol.

parallel toward the lower concentration range ($7 \times 10^{-7}M$–$4 \times 10^{-5}M$) by more than one decade compared with that ($2 \times 10^{-5}M$–$7 \times 10^{-4}M$) obtained by buffer solution without dithiothreithol, and the detection limit was decreased by $2 \times 10^{-7}M$ from $8 \times 10^{-6}M$.

When reactants of dithiothreithol are contained in the sample solution, these would interfere because the concentration of dithiothreithol in an enzyme solution is decreased. But serious interference can be avoided by the dissolution of a large amount of dithiothreithol in the enzyme solution, or if large amounts of reactants consuming dithiothreithol are present, these reactants can be eliminated in advance by the addition of dithiothreithol into the sample solutions prior to measurement.

From the results, it can be expected that the sensitivity of an L-ascorbic acid sensor using immobilized ascorbate oxidase membrane would be significantly increased by using the described cyclic reaction of vitamin C and such a sensor system would be very effective for the measurement of not only L-ascorbic acid but also dehydroascorbic acid.

Acknowledgements—The author thanks Mr. Masahiro Yoshino and Mr. Yoshihiro Watanabe for their experimental assistance.

REFERENCES

1. K. Matsumoto, K. Yamada and Y. Osajima, *Anal. Chem.*, 1981, **53**, 1974.
2. B. J. Vincke, M. J. Devleeshouwer and G. J. Patriarche, *Anal. Lett.*, 1985, **18**, 1593.
3. G. J. Patriarche, J-M. Kauffmann, J-C. Vire and B. J. Vincke, in *Analytical Uses of Immobilized Biological Compounds for Detection, Medical and Industrial Uses*, G. G. Guilbault and M. Mascini (eds.), p. 62–63. Reidel, 1988.
4. S. Uchiyama, Y. Tofuku and S. Suzuki, *Anal. Chim. Acta*, 1988, **208**, 291.
5. S. Uchiyama and Y. Umetsu, *ibid.*, 1991, **255**, 53.
6. S. Uchiyama, T. Yamaguchi, O. Hamamoto and S. Suzuki, *Bunseki Kagaku*, 1989, **38**, 286.
7. M. Okamura, *Clin. Chim. Acta*, 1980, **103**, 259.
8. S. Uchiyama and S. Suzuki, *Bunseki Kagaku*, 1990, **39**, 793.
9. S. Uchiyama, Y. Kobayashi, O. Hamamoto and S. Suzuki, *Anal. Chem.*, 1991, **63**, 2259.

Talanta, Vol. 39, No. 10, pp. 1293–1298, 1992
Printed in Great Britain.

0039-9140/92 $5.00 + 0.00

APPLICATION OF APCD/DIBK EXTRACTION SYSTEM IN STRONGLY ACIDIC MEDIA: DETERMINATION OF TRACES OF COPPER AND NICKEL IN TITANIUM METALS BY EXTRACTION–FLAME ATOMIC-ABSORPTION SPECTROMETRY

MASAHIKO MURAKAMI and TAKEO TAKADA

Department of Chemistry, College of Science, Rikkyo (St. Paul's) University, Nishi-Ikebukuro, Toshima-ku, Tokyo 171, Japan

(*Received* 6 *August* 1991. *Revised* 7 *April* 1992. *Accepted* 10 *April* 1992)

Summary—Extraction of nickel in strongly acidic solution (0.01 ~ 8*M* hydrochloric acid) with ammonium 1-pyrrolidinecarbodithioate (APCD) into di-isobutyl ketone (DIBK) has been studied, and the APCD/DIBK system has been applied to simultaneous extraction and flame atomic-absorption spectrometric determination of trace amounts of copper and nickel in titanium metal. Nickel could be extracted with copper from strongly acidic solution such as up to 5*M* hydrochloric acid with APCD/DIBK system. The extraction from such a strongly acidic media made it possible to extract nickel with copper, since it did not require the addition of a large amount of the masking agent which prevents the hydrolysis of the matrix titanium and also prevents the extraction of nickel. Thus, they could be extracted directly from the titanium metal sample digested by concentrated hydrochloric acid with a small amount of tetrafluorohydroboric acid. Effect of coexistence of a large amount (at least 0.2 g) of iron on the extraction of both elements could be prevented by keeping most of the matrix titanium as Ti(III). With the method described here, μg/g levels of copper and nickel in titanium metal could be rapidly determined with good precision and accuracy.

The solvent extraction of various elements with ammonium 1-pyrrolidinecarbodithioate (APCD) into isobutyl methyl ketone (IBMK) is most widely used for matrix separation and preconcentration prior to their determination by atomic-absorption spectometry (AAS). The application of the APCD/IBMK system has been studied for various elements and the conditions for their extraction with this system, such as a pH range of the system which can be used have also been investigated.[1–4] In these reports, most of the workers stated that the pH range of 2 ~ 11 had been considered as the standard procedure for extraction of metals with the APCD/IBMK system, although the APCD/$CHCl_3$ system can be used in a very low pH region (< 1); in early work it was reported that Cu(II), Sb(III), and Sn(II) can be quantitatively extracted into $CHCl_3$ with APCD even from 6*M* hydrochloric acid solution.[5] Although there are only a few reports that suggest the possibility for the use of the APCD/IBMK system in the very low pH region (< 1) or that mention the effect of hydrogen-ion concentration on the extraction of various elements,[6,7] in both reports, there is no positive intention to use this system in such a region.

However, it is expected that the extraction of elements from such a strongly acidic media has significant analytical advantages. Because it permits direct extraction of analytes from a solution of sample decomposed by concentrated mineral acid without any neutralization or pH adjustment, the time and labour needed for the analysis can be decreased, and the contamination by impurities contained in the reagent can be reduced. With this aim, we have systematically studied the extraction of copper(II) from strongly acidic solution (0.01–8*M* hydrochloric and nitric acids) with APCD, to apply this system to the extraction of some elements from very acidic solution.[8–11] We found that if di-isobutyl ketone (DIBK) is used as an alternative to IBMK and a large excess of the reagent is used, the decomposition of Cu(II)–PCD chelate in the extract can be effectively suppressed and copper can be quantitiatively extracted from up to 8*M* hydrochloric or 4*M* nitric acids.

We believe that a good case which demonstrates the excellent characteristics of the APCD/DIBK system in strongly acidic media is the analysis of some trace elements in a matrix which tends to be hydrolyzed in aqueous solution, such as titanium metal. In such a case, when the pH of the solution of the decomposed sample is adjusted to 2–11 for conventional extraction procedures, masking of the matrix by the use of a large amount of a reagent such as EDTA is required, in order to prevent the coprecipitation of traces caused by the precipitation of the matrix element due to its hydrolysis. However, besides being tedious, use of a large amount of the masking agent prevents the simultaneous extraction of some desired elements; for example, when EDTA is used as the masking agent in the ASTM method for the determination of copper in titanium metal,[12] some traces other than Cu(II) are masked and cannot be simultaneoulsy extracted with APCD. On the other hand, if the desired elements can be extracted from a solution of hydrochloric or nitric acids at a strength of at least $1 \sim 2M$, they can be extracted directly from such acidic sample solution without hydrolysis of the matrix and coprecipitation of analytes.

Hence, in this paper, we studied the extraction of nickel(II) from strongly acidic media (0.01–8M hydrochloric acid) with the APCD/DIBK system, and applied the APCD/DIBK extraction to the simultaneous extraction–AAS determination of trace amounts of copper and nickel in titanium metal, to demonstrate a validity of this system.

EXPERIMENTAL

Reagents

All chemicals used were of reagent grade. Water was redistilled from an all-glass apparatus. The standard stock solutions (1000 μg/ml) of copper and nickel were prepared from 99.99% pure metals of each element and their acidities were adjusted to 0.1M hydrochloric acid, respectively. The solution of iron(III) (Fe 0.4 mg/ml) was prepared from $FeCl_3.6H_2O$. All solvents were used without further purification.

Sample preparation

A 2-g portion of the titanium metal sample was transferred to a 200-ml conical flask, and 80 ml of concentrated hydrochloric acid and 2 ml of 42% tetrafluorohydroboric acid solution were added. The mixture was heated gently until the sample was dissolved. To prepare the "unoxidized" sample, the mixture was directly diluted to 100 ml with water. The "oxidized" sample was prepared by the dropwise addition of concentrated nitric acid until the purple colour of the mixture had completely disappeared, and it was boiled gently to expel oxides of nitrogen. After oxidation, it was diluted to 100 ml with water. The strength of acid of both sample solutions was about $5 \sim 6M$.

Extraction procedures

Optimum time and APCD concentration for Ni(II) extraction. A 20-ml portion of hydrochloric acid of desired concentration, and 2.5 ml of a 10-μg/ml nickel solution were transferred to a 100-ml separating funnel, and 10 ml of DIBK were added. Portions (2.5 ml) of different concentrations of APCD solution ($1.6 \times 10^{-3} \sim 8.0 \times 10^{-2}M$) were added to the mixture just before the extraction to avoid the decomposi tion of the reagent, and the mixture was mechanically shaken vigorously for different periods of time ($30 \sim 300$ sec). Immediately after the aqueous phase had been withdrawn, the extract was washed with water; 25 ml of water was added to the separating funnel and the mixture was mechanically shaken for 180 sec. The washed extract was filtered with dry filter paper.

Extraction of Cu and Ni in titanium metal. A 10-ml aliquot of the sample solution was transferred to a 100-ml separating funnel, and 10 ml of DIBK were added. In recovery tests, $0 \sim 0.3$ ml of a 10-μg/ml copper solution and $0 \sim 0.3$ ml of a 100-μg/ml nickel solution were also added to the titanium sample solution. To study the effect of iron on the recovery, 0.35 ml of a 100-μg copper solution and 0.15 ml of a 100-μg nickel solution (final amount of each element in the sample solution is 40-μg), and $0.1 \sim 5$ ml of 40-mg/ml iron(III) solution were added to the titanium sample solution; in this case, an appropriate volume of 10M hydrochloric acid was added to the mixture, to adjust the final acid concentration to 3M. A $1 \sim 10$ ml portion of $8 \times 10^{-2}M$ APCD was added to the mixture just before the extraction, and extraction was performed for 300 sec. Immediately after the aqueous phase had been drained off, the organic phase was washed with 25 ml of water and was filtered with dry filter paper.

Determination of Cu and Ni in titanium metal samples

The titanium strip (Nippon Mining Co, LTD, CP–Ti) was digested according to the above-

mentioned procedure for "unoxidized" sample preparation, and the extraction was done as mentioned above, with addition of 10 ml of $8 \times 10^{-2}M$ APCD.

For the high purity titanium standard TAS-104 (Japan Titanium Society), the sample preparation and the extraction were done as follows: a 1-g portion of the sample metal was transferred to a 100-ml conical flask, and 20 ml of concentrated hydrochloric acid and 0.5 ml of 42% tetrafluorohydroboric acid solution were added. The mixture was heated gently until the sample was dissolved. After the solution was cooled, 10 ml of water and 10 ml of DIBK was added to the flask. A 10-ml portion of $8 \times 10^{-2}M$ APCD solution was added to the mixture just before the extraction, and the mixture was extraced for 300 sec. To avoid a contamination and loss of the analytes, the extraction was directly performed in the flask. After the aqueous phase has been drained off with a 50-ml syringe, the organic phase was washed with 25 ml of water and filtered with dry filter paper.

Measurements

UV–Visible spectra of the extract were measured with a 10-mm quartz cell. For AAS measurements, an air-acetylene flame atomizer was used. The absorption line of 324.75 nm was used for copper. For nickel, the absorption line of 341.48 nm, which is not the most sensitive line, was selected since relatively large amounts of nickel were contained in the present titanium samples.

RESULTS AND DISCUSSION

Optimum time and APCD concentration for Ni(II) extraction

The shaking time and the reagent concentration needed for quantitative extraction of 25 μg of nickel from $0.01 \sim 8M$ hydrochloric acid with the APCD/DIBK system were studied.

Shaking time. The studies were performed in the range $0.01 \sim 5M$ hydrochloric acid with APCD at $8 \times 10^{-3}M$. In the whole range of acid concentrations, the nickel chelate could be quantitatively extracted into DIBK with shaking for $30 \sim 300$.

APCD concentration and acidity range. In the preceding paper,[11] it was observed that the limiting acidity of the quantitative extraction of the copper chelate was directly dependent on the concentration of the reagent added. Hence, the the acidity range of the nickel chelate extraction was studied with various concentrations of APCD. Figure 1 shows the percentage extraction of nickel chelate as a function of hydrochloric acid concentration of the aqueous phase, with $1.6 \times 10^{-4}M$, $3.2 \times 10^{-4}M$, and $8.0 \times 10^{-3}M$ of APCD. Similar to the copper extraction, the acidity range depends on the concentration of the reagent added. The limiting hydrochloric acid concentrations for quantitative extraction of the nickel chelate were taken as follows: $0.5M$ with $1.6 \times 10^{-4}M$ APCD (9.4-fold ratio to nickel), $1M$ with $3.2 \times 10^{-4}M$ (19-fold), and $5M$ with $8.0 \times 10^{-3}M$ APCD (470-fold).

Hence, the shaking time of $60 \sim 300$ sec and the reagent concentration of $8 \times 10^{-3}M$ or more were selected as the optimum conditions for the extraction of nickel from up to $5M$ hydrochloric acid solution. They are also taken as optimum for the simultaneous extraction of copper and nickel from such a medium, since copper could also be quantitatively extracted under the present conditions.[10,11]

Extraction of Cu and Ni in titanium metal

Effect of oxidation state of matrix titanium. Simultaneous extraction of copper and nickel contained in the titanium metal sample (Nippon Mining Co, LTD, heat No. 81475) with the APCD/DIBK system was examined. This titanium metal contains about 10 μg/g and 110 μg/g of copper and nickel, respectively, and also contains a relatively large amount (about 2.5 mg/g) of iron.

Figure 2 shows the percentage extraction of each element from a sample solution in which the matrix titanium was oxidized to Ti(IV)

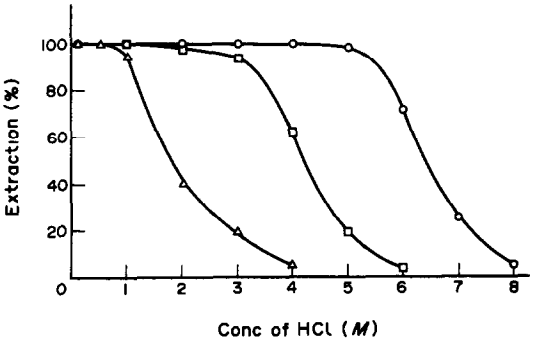

Fig. 1. Extraction range of Ni(II) with APCD/DIBK system in hydrochloric acid media: [APCD] $1.6 \times 10^{-4}M$(△), $3.2 \times 10^{-4}M$(□), $8.0 \times 10^{-3}M$(○); [Ni] $1.5 \times 10^{-5}M$; shaking time 180 sec.

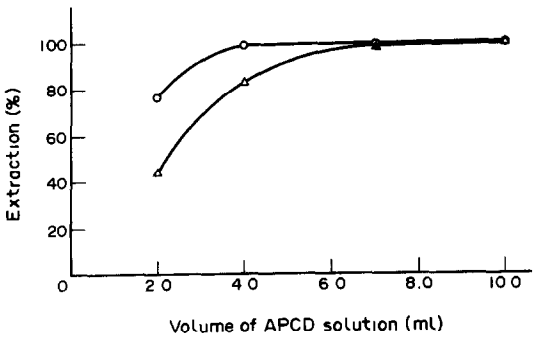

Fig. 2. Effect of volume of APCD solution on Cu and Ni extraction from the "oxidized" titanium sample: Cu(○), Ni(△); [APCD] $8.0 \times 10^{-2}M$; shaking time 300 sec.

according to the conventional sample preparation, as a function of the volume of $8 \times 10^{-2}M$ APCD solution. The strength of acid of the aqueous phase was about $2 \sim 3M$ with hydrochloric acid, during the extraction. The copper and nickel could be quantitatively extracted when 7 ml or more of the reagent was added. This suggests that the APCD/DIBK system has the obvious potential for the simultaneous extraction of some trace metals from samples requiring high acidity to prevent hydrolysis of the matrix element.

However, when nickel and copper were extracted from a sample solution in which the matrix titanium was oxidized to Ti(IV), considerable amounts of the iron chelate were also extracted. In the UV–Vis spectrum of the DIBK extract, characteristic absorption peaks of $Fe(PCD)_3$ were observed at 510 and 595 nm, and a large amount of iron was detected by AAS. There was concern that the co-existence of a large amount of iron would affect the extraction of copper and nickel due to consumption of the reagent. Although both elements could be quantitatively extracted in the above case, it may be assumed that the coexistence of iron affects the amount of available reagent; the amount of the reagent needed for the quantitative extraction of both elements is larger than that expected from the studies on the extraction conditions of copper and nickel.

It is known that some dithiocarbamato complexes of divalent iron were unstable,[13] and it was also reported that Fe(II) cannot be extracted from acidic solution (<pH 1) with diethylammonium diethyldithiocarbamate into $CHCl_3$.[14] Therefore, to avoid the chelation of iron it is preferable to keep the iron in the divalent state. Hence, we have tried to extract copper and nickel from a sample solution prepared by the procedure omitting oxidation of the titanium. In this "unoxidized" case, most of the titanium probably remains in the trivalent state, and it is expected that the iron is kept in the divalent state during the extraction since Ti(III) matrix acts as a reducing agent for iron.

Figure 3 shows the percentage extraction of each element in the "unoxidized" case, as a function of the volume of $8 \times 10^{-2}M$ APCD. In the "unoxidized" case, the volume of the APCD solution needed for complete extraction of each element was considerably less than that observed in the "oxidized" case (Fig. 2); the percentage extraction of copper and nickel were maximum when 1 and 4 ml of the reagent was added, respectively. In this case, the characteristic absorption spectrum of $Fe(PCD)_3$ was only slightly observed in the extract, and iron was not detected by AAS. These facts indicate that the chelation of large amounts of Fe(III) causes an increase in the amount of APCD needed for complete extraction of both elements, and that such an effect of iron can be suppressed provided that the matrix titanium is not oxidized to Ti(IV). We have therefore extracted the copper and nickel chelate from strongly acidic conditions without oxidation of matrix titanium.

Figure 3 also shows that adding 4 ml or more of $8 \times 10^{-2}M$ APCD is enough for the extraction of copper and nickel in the present sample, if titanium is not oxidized. However, in our previous studies it was found that the kinetic stability of the copper chelate in the extract, and therefore the limit of acidity for its extraction, could be increased by increasing the amount of APCD added.[10,11] Therefore, addition of 10 ml of APCD solution was selected for later studies.

Recoveries. To make sure of the effect of titanium matrix on the extraction–AAS deter-

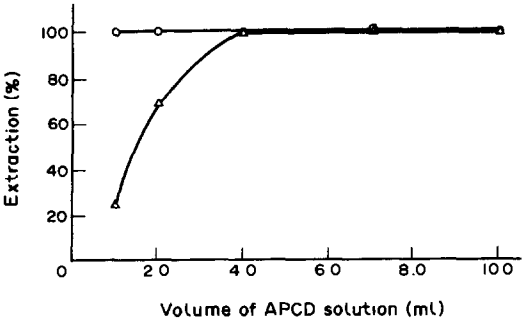

Fig. 3. Effect of volume of APCD solution on Cu and Ni extraction from the "unoxidized" titanium sample: Cu(○), Ni(△); [APCD] $8.0 \times 10^{-2}M$; shaking time 300 sec.

mination and the amounts of copper and nickel which can be extracted with the present condition, the recoveries of copper and nickel from the "unoxidized" titanium sample solution were studied. The studies were carried out by standard additions of each element to the sample solution during its preparation. The slopes and the linear ranges of the plots of AAS intensity against the added amount of each element were compared with those of working curves. The working curves were prepared by extracting the appropriate volume of the standard solutions of each element, in the absence of the titanium matrix.

The results are shown in Table 1. The slopes of the curves for each element agreed very closely with each other, indicating that both elements were satisfactorily recovered with this method. The linearity of the standard addition curves for each element remained throughout addition of 36 μg or more and 41 μg or more of copper and nickel, respectively. Since the present sample contains about 2 μg of copper and 22 μg of nickel, with the addition of 10 ml of the reagent solution, about 38 μg of copper and about 63 μg of nickel can be recovered from the sample solution containing about 0.2 g of titanium.

Effect of Fe. The effect of iron on the recoveries of copper and nickel were studied by adding various amounts of iron(III) ion to the above sample solution. In this study, the contents each of copper and nickel in the sample solution were adjusted to about 37 μg by addition of appropriate amounts of the standard solutions of each element. It is assumed that such an amount of both elements must be satisfactorily recovered with the present extraction, because it is approximately equivalent to the upper limit of the linear calibration of each element in this system; this is about 40 μg for both elements when the most sensitive absorption line of each element (324.75 nm for Cu and 232.00 nm for Ni) used.

Table 1. Slope and linear range of the standard addition plots and the working curve

Method	Slope (mm/μg)		Linear range (μ/g)	
	Cu	Ni*	Cu	Ni*
Std. add. plots ("unoxidized")	11.3	1.16	>38.2	>63.0
Working curve (no Ti contained)	11.1	1.18	≦40	≦65.0

*For AAS measurement of nickel, the absorption line of 341.48 nm was used.

Table 2. Determination of copper and nickel and titanium strip (CP–Ti) and standard sample of high purity titanium (TAS–104)

	CP–Ti		TAS–104	
	Cu	Ni	Cu	Ni
Certificate value (μg/g)	11	80	2*	28
Found (μg/g)	10.8	82.4	1.65	28.2
R.S.D. (%)	1.6	0.36	1.1	1.1

*This is the reference (non-certified) value.

The extraction of copper and nickel were not affected by the Fe(III) ions which were added in a 0.2-g weight, although extraction of considerable amounts of the iron chelate was observed. The copper and nickel chelates were stable at least for one week when the extract was kept in the light.

Therefore, it can be concluded that the amount of reagent is sufficient for the determination of copper and nickel by the proposed extraction-flame AAS. Hence, 10 ml of $8 \times 10^{-2}M$ APCD solution was selected for the determination of copper and nickel in titanium metal samples.

Determination of Cu and Ni in titanium metal samples

The method was applied to the simultaneous extraction–AAS determination of trace amounts of copper and nickel in titanium metal samples. The determination of both elements was carried out by the working curve method.

The results of five replicate analyses of both the titanium strip (Nippon Mining Co, CP–Ti) and the standard reference sample of high purity titanium (Japan Titanium Society, TAS–104) are shown in Table 2. As can be seen, the μg/g levels of copper and nickel in titanium metal can be determined by the present method, with good precision.

CONCLUSION

The APCD/DIBK system made its possible to extract both copper and nickel together directly from the strong hydrochloric acid solution (about $5M$) of digested titanium sample. In this case, the time required to prepare the sample solution could be reduced by about 50% or more. Furthermore, taking into consideration that copper and nickel can be simultaneously extracted from the same solution, further saving of time is achieved.

It was also found that co-extraction of iron can be avoided if the extraction of desired element is carried out in the strongly acidic medium under the existence of an appropriate reducing agent [not only Ti(III)] to keep iron in the Fe(II) state during the extraction. We believe this will be one of the significant advantages for the practical application of the APCD/DIBK system in the strongly acidic media.

Acknowledgement—The authors are grateful to Mr. Y. Tegawa, Nippon Mining Co., Ltd., for providing us with the samples of titanium.

REFERENCES

1. E. Lakanen, *At. Absorpt. News* 1., 1966, **5**, 17.
2. C. E. Mulford, *ibid.*, 1966, **5**, 88.
3. S. R. Koirtyohann and J. W. Wen, *Anal. Chem.*, 1973, **45**, 1986.
4. J. D. Kinrade and J. C. Van Loon, *ibid.*, 1974, **46**, 1894.
5. H. Malissa and S. Gomiscek, *Z. Anal. Chem.*, 1960, **177**, 97.
6. R. J. Everson and H. E. Parker, *Anal. Chem.*, 1974, **46**, 1966.
7. I. Dellien and L. Persson, *Talanta*, 1979, **26**, 1101.
8. T. Takada, *ibid.*, 1982, **29**, 799.
9. M. Murakami and T. Takada, *ibid.*, 1985, **32**, 513.
10. *Idem*, *ibid.*, 1990, **37**, 229.
11. *Idem*, *ibid.*, 1991, **38**, 1129.
12. American Society for Testing Materials, Standard Methods for Chemical Analysis of Titanium and Titanium Alloys, E120-75, 1979, 377.
13. K. Glue and R. Schwab, *Angew. Chem.*, 1950, **62**, 320.
14. H. Bode and F. Neuman., *Z. Anal. Chem.*, 1960, **172**, 1.

Talanta, Vol. 39, No. 10, pp. 1299–1306, 1992
Printed in Great Britain.

0039-9140/92 $5.00 + 0.00

COMPLEXATION, EXTRACTION AND DETERMINATION OF THE H_3CHg^+ ION WITH CADION [1-(*p*-NITROPHENYL)-3-(*p'*-AZOBENZENE)-TRIAZENE]

ANDREI F. DĂNEȚ* and VASILE DAVID

Department of Analytical Chemistry, Faculty of Chemistry, University of Bucharest, Bul. Republicii 13, Bucharest 70.031, Romania

(*Received* 24 *June* 1991. *Revised* 20 *February* 1992. *Accepted* 3 *March* 1992)

Summary—The partition constants of Cadion, *i.e.*, 1-(*p*-nitro-phenyl)-3-(*p'*-azobenzene)-triazene, of its complex with the methylmercuric ion, and of methylmercury chloride were determined in the system toluene/aqueous phase containing 40 vol.% methyl alcohol; they have the values of 4.3×10^3, 3.0×10^3, and 2.6 respectively. The reagent has an absorption maximum at 406 nm, whereas the methylmercury complex at 460 nm. The K_{HR} value corresponding to the $H^+ + R^- \rightleftharpoons HR$ equilibrium is $10^{10.85}$, HR being the reagent molecule and H belongs to the –NH– of the triazenic group (–N=N–NH–). The K_{ext} value corresponding to the equilibrium $H_3CHg^+ + (HR)_o \rightleftharpoons (H_3CHgR)_o + H^+$ is 1.0, where the "o" indicates the species present in the organic phase. The reagent/H_3CHg^+ combination ratio is 1/1. The formation constant of the methylmercury complex, K_{H_3CHgR}, which corresponds to the equilibrium $H_3CHg^+ + R^- \rightleftharpoons H_3CHgR$, has a value of $10^{10.8}$ as estimated by means of two different methods. The IR spectra allowed some conclusions to be drawn concerning the formation of the complex. The complex is stable up to 180°, and the reagent up to 140°. The molar absorptivity is of 3.46×10^4 $l \cdot mole^{-1} \cdot cm^{-1}$ and the H_3CHg^+ can be determined in the range 0.025–4 ppm. The determination is highly selective.

Methylmercury is one of the most toxic forms of mercury. In the environment, this compound can be formed from inorganic mercury by biological methylation; it then accumulates in living organisms by a series of processes taking place along the food chain.[1,2] This would account at least partially for the attention being paid to the chemistry of the complexes that methylmercury can form with a series of ligands[3–8] to the determination of methylmercury[9–13] and also to the study of the stability of the aqueous solutions containing this ion.[14–16]

The 1,3-diaryltriazenic derivatives have the property of forming very stable complexes with the mercury(II) and phenylmercury(I) ions, which can be extracted in organic solvents from a neutral or very slightly alkaline medium. Based on this property, sensitive and selective spectrophotometric methods of determining these ions with 1,3-diphenyltriazene[17,18] and 1-(*p*-nitro-phenyl)-3-(*p'*-azobenzene)-triazene (Cadion)[19,20] were proposed; these methods are neatly more selective than the method proposed originally with the latter of these two reagents,[22] in which the determinations have been made in a basic water–alcohol medium. The sensitivity, but particularly the high selectivity of these determination methods prompted us to investigate the equilibria involved in complexation and extraction, in order to establish the optimal conditions for the determination of methylmercury with Cadion.

The literature reports very few data on the reaction of methylmercury with organic reagents, especially with dithizone.[23,24] However, dithizone reacts with a large number of ions and its use for analysing methylmercury requires very pure reagents or their prior purification; moreover, the determination has poor selectivity, and the formed complex between the methylmercuric ion and dithizone is photosensitive. The reagent proposed by us does not show such disadvantages.

EXPERIMENTAL

Apparatus and reagents

The absorption spectra were recorded with the UV-Vis and 75IR Specord spectrophotometers, and the measurements at fixed wavelengths were carried out with the VSU 2G spectrometer, all these intruments being provided by Carl Zeiss Jena (Germany). The pH measurements were carried out with the MV85

*Author for correspondence.

pH-meter (Germany), whereas the thermograms were recorded with a system derivatograph (J. Paulik, F. Paulik and L. Erdey, Hungary).

All the used reagents were analytically pure. A 0.015% stock solution of 1-(*p*-nitrophenyl)-3-(*p'*-azobenzene)-triazene (Austranal) in methanol and 100 μg H_3CHg^+/ml of solution of methylmercury chloride (Merck) in water were prepared. The solution of methylmercury chloride was obtained by dissolving first the weighed amount of solid substance in 3 or 4 ml of acetone, then diluting with water. From these, solutions of necessary concentrations were obtained by dilution.

The working procedure

The following procedure was pursued in order to carry out the complexation and extraction studies. A 1-ml aliquot of 2*M* sodium acetate, the solution containing methylmercury chloride, distilled water, methanol, and the solution of the reagent were introduced into a 50-ml graduated cylinder provided with ground-glass stopper, so that the final volume was 10 ml and the methanol concentration was 40 vol.%. The solution was stirred for homogenization and then left to stand for 10 min. Toluene (5 ml) was added and the cylinder was stirred vigorously for one minute. After phase separation, an adequate amount of the organic phase was taken out with a dry pipette to fill up the spectrophotometer cell, and its absorbance was measured. In all cases 1-cm thick cells were used.

In order to draw the calibration curve and to determine methylmercury, the procedure described above was preserved, but 4 ml of reagent were introduced in all samples, and the absorbances were measured relative to a reference sample at 480 nm.

The complex of methylmercury with the investigated reagent was prepared as follows: stoichiometric amounts of methylmercury chloride and reagent, corresponding to a 1/1 combination ratio and calculated to yield 1 g of complex, were dissolved by heating in 10 ml and in 100 ml of acetone. The solution of methylmercury chloride was introduced over the hot solution of reagent, then 10 g of solid $H_3CCOONa \cdot 3H_2O$ were added, stirring until its complete dissolution. The solution was left to cool down, when at the bottom of the beaker a slightly coloured liquid phase separated, which contained most of the sodium acetate dissolved in its own crystallization water; the formed complex precipitated from acetone and separated at the interface between the two phases. The solution was filtered through a G4 sintered-glass filter, the precipitate was washed with hot water and then with a small amount of acetone; it was dried in an oven at 105°. The obtained solid complex was a microcrystalline structure and is red-violet in colour. The yield was 80%.

The partition constants of the reagent and of the complex were estimated on the basis of their solubilities in toluene and in an aqueous phase having identical composition to that used in the extraction studies. In order to do this, 50 ml of aqueous phase and 10 ml of toluene and reagent or solid methylmercury complex, taken in excess, were brought into contact in 100-ml separating funnels. The samples were stirred for 20 min, then the phases were separated and filtered. The reagent and the complex were extracted from their saturated aqueous phases by using volumes of toluene 2 and 10 times less, respectively for the reagent and the complex. The organic phases, which are saturated solutions of reagent and of complex, were diluted 1000 and 300 times, respectively. Absorbance measurements were made at the wavelengths of the absorption maxima of the reagent and of the complex. The partition constants were estimated from the values of the absorbances, taking into account the dilution.

The partition constant of methylmercury chloride between toluene and an aqueous phase having an identical composition to that used in the extraction studies was estimated similarly as for the partition constants of the reagent and the complex; finally, methylmercury was oxidized to Hg^{2+} and determined spectrophotometrically, with Cadion.[19]

RESULTS AND DISCUSSION

The absorption spectra of a $2.5 \times 10^{-5}M$ solution of reagent extracted in toluene (curve 1) and of a series of solutions containing the same amount of reagent and increasing amounts of methylmercuric ions (curves 2–6) are given in Fig. 1. As can be seen, the reagent has an absorption maximum at 406 nm (24,630 cm^{-1}), whereas the formed complex, at 460 nm (21,740 cm^{-1}). The spectra have a single isosbestic point, which suggests that a single complex is formed. However, the curve for the highest reagent concentration does not pass through the isosbestic point. This would indicate that some

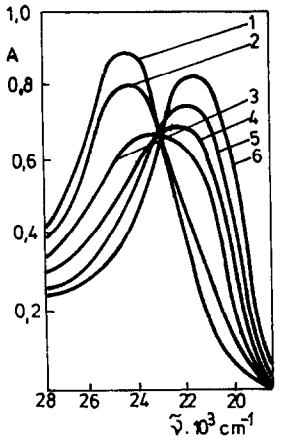

Fig. 1. The absorption spectra of the reagent and of the methylmercury complex, extracted in toluene: (1) reagent, $2.5 \times 10^{-5}M$; (2–6) the same concentration of reagent and increasing concentrations of CH_3Hg^+, with the following $[HR]/[H_3CHg^+]$ ratios: (2) 4/1; (3) 1/1; (4) 1/2; (5) 1/4 and (6) 1/8.

higher complex may also be formed. The difference between the absorbance of the complex and that of the reagent is maximum at 480 nm (20,830 cm^{-1}).

The influence of methyl alcohol concentration in the aqueous phase, of pH values of the aqueous phase, of phase stirring duration and of time on the absorbance of the complex extracted in toluene has been studied.

A variation of methyl alcohol concentration between 10–50 vol.% did not lead to a change in the absorbance of the methylmercury complex extracted in toluene. In general, the extraction studies were carried out in a medium of water–40 vol.% methanol.

Figure 2 shows the absorbance variation of the complex extracted in toluene as a function

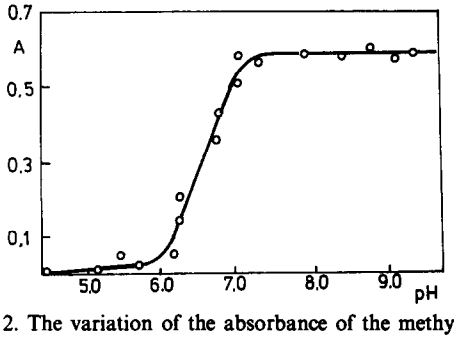

Fig. 2. The variation of the absorbance of the methylmercury complex extracted in toluene, as a function of the pH value of the aqueous phase. The concentration of the reagent in the organic phase = $2 \times 10^{-4}M$. The concentration of methylmercury chloride introduced initially in aqueous phase = $9.5 \times 10^{-6}M$.

of the pH. One can see that the absorbance remains constant for pH values larger than 7 in the aqueous phase, whereas the complex is extracted practically quantitatively in toluene. The pH-meter was calibrated with buffer solutions in 40 vol.% methyl alcohol, while the pH concept in this case has the same significance as that attributed to it in the book.[30] The reagent extraction in the organic phase as the non-dissociated form, HR, is practically not affected by the pH values within the 4.5–9 range.

One minute of vigorous stirring is quite enough for extracting the complex in toluene.

The complex absorbance remains constant for more than 2 hr provided that the organic extract is not submitted to very strong light.

The H_3CHg^+/reagent combination ratio, as well as both extraction and stability constants of the methylmercury complex (the latter by two different methods) were determined.

The H_3CHg^+/reagent combination ratio was determined by the spectrophotometric titration method and also using the method of continuous variations; it has the value of 1/1, in full agreement with the coordinative properties of methylmercury.[3,8]

The extraction constant of the complex was estimated from the influence of pH on the extraction yield (Fig. 2). It was considered that the extraction takes place according to the equilibrium:

$$H_3CHg^+ + (HR)_o \rightleftharpoons (H_3CHgR)_o + H^+ \quad (1)$$

where the "o" indicates the species present in the organic phase. The extraction constant is given by

$$K_{ext} = \frac{[H_3CHgR]_o[H^+]}{[H_3CHg^+][HR]_o} = D\frac{[H^+]}{[HR]_o} \quad (2)$$

where D is the partition ratio of mercury between the two phases and is equal to 1 at the pH of half-extraction. The half-extraction pH ($pH_{1/2}$) determined from Fig. 2 has the value 6.6. In the aqueous phase from which the extraction was made, methylmercury can however also be present as a complex with chloride, hydroxide and acetate ions, these having formation constants equal to $10^{5.25}$, $10^{9.37}$ (Refs. 3 and 4) and $10^{3.18}$ (Ref. 4), respectively. Taking account of the formation of these complexes, the concentration $[H_3CHg^+]$ of free methylmercury in the aqueous phase, at pH 6.6, will

have the value

$$[H_3CHg^+] = \frac{[H_3CHg^+]_t}{2} \times \frac{1}{1 + K_{H_3CHgOH}[OH^-] + K_{H_3CHgOOCH_3}[H_3CCOO^-]} \quad (3)$$

where $[H_3CHg^+]_t$ is the initial concentration of methylmercury ions introduced in the aqueous phase. (It was assumed that in the aqueous phase the species H_3CHgCl and the methylmercury complex of the reagent are practically absent). By estimating the value of $[H_3CHg^+]$ from equation (3) and substituting it in (2), it was found that $K_{ext} = 1.0$.

It is considered that the formation of the methylmercury complex in the aqueous phase takes place according to the equilibrium:

$$H_3CHg^+ + R^- \rightleftharpoons H_3CHgR \quad (4)$$

where R^- is the anion formed after the dissociation of the –NH– bond of the triazenic group (–N=N–NH–) of the reagent. The stability constant of the complex can be computed by means of the following relation:

$$K_{H_3CHgR} = \frac{[H_3CHgR]}{[H_3CHg^+][R^-]} = \frac{K_{HR} K_{ext} P_{HR}}{P_{H_3CHgR}} = 10^{11.0} \quad (5)$$

where

$$K_{HR} = \frac{[HR]}{[H^+][R^-]} = 10^{10.85}$$

and it corresponds to the equilibrium $H^+ + R^- \rightleftharpoons HR$, HR being the reagent molecule and H belongs to the –NH– of the triazenic group (–N=N–NH–). K_{HR} was determined from the influence of pH on the reagent's dissociation.

$$P_{HR} = \frac{[HR]_o}{[HR]} = 4.3 \times 10^3$$

and

$$P_{H_3CHgR} = \frac{[H_3CHgR]_o}{[H_3CHgR]} = 3.0 \times 10^3$$

are the partition constants of the reagent and the methylmercury complex, respectively, as determined from the solubility ratio. The "o" indicates the species present in the organic phase.

The stability constant of the methylmercury complex was also determined by a second method. This method is based upon the competing equilibria which occur when introducing a second ligand for the methylmercury ion. To this purpose, the Cl^- ion was used. The variation of the absorbance of the methylmercury complex extracted in toluene, as a function of the $[Cl^-]/[H_3CHg^+]$ ratio, is given in Fig. 3. From the data in this figure, one can infer that the competing equilibrium of the formation of the H_3CHgCl species is only to a little extent affected by the methyl alcohol in the aqueous phase. This leads to the conclusion that the constants of formation of the H_3CHgCl species are not appreciably modified under the influence

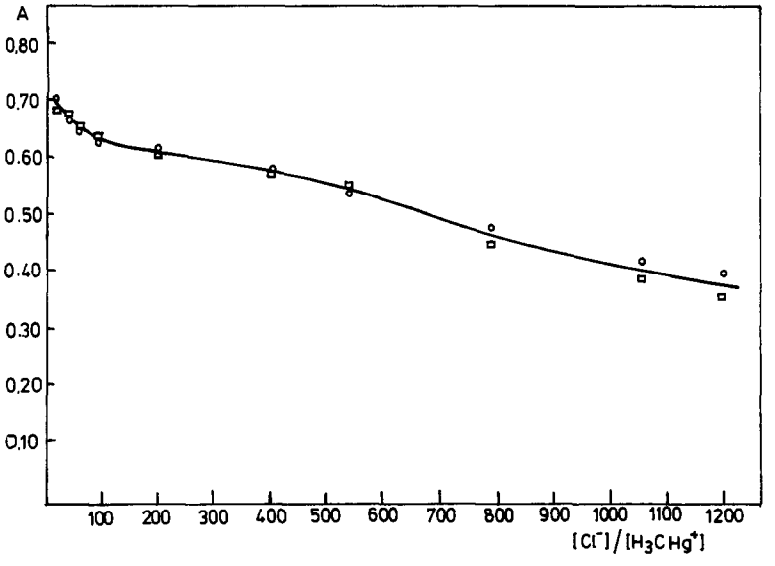

Fig. 3. The variation of the absorbance of the complex extracted in toluene as a function of the $[Cl^-]/[H_3CHg^+]$ ratio. The concentration of the reagent initially in the organic phase = $1.4 \times 10^{-4} M$; the concentration of methylmercury initially introduced in the aqueous phase = $2.0 \times 10^{-5} M$. In the presence of 40 vol.% of methyl alcohol (□) and in the absence of methyl alcohol (○). Equal volumes of the phases.

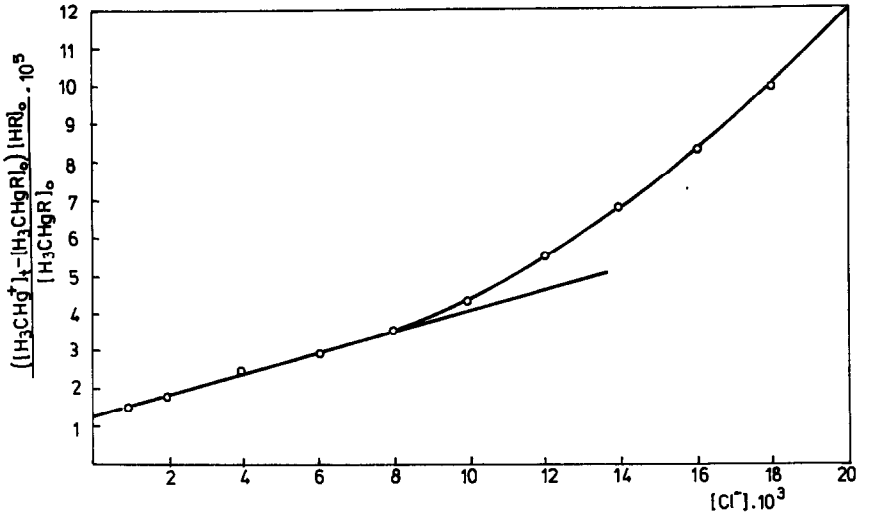

Fig. 4. The plot of $([H_3CHg^+]_t - [H_3CHgR]_o)\,[HR]_o/[H_3CHgR]_o$ as a function of $[Cl^-]$.

of methyl alcohol introduced in the aqueous phase, since the decrease in the methylmercury complex absorbance with studied reagent in Cl^- ion presence occurs similarly as much in presence as in absence of the methyl aclohol from the aqueous phase (Fig. 3).

The K_{H_3CHgR} value has been computed according to the following considerations. The sum of concentrations of all species (neglecting H_3CHgR) of the methylmercury in the aqueous phase is given by the relation:

$$[H_3CHg^+] + [H_3CHgCl] + [H_3CHgOH] = [H_3CHg^+]_t - [H_3CHgR]_o - 2.6[H_3CHgCl] \quad (6)$$

since the $[H_3CHgCl]_o/[H_3CHgCl]$ partition constant has the value of 2.6, as determined from the solubility ratio.

Substituting in (6) the values of $[H_3CHgCl]$ and $[H_3CHgOH]$ as functions of the stability constants of the corresponding complexes and taking account of the other determined quantities, one can write:

$$K_{H_3CHgR} = \frac{P_{HR} K_{HR} [H^+][H_3CHgR]_o}{P_{H_3CHgR}[HR]_o} \times \frac{1 + 3.6K_{H_3CHgCl}[Cl^-] + K_{H_3CHgOH}[OH^-]}{[H_3CHg^+]_t - [H_3CHgR]_o} \quad (7)$$

Rearranging equation (7) and plotting

$$\frac{([H_3CHg^+]_t - [H_3CHgR]_o)[HR]_o}{[H_3CHgR]_o}$$

against the concentration of the Cl^- ions, a straight line is obtained (Fig. 4) whose slope is

$$\frac{3.6P_{HR}K_{HR}[H^+]K_{H_3CHgCl}}{P_{H_3CHgR}\,K_{H_3CHgR}}$$

where all quantities are known, except the value of K_{H_3CHgR}, which can then be found. It may be seen that the plot in Fig. 4 is linear only on its first side, which corresponds to lower concentrations of Cl^- ions; for high Cl^- concentrations, the points no longer belong to the straight line, most likely because of the formation of higher complexes of H_3CHg^+ with Cl^- ions. For K_{H_3CHgR} the value of $10^{10.6}$ was found, which is close to the value determined by the previous method.

The IR spectra of the reagent and of the methylmercury complex, recorded in the range 4000–400 cm^{-1}, are given in Fig. 5. One can see that the bands located at 3260 and 1526 cm^{-1}, assigned, respectively, to the valence and bending vibrations of the -NH- bond of the triazenic group,[21] no longer appear in the spectrum of the complex; this indicates that the bonding between the H_3CHg^+ ion and the reagent's molecule is achieved by the replacement of the hydrogen atom of the triazenic group, which means, in fact, that the extraction and complexation equilibria represented by equations. (1) and (4) are correct.

The thermogravimetric (TG), differential thermal analysis (DTA) and differential thermogravimetric (DTG) curves for the reagent (curve 1) and its methylmercury complex (curve 2) are shown in Fig. 6. One can see that the reagent is stable up to 140°, and its methylmercury complex up to 180°; thus, the reagent could

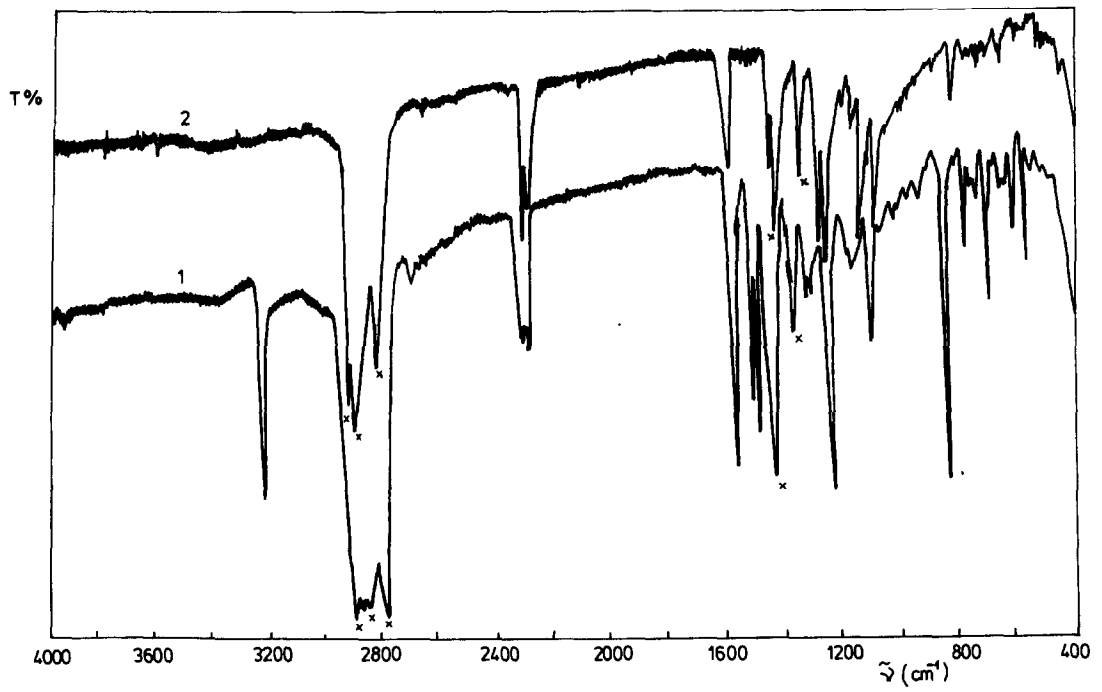

Fig. 5. The IR spectra of the reagent (1) and of the methylmercury complex (2). The samples were prepared as nujol mulls. The bands of nujol are marked by x on the spectra.

also be used for determining methylmercury gravimetrically.

Verification of the validity of Beer-Lambert's law

The procedure used was similar to that already described. The spectra obtained for the complex-containing solutions, recorded by using as reference a comparison sample, are given in Fig. 7; the variation of the absorbance as a function of concentration is also given. The value of the molar absorptivity is of 3.46×10^4 $l \cdot mole^{-1} \cdot cm^{-1}$. By using 1-cm thickness cells, methylmercury can therefore be determined in the range 0.025–4 ppm.

Interferences

Based on the detailed study of the interferences occurring in the determination of mercury(II) with the considered reagent, described in Ref. 19, one can estimate that the errors which may affect the methylmercury determination are less than 3% for [ion]/[H_3CHg^+] ratios larger or equal to 1000 for the ions: Li^+, Na^+, K^+, Fe^{3+}, Co^{2+}, Ni^{2+}, Be^{2+}, Mg^{2+}, Sr^{2+}, Ba^{2+}, Zn^{2+}, Cd^{2+}, Ga^{3+}, In^{3+}, Tl^+, UO_2^{2+}, Pb^{2+}, SO_4^{2+}, citrate and tartrate, larger or equal to 500 for the ions: Cu^{2+}, Bi^{3+}, Cr^{3+}, Mn^{2+} and CrO_4^{2-}, and larger or equal to 100 for the ions Rh^{3+}, Au^{3+}, Pd^{2+} and Pt^{4+}. The ions: Hg^{2+}, Hg_2^{2+}, Cl^-, Br^-, I^-, SCN^-, CN^- and S^{2-} do interfere, either by forming complexes with the reagent, or precipitating or complexing the methylmercuric ion. The Ag^+ ion interferes by forming a red complex with the reagent, but which can only be extracted with difficulty in toluene. Its interference can be eliminated by precipitation as silver(I) chloride, but the excess of Cl^- ions must be avoided. The interference of the Hg^{2+} and Hg_2^{2+} can be eliminated by their prior reduction with stannous chloride[9]. The H_3CHg^+ ion is stable under these conditions. The cations were introduced as nitrates, sulphates or acetates, and the anions as salts with alkali metals.

There are also other organomercuric compounds, such as $C_2H_5Hg^+$ and $C_6H_5Hg^+$, which react with Cadion with interferences. However, literature data[1,2] suggest that in samples in which methylmercury is usually determined (biological products, some foodstuffs) mercury is found only as inorganic compounds and as CH_3Hg^+. This is because methylmercury is a compound which forms even in living organisms from inorganic mercury.

We used cold-vapour atomic-absorption spectrometry as a reference method for comparing our results;[25] in this method reduction of

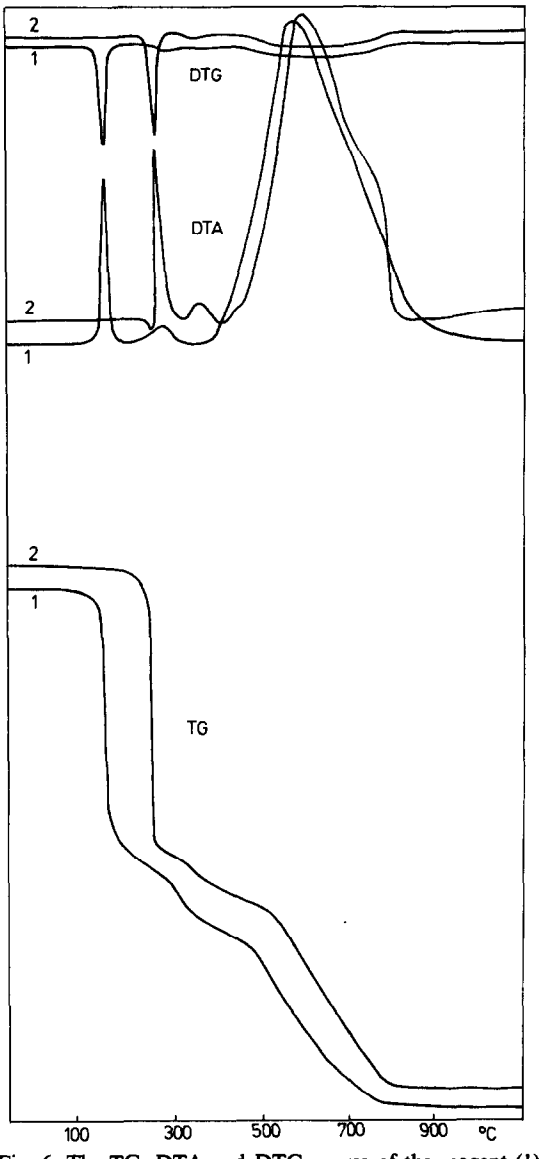

Fig. 6. The TG, DTA and DTG curves of the reagent (1) and of the methylmercury complex (2).

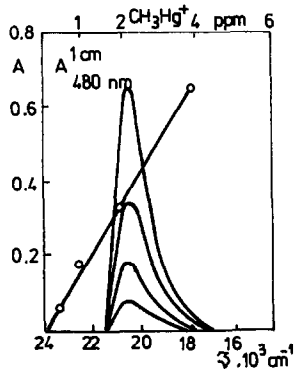

Fig. 7. The absorption spectra of the samples which contain the complex, vs. a reference sample, and the calibration curve used for determining methylmercury.

methylmercury is made with sodium borohydride. The results obtained by these methods are in good agreement.

CONCLUSIONS

The partition constants of the reagent, of its complex with the methylmercuric ion, and of methylmercury chloride were determined in the system toluene-aqueous phase containing 40 vol.% methyl alcohol. The optimum wavelength for carrying out the determinations were found based on the UV/Visible absorption spectra of the reagent and of its methylmercury complex. The extraction constant was determined from the half-extraction pH value and the formation constant of the methylmercury complex was estimated by two different methods, taking into account the main competing equilibria occurring in the aqueous phase and upon extraction. Based on the IR spectra and taking into account the value of the reagent/H_3CHg^+ combination ratio, the type of bonding of H_3CHg^+ ion to the reagent molecule could be determined. The range of thermal stability of the reagent and of the complex was established based on their derivatograms. The investigated reagent allows the determination of the methylmercuric ion with good sensitivity and high selectivity.

Even though the proposed method for determining methylmercury is less sensitive than the method based on the reduction of mercury and its determination by cold-vapour atomic absorption it has some advantages. Thus, a preliminary separation of methylmercury by extraction in benzene or toluene[26,27] could be carried out for typical samples (biological products, some foodstuffs). After separation, methylmercury can be determined directly in the organic phase by contacting it with an aqueous phase containing the reagent and then applying the described manner of analysis. The determination by atomic absorption is much more difficult in this case, since it requires the removal of the organic solvent (during which losses of mercury may occur) and the oxidation of methylmercury to inorganic mercury. The method of determining methylmercury described in this paper has been applied for determining this compound in seafish,[28] after its preliminary separation by distillation from the samples to be analyzed.[29]

REFERENCES

1. R. Hartung and B. D. Dinman, *Environmental Mercury Contamination*, Ann Arbor Science Publishers, Ann Arbor, 1972.
2. P. A. D'Itri and F. M. D'Itri, *Mercury Contamination: A Human Tragedy*, Wiley, New York, 1977.
3. G. Schwarzenbach and M. Schellenberg, *Helv. Chim. Acta*, 1965, **48,** 28.
4. S. Libich and D. L. Rabenstein, *Anal. Chem.*, 1973, **45,** 118.
5. D. L. Rabenstein, M. C. Tourangeau and Ch. A. Evans, *Can. J. Chem.*, 1976, **54,** 2517.
6. D. L. Rabenstein, *Acc. Chem. Res.*, 1978, **11,** 100.
7. O. Budevski, F. Ingman and D. H. Liem, *Acta Chem. Scand.*, 1973, **27,** 1277.
8. M. Jawavd, F. Ingman, H. D. Liem and T. Wallin, *ibid.*, Ser. A, 1978, **A32,** 7.
9. C. Luca, I. Tănase, A. F. Dănet and I. Ioneci, *Rev. Anal. Chem.*, 1987, **9,** 1.
10. D. L. Collett, D. E. Fleming and G. A. Taylor, *Analyst*, 1980, **105,** 897.
11. J. Ireland-Ripert, A. Bermond and C. Ducauze, *Anal. Chim. Acta*, 1982, **143,** 249.
12. W. K. Panaro, D. Erickson and I. S. Krull, *Analyst*, 1987, **112,** 1097.
13. D. S. Bushee, *ibid.*, 1988, **113,** 1167.
14. Ch. J. Cappon and J. Cr. Smith, *Anal. Chem.*, 1980, **52,** 1527.
15. R. Ahmed and M. Stoeppler, *Analyst*, 1986, **111,** 1371.
16. P. Lansens, C. Meuleman and W. Baeyens, *Anal. Chim. Acta*, 1990, **229,** 281.
17. A. F. Dănet, R. Dreptu and Gh. Nicolae, *Rev. Roum. Chim.*, 1979, **24,** 1229.
18. A. F. Dănet and A. M. Bercaru, *ibid.*, 1982, **27,** 459.
19. Gr. Popa, A. F. Dănet and M. Popescu, *Talanta*, 1978, **25,** 546.
20. A. F. Dănet, A. M. Bercaru and M. Popescu, *Rev. Chim. (Bucharest)*, 1982, **33,** 1133.
21. T. V. Ershova, E. C. Ruhadze and A. P. Terentiev, *Zh. Obshch. Khim.*, 1969, **39,** 59.
22. P. Chavanne and Cl. Geronimi, *Anal. Chim. Acta*, 1958, **19,** 442.
23. H. M. N. H. Irving and A. M. Kiwan, *ibid.*, 1969, **45,** 255.
24. J. Stary, K. Kratzer and J. Prasilova, *ibid.*, 1978, **100,** 627.
25. C. Luca, A. F. Dănet and C. Radu, *Rev. Chim. (Bucharest)*, 1985, **36,** 856.
26. S. C. Hight, *J. Assoc. Off. Anal. Chem.*, 1987, **70,** 667.
27. S. C. Hight and M. T. Corcoran, *ibid.*, 1987, **70,** 24.
28. A. F. Dănet and V. David, *Bul. Inst. Politeh. Bucureşti*, 1991, in the press.
29. L. W. Margler and R. A. Mah, *J. Assoc. Off. Anal. Chem.*, 1981, **64,** 1017.
30. R. G. Bates, *Determination of pH*, Wiley, New York, 1964.

Talanta, Vol. 39, No. 10, pp. 1307–1312, 1992
Printed in Great Britain.

0039-9140/92 $5.00 + 0.00

EXTRACTION OF Fe(III), Cu(II), Co(II), Ni(II) AND Pb(II) WITH THENOYLTRIFLUOROACETONE USING THE TERNARY SOLVENT SYSTEM WATER/ETHANOL/METHYLISOBUTYLKETONE

JOSÉ F. DA SILVA
Universidade do Amazonas, Manaus, Amazonas, Brazil

WALTER MARTINS*
Instituto de Química, Unicamp, C.P. 6154 13.081 Campinas, SP, Brazil

(*Received* 8 *October* 1991. *Revised* 26 *February* 1992. *Accepted* 29 *February* 1992)

Summary—Single-phase solutions ($1.72 \times 10^{-2} M$ in TTA) of water/ethanol/MIBK, when added to an excess of water, break down into two immiscible liquid layers and TTA complexes of Fe(III), Co(II), Ni(II), Cu(II) and Pb(II) are extracted into the organic layer. Quantitative extractions were obtained for the five metals and separations of Fe(III) from a 1000-fold excess of Co(II), Ni(II) or Pb(II) are obtained. The reactions of the metal ions with TTA were studied in the single-phase solutions before the extraction step, giving useful information as to their complexation behavior.

Several liquid–liquid extraction methods using the phenomenon of phase separation have appeared from time to time in the literature. The authors of these methods have made use of diverse physicochemical procedures in order to obtain phase separations.

The homogeneous extraction method of Murata and Ikeda,[1] in which a liquid phase of propylene carbonate coalesces with an aqueous phase at 80°, could extract Mo, after phase separation at room temperature, as an ion association complex.[2]

Workers have also studied the immiscibilization of some otherwise water-miscible solvents. By the use of the salting out effect, Matkovich and Christian[3] were able to separate an acetone phase, which is totally miscible with water, by saturating the aqueous phase with sucrose or any of a series of salts; Nagaosa[4] and Fujinaga and Nagosa[5] separated an acetonitrile phase, and verified the possibility of performing extractions of metal ions.

There is also the procedure of Fujinaga *et al.*[6] who used, instead of the salting out effect, the addition of a small volume of a third solvent to promote the separation of an immiscible ternary phase, made up almost entirely of the water-miscible solvent.

Finally, there is the single-phase technique in which an aqueous phase (A) is made totally miscible with an extractor solvent (B; *e.g.*, benzene, cyclohexane or MIBK), by the addition of a consolute solvent (C) such as acetone or ethanol. After preparing this single-phase solution, the homogeneous system is broken down by the addition of an excess of water, thus separating the solution into two liquid layers. Belcher *et al.*[7] made use of this extraction to obtain an organic phase containing the chelate of interest; nevertheless, they used the technique only in a preparative way, in order to obtain an organic extract for injection in a gas chromatograph. Our study, on the other hand, was primarily directed to the use of the process as an analytical technique.[8]

Although the last two cited techniques, the one of Fujinaga *et al.*[6] and the single-phase, seem to be similar, they are nevertheless quite different. In the former process, an auxiliary solvent must be empiricallly chosen and a volume phase diagram must be constructed[9] in order to determine the small volume of this solvent to be added to the one-phase, binary solution in order to separate the system into two well-defined phases, thus bringing about the extraction. In the single-phase technique a specific auxiliary solvent is not needed nor is it necessary to construct a (volume) phase

*Author for correspondence.

diagram. The system starts in the one-phase region of a ternary diagram, with a mixture of the three components, and by adding a large amount of water, we bring the system to the two-phase region where the extraction occurs. Therefore, the single-phase procedure is applicable to any three A, B and C solvents, defined as above.

To our knowledge, few practical applications[10] have been made for any of the extraction systems mentioned above, although a drastic difference in metal ion extraction is known to exist when they are compared to the conventional binary technique.

This paper reports a study of some practical applications for the single-phase method. From low-acidic single-phase solutions all five metals are extracted together into MIBK by the use of thenoyltrifluoroacetone (TTA), a fact that may be useful in group separations of metal ions, while from high-acidic single-phase solutions, iron(III) is separated from a 1000-fold excess of cobalt(II), nickel(II) and lead(II).

EXPERIMENTAL

Apparatus

A Zeiss atomic-absorption spectrophotometer model FMD-3 was used for the metal ion determinations and a UV–V Zeiss PMQ-II spectrophotometer was used for the photometric measurements with 10- and 50-mm quartz cells. Electrometric measurements were made with a Metrohm E-517 pH meter with a combined set of glass and calomel electrodes. A piston-microburette from Metrohn, using a 0.5000-ml tip, was used to deliver the metal ion solutions.

Reagents

Thenoyltrifluoroacetone, used without further purification, and methyl isobutyl ketone (MIBK) were analytical grade reagents from Carlo Erba.

The metal ion solutions were prepared from the pure metal (Baker), with the exception of cobalt which was prepared from cobalt(II) chloride, dried twice to fumes with nitric acid and standardized by titration with EDTA solution. All solutions contained *ca.* 2000 μg/ml of metal ion and have a pH near 1.

Metal ion cocktail solution. In a steam bath, 100-ml aliquots of the five metal ion solutions were evaporated to dryness and then transferred to a 100-ml standard flask. Enough nitric acid was added in order to make the pH *ca.* 1.

Phase titrations. Solutions (5 ml) of two miscible solvents, either MIBK/ethanol or water/ethanol, were titrated with the third solvent until the appearance of a turbidity, characteristic of the point of opalescence. These titrations were made at room temperature, since the objective was only to verify the position of the two regions of interest, namely those of the single-phase and of the system after phase separation.

Procedure to single-phase extraction. To 2 ml of water, the desired amount of the metal ion solution plus 10 drops of concentrated nitric acid were added, followed by the addition of 7.5 ml of ethanol and 5 ml of MIBK containing TTA. The acidity was adjusted to the desired value, first with concentrated and then with diluted ammonium hydroxide solutions while reading the pH_{sp} (see below) with a pH meter.

Single-phase solutions were always prepared by adding the solvents in the order given above, so as to have at all times a homogeneous solution.

In the extraction step, the prepared single-phase solution (a, in Fig. 1) was added through a filtration funnel (b), which had its bore reduced so as to deliver 30 ml of water in *ca.* 20 sec, to 80 ml of water in a pear-shaped separatoring funnel (c) that had its top removed at the point of its maximum circumference.

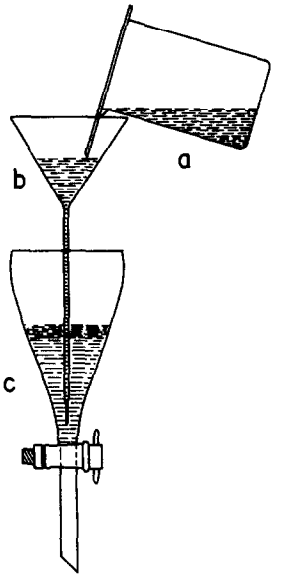

Fig. 1. Set-up for single-phase extractions. Single-phase solution in *a* is delivered through *b* into 80 ml of water at 40° (*c*).

In the successive extractions, after the initial one, 80 ml of water were poured into the funnel from a beaker with the help of a glass rod. The temperature of the separating water was always 40°.

RESULTS AND DISCUSSION

Acidity scale in single-phase solution

Many authors express the acidity of aquo-organic solutions for analytical purposes by nominal pH value. Thus, the pH readings of mixtures of water and acetone of high ionic strengths have been denoted by Matkovich and Christian as a nominal scale.[3] We will use the same procedure in this work but in order to avoid confusion, we shall designate this nominal pH scale as the pH_{sp}, which means that it refers exclusively to readings taken from the single-phase solutions.

Phase diagram of the water/ethanol/MIBK system

The results from the phase titrations were plotted on a ternary Roozeboom[11] diagram (Fig. 2). Point A in the diagram represents the single-phase solution we used in our work, and point B represents the two-phase region of the system after phase separation with water. Point A is well inside the one-phase region, so we can safely add aqueous acids or base solutions without the risk of starting an incipient phase separation. These results were obtained at room temperature, but separations of the single-phase solution with water at 30 and 40° also gave the same volume of the organic (MIBK) phase,

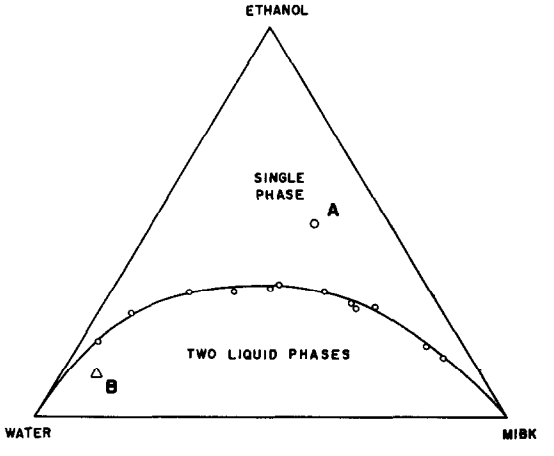

Fig. 2. Ternary phase-diagram for water/ethanol/methylisobutylketone. Point A: single-phase solution used in this work; point B: localization of the system after phase separation with water.

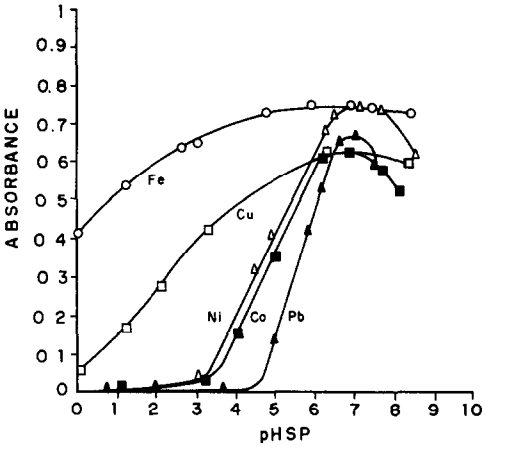

Fig. 3. Complexation curves of Fe, Cu, Ni, Co and Pb in single-phase solution. TTA: $1.72 \times 10^{-2}M$. Metal ions 500 μg each.

indicating that the system is not much affected by this change in temperature.

Complexation curves

An interesting feature of single-phase extractions is that we can normally follow the complexation of the metal ion in the single-phase solution by monitoring a suitable wavelength in which the complex is the only absorbing species. This permits one to study the complexation of each metal ion. To obtain these curves, a series of single-phase solutions with diverse pH_{sp} were prepared and their absorbances were measured in a spectrophotometer. The complexation curves of iron(III), cobalt(II), nickel(II), copper(II) and lead(II) (Fig. 3) show that iron is readily complexed at low acidities and that all complexation curves attain a maximum around pH_{sp} 5.5–7.

To construct the curves, absorbance readings in the range of 400–420 nm were used where the absorption of TTA is quite low and the metal ion complexes have their maximum. The TTA concentration in the single-phase solutions was $3.4 \times 10^{-2}M$. The complexation with TTA in single-phase solutions are very fast, a fact that has already been observed,[8] and specifically in the case of strongly coloured complexes like that of iron, it can be seen visually that as soon as a base is added to an acidic single-phase solution it becomes immediately coloured, the intensity depending, of course, on the amount of metal ion present.

Extraction curves

Extraction curves for the five metals studied are presented in Fig. 4. If we compare these

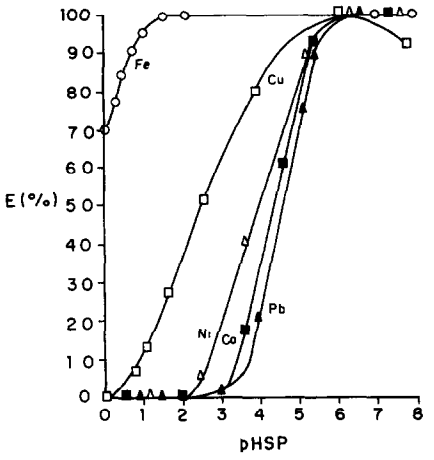

Fig. 4. Extraction curves of Fe, Cu, Ni, Co and Pb. SP solution separated with 80 ml of water at 40°. TTA: $1.72 \times 10^{-2}M$. Metal ions 500 μg each.

curves with the complexation curves, we can see some differences in behavior worth noting. Iron increases its complexation with TTA from pH_{sp} 0 up to pH_{sp} 5–6, while its extraction is already quantitiative at pH_{sp} 1.5. The extraction curve for copper lies between that of iron and those of the other metal ions and has its complexation decreased during the extraction step: its extraction is zero at pH_{sp} zero, while its absorbance at this pH_{sp} values is already more than 0.05. Around pH_{sp} 6, all metals are quantitatively extracted.

The behavior of these metals relative to MIBK and TTA, in the conventional, two-phase solvent extraction[12] and in the single-phase technique is similar: the order of extraction is about the same, Fe–Cu then Ni–Co and then Pb (in the conventional technique the pH of 50% extraction for each is respectively: 1.7–1.6, 3.3–3.8 and 4.0). The only important difference is that in single-phase extraction, the curve of Fe is quite far from that of Cu and also from those of Ni–Co, while in the conventional extraction they are much closer, those of Fe and Cu being almost superimposed.

Extractions

Successive extractions. After the initial single-phase extraction, the volume of the aqueous phase is very large (the phases were separated with 80 ml of water) so it would be time consuming to make a second extraction of the aqueous phase since one should reduce its volume to 2 ml again. Nevertheless, it is simple and in some cases advantageous to extract the organic phase again. If we add 7.5 ml of ethanol plus 2 ml of water, to this organic phase, and adjust the pH_{sp} to the same value as before, we have regenerated the single-phase solution. This new single-phase solution contains the metals extracted in the first organic layer, but now the metals are again dispersed in the single-phase solution, so that if we again perform a phase separation, it is proper to call it "a second single-phase extraction from the organic phase". This regeneration may be executed several times, as indicated in Fig. 5.

Performance of the successive extractions. If a metal A is highly extracted and another B poorly extracted, the application of the successive extractions on the organic phase will lead to purification of A from B. It was important to know whether these subsequent extractions, following a quantitative extraction, would still be quantitative. We have used Ni as a test, at a pH_{sp} of 6, and it was extracted consecutively four times, giving a total recovery of more than

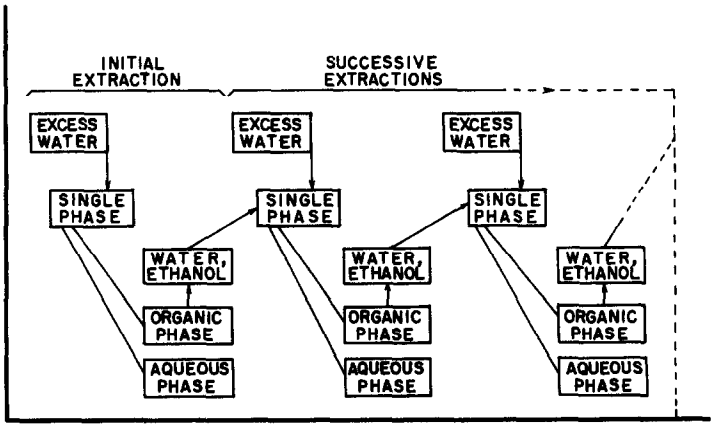

Fig. 5. Block diagram showing the procedure to perform the successive single-phase extractions from the organic phase.

Table 1. Single-phase extraction of metal ions as a function of the TTA concentration. Amount: 500 μg each

Acidity (pH_{sp})	TTA, M ($\times 10^3$)	E%				
		Fe	Co	Ni	Cu	Pb
1.5	34.5	>99	0.0	0.0	32	0.0
	17.2	>99	0.0	0.0	16	0.0
	3.45	>44	0.0	0.0	0.0	0.0
6.4	34.5	>99	>99	>99	>99	>99
	17.2	>99	>99	>99	>99	>99
	3.45	86	51	82	95	18

99.8%. This result justifies the use of the successive extractions from the organic phase in order to promote metal ion separations.

Extractions varying the TTA concentration. At pH_{sp} 6.4 and for TTA concentrations of 3.45×10^{-2} (I) and $1.72 \times 10^{-2}M$ (II) in the single-phase solution, all the studied metals are quantitatively extracted; the extraction being reduced only when the TTA concentration is ten times smaller (III) than I (Table 1).

When the pH_{sp} is lowered to 1.5, only iron continues to show quantitative results for TTA concentrations I and II and the extraction of the other metals is near zero, with the exception of copper which presents and intermediate extraction (16–32%); for the lowest TTA concentration, even iron is not quantitatively extracted (44%).

These results are confirmed when use is made of the cocktail solution employing TTA concentrations I and II; at pH_{sp} 1.5, iron is completely extracted, copper only partially (16–32%) and the other metals are not extracted, while at pH_{sp} 6.4, the extraction is quantitative for all metals.

Therefore, for Co(II), Ni(II) and Pb(II) in the range of a few hundred micrograms, Fe(III) is completely separated with just one single-phase extraction. Cu(II) can also be separated from Fe(III) if a series of four successive single-phase extractions from the organic phase is done after the initial one, its amount then being reduced to 0.2%.

Table 2. Separation of iron from a thousand-fold excess of Co, Ni or Pb with TTA by single-phase extractions (initial extraction followed by three more extractions from the organic phase). Fe: 100 μg. Co, Ni and Pb 100 mg each. TTA: $1.72 \times 10^{-2}M$. pH_{sp}: 2.1

Pair	E%			
	Fe	Co	Ni	Pb
Fe/Co	>99	<0.01	—	—
Fe/Ni	>99	—	<0.01	—
Fe/Pb	>99	—	—	<0.02

Separation of iron from large amounts of cobalt, nickel and lead. Table 2 shows the results for single-phase extractions of the pairs Fe/Co, Fe/Ni and Fe/Pb. They were made by taking 100 μg of Fe(III) and a thousand-fold excess (100 mg) of the other metals with a TTA concentration of $1.72 \times 10^{-2}M$ and a pH_{sp} value of 2.1. The initial single-phase extraction was followed by three additional successive single-phase extractions from the organic phase; the percent extraction of iron amounted to 99% while those of cobalt and nickel dropped to less than 0.01%, and that of lead to 0.02%.

CONCLUSION

One disadvantage of the method is that the single-phase solutions do not allow us to deal with concentrated solutions of any salt and that some species such as sulfates, phosphates and EDTA have a reduced solubility.

As to the applications, many colorimetric methods for the determination of iron call for a very reduced amount of Co and Ni as contaminants[13] and the single-phase technique could be used with advantage in such cases. The method is quite simple and fast. On the other hand, when extractions are done at high pH_{sp} values (around 6) it is possible to pass all the five studied metals to the MIBK phase, which may be interesting in the case where we want to extract a group of metal ions together. Studies are under way to verify how many other metal ions could be extracted together at this same pH_{sp}, and then to re-extract them selectively.

Acknowledgements—We are indebted to Fred Fujiwara for correcting and improving the manuscript, and one of us (FJS) is grateful for a grant from CAPES, a government agency of Brazil.

REFERENCES

1. K. Murata and S. Ikeda, *Bunseki Kagaku*, 1969, **18**, 1137.

2. *Idem, J. Inorg. Nucl. Chem.*, 1970, **32,** 267.
3. C. E. Matkovich and G. D. Christian, *Anal. Chem.* 1974, **46,** 102.
4. Y. Nagaosa, *Mikrochim. Acta*, 1979 **I,** 495.
5. T. Fujinaga and Y. Nagaosa, *Bull. Chem. Soc. Japan*, 1980, **53,** 416.
6. T. Fujinaga, A. Shuhara and T. Hori, *Bunseki Kagaku*, 1984, **33,** 159.
7. R. Belcher, R. J. Martin, W. I. Stephen, D. E. Henderson, A. Kamalizad and P. C. Uden, *Anal. Chem.*, 1973, **45,** 1197.
8. W. Martins, Ph.D. thesis, Unicamp, 1974.
9. T. Hori and T. Fujinaga, *Talanta*, 1985, **32,** 735.
10. V. I. Kofanov and L. V. Nevinnaya, Paper presented at IInd URSS-Japan Symposium Anal. Chem., Moscow, 1984.
11. W. J. Moore, *Physical Chemistry*, 2nd Ed., p. 153. Prentice-Hall, Englewood Cliffs, N.J., 1959.
12. W. M. Jackson and G. I. Gleason, *Anal. Chem.*, 1973, **45,** 2125.
13. S. Bhattacharya, S. K. Roy and A. K. Chakraborty, *Talanta*, 1990, **37,** 1101.

Talanta, Vol. 39, No. 10, pp. 1313–1316, 1992
Printed in Great Britain.

0039-9140/92 $5.00 + 0.00

DETERMINATION OF CARBOHYDRAZIDE AT TRACE AND SUBTRACE LEVELS

M. BLANCO,* J. COELLO, H. ITURRIAGA, S. MASPOCH and E. ROVIRA

Departamento de Química, Unidad de Química Analítica, Facultad de Ciencias, Universidad Autónoma de Barcelona, E-08193 Bellaterra, Barcelona, Spain

(*Received* 20 *January* 1992. *Revised* 23 *March* 1992. *Accepted* 3 *April* 1992)

Summary—We developed three analytical methods for the determination of carbohydrazide at different concentration levels. One involves the volumetric titration of the analyte with bromate ion and dead-stop end-point detection, and is applicable to concentrations above 10 mg/l., so it can be used for standardizing carbohydrazide solutions. A second, spectrophotometric method is based on the reduction of Fe(III) and measurement of the absorbance of the Fe(II)–ferrozine complex, and features an applicability range of 25–700 μg/l. carbohydrazide. The third method uses differential pulse polarography and the oxidation of carbohydrazide in a basic medium at a dropping mercury electrode to determine the analyte. This last method is the most sensitive of the three and also that offering the widest determination range: from 4 to 3000 μg/l. carbohydrazide.

Carbohydrazide is a hydrazine derivative that frequently replaces hydrazine as oxygen scavenger for all types of boiler. Its reaction with oxygen is similar to that of hydrazine, though somewhat more complex; in fact, the numerous intermediate steps involved in the deoxygenation of carbohydrazide result in higher reactivity and improved metal passivation. Unlike hydrazine, which is a suspected carcinogen, carbohydrazide is not toxic.

A literature scan revealed no analytical reports on carbohydrazide itself, and only a few papers on hydrazine providing some analytical information on carbohydrazide among a few derivatives of the parent compound.[1–4] There was thus an obvious need for methods allowing the determination of carbohydrazide not only at the high concentrations typically found in steam generation systems, but also at the lower concentrations encountered in boilers.[5,6]

In this work we determined carbohydrazide at different concentration levels by a titrimetric, a spectrophotometric and a differential pulse polarographic (DPP) method. The titrimetric method relies on the oxidation of the analyte by BrO_3^- with dead-stop end-point detection.[7] While using a coloured dye would seem appropriate, the fact that the analytical reaction is often slower than the indicator reaction in dilute solutions may result in the indicator being decomposed before the equivalence point is reached, thereby introducing a negative error in the determination. The spectrophotometric method is based on the reducing power of carbohyrazide, which yields the coloured complex Fe(II)–ferrozine with clearly higher sensitivity than other chromophores. Finally, the DPP method entails the oxidation of carbohydrazide at a dropping mercury electrode under conditions where the analyte is electroactive.

EXPERIMENTAL

Reagents

The solutions used in this work included the following: 0.1/6*M* potassium bromate, prepared by weighing from commercially available AR grade reagent (As_2O_3 can be used alternatively for standardization by biamperometric titration); 1 g/l. potassium bromide; 50 mg/l. iron (III), prepared by weighing from Merck iron (III) nitrate [$Fe(NO_3)_3 \cdot 9H_2O$]; aqueous 0.3% w/v ferrozine [3-(2-pyridyl)-5,6-bis(4-phenylsulphonic acid)-1,2,4-triazine]; and 1000 mg/l. stock carbohydrazide from Fluka, standardized with Merck AR grade $KBrO_3$.

All other chemicals used were Merck AR grade.

Apparatus

Biamperometric measurements were made with a Radiometer PHM29b pH-meter (polarization voltage 0–700 mV) furnished with a

*Author for correspondence.

Radiometer PP1311 dual platinum electrode. Spectrophotometric measurements were made on a Hewlett-Packard HP8451A diode array spectrophotometer. Finally, all polarographic measurements were made on a Metrohm Polarecord E506 instrument fitted with a VA E663 stand, also from Metrohm.

Procedure

Titrimetric determination. Once the polarization voltage of the pH-meter has been set to 50 mV, to 25 ml of the carbohydrazide solution are added 10 ml of potassium bromide and 4 ml of 6*M* hydrochloric acid, and the mixture is titrated with 0.1/6*M* potassium bromate. The end-point of the titration is signalled by a potential jump from 50 to *ca.* 300 mV. Very dilute carbohydrazide solutions are best titrated by using more dilute potassium bromate and adding 80–90% of the estimated titrant volume required at once and then continuing to add it more gradually in the vicinity of the equivalence point.

Spectrophotometric determination

A volume of 15 ml of the carbohydrazide stock solution, 2 ml of ferrozine and 2 ml of the Fe(III) solution are mixed and the pH of the mixture is adjusted to 1.6–1.9 with diluted sulphuric acid. Then, the mixture is heated in a water bath at 80–90° for 10 min and allowed to cool to room temperature, after which the pH is adjusted to 3.2 with sodium acetate and the mixture is finally transferred into a 25-ml standard flask. The absorbance of the mixed solution is measured at 562 nm against a blank containing all of the mixture ingredients except carbohydrazide.

The pertinent calibration graph is constructed by using carbohydrazide standards of known concentration.

Polarographic determination

The polarographic determination of hydrazide is carried out with an Ag/AgCl/KCl (3*M*) reference electrode and a platinum auxiliary electrode by using a drop time of 0.8 sec, a scan rate of 1.25 mV/sec and a pulse height of 70 mV.

The recording baseline is obtained by polarographing a solution of 25 ml of distilled water plus 2 ml of 0.5*M* sodium hydroxide between 0.4 and 0.1V after bubbling nitrogen through it for *ca.* 15 min. Then, the carbohydrazide solution is deoxygenated by passing N_2 for 5 min and the corresponding polarogram is recorded. A calibration graph is finally constructed by plotting the peak height against the concentration.

RESULTS AND DISCUSSION

Titrimetric determination

The chemical reactions involved in the redox titrimetric determination of carbohydrazide with bromate are as follows:

$$CO(NHNH_2)_2 + H_2O - 8e^- \rightleftarrows CO_2 + 2N_2 + 8H^+ \quad (1)$$

$$BrO_3^- + 6H^+ + 6e^- \rightleftarrows Br^- + 3H_2O \quad (2)$$

$$2Br^- - 2e^- \rightleftarrows Br_2 \quad (3)$$

Half-reactions (1) and (2) represent the titration process, while (3) corresponds to the end-point detection by the dead-stop end-point technique.

The process is quite slow for dilute carbohydrazide solutions, but can be expedited by initially adding 80–90% of the estimated titrant volume required and then continuing to add it dropwise at 20-sec intervals in the vicinity of the end-point.

The lower limit of determination of this method is 10 mg/l. carbohydrazide.

Table 1 lists the percent recoveries obtained in the titration of different analyte concentrations by using various titrant concentrations. As a rule, the method results in errors less than 2% for samples with concentrations of *ca.* 10 mg/l. As can be inferred from Table 1, the titrant solution should be very dilute—otherwise, the end-point is detected before the equivalence point and a negative error is introduced in the results. The influence of the titrant concentration decreases with increasing carbohydrazide concentration. Thus, recoveries from 25 mg/l. solutions of carbohydrazide are quite good whether 0.025/6 or 0.10/6*M* titrant is used.

Spectrophotometric determination

We optimized the conditions for the colorimetric determination of carbohydrazide by using

Table 1. Percent carbohydrazide recoveries obtained under different titration conditions

$[CO(NHNH_2)_2]$ *mg/l.*	$[KBrO_3]$ $M \times 6$	Number of titrations	Recovery %
100	0.1	6	100.7 ± 1.6
25	0.1	5	101.1 ± 2.2
25	0.025	9	98.2 ± 2.3
10	0.1	6	95.7 ± 4.2
10	0.025	4	98.9 ± 2.0

the univariate method to study the influence of the Fe(III) and ferrozine concentrations, temperature, reaction time and pH. The Fe(III) concentration was found not to alter the results provided the ion was in excess over carbohydrazide. We thus used Fe(III) solutions 100 times more concentrated than those of carbohydrazide and ferrozine solutions in 10-fold excesses over those of Fe(III). Beyond these concentrations the blank signal was too tall for practical purposes.

The temperature was found to have a marked effect on the reaction rate. We chose 80–90° as a compromise.

Under the above conditions, the reaction time had no appreciable effect after 5 min, so we chose 10 min as optimal.

Finally, the optimum pH for the reduction of Fe(III) was found to be 1.6–2.0. Since the maximum sensitivity to the complex was obtained at pH 3.2,[8] the pH of the medium was adjusted to this value with sodium acetate immediately after ferric ion was reduced.

The calibration graph obtained by plotting the absorbance at 562 nm of various carbohydrazide standards against their concentration conformed to the following equation

$$A = -0.0017(\pm 0.0049) + 6.08(\pm 0.13) \times 10^4 C$$

$$(r = 0.99993)$$

where C is expressed in M. Beer's law was obeyed over the range 25–700 μg/l. and the detection limit achieved was 10.7 μg/l.

We determined the molar absorptivity of the Fe(II)-ferrozine complex from the calibration curve obtained by reducing Fe(III) with hydroxylamine,[8] which was found to be $3.2(\pm 0.6) \times 10^4$ l.mol^{-1} cm^{-1}. Therefore, on the basis of reaction (1) as theoretical reference for the oxidation of carbohydrazide, the yield achieved was 24%. Improving the yield beyond this limit could only be accomplished at the expense of increased blank absorbance and hence of a higher the detection limit.

Polarographic determination

We carried out a preliminary study of the electroactivity of carbohydrazide at a dropping mercury electrode by recording a single oxidation wave in an alkaline medium. We used the differential pulse technique in order to ensure a high sensitivity. This provided two polarographic peaks at −0.304 and −0.230 V (Fig. 1). Only the height of the former was proportional to the analyte concentration at subtrace levels, so this peak was chosen for quantitation purposes.

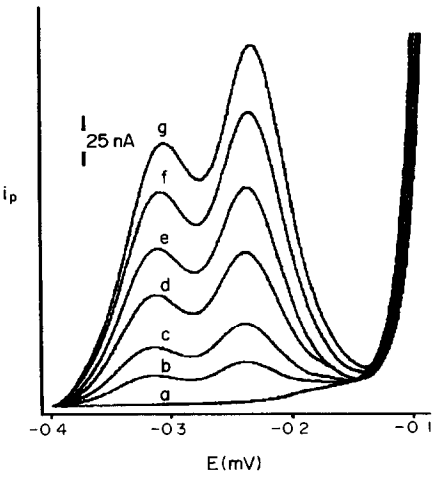

Fig. 1. Differential pulse polarograms of blank (a), 0.36 (b), 0.69 (c), 1.29 (d), 1.82 (e), 2.50 (f) and 3.08 (g) mg/l. solutions of carbohydrazide. Recording sensitivity = 2.50 nA/cm.

Figures 1 and 2 show the polarographic recordings obtained at various instrumental sensitivities from a series of calibration samples containing different amounts of carbohydrazide.

We studied the influence of the sodium hydroxide concentration and various instrumental parameters on the peak height. As far

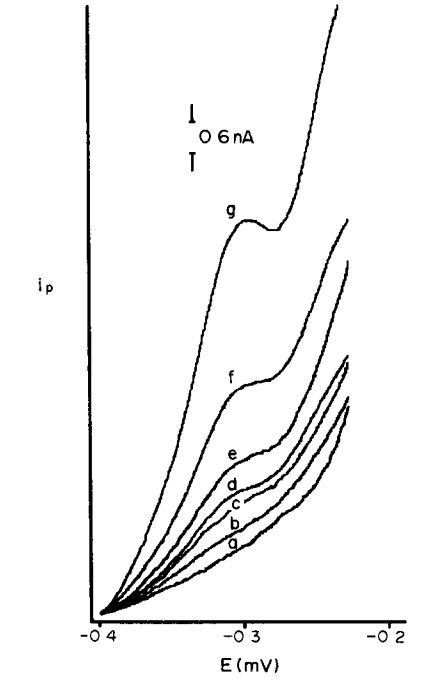

Fig. 2. Differential pulse polarograms of blank (a), 3.57 (b), 6.90 (c), 10.00 (d), 12.90 (e), 25.00 (f) and 51.35 (g) μg/l. solutions of carbohydrazide. Recording sensitivity = 0.06 nA/cm.

Table 2. Figures of merit of the polarographic calibration curves

Recording senstivity (nA/cm)	Concentration range (μg/l)	Regression equation $I_p = a + bC$ (I_p, nA; C, μg/l)	Regression coefficient	Regression standard deviation, $S_{y/x}$
0.06	3.6–51.4	$I_p = -0.075(\pm 0.174) + 0.120(\pm 0.007)C$	0.9993	0.09
0.10	37.2–82.0	$I_p = 0.048(\pm 1.096) + 0.110(\pm 0.018)C$	0.9998	0.09
0.15	100.0–235.0	$I_p = -0.181(\pm 1.529) + 0.106(\pm 0.009)C$	0.9999	0.11
2.50	360.0–3080	$I_p = -4.268(\pm 4.133) + 0.094(\pm 0.002)C$	0.9999	1.62

as the base concentration is concerned, the peak sensitivity increased with increasing concentration up to a maximum value. The scan rate influenced the baseline features, so the chosen working value was a compromise between smoothness and rapidity. Increasing pulse heights resulted in increased signal sensitivity up to a limit above which the resolving power started to decline. The optimal values of the different variables were given above.

Once the optimal working conditions were established, we ran a calibration graph for carbohydrazide concentrations between a few μg/l. and a few mg/l. Table 2 lists the equations and figures of merit of the four calibration curves obtained from the polarograms of 21 standards containing between 3.6 and 3080 mg/l. carbohydrazide. A random residual distribution was used in every case. The detection limit achieved[9] was 2.2 μg/l. As can be seen, the calibration curves were of a high quality and encompassed a few orders of magnitude in the concentration.

According to the reproducibility results obtained at the subtrace level, recordings made on different days or sensitivity scales resulted in small variations in the calibration curves, so standards and samples should be measured under similar instrumental conditions.

CONCLUSIONS

The results obtained in this work show the titrimetric determination of carbohydrazide with bromate ion and biamperometric end-point detection to be appropriate for the standardization of carbohydrazide solutions.

On the other hand, the proposed indirect spectrophotometric determination of carbohydrazide by reduction of Fe(III) and formation of the Fe(II)–ferrozine complex allows the analyte to be determined over the range 25–700 μg/l. In addition, the method is highly sensitive and provides high-quality calibrations despite the previous reduction involved.

Finally, the differential pulse polarographic method offers excellent features such as a very broad linear response range (between a few μg/l. and a few mg/l. at the recording sensitivities used in this work), which makes it applicable to samples with concentrations varying by up to 3 orders of magnitude or even more if a higher recording sensitivity is employed.

Acknowledgements—The authors are grateful to the DGICyT for financial support granted for the realization of this work as part of Project PB88-0242.

REFERENCES

1. P. E. Iversen and H. Lund, *Anal. Chem.*, 1969, **41**, 1322.
2. J. A. Plaizier, J. G. Van Damme and R. E. De Nève, *ibid.*, 1976, **48**, 1536.
3. N. M. Ratcliffe, *Anal. Chim. Acta*, 1990, **239**, 257.
4. W. Hou, H. Ji and E. Wang, *Talanta*, 1992, **39**, 45.
5. W. D. Basson and J. F. Van Staden, *Analyst*, 1978, **103**, 998.
6. M. L. Balconi, F. Sigon, M. Borgarello, R. Ferraoli and F. Realini, *Anal. Chim. Acta*, 1990, **234**, 167.
7. Vogel's, *Text-book of Quantitative Inorganic Analysis*, p. 685. Longman, 1981.
8. F. Dias, A. S. Olajola and B. Jaselskis, *Talanta*, 1979, **26**, 47.1.1.
9. J. C. Miller and J. N. Miller, *Statistics for Analytical Chemistry*, p. 99. Ellis Horwood, Chichester, 1986.

Talanta, Vol. 39, No. 10, pp. 1317–1321, 1992
Printed in Great Britain

0039-9140/92 $5.00 + 0.00
Pergamon Press Ltd

A NOVEL AND HIGHLY SENSITIVE CATALYTIC METHOD WITH OSCILLOPOLAROGRAPHIC DETECTION FOR THE DETERMINATION OF ULTRATRACE AMOUNTS OF IRIDIUM

JIANG ZHI-LIANG

Laboratory of Instrumental Analysis, Department of Chemistry, Guangxi Normal University, Guilin, People's Republic of China

(*Received* 5 *November* 1991. *Revised* 19 *March* 1992. *Accepted* 23 *March* 1992)

Summary—Iridium(IV) has a strong catalytic effect on the slow redox reaction between Malachite Green and periodate ion in pH 4.2 acetate buffer solution at 100°, and Malachite Green exhibits a sensitive single-sweep oscillopolarographic wave at −0.65 V *vs.* SCE. This provides the basis for a novel and highly sensitive and selective catalytic method with oscillopolarographic detection for iridium. The effect of pH, potassium periodate and Malachite Green concentrations, reaction temperature and reaction time and other variables are investigated. The detection limit is 8 ng/l. with a fixed-reaction time of 10 min. A linear calibration graph from 24 to 1600 ng/l. is obtained. Possible interferences by co-existing ions are examined.

Precious metals have many desirable properties, and have been widely applied to modern technological fields.[1] However, their content in the earth's shell is very low. It is important to develop highly sensitive and selective methods for the determination of precious metals.

Because of the stability of iridium compounds, polarographic methods are few and not completely satisfactory.[2,3] Ezerskaya *et al.*[4] have reported a polarographic method for the determination of $1–10 \times 10^{-7}M$ Ir with thiosemicarbazide. A procedure has been suggested for determining $5–50 \times 10^{-8}M$ Ir, based on the complex of Ir(III) with 2-furylmonooxime which exhibits a catalytic polarographic wave.[5] Bao *et al.*[6] have found that Ir(IV) exhibits a sensitive catalytic polarographic wave in a supporting electrolyte of $0.07M$ thiourea–$0.2M$ potassium iodide–$2M$ hydrochloric acid, with a detection limit of $5 \times 10^{-8}M$ Ir.

Catalytic methods for silver,[7] osmium[8,9] and ruthenium[10,11] with oscillopolarographic detection have been proposed. However, a catalytic method for iridium with oscillopolarographic detection does not seem to have been reported to date. To develop such a method, many catalytic reaction systems of Ir(IV)–potassium periodate–organic reagent were tested. The results demonstrate that some of the Ir(IV)–potassium periodate–triphenylmethane dyes and Ir(IV)–potassium periodate–azocompound systems can be utilized. In the present work, we studied the Ir(IV)–potassium periodate–Malachite Green system in detail by single-sweep oscillopolarography. A very sensitive and selective catalytic method with oscillopolarographic detection was developed for Ir, with a detection limit of 8 ng/l. and a determination range of 24–1600 ng/l. by the fixed-reaction time procedure.

EXPERIMENTAL

Apparatus

A model JP-2 single-sweep oscillopolarograph (Chendu Instrumental Factory) was used for the polarographic measurements. The settings on the JP-2 single-sweep oscillopolarograph were: dropping mercury period 7 sec; scanning rate 250 mV/sec; scanning potential range 500 mV in the negative direction; initial scanning potential −400 mV; I_p'' (second derivative weave); and a three-electrode system–DME, SCE, and platinum electrode. A model JY-501B thermostat and a pHS-2 pH meter were used.

Reagents

A standard solution of Ir(IV) (100 μg/ml) was prepared according to the following procedure: weigh out 22.94 mg $(NH_4)_2IrCl_6$ and place in a 250-ml beaker. Add about 20 ml of $5M$ hydrochloric acid solution, heat to dissolve, cool, then transfer to a 100-ml standard flask

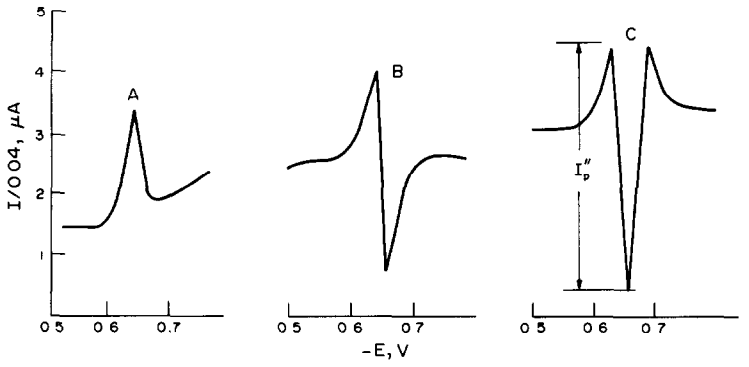

Fig. 1. The single-sweep oscillopolarographic wave of $8.00 \times 10^{-6}M$ Malachite Green in pH 4.2 of acetate buffer solution. A: Normal wave; B: First derivative; C: Second derivative.

and dilute to the mark with doubly distilled water. Prepare working solutions by dilution shortly before use.

A $1.00 \times 10^{-4}M$ Malachite Green solution and a $1.5 \times 10^{-2}M$ potassium periodate solution were prepared by dissolving the reagents in water. A pH 4.2 acetate buffer solution was used.

Procedure

Into a 25-ml graduated test-tube fitted wtih a glass stopper, 1.0 ml of pH 4.2 acetate buffer solution, 2.3 ml of $1.5 \times 10^{-2}M$ potassium periodate and 1.0 ml of $1.00 \times 10^{-4}M$ Malachite Green were added, and the solution was diluted accurately to 10 ml with water, then 2.5 ml of $0.10M$ ascorbic acid solution was added, and mixed well. A portion of the solution was transferred into a polarographic cell and the second derivative peak current $(I''_p)_i$ was measured. This represents current at reaction time zero.

Into a 25-ml graduated test-tube fitted with a glass stopper, 1.0 ml of 5.0 ng/ml Ir(V) solution, 1.0 ml of pH 4.2 buffer solution, 2.3 ml of $1.5 \times 10^{-2}M$ potassium iodate and 1.0 ml of $1.00 \times 10^{-4}M$ Malachite Green were transferred, and the solution was diluted accurately to 10 ml with water, and mixed well. The tube was placed in the boiling water bath (100°), while the stopwatch was started. After 10 min the reaction was quenched by cooling with tap-water, then 2.5 ml of $0.10M$ ascorbic acid solution was added, and mixed well. The second derivative peak current $(I''_p)_{cat}$ was measured. The log $[(I''_p)_i/(I''_p)_{cat}]$ value was obtained. The $(I''_p)_{uncat}$ for the uncatalysed (blank) reaction was measured in a similar manner. And the log$[(I''_p)_i/(I''_p)_{uncat}]$ (that is, blank value) was obtained.

The log $[(I''_p)_{uncat}/(I''_p)_{cat}]$ values for a range of Ir concentrations were plotted as a function of Ir concentration to prepare a calibration graph.

RESULTS AND DISCUSSIONS

The oscillopolarographic behaviour of Malachite Green

The oscillopolarographic behaviour for many organic compounds has been studied.[12] However their applications in inorganic oscillopolarographic analysis are few.[13-15] In the present work, the oscillopolarographic character of Malachite Green was investigated for the application of Malachite Green to the catalytic determination of iridium.

In pH 4.2 acetate buffer solution, Malachite Green exhibits a sensitive single-sweep oscillopolarographic wave at −0.65 V *vs.* SCE. Figure 1 shows the normal wave, first derivative wave and second derivative wave. The second derivative peak current is biggest, and was chosen for use, although at lower concentrations the signal-to-noise ratio will deteriorate. The I''_p is proportional to the Malachite Green concentration between 4×10^{-7} and $4 \times 10^{-5}M$. The electrocapillary curve is lower in the presence of $5.0 \times 10^{-6}M$ Malachite Green than in its absence, owing to adsorption of Malachite Green on the surface of the DME changing the surface tension of the mercury drop. No wave was observed when scanning in the positive direction. The mean temperature coefficient is −0.95%/deg in the range of 20–40°. The I''_p decreases substantially when the surfactants polyvinyl alcohol, cetyltrimethylammonium bromide, Triton X-10, Triton X-100 and sodium dodecyl sulphate are added.

The experiments show that IO_4^- and IO_3^- ions interfere with the oscillopolarographic

measurements of Malachite Green, because both exhibit waves near the Malachite Green wave. To eliminate the interferences, several reduction reagents were considered. The results demonstrate that ascorbic acid can mask the interferences and does not affect the oscillopolarographic measurements of Malachite Green.

Ir(IV)–KIO_4–Malachite Green catalytic reaction system

Many catalytic methods for Ir have been reported.[16] The use of Malachite Green for the catalytic determination of Ir has not been reported. We first found that Ir(IV) catalysed the slow decolourization reaction of Malachite Green and potassium periodate in pH 4.2 acetate buffer solution at 100°. Malachite Green concentration in the reaction system can be measured spectrophotometrically or oscillopolarographically. Our experiments show that oscillopolarography is more sensitive than spectrophotometry. Oscillography was chosen as the detection technique for Malachite Green.

In the catalytic reaction solution, the catalytic and uncatalysed reactions occur simultaneously.

$$IO_4^- + \text{Malachite Green} \xrightarrow[H^+,\ 100^\circ]{\text{Ir(IV) cat., fast}} IO_3^- + \text{Products} \quad (1)$$

$$IO_4^- + \text{Malachite Green} \xrightarrow[H^+,\ 100^\circ]{\text{slow}} IO_3^- + \text{Products} \quad (2)$$

Under the chosen conditions, the periodate concentration is greater than the Malachite Green concentration, and it is presumed that a pseudo first-order reaction (with respect to Malachite Green) occurs. The rate equation of the overall reaction is

$$V_{cat} = -\mathrm{d}[MG]/\mathrm{d}t = k_c[MG][Ir] + k_{un}[MG] \quad (3)$$

or

$$-\mathrm{d}[MG]/[MG] = (k_c[IR] + k_{un})\,\mathrm{d}t. \quad (4)$$

where k_c and k_{un} are the rate constants of the catalytic and uncatalysed reactions, respectively, for use of a fixed concentration of periodate and pH, and MG is Malachite Green. Since

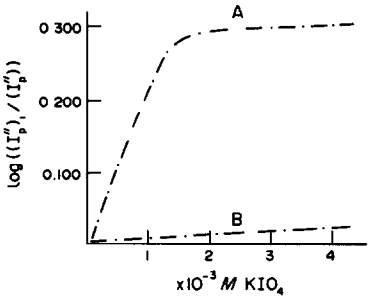

Fig. 2. Effect of KIO_4 concentration on $\log[(I''_p)_i/(I''_p)]$. A: Catalytic reaction (0.4 ng/ml Ir). B: Uncatalysed reaction. For other conditions see the procedure.

$I''_p = k'[MG]$, where k' is a constant, equation (4) may be rewritten as

$$-\mathrm{d}[(I''_p)_{cat}]/(I''_p)_{cat} = (k_c[Ir] + k_{un})\,\mathrm{d}t \quad (5)$$

Integration of equation (5) gives

$$\log[(I''_p)_i/(I''_p)_{cat}] = (k_c[Ir] + k_{un})t \quad (6)$$

where $(I''_p)_i$ and $(I''_p)_{cat}$ are the second derivative peak currents of Malachite Green in the catalytic reaction solution at time 0 and t min, respectively. When [Ir] = 0, only the uncatalysed reaction takes place, and equation (6) has the form

$$\log[(I''_p)_i/(I''_p)_{uncat}] = k_{un} \cdot t \quad (7)$$

where the $(I''_p)_{uncat}$ is the (I''_p) of MG in the uncatalysed reaction solution at time t min. Combining (6) and (7), we obtain

$$\log[(I''_p)_{uncat}/(I''_p)_{cat}] = k_c[Ir]t \quad (8)$$

Equation (8) shows that the logarithmic term is proporational to the Ir concentration, with the other variables held constant for the given system.

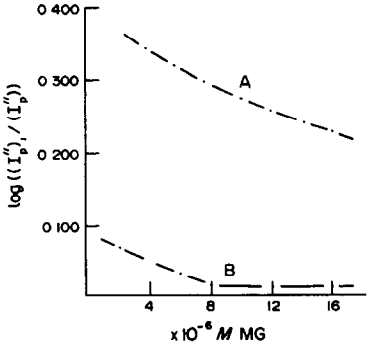

Fig. 3. Effect of MG concentration on $\log[(I''_p)_i/(I''_p)]$. A: Catalytic reaction (0.4 ng/ml Ir). B: Uncatalysed reaction.

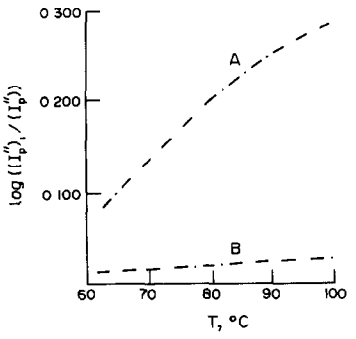

Fig. 4. Effect of reaction temperature on $\log[(I''_p)_i/(I''_p)]$. A: Catalytic reaction (0.4 ng/ml Ir). B: Uncatalysed reaction.

Table 1. Influence of foreign ions

Tolerance limit (Ion)/(Ir)	Ion added
3.0×10^6	SO_4^{2-}, ClO_4^-, PO_4^{3-}, Cl^-
1.0×10^5	SiO_3^{2-}, ClO_3^-
2.5×10^4	Ca^{2+}, Mg^{2+}, Al^{3+}, Zn^{2+}
1.0×10^4	Au^{3+}, Pt^{4+}, Pb^{2+}, Fe^{3+}, Hg^{2+}, Ba^{2+}, NH_4^+
6.0×10^3	Ag^+, Ni^{2+}, As^{3+}, La^{3+}, V^{5+}
2.0×10^3	Os^{4+}, Pd^{2+}, Mo^{6+}, W^{6+}
5.0×10^2	Co^{2+}, Cr^{6+}
1.0×10^2	Mn^{2+}*
20	Ru^{3+}*
4	Rh^{3+}*

*Excess also has catalytic effect on the reaction.

Effects of variables

The effects of the concentrations of periodate and Malachite Green, pH, reaction temperature and time on $\log[(I''_p)_i/(I''_p)_{cat}]$ and $\log[(I''_p)_i/(I''_p)_{uncat}]$ were studied. In general the effect of each factor leads to higher $\log[(I''_p)_i/(I''_p)_{cat}]$ and lower $\log[(I''_p)_i/(I''_p)_{uncat}]$ which is to be recommended.

The reaction media tested were sulphuric acid, hydrochloric acid, perchloric acid and acetate buffer solution. The results show that pH 4.2 acetate buffer solution gives a bigger $\log[(I''_p)_i/(I''_p)_{cat}]$ value and a lower blank value than the others and was selected for use.

The effect of variation of the potassium periodate concentration on the logarithmic terms is shown in Fig. 2. The $\log[(I''_p)_i/(I''_p)_{uncat}]$ increases slowly with potassium periodate concentration; but that of the $\log[(I''_p)_i/(I''_p)_{cat}]$ increases substantially with potassium periodate concentration (less than $0.0013M$), and the logarithmic value reaches a limiting value not affected by potassium periodate concentration (more than about $1.5 \times 10^{-3}M$). A concentration of $2.76 \times 10^{-3}M$ potassium periodate, which gave the largest $\log[(I''_p)_i/(I''_p)_{cat}]$ value was chosen for use.

Figure 3 shows the relationship of the logarithmic terms and the Malachite Green concentration (i.e., the indicator species). The $\log[(I''_p)_i/(I''_p)_{cat}]$ decreases as the Malachite Green concentration increases as does the $\log[(I''_p)_i/(I''_p)_{uncat}]$ value for concentrations less than $6.4 \times 10^{-6}M$. A Malachite Green concentration of $8.00 \times 10^{-6}M$, which gives a lower blank, was chosen.

The relationship of logarithmic terms and reaction temperature is shown in Fig. 4. The $\log[(I''_p)_i/(I''_p)_{cat}]$ increases substantially with the reaction temperature, and the blank value increases slowly with the temperature. A temperature of 100°, which gives a higher sensitivity, was chosen. A fixed-reaction time of 10 min was selected for use, giving a good compromise between high sensitivity and short analysis time.

Effect of foreign ions

The influence of 31 foreign ions on the catalytic determination of 0.40 ng/ml Ir was examined. The results are summarized in Table 1. The tolerance limit is that giving not more than ±5% error. Most common ions do not interfere with the catalytic determination of Ir. The precious metal ions Rh(III) and Ru(III) also have catalytic effects on the redox reaction when exeeding their tolerence limits 4 and 20 times, respectively. Table 1 indicates that this catalytic method for iridium has good selectivity.

Calibration graph

The fixed-reaction time procedure under optimal experimental conditions gave a calibration

Table 2. Analysis of Ir in synthetic samples

Composition, μg/ml	Ir found, ng/ml	Mean value, ng/ml	RSD, %	Relative error, %
$0.001Ir^{4+}$–$1Pd^{2+}$–	0.960 0.960			
$1Pt^{4+}$–$0.5Au^{3+}$–	0.890 1.00	0.997	3.68	−0.30
$0.2Ag^-$–$0.1Os^{4+}$	1.04 1.04			
$0.001Ir^{4+}$–$1Fe^{3+}$–	1.00 1.00	1.02	1.52	+2.0
$0.5Cr^{6+}$–$0.5Hg^{2+}$–	1.02 1.02			
$0.2Ni^{2+}$–$5Si^{4+}$	1.02 1.04			

graph that was linear for iridium concentrations from 24 to 16000 ng/l. The relative standard deviation (RSD) of the $(I''_p)_{uncat}$ is 0.53%. The RSD of the method for 0.40 ng/ml and 0.80 ng/ml Ir was 3.6% and 2.4% (10 replication), respectively. The detection limit is 8 ng/l. The method is the most sensitive oscillopolarographic method for Ir and the most sensitive catalytic method at present.[2-6,16-18]

Analysis of synthetic sample

The method was directly applied to analysis of synthetic samples, with various mixtures of ions and good results were obtained (see Table 2).

REFERENCES

1. Tian Guang-Rong, *Guijinshiu*, 1991, **12**, 64.
2. Gao Xiao-Xia and Yao Xiu-Ren, *Polarographic Catalytic Waves of Platinum Metals*, p. 143. Kexue Publishing House, Beijing, 1977.
3. Yao Xiu-Ren and Zhang Li-Qu, *Atlas of Polarographic Catalytic Waves*, p. 313. Dizhi Publishing House, Beijing, 1988.
4. N. A. Ezerskaya, I. Nkiselva and L. K. Shubochim, *Zh. Analit. Khim.*, 1976, **31**, 1274.
5. N. A. Ezerskaya, G. V. Prokhorova and L. K. Shubochim, *idid.*, 1981, **36**, 523.
6. Bao Qi-Er, Yao Xiu-Ren, Chen Hui-Xian, Jin Long-Ju and Gao Xiao-Xia, *Fenxi Huaxue*, 1974, **2**, 10.
7. Jiang Zhi-Liang, *Guijinshu*, 1991, **12**, 24.
8. Jiang Zhi-Liang and Liang Ai-Hui, *Talanta*, 1990, **37**, 1077.
9. Qin Chen-Zhen, Li Xiao-Jin and Jiang Zhi-liang, *Chinese Chemical Letters*, 1991, 2, 641.
10. Jiang Zhi-Liang, *Talanta*, 1991, **38**, 621.
11. *Idem*, *Electroanalysis*, 1991, **3**, 823.
12. Li Nan-qiang, *Fenxi Shiyanshi*, 1987, 6(5–6), 62.
13. Jhiang Zhi-Liang and Lu Ba, *Fenxi Huaxue*, 1991, **19**, 111.
14. Jiang Zhi-Liang, *ibid.*, 1991, **19**, 339.
15. *Idem*, *Xiyou Jinshu*, 1988, **12**, 310.
16. K. B. Yatsimirskii and L. P. Tikhonova, *Talanta*, 1987, **34**, 69.
17. Chen Si-Zhen, *Fenxi Huaxue*, 1978, **6**, 42.
18. Chen Guo-Shu, *Cuihua Donglixue Fenxifa Jiqi Yingyong*, p. 294. Jiangxi Gaoxiao Publishing House, Nanchang, 1991.

Talanta, Vol. 39, No. 10, pp. 1323–1327, 1992
Printed in Great Britain.

0039-9140/92 $5.00 + 0.00

STABILITY-INDICATING METHOD FOR THE DETERMINATION OF CLORAZEPATE DIPOTASSIUM—II. VIA *N*-DESMETHYLDIAZEPAM AND DETERMINATION OF ITS DEGRADATION PRODUCTS

M. G. EL-BARDICY, L. I. BEBAWY and M. M. AMER
Analytical Chemistry Department, Faculty of Pharmacy, Cairo University, Cairo, Egypt

(*Received* 26 *September* 1991. *Revised* 27 *March* 1992. *Accepted* 27 *March* 1992)

Summary—A spectrophotometric method for the determination of the intact clorazepate dipotassium in the presence of its degradation products is developed. It depends upon preliminary hydrolysis of clorazepate dipotassium—thus liberating its equivalent of *N*-desmethyldiazepam which is extracted, with benzene–methylene chloride (9:1). The extract is evaporated, the residue dissolved in methanol and its absorbance measured at about 315 nm. The procedure determines 0.4–1.6 mg of clorazepate dipotassium with an accuracy of $100.2 \pm 0.7\%$. The procedure is applied successfully for the determination of clorazepate dipotassium in bulk powder and in capsules; retaining its accuracy in the presence of up to 80% degradation. Determination of the different degradation products is also possible. Thus, *N*-desmethyl diazepam is determined after preliminary extraction with benzene–methylene chloride mixture, followed by TLC separation, 2-amino-5-chlorobenzophenone by directly applying the first derivative spectrophotometric technique, and glycine in the aqueous layer determined colorimetrically with ninhydrin reagent in the presence of pyridine.

Clorazepate dipotassium, 7-chloro-1,3-dihydro-2-oxo-5-phenyl-1H-1,4-benzodiazepine-3-carboxylic acid, dipotassium salt, degrades to *N*-desmethyldiazepam below pH 4 but is relatively stable at pH 7.4 and above.[1]

Several methods have been reported for the determination of clorazepate dipotassium, including fluorimetric,[2] colorimetric,[3] polarographic,[4] GLC,[5] TLC[6] and high performance liquid chromatographic procedures.[7]

The purpose of the present investigation is to develop a simple spectrophotometric method for the determination of only the intact clorazepate dipotassium in bulk powder and pharmaceutical preparations.

EXPERIMENTAL

Apparatus

The following apparatus was used: a UV/Vis spectrophotometer (Shimadzu UV-120); a Du.7 spectrophotometer Beckman; a UV short wavelength lamp (254 nm) and TLC plates (20 × 20 cm with 0.25 mm thickness silica gel GF 254, E Merck).

Reagents

All chemicals are of analytical grade. Clorazepate dipotassium, working standard was kindly supplied by the Nile pharmaceutical Co, Cairo, Egypt, and *N*-desmethyldiazepam, working standard, was kindly supplied by Arab Drug Co., Cairo, Egypt.

Other reagents used were: 2-amino-5-chlorobenzophenone (Aldrich); glycine (B.D.H.); dilute hydrochloric acid, about 2*N* aqueous solution; dilute sodium hydroxide, about 4*N* aqueous solution; benzene (A.R., Prolabo); methylene chloride (A.R., Prolabo); benzene–methylene chloride mixture (9:1); spectroscopic grade methanol (E. Merck); development system; heptane–chloroform–ethanol (50:50:5); citric acid–citrate buffer, pH 5;[8] ninhydrin–citrate reagent; 5% solution in citric acid–citrate buffer, pH 5; and pyridine; C.P. (E. Merck).

Procedure

Determination of clorazepate dipotassium via its quantitative degradation to N-desmethyldiazepam. Bulk Powder. Weigh, accurately, about 20–80 mg of clorazepate dipotassium, dissolve in 10 ml of water, add about 25 ml of dilute hydrochloric acid solution and leave each

*National Organization of Drug Control and Research.

at room temperature (18–22°) for 30–45 min. At the end of this interval, make alkaline with dilute sodium hydroxide solution, cool and extract with 3 × 20 ml portions of benzene–methylene chloride (9:1). Evaporate the combined extracts just to dryness, dissolve the residue in 20 ml of methanol, transfer into a 50-ml standard flask and complete to volume with methanol.

Transfer 1 ml of this solution, into a 10-ml standard flask, complete to the mark with methanol, and measure the absorbance at 315 nm against a blank prepared as for the test solution but without previous hydrolysis. This can be achieved by adding the same volume of dilute hydrochloric acid and dilute sodium hydroxide solutions together to the sample solution and completing as under "Bulk Powder", beginning with the words " . . . Cool and extract with 3 × 20-ml portions of benzene–methylene chloride (9:1) . . . ".

Calculate the concentration of clorazepate dipotassium in the sample from a calibration curve simultaneously prepared or from the A (1%, 1 cm) calculated to be 54.29 or from the following regression equation: $Y = 0.54x + 0.004$, $r = 0.998$ where Y is absorbance, X is concentration of the final solution in mg and r is the correlation coefficient.

Capsules. Evacuate the contents of 20 capsules, mix thoroughly, weigh, and calculate the average weight in each capsule. Transfer an accurate weight of the mixed sample, equivalent to about 20–80 mg of clorazepate dipotassium, shake with 10 ml of water, filter through a filter paper, add 25 ml of dilute hydrochloric acid solution to the filtrate and proceed as mentioned under Bulk Powder above, starting with the words " . . . allow to stand at room temperature for 30–45 min . . . ".

Determination of clorazepate dipotassium and its degradation products in laboratory prepared mixtures. Intact clorazepate dipotassium. Proceed as for Bulk Powder.

Degradation products. Weigh accurately about 20–80 mg of clorazepate dipotassium, dissolve in 10 ml of water and extract with 3 × 20-ml portions of benzene–methylene chloride (9:1). Combine the organic extracts together for the determination of *N*-desmethyldiazepam and 2-amino-5-chlorobenzophenone, and keep the aqueous layer for the determination of glycine.

Evaporate the combined organic extracts just to dryness and dissolve the residue in about 5 ml of methanol. Transfer, quantitatively, into a 10-ml standard flask, complete to volume with methanol and mix well (solution A). For *N*-desmethyldiazepam apply a band of 0.2 ml of the methanolic solution (above) onto a starting line on the silica gel glass plate and simultaneously apply on the same plate a parallel spot of a reference *N*-desmethyldiazepam methanolic solution. Develop with the developing solvent and mark the band corresponding to the spot of *N*-desmethyldiazepam under UV light (254 nm). Scratch, then extract, the band with 3 × 3 ml of methanol, passing the extracts through a filter paper moistened with methanol into a 10-ml standard flask and complete to volume with methanol. Measure the absorbance at 315 nm against a blank prepared by extraction of an area of silica gel equivalent to the sample spot. Calculate the concentration of the sample from a calibration curve simultaneously prepared from 0.2–1.2 mg of *N*-desmethyldiazepam, or from the *A* (1%, 1 cm) which amounts to 75.42, or from the following regression equation: $Y = 0.75x + 0.005$, $r = 1$.

For 2-amino-5-chlorobenzophenone transfer 5 ml of the methanolic solution A into a 25-ml standard flask and complete to volume with methanol. Introduce 1 ml of this solution into a 10-ml standard flask, complete to volume with methanol and record the corresponding first derivative curve against methanol as a blank. Measure the absolute trough amplitude at 362 nm as shown in Fig. 1. Calculate the concentration of the sample from a previously constructed curve using an authentic sample of 2-amino-5-chlorobenzophenone, or from the following regression equation $Y = 63.57x + 0.64$, $r = 0.999$, where Y is height in mm, X is concentration and r is correlation coefficient.

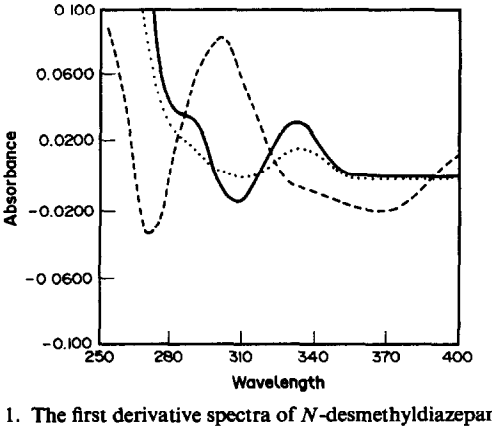

Fig. 1. The first derivative spectra of *N*-desmethyldiazepam (———), 2-mino-5-chlorobenzophene (– – –), and clorazepate dipotassium (· · ·), 0.15 mg/10 ml.

For determination of glycine[9] transfer the aqueous layer quantitatively into a 100-ml standard flask and complete to volume with citric acid–citrate buffer of pH 5 ± 0.2. Introduce 1 ml of the diluted solution into a 25-ml standard flask, add 4–4.5 ml of citrate buffer, 1 ml of ninhydrin reagent, 1 ml of pyridine and heat in a boiling water bath for 15–20 min. Complete to volume with water and measure the absorbance at 560 nm against a blank prepared simultaneously using 5 ml of citrate buffer. Calculate the concentration of glycine from a standard calibration curve, or from the A (1%, 1 cm) which was calculated to be 959.9 or from the following regression equation: $Y = 3.5x + 0.05$, $r = 0.959$ for glycine.

RESULTS AND DISCUSSION

Although clorazepate dipotassium is stable in alkaline medium, it is readily hydrolysed in acid medium. Upon standing at room temperature for half an hour in 2*N* hydrochloric acid it is completely degraded to *N*-desmethyldiazepam.[4] Under more drastic conditions, *i.e.*, heating with 6*N* hydrochloric acid at 100° for one hour, it is completely degraded yielding 2-amino-5-chlorobenzophenone and glycine.[10]

The proposed procedure depends upon the determination of clorazepate dipotassium via its degradation products, namely, *N*-desmethyldiazepam after hydrolysis with 2*N* hydrochloric acid for 30–45 min at room temperature (18–22°). The optimum conditions for quantitative hydrolysis of clorazepate dipotassium to *N*-desmethyldiazepam were studied and confirmed by TLC using silica gel glass plate GF 254 and heptane–chloroform–ethanol (50:50:5) as developing system, when only one spot corresponding to the *N*-desmethyldiazepam was detected under U.V. However, longer standing even at room temperature extends hydrolysis further to 2-amino-5-chlorobenzophenone and glycine; this has been evidenced by the formation of a precipitate of the benzophenone derivatives upon rendering the solution alkaline with 4*N* sodium hydroxide.

After hydrolysis, the solution was extracted with a mixture of benzene–methylene chloride (9:1), which extracted, not only the quantitatively produced *N*-desmethyldiazepam, but also any 2-amino-5-chlorobenzophenone and *N*-desmethyldiazepam, originally presented as degradation products. The absorption spectrum of an authentic sample of *N*-desmethyldiazepam was found to possess a maximum at about 315 nm as shown in Fig. 2. On the other hand, it overlaps with the spectral curves of 2-amino-5-chlorobenzophenone and clorazepate dipotassium (Fig. 2). Thus, to overcome interferences due to overlapping, a blank was done by extracting a similar amount of clorazepate dipotassium, with benzene–methylene chloride mixture, without preliminary hydrolysis. This would extract any *N*-desmethyldiazepam and 2-amino-5-chlorobenzophenone originally present as degradation products and would eliminate their interferences, it is only the *N*-desmethyldiazepam produced from the hydrolysis of the intact clorazepate dipotassium that is determined.

Different concentrations of an authentic sample of clorazepate dipotassium were analysed by the proposed procedure and the linear concentration–absorbance relationship is obtained.

To assess the efficiency of the proposed procedure, the degradation products, *N*-desmethyldiazepam, 2-amino-5-chlorobenzophenone and glycine were mixed with an authentic sample of clorazepate dipotassium in different ratios and analysed by the proposed procedures. It is obvious from the results in Table 1 that the presence of up to 80% degradation products does not affect the accuracy of the proposed procedure, while the reported procedure[11] gives much higher results.

Pharmacologically speaking, clorazepate dipotassium is the precursor of *N*-desmethyldiazepam; the latter being produced *in vivo* from the former[12] and is equally active. Yet, pharmaceutically speaking, formulation of partially degraded clorazepate dipotassium in a

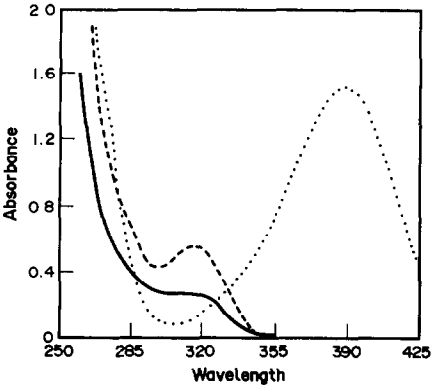

Fig. 2. Absorption spectra of clorazepate dipotassium (———), *N*-desmethyldiazepam (– – –), and 2-amino-5-chlorobenzophenone (· · ·), 6 mg/100 ml.

Table 1. Determination of mixtures of authentic samples and acid degradation products* by the proposed procedures and compendial method[11]

Mixtures, No.	Clorazeptate dipotassium Proposed procedure Found, %	Clorazeptate dipotassium Compendial method Found, %	*N*-Desmethyldiazepam Found, %	2-Amino-5-chloro-benzophenone Found, %	Glycine Found, %
1	100.3	191.7	99.3	100.2	99.6
2	99.5	180.0	100.4	100.3	99.9
3	100.0	120.0	100.6	99.8	100.3
4	99.6	113.0	99.5	100.2	99.7
5	100.7	105.0	99.2	100.4	100.2
Mean	100.2%		99.8%	100.2%	99.9%
C.V.	0.6%		0.7%	0.2%	0.3%

*Five mixtures were prepared containing clorazepate dipotassium, *N*-desmethyldiazepam, 2-amino-5-chlorobenzophenone and glycine respectively:

1) 20:30:25:25
2) 30:25:30:15
3) 40:20:20:20
4) 50:15:15:20
5) 80:10: 5: 5

pharmaceutical preparation would result in an increase of the dose concentration; the molecular weight of clorazepate dipotassium being 408.9 and that of *N*-desmethyldiazepam being 270.7. On the other hand, a clorazepate stability-indicating method without simultaneous determination of its pharmacologically-active first degradation product *N*-desmethyldiazepam, would be inadequate. The presence of an undetermined amount of *N*-desmethyldiazepam would result in an overdose.

The proposed procedure was applied to determine the concentration of clorazepate dipotassium in its capsules and the results obtained are shown in Table 2. The accuracy of the procedure was assured by applying the standard addition technique. The results are shown in Table 2.

By applying the proposed procedure it is also possible to determine the different degradation products expected to be present with clorazepate dipotassium. *N*-desmethyldiazepam and amino-chlorobenzophenone were extracted from the aqueous solution of clorazepate dipotassium with benzene–methylene chloride mixture before hydrolysis. Due to the significant overlapping of the absorption spectra of *N*-desmethyldiazepam and aminochlorobenzo it

Table 2. Accuracy of the recovery of standard addition of clorazepate dipotassium to some market preparations using the proposed procedure

Pharmaceutical preparation	Manufacture	Standard clorazepate dipotassium added, *mg*	Found, *mg*	Accuracy, %
Tranxene capsules	Nile Co.	0		99.7*
5 mg/capsule	B.N 831489	25	24.96	99.8
		40	40.10	100.3
		50	49.89	99.8
			Mean	100.0
			C.V	±0.3%
Tranxene capsules	Nile Co.	0		99.9*
5 mg/capsule	B.N 861371	25	25.05	100.2
		40	40.06	100.2
		50	50.15	100.3
			Mean	100.2
			C.V	±0.1%
Tranxene capsules	Nile Co.	0		99.7*
5 mg/capsule	B.N 83053	30	30.16	100.5
		40	40.26	100.7
		50	49.93	99.9
			Mean	100.4
			C.V	±0.4%

was only possible to determine 2-amino-5-chlorobenzo-phenone in the presence of *N*-desmethyldiazepam by first derivative spectrophotometry (but not the reverse) as shown in Fig. 1. A linear relationship was found between the concentration of amino chlorobenzophenone and the trough amplitude over the range 0.1–0.7 mg/10 ml.

In order to determine *N*-desmethyldiazepam in the presence of 2-amino-5-chlorobenzophenone, it was inevitable to separate *N*-desmethyldiazepam by TLC before its determination.

Glycine, in the aqueous layer, was determined colorimetrically[9] by using ninhydrin in the presence of pyridine which has been found to accelerate the production of colour and stabilizes it for a longer period. The procedure was found to be applicable to the range 0.027–0.275 mg with an average accuracy of $99.9 \pm 0.3\%$.

The suggested procedures for the determination of degradation products were applied in the range 0.2–1.2 mg of *N*-desmethyldiazepam, with an average accuracy of $99.8 \pm 0.7\%$, and from 0.1–0.7 mg of 2-amino-5-chlorobenzophenone with an average accuracy of $100.2 \pm 0.2\%$.

Comparing the results of the proposed procedure with the compendial method,[11] it was found that the suggested procedure is more selective, since the nonaqueous procedure does not differentiate between the intact molecule and its degradation products.

REFERENCES

1. M. A. Brooks, M. R. Hackman, R. E. Weinfeld and T. C. Macasieb, *J. Chromatog.*, 1977, **135**, 123.
2. J. Troschutz, *Arch. Pharm.* 1981, **314**, 204.
3. J. Manes, J. Civera, G. Font and F. Bosch, *Cienc. Ind. Farm.*, 1987, **6**, 333.
4. W. F. Smyth and B. Leo, *Anal. Chim. Acta*, 1975, **76**, 289.
5. D. M. Hailey, *J. Chromatog.*, 1974, **98**, 527.
6. J. Th. M. Groenewegen and P. J. P. De Meijer, *Pharm. Weekbl*, 1980, **115**, 965.
7. L. Elrod, Jr., D. M. Shada and V. E. Taylor, *J. Pharm. Sci.* 1981, **70**, 793.
8. F. Welcher, *Chemical Solutions*, p. 65, Van Nostrand, New York, 1966.
9. M. G. El-Bardicy, L. I. Bebawy, M. M. Amer, in the press.
10. D. J. Hoffman and A. H. C. Chun, *J. Pharm. Sci.* 1975, **64**, 1668.
11. K. Florey (ed.), *Analytical Profiles of Drug Substances*, Vol. 4, pp. 92–112. Academic Press, New York, 1975.
12. A. G. Gilman, L. S. Goodman, Th. W. Rall and F. Murad, *The Pharmacological Basis of Therapeutics*. 7th Ed., pp. 435, 465. Collier Macmillan, New York, 1985.

Talanta, Vol. 39, No. 10, pp. 1329–1335, 1992
Printed in Great Britain.

0039-9140/92 $5.00 + 0.00

LIQUID AND POLY (VINYL CHLORIDE) MATRIX MEMBRANE ELECTRODES FOR THE SELECTIVE DETERMINATION OF COCAINE IN ILLICIT POWDERS

EMAN M. ELNEMMA and MARAWAN A. HAMADA
Department of Chemistry, Faculty of Science, Qatar University, Doha, Qatar

SAAD S. M. HASSAN*
Department of Chemistry, Faculty of Science, Ain Shams University, Cairo, Egypt

(*Received* 2 *January* 1992. *Revised* 16 *March* 1992. *Accepted* 27 *March* 1992)

Summary—The construction of liquid membrane and PVC matrix-type cocainium ion selective electrodes and their use for direct potentiometry and potentiometric titration of cocaine are described. The ion-pair complexes of cocaine cation with reineckate and tetraphenylborate anions are either dissolved in nitrobenzene solvent or dispersed in a PVC matrix, with DOP or DBS plasticizer, and used as the ion-exchange membranes. The electrochemical response characteristics of electrodes incorporating these types of membranes are evaluated with regard to the effect of pH, foreign basic compounds, temperature and γ-radiation. The electrodes display a stable fast Nernstian response for 10^{-2}–$10^{-5}M$ cocainium cation over the pH range 3–7, the lower limit of detection being 1 μg/ml. Determination of as low as 20 μg/ml cocaine hydrochloride shows an average recovery of 98% and a mean standard deviation of $\pm$0.6%. The electrodes exhibit useful analytical characteristics for determining cocaine in some illicit powders. The results agree fairly well with those obtained by gas–liquid chromatography.

There has been an increasing world-wide availability and abuse of cocaine in recent years. This necessitates the development of suitable methods for determining cocaine in samples which are seized. The British and United States Pharmacopoeias give an assay method for cocaine hydrochloride based on the repeated extraction of cocaine base from an alkaline solution and subsequent non-aqueous titration.[1,2] This method besides being tedious, suffers from severe interference by various organic bases. Other techniques used for determining cocaine include polarimetry,[3] circular dichroism,[4] fluorescence polarization immunoassay,[5] nuclear magnetic resonance,[6] Fourier-transform infrared spectrometry,[7] gas–liquid chromatography,[8,9] gas chromatography–mass spectrometry,[10] high performance thin layer chromatography,[11] high pressure liquid chromatography,[12] and enzyme and radio immunoassays.[13] Many of these methods, however, require several time-consuming manipulation steps, sophisticated instruments and special training.

Ion selective membrane electrodes have been extensively used for monitoring various pharmaceutical preparations[14,15] and offer prospects for the determination of some illicit drugs.[16,17] However, little is known about the use of these sensors for determining cocaine. Potentiometric titrations of cocaine hydrochloride with silver(I),[18] picrate,[19] and tetraphenylborate[20] (TPB) ions have been described using chloride, picrate, and tetraphenylborate membrane electrodes, respectively. The methods are not selective for cocaine because the halides of various amines are similarly titrated. A coated wire membrane electrode for direct determination of cocaine based on the use of cocaine–dinonylnapthalene sulphonate ion-pair complex in poly (vinyl chloride) matrix has been suggested.[21] Selectivity data for this sensor have been evaluated for only three basic compounds and determination of cocaine in complex mixtures or illicit powders has not been tested.

The present work describes simple potentiometric sensors for the determination of cocaine in illicit powders. Electrodes with reineckate and tetraphenylborate ion pair complexes in liquid and poly (vinyl chloride) membranes have been prepared, characterized, compared and examined for determining cocaine. These electrodes display stable fast and linear response for 10^{-2}–$10^{-5}M$ cocaine hydrochloride over the pH

*Author for correspondence.

range 3–7 with minimum interference from many related basic compounds.

EXPERIMENTAL

Reagents

All the chemicals were of analytical reagent grade and doubly distilled water was used throughout. Sodium tetraphenylborate (NaTPB) and ammonium reineckate were obtained from Sigma (St. Louis, MO, U.S.A.). Poly (vinyl chloride) (PVC), dioctylphthalate (DOP), dibutyl sebacate (DBS) and tetrahydrofuran (THF) were obtained from Aldrich Chem. Comp., Inc., (Milwaukee, WI, U.S.A.). A Standard World Health Organization (WHO) cocaine hydrochloride sample of purity not less than 97% and different illicit cocaine powders of different origins were obtained through the Department of Narcotics, Criminal Laboratory, Ministry of Interior, Doha, Qatar.

A $10^{-2}M$ cocaine hydrochloride stock solution was prepared by dissolving 0.3398 g of pure cocaine hydrochloride in 100 ml of water. Dilute solutions (10^{-3}–$10^{-6}M$) were prepared fresh by appropriate dilution and kept in air-tight bottles. A standard $10^{-2}M$ NaTPB solution was prepared by dissolving 3.42 g in the minimum volume of water, followed by filtration and dilution to one litre. The solution was standardized by potentiometric titration with standard $10^{-2}M$ silver nitrate solution using an Orion Ag/Ag_2S membrane electrode (Model 94-16) for end-point detection.

Apparatus

All potentiometric measurements were carried out at $25 \pm 1°$ with an Orion pH/mV meter (Model SA 720) and cocaine membrane electrodes in conjunction with an Orion Ag/AgCl double junction reference electrode (Model 90-02) with 10% w/v potassium nitrate in the outer compartment. An Orion combination pH electrode (Model 91-02) was used for pH adjustments.

The electrical conductivities of the liquid membrane solutions were measured by means of a Tacussel conductivity cell (Type CM 0.05/G) and a Prolabo conductivity meter (Type CD 6N). A gamma cell 220 (Atomic Energy of Canada Ltd) was used for irradiation of the PVC membranes.

Gas–liquid chromatographic measurements were made using a Pye Unicam GLC instrument (Model 104) operated under the following conditions: column glass, 6 ft. × 1/4 in. i.d., packed with 3% OV-17 on Gas-Chrom Q (100–200 mesh), column temperature, 250°, injection temperature 270°, carrier gas, nitrogen at a flow-rate 25 ml/min; detector, flame ionization; and detector temperature 270°.

Cocaine ion-pair complexes

The ion association complexes of cocaine with tetraphenylborate and reineckate were prepared by mixing 10 ml of $10^{-2}M$ aqueous cocaine hydrochloride solution and 10 ml of $10^{-2}M$ of either sodium tetraphenylborate or ammonium reineckate. The precipitates were filtered off, washed with demineralized water, dried at room temperature and ground to fine powders. These complexes were used as electroactive materials in PVC and liquid membranes. Elemental analysis of the complexes gave C 78.7, H 6.6, N 2.2% for the cocaine–TPB ion-pair complex (C_{41} H_{42} P_4 NB, C 78.97, H 6.79, N 2.25%) and C 40.1, H. 4.7, N 16.1% for the cocaine–reineckate ion-pair complex (C_{21} H_{28} O_4 N_7 S_4 Cr, C 40.50, H. 4.53, N 15.74%).

Cocaine–PVC membrane electrodes

The membrane of the electrodes was prepared with the composition 2.0% cocaine ion pair complex, 28.3% PVC and 69.7% plasticizer (DOP or DBS). The master membrane was fabricated by dissolving 150 mg of powdered PVC, 370 mg of plasticizer and 10 mg of cocaine ion pair complex in 6 ml of THF. The solution was poured into a petridish (3 cm diameter and the solvent was evaporated at room temperature. Discs were cut from the membrane for the electrode assembly. The electrodes were constructed as previously described[15,22] with a mixed internal reference solution of sodium chloride ($2 \times 10^{-3}M$) and cocaine hydrochloride ($2 \times 10^{-3}M$).

Cocaine liquid membrane electrodes

An Orion liquid membrane electrode body (Model 92) was used in conjunction with an Orion porous membrane (92-81-04). The internal reference solution was a mixture of equal volumes of $2 \times 10^{-3}M$ sodium chloride and $2 \times 10^{-3}M$ cocaine hydrochloride. The liquid membrane was a solution of $5 \times 10^{-3}M$ ion association complex of cocaine in a nitrobenzene solvent. The liquid and PVC matrix membrane electrodes were preconditioned after preparation by soaking for at least 24 hr in

$5 \times 10^{-3}M$ aqueous cocaine hydrochloride solution and stored in the same solution when not in use.

Calibration of cocaine electrodes

The cocaine electrodes were calibrated by pipetting 5.0-ml portions of 10^{-2}–$10^{-5}M$ aqueous cocaine hydrochloride solutions into 100-ml beakers containing 45 ml of $0.1M$ potassium nitrate background. The cocaine electrode in conjunction with a double junction Ag/AgCl reference electrode was immersed in the solution. The emf readings were recorded after stabilization to ± 0.5 mV and plotted *vs.* log [cocaine. hydrochloride]. The calibration graph was used for subsequent measurement of cocaine in illicit powders.

Direct potentiometric determination of cocaine

A portion of illicit cocaine powder (*ca.* 10 mg) was finely powdered and dissolved in doubly distilled demineralized water. The pH of the solution was adjusted to 4–5, the solution diluted with $0.1M$ potassium nitrate in a 25-ml calibration flask to the mark, shaken for 5 min and transferred to a 100-ml beaker. The cocaine membrane electrode in conjunction with an Orion double junction Ag/AgCl reference electrode was immersed in the test solution. The e.m.f. was recorded after stabilization to ± 0.5 mV and compared with the calibration graph. Alternatively, the standard known addition (spiking) technique was used by recording the e.m.f. before and after the addition of 2.50 ml of a standard aqueous $5 \times 10^{-3}M$ cocaine hydrochloride solution to the above test solution. The change in the potential readings was recorded and used for calculation of the cocaine content.

Potentiometric titration of cocaine

A 50-ml aliquot of aqueous cocaine hydrochloride solution (containing 3–20 mg) was pipetted into a 100-ml beaker. The cocaine and reference electrodes were immersed in the solution. The titration was performed with constant stirring using a standard $10^{-2}M$ NaTPB solution. The titration curves were recorded and the equivalence points calculated from the maximum slope ($\Delta E/\Delta V$). Alternatively, 3 to 6 aliquots of the titrant (0.5–1.0 ml each) were successively added and the potentials were recorded after each addition. The results were plotted on the Gran's plot paper (Orion 90-00-90) marking off the major divisions on the vertical axis in 5 mV. A blank experiment was carried out under identical conditions.

Gas liquid chromatographic determination of cocaine

An accurately weighed portion of illicit cocaine powder (*ca.* 20 mg) was finely powdered, dissolved in 5 ml of doubly distilled demineralized water and transferred to a 25-ml separating funnel. The solution was rendered slightly alkaline with $6M$ aqueous ammonia followed by addition of 5 ml of diethylether. The mixture was shaken for 5 min, centrifuged and the organic layer removed. The extraction was repeated 3 times, the organic phase was collected and evaporated on a water-bath. The residue was dissolved in 10 ml of chromatographic grade chloroform. After shaking, a 2–5 μl portion of the chloroform solution was injected on the GLC column. The peak heights for five replicate injections for each sample were recorded and their average value was compared with a standard calibration graph prepared for pure cocaine hydrochloride under similar conditions.

RESULTS AND DISCUSSION

Nature and composition of cocaine membranes

Cocaine cation reacts with tetraphenylborate and reineckate anions to form 1:1 water insoluble ion-association complexes. These complexes were tested as electroactive materials in liquid and poly (vinyl chloride) matrix (PVC) membranes responsive for cocaine. The typical cell used for potentiometric measurements was: Ag–AgCl/$10^{-3}M$ cocaine hydrochloride, $10^{-3}M$ sodium chloride//cocaine liquid or PVC membrane//Ag/AgCl reference electrode. The liquid membranes were prepared from $5 \times 10^{-3}M$ nitrobenzene solution of the complexes. Cocaine–tetraphenylborate and cocaine–reineckate liquid membranes displayed specific conductances of 13.8×10^{-6} ohm^{-1} cm^{-1} (1.35×10^{4} Ω) amd 18.7×10^{-6} ohm^{-1} cm^{-1} (1.0×10^{4} Ω), respectively. The PVC membranes were prepared by using casting solutions of the composition 28:2:70 w/w PVC, cocaine ion-association complex and dioctylphthalate (DOP) or dibutylsebacate (DBS) plasticizer, respectively.

Potential response of cocaine electrodes

The electrochemical response characteristics of liquid and PVC membrane electrodes were

Table 1. Response characteristics of the cocaine liquid and PVC matrix membrane electrodes

Parameter	Cocaine–TPB membrane			Cocaine–reineckate		
	Nitrobenzene	PVC–DOP	PVC–DBS	Nitrobenzene	PVC–DOP	PVC–DBS
Slope, mV/log C	60.0 ± 0.5	54.0 ± 0.4	60.5 ± 0.6	63.0 ± 0.5	54.0 ± 0.4	53.5 ± 0.4
Correlation coefficient, r	0.998	0.999	0.997	0.998	0.999	0.998
Intercept, mV	269 ± 0.7	258 ± 0.7	256 ± 0.6	259 ± 0.5	226 ± 0.7	170 ± 0.6
Lower limit of detection, M	2×10^{-5}	4.5×10^{-6}	1.5×10^{-5}	2×10^{-5}	7×10^{-6}	7×10^{-6}
Working acidity range, pH	3.2–7	3–7.5	2.5–7	3–7	3–6.8	2.5–7.5
Response time for $10^{-3}M$, *sec*	35	48	50	30	45	60

evaluated according to IUPAC recommendations[23] and compared. Data collected over a period of 3 months from 5 different electrode assemblies for each membrane type are summarized in Table 1. The responses of all electrode systems at pH 5 are linear over the concentration range 10^{-2}–$10^{-5}M$ (Fig. 1). The slopes of the calibration plots are typically 53.5–63 mV/concentration decade. Deviation from the ideal Nernstian slope stems from the fact that the electrodes respond to the activity of cocainium ion rather than the concentration. The lower limit of detection, defined as the concentration of cocaine corresponding to the intersection of the extrapolated linear segments of the calibration graphs, ranges between $2 \times 10^{-5}M$ and $4.5 \times 10^{-6}M$ (1–6 ppm).

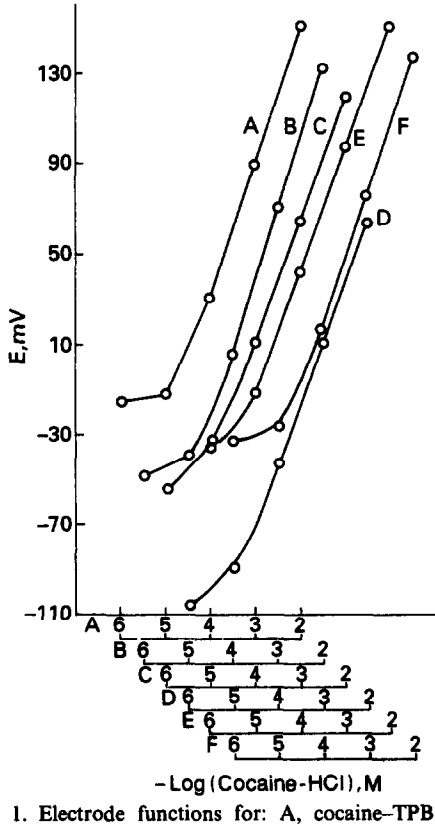

Fig. 1. Electrode functions for: A, cocaine–TPB liquid; B, cocaine–reineckate liquid; C, cocaine reineckate PVC (DOP); D, cocaine–TPB PVC (DOP); E, cocaine–TPB (DBS), and F, cocaine-reineckate PVC (DBS) membrane electrodes.

To check the pH dependence of the electrodes, potential–pH curves at various cocaine concentrations (10^{-2}–$10^{-4}M$) were constructed. For all electrodes, the potentials are stable and practically unaffected by pH fluctuations over the working pH range 3–7 (Table 1). Above pH 8, the potentials displayed by the electrode systems sharply decrease due to the formation of either a non-protonated cocaine base or cocaine-hydrolyzed products. On the other hand, the time required by the PVC matrix membrane electrodes to achieve steady potential readings within ±0.2 mV, after a rapid 10-fold increase in the concentration of $10^{-3}M$ cocaine hydrochloride, ranges from 0.5 to 1 min. Faster and more stable responses are obtained with the liquid membrane electrodes. Calibration curves for the PVC and liquid membrane electrodes are reasonably reproducible within ±1 mV from day to day. Ageing of the electrodes up to 8 weeks does not influence the response time, calibration slope and selectivity characteristics.

Effect of foreign compounds

The influence of 29 different inorganic and organic cations, including narcotics, anaesthetics, amides and amino acids, was investigated on the electrode response. Selectivity coefficients measured by the separate solutions method[15,23] using a $10^{-3}M$ concentration of both cocaine hydrochloride and the interferents are recorded in Table 2 as $-\log k^{pot}_{coc,B}$. The results reveal that the PVC matrix membrane electrodes are generally less susceptible to interference from many foreign compounds. The selectivity of TPB and reineckate based PVC membranes with DOP

Table 2. Potentiometric selectivity coefficients for cocaine liquid and PVC matrix membrane electrodes

	Pot $-\log k$ coc, B					
	Cocaine–TPB membrane			Cocaine–reineckate membrane		
Interferent, B	Nitrobenzene	PVC–DOP	PVC–DBS	Nitrobenzene	PVC–DOP	PVC–DBS
Morphine	1.31	2.23	1.61	1.05	2.00	2.40
Diacetyl morphine	0.18	1.70	1.60	0.72	1.56	1.58
Codeine	1.90	2.20	2.10	1.16	2.10	2.07
Acetyl codeine	0.54	1.12	1.20	0.67	0.48	0.74
Procaine	0.49	0.67	0.74	0.73	0.51	0.67
Lidocaine	0.49	0.67	0.74	0.73	0.51	0.67
Papaverine	−0.83	−0.38	−0.63	−0.52	−0.50	−0.70
Narcotine	−0.61	−0.20	−0.51	−0.02	−0.25	−0.01
Amphetamine	0.67	1.20	0.90	1.03	0.85	0.86
Nicotine	0.90	3.13	1.96	1.28	2.41	1.21
Brucine	0.80	2.67	1.94	1.12	1.76	1.35
Caffeine	1.83	2.33	2.31	1.75	1.92	2.23
Ephedrine	0.94	1.93	1.53	1.34	2.34	1.09
Pilocarpine	0.89	2.16	1.68	1.08	0.63	1.31
Quinine	0.25	2.82	2.02	1.77	2.06	1.76
Cinchonine	0.20	0.65	0.16	0.60	0.43	0.03
Diethylamine	3.25	3.57	3.35	4.08	1.16	2.26
Propylamine	4.52	3.85	3.67	4.33	1.50	2.57
Alanine	1.83	2.23	2.23	1.85	1.88	2.12
Phenylalanine	2.14	2.16	2.29	2.38	1.69	2.10
Anthranilic acid	4.10	4.69	3.18	4.80	3.43	2.91
Sulphanilic acid	0.78	2.69	2.12	1.08	1.80	1.90
Acetamide	2.10	2.58	2.18	1.65	2.02	1.16
Urea	1.80	2.05	2.23	1.73	1.71	1.82
NH_4^+	1.43	2.58	2.31	1.77	0.74	2.27
Na^+	1.71	2.35	2.23	2.31	2.02	2.16
K^+	2.00	2.40	2.23	2.20	2.02	2.04
Ca^{2+}	1.63	2.33	2.18	2.18	1.98	2.16
Ba^{2+}	1.51	2.43	2.21	2.00	1.99	2.20

plasticizer is generally better than those containing DBS plasticizer or liquid membranes. Narcotine and papaverine, however, are the most serious interferents with all membranes. These opium alkaloids are seldom associated with cocaine. On the other hand, interference from adulterants commonly added to cocaine samples illegally sold at the street level such as lactose, starch, inositol and mannitol on the response of the proposed electrode systems is negligible. Selectivity coefficient values measured for some interferents (*e.g.*, NH_4^+, K^+, Ca^{2+}, ephedrine, and alanine) by the mixed solutions method are very close to those obtained by the separate solutions method.

Effect of temperature

The potential response displayed by liquid and PVC cocaine membrane electrodes was monitored as a function of temperature of cocaine hydrochloride test solutions in the range 20–50°. All electrodes exhibit a slight gradual increase in their potentials as the temperature increases. The calibration graphs at different temperatures are essentially parallel. The temperature coefficients of the potentials are 0.5, 0.28 and 0.04 mV per degree for membranes consisting of PVC–DOP, PVC–DBS and nitrobenzene matrices, respectively. The limit of detection and response time do not significantly vary due to the change of temperature indicating reasonable thermal stability of the cocaine membranes up to 50°. These data show that the change of potentials due to the variation of temperature depends on the nature of the membrane solvent and is independent of the nature of the membrane ion pair complex.

Effect of γ radiation

The potential response of cocaine PVC matrix membranes was studied after exposure to various doses of cobalt-60 γ rays. Membranes incorporating the cocaine–TPB ion pair complex with either DOP or DBS plasticizer display a negative potential shift of ~3 mV upon increasing the radiation doses from 10^3 to 10^8 rad. Membranes containing cocaine reineckate ion pair complex with DOP or DBS plasticizer are significantly affected by γ radiation. Increasing the radiation doses from 10^3 to 10^8 rad is

associated by a positive potential shift (~25 mV) of the electrode response. All radiated membranes essentially exhibit the same calibration slope and linear response range as those displayed by the non-irradiated membranes. Contrary to the influence of temperature, variation of electrode potential due to the change of radiation doses depends on the nature of the membrane ion pair complex and is independent of the nature of the membrane solvent.

Determination of cocaine

The reliability of cocaine–TPB (DOP) membrane electrode for quantification of cocaine was assessed by determining 20–300 μg/ml standard cocaine hydrochloride (5 replicates each) at pH 5 using the standard addition method. The results depicted in Table 3 show an average recovery of 97.8% and a mean standard deviation of 0.5% ($n = 7$). Cocaine was also determined by potentiometric titration with standard sodium tetraphenylborate (NaTPB) using the same electrode system. Typical S-shape titration curve and linear Gran's plot are shown in Fig. 2. The S-shape titration curves (inflection break ~120 mV) are generated by addition of at least 20 increments of the titrant whereas Gran's plots are obtained by only 3–5 data points, before or after the equivalence point, on a semi-antilog paper.[15] The equivalence points are reproducibly and consistently obtained at points equivalent to the consumption of 1.00 ± 0.01 mole NaTPB per mole of cocaine ($n = 7$). The average recovery is 98.1% and the mean standard deviation being 0.3% (Table 3).

Cocaine in some real illicit samples from different sources was similarly determined by direct potentiometry. The results obtained are given in Table 4. A mean standard deviation of ±1.2% reveals reasonable precision of the electrode method for such complex mixtures. The accuracy of these data was evaluated by comparison with results obtained using gas–liquid chromatography (GLC). There is fairly good agreement between the results obtained by both techniques. The *t*-test reveals that the mean of 5 runs obtained for each sample by the electrode method as compared to the GLC method is not different at the 0.05 significant level. The *F*-test reveals no significant difference between means and variances of results obtained by the potentiometric and GLC methods. On the other hand, the uses of the Pharmacopoeial methods,[1,2]

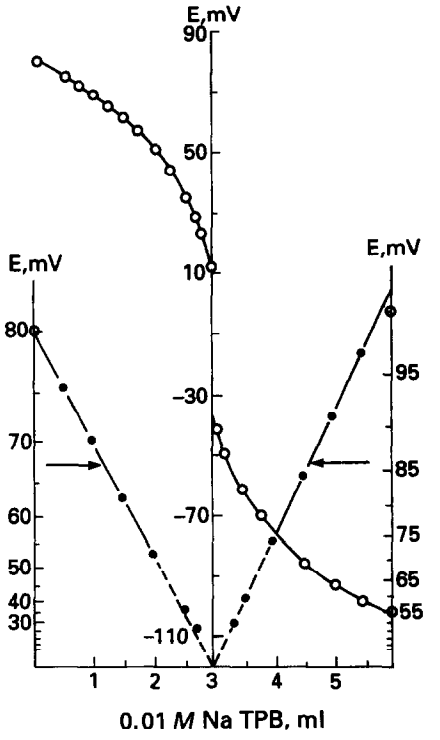

Fig. 2. Typical potentiometric titration curve (○) and Gran's plot (●) for 10.2 mg of cocaine hydrochloride with standard $10^{-2}M$ NaTPB using a cocaine–PVC membrane electrode (ion-pair complex: cocaine–TPB; plasticizer; DOP).

Table 3. Determination of cocaine hydrochloride by direct potentiometry and potentiometric titration with NaTPB using PVC cocaine–TPB membrane electrode

Direct potentiometry cocaine, μg/ml		Potentimetric titration cocaine, mg/ml	
Added	Recovery, %*	Added	Recovery, %*
20.0	98.0 ± 0.6	3.0	98.2 ± 0.4
50.0	97.6 ± 0.5	5.0	98.0 ± 0.4
100.0	98.3 ± 0.5	7.0	98.3 ± 0.3
150.0	97.9 ± 0.6	9.0	97.8 ± 0.3
200.0	97.1 ± 0.4	12.0	97.9 ± 0.3
250.0	98.0 ± 0.5	15.0	98.2 ± 0.2
300.0	97.6 ± 0.6	20.0	98.0 ± 0.3

*Average of 5 measurements.

Table 4. Determination of cocaine in illicit cocaine powders using the PVC cocaine–TPB membrane electrode and GLC methods

	Cocaine found, %(w/w)*	
Sample number	Electrode method	GLC method
1	18.6 ± 1.3	18.2 ± 1.5
2	27.4 ± 1.1	27.0 ± 1.4
3	31.1 ± 1.2	30.9 ± 1.3
4	42.0 ± 1.2	41.7 ± 1.2
5	55.0 ± 1.1	54.8 ± 1.4

*Average of 5 measurements.

which involve treatment with alkalis and extraction in organic solvent followed by acid-base titration, are not suitable for the analysis of real cocaine illicit samples due to the presence of many interfering basic compounds. Without a prior separation, such compounds are extracted and titrated with the cocaine base.

In conclusion, the proposed potentiometric procedure for determination of cocaine involves little manipulation or pretreatment steps compared to other methods.[1,2,5,13] The proposed membrane electrode systems offer the advantages of simple design, fast response, good selectivity and applicability to real illicit cocaine powders.

REFERENCES

1. *United States Pharmacopeia XXII, National Formulary XVII*, pp. 343–344. United States Pharmacopeial Convention, Rockville, MD, 1989.
2. *British Pharmacopoeia*, Vol. 1., pp. 150–151, University Press, Cambridge, 1988.
3. R. J. Palma, J. M. Young, and M. W. Espenscheid, *Anal. Lett.*, 1985, **8**, 641.
4. W. M. Atkinson, J. M. Bowen and N. Purdie, *J. Pharm. Sci.*, 1984, **73**, 1827.
5. K.-H. Beyer and S. Martz, *Dtsch. Apoht.-Ztg.*, 1987, **127**, 2037.
6. A. S. Gonzalez and E. Uriarte, *Farmaco, Ed. Prat.*, 1987, **42**, 281.
7. M. Ravreby, *J. Forensic Sci.*, 1987, **32**, 20.
8. *P. Jacob (III), B. A. Elias-Baker, R. T. Jones and N. L. Benowitz, J. Chromatogr., Biomed. Appl.*, 1987, 61, 277.
9. S. Goenechea, G. Ruecker, M. Neugebauer and U. Zerell, *Fres. Z. Anal. Chem.*, 1986, **323**, 326.
10. S. J. Mule and G. A. Casella, *J. Anal. Toxicol.*, 1988, **12**, 153.
11. E. Dellacase and G. Martone, *Forensic Sci. Int.*, 1986, **32**, 117.
12. R. Gill, R. W. Abbott and A. C. Moffat, *J. Chromatogr.*, 1984, **301**, 155.
13. J. E. Wallace, H. E. Hamilton, J. G. Christenson, E. L. Shimek (Jr.), P. Land and S. C. Harris, *J. Anal. Toxicol.*, 1977, **1**, 20.
14. V. V. Cosofret, *Membrane Electrodes in Drug Substances Analysis*, Pergamon Press, Oxford, 1982.
15. T. S. Ma and S. S. M. Hassan, *Organic Analysis Using Ion Selective Electrodes*, Volumes I and II, Academic Press, London, 1982.
16. C. R. Martin and H. Freiser, *Anal. Chem.*, 1980, **52**, 1772.
17. S. S. M. Hassan and M. A. Hamada, *Analyst*, 1990, **115**, 623.
18. S. Zommer-Urbanska and H. Bojarwicz, *Farm. Pol.*, 1984, **40**, 657.
19. E. P. Diamandis and T. P. Hadjiioannou, *Anal. Chim. Acta*, 1981, **123**, 341.
20. T. K. Christopoulose, E. P. Diamandis and T. P. Hadjiioannou, *ibid.*, 1982, **143**, 143.
21. L. Cunningham and H. Freiser, *ibid.* 1982, **139**, 97.
22. A. Craggs, G. J. Moody and J. D. R. Thomas, *J. Chem. Ed.*, 1974, **51**, 541.
23. IUPAC Analytical Chemistry Division, Commission on Analytical Nomenclature, *Pure Appl. Chem.*, 1978, **48**, 127.

Talanta, Vol. 39, No. 10, pp. 1337–1341, 1992
Printed in Great Britain.

0039-9140/92 $5.00 + 0.00

EXTRACTION AND ENRICHMENT OF CADMIUM AND MANGANESE FROM AQUEOUS SOLUTION USING A LIQUID MEMBRANE

YONGTAO LI* and AIXIA WANG
Department of Chemistry, Northeast Normal University, Changchun 130024, People's Republic of China

J. C. VAN LOON and R. R. BAREFOOT
Department of Geology, University of Toronto, Toronto, Ontario, M5S 3B1, Canada

(*Received* 23 *October* 1991. *Revised* 6 *February* 1992. *Accepted* 29 *February* 1992)

Summary—A liquid membrane containing 4% di-2-ethylhexyl phosphoric acid and 5% sorbitan monooleate in kerosene is used in the form of an emulsion for the simultaneous extraction and concentration of cadmium and manganese from aqueous solutions. When 4% tri-n-octylamine is included in the membrane composition, only manganese is extracted while cadmium remains in the sample solution. The extracted elements in the concentrate are recovered by breaking the emulsion with n-butanol. Recoveries of cadmium and manganese range from 92–104% for 60-ml samples containing 2–9 μg of each element.

The accurate determination of trace elements such as cadmium, manganese, mercury, zinc and copper in natural waters is important because of the toxic properties of the elements. Very sensitive analytical methods based upon furnace atomic-absorption spectrometry, plasma source mass spectrometry and neutron activation analysis have been employed for direct measurements of trace elements in water. However, these expensive instruments are not readily available in many laboratories. Thus, techniques for the separation and preconcentration of trace elements are very valuable because the concentrate can be analyzed with other, less expensive instruments such as flame atomic-absorption spectrometers and UV/Vis spectrometers.

Liquid membranes in emulsion forms have proven useful as a means of extraction and concentration of trace elements in aqueous solutions. Li[1] patented a liquid membrane emulsion separation process. Industrial applications of liquid membrane emulsions have included the removal of elements such as copper from waste water[2] and the purification of brines. More recently, liquid membrane emulsions have been applied in analytical chemistry. Liquid membrane compositions and experimental conditions have been recommended for the quantitative extraction and concentration of rare earth elements,[3] manganese[4] and iron[5] in water.

In this report, new liquid membrane emulsions are described for the simultaneous extraction and concentration of cadmium and manganese in aqueous solution, and for the extraction of manganese from solutions containing both elements. The extracted elements are recovered from the emulsion rapidly and efficiently by chemical demulsification with n-butanol. The elements are determined by flame atomic-absorption spectrometry.

Principle of the method

A liquid membrane consists of an extraction reagent (or carrier), and a surfactant dissolved in kerosene. The kerosene solution is mixed with an acidic or a basic aqueous solution (internal phase or stripper) to form a stable water-in-oil emulsion. The droplets of internal phase of the emulsion are 1–10 μm in diameter. The emulsion is then mixed

*Author for correspondence.

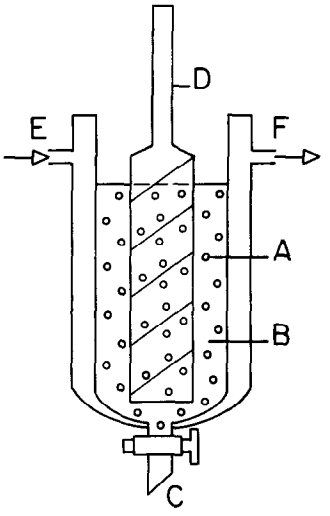

Fig. 1. Glass extraction vessel: A, liquid membrane; B, sample; C, drain; D, Stirrer; E, F, water in, out.

with an aqueous sample whose pH is adjusted in order to establish a pH gradient between the sample and the internal phase of the emulsion. The size of the kerosene droplets in this mixture range from 0.5–2 mm. While the phases are in contact, ions in the sample solution pass through the membrane and are concentrated in the internal phase of the emulsion. After the mixing is terminated, the phases separate and the emulsion is removed. The aqueous concentrate is recovered by means of chemical demulsification.

The extraction and concentration processes are illustrated in equation (1)

$$M^{2+}_{aq} + 2H_2A_{2_{org}} \underset{\text{stripping}}{\overset{\text{extraction}}{\rightleftharpoons}} M(HA_2)_{2_{org}} + 2H^{+}_{aq}$$

Cations (M^{2+}) in the aqueous solution react with the extraction agent (H_2A_2) in the kerosene. In this work, the extraction agent or carrier, di-2-ethylhexyl phosphoric acid, exists as a dimer. The cations enter the membrane in the form $M(HA_2)_2$. This is the extraction step. The complex diffuses to the surface of the membrane in contact with the internal aqueous phase. The metal ions pass into the aqueous phase. This is the concentration or stripping step shown in equation (1). The selectivity of the process depends upon the composition and physical properties of the membrane, and with the pH conditions of the sample and the internal aqueous phase. The pH gradient serves as the driving force. Because of the continuous transfer of M^{2+} ions from the sample to the internal phase, "multiple" extractions are achieved. This is contrasted with single extraction/stripping reactions in conventional extraction methods which must be repeated one at a time. Thus, extraction with a liquid membrane emulsion are highly efficient.

EXPERIMENTAL

Apparatus

The following equipment was used: Perkin–Elmer model 3030 atomic-absorption spectrometer; motor driven stirrers (ranges 0–600 rpm and 0–6000 rpm); pH meter; temperature controller; extractor shown in Fig. 1.

Reagents

Standard solutions of cadmium and manganese were prepared from reagent grade chemicals and distilled, demineralized water. Hydrochloric acid and n-butanol were reagent grade chemicals. Span 80 or sorbitan monooleate was obtained form Public Pharmacy Factory, Tianjing, P.R.C. D2EHPA or di-2-ethylhexyl phosphoric acid and TOA or tri-n-octylamine were obtained from the Organic Chemical Institute, Shanghai, P.R.C. Purified kerosene was used as the membrane solvent. Twenty percent (v/v) solutions of Span 80, D2EHPA and TOA in kerosene were used in this work.

Procedures

Preparation of liquid membrane emulsion. For the simultaneous extraction of cadmium and manganese, prepare the organic phase by combining 6 ml of Span 80 solution (surfactant), 4 ml of D2EHPA solution (carrier) and 90 ml of kerosene. Transfer 20 ml of the organic solution and 20 ml of 2*M* hydrochloric acid (internal aqueous phase) to a flask. Stir the contents at 2000–3000 rpm for 10 min to form the liquid membrane emulsion. For the extraction of manganese from samples containing both cadmium and manganese, combine 6 ml of Span 80 solution, 4 ml of D2EHPA solution, 5 ml of TOA (carrier) solution and 85 ml of kerosene. Transfer 20 ml of the organic solution and 20 ml of 2*M* hydrochloric acid to a flask. Form the liquid

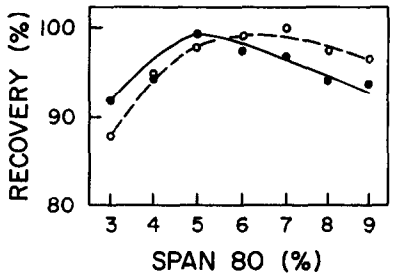

Fig. 2. Relationship between concentration of Span 80 and recovery of cadmium and manganese: ● cadmium; ○ manganese.

membrane emulsion by stirring as described previously.

Extraction of cadmium and manganese. Aqueous solutions contained 0.1 μg/ml of each cation. Adjust the pH of the sample solution to 5 by means of a sodium acetate–acetic acid buffer. Combine 60 ml of sample solution with 10 ml of liquid membrane emulsion in a flask. Stir the contents of 200–300 rpm for 10 min. Allow the phases to separate (1–2 min). Remove the liquid membrane emulsion and transfer it to a flask. Prepare a blank by treating 60 ml of pure water in the same manner as the sample.

Demulsification. Add 0.5–1 ml of n-butanol to the liquid membrane emulsion. After the phases have separated (2–5 min) remove the aqueous phase and measure its volume.

Determination of cations. Measure the concentrations of cadmium (wavelength 222.8 nm, 0.7 nm slit, 4 mA current) and manganese (279.5 nm wavelength, 0.2 nm slit, 10 mA current) in the separated aqueous phase by flame atomic-absorption spectrometry, using an acetylene : air ratio of 8 : 1. The recovery (R) of the cations from the sample was calculated by the following formula:

$$R\ (\%) = \frac{C_i V_i - C_{ib} V_{ib}}{C_e V_e}$$

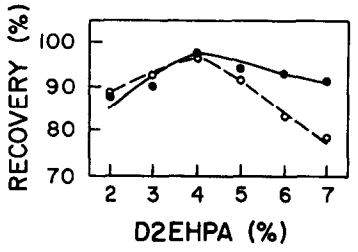

Fig. 3. Relationship between concentration of D2EHPA and recovery of cadmium and manganese: ● cadmium; ○ manganese.

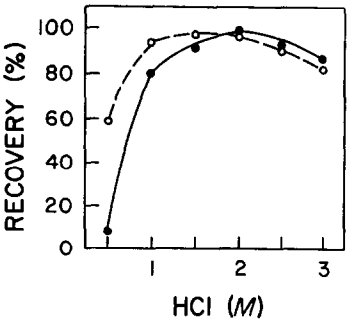

Fig. 4. Effect of acidity of stripping solution on the recovery of cadmium and manganese: ● cadmium; ○ manganese.

where C_i and V_i are the concentration of the cation in the stripping solution (internal aqueous phase of the membrane) and the volume of stripping solution, respectively. C_{ib} and V_{ib} are the corresponding concentration of ca ion and volume of stripping solution in the blank: C_e and V_e are the concentration of cation in the sample and the volume of the sample.

RESULTS AND DISCUSSION

Characteristics of the liquid membrane emulsion

Both the stability of the emulsion and the viscosity of the liquid membrane were altered by the proportion of surfactant in the organic phase. An increase in the concentration of Span 80 (surfactant) increased the stability of the emulsion. However the rate of transfer of the cations decreased. The relationship between the concentration of Span 80 in the organic phase and the recovery of the cations is shown in Fig. 2. A concentration of 5–6% by volume in the organic phase resulted in good recoveries of cations and rapid demulsifications. The effect of the concentration of D2EHPA (carrier) in the organic phase on the recovery of cadmium and manganese is shown in Fig. 3. The optimum concentration of carrier was 4% by volume. The relationship between the concentration of hydrochloric acid in the stripping solution and the recoveries of the cations is shown in Fig. 4. An acid concentration of 2M resulted in the best recoveries. There was a large decrease in the recovery of cadmium at a low acid concentration.

Sample solution

In order to establish a pH gradient between the sample solution and stripping solution and

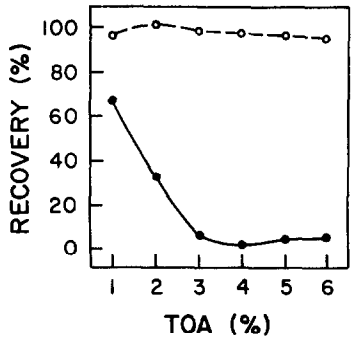

Fig. 5. Relationship between concentration of TOA and the recovery of cadmium and manganese: ● cadmium; ○ manganese.

thus ensure an efficient recovery of cations, the pH of the sample should be higher than 4. A pH of 5 was established by means of a sodium acetate–acetic acid buffer.

Analysis of samples

Samples containing known amounts of cadmium (7.2–1.6 μg) and manganese (5.7–8.5 μg) were extracted using the optimum conditions listed in the Procedures section for the simultaneous concentration of the two elements. Recoveries ranged from 92 to 104%. In the analysis of dilute solutions, it may be necessary to increase the concentrations of elements in the stripping solution to levels above those obtained from the treatment of a single sample with a liquid membrane emulsion. The same batch of liquid membrane emulsion (10 ml) can be used to treat several aliquots (60 ml) of sample solution. In order to describe the increases in concentration by means of the extraction of several aliquots of sample, the term enrichment multiple is used. It is defined as the ratio of the concentration of an analyte in the stripping solution of a liquid membrane emulsion to the initial concentration of the analyte in the sample solution. In this work, the same batch of liquid membrane emulsion was used to extract up to six aqueous samples containing 0.02 μg/ml cadmium and manganese. After each aliquot was extracted, the depleted sample solution was replaced by the same volume of fresh sample solution, and the extraction was repeated. The enrichment multiples increased with the number of extractions, as expected, from 10 for one extraction to *ca.* 50 for six extractions. The enrichment multiple increased by about 10 for 2 and 3 extractions and then about 5 for each subsequent extraction. Also four successive extractions yielded enrichment multiples of about 40 for each element without significant declines in recoveries. However, five and six successive extractions resulted in poor recoveries.

Separation of manganese from cadmium

The inclusion of TOA as a second carrier in the organic phase produced a liquid membrane which was used for the concentration of manganese, while cadmium was retained in the sample. The effects of increasing concentrations of TOA (in the presence of 4% D2EHPA) in the organic phase on the recoveries of both elements are shown in Fig. 5. As the proportion of TOA in the membrane increased from zero to 4%, the extraction of cadmium decreased until no cadmium passed through the liquid membrane. Recoveries of manganese from sample solutions containing 5–6 μg of manganese and 2–18 μg of cadmium ranged from 93 to 102%. Neither element was extracted from solutions by liquid membrane emulsions containing TOA as the sole extracting reagent. Thus, a liquid membrane containing both extracting reagents was selective in extracting manganese when both cadmium and manganese were present in the sample.

CONCLUSIONS

Cadmium and manganese in concentrations ranging from 0.03 to 0.15 μg/ml of each element in aqueous solution can be extracted and concentrated by means of a liquid membrane emulsion. Recoveries are in the range of 92–104%. A liquid membrane emulsion is also effective in the quantitative separation of manganese from cadmium. The procedures are rapid, and no expensive equipment other than an atomic-absorption spectrometer is required for the determination of these elements.

Acknowledgements—We thank the National Natural Science Fund of China and Dr. A. N. Bourns and the World Bank through the International Advisory Panel—Chinese Provincial Universities Development Project for financial support of this work.

REFERENCES

1. N. N. Li, U.S. Patent 3, 1968, 410, 794.
2. N. N. Li, R. P. Cahn, D. Naden and R. W. M. Lai, *Hydrometallurgy*, 1983, **9**, 277.
3. Y. Li and S. Xu, *Chem. J. Chinese Univ.*, 1989, **5**, 190.
4. S. Xu, Y. Li and J. Tian, *J. Anal. Chem.*, 1989, **17**, 1028.
5. Z. Wang, J. Li, J. C. Van Loon and R. R. Barefoot, *Anal. Chim. Acta*, 1991, **252**, 205.

Talanta, Vol. 39, No. 10, pp. 1343–1348, 1992
Printed in Great Britain

0039-9140/92 $5.00 + 0.00
Pergamon Press Ltd

GENERATION OF AsH_3 FROM As(V) IN THE ABSENCE OF KI AS PREREDUCING AGENT: SPECIATION OF INORGANIC ARSENIC

A. LOPEZ, R. TORRALBA,* M. A. PALACIOS and C. CAMARA

Department of Analytical Chemistry, Faculty of Chemistry, Complutense University of Madrid, 28040 Madrid, Spain

(*Received* 16 *September* 1991. *Revised* 20 *February* 1992. *Accepted* 20 *February* 1992)

Summary—It is shown that the potassium iodide to the samples to reduce As(V) to As(III) is not essential when total inorganic arsenic is determined by molecular spectrophotometry (trapping AsH_3 in Ag–DDTC) or by atomic-absorption spectrometry (if Ar flow-rate and $NaBH_4$ addition rate are controlled in 6*M* hydrochloric acid medium). Furthermore, in the presence of low concentration of organic arsenic, a method is reported for the selective determination of inorganic As(III) and As(V), based on the use of citrate/citric acid medium to determine As(III) and hydrochloric acid to determine total inorganic As. As(V) is determined by the difference between total inorganic As and As(III). The interference level of organic arsenic species (monomethylarsenic acid and dimethylarsenic acid) in the determination of total inorganic arsenic and As(III) in 6*M* hydrochloric acid and citrate/citric acid medium respectively, is reported in the text. The developed method is applied to determine As(III) and As(V) in spiked, tap and waste waters and in lake sediments.

Hydride generation atomic-absorption spectrometry (HG–AAS) has been used for the determination of hydride forming elements in many kinds of sample analyses. Some of these elements can exist in various oxidation states, *e.g.*, As(III) and As(V).

The speciation of arsenic with respect to oxidation state is important from the points of view of bioavailability and toxicity, As(III) being more toxic than As(V).[1]

A great difference in sensitivity for these two oxidation states under the usual HG–AAS conditions (in batch and flow-injection analysis systems) has been reported.[2]

For the prereduction of pentavalent arsenic to the trivalent state before the hydride generation step, potassium iodide solution with or without ascorbic acid has gained acceptance as the most suitable reagent. However, some disadvantages are found.

(i) In samples treated with strong oxidizing acid or containing oxidizing agents (as Fe^{3+}), large amounts of I_2 are formed and a high potassium iodide concentration is needed. The presence of I_2 (or I_3^-) in the sample solution is objectionable for two reasons: (a) the I_2, a strongly absorbing agent, could be stripped from the solution prior to the addition of the sodium tetrahydroborate, changing the base line; and (b) loss of a volatile As(III)–iodine adduct in the generator can also be observed.[3]

(ii) Usually, ascorbic acid is also added to prevent the inevitable I^- oxidation by atmospheric oxygen.

(iii) The speed of As(V) reduction to As(III) even in very high acid concentration is sometimes very low and measurement is therefore time consuming (references and standard solutions must be treated in the same manner).

(iv) The most common derivatization method for arsenic speciation is hydride formation after separation of species by high pressure liquid chromatography or ion-chromatography. The analytical difficulties dealing with the potassium iodide prereduction step are difficult to avoid. Therefore, it would be highly desirable to find conditions where addition of potassium iodide is not required. The redox potential of the sodium tetrahydroborate solution is highly dependent on pH and some authors therefore propose combining suitable concentrations of $NaBH_4$ and hydrochloric acid to ensure rapid and efficient generation of the As(V) and As(III) hydride.[4]

In order to further characterize the conditions for the reduction of As(V) to AsH_3 without a potassium iodide prereduction step, we carried out experiments at the part per billion (ppb) and

*Author for correspondence.

part per million (ppm) arsenic level. For the ppm level, the reaction was followed by molecular visible spectrophotometry using silver–diethyl-dithiocarbamate (Ag–DDTC). The red chromophore formed in the determination of As with Ag–DDTC is a polynuclear dithiocarbamate complex containing silver metal and As(III) as central atoms.[5] This technique is in principle not affected by the possible slow kinetics of As(V) reduction by sodium tetrahydroborate. For the ppb level of As, the reaction was followed by hydride generation atomic-absorption spectrometry (HG–AAS).

EXPERIMENTAL

Apparatus

A Perkin–Elmer model 2380 atomic-absorption spectrometer equipped with an electrodeless discharge lamp operated at 8 W from an external power supply was used for all determinations.

A spectral band width of 0.7 nm was selected to isolate the 193.7–nm As line. The signals were recorded on a Perkin–Elmer model 56 recorded set at the 10-mV range.

A laboratory-made hydride system with three valves which allow control of the three Ar flows (purge, mixing and $NaBH_4$ addition), was used.[6]

Visible spectra were obtained with a HP8452 diode-array spectrophotometer. A domestic microwave oven (Balay Bahhm-III) with nine power settings (starting at 80 W and increasing by 80 W increments to 720 W) was used. The teflon–PFA vessels used for sample mineralization had a volume of approximately 150 ml and tight-fitting screw cap lids.

Chemicals

Stock solutions (1000 mg/l.) in As(III), As(V), monomethylarsenic acid (MMA) and dimethylarsenic acid (DMA) were prepared by dissolving the appropriate amount of ultrapure As_2O_3 (Merck), As_2O_5 (Aldrich), disodium salt of monomethylarsenic acid (Carlo Erba) and sodium salt of dimethylarsenic acid (Sigma) respectively; As(III) was dissolved in 20 ml of 1*M* sodium hydroxide, the solution was neutralized using 2*M* hydrochloric acid and finally diluted to one litre with 0.6*M* hydrochloric acid. As(V), MMA and DMA was prepared by dissolving the reagent in distilled water from a milli Q-system.

Sodium tetrahydroborate(III), Aldrich reagent-grade, was prepared as a 3% w/v solution in 0.1% sodium hydroxide.

Silver diethyldithiocarbamate solution was obtained by dissolving 0.5 g of Ag–DDTC in 100 ml of pyridine and stored in an amber bottle.

Buffer solutions for the pH range 2–5 were prepared from citric (40%) w/v, acetic (50%) w/v and tartaric acids (30%) w/v, and adjusted to the required pH with sodium hydroxide.

All other reagents were of analytical reagent grade.

Procedures

Sample aliquots containing about 10 μg of arsenic as As(III), As(V) or both in 2*M* hydrochloric acid (for molecular spectrophotometric method) or about 50 ng of arsenic as As(III) and As(V) or both in 6*M* hydrochloric acid (for the atomic-absorption method) and at pH 4.5 [for As(III) determination in both methods] were placed in a reaction flask and the following procedures were carried out.

Spectrophotometric method. The arsine generated at the μg level with 3 ml/min of $NaBH_4$ and 100 ml/min Ar flow was absorbed for 5 min in 3 ml of Ag–DDTC in pyridine. The molecular absorbance of the red complex formed was measured at 536 nm against its blank.

Atomic-absorption spectrometric method. Arsenic generated as arsine at the ng level with 3 ml/min of $NaBH_4$ and a 50-ml/min Ar flow was determined by measuring the absorbance as peak height at 193.7 nm using a quartz cell heated by an air–acetylene flame.

In both methods only peak height was possible with the equipment used, and thus peak height was therefore not compared with peak area.

Microwave oven mineralization. About 3 g of spiked waste-water (or 0.5 g of sediment) and 5 ml of 6*M* hydrochloric acid were placed in a teflon reactor. The samples were mineralized in the microwave oven in sets of three according to the following programme: 4 min at 40% P (280 W), 5 min at 30% P(210 W) and 10 min at 40% P (280 W).

Between each step, the samples were cooled in an ice bath, and depressurized in order to avoid overpressurization problems. The sample solution was made up to 25 ml with water and stored in plastic bottles until analysis.

Table 1. Effect of flow-rate $NaBH_4$ purge on the efficiency of AsH_3 generation for As(III) and As(V) in 6*M* hydrochloric acid by atomic-absorption spectrometry

Flow-rate $NaBH_4$; purge Ar	Peak height As(III) $X \pm S$	Peak height As(V) $X \pm S$	% difference	As(III) + KI $X \pm S$	As(V) + KI $X \pm S$
0.3 ml/sec; 100 ml/min	0.120 ± 0.004	0.076 ± 0.004	37	0.150 ± 0.007	0.150 ± 0.004
0.4 ml/sec; 100 ml/min	0.133 ± 0.007	0.089 ± 0.002	34	0.157 ± 0.005	0.153 ± 0.005
0.5 ml/sec; 100 ml/min	0.174 ± 0.003	0.108 ± 0.002	38	0.160 ± 0.006	0.160 ± 0.005
0.5 ml/sec; 66.7 ml/min	0.159 ± 0.009	0.121 ± 0.007	24	0.163 ± 0.004	0.160 ± 0.006
0.5 ml/sec; 50 ml/min	0.104 ± 0.007	0.104 ± 0.007	—	0.174 ± 0.006	0.169 ± 0.005
0.5 ml/sec; 25 ml/min	0.101 ± 0.005	0.099 ± 0.005	—	0.179 ± 0.004	0.171 ± 0.004
0.5 ml/sec; 0 ml/min	0.090 ± 0.010	0.090 ± 0.010	—	0.170 ± 0.008	0.169 ± 0.008

$X \pm S$ = means and standard deviation of 5 measurements.

RESULTS AND DISCUSSION

Effect of HCl concentration, Ar flow rate and $NaBH_4$ addition rate on the efficiency of arsine generation from As(III) and As(V)

The efficiency of reduction of arsenic species to arsine is highly dependent on pH and kinetics.[7]

When measurements were made by atomic-absorption spectrometry, the slow kinetics of the reduction reaction made it necessary to carefully control the $NaBH_4$ addition rate to the reaction flask in arsine generation as can be seen in Table 1. Thus, for both inorganic arsenic oxidation states, the analytical signal measured as peak height is clearly dependent on the $NaBH_4$ addition and Ar purge flow-rates. The peak height increases with increasing $NaBH_4$ flow-rate at constant purge flow-rate, the difference in sensitivity for As(III) and As(V) being about 35%. This difference may be attributed to the lower reaction rate between As(V) and $NaBH_4$. If the purge flow is decreased at constant $NaBH_4$ flow, it is possible to achieve identical, but lower, signal for the same concentration of As(III) and As(V). Thus, we conclude that the efficiency of the AsH_3 formation from As(III) and from As(V) is the same, when high $NaBH_4$ flow and low purge flow are used (3 ml/min of $NaBH_4$ and 50 ml/min Ar flow).

The addition of 2 ml of 1*M* potassium iodide to both As(III) and As(V) test solutions 15 min before hydride generation significantly increased the efficiency of AsH_3 formation, with similar signal intensities being measured for the two oxidation states (Table 1). However, if the signal was recorded as soon as the potassium iodide was added, the approx 35% difference in sensitivity achieved without addition of potassium iodide remained constant.

Experiments carried out in parallel using the molecular spectrophotometric method (8 μg of As), Fig. 1, clearly demonstrate that increasing the concentration of hydrochloric acid from 1 to 6*M* results in a marked decrease in the As(III) and As(V) absorbance signal. This decrease in the absorbance signal is not attributed to a difference in hydride efficiency generation but rather to competition (between arsine and hydrogen for the Ag–DDTC). No differences were observed between the two oxidation states between 2–6*M* hydrochloric acid. Table 2 shows that the slopes for As(III), As(V) and As(V) plus potassium iodide in 2*M* hydrochloric acid are identical after a 2-min arsine collection time in the Ag–DDTC solution.

Effect of different buffers

Different buffer solutions were used for AsH_3 generation in the molecular spectrophotometric method. The results, Fig. 2, show that in citric/citrate buffer at pH 4.5 it is possible to inhibit the reduction of As(V) to AsH_3 and hence to selectively obtain arsine from the As(III) oxidation state. These results agree with those obtained by the HG–AAS method (Fig. 3) in citric/citrate buffer. Thus, speciation of As(III) and As(V) can be carried out using this medium.

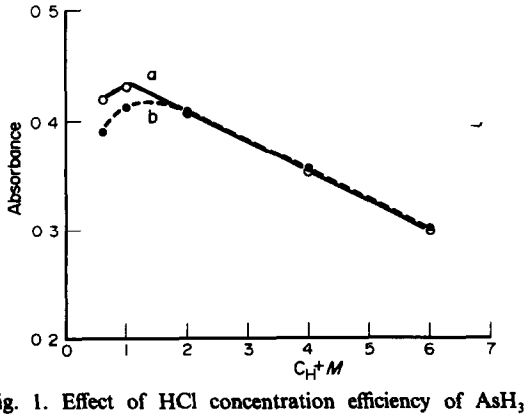

Fig. 1. Effect of HCl concentration efficiency of AsH_3 formation measured by molecular spectrophotometric method (8 μg of As). (a) HCl and As(III). (b) HCl and As(V).

Table 2. Calibration for As(III), As(V) and As(V) + KI in 2*M* HCl by molecular absorption spectrometry

μg As	As(III)	Absorbance As(V)	As(V) + KI
0.0	0.008 ± 0.001	0.008 ± 0.001	0.008 ± 0.001
4.0	0.170 ± 0.002	0.176 ± 0.001	0.174 ± 0.003
8.0	0.339 ± 0.002	0.338 ± 0.002	0.336 ± 0.002
12.0	0.511 ± 0.002	0.513 ± 0.003	0.512 ± 0.002
16.0	0.701 ± 0.001	0.704 ± 0.002	0.709 ± 0.002
	Slope: 0.0431	Slope: 0.0432	Slope: 0.0435
	S.STD: 0.0007	S.STD: 0.0008	S.STD: 0.001
	Intercept: 0.001	Intercept: 0.002	Intercept: 0.001
	I.STD: 0.007	I.STD: 0.008	I.STD: 0.009
	r: 0.9995	*r*: 0.9995	*r*: 0.9992

$n = 5$.

Similar results were obtained in acetic/acetate medium for the molecular spectrophotometric method but the sensitivity for As(III) was lower than in citric/citrate buffer. Other buffer solutions, such as tartaric/tartrate, resulted in a negligible As(V) signal at pH 4.5 (Fig. 2). The ability of citric/citrate medium to distinguish between As(III) and As(V) using the molecular spectrophotometric method can be seen in Fig. 4, where the calibration curve slope for As(V) is negligible. The same results were obtained by atomic-absorption spectrometry.

Effect of MMA and DMA on AsH_3 generation from As(III)

The interferent effect of different amounts of MMA and DMA on arsine generation from As(III) at the 60 ppb level using atomic-absorption spectrometric detection has been tested.

The presence of MMA in citrate/citric medium up to 180 ppb (maximum concentration assayed) does not interfere, whereas in 6*M* hydrochloric acid concentrations higher than 30 ppb interferes (60 ppb enhances the signal about 20%).

The interference level of DMA in citrate/citric medium is higher than MMA, in which 60 ppb is the maximum concentration allowed without interference (120 ppb enhances the absorbance by about 20%). On the contrary in 6*M* hydrochloric acid its interfering effect is significantly

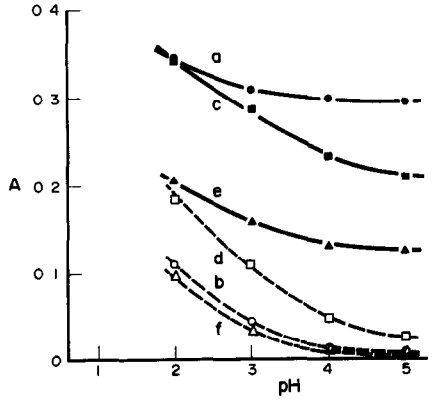

Fig. 2. Effect of buffer solution on Ag–As-DDTC absorbance signal using molecular spectrophotometric method (8 μg of As). (a) citric/citrate and As(III). (b) citric/citrate and As(V). (c) tartaric/tartrate and As(III). (d) tartaric/tartrate and As(V). (e) acetic/acetate and As(III). (f) acetic/acetate and As(V).

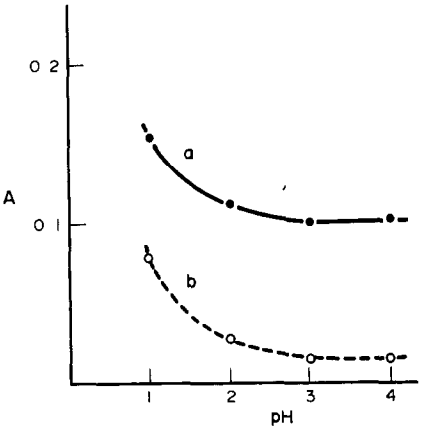

Fig. 3. Effect of citric/citrate buffer on 50 ng of As(III) (a) and As(V) (b) using hydride generation atomic-absorption spectrometric method.

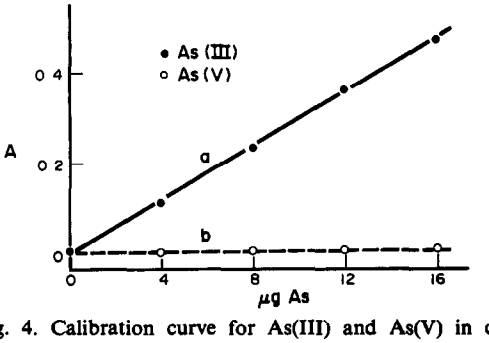

Fig. 4. Calibration curve for As(III) and As(V) in citric/citrate medium at pH 4.5 by molecular spectrophotometry.

Table 3. Absorbance for different As(III):As(V) proportions in 2*M* HCl and pH 4.5 citric/citrate media by molecular absorption spectrophotometry

As(III):As(V)	Absorbance HCl	μg As	Absorbance Citric/citrate	μg As(III)
Blank	0.004 ± 0.001	—	0.004 ± 0.001	—
0:8 (8 μg)	0.339 ± 0.002	8.016 ± 0.002	0.005 ± 0.002	0.172 ± 0.002
2:6 (8 μg)	0.336 ± 0.003	7.957 ± 0.003	0.060 ± 0.001	2.077 ± 0.001
4:4 (8 μg)	0.339 ± 0.002	8.028 ± 0.002	0.113 ± 0.003	3.869 ± 0.003
6:2 (8 μg)	0.338 ± 0.001	7.995 ± 0.001	0.178 ± 0.002	6.108 ± 0.002
8:0 (8 μg)	0.338 ± 0.002	8.000 ± 0.001	0.233 ± 0.001	8.000 ± 0.001

$n = 5$.

lower than that of MMA (presence of 60 ppb produces an increase in absorbance by about 11%).

Application

Because of the difficulty in obtaining certified materials for As(III) and As(V), five synthetic samples for the molecular spectrophotometric method were prepared in 2*M* hydrochloric acid and pH 4.5 citric/citrate media, over a range of As(III)/As(V) ratios. Table 3 shows that the 2*M* hydrochloric acid medium, allowed the determination of total As independently of the oxidation state, while in citric/citrate at pH 4.5 only As(III) is determined. The concentration of As(V) can be calculated as the difference between total inorganic arsenic and As(III).

The proposed chemical method for differentiating inorganic As species was applied in both molecular spectrophotometry and atomic-absorption spectrometry. It can be used for As(III) and As(V) speciation when the presence of methylated arsenic compounds is not higher than 40% total arsenic. Thus, it can be useful for some environmental water samples in which methylated arsenic compounds are reported to be as high as 16–54% of the total arsenic.[8] As the As level content in tap water was too low to be detected, the developed method was applied to the speciation of As(III) and As(V) in spiked tap and waste (paper mill effluent) waters, and sediments. Spiked tap waters were analysed without any previous sample treatment, while spiked waste waters and sediments were treated with hydrochloric acid in a microwave oven as described in the procedure. Solid residue was discarded and only the supernatant was analysed.

When a known amount of As(III) and As(V) was added to waste water, all the arsenic was determined as As(V) and none as As(III). This fact can be attributed to the large amount of oxidant material in the matrix, which changed As(III) to As(V). The amount of As(III) measured in the sediment sample was about 85% of the total As (Soil 7-OIEA, RM). The amount of As(V) measured was negligible.

The presence of organic arsenic in sediments by molecular spectrometry was not detected as absorbance of the complex at 525 nm (maximum λ of Ag–DDTC-organic arsenic or/and As(V) complex[7]) was negligible. The 15% of the As that was unrecovered could be in the sediment attached to silicates not extracted by our procedure.

The analytical characteristics of both the atomic and molecular methods are included in Table 4.

Table 4. Analytical characteristics of atomic and molecular methods by hydride generation

	DL*	Linearity range	C.V.† Within run	C.V.† Between run	Recovery As(III)	Recovery As
AAS	0.5 ppb	0–100 ng	3%	5%	98 ± 3%	95 ± 6%
MAS	0.2 ppm	0–100 μg	3%	3%	98 ± 3%	98 ± 3%

$n = 10$.

AAS = atomic absorption spectrometry.

MAS = molecular absorption spectrometry.

*Calculated using the IUPAC recommendation (3σ).

†At the 8 ppm and 30 ppb levels.

CONCLUSIONS

We have demonstrated that in HG–AAS the addition of potassium iodide when the arsenic hydride is generated in 6*M* hydrochloric acid medium using adequate Ar flows and $NaBH_4$ is not necessary because identical signals for As(III) and As(V) can be obtained. This clarifies the controversial literature published on this topic.

The speciation of inorganic As(III) and As(V) in the absence of organic arsenic is possible by determining As(III) in citric/citrate media at pH 4.5 and total As in 2*M* and 6*M* hydrochloric acid for molecular and atomic methods respectively. As(V) is determined by the difference between total inorganic As and As(III).

Acknowledgements—The authors wish to thank DGCYT for their financial support under project PB 88/0094 and Max Gormann for the revision of this manuscript.

REFERENCES

1. G. A. Cutter, *Anal. Chem.*, 1985, **57**, 2951.
2. H. W. Sinemus, M. Melcher and B. Welz, *At. Spectrosc.* 1981, **3**, 81.
3. D. Siemer, P. Kottel and V. Jariwala, *Anal. Chem.* 1976, **48**, 836.
4. L. Ebdon, J. R. Wilkinson and K. W. Jackson, *Anal. Chim. Acta*, 1982, **136**, 191.
5. A. Csikkil-Szolvoki, E. Csaki-Tombacz, S. Veres and K. Burger, *Acta Chim. Hung.* 1986, **123**, 45.
6. Y. Madrid, M. Bonilla and C. Cámara, *Journal of Anal. Atom. Spectr.*, 1987, **2**, 157.
7. A. G. Howard and M. H. Arbab-Zavar, *Analyst*, 1980, **105**, 338.
8. T. A. Hinners, *ibid.*, 1980, **105**, 751.

Talanta, Vol. 39, No. 10, pp. 1349–1354, 1992
Printed in Great Britain.

0039-9140/92 $5.00 + 0.00

COLUMN PRECONCENTRATION OF TITANIUM IN ALUMINIUM AND ZINC ALLOYS WITH OXALIC ACID–ASCORBIC ACID AND THE ION-PAIR OF SODIUM 1,2-DIHYDROXYBENZENE-3,5-DISULPHONIC ACID AND TETRADECYLDIMETHYLBENZYLAMMONIUM CHLORIDE SUPPORTED ON NAPHTHALENE USING SPECTROMETRY

M. SATAKE*
Faculty of Engineering, Fukui University, Fukui 910, Japan

T. NAGAHIRO
Department of Chemistry, Himeji Institute of Technology, Himeji 671–22, Japan

B. K. PURI
Department of Chemistry, Indian Institute of Technology, Huaz Khas, New Delhi-110016, India

(*Received* 6 *December* 1991. *Accepted* 27 *January* 1992)

Summary—A solid ion-pair compound produced from sodium 1,2-dihydroxybenzene-3,5-disulphonic acid (Tiron) and tetradecyldimethylbenzylammonium chloride(TDBA) supported on naphthalene in a simple glass-tipped funnel tube provides a simple adsorbent system for preconcentrating titanium from some alloys. Titanium reacts with Tiron to form a water-soluble coloured chelate anion which in turn forms a water-insoluble stable titanium/Tiron/TDBA complex with the ion-pair on the surface of naphthalene packed in a column. Titanium is quantitatively retained on the naphthalene in the presence of *L*-ascorbic acid and oxalic acid in the pH range 3.0–4.5 and at a flow-rate of 1 ml/min. The metal complex and naphthalene were dissolved from the column with 5 ml of dimethylformamide(DMF), and the absorbance of the solution was measured at 398 nm. A calibration graph was linear over the range 1–18 μg of titanium in 5 ml of the final DMF solution. The complex has a molar absorptivity of 1.39×10^4 l. mole^{-1}. cm^{-1} and a sensitivity of 3.44×10^{-3} μg/cm^2 for 0.001 absorbance. Eight replicate determinations for a sample containing 12 μg of titanium gave a mean absorbance of 0.697 with a relative standard deviation of 0.82%. The interference of various ions was studied and optimum conditions were developed for the determination of titanium in various aluminium and zinc alloys.

Numerous quaternary ammonium salts such as cetyltrimethylammonium chloride, trioctylmethylammonium chloride, and tetradecyldimethylbenzylammonium chloride(TDBA) have been widely used as the counter ions of anionic metal complexes or metal chelates in the solvent extraction–spectrophotometric determination of metals.[1,2] The use of high molecular weight amines provides high sensitivity and selectivity.

Tiron is a well-known chelating agent for the colorimetric determination of titanium,[3] molybdenum,[4] niobium,[5] vanadium,[6] *etc.* This reagent has two sulphonic acid groups and reacts with various metal ions to form anionic chelates. The metal chelate anions form water-insoluble complexes with quaternary ammonium salts like TDBA which can be extracted into nonaqueous solvents. Matsuo *et al.*[7] have reported the spectrometric determination of iron with SCN in the presence of TDBA. The sensitivity and selectivity of the method are greatly enhanced over the conventional thiocynate method and interference due to foreign ions is also diminished. However, some of the organic solvents are miscible with water to a certain extent, hence the degree of the concentration of the metal ion into the organic solvent is limited.

Recently some column methods have been reported for the preconcentration of metals with different adsorbents such as activated carbon,[8] thiol cotton,[9] green tea leaves,[10] chelating resin,[11] cellulose,[12] polythioether foam,[13] *etc.* Although some of these methods are fairly efficient, once prepared the adsorbents are not reuseable, unlike the material used in this procedure. Furthermore, introduction of a Chelex-100[14] and ion-exchange resin[15] minicolumn into a

*Author for correspondence.

flow-injection system increases the sensitivity to trace levels (ng/ml-pg/ml) thus allowing natural waters to be analysed.

Solvent extraction is a simple and convenient technique, but is inconvenient if emulsion forms or the solubility of the complex in the organic solvent is poor. These difficulties may be overcome by using molten naphthalene,[16] naphthalene adsorption[17] and benzophenone.[18] The only inconvenience of the methods are in the filtration and drying, which increase the number of the operation steps and thus make the method more time-consuming.

We have developed a new column method for the preconcentration of trace metals using various adsorbents supported on naphthalene.[19-21] In the present study, an efficient method has been described for the preconcentration of titanium with Tiron–TDBA adsorbed on naphthalene. The metal retained in the column is dissolved along with the naphthalene, and trace titanium is determined spectrophotometrically. The conditions have been optimized and the method has been used for the determination of titanium in standard aluminium and zinc alloys.

EXPERIMENTAL

Apparatus and reagents

A Hitachi Model 200-20 double beam spectrophotometer and a Toa-Dempa HM-5A pH meter were used. A funnel-tipped glass tube (60 × 6 mm i.d.) was used as a column. The column was plugged with coarse polypropylene fibres and then filled with the adsorbent to a height of 1.2–1.5 cm, compressed lightly with a flattened glass rod.

Standard titanium solution (3 μg/ml) was prepared by diluting 1000 ppm atomic-absorption standard titanium sulphate, $Ti(SO_4)_2$ solution with distilled water. Buffer solutions were prepared by mixing appropriate ratios of 0.5*M* acetic acid and 0.5*M* ammonium acetate solutions 0.5*M* aqueous ammonia and 0.5*M* ammonium acetate solutions, and 0.1*M* potassium dihydrogen phosphate and 0.1*M* disodium hydrogen phosphate solutions. TDBA, naphthalene, DMF, Tiron and all other reagents were of analytical reagent grade.

Preparation of Tiron/TDBA/naphthalene adsorbent

A solution of naphthalene was prepared by dissolving 20 g of naphthalene in 40 ml of acetone on a hotplate stirrer at 35°. This was transferred to 1400 ml of distilled water containing 3.5 g (0.0098 moles) of TDBA, with constant stirring at room temperature, and to it was added a 500-ml solution of Tiron (1.5 g, 0.0048 moles). The naphthalene mixture coprecipitate was stirred for a few hours and allowed to stand for one night. It was drained off by decantation and then the mixture was washed twice with distilled water in the same way. The slurry of naphthalene in water was stored in a bottle.

General procedure

To an aliquot of solution containing 1–18 μg of titanium were added 12 ml of distilled water, 0.7 ml of 1.0% *L*-ascorbic acid solution, 0.4 ml of 1.0% oxalic acid solution and 0.5 ml of the buffer (pH 4.0). The sample solution was passed through the column packed with naphthalene/Tiron/TDBA. The solid mass in the column was washed with a small volume of distilled water and then aspirated for *ca.* 30 sec, compressing the naphthalene material with a flat glass rod. This was dissolved from the column with 5 ml of DMF. The absorbance of this solution was measured at 398 nm with a spectrophotometer against the reagent blank.

RESULTS AND DISCUSSION

Retention characteristics of Tiron/TDBA

TDBA is used as a counter cation for the metal chelate anion. Tiron has two sulphonic acid groups capable of dissociation and it is considered to form an ion-pair (Tiron:TDBA = 1:2) with a quaternary ammonium cation as shown in the following reaction.

$$C_6H_2(OH)_2(SO_3^-)_2 + 2(R)_4N^+ = [C_6H_2(OH)_2(SO_3^-)_2][R_4N^+]_2$$

The experimental observation revealed that the ion-pair coprecipitated with naphthalene. The co-precipitated ion-pair forms a chelate ring between a metal ion and two OH groups, on the inactive surface of naphthalene. From the stoichiometry in the above reaction, the mole ratio of Tiron and TDBA should be 1:2. For the preparation of adsorbent, use of Tiron (1.5–2.0 g) and TDBA (2.5–4.0 g) for 25 g of naphthalene was quite adequate for the complete retention of metal ions. In the present work, 1.7 g of Tiron and 3.6 g of TDBA were used.

Various ion-pair reactions of Tiron with quaternary ammonium salts were examined.

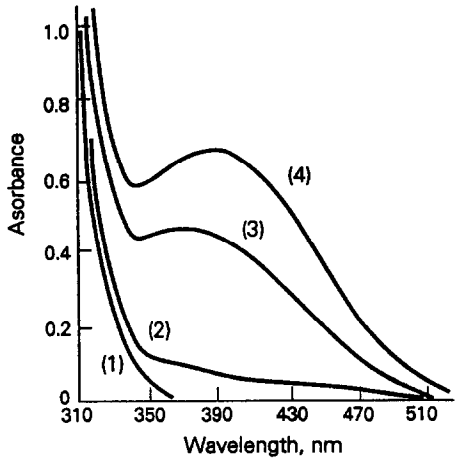

Fig. 1. Absorption spectra of the reagent blank and titanium complex in naphthalene–dimethylformamide solution. Ti: 12 μg, pH: 4.0, 1.0% *L*-ascorbic acid: 0.7 ml, 1.0% oxalic acid: 0.4 ml. Reference: water. (1) Reagent blank, with ascorbic acid and oxalic acid. (2) Titanium complex, without *L*-ascorbic acid and oxalic acid. (3) Titanium complex, with *L*-ascorbic acid. (4) Titanium complex, with *L*-ascorbic acid and oxalic acid.

Among the salts tested, cetylpyridinium chloride (CPC), cetyltrimethylammonium bromide (CTMA), trioctylmethylammonium chloride (TOMA) and TDBA formed ion-pairs with Tiron and coprecipitated with naphthalene. TDBA was recommended as a counter ion for Tiron because it is economical and available in high purity, and shows excellent retention characeristics for metal ions.

Absorption spectra

The absorption spectra of the reagent blank and the titanium/Tiron/TDBA complex in naphthalene–DMF solution were recorded against water (Fig. 1). The complex showed an absorption maximum at 398 nm in the presence of ascorbic acid and oxalic acid, and the absorption of the reagent blank is negligible at this wavelength. The complex showed absorption maxima at 375 and 398 nm in the presence of ascorbic acid and oxalic acid–ascorbic acid, respectively, whereas its absorption is very small in the absence of both acids. Thus, all absorbance measurements were made at 398 nm in subsequent works.

Effect of pH

Experiments were carried out by using 12 μg of titanium. The complex was quantitatively retained on this adsorbent in the pH range 3.0–4.5 (Fig. 2). The retention was incomplete at lower and higher pH values. The addition

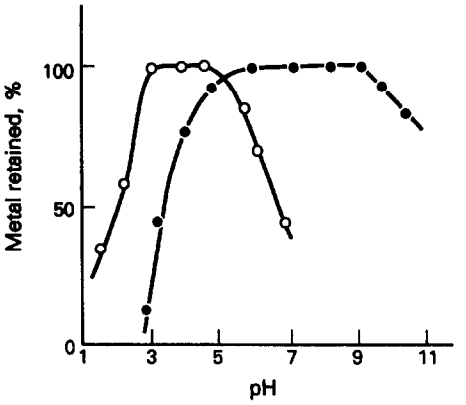

Fig. 2. Effect of pH. ○: Ti: 12 μg, 1.0% *L*-ascorbic acid: 0.7 ml, 1.0% oxalic acid: 0.4 ml. Wavelength: 398 nm. Fe: 15 μg, 0.5% potassium sodium tartrate: 1.0 ml. Wavelength: 248 nm (AAS method). Reference: reagent blank.

of 0.3–2.0 ml of the acetate buffer did not affect the retention of titanium and thus 0.5 ml was recommended in the present work.

Effect of L-*ascorbic acid and oxalic acid concentration*

Various amounts of ascorbic acid and oxalic acid were added to the solution containing 12 μg of titanium and the general procedure was followed. The results are given in Fig. 3. The absorbance of the complex increased with increasing amounts of 1% *L*-ascorbic acid and became constant with 0.6–1.0 ml of this solution. Keeping the *L*-ascorbic acid concentration (1.0%, 0.7 ml) constant, the absorbance remained constant over the range 0.2–1.0 ml of 1% oxalic acid. The absorbance of the complex was very small in the absence of both acids.

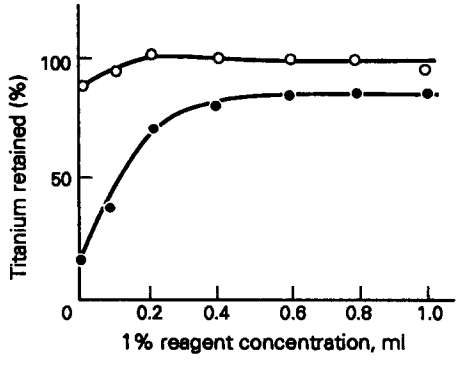

Fig. 3. Effect of reagent concentration. Ti: 12 μg, pH: 4.0, 1.0% *L*-ascorbic acid: 0.7 ml, 1.0% oxalic acid: 0.4 ml. Reference: reagent blank. ●: Varying *L*-ascorbic acid concentration; no oxalic acid. ○: Varying oxalic acid concentration, keeping *L*-ascorbic acid concentration (1.0%, 0.7 ml) constant.

Thus 0.7 ml of *L*-ascorbic acid and 0.4 ml of oxalic acid was used in further work.

Effect of flow-rate, standing time and aqueous volume

The flow-rate was examined from 0.5 to 10 ml/min under the optimum conditions. This range did not cause any effect on the absorbance. Thus, a flow-rate of 1 ml/min was selected. This rate is a natural rate of falling through the column. The colour of the complex in naphthalene–DMF solution was stable for 60 min. The volume of aqueous phase was varied from 15 to 150 ml. The absorbance remained constant when the aqueous phase volume did not exceed 80 ml. In subsequent work, 15 ml of the aqueous phase was used for convenience.

Choice of solvent

Different organic solvents were studied for dissolving the naphthalene/Ti/Tiron/TDBA complex from the column. Since the solid mass should be dissolved in a small volume of solvent, it is essential to select a solvent in which it has high solubility. The solid material was very soluble in DMF, methanol, ethanol, acetonitrile, 4-methyl-2-pentanone, dimethyl sulphoxide and acetone. The sensitivity and precision for measurement of the complex were the highest in DMF solution. Three millilitres of DMF were sufficient to dissolve the mixture, thus providing maximum sensitivity.

Beer's law, sensitivity and precision

Beer's law was obeyed over the concentration range 1–18 μg of titanium in 5 ml of DMF solution. The molar absorptivity of the complex was 1.39×10^4 l. mole^{-1}. cm^{-1} and the sensitivity was 3.44×10^{-3} μg/cm^2 for absorbance of 0.001. Eight replicate determinations containing 12 μg of titanium gave a mean absorbance of 0.697 with a relative standard deviation of 0.82%.

Effect of diverse ions

Different amounts of alkali metal salts of different anions and metal ion solutions were added individually to a solution containing 12 μg of titanium and the general procedure was applied. The tolerance limit was set as the amount which caused an error of $\pm 3\%$ in the recovery of 12 μg of titanium. The results are given in Tables 1 and 2. Among the salts examined, most of them could be tolerated up to 50 mg–1 g levels. KCN and EDTA interfered seriously. Anions like SCN^- and ClO^{4-} react with TDBA to form water-insoluble ion-pairs and cause errors in the determination. Larger amounts of Cl^- and ClO_4^- affect the determination, and thus for wet-ashing decomposition of practical samples, the samples must be completely evaporated to dryness on a water-bath to eliminate these ions. Most of the metal ions did not interfere in the determination of titanium at the one milligram level. W(VI), Cd(II), Cr(VI) and Pb(II) could be tolerated even in amounts of 20–40-fold more than titanium. The effects of

Table 1. Effect of diverse salts

Salt or ion	Tolerance limit*
$CH_3COONa.3H_2O$, Na_2SO_4, $Na_2C_2O_4$, thiourea, *L*-ascorbic acid, CH_3COONH_4	1 g†
NaCl	500 mg
KNO_3	100 mg
KH_2PO_4	50 mg
Potassium sodium tartrate, NH_4Cl	20 mg
KI, $Na_2S_2O_3$	5 mg
Ammonium citrate	800 μg
KSCN, NaF	500 μg
$NaClO_4.H_2O$	300 μg
Disodium EDTA, KCN	10 μg

*Amount causing $\pm 3\%$ error in recovery of 12 μg of Ti.
†Maximum value tested. Ti: 12 μg. pH: 4.0. 1.0% *L*-ascorbic acid: 0.7 ml, 1.0% oxalic acid: 0.4 ml. Adsorbent: [Tiron^{2-}] [TDBA$^+$]$_2$[Naph].

Table 2. Effect of metal ions

Ion	Tolerance limit: Without masking agent	Tolerance limit: With masking agent
Ca(II), Mg(II), Mn(II), Al(III), Co(II) Hg(II), Co(II), Cu(II), Ru(III)	1 mg†	
V(V)	5 μg	1 mg[a]
Pt(IV)	50 μg	800 μg[b]
Fe(II)	50 μg	700 μg[c]
W(VI)	600 μg	
Ag(I)	10 μg	500 μg[d]
Cd(II), Cr(III)	400 μg	
Bi(III)	50 μg	400 μg[e]
Pb(II)	300 μg	
Pd(II)	5 μg	200 μg[f]
Zn(II)	100 μg	
Mo(VI)	10 μg	

*Amount causing $\pm 3\%$ error in recovery of 12 μg of Ti.
†Maximum value tested. Ti: 12 μg. pH: 4.0. 1.0% *L*-ascorbic acid: 0.7 ml, 1% oxalic acid: 0.4 ml. Masking agents were as following: [a]$Na_2C_2O_4$: 200 mg; [b]thiourea: 300 mg; [c]KSCN: 400 μg or $Na_2C_2O_4$: 50 mg; [d]$Na_2S_2O_3$: 4 mg; [e]thiourea: 400 mg; [f]KSCN, 400 μg. Adsorbent: [Tiron^{2-}] [TDBA$^+$]$_2$[Naph].

Table 3. Analysis of samples for titanium

Sample and composition, %	Titanium,*% Certified value	Amount found
Aluminium alloy (NKK, 916) Si:0.41; Cu:0.27; Mn:0.11; Mg:0.10; Cr:0.05; Ni:0.06; Zn:0.30; Fe:0.54; Zn:0.05; Pb:0.04; V:0.02; Zr:0.05; Bi:0.03; Ga:0.03; Co:0.03; Sb:0.01; Ca:0.03; B:0.0006	0.10	$0.11 \pm 0.005^{a,c}$
Aluminium alloy (NKK, 920) Si:0.78; Cu:0.71; Mn:0.20; Mg:0.46; Cr:0.27; Ni:0.29; Zn:0.80; Fe:0.72; Sn:0.20; Pb:0.10; V:0.15; Bi:0.06; Ga:0.05; Co:0.10; Sb:0.01; Ca:0.03	0.15	$0.149 \pm 0.003^{b,c}$
Aluminium alloy (NKK, 1021) Si:5.56; Fe:0.99; Cu:2.72; Mn:0.20; Mn:0.20; Mg:0.29; Cr:0.03; Ni:0.14; Zn:1.76; Sn:0.10; Pb:0.18; V:0.007; Zr:0.01; Bi:0.01; Sb:0.01; Ca:0.004	0.04	0.039 ± 0.004^{c}
Sumitomo (M-2-1) Cr:0.23; Be:0.0013; B:0.0002; Si:0.29; Cu:0.0042; Mn:0.0025; Fe:0.071; Mg:4.90; Zn:0.04; Bi:0.022	0.14	0.143 ± 0.003^{d}
Zinc alloy (N.B.S, SRM-85b) Mn:0.61; Si:0.18; Cu:3.99; Ni:0.084; Cr:0.211; V:0.006; Ga:0.019; Fe:0.24; Pb:0.021; Mg:1.49; Zn:0.030	0.022	$0.0225 \pm 0.0008^{a,e}$

*Mean of 4 determinations. 1.0% *L*-ascorbic acid (0.7 ml) and 1.0% oxalic acid (0.4 ml) were added. Masking agents were as follows: [a]$Na_2C_2O_4$ (50 mg), [b]$Na_2C_2O_4$ (50 mg), [c]KSCN (400 μg), [d]$Na_2C_2O_4$ (20 mg), [e]KSCN (400 μg). NIES: National Institute for Environmental studies (values in parentheses are approximate and not certified).

V(V), Pt(IV), Fe(II), Ag(I), Bi(III) and Pd(II) were greatly improved by using suitable masking agents, but Mo(VI) was not masked with the complexing agents described (Tables 1 and 2). The proposed method is quite selective and can be applied to the determination of titanium in standard aluminium and zinc alloys.

Analysis of alloys for titanium

The proposed method has been successfully applied to the determination of titanium in aluminium and zinc alloy. The results in Table 3 are in reasonable agreement with the certified values. For analysis of alloy samples, a 0.1-g mass of alloy was completely dissolved in 10 ml of *aqua regia* on a water-bath. The solution was evaporated to dryness to eliminate the excess acids. The residue was dissolved in a few drops of concentrated nitric acid and distilled water. The mixture was cooled and filtered through filter paper. The filtrate was diluted to 100 ml with distilled water in a standard flask. An aliquot (1–4 ml) of this sample was taken in a beaker and the general procedure applied.

CONCLUSION

A solid ion-pair compound produced from Tiron and TDBA on naphthalene provides a simple and rapid method for the preconcentration of trace titanium. The proposed method is the first attempt to separate titanium using the reaction of Ti/Tiron complex anion with the quaternary ammonium cation. Solvent extraction is difficult to separate metal ions in the presence of cationic surfactant due to the formation of emulsions in the two phases on shaking. In such cases, larger amounts of the salting-out agent must be added in the solution or both phases must be left to stand for a long time, thus making the method more tedious. The proposed method is free from these problems and needs only simple glassware such as funnel-tipped glass and small volume beakers. The sensitivity of the proposed method may be further improved by combination with an HPLC ultraviolet–visible flow detector.

REFERENCES

1. S. Bandyopadhyay and A. K. Das, *Indian J. Chem.*, 1989, **66**, 427.
2. K. C. Bayan and H. K. Das, *ibid.*, 1990, **67**, 579.
3. F. H. P. Konig, G. D. Baef and H. Poppe, *Z. Anal. Chem.*, 1971, **256**, 270.
4. J. H. Yoe and F. Will, *Anal. Chim. Acta*, 1952, **6**, 450.
5. H. Flashka and E. Lassner, *Mikrochim. Acta*, 1956, **I**, 783.

6. S. Nishikawa, Y. Nakagawa, M. Satake and T. Matsumoto, *Bunseki Kagaku*, 1966, **15**, 944.
7. H. Matsuo, S. Chaki and S. Hara, *Japan Analyst*, 1965, **14**, 935.
8. B. M. Vanderborght and R. E. van Grieken, *Anal. Chem.*, 1977, **40**, 311.
9. M. Q. Yu, G. Q. Liu and Q. Jin, *Talanta*, 1983, **30**, 265.
10. K. Kimura, H. Yamashita and J. Komada, *Bunseki Kagaku*, 1986, **35**, 400.
11. D. G. Biechler, *Anal. Chem.*, 1965, **37**, 1054.
12. P. Burba and P. G. Willmer, *Talanta*, 1983, **30**, 381.
13. A. S. Khan and A. Chow, *ibid.*, 1986, **33**, 182.
14. S. Olsen, L. C. R. Pessenda, J. Ruzicka and E. H. Hansen, *Analyst*, 1983, **106**, 905.
15. O. F. Kamson and A. Townshend, *Anal. Chim. Acta*, 1983, **155**, 253.
16. M. Satake, T. Nagahiro and B. K. Puri, *Analyst*, 1984, **109**, 31.
17. M. Satake, G. Kano, M. C. Mehra, M. Katyal and B. K. Puri, *Annali di Chimica*, 1986, **76**, 45.
18. D. Thorburn Burns and N. Tungkananuruk, *Anal. Chim. Acta*. 1989, **219**, 323.
19. M. Satake, J. Miura, S. Usami and B. K. Puri, *Analyst*, 1989, **114**, 813.
20. S. Usami, S. Yamada, B. K. Puri and M. Satake, *Mikrochim. Acta*, **I**, 263.
21. J. Miura, S. Arima and M. Satake, *Anal. Chim. Acta*, 1990, **237**, 201.

Talanta, Vol. 39, No. 10, pp. 1355–1359, 1992
Printed in Great Britain.

0039-9140/92 $5.00 + 0.00

KINETIC ANALYSIS OF SECOND ORDER REACTIONS USING UV–VIS SPECTROSCOPY

J. POLSTER

Lehrstuhl für Allgemeine Chemie und Biochemie der Technischen Universität München, D-8050 Freising-Weihenstephan, Germany

H. MAUSER

Institut für Physikalische und Theoretische Chemie der Universität Tübingen, Auf der Morgenstelle, D-7400 Tübingen, Germany

(*Received* 21 *November* 1991. *Revised* 6 *March* 1992. *Accepted* 6 *March* 1992)

Summary—A new method was recently developed for the spectroscopic kinetic analysis of reactions with two linearly independent concentration variables. Firstly, the results of this theory applied to experimental data are represented. For this investigation, reactions of the mechanism type

$$A + B \xrightarrow{k_1} C + D \text{ and } A + E \xrightarrow{k_2} F + G$$

were chosen since both reaction steps can be studied separately. The evaluation of the reaction system consisting of both reaction steps gives satisfactory results when the methods of "formal integration" and "singular value decomposition" (SVD) are used. Absorption coefficients of absorbing species are not needed for the evaluation. Only time dependent spectroscopic measuring values and initial concentrations are used in the presented practical example.

It has been demonstrated in a previous paper[1] that non-linear reaction systems with two linearly independent reaction steps can be analysed by spectroscopic methods. The following differential equations in matrix notation hold generally for the absorbances of those reactions:

$$\dot{\mathbf{A}} = \dot{\mathbf{A}}_0 + \mathbf{Z}\ \Delta\mathbf{A} + \mathbf{Y}\ \Delta\mathbf{A}^2$$
$$\mathbf{A} = \mathbf{Z}'(\mathbf{A} - \mathbf{A}_\infty) + \mathbf{Y}(\mathbf{A} - \mathbf{A}_\infty)^2 \qquad (1)$$

The vectors have the following meaning

$$\dot{\mathbf{A}} = \begin{pmatrix} \dot{A}_1 \\ \dot{A}_2 \end{pmatrix} \quad \dot{\mathbf{A}}_0 = \begin{pmatrix} \dot{A}_{01} \\ \dot{A}_{02} \end{pmatrix} \quad \Delta\mathbf{A} = \begin{pmatrix} A_1 - A_{01} \\ A_2 - A_{02} \end{pmatrix}$$

$$(\mathbf{A} - \mathbf{A}_\infty) = \begin{pmatrix} A_1 - A_{\infty 1} \\ A_2 - A_{\infty 2} \end{pmatrix} \quad \Delta\mathbf{A}^2 := \begin{pmatrix} \Delta A_1^2 \\ \Delta A_2^2 \\ \Delta A_1\, \Delta A_2 \end{pmatrix}$$

$$(\mathbf{A} - \mathbf{A}_\infty)^2 := \begin{pmatrix} (A_1 - A_{1\infty})^2 \\ (A_2 - A_{2\infty})^2 \\ (A_1 - A_{1\infty})(A_2 - A_{2\infty}) \end{pmatrix} \qquad (2)$$

and the following matrices are introduced

$$\mathbf{Z} := \mathbf{Q}\mathbf{k}\mathbf{Q}^{-1}, \quad \mathbf{Z}' := \mathbf{Q}\mathbf{k}'\mathbf{Q}^{-1} \quad \mathbf{Y} := \mathbf{Q}\mathbf{k}''\mathbf{P} \qquad (3)$$

The matrix **Q** transforms the two degrees of advancement X_1 and X_2 into the absorbance differences $(A_1 - A_{10})$ and $(A_2 - A_{20})$. The indices 1 and 2 indicate the two different measuring wavelengths of the observation light. These wavelengths have to be chosen in such a way that the matrix **Q** is regular. The matrices **k** and **k′** are the Jacobian matrices:

$$\mathbf{k} = \begin{pmatrix} \partial\dot{X}_1/\partial X_1 & \partial\dot{X}_1/\partial X_2 \\ \partial\dot{X}_2/\partial X_1 & \partial\dot{X}_2/\partial X_2 \end{pmatrix}_{t=0}$$

and

$$\mathbf{k}' = \begin{pmatrix} \partial\dot{X}_1/\partial X_1 & \partial\dot{X}_1/\partial X_2 \\ \partial\dot{X}_2/\partial X_1 & \partial\dot{X}_2/\partial X_2 \end{pmatrix}_{t\to\infty}.$$

The matrix **k″** is defined by

$$\mathbf{k}'' = \begin{pmatrix} \partial^2\dot{X}_1/\partial X_1^2 & \partial^2\dot{X}_1/\partial X_2^2 & 2\partial^2\dot{X}_1/\partial X_1\, \partial X_2 \\ \partial^2\dot{X}_2/\partial X_1^2 & \partial^2\dot{X}_2/\partial X_2^2 & 2\partial^2\dot{X}_2/\partial X_1\, \partial X_2 \end{pmatrix} \Big/ 2. \qquad (4)$$

The matrix **P** transforms the square elements of the degrees of advancement into the corresponding absorbance quantities.[2,3] This matrix

can be calculated by means of the elements of the matrix **Q**:

$$\mathbf{P} = \begin{pmatrix} Q_{22}^2 & Q_{12}^2 & -2Q_{22}Q_{12} \\ Q_{21}^2 & Q_{11}^2 & -2Q_{11}Q_{21} \\ -Q_{21}Q_{22} & -Q_{11}Q_{12} & Q_{11}Q_{22}+Q_{12}Q_{21} \end{pmatrix} \Big/ |\mathbf{Q}|^2 \tag{5}$$

$|\mathbf{Q}|$ is the determinant of **Q**.

The matrices of equation (4) obtain the information which characterize the single systems. Only the elements of the transformed matrices **Z**, **Z'** and **Y** can be obtained from spectroscopic measurements according to equation (1). The differential equation (1) written as a system of usual differential equations is:

$$\begin{aligned} \dot{A}_1 &= z_{01} + z_{11}\,\Delta A_1 + z_{12}\,\Delta A_2 + y_{11}\,\Delta A_1^2 \\ &\quad + y_{12}\,\Delta A_2^2 + y_{13}\,\Delta A_1\,\Delta A_2 \\ \dot{A}_2 &= z_{02} + z_{21}\,\Delta A_1 + z_{22}\,\Delta A_2 + y_{21}\,\Delta A_1^2 \\ &\quad + y_{22}\,\Delta A_2^2 + y_{23}\,\Delta A_1\,\Delta A_2 \end{aligned} \tag{6}$$

or

$$\begin{aligned} \dot{A}_1 &= z'_{11}(A_1 - A_{1\infty}) + z'_{12}(A_2 - A_{2\infty}) \\ &\quad + y_{11}(A_1 - A_{1\infty})^2 + y_{12}(A_2 - A_{2\infty})^2 \\ &\quad + y_{13}(A_1 - A_{1\infty})(A_2 - A_{2\infty}) \\ \dot{A}_2 &= z'_{21}(A_1 - A_{1\infty}) + z'_{22}(A_2 - A_{2\infty}) \\ &\quad + y_{21}(A_1 - A_{1\infty})^2 + y_{22}(A_2 - A_{2\infty})^2 \\ &\quad + y_{23}(A_1 - A_{1\infty})(A_2 - A_{2\infty}) \end{aligned} \tag{7}$$

The constants z_{ik} and y_{ik} or z'_{ik} and y_{ik} can be determined by means of an appropriate linear regression method when the absorbances A_1 and A_2 are measured as a function of time. These constants can be used for the kinetic analysis of the investigated reactions as shown in [1] and in the following examples.

Generally, a reaction mechanism cannot be proved by kinetic analysis of absorbance–time curves. It is only possible to show that the postulated mechanism (theory) does not contradict the experiment. If theory and experiment are inconsistent the theory has to be replaced. These facts can be expressed by Theorem 1:

Proving a reaction mechanism only by kinetic analysis is not possible.

Equation (1) is the basis of absorbance differential equations for about 100 different reaction mechanisms where at least one reaction is second order (all systems were theoretically studied in detail). It can be distinguished in suitable cases between different reaction mechanisms when the constants z_{ik} or z'_{ik} and y_{ik} are used as demonstrated by Mauser.[1]

A THEORETICAL EXAMPLE

Assuming that an investigated reaction runs according to the mechanism

$$A + B \xrightarrow{k_1} C \xrightarrow{k_2} D \tag{8}$$

the equations for **k**, **k'** and **k''** lead to

$$\mathbf{k} = \begin{pmatrix} -k_1(a_0+b_0) & 0 \\ k_2 & -k_2 \end{pmatrix},$$

$$\mathbf{k}' = \begin{pmatrix} -k_1(a_0-b_0) & 0 \\ k_2 & -k_2 \end{pmatrix},$$

$$\mathbf{k}'' = \begin{pmatrix} k_1 & 0 & 0 \\ 0 & 0 & 0 \end{pmatrix}. \tag{9}$$

It is true that the elements of the matrices **Z** and **k** are different as those of **Z'** and **k'** but the corresponding matrices are similar matrices, *i.e.*, they have the same rank, the same trace and therefore the same eigenvalues. The matrices **Y** and **k''** are equivalent matrices which have the same rank. From this it follows that for reaction (8) the rank of **Z** and **Z'** has to be two and the rank for **Y** is one. Furthermore it follows (S = trace of **Z**, D = determinant of **Z**)

$$\begin{aligned} S &= z_{11} + z_{22} = -k_1(a_0+b_0) - k_2, \\ D &= z_{11}z_{22} - z_{12}z_{21} = k_1k_2(a_0+b_0) \end{aligned} \tag{10}$$

These equations lead to

$$-S = k_1 + D/k_1 \tag{11}$$

Analogously, the following equations are true (S' = trace of **Z'**, D' = determinant of **Z'**)

$$\begin{aligned} S' &= z'_{11} + z'_{22} = -k_1(a_0-b_0) - k_2 \\ D' &= z'_{11}z'_{22} - z'_{12}z'_{21} = k_1k_2(a_0-b_0) \end{aligned} \tag{12}$$

and

$$-S' = k_1 + D'/k_1. \tag{13}$$

The existence of the equations (10)–(13) can be verified and their relations used for the determination of rate constants when various series of

measurements with different initial concentrations are carried out.

$$y_{11}/y_{12} = y_{21}/y_{22} = y(h) = (Q_{22}/Q_{12})^2 \quad (14)$$

$$y_{11}/y_{13} = y_{21}/y_{23} = y(h') = -Q_{22}/2Q_{12} \quad (15)$$

$$y_{12}/y_{13} = y_{22}/y_{23} = y(h'') = -Q_{12}/2Q_{22} \quad (16)$$

$$y_{11}/y_{21} = y_{12}/y_{22} = y_{13}/y_{23} = y(v) = Q_{11}/Q_{21} \quad (17)$$

The four quantities from $y(h)$ to $y(v)$, on the right hand side above, have close connections to the elements of the matrix **Q**. They indicate the directions of the axis X_1 and X_2 in the "absorbance (A)-diagram".[1-7] Experimental examples are given for evaluating this reaction type as a "quasilinear reaction" by Lachmann *et al.*[2,3] and Polster.[4]

The treated consecutive reaction mechanism A + B→C→D consists of one reaction step being of second order and one step of first order. This mechanism has to be distinguished from the system A→B→C where only reactions of first order take place. Both reaction systems lead to bent curves in the A-diagrams and to straight lines in the ADQ-diagrams.[1-4] Therefore, it is not possible to distinguish a priori between the system A + B→C→D and the system A→B→C. The situation is yet more complicated because of Theorem 2[8,9]

Two linear reactions the Jacobian matrices of which have the same rank cannot be distinguished alone by spectroscopic means.

For example, this means that the system A→B→C cannot be distinguished from the system A→B, C→D by spectroscopic kinetic analysis except by using additional information. However, the absorbance differential equations of linear systems[9] are completely different from those having at least one reaction step of second order [compare equation (1)]. This means that in practice "pure" linear reaction systems can be kinetically distinguished in most cases from those having reaction steps of second order. For example, the equation analogous to equation (10) holds for the system A→B→C or A→B, C→D[2,3,7,9]

$$S = z_{11} + z_{22} = -(k_1 + k_2)$$

and

$$D = z_{11}z_{22} - z_{12}z_{21} = k_1k_2$$

indicating that S and D are independent concentrations. S and D here are the trace and determinant of the matrix **Z** according to Lachmann *et al.*[2,3] and Mauser and Polster[9]

$$\dot{\mathbf{A}} = \mathbf{Z}(\mathbf{A} - \mathbf{A}_\infty)$$

is the basic equation for linear reaction systems.

Table 1. Results of evaluation according to equations (20) and (21) using different wavelength combinations λ_1/λ_2

Wavelengths *nm*	$k_1(20)$	$k_2(21)$	$k_2(20)$
370/350	(2.0)	0.39	–
370/330	2.89	0.34	0.39
370/310	2.81	(0.30)	–
350/330	2.85	0.35	0.39
350/310	2.78	(0.27)	–
330/310	2.82	(0.42)	–

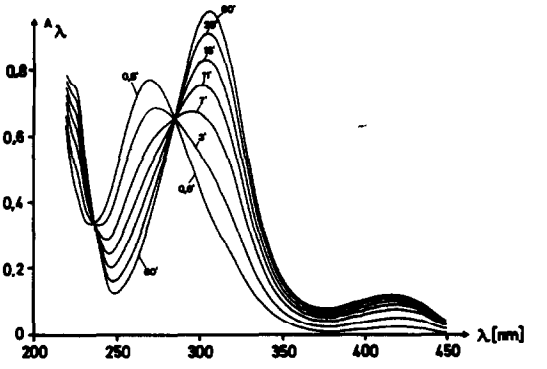

Fig. 1. Reaction spectra of the first reaction step: t-BOC-glycine p-nitrophenyl ester ($1 \times 10^{-4}M$) and n-butylamine ($6 \times 10^{-4}M$) in acetonitrile (25°). The reaction time is given.

A PRACTICAL EXAMPLE

Spectroscopically measured reaction systems can be analysed by means of the relations presented by Mauser.[1] However, a prerequisite is that methods can be found for determining the characteristic matrices with sufficient accu-

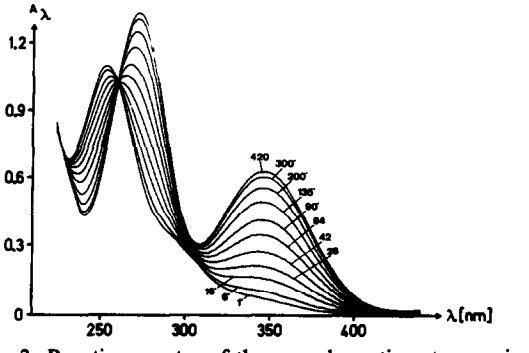

Fig. 2. Reaction spectra of the second reaction step: o-nitrophenyl acetate ($2 \times 10^{-4}M$) and n-butylamine ($6 \times 10^{-4}M$) in acetonitrile (25°). The reaction time is presented.

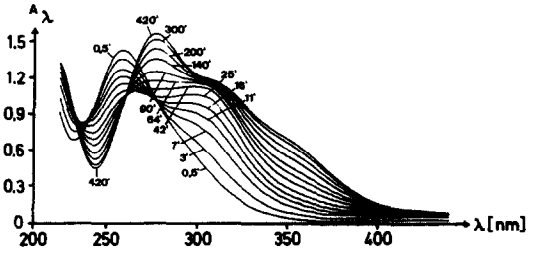

Fig. 3. Reaction spectra of the full reaction system (t-BOC-glycine *p*-nitrophenyl ester = $1 \times 10^{-4}M$, *o*-nitrophenyl acetate = $2 \times 10^{-4}M$, n-butylamine = $6 \times 10^{-4}M$; solvent = acetonitrile; 25°.

racy. At first glance it appears hopeless because six constants have to be determined simultaneously in each equation of (6) and in the case of equations (7) there are five constants for each equation. Firstly, in order to test the new method the following reactions were chosen:

$$\begin{aligned} A + B &\xrightarrow{k_1} C + D \\ A + E &\xrightarrow{k_2} F + G \end{aligned} \qquad (18)$$

The reactants are: A = n-butylamine; B = tert. butoxycarbonyl (t-BOC)-glycine *p*-nitrophenyl ester; C = t-BOC-glycine n-butylamide; D = *p*-nitrophenol; E = *o*-nitrophenyl acetate; F = *N*-acetyl-n-butylamide; G = *o*-nitrophenol. The solvent is acetonitrile (for UV-spectroscopy, Fluka). The experimental procedure has been described earlier.[2-6]

This reaction was chosen because both reaction steps can be studied separately in an easy way.[5,6] At first it was attempted to evaluate the spectroscopically measured values by the method of "formal integration".[2-7] Using common regression methods the results were totally unsatisfactory. Then the "singular value decomposition method" (SVD) developed in the seventies was applied for determining the constants of equations (6) on basis of the formal integration. Both FORTRAN and PASCAL programs were developed for this method.[10,11] Using the SVD method the results were encouraging. The matrix **k** has the form

$$\mathbf{k} = \begin{pmatrix} -k_1(a_0 + b_0) & -k_1 b_0 \\ -k_2 e_0 & -k_2(a_0 + e_0) \end{pmatrix} \qquad (19)$$

The determinant D and trace S were calculated from the computed values z_{ik} according to equation (10). The rate constants k_1 and k_2 can be determined from the equations

$$D = \text{determinant} = k_1 k_2 a_0 (a_0 + b_0 + e_0)$$

and

$$S = \text{trace} = -k_1(a_0 + b_0) - k_2(a_0 + c_0).$$

With the abbreviations of the known combinations of the initial concentrations

$$\sigma_1 = a_0(a_0 + b_0 + e_0)$$

$$\sigma_2 = a_0 + b_0,$$

$$\sigma_3 = a_0 + e_0,$$

it follows from the equations for D and S:

$$k_{1,2} = \frac{-\sigma_1 S \pm \sqrt{(\sigma_1 S)^2 - 4\sigma_1 \sigma_2 \sigma_3 D}}{2\sigma_1 \sigma_2} \qquad (20)$$

More accurate values for k_2 are obtained using the relationship

$$k_2 = D/k_1\sigma_1. \qquad (21)$$

The results of evaluation are presented in Table 1. The dimensions of k_1 and k_2 are

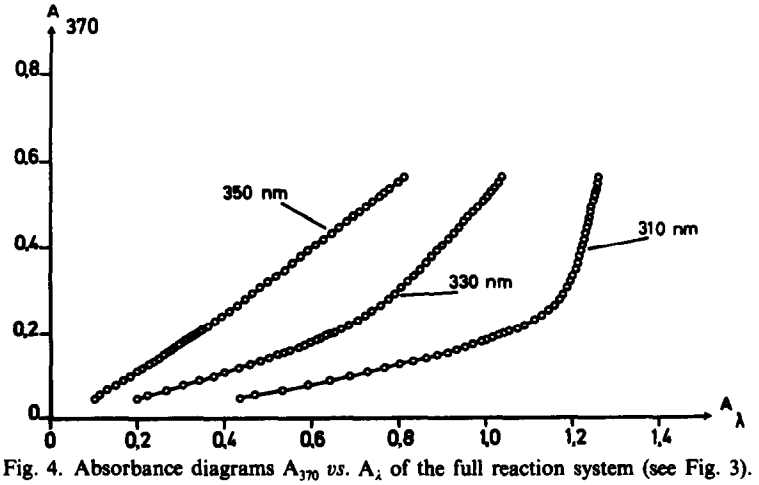

Fig. 4. Absorbance diagrams A_{370} *vs.* A_λ of the full reaction system (see Fig. 3).

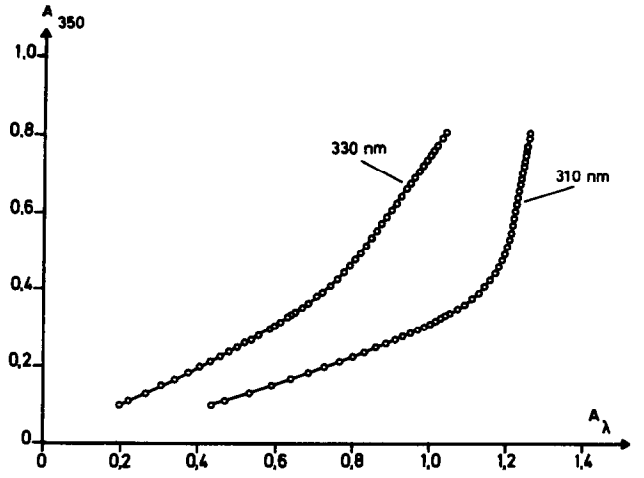

Fig. 5. Absorbance diagrams A_{350} *vs.* A_λ of the full reaction system (see Fig. 3).

$M^{-1}\,sec^{-1}$. The evaluation of the single reactions measured separately led to the values

$$k_1 = 2.86 \quad \text{and} \quad k_2 = 0.35$$

The 'reaction spectra'[2–7] of the first and second reaction step as well as of the full reaction system are presented in Figs. 1, 2 and 3. The A-diagrams for selected wavelength combinations are shown in Figs. 4 and 5. As Fig. 2 shows, the reactants of the second reaction step do not absorb strongly near 310 nm. Therefore, the quantities k_2 of this reaction determined by combining different wavelengths with 310 nm are relatively inaccurate (about 10–30%); these values are noted in the brackets in Table 1. It is astonishing that the k_i values calculated from the wavelength combination 370/350 nm are fairly reasonable though the corresponding A diagram shows only a weakly curved trend (see Fig. 4).

As shown by this practical example the knowledge of absorption coefficients is not a prerequisite for the application of the theory. During the reactions all or nearly all components may be absorbing. The only requirement for the evaluation is that enough components absorb, *i.e.*, that the single reactions of the system are individually registered spectroscopically. (Thus, in the case of the practical example it would be sufficient if only the components D and G were light absorbing.)

The practical procedure described here is typical for the analysis of about 100 different reaction systems obeying equation (1). The spectroscopically kinetic analysis involving reaction steps of second order is more complicated than that of systems consisting of only linear reactions. More constants have to be determined significantly in the case of reactions of second order at the same number of linearly independent reactions. However, it is possible to distinguish here between different reaction systems using consequently the criteria of equations (10)–(17) and other criteria described by Mauser.[1]

REFERENCES

1. H. Mauser, *Z. Naturforsch*, 1987, **42a**, 713.
2. G. Lachmann, H. Lachmann and H. Mauser, *Z. Physik. Chem. N.F.*, 1980, **120**, 9.
3. *Idem*, *ibid.*, 1980, **120**, 19.
4. J. Polster, *GIT Fachz. Lab.*, 1985, **9**, 869.
5. *Idem*, Dissertation 1974, Tübingen.
6. H. Mauser and J. Polster, *Z. Physik. Chem. N.F.*, 1974, **91**, 108.
7. H. Mauser, *Formale Kinetik*, Bertelsmann, Universitätsverlag, Düsseldorf, 1974.
8. H. Mauser and J. Polster, *Z. Physik. Chem. N.F.*, 1983, **138**, 87.
9. *Idem*, *Z. Physik. Chem. Leipzig*, 1987, **268**, 481.
10. J. H. Wilkinson, in *Numerical Software—Needs and Availability*, Academic Press, New York, 1978.
11. W. H. Press, B. R. Flannery, S. A. Teukolsky and W. T. Vetterling, *Numerical Recipes in PASCAL*, Cambridge University Press, 1989.

Talanta, Vol. 39, No. 10, pp. 1361–1367, 1992
Printed in Great Britain.

0039-9140/92 $5.00 + 0.00

CHARACTERIZATION OF REACTION PRODUCTS FORMED DURING THIN-LAYER CHROMATOGRAPHIC DETECTION OF THIOCARBAMATE HERBICIDES

KATALIN FODOR-CSORBA
Research Institute for Solid State Physics of the Hungarian Academy of Sciences, H-1525 Budapest, P.O. Box 49, Hungary

SÁNDOR HOLLY and ANDRÁS NESZMÉLYI
Central Research Institute for Chemistry of the Hungarian Academy of Sciences, H-1525 Budapest, P.O. Box 17, Hungary

GYÖRGY BUJTÁS
National Office of Inventions, H-1370 Budapest, P.O. Box 552, Hungary

(*Received* 26 *September* 1990. *Revised* 27 *February* 1991. *Accepted* 1 *July* 1991)

Summary—The reaction between thiocarbamate herbicides and 2,6-dichlorobenzoquinone-*N*-chloroimine or 2,6-dibromobenzoquinone-*N*-chloroimine is suitable for the detection of these herbicides on thin-layer plates with high sensitivity. The reactions were followed by infrared, nuclear magnetic resonance and mass spectrometry. We have established the formation of 2,6-dichlorobenzoquinone-*S*-alkyl sulphenylimines. In the case of the bromo-derivative, halogen exchange and substitution on the quinone ring took place simultaneously leading to the formation of mixed halogenated 2,6-dihalo- and, in addition, 2,3,6-trihalobenzoquinone-*S*-alkyl sulphenylimines. The final product of the detection reaction, *i.e.*, 2,6-dichlorobenzoquinone-*S*-alkyl sulphenylimine was reacted with 2,6-dibromobenzoquinone-*N*-chloroimine where 2,6-dichloro-3-bromobenzoquinone-*S*-alkyl sulphenylimine formed as a consequence of the looser bromine–carbon linkage on the 2 and 6 positions of the quinone ring.

Gibbs[1,2] introduced the 2,6-dichlorobenzoquinone-*N*-chloroimine (**I**) and the 2,6-dibromobenzoquinone-*N*-chloroimine[3] (**II**) for the detection of phenols in alkaline solution, leading to the formation of indophenols.[4,5] This method was extended for the analysis of anilines, adrenalins and noradrenaline.[6–8]

The compounds **I** and **II** were supposed to react with thiophenols forming thioindophenols. Surprisingly, the products were 1,4-benzoquinone-4-aryl sulphenylimines[9] which could be converted by heat treatment into the expected thioindophenols. Thioketons, sulphur containing pesticides, alkyl-, and aryl heterocyclic mercapto compounds can also be detected by **I** and **II** in alkaline conditions.[10,11]

Cuzzoni and Pietra Lissi[12] studied the reaction of Gibbs reagents with alkyl and aryl disulphides pointing out the formation of sulphenylimines followed by Cl_2 evolution. In these reactions of **II**, anomalous mixed halogenated benzoquinone derivatives were observed.

More recently, sulphydryl groups were detected in histochemical studies by these reagents.[13] Analogously, glyoxaline-2-thiol gave also sulphenylimine derivatives[14] in the reaction with **I** or **II**.

Thiocarbamate herbicides can be visualized by different detection methods. Some of them are summarized in Table 1. Ninhydrine,[17] palladium chloride in acidic solution[18] detect these compounds with the same detection limit. Less sensitive is the reaction of 4-(dimethylamino)-benzaldehyde but *o*-toluidine–KI system[19] detects thiocarbamates with two orders of magnitude higher sensitivity than the former one. Insecticides are very effective inhibitors of acetylcholine esterases. Surprisingly, thiocarbamates have some inhibitory effect on these enzymes[19,20] but their detection limits are two or three orders of magnitude higher. NBD-Cl (4-chloro-7-nitrobenzo-2,1,3-oxadiazole)[21] can be used for fluorogenic labelling. This agent reacts with the amino part of the carbamates and thiocarbamates after hydrolysis, giving fluorescent spots on a non-fluorescent background.

Table 1. Sensitivity of the thin-layer chromatographic detection methods for thiocarabamate herbicides

Reagents	Sensitivity (μg/spot)	Ref.
Ninhydrine	2.0	17
$PdCl_2$ + HCl	2.0	18
4-(Dimethylamino)-benzaldehyde	10.0	19
o-Toluidine + KI	0.3	19
Bee head esterase + 2-naphthylacetate	1.0	20
Drosophyla esterase + 2-naphthylacetate	1.0	20
Horse serum esterase + 2-indoxylacetate	0.5 (Butylate)	19
NBD–Cl	0.1	21
I	0.05	15
II	0.05	15

In our previous works[15,16] Gibbs reagents (**I, II**) were reported as sensitive thiocarbamate (**III**) detecting agents (Table 1). These compounds gave yellow spots with **III** on the thin-layer chromatographic (TLC) plates in strong acidic conditions. We have extended this method for the quantitative determination of **III** by *in situ* densitometry.[22,23] The absorption maximum of the coloured spots obtained with **I** was constantly at 450 nm, but it was less reproducible when **II** was applied.

In order to understand this changing absorption maximum of the coloured spots, we investigated the colour reaction. We used the same conditions in the synthesis of the compounds responsible for the detection, as was used in the analytical procedure. The only difference was heat treatment of the plates at the nanogram range which completed the colour formation. The isolated coloured compounds were studied by infrared (IR) nuclear magnetic resonance (NMR) and mass (MS) spectrometry.

EXPERIMENTAL

Apparatus

Infrared spectra were taken with a Nicolet 170 SX FTIR spectrometer in carbon tetrachloride solution, in nujol and/or potassium bromide pellets. Solid state Raman spectra were recorded with a Cary 82 spectrometer with an argon ion laser (exciting line 514.5 nm).

^{1}H NMR spectra were measured with a Varian XL-100-15 FT spectrometer at 25°, and ^{13}C spectra at 50°, the chemical shifts (δ) are with reference to internal tetramethylsilane. The multiplicities of the carbon lines were determined by the attached proton test (APT) technique.[24]

The mass spectra were taken by an AEI–MS 902 spectrometer with the following settings: ion accelerating voltage 8 kV, ionizing voltage 8 kV, stop current 100 μA, direct introduction, 180°. All mass numbers are given in daltons calculated for ^{35}Cl and ^{79}Br isotopes, respectively.

For TLC detection, the TLC plates were dipped or sprayed with 1% solution of **I** or **II** in acetic acid (96%) and heated at 110° for 2–10 min after drying. The yellow spots of the thiocarbamates appeared against the white background.

Densitometric measurements were carried out with a Shimadzu CS-920 high speed scanner at the absorption maximum of 2,6-dichlorobenzoquinone-*S*-alkyl sulphenylimine (λ_{max} 450 nm) determined *in situ* on Silufol plates (Kavalier, Czechoslovakia).[22,23] When the detection was carried out by **II**, the λ_{max} value had to be determined *in situ* in each case separately, and was found to be between 450–455 nm.

Melting points (uncorrected) were determined with a Boetius micro melting point equipment.

Chemicals

2,6 - Dichlorobenzoquinone - *N* - chloroimine was purchased from Janssen Chimica (Beerse, Belgium) and 2,6-dibromobenzoquinone-*N*-chlorimine from Merck (Darmstadt, Germany). EPTC (*S*-ethyl dipropylthiocarbamate), butylate (*S*-ethyl diisobutylthiocarbamate), cycloate (*S*-ethyl cyclohexyl *N*-ethyl-thiocarbamate), pebulate (*S*-propyl butylethylthiocarbamate), vernolate (*S*-propyl dipropylthiocarbamate) were commercial products supplied by (Nitrokémia Fűzfőgyártelep, Hungary) and purified by distillation. Kieselgel 60 (0.063–0.040 mm) stationary phase and Kieselgel 60 TLC plates were purchased from Merck (Darmstadt, Germany) while Silufol F_{254} plates were from Kavalier (Votice, Czechoslovakia). Solvents were obtained from Reanal (Budapest, Hungary) and distilled from glass before use.

Reagents

2,6-Dichlorobenzoquinone-N-*chloroimine (I).* Purified by recrystallization from ethyl alcohol:[24] m.p. 67°. ^{13}C NMR ($CDCl_3$) 124.5 (C_3), 136.5 (C_2), 134.6 (C_5), 141.9 (C_6), 165.2 (C_4), 172.6 (C_1) ppm. Found C 34.22, H 0.94, Cl 50.56, N 6.65, $C_6H_2Cl_3NO$ requires C 34.24, H 0.96, Cl 50.54, N 6.66

2,6-dibromobenzoquinone-N-*chloroimine (II).* Purified by recrystallization from ethyl alcohol:

m.p. 79–80° (chromatographic purity). Found C 24.09, H 0.70, Cl 11.82, Br 53.35, N 4.67, $C_6H_2ClBr_2NO$ requires C 24.07, H 0.67, Cl 11.84, Br 53.38, N 4.68 ^{13}C NMR ($CDCl_3$) 128.8 (C_3), 127.6 (C_2), 134.3 (C_6), 138.7 (C_5), 166.0 (C_4) ppm; $^3J_{CH}(C_3)$ 5.9, $^1J_{CH}(C_3)$ 175.5, $^2J_{CH}(C_2)$ 5.4, $^2J_{CH}(C_6)$ 6.0, $^3J_{CH}(C_5)$ 5.5, $^1J_{CH}(C_5)$ 175.6 Hz.

Synthesis

*2,6-Dichlorobenzoquinone-S-ethyl sulphenylimine (IVa).** The solution of 1.0 g (5 mmoles) of 2,6-dichlorobenzoquinone-*N*-chloroimine (**I**) in 10 ml (96%) acetic acid was added dropwise to the stirred solution of 0.9 g (5 mmoles) of EPTC (**III**) in 10 ml of $CHCl_3$ at room temperature. In the slightly exothermic reaction gas evolved, a yellowish precipitate formed, and the pale yellow solution turned deep brownish–red. After 30 min the precipitate was filtered off and the filtrate was poured on ice. The organic layer was washed with 3 × 10 ml of water, 3 × 10 ml of 5% $NaHCO_3$, 3 × 10 ml of water, dried (with magnesium sulphate) and evaporated under reduced pressure. The residue was purified on a Florisil column (inner diameter 22 mm), deactivated by 5% w/w H_2O eluted with cyclohexane:ethylacetate (9:1). The elution was followed by TLC on Silufol F_{254} plates developed in xylene. Fractions, containing the compound which appeared on the TLC plate at R_f 0.35, were evaporated and the residue crystallized from cyclohexane, giving orange-red needles [1 g (84.75%), m.p. 82.5–83°]. Found: C 40.05, H 2.94, N 5.87, S 13.45, Cl 30.00, $C_8H_7Cl_2NOS$ requires C 39.95, H 2.90, N 5.63, S 13.29, Cl 30.10 IR (CCl_4) 3000–2800 (νCH_{aliph}, *S*-ethyl), 1665 ($\nu C{=}O$), 1559 ($\nu C{=}N$), 1277 ($=C_3H$ and $=C_5H$ in plane deformation), 1265 [(*S*)—CH_2 wagging], 1056 ($=C_3H$ and $=C_5H$ in plane deformation), 900 ($=C_3H$ and $=C_5H$ out of plane wagging) cm^{-1}. ^1H NMR ($CDCl_3$) 1.4(t), 3.1(q), 7.46(d) (overlapping doublets) $J_{3,5} = 2.5$ Hz (DMSO) 1.45(t), 3.36(q), 7.73(d) (overlapping doublets) ppm. $J_{3,5} = 2.5$ Hz. ^{13}C NMR ($CDCl_3$) 13.5(q), 35.9(t), 123.5 (C_3), 128.3 (C_3), 133.8 (C_6), 136.1 (C_5), 150.9 (C_4), 173.5 (C_1) ppm MS m/e (I%): 235 M(100), 207 M-C_2H_4(100), 179 M-C_2H_4—CO(9), 172 M-C_2H_4—Cl(20), 144 M-C_2H_4—Cl—CO(17), 60 C_2H_4S(20). When cycloate or butylate were reacted with **I** instead of EPTC, the same product **IVa** was isolated.

2,6-Dichlorobenzoquinone-S-propyl sulphenylimine (IVb).† Pebulate (**III**) (5 mmoles) was reacted with **I** (5 mmoles) according to the procedure described in **IVa**, giving the product **IVb**. R_f 0.39 (xylene, Kieselgel 60), 0.9 g (71.9%) m.p. 72–73°. Found C 43.10, H 3.78, N 5.53, S 12.86, Cl 28.37, $C_9H_9Cl_2NOS$ requires C 43.21, H 3.62, N 5.59, S 12.81, Cl 28.34 IR (CCl_4) 3000–3800 (νCH_{aliph}, *S*-propyl), 1660 ($\nu C{=}O$), 1559 ($\nu C{=}N$), 1276 ($=C_3H$ and $=C_5H$ in plane deformation), 1240 [(*S*)—CH_2 wagging], 1050 ($=C_3H$ and $=C_5H$ in plane deformation), 901 ($=C_3H$ and $=C_5H$ out of plane wagging) cm^{-1}. ^1H NMR ($CDCl_3$) 1.13(t), 1.86(m), 3.3(t), 7.46(d) (overlapping doublets) ppm, $J_{3,5} = 2.5$ Hz. ^{13}C NMR ($CDCl_3$) 12.90(q), 21.954(t), 43.961(t), 123.392(d), 136.062(d), 150.888(s), 173.3(s) ppm MS m/e (I%): 249 M(50), 207 M-C_3H_6(50), 202 M-CH_3S(20), 179 M-C_3H_6—CO(13), 172 M-C_3H_6—Cl(20), 144 M-C_3H_6Cl—CO(10), 74 C_3H_6S(90), 73 C_3H_5S(25), 43 C_3H_7(100). When vernolate was reacted with **I** instead of pebulate, the same product, **IVb**, was isolated.

2,6-Dibromobenzoquinone-S-ethyl sulphenylimine (Va). To the stirred and cooled solution of EPTC (5 mmoles) in 5 ml of chloroform, 1.45 g (5 mmol) **II** in 10 ml (96%) of acetic acid was added. After 30 min of stirring the precipitate was filtered off. The organic phase was poured on ice and washed with 3 × 10 ml of water, 3 × 10 ml of 5% $NaHCO_3$, 3 × 10 ml of water, dried on anhydrous magnesium sulphate and concentrated to 2 ml. This solution was checked by TLC. Two yellow spots were visible on Kieselgel 60 plates eluted with xylene. According to MS results the first one at R_f 0.58 was the mixture of **VIIa–IXa**, and the second one at R_f 0.31 contained the desirable **Va** but **VIa, VIIa** were also present (see later).

Preparative chromatographic separation of R_f 0.58 and R_f 0.31 was carried out by flash chromatography on a column (inner diameter 50 mm) packed with 300 g Kieselgel 60 (0.063–0.040 mm) under 0.2 bar overpressure, using xylene as an eluant. *Rf* 0.58 (**VIIa–IXa**), 0.3 g m.p. 101–103°, after crystallization from cyclohexane 0.2 g m.p. 105–106°; MS 2,3,6-tribromobenzoquinone-*S*-ethyl sulphenylimine (**VIIIa**) $C_8H_6Br_3NOS$ M = 401, 2-chloro-3,6-dibromobenzoquinone-*S*-ethyl sulphenylimine (**VIIIa**) $C_8H_6Br_2ClNOS$ M = 357 as main product, 2,6-dichloro-3-bromo-benzoquinone-

*"a" denotes the *S*-ethyl derivative.
†"b" denotes the *S*-propyl derivative.

S-ethyl sulphenylimine (**IXa**) $C_8H_6BrCl_2NOS$ M = 313. Each component exhibited fragment ions analogous to those of **IVA**. IR (CCl_4) 3000–2800 (νCH_{aliph}, *S*-ethyl), 1662 ($\nu C{=}O$), 1553 ($\nu C{=}N$), 1267 [(*S*)—CH_2 wagging] cm^{-1}. ^1H NMR ($CDCl_3$): 1.53(t), 3.36(q), 7.68 and 7.95(s) ppm (DMSO): 1.40(t), 3.36(q), 8.00 and 8.20(s) ppm

R_f 0.31. (**IVa–VIa**) 1.1 g m.p. 89–91°, crystallized from cyclohexane 0.96 g m.p. 91–91.5°; as minor component. MS 2,6-di bromobenzoquinone-*S*-ethyl sulphenylimine (**Va**) $C_8H_7Br_2NOS$ M = 323, 2-bromo-6-chlorobenzoquinone-*S*-ethyl sulphenylimine (**VIa**) $C_8H_7BrClNOS$ M = 279, 2,6-dichloro-benzoquinone-*S*-ethyl sulphenylimine (**IVa**) $C_8H_7Cl_2NOS$ M = 235. Each component exhibited fragment ions analogous to those of **IVa**. IR (CCl_4): 3000–2800 (νCH_{aliph}, *S*-ethyl), 1660 ($\nu C{=}O$), 1553 ($\nu C{=}N$), 1276 ($=C_3H$ and $=C_5H$ in plane deformation), 1267 [(*S*)—CH_2 wagging], 1057 ($=C_3H$ and $=C_5H$ in plane deformation), 903 ($=C_3H$ and $=C_5H$ out of plane wagging) cm^{-1} ^1H NMR: ($CDCl_3$) 1.53(t), 3.29(q), 7.43 and 7.76(d) (overlapping doublets) ppm $J_{3,5}$ = 2.5 Hz. (DMSO) 1.33(t) 3.4(q), 7.73 and 7.92(d) ppm. Densitometry of the separated **IVa–VIa** and **VIIa–IXa** was carried out on Silufol plates eluted with xylene and scanned 30 min after development. The ratio of **IVa–VIa** to **VIIa–IXa** was 3:1.

2,6-Dichloro-3-bromobenzoquinone-S-ethyl sulphenylimine (IXa). To the solution of 0.5 g (1.18 mmol) 2,6-dichloro-benzoquinone-*S*-ethyl sulphenylimine (**IVa**) in 5 ml of $CHCl_3$, 0.6 g (2 mmoles) **II** in 5 ml of 96% acetic acid was added and stirred for four hours. The precipitate was fitered off and recrystallized from 70% ethyl alcohol. According to the elemental analysis the precipitate was a mixed salt of ammonium chloride and ammonium bromide. After pouring the reaction mixture on iced water and extracting with chloroform, washing with $NaHCO_3$ (5%) and water, it was evaporated and purified by flash chromatography on Kiesegel 60 (0.063–0.040 mm) column eluted with xylene under 0.2 bar overpressure. 2,6-dibromo-, 2-bromo-6-chloro-, 2,6-dichlorobenzoquinone and unreacted **IVa** were separated from **IXa**. 0.1 g **IXa** m.p. 69–70° cafter crystallization from cyclohexane. IR 3000–2800 (νCH_{aliph}, *S*-ethyl), 1666 ($\nu C = O$), 1553 ($\nu C = N$) cm^{-1}. ^1H NMR ($CDCl_3$) 1.53(t), 3.33(q), 7.66(d) ppm. MS m/e (I%) $C_8H_6BrCl_2NOS$: 313 M(100); 285 M-C_2H_4(100).

Preparation of food extracts

Method A. Samples (100 g) with high water (>70%) and low sugar content (<5%) were extracted with acetonitrile (100 ml) in the presence of Hyflosupercel (10 g) in a high speed blender. After suction the remaining material was washed with acetonitrile (2 × 20 ml). The filtrate was partitioned with petroleum ether (100 ml). After 2 min of shaking, saturated sodium chloride solution (50 ml) and water (300 ml) was given to the mixture. After shaking and separation, the organic layer was washed with water (2 × 100 ml) dried on anhydrous sodium sulphate (15 g) and concentrated on a Kuderna-Danish evaporator. The obtained solution was cleaned on a Florisil column (20 g, 60–100 mesh), deactivated in 5% with water (w/w). The evaporated extract was eluted with 6 and 15% ether containing petroleum ether. The eluates were concentrated to 1 ml in Kuderna-Danish equipment and analysed by TLC.

Method B. High water (>70%) and 5–15% sugar containing samples (100 g) were extracted as given above but 25 ml of water was added before blending.

Deep frozen spinach and potato samples were analysed by method A and green pea and green bean samples by method B.[23]

RESULTS AND DISCUSSIONS

We studied the chemical reaction responsible for the detection of thiocarbamate herbicides (Fig. 1). The thiocarbamates (**III**) (EPTC, butylate, cycloate) reacted with the formation of the same derivative: 2,6-dichloro-benzoquinone-*S*-ethyl sulphenylimine (**IVa**), while pebulate and vernolate gave the *S*-propyl analogue (**IVb**) according to their IR, ^1H, ^{13}C NMR and mass spectra.

The highly pure **II** (controlled by elemental analysis, IR, NMR and MS) was reacted with **III** and an unexpected reaction was observed. In spite of the fact that, the product obtained in the reaction between **II** and **III** seemed to be chromatographically pure in several solvents and solvent systems having different polarity and selectivity (benzene, toluene, xylene, mesitylene, cyclohexane, cyclohexene and their mixtures),[22] the results of elemental analysis did not correspond to the expected 2,6-dibromobenzoquinone-*S*-alkyl sulphenylimine. The potentiometric halogen determination[26] gave evidence of the presence of chlorine and bromine in the product, suggesting the formation of a mixture.

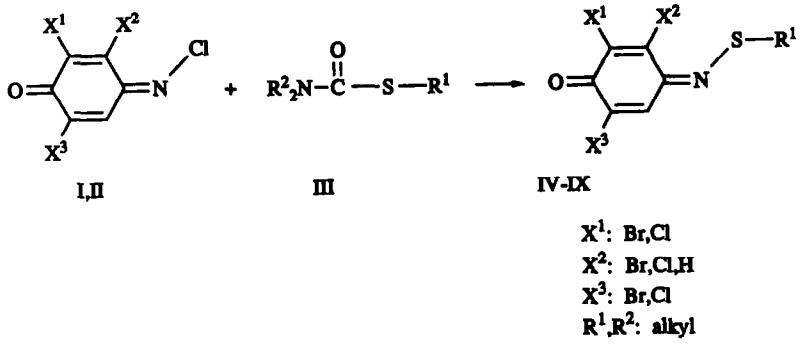

Fig. 1. Formation of halogen substituted benzoquinone-*S*-alkyl sulphenylimines in the detection process.

MS showed on the basis of the molecular ions that the separated materials were mixtures of dihalogenated (**IVa–VIa, IVb–VIb**) and trihalogenated (**VIIa–IXa, VIIb–IXb**) benzoquinone-*S*-alkyl sulphenylimines.

The molecular ions of the products undergo simultaneous fragmentation routes: cleavage of the mercapto group and elimination of ethylene or propylene, followed by the loss of the carbonyl group or a halogen atom (*cf.* mass spectral data of **IVa** and **IVb** in the experimental part). The molecular ions together with these fragment peaks enabled us to recognize the components of the mixture of **IVa–VIa, IVb–VIb, VIIa–IXa, VIIb–IXb**. Tetrahalogenated derivatives were never detected in the spectra of the above mixture.

As the MS analysis showed the reaction of **II** and **III** led not only to the formation of **Va** or **Vb**, but two simultaneous side reactions took place also: halogen exchange (**IV** and **VI**), and proton→halogen substitution (**VII–IX**) on the quinone ring.

The halogen exchange proceeds in the opposite direction of the Finkelstein reaction.[27] Earlier Cuzzoni and Pietra Lissi[12] found the formation of a mixture of dibromo-, dichloro- and Br,Cl-containing sulphenylimines, nevertheless the positions of these substituents were not established, furthermore no trihalogenated derivative was assumed. Presumably, this side reaction took place in that case as well.

In the literature there are some examples on halogen exchange in the unexpected direction: Lyons and Thompson[28] found the formation of 3,6-dichloronaphthoquinone from 3-bromo-6-chloronaphthoquinone in alcoholic hydrochloric acid solution; the same reaction took place with 3-bromo-6-methylnaphthoquinone, where the chloro atom entered at position 3. An ionic mechanism was assumed.

The halogen atoms attached to a quinone ring are exchangeable by fluorine as well: tetrachloro-1,4-benzoquinone can be transformed at high temperature to 6-fluoro-2,3,5-trichloro- and 3,6-difluoro-2,5-dichloro-1,4-benzoquinone.[29] Further on, the tetrabromo derivative can easily be transformed to a 2,6-di- or tetraiodo derivative.[30] Simultaneously Cl→Br, and H→Br substitutions are described on 2-chloro-1,4-naphthoquinone.[31] These few examples support that the Br→Cl exchange is not unprecedented, however, we have to verify that the halogen exchange on the quinone ring takes place at 2,6-position. This is supported by the results of ^{1}H, ^{13}C NMR and IR spectroscopy.

Because of the trigonal hybrid state of nitrogen in **II**, the chloroatom attached to nitrogen eliminates the equivalency of the protons at the 3 and 5 positions. Their signals can be assigned as doublets with the coupling constant $J_{3,5} = 2.5$ Hz[32,33]. The doublets of the protons at the 3 and 5 positions of the dihalogenated products (**Va, VIa** or **Vb,VIb**) were resolved in dimethyl sulphoxide. **IVa** was present only in a very small amount so it had no disturbing effect. The coupling constant was characteristic for the meta position. In the IR spectra of the dihalogenated compounds (**IVa, b–VIa,b**) the coupled in plane deformation vibrations of the protons at 3 and 5 positions showed changes. **I** and **IVa** have this vibration at 1277 cm^{-1}. In the spectrum of **II** this appeared at 1271 cm^{-1}, but after a short reaction time with **III** the product has it at 1265 cm^{-1}. After longer time a band appeared at 1277 cm^{-1} showing the formation of **IVa**.

In 30 min **I** or **II** reacted with **III** completely, but in the reaction of **II** trihalogenated benzoquinone sulphenylimine derivatives appeared (**VII–IX**). The ratio of di- and trihalogenated sulphenylimines was measured by *in situ* densit-

ometry and was found to be 3:1. The longer the reaction time the more **IVa,b**, **VIa,b** and **VIIa,b–IXa,b** formed simultaneously.

Steric hindrance of the *S*-propyl group on the 3 and 5 positions of the quinone ring causes the formation of **VIIb–IXb** in smaller quantities than that of **VIIa–IXa**. It should be remarked that the coupled deformation vibrations of the 3 and 5 protons disappeared from the IR spectra of **VIIa,b–IXa,b**. So we can establish that the bromine–carbon linkage on the quinone ring in the 2 and 6 positions is less stable than the chlorine–carbon one and therefore replacement of bromine by another halogen atom was observed. Spectroscopic data of this substitution reaction were supported by chemical reaction too.

We can study this substitution reaction separately from the formation of the sulphenylimine derivatives if the final product (**IVa**) of the reaction between **I** and **III** is reacted with **II**. On the basis of our results we expected the formation of 2,6-dichloro-3-bromo-benzoquinone-*S*-ethyl sulphenylimine (**IXa**) (Fig. 2) which was isolated.

Substitution took place only when the reaction was carried out for a longer time (several hours) while **II** suffered some decompositions leading to 2,6-dihalobenzoquinones.[34] These byproducts were identified by IR spectroscopy. The tetrahalogenated compound was never observed.

In the analysis of thiocarbamates, more reproducible results were obtained with the use of **I** than with **II**. The chemical investigations on the colour formation of **II** can explain this phenomenon. The thiocarbamate herbicide content of biological extracts was determined by densitometry with the application of the above discussed chemical colour detection method using reagent **I** on Silufol plates.[35] This detection was selective for the thiocarbamates in several biological samples. Figure 3 depicts a densitogram of deep frozen green peas extract where no interfering coextracts disturbed the quantitative determination.

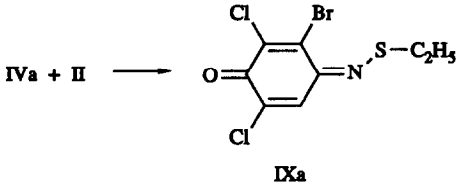

IXa

Fig. 2. Chemical evidence of substitution.

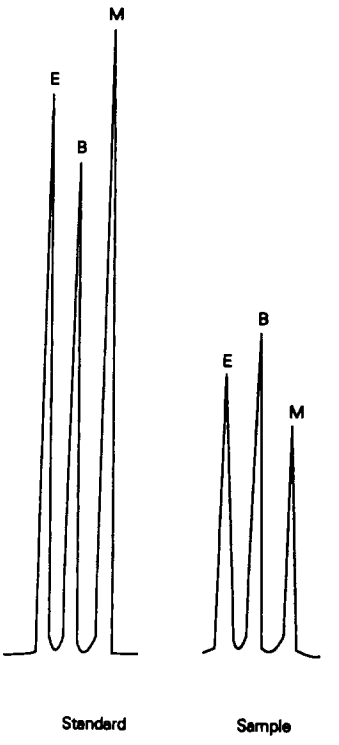

Fig. 3. Densitogram of deep frozen green peas extract. E: EPTC, B: butylate M: molinate.

Acknowledgement—We are thankful to Dr. I. Gács, for potentiometric halogen determination.

REFERENCES

1. H. D. Gibbs, *J. Biol. Chem.*, 1927, **71**, 445.
2. *Idem, ibid.*, 1927, **72**, 649.
3. R. Castle, *Chem. Ind. (London)*, 1950, 313.
4. M. B. Ettinger and C. C. Ruchhoft, *Anal. Chem.*, 1948, **20**, 1191.
5. P. D. Josephy and R. E. Lenkinski, *J. Chromatogr.*, 1984, **294**, 375.
6. H. Thielemann, *Z. Anal. Chem.*, 1973, **267**, 46.
7. *Idem, Sci. Pharm.*, 1980, **48**, 170.
8. H. Ulrich and R. Richter, *Methoden der Organischen Chemie*, E. Muller and C. Grundmann (eds.), 4th Ed., Vol. VIII/3a, p. 724. Georg Thieme Verlag, Stuttgart, 1977.
9. D. N. Kramer and R. M. Gamson, *J. Org. Chem.*, 1959, **24**, 1154.
10. Shozo Kamiya, *Bunseki Kagaku*, 1959, **8**, 596; *Chem. Abstr.*, 1963, **58**, 9612h.
11. J. H. V. Stenersen, *Bull. Environ. Contam. Toxicol.*, 1967, **2**, 364.
12. M. T. Cuzzoni and T. Pietra Lissi, *Farmaco, Ed. Sci.*, 1964, **19**, 981.
13. Z. Hallit and D. Damas, *Microsc. Acta*, 1981, **84**, 1.
14. C. E. Searle, *J. Appl. Chem.*, 1955, **5**, 313.
15. K. Fodor-Csorba, T. Kőmives, A. F. Márton and F. Dutka, *Magy. Kem. Foly.*, 1978, **84**, 526; *Chem. Abstr.*, 1979, **90**, 34805q.
16. K. Fodor-Csorba, T. Kömives, A. F. Márton and F. Dutka, *Nahrung*, 1980, **24**, 963; *Chem. Abstr.*, 1981, **94**, 82334q.

17. J. E. Casida, E. C. Kimmel, H. Ohkawa and R. Ohkawa, *Pestic. Biochem. Physiol.*, 1975, **5**, 1.
18. W. Ebing, *J. Chromatogr.*, 1972, **65**, 533.
19. A. Ambrus, E. Hargitai, Gy. Károly, A. Fülöp and J. Lantos, *J. Assoc. Off. Anal. Chem.*, 1981, **64**, 743.
20. G. F. Ernst, C. Pieterse and L. J. H. Martens, *J. Chromatogr.*, 1977, **133**, 245.
21. F. Van Hoof and A. Heyndrickx, *Meded. Fac. Landbouwwetensch., Rijksuniv. Gent*, 1973, **38**, 911; *Chem. Abstr.*, 1974, **81**, 22122r.
22. K. Fodor-Csorba, F. Dutka and M. Vajda, in *Proceedings of International Symposium on TLC with Special Emphasis on OPLC*, E. Tyihák (ed.), p. 164. Labor MIM, Szeged, 1984.
23. K. Fodor-Csorba and F. Dutka, *J. Chromatogr.*, 1986, **365**, 309.
24. S. L. Patt and J. N. Shoolery, *J. Magn. Reson.*, 1982, **46**, 535.
25. P. Venuvanalingam, U. Chandra Singh, N. R. Subbaratman and V. K. Kelkar, *Spectrochim. Acta*, 1980, **36A**, 103.
26. A. Campiglio and G. Traverzo, *Mikrochim. Acta*, 1980, **1**, 495.
27. H. Finkelstein, *Chem. Ber.*, 1910, **43**, 1528.
28. J. M. Lyons and R. H. Thompson, *J. Chem. Soc.*, 1953, 2910.
29. K. Wallenfels and W. Draber, *Chem. Ber.*, 1957, **90**, 2819.
30. H. A. Torrey and W. H. Hunter, *J. Am. Chem. Soc.*, 1912, **34**, 707.
31. R. F. Silver and H. L. Holmes, *Can. J. Chem.*, 1968, **46**, 1859.
32. J. F. Bagli, *J. Am. Chem. Soc.*, 1962, **84**, 177.
33. H. Saito and K. Nukada, *Can. J. Chem.*, 1968, **46**, 2989.
34. P. A. Morozov, A. A. Lugovskoi, N. K. Morozova, V. P. Bukalov and A. P. Tuseev, *Zh. Strukt. Khim.*, 1978, **19**, 755; *Chem. Abstr.*, 1979, **90**, 5459z.
35. K. Fodor-Csorba, in *Handbook of Thin-Layer Chromatography*, J. Sherma and B. Fried (eds.), Vol. 55, Chapter 22, p. 685. Marcel Dekker, New York, 1990.

Talanta, Vol. 39, No. 10, pp. 1369–1375, 1992
Printed in Great Britain.

0039-9140/92 $5.00 + 0.00

SPECTROFLUORIMETRIC DETERMINATION OF GUANETHIDINE SULPHATE, GUANOXAN SULPHATE AND AMILORIDE HYDROCHLORIDE IN TABLETS AND IN BIOLOGICAL FLUIDS USING 9,10-PHENANTHRAQUINONE

MOHAMED H. ABDEL-HAY, SHEREEN M. GALAL, MONA M. BEDAIR, AZZA A. GAZY and ABDEL AZIZ M. WAHBI

Faculty of Pharmacy, University of Alexandria, Pharmaceutical Analytical Chemistry Department, Alexandria, 21521, Egypt

(*Received* 27 *May* 1991. *Revised* 9 *March* 1992. *Accepted* 23 *March* 1992)

Summary—A highly sensitive spectrofluorimetric method for the determination of some drugs of the monosubstituted guanidine derivatives in laboratory made tablets, in spiked human serum and in urine samples is presented. The method is based on the reaction of guanethidine sulphate (I), guanoxan sulphate (II) and amiloride hydrochloride (III) with 9,10-phenanthraquinone (IV) to give highly fluorescent derivatives. The linearity ranges were found to be 0.06–0.96 μg/ml for (I) and (II) and 0.04–0.28 μg/ml for (III), with relative standard deviation less than 2%. Mean percentage recoveries for tablets were found to be 99.9 ± 1.3, 100.5 ± 1.1 and 100.0 ± 1.6 for I, II and III, respectively. For I and III the results are highly correlated with the B.P. methods. Using the synchronous fluorimetry, differentiation between I and II was possible. Chloroform, dichloromethane and ethyl acetate have been used to extract I, II and III, respectively from serum and urine at basic pH, followed by applying the proposed fluorimetric method. Percentage recoveries were found to be 95.7–102.2%. The limit of detection is 0.04 μg/ml for I and II and 0.02 μg/ml for III.

The fluorescence reaction of 9,10-phenanthraquinone as a very sensitive test for arginine and arginine-containing peptides was first introduced by Itano and Yamada.[1] The mechanism of the fluorescence reaction of benzylguanidine as monosubstituted guanidines with 9,10-phenanthraquinone was investigated.[2] Biguanides reacted similarly giving highly fluorescent products.[3]

Guanethidine and guanoxan sulphates have been widely used as antihypertensive agents. They exhibit marked neuron blocking effects in the treatment of moderate and severe hypertension. Several methods have been reported for their determination, including spectrophotometry,[4] oxidimetry,[5] complexometry,[6] colorimetry,[7–10] fluorimetry,[11–13] and high-performance liquid chromatography.[14–16] Amiloride hydrochloride is used as potassium-sparing diuretic in edema, renal and liver disorders. It interferes with the process of cationic exchange in the distal tubule by blocking the resorption of sodium ion and the secretion of potassium ion. It has been determined colorimetrically using sodium nitroprusside,[17] methylbenzothiazolin hydrazone[18] and *N*,*N*-dimethyl–phenylenediamine.[19] Second derivative spectrophotometric determination of amiloride hydrochloride in a two component mixture was described.[20] Methylguanidine and guanidine in physiological fluids have been determined by high-performance liquid chromatography with fluorescence detection[21] and determination[22] using their reaction with phenanthrene-9,10-dione. Guanethidine and guanoxan have been determined in biological fluids by gas chromatography after selective extraction procedures.[23]

The official methods[24] for the assay of the above-selected drugs are, (i) a colorimetric procedure using sodium nitroprusside and potassium hexacyanoferrate for guanethidine sulphate and (ii) a spectrophotometric measurement at 363 nm for amiloride hydrochloride using tributylorthophosphate as a solvent.

The present work deals with the determination of guanethidine sulphate, guanoxan sulphate and amiloride hydrochloride using the

condensation reaction of the guanidino group with 9,10-phenanthraquinone with the purpose of increasing sensitivity and selectivity. In urine and serum these drugs were first extracted according to the GC method[23] followed by applying the proposed fluorimetric method.

EXPERIMENTAL

Apparatus

All fluorimetric measurements were performed on a Perkin–Elmer Model 650-10S fluorescence spectrophotometer equipped with 1.0 × 1.0 cm quartz cells, a 150-W xenon lamp, excitation and emission grating monochromators and a Perkin–Elmer Model 56 recorder. The spectra were measured with the normal instrument gain and minimum ratio mode. The sensitivity ranges used were 0.1 and 0.3 according to the concentration level.

Reagents and samples

All reagents were of AnalaR grade, and were checked before use for the presence of fluorescent contaminants.

9,10-Phenanthraquinone reagent, 2 μg/ml in dimethylformamide, Gold label, free of anthraquinone, Aldrich Chemicals Co., Inc. The solution was kept in a refrigerator. Fresh solutions were prepared every week.

Authentic samples of guanethidine sulphate (Ciba–Geigy, Basle, Switzerland), guanoxan sulphate (Pfizer, Kent, England) and amiloride hydrochloride (Kahira Pharmaceuticals & Chemical Industries Co., Cairo, Egypt) were kindly donated by the manufacturer and were used without further purification.

Biological samples. Serum and urine specimens are collected from adult healthy volunteers who are not under medical treatment. The samples were first analysed by the proposed method to ensure that there is no interference from endogenous compounds.

Fluorimetric procedure

Preparation of calibration graphs. Prepare a solution containing 50 mg of either guanethidine sulphate, guanoxan sulphate or amiloride hydrochloride in 50 ml of distilled water. Place in a 25-ml calibrated flask, an appropriate volume of the drug solution (6–24 μl) for guanethidine sulphate and guanoxan sulphate and (2–8 μl) for amiloride hydrochloride so that the final content is between 6–24 μg for I and II and 2–8 μg for III. Add 2.5 ml of 9,10-phenanthraquinone reagent (2 μg/ml) and 0.25 ml of 1*M* sodium hydroxide solution. Allow the mixture to stand at room temperature for 45 min, then add 0.25 ml of concentrated hydrochloric acid. Make up to volume with distilled water and measure the fluorescence intensity. Correct the observed fluorescence by subtracting the fluorescence intensity measured using the same procedure on a reagent blank. Make the fluorimetric measurements using an excitation wavelength of 310 nm for I and II and 360 nm for III and an emission wavelength of 395 nm for I and II and 420 nm for III (Figs. 1 and 2).

Determination of Guanethidine sulphate, Guanoxan sulphate and Amiloride hydrochloride in laboratory prepared tablets. Weigh and powder 20 tablets. Weigh accurately a quantity of the powdered tablets equivalent to about 50 mg of each of the three drugs. Extract with three 10-ml portions of distilled water and filter (using Whatman No. 1) the combined extracts into a 50-ml calibrated flask. Complete to volume with distilled water. Apply the above procedure, using 20 μl of the final tablet solution for I and II and 5 μl of the final tablet solution for III beginning at "Add 2.5 ml of 9,10-phenanthraquinone...".

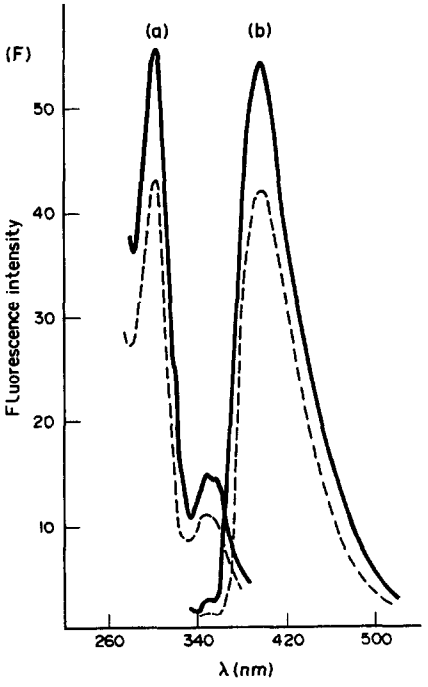

Fig. 1. (a) Excitation and (b) emission spectra of 9,10-phenanthraquinone derivatives of (——) guanethidine (0.60 μg/ml) and (– – –) guanoxan (0.36 μg/ml). (λ_{ex} = 310 nm, λ_{em} = 395 nm).

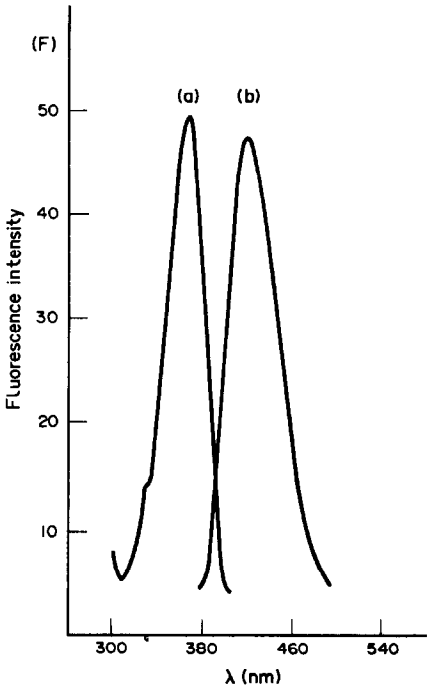

Fig. 2. (a) Excitation and (b) emission spectra of 9,10-phenanthraquinone derivatives of amiloride (0.16 μg/ml) (λ_{ex} = 360nm, λ_{em} = 420 nm).

Determination of the selected guanidino drugs in urine and serum. Adjust the pH of urine to 10.0 and of serum to 7.0. Place 5 ml of serum or urine in 50-ml stoppered shaking tube. Add a 6.0-ml aliquot of I and II and 2.0 ml of III. Add 20 ml of toluene in the case of urine and 20 ml diethyl ether in the case of serum, shake the tube for 10 min and centrifuge. Reject the organic layer. Add 0.5 ml of 50% sodium hydroxide, extract for 20 min using 30 ml of each of chloroform for I, dichloromethane for II and ethyl acetate for III. Centrifuge and remove the upper aqueous layer. Transfer the organic phase to another shaking tube containing 10 ml of 0.1*N* hydrochloric acid, shake the tube for 10 min and centrifuge. Transfer the aqueous layer to a 100-ml standard flask and complete to the mark with distilled water. Pipette 0.1–0.2 ml of this solution into a 25-ml standard flask, follow exactly as in "Calibration graphs above beginning at "Add 2.5 ml of 9,10-phenanthraquinone...". Calculate the concentration from a calibration graph prepared similarly using aqueous solutions in place of the urine and serum.

RESULTS AND DISCUSSION

9,10-Phenanthraquinone (IV) reacts with guanidino compounds in an alkaline medium to give an intermediate compound which can easily undergo hydrolysis in acid medium to give a fluorescent product and aldehyde.[2] Similarly, the reaction between guanethidine (I) and guanoxan (II) with IV can be explained to follow scheme I in the present work. The excitation and emission wavelengths of the fluorescent product (VI) were found to occur at 310 and 395 nm, respectively[13] (Fig. 1). These findings differ slightly from the previously reported wavelengths using simple guanidines.[2]

The reaction of 9,10-phenanthraquinone (IV) with amiloride (III) in alkaline medium is suggested to give another intermediate substance VII containing amide linkage. The latter (VII) cannot undergo hydrolysis in acid medium at room temperature. The excitation (360 nm) and emission (420 nm) wavelengths of the product (Fig. 2) were found to be completely different from those of compound VI. Moreover, the reaction product with amiloride was found to be 10 times more sensitive than VI (Table 1). Accordingly, we suggest that a further condensation of VII with another molecule of IV would occur to give a highly fluorescent compound VIII as shown in scheme 2.

Factors affecting the fluorimetric procedure

Influence of reagent concentration and reaction time. The effect of 9,10-phenanthraquinone concentration and reaction time selected for the recommended method was studied by carrying out the fluorimetric procedure using 0.72 μg/ml

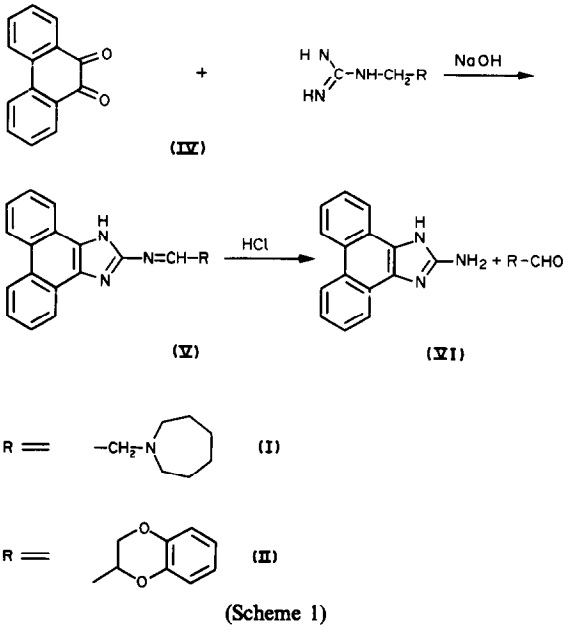

(Scheme 1)

Table 1. Analytical data for guanethidine sulphate, guanoxan sulphate and amiloride hydrochloride using the proposed fluorimetric method

Compound	Wavelength, nm λ_{exc}	Wavelength, nm λ_{em}	Concentration range μg/ml	Sensitivity setting	Linear† regression *a*	Linear† regression *b*	Corr. Coeff. *r*	RSD*, %
Guanethidine sulphate	310	395	0.24–0.96	0.1	−0.36	90.27	0.9997	1.30
			0.06–0.36	0.3	−3.83	255.40	0.9998	0.96
Guanoxan sulphate	310	395	0.24–0.84	0.1	0.58	102.19	0.9995	1.06
			0.06–0.36	0.3	−5.18	310.00	0.9999	1.33
Amiloride hydrochloride	360	420	0.12–0.28	0.1	−1.76	373.00	0.9992	1.70
			0.04–0.24	0.3	−5.39	1079.50	0.9990	1.60

*Relative standard deviation (six replicate determinations).
†Relative digital units, where (a) is the intercept and (b) is the slope.

of I, 0.60 μg/ml of II and 0.12 μg/ml of III. Changing the concentration of 9,10-phenanthraquinone over the range 0.04–0.32 μg/ml showed that the optimum concentration to be used is 0.20 μg/ml. Maximum fluorescence intensity for all three was developed within 45 min and remained stable for 60 min at room temperature.

Effect of temperature, sodium hydroxide and hydrochloric acid concentrations. An experiment has been designed to study the effect of carrying out the reaction at 20° (room temperature), 40° and 60°. It was found that as the temperature increases, the fluorescence decreases with loss of sensitivity. Accordingly, the reaction was maintained at room temperature. The effect of sodium hydroxide and hydrochloric acid concentrations on the fluorescence intensity has been carried out separately. It was found that for maximum fluorescence intensity associated with a minimum blank reading, 1*M* sodium hydroxide and 10*M* hydrochloric acid solutions should be used.

Sensitivity, precision, limits of detection and accuracy of the procedure. Calibration graphs were constructed from five points covering the concentration ranges 0.24–0.96 μg/ml for I and II and 0.04–0.24 μg/ml for III using a sensitivity setting of 0.1. For the analysis in urine and serum, the concentration ranges for the linearities were prepared to be 0.06–0.36 μg/ml for I and II and 0.02–0.10 μg/ml for III using sensitivity setting at 0.3. Regression analysis indicated a linear relationship between fluorescence intensity and concentration (Table 1). The correlation coefficients were found to range between 0.9990 and 0.9997. Six replicate determinations at different concentration levels were carried out to test the precision of the method. The relative standard deviations were found to be less than 2%, indicating excellent reproducibility of the method. The limits of detection, where the fluorescence of the sample reading was double the blank reading, were found to be 0.04 μg/ml for I and II and 0.02 μg/ml for III. The accuracy of the procedure was tested by assaying the selected drugs in laboratory prepared tablets (prepared to contain 10 mg, 10 mg

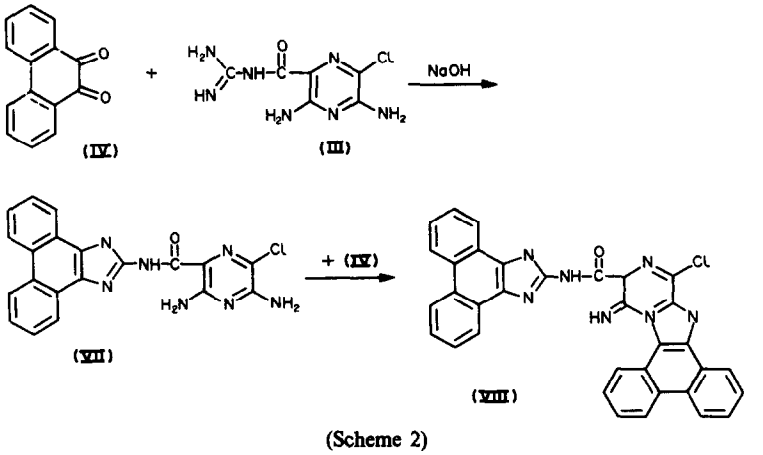

(Scheme 2)

Table 2. Determination of guanethidine sulphate, guanoxan sulphate and amiloride hydrochloride in prepared tablet using the proposed fluorimetric method and official methods

Drug	Percentage of expected*		Official method
	Fluorimetric method		
Guanethidine sulphate	100.20 ± 1.18	t† = 0.17 F‡ = 2.12	100.30 ± 0.81
Guanoxan sulphate	100.30 ± 1.24	t† = 0.17 F‡ = 2.75	100.20 ± 0.75
Amiloride hydrochloride	100.10 ± 1.28	t† = 0.31 F‡ = 1.78	100.30 ± 0.96

*Average of six determinations ± standard deviation.
†Theoretical value: $t = 2.23$ at the 95% confidence level.
‡Theoretical value: $F = 5.05$ at the 95% confidence level.

and 5 mg per tablet, respectively) and in spiked human urine and serum. The mean percentage recoveries were found to be around 100.00% (mean of 5-replicates) for tablets (Table 2) and between 95.7–102.2% (mean of 5-replicates) for urine and serum (Tables 3 and 4).

The official methods (B.P. 1988) have been applied to assay the laboratory prepared tablets and the results were found to be in good agreement with the proposed fluorimetric method. The calculated t- and F-values did not exceed the theoretical values, indicating that there is no significant difference between the mean recoveries obtained by either method (Table 2).

Stability indicating assay. The fluorimetric method has been tested as a stability indicating assay of the studied guanidines. The effect of heating at 40, 50, 60 and 70° with 4*M* sodium hydroxide solution with subsequent fluorimetric determination has been carried out. Compounds I and II did not show any degradation indicating good stability. Rate of degradation of amiloride (III) in 4*M* sodium hydroxide solution at 40–70° using the fluorimetric method was found to be first order (Fig. 3). A typical Arrhenius plot was obtained for III with a degradation rate constant 0.000195 min^{-1} and $t_{1/2}$ of 59.26 hr. Degradation of III has been reported[25] to occur in the guanidine side chain. This is in good agreement with the fact that the proposed fluorimetric method can be considered a stability indicating assay.

The official B.P. method has been proven to be non-specific when applied to III in 4*M*

Table 3. Precision and relative recovery in the determination of guanethidine sulphate, guanoxan sulphate and amiloride hydrochloride in spiked human urine

Guanethidine sulphate		Guanoxan sulphate		Amiloride hydrochloride	
Added μg/ml	% Recovery* (C.V.%)*	Added μg/ml	% Recovery* (C.V.%)*	Added μg/ml	% Recovery* (C.V.%)*
0.06	95.7 (1.46)	0.06	99.3 (0.63)	0.02	96.3 (0.82)
0.12	99.7 (0.31)	0.12	99.9 (0.26)	0.04	100.7 (0.19)
0.18	100.7 (0.20)	0.18	100.1 (0.11)	0.06	101.7 (0.09)
0.24	101.3 (0.09)	0.24	100.2 (0.12)	0.08	101.0 (0.07)
0.36	99.3 (0.10)	0.36	97.0 (0.05)	0.10	101.9 (0.08)
0.48	100.4 (0.17)	0.48	99.3 (0.12)	0.12	100.6 (0.19)
0.60	101.2 (0.16)	0.60	101.4 (0.07)	0.16	97.6 (0.10)
0.72	99.9 (0.09)	0.72	98.7 (0.12)	0.20	102.2 (0.07)
0.84	100.9 (0.08)	0.84	99.6 (0.11)	0.24	99.9 (0.06)
0.96	100.9 (0.10)	—	— —	0.28	99.2 (0.05)

*Mean the five experiments.

Table 4. Precision and relative recovery in the determination of guanethidine sulphate, guanoxan sulphate and amiloride hydrochloride in spiked human plasma

Guanethidine sulphate		Guanoxan sulphate		Amiloride hydrochloride	
Added μg/ml	% Recovery* (C.V.%)*	Added μg/ml	% Recovery* (C.V.)*	Added μg/ml	% Recovery* (C.V.%)*
0.06	95.1 (1.06)	0.06	94.4 (0.66)	0.02	92.4 (0.68)
0.12	97.8 (0.17)	0.12	97.1 (0.18)	0.04	97.0 (0.15)
0.18	98.2 (0.13)	0.18	98.1 (0.17)	0.06	98.4 (0.15)
0.24	98.6 (0.09)	0.24	98.9 (0.08)	0.08	98.6 (0.13)
0.36	98.0 (0.10)	0.36	98.4 (0.05)	0.10	97.2 (0.09)
0.48	97.9 (0.14)	0.48	97.9 (0.19)	0.12	98.1 (0.24)
0.60	97.8 (0.18)	0.60	98.9 (0.09)	0.16	98.2 (0.10)
0.72	98.4 (0.14)	0.72	98.2 (0.08)	0.20	99.3 (0.10)
0.84	98.6 (0.12)	0.84	98.9 (0.07)	0.24	98.0 (0.06)
0.96	98.4 (0.10)	—	— —	0.28	98.2 (0.08)

*Mean of five experiments.

sodium hydroxide solution at 40–70°. Thus a solution of 1 mg %w/v of III after complete degradation was found to read 0.406 at the analytical wavelength used.

Differentiation between guanethidine and guanoxan has been carried out using synchronous fluorimetry.[26,27] Thus, by scanning the synchronous fluorescence of the reaction products at a starting excitation wavelength 220 nm with $\Delta\lambda = 40$ nm (*i.e.*, emission wavelength at 260 nm), II was found to exhibit a Gaussian band at 280, 320 nm (Fig. 4), whereas I did not show such a band.

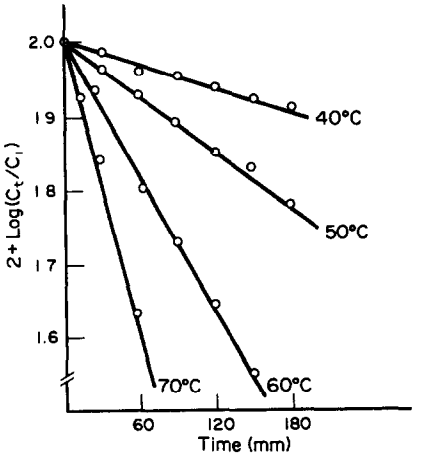

Fig. 3. Apparent first order degradation of amiloride hydrochloride in 4*M* sodium hydroxide solution at different temperatures. (C_1 = initial concentration, 0.16 μg/ml, C_t = remaining concentration in μg/ml after time, t).

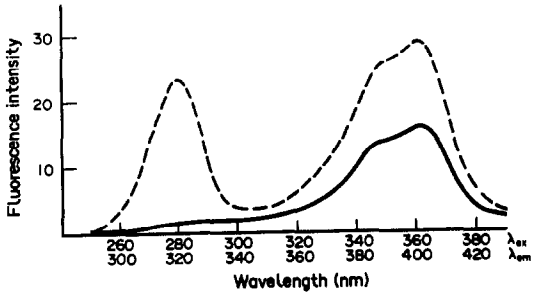

Fig. 4. Synchronous fluorescence spectra of 9,10-phenanthraquinone derivatives of 0.48 μg/ml guanethidine sulphate (——) and 0.48 μg/ml guanoxan sulphate (– – –).

In conclusion, the proposed spectrofluorimetric method, being simple, accurate, precise and highly sensitive is suitable for determination of the investigated drugs in dosage forms and in different biological fluids. In particular, the method is much simpler in technique than the GC method previously reported for biological fluids.[23] Furthermore the method can be used for the determination of amiloride hydrochloride in the presence of its degradation products, an advantage over the official method, and for the differentiation between guanethidine sulphate and guanoxan sulphate utilizing the synchronous spectrofluorimetry.

Acknowledgements—The authors wish to thank Ciba-Geigy Co., for providing guanethidine sulphate, Pfizer Co. for providing guanoxan sulphate and Kahira Co. for providing amiloride hydrochloride as pure authentic samples.

The authors also thank the Alexander von Humboldt foundation in Germany for the donation of the spectrofluorimeter.

REFERENCES

1. H. A. Itano and S. Yamada, *Anal. Biochem.*, 1972, **48**, 483.
2. S. Tanabe and T. Sakaguchi, *Chem. Pharm. Bull.*, 1978, **26**, 337.
3. *Idem, ibid.*, 1978, **26**, 423.
4. R. D. Kadyrova, L. T. Ikramov and E. T. Tegisbaev, *Farmatsiya (Moscow)*, 1988, **37**, 44.

5. I. Ganescu, G. Brinzar and C. Verhelyi, *Chem. Anal. (Warsaw)*, 1984, **29**, 549.
6. E. Zollner, *Acta Pharm. Hung.*, 1978, **48**, 76.
7. G. R. Rao and S. Raghuveer, *Indian J. Pharm. Sci.*, 1980, **42**, 141.
8. I. Ganescu, I. Papa and M. Preda, *Pharmazie*, 1985, **40**, 495.
9. S. Tanabe, T. Oya and T. Sakaguchi, *Chem. Pharm. Bull.*, 1975, **23**, 1657.
10. M. A. Arustamyan, L. E. Zel'tser, D. Kh. Yunusov and N. Suleimanova, *Zh. Analit. Khim.*, 1983, **38**, 129.
11. M. Kai, T. Miura, K. Kohashi and Y. Ohkura, *Chem. Pharm. Bull.*, 1981, **29**, 1115.
12. M. A. Parniak, G. Lange and T. Viswanatha, *J. Biochem. Biophys. Methods*, 1983, **7**, 267.
13. S. Takeichi, T. Shinzo, Y. Hisako, M. Tomoko and S. Akemi, *Yakugaku Zasshi*, 1977, **97**, 1053.
14. Y. Kobayashi, H. Kubo and T. Kinoshita, *Anal. Sci.*, 1987, **3**, 363.
15. Y. Hiraga and T. Kinoshita, *J. Chromatogr.*, 1985, **342**, 269.
16. M. Kai, T. Miyazaki and Y. Ohkura, *J. Chromatog.*, 1984, **311**, 257.
17. J. Vachek, *Cesk. Farm.*, 1985, **34**, 226.
18. C. S. P. Sastry, T. N. V. Prasad, B. S. Sastry and E. V. Rao, *Analyst*, 1988, **113**, 255.
19. C. S. P. Sastry, M. V. Suryanarayana and A. S. R. P. Tipirneni, *Talanta*, 1989, **36**, 491.
20. M. Parissi-Poulou, V. Reizopoulou, M. Koupparis and P. Macheras, *Int. J. Pharm.*, 1989, **51**, 169.
21. Y. Yukio, S. Akira, M. Tadatomi, M. Kenji and O. Kazuhiro, *J. Chromatog.*, 1979, **162**, 23.
22. S. Higashidate, T. Maekubo, M. Saito, M. Senda and T. Hoshino, *Bunseki Kagaku*, 1984, **33**, 366.
23. J. H. Hengstmann, F. C. Falkner, J. Throk Watson and J. Oates, *Anal. Chem.*, 1974, **46**, 34.
24. The British Pharmacopoeia, HMSO, London,1980.
25. K. Florey, *Analytical Profiles of Drug Substances*, 1986, **15**, 26.
26. J. B. F. Lloyd and I. W. Evett, *Anal. Chem.*, 1977, **49**, 1710.
27. T. Vo-Dinh, *ibid.*, 1978, **50**, 396.

Talanta, Vol. 39, No. 10, pp. 1377–1382, 1992
Printed in Great Britain.

0039-9140/92 $5.00 + 0.00

THE SEPARATION OF W(V) FROM HCl–KSCN MEDIUM ON POLYURETHANE FOAM SORBENTS FOR ITS SPECTROPHOTOMETRIC DETERMINATION IN STEELS AND SILICATES

ALAKANANDA RAYCHAUDHURI and S. K. ROY
Analytical Chemistry Division, Central Glass & Ceramic Research Institute, Calcutta 700 032, India

A. K. CHAKRABURTTY
Chemistry Department, Jadavpur University, Calcutta 700 032, India

(*Received* 12 *December* 1991. *Revised* 9 *April* 1992. *Accepted* 11 *April* 1992)

Summary—A simple procedure for selective sorption of tungsten is described. The method involves reduction of W(VI) to W(V) with tin(II) chloride (2%, w/v) at 8–9*M* hydrochloric acid, formation of the W(V)–SCN complex with 0.2*M* KSCN and its sorption on polyurethane foam within 20 min. The sorbed complex is then eluted with acidified acetone (1 ml of 1*M* hydrochloric acid and 8 ml of acetone) followed by addition of 1 ml of 0.1*M* KSCN to the eluent. The method has been applied to the spectrophotometric determination of tungsten in steels and silicates by measuring the absorbance of the eluted solution at 400 nm. Beer's law is obeyed for the range 0.1–12 μg W/ml. Other elements, *e.g.*, Co^{III} (50 μg/ml), Cu^{II} (10 μg/ml), Ti^{IV} (20 μg/ml), V^{V} (10 μg/ml) and Mo^{VI} (0.5 μg/ml) have no effect on the method. Interference of copper, up to 100 μg/ml has been eliminated by masking with thiourea and that due to molybdenum by prior separation with thioglycollic acid on PUF. The method has been verified with standard samples.

Thiocyanate has been used for several decades as a means of extracting W(V) into organic solvents.[1–6] After the pioneering work of Bowen,[7,8] Braun and Farag,[9–11] Chow and co-workers,[12–14] the use of polyurethane foam (PUF) has been established and found wide application in different separation procedures. Furthermore, the resilient character of PUF allows its use in a batch squeezing operation.[15] The resilient property combined with high retention capacity due to large surface area has made PUF preferred over conventional solvent and other extraction techniques for certain applications and the separation of elements by selective sorption on PUF has been the subject of various studies.

Systematic studies on the retention behaviour of W(VI) have been reported by Caletka *et al.*[16] using tracer techniques. They reported that the maximum sorption of W(VI) was reached at high hydrochloric acid concentration (4*M*). But till now hardly any method has been reported for the determination of small amounts of tungsten in silicates and other materials using the sorption technique with PUF. Moreover, the studies by Caletka *et al.*[16] possibly cannot be utilized for spectrophotometric determination of tungsten due to the poor colour sensitivity of the W(VI)–SCN complex in 4*M* hydrochloric acid.

However, available spectrophotometric methods[1–2,17–21] are based upon the formation of the yellow–green W(V)–SCN complex and its extraction with suitable solvents, but the retention behaviour of W(V) from HCl–SCN medium with PUF is yet to be studied. In the present work the parameters for quantitative sorption of W(V) from HCl–SCN medium with PUF were studied and established in order to develop a method for spectrophotometric determination of tungsten in silicates and steels.

EXPERIMENTAL

Apparatus and reagents

A Spectromom model 360 spectrophotometer was used. All reagents and chemicals were of analytical grade. Bidistilled water was used throughout.

Standard tungsten solution, 100 μg *W/ml*. A 0.08971-g amount of sodium tungstate,

$Na_2WO_4 \cdot 2H_2O$ (mol.wt 329.86) was dissolved in water and diluted to 500 ml in a calibrated flask. Working tungsten solutions (20 and 1 μg/ml) were prepared by diluting the above stock solution.

Potassium thiocyanate solution 2M. Iron (as impurity) was removed from a stock (2*M*) potassium thiocyanate solution by extracting with amyl alcohol. Working potassium thiocyanate solution (0.1*M*) was prepared by diluting the above solution.

Stannous chloride: 10% (w/v) in hydrochloric acid.

Preparation of foam chips

Polyether type polyurethane foam chips were cut from commercial 'U' foam sheet in the form of cylinders (6 mm diameter and 2 cm length, average weight 12 mg/chip), cleaned by soaking in 4*M* hydrochloric acid for 24 hr, washed thoroughly with distilled water and then refluxed with acetone in a Soxhlet apparatus for 6 hr. Washed foam chips were then air-dried at room temperature and stored in a dark coloured bottle.

Procedure

An aliquot of tungstate solution containing 1–120 μg of tungsten was transferred into a 50-ml beaker and evaporated on a water bath down to nearly 3 ml. Then 10 ml of hydrochloric acid followed by 4 ml of 10% (w/v) tin(II) chloride were added to the beaker. The solution was allowed to stand for 20 min for complete reduction of W(VI) to W(V). A 2-ml portion of 2*M* potassium thiocyanate was then added and the mixture diluted to 20 ml with water. Four pieces of foam chips were added to the solution and squeezed thoroughly with a glass plunger. The solutions were equilibrated with the foam chips from 20 min by squeezing every 5 min. The chips were removed from the solution and transferred into a 5-ml disposable syringe. The foam chips were thoroughly washed by squeezing 4 times with 4 ml of water. Finally the sorbed complex was eluted from the foam by washing 4 times with 2-ml portions of acidified acetone (1 ml of 1*M* hydrochloric acid 8 ml of acetone) into a 10-ml calibrated flask. A 1-ml portion of 0.1*M* potassium thiocyanate was added to each flask and diluted up to the mark with the acidified acetone added by the same syringe. The absorbance of the solution was measured at 400 nm within 45 min against a reagent blank.

RESULTS AND DISCUSSION

During preliminary studies, it was observed that the yellow–green complex of W(V)–SCN formed after reduction of W(VI) with tin(II) chloride in strong hydrochloric acid medium ($\sim$9*M*) in the presence of potassium thiocyanate could be sorbed on PUF within a short period of time. The sorbed complex on the foam matrix after washing with water using a syringe could also be eluted with acidified acetone, but not with acetone only. Further, it was observed that the eluted complex in acidified acetone medium could be stabilized by addition of small amounts of potassium thiocyanate solution. The absorption spectrum of the yellow–green W(V)–SCN complex in acetone–hydrochloric acid–potassium thiocyanate medium showed an absorption maximum at 400 nm at which the reagent blank did not absorb significantly. These observations lead to further investigations for establishing different parameters affecting the extraction of the W(V)–SCN complex on PUF, its quantitative elution and stability of the eluted complex, *i.e.*, acid concentration during extraction, time of reduction of W(VI) to W(V), concentration of stannous chloride and thiocyanate, time of equilibration and final acid and thiocyanate concentration in acetone medium.

Effect of reducing agent and hydrochloric acid concentration

The reduction of W(VI) with tin(II) chloride was found to be dependent on the hydrochloric acid concentration. Therefore, it was imperative to determine the optimum acid concentration for quantitative reduction of W(VI) to W(V) and subsequent sorption of the W(V)–SCN complex on PUF. The hydrochloric acid concentration was varied over a wide range of 1–9*M* hydrochloric acid and it was observed that a waiting time of 20 min was necessary for quantitative reduction of W(VI) to W(V) at 8–9*M* hydrochloric acid. The extent of formation as well as the sorption of the W(V)–SCN complex on PUF was found to be maximum in the acid range of 8–9*M* hydrochloric acid. However, the extent of sorption on PUF was found to decrease at acid concentration $<8M$. Therefore, the concentration of hydrochloric acid and time of reduction were maintained at 8–9*M* and 20 min for subsequent experiments.

The effects of the tin(II) chloride concentration on the reduction of W(VI) and on the sorption of the complex were also studied. The optimum

concentration of tin(II) chloride for achieving both was found to be 1%, and above this concentration, the further addition of the reducing agent up to 6% did not result in any change in the absorbance.

Effect of thiocyanate

The concentration of potassium thiocyanate was found to have a great influence on the formation and sorption of the W(V)–SCN complex on PUF. The formation as well as sorptions of the complex was found to be maximum at 0.2*M* potassium thiocyanate. But at concentration $>0.2M$ the sorption was found to decrease, probably due to the formation of unextractable species.

Effect of equilibration time

The sorption of the W(V)–SCN complex with PUF under the above mentioned conditions was found to be maximum after 20 min equilibration and no further sorption took place after that period (Fig. 1). The sorption of the W(V)–SCN complex was found to be more than 99% under the experimental conditions. But, in any case, equilibration time could not be extended beyond 30 min, as thiocyanate itself undergoes gradual decomposition in strong acid medium.[2] Gradual decomposition of PUF was also observed when it was subjected to strong acid ($>9M$) for more than one hour.

As reported by Caletka *et al.*[16,22] WO_2^{2+} is converted to WO^{4+} at high acidity but on reduction with tin(II) chloride this WO^{4+} is reduced to WO^{3+}. This reduced WO^{3+} reacts with SCN^- to form anionic species $[WO(SCN)_n]^{3-n}$ which are sorbed on PUF through a cation chelation mechanism.[13] According to this mechanism, complexation of cations, *e.g.*, K^+ or H_3O^+, takes place in the PUF cavities through ion-dipole interaction or hydrogen bonding or both.[14] Then the anionic species, *i.e.*, $[WO(SCN)_n]^{3-n}$, are extracted as counter ions to the captured cations in the PUF cavities.

Elution and stability of the eluted complex in acetone

It was observed during the study that the complex can only be quantitatively eluted from the foam matrix with acidified acetone, *i.e.*, acetone protonated with hydrochloric acid (8 ml of acetone +1 ml of 1*M* hydrochloric acid), which also established the anionic nature of the complex. The optimum acid concentration for quantitative elution and stability of the eluted complex was found to be 0.1*M* hydrochloric acid in acetone (Fig. 2). It can further be seen from Fig. 2 that below 0.1*M* hydrochloric acid, the elution of the complex from foam is not quantitative while at $>0.1M$ the complex tends to dissociate with time and yields lower absorbance values as obtained with 0.3, 0.6 and 1.2*M* acid concentrations.

The stability of the eluted complex can be increased further by the addition of fresh potassium thiocyanate solution to the eluted solution. Therefore, the concentration of

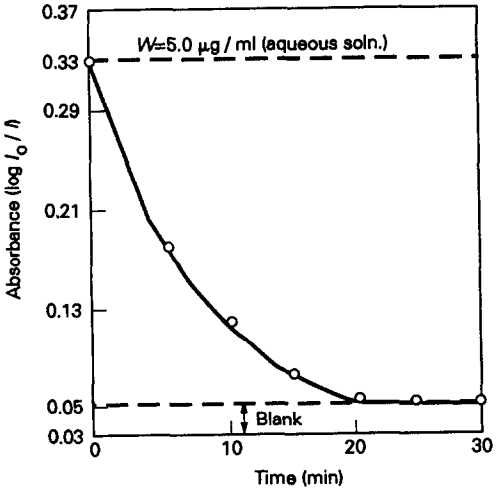

Fig. 1. Effect of time on the equilibration of W(V)–SCN complex with PUF at 8.5*M* HCl containing 2% $SnCl_2$ and 0.2*M* KSCN.

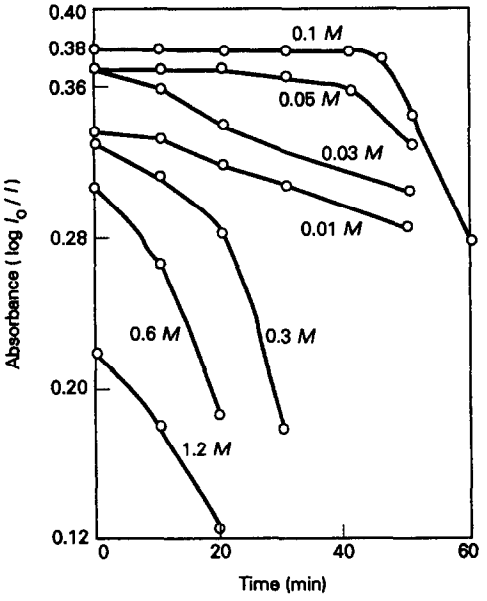

Fig. 2. Effect of HCl concentration in acetone on the quantitative elution and stability of the eluted W(V)–SCN complex.

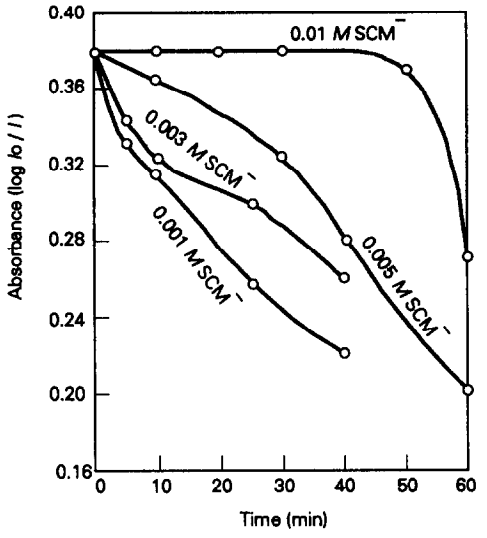

Fig. 3. Effect of KSCN concentration in acetone on the stability of W(V)–SCN complex after elution at 0.1*M* HCl.

potassium thiocyanate in the eluted solution was varied to establish its optimum concentration for stability of W–SCN complex. Figure 3 shows that the colour of the eluted complex is stable up to 45 min in 0.01*M* SCN^-. These observations suggested that a minimum concentration of 0.01*M* potassium thiocyanate was essential over the stoichiometric amount for increasing the stability of the colour in acetone–hydrochloric acid medium. However, a ratio between acetone:HCl:KSCN solution has to be maintained at 8:1:1 to avoid turbidity in the acetone–hydrochloric acid medium.

Validity of Beer's law

The effect of tungsten concentration was studied under the experimental conditions set up and Beer's law was found to be obeyed in the range 0.10–12 μg/ml tungsten. The molar extinction coefficient for W has been calculated to be 1.3×10^4 l. $mole^{-1}$. cm^{-1} at 400 nm. From the regression analysis of the calibration plot of absorbance against W concentration, the correlation coefficient was found to be 0.999. The Sandell's sensitivity was calculated to be 0.012 μg/cm against 0.001 absorbance.

Effect of foreign elements

The effect of diverse ions on the determination of 5 μg/ml W(V) was examined following the procedure and is presented in Table 1. The elements which remained in the solution along with tungsten after caustic soda separation, *e.g.*, Mo, V, Mn, Al and Zn, are of practical importance. But the elements Al, Mn and Zn did not interfere with the determination of tungsten. However, molybdenum could be tolerated only up to 0.5 μg/ml above which it interferes seriously by producing a positive error. The adverse effect of molybdenum (>0.5 μg/ml) could be eliminated by previously extracting its thiogycollate complex on PUF from 0.1*M* hydrochloric acid in the presence of oxalate,[23] and after sorption of the molybdenum, the acidity of the solution could be increased for sorption of tungsten by the given procedure. Vanadium up to 10 μg/ml did not interfere in the method. Further, the study (Table 1) indicates that copper up to 10 μg/ml, did not interfere in the determination of tungsten (5 μg/ml), but its adverse effect at higher concentration (up to 100 μg/ml) could be eliminated by masking with thiourea.

Table 1. Effect of foreign elements on the sorption of tungsten. Conditions: Tungsten (VI)—5 μg/ml, acid—8.5*N* HCl, $SnCl_2$—2% (w/v), KCNS—0.2*M*, sorbent—PUF, elutant—acidified acetone (8 ml acetone +1 ml 1*M* HCl), KCNS (in acetone medium)—0.01*M*

Foreign ion	Amount added (μg/ml)	Absorbance
Nil	—	0.380
Fe^{III}	200	0.380
Co^{II}	50	0.385
Ni^{II}	200	0.380
Cu^{II}	10(100)*	0.380
Cr^{III}	100	0.390
Ti^{IV}	20	0.380
V^{V}	10	0.385
Mn^{II}	200	0.380
Mo^{VI}	0.5	0.380
Zn^{II}	200	0.380
Al^{III}	200	0.380
Ca^{II}	200	0.380
Mg^{II}	200	0.380

*In the presence of 0.1% thiourea (w/v).

Application of the method

The developed method was checked with indigenous plain carbon steel samples without tungsten spiked with known amounts of tungsten (Table 2). The method was then applied to the determination of tungsten in standard steel

Table 2. Determination of tungsten in stimulated steel solutions (results are averages of eight determinations)

Sample	Tungsten* added, %	Tungsten found, %	Standard deviation
Steel (1)	0.04	0.038	±0.0024
Steel (2)	0.10	0.098	±0.0031
Steel (3)	0.20	0.19	±0.022
Steel (4)	0.60	0.59	±0.015
Steel (5)	0.50	0.48	±0.008

*Calculated amount of tungsten were added to each steel sample during decomposition.

Table 3. Determination of tungsten in steel samples and silicate materials (molybdenum was separated with thioglycollic acid prior to sorption of tungsten by the reported procedure[23])

Sample	Certified values of tungsten, %	Tungsten found, *%	Standard deviation
Steel (BCS–219/2)	0.19	0.183	±0.0046
Steel (SS–455/1)	0.20	0.194	±0.0062
Silicate Rock (Canmet–Canada)	0.68	0.674	±0.0054

*Results are averages of nine determinations.
BCS: British Chemical Standards, U.K.
SS: Primary Spectroscopic standards, U.K.
CANMET CANADA: Geological Survey of India (Reference material from Geological Survey, Canada).

and silicate material samples after preparation of sample solution by following the procedures given below. Results are presented in Table 3.

Preparation of sample solution

Steel. A 0.1-g steel sample was decomposed with 10 ml of hydrochloric acid and 10 ml of nitric acid in a 200-ml glass beaker. The solution was evaporated on a water bath to near dryness. This process was thus repeated twice and evaporated to expel all the oxides of nitrogen. The residue was dissolved in 10 ml of hydrochloric acid (1 + 2) by boiling and poured into a 100-ml beaker containing 15 ml of hot 5*M* sodium hydroxide solution with stirring. It was then filtered through Whatman No. 41 filter paper. The residue was washed first with hot 1*M* sodium hydroxide and then with hot water. The filtrate was just acidified with dilute hydrochloric acid, transferred into a 100-ml calibrated flask, cooled and diluted up to the mark with water.

Silicates

A 0.1-g sample (dried at 110°) was placed in a PTFE basin and digested on a sand bath with 5 ml of nitric acid and 5 ml of HF to near dryness. The basin was cooled, a further 5 ml of nitric acid, 5 ml of HF and 1 ml of sulphuric acid (1 + 1) were added and the process repeated until fumes of SO_3 were evolved. The acid was almost driven off and the residue taken up in 10 ml of hydrochloric acid (1 + 2), boiled and poured into 15 ml of hot 5*M* sodium hydroxide solution, with stirring. It was then filtered through Whatman No. 41 filter paper. The residue was washed first with hot 1*N* sodium hydroxide and then with hot water. The filtrate was just acidified with dilute hydrochloric acid, transferred into a 100-ml calibrated flask, cooled and diluted up to the mark with water.

A 5-ml aliquot of the above sample solution was transferred to a 50-ml beaker and evaporated on a water bath almost to dryness. Then 2 ml of water were added and the determination procedure was applied.

Calibration

Standard tungstate working solutions (1–10 ml) containing 1–120 μg of W were added into 50-ml glass beakers and evaporated on a water bath to about 3 ml. The procedure for the determination of tungsten was then followed. The absorbance of each solution was obtained at 400 nm against a reagent blank and a calibration curve was plotted.

Calculation

The absorbance of the test solution was compared with the calibration curve and converted to the quantity of tungsten in μg, from which its concentration in the sample is calculated:

$$W = 2 \times 10^{-2} A / W\%$$

where A is the number of μg of W corresponding to the absorbance measured and the sample weight is in g.

Acknowledgement—The authors are thankful to Dr B. K. Sarkar, Director, Central Glass and Ceramic Research Institute, Calcutta 700032 for his kind permission to publish the paper.

REFERENCES

1. E. B. Sandell, *Colorimetric Determination of Traces of Metals*, 3rd Ed., p. 886. Interscience, New York, 1959.
2. E. Upor, M. Mohai and Gy. Novak, *Photometric Methods in Inorganic Trace Analysis*, Vol. XX p. 251. Elsevier, Amsterdam, 1985.
3. G. GottSchalk, *Z. Anal Chem*, 1962, **187**, 164.
4. H. E. Affsprung and J. W. Murphy, *Anal. Chim. Acta*, 1964, **30**, 501.
5. W. E. M. Donaldson, *Talanta*, 1975, **22**, 837.
6. J. J. Topping, *ibid*, 1978, **25**, 61.
7. H. J. M. Bowen, *J. Chem. Soc. A*, 1970, 1082.
8. *Idem, British Patent 1*, 1973, **305**, 375.
9. T. Braun and A. B. Farag, *Anal. Chim. Acta*, 1972, **61**, 265.
10. *Idem, Talanta*, 1972, **19**, 828.
11. T. Braun, *Z. Anal. Chem.*, 1989, **333**, 785.
12. A. Chow and D. Buksak, *Can. J. Chem.*, 1975, **53**, 1373.
13. R. F. Hamon, A. S. Khan and A. Chow, *Talanta*, 1982, **29**, 313.
14. Sargon J. Al-Bazi and A. Chow, *ibid.*, 1982, **29**, 507.
15. T. Braun, A. B. Farag and J. Navratil, *Polyurethane Foam Sorbents in Separation Chemistry*, p. 15. CRC Press, Boca Raton, 1985.

16. R. Caletka, R. Hausbeck and V. Krivan, *Talanta*, 1986, **33**, 315.
17. W. T. Elwell and D. F. Wood, *Analytical Chemistry of Molybdenum and Tungsten*, 1st Ed., p. 103. Pergamon Press, Oxford, 1971.
18. B. F. Quinn and R. R. Brooks, *Anal. Chim. Acta*, 1975, **74**, 75.
19. K. M. Chan and J. P. Riley, *ibid.*, 1967, **39**, 103.
20. B. F. Quinn and R. R. Brooks, *ibid.*, 1972, **58**, 301.
21. A. G. Fogg, D. R. Marriott and D. Thorburn Burns, *Analyst*, 1970, **95**, 848.
22. R. Caletka, R. Hausbeck and V. Krivan, *Anal. Chim. Acta*, 1990, **229**, 127.
23. A. Roy, S. K. Roy and A. K. Chakraburtty, *Glass Technology*, 1991, **32**, 20.

Talanta, Vol. 39, No. 10, pp. 1383–1385, 1992
Printed in Great Britain

0039-9140/92 $5.00 + 0.00
Pergamon Press Ltd

RAPID AND SELECTIVE SPECTROPHOTOMETRIC DETERMINATION OF MANGANESE IN STEELS AND ALLOYS USING RESACETOPHENONE OXIME

C. KESAVA RAO, O. BABAIAH, V. KRISHNA REDDY and T. SREENIVASULU REDDY
Department of Chemistry, Sri Krishnadevaraya University, Anantapur 515 003, India

(*Received* 11 *July* 1991. *Revised* 25 *September* 1991. *Accepted* 25 *September* 1991)

Summary—A sensitive spectrophotometric method is developed for the determination of manganese in aqueous medium. The metal ion forms a yellowish brown coloured complex with resacetophenone oxime (RPO) in ammonium chloride and ammonium hydroxide buffer of pH 10.5. The 1:1 complex shows maximum absorbance at 380 nm with a Beer's law range of 0.09–1.7 ppm. The molar absorptivity and the Sandell sensitivity are found as 2.5×10^4 l.mole^{-1}.cm^{-1} and 0.002 μg/cm^2, respectively. The stability constant of the complex calculated by Job's method is 7.5×10^5. The interfering effects of various cations and anions are studied. The present method is applied to the determination of manganese in some steel and alloy samples.

Oximes have found wide application as analytical reagents. They form the most selective class of reagents commonly employed as spectrophotometric reagents for a variety of metal ions.[1] Several methods using oxime reagents for the determination of manganese have been reported.[2] Among them, formaldoxime (stability constant = 1.12×10^4 at 455 nm)[3] is the most sensitive. The other oximes are generally insensitive, being suitable only for the determination in the mg/l. range. Among other methods, most of them are of the extraction type. In the present paper a simple, rapid and sensitive method is reported for the direct spectrophotometric determination of trace amounts of manganese in aqueous medium by complexing with 2,4-dihydroxy acetophenone oxime (resacetophenone oxime, RPO). The method is highly selective for the determination of manganese in steels in the presence of EDTA.

EXPERIMENTAL

Apparatus

An ELICO Digital spectrophotometer model CL-27 and a Philips Digital pH meter model PP9046 were used for absorbance and pH measurements respectively.

Reagents

Analytical reagent grade chemicals were used throughout without further purification. Standard manganese chloride (1 g/l. Mn) was prepared and standardized complexometrically.[4] Working solutions were prepared daily by diluting the stock solutions to appropriate concentrations.

Resacetophenone oxime was prepared using the reported procedure.[5] A stock solution (0.1*M*) in 40% aqueous methanol was used in the studies.

Buffer solutions

For the preparation of buffer solutions 2.0*M* ammonium hydroxide–2.0*M* ammonium chloride were uses.

Preparation of sample solutions

A 0.5-g sample was treated with 2 ml of concentrated nitric acid. When the reaction was almost over, the mixture was warmed on a hot plate to complete the dissolution. After the addition of 1 ml of concentrated sulphuric acid the mixture was evaporated until white fumes appear, then cooled and diluted to about 20 ml with 0.3*M* hydrochloric acid. The solution was heated almost to boiling and hydrogen sulphide was passed through it to precipitate copper. The copper sulphide was filtered off and washed and the filtrate was boiled to remove the dissolved hydrogen sulphide, and then evaporated to dryness. The residue was dissolved in distilled water and diluted to the required volume.

Procedure

In each of a set of different 25-ml standard flasks, 10 ml of buffer solution (pH 10.5),

various volumes of ($2 \times 10^{-4}M$) manganese solution, 4 ml of $2 \times 10^{-3}M$ RPO solution and 2.0 ml of $0.01M$ potassium persulphate were added and heated on a water bath for 10 min. The contents were cooled and made up to the mark with distilled water. The absorbance was measured at 380 nm against a reagent blank. A linear plot passing through the origin was obtained when absorbance was plotted against the amount of manganese.

RESULTS AND DISCUSSION

Manganese reacts with RPO in ammoniacal buffer medium to form a soluble yellowish brown coloured complex. The probable structure of the complex may be drawn as

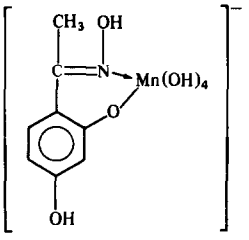

The colour intensity increased with time and attained a constant value after about 5 days. The complex attains maximum and constant absorbance when it is heated on a water bath for 2 hr, as the manganese is air oxidized to Mn(IV). However, in the presence of 0.035% persulphate, the maximum absorbance could be attained when the reaction mixture is heated for 10 min.

Figure 1 shows the absorption spectra of the reagent and metal complex. The figure indicates that the reagent absorbance is small at 380 nm while the complex has maximum absorbance. Hence the studies are carried out at 380 nm. The complex shows maximum absorbance in the pH range 10.2–10.7. Hence further studies are made at pH 10.5. A 20-fold excess RPO is necessary to obtain maximum colour intensity. Beer's law is obeyed up to 1.7 ppm manganese. The practical range of determination of manganese obtained from Ringbom's method is 0.09–1.7 ppm. The complex has molar absorptivity of $2.0 \pm 0.5 \times 10^4$ $1.mole^{-1}.cm^{-1}$ at 380 nm. The Sandell's sensitivity is found to be 0.002 $\mu g/cm^2$. The relative standard deviation is 0.002 ppt. Comparing the mean determined values against the standard amount of manganese taken, the 't' value calculated (2.20) for 10 measurements is found to be less than the tabulated value (2.23) at the 95% confidence interval.

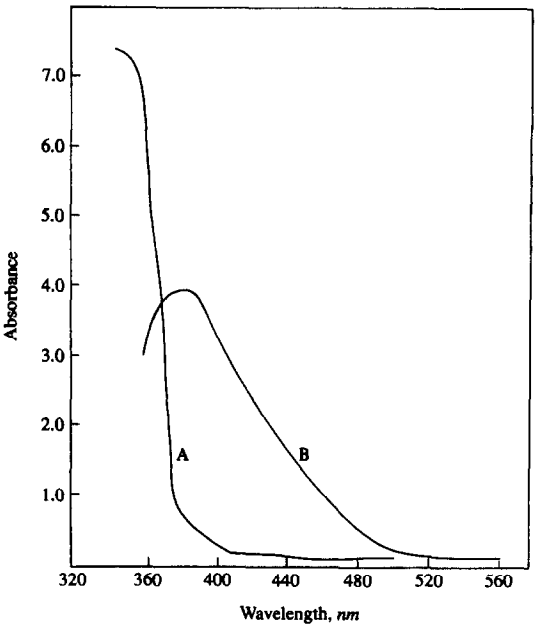

Fig. 1

The studies based on Job's continuous variation, mole ratio and slope ratio methods indicate a 1 : 1 complex formation between the metal and reagent. The stability of the complex calculated from Job's continuous method is 7.5×10^5.

The interference of various anions and cations normally found in association with manganese was studied. The amount of the diverse ion which brings about 2% variation in absorbance was taken as its tolerance limit.

In the determination of 0.9 ppm manganese, the tolerance limit (given in ppm) of various ions is as follows, EDTA (1600); thiosulphate (440); oxalate (350); tartrate (300); thiocyanate (300); iodide (135); nitrate (135); fluoride (130); carbonate (85); phosphate (70); thiourea (70); ascorbic acid (70); Zn(II) (700); Mo(VI) (700); V(V) (700); W(VI) (100); Cd(II) (100); Th(IV) (100); Pb(II) (86); Cr(VI) (60); Pd(II) (56); Ag(I) (30); Mg(II) (20); U(VI) (20); Ce(IV) (16); Pt(IV) (10); Hg(II) (8). In the presence of EDTA, Fe(III), Cu(II), Co(II) and Ni(II) are tolerable up to 210 ppm 25 ppm, 120 ppm and 120 ppm respectively. Hence in the presence of EDTA, the present method becomes highly selective for the determination of manganese.

Analysis of alloys and steel samples

Manganese present in various standard steel and alloy samples was determined by the present method.

Table 1. Analysis of alloy and steel samples

Sample	Composition (%)	Manganese Taken, *ppm*	Manganese Found,* *ppm*
BAS No. 180/2	Cu: 68.12, Fe: 0.68	0.140	0.141
	C: 0.04, Ni: 30.35	0.420	0.418
	Mn: 0.75, S: 0.006	0.630	0.629
BAS No. 179/2	Mn: 0.86, Cu: 58.5	0.165	0.166
	Ni: 0.56, Sn: 0.70	0.495	0.496
	Fe: 1.02, Si: 0.044	0.990	0.989
	Zn: 35.8, Pb: 0.35		
	Al: 2.22		
BCS No. 406	Mn: 0.53, Ni: 1.69	0.346	0.344
	Mo: 1.03, V: 0.02	0.965	0.963
	Cr: 2.12, Cu: 0.32	1.038	1.036
BCS No. 219/4	Mn: 0.81, Cr: 0.66	0.176	0.177
	Mo: 0.58, Ni: 2.55	0.352	0.351
	Cu: 0.088, Sn: 0.011	1.408	0.406
	Fe: 95.0		

*Average of six determinations.

A known aliquot of steel solution was transferred into a 25-ml standard flask containing 10 ml of buffer solution, 1 ml of reagent ($1 \times 10^{-3}M$), 2 ml of potassium persulphate ($1 \times 10^{-2}M$) and 1.5 ml of EDTA ($0.1M$) and made up to the mark with distilled water. After 10 min, the absorbance of the solution was measured at 380 nm. The amounts of manganese present were computed from the predetermined calibration plot. The results obtained are presented in Table 1.

For steel samples containing copper in amounts less than 25 times the manganese, prior separation with sulphide was not needed, as the copper could be masked with EDTA. In BAS No. 180/2 and BAS 179/2, sulphide precipitation was necessary.

Comparison with other reagents

Among the methods reported[2] using oximes, the present method is the most sensitive. It is also more highly sensitive than the most widely employed procedure based on the oxidation of Mn(II) to Mn(VII). Though the sensitivity is lower than those of other reagents such as PAR[6] or PAN,[7,8] the method has the advantage of higher selectivity in the presence of EDTA. Further, most of the more sensitive methods involve extraction.

Acknowledgement—The authors are thankful to the authorities of Sri Krishnadevaraya University, Anantapur, India, for providing the necessary facilities to carry out the research work.

REFERENCES

1. R. B. Singh, B. S. Garg and R. P. Singh, *Talanta*, 1979, **26**, 425.
2. B. Chiswell and G. Rauchle, *ibid.*, 1990, **37**, 237.
3. Z. Marczenko, *Anal. Chim. Acta*, 1964, **31**, 224.
4. A. I. Vogel, *A Text Book of Quantitative Inorganic Analysis*, 3rd Ed., p. 434. 1975.
5. D. E. Dey and M. V. Sitaraman, *Laboratory Manual of Organic Chemistry*, p. 264. 1952.
6. E. Donaldson and W. Inman, *Talanta*, 1966, **13**, 489.
7. T. Yoytsuyanagi, K. Goto, M. Nagayama and K. Aamura, *Bunseki Kagaku*, 1969, **18**, 477.
8. K. Ueda, Y. Yamamoto and S. Ueda, *Nippon Kagaku Zasshi*, 1969, **90**, 903.

Talanta, Vol. 39, No. 10, pp. 1387–1390, 1992
Printed in Great Britain

0039-9140/92 $5.00 + 0.00
Pergamon Press Ltd

SPECTROPHOTOMETRIC ASSAY OF ISOPROTURON AND METOXURON IN TECHNICAL GRADE AND FORMULATION SAMPLES USING 3-METHYLBENZOTHIOZOLIN-2-ONE HYDRAZONE HYDROCHLORIDE

K. RAMAKRISHNAM RAJU, T. N. PARTHASARATHY,* S. R. K. M. AKELLA and U. T. BHALERAO
Indian Institute of Chemical Technology, Hyderabad 500 007, India

(*Received* 9 *October* 1991. *Revised* 12 *February* 1992. *Accepted* 22 *February* 1992)

Summary—A spectrophotometric method for the assay of Isoproturon and Metoxuron in technical grade and formulation samples has been developed using the oxidative coupling reaction with 3-methylbenzothiozolin-2-one hydrazone hydrochloride (MBTH). The reaction variables have been optimized and the reaction mechanism is discussed. The method is simple, rapid and has been successfully applied for the assay of Isoproturon and Metoxuron in commercial grade technical and formulated samples. The percent relative standard deviation is found to be in the range 0.34–1.00 for Isoproturon and 0.33–0.57 for Metoxuron.

Isoproturon (IPN) and Metoxuron (MTN) belong to the phenylurea class of compounds, widely used as pre or post emergent herbicides for control of different weed species in cereals and carrots. Simple methods for their assay in technical grade and formulation samples are necessary for routine analysis and quality evaluation. The chemical[1] and GC[2] methods reported in the literature are time consuming and unsuitable for routine analysis. To overcome some of the difficulties we have reported a spectrophotometric method recently.[3] In search of more convenient methods, we have carried out further spectrophotometric investigations of the chromogenic reaction between these herbicides and 3-methylbenzothiozolin-2-one hydrazone hydrochloride (MBTH) based on oxidative coupling and application to technical grade and formulation samples and the results are presented here.

EXPERIMENTAL

Apparatus

Shimadzu Model UV-240 and 210 spectrophotometers, and matched 1.0-cm glass cells were used.

Reagents and materials

A 0.4% solution of MBTH (Loba Chemicals, Bombay, India) in water and a 0.1% solution of ceric ammonium sulphate in 10 and 6.5% sulphuric acid were prepared. All other chemicals used were of reagent grade.

IPN (99.65%) was supplied by Bharat Pulverizing Mills, Bombay, India and used as such. MTN supplied by Pesticides Division, IICT, Hyderabad, India, was used after recrystallisation in hot water and the purity was checked by HPLC (99.7%).

Standard herbicide solutions were prepared by dissolving about 20 mg (accurately weighed) in methanol, diluted to 100 ml with methanol and used as working solutions.

General procedure

Working sample solutions (1.0 ml) were transferred into 10-ml standard flasks. Portions of 5.0 and 2.0 ml of 0.1% ceric ammonium sulphate solution in 10 and 6.5% sulphuric acid respectively, were added for IPN and MTN and kept aside for 5 min, after which 2.5 ml and 3.5 ml of 0.4% MBTH reagent were added for IPN and MTN, respectively. The flasks were heated in a water bath at 60° for about 25 min for IPN and 4 min for MTN. After heating the flasks were removed from the water bath, cooled to room temperature and diluted to 10 ml with

*Author for correspondence.
†IICT Communication No. 2901.

water. The absorbances of these solutions were measured at 510 nm for IPN and 490 nm for MTN against a reagent blank.

Technical grade samples

About 20 mg of technical grade samples were weighed accurately and dissolved in 50 ml of methylene chloride, treated with 1*N* hydrochloric acid and the organic layer was evaporated.[1] The residue after evaporation was dissolved in 5.0 ml of methanol and diluted to 100 ml with this solvent. A 1.0-ml portion was subjected to analysis using the general procedure.

Formulation samples

About 40 and 30 mg of well mixed formulations of IPN and MTN, respectively, were weighed accurately and 50 ml of methylene chloride was added and the mixture centrifuged. The organic layer after treatment with 1*N* hydrochloric acid was evaporated. The residue was dissolved in methanol and 1.0 ml was subjected to analysis using the general procedure after dilution to 100 ml.

In the case of MTN, formulations were not available and hence synthetic formulations (80%) were prepared and analysed.

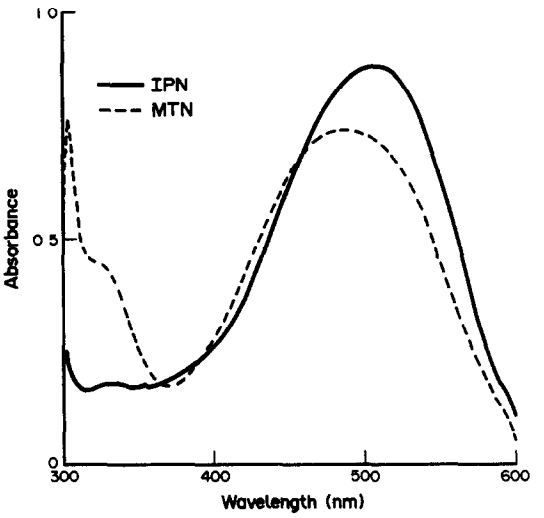

Fig. 1. Absorption spectra of IPN and MTN. —— IPN, --- MTN. 1.0 ml of 0.02% IPN + 5.0 ml of 0.1% ceric ammonium sulphate in 10% H_2SO_4 + 2.5 ml of 0.4% MBTH, against reagent blank. Heating at 60° for 25 min. 1.0 ml of 0.02% MTN + 2.0 ml of 0.1% ceric ammonium sulphate in 6.5% H_2SO_4 + 3.5 ml of 0.4% MBTH, against reagent blank. Heating at 60° for 4 min.

RESULTS AND DISCUSSION

Optimization of reaction variable

The absorption spectra of IPN and MTN are shown in Fig. 1. The reaction variables have been optimized by varying each profile, keeping others constant for obtaining maximum colour development as shown in Figs. 2–4. It is clear that 20 min (IPN), 3 min (MTN) reaction time in a water bath at 60°; 4.0 ml, 1.5 ml of 0.1% ceric ammonium sulphate in 10% (IPN) and 5% (MTN) sulphuric acid and 2.0 ml (IPN) 3.0 ml (MTN) of 0.4% MBTH reagent, respectively, were necessary for maximum colour development.

Beer's law precision and accuracy

The λ max, the molar absorptivities, Beer's law range, slopes, correlation coefficients, precision and accuracy of the method are given in Table 1. The colour is stable for more than two hours for IPN and one hour for MTN.

Reaction mechanism

Under acidic conditions the hydrolysed products of the corresponding amines of IPN (4-isopropyl-aniline) and MTN (3-chloro-4-methoxy aniline) coupled with MBTH in the presence of Ce(IV) to yield coloured oxidizing products, as reported in the literature.[4,5] As the *p*-position in both compounds is blocked, it is assumed that coupling would have taken place in the *o*-position (Scheme 1). The absorption maxima and low molar absorptivities also

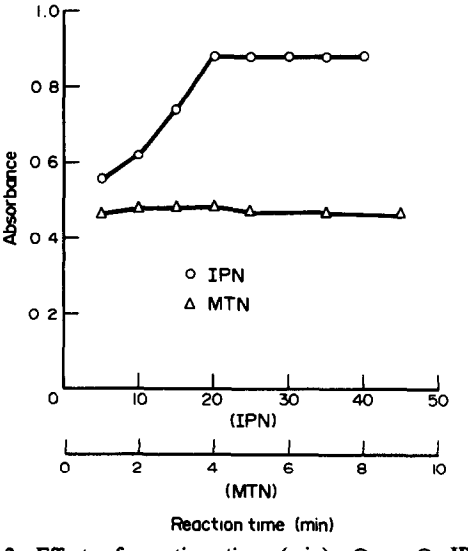

Fig. 2. Effect of reaction time (min). O——O IPN, Δ——Δ MTN. 1.0 ml of 0.02% IPN + 4.0 ml 0.1% ceric ammonium sulphate in 10% H_2SO_4 + 1.0 ml of 0.4% MBTH. Heating at 60°. 1.0 ml of 0.02% MTN + 2.0 ml 0.1% Ceric Ammonium Sulphate in 6.5% H_2SO_4 + 1.0 ml of 0.4%, MBTH. Heating at 60°.

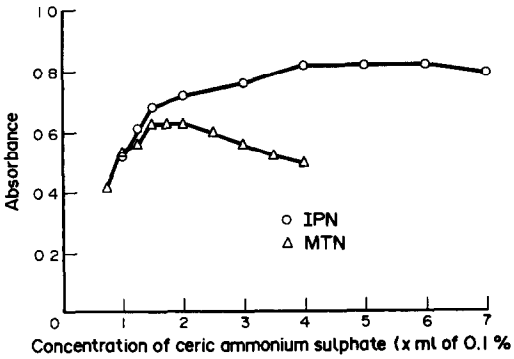

Fig. 3. Effect of ceric ammonium sulphate. O——O IPN, Δ——Δ MTN. 1.0 ml of 0.02% IPN + 1.0 ml of 0.4% MBTH + varying amounts of ceric ammonium sulphate in 10% H_2SO_4, heating at 60° for 25 min. 1.0 ml of 0.02% MTN + 3.5 ml of 0.4% MBTH + varying amounts of ceric ammonium sulphate in 6.5% H_2SO_4, heating at 60° for 4 min.

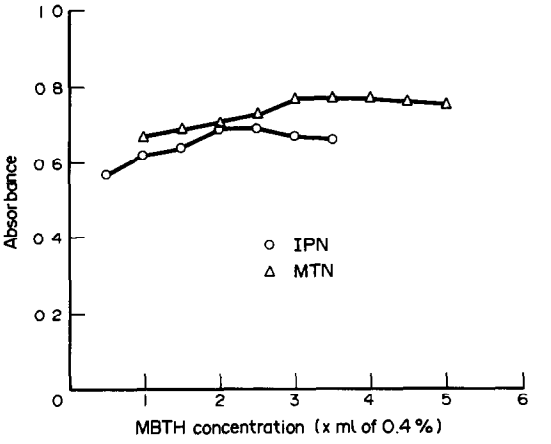

Fig. 4. Effect of MBTH concentration. O——O IPN Δ——Δ MTN. 1.0 ml of 0.02% IPN + 1.0 ml of 0.5% ceric ammonium sulphate in 10% H_2SO_4 + varying amounts of MBTH. Heating at 60° for 25 min. 1.0 ml of 0.02% MTN + 2.0 ml of 0.1% ceric ammonium sulphate in 6.5% H_2SO_4 + varying amounts of 0.4% MBTH. Heating at 60° for 4 min.

support this.[6] The slow reaction in the case of IPN (20 min) may be attributed to the out of plane arrangement of the bulky alkyl group in the *p*-position. However, in the case of MTN, the reaction is fast (3 min) which may be accounted for by the combined effects of Cl- and OMe-groups.

Interferences

Free amines which interfere with the method are removed by extracting into 1*N* hydrochloric acid. However, phenylurea derivatives if present cause interference.

Application

A number of technical grade and formulation samples of IPN and MTN have been subjected to analysis using the developed method and the results are shown in Tables 2 and 3. The percent relative standard deviations are in the range of 0.34–1.00 for IPN and 0.33–0.57 for MTN.

Table 1. Beer's law, precision and accuracy

	IPN	MTN
λ Max (*nm*)	510	490
Beer's law limit (*μg/ml*)	30	40
Molar adsorptivity ($l.mole^{-1}.cm^{-1}$)	8.34×10^2	5.85×10^2
Slope (*A*/*μg/ml*)	0.000024	0.002072
Intercept/*A*	−0.00359	0.0791
Correlation coefficient	0.9998	0.9934
Relative error (%)	<1	<1

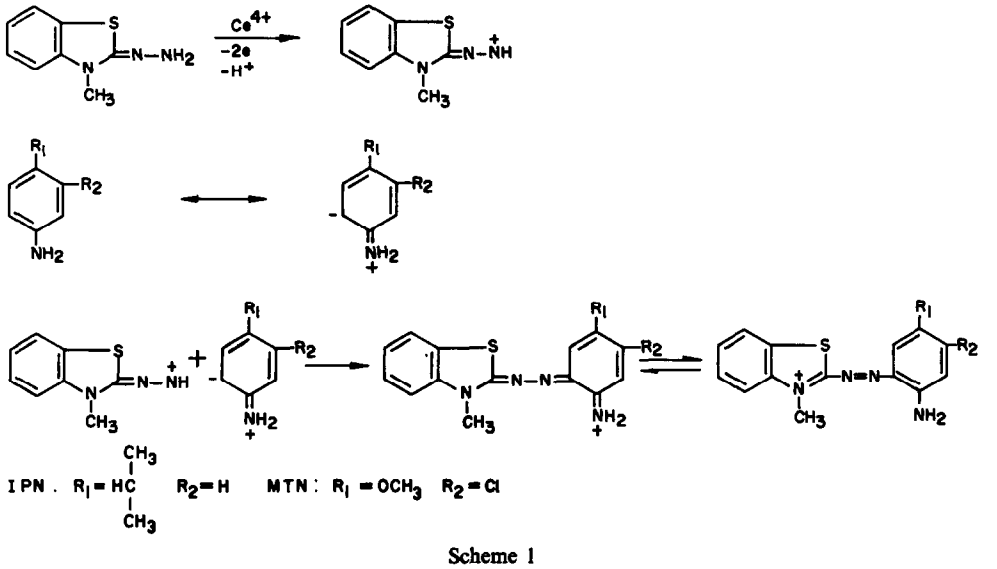

Scheme 1

Table 2. Assay of IPN

Sample	Comparison method[1] ($n = 4$)	Present method ($n = 10$)	Recovery, %	Relative standard deviation, %
Technical grade	99.60	99.10	99.50	0.62
	99.60	99.61	100.01	0.41
	98.40	98.37	99.97	0.35
	99.70	99.57	99.87	0.34
Formulation	50.90	50.34	98.90	1.00
(labelled 50%)	48.90	49.48	101.10	0.94
	49.90	50.00	100.20	0.86
	49.60	49.99	100.80	0.89

Table 3. Assay of MTN

Sample	Comparison method[1] ($n = 4$)	Present method ($n = 10$)	Recovery, %	Relative standard deviation, %
Technical grade	99.30	99.43	100.13	0.33
	99.90	99.64	99.74	0.33
	93.50	93.50	100.00	0.42
Formulation	78.00	78.79	101.01	0.50
(80%)	80.90	80.00	98.89	0.48
	80.80	80.12	99.16	0.57

Advantages

The method does not involve time consuming distillation and photodecomposition.[1] Further, the present method is superior to our earlier method[3] as analysis is faster and eliminates the hydrolysis step; but it is inferior with regard to sensitivity. Therefore, the method is simple, rapid and can be employed for routine analysis of technical grade and formulation samples of IPN and MTN.

Acknowledgements—The authors gratefully acknowledge Dr R. V. Venkataratnam and Dr M. Panduranga Rao for providing MTN samples and Dr B. S. N. Murthy for regression data. The authors also acknowledge Bharat Pulverising Mills, India for a gift of IPN samples.

REFERENCES

1. Z. Gunthar, *Analytical methods for pesticides and plant growth regulators* Vol. 8, p. 417, Academic Press, New York, 1976.
2. H. Buser and K. Grolimund, *J. Assoc. Anal. Chem.*, 1974, **57**, 1294.
3. K. Ramakrishnam Raju, T. N. Parthasarathy and S. R. K. M. Akella, *Analyst*, 1990, **115**, 455.
4. C. S. P. Sastry, T. N. V. Prasad, B. S. Sastry and E. Venkata Rao, *ibid.*, 1988, **113**, 255.
5. M. E. El-Kommos, *ibid.*, 1987, **112**, 101.
6. E. Sawicki, T. Stanley, T. R. Hauser, W. Elbert and J. L. Noe, *Anal. Chem.*, 1961, **33**, 722.

Talanta, Vol. 39, No. 10, pp. 1391–1394, 1992
Printed in Great Britain.

0039-9140/92 $5.00 + 0.00

SPECTROPHOTOMETRIC DETERMINATION OF AMPICILLIN AND ITS DOSAGE FORMS

M. B. DEVANI, ILA T. PATEL* and T. M. PATEL
Department of Pharmaceutical Chemistry, L. M. College of Pharmacy, Ahmedabad-380 009, India

(*Received* 15 *January* 1991. *Revised* 8 *January* 1992. *Accepted* 15 *January* 1992)

Summary—A new spectrophotometric procedure is described for the determination of ampicillin. The method is based on the reaction of ampicillin with acetylacetone–formaldehyde reagent to give a yellow coloured product having λ max at 400 nm. A variety of pharmaceutical dosage forms containing ampicillin are successfully analysed by the proposed procedure.

Several spectrophotometric methods for assay of ampicillin are cited in the literature.[1–8] The reported titrimetric procedures for estimation of ampicillin[9,10] are not satisfactory for microgram quantities. Acetylacetone–formaldehyde reagent has been found to be a valuable reagent for the determination of primary amines in the UV region. Csiba[4] has reacted ampicillin with acetylacetone and formaldehyde in acidic medium. The chromophore formed has λ max at 339 nm. This paper describes a modification of the acetylacetone–formaldehyde reagent method for colorimetric estimation of ampicillin, in which ampicillin is reacted with a buffered reagent (pH 4.3) to obtain an additional peak in the visible region at 400 nm. The procedure has been successfully applied to analyse a variety of pharmaceutical preparations of ampicillin.

EXPERIMENTAL

Apparatus

A Beckman Model-25 spectrophotometer with matched 1.0-cm quartz cells was used for absorbance measurements.

pH measurements were made on a Systronic digital pH meter Model-355, equipped with glass and calomel electrodes.

Reagents

All chemicals and reagents used were of analytical or pharmaceutical grade. All solutions were prepared in doubly distilled water.

The acetylacetone–formaldehyde reagent solution was prepared by mixing freshly distilled acetylacetone (7.8 ml), and formaldehyde (15.0 ml; 36% w/w) with sodium acetate (16.0 ml; 0.2*M*) and acetic acid (34.0 ml; 0.2*M*). After keeping the solution in a boiling water bath for 5 min, it was cooled to room temperature, the pH was adjusted to 4.3 and the solution was diluted with water to 100 ml. The reagent solution was prepared freshly.

Ampicillin solution (0.005*M*) was used as stock.

Procedure

Bulk samples. A portion of ampicillin solution (0.5–1.5 ml) was pipetted into a 25-ml standard flask. After addition of the reagent solution (4.0 ml), the reaction mixture was kept in a water bath at $35 \pm 1°$ for 30 min. The solution was then diluted to the mark with water and the absorbance measured at 400 nm against a reagent blank prepared in a similar manner. The drug concentration was read from the calibration graph prepared under identical conditions.

Pharmaceutical preparations. An amount of powdered tablet, capsule, injection, paediatric drops or oral suspension equivalent to 200 mg of ampicillin was extracted with water (four 15-ml portions). The combined extracts were collected in a 100-ml standard flask and the volume was made up to the mark with water. This solution was then analysed as above. The results were compared with the official method and are summarized in Table 1.

RESULTS AND DISCUSSION

Absorption spectra

The absorption spectrum of the reaction product from ampicillin and acetylacetone–formaldehyde reagent shows characteristic

*Author for correspondence.

Table 1. Analysis of ampicillin and its dosage forms.

Drug/dosage form	Nominal amount,* mg	Found,† mg		Recovery by proposed method‡, % ± SD
		Official method[11]	Proposed method	
Ampicillin anhydrous		98	98	
Ampicillin sodium		87	87	
Ampicillin trihydrate		99	100	
Tablets				
Ampicillin	125	129	128	102 ± 0.5
Ampicillin	250	252	254	102 ± 0.5
Capsules				
Ampicillin	250	246	247	99 ± 0.3
Ampicillin	500	506	506	101 ± 0.4
Ampicillin + CL	250	248	249	100 ± 0.4
Ampicillin + PR	250	252	251	100 ± 0.5
Ampicillin + LA	500	495	495	99 ± 0.5
Injections				
Ampicillin	100	99	99	99 ± 0.2
Ampicillin	250	251	252	101 ± 0.2
Ampicillin	500	504	503	101 ± 0.2
Ampicillin + CL	250	249	250	100 ± 0.2
Oral suspensions				
Ampicillin	125	130	129	103 ± 0.5
Ampicillin	250	262	262	105 ± 0.6
Ampicillin + CL	125	125	125	100 ± 0.4
Ampicillin + CL	250	253	253	101 ± 0.4
Paediatric drops				
Ampicillin	100	110	110	110 ± 0.6

†Mean of 5 determinations.
*Equivalent to ampicillin anhydrous.
‡Assuming nominal amount correct.
CL = Cloxacillin sodium 125 mg or 250 mg.
PR = Probenecid 250 mg.
LA = Lactobacillus sporogenes 1G.

maxima at 339 ($\epsilon 2.20 \times 10^3$) (UV) and 400 ($\epsilon 2.11 \times 10^3$) (visible region). All the measurements were made at 400 nm.

The calibration graph is linear over a concentration range (μg/ml) of 8.0–140. The coloured species are stable for 15 min–3 hr.

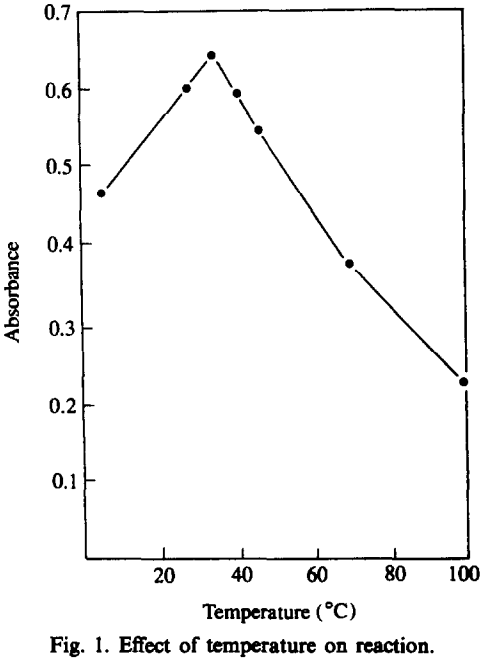

Fig. 1. Effect of temperature on reaction.

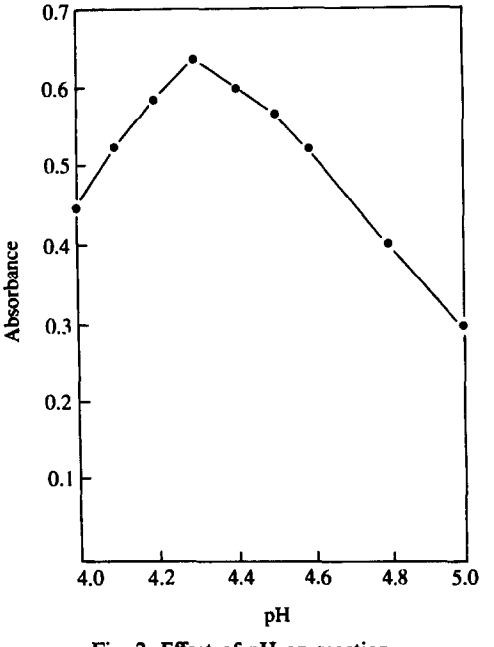

Fig. 2. Effect of pH on reaction.

Table 2. Optical characteristics, precision and accuracy

Parameters	Ampicillin
Beer's law limits, $\mu g/ml$	8.0 – 140
Molar absorptivity, $l.mol^{-1}.cm^{-1}$	2.82×10^3
Sandell's sensitivity, $\mu g.cm^{-2}/0.001A$	0.115
Regression equation*	
Slope (b)	0.53
Intercept (a)	0.027
Correlation coefficient (r)	0.9986
Relative standard deviation, %	0.7
Range of error, %	±0.25
Calculated 't' value = 1.728 (2.310)†	
Calculated 'F' value = 1.573 (2.450)†	

*$A = a + bC$, where C is the concentration in μg/ml.
†95% confidence limit.

The reaction conditions were established by variation of one parameter at a time. For the reaction, use of acetate buffer (pH 4.1–4.5) was found optimal. This compares with the pH range of 1.5–2 used by Csiba[4] for the UV method. The reaction time was established by increasing it in increments of 5 min, and it was found that 30 min is sufficient to yield maximum absorbance. The use of 3.0–5.0 ml of reagent solution and temperature $35 \pm 1°$ for the reaction was considered optimal. The final temperature after dilution was not critical.

Analytical data

The optical characteristics and figures of merit are given in Table 2. The values obtained by the proposed and official[11] methods for pharmaceutical preparations are compared in Table 1. Table 3 shows the results of recovery experiments.

Table 4. Determination of ampicillin* in the presence of combination drugs and excipients by the proposed method

Combination, *mg*		% Recovery*
I. Cloxacillin sodium	250	99
	500	99
	750	99
	1000	99
	1500	99
II. Probenecid	250	100
	500	99
	1000	99
	1500	99
	2000	99
III. Lactobacillus Sporogenes†	250	100
	500	100
	1000	100
	1500	99
	2000	99
IV. Excipients Starch	1000	99
Dicalcium phosphate	1000	99
Talc	1000	100
Magnesium sterate	1000	100
Lactose	1000	99

*Mean of 5 determinations.
†1G Lactobacillus sporogenes contain 60 million spores.

Table 4 indicates that other active components such as cloxicallin sodium, probenecid or lactobacillus sporogenes which are generally present in combined formulations did not interfere. Commonly encountered excipients such as starch, talc, lactose, magnesium stearate and dicalcium phosphate also did not interfere.

Table 3. Recovery of ampicillin in pharmaceutical formulations by official and proposed methods

Sample	Label claim	Ampicillin added, *mg*	Found, *mg** Official method	Found, *mg** Proposed method	Recovery†, % ± SD
Tablet	250 mg/tab	25	247	274	96 ± 0.3
	250 mg/tab	50	298	300	96 ± 0.3
	500 mg/tab	25	524	524	96 ± 0.3
	500 mg/tab	50	549	550	100 ± 0.4
Capsule	250 mg/cap	25	274	275	100 ± 0.4
	250 mg/cap	50	300	300	100 ± 0.3
	500 mg/cap	25	523	524	96 ± 0.4
	500 mg/cap	50	550	550	98 ± 0.4
Injection	100 mg/vial	25	125	127	100 ± 0.2
	100 mg/vial	50	149	149	98 ± 0.2
	250 mg/vial	25	274	275	100 ± 0.1
	250 mg/vial	50	299	299	98 ± 0.2
	500 mg/vial	25	525	525	100 ± 0.2
	500 mg/vial	50	649	549	98 ± 0.1
Suspension	100 mg/5 ml	25	124	125	100 ± 0.3
	100 mg/5 ml	50	150	150	100 ± 0.4
	125 mg/5 ml	25	149	149	96 ± 0.4
	125 mg/5 ml	50	174	175	100 ± 0.5
	250 mg/5 ml	25	275	275	100 ± 0.4
	250 mg/5 ml	50	301	300	100 ± 0.6

*Mean of 5 determinations.
†Recovery of added amount, assuming label claims correct.

The present method has advantages over the pharmacopeial and other reported methods in terms of simplicity, sensitivity and freedom from interferences.

The chemistry of the colour reaction may be suggested on the basis of earlier reports[4] and our findings as follows:

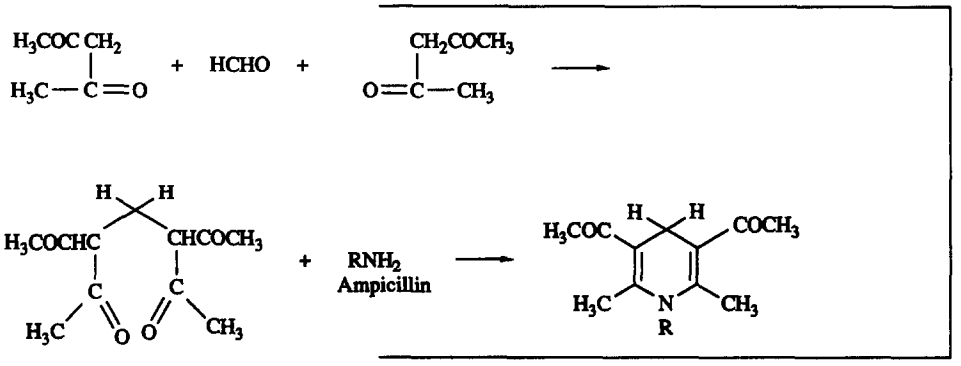

Applications

The method was applied to the assay of ampicillin in drug formulations (commercial products randomly collected from local pharmacies). Typical results are given in Table 1 and show good agreement with those obtained by official methods.[11] The method can possibly be extended to the determination of other amino β-lactam penicillins, as described by Csiba.[4]

REFERENCES

1. J. W. G. Smith, G. E. de Grey and V. J. Patel, *Analyst*, 1967, **92**, 247; *Chem. Abstr.*, 1967, **67**, 5713c.
2. M. Llena, V. Girona, J. De Bolos and M. Castillo, *Cienc. Ind. Farm.*, 1985, **4**, 13; *Chem. Abstr.*, 1985, **103**, 59372w.
3. A. Burr and H. Bundgaard, *Arch. Pharm. Chem. Sci. Ed.*, 1983, **11**, 897; *Chem. Abstr.* 1985, **102**, 67451r.
4. A. Csiba, *Proc. Hung. Annu. Meet. Biochem.*, 1979, **19**, 291; *Chem. Abstr.*, 1980, **92**, 64836j.
5. P. Celletti, G. P. Moretti and B. Petrangeli, *Farmaco, Ed. Prat.*, 1972, **27**, 688; *Chem. Abstr.*, 1973, **78**, 102074e.
6. W. K. Lee, B. T. Yoo and G. J. Kang, *Yakhak Hoe Chi*, 1974, **18**, 190; *Chem. Abstr.*, 1975, **82**, 116152y.
7. K. J. Mills, *Spectrovision*, 1971, **25**, 3; *Chem. Abstr.*, 1973, **79**, 83505y.
8. P. B. Issopoulos, *J. Pharm. Biomed. Anal.*, 1988, **6**, 321.
9. J. Talegaonkar and K. S. Bopari, *Indian Drugs*, 1981, **18**, 410.
10. S. D. Leo and G. Pitrolo, *Bull. Chim. Farm.*, 1973, **112**, 487; *Chem. Abstr.*, 1974, **80**, 63887s.
11. *British Pharmacopoeia*, H.M. Stationery Office, London, 1988.

Talanta, Vol. 39, No. 10, pp. 1395–1398, 1992
Printed in Great Britain

0039-9140/92 $5.00 + 0.00
Pergamon Press Ltd

1-(4-NITROPHENYL)-3-(2-QUINOLYL) TRIAZENE AS AN EXTREMELY SENSITIVE REAGENT FOR SPECTROPHOTOMETRIC DETERMINATION OF MERCURY

CAO SHITI* and LI XU†
Changsha Research Institute of Mining and Metallurgy, Changsha, Hunan, 410012, People's Republic of China

(*Received* 2 *December* 1988. *Revised* 17 *August* 1991. *Accepted* 1 *October* 1991)

Summary—1-(4-Nitrophenyl)-3-(2-quinolyl)triazene has been synthesized, and used as an extremely sensitive reagent for the spectrophotometric determination of mercury by the decrease in the absorbance of the reagent at 490 nm and pH 9.0–10.8 in the presence of cetylpyridinium bromide. Beer's law is obeyed over the range 0–120 ng/ml Hg(II), the apparent molar absorptivity being 1.0×10^6 l. mole^{-1}. cm^{-1}. The effect of 69 ionic species or compounds has been examined. Trace mercury in waste water has been determined satisfactorily.

4,4′-Dinitrodiazoaminobenzene (DNAAB),[1–6] 2,2′-dichloro-4,4′-dinitrodiazoaminobenzene (2,2′-diCl-DNAAB)[7–11] and 1-(4-nitrophenyl)-3-(2-pyridyl)triazene (NPPyT)[12] have been investigated as reagents for spectrophotometric determinations, and the use of triazenes in spectrophotometry has been reviewed.[13] In this paper the use of 1-(4-nitrophenyl)-3-(2-quinolyl)triazene (NPQT) as a spectrophotometric reagent for the determination of mercury(II) is reported.

EXPERIMENTAL

Synthesis of NPQT

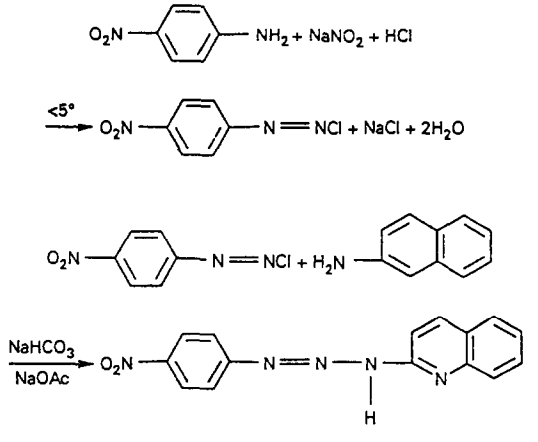

Concentrated hydrochloric acid (20 ml) and water (120 ml) were added to 4-nitroaniline (4.8 g) in a 500-ml flask and heated gently until the 4-nitroaniline dissolved. The solution was cooled in an ice-bath to below 5°, and a solution of 2.5 g of sodium nitrite in 20 ml of water (at <5°) was added with stirring. This solution was then mixed with a solution (cooled to <5°) of 5 g of 2-aminoquinoline in a mixture of 10 ml of concentrated hydrochloric acid and 20 ml of water. After half an hour sodium bicarbonate (30–40 g) was added in small portions, and after 24 hr about 40 g of sodium acetate was added with stirring until the pH of the solution rose to about 6. After another 24 hr the yellow solid was filtered off and dried in air. The crude product was recrystallized twice from ethanol, to yield bright yellow crystals, m.p. 216°.

The composition of NPQT was established from its low-resolution mass spectrum (Fig. 1) in which the molecular peak appears at m/z 293. The base peak at m/z 122 is due to

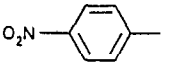

and the second most intense peak at m/z 150 is due to

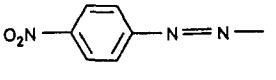

*Author for correspondence.
†Present address: Zhuzhou Institute of Technology, Zhuzhou, Hunan, 412008, P.R.C.

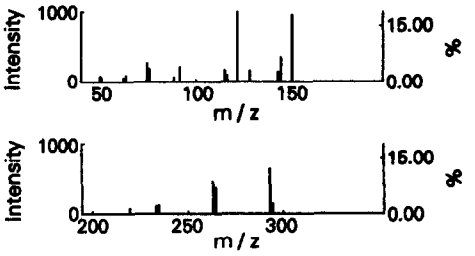

Fig. 1. Low-resolution mass spectrum of NPQT.

and the two weak peaks at m/z 128 and 143 are due to

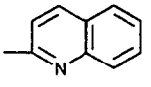

and

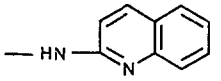

respectively.

Analysis gave C 61.3%, H 3.8%, N 23.4%; $C_{15}H_{11}N_5O_2$ requires C 61.43%, H 3.78%, N 23.88%.

NPQT has good stability. It is sparingly soluble in water, but easily soluble in ethanol and in acids and alkalis. Its solution in alkaline aqueous alcohol is yellow and stable for at least a year.

In aqueous alcohol solution its dissociation equilibria are

$$H_2L^+ \underset{+H^+}{\overset{+OH^-}{\rightleftharpoons}} HL \underset{+H^+}{\overset{+OH^-}{\rightleftharpoons}} L^-$$

pH 1.5	pK_1 2.08	pH 2.5–11.5	pK_2 11.92	pH 12.5–14
yellow		greenish-yellow		orange

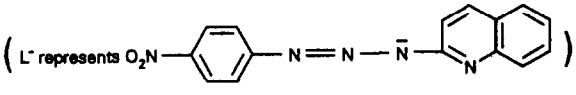

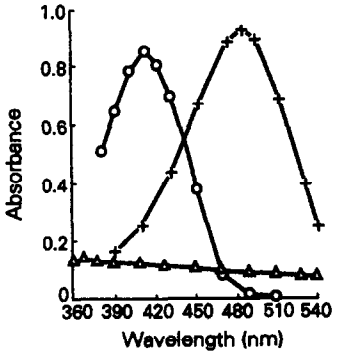

Fig. 2. Absorption curves of NPQT solution ($2.4 \times 10^{-5}M$) with HCl or / and NaOH present at pH 1.6 (○), 9.63 (△) and 14(+).

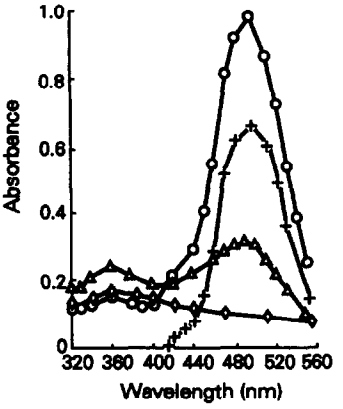

Fig. 3. Absorption spectra with $6.4 \times 10^{-7}M$ Hg(II)–NPQT (◇), NPQT–CPB (○) and NPQT–CPB–Hg(II) (△) solutions measured against H_2O and NPQT–CPB solution measured against NPQT–CPB–Hg(II) solution (+).

NPQT decomposes to give a greyish precipitate when the basicity of the solution is $>1M$ sodium hydroxide. The absorption spectra of NPQT at different pH values are shown in Fig. 2. The maximum absorption was at 412 and 481 nm at pH $\leqslant$ 1.5 and 12.5–14 respectively. There was no absorption maximum when the pH was 2.5–11.5.

RESULTS AND DISCUSSION

Spectrophotometric determination of Hg(II)

NPQT solution (1.5×10^{-4}M). In a 2-litre standard flask, dissolve 0.0898 g of NPQT in 1 litre of 95% ethanol and 5 ml of $2.5M$ sodium hydroxide, and dilute to the mark with water.

Standard mercury solution (5 mg/ml). Dissolve 6.891 g of mercuric chloride in 1 litre of 0.5% v/v hydrochloric acid. Prepare a working standard solution (1.0 μg/ml Hg) by diluting the stock solution with water just before use.

Buffer solution (pH 10.5). Prepare with $0.1M$ borax and $2.5M$ sodium hydroxide.

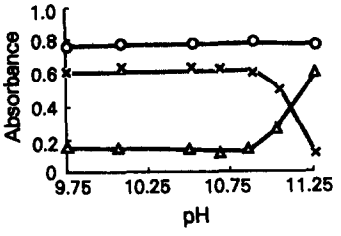

Fig. 4. Effect of pH on absorbance of NPQT–CPB (○) and NPQT–CPB–Hg(II) (△) solutions measured against H_2O and NPQT–CPB solution measured against NPQT–CPB–Hg(II) solution (+); (conditions as for Fig. 3).

Table 1. Results of determination of trace mercury in water

Sample	Found, *ppm*	Average, *ppm*	Std. devn., *ppm*
[5 ml of tap water+ 1.6 μg of Hg(II)]/25 ml	0.064, 0.062 0.063, 0.065 0.064, 0.062	0.063	0.001
Industrial waste water (2.36 ppm*)	2.32, 2.31 2.34, 2.31 2.38, 2.30	2.33	0.03

*Determined with a mercury analyser.

Cetylpyridinium bromide (CPB) solution (5×10^{-3}M)

Procedure. In a 25-ml standard flask place 4.0 ml of the buffer solution, 3.5 ml of NPQT solution and a known volume of standard or sample solution (containing up to 3.0 μg of mercury), in that order, and mix. After 5 min add 5.0 ml of CPB solution and dilute to the mark with water. Prepare a reagent blank in the same way. Keep both solutions at 25° and after 15 min measure the absorbance of the reagent blank against the sample solution at 490 nm, in 1-cm cells.

The absorption spectra for the reagent and the complex system are shown in Fig. 3. NPQT itself has no absorption maximum in the visible spectrum at the pH used, but has a strong absorption peak at 490 nm in the presence of CPB (curve 1) and this is decreased by Hg(II) (curve 2) owing to formation of the Hg(II)–NPQT–CPB complex. The absorption maximum of the Hg(II)–NPQT–CPB complex is at 360 nm, and the apparent molar absorptivity for Hg(II) at this wavelength is 1.5×10^5 l.mole^{-1}.cm^{-1}, but the reagent blank is rather high. Moreover the sensitivity is considerably increased by use of the decrease in the reagent absorbance at 490 nm.

The absorbances of the reagent and the ternary complex vary slightly with the pH of the solution in the ranges 9.8–11.3 and 9.8–10.8 respectively (Fig. 4), but the difference between the two varies only slightly in the pH range 9.8–10.8. Therefore, pH 10.5 is chosen for the determination.

The absorbance of 25 ml of solution containing 1.6 μg of mercury is maximum and constant with 2.3–7.0 ml of $1.5 \times 10^{-4}M$ NPQT and 2–6 ml of buffer solution. The absorbance appears to be maximal with about 1.5 ml of $5 \times 10^{-3}M$ CPB and then decreases, but is constant with 3.5–5.5 ml of CPB solution. The absorbance of the reagent blank (measured against water) is constant for about 2 hr, but the absorbance for the mercury system (measured against water) increases slightly with time. However, the difference between them decreases by less than 5% per hr, so the spectrophotometric measurement should be made at a fixed time (in the range 15–45 min) after all the reagents have been added.

The absorbance for NPQT–CPB measured against water does not change with temperature, but that for Hg(II)–NPQT–CPB measured against water increases by about 34% when the temperature rises from 15° to 40°. Hence we recommend keeping the temperature at 25°.

Less than 3 ml of extra ethanol added together with the NPQT solution does not affect the sensitivity for the determination of mercury.

The effect of the temperature, time and other factors on the decrease of the absorbance of NPQT by mercury(II) is serious, so it is very important to control all conditions precisely in the determination of mercury. In particular, the sample and reference solutions have to be made up with as nearly as possible exactly the same amount of NPQT in each.

The calibration curve is constructed at 490 nm in the usual way, according to the general procedure. Beer's law is obeyed for 0–3 μg of Hg(II) in 25 ml of solution. The apparent molar absorptivity is 1.0×10^6 l.mole^{-1}.cm^{-1}. The method is one of the most sensitive spectrophotometric methods for mercury.

Effect of foreign ions

Cd(II), Ag(I), Cu(II) and Pd(II) behave like Hg(II), and cause positive interference, but 1 μg of Cd(II) or 3 μg of Cu(II) or Pd(II) can be tolerated if 1 mg of potassium bromide and 2 mg of citrate as masking agents are added for the determination of 1.6 μg of Hg(II). CNS^-, I^-, ClO_4^-, ascorbic acid, salicylic acid and $S_2O_3^{2-}$ interfere seriously and large amounts of EDTA, DCTA, $C_2O_4^{2-}$, F^-, NTA, tartrate, H_2O_2, $NH_2OH \cdot HCl$, $(NH_2OH)_2 \cdot H_2SO_4$ and thiourea interfere. Less than ±5% deviation in the determination of 1.6 μg of mercury(II) results from the following amounts (μg) of various ionic or molecular species: Na^+, K^+ (5000);

NH_4^+ (2000); V(V), Mn(II) (1000); Ba(II), Ca(II), Mg(II) (500); W(VI) (100); Ga(III), As(V), In(III), Sr(II), Cr(VI), Mo(VI), Al(III), Pt(II) (50); Ni(II), Co(II), Bi(III), Tl(III), Ge(IV), Sn(IV) (30); Zr(IV), Ti(IV), Fe(III), Au(III), Nb(V), Ta(V), Pb(II), Te(IV), lanthanides, Th(IV), Zn(II) (10); Rh(III) (5); Ir(III) (2); Sb(V) (1); Cl^-, SO_4^{2-}, $S_2O_7^{2-}$, TEA, citrate, PO_4^{3-} (20,000); tartrate, CO_3^{2-}, $S_2O_8^{2-}$, NO_3^- (2000); Br^-, NO_2^-, $C_2O_4^{2-}$, $CH_3CO_2^-$, H_2O_2 (1000); $NH_2OH \cdot HCl$, $(NH_2OH)_2 \cdot H_2SO_4$, thiourea (500); F^-, DCTA, NTA (100).

Determination of mercury in water

The mercury content of a waste water sample was determined by the proposed method (1 mg of potassium bromide and 2 mg of sodium citrate were added as masking reagents). The result was in reasonable agreement with that obtained with a mercury analyser. A mercury-free tap water was spiked with known amounts of mercury and analysed. The results are shown in Table 1.

REFERENCES

1. Cao Shiti, Ma Qiang and Yan Xiuqin, *Acta Chimica Sinica*, 1966, **32**, No. 1, 82.
2. Cao Shiti and Zhing Ling, *Mining and Metallurgical Engineering*, 1986, **6**, No. 1, 36.
3. Cao Shiti and Sun Qin, *Fenxi Huaxue*, 1983, **11**, 863.
4. Cao Shiti and Cao Bonan, *Huaxue Shiji*, 1983, **5**, 370.
5. Cao Shiti and Gu Yuween, *Mining and Metallurgical Engineering*, 1984, **4**, No. 1, 48.
6. Cao Shiti and Zeng Xiaoping, *Hunan Yejin*, 1986, No. 1, 43.
7. Cao Shiti, Ma Taiyu and Yuan Xizhao, *Huaxue Shiji*, 1984, **6**, 337.
8. Cao Shiti and Sun Qin, *ibid.*, 1984, **6**, 216.
9. Cao Shiti and Cao Bonan, *Fenxi Shiyanshi*, 1985, **4**, No. 11, 11.
10. Cao Shiti and Cai Bosheng, *J. Maanshan Inst. Iron and Steel Technol.*, 1985, No. 3, 75.
11. Cao Shiti and Wang Jiajun, *Fenxi Shiyanshi*, 1986, **5**, No. 3, 4.
12. Cao Shiti, Li Xu and Qu Long, *ibid.*, 1987, **6**, No. 9, 1.
13. Cao Shiti and Li Xu, *ibid.*, 1987, **6**, No. 4, 26.

Talanta, Vol. 39, No. 10, pp. 1399–1401, 1992
Pergamon Press Ltd. Printed in Great Britain

BOOK REVIEWS

Dual Diagnosis in Substance Abuse: M. S. GOLD and A. E. SLABY (editors), Dekker, 1991. Pages x + 341. $89.75 (US and Canada), $103.00 (Elsewhere).

It has been a privilege for me as a psychiatrist to review this volume. The title is mildly misleading as not all patients will have only two diagnoses. However, if the title is designed to convey the occurrence of some substance misuse disorder with any other combination of diagnoses then the editors have succeeded in their task.

Three sections have been presented, namely an introduction, a section on clinical presentation of other diagnoses in substance misuse and a section on treatment. The chapters in these sections have been written by a number of physicians from the United States of America, some being better known than others, and two counsellors. Generally, these authors have presented their material well, though the editors have allowed some repetition across chapters. Unfortunately, the style in the chapter on "Diagnosing Dual Diagnosis Patients" is greatly at odds with that used throughout the rest of the volume. The authors have used quite a few unexplained initials and introduced jargon. Inclusion of case histories to illustrate the diagnostic criteria help to offset what might otherwise ruin this chapter completely.

For those who are looking for a word on the role and usefulness of chemical analysis, what a clinician wants and problems that might arise, there is not a whisper. There are at most three pages which mention thin-layer chromatography, gas chromatographic mass spectrometry, radio immunoassay and enzyme immunoassay in the chapter on pharmacotherapy. I respectfully suggest that while psychiatrists would find this book worth reading those who deal with chemical analysis might wish only to glance at the chapter on pharmacotherapy and read further only if wishing to have some background understanding of what is a complicated area in the substance misuse field.

A. D. T. ROBINSON

Instrumentation in Analytical Chemistry, volume 1: J. ZÝKA (editor), Ellis Horwood, 1991. Pages 368. £53.00.

This is volume one of a two-part work intended to provide students of analytical chemistry, industrial chemists and workers in other scientific fields with an up-to-date overview of a wide range of modern instrumental techniques. In recent years the pace of development in instrumentation, automation and computerisation and the increasingly diverse and complex nature of many contemporary analytical problems, some requiring an interdisciplinary approach, has made it difficult for students, industrialists, environmentalists, *etc.*, to keep fully abreast of such advances. The editor and authors have addressed this problem by planning two volumes of suitably condensed information on a variety of modern analytical techniques with extensive references to monographs and other specialised literature.

The sixteen chapters cover a quite diverse range of topics, *viz.*

1. Analytical isotachophoresis
2. Differential pulse polarography and voltammetry
3. Advances in ion-selective electrode potentiometry
4. Analytical measurements in flowing liquids
5. The use of computers in gas chromatography
6. The long-range detection of atoms, molecules and aerosols with lasers
7. New sources in optical emission spectrometry
8. Modern radioanalytical methods
9. Modern methods of decomposition of inorganic substances
10. Gas chromatography and headspace analysis
11. Inclusion compounds in chromatography
12. Chromatographic methods in the analysis of phenols
13. X-ray spectroscopy
14. Mössbauer spectroscopy
15. Neutron activation analysis
16. The analytical application of characteristic X-rays excited by charged particles (the PIXE method).

These are in the main well-structured and concisely written covering essential theory, instrumentation and practical applications. Diagrams are generally clear and long lists of more detailed and specialised references are given at the end of each chapter. Although some recent references are cited the number from the late eighties and nineties in many chapters is small and, coupled with the omission of such topics as radioimmunoassay and ICP-Mass spectrometry, this gives the book a somewhat dated feel. Nevertheless, the idea for this type of work is a good one but it must also be said that the choice of

Talanta, Vol. 39, No. 10, pp. 1399–1401, 1992
Pergamon Press Ltd. Printed in Great Britain

BOOK REVIEWS

Dual Diagnosis in Substance Abuse: M. S. GOLD and A. E. SLABY (editors), Dekker, 1991. Pages x + 341. $89.75 (US and Canada), $103.00 (Elsewhere).

It has been a privilege for me as a psychiatrist to review this volume. The title is mildly misleading as not all patients will have only two diagnoses. However, if the title is designed to convey the occurrence of some substance misuse disorder with any other combination of diagnoses then the editors have succeeded in their task.

Three sections have been presented, namely an introduction, a section on clinical presentation of other diagnoses in substance misuse and a section on treatment. The chapters in these sections have been written by a number of physicians from the United States of America, some being better known than others, and two counsellors. Generally, these authors have presented their material well, though the editors have allowed some repetition across chapters. Unfortunately, the style in the chapter on "Diagnosing Dual Diagnosis Patients" is greatly at odds with that used throughout the rest of the volume. The authors have used quite a few unexplained initials and introduced jargon. Inclusion of case histories to illustrate the diagnostic criteria help to offset what might otherwise ruin this chapter completely.

For those who are looking for a word on the role and usefulness of chemical analysis, what a clinician wants and problems that might arise, there is not a whisper. There are at most three pages which mention thin-layer chromatography, gas chromatographic mass spectrometry, radio immunoassay and enzyme immunoassay in the chapter on pharmacotherapy. I respectfully suggest that while psychiatrists would find this book worth reading those who deal with chemical analysis might wish only to glance at the chapter on pharmacotherapy and read further only if wishing to have some background understanding of what is a complicated area in the substance misuse field.

A. D. T. ROBINSON

Instrumentation in Analytical Chemistry, volume 1: J. ZÝKA (editor), Ellis Horwood, 1991. Pages 368. £53.00.

This is volume one of a two-part work intended to provide students of analytical chemistry, industrial chemists and workers in other scientific fields with an up-to-date overview of a wide range of modern instrumental techniques. In recent years the pace of development in instrumentation, automation and computerisation and the increasingly diverse and complex nature of many contemporary analytical problems, some requiring an interdisciplinary approach, has made it difficult for students, industrialists, environmentalists, *etc.*, to keep fully abreast of such advances. The editor and authors have addressed this problem by planning two volumes of suitably condensed information on a variety of modern analytical techniques with extensive references to monographs and other specialised literature.

The sixteen chapters cover a quite diverse range of topics, *viz.*

1. Analytical isotachophoresis
2. Differential pulse polarography and voltammetry
3. Advances in ion-selective electrode potentiometry
4. Analytical measurements in flowing liquids
5. The use of computers in gas chromatography
6. The long-range detection of atoms, molecules and aerosols with lasers
7. New sources in optical emission spectrometry
8. Modern radioanalytical methods
9. Modern methods of decomposition of inorganic substances
10. Gas chromatography and headspace analysis
11. Inclusion compounds in chromatography
12. Chromatographic methods in the analysis of phenols
13. X-ray spectroscopy
14. Mössbauer spectroscopy
15. Neutron activation analysis
16. The analytical application of characteristic X-rays excited by charged particles (the PIXE method).

These are in the main well-structured and concisely written covering essential theory, instrumentation and practical applications. Diagrams are generally clear and long lists of more detailed and specialised references are given at the end of each chapter. Although some recent references are cited the number from the late eighties and nineties in many chapters is small and, coupled with the omission of such topics as radioimmunoassay and ICP-Mass spectrometry, this gives the book a somewhat dated feel. Nevertheless, the idea for this type of work is a good one but it must also be said that the choice of

techniques (the chapter on phenols is all chromatography) is curious in that there is no apparent logic to it. Some of the techniques selected are in the mainstream of modern analytical chemistry whilst others are highly specialised and are likely to be of very little or no interest to many potential readers. Given the two-volume nature of the work, it might have been more prudent, and commercially adroit, to have grouped mainstream techniques in volume one and the more peripheral ones in volume two. The scope of the latter is as yet unknown but there are certainly many more widely-used techniques that could and should be covered.

Inevitably one must compare this book with the established and more detailed volumes on instrumental analysis several of which are up-dated frequently and are generally available in relatively cheap student editions. However, the attraction (but possibly the weakness) of this book is that it includes more diverse and esoteric techniques. It is not a book for the individual but will provide libraries with useful and reasonably up-to-date introductory material and a source of references to more detailed information.

D. KEALEY

The Important Peak Index of the Registry of Mass Spectral Data: Volumes 1–3. F. W. MCLAFFERTY and D. B. STAUFFER, Wiley-Interscience, New York, 1991. Pages: viii + 1352 (Volume 1), 1353–2708 (Volume 2) and 2709–4057 (Volume 3). £576.50.

This three-volume Index is derived from the "Registry of Mass Spectral Data", published in 1989, which contains spectra of over 115,000 different compounds of established structure.

With the proliferation of combined GC/MS and LC/MS instrumentation, reliable mass spectral data can now be routinely obtained on individual components of complex mixtures, without the need for isolation of the compounds themselves. This has generated an urgent need to identify the types of compounds which give rise to peaks at the masses found in the spectrum of a compound of unknown structure. Computer searching of MS databases does provide an efficient method for the matching of mass spectra, and recent advances have reduced costs in this area, but additional aids to interpretation are still required. One such adjunct is the widely used "Eight Peak Index" (RSC, 1983), which lists the most abundant peaks by m/z value. In this new Index, the peaks listed are chosen on the basis of their statistical importance, rather than just their abundance, according to a probability-based matching system. This more sophisticated system affords greater reliability in the matching of peaks for two main reasons (i) it eliminates all the commonly occurring low m/z peaks (which are usually the most abundant and the most infuriating) from the analysis, and (ii) it allows attention to be focussed upon those peaks which are of the greatest value in identifying an unknown compound. These innovations allow the number of possible structures to be narrowed down dramatically when higher m/z peaks are considered.

The probability of occurrence of ions in the Registry database has been tabulated in terms of the "uniqueness value" ("U") used in the probability based matching algorithm, U representing the log base 2 value for the probability that a reference will contain a peak of this m/z value of $\geqslant 1\%$ abundance. The "importance" rating of each peak for this Index is based upon the sum of the uniqueness and abundance values (U + A), thereby allowing ions of low to moderate abundance in the upper m/z range of a mass spectrum to be rated as highly as a base peak of low m/z value. As an aid, a one-line summary of approximate U and A values appears at the bottom of each page of the Index.

The Index has been found to be extremely useful in identifying aroma volatiles from various sources by GC/MS headspace analysis. The rating system provides a mechanism for allowing for the differences between mass spectra obtained with different instruments and conditions, particularly as abundance variability can sometimes be considerable. Of course it is not possible to identify new compounds using this Index, but its novel features ensure that existing compounds in the molecular weight range of an unknown can rapidly be identified and eliminated from consideration.

Each of these three volumes weighs no less than 5lb 5oz. Although the published price may seem high, it represents a rare bargain, for they are worth their weight in gold.

A. B. TURNER

Chromatographic Enantioseparation—methods and applications, 2nd edition: S. ALLENMARK, Ellis Horwood, 1991. Pages 282. £55.00.

The second edition of this book appears three years after the first. The original work was well received (for a review by J. L. Wardell see *Talanta*, 1989, **36**, No. 4) and the rapidly advancing field of chiral chromatography has provided the reason for this new edition. If you are new to this area of separation science and wish a good introductory text which also covers some recent work then this book is highly recommended. If you are an experienced practitioner in chromatography and have already purchased the first edition do you also buy this edition? If you wish to keep up to date then the answer must be "yes". However, a comparison with the first edition may be of interest.

The topics covered are essentially the same as in the first edition (the chapters have identical headings) but have been updated where necessary by reference to more recent literature. The most obvious difference between editions is the inclusion of additional experimental procedures for the synthesis of chiral sorbents. In particular, several techniques used for the binding of chiral selectors to silica are now presented. Chapter 10 on "future trends" is also of interest as the newly developed diode-laser-based micropolarimetric detectors (a "future trend" in the first edition) is now mentioned

techniques (the chapter on phenols is all chromatography) is curious in that there is no apparent logic to it. Some of the techniques selected are in the mainstream of modern analytical chemistry whilst others are highly specialised and are likely to be of very little or no interest to many potential readers. Given the two-volume nature of the work, it might have been more prudent, and commercially adroit, to have grouped mainstream techniques in volume one and the more peripheral ones in volume two. The scope of the latter is as yet unknown but there are certainly many more widely-used techniques that could and should be covered.

Inevitably one must compare this book with the established and more detailed volumes on instrumental analysis several of which are up-dated frequently and are generally available in relatively cheap student editions. However, the attraction (but possibly the weakness) of this book is that it includes more diverse and esoteric techniques. It is not a book for the individual but will provide libraries with useful and reasonably up-to-date introductory material and a source of references to more detailed information.

D. KEALEY

The Important Peak Index of the Registry of Mass Spectral Data: Volumes 1–3. F. W. MCLAFFERTY and D. B. STAUFFER, Wiley-Interscience, New York, 1991. Pages: viii + 1352 (Volume 1), 1353–2708 (Volume 2) and 2709–4057 (Volume 3). £576.50.

This three-volume Index is derived from the "Registry of Mass Spectral Data", published in 1989, which contains spectra of over 115,000 different compounds of established structure.

With the proliferation of combined GC/MS and LC/MS instrumentation, reliable mass spectral data can now be routinely obtained on individual components of complex mixtures, without the need for isolation of the compounds themselves. This has generated an urgent need to identify the types of compounds which give rise to peaks at the masses found in the spectrum of a compound of unknown structure. Computer searching of MS databases does provide an efficient method for the matching of mass spectra, and recent advances have reduced costs in this area, but additional aids to interpretation are still required. One such adjunct is the widely used "Eight Peak Index" (RSC, 1983), which lists the most abundant peaks by m/z value. In this new Index, the peaks listed are chosen on the basis of their statistical importance, rather than just their abundance, according to a probability-based matching system. This more sophisticated system affords greater reliability in the matching of peaks for two main reasons (i) it eliminates all the commonly occurring low m/z peaks (which are usually the most abundant and the most infuriating) from the analysis, and (ii) it allows attention to be focussed upon those peaks which are of the greatest value in identifying an unknown compound. These innovations allow the number of possible structures to be narrowed down dramatically when higher m/z peaks are considered.

The probability of occurrence of ions in the Registry database has been tabulated in terms of the "uniqueness value" ("U") used in the probability based matching algorithm, U representing the log base 2 value for the probability that a reference will contain a peak of this m/z value of $\geqslant 1\%$ abundance. The "importance" rating of each peak for this Index is based upon the sum of the uniqueness and abundance values (U + A), thereby allowing ions of low to moderate abundance in the upper m/z range of a mass spectrum to be rated as highly as a base peak of low m/z value. As an aid, a one-line summary of approximate U and A values appears at the bottom of each page of the Index.

The Index has been found to be extremely useful in identifying aroma volatiles from various sources by GC/MS headspace analysis. The rating system provides a mechanism for allowing for the differences between mass spectra obtained with different instruments and conditions, particularly as abundance variability can sometimes be considerable. Of course it is not possible to identify new compounds using this Index, but its novel features ensure that existing compounds in the molecular weight range of an unknown can rapidly be identified and eliminated from consideration.

Each of these three volumes weighs no less than 5lb 5oz. Although the published price may seem high, it represents a rare bargain, for they are worth their weight in gold.

A. B. TURNER

Chromatographic Enantioseparation—methods and applications, 2nd edition: S. ALLENMARK, Ellis Horwood, 1991. Pages 282. £55.00.

The second edition of this book appears three years after the first. The original work was well received (for a review by J. L. Wardell see *Talanta*, 1989, **36**, No. 4) and the rapidly advancing field of chiral chromatography has provided the reason for this new edition. If you are new to this area of separation science and wish a good introductory text which also covers some recent work then this book is highly recommended. If you are an experienced practitioner in chromatography and have already purchased the first edition do you also buy this edition? If you wish to keep up to date then the answer must be "yes". However, a comparison with the first edition may be of interest.

The topics covered are essentially the same as in the first edition (the chapters have identical headings) but have been updated where necessary by reference to more recent literature. The most obvious difference between editions is the inclusion of additional experimental procedures for the synthesis of chiral sorbents. In particular, several techniques used for the binding of chiral selectors to silica are now presented. Chapter 10 on "future trends" is also of interest as the newly developed diode-laser-based micropolarimetric detectors (a "future trend" in the first edition) is now mentioned

techniques (the chapter on phenols is all chromatography) is curious in that there is no apparent logic to it. Some of the techniques selected are in the mainstream of modern analytical chemistry whilst others are highly specialised and are likely to be of very little or no interest to many potential readers. Given the two-volume nature of the work, it might have been more prudent, and commercially adroit, to have grouped mainstream techniques in volume one and the more peripheral ones in volume two. The scope of the latter is as yet unknown but there are certainly many more widely-used techniques that could and should be covered.

Inevitably one must compare this book with the established and more detailed volumes on instrumental analysis several of which are up-dated frequently and are generally available in relatively cheap student editions. However, the attraction (but possibly the weakness) of this book is that it includes more diverse and esoteric techniques. It is not a book for the individual but will provide libraries with useful and reasonably up-to-date introductory material and a source of references to more detailed information.

D. KEALEY

The Important Peak Index of the Registry of Mass Spectral Data: Volumes 1–3. F. W. MCLAFFERTY and D. B. STAUFFER, Wiley-Interscience, New York, 1991. Pages: viii + 1352 (Volume 1), 1353–2708 (Volume 2) and 2709–4057 (Volume 3). £576.50.

This three-volume Index is derived from the "Registry of Mass Spectral Data", published in 1989, which contains spectra of over 115,000 different compounds of established structure.

With the proliferation of combined GC/MS and LC/MS instrumentation, reliable mass spectral data can now be routinely obtained on individual components of complex mixtures, without the need for isolation of the compounds themselves. This has generated an urgent need to identify the types of compounds which give rise to peaks at the masses found in the spectrum of a compound of unknown structure. Computer searching of MS databases does provide an efficient method for the matching of mass spectra, and recent advances have reduced costs in this area, but additional aids to interpretation are still required. One such adjunct is the widely used "Eight Peak Index" (RSC, 1983), which lists the most abundant peaks by m/z value. In this new Index, the peaks listed are chosen on the basis of their statistical importance, rather than just their abundance, according to a probability-based matching system. This more sophisticated system affords greater reliability in the matching of peaks for two main reasons (i) it eliminates all the commonly occurring low m/z peaks (which are usually the most abundant and the most infuriating) from the analysis, and (ii) it allows attention to be focussed upon those peaks which are of the greatest value in identifying an unknown compound. These innovations allow the number of possible structures to be narrowed down dramatically when higher m/z peaks are considered.

The probability of occurrence of ions in the Registry database has been tabulated in terms of the "uniqueness value" ("U") used in the probability based matching algorithm, U representing the log base 2 value for the probability that a reference will contain a peak of this m/z value of $\geqslant 1\%$ abundance. The "importance" rating of each peak for this Index is based upon the sum of the uniqueness and abundance values (U + A), thereby allowing ions of low to moderate abundance in the upper m/z range of a mass spectrum to be rated as highly as a base peak of low m/z value. As an aid, a one-line summary of approximate U and A values appears at the bottom of each page of the Index.

The Index has been found to be extremely useful in identifying aroma volatiles from various sources by GC/MS headspace analysis. The rating system provides a mechanism for allowing for the differences between mass spectra obtained with different instruments and conditions, particularly as abundance variability can sometimes be considerable. Of course it is not possible to identify new compounds using this Index, but its novel features ensure that existing compounds in the molecular weight range of an unknown can rapidly be identified and eliminated from consideration.

Each of these three volumes weighs no less than 5lb 5oz. Although the published price may seem high, it represents a rare bargain, for they are worth their weight in gold.

A. B. TURNER

Chromatographic Enantioseparation—methods and applications, 2nd edition: S. ALLENMARK, Ellis Horwood, 1991. Pages 282. £55.00.

The second edition of this book appears three years after the first. The original work was well received (for a review by J. L. Wardell see *Talanta*, 1989, **36**, No. 4) and the rapidly advancing field of chiral chromatography has provided the reason for this new edition. If you are new to this area of separation science and wish a good introductory text which also covers some recent work then this book is highly recommended. If you are an experienced practitioner in chromatography and have already purchased the first edition do you also buy this edition? If you wish to keep up to date then the answer must be "yes". However, a comparison with the first edition may be of interest.

The topics covered are essentially the same as in the first edition (the chapters have identical headings) but have been updated where necessary by reference to more recent literature. The most obvious difference between editions is the inclusion of additional experimental procedures for the synthesis of chiral sorbents. In particular, several techniques used for the binding of chiral selectors to silica are now presented. Chapter 10 on "future trends" is also of interest as the newly developed diode-laser-based micropolarimetric detectors (a "future trend" in the first edition) is now mentioned

as a commercial reality. Chapter 10 also contains new details of computer-aided optimization of mobile-phase systems.

Overall the book length has increased from 224 to 282 pages, some new exercises (without answers) have been added and references are now quoted up to 1991.

P. J. Cox

Talanta, Vol. 39, No. 11, pp. 1403–1405, 1992
Printed in Great Britain.

0039-9140/92 $5.00 + 0.00

TRIBUTE

THOMAS SUMMERS WEST—"Tom" to his many friends throughout the world—was born at Peterhead, Scotland, on 18th November 1927. When he was about six years old he moved with his parents to Portmahomack, a small fishing village on the Dornoch Firth. His father was a fisherman, indeed all his forebears were seafaring folk. In Portmahomack his primary education was at Tarbat Old Public School, after which he attended the nearby Tain Royal Academy.

In 1945 West entered the University of Aberdeen as a Highlands and Islands Bursary Scholar, graduating with first class honours in chemistry in 1949. He had been interested in analytical chemistry since his school days, and his future scientific path was confirmed while he was living at the YMCA in Aberdeen, where he met Ronald Belcher, Lecturer in Inorganic and Analytical Chemistry at the University. When Belcher moved with Prof. H. W. (now Sir Harry) Melville to the University of Birmingham in 1948, West followed in 1949. There he helped to form the nucleus of Belcher's Birmingham School of Analytical Chemistry. West duly received his Ph.D. (1952), was subsequently awarded a Senior DSIR Fellowship (1952–1955), and then became a Lecturer in Chemistry (1955–1963). His D.Sc. was conferred in 1962.

At Birmingham Belcher built up an international centre for microanalysis. West's early contribution to that was work on a quartz fibre torsion ultramicrobalance and on a system of ultramicro organic elemental and functional group methodology. With the award of his Ph.D, he started up his own group, pursuing an independent line of research into analytical chelate chemistry. Also, he did exploratory work on solvent extraction and polarography. A highlight was the specific chromogenic ternary complex reaction between fluoride, either of the first two members of the lanthanides and 3-dicarboxymethylaminomethyl-1,2-dihydroxyanthraquinone, and the interpretation of the mode of action of this only known positive colour reaction of the fluoride ion. It has subsequently replaced all other spectrophotometric reactions for fluoride. Another important discovery was the unique conditionally specific reaction between calcium and a new specially synthesized trishydroxytriazo clathrate cage dyestuff molecule.

West moved in 1962 to succeed Mr. L. S. Theobald as Reader in Analytical Chemistry at Imperial College of Science and Technology in London. There he found himself junior to Prof. F. C. Tomkins (Physical Chemistry and long-time Secretary of the Faraday Society), Prof. G. (later Sir Geoffrey) Wilkinson (Inorganic Chemistry and Nobel Laureate 1973), Prof. D. H. R. (later Sir Derek) Barton (Organic Chemistry and Nobel Laureate 1969), and Prof. R. M. Barrer (Head of Department and Physical Chemistry, renowned for his work on molecular sieve action and coincidentally Professor of Chemistry in West's final year at Aberdeen). Undeterred, and together with three young post-doctorates from Birmingham—Roy Dagnall, Bernard Fleet, and Gordon Kirkbright—he quickly set up a thriving team, and in 1965 was promoted to Professor of Analytical Chemistry. Over the course of some ten years, West established an international reputation for his analytical chemistry research work at IC.

This work was largely centred in analytical atomic and molecular absorption and fluorescence spectroscopy. In Australia Alan Walsh had opened a new era by demonstrating first an easy laboratory technique of atomic absorption spectrophotometry (AAS), and then showing its unique specificity for the determination of most metal ions. It was a far cry from classical analysis, but West in the U.K. and Jim Robinson in the U.S.A., another former Belcher student, made rapid advances in the new field. It proved to be very popular with West's students, extending AAS to pioneering studies in atomic spectroscopy by carbon rod electrothermal atomization, microwave-excited high intensity atomic line sources, low emissitivity separated flames, chemiluminescence in diffusion flames, atomic fluorescence spectroscopy, and atom trapping atomic absorption spectroscopy. He received widespread international recognition and awards.

In 1975 West returned to Scotland as Director of the Macaulay Institute for Soil Research at Aberdeen. The Institute's role was to evaluate the whole of Scotland's land and to determine how

best it might be used or developed. It carried out remote sensing and image processing, and used ESCA, photoacoustic and spectroscopic methods. The applied focus of the programme stimulated West to new experiments. He continued to evolve the technique of atom trapping atomic absorption spectroscopy, and made contributions to piezo-electric crystal sensor systems for minute traces of airborne pollutants and to the study of interfacial optical absorption and emission phenomena at platinum electrode surfaces under conditions of diffusion controlled electrolysis in aqueous solutions. Work on biosignificant and toxic trace elements in the soil–plant ecosystem and acidification phenomena led to his participation in the U.K. Royal Society's SWAP (Surface Water Acidification Programme) team together with the Royal Academies of Science in Norway and Sweden. His final years at MI were much taken up with the painful necessity, imposed by the Department of Agriculture and Fisheries for Scotland, to reduce the Institute staff by about 25% and with the battle to avoid closure of the Institute in Aberdeen for amalgamation with another Institute near Edinburgh. He was able to secure jobs elsewhere for all but a few, and mounted a campaign, mobilizing all the considerable scientific community in Aberdeen, members of Parliament and the House of Lords, plus a continuous stream of letters from some 200 former visitors from all over the world, who had worked at MI. In the end the civil service mandarins of the Scottish Office in Edinburgh were obliged to give way. Amalgamation took place on the Aberdeen site.

In the laboratory West was held in great affection and respect by his students. The ladies were much affected by his Scottish burr and good looks, although there is no record of them swooning or leaving poems behind at the end of a lecture. He is a committed internationalist, and always provided a warm welcome to students from abroad throughout his career. The sentiments of many are captured by Sameer Rahim, who writes "I found him a great-hearted and experienced head of the department, admired by everyone. I was very happy when told that I was lucky because Prof. West is your supervisor. He was very humanitarian: father, brother, and friend, especially to overseas students, who face special problems during their period of stay in Britain. Prof. West did his best to minimize such problems. When we visited his home, we found him an ideal family man, which helped him to be a great scientist. We were astonished to see a dish of Iraqi rice, and also learned that he was an expert in making tea."

At Birmingham he tolerated the brewing sub-industry of his students. Dai Rees, on loan from the Food Research Laboratory, set a high standard in this respect. Bob Close filled the laboratories with fermenting and exploding bottles, whose contents were usually deemed unspeakable and undrinkable. At IC West was not amused when, according to Godfrey Everett, some of his students caught a mouse, and it was incarcerated in a large round-bottomed flask with an ample supply of water, bedding, and food. He arrived earlier than usual the next day, and commented that his research laboratory "was not a menagerie". From then on mice and roosting pigeons were left in peace. He banned noisy radios, but supported ball-by-ball commentary through the cricket season. The social scene moved with members of his staff and former students, who set up Electrodeless Discharge Tubes (EDT) as a company to exploit inventions of the research team.

West encouraged open thinking and experimentation in new fields. In his Birmingham days, the analytical team had one of the very few spectrophotometers owned by the Department of Chemistry. West encouraged the use of all the techniques scattered throughout the Department. As he put it "All those other fellows (organic and physical chemists) are basically stuck with one set of apparatus or one measurement technique. In analytical chemistry we can use the lot." It is a vision which has resulted in his students being leaders in many fields of analytical science and in domains well away from chemistry.

Within the Royal Society of Chemistry West holds the Meldola Medal (1956), Perkin-Elmer Medal for Instrumentation and Analytical Chemistry (1976). Gold Medal for Analytical Chemistry (1977), and Redwood Lectureship (1974). Overseas awards include the Interan Medal (1977) of the Czechoslovak Chemical Society, Johannes Marcus Medal for Spectroscopy (1977) of the Spectroscopic Society of Bohemia, and Honorary Membership (1981) of the Japan Society of Analytical Chemistry. He became a Fellow (1979) of the Royal Society of Edinburgh and in 1989 a Fellow of the Royal Society of London. In the Queen's New Year's Honours List for 1988 he was made a Commander of the Order of the British Empire (CBE) for his contributions to chemistry and international science.

During his Birmingham days West had already become a member of the Council of the Society for Analytical Chemistry (1956–1972), serving on various of its Committees. This culminated in his election to the Presidency of the Society during 1969–1971. Whilst he was in London, West became increasingly involved in the wider scientific community. Within the Chemical Society (later Royal Society of Chemistry), he served as Honorary Secretary (1972–1975) and on some important committees. He played a prominent role in the negotiations which led to the amalgamation in the U.K. of the Chemical Society, Royal Institute of Chemistry, Faraday Society, and Society of Analytical Chemistry.

Also, West has worked within the committee structure of the Royal Society, serving on analytical international matters. More recently his role has broadened, and he served on the Department of Health and Social Security's Expert Group on Sudden Infant Death Syndrome (Cot Death), the Ministry of Defence's Gruinard Island (Anthrax) Group, and is chairing the recently formed Scientific Advisory Committee to the Guildford and Woolwich Enquiry.

In November 1987, having reached the statutory age of sixty, West retired from MI and was given the status of Professor Emeritus by the University of Aberdeen. His release from the duties of Director enabled him to devote more time to international science. He had already been an active Commission and Division member in the International Union of Pure and Applied Chemistry (IUPAC) since 1963, rising to President of the Analytical Chemistry Division (1977–1981). After a period as Assistant Secretary General (1981–3), he was elected Secretary General of the Union and served two four-year periods in that office (1983–1991). During this time he was responsible for introducing the scheme of Affiliate (individual) Membership, and helping to broaden the scope of the classically-oriented Divisional activities of IUPAC into interdisciplinary areas, such as chemistry and the environment. In addition, acting as the official representative to the General Committee of the International Council of Scientific Unions (ICSU), West strove to increase the involvement of the Union—and chemistry as the central science—in the activities of ICSU, which had been rather neglected for several years. Two initiatives of his are presently under consideration of implementation by ICSU, namely the consequences of use of chemical weapons and a study of the world's future energy supplies. In 1990–2 West became Chairman of the Standing Finance Committee of ICSU and a member of the Executive Board.

Several of West's former research students from Birmingham and IC now hold Chairs of Chemistry in Canada, Japan, the U.K., and U.S.A., and prominent positions in a wide range of industries. For instance, Lay Har Tan Ng comments "Through his inspiration a good number of his students and postdoctoral associates have carried his influence to Hong Kong, and made reputations for themselves in the civil service, in industry, and in the academic circles here. Prof. West's sound judgement and fairmindedness have made him much sought after as an external examiner." West has published over 400 research papers, books, and monographs (see pages 1411–1428 for details), and lectured worldwide on his research work.

Tom West is a devoted family man, having married Margaret Officer Lawson, a mathematics student who he met while a student himself at the University of Aberdeen. Their three children—Ann, Ruth and "young" Tom—were all born in Birmingham and, although they are now themselves all married and living as far away as in northern France, Tom and his wife are regular visitors each year to their various homes and their four grandchildren, Alexander and Marianne Cochennec and Catherine and Sarah West.

D. Betteridge

British Petroleum Co.,
1 Finsbury Circus,
London EC2M 7BA, U.K.

M. Williams

IUPAC Secretariat,
2–3 Pound Way, Cowley Centre,
Oxford OX4 3YF, U.K.

Talanta, Vol. 39, No. 11, pp. 1407–1410, 1992
Printed in Great Britain.

0039-9140/92 $5.00 + 0.00

SOME MEMOIRS ABOUT PROFESSOR T. S. WEST

In the biography "Thomas Summers West", earlier in this issue, we have distilled the essence of his work and style of life. This has been done with the help of several former students and colleagues, who have contributed their reminiscences. Inevitably, some of the flavour has been lost in the process of condensing a full life into a brief account. The following letters, reproduced in their entirety, go some way towards redressing the balance. They capture the sense of his personal impact from different perspectives.

* * *

I consider this a great opportunity to write some of my best memories of Tom West in honour of his 65th birthday.

Tom West is a person who has made a lasting impression on me. I had the honour of being one of his research students at Imperial College London for about eighteen months in the early 1970s on my first overseas visit.

During that period of time, we had many brief discussions, and each time I would become a little wiser. He was very caring, meticulous and at the same time very precise in his methods of approach; at times he sparkled with brilliance. Although my research was of no great significance, what I learned, particularly from him, did turn out to be of much significance to me later.

I recall some of the everyday conversation. One day in his room, I happened to smoke a small-sized cigarette, rather unenthusiastically. He smiled and remarked "You are like me". This, I could understand, because he too smoked only sparingly. But what I could not understand was when he remarked the same thing when I was just returning after delivering a talk about our research work, the programme having been arranged under his guidance. To be told after the talk that I was like him left me wondering; in my view there is no comparison between him and me.

In 1972 at an SAC symposium in Glasgow, while delivering a paper, he howled from a top back-bench and many heads turned around. I did not know that he himself was running a short strip of film about my research work. While the film was running I looked silently at the screen without explaining the action. The loud shout jerked me to attention, and I realised my mistake.

During conversations, I was used to addressing him as "Professor West/Sir". One day, he stoutly told me "From now on call me Tom"; I do not remember that I took his advice.

I enjoyed and gained greatly from being associated with him.

Thank you Tom. I wish you many happy returns of the day.

Iswori Lal Shrestha
Deputy Director General
Department of Mines and Geology
Kathmandu, Nepal

6th March 1992

* * *

For many of those who studied under Prof. West at Imperial College, the portals of the Advanced Analytical Laboratory marked the entrance to a career in one branch or another of science, in which analysis would play a part. I imagine Tom always thinks of those who followed so directly in his footsteps, even though perhaps not to the topmost heights he occupied, as his best and most worthy products. The exponential flowering of a multitude of research papers, each with a name or two known to have been students of the master, must have given and continue to give him inordinate satisfaction.

Sadly, I cannot claim to be numbered among this favoured band, since directly from Imperial College I was claimed by Mammon, destined ever after to earn my corn in the halls of commerce and finance. I am now able to reveal that one of the best kept secrets in this area of human

endeavour is that many of its problems are susceptible to Tom's type of analytical treatment. By this, I mean the application of tried and tested methods, clear labelling, the careful collection of data, rigorous and unbiased processing into final form, and due noting of negative results.

Many are the examples I can cite: the coal exploration prospect in Latin America, where my short demonstration of the "alternate quarter and shovel" sampling technique struck fear into all concerned; the fascinating discussion with the clerk in the Punjab cotton ginning plant on the distinction between accuracy and precision; the Andean economist gathering the tin mine assay information, whose only question was "What answer do you want?"; the African broker who needed persuading that 90% of his clients could not all be above average; and the Eastern European banker requiring confirmation that his new bank could profitably lend at 6% while borrowing at 8%.

Tom West's special way of letting the lowliest 3rd year dissertation student in on the mysteries of experimental discipline or of curbing some flight of fancy by a desperate would-be PhD student searching for that nugget of knowledge, stayed with me sufficiently for application (he might say distortion) to these other worldly uses.

His use of metaphor and allegory would likewise have come in handy in some of the tighter spots, my only recorded success being to explain spectroscopy to an unsmiling audience in Egypt by quoting from Omar Khayyam:

"In and out, above, about, below,
'Tis nothing but a Magic Shadow show,
Held in a box whose candle is the Sun,
Round which we phantom figures come and go."

To conclude, my message is a simple one: the great teachers, such as Tom West, so influence their pupils that not only is the effect seen in their area of immediate specialisation, but also other apparently distant spheres are guided by the unseen hand.

David J. Smith
Higham House, Higham
Colchester, UK

19th March 1992

* * *

I met Tom West many years ago in one of the biennial general assemblies of IUPAC. He was heavily involved with the work of the analytical chemistry division. Tom represents the very best traditions of modern analytical chemistry, and his personality is ideally suited to the demanding requirements of the subject. He is meticulous and gives attention to every detail in all his work—the outcome is that he has always produced very good and useful results.

Tom is a warm-hearted, cheerful person and works well with other colleagues. He is also highly committed to his work and loyal to friends and to institutions. These qualities became further underlined when I came to know him closely in the late 1970's and early 1980's.

I recollect a rather awkward day during the IUPAC general assembly at Lyngby in 1983, when I was rather depressed. I was a candidate for the post of Vice-President of IUPAC. There was a suggestion that I withdraw from the election, to avoid certain misunderstandings. However, many gave me support and urged me to go through the democratic process. I remember Tom's wise counsel at that time. After I was elected as Vice-President, I worked closely with Tom on various aspects of the Union. He was then Secretary General. When I became President in 1985, Tom's advice and support became invaluable. There he was like a rock, always dependable and available. I enjoyed working with him and treasure his friendship. His urge to contribute constructively and with humility has endeared him to all his colleagues and associates.

My association with Tom continued later as Past-President of IUPAC and also as coordinator of the horizontal programme on chemistry and advanced materials. I believe that in Tom I have found a fine friend of great talent and indisputable human qualities.

C. N. R. Rao
Director
Indian Institute of Science
Bangalore-560012, India

4th March 1992

My first contact with Tom was after graduating in the early 1960's, when I decided to look for graduate work in analytical chemistry. In those opulent times, I was trying to decide between the abundance of offers I had received from graduate schools in the United States, when I happened to read an excellent review that Tom had written for the Royal Institute of Chemistry monograph series on advances in analytical chemistry. It was this article more than anything else that prompted me to apply to Birmingham, and eventually to join the Belcher-West group there. Whether Tom can be accused of stemming the brain drain or of promoting it is an open question

At Birmingham, even though I was not working for Tom, I have a keen recollection of his accessibility and of the fact that he was always willing to spend a few minutes discussing your work. These discussions were very important to me in shaping my research interests and future career direction, and consequently I was very honoured a few years later to be invited to join Tom's group at Imperial College.

During my early years at Imperial, I must also say that Tom gave me enormous support and encouragement in starting my research in electroanalytical chemistry, even though it was outside his own main interests and those of the rest of the research group there.

I have many happy memories of our time together at Imperial. Of the many social events, a dinner organized by the late Peter Keliher, at which Tom was to be the guest of honour, stands out. This was held at an infamous Chelsea Bistro, noted for its ambience and cheap wine. The dinner was indeed famous for the amount of wine consumed and for a rendition by Peter of "we are poor little lambs who have lost our way" not calculated to inspire hope in fresh graduate students. Unfortunately, in those pre-plastic days, when the bill finally arrived, the budget had been well and truly blown and, after much pocket searching, the guest of honour was prevailed upon to dig into his sporran and bail us out.

A more recent event was held here in Toronto during the 1988 North American Chemical Congress. This was the first TS West Group North American reunion at which TSW was the guest of honour. Unfortunately, at the last minute, due to an unexpected IUPAC commitment, Tom was unable to attend. Not to be thwarted, his devoted followers pressed ahead with the event, and a life-sized model of the boss was constructed to fill his place and is still available, for hire, for future events.

On a more serious note, like most of his students, I owe Tom a deep debt of gratitude for his support, advice and guidance over the years. May his semi-retirement years be long, happy and healthy.

Bernard Fleet
Toxics Recovery Systems International
44 Fasken Drive, Units 14 & 15
Rexdale, Ontario
Canada M9W 5M8

5th May 1992

* * *

Working with the International Union of Pure and Applied Chemistry gave me the opportunity to meet many wonderful and very interesting people. Among all these chemists, one of them immediately struck me by his kindness, by his very open mind, by his simple approach. That was Thomas West, that was in 1979.

For twelve years, we worked together for the Union. We both served as Bureau members. Then Tom West became Secretary General, and later I was elected Vice-President and became President. This four-year period of office for me (1987–1991) merits special mention.

During this time I received continuous support and friendly help from Tom West to fulfill the presidential duties, which are not always easy. But that was only part of his contribution: the visible part of the iceberg. I found a man of exception, the main qualities of whom were generosity and full devotion to his duty.

He never made a move or gave his opinion on a problem dealing with the Union, without giving deep thought to it and without considering the benefit it might bring to the Union. Actually, when I say to the Union, this is not the right way to describe things. Tom West always thought first about people, about Union members, about our fellow chemists.

May I take as an example the tremendous efforts he made to set up the IUPAC Affiliate Membership Scheme (later termed Programme). Undoubtedly, the development of AMP was his very own work. The way he presented the Programme and its progress to the Council at general assemblies in warm words was a perfect example of his behaviour. He strongly supported a way to associate more chemists with the work of the Union, especially those from developing countries. Indeed, they have chemists who are so isolated and who need so much help. This action was typical of the generosity of Tom West.

One of the duties of our Secretary General is to maintain the Secretariat of the Union in good shape and to support its activities. He took great care of our Oxford Secretariat and of its staff, again with his personal touch, paying great attention to personal problems. Doing this he greatly contributed to the development of its work.

This presentation could be continued with other examples. Meeting Tom West was very rewarding to me and I am sure he will allow me to say that, thanks to IUPAC, we became good friends. One day, he described to me his visit to South Africa, and particularly to the Krüger National Park. He told me: you will be surprised if you go there, to see how clear is the sky and how bright are the stars during the night. They are so brilliant that they look very close indeed. One could say that every time Tom West presented his views on a problem, he had such a way to explain the problem, that the solution appeared quite clearly, just like the stars in the sky of South Africa.

On behalf of the International Union of Pure and Applied Chemistry I am pleased to acknowledge his invaluable contribution.

Y. P. Jeannin
Laboratoire de Chemie des Métaux
de Transition
Université Pierre et Marie Curie
4, Place Jussieu
75252 Paris Cedex 05, France

13th July 1992

Talanta, Vol. 39, No. 11, pp. 1411–1428, 1992
Printed in Great Britain.

0039-9140/92 $5.00 + 0.00

PUBLICATIONS

(In Chronological Order)

THOMAS S. WEST

1. The Determination of Trace Amounts of Hydroquinone. *Anal. Chim. Acta*, 1951, **5**, 599. (with R. Belcher)
2. Mercurous Nitrate as a Reductimetric Reagent. Part I. Stoicheiometry of Reaction. *Anal. Chim. Acta*, 1951, **5**, 260. (with R. Belcher)
3. Mercurous Nitrate as a Reductimetric Reagent. Part II. The Interference of the More Common Cations and Anions in the Determination of Iron. *Anal. Chim. Acta*, 1951, **5**, 268. (with R. Belcher)
4. Mercurous Nitrate as a Reductimetric Reagent. Part III. The Titration of Various Oxidising Agents. *Anal. Chim. Acta*, 1951, **5**, 360. (with R. Belcher)
5. Mercurous Nitrate as a Reductimetric Reagent. Part IV. The Determination of Copper. *Anal. Chim. Acta*, 1951, **5**, 364. (with R. Belcher)
6. Mercurous Nitrate as a Reductimetric Reagent. Part V. The Titration of Iron on the Micro-scale. *Anal. Chim. Acta*, 1951, **5**, 472. (with R. Belcher)
7. Mercurous Nitrate as a Reductimetric Reagent. Part VI. The Determination of Hg(I) [in presence of Hg(II)]. *Anal. Chim. Acta*, 1951, **5**, 474. (with R. Belcher)
8. Mercurous Nitrate as a Reductimetric Reagent. Part VII. The Determination of Hydroxylamine and Nitrates. *Anal. Chim. Acta*, 1951, **5**, 546. (with R. Belcher)
9. Mercurous Nitrate as a Reductimetric Reagent. Part VIII. The Potentiometric Titration of Ferric Iron in Presence of Ions Forming Highly Coloured Thiocyanates. *Anal. Chim. Acta*, 1952, **7**, 470. (with R. Belcher)
10. Trivalent Manganese as an Oxidimetric Reagent. *Anal. Chim. Acta*, 1952, **6**, 322. (with R. Belcher)
11. The Gravimetric Determination of Copper(II) as Copper(I) Thiocyanate. *Anal. Chim. Acta*, 1952, **6**, 337. (with R. Belcher)
12. A New Reagent for the Titration of Water. *J. Chem. Soc.*, 1953, 1772. (with R. Belcher)
13. Quadrivalent Uranium as a Reducing Titrant. *Anal. Chem.*, 1954, **26**, 1025. (with R. Belcher and D. Gibbons)
14. The Evaluation of Barium Sulphate Precipitates by a Titrimetric Method. *Chem. & Ind.*, 1954, 127. (with R. Belcher and D. Gibbons)
15. The Indirect Determination of Sulphate Ion Using Ethylenediamine Tetraacetic Acid. *Chem. & Ind.*, 1954, 850. (with R. Belcher and D. Gibbons)
16. Analytical Chemistry: Instrumental Methods: Separation Methods. *Ann. Repts. Chem. Soc.*, 1954, **51**, 349.
17. Microchemistry Applied to Chemical Analysis. *Research*, 1954, **7**, 60.
18. The Determination of Sulphur in Plain Carbon Steel. *Analyst*, 1955, **80**, 751. (with R. Belcher and D. Gibbons)
19. The Effect of Ethylenediaminetetraacetate on the Fe^{3+}/Fe^{2+} and Cu^{2+}/Cu^{+} Redox Systems. *Anal. Chim. Acta*, 1955, **12**, 107. (with R. Belcher and D. Gibbons)
20. The Potentiometric Determination of Copper by Complexometric Titration with Ethylenediamine Tetraacetic Acid. *Anal. Chim. Acta*, 1955, **13**, 226. (with R. Belcher and D. Gibbons)
21. Analytical Chemistry: Instrumental Methods: Separation Methods. *Ann. Repts. Chem. Soc.*, 1955, **52**, 357.
22. A Simple Robust Ultramicrobalance. *Mikrochim. Acta*, 1956, 598. (with H. Astbury and R. Belcher)
23. Analytical Chemistry: Instrumental Methods: Separation Methods. *Ann. Repts. Chem. Soc.*, 1956, **53**, 358.

24. Submicro Methods of Organic Analysis. Part I. The Determination of Nitrogen. *J. Chem. Soc.*, 1957, 4323. (with R. Belcher and M. Williams)
25. Submicro Methods of Organic Analysis. Part II. The Determination of Alkoxyl Groups. *J. Chem. Soc.*, 1957, 4480. (with R. Belcher and M. K. Bhatty)
26. Fast Sulphon Black F as Indicator for the EDTA Titration of Copper(II). *Chem. & Ind.*, 1957, 1647. (with R. Belcher and R. A. Close)
27. Some Ortho-ortho′-dihydroxyazo Dyes for EDTA Titrations. *Chemist Analyst*, 1957, **46**, 86. (with R. Belcher and R. A. Close)
28. Scheme of Qualitative Inorganic Analysis (with W. M. Dowson and R. Harrison). Stanford and Mann Ltd., 5 editions dating from 1956 to 1960.
29. Further Ortho-ortho′-dihydroxyazo dyes for EDTA Titrations. *Chemist Analyst*, 1958, **47**, 2. (with R. Belcher and R. A. Close)
30. The Preparation and Analytical Properties of N,N-di(carboxymethyl) Aminomethyl Derivatives of Some Dihydroxyanthraquinones. *J. Chem. Soc.*, 1958, 2390. (with R. Belcher and M. A. Leonard)
31. Submicro Methods of Organic Analysis. Part III. The Determination of *N*-methyl Groups and Simultaneous Determination of Alkoxyl and *N*-methyl Groups. *J. Chem. Soc.*, 1958, 2392. (with R. Belcher and M. K. Bhatty)
32. Submicro Methods of Organic Analysis. Part IV. The Determination of Iodine and Bromine. *J. Chem. Soc.*, 1958, 2998. (with R. Belcher and R. A. Shah)
33. Submicro Methods of Organic Analysis. Part V. The Determination of Sulphur. *J. Chem. Soc.*, 1958, 4054. (with R. Belcher, R. L. Bhasin and R. A. Shah)
34. The Complexometric Titration of Calcium in Presence of Magnesium. A Critical Study. *Talanta*, 1958, **1**, 238. (with R. Belcher and R. A. Close)
35. New Reagents in Complexometric Analysis. *Proc. Int. Symp. Microchemistry*, Birmingham (1958). Pergamon Press, 1959. 455.
36. New Colour Reactions of Phthalein Complexone. *Chem. & Ind.*, 1958, 128. (with R. Belcher and M. A. Leonard)
37. Succinyl Chloride as a Hydrolytic Reagent for Water. *Anal. Chim. Acta*, 1958, **19**, 148. (with R. Belcher and J. H. Thompson)
38. The Determination of Metals in Organic Compounds by the Closed-flask Method. *Talanta*, 1958, **1**, 408. (with R. Belcher and A. M. G. Macdonald)
39. The Synthesis of Vic-dioximes from Symmetrical Ketones. *J. Chem. Soc.*, 1958, 2743. (with R. Belcher and W. Hoyle)
40. Studies in Inorganic Qualitative Analysis. A Test for the Detection of Tin(IV). *Mikrochim. Acta*, 1958, 137. (with D. Bailey, W. M. Dowson and R. Harrison)
41. Analytical Applications of Diaminoethanetetraacetic Acid. (with A. S. Sykes). British Drug Houses. First Ed., pp. 106. 1958.
42. The Titrimetric Determination of Carbon Dioxide with Special Reference to the Determination of Carbon in Organic Compounds. *Anal. Chim. Acta*, 1958, **19**, 309. (with R. Belcher and J. H. Thompson)
43. Submicro Methods or Organic Analysis. Part VI. The Determination of Carbon. *J. Chem. Soc.*, 1959, 2582. (with C. W. Ayers and R. Belcher)
44. Submicro Methods of Organic Analysis. Part VII. The Determination of Nitrogen in Heterocyclic Compounds, Azo, Hydrazo and Nitro Compounds, and in the Presence of Other Elements. *J. Chem. Soc.*, 1959, 2585. (with R. Belcher and R. L. Bhasin)
45. Submicro Methods or Organic Analysis. Part VIII. Factors Associated with Submicrotitration in Glacial Acetic Acid. *J. Chem. Soc.*, 1959, 2877. (with R. Belcher and J. Berger)
46. Submicro Methods of Organic Analysis. Part IX. Titration of Organic Bases and Amine Hydrohalides in Glacial Acetic Acid. *J. Chem. Soc.*, 1959, 2882. (with R. Belcher and J. Berger)
47. Submicro Methods of Organic Analysis. Part X. The Determination of Fluorine. *J. Chem. Soc.*, 1959, 3577. (with R. Belcher and M. A. Leonard)
48. Isomeric Complexans. The *dl* and *meso* Forms of 2,3-Butanediamine-N,N,N′,N′-tetraacetic Acid. *Talanta*, 1959, **3**, 201. (with R. Belcher and W. Hoyle)

49. Polarographic Examination of Chelating Power of Ethylenediamine Tetraacetic Acid and Some Closely Related Agents. *Talanta*, 1959, **2**, 158. (with W. Hoyle)
50. Application of Zone Electrophoresis and Polarography to the Analysis of Complexone Mixtures. *Talanta*, 1959, **3**, 47. (with W. Hoyle)
51. A New Spot-test for the Detection of Fluoride Ion. *Talanta*, 1959, **2**, 92. (with R. Belcher and M. A. Leonard)
52. Recent Developments in Inorganic and Organic Analytical Chemistry. *R. Inst. Chem.* Monograph No. 1, 1959.
53. Submicro Methods of Organic Analysis. Part XI. The Determination of Tertiary Nitrogen by Use of an Ion Exchange Resin. *J. Chem. Soc.*, 1960, 2473. (with R. Belcher and M. K. Bhatty)
54. Submicro Methods of Organic Analysis. Part XII. The Determination of Carboxyl Groups. *J. Chem. Soc.*, 1960, 3830. (with R. Belcher and L. Serrano-Berges)
55. Acid Chlorides of Substituted Succinic and Glutaric Acids as Hydrolytic Reagents for the Determination of Water. *Talanta*, 1960, **4**, 166. (with R. Belcher and L. Ottendorfer)
56. Acid Alizarin Black SN. Metallochromic Indicator for Calcium. *Anal. Chim. Acta*, 1960, **23**, 261. (with R. A. Close)
57. Photometric Titration of Calcium in Blood Serum with Acid Alizarin Black SN as Metallochromic Indicator. *Anal. Chim. Acta*, 1960, **23**, 370. (with R. A. Close)
58. A New Selective Metallochromic Reagent for the Detection and Chelatometric Determination of Calcium. *Talanta*, 1960, **5**, 221. (with R. A. Close)
59. Chelating Reactions of 1,2 dihydroxyanthraquinon-3-ylmethylamine-N,N-diaceticacid with Metal Ions. *J. Chem. Soc.*, 1960, 4477. (with M. A. Leonard)
60. Monograph on Titrations in Non-Aqueous Media, in "Comprehensive Analytical Chemistry". Wilson and Wilson, Elsevier Publishing Co., Amsterdam. Vol. IB, 1960, pp. 767.
61. An Examination of Some Aspects of Increasing Selectivity in Chelatometry. *Anal. Chim. Acta*, 1961, **25**, 301.
62. The Spectrophotometric Determination of Trace Amounts of Silver. *Talanta*, 1961, **8**, 711. (with R. M. Dagnall)
63. A Study of the Ce(III)-alizarin Complexan Fluoride Reaction. *Talanta*, 1961, **8**, 853. (with R. Belcher)
64. A Comparative Study of Some Lanthanon Chelates of Alizarin Complexan as Reagents for Fluoride Ion. *Talanta*, 1961, **8**, 863. (with R. Belcher)
65. Direct Polarographic Resolution of Mixtures of Complexones. *J. Electroanal. Chem.*, 1961, **2**, 166. (with W. Hoyle and I. P. Sanderson)
66. Chloridionenübergänge in Phenylphosphoroxychlorid, 2 Mitt. *Monatsh. f. Chemie*, 1961, **92**, 150. (with M. Baaz, V. Gutmann and M. Y. A. Talaat)
67. Chloridionenübergänge in Phenylphosphoroxychlorid, 3 Mitt. *Monatsh. f. Chemie*, 1961, **92**, 164. (with M. Baaz and V. Gutmann)
68. Über das Amphotere Verhalten von Aluminium Chlorid in Phosphoroxychlorid und Phenylphosphoroxychlorid. *Z. anorg. Allgem. Chemie*, 1961, **31**, 302. (with M. Baaz, V. Gutmann, L. Hubner and F. Mairinger)
69. Separation of Traces of Inorganic Ions from Aqueous Solution by Gas-Liquid and Solid-Phase Distribution Procedures. *Anal. Chim. Acta*, 1961, **25**, 405.
70. Analytical Applications of Diaminoethanetetraacetic Acid. (with A. S. Sykes). British Drug Houses, pp. 127. Second Ed., 1961.
71. The Synthesis of Chelating Agents Related to Cyclohexane-1,2-diamine-N,N,N′,N′-tetraacetic Acid. *J. Chem. Soc.*, 1961, 667. (with R. Belcher and W. Hoyle)
72. Selective Chelatometry of Copper(II) with Ethylenediamine-N,N,N′,N′-tetra-n-propionic Acid. *Talanta*, 1962, **9**, 71. (with I. P. Sanderson)
73. Chelating Action of Thioglycollic Acid with Silver and Some Common Bivalent Cations. *Talanta*, 1962, **9**, 730. (with A. M. Cabrera)
74. Direct Spectrophotometry of Silver in a Non-Aqueous Medium. *Anal. Chim. Acta*, 1962, **27**, 9. (with R. M. Dagnall)
75. An Ion Association System for the Selective Extraction of Microgram Amounts of Silver from Aqueous Solution. *Anal. Chim. Acta*, 1962, **26**, 101. (with D. Betteridge)

76. The Effect of Some Anions on the Spectrophotometric Absorption of bis(di-*n*-octylethylenediamine)–Cu(II) Complexes in Aqueous Solution. *Talanta*, 1962, **9**, 457. (with D. Betteridge)
77. The Search for New Reagents for Spectrophotometry: Some Practical Considerations. *Analyst*, 1962, **87**, 630.
78. Masking Action of Complexans on Qualitative Inorganic Reactions. *Anal. Chim. Acta*, 1962, **26**, 290. (with W. Hoyle and I. P. Sanderson)
79. The Polarographic Determination of Silver. *Talanta*, 1962, **9**, 925. (with R. M. Dagnall)
80. Analytical Chemistry 1962. (co-editors: P. W. West and A. M. G. MacDonald). pp. 411. Elsevier Publishing Co., 1963.
81. Spectrophotometric Determination of Traces of Silver and Chloride Ions. *Proc. Int. Symp. on Anal. Chem.*, pp. 188. Elsevier, 1962. (with R. M. Dagnall)
82. A New Spectrophotometric Reaction of Beryllium. *Analyt. Chem.*, 1963, **35**, 311. (with A. M. Cabrera)
83. An Investigation of the Chelatometry of Copper(II) with Ethylenediamine-*N*,*N*,*N*′,*N*′-tetra-*n*-proprionic Acid. *Talanta*, 1963, **10**, 247. (with I. P. Sanderson)
84. 4(2-pyridylazo)resorcinol as a Selective and Sensitive Spectrophotometric Reagent for Niobium(V). *Talanta*, 1963, **10**, 1013. (with R. Belcher and T. V. Ramakrishna)
85. Cyclo-tris-7-(1-azo-8-hydroxynaphthalene-3,6-disulphonic acid) as Spectrophotometric Determination of Small Amounts of Calcium. *Analyt. Chem.*, 1963, **35**, 2131. (with M. L. Herrero)
86. Nueva Reaccion Espectrofotometrica, Selectiva Para Cobre(II). *Anales Soc. Real Espan. Fis y. Quim.*, 1963, **596**, 281. (with R. Belcher and A. M. Cabrera)
87. A New Colour Reaction of Nb(V) with Bromopyrogallol Red. *Chem. & Ind.*, 1963, 531. (with R. Belcher and T. V. Ramakrishna)
88. A Selective and Sensitive Colour Reaction for Silver. *Talanta*, 1964, **11**, 1533. (with R. M. Dagnall)
89. The Selective Solvent Extraction of Trace Amounts of Silver. *Talanta*, 1964, **11**, 1627. (with R. M. Dagnall)
90. The Determination of Trace Amounts of Silver by Atomic Absorption Spectroscopy. *Talanta*, 1964, **11**, 1257. (wtih R. Belcher and R. M. Dagnall)
91. Observations on the Atomic-Absorption Spectroscopy of Lead in Aqueous Solution in Organic Extracts and in Gasoline. *Talanta*, 1964, **11**, 1553. (with R. M. Dagnall)
92. New Methods in Analytical Chemistry. (with R. Belcher and C. L. Wilson) Chapman and Hall, London, pp. 366. Third Ed., 1964.
93. Submicro Methods of Organic Analysis. Part XX. The Determination of Phosphorus and Arsenic. *J. Chem. Soc.*, 1965, 2044. (with R. Belcher and A. M. G. MacDonald)
94. A Method for the Direct Determination of Oxygen in Organic Compounds. *Talanta*, 1965, **12**, 43. (with R. Belcher and D. H. Davies)
95. The Determination of Niobium by Bromopyrogallol Red. *Talanta*, 1965, **12**, 681. (with R. Belcher and T. V. Ramakrishna).
96. A Spectrophotometric Method for the Determination of Thorium. *Anal. Chim. Acta*, 1965, **32**, 301. (with P. Kusakul)
97. A Spectrofluorimetric Method for the Determination of Beryllium and Aluminium in Submicrogram Amounts. *Analyt. Chem.*, 1965, **37**, 137. (with G. F. Kirkbright and C. L. Woodward)
98. El Negro Sulfon Solido F Como Reactivo Espectrofotometrico de Cationes. Effecte del Ion Manganoso Sobre la Reaccion con Differentes Cations. *Anales Real Soc. Espan. Fis y Quim.*, 1965, **61B**, 701. (with F. Burriel and A. M. Cabrera)
99. El. Negro Sulfon Solido F Como Reactivo Espectrofotometrico de Cationes. III. Aplicacion a la Determinacion de Co(II). *Anales Real Soc. Espan. Fis y Quim.*, 1965, **61B**, 703. (with F. Burriel and A. M. Cabrera)
100. El Negro Sulfon Solido F. Como Reactivo Espectrofotometrico de Cationes. IV. Aplicacion a la Determinacion de Niquel. *Anales Real Soc. Espan. Fis y Quim.*, 1965, **61B**, 839. (with F. Burriel Marti and A. M. Cabrera)
101. Determination of Lead with 4-(2-pyridylazo)-resorcinol. I. Spectrophotometry and Solvent Extraction. *Talanta*, 1965, **12**, 583. (with R. M. Dagnall and P. Young)

102. Determination of Lead with 4-(2-pyridylazo)-resorcinol. II. Application to Steel, Brass and Bronze. *Talanta*, 1965, **12**, 589. (with R. M. Dagnall and P. Young)
103. The Spectrofluorimetric Determination of Microgram Amounts of Scandium with Salicylaldehyde Semicarbazone. *Proc. S.A.C. Conf., Nottingham*, Society for Analytical Chemistry, 1965, 474. (with G. F. Kirkbright and C. Woodward)
104. Spectrophotometric Determination of Copper(II) with Acid Alizarin Black S.N. *Anal. Chim. Acta*, 1965, **33**, 164. (with M. L. Hosain)
105. Spectrofluorescence of Aluminium and Gallium with Salicylidene-o-aminophenol. *Chem. & Ind.*, 1965, 1499. (with R. M. Dagnall and R. Smith)
106. Spectrofluorimetry of Microgram Amounts of Thallium I. *Talanta*, 1965, **12**, 517. (with G. F. Kirkbright and C. Woodward)
107. Spectrofluorimetry as a Trace Analytical Technique. I. General Considerations. *Lab. Practice*, 1965, 922.
108. Spectrofluorimetry as a Trace Analytical Technique. II. Apparatus and Techniques. *Lab. Practice*, 1965, 1030.
109. The Determination of Aluminium in Steel. *The Analyst*, 1965, **90**, 13. (with R. M. Dagnall and P. Young)
110. Analytical Applications of Ternary Complexes. II. Spectrophotometric Determination of Copper as Rose Bengal Bisphenanthrolinium Copper (II). *Talanta*, 1966, **13**, 753. (with B. W. Bailey and R. M. Dagnall)
111. Analytical Applications of Ternary Complexes. III. A Spectrofluorimetric Method for the Determination of Submicrogram Amounts of Copper. *Talanta*, 1966, **13**, 1661. (with B. W. Bailey and R. M. Dagnall)
112. Analytical Applications of Ternary Complexes. IV. Titration of Macro and Micro Amounts of Cyanide. *Talanta*, 1966, **13**, 1667. (with R. M. Dagnall and M. T. El Ghamry)
113. Carminic Acid as a Reagent for the Spectrofluorimetric Determination of Molybdenum and Tungsten. I. Development of Procedures. *Talanta*, 1966, **13**, 1637. (with G. F. Kirkbright and C. Woodward)
114. Carminic Acid as a Reagent for the Spectrofluorimetric Determination of Molybdenum and Tungsten. II. Determination of Molybdenum in Mild Steel. *Talanta*, 1966, **13**, 1645. (with G. F. Kirkbright and C. Woodward)
115. Spectrophotometric Determination of Antimony with Bromopyrogallol Red. *Talanta*, 1966, **13**, 507. (with D. H. Christopher)
116. Some Spectrofluorimetric Applications of the Cerium(IV)–Cerium(III) System. *Anal. Chim. Acta*, 1966, **36**, 298. (with G. F. Kirkbright and C. Woodward)
117. Spectrofluorimetric Determination of Microgram Amounts of Scandium and Separation by Solvent Extraction. *The Analyst*, 1966, **91**, 23. (with G. F. Kirkbright and C. Woodward)
118. A Sensitive and Selective Spectrophotometric Procedure for the Determination of Phosphorus. *The Analyst*, 1966, **91**, 89. (with V. Djurkin and G. F. Kirkbright)
119. Spectrofluorimetric Determination of Submicrogram Amounts of Aluminium Using Salicylidene-o-aminophenol. *Talanta*, 1966, **13**, 609. (with R. M. Dagnall and R. Smith)
120. Spectrofluorescence of the Magnesium Complexes of Some Quadridentate-azomethines. *J. Chem. Soc.*, 1966, 1595. (with R. M. Dagnall and R. Smith)
121. Some Sensitive and Selective Reactions in Inorganic Spectroscopic Analysis. *The Analyst*, 1966, **91**, 69.
122. Inorganic Trace Analysis. (Inaugural Lecture, Imperial College.) *Chem. & Ind.*, 1966, 1005.
123. The Determination of Trace Amounts of Copper in Niobium and Tantalum by Atomic-Absorption Spectroscopy. *The Analyst*, 1966, **91**, 411. (with G. F. Kirkbright and M. K. Peters)
124. Rapid Determination of Molybdenum in Alloy Steels by Atomic-Absorption Spectroscopy in a Nitrous Oxide-Acetylene Flame. *The Analyst*, 1966, **91**, 700. (with G. F. Kirkbright and A. M. Smith)
125. Determination of Trace Amounts of Lead in Steels, Brass and Bronze Alloys by Atomic-Absorption Spectroscopy. *Anal. Chem.*, 1966, **38**, 358. (with R. M. Dagnall and P. Young)

126. Determination of Cadmium by Atomic-Fluorescence and Atomic-Absorption Spectrophotometry. *Talanta*, 1966, **13**, 803. (with R. M. Dagnall and P. Young)
127. An Investigation of Some Experimental Parameters in Atomic Fluorescence Spectrophotometry. *Anal. Chim. Acta*, 1966, **36**, 269. (with R. M. Dagnall and K. C. Thompson)
128. Novye Visokizbivateznye i. Chuvstviteznye Spectrophotometricheskye Reagenty. *Zuhrnal Analiticheskoi Khimi (USSR)*, 1966, **21**, 913.
129. The Catechol Violet Colour Reaction for Tin(IV) Sensitized by Cetyltrimethylammonium Bromide. *The Analyst*, 1967, **92**, 27. (with R. M. Dagnall and P. Young)
130. The Spectrofluorimetric Determination of Magnesium with *N,N'*-bis-salicylidene-2,3-diaminobenzofuran. *The Analyst*, 1967, **92**, 20. (with R. M. Dagnall and R. Smith)
131. A Linear to Logarithmic Signal Converter for Use with Recording Spectrophotometers. *Anal. Chim. Acta*, 1967, **39**, 125. (with D. Alger, G. F. Kirkbright and M. D. Mayhew)
132. A Specific Spectrofluorimetric Determination of Terbium as its EDTA/Sulphosalicylic Acid Complex. *The Analyst*, 1967, **92**, 358. (with R. M. Dagnall and R. Smith)
133. Studies in Atomic-Fluorescence Spectroscopy. III. Microwave Electrodeless Discharge Tubes as Spectral Sources for Atomic-Fluorescence and Atomic-Absorption Spectroscopy. *Talanta*, 1967, **14**, 551. (with R. M. Dagnall and K. C. Thompson) (Part I see ref. 126, Part II see ref. 127)
134. Studies in Atomic-Fluorescence Spectroscopy. IV. The Atomic-Fluorescence Spectroscopic Determination of Selenium and Tellurium. *Talanta*, 1967, **14**, 557. (With R. M. Dagnall and K. C. Thompson)
135. Studies in Atomic-Fluorescence Spectroscopy. V. The Spectroscopic Behaviour and Analytical Determination of Antimony. *Talanta*, 1967, **14**, 1151. (with R. M. Dagnall and K. C. Thompson)
136. Studies in Atomic-Fluorescence Spectroscopy-VI. The Spectroscopic Behaviour and Analytical Determination of Bismuth. *Talanta*, 1967, **14**, 1467.
137. Molecular Emission Spectroscopy in Cool Flames. I. The Behaviour of Sulphur Species in a Nitrogen-Hydrogen Flame. *The Analyst*, 1967, **92**, 506. (with R. M. Dagnall and K. C. Thompson)
138. The Determination of Trace Amounts of Calcium, Magnesium, Iron and Nickel in Aluminium Salts by Atomic-Absorption Spectrophotometry with a Microwave Excited Source and Hollow-Cathode Lamps. *Talanta*, 1967, **14**, 823. (with G. B. Marshall)
139. The Emission Spectra of Nitrous Oxide-Supported Acetylene Flames at Atmospheric Pressure. *Talanta*, 1967, **14**, 789. (with G. F. Kirkbright and M. K. Peters)
140. An Indirect Sequential Determination of Phosphorus and Silicon by Atomic-Absorption Spectrophotometry. *The Analyst*, 1967, **92**, 411.
141. The Use of Separated Flames in Absorption, Emission and Fluorescence Studies in Flame Spectroscopy. *Talanta*, 1967, **14**, 1011. (with G. F. Kirkbright and A. Semb)
142. Determination of Small Amounts of Molybdenum in Niobium and Tantalum by Atomic-Absorption Spectroscopy in a Nitrous Oxide-Acetylene Flame. *The Analyst*, 1966, **91**, 705. (with M. K. Peters and G. F. Kirkbright)
143. Monograph "Chemical Spectrophotometry in Trace Characterisation" in "Trace Characterisation, Chemical and Physical" Editors: W. W. Meinke and B. F. Scribner. Monograph No. 100. National Bureau of Standards, Washington, D.C., U.S.A., 1967, pp. 215–301.
144. Atomic Analysis in Flames. *Endeavour*, 1967, **26**, 44.
145. The Use of Microwave Excited Electrodeless Discharge Tubes as Spectral Sources in Atomic Absorption Spectroscopy. *Atomic Absorption Newsletter*, 1967, **6**, 117. (with R. M. Dagnall and K. C. Thompson)
146. Preparation of Metal Halide-Mercury Microwave-Excited Electrodeless Discharge Tubes as Spectral-Line Sources. *The Analyst*, 1967, **92**, 597. (with M. J. Al. Ani and R. M. Dagnall)
147. Rapid Visual Complexiметric Titration of Calcium in Natural Waters. *Talanta*, 1968, **15**, 333. (with B. Fleet and Soe Win)
148. Analytical Application of Ternary Complexes. V. Indirect Spectrophotometric Determination of Cyanide. *Talanta*, 1968, **15**, 107. (with R. M. Dagnall and M. T. El-Ghamry)

149. 1-Dicarboxymethylaminomethyl-2-hydroxy-3-naphthoic Acid as a Sensitive and Selective Fluorimetric Reagent for Beryllium, and for Lanthanum and Lutetium in Presence of the Other Lanthanides. *Anal. Chim. Acta*, 1968, **42**, 455. (with B. Budešinsky)
150. Preparation of Microwave Excited Electrodeless Discharge Tubes for Titanium, Vanadium and Zirconium for Use as Spectral-Line Sources. *The Analyst*, 1968, **93**, 281. (with R. M. Dagnall and R. Přibil)
151. An Indirect Amplification Procedure for the Determination of Niobium by Atomic-Absorption Spectroscopy. *The Analyst*, 1968, **93**, 292. (with G. F. Kirkbright and A. M. Smith)
152. The Thermal and Atomic-Fluorescence Emission of Germanium in a Nitrogen–Oxygen–Acetylene Flame. *Anal. Chim. Acta*, 1968, **41**, 551. (with R. M. Dagnall and K. C. Thompson)
153. Spectroscopy in Separated Flames. II. The Use of the Separated Air-Acetylene Flame in Long Path Atomic Absorption Spectroscopy. *Talanta*, 1968, **15**, 199. (with D. N. Hingle and G. F. Kirkbright)
154. Spectroscopy in Separated Flames. III. Use of the Separated Nitrous Oxide-Acetylene Flame in Thermal Emission Spectroscopy. *Talanta*, 1968, **15**, 441. (with G. F. Kirkbright and A. Semb)
155. The Separated Nitrous Oxide-Acetylene Flame as an Atom Reservoir in Thermal Emission Spectroscopy. *Spectroscopy Letters*, 1968, **1**, 7. (with G. F. Kirkbright and A. Semb)
156. Detection Limits for Thermal Emission Spectroscopy in a Separated Nitrous Oxide-Acetylene Flame. *Spectroscopy Letters*, 1968, **1**, 97. (with G. F. Kirkbright and A. Semb)
157. Temperature Profiles in Nitrous Oxide Supported Acetylene Flames at Atmospheric Pressure. *Talanta*, 1968, **15**, 663. (with G. F. Kirkbright, M. K. Peters and M. Sargent)
158. Molecular Emission Spectroscopy in Cool Flames. II. The Behaviour of Phosphorus-Containing Compounds. *The Analyst*, 1968, **93**, 72. (with R. M. Dagnall and K. C. Thompson)
159. Molecular Emission Spectroscopy in Cool Flames. III. The Emission Characteristics of Tin in Diffusion Flames. *The Analyst*, 1968, **93**, 518. (with R. M. Dagnall and K. C. Thompson)
160. Some Preliminary Studies of the Analytical Potentialities of the Atomic-Hydrogen Plasma Torch. *Anal. Chim. Acta*, 1968, **41**, 380. (with K. M. Aldous, K. C. Thompson and R. M. Dagnall)
161. The Determination of Beryllium by Thermal Emission and Atomic Fluorescence Spectroscopy in a Separated Nitrous Oxide-Acetylene Flame. *The Analyst*, 1968, **93**, 522. (with D. N. Hingle and G. F. Kirkbright)
162. Studies in Atomic Fluorescence Spectroscopy. VII. Fluorescence and Analytical Characteristics of Arsenic, with a Microwave Excited Electrodeless Discharge Tube as Source. *Talanta*, 1968, **15**, 677. (with R. M. Dagnall and K. C. Thompson)
163. The Nitrous Oxide Hydrogen Flame in Spectroscopic Analysis. *The Analyst*, 1968, **93**, 153. (with R. M. Dagnall and K. C. Thompson)
164. The Application of Separated Flames in Analytical Flame Spectroscopy. *Applied Optics*, 1968, **7**, 1305. (with G. F. Kirkbright)
165. Some Applications of Microwave Excited Electrodeless Discharge Tubes in Atomic Spectroscopy. *Applied Optics*, 1968, **7**, 1287. (with R. M. Dagnall)
166. Atomic-Fluorescence Spectroscopy of Magnesium with a High-Intensity Hollow-Cathode Lamp as Line Source. *Anal. Chim. Acta*, 1968, **42**, 29. (with X. K. Williams)
167. Analytical Applications of Ternary Complexes. VI. Spectrophotometric Determination of Trace Amounts of Palladium. *Talanta*, 1968, **15**, 1353. (with R. M. Dagnall and M. T. El Ghamry)
168. Analytical Applications of Ternary Complexes. VII. Elucidation of Mode of Formation of Sensitized Metal-Chelate Systems and Determination of Molybdenum and Antimony. *Talanta*, 1968, **15**, 1359. (with B. W. Bailey, J. E. Chester and R. M. Dagnall)
169. A Selective Amplification-Titration Procedure for the Determination of Microgram Amounts of Phosphate. *Analyst*, 1968, **93**, 224. (with G. F. Kirkbright and A. M. Smith)
170. Rapid Visual Compleximetric Titration of Calcium in Natural Waters. *Talanta*, 1968, **15**, 333. (with B. Fleet and Soe Win)

171. Studies in the Analytical Chemistry of Selenium: Absorptiometric Determination with 2-mercaptobenzoic Acid. *Analyst*, 1968, **93**, 595. (with M. S. Cresser)
172. The Fluorescence Quantum Efficiencies of Some Analytically Useful Chelate Complexes. *Analyst*, 1968, **93**, 638. (with R. M. Dagnall, L. Pratt and R. Smith)
173. Spectroscopy in Separated Flames. IV. Application of the Nitrogen-Separated Air-Acetylene Flame in Flame-Emission and Atomic-Fluorescence Spectroscopy. *Talanta*, 1968, **15**, 997. (with R. S. Hobbs, G. F. Kirkbright and M. Sargent)
174. Determination of Trace Amounts of Cobalt in Alumina by Atomic-Absorption Spectroscopy. *Analyst*, 1968, **93**, 701. (with B. Fleet and K. V. Liberty)
175. Atomic Fluorescence Spectroscopy of Silver Using a High-Intensity Hollow Cathode Lamp as Source. *Anal. Chem.*, 1968, **40**, 335. (with X. K. Williams)
176. An Indirect Amplification Procedure for the Determination of Niobium by Atomic-Absorption Spectroscopy. *Analyst*, 1968, **93**, 202. (with G. F. Kirkbright and A. M. Smith)
177. Atomic Absorption and Fluorescence Spectroscopy. British Patent Application 2590/69, 1969; Complete Specification 1221172, 1971.
178. Complexometry with EDTA and Related Reagents. B.D.H. Publications, pp. 235. 1969.
179. The Polarographic Behaviour of Ethyleneglycol-Bis-β-aminoethylether-*N*,*N*,*N*′,*N*′-Tetra-acetic Acid. *J. Electroanal. Chem.*, 1969, **21**, 541. (with B. Fleet and Soe Win)
180. Polarographic Determination of Calcium and Magnesium. *Analyst*, 1969, **94**, 269. (with B. Fleet and Soe Win)
181. A Rapid Indirect Titrimetric Determination of Microgram Amounts of Orthophosphate. *Analyst*, 1969, **94**, 321. (with G. F. Kirkbright and A. M. Smith)
182. Solvent Extraction—Absorptiometric Determination of Niobium in Steels with Bromopyrogallol Red. *Talanta*, 1969, **16**, 847. (with T. V. Ramakrishna and S. A. Rahim)
183. Spectrophotometric Determination of Microgram Amounts of Tantalum with Victoria Blue B. *Anal. Chem.*, 1969, **40**, 2210. (with G. F. Kirkbright and M. D. Mayhew)
184. Fluorescence Characteristics of Inorganic Complexes in Hydrochloric Acid Medium at Liquid-Nitrogen Temperature. *Talanta*, 1969, **16**, 65. (with G. F. Kirkbright and C. G. Saw)
185. Low-Temperature Fluorescence of Some Bromide-Ion Association Complexes in Hydrobromic Acid Glasses at − 196°C. *Analyst*, 1969, **94**, 538. (with G. F. Kirkbright and C. G. Saw)
186. Determination of Trace Amounts of Antimony by Spectrofluorimetry in Hydrobromic Acid Medium at Liquid Nitrogen Temperature. *Talanta*, 1969, **16**, 1081. (with G. F. Kirkbright, C. G. Saw and K. C. Thompson)
187. The Determination of Trace Amounts of Tellurium by Inorganic Spectrofluorimetry at Liquid Nitrogen Temperature. *Analyst*, 1969, **94**, 457. (with G. F. Kirkbright and C. G. Saw)
188. Kinetochromic Spectrophotometry. I. Determination of Fluoride by Catalysis of the Zirconium-Xylenol Orange Reaction. *Talanta*, 1969, **16**, 781. (with M. L. Cabello-Tomas)
189. Kinetochromic Spectrophotometry. II. Determination of Sulphate by Catalysis of the Zirconium-Methylthymol Blue Reaction. *Talanta*, 1969, **16**, 789. (with R. V. Hems and G. F. Kirkbright)
190. Recommendations for the Presentation of the Results of Chemical Analysis. *J. Pure & Applied Chem.* (IUPAC), 1969, **18**, 439. (with R. W. Fennell)
191. 3,5′Bis(dicarboxymethylaminomethyl)-4,4′-dihydroxy-*trans*-stilbene as a Selective Spectrofluorimetric Reagent for Cadmium. *Analyst*, 1969, **94**, 182. (with B. Budesinsky)
192. 1,5-Bis(Dicarboxymethylaminomethyl)-2,6-dihydroxynaphthalene as a Selective Spectrofluorimetric Reagent for Calcium. *Talanta*, 1969, **16**, 399. (with B. Budesinsky)
193. Spectrophotometric Determination of Selenium with Cyclohexanone. *Talanta*, 1969, **16**, 416. (with M. S. Cresser)
194. The Determination of Silicon by Flame Photometry and Atomic Fluorescence Spectroscopy with a Separated Nitrous Oxide-Acetylene Flame. *Anal. Chim. Acta*, 1969, **47**, 406. (with R. M. Dagnall, G. F. Kirkbright and R. Wood)
195. The Determination of Iron by Atomic Fluorescence Spectroscopy with a Modulated Microwave-Excited Electrodeless Discharge Tube. *Anal. Chim. Acta*, 1969, **47**, 563. (with L. Ebdon and G. F. Kirkbright)

196. The Determination of Tin by Atomic Fluorescence Spectroscopy with an Electronically Modulated Electrodeless Discharge Tube as Source. *Anal. Chim. Acta*, 1969, **46**, 207. (with R. F. Browner and R. M. Dagnall)
197. Preparation and Spectral Characteristics of Microwave-Excited Electrodeless Discharge Tubes for Palladium, Silver, Platinum and Gold. *Analyst*, 1969, **94**, 347. (with K. M. Aldous and R. M. Dagnall)
198. The Preparation of Electrodeless Discharge Tubes for Some Alkali and Alkaline Earth Elements. *Anal. Chim. Acta*, 1969, **44**, 457. (with K. M. Aldous and R. M. Dagnall)
199. An Investigation of the Performance of the Separated Air-Acetylene Flame in Thermal-Emission Spectroscopy. *Analyst*, 1969, **94**, 554. (with R. S. Hobbs and G. F. Kirkbright)
200. Spectroscopy in Separated Flames. V. The Argon- or Nitrogen-Sheathed Nitrous Oxide-Acetylene Flame in Flame Emission Spectroscopy. *Talanta*, 1969, **16**, 245. (with G. F. Kirkbright and M. Sargent)
201. Spectroscopy in Separated Flames. VI. The Argon or Nitrogen-Sheathed Nitrous Oxide-Acetylene Flame in Atomic Absorption Spectroscopy. *Talanta*, 1969, **16**, 1467. (with G. F. Kirkbright and M. Sargent)
202. The Atomic Fluorescence Spectroscopy of Cobalt with a High-Intensity Hollow-Cathode Lamp and a Microwave-Excited Electrodeless Discharge Tube as Sources. *Anal. Chim. Acta*, 1969, **45**, 205. (with B. Fleet and K. V. Liberty)
203. An Indirect Amplification Procedure for the Determination of Titanium by Atomic-Absorption Spectroscopy. *Analyst*, 1969, **94**, 754. (with G. F. Kirkbright, A. M. Smith and R. Wood)
204. Shielded Flame Emission Burner Assembly for Use with Atomic Absorption Spectrophotometers. *Laboratory Practice*, 1969, **18**, 1069. (with D. N. Hingle, G. F. Kirkbright and M. Sargent)
205. The Determination of Silicon in Low Alloy Steels by Atomic Fluorescence Spectroscopy in a Separated Nitrous Oxide-Acetylene Flame. *Analytical Letters*, 1969, **2**, 465. (with G. F. Kirkbright and A. P. Rao)
206. Comparison of Sensitivity of Atomic-Absorption and Atomic-Fluorescence Spectroscopy. *Spectroscopy Letters*, 1969, **2**, 179.
207. Electronically Modulated Microwave-Excited Electrodeless Discharge Tubes as Sources in Atomic Absorption Spectroscopy. *Anal. Chim. Acta*, 1969, **45**, 163. (with R. F. Browner and R. M. Dagnall)
208. Studies in Atomic Fluorescence Spectroscopy. VIII. Atomic Fluorescence and Atomic Absorption of Thallium and Mercury with Electrodeless Discharge Tubes as Sources. *Talanta*, 1969, **16**, 75. (with R. F. Browner and R. M. Dagnall)
209. Atomic Absorption and Fluorescence Spectroscopy with a Carbon Filament Atom Reservoir. Part I. Construction and Operation of Atom Reservoir. *Anal. Chim. Acta*, 1969, **45**, 27. (with X. K. Williams)
210. The Atomic-Emission Spectroscopy of the Rare Earth Elements in a Separated Nitrous Oxide-Acetylene Flame. *Analyst*, 1969, **94**, 864. (with D. N. Hingle and G. F. Kirkbright)
211. Indirect Amplification Determination of Thorium by Atomic Absorption Spectroscopy. *Spectroscopy Letters*, 1969, **2**, 69. (with G. F. Kirkbright and A. P. Rao)
212. Molecular-Emission Spectroscopy in Cool Flames. Part IV. The Determination of Chloride, Bromide and Iodide by Thermal-Emission Spectroscopy in the Presence of Indium Salts. *Analyst*, 1969, **94**, 643. (with R. M. Dagnall and K. C. Thompson)
213. The Microwave-Excited Emissive Detector in Gas-Phase Chromatography—I. *Talanta*, 1969, **16**, 797. (with R. M. Dagnall, S. J. Pratt and K. C. Thompson)
214. Emission Spectra Obtained from the Combustion of Organic Compounds in Hydrogen Flames. *Analyst*, 1969, **94**, 871. (with R. M. Dagnall, D. J. Smith and K. C. Thompson)
215. Microwave Excited Electrodeless Discharge Tubes Containing Organo-Sulphur and Phosphorus Compounds. *Analytical Chemistry*, 1969, **41**, 1851. (with R. M. Dagnall, K. M. Aldous and S. J. Pratt)
216. Recommended Nomenclature for Titrimetric Analysis. *J. Pure & Applied Chem.*, 1969, **18**, 429. (with E. B. Sandell)

217. Atomic Flame Spectroscopy in Trace Analysis. Part 1: Atomic-Absorption Spectroscopy. *Minerals Science & Engineering*, 1969, **1**, 44.
218. Determination of Chromium in Aluminium Salts by Atomic Absorption Spectroscopy. *Analyst*, 1970, **95**, 343. (with G. B. Marshall)
219. The Flame Spectroscopic Determination of Sulphur and Phosphorus in Organic and Aqueous Matrices by Using a Simple Filter Photometer. *Analyst*, 1970, **95**, 417. (with K. M. Aldous and R. M. Dagnall)
220. Recent Developments en Spectroscopie Atomique avec References Particulieres au Flammes et aux Sources Spectrales. *Methods Physiques D'Analyse* (GAMS) 1970, **6**, 3.
221. The Fluorescence and Phosphorescence Characteristics of Some Antioxidants and Ultraviolet Absorbers. *Anal. Chim. Acta*, 1970, **52**, 237. (with G. F. Kirkbright and R. Narayanaswamy)
222. Observations on the Preparation and Operation of Microwave Excited Electrodeless Discharge Tubes for Use in Atomic Spectroscopy. *Laboratory Practice*, 1970, **19**, 587. (with K. M. Aldous, D. Alger and R. M. Dagnall)
223. A Study of Some Matrix Effects in the Determination of Beryllium by Atomic Absorption Spectroscopy in Nitrous Oxide Acetylene Flames. *Talanta*, 1970, **17**, 203. (with B. Fleet and K. V. Liberty)
224. Determination of Very Small Amounts of Materials by the Techniques of Atomic Absorption and Atomic Fluorescence Spectroscopy. *Proc. Int. Symposium on Microtechniques, Graz*, 1970, **5**, 5–8.
225. Flame Emission and Atomic Absorption Spectrometry. *Chemistry & Industry*, 1970, 387.
226. Some Interference Studies in Atomic Fluorescence Spectroscopy with a Continuum Source. *Spectrochimica Acta*, 1970, **25B**, 61. (with M. S. Cresser)
227. Atomic Flame Spectroscopy in Trace Analysis. Part II. Atomic Fluorescence Spectroscopy. *Minerals Science & Engineering*, 1970, **2**, 31.
228. Kinetochromic Spectrophotometry. III. Determination of Fluoride by Catalysis of the Zirconium-Methylthymol Blue Reaction. *Talanta*, 1970, **17**, 433. (with R. V. Hems and G. F. Kirkbright)
229. A Solid Sample Reactor Injection Vessel for Gas Chromatography. *Anal. Lett*, 1970, **3**, 143. (with R. M. Dagnall and T. H. Risby)
230. Analytical Applications of Ternary Complexes. VIII. An Improved Reagent System for the Spectrophotometric Determination of Aluminium. *Talanta*, 1970, **17**, 13. (with J. E. Chester and R. M. Dagnall)
231. Some Observations on the Chemiluminescence of Atoms in Acetylene Flames Supported by Air and Argon-Oxygen Mixtures. *Anal. Chim. Acta*, 1970, **50**, 383. (with J. F. Alder and K. C. Thompson)
232. Some Preliminary Studies Concerning the Analytical Potentialities of an Augmented Diffusion Flame. *Anal. Chim. Acta*, 1970, **50**, 335. (with K. M. Aldous, R. M. Dagnall and L. C. Ebdon)
233. The Determination of Lead by Atomic Fluorescence Spectroscopy. *Anal. Chim. Acta*, 1970, **50**, 375. (with R. F. Browner and R. M. Dagnall)
234. An Investigation of the Determination of Germanium by Flame Photometry and Atomic Fluorescence Spectroscopy by Using a Separated Nitrous Oxide-Acetylene Flame. *Analyst*, 1970, **95**, 425. (with R. M. Dagnall, G. F. Kirkbright and R. Wood)
235. Spectrofluorimetric Determination of Submicrogram Amounts of Zirconium with Calcein Blue. *Anal. Chem.*, 1970, **42**, 784. (with R. V. Hems and G. F. Kirkbright)
236. Analysis by Flames. *British Science News*, 1970, **76**, 1.
237. Some Observations on the Determination of Zinc by Atomic Fluorescence Spectrometry Under Conditions Favourable for Analysis. *Anal. Chim. Acta*, 1970, **50**, 517. (with M. S. Cresser)
238. Absorptiometric Determination of Sulphide Ion. *Talanta*, 1970, **17**, 851. (with S. A. Rahim)
239. Atomic Absorption and Fluorescence Spectroscopy with a Carbon Filament Atom Reservoir. Part II. The Use of the Atom Reservoir in Atomic Fluorescence Spectroscopy. *Anal. Chim. Acta*, 1970, **51**, 355. (with R. G. Anderson and I. S. Maines)

240. Multi-Element Atomic Fluorescence Spectroscopy. Part I. Stimulation of Atomic Fluorescence of Mixtures of Bismuth, Mercury, Selenium and Tellurium, Cadmium and Zinc, Gallium and Indium by Means of Multi-Element Microwave Excited Electrodeless Discharge Tubes. *Anal. Chim. Acta*, 1970, **51**, 179. (with G. B. Marshall)
241. Multi-Element Atomic Fluorescence Spectroscopy. Part II. A Duel-Element Arsenic-Antimony Electrodeless Discharge Tube Spectral Line Source for Atomic Fluorescence and Atomic Absorption Spectroscopy. *Anal. Chim. Acta*, 1970, **51**, 272. (with A. Fulton and K. C. Thompson)
242. Atomic Absorption and Fluorescence Spectroscopy with a Carbon Filament Atom Reservoir. Part III. A Study of the Determination of Cadmium by Atomic Fluorescence Spectroscopy with an Unenclosed Atom Reservoir. *Anal. Chim. Acta*, 1970, **51**, 365. (with J. F. Alder)
243. The Selection of Line Pairs for the Iron 'Two-Line' Method of Flame Temperature Measurement. *Spectrochimica Acta*, 1970, **25B**, 465. (with G. F. Kirkbright and M. Sargent)
244. Multi-Element Atomic Fluorescence Spectroscopy. Part III. A New Type of Dual Element Microwave Excited Electrodeless Discharge Tube. *Anal. Chim. Acta*, 1970, **51**, 530. (with M. S. Cresser)
245. Atomic Fluorescence Spectrometry of Aluminium, Molybdenum, Titanium, Vanadium and Zirconium in Inert Gas Separated Nitrous Oxide-Acetylene Flames. *Anal. Chem.*, 1970, **42**, 1029. (with R. M. Dagnall, G. F. Kirkbright and R. Wood)
246. Spectrophosphorimetric Measurement of Niobium Oxinate at Liquid Nitrogen Temperature for Determination of Microgram Amounts of Niobium. *Anal. Chem.*, 1970, **42**, 782. (with G. F. Kirkbright and J. V. Thompson)
247. Application of Capillary Burners in Flame Spectrometry. *Anal. Chem.*, 1970, **42**, 939. (with K. M. Aldous, R. F. Browner and R. M. Dagnall)
248. A Microwave Excited Emissive Detector for Gas Chromatography. Further Studies with Sulphur Compounds. *Talanta*, 1970, **17**, 1009. (with R. M. Dagnall and S. J. Pratt)
249. Atomic Fluorescence Characteristics and Analytical Determination of Manganese in an Air-Acetylene Flame. *Talanta*, 1970, **17**, 965. (with L. Ebdon and G. F. Kirkbright)
250. The Applications of a Piezoelectric Scanning Fabry-Perot Interferometer to the Study of Atomic Line Sources. I. Assembly and General Application of the Instrumental System. *Spectrochimica Acta*, 1970, **25B**, 577. (with G. F. Kirkbright)
251. Vlam-Analyse. *Instrumentatie*, 1970, **4**, 11.
252. Developments in Atom Reservoirs and Line Sources for Atomic Absorption and Atomic Fluorescence Spectroscopy. *Pure & Appl. Chem.*, 1970, **23**, 99.
253. High Voltage Spark Excitation of Some Organic Molecules in Nitrogen and Argon Atmospheres. *Anal. Letts*, 1970, **3**, 475. (with R. M. Dagnall and D. J. Smith)
254. Some Analytical Aspects of Environmental Pollution: An Introduction. *Laboratory Practice*, 1971, **20**, 2.
255. Spectrofluorimetric Determination of Traces of Fluoride Ion by Ternary Complex Formation with Zirconium and Calcein Blue. *Anal. Chem.*, 1971, **43**, 136. (with Lay Har Tan)
256. A Spectrofluorimetric Method for the Determination of Small Amounts of Sulphate Ion. *Analyst*, 1971, **96**, 281. (with Lay Har Tan)
257. A Dewar Tube Sample Cell Assembly for Low Temperature Fluorimetry. *Anal. Chim. Acta*, 1971, **54**, 353. (with G. F. Kirkbright and P. J. Mayne)
258. A Microwave-Induced Argon Plasma System Suitable for Trace Analysis. *Anal. Chim. Acta*, 1971, **54**, 233. (with K. M. Aldous, R. M. Dagnall and B. L. Sharp)
259. Optimisation of Some Experimental Parameters in the Preparation and Operation of Microwave-Excited Electrodeless Discharge Lamps. *Anal. Chim. Acta*, 1971, **54**, 381. (with D. O. Cooke and R. M. Dagnall)
260. Emission Spectroscopy of Trace Impurities in Powdered Samples with a High-Frequency Argon Plasma Torch. *Anal. Chim. Acta*, 1971, **54**, 397. (with R. M. Dagnall and D. J. Smith)
261. The Application of Photon Counting as a Detection System in Atomic Fluorescence and Emission Spectrometry. *Spec. Letters*, 1971, **4**, 91. (with D. O. Cooke, R. M. Dagnall and B. L. Sharp)

262. The Determination of Very Small Amounts of Materials by the Technique of Atomic Absorption and Atomic Fluorescence Spectroscopy. *Pure & Appl. Chem.*, 1971, **25,** 47.
263. Atomic Absorption and Fluorescence Spectroscopy with a Carbon Filament Atom Reservoir. Part IV. The Determination of Gold by Atomic Fluorescence and Atomic Absorption Spectroscopy with an Unenclosed Atom Reservoir. *Anal. Chim. Acta*, 1971, **55,** 349. (with A. J. Aggett)
264. Multi-Element Atomic Fluorescence Spectroscopy. Part IV. The Determination of Cobalt and Nickel by Atomic Fluorescence Spectroscopy in a Separated Air-Acetylene Flame with a Dual-Element Electrodeless Discharge Lamp. *Anal. Chim. Acta*, 1971, **55,** 359. (with J. D. Norris)
265. Versatile Atomic Fluorescence Spectroscopy. *Chem. in Britain*, 1971, **7,** 378.
266. Evaluation of Some Three-Quarter Wave Microwave Cavities for the Operation of Electrodeless Discharge Lamps. *Anal. Chim. Acta*, 1971, **56,** 17. (with D. O. Cooke and R. M. Dagnall)
267. Spectrofluorimetric Determination of Orthophosphate as Rhodamine B Molybdophosphate. *Anal. Chem.*, 1971, **43,** 1434. (with G. F. Kirkbright and R. Narayanaswamy)
268. Spectroscopy in Separated Flames. VII. Determination of Bismuth by Atomic Fluorescence Spectroscopy in a Separated Air-Acetylene Flame with Electronically Modulated Electrodeless Discharge Tube Sources. *Talanta*, 1971, **18,** 859. (with R. S. Hobbs and G. F. Kirkbright)
269. Atomic Spectroscopy in Flame Media—History and Development "Advances in Automated Analysis". *Proceedings Technicon International Congress*, 1970. Vol. II. Thurman Associates, Miami, 1971. pp. 487–495.
270. Electronic Modulation of Microwave-Excited Electrodeless Discharge Lamps for Use in Atomic Fluorescence Spectrometry. *Talanta*, 1971, **18,** 1103. (with R. M. Dagnall and M. D. Silvester)
271. The Design and Operation of a Photon-Counting System for Analytical Atomic Spectrometry. *Anal. Chim. Acta*, 1971, **57,** 1. (with D. Alger, R. M. Dagnall and B. L. Sharp)
272. Atomic Absorption and Fluorescence Spectroscopy with a Carbon Filament Atom Reservoir. Part V. Determination of Elements in Organic Solvents. *Anal. Chim. Acta*, 1971, **57,** 15. (with J. Aggett)
273. Atomic Absorption and Fluorescence Spectroscopy with a Carbon Filament Atom Reservoir. Part VI. A Study of Some Matrix Effects. *Anal. Chim. Acta*, 1971, **57,** 271. (with D. Alger, R. G. Anderson and I. S. Maines)
274. Atomic Absorption and Fluorescence Spectroscopy with a Carbon Filament Atom Reservoir. Part VII. Atomic Absorption Under Limited Field Viewing Conditions. *Anal. Chim. Acta*, 1971, **57,** 281. (with R. G. Anderson and H. N. Johnson)
275. Multichannel Atomic Fluorescence and Flame Photometric Determination of Calcium, Copper, Magnesium, Manganese, Potassium and Zinc in Soil Extracts. *Anal. Chem.*, 1971, **43,** 1765 (with R. M. Dagnall, G. F. Kirkbright and R. Wood)
276. Simplified Photon Counting System for Measurement of Low Radiation Levels. *Nature* (Phys. Sciences), 1972, **235,** 65. (with R. M. Dagnall and B. L. Sharp)
277. Atomic Absorption and Fluorescence Spectroscopy with a Carbon Filament Atom Reservoir. Part VIII. The Determination of Manganese by Atomic Absorption Spectroscopy. *Anal. Chim. Acta*, 1972, **58,** 39. (with L. Ebdon and G. F. Kirkbright)
278. Atomic Absorption and Fluorescence Spectrophotometry with a Carbon Filament Atom Reservoir. Part IX. The Direct Determination of Silver and Copper in Lubricating Oils. *Anal. Chim. Acta*, 1972, **58,** 331. (with J. F. Alder)
279. The Determination of Mercury by Atomic Absorption Spectrophotometry with the 'Delves Sampling Cup' Technique. *Anal. Chim. Acta*, 1972, **58,** 339. (with D. Clark and R. M. Dagnall)
280. Atomic Absorption and Fluorescence Spectroscopy with a Carbon Filament Atom Reservoir. Part X. The Determination of Nickel with an Unenclosed Atom Reservoir. *Anal. Chim. Acta*, 1972, **59,** 187. (with K. W. Jackson)
281. The Spectrofluorimetric Determination of Orthophosphate as Quinine Molybdophosphate. *Analyst*, 1972, **97,** 174. (with G. F. Kirkbright and R. Narayanaswamy)
282. Multi-Element Atomic Fluorescence Spectroscopy. Part V. The Determination of Chromium and Manganese in Steels in a Separated Air-Acetylene Flame with a Dual-Element Electrodeless Discharge Lamp. *Anal. Chim. Acta*, 1972, **59,** 474. (with J. D. Norris)

283. The Atomic Fluorescence Characteristics and Determination of Chromium in an Argon Separated Air-Acetylene Flame. *Anal. Chim. Acta*, 1972, **59**, 355. (with J. D. Norris)
284. The Simultaneous Determination of Six Metals in Aluminium Alloys by Atomic Fluorescence Spectrophotometry. *Analyst*, 1972, **97**, 245. (with R. M. Dagnall, G. F. Kirkbright and R. Wood)
285. The Occurrence of Multiple Peaks in the Determination of Various Elements by the 'Delves Sampling Cup' Method. *Anal. Chim. Acta*, 1972, **60**, 219. (with D. Clark and R. M. Dagnall)
286. A Simple Atmospheric Microwave-Excited Emissive Detector for Gas Chromatography. *Anal. Chim. Acta*, 1972, **60**, 25. (with R. M. Dagnall and P. Whitehead)
287. The Use of Triple Pass Optical Arrangement for Determination of As and Se by AAS in an Inert Gas Shielded Nitrous Oxide-Acetylene Flame. *Spec. Letters*, 1972, **5**, 25. (with G. F. Kirkbright and L. Ranson)
288. The Direct Determination of Iodine by Atomic Absorption Spectroscopy in a Nitrogen Separated Nitrous Oxide-Acetylene Flame. *Atom. Absorp. Newsl.*, 1972, **11**, 53. (with G. F. Kirkbright and P. J. Wilson)
289. Some Optical Studies with the Air-Acetylene Flame. *Talanta*, 1972, **19**, 927. (with K. M. Aldous, R. F. Browner, D. Clark and R. M. Dagnall)
290. Atomic Absorption and Fluorescence Spectroscopy with a Carbon Filament Atom Reservoir. Part XI. The Determination of Iron by Atomic Absorption Spectroscopy. *Anal. Chim. Acta*, 1972, **61**, 15. (with L. Ebdon and G. F. Kirkbright)
291. Atomic Absorption and Fluorescence Spectroscopy with a Carbon Filament Atom Reservoir. Part XII. The Determination of Nickel in Crude and Residual Fuel Oils by Atomic Absorption Spectrometry. *Anal. Chim. Acta*, 1972, **61**, 132. (with J. F. Alder)
292. Determination of Trace Amounts of Metals in Soils by Ultramicro Atomic-Absorption Spectrometry. *Proc. Soc. Analyt. Chem.*, 1972, **9**, 198. (with A. C. Oborne)
293. An Indirect Amplification Procedure for the Determination of Vanadium in Aluminium Alloys by Atomic Absorption Spectroscopy. *Analyst*, 1972, **97**, 696. (with H. N. Johnson and G. F. Kirkbright)
294. Photo-Oxidation of Thallium(I) with the Production of Hydrogen Peroxide. *J. Chem. Soc., Dalton Trans.*, 1972, 1918. (with G. F. Kirkbright and P. J. Mayne)
295. A Simple Non-Selective Detector for Gas-Phase Chromatography Using the Measurement of Reflected Microwave Power. *Talanta*, 1972, **19**, 1226. (with R. M. Dagnall, M. D. Silvester and P. Whitehead)
296. Some Applications of Heteropoly Acids for Amplification Procedures in Atomic Absorption Spectroscopy. *Proc. Soc. Analyt. Chem.*, 1972, **9**, 259. (with H. M. Johnson and G. F. Kirkbright)
297. Emission Spectroscopy of Atoms in the Secondary Interconal Zone of the Argon-Oxygen-Acetylene Flame. *Chemia Analityczna*, 1972, **17**, 1091. (with J. F. Alder and K. C. Thompson)
298. Atomic Fluorescence for Chemical Analysis. *Chem. in Britain* 1972, **8**, 428. (with G. F. Kirkbright)
299. Application of Photon-Counting in Atomic-Absorption Spectrophotometry. *Talanta*, 1972, **19**, 1442. (with R. M. Dagnall and B. L. Sharp)
300. Determination of Manganese by Atomic Fluorescence Spectroscopy Using a Carbon-Filament Atom-Reservoir. *Talanta*, 1972, **19**, 1301. (with L. Ebdon and G. F. Kirkbright)
301. The Determination of Sulphur and Phosphorus by Atomic Emission Spectrometry with an Induction-Coupled High-Frequency Plasma Source. *Anal. Chim. Acta*, 1972, **62**, 241. (with F. G. Kirkbright and A. F. Ward)
302. The Application of the Leipert Amplification to Increase Sensitivity in the Direct Determination of Iodine by Atomic Absorption Spectrometry. *Atomic Absorption Newsletter*, 1972, **6**, 11. (with G. F. Kirkbright and P. J. Wilson)
303. Direct Determination of Sulfur in Oils by Atomic Absorption Spectrometry Using an Inert Gas Shielded Nitrous Oxide-Acetylene Flame. *Anal. Chem.*, 1972, **44**, 2379. (with G. F. Kirkbright and M. Marshall)

304. Some Analytical Properties of Low Pressure Flames. *Spectrochim. Acta*, 1972, **27B**, 515. (with R. Stephens)
305. A Scanning Technique for Multielement Analysis by Flame Atomic Emission Spectroscopy. *Lab. Practice*, 1972, **21**, 171. (with D. O. Cooke, R. M. Dagnall, H. N. Johnson and G. F. Kirkbright)
306. Switched Resistor Modulation of Microwave Excited Electrodeless Discharge Lamps. *Anal. Chem.*, 1972, **44**, 2255. (with D. Alger, R. M. Dagnall and M. D. Silvester)
307. Use of a Microwave Excited Emission Detector in Gas Chromatography for the Quantitative Measurement of Inter Element Ratios. *Anal. Chem.*, 1972, **44**, 2074. (with R. M. Dagnall and P. Whitehead)
308. Some Recent Developments in Electronically Modulated and Pulsed Electrodeless Discharge Lamps Used in Flame Fluorescence Spectrometry. *Rept. Colloquium Spectroscopicum Internationale XVI*, Adam Hilger (London), 1971 (2), 244. (with R. M. Dagnall & M. D. Silvester)
309. International Review of Science T. S. West (Ed.). Analytical Chemistry, Part 1. Physical Chemistry, Series One Volume 12. pp. 307. Butterworths, 1973.
310. Some Considerations on Spectral Line Profiles of Microwave-Excited Electrodeless Discharge Lamps. *Talanta*, 1972, **19**, 1309. (with R. M. Dagnall and D. O. Cooke)
311. The Simultaneous Determination of Traces of Cobalt, Chromium, Copper, Iron, Manganese and Zinc by Atomic Fluorescence Spectrometry with Preconcentration by an Automated Solvent Extraction Procedure. *Anal. Chim. Acta*, 1973, **63**, 210. (with M. Jones, G. F. Kirkbright and L. Ranson)
312. The Direct Determination of Mercury by Atomic-Absorption Spectrophotometry at 184.9 nm by Using a Nitrogen-Separated Nitrous Oxide-Acetylene Flame. *Analyst*, 1973, **98**, 49. (with G. F. Kirkbright and P. J. Wilson)
313. Determination of Vanadium in Titanium Dioxide by Ultramicro Atomic Absorption Spectrometry on a Carbon Filament Atom Reservoir. *Anal. Chem.*, 1973, **45**, 249. (with K. W. Jackson and L. Balchin)
314. Application of a Wavelength Scanning Technique to Multi-Element Determinations by Atomic Fluorescence Spectrometry. *Anal. Chem.*, 1973, **45**, 226. (with J. D. Norris)
315. The Use of a Wavelength Scanning Technique for Multi-Element Determinations by Atomic Fluorescence Spectroscopy. *Z. Anal. Chem.*, 1973, **263**, 128. (with J. D. Norris)
316. A Method for the Determination of Carbon Monoxide, Carbon Dioxide, Nitrous Oxide and Sulphur Dioxide in Air by Gas Chromatography Using an Emissive Helium Plasma Detector. *Spec. Letts.*, 1973, **6**, 87.
317. Atomic Absorption and Emission Spectrometry of Mercury at 184.9 nm. *Spec. Letts.* 1973, **6**, 183. (with R. M. Dagnall, J. M. Manfield and M. D. Silvester)
318. The Atomic Absorption Determination of Zinc with a Graphite Furnace. *Anal. Chim. Acta*, 1973, **63**, 11. (with D. Clark and R. M. Dagnall)
319. Some Intense Sources of Radiation for the Alkali and Alkaline Earth Elements. *Spectrochim. Acta*, 1973, **28B**, 51. (with R. M. Dagnall and M. D. Silvester)
320. Ultramicro Atomic-Absorption Spectroscopy with a Tungsten-Filament Atom-Reservoir. *Talanta*, 1973, **20**, 459. (with J. E. Cantle)
321. Atomic Absorption and Fluorescence Spectrometry with a Carbon Filament Atom Reservoir. Part XIII. The Determination of Chromium with a Fully Enclosed Atom Reservoir. *Anal. Chim. Acta*, 1973, **64**, 363. (with K. W. Jackson)
322. Atomic Emission Spectrometry with an Induction-Coupled High-Frequency Plasma Source. The Determination of Iodine, Mercury, Arsenic and Selenium. *Anal. Chim. Acta*, 1973, **64**, 353. (with G. F. Kirkbright and A. F. Ward)
323. The Direct Determination of Mercury by Atomic Fluorescence Spectrometry in a Nitrogen-Separated Air-Acetylene Flame with Excitation at 184.9 nm. *Anal. Chim. Acta*, 1973, **66**, 130. (with G. F. Kirkbright and P. J. Wilson)
324. Atomic Absorption and Fluorescence Spectrometry with a Carbon Filament Atom Reservoir. Part XIV. The Determination of Vanadium in Fuel Oils. *Anal. Chim. Acta*, 1973, **66**, 301. (with G. L. Everett)

325. The Determination of Germanium by Atomic Absorption Spectrometry with a Graphite Tube Atomizer. *Anal. Chim. Acta*, 1973, **67**, 79. (with D. J. Johnson and R. M. Dagnall)
326. Atomic Fluorescence Spectrometry. *Appl. Spec. Rev.*, 1973, **7**, 79. (with M. S. Cresser)
327. The Determination of Volatile Metal Chelates by Using a Microwave-Excited Emissive Detector. *The Analyst*, 1973, **98**, 647. (with R. M. Dagnall and P. Whitehead)
328. Microwave Plasma Detector System for Measurement of Trace Levels of Carbon Monoxide in Air. *Proc. Soc. Anal. Chem.*, 1973, **10**, 192. (with J. Moore and R. M. Dagnall)
329. Investigation of Spectral Overlap of the Neon 359.352 nm and Chromium 359–349 nm Spectral Lines in AA and AFS of Chromium. *Anal. Chem.*, 1973, **45**, 2148. (with J. D. Norris)
330. Non-Dispersive Atomic Fluorescence Using a Non-Flame Atom Reservoir: Determination of Bismuth. *Proc. Soc. Analyt. Chem.*, 1973, **10**, 271. (with R. P. Mounce, R. M. Dagnall and B. L. Sharp)
331. Time-resolved non-dispersive atomic fluorescence by the carbon filament atomisation technique. *Proc. Soc. Analyt. Chem.*, 1973, **10**, 279. (with A. F. King)
332. A Comparative Study of the Determination of Zinc and Molybdenum by Atomic Absorption Spectrometry in a Carbon Filament Atom Reservoir. *Anal. Chim. Acta*, 1973, **66**, 171. (with D. J. Johnson)
333. International Review of Science. T. S. West (Editor) Analytical Chemistry. Part 2. Physical Chemistry. Series One Volume 13, pp. 263. Butterworths, 1973.
334. 'Time Resolved Non-Dispersive Atomic Fluorescence Spectroscopy' British Patent, 1973, 49949/73.
335. 'Free Atom Spectrometry' British patent, 1973, 50038/73.
336. Determination of Sodium by Atomic Emission Spectrometry Using a Carbon Filament Atom Reservoir. *Spectroscopy Letters*, 1973, **6**, 767. (with G. L. Everett and R. W. Williams)
337. Trace Analysis for Sulphur and Phosphorus in Aqueous Solution by the Carbon Filament Atom Reservoir Technique. *Anal. Chim. Acta*, 1974, **68**, 387. (with G. L. Everett and R. W. Williams)
338. Determination of Iodine by Atomic Absorption and Emission Spectrometry with a Cathode Sputtering Cell. *Anal. Chim. Acta*, 1974, **68**, 462. (with G. F. Kirkbright and P. J. Wilson)
339. Silver Chloride-Silver Sulphide Amplification Reaction for the Micro-Determination of Chloride Ion. *Mikrochim. Acta*, 1974, 111. (with S. A. Rahim and H. Abdulahad)
340. The Determination of Tin by Carbon Filament Atomic Absorption Spectrometry. *Anal. Chim. Acta*, 1974, **70**, 291. (with G. L. Everett and R. W. Williams)
341. The Determination of Manganese in Lubricating Oils by Carbon Filament Atomic Absorption Spectrometry. *Anal. Chim. Acta* 1974, **70**, 204. (with G. L. Everett and R. W. Williams)
342. Direct Determination of Nanogram Amounts of Iodine by Atomic Absorption Spectrometry Using a Graphite Tube Atomizer. *Talanta*, 1974, **21**, 573. (with M. J. Adams and G. F. Kirkbright)
343. Determination of Iodine by Atomic Absorption Spectrometry Using the Platinum Loop Technique. *Talanta*, 1974, **21**, 787. (with J. M. Mansfield and R. M. Dagnall)
344. Use of an Argon-Hydrogen Flame for the Atomic Absorption and Atomic Fluorescence Spectrometry of Antimony. *Anal. Chim. Acta*, 1974, **71**, 458. (with J. D. Norris)
345. Use of a Non-Dispersive Atomic Fluorescence Spectrometer for the Determination of Zinc in Soils and Non-Ferrous Metal Alloys. *Anal. Chim. Acta*, 1974, **71**, 289. (with J. D. Norris)
346. Optical Absorption Phenomena at Electrode Surfaces. *Nature*, 1974, **250**, 139. (with J. F. Tyson)
347. Some Applications of Spectral Overlap in Atomic Absorption Spectrometry. *Anal. Chem.*, 1974, **46**, 1423. (with J. D. Norris)
348. Determination of Lead in Instant Coffee and Tea Powders by Carbon Filament Atomic Absorption Spectrometry. *Anal. Chim. Acta*, 1974, **73**, 180. (with J. K. Kapur)
349. Atomic Fluorescence and Atomic Absorption Spectrometry for Chemical Analysis. *Analyst*, 1974, **99**, 886.
350. Stable Direct-Current Capillary Arc Plasma for Solution Analysis. *Talanta*, 1975, **22**, 379. (with H. Denton and B. L. Sharp)

351. Some Observations on the Vaporization and Atomization of Samples with a Carbon Filament Atomizer. *Anal. Chem.*, 1975, **47**, 1234. (with P. J. Johnson, B. L. Sharp and R. M. Dagnall)
352. Investigation of Submicro Analysis of Metal Surfaces by Electrography and Carbon Filament Atomic Absorption Spectrometry. *Bull. Soc. Chem. Belge*, 1975, **84**, 549. (with I. L. Shresta)
353. International Review of Science. T. S. West (Ed.) Analytical Chemistry, Part I. Physical Chemistry, Series Two, Vol. 12. pp. 334. Butterworths, 1976.
354. International Review of Science. Analytical Chemistry. Part II. Physical Chemistry. Series Two. Vol. 13. pp. 271. Butterworths, 1976.
355. Rapid Determination of Sulphur in Oils and Fuels by Cool Flame Molecular Emission Spectrometry. *Lab. Practice*, 1976, **25**, 455. (with J. F. Alder, M. A. Pinches and R. W. Williams)
356. Determination of Anionic Detergents at ppb Levels by Graphite Furnace Atomic Absorption Spectrometry. *Anal. Chim. Acta*, 1976, **87**, 97. (with P. T. Crisp, J. M. Eckert, N. A. Gibson & G. F. Kirkbright)
357. Development and Design of a Multi-Channel Atomic Absorption Spectrometer for the Simultaneous Determination of Trace Metals in Hair. *Anal. Chim. Acta*, 1976, **87**, 301. (with J. F. Alder, D. Alger and A. J. Samuel)
358. Single Element Determination of Trace Metals in Hair by Carbon Furnace Atomic Absorption Spectrometry. *Anal. Chim. Acta*, 1976, **87**, 313. (with J. F. Alder and A. J. Samuel)
359. Practical Developments in Atomic Fluorescence Spectroscopy. *Proc. Soc. Anal. Div. Chem. Soc.*, 1976, **13**, 257.
360. Fluorescencia Atomica No Dispersiva Utilizando un Filamento de Carbon Como Dispositivo Atomizador. I. Descripcion del Aparato de Medida y su Aplicacion a la Determinacion de Mercurio. *Anal. Quim. Real. Soc. Espan. Fis. y Quim.*, 1977, **73**, 849. (with A. Sanz Medel and J. A. Perez Bustamante)
361. Fluorescencia Atomica no Dispersiva Utilizando un Filamento de Carbon Como Dispositivo Atomizador. II. Determinacion de Cadmio y Cinc. *Anal. Quim. Real. Soc. Espan. Fis. y Quim.*, 1977, **73**, 988. (with A. Sanz Medel and J. A. Perez Bustamante)
362. Fluorescencia Atomica no Dispersiva Utilizando un Filamento de Carbon Como Dispositivo Atomizador. III. Elementes Menos Volatiles. Determinacion de Plobo y Bismuto. *Anal. Quim. Real. Soc. Espan. Fis. y Quim.*, 1977, **73**, 995. (with A. Sanz Medel and J. A. Perez-Bustamante)
363. Sample Atomization in Low Pressure Flames. Analytical Chemistry—Anders Ringbom Memorial Volume. Pergamon Press, Oxford, 1977, 477. (with R. Stephens)
364. The Anatomical and Longitudinal Variation of Trace Element Concentrations in Human Hair. *Anal. Chim. Acta*, 1977, **92**, 217. (with J. F. Alder and A. J. Samuel)
365. The Use of Silk and Animal Hairs as Standards for Hair Analysis. *Anal. Chim. Acta*, 1977, **91**, 407. (with J. F. Alder, C. A. Pankhurst and A. J. Samuel)
366. Compendium of Analytical Nomenclature (IUPAC) Pergamon Press, Oxford, 1978. pp. 223. (with H. M. N. H. Irving and H. Freiser)
367. The Determination of Copper in Alloys by Electrography and Atomic Absorption Spectrometry. *Anal. Chim. Acta*, 1977, **90**, 267–270. (with J. F. Alder and A. E. Baker)
368. Use of a Twin-Port Power Divider and Attenuator in the Operation of Electrodeless Discharge Lamps for Multi-Element Atomic Fluorescence Spectrometry. *Spectroscopy Letters*, 1978, **11(9)**, 708. (with J. D. Norris)
369. Thermostated Electrodeless Discharge Lamps in Atomic Spectrometry. *Reviews in Anal. Chem.*, 1978, **1**, 19. (with D. F. Bartlet, T. Hurst and J. D. Norris)
370. Some Recent Developments in Atomic Fluorescence Spectroscopy. *Pure & Appl. Chem.*, 1978, **50**, 837.
371. Recommended Nomenclature for Scales of Working in Analysis. *Pure & Appl. Chem.*, 1979, **51**, 43. (with E. B. Sandell)
372. Non-Dispersive Atomic Fluorescence Spectrometry with a Carbon Filament Atom Reservoir. *Anal. Chim. Acta*, 1979, **104**, 85. (with M. Hargreaves, A. F. King, J. D. Norris and A. Sanz-Medel)
373. Analytical Aspects of Absorption Spectroelectrochemistry at a Platinum Electrode—I. Study of Metal Ions. *Talanta*, 1979, **26**, 117. (with J. F. Tyson)

374. The Atomic Absorption Spectrophotometric Determination of Palladium with a Carbon Filament Electrothermal Atomizer. *Anal. Chim. Acta*, 1979, **104,** 385. (with E. A. Bound, J. D. Norris and A. Sanz-Medel)
375. Trace Element Determination (in Soils). *Education in Chemistry*, 1979, **16,** 62.
376. The Determination of Selenium in Soils and Plants by Differential Pulse Cathodic Stripping Voltammetry. *Talanta*, 1979, **26,** 473. (with S. Forbes and G. P. Bound)
377. An Investigation of Atom Collection Phenomena in the Atomic Absorption Spectrometry of Copper. *Anal. Chim. Acta*, 1979, **107,** 191. (with J. Khalighie and A. M. Ure)
378. Biosignificance and Analysis of Trace Elements in Agricultural Soils. (1st T. B. Miller Memorial Lecture). Special Publication, North of Scotland College of Agriculture, 1979.
379. Uptake of Major Mineral Elements by Plants. In 'Food Chains in Human Nutrition', Ed. Sir Kenneth Blaxter, Applied Science Publishers Ltd., 1979, 223. (with B. W. Bache)
380. Atomic Spectrochemical Analysis in Soil Science Research. In Proc. Euroanalysis III Conference 1978, Eds. D. M. Carroll and D. T. Burns, Applied Science Publishers Ltd., 1979, 93.
381. A Quartz Crystal Piezoelectric Device for Monitoring Organic Gaseous Pollutants. *Anal. Chim. Acta*, 1980, **117,** 147. (with T. E. Edmonds)
382. Some Observations on the Mechanisms of Atomization in Atomic Absorption Spectrometry with Atom-Trapping and Electrothermal Techniques. *Anal. Chim. Acta*, 1980, **117,** 257. (with J. Khalighie and A. M. Ure)
383. The Differential Pulse Anodic Stripping Voltammetry of Copper and Lead and Their Determination in EDTA Extracts of Soils with the Mercury Film Glassy Carbon Electrode. *Anal. Chim. Acta*, 1980, **120,** 41. (with T. E. Edmonds and Pu Guogang)
384. Use of a Piezoelectric Sensor as a Continuous Monitor of Atmospheric Pollutants. *Chem. Soc. Anal. Proc.*, 1980, **17,** 2. (with S. Cooke and P. Watts)
385. Analytical Aspects of Absorption Spectroelectrochemistry at a Platinum Electrode—II. Quantitative Basis and Study of Organic Compounds. *Talanta*, 1980, **27,** 335. (with J. F. Tyson)
386. Electrolytic Determination of Micromolar Concentration of Copper (II) with a Piezoelectric Quartz Crystal. *Bunseki Kagaku, Japan Society for Analytical Chemistry*, 1981, **30,** 494. (with T. Nomura, T. Nagamune and K. Izutsu)
387. Comparison of Sample Introduction Techniques with a Continuously Heated Graphite-Furnace Atomizer for Atomic-Absorption Spectrophotometry. *Talanta*, 1980, **27,** 867. (with M. Chamsaz and B. L. Sharp)
388. The Determination of the Ionisation Constants of Polymaleic Acid and the Stability Constants of its Complexes with Copper. *Anal. Chim. Acta*, 1981, **129,** 69. (with T. E. Edmonds and Pu Guogang)
389. Soil as the Source of Trace Elements. *Phil. Trans. R. Soc. Lond.*, 1981, **B294,** 19.
390. Atom Trapping Atomic Absorption Spectrometry of Arsenic, Cadmium, Lead, Selenium and Zinc in Air-Acetylene and Air-Propane Flames. *Anal. Chim. Acta*, 1981, **131,** 27. (with J. Khalighie and A. M. Ure)
391. The Atomic Spectroscopy of Biosignificant Trace Elements in Soils in Relation to Plant and Animal Nutrition. *Bunseki Kagaku*, 1981, **30,** 103.
392. Atom Trapping Absorption Spectrometry with Water-Cooled Metal Collector Tubes. *Anal. Chim. Acta*, 1982, **134,** 271. (with J. Khalighie and A. M. Ure)
393. Spectroelectrochemistry of Morphine and Related Alkaloids and their Investigation by Fluorescence in a Gold Micromesh Cell. *The Analyst*, 1982, **107,** 1. (with C. M. W. McLeod)
394. *Collaborative Interlaboratory Studies in Chemical Analysis* (Proc. IUPAC Discussion meeting Helsinki, Aug. 1981). Pergamon Press, Oxford 1982, pp. 8 + 171 (Joint Editorship with H. Egan)
395. The Determination of Selenium by Atom-Trapping Atomic Absorption Spectrometry. *Anal. Chim. Acta*, 1982, **141,** 213. (with C. M. Lau and A. M. Ure)
396. *Recent Advances in Analytical Chemistry* (Proc. Roy. Soc. Discussion Group Meeting Dec. 1981) The Royal Society, London 1982, pp. vi + 219 (Joint Editorship with J. M. Thomas and R. Belcher)

397. Biosignificant Trace Elements in Soils: The Role of Biosignificant Trace Elements in Soils in Relation to Plant and Animal Nutrition as Revealed by the Techniques of Atomic Spectroscopy. *Anal. Proc.*, 1982, **19,** 436.
398. The Determination of Lead by Adsorption of the Extracted 8-Quinolinolate on the Electrodes of a Piezoelectric Quartz Crystal. *Anal. Chim. Acta*, 1982, **143,** 243. (with T. Nomura and T. Yamashita)
399. The Determination of Lead and Cadmium in Soils by Atom Trapping Atomic Absorption Spectrometry. *Anal. Chim. Acta*, 1983, **146,** 171. (with C. M. Lau and A. M. Ure)
400. Nicolae Teclu—A Pioneer of Flame Spectroscopy. *Talanta*, 1983, **30,** 135. (with G. E. Baiulescu and S. Moldoveanu)
401. Atom Trapping Atomic Absorption Spectrometry. *Anal. Proc.*, 1982, **20,** 114. (with C. M. Lau and A. M. Ure)
402. Column Cementation on Aluminium Powder as a Preconcentration Technique for Trace Element Determination by Spark Source Mass Spectrometry. Part 1. Copper, Lead, Ruthenium and the Noble Metals. *Anal. Chim. Acta*, 1983, **152,** 95. (with B. Fu and A. M. Ure)
403. Behaviour of Piezoelectric Quartz Crystals in Solutions with Application to the Determination of Iodide. *Anal. Chim. Acta*, 1985, **175,** 107. (with T. Nomura and M. Watanabe)
404. Scotland's Land and Soils. *Proc. Roy. Soc. Edinburgh*, 1986, **87B,** 125.
405. Determination of Cadmium in Calcium Chloride Extracts of Soils by Atom Trapping Atomic Absorption Spectrometry. *J. Anal. Atomic Spectrometry*, 1986, **1,** 19. (with S. M. Fraser, A. M. Ure and M. C. Mitchell)
406. Optical Electron and X-Ray Spectrometry in Soil Analysis. *Anal. Chim. Acta*, 1986, **180,** 163. (with D. C. Bain, M. L. Berrow, W. J. McHardy, E. Paterson, J. D. Russell, B. L. Sharp and A. M. Ure)
407. Spectrophotometric Determination of Traces of Fluoride Ion by Ternary Complex Formation with Zirconium and Acid Alizarin Black SN. *Arab Gulf J. Scientific Research*, 1986, **4,** 105. (with S. B. Salama)
408. Development of a Multi-Sensor System Using Coated Piezoelectric Crystal Detectors. *Analyst*, 1986, **111,** 1183. (with S. M. Fraser and T. E. Edmonds)
409. The Determination of Trace Elements in Natural Waters, Blackwell Scientific Publications, Oxford, 1988, **18,** 1362. (Joint Editorship with H. W. Nüruberg)
410. An Examination of Some Scientific Issues in the Case of the Maguire Seven, Guildford and Woolwich Enquiry, London, 1992, 74.

Talanta, Vol. 39, No. 11, pp. 1429–1435, 1992
Printed in Great Britain.

0039-9140/92 $5.00 + 0.00

EVALUATION OF SOME *AS*-TRIAZINES AND RE-EVALUATION OF PDT AND FERROZINE AS REAGENTS FOR SPECTROPHOTOMETRIC DETERMINATION OF RUTHENIUM

M. A. ISLAM
Department of Chemistry, University of Dhaka, Dhaka 1000, Bangladesh

W. I. STEPHEN†
School of Chemistry, University of Birmingham, Edgbaston, Birmingham, B15 2TT, U.K.

(*Received* 14 *April* 1992. *Accepted* 14 *May* 1992)

Summary—A sensitive method for the spectrophotometric determination of ruthenium with the ferroin-yielding *as*-triazines has been developed. This method has several advantages; complete reduction of ruthenium species to ruthenium(II) can be achieved by the recommended procedure, which shortens the colour development time, saves the unnecessary use of several-fold excess of the reagent and the molar absorptivity is increased significantly. A few of the new *as*-triazines together with the commercially available Ferene® have been evaluated as ruthenium(II) chromogens. 3-(2-Pyridyl)-5,6-diphenyl-*as*-triazine (PDT) and ferrozine, a sulphonated derivative of PDT, have been re-evaluated by the new method. It has been observed that the *as*-triazine acting as a bidentate ligand forms a tris-complex with ruthenium(II) similar to its reaction with iron(II).

A variety of chromogenic reagents has served as the basis for the spectrophotometric determination of ruthenium. Recent reference works[1,2] list more than forty reagents for ruthenium and the number of methods for the spectrophotometric determination of ruthenium is steadily increasing because of its commercial importance. The various methods differ considerably in sensitivity, tolerance to other ions, rate of reaction, useful concentration range and availability of the reagents, and there appears to be scope for the development of further procedures with readily available chromogenic reagents which give good sensitivity.

Recently, certain 3,5,6-trisubstituted-1,2,4-triazines have been prepared and evaluated as highly sensitive chromogenic reagents for the spectrophotometric determination of iron(II).[3] In the present study, consideration was given to the possible reaction of ruthenium with these chromogens in the light of its position in the periodic table and the analytical resemblance of certain compounds of ruthenium to those of iron. The behaviour of three new chromogens; 3-(2-py)-5,6-bis(*p*-methoxyphenyl)-*as*-triazine (PBMPT), 3-(2-py)-5,6-bis(4-biphenyl)-*as*-triazine (PBBT), 3-(2-py)-5,6-bis(4-biphenyl-4′-sulphonic acid)-*as*-triazine, diammonium salt (PBBT–DAS) with ruthenium has now been studied and their potential as analytical reagents has been assessed.

Sporadic attempts have been made to apply this class of spectrophotometric reagent for iron, based on its reaction with the ferroin-yielding functional group, to the spectrophotometric determination of ruthenium. However, all these methods suffer from certain difficulties.

The method of Banks and O'Laughlin[4] which utilises 1,10-phenanthroline is very sensitive to the amount of the reducing agent (hydroxylammonium chloride) and requires more than 20 hours heating for full colour development. The larger the amount of reducing agent present, the lower is the rate of formation of the complex and apparent shift in the wavelength of maximum absorbance towards higher wavelengths. The absorption maximum at longer wavelength was greater when the amount of hydroxylammonium chloride added was increased, or the amount of 1,10-phenanthroline was decreased. This was explained by postulating that a species might be formed involving the hydroxylammonium ion. The method with 4,7-diphenyl-1,10-phenanthroline[5] in the presence of the reducing agent, hydroxylammonium chloride, and using

†Author for correspondence. Present address: The Garden House, Binghill, Milltimber, Aberdeen AB1 0JL, U.K.

a buffer system containing sodium acetate and ammonium hydroxide, produces a broad absorption band of the ruthenium complex at 445–470 nm. Embry and Ayres[6] attempted to develop the colour of the 2,4,6-tris (2-py)-*s*-triazine–ruthenium complex with hydroxylammonium chloride as a reducing agent following the work of Banks and O'Laughlin;[4] however, lower values of absorbances were obtained. The colour was therefore developed in the presence of 20–50% by volume of ethanol without the addition of another reducing agent. They report that the complex contains the ruthenium(III) species. Karma and Ayres[7] have also reported that ruthenium(III) reacts with 3-(2-py)-5,6-diphenyl-*as*-triazine (PDT) in aqueous ethanol medium at pH 5 to give a magenta coloured $[Ru(PDT)_2]^{2+}$ complex. The molar absorptivity at 485 nm was 2.1×10^4 $l \cdot mole^{-1} \cdot cm^{-1}$. They also noted that the PDT appears to reduce ruthenium(III) under their experimental conditions, because the same value of absorbance was obtained in the presence of any added reducing agent and with only the complexing agent present under the experimental conditions, and again when reducing agents such as hydroxylammonium chloride or hypophosphite were present. The composition of the complex in solution was determined by continuous variation and mole-ratio methods and it was reported that PDT acts as a tridentate ligand and forms a bis-complex with ruthenium(II). However, it is well known that reagents of this class acting as bidentate ligands tend to form tris-chelates with iron(II).[8,9] Kundra and his coworkers[10] have developed a method for the spectrophotometric determination of ruthenium(III) with the widely used iron reagent, ferrozine, a sulphonated derivative of PDT. They reported that ruthenium(III) forms a bis-complex with ferrozine having a molar absorptivity of 3.1×10^4 $l \cdot mole^{-1} \cdot cm^{-1}$ at 480 nm. Three hours of heating and a 120-fold excess of ferrozine were needed for full colour development.

In this study, we have taken the opportunity of re-evaluating PDT and ferrozine as ruthenium(II) chromogens because in earlier work incomplete reduction and variable composition with ferroin analogues may have occurred. A sensitive iron(II) chromogen: 3-(2-py)-5,6-bis[2-(5-furylsulphonic acid)]-*as*-triazine, disodium salt (Ferene)[11] has also been evaluated as a ruthenium(II) chromogen.

EXPERIMENTAL

Reagents

PBMPT, PBBT, PBBT–DAS and PDT were synthesised in this laboratory;[3] ferrozine® and Ferene® were obtained from Aldrich and Sigma Chemical Companies respectively and were used as received. A typical stock solution (0.005*M*) of the organic reagents was prepared by dissolving the requisite amounts in a small volume of ethanol, in some cases a drop or more of concentrated AR hydrochloric acid was added to dissolve the reagent. The solution was then diluted to volume with spectroscopic grade ethanol. Sulphonated derivatives of organic reagents were dissolved in distilled water. Dilution of the stock solution was made for the determination of the composition of the complexes.

A standard solution of ruthenium(III) chloride in 5% hydrochloric acid (containing 1000 μg/ml and prepared as a standard for atomic absorption use) was obtained from Aldrich Chemical Company. This solution was diluted to obtain the required concentration.

A range of conventional buffer solutions, nominally 1*M* in strength was prepared containing, where appropriate, one or more of the following analytical grade chemicals: hydrochloric acid, acetic acid, sodium acetate, ammonium acetate, ammonium chloride and aqueous ammonia solution. Solutions at different pH intervals in the range 2.5–11 were thus obtained.

All other reagents were of analytical grade.

Effect of variables

Systematic investigations were made of the effect of variables (such as the choice of reducing agent and pH of the buffer solution, length of heating time and excess of complexing agent) on the rate and completeness of complexation. This was done by preparing a series of solutions in which all but one variable were held constant.

Analytical procedures

Recommended procedures for the reduction of ruthenium(III) to ruthenium(II). Place 5 ml of standard ruthenium(III) chloride solution in 5% hydrochloric acid (1000 μg/ml) and a weighed amount, 0.15–0.20 g, of AR metallic zinc shot (8–30 mesh) in a 100-ml stoppered conical flask. Add 2 ml of concentrated acetic acid to this mixture. Gently swirl the flask for 8-10 min (the solution turns completely blue within this time). Carefully transfer the solution into a 250-ml

Table 1. Summary of the results of spectrophotometric reactions of some *as*-triazines with ruthenium(II)

Photometric reagent	Colour dev. time (hr)	λ_{max}/nm	Composition M: L	ϵ/l · mole^{-1} · cm^{-1}	Solution medium	Colour stability
PDT	1.0	475 (485)*	1:3 (1:2)*	3.5×10^4 (2.1×10^4)*	EtOH-H_2O	Excellent
Ferrozine	1.0	478 (480)†	1:3 (1:2)†	3.56×10^4 (3.15×10^4)†	Aqueous	Excellent
PBBT	1.5	484	1:3	4.63×10^4	EtOH-H_2O	Excellent
PBBT-DAS	2.0	485	1:3	5.50×10^4	EtOH-H_2O	Excellent
PBMPT	1.5	483	1:3	4.70×10^4	EtOH-H_2O	Excellent
Ferene	2.0	505	1:3	4.63×10^4	Aqueous	Good (around 48 hours)

*Ref. 7.
†Ref. 10.

standard flask. Wash the unused metallic zinc with 5 ml of concentrated acetic acid and then several times with distilled water and transfer the washings into the flask. Dry the unused zinc and weigh. Dissolve an exact amount of zinc used in the reduction process in acetic and hydrochloric acids and dilute to 250 ml keeping the same acid concentrations for this reagent blank solution.

Recommended procedure for colour development. Add 0.5–2.5 ml of ruthenium(II) solution (20 μg/ml), 5 ml of complexing agent solution and 5 ml of pH 3 buffer solution to a 25-ml standard flask in the above order and heat for different lengths of time (Table 1) for each complexing agent at a boiling water bath temperature and make up the volume with either ethanol (spectroscopic grade) or distilled water (Table 1). In the case of the PBBT-complex, the colour should be developed by refluxing, rather than heating, because of its low solubility in aqueous-ethanol medium. Similarly, prepare the reagent blank solution with metallic zinc solution taking the highest equivalent amount of ruthenium solution.

Spectra of all solutions in the visible region were recorded with a Shimadzu UV–Vis recording spectrophotometer, UV-240 against reagent blanks in the appropriate solvents. Absorbance measurements at fixed wavelength were made on a CE 505 (Cecil Instrument) spectrophotometer using 1-cm matched glass cells.

Sensitivity Determination

With each complexing agent, a series of metal complex solutions was prepared following the recommended procedure. Absorbances of the solutions were recorded at wavelength of maximum absorbance (Table 1) against the similarly prepared reagent blank solution. In all cases at least five different solutions of each complex were prepared and the molar absorptivity (ϵ) of the complex at the wavelength of maximum absorbance (λ_{max}) was calculated from the linear regression coefficient.

Determination of composition of the complex

The composition of all complexes in solution was determined by the mole-ratio method; once by varying the amount of complexing agent, keeping the amount of ruthenium constant; and again by varying the amount of ruthenium, keeping the complexing agent constant. The results of this study are summarised in Table 1.

Colour stability of the complexes

The colour stability of the solution of the complexes was observed by measuring the absorbances at different time intervals and the results are summarised in Table 1.

Table 2. Effect of reducing agent on the formation of PDT-ruthenium(II) complex

Ruthenium solution 1.6 μg/ml	Reducing agent added	Corresponding λ_{max}	Corresponding absorbance (1 cm cell)
Ru(III)	2 ml of 10% hydroxylammonium chloride	480 nm	0.42
Ru(III)	10–15 mg of ascorbic acid	475 nm	0.54
Ru(III)	10–15 mg of sodium hypophosphite	475 nm	0.50
Ru(III)	None	475 nm	0.56
Ru(II)	Metallic zinc and acetic acid	475 nm	0.61

Table 3. Effect of pH on the formation of PDT-ruthenium(II) complex

pH of the buffer soln.	Buffer system	Corresponding λ_{max}	Absorbance at λ_{max}
2.5	Sodium acetate acetic acid and hydrochloric acids	475 nm	0.560
3.0	Sodium acetate/ acetic acid and hydrochloric acids	475 nm	0.575
4.0	Sodium acetate and acetic acid	475 nm	0.530
5.0	Sodium acetate and acetic acid	475 nm	0.450
6.0	Sodium acetate and acetic acid	475 nm	0.350
6.48	1*M* ammonium acetate	490–535 nm	0.290
9.0	1*M* ammonium chloride and ammonia solution	470–530 nm	0.240
11.0	Ammonia solution	510–540 nm	0.140

RESULTS AND DISCUSSION

Typical examples of the effect of variables on the rate and completeness of complexation are given in Tables 2–5. During the preliminary study, following the work of Banks and O'Laughlin[4], it was revealed that hydroxylammonium chloride seems to be quite unsuitable for the reduction of ruthenium(III) to ruthenium(II) prior to complexation with this type of reagent. It always gave variable absorbances and different wavelengths of maximum absorbance (λ_{max}) depending on the amount of reducing agent and heating time. The shift of the absorption maxima towards longer wavelengths was greater when the amount of hydroxylammonium chloride added was increased, or the amount of complexing agent was decreased. The value of absorbance also decreases with an increase of hydroxylammonium chloride. When no reducing agent, other than the complexing agent is present, ruthenium(III) always gives higher absorbances than with hydroxylammonium chloride and the wavelength of maximum absorbance remains constant.

Table 4. Effect of heating time on the formation of PDT-ruthenium(II) complex

Heating time (hours)	Corresponding absorbance at λ_{max}
0.25	0.490
0.50	0.515
0.75	0.530
1.00	0.550
1.50	0.550
2.00	0.560
2.50	0.560
3.00	0.560
3.50	0.565

With the hope of finding a suitable reducing agent for the reaction conditions, ascorbic acid and sodium hypophosphite were tried. With both reductants, the same wavelength of maximum absorbance was obtained as when no reducing agent was added. However the absorbances were lower than with it. At this stage, it was considered that either a ruthenium(III) complex was forming or the complexing agent itself was acting as a reducing agent. To clarify the matter, the 1,10-phenanthroline complex of ruthenium(III) or ruthenium(II) was formed with and without a reducing agent; each complex gave the same wavelength of maximum absorbance. Then the ruthenium(II) complex of 1,10-phenanthroline was prepared following the method of Dwyer and his coworkers.[12] The absorption spectrum of this complex solution and the complex solution developed without any added reducing agent were exactly the same. These observations suggest that the complexing agent and ethanol are enough to reduce ruthenium(III) to ruthenium(II).

During further study, it was observed that the freshly diluted solution of ruthenium(III) gives higher absorbances. This may be due to oxidation of ruthenium(III) to (IV) and/or to hydrolysis of the ruthenium(III) ions. Either the

Table 5. Effect of the amount of PDT on the formation of PDT–ruthenium (II) complex

X fold excess of PDT added	Corresponding absorbance at λ_{max}
8	0.555
16	0.555
24	0.560
32	0.560
40	0.570
48	0.575

hydrolysed species or ruthenium(IV), or both, may not be reduced to ruthenium(II) by the complexing agent or ethanol for complexation. To overcome this problem of hydrolysis or of oxidation, metallic zinc in the presence of acetic acid was tried for the reduction of ruthenium (III) or (IV). It always gave reproducible results and even higher values of absorbance than without any added reducing agent with the freshly diluted solution. Further studies were then carried out in which reduction with metallic zinc was incorporated into the experimental procedure.

These observations suggest the following possibilities: (i) the triazine molecule and ethanol are able to reduce ruthenium(III) to ruthenium (II), the preferred form for complexation, (ii) since all reducing agents used in this study except hydroxylammonium chloride give the same absorbance maxima, the hydroxylammonium ion may participate with the complexing agent to form a different ruthenium(II) complex, (iii) the lowering of the absorbance and the bathochromic shift of the λ_{max} with an increase of the hydroxylammonium ion and a lowering of the amount of triazine suggest that the hydroxylammonium ion is competing with the triazine molecule for complexation with ruthenium(II) under the experimental conditions and (iv) complete reduction of ruthenium species to ruthenium(II) by metallic zinc in the presence of acetic acid allows unhindered complexation with the triazine molecule and provides the highest overall absorption.

When the pH was varied by adding different buffer solutions, it was observed (Table 2) that in the case of the buffer system containing sodium acetate and acetic acid or hydrochloric acid within the pH range 2.5–6.0, the same absorption maximum was always obtained. The maximum absorbance occurred between 2.5-3.0 pH units. At higher pH, the absorbance gradually decreased. Buffer systems containing nitrogen species lead to further decreases in the absorbances and shifts of the absorption maxima towards longer wavelengths. Apparently, the larger the amount of the nitrogen-containing species in the buffer system, the lower is the absorbance and more pronounced is the bathochromic shift of the λ_{max}. It is clear from this observation that nitrogen-containing species in the buffer system are also taking part in complex formation with the ruthenium(II), as was the case with hydroxylammonium ion, resulting in a bathochromic shift of the λ_{max} and a lowering of the absorbance. The effect of heating time on the development of the colour suggests that the larger the complexing agent, the longer the heating time required for full colour development (Table 1); also that there is no advantage in prolonged heating. Since the ruthenium species is being reduced to ruthenium(II) prior to complexation, only a small excess of the reagent is required for full colour development. Kundra and his coworkers[10] report the use of a several-fold excess of ferrozine® and a three hour heating time for full colour development. This may be explained on the basis of its dual functionality as reducing and complexing agent. The results of the spectrophotometric measurements are summarised in Table 1.

Ruthenium(II) chromogens

3-(2-Pyridyl)-5,6-diphenyl-as-*triazine (PDT).* This compound has been re-evaluated as a ruthenium chromogen by the recommended procedures. It is by far the poorest of the ruthenium(II) chromogens tested in this study. The visible absorption spectrum of its ruthenium(II) complex [Fig. 1(a)] shows a single absorption peak at 475 nm with a molar absorptivity of 3.5×10^4. The composition of the complex has been determined by the mole-ratio method and it was observed that the ferroin-yielding PDT forms a tris-complex with ruthenium(II) acting as a bidentate ligand similar to its reaction with iron(II).[13] Incomplete reduction of ruthenium species to ruthenium(II) by the complexing agent and ethanol and hence incomplete complexation resulted in Karma and Ayres[7] obtaining a lower molar absorptivity of

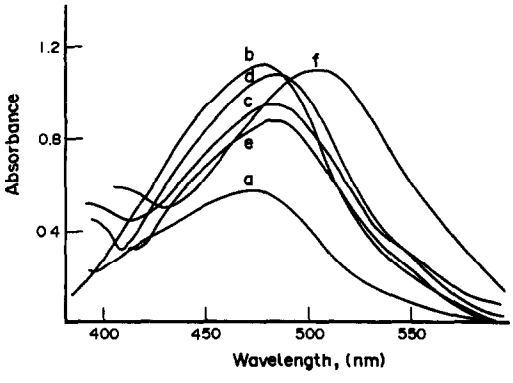

Fig. 1. Visible absorption spectra of ruthenium(II) complexes of (a) PDT, (c) PBBT, (d) PBBT–DAS and (e) PBMPT in aqueous-ethanol medium and (b) Ferrozine® and (f) Ferene® in aqueous medium recorded against reagent blanks in 1 cm glass cells at ruthenium concentrations of (a) 1.6 ppm, (b) 3.2 ppm, (c) 2.4 ppm, (d) 2.0 ppm, (e) 2.0 ppm and (f) 2.4 ppm.

2.1×10^4 at 485 nm. This also led them to the formulation of a bis-complex. The colour of the complex shows excellent stability.

Ferrozine®, the sulphonated derivative of PDT. The visible absorption spectrum of the ferrozine–ruthenium(II) complex shows a single absorption peak [Fig. 1(b)] at 478 nm with a molar absorptivity of 3.56×10^4 in aqueous medium. The sensitivity of this compound is comparable with that of PDT towards ruthenium(II) but its aqueous solubility is a significant advantage. It also forms a tris-complex with ruthenium(II) as with iron(II).[14] The reported λ_{max} (480 nm) by Kundra and his coworkers[10] is almost the same, but their molar absorptivity is lower. The higher value obtained and the lower heating time required in this study occur because the reagent itself is not sufficient to reduce the ruthenium species completely to ruthenium(II) for complexation. Incomplete reduction and hence complexation led them also to the formulation of a bis-complex. The commercial availability of the ferrozine® reagent, the high molar absorptivity and extreme stability of the complex in aqueous medium make the compound an effective chromogenic reagent for the determination of ruthenium.

3-(2-Pyridyl)-5,6-bis(4-biphenyl)-as-*triazine (PBBT).* This new compound, which contains a ferroin-functionality shows considerable promise as a ruthenium(II) chromogen. The molar absorptivity of 4.63×10^4 at 484 nm in aqueous-ethanol medium is much higher than PDT. The higher sensitivity and lower solubility in aqueous-ethanol medium compared to PDT system was predictable because of the presence of more phenyl groups. The biphenyl groups enhance the delocalisation of electrons in the molecule more than the phenyl groups and result in an increase in sensitivity and bathochromic shift of the λ_{max}. This reagent also forms a tris-complex of excellent colour stability.

PBBT–DAS, the sulphonated derivative of PBBT. This is the most sensitive reagent in this particular study. The spectrum of the ruthenium (II) chelate has a maximum at 485 nm [Fig. 1(d)] with a molar absorptivity of 5.5×10^4 in an aqueous-ethanol medium. The spectrum of the aqueous solution is very similar to that of an aqueous-ethanolic solution, but with a much lower sensitivity and solution stability. The molar absorptivity in aqueous medium is 4.3×10^4 at 485 nm. Precipitation of the complex was first noticed after about 12 hr of colour development. This may arise from the involvement of more aromatic rings. However, by developing the colour in aqueous medium and then diluting with ethanol, two advantages accrue: it gives excellent stability to the colour and increases the sensitivity from 4.3×10^4 to 5.5×10^4. This reagent also forms a tris-complex with ruthenium(II). The very high molar absorptivity and extreme stability of the complex in aqueous-ethanol medium make the compound the most effective spectrophotometric reagent so far reported for the determination of trace amounts of ruthenium. Ease of preparation of the parent compound and its sulphonation is an extra advantage.

*3-(2-Pyridyl)-5,6-bis(*p*-methoxyphenyl)*-as-*triazine (PBMPT).* The results for this compound (Table 1) show it to be an effective reagent for ruthenium(II). Its sensitivity, 4.7×10^4 at 483 nm, compares well with PBBT, which indicates that the methoxy group *para* to the phenyl group (*p*-methoxyphenyl) is as active or even better than the phenyl group (4-biphenyl) in enhancing the sensitivity of the reagent. This phenomenon has also been observed with iron(II).[3] Owing to the presence of the methoxy group, the compound and its metal chelate are highly soluble in aqueous-ethanol media. The colour of the complex solution is extremely stable; it will give the same absorbance, within experimental error, even after 45 days. The sensitivity, high solubility and ease of preparation of the compound[3] make this a particularly useful chromogenic reagent for ruthenium.

Ferene®. The spectrum of this ruthenium(II) chelate [Fig. 1(f)] has a maximum at 505 nm with a molar absorptivity of 4.63×10^4. Ferene forms a tris-complex with ruthenium(II) acting as a bidentate ligand similar to its reaction with iron(II).[11] Its sensitivity compares well with PBBT and PBMPT with an extra feature of aqueous solubility. Its sensitivity towards ruthenium(II) is much higher than ferrozine, but the colour of the complex is much less stable (around 48 hr). During this present investigation it has been observed that the ferene solution itself appears to be somewhat unstable under normal conditions and requires storage in the refrigerator. This lesser colour stability of the complex solution may be due to the decomposition of or change in the excess ferene molecules present in the system. However, commercially available Ferene® shows great promise as a possible chromogenic reagent for ruthenium.

CONCLUSION

Certain reagents with the ferroin-functional group can also serve as suitable and sensitive colour-forming reagents for the spectrophotometric determination of ruthenium(II). Complete reduction of ruthenium species to ruthenium(II) can be achieved before complexation by metallic zinc and acetic acid. The main conclusion to be drawn from the present study is that nitrogen-containing species either as a reducing agent or buffer component should not be used during the spectrophotometric determination of ruthenium with these type of reagents. The hydroxylammonium ion and perhaps the ammonium ion compete with the triazine molecule for complexation with the ruthenium(II) species under the experimental conditions. This casts doubt on the reliability of the existing procedures for the determination of ruthenium with this type of reagent. Some of the reagents employed are already commercially-available and others can be prepared easily from commercially-available reactants. The ease of preparation of PBBT, PBBT–DAS and PBMPT, the very high sensitivity and exceptional colour stability of their chelates make these and others very effective reagents for the spectrophotometric determination of trace amounts of ruthenium.

Acknowledgements—M. A. Islam thanks the Association of Commonwealth Universities for the award of a scholarship and the University of Dhaka, Bangladesh for granting leave of absence after the scholarship. He also gratefully acknowledges the help, encouragement and keen interest of Dr. Colin L. Graham in the final year of study.

REFERENCES

1. B. Morelli, *Analyst*, 1983, **108**, 386.
2. *Idem*, *Anal. Letters*, 1986, **19**, 503.
3. M. A. Islam, Ph.D. Thesis, University of Birmingham, 1990.
4. C. V. Banks and J. W. O'Laughlin, *Anal. Chem.*, 1957, **29**, 1412.
5. O. A. Vita and C. F. Trivisonno, *Nucl. Appl.*, 1965, **1**, 375.
6. W. A. Embry and G. H. Ayres, *Anal. Chem.*, 1968, **40**, 1499.
7. L. C. Karma and G. H. Ayres, *Anal. Chim. Acta*, 1975, **78**, 423.
8. A. A. Schilt, W. E. Dunbar, B. W. Gandrud and S. E. Warren, *Talanta*, 1970, **17**, 649.
9. A. A. Schilt, C. D. Chriswell and T. A. Fang, *ibid.*, 1974, **21**, 831.
10. S. K. Kundra, M. Katyal and R. P. Singh, *Curr. Sci.*, 1975, **44**, 548.
11. F. E. Smith and S. L. Thompson, D. J. Hennessy and G. R. Reid, *Can. J. Chem.*, 1984, **82**, 721.
12. F. P. Dwyer, J. E. Humpoeltz and R. S. Nyholm, *J. Proc. Roy. Soc. N.S. Wales*, 1947, **80**, 212.
13. C. D. Chriswell and A. A. Schilt, *Anal. Chem.*, 1974, **46**, 992.
14. L. L. Stookey, *ibid.*, 1970, **42**, 779.

Talanta, Vol. 39, No. 11, pp. 1437–1442, 1992
Printed in Great Britain.

0039-9140/92 $5.00 + 0.00

REVERSED-PHASE LIQUID CHROMATOGRAPHY OF ALKALOIDS: MASKING EFFECTS OF INORGANIC SALTS

WASSILY NOWICKY, LIANG-FENG HAN, WLADYSLAWA NOWICKY, VIKTOR GUTMANN* and WOLFGANG LINERT

Institute of Inorganic Chemistry, Technical University of Vienna, Getreidemarkt 9, A-1060 Vienna, Austria

(*Received* 19 *February* 1992. *Accepted* 5 *March* 1992)

Summary—The addition of salts (investigated cations Na^+, NH_4^+, K^+, KBu_4^+ combined with the anions acetate, Br^-, SCN^- and I^-) can be used to eliminate peak tailing and to decrease retention of cationic species in the course of the separation of alkaloids from Chelidonium majus L. by reversed-phase chromatography on a ODS Hypersil column, using water–acetonitrile–methanol mixture as eluent. These findings are interpreted in terms of a silanol masking effect. The extended donor–acceptor concept is used to interpret the effectiveness of different salts in masking the active sites of the stationary phase.

Reversed-phase high-performance liquid chromatography is usually not applicable to compounds with unprotected basic atoms.[1] This is believed to be due to interactions between the basic compounds and the acidic silanol groups at the stationary phase surface.[2–6] By addition of organic amines or ammonium salts to the mobile phase the separation behaviour can be improved, and in some cases the selectivity of the stationary phase is altered.[2,5–15] Recently, it has been shown that for the separation of alkaloids in chelidonium majus L. by means of reversed phase liquid chromatography, peak shape and resolution are improved in the presence of potassium iodide.[15] The effect of such addition can be explained on the basis of masking active silanol groups of the stationary phase. This led us to investigate the influence of salts–additives with cations and anions of different softness, namely Na^+, NH_4^+, K^+ and NBu_4^+ and acetate, Br^-, SCN^- and I^-, respectively.[16–18]

EXPERIMENTAL

Apparatus and materials

The chromatographic system consisted of a Hewlett-Packard (Palo Alto, CA., U.S.A.) Model 1090 Liquid Chromatograph, equipped with a HP Model DR5 Solvent Delivery System, and a HP 1090 option 44 Auto-injector. Detection was performed with a HP 1090 option 80 UV Diode-array Detector. An ODS Hypersil column (RP C^{18}, Hewlett-Packard) (100 × 4.6 mm I.D., 5-μm particle size) was used.

Acetonitrile (LiChrosolv, Merck, Darmstadt, F.R.G.), methanol (Reinst, Merck) and water (Chromasolv for gradient elution, Riedel-de Haen, Seelze, F.R.G.), sodium thiocyanate (Merck), potassium thiocyanate (Merck), sodium acetate (Merck), ammonium acetate (Merck) and potassium bromide (Merck) were of analytical reagent grade. Tetrabutylammonium iodide (NBu_4I) was prepared in our laboratory. The following standard alkaloids have been kindly supplied, namely: sanguinarine, allocryptopine by L. Jusiak (Lublin, Poland); methoxychelidonine, oxysanguinarine, dihydrosanguinarine, dihydrochelerythrine, (−)-stylopine by J. Slavik and L. Slavikova (Brno, CSFR.); berberine and protopine by W. Debska (Poznan, Poland); chelidonine by the late F. Kuffner (Vienna, Austria). The structures of these alkaloids are given in Fig. 1.

Plants of Chelidonium majus L. were collected from fields near Vienna, Austria. The extraction of the alkaloids from Chelidonium majus L. was carried out as described recently.[18] Standard alkaloids were dissolved in methanol at concentrations of 0.3 mg/ml and stored in airtight flasks in the dark. Water was adjusted to pH 3.6 with acetic acid (3.8m*M*) or to pH 8.5 with sodium hydroxide. Methanol contained appropriate concentrations of the respective inorganic salt. A mixture of 45% water, 25% acetonitrile and 30% methanol was used and a flow-rate of

*Author for correspondence. Dedicated to Prof. Tom S. West on the occasion of his 65th birthday in grateful memory of his stay in Vienna in 1961 and 1962.

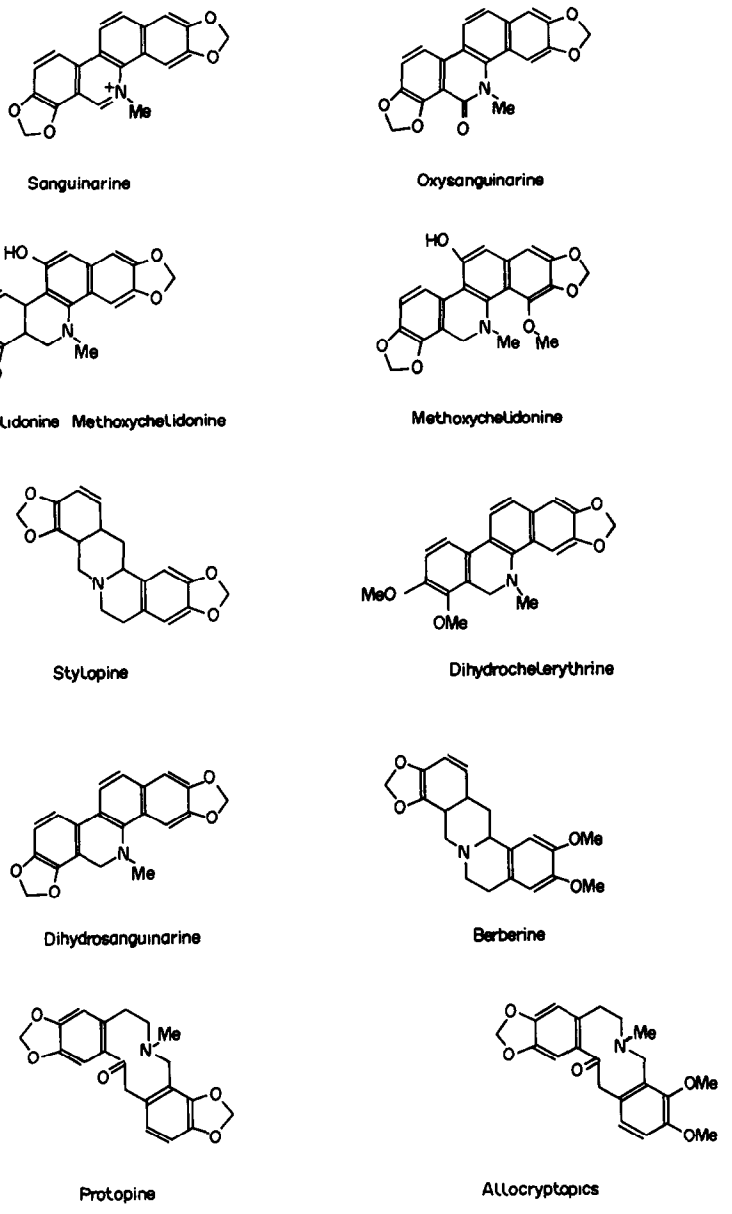

Fig. 1. Structures of the ten alkaloids from Chelidonium majus L.

1.2 ml/min employed, unless stated otherwise. Because of the low buffering capacity of the mobile phases, only 0.1–2 μl of the solute were injected. The chromatograms were taken at 30° and monitored at 285 nm with a band-width of 30 nm. The reference wavelength was 400 nm with a band-width of 100 nm. Retention time data were measured from the peak minima.

RESULTS AND DISCUSSION

Effect of type and concentration of the added salts

Without addition of salts strong peak tailing was found for most of the cationic alkaloids. Many of them could not be eluted with salt free water–acetonitrile–methanol mixtures. Uncharged alkaloids, produce almost symmetrical peaks without added salt and the peak performance is not affected by the addition of salts. Figure 2 shows the influence of increasing concentration of the investigated salts in the mobile phase on the retention of allocryptopine, at pH = 3.6 and at pH = 8.5. Allocryptopine was selected as a test compound because of its wide spread of retention properties at pH = 3.6–8.5. In all cases the capacity factor k' of the alkaloid was decreased and the peak tailing becomes smaller with increasing salt concentration. Salts with soft anions or soft cations

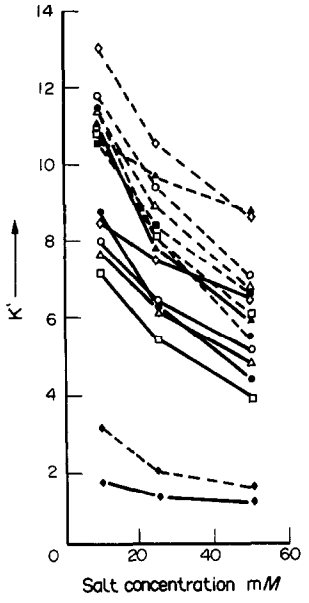

Fig. 2. Effect of the nature of the salt additives in the mobile phase on the capacity factor of allocryptopine. Eluent: 3.8m*M* acetic acid (pH 3.6)–acetonitrile–methanol (45:25:30 —full lines); water (pH 8.5)–acetonitrile–methanol (45:25:30 —dashed lines). Salts: --◇-- NaOAc; --○-- KBr; --△-- KI; --□-- NH_4OAc; --▲-- NaSCN; --■-- NH_4SCN; --○-- KSCN; --◆-- NBu_4I.

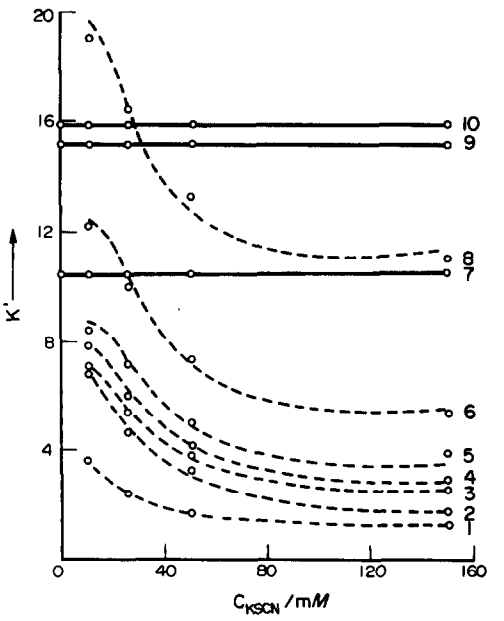

Fig. 3. Influence of potassium thiocyanate concentration on the capacity factors, *k'*, for the ten alkaloids. Compounds: 1 = methoxychelidonine; 2 = chelidonine; 3 = allocryptopine; 4 = protopine; 5 = (-)-stylopine; 6 = berberine; 7 = oxysanguinarine; 8 = sanguinarine; 9 = dihydrochelerythrine; 10 = dihydrosanguinarine. Eluent: 3.8m*M* acetic acid–acetonitrile–methanol (45:25:30; pH 3.6). Dashed lines represent calculated curves.

(*e.g.*, tetrabutylammonium iodide) have greater influence than salts with hard anions or hard cations (*e.g.*, sodium acetate). The influence was greater as the softness of both cations and anions was increased.

Figure 3 shows the variation of capacity factors, *k'*, with the mobile phase concentration of potassium thiocyanate for ten alkaloids from Chelidonium majus L. Addition of potassium thiocyanate decreases the capacity factor for most of the alkaloids. The retention times of most alkaloids is also decreased with increasing concentration of potassium thiocyanate but dihydrochelerythrine, dihydrosanguinarine and oxysanguinarine were not affected. Because the latter alkaloids can be extracted easily into organic solvents even from acidic aqueous solution[19] they may be present as free bases under the above given chromatographic conditions. Potassium thiocyanate (Fig. 4) effects the retention of chelidonine, sanguinarine, allocryptopine and protopine. Methoxychelidonine and (−)-stylopine are not affected at this pH value, indicating again their presence as free bases. At a pH = 8.5 and $c_{KSCN} > 130$m*M* the alkaloids allocryptopine and protopine were eluted before methoxychelidonine. This indicates that the unprotected nitrogen atoms play an important role in the retention mechanism of the nitrogen-containing samples in a reversed-phase system.

At an unmodified silica surface the retention of the cationic alkaloids approaches zero as the concentration of sodium acetate is drastically increased.[20] This suggests two kinds of adsorption

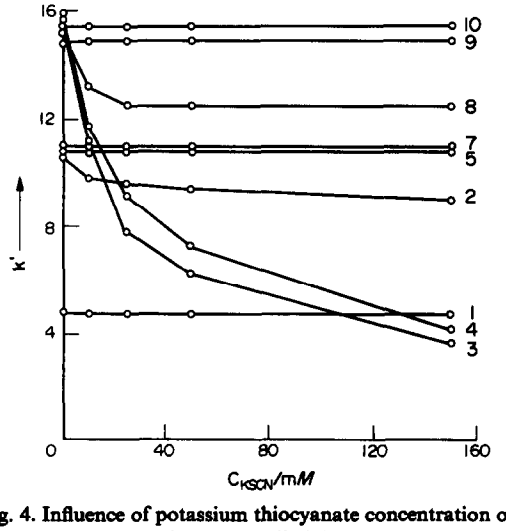

Fig. 4. Influence of potassium thiocyanate concentration on the capacity factors, *k'*, for the alkaloids. Compounds as in Fig. 3. Eluent: water–acetonitrile–methanol (45:25:30; pH 8.5).

sites in the reversed-phase system, one on which uncharged samples are predominantly retained with potassium thiocyanate, and a second one on which potassium thiocyanate competes with the cationic samples.

According to these findings the following equilibria may influence the retention procedure:

$$Q_m^+ + Z_m^- + A_s \rightleftarrows QZA_s \quad (1)$$

$$Q_m^+ + A_s^* \rightleftarrows QA_s^* \quad (2)$$

$$B_m^+ + Z_m^- + A_s^* \rightleftarrows BZA_s^* \quad (3)$$

In this Q_m^+ represents a cationic alkaloid present in the mobile phase. Z_m^- and B_m^+ are anions and cations respectively of an added salt. A_s are adsorption sites, which remain unaffected by added salt and A_s^* are salt-influenced adsorption sites. The subscripts m and s refer to mobile phase or stationary surface, respectively. The species in the mobile phase are distributed to the stationary phase where they occupy areas, A_s or A_s^*. The equilibrium constants for these processes are:

$$K_{QZ} = [QZA_s]/\{[Q_m^+][Z_m^-][A_s]\} \quad (3)$$

$$K_Q^* = [QA_s^*]/[Q_m^+][A_s^*] \quad (4)$$

$$K_{BZ}^* = [BZA_s^*]/\{[B_m^+][Z_m^-][A_s^*]\} \quad (5)$$

Quantities with and without asterisk refer to adsorption sites A_s and A_s^*, respectively. Concentrations in the mobile phase are in molar and concentrations in the stationary phase are expressed in moles/g of solid phase. $[A_s]$ and $[A_s^*]$ are the concentration of free adsorption sites of moles/g of solid phase at equilibrium. (Acetate is omitted in the case pH = 3.6 because it has only small effect on the peak tailing.)

It can be assumed that the capacity factor, k'_Q, of the eluate Q^+ bound to the stationary phase can be expressed as the sum of the capacity factors for the two processes:

$$k'_{Q'} = k'_{Q,A} + k^*_{Q,A} \quad (6)$$

The capacity factors of Q^+ ($k'_{Q,A}$) depend on the phase-ratio W_s/V_m and the distribution ratios:

$$k'_{Q,A} = \frac{W_s[QZA_s]}{V_m[Q_m^+]} \quad (7)$$

$$k'_{Q,A^*} = \frac{W_s[QA_s^*]}{V_m[Q_m^+]} \quad (8)$$

where the phase-ratio is the ratio of the solid phase to the mobile phase in the column given in g/l. The stationary phase has limited adsorption capacities which are characterized by K_0 and K_0^*, respectively:

$$K_0 = [A_s] + [QZA_s] \quad (9)$$

$$K_0^* = [A_s^*] + [QA_s^*] + [BZA_s^*] \quad (10)$$

A combination of equations (3)–(10) yields

$$k'_Q = \frac{W_s K_0 K_{QZ}[Z_s^-]}{V_m(1 + K_{QZ}[Q_m^+])} + \frac{W_s K_0^* K_Q^*}{V_m(1 + K_Q^*[Q_{mm}^+] + K_{BZ}^*[B_m^+][Z_m^-])} \quad (11)$$

It is assumed that $K_{QZ}[Q_m^+]$ in the first term can be omitted at sufficiently low sample concentration leading to:

$$k'_Q = \frac{W_s K_0 K_{QZ}[Z_m^-]}{V_m} + \frac{W_s K_0^* K_Q^*}{V_m\{1 + K_Q^*[Q_m^+] + K_{BZ}^*[B_m^+][Z_m^-]\}} \quad (12)$$

Equation (12) shows that the capacity factor increases with decreasing alkaloid concentration and leads to peak tailing. The competing effect by an added salt on the distribution of the sample at the adsorption sites A_s^* decreases the influence of the term containing the sample concentration in equation (12), because the significance in equilibrium (2) is decreased. At sufficiently high concentration of an added salt, the second term in equation (12) can be simplified so that peaks become symmetrical as observed:

$$k'_Q = \frac{W_s K_0 K_{QZ}[Z_m^-]}{V_m} + \frac{W_s K_0^* K_Q^*}{V_m\{1 + K_{BZ}^*[B_m^+][Z_m^-]\}} \quad (13)$$

Equation (13) is non-linear in $[B^+]$ and $[Z^-]$ and contains the concentrations of the added salt in its cationic and anionic form as independent variables. For a given solute, when the eluent composition and flow-rate are unchanged at constant temperature with a fixed column, the terms $W_s K_0 K_{QZ}/V_m$, $W_s K_0^* K_Q^*/V_m$ and K_{BZ}^* are invariant. Hence, for each cationic solute the values of $W_s K_0^* K_{QZ}^*/V_m$, $W_s K_0^* K_Q^*/V_m$ and K_{BZ}^* can be fitted by a non-linear least square regression. The fitted lines show good agreement with the experimental values (dashed lines in Fig. 3). The term K_{BZ}^*, which is the equilibrium constant for the adsorption of the added salt on the adsorption sites A_s^*, remains fairly constant, whereas the other two terms changes for different samples. The values of $W_s K_0 K_{QZ}/V_m$,

Table 1. $W_s K_0 K_{QZ}/V_m$, $W_s K_0^* K_Q^*/V_m$ and K_{BZ}^* values calculated to produce the best fit of experimental data. For chromatographic conditions see Fig. 4

Solute	$W_s K_0 K_{QZ}/V_m$	$W_s K_0^* K_Q^*/V_m$	K_{BZ}^*
Methoxychelidonine	32	2.9	8175
Chelidonine	57	5.7	564
Allocryptopine	69	6.1	9
Protopine	76	6.7	7655
(−)-Stylopine	129	7.1	6935
Berberine	175	10.5	7606
Sanguinarine	383	15.0	6922

$W_s K_0^* K_Q^*/V_m$ and K_{BZ}^* calculated for the cationic solutes of the alkaloids at pH of 3.6 are summarized in Table 1. On the other hand it should be pointed out that an ion-pair formation model[12] leads to equations which cannot be brought into accordance with the experimental results.

The less satisfactory curve fits for both tertiary and quarternary alkaloids at higher pH value may be due to heterogeneity of the stationary phase in the presence of residual silanol groups. At pH > 4.5 a dissociation of the acidic silanol groups may occur. This results in a retardation owing to the ion-exchange effect.[21] The general retention decreases for the cationic alkaloids at lower pH values (Figs. 2–4). This can be explained by decreasing dissociation of the acidic silanol groups at lower pH value so that the ion-exchange effect is mainly prevented in this case. In contrast to the cationic species the retention of the uncharged species was found to be independent from the pH values (Figs. 3 and 4).

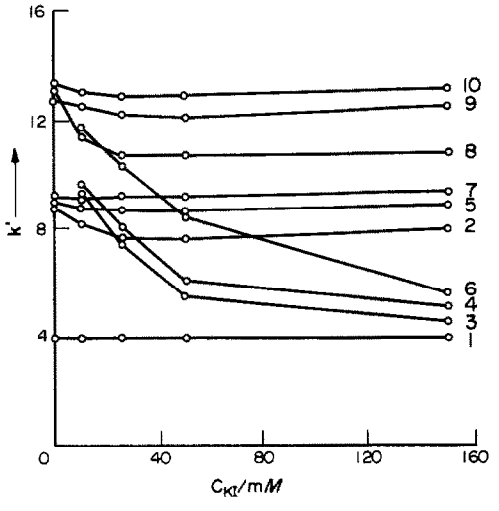

Fig. 5. Influence of potassium iodide concentration on the capacity factors, k', for the alkaloids. Compounds as in Fig. 3. Mobile phase: water (pH 8.5)–acetonitrile–methanol. Potassium iodide was added to methanol. Gradient: water–acetonitrile–methanol = 50:20:30 to 20:50:30 in 15 min. Flow-rate 0.8 ml/min to 1.5 ml/min in 15 min.

Selectivity of separation

It has been noted, that with an inorganic salt added to the mobile phase the alkaloids were eluted faster, together with better peak symmetry and increase in peak resolution. In our previous study[18] good separation was achieved by adding 150mM potassium iodide to the eluent and by using an appropriate gradient elution program. Figure 5 illustrates the capacity factors of ten alkaloids from Chelidonium majus L. obtained after addition of potassium iodide to the eluent and application of a gradient elution program. It can be seen that the alkaloids, except for allocryptopine, berberine and protopine, are eluted in the same order with all concentrations of potassium iodide. Elution times of the cationic samples decrease as the concentration of the added salt is increased while alkaloids presumably present as free bases show only small changes. Thus retention can be controlled by

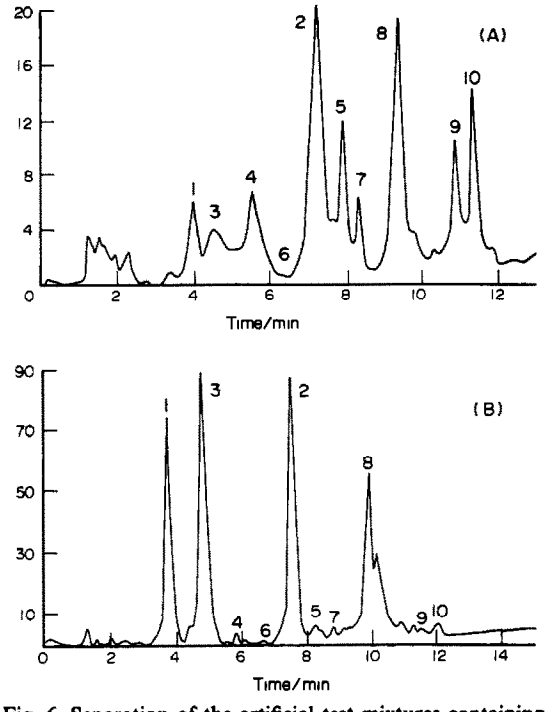

Fig. 6. Separation of the artificial test mixtures containing ten alkaloids and the crude drug extract of Chelidonium majus L. by reversed-phase HPLC. Chromatographic conditions as in Fig. 6. (A) Chromatogram of the artificial test mixture containing ten alkaloids. Potassium iodide 0.15M was added to methanol; (B) chromatogram of the crude drug extract of Chelidonium majus L. 0.15M potassium iodide was added to methanol.

selection of an appropriate salt concentrtion. Figure 6(a) shows a chromatogram of a test mixture of ten alkaloids from Chelidonium majus L. at a potassium iodide concentration of 150m*M*. Figure 6(b) shows a chromatogram of a crude extract from Chelidonium majus L. under the same chromatographic conditions as in Fig. 6(a).

Buytenhuys *et al.*[22] have shown that sodium chloride, sodium acetate, ammonium acetate, potassium acetate and tetramethylammonium acetate are increasingly adsorbed in the given order at pH of 5 on unmodified silica in aqueous solvents. The salts are adsorbed on the silica surface as neutral molecules because under the above-given conditions no ion-exchange process accrues [this is also confirmed by the good fit of the experimental data with equation (13)].[21] According to the similarity rules of the HSAB-concept, hard–hard interactions and soft–soft interactions lead to more stable compounds than hard–soft interactions. The "softer" the cation of the salt with a given anion, the stronger pronounced is its acceptor ability towards the oxygen atom of the silanol group. Consequently, the "softer" the cation, the stronger it will reduce the retention of the alkaloids.[22] The retention order of allocryptopine upon added salts is in agreement to the adsorption ability of the respective salts (Fig. 2).

Acknowledgement—This investigation has been carried out under contract by the "Bundesministerium für Wissenschaft und Forschung" in Österreich.

REFERENCES

1. P. J. Twitchett and A. C. Moffat, *J. Chromatogr.*, 1975, **111**, 149.
2. F. P. B. Van der Maeden, P. T. Van Rens and F. A. Buytenhuys, *ibid.*, 1977, **142**, 715.
3. W. R. Melander, J. Stoveken and Cs. Horvath, *ibid.*, 1980, **199**, 35.
4. A. Nahum and Cs. Horvath, *ibid.*, 1981, **203**, 53.
5. K. Bij, Cs. Horvath, W. Melander and A. Nahum, *ibid.*, 1981, **203**, 65.
6. R. Grill, S. P. Alexander and A. C. Moffat, *ibid.*, 1982, **247**, 39.
7. I. M. Johansson, K. G. Wahlund and G. Schill, *ibid.*, 1978, **149**, 281.
8. K. G. Wahlund and A. Sokolowski, *ibid.*, 1978, **151**, 299.
9. W. R. Melander, J. Stoveken and C. Horvath, *ibid.*, 1979, **185**, 111.
10. D. Westerlund and E. Erixson, *ibid.*, 1979, **185**, 593.
11. M. G. M. de Ruyter, R. Cronelly and N. Castagnoli *ibid.*, 1980, **183**, 193.
12. A. Sokolowski and K. G. Wahlund, *ibid.*, 1980, **189**, 299.
13. C. T. Hung, R. B. Taylor and N. Paterson, *ibid.*, 1982, **240**, 61.
14. A. Wehrli, J. C. Hildenbrand, H. P. Keller, R. Stampfi and R. W. Frei, *ibid.*, 1978, **149**, 199.
15. L. F. Han, W. Linert and V. Gutmann, *Chromatogr. Sci*, 1992, in the press.
16. V. Gutmann, *The Donor Acceptor Approach to Molecular Interactions*. Plenum Publ. Co., N.Y., 1978.
17. R. G. Pearson, *J. Am. Chem. Soc.*, 1963, **85**, 3533.
18. L. F. Han, W. Nowicky and V. Gutmann, *J. Chromatogr.*, 1991, **543**, 123.
19. J. Slavik and L. Slavikova, *Coll. Czech. Chem. Commun.*, 1977, **42**, 2686.
20. C. Bugatti, M. L. Colombo and F. Tome, *J. Chromatogr.*, 1987, **393**, 312.
21. J. H. Knox and A. Pryde, *ibid.*, 1975, **112**, 171.
22. F. A. Buytenhuys and F. P. B. Van der Maeden, *ibid.*, 1978, **149**, 489.

Talanta, Vol. 39, No. 11, pp. 1443–1448, 1992
Printed in Great Britain.

0039-9140/92 $5.00 + 0.00

COMPARISON OF A MODIFICATION OF THE ELLMAN METHOD TO MEASURE CARBAMATE INHIBITION OF ACETYLCHOLINESTERASE IN PLASMA, ERYTHROCYTES AND BRAIN TISSUES IN SPRAGUE DAWLEY RATS USING TWO ANALYTICAL SYSTEMS

ROY M. DAGNALL,* SUSAN M. BJORN, GLORIA T. LAU, JANET A. TRUTTER, RICHARD D. ALSAKER and SUSAN A. LEWIS

Hazleton Washington, Inc., 9200 Leesburg Pike, Vienna, VA 22182, U.S.A.

HELEN C. CUNNY

Rhone-Poulenc, 2 TW Alexander Drive, Research Triangle Park, NC 27709, U.S.A.

(*Received* 15 *March* 1992. *Accepted* 31 *March* 1992)

Summary—Inhibition of the enzyme acetylcholinesterase (AChE) using a carbamate compound was measured in 30 Crl: CD®BR Sprague Dawley rats. Erythrocyte, plasma, and brain tissues were analyzed using modifications of the Ellman technique[1] on two different clinical chemistry analyzers. Both EDTA and heparin anticoagulated whole blood were used for the erythrocyte and plasma tests. Results demonstrated similar inhibition of the enzyme in all three tissues between the control and dosed groups using the two technique modifications and instruments. Final inhibition of plasma and erythrocyte AChE for the control *vs.* treated groups (males and females combined) was 89.5% *vs.* 82% and 39% *vs.* 38% for the Technicon AutoAnalyzer® *vs.* the Boehringer Mannheim Hitachi® 704, respectively. Inhibition of the left and right brain segments for the control *vs.* treated groups (males and females combined) was 35% *vs.* 39% and 33.2% *vs.* 29% for the Technicon and the Hitachi, respectively. All inhibitions were significant at the 5% level using two tailed Dunnett's *t*-Test. Hemolysates prepared from EDTA whole blood packed cells gave more consistent results on the Hitachi 704.

In the product safety and effectiveness testing arena, evaluation is traditionally assessed by determining the effects of the test material on changes in the physiologic parameters of the animal model. Compounds tested range from materials that will be added to foods for consumption, pharmaceuticals and agricultural chemicals. In the latter case, the evaluations of compounds that will be used in pesticides must assure both the safety of the user and the efficacy of the pesticide. A high-profile test in pesticide evaluation, particularly in carbamate- and organophosphate-based compounds, is the measurement of the inhibition of the enzyme, AChE.

A number of techniques, both manual and automated, are currently used to measure AChE activity in erythrocytes, plasma and the brain. Several kits are manufactured, and most commonly, the methodology is based on the Ellman technique or modification of that technique.[1] Some investigators using this basic technique maintain that measurement of whole blood hemolysates rather than packed cell hemolysates is more effective in measuring erythrocyte AChE inhibition. Considerable controversy exists in the industry concerning appropriate analytical methods that will standardize the assay of AChE. However, automated analysis provides a cost effective method for evaluating the enzyme inhibition on large numbers of samples collected at one time.

The accurate measurement of inhibition induced by carbamate-based compounds presents unique challenges because of the rapid reversal of this effect. Rapid processing and automated analytical methods are thus preferred. A further difficulty in the testing of the animal model is the occurrence of varied responses in tissues from different animal species. Techniques generally require adjustment of the original substrate concentrations, reaction temperature, and pH of the reaction system to maximize the AChE inhibition in given tissues and species.

*Author for correspondence.

This investigation was designed to compare inhibition of the AChE in plasma, erythrocyte, and brain tissue of rats using both an internally developed modification of the Ellman technique on a Technicon Single channel AutoAnalyzer System (considered the reference system in this case) and a modification of the Reagent Set Cholinesterase® Kit by Boehringer Mannheim Corporation, Inc.[2] on the Boehringer Mannheim Hitachi 704 Chemistry Analyzer.

EXPERIMENTAL

Equipment and materials

The following equipment and materials were used: Hitachi 704 Chemistry Analyzer, Boehringer Mannheim Corporation, Indianapolis, IN, U.S.A. Technicon AutoAnalyzer, Technicon Corporation, Tarrytown, NY, U.S.A. BMD Reagent Set Cholinesterase Kit No. 124117, Boehringer Mannheim Corporation, Indianapolis, IN, U.S.A. Potassium phosphate, monobasic, anhydrous, Sigma Chemical Co., St Louis, MO, U.S.A. Sodium phosphate, dibasic, anhydrous, Sigma Chemical Co., St. Louis, MO, U.S.A. Triton-X-100, Sigma Chemical Co., St Louis, MO, U.S.A. Precitrol Normal and Precitrol Abnormal Control Sera, Boehringer Mannheim Corporation, Indianapolis, IN, U.S.A. ICN Digiflex® Automatic Pipette Dilutor. Temperature controlled centrifuge. Analytical balances. Magnetic and vortex mixers. Adjustable semiautomated pipette and pipette tips. Volumetric and serolog ical pipettes. Electric tissue grinder. Trizma Base, (Tris[hydroxymethyl]amino-methane) Sigma Chemical Co., St Louis, MO, U.S.A. 5,5-Dithiobis-(2-nitrobenzoic acid), DTNB Sigma Chemical Co., St Louis, MO, U.S.A. Cholinesterase Acetyl (EC 3.1.1.7) Sigma Chemical Co., St Louis, MO, U.S.A. Reduced Glutathione, Sigma Chemical Co., St Louis, MO, U.S.A. Sodium Chloride, Sigma Grade, Anhydrous, Sigma Chemical Co., St Louis, MO, U.S.A. Demineralized water. Brij®-35, 30% Solution Aqueous, Fisher Scientific.

Procedure for the Hitachi 704 Chemistry Analyzer

Reagents. Stock phosphate buffers were prepared by dissolving 9.0727 grams of monobasic potassium phosphate in one litre of demineralized water and 14.2 grams of anhydrous dibasic sodium phosphate in one litre of demineralized water. The working phosphate buffer was prepared by mixing 55 ml of the potassium phosphate stock with 945 ml of the sodium phosphate solution, adjusting the final pH to 8.0 (+/−0.05) and adding 100 μl of Triton X-100 to each 100 ml.

Triton-saline solution, used in the processing of brain tissue, was prepared by adding 100 μl of Triton X-100 to 100 ml of isotonic saline and mixing until complete dissolution was achieved.

The Hitachi analyzer procedure required two reagents, R1 and R2. These are prepared from reagents supplied in the BMD Reagent Set Cholinesterase Kit.

R1 working solution was prepared by dissolving the contents of one bottle (buffer/chromogen) with 100 ml of demineralized water.

Stock R2, the substrate, was prepared by dissolving the substrate provided with the kit with 30 ml of demineralized water. For working R2 substrates, one ml of the working substrate solution was diluted with two ml of demineralized water.

Procedure for the Technicon AutoAnalyzer

Reagents. Tris buffer was prepared using 6.05 g of Tris[hydroxymethylamino]methane, 6.65 g of sodium chloride, 40 ml of 1*N* hydrochloric acid, and approximately 975 ml of demineralized water. The buffer was adjusted to a pH of 7.50 (+/−0.05) at room temperature and adjusted to a volume of one litre with demineralized water. Immediately prior to use, 0.5 ml of Brij-35 was added to the buffer.

DTNB was prepared by dissolving 100 mg of DTNB in one litre of the Tris buffer adding the Brij-35 just prior to use. This was prepared fresh for each run.

Acetylthiocholine iodide (5m*M*) was prepared for use as the substrate in the analysis of the brain tissue. Acetylthiocholine iodide (10m*M*) was prepared for use as the substrate in the analysis of the plasma and erythrocyte samples.

A stock 100μM/ml reduced glutathione standard was prepared with demineralized water. Working standards of 1, 3, 5, 7, 9 and 10μM were prepared from the stock standard just prior to a run and were used to prepare the standard curve. Standards were run approximately every 30 samples, along with controls and water blanks to minimize carry over from the 10μM standard.

Table 1. Instrument settings for the Hitachi 704

Chemistry parameters	
Test name	[PCHE] or [RBCHE] or [BCHE]
Assay code	[RATE-A]:[19]-[22]
Sample volume	[5]
R1 volume	[500][50][NO]
R2 volume	[50][20][NO]
Wavelength 1	[660][480]
Calib. method	[K FACTOR] [0][0]*
STD. (1)	[0]-[1]
STD. (2)	[0]-[0]
STD. (3)	[0]-[0]
STD. (4)	[0]-[0]
STD. (5)	[0]-[0]
STD. (6)	[0]-[0]
UNIT	[U/L]
SD Limit	[0.1]
Duplicate limit	[100]
Sensitivity limit	[0]
Abs.limit (INC/DEC)	[25000][INCREASE]
Prozone limit	[0][LOWER]
Expected value	[0]-[999]
Instrument factor	[1.0]
Temperature	37°

*Calculation based on total reagent volume per analysis.

Study design

Thirty animals, fifteen males and fifteen females, were selected for the study. Animals weighing less than 300 grams were not used. The study animals were assigned to two groups (Groups 1 and 2) using computer-generated random numbers: five males and five females to control group 1; 10 males and 10 females to treatment group 2. The treatment dose carbamate of an insecticide was selected to produce significant AChE inhibition with no morbidity, and blood and brain samplings were performed after at least 12 (males) or 5 (females) weeks of dosing. Blood was collected from the orbital sinus after animals were anesthetized with CO_2/O_2 and assayed for plasma and erythrocyte AChE activities. There were two blood sampling intervals six days apart. Brain tissues were harvested from all animals sacrificed (using sodium pentobarbital anesthesia and exsanguination) on the day of the second blood collection. Left and right brains were isolated, placed in 50-ml screw cap conical centrifuge tubes and snap frozen in a preparation of methanol and dry ice. They were transported on dry ice to the laboratory and stored in a −70°F freezer pending analysis.

Sample processing

Samples for the erythrocyte and plasma analyses were collected in both EDTA and heparin anticoagulants. The Technicon procedure uses heparinized whole blood. The Boehringer Mannheim Diagnostics procedure recommends EDTA anticoagulated whole blood. Consequently, parallel testing involved analyzing both types of anticoagulated whole blood for the isolation of plasma and erythrocytes to determine if either offered a significant advantage.

The orbital sinus plexus was used as the collection site for all plasma and erythrocyte AChE assays. Animals were not fasted (feed and water) prior to sample collection. Samples were collected and transported on a slurry of crushed ice and water to help retard reversal of the carbamate inhibition. Transport to the clinical laboratory occurred within 15 min of collection. Samples were centrifuged upon arrival at 5° at 4000 rpm for 10 min to separate the plasma. For the Technicon procedure, male rat plasma was diluted 1:2 prior to analysis and female plasma was diluted 1:4. No dilution of the plasma was required for the assay on the Hitachi 704. Plasma samples were analyzed immediately after appropriate processing.

The standard procedure for the Technicon required washing the erythrocytes in isotonic saline in graduated conical centrifuge tubes prior to analysis. The supernatant was removed after recording of the packed cell volume (PCV), and saline was added to the cells to achieve a 1:4 dilution. All cell preparations were maintained at 5° and mixed with a transfer pipette just prior to uptake by the analyzer. This dilution was then analyzed at 37° on the AutoAnalyzer.

A 1:21 dilution of the original packed cells was prepared for the Hitachi 704 analysis. Using the Digiflex® Automatic Dilutor, 100 μl of packed cells and 2000 μl of pH 8.0 phosphate buffer with 0.1% Triton X-100 were flushed into a 13 mm × 100 mm test tube. The resulting hemolysate was vortexed to ensure clarity. Samples were maintained at 5° throughout the diluting and processing steps. Each hemolysate was again vortexed briefly immediately prior to placing in the instrument sample cup in position for sample uptake by the instrument. The analysis then proceeded at 37° based on programmed sample and reagent volumes and incubation times, as shown in the outline of the System Parameters in Table 1.

The brain tissues homogenates were prepared in cold isotonic saline with 0.1% Triton X-100 using a Wheaton® tissue grinder. The resulting dilution in saline was 1:20 based on brain weight. The homogenates were maintained at 5° throughout the grinding and diluting process.

Table 2. Plasma and erythrocyte AChE Technicon AutoAnalyzer, μM/ml

Sample 1 males	Plasma controls	Treated	RBC controls	Treated	Sample 2 males	Plasma controls	Treated	RBC Controls	Treated
X	2.0	0.3	6.4	3.5	X	1.7	0.2	6.8	4.0
SD	0.4	0.1	0.5	0.5	SD	0.2	0.1	0.9	0.7
N	5	8	5	8	N	4	8	4	9
P		0.0000		0.0000	P		0.0000		0.0001
%		85.00%		45.00%	%		88.00%		41.00%
Sample 1 females	Plasma controls	Treated	RBC controls	Treated	Sample 2 females	Plasma controls	Treated	RBC Controls	Treated
X	8.5	1.1	6.3	3.6	X	7.9	0.7	6.7	4.2
SD	2.9	0.7	0.9	0.3	SD	1.8	0.1	0.7	0.3
N	5	10	5	10	N	5	8	5	8
P		0.0000		0.0000	P		0.0000		0.0000
%		87.00%		43.00%	%		91.00%		37.00%

The homogenates were mixed and then filtered into the Technicon AutoAnalyzer cups immediately prior to analysis for subsequent determination at 37°. For analysis on the Hitachi 704, a portion of the homogenate was centrifuged at 4000 rpm at 5° for 10 min. The resulting supernatant was maintained between 2 and 8° until the preparation was placed in the Hitachi sample cup immediately prior to sample uptake. The analysis proceeded at 37° with the addition of reagents and reaction times controlled by the previously determined system parameters set for the instrument, as shown in Table 1.

RESULTS AND DISCUSSION

Results shown for the erythrocyte and plasma determinations were carried out on samples of heparinized whole blood for the Technicon AutoAnalyzer procedure and on EDTA whole blood for the Hitachi 704 procedure. Previous comparison of the two anticoagulants showed no significant difference in the plasma determinations on the Hitachi 704 using heparin and EDTA. Hemolysates prepared from EDTA whole blood packed cells gave more consistent results on the Hitachi 704. EDTA was therefore determined to be the anticoagulant of choice for the Hitachi 704 analyses based on this experience and the manufacturer's recommendations.

Inhibition of plasma AChE at the first sampling interval was 85% for male rats and 87% for female rats on the Technicon AutoAnalyzer (Table 2). At the second sampling interval, plasma AChE inhibition was 88 and 91% in males and females, respectively (Table 2). Plasma AChE inhibition on the Hitachi 704 showed the same pattern but was less than the Technicon AutoAnalyzer. Inhibition of the first interval was 79% for male rats and 84% for female rats. On the second interval, inhibition was 80 and 84% for males and females, respectively (Table 3).

Erythrocyte AChE inhibition measured on the AutoAnalyzer was 45 and 43% in male and female rats, respectively, on the first interval. On the second interval, the inhibition was 41 and 37%, for males and females, respectively (Table 2). A similar pattern was demonstrated in the results from the Hitachi 704. The inhibition in

Table 3. Plasma and erythrocyte AChE BMD Hitachi 703 U/l

Sample 1 males	Plasma controls	Treated	RBC controls	Treated	Sample 2 males	Plasma controls	Treated	RBC Controls	Treated
X	437	90.9	1456.8	944.1	X	473.2	96.5	1550.0	1025.7
SD	85.6	15.3	92	216	SD	78.5	16.6	78.3	78.8
N	5	10	5	10	N	5	10	5	10
P		0.0000		0.0002	P		0.0000		0.0000
%		79.00%		35.00%	%		80.00%		34.00%
Sample 1 females	Plasma controls	Treated	RBC controls	Treated	Sample 2 females	Plasma controls	Treated	RBC Controls	Treated
X	1947.8	303.1	1492.0	845.0	X	2071.6	329.2	1573.4	909.2
SD	696.1	79.2	88.4	56.4	SD	632.2	93.9	352.1	143.2
N	5	10	5	10	N	5	10	5	10
P		0.0000		0.0000	P		0.0000		0.0001
%		84.00%		43.00%	%		84.00%		42.00%

Table 4. Left and right brain AChE Technicon AutoAnalyzer and Hitachi 704

Technicon auto analyzer-μM/ml					BMD Hitachi 704-U/l				
	Left brain		Right brain			Left brain		Right brain	
Males	Controls	Treated	Controls	Treated	Males	Controls	Treated	Controls	Treated
X	61.2	42.1	68.2	47.5	X	1436.4	820.8	7537.2	5533.5
SD	3.7	10	3.1	11.9	SD	385.1	307.2	143.4	1149.2
N	5	10	5	10	N	5	10	5	10
P		0.0013		0.0008	P		0.0050		0.0002
%		31.00%		30.35%	%		43.00%		27.00%
	Left brain		Right brain			Left brain		Right brain	
Females	Controls	Treated	Controls	Treated	Females	Controls	Treated	Controls	Treated
X	63.1	38.2	68.7	44.3	X	1314.8	851.2	7548.2	5233.7
SD	3.7	10.9	2.6	13	SD	385.3	241.1	171	1383.3
N	5	10	5	10	N	5	10	5	10
P		0.0001		0.0012	P		0.0127		0.0011
%		39.00%		36.00%	%		35.00%		31.00%

erythrocytes of male and female rats on the first interval was 35 and 43%, and the second interval, 34 and 42%, respectively (Table 3).

The left and right brain segments were both used to compare inhibition in this study. Inhibition of brain AChE for the left brain was 31 *vs.* 43% for the AutoAnalyzer and the Hitachi 704, respectively, in male rats. Inhibition of AChE in the right brain segment for males was 30 *vs.* 27% for the two instruments, respectively (Table 4). In the female rats, inhibition of left brain AChE was 39 *vs.* 35% for the AutoAnalyzer and the Hitachi 704, respectively. Right brain inhibition was 36 *vs.* 31% (Table 4). More inhibition of left brain AChE than of right brain AChE was demonstrated by both instrumental techniques; however, the range between brain segments was broader for the Hitachi 704 than for the AutoAnalyzer. No apparent sex related pattern was evident.

Inhibition of plasma AChE, within and between instrument systems, was very consistent. Lower values were noted in males *vs.* females, which has been shown historically in this laboratory to be characteristic of the rat. Therefore, a lower dilution was required for male *vs.* female plasma in the AutoAnalyzer method. The ability of the Hitachi 704 to measure the activity in units/litre made this dilution step unnecessary for either sex in plasma measurements. The typical pattern, however, was maintained. Values for percent inhibition were similar for both systems. More variation was found in the AutoAnalyzer measurement between days 51 and 57 than on the Hitachi system. This may be attributed to the more cumbersome and lengthy processing steps necessary to prepare the samples for the AutoAnalyzer. Consequently, the decrease shown between days 51 and 57 is probably spurious and caution should be exercised in over-interpretation of the apparent decrease.

The AutoAnalyzer measured less erythrocyte AChE inhibition at the second interval than at the first. In contrast, the Hitachi measured the same inhibition of erythrocyte AChE at both intervals. Caution must again be applied in over-interpreting the variation shown by the AutoAnalyzer, probably due to inherent variation in the procedure. Erythrocyte measurements were more varied between the instruments than the plasma measurements. In general, measurement in erythrocytes is hampered by the color (hemoglobin) of the hemolysates and the difficulty in achieving a clear hemolysate that is free of erythrocyte ghosts. The incorporation of dialysis within the Technicon analysis allows for reduction in both membrane ghosts and for dilution of the hemoglobin color.

Measurement of AChE inhibition in the left and right brain segments demonstrated less inhibition in the right segment than in the left segment. There appeared to be a possible sex related pattern in the AutoAnalyzer method. This pattern was reversed in the left brain measurements on the Hitachi. A similar, though less marked pattern was shown in the right brain measurement for the Hitachi. Again, caution must be exercised in over-interpretation.

CONCLUSION

There are definite advantages to rapid measurement of AChE inhibition, especially in

the diagnosis and treatment of acute carbamate poisoning. Both analytical systems demonstrated AChE inhibition of similar magnitude between control and treated groups of the rats, regardless of sex, and in all three types of samples. However, optimization and standardization of the assay are still controversial since membrane-bound enzyme may still not be completely measured in supernatant of brain homogenates or in hemolysates that may contain considerable numbers of erythrocyte-membrane ghosts. The Hitachi method developed here for this study, compared well with this laboratory's reference method on the Technicon Auto-Analyzer. Therefore, the combined advantages in reduced analytical time, higher sample through-put, less sample manipulation, increased ability to control temperature and cost effective automation make the Hitachi 704 our system of choice.

Acknowledgements—Dr Robert Hall, D. V. M., Mr Ronald Markevitch of Hazleton Wisconsin, Mrs Julieta M. Bool and Mr Thomas S. Skyta of Hazleton Washington are thanked for their technical assistance.

REFERENCES

1. G. L. Ellman, *et al. Biochem. Pharmacol.*, 1961, **7**, 88.
2. Boehringer Mannheim Corporation Insert #124117, 9115 Hague Road, Indianapolis, IN 46250, Nov. 1990.
3. J. B. Levine, R. A. Scheidt, V. A. Nelson, Technicon Symposium 1965, *Automation in Analytical Chemistry*. pp. 582–585, New York, NY: Mediad, Inc., 1966.
4. H. J. Mersmann, M. C. Sanguinetti, *Am. J. Vet. Res.*, 1974, **35**, 579, 1974.
5. W. Pilz, *Methods of Enzymatic Analysis*. 2nd English Ed., HU Bergmeyer (ed.) Academic Press Inc., New York, pp. 845, 1974.
6. Technicon Instruments Corporation, General Operating Instruction Manual, Sec. C-R, Chaucey, NY, Technicon Instruments Corporation, 1966.
7. N. Tietz, *Fundamentals of Clinical Chemistry*. 2nd Ed. p. 47, Saunders, 1976.
8. *Idem, ibid* 3rd Ed. p. 407, Saunders, Philadelphia, PA, 1987.

Talanta, Vol. 39, No. 11, pp. 1449–1457, 1992
Printed in Great Britain.

0039-9140/92 $5.00 + 0.00

ELECTROCHEMICAL SENSORS FOR MONITORING ENVIRONMENTAL POLLUTANTS

BERNARD FLEET*

Department of Chemistry/Institute for Environmental Studies, University of Toronto, St. George St., Toronto, Ontario, Canada M5S 1A1*, and Toxics Recovery Systems International (TRSI) Inc, Rexdale, Ontario

HARI GUNASINGHAM

Eutech Cybernetics Pte. Ltd. and Department of Chemistry, National University of Singapore, Singapore, Malaysia

(*Received* 13 *April* 1992. *Accepted* 14 *May* 1992)

Summary—Stricter environmental controls on the emission and discharge of chemical pollutants are creating an increased demand for the development of improved chemical sensor devices. Although electrochemical sensors show great promise for this task, their utility has been constrained by a number of practical problems, the most serious being the effect of surface adsorption of impurities leading to non-reproducible response. This review presents a survey of recent advances in electrochemical sensor technology which have attempted to improve the performance of these devices. Three main areas of development have been addressed; advances in sensor design and measurement techniques, novel approaches to conferring electrode selectivity and the use of microminiaturization and microelectronics fabrication techniques. Recent applications and future prospects for the measurement of toxic metals, organics and gases including volatile organic compounds are surveyed.

The invention of polarography by Heyrovsky[1] in 1923, by introducing a readily polarizable, microelectrode with a constantly renewed surface provided the creative spark from which the development of most electrochemical sensors have been derived. Although polarography has played an important role in chemical analysis, it was the limitations of the dropping mercury electrode, its limited sensitivity, poor mechanical stability and especially its limited anodic range, that provided the original impetus for the development of new designs of electrochemical sensors. During the last three decades the need for sensors of all types has increased dramatically with their critical involvement in most areas of our technological society including industrial automation, process control, medicine and public health, energy control and environmental quality monitoring.

In many of these applications, especially in process control and environmental quality, monitoring sensors are required to operate in a continuous monitoring mode, either in-line or on-line. Electrochemical sensors have played an important role in the measurement of both chemical and biological substances and it is worth noting here that Tom West's group at Imperial College were among the first to study the application of these devices in continuous analysis.[2–4]

The purpose of the present brief review is to focus on the major requirements for chemical or electrochemical sensors in environmental pollution monitoring in three main areas of toxics in water, organics and gases including volatile organics (VOCs). Rather than attempt a comprehensive review of electrochemical sensors in the environmental area, the aim has seen to focus on the most significant developments and on those areas and technologies which show the most promise for meeting future needs.

The last 15 years has seen enormous advances in sensor technology, especially in the development of sensor devices for measuring physical parameters such as pressure, flow, or temperature, motion or position. This has resulted mainly from the application of the mass production techniques of microelectronics to sensor manufacturing. The use of microfabrication, micromachining and photolithography has enabled the development of small relatively low

*Author address for correspondence.

cost solid state devices and has largely eliminated the specialist construction methods of the past.[5] Microelectronic sensors are now available for measurement of parameters such as pressure, temperature, humidity and flow where both the sensing element and the electronics are incorporated at the chip level. These trends also had the goal of developing so-called "intelligent sensors" where the measurement step and some level of decision making would be incorporated in the sensor-microchip unit[6] although with current advances in distributed process control this goal is no longer so critical.

Comparable advances in chemical sensor technology have been far less dramatic, reflecting the complexity of the chemical sensing process, especially the multiple levels of interactions at the sensor-sample interface.[7,8] A major trend in chemical sensor research has attempted to emulate the developments in physical sensors using solid state technology. This has generated somewhat mixed results; on the one hand, two decades of research into CHEMFET and ISFET devices[9] has failed to spawn any significant introduction of commercially viable sensors. In contrast, these efforts have generated an enormous level of interest in microelectronic approaches to sensor design including microfabrication and the use of microstructures. It is undoubtedly this line of research which is providing one of the most fruitful avenues of current developments in chemical sensors.[10]

As a result, the earlier classification of electrochemical sensors as either potentiometric, conductimetric or amperometric devices has now been expanded to include various hybrid devices including solid state, electrocatalytic and membrane phenomena.[11] This expanded research horizon is also required in order to solve the formidable barriers of conferring sensor selectivity, eliminating problems of surface contamination and also developing devices that are capable of operating in real world harsh environments. Despite these barriers, electrochemical sensors have generated a high level of interest both for the monitoring and the destruction of pollutants.[12,13]

Sensor requirements

Researchers frequently ignore market needs when developing new sensor devices. In this context it is worth noting that the target application for a sensor will significantly affect the performance requirements of sensitivity, selectivity, accuracy, precision, long term stability and ease of maintenance. In research applications, sensor specifications may not be too critical due to the nature of the measurements and the high skill level of research operators. In contrast, for on-line measurements, especially for process control applications, the sensor performance is much more critical. Even within various types of process control applications the sensor requirements may vary widely. The operating criteria for devices which are used in an alarm or warning situation may not be too critical since an alarm event would normally be monitored by an operator. With online analytical instrumentation, where analytical data may be required for environmental regulatory authorities, a higher level of performance may be required although frequent calibration is often possible. The most rigorous requirements are those in process control where the sensor signal is used to trigger an external action, for example, the use of a pH sensor to activate the discharge of a waste treatment tank. It is interesting to note that electrochemical sensors have been used in the first two of these examples, whereas to date, only the pH electrode has found use in the latter area.

One of the major problems in operating electrochemical sensors in continuous monitoring applications has been the difficulty of maintaining electrode stability and long-term performance. Surface contamination by solution impurities and electrolysis products has long been the bane of electroanalytical chemists. The problem has been most exhaustively studied in classical solid electrode voltammetry but the conclusions are fairly general. The most comprehensive study of this problem has been made by Tenygl,[14] who recommends the use of practical common sense, ensuring purity of solvents and supporting electrolytes and minimising concentration of analytes. In addition he describes a wide variety of approaches to maintaining electrode stability and reproducibility, including mechanical cleaning, potential cycling or the use of a semi-permeable membrane to protect the sensor surface. Even intermittent pyrolysis has been used as a cleaning method. However, while each of the above methods has found success in specific cases, they do not provide a universal solution to the problem. Perhaps the approach recommended by the present authors of using low-cost, single analysis, disposable sensors may be the most effective approach.[15]

TRENDS AND DEVELOPMENTS

Overlaying all recent develpments in electrochemical and chemical sensor design has been the rapid advances in microcomputer based instrumentation which has made high levels of data acquisition and processing readily accessible at very modest cost. In parallel, at least three major paths have been followed in sensor development which are in many cases overlapping. The first is the improvements in classical electrochemical sensor designs and construction, including flow-through devices and improvement in sensor selectivity by using selective membranes or interposed chemical reaction layers. These ideas are not new, however, and have been actively explored for more than 20 years. More fundamental are the approaches to conferring sensor selectivity by the use of chemical, biological processes or modified electrode surfaces. A third area is the developments in solid state technology and the use of microminiaturization with its spin-offs in the development of microelectrodes and micro sensor arrays.

Hydrodynamic voltammetry

Since amperometric devices dominate the applications of electrochemical sensors in pollution control, it is worthwhile to briefly review the basic principles governing the operation of these devices in a flowing stream. The general technique describing the application of amperometric processes in continuous analysis is hydrodynamic voltammetry (HDV). During the 1970s limiting current-mass transfer relationships were derived for various electrode geometries under varying mass-transfer conditions and cell geometries.[16] As the review by the present authors[16] points out, these studies do have relevance to sensor design since they theoretically indicate the most promising geometries by defining the effect of operating parameters such as electrode area and solution flow dynamics on the measured response.

Most of the sensors in this class operate as hydrodynamic chronoamperometric devices [measurement of current (i) *vs.* time (t) in a flowing stream]. In this approach only a small fraction of the electroactive component in the sample stream is actually reduced or oxidized. A question which is often raised is whether coulometric devices in which 100% of the analyte is consumed in the measurement step should be more sensitive. At first sight it might be predicted that coulometry should provide a more sensitive technique than amperometry, but in fact the reverse is true. There are several reasons for this; first, the signal from coulometric sensors is a step function rather than a peak and second, the signal/noise ratio for coulometric detectors is generally poor due to the effect of the large background charging current resulting from the expanded surface area of the coulometric electrode. In reality, as the electrode area increases, the current increase per increment in area actually decreases since it is only the first, smallest part of the electrode that senses the peak and does most of the work. Also, the background current (noise, charging current, H_2O reduction, *etc.*) increases almost linearly with area. The overall result is that the S/N is actually worse at higher electrode areas compared to lower.

Apart from sensitivity, the ease of manufacture and maintenance and long term response stability are also important factors in the selection of sensor design. Although originally it was the limitations in the dropping mercury electrode which stimulated the search for alternative electrode materials and structures, recent work at the Heyrovsky Institute has given a new impetus to classical polarography.[17] This work has resulted in significant improvements in capillary design and advances in programmable electrode drop geometry including microdrops, drops with stepwise growing area and variable meniscus area drops. These developments should reflect in the wider application of polarography in environmental analysis.

The practical consequences of hydrodynamic voltammetry is evidenced by the wide range of electrode structures and cell geometries that have been used in continuous analysis. The most significant of these is the use of electrochemical sensors as detectors in HPLC which has included numerous clinical and environmental applications.[18] However, it is worth noting that the most widely used electrode configuraton, the wall-jet cell, was first demonstrated as a practical flow sensor in Tom West's laboratory.[19]

Approaches to conferring electrode selectivity

The second major area of research in the chemical sensor field has been directed towards

a study of methods for conferring sensor selectivity. Various approaches have been adopted including the development of ion or molecular sensitive ligands, the modification of electrode surfaces to adapt selective chemistry and the use of multiple, less selective sensor arrays linked to a pattern recognition process.

The driving force for these concepts was undoubtedly the elegant work of Simon and colleagues[20] who designed and synthesized a range of cationic responsive macrocyclic polyether compounds exhibiting strong selectivity to a range of cations, including K^+, Ca^{2+}, Mg^{2+} and Na^+. This work has translated into the development of a number of practical, commercial ion-selective electrodes which have found important applications in laboratory and clinical analysis.

Comparable research efforts in the field of biosensors, which has aimed to develop receptors selective to a wide range of organic or biochemical analytes has been interesting, but in general far less commercially successful. This situation simply reflects the complexity of the interfacial reactions involved in this type of measurement.

Thompson and Krull have reviewed the problems of molecular recognition in chemical sensors and the impact on the development of biosensors.[21] They have discussed the principles of selective binding in the biosensor concept and outline the techniques for measuring the change in surface free energy associated with a selective chemical reaction. The interaction between the substrate and the biosensor causes a change in surface free energy which may be monitored by observing the electrochemical potential changes. However, the magnitude of this change is small, being governed by the Nernstian relationship so that it may be preferable to allow this chemical reaction to modulate a larger amount of signal energy. This can be achieved using either amperometry or by measuring the change in mechanical motion via the piezoelectric effect.

Most of the developments in biosensor research has focussed on biological molecular recognition systems such as enzyme/substrate or antibody/antigen reactions. In order to develop a sensor for a specific organic analyte it may be necessary to bind it to one of these processes. To date, applications in the area of environmental monitoring have been limited. Examples include the use of immobilized enzyme ion-selective electrodes to measure pesticides which are able to inhibit enzyme reactions.[22] In general, although the practical problems facing the development of biosensors are formidable, there is an enormous demand for this type of device. In the environmental area, for example, we can expect future advances to have important applications in public health screening, for example in the monitoring of the effects of toxic chemicals in the workplace.

The other major development in the approach to electrode selectivity has been based on the concept of chemically modified electrodes.[23] In this approach, ionic interaction, complexation, catalytic or size exclusion effects are used to confer increased selectivity and/or sensitivity for the analyte. Modified surfaces may be formed by chemisorption, covalent bonding or *in situ* polymerization of the selective agent or by mixing the electrode material with the ligand and pressing to form a composite. Applications cover a broad spectrum; for example, dithiocarbamate modified electrodes have been used to determine trace levels of mercury.[24] One interesting process which uses this approach is the application of metal doped electrocatalysts which have shown promise for the anodic oxidation of organics.[25] These materials operate by stabilizing the anodic $O_2/^{\cdot}OH$ hydroxyl free radical couple which is the critical step in the oxidation process.

Solid state technology

Following Bergveld's report on the first prototype chemically sensitive semiconductor device[26] the field of solid state technology became one of intense research activity, especially in the biosensor area. However, as Buck pointed out,[10] many of the electrical engineers and solid state physicists, and indeed many of the chemists who enthusiastically embraced this field, overlooked two critical factors. The first is that these devices often have to work in a harsh environment, much more aggressive than that for corresponding physical devices. The second factor was that the market for these devices is not only much smaller than for physical sensors but is also much more specialized and fragmented.

The early enthusiasm was for the use of the field effect transistor as the measuring step. While applications to the measurement of gases (hydrogen, hydrogen sulphide and ammonia)

have been successful,[27] serious problems have been encountered in measurements in liquids primarily due to difficulties in encapsulation. There would seem to be no obvious justification for using the FET route since microfabrication offers much better options using other measurement steps. Amperometric and potentiometric sensors have, for example, been made on SiO_2 or Si_3N_4 passivated silicon chips using photolithography and microfabrication.[28] According to Buck,[10] microminiaturization techniques should be much more effective when applied to faradaic rather than the non-faradaic, blocked electrode field effect processes.

This is evidenced by the fact that the application of microminiaturization techniques to traditional amperometric devices is already showing great promise. Ultramicroelectrodes which may typically have an electrode diameter of 10–30μM offer a number of important advantages over conventional sized electrodes including reproducible geometries, and ease of mass production. Carbon fibre microelectrodes, for example[29] show faster response times and higher sensitivities than macro electrodes and give typical S-shaped response curves. The rate of electrolysis at ultramicroelectrodes is also comparable to the rate of diffusion. Consequently, the diffusion zone is much more stable and does not move out into the solution as is the case with macro electrodes.

Another major advantage of the microminiaturization approach is the ability to construct multisensor arrays. These may be designed with individual sensors selective to different species or they may be relatively non-selective elements where multicomponent analysis is effected by the use of pattern recognition methods. Examples of this approach include the use of an array of electrocatalyst filaments and amperometric sensors to monitor organic gases at a hazardous waste site[30] and the analysis of electroplating wastes used an array of thin film mercury sensors to measure Ni^{2+}, Cd^{2+}, Pb^{2+} and Cu^{2+} and a hydrated iridium oxide substrate as pH sensor.[31] Recently, the construction of electrodes with a diameter of 0.2 μm (2000Å) has been reported.

APPLICATIONS

From the perspective of both problem area and type of instrumentation required, three major areas of applications can be identified. These cover methods for toxic metals and inorganics in water, the measurement of toxic organics in liquids, and the measurement of toxic gases and volatile organics (VOCs).

On-line monitoring of toxic metals and inorganics

Contamination of drinking water and the natural environment by toxic metals is a serious problem. In the US alone there are over 30,000 abandoned chemical dump sites, many of which are leaking various pollutants into local water courses. The Comprehensive Environmental Response and Cleanup Liability Act (CERCLA) is directed at the clean-up of all of these sites and is estimated to cost over $200 billion although, unfortunately, a large portion of the $12 billion spent so far has gone to lawyers. Apart from legal fees, the initial plan for orphan site clean-up calls for a site assessment and for monitoring all water runoffs for many of the priority pollutants. This is providing a strong incentive for the development of continuous metals analyzers. The other major incentive is for monitoring effluents from existing waste generators such as electroplating plants, electronics products manufacturers and some mining operations. In these applications two types of analytical measurement are generally required; monitoring of the performance of waste treatment equipment to detect either malfunction or for example, saturation of an ion exchange column. The second type of measurement is an end-of-pipe analysis to ensure that the plant discharge meets compliance. In the former case, fairly simple metal monitors which can provide an alarm response in the range 5–20 ppm are adequate whereas the requirements for discharge monitoring are much more rigorous. These may be required to accurately measure lead to local discharge standards which in California, for example, are 0.1 ppm for Pb and 0.5 ppm for Cu. A third application area is in the monitoring of drinking water where permissible metal levels are much lower, generally in the ppb levels (USEPA recommended standards are Pb 0.005 and Cu 0.02 ppm).

During the last decade, in the area of trace and ultratrace inorganic analysis, polarographic techniques, especially pulse, differential pulse

and anodic stripping voltammetry have provided strong competition for spectroscopic techniques. For automated trace metals analysis it would seem that online anodic stripping voltammetry is now the technique of choice. The practical viability of the approach was demonstrated by Fleet *et al.*[3] and Vydra *et al.*[32] in the mid-1970s. However, during the last few years there have been some major advances in cell design, instrumentation and control systems. An improved version of the wall-jet cell using microprocessor control has been used in continuous flow ASV[33] while a similar approach using a thin-layer cell and the flow injection principle has also been described.[34]

These developments have led to the introduction of several commercial instruments designed for field analysis of toxic metals. Two examples illustrate alternate design approaches. A portable, semi on-line voltammetric analyzer developed by Chemtronics[35] uses a glassy carbon working electrode, operates on 0.1–5-ml batch samples and provides automatic deaeration and system calibration. Targetted at industrial effluent and domestic water supply analysis, measureable metals include Sb, As, Bi, Cd, Cu, Au, Pb, Hg, Tl and Zn over the concentration range down to 10 ppb. A different approach has been developed by the Singapore group, Eutech Cybernetics which has developed a hand held metal monitor, also based on the ASV principle. A novel feature of this system is the use of disposable electrode strips on which the electrodes have been screen printed. Designed as a dedicated metal monitor for copper or lead, each unit has high and low operating ranges; 0.01 to 0.7 ppm and 0.5 to 3.0 ppm. The main applications of the Electrascan are also drinking water and industrial effluent monitoring. The use of disposable electrodes, as was discussed earlier has some significant advantages including elimination of the need for electrode pre-conditioning which is a tedious feature of most stripping voltammetric methods. It also avoids problems of cross contamination of samples which may occur in continuous flow systems. The simplified operating procedure aims to eliminate the need for skilled technicians which is a pre-requisite for most electrochemical techniques. A two-point calibration is first carried out on one of the two electrodes in the Electrascan sample chamber, using calibrating standards. Next, one drop of activating solution is added to a 1.0-ml sample then a 100-μl aliquot introduced into the cell chamber (a small depression above the electrode strip) and the analysis is completed and the result displayed in approximately 100 sec.

Two other important advances in this area, briefly referred to earlier, should also be noted. Improvements in the design and fabrication of the dropping mercury electrode by Novotny *et al.*[17] has provided a much more robust, versatile sensor with wide ranging applications in environmental monitoring. The second area is the work of Glass *et al.* at Lawrence Livermore Laboratories on the development of metal sensing sensor arrays.[31] This approach offers another approach to the development of a relatively low cost, multicomponent analyzer with cheap, disposable electrodes.

Organics

Monitoring of organic pollutants presents a formidable challenge, partly due to the large number of toxic substances and also to the complexity of the sample medium in many applications. The list of toxic organics defined as priority pollutants by the EPA includes over 120 compounds while the EC Priority List contains a similar number. Toxic organics result from a variety of sources; pesticides, insecticides and herbicides are found in runoffs from agricultural land where they may contaminate water supplies and enter the biological food chain. Residues of these materials are also found in soils, plant and animal tissues. Industrial sources include residues and waste by-products from chemical, pharmaceutical and a variety of manufacturing processes, aqueous effluents containing typically low levels of organics and volatile organic compounds (VOCs) in atmospheric emissions. Another major source of organic pollutants are the vast number of abandoned chemical dump sites where often a complex soup of toxic chemicals is present in the runoffs.

Electrochemical approaches have found wide application to monitoring organic pollutants since in the majority of cases the toxic or reactive grouping in a pollutant will also exhibit electrochemical activity. The basic techniques of classical polarography, solid electrode voltammetry, cathodic and anodic stripping voltammetry and a.c. polarography or tensammetry have all found wide application of organic pollution monitoring.[12] For example, polarography has

been used to measure a range of toxic substances which contain reducible functional groupings including carcinogens such as polycyclic aromatics, nitroso and azo dyes. Anodic voltammetry using solid electrodes has been used to analyze toxic and carcinogenic organics, phenols, amines, benzidines and chlorophenols. The two main problems faced in this type of analysis are first the need for pre-concentration, and second the elimination of interferences from other electroactive impurities. The most successful approach to solving both of these problems has been the use of high performance liquid chromatography with electrochemical detection.[18]

Other polarographic variants which have found use in organic pollutant analysis are the techniques of cathodic and anodic stripping voltammetry. Some of the early work on cathodic stripping voltammetry was carried out in Tom West's laboratory. Determination of the sulphur and chlorine containing pesticides, for example, was carried out by first pre-concentrating onto a mercury film electrode as an insoluble Hg-complex surface layer.[36] This adsorbed layer is then stripped off during the cathodic voltage scan. Another example is the determination of organotin fungicides which are used as antifouling agents. In the determination of this type of compound by anodic stripping voltammetry the pre-concentration step involves the formation of an organotin free radical which is adsorbed onto the mercury electrode and subsequently stripped off in the anodic voltage scan.[37]

A further class of electrochemical measurements uses a.c. or tensammetric methods to measure adsorption/desorption processes.[12] These have been used as a general indication of water quality, and also to measure specific surfactants, for example in sea water after the clean up of an oil spill.[38] In this method, an a.c. signal is superimposed on the normal d.c. waveform using phase selective detection. The presence of surfactants results in adsorption/desorption peaks with the peak potential giving some indication of the surfactant type. All of these polarographic or amperometric based approaches offer the possibility of developing specific detector systems for organic pollutants. The examples of portable, low cost, single or multiparameter instruments described earlier[13,28,35] clearly demonstrate the possibilities.

A number of other electrochemical approaches to monitoring of organics show promise. The measurement of complex organic vapour emissions from hazardous waste sites has been attempted using a sensor array system comprising two electrocatalyst filaments and two voltammetric detectors, one platinum and one rhodium. By carrying out a series of analyses using varying settings of filament current and electrode potential, a response pattern is generated from which the presence of chlorinated hydrocarbons, particularly chloroform and 1,1,1,-trichlorethylene can be confirmed.[30]

Another area showing promise is the various organic electrode processes developed from industrial electrosynthesis and more recently adapted to the destruction of toxic organics.[39] Reductive dechlorination of polychlorinated biphenyls can be carried out on a carbon filter cathode[40] and should provide an amenable route for the measurement of this important class of pollutants. The direct oxidation of organics using metal doped catalytic electrodes was mentioned earlier[25] and also shows considerable promise. A process which could have wide application to the coulometric analysis of toxic organics is anodic oxidation via the use of Ag(II) generated in a $AgNO_3/HNO_3$ analyte. The Ag(II) intermediate reacts with water to form hydroxyl free radicals which are highly oxidizing species. This process has already been used to detoxify organic waste streams at pilot scale level.[41] As a final example, amperometric or coulometric oxygen sensors are now routinely used to measure oxygen uptake in 5-day biological oxygen demand (BOD) measurements. An accelerated, 3-minute measurement has recently been proposed as a rapid screening method for organic pollutant levels in wastewaters.

Gases and VOCs

The rigorous requirements of the Clean Air Act and similar legislation in other industrialised nations has created a strong demand for reliable, low cost gas sensors. Environmental legislation based on the "command and control" approach having failed to bring about desired improvements in air quality, alternative, market based approaches including the trading of pollution permits are now being introduced. These approaches present even greater demands on sensor technology. For example, the Southern California Air Quality District is proposing to link NO_2

sensors from more than 100 electrical utility companies, directly to its computer tracking system. Although current technology relies on chemiluminescence methods, as emission standards are reduced there are prospects for the use of sensitive electrochemical devices. Plans to monitor VOC emissions in a similar fashion are facing obstacles due to the lack of available sensors and an indirect approach based on chemicals usage has been proposed.

Electrochemical sensors have already demonstrated considerable success for monitoring air pollutants[42] and show great promise for meeting future more rigorous legislation. The main gases of interest are O_2, CO, H_2S, NO, NO_2, HCN, NH_3, Cl_2 and HCl; other pollutant gases for which sensors are required and are currently being developed include HF, O_3, arsine and phosphine along with a range of volatile organic compounds. The whole spectrum of electrochemical techniques has found application in gas analysis, reflecting the less aggressive conditions in gaseous media compared to measurements in liquids. The application of potentiometry (with interposed chemical reaction layers), amperometry, chemical field effect transistors, semiconductor and electrocatalytic devices have all been described.

The potentiometric pH electrode modified with the inclusion of an interposed reaction layer has been widely used for the measurement of NH_3, SO_2 or NO_2 which diffuse into the reaction layer and effect a pH change.[12] Applications of potentiometric devices, however, are limited both in versatility and via the Nernstian response in terms of sensitivity. Amperometric devices, in contrast, have demonstrated a much wider range of applications and superior sensitivity, especially for the ppm/sub-ppm range required for most gaseous pollutants.[42,43] The use of a semi-permeable membrane to allow selective transport of the electroactive material and at the same time protect the electrode from contamination by the sample solution originates from the work of Clark in the 1950s.[44] Since then major advances in electrode construction have been made including novel electrode/electrocatalytic materials, the use of 3-electrode potentiostatic construction to reduce consumption of electroactive material and the use of solid polymer electrolytes to improve the robustness of the devices. The use of selective chemical filters for example, has been used to extend both the selectivity and sensitivity of amperometric gas sensors.[42]

The development of semiconductor gas sensors has also been an active area of research.[8,9] In these devices a catalytic coating is placed over the gate of the semiconductor device and the adsorption of the gas alters the drain current. The earliest of this principle are the CHEMFET devices which used the field effect transistor with gates constructed out of palladium or iridium and which showed a selective response to hydrogen and hydrogen containing molecules such as ammonia or hydrogen sulphide.[27,45] These devices show detection limits of around 1 ppm in air. Other types of integrated thin film semiconductor devices have since been developed using a range of electrocatalyst coatings. SnO_2 is the most common catalyst coating but ZnO_2, ZrO_2, WO_3, In_2O_3 and TiO_2 have also been used for specialized applications.[46] Semiconductor detectors are now finding widespread application in gas analysis either as selective detectors or for multicomponent analysis using pattern recognition. Simplified designs are also used as thermistor detectors in the "Figaro" type of smoke detector. Selective detection of ozone has been reported using In_2O_3 as catalyst coating,[47] while a Ru supported TiO_2 electrocatalyst has been used in the selective detection of trimethylamine which is used to monitor the freshness of fish.[48] An important example of multicomponent analysis is the report of a multicatalyst sensor array which acts as a "chemical nose".[46]

CONCLUSIONS

Increasingly stringent environmental legislation has created a large demand for chemical pollution sensors. In turn, electrochemical sensors are showing great promise for monitoring a wide range of pollutants including trace toxic metals in water, organics and gases. Although advances in the last two decades have not been as dramatic as those in other areas of sensor technology, future prospects are extremely bright. In particular, new techniques of electrode fabrication such as the use of ultramicro sensors or disposable electrodes offer real promise for overcoming the bane of electrochemical analysis, lack of stability due to sensor passivation.

Other advances, such as the development of sensor arrays provide an innovative approach

to the design of instrumentation for low cost multiparameter pollution monitoring. This approach could result in the development of moderately priced pollution monitoring equipment capable of working in a field environment and which could compete strongly with the much more costly, laboratory based techniques such as ion-chromatography or GC coupled mass-spectrometry.

REFERENCES

1. J. Heyrovsky, *Chem. Listy*, 1922, **16**, 256; *Philos. Mag. J. Sci.* 1923, **45**, 303.
2. M. D. Booth, B. Fleet, Soe Win and T. S. West, *Anal. Chim. Acta*, 1969, **48**, 329.
3. B. Fleet, H. Gunasingham, T. A. Berger, G. de Damia and S. Das Gupta, in *Proc. Int. Conf. on Physiochemical Hydrodynamics*, B. Spalding (ed.), p. 393. Advance Publications, London, 1977.
4. J. F. Alder, B. Fleet and P. O. Kane, *J. Electroanal. Chem.*, 1971, **30**, 427.
5. H. Woltjen, *Anal. Chem.*, 1984, **56**, 87A.
6. S. Middlehoek and D. J. W. Noorlag, *Sensors and Actuators*, 1982, **2**, 211.
7. T. Edmonds, *Chemical Sensors*, Blackie, London, 1988.
8. *Chemical Sensor Technology*, T. Seiyama (ed), Vol. 1, 1988 and Vol. 2, 1989, N. Yamazoe (ed), Vol. 3, 1991, Kodansha, Elsevier.
9. J. Janata and R. J. Huber (eds.), *Solid State Chemical Sensors*, Academic Press, New York, 1985.
10. R. P. Buck, *Electrochim. Acta.*, 1991, **36**, 243.
11. B. Fleet, *Proc. J. Heyrovsky Centenary Congress*, Prague, 1990.
12. R. Kalvoda, *Selective Electrode Rev.*, 1988, **10**, 127.
13. B. Fleet, *Coll. Czech. Chem. Commun.*, 1988, **53**, 1107.
14. J. Tenygl, in T. H. Ryan (ed.), *Electrochemical Detectors*, Proceedings of Fifth Anglo-Czech Symposium, Plenum, New York, 1984, 89.
15. B. Fleet, H. Gunasingham, R. R. Delangin, B. Narayanan and T. F. Tang, *Proc. Pittsburgh Conf. Anal. Chem.*, Paper # 922, 1991.
16. H. Gunasingham and B. Fleet, Hydrodynamic Voltammetry, in A. J. Bard (ed.), *Electroanalytical Chemistry* pp. 16, 89–180. Marcel Dekker, 1989.
17. L. Novotny and M. Heyrovsky, *Trends in Anal. Chem.*, 1987, **6**, 176.
18. Bioanalytical Systems Inc., West Lafayette, IN, U.S.A.
19. B. Fleet and C. J. Little, *J. Chromat. Sci.*, 1974, **12**, 747.
20. E. Pretsch, M. Badertscher, M. Welti, T. Maruzumi, W. E. Morf and W. Simon, *Pure Appl. Chem.*, 1988, **60**, 657.
21. M. Thompson and U. J. Krull, *Anal. Chem.*, 1991, **63**, 393A.
22. C. Tran Minh, *Ion-Selective Electrode Revs.*, 1985, **7**, 41.
23. G. Wallace, in T. Edmonds (ed.), *Chemical Sensors*, Blackie, London, 1988.
24. D. M. T. O'Riordan and G. G. Wallace, *Anal. Proc.*, 1986, **23**, 14.
25. D. C. Johnson, J. Feng, H. Chang, Y. L. Hsiao, J. S. Gordon, L. A. Larew, *Proc. Pittsburgh Conf. Anal. Chem.*, 1991, Paper #275.
26. P. Bergveld, *Biomed Eng.*, 1970, BME-17, 70.
27. A. Spetz, M. Armgarth and I. Lundstrom, *Sensors and Actuators*, 1987, **11**, 349.
28. I.Lauks, J. van der Spiegel, W. Sansen and M. Steyaert, *Digest of Technical Papers, International Conference on Sensors and Actuators*, Philadelphia, 1985, p. 122 (check I-Stat Corp tel 613-8312725).
29. J. Osteryoung and J. J. O'Dea, in A. J. Bard (ed.), *Electroanalytical Chem.*, p. 209. Marcel Dekker, New York, 1986.
30. M. W. Findlay, J. R. Stetter and T. Pritchett, Proc. Hazmat Conf., *Environmental Hazards Management Institute*, P.O. Box 932, Durham, NC 1990.
31. R. S. Glass, S. P. Perone and D. R. Ciarlo, *Anal. Chem.*, 1990, **62**, 1914.
32. F. Vydra, K. Stulik and E. Julakova, *Electrochemical Stripping Analysis*, Halstead Press, New York, 1976.
33. H. Gunasingham, K. P. Ang, C. C. Ngo, P. C. Thiak and B. Fleet, *J. Electroanalytical Chem.*, 1985, **186**, 51.
34. J. A. Wise, W. R. Heineman and P. T. Kissinger, *Anal. Chim. Acta.*, 1985, **172**, 1–12.
35. A. W. Mann and M. J. Lintern, *J. Geochem. Exploration*, 1984, **22**, 333.
36. M. J. D. Brand and B. Fleet, *Analyst*, 1968, **93**, 498.
37. D. M. Booth, M. J. Brand and B. Fleet, *Talanta*, 1970, **17**, 1059.
38. Z. Kozarac, B. Cosovic and M. Branica, *J. Electroanal. Chem.*, 1976, **68**, 75.
39. B. Fleet, R. Brazao Gomes and C. E. Small, *Environ. Sci. Eng.*, 1992, **22**, 12.
40. D. Schmaal, J. Van Erkel, A. M. C. P. de Jong and J. P. Van Duin, Environmental Technology Report R87/037 of MT-TNO to the Commission of the EC, 1987, and Assessment of International Technologies for Superfund Applications, USEPA Report EPA-540-2-88-033, September 1988.
41. D. F. Steele, D. Richardson, J. D. Campbell, D. R. Craig and J. D. Quinn, *I Chem. E. Symp. Ser.*, 1990, **116**, 237.
42. J. R. Stetter, *ACS Symp. Ser.*, 1986, **309**, 299.
43. J. R. Stetter, S. Zaromb and M. W. Findlay Jr., *Sensors and Actuators*, 1984, **6**, 269.
44. L. C. Clark, R. Wolf, D. Granger and Z. Taylor, *J. Appl. Physiol.*, 1953, **6**, 189.
45. I. Lundstrom and C. Svennson, in Ref. 9, 1985. 1.
46. T. Nakahara and H. Koda in Ref. 8, Vol. 3, 1991, 19.
47. Y. Shimazu, T. Takao and M. Egashira, *J. Electrochem. Soc.*, 1988, **135**, 2539.
48. T. Nakahara and H. Koda, in ref. 8, **1**, 19–32.

Talanta, Vol. 39, No. 11, pp. 1459–1462, 1992
Printed in Great Britain.

0039-9140/92 $5.00 + 0.00

INDIVIDUAL AND SIMULTANEOUS DETERMINATION OF URIC ACID AND ASCORBIC ACID BY FLOW INJECTION ANALYSIS

ALA'DDIN M. ALMUAIBED and ALAN TOWNSHEND*
School of Chemistry, University of Hull, Hull HU6 7RX, U.K.

(*Received* 18 *February* 1992. *Accepted* 5 *March* 1992)

Summary—Flow injection methods for the individual and simultaneous determination of ascorbic acid and uric acid are proposed. A spectrophotometer and a miniamperometric detector are connected in sequence. The calibration graphs for uric acid obtained by measuring its absorbance at 293 nm and its current at +0.6 V are linear up to at least 80 and 70 μg/ml, respectively, with an rsd ($n = 10$) of 1% for both methods at mid-range concentrations. The calibration graph for ascorbic acid with amperometric detection is linear up to 80 mg/l. with an rsd ($n = 10$) of 0.8% at 30 mg/l. The simultaneous determination of uric acid and ascorbic acid is based on measurement of the absorbance of uric acid at 393 nm and amperometric determination of both analytes at +0.6 V. The average relative errors of the analysis of binary mixtures of uric acid and ascorbic acid are 2.2 and 4.2%, respectively.

The determination of ascorbic acid has received great attention in analytical chemistry due to the wide use of ascorbic acid in soft drinks, human and animal food, and drugs. It is also important clinically to determine its concentration in blood, urine and in some tissues. Many flow injection methods have been proposed for determination of ascorbic acid. Each has its advantages and disadvantages. For instance two spectrophotometric procedures for determination of ascorbic acid using chloramine T have been described by Lazaro *et al.*[1] The first is carried out in the presence of potassium iodide and starch (linear range 15–150 mg/l.), the second in the presence of potassium bromide and bromide/methyl red using a flow injection titration. The same authors[2] also applied the above procedures for determination of ascorbic acid in urine. Another spectrophotometric assay has been described by Hernandez-Mendez *et al.*[3] in which iodine is generated in the flow system as triiodide or the triiodide/starch complex giving a steady absorbance at 350 or 580 nm, respectively. The decrease in the absorbance caused by ascorbic acid was measured. Amperometric detection has also been used for determination of ascorbic acid. For example, Fogg *et al.*[4] reported a procedure in which the measurement is made at +0.19 V *vs.* SCE in pH 5.5 acetate buffer. The calibration graph is rectilinear up to *ca.* 60 mg/l. A reticulated, vitreous carbon, flow-through electrode has been used by Strohl and Curran in an amperometric method for ascorbic acid.[5]

Owing to the demand for measurements of uric acid in biological fluids, many enzymatic[6–8] and nonenzymatic[9] flow injection methods have been reported for its determination. For example, a recent flow coulometric detector involving an immobilized uricase reactor and an electrolyte cell was fabricated and used for determination of uric acid.[8] The calibration graph is linear over the range 1×10^{-4}–$1 \times 10^{-3} M$ with a relative standard deviation (RSD) of <1%.

Ascorbic acid and uric acid are both present in biological fluids such as blood and urine. There is no flow injection method reported so far to measure both analytes simultaneously. Therefore, the present paper describes a combination of spectrophotometry and amperometry for simultaneous determination of ascorbic acid and uric acid. The procedure is based on measurement of the absorbance of uric acid at 293 nm[10] and amperometric detection of both analytes at +0.6 V.

EXPERIMENTAL

Reagents and chemicals

Distilled, demineralized water was used throughout. Ascorbic acid (AnalaR, BDH), ethanol and urea were obtained from BDH.

*Author for correspondence.

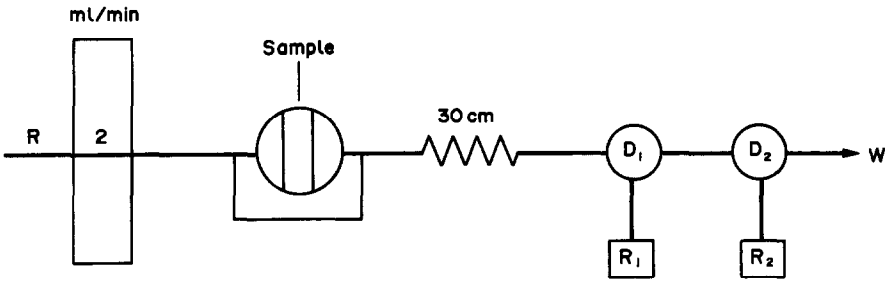

Fig. 1. Manifold used for individual and simultaneous determination of uric acid and ascorbic acid: R, carrier stream (0.05*M* succinate buffer, pH 3.0); D_1, spectrophotometer; D_2, miniamperometric detector; R_1 and R_2 are recorders; W, waste.

Xanthine, hypoxanthine and cysteine were obtained from Sigma Chemical Co. and uric acid from Hopkin and Williams. Succinate buffer (0.05*M*) (AnalaR, BDH) was used throughout.[11]

Apparatus

Spectrophotometric measurements were made with an LKB Ultrospec II spectrophotometer equipped with a flow cell (volume 18 μl, light path 10 mm). Amperometric measurements were made with a miniamperometric detector constructed by Masoom and Townshend[12] and used later by Almuaibed and Townshend for enzymatic determination of oxalate.[13] The components, including injection valve, pump, manifold and reaction coil tubing, were as reported earlier.[14]

Flow injection manifolds and procedures

The manifold used for determination of individual and simultaneous determination of uric acid and ascorbic acid is shown in Fig. 1. The spectrophotometer and a miniamperometric detector were connected in-line. Two recorders were used as shown in Fig. 1. When uric acid solutions were injected into the carrier stream (0.05*M* succinate buffer, pH 3.0), the absorbance and amperometric signals were measured at 293 nm and +0.6 V, respectively. When ascorbic acid solutions were injected into the same carrier stream, the amperometric signal was also measured at +0.6 V. For mixtures of uric acid and ascorbic acid, therefore, the uric acid was measured at 293 nm, and the sum of the two acids by the response at 0.6 V. A 30-μl injection was used for all measurements.

RESULTS AND DISCUSSION

Optimization studies for uric acid with spectrophotometric and amperometric detection

The effect of flow rate on the response for 50 μg/ml uric acid was investigated over the range 0.8–2 ml/min. The peak height absorbance decreases by *ca.* 25% as the flow rate increases from 1 to 2 ml/min, probably because of dispersion. The amperometric peak height for 50 mg/l. uric acid was nearly constant as the flow rate increased from 0.8 to 2 ml/min. Thus, 2 ml/min was used in subsequent experiments in order to increase the sample throughput rate.

The effect of pH was investigated by using 0.05*M* succinate buffer over the pH range 3–7 as the carrier stream. It was found that there was no significant effect on the amperometric peak height for 50 μg/ml uric acid over the above range. The peak height absorbance increased by 60% as the pH increased from 3 to 7. It was also found that ascorbic acid (40 mg/l.) absorbance increased significantly as the pH increased from 3 to 7; ascorbic acid does not absorb at pH 3, which was selected for further work.

The effect of the coil length was examined over the range 10–70 cm. It was found that the spectrophotometric peak height for 50 μg/ml uric acid decreased by 30% as the coil length increased from 30 to 70 cm. The amperometric signal also decreased, by 20%, as the coil length increased from 30 to 70 cm. Thus 30 cm was selected for subsequent work.

The effect of ascorbic acid on the peak height absorbance for 60 mg/l. uric acid was examined over the range 10–50 mg/ml. There was no effect.

Analytical performance

Under the conditions established, the calibration graph for uric acid using spectrophotometric detection was linear up to at least 80 μg/ml. The calibration graph and peaks are shown in Fig. 2. The least-squares linear equation over the range was: peak height absorbance $= 8.2 \times 10^{-3}$ [uric acid] (mg/ml) + 2.1×10^{-3} ($r = 0.999$, $n = 6$). The detection limit (2 × noise) and sample throughput rate

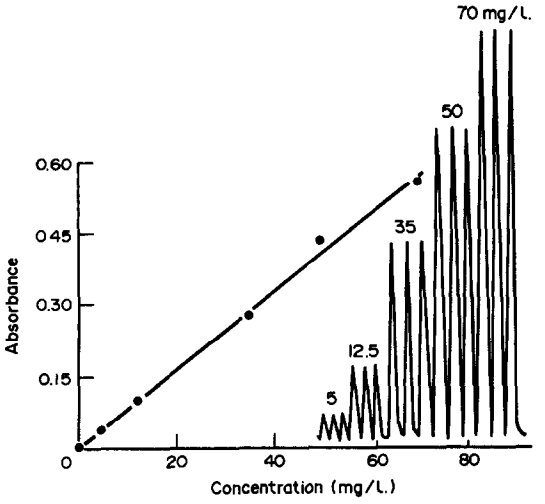

Fig. 2. Calibration graph and peaks for uric acid (spectrophotometric detection).

were 0.1 μg/ml and 100/hr, respectively. The RSD for 10 replicate injections of 30 μg/ml uric acid was 1%.

The calibration graph for uric acid using amperometric detection under the optimized conditions is linear over the range 0–70 μg/ml. The least-squares linear equation was: peak height (mm) = 1.27[uric acid](mg/ml) + 1.16 ($r = 0.998$, $n = 6$). The detection limit (2 × noise) and sample throughput rates were 0.12 μg/ml and 80/hr, respectively. The RSD for 10 replicate injections of 40 μg/ml uric acid was 1%.

Optimization studies for ascorbic acid with amperometric detection

The effect of the pH of the succinate buffer pH on the peak height for 50 μg/ml ascorbic acid was studied over the range 3–7. It was found that there was no significant effect on the peak height, so pH 3.0 was used for further work, as for uric acid.

The effect of flow rate over the range 0.8–2 ml/min on the responses for 50 mg/l. ascorbic acid was also investigated. The peak height was nearly constant over the above range, so 2.0 ml/min was selected for further work, as for uric acid.

Analytical performance

When the optimized conditions were used, the calibration graph for ascorbic acid was linear up to at least 80 μg/ml. The calibration graph and peaks are shown in Fig. 3. The least-squares linear equation was: peak height (mm) = 1.14[ascorbic acid](mg/ml) − 0.45 ($r = 0.999$, $n = 6$). The detection limit (2 × noise) and sample throughput rate were 0.15 μg/ml and 80/hr, respectively. The RSD for 10 replicate injections of 30 μg/ml ascorbic acid was 0.8%.

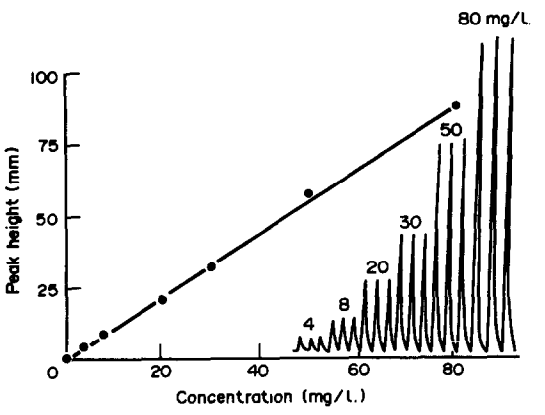

Fig. 3. Calibration graph and peaks for ascorbic acid.

Simultaneous determination of ascorbic acid and uric acid

The manifold shown in Fig. 1 was used for this determination. Succinate buffer (0.05M) (pH 3.0) was again used as carrier stream at a flow rate of 2 ml/min for this determination. The concentration of uric acid in the mixture was determined directly from the calibration graph shown in Fig. 2. Ascorbic acid was determined as follows. The amperometric signal equivalent to the uric acid concentration obtained from the spectrophotometric measurement was estimated from the amperometric calibration results for uric acid alone. This signal was subtracted from the total amperometric signal for the mixture and the remaining signal used to ascertain the ascorbic acid concentration from the ascorbic acid calibration graph (Fig. 3). Three synthetic mixtures of uric acid and ascorbic acid were analyzed. The results are shown in Table 1. Relative errors for uric acid were all $<3\%$, and those for ascorbic acid $\leqslant 5\%$.

Table 1. Simultaneous determination of uric acid and ascorbic acid

Conc. taken (*mg/l.*)		Conc. found (*mg/l.*)*			
Uric acid	Ascorbic acid	Uric acid	RE (%)	Ascorbic acid	RE (%)
5.00	5.00	5.13	2.6	4.75	5.0
5.00	10.00	5.11	2.2	10.31	3.1
10.00	5.00	10.17	1.7	4.78	4.4

*Mean of 3 readings.
RE, relative error.

Interference study

Uric acid and ascorbic acid are present in some biological fluids such as urine and blood. These types of fluids are very complex due to the presence of a variety of species at a variety of concentrations. Thus some compounds were selected, which are normally present in such biological fluids, to study the selectivity of the proposed system. Glucose (50 mg/l.), ethanol (60 mg/l.), urea (100 mg/l.), xanthine (20 mg/l.), hypoxanthine (20 mg/l.), cysteine (50 mg/l. with spectrophotometry, 1 mg/l. with amperometric) were injected into the system individually and with 20 mg/l. uric acid or ascorbic acid. They had no effect.

CONCLUSIONS

An on-line combination of spectrophotometry and amperometry has been successfully applied for determination of uric acid and ascorbic acid together in flow injection analysis. The method is simple, rapid, reproducible and sensitive.

REFERENCES

1. F. Lazaro, A. Rios, M. D. Luque de Castro and M. Valcarcel, *Analyst*, 1986, **111**, 163.
2. *Idem, ibid.*, 1986, **111**, 167.
3. J. Hernandez-Mendez, A. Alonso Mateos, M. J. Almendral Parra and C. Garcia de Maria, *Anal. Chim. Acta*, 1986, **184**, 246.
4. A. G. Fogg, A. M. Summan and M. A. Fernandez-Arciniega, *Analyst*, 1985, **110**, 341.
5. A. N. Strohl and D. J. Curran, *Anal. Chem.*, 1979, **51**, 1045.
6. M. Ohyabu, M. Fujimura, K. Tanimizu, Y. Okuno, M. Tabata, M. Totani and T. Murachi, *Anal. Sci.*, 1987, **3**, 277.
7. M. Tabata, C. Fukunaga, M. Ohyabu and T. Murachi, *J. App. Biochem.*, 1984, **9**, 251.
8. S. Uchiyama, F. Umesato, S. Suzuki and T. Sato, *Anal. Chim. Acta*, 1990, **230**, 195.
9. B. Bouzid and A. M. G. Macdonald, *ibid.*, 1988, **211**, 175.
10. P. Scheibe, E. Bert and H. U. Bergmeyer (eds.), *Methods of Enzymatic Analysis*, 2nd Ed., Vol. 4, Verlag Chemie, Weinheim, 1971.
11. D. D. Perrin, *pH and Metal Ion Control*, Chapman and Hall, London, 1974.
12. M. Masoom and A. Townshend, *Anal. Chim. Acta*, 1984, **166**, 111.
13. A. M. Almuaibed and A. Townshend, *ibid.*, 1989, **218**, 1.
14. *Idem, ibid.*, 1987, **198**, 37.

Talanta, Vol. 39, No. 11, pp. 1463–1469, 1992
Printed in Great Britain.

0039-9140/92 $5.00 + 0.00

DETERMINATION OF NITRIC ACID IN AMBIENT AIR USING DIFFUSION DENUDER TUBES

G. B. MARSHALL* and N. A. DIMMOCK
National Power PLC, Technology & Environmental Centre, Kelvin Avenue, Leatherhead, Surrey KT22 7SE, U.K.

(*Received* 22 *January* 1992. *Accepted* 5 *March* 1992)

Summary—A method has been developed for the determination of gaseous nitric acid in air based on its separation from particulate nitrate aerosol using diffusion denuder tubes. An integrated value of nitric acid concentration in air is obtained. The experimentally derived absorption efficiencies of the diffusion denuder tubes ranged from 87.6 to 96.9%. The standard deviation of the method was calculated as 0.10 $\mu g/m^3$ for nitric acid concentrations in the range 0.54–1.72 $\mu g/m^3$. A correction procedure, using two diffusion denuders in series, should be applied if measurements are made in the presence of high levels of nitrogen oxides.

The measurement of gaseous nitric acid in ambient air is important in atmospheric chemistry studies. Together with particulate nitrate aerosol, and peroxyacetyl nitrate (PAN), it is a sink for oxides of nitrogen which are emitted by both coal fired power stations and automobiles. It is a precursor in the formation of ammonium nitrate particles, which cause visibility reduction, and is also a contributor to direct acid and nitrogen deposition.

Methods for the determination of nitric acid in the atmosphere are complicated by the need to differentiate it from particulate nitrate aerosol which is present at similar concentrations. Early attempts to measure nitric acid (and particulate nitrate) used filter pack assemblies.[1] The first filter of Teflon or quartz removes nitrate aerosol, while nitric acid passes through unabsorbed and is collected on a second filter of either nylon, or sodium chloride impregnated on an inert material.

Doubts exist as to whether filter methods are effective in separating nitric acid from nitrate aerosol. Because of shifts in the nitric acid, ammonia, ammonium nitrate equilibrium (caused by temperature, relative humidity or acidity change) on the filter, compared with that in the atmosphere, erroneous results can occur.[2,3] Ammonium nitrate absorbed on the first filter can volatilize to release nitric acid, which is subsequently absorbed on the second filter to give positively biased nitric acid concentrations.

Ammonium nitrate can also react with acidic particles on the first filter to yield nitric acid, again leading to positively biased nitric acid values.

In addition nitric acid can be absorbed by basic particles on the first filter leading to negatively biased nitric acid concentrations.[4]

Because of the difficulties experienced with filter packs, workers are turning increasingly to the use of diffusion denuder tubes to determine nitric acid. These are based on the principle that, when air is drawn through a tube coated with a selective absorbent, separation of particles from gaseous species is achieved due to the much more rapid diffusion of gaseous species to the tube wall compared with that of the particles. Hence nitric acid gas diffuses rapidly to the wall of the diffusion denuder tube and is retained, whereas nitrate aerosol particles pass through unabsorbed. The theory and operation of diffusion denuder tubes has recently been reviewed.[5]

Previously, coatings of magnesium oxide,[6] sodium carbonate[7,8] and nylon[9] have been used to absorb nitric acid. In a previous paper from these laboratories[10] a coating of sodium fluoride, chosen because of its alkalinity and inertness, was found effective in absorbing hydrogen chloride in a diffusion denuder tube. This paper describes the development of a method, and its performance characteristics, for

*Author for correspondence. Present address: Chemistry Department, Birkbeck College, University of London, 29 Gordon Square, London WC1, U.K.

nation of nitric acid in ambient air with a similar diffusion denuder tube.

THEORY

The theory of diffusion–denuder tubes has been discussed fully by ourselves.[11] In brief, the air sample is drawn through a cylindrical tube coated with a selective absorbent, and the molecules of nitric acid diffuse to the wall according to the mathematical model first developed by Gormley and Kennedy.[12]

$$\frac{C}{C_0} = 0.819 \exp\left(-14.6272 \frac{\pi DL}{4F}\right) \quad (1)$$

where C = mean concentration of nitric acid in the air leaving the tube, C_0 = concentration of nitric acid in the incoming air, D = diffusion coefficient of nitric acid in air, L = length of the coated tube and F = flow rate of air.

Separation of gaseous nitric acid from particulate nitrate aerosol is achieved because of the much more rapid diffusion of gaseous nitric acid molecules to the wall of the tube than particulate nitrate—the latter passing through the tube unabsorbed. For particulate absorption to be avoided it is important that the flow of air through the coated part of the tube is laminar and this is so if the Reynolds Number is <2000. For the experimental conditions used in this work (air flow 2 litre/min and tube diameter 3 mm) the Reynolds Number is calculated to be 988. To ensure laminar flow through the coated region of the tube there should be an uncoated section of tubing of length 15 cm upstream of the coated tube. Deposition of particles by gravitation can be avoided by sampling with the tube in a vertical position (with either downward or upward flow) and Brownian diffusion of particles to the tube walls can be considered insignificant because of the relatively small diffusion coefficients of the particles of size 0.01 μg → 10 μm expected to be present in ambient air.

EXPERIMENTAL

Sampling apparatus

The diffusion–denuder tubes consisted of glass tubes of length 95 cm and i.d. 3 mm. An etch mark was made 15 cm from one end, and into this 15-cm length of tube was placed a PTFE tubular insert of diameter sufficient to make a gas-tight fit. The remaining 80-cm length was coated with the selective absorbent. Before initial use, the tubes were soaked overnight in a chromic acid cleaning solution, washed with demineralized distilled water and stored completely submerged under water in a specially prepared storage cylinder. The air sampling apparatus is shown in Fig. 1. Air was drawn through the diffusion-denuder tube by a diaphragm pump (Capex 2D, Charles Austen Ltd) and the volume measured by a gas meter (Model G4, UGI Meters Ltd). The flow of air was controlled by a needle valve (Fisher Controls Ltd).

Nitrate measurement

Nitrate measurements were made on the aqueous extracts from the diffusion denuder tube by ion chromatography (Dionex). A standard AS4 separator column was used with micromembrane suppressor (AMMS). Loop size was 0.5 ml and the eluent was a mixture of 2.25mM sodium carbonate and 2.80mM sodium bicarbonate.

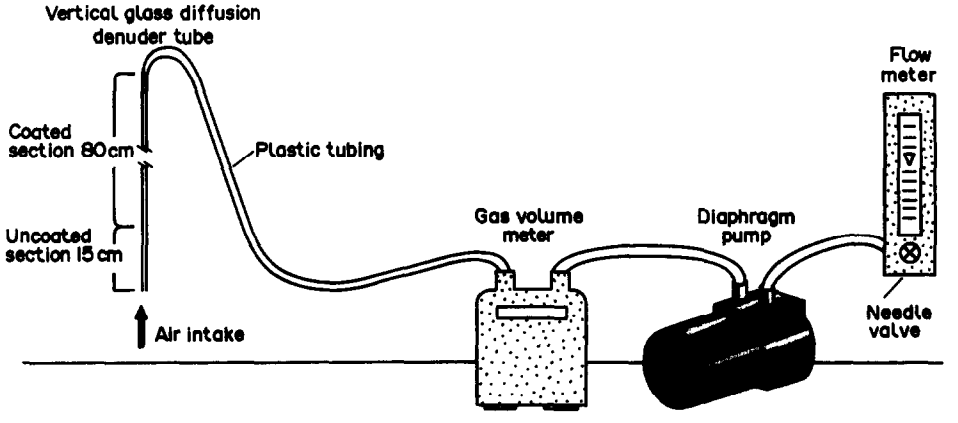

Fig. 1. Apparatus for sampling gaseous nitric acid in ambient air by diffusion denuder tube.

Reagents

Sodium fluoride stock solution, 40 g/l. A 40-g weight of sodium fluoride (BDH Analar grade) was dissolved in demineralized distilled water and made up to one litre with demineralized distilled water.

Ethanolic sodium fluoride coating solution. A 0.5-ml portion of the 40 g/l. fluoride stock solution was diluted to 10 ml with ethanol (BDH Spectrosol grade). This coating solution was prepared fresh every day for each batch of tubes to be coated.

Procedure

Before coating, the diffusion–denuder tube was washed successively with dimineralized distilled water, methanol (BDH Analar grade), and ethanol (BDH Spectrosol grade). The open end of the 80-cm section of the tube was then placed in the ethanolic sodium fluoride coating solution and, with the aid of a pipette filler, was filled to the etch mark and then allowed to drain back into the sodium fluoride container. This operation was repeated five times. The coated tube was then allowed to drain for 20 sec and was then dried by pumping dry air through it for 20 sec with a diaphragm pump. (If left to store both ends of the tube were then sealed immediately with Parafilm (Gallenkamp Ltd).) The unsealed diffusion–denuder tube was then placed in position in the sampling apparatus (see Fig. 1) and sampling commenced at about 2 litres/min. At the end of the sampling period the tube was removed, sealed at both ends with Parafilm, and the volume sampled was recorded.

Immediately before analysis the Parafilm was removed from both ends with a scalpel (care was taken to avoid contamination). The open end of the coated section of the exposed diffusion–denuder tube was then placed in 5 ml of demineralized distilled water contained in a small sample vial. With the aid of the pipette filler the water was drawn into the tube to the etch mark and then allowed to drain out. This operation was repeated five times.

The concentration of nitric acid in air (assuming 100% efficiency of absorption) is given by:

$$C_0 = \frac{aw}{v}$$

where

C_0 = concentration of nitric acid in air, $\mu g/m^3$.

a = concentration of nitric acid in the washing solution, $\mu g/l$.

v = volume of air sampled, litres.

w = volume of washing solution, ml, this is typically 5 ml.

RESULTS

Method development

The method was developed and tested by sampling laboratory air.

The appropriate tube length and flow rate were selected by reference to equation (1). For a 95% absorption efficiency, *i.e.*, $C/C_0 = 0.05$, the required length of coated tube can be calculated (given a flow rate of 2 litres/min (3.33×10^{-5} m^3/sec) and a diffusion coefficient of 1.15×10^{-5} m^2/sec for nitric acid in air[7] to be 70 cm. To maintain consistency with previous work with hydrogen chloride measurements in air[10] all diffusion denuder tubes were 95 cm in total length with a coated section of 80 cm. In addition, this increased length of coated section will allow for lower values of the diffusion coefficient as has subsequently been reported by Benner *et al.*[13] A flow rate of 2 l./min was used in all work.

Absorption efficiencies for a single tube were calculated as previously[11] by connecting two tubes in series and analysing separately after exposing to sample air. Absorption efficiency was then calculated as

$$\frac{\text{first tube concentration} \times 100}{\text{first tube} + \text{second tube concentration}}$$

Absorption of nitric acid on glass

Early work revealed that nitric acid can be absorbed by glass. For instance, when two diffusion denuder tubes, one coated with sodium fluoride and the other uncoated, were exposed to a source of nitric acid from a permeation tube calibrator, the coated tube gave a nitric acid concentration of 0.30 $\mu g/m^3$ while the uncoated one gave 0.25 $\mu g/m^3$.

In addition, further experiments showed that nitric acid (or perhaps particulate nitrate) was absorbed on the 15 cm pre-laminar flow region of the diffusion-denuder tube, as shown by positive nitrate concentrations measured in the washing solutions by ion chromatography. An attempt was made, by analysing separate sections of the tube, to determine if a constant proportion of the total nitric acid present had been absorbed on the pre-laminar flow region.

If this was so it would allow the true nitric acid concentration to be calculated by applying a correction factor to the results from the coated section. *i.e.*, that section where it can be assumed that no nitrate particles had been absorbed. No such constant ratio was found.

Ferm[7] found with sodium carbonate coated diffusion denuder tubes that there was similar deposition of nitric acid on the uncoated pre-laminar flow region. His solution was to analyse all the diffusion denuder tube rather than just the coated section and assume that no nitrate aerosol particles would be deposited, and hence analysed as nitric acid, in the pre-laminar flow region.

Rather than make this assumption the possibility of coating the pre-laminar flow region with a material with a negligible sorption efficiency for nitric acid was investigated. Spicer and Schumacher[14] and Appel *et al.*[15] have reported that, of the materials tested, PTFE has the lowest sorption efficiency for nitric acid.

Accordingly, PTFE sleeves of length 15 cm were prepared (Polypenco TW12), and inserted into the pre-laminar flow region of the diffusion denuder tube. It was assumed that the change in flow, caused by the reduced diameter of the pre-laminar flow tubing, did not induce turbulence. Before use they were thoroughly washed with demineralized distilled water and dried in an oven at 130°.

Table 1 shows results for diffusion denuder tubes prepared with PTFE inserts in the pre-laminar flow region of the tube and exposed to varying levels of nitric acid. The percentage of nitric acid (1.0 → 3.6%) absorbed in the pre-laminar flow region is very much lower than the levels, (up to 40% and variable) recorded for tubes with no inserts. Accordingly, in all subsequent work, measurements were made with PTFE inserts in the 15-cm pre-laminar flow region of the diffusion denuder tube.

Table 1. Absorption of nitric acid in the coated and uncoated (PTFE lined) sections of diffusion denuder tubes

	Coated section		Uncoated section	
	$\mu g/m^3$	Percentage of total	$\mu g/m^3$	Percentage of total
1	10.25	98.3	0.18	1.7
2	8.75	98.7	0.12	1.3
3	9.74	97.7	0.23	2.3
4	8.36	97.9	0.18	2.1
5	8.77	99.0	0.09	1.0
6	9.91	96.4	0.37	3.6

Nitric acid measurements in the presence of nitrate aerosol particles

In our previous work[10] it was shown that for particles of size range 0.01–4 μm there should be insignificant deposition and hence interference from these particles with the experimental conditions used. Larger particles can be precluded from entering the diffusion denuder tube and depositing by gravitation by orientating the tube in a vertical position.

Attempts were made to confirm these findings experimentally with an aerosol generator, as described previously.[10] Nitric acid measurements were made at the air intake point of the aerosol generator and compared with measurements made, in the presence of varying concentrations of ammonium nitrate aerosol, at the exit from the generator. In the presence of no added aerosol, nitric acid measurements at the exit of the generator tube were significantly less than those in the air intake to the tube. It can be concluded that nitric acid was being absorbed on the walls of the generator and so rendering comparisons of nitric acid measurements in ambient air with nitric acid measurements in the presence of added aerosol invalid. Quantitative comparisons of nitric acid in the presence and absence of aerosol cannot therefore be made in the same way as in our earlier work.[10] Nevertheless an indication of whether aerosols are deposited on the coated section of the diffusion denuder tube can be made by generating successively increasing concentrations of aerosol and comparing measured nitric acid concentrations as before. The levels of ammonium nitrate aerosol were increased from 4.2–22.6 $\mu g/m^3$ but no concomitant increase in measured nitric acid concentration was evident, from which it can be concluded that nitric acid measurements by diffusion denuder tube are free from interference from particulate aerosol.

Diffusion denuder tube storage

Experiments were performed to ascertain whether coated diffusion denuder tubes could be stored, both before use, and after exposure prior to analysis. It is important that the ends of the coated tubes are sealed with Parafilm immediately after preparation. When this was done, sealed tubes could be left unexposed for several days, with neither deterioration in absorption capacity nor contamination.

To ascertain whether exposed tubes could be left standing before analysis, room air (seeded

artificially with nitric acid, by opening a bottle of concentrated nitric acid for a few seconds) was sampled through two separate tubes in parallel. One tube was analysed immediately and the other tube was left for a period of time before analysis. All determinations were performed in duplicate. Results are given in Table 2.

From these results it can be concluded that exposed tubes can be left for at least eight days before analysis but for the most precise work it is recommended that tube preparation be done immediately before exposure and then analysis carried out immediately afterwards.

Interferences

Measurements of gaseous nitric acid in ambient air will be taken in the presence of varying levels of nitrogen oxides, peroxyacetyl nitrate (PAN), and nitrous acid. These gases present a potential interference because of their possible deposition on the diffusion denuder tube wall and subsequent conversion to nitrate giving positively. biased nitric acid concentrations.

Nitrogen oxides

All acid gases can be deposited, to a certain extent, on sodium fluoride coated diffusion denuder tubes. To test for the effect of nitrogen dioxide, relatively high levels (50 ppb) were passed from a permeation tube calibrator into diffusion denuder tubes for periods ranging from 12 to 24 hours. The tubes were then processed for nitrate determination in the normal manner. The experiment was carried out on three occasions and 0.42 and 1.44% of the incoming nitrogen dioxide was measured as apparent nitric acid.

It is likely that NO_2 will be converted to nitrite on the diffusion denuder tube wall and Perrino *et al.*[16] have postulated the following reaction

$$2NO_2 + H_2O \rightarrow HNO_2 + HNO_3$$

Table 2. Effect of storage on exposed denuder tubes

Nitric acid concentration $\mu g/m^3$ for storage period (days)						
Immediate analysis	One	Two	Three	Four	Six	Eight
1.01	1.00					
1.13		1.13				
1.13			1.18			
1.14				1.17		
0.29					0.27	
0.29						0.25

Nitrite can then be oxidised to nitrate on the diffusion denuder surface depending on the levels of photochemical oxidants present, in particular, ozone. Perrino *et al.*[16] estimated that in the presence of 45 ppb O_3, and with a two hour exposure, there was a 13% oxidation of nitrite to nitrate. This increased to 84% in the presence of 500 ppb O_3 with the same exposure. It can therefore be concluded that nitric acid measurements would be difficult in photochemical smog episodes unless appropriate corrections are made.

Eatough *et al.*[17] have suggested a procedure to correct for interference from nitrogen oxides. Given that the percentage deposition of NO_2 is relatively small the amount of NO_2 deposited in a second diffusion denuder placed in series with the first will be the same as that on the first denuder. Therefore if the nitrate formed in the second tube is taken from that in the first the net figure gives nitrate due to nitric acid deposition alone. (Nitric acid will be fully deposited in the first tube.)

Peroxyacetyl nitrate

PAN can undergo alkaline hydrolysis to yield acetate and nitrite ions[18] and it is feasible that this reaction could occur on the diffusion denuder tube wall.

$$CH_3C(O)OONO_2 + 2OH^- \rightarrow CH_3COO^- + NO_2^- + O_2 + H_2O$$

Because of the oxidation of nitrite to nitrate on the diffusion denuder tube wall (especially in the presence of high levels of ozone) PAN is a potential source of positive bias in nitric acid measurements. In an attempt to assess the amount of PAN deposition in the sodium fluoride coated diffusion denuder tube and the resultant amount of extractable nitrate, large concentrations (100 ppm and 250 ppm) of PAN were drawn into a diffusion denuder tube from a 200-ml container on separate occasions. PAN was generated by the photolysis of acetone in the presence of NO_2 and air.[19] The apparent concentration of nitric acid was equivalent to 1.7 and 1.0% of the 100 and 250 ppm original PAN. If required, this can be corrected for in an exactly similar way as for NO_2 but because the concentrations of PAN in ambient air are comparable to those of nitric acid its potential interference effect can, in most situations, be considered to be insignificant.

Nitrous acid

Ferm and Sjodin[20] obtained quantitative recovery of nitrous acid in sodium carbonate coated diffusion denuder tubes, and similar absorption within sodium fluoride coated tubes can be expected. Nitrous acid is converted to nitrite ion on the diffusion denuder wall which can then be oxidised to nitrate ion as previously discussed. High levels of nitrous acid are therefore a potential interference and will give positively biased nitric acid concentrations. Nitrous acid concentrations in air are, however, usually significantly less than nitric acid concentrations, particularly during the day and in summer, and so can probably be ignored. Concurrent measurements of nitrite ion by ion chromatography will indicate whether its effect needs to be considered.

Performance characteristics

The performance characteristics of the analytical method were assessed. In all cases the procedure as described previously was followed.

Calibration line

A fresh calibration line was prepared for each batch of samples. Calibration standards were prepared from Analar sodium nitrate at concentrations between 1 and 12 μmol/l. (62–744 μg/l.[3] NO_3^-). Within this range the calibration was linear.

Diffusion denuder tube absorption efficiency

The percentage of nitric acid absorbed on the coated diffusion denuder tube was measured by connecting two tubes in series and analysing each tube separately. Different volumes of room air were analysed on separate occasions and the results are given in Table 3. Absorption efficiencies ranged from 87.6 to 96.9%. This scatter is probably due to the difficulty of accurately measuring the low levels of nitric acid in the upper tube, *i.e.*, a relatively large error was introduced because the nitrate levels in the upper tube were at or near the blank level.

Table 3. Absorption efficiency of nitric acid denuder tubes

No	Volume sampled (litres)	Measured concentration of nitric acid: Upper tube, $\mu g/m^3$	Measured concentration of nitric acid: Lower tube, $\mu g/m^3$	Absorption efficiency, %
1	2478	0.032	0.725	95.8
2	2541	0.024	0.746	96.9
3	3267	0.014	0.237	94.4
4	2791	0.018	0.296	94.3
5	2798	0.014	0.248	94.7
6*	638	0.079	2.249	96.7
7*	638	0.167	2.167	92.8
8	2597	0.017	0.12	87.6
9	3314	0.009	0.128	93.4
10	3330	0.022	0.191	89.7

*Air sampled from a nitric acid permeation tube calibrator.

Precision

The precision of the analytical method was estimated by sampling room air through two tubes in parallel on separate occasions. The nitric acid concentration in the air samples ranged from 0.54 to 1.72 $\mu g/m^3$ and the standard deviation was estimated to be 0.10 $\mu g/m^3$.

Tube blank

It is important that blank diffusion–denuder tubes are included in any series of measurements, by coating, sealing and analysing in exactly the same way as sample tubes. The levels of nitric acid found in the 5 ml of demineralized distilled water used for dissolution of the coating should be $\ll 10$ $\mu g/l$.

Acknowledgements—The work was carried out at National Power Technology & Environmental Centre and the paper is published with permission of National Power.

REFERENCES

1. J. Forrest, R. L. Tanner, D. Spandau, T. D'Ottavio and L. Newman, *Atmos. Environ.*, 1980, **14**, 137.
2. A. W. Stelson and J. H. Seinfeld, *ibid.*, *1982*, **16**, 983.
3. *Idem*, *ibid.*, 1982, ***16***, 993.
4. J. Forrest, D. J. Spandau, R. L. Tanner and L. Newman, *ibid.*, 1982, **16**, 1473.
5. Z. Ali, C. L. P. Thomas and J. F. Alder, *Analyst*, 1989, **114**, 759.
6. R. W. Shaw, R. K. Stevens, J. Bowermaster, J. W. Tesch and E. Tew, *ibid.*, 1982, **16**, 845.
7. M. Ferm, *ibid.*, 1986, **20**, 1193.
8. I. Allegrini, F. De Santis, V. Di Palo, A. Febo, C. Perrino, M. Possanzini and A. Liberti, *The Science of the Total Environment*, 1987, **67**, 1.
9. P. A. Mulawa and S. H. Cadle, *Atmos. Environ.*, 1982, **16**, 845.
10. N. A. Dimmock and G. B. Marshall, *Anal. Chim. Acta*, 1987, **202**, 49.
11. *Idem*, *ibid.*, 1986, **185**, 159.
12. P. G. Gormley and M. Kennedy, *Proc R I A*, 1949, **52**, (A) 163.
13. C. L. Benner, N. L. Eatough, E. A. Lewis, D. J. Eatough, A. A. Huang and E. C. Ellis, *Atmos. Environ.*, 1988, **22**, 1669.
14. C. W. Spicer and P. M. Schumacher, *ibid.*, 1979, **13**, 543.
15. B. R. Appel, Y. Tokiwa, M. Haik and E. L. Kothny, *ibid.*, 1984, **18**, 409.

16. C. Perrino, F. De Santis and A. Febo, *ibid.*, 1988, **22**, 1601.
17. N. L. Eatough, S. McGregor, E. A. Lewis, D. J. Eatough, A. A. Huang and E. C. Ellis, *ibid.*, 1988, **22**, 1601.
18. D. Grosjean, K. Fung, J. Collins, J. Harrison and E. Breitung, *Anal. Chem.*, 1984, **56**, 569.
19. H. J. Allen, Private Communication, 1989.
20. M. Ferm and A. Sjodin, *Atmos. Environ.*, 1985, **19**, 979.

Talanta, Vol. 39, No. 11, pp. 1471–1478, 1992
Printed in Great Britain.

0039-9140/92 $5.00 + 0.00

AUTOMATED DETERMINATION OF SULPHITE AND SULPHUR DIOXIDE BY COOL FLAME MOLECULAR EMISSION SPECTROMETRY AFTER REDUCTION TO HYDROGEN SULPHIDE WITH SODIUM TETRAHYDROBORATE III

TOYIN A. AROWOLO and MALCOLM S. CRESSER*

Department of Plant and Soil Science, University of Aberdeen, Meston Building, Aberdeen, AB9 2UE, U.K.

(*Received* 14 *April* 1992. *Accepted* 14 *May* 1992)

Summary—An automated method for the determination of sulphite and sulphur dioxide by cool flame molecular emission spectrometry is described. The method is based on the reduction of both compounds to hydrogen sulphide with sodium tetrahydroborate III. The sample which is mixed with $NaBH_4$ is acidified with 6*M* hydrochloric acid and carried by a continuous-flow stream into a gas–liquid separator where the evolved hydrogen sulphide is swept by nitrogen into a cool, hydrogen–nitrogen-entrained air flame. The intensity of the blue diatomic S_2 emission generated is measured at 384 nm. The proposed method has a detection limit for sulphite of 0.029 μg/ml and relative standard deviations of 1.2 and 1.5% for 1 and 5 μg/ml respectively. The calibration graph is linear up to 24 μg/ml sulphite and samples can be analysed at a rate of about 40/hr. The method has been applied to the determination of SO_2 in air and sulphite in wines.

Sulphur dioxide is one of the most important gaseous pollutants causing widespread concern. It is emitted into the atmosphere during various industrial processes and by the burning of fossil fuels. Its adverse effects on living organisms are well known.[1] Sulphite, an anion of major importance, is widely used as an antioxidant in the pharmaceutical and food industries, as an oxygen scavenger in water for steam generation, and in the production of paper pulp. Sulphite is also often produced as an intermediate in the analysis of sulphur-containing materials and strict control over its concentration in industrial products is necessary. Consequently, the development of analytical methods for the determination of both sulphur dioxide and sulphite has attracted considerable attention.

Several methods[2–4] have been described for the analytical determination of both compounds, including ion-chromatography,[5] conductimetry,[6] amperometry,[7] flame photometry,[8] meca,[9] chemiluminescence,[10] UV/Vis spectrophotometry,[11,12] and flow injection analysis.[13] Several workers[9,14–16] have shown that temperature enhances the sensitivity obtained in analytical techniques employing gas-phase sample introduction for the determination of sulphite or SO_2. This is because of the increase in the rate of reaction, reduction in solubility of SO_2 with increasing temperature and reduction in the viscosity of the reaction mixture. All these factors lead to an increase in the evolution rate of SO_2 at high temperature (*e.g.*, 50°) and hence an improvement in the sensitivity. A major drawback in this approach is the condensation of water vapour at the top of the gas–liquid separator and sometimes in the connection tubing leading to the absorption cell or flame. This leads to poor precision because of the reabsorption of the sulphur dioxide by the water droplets and the obstruction of the smooth flow of the gas. In the automated gas phase molecular absorption spectrometric method (GPMAS) for sulphite which we reported earlier,[16] this problem was solved by wrapping the gas–liquid separator with a heating tape. Alder and Kargosha[14] attached a small Liebig condenser at the outlet of their apparatus to prevent the steam from reaching the flame. These alterations make the set-up cumbersome, and it is desirable to develop a sensitive gas-phase sample introduction method for SO_2 determination that can readily be carried out at room temperature.

Techniques using gas-phase sample introduction have commonly been applied to both sulphide and sulphite because acidification of

*Author for correspondence.

solutions of these ions readily produces hydrogen sulphide and sulphur dioxide respectively. However, the literature shows that, whenever the same technique is applied to both ions, sulphide determination always yields better sensitivity and a lower detection limit than that of sulphite.[16–19] For example in a recent paper from this laboratory describing a simple and sensitive automated method for the determination of sulphide in environmental samples by cool flame molecular emission spectrometry,[20] sulphite interfered. The technique was based on passing the hydrogen sulphide liberated on acidification of samples with 3*M* hydrochloric acid into a cool, nitrogen–hydrogen diffusion flame and the resulting S_2 molecular emission was measured at 384 nm. The technique was more than an order of magnitude less sensitive for sulphite than for sulphide and analysis at 50° did not substantially improve the sensitivity. As an alternative way of enhancing the sensitivity of sulphur dioxide determination at room temperature using a gas-phase sample introduction technique, converting sulphite to hydrogen sulphide appeared potentially attractive, because of the better sensitivity which can be obtained.

Tin(II) chloride[21] and Raney nickel[22] have been proposed as reducing agents for sulphite. However, sodium tetrahydroborate(III) has been used extensively in the generation of covalent hydrides in atomic absorption spectroscopy.[23] In this paper, an improved and automated method for the determination of sulphite and sulphur dioxide is described. The method involves the reduction of both species with $NaBH_4$ and acidification with 6*M* hydrochloric acid. The released hydrogen sulphide is swept into a cool, nitrogen–hydrogen flame and the resulting S_2 molecular emission is measured at 384 nm. The method has been successfully applied to the determination of sulphur dioxide in air and sulphite in wine.

EXPERIMENTAL

Reagents

All reagents were of analytical-reagent grade.

Sulphite stock solution, 500 μg/ml. This solution was prepared by dissolving 0.197 g of anhydrous sodium sulphite, Na_2SO_3 [Merck (formerly BDH)], in 250 ml of antioxidant solution. Working standards were freshly prepared each day in antioxidant solution[16] by the least number of dilution steps possible.

*Stock sodium tetrachloromercurate(II) (TCM) solution, 0.04*M. Prepared by dissolving 10.86 g of mercury(II) chloride, 5.96 g of potassium chloride, and 0.066 g of disodium dihydrogen ethylenediaminetetraacetate (Na_2H_2EDTA) in water, and diluting to the mark in a one-litre standard flask.

Stock sulphamic acid solution, 0.6%. Prepared by dissolving 0.6 g of sulphamic acid in 100 ml of water.

Sodium tetrahydroborate(III) solution, 0.2%. Prepared by dissolving 2 g of $NaBH_4$ in one litre of 0.1*M* sodium hydroxide. After filtration, this solution was stored in a dark glass bottle. The solution remains usable for 2–3 days.

Interferent solutions, 1000 μg/ml. Solutions of a range of cations and anions were prepared from analytical-reagent grade salts.

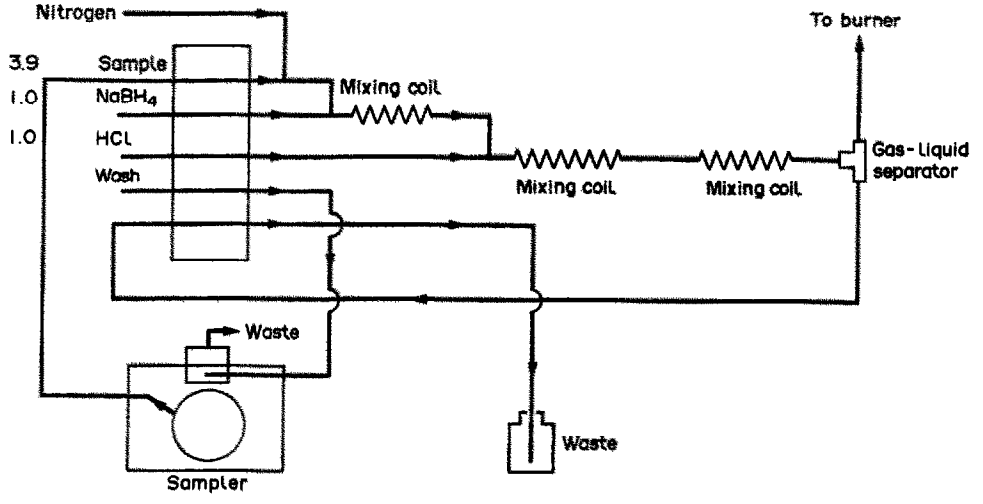

Fig. 1. Schematic diagram of the manifold for the automated cool flame emission spectrometric method for sulphite and sulphur dioxide. Flow rates in ml/min.

Table 1. Optimum conditions used for the determination of sulphite and sulphur dioxide by Automated Cool Flame Emission Spectrometry

Conditions	Optimum value
Flow rates (l./min):	
H_2 flow rate	0.65
N_2 flow rate	2.31
N_2 (carrier gas) flow rate	0.075
Wavelength	384 nm
Slit width	1.0 mm
Bandpass	3.0 nm
Hydrochloric acid	6*M*
Sample time	45 sec
Wash time	45 sec

Apparatus

The atomic absorption spectrometer, burner and other apparatus used in this study have been described elsewhere.[20] A diagram of the flow manifold used is shown in Fig. 1 and the operating parameters for the various parts of the instrument and manifold are shown in Table 1.

Instrumental operation

To obtain optimum sensitivity, the different parameters affecting the generation, and hence the subsequent determination of H_2S, such as concentration of acid, carrier gas flow, concentrations and volume of the sodium tetrahydroborate(III) solution and volume of sample solution were studied.

There was no significant difference in the emission intensity obtained from 5 μg/ml of sulphite when $NaBH_4$ was mixed with the sample first before the addition of hydrochloric acid and vice-versa. However, the former approach was used in this study. It was important to mix the reagents thoroughly; hence the need for three mixing coils (28 turns each) as shown in Fig. 1. The flow rate of the carrier gas and the point at which it was introduced into the system led to a fast and efficient mixing of the reagents and also to the efficient stripping of the evolved hydrogen sulphide.

Procedure

Except where otherwise stated, the experimental procedure is the same as previously reported for sulphide.[20] A maximum sampling rate of 40 samples per hour was possible because the baseline was re-established quickly between consecutive peaks.

RESULTS AND DISCUSSIONS

Optimization of experimental conditions

Effect of HCl concentration. The effect of hydrochloric acid concentrations (between 1 and 8*M*) on the emission intensity of hydrogen sulphide obtained from the reduction of 5 μg/ml sulphite was investigated. The results, which are shown in Fig. 2, indicate that the volume of hydrogen sulphide evolved from a given sulphite solution depends on the molarity of hydrochloric acid introduced into the manifold. The relative emission intensity increases gradually at the beginning, then sharply until about 6*M* when it approaches a plateau. Hydrochloric acid at a concentration of 6*M* was selected as the best compromise for subsequent work. This corresponds to a molarity of 1.02*M* in the final solution.

Effect of $NaBH_4$ concentration. The effect of varying the concentration of sodium tetrahydroborate(III) on the emission intensity of hydrogen sulphide obtained when 5 μg/ml of sulphite was taken through the procedure is shown in Fig. 3. When higher concentrations of $NaBH_4$ were used, rapid evolution of hydrogen bubbles was observed in the waste manifold tube. These hydrogen bubbles later formed small gas pockets which segment the waste liquid stream and prevent the smooth flow of the waste liquid. Since accumulation of the waste liquid in any part of the system is not desirable (except in the waste bottle) and for economic reasons, a concentration of 0.2% $NaBH_4$ at a flow rate of 1.0 ml/min was used subsequently in this study.

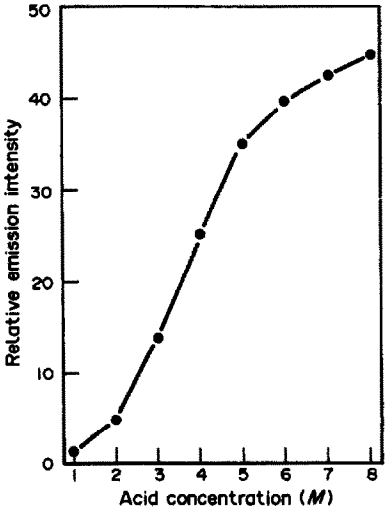

Fig. 2. Effect of HCl concentration on the emission intensity of 5 μg/ml sulphite.

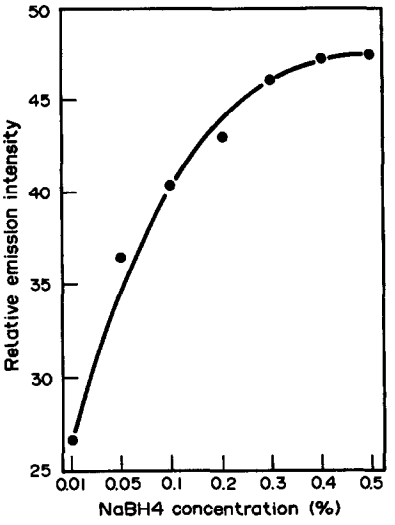

Fig. 3. Effect of $NaBH_4$ concentration on the emission intensity of 5 μg/ml sulphite.

Optimization of flame composition. The effect of flame composition on the emission intensity of hydrogen sulphide was studied. Hydrogen flow rates were held constant while the nitrogen flow rate was varied. The results, which are shown in Fig. 4, were obtained by monitoring the emission at 384 nm of hydrogen sulphide obtained from a 5-μg/ml sulphite standard solution. The optimal composition of the flame was 0.65 l. H_2/min and 2.31 l. N_2/min.

Analytical parameters. Using the optimized conditions shown in Table 1, the calibration graph ($\log I$ *vs.* $\log C$) of the proposed method was linear up to 24 μg/ml of sulphite ($\log I = -1.56 + 1.82 \log C$ with $r = 0.9994$). When aqueous sulphite solutions (as SO_2) stabilized by alkaline antioxidant reagent [(AAR) – 0.1*M* NaOH/0.001*M* EDTA] or 0.005*M* TCM or 0.01*M* TCM were analysed by the proposed procedure, straight line calibration graphs were obtained as shown in Fig. 5. This confirms that the method is applicable to aqueous solutions of sulphite which are stabilized by the two antioxidants. The limit of detection (signal to noise ratio = 3) was 0.029 μg/ml sulphite and the relative standard deviations for 1 and 5 μg/ml sulphite were 1.2 and 1.5%, respectively ($n = 10$). A comparison of this approach (involving the use of $NaBH_4$) with our earlier approach of simple acidification of sulphite samples and sweeping the SO_2 generated into flame was investigated by analysing standard sulphite solutions by both techniques. The results shown in Fig. 6 indicate that the use of $NaBH_4$ increases the sensitivity very substantially. When aqueous standard solutions of sulphite (0–7.5 μg/ml sulphur dioxide) were analysed by the proposed procedure, the equation of the graph obtained by the method of least squares was:

$$\log I = -0.59 + 1.99 \log C$$

with $r = 0.9999$ ($n = 6$)

The slope is very close to the theoretical slope of 2. Comparison of the detection limit, sensitivity and linear range from this work with the corresponding parameters quoted in the literature for sulphite determination by other

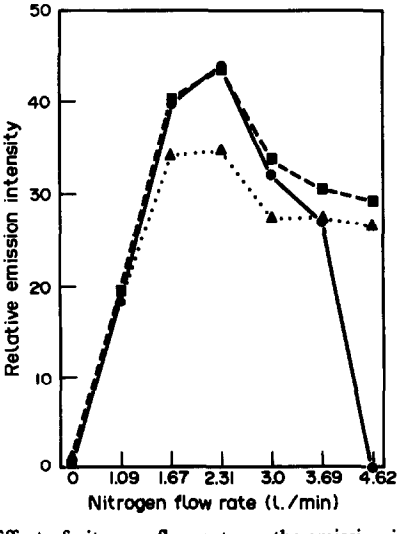

Fig. 4. Effect of nitrogen flow rate on the emission intensity of 5 μg/ml sulphite. Hydrogen supplied to the flame: ● 0.65 l./min, ■ 1.03 l./min, ▲ 1.76 l./min.

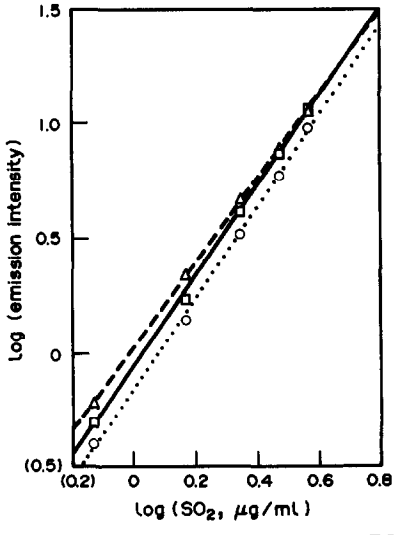

Fig. 5. Calibration graphs for sulphite in TCM and AAR (0.1*M* NaOH/0.001*M* EDTA): △ 0.005*M* TCM (slope = 1.82), □ 0.01*M* TCM (slope = 1.96), ○ AAR (slope = 1.97).

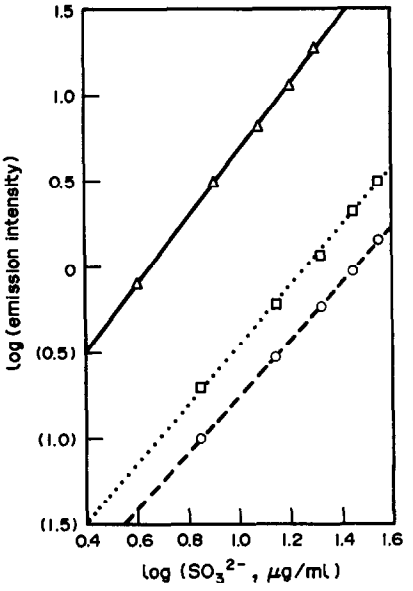

Fig. 6. Comparison of calibration graphs for sulphite: ○ without $NaBH_4$—temp. 24° (slope = 1.64), □ without $NaBH_4$—temp. 50° (slope = 1.71), △ with $NaBH_4$ temp. 24° (slope = 1.94).

techniques[16,18,19] indicate the usefulness of the proposed approach.

Interferences

Interferences from anions were studied by analysing a 5 μg/ml standard solution of sulphite spiked with known amounts of the ions. The responses were compared with those obtained from an uncontaminated sulphite solution. No significant interference was observed from 100 μg/ml Cl^-, Br^-, I^-, CO_3^{2-}, NO_3^-, PO_4^{3-} and SO_4^{2-}. The effect of nitrogen dioxide, a common interferent in the determination of atmospheric SO_2 was also studied. A 100-μg/ml concentration of nitrite depresses the signal of 5 μg/ml sulphite by approximately 16%. Addition of 0.6% sulphamic acid to the solution containing sulphite and nitrite (100 μg/ml) prior to analysis did not restore the peak. However, up to 60 μg/ml nitrite could be tolerated in the determination of 5 μg/ml sulphite. This is an improvement on the very low allowable concentration of nitrite reported earlier for sulphite determination by GPMAS.[16] No emission was observed when pure solutions of the anions were introduced into the manifold.

As expected, sulphide interferes with the proposed method. Solutions containing sulphite and sulphide should be divided into two, one stabilised with sulphide antioxidant buffer[17] (SAOB) and the second with alkaline antioxidant reagent (AAR). The two solutions should then be analysed by the proposed method with and without $NaBH_4$. Sulphide is not affected significantly by SAOB or AAR or whether $NaBH_4$ is included in the manifold or not. However, sulphite does not give a peak when stabilized by SAOB (possibly because it contains ascorbic acid). Therefore, stabilizing a sample containing sulphide and sulphite with SAOB and analysing without adding $NaBH_4$ will ensure that the sulphite peak is suppressed and hence the amount of sulphide in the mixture can be determined. Results of the total amount of both ions present in the mixture can be obtained by stabilizing with AAR and analysing, using $NaBH_4$ as the reducing agent. The amount of sulphite in the mixture can then be obtained by difference.

The effects of cations on the determination of 5 μg/ml sulphite in the proposed method were also investigated. Since the extent to which some metal ions interfere in the determination of sulphite depends on the method, it is important to determine the threshold concentrations at which these metal ions start to interfere. Standard solutions of sulphite were therefore spiked with known amounts of the interfering metal ions and taken through the analytical procedure. No emission was observed when pure solutions of any of the metal ions were introduced into the manifold. A summary of the results obtained, which is shown in Table 2, indicates that disodium EDTA at concentrations in the range 0.001–0.01*M* is effective in removing the interferences of some metal ions. Of all the cations investigated, only Mn^{2+} and Fe^{2+} interfered significantly with the proposed method. The results in Table 2 show that only 2.5 μg/ml Fe^{2+} and 5 μg/ml Mn^{2+} can be

Table 2. Effect of various ions on the determination of 5 μg/ml sulphite by the proposed method

Ions	Masking agent (EDTA)	Allowable* concentrations, μg/ml
Na^+, K^+, Ca^{2+}, Al^{3+}, Ba^{2+}, Pb^{2+}	0.001*M*	100
Mg^{2+}, Zn^{2+}, Cd^{2+}, Ni^{2+}	0.01*M*	100
Cr^{3+}	0.01*M*	50
Fe^{3+}, Co^{2+}	0.01*M*	40
Cr(VI)	0.001*M*	15
Cu^{2+}	0.01*M*	15
Mn^{2+}	†	5
Fe^{2+}	†	2.5

*100(±4)% recovery of 5 μg/ml of sulphite was obtained in the presence of the stated concentrations.
†No significant improvement when EDTA was used.

tolerated in the determination of 5 μg/ml sulphite by the proposed method. Since the maximum reported values[12] of these ions in the atmosphere are low, they should not interfere significantly with the determination. These cationic interferences are due to the formation of stable complexes or insoluble compounds with sulphite.

Application

Determination of sulphur dioxide in air. The proposed method looks attractive particularly for SO_2 determination in air because it does not suffer seriously from nitrogen dioxide interference. Some methods in the literature have this major set-back. It was therefore decided to investigate the application of the proposed method to SO_2 determination in air.

The most widely applicable method for the collection and determination of sulphur dioxide in air is that of West and Gaeke.[4,11,12] The gaseous sulphur dioxide is absorbed into a solution of potassium or sodium tetrachloromercurate, TCM. The retention of the sulphur dioxide is due to the formation of monochlorosulphonato–mercurate(II) complex. The latter is treated with formaldehyde and specially purified, acid bleached pararosaniline, to form a red–violet complex, pararosanilinemethylsulphonic acid, and the absorbance is measured at 548 or 575 nm.

The application of the proposed method to the determination of sulphur dioxide stabilized by various concentrations of TCM was investigated in an attempt to establish the optimum TCM concentration that would be suitable for absorbing sulphur dioxide from air. The results in Fig. 7 indicate that TCM concentrations in the range 2–10mM did not affect significantly the emission intensity from 5 μg/ml of sulphite while concentrations greater than 0.01M reduced the emission intensity drastically. Therefore, complete recovery of sulphite occurs from TCM concentrations $<0.01M$. When 30mM was used, the emission intensity from 5 μg/ml sulphite was quenched completely. It was therefore decided that the final concentration of TCM in the analyte solution should not exceed 0.01M TCM. If air is purged through higher concentrations of TCM, then appropriate dilution should be made to ensure that the final concentration of TCM does not exceed 0.01M.

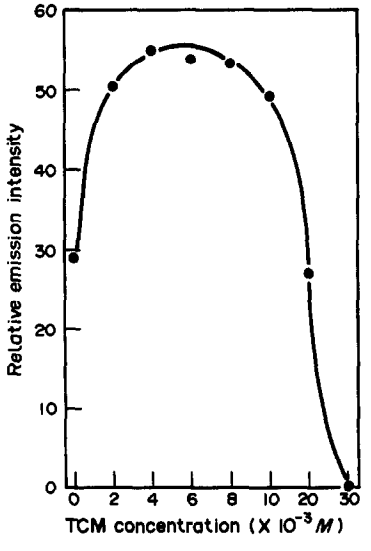

Fig. 7. Effect of TCM concentration on the emission intensity of 5 μg/ml of sulphite.

Table 3. Determination of sulphur dioxide in air

Sample No	Sulphur dioxide/μg/m³ West–Gaeke Method	CFES Method
1	16.5	16.8
2	15.7	15.6
3	19.9	20.3
4	17.4	17.1
5	14.4	14.6

Analysis of atmospheric sulphur dioxide in the vicinity of the University Chemistry laboratory was carried out by both the conventional West–Gaeke method and the proposed method. One cubic meter of air was sampled from outside the laboratory window. The air was pulled through a fritted glass bubbler containing 20 ml of the absorbing solution for a period of about 1 hr at a flow rate of about 15 l./min. The

Table 4. Determination of sulphur dioxide in diluted samples obtained from the permeation tube device

Sample No	Sulphur dioxide/μg/ml West–Gaeke Method	CFES Method
1	3.85	3.87
2	3.50	3.40
3	1.60	1.64
4	5.33	5.23
5	2.25	2.15
6	1.70	1.74
7	2.15	2.21
8	3.35	3.31
9	4.45	4.55
10	6.50	6.43

Linear regression: y (W–G) = 0.04 + 0.98x (CFES); r = 0.9990.

absorbing solution was then transferred to a 25-ml standard flask and made to the mark with TCM. Aliquots of the solution were subsequently analysed by the method of West–Gaeke[4] and by the proposed method. The results obtained by both methods are in good agreement as shown in Table 3. Also, samples collected from a permeation tube system were diluted with TCM and analysed by the proposed method and the West–Gaeke method. The results are shown in Table 4. Again the agreement is good.

Determination of sulphur dioxide in wines. The proposed method was also applied to the determination of total SO_2 in wines. A 50 ml aliquot of the wine sample was first reacted with 10 ml of 25% sodium hydroxide for 10 min[24] at room temperature to liberate aldehyde-bound sulphite. Aliquots of the treated wine were then diluted twenty times with 0.01*M* TCM and analysed by the proposed method. However, analysis of some samples of wines at this level of dilution gave poor and unreproducible results. This is because some of the evolved gaseous SO_2 were trapped by liquid droplets and consequently prevented from reaching the flame. This is possibly due to a matrix effect of the wine which limits the diffusion of sulphur dioxide. Fifty-fold dilution of such wine samples with 0.01*M* TCM solved the problem. The results are compared with those obtained by the standard method recommended by the EEC[25] which involves the direct titration with iodine after a prior alkaline hydrolysis. The results in Table 5 show reasonable agreement between the two methods. Recovery studies were carried out by analysing, using the proposed method, aliquots of the treated wine samples spiked with known amounts of the standard solution. The results which are shown in Table 6, indicate recovery in the range 95.4–105.4%, with a mean recovery of 100.7% and a relative standard deviation of 2.4%.

Table 5. Comparison between the proposed and the recommended methods for the determination of total sulphite (μg/ml SO_2) in wines

Wine	Recommended* method	CFES† method
White—sweet	83.8	81.9
White—sweet	120.3	118.4
White—dry	91.2	88.4
Red	70.4	72.0
Red	105.6	102.1

*Mean of three values.
†Mean of five values.

Table 6. Recovery of sulphite added to wine samples

Type of wine	Sulphur dioxide,* μg/ml: Initially present	Added	Found	Recovery, %
1		0.92	5.03	102.2
		1.84	5.97	102.2
White—sweet	4.09	2.76	6.87	100.7
		3.68	7.73	98.9
2		0.92	3.32	103.3
		1.84	4.20	99.5
White—sweet	2.37	2.76	5.18	101.8
		3.68	6.10	101.4
3		0.92	3.59	102.2
		1.84	4.53	102.2
White—dry	2.65	2.76	5.35	97.8
		3.68	6.32	99.7
4		0.92	4.50	97.8
		1.84	5.42	98.9
Red	3.60	2.76	6.37	100.4
		3.68	7.09	95.4
5		0.92	3.01	105.4
		1.84	3.89	100.5
Red	2.04	2.76	4.78	99.3
		3.68	5.88	104.3

*Mean of three values.

CONCLUSION

The conversion of sulphite and sulphur dioxide [fixed as disulphitomercurate(II)] to hydrogen sulphide by reduction with $NaBH_4$ has been used to provide a sensitive, cool flame emission spectrometric method for the determination of sulphur dioxide and sulphite. The proposed method, which is more sensitive than some of the earlier reported methods, is simple, versatile and capable of good precision. It offers speed and convenience of operation for the routine analysis of large numbers of samples. Interferences are known but their effects may be minimized if not totally eliminated. An attractive feature of the method is its relative freedom from nitrogen dioxide interference (added as nitrite) and its selectivity in the presence of sulphate which is not reduced. A maximum of forty samples can be analysed in one hour and the results obtained by the proposed method correlate well with those obtained using an official method. Considering the excellent sensitivity obtained in this work because of the use of $NaBH_4$ and the large number of techniques based on acidification of sulphite and SO_2 stabilized samples prior to their determination, the adoption of the proposed approach is to be recommended.

Acknowledgements—The authors thank the Commonwealth Scholarship Commission and the University of Agriculture, Abeokuta, Nigeria for financial support and leave of absence, respectively, for T.A.A.

REFERENCES

1. Environmental Health Criteria 8—*Sulphur Oxides and Suspended Particulate Matter*, WHO, Geneva, 1979.
2. W. J. Williams, *Handbook of Anion Determination*, 1st Ed., p. 587. Butterworth, London, 1979.
3. J. E. Sickles, II and P. M. Grohse, *Sampling and Analysis Methods for Sulfur Dioxide and Nitrogen Dioxide: A Literature Review*. Research Triangle Institute Report No RTI/2823/00-011, Research Triangle Institute, Research Triangle Park, North Carolina, 1984.
4. American Public Health Association, Intersociety Committee, *Method of Air Sampling and Analysis*, 2nd Ed., Washington, DC, 1977.
5. C. D. Frezier, *Ion Chromatogr. Anal. Environ. Pollut.*, 1979, **2**, 211; *Chem. Abstr.*, 1980, **93**, 30944y.
6. J. Janak and Z. Vezera, *Mikrochim. Acta*, 1990, **III**, 29.
7. G. Schiavon, G. Zotti, R. Toniolo and G. Bontempelli, *Analyst*, 1991, **116**, 797.
8. S. S. Brody and J. E. Chaney, *J. Gas Chromatogr.*, 1966, **4**, 42.
9. A. C. Calokerinos and A. Townshend, *Z. Anal. Chem.*, 1982, **311**, 214.
10. S. A. Al-Tamrah, A. Townshend and A. R. Wheatley, *Analyst*, 1987, **112**, 883.
11. P. W. West and G. C. Gaeke, *Anal. Chem.*, 1956, **28**, 1816.
12. F. P. Scaringelli, B. E. Saltzman and S. A. Frey, *ibid.*, 1967, **39**, 1709.
13. P. MacLaurin, K. S. Parker, A. Townshend, P. J. Worsfold, N. W. Barnett and M. Crane, *Anal. Chim. Acta*, 1990, **238**, 171.
14. J. F. Alder and K. Kargosha, *ibid.*, 1979, **111**, 145.
15. N. Grekas and A. C. Calokerinos, *Analyst*, 1985, **110**, 335.
16. T. A. Arowolo and M. S. Cresser, *ibid.*, 1991, **116**, 1135.
17. *Idem*, *ibid.*, 1991, **116**, 595.
18. N. Grekas and A. C. Calokerinos, *Anal. Chim. Acta*, 1989, **225**, 359.
19. D. D. Nygaard, *ibid.*, 1981, **127**, 257.
20. T. A. Arowolo and M. S. Cresser, *Microchem. J.*, 1992, **45**, 97.
21. M. N. Brenner, J. L. Owades and T. Fazio, *Proc. Amer. Soc. Brewing Chem.*, 1955, 133.
22. W. Kijowski and P. A. Steudler, *Limnol. Oceanogr.*, 1982, **27**, 975.
23. R. G. Godden and D. R. Thomerson, *Analyst*, 1980, **105**, 1137.
24. S. F. Lewis and A. Syty, *Atom. Spectrosc.*, 1983, **4**, 199.
25. *Off. J. Eur. Comm.*, 14 May 1982, **L133**, 55.

Talanta, Vol. 39, No. 11, pp. 1479–1487, 1992
Printed in Great Britain.

0039-9140/92 $5.00 + 0.00

DETERMINATION OF DISSOLVED ORGANIC PHOSPHORUS IN SOIL SOLUTIONS BY AN IMPROVED AUTOMATED PHOTO-OXIDATION PROCEDURE

M. D. RON VAZ, A. C. EDWARDS, C. A. SHAND
Plants Division, Macaulay Land Use Research Institute, Craigiebuckler, Aberdeen AB9 2QJ, U.K.
M. CRESSER*
Department of Plant and Soil Science, University of Aberdeen, Aberbeen AB9 2UE, U.K.

(*Received* 2 *December* 1991. *Revised* 28 *February* 1992. *Accepted* 28 *February* 1992)

Summary—An improved automated photo-oxidation procedure to determine dissolved organic phosphorus in soil solutions is described. Organically combined phosphorus is converted quantitatively to orthophosphate under UV radiation and an excess of dissolved oxygen. The orthophosphate is determined spectrophotometrically using the Murphy and Riley procedure, modified by increasing the concentration of ascorbic acid. Fluoride was added to the system to overcome potential interference when working with soil solution. The limit of detection was 0.64 μg/l. PO_4^{-3} – P and calibration was linear over the range studied (5–1000 μg/l. PO_4^{-3} – P).

An adequate supply of soil phosphorus in a plant-available form is essential to sustain current levels of agricultural production. Despite the low solubility of soil phosphorus (P) compared to several other nutrients, some is still lost naturally through weathering and leaching processes.[1] Organic phosphorus may account for 3–75% of the total P in soil.[2] Organically-bound P is generally only available to plants once it has been mineralized and the rapid mineralization of simple organic compounds such as phospholipids, phosphosugars, nucleotides and nucleic acids is therefore of considerable importance.[3]

Several workers have reported that organic P occurs in soil solution at concentrations up to 20 times those of inorganic P.[4] In such solutions and in surface waters, phosphorus occurs in both particulate and dissolved forms. Analytically it is useful to further subdivide the dissolved phosphorus fraction. The fractions commonly used to characterize dissolved phosphorus include:[5]

(i) Total dissolved phosphorus (TDP), conventionally defined as the phosphorus which may be filtered through a membrane filter (0.45 μm). Such filtrate may include colloidal material in addition to dissolved phosphorus. TDP may be determined by converting all forms of P present after filtration to orthophosphate (using hydrolysis and oxidation) and subsequent spectrophotometric determination of the orthophosphate. Alternatively TDP can be determined by an atomic spectrometry technique such as inductively coupled plasma–atomic emission spectroscopy.

(ii) Dissolved reactive phosphorus (DRP), defined as the fraction of dissolved phosphorus which will react directly with molybdate ions to form a phosphomolybdate complex. This fraction contains primarily orthophosphate and any readily acid-hydrolysable phosphate compounds.

(iii) Dissolved unreactive phosphorus (DUP), defined as what is left when DRP is substracted from TDP. This fraction includes condensed phosphates (poly-, meta- and ultraphosphates) and resistant dissolved organic phosphorus (several organic acids and a variety of phosphate esters).

To study the transfer of P fluxes in ecosystems it is necessary, especially for nutrient-poor, organic soils to be able to determine these three P fractions. Furthermore, there is a need for a technique for determination of dissolved organic P (DOP) in its own right.

The use of UV photochemical oxidation as a first step towards detecting low levels of organic

*Author for correspondence.

material in water is convenient.[6] Armstrong *et al.*[7] reported the complete oxidation of organic carbon to carbon dioxide and the release of organically bound phosphorus and nitrogen under the action of UV radiation at wavelengths below 250 nm. Further investigations of the oxidation of organic matter and the release or organic phosphorus, nitrogen and iron have demonstrated that photo-oxidation in the presence of oxygen, or oxygen-releasing compounds, is at least as efficient as chemical oxidation.[8–10] A segmented-flow AutoAnalyser system, using a silica coil irradiated with UV light, has been adapted by a number of workers for determination of the organic carbon component in water samples.[11–13] One potential advantage of photochemical oxidation for organic P determination is that condensed phosphates are not broken-down except in strong acid solutions.[14] The organically combined phosphorus is converted quantitatively to orthophosphate under UV radiation in the presence of dissolved oxygen. Therefore, if dissolved reactive phosphorus (DRP) is determined colorimetrically before irradiation, and DRP plus oxidized organic P after irradiation, the difference between the two values should give the amount of DOP in the sample.

Most automated methods for the determination of phosphate following UV radiation are concerned primarily with the determination of TDP, which can only provide a limited amount of information on P cycling. The determination involves the hydrolysis of condensed phosphates either by photo-oxidation in the presence of acid or by heating irradiated samples in the presence of diluted acid.

McKelvie *et al.*[15] developed a semi-automated system for the spectrophotometric determination of DOP in natural waters using flow injection (FI) and in-line photo-oxidation. They used tin(II) chloride reduction of phosphomolybdate for the spectrophotometric determination of the dissolved reactive phosphorus (DRP) produced by the photo-oxidation. However, the use of tin(II) chloride as a reductant in the determination of DRP has some shortcomings:[16] the absorbance is markedly temperature-dependent, the colour is relatively unstable, large amounts of soluble salts, arsenates and copper interfere, and the method is unsatisfactory at high concentrations.

The semi-automated flow injection procedure proposed by McKelvie *et al.*[15] appears to suffer from several limitations which make it inadequate for analysis of soil extracts. When their procedure was applied to "real samples", the relationship between TDP, DOP and DRP was given by:

$$[\mathrm{TDP}] = 1.200([\mathrm{DOP}] + [\mathrm{DRP}]) - 0.001$$

The high slope value was attributed to the probable occurrence of condensed phosphates in some samples, although no direct experimental evidence was presented to support this suggestion. The equation implies a linear relationship between condensed phosphate P and ([DOP] + [DRP]), a surprising observation if correct. Only when data for 16 of the 25 samples analysed was rejected was a slope close to unity (1.013) obtained.

An alternative explanation is that organic matter photochemical oxidation was incomplete for more organic-rich samples under the chemical conditions and with the photoreactor eventually used.

McKelvie *et al.*[15] went to considerable lengths to overcome problems of bubble production from the autodecomposition of irradiated, strongly alkaline persulphate in the FI manifold, but still found that precision was adversely effected by bubble production effects. Moreover, orthophosphate and gluscose-6′-phosphate gave significantly different calibration graphs as a consequence of interruption of flow by bubble production.

In McKelvie's work, it was assumed that inorganic concomitants did not interfere, but the present authors encountered problems from aluminium released from organic complexes following photo-oxidation. This aluminium could be retained in the oxidation coil, probably as hydrous oxide, which subsequently retained phosphate, causing low recoveries and calibration drift. Such an effect could also have contributed to the high slope of the [TDP] *vs.* ([DOP] + [DRP]) plot mentioned above.

The present authors therefore decided to evaluate a segmented-flow system, in which bubble removal should be greatly facilitated, and a method for overcoming aluminium interference. It was further decided to attempt to minimise unnecessary dilution, and to exploit the improved precision attainable by the Murphy and Riley[17] procedure, rather than the tin(II) chloride method, for colorimetric orthophosphate determination, in an attempt to push the detection limit below that of 10 μg/l. claimed by McKelvie *et al.*[15]

EXPERIMENTAL

Instrumentation

DOP manifold. The manifold developed is shown in Fig. 1. It was set up taking into consideration the required mixing volume ratios, colour development time and the need for thorough mixing of samples and reagents. Mixing coils used were 15-turn and 45-turn respectively (20-mm coil diameter, 2-mm i.d.); the delay coil was 22-turn (165 mm coil diameter, 2 mm i.d.). A Sterilin Instruments autosampler (10 samples/hr) and a Chemlab CPP 15 peristaltic pump were used for sampling and reagent delivery.

The UV irradiation system consisted of a 50-turn silica coil (32-mm coil diameter, 1-mm i.d.) irradiated by a Voltarc UV-Lux tube.

Orthophosphate determination (DRP) in irradiated samples was carried out using a procedure modified from Murphy and Riley.[17] The absorbance of the phosphomolybdenum blue was measured at 882 nm using a 40-mm flow cell in a CE 393 Digital Grating Spectrophotometer connected to a 2 pen Kompensograph X-T C1012 Recorder.

The difference in DRP values for irradiated and non-irradiated sample (UV lamp on and off) gives the amount of dissolved organic P present in the sample.

Reagents

All aqueous solutions were prepared with milli-Q ultra pure water. Unless otherwise indicated, all reagents were AnalaR grade or equivalent.

DOP Manifold

Fluoride. A 1.105-g weight of sodium fluoride was dissolved in 100 ml of water.

Saturated potassium persulphate. A 6.4-g weight of potassium persulphate was dissolved in 100 ml of water. Warm to dissolve, and allow to cool to room temperature; stand to allow some crystallization, otherwise it will crystallize in the manifold tube.

Mixed reagent. Potassium antimonyl tartrate solution (a): dissolve 0.2908 g of $K(SbO)C_4H_4O_6.\frac{1}{2}H_2O$ in 100 ml of water. Ammonium molybdate solution (b): dissolve 12 g of $(NH_4)_6Mo_7O_{24}.4H_2O$ in 250 ml of water. Sulphuric acid (2.5*M*) (c): dilute 148 ml of concentrated sulphuric acid to one litre with water. Mix the three solutions thoroughly and make up to two litres with water. This reagent must be kept in a dark cupboard.

Ascorbic acid. Dissolve 11 g of $C_6H_8O_6$ in 250 ml of water and add 150 μl of aerosol 22 as wetting agent. This solution is stable for about one week at 4° in the dark.

Phosphorus model compounds

A range of phosphorus compounds found in natural waters was analysed by the proposed method to quantify individual responses to

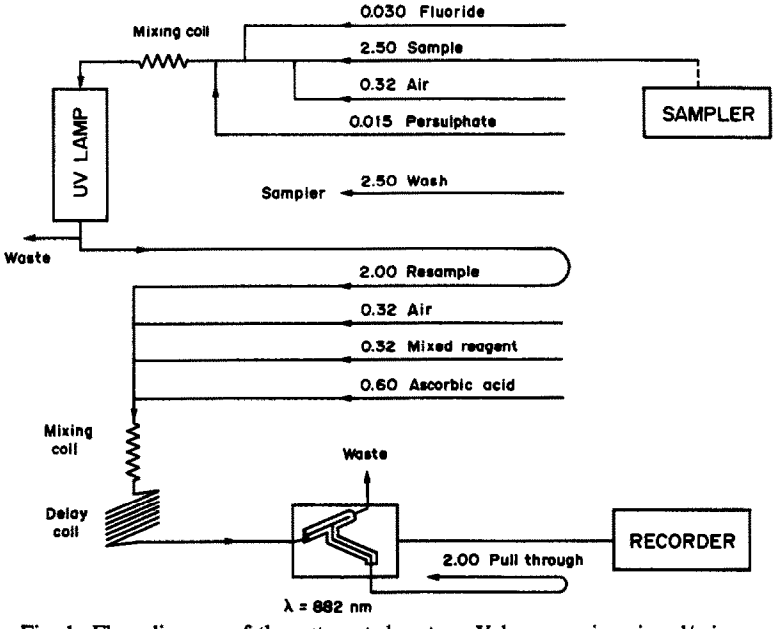

Fig. 1. Flow diagram of the automated system. Values are given in ml/min.

the method. The compounds studied were potassium dihydrogen phosphate, trimetaphosphate trisodium salt, tetrasodium pyrophosphate, α-D-glucose-1-phosphate, β-glycerophosphate, phytic acid, 2-aminoethylphosphonic acid, adenosine-2′(3′)-phosphoric acid monohydrate, nicotinamide adenine dinucleotide (reduced form), and adenosine-5′-triphosphoric acid disodium dihydrogen salt (general purpose reagent grade).

Working standard solutions of these compounds were prepared in the range 5–1,000 μg/l. P by dilution of the stock solutions. All the solutions were stored at 4° to minimize risk of microbial growth.

Optimization of the method

To optimize the signal:noise ratio, the Murphy and Riley procedure was modified by increasing the amount of ascorbic acid, and using persulphate as an oxidizing agent. Fluoride was added to the system to prevent interference from Al released upon organic matter breakdown. These aspects are discussed later.

Soil extracts and suction cup lysimeter samples: TDP, DOP and DRP analysis

Samples were collected at Glensaugh Research Station (National Grid Reference NO 660803). The soil is a peaty podzol (Typic placaquad, Strichen association, Gaerlie series) typical of the area. Porous ceramic suction cup samplers[18] were installed and samples collected every two weeks when water had been sucked into the cups. Soil cores, 100 mm in diameter and 120 mm deep, were collected at monthly intervals. All soil was sieved (< 6 mm) immediately on return to the laboratory, and stored field-moist at 4°.

Water extracts were obtained by shaking soil and water at a 1:10 ratio (m:v). Solutions were centrifuged at 2000 *g* for 15 min, and the supernatant solutions were further centrifuged (19000 *g*, 30 min), then filtered through a No. 42 filter paper to remove traces of suspended material. Solutions were stored at 4° prior to chemical analysis. Blanks were prepared similarly.

Total dissolved phosphorus values were obtained following a persulphate digestion method.[19] Dissolved organic phosphorus and dissolved reactive phosphorus values were obtained by the proposed method.

RESULTS AND DISCUSSION

Optimization of the method

Colour development. The automated method consists of two stages:

(1) Photo-oxidation of the sample; the sample is exposed to UV radiation in the presence of an oxidizing agent. Organically-bound phosphorus is released as inorganic phosphate.

(2) Determination of DRP; by the spectrophotometric determination as a reduced phosphomolybdate complex in acid solution after irradiation of the sample.

The amount of ascorbic acid used had to be increased to overcome residual effects of the oxidizing agent used in the first stage. To optimize the concentration of ascorbic acid, 4.2 ml of 500 μg/l. $PO_4^{-3} - P$, spiked with 20 μl of 30% m/v hydrogen peroxide solution (100 volume), was passed through the silica coil, with the UV lamp either on or off. The solution was collected and analysed colorimetrically (manually) using different concentrations of ascorbic acid. A 10-mm flow cell was used in this experiment [Fig. 2(a)].

In Fig. 2(a), the horizontal axis represents the final concentration of ascorbic acid in the sample, before any oxidation. The concentration of ascorbic acid required to give maximum absorbance in the presence of 20 μl of 30% m/v hydrogen peroxide should be $> 0.04M$ with the lamp on and $> 0.064M$ with the lamp off. When the UV lamp is on, hydrogen peroxide will be partially decomposed to O_2, and partially used in the decomposition of the organic matter. Therefore, less ascorbic acid is required compared to the amount needed when the UV lamp is off. In normal working conditions, the UV lamp will be on and, therefore, the minimum concentration of ascorbic acid required would be $0.04M$.

A similar experiment was carried out using a saturated persulphate solution as an alternative oxidizing agent; 4.2 ml of 250 μg/l. $PO_4^{-3} - P$ solution was spiked with 30 μl of saturated potassium persulphate; the sample was analysed colorimetrically (40-mm flow cell) using the same range of concentration of ascorbic acid as in the previous experiment, but the UV lamp was always off. In this case, the minimum concentration of ascorbic acid required to give maximum absorbance in the presence of persulphate was $> 0.016M$ [Fig. 2(b)]. An excess of

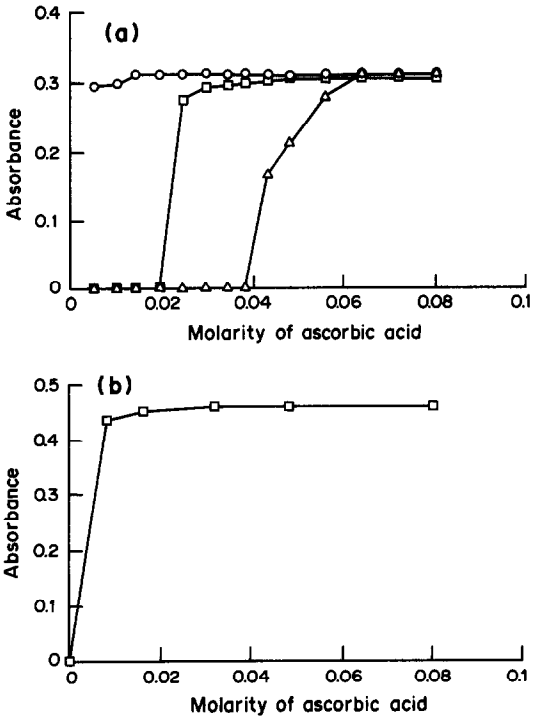

Fig. 2. Optimization of the final concentration of ascorbic acid in the assay (a) with hydrogen peroxide and UV lamp switched on (—□—), with hydrogen peroxide but the UV lamp switched off (—△—) and without hydrogen peroxide or UV illumination (—○—); (b) with potassium persulphate and UV lamp switched on (—□—).

ascorbic acid (0.046*M*) was chosen as final concentration in the sample stream.

Oxidizing agent

Initially, hydrogen peroxide was chosen as oxidizing agent to provide a source of hydroxyl radicals which, in addition to ultraviolet radiation, will decompose dissolved organic matter and convert organic phosphorus to inorganic phosphate. The amount of hydrogen peroxide added to the system was optimized in order to maximize the signal: noise ratio and to avoid the formation of unwanted products which could be produced in the presence of an excess of hydrogen peroxide. Phytic acid and several soil extract samples were run using different concentrations of hydrogen peroxide prepared by dilution of a 30% m/v hydrogen peroxide solution (100 volume). Peak heights were recorded (Fig. 3).

The optimum concentration of hydrogen peroxide was found to be between 3 and 4.5% m/v (Fig. 3). Peak heights decreased when using a 6% m/v concentration and peak shapes were not clearly defined when the amount of hydrogen peroxide was increased to 9% m/v (Fig. 4). From 3 to 4.5% m/v hydrogen peroxide, the

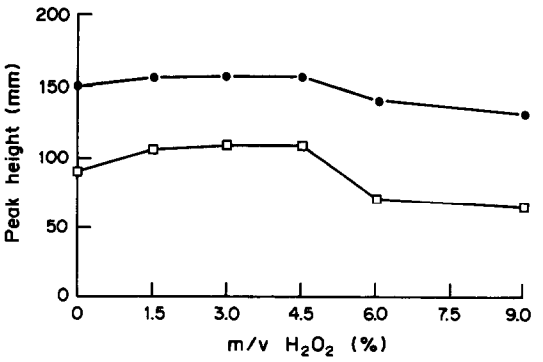

Fig. 3. Optimization of the amount of hydrogen peroxide (a) using phytic acid as a standard (—●—) and (b) using a soil extract sample (—□—).

peak heights were constant, but the baseline was less stable when using hydrogen peroxide solutions stronger than 3.75% m/v; therefore the optimum hydrogen peroxide concentration was found to be 3% m/v. However, when samples from suction cup lysimeters were run through the system, the analytical response for DOP + DRP was generally smaller than the one obtained for DRP alone. This phenomenon did not occur with a saturated potassium persulphate solution as oxidizing agent (Table 1). It is probable that oxygen gas release rates from hydrogen peroxide upon irradiation are different in the presence and absence of soil organic matter in the suction cup samples. This may be due to the presence of particulates acting as nucleation centres, thus causing different mixing patterns between samples and the organic-free standards. Persulphate was therefore used in subsequent work, rather than hydrogen peroxide.

Addition of fluoride

When soil solution samples were run through the system, following synthetic standards, a decrease in the peak heights for the next batch

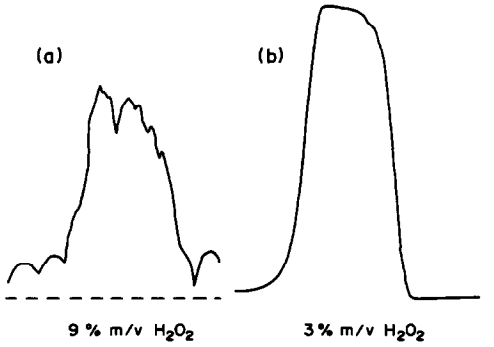

Fig. 4. The deformation in the peak shape when using a high concentration of hydrogen peroxide.

Table 1. Comparison of DOP values obtained for suction cup lysimeter samples using different oxidizing agents

Sample	DRP	DOP + DRP*	DOP*	DOP + DRP†	DOP†
1	194	152	−42	217	+23
2	190	152	−38	209	+19
3	152	166	−40	169	+17
4	160	122	−38	174	+14
5	256	272	+16	286	+30
6	313	305	−8	359	+46

*Hydrogen peroxide,
†Potassium persulphate.
Values are in μg/l. P.

of standards run after the samples was observed (Table 2). Thus running the samples resulted in a source of phosphorus removal, possibly via contamination of either manifold tubes and/or of the silica coil. Manifold tubes were replaced but the loss of phosphorus was still observed indicating that the silica coil was contaminated.

One possible explanation for this source of phosphorus loss could be aluminium interference. When organic matter of acid organic soil origin is decomposed under UV radiation in the presence of hydrogen peroxide or potassium persulphate, aluminium is liberated, and may be adsorbed on the surface of the silica coil in the form of hydrous aluminium oxide which then strongly adsorbs phosphorus: $Al(OH)_2^+ + H_2PO_4^- \rightarrow Al(OH)_2H_2PO_4$. The problem was solved using a new silica coil and spiking the standards with a concentrated solution of fluoride. Fluoride forms a strong complex with aluminium and therefore prevents the aluminium oxide accumulation and subsequent loss of phosphorus. Experiments were carried out to establish that aluminium was the source of contamination by adding 1,000 μg/l. Al^{3+} to standards and passing them through a clean silica coil, then looking at the difference in the absorbance between standards with and without aluminium. The results proved that aluminium was the problem.

The stability of the colour developed in the modified phosphomolybdenum blue reaction in the presence of a large amount of fluoride was studied. No differences in absorbance values occurred, but it was found that the rate of reaction decreased in the presence of fluoride. A delay coil was incorporated into the manifold to give around 12 min of colour development time which was sufficient to reach maximum absorbance.

Table 2. Concentration of P in standards run before and after samples

μg/l. $PO_4^{-3}-P$	μg/l. PO_4^{-3} before sample run	μg/l. $PO_4^{-3}-P$ after sample run
50	47	—
100	99	47
200	203	138
300	296	241
400	416	351
500	489	413

Recovery, linearity and limit of detection

The recovery of phosphorus from different phosphorus compounds was measured using the proposed method. Firstly, 200 μg/l. P solutions of each compound were run using the autoanalyzer procedure with the UV lamp off to ensure that the analytical response for DOP was not due to DRP impurities. The same solutions were run with UV lamp on and without persulphate, and with UV lamp on with persulphate. The results (Table 3) show that complete recovery was achieved for several compounds but very low recovery was obtained for the inorganic condensed phosphorus (trimetaphosphate, pyrophosphate) and for the condensed organic compounds (adenosine triphosphate (ATP), nicotinamide adenine dinculeotide, reduced form (NADH)]. The apparent recoveries, in addition to DRP for the condensed organic compounds (Table 3), could be due to organic impurities. Furthermore, total recovery was achieved without using persulphate, which means that UV radiation, in addition to the dissolved oxygen present either from the air bubbles or in the water, was enough to release organic phosphorus bound in the ester form [phytic acid, α-*D*-glucose-1-phosphate, β-glycerophosphate, adenosine-2′(3′)-phosphoric acid], or via a C—P bond (2-aminoethylphosphonic acid). The recovery values for adenosine-2′(3′)-phosphoric acid (AMP) and adenosine-5′-triphosphoric acid show that the UV radiation, in addition to hydroxyl radicals, will release the organic phosphorus but as an orthophosphate group for AMP and probably as

Table 3. Recovery of model phosphorus compounds

Compounds	Recovery 1 (%)	$\sigma(n-1)$ (%)	Recovery 2 (%)	$\sigma(n-1)$ (%)
Phytic acid	100.50	0.10	101.50	0.02
β-Glycerophosphate	99.33	0.12	99.00	0.00
α-*D*-Glucose-1-phosphate	100.30	0.12	99.50	0.12
2-Aminoethylphosphonic ac	100.50	0.00	99.83	0.12
Adenosine-2′(3′)-phosphoric acid.	97.50	0.00	96.50	0.00
Mixture*	99.47	0.00	99.34	0.00
Nicotinamide adenine dinucleotide.	8.00	0.12	8.00	0.02
Adenosine-5′-triphosphoric acid	8.00	0.12	8.00	0.02
Trimetaphosphate†	7.00	0.00	7.00	0.00
Pyrophosphate†	6.00	0.10	6.00	0.00

Recovery 1 = UV light + persulphate
Recovery 2 = UV light
$n = 3$
*Mixture = 50 μg/l. P as Phytic acid + 50 μg/l. AMP − P + 50 μg/l. P as glycerophosphate + 50 μg/l. P as glucosephosphate.
†Due to DRP impurities.

a triphosphate group for ATP, and the latter cannot be determined by the colorimetric phosphomolybdenum blue method. The same explanation could be applied to NADH. In other words UV radiation in addition to the hydroxyl radicals does not break P–O–P bonds. If it did, the analytical response would be total dissolved phosphorus.

The complex chemical nature of phosphorus containing organic compounds likely to be encountered in soil solution requires the use of persulphate to ensure complete photo-oxidation (Table 4).

Sugimura and Suzuki[21] reported that neither UV photo-oxidation methods or low temperature chemical oxidation methods are 100% efficient for oxidizing organic carbon in seawater. However, a comparison of total organic carbon determined either by an automated photo-oxidation procedure (similar to the one described here) and a furnace combustion procedure (TOCsin II, Phase Sep.) showed a high degree of correlation for a range of natural water samples containing up to 52 μg/ml.[22]

Table 4. Comparison of DOP values obtained for soil extract samples

Sample	DOP*	DOP†
1	49	85
2	53	87
3	43	68
4	57	89
5	45	61
6	36	64
7	66	92
8	58	79
9	55	75
10	86	99

*UV lamp on and without potassium persulphate.
†UV lamp on and with potassium persulphate.
Values are in μg/l. P

The linearity of the DOP automated procedure was checked (Fig. 5). The range studied was from 5 to 1,000 μg/l. $PO_3^{-3} - P$. The calibration shows good linearity over this range ($r^2 = 0.9999$, peak height (mm) $= -9.14 + 2.12[\mu g$ 1. P]). Limit of detection[20] (defined as the determinant concentration giving a signal equal to the blank signal, Y_B, plus three standard deviations of the blank, S_B) was 0.64 μg/l. P which could be improved by using a 50-mm flow cell.

Soil extract and suction cup lysimeter samples: TDP and (DOP + DRP) analysis

Analyses for TDP (acid persulphate digestion) and DOP + DRP (autoanalyser) were

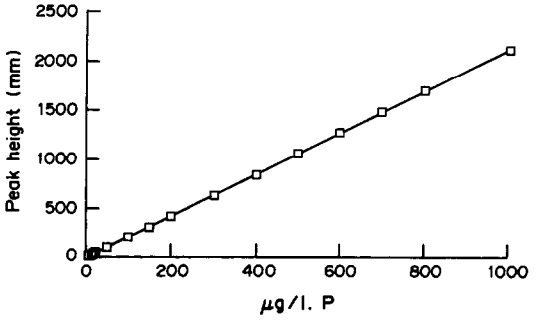

Fig. 5. Calibration graph using orthophosphate standards. Orthophosphate was run as standard.

carried out in twenty suction cup lysimeter samples and twenty soil extract samples.

Comparison of TDP values with DRP + DOP values in both types of sample are represented in Fig. 6(a) and 6(b). For suction cup lysimeters a good correlation was obtained ($r^2 = 0.998$, TDP = 1.8 + 1.048[DOP + DRP]); in this type of sample TDP and DOP + DRP values are almost equal which means that the DUP fraction is formed almost entirely of DOP. However, for soil extract samples the values obtained for TDP were higher than the ones obtained for DOP + DRP {Fig. 6(b), $r^2 = 0.982$, TDP = 56.2 + 1.005 [DOP + DRP]}; therefore in this type of sample the DUP fraction is formed primarily by DOP and a residual fraction formed by dissolved condensed P compounds (DCP). The relationship between each of the different phosphorus fractions (TDP, DRP, DOP and DCP) will be expected to vary with factors such as soil type, climate and fertilizer additions.

CONCLUSIONS

The detection limit obtained with the proposed procedure, 0.64 μg/l., was substantially better than the detection limit of 10 μg/l. obtained by McKelvie *et al.*[15] Such a low detection limit was necessary for analysis of some of the soil solution samples studied. A satisfactory and simple procedure has been found for overcoming interference from aluminium. The segmented flow system obviates the need for adding a high pH sodium tetraborate buffer to absorb evolved carbon dioxide. Results for lysimeter samples suggested that condensed phosphate concentrations were negligible in all the samples tested, and very small for the soil extracts. This is in marked contrast to the results of McKelvie *et al.*[15] for waters. They needed to suggest, for effluent-rich samples, a linear relationship between condensed phosphate and ([DOP] + [DRP]). The results reported in this work require no such assumption.

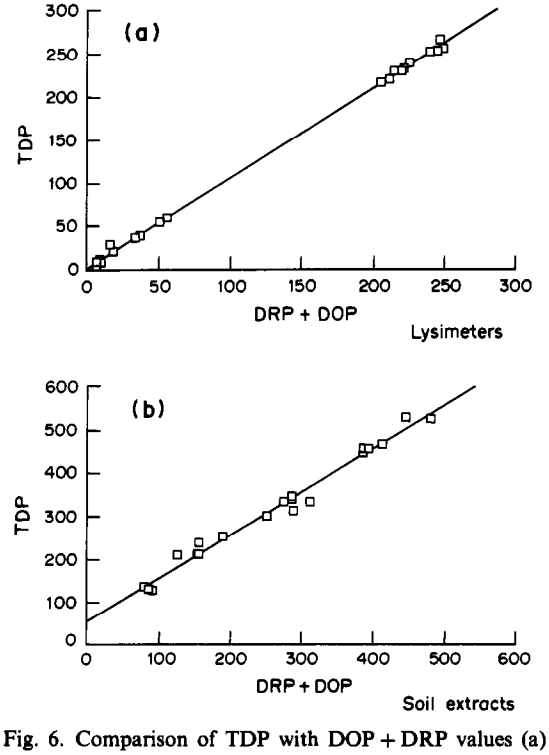

Fig. 6. Comparison of TDP with DOP + DRP values (a) when working with suction cup lysimeter samples and (b) when working with soil extract samples. Values are given in μg/l. P.

Acknowledgements—M. D. Ron Vaz acknowledges receipts of a research grant from the Ministerio de Educacion y Ciencias (Spain).

REFERENCES

1. G. W. Thomas, *Nutrient Mobility in Soils: Accumulations and Losses* O. P. Engelstad (ed.), Soil Sci. Soc. Am., Wisconsin, 1970.
2. S. R. Olsen and N. Fried, *The 1957 Yearbook of Agriculture*, A. Stefferud (ed.), p. 94. USDA, Washington, 1957.
3. A. F. Harrison, *Soil Organic Phosphorus, A Review of a World Literature*, p. 87. C. A. B. International, 1987.
4. A. F. Harrison, *ibid.*, p. 67. C. A. B. International, 1987.
5. O. Broberg and Persson, *Phosphorus in Freshwater Ecosystems*, G. Persson and M. Jansson (ed.), Academic Publishers, 1985.
6. J. Beattie, C. Bricker and G. Garvin, *Anal. Chem.*, 1961, **33**, 1890.
7. F. A. J. Armstrong, P. M. Williams and J. D. H. Strickland, *Nature*, 1966, **211**, 481.
8. F. A. J. Armstrong and S. Tibbitts, *J. Mar. Biol. Ass. U. K.*, 1968, **48**, 143.
9. A. Henriksen, *Analyst*, 1970, **95**, 601.
10. L. Zaiyou and W. Limin, *Talanta*, 1986, **33**, 98.
11. K. Grasshoff, *Automation in Analytical Chemistry, Technicon Symposium*, Vol. 1, p. 573. 1966.
12. M. Ehrhardt, *Deep-Sea Res.*, 1969, **16**, 393.
13. J. H. Lowry and R. H. Mancy, *Water Res.*, 1978, **12**, 471.
14. L. Solorzano and J. D. Strickland, *Limnol. Oceanogr.*, 1968, **13**, 515.
15. I. D. McKelvie, B. T. Hart, T. J. Cardwell and R. W. Cattrall, *Analyst*, 1989, **114**, 1459.
16. J. E. Harwood and W. H. J. Hatting, *Environmental Phosphorus Handbook* (ed.), E. J. Griffith, A. M. Beeton, J. M. Spencer, and D. I. Mitchell, p. 289. Wiley, New York, 1973.
17. J. Murphy and J. P. Riley, *Anal. Chim. Acta*, 1962, **27**, 31.

18. T. L. Chow, *Soil Sci.*, 1977,**124**, 173.
19. *Standard Methods for the Examination of Water and Wastewater*, American Public Health Association, American Water Works Association and Water Pollution Control Federation. 15th Ed., 1980, 415.
20. J. N. Miller, *Analyst*, 1991, **116**, 3.
21. Y. Sugimura and Y. Suzuki, *Marine Chemistry*, 1988, **24**, 105.
22. M. D. Ron Vaz, MSc. Thesis (unpublished), Aberdeen University, 1989.

Talanta, Vol. 39, No. 11, pp. 1489–1491, 1992
Printed in Great Britain.

0039-9140/92 $5.00 + 0.00

COLORIMETRIC DETERMINATION OF ETHANOL IN THE PRESENCE OF METHANOL AND OTHER SPECIES IN AQUEOUS SOLUTION

S. A. RAHIM* and S. G. GEESO
Department of Chemistry, College of Science, Mosul University, Mosul, Iraq

(*Received* 1 *March* 1992. *Accepted* 31 *March* 1992)

Summary—Ethanol is coupled with diazotized *p*-aminobenzoic acid, to give a coloured product with maximum absorption at 436 nm. The coloured product has a molar absorptivity of 1.02×10^4 l.mole^{-1}.cm^{-1} and Beer's law is obeyed over the range 0.5–4.0 μg/ml. The relative standard deviation is less than 4.76% and the relative errors are within −2.89–3.9%. The suggested method is rapid, simple, selective and sensitive.

The official AOAC method[1] for the quantitative determination of ethanol in distilled spirits is based on distillation and measurement of specific gravity. This method cannot be used if other alcohols such as methanol are present. Determination of alcohol by measuring its volume in pure form[2] is a lengthy procedure that requires considerable technique and is not suitable for routine analysis. Determination of alcohol in the distillate by measuring physical properties such as specific gravity and refractive index[3–5] is not well suited to very small quantities, or to mixtures containing other volatile ingredients. There are a number of methods based on oxidation with potassium permanganate,[6] iodine pentoxide,[7] or potassium dichromate.[8–19] Other methods include bromometric measurement of ethylene alcohol vapors,[20] conversion of alcohol to ethylnitrite and formed by pyrolytic dehydration of measurement of nitrite formed,[21] spectrophotometric determination of reduced trivalent chromium,[5] or determination by enzymic,[22] amperometric,[23] interferometric,[24] and spectrophotometric[18,19,25,26] methods. These methods are not specific because compounds such as methyl alcohol, ether, chloroform, or formaldehyde interfere. The spectrophotometric methods based on oxidation with potassium dichromate[18,19] and on conversion of ethanol to ester[26] are lengthy and need heating.

This paper presents a novel, simple, rapid, selective and sensitive procedure for the estimation of ethanol, by coupling with diazotized *p*-aminobenzoic acid in alkaline aqueous solution.

EXPERIMENTAL

Reagents

All reagents used were of analytical or microanalytical reagents grade.

Hydrochloric acid, 0.5M aqueous solution.

p-*Aminobenzoic acid, 1.25%*. Freshly prepared in 0.5*M* hydrochloric acid.

Sodium nitrite, 7.5%. Freshly prepared, aqueous solution.

Diazotized p-*aminobenzoic acid.* Freshly prepared by cooling both *p*-aminobenzoic acid and sodium nitrite solutions to about 5°, then mixing 100 ml of *p*-aminobenzoic acid and 10 ml of sodium nitrite solutions, and stirring the mixture for about 5 min. The reagent is stable for more than 20 hr, when stored in a dark and cold place (about 5°).

Sodium hydroxide, 30% aqueous solution.

Stock standard ethanol solution (1 mg/ml). Prepared in water by accurate dilution of an absolute ethanol (99.8%).

Working standard ethanol solution, (0.05 mg/ml). Prepared in water by dilution of stock standard ethanol solution.

Interferent solutions were aqueous.

*Author for correspondence.

Table 1. The optimization of the reagents used in the recommended procedure

Studied property	Optimum value
Concentration of *p*-aminobenzoic acid solution	1.25%
Concentration of sodium nitrate solution	7.5%
Concentration of hydrochloric acid solution	0.5*M*
Stability period of diazotized *p*-aminobenzoic acid Solution	>20 hr
Volume of diazotized *p*-aminobenzoic acid solution	3 ml
Concentration of sodium hydroxide solution	30%
Volume of sodium hydroxide solution	1 ml

Procedure for calibration graph

Pipette 0.1–0.8 ml of working standard ethanol solution into 10-ml standard flasks. Add 3 ml of diazotized *p*-aminobenzoic acid solution and 1 ml of sodium hydroxide solution to each, then dilute to volume with (5–10°) distilled water. Prepare a reagent blank by diluting 3 ml of diazotized *p*-aminobenzoic acid solution and 1 ml of sodium hydroxide solution to 10 ml with (5–10°) distilled water. Measure the absorbance of the standards against the reagent blank within 10 min after dilution in 1-cm cells at 436 nm.

Effect of interferences

In order to study the effect of interferences on the proposed method for the determination of ethanol, pipette suitable aliquot of interferent solutions, each into 10 ml standard flask containing 0.5 ml of working standard ethanol solution, and apply the general procedure on each one.

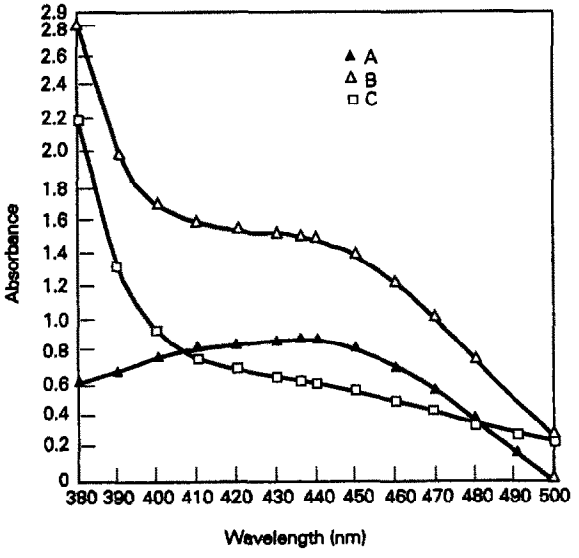

Fig. 1. Absorption spectra of ethanol (2.5 μg/ml)–diazotized *p*-aminobenzoic acid complex against reagent blank (A) and against water (B) and reagent blank against water (C).

RESULTS AND DISCUSSION

Ethanol can be coupled with diazotized *p*-aminobenzoic acid in strongly alkaline medium to produce an orange–yellowish compound. This reaction can be used for spectrophotometric determination of ethanol.

Under the optimum conditions (Table 1) the colour developed instantly and remained stable for about 10 min. The absorbance maximum was at 436 nm (Fig. 1) and Beer's law was obeyed over the range 0.5–4 μg/ml. The molar absorptivity of the product was 1.02×10^4 $l.mole^{-1}.cm^{-1}$.

Methanol, propanol, isopropanol, *t*-butylalcohol, ethyl acetate, acetic acid and acetone, were found not to interfere in the analysis (Table 2).

The values of relative standard deviation (3.2–4.76%) and relative errors (−2.89-3.9%) (for 4 results), show that the method has good precision and accuracy.

The proposed method has the advantages of being simple, rapid, selective and sensitive. The method has the additional advantage that the coloured product is soluble in water, so it does not precipitate and needs no extraction. The method also has advantage over the spectrophotometric methods[18,19,25,26] that no heating is required.

Table 2. Effect of methanol and other organic species on the determination of 0.025 mg of ethanol

Organic compound	Taken, mg	Ratio of interferent to ethanol	Ethanol recovery, %
Methanol	112.5	450	102.7
Propanol	62.5	250	100
Isopropanol	62.5	250	98.55
t-Butylalcohol	125	500	95.7
Ethyl acetate	187.5	750	95.5
Acetic acid	187.5	750	101.56
Acetone	0.025	1	97.4

*Average of 3 results.

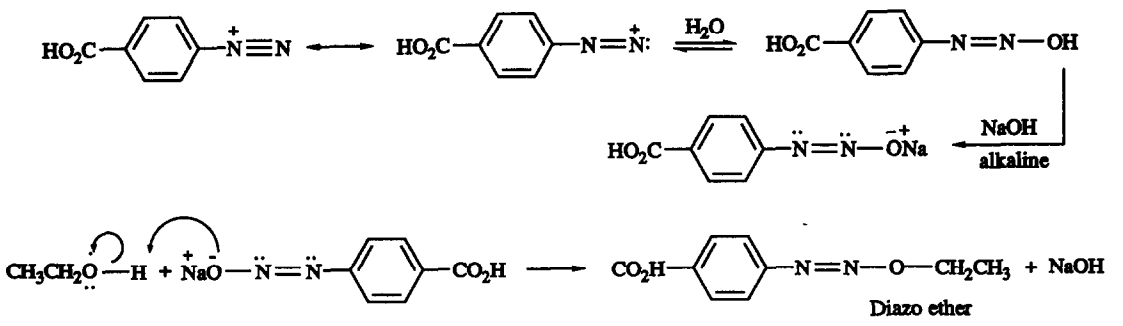

Scheme I

Scheme I represents a possible reaction pathway for the formation of the diazo ether compound.

REFERENCES

1. Official Methods of Analysis, 13th Ed., Sections 9.012, 52.003, AOAC, Arlington, VA, U.S.A., 1980.
2. A. O. Getter and H. Siegel, *Am. J. Clin. Pathol.*, 1937, **7**, 85.
3. J. C. Bock, *J. Biol. Chem.*, 1931, **93**, 645.
4. H. Decker, *Dtsch. Z. Gesamte Gerichtl. Med.*, 1940, **33**, 33.
5. R. B. H. Gradwohl (ed.), *Legal Medicine*, pp. 770. C. V. Mosby and Co., St. Louis, MO, 1954.
6. T. E. Friedemann and R. Klaas, *J. Biol. Chem.*, 1936, **115**, 42.
7. H. W. Haggard and L. A. Greeberg, *J. Pharmacol. Exper. Therap.*, 1934, **52**, 137.
8. R. J. Henry, *J. Lab. Clin. Med.*, 1948, **33**, 241.
9. M. Boudot, in *Stimulants and Narcotics*, E. F. Anstie (ed.), pp. 360–361, Lindsay and Blakiston, Philadelphia, PA, U.S.A., 1865.
10. R. N. Harger, *J. Lab. Clin. Med.*, 1935, **20**, 746.
11. H. W. Smith, *ibid.*, 1951, **38**, 762.
12. A. Hemingway, L. A. Barnet and J. Maschmeyer, *J. Lab. Clin. Med.*, 1948, **33**, 126.
13. E. Widmark, *Biochem. Z.*, 1922, **131**, 473.
14. J. W. Cavett, *J. Lab. Clin. Med.*, 1938, **23**, 543.
15. F. L. Kozelka and C. H. Hine, *Analyst (London)*, 1942, **67**, 174.
16. F. L. Kozelka and C. H. Hine, *Ind. Eng. Chem.*, 1941, **13**, 905.
17. H. S. Mahal, *Anal. Chem.*, 1959, **31**, 1908.
18. D. Eskes, *Mikrochim. Ichonoanalyt. Acta*, 1965 (5–6), 1065; *Anal Abstr.* 1967, **14**, 2107.
19. R. T. Sone, S. S. Kamat and M. D. Pandit, *J. Assoc. Off. Anal. Chem.*, 1981, **64**(5), 1145.
20. E. Schifferli, *Ann. Med. Leg.*, 1951, **31**, 79.
21. I. Y. Shaferstein, *J. Appl. Chem., USSR*, 1934, **7**, 239.
22. R. K. Bonnichsen and H. Theorell, *Scand. J. Clin. Lab. Invest.*, 1931, **3**, 58.
23. M. D. Smith and C. L. Olson, *Anal. Chem.*, 1975, **47**, 1074.
24. M. P. Kurhekar and B. N. Mattoo, *Curr. Sci.*, 1974, **43**, 45.
25. A. Caputi, M. Ueda and T. Brown, *Am. J. Enol. Vitic.*, 1968, **19**, 160.
26. V. Klingmueller, W. Nuglish and N. Weyss, *Clin. Chim. Acta*, 1968, **22**, 317; *Anal. Abstr.*, 1970, **18**, 1819.

Talanta, Vol. 39, No. 11, pp. 1493–1498, 1992
Printed in Great Britain.

0039-9140/92 $5.00 + 0.00
Pergamon Press Ltd

SEPARATION AND IDENTIFICATION OF SUGARS AND MALTODEXTRINES BY THIN LAYER CHROMATOGRAPHY: APPLICATION TO BIOLOGICAL FLUIDS AND HUMAN MILK

F. BOSCH-REIG, M. J. MARCOTE, M. D. MINANA
Departamento de Química Analítica, Facultad de Ciencias Químicas, Valencia, Spain

M. L. CABELLO*
Unidad de Metabolopatías Congénitas, Hospital Universitario "La Fe", Avda. Campanar, 46009 Valencia, Spain

(*Received* 27 *March* 1992. *Accepted* 1 *April* 1992)

Summary—A monodimensional thin layer chromatography method to separate several sugars of clinical interest is described. The separation and identification of 14 sugars (*L*-fucose, *D*-galactose, *D*-glucose, lactose, *N*-acetylglucosamine, *D*-maltose, *D*-manose, *L*-sorbase, fructose, *D*-xylose, glucuronic acid, *N*-acetyllactosamine, 3′ and 6′ sialyllactose) and maltodextrines (G_2–G_8) is possible by using two different eluents mixtures, as well as two different detection reagents. The method has been applied to separate sugars, maltodextrines and oligosaccharides in several biological fluids (blood, urine and faeces), in an infant milk and in human milk. It is a very simple technique (with a high sensitivity) that can be used in any lab.

The presence of anomalous amounts of carbohydrates can be detected in blood, urine and faeces of patients with inborn errors in the metabolism of carbohydrates, such as essential fructosuria and others.[1–7]

In the present method, urine does not need to be desalted as in most cases, either by column[4–8] or by precipitation.[5,9]

Over the last few years, the increasing popularity of breastfeeding has stimulated interest in the sugar content of human milk.

It is known that the carbohydrate concentration of human milk is about 7 g/100 ml; 80% lactose and the rest oligosaccharides (1–1.2 g/100 ml in nature milk, 2–2.5 g/100 ml in colostrum).[14]

It has not yet been possible to reproduce the structure of these oligosaccharides. They are substituted by maltodextrines in "adapted" milk formula, keeping the total sugar concentration at 7–8 g/100 m.[15]

The biological role of human milk oligosaccharides is not completely understood, but it seems clear that they have a very important anti-infective action for breast-fed infants.[16]

Kobata *et al.* isolated and characterized most of the oligosaccharides in human milk using very sophisticated technology.[9–18] At first they used pooled milk from several donors as starting material, but then observed that the type of oligosaccharides present in individual samples of milk can vary with the ABO or Lewis blood type of the donor. The enzymes involved in their synthesis are also responsible for the formation of the structural determinants of these blood types.

All oligosaccharides in human milk have some general structural principles in common, they all derive from lactose and contain, besides galactose and glucose, *N*-acetylglucosamine and/or more of *L*-fucose and *N*-acetyl-neuraminic acid molecules.

Another advantage of the method is that sugars may be identified without using internal standards.

Thin layer chromatography has been applied specifically to the study of the role placed by the oligosaccharides obtained from human blood, urine and milk[10,11,13] in metabolic pathways.

*Author for correspondence.

Several sugars obtained from animal urines have been studied by thin layer chromatography and high pressure liquid chromatography.[12] It can be seen in the references in the literature that certain sugars have been studied, however a complete study of separation, identification and application to biological fluids of carbohydrates has not been done.

EXPERIMENTAL

Samples and solvent systems

Aqueous solutions of the following sugars were prepared:

L-fucose, *D*-galactose, *D*-glucose, lactose, *N*-acetylglucasamine, *D*-maltose, *D*-manose, *L*-sorbose, *D*-xylose, fructose (0.7 g/100 ml), glucuronic acid (0.21 g/100 ml), *N*-acetyllactosamine (5.00 g/100 ml) 3′ and 6′ sialyllactose (1.70 g/100 ml) and maltodextrines (G_2–G_{10}) (8.33 g/100 ml).

All sugars were obtained from commercial sources (Merck, Sigma). Less concentrated solutions were obtained by diluting the original ones.

Blood samples, as well as fresh and twenty-four hour urine samples were taken from the ones available in the laboratory.

Faeces samples belonged to preterm infants. The milk samples used were from either one donor, 15 days and 45 days after the delivery, or several donors, 15 days after the delivery.

An infant milk formula containing lactose and maltodextrines (56.9 g/100 g milk), 15% in water.

Blood was delipidated using a chloroform: metanol 2:1 mixture in a ratio 1:10, mixed for 5 min and centrifuged for 25 min at 5000 rpm. Then it was ready to be applied to the plate.

Urine required no previous treatment and could be directly applied to the plate.

Faeces were analysed after being diluted in distilled water 1:2 and centrifuged 25 min at 5000 rpm. The supernatant was applied to the plate.

Milk samples were delipidated by centrifugation at 1500 rpm for 30 min and diluted 1:2 with distilled water. One-millilitre aliquots were kept at −20° until they were analysed.

Two elements mixtures were used: in-butanol/ethanol/water (3:2:1) and pyridin/ethyl acetate/acetic acid/water (5:5:3:1).

Chromatography

Cellulose plates (20 × 20 cm, 0.1-mm thick) were used (Merck Art. 5716). Cellulose plates (20 × 20 cm, 0.5-mm thick) were used for preparative chromatography (Merck Art.).

Aliquots (3 μl), were spotted on the 0.1-mm plates with a micro syringe, at 1.5-cm intervals and 2 cm from the lower edge of the plates. Then they were developed by the ascending technique. A three-fold development, with the same eluent mixture, is used in order to improve separation. A good separation was obtained when the eluent was allowed to run 14.5 cm from the edge of the plate. The time required for a single run is approximately two and a half hours.

In the preparative chromatography milk samples aliquots (850 μl) were applied as a streak on the 0.5-mm plate. A three-fold development was also used. Guide strips were developed with silver nitrate reagent to locate the bands. The required bands on the unsprayed area were scrapped off onto test tubes, 1 ml of distilled water was added to each and tubes were shaken thoroughly. Sugar was separated from cellulose powder by centrifugation at 4.500 rpm for 5 min.

Detection reagents

The following reagents were used: silver nitrate solution prepared by dissolving 3 g of silver nitrate in 12 ml of distilled water adding 500 ml of acetone.

Ethanolic sodium hydroxide solution prepared by diluting 50 ml of 10*N* sodium hydroxide in 450 ml of ethanol.

Sodium thiosulphate (5%) was also used.

The developed plates were allowed to dry at room temperature and dipped into AgNO solution for one minute. When dry they were sprayed with the ethanolic sodium hydroxide solution until dark brown spots appeared on a light brown background.

If the plates must be kept for a long time, they must be sprayed with a 5% $Na_2S_2O_3$ solution once they are dry.

Elson-Morgan reagent

1% Acetillacetone in butanol is treated with a 1/20 volume of 50% potassium hydroxide–ethanol (1:4 v/v).

p-Dimethylaminobenzaldehide solution: 1 g of *p*-dimethylbenaldehide is dissolved in 30 ml

of ethanol of concentrated HCl and 30 ml of *N*-butanol.

When the plate was dry, it was sprayed with the acetylacetone solution, heated at 100° for 5 min and then sprayed with *p*-dimenthylbenzaldehide solution. *N*-Acetylaminated sugars appear immediately as violet spots.

RESULTS AND DISCUSSION

Aqueous solutions of the following sugars were chromatographed on 0.1-mm cellulose plates: *N*-acetylglucosamine, fucose, xylose, manose, sorbose, glucose, galactose, *N*-acetyllactosamine, glucuronic acid, maltose, lactose, 3′-sialyllactose and 6′-sialyllactose, using *N*-butanol/ethanol/water (3:2:2) as eluent and with a 3-fold development. All sugars were detected with both silver nitrate and Elson-Morgan reagents. The R_f values and sensitivities are shown in Table 1.

Similarly, an aqueous solution of maltodextrines was also chromatographed using two different eluents: (1) n-butanol/ethanol/water (3:2:2) and (2) pyridine/ethyl acetate/acetic acid/water (5:5:1:3). Then maltodextrines were located with silver nitrate reagent. The method sensitivity for maltodextrines is 6.25 μg and the R_f values are shown in Table 2.

As can be seen in Table 1 fucose and *N*-acetylglucosamine have the same R_f but they could be identified by the detection reagents. Both of them can be visualized with silver nitrate reagent, but only *N*-acetylglucosamine can be detected with Elson-Morgan reagent.

Table 2 shows that only G_2 to G_7 components of maltodextrines can be separated with eluent (2). G_2 to G_8 can be separated with eluent (1).

Table 2. R_f values, using two different eluents mixtures, of maltodextrines in aqueous solutions

Sugar	R_f (eluent 1)	R_f (eluent 2)
G_2	0.73	0.48
G_3	0.65	0.35
G_4	0.56	0.26
G_5	0.46	0.19
G_6	0.38	0.14
G_7	0.31	0.10
G_8	0.24	—

However G_9 and G_{10} components cannot be separated either with eluent (1) or with eluent (2).

It can be said that the described aqueous solutions of sugars and maltodextrines have been identified either by their R_f or by selecting the suitable detection reagent.

When sugars were added to blood, fresh urine, twenty-four hour urine and faeces, these biological fluids were chromatographed and it was seen that there is very good agreement between the R_f of the standard solutions and those of the biological fluids, as shown in Table 3.

Samples of infant milk were also chromatographed. Its sugar content according to the manufacturer was lactose and maltodextrines. *N*-Butanol/ethanol/water (3:2:2) was used as eluent and the detection reagent was silver nitrate. On the chromatogram shown in Fig. 1 can be seen that lactose and maltodextrines were identified, as well as minor sugars like galactose and glucose. Therefore, this procedure allows the identification of sugars with a sensitivity that may be considered high.

Seven spots were detected when samples of milk from a donor who had delivered a full term infant 15 days before, were chromatographed.

Table 1. R_f values and sensitivity in μg of sugars in aqueous solutions

Sugar	R_f	μg ($AgNO_3$ R.)	μg (Elson-MorganR.)
6′-Sialillactose	0.35	3.19	—
3′-Sialillactose	0.42	3.19	—
Lactose	0.48	0.56	—
Maltose	0.48	0.21	—
Glucuronic Acid	0.55	0.09	—
N-Acetillactosamine	0.58	3.0	3.0
Galactose	0.65	0.14	—
Glucose	0.69	0.11	—
Sorbose	0.70	0.21	—
Manose	0.73	0.21	—
Xilose	0.78	0.11	—
Function	0.74	0.11	—
Fucose	0.81	0.11	—
N-Acetilglucosamine	0.81	0.42	2.1

Table 3. R_f values of sugars in several biological fluids (blood, faeces and urine)

Sugar	R_f values		
	Aqueous solution	Blood	Faeces
Xilose	0.78	0.78	0.78
Fructose	0.74	0.73	0.74
Glucose	0.69	0.69	0.69
Galactose	0.65	0.65	0.65
Glucuronic Acid	0.55	0.53	0.54
Lactose	0.48	0.47	0.48
Sugar	Fresh urine	Twenty-four hour urine	
Xilose	0.78	0.78	
Fructose	0.74	0.74	
Glucose	0.69	0.69	
Galactose	0.66	0.66	
Glucuronic Acid	0.55	0.55	
Lactose	0.48	0.48	

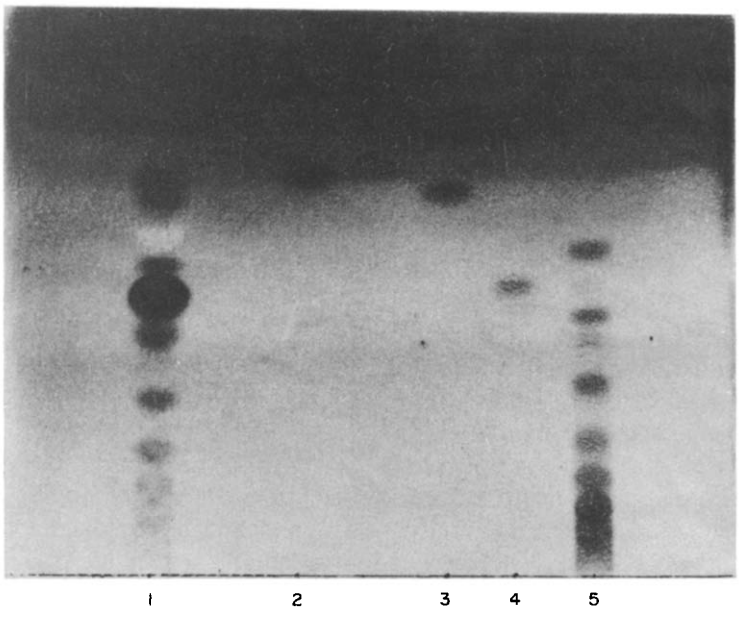

Fig. 1. Chromatogram of sugars of an infant milk; 1: infant milk:water (1:1); 2: glucose: 14 mg/100 ml; 3: galactose: 14 mg/100 ml; 4: lactose: 70 mg/100 ml; 5: maltodextrines: 830 mg/100 ml.

As shown in Fig. 2, spots 1, 2, 3 and 4 were confirmed to be glucose, lactose, 3′-sialyllactose and 6′-sialyllactose respectively. Spots 5, 6 and 7 were confirmed to be fractions of oligosaccharides. They were isolated by preparative chromatography and they all released glucose, galactose and fucose when mild hydrolysis was carried out. Spot 5 also contains *N*-acetyl glucosamine as it reacts with Elson-Morgan reagent.

Samples of milk of the same donor 45 days after she gave birth were also chromatographed (Fig. 3). The chromatogram was quite similar to the former. However, the fractions of oligo-

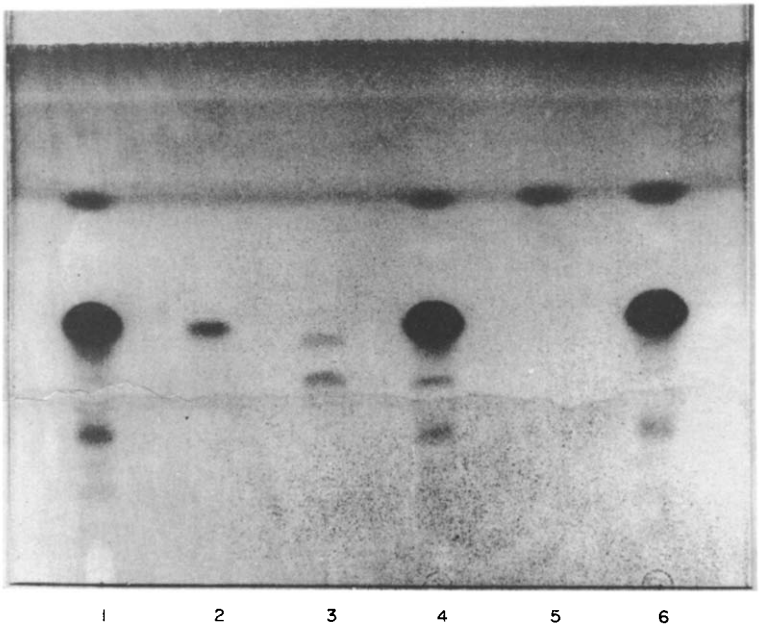

Fig. 2. Chromatogram of human milk; 1: human milk:water (1:1); 2: lactose: 70 mg/100 ml; 3: 3′ and 6′ sialyllactose: 210 mg/100 ml; 4: human milk: 3′ and 6′ sialyllactose (1:1); 5: glucose: 14 mg/100 ml; 6: human milk: glucose (1:1)

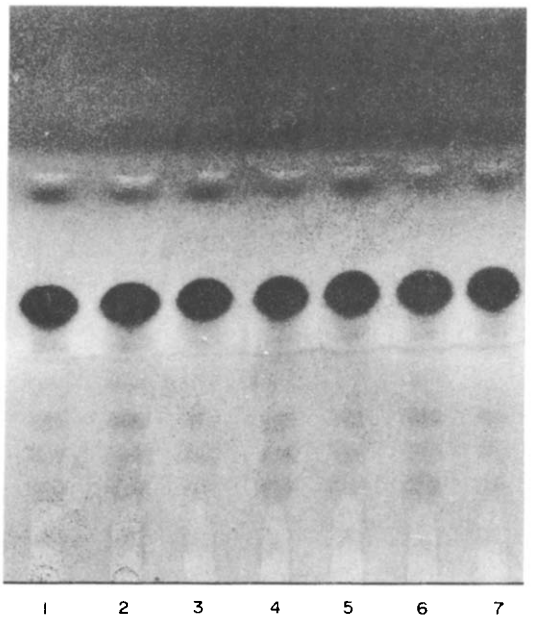

Fig. 3. Chromatogram of human milk from the same donor 1, 3, 5 and 7: sample of milk after 45 days of delivery. 2, 4 and 6: sample of milk after 15 days of delivery.

saccharides were in less concentration and subsequently the glucose concentration was increased.

When samples of milk from different donors, who had delivered babies 15 days before, were chromatographed, strong differences were observed in the chromatogram as a function of the donors (Fig. 4).

Therefore, it can be said that the chromatogram of sugars from milk depends fundamentally on the donor, the maturity of the milk and its origin (human and infant milk formula). All of that can be detected by thin layer chromatography which is a very simple technique that can be used in any laboratory.

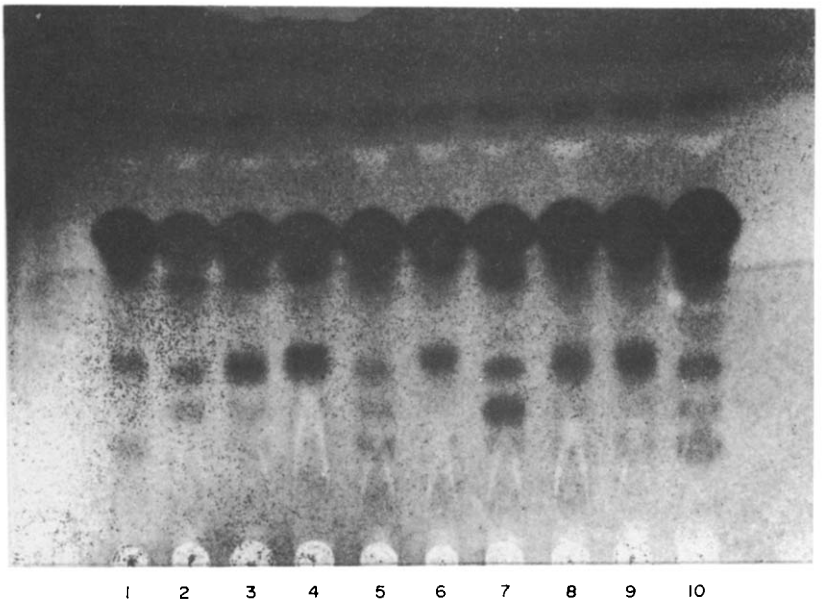

Fig. 4. Chromatogram of sugars of milks from several donors 1–10 spots belong to milks from different donors.

REFERENCES

1. I. Lytt, Gardner. Salvat., *Enfermedades congénitas y endocrinas de la infancia.*
2. Lynch, Raphael, Mellor, Spare, Inwood, *Laboratory Methods*, 2nd ed.
3. M. Ghebregzabher, S. Rufini, B. Monaldi and M. Lato, *J. Chromatogr.*, 1976, **127,** 133.
4. Vladimir Vitek and Kveta Vitek, *ibid.*, 1971, **60,** 381.
5. *Idem, ibid.*, 1977, **143,** 65.
6. Gerard Strecker and Anick Lemaire-Poitau, *ibid.*, 1977, **143,** 65.
7. M. Lato, B. Brunelli and G. Ciuffini and T. Mezzetti, *ibid.*, 1968, **36,** 191.
8. Wolfgang Prinz, William Meldrum and Lynne Wilkinson, *Clin. Chim. Acta*, 1978, **82,** 229.
9. Zeljko Zilic and Nenad Blau and Margarethe Knob, *J. Chomatogr.*, 1979, **164,** 91.
10. R. Ramphal, C. Carnoy, S. Fieure, J. C. Michalski, N. Hondret, G. Lamblin, G. Strecker and P. Roussel, *Intect. Iunmnn.*, 1991, **59,** 700.
11. P. Scudder, A. M. Lawson, E. F. Hounsell, R. A. Carruthern, R. A. Childs and T. Feiz, *Eur. J. Biochem.*, 1978, **163,** 585.
12. C. D. Warren, S. Sadeh, P. F. Daniel, B. Bugge, L. F. James and R. W. Jeanloz, *Febs Lett.*, 1983, **163,** 99.
13. A. Cahour, P. Debeire, L. Hartmann and J. Montrenil, *Biochem. J.*, 1983, **211,** 55.
14. Comite sobre nutrición ESPAGN (1982). Acta Paediatr. Scand. Suplemento 302.
15. Comite sobre nutrición ESPAGN (1977). Acta Paediatr. Scand. Suplemento 262.
16. J. Cruz and C. Arevalo, *Pedriatric Infections* Disease 5, S-148.
17. A. Kobata, E. Grollman and V. Ginsburg, *Biochem. Biophys. Res. Commun.*, 1968, **32,** 272.
18. A. Kobata and V. Ginsburg, *Arch. Biochem. Biophys.*, 1969, **130,** 509.
19. *Idem, J. Biol. Chem.*, 1969, **244,** 5496.
20. *Idem, ibid.*, 1970, **245,** 1984.
21. *Idem, ibid.*, 1972, **247,** 1525.
22. *Idem, Arch. Biochem. Biophys.*, 1972, **150,** 273.
23. K. Yamashita and A. Kobata, *ibid.*, 1974, **161,** 164.
24. K. Yamashita, Y. Tachibana and A. Kobata, *ibid.*, **174,** 582.
25. A. Kobata, *Methods in Enzymology*, 1972, **28,** 262.
26. A. Kobata, K. Yamashita and Y. Tachibana, *Methods in Enzymology*, 1978, **50,** 216.

Talanta, Vol. 39, No. 11, pp. 1499–1503, 1992
Printed in Great Britain.

0039-9140/92 $5.00 + 0.00
Pergamon Press Ltd

A FLOW-CELL OPTOSENSOR FOR LEAD BASED ON IMMOBILIZED DITHIZONE

WALACE A. DE OLIVEIRA* and RAMAIER NARAYANASWAMY†
Department of Instrumentation and Analytical Science, UMIST., P.O. Box 88, Manchester M60 1QD, U.K.

(*Received* 24 *March* 1992. *Accepted* 31 *March* 1992)

Summary—Dithizone immobilized on XAD-4 resin has been studied as a sensor element of an optical sensor for lead using a flow-cell. Using this arrangement, lead in solution has been determined in the concentration range 1×10^{-5}–$3 \times 10^{-7}M$ with a detection limit of $1 \times 10^{-8}M$ (*i.e.*, 2 μg/l.). The standard deviation of the method for the measurement of lead at a concentration of $1 \times 10^{-6}M$ was found to be 7%. The response of the sensor was reproducible and can be regenerated using 0.01*M* hydrochloric acid followed by citrate-hydroxylamine solution.

The toxicity of heavy metals is very high and their adverse effects upon human life are well recognized.[1] Among the heavy metals, lead is one which merits great environmental concern[2] because it is widespread and has contaminated the whole biosphere. It is believed that no other chemical pollutant has accumulated in humans so close to the threshold of potential clinical poisoning.[3] Therefore, there is a great need of monitoring the concentration of lead in the environment.

Determination of lead in environmental samples is usually performed by atomic absorption spectrometry or other methods.[2] In some instances, however, it is desirable to perform the analysis *in situ*, or to monitor the pollutant concentration continuously and remotely. Optical fibre chemical sensors have the potential to meet this demand[4,5] provided characteristics such as sensitivity and reliability can be achieved.

The mostly widely studied spectrophotometric reagent for lead is probably dithizone (diphenylthiocarbazone). The spectrophotometric procedure based on this reagent and solvent extraction technique was an official method for many years[6,7] and has proved to be reliable. Though other reagents such as immobilised Xylenol Orange[8] has been studied in the development of optical lead sensors, the possibility of using the dithizone reaction as the basis in the development of an optical sensor for lead was pursued.

EXPERIMENTAL

Instrumentation

The instrumentation employed in this work was similar to that previously reported.[9] It comprises a quartz-halogen lamp (12V, 30W) whose optical radiation was modulated by an optical chopper (Bentham 218) set at a frequency of 430 Hz and focused onto the end of a bifurcated optical fibre (Optronics). The optical fibre was inserted perpendicular to the axis of a cylindrical compartment of a flow cell (4 mm long and 3 mm in diameter) fabricated from a perspex block. A fine wire mesh was placed at one end of this compartment to block the reagent phase, which was loaded into the flow cell with the aid of a peristaltic pump (Watson-Marlow 202V).

Light reflected from the reagent phase was collected by the optical fibre and guided to a monochromator (ISA Instruments H-1061) and subsequently detected by a photomultiplier (Hamamatsu R446). The signal was enhanced by a current amplifier (Bentham 286) and a lock-in amplifier (Bentham 223) synchronized with the optical chopper frequency, and was recorded on a chart recorder (BBC SE120).

Reagents and solutions

All chemicals were of analytical reagent grade. The citrate (0.01*M*)/hydroxylamine

*Permanent address: Instituto de Quimica, Universidade Estadual de Campinas, CP 6154, 13081 Campinas, SP, Brazil.
†Author for correspondence.

hydrochloride (0.05M) solution was made by dissolving appropriate amounts of these chemicals in demineralized, distilled water and adjusting the pH to 8.0 with ammonia solution.

The standard solutions of lead were freshly prepared by dissolving dried lead nitrate in the citrate/hydroxylamine hydrochloride solution.

Procedure

A calibration curve was obtained by the following procedure: to 10.0 mg of Amberlite XAD-4 (mesh < 70 μm), 10 ml of a saturated solution of dithizone in methanol was added and allowed to stand for about one hour. The whole suspension was then sucked into the flow cell with the help of the peristaltic pump. About 5 ml of the citrate/hydroxylamine solution was passed through the reagent phase before measurements were taken.

The measurements were carried out using two procedures as described below. In the method of 'kinetic analysis', the standard solutions of lead were allowed to flow at a constant flow-rate, and the analytical signal was recorded as a function of time. For measurements using the 'concentration procedure', only the initial and final values of reflectance were recorded. The light path was blocked during the addition of lead solutions and the regeneration of the reagent phase to avoid any photodegradation. The reagent phases were regenerated by passing about 5 ml of 0.01M hydrochloric acid followed by about 5 ml of citrate/hydroxylamine solution through the flow-cell.

The measurements were expressed as the relative reflectance, defined as the reflectance of the lead complex minus that of the immobilized dithizone alone.

RESULTS AND DISCUSSION

Immobilization

Immobilization of dithizone was carried out with both non-ionic (Amberlite XAD-2, XAD-4 and XAD-7) and ionic (Amberlite IRA-400) resins. Best results were obtained with the Amberlite XAD-4 which was chosen for further investigations. The effect of experimental parameters on immobilization was studied by varying the time (in the range 60–210 min), concentration of dithizone (from $1 \times 10^{-5}M$ to saturated solutions) and particle size of the resin (<70 to 200 μm). It was observed that reagent phases with lower concentrations of dithizone yielded good sensitivity but lower stability, whereas those with higher concentrations of the reagent produced more stability but sluggish response. Optimum conditions of response were determined using a time of 60 min, fresh saturated solutions of dithizone and XAD-4 beads with diameter less than 70 μm. No leaching of the reagent was observed upon passage of aqueous solutions (citrate–hydroxylamine solution or dilute hydrochloric acid) through the immobilized dithizone.

Figure 1 shows the diffuse reflectance spectrum of the immobilized dithizone and that of the lead complex. It can be noted that the formation of the complex causes a large increase in reflectance, which is due to a sharp change in colour of the reagent phase from green to red. The maximum divergence between the two spectra was observed at 650 nm and this wavelength was, therefore, used for the analytical measurements.

Photodecomposition studies

It was observed that the immobilized dithizone was susceptible to photodecomposition caused by the light from the quartz-halogen lamp. This resulted, with time, in an increase in reflectance which affected the accuracy of the measurements. The sensitivity to light of solutions of dithizone has been frequently studied.[7,10] Meriwether *et al.*,[11] for example, found that in benzene solutions decomposition was fast with a radiation of low wavelength, but with light of wavelengths above 400 nm there

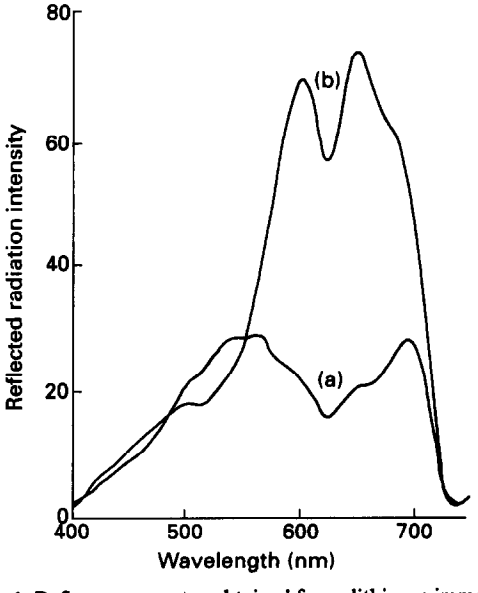

Fig. 1. Reflectance spectra obtained from dithizone immobilized on XAD-4, (a) before and (b) after reaction with lead ions.

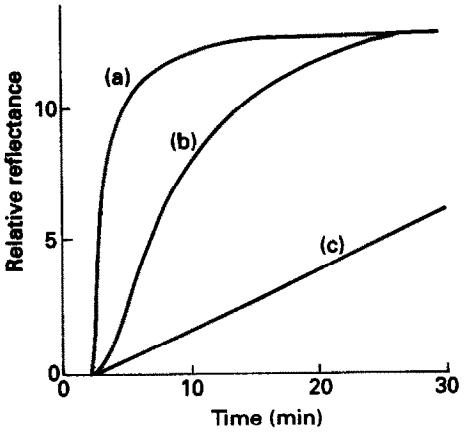

Fig. 2. The variation of relative reflectance with time obtained by using solutions of lead ions at concentrations of (a) $1.0 \times 10^{-4}M$; (b) $1.0 \times 10^{-5}M$ and (c) $1.0 \times 10^{-6}M$, in the flow-cell at a flow-rate of 0.65 ml/min.

was no decomposition. Accordingly, an attempt to avoid photodecomposition was made by inserting a coloured glass filter in front of the light source which eliminated light below 580 nm. This, however, diminished the photodecomposition rate but did not eliminate it. It appears that the adsorption of dithizone on the cross-linked copolymer (styrene–divinylbenzene) has created an environment that is more susceptible to photodecomposition than in solution. However, photodecomposition was almost eliminated by installing a band-pass filter (Ealing Electro Optics) which allows only a narrow passage of radiation with a peak at 650 nm. With this filter, the increase in relative reflectance due to photodecomposition, during a period of three hours, was about 1% of the magnitude of the average analytical signal. For much shorter exposure times used during the measurement in this work, therefore, this error can be neglected.

Dynamic range

Typical analytical curves of signal response as a function of lead concentration are shown in Fig. 2. It can be noted that the slopes of the curves are smaller at lower concentrations. All curves, however, were observed to reach the same constant value in reflectance at which further passage of lead solutions caused no more increase in the relative reflectance. This point represents the state where all of the immobilized dithizone had been consumed by reaction with lead ions. Under this circumstance it is preferable to use a kinetic analysis approach. This can be done by choosing a specific time that embraces the range of concentration of interest. Setting, for example, a time of 15 min enables determination of lead in the range 1.0×10^{-5} to $1.0 \times 10^{-6}M$. As can be seen in Fig. 3(a), a linear relationship between the relative reflectance and the logarithm of concentration, was obtained within this concentration interval with a correlation coefficient of 0.993.

In order to extend the dynamic range to lower concentrations without overexposing the dye to the light source, the concentration procedure was used. It consists of measuring the relative reflectance before and after the passage of a fixed volume of sample solution. This volume is chosen to encompass the desired range of sample concentration. In order to evaluate the possibility of lead determinations at lower concentrations, a volume of 100 ml was used. Figure 4 shows a typical experimental response. Between each measurement, the light path was blocked in order to reduce the photodegradation of reagent. The standard (or regenerating) solutions were allowed to flow through the reagent phase and the relative reflectances were

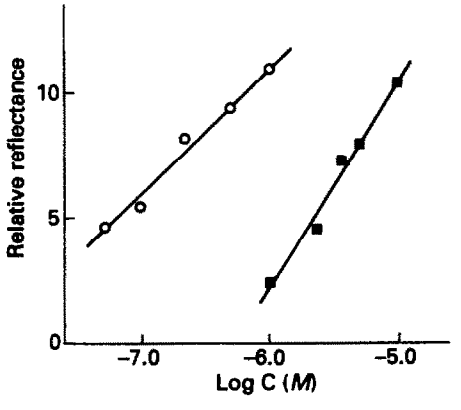

Fig. 3. Calibration plots obtained by the kinetic approach (■) and the concentration procedure (○).

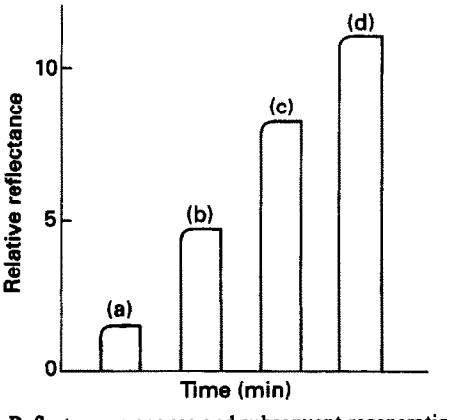

Fig. 4. Reflectance response and subsequent regeneration of the sensor obtained at lead concentrations of (a) $0.0M$; (b) $5.0 \times 10^{-8}M$; (c) $2.2 \times 10^{-7}M$ and (d) $1.0 \times 10^{-6}M$.

recorded. A linear relationship between the relative reflectance and concentration was observed [Fig. 3(b)] with a correlation coefficient of 0.990.

The limit of detection of lead, defined here as the concentration equivalent to a signal four times the standard deviation of the blank, was estimated as $1 \times 10^{-8}M$. The reproducibility of the response was evaluated by performing several measurements using the same standard solution and reagent phase. This resulted in the relative standard deviation for 7 samples containing $1.0 \times 10^{-6}M$ lead solution of 7%.

Regeneration of sensor

Regeneration of the reagent phase can be accomplished by passing about 5 ml of $0.01M$ hydrochloric acid followed by about 5 ml of citrate–hydroxylamine solution. The passage of dilute solution of hydrochloric acid washed out lead instantly and completely. This is not surprising because lead ions react with the basic form of dithizone (HDz) and the lead dithizonate, $Pb(HDz)_2$, is formed only in neutral and basic media. Using the concentration procedure, more than 10 cycles of complexation and decomplexation of lead were possible without any sign of decreasing response.

The immobilized dithizone is best stored in the dark in the refrigerator, and in a solution of citrate–hydroxylamine or dilute hydrochloric acid. Under these conditions the reagent phase was found to be stable for at least one month.

Load of the immobilised reagent

The amount of the dithizone immobilised on XAD-4 was determined by desorbing the dye with chloroform and determining its concentration spectrophotometrically. Thus, 10 μmole of dithizone was found per 1.0 g of XAD-4. This value can be compared with the amount of lead ion necessary to saturate the reagent phase. From Fig. 2 it can be noted that about 16 ml of $1.0 \times 10^{-5}M$ solution of lead were required to reach the constant value in relative reflectance. This indicates that approximately 0.16 μmole of Pb^{2+} ions were necessary to saturate the dithizone contained in 10 mg of resin. This is higher than the stoichiometric value (0.05 μmole) and seems to indicate that, at the operating conditions of the peristaltic pump, some of the lead ions pass through the flow cell without reacting with the reagent phase. However, at saturation, a complete change of colour of the reagent phase (from green to red) is noted and it can be assumed that all of the immobilized dithizone has formed the metal complex. Furthermore, one can visualize that the molecules of dithizone adsorbed on the polymeric matrix as having a structure that favours the metal complex formation.

Comparison with solvent extraction

The behaviour of the immobilized dithizone resembles that observed in the solvent extraction method. Although, in the basic medium dithizone becomes yellow in colour, the immobilized form remains green in the citrate solution at pH 8.0. Furthermore, the colour change due to complex formation on the surface of the solid matrix is similar to that found in the solvent extraction procedure. It appears that the immobilized reagent can be considered as a solid solution phase capable of extracting a number of metal ions from the aqueous phase. Vast amounts of literature available on such extraction procedures[7,12] may be used as a guidance in the development of sensors for these metal ions and also in the study of interferents in a particular sensor, which will be similar to that reported in the literature.

CONCLUSIONS

The experimental procedures developed in the present work have enabled the determination of lead ions in solution over a wide concentration range (about 3–4 orders of magnitude). The low detection limit for lead determination is suitable in the analysis of most environmental samples including drinking water (for which the recommended upper safe limit is 50 μg/l.).[13] Dithizone has been used as a preconcentrating reagent in conjunction with other techniques such as atomic absorption spectrophotometry.[14,15] The advantage of the method reported here is that it can be operated remotely and in a real-time basis. The method can find application in flow injection analysis[16] and in on-line as well as field applications of lead analysis.

Acknowledgements—The authors wish to express their gratitude to FAPESP-Brazil, for the financial support to one of us (W.A.O.).

REFERENCES

1. R. A. Horne, *The Chemistry of Our Environment*, Wiley, New York, 1978.
2. W. R. Boggess, (ed.), *Lead in the Environment*, National Science Foundation RA-770214, Washington, DC, 1977.

3. D. Bryce-Smith, *Heavy Metals as Contaminants of the Human Environment*, Chemistry Cassettes, ETSG-The Chemical Society, London, 1975.
4. R. Narayanaswamy and F. Sevilla III, *J. Phys. E: Sci. Instrum.*, 1988, **21**, 10.
5. W. R. Seitz, *CRC Crit. Rev. Anal. Chem.*, 1988, **19**, 135.
6. Official Methods of Analysis of the AOAC, 11th Edition, Association of Official Analytical Chemists, Washington, DC, 1970.
7. H. M. N. H. Irving, *Dithizone*, The Chemical Society, London, 1977.
8. L. M. Trutneva, O. P. Shvoeva and S. B. Savvin, *Zh. Anal. Khim.*, 1989, **44**, 1804.
9. R. Narayanaswamy and F. Sevilla III, *The Analyst*, 1986, **111**, 1085.
10. H. M. N. H. Irving and D. C. Rupainwar, *Anal. Chim. Acta*, 1969, **48**, 187.
11. L. S. Meriwether, E. C. Breitner and C. L. Sloan, *J. Amer. Chem. Soc.*, 1965, **87**, 4441.
12. E. B. Sandell and H. Onishi, *Photometric Determination of Traces of Metals*, Part I, Wiley, New York, 1977.
13. *EC Directive Relating to the Quality of Water Intended for Human Consumption*, 80/778/EEC, *Off. J. Eur. Commun.*, July 1980; OJL 229, 30 Aug. 1980.
14. S. L. Sachdev and P. W. West, *Anal. Chim. Acta*, 1969, **44**, 301.
15. J. Aggett and T. S. West, *ibid.*, 1971, **57**, 15.
16. D. Klinghoffer, J. Růžička and E. H. Hansen, *Talanta*, 1980, **27**, 169.

Talanta, Vol. 39, No. 11, pp. 1505–1509, 1992
Printed in Great Britain.

0039-9140/92 $5.00 + 0.00
Pergamon Press Ltd

WATER SORPTION ISOTHERMS ON AMINOPROPYLTRIETHOXYSILANE COATED SURFACE ACOUSTIC WAVE SENSORS

JULIE T. WOOD and JOHN F. ALDER*
Department of Instrumentation and Analytical Science, UMIST, P.O. Box 88, Manchester M60 1QD, UK

(*Received* 1992. *Accepted* 14 *May* 1992)

Summary—Water sorption isotherms were obtained on surface acoustic wave sensors (SAWS) coated with aminopropyltriethyoxysilane (APTES), and on uncoated SAWS of which the substrate material was polished ST-quartz. The isotherms were obtained at 25°, 30° and 40° over the range 1–80% relative humidity (RH). The isotherms exhibit BDDT type III characteristics typical of weak gas–solid interaction. The isotherms showed good fit to quadratic equations relating frequency change on exposure to humid air with relative humidity. There was no significant hysteresis in the isotherms when the SAWS was taken through a cycle of relative humidity at any of the three temperatures employed. These results are similar to those obtained in earlier work on FPOL and polyvinylpyrollidone coated SAWS. They demonstrate that a correction algorithm based on a quadratic equation should be possible to overcome water vapour response of coated SAWS.

Surface acoustic wave sensors (SAWS) have been employed widely over the last decade and are still the subject of active research. In this laboratory, and previously in the analytical chemistry laboratories at Imperial College under the direction of Professor T. S. West, we have carried out extensive studies on the interaction of gaseous species with coated quartz bulkwave piezoelectric crystals (PZX)[1,2] and latterly their more recent SAWS counterparts.[3]

All sensors that rely upon reversible sorption of gas onto their surface as a prerequisite to the sensing process, will exhibit a response which is closely related to the sorption isotherm of the gas over the surface. It may not be exactly the same, because of non-linear response in the relationship between partial pressure of the gas (p) over the surface, mass of material sorbed (m) and the response function of the sensor R(m.p). In the work ongoing in this laboratory a series of experiments is being carried out to determine the nature of the response isotherms of SAWS coated with materials which exhibit selectivity towards target species, but also, and almost inevitably, exhibit response to water vapour. Previous work has specifically addressed the sorption of water vapour onto polyvinylpyrrolidone and F-POL (a fluorinated polyether-polyol),[4] which are known to respond to organophosphonate compounds[5–7] and it was demonstrated that the isotherms for water resembled the BDDT type III, characteristic of weak gas–solid interactions, and could be modelled using a quadratic equation relating SAWS frequency change to the relative humidity of the challenge gas.

The present work studied the response of aminopropyltriethyoxysilane (APTES) coated SAWS, which is known to sorb nitrobenzene,[8] to water vapour. This was the preliminary step in a continuing programme to study the interaction between the surface of coated SAWS and a two-component vapour system, nitrobenzene and water, in air.

EXPERIMENTAL

The experimental rig used to generate the humidified atmospheres was in all respects identical to that described by Fox and Alder.[4] The SAWS employed were manufactured for the authors by Plessey (Towcester, U.K.) and comprised a pair of 70 MHz delay lines on a quartz substrate. The SAWS and its associated oscillator have been described elsewhere.[9] The output of each SAWS controlled oscillator was to a Philips PM6673 frequency counter (Philips, Cambridge, U.K.) with digital-analogue converter output to a strip chart recorder.

*Author for correspondence.

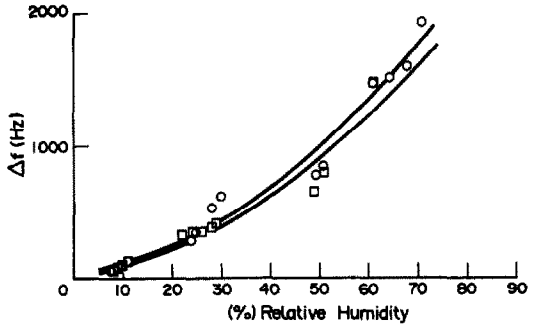

Fig. 1. Sorption isotherm at 25° onto APTES coated (side 1 —□—) and notionally uncoated (side 2 —○—) SAWS. It can be seen that there is no significant difference between the responses of the two sides, almost certainly an indication that the coating had crept from side 1 to side 2. Error bars are standard deviation.

The rig ran continuously throughout the period of the experiments. Relative humidity could be maintained to within ±0.5% and temperature within ±0.5° over a period of 9 months. Equilibrium of the SAWS to switched dry–wet air stream was of the order 15–100 min, depending on the actual change imposed.

Coating of the SAWS with APTES was achieved using a fine (00000 grade) paintbrush (available from model makers shops). A 20% solution of APTES in toluene was brushed on to the area in between the electrodes on one side of the SAWS only. The procedure employed was to first wash the SAWS free of grease using methylene chloride in a clean glass beaker and then allow it to dry in the oven at 60°, and cool in a desiccator. It was then placed in the oscillator circuit and maintained in the test cell at 25° and 1% relative humidity (RH) (±0.5% RH) as read on a Vaisala HMP123 humidity meter (Vaisala, Cambridge, U.K.). When the frequency of the SAWS had become stable, the side of SAWS exhibiting the lower frequency was coated. This caused the frequency difference between the coated and uncoated sides to separate further, thus minimising the problem of the oscillators associated with the two sides, locking

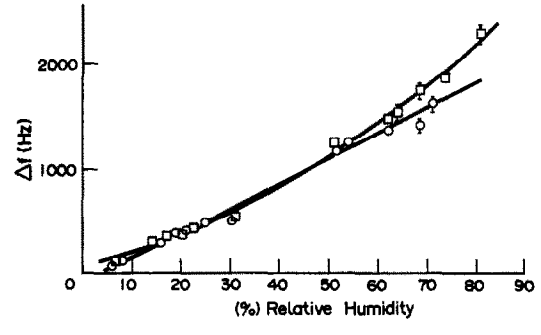

Fig. 2. Sorption isotherm at 30°; see legend to Fig. 1.

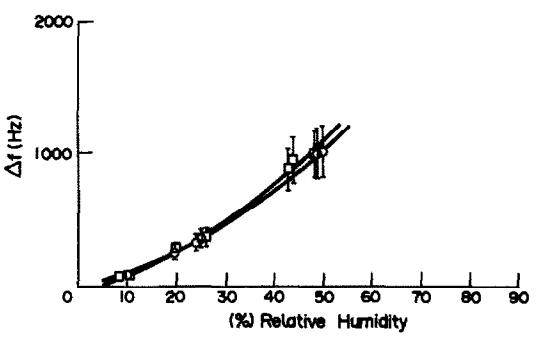

Fig. 3. Sorption isotherm at 40°; see legend to Fig. 1.

together. The coated SAWS was then placed in an oven at 45 ± 2° overnight to evaporate volatile materials and allow the coating to relax. The SAWS was then brought to equilibrium in the last cell at 25° 1% RH and the new frequencies noted. The resonant frequency of the uncoated side was virtually unchanged (±100 Hz) whereas the frequency of the coated side had reduced. On one occasion, for example, this was −5.39 kHz which corresponded to a coating of approximately 21 ± 3 molecular layers, calculated from the equation

$$\Delta f = (k_1 + k_2)\, f_o^2\ \text{m/A}$$

where k_1 and k_2 are the material constants for quartz,[10,11] f_o is the unperturbed frequency, m is the mass of coating and A is the surface area over which the coating was applied. Much of the work reported here was carried out with the 21 layer coated SAWS.

The coated SAWS was maintained in the test chamber[4] in a stream of air maintained at different relative humidities and one of the temperatures 25,30 or 40° (±0.5°). The flow rate chosen was 410 cm³/min which was shown to give reasonable response time between the humid and dry air flows (approximately 1 min on switchover to 95% change of frequency).

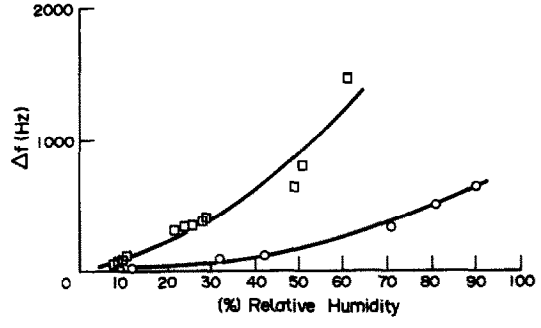

Fig. 4. Sorption isotherm at 25° onto APTES coated side 1 (—□—) of the same SAWS as in Fig. 1, (same data) compared with sorption isotherm onto a clean, uncoated SAWS at the same temperature, (—○—).

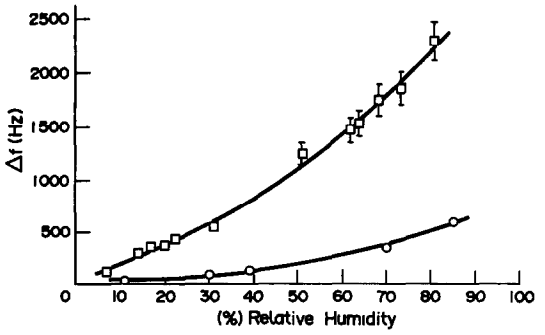

Fig. 5. Sorption isotherm at 30° onto APTES coated side 1 (—□—) of the same SAWS as Fig. 2, (same data) compared with sorption isotherm onto a clean, uncoated SAWS at the same temperature, (—○—).

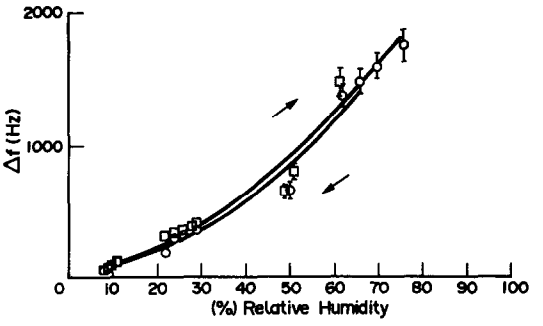

Fig. 7. APTES coated SAWS (side 1 as in previous figures) exposed to relative humidity cycle at 25°. Isotherms drawn (—○—) for ascending RH: (—□—) for descending RH.

The changes in relative humidity took longer to stabilize (15 min typically). RH could be maintained to within about 0.5% RH. The whole system was maintained in this regime for several months during the course of the experiments.

The sorption isotherms were obtained by first stabilizing the SAWS in a dry (1% RH) atmosphere at the chosen temperature and noting the frequency and the frequency stability. The flow was then switched to the humid air at the same temperature and allowed to stabilize again. These cycles were then repeated, each taking about 15 min. The RH was then changed and the cycles repeated to obtain the data points on the isotherms. Each isotherm took between one and three weeks to obtain.

RESULTS AND DISCUSSION

It was noted that the frequency stability degraded as the temperature of the SAWS increased from 25 to 40°, being typically ±2 Hz p-p at 25° degrading to ±10 Hz p-p at 40° for the uncoated, and ±15 Hz for the coated side, in dry air. In humid air the problem was worse, for example, the SAWS exposed to 80% RH at 40° for 2 hr exhibited noise of about ±15 Hz p-p, rendering it virtually unusable as a sensor. The authors are not sure what causes this effect, but it is at least in part influenced by the presence of the coating, as the noise is greater on the coated side of the sensor.

Isotherms were initially obtained using the dual SAWS described above, one side coated with APTES and the other side notionally uncoated. Figures 1–3 show the isotherms for 25°, 30° and 40° respectively. One notes however, that the two sides of the SAWS behaved in a very similar manner, with hardly any significant difference between them. This was not thought to be a true result. The isotherms were obtained for another SAWS device which had been thoroughly cleaned with methylene chloride, and indeed had never been coated with APTES. The isotherms at the three temperatures are given in Figs 4–6, for the uncoated, second SAWS, and the truly coated side of the first SAWS. The initial frequencies [$f_0 x$) of the two SAWS oscillators were very similar. One can clearly see a difference between the sorption isotherms onto the uncoated SAWS and the coated device in these figures. This indicates that some of the coating had crept from the coated, to the uncoated side of the dual SAWS. One would expect to detect an APTES monolayer

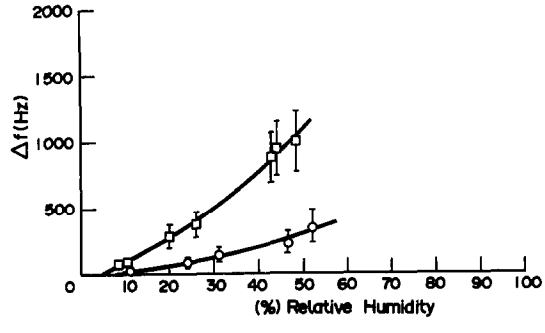

Fig. 6. Sorption isotherm at 40° onto APTES coated side 1 (—□—) of the same SAWS as Fig. 3, (same data) compared with sorption isotherm onto a clean, uncoated SAWS at the same temperature, (—○—).

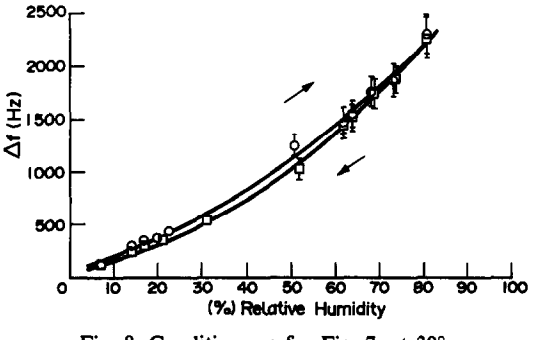

Fig. 8. Conditions as for Fig. 7, at 30°.

coverage on a 70 MHz SAWS as it represents about a 240 Hz frequency shift. Irreproducibility in manipulating and fitting the SAWS in its socket however, somewhat blurs these small changes in frequency, and a partial monolayer could readily be missed using this method of diagnosis. The water sorption isotherms onto the uncoated SAWS were similar in shape and magnitude to those obtained in previous studies in this laboratory, using 158 MHz devices.[4] The fact that creep was not evident using the FPOL and polyvinylpyrrolidone coatings in the previous work[4] was possibly due to the much higher molecular weight and viscosity/lower mobility of the polymers compared to the lower molecular weight APTES.

As was found in previous studies,[4] the sorption isotherms resemble the BDDT type III behaviour[12] which are characteristic of weak gas–solid interactions, particularly where the sorbed gas is polar and acts as sites for stronger polar-polar sorption of further water molecules. One would expect therefore a quadratic relationship between the frequency change on exposure of the SAWS to water vapour, and the relative humidity. Using a curve fitting routine "Techcad", quadratic functions of the form $y = ax^2 + bx + c$ were fitted to the data points obtained, and the best fit curves are shown as the solid lines in the Figs 1–6. It must be emphasized that these are purely empirical fits and although they show good regression analysis coefficients to the measured data, they have no detailed quantitative relationship to the underlying isotherm theory.[12] Table 1 shows the equation coefficients and the regression coefficient for the Figs 4–6. The effect of cycling the coated SAWS through a range of relative humidity was essayed at 25°, 30° and 40°. Quadratic functions were fitted to the data in ascending and descending order and the data shown in Figs 7–9. From the data it can be seen that there is no significant hysteresis in the cycle.

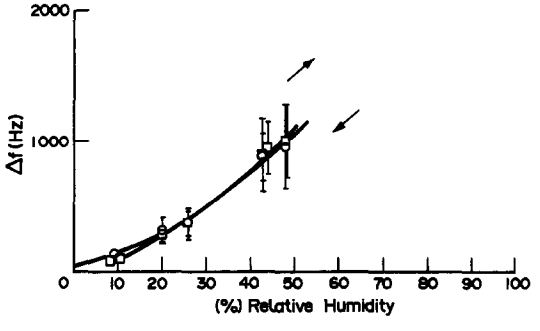

Fig. 9. Conditions as for Fig. 7, at 40°.

Table 1. Table of water sorption isotherm equation coefficients. Fitting the isotherm data to an equation of the form $y = ax^2 + bx + c$ where y represents frequency change (Δf/Hz) and x represents relative humidity (% RH)

Data from Figure	Coating	Temp (°C)	Equation coefficients (c)	(b)	(a)	Regression coefficient
4	APTES	25	9.6	5.74	0.24	0.978
4	Uncoated	25	68.3	−3.21	0.10	0.996
5	APTES	30	65.3	11.95	0.18	0.998
5	Uncoated	30	71.0	−2.31	0.10	0.995
6	APTES	40	−41.0	11.24	0.23	0.997
6	Uncoated	40	0.79	1.66	0.09	0.989

CONCLUSIONS

This work has shown that SAWS coated with APTES demonstrate sorption isotherms for water vapour which can be represented by quadratic equations which fit well over the range 1–70% RH at 25–30° and up to 50% RH at 40°. At higher temperatures and higher RH the frequency response becomes increasingly noisy for reasons which are at present not clear. Hysteresis in the adsorption and desorption curves is almost indiscernible at 25, 30 or 40° with the coating employed (21 ± 3 monolayers). These results indicate that it should be possible to partially correct the response of an APTES coated SAWS for water vapour adsorption up to 30° and 70% RH by data processing. There is bound to be a further effect due to competition between water vapour and competing target analytes for active sites, which will further complicate the response characteristics of coated SAWS. Current work in this laboratory is investigating the response of APTES coated SAWS to nitrobenzene, in atmospheres of varying relative humidity and temperature.

Acknowledgements—We are grateful to the Plessey Company for the gift of the 70 MHz SAWS.

REFERENCES

1. J. F. Alder and J. J. McCallum, *Analyst*, 1983, **108**, 1169.
2. J. J. McCallum, *Analyst*, 1989, **14**, 1173.
3. C. G. Fox and J. F. Alder, *ibid.*, **114**, 1989, 997.
4. *Idem*, *Anal. Chim. Acta*, 1991, **248**, 337.
5. J. W. Grate, A. Snow, D. S. Ballantine, H. Wohltjen, M. H. Abraham, R. A. McGill and P. Sasson, *Anal. Chem.*, 1988, **60**, 869.

6. D. S. Ballantine, S. L. Rose, J. W. Grate and H. Wohltjen, *ibid.*, 1986, **58**, 3058.
7. S. L. Rose-Pehrsson, J. W. Grate, D. S. Ballantine and P. C. Jurs, *ibid.*, 1988, **60**, 2801.
8. W. M. Heckl, F. M. Marassi, K. M. R. Kallery, D. C. Stone and M. Thompson, *ibid.*, 1990, **62**, 32.
9. J. F. Alder, C. G. Fox, A. R. M. Przybylko, N. D. Rezgui and R. D. Snook, *Analyst*, 1989, **114**, 1163.
10. H. Wohltjen, *Sensors Actuators*, 1984, **5**, 307.
11. B. A. Auld, *Acoustic Fields and Waves in Solids*, Vol. 2, Chap. 13. Wiley Interscience, New York, 1973.
12. S. J. Gregg and K. S. W. Sing, *Adsorption, Surface Area and Porosity*, 2nd Edn., p. 249. Academic Press, New York, 1982.

Talanta, Vol. 39, No. 11, pp. 1511–1516, 1992
Printed in Great Britain.

0039-9140/92 $5.00 + 0.00

POLARIMETER DESIGN FOR A NITROGEN LASER SOURCE

ROGER STEPHENS
Department of Chemistry, Dalhousie University, Halifax, Canada B3H 4J3

(*Received* 12 *March* 1992. *Accepted* 31 *March* 1992)

Summary—The system uses a Brewster angle reflector as a passive amplifier. This device reduces intensity without causing a serious reduction in either the signal of interest or the signal-to-noise ratio. It also reduces the need for a high quality analyser. However, polariser quality is critical and determines the background light level at the detector. The present work allowed shot-noise-limited operation to be attained. However full optimization was not achieved because of excessive background transmission at optimum alignment.

Laser sources have been used in polarimetry to achieve high sensitivity, for example in the detection of optically active compounds by liquid chromatography.[1,2] The sensitivity which is obtained is the result of the good signal-to-shot-noise ratio inherent in a high photon count. In practice however the task of designing a laser polarimeter to actually reach the shot noise limit is not trivial, because of the need to reject flicker noise: a requirement which becomes progressively more difficult to meet as the source intensity is increased. Various ways to approach this problem have been described.[3–5]

The difficulty of reaching the shot noise limit is compounded if a pulsed source such as a nitrogen laser is used. Flicker noise associated with pulse-to-pulse variability is high. Severe demands are placed on optical and electronic linearity. Selective modulation and synchronous detection cease to be easily employed. Finally, Davis *et al.* have warned of a risk of degraded polariser performance at the flux levels produced by a nitrogen laser,[6] which means that a high background can be expected at the detector even if polariser and analyser are exactly crossed.

Although obvious difficulties are involved in the use of a pulsed source for polarimetric measurements, such a system is potentially interesting for several reasons: examination of transient phenomena becomes easier; ultraviolet observation becomes more accessible; and optical rotation caused by non-linear interactions can be expected.[7–9] With these benefits in mind the present work was carried out to look at the feasibility of building an instrument around a nitrogen laser source and to examine its capacity to reach the shot noise limit. The method of design used the technique of passive amplification.[10,11]

THEORY

In the system employed here a linearly polarized laser beam undergoes optical rotation in the medium of interest and is then reflected from a glass plate aligned close to the Brewster angle. The effect of the plate is to amplify the angle of optical rotation at the cost of a reduction in beam intensity.[12] This is precisely the combination of characteristics needed to deal with an intense pulse, giving high sensitivity towards the signal of interest while avoiding an overload of the detector.

The schematic optical train shown in Fig. 1 will be described by means of the Jones calculus.[13] Preliminary experimental examination showed that the Jones matrices of polariser P_x and of the glass plate G could be written:

$$P_x = \begin{pmatrix} 1 & iA \\ iA & 0 \end{pmatrix} \quad (1)$$

and

$$G = \begin{pmatrix} K_x & 0 \\ 0 & K_y \end{pmatrix} \quad (2)$$

where $i = \sqrt{-1}$ and all other variables are real. Hence the Jones vector of light reflected from the plate G is given by:

$$\begin{pmatrix} E_x \\ E_y \end{pmatrix} = \begin{pmatrix} K_x \cos\Theta & 0 \\ K_y(iA\cos\Theta - \sin\Theta) & 0 \end{pmatrix} \begin{pmatrix} E_x^\circ \\ 0 \end{pmatrix} \quad (3)$$

where E_x° is the amplitude of light emerging from P_x and second order terms, involving

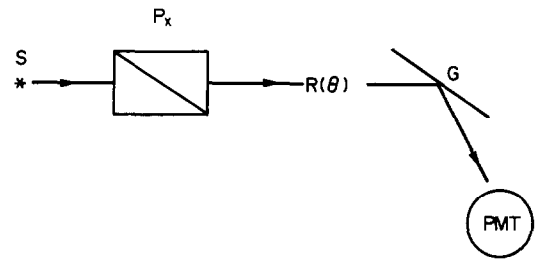

Fig. 1. Schematic optical train. S = source, P_x = polariser, G = glass reflector plate, PMT = photomultiplier.

AK_x for instance, have been neglected since K_x is small when G is aligned close to the Brewster angle. If

$$A \ll K_y \sin \Theta \tag{4}$$

then equation (3) describes light of an intensity reduced from its incident value by a factor of $K_x^2 \cos^2 \Theta + K_y^2 \sin^2 \Theta$ and an angle of optical rotation which has been amplified by K_y/K_x. Thus it is essential for A to be as small as possible in order to satisfy equation (4), and hence to maximise the amplifying effect of the glass reflector plate G and to minimise the background transmission of the system. The level to which A can be reduced is a measure of the purity of the linear polarization of the source.

Interestingly equation (3) remains valid even when an imperfect analyser is used to measure the Jones vector

$$\begin{pmatrix} E_x \\ E_y \end{pmatrix}.$$

For instance, a Wollaston prism will serve to spacially separate E_x and E_y. By analogy with equation (1) the Jones matrix, **W**, of the Wollaston prism becomes:

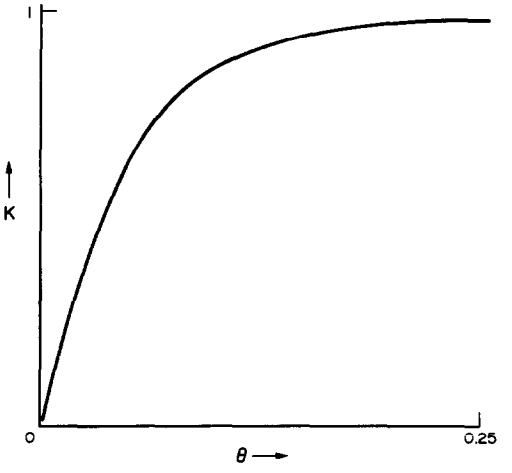

Fig. 2. K *vs.* Θ; K calculated as the ratio of equation (9)/equation (10) in units of $\sqrt{N^\circ}\,\Delta\Theta$.

$$\mathbf{W} = \begin{pmatrix} 1 & iB \\ iB & 1 \end{pmatrix} \tag{5}$$

and the Jones vector of light emerging from **W** remains the same as in equation (3) when second order terms are neglected.

The intensities corresponding to the Jones vector of equation (3) are:

$$I_x = K_x^2 \cos^2 \Theta I_x^\circ \tag{6}$$

$$I_y = K_y^2(\sin^2 \Theta + A^2 \cos^2 \Theta) I_x^\circ \tag{7}$$

where $I^\circ = E_x^{\circ 2}$.

The ratio, R, of the photon count on I_x, I_y over an integration time t is:

$$R = (I_y t \pm \sqrt{(I_y t)})/(I_x \pm \sqrt{(I_x t)})$$

$$= (N_y \pm \sqrt{N_y})/(N_x \pm \sqrt{N_x}) \tag{8}$$

Table 1. Summary of optical parameters

Reflector plate, G	$K_x = 3 \times 10^{-3}$, $K_y = 0.25$
Transmission efficiency of optical train, excluding G	15%
A^2 [equation (1)]	1×10^{-6}
X-channel photomultiplier characteristics:	
Photomultiplier quantum efficiency	15%
Gain (fixed)	4200
Output	1 volt across 0.001 μF
Half-width of output pulse	2 μsec
Estimated average cathode current	5 mA
Average anode current	0.5 mA
Laser output	5 μJ, 2 nsec duration
N^0 [equation (11)]	5×10^{12}
Calculated value of $\Delta\theta$ for unity signal-to-noise ratio from equation (11)	2×10^{-4}

Transmission and gain measurements were made using dc emission at 338 nm from a silver hollow cathode lamp. Photomultiplier characteristics were measured on the I_x channel at the same (fixed) gain used during data acquisition. The y-channel output at zero offset was 0.45 V across 0.001 μF, rising to 1 V at 0.06° offset at a gain of 4×10^5.

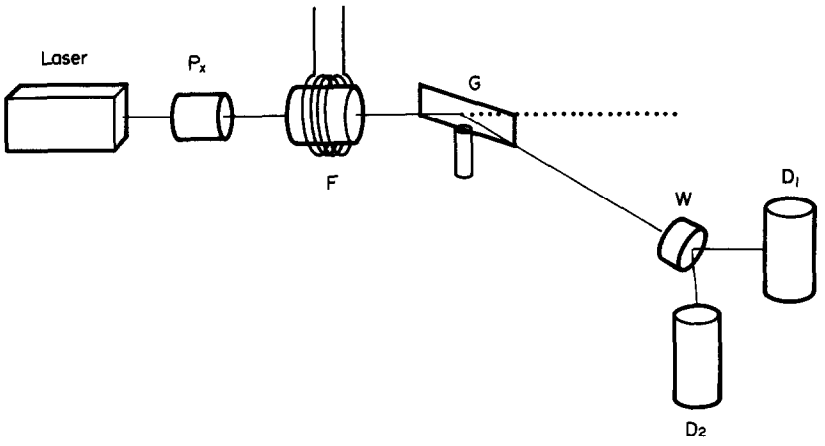

Fig. 3. Apparatus. P_x = polariser, F = Faraday cell, G = glass reflector plate, W = Wollaston prism, D1 and D2 = x- and y-polarisation detectors.

for a photon count $N = It$

$$\approx (N_y/N_x)(1 \pm 1/\sqrt{N_y})(1 \pm 1/\sqrt{N_x})$$

Hence

$$\frac{dR}{d\Theta} = 2K_y^2 \sin\Theta / K_x^2 \cos^3\Theta$$

i.e., the signal of interest, ΔR, is:

$$\Delta R \approx 2K_y^2 \sin\Theta \, \Delta\Theta / K_x^2 \cos^3\Theta \qquad (9)$$

with a shot noise level on R of

$$\sqrt{(N_y(N_x + N_y)/N_x^3)} \qquad (10)$$

The signal-to-noise ratio, r, is given by the ratio of equation (9) to equation (10) and can be written in the form

$$r = K\sqrt{N^\circ}\,\Delta\Theta \qquad (11)$$

where $N^\circ = I^\circ t$ is the source count. The limiting value of K for $A \to 0$, $\Theta \to 0$ is $2K_y$. Figure 2 shows values of K, calculated as the ratio of equation (9)/equation (10) and using experimental values of A^2, K_x^2, K_y^2 from Table 1, plotted against Θ. The maximum value of K in Fig. 2 is 0.99, corresponding to a minimum value of $\Theta \approx 1/\sqrt{N^\circ}$ for $r = 1$. The reduction in K from its upper limit of $2K_y$ results from the drop in signal-to-noise ratio, relative to an ideal system, which occurs when optical linearization is used to minimize the effect of background transmission.

In terms of the signal-to-noise ratio the procedure described above is equivalent to measuring the optical rotation signal of interest while simultaneously generating a reference pulse to correct for variations in source intensity. The present method of description is advantageous in that it identifies an optical geometry which will tolerate spatial inhomogeneity of the beam and which minimizes the intensities to which the detectors are subject. Both of these factors are important in allowing a full correction for laser power fluctuations to be obtained.

EXPERIMENTAL

The apparatus is shown in Fig. 3. The x- and y-polarised beams emerging from the Wollaston prism, W, corresponding to I_x and I_y in equations (6) and (7), were directed onto two 1P28 photomultipliers (detectors D1, D2 in Fig. 3). Dynode voltages were drawn from conventional divider chains using 100 K resistors for voltage division.

Following the procedure described earlier,[12] the plate G was aligned initially at the Brewster angle. The angle was then increased until the

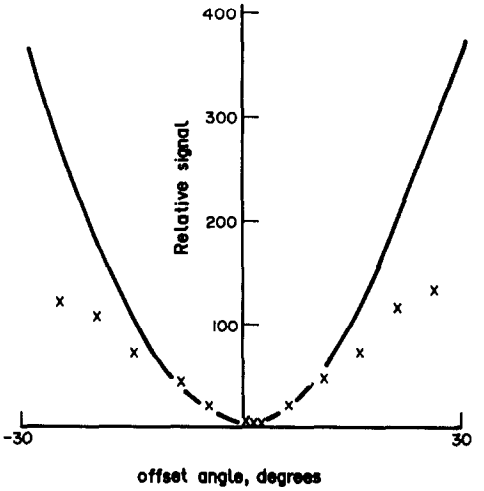

Fig. 4. Signal versus offset angle of polariser P_x. Solid curve: quadratic fit on lowest 6 point.

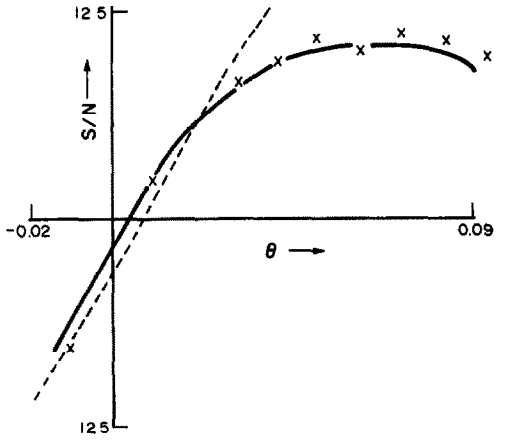

Fig. 5. Signal-to-noise ratio versus offset angle of polariser P_x. Solid curve: experimental. Dashed curve: signal-to-noise ratio calculated from equation (11) using the K values from Fig. 2 and the data in Table 1.

intensity of the x-polarised signal increased about 10-fold. Similarly, the y-polarised signal was raised above background by applying a small, known offset angle to polariser P_x, corresponding to the value of Θ in equation (9). The signal of interest, $\Delta\Theta$, was generated by the Faraday cell shown in Fig. 3. Construction of the cell has been described.[12]

All measurements were made on a laboratory-built dual channel boxcar integrator with delay and window times optimized to match the anode pulses of the photomultipliers. The two signals from the boxcar output channels went to a DEC MINC 11 computer, which calculated their ratio after each laser pulse; *i.e.*, the ratio corresponding to R in equation (8). Values of R and the R-to-noise ratio were

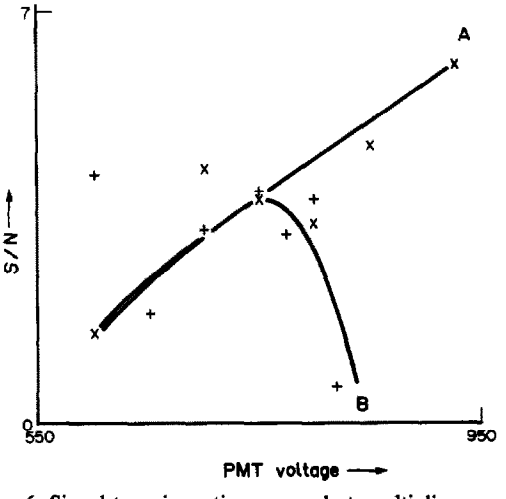

Fig. 6. Signal-to-noise ratio versus photomultiplier supply voltage. Curve A: offset angle on polariser $P_x = 0.02°$. Curve B: offset angle = 0.1°.

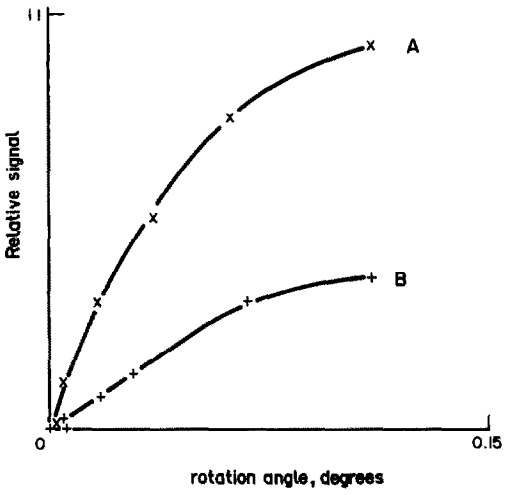

Fig. 7. Signal dependence on angle of rotation in Faraday cell. Curve A: photomultiplier supply voltage = 800 V. Curve B: 750 V.

displayed as the mean and standard deviation of up to 25 laser pulses. In order to minimize errors caused by detector non-linearity on the I_x channel the computer program rejected pulses with a value of N_x differing by more than 15% from the mean. Values of R were transferred to a chart recorder for a visual record as in Fig. 8 below.

RESULTS AND DISCUSSION

Light levels at the detectors

Some relevent characteristics of the apparatus are summarized in Table 1. The data in the Table lead to estimates for the photocathode and anode currents of 5 and 0.5 mA respectively for the I_x channel photomultiplier. The anode current is lower than the cathode current because of the increased pulse width at the anode. However, and even when the increased pulse width is considered, the current ratio is clearly inconsistent with the measured steady state gain. Therefore it was assumed that flux levels at the x-channel detector were high enough to cause the device to operate outside its usual linear response range, and to require the software correction mentioned above to limit the variation in I_x which would be accepted.

Detector non-linearity

Figures 4–7 show the observations which were made to determine the extent to which photomultiplier non-linearity was likely to affect the y-channel.

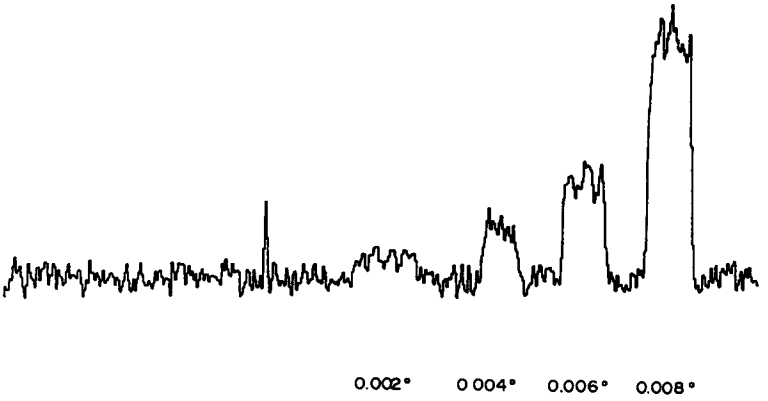

Fig. 8. Experimental signals from Faraday cell measured on single pulses from the laser.

Figure 4 shows the signal from the y-channel detector versus the angle of rotation of P_x. The solid line is the ideal $\sin^2 \Theta$ response curve fitted to the points close to the origin. Deviations at high light levels are obvious. That detector non-linearity is significant even at low offset angles is suggested by the results of Fig. 5, which shows that the signal-to-noise ratio falls off from the expected value, calculated on the basis of the curve in Fig. 2, at values of Θ above about 0.02°. Detector non-linearity means that pulse-to-pulse variations are no longer cancelled by the division of x- and y-channel signals: *i.e.*, flicker noise starts to degrade the signal-to-noise ratio.

Figure 6 shows the signal-to-noise ratio versus photomultiplier supply voltage at values of Θ of 0.02° and 0.1°. If the quantum efficiency of the photocathode is assumed to be independent of voltage then the maximum observed in curve B appears to represent an electron loss within the tube which occurs at higher voltages. Comparison of curves A and B shows the loss to be associated with the higher offset angle and, hence, the higher intensity. The data in Fig. 6 are one of several sets which were taken on successive days to determine that the pattern was consistent.

Similar behavior is evident in Fig. 7, which shows calibration curves at the two photomultiplier voltages used in Fig. 6. The upper curve shows the output stages to be able to handle a higher current than is demanded by the lower curve: nevertheless non-linearity on both curves is still apparent.

Capacitive de-coupling of the dynode load resistors and de-focussing of the incident beam, to cover a larger area of the photocathode, failed to change these observations. It is thought that they arise as a result of electron loss during transit through the tube when electron repulsion at high current densities overcomes the focussing effect of the dynode fields and allows spatial spreading of the electron beam to occur.

Signal optimization

The curve in Fig. 2 shows that the offset angle, Θ, should be sufficiently large for the effect of background transmission, [caused by incomplete source polarization; the 'A' term in equations (1) and (4)], to be insignificant. At the same time Θ should be small enough to avoid the detector non-linearity and degradation of signal-to-noise performance seen above. These requirements cannot be met simultaneously if the background transmission is too high. In the case of the present apparatus and with the laser output reduced to a level close to threshold the first condition requires Θ to be above about 0.1° (Fig. 2); the second requires Θ to be below about 0.02° (Fig. 5): *i.e.*, the degree of polarization of the source is a little below the limit of compromise.

Figure 8 shows experimental signals for Θ fixed at 0.05°. Unity signal-to-noise ratio is about 1×10^{-3}°. The noise dependence on intensity, under the same conditions, was determined by means of a variable aperture located between the laser and polariser P_x to vary the power delivered by the beam. Slopes of the resulting log plots of noise versus intensity varied between 0.4 and 0.7. Thus shot noise still appears to be dominant for the compromise value $\Theta = 0.05$°. However the response function K now falls below the optimum by a factor of about 3, using the curve in Fig. 2. Increasing the offset angle Θ improves K but degrades the signal-to-noise ratio, and vice versa: *i.e.*, the results shown in Fig. 8 are considered to be

essentially optimal for the particular combination of components used in the present apparatus.

CONCLUSIONS

It is considered that the instrumental design described here offers a viable way to use a photomultiplier to detect optical rotation on kilowatt-level light pulses. Operation close to the shot noise limit was found to be possible, although the present system failed to achieve an optimum signal-to-noise ratio. The reason for the shortfall lies in the need to avoid intensities where detector non-linearity and correspondingly increased flicker noise become evident. For the same reason higher laser power cannot be usefully employed with the existing arrangement.

Detector non-linearity is thought to be the result of electron scatter at high photocathode currents. Although appropriate modification and correction for this effect is possible, for example by an extension of the software correction used here, it is felt that the problem of detector non-linearity can probably be dealt with more satisfactorily by modification of the optical train. Equations (1)–(4) show that such modification can be approached through an improvement to the polarization quality of the source.

REFERENCES

1. D. R. Bobbitt and E. S. Yeung, *Anal. Chem.*, 1984, **56**, 1577.
2. K. C. Chan and E. S. Yeung, *J. Chromatog.*, 1988, **457**, 421.
3. H. Adams, P. Reinert, P. Kalbert and W. Urban, *Appl. Phys. B*, 1984, **34**, 179.
4. J. J. Kankare and R. Stephens, *Talanta*, 1986, **33**, 571.
5. D. R. Bobbitt and E. S. Yeung, *Appl. Spectrosc.*, 1986, **40**, 407.
6. L. A. Davis, R. J. Kruppa and J. D. Winefordner, *Spectrochim. Acta B*, 1986, **41**, 1167.
7. C. Wieman and T. Hansch, *Phys. Rev. Lett.*, 1976, **36**, 1170.
8. R. J. M. Anderson, T. M. Stachelek and W. M. McClain, *Chem. Phys. Lett.*, 1978, **59**, 100.
9. A. Giraud-Cotton and V. P. Kaftandjian, *Phys. Rev. A*, 1985, **23**, 2211.
10. V. S. Zapasskii, *Opt. Spektrosk.* 1979, **47**, 810.
11. R. Stephens, *Can. J. Applied Spectrosc.*, 1990, **35**, 110.
12. *Idem ibid.*, 1991, **36**, 140.
13. D. S. Kliger, J. W. Lewis and C. E. Randall, *Polarised Light in Optics and Spectroscopy*, Ch. 4, Academic Press, 1990.

Talanta, Vol. 39, No. 11, pp. 1517–1523, 1992
Printed in Great Britain.

0039-9140/92 $5.00 + 0.00

DETERMINATION OF ARSENIC BY INDUCTIVELY-COUPLED PLASMA ATOMIC EMISSION SPECTROMETRY ENHANCED BY HYDRIDE GENERATION FROM ORGANIZED MEDIA

B. AIZPUN FERNANDEZ, C. VALDES-HEVIA Y TEMPRANO, M. R. FERNANDEZ DE LA CAMPA and A. SANZ-MEDEL*

Department of Physical and Analytical Chemistry, Faculty of Chemistry, University of Oviedo, C/Julián Clavería 8, Oviedo, Spain

P. NEIL

Unicam Analytical Systems, Cambridge, England, U.K.

(*Received* 15 *March* 1992. *Accepted* 31 *March* 1992)

Summary—A method is described for the determination of arsenic, which combines a continuous flow hydride generation technique with an inductively coupled plasma atomic emission detection system. Some atomic absorption preliminary studies are described as well. Arsine is generated with $NaBH_4$ from a didodecyldimethylammonium bromide (DDBA) vesicular medium. The analytical performance of this vesicles-enhanced method is superior to the generation of the hydride from aqueous media: the detection limit (0.6 ppb) is improved by a factor of 2 and greater tolerance to interferences is observed for arsine generation from DDBA vesicles. Precision of As determinations is also improved. The proposed method has been validated for low As levels determinations in two Certified Reference Materials (CRM) sediments with satisfactory results. The potential of organized media to improve hydride generation is addressed.

The toxicity of arsenic to humans is widely recognised and consequently its determination in the environment and foodstuffs is of great importance. In sea and estuarine water, most arsenic is present as arsenate [As(V)], although low levels of arsenite [As(III)] and organoarsenicals (monomethylarsonic acid, dimethylarsinic acid, arsenobetaine, arseno-sugars, etc.) are also found.[1] These species are also found in marine organisms and terrestrial plants.

Although it is widely recognised that inductively coupled plasma atomic emission spectrometry offers adequate sensitivity for most environmental and clinical analyses, arsenic concentration levels in water samples are too low to be detected by ICP–AES.[2]

The necessarily low efficiency of nebulization, to prevent quenching of the plasma, is a serious drawback in the determination of toxic metals by ICP–AES due to the high sample consumption and its wastage before the measuring process. The introduction of samples in the vapour phase to the plasma provides a solution to these problems. Sensitivity is improved due to the increase of the transport efficiency and interferences may be overcome by the vapour generation.

Thompson *et al.*[3–5] first reported the combination of hydride generation techniques with ICP. Since then, a number of reports have appeared that discuss fundamental studies and applications[6–10] and theoretical aspects of hydride generation with ICP–AES. Particularly, the determination of arsenic by ICP based on arsine generation has been demonstrated to be subject to interferences, particularly from transition metal ions, which may affect the hydride generation process.[4,10–12] An approach to improve the selectivity could be a previous liquid–liquid separation of arsenic from interfering elements,[13] or a continuous on-line separation/hydride generation in the so-called "tandem on-line" technique used for As determination by ICP–AES and where the hydride is generated directly from the organic phase.[14]

The introduction of organic solvents into the ICP, however, continues to present particular difficulties[15] and therefore the use of micelles and other organised media, with a hybrid aqueous/organic character, could prove advantageous. In fact, we found that the presence of liquid solutions of "organized media", *e.g.*,

*Author for correspondence.

micelles and vesicles, may enhance the kinetics of the hydride generation.[16]

The singular characteristics of "organized media" such as solubilizing power, ability to build up a new "microenvironment", organizing reactants at molecular level, capacity to change the kinetics of a process, could provide a powerful tool for enhancing the sensitivity of arsenic and other hydride forming elements. In addition, their availability to react selectively with opposite charged reagents could also be used to improve the selectivity.

The purpose of the present work was to examine the ability of "organized media" to improve the analytical performance of hydride generation–ICP–AES technique by using arsenic as a model element.

As a result of our studies, a sensitive and selective analytical method for the determination of arsenic by ICP–AES has been developed. This method is based on continuous flow arsine generation from vesicles of didodecyldimethylammonium bromide (DDBA). The validity of the method for real sample analysis has also been tested through the successful determination of low levels of arsenic in some environmental samples.

EXPERIMENTAL

Apparatus

ICP–AES measurements. A Unicam ICP, model PU7000 spectrometer was used for emission measurements. It has a 40.68 MHz free-running radio-frequency generator, which includes an internal voltage regulator. A fixed quartz torch is used. The spectrometer uses a coarse-ruled echelle grating, and cross dispersion with a quartz prism for order sorting, resulting in a two dimensional spectrum, at the focal plane.[17] The nebuliser used consists of two platinum screens (dual platinum grid nebuliser): as the sample is nebulised from the first screen a primary aerosol is formed; the particle size is further reduced by impaction on a second screen. The nebuliser can act as an on-line gas–liquid separator when properly adjusted. As the liquid flows over the screens the hydride gases are entrained in an argon stream and are carried to the torch. The liquid is pumped through the drain to waste (Fig. 1). (This system is similar to that used by Watting and Collier[2]).

Flame AAS measurements. A Perkin-Elmer Model 2280 atomic absorption spectrophotometer equipped with an electrodeless discharge lamp operated at 7 mA from an external power supply and a deuterium background corrector was used for AAS measurements. In this case, a laboratory-made hydride generator/gas–liquid separator system previously described[13] was used throughout for sample introduction of arsine (Fig. 2). A Perkin–Elmer MS-10 hydride generator was used for non-continuous (batch) measurements.

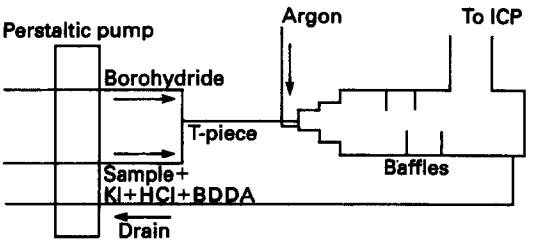

Fig. 1.

An ultrasonic device Sonics & Materials, Model VC500, 250 Watts was used to prepare the vesicle solutions.

Reagents

A stock solution of arsenic (1000 μg/ml) was prepared by dissolving 1.320 g of As_2O_3 in 25 ml of 0.1*M* sodium hydroxide, hydrochloric acid was then added until pH 7.0 and this solution was made up to 1.0 litre with redistilled water. The working solutions were prepared fresh by diluting appropriate aliquots from the stock solution.

Sodium tetrahydroborate (III) solution (1.5% w/v) was prepared by dissolving tetrahydroborate (III) powder (Carlo Erba) in demineralized Milli-Q water stabilized by 0.1% sodium hydroxide. Working solutions were prepared weekly and filtered before use.

Potassium iodide stock solution (10% w/v) was prepared by dissolving 25 g of potassium iodide in 250 ml of demineralized Milli-Q water.

Hexadecyl-trimethylammonium bromide (CTAB) solution ($10^{-2}M$) was prepared by dissolving the surfactant in water by gentle warming. The other surfactants assessed were prepared in a similar way.

Didodecyldimethylammonium bromide (DDAB) solution ($10^{-2}M$) was prepared by dissolving the surfactant powder in water and then sonicating for 12 min in an ultrasonic device, in order to obtain vesicles.

All reagents used were of analytical-reagent grade and redistilled or Milli-Q water was used throughout.

Procedures

Sample preparation. A 0.5-g weight of the sediment sample is weighed and placed into a nickel crucible, with 4 grams of potassium hydroxide. The crucible is then introduced into a furnace and heated at 500° for 30 min. The ashes are dissolved in 50 ml of 1*M* hydrochloric acid, and filtered before analysis. This solution is made up to 100 ml and analysed by ICP–AES.

Non-continuous (batch) measurements. The sample is transferred into a 10-ml flask and made up to volume with demineralized Milli-Q water. An aliquot is placed into the reaction vessel and hydrochloric acid and potassium iodide are added. It is then mixed with a 8% $NaBH_4$ solution in the MS-10/HG system. The generated arsine is swept into the heated quartz T-tube by a continuous stream of argon.

Continuous measurements. An aliquot of 5 ml is placed into a 50-ml flask and 4.2 ml of hydrochloric acid, 1 ml of 10% potassium iodide and 4.2 ml of $10^{-2}M$ DDAB are added and this solution is made up to volume with demineralized Milli-Q water. This solution was continuously pumped through one of the channels of the peristaltic pump, while a 1.3% solution of $NaBH_4$ was pumped through the second channel. Both flows were mixed at a T-piece where the hydride formation takes place. The gaseous and liquid mixture is passed through the grid nebuliser; the liquid is drained and the gaseous products are swept into the plasma, by the argon flow across the nebuliser.

RESULTS AND DISCUSSION

AAS studies

In our study of hydride generation methodology using organized media instead of aqueous media, the ability of different "organized media"[16] to enhance the sensitivity of As determinations was investigated. Arsine generation was carried out in a Perkin-Elmer MS10 commercial hydride generator. Optimum instrumental conditions selected for such determination are summarized in Table 1.

Table 1. Instrumental conditions in AAS measurements for As

Lamp current	7 mA
Spectral band width	0.7 nm
Wavelength selected	193.7 nm
Air/acetilene flow ratio	4

The following organised media were tested in concentrations below and above their critical micellar concentrations (cmc's):

—Cationic surfactant: CTAB (Hexadecyl-trimethylammonium bromide). (cmc = $9.2 \times 10^{-3}M$)
—Anionic surfactant: SDS (Sodium Dodecyl Sulphate). (cmc = $8.1 \times 10^{-3}M$)
—Non-ionic surfactant: TX-100 (TritonX-100). (cmc = $2\ 10^{-4}M$)
—Vesicles: DDAB (Didodecyldimethylammonium Bromide).

The net signals obtained generating the arsine from these four media, were compared with those obtained from aqueous media. Results showed that maximum Abs_s/Abs_b ratios (where Abs_s is the absorption due to the sample and Abs_b the absorption due to the blank), were obtained with DDAB vesicles.

To evaluate the relative merits of this methodology, we compared the sensitivity under optimized conditions of arsine generation AAS from water, DDBA and TX-100 (the three media which provided higher signals). These experiments were performed in both, continuous and non-continuous hydride generation systems, and the results observed were as follows:

Generation from a batch device (Perkin-Elmer MHS-10). An aliquot of the sample solution is placed in the sample reservoir, along with hydrochloric acid and potassium iodide. An 8% borohydride solution and an argon stream were used to generate and transport the arsine to a quartz tube placed on the flame of the AAS spectrometer.

Results obtained for the three media are given in Table 2. As shown in the Table, the precision was relatively poor when using a non-continuous generation system. Better results seemed to be obtained using vesicles of DDAB. To increase the precision of measurements a continuous generation system was investigated.

Table 2. Comparison of analytical performance of arsine generation–AAS in various media

	L.D.		Precision (%)	
Media	*A*	*B*	*A*	*B*
Water	36 ng	4 ppb	25	6.7
BDDA	17 ng	1 ppb	23	6.9
TX-100	136 ng	—	39	—

A: Batch.
B: Continuous.

Generation from a continuous hydride generation device. A schematic diagram of this hydride generator is shown in Fig. 2. The liquid streams of sample solution, or blank, in 0.2% potassium iodide solution [to ensure that all arsenic is in the As (III) form], 1*M* hydrochloric acid solution and the reducing reagent, 1% $NaBH_4$ were pumped continuously and merged at a T-piece where the hydride formation takes place. The mixture of liquid and gas then arrives to an interface vessel (filled with 3-mm o.d. Pyrex beads) which provides a smooth separation of liquid and gas. The gaseous products, arsine and hydrogen, are swept through the vessel into the quartz tube of the AAS system by a continuous stream of argon. This argon stream was optimized and fixed at 0.045 l./min. The waste liquid is drained via a U-tube system, as can be seen in Fig. 2.

Using this system, we compared the analytical characteristics of arsine generation, in terms of detection limit and precision, from the two better media, that is DDAB vesicles and water. As shown in Table 2, detection limits (3 σ_b where σ_b is the standard deviation of blanks) found were: 1 ng/ml of As using BDDA and 4 ng/ml generating AsH_3 from aqueous media, the precision being similar in both cases (around $\pm$ 7% for 12 ppb solutions of As).

Thus, organized media do enhance the analytical characteristics of hydride generation-AAS determination of As.

The use of micelles and other organized media are particularly useful in ICP–AES, because they provide a microenvironment similar to that of organic solvents for reactions.[16] However, they offer superior performance and are more compatible with plasma operation; in fact, extinguishing, de-stabilization and background levels of the ICP, are all minimized by using micellar solutions instead of organic solvents.[13,18]

Therefore the use of organized media was also tested for hydride generation–ICP–AES determination of As.

HG–ICP studies

The first step was to optimize the experimental generation of AsH_3 and its continuous introduction into the plasma using a Philips HG system (see Fig. 1). In a second step, the following organised media: Tritón X-100, CTAB, and DDAB were assayed and compared with aqueous AsH_3 generation. Preliminary studies showed that CTAB produces a slight precipitate with potassium iodide, while TX-100 did not produce any improvement in the ICP–AES signal (as observed by AAS). Therefore, an

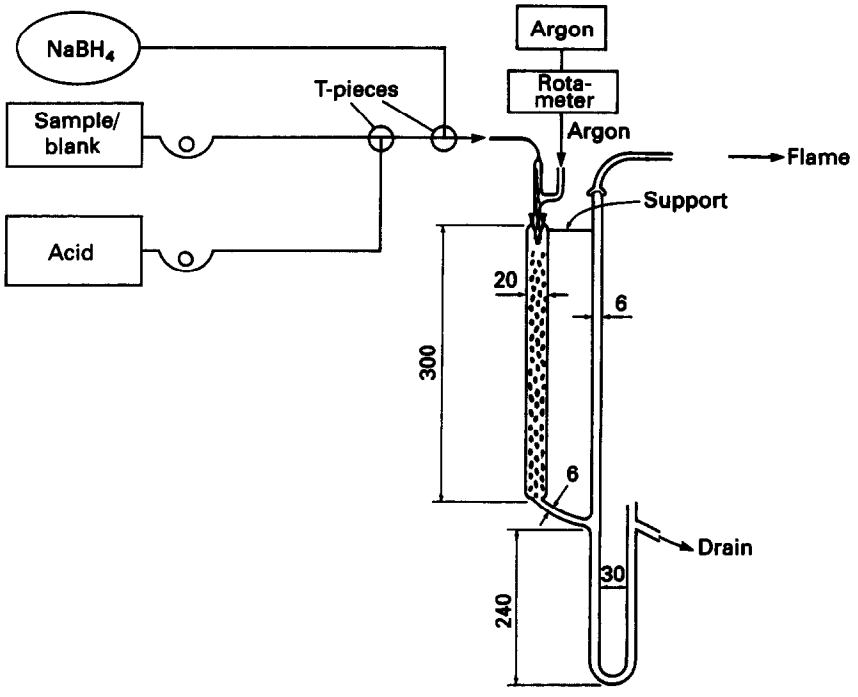

Fig. 2.

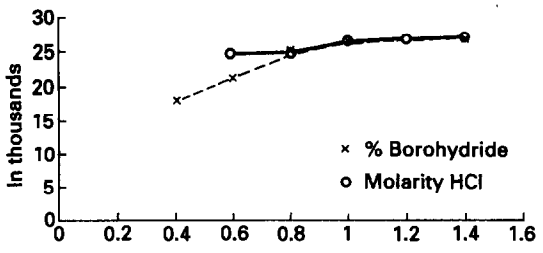

Fig. 3.

organized media of vesicles of DDAB was finally selected for further experiments.

Optimization of the instrumental parameters

The criterion for optimization was taken to be the best signal-to-background ratio, $SBR = (I_e - I_b)/I_b$ (where I_e is the intensity for the sample, and I_b for the blank).

Selection of the analytical line. The two most sensitive analytical emission lines for arsenic were tested: 193.695 nm and 197.198 nm. The observed values of SBR were 7.2 for the former and 6.5 for the latter analytical line, using a 50-ppb standard.

Optimization of chemical parameters for AsH_3 generation. Optimum hydrochloric acid and $NaBH_4$ concentrations were investigated using 50 ppb arsenic, a 0.5% potassium iodide solution as reducing agent and working at both emission lines sequentially. A univariant search was used in this instance to establish the optimum hydrochloric acid and $NaBH_4$ concentrations in the aqueous phase. The emission intensities obtained for each hydrochloric acid and $NaBH_4$ concentrations, are given in Fig. 3. It can therefore be seen why $1M$ hydrochloric acid and 1.3% $NaBH_4$ were selected for the subsequent work.

It was observed that the ICP signal became higher with higher DDAB concentration. However, above $8.4 \times 10^{-4}M$ of the surfactant a precipitate formed in the presence of potassium iodide. Therefore, reductants other than potassium iodide were assayed in order to reduce As (V) to As (III). The behaviour of potassium iodide, titanium (III) chloride and sodium sulphite compared in vesicles of DDAB. Figure 4 summarizes the observed results which showed that the signal obtained when using $TiCl_3$ or Na_2SO_3 was always lower than that obtained for potassium iodide. For this reason, a potassium iodide concentration of 0.5% was selected to ensure that all arsenic is in the As (III) form.

Table 3. Optimum operating conditions in ICP–OES measurements

Plasma	
Coolant gas flow	11 l./min
Pressure of Ar in nebuliser	35 psi
Forward power	1.5 kW
Hydride generation system	
$NaBH_4$ concentration	1.3% m/v in 0.1% NaOH
$NaBH_4$ uptake rate	2.1 ml/min
Sample acidity	$1M$ in HCl
Sample uptake rate	4.2 ml/min
DDAB conc.	$8.4 \times 10^{-4}M$

The overall optimum conditions found are summarized in Table 3, and they happened to be the same in both media tested (water and DDAB).

Analytical performance, characteristics of the DDAB–HG–ICP–AES determination of arsenic. Using the optimum conditions previously obtained (Table 3), sensitivity, selectivity, and precision of As determination by HG–ICP–AES using aqueous or DDAB media were evaluated.

Calibration graphs obtained in both media are shown in Fig. 5 and show that the sensitivity (slope of calibration curve) is twice when using vesicles; the linear analytical range obtained extended from 6 ng/ml to, at least 100 μg/ml using DDAB and from 13 ng/ml to 100 μg/ml for water media, while the detection limts ($3\sigma_b$) were 0.6 ng/ml for BDDA and 1.3 ng/ml for aqueous media.

The precision was evaluated by analysing ten replicates of a solution containing 50 ng/ml of arsenic with AsH_3 generation from aqueous and DDAB media. Relative standard deviation observed were $\pm 3.2\%$ using aqueous and $\pm 2.3\%$

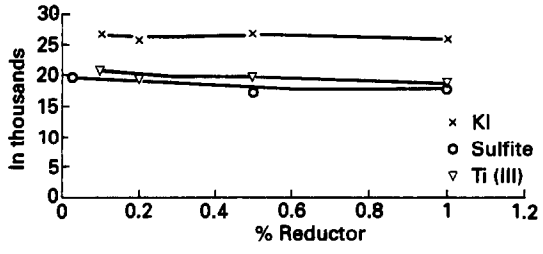

Fig. 4.

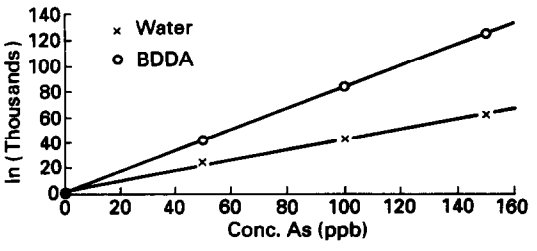

Fig. 5.

in DDAB media. Therefore, the precision of arsine generation (see Table 2 for similar AAS measurements) seems to be clearly improved by adding vesicles to aqueous solutions.

Interference studies

In order to investigate potential interferences from aqueous and DDAB media, solutions containing 25 ng/ml of arsenic (III) with various amounts of foreign ions were prepared. These solutions were analysed for As following the recommended procedure in the presence and absence of DDAB vesicles.

All the results obtained are summarized in Table 4 in a comparative manner. As it can be seen in this table, some interferences are reduced (as in the case of Bi, for instance) or eliminated (in the case of Ti) when hydride generation is performed from DDAB vesicles. There is, however, an important interference in DDAB: when Sb is present in concentrations above 20 μg/ml, it produces precipitates (with DDBA) which seriously inhibit the introduction of the sample due to blocking of tubing.

Table 4. Interferences of some elements in As determination by HG–ICPAES

Interferent	Relationship	Recovery (1) (Water)	Recovery (2) (DDBA medium)
Bi	1:1000	50	
	1:500	52	75
	1:300	54	98
	1:100	55	
	1:50	85	
Ca	1:1000	110	
	1:500	101	98
Co	1:1000	101	
Cr	1:1000	108	
	1:500	93	97
Cu	1:1000	88	
	1:500	98	
Fe	1:1000	103	
	1:500		107
	1:300		100
Hg	1:1000	115	
	1:500	106	102
	1:300	105	
K	1:1000	100	100
Li	1:1000	111	
	1:500	96	
Mn	1:1000	97	
Na	1:1000	111	
	1:500	99	
Ni	1:1000	99	
	1:500	100	
Pb	1:1000	102	
Sb	1:300	105	
	1:200	97	
	1:100	95	
Sn	1:500	122	90
	1:300	102	100
Te	1:1000	100	
Ti	1:1000	65	
	1:500	75	100
	1:300	103	
Zn	1:1000	100	
	1:500		101

Table 5. Results of the analysis of some sediments (reference materials)

Sediment	Observed value (μg/g)	Certified value (μg/g)
CRM 277	47.6 ± 1.0	47.3 ± 1.6
CRM 320	74.1 ± 3.3	76.7 ± 3.4

Results show that in general terms the method proposed using DDAB seems to be more selective than the method using aqueous solution and thus it can be favourable for the determination of As in real samples.

Application to real samples

In order to test the analytical usefulness of the proposed method for the determination of low levels of As in environmental samples, we analysed two different certified sediments, namely, CRM 227 and CRM 320 (estuarine and river sediment respectively) from B.C.R. (E.C.).

Sample dissolution and preparation was carried out as described elsewhere[11] with hydride production and determination using the developed methodology.

The results obtained are given in Table 5 (each value given is the average of three determinations) and demonstrate that the DDAB–HG–ICP–AES procedure proposed here provides good accuracy and precision for this type of analytical problem.

CONCLUSIONS

Long-chain surfactants have been proposed to improve the sensitivity of many analytical methods of atomic spectrometry. Sample transport in nebulizers and atomization efficiency enhancements in the flame had been invoked to rationalize the observed sensitivity improvements. Other workers, however, found very little or no sensitivity enhancement by surfactants, while recent research on the topic[18,19] tends to indicate that transport efficiency does not increase on addition of most varied surfactants.[18] Micelles thus appear to have limited application for ICP–AES conventional nebulisation.[19]

Conversely, micelles, and other organized media such as vesicles, could be most helpful in atomic methods based on hydride generation. As we have shown in a preliminary communication[16] the hydride generation is a chemical

reaction which can be improved in the presence of such "organized" media, at least from two different points of view:

(a) Micelles, vesicles, *etc.*, are able to "organize" reagents at a molecular level, as has been repeatedly shown[20] for coloured and photoluminiscent reactions. This could affect sensitivity (effective concentration of reactants is higher in the microenvironment created by the organized medium than in water) and selectivity of hydride generation (*i.e.*, by selecting oppositely or identically charged micelles for the analyte and interferences respectively).

(b) Not only thermodynamic constants but kinetics of the reactions can also be altered by organized media.

Our results for As have shown that, at least modestly, all the expected improvements (detection limits, selectivity and precision) have been realized using vesicles of DDAB in the continuous (and batch) generation of arsine.

The "organized medium"-enhanced technique for hydride generation allows a fast and precise determination of As by ICP–AES and could be extended to other hydride forming elements. Moreover, analysis of environmental samples using the developed method gives results close to the certified values. Speciation of As is an important requirement for this application; this challenge could be approached using micellar chromatography[21] for separation of species and the proposed DDAB-arsine generation ICP–AES for detection.

Research in this direction of As speciation is currently in progress in our laboratory.

REFERENCES

1. A. G. Howard and M. H. Arbab-Zavar, *Analyst*, 1981, **106**, 213.
2. R. J. Watting and A. R. Collier, *ibid.*, 1988, **113**, 345.
3. M. Thompson, B. Pahlavanpour, S. J. Walton and G. F. Kirkbright, *ibid.*, 1978, **103**, 568.
4. M. Thompson, B. Pahlavanpour, S. J. Walton and G. F. Kirkbright, *ibid.*, 1978, **103**, 705.
5. H. Thompson and B. Pahlavanpour, *Anal. Chim. Acta*, 1979, **109**, 251.
6. E. De Oliveira, J. W. McLaren and S. S. Berman, *Anal. Chem.*, 1983, **55**, 2047.
7. R. R. Liversage, J. C. Van Loon and J. C. De Andrade, *Anal. Chim. Acta*, 1984, **161**, 275.
8. G. S. Pyen and R. F. Browner, *Appl. Spectrosc.*, 1988, **42**, 508.
9. F. Nakata, H. Sunahara, H. Fujimoto, M. Yamamoto and T. Kumamaru, *J. Anal. At. Spectrom.*, 1988, **3**, 579.
10. T. Nakahara, *Appl. Spectrosc.*, 1983, **37**, 539.
11. J. Wilson Wershey and P. Keliher, *Spectrochim. Acta.*, 1986, **41B**, 713.
12. L. Halic and G. H. Rusell, *Analyst*, 1986, **111**, 15.
13. A. Menéndez García, J. E. Sánchez Uría and A. Sanz-Medel, *J. Anal. At. Spectrom.*, 1989, **4**, 581.
14. J. Aznarez, F. Palacios, M. S. Ortega and J. C. Vidal, *Analyst*, 1984, **109**, 713.
15. P. Changkan, Z. Guangxuan and R. F. Browner, *J. Anal. At. Spectrom.*, 1990, **5**, 537.
16. R. Fernández de la Campa, C. García Ortiz, M. Díaz García and A. Sanz-Medel, Conference presentation, XII National Congress of Spectroscopy, Barcelona (Spain), 1990.
17. T. C. Dymott, International Laboratory, March 26, 1989.
18. J. Mora, A. Canals and V. Herandis, *J. Anal. At. Spectrom.*, 1991, **6**, 143.
19. Z. Yin Yan and Z. Wuming, *ibid.*, 1989, **4**, 797.
20. A. Sanz-Medel, P. L. Martinez and M. E. Díaz García, *Anal. Chem.*, 1987, **59**, 774.
21. W. L. Hinze and D. W. Armstrong (ed.), *Ordered Media in Chemical Separations*, ACS Symposium Series 342, Washington 1987.

Talanta, Vol. 39, No. 11, pp. 1525–1530, 1992
Printed in Great Britain.

0039-9140/92 $5.00 + 0.00

CLOSED-LOOP RECIRCULATING MANIFOLD FOR MATRIX ISOLATION IN FLOW INJECTION FLAME ATOMIC ABSORPTION SPECTROMETRY. ANALYSIS OF SILVER ELECTROLYSIS SOLUTIONS

EBENEZER DEBRAH and JULIAN F. TYSON*
Department of Chemistry, University of Massachussets, Amherst, MA 01003, U.S.A.

MICHAEL W. HINDS
Royal Canadian Mint, 320 Sussex Drive, Ontario, Ottawa, Canada K1A 0G8

(*Received* 27 *March* 1992. *Accepted* 31 *March* 1992)

Summary—Two flow injection procedures have been investigated for the determination of some elements in silver electrolysis solutions, for which the problem of the formation of silver acetylide needs to be addressed. A single line manifold was found to give acceptable results for limited time periods, but for prolonged operation it was necessary to remove the silver. This was achieved with a recirculating reactor in which the silver was precipitated as the chloride and retained on a filter of nylon fibers. Good recoveries of copper, iron, nickel and zinc from solutions containing up to 100 g/l. silver were obtained with over 95% of the silver retained on the filter. The filter was regenerated rapidly by flushing with ammonia solution.

A major driving force in research in analytical atomic spectrometry is the need to remove matrix interferences. The use of flow injection (FI) techniques for the separation of analyte and matrix species is proving to be of considerable versatility and several methods of FI separation and preconcentration have recently been reviewed.[1] Although most of the FI procedures have already been described in an off-line batch mode, there are some practical problems associated with their use which have mitigated against their use in favor of some instrumental based methods of interference removal or compensation. As well as the dangers of contamination and loss, batch procedures are often labor intensive and time consuming. Flow injection methodology, as an approach to automation, is a versatile alternative to manual procedures. Due to the inherent high precision of flow-based procedures, most of the physical and chemical manipulations of the sample can be reduced to the actions of filling and injecting the contents of a sample loop. Flow injection techniques also have the additional benefit of providing a safe, contamination-free enclosed sample handling system.

*Author for correspondence.

Precipitation is the oldest method of chemical separation.[2] Precipitation methods are satisfactory for macro separations, although precipitates are usually contaminated with foreign ions present in solution, although these would not themselves have been precipitated under the given experimental conditions. Developments in trace analysis and the methods of separation and preconcentration have led to the study of the possibility of using precipitation techniques for matrix isolation. Precipitation is useful for removing the major constituent of a sample if this interferes with the subsequent determination of trace components. Conditions can be chosen such that a considerable amount, if not all, of the major constituent can be precipitated without causing losses, by co-precipitation, of the trace constituents to be determined. For example, Karabash *et al.*[3] studied coprecipitation of trace elements with the aid of radio-tracers and have shown that in the precipitation of lead sulfate from a 6*M* nitric acid solution, many trace elements remained (85–100%) in solution, which is sufficient for trace analysis purposes.

Several groups of workers have shown tha it is possible to use precipitation and redissolution in a flow injection manifold for the purposes of preconcentration of trace

components and the removal of potentially interfering matrix components. For the small quantities of precipitate involved it is possible to retain the solid phase on an in-line filter of either stainless steel,[4] cellulose acetate[5] or even to retain the analyte element co-precipitated on the interior of an open knotted tube reactor.[6]

The insertion of a filter directly in-line does not cause a problem when the amount of precipitate is small, but for large amounts of solid the use of a precipitation manifold with direct coupling to an atomic spectrometer presents some difficulties due to the changes in flow rate which occur as the precipitate collects on the filter medium. This is particularly true if a high concentration of a matrix species is to be removed by precipitation.

To overcome this problem, the use of a recirculating, closed-loop manifold for sample pretreatment is described. The use of closed loop recirculating systems in flow systems predates flow injection methodology[7] and continuous flow recirculation manifolds have been used as part of sample pretreatment procedures. Carbonell *et al.*[8] have described the digestion of sewage sludge samples in a continuous flow reactor. The aim of the study was the on-line digestion and the determination of trace metallic elements in solid samples using the slurry approach coupled with microwave oven digestion in an FIA system. In this procedure the partially digested sample was returned into a sample reservoir and a subsample was injected into a single line manifold for transport to the flame atomic absorption spectrometer. Lazaro *et al.*[9] described a procedure for the on-line leaching of iron from plant material with the aid of ultrasound and the entire recirculating loop formed the loop of the injection valve. On injection, the sample stream merged with a reagent stream containing 1,10-phenanthroline and the product of the reaction was detected spectrophotometrically at 512 nm. The use of recirculating loops for several different flow injection sample pretreatment procedures has recently been discussed by Tyson *et al.*[10] These procedures concerned dilutions for calibration purposes, on-line extraction and matrix isolation.

The determination of metals in solution with high concentrations of silver by flame atomic-absorption spectrometry with an air/acetylene flame can be problematical due to the formation of solid silver acetylide in the spray chamber. This leads to blockage of both the nebulizer and the burner and it is a serious hazard as it may detonate if allowed to dry.[11]

The aim of these studies was to investigate the possibilities for determining trace amounts of metals in silver electrolysis solutions by matrix removal of the silver by precipitation and retention on an on-line filter.

EXPERIMENTAL

Two atomic absorption spectrometers with continuum source background correction (Perkin-Elmer models 5000 and 1100B) were used. For the model 5000, the signal was recorded on a Houston Instrument Model 200 XY recorder connected to the analog signal output of the spectrometer. For the model 1100B, the signal was printed on an Epson model LQ-850 printer. Hollow cathode lamps were operated at the manufacturer's recommended currents. Wavelengths of 324.8 nm for copper, 232 nm for nickel, 248.3 nm for iron, 213.7 nm for zinc and 328.1 nm for silver were used and the appropriate single element hollow cathode lamp was used in each case. An air–acetylene flame was used in all determinations. The instruments were used for each element according to the manufacturers' specification.

The single line manifold is shown in Fig. 1. A Gilson Minipuls 3 variable speed peristaltic pump was used with a Rheodyne model 5020 6-way injection valve. Teflon tubing (0.08 mm i.d.) tubing and flangeless fittings (Supelco) were used to complete the manifold. The injection loop volume was 70.7 μl. The recirculating flow manifold (see Fig. 2) was constructed from PTFE tubing of 0.8 mm or 0.5 mm internal diameter. The filter column consisted of a borosilicate glass column 50 mm × 3 mm (Omnifit) filled with nylon fibers (PolyScience Inc., Pennsylvania). A multichannel variable speed peristaltic pump (Ismatec model MS-4 Reglo 8-100, Cole Parmer, Chicago, IL, U.S.A.) was used to pump liquid in the manifold. Valves were either 6-port rotary valves (Rheodyne model 50, Alltech, South College, Pennsylvania) for sample introduction into the manifold and

Fig. 1. Single line manifold. C is a distilled water carrier stream, S is the sample injection valve and AA is the model 5000 spectrometer. The connection between the valve and the detector was the minimum length of tubing possible.

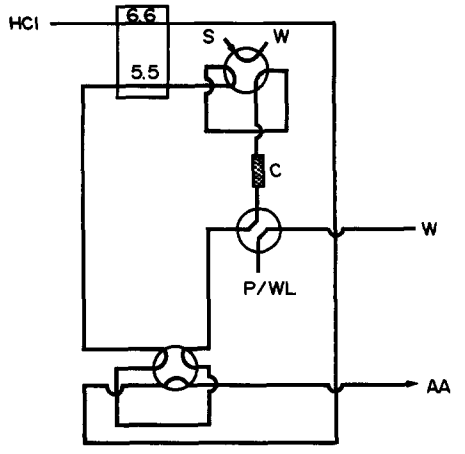

Fig. 2. Recirculation closed loop manifold for the matrix isolation of silver in the determination of trace metals. AA is the model 1100B Spectrometer, S is the sample injection valve, P/WL is the precipitant/wash liquid, HCl is 2*M* hydrochloric acid solution and W is waste.

the injection of subsamples into the spectrometer or 4-port distribution valve (Omnifit, model 1114) for introduction of the precipitant or the wash liquid into the manifold.

The manifold was operated by first filling the loop with the precipitant (hydrochloric acid) via the four way selection valve and then injecting the sample into the manifold at the point labelled S in Fig. 2 and turning the valve so that the precipitant flowed through the sample loop. The precipitate formed was retained on the filter column labelled C and the sample was allowed to circulate for a predetermined period of time after which a subsample of the contents in the recirculation loop was injected into the spectrometer via a single line manifold. After injection of the subsample, the loop was filled via the selection valve with ammonium hydroxide solution (1 + 1) to dissolve precipitate on the column and wash the loop. The loop was then rinsed with distilled demineralized water and was then filled with fresh precipitant and the procedure repeated.

Copper, iron, nickel and zinc standards were made from the dilution of 1000 mg/l. standards (Fisher Scientific). The silver solutions were prepared from silver nitrate crystals (Fisher Scientific). Hydrochloric acid (Baker Instra-analyzed, Fisher Scientific) was used for the precipitation reactions and ammonium hydroxide (ACS Certified, Fisher Scientific) was used for all washings. Distilled dimineralized water (Barnstead Inc.) was used for all dilutions and washing of the manifold. All solutions were stored in high density polyethylene bottles.

Procedures

Single line manifold. The effect of flow and the concentration of dissolved silver on copper absorbance were investigated. To investigate the effect of the formation and build-up of precipitate in the spray chamber a 2.0-ppm copper solution was introduced continuously at a fixed flow rate of 2.5 ml/min between each change in silver concentration. The calibration solutions covered the range 0–60 ppm copper. Two samples were analyzed by the single line flow injection procedure and by EDTA titration.

Recirculating loop manifold

Effect of the recirculation time. This was studied by filling the loop with demineralized water and injecting samples of 10 mg/l. Cu and allowing them to recirculate for different lengths of time between 1.5 and 10 min.

Effect of the concentration of the precipitant. The effect of the concentration of the HCl precipitant over the range 0.2 to 2.0*M* was studied for a solution containing 10 mg/l. Cu and 50 g/l. Ag.

Tolerable level of silver in the sample injected. The effect of varying the silver concentration between 1 and 100 g/l. was studied for a fixed concentration of copper.

Optimization of the flow parameters. The flow rate of the carrier to the spectrometer was optimized by injecting a subsample of the solution into the spectrometer at varying flow rates. The flow rate was varied between 3.2 and 8.6 ml/min. The flow rate within the loop was also varied between the same values.

Effect of the sample volume injected. The volume of sample solution injected into the manifold was varied between 70 and 185 μl.

Effect of subsample injected into the spectrometer. Volumes of the subsample injected into the carrier stream for transport to the spectrometer were varied between 111 and 462 μl.

Recovery studies. The recovery of copper, zinc, nickel and iron at concentrations of 10 mg/l. in the presence of varying amounts of silver between 1 and 100 g/l. were studied.

Breakthrough of silver. The amount of silver that was not retained on the filter column was investigated by monitoring the silver absorbance for the same samples used for the recovery studies.

Calibration. Under the optimum conditions, a 163-μl sample volume and a subsample of

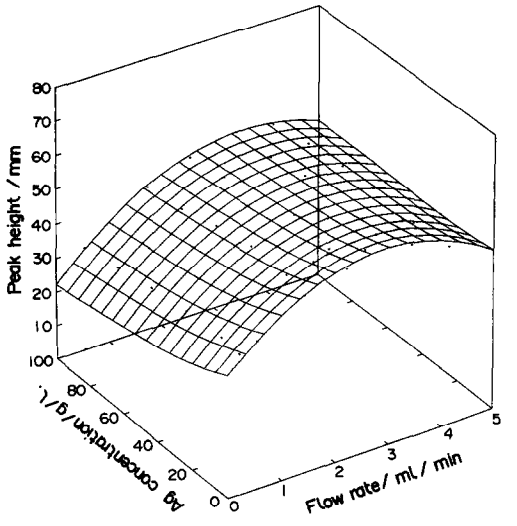

Fig. 3. Response surface for variation of flow rate and silver concentration for the single line manifold.

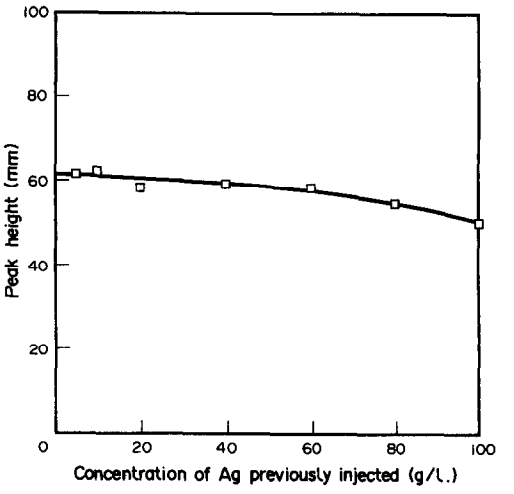

Fig. 4. Response of a constant concentration of copper as a function of the concentration of silver injected.

237 μl, calibration plots were generated for copper, nickel, iron and zinc in the range of 0 to 30 mg/l. and the amounts of these trace elements in synthetic samples with silver matrix determined. Three samples from the Royal Canadian Mint (RCM 1, RCM 2 and RCM 3) were also analyzed for copper by the standard addition method. Both the normal calibration plots and the standard additions plots were generated using standard solutions containing 1000 mg/l. silver.

RESULTS AND DISCUSSION

Single line manifold

The effects of the flow rate and silver concentration are shown in Fig. 3. The surface plot shows the variation of the peak height with changes in both flow rate and Ag concentrations. Peak height remained independent of the silver concentration except at very high concentrations. Changes in flow rate affected the measured absorbance. A decrease in the flow rate below 2.5 ml/min caused a significant decrease in the peak heights observed. The effect of the build up of precipitate is shown in Fig. 4. There was a small change in response over the silver concentration range indicating that the amount of this type of material deposited in the nebulizer does not seriously impede the solution from reaching the flame in the short term. However, over prolonged periods of operation it was found necessary to clean the system.

A typical analysis sequence is shown in Fig. 5. The values for the copper concentrations of two samples determined by this procedure were 0.44 and 5.13 g/l. whereas the values obtained by EDTA titration were 0.441 and 5.36 g/l., respectively.

Recirculating loop manifold

Peak height was used to characterize the absorbances. All the standard deviations and relative standard deviations quoted are based on four replicate measurements. The total volume of the recirculation loop was 660 μl, the optimum volume of sample injected in the manifold

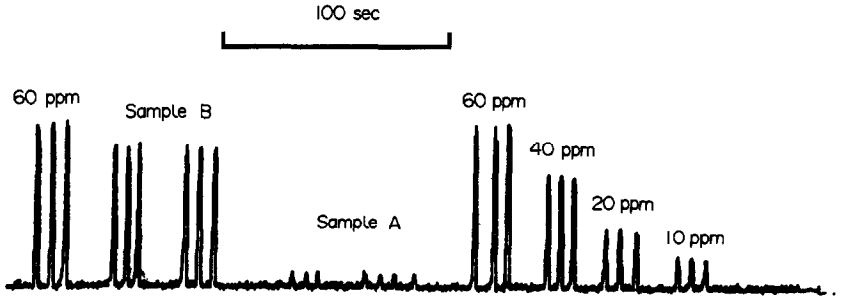

Fig. 5. Recorder trace for single line manifold for the determination of copper at 222.6 nm in diluted (100 fold) silver electrolysis solutions.

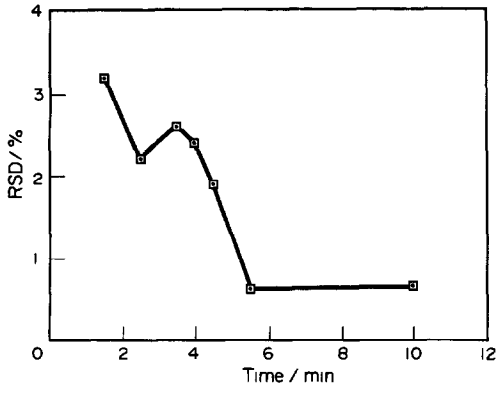

Fig. 6. Variation of precision with recirculation time.

Table 2. Calibration plots

	r^2
Nickel Absorbance = $1.3500 \times 10^{-3} + 3.4510 \times 10^{-3}$ [Ni]	0.998
Copper Absorbance = $4.9493 \times 10^{-3} + 4.0174 \times 10^{-3}$ [Cu]	0.995
Zinc Absorbance = $1.8911 \times 10^{-2} + 1.6589 \times 10^{-2}$ [Zn]	0.991
Iron Absorbance = $1.8893 \times 10^{-3} + 4.5314 \times 10^{-3}$ [Fe]	0.996

was 163 μl and the optimum subsample volume injected into the spectrometer was 237 μl. It was observed that circulating the sample in the manifold for 4.5 min was sufficient to let the contents of the sample mix so that a reasonable reproducibility could be obtained, see Fig. 6. For times of less than 4.5 min the reproducibility was poor. In effecting a good filtration for these studies the differences between the two principal types of colloidal precipitates, hydrophobic and hydrophilic, is important. Hydrophilic precipitates are difficult to separate by filtration and to wash and are likely to coprecipitate numerous substances. On the other hand, hydrophobic precipitates, such as silver chloride, have a low water affinity and are purer and more readily filterable.[2] It was observed that the precipitation was very efficient at a hydrochloric acid concentration of 2*M* and this was chosen for further experiments. This concentration was high enough such that only a small amount of precipitate was not retained on the first pass of the precipitate through the filter column. The recoveries obtained are shown in Table 1. These results indicate there is no problem with coprecipitation and also varying silver concentrations do not give significantly different recoveries. The recoveries for nickel were higher than for the other elements and to investigate a possible enhancement by silver or iron, solutions containing varying amounts silver or iron in a fixed concentration of nickel were nebulized directly into the spectrometer. However, no significant difference between the absorbance of the sample containing no silver and the samples containing the largest amount of silver (1000 mg/l.) or iron (500 mg/l.) was observed.

There was no significant difference between the peak heights obtained for the different flow rates in the recirculating loop. A flow rate of 5.5 ml/min was chosen for further experiments. It was observed that large volumes of samples did not significantly affect the peak height, although peak area increased proportionately. In a manner similar to that observed with the single line manifold, as the flow rate of the carrier was varied it was observed that the peak height increased in a direct proportion. The highest flow rate used, 8.6 ml/min, gave the highest mean absorbance but the precision was poor so a flow rate of 6.6 ml/min was used throughout the experiment.

The manifold can accommodate a silver concentration of up to 90 g/l. but above this concentration the flow in the manifold is impeded and the precision of the measurements get worse. For example the RSD for the recovery of copper in the presence of 100 g/l. silver was 15% compared with 4% in the presence of 90 g/l. silver. The precision (measured as the relative standard deviation of 4 replicate determinations) was below 5% for almost all the measurements made at or below this concentration of silver. It was observed that even for a sample containing 90 g/l. silver, more than 95% of the silver was retained on the column. It was noted that proportion of the precipitate retained increased as the silver content in the solution analyzed increased. This was

Table 1. Recoveries (%) of metals from a silver matrix

Element	50 g/l. Ag	60 g/l. Ag	70 g/l. Ag	80 g/l. Ag	100 g/l. Ag
Zn	112.0	—	114.0	—	—
Cu	97.2	—	106.5	—	95.0
Fe	99.8	—	96.5	—	—
Ni	101.4	129.0	—	129.0	—

Table 3. Determination of trace elements in synthetic samples

	Added (mg/l.)	Found (mg/l.)*	RSD (%)
Iron sample 1	18	18.67 ± 0.74	4.0
Iron sample 2	12	12.23 ± 0.35	2.9
Zinc sample 2	15	16.53 ± 0.24	1.5
Copper sample 1	15	16.53 ± 0.24	1.5
Copper sample 2	12	11.34 ± 0.30	2.6
Nickel sample 1	15	14.60 ± 0.35	2.4
Nickel sample 2	18	8.11 ± 1.77	9.8

* ± terms are standard deviation based on 4 replicate measurements.

considered to be related to an increased rate of crystal growth at higher concentrations. The calibration plots for all the elements were linear (see Table 2) and the results obtained for the synthetic samples are shown in Table 3. Two samples previously analyzed by the Royal Canadian Mint and found to have 3.65 and 3.00 g/l. copper were analyzed and found to contain 3.72 ± 0.12 and 3.10 ± 0.12 g/l. copper, respectively. The ± terms are standard deviations calculated from the calibration plots.[12]

CONCLUSION

The coupling of a chemical pretreatment whose kinetic character would make interfacing a flow injection manifold directly with a flame atomic absorption spectrometer difficult has been achieved by the use of a flow injection valve as interface between the reactor and the carrier stream for delivery to the instrument. In this manner, the kinetics of the two operations are decoupled and each procedure can be optimized separately. It has been demonstrated that it is possible to remove substantial proportions of a potentially interfering matrix by precipitation in a flow injection system.

Acknowledgement—Financial support from the Royal Canadian Mint is gratefully acknowledged.

REFERENCES

1. J. F. Tyson, *Spectrochimica Acta Rev.*, 1991, **14**, 169.
2. J. Minczewski, J. Chwastowska and R. Dybczynski, *Separation and Preconcentration Methods in Inorganic Trace Analysis*, Ellis Horwood, Chichester, 1982.
3. A. G. Karabash, L. S. Bondarenko, G. G. Morozova and Sh. I. Peizulaev, *Zh. Analit, Khim.*, 1960, **15**, 623.
4. P. Martinez-Himinez, M. Gallego and M. Valcarcel, *Analyst*, 1987, **112**, 1233.
5. E. Debrah, C. E. Adeeyinwo, S. R. Bysouth and J. F. Tyson, *ibid.*, 1990, **115**, 1543.
6. Z. Fang, M. Sperling and B. Welz, *J. Anal. At. Spectrom.*, 1991, **6**, 301.
7. H. U. Bergmeyer and A. Hagen, *Z. Anal. Chem.*, 1972, **261**, 333.
8. V. Carbonell, M. de la Guardia, A. Salvador, J. L. Burguera and M. Burguera, *Anal. Chim. Acta*, 1990, **238**, 417.
9. F. Lazaro, M. D. Luque de Castro and M. Valcarcel, *ibid.*, 1991, **242**, 283.
10. J. F. Tyson, S. R. Bysouth, E. Grzeszczyk and E. Debrah, *Anal. Chim. Acta*, 1992, **261**, 75.
11. G. D. Muir (ed.), *Hazards in the Chemical Laboratory*, The Chemical Society, London, 1977.
12. J. C. Miller and J. N. Miller, *Statistics for Analytical Chemistry*, Ellis Horwood, Chichester, 1984.

Talanta, Vol. 39, No. 11, pp. 1531–1535, 1992
Printed in Great Britain.

0039-9140/92 $5.00 + 0.00

KINETICS OF ALUMINIUM FLUORIDE COMPLEXATION IN SINGLE- AND MIXED-LIGAND SYSTEMS

GEOFFREY S. TOWNSEND and BRYON W. BACHE*
Department of Geography, The University, Cambridge, CB2 3EN, U.K.

(*Received* 30 *March* 1992. *Accepted* 9 *April* 1992)

Summary—The complexation reaction between Al^{3+} and fluoride was studied over concentration ranges 2–50μM fluoride, 0.5–500μM aluminium, pH 2.5–5.0, at ionic strength 0.1 and temperatures of 298 and 283 K. The initial rate of formation of AlF^{2+} was strongly dependent on pH, reaching a minimum at pH 3, and was considerably slower at the lower temperature. Addition of salicylate increased the reaction rate, probably because of the corresponding increase in the initial concentration of $AlOH^{2+}$. These effects of pH, temperature and competing ligands will therefore be critical in determining the composition of acid natural water systems and in particular the speciation of soluble aluminium.

Aluminium is a key element in acid ecosystems because its ionic forms, which begin to dissolve as pH drops below 6, are toxic to many organisms. In acid waters where aluminium toxicity has been associated with poor biological productivity, a number of inorganic and organic ligands are present that affect the speciation of the aluminium ions in solution.[1] Furthermore, the mobilization and transport of aluminium from sparingly soluble forms in soils into percolating waters and thus into streams and lakes depends critically on both the chemical combinations of aluminium and the rates of flow of water.[2] One is frequently dealing with non-equilibrium conditions in these systems. As part of a wider study on rate processes in aluminium mobilization from soils to surface waters,[3] it became necessary to study the kinetics of the complexation of aluminium ions in solution with soluble ligands that affect its speciation. The most important of these are the fluoride ion and organic ligands. Organic matter soluble in acid solutions is frequently called "fulvic acid", but this is poorly defined chemically apart from containing COOH and phenolic OH functional groups. Salicylic acid is commonly used as a surrogate for fulvic acid because it contains these functional groups, and it is particularly useful in the present study because it can be easily determined by fluorimetry.

The relative rates at which aluminium complexes are formed may determine their biological activity, particularly as thermodynamic equilibrium is believed to be attained only rarely in natural waters.[4] Previous studies of the rates of complex formation of aluminium with fluoride[5] and salicylic acid[6] were conducted at higher concentrations, ionic strengths and temperatures than are relevant in natural water systems. These also considered only a single ligand at a time whereas natural systems contain a mixture of ligands. The difference between ligands in the temperature dependence of their reaction rates may also result in a competitive advantage being given to the formation of one particular complex, and this effect will be superimposed on other factors such as the concentrations of the ligands concerned and the solution pH.

Because fluoride complexes are more stable than any of the other expected soluble aluminium complexes, the approach adopted here was first to study their rate of formation, and then to study the competitive complexation reactions with the addition of salicylate.

EXPERIMENTAL

Reagents

Three stock solutions (1×10^{-4}, 1×10^{-3} and $5 \times 10^{-3} M$) of sodium fluoride were prepared from Analar grade salt after drying at 373 K for 24 hr, and transferred to polyethylene bottles. All subsequent fluoride solutions were prepared fresh daily from these stock solutions. Aluminium solutions were prepared fresh each day from Spectrosol aluminium nitrate solution, and their concentrations verified by the catechol violet colorimetric method. Salicylic acid

*Author for correspondence.

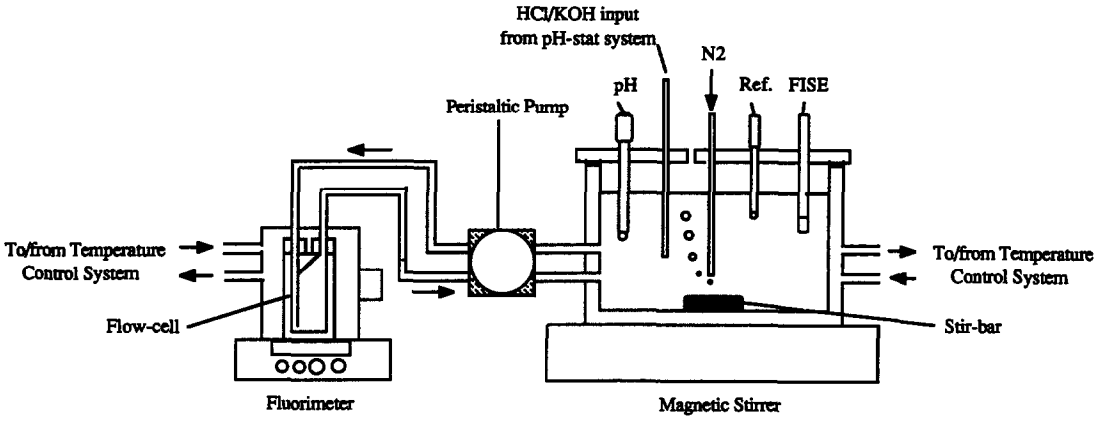

Fig. 1. Experimental reaction system for simultaneous determination of fluoride and salicylate. (FISE = fluoride ion selective electrode).

solutions were prepared fresh each day to prevent possible polymerization[7] and were standardized by potentiometric titration with potassium hydroxide.

Apparatus

All containers used were washed by soaking in 10% nitric acid and rinsed with distilled and demineralized water prior to use. Experiments were performed in the reaction vessel shown on the right of Fig. 1 when using inorganic components alone, with the addition on the left of Fig. 1 to measure salicylate concentrations by fluorimetry for the competitive complexation reactions. The combination of the two systems allowed the fluoride and the salicylate complexation reactions to be monitored simultaneously. Fluoride activities were determined with a Philips fluoride ion-selective electrode and a saturated calomel reference electrode with an E.D.T. ECM202 digital voltmeter. The pH was controlled with a Radiometer TTT 85 pH-stat system with a combined pH electrode, adding hydrochloric acid or potassium hydroxide to maintain a specific pH. Hydrogen ion concentrations were calculated from pH measurements using the Debye-Huckel approximations. The volumes of HCl/KOH required were predetermined so that the amounts of potassium chlorate required to maintain the required ionic strength could be calculated for each experiment. The reaction vessel was surrounded by a thermostatted water jacket connected to a Grant constant temperature water bath and purged with oxygen-free nitrogen. Salicylate concentrations were measured with a Zeiss model DMR21 spectrofluorimeter equipped with two grating monochromaters each with a fixed 10-nm band pass, which was used with a 10-mm flow-through quartz cuvette and Watson Marlow peristaltic pump. Outputs from the pH meter, the spectrofluorometer and the voltmeter were recorded by Linseis chart recorders.

Procedures

Before each run, the fluoride ISE was calibrated for the appropriate concentration range and pH with eight standard solutions. The response time of this electrode was less than one second and so was well able to monitor the slower Al-F complexation reactions. For each kinetic run, 500 ml of the fluoride reaction mixture was placed in the reaction vessel, and stirred to the desired constant temperature with a Teflon stir bar.

Two separate procedures were used in the experiments: (i) aluminium solutions were added to fluoride in the reaction vessel in discrete steps, and the reaction monitored until equilibrium was attained between successive additions. (ii) A single aluminium addition, of concentration 10× the fluoride concentration, was injected into the solution and the reaction monitored to equilibrium. Initial fluoride concentrations were 2×10^{-6} to $50 \times 10^{-6} M$, initial aluminium concentrations were 5×10^{-7} to $5 \times 10^{-4} M$, pH was controlled within the range 2.5–6.0, ionic strength was 0.10 and temperature 298 K. Some experiments were also performed at ionic strength 0.05, and some at 283 K. For the competitive complexation experiments, an initial fluoride concentration of $10^{-5} M$ was used, with salicylate concentrations from 10^{-6} to $10^{-4} M$, pH between 3.0 and 6.0 and ionic strength 0.10. Each experiment was performed in duplicate and the means are reported in the results.

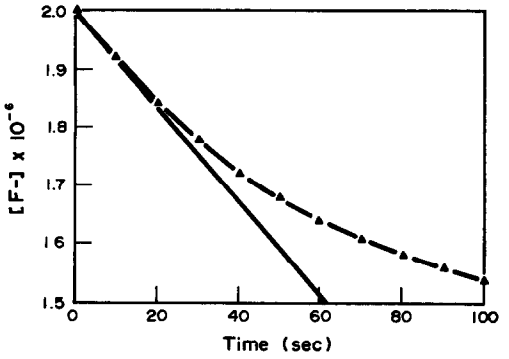

Fig. 2. Typical plot of fluoride concentration as a function of time, with tangent drawn at $t = 0$, from which initial rate was derived.

RESULTS AND DISCUSSION

Reaction rate for aluminium-fluoride complexation

Determining rate laws and constants from integrated equations is fraught with problems, particularly if secondary or reverse reactions may be involved. It is preferable to use initial reaction rates, for which the concentration of reactant or product is plotted against time for the short initial period of the reaction during which concentrations change so little that the instantaneous rate is hardly affected.[8]

During the titrations, the potential of the fluoride ISE becomes more positive with respect to the calomel electrode, indicating a decrease in the free F^- concentration resulting from the formation of the complex ion AlF^{2+}. The tangent to the rate curve at time = 0 then gives the initial reaction rate. We used this initial rate (IR) method, used previously for fluoride kinetics by Srinivasan and Rechnitz.[5] The majority of the kinetic runs gave plots whose tangents could be drawn with a reproducibility of about ±3%. The method is illustrated for a typical experimental run in Fig. 2. To calculate a rate constant, it is preferable to define the rate of formation of AlF^{2+} rather than the rate of free fluoride consumption. This was done and the results for all 26 experiments are summarized in Table 1.

Table 1. Initial rates of AlF^{2+} formation as a function of H^+ ion concentration, Al concentration, ionic strength and temperature

I (M)	$[H^+]$ (M)	$[Al^{3+}]$ (M)	$[F^-]$ (M)	$(d[AlF^{2+}]/dt)_{t=0}$ (M/sec)
		298 K		
0.01	1.09×10^{-6}	1.00×10^{-4}	1.00×10^{-5}	7.69×10^{-6}
		5.00×10^{-4}	5.00×10^{-5}	1.38×10^{-4}
0.01	3.47×10^{-6}	1.00×10^{-4}	1.00×10^{-5}	3.43×10^{-6}
		5.00×10^{-4}	5.00×10^{-5}	6.47×10^{-5}
0.01	1.09×10^{-5}	2.00×10^{-5}	2.00×10^{-6}	1.89×10^{-7}
		1.00×10^{-4}	1.00×10^{-5}	2.09×10^{-6}
		5.00×10^{-4}	5.00×10^{-5}	3.81×10^{-5}
0.01	3.48×10^{-5}	2.00×10^{-5}	2.00×10^{-6}	4.22×10^{-8}
		1.00×10^{-4}	1.00×10^{-5}	6.32×10^{-7}
		5.00×10^{-4}	5.00×10^{-5}	1.17×10^{-5}
0.01	1.09×10^{-4}	2.00×10^{-5}	2.00×10^{-6}	2.07×10^{-8}
		1.00×10^{-4}	1.00×10^{-5}	3.23×10^{-7}
		5.00×10^{-4}	5.00×10^{-5}	5.81×10^{-6}
0.01	3.48×10^{-4}	2.00×10^{-5}	2.00×10^{-6}	1.25×10^{-8}
		1.00×10^{-4}	1.00×10^{-5}	1.17×10^{-7}
		5.00×10^{-4}	5.00×10^{-5}	2.11×10^{-6}
0.01	1.90×10^{-3}	1.00×10^{-4}	1.00×10^{-5}	5.92×10^{-7}
		5.00×10^{-4}	5.00×10^{-5}	2.59×10^{-6}
0.01	3.48×10^{-3}	1.00×10^{-4}	1.00×10^{-5}	9.63×10^{-7}
		5.00×10^{-4}	5.00×10^{-5}	1.33×10^{-5}
0.05	1.09×10^{-5}	1.00×10^{-4}	1.00×10^{-5}	9.82×10^{-7}
0.10		1.00×10^{-4}	1.00×10^{-5}	6.89×10^{-7}
0.05	1.09×10^{-4}	1.00×10^{-4}	1.00×10^{-5}	1.34×10^{-7}
0.01		1.00×10^{-4}	1.00×10^{-5}	9.97×10^{-8}
0.05	1.09×10^{-3}	1.00×10^{-4}	1.00×10^{-5}	1.97×10^{-7}
0.01		1.00×10^{-4}	1.00×10^{-5}	1.21×10^{-7}
		283 K		
0.01	1.09×10^{-5}	2.00×10^{-5}	2.00×10^{-6}	6.41×10^{-8}
		1.00×10^{-4}	1.00×10^{-5}	7.14×10^{-7}
		5.00×10^{-4}	5.00×10^{-5}	1.28×10^{-6}
	3.48×10^{-4}	2.00×10^{-5}	2.00×10^{-6}	7.94×10^{-9}
		1.00×10^{-4}	1.00×10^{-5}	7.28×10^{-8}
		5.00×10^{-4}	5.00×10^{-5}	1.27×10^{-6}

Rate equation and mechanisms of complex formation

In all cases the initial rate of formation of AlF^{2+} was first order with respect to $[Al^{3+}]$ but not with respect to [F]. At constant initial fluoride concentration, rate/[F] increased with $[F^-]$, an effect that was more pronounced at higher pH, (Fig. 3) indicating the need for fluoride concentration terms in the rate equation. At constant pH the rate/$[Al^{3+}]$ values were approximately constant, so that a rate equation of the following form was indicated:

$$\text{Initial rate (IR)} = (d[AlF^{2+}]/dt)_{t=0}$$
$$= K_1[Al^{3+}][F^-] + K_2[Al^{3+}][F^-]^2$$

This equation was tested between pH 2.5–6.0 over the entire range of concentrations investigated using a non-linear least squares programme; the comparison between the observed rates and the calculated rates gave a standard deviation of 3.7%. The same rate equation resulted from a detailed theoretical consideration of possible reaction mechanisms[3,5,9,10] where K_1 and K_2 are defined in terms of the rates of a number of possible reactions in which HF, F^- and OH^- penetrates the $Al(H_2O)_6^{3+}$ aquo ion.

Effect of pH on reaction rate

Figure 3 indicated the importance of pH on the reaction rate, but this is further demonstrated in Fig. 4 by the dependence of both K_1 and K_2 on pH, both reducing rapidly as pH drops from 5.5 to about 3, but then whereas K_2 drops to zero K_1 increases at pH below 3. The combined effect is to give a minimum rate of Al-F complexation at pH about 3. The consequences of this for natural water systems are considerable, indicating that fluoride will be important for mobilizing aluminium into soluble complexes at pH values around 5, but it is likely to be much less effective in more acid systems.

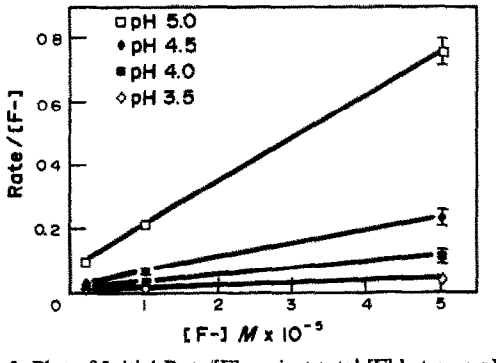

Fig. 3. Plot of Initial Rate/[F] against total [F] between pH 3.5 and 5.0. $[Al^{3+}] = 5 \times 10^{-4} M$. Error bars = ±S.E.

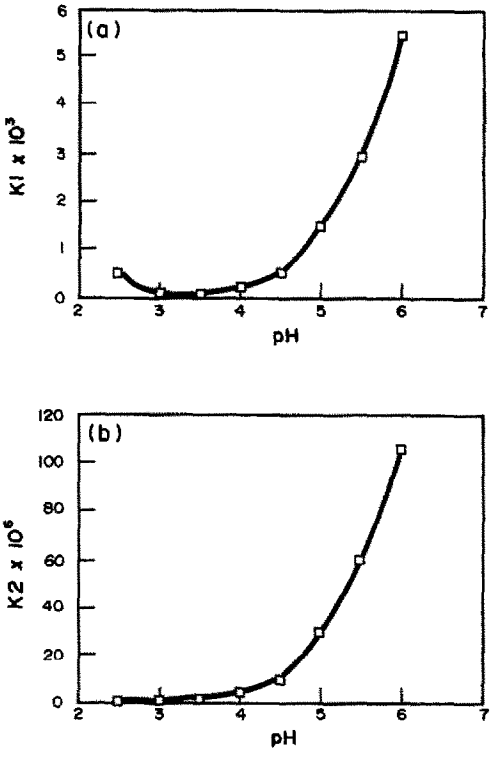

Fig. 4. Dependence of (a) K_1, and (b) K_2 on pH at 298 K.

Effect of salicylate on fluoride complexation rate

Plots were made of the initial reaction rate (IR) against the other variables in the system. The following plots were found to be linear, with slopes from 0.92 to 1.1

log(IR) vs. $[Al^{3+}]$,

at constant pH, [F] and $[SA_{tot}]$.

log(IR) vs. $[F^-]$,

at constant pH, [Al] and $[SA_{tot}]$.

This is good evidence of first order dependence on both $[Al^{3+}]$ and $[F^-]$. However, plots of log(IR) against log(SA) were not linear which suggests a fractional order with respect to [SA]. These results, together with a non zero intercept for a plot of IR/[Al][F] against $[SA_{tot}]$ at constant pH, suggest that a suitable experimental rate equation for the complexation of fluoride with aluminium in the presence of salicylic acid can be expressed as:

$$IR = (-d[F^-]/dt)_{t=0}$$
$$= k_i[Al^{3+}][F^-] + k_{ii}[Al^{3+}][F^-][SA_{tot}],$$

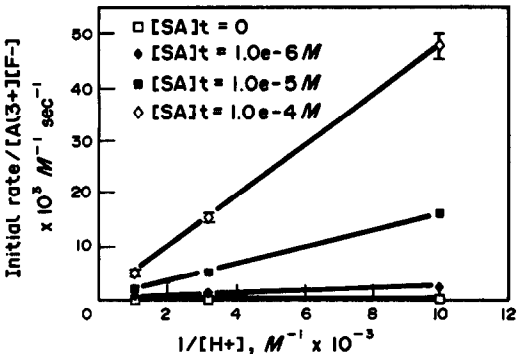

Fig. 5. Plot of Initial Rate/$[Al^{3+}][F^-]$ against $1/[H^+]$ for various total salicylate concentrations, $[SA]_t$. Error bars = ±S.E.

where k_i and k_{ii} are observed rate constants that are functions of the hydrogen ion concentration. Detailed mechanisms for these reactions according to the Eigen[9] treatment were proposed and these gave a rate equation similar in form to the above experimental rate equation.

The effect of salicylate on the fluoride complexation rate is demonstrated effectively in Fig. 5, where $IR/[Al^{3+}][F^-]$ is plotted against $1/[H^+]$. It can be seen that the presence of salicylate *increases* the rate of fluoride complexation at a constant pH, and that this increase is pH dependent. The theoretical derivation indicates that the reactions that either produce or utilize $AlOH^{2+}$ become increasingly important at the expense of reactions which produce or utilize Al^{3+}. It appears that the increase in the initial rate of fluoride complexation is caused by a significant increase in the initial concentration of $AlOH^{2+}$. Other evidence[10] also suggests that $AlOH^{2+}$ complexes with ligands faster than does Al^{3+}.

These results are at variance with opinions on the kinetics of concurrent reactions in natural water chemistry, which are thought to proceed independently in relative isolation.[11] Clearly, the presence of a third component that alters the speciation of one or both of the reactants can have a considerable effect on the system as a whole.

Temperature dependence

The data in Table 1 show that the initial rate of fluoride complexation is at least an order of magnitude slower at 10° than at 25°. Comparable data for salicylic acid are not available, but data for fulvic acid[3] show that its rate of complexation with aluminium is less temperature dependent. In mixed ligand systems lower temperatures may favour the more rapid organic complexations, depending on the temperature coefficient of the competing reactions, and so can be an important determinant of aluminium speciation.

REFERENCES

1. C. T. Driscoll, J. P. Baker, J. J. Bisogni and C. L. Schofield, *Nature*, 1980, *284*, 161.
2. B. W. Bache, in J. W. S. Longhurst, *Acid Deposition: Origins, Impacts and Abatement Strategies*, p. 91, Springer, Berlin, 1991.
3. G. S. Townsend, Ph. D. Thesis, Cambridge, 1991.
4. J. F. Pankow and J. J. Morgan, *Environmental Science and Technology*, 1981, *20*, 160.
5. K. Srinivasan and G. A. Rechnitz, *Analytical Chemistry*, 1968, **40**, 1818.
6. F. Secco and M. Venturini, *Inorganic Chemistry*, 1975, **14**, 1978.
7. J. Miceli and J. Stuher, *J. Amer. Chem. Soc.*, 1968, **90**, 6967.
8. J. F. Bunnet in C. F. Bernosconi, *Investigations of Rates and Mechanisms of Reactions*, 4th Edn., Wiley, New York, 1980.
9. M. Eigen, *Pure and Applied Chemistry*, 1963, **6**, 97.
10. B. Perlmetter-Hayman and E. Tapuhi, *Inorganic Chemistry*, 1977, **16**, 2742.
11. W. Stumm and J. J. Morgan, *Aquatic Chemistry*, 2nd Ed., Wiley, New York, 1981.

Talanta, Vol. 39, No. 11, pp. 1537–1542, 1992
Printed in Great Britain.

0039-9140/92 $5.00 + 0.00

RAPID SEQUENTIAL DETERMINATION OF INORGANIC MERCURY AND METHYLMERCURY IN NATURAL WATERS BY FLOW INJECTION—COLD VAPOUR-ATOMIC FLUORESCENCE SPECTROMETRY*

WEI JIAN and C. W. MCLEOD†

Chemical Analysis Research Centre, Division of Chemistry, Sheffield City Polytechnic, Sheffield, S1 1WB, U.K.

(*Received* 10 *July* 1992. *Accepted* 10 *July* 1992)

Summary—A novel method for the rapid sequential determination of inorganic mercury and methylmercury in natural waters at the ng/l. level has been developed. Trace enrichment and separation of mercury species are achieved using a microcolumn of sulphydryl cotton which has a relatively high affinity for methylmercury. The limit of detection for methylmercury based on processing of a 0.5-ml sample volume was 6 ng/l. Application to river waters is demonstrated.

The past two decades have seen a remarkable increase in our understanding of the impact of trace elements in environmental and biological systems. The toxicity of mercury and its compounds is well known but differences in relative toxicity demand, for regulatory purposes, that species sensitive methodology is available. Substantial literature on mercury speciation exists[1] with many schemes based on original work of Westöö,[2] *i.e.*, conversion of organic bound mercury to the halide derivative, isolation of the organic mercury halide via multiple extractions with benzene or toluene and quantitation by diverse techniques viz gas chromatography (GC) with electron capture detection,[3] plasma emission spectrometry,[4,5] GC–mass spectrometry[6] and flow injection–ICP mass spectrometry.[7]

Some of the most promising speciation procedures for mercury are based on cold vapour atomic spectrometry. In the scheme of Oda and Ingle,[8] tin chloride and sodium borohydride were used to selectively reduce inorganic and organomercury species, respectively, and achieve a rapid (3 min) sequential monitoring capability. Limits of detection, based on processing a 1-ml sample were 3–5 ng/l. Birnie[9] developed a flow injection–cold vapour–atomic absorption (FI–CV–AFS) procedure for automated continuous monitoring of inorganic and total mercury in wastewater. On-line oxidation of organic mercury was effected by potassium persulphate reagent using a heated reaction coil and differential measurements (i.e., inorganic and total; organomercury by difference) corresponded to analysis with and without oxidant stream flowing. Determination of inorganic and total mercury using flow injection-cold vapour-atomic fluorescence spectrometry has also been proposed,[10] a novel aspect of the work being the use of a flow-through UV irradiation cell for sample digestion/oxidation.

The present investigation utilises a FI–CV–AFS system and speciation measurement is based on time-resolved detection of inorganic and methylmercury species after separation/enrichment on a microcolumn of sulphydryl cotton. The microcolumn, essentially a scaled-down version of that utilized by Lee[11] for trace enrichment of methylmercury in lake waters (prior to GC analysis), proved extremely effective in the FI–AFS system. Method development studies aimed at system characterization/optimization are presented together with basic analytical performance data and speciation results for mercury in rivers.

EXPERIMENTAL

Apparatus

Flow injection–cold vapour–atomic fluorescence measurements were performed with a Merlin mercury detector (P S Analytical)

*Presented in part at Euroanalysis VII, Vienna 1990.
†Author for correspondence.

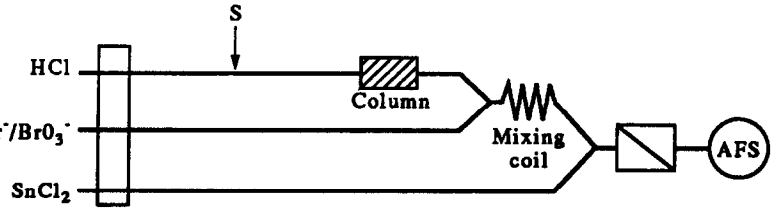

Fig. 1. Flow injection–cold vapour–atomic fluorescence system.

equipped with a peristaltic pump (Ismatec) and a rotary injection valve (Omnichem). A microcolumn (PTFE tubing, 6 cm × 1.5 mm ID) with sulphydryl cotton fibre (~0.015 g) was used for trace enrichment of methylmercury. A schematic diagram of the FI–CV–AFS system is shown in Fig. 1.

Reagents and materials

Tin chloride solution (3% w/v) in hydrochloric acid (15% v/v) was freshly prepared from tin chloride 2-hydrate salt (Spectrosol, BDH), concentrated hydrochloric acid (Aristar, BDH) and high purity water (Millipore). A bromide/bromate solution (0.5% KBr + 0.14% $KBrO_3$ w/v) was made by dissolving potassium bromide/potassium bromate salts (Analytical reagents, Fisons) in Millipore water. Hydrochloric acid solution (0.01*M*) was prepared from concentrated hydrochloric acid (Aristar, BDH) and Millipore water. Inorganic mercury working solutions were prepared by dilutions of commercial stock solution (Spectrosol, BDH, 1000 mg/l.). Methylmercury stock solution was prepared by dissolving methylmercury chloride salt (Organics, BDH) with a small amount of acetone (Analar, BDH) and then diluting with Millipore water. Methylmercury standard solutions for calibration were freshly prepared from serial dilution of the stock. Sulphydryl cotton, prepared according to the method of Lee,[11] was evenly packed into microcolumns. adjusted to 3 immediately prior to analysis (the time delay between sampling and analysis was less than 4 hr).

Analytical procedure

The carrier (0.01*M* HCl), oxidant (Br^-/BrO_3^-) and reductant ($SnCl_2$) streams were continuously pumped at flow rates of 1.5 ml/min each. On injection of sample (0.5 ml) into the carrier stream, inorganic mercury passed through the column and underwent reduction/phase separation before atomic fluorescence detection. Hydrochloric acid (3*M*) was then injected to elute methylmercury from the column, the species first being oxidized by bromide/bromate solution and then reduced as before. In this way, a rapid sequential monitoring of methylmercury and inorganic mercury was achieved.

RESULTS AND DISCUSSION

Deposition/elution of methylmercury

It is well known that the sulphydryl group (−SH) has a relatively high affinity for mercury. This prompted us to investigate the possibility of preparing and utilizing microcolumns packed with sulphydryl cotton to effect on line enrichment/separation of mercury species. It was suspected that the deposition/elution process for methylmercury would proceed in the FI system according to the scheme:

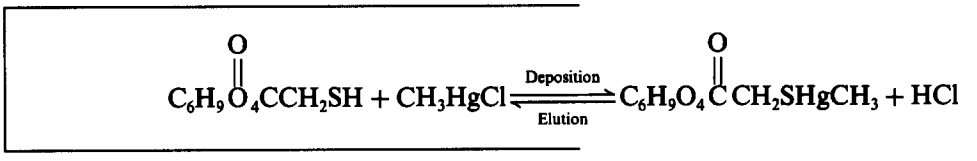

Sample collection and pretreatment

River water samples, collected in a precleaned polypropylene bucket, were filtered (0.45 μm) at site using on-line filter apparatus. The filtrate was collected in precleaned glass volumetric flasks (200 ml capacity) which contained 1 ml of concentrated nitric acid (Aristar, BDH). On return to the laboratory sample pH was ad-

To study relative affinity of the mercury species synthetic standard solutions of methylmercury and inorganic mercury were injected into the FI system while monitoring fluorescence as a function of time. The fluorescence-response curves given in Fig. 2 clearly indicate that inorganic mercury was not retained on the microcolumn since immediately after sample

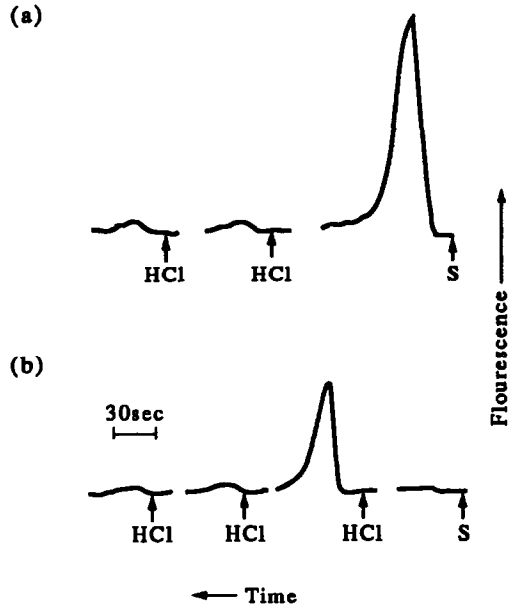

Fig. 2. Fluorescence *vs.* time response for (a) inorganic mercury (0.5 ml, 2.0 μg Hg/l.) and (b) injection/elution of methylmercury chloride (0.5 ml, 2.0 μg Hg/l.). Operating conditions, see Experimental.

injection a breakthrough signal is evident. In contrast methylmercury underwent deposition and a subsequent injection of eluant (3*M* HCl) was required to effect elution. Thus in the case of a solution containing a mixture of inorganic mercury and methylmercury it is possible to achieve a rapid sequential monitoring capability for the two species (Fig. 3).

The reduced signal strength in the case of the response for methylmercury suggests incomplete recovery/analyte losses associated with the deposition/elution process and/or subsequent redox reactions. Systematic studies were, therefore, performed in an attempt to characterize and optimize key system parameters.

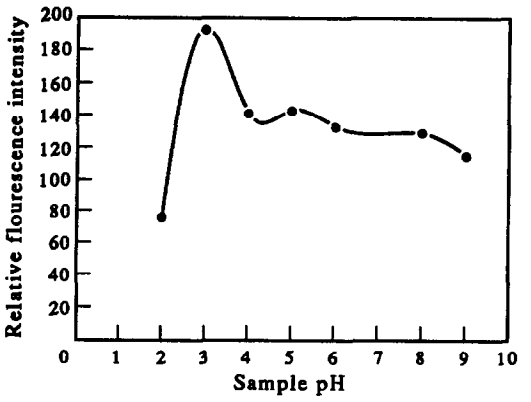

Fig. 4. Effect of sample pH on analytical response. Sample, 0.5 ml of methylmercury chloride (2.0 μg Hg/l.). Eluant, 0.5 ml HCl (3*M*). Operating conditions, see Experimental.

Effect of sample pH

The affinity of sulphydryl cotton for methylmercury was dependent on sample pH. Using the operating procedures as specified in the Experimental section it was found that methylmercury underwent deposition/elution over a wide pH range while inorganic mercury was not retained. Fluorescence response, as a function of pH, given in Fig. 4 reveals maximum signal strength for methylmercury at about pH 3 while the reduced response at pH 2 is an indication of analyte breakthrough during the deposition stage. Subsequent studies were performed with solutions adjusted to pH 3.

Effect of eluant volume

Hydrochloric acid (3*M*) was effective in eluting methylmercury from the microcolumn. However residual signals on subsequent (repeat) injections of eluant (see Fig. 2) were registered unless volumes of at least 0.5 ml were used. Typical results for processing of methylmercury

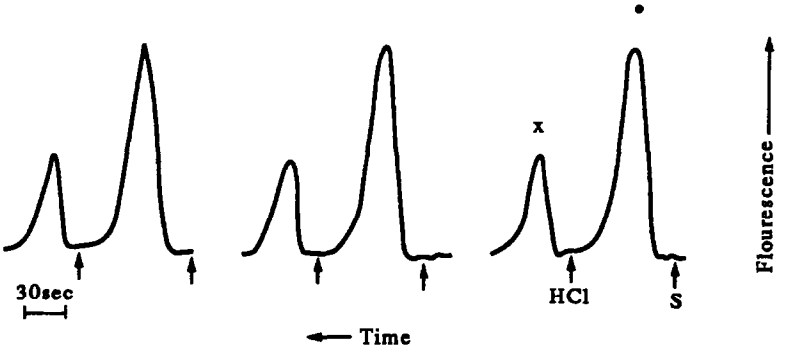

Fig. 3. Fluorescence *vs.* time response (in triplicate) for injection/elution of mixed standard solution–0.5 ml methylmercury chloride (2.0 μg Hg/l.)/inorganic mercury (2.0 μg Hg/l.): ● inorganic mercury x methylmercury. Operating conditions, see Experimental.

Table 1. Analysed values for methylmercury for various eluant volumes

Volume of Eluant (HCl, 3*M*)	Concentration of methylmercury (μg Hg/l.) 1st injection	2nd injection
0.25 ml	1.88, 1.85	0.117, 0.159
0.50 ml	2.10, 1.92	Not Detected, Not Detected
1.0 ml	1.99, 2.02	Not Detected, Not Detected

standard solution (2.0 μg Hg/l.) are presented in Table 1 and it is seen that an eluant volume of 0.25 ml achieves an elution efficiency of about 93% relative to 0.5- and 1.0-ml injections. In subsequent work an eluant volume of 0.5 ml was selected and 2 sequential injections were used to guard against the possibility of residual signals/memory effects.

Effect of mixing coil length

A critical aspect of method development was mixing coil length since this controls to a considerable extent the degree of mixing of eluate and oxidant streams and hence oxidation efficiency and signal strength. There was concern that the rate of oxidation in the FI system might not be sufficiently rapid given that official methods for total mercury determination in waters using batch techniques specify, after addition of oxidant to sample, a reaction time of at least one hour.[12] As shown in Fig. 5, a significant enhancement in signal strength was realised by employing a mixing coil at least 3 m in length. Thus, in the present FI system, on-line oxidation of methylmercury using bromide /bromate reagent proceeded rapidly and with high conversion efficiency (>80%). Subsequent work utilized a mixing coil 4 m in length.

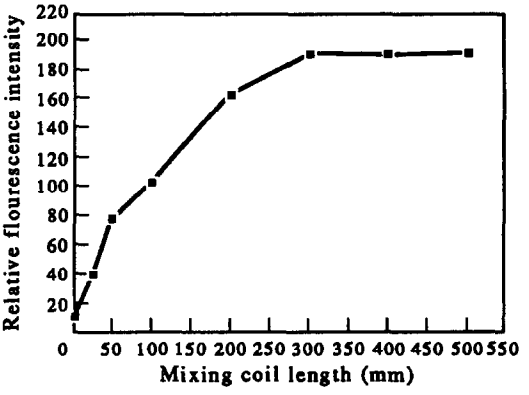

Fig. 5. Effect of mixing coil length on analytical response. Sample, 0.5 ml of methylmercury chloride (2.0 μg Hg/l.). Eluant, 0.5 ml HCl (3*M*). Operating conditions, see Experimental.

Analytical performance

Calibration and limit of detection. A calibration graph, based on processing standard solutions of methylmercury chloride, was linear over the concentration range examined (50 ng/l.–10 μg/l.; sample volume, 0.5 ml). The limit

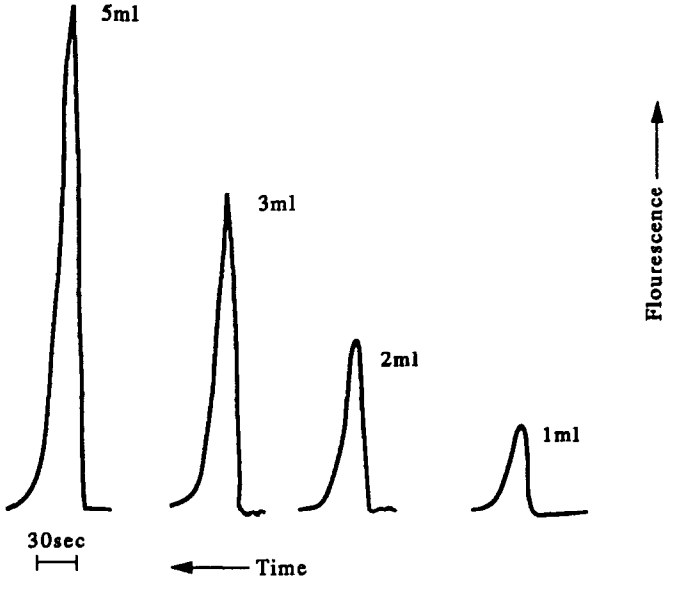

Fig. 6. Effect of sample injection volume on analytical response. Sample, methylmercury chloride (2.0 μg Hg/l.). Eluant, 0.5 ml HCl (3*M*). Operating conditions, see Experimental.

of detection based on 10 replicate injections of eluant and 3 × the standard deviation of the corresponding background signals was calculated as 6 ng/l. methylmercury.

An important feature of the FI system is the in-built trace enrichment capability. As shown in Fig. 6, processing of moderate sample volumes (1–5 ml) results in significant improvements in method sensitivity such that determinations at the ng/l. level and below are realistic. As a performance indicator processing of a 50-ml sample resulted in an enrichment factor of about 200.

Interferences

The possibility of a reduced deposition efficiency for methylmercury in the presence of diverse foreign ions was examined since metal ions are retained by the sulphydryl cotton microcolumn.[13] A methylmercury standard solution (2.0 μg Hg/l.), a tap water sample spiked with methylmercury (2.0 μg Hg/l.) and a methylmercury standard solution (2.0 μg Hg/l.) spiked with multielement solution (Al, Mg, Fe, Zn: 20 mg/l; As, Cd, Cr, Cu, Mn, Pb: 4 mg/l.) were processed as previously and fluorescence intensities for the three solutions are presented in Table 2. It is clear that no significant enhancements/suppressions occurred for the spiked samples. It can be concluded, therefore, that the presence of co-existing metal ions did not impair uptake of methylmercury and the proposed method may be suitable for natural waters analysis.

Analysis of waters

The FI method was applied to the analysis of a tap water and a series of river water samples. All samples were filtered (Millipore, 0.45 μ) before analysis and also spiked with methylmercury chloride (at the 10 or 20 ng/l. level) to check recovery. A sampling volume of 20 ml was used to achieve preconcentration in the case of the methylmercury species. The results obtained are presented in Table 3 and reveal relatively low concentrations of methylmercury with acceptable precision and recovery. Unfortunately due to lack of sensitivity it was not possible to quantify inorganic mercury directly (on-line preconcentration applicable only for methylmercury) and thus a total mercury determination was performed after acid digestion and conventional AFS measurement. The data are consistent with literature values for mercury in fresh water (150–700 ng/l. for industrial regions) and indicate a predominance of the inorganic fraction relative to methylmercury.

Table 2. Analysed values for methylmercury in standard solutions and spiked samples

Concentration of methylmercury (μg Hg/l.)		
Standard solution+	2.08	2.17
Spiked tap water+	1.99	2.14
Standard solution-multielement spike+*	2.16	2.15

+Concentration of CH_3 Hg Cl, 2 μg Hg/l.
*See text for composition.

Table 3. Analytical values for methylmercury and total mercury in waters

	Methylmercury Concentration, μg Hg/l.	Total mercury
Tap Water	0.013 ± 0.001 (90%)	0.053
River Water-1	0.006 ± 0.001 (125%)	0.040
River Water-2	0.017 ± 0.001 (100%)	0.412
River Water-3	0.012 ± 0.001 (110%)	0.081

Data in parentheses, spike recoveries (see text).
Uncertainties, $\pm 1\sigma$; $n = 5$.

CONCLUSIONS

An FI–AFS system incorporating a microcolumn of sulphydryl cotton has provided a novel route for rapid sequential measurement of inorganic mercury and methylmercury. On-line preconcentration affords high sensitivity in the case of methylmercury determination. Although application to river waters was demonstrated there is some concern regarding reliability of data given the notorious instability of methylmercury species.[8] It is proposed to investigate and evaluate the possibility of stabilizing methylmercury species at the sampling stage by passage of water samples through sulphydryl cotton microcolumns. The microcolumns are then returned to the laboratory and inserted into the FI–AFS system for elution/quantitation. Preliminary data for this new field sampling/flow injection measurement approach are promising.[14] The suitability of sulphydryl cotton microcolumns for multielement field sampling/flow injection/ICP analysis is also receiving attention.

Acknowledgements—We are grateful for the assistance of Mr J. Rollins and staff of National Rivers Authority, Warrington, U.K., and to P S Analytical Ltd.

REFERENCES

1. S. Rapsomanikis in *Environmental Analysis using Chromatography Interfaced with Atomic Spectrometry*, p. 299. 1988, Ellis Horwood, Chichester.

2. G. Westöö, *Acta. Chem. Scand.*, 1966, **20**, 2131.
3. *AOAC Official Methods of Analysis*, Section 25, 146–152, 1984, Arhryton, U.S.A.
4. Y. Talmi, *Anal. Chim. Acta*, 1975, **74**, 107.
5. K. Chiba, K. Yoshida, K. Tanabe, H. Haraguchi and K. Fuwa, *Anal. Chem.*, 1983, **55**, 450.
6. K. Fujiwara, Y. Tamaura and T. Katsura, *Bunseki Kagaku* 1984, **33**, T87–T91.
7. D. Beauchemin, K. W. M. Sin and S. S. Berman, *Anal. Chem.*, 1988, **60**, 2587.
8. C. E. Oda and J. D. Ingle Jr, *ibid.*, 1981, **53**, 2305.
9. S. E. Birnie, *J. Autom. Chem.*, 1988, **10**, 140.
10. H. Morita, M. Sugimoto and S. Shimomura, *Anal. Sciences*, 1990, **6**, 91.
11. Y. H. Lee, *Inter. J. Environ. Anal. Chem.* 1987, **29**, 263.
12. Yorkshire Water, *Methods of Analysis*, 5th Ed. 1989, Yorkshire Water, Leeds.
13. Unpublished work, Wei Jian and C. W. McLeod.
14. Wei Jian and C. W. McLeod, *Anal. Proced.*, 1991, **28**, 293.

Talanta, Vol. 39, No. 11, pp. 1543–1547, 1992
Printed in Great Britain.

0039-9140/92 $5.00 + 0.00

INVESTIGATIONS OF V_2O_5–BASED LPG SENSORS*

A. R. RAJU, KANNAN SESHADRI and C. N. R. RAO†

CSIR Centre of Excellence in Chemistry and Materials Research Centre, Indian Institute of Science, Bangalore 560012, India and
Jawaharlal Nehru Centre for Advanced Scientific Research IISc campus, Bangalore 560012, India

(*Received* 20 *March* 1992. *Accepted* 1 *April* 1992)

Summary—Sensor characteristics of V_2O_5 dispersed on oxide supports such as Al_2O_3, TiO_2 and ZrO_2 with respect to various gases and vapours including liquefied petroleum gas (LPG) have been investigated. Of all the systems studied, 20 mol% V_2O_5 dispersed on ZrO_2 shows the highest sensitivity for LPG, the log sensitivity–log concentration (in ppm) plots being linear up to 1000 ppm or more. The sensitivity is not affected by humidity or recycling. Addition of P_2O_5 to V_2O_5 however destroys the sensitivity. Considering all aspects, 20 mol% V_2O_5/ZrO_2 is suggested for use as a practical LPG sensor. ESR spectroscopy indicates the formation of V^{4+} species on exposure of V_2O_5/ZrO_2 or TiO_2 to LPG. *In-situ* high-temperature x-ray diffraction measurements show the formation of an unusual monoclinic form of VO_2 on exposure to LPG at 625 K which gets oxidized back to V_2O_5 on exposure to air.

Hydrocarbon gases, widely used as industrial and domestic fuels, have often proved to be hazardous because of explosions caused by leaks. It is therefore of vital importance to develop good sensors for hydrocarbon gases. While there have been attempts to use different materials as hydrocarbon sensors, good sensitivity has been obtained only with platinum supported on ZnO or SnO_2.[1–4] Supported Pt is not as selective as one would desire since it also acts as a sensor for H_2, alcohol and possibly other gases and vapours as well. Palladium dispersed on Fe_2O_3 detects hydrocarbons, but with considerably lower sensitivity.[5] We have been interested in finding a suitable sensor for liquefied petroleum gas (LPG) which is essentially a mixture of n-propane and n-butane by employing catalytic oxides and avoiding the use of noble metals. We have found that V_2O_5 dispersed on ZrO_2 serves this purpose excellently. We have carried out detailed experiments to determine the sensor characteristics of pellets or wafers of V_2O_5 dispersed on Al_2O_3, TiO_2, ZrO_2 and other oxide supports for different gases and vapours. We have also examined the dependence of the sensitivity on the pellet thickness as well as humidity. In order to understand the nature of interaction of aliphatic hydrocarbons (LPG) with the active surface of V_2O_5, we have employed electron spin resonance (ESR) spectrocopy and *in-situ* x-ray diffraction. The study has shown that hydrocarbon-sensing by V_2O_5 dispersed on oxide supports involves facile reduction to a novel monoclinic form of VO_2.

EXPERIMENTAL

Fine powders of ZrO_2, TiO_2 (anatase), γ-Al_2O_3 and ZnO were prepared by hydrolysing zirconium nitrate, titanium tetrachloride, aluminium nitrate and zinc nitrate respectively with liquid ammonia followed by calcination in air at 670 K for 6 hr. Fumed silica was used as the starting material for SiO_2. $LaCoO_3$ powder was prepared by solid state reaction of La_2O_3 and CoO at 1300 K for 24 hr. Vanadium oxide was supported on these metal oxides by wet impregnation with oxalic acid solution of ammonium meta-vanadate.[6-9] Sb_6O_{13}[10] and P_2O_5[11] were supported by using antimony chloride and ammonium dihydrogen phosphate solutions respectively. Wet impregnation was carried out at 350 K for 12 hr followed by drying at 370 K. The final products were heated slowly to 670 K and kept for 6 hr and then cooled to room temperature in air.

The powders obtained after wet impregnation were made into pellets (10 mm diameter and 1, 2 and 5 mm thick) under 20 KPa/cm^2 pressure. The pellets were heated at 770 K for 12 hr. Thick films were made by using pastes prepared by mixing equal amounts of nitrocellulose and amyl acetate to the dispersed powders. The

*Dedicated to Professor T. S. West, a dear friend of the senior author (C.N.R.R.) who worked closely with Tom for several years in IUPAC.

†Author for correspondence.

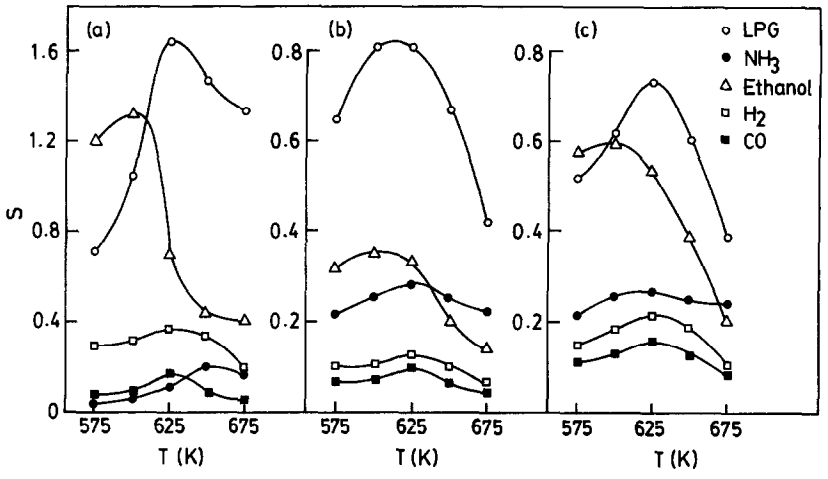

Fig. 1. Temperature-variation of the sensitivity of 20 mol% V_2O_5 dispersed on (a) ZrO_2, (b) TiO_2 and (c) Al_2O_3 for different gases and vapours (400 ppm).

paste was screen-printed on alumina (99%) substrates followed by heat treatment at 850 K for 6 hr. Conducting silver paint (Acheson Electrodag 915, England) was used for contact purposes. The thick films did not show good sensitivity (usually $<50\%$ of the pellets of the same composition) and were therefore abandoned in preference to the pellets.

Sensitivity of the gas sensors was measured by applying 9 V (DC) across the sensor and monitoring the current through the sensor element. The experimental set-up used for the measurements had been described elsewhere.[12] The sensitivity, S, of the sensor was calculated by using the expression

$$S = (\sigma g - \sigma a)/\sigma a$$

where, σg and σa are the conductivities of the sensor in the presence of test gas and dry air respectively. The effect of humidity on the sensitivity was studied by passing air with known humidity content through the cell.

Electron spin resonance (ESR) studies were carried out with a Varian E-109 x-band spectrometer. High-temperature x-ray diffraction measurements were made by employing a JEOL JDX-8P diffractometer fitted with an *in-situ* cell designed and fabricated in the laboratory.[13]

RESULTS AND DISCUSSION

In Fig. 1 we show plots of the sensitivity of 20 mol% V_2O_5 dispersed on ZrO_2, TiO_2 and Al_2O_3 supports to various gases and vapours including LPG, ethanol, CO and H_2. We generally find that the sensitivity is not high for NH_3, CO and H_2 independent of the oxide support, but is good for ethanol, specially at 600 K. The

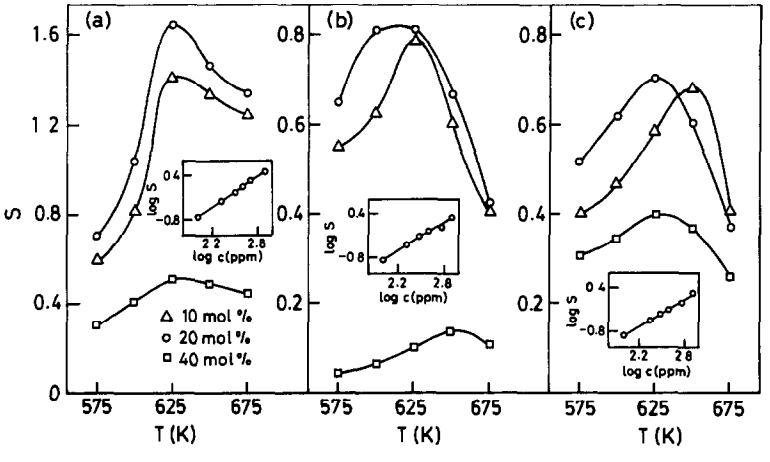

Fig. 2. Temperature-variation of the sensitivity to LPG (400 ppm) for different loadings of V_2O_5 on (a) ZrO_2, (b) TiO_2 and (c) Al_2O_3. Insets show the log sensitivity–log concentration (ppm) plots for 20 mol% V_2O_5 dispersed on oxide supports.

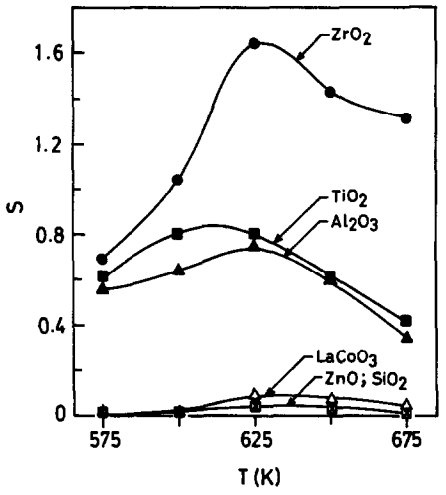

Fig. 3. Temperature-variation of the sensitivity of 20 mol% V_2O_5 dispersed on ZrO_2, TiO_2, Al_2O_3, $LaCoO_3$, ZnO and SiO_2 supports to LPG (400 ppm).

sensitivity is highest for LPG around 625 K with all the supports studied. Sensitivity for LPG is highest with 20 mol% V_2O_5/ZrO_2, although 20 mol% V_2O_5/TiO_2 is also satisfactory; it appears that either of the two supports will be adequate. We have examined the dependence of the sensor characteristics (Fig. 2) on V_2O_5 loading and found 20 mol% V_2O_5 to possess maximum sensitivity for LPG, specially when dispersed on ZrO_2. In Fig. 3 we compare the sensitivity of 20 mol% V_2O_5 dispersed on various oxide supports. The sensitivity is negligible in the case of ZnO, SiO_2 and $LaCoO_3$ supports. In the insets of Fig. 2 we have shown the variation of the sensitivity with the concentration for 20 mol% V_2O_5 dispersed on ZrO_2, TiO_2 and Al_2O_3. The log S–log C (in ppm) plots are linear up to 1000 ppm or more, the minimum detection limit for LPG in air being 10 ppm. Since the lower flammability limit for LPG in air is 1000 ppm, the sensitivity of 20 mol% V_2O_5/ZrO_2 is more than adequate for sensing purposes. At 1000 ppm of LPG, the sensitivity of 20 mol% V_2O_5/ZrO_2 is 2.7 compared to 0.9 for Pd/γ-Fe_2O_3, 0.7 for γ-Fe_2O_3 and 3.0 for Pt/ZnO.

In Fig. 4(a) we show the variation of the sensitivity of 20 mol% V_2O_5/ZrO_2 to LPG after repeated cycling. We see negligible fatigue after 30 days, after repeated cycling. The effect of humidity on the sensitivity of 20 mol% V_2O_5/ZrO_2 to LPG is shown in Fig. 4(b). The sensitivity is not affected significantly even up to 80% relative humidity. We have studied the effect of other oxide additives on the sensitivity of the V_2O_5 dispersed on ZrO_2 and TiO_2. In Fig. 5 we compare the sensitivity plots for 10 mol% Sb_6O_{13} and V_2O_5:P_2O_5 solid solutions (total loading of the oxides, 20 mol%) with those of 20 mol% V_2O_5. Addition of P_2O_5 destroys the sensitivity of V_2O_5; sensitivity of Sb_6O_{13} is much lower than that of V_2O_5. The high selectivity of 20 mol% V_2O_5/ZrO_2 pellets to LPG as well as the negligible fatigue found by us, when subjected to repeated cycling and high humidity makes it viable as a practical LPG sensor.

All the measurements obtained hitherto pertained to pellets 2 mm thick. We have examined the dependence of the sensitivity on the pellet thickness. In Fig. 6 we show the sensitivity of pellets of 20 mol% V_2O_5/ZrO_2 of different thicknesses. The sensitivity essentially remains the same for pellets in the thickness range of 1–5

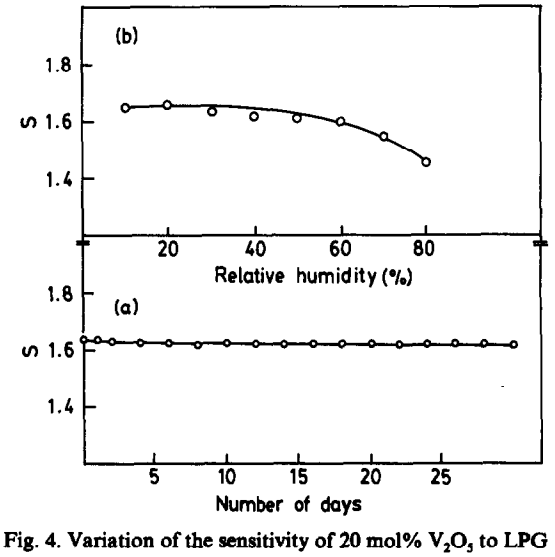

Fig. 4. Variation of the sensitivity of 20 mol% V_2O_5 to LPG (400 ppm) with (a) the number of days repeated cycling and (b) relative humidity.

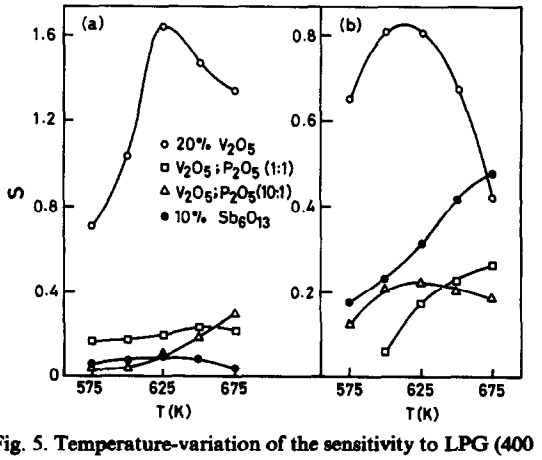

Fig. 5. Temperature-variation of the sensitivity to LPG (400 ppm) for different oxide loadings on (a) ZrO_2 and (b) TiO_2 supports.

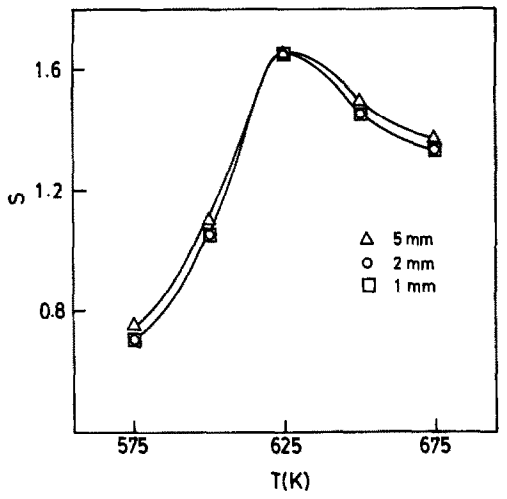

Fig. 6. Variation of the sensitivity of 20 mol% V_2O_5/ZrO_2 to LPG (400 ppm) with pellet thickness.

mm. The 1-mm thick pellets would be best for practical applications, since they would require least electric power.

We were interested in understanding the mechanism of gas sensing of V_2O_5 dispersed on oxide supports. For this purpose, we have employed ESR spectroscopy to monitor the interaction between V_2O_5 and LPG. In Fig. 7 we compare the ESR spectra of 20 mol% V_2O_5 dispersed on ZrO_2 and TiO_2 before and after exposure to LPG vapours. Both V_2O_5/ZrO_2 and V_2O_5/TiO_2 show signals due to V^{4+} present on the surface; after exposure to LPG at 625 K, the

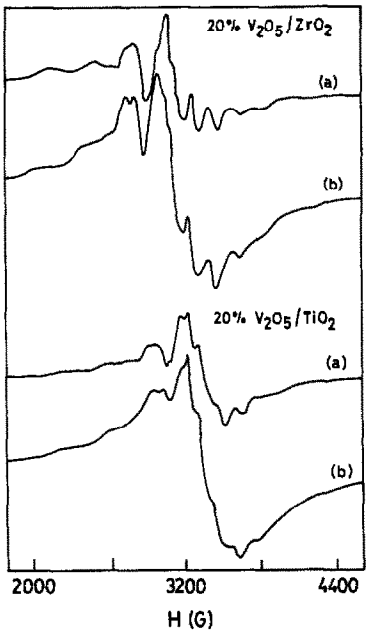

Fig. 7. ESR spectra of 20 mol% V_2O_5 dispersed on ZrO_2 and TiO_2 at 625 K. Spectra (a) and (b) are before and after exposure to LPG vapours.

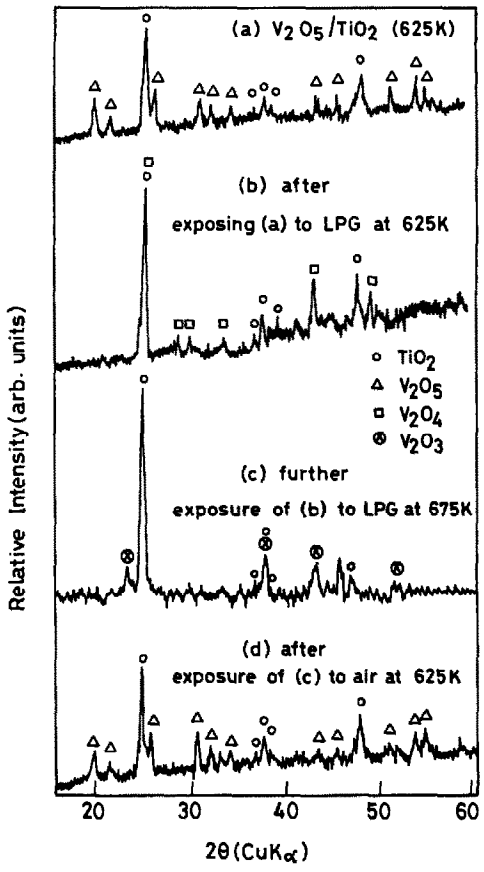

Fig. 8. X-ray diffraction patterns of 20 mol% V_2O_5/TiO_2: (a) at 625 K in air; (b) after exposure to LPG at 625 K; (c) further exposure of (b) to LPG at 675 K; (d) after exposure of (c) to air at 625 K.

intensity of the V^{4+} signal increases markedly showing that the aliphatic hydrocarbons reduce V_2O_5 to VO_2. When such a surface is again exposed to air at the same temperature, VO_2 is oxidized back to V_2O_5.

In order to investigate the nature of the reduction–oxidation of the vanadium oxides, we have carried out an *in-situ* x-ray diffraction study of 20 mol% V_2O_5/TiO_2 in the 625–675 K range. In Fig. 8 we show the x-ray diffraction patterns of V_2O_5/TiO_2 before and after exposure to LPG at 625 K. We clearly see features of VO_2 emerging after exposure to LPG at 625 K. The VO_2 so formed has a unique B′ monoclinic structure[14] ($a = 12.03$, $b = 3.693$, $c = 6.42$ Å, $\beta = 107°$, space group C2/m) which is different from the stable room temperature monoclinic structure ($a = 5.752$, $b = 4.538$, $c = 5.383$ Å, $\beta = 122.6°$, space group $P2_1C$) or the well-known 340 K rutile structure ($a = 4.551$, $c = 2.851$ Å, space group P4/mmm). The B′ monoclinic phase is related to V_6O_{13} and transforms to the stable monoclinic structure on

cooling. When V_2O_5/TiO_2 is exposed to LPG at a slightly higher temperature (675 K) or at 625 K for long periods, V_2O_3 is formed (Fig. 8). However, on exposure to air at 625 K, the surface is regenerated within two minutes and we get back V_2O_5. From these studies we conclude that sensing of LPG by V_2O_5 dispersed on oxide supports involves reduction–oxidation of V_2O_5.

Acknowledgements—The authors thank Mr. K. R. Kannan for the *in-situ* high-temperature x-ray diffraction cell and Ram Seshadri for his assistance in carrying out measurements.

REFERENCES

1. T. Seiyama and S. Kagawa, *Anal. Chem.*, 1966, **38**, 1069.
2. M. Nitta, S. Kanefusa and M. Haradome, *J. Electrochem. Soc.*, 1978, **125**, 1876.
3. S. Saito, M. Miyayama, K. Koumoto and H. Yanagida, *J. Am. Ceram. Soc.*, 1985, **68**, 40.
4. D. Kohl, *Sensors and Actuators*, 1989, **18**, 71.
5. D. D. Lee and D. H. Choi, *ibid.*, 1990, **B1**, 231.
6. L. Y. A. Margolis, *Adv. Catal.*, 1963, **14**, 429.
7. H. Miyata, K. Fujii, T. Ono, Y. Kubokawa, T. Ohno and F. Hatayama, *J. Chem. Soc. Faraday Trans. I*, 1987, **83**, 675.
8. T. Ono, H. Miyata and Y. Kubokawa, *J. Chem. Soc. Faraday Trans. I*, 1987, **83**, 1761.
9. R. B. Bjorki, C. U. I. Odenbrand, J. G. M. Brandin, L. A. H. Andersson and B. Liedberg, *J. Catal.*, 1989, **119**, 187.
10. T. Ono, M. Kiryu, M. Komiyama and R. L. Kuczkowski, *ibid.*, 1991, **127**, 698.
11. F. Garbassi, J. C. J. Bart, R. Tassinari, G. Vlaic and P. Lagarde, *ibid.*, 1986, **98**, 317.
12. A. R. Raju and C. N. R. Rao, *Sensors and Actuators*, 1991, **B3**, 305.
13. K. R. Kannan, M.Sc (Engineering) Thesis, Indian Institute of Science, 1992.
14. F. Theobald, R. Cobala and J. Bernard. *J. Solid State Chem.*, 1976, **17**, 431.

Talanta, Vol. 39, No. 11, pp. 1549–1554, 1992
Printed in Great Britain.

0039-9140/92 $5.00 + 0.00

CALIXARENE-BASED POTENTIOMETRIC ION-SELECTIVE ELECTRODES FOR SILVER

KATHERINE M. O'CONNOR and GYULA SVEHLA*
Department of Chemistry, University College, Cork, Ireland

STEPHEN J. HARRIS
School of Chemical Sciences, Dublin City University, Dublin, Ireland

M. ANTHONY MCKERVEY
School of Chemistry, Queens' University, Belfast, Northern Ireland, U.K.

(*Received* 12 *March* 1992. *Accepted* 31 *March* 1992)

Summary—Four lipophilic sulphur and/or nitrogen containing calixarene derivatives have been tested as ionophores in Ag(I)-selective poly (vinyl chloride) membrane electrodes. All gave acceptable linear responses with one giving a response of 50 mV/dec in the Ag(I) ion activity range 10^{-4}–$10^{-1}M$ and high selectivity towards other transition metals and sodium and potassium ions. This ionophore was also tested as a membrane coated glassy-carbon electrode where the sensitivity and selectivity of the conventional membrane electrode was found to be repeated. The latter electrode was then used in potentiometric titrations of halide ions with silver nitrate.

Calixzarenes[1] are cyclic oligmers of phenol–formaldehyde condensates which when derivatized at the phenolic oxygen group show receptor inophoric activity. Derivatives containing a wide range of functional groups have been synthesized and have been shown to have the ability to complex alkali and alkali-earth metal cations selectively into the cavity present in the cone conformation.[2] A number of calixarene derivatives have been incorporated as neutral carriers into ion-selective electrodes sensitive to sodium ions,[3–6] potassium ions[7] and ceasium ions.[8,9] The sodium selective electrodes have been used successfully in the determination of sodium in human blood[4,10] and recently a sodium selective CHEMFET has been reported.[11] A polymeric tetrameric calixarene has been used in a modified carbon paste electrode for the stripping voltammetry of copper, lead and mercury.[12] Due to the success of these calixarene derivatives a number have been patented. However, calixarene based ion-selective electrodes sensitive to transition metal ions have not yet been reported as they would suffer interference from alkali metal ions. Crown compounds containing nitrogen and sulphur atoms in the ring have been incorporated into poly (vinyl chloride) membranes to give electrodes sensitive to Ag(I) ions with some Hg(II) interference.[13,14] By using calixarene derivatives with functional groups containing nitrogen and sulphur atoms the interference from alkali metal ions is expected to be significantly reduced.[15]

In this paper the performance of four calixarene derivatives, tested as ionophores for silver selective electrodes, is described. The most promising is also tested as a membrane-coated glassy carbon electrode. There are many descriptions on the usage of glassy carbon electrodes in voltammetry, amperometry, potentiometry and coulometry[16] but there are a limited number of reports on the usage as a substrate of the sensor phase in ion-selective electrodes. It has been recently used successfully in dip coated enzyme sensors[17] and tested as a substrate for a variety of sensor phases by Jovanoić *et al*[18]. Also carbon rods have been dip coated for use in lead(II) selective electrodes.[19] An application of these types of electrodes in potentiometric titrations of halide ions with silver nitrate is also described.

*Author for correspondence.

EXPERIMENTAL

Materials

The ionophores employed in this work were synthesized by S. J. Harris and M. A. McKervey and are shown in Fig. 1.

The membrane components, PVC (ISE grade), potassium tetrakis (4-chlorophenyl) borate (KTpClPB), 2-nitrophenyl octyl ether (2-NPOE) and AnalaR grade tetrahydrofuran (THF) were obtained from Fluka. The nitrates of sodium, potassium, nickel, copper(II), lead(II), cadmium(II), cobalt(II) and mercury(II) were of AnalaR grade as were the potassium chloride, bromide and iodide. The silver nitrate was obtained from Johnson Matthey Chemicals Ltd. All solutions and standards were made up with doubly distilled water.

Electrode preparation

The membrane components, [0.66% m/m ionophore, 0.17% m/m KTpClPB, 65.84% m/m 2-NPOE and 33.33% m/m PVC] were mixed and dissolved by stirring in THF overnight.

For the preparation of a conventional membrane electrode the resulting PVC–THF syrup was poured into a glass mould,[20] and the solvent was allowed to evaporate off at room temperature, over a period of 24 hr. A semi-transparent flexible membrane was obtained from which discs of 7 mm diameter were cut using a cork borer. These discs could be pasted, using THF, to an interchangeable PVC tip clipped to the end of the electrode body which consisted of an Ag–AgCl wire immersed in an internal solution of 5×10^{-4}M silver nitrate and 10^{-2}M nitric acid.

A membrane-coated glassy-carbon electrode was prepared as follows. Initially, the end of a glassy-carbon electrode (3 mm in diameter) was polished on Al_2O_3 slurry and air dried. It was then dip coated to a depth of 10 mm in a PVC–THF syrup and dried at room temperature. This was repeated three times. The PVC-THF syrup was of the same composition as that for the conventional membrane electrodes.

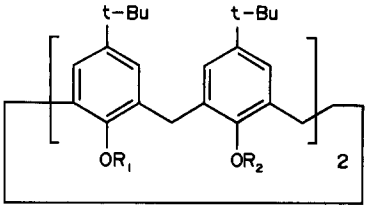

Ionophore.	R_1	R_2
(i)	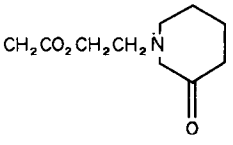	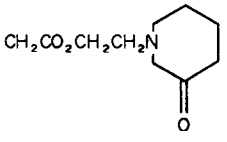
(ii)	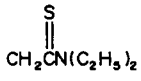	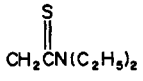
(iii)	$CH_2CO_2CH_2CH_2SCH_3$	$CH_2CO_2C_2H_5$
(iv)	$CH_2CO_2CH_2CH_2SCH_3$	$CH_2CO_2CH_2CH_2SCH_3$

Fig. 1. Structure of ionophores.

Measurement of electrode potentials

All measurements were carried out at 25° in a thermostatted potentiometric cell. The electrochemical systems for the study were as follows:

Ag,AgCl|int. soln.(5×10^{-4}M $AgNO_3 + 10^{-2}$M HNO_3)|PVC membrane|sample|salt bridge ($1M$ KNO_3)|$1M$ KNO_3)$1M$ KNO_3|Hg_2Cl_2,Hg.

Carbon|PVC membrane|sample|salt bridge ($1M$ KNO_3)|Hg_2Cl_2,Hg.

The potential readings were measured using a Metrohm 654 millivot/pH meter and registered on a Linseis LM 24 chart recorder. The reference electrode was a Metrohm saturated calomel. The performance of the electrodes were assessed by measuring parameters such as slope, limit of detection, selectivity, response times and temperature dependence of the electrode. Selectivity coefficients (log $K_{Ag,M}$) were determined using the separate solution method[21] at a concentration of $0.1M$. Dynamic responses were measured by injection of 90.9 μl; of $1M$ silver nitrate solution into 10 ml of $10^{-3}M$ silver nitrate on a fast chart speed (10 cm/min) thus producing a $1 \times 10^{-3}M$ to $1 \times 10^{-2}M$ change in concentration. The temperature dependence was investigated by noting the potential change in solutions of $10^{-3}M$, $10^{-2}M$ and $10^{-1}M$ silver nitrate respectively over a temperature range of 5–45° (278–318 K). Lifetime of the electrodes was investigated by recalibrating them periodically and calculating the response over the linear range Reproducibility studies were carried out by determining the coefficient of variation for five consecutive potential readings in solutions of $10^{-3}M$ and $10^{-2}M$ silver nitrate respectively. The instruments used for the potentiometric titrations were a Metrohm E 536 Potentiograph and E 535 Dosimat.

RESULTS AND DISCUSSION

Four nitrogen and/or sulphur containing calixarene derivatives, shown in Fig. 1 were incorporated into poly (vinyl chloride) membrane electrodes and were shown to give acceptable linear responses to Ag(I) ion activity with limits of detection of between $10^{-3.8}$ and 10^{-4}M. The calibration graphs of Fig. 2(a) indicate that the degree of linearity of the response occurs in the order of:

ionophore (iv) > (iii) > (ii) > (i)

with ionophore (i) giving the lowest response of 38.26 mV/dec in the limited range of $10^{-3.8}$ to $10^{-1.8}$ M. This trend may be simply attributed to the number and type of "soft" donor atoms present within each ionophore. It should be noted that ionophore (iv) contains S atoms and no N atoms where as in ionophore (i) the opposite is true. When comparing the selectivity coefficients (log $K^{pot}_{Ag/M}$) for the electrodes based on ionophores (i) to (iv) in Fig. 2(b) it can be seen that Hg^{2+} and Na^+ ions are the major

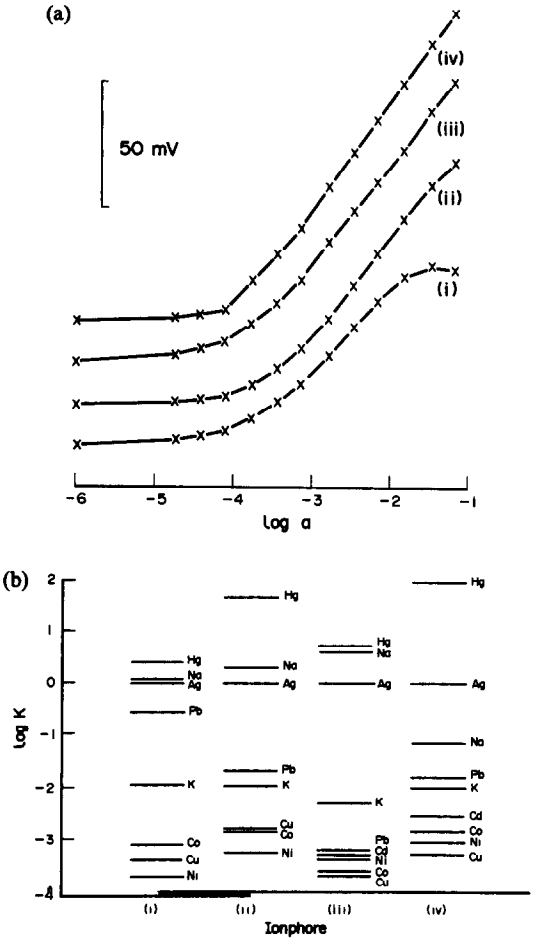

Fig. 2. (a) Potential responses of conventional membrane electrodes incorporating ionophores (i)–(iv) to silver (I) ion activity. (i) 38.26 mV/dec, (ii) 45.67 mV/dec, (ii) 47.64 mV/dec and (iv) 50.01 mV/dec. (b) Comparison of selectivity coefficients (log $K^{pot}_{Ag/M}$) for conventional membrane electrodes incorporating ionophores (i)–(iv).

interferents followed closely by Pb^{2+} ions. Phase transfer and stability studies on a wide range of tetrameric calixarene derivatives have shown them to be excellent complexing agents for alkali and alkali-earth metal ions with, in the majority of cases, a clear preference for sodium ions[2]. However, very little work has been reported on tetrameric calixarene derivatives with functional groups containing "soft" donor atoms such as N and S atoms which according to Pearson[15] are more likely to complex heavy metal ions such as Ag^+, Hg^{2+} and Pb^{2+}. With ionophores (i) to (iv) the soft donor atoms are imparting some selectivity to heavy metals but there is still a significant response to Na^+ ions. Ionophore (iii) is a calixarene with mixed ligating functional groups, one being the ethyl ester. In general the trends in extraction and stability constants observed in a homo calixarene containing a certain functional group are still discernible in the mixed calixarene.[2] Since the homo calixarene containing the ethyl ester has been incorporated into a poly (vinyl chloride) membrane and has been shown to be a successful sodium ion-selective electrode,[6,8,22] it is not surprising that ionophore (iii) has the most severe Na^+ interference. The Hg^{2+} interference is caused most strongly by the S donor atom as Hg^{2+} is a strongly thiophilic metal ion.[23] When the membranes came in contact with Hg^{2+} and Pb^{2+} ions the silver response was tested immediately afterwards and also after 3 and 24 hr respectively, the electrodes being stored in $0.1M$ silver nitrate when not in use. The effect of the ions on the membranes was in the following orders;

Pb^{2+} effect. ionophore (ii)$\gg$(iv) > (i) > (iii)

Hg^{2+} effect. ionophore (ii)$\gg$(i) > (iv) > (iii)

Ionophore (ii) did not have its full silver response back after 24 hr after contact with Pb^{2+} ions but in the case of contact with Hg^{2+} ions it had almost its full response back. Ionophores (ii) to (iv) were all regenerated in less than 3 hr but the Hg^{2+} ions in general had a stronger poisoning effect than the Pb^{2+} ions. It must be borne in mind that these membranes were in contact with interfering ions up to concentration of $0.1M$. Smaller concentrations would have a less detrimental effect. Na^+ ions had no poisoning effect on the membrane with it's response being totally reversible.

Further work was carried out on ionophore (iv) as it gave the best Ag(I) ion calibration slope and the best selectivity towards all the ions tested with the exception of Hg^{2+} ions. A membrane-coated glassy carbon electrode (B) was tested under the same conditions as the conventional membrane electrode (A). The properties of the two types are summarized in Table 1. The sensitivities and selectivities of the two electrodes are very alike with B being slightly more sensitive, with a higher Ag(I) ion response slope. In comparing the full responses (in the concentration range of 10^{-6} to $10^{-1}M$) against all the interfering ions, in Fig. 3, it can be seen that the responses are almost identical. Most of the ions gave practically no response but the Na^+ response had a slope of 25 mV/dec and Pb^{2+} a slope of 17 mV/dec. The Hg^{2+} response behaved relatively linearly up to a concentration $10^{-1.8}M$ where it became anionic in nature. This is known as the "anion effect"[24] and is usually reduced by the addition of incorporated ion exchangers within the membrane. In the case of our membrane which has KTpClPB as an incorporated ion exchanger the transition of the response into an anionic function is obtained only when complete consumption of free

Table 1. Properties of silver-selective membrane electrodes based on ionophore (iv). (a) conventional membrane electrodes. (b) membrane-coated glassy carbon electrode.

	(a)	(b)
Detection limit M	10^{-4}	10^{-4}
Slope, mV/dec	50.01	51.74
Log $K^{pot}_{Ag/M}$		
Na^+	−1.16	−1.21
K^+	−2.01	−2.14
Ni^{2+}	−3.08	−3.02
Co^{2+}	−2.85	−3.02
Cu^{2+}	−3.3	−2.59
Pb^{2+}	−1.81	−1.86
Cd^{2+}	−2.57	N/A
Hg^{2+}	+1.93	+1.79
Response Time/sec	3	2
Temp. Coeff. $\delta E/\delta T$.		
$10^{-3}M$	−0.180	+.031
$10^{-2}M$	+0.116	−0.057
$10^{-1}M$	+0.397	+0.028
Slope/mV/dec		
day 14	46.04	N/A
day 22	N/A	42.42
day111	38.61	N/A
Coeff. of. var. ($n = 5$)		
Day 1		
10^{-3} M	0.400%	0.474%
10^{-2} M	0.218%	0.212%
Day 6		
10^{-3} M	N/A	3.087%
10^{-2} M	N/A	16.609%
Day 111		
10^{-3} M	0.109%	N/A
10^{-2} M	0.123%	N/A

carriers has occurred.[25] In the linear range of the Hg^{2+} response a slope of 80–90 mV/dec is obtained compared to the expected Nernstian slope of 29.6 mV/dec for a divalent metal cation. This response characteristic may be due to the formation of charged associates within the membrane[26] and has been noticed previously in Hg(II) and Ag(I) selective poly (vinyl chloride) membrane electrodes based on dithia crown ethers[13] where this unusual response was attributed to the formation of $Hg(TPB)^+$ ions in the membrane so perhaps the response in this case is due to $Hg(TPClB)^+$ ions. On preparation of a membrane containing no ion exchanger there is a large increase in anion interference, the Ag(I) ion response has a slope of < 10 mV/dec and the membrane has a very dark brown/yellow colour (characteristic of a very old stored membrane) after a few days. However, the Hg^{2+} response is nearer to divalent in nature. Electrode type B has a marginally shorter response time than type A which is probably due to the much thinner film (0.2 mm) formed on the carbon surface. Temperature studies indicate that both electrodes are affected very little by temperature, with type B being slightly more stable. Examining the lifetime calibration slopes in Table 1 it can be seen that at day 22 electrode type B gives a slope of 42.42 mV/dec but the potential readings for this slope have shifted up by 230 mV from the original potential readings. On day 111 electrode A had a calibration slope which differed by only 20 mV from the original potential readings. Reproducibility studies on new and old membranes of both types show that type A membranes have steady readings even after 111 days whereas after only 6 days type B membranes have erratic readings. The initial readings of both are very similar.

Membrane electrodes of type B were used in potentiometric titrations of halide ions against silver nitrate as these electrodes were easier and quicker to prepare and did not require long conditioning times. Figure 4 shows that the membrane was successful in resolving a mixture of Cl, Br and I ions. The reversal of potential occurring in the presence of iodide and to a lesser extent of bromide ions is reproducible and does not affect the accuracy of the titrations. Though we did not investigate this matter further, it can probably be attributed to the adsorption of precipitate particles on the electrode surface, causing increased cell resistance. By physically removing the precipitate from the electrode surface, potential readings can be restored more or less to their expected values.

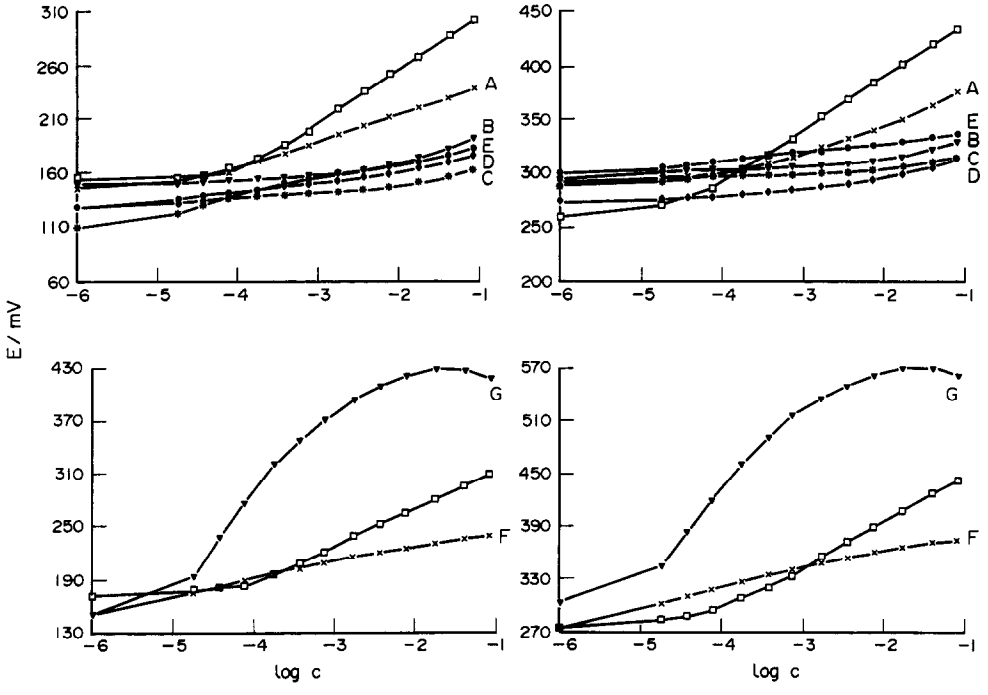

Fig. 3. Response of silver-selective electrodes to metal cations. (A) Na, (B) K, (C) Ni, (D) Co, (E) Cu, (F) Pb and (G) Hg. (unlabelled response) Ag. (a) conventional membrane electrode. (b) membrane-coated glassy carbon electrode.

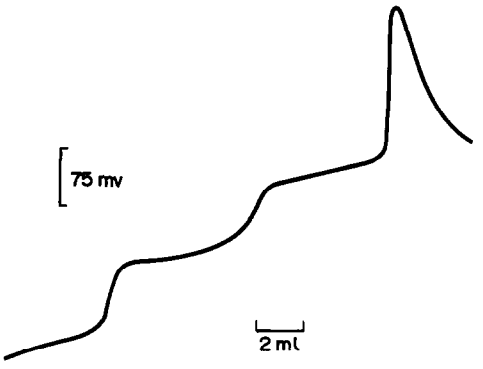

Fig. 4. Potentiometric titration of a mixture of 4.5 ml KI, 5.5 ml KBr and 6.5 ml KCl (all 0.1*M* concentration) with 0.1*M* $AgNO_3$ using a membrane-coated glassy carbon electrode incorporating ionophore (iv).

CONCLUSIONS

Conventional membrane electrodes and membrane-coated glassy-carbon electrodes based on ionophore (iv) were found to be successful Ag(I) selective electrodes. Both types exhibited good linear responses and good sensitivity and selectivity. They responded quickly and reversibly and gave good temperature stability. However conventional membrane electrodes were more beneficial for long-term use as they were found to be more stable and reproducible with time.

REFERENCES

1. C. D. Gutsche, *Calixarenes: Monographs in Supramolecular Chemistry*, No. 1, RSC, Cambridge (U.K.), 1989.
2. Marie-José Schwing and M. Anthony McKervey, *Chemically Modified Calixarenes as New Selective Receptors for Monovalent Cations*, in J. Vicens and V. Böhmer (eds.), *Calixarenes: A Versatile Class of Macrocylic Compounds*. Kluwer Academic Publishers, Dordrecht 1991, p. 139.
3. K. Kimura, M. Matsuo and T. Shona, *Chem. Lett.*, 1988, 615.
4. K. Kimura, T. Miura, M. Matsuo and T. Shona, *Anal. Chem.*, 1990, **62**, 1510.
5. K. Cunningham, G. Svehla, M. A. McKervey and S. J. Harris, *Anal. Proc.*, 1991, **28**, 294.
6. A. Cadogan, D. Diamond, M. R. Smyth, M. Deasy, M. A. McKervey and S. J. Harris, *Analyst*, 1989, **114**, 1551.
7. A. Cadogan, D. Diamond, S. Cremin, M. A. McKervey and S. J. Harris. *Anal. Proc.*, 1991, **28**, 13.
8. D. Diamond, in M. R. Smyth and J. G. Vos, (eds.), *Electrochemistry, Sensors and Analysis*. Analytical Chemistry Symposium Series. Volume 25, p. 155. Elsevier, Amsterdam, 1986.
9. A. Cadogan, D. Diamond, M. R. Smyth, G. Svehla, E. M. Seward, M. A. McKervey and S. J. Harris, *Analyst*, 1990, **115**, 1207.
10. M. Telting-Diaz, D. Diamond, M. R. Smyth, G. Svehla, E. M. Seward, M. A. McKervey and S. J. Harris, *Anal. Proc.*, 1989, **26**, 29.
11. J. Brunink, J. R. Haak, J. G. Bomer, D. N. Reinhoudt, M. A. McKervey and S. J. Harris, *Anal. Chim. Acta.*, 1991, **254**, 75.
12. D. W. M. Arrigan, G. Svehla, M. A. McKervey and S. J. Harris, *Anal. Proc.*, 1992, **29**, 27.
13. M. Lai and J. Shih, *Analyst*, 1986, **111**, 891.
14. M. Oue, K. Kimura, K. Akama, M. Tanata and T. Shona, *Chem. Lett.*, 1988, **409**.
15. P. R. Pearson, *J. Am. Chem. Soc.*, 1963, 85, 22, 3533.
16. W. E. Van der Linden and J. W. Dieker, *Anal. Chim. Acta*, 1980, **119**, 1.
17. C. Chen, Y. Sakai, J. Hasebe, J. Anzai, A. Ueno and T. Osa, *Chem. Pharm. Bull.*, 1989, **37**, 3316.
18. S. M. Stankovic, V. M. Jovanović and M. S. Jovanović, *J. Serb. Chem. Soc.*, 1990, **55**, 125.
19. S. Kamata and K. Onoyama, *Anal. Chem.*, 1991, **63**, 1295.
20. G. J. Moody, J. D. R. Thomas and T. E. Edmonds, (ed.) *Chemical Sensors*, Blackie, London, 1988.
21. G. G. Guilbault, R. A. Durst, M. S. Frant, H. Freiser, E. H. Hansen, T. S. Light, E. Pungor and J. D. R. Thomas, *Pure Appl. Chem.*, 1976, **48**, 127.
22. D. Diamond, G. Svehla, E. M. Seward and M. A. McKervey, *Anal. Chim. Acta.*, 1988, **204**, 223.
23. G. Wu, W. Jiang, J. D. Lamb, J. S. Bradshaw and R. M. Izatt, *J. Am. Chem. Soc.*, 1991, **113**, 6538.
24. W. E. Morf, *The Principles of Ion-selective Electrodes and of Membrane Transport*, Chap. 12, p. 296. Elsevier, Amsterdam. 1981.
25. Ref. 24, p. 311.
26. Ref. 24, p. 307.

Talanta, Vol. 39, No. 11, pp. 1555–1559, 1992
Printed in Great Britain.

0039-9140/92 $5.00 + 0.00
Pergamon Press Ltd

COULOMETRIC TITRATION IN THE STUDY OF METAL ION-LIGAND EQUILIBRIA

STANISŁAW GŁĄB and ADAM HULANICKI*
Department of Chemistry, Warsaw University, Pasteura 1, 02-093 Warsaw, Poland

URSZULA NOWICKA
Department of Chemistry, University of Teachers College, 08-110 Siedlce, Poland

(*Received* 16 *March* 1992. *Accepted* 31 *March* 1992)

Summary—The coulometric titration technique is applied to evaluation of stability constants of metal complexes with ligands which have protolytic properties. The validity of the procedure was checked by studying several well-known systems. The proposed method can be used with success when metal ions are not reduced at the working cathode. Constants for calcium and magnesium complexes with components of some biologically important buffers, so-called Good buffers, were evaluated under experimental conditions (ionic strength of 0.16*M*, 37°) used in clinical analysis.

The most commonly used method for determination of stability constants of metal complexes with ligands which have protolytic properties is based on alkalimetric titration of solution containing the protonated form of ligand alone and in the presence of metal ion.[1] The changes in hydrogen ion-activity or concentration are followed with a glass electrode calibrated with appropriate standards. In the latter case for calibration of glass electrode the so-called "E^0-titration"[2] is used, in which a strong acid is titrated with a strong base. At constant ionic strength the EMF of a cell linearly depends on the logarithm of the hydrogen ion concentration.

In the alkalimetric titration of the protonated form of the ligand necessary for the determination of the ligand protonation constant a strong base used as a titrant may be successfully generated coulometrically. The advantages of the application of coulometric titrant generation for determination of protonation constants were pointed out previously.[3–5]

There are only a few papers in the literature in which the ligand in the presence of metal ion is alkalimetrically titrated by an electrolytically generated titrant. Such a procedure was used by Paris and Gregoire[6,7] who have determined the hydrolysis constants of beryllium(II)[6] and titanium(III).[7]

The aim of this paper is to check the possibility of the coulometric titration in studies of complexation equilibria. It requires more systematic studies of the titrant (strong base) electrogeneration efficiency in solutions containing metal ions with various redox properties. In order to check the applicability of coulometric titration for determination of stability constants of complexes some well-known metal–ligand systems were studied for comparison. The proposed method was used for the study of calcium and magnesium complexes with components of some biologically important buffers, so-called "Good" buffers,[8] for which stability constants, until now, have not been determined under experimental conditions (ionic strength—0.16*M*, 37°) used in examination of biological samples and in clinical analysis. Some buffers from this group are used as components of calibration standards for blood electrolyte measurements with calcium and magnesium ion-selective electrodes. Such buffer components should either not complex these metal ions or form complexes of known stability constants.

Among advantages in this procedure the simplicity as well as extreme precision and accuracy should be mentioned and make such procedure especially useful even for low-stability complexes.

*Author for correspondence.

EXPERIMENTAL

Reagents

Analytical grade acids. Citric, nitrilotriacetic (NTA), perchloric, succinic and tartaric acids were used.

Ethylenediaminetetraacetic acid, disodium salt dihydrate (EDTA). Analytical grade.

Cadmium nitrate tetrahydrate, copper(II) nitrate hydrate, calcium nitrate tetrahydrate, iron(III) nitrate nonahydrate, magnesium nitrate hexahydrate, sodium perchlorate monohydrate were all analytical grade reagents.

Components of buffer for the physiological pH range were *N*-(2-acetamido)- 2-aminoethanesulphonic acid (ACES), 4-morpholineethanesulphonic acid (MES), 3-{[Tris-(hydroxymethyl)methyl]-amino}-1-propanesulphonic acid (TAPS), (2-{[Tris(hydroxymethyl)-methyl]amino}-1-ethanesulphonic acid (TES) (Aldrich).

Apparatus

Coulometric analyser OH-404 Radelkis, pH-meter OP-208/1, Radelkis with the glass indicator electrode and the silver–silver chloride reference electrode (Ingold P 1883).

Measurements were carried out at 25 and 37° in a two-compartment coulometric cell equipped with a magnetic stirrer. The solutions were deaerated and kept under argon gas.

Procedures

The anode and cathode (2 ml) compartments of the coulometric cell were separated by two G-4 sintered glass discs and the space between them was filled with 3% aqueous sodium perchlorate in 3% agar-agar. Both electrodes of the generating system were platinum, the surface area of the working electrode was $A = 0.25$ cm^2. The reference electrode of the indicator system was connected through an electrolytic bridge containing 0.1 or 0.16*M* sodium chloride depending whether the ionic strength of titrated solution adjusted with sodium perchlorate was equal to 0.1 or 0.16. The current $i = 3$ mA provides 100% generation efficiency of the base in sodium perchlorate solutions.[3]

The solutions titrated coulometrically contained approximately 5 μmoles of perchloric acid for calibration of indicator electrode system, or 5 μmoles of protonated ligand in the case of determination of the protonation constant.

For determination of stability constants the solutions contained a mixture of protonated ligand (approx. 5 μmoles) and the examined metal ions, approx. 5 or 50 μmoles depending whether the studied complexes are strong or very weak.

Solutions of metal ions were standardized by volumetric complexometric methods.[9]

The current potential curves were obtained by measuring the current *vs.* potential of the working cathode measured against a silver-silver chloride electrode.

RESULTS AND DISCUSSION

Experimental data obtained in the course of coulometric titration of the protonated ligand with electrogenerated strong base were used for protonation constant calculations.[3] The protonation constant of a ligand (K_H) is evaluated from the Henderson-Hasselbach equation:

$$\log k_H = -\log[H^+] + \log \frac{[HL]}{[L]}$$

which was transformed into a form directly applicable to coulometric titration:

$$\log K_H = -\log[H^+] + \log \frac{Q_{ep} - Q - FV([H^+] - [OH^-])}{Q + FV([H^+] - [OH^-])}$$

where V is the volume of solution, F is the Faraday constant, and Q_{ep} is the charge consumed until the titration end-point. The pairs of values Q and $[H^+]$ (or $[OH^-]$) were evaluated from the coulometric titration curve, $E = f(Q)$, of an acid examined.

In the case of diprotic acids, when $\log K_{1H} - \log K_{2H} < 2.3$ the constants were calculated from the titration curve using the least square-procedure.[10]

The evaluation of hydrogen ion concentration $[H^+]$ requires the calibration of the indicator electrode, because:

$$\log[H^+] = (E_a^0 - E)F/2.3RT$$

where E_a° is a calibration constant. This constant is evaluated from coulometric titration of perchloric acid carried out at a given temperature and ionic strength.[3] Stability constants of metal–ligand complexes were calculated from the experimental data obtained in the course of alkalimetric titration of solution containing a mixture of protonated ligand and metal ion. The stability constants were calculated from an equation given by Yoshino *et al.*[11] For the

system of ligand $H_M L$ and metal ion where a series of complexes MH_iL ($i = 0, 1, \ldots N$) is formed, the stability constant of the complex MH_nL is given by the equation:

$$K^{M}_{MH_nL} = \frac{[MH_nL]}{[M][H_nL]} = \frac{(B_nC_n - A_nD_n)(C_nC_L - A_nC_H)}{(B_nC_H - D_nC_L)(A_nB_nC_H + D_nC_nC_M - A_nD_nC_M - B_nC_nC_L)}$$

where

$$A_n = \sum_{i=0}^{N} \frac{[H^+]^i K_i}{[H^+]^n K_n}$$

$$B_n = \sum_{i=0}^{N} \frac{[H^+]^i K^1_i}{[H^+]^n K^1_n}$$

$$C_n = \sum_{i=0}^{N} \frac{i[H^+]^i K_i}{[H^+]^n K_n}$$

$$D_n = \sum_{i=0}^{N} \frac{i[H^+]^i K^1_i}{[H^+]^n K^1_n}$$

$$C_H = (N - a)C_L - [H^+] + [OH^-],$$

where C_L is the total concentration of ligand, C_M is the total metal ion concentration, and a is the titration fraction;

$$a = NQ/Q_{ep}$$

$$K^1_i = K^H_{MHL}\, K^H_{MH_2L} \cdot \ldots \cdot K^H_{MH_2L} \quad (K^1_0 = 1)$$

$$K_i = K_{1H}\, K_{2H} \ldots . K_{iH} \quad (K_0 = 1)$$

The calculation of $K^M_{MH_nL}$ requires the knowledge of protonation constants of complexes:

$$K^H_{MH_iL} = \frac{[MH_iL]}{[MH_{i-1}L][H]}$$

These constants can be evaluated from the dependence of the average number of hydrogen ions bound to complexes on hydrogen ion concentration (formation curve).

Before applying the procedure of coulometric determination of protonation constants and stability constants to the Good buffers and their complexes with calcium and magnesium some ligand–metal ion systems were used to check the applicability of methods and to compare the calculated values with literature data. The undesirable electrode reactions which can obviously influence the current efficiency of the electrogeneration of a base may appear when studying complexes of metal ions being easily reduced at the cathode. Therefore cations with various redox properties (Ca^{2+}, Mg^{2+}, Cd^{2+}, Cu^{2+}, Fe^{3+}) were chosen to check the applicability of the use of coulometry for determination of stability constants of their complexes. A current–potential curve recorded for the supporting electrolyte (0.1*M* sodium perchlorate) alone and in the presence of investigated metal ions allows one to check whether 100% current efficiency of titration processes is obtainable. Experiments made at pH 2.5 and 6.0 (these values are within the pH range of metal ion–ligand mixtures titrated coulometrically) indicated clearly for which system that proposed method can be used (Figs. 1 and 2). No disturbance in 100% base electrogeneration occurs for solutions of Ca^{2+}, Mg^{2+} and Cd^{2+}. Only reduction of water or reduction of hydrogen ions (in the case of more acidic solutions) and water occur at the platinum cathode. Therefore, coulometry cannot be used for the study of complexation of easily reduced metal ions, *e.g.*, Cu^{2+} and Fe^{3+}. Reduction of metal ions at the working cathode results not only in current efficiency of titration processes below 100% but also decreases the

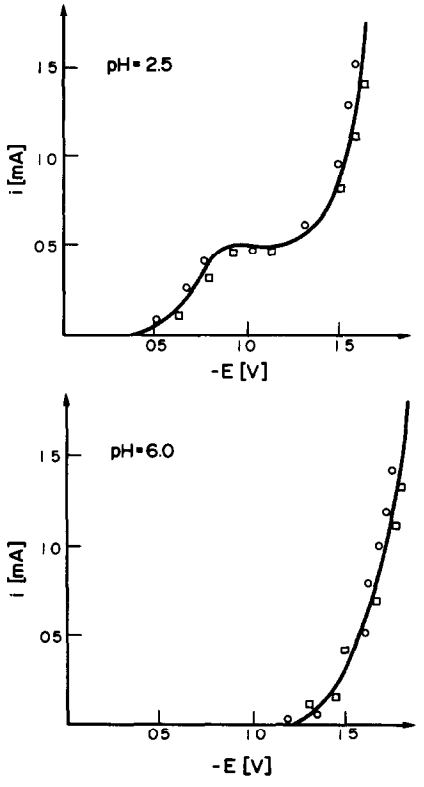

Fig. 1. Current–potential curves for 0.1*M* $NaClO_4$ (solid lines), 0.1*M* $NaClO_4 + 2 \times 10^{-3}M$ Ca^{2+} (○), and 0.1*M* $NaClO_4 + 2 \times 10^{-3}M$ Mg^{2+} (□).

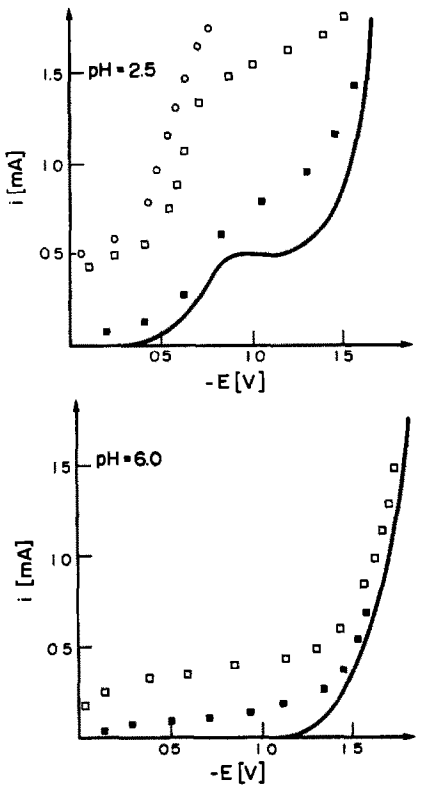

Fig. 2. Current–potential curves for 0.1 M $NaClO_4$ (solid lines), 0.1 M $NaClO_4 + 2 \times 10^{-3}$ M Cu^{2+} (□), 0.1 M $NaClO_4 + 2 \times 10^{-3}$ M $Cu^{2+} + 2 \times 10^{-3}$ M NTA (■), and 0.1 M $NaClO_4 + 2 \times 10^{-3}$ M Fe^{3+} (○).

total metal ion concentration in the course of measurement. The obtained results compared to literature data (Table 1) confirm the statement and indicate that coulometry can be used with success not only for determination of protonation constants but also stability of metal complexes when metal ions are not reduced.

The coulometric method is especially valuable when the complexes are very weak and the error of the conventional titration procedure becomes significant. This is the case of some buffers which are used for biological experiments and form weak complexes with calcium and magnesium. In those systems the stability constants of calcium and magnesium complexes are below 10. In such a case the difference between the titration curves in the presence and absence of metal ion is small. This is clearly shown in Fig. 3 where curves for one of the Good buffers (MES) as well as for EDTA in the absence and in the presence of calcium ions are presented. The estimated smallest value of the constant which can be evaluated equals approximately 1 when we assume that a minimal reasonable shift of the titration curve of the ligand in the presence and absence of excess of metal ion is equal to 1 mV. The protonation constants of Good buffer components as well as stability constants of their complexes with calcium and magnesium, determined under conditions used in biological and clinical measurements, are collected in Table 2. When the literature data for comparable conditions were available the agreement was found quite satisfactory.

Table 1. Protonation constants of ligands and stability constants of their complexes determined by coulometric titration at $I = 0.1$ and 25°. In brackets literature data[12] are given

Ligand	log K_H	log K_{CaL}	log $_{CaL}$
EDTA	10.15 (10.08)	10.75 (10.62)	15.9 (16.3)
	6.00 (6.03)		
NTA	9.40 (9.49)	6.3 (6.4)	10.99 (11.25)
	2.65 (2.67)		
	2.95 (2.08)		
Citrate	5.70 (5.68)	3.5 (3.4)	4.12 (4.22)
Succinate	5.24 (5.24)	1.33 (1.20)	
	3.93 (4.00)		
Tartrate	3.91 (3.78)	1.83 (1.80)	
	2.70 (2.73)		

CONCLUSIONS

The coulometric generation of a strong base was adapted for determination of stability constants of metal complexes with ligands having protolytic properties. The proposed method of determination of stability constants offers several advantages, some worth mentioning are:

No need for preparation of standard solutions.

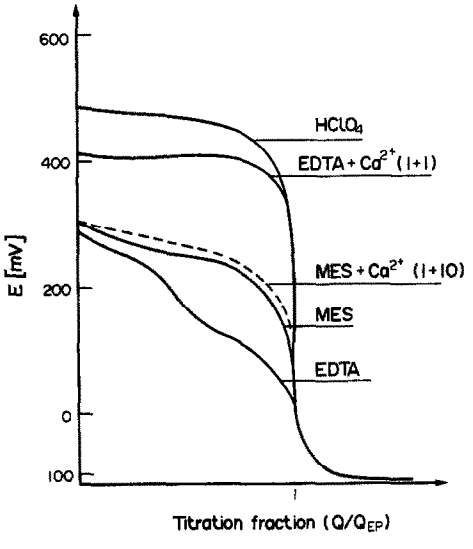

Fig. 3. Coulometric titration curves of $HClO_4$, EDTA, EDTA + Ca^{2+}, MES, and MES + Ca^{2+}.

Table 2. Protonation constants of some buffer components and stability constants of their calcium and magnesium complexes determined by coulometric titration at $I = 0.16$ and 25 or 37°. Data in brackets[8] at $I = 0.1$ and 20 or 37° [a] are given for comparison

	$\log K_H$		$\log K_{CaL}$		$\log K_{MgL}$	
Compound	25°	37°	25°	37°	25°	37°
ACES	6.62 (6.9)	6.35 (6.56)[a]	0.4 (0.4)	0.2	0.4 (0.4)	0.3
MES	6.02 (6.1)	5.96 (5.98)[a]	0.5 (0.7)	0.3	0.6 (0.8)	0.5
TAPS	8.21	7.98	No complexation*		No complexation	
TES	7.30 (7.5)	7.08 (7.14)[a]	No complexation		No complexation	

*Titration curve in presence of metal ion to the titration curve of the ligand alone was not shifted or the shift was lower than 1 mV.

Better precision than that obtained in a standard procedure.

Applicability to weak complexes.

Applicability to microsamples.

The most important disadvantage is the limitation of the method to such complexation systems in which the metal ions are not reduced in the potential range used for reduction of water at the working electrode of the generation system.

REFERENCES

1. J. Inczedy, *Analytical Applications of Complex Equilibria*, Horwood, Chichester, 1973.
2. L. Persson, F. Ingman and A. Johansson, *Talanta*, 1976, **23**, 76.
3. S. Głąb, E. Skrzydlewska and A. Hulanicki, *ibid.*, 1987, **34**, 411.
4. S. Głąb and U. Nowicka, *Mikrochim. Acta*, 1987 **II**, 229.
5. V. I. Vajgand, R. P. Michajlovic and R. M. Dzudovic, *Talanta*, 1989, **36**, 1154.
6. M. R. Paris and C. L. Gregoire, *Anal Chim. Acta*, 1968, **42**, 431.
7. *Idem, ibid.*, 1968, **42**, 439.
8. N. E. Good, G. D. Winget, W. Winter, T. N. Connoly, S. Izawa and R. M. M. Singh, *Biochem.*, 1966, **5**, 467.
9. R. Pribil, *Komplexone in der Chemischen Analyse*, VEB Deutscher Verlag der Wissenschaften, Berlin 1961.
10. A. Albert, E. P. Serjeant, *The Determination of Ionization Constants*, Chapman and Hall, London, 1971.
11. T. Yoshino, S. Murakami, M. Kagawa and T. Araragi, *Talanta*, 1974, **21**, 79.
12. A. E. Martell and R. M. Smith, *Critical Stability Constant*, Plenum Press, New York and London 1977.

Talanta, Vol. 39, No. 11, pp. 1561–1567, 1992
Printed in Great Britain.

0039-9140/92 $5.00 + 0.00

APPLICATION OF FREE-RADICAL CHROMOGENS TO DETERMINATION OF NITRITE AND NITRATE IONS BY EPR SPECTROMETRY

ERIC P. K. TSANG, D. THORBURN BURNS and BRIAN D. FLOCKHART*
School of Chemistry, Queen's University of Belfast, Belfast, BT9 5AG, U.K.

(*Received* 27 *February* 1992. *Accepted* 21 *April* 1992)

Summary—Various azines and substituted phenylene diamines are oxidized by the nitrite ion to give stable radicals in an autocatalytic reaction. This finding has now been developed into highly sensitive methods for nitrite determination by EPR spectrometry. Thus, when the reagent is phenothiazine, the detection limit for nitrite is 0.012 ppm, the relative standard deviation at 0.05 ppm is 1.9%, and the analytical range is 0–1.5 ppm. With *N,N,N′,N′*-tetramethyl-*p*-phenylenediamine as the reagent, the corresponding values are 0.025 ppm, 2.6%, and 0–1.3 ppm. Nitrate can be determined after prior reduction to nitrite. A mixture of nitrite and nitrate ions can also be quantitatively analysed. The EPR methods were applied to the determination of the nitrite and nitrate contents of prepacked cooked ham and of soft-spreading cheese. The results agreed well with those obtained by ISO and AOAC standard methods for these samples.

Electron paramagnetic resonance (EPR) as a quantitative analytical tool has not been greatly exploited. Its present applications lie mainly in the determination of selected metals, either by their natural paramagnetic states[1] or through the use of spin labels.[2] Several factors may explain this limited use. An EPR spectrometer is seldom situated in the laboratory dedicated to analytical chemistry; only paramagnetic substances, and substances that can be converted to a paramagnetic form with sufficient stability for a spectrum to be recorded, are suitable for analysis by EPR spectrometry; the analytical basis of the technique has been less well researched than those of most other spectroscopic methods.

Alkali nitrites and nitrates are used as additives in a variety of foods to prevent bacterial spoilage and food poisoning. However, concern exists over the presence of nitrate in the diet, not because of any intrinsic behaviour of the ion itself, but rather in its ability to form nitrite by microbiological or other biochemical reduction processes. Consequently, whenever nitrate is ingested in food, there is always the possibility that some of it will be reduced to nitrite. Under the acidic conditions in the stomach the nitrite ion can react with dietary components to form products that are often associated with carcinogenesis.[3] It is therefore highly desirable that the amounts of nitrite and nitrate in foodstuffs should be closely monitored. Various methods are available for this purpose.[4–6] The present paper describes the application of EPR spectrometry to the determination of these ions, individually and in admixture. A preliminary account of the work has been published.[7]

The early research of Michaelis *et al.*[8] on one-electron oxidation–reduction processes revealed many classes of organic compound that exhibit this behaviour. Compounds investigated included phenothiazine and its derivatives. Subsequently, other workers studied the stable radical obtained from the oxidation of phenothiazine.[9–11] Stable radicals are also formed when the *p*-phenylenediamines are oxidized.[12,13] Sawicki *et al.*[14] showed that nitrite can oxidize such compounds to give coloured products suitable in some cases for spectrophotometric determinations and they concluded that free radicals are present. The present EPR methods for the determination of nitrite and nitrate ions are based on this principle, *viz.*,

Nitrite + reagent → stable free radical.

(capable of one-electron oxidation)

The formation of the free radical is autocatalytic[14] and hence nitrite can be determined at trace levels by EPR spectrometry.

*Author for correspondence.

EXPERIMENTAL

Apparatus

The EPR measurements were made with a Varian E-109 spectrometer operated at *ca.* 9.5 GHz with a magnetic field modulation of 100 kHz. The resonator was a Varian E-231 rectangular cavity operating in the TE102 mode. The spectrometer was interfaced to a Varian E-900 data processing system. The sample cells were quartz tubes with an internal diameter of 2.0 mm and a wall thickness of 3 mm. Spectra were recorded at room temperature (20°).

Reagents

The stock nitrite solution was obtained by dissolving analytical reagent grade sodium nitrite (dried to constant weight at 110°) in demineralized water. Other nitrite solutions were obtained by dilution. The stock nitrate solution was prepared by dissolving analytical reagent grade potassium nitrate in demineralized water. Phenothiazine was recrystallized twice from heptane–ethylcyclohexane and *N,N,N′,N′*-tetramethyl-*p*-phenylenediamine once from methanol, before use. Glacial acetic acid, of analytical reagent grade, was distilled twice; it was degassed before use by bubbling nitrogen through it and then subjecting it to a freeze-evacuate-thaw cycle.

Preparation of spongy cadmium

Zinc rods were immersed in aqueous cadmium sulphate (AnalaR, 80 g, dissolved in one litre of water). After two hours the deposit of cadmium was scraped off the rods and was washed by decantation using two one litre volumes of water. Care was taken that the cadmium sponge was always covered with water. It was transferred to a food blender using 0.1*M* hydrochloric acid and the bulk of the sponge was reduced to *ca.* 40 mesh. It was again washed with water, allowed to stand overnight under water, and then transferred to a column of height 2 dm and internal diameter 8 mm. The cadmium was activated by passing successively through the column 25 ml of 0.1*M* hydrochloric acid, 50 ml of water, and 25 ml of buffer of pH 9.6. This buffer was prepared by diluting 20 ml of concentrated hydrochloric acid to 500 ml with water, adding 50 ml of aqueous ammonia and then bringing the total volume to one litre.

Finalised procedures

Determination of nitrite. Phenothiazine. A 0.1-ml volume of test solution, delivered from an Agla micrometer syringe, was diluted to 10 ml with a solution of 0.05% (w/v) phenothiazine in glacial acetic acid. The EPR measurements were made 50 min after mixing.

A 0.01% solution of the reagent was used for test solutions that contained <0.1 ppm nitrite. All solutions of the reagents were stored in the dark. Nitrite solutions to which the reagent had been added were kept in the dark until the due time to record the spectrum.

N,N,N′,N′-Tetramethyl-*p*-phenylenediamine. A 0.1-ml volume of test solution, delivered from an Agla micrometer syringe, was diluted to 10 ml with a 0.05% (w/v) solution of the reagent in glacial acetic acid. One millilitre of sulphamic acid (0.1% solution of the acid in ethanol) was added after 40 min to stabilize the signal. EPR measurements were taken 10 min later. A 0.01% solution of the reagent was used for solutions that contained <0.1 ppm nitrite.

Determination of nitrate. An aliquot quantity of the test solution was added to the column of spongy cadmium, the flow rate through the column was adjusted to 4–6 ml/min, and the eluate was collected in a 100-ml standard flask. As the column emptied, the reservoir and column wall were washed with three 15-ml volumes of water. The flask was removed and the volume made up to 100 ml. The nitrite content was determined by one of the methods described.

Determination of an admixture of nitrite and nitrate

A 50-μl volume of 12*M* hydrochloric acid was added to 2 ml of test solution and the nitrite was removed by volatilization as nitrosyl chloride, nitrogen being blown over the solution for 5 min.[15] The nitrate was then determined after prior reduction to nitrite by spongy cadmium. The nitrite plus nitrate content of another 2-ml sample of the test solution was obtained by reduction followed by determination of the total nitrite present.

RESULTS AND DISCUSSION

Instrumental variables

A linear relationship between the signal amplitude (peak-to-peak height of the first derivative absorption curve) and the amplitude of the magnetic field modulation held up to 10 G (1 mT). This latter modulation amplitude was subsequently used in the quantitative measurements and it removed the resolution of the

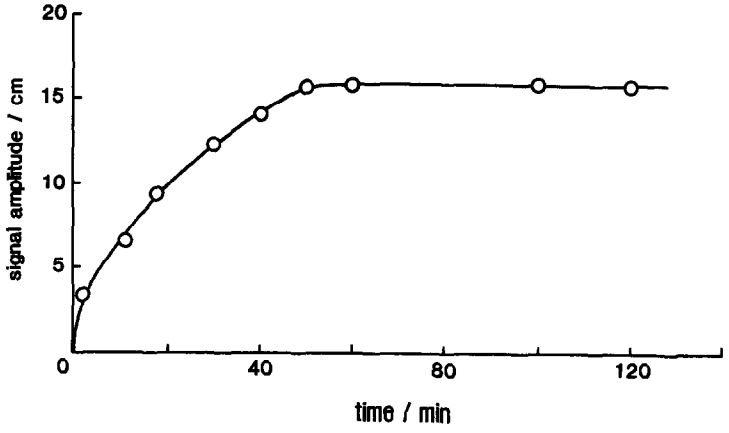

Fig. 1. Signal amplitude of the phenothiazine–nitrite–acetic acid system as a function of time.

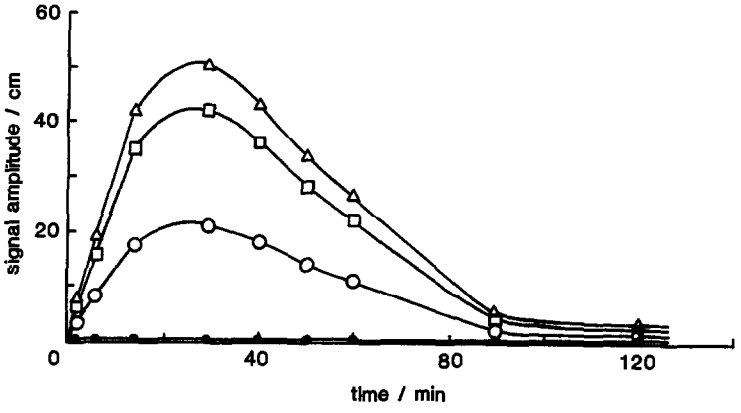

Fig. 2. Signal amplitude of phenothiazine in acetic acid as a function of time: solution kept in the dark (●); solution exposed to daylight (○); solution irradiated with light from a xenon lamp for 2 min (□) and for 4 min (△).

spectra.* The relative standard deviation of the measurements was lower for over-modulated spectra whether signal amplitudes or signal intensities (obtained by double integration of the first derivative curves) were used, and this is especially advantageous when the concentration of the analyte is low.

A microwave power level of 160 mW, which produced no observable saturation, and a scan time of 2 min, were employed.

Determination of nitrite

Phenothiazine. The variation of signal amplitude with time when phenothiazine was added to a nitrite solution is shown in Fig. 1. Little change in amplitude occurred after ~50 min. The radical remained stable for at least 4 hr. Glacial acetic acid is a better solvent than either ethanol or an ethanol–glacial acetic acid mixture with respect to the amplitude of the signal and the stability of the radical associated with the phenothiazine–nitrite system. Degassing of the solvent was necessary to reduce the signal attributable to the reagent itself to a barely detectable resonance.

In the determination of nitrite with phenothiazine as the reagent, exclusion of light is of critical importance. When a degassed reagent solution was exposed to daylight, an EPR signal developed and reached a maximum after ~30 min of exposure (Fig. 2). Another portion of the solution that had been kept in the dark gave a signal scarcely larger than the inherent low noise level of the spectrometer setting (Fig. 2). A flat quartz cell (faces *ca.* 0.3 mm apart) was filled with reagent solution, mounted in the cavity, and irradiated with light from a xenon lamp (Osram XBO, 150 W), the light being focused onto the cell by means of a quartz lens. One

*The phenothiazine-nitrite system and the phenylenediamine-nitrite system gave well-resolved EPR spectra. These and other related spectra will be the subject of a later publication.

Fig. 3. EPR spectrum (first derivative) of phenothiazine in acetic acid after irradiation with light from a xenon lamp.

sample of solution was irradiated for 2 min, another sample for 4 min; the results are presented in Fig. 2. Irradiation with light from a xenon arc lamp produced the same pattern of results as observed with samples exposed to daylight, but the effects were more pronounced. Figure 3 shows the spectrum given by irradiated solutions; a similar spectrum was obtained from solutions exposed to daylight. Clearly, when working with solutions of this reagent, light must be excluded until the analysis has been completed.

The concentration of phenothiazine was not critical in the range 0.05–0.4% for solutions containing more than 0.1 ppm of nitrite. With a reagent concentration of 0.05% the plot of signal amplitude versus nitrite concentration was linear in the range 0.1–1.5 ppm, but curvature was present in the range 0–0.1 ppm. By reducing the reagent concentration to 0.01%, a linear calibration plot was also obtained in the latter range. For both the higher and lower ranges of nitrite concentration, the correlation coefficient was 0.999.

The relative standard deviation at 0.3 ppm was 1.2% (ten signal amplitude measurements); the corresponding value for a solution containing 0.05 ppm nitrite was 1.9%. The detection limit at three times the standard deviation of the field blank was 0.012 ppm. The relative standard deviation of the measurements based on signal intensities was 2.8% at 0.3 ppm nitrite.

Inorganic oxidizing agents such as chlorate and perchlorate interfered with the determination of nitrite; low results were obtained. Nitrate had a similar effect. Sulphite could be tolerated up to a sulphite-to-nitrite mole ratio of 2000 to 1.

The volume of nitrite solution (aqueous) employed for an analysis was set at 0.1 ml. The signal amplitude decreased as the volume of this solution was increased in the range 0.1–1 ml. Water with its high dielectric constant results in electric loss and a marked lowering of the cavity Q.

N,N,N′,N′-*Tetramethyl*-p-*phenylenediamine*. The variation of signal amplitude with time when the reagent was *N,N,N′,N′*-tetramethyl-*p*-phenylenediamine is shown in Fig. 4. Even after 2 hr the signal was still increasing. The addition of sulphamic acid (1 ml of 1% solution in ethanol) effectively stabilized the signal. This effect is illustrated in Fig. 4 which incorporates the results of several separate experiments. The compromise chosen for the analytical measurements was to add the sulphamic acid 40 min after mixing the nitrite and reagent solutions, and to record the spectrum 10 min later. Daylight had no noticeable effect on the reagent solution.

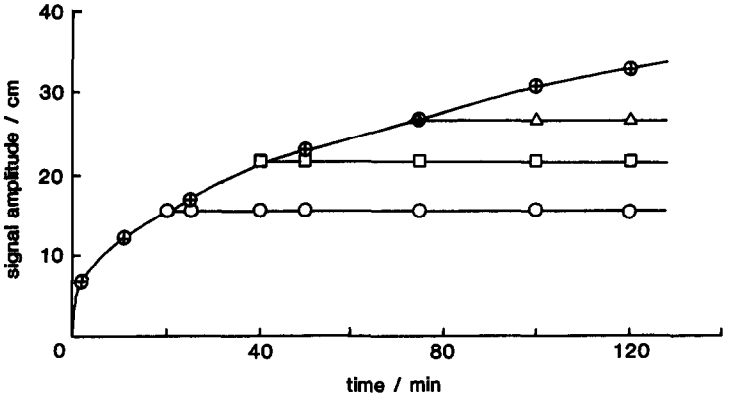

Fig. 4. Signal amplitude of the *N,N,N′,N′*-tetramethyl-*p*-phenylenediamine–nitrite–acetic acid system as a function of time (⊕). Signal amplitude of the *N,N,N′,N′*-tetramethyl-*p*-phenylenediamine–nitrite–acetic acid–sulphamic acid system as a function of time. Sulphamic acid added after: 20 min (○); 40 min (□); 75 min (△).

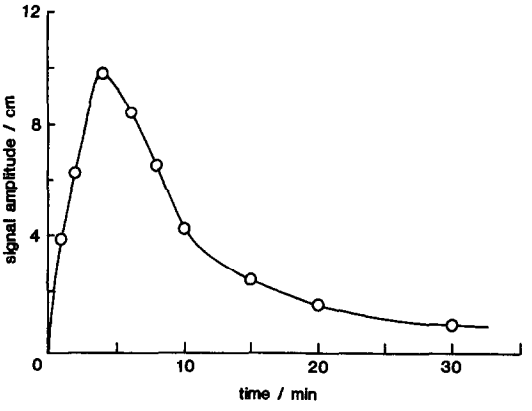

Fig. 5. Signal amplitude of the *N,N,N′,N′*-tetramethylbenzidine–nitrite–acetic acid system as a function of time.

When a reagent concentration of 0.05% was used, a linear calibration graph was obtained in the range 0.1–1.3 ppm, whereas curvature was present in the range 0–0.1 ppm. By reducing the reagent concentration to 0.01%, linearity was also produced in the latter range. For both the higher and lower ranges of nitrite concentration, the correlation coefficient was 0.998.

The relative standard deviation at 0.3 ppm was 1.5% (ten signal amplitude measurements). The detection limit at three times the standard deviation of the field blank was 0.025 ppm. The relative standard deviation of the measurements based on signal intensities was 3.1% at 0.3 ppm nitrite.

The presence of strong oxidizing agents produced high results for nitrite; low results were obtained when nitrate was present; sulphite did not interfere with the determination up to a mole ratio of at least 1000 to 1.

Other reagents. When the reagent was *N,N,N′,N′*-tetramethylbenzidine the signal amplitude reached a maximum *ca.* 3 min after the reagent was added to a nitrite solution and it then decreased rapidly (Fig. 5). Attempts to stabilize the signal by adding sulphamic acid were unsuccessful. Measurements had therefore to be made 3 min after mixing. When a reagent concentration of 0.05% was used, a linear calibration graph was obtained in the range 0.1–0.5 ppm. Curvature was present in the range 0–0.08 ppm, but this was removed when the reagent concentration was reduced to 0.01%. The relative standard deviation at 0.3 ppm was 5.4%, and the detection limit at three times the standard deviation of the field blank was 0.035 ppm. The poor reproducibility is consistent with the signal amplitude-time curve. Low results were obtained in the presence of nitrate, chlorate and perchlorate. At a mole ratio of 60 to 1, sulphite did not interfere with the determination.

Two compounds related to phenothiazine, namely, phenoxazine and chloropromazine, were investigated as possible reagents for nitrite determination. Phenoxazine was less sensitive than phenothiazine and more prone to interferences, although the EPR signal reached its maximum amplitude in a shorter time (~25 min). The EPR signal from a chloropromazine-nitrite system decayed rapidly, rendering this compound unsuitable for nitrite determination. The *N,N,N′*-trimethyl-*p*-phenylenediamine-nitrite system gave a weak signal even at 4 ppm nitrite and was not investigated further.

Determination of nitrate

Nitrate solutions of known concentration were passed through the reduction column and the nitrite content was determined by both the phenothiazine method and the *N,N,N′,N′*-tetramethyl-*p*-phenylenediamine method (subsequently referred to as the phenylenediamine method). The results are summarized in Table 1.

Determination of admixtures of nitrite and nitrate

Solutions containing known amounts of nitrite and nitrate were analysed according to the procedure described in the experimental section. Both the phenothiazine method and the phenylenediamine method were used for nitrite determination. The results are summarized in Table 2.

Table 1. Determination of nitrate

Method	Nitrate added (ppm)	Nitrate found* (ppm)	Recovery (%)
Phenothiazine	0.050	0.0494	98.8
	0.100	0.0990	99.0
	1.00	0.990	99.0
N,N,N′,N′-Tetramethyl-*p*-phenylenediamine	0.050	0.0495	99.0
	0.100	0.0992	99.2
	1.00	0.991	99.1

*Mean of three measurements.

Table 2. Determination of admixtures of nitrite and nitrate

Method*	Amount added (ppm) Nitrite	Nitrate	Amount found (ppm)† Nitrite	Nitrate	Recovery (%) Nitrite	Nitrate
(i)	0.100	0.050	0.0994	0.0496	99.4	99.2
	0.50	0.100	0.495	0.0993	99.0	99.3
	1.00	0.100	0.993	0.0992	99.3	99.2
(ii)	0.100	0.050	0.0991	0.0495	99.1	99.0
	0.50	0.100	0.496	0.0991	99.2	99.1
	1.00	0.100	0.992	0.099	99.2	99.0

*(i) phenothiazine method; (ii) phenylenediamine method.
†Mean of three measurements.

Table 3. Nitrite and nitrate content of cooked ham

Method*	Nitrite content (ppm)† Sample 1	Sample 2	Nitrate content (ppm)† Sample 1	Sample 2
(i)	50.2	67.5	65.2	85.1
(ii)	49.8	67.2	64.9	84.8
ISO	50.5	67.8	65.6	85.4

*(i) Phenothiazine method; (ii) phenylenediamine method.
†Mean of three measurements.

Table 4. Nitrite and nitrate content of soft cheese

Method*	Nitrite content (ppm)† Sample 1	Sample 2	Nitrate content (ppm)† Sample 1	Sample 2
(i)	18.5	32.5	62.4	75.8
(ii)	18.2	32.1	61.6	75.4
AOAC	18.8	32.7	62.6	76.0

*(i) Phenothiazine method; (ii) phenylenediamine method.
†Mean of three measurements.

Applications

The EPR methods were applied to the determination of the nitrite and nitrate contents of pre-packed cooked ham and of soft-spreading cheese. In Tables 3 and 4 the results obtained by the EPR methods are compared with those given by International Standards Organization (ISO)[16] and Association of Official Analytical Chemists (AOAC)[17] standard methods for these samples. The samples were prepared for analysis by the respective ISO and AOAC procedures.[16,17] Statistical analysis (students' *t* test) between the EPR and ISO results and between the EPR and AOAC results revealed no significant difference between the methods (at the 95% confidence level).

CONCLUSION

A large number of spectrophotometric methods are available for the determination of nitrite ion.[14] The EPR methods now described provide alternative viable analytical methods of high sensitivity and with an accuracy that compares favourably with the other procedures. Moreover, the new methods are simple and extraction is not required. Further, these methods can tolerate large amounts of reducing agents which should permit their application to pollution studies, such as the determination of nitrogen dioxide in the presence of sulphur dioxide. An additional advantage is that they are applicable to coloured solutions. A drawback of the EPR methods herein is the long procedural time (50 min).

A preliminary investigation has shown that the EPR methods are also suitable for other oxidizing agents such as perchlorate, although they are less sensitive when applied to ions other than the nitrite ion.

REFERENCES

1. I. B. Goldberg, in *Specialist Periodical Report: Electron Spin Resonance*, Vol. 6, Chap. 1, p. 1 (The Chemical Society, London, 1981) for many references.
2. V. Yu. Nagy, O. M. Petrukhin and Yu. A. Zolotov, *CRC Crit. Rev. Anal. Chem.*, 1987, **17**, 265.
3. C. Glidewell, *Chem. Brit.*, 1990, **26**, 137.
4. W. J. Williams, *Handbook of Anion Determination*, Butterworths, London, 1979.
5. F. D. Snell, *Photometric and Fluorometric Methods of Analysis—Non Metals*, Wiley, New York, 1981.
6. Z. Marczenko, *Separation and Spectrophotometric*

Determination of Elements, Ellis Horwood, Chichester, 1986.
7. E. P. K. Tsang, D. T. Burns and B. D. Flockhart, *Anal. Proc.*, 1991, **28**, 10.
8. L. Michaelis, S. Granick and M. P. Schubert, *J. Amer. Chem. Soc.*, 1941, **63**, 351.
9. H. J. Shine, C. Veneziani and E. E. Mach, *J. Org. Chem.*, 1966, **31**, 3395.
10. C. Jackson and N. K. D. Patel, *Tetrahedron Lett.*, 1967, No. 24, 2255.
11. M. F. Chiu, B. C. Gilbert and P. Hanson, *J. Chem. Soc., B*, 1970, 1700.
12. M. T. Melchior and A. H. Maki, *J. Chem. Phys.*, 1961, **34**, 471.
13. J. R. Bolton, A. Carrington and J. dos Santos-Veiga, *Mol. Phys.*, 1962, **5**, 615.
14. E. Sawicki, T. W. Stanley, J. Pfaff and H. Johnson, *Anal. Chem.*, 1963, **35**, 2183.
15. N. Velghe and A. Claeys, *Analyst*, 1983, **108**, 1018.
16. Meat and Meat Products, *Determination of Nitrite Content*, *International Standards Organization*, ISO 2918-1975(E), Sections 7.1-2, 8.1, 8.3.1-5 and 8.4.1-4.
17. Official Methods of Analysis of the Association of Official Analytical Chemists, S. Williams (ed.), Association of Official Analytical Chemists, Arlington, VA, 14th Ed., 1984, Nitrate and Nitrite in Cheese, Section 16.278–16.283.

Talanta, Vol. 39, No. 12, pp. 1569–1573, 1992
Printed in Great Britain.

0039-9140/92 $5.00 + 0.00

STABILITY-INDICATING METHOD FOR THE DETERMINATION OF CLORAZEPATE DIPOTASSIUM—I. VIA ITS FINAL DEGRADATION PRODUCTS

M. G. EL-BARDICY, L. I. BEBAWY* and M. M. AMER
Analytical Chemistry Department, Faculty of Pharmacy, Cairo University, Cairo, Egypt

(*Received* 22 *April* 1991. *Revised* 7 *August* 1991. *Accepted* 9 *August* 1991)

Summary—A sensitive spectrophotometric procedure is described for the determination of 1,4-benzodiazepine (clorazepate dipotassium) in the presence of its degradation products. The procedure is based on acid hydrolysis of clorazepate dipotassium to yield its final degradation products *viz.*, 2-amino-5-chlorobenzophenone and glycine. The amino-chlorobenzophrenone is extracted from the neutralized hydrolysate with diethyl ether, the extract is evaporated, the residue is dissolved in methanol and its absorbance measured at about 240 nm or 380 nm. Glycine, left in the aqueous layer after etherial extraction of aminochlorobenzophenone, is treated with ninhydrin reagent in the presence of pyridine and the bluish violet colour formed is measured at about 560 nm. The suggested procedures determine 20–100 mg of clorazepate dipotassium via its degradation products aminochlorobenzophenone and glycine with mean accuracies of 100.0 ± 0.5% at 560 nm, 100.2 ± 0.6% at 380 nm and 99.8 ± 0.5%. The suggested procedures are suitable for stability-testing of clorazepate dipotassium in bulk powder and in pharmaceutical preparations.

Clorazepate dipotassium,7-chloro-1,3-dihydro-2-oxo-5-phenyl-1H-1,4-benzodiazepine-3-carboxylic acid, dipotassium salt, is the active ingredient in tranxene® which is marketed as an anti-anxiety agent.[1] Several methods have been reported for the quantitative analysis of clorazepate dipotassium, including GLC,[2–4] HPLC,[5–7] TLC,[8] colorimetry,[9] fluorimetry,[10] spectral methods and polarography.[11] In the present communication, two procedures, spectrophotometric and colorimetric are described for the determination of clorazepate dipotassium after hydrolysis to amino chlorobenzophrenone and glycine.

EXPERIMENTAL

Apparatus

U.V./Vis spectrophotometer (Shimadzu UV-120) was used.

Reagents

All chemicals were of analytical grades.

Clorazepate dipotassium. Working standard, kindly supplied by Nile Pharmaceutical Co., Cairo, Egypt.

Hydrochloric acid, ~6N Aqueous solution.

Sodium hydroxide, ~6N Aqueous solution.

Diethyl ether. Chemically pure (Prolabo.).

Methanol. Spectroscopic grade (Merck).

Citric acid–citrate buffer, pH 5.[12]

Ninhydrin–citrate reagent. A 5% solution in citric acid–citrate buffer, pH 5.

Pyridine. Chemically pure (Merck) containing no ammonia and gives no colour with ninhydrin–citrate reagent when heated in a boiling water bath for 15–20 min.

Benzene–methylene chloride; 9:1. (Prolabo.)

N-desmethyldiazepam working standard. Kindly supplied by Arab Drug Co., Cairo, Egypt.

2-Amino-5-chlorobenzophenone (Aldrich).

Glycine. (B.D.H.)

Procedure

Bulk powder. To prepare the sample solution accurately, weigh about 20–100 mg of clorazepate dipotassium, dissolve in 10 ml of water and extract with 3 × 20 ml of a mixture of benzene–methylene chloride (9:1). Transfer the aqueous layer into a 100-ml loosely stoppered (or covered) conical flask, add 25 ml of 6*N* hydrochloric acid, stopper the flask and heat at 100° for 1 hr. Cool to room temperature and add 25 ml of 6*N* sodium hydroxide; assure that the solution

*From National Organization of Drug Control and Research.

is just alkaline to litmus. Cool again and quantitatively transfer the contents into a 150-ml separating funnel. Extract with 3 × 20 ml of diethyl ether and combine the etherial extracts together for the determination of aminochlorobenzophrenone. Retain the aqueous layer for the determination of glycine.

Determination of aminochlorobenzophenone. Evaporate the combined etherial extracts just to dryness and dissolve the residue in 20 ml of methanol. Transfer the methanolic solution into a 50-ml standard flask, dilute to volume with methanol and mix well.

1. Pipette an aliquot of the methanolic solution corresponding to 0.4–2 mg of clorazepate dipotassium into a 25-ml standard flask and dilute to volume with methanol. Measure the absorbance of the solution at 380 nm against methanol as a blank.

2. Transfer an aliquot volume (equivalent to 2 mg) from the above solution into a 25-ml standard flask and dilute to the mark with methanol. Pipette an aliquot volume corresponding to 0.08–0.56 mg of clorazepate dipotassium into a 25-ml standard flask and dilute to volume with methanol. Measure the absorbance of this solution at 240 nm against methanol as a blank.

Calculate the concentration of clorazepate dipotassium from a calibration curve prepared simultaneously, or from the A (1%, 1 cm) = absorbance of 1% solution in a 1 cm cell, which amounts to (1) 106.9 at 380 nm or 469.26 at 240 nm for clorazepate dipotassium or (2) 188.5 at 380 nm or 827.62 at 240 nm for 2-amino-5-chlorobenzophenone; the result of amino-chlorobenzophenone can be expressed as clorazepate dipotassium if multiplied by 0.567, or from the following regression equations: at 240 nm: $y = 1.85x + 0.006$, $R = 1$ for clorazepate dipotassium and $y = 3.17x + 0.027$, $R = 0.984$ for 2-amino-5-chlorobenzophenone and at 380 nm: $y = 0.42x - 0.005$, $r = 1.001$ for clorazepate dipotassium, and $y = 0.37x + 0.003$, $r = 0.994$ for 2-amino-5-chlorobenzophenone, where y is absorbance, x is concentration and r is correlation coefficient.

Determination of glycine. Transfer the aqueous layer, quantitatively, into a 100-ml standard flask and complete to volume with citric acid–citrate buffer solution (pH 5). Introduce an aliquot volume of the solution, corresponding to 0.3–1.5 mg of clorazepate dipotassium, into a 25-ml standard flask, add 3.5–4 ml of the citric acid–citrate buffer, 1 ml of the ninhydrin–citrate reagent, 1 ml of pyridine and heat in a boiling water bath for 15–10 min. Cool to room temperature, complete to volume with water and measure the absorbance of the violet colour at 560 nm against a blank prepared by treating 20–100 mg as described for preparing the sample solution above, but omitting heating at 100° for 1 hr, adding 25 ml of 6*N* hydrochloric acid and 25 ml of 6*N* sodium hydroxide to the aqueous layer, and instead using the aqueous layer as described under determination of glycine above.

Calculate the concentration of glycine from a calibration curve prepared simultaneously or from the A (1%, 1 cm) = absorbance of 1% solution in a 1 cm cell, which amounts to: (1) 175.7 for clorazepate dipotassium, or (2) 959.9 for glycine; the result of glycine can be expressed as clorazepate dipotassium if multiplied by 0.183, or from the following regressing equations: $y = 0.699 + 0$ and $r = 1$ for clorazepate dipotassium or $y = 3.5x + 0.05$ and $r = 0.959$ for glycine.

*For capsules**

Evacuate the contents of 20 capsules, mix thoroughly, weigh and calculate the average weight in each capsule. Transfer an accurate weight of the mixed sample, equivalent to about 20–100 mg of clorazepate dipotassium, dissolve in 10 ml of water and extract with 3 × 20 ml of a mixture of benzene–methylene chloride (9:1). Filter the aqueous layer through a filter paper into a 100-ml conical flask and proceed as mentioned for preparation of the sample solution for bulk powder, starting at the point "... add 25 ml of 6*N* hydrochloric acid, stopper the flask and heat at 100° for 1 hr ...".

RESULTS AND DISCUSSIONS

Although clorazepate dipotassium is stable in alkaline medium, it is readily hydrolysed in acid medium. Upon standing at room temperature for half an hour in 2*N* hydrochloric acid it is completely degraded to *N*-desmethyldiazepam.[11] Under more drastic conditions, *i.e.* heating with 6*N* hydrochloric acid at 100° for 1 hr, it is completely degraded yielding 2-amino-5-chlorobenzophenone and glycine.[2]

The proposed procedure depends upon the determination of clorazepate dipotassium via

*The drug is available in the Egyptian market as capsules only.

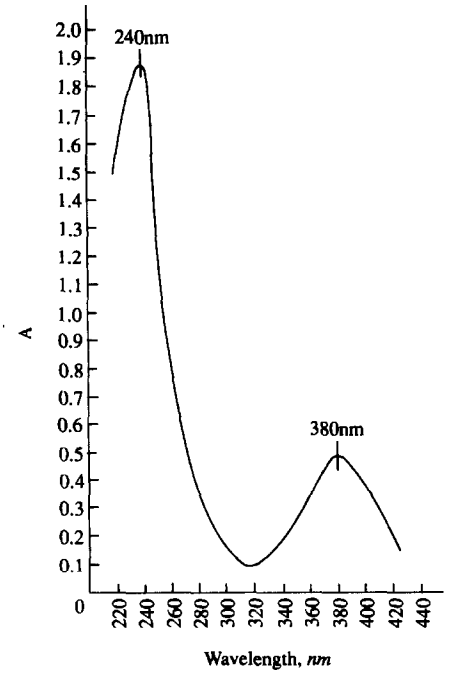

Fig. 1. Spectrum of 2-amino-5-chloropenzophenone in methanol after the hydrolysis of clorazepate dipotassium (1.2 mg/25 ml).

its degradation products, namely, 2-amino-5-chlorobenzophenone and glycine, after hydrolysis with 6*N* hydrochloric acid at 100° for 1 hr.

Before hydrolysis, the solution is extracted with a mixture of benzene–methylene chloride to extract 2-amino-5-chlorobenzophenone and *N*-desmethyldiazepam which might be present due to partial degradation, and which will be hydrolysed to give 2-amino-5-chlorobenzophenone and glycine.

The first procedure is spectrophotometric, and depends upon the determination of 2-amino-5-chlorobenzophenone which is produced quantitatively by drastic aicd hydrolysis of clorazepate dipotassium. The absorption spectrum

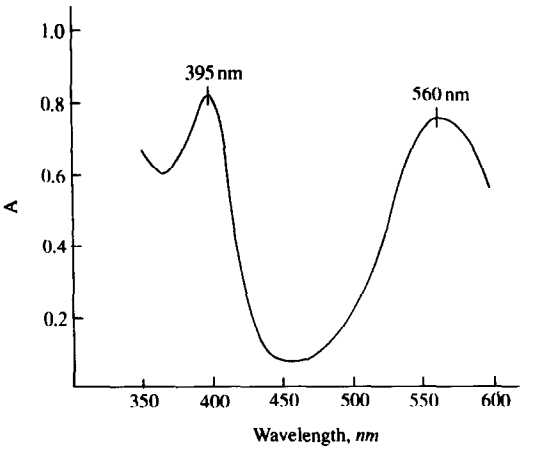

Fig. 2. Spectrum of glycine–ninhydrin pyridine complex.

is shown to possess two maxima at 240 nm and at 380 nm, Fig. 1.

A linear relationship prevails between the concentration of the hydrolysed clorazepate dipotassium or 2-amino-5-chlorobenzophenone and the absorbance at 240 and 380 nm.

The optimum conditions for quantitative degradative hydrolysis of clorazepate dipotassium to yield 2-amino-5-chlorobenzaphenone and glycine were studied and confirmed by TLC.

On analysing different concentrations 0.08–0.56 mg at λ_{max} 240 nm and 0.4–2.0 mg at λ_{max} 380 nm of an authentic sample of clorazepate dipotassium, the results in Table 1 were obtained.

The second procedure is colorimetric, and depends upon the determination of glycine in the aqueous layer left after the extraction of amino-chlorobenzophenone by reaction with ninhydrin in the presence of pyridine. The spectrum of the violet colour produced has two maxima at 560 nm and 395 nm (Fig. 2).

The experimental conditions for maximum colour development were optimized. The use of

Table 1. Determination of authentic samples of clorazepate dipotassium using the proposed procedures

	Spectrophotometric procedure (via 2-amino-5-chlorobenzophenone)						Colorimetric procedure (via glycine)		
	At 240 nm			At 380 nm			At 560 nm		
Exp. Mo.	Taken, *mg*	Found, *mg*	Recovery, %	Taken, *mg*	Found, *mg*	Recovery, %	Taken, *mg*	Found, *mg*	Recovery, %
1	0.08	0.804	100.5	0.4	0.402	100.5	0.3	0.299	99.7
2	0.16	0.159	99.5	0.6	0.599	99.8	0.45	0.452	100.4
3	0.24	0.239	99.6	0.8	0.798	99.8	0.6	0.597	99.6
4	0.32	0.322	100.5	1.0	0.993	99.3	0.75	0.755	100.7
5	0.40	0.40	100.0	1.4	1.414	101.0	1.05	1.047	99.7
6	0.48	0.482	100.4	1.6	1.61	100.6	1.2	1.195	99.6
7	0.56	0.558	99.6	2.0	2.005	100.3	1.5	1.487	99.1
	Mean		100.0			100.2			99.8
	C.V.		0.5%			0.6%			0.5%

Table 2. Determination of mixtures of authentic sample and acid degradation products by the proposed procedures and non-aqueous method[13]

Exp. No.	Authentic sample mg	Degradation products: N-Desmethyl diazepam, mg	Degradation products: 2-Amino-5-chloro-benzophenone mg	Degradation products: Glycine, mg	Spectrophotometric procedure: At 240 nm Recovery, %	Spectrophotometric procedure: At 380 nm Recovery, %	Colorimetric procedure recovery, %	Non-aqueous method (for bulk powder) recovery, %
1	20	0	0	0	100.5	100.5	100.0	99.9
2	20	40	20	20	100.3	101.1	98.5	191.7
3	30	35	20	15	99.8	100.8	101.6	180.0
4	40	40	17.5	17.5	99.9	99.8	99.8	134.0
5	50	25	12.5	12.5	100.2	99.7	98.1	119.0
6	60	20	10	10	100.0	100.7	99.6	113.6
7	70	15	7.5	7.5	100.4	101.4	99.4	110.8
8	80	10	5	5	100.0	99.6	101.2	105.0
	Mean				100.1	100.5	99.8	
	C.V.				0.2%	0.7%	1.2%	

1 ml of 5% ninhydrin and 1 ml of pyridine gave the highest colour intensity upon heating for 15–20 min on a boiling water bath. The citric acid–citrate buffer solution of pH 5 ± 0.2 proved to be a suitable medium for maximum colour formation, which is then stable for up to 1 hr.

A linear relationship was found between the concentration and the absorbance at 560 nm. On applying the proposed procedure to different concentrations (0.3–1.5 mg) of an authentic sample of clorazepate dipotassium, the results in Table 1 were obtained.

The blank used in the spectrophotometric procedure is methanol, because extraction with benzene–methylene chloride mixture before hydrolysis removes any degradation products, if present, except glycine. In the colorimetric procedure however, the blank used is prepared as for sample solution but without previous hydrolysis, because glycine is not extracted in the solvent mixture and remains in the aqueous layer.

To assess the stability-indicating efficiency of the proposed procedure, the degradation products, *N*-desmethyldiazepam, 2-amino-5-chlorobenzophenone and glycine, were mixed with the authentic sample of clorazepate dipotassium in different ratios and analysed by the proposed procedures. The results obtained are shown in Table 2. It is clear that the accuracy of the proposed procedure is not affected by the presence of 20–80% of these degradation products and the results are nearly the same as in Table 1.

Applying the proposed procedures to the analysis of tranxene capsules, the results obtained are shown in Table 3.

The validity of both procedures was assessed by applying the standard addition technique. The results are presented in Table 4.

It is obvious from the results shown in Table 1 that the suggested procedures can determine 0.08–0.56 mg and 0.4–2.0 mg of clorazepate

Table 3. Analysis of some pharmaceutical preparations of clorazepate dipotassium by the proposed procedures and a compendial method*

Preparations†	% Recovery: Spectrophotmetric procedure: At 240 nm	Spectrophotmetric procedure: At 380 nm	Colorimetric procedure	Compendial method*
Tranxene capsules, 5 mg/capsule	99.8	99.5	99.3	101.0
Tranexene capsules, 5 mg/capsule	99.9	99.7	99.2	99.1
Tranxene capsules, 5 mg/capsule	100.7	101.2	99.8	99.7
Treanxene capsules, 10 mg/capsule	100.5	99.7	99.6	99.3

*Spectrophotometric procedure. Carried out in 0.03% aqueous potassium carbonate; exhibits a maximum at 230 nm ($\epsilon = 35{,}000\ l \cdot mole^{-1} \cdot cm^{-1}$).[13]

†The three first samples were of different batch numbers.

Table 4. Accuracy of the recovery of standard additions of clorazepate dipotassium to some market preparations using the proposed procedures

Pharmaceutical preparations	Standard added, *mg*	% Recovery		
		Spectrophotometric procedure		Colorimetric procedure
		At 240 nm	At 380 nm	
Tranxene capsules, 5 mg/capsule	20	99.9	100.7	100.4
Batch No. 831489	30	100.2	99.7	99.6
	40	99.9	100.4	100.2
	Mean	100.0	100.3	100.1
	C.V.	0.2%	0.5%	0.4%
Tranxene capsules, 5 mg/capsule	20	100.1	100.3	100.0
Batch No. 861371	30	100.0	100.1	100.3
	40	100.0	100.5	99.8
	Mean	100.0	100.3	100.0
	C.V.	0.1%	0.2%	0.3%
Tranxene capsules, 5 mg/capsule	20	99.9	99.9	100.1
Batch No. 387	30	100.0	99.9	99.7
	40	99.6	100.2	100.6
	Mean	99.8	100.0	100.1
	C.V.	0.2%	0.2%	0.5%
Tranxene capsules, 10 mg/capsule	20	99.8	100.1	99.7
Batch No. 83053	30	100.0	99.7	99.8
	40	99.9	100.2	100.3
	Mean	99.9	100.0	99.9
	C.V.	0.1%	0.3%	0.3%

dipotassium with accuracies of $100.0 \pm 5\%$ and $100.2 \pm 0.6\%$ at λ_{max} 240 nm and 380 nm respectively by spectrophotometry and 0.3–1.5 mg with an accuracy of $99.8 \pm 0.5\%$ by the colorimetric method.

Comparing the results by the proposed procedure with those from the non-aqueous titration procedure for bulk powder,[13] it is evident that this latter procedure is not selective for the intact molecule, since it also determines the degradation products.

The most important advantage of the suggested method over other methods is that, with the exception of the HPLC method, it determines only the intact clorazepate dipotassium in the presence of its degradation products. Moreover, the method is inexpensive, rapid, sensitive and applicable over a convenient range of clorazepate dipotassium concentrations.

REFERENCES

1. M. A. Brooks, M. R. Hackman, R. E. Weinfeld and T. C. Macasieb, *J. Chromatog.*, 1977, **135**, 123.
2. D. J. Hoffman and A. H. C. Chun, *J. Pharm. Sci.*, 1975, **64**, 1668.
3. D. M. Hailey, *J. Chromatog.*, 1974, **98**, 527.
4. Aviala, J. P. Cano, J. P. Reynier and R. Rispe, *ibid.*, 1978, **147**, 349.
5. L. Elrod, Jr., D. M. Shada and V. E. Taylor, *J. Pharm. Sci.*, 1981, **70**, 793.
6. P. M. Kabra, G. L. Stevens and L. J. Marton, *J. Chromatog.*, 1978, **150**, 355.
7. R. J. Perchalski and B. J. Wilder, *Anal. Chem.*, 1978, **50**, 554.
8. J. Th. M. Groenwegen and P. J. P. de Meijer, *Pharm. Weekbl.*, 1980, **115**, 965.
9. R. W. T. Seitzinger. *Pharm. Weekbl.*, 1975, **110**, 1073.
10. J. Troschutz, *Arch. Pharm.*, 1981, **314**, 204.
11. W. F. Smyth and B. Leo, *Anal. Chim. Acta*, 1975, **76**, 289.
12. F. Welcher, *Chemical Solutions*, p. 65, Van Nostrand, New York, 1966.
13. K. Florey (Ed.), *Analytical Profiles of Drug Substances*, Vol.4, pp. 92–112. Academic Press, New York, 1975.

Talanta, Vol. 39, No. 12, pp. 1575–1577, 1992
Printed in Great Britain.

0039-9140/92 $5.00 + 0.00

SUBSTITUTIONAL COMPLEXOMETRIC DETERMINATION OF MAGNESIUM IN HOMOGENEOUS WATER–DIOXAN MEDIUM, BASED ON DECOMPOSITION OF MgEDTA WITH 8-QUINOLINOL AND TITRATION OF RELEASED EDTA WITH CALCIUM

ASSEN KAROLEV
Institue of Ferrous Metallurgy, Sofia 1870, Bulgaria

(*Received* 31 *July* 1989. *Revised* 5 *December* 1991. *Accepted* 15 *December* 1991)

Summary—A method based on a substitution reaction between MgEDTA and 8-quinolinol, and titration of the liberated EDTA with calcium is proposed. The reaction is performed in homogeneous 50–60% dioxan medium at pH 10, in which magnesium forms a soluble and stable 8-quinolinol complex.

Sinha and Roy[1] have proposed a complexometric determination of magnesium by selective conversion of the MgEDTA complex into the insoluble magnesium 8-quinolinolate, liberating an equivalent quantity of EDTA. The mixture is first titrated with EDTA to determine the sum of the two metal ions, then heated to 50–60° after addition of excess of 8-quinolinol and a known amount of calcium chloride. The calcium and magnesium 8-quinolinolate complexes are formed. The calcium precipitate is dissolved with excess of EDTA, the surplus of which is then titrated with a standard calcium solution.

In a second paper[2] these authors reported that the method was improved by extraction of the magnesium 8-quinolinolate into chloroform. Calcium remained in the aqueous solution as CaEDTA and the EDTA liberated from MgEDTA was titrated in the aqueous solution with calcium.

From a practical point of view, it would be better to perform the second titration in homogeneous medium, such as a 50–60% dioxan solution in water, in which the magnesium 8-quinolinolate complex is stable and soluble. Calcium can also form an 8-quinolinolate complex but this is less stable than the EDTA complex and is not produced under the conditions used. A preliminary evaluation of the equilibrium constant for the susbstitution reaction

$$MgY^{2-} + 2Ox^{-} + Ca^{2+} = CaY^{2-} + Mg(Ox)_2 \quad (1)$$

is necessary (Ox^{-} represents the 8-quinolinolate anion). Under the back-titration conditions (pH = 10 and considerable excess of 8-quinolinol), the conditional equilibrium constant is:

$$K'_{eq} = \frac{[CaY][Mg[Ox]_2]}{[MgY][Ca']^2[Ox']^2} = \frac{\beta_{CaY}\beta_{Mg(Ox)_2}}{\beta_{MgY}\alpha_{Ca(Ox)}\alpha^2_{Ox(H)}} = \frac{10^{10.7} \times 10^{11}}{10^{8.7} \times 255 \times 32.6^2} = 3.7 \times 10^7 \quad (2)$$

where primes indicate conditional quantities[3] and charges are omitted for simplicity.

The CaEDTA and MgEDTA stability constants (for aqueous solution, ionic strength 0.1) are taken from Ringbom.[3] It is assumed that they both change to the same extent in the water–dioxan medium. The stability constants for the magnesium 8-quinolinolate and the protonation constants for EDTA and 8-quinolinol in 60% dioxan medium are taken from Perrin.[4] The value of $\alpha_{Ca(Ox)}$ is calculated for a typical $0.05M$ initial concentration of 8-quinolinol (C_{Ox}) and $0.001M$ initial concentration of magnesium (C_{Mg}) in the solution obtained after the EDTA titration of Mg + Ca and addition of dioxan and 8-quinolinol:

$$\alpha_{Ox(H)} = 1 + \beta^H_1[H] + \beta^H_2[H]^2 = 1 + 10^{11.5} \times 10^{-10} + 10^{15.5} \times 10^{-20} = 32.6 \quad (3)$$

$$\alpha_{Ca(Ox)} = 1 + \beta_{Ca(Ox)}[Ox] + \beta_{Ca(Ox)_2}[Ox]^2 \quad (4)$$

and since at the equivalence point of the back-titration

$$[Ox] = \frac{[Ox']}{\alpha_{Ox(H)}} \approx \frac{C_{Ox} - 2C_{Mg}}{\alpha_{Ox(H)}} \quad (5)$$

$\alpha_{Ca(Ox)}$ is given by

$$\alpha_{Ca(Ox)} = 1 + \frac{10^{4.4} \times 4.8 \times 10^{-2}}{32.6} + \frac{10^{8.0} \times (4.8 \times 10^{-2})^2}{32.6^2} = 255 \quad (6)$$

Although the value of the conditional equilibrium constant (K'_{eq}) is large, it is smaller than that corresponding to 99.9% completion of the substitution reaction ($K'_{99.9}$) at the equivalence point for a titration involving 0.001*M* concentrations of calcium and magnesium:

$$K'_{99.9} \sim \frac{(C_{Ca} + C_{Mg}) \times C_{Mg}}{0.001C_{Mg} \times 0.001(C_{ca} + C_{Mg}) \times (C_{Ox} - 2C_{Mg})^2}$$

$$= \frac{2 \times 0.001 \times 0.001}{0.001 \times 0.001 \times 0.001(0.001 + 0.001) \times (0.050 - 0.002)^2}$$

$$= 4.3 \times 10^8 \quad (5)$$

The theoretical value of [Ca'] (which would be nearly equal to [MgY]) at the equivalence point of the back-titration is calculated by use of the equation:

$$K'_{eq} = \frac{[CaY][Mg(Ox)]}{[MgY][Ca'][Ox']^2} = \frac{(C_{Ca} + C_{Mg} - [Ca'])(C_{Mg} - [Ca'])}{[Ca']^2(C_{Ox} - 2C_{Mg})^2}$$

$$= 3.7 \times 10^7 \quad (6)$$

Hence

$$3.7 \times 10^7(C_{Ox} - 2C_{Mg})^2[Ca']^2 = C_{Ca}C_{Mg} + C_{Mg}^2 - 2C_{Mg}[Ca'] - C_{Ca}[Ca'] + [Ca']^2 \quad (7)$$

Since $[Ca']^2 \ll 3.7 \times 10^7(C_{Ox} - 2C_{Mg})[Ca']^2$ it can be neglected. Then

$$3.7 \times 10^7(0.050 - 0.002)^2[Ca']^2 + 0.003[Ca'] - 2 \times 10^{-6} = 0 \quad (8)$$

and the calculated

$$[Ca'] \approx [MgY] = 0.5 \times 10^{-5}M.$$

Consequently the concentration of unchanged MgEDTA is only $100 \times 0.6 \times 10^{-5}/10^{-3} = 0.5\%$ of the initial MgEDTA concentration, and substitution reaction (1) is 99.5% complete.

If the initial molar concentration of the calcium is ten times that of the magnesium the substitution reaction will be less complete (99.0%), but for determination of relatively low concentrations of magnesium this is acceptable. A similar calculation for $10^{-3}M$ calcium and magnesium but only 0.025*M* 8-quinolinol shows that the reaction would be 99.5% complete, indicating that the 8-quinolinol concentration is not critical provided it does not exceed about 0.05*M*.

EXPERIMENTAL

Reagents

Titrants. Standardized 0.025*M* Na_2EDTA and calcium chloride solutions.

Buffer solution, pH 10. Dissolve 70 g of ammonium chloride in about 300 ml of water, mix the solution with 570 ml of concentrated ammonia solution (s.g. 0.880) and dilute to 1 litre with water.

8-Quinolinol. A 0.25*M* solution in 1,4-dioxan.

Methylthymol Blue indicator. A 1% solid mixture with potassium nitrate.

Procedure

To a nearly neutral solution containing calcium and up to 6–7 mg of magnesium, add 10 ml of buffer and about 100 mg of indicator mixture, and titrate with EDTA until the colour changes from blue to pale grey. This titration gives the sum of the calcium and magnesium. Add a slightly greater volume of dioxan than that of the titrated solution, and 5–20 ml of the 8-quinolinol solution, depending on the magnesium content expected. Add another portion of indicator and titrate with standard calcium solution until the colour changes to greenish yellow. The amount of calcium consumed is equivalent to the magnesium content.

Table 1. Complexometric determination of magnesium and calcium in synthetic solutions

Mg added, *mg*	Ca added, *mg*	Mg found,* *mg*	Ca found,* *mg*
1.00	1.00	1.03 ± 0.02	1.02 ± 0.04
1.00	10.00	0.97 ± 0.03	10.08 ± 0.04
1.00	30.00	0.96 ± 0.03	30.15 ± 0.06
5.00	10.00	4.97 ± 0.04	10.05 ± 0.06
5.00	30.00	5.06 ± 0.05	29.88 ± 0.08

*Mean ± standard deviation of 6 replicates.

Table 2. Magnesium and calcium determination in standard samples*

Sample	Certified values % MgO	Certified values % CaO	MgO found,* %	CaO found,† %
SOD 116-83 VR8 limestone	0.56	54.98	0.58	55.1
S 2 USSR slag	2.71	44.2	2.62	44.0
SM 3 DDR slag	7.73	45.43	7.61	45.3
AN DDR calcium sulphate	0.32	40.73	0.31	40.8

*Ca and Mg in the slags were determined after preliminary separation of Fe, Al and Mn by hydroxide precipitation. The Fe, Al and Mn content in the limestone and calcium sulphate being very low, the calcium and magnesium titrations were performed in the presence of the hydroxide precipitates.

†Mean of 3 replicates.

RESULTS AND DISCUSSION

Typical results for analysis of mixtures of standard magnesium and calcium solutions are shown in Table 1, and those for analysis of some standard samples are shown in Table 2.

The amount of 8-quinolinol to be added is not critical, but the concentration in the final solution should not exceed 0.05*M*, and the quantity added must provide an adequate excess relative to the amount of magnesium present.

The procedure given will provide a back-titration of about 10 ml of 0.025*M* calcium solution for 6 mg of magnesium, and for smaller amounts of magnesium better precision can be obtained by use of 0.01*M* calcium solution, but lower concentrations than this should not be used, as the end-point is then difficult to detect.

Methylthymol Blue is preferred as the indicator, since it gives a sharper end-point than other indicators do. At pH 10, pCa_{trans} ($=\log \beta'_{CaInd}$) is 5.5 for Methylthymol Blue, 4.0 for murexide and 4.5 for Metalphthalein.[5] It is convenient to make a glass scoop to hold 100–120 mg of the solid indicator.

The method has good reproducibility and accuracy and is especially suitable for samples containing much more calcium than magnesium. If desired, photometric detection of the end point can be used (at $\lambda = 610$ nm).

REFERENCES

1. B. C. Sinha and S. K. Roy, *Analyst*, 1980, **105**, 720.
2. *Idem, ibid.*, 1982, **107**, 965.
3. A. Ringbom, *Complexation in Analytical Chemistry*, Interscience, New York, 1963.
4. D. D. Perrin, *Stability Constants of Metal-ion Complexes* Part B, *Organic Ligands*, Pergamon Press, Oxford, 1979.
5. E. Bishop, *Indicators*, Pergamon Press, Oxford, 1972.

Talanta, Vol. 39, No. 12, pp. 1579–1582, 1992
Printed in Great Britain.

0039-9140/92 $5.00 + 0.00

SPECTROPHOTOMETRIC DETERMINATION OF CHROMIUM(III, VI) BY USE OF CHROMIUM(III, VI)–CHROME AZUROLS–CETYLPYRIDINIUM BROMIDE–HYDROXYLAMINE HYDROCHLORIDE–ZINC(II) SYSTEM

FANG GUOZHEN and LUO JIKUEN

Department of Chemistry, Sichuan University, Chengdu, Sichuan, 610064, People's Republic of China

(*Received* 9 *November* 1989. *Revised* 9 *November* 1991. *Accepted* 27 *December* 1991)

Summary—This paper shows that the sensitivity of the Cr(III, VI)–Chrome Azurol S (CAS)–cetylpyridinium bromide (CPB)–hydroxylamine hydrochloride system can be increased and the wavelength of maximum absorption slightly shifted by addition of zinc(II) and that the analytical data are practically identical for both Cr(III) and Cr(VI), indicating that under the conditions used both initial oxidation states of chromium yield the same final oxidation state, Cr(III). On the basis of the Cr(III, VI)–CAS–CPB–$NH_2OH \cdot HCl$–Zn systems a new, highly sensitive and selective method for spectrophotometric determination of microamounts of Cr(III, VI) has been developed, with molar absorptivity of 1.27×10^5 l. mole^{-1}. cm^{-1} for the complex at 620 nm and linear calibration up to 0.4 μg/ml chromium. Various foreign ions do not interfere. The method can be applied to direct determination of chromium in steels.

Existing spectrophotometric methods for determining chromium(III) are not very sensitive ($\epsilon < 10^5$ l. mole^{-1}. cm^{-1}.[1] The sensitivity of the Cr(III)–Chrome Azurol S (CAS) system may be increased by addition of cetyltrimethylammonium bromide (CTMAB)[2] or cetylpyridinium bromide (CPB).[3] The purpose of this paper is to explore another path for increasing the sensitivity of determination of chromium. One such possibility is by formation of mixed-metal complexes, as shown for the chromium–Eriochrome Cyanine R–manganese system,[4] the lanthanide–Bromopyrogallol Red–yttrium system[5–8] and the scandium–Arsenazo III–molybdenum system.[9]

Horiuchi and Nishida[10] have developed a spectrophotometric method for zinc with CAS and zephiramine. We have found that (*a*) the sensitivity of the spectrophotometric determination of Cr(VI) by means of the Cr(VI)–CAS–CPB system can be increased by adding $NH_2OH \cdot HCl$; (*b*) the sensitivity of the Zn–CAS–CPB–$NH_2OH \cdot HCl$ system at pH 5.7 is very low ($\epsilon = 37.1$ l. mole^{-1}. cm^{-1} at 500 nm, and 5.5 at 620 nm), but the Zn–Cr(III, VI)–CAS–CPB–$NH_2OH \cdot HCl$ system ($\epsilon = 1.27 \times 10^5$ at 620 mm) is much more sensitive than the Cr(III, VI)–CAS–CPB–$NH_2OH \cdot HCl$ system ($\epsilon = 5.6 \times 10^4$ at 620 nm); (*c*) with the Zn/Cr mixed-metal system the absorption spectra, calibration graphs and complex compositions obtained with Cr(III) and Cr(VI) are nearly identical, so the same procedure may be used for determination of either Cr(III) or Cr(VI) alone or of total chromium(III, VI) without prior oxidation or reduction treatment.

The proposed method is a new, highly sensitive and selective procedure for determination of chromium.

EXPERIMENTAL

Apparatus

Absorbance measurements were made with a type 72 photoelectric spectrophotometer (made in China) suitable for measuring absorbance at wavelengths from 420 to 700 nm. Absorption spectra were obtained with a Shimadzu UV-240 recording spectrophotometer.

Reagents

All reagents were of analytical grade unless specified otherwise, and demineralized water was used throughout.

Chromium(III) standard solution, 2 μg/ml. Dissolve 0.5000 g of chromium metal (purity 99.99%) in 20 ml of concentrated hydrochloric acid and a small quantity of water (with warming) and cool. Transfer the solution to a

500-ml standard flask, make up to the mark with water, and mix well.

Chromium(VI) standard solution, 2 μg/ml. Dissolve 0.2830 g of $K_2Cr_2O_7$ (previously dried at 140°) in water, and dilute the solution with water to volume in a 1-litre standard flask and mix well. Dilute 5.00 ml of this solution to 500 ml.

Chrome Azurol S (CAS) solution, $3.2 \times 10^{-3}M$.

Cetylpyridinium bromide (CPB) solution, $5.0 \times 10^{-3}M$. Dissolve 0.96 g of CPB in 500 ml of hot water and cool.

Hydroxylamine hydrochloride solution, 50 mg/ml.

Disodium ethylenediaminetetra-acetate (Na_2 EDTA) solution, 20 mg/ml.

Zinc(II) solution, 10 mg/ml. Dissolve 11.04 g of $ZnSO_4 \cdot 7H_2O$ in 250 ml of water containing 1 ml of $0.25M$ sulphuric acid.

Iron(III) solution, 1 mg/ml Fe(III). Dissolve 4.32 g of $NH_4Fe(SO_4)_2 \cdot 12\ H_2O$ in 500 ml of water slightly acidified with sulphuric acid.

Acetic acid–sodium acetate buffer, pH 5.7. Dissolve 109 g of $CH_3COONa \cdot 3H_2O$ in 500 ml of water containing 5.65 ml of glacial acetic acid and mix.

Saturated aqueous 2,4-dinitrophenol solution.

Calibration

(*i*) Pure solution: transfer known volumes of standard solution containing up to 10 μg of chromium(III or VI) to 25-ml standard flasks [if chromium(III) is used add 1 drop of 2,4-dinitrophenol solution and adjust the colour of the solution to slightly yellow with $0.5M$ sodium hydroxide to make the solution nearly neutral]. To each flask add 1.5 ml of pH 5.7 buffer, 1.4 ml of CAS solution, 2.0 ml of CPB solution, 1.5 ml of Zn(II) solution and 1.5 ml of $NH_2OH \cdot HCl$ solution and mix well. Heat the flasks in a gently boiling water-bath for 20 min, then cool them rapidly to room temperature. Dilute each solution to the mark with water. Measure the absorbance in a 1-cm cell at 620 nm against a reagent blank containing 15 mg of Zn(II).

(*ii*) Steel analysis: proceed as described above, but in addition to each portion of chromium(III or VI) standard solution add 1 ml of 1 mg/ml Fe(III) solution.

Analysis of steel samples

Dissolve an appropriate amount of sample in warm $3M$ hydrochloric acid, decompose any carbides by addition of the minimum of concentrated nitric acid needed, boil off nitrous fumes, cool, filter if necessary and dilute to volume in a suitable size of standard flask. Transfer a known volume of this solution, containing up to 10 μg of chromium, to a 25-ml standard flask. Add 1 drop of 2,4-dinitrophenol solution, then $0.5M$ sodium hydroxide until the solution is slightly yellow. Add 1.5 ml of hydroxylamine hydrochloride solution, swirl for 1 min, add 1.5 ml of pH-5.7 buffer, 1.4 ml of CAS solution, 2.0 ml of CPB solution and 1.5 ml of Zn(II) solution. Heat the flask in a boiling water-bath for 20 min, then add 5.5 ml of EDTA solution. Shake the solution for 1 min, allow to stand for 4 min, then cool it rapidly. Dilute the solution to the mark with water and mix. Measure the absorbance at 620 nm in a 1-cm cell against a reagent blank containing 1 mg of Fe(III) and 15 mg of Zn(II).

RESULTS AND DISCUSSION

Preliminary experiments

Qualitative tests showed that a large amount of Mn(II), As(V) or Zn(II) gives a weak colour reaction with CAS, CPB and $NH_2OH \cdot HCl$ in the absence of chromium(III or VI), but the colour intensity of the Cr(III or VI)–CAS–CPB–$NH_2OH \cdot HCl$ system is increased by addition of Zn(II).

The wavelengths of maximum absorption of the Zn(II)–CAS–CPB–$NH_2OH \cdot HCl$, Cr(III or VI)–CAS–CPB–$NH_2OH \cdot HCl$ and Cr(III or VI)–Zn(II)–CAS–CPB–$NH_2OH \cdot HCl$ systems are 500, 610 and 620 nm, respectively (Fig. 1). The sensitivity of the Cr(III or VI)–CAS–CPB–$NH_2OH \cdot HCl$ colour reaction is increased by a factor of *ca.* 2 by the presence of Zn(II). For this combined system, however, the total absorbance is not equal to the sum of the individual Cr–CAS–CPB and Zn–CAS–CPB absorbances, when the reference solution is a reagent blank that does not contain zinc (Fig. 1, curves 2–6), but when the reference solution is a reagent blank containing the same amount of zinc as is present in the test solutions, the total absorbance is increased by an amount equal to the difference between the absorbance of the reagent blank (Fig. 1, curve 1) and the Zn–CAS–CPB absorbance (Fig. 1, curve 2). In addition to this, the absorption spectrum obtained is practically the same, irrespective of the initial oxidation state of the chromium.

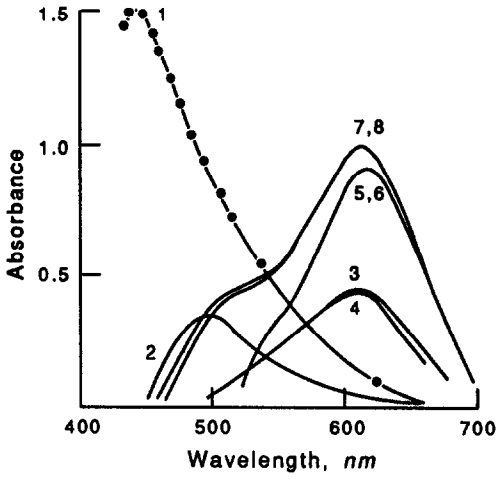

Fig. 1. Absorption spectra: (1) reagent blank (buffer, CAS, CPB, $NH_2OH \cdot HCl$) *vs.* water; (2) Zn(II) + reagent blank *vs.* reagent blank; (3) Cr(III) + reagent blank *vs.* reagent blank; (4) Cr(VI) + reagent blank *vs.* reagent blank; (5) Cr(III) + Zn(II) + reagent blank *vs.* reagent blank; (6) Cr(VI) + Zn(II) + reagent blank *vs.* reagent blank; (7) Cr(III) + Zn(II) + reagent blank *vs.* Zn(II) + reagent blank; (8) Cr(VI) + Zn(II) + reagent blank *vs.* Zn(II) + reagent blank. Conditions: Zn(II) 15 mg; Cr(III) 10.6 μg; Cr(VI) 10.0 μg; pH 5.7 buffer 1.5 ml; 3.2×10^{-3} *M* CAS 1.4 ml; 5×10^{-3} *M* CPB 1.5 ml; $NH_2OH \cdot HCl$ 75 mg; total volume 25 ml; 1-cm cells.

These facts indicate that a mixed-metal Cr(III)–CAS–CPB–Zn(II) complex is formed, and that the excess of CAS is all bound in a Zn(II)–CAS–CPB complex. The zinc added therefore performs two functions, increasing the sensitivity by (a) forming a chromium complex having a higher molar absorptivity than the simpler Cr–CAS–CPB complex, and (b) reducing the absorbance of the reagent blank by complexing with the excess of CAS. The role of the hydroxylamine appears to be solely the reduction of Cr(VI) to Cr(III).

Choice of conditions

Zinc concentration. Figure 2 shows that a large amount of zinc is needed, indicating that

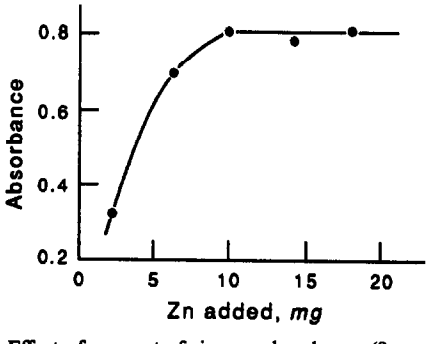

Fig. 2. Effect of amount of zinc on absorbance (8 μg of Cr).

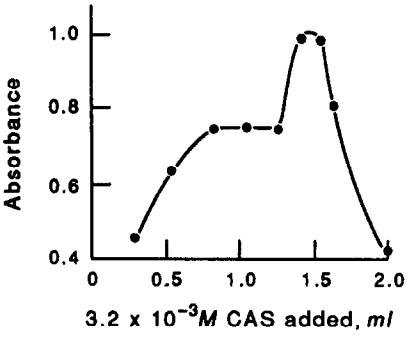

Fig. 3. Effect of CAS concentration on absorbance (10.6 μg of Cr).

the mixed-metal complex is not very much more stable than the parent chromium complex.

CAS and CPB concentrations. Figures 3 and 4 show the effect of the concentration of these two reagents. The optimum range is 1.4–1.5 ml of $3.2 \times 10^{-3}M$ CAS and 1.5–4.0 ml of $5 \times 10^{-3}M$ CPB per 25 ml of final solution. The apparent irregularity with lower amounts of CPB is presumably associated with the critical micelle concentration of this surfactant.

$NH_2OH \cdot HCl$ concentration. This was found not to be critical in the range 1.5–2.5 ml of 50-mg/ml solution per 25 ml of final solution.

Buffer solution. Maximal absorbance is obtained with 1.0–1.5 ml of buffer solution per 25 ml; larger amounts of buffer give lower absorbance, presumably because of competitive side-reactions with chromium(III).

Heating time. Maximal absorbance is obtained with heating times of 20–30 min at 100°.

Characteristics of the complex

The composition of the mixed-metal complex cannot be determined by the usual spectrophotometric methods, because of the nature of the system and the large excess of zinc necessary.

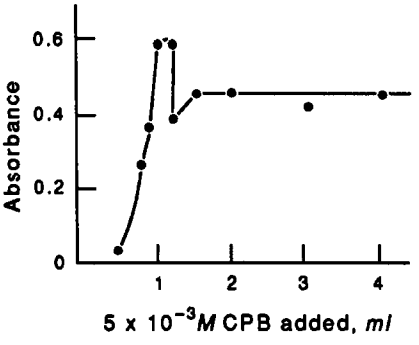

Fig. 4. Effect of CPB concentration on absorbance (5 μg of Cr).

Table 1. Determination of total chromium in some synthetic solutions

Cr(III)/Cr(VI) mole ratio	Total Cr taken, μg/25ml	Total Cr found,* μg/25ml
1:4	10.0	9.9 ± 0.1
1:1	10.0	10.0 ± 0.2
4:1	10.0	9.8 ± 0.2

*Mean ± standard deviation of 5 replicates

Table 2. Determination of chromium in some standard alloy steels

Samples	Certified value, %	Cr found,*
Chromium–silicon steel	1.38	1.43 ± 0.05
Low alloy steel	1.00	0.96 ± 0.04
Chromium–vanadium steel	0.77	0.76 ± 0.22

*Mean ± standard deviation of 6 replicates.

Once formed, the complex has constant absorbances for at least 2-hr.

Effect of foreign ions

The limiting concentration of foreign ions was taken as that concentration which caused an error of not more than 5%. In 25 ml of final solution the presence of at least 1 mg of Mn(II) and V(V), 0.8 mg of As(V), 0.5 mg of Ni(II), 0.4 mg of W(VI), 0.33 mg of Mo(VI) and 0.1 mg of Sn(IV) caused no interference. Addition of an appropriate amount of EDTA as masking agent after development of the colour allows up to 1 mg of Fe(III), 0.3 mg of Al(III) and Co(II) and 0.1 mg of Pb(II) to be tolerated.

Precision and accuracy

The method has been satisfactorily used to analyse synthetic solutions containing various ratios of chromium(III) and chromium(VI), and several alloy steels, with the results shown in Tables 1 and 2.

REFERENCES

1. G. Fang and C. Miao, *Analyst*, 1985, **110**, 65.
2. G. Fang and J. Luo, *Huaxue Shiji*, 1985, **7**, 362.
3. *Idem*, *Fenxi Huaxue*, 1985, **13**, 769.
4. D. Xia, *ibid.*, 1981, **9**, 196.
5. H. Shen and G. Xu, *ibid.*, 1981, **9**, 17.
6. *Idem*, *ibid.*, 1981, **9**, 441.
7. H. Shen and Z. Wang, *ibid.*, 1981, **9**, 711.
8. H. Shen, Z. Liu and Z. Wang, *ibid.*, 1982, **10**, 324.
9. P. K. Spitsyn, *Zavodsk. Lab.*, 1980, **46**, 582.
10. Y. Horiuchi and H. Nishida, *Bunseki Kagaku*, 1968, **17**, 756.

Talanta, Vol. 39, No. 12, pp. 1583–1586, 1992
Printed in Great Britain.

0039-9140/92 $5.00 + 0.00

PHASE COMPOSITION ANALYSIS OF HYDROUS ALUMINIUM OXIDES BY THERMAL ANALYSIS AND INFRARED SPECTROMETRY

Zs. WITTMANN, E. KÁNTOR, K. BÉLAFI, L. PÉTERFY and L. P. FARKAS
Hungarian Oil and Gas Research Institute, József A. u. 34, H-8200 Veszprém, Hungary

(*Received* 22 *December* 1989. *Revised* 18 *February* 1992. *Accepted* 26 *February* 1992)

Summary—A general method for determination of the phase composition of hydrous aluminium oxides by thermal analysis and infrared spectrometry, and determination of the transformation temperature of mixtures of $Al(OH)_3$ and AlOOH into α-Al_2O_3 are described.

Six methods are available for production of high-purity alumina (purer than 99.9%): thermal cracking of ammonium alum; hydrolysis of organometallic compounds; the ethylene chlorohydrin process; thermal cracking of ammonium aluminium carbonate; the spark discharge process and the so-called modified Bayer process.[1] The properties of high-purity alumina depend on the different oxide phases obtained during calcination, and the crystal structure of these oxides depends on the mode of dehydration of the original hydrous aluminium oxide.

The transformation of different $Al(OH)_3$ and AlOOH samples into Al_2O_3 is shown in Fig. 1.[2–4] Bayerite, nordstrandite and pseudoamorphous aluminium hydroxide transform into α-Al_2O_3 through η- and θ-Al_2O_3. α-Al_2O_3 can be formed through χ- and κ-Al_2O_3 from gibbsite. The H_2O/Al_2O_3 mole ratios are 3 in gibbsite, bayerite, the rare nordstrandite and pseudoamorphous aluminium hydroxide. The hydrous aluminium oxides begin to lose water at about 200° and the loss is complete by about 500°. The different modifications of Al_2O_3 are produced at temperatures up to 1000–1200°, but at above 1200° there is only α-Al_2O_3.

The forms of AlOOH are boehmite and the rarely occurring diaspore. Boehmite transforms into α-Al_2O_3 through γ-, δ- θ-Al_2O_3, and diaspore is converted directly into α-Al_2O_3. The H_2O/Al_2O_3 mole ratios are 1 in both boehmite and diaspore. The loss of water from both is completed over the temperature range 380–550°.

The phase composition of a hydrous aluminium oxide can be determined by means of thermal analysis. In this paper a phase-composition analysis and the determination of the transformation temperature of the hydrolysis product of an organoaluminium into α-Al_2O_3 are described.

EXPERIMENTAL

A Derivatograph (5°/min heating rate, maximum temperature 1500°) was used. The DTA/DTG sensitivity ratio was 1:3. (500 mg) were placed in covered platinum cups and an air atmosphere was used throughout.

DTA and DTG curves for $Al(OH)_3$ (bayerite, gibbsite) and AlOOH (boehmite) were recorded and used for qualitative and quantitative analysis of the phase composition (Fig. 2).

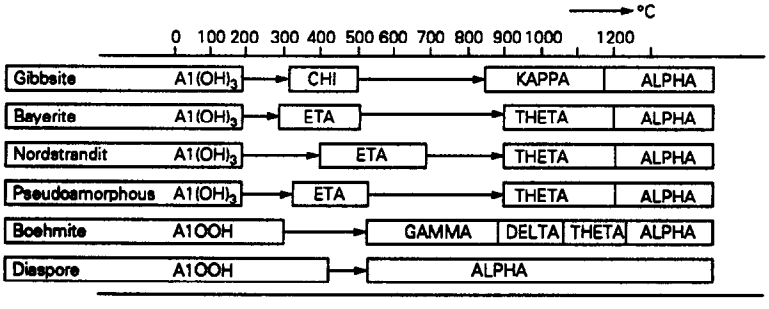

Fig. 1. Dehydration sequence of alumina hydrates (from Refs. 2–5).

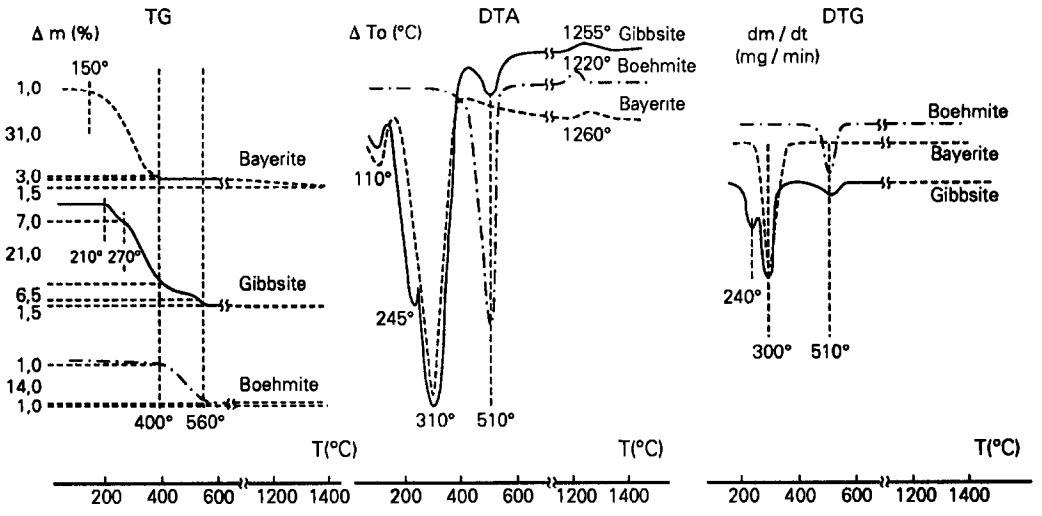

Fig. 2. Thermoanalytical curves of bayerite, gibbsite and boehmite.

The decomposition of bayerite is almost complete at 390°, with a peak temperature of 300°. There is 31% weight loss over the temperature range 150–390°, a further 3% at 390–560° and a final 1.5% at >560°. The dehydration of gibbsite proceeds in two major steps with 28% weight loss at 150–390° and 6.5% at 390–560°, and a final 1.5% at >560°. Boehmite loses 1% in weight up to 390° and a further 14% in the range 390–560°. These results (the averages of three replicate measurements) are in good agreement with the literature values.[5–8]

Water is evolved from $Al(OH)_3$ and AlOOH over two different temperature intervals, 150–390° and 390–560°.

The qualitative composition of a mixture of $Al(OH)_3$ and AlOOH can be determined on the basis of the weight losses over particular temperature intervals. A mixture of boehmite with either gibbsite or bayerite can be quantitatively analysed from the weight losses (Δm), as follows:

$$\begin{cases} \text{Bayerite} \quad (\%, \text{w/w}) = 100\ \Delta m \text{ (at 150–390°)}/31 \\ \text{Boehmite} \quad (\%, \text{w/w}) = 100\ [\Delta m \text{ (at 390–560°)} - 0.03 \times \%\ \text{bayerite}]/15 \end{cases}$$

$$\begin{cases} \text{Gibbsite} \quad (\%, \text{w/w}) = 100\ \Delta m \text{ (at 150–390°)}/28 \\ \text{Boehmite} \quad (\%, \text{w/w}) = 100\ [\Delta m \text{ (at 390–560°)} - 0.065 \times \%\ \text{gibbsite}]/15 \end{cases}$$

The thermoanalytical curves (Fig. 2) show the transformation temperatures into α-Al_2O_3 to be 1255° for gibbsite, 1220° for boehmite and 1260° for bayerite.

Table 1 gives the results obtained for various mixtures of bayerite, gibbsite and boehmite. The detection limits were examined with a mixture of known amounts of boehmite, bayerite and gibbsite and found to be 2%.

Table 1. Thermoanalytical analysis of bayerite, gibbsite and boehmite mixtures

Taken, % w/w			Found, % w/w		
Bayerite	Gibbsite	Boehmite	Bayerite	Gibbsite	Boehmite
90.0	—	10.0	90.3	—	9.3
10.0	—	90.0	9.5	—	91.4
50.0	—	50.0	50.3	—	50.0
—	30.0	70.0	—	31.3	68.5
20.0	40.0	40.0	20.5	40.9	38.7

The reproducibility obtained with two instruments was ±5% relative, and the repeatability for the same instrument and operator was ±3% relative.

The samples were also analysed by infrared spectrometry. The spectra of $Al(OH)_3$ (bayerite, gibbsite) and AlOOH (boehmite) are shown in Figs. 3 and 4 and the characteristic vibration bands are given in Table 2.

CONCLUSIONS

The thermoanalytical data for some samples are shown in Table 3 and the thermoanalytical curves of two different samples in Fig. 5. Moisture and any organic residues in the samples

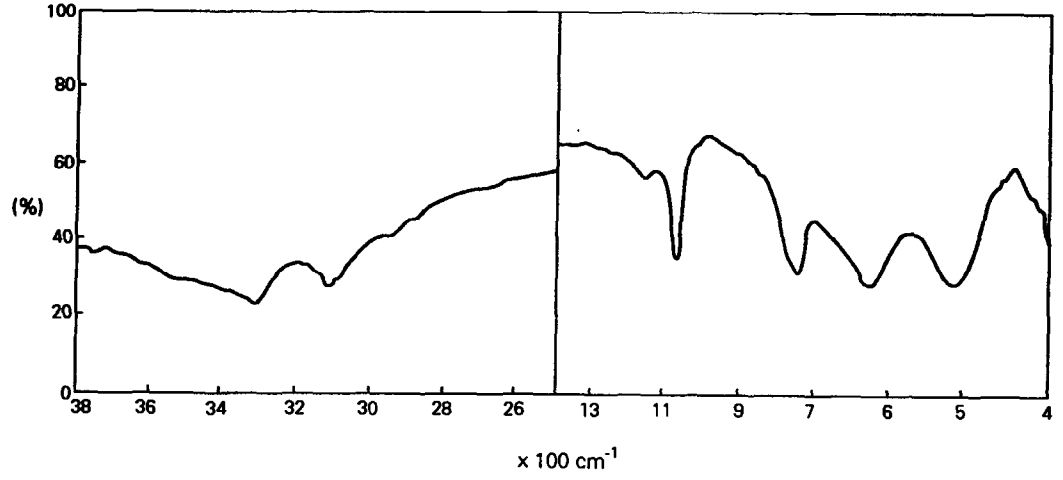

Fig. 3. Infrared spectrum of AlOOH.

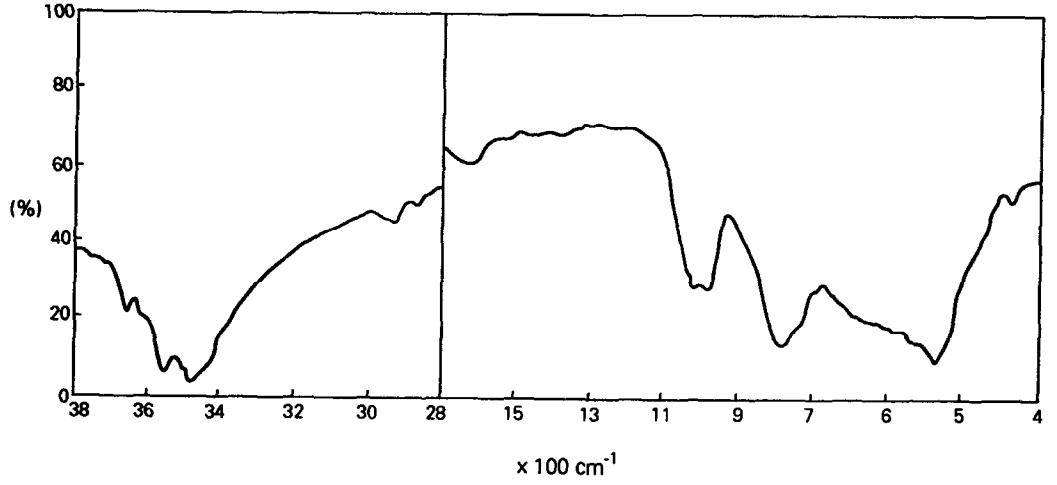

Fig. 4. Infrared spectrum of $Al(OH)_3$.

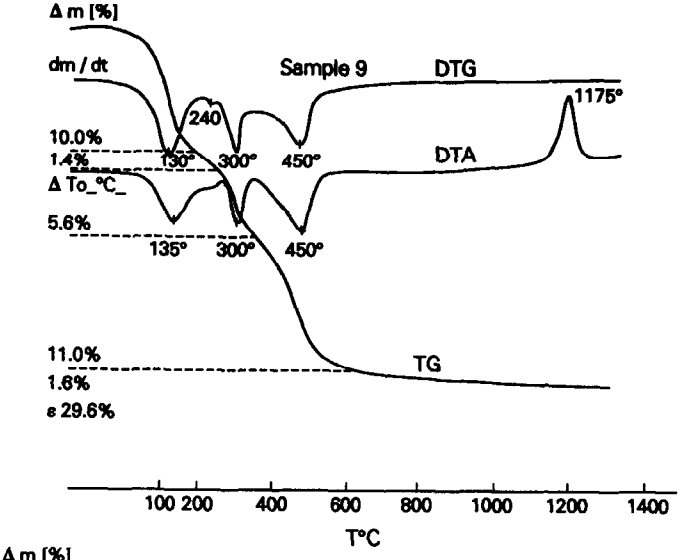

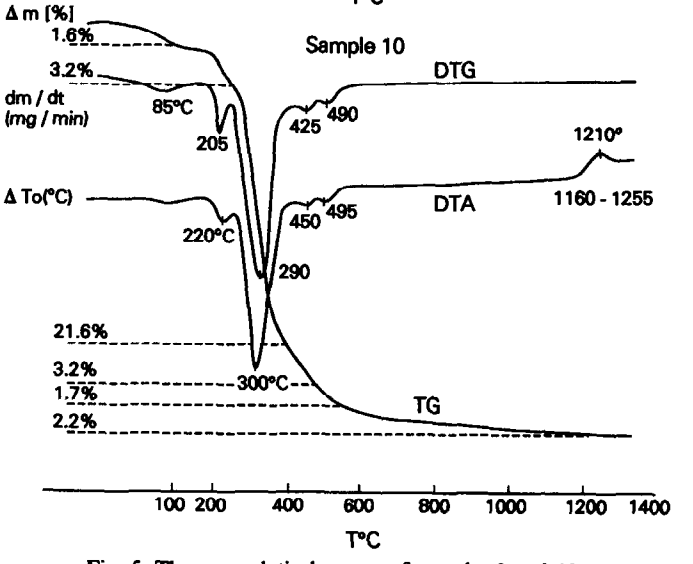

Fig. 5. Thermoanalytical curves of samples 9 and 10.

Table 2. Characteristic vibration bands (cm^{-1}) of AlOOH and $Al(OH)_3$

Vibrations	AlOOH	$Al(OH)_3$
Vibrational bands of AlO_6 octahedra	500, 630, 740	520, 770
OH deformation vibration	1160	980, 1020
OH stretching vibration	3100, 3300	3440, 3560, 3670

Table 3. Thermoanalytical and infrared results for aluminium hydrate samples

Sample	Moisture and organics	Thermoanalysis, % w/w		Infrared	
		$Al(OH)_3$	AlOOH	$Al(OH)_3$	AlOOH
1	4.0	71	25	+++	+
2	3.5	55	40	++	++
3	3.0	64	32	+++	++
4	3.0	76	21	+++	–
5	3.5	75	21	+++	–
6	8.0	43	48	++	++
7	3.0	50	48	++	++
8	10.0	23	67	+	+++
9	10.0	21	69	+	+++
10	1.6	89	9	+++	–

were lost at 120–130°. In the temperature interval 150–390° there are two dehydration steps, at 210–270° and 270–380°, characteristic of gibbsite. The amount of $Al(OH)_3$ can be calculated from the weight losses in both temperature intervals. In the temperature interval 390–560° boehmite is dehydrated.

The temperatures of transformation into α-Al_2O_3 depend on the proportions of $Al(OH)_3$ and AlOOH in the samples, and are shown in Fig. 6 as a function of the composition. The transformation temperature into α-Al_2O_3 seems to be $1170 \pm 5°$ over a very wide range of composition: 20–80% w/w $Al(OH)_3$ or AlOOH containing hydrated alumina. In the presence of about 10% w/w $Al(OH)_3$ or AlOOH the

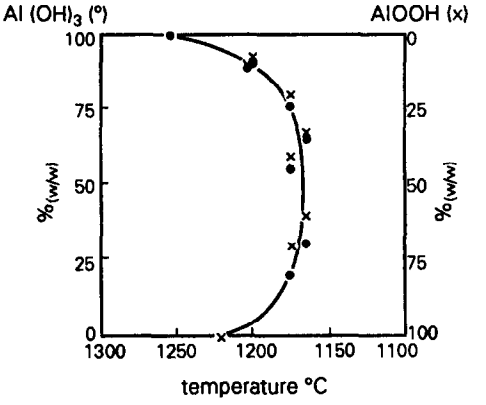

Fig. 6. Transformation temperature into α-Al_2O_3 from different $Al(OH)_3$ and AlOOH mixtures.

transformation temperature of the mixture is about 40° lower than that of the main component.

Only a semiquantitative estimation can be achieved on the basis of the infrared spectra. In Table 3 +++ indicates >60% w/w of a component, ++ about 40–50% w/w and + <25% w/w. The estimates found are in agreement with the results of the thermoanalytical measurements.

REFERENCES

1. T. Hashimoto, K. Nakano and M. Hama, *Chem. Econ. Eng. Rev.*, 1985, **17**, 3, 38
2. E. Dörre and H. Hübner, *Alumina, Processing, Properties, and Applications*, Springer-Verlag, Berlin, 1984.
3. *Ullmanns Encyklopädie der Technischen Chemie*, Band 7, Verlag Chemie, Weinheim/Bergstr., 1974.
4. F. Tamás, *Szilikát ipari kézikönyv*, Müszaki Könyvkiadó, Budapest, 1982.
5. G. Liptay, *Atlas of Thermoanalytical Curves 2.* Akadémiai Kiadó, Budapest, 1973.
6. M. Földvári-Vogl and B. Kliburszky, *Geologie*, 1957, **6**, 542.
7. C. Duval, *Inorganic Thermogravimetric Analysis*, 2nd Ed., pp. 228–229. Elsevier, Amsterdam, 1963.
8. L. Erdey and F. Paulik, *Acta Chim. Acad. Sci. Hung.*, 1957, **13**, 117.

Talanta, Vol. 39, No. 12, pp. 1587–1590, 1992
Printed in Great Britain.

0039-9140/92 $5.00 + 0.00

COULOMETRIC TITRATIONS OF BASES IN PROPYLENE CARBONATE USING HYDROGEN–PALLADIUM AND DEUTERIUM–PALLADIUM GENERATOR ELECTRODES

RANDJEL P. MIHAJLOVIĆ
Faculty of Science, Kragujevac, R. Domanovića 12, Yugoslavia

LJILJANA N. JAKŠIĆ
Faculty of Science, Priština, Yugoslavia

VILIM V. VAJGAND
Faculty of Science, Belgrade, Yugoslavia

(*Received* 1 *November* 1991. *Revised* 16 *March* 1992. *Accepted* 23 *March* 1992)

Summary—The application of hydrogen and deuterium ions obtained by anodic oxidation of hydrogen and deuterium dissolved in palladium, for the coulometric determination of bases (both individual and in mixtures) in propylene carbonate, is described. The current-potential curves at a palladium anode for supporting electrolyte indicator, titrated bases, hydrogen dissolved in palladium and deuterium dissolved in palladium showed that hydrogen and deuterium are oxidized at much less positive potentials than the oxidation potentials of other substances present in the solution. The generated H^+ and D^+ ions were used for the titration of bases (pyridine, quinoline, triethylamine, n-butylaniline, 2,2′-dipiridyl and aminopyrine) with visual and potentiometric detection. The oxidation of hydrogen and deuterium proceeded with 100% current efficiency. Two-component mixtures of bases (aliphatic + aromatic amine) were titrated successfully by using two indicators, Eosin and Crystal Violet. The relative error of the determination with respect to each individual base determination, was less than 2.5% for quantities of bases ranging from 1 to 3 mg.

Propylene carbonate (PC) is an aprotic dipolar solvent with a high permittivity ($\epsilon = 64$) and relatively large acidity scale; it dissolves many organic compounds and is not toxic.[1] However, solutions of strong mineral acids in PC are not stable which makes the classical volumetric determinations of bases in this solvent difficult. For potentiometric titration of bases in PC, Baranov *et al.*[2] used a standard solution of perchloric acid in PC–methanol/5 + 1, v/v mixture.

In our previous paper[3] it was shown that the difficulties encountered in the classical titrations of bases in PC can be avoided by using hydrogen ions obtained by anodic oxidation of various organic compounds (esters of gallic acid, phenols and ascorbic acid).

In comparison with the classical depolarizers, hydrogen and deuterium dissolved in palladium have advantages, since, by their applications, no foreign substances which can make worse the conditions for the titration of bases, are introduced into the solution. Hydrogen–palladium and deuterium–palladium electrodes have so far been successfully used in coulometric titrations of bases in water[4] and some non-aqueous solvents.[5–7]

Taking into account all good properties of propylene carbonate as a medium for the titration of bases, as well as the advantages of hydrogen and deuterium dissolved in palladium with respect to other depolarizers, in this paper we have investigated the behaviour of hydrogen–palladium and deuterium–palladium generator electrodes in coulometric titrations of bases in propylene carbonate as solvent.

EXPERIMENTAL

Reagents

All chemicals were of analytical reagent grade from Merck and Fluka. Liquid bases were first dried over fused potassium hydroxide and then distilled under reduced pressure. The concentration of organic bases was previously determined coulometrically with H^+ ions obtained

by the oxidation of hydroquinone at a platinum anode, in acetonitrile as solvent. The supporting electrolyte was 0.2*M* sodium perchlorate in propylene carbonate.

A saturated solution of Eosin in propylene carbonate or a 0.1% solution of Crystal Violet in the same solvent were used as indicators.

Propylene carbonate was used without purification. Deuterium oxide (heavy water), 99.8%, was purchased from the Radioisotope Division of IGN Chemicals.

Electrodes

The $(H_2/Pd)_{gener}$ and $(D_2/Pd)_{gener}$ electrodes were palladium plates (1 × 2 × 0.5 cm) saturated with hydrogen or deuterium obtained by electrolysis. The apparatus used is described in our previous paper.[6] The indicator electrode was a glass electrode and the reference electrode was SCE.

Procedure

Visual end-point detection. The supporting electrolyte is placed into the anode (2–3 cm^3) and cathode (3–5 cm^3) compartments of the electrolytic vessel up to the same level. A platinum spiral is dipped into the catholyte, a drop of Crystal Violet solution is added to the anolyte, and a $(H_2/Pd)_{gener}$ electrode is immersed into the anolyte. The current is turned on and the supporting electrolyte is titrated. A weighed amount of the base being determined is then added to the anolyte, and by simultaneously switching on the current and the chronometer H^+ ions are generated until the indicator color is changed. A further aliquot of the base is then added to the anolyte and the solution is again titrated. Several samples can be analyzed in the same supporting electrolyte.

Potentiometric end-point detection. The supporting electrolyte was poured into the cathode and anode compartments of the electrolyte vessel up to the same level.[6] The platinum cathode was dipped into the catholyte and $(H_2/Pd)_{gener}$ electrode, or $(D_2/Pd)_{gener}$ electrode, a glass electrode and an SCE were immersed in the anolyte. A weighed amount of the base being determined was added to the anolyte, the current was switched on; H^+/or D^+ ions were generated and the potentials were read. The titration end point was determined from the second derivative.

Determination of two component mixture of amines. In the determination of dicomponent mixtures of amines (an aliphatic and an aromatic amine) the supporting electrolyte is also placed into the cathode and anode compartments up to the same level. A drop of Eosin solution is added to the anolyte and the supporting electrolyte is titrated until the indicator colour changes. Then, a weighed amount of a mixture of bases is added to the anolyte and H^+ ions are generated until the color of Eosin is changed, whereby the aliphatic amine is titrated. An aliquot of the same mixture of bases is then titrated in the same way but by using Crystal Violet as indicator. The amount of the aromatic amine is determined from the difference.

RESULTS AND DISCUSSION

In order to check the possibility of applying H^+ ions obtained by anodic oxidation of hydrogen dissolved in palladium for the titration of organic bases in propylene carbonate, the current–potential curves for the supporting electrolyte indicator, titrated bases and hydrogen dissolved in palladium were first recorded. The current-potential curves (Fig. 1) for propylene carbonate, Crystal Violet, pyridine and hydrogen dissolved in palladium showed that hydrogen dissolved in palladium is oxidized at a more negative potential than the oxidation potentials of other components present in the solution. H^+ ions generated at the palladium anode were used for the titration of triethylamine, *n*-butylaniline, quinoline, pyridine, 2,2′-dipyridyl and aminopyrine in the presence of Crystal Violet indicator. The results obtained (Table 1) indicate

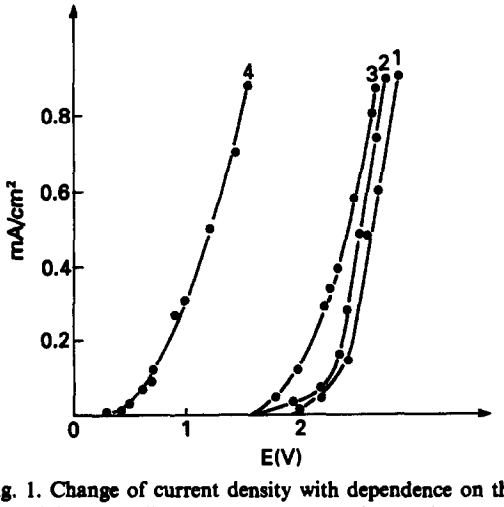

Fig. 1. Change of current density with dependence on the potential at the palladium anode: 1) propylene carbonate; 2) Crystal Violet; 3) pyridine and 4) $H_2(D_2)$ dissolved in palladium.

Table 1. Results of coulometric titrations of bases with H^+ ions obtained by anodic oxidation of hydrogen dissolved in palladium, in propylene carbonate. $C_B = 0.01M$. Supporting electrolyte, $0.2M$ sodium perchlorate; $I = 0.010$ A.

Titrated base	Taken mg*	Number of determination	Found % $(H_2/Pd)_{gener.}$	Found % $(D_2/Pd)_{gener.}$
Triethylamine	2.19	7	100.2 ± 0.2†	100.1 ± 0.2†
Triethylamine	10.92	5	100.1 ± 0.5‡	
n-Butylaniline	4.33	6	100.1 ± 0.4†	100.0 ± 0.3†
n-Butylaniline	14.98	5	99.6 ± 0.6†	
Quinoline	2.86	6	100.0 ± 0.3†	100.2 ± 0.4†
Quinoline	14.59	5	99.5 ± 0.5†	
Pyridine	2.29	9	100.1 ± 0.5†	100.1 ± 0.6
2,2′-dipyridil	7.20	6	100.1 ± 0.3†	99.9 ± 0.4†
2,2′-dipyridil	8.79	6	100.3 ± 0.6†	
Piperidine	2.27	6	99.9 ± 0.5†	99.9 ± 0.4†
Aminopyrine	7.18	5	100.2 ± 0.7†	100.0 ± 0.5†

*The volume of the electrolytic vessel for potentiometric end-point detection is 4–5 times that for visual end point detection. Therefore, the concentration of the titrated bases are in each case approximately the same

†Visual end-point detection.

‡Potentiometric end-point detection (glass electrode—modified SCE).

that the current efficiency was 100%, when 2–7 mg of the investigated bases were titrated. With D_2/Pd generator electrode the current efficiency was also 100%.

In coulometric titrations of triethylamine, quinoline, *n*-butylaniline and 2,2′-dipyridil, respectively, the titration end-point was detected also by the potentiometric method, using the electrode couple: glass electrode-SCE. The titration curves obtained are shown in Fig. 2. The highest potential changes were detected in the titration of triethylamine (about 300 mV for 30 sec), whereas the lowest one in the titration of *n*-butylaniline (about 100 mV for 30 sec).

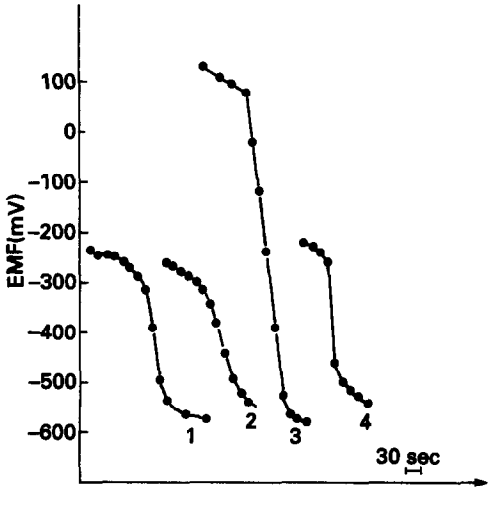

Fig. 2. Coulometric titrations curves for bases in propylene carbonate with a glass electrode and SCE: 1) quinoline; 2) n-butylaniline; 3) triethylamine; 4) 2,2′-dipiridyl.

The determination of dicomponent mixtures of bases

Since propylene carbonate has a differentiating effect on the strength of bases, in this solvent it is possible to titrate a mixture of bases differentially with perchloric acid, provided their pK values in water differ at least for 1.4 pK units.[2] In our previous paper,[8] two component mixtures of aliphatic and aromatic amines were coulometrically determined in acetonitrile as solvent, using two indicators (Eosin and Crystal Violet).

By using the differentiating effect or propylene carbonate on the strength of bases and the possibility of direct generation of H^+ ions by the oxidation of hydrogen dissolved in palladium, we have determined coulometrically mixtures of an aliphatic and aromatic amine in propylene carbonate visual end-point detection using Eosin and Crystal Violet (Table 2) as indicators.

Table 2. Coulometric determination of mixtures of aliphatic and promatic amines with H^+ ions generated by the oxidation of hydrogen dissolved in palladium with visual end-point detection using Eosin and Crystal Violet as indicator. $I = 0.010$ A.

Titrated bases	Taken, *mg*	Number of determination	Found, %
Triethylamine+	1.31	6	98.9 ± 1.6
2,2′-dipiridil	2.02	6	98.0 ± 1.0
Triethylamine+	1.15	6	100.6 ± 1.3
Quinoline	2.24	6	100.2 ± 2.5
Butylamine+	2.38	6	99.4 ± 0.2
Quinoline	1.44	6	100.9 ± 2.7
Butylamine+	3.00	6	101.1 ± 1.2
2,2′-dipirydil	2.99	6	99.0 ± 1.9

The results presented in Table 2 show that the relative error of the determination with respect to each individual base determination was less than 2.5% for base quantities ranging from 1 to 4 mg.

On the basis of these results it may be concluded that the oxidation of hydrogen and deuterium dissolved in palladium, in propylene carbonate as solvent, proceeds with 100% current efficiency and that the generated H^+ ions can be applied to the determination of two-component mixtures of bases. By using hydrogen and deuterium as anodic depolarizers it is possible to eliminate the use of standard solutions of acids which are unstable in propylene carbonate. Furthermore, their application brings no foreign organic compounds into the solution being investigation. At a current of 10 mA, a palladium plate with a volume of 1 cm^3 saturated with hydrogen can generate H^+ ions for more than 100 hr.

REFERENCES

1. Yu. A. Karapetyan and V. N. Eichis, *Fiziko-khimicheskie Svoistva Elektrolitnykh Nevodnikh Rastvorov*, Khimiya, Moskva, 1989.
2. N. A. Baranov, N. A. Vlasov, L. P. Potehina and O. F. Shepotko, *Zh. Analit. Khimii*, 1970, **25**, 2069.
3. R. P. Mihajlović, V. J. Vajgand, Lj. N. Jakšić and M. S. Manetović, *Anal. Chim. Acta*, 1990, **229**, 287.
4. R. P. Mihajlović, V. J. Vajgand and Lj. N. Jakšic, *Talanta*, 1991, **38**, 333.
5. V. J. Vajgand, R. P. Mihajlović, R. M. Džudovic and Lj. N. Jakšic, *Anal. Chim. Acta*, 1987, **202**, 231.
6. R. P. Mhiajlović, Lj. V. Mihajlović, V. J. Vajgand and Lj. N. Jakšic, *Talanta*, 1989, **36**, 1135.
7. R. P. Mihajlović, V. J. Vajgand and R. M. Džudović, *ibid.*, 1991, **38**, 673.
8. V. J. Vajgand, R. P. Mihajlović and M. Rakočević, *J. Serb. Chem. Soc.*, 1972, **37**, 269.

Talanta, Vol. 39, No. 12, pp. 1591–1595, 1992
Printed in Great Britain.

0039-9140/92 $5.00 + 0.00

APPLICATION OF *p*-XYLENESULPHONIC ACID AS ASHING REAGENT IN THE DETERMINATION OF TRACE METALS IN CRUDE OIL

A. P. UDOH,* S. A. THOMAS and E. J. EKANEM†
Department of Chemistry, Ahmadu Bello University, Zaria, Nigeria

(*Received* 15 *July* 1991. *Revised* 9 *March* 1992. *Accepted* 23 *March* 1992)

Summary—The *p*-xylenesulphonic acid ashing procedure was applied to the determination of Ca, Cu, Fe, Mg, Na, Ni and Zn in crude petroleum. The optimum acid ratio was 1.0 g per gram of oil for determining Na and Ni and 0.5 g per gram of oil for the other metals determined. The simultaneous ignition of the oil-acid mixture while boiling prevented volatilization losses for Fe, Na and Ni, eliminated the coke residue and reduced the ashing time. The minimum sample size for efficient metal release was 15.0 g. Satisfactory recoveries of added Na and Ni and highly reproducible results were obtained. Results obtained by this method were similar to those obtained by standard methods for the same samples.

The determination of trace metals in petroleum oils has relied on ashing methods that aim at preventing metal losses by volatilization during the ignition of samples.[1–13] Benzenesulphonic acid destroys the porphyrin metallocomplexes present in an oil and renders the metals non-volatile.[14] A procedure for determining nickel and vanadium in petroleum distillates using this compound as ashing reagent has been reported[6,14] and was adopted by the Institute of Petroleum.[15] An extension of this procedure using *p*-xylenesulphonic acid as the ashing reagent for the determination of copper, iron, nickel and vanadium in refinery fluid catalytic cracking feedstock has been reported.[8] The application of this reagent to crude petroleum has not been reported: an examination of this reagent in the ashing of petroleum crude is presented in this article.

EXPERIMENTAL

Reagents and apparatus

All reagents used were of analytical reagent grade. Doubly distilled water was used to prepare all solutions. Stock solutions (1000 ppm) of Ca, Cu, Fe, K, Mg, Na, Ni and Zn were prepared from their carbonate (Ca), chlorides (K, Mg, Na), nitrates (Cu, Ni), oxide (Zn) or ammonium sulphate (Fe) and stored in polythene bottles; each was appropriately diluted to obtain working solutions. Lanthanum [5% (m/v)] as the nitrate was introduced in the working solutions used for determining Ca and Mg as buffer to minimize the interferences of ions like phosphate, aluminate and silicate.

The muffle furnace was a Carbolite (Sheffield, U.K.) capable of maintaining a constant temperature in the range 20–1200°.

K and Na were determined with a Corning-EEL flame photometer.

Other metals were determined with a Pye-Unicam SP 1900 atomic-absorption spectrometer equipped with a premix chamber and a 10-cm single slot burner head operated on the air-acetylene flame applying single element hollow cathode lamps as sources. Instrument parameters were appropriately optimized for each element determined.

Crude oil samples

The samples analysed were obtained from various Nigerian oil-drilling and refining companies. They were blends from particular production fields and were for either export or local refining. All samples were stored in polythene bottles and were assigned numbers to differentiate them in this work.

p-*Xylenesulphonic acid*

This ashing reagent was prepared as recommended by Vogel[16] and stored in a desiccator for use as required.

*Present address: University of Cross River State, Uyo, Nigeria.
†Author for correspondence.

Table 1. Optimization of *p*-Xylenesulphonic acid ratio

Acid ratio (g/g oil)	Concentration (ppm) of metal measured							
	Ca	Cu	Fe	K	Mg	Na	Ni	Zn
0.1	0.9	0.2	4.0	0.4	0.2	5.0	6.9	0.2
0.3	1.3	0.3	9.0	0.7	0.6	6.8	8.6	0.3
0.5	1.9	0.3	10.5	0.8	0.7	11.6	10.1	0.5
0.7	1.8	0.3	10.5	0.8	0.8	14.8	12.5	0.5
1.0	2.0	0.2	10.5	0.8	0.9	16.2	13.6	0.5
1.5	2.0	0.3	10.6	0.8	0.8	16.6	13.4	0.5
2.0	2.1	0.3	10.5	0.9	0.7	16.2	13.8	0.5
3.0	1.9	0.3	10.4	0.8	0.8	16.2	13.6	0.4
4.0	2.0	0.3	10.6	0.8	0.8	16.0	13.7	0.5
5.0	1.9	0.3	10.6	0.8	0.8	16.2	13.7	0.5

Sampling for analysis

The sampling procedure was to ensure even distribution of particles, sludge and water in the crude when a sample was taken for analysis. The crude was heated on a steam bath for at least thirty minutes; the container was then shaken vigorously to mix the oil before any sample was taken with a dropper.

Optimization of the ratio of p-*xylenesulphonic acid*

A 20.0-g oil sample, in each case, was mixed with varying masses of *p*-xylenesulphonic acid; the mixture was coked, charred and muffled at 500°; the resulting ash was digested and dissolved using 50% hydrochloric acid by the method reported later under 'proposed procedure' and the solution analysed for metals as presented in Table 1 for sample 1.

Heating procedure and muffling temperature

The acid–oil mixture was brought gently to boil on a heating mantle. It was then ignited with a flame as recommended by Row and Yates[8] until a charred mass was obtained. This charred mass was muffled at 500°.

The effect of igniting during coking

The acid–oil mixture was prepared in replicate in different beakers; each mixture was ignited at a different time interval after it was brought to the boil. The effect of this ignition is indicated in Table 2 for one of the four samples investigated.

Table 2. Effect of ignition during coking on metal recovery

Stage of ignition	Concentration (ppm) of metal measured							
	Ca	Cu	Fe	K	Mg	Na	Ni	Zn
Immediately on boiling	4.4	0.1	6.5	1.2	2.5	6.5	7.4	0.4
One hour after onset of boiling	4.3	0.1	6.4	1.2	2.4	6.1	7.4	0.3
No ignition applied at all	4.3	0.1	4.9	1.4	2.5	5.4	6.0	0.3

Optimization of the sample size

Varying masses of sample 5 were mixed with 1.0 g of *p*-xylenesulphonic acid per gram of oil, coked, charred and ashed before the metals were determined. The results are presented in Table 3.

Proposed procedure

A 20.0-g sample of crude oil is mixed with 1.0 g of *p*-xylenesulphonic acid per gram of oil in a 500-ml pyrex beaker. The mixture is brought to the boil, ignited and charred, and the carbon burnt off in a muffle furnace at 500°. The resultant ash is digested in 20.0 ml of hydrochloric acid (1 + 1) on a steam bath until the volume decreases to about 5.0 ml. This solution is transferred quantitatively and made up to 25 ml introducing 5.0 ml of 5% lanthanum solution. Flame photometry and flame atomic-absorption spectrometry were then applied to determine Ca, Cu, Fe, K, Mg, Na, Ni and Zn against a blank solution derived from only *p*-xylenesulphonic acid in the absence of oil.

Evaluation of the procedure

The reproducibility of the procedure was determined by applying the proposed procedure nine times in turn on sample 5. The reproducibility in the determination of the various determinant elements is indicated in brackets as percent relative standard deviations (RSD) in Table 3.

Table 3. Effect of sample size on metal release

Sample size, g	Concentration (ppm) of metal measured							
	Ca	Cu	Fe	K	Mg	Na	Ni	Zn
10.0	5.0	0.0	4.3	0.5	2.4	6.0	6.3	0.3
15.0	6.2	0.1	6.5	0.9	2.5	6.5	6.7	0.3
20.0	8.6	0.1	6.4	1.2	2.5	6.4	7.4	0.3
(RSD) (%)	(0.7)	(10.0)	(1.5)	(14.5)	(3.6)	(2.5)	(0.7)	(23.3)
25.0	8.8	0.1	6.6	1.0	2.3	6.7	7.5	0.4

Table 4. Recovery of added metal from a spiked crude oil sample

Metal added	Metal level (ppm) Added	Recovered	Recovery (%)
Na	2.0	1.8	91.0
	10.0	9.0	90.0
	100.0	95.0	95.0
Ni	2.0	1.9	95.0
	10.0	9.5	95.0
	100.0	97.0	97.0

To study the recovery of added determinant, 20.0-g replicates of sample 5 were spiked with various levels of sodium and nickel added as the cyclohexanebutyrates in amyl alcohol. Each mixture was then treated by the proposed procedure and Na and Ni determined; the results, after discounting the known sample level, are presented in Table 4.

In a comparison of methods, various crude oil samples were analysed for the same trace metals using the *p*-xylenesulphonic acid procedure described in this article, the sulphuric acid ashing procedure,[12,13] and the Institute of Petroleum (IP) procedure.[15] Samples were prepared and analysed in duplicate by each procedure and the mean results are compared in Table 5.

Table 5. Comparison of sample results obtained by three ashing procedures

Sample No.	Analyte	Measured levels (ppm) Proposed procedure	Sulphuric acid procedure	IP procedure
1	Ca	2.0	2.2	3.0
	Cu	0.3	0.2	0.2
	Fe	10.5	11.6	9.5
	K	0.8	0.6	0.9
	Mg	0.8	1.1	1.2
	Na	16.2	14.8	15.3
	Ni	13.6	12.3	12.2
	Zn	0.5	0.3	0.4
2	Ca	3.5	3.6	4.3
	Cu	0.1	0.1	0.1
	Fe	2.7	3.4	3.0
	K	0.6	0.6	0.7
	Mg	0.6	0.7	0.9
	Na	9.5	11.1	7.8
	Ni	3.9	2.8	3.0
	Zn	0.5	0.3	0.5
3	Ca	5.7	5.0	8.9
	Cu	0.1	0.1	0.2
	Fe	1.0	0.9	0.8
	K	0.9	0.7	1.1
	Mg	2.3	2.5	2.7
	Na	57.3	51.5	63.8
	Ni	2.0	1.8	1.7
	Zn	0.4	0.5	0.3
4	Ca	6.6	5.9	8.3
	Cu	0.1	0.1	0.1
	Fe	6.3	8.4	7.7
	K	0.5	0.7	0.8
	Mg	1.1	1.2	1.5
	Na	44.5	47.0	35.0
	Ni	5.1	3.3	3.6
	Zn	0.3	0.4	0.1
5	Ca	8.6	6.1	9.9
	Cu	0.1	0.1	0.3
	Fe	6.5	7.8	7.6
	K	1.1	1.0	1.3
	Mg	2.5	2.7	1.5
	Na	6.4	9.7	13.6
	Ni	7.4	6.6	7.2
	Zn	0.3	0.2	0.2
6	Ca	b.d	b.d	b.d
	Cu	0.1	0.1	0.1
	Fe	1.2	0.9	1.6
	K	1.5	0.8	1.2
	Mg	2.3	2.2	4.6
	Na	14.8	16.1	16.3
	Ni	19.8	20.3	19.8
	Zn	0.3	0.2	0.2

b.d. = below detection.

RESULTS AND DISCUSSION

The concentration of each element indicated in the ash increased with the ratio of *p*-xylenesulphonic acid per gram of oil until a peak concentration was obtained. The peak concentration was attained for sodium and nickel with 1.0 g of *p*-xylenesulphonic acid per gram of oil but for the other metals measured, the peak was attained with 0.5 g of *p*-xylenesulphonic acid per gram of oil. Once attained, the peak concentration remained unchanged when higher acid ratios were applied. Plotted against increasing *p*-xylenesulphonic acid ratios, the concentration of each element observed increased linearly to the peak value and, thereafter, maintained a plateau up to an acid ratio of 5.0 g per gram of oil. The same trend was observed for samples other than sample 1 to which the results of Table 1 relate. The two peak reagent: oil ratios were characteristic for the determinants investigated in this work. The differences in the acid ratio required to achieve maximum release of each metal have been explained[17] in terms of corresponding differences in the thermodynamic stabilities of the complexes of the metals in the oils. The trends observed in this work suggest that the complexes of sodium and nickel are thermodynamically more stable than those of the other elements.

The burning of the sample while boiling offered the advantage that the large volume of

coke produced in methods like the sulphuric acid ashing procedure[12,13] was eliminated; the ashing time was also much shorter, decreasing to about five hours. The muffling temperature of 500° was selected from a range of effective values to permit the use of ordinary pyrex beakers; they get disfigured at much higher muffling temperatures. A qualitative examination of the ash solution in (1 + 1) hydrochloric acid gave a negative test for SO_4^{2-} ion indicating that the metal sulphonates were converted already at 500° to the oxides of the metals.

Table 2 shows that similar results were obtained for Ca, Cu, K, Mg and Zn when ignition was started immediately on boiling and long (1 hour) after boiling had commenced as when ignition was not applied at all; slightly lower values were obtained for Fe, Na and Ni when there was no ignition at all than when ignition was applied. This trend was observed consistently for four samples included in this investigation. In all cases, delaying the ignition offered no advantage at all. These results provide some idea of the elements in crude oils that are more prone to volatilization losses; the simultaneous burning of the oil–acid mixture is important for these elements. The burning generally shortened the time required for charring the sample.

The results of element analysis of the ash presented in Table 3 indicate that at least 15.0 g of the oil is required for maximum release of most of the elements. For this work, 20.0 g of oil was applied to allow some safe margin. The Q-test showed that the value obtained for iron using 10.0 g of oil was divergent.

The RSD values inserted in Table 3 show that this technique yields highly reproducible analysis on crude oil samples, at least for most of the elements measured. The higher relative standard deviation (RSD) values observed for elements like copper, potassium and zinc arise from their rather low levels in the sample analysed.

The high recoveries reported in Table 4 indicate the merit of this method. Besides, Table 5 shows that the results from the procedure compare well with those from the sulphuric acid and the standard Institute of Petroleum ashing procedures. At the 98% confidence level, the Student t-test showed that there was no significant difference between the results obtained by the three procedures.

With particular reference to benzenesulphonic acid, the procedure and reagent presented in this article offer the following advantages. Whereas the benzenesulphonic acid method has been applied only to distillate fractions,[6,15] the p-xylenesulphonic acid reagent and method, hitherto reported only for ashing petroleum distillate fractions, are suitable also for whole crudes; to provide an alternative reagent, even with a capacity to cope with a more complex matrix, is an advantage of the p-xylenesulphonic acid method. Besides, benzenesulphonic acid is very hygroscopic and requires special handling such as storing in an oven at 90° and using special materials for transferring it; p-xylenesulphonic acid offers an advantage in that it can be prepared simply and maintained solid over a long period in a desiccator at room temperature. With the simultaneous ignition of the crude, the p-xylenesulphonic acid procedure yields a drastic reduction in ashing time to about 5 hr in the benzenesulphonic acid procedure,[6,15] a filtration stage which is delayed overnight for an element like zinc is included; the p-xylenesylphonic acid procedure described in this article removes the need for filtration as the ash is rendered carbon-free in about three hours of muffling. In addition to the advantage in speed of analysis, the exclusion of the filtration eliminates the associated chance of error arising from either contamination during the filtration or loss by removal of determinant with the particles filtered out. One sample preparation is adequate for the determination of all the elements included in this work, whereas, in the benzenesulphonic acid procedure, modifications are required for specific elements.

CONCLUSION

The p-xylenesulphonic acid ashing procedure has hitherto been applied mainly for the determination of trace and additive metals in petroleum distillate fractions. Its merits for the determination of Ca, Cu, Fe, K, Mg, Na, Ni and Zn and perhaps other metals in whole crudes have been demonstrated in this article. The procedure is fast, reproducible and accurate; it precludes the profuse formation of coke which is a nuisance in other similar methods. The much reduced ashing time renders the method particularly suitable for progressive monitoring of on-going blending processes in addition to quick determination of constituents in crudes.

REFERENCES

1. J. H. Karchmer and E. L. Gunn, *Anal. Chem.*, 1952, **24**, 1733.

2. O. I. Milner, J. R. Glass Jnr., J. P. Kirchner and A. N. Yurich, *ibid.*, 1952, **24,** 1728.
3. E. N. Davis and B. C. Hoeck, *ibid.*, 1955, **27,** 1880.
4. L. W. Gamble and W. H. Jones, *ibid.*, 1955, **27,** 1456.
5. J. T. Horeczy, B. N. Hill, A. E. Walters, H. G. Schutze and W. H. Bonner, *ibid.*, 1955, **27,** 1899.
6. J. E. Shott Jnr., T. J. Garland and R. O. Clark, *ibid.*, 1961, **33,** 506.
7. E. J. Agazzi, D. C. Burtner, D. J. Crittenden and D. R. Patterson, *ibid.*, 1963, **35,** 332.
8. W. A. Row and K. P. Yates, *ibid.*, 1963, **36,** 368.
9. Z. Skorko-Trybula, *Nafta Krakow*, 1966, **22,** 141; *Anal. Abstr.*, 1967, **14,** 5505.
10. J. G. Bergman, C. H. Ehrhardt, L. Granatelli and J. L. Janik, *Anal. Chem.*, 1967, **39,** 1258.
11. S. Banerjee, B. P. Sinha and R. K. Dutta, *Talanta*, 1975, **22,** 689.
12. A. P. Udoh, Ph.D. Thesis, Ahmadu Bello University, Zaria, 1989.
13. A. P. Udoh, S. A. Thomas and E. J. Ekanem, *Bull. Chem. Soc. Ethiopia.*, 1990, **4,** 13.
14. J. G. Erdman, in J. E. Shott, T. J., Garland and R. O. Clark, *Anal. Chem.*, 1961, **33,** 506.
15. Institute of Petroleum, Method IP 286/77(85), IP Standards for Petroleum and its Products, Part I: Methods for Analysis and Testing, Vol. 2, p. 286, Institute of Petroleum, London, 1985.
16. A. I. Vogel, *A Textbook of Practical Organic Chemistry*, 4th Ed., p. 644. Longman Groups Ltd., London, 1978.
17. R. H. Filby, in *The Role of Trace Metals in Petroleum*, T. F. Yen (ed.), p. 31. Ann Arbor Science Publishers Inc., Ann Arbor, Michigan 1975.

Talanta, Vol. 39, No. 12, pp. 1597–1603, 1992
Printed in Great Britain.

0039-9140/92 $5.00 + 0.00

AN IMPROVED COMPUTER MODEL OF STRUVITE SOLUTION CHEMISTRY

T. J. WRIGLEY, W. D. SCOTT and K. M. WEBB

Environmental Science, School of Biological and Environmental Sciences, Murdoch University, Murdoch 6150, Western Australia

(*Received* 5 *December* 1991. *Revised* 9 *April* 1992. *Accepted* 11 *April* 1992)

Summary—The computer model of the solution chemistry of struvite has been improved. Firstly, with ammonia as the prime calculation point in the liquid phase, the algorithm is smaller and faster. Secondly, the incorporation of distilled magnesium hydrogen phosphate in the model significantly increased the concentrations in solution. Thirdly, estimates of the activity coefficients are included. These improvements have but a marginal (5–10%) improvement in the fit. However, proceeding with this flexible modelling procedure using the symbolic manipulator, Maple, easily allows the inclusion of all possible species. The addition of associated ammonium phosphates improves the fit. The relative standard deviation of the fit of both Taylor's data and the data of Webb is improved from 0.5 to 0.2. Estimates of the association constants are included.

Magnesium ammonium phosphate hexahydrate ($MgNH_4PO_4 \cdot 6H_2O$, struvite) is found in wastewaters, soils and is responsible for up to 16 per cent of urinary calculi. Conditions required for struvite precipitation in wastewaters and growth in human urine have not been well described. The literature on the basic chemistry is sparse.[1] The solubility of struvite was computed by Verplaetse *et al.*[2] and improvements have been completed by Scott *et al.*[3] This latter model includes the electro-neutrality equation and allows full expression of the inherent two degrees of freedom in this system. This means that the output should characterise precipitation in the general sense, *i.e.*, when the component ratios are not just 1:1:1.

In this paper, further improvements of the model are described. Firstly, the programme has been reconstructed using ammonia (NH_3) as the first calculation point to decrease the size and improve the running of the original programme. Secondly, the effects of associated magnesium hydrogen phosphate and ammonium phosphate ions and other possible species were investigated. Thirdly, a routine to calculate activity coefficient corrections was included.

The final aim of this study is to develop a predictive model incorporating all present knowledge of the system and to determine the amount of solid (*i.e.*, all possible solid compounds) formed from solution following the additions of arbitrary amounts of N, Mg and P. This paper is intended for design and calculation at 30° for waste-water treatment in the tropics; the baseline data of Webb[4] is the primary comparison.

EXPERIMENTAL

Materials and methods

Dissolved magnesium hydrogen phosphate (dMHP). The original algorithm[3] fitted the data of Taylor *et al.*,[5] but a large error remained. This deficiency was partly removed when a soluble component of magnesium hydrogen phosphate (MHP) was considered in the algorithm. Taylor *et al.*[5] suggested that this species is present in such systems and they provide an estimate of the appropriate equilibrium constant. The incorporation of dMHP into the model required a restructuring of the Maple algorithm, adding an additional equilibrium constant for this dissolved/solid equilibrium. The data for 30° are listed in Table 1. The constants listed in the second column of the table are the best values using a least squares fit of the data from Webb[4] (see Scott *et al.*[3]). The mass balance equations for magnesium and phosphorus were also amended to include the dissolved species. It was not necessary to change the solid mass balances or the electro-neutrality equation, however the direct calculation of Plqd from a quadratic was not possible, in contrast to the model reported previously.[3]

Table 1. Solubility constants with derived values for ionic equilibrium during model calibration

Equilibrium	Literature K[8]	Predicted K values
$Mg^{2+} + NH_4^+ + PO_4^{3-} = MgNH_4PO_4$	1.41×10^{13}	6×10^{13}
$H^+ + H_2PO_4^- = H_3PO_4$	77.4	77
$H^+ + HPO_4^{2-} = H_2PO_4^-$	1.86×10^6	9×10^7
$H^+ + PO_4^{3-} = HPO_4^{2-}$	7.08×10^{10}	1.8×10^{12}
$3Mg^{2+} + 2PO_4^{3-} + 8H_2O = Mg_3(PO_4)_2 8H_2O$	1.58×10^{25}	1.0×10^{24}
$Mg^{2+} + OH^- = Mg(OH)^+$	380	1.4×10^6
$Mg^{2+} + 2OH^- = Mg(OH)_2$	7.94×10^{10}	7.94×10^{10}
$Mg^{2+} + HPO_4^{2-} = MgHPO_4$	6.6×10^5	1.7×10^6
$MgHPO_4(s) = MgHPO_4(aq)$	98×10^{-3}	98×10^{-3}

An improved algorithm. The reconstruction made it necessary to check the effect of structure on the calculation. Hence calculations were made in which the logic and the algorithm were deliberately changed. Generally this resulted in a faster algorithm that showed no significant change in computed values. All calculations were done in double precision with an accuracy of at least 15 digits and a range of 10^{-307} to 10^{+307} using Absoft Fortran on an Amiga 2000. Two different algorithms evolved; one based on the original calculation of the total phosphorus concentration in the liquid, Plqd, the other based on calculating the concentration of dissolved NH_3 in the liquid.

When Plqd is calculated, the [H] and total magnesium in the liquid, Mlqd, are the independent inputs. The calculation uses the mass and charge balance equations to produce a quadratic equation in Plqd. From this point $[PO_4^{3-}]$ is calculated from a version of the liquid P balance equation, $[Mg^{2+}]$ from the Mg liquid balance equation and $[NH_4^+]$ from a version of the electro-neutrality equation. The remaining concentrations are calculated as simple ratios from the equilibrium constants. Later it was discovered that greater deficiency was achieved by using the dissolved magnesium ion concentration $[Mg^{2+}]$ rather than Mlqd as one of the input independent arguments. Mlqd is the total of all dissolved magnesium containing ions in the liquid, in gram-atoms/litre. The results of this calculation were the same as the original but approximately one-half the number of terms was used and less time was required for the calculations.

The greatest efficiency was achieved when $[NH_3]$ was calculated first. In this case, [H] and $[Mg^{2+}]$ were input arguments as well as all species that can be directly calculated from these values including [OH], $[MgOH]^+$ and the solid mole fraction of $Mg(OH)_2$. A flow sheet of the improved programme is listed in Table 2. The concentration of dissolved ammonia $[NH_3]$ is calculated from the solid mass balance equation using Maple with $[PO_4^{3-}]$, in turn, calculated from the electroneutrality equation.

Activity coefficients. There are many theoretical methods of calculating activity coefficients.[6,7] All have deficiencies but they generally acknowledge a dependence of the activity coefficient of a single ionic compound on the ionic strength; I where,

$$I = 0.5 \sum m_i z_i^2$$

m_i is the molarity

and z_i is the charge of species i.

The classic approximation is the Debye-Huckel equation (for $I < 0.01$). This equation relates the mean molar activity coefficient $\gamma \pm$ for both positive and negative ionic components to the charge on the ion, the charge on the ionic

Table 2. Flow sheet of the improved programme

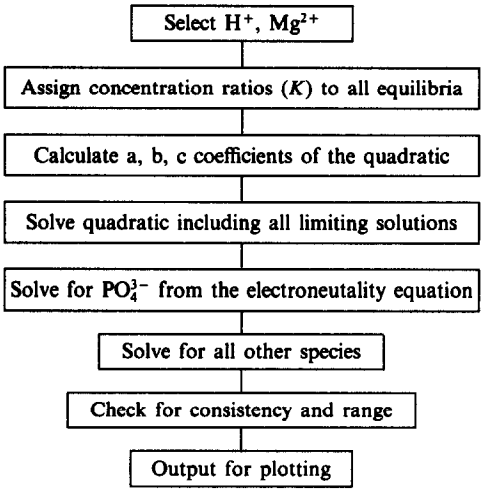

Note: intermediate concentrates of species are calculated as necessary. The final algorithm includes an algorithm for calculating activity coefficients by iteration. It covers 18 equilibria and requires the solution of a quadratic for NH_3 using a Newton–Raphson technique.

environment and the ionic strength. In our case, $\gamma \pm$ values are used for individual ions in a multivalent solution. For this, we chose an *ad hoc* approach that allows for a complete mixture of ions in solution; a formula which reverts to the original Debye-Huckel form when only a simple equivalent salt is present. The equation used is

$$\gamma_i = 0.5\, z_i z_e \log I^{1/2} \qquad (1)$$

where $z_e = \Pi\, z_J^{y_J}$ is the equivalent charge of the environmental field of ion i, $y_J = m_J/\Sigma m_J$ is the fraction of charge contributed by ions of charge J to the 'pool' of ions of charge opposite in sign to ion i. Π is the overall product from ions that have the opposite charge to i. Σm_J is the sum over all ions of charge J.

The final, complete programme follows the general flow of Table 2 but includes an iteration to estimate activity coefficients. The algorithm begins to calculate concentrations with all activity coefficients equal to 1. Concentrations are estimated, then the activity coefficient ratios are estimated from equation (1) and new estimations of the concentration based on "corrected" equilibrium constants are found. Initially, the calculation was repeated twice with estimated activity coefficient values. Later with the inclusion of further ionic species the calculation was repeated until the activity coefficients came to final limiting values. The procedure includes various tests to assure that realistic concentrations and activity coefficients are calculated.

Changes to the contour plots

A series of plots incorporating combinations of (a) dissolved NH_3 as the prime variable (b) the inclusion of dMHP and (c) the influence of activity coefficients are presented in Figs. 1–3. Note that these data are all for 30°. Little change in the concentration of both Plqd and Nlqd was apparent when compared with the original algorithm at >30°. The curves show an increase in concentration of about an order of magnitude over the 25° values (see Fig. 1 in Ref. 3). Also, they have a different shape because the equilibrium constant values were rederived and the contouring package (Surface II) has difficulty fitting the limits of the curve.

The inclusion of dMHP increased the solubility of phosphorus and nitrogen. At a pH of 9, the inclusion of dMHP in the new algorithm increased the phosphorus from $10^{-1.8}$ to $10^{-1.3}$ when the total magnesium in the liquid is 10^{-6}.

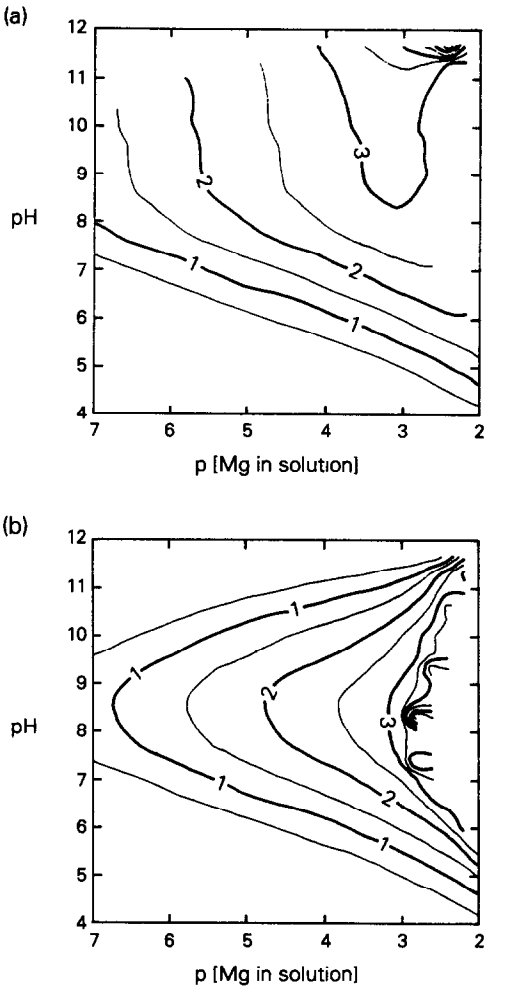

Fig. 1 (a). Concentration curve for the solubility of phosphorus and magnesium in solution when ammonia (NH_3) is the key variable. 30° lines are constant p [phosphorus in solution]. (b). concentration curve for the solubility of nitrogen and magnesium in solution when ammonia (NH_3) is the key variable. 30° lines are constant p [nitrogen in solution].

Nitrogen in solution Nlqd similarly increased from $10^{-1.3}$ to $10^{-0.8}$ [compare Figs. 1(a) and 1(b), and 2(a) and 2(b)].

The inclusion of activity coefficients in the new algorithm [Fig. 3(a) and (b)] had a more marked influence. In broad terms both Plqd and Nlqd increased in concentration by an order of magnitude. This shows more free ions with less dissolved solid; the inclusion of dMHP was somewhat overwhelmed by the inclusion of activity coefficients.

RESULTS AND DISCUSSION

Final algorithm

These changes did improve the fit, particularly at low concentrations, including the fitting

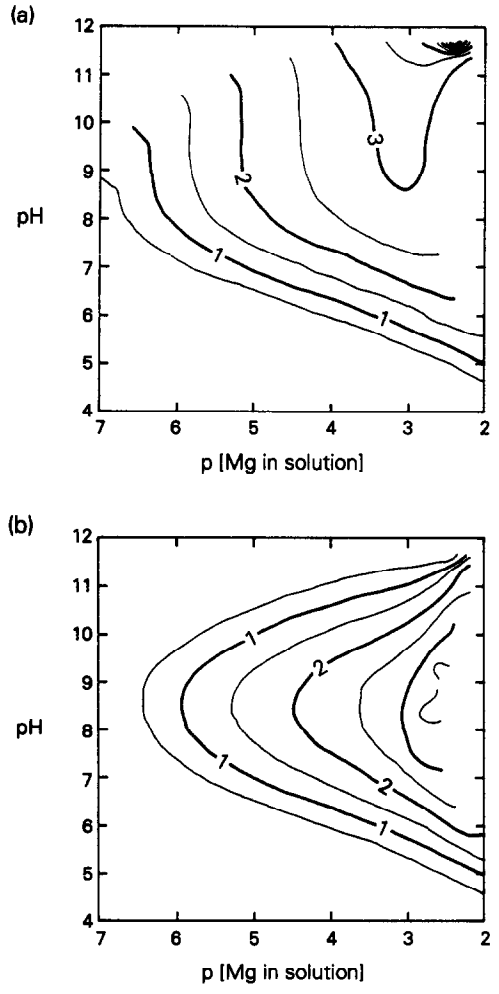

Fig. 2. (a) Concentration curve for the solubility of phosphorus and magnesium in solution with the inclusion of dMHP in the new algorithm. 30° lines are constant p [phosphorus in solution]. (b) Concentration curve for the solubility of nitrogen and magnesium in solution with the inclusion of dMHP in the new algorithm. 30° lines are constant p [nitrogen in solution].

of the data of Taylor *et al.*[5] at 25°. Still remaining, however was a general disparity between the absolute values of the calculated and measured values of phosphorus. This is apparent in Fig. 4 of Scott *et al.*[3]. Although there is a good correlation between the values ($r^2 = 0.85$), there is a difference between the absolute values which produce a relative standard error of about 0.5. This is unacceptable considering the exact nature of the calculation and the simple inorganic constituents involved. The above improvements only decrease the relative standard error by 5–10%. To find a reason for this disparity, every conceivable species was introduced into the algorithm. At this point the structure easily accommodated the changes; up to 18 different equilibria were considered.

This effort was rewarded by a lowering of the relative standard error by a factor of two. This was mostly a result of the inclusion of an associated ammonium phosphate ion. In the fitting of equilibrium constants, approximately 8 new values were predicted. Table 3 presents a summary of the results together with equilibrium constants and statistics. NH_3 is still a primary calculating variable but now the calculation requires the solution of a quartic equation. The 5 coefficients a, b, c, d and e required are complex functions of the equilibrium constants and the known concentrations of H^+, Mg^{2+}, OH^-, $MgOH^+$ and $Mg(OH)_2$

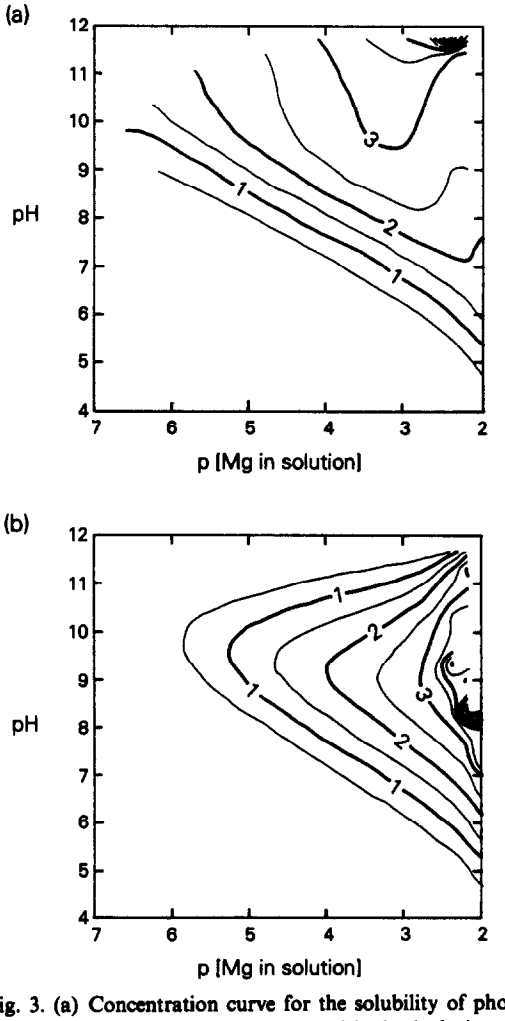

Fig. 3. (a) Concentration curve for the solubility of phosphorus and magnesium in solution with the inclusion of activity coefficients and dMHP in the new algorithm. 30° lines are constant p [phosphorus in solution]. (b) Concentration curve for the solubility of nitrogen and magnesium in solution with the inclusion of activity coefficients and dMHP in the new algorithm. 30° lines are constant p [nitrogen in solution].

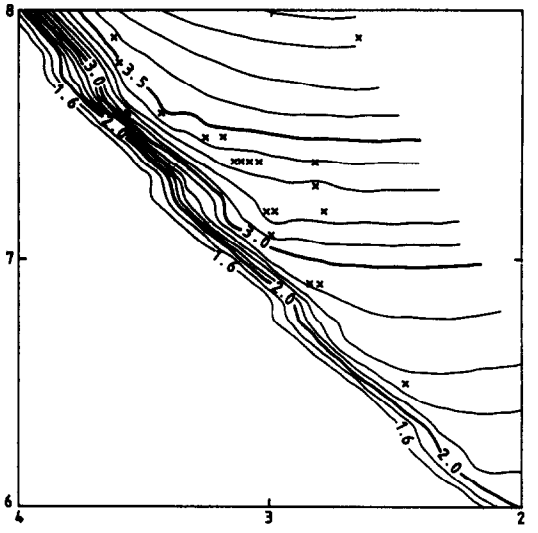

Fig. 4. Contours of constant dissolved nitrogen as p values; + = the data points from Webb[4] for 30°.

found from a Maple programme. Copies of these functions and the entire programme used are available on request. The solution of the quartic follows a Newton–Raphson technique. Checks are built into the programme to disallow negative values of roots and also disallow concentrations to rise larger than molarities of one or mole fractions of one.

Table 3. Formation constants derived and used

	Taylor's data (25°)		Webb's data (30°)		
	Earlier value	Present value	Earlier value	Present value	
K1 =	2.6D14	1.3D14	4.0D12	5.9D14	Struvite
K2 =	2.0D9*	2.0D9*	1.0D9*	1.0D09*	Ammonium
K3 =	1.1D7	1.6D7*	1.5D2*	1.5D02*	Phosphoric acid
K4 =	1.7D8	6.7D7	5.0D6	1.6D07	Dihydrogen phosphate ion
K5 =	2.2D12	2.0D12	1.8D12	1.8D12	Hydrogen phosphate ion
K6 =	1.6D25#	6.2D24#	1.2D26#	1.0D25#	Magnesium phosphate solid 8H20
K7 =	1.3D23#	4.9D22#	1.0D23#	8.0D22#	Magnesium phosphate solid 22H20
K8 =	2.4D7	6.0D7#	1.0D3#	5.0D04#	Magnesium hydroxide ion
K9 =	5.0D10*	5.0D10*	5.0D10*	5.0D10*	Magnesium hydroxide solid
K10 =	2.9D6	1.9D6	1.1D5	5.0D05	Magnesium hydrogen phosphate solid
K11 =	1.0D14*	1.0D14*	7.1D13*	7.1D13*	H20
K12 =	5.0D-4	2.8D-3#	1.0D-2	7.0D-1#	MHP solid forming NHP in solution
K13 =			no effect	1.3D03*	Magnesium phosphate ion
K14 =			no effect	1.3D01*	Magnesium dihydrogen phosphate ion
K15 =			1.0D-4	2.7D-5#	Dissolved struvite
K16 =			no effect	8.0D03#	Ammonium phosphate ion
K17 =			no effect	7.0D06#	Diammonium phosphate ion
K18 =			1.1D1#	2.0D01#	Ammonium hydrogen phosphate ion
Data Points	19	16	31	25	
Coefficient of Determination (r^2)	0.51	0.76	0.84	0.96	
Standard Relative Error	45%	26%	49%	22%	

Note: Earlier value refers to the algorithm with 12 constants and activity coefficient iteration, not the constants given by Scott *et al.* (1991). Present value refers to the algorithm with all features. The symbol* refers to a value derived from the literature; #, to a value that affects the fit but either has little effect on reducing the error or the number of data points that can be used in the fit are reduced. In the values given for the two solid magnesium phosphates, their ratio was retained at the known literature values; they had little effect on the fitting process. All the remaining constants were fit to the data by a trial and error procedure to minimise the relative value of the sum of the squares of the differences.

The main problem with this full algorithm, which also includes a multiple iteration for activity coefficient adjustment, is that the chance of success is small unless the initial trial is a good estimate. That means that a broad sweep of the input variable, H^+ and Mg^{2+} only gives a small number of successful results. A calculation to fit known data however is relatively easy. Figure 4 presents the calculated nitrogen in solution as contours at a given pH and pMlqd. The data for 30°, the experimental values of Webb,[4] are shown on the graph. Note that these data were used to drive the contours and the experimental Nlqd is about $0.1M$ for all points. The data also includes excess chloride ions at approximately $0.13M$.

In the final analysis, the improvement included dissolved ammonium magnesium phosphate and associated ammonium phosphate ions. Table 3 presents a summary of the values of equilibrium constants fitted to both the data of Taylor *et al.*[5] and Webb.[4] The coefficient of determination becomes 0.96 with Webb's data with a 22% standard relative error in the computed phosphorus values. The fit of the more dilute 25° data of Taylor *et al.*[5] is not as good with a coefficient of determination of 0.76 and a standard relative error of 26%. Considering that the algorithm of Scott *et al.*[3] shows a relative standard error of about 50% for both data sets; this is a marked improvement.

This is not totally clear as the computer algorithm is more difficult to fit to the data and fewer data points are actually used. Also more constants are calculated from the data; rather than 6, now we calculate about 8. Several of the constants have only a minor effect on the fit. Removal of outliers from the data set was explored and roughly half of the error is removed by the removal of 5 data points. The lowering of the degrees of freedom by about 2 due to the additional estimates is unlikely to be responsible for the better fit.

Points to be noted in reference to Table 3 include:

1. The data of Taylor *et al.*[5] are rather dilute, compared to Webb.[4] As would be expected, the associated ammonium phosphate ions are essentially absent. The expected formation constant for struvite from both studies is comparable to values quoted in the literature. We would suggest that the present algorithm should give best values of the solubility product at 25 and 30°.
2. Taylor *et al.*[5] delude to various constants for the solubility of ammonia hydrogen phosphate. The present values are of the same order of magnitude. Again, in this complex set of equilibria, it is most likely that the present algorithm compensates properly and can produce a satisfactory solubility constant for this species.
3. Many of the formation constants are only known to an order of magnitude. The effect is apparent when one adjusts the hydrogen phosphate constants for a best fit. The dihydrogen phosphate constant, in particular, varies by a factor of two or three with difference choices of the other constants.
4. The dissolved struvite is insignificant around 10^{-4} to 10^{-5}, in the presence of pure solid. The associated ammonium phosphate and associated ammonium phosphate ions are appreciable. At 1 millimolar NH_4^+ the associates $NH_4PO_4^{2-}$ and $(NH_4)_2PO_4^-$ are approximately in equal proportions and most of the PO_4^{3-} is associated. Note that the associates have no influence on the 25° data.[5] This is significant and needs to be checked using appropriately designed experiments.

A final graph is presented in Fig. 4. These are the standard curves showing dissolved nitrogen contours as used earlier to show the trends of the data, except they only show the two orders of magnitude exhibited by the data of Webb.[4] The figure shows minimal extrapolation and the limits of the information presented so far. The dissolved nitrogen contours exhibit an extraordinary "L" shape, that is extremely sensitive to the dissolved nitrogen. As the nitrogen varies by about a factor of 30% in the experiment, the H and Mlqd concentrations vary by about 2 orders of magnitude. Also the trend bifurcates so that no sensible relationship exists. Again further experiments are needed that pay great attention to holding the nitrogen levels constant. The experimental error of Webb[4] easily accounts for the 11% relative standard error observed and suggests that even greater control is necessary.

Speciation has not been reported in detail in the present work because of the numbers of individual species and an operational engineering requirement to see an overview. The curves suggest that gross changes occur in speciation in two decades of pH. Added excess passive anions and cations could easily limit the region in which the solid is in equilibrium with

the liquid. This is of great interest in kidney stone studies and the wastewater industry.

The final algorithm, including associated species, does improve the standard relative error and gives an acceptable fit. The standard relative error of the 25° data lowers to 26%; that of the 30° data lowered to 22%. There are many reasons for this including the increased degrees of freedom of the fit, the fact that not all of the set were considered and importantly the inclusion of the associated species. The actual number of the fitted constants is increased to about 8 since most of the species included had no effect (see Table 3, column 2). The dramatic change in the fit is most likely the effect of an associated ammonium phosphate in the solution, possibly ammonium phosphate ion.

CONCLUSIONS

The improvements incorporated into the model include a more efficient algorithm; all the known species as well as estimates of the activity coefficients. The inclusion of all possible species has pinpointed the need for associated ammonium phosphate ions. The fit is good in both a relative and an absolute sense with data sets at 25°[5] and 30°.[4] The presence of these species needs collaboration.

Clearly it is necessary to know all the species present in significant amounts to predict the amount of solid that will be formed and the present theoretical effort, with its variations and sensitivity, tests should at least give guidance to further laboratory and field experimentation. Preliminary design calculations are now possible; these will be the subject of a follow-up paper.

REFERENCES

1. J. R. Burns and B. Finlayson, *J. Urol*, 1982, **128**, 426.
2. H. Verplaetse, R. M. H. Verbeeck, H. Minnaert and W. Oosterlinck, *Eur. Urol.* 1985, **11**, 44.
3. W. D. Scott, T. J. Wrigley and K. M. Webb, *Talanta* 1991, **38**, 889.
4. K. M. Webb, *The Solubility of Struvite and its Application to a Piggery Effluent Problem*, Honours Thesis, Murdoch University.
5. A. W. Taylor, A. W. Frazier and E. L. Gurney, *Trans Faraday Soc.*, 1963, **59**, 1580.
6. R. Robinson and R. Stokes, *Electrolyte Solutions*, Butterworths, London, 1959.
7. S. H. Eberle, *Wat. Res.* 1989, 1373.

Talanta, Vol. 39, No. 12, pp. 1605–1609, 1992
Printed in Great Britain.

0039-9140/92 $5.00 + 0.00

EXTRACTION AND SENSITIVE SPECTROPHOTOMETRIC DETERMINATION OF YTTERBIUM WITH 2-(3,5-DICHLORO-2-PYRIDYLAZO)-5-DIMETHYLAMINOPHENOL

LILIANA FERNANDEZ and ROBERTO OLSINA

Department of Analytical Chemistry (Dr Carlos B. Marone) Faculty of Chemistry, Biochemistry and Pharmacy, University of San Luis, Argentina

(*Received* 2 *April* 1992. *Revised* 13 *April* 1992. *Accepted* 13 *April* 1992)

Summary—The operating conditions for the absorptiometric determination of Yb(III) with the reagent 2-(3,5-dichloro-2-pyridylazo)-5-dimethylaminophenol (3,5-diClDMPAP) by a liquid–liquid extraction technique are presented. The complex yields a molar absorptivity of 1.54×10^5 l.mole^{-1}.cm^{-1} (λ_{max} = 588 nm) and an optimum concentration range of 0.025–1.360 mg/l., at pH = 10. The method developed has been applied to the determination of Yb(III) in synthetic and concrete mixtures.

At present only a small number of organic reagents allow the absorptiometric determination of ions belonging to the group of the rare earths, in high sensitivity conditions, by means of extractive techniques.[1–6] Most of these techniques are based on the formation of ionic pairs[7–9] or ternary complexes[10,11] with molar absorptivity in the order of 10^4 l.mole^{-1}.cm^{-1}.

One of the features of partition processes between two immiscible phases is that they cause the sensitivity and the selectivity of the chromatic reaction to be increased.

It is considered of interest to develop techniques involving liquid–liquid extractions with new organic reagents, which allow the determination of the above-mentioned ions by means of simple and high sensitivity methods.

In previous work,[12] we have pointed out the very good sensitivity showed by the chromatic reactions between the reagent 2-(3,5-dichloro)-2-pyridylazo-5-dimethylaminophenol (3,5-diClDMPAP) and several rare earth ions. This reagent has been used in the determination of La(III) in synthetic samples with highly satisfactory results.[13]

According to the very good results obtained, in the present work the study of Yb-3,5-diClDMPAP for an extractive-spectrophotometric methodology is proposed. The purpose is to obtain a better selectivity and then to study its potentiality as base of kinetic aspects.

Considering the importance of ytterbium in the production of X-ray sources, magnet alloys and in geochemical prospecting for the determination of rock genesis, the methodology developed will be applied to the determination of it in synthetic and concrete samples.

EXPERIMENTAL

Apparatus

A Varian UV–visible spectrophotometer with 10-mm optical-path glass cells was used for absorptiometric measurements. The pH measurements were carried out with an Orion 701-A pHmeter, equipped with a combined glass electrode and Ag-AgCl reference. The liquid–liquid extraction experiences were carried out in a mechanical shaker with up to 300 shakings/minute.

Reagents

Standard solution of 3,5-diClDMPAP. The reagent 3,5-diClDMPAP was synthesized in our laboratory according to usual synthesis and purification techniques.[12]

A $3 \times 10^{-3}M$ solution of the purified reagent dissolved in absolute ethanol was prepared.

Standard solution of Yb(III). A 1-mg/ml solution of Yb(III) was prepared from Yb_2O_3 of certified purity, dissolved in nitric acid and made up to volume with bidistilled water. The normalization was carried out according to the procedure described by Ryabchikov and Ryabukhin.[14]

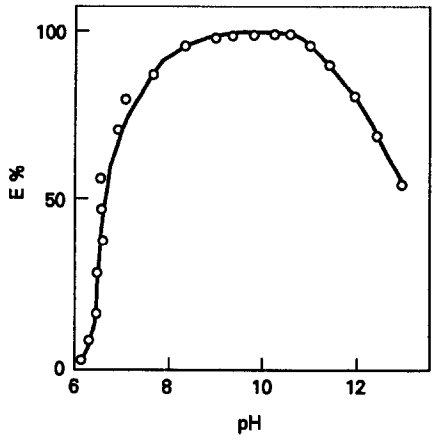

Fig. 1. Extraction curve of Yb(III)–3,5-diClDMPAP complex. $C_{Yb} = 4.5 \times 10^{-6}M$; $C_{organic\ reagent} = 9.0 \times 10^{-5}M$; equilibration time = 5 min; organic phase = benzene; working wavelength = 588 nm.

Buffer solution. A $1M$ solution of NH_4Cl was prepared, reaching the desired pH by the addition of the required volume of NH_4OH(c).

Other rare earths. All the reagents used were of analytical grade.

Extractive–absorptiometric procedure

An adequate aliquot of sample containing between 0.025 and 1.360 mg/l. Yb(III) is put into an extractive tube, then, the reagent dissolved in a minimum quantity of ethanol (reagent excess 10:1 with respect to metal ion concentration) and NH_4^+/NH_3 pH = 10 buffer solution (final concentration approximately $0.1M$) are added. The system is left to react for 10 min; the volume is made up to 0 cm^3 with bidistilled water and the solution mixed.

Next, 10 cm^3 of benzene are added and the system is manually shaken for 30 sec. The phases are separated and the absorbance of organic phase is measured at 588 nm against reagent blank.

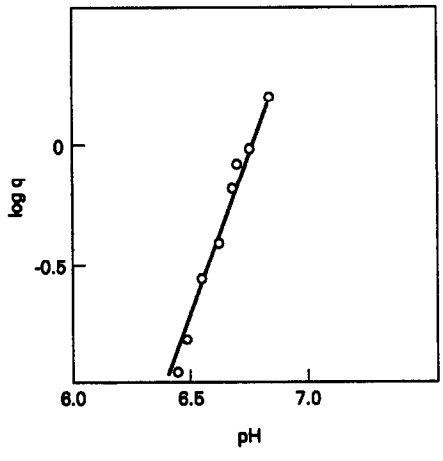

Fig. 2. Determination of n (number of displaced protons).

Procedure for the ytterbrium determination in samples

A column with strongly basic anion exchange resin Dowex 1 × 8 in the Cl^- form, 200 mesh was used. The resin was conditioned by means of successive washing with $1M$ hydrochloric acid, $1M$ sodium hydroxide, $1M$ hydrochloric acid and $0.2M$ EDTA disodic salt (Na_2H_2Y), until no Cl^- ions could be detected in the effluent. The resin was placed in a column of 6 mm diameter and 7 cm high.

An adequate aliquot of rare earth mixture, from the sample dissolution and later elimination of the matrix elements,[15] was evaporated to dryness and quantitatively turned into the respective anionic complexes with EDTA. It was dissolved at a volume of 200 μl of $5 \times 10^{-3}M$ Na_2H_2Y, pH = 4.7, and the sowing was carried out to the top of the column. Elution was performed with $5 \times 10^{-3}M$ Na_2H_2Y at a flow rate of 1 cm^3/min.

Fractions of 1.5 cm^3 were collected and analysed after removing organic matter with a HCl–HNO_3 mixture by an extractive–absorptiometric proposed procedure.

In the present working conditions Yb(III) is found in the first 37 cm^3 of elution.

RESULTS AND DISCUSSION

Extraction of the Yb(III)–3,5-diClDMPAP complex

The reagent 3,5-diClDMPAP reacts with the Yb(III) ion giving a dark red complex in excess of reagent ($\lambda_{max} = 588$ nm), which is hardly soluble in aqueous solution. If the system comes into contact with a non-aqueous solvent, the quantitative extraction of the complex is achieved after a few minutes of mechanical shaking. Benzene proved to be the most suitable solvent for this purpose, since it allows one to obtain higher absorptiometric sensitivity and stability.

Influence of pH. Extraction curve

In the absence of complexing agents in the aqueous phase, the Yb(III)–3,5-diClDMPAP complex begins to be extracted at pH = 6.2 and starts to decrease above pH = 11, which is expected due to the incipient hydrolysis of the metal ion (Fig. 1).

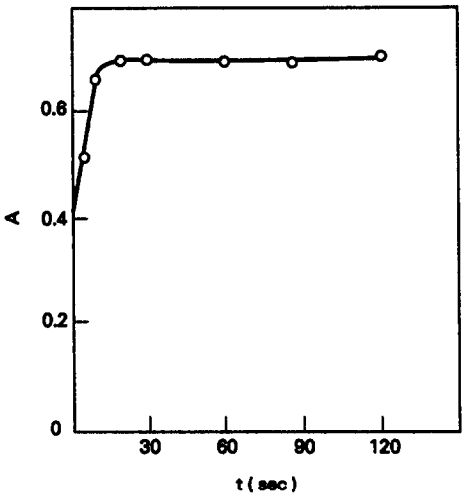

Fig. 3. Determination of equilibration time. $C_{Yb} = 4.5 \times 10^{-6}M$; $C_{organic\ reagent} = 9.0 \times 10^{-5}M$; reaction time = 10 min; organic phase = benzene; working wavelength = 588 nm.

The $pH_{1/2}$ value[16] for the reagent concentration of $1M$ is 2.68. The complexation–extraction equilibrium between the two immiscible phases can be expressed by:

$$Yb(III)_{aq} + [(n+r)HL]_{org} \rightleftharpoons [YbL_n(HL)_r]_{org} + n(H^+)_{aq}$$

and the logarithmic expression of the extraction constant is:

$$pK_{ext} = (n+r)\log(HL)_{org} + \log(HL)_{org} + n\ pH - \log q$$

where HL and q represent the organic reagent and the concentration ratio of the solute, respectively.

The results obtained after applying the equilibrium shift method[16] proved that $(n+r) = 3$; $n = 3$; $pK_{ext} = -8.05$ (Fig. 2), from which the following conclusions can be drawn:

(a) The stoichiometry of the extracted chelate is 3:1 (reagent:metal ion).
(b) No formation of adducts is observed.

Reaction and equilibrium time

It has been found previously that a minimum reaction time of 20 min is required for the quantitative formation of the La(III)–3,5-diClDMPAP complex.[13] This variable is investigated in detail.

In this experiment, the pH value was kept at 10, the Yb(III) concentration was set at $4.5 \times 10^{-6}M$. The reagent excess was 20:1 with respect to the metal ion, and it was added to the system dissolved in a minimum quantity of ethanol. This methodology was adopted in order to obtain an adequate extraction rate. Otherwise, following the conventional techniques of adding the reagent dissolved in the organic solvent, a quantitative extraction is only obtained after 3 hr of shaking.

The system was left to react for 1–30 min. Then, the solvent was added and the extraction was performed. Shaking was applied for 15 min. After separating the phases, the absorbance of organic phase was measured at 588 nm against reagent blank.

The results obtained showed that 5 min of reaction are needed prior to the extraction to allow for the quantitative formation of Yb(III)–3,5-diClDMPAP complex.

In an experiment analogous to the one described above, the reaction time was set at 10 min and the equilibration time was changed. It was determined that the system requires a minimum of 25 sec of manual shaking to obtain a quantitative extraction (Fig. 3).

Excess of reagent. Ionic strength

In order to verify the influence of the excess of reagent, an experiment was carried out in which the Yb(III) concentration was kept constant at $4.5 \times 10^{-6}M$, the reaction time was 10 min, the equilibrium time was 30 sec, the working pH was 10 ($0.1M$ NH_4^+/NH_3 buffer), and the reagent concentration was varied from 4×10^{-6} to $9 \times 10^{-5}M$.

Above a reagent to metal ion excess of 10:1 no variation took place in the complex absorbance. With respect to ionic strength it could be verified that it has no considerable effect upon the magnitude of the extraction within the interval 0.1 to $1M$.

Beer's law

Table 1 summarizes the experimental conditions which are most important for the spectrophotometric determination of Yb(III) with 3,5-diClDMPAP.

Table 1. Determination of Yb(III) with 3,5-diClDMPAP

Experimental conditions	
Working pH	10.0
Buffer solution	$0.1M$ NH_4^+/NH_3
Organic solvent	benzene
Maximum of reagent absorption	450 nm
Maximum of complex absorption	588 nm
Bathochromic shift	138 nm
fulfillment of Beer's law	0.025–1.363 mg/l
Molar absorptivity	$1.54 \times 10^5 \pm 2350$ $l.mole^{-1}.cm^{-1}$
Detection limit[17]	0.005 mg l.

Table 2. Determination of Yb(III) 3,5-diClDMPAP. Ternary mixtures

Samples		% Composition (w/w) molar relation	Yb(III) found	% Relative error
	Yb(III)	33.3	32.6 ($n = 6$)	
1	La(III)	33.3	$s = 0.141$	+2.0
	Ce(III)	33.3	$CL_{\alpha=0.05} = 32.6 \pm 0.05$	
	Yb(III)	50.0	49.2 ($n = 6$)	
2	La(III)	49.0	$s = 0.023$	−1.5
	Ce(III)	1.0	$CL_{\alpha=0.05} = 49.2 \pm 0.02$	
	Yb(III)	5.0	4.7 ($n = 6$)	
3	La(III)	45.0	$s = 0.23$	−5.2
	Ce(III)	50.0	$CL_{\alpha=0.05} = 4.7 \pm 0.19$	

It is important to note that by means of flame atomic absorption techniques, the detection limit for Yb(III) is 0.01 mg/l. against 5×10^{-3} mg/l. by the proposed technique.

Although the methodology developed here is inferior to techniques that make use of ovens (Electrothermal Atomization Technique: detection limit 2×10^{-4} mg/l.), it is, however, much simpler.

Resolution of rare earth mixtures

The reagent 3,5-diClDMPAP presents an adequate sensitivity for the absorptiometric determination of rare earth ions, but it is not highly selective.

Synthetic binary mixtures of Yb(III) and La(III) containing different proportions of both substances were solved with excellent results. This is due to the fact that the Yb(III) ion is selectively extracted with respect to La(III).

It is also possible to solve ternary mixtures of Yb(III), La(III) and Ce(III) with the results shown in Table 2.

The lanthanide determinations in geological and other samples require a preceding separation step, even though determination techniques such as ICP[18] are used. These separative procedures are time-consuming processes. Methods such as that of Crock *et al.*[15] based on ion exchange chromatography by sequential acid elution can be used for the initial separation of the lanthanides from the matrix elements (this yields to a relative error of 2% in the individual Yb determination).

In order to solve multielement lanthanide samples, chromatography of ionic exchange was used. Minczewsky and Dybczynski,[19] taking as a basis the formation of anionic complexes of rare earth elements with several organic ligands, have investigated

Table 3. Determination of Yb(III) with 3,5-diClDMPAP. Multielement samples

Samples		% Composition (w/w) molar relation	Yb(III) found	% Relative error
	Yb(III)	50.0	49.8 ($n = 6$)	
1*	Other REE	50.0	$s = 0.032$	−0.31
			$CL_{\alpha=0.05} = 49.8 \pm 0.03$	
	Yb(III)	10.0	10.1 ($n = 6$)	
2*	Other REE	90.0	$s = 0.136$	+1.00
			$CL_{\alpha=0.05} = 10.1 \pm 0.11$	
	Yb(III)	50.0	51.6 ($n = 6$)	
3*	Other REE (with Y)	50.0	$s = 0.20$	+3.21
			$CL_{\alpha=0.05} = 51.6 \pm 0.16$	
	Magnet alloy[20]		24.9 ($n = 6$)	
4	Yb	25.0	$s = 0.070$	−0.40
			$CL_{\alpha=0.05} = 25.0 \pm 0.07$	
	Perovskite[21]		9.45 ($n = 6$)	
5	Ba $Na_{1/2}$ $Yb_{1/2}$ Te O_6 type		$s = 0.044$	+0.53
	Yb	9.4	$CL_{\alpha=0.05} = 9.45 \pm 0.045$	
	Perovskite[22]		17.1 ($n = 6$)	
6	Ba_3 Yb Ru Ir O_9 type		$s = 0.136$	+1.18
	Yb	16.9	$CL_{\alpha=0.05} = 17.1 \pm 0.014$	

*Synthetic samples.

the possibility of separating them, using anionic resins. This is a rapid and effective method.

According to the results obtained by Minczewsky, the elution order is: Lu < Yb < Tm < Y < Ho < La < Ce < Tb < Pr < Gd < Pm < Eu.

The experiment showed that the separation of Yb(III) from La(III) is possible by the methodology described here (% relative error < 1%). Yb(III) was separated from Y(III) with an error of 3%. The elution order obtained by Minczewksy was confirmed, which guarantees the quantitative separation of Yb(III) from the rest of the lanthanides. Table 3 shows the results obtained in the processing of synthetic samples and other materials.

CONCLUSIONS

The reagent 2-(3,5-dichloro-2-pyridylazo)-5-dimethyl aminophenol has been used in the spectrophotometric-extractive determination of the Yb(III) ion. The results obtained have been highly satisfactory taking into account the high sensitivity reached and the simplicity of the operation. The proposed methodology is applicable to the analysis of concrete samples of interest.

Acknowledgements—The authors wish to thank CONICET and the Government of San Luis for their financial support.

REFERENCES

1. S. Shibata, *Anal. Chim Acta*, 1963, **28**, 388.
2. H. A. Mottola and H. Freiser, *Talanta*, 1966, **13**, 55.
3. Yu. A. Zolotov and V. G. Lambrev, *Zh. Anal. Khim.*, 1965, **20**, 1153.
4. I. S. Kalmykova and L. V. Kukarina, *ibid.*, 1978, **33**, 909.
5. L. M. Antsiferova, L. V. Kukarina, I. S. Kalmykova and A. M. Shavrin, *ibid.*, 1977, **32**, 526.
6. W. B. Brown, J. F. Steinbach and W. F. Wagner, *J. Inorg. Nucl. Chem.*, 1960, **13**, 119.
7. L. S. Serdyuk, L. B. Karaseva, L. A. Albota and V. P. Denisenko, *Zh. Anal. Khim.*, 1977, **32**, 2361.
8. V. T. Mishchenko, E. Tselik and N. S. Alekseeva, *Ukr. Khim. Zh.*, 1977, **43**, 1322.
9. M. A. Akhmedli, P. B. Granovskaya and E. G. Melikeva, *Zh. Anal. Khim.*, 1973, **28**, 1304.
10. V. K. Manchanda and C. Allen Chang, *Anal. Chem.*, 1987, **59**, 813.
11. *Idem*, *ibid.*, 1986, **58**, 2269.
12. L. Fernández and R. Olsina, *Talanta*, 1991, **38**, 339.
13. L. Fernández and R. Olsina, *Anal. Sci.*, 1990, **6**, 411.
14. D. I. Ryabchikov and V. A. Ryabukhin, in *Analytical Chemistry of Yttrium and the Lanthanide Elements*, Ann Arbor, London, 1970.
15. J. C. Crock, F. E. Lichte, G. O. Riddle and C. L. Beech, *Talanta*, 1986, **33**, 601.
16. Yu. A. Zolotov, in *Extraction of the Chelate Compounds*, Ann Arbor, London 1970.
17. L. Sommer and G. Ackermann, *Pure and Appl. Chem.*, 1986, **58**, No 7, 1015.
18. Z. Sulcek, I. Rubeska, V. Sixta and T. Pauket, *At. Spectrosc.*, 1989, **10**, No 1, 4.
19. J. Minczewsky and R. Dybczynski, *J. Chromatog.*, 1962, **7**, 98.
20. Y. Inokoshi and M. Hata, *Jpn. Kokai Tokkyo Koho JP* 61 37, 940, 1986; *Chem. Abstr.*, 105, 28415z.
21. H. Roller and S. Kemmler-Sack, *Z. Anorg. Allg. Chem.*, 1980, **466**, 103; *Chem. Abstr.*, 93, 123997h.
22. E. Duerrschmidt and S. Kemmler-Sack, *ibid.*, 1980, **470**, 109; *Chem. Abstr.*, 94, 39820h.

Talanta, Vol. 39, No. 12, pp. 1611–1617, 1992
Printed in Great Britain.

0039-9140/92 $5.00 + 0.00

SENSITIVE SIMULTANEOUS DETERMINATION OF BENZO(A)PYRENE, PERYLENE AND CHRYSENE BY SYNCHRONOUS SPECTROFLUOROMETRY IN NONIONIC MICELLAR MEDIA

J. J. SANTANA RODRIGUEZ and Z. SOSA FERRERA
Department of Chemistry, Facultry of Marine Sciences, University of Las Palmas de Gran Canaria, 35017 Las Palmas, Spain

A. AFONSO PERERA and V. GONZALEZ DIAZ*
Department of Analytical Chemistry, Food Science and Toxicology, University of La Laguna, 38204 La Laguna, Spain

(*Received* 5 *December* 1991. *Revised* 13 *April* 1992. *Accepted* 13 *April* 1992)

Summary—A synchronous spectrofluorometric method was developed for the simultaneous determination of benzo(a)pyrene, perylene and chrysene in a POLE micellar medium, with detection limits of 0.05 ng/ml, 0.28 ng/ml and 0.64 ng/ml, respectively. Good recoveries were obtained for sea water samples spiked with each hydrocarbon.

Polycyclic aromatic hydrocarbons (PAHs) are present in complex environmental matrices, such as crude oils and sediment extracts, often in association with other organic compounds.[1] Increased attention has recently been paid to these compounds in environmental chemistry due to the mutagenic character of some of these molecules.[2] Therefore, a highly selective analytical method is required for assessment of pollution in the environment.

Synchronous scan luminiscence spectrometry has been developed by Lloyd to simplify a fluorescence spectrum;[3] the excitation and fluorescence wavelengths are synchronously scanned under the optimized separation of these wavelengths. This technique has been used to characterize crude oils[4-6] and to identify and quantify polycyclic aromatic compounds.[7-12]

Although aqueous micellar systems continue to be the focus of intensive study in many disciplines[13,14] they have had few practical applications in the analyses of organic species.[15] Three major potential advantages can be accrued by the use of micelles in fluorometry. These include improved sensitivity, diminution of interferences, and greater experimental convenience.[16] However, the solutions of some surfactants exhibit fluorescence which may cause important disturbances in analytical signals.

In a former paper[12] it was established that fluorescence emitted by PAHs benzo(a)pyrene and perylene increases considerably in the presence of Triton X-100 micelles. However, the fluorescence due to this surfactant, may considerably affect analytical determinations of some PAHs.

This paper shows that the substitution of Triton X-100 (the most important non-ionic surfactant used for analytical purposes), for another non-ionic surfactant may result advantageous. By using Polyoxyethylene 10 lauryl ether (POLE) micelles, a sensitive method for simultaneous determination of a mixture of three PAHs, benzo(a)pyrene, perylene and chrysene by synchronous fluorescence spectrometry is proposed.

EXPERIMENTAL

Reagents

Stock solutions (0.23 mg/ml) of chrysene (Aldrich) and (0.25 mg/ml) of benzo(a)pyrene, B[a]P, (Aldrich) and of perylene (Sigma) were prepared in ethanol. Working solutions were prepared by appropriate dilution with ethanol.

The surfactants Brij-96 and Polyoxyethylene 10 lauryl ether (POLE) were obtained from Aldrich.

*Author for correspondence should be addressed.

Apparatus

Synchronous fluorescence measurements and spectra were made with a Perkin-Elmer MPF-44A recording spectrofluorometer equipped with a 150-W Osram XBO xenon arc, a Sabtronics 2010A digital read-out, a Selecta Frigitherm S382 thermostat and 1-cm quartz cells. The emission measuring system was calibrated daily via use of the Perkin-Elmer set of fluorescent polymer blocks.

General procedure for the determination of mixtures of benzo(a)pyrene, perylene and chrysene

To an aliquot containing 12.5 ng–2.5 μg of chrysene, 2.5 ng–2.5μg of benzo(a)pyrene and perylene, in the allowed ratios, in a 25-ml calibrated flask, add 5 ml of $1.0 \times 10^{-2}M$ POLE solution and the necessary volume of ethanol so that the final solution contains 2% (v/v) of organic solvent, and dilute to volume with demineralized water. The fluorescence intensity measures are made to synchronous maxima of each PAH: for chrysene $\lambda^0_{s,em} = 320$ nm ($\Delta\lambda = 42$ nm), for benzo(a)pyrene $\lambda^0_{s,em} = 386$ nm ($\Delta\lambda = 17.5$ nm) and for perylene $\lambda^0_{s,em} = 432$ nm ($\Delta\lambda = 17.5$ nm). The quantities of all hydrocarbons are determined from calibration curves obtained under the same experimental conditions.

Recovery of benzo(a)pyrene, perylene and chrysene in sea water

Sea water samples were passed successively through filters of different porosity (50, 30 and 5 μm) and by UV radiation. After verifying that they do not present fluorescence, they were spiked by suitable amounts of each PAH and analysed according to the above method.

RESULTS AND DISCUSSION

Conventional spectra

Polycylic aromatic hydrocarbons are slightly soluble in water. In order to study the spectrofluorometric behaviour of benzo(a)pyrene, perylene and chrysene, ethanol–water solutions were used.

We refer to aqueous solutions as containing 2% (v/v) ethanol–water. Solutions containing the same volume of ethanol, to which sufficient surfactant is added in order to ensure a surfactant concentration greater than its critical micellar concentration, are referred to as micellar solutions.

I_F–$C_{surf.}$ curves allow one to select such a surfactant concentration and additionally, confirm that the changes observed in the fluorescence of PAHs are directly related to the formation of a micellar system. This can be seen for POLE in Fig. 1.

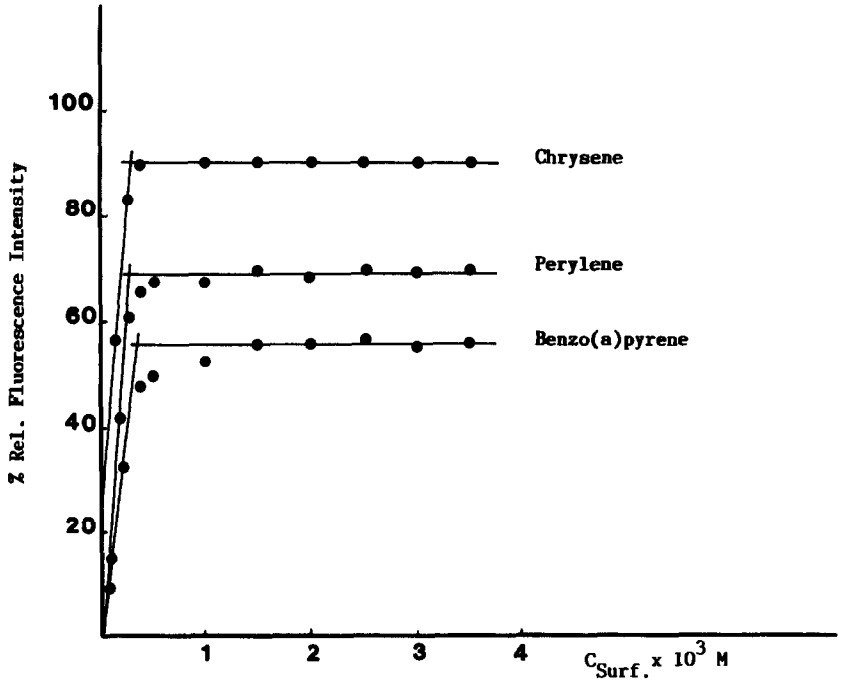

Fig. 1. Effect of POLE concentration on the fluorescence intensity of benzo(a)pyrene, perylene and chrysene. $C_{PAH} = 2.0 \times 10^{-6}M$.

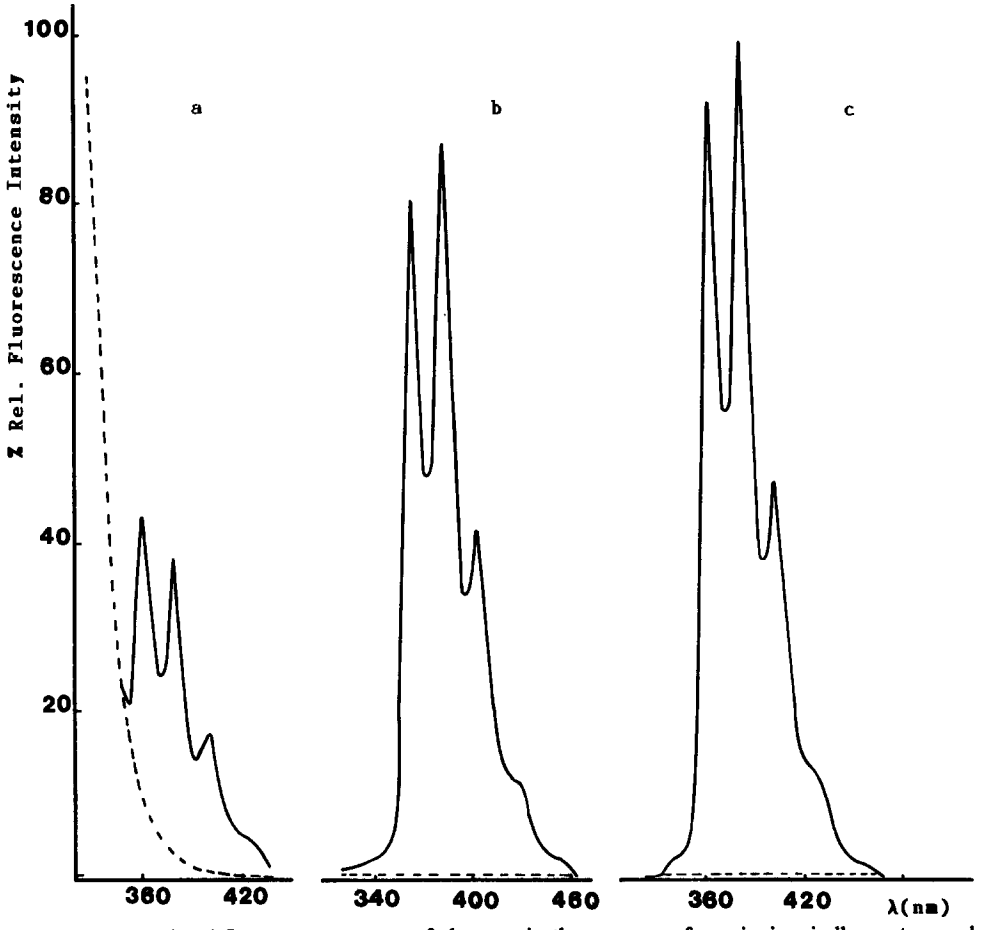

Fig. 2. Conventional fluorescence spectra of chrysene in the presence of non-ionic micellar system and of each surfactant. Triton X-100 (a), Brij-96 (b) and POLE (c). $C_{PAH} = 2.0 \times 10^{-6} M$, $C_{Surf.} = 1.0 \times 10^{-3} M$. $\lambda_{exc} = 273$ nm.

Figure 2 shows the emission spectra of chrysene in the presence of a non-ionic micellar system, as well as of each surfactant. In high concentrations, Triton X-100 originates a fluorescence emission that interferes remarkably with the chrysene emission. It does not occur

Table 1. Spectrofluorometric characteristics of chrysene, benzo(a)pyrene and perylene in different media

PAH	Aqueous λ_{exc}	Aqueous λ_{em}	POLE λ_{exc}	POLE λ_{em}	POLE I_M/I_A*	Brij-96 λ_{exc}	Brij-96 λ_{em}	Brij-96 I_M/I_A*
Chrysene	285 (32)	364 (6)	273 (15)†	363 (12)	38	274 (15)†	362 (13)	33
	307 (—)	391 (—)	300 (—)	382 (16)‡		312 (35)	382 (16)‡	
	318 (20)†	403 (12)‡	310 (36)	402 (24)		324 (20)	402 (20)	
	334 (18)	428 (—)	324 (24)	426 (—)		425 (—)		
	349 (—)							
Benzo(a)pyrene	266 (—)	406 (16)‡	353 (—)	406 (12)‡	186	356 (—)	406 (12)‡	170
	288 (—)	428 (23)	370 (22)	430 (16)		372 (20)	430 (16)	
	296 (14)	456 (66)	388 (18)†	455 (—)		391 (19)†	456 (20)	
	350 (—)	480 (102)						
	366 (26)							
	384 (24)†							
Perylene	282 (26)†	442 (18)‡	372 (—)	443 (18)‡	89	365 (—)	444 (18)‡	75
		471 (25)	396 (—)	472 (25)		396 (—)	473 (24)	
		503 (—)	415 (26)†	503 (—)		415 (25)†	504 (—)	
			440 (—)			441 (—)		

*Ratio of fluorescence intensity in micellar and aqueous media.
†Wavelengths of excitation.
‡Wavelengths of emission.
Values in parentheses refer to the peak half-widths; dash (—) indicates that the peaks were extensively overlapped.

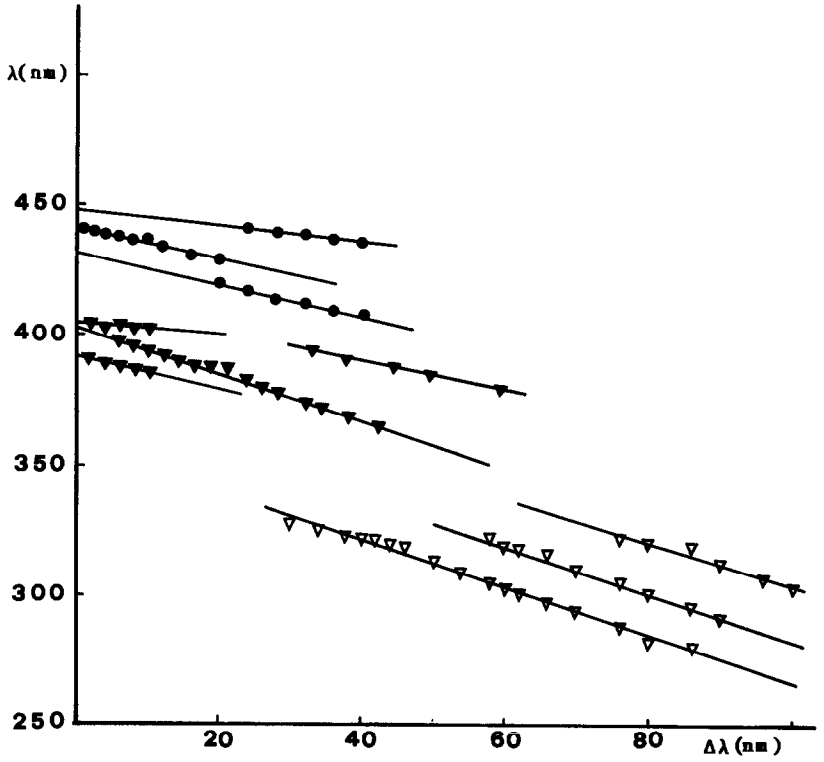

Fig. 3. Effect of $\Delta\lambda$ on the values $\lambda_{s,em}$. $C_{PAH} = 2.0 \times 10^{-6}M$. $C_{PAH} = 2.0 \times 10^{-6}M$, $C_{POLE} = 1.0 \times 10^{-3}M$. Benzo(a)pyrene (▼), perylene (●) and chrysene (▽).

with perylene and benzo(a)pyrene because the wavelengths of its excitation and emission maxima are above 350 nm and 400 nm respectively.

Some important characteristics of the excitation and emission spectra are summarized in Table 1. The excitation and emission spectra of PAHs in neutral micellar media of POLE and Brij-96 are similar with regard to the number of peaks and wavelengths of maximum intensity.

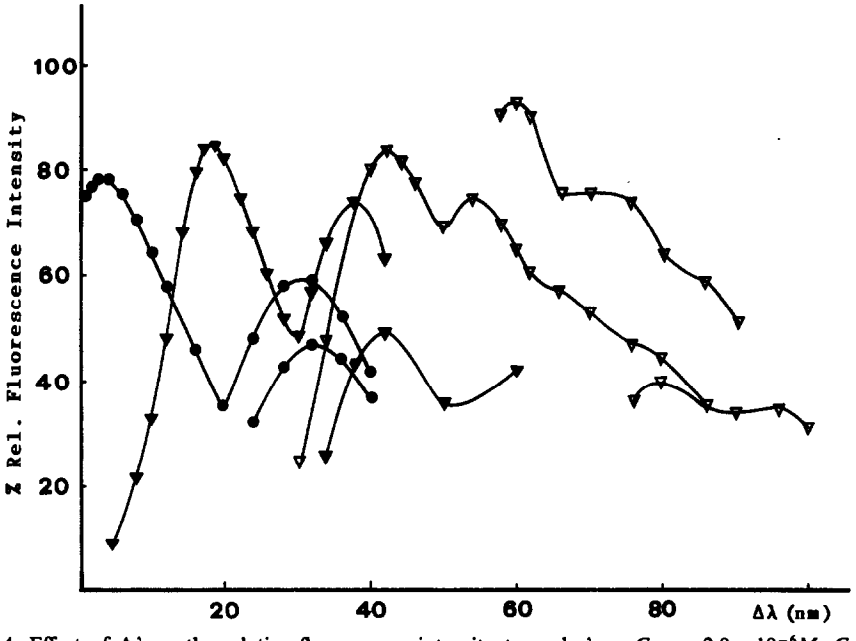

Fig. 4. Effect of $\Delta\lambda$ on the relative fluorescence intensity to each $\lambda_{s,em}$. $C_{PAH} = 2.0 \times 10^{-6}M$, $C_{POLE} = 1.0 \times 10^{-3}M$. Benzo(a)pyrene (▼), perylene (●) and chrysene (▽).

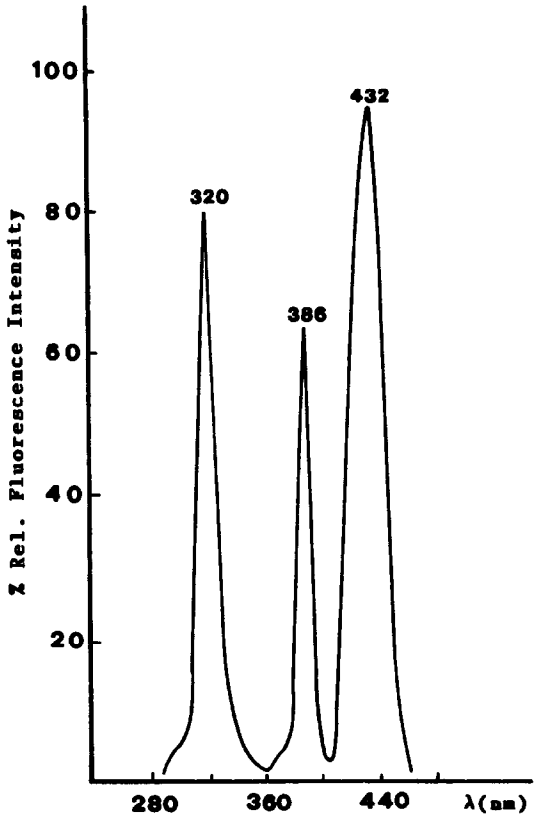

Fig. 5. Synchronous fluorescence spectra of a mixture of benzo(a)pyrene, perylene and chrysene in micellar medium. $C_{POLE} = 2.0 \times 10^{-3} M$. Chrysene: $\Delta\lambda = 42$ nm, $C_{PAH} = 2.0 \times 10^{-6} M$. Benzo(a)pyrene and perylene: $\Delta\lambda = 17.5$ nm, $C_{PAH} = 2.0 \times 10^{-8} M$.

Comparing both media, aqueous and micellar, the most important differences are observed in the excitation spectra. It slightly enhances the definition of chrysene and benzo(a)pyrene in micellar medium. Quite the reverse of perylene, in which an important shift towards longer wavelengths is produced. This shift has a great analytical interest because it introduces a differential factor between perylene and the other two PAHs. The half-widths obtained in micellar medium are similar or narrower than those obtained in aqueous medium.

With the same experimental conditions, the use of micellar media produces an important increase in fluorescence intensities emitted by the three PAHs and in particular by perylene. This sensitivty is higher when POLE is used as a surfactant.

Synchronous spectra

In aqueous medium, the synchronous spectra of the three PAHs show several bands of different intensity only slightly defined. The introduction of a micellar medium, not only produces an important sensitivity but also allows synchronous spectra, in which the correct selection of $\Delta\lambda$ would let the analysis of each PAH in the presence of the others.

Between the maximum of emission at the shortest wavelength and the maximum of excitation at the longest wavelength ($\lambda^0_{em} - \lambda^0_{exc}$) of conventional spectra, differences of 38–41 nm, 15–18 nm and 3 nm are produced for chrysene, benzo(a)pyrene and perylene, respectively, in micellar media of Triton X-100, Brij 96 and POLE. These values of $\Delta\lambda$ could be adequate for the determination of the three PAHs by synchronous spectrofluorometry. However, as for Triton X-100, $\lambda^0_{em} - \lambda^0_{exc} = 48$ nm, the synchronous spectra of Triton X-100 and chrysene overlap. The highest intensity of the signals obtained in the presence of POLE recommend the use of this surfactant with analytical purposes. In order to modify the spectral bandwidth of the synchronous signal, $\Delta\lambda$ and Stokes shift parameters can be varied experimentally. The most important parameter in the simultaneous analysis of mixtures is the selection of the optimum wavelength difference between both monochromators.

Table 2. Simultaneous analysis of synthetic binary mixtures of benzo(a)pyrene, perylene and chrysene

Mixture	Ratio	Benso(a)pyrene μg/ml Given	Found*	Perylene μg/ml Given	Found*	Chrysene μg/ml Given	Found*
B[a]P:Perylene	1:5	2.0	2.05	10.0	9.70		
	1:4	2.0	2.13	8.0	8.40		
	1:1	1.0	1.03	1.0	0.90		
	5:1	5.0	5.22	1.0	0.94		
	8:1	8.0	7.99	1.0	0.99		
B[a]P:Chrysene	1:5	2.0	2.08			10.0	9.16
	1:4	2.0	2.02			8.0	8.36
	1:1	1.0	0.99			1.0	1.00

*Mean of three determinations.

Table 3. Simultaneous analysis of synthetic ternary mixtures of benzo(a)pyrene, perylene and chrysene

Ratio	Benzo(a)pyrene ppb		Perylene ppb		Chrysene ppb	
	Given	Found*	Given	Found*	Given	Found*
1:1:1	5.0	4.67	5.0	5.06	5.0	4.66
1:10:10	1.0	0.95	10.0	9.26	10.0	10.71
10:1:10	10.0	9.27	1.0	0.99	10.0	9.83
3:1:4	6.0	5.86	2.0	1.79	8.0	7.95
1:3:1	2.0	1.99	6.0	5.83	2.0	2.04

*Mean of three determinations.

For chrysene, perylene and benzo(a)pyrene, synchronous fluorescence spectra were obtained over a range of $\Delta\lambda$ from 1 to 100 nm. The results found are shown in Figs. 3 and 4 from which the following considerations can be made: the spectral distribution is a function of $\Delta\lambda$ and the fluorescence intensity depends strongly on $\Delta\lambda$.

The experimental results show that it is necessary to use $\Delta\lambda = 30$–45 nm for chrysene, $\Delta\lambda = 12$–32 for benzo(a)pyrene and $\Delta\lambda < 19$ nm for perylene, to obtain synchronous spectra of only one peak and an adequate fluorescence intensity. In these intervals of wavelengths, maxima intensities were obtained for $\Delta\lambda = 42$ nm, $\Delta\lambda = 17$–19 nm and $\Delta\lambda = 3$–4 nm, for chrysene, benzo(a)pyrene and perylene, respectively. These values of $\Delta\lambda$ correspond to $\lambda^0_{s,em} = 322$ nm, $\lambda^0_{s,em} = 386$ nm and $\lambda^0_{s,em} = 439$ nm.

A great concordance exists between $\Delta\lambda$ deduced from the conventional fluorescence spectra and the experimental $\Delta\lambda$. In addition, it must be stressed that the values of $\lambda^0_{s,em}$ are practically the same as the peak wavelength of the maximum of excitation at the longest wavelength on the conventional spectrum (λ^0_{exc}).

Figure 5 shows the synchronous spectrum of a synthetic mixture of the three PAHs using the same $\Delta\lambda$ for benzo(a)pyrene and perylene.

Analytical considerations

In order to develop a procedure for the analysis of binary and ternary mixtures of PAHs, the analytical characteristics were evaluated.

For chrysene and benzo(a)pyrene its optimum $\Delta\lambda$ was selected whereas for perylene the same $\Delta\lambda$ was chosen as for benzo(a)pyrene in order to simplify the experimental process.

In the presence of POLE, linear calibration graphs for each PAH were obtained by plotting the fluorescence intensity measures on the synchronous spectra against hydrocarbon concentration. The linear concentration ranges are 0.1–100 ng/ml for benzo(a)pyrene and perylene and 0.5–100 ng/ml for chrysene. The detection limits[17] are 0.05 ng/ml, 0.28 ng/ml and 0.64 ng/ml for benzo(a)pyrene, perylene and chrysene, respectively.

When the method was applied to two series of eleven samples containing 5 and 50 ng/ml for each PAH, the relative standard deviations obtained were $\pm 3.1\%$ and $\pm 0.95\%$ for benzo(a)pyrene, $\pm 3.8\%$ and $\pm 0.28\%$ for perylene, and 0.8% and 0.65% for chrysene.

The analysis of samples containing various ratios of two of these hydrocarbons shows that the determination of their mixtures is feasible up to the following ratios. B[a]P:Perylene = 1:25; Perylene:Chrysene = 1:5; B[a]P:Chrysene = 1:100 and Chrysene:B[a]P = 1:1. The criterion for interference was a variation of more than $\pm 4\%$ in the hydrocarbon concentrations found.

Table 4. Simultaneous analysis of synthetic binary mixtures of benzo(a)pyrene, perylene and chrysene in sea water

Mixture	Ratio	Benzo(a)pyrene μg/ml		Perylene μg/ml		Chrysene μg/ml	
		Given	Found*	Given	Found*	Given	Found*
B[a]P:Perylene	1:2	2.0	1.96	4.0	3.68		
	1:1	3.0	2.86	3.0	2.74		
	3:1	6.0	5.73	2.0	1.95		
B[a]P:Chrysene	1:3	2.0	2.09			6.0	5.81
	1:1	1.0	0.92			1.0	0.97
	1:7	1.0	1.07			7.0	7.15

*Mean of three determinations.

Table 5. Simultaneous analysis of synthetic ternary mixtures of benzo(a)pyrene, perylene and chrysene in sea water

Ratio	Benzo(a)pyrene ppb		Perylene ppb		Chrysene ppb	
	Given	Found*	Given	Found*	Given	Found*
1:1:1	5.0	4.68	5.0	4.90	5.0	4.52
1:10:1	1.0	0.92	10.0	10.30	10.0	9.00
10:1:10	10.0	9.80	1.0	1.00	10.0	9.75
2:1:3	6.0	5.69	3.0	3.26	9.0	8.60
1:3:1	3.0	2.90	9.0	9.30	3.0	2.75

Mean of three determinations.

Determination of mixtures of benzo(a)pyrene, perylene and chrysene

The procedure is not only very sensitive for the determination of benzo(a)pyrene, perylene and chrysene but also allows the analysis of binary and ternary mixtures. Tables 2 and 3 show the results obtained for some synthetic samples.

The method was applied to the simultaneous determination of benzo(a)pyrene, perylene and chrysene in sea-water spiked with suitable amounts of each hydrocarbon. The results shown in Tables 4 and 5 indicate good recovery data.

Acknowledgements—The authors wish to acknowledge financial support of this work by the Gobierno Autónomo de Canarias (Research Project No 20-31.07.89) and CICYT (Spain) grant PB88-0427.

REFERENCES

1. W. H. Griest and J. E. Caton, *Handbook of Polycyclic Aromatic Hydrocarbons*, p. 95–148. Marcel Dekker, New York, 1983.
2. *Polycyclic Aromatic Hydrocarbons and Carcinogenesis*, p. 185. Adv. Chem. Series 283, ACS, Washington, 1985.
3. J. B. F. Lloyd, *Nature* (London) 1971, **64**, 231.
4. *Idem, J. Forensic Sci. Soc.*, 1971, **11**, 235.
5. *Idem, Analyst*, 1980, **105**, 97.
6. P. John and I. Soutar, *Anal. Chem.*, 1976, **48**, 520.
7. T. Vo-Dinh, R. B. Gammage, A. R. Hawthorne and J. H. Thorngate, *Environ. Sci. Technol.*, 1978, **12**, 1297.
8. E. L. Inman and J. D. Winefordner, *Anal. Chem.*, 1982, **54**, 2018.
9. T. Vo-Dinh, R. B. Gammage and P. R. Martínez, *ibid.*, 1981, **53**, 253.
10. M. J. Kerkhoff, T. M. Lee, E. R. Allen, D. A. Lundgren and J. D. Winefordner, *Environ. Sci. Technol.*, 1985, **19**, 695.
11. L. A. Files, B. T. Jones, S. Hanamura and J. D. Winefordner, *Anal. Chem.*, 1988, **58**, 1440.
12. J. J. Santana Rodriguez, Z. Sosa Ferrera, A. Afonso Perera and V. González Díaz, *Anal. Chim. Acta*, 1991, **255**, 107.
13. J. H. Fendler, *Membrane Mimetic Chemistry*, Wiley, New York, 1982.
14. D. Attwood and A. T. Florence, *Surfactant Systems*, Chapman & Hall, New York, 1983.
15. J. Georges, *Spectrochimica Acta Rev.*, 1990, **33**, 27.
16. W. L. Hinze, H. N. Singh, Yoshima Baba and N. G. Harvey, *Trends Anal. Chem.*, 1984, **3(8)**, 193.
17. G. L. Long and J. D. Winefordner, *Anal. Chem.*, 1983, **55**, 712A.

Talanta, Vol. 39, No. 12, pp. 1619–1623, 1992
Printed in Great Britain.

0039-9140/92 $5.00 + 0.00

HPLC ANALYSIS OF THIMEROSAL AND ITS DEGRADATION PRODUCTS IN OPHTHALMIC SOLUTIONS WITH ELECTROCHEMICAL DETECTION

JESUS R. PROCOPIO, Mª PILAR DA SILVA, Mª DEL CARMEN ASENSIO, Mª TERESA SEVILLA and LUCAS HERNANDEZ

Department of Analytical Chemistry and Instrumental Analysis, Autonoma University of Madrid, 28049 Madrid, Spain

(*Received* 3 *February* 1992. *Revised* 13 *April* 1992. *Accepted* 13 *April* 1992)

Summary—A reverse-phase high-performance liquid chromatographic assay using amperometric detection on a glassy-carbon electrode has been developed for analysis of thimerosal and its main degradation products, thiosalicylic acid and dithiodibenzoic acid, in ophthalmic formulations. A potential value of 0.9 V *vs.* Ag/AgCl was chosen for simultaneous detection of thimerosal and thiosalicylic acid, obtaining limits of detection of 1.0 and 0.2 ng injected, respectively. A potential value of 1.2 V was applied for simultaneous determination of all three compounds studied, obtaining in this case limits of detection of 3, 4 and 4 ng injected for thimerosal, thiosalicylic acid and dithiodibenzoic acid, respectively. The results obtained reveal the utility of the HPLC method in quality control of commercial products containing thimerosal with good detectability.

Thimerosal (sodium ethylmercurythiosalicylate) [TMS] is an organomercurial compound widely used as both topical antiseptic and antimicrobial preservative. It is the preservative used for soft contact lens care solutions. Stability studies have revealed that this compound is unstable in aqueous solution,[1,2] mainly in glass bottles, though thimerosal can be lost from ophthalmic solutions stored in plastic containers.[3,4] It has also been reported that the presence of halides can have an adverse influence on its stability.[5]

The decomposition of thimerosal in aqueous solution has been reported previously,[2,4] and it was shown that the major degradation products were thiosalicylic acid [TSA] and ethylmercury salts (Fig. 1). Thiosalicylic acid can also undergo irreversible oxidation to 2,2′-dithiodibenzoic acid [DTDBA].

Analytical methods previously developed for thimerosal determination in ophthalmic solutions have included polarography,[6] atomic-absorption spectrometry using a carbon rod atomiser,[7] and colorimetry.[8] These techniques, based on total mercury or total organic mercury, do not indicate accurately the amount of intact thimerosal present in solution. High-pressure liquid chromatography has been suggested as a simple, specific method for analysis of intact thimerosal and its degradation compounds.[9–13] In previous works, several HPLC methods have been developed for simultaneous determination of TMS and its degradation products. Meyers and Colm[10] reported a method, using an ODS reverse-phase column, for separation of TMS and TSA, but the method was poor in sensitivity (>5 μg/ml) and it did not provide adequate resolution of both compounds. Reader and Lines[4] obtained an adequate resolution of TMS and its major decomposition products and good sensitivity on a ODS reverse-phase HPLC using ionic suppression. In all these methods UV detection was used. Coulometric detection has been applied to HPLC analysis of TMS alone in an ophthalmic solution, obtained a detection limit of 0.4 ng (at signal/noise ratio = 2) for an injection volume of 50 μl.[13]

Because thimerosal and its degradation compounds are often present in microquantities (usually less than 10 μg/ml or 40 μg/ml for TMS, depending on sample type, and less than 1 μg/ml for TSA and DTDBA), and the poor utility of methods found in the bibliography for analysis of three compounds in real samples, it was necessary to develop a suitable method with a low detection limit. The objectives of this study were to develop an HPLC assay for thimerosal and its degradation compounds, in ophthalmic solutions, using amperometric detection. The choice of this detection mode

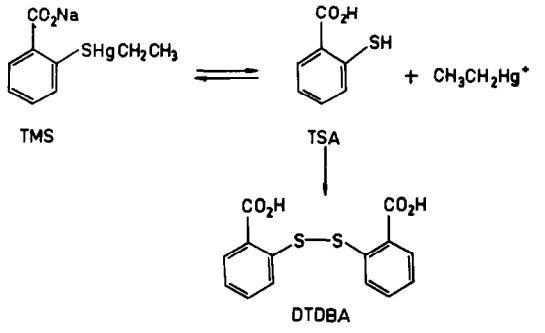

Fig. 1. Scheme for the decomposition of thimerosal in aqueous solutions.

presents several advantages: wide linear dynamic range, good reproducibility and detection limits in the low nanogram to picogram range. Additionally, response selectivity can be controlled by appropriate choice of the working potential.

EXPERIMENTAL

Reagents

Thimerosal TMS (Alcon Iberhis, Spain), thiosalicyclic acid TSA and 2,2′-dithiodibenzoic acid DTDBA (Sigma, U.S.A.) were used without further purification. Methanol, phosphoric and acetic acids were analytical reagent grade (Carlo ERBA, Italy). A stock solution of thimerosal was made up in water whereas stock solutions of other compounds were made up in methanol, in the concentration range 1000–2000 μg/ml. The solutions were stored at 4°, preserved from light.

Apparatus

The HPLC system consisted of a Gilson model 302 pumping system, equipped with a membrane damper, and a Rheodyne model 7125 injector equipped with a 20-μl loop. The detector was a Methrom model 461 amperometric detector, equipped with a Methrom model 656 flow cell of less than 1-μl volume. A glassy carbon electrode (Methrom 6.0805.010) with an area of 7 mm^2 was used as working electrode. The column temperature was thermostated at $25.0 \pm 0.2°$ with a glass jacket using a Selecta model Digiterm S-613 thermostat. A Spectra physics SP-4290 integrator was used to record and integrate all chromatograms.

Chromatographic condition

The column was a 150 × 4 mm stainless steel prepacked reverse-phase column containing 5-μm Spherisorb C18 particles (Tracer). The mobile phase was methanol–water (60:40, v/v) containing 0.02*M* acetic acid or phosphoric acid. This solution was filtered through a Millipore (Waters) Durapore filter (0.45-μm pore size) and deareated by stirring under vacuum for 10 min. The pressure at a flow rate of 1 ml/min was 140 bar. The detector was operated both 0.9 and 1.2 V *vs.* Ag/AgCl, with a sensitivity of 10 nA full scale. Quantification was carried out by comparison of the peak areas and heights obtained from test solutions with the peak areas and heights obtained from standard solutions registered in the same conditions.

As TSA suffers a quick decomposition by light in the chromatographic conditions, injection of the samples at neutral pH was necessary in order to obtain a good response for this compound.

Determination of TMS in ophthalmic solutions by HPLC method

The samples were made homogeneous by stirring for 5 min. Samples containing 0.001% TMS (10 μg/ml) were filtered and directly injected into the chromatographic system. For the samples containing 0.004% TMS (40 μg/ml) a dilution (1 ml of sample to 10 ml in water) was made previous to injection.

RESULTS AND DISCUSSION

Electrochemical studies

The electrochemical behaviour of TMS and its main decomposition products, TSA and DTDBA, was characterized by both cyclic and hydrodynamic voltammetry on glassy carbon electrode, in order to choose the operating parameters. Figure 2 shows the cyclic voltamperograms of the studied compounds at the 60 μg/ml concentration level in 0.02*M* phosphoric acid and in the presence of 60% (v/v) methanol. For TMS and DTDBA the voltamperograms reveal a single anodic wave with peak potentials at 1.08 and 1.20 V (*vs.* SCE) respectively. The TSA presents two peaks in the voltamperograms at 0.64 and 1.18 V. Absence of cathodic waves during the reverse scan of the CV cycle indicates an irreversible oxidation for all compounds.

By comparison of the peak heights of each compound, the electrochemical oxidation mechanism of TMS probably involves one electron transfer from a sulphur atom to the electrode surface yielding a transient radical cation.

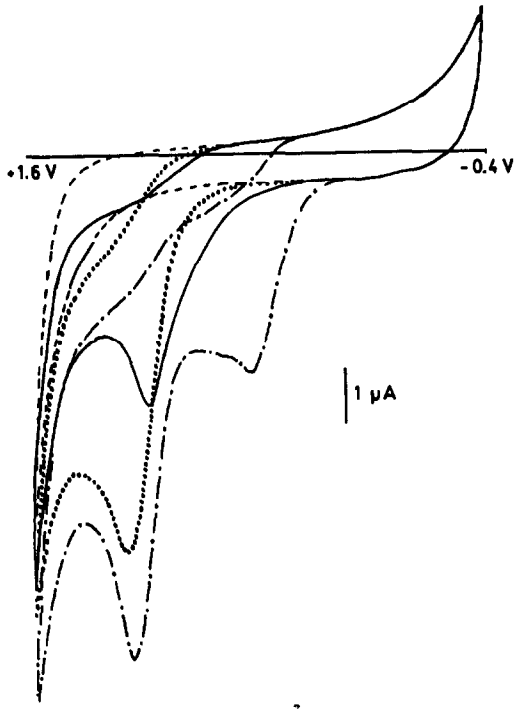

Fig. 2. Cyclic voltamperograms of studied compounds at the 60 μg/ml concentration level in chromatographic conditions. TMS (—) TSA (-·-·-); DTDBA (···); background (---).

The first wave observed for TSA is probably due to a one electron transfer with subsequent dimerization to form thiuram disulphide, DTDBA, which is subsequently oxidized at higher potentials in a two-electron transfer, giving the second anodic peak. According to this assumption, the wave observed at 1.2 V for DTDBA corresponds to oxidation of disulphide linkage. The electrochemical behaviour of all compounds studied is presently under investigation.

As shown in the cyclic and hydrodynamic voltamperograms, TMS reaches a better signal at potentials higher than 1.0 V, while for DTDBA a maximum signal is obtained at 1.2 V. TSA can be efficiently oxidized at potentials higher than 0.8 V, obtaining an optimal signal at potentials higher than 1.1 V. According to these results an average potential of 0.9 V for simultaneous detection of TMS and TSA, and a potential of 1.2 V for TMS, TSA and DTDBA can be chosen. Detection limits and linearities, for concentrations ranging between 0.10 and 10.0 μg/ml, were evaluated at these values of potentials. The results of sensitivity, limits of detection and linearities found are shown in Table 1. Better detection limits and higher linearities for TMS and TSA were obtained at 0.9 V, because of lower backgrounds and noises found at this potential value, obtaining better signal-to-noise ratios. The limit of detection found for TMS at 0.9 V is in the same order of magnitude than in the bibliography,[13] using a coulometric detector.

Replicate samples of three compounds were injected at the 1-μg/ml concentration level, in order to obtain a measure of method reproducibility. The method exhibits good reproducibility with relative standard deviation of 1.4 and 2.9% for TMS and TSA at 0.9 V, respectively. At a potential of 1.2 V, the relative standard deviation was higher than at 0.9 V, obtaining values of 2.9, 4.1 and 3.5% for TMS, TSA and DTDBA, respectively. Typical chromatograms are shown in Fig. 3.

Determination of TMS in ophthalmic solutions

Several soft lens products containing TMS in concentrations of 0.001 (10 μg/ml) and 0.004% (40 μg/ml) (Alcon Iberhis, Spain) were analysed using the proposed method, some of these at the time of their manufacture and others up to three years old. Concomitants present in samples do not interfere, only a slow decrease of retention times of TMS because of presence of polymers in samples that can coat the column packing was observed, as it was previously reported.[10] No change was observed for TSA and DTDBA. In addition, an increase of the analytical signal of TMS was observed without an increase of background or noise, when successive sample solutions were injected. Figure 4 shows chromatograms obtained for real samples in these conditions.

Table 1. Statistical treatment of calibration graphs and limits of detection (signal-to-noise 1:3)

Compounds	Detection potential, V	Sensitivity, nA ml/μg	L.D.* ng	Correlation coefficient
TMS		33.5	3	0.9985
TSA	+1.2	48.9	4	0.9907
DTDBA		34.5	4	0.9988
TMS	+0.9	9.3	1	0.9994
TSA		65.9	0.2	0.9996

*Injection volume: 20 μl.

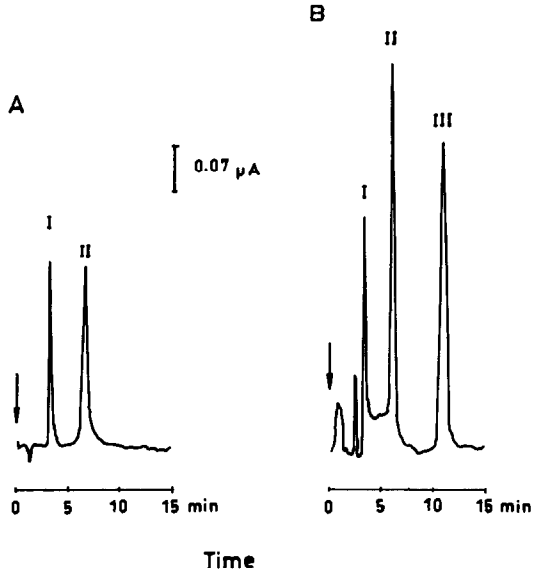

Fig. 3. Chromatograms of thiosalicyclic acid (I), thimerosal (II) and dithiodibenzoic acid (III). Potential of the detector: (A) 0.9 V and (B) 1.2 V *vs.* Ag/AgCl.

The results obtained for TMS concentrations by the HPLC method are compared in Table 2 with those obtained by the cold-vapour atomic absorption spectrophotometric (CVAAS) standard method. The products assayed at the time of manufacture gave similar results by the HPLC and CVAAS methods, however older products contained, according to the HPLC method, significatively less TMS than the initial amount, specially the product type B.

These results indicate that the CVAAS method is not adequate for checking the ageing of the ophthalmic solutions by degradation of TMS. In most cases, as can be deduced from Table 2, only a light diminution of TMS amount is observed in comparison with the diminution observed by the HPLC method. The CVAAS technique detects only the total amount of mercury in the sample but, as a consequence of the degradation process, the total concentration of mercury does not vary, because the decomposition compound, ethyl mercury ions contains mercury as the intact TMS. Lower concentrations of mercury encountered for TMS by the CVAAS method in relation to the initial content in most of the samples may be due to adsorption processes of TMS or ethylmercury on the container walls.[4]

Table 2 shows TMS concentrations obtained for different formulations stored in similar conditions. From the results, an important effect of concomitant nature in each formulation on the degradation rate of TMS could be inferred. Also it was observed that samples stored in the darkness keep their TMS level larger than samples stored in subdued sunlight.

With the proposed method it is also possible to distinguish between TMS and its decomposition products, TSA and DTDBA. So, samples that seem unaltered by the CVAAS technique, by the HPLC method show an important diminution of TMS concentration and appreciable amounts of degradation products. In Table 3 the results obtained in the determination of TSA and DTDBA content in some significant samples are shown. It is observed that in the darkness TSA is the main degradation compound, but in presence of light DTDBA is the principal degradation compound from both TMS and TSA.

All these results reveal the utility of the HPLC method with electrochemical detection in the quality control of commercial products containing TMS. This is an easy, quick and feasible method not only for determination of TMS

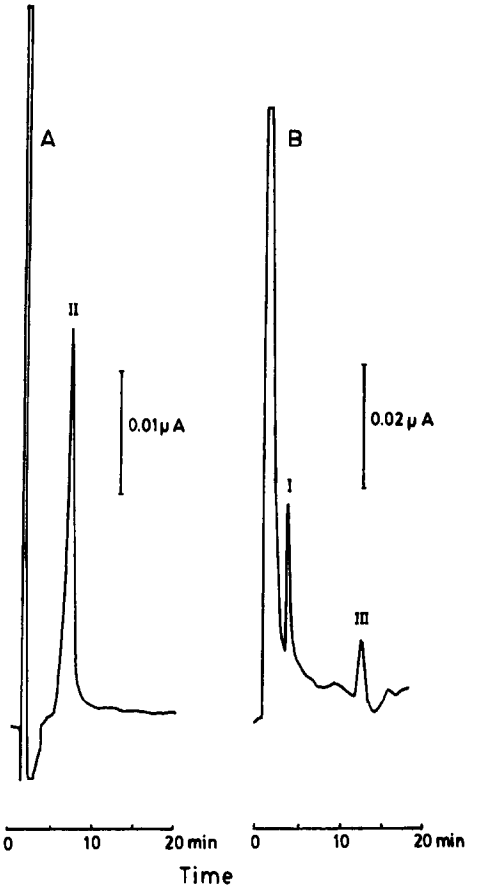

Fig. 4. Chromatograms of real samples. (A) sample B1, electrode potential 0.9 V. (B) sample A6, assay data 10/91, electrode potential 1.2 V. Compounds: TSA (I), TMS (II) and DTDBA (III).

Table 2. Thimerosal assay in soft contact lens products ($n = 3$)

Sample	Manufacture date	TMS concentration, μg/ml			
		HPLC		CVAA	
		I	II	III	IV
A1	4/91	10.6 ± 0.2	—	10.7 ± 0.1	—
A2	4/91	10.6 ± 0.1	—	10.6 ± 0.1	—
A3	11/90	9.53 ± 0.05	7.67 ± 0.05	10.2 ± 0.1	10.4 ± 0.2
A4	11/90	8.70 ± 0.05	5.7 ± 0.1	9.9 ± 0.2	10.4 ± 0.2
A5	5/89	7.9 ± 0.2	N.D.	10.7 ± 0.2	11.7 ± 0.2
A6	1/89	3.41 ± 0.01	1.41 ± 0.04	8.6 ± 0.2	10.4 ± 0.1
B1	6/90	7.7 ± 0.2	—	9.9 ± 0.1	10.5 ± 0.2
B2	4/90	7.4 ± 0.1	—	9.4 ± 0.1	10.3 ± 0.1
B3	5/89	6.4 ± 0.1	5.77 ± 0.05	8.4 ± 0.3	11.0 ± 0.3
B4	5/89	6.9 ± 0.1	5.11 ± 0.06	9.8 ± 0.1	11.1 ± 0.1
B5	9/88	3.5 ± 0.2	3.9 ± 0.1	9.0 ± 0.2	10.5 ± 0.2
B6	5/88	1.23 ± 0.05	0.90 ± 0.01	9.3 ± 0.1	11.2 ± 0.2
C1	4/91	11.2 ± 0.2	—	11.2 ± 0.1	—
C2	4/91	11.1 ± 0.1	—	11.1 ± 0.1	—
C3	6/89	2.53 ± 0.07	—	9.8 ± 0.1	10.0 ± 0.1
D	5/91	43.0 ± 1.3	—	—	42.8 ± 0.4
E	4/91	42.2 ± 1.5	—	—	42.2 ± 0.6
F	4/91	39.7 ± 1.2	—	—	42.0 ± 0.8
G	5/91	44.4 ± 1.2	—	—	43.6 ± 0.9

I: samples stored in darkness. Assay date: 5/91.
II: the same samples as I but stored at subdued sunlight. Assay data: 10/91.
III: the same samples as I.
IV: Concentration data by CVAA at manufacture date.
Manufacturer concentration level: 10 μg/ml (0.001% p/v), samples A, B and C; 40 μg/ml (0.004% p/v), samples D, E, F and G.

Table 3. Thiosalicilic and dithiodibenzoic acid assay in soft contact lens products ($n = 3$)

Sample	TSA concentration μg/ml		DTDBA concentration, μg/ml	
	I	II	I	II
A3	0.30 ± 0.02	0.90 ± 0.05	N.D.	N.D.
A4	0.61 ± 0.03	1.62 ± 0.05	N.D.	0.12 ± 0.01
A5	0.83 ± 0.05	N.D.	0.08 ± 0.01	0.24 ± 0.09
A6	0.90 ± 0.06	0.90 ± 0.05	0.30 ± 0.03	0.72 ± 0.04
B3	1.02 ± 0.05	0.80 ± 0.05	0.50 ± 0.03	1.12 ± 0.07
B4	1.13 ± 0.07	0.83 ± 0.07	0.38 ± 0.02	1.12 ± 0.08
B5	1.68 ± 0.09	1.04 ± 0.05	N.D.	N.D.
B6	0.65 ± 0.03	0.64 ± 0.03	N.D.	N.D.
C3	1.8 ± 0.1	0.54 ± 0.02	N.D.	0.84 ± 0.01

I and II as in Table 2.

concentration but also to obtain information about the decomposition degree of the samples.

Acknowledgements—The authors thank the Autonoma University of Madrid for the financial support of this work (aids to precompetitive groups), the Autonoma Community of Madrid for the research grant of one of the authors (Mª Carmen Asensio), and Alcon Ibheris for samples supply.

REFERENCES

1. K. Tsuji, Y. Yamawaki and Y. Miyazaki, *Arch. Pract. Pharm.*, 1951, **24**, 110.
2. E. O. Davisson, H. M., Powell, J. O. MacFarlane, R. Hodson, R. L. Stone and C. G. Culbertson, *J. Lab. Clin. Med.*, 1956, **47**, 8.
3. N. E. Richardson, D. J. G. Davies, B. J. Meakin and D. A. Norton, *J. Pharm. Pharmacol.*, 1977, **29**, 717.
4. M. J. Reader and C. D. Lines, *J. Pharm. Sci.*, 1983, **72**, 1406.
5. E. Lüdtke, H. Darsow and R. Pohlovdek-Fabini, *Pharmazie*, 1977, **32**, 99.
6. S. Pinzanti and M. Casini, *Farmaco*, 1980, **2**, 92.
7. P. G. Takla and V. Valajanian, *Analyst* 1982, **107**, 378.
8. J. Viska and A. Okac, *Cesk. Farm.*, 1967, **16**, 29.
9. C. Fu and M. J. Sibley, *J. Pharm Sci.*, 1977, **66**, 738.
10. R. C. Meyer and L. D. Cohn, *ibid.*, 1978, **67**, 1636.
11. S. W. Lam, R. C. Meyer and L. T. Takahashi, *J. Parent. Sci. Tech.*, 1981, **35**, 262.
12. D. S. Bushee, *Analyst*, 1988, **133**, 1167.
13. G. C. Visor, R. A. Kenley, J. S. Fleitman, D. A. Neu and I. W. Partridge, *Pharm. Res.*, 1985, **2**, 73.

Talanta, Vol. 39, No. 12, pp. 1625–1628, 1992
Printed in Great Britain.

0039-9140/92 $5.00 + 0.00

POTENTIOMETRIC STUDIES OF BINARY AND TERNARY COMPLEXES OF AMOXYCILLIN

MOHAMED M. SHOUKRY
Department of Chemistry, Faculty of Science, Cairo University, Giza, Egypt

(*Received* 1 *May* 1991. *Revised* 3 *March* 1992. *Accepted* 13 *April* 1992)

Summary—The formation equilibria for the binary complexes of copper(II), nickel(II), cobalt(II) and zinc(II) with amoxycillin (Amx) and for the ternary complexes M(Arm)(Amx), where Arm refers to aromatic amines, namely 2,2′-dipyridyl or 1,10-phenanthroline, were investigated by a potentiometric technique. The protonation constants of amoxycillin and conditional stability constants of the formed complexes were determined at 25° (=0.1*M* $NaNO_3$). Probable mode of chelation with amoxycillin is discussed.

Lactam antibiotics, such as amoxycillin, represent the most important class of drugs against infection diseases caused by bacteria.[1,2] It is known that the antibiotic action is related to the ability of these compounds to form complexes with metal ions. This stimulated a great deal of investigation on the complexing properties of the antibiotics as ligands.[3,4] Investigation of the binary and ternary complexes of amoxycillin may therefore help toward understanding the driving forces which lead to the formation of such complexes in biological systems. In connection with our previous studies of the binary and ternary complexes of biological significance,[5,7] the present investigation reports potentiometric studies of the binary and ternary complexes of some transitional metal ions with amoxycillin and aromatic amines, 2,2′-dipyridyl (Dpy) and 1,10-phenanthroline (Phen), as secondary ligands.

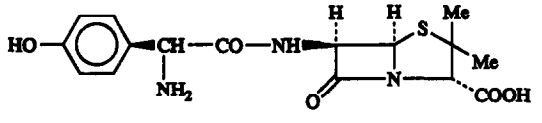

Scheme 1. Amoxycillin

EXPERIMENTAL

Apparatus

Potentiometric titrations were performed with a Metrohm 686 Titroprocessor equipped with a 665 Dosimat (Metrohm, Herisau-S.). The titroprocessor and electrode were calibrated with standard buffer solutions prepared according to NBS specifications.[8] All titrations were carried out at 25 ± 0.1°, in a purified nitrogen atmosphere using a titration vessel described previously.[9]

Materials and reagents

Amoxycillin trihydrate is (6R)-6-(α-*D*-*p*-hydroxyphenylglycylamino)penicillanic acid trihydrate. It was obtained from Gulphar Pharmaceutical Co. (Ras El-khima, U.A.E.). 2,2′-Dipyridyl and 1,10-phenanthroline monohydrate (Merk Chem. Co., Darmstadt-D) were utilized as supplied. Solutions of metal ions were prepared from their nitrate salts (BDH, U.K.). Amoxycillin solution was prepared, immediately before use, by exact weighing of the substance, which was then dissolved in aqueous equimolar nitric acid solution. The aromatic amines were in diprotonated form by dissolution in nitric acid. Concentrations of stock solutions of the metal ions were determined by conventional analytical methods.[10] All solutions were prepared in demineralized water.

Procedure and measuring techniques

Prepare the following mixtures (A–D) and titrate potentiometrically with standardized sodium hydroxide solution (0.25*M*).

(A) 40 ml of solution containing $5.0 \times 10^{-3}M$ Amx and 0.1*M* $NaNO_3$.
(B) 40 ml of solution containing $2.5 \times 10^{-3}M$ metal ion, $5.0 \times 10^{-3}M$ Amx and 0.1*M* $NaNO_3$.
(C) 40 ml of solution containing $5.0 \times 10^{-3}M$ metal ion, $5.0 \times 10^{-3}M$ Arm and 0.1*M* $NaNO_3$.

(D) 40 ml of solution containing $5.0 \times 10^{-3}M$ metal ion, $5.0 \times 10^{-3}M$ Arm, $5.0 \times 10^{-3}M$ Amx and $0.1M$ $NaNO_3$.

The protonation constants of amoxycillin were determined by titrating mixture (A). The formation constants of the binary complexes formed in solution were determined by titrating mixture (B). With the concentrations in mixture (B), the 1:1 and higher complexes are allowed to form. The stability constants, $K^{M(Arm)}_{M(Arm)(Amx)}$, for the ternary complexes were determined by titration of mixture (D), utilizing the data obtained within the pH range corresponding to the complete formation of the $[M(Arm)]^{2+}$ complex.

The calculations were performed using the computer program MINIQUAD-75[11] loaded on an IBM-4331 computer. The model selected was that which gave the best statistical fit to, and proved chemically consistent with the titration data, without showing any systematic bias in residuals, as elsewhere described.[11] Tables 1 and 2 summarize the obtained results.

RESULTS AND DISCUSSION

Protonation of amoxycillin

Amoxycillin protonation constants were determined by direct potentiometric, pH measurements because all protonation reactions were observed to take place within the potentiometrically measurable pH range (2–11). Amoxycillin behaves as triprotonic acid $[H_3L^+]$, where the differential log protonation constants were found to be 2.41, 7.19 and 9.38. In considering the nature of the donor groups involved in successive protonation reactions, it is helpful to invoke the protonation constants of cephalexin (7.18 and 2.62)[12] analogue, where the protonation centres are the amino and carboxylic groups. In acid medium amoxycillin is protonated to give a cationic species H_3L^+. Addition of base produces, in a first stage, the deprotonation of carboxylic group ($pK_{a1} = 2.41$) yielding the zwitter ion species $H_2L^{\pm}$, existent in the pH range 4–6. When the pH is increased the deprotonation of the amino group $-NH_3^+$ ($pK_{a2} = 7.19$), followed by that of the phenolate group ($pK_{a3} = 9.38$).

Table 1. Formation constants of the binary complexes of amoxycillin

System	l	*p*	*q**	log B†	n‡	S§
Amoxycillin	0	1	1	9.38 (0.01)	211	1.6×10^{-6}
	0	1	2	16.57 (0.01)		
	0	1	3	18.98 (0.02)		
Copper(II)	1	1	1	15.51 (0.03)	64	1.7×10^{-6}
Nickel(II)	1	1	1	13.01 (0.06)	125	2.0×10^{-6}
	1	1	0	5.46 (0.05)		
	1	1	−1‖	−3.29 (0.06)		
Cobalt(II)	1	1	1	12.98 (0.07)	126	2.6×10^{-6}
	1	1	0	4.95 (0.06)		
	1	1	−1	−3.47 (0.07)		
Zinc(II)	1	1	1	12.12 (0.06)	126	1.1×10^{-6}
	1	1	0	4.13 (0.07)		
	1	1	−1	−3.10 (0.03)		

*The symbols 1, *p* and *q* are the stoichiometric coefficients corresponding to the metal ion, amoxycillin and H^+ respectively.

†Standard deviations are given in parentheses.

‡Number of data points.

§Sum of square of residuals.

‖The coefficient −1 refers to a complex losing H^+ *i.e.*, producing the hydroxo-complex.

Binary complexes of amoxycillin

The model that best fits the potentiometric data of the nickel(II), cobalt(II) and zinc(II) complexes is found to consist of $[MHL]^+$, [ML] and $[ML(OH)]^-$ species. The validity of the

Table 2. Formation constants of the ternary complexes involving aromatic amines and amoxycillin

System	l	*p*	*q**	log B	n	S	Δlog *K*
Cu–Phen–Amx	1	1	1	14.38 (0.04)	46	8.8×10^{-7}	
	1	1	0	7.92 (0.03)			
Cu–Dpy–Amx	1	1	1	14.44 (0.05)	30	8.1×10^{-7}	
Ni–Phen–Amx	1	1	1	12.43 (0.03)	47	5.5×10^{-7}	−1.08
	1	1	0	4.38 (0.02)			
Ni–Dpy–Amx	1	1	1	12.51 (0.03)	68	6.4×10^{-7}	−0.88
	1	1	0	4.58 (0.02)			
Co–Phen–Amx	1	1	1	11.76 (0.04)	46	4.8×10^{-7}	−1.40
	1	1	0	3.55 (0.03)			
Co–Dpy–Amx	1	1	1	11.98 (0.03	68	8.2×10^{-7}	−1.12
	1	1	0	3.83 (0.02)			
Zn–Phen–Amx	1	1	1	11.60 (0.04)	47	1.2×10^{-7}	−0.07
	1	1	0	4.06 (0.03)			
Zn–Dpy–Amx	1	1	1	11.66 (0.07)	68	1.4×10^{-7}	−0.15
	1	1	0	3.98 (0.02)			

*The symbol 1 is the stoichiometric coefficient corresponding to [M–Arm] species.

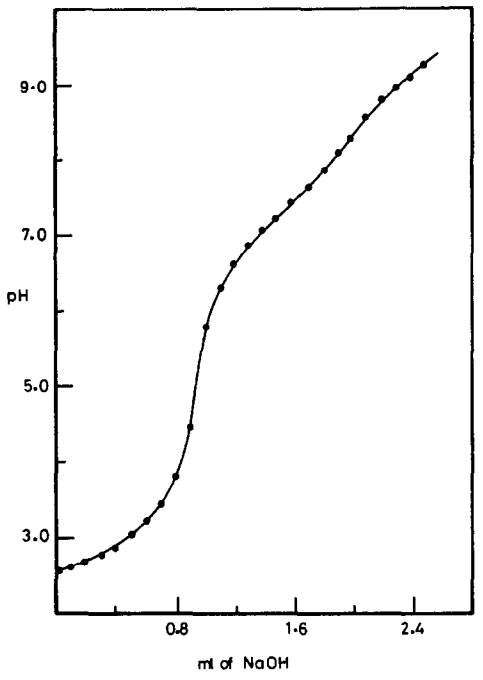

Fig. 1. Potentiometric titration curve of nickel(II)–amoxycillin complex. The solid curve through the experimental points is the theoretical curve. Approximately one-fifth of the experimental points are shown.

same is proven in Fig. 1, where an excellent fit can be observed between the experimental data points from the titration of nickel–amoxycillin complex, taken as a representative, and the theoretical curve calculated from the values of protonation constants of amoxycillin and formation constants of the corresponding complexes. The potentiometric results of the copper–amoxycillin system reveals the formation of $[CuHL]^+$ complex species. The [CuL] species was not detected as the solution turned turbid at pH 4.7.

The acid dissociation constant of the protonated complex species is given by relation (1);

$$pK^{H}_{(M)(L)(H)} = \log K^{(M)}_{(M)(L)(H)} - \log K^{(M)}_{(M)(L)} \quad (1)$$

The value of pK^H of the protonated complexes is in the range 7.55–8.03. This value may compare with the protonation constant (pK_{a3}) of the phenolate group if the increase of its acidity as a result of metal complex formation with the amino group would be considered.

Ternary complexes of amoxycillin

The potentiometric titration curves of M^{II}–Arm system in the presence (mixture D) and absence (mixture C) of amoxycillin reveals their coincidence in the region $0 \leqslant a \leqslant 2$, ($a$ = number of moles of base added per mole of ligand), where the 1:1 M^{II}–Arm complex is formed. The formation of a ternary complex is ascertained by comparison of the mixed-ligand titration curve with the composite curve obtained by graphical addition of the amoxycillin titration data to that of the M^{II}–Arm titration curve. The mixed-ligand system was found to deviate considerably from the resultant composite curve indicating the formation of a ternary complex.[13] Therefore, it is assumed that in the presence of both ligands, the aromatic amine is ligated to the metal ion, then followed by ligation of amoxycillin, *i.e.*, the ternary complex formation could be considered in stepwise equilibria [equations (2) and (3)]

$$M + Arm \rightleftharpoons [M\text{–}Arm] \quad (2)$$

$$[M\text{–}Arm] + Amx \rightleftharpoons [M\text{–}Arm\text{–}Amx] \quad (3)$$

The relative stability of the ternary complexes, as compared to that of the corresponding binary complexes, can be quantitatively expressed in different ways. A review on those methods[14] has shown that, for a variety of reasons, the most suitable comparison is in terms of $\Delta \log K$. Table 2 demonstrates the difference in stabilities of the binary and ternary complexes in terms of $\Delta \log K$ as defined by equation (4):

$$\Delta \log K = \log K^{(M)(Arm)}_{(M)(Arm)(Amx)} - \log K^{(M)}_{(M)(Amx)}. \quad (4)$$

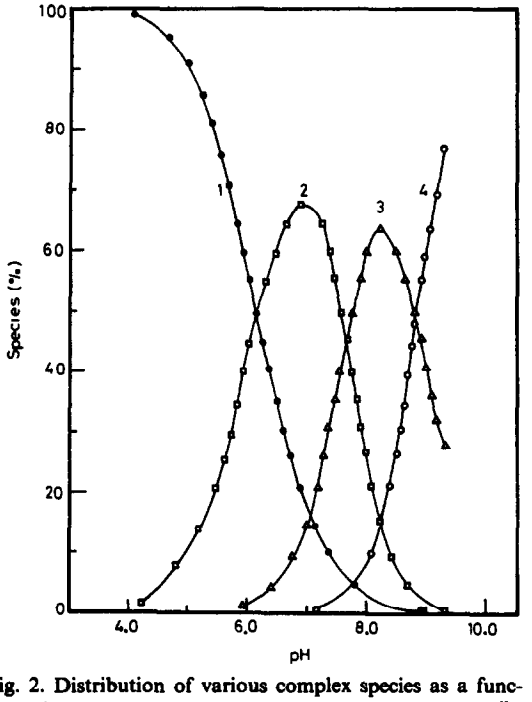

Fig. 2. Distribution of various complex species as a function of pH for the nickel(II)–amoxycillin system: (1) $[Ni^{II}]$, (2) [Ni(HL)], (3) [Ni(L)] and (4) [Ni(L)(OH)].

Table 3. Maximum proportions of the amoxycillin complexes

Species	% Proportion of species	pH
Amoxycillin		
$[H^3L]^+$	45	2.6
$[H^2L]$	98	4.8
$[HL]^-$	84	8.3
$[L]^{2-}$	90	10.5
Binary complexes		
$[Cu(HL)]^+$	94	4.6
$[Ni(HL)]^+$	69	6.9
$[Co(HL)]^+$	79	7.0
$[Zn(HL)]^+$	39	7.2
[Ni(L)]	63	8.3
[Co(L)]	43	8.3
[Zn(L)]	10	7.5
$[Ni(L)(OH)]^-$	75	9.2
$[Co(L)(OH)]^-$	76	9.0
$[Zn(L)(OH)]^-$	64	7.9
Ternary complexes		
$[Cu(Phen)(HL)]^+$	67	5.6
$[Cu(Dpy)(HL)]^+$	53	4.9
$[Ni(Phen)(HL)]^+$	49	7.5
$[Ni(Dpy)(HL)]^+$	50	7.2
$[Co(Phen)(HL)]^+$	30	7.6
$[Co(Dpy)(HL)]^+$	33	7.5
$[Zn(Phen)(HL)]^+$	21	7.4
$[Zn(Dpy)(HL)]^+$	23	7.3
[Cu(Phen)(L)]	45	6.5
[Ni(Phen)(L)]	48	8.4
[Ni(Dpy)(L)]	38	8.0
[Co(Phen)(L)]	38	8.6
[Co(Dpy)(L)]	36	8.4
[Zn(Phen)(L)]	35	8.0
[Zn(Dpy)(L)]	29	8.0

In general, one expects to observe negative values for $\Delta \log K$, because more coordination positions are available for bonding of amoxycillin in the binary than in the ternary complexes. The $\Delta \log K$ values are found to be invariably negative. This means that the amoxycillin forms a more stable complex with the free metal ion than with the M^{II}–Arm one.

The concentration distribution diagrams in terms of formation percent as a function of pH were obtained for complexes formed in solution in the metal ion–amoxycillin and metal ion–aromatic amine–amoxycillin systems. Figure 2 shows the distribution diagram of nickel–amoxycillin complex, as a representative example. The maximum percent of formation of the protonated (H_3L^+) and deprotonated (L^{2-}) forms of amoxycillin, given in Table 3, are obtained under the prevailing experimental conditions. The same is true for the hydrxo-complex species [M(L)(OH)]. The maximum proportions of the complexes formed in solution are given in Table 3.

Based on the potentiometric results, the formation of the metal chelates with amoxycillin can take place through the vicinal amino and carbonyl groups as proposed. Such a suggestion is supported by the literature data[15,16] reported for cephalexin, which is structurally related to amoxycillin. Attempts made to isolate the complexes in a pure state were unsuccessful. Supportive structural elucidation on the mode of coordination of the metal ions in binary and ternary complexes needs further studies, *e.g.*, nuclear magnetic resonance studies of the solution chemistry of diamagnetic metal complexes. However, such studies are not available now and will be considered in the future.

REFERENCES

1. F. A. Jung, W. R. Pilgrim, J. P. Poyser and P. J. Siret, *Top. Antibiot. Chem.*, 1980, **4**, 1.
2. M. I. Page, *Acc. Chem. Res.*, 1984, **17**, 144.
3. W. A. Baker Jr and P. M. Brown, *J. Am. Chem. Soc.*, 1966, **88**, 1314.
4. L. A. Mitscher, A. C. Bonacci, B. Slater-Eng, A. K. Hacker and T. D. Sokoloski, *Antimicrob. Agents Chemother.*, 1969, 111.
5. M. M. Shoukry, *Transition Met. Chem.*, 1990, **15**, 1.
6. *Idem*, *Talanta*, 1989, **36**, 1151.
7. M. M. Shoukry, B. V. Cheesman and D. L. Rabenstein, *Can. J. Chem.*, 1988, **66**, 3184.
8. R. G. Bates, *Determination of pH—Theory and Practice*, 2nd Edn., p. 73. Wiley Interscience, New York, 1973.
9. M. M. Shoukry, M. M. Khater and E. M. Shoukry, *Indian J. Chem.*, 1986, **25A**, 488.
10. F. J. Welcher, *The Analytical Uses of Ethylenediaminetetraacetic Acid.*, 4th Edn., p. 149–217, Van Nostrand, Princeton, 1965.
11. P. Gans, A. Sabatini and A. Vacca, *Inorg. Chim. Acta*, 1976, **18**, 237.
12. J. M. Moratal, J. Borras, A. Donaire and M. Martinez, *ibid.*, 1989, **162**, 113.
13. M. M. Shoukry, A. E. Mahgoub and W. M. Hosny, *Transition Met. Chem.*, 1987, **12**, 77.
14. R. B. Martin and R. J. Prados, *J. Inorg. Nucl. Chem.* 1974, **36**, 1665.
15. G. V. Fuzakerley and G. C. Jackson, *ibid.*, 1975, **37**, 2371.
16. J. Hernandez and A. Sanchez, *Anal. Chim. Acta*, 1984, **160**, 335.

Talanta, Vol. 39, No. 12, pp. 1629–1636, 1992
Printed in Great Britain.

0039-9140/92 $5.00 + 0.00

APPLICATION OF RIDGE TRACE ANALYSIS IN DIRECT SPECTROPHOTOMETRIC CALIBRATION

WEI WANZHI, ZHU WENHONG and YAO SHOUZHUO

Department of Chemistry and Chemical Engineering, Hunan University, Changsha 410012, People's Republic of China

(*Received* 6 *December* 1991. *Revised* 23 *April* 1992. *Accepted* 24 *April* 1992)

Summary—The use of ridge trace analysis for multivariate calibration problems is described. Application is made to the simultaneous quantitative determination of components for several pharmaceutical systems with unknown sample UV spectra by the direct calibration technique. The results indicate that with the help of ridge trace analysis and ridge regression, the parameter k can be selected to obtain estimation of the colinearity of a system based on the stability of relative concentration as a function of k. Much information about the system to be analyzed can be obtained, such as whether there is colinearity among the variables, which measurement wavelength range is suitable for performing quantitative analysis, which components cannot be measured and which components can only be measured as a sum, and whether the quantitative model is correct.

For quantitative analysis of complex samples containing more than one component, multiple calibration techniques must be used and the widespread availability of computers makes their application possible. By far the most commonly used statistical methods for multicomponent determinations are multiple linear calibration procedures.[1] They are utilized to establish quantitative models between analyte concentration and instrumental response through regression analysis on the data of a calibration set, and then to estimate the component concentrations in unknown samples with the model and the response of the samples, when the number of analytes is known and they possess different distinct characteristics in the measurement. Unfortunately, many components to be analyzed in multicomponent samples have almost the same measurement characteristics, due to the limitation of analysis methods. For these cases, some special regression techniques must be adopted to gain more stable parameter estimation,[2] and ridge regression is one of the most generally used techniques.[3–5] Recently, ridge regression was introduced for chemical analyses[6,7] but there is no literature concerning the wider application of ridge trace analysis in analytical chemistry.

To detect and quantify analytes in multicomponent samples by spectrophotometry, the direct calibration process can be applied, *i.e.*, the pure spectra of analytes to be determined are utilized for obtaining coefficients to build a linear model of the relationship between concentration of the analytes and response. Then the spectrum of an unknown sample is placed into the model and the concentrations can be estimated through the following linear model with regression at the same time:

$$[\mathbf{R}] = [\mathbf{K}][\mathbf{C}] + [\mathbf{E}] \quad (1)$$

where $[\mathbf{K}]$ is an $m \times p$ coefficient matrix of p analytes pure spectra in m measurement wavelengths; $[\mathbf{R}]$ is an $m \times 1$ vector of unknown sample spectrum in m measurement wavelengths; $[\mathbf{C}]$ is a $p \times 1$ vector of the concentrations for p analytes in the sample and $[\mathbf{E}]$ is an $m \times 1$ residual vector. When MLR (multiple linear regression) is used to estimate the component concentrations of an unknown sample, equation (1) is rearranged to solve for $[\mathbf{C}]$

$$[\mathbf{C}] = ([\mathbf{K}]^{\mathrm{T}}[\mathbf{K}])^{-1}[\mathbf{K}]^{\mathrm{T}}[\mathbf{R}] \quad (2)$$

The main difficulty with the use of MLR for model (1) is the inversion of $[\mathbf{K}]^{\mathrm{T}}[\mathbf{K}]$ when there is a high degree of colinearity.[4] Colinearity is the lack of independence between the columns of $[\mathbf{K}]$. The less independent these columns, the more error or instability is produced when determining the inverse.

Ridge regression, on the other hand, is a procedure with which a more stable estimation

of [C] can be achieved. Ridge regression can be defined from

$$[\mathbf{C}](k) = ([\mathbf{K}]^{\mathrm{T}}[\mathbf{K}] + k[\mathbf{I}])^{-1}[\mathbf{K}]^{\mathrm{T}}[\mathbf{R}] \quad (3)$$

where k is a constant ($0 < k < \infty$) and [I] is a $p \times p$ unit square matrix. Since the eigenvalues of $[\mathbf{K}]^{\mathrm{T}}[\mathbf{K}]$ and $[\mathbf{K}]^{\mathrm{T}}[\mathbf{K}] + k[\mathbf{I}]$ are $\lambda_1, \ldots, \lambda_p$ and $\lambda_1 + k, \ldots, \lambda_p + k$, respectively, when some λ_i approaches zero, *i.e.*, there is colinearity in the system, $\lambda_i + k$ will be larger than λ_i and it can be expected that $[\mathbf{C}](k)$ is more stable than [C]. Particularly, some $k > 0$ is found to make

$$E(\| [\mathbf{C}](k) - [\tilde{\mathbf{C}}] \|^2) < E(\| [\mathbf{C}] - [\tilde{\mathbf{C}}] \|^2) \quad (4)$$

where $[\tilde{\mathbf{C}}]$ is a $p \times 1$ vector of the true concentrations of the analytes, and the left of equation (4) is as small as possible. In practice, the optimum value of k relies on the unknown model parameters [C] and σ^2, and the relation between k, [C], and σ^2 is unknown. Therefore, it cannot be known before regression and must be determined from the experimental data, which makes the estimation of $[\mathbf{C}](k)$ complex. There are many techniques to select a suitable k,[8] and ridge trace analysis is an important and basic technique to determine k. So called ridge traces are a group of curves which indicate that for each i ($i = 1, \ldots, p$) when k increases from zero to ∞, $C_i(k)$, as a function of k, varies with k. Because ridge traces reflect some properties of a multiple linear system to be analyzed, much valuable information can be obtained with the ridge trace analysis.

The purpose of this study was to provide evidence that ridge trace analysis, as a helpful tool for linear multivariate analysis, can be used to obtain some useful quantitative and qualitative information for linear systems of analytical chemistry, such as spectrophotometric systems. This study also investigated how to obtain ridge traces and how to perform ridge trace analysis through several known analysis systems. Since the characteristics about the system are important for acquiring correct analytical results, ridge trace analysis is of considerable interest for analysts.

EXPERIMENTAL

Instrument and reagents

A Hitachi 557 double wavelength/double beam spectrophotometer was used to obtain the pure spectra of components and the spectra of all samples, and an IBM PC/XT computer was used to treat the experimental data. Analytical reagent grade chemicals and distilled water were used. Salicylic acid, thymol, phenol, benzoic acid, resorcinol, theobromine, theophylline, caffeine, amidopyrine, phenacetin, phenobarbital and ephedrine were of Pharmacopoeia (1985, P. R. China) quality.

Procedure

Salicylic acid, thymol, phenol, benzoic acid and resorcinol, accurately weighed, were dissolved in minimum volumes of 95% alcohol and then the five solutions were diluted with suitable volumes of water, respectively. The pure spectra of the five components were obtained by scanning the five solutions from 250 to 330 nm in the spectrophotometer. Two samples of salicylic acid, thymol, phenol and benzoic acid, two samples of salicylic acid, thymol and phenol, and ten samples containing different quantities of the above five components were prepared and fourteen sample spectra were obtained in the same wavelength range. The seven other pharmaceutical samples, accurately weighed, were dissolved in water to form seven single-component solutions, and then seven pure spectra from 230 to 300 nm were obtained. Eight samples, the composition proportions according to the prescription of some tablets, were compounded and eight spectra were obtained in the same wavelength range. At the same time, the spectral stability for both single component and mixture samples was tested.

Computation

Ridge traces can be obtained with equation (3), but an inversion must be determined for each k. Here, a simple computation method is introduced for ridge traces. [U] is defined as

$$[\mathbf{U}] = \begin{bmatrix} [\mathbf{R}]^{\mathrm{T}}[\mathbf{R}] + k & [\mathbf{R}]^{\mathrm{T}}[\mathbf{K}] \\ [\mathbf{K}]^{\mathrm{T}}[\mathbf{R}] & [\mathbf{K}]^{\mathrm{T}}[\mathbf{K}] + k[\mathbf{I}] \end{bmatrix} \quad (5)$$

If [A] is a $(p+1) \times (p+1)$ orthogonal square matrix and

$$[\mathbf{A}][\mathbf{U}][\mathbf{A}]^{\mathrm{T}} = [\Lambda] = \mathrm{diag}(\lambda_1 + k, \ldots, \lambda_{p+1} + k) \quad (6)$$

then the following equations give the $[\mathbf{C}](k)$ as a function of k

$$C_{j-1}(k) = -\left(\sum_{i=1}^{p+1} \frac{a_{i1}a_{ij}}{\lambda_i + k}\right) \Big/ \left(\sum_{i=1}^{p+1} \frac{a_{i1}^2}{\lambda_i + k}\right) \quad (7)$$

for $j = 2, \ldots, p+1$, where a_{ij} is the element of [A]. The computation in this work was carried out on an IBM PC/XT computer and all

programs were written in BASIC. All spectra were disintegrated at intervals of 2 nm to form spectral vectors and the data vectors and matrices were mean-centered and scaled to unit variance in each column. All estimated concentrations in the plots of ridge traces were the relative concentrations for the pure spectra, so that all components possess almost the same sensitivity. Copies of the data and programs are available from the authors.

RESULTS AND DISCUSSION

Colinearity for a four component system by ridge trace analysis

Ridge trace analysis is a useful means to analyze the system behaviour, and the interaction and relation among the variables. A basic application is that it can be used to judge whether there is colinearity for a given system. In spectrophotometry, direct calibration, when the composition of a system is known, can be used to determine a suitable measurement wavelength range to improve the stability of concentration estimation. For a pharmaceutical sample containing 20.05 mg/l. salicylic acid, 12.42 mg/l. thymol, 10.36 mg/l. phenol and 29.55 mg/l. benzoic acid (the pure spectra of the four components are in Fig. 1), 250–270 nm was selected to determine them quantitatively. From the ridge trace plot, Fig. 2, it can be seen that the four curves change morbidly with a slight increase of k, so the wavelength range was poor for the simultaneous determination. When the range of 250–290 nm was used, the curves (Fig. 3) were

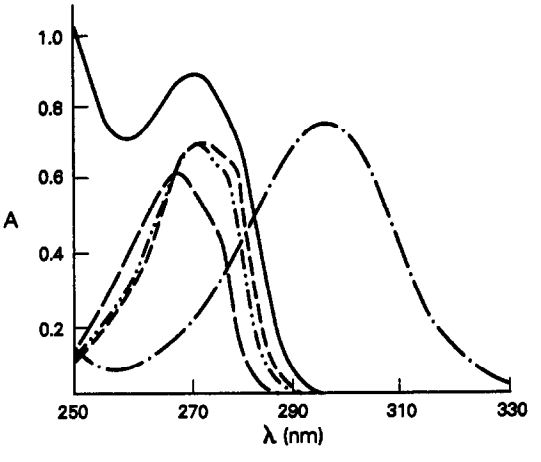

Fig. 1. Pure spectra of salicylic acid, thymol, phenol, benzoic acid and resorcinol. (—·—) salicylic acid (30.65 mg/l.); (– – –) thymol (54.70 mg/l.); (— —) phenol (40.12 mg/l.); (——) benzoic acid (127.4 mg/l.); (—··—) resorcinol (43.45 mg/l.).

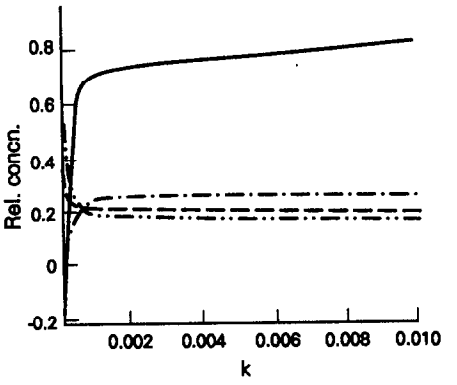

Fig. 2. Ridge traces of the four-component sample with wavelength range from 250 to 270 nm. (——) salicylic acid (rel.con. 0.06542); (—··—) thymol (rel.con. 0.2271); (—·—) phenol (rel.con. 0.2582); (– – –) benzoic acid (rel.con. 0.2319).

all smooth and steady, which shows that the colinearity had been removed from the system, and hence this wavelength range was suitable for quantitative analysis of the components, with the techniques based on the principle of least squares.

From practice, for good linear (*e.g.*, spectrophotometric) systems, when there is obvious colinearity among the variables, the change of ridge traces is obvious with the increase of k from 0 to 0.005, with the largest relative errors far larger than 0.1. The estimated concentrations were −6.49, 30.43, 0.89 and 46.04 mg/l. with the first wavelength range, and 19.92, 11.89, 9.96 and 29.30 mg/l. with the second wavelength range, respectively, when MLR was used. The results of the latter were far better than those of the former. Of course, if a better wavelength range cannot be found, MLR cannot be used, and biased estimators must be adopted. In multicomponent determination with an array of sensors, colinearity is an important factor which affects the quantitative precision,[9] hence ridge

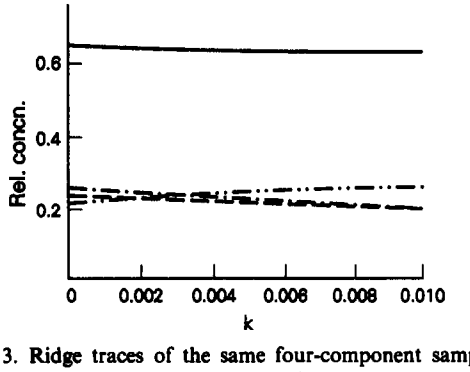

Fig. 3. Ridge traces of the same four-component sample as in Fig. 2 with wavelength range from 250 to 290 nm.

Table 1. Multivariate prediction with ridge regression for five-component system

Sample no.	Actual concn., *mg/l.*					Ridge regression predicted concn. ($k = 0.005$), *mg/l.*					Recovery, %				
	A	B	C	D	E	A	B	C	D	E	A	B	C	D	E
1	20.01	12.07	20.96	24.70	21.16	19.98	13.18	21.01	25.05	20.03	99.85	109.19	100.24	101.42	94.66
2	20.01	12.07	10.48	49.40	10.58	19.74	13.01	9.96	48.01	10.32	98.65	107.78	107.78	97.19	97.54
3	20.01	12.07	10.48	49.40	21.16	19.92	13.11	10.52	49.02	19.63	99.55	108.62	100.38	99.23	92.79
4	20.01	12.07	10.84	24.70	21.16	20.00	12.03	10.99	24.17	19.55	99.95	103.65	105.34	97.85	94.28
5	40.02	12.07	20.96	24.70	21.16	38.90	13.20	19.59	24.91	19.92	97.20	109.36	93.46	100.80	94.14
6	40.02	24.14	10.48	24.70	21.16	38.59	25.13	10.73	23.80	19.98	96.43	104.10	102.39	96.36	94.42
7	20.01	12.07	20.96	49.40	21.16	19.95	13.62	20.68	49.30	18.55	99.70	112.84	98.66	99.80	87.66
8	20.01	24.14	10.48	24.70	21.16	19.98	24.25	10.82	25.30	19.35	99.85	100.46	103.32	102.43	91.45
9	20.01	24.14	20.96	24.70	21.16	19.98	24.98	20.33	25.40	19.61	99.85	103.48	96.99	102.83	92.67
10	20.01	24.14	10.48	49.40	21.16	19.95	24.91	10.23	49.01	19.44	99.70	103.19	97.61	99.21	91.87
av											99.07	106.27	100.12	99.71	93.15
standard deviation (%)											1.26	3.82	4.24	2.18	2.59

A—salicylic acid; B—thymol; C—pehnol; D—benzoic acid; E—resorcinol.

Table 2. Multivariate prediction with ridge regression for seven-component system

Sample no.	Actual concn. *mg/l.*				Ridge regression predicted concn. ($k = 0.015$) conc., *mg/l.*				MLR predicted concn. *mg/l.*				Recovery with ridge regression, %				Recovery with MLR, %			
	A*	B	C	D†	A*	B	C	D†	A*	B	C	D†	A*	B	C	D†	A*	B	C	D†
1	4.44	1.24	8.08	8.56	4.74	1.27	7.50	8.29	4.34	1.81	7.70	8.69	106.8	102.4	92.8	104.2	96.9	146.0	95.3	101.5
2	5.32	1.48	9.70	10.18	5.52	1.57	9.03	10.62	4.95	2.11	9.61	10.11	103.8	106.1	93.1	104.3	93.0	142.3	99.1	99.3
3	5.76	1.61	10.50	11.04	5.88	1.71	9.77	11.41	5.38	2.40	8.92	11.66	102.1	106.5	93.0	103.3	93.4	148.8	85.0	105.6
4	4.87	1.36	8.89	9.34	5.06	1.44	8.36	9.77	5.06	1.81	7.82	9.94	104.0	105.6	94.1	104.6	104.0	133.3	88.0	106.4
5	5.32	1.48	9.70	10.18	5.48	1.64	9.06	11.26	4.96	2.42	9.06	10.40	103.0	110.8	93.4	110.6	93.2	178.3	93.4	102.2
6	6.20	1.73	11.31	11.88	6.40	1.87	10.51	12.38	5.62	2.91	10.71	11.97	103.2	109.0	92.9	104.3	90.7	168.3	97.4	100.7
7	4.38	1.23	12.09	12.61	4.66	1.49	11.16	13.29	4.30	2.85	9.49	13.80	106.3	121.0	92.3	105.4	98.2	231.7	78.5	109.4
8	4.44	1.24	12.12	12.48	4.56	1.38	11.04	13.20	4.53	2.09	10.74	13.19	102.7	111.0	91.1	105.7	102.1	168.2	88.6	105.7
av													104.0	109.1	92.8	105.3	96.4	164.6	90.3	103.9
standard deviation %													1.68	5.60	0.86	2.26	4.74	31.15	6.62	3.43

A—theobromine; B—caffeine; C—amidopyrine; D—phenacetin.

*Concn. sum of theobromine and 1.15 times theophylline.

†Concn. sum of phenacetin and 0.850 times phenobarbital.

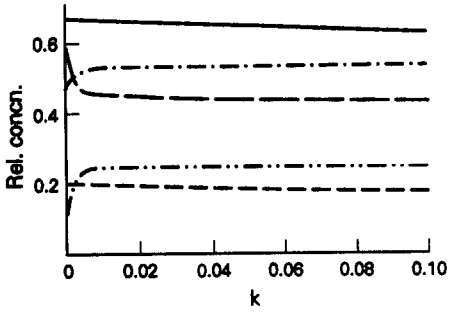

Fig. 4. Ridge traces of sample one for the five-component system. (——) salicylic acid (rel.con. 0.6529); (— · · —) thymol (rel.con. 0.2207); (— · —) phenol (rel.con. 0.5224); (– – – –) benzoic acid (rel.con. 0.1939); (— —) resorcinol (rel.con. 0.1475).

trace analysis can be used to select a suitable array for a given system.

Ridge regression of a five-component system

Ridge regression, as an important biased estimator, can be utilized to obtain a more stable concentration estimation for colinearity systems and ridge trace analysis is a basic technique to acquire the ridge regression parameter k. Ten samples, Table 1, of five ingredients were analyzed with ridge regression. The pure spectra of the components are in Fig. 1. The ridge traces of sample one, Fig. 4, indicated there was colinearity in the system since the ridge traces of thymol, phenol and resorcinol change obviously with a slight increase in k from zero. When k increases from 0 to 0.005, the percentages of estimation change were 87 for thymol, 8 for phenol and −21 for resorcinol, only 1 for salicylic acid and 3 for benzoic acid respectively. The reason the former three curves changed markedly can be assessed qualitatively from Fig. 1, where the pure spectra of thymol and resorcinol are very similar and the spectrum of phenol is slightly similar to them. From Fig. 4, it can be seen that when k was larger than 0.005, the five curves were all stable, so $k = 0.005$ can be selected to gain a biased concentration estimation for the components with ridge regression. The results of ridge regression with $k = 0.005$ for ten samples are listed in Table 1. The average recoveries and standard deviations of the five components were 99.01% (1.27%), 106.27% (3.59%), 100.12% (4.21%), 99.71% (2.19%) and 93.15% (2.78%) with ridge regression and 99.69% (1.34%), 56.17% (21.91%), 84.86% (11.18%), 101.48% (2.50%) and 131.86% (20.67%) with MLR, respectively, which show that though the estimation with ridge regression was biased, it was more precise and accurate than that with MLR.

Ridge trace analysis of seven-component system

For more complex colinearity systems, for which the qualitative composition is known, ridge trace analysis can be used to quantitatively determine the ingredients which ordinarily cannot be measured due to their low contribution to a sample spectrum. Using ridge trace analysis, we can know which ingredients can only be measured as a sum and which ingredients can be measured individually with biased estimators.

A common pharmaceutical tablet preparation contains theobromine, theophylline, caffeine, amidopyrine, phenacetin, phenobarbital and ephedrine. The pure spectra of these components is plotted in Fig. 5. Eight samples, Table 2, were prepared, the compositions of which were according to the prescription proportion of tablets.

The ridge trace of sample one (Fig. 6) can give the following information. First, the concentration estimation of ephedrine approaches zero stability for any k, so it cannot be determined accurately with the measured data, and the variable can be removed from the regression model. Whether a variable can be considered close to zero depends on many factors, *e.g.*, the analysis requirement and the instrumental noise level. For spectrophotometry, if the absolute concentration estimation is always smaller than 0.02, the variable can be safely treated as zero. Second, the other six curves changed markedly with an increase in k from 0 to 0.005, which

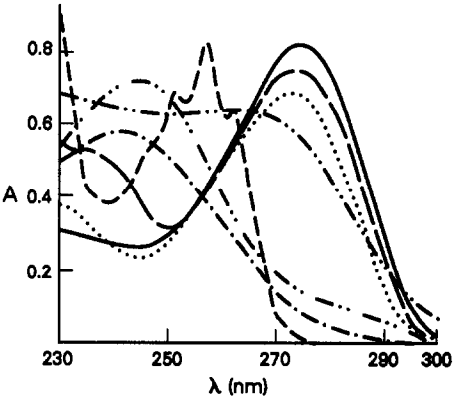

Fig. 5. Pure spectra of the seven-component system. (— —) theobromine (13.28 mg/l.); (——) theophylline (12.68 mg/l.); (· · · ·) caffeine (16.36 mg/l.); (— · · —) amidopyrine (18.22 mg/l.); (— · · · —) phenacetin (11.02 mg/l.); (— · —) phenobarbital (17.51 mg/l.); (– – – –) epherdine (836.0 mg/l.).

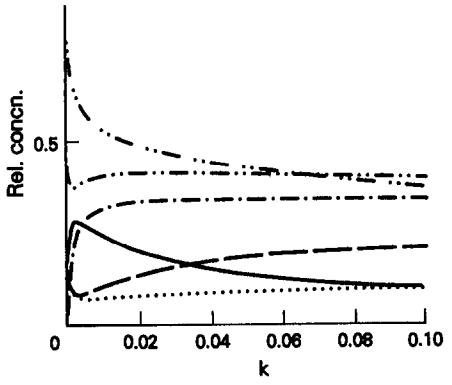

Fig. 6. Ridge traces of sample one for the seven-component system (— —) theobromine (rel.concn. 0.155); (——) theophylline (rel.concn. 0.163); (· · ·) caffeine (rel.concn. 0.0758); (— · · —) amidopyrine (rel.concn. 0.443); (— · · · —) phenacetin (rel.concn. 0.727); (— · —) phenobarbital (rel.concn. 0.0425); (– – – –) ephedrine (rel.concn. 0.00099).

shows that there was colinearity in the system, so biased estimators must be used to achieve a good concentration estimation. On the other hand, the traces of caffeine, amidopyrine, phenacetin and phenobarbital were more stable when k was larger than 0.015, and hence 0.015 can be selected as the ridge regression parameter. Third, although the curves of theophylline and theobromine were unstable, the sum of the two traces was basically equal at any k, so only the sum of them can be estimated.

Additionally, it can be seen from Fig. 6 that when $k = 0.015$, the concentration estimation proportion for caffeine, amidopyrine and the sum of theophylline and theobromine approached the composition of the tablet. That of phenacetin and phenobarbital was not reasonable, *i.e.*, the former was too low and the latter was too high, which did not conform to the prior information about the system. However, the two ridge traces showed that the concentration estimation sum of them is more stable with the change of k, so the total quantity of them can be estimated with ridge regression. Of course, for this situation, there is no common law that can be obeyed, but the analyst's experience and the signal of estimation are both helpful for obtaining the correct conclusion. From our practice, the situation is rare, and the situation where the concentration estimation is closer to the true concentration with the k slightly larger than zero for colinearity systems is common.

For more complex systems, the pure spectra of components cannot give the above information. For example, the spectral behaviours of theobromine and caffeine were closer than those of theobromine and theophylline, but ridge analysis shows that caffeine can be individually quantified and theobromine and theophylline can only be measured as a sum.

From the analysis, it can be seen that for the theophylline compound tablet system with UV spectrophotometry, there are four ingredients that can be simultaneously quantified, *i.e.*, caffeine, amidopyrine, the sum of theobromine and theophylline, and the sum of phenacetin and phenobarbital. Based on this, the model of six variables was used to estimate their concentrations for eight unknown samples with ridge regression and $k = 0.015$. The results are listed in Table 2, where the concentrations of theobromine and phenacetin were, respectively, the concentration sums of theobromine and 1.15 times theophylline, and phenacetin and 0.850 times phenobarbital. Values of 1.15 and 0.850 were the maximum absorption coefficient ratios of the latter to the former, respectively. The average recoveries and standard deviations were 103.99 (1.63%), 109.5 (45.60%), 92.83 (0.86%) and 105.3 (2.26%) with ridge regression and 96.44 (4.74%), 164.60 (31.15%), 90.30 (6.62%) and 103.86 (3.43%) with MLR for theobromine, caffeine, amidopyrine and phenacetin respectively. The estimation improvement with ridge regression for caffeine and amidopyrine was obvious and the estimation for the two sums with ridge regression was more stable than that with MLR.

With the help of ridge trace analysis, some qualitative information about a system to be analyzed can be obtained, when the composition of analytes is partially known.

Ridge trace analysis of three-component system with four-component model

When there is obvious absorption interference in a sample spectrum, more pure spectra can be used to build a calibration model to determine the composition of the sample and after the determination of a suitable model, a better concentration estimation can be reached. When the estimations of some components are stable about zero or close to zero with a slight increase of k, the variables can be removed from the model to achieve higher estimation precision for the components which can be quantified.

The pure spectra of salicylic acid, thymol, phenol and benzoic acid were used to set up a model of four variables to regress the spectrum of a sample containing 26.15 mg/l. salicylic acid,

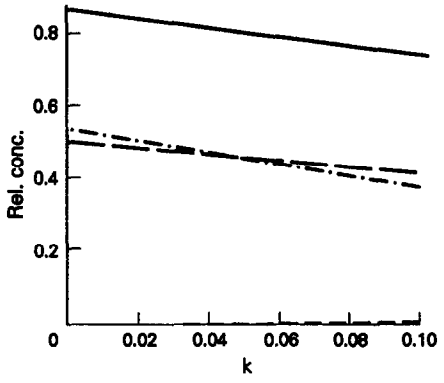

Fig. 7. Ridge traces of the three-component system with the four-component model. (——) salicylic acid (rel.concn. 0.8532); (— —) thymol (rel.concn. 0.4649); (— · —) phenyl (rel.concn. 0.5621); (– – – –) benzoic acid (rel.concn. 0.0000).

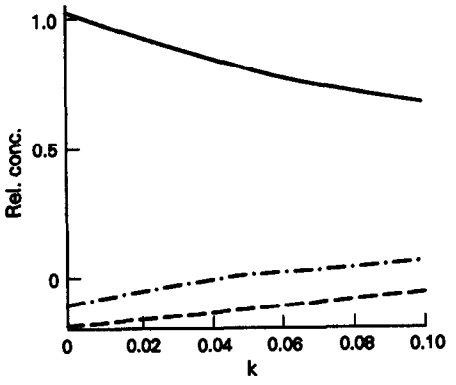

Fig. 9. Ridge traces of the incorrect three-component model for the three-component sample. (——) thymol; (— · —) phenol; (– – – –) benzoic acid.

25.43 mg/l. thymol and 22.55 mg/l. phenol. Figure 7 shows that the four curves were all stable, so the system was linear and there was no colinearity among the variables, and a good estimation can be obtained with MLR. The benzoic acid curve was negative when $k = 0$, then rapidly became positive with increased k, stabilizing at about zero. This indicates that there was no benzoic acid in the sample. The results of the four-variable model and three-variable model with MLR were 26.25 and 26.20 mg/l. for salicylic acid; 26.82 and 26.58 mg/l. for thymol; and 21.37 and 21.40 mg/l. for phenol respectively. The latter was slightly better than the former. This fact indicates that the correct determination of variables and models with ridge trace analysis is valuable for acquiring both qualitative information and a better quantitative estimation.

Ridge trace analysis of unknown systems

Another use of ridge trace analysis is the determination of whether a system obeys a given model built with some pure spectra when the composition of the system is unknown. To illustrate how to perform the analysis, two samples were prepared, *i.e.*, sample 1 containing 20.05 mg/l. salicylic acid, 12.43 mg/l. thymol, 20.72 mg/l. phenol and 59.1 mg/l. benzoic acid, and sample 2 containing 20.01 mg/l. salicylic acid, 28.04 mg/l. thymol and 24.08 mg/l. phenol. The two sample spectra were both the linear combinations of the component pure spectra. For the first sample, the model of three variables (thymol, phenol and benzoic acid) was used in the regression. The ridge traces (Fig. 8) possess the following characteristics: when k increased from 0 to 0.005, the three curves were all stable, *i.e.*, there was no colinearity for the model. The estimation of phenol was far smaller than zero with $k = 0$ and still smaller than zero with $k < 0.03$ and, except for benzoic acid, the other two curves changed gradually with an increase in k. Since the negative concentration was not caused by colinearity and the ridge traces of phenol and thymol were not very stable, it can be concluded that the model was not correct. For sample 2, the model of three pure spectra (thymol, phenol and benzoic acid) was utilized, and a similar ridge trace plot (Fig. 9) was obtained, so the same result can be achieved.

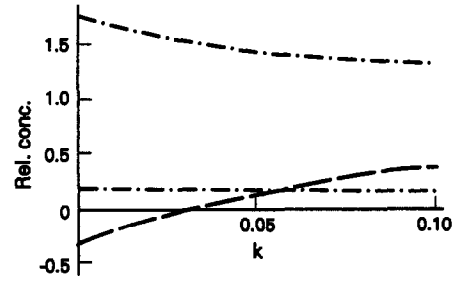

Fig. 8. Ridge traces of the three-component model for the four-component sample. (——) thymol; (— —) phenol; (— · —) benzoic acid.

CONCLUSION

The main advantage of ridge trace analysis is its presentation and its relative simplicity. A group of curves reflects many system behaviour characteristics, such as the relation and interaction among the variables, and gives much valuable system information not convenient with other single multivariate analysis techniques.

Furthermore, the ridge trace algorithm is easy to program and the ridge trace plot is easy to obtain with microcomputers. Since multivariate analysis, especially multivariate linear analysis, is an important tool for obtaining qualitative and quantitative information from experimental data, ridge trace analysis has general importance for analytical chemistry, though it was only used for UV spectrophotometry in this paper. Of course, because of the complexity of systems and analysis demands, it is sometimes difficult to acquire totally correct results with only ridge trace analysis.

On the other hand, it should be noted that ridge trace analysis is only one of many possible multivariate analysis techniques that can be used for obtaining the same information as in this paper. There are several methods for selecting a suitable wavelength range[10] and the calibration matrix condition number is the most general measure of selectivity.[11] A number of research works indicate that many procedures, such as principal component regression, partial least-squares, and stepwise regression, can all perform well for colinearity and for building correct models,[1,12] while many techniques can be used to select a set of suitable variables for models and to obtain optimal models with the PRESS and *F*-tests.[2,13] The ability to combine these techniques with multivariate data provides a high-power analysis tool that may give far more correct and far more qualitative and quantitative information than individual techniques.

REFERENCES

1. S. D. Brown, *Anal. Chem.*, 1990, **62**, 84R.
2. N. R. Draper and H. Smith, *Applied Regression Analysis*, 2nd Ed., Wiley, New York, 1981.
3. A. E. Hoerl. and R. W. Kennard, *Technometrics*, 1970, **12**, 55.
4. *Idem, ibid.*, 1970, **12**, 69.
5. *Idem, ibid.*, 1987, **29**, 161.
6. E. Sanchez and B. R. Kowalski, *J. Chemom.*, 1988, **2**, 247.
7. *Idem, ibid.*, 1988, **2**, 265.
8. D. W. Wichern and G. A. Churchiu, *Technometrics*, 1978, **20**, 1978.
9. W. P. Carey, K. R. Beeke and B. R. Kowalski, *Anal. Chem.*, 1987, **59**, 1529.
10. J. H. Kalivas, N. Roberts and J. M. Sutter, *ibid.*, 1989, **61**, 2024.
11. M. Otto and W. Wegscheider, *Anal. Chim. Acta*, 1986, **180**, 347.
12. S. D. Brown, T. Q. Barker, R. J. Larivee, S. L. Monfre and H. R. Wilk, *Anal. Chem.*, 1988, **60**, 252R.
13. D. W. Osten, *J. Chemom.*, 1988, **2**, 39.

Talanta, Vol. 39, No. 12, pp. 1637–1642, 1992
Printed in Great Britain.

0039-9140/92 $5.00 + 0.00

BIOACCUMULATION AND VOLTAMMETRY OF GOLD AT FLOWER-BIOMASS MODIFIED ELECTRODES

JOSEPH WANG,* BAOMIN TIAN and GARY D. RAYSON
Department of Chemistry, New Mexico State University, Las Cruces, NM 88003, U.S.A.

(*Received* 30 *April* 1992. *Accepted* 1 *May* 1992)

Summary—The bioaccumulation of gold at antheral cells from the flower *Datura innoxia* is investigated by incorporating these plant cells into a carbon paste matrix. The resulting plant-modified electrode offers a preferential uptake of gold from dilute solutions. The voltammetric behavior of the surface-bound gold is examined under different preconcentration conditions. Scanning electron microscopy offers useful insights into the gold collection process. Convenient measurements of micromolar gold concentrations are possible, with effective self cleaning allowing the use of a single electrode in multiple determinations (R.S.D. of 4.8% for 50 repetitions). The sensitivity and selectivity enhancements associated with the preferential bioaccumulation process, and the convenient surface regeneration, offer the prospect of using the flower-biomass containing electrodes as sensors for gold.

Biological organisms have the potential to preferentially accumulate specific elements.[1,2] The incorporation of such organisms onto electrode surfaces can shed useful insights into their interaction with these metals, and offers a great promise for electroanalytical work. In particular, chemically modified electrodes (CMEs) have been used for studies of metal uptake by nonliving algal biomass, and demonstrated applicability for electroanalysis[3,4] and electrocatalysis.[5] Recent work illustrated the utility of higher plant cells from lichens[6] and peat mosses,[7] as surface modifiers for preconcentration/voltammetric measurements.

The present article describes the bioaccumulation and voltammetric behaviour of gold at flower-cells modified electrodes. In particular, carbon paste electrodes containing antheral cells from *Datura innoxia* are used to effectively bind gold from dilute solutions. Early spectroscopic studies have illustrated the biosorption of cadmium and europium onto the cell walls of the *Datura innoxia* biomass.[8,9] Such bioaccumulation has been attributed to several types of binding sites on the *Datura innoxia* wall. The collection and voltammetry of gold at *Datura innoxia* modified electrodes, as reported in the following sections, hold great promise for electrochemical sensing applications, as well as for elucidating the metal/plant interactions.

*Author for correspondence.

EXPERIMENTAL

Apparatus

Two 10-ml cells were used for the preconcentration and measurement steps; these contained the gold/0.01*M* hydrochloric acid solution and 0.1*M* perchloric acid, respectively. The modified working electrode, the Ag/AgCl reference electrode (Model RE-1, BAS) and a platinum wire auxiliary electrode joined the measurement cell through holes in its Teflon cover. A voltammetric system (EG&G PAR 264A) was used to conduct the experiment. Data were recorded on a EG&G PAR Model 0073 X-Y recorder. Scanning electron microscopy was done with a Phillips 501B SEM.

Electrode preparation

Antheral cells from *Datura innoxia* were obtained and prepared as previously reported.[8,9]

The flower-cells modified carbon paste electrode (11% plant by weight) was prepared by throughly mixing 80 mg of mineral oil (Aldrich) with 26 mg of the plant powder, and then adding 125 mg of graphite powder (Acheson 38, Fisher) and mixing again until a uniform paste was achieved. A portion of the plant-containing paste was packed into the end of a glass tube (3-mm i.d.); a copper wire was inserted through the opposite end to establish electrical contact. The paste surface was smoothed on a weighing paper.

Procedure

The first smooth electrode surface was preconditioned by immersing the electrode in a stirred 25 mg/l. gold solution (in 0.01*M* hydrochloric acid) for 4 min, recording the differential pulse voltamperogram (from +0.85 to +0.20 V) in a 0.1*M* perchloric acid solution, and repeating these steps (*ca.* 5–7 times) until a stable gold peak was obtained.

The preconcentration/medium-exchange/voltammetric scheme[3] was used in all experiments. For the preconcentration step, the modified electrode was immersed in a stirred 10-ml gold test solution (in 0.01*M* hydrochloric acid) for a given period of time; the preconcentration proceeded at open circuit. The electrode was then removed from the preconcentation solution, rinsed with water, and placed in the measurement cell (containing 0.1*M* perchloric acid). After 15 sec the initial potential (+0.85 V) was applied for 10 sec before the voltamperogram was recorded. The scan was terminated at −0.4 V. The scan was repeated to verify the absence of the gold peak. The electrode was then rinsed and placed in the preconcentration cell for the next cycle.

RESULTS AND DISCUSSION

Surface-bound *Datura innoxia* cells incorporate gold(III) onto the electrode. Figure 1 compares cyclic voltamperograms obtained with the plain (A) and plant biomass (B) carbon paste

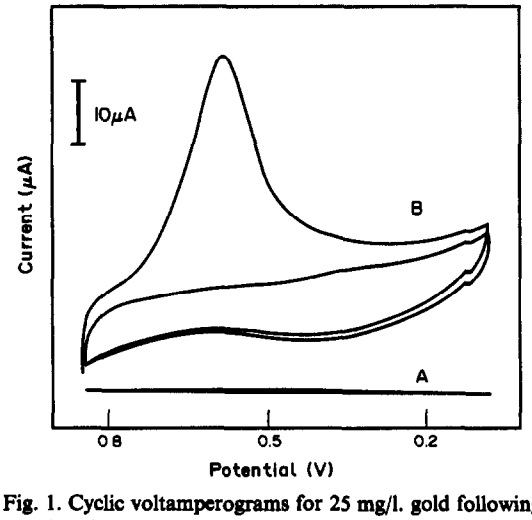

Fig. 1. Cyclic voltamperograms for 25 mg/l. gold following 10-min stirring at the unmodified (A) and plant biomass modified (B) carbon paste electrodes. Scan rate, 10 mV/sec. Accumulation solution, 0.01*M* HCl; measurement solution, 0.1*M* $HClO_4$.

electrodes following 10 min stirring (open-circuit conditions) in a 25 mg/l. gold solution and transfer of the electrode to a perchloric acid blank solution.

Voltammetric peaks are not observed when the unmodified electrode is used, as expected in the absence of gold collection. In contrast, the first scan (designated as 1) at the modified electrode exhibits a distinct current response (E_p = +0.58 V), corresponding to the reduction of the surface-bound gold(III). Reoxidation is not observed upon scanning in the positive direction. No peaks are observed upon subsequent scans. A similar redox behavior was reported for bioaccumulation/voltammetric experiments at algae-containing carbon pastes,[4] but using significantly higher gold concentrations.

Scanning electron microscopy can offer valuable insights into the collection of gold at *Datura innoxia* modified electrodes. Figure 2 shows scanning electron micrographs of the biomass modified electrode following immersion in the blank (a) and 20 mg/l. gold (b, c) solutions for 10 (b) and 60 (a, c) min, and scanning the potential from +0.85 to +0.20 V (to reduce the accumulated species). The open-circuit "collection" from the diluted gold solution resulted in the appearance of surface-bound gold particles. The size of these metallic particles is greatly influenced by the accumulation period, from *ca.* 0.5 μm following 10 min preconcentration to about 5–10 μm after 60 min accumulation. In contrast, the analogous micrograph following immersion in the blank solution revealed no gold particles.

The collection of gold(III) on a flower biomass electrode can be used as an effective preconcentration step prior to the voltammetric measurement. Figure 3(A) shows differential pulse voltamperograms for 25 mg/l. gold after different preconcentration times. Short accumulation periods yield well-defined peaks for mg/l. (ppm) concentrations. The longer the preconcentration time, the more gold is collected, and the larger the peak current. For a 5-min preconcentration period, a 9-fold enhancement of the peak height is observed over that attained following 20-sec stirring [compare curves (a) and (h)]. Although such sensitivity enhancement is important, the procedure also offers improved selectivity based on the discriminative properties of the preconcentration and the medium-exchange steps (see interference study below). Also shown in Fig. 3(B) are plots of peak

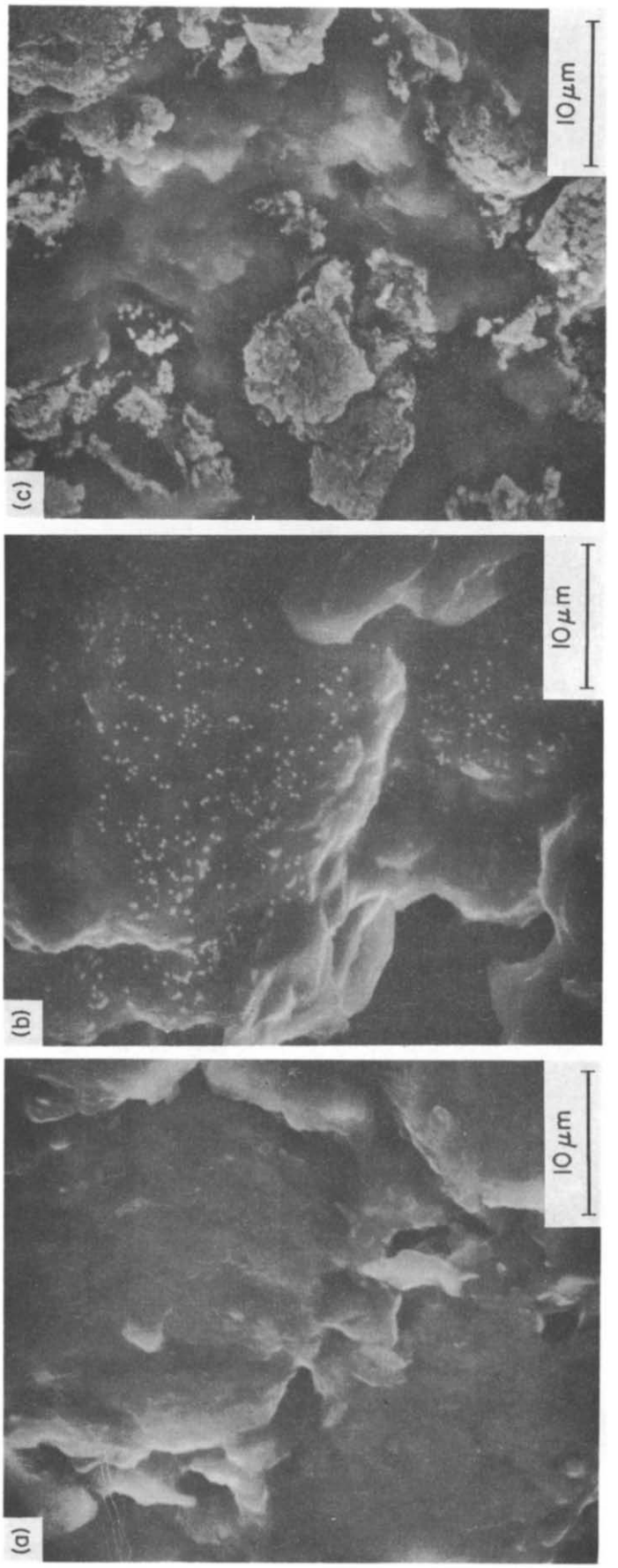

Fig. 2. Scanning electron micrographs of the plant biomass electrode following immersion (stirring) in the blank (a) and 20 mg/l. gold (b, c) solutions for 60 (a, c) and 10 (b) min. Magnification, 2500×.

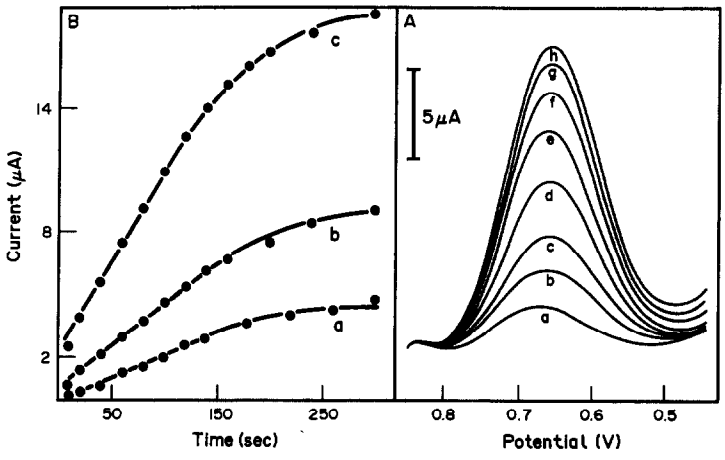

Fig. 3. (A) Differential pulse voltamperograms for 25 mg/l. gold after different preconcentration times. 10 (a), 40 (b), 60 (c), 100 (d), 140 (e), 180 (f) and 240 (g) sec. (B) Resulting peak current *vs.* preconcentration time plots for 5 (a), 10 (b), and 25 (c) mg/l. gold. Differential pulse waveform with 10 mV/sec scan rate and 50 mV amplitude. Details of the preconcentration/medium-exchange voltammetric scheme are given in the Experimental section.

current *vs.* preconcentration time for different gold concentrations [5 (a), 10 (b), and 25 (c) mg/l.]. The rate of gold biosorption is independent on the concentration. The peak currents rise rapidly at first and then more slowly. Apparently, the binding reached equilibrium in accumulation for 4 min.

The solution pH has a profound effect upon the uptake (and hence the voltammetric response) of gold. As illustrated in Fig. 4 a large response is obtained following accumulation from highly acidic solutions. A rapid decrease in the peak is observed upon increasing the pH between 2 and 6; no response is obtained at higher pH values. Such a profile is characteristic of an anion-exchange binding process, as expected for the tetrachloroaurate anion. A similar pH profile was reported for the collection of this gold anion at algae-modified electrodes.[4] The exact identity of the positively charged sites on the *Datura innoxia* cells remains to be elucidated. Various negatively charged groups have been identified earlier on the *Datura innoxia* cells in connection with electrostatic uptake of cations.[8,9] A medium-exchange step, *i.e.*, transfer of the electrode (following the accumulation) to a more favorable electrolyte can be used to improve the selectivity of preconcentrating CMEs.[10] The most favorable response was obtained using a 0.1*M* perchloric acid solution in the voltammetric cell.

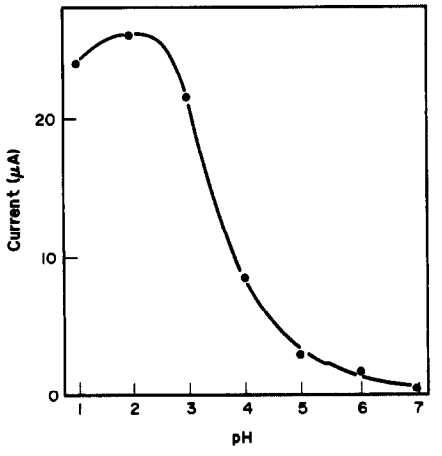

Fig. 4. Dependence of the gold peak (25 mg/l.) on the pH of the preconcentration solution. Four min accumulation. Other conditions, as in Fig. 3.

Most preconcentrating modified electrodes require a "cleaning" step (before the next preconcentration/voltammetric cycle) to eliminate memory effects.[10] Such a step is not needed with the flower biomass electrode, since the metallic gold product of the voltammetric scan does not contribute to the subsequent voltammetric response. (No peak is observed by repeating the scan in the measurement solution.) In addition, despite the presence of metallic gold, the bioaccumulation continues in a reproducible fashion, due to the very large gold(III) binding capacity. The reproducible accumulation and effective self-cleaning are illustrated in Fig. 5, from a prolonged series of 50 preconcentration/voltammetric repetitions with 10 mg/l. gold, during a continuous 5-hr period. Such a long operation yielded a highly stable response, with a mean peak current of 11.0 μA,

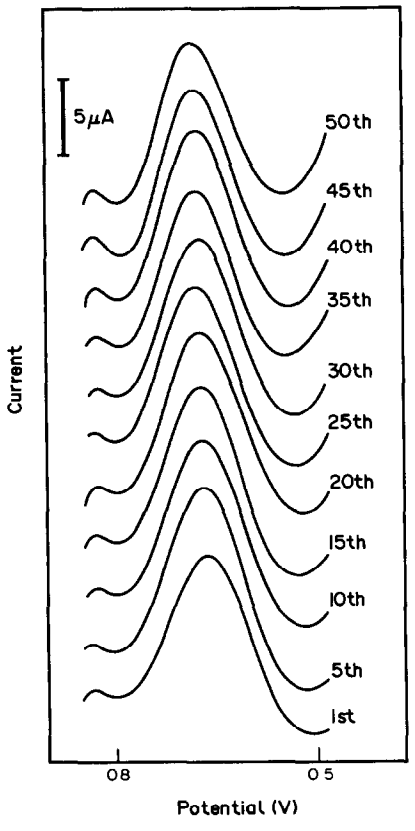

Fig. 5. Sensor performance under continuous use. Repetitive measurement of 10 mg/l. gold over a five hour period. Four min accumulation. Other conditions, as in Fig. 3.

a range of 10.4–11.9 μA, and a relative standard deviation of 4.8%. Analogous measurements of gold at algae-modified electrodes required surface regeneration via immersion in a sodium cyanide solution.[4] The high stability and simple operation of the flower-biomass electrodes hold great promise for their use in voltammetric sensing of gold.

High selectivity is also essential for such sensing applications. Co-existing metal ions (whether electroactive or not) can interfere with the determination of gold if they compete for binding sites. The following metal ions (20 mg/l.) were tested and found not to affect the 10 mg/l. gold response: Cu(II), Pb(II), Zn(II), Ni(II), Ti(IV), In(III), Fe(III), Hg(II), and Mn(II). In contrast, additions of 20 mg/l. Cd(II), Tl(I) and V(V) resulted in 18, 25 and 34% diminutions, respectively, of the 10 mg/l. gold response. The interference study suggests a relatively high selectivity associated with the coupling of preferential binding (to the flower biomass) and the medium-exchange step.

Figure 6 displays pulse voltamperograms for gold solutions of increasing concentration [2.5–25 mg/l. (a)–(h)], following 4 min accumulation (A), along with the resulting calibration plot (B). The well-defined peaks increase linearly with the gold concentration up to 15 mg/l., and then start to level off. The slope of the linear portion corresponds to 1.12 μA . l./mg (correlation coefficient, 0.999). A detection limit of 0.5 mg/l. gold can be estimated from the signal-to-noise characteristics (S/N = 3) of these data. In contrast, a higher detection limit of 4.8 mg/l. gold was reported for analogous measurements at the algae modified electrode.[4]

In conclusion, this work has illustrated the utility of flower cells as surface modifiers in connection with preconcentration/voltammetric measurement schemes. The unique bioaccumulation process at this flower biomass permits effective preconcentration of gold from dilute solutions. Lower detection limits are obtained in comparison to electrodes modified by algal biomass. The electrodes are simple and inexpen-

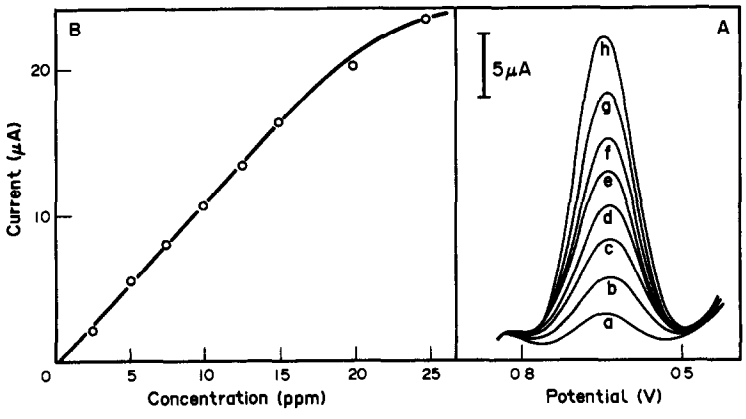

Fig. 6. Dependence of the peak current on the gold concentration. Voltamperograms for increasing gold concentration [2.5 (a), 5.0 (b), 7.5 (c), 10 (d), 12.5 (e), 15 (f), 20 (g) and 25 (h) mg/l. (A), along with the resulting calibration plot (B).

sive to prepare. Besides its sensing implications, the voltammetric study offers a better understanding of the gold collection process (although the exact binding mechanism is still not clear). This work serves as a basis for future work on using higher plant cells in electroanalytical (preconcentration/voltammetric) applications.

Acknowledgement—This work was supported by grants from Sandia NL (to J.W.) and the DOE-NM-WERC program (to G.D.R.). T.B. acknowledges a fellowship from Sichuan University (PR China).

REFERENCES

1. M. Shengjun and J. Holocombe, *Talanta*, 1991, **38**, 503.
2. K. Tanaka, *Bioelectrochem. Bioenerg*, 1991. **26**, 403.
3. J. Gardea-Torresdey, D. Darnall and J. Wang, *Anal. Chem.*, 1988, **60**, 72.
4. J. Gardea-Torresdey, D. Darnall and J. Wang, *J. Electroanal. Chem.*, 1988, **252**, 197.
5. J. Wang, T. Martinez and D. Darnall, *J. Electroanal. Chem.*, 1989 **259**, 295.
6. M. Connor, E. Dempsey, M. R. Smyth and D. H. S. Richardson, *Electroanalysis*, 1991, **3**, 331.
7. J. Wang, N. Naser, D. Darnall and J. Gardea-Torresdey, *ibid.*, 1992, **4**, 71.
8. H. D. Ke and G. Rayson, Environ. *Sci. Technol.*, in the press.
9. H. D. Ke, E. Birnbaum, D. Darnall and G. Rayson, *J. Appl. Spectroscopy*, in the press.
10. J. Wang, in A. J. Bard (ed.), *Electroanalytical Chemistry*, Vol. 16, pp. 1–88. Marcel Dekker, New York, 1989.

Talanta, Vol. 39, No. 12, pp. 1643–1645, 1992
Printed in Great Britain.

0039-9140/92 $5.00 + 0.00

DETERMINATION OF CADMIUM IN RIVER WATER BY SEQUENTIAL METAL VAPOR ELUTION ANALYSIS

KIYOHISA OHTA,* NOBUYUKI NAKAJIMA and SYN-YA INUI
Department of Chemistry for Materials, Mie University, Mie, Tsu, 514, Japan

JAMES D WINEFORDNER
Department of Chemistry, University of Florida, Gainesville, FL 32611, U.S.A.

TAKAYUKI MIZUNO
Department of Chemistry for Materials, Mie University, Mie, Tsu, 514, Japan

(*Received* 11 *March* 1992. *Revised* 20 *May* 1992. *Accepted* 20 *May* 1992)

Summary—Determination of cadmium in river water by sequential metal vapor elution analysis (column temperature; >1500 K) with argon and hydrogen carrier gas and with atomic absorption spectrometric detection is described. The column is made of a molybdenum capillary tube (i.d. 1.22 mm) and the temperature is 1760 K. The cadmium vapor was separated from those of calcium, iron and sodium. The calibration graph was linear up to 15 μg/ml. Relative standard deviations of 0.8–4.3% were obtained in the range 1 to 15 μg/ml. Cadmium in spiked samples (river water) was determined. The results were in good agreement with the amount spiked.

Sequential metal vapor elution analysis (SMVEA) or super high temperature gas chromatography with atomic absorption spectrometric detection (SHTGC–AAS) has been recently developed. The potential of this technique for the separation of gaseous species at high temperatures (>1500 K) has been recognized by us.[1–3] Yanagisawa *et al.*[4–7] have reported the separation of some volatile elements in argon carrier gas by use of a separative column atomizer and detection by an atomic absorption or emission spectrometer. However, few SMVEA studies for various elements have been reported.

In this study, the separation of cadmium from calcium, iron and sodium by SMVEA–AAS with argon and hydrogen carrier gas is evaluated. The determination of cadmium in river water by SMVEA–AAS is described.

EXPERIMENTAL

Apparatus

The high temperature column unit of SMVEA were reported in detail in a previous paper.[1] An open tubular column is made of a molybdenum tube (i.d. 1.22 mm, wall thickness 0.406 mm, length 250 mm) (99.95% purity, Goodfellow). The column consisted of three portions; atomization, separation, and detection portions. A 0.5-mm diameter hole is drilled at the midpoint of the atomization portion to inject the sample solution. The detection portion has a 0.8-mm hole, perpendicular to the hole in the atomization portion, for atomic absorption measurement. A monochromator (Nippon Jarrell-Ash 0.5 m Ebert-type), a lock-in amplified (NF LI-575), a memoriscope (Kikusui 5516ST), and a microcomputer (NEC, PC-9801RX) are used for AA signal detection in this study. The absorption signal from the amplifier was fed into the microcomputer. The column temperature was measured with an optical pyrometer (Chino Works). Two pinhole apertures were placed in front of and in the rear of the detection hole portion to provide a narrow beam of light about 0.8 mm in diameter and to remove background emission from the column surface.

Hollow-cathode lamps (Hamamatsu Photonics Co.) were used as light sources. The atomic resonance lines for measuring the absorption signal were 228.8, 422.7, 248.3 and 589.0 nm

*Author for correspondence.

for cadmium, calcium, iron and sodium, respectively.

Reagents

Stock solution (1 mg/ml) of cadmium, calcium, iron, and sodium were prepared as chlorides in 0.1*M* hydrochloric acid. The test solutions for the measurement were mixed and diluted from the stock solutions with distilled-demineralized water just before use. All chemicals used were of analytical grade purity.

Procedure

The column temperature was in the range 1760–1870 K. The atomization temperatures were in the range 1760–1940 K. The carrier gas was argon (1.0 ml/min) and hydrogen (0.5 ml/min). The purge gas flow rates in the column chamber were 3.0 l/min for argon and 200 ml/min for hydrogen. The slight hydrogen flow rate was needed to protect the metal column from oxidization by residual oxygen in the column chamber and in the argon.

After stopping the carrier gas, a 1-μl aliquot of sample solution was pipetted into the atomization portion. The sample was dried at 400 K for 10 sec and pyrolysed 760 K for 10 sec. After allowing the carrier gas to flow, the column was heated at 1760 K and the residue in the atomization portion was atomized at 1760 K for >1 min.

RESULTS AND DISCUSSION

The separation of cadmium from calcium, iron and sodium by SMVEA–AAS with argon and hydrogen carrier gas was evaluated. Calcium, iron and sodium are relatively rich in river water; these species interfere with determinations of cadmium by conventional AAS with metal atomizers,[8-9] and so they were selected for the present study. In the separation study, the amounts of Cd, Ca, Fe and Na introduced into the column were 15 ng, 200 ng, 10 ng and 1 ng, respectively.

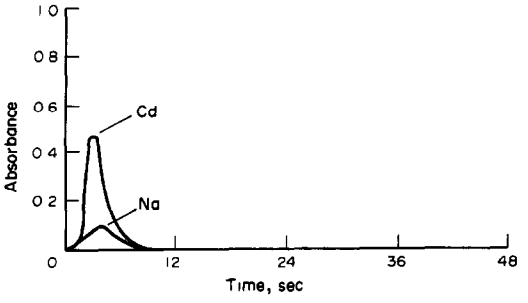

Fig. 1. Profile at the column temperature of 1870 K by sequential metal vapor elution analysis. Atomization temperature; 1940 K, carrier gas; Ar 1.0 and H_2 0.5 ml/min, purge gas; Ar 3000 and H_2 200 ml/min.

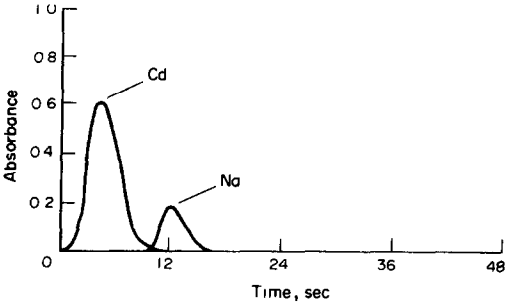

Fig. 2. Profile at the column temperature of 1760 K by sequential metal vapor elution analysis. Atomization temperature; 1760 K, carrier gas; Ar 1.0 and H_2 0.5 ml/min, purge gas; Ar 3000 and H_2 200 ml/min.

In general, the column temperature influences retention time and separation power. Therefore, the performance characterization of the metal column in the SMVEA-AAS was evaluated at column temperatures between 1760–1870 K and atomization temperatures between 1760–1940 K. Figure 1 shows a typical unseparated graph was obtained with a column temperature of 1870 K and with an atomization temperature of 1940 K. The cadmium vapor in the argon and hydrogen carrier gas was separated from Ca, Fe and Na at 1760 K of column and atomization temperatures, as shown in Fig. 2. The retention times (t_r) and the relative standard deviations under the optimal conditions are listed in Table 1. From Figs 1 and 2, the separation of cadmium at relatively low column temperature is preferable to high temperature. Even though the relative standard deviation of the t_r values for cadmium was poor, cadmium could still be separated and determined. Profiles for Ca and Fe were not detected in the capillary tube column. At atomization and column temperatures higher than 1940 K, Ca and Fe were separated, but cadmium was then not separated from sodium. At 1760 K, it seems that the residue of Ca and Fe remained in the column. By continual heating of the column, however,

Table 1. Retention time of peak by sequential metal vapor elution analysis

Element	Retention time t_r, *sec*	r.s.d. of t_r %
Cd	4.1	14
Na	12	3.9
Ca	—	—
Fe	—	—

Table 2. Determination of cadmium in river water

Sample	Cd, μg/ml		
	Added*	Found	Recovery, %
Anou river	0.00	—	—
	1.00	1.01 ± 0.08	101
	5.00	5.45 ± 0.18	109
Iwata river	0.00	—	—
	1.00	1.01 ± 0.09	101
	5.00	5.21 ± 0.21	104
Shitomo river	0.00	—	—
	1.00	1.05 ± 0.10	105
	5.00	4.85 ± 0.69	97.0

*The number of analysis; 3.

no memory effect for these elements was observed in the system.

From these results, the separation mechanism of Cd and Na at the column temperature of 1760 K may be due to the differential vapor pressure between cadmium (b.p. 1040 K) and sodium (b.p. 1156 K).[10] However, by considering the void volume (150 mm column; 0.175 ml), the actual flow rate of the carrier gas (9.01 ml/min = 0.150 ml/sec at 1760 K) and the atomization rate (<1 sec at 1760 K), the signals of Cd and Na appear in a much longer time than the throughput time (<1.17 sec) of the carrier in the column. Therefore, the separation mechanism may be the differential vapor pressure of analyte and the interaction of the elements and the inside surface of the column.

The relative standard deviation for peak area calculated for 6 repeated measurements of 15 ng cadmium was 0.8%.

Under optimal experimental conditions, cadmium in river water was determined. The calibration curve was prepared from cadmium standard solutions and the peak areas of the absorbance. The calibration graph was linear up to 15 ng. Relative standard deviations of 0.8–4.3% were obtained in the range 1–15 ng of Cd. Cadmium in spiked samples (river water) was determined. The recoveries were found to be excellent (Table 2).

As described above, the major benefits of the SMVEA with a high temperature column were; (1) direct separation of metal vapor, (2) elimination of chemical interference occurring in conventional AAS, (3) simplicity and low-cost, (4) possibility of using tandem mass spectrometry as a detector.

Consequently, the remarkable performance of SMVEA with the metal column may allow accurate determination of various elements in complex samples.

Acknowledgements—This work was supported financially by the Ministry of Education, Science and Culture of Japan and Okasan katou bunka sinkou zaidan. The authors wish to thank Mr. Takehiko Sugiyama for the technical assistance.

REFERENCES

1. K. Ohta, B. W. Smith, M. Suzuki and J. D. Winefordner, *Spectrochim. Acta*, 1982, **37B**, 343.
2. K. Ohta, B. W. Smith and J. D. Winefordner, *Anal. Chem.*, 1982, **54**, 320.
3. *Idem, Microchem. J.*, 1985, **32**, 50.
4. M. Yanagisawa, K. Ida and K. Kitagawa, *Anal. Sci.*, 1989, **5**, 765.
5. K. Kitagawa, T. Takeuch and M. Yanagisawa, *ibid.*, 1989, **5**, 445.
6. *Idem, ibid.*, 1989, **5**, 539.
7. M. Yanagisawa, K. Katoh and K. Kitagawa, *ibid.*, 1990, **6**, 471.
8. K. Ohta, W. Aoki and T. Mizuno, *Talanta*, 1988, **35**, 831.
9. K. Ohta, S. Itoh and T. Mizuno, *ibid.*, 1991, **38**, 871.
10. D. R. Lide (ed.), *Handbook of Chemistry and Physics*, 72nd Ed., pp. 4–122, 4–123. CRC Press, Boston, 1991.

Talanta, Vol. 39, No. 12, pp. 1647–1652, 1992
Printed in Great Britain.

0039-9140/92 $5.00 + 0.00

ANALYTICAL DATA

SPECTROPHOTOMETRIC DETERMINATION OF THE STABILITY CONSTANT OF THE Eu(III)–MUREXIDE COMPLEX

SHASHI JAIN and PINAKI GUPTA-BHAYA*
Department of Chemistry, Indian Institute of Technology, Kanpur, Kanpur 208 016 (UP), India

(*Received* 24 *September* 1988. *Revised* 16 *December* 1991. *Accepted* 24 *December* 1991)

Summary—The values of the stability constants of the Ca(II) and lanthanide(III) complexes of murexide reported in the literature were determined without proper correction for binding of buffer ions to the metal ion. The constants are best determined without a buffer present. Accurate values of conditional stability constants for the Eu(III)–murexide complex (relative standard deviation better than 3%), of the differential molar absorptivity of the Eu(III)–murexide complex with respect to murexide at 480 nm (relative standard deviation better than 0.5%) and of the molar absorptivity of murexide at 520 and at 506 nm (precision better than 0.4%) at pH 5.0 and 6.5 at 15, 25 and 35° are reported. The accuracy and precision of the concentration of metal ion in solution determined by using these conditional stability constants are discussed.

The stability constants of metal–dyestuff complexes are important for the detection and determination of low concentrations of metal ions. Besides their analytical use, metallochromic indicators are used to determine concentrations of free metal ion in a mixture of metal ion and ligand for determination of stability constants and rate constants of metal–ligand systems. Murexide has been used in this way for various metal ions, in particular calcium(II) and lanthanide(III), but accurate values of metal–murexide (MMu) stability constants are not always available.

In earlier determinations of metal–murexide stability constants,[1–3] buffers were used to keep the pH constant when the absorbances of mixtures of metal ions at different concentrations with murexide at fixed concentration were measured against murexide at the same total concentration, but side-reactions of the metal ion with the buffer or other background anions (from electrolytes added to keep the ionic strength constant) were ignored. The stability constants thus obtained[1–3] were therefore conditional constants. The free metal ion concentrations in solution calculated by using these conditional constants are incorrect. Balaji *et al.*[1] pointed out that the true stability constants (K) can be obtained from the conditional values K' (calculated by ignoring metal-binding by the buffer) by means of the relation

$$K = K'(1 + \sum_i K_{MB_i}[M][B]_t^i) = K'\alpha,$$

where the K_{MB_i} values are the metal–buffer stability constants and $[B]_t$ is the total concentration of buffer. It is assumed that the free buffer concentration $[B]_f$ is approximated by $[B]_t$ since $[B]_t \gg [M]_t$. If α is incorrectly determined, K may have high precision, but will have low accuracy. The authors used literature values (corrected for changes in experimental conditions) of K_{MB} to calculate α. These K_{MB} values had been obtained from pH titrations, and had good precision, but also a large systematic error arising from lanthanide hydrolysis.[4] Also, they were based on use of high concentrations of buffers (acetate and phosphate) that bind certain metal ions fairly strongly, making $\alpha \gg 1$. Even a small error in the values of K_{MB_i} makes α inaccurate to a significant extent. This could be ignored for

$$\sum_i K_{MB_i}[M]_f[B]_t^i \ll 1.$$

$[M]_f$ is calculated from

$$[M]_f = [M]_t - [MMu] - \sum_i [MB_i].$$

*Author for correspondence.

In the experiments of Balaji *et al.*[1] the minimum error in the values of K_{MB} used is 10%.[5] Since $[B]_t$ is large, the error in

$$\sum_i [MB_i]$$

is of the order of $[M]_f$. This leads to a very large relative error in $[M]_f$ and therefore in K_{MMu}. The effect of metal ion–chloride association was not considered.

The ideal buffer would have a small but accurately and precisely known stability constant for its metal-complex, and a pK value close to the desired pH, so that its concentration can be kept low. The pH values used here were 5.0 and 6.5. Some good buffers for these values weakly bind metal ions.[6] Many nitrogenous heterocycle buffers, *e.g.*, Pipes [piperazine-di(ethanesulfonic acid)] react with murexide, and Tes [*N*-tris(hydroxymethyl)methyl-2-aminoethanesulfonic acid], pK 7.5, seems the only choice for use at pH 6.5, but is poor because a high Tes concentration is necessitated by its low buffer capacity at this pH. The binding constant of Tes and Eu(III) is not known, but its effect cannot be ignored even if it is small, because of the high Tes concentration needed. If [Tes] is ~ 100 mM and K_{MB} is ~ 10, then if $[B]_f = [B]_t$, [MB] is $\sim 7\%$ of [MMu] (assuming use of typical concentrations). At pH 5.0, Bistris [bis(2-hydroxyethyl)imino-tris(hydroxymethyl)methane] or acetate buffer can be used, but Bistris binds several metal ions strongly.[7] A preliminary experiment (with murexide to indicate the free metal concentration) showed that the stability constant of the Eu(III)–Bistris complex is $\sim 10^5$. The stability constant of the Eu(III)–acetate complex is large,[5] with an error of 10% as estimated by the authors. The effect of lanthanide hydrolysis introduces an additional unestimated error.[4] An accurate value of the Eu(III)–acetate equilibrium constant is thus not available.

In view of all this, the Eu(III)–murexide equilibrium is best examined in the absence of a buffer. The accuracy depends on having the same pH and total murexide concentration in both cuvettes, one containing Eu(III) and the other not, since otherwise $\Delta A = \Delta\epsilon[MMu]$ will not hold for the difference in absorbance (ΔA); $\Delta\epsilon$ is the difference between the molar absorptivities of murexide and the complex. Addition of a metal solution to unbuffered murexide solution will change the pH, and restoration of this to the original value while keeping the total murexide concentrations equal must be done directly in the cuvette. The error in so doing is insignificant and less than that due to the uncertainty in K_{MB}. The values of K_{MMu} however, should be determined at a definite ionic strength maintained by a sufficiently high inert electrolyte concentration (0.100M KCl is recommended by IUPAC and IUPAB[8]). The values of K_{MMu} reported in this paper can only be used in calculating the free metal ion concentration in metal–ligand titration experiments aimed at determination of metal–ligand stability constants if these are conducted at a sufficiently high ionic strength. This is because in such titrations the concentrations of metal and ligand are varied over as wide a range as possible, and in the absence of an ionic-strength adjuster the ionic strength of the metal–ligand mixture will change considerably, since the metal ion and quite often the ligand will be charged. Such an adjustment, however, introduces the risk of side-reactions of the cation and anion of the "inert" electrolyte with the ligand and the test metal ion, respectively.

EXPERIMENTAL

Reagents

Eu_2O_3 (purity 99.9%, Sigma); murexide (analytical grade, Koch-Light) with purity checked by C,H,N analysis (Ca^{2+} was found to be absent). Other chemicals were analytical grade. All the reagent solutions were prepared in the appropriate buffer (acetate for pH 5, Tes for pH 6.5) and adjusted to ionic strength 0.100M with potassium chloride.

Europium solution. Eu_2O_3 was dissolved in hydrochloric acid and the solution evaporated to dryness. This step was repeated 3 or 4 times and the $EuCl_3$ obtained was dissolved in the buffer. The solution was standardized by weight titration of 100 μl with EDTA at pH 5.0, with Xylenol Orange as indicator.[9] The [EDTA]/[Eu] ratio was about 0.25, and the standardization error was about 0.5%.

In this and all the other experimental work, high precision was achieved by weighing to find the volumes of reagents dispensed, with careful adjustment to the desired values by dispensing from μl-pipettes. The maximum error was ~ 1 μl.

Murexide solution. A freshly prepared solution of murexide (in demineralized water) was filtered, then lyophilized. Thermogravimetry showed that the product contained no water of

hydration. A buffered solution in 0.1*M* potassium chloride at 25° deteriorated in ~1.5 hr at pH 5 and ~3.5 hr at pH 6.5. Calculation of the concentration requires the molar absorptivity (ϵ) to be known. Schwarzenbach and Gysling[2] reported its value at 520 nm, pH 8.53 and an unspecified temperature. It is expected to be dependent on pH and may depend on temperature owing to a change in solvation. We have redetermined ϵ under the experimental conditions of interest, by dissolving a weighed quantity of lyophilized murexide in 1000 ml of buffer solution (15m*M* acetate buffer at pH 5.0 and 100m*M* Tes buffer at pH 6.5) of ionic strength 0.100 (adjusted with potassium chloride) and measuring the absorbance at 520 and 506 nm against the corresponding buffer blank. The molecular weight of non-hydrated murexide was used to calculate the concentration. Two independent measurements agreed within ~0.1%.

Determination of $\Delta\epsilon$

Identical volumes of murexide solution in the acetate or Tes buffers just mentioned, of ionic strength adjusted to 0.100*M* (KCl), were added to the reference and sample cuvettes. A preliminary experiment was used to find what concentration of europium chloride solution would be needed for 100 μl of it to convert all the murexide into its europium complex, and 100 μl of the appropriate solution (in the correct buffer) was added to the murexide solution in the sample cell. An identical volume of buffer/KCl solution was added to the murexide solution in the reference cell. The absorbance of the sample solution was measured (ΔA) and divided by the total murexide concentration (which was equal to the concentration of the europium complex) to give $\Delta\epsilon$. The value was checked by making further 100-μl additions of europium solution to the sample cell and buffer/KCl solution to the reference cell and redetermining ΔA.

The following considerations show that $\Delta\epsilon$ values reported here can be used at a given pH even when the buffer and KCl are absent. (*a*) We have found that the molar absorptivity of murexide at 480 nm is 2% higher in 100m*M* potassium chloride than in Tes buffer alone. The same is true for the europium complex. Thus $\Delta\epsilon$ (EuMu – Mu) at 480 nm is not affected significantly by the presence of potassium chloride. (*b*) The Eu(III)–Tes complex, free Eu(III) and Eu(III)–Cl^- complex absorb negligibly at 480 nm. The buffer contributes very little sodium ion compared to the amount of potassium present. Thus the presence of buffer also does not affect $\Delta\epsilon$ at 480 nm. (*c*) $[K^+]_f$ nearly equals $[K^+]_t$ in both cuvettes. The value of $[Mu]_f$, however, is nearly zero in one cuvette and is non-zero in the other. Thus [KMu] is different in the two cells, but this is of negligible consequence since 480 nm is at the tail end of the difference spectrum of murexide in the presence and absence of 100m*M* potassium chloride (the difference is only ~2%). The maximum of the difference spectrum is at 518 nm, where the difference is ~8%). Values of $\Delta\epsilon$ determined in the absence of buffer agreed with those reported in Table 2, within experimental error.

Metal–murexide stability constant

Identical volumes of murexide solution were added to the two cuvettes, the concentration of murexide being such that the absorbance at 520 nm was between 0.65 and 1.05. Metal solution was then added to the sample cell and an identical volume of water to the reference cuvette, followed by enough potassium chloride solution to make the ionic strength 0.100*M* in both cuvettes. The concentration of metal was chosen so that [MMu] and $[Mu]_f$ were similar.

The pH of the test solution was adjusted by addition of dilute sodium hydroxide solution (pH ~8), the approximate volume of base needed having already been estimated in a separate experiment. The solution was mixed and the final pH checked with a microelectrode inserted into the cuvette. The pH was almost always within 0.05 of the pH of the murexide solution in the reference cuvette. If it was slightly outside this range, a measured small volume (1–2 μl) of base or acid was added by μl-pipette to bring the pH closer to the desired value, and an identical volume of potassium chloride solution ($\mu = 0.100M$, pH equal to that of the solution in the reference cuvette) was added to the reference cuvette. The liquid lost when the microelectrode is removed after the pH measurement does not affect the accuracy, because it does not alter the concentration. In spite of a small difference in pH (~0.05) between the two cuvettes the reproducibility is 1–3%. The analysis of errors given later shows that inaccurate adjustment of pH does not significantly contribute to the error.

The Hellma cells have small openings and were kept tightly stoppered during spectral

measurements and weighings. The loss by evaporation was negligible.

The absorbance of the test solution (ΔA) was measured against the murexide reference solution at the desired temperature (thermostatically controlled cell compartment) at 480 nm (the wavelength of the maximum in the difference spectrum) in a Cary 17D spectrophotometer. The mean absorbance and its standard deviation were noted from the digital read-out. The reagent concentrations were chosen to make ΔA high (>0.5) so that its standard deviation of 0.002 was insignificant.

Table 2. Differential molar absorptivity ($\Delta\epsilon$)

pH	Temperature, °C	$\Delta\epsilon \pm s$,* 10^4 l.mole^{-1}.cm^{-1}
6.5	15	1.312 ± 0.003
	25	1.289 ± 0.005
	35	1.264 ± 0.005
5.0	15	1.385 ± 0.006
	25	1.351 ± 0.006
	35	1.325 ± 0.004

*Average of six independent measurements. Concentration of murexide being saturated is in the range 3.39–$6.7 \times 10^{-5}M$. The $\Delta\epsilon$ values are independent of the absolute value of the concentration of murexide and the presence of KCl and buffer salts.

RESULTS AND DISCUSSION

Trends and comparison with literature values

The values of ϵ, $\Delta\epsilon$ and K_{MMu} are given in Tables 1, 2 and 3 respectively. The values of ϵ at pH 5.0 and 6.5 are equal within experimental error, as expected in view of the pK value of murexide. There is a small but significant decrease in ϵ with increasing temperature at both 520 and 506 nm. The ratio of the two values of ϵ can be used as an indicator of the quality of the murexide sample. Schwarzenbach and Gysling[2] reported a value of 1.35×10^4 l.mole^{-1}.cm^{-1} for ϵ at 520 nm in veronal buffer (pH 8.53) at an unspecified temperature. This value lies between the values determined by us at 15° and 25°. Schwarzenbach[10] has published the spectra of murexide at pH 7 and 13, without giving numerical values of the absorbance. An approximate estimate made from the plot shows that the difference in ϵ is $\sim 5\%$ at λ_{max}. At pH 13 two protons (p$K_{a1} = 9.2$, p$K_{a2} = 10.5$) are completely dissociated; at pH 8.53 the first dissociation is only about 17% complete, so a difference of only $\sim 1\%$ is expected between the spectrum at pH 8.53 and that at pH ≤ 7.0. The difference between the ϵ values determined by us and those reported by Schwarzenbach and Gysling[2] is of that order. The values of $\Delta\epsilon$ decrease with increase in temperature or pH, whereas the values of K_{MMu} decrease with decrease in pH or increase in temperature. The values differ significantly from those determined by Balaji *et al.*,[1] who took into account the effect of metal–buffer interaction incorrectly. For 25°, pH 5.0 and $\mu = 0.100M$, they reported $\log K = 5.42$. The value reported here is $\log K = 4.20$. The value reported by Geier[3] for 12°, pH 4.0, $\mu = 0.100M$, without consideration of metal–buffer interaction (the chemical nature of the buffer was not specified) was $\log K = 4.18$. At 15°, pH 5.0, $\mu = 0.100M$, we found $\log K = 4.28$. As $\log K$ decreases with decrease in pH our result seems in good accord with Geier's.

Table 1. Molar absorptivity of murexide

Temperature, °C	ϵ*, 10^4 l.mole^{-1}.cm^{-1}	
	At 506 nm	At 520 nm
15	1.260 ± 0.0005	1.365 ± 0.002
25	1.247 ± 0.001	1.341 ± 0.002
35	1.233 ± 0.001	1.323 ± 0.002

*Range of two independent measurements, one for $7.672 \times 10^{-5}M$ murexide and the other for $7.995 \times 10^{-5}M$.

Nature of the constants and their range of validity

In the calculation of K, we consider Mu and MMu as single species without regard to protonation. These constants are thus conditional constants dependent on pH. As is shown below, binding of K^+ to Mu and metal ion to Cl^- causes further complications. The values of K are calculated assuming that a 1:1 complex is

Table 3. Log$K$ of Eu(III)–murexide association equilibria

pH	Temperature, °C	$\log K \pm s$*
5.0	15	$5.278_4 \pm 0.006_4$
	25	$5.205_0 \pm 0.007_7$
	35	$5.143_6 \pm 0.004_6$
6.5	15	5.525 ± 0.013
	25	5.435 ± 0.011
	35	5.365 ± 0.012

*Average of 6 or 7 measurements; titration points for [MMu] = 60% of [Mu]$_t$ or [M]$_t$ are omitted. Inclusion of these points increases the value of s. These values do not include the effect of binding of K^+ to murexide and that of Eu(III) to Cl^-, but these conditional stability constants yield correct values of free Eu(III) in solution (see Results and Discussion).

formed, which appears to be valid over the range of concentrations explored ($3–4 \times 10^{-5}M$ [MMu], $2.5–5 \times 10^{-5}M$ $[M]_f$, $3–5 \times 10^{-5}M$ $[Mu]_f$) because the K_{MMu} values obtained are the same within 1–3% at a given temperature and pH.

Estimate of precision

The maximum error of the volume measurements made by weighing was 5×10^{-5} ml (maximum weighing error 0.05 mg) and is negligible. The error in absorbance measurement was estimated from the fluctuation in the digital read-out, and an absorbance of 0.6 or above had a maximum error of ~0.3%, equivalent to a relative standard deviation (s) of ~0.1% (99% confidence). The europium concentration has a relative standard deviation of ~0.5%, which is wholly due to the end-point error and the burette reading error. The EDTA concentration has a maximum error of ~0.5%, arising from the purity of the EDTA used, the weighing error and the error in making up the solution to standard volume. This error does not affect the precision but alters the accuracy since only one EDTA solution is made. The error in the volume of europium solution taken for titration is negligible because the volume is measured by weighing. The error in measuring the molar absorptivity depends on the absorbance (maximum error ~0.3%) and the murexide concentration error (weighing error ~0.2%, volume error in dilution to 1000 ml ~0.04%), and thus is ~0.3% maximum, equivalent to a relative standard deviation of ~0.1% (the value observed, Table 1).

From these values it can be calculated that the relative standard deviation of K_{MMu} is about 1.2%, in agreement with the precision found experimentally. We conclude that adjustment of the pH directly in the cuvette does not lead to any additional error. The maximum error in the pH was ±0.05, the reading error of the pH-meter.

The values of $\log K_{MMu}$ in Table 3 are quoted to four (pH 5.0) and three (pH 6.5) decimal places even though the third (pH 5.0) and the second (pH 6.5) places respectively are in error. This is done to avoid truncation errors. The quantity of eventual interest to us is $[M]_f$, which is calculated from $[M]_f = [MMu]/[Mu]_f K_{MMu}$ and has a calculated error of ~1.6%. Any truncation should be done at this stage.

Effect of binding of potassium by murexide

Potassium chloride at $0.1M$ concentration was used to maintain the ionic strength constant. Though the affinity of murexide for potassium is less than that for Eu(III), it cannot be ignored. The difference $[Mu]_t - [MMu]$ gives only the apparent concentration of free murexide, $[Mu]'_f$. The true value is $[Mu]_f = [Mu]'_f - [KMu]$. [KMu] is given by $K_{KMu}[K^+]_f[Mu]_f$; since $[K^+] \sim 10^4[Mu]$, $[K^+]_f \simeq [K^+]_t$ and $[Mu]_f = [Mu]'_f/(1 + K_{KMu}[K^+]_t) = [Mu]'_f/\alpha_{Mu(K^+)}$. As the value of K_{KMu} in aqueous medium is not known, $[Mu']_f$ of necessity remains a conditional concentration. However, a crude value for the constant might be estimated from the reported values for non-aqueous media[11] and the difference in dielectric constant, and appears likely to be in the range 1–25. If so, $\alpha_{Mu(K^+)}$ would be in the range 0.1–2.5 and would change $[Mu]_f$ by a factor of between ~0.3 and 0.9.

Inability to calculate α prevents us from calculating the true value of $K_{EuMu'}$ but does not affect the value of free Eu(III) ion concentration determined in a solution by use of murexide as indicator. It can be readily shown, using $[Mu]'_f = \alpha_{Mu(K^+)}[Mu]$ that the measured values of $\Delta\epsilon$ (Table 2) equal $\{\epsilon_{EuMu} - [\epsilon_{Mu}(1/\alpha) - \epsilon_{KMu}(1 - 1/\alpha)]\}$, where $\alpha = \alpha_{Mu(K^+)}$, and that $\Delta A = \Delta\epsilon[EuMu]$ holds, even if $\epsilon_{Mu} \neq \epsilon_{KMu}$. At 480 nm, however, ϵ_{Mu} differs negligibly from ϵ_{KMu}. Therefore [EuMu] calculated as $(\Delta A/\Delta\epsilon)$ is correct and is unaffected by $\alpha_{Mu(K^+)}$. The conditional K_{EuMu} reported in Table 3 uses $[Mu]'_f$ for calculation. If $[Mu]_f$ were used instead, we would obtain $K_{EuMu}(\text{corrected}) = \alpha_{Mu(K^+)}K_{EuMu}$ (conditional). Then $[Mu]'_f K_{EuMu}(\text{conditional}) = [Mu]_f K_{EuMu}(\text{corrected})$. We conclude that $[Eu]_f$ calculated as $[EuMu]/\{[Mu]'_f K_{EuMu}(\text{conditional})\}$ is unaffected by the factor $\alpha_{Mu(K^+)}$.

Effect of side-reactions of Eu(III)

The value of the free europium concentration used in calculating K_{MMu} obtained by subtracting [MMu] from $[M]_t$ is not its true value, but is a conditional quantity $[M']_f$, because of side-reactions with chloride. $[M']_f = \alpha_{M(Cl)}[M]_f$ where $\alpha_{M(Cl)} = \{1 + \beta_1[Cl^-]_t + \beta_2[Cl^-]_t^2\}$ (β_1 and β_2 are the stability constants for $EuCl^{2+}$ and $EuCl_2^{2+}$). The reported values[12–18] of β_1 and β_2 were determined at high ionic strengths, and after being corrected to $\mu = 0.1M$ yield a temperature-independent mean value of $\alpha = 1.088 \pm 0.01$ for $\mu = 0.1M$ (KCl).

In contrast to the effect of $\alpha_{Mu(K+)}$, that of $\alpha_{M(Cl)}$ can be corrected for, but since inability to calculate $\alpha_{Mu(K+)}$ already prevents us from calculating the true K_{EuMu}, we do not apply the correction due to $\alpha_{M(Cl)}$. It turns out once again, that the value of $[Eu]_f$ in a solution, determined by use of murexide as indicator, is not seriously affected by $\alpha_{M(Cl)}$. If we use the conditional K_{EuMu} value reported in Table 3 in calculating the ratio $[EuMu]/\{[Mu]'_f K_{EuMu}\}$ we obtain $[Eu]'_f$. The desired quantity $[Eu]_f$ can then be calculated from $[Eu]'_f$ by using the value of $\alpha_{M(Cl)}$. The precision of $[Eu]'_f$ is only slightly worse than that of K_{EuMu} (the worst is ~3%, Table 3). The precision of $\alpha_{M(Cl)}$ as calculated from the mean values of $\beta_{1,2}$ for the Eu(III)–Cl^- association given in 16 reports is ~1%. Twelve of these values differ from the mean value by ~1%, 3 by ~3%, and only one[18] differs from it significantly (~7%), but that work perhaps detected only one of several Eu(III)–Cl^- complexes. The precision of $\beta_{1,2}$ in the individual reports varies, the best being ±4%.[14] The accuracy and precision of $[Eu]_f$ is thus slightly inferior to that of $[Eu]'_f$.

Potential use of K_{MMu}

In metal–ligand mixtures of various concentrations of metal and ligand, values of $[M]'_f$ and $[M]_f$ can be calculated from K_{MMu}. The titration data can then be analysed by a computer program to obtain the best values of the stability constants of the metal–ligand complexes. In our laboratory, we have successfully used this technique to determine the β-values for Eu(III)–amino-acid complexes.[19] Determination of $[M]_f$ by use of murexide as a metallochromic indicator is also useful in stopped-flow or temperature-jump relaxation experiments aimed at the determination of the rate constants of metal–ligand interaction.

Acknowledgement—The authors express their gratitude to the referees and Dr. R. A. Chalmers, whose criticism and suggestions have added to the value of the paper.

REFERENCES

1. K. S. Balaji, S. D. Kumar and P. Gupta-Bhaya, *Anal. Chem.*, 1978, **50**, 1972.
2. G. Schwarzenbach and H. Gysling, *Helv. Chim. Acta*, 1949, **32**, 1314.
3. G. Geier, *Ber. Bunsenges.*, 1965, **69**, 617.
4. R. Prados, L. G. Stadtherr, H. Donato, Jr and R. B. Martin, *J. Inorg. Nucl. Chem.*, 1974, **36**, 689.
5. R. S. Kolat and J. E. Powell, *Inorg. Chem.*, 1962, **1**, 293.
6. D. E. Gueffroy (ed.), *A Guide for the Preparation and Use of Buffers in Biological Systems*. Calbiochem, California, 1975.
7. K. H. Scheller, T. H. J. Abel, P. E. Polanyi, P. K. Wenk, B. E. Fischer and H. Sigel, *Eur. J. Biochem.*, 1980, **107**, 455.
8. Interunion Commission on Biothermodynamics, *J. Biol. Chem.*, 1976, **251**, 6879.
9. I. M. Kolthoff and P. J. A. Elving (eds.), *Treatise on Analytical Chemistry*, Part II, p. 57. Interscience, New York, 1963.
10. G. Schwarzenbach, *Complexometric Titrations*, p. 36. Methuen, London and Interscience, New York, 1960.
11. M. Shamsipur, S. Madaeni and S. Kashanian, *Talanta*, 1989, **36**, 773.
12. G. R. Choppin and P. J. Unrein, *J. Inorg. Nucl. Chem.*, 1963, **25**, 387.
13. H. M. N. H. Irving and P. K. Khopkar, *ibid.*, 1964, **26**, 1561.
14. P. K. Khopkar and P. Narayanankutty, *ibid.*, 1971, **33**, 495.
15. T. Sekine, *ibid.*, 1964, **26**, 1463.
16. D. F. Peppard, G. W. Mason and I. Hucher, *ibid.*, 1962, **24**, 881.
17. B. M. L. Bansal, S. K. Patil, H. D. Sharma, *ibid.*, 1964, **26**, 993.
18. P. J. Breen and W. DeW. Horrocks, Jr., *Inorg. Chem.*, 1983, **22**, 536.
19. S. Jain, *Ph.D. Thesis*, Department of Physics, I.I.T., Kanpur, 1983.

Talanta, Vol. 39, No. 12, pp. 1653–1656, 1992
Printed in Great Britain.

0039-9140/92 $5.00 + 0.00

A LEAD(II) ION SELECTIVE ELECTRODE VIA A METAL COMPLEX OF POLY(HYDROXAMIC ACID)

K. ANUAR* and S. HAMDAN

Department of Chemistry, Faculty of Science and Environmental Studies, Universiti Pertanian Malaysia, 43400 UPM Serdang, Selangor, Malaysia

(*Received* 6 *September* 1991. *Revised* 6 *November* 1991. *Accepted* 6 *November* 1991)

Summary—A new lead(II) electrode has been constructed with poly(hydroxamic acid) (PHXA) as the active material and silicone rubber as the supporting material. The electrode gave near Nernstian response over the concentration range 4×10^{-5}–$1 \times 10^{-2}M$ lead(II). The detection limit of the electrode is approximately $4 \times 10^{-6}M$ and the electrode works well in the pH range 4.5–6.0. The response time was 50–120 sec over the whole concentration range and the electrode has a working life of at least 4 weeks. Iron(III) severely poisoned the electrode membrane. Nickel(II) and mercury(II) gave very strong interference compared to copper(II), silver(I), cobalt(II), sodium(I), potassium(I), zinc(II) and cadmium(II) which gave some or little interference. Values determined with atomic absorption (AAS) and a commercial lead(II) electrode were in good agreement with those measured with the lead(II) electrode reported here.

Ion selective electrodes (ISE) have been the subject of great interest over the past few years and their development has opened up the field of potentiometry. The field has developed rapidly because the analysts need rapid, accurate and low-cost analysis. Many compounds, either organic or inorganic, have been used for molecular recognition in ion selective electrodes[1–6] and some of these have been successfully developed commercially.[7–9] The aim of this study was to explore the use of a metal complex of the compound poly(hydroxamic acid) as a cationic sensor in ion selective electrodes. It is known that poly(hydroxamic acid) forms stable complexes with many metal ions.[10,11] Its use in analytical applications has been extensively demonstrated in extraction, purification and separation of metal ions.[12–14]

EXPERIMENTAL

Reagents

All reagents including lead nitrate were analytical grade. Solutions were prepared with doubly distilled water. Poly(hydroxamic acid) (PHXA) was prepared as described in the literature.[15] Silicon rubber (Selleys) is commercially available and was directly used.

Instruments

The emf values were measured with an Orion Research Model 601A/digital/Ionalyzer and a TOH pH meter HM7B was used for pH measurements. In the comparison study, an atomic-absorption spectrometer model IL 651 was used. A saturated calomel electrode (SCE) was used as reference electrode for all emf readings.

Preparation of membranes and electrode

Poly(hydroxamic acid) is not soluble in most organic solvents, so it is impossible to prepare a thin membrane by solvent casting such solvents. Preparations of homogenous membranes made with PHXA were not stable. Hence, heterogenous membranes were made by using silicon rubber as a supporting matrix and were found to be satisfactory.

PHXA was ground in a mortar and then mixed with silicone rubber. The mixture was spread on a filter paper, covered with another filter paper and pressed gently between two glass plates before leaving to dry. When the membrane had dried and hardened, a disc of 1.0-cm diameter was cut out and the filter papers were detached. A large number of membranes of different compositions (thickness 0.5–0.8 mm) were prepared. The membranes were fixed at

*Author for correspondence.

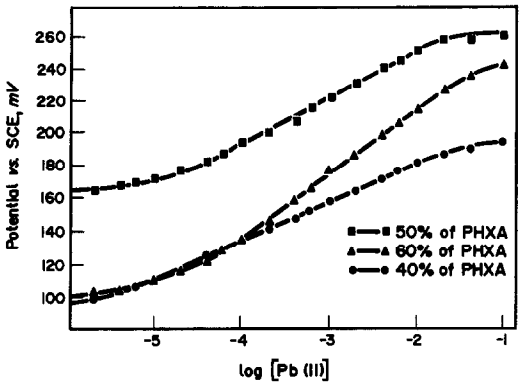

Fig. 1. Response curves of lead selective electrode for different composition of PHXA in the membrane.

one end of a glass tube with silicon rubber and left to dry.

The dried membrane was then equilibrated with 0.1M lead nitrate solution for a week and clean platinum was used as the internal electrode. The 0.1M lead nitrate solution was used as reference solution for the lead selective electrode and a saturated calomel electrode (SCE) was used as reference for all emf measurements at $27 \pm 0.1°$.

RESULTS AND DISCUSSION

Dependence of electrode potential on log [lead(II)]

Typical calibration curves of lead selective electrodes in the concentration range 1×10^{-6}–$1 \times 10^{-1}M$ lead(II), using different compositions of PHXA in the membranes are shown in Fig. 1. The slope, Nernstian limit and detection limit for each composition of the electrode are presented in Table 1.

Results from Table 1 showed that membranes with 50% PHXA content gave slopes which are closest to the theoretical Nernstian slope. This was then selected for further studies. Although membranes with 40 and 60% give a non-Nernstian slope, the responses are linear over the concentration range 4×10^{-5}–$1 \times 10^{-2}M$. However a membrane with 40% PHXA content shows a better Nernstian response. The table also shows that after a few weeks the slope changed for specific compositions. This is probably due to the effect of ageing on the asymmetry potential of the membranes, as observed by Wilson *et al.*[16]

Response time, reproducibility and stability

The response time for emf measurements during calibration of lead selective electrode was not studied in detail. At concentrations of 1×10^{-4} and $1 \times 10^{-5}M$, stable readings were obtained in about 50 sec or less. With more dilute solutions a 1–2 min period was required to obtain stable readings. The potential remains stable for at least 10 min. It was found that measurements were more stable with slow rather than fast stirring.

The standard potentials (E') of the electrode were reproducible to ± 1 mV over 5 hr. The standard potentials drifted about ± 7 mV over the first three weeks of its usage. After 3 weeks of its usage, the performance of these electrodes

Table 1. Slope, Nernstian limit and detection limit[17] of lead selective electrodes using various membrane compositions

Composition of PHXA		1st week	2nd week	3rd week
40%	Slope (mV/decade)	22.2	21.7	22.2
	Nernstian limit ($\times 10^{-5}M$)	0.9	1.0	0.5
	Detection limit ($\times 10^{-6}M$)	1.1	1.5	1.0
50%	Slope (mV/decade)	29.6	28.1	26.5
	Nernstian limit ($\times 10^{-5}M$)	4.0	1.8	2.0
	Detection limit ($\times 10^{-6}M$)	8.0	4.8	2.4
60%	Slope (mV/decade)	39.3	36.1	35.0
	Nernstian limit ($\times 10^{-5}M$)	4.4	4.2	9.5
	Detection limit ($\times 10^{-6}M$)	10.0	6.5	22.0

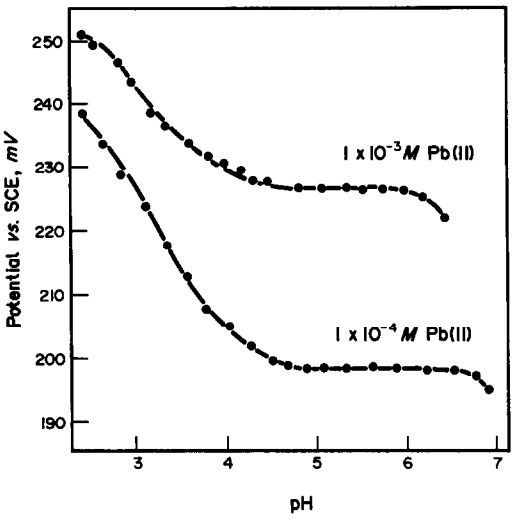

Fig. 2. Response curves of pH dependence of lead selective electrode on membrane potential.

deteriorated and reconditioning of the membrane was necessary. The life-time of these electrodes is approximately 3 to 4 weeks.

Effect of pH on membrane potential

The pH-dependence of the electrode response has been investigated at two lead(II) concentrations, 1×10^{-4} and $1 \times 10^{-3}M$, and the results are shown in Fig. 2. This figure shows that the pH working range of the electrodes is between pH 4.5 and 6. The positive shift of potential at pH below 4.5 is most probably caused by the proton interference and the negative potential shift in basic solution is observed at a pH greater than 6, where the lead hydroxide starts to precipitate.

Table 2. Selectivity coefficient, K^{pot}_{PbB}, for lead selective electrode in $1 \times 10^{-3}M$ solutions of interfering ions B

Interfering ions B	K^{pot}_{PbB}
Ni(II)	0.640
Cd(II)	0.023
Zn(II)	0.032
Cu(II)	0.20
Ag(I)	0.061
Hg(II)	0.830
Co(II)	0.070
Na(I)	0.120
K(I)	0.240

Selectivity of electrodes

The selectivity of the electrode with respect to copper(II), cadmium(II), nickel(II), zinc(II), iron(III), silver(I), mercury(II), cobalt(II), sodium(I) and potassium(I), were checked by the mixed solution method in lead(II) in the presence of a fixed concentration ($1 \times 10^{-3}M$) of the interfering ions.[17] The selectivity coefficient, K^{pot}_{PbB} of the electrode for each interfering ion is presented in Table 2. It was observed that in the presence of iron(III) at a concentration of $1 \times 10^{-3}M$, there was no emf response for various concentrations of lead(II) used. This suggests that iron(III) severely poisoned the electrode membrane and may be due to the strong complexation of iron(III) with PHXA compared to lead(II). Nickel(II) and mercury(II) gave very strong interference compared to copper(II), cobalt(II), silver(I), sodium(I), potassium(I), zinc(II) and cadmium(II) which gave some or little interference. This indicates that the electrode can give a good

Table 3. Comparison study for determination of lead(II) prepared sample solution by using atomic absorption spectroscopy (AAS), Orion commercial lead(II) selective electrode (OPb-SE) and prepared lead(II) selective electrode (Pb-SE)

		Concentration of lead(II), M			
		Sample I		Sample II	
Method	No. of replicates	Prepared ($\times 10^{-4}$)	Observed* ($\times 10^{-4}$)	Prepared ($\times 10^{-5}$)	Observed* ($\times 10^{-5}$)
Pb-SE	3	4.03	4.01 (99.50%)† (1.93%)‡	5.95	5.87 (98.76%)† (1.94%)‡
OPb-SE	3	4.03	4.00 (99.25%) (2.50%)	5.95	5.90 (98.33%) (1.70%)
AAS	3	4.03	4.10 (101.74%) (1.10%)	5.95	5.90 (99.17%) (1.61%)

*Average of triplicate observations.
†Percentage of recovery.
‡Standard deviation (mean).

selectivity of iron(II) in the presence of these ions.

Comparison study with atomic-absorption spectrometry (AAS) and Orion lead selective electrode (commercial electrode)

A comparison of the results obtained for lead(II) determination of prepared sample solutions with other procedures is given in Table 3. From Table 3, it is shown that the lead selective electrode prepared (Pb–SE) performed well as compared with Orion commercial electrode (OPb–SE) and with atomic absorption spectrometry. Our electrode provides an excellent alternative to the more expensive commercial electrodes, especially when the risk of damage to the membrane is high.

CONCLUSION

From the study, it was found that the PHXA metal complex of lead(II) has the ability to perform as a sensor in lead selective electrodes. It is cheap and can be easily constructed in a normal analytical laboratory. Its performance is satisfactory and it provides an excellent alternative to the more expensive commercial electrodes.

Acknowledgement—The authors would like to thank Mr Rani Zaman and Mr Bahrudin Ismail for their assistance and the Universiti Pertanian Malaysia for awarding the grant No. 50205 (1989) for this project.

REFERENCES

1. A. K. Covington, *CRC Crit. Rev. Anal. Chem.*, 1974, 355.
2. E. Pungor and K. Toth, *Pure Appl. Chem.*, 1973, **34**, 105.
3. G. J. Moody and J. D. R. Thomas, *Selective Ion Sensitive Electrode*, Merrow, Watford, 1971.
4. E. Pungor, *Ion-selective electrodes, 4*, Vol. 22, Elsevier, Amsterdam, 1985.
5. M. D. Hampton, C. A. Peters and L. A. Wellington, *Anal. Chim. Acta*, 1987, **194**, 171.
6. N. Takisawa, D. G. Hall, E. W. Jones and P. Brown, *J. Chem. Soc., Faraday Trans. I*, 1988, **84**, 3059.
7. M. S. Frank and J. W. Ross, *Science N.Y.*, 1966, **154**, 3756.
8. J. W. Ross, *ibid.*, 1967, **156**, 3780.
9. L. A. R. Pioda, V. Stankova and W. Simon, *Anal. Lett.*, 1969, **2**, 665.
10. V. C. Boss and J. H. Yoe, *Talanta*, 1966, **13**, 735.
11. T. J. King and P. G. Horrison, *J.C.S. Chem. Comm.*, 1972, 815.
12. F. Vernon, *Pure Appl. Chem.*, 1980, **11**, 54.
13. A. Shah and S. Devi, *Analyst*, 1985, **110**, 12.
14. *Idem, ibid.*, 1987, **112**, 3.
15. W. M. Zin and A. Zaharudin, *Pertanika*, 1988, **11**, 2.
16. M. F. Wilson, E. Haikala and P. Kivalo, *Anal. Chim. Acta*, 1957, **74**, 395.
17. P. L. Bailey, *Analysis and Ion-Selective Electrodes*, p. 44. Heydan, London, 1976.
18. M. E. Meyerhoff and Y. M. Fraticelli, *Anal. Chem.*, 1982, **54**, 27.

Talanta, Vol. 39, No. 12, pp. 1657–1667, 1992
Printed in Great Britain.

0039-9140/92 $5.00 + 0.00

AN OPTICAL WAVEGUIDE ACID VAPOR SENSOR

DAVID S. BALLANTINE, JR.* and DANIEL CALLAHAN
Chemistry Department, Northern Illinois University De Kalb, IL 60115, U.S.A.

G. JORDAN MACLAY* and JOSEPH R. STETTER
Transducer Research, Inc. Naperville, IL 60540, U.S.A.

(*Received* 25 *November* 1991. *Revised* 9 *January* 1992. *Accepted* 7 *February* 1992)

Summary—An optical waveguide sensor for the detection of acid vapors is described. The chemically sensitive reagent coating consists of bromothymol blue indicator suspended in a Nafion polymer film. The sensor uses a 562 nm LED source and a phototransistor detector. Response to hydrochloric acid and hydrogen sulphide vapors is both rapid and reversible, with an estimated detection limit for hydrogen sulphide of less than 15 ppm. The sensor exhibits generalized response to protonic acid vapors, but does not produce an indicator response to carbon dioxide, even at large concentrations (1100 mg/l.) in the presence of water vapor. The sensor exhibits a systematic interference from water vapor which may be corrected by a differential approach, either using a reference sensor (Nafion/no indicator) or by monitoring sensor response at two wavelengths.

Chemical sensor technologies have been used increasingly for the detection or monitoring of toxic/hazardous vapors in the workplace environment. Applications include portable sensors or dosimeters to monitor individual personnel exposure, or fixed-site sensors to monitor ambient concentrations of chemical species. Sensors under development include elecrochemical piezoelectric and optical sensors.[1-5] The great attraction toward these technologies is their capability for rapid, sensitive response at low cost.

The need for a reliable sensor for the detection of toxic acid vapors in ambient atmospheres has led to the research efforts reported herein. The specific application of interest was the development of an end-of-service sensor/alarm for protective equipment, such as gas masks, *etc.* Some of the technologies mentioned above have demonstrated ability to detect acid vapors.[6-13] Optical techniques have the advantage of being potentially less expensive, more selective and less susceptible to electromagnetic interference.[3,14] An absorbance-based optical sensor for the detection of acid vapors has been developed and evaluated using optical waveguide (OWG) technology. Relevant information concerning the OWG operating principles and the chemical reagents employed are presented, as well as discussions of possible sensor configurations to correct for interferences and/or humidity effects.

THEORY AND DESIGN CONSIDERATIONS

Theory

The sensitivity of the sensor is dependent on the optical properties of the reagent and/or analyte, and on the concentration of the optically active component in the light path.[14] Fiber optic or optical waveguide (OWG) sensors can be classified as absorbance/reflectance, or fluorescence-based sensors. The sensitivity of the former techniques can be improved by (1) increasing the concentration of absorbing species, or (2) maximizing the interaction of the incident light with the reagent, *i.e.*, by taking advantage of multiple internal reflection (MIR) light propagation. A typical MIR waveguide sensor consists of a thin, optically transparent substrate coated with a chemically sensitive reagent film. A light source focused on one end of the waveguide introduces radiant energy of an appropriate wavelength (and bandwidth) to the waveguide. This radiant energy then propagates by multiple internal reflection along the length of the waveguide. At the opposing end of the waveguide, the exiting light is focused onto an optical detector. The light wave can interact with the reagent film either directly as it passes through the film, or via an evanescent wave perpendicular to the direction of propagation if the light wave is reflected at the film/substrate

*Authors for correspondence.

interface.[15] Any change in the optical properties of the reagent film that result in a change in the intensity of light reaching the detector constitutes a sensor response. These changes can include absorbance, scattering, and fluorescence/luminescence. If these changes occur in response to chemical stimuli, then the OWG acts as a chemical sensor. The use of such devices as chemical sensors has been described previously.[16–18]

The ideal sensor characteristics include the following: rapid, sensitive response; reproducibility; selectivity; small size/portability; low cost and low power consumption. For optical sensing systems, the critical components include the colorimetric reagent(s), the radiative source, the waveguide and its geometry, and the detector. Each of these system components will be considered with respect to the impact on the desirable sensor characteristics listed above.

Source/detectors

The ideal source must exhibit stable output of sufficient intensity in the spectral region of interest. Light emitting diodes (LEDs) are readily available at low cost from commercial sources, having maximum emission output in the spectral region between 550–680 nm. The LEDs have a squarewave output, which provides higher optical output than sine wave outputs. Typical bandwidths for these sources are in the order of 10–50 nm. While these sources are not as intense as others (*e.g.*, lasers or tungsten lamps), they are of sufficient intensity to achieve the required response sensitivity/detectability for the absorbance-type sensor considered here.[16–18] As detectors, inexpensive phototransistors are available which provide adequate sensitivity to light in the visible region.

Colorimetric reagents

The most familiar acid sensitive colorimetric reagents are pH indicators. These materials exhibit changes in their absorbance properties in the visible region upon exposure to acid vapors.[3] Thus, these materials were studied initially to determine whether any suitable reagents could be identified for use with the OWG sensor. The following criteria were used in the selection process:

(1) The reagent must be stable in air.

(2) The reagent must form thin films with good adhesive properties when suspended in polymer films.

(3) The spectral properties of the reagent indicator must be compatible with the sensor source/detector components under consideration; *i.e.*, the resulting film must exhibit a color change in the visible region upon exposure to acid vapor.

EXPERIMENTAL

Materials

A variety of polymers and pH indicators were tested as potential sensor films and are listed in Table 1(a). Among the selected polymers were polyisobutylene (PIB), polyvinyl alcohol (PVA), polyvinylpyrrolidone (PVP), polyethylene glycol (PEG), polyethyleneimine (PEI), and a perfluorinated sulphonic acid polymer,

Table 1. Indicator and polymer properties

A. Coating materials—polymers and indicators

Polymers	*MW range*	*Indicators*	*pH transition range*
PIB	380,000	Thymol Blue	1.2–2.8; 8.0–9.6
PVA	31–50,000	Bromothymol Blue	6.0–7.6
PVP	40,000	Bromcresol Green	3.8–5.4
PEG	600/1500	Litmus	5.0–8.0
PEI	50–60,000	Methyl Red	4.8–6.0
Nafion	(unknown)	Bromcresol Purple	5.2–6.8
		Phenolphthalein	8.0–9.6

B. Indicator/polymer film behavior

Coating	*Dry color*	*Acid exposure**	*Base exposure*
BTB/NAF†	violet	yellow → violet(R)	yellow → blue (R)
BCG/PVP	blue/green	blue → yellow (N)	yellow → blue (R)
MR/PEG	red orange	orange → purple (R)	orange → yellow (R)
BCG/PEG	yellow	yellow → colorless (R)	yellow → blue (R)

*The acid and base responses were reversible (R) or non-reversible (N), as indicated.

†The BTB–NAF film dries in the R form, but can be converted to the Y^- form by exposure to water vapor.

Nafion (NAF; 5% solution in alcohol). The Nafion was obtained from Solution Technologies; the remaining polymer materials were obtained from Aldrich. All materials were used as received. With the exception of PIB, these polymers contain proton donor and/or proton acceptor functionalities. One of these polymers (Nafion) is an ionomer containing sulphonic acid groups attached to a perfluorinated polyethylene backbone.[19] Nafion is of particular interest because it can be processed into thin membranes that would be well suited to an optical sensor. These materials were evaluated on the quality of the resulting films when cast on a glass surface.

Indicators were selected based on the observed color transitions and on the pH transition ranges. Available indicators included thymol blue, bromothymol blue, litmus, phenolphthalein, Methyl Red, bromcresol purple, and bromcresol green (see Table 1). The majority of these indicators undergo a visible color change when exposed to slightly acidic conditions. The notable exceptions are phenolphthalein (transition in the basic range) and thymol blue (transition in the low pH/strong acid range).

Optical electronic components (LEDs, phototransistors) for the construction of the OWG were obtained from Newark Electronics.

Equipment

UV–Vis absorbance spectra (300–750 nm) were obtained in the NIU Chemistry department with a Minichrom Scanning Monochromator (Optometrics), using a tungsten lamp source and a PM tube detector. A sample flow cell was constructed using 1.0 cm × 1.0 cm quartz tubing, with inlet and outlet tubes fixed onto the cell to permit introduction of acid vapors during the spectral scan.

Waveguide studies were performed using an OWG electronics module built by the NIU Chemistry Electronics shop (schematic available upon request). The circuitry is similar in design to that described previously.[16] It consists of a pulsed LED source to minimize thermal drift, and a series of amplification/rectification stages to filter and amplify the PT detector output signal. Amplification of the signal can be controlled using a 10-turn 100 K variable resistor (GAIN), and the zero can be adjusted with a NULL OFFSET potentiometer. The 0% and 100% transmittance signals are adjusted to be compatible with the data acquisition computer. Data collection for the spectral and waveguide studies was performed with a Hyundai 286 microcomputer via an IBM data acquisition and control adapter (DACA) card using software developed at the NIU Chemistry department.

Coating selection/screening

Solutions were prepared by dissolving the polymers and indicators in suitable solvents, usually methanol or methanol/water. Final solutions contained approximately 1 mg/ml each of polymer and indicator. Test films were prepared by casting a small volume of the solution(s) on the surface of clean glass slides and allowing the solvent to evaporate. The resulting films were then evaluated based on film quality and response characteristics, as described below. These films were then exposed to HCl vapor to determine relative response behavior. The results of these preliminary screening tests are summarized in Table 1(b). Several of the indicators failed to exhibit an acceptable color change upon exposure to the acid (phenolphthalein, litmus). The remaining indicators gave good visible color-change response to acid vapor in some polymers but not in others; PIB-indicator films gave no response, which supports the observation that the supports the observation that the support polymer must exhibit some proton donor–acceptor behavior in order to activate the proton-transfer indicator color change. Some acid response was exhibited by the PEG-indicator films, but the PEG produced viscous, oily films that were difficult to work with in our sensor application. Previous work using thymol blue in PVA-clad optical fibers cited good sensitivity to acid vapors;[10] preliminary results using PVA films in our lab, however, showed poor reversibility. The most promising results were obtained using the bromcresol green/polyvinylpyrrolidone (BCG–PVP) and bromothymolblue/Nafion (BTB–NAF) films. Both of these indicator films had good adhesion properties and dried to produce robust thin films exhibiting uniform surface coverage. The BCG–PVP film exhibited a blue color upon drying, typical of the basic form of the indicator. Exposure to acid resulted in an irreversible conversion to the acid form (yellow) which persisted after removal from the acid vapor. Subsequent exposure to NH_3 vapors produced a blue color, which reverted to yellow upon exposure to dry air. This indicator film would be suitable as a dosimeter for acid gases or for

on/off alarm applications, but was not considered further for these studies. In its acid-treated form, the BCG–PVP film might be used as a reversible NH_3 sensor.

The various structures for the bromothymol blue indicator dye are given in Fig. 1, along with the absorbance maxima, λ_{max}, the approximate pK_a for transitions between forms (in aqueous solution), and the associated visual colors. It is worth noting that the transition from the blue form (B^{2-}) to the yellow form (Y^-) takes place under very slightly basic conditions in aqueous solution, but the transition from the Y^- form to the red (R) form requires very acidic (4–5*M*) conditions. The BTB–NAF film dried in the fully protonated form (R) which is red–violet in color, but exposure to water resulted in conversion to the yellow form (Y^-). This film exhibited reversible response to hydrochloric acid vapor. Subsequent exposure to acid vapor resulted in conversion to the R form, which recovered slowly to the Y^- form after removal from the acid vapor. Because of the reversible nature of this indicator film to acids, it was selected for futher evaluation as an acid vapor sensor.

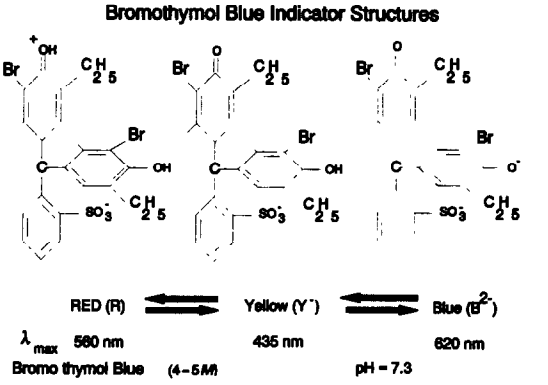

Fig. 1. Structural formulas for the three forms of bromothymol blue dye indicator, with corresponding absorbance maxima λ_{max} and transition ranges in aqueous solution.

Spectral studies

The BTB–NAF coating was studied by UV–Vis spectrophotometry to determine appropriate wavelengths to be used for the selection of components in the construction of an OWG sensor. A thin film was coated on a quartz slide, which was placed inside the flow cell. Spectral scans were performed while acid vapors of varying concentrations were passed through the cell. Acid vapors were generated by bubbling dry air carrier through a flask containing hydrochloric acid solutions of varying concentrations.

The spectra for the film are shown in Fig. 2 under exposure to hydrochloric acid vapors from solutions of different concentration. The BTB–NAF film exhibits two absorbance maxima, each of which exhibits acid vapor concentration dependence. The first maxima occurs at 435 nm and corresponds to the Y^- form of the indicator. As the film is exposed to increasing concentrations of acid vapor, the 435-nm peak decreases and undergoes an apparent slight blue shift, while there is a corresponding increase in absorbance at 562 nm corresponding to the

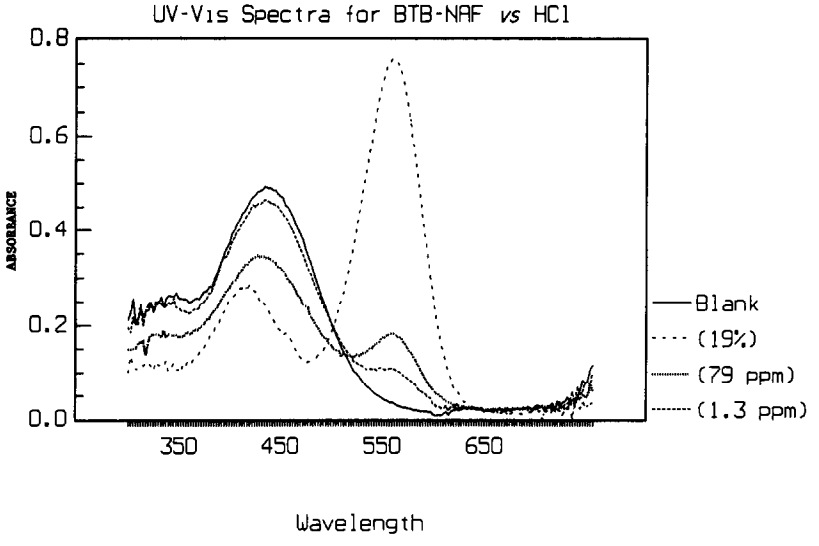

Fig. 2. UV–Vis spectra of bromothymol blue indicator in Nafion film exposed to (1) dry air (2) 12*M* HCl (19% vapor) (3) 5*M* HCl (79 ppm vapor) and (4) 2*M* HCl (1.3 ppm vapor).

R form of the indicator. The absorbance wavelengths for the indicator suspended in the Nafion film are essentially identical to the corresponding λ_{max} for the aqueous forms of the indicator.

OWG sensor construction

Using the results of the spectral studies, a yellow LED having maximum emission intensity at 562.5 nm was selected as the source. This wavelength corresponds to the absorbance maximum for the indicator film in the R form. The detector consists of a phototransistor (PT). The OWG substrate consists of a thin-walled glass capillary tube (75 mm long, 1.2 mm o.d., 0.2 mm wall thickness) coated with the film. A small diameter plug was inserted inside the capillary to block light travelling down the center of the tube. Thus, only light that has traversed the waveguide via reflection inside the capillary walls will reach the photodetector. The LED–OWG–PT components are held in rigid contact using plastic rods that have been drilled out to accommodate the optical components and the waveguide. The entire sensor configuration is enclosed by a glass tube having inlet/outlet ports to introduce/vent the carrier/acid vapor gas streams.

OWG test procedures

Acid vapor studies at NIU were performed by bubbling carrier gas (dry N_2) through a vessel containing hydrochloric acid solutions of varying concentration. The voltage output from the OWG electronics was monitored using the computer data acquisition system while the sensor was alternately exposed to dry air and acid vapor. Increases in acid (H^+) concentration in the film will shift the indicator from the Y^- to the R form, with a corresponding increase in absorbance at the 562-nm wavelength. This translates into a decrease in light reaching the PT detector (decreased voltage output). Typical data curves are presented and discussed in the Results and Discussion section.

Additional tests were performed at Transducer Research, Inc. facilities (Naperville, IL).

RESULTS AND DISCUSSION

Sensor response is determined by an increase in absorbance at 562 nm for the R form of the indicator, which will produce a decrease in light intensity reaching the PT detector. The long-term and short-term waveguide response to acid vapors is not straightforward, and appears to be dependent on three separate phenomena. These phenomena include water sorption by the Nafion, irreversible interactions between the acid vapor and the Nafion, and the interaction between the indicator and the acid vapor. These factors are discussed in more detail below.

Nafion–water response

Acid vapors were generated by bubbling dry carrier gas through an aqueous solution of hydrochloric acid. The concentration of hydrochloric acid in the vapor phase was varied by serial dilution of the hydrochloric acid solution in the bubbler. This procedure obviously produces water vapor as well as acid vapor. Thus, it was necessary to determine the sensor response to water vapor, if any, to determine possible interference effects. The water tests are summarized graphically in Fig. 3. In Fig. 3(a) (insert) the response of a Nafion film to water vapor is presented. The introduction of only water vapor to the Nafion coated waveguide results in an increase in PT signal of nearly 40%, or 2 V. This increase in signal is reproducible upon repeated exposure to water vapor. To determine if this effect is due to condensation of water from a nearly saturated vapor stream, tests were performed, using water bubblers at two different temperatures. The results are shown for a BTB–NAF coated sensor in Fig. 3(b). The first 4 exposures represent responses to nearly saturated water vapor, produced from a bubbler at room temperature, and produced significant increases in OWG sensor signal. Five subsequent exposures were made using a bubbler that was maintained in an ice bath, and produced only a slight increase in signal. This increase in response to water vapor constitutes a potential interference, and also prevents us from determining the inherent sensitivity of the sensor to acid vapor. Initial attempts to dry the vapor stream with a desiccating agent were successful in reducing the response to water vapor. However, these drying agents also appeared to remove acid vapor, and response of the sensor to acid streams was dramatically reduced when drying tubes were utilized in-line. All subsequent acid vapors were generated from solutions maintained in an ice bath to reduce the response from water vapor.

Acid vapor generation

Vapor streams of hydrochloric acid (g) were produced by bubbling carrier gas (N_2) through

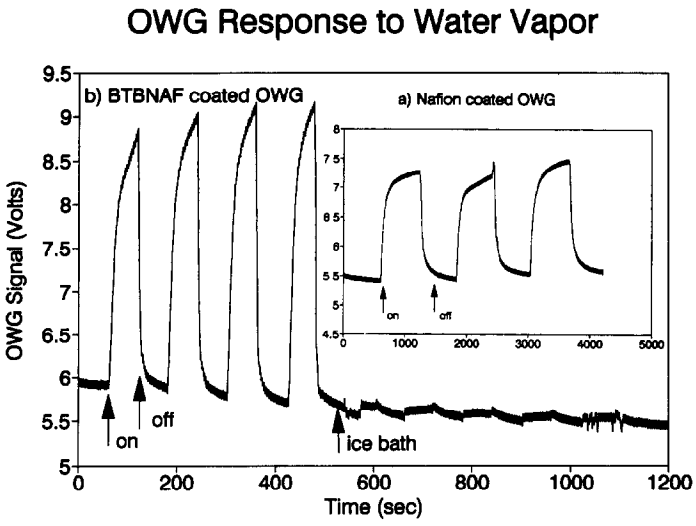

Fig. 3. Response of the OWG to water vapor. In the insert (a), the response of a Nafion coated waveguide to water vapor from a bubbler at room temperature; (b) the response of a BTB–NAF coated waveguide to water from a bubbler at room temperature, and the reduced response when the bubbler temperature is reduced to 0° in an ice bath.

hydrochloric acid solutions of varied concentration. The concentration of hydrochloric vapors produced in this manner have been estimated using thermodynamic data (free energy, activity coefficients) and equations from Ref. 20 and 21 and are summarized in Table 2. The efficiency of vapor generation was estimated by bubbling nitrogen at a constant flowrate (155 ± 5 ml/min) through a known volume of 6.0*M* hydrochloric acid solution over a 24-hr period, at an ambient temperature of $\approx 19.5°$. The amount of hydrochloric acid stripped from the solution was determined by titrating aliquots of the hydrochloric acid solution before and after bubbling. After correcting for volume changes in the bubbler solution, the hydrochloric acid vapor generated from a 6.0*M* hydrochloric acid solution was calculated to be 0.34 mg/l. (228 ppm). This can be compared to the value of 0.52 mg/l. calculated at 25° from thermodynamic data,[20] and corrected for the variation in activity coefficients as a function of temperature.[21] Taking into consideration the difference in temperature, the vaporization efficiency at 20° for the 6.0*M* hydrochloric acid solution is in the order of 80%. Thus, the estimated concentrations in Table 2 represent upper limits only; hydrochloric acid vapor concentrations reported in this work have been corrected to account for vaporization efficiency.

Based on the estimations discussed above, a 2.0*M* bubbler solution (16% v/v solution; 2.08 molal) at room temperature (20°) will produce an acid vapor concentration of approximately 0.0019 mg/l. (1.3 ppm). Thus, the estimated hydrochloric acid vapor concentrations used to construct Fig. 2 are as follows: blank (0.0 mg/l.; 0.0 ppm), 2.0*M* (0.0019 mg/l.; 1.3 ppm), 5.0*M* (0.12 mg/l.; 79 ppm), 12.0*M* (290 mg/l.; 19%). For the single pass absorbance measurements presented in Fig. 2, a detection limit for hydrochloric acid vapor of < 1 ppm is estimated,

Table 2. Estimated HCl vapor concentrations

Molarity, *M*	Molarity, *mole/kg*	*[HCl(g)] @ 25°** *mg/l.*	*[HCl(g)] @ 20°†* *mg/l.*	*Estimated [HCl(g)]* (0.80 vaporization)
0.05	(0.5)	1.3×10^{-6}	9.7×10^{-7}	7.7×10^{-7} (0.5 ppb)
0.10	(0.102)	4.7×10^{-6}	3.5×10^{-6}	2.8×10^{-6} (2 ppb)
0.50	(0.505)	1.1×10^{-4}	8.2×10^{-5}	6.6×10^{-5} (44 ppb)
1.00	(1.02)	4.8×10^{-4}	3.6×10^{-4}	2.9×10^{-4} (0.2 ppm)
2.00	(2.07)	0.003	0.0024	0.0019 (1.3 ppm)
4.00	(4.37)	0.058	0.045	0.040 (27 ppm)
6.00	(6.72)	0.52	0.42	0.34‡ (230 ppm)

*Calculated from thermodynamic data in reference (19).
†Calculated based on activity coefficient data in reference (20).
‡Calculated from titration data as described in the text.

which corresponds to vapor produced from a bubbler containing $\simeq 1.5M$ hydrochloric acid. It should be noted that the detection limit gives above represents an upper limit for a single pass optical detection system. Application of this reagent system to a multiple internal reflection OWG device would be expected to provide an improvement in sensitivity and detection limits of several orders of magnitude due to an increase in the effective cell path length.

Indicator–acid response

For the OWG sensor, any change in the optical properties of the film that translates into a change in light intensity reaching the photodetector will affect the analytical signal. A typical response of the BTB–NAF optical waveguide sensor to hydrochloric acid is given in Fig. 4 ($1.2M$ hydrochloric acid solution at 0°; 0.4 ppm). Upon exposure to the acid vapor, the signal from the phototransistor decreases rapidly, consistent with the increase in absorbance at 562 nm by the R form of the indicator. Removal of the acid vapor results in a slow return to the Y^- form. A more rapid recovery could be accomplished by exposing the sensor to base and/or water vapor; in any event, the signal fails to return completely to the original baseline response. Repeated exposure to high acid concentrations results in a gradual decrease in the baseline signal intensity. It is worth noting that repeated exposure of these sensors to acid vapor produced a very reproducible minimum signal, even though the sensor signal did not return to the original baseline after removal of the acid vapor.

To verify that the observed response was, in fact, the result of absorbance by the indicator, the following experiment was performed. The sensor was exposed to acid vapor from $0.06M$ hydrochloric acid in an ice bath (0.01 ppm vapor) while the sensor output was monitored upon illumination of the OWG with a yellow-green LED (562 nm). This experiment was repeated with a red LED source, having a maximum emission intensity at 680 nm. This wavelength is well removed from the absorbance λ_{max} for the R form (562 nm) and Y^- form (435 nm) of the indicator. The results are presented in Fig. 5. At the 680-nm wavelength there is minimal change in signal upon exposure to acid (bottom trace) whereas the sensor exhibits significant decrease in signal at 560 nm, confirming that the observed signal is due to absorbance by the R form of the indicator.

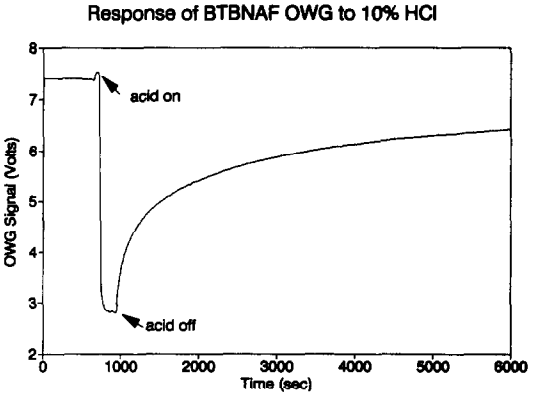

Fig. 4. Response of BTB–NAF OWG to HCl vapor produced from a 10% (v/v) solution ($1.2M$; 0.4 ppm).

Nafion–acid response

Repeated exposure of films resulted in a gradual decrease in sensor response in the form of a long term reduction in the sensor baseline signal. It was postulated that the Nafion was undergoing fatigue upon acid exposure, resulting in an irreversible decrease in transmittance properties.

Waveguides coated with Nafion films (no indicator) were exposed to acid vapors, and the transmittance at 562 nm was monitored. These results are presented in Fig. 6. The test was performed using an 8% hydrochloric solution maintained in an ice bath (0.24 ppm hydrochloric acid vapor) to reduce the effects of water on the sensor response, as discussed previously. As the Nafion film was exposed to repeated one minute cycles of dry air/acid vapor the sensor baseline steadily decreased. Upon exposure to acid vapor, the sensor response undergoes a reproducible decrease of approx. 170 mV.

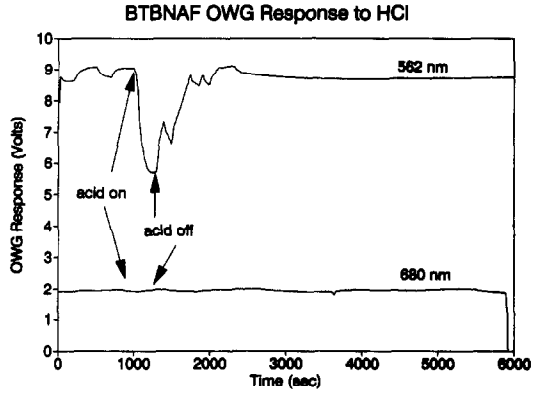

Fig. 5. BTB–NAF OWG response to vapor from 0.5% HCl solution ($0.06M$; 0.8 ppb) using 560-nm yellow LED (top trace) and 680-nm LED (bottom trace).

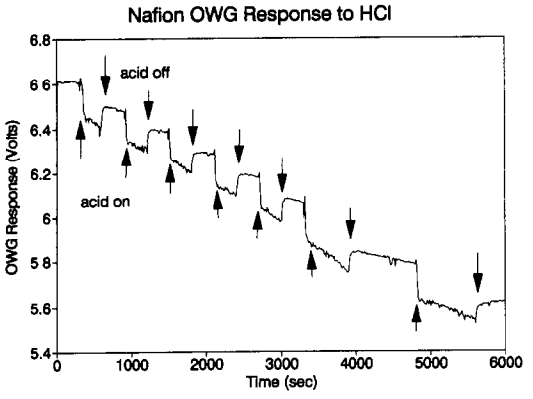

Fig. 6. Change in transmittance of Nafion coated OWG upon repeated exposures to vapor from 8% HCl solution (1*M*; 200 ppb).

Returning to dry air results in partial recovery of sensor signal, but there is still a net irreversible signal change of approx. 110 mV. The extent of irreversible signal decrease seems to increase as the acid concentration increases, and constitutes a dosimetric response. The 170-mV response of the Nafion OWG to 0.24 ppm hydrochloric acid (Fig. 6) can be compared with the nearly 4.5 V response of the BTB–NAF film to 0.4 ppm hydrochloric acid (Fig. 4). Obviously, the indicator response is nearly 20 times more sensitive to acid vapor than the Nafion alone, and will be the predominant response mechanism of the OWG sensor.

Changes in the optical properties in the Nafion film upon exposure to acid vapor may be the result of several phenomena. First, the decrease in light intensity reaching the PT detector may be due to changes in the refractive index of the polymer film; second, the introduction of acid vapor may result in increased scattering losses in the film. If there is an irreversible absorption of a small amount of acid vapor, these mechanisms could result in the long term decrease in the transmittance baseline of the sensor.

OWG response to CO_2

One of the proposed uses of this sensor is as a monitor in protective equipment, such as a gas mask. In such an environment, the sensor could also be exposed to exhaled gases, including CO_2 and water vapor. This combination of gases could potentially form an acidic mixture. The sensor response to combinations of these gases was investigated, and is displayed in Fig. 7.

Sample streams of dry nitrogen, water vapor and CO_2 were generated in the following manner. Dry nitrogen was supplied from a gas cylinder. This dry gas stream could be sent directly to the sensor or diverted through a water bubbler. A vessel containing dry ice was incorporated into the vapor flow system via a T-junction. The flow of CO_2 vapor into the flow stream could be controlled by opening or closing a restrictor. With the restrictor completely open, the flow of CO_2 from the vessel was $\approx$750 ml/min. Opening the restrictor 2 turns would permit a CO_2 flow-rate of $\approx$200 ml/min. The flow of dry nitrogen in the system was 160 ± 5 ml/min. Thus, when CO_2(g) was bled into the vapor stream the approx. [CO_2(g)] was 55% (by volume) or 1100 mg/l. (62%). [For comparison, the CO_2 concentration in the atmosphere is a fairly constant 300 ppm, and the content of exhaled air is $\approx$70 mg/l. (4%).]

Vapor streams of dry nitrogen, dry nitrogen + CO_2, and water vapor + CO_2 were sent to the OWG. Upon exposure to dry air + CO_2 there is a slight increase in the sensor signal, and a return to the original baseline when the CO_2 is removed. When water vapor is included in the CO_2 stream there is an additional small increase in signal. This is consistent with the OWG response to water vapor as noted above. The total response to CO_2(g) under the test conditions was an increased signal of $\approx$100–150 mV. To counteract this increase in signal would require an indicator response (signal decrease) equivalent to 3×10^{-4} ppm hydrochloric acid. From these results, it is concluded that CO_2 alone does not constitute a significant interference. The CO_2 with water could produce a protonic acid which would be expected to produce an indicator response, since the indicator undergoes a transition as a result of a proton transfer reaction. The fact that no response is

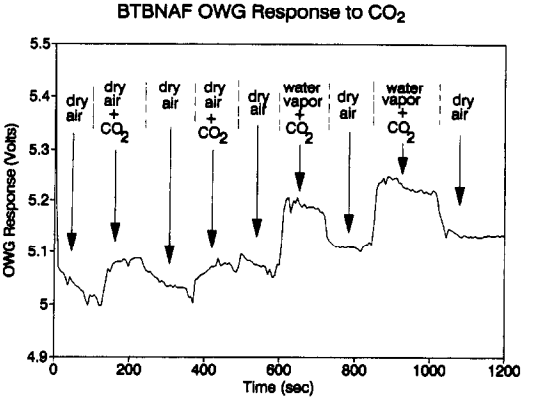

Fig. 7. Response of BTB–NAF OWG to CO_2 (1100 mg/l.) in dry nitrogen, and in water vapor.

observed, even in the presence of water, may be due to the fact that carbonic acid (H_2CO_3) is a very weak acid ($K_a = 4.3 \times 10^{-7}$). Alternatively, it is possible that H_2CO_3 is not formed to any great extent upon the addition of CO_2 and H_2O to the Nafion film. Without formation of the protonic acid, no indicator response would be expected.

Minimum detectability

In order to determine the minimum detectability of the sensor, the sensor response to a calibrated acid vapor source was necessary. The vapor generating apparatus used at NIU could not be calibrated at low acid concentrations for reasons discussed above. Further testing was performed at the TRI facilities to determine the minimum detectability of the sensor using a calibrated hydrogen sulphide dry gas mixture (228 ppm in N_2). The choice of hydrogen sulphide as the test gas was based on the fact that it is a highly toxic, acidic vapor. As such it would be among the class of vapors that the OWG sensor was designed to detect. The sensor output (in mV) was monitored with a strip chart recorder as the sensor was exposed to alternating streams of dry air and H_2S/N_2 mixtures of varying concentrations at flow-rates of approx. 200 ml/min. The H_2S/N_2 gas mixture was diluted with laboratory air that was scrubbed with a charcoal/molecular sieve trap. Thus, the final mixture contained some O_2 but water vapor (RH) was minimized. The results are summarized in Fig. 8. As was the case upon exposure to hydrochloric acid, the OWG sensor signal decreased upon exposure to hydrogen sulphide (note that the y-axis in Fig. 8 gives the OWG signal in negative mV), indicating an increase in absorbance at 562 nm. The sensor exhibits good linearity of response over the concentration range studied (0–228 ppm). Assuming a S/N equal to three as the detection limit, and using a value of 5 mV for rms noise for the OWG sensor, a minimum detectability of 15 ppm hydrogen sulphide is calculated.

The actual detection limit is probably lower than this figure for several reasons. The gas canister used for the calibration was nearly 2 years old, and the concentration of H_2S normally decreases 1–5% per year.[22] Further, the response of the sensor to hydrogen sulphide directly from the canister was significantly higher (nearly a factor of 2) than the response to undiluted hydrogen sulphide that had been diverted through the dilution apparatus. The hydrogen sulphide vapor stability in contact with many surfaces is poor. Thus, the concentration of hydrogen sulphide actually delivered to the sensor is probably less than calculated based on the concentration of hydrogen sulphide calibration gas and the performed dilutions.

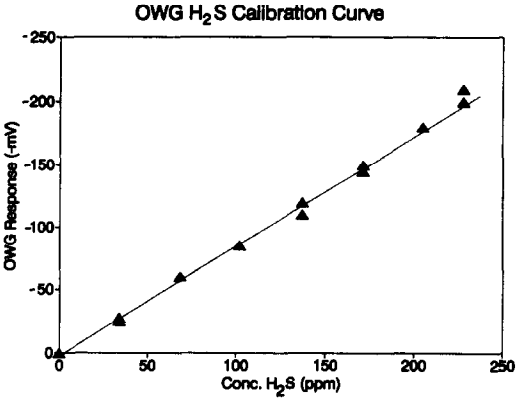

Fig. 8. Calibration curve for BTB–NAF OWG sensor, demonstrating linear response (−mV) to H_2S vapor between 0 and 228 ppm.

Interpretation of indicator response

The observed OWG signal is likely to be the net result of interactions between the indicator, the Nafion polymer (assumed to be in the acid form), and the acid vapor. From the hydrochloric acid spectral studies it is obvious that small concentrations of hydrochloric acid in the BTB–NAF film are sufficient to shift the indicator from the Y^- to the R form via proton donation from the acid to the indicator. Although these indicator dyes were originally designed for use in aqueous systems, it is worth noting that this response is observed even in the absence of water vapor. Apparently the Nafion matrix is sufficiently polar to permit proton transfer processes without significant water concentration in the membrane. Although no spectral studies were performed to verify this transition for the weak acid hydrogen sulphide exposure, the decrease in OWG sensor signal is consistent with an increase in absorbance at the 562-nm wavelength of the LED source. If hydrogen sulphide also donates a proton to the indicator, formation of the R form would result. Loss of a proton from hydrogen sulphide produces HS^-, which is a proton acceptor. If the proton from hydrogen sulphide is donated instead to the sulphonic acid group on the Nafion polymer then it is possible that the HS^- might

accept a proton from the Y^- form to produce the B^{2-} form. It should be noted that the λ_{max} for the B^{2-} form of the indicator at 620 nm is very broad and overlaps the 562-nm band considerably. Thus, a transition to the B^{2-} form would also produce absorbance at 562 nm with a corresponding decrease in the observed OWG signal. Further studies are planned to determine the exact nature of the response mechanism for weak acids.

Sensor configurations

The sensitivity of the OWG can be compromised by the presence of water vapor. The polymer used as the supporting matrix for the indicator reagent interacts with water vapor to produce an increase in OWG signal which constitutes a systematic interference. The normal indicator-acid response produces a decrease in the sensor signal. Two possible dual-sensor configurations are presented here that may correct for the systematic water vapor interference.

In one configuration, two waveguides can be coated with identical BTB–NAF films, with each waveguide having its own photodetector and LED. One waveguide will use an LED at 562 nm, while the other waveguide will use an LED at 680 nm. The 562-nm sensor response will be the net result of both water and acid, whereas the 680 LED response will be due only to water effects. Taking the difference between the two waveguide responses will correct for the effects of water on the acid sensor response. A potential problem with this approach is that it uses two different LEDs; long term drift or differences in LED intensities will produce discrepancies in the difference signal over time. The second configuration would circumvent this problem by using only one LED of 562 nm. The two waveguides will be coated with BTB–NAF and Nafion films respectively, and each will have its own photodetector. The Nafion film would respond to water, while the BTB–NAF film would respond to water and acid. Again, the difference between the two signals would correspond to the acid response.

Water vapor may also constitute a chemical interference if the presence of water vapor interrupts the acid–indicator interactions. Preliminary results indicate that the nature of the acid/indicator interaction is significantly affected by the polymer matrix.[23] Additional studies are planned to further investigate the nature of this interference.

CONCLUSIONS

Results indicate that the BTB–NAF indicator film provides a sensitive response in an optical waveguide configuration, particularly when the multiple internal reflection system is employed. The Nafion acts as a supporting film for the bromothymol blue reagent, providing good contact with the substrate surface. In addition, the ionic nature of the Nafion polymer facilitates transport of the polar acidic vapors to the indicator. It exhibits general sensitive and reversible response to the protonic acid vapors, hydrochloric acid and hydrogen sulphide, but does not exhibit a measurable indicator response to carbon dioxide. The detection limit for hydrogen sulphide is estimated as <15 ppm. The lowest hydrochloric acid vapor reported during this work, from $0.06M$ hydrochloric acid (0.01 ppm) produces a signal of nearly 3 volts. The OWG sensor is clearly several orders of magnitude more sensitive towards hydrochloric acid. This variable sensitivity for acid vapors may be due to the relative strength of the acid (hydrogen sulphide has a K_a of 1.0×10^{-7}).

The potential interferences from water and the acid effects on Nafion must be considered. While long term acid exposure will produce a decrease in baseline signal this effect is not considered to be a serious problem for several reasons. First, the magnitude of signal decrease is smaller than the indicator acid response by a factor of 20 or more. Second, the time frame over which this effect would become a problem is long compared to the time frame in which the indicator response to acid would signal the end of service of an acid-scrubbing filter. Finally, both the acid effect on Nafion and the acid indicator response produce a decrease in signal, so the cumulative effect would be a long term decrease in signal in the presence of acid. This effect will be more dramatic at higher acid concentrations. If this sensor is used as an alarm device to signal the end of service for protective equipment (gas masks) then it would produce an alarm response before high acid concentrations are present. Thus, the useful lifetime of the sensor would not be affected by this phenomenon.

The effect of water as a systematic interference is more serious, but can be dealt with instrumentally as discussed above. Future work should focus on the stability and sensitivity of these sensors. Specifically, the effects of polymer–indicator interactions on the response

mechanism of the sensor should be determined more quantitatively. In addition, further characterization of the response mechanism is planned. A more thorough understanding of polymer–indicator–acid vapor interactions/reactions will lead to significant analytical improvements in sensitivity and long-term stability.

Acknowledgements—The authors would like to acknowledge the efforts of Larry Gregerson of the NIU/Chemistry Department machine shop, Charles Caldwell of the NIU/Chemistry electronics shop, and Ed Hyland of the NIU/Chemistry glass blowing shop for all their assistance in the design and construction of the OWG sensor cells and electronics. In addition, the authors wish to thank W. R. Seitz for helpful discussions/suggestions regarding indicator chemistry. This project has been supported in part by NIOSH grant No. 2 R44 OHO2312-02.

REFERENCES

1. D. S. Ballantine, Jr. and H. Wohltjen, *Anal. Chem.*, 1989, **61**, 704A.
2. J. Janata, *ibid.*, 1988, **60**, 62R.
3. W. R. Seitz, in *CRC Crit. Rev. Anal. Chem.*, 1988, **19**, 135.
4. R. E. Dessy, *Anal. Chem.*, 1989, **61**, 1079.
5. Z. Cao, W. J. Buttner and J. R. Stetter, *Electroanalysis*, 1991, in the press.
6. J. Hlavay and G. G. Guilbault, *Anal. Chem.*, 1977, **49**, 1890.
7. J. F. De Andrade, A. A. Suleiman and G. G. Guilbault, *Anal. Chim. Acta*, 1989, **217**, 187.
8. G. G. Neuburger, *Anal. Chem.*, 1989, **61**, 1559.
9. E. C. Hahn, A. A. Suleiman and G. G. Guilbault, *Anal. Lett.*, 1989, **22**, 213.
10. S. Muto, A. Ando, T. Ochiai, H. Ito, H. Sawasa and A. Tanaka, *Jap. J. Appl. Phys.*, 1989, **28**, 125.
11. R. Narayanaswamy and F. Sevilla, *Analyst*, **113**, 661.
12. E. T. Hayes, O. Y. Ataman, A. E. Karagozler, Y. L. Zhang, D. P. Hautman, R. T. Emerich, A. G. Ataman, H. Zimmer and H. B. Mark, Jr., *Microchem. J.*, 1990, **41**, 98.
13. R. B. Beswick and C. W. Pitt, *J. Coll. Interf. Sci.*, 1988, **124**, 147.
14. W. R. Seitz, *Anal. Chem.*, 1984, **56**, 16.
16. D. S. Ballantine, Jr. and H. Wohltjen, *ibid.*, 1986, **58**, 2883.
17. R. R. Smardzewski, *Talanta*, 1988, **35**, 95.
18. M. W. Nevergold and K. Abel, *Spectroscopy*, 1990, **5**, 46.
19. S. J. Sondheimer, N. J. Bunce and C. A. Fyfe, *Rev. Macromol. Chem. Phys.*, 1986, **C26(3)**, 353.
20. G. N. Lewis and M. Randall, *Thermodynamics*, McGraw-Hill, 2nd Ed., Chap. 22, pp. 312–319, 1961.
21. Data taken from *Gmelin Handbook of Inorganic Chemistry*, Vol. 6 Chlorine (B1), pp. 240–243, 1964.
22. R. B. Denyszn, G. W. Bean and R. C. Geib, *Amer. Lab.*, **1990**, 24.
23. D. S. Ballantine, Unpublished data. Presented at FACCS Meeting, Anaheim, CA, October 1991.

Talanta, Vol. 39, No. 12, pp. 1669–1673, 1992
Printed in Great Britain.

0039-9140/92 $5.00 + 0.00

RELEASE OF COPPER FROM COMMERCIAL SOLID-STATE COPPER ION-SELECTIVE ELECTRODES

BOY HOYER
Department of Chemistry, Aarhus University, Langelandsgade 140, 8000 Åarhus C, Denmark

(*Received* 9 *December* 1991. *Revised* 30 *March* 1992. *Accepted* 30 *March* 1992)

Summary—The release of copper from two commercial solid-state cupric ion-selective electrodes [Orion 94-29 Cupric Electrode (I) and Radiometer F1112 Selectrode (II)] was measured by immersion in the following media: 0.1*M* potassium nitrate (pH = 4.7), 0.5*M* sodium chloride (pH = 4.7) and 0.1*M* nitric acid. In the 0.1*M* potassium nitrate medium, the amount of copper released from both electrodes causes interference when they are used for the determination of cupric ion at the $10^{-7}M$ level. In comparison with the 0.1*M* potassium nitrate medium, the copper release in the 0.5*M* sodium chloride and 0.1*M* nitric acid media was increased for electrode II but not for electrode I. The release of copper was not affected by removal of oxygen from the media but can be substantially lowered by coating the electrodes with a thin cation-exchange membrane (Nafion). The mechanism of copper dissolution is investigated.

It has been known for many years that the use of a solid-state cupric ion selective electrode (Cu–ISE) can cause sample contamination owing to dissolution of copper from the membrane material.[1] For prototype electrodes prepared from CuS it has been shown that copper dissolution is accelerated by oxidants,[2] chloride[3] and copper-binding ligands,[4] while reductants have the opposite effect.[2]

In spite of the relevance to practical analysis, no systematic and quantitative study on the dissolution of copper from commercially available Cu–ISE's under realistic measuring conditions has been undertaken. It is the aim of the present study to provide such data. The electrodes selected for study were an Orion and a Radiometer Cu–ISE which employ different ion-sensing materials. The copper dissolution was also measured after coating the electrodes with a cation-exchange membrane (Nafion) which has previously proven beneficial for suppression of the chloride interference effect without impairing the functioning of the electrode.[5]

The procedures used complied with the recommendations of the manufacturers of the Cu–ISE's and no special measures such as chemical pretreatment were taken to either reduce or enhance the copper dissolution. The corrosion of the Cu–ISE's was measured in a non-interfering medium, a medium resembling seawater with a high chloride content, and an acidic medium.

EXPERIMENTAL

Apparatus

The Cu–ISE's were a new Orion 94-29 Cupric Electrode and a Radiometer F1112 Selectrode which had been in regular use for four years. The Radiometer electrode was kept dry with the sensing element covered with a rubber cap, when not in use. The copper-selective membranes in the Radiometer and the Orion electrodes are respectively a $Cu_{1.8}Se$ monocrystal and a CuS–Ag_2S pressed pellet with diameters of 5.5 mm and 7.5 mm respectively. Both electrodes employ a solid state internal contact. During corrosion experiments, the Cu–ISE was immersed in a cell thermostatted to 28 ± 2° with a water jacket.

Determination of cupric ion was done by potentiometric stripping analysis (PSA) using a programmable electrochemical analyzer.[6] The working electrode was a mercury-plated glassy carbon electrode, while the reference electrode and the counter electrode were a Radiometer K401 saturated calomel electrode (SCE) and a platinum rod, respectively.

Reagents

All electrolyte media were prepared from Merck Suprapur chemicals and triply distilled water. Other reagents were of analytical grade. Cupric ion standards were prepared from Merck Titrisol stock solution. A 5% solution of the Nafion perfluorosulphonate ionomer (1100

equiv. wt.) was obtained from Solution Technology (Mendenhall, Pennsylvania, U.S.A.). The 0.1*M* potassium nitrate and 0.5*M* sodium chloride media were buffered to pH 4.7 by addition of $10^{-2}M$ acetate buffer prepared from acetic acid and sodium hydroxide.

Procedure

The Radiometer Cu–ISE was maintained by regular polishing with Radiometer D709 abrasive agent and 0.25-μm diamond paste, while the Orion electrode was polished with Orion 948201 polishing strips. After abrasion, the electrodes were rinsed copiously with ethanol and distilled water. Overnight, the Cu–ISE's were stored in distilled water.

Corrosion experiments were carried out by immersing the Cu–ISE in a polyethylene beaker containing 10 ml of solution. Stirring was done by means of a Teflon-coated magnetic bar. For deaeration, the measuring cell was closed with plastic film, and argon was bubbled through the solution for 10 min prior to and also during the immersion of the Cu–ISE. The Cu–ISE was preconditioned for at least 15 min in the same medium used in the subsequent corrosion experiment. This medium was also used for storage between repetitive measurements and for rinsing of the electrode.

Coating of the Cu–ISE's with Nafion was carried out as previously described.[5]

The instrumental settings for PSA were as follows: plating potential, −700 mV *vs.* SCE, plating time, 60 sec; rest potential, 0 mV *vs.* SCE; rest time, 15 sec; background electrolysis time; 1 sec. In the 0.5*M* sodium chloride medium, the rest potential was decreased to −100 mV *vs.* SCE. Prior to PSA, all samples were spiked with 250μM of Hg(II) while $1.3 \times 10^{-2}M$ sodium chloride was added to the 0.1*M* potassium nitrate and 0.1*M* nitric acid media. Quantitation of copper was done by standard addition.

All experimental work was carried out in a clean bench. The blank value of the overall analytical procedure was routinely determined and was found to be insignificant in comparison with the copper concentrations determined.

RESULTS AND DISCUSSION

In Table 1, the copper ion concentrations resulting from dissolution of the Cu–ISE's are summarized. The oxidation state of the copper ions released is not known, and the signal obtained in PSA may therefore be made up of contributions from Cu(I) as well as Cu(II). Generally, the sensitivity in PSA is dependent on the chemical form of the metal determined. However, with the preelectrolysis potential used the sensitivity towards copper is governed by mass transport, and the PSA signal is proportional to $D^{2/3}$, where D is the diffusion coefficient of the metal species being preconcentrated onto the working electrode.[7] Equilibrium calculations showed that the addition of Hg(II) prior to PSA ensures quantitative oxidation of Cu(I) to Cu(II) in the 0.1*M* nitric acid and 0.1*M* potassium nitrate media, but not in the 0.5*M* sodium chloride medium owing to the stabilization of Cu(I) and Hg(II) by chloride. However, Cu(I) as well as Cu(II) are predominantly

Table 1. Release of copper from commercial Cu–ISE's in various media

Electrode and medium	Release of cupric ion/n*M**			
	bare, no deaeration	bare, deaeration	Nafion-coated, no deaeration	Nafion-coated, deaeration
Radiometer 0.1*M* KNO_3 (pH = 4.7)	65	66	60	51
Radiometer 0.5*M* NaCl (pH = 4.7)	210	210	64	53
Radiometer 0.1*M* HNO_3	290	240	150	110
Orion 0.1*M* KNO_3 (pH = 4.7)	71	46	< 30	< 30
Orion 0.5*M* NaCl (pH = 4.7)	67	81	< 30	< 30
Orion 0.1*M* HNO_3	82	89	44	42

*Electrodes were immersed for 5 min in 10 ml of the medium. The values quoted are averages of four or more separate corrosion experiments. The relative standard deviation of the copper concentration obtained in such repeated experiments was typically 15%.

present as chloride complexes in the latter medium and the difference in their diffusion coefficients will be small.

Even in a non-corrosive medium (0.1*M* potassium nitrate), the release of copper ion from both electrodes is sufficient to seriously affect measurements of cupric ion at the $10^{-7}M$ level. No systematic change in the copper release was observed during repetitive corrosion experiments which implies that a steady-state situation is established. The response time of the Orion Cu–ISE is at least 5 min at a cupric ion concentration of $10^{-7}M$ (Ref. 8) which equals the immersion time in the measurements on which Table 1 is based. As the response time increases dramatically with decreasing concentration below the $10^{-7}M$ level,[8] the results in Table 1 should be considered as a lower limit to sample contamination when using the Cu–ISE's for measurement of Cu(II) in the submicromolar range.

In contrast to the Orion Cu–ISE, the release of copper from the Radiometer Cu–ISE in the 0.5*M* sodium chloride and 0.1*M* nitric acid media was much higher than in the 0.1*M* potassium nitrate medium. This difference between the electrodes is even more pronounced when the areas of the ion-sensing elements are taken into consideration. Sample deaeration prior to and during immersion of the electrodes has surprisingly little effect on the results which implies that oxidation of the membrane during immersion is not the dominating mechanism of copper dissolution. The soluble copper species must therefore be present in the bulk or on the surface of the electrode material prior to immersion. The cases where the release of copper is increased by deaeration can be explained by increased convection in the solution due to argon bubbling. However, sample dearation is still important with the Radiometer Cu–ISE in measurements of micromolar or submicromolar concentrations of Cu(II) owing to the high redox sensitivity of the membrane.[9]

Table 2. Rate of copper release from commercial Cu–ISE's

Electrode and medium	Dissolution rate* of copper ion/n*M*/min	Correlation coefficient
Radiometer ÷ Nafion in 0.5*M* NaCl (pH = 4.7)	16	0.96
Radiometer + Nafion in 0.5*M* NaCl (pH = 4.7)	3.0	0.99
Radiometer ÷ Nafion in 0.1*M* HNO_3	50	0.99
Radiometer + Nafion in 0.1*M* HNO_3	14	0.96
Orion ÷ Nafion in 0.5*M* NaCl (pH = 4.7)	5.5	0.98
Orion ÷ Nafion in 0.1*M* HNO_3	15	0.99
Orion + Nafion in 0.1*M* HNO_3	3.1	0.98

*The dissolution rate was calculated by linear regression on a ($[Cu]_T$, $T_{immersion}$) data set with $T_{immersion}$ = 5, 10, 15 and 20 min. The media were not deaerated.

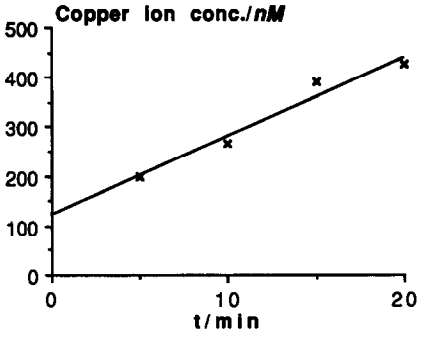

Fig. 1. Effect of immersion time on the release of copper from a Radiometer Cu–ISE. Experimental conditions: bare electrode immersed in 10 ml of non-deaerated 0.5*M* NaCl (pH = 4.7).

Nafion-coating of the Cu–ISE's suppressed the release of copper in all combinations of Cu–ISE and medium. A polymer membrane poses a diffusional barrier to mass transport, and it is therefore to be expected that transport-related processes such as the dissolution of the Cu–ISE will be slower, but this advantage is partially offset by the increased response time of the electrode.[8] Furthermore, the Nafion polymer is a cation-exchange resin which selectively hinders the permeation of anions by Donnan exclusion. The latter mechanism explains the particularly large decrease in copper release from the Radiometer Cu–ISE in the 0.5*M* sodium chloride medium obtained by Nafion-coating. This polymer has previously been employed to suppress the chloride interference on a Cu–ISE.[5] Also, the Donnan exclusion effect of the Nafion coating causes an accumulation of anionic dissolution products from the Cu–ISE which counteracts the dissolution process.

In order to measure the dissolution rate of copper the increase in copper ion concentration was measured for immersion times between 5 and 20 min in the 0.1*M* nitric acid and 0.5*M* sodium chloride media. The results are given in Table 2, and a typical data set is plotted in Fig. 1. In all cases, a highly significant linear relationship (*cf.* Table 2) and a positive intercept

on the concentration axis was obtained. Clearly, a considerable fraction of the copper contamination from the Cu–ISE is constant and not related to the immersion time. This observation is in agreement with previous work of Blaedel and Dinwiddie,[8] who showed that the exposure of a moist Orion Cu–ISE to air (associated with transfer between solutions) corroded the electrode and caused copper contamination of the solution in which the electrode was subsequently immersed.

It has been shown[10] that the sensing element of the Orion Cu–ISE is composed of the minerals jalpaite ($Ag_{1.55}Cu_{0.45}S$) and acanthite (Ag_2S), while the sensing element of the Radiometer Cu–ISE is composed of berzelianite ($Cu_{1.8}Se$) and a surface layer of umagite (Cu_3Se_2) generated by prolonged use. Unfortunately, no solubility data on the mentioned copper-containing minerals could be found. For comparison, the solubilities of CuS, Cu_2S, CuSe and Cu_2Se were calculated in the media employed with the relevant side reactions of S^{2-}, Se^{2-}, Cu^{2+} and Cu^+ taken into account. Thermodynamic data were taken from Smith and Martell.[11] In all cases, the copper concentrations resulting from dissolution of the Cu–ISE by far exceeded the calculated equilibrium values. This discrepancy can be explained by two mechanisms. Firstly, the membrane material itself may contain traces of soluble copper compounds which are either introduced in the fabrication process or formed during storage of the electrode. Secondly, such compounds may be generated by surface oxidation of the membrane material during use of the electrode. As discussed above, surface oxidation of the membrane was evident in the present study, but the leaching mechanism must also be involved because the amount of copper released increased linearly with immersion time in a non-oxidizing medium such as 0.5*M* sodium chloride (*cf.* Fig. 1). Although this medium contained dissolved oxygen, surface oxidation of the Cu–ISE can still be ruled out because deaeration of the immersion medium did not suppress the release of copper from the Cu–ISE's (*cf.* Table 1). These findings are in agreement with previous work on laboratory-made Cu–ISE's. Heine and Van der Linden[12] showed that copper sulphate is slowly formed by oxidation of jalpaite in dry air and even more so in ambient air. Problems with oxidation of sulphides in connection with preparation of pressed-pellet CuS electrodes have also been reported.[2,13] No analogous investigations have been performed for the copper selenide minerals, but the relative susceptibilities of the sulphide- and selenide-based electrodes towards oxidation can be estimated from the following standard potentials:

$$S(o) + 2e^- \leftrightarrow S^{2-};\ E^0 = -0.51\ V$$

$$Se(o) + 2e^- \leftrightarrow Se^{2-};\ E^0 = -0.78\ V$$

$$SO_4^{2-} + 4H_2O + 8e^- \leftrightarrow S^{2-} + 8OH^-;\ E^0 = -0.69\ V$$

$$SeO_4^{2-} + 4H_2O + 8e^- \leftrightarrow Se^{2-} + 8OH^-;\ E^0 = -0.36\ V$$

Thus, selenium is more easily oxidized from state −II to 0 than sulfur, while the opposite holds for the oxidation from state −II to +VI. In the present study, the Radiometer Cu–ISE did release more copper than the Orion Cu–ISE in the 0.5*M* sodium chloride and 0.1*M* nitric acid media, but the difference may also be attributed to the different history of the electrodes as the Radiometer Cu–ISE was older, had been in prolonged use and was kept in an ambient laboratory atmosphere. Therefore, it is possible that the layer in which oxidation of the membrane had occurred was so thick that the polishing procedure did not fully remove it.

Harsányi *et al.*[14] measured the release of copper in acetate buffer from a laboratory-made, pressed-pellet CuS electrode which had been pretreated in a reducing medium. After normalization with respect to immersion time, immersion volume and electrode area, this electrode released at least 20 times as much copper as the Radiometer and Orion electrodes did in the 0.1*M* potassium nitrate medium. However, the copper release could to a large extent be remedied by treatment of the precipitate with sulphide prior to pressing.[14]

In conclusion, the detection limit of commercial Cu–ISE's is limited not only by their Nernstian range, but also by sample contamination from dissolution of the membrane material. Measurements of Cu(II) in the micromolar and submicromolar range with these electrodes must therefore be critically evaluated. Apart from future improvements in the fabrication procedures of the Cu–ISE's, sample contamination by copper can be minimized by use of large sample volumes and by Nafion-coating of the Cu–ISE. The contamination problem can also be remedied by mounting of

the Cu–ISE in a flow configuration, and Nernstian calibration to very low cupric ion levels[15] can be achieved. However, large sample volumes must be available.

REFERENCES

1. D. Midgley, *Anal. Chim. Acta*, 1976, **87**, 7.
2. E. Pungor, K. Tóth, M. K. Pápay, L. Pólos, H. Malissa, M. Grasserbauer, E. Hoke, M. F. Ebeland and K. Persy, *ibid.*, 1979, **109**, 279.
3. E. G. Harsányi, K. Tóth, E. Pungor and M. F. Ebel, *Mikrochim. Acta*, 1987, **II**, 177.
4. Y. Umezawa, K. Ito, H. Hata, M. Sugawara, E. G. Harsányi, K. Tóth, E. Pungor, M. Soma and A. Tanaka, *ibid.*, 1990, **I**, 231.
5. B. Hoyer and M. Loftager, *Anal. Chem.*, 1988, **60**, 1235.
6. K. N. Thomsen, H. J. Skov and L. Kryger, *Anal. Chem. Acta*, 1989, **219**, 105.
7. A. J. Bard and L. R. Faulkner, *Electrochemical Methods. Fundamentals and Applications*, Wiley, New York, 1980.
8. W. J. Blaedel and D. E. Dinwiddie, *Anal. Chem.*, 1974, **46**, 873.
9. J. Vesely, *Collect. Czech. Chem. Commun.*, 1971, **36**, 3364.
10. J. Siemroth and I. Henning, *Anal. Chem. Symp. Ser.*, 1981, **8**, 339.
11. R. M. Smith and A. E. Martell, *Critical Stability Constants*, Vols. 1–6, Plenum Press, New York, 1974–1989.
12. G. J. M. Heine and W. E. Van der Linden, *Anal. Chim. Acta*, 1977, **93**, 99.
13. E. Gráf, K. Tóth, K. Varga, E. Pungor and M. F. Ebel, in *Ion-Selective Electrodes*, E. Pungor (ed.), Vol. 5, p. 367. Pergamon Press, Oxford 1989.
14. E. G. Harsányi, K. Tóth and E. Pungor, *Anal. Chim. Acta*, 1983, **152**, 163.
15. W. J. Blaedel and D. E. Dinwiddie, *Anal. Chem.*, 1975, **47**, 1070.

Talanta, Vol. 39, No. 12, pp. 1675–1679, 1992
Printed in Great Britain.

0039-9140/92 $5.00 + 0.00

OPTICAL HUMIDITY AND AMMONIA GAS SENSORS USING REICHARDT'S DYE-POLYMER COMPOSITES

YOSHIHIKO SADAOKA,* YOSHIRO SAKAI and YU-UKI MURATA
Department of Applied Chemistry, Faculty of Engineering, Ehime University, Matsuyama 790, Japan

(*Received* 17 *March* 1992. *Revised* 10 *April* 1992. *Accepted* 10 *April* 1992)

Summary—Optical intensity reflected at 750 nm by Reichardt's betain dye-polymer (PMMA or PEO) composite increased with an increase in humidity and was not affected by ammonia vapor. For the composites treated with hydrochloric acid, the intensity at around 590 nm decreased with an increase in ammonia concentration, and the sensitivity was enhanced by the presence of water vapor. The treatment with hydrochloric acid induced the formation of phenolic group, O^-–H^+ and N^+–Cl^- in the dye. The sorption of NH_3 decreases the ionic interactions.

A number of optical fibre sensors have been devised for the measurement of physical parameters like temperature and displacement. There has been an increasing interest in optical sensors to detect gas species in the atmosphere such as H_2O, NH_3, NO_2, organic vapor.[1–7] Chemical sensors based on optical fibres offer several advantages, *i.e.*, the sensors are electrically safe, their signals are not influenced by electrical disturbances, and the separation of the sensor element and actuators is easy. Most optochemical sensors are composed of polymer thin films with dyes whose absorption or fluorescence characteristics are a function of the concentration of chemical species. It is well known that Reichardt's dye exhibits one of the largest solvatochromic effects of any known molecule.[8] It is extremely sensitive to solvent polarity. The absorption peak of Reichardt's dye dissolved in non-polar solvent such as hexane, toluene, benzene is observed at around 850 nm and the coexistence of polar molecules such as water, alcohol and acetone induces the blue shift. The degree of the blue shift is expected to increase with increasing hydrogen bond donor strength and polarity of solvent.[9] The electronic transition leading to the solvatochromic band involves charge delocalization from the phenoxide oxygen into the pyridium ring and the phenyl groups attached thereto.[10] Recently, Paley *et al.*[11] have reported that the absorption wavelength of Reichardt's dye dispersed in a polymer matrix is very sensitive not only to the solid polymer matrix but also to humidity in ambient air since the sorbed water acts as acidic site which binds to the basic $-O^-$ site on Reichardt's dye. It seems that dye-polymer composites are useful materials to fabricate chemical sensor's that are selective for ambient gases since the position of absorption bands is a function of hydrogen bond acidity or polarity of sorbed molecules. Furthermore, it is expected that the selectivity can be controlled by the polarizability and/or acidity of the polymer matrix.

We propose a new type of optochemical sensor fabricated with Reichardt's dye for determining humidity and ammonia concentration in ambient air. This sensor can be operated in the longer wavelength range and at room temperature.

EXPERIMENTAL

Reichardt's betain [2,6-diphenyl-4-(2,4,6-triphenylpyridino)phenolate], poly(methyl methacrylate) (PMMA, MW = 12,000) and poly (ethylene oxide) (PEO, MW = 5,000,000) were obtained from Aldrich. For thin film preparation, Reichardt's dye was dissolved in acetone–water mixture with PEO (dye:PEO = 20:5 in weight) and in acetone with PMMA (dye:PEO = 20:5 in weight). Thin films were formed on alumina plates and quartz oscillating element (4 MHz) by solvent casting. The humidity and/or ammonia concentrations of test gases were controlled by mixing 1% ammonia diluted with standard air (21% O_2 + 79% N_2), humid air prepared by bubbling standard air through water, and standard air. The impurity con-

*Author for correspondence.

centration in standard air was as follows: CO < 1 ppm, CO_2 < 2 ppm, HCl < 1 ppm and H_2O < 10 ppm. The desired concentration of ammonia and humidity was achieved within 20 sec by using a special chamber (volume less than 20 cm^3) to measure optical response and weight gain of the film. The Y-type bundled flexible quartz fibre (2 mm in diameter) was fixed just in front of the film. Light from a D_2/I_2 lamp was guided into the fibre and directed to the film; the reflected light was collected by the same optical fibre. The collected light was analyzed by using a photospectrum analyzer (MCPD-1000, Otsuka electronics) in the region of 400–1100 nm. The water and/or ammonia contents were measured using a quartz oscillator as a microbalance. The weight and weight gain for the film exposed to the test gases were estimated from the oscillating frequency of the quartz oscillating element coated with film. All of the measurements were performed at 30°.

RESULTS AND DISCUSSIONS

Humidity sensing characteristics

In Fig. 1, the reflection spectra in dry air and in 50% RH (relative humidity) air for the composite films formed on alumina substrate are shown. In these cases, the spectrum observed for the uncoated alumina substrate (plate) was used as a reference. The position of the absorption band of Reichardt's dye dispersed in polymer was influenced by the polymer matrix, *i.e.*, the wavelength of the peak was 700 nm in dry air and 600 nm in 50% RH air for PMMA composite and 660 nm in dry air

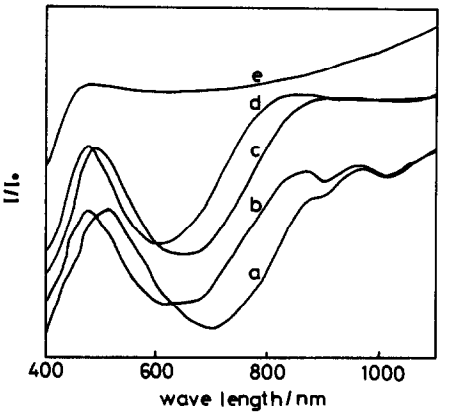

Fig. 1. Spectra of dye-polymer composites. (a) PMMA, in dry air, (b) PMMA, in 50% RH air (c) PEO, in dry air, (d) PEO, in 50% RH air (e) PEO treated with HCl, in 50% RH air.

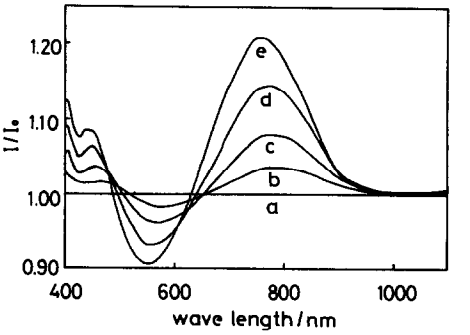

Fig. 2. Humidity dependence of spectrum in reflection mode for the PMMA composite untreated with HCl. (a) 0, (b) 5, (c) 13, (d) 38, (e) 71 in %RH.

and 600 nm in 50% RH air for PEO composite, respectively. The absorption peak was dependent on the polymer matrix even in a humid atmosphere and the humidification induced the blue shift. It is well known that the absorption peak of Reichardt's dye dissolved in solvent appears at 453 nm for water, 515 nm for methanol, 550 nm for ethanol, 677 nm for acetone, and 828 nm for benzene. For the polymer composites, the absorption peak in a humid atmosphere appeared at a longer wavelength than that of the dye dissolved in water. The hydrogen bond acidity or polarizability of the sorbed water is less than the liquid water. Since the water sorption ability can be controlled by the hydrophilicity of the polymer, the wavelength of reflection peak for humidity detection is easily controlled by the selection of polymer species. In Fig. 2, the spectral changes are shown as a function of the humidity for PMMA composite. In this case, the spectrum observed for the composite film in dry air was used as a reference. The optical intensity of the reflection peak observed around 770 nm increased with humidity and the wavelength of the peak became shorter while that of the reflection peak appeared at around 550 nm was decreased. The reflection peak observed at around 770 nm is more sensitive to the humidity than that at 550 nm. Humidity dependence of the wavelength of the peak appeared at around 770 nm and it's optical intensity is shown in Fig. 3. Similar dependencies were observed for the PEO composite (Fig. 4). The sensitivity for humidity in the optical intensity and in the wavelength of the peak of PMMA composite is higher than that of PEO composite. The difference in the sensitivity to humidity may be caused by the difference of hydrophobicity of polymer species.

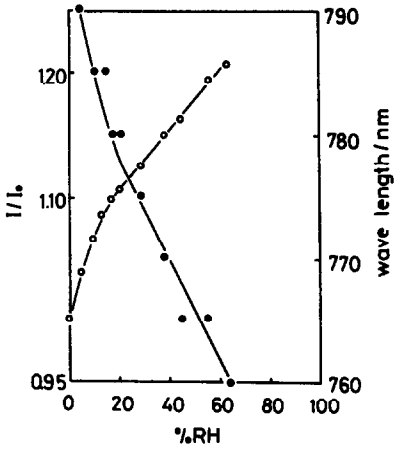

Fig. 3. Humidity dependence of the wavelength of maximum and it's optical intensity for PMMA composite untreated with HCl. (○) I/Io, (●) λ max.

Ammonia sensing characteristics

While for PEO composite, an absorption band appeared at 700 nm in atmosphere, the treatment with hydrochloric acid vapor induced a disappearance of the absorption band as shown in Fig. 1. A similar phenomenon was confirmed for the composite treated with nitric acid vapor. The treatment with hydrochloric acid caused the formation of phenolic OH, which was confirmed by infra-red spectroscopy. For the PEO composite treated with hydrochloric acid vapor, the spectra in the range between 400 and 1100 nm was only slightly influenced by the humidification but strongly affected by the ammonia vapor. The position of the absorption peak was only slightly affected by the concentration of ammonia. The results observed in dry air and in air with 50% RH are

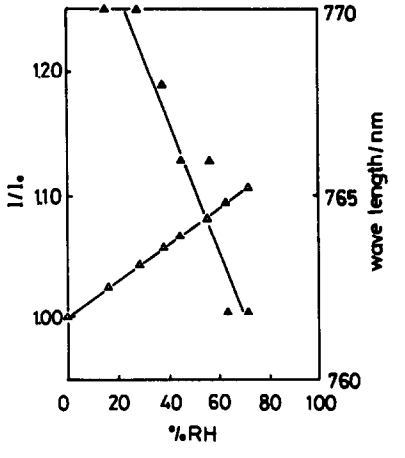

Fig. 4. Humidity dependence of the wavelength of maximum and it's optical intensity for PEO composite untreated with HCl. (○) I/Io, (●) λ max.

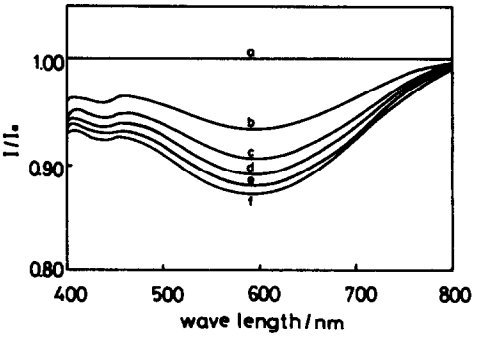

Fig. 5. NH_3 concentration dependence of spectrum in reflection mode for the PEO composite treated with HCl. (a) 0, (b) 1000, (c) 2000, (d) 3000, (e) 4000, (f) 5000 ppm NH_3 in dry air.

shown in Figs. 5 and 6. As a reference, the spectrum observed for the composite film in ammonia-free air was used. The introduction of ammonia induced a decrease in the optical intensity at around 600 nm. The peak wavelength was not affected by concentration and was the same as observed for untreated-dye–PEO composite. It seems that the bond strength of O^-–H^+ and of N^+–Cl^- was weakened by the sorption of ammonia. Ammonia concentration dependence of the optical intensity at 590 nm is shown in Fig. 7 for the PEO composite treated with hydrochloric acid. The sensitivity and it's response time for ammonia was accelerated by the coexistence of water vapor. The 90% response time in the optical intensity for ammonia was about 120 sec in dry air and 30 sec or less in 50% RH air. For the PMMA composite treated with hydrochloric acid vapor, the optical intensity at around 600 nm also became sensitive to ammonia and the sensitivity was accelerated by the water vapor while the sensitivity was considerably less than these for the PEO composite. The humidifi-

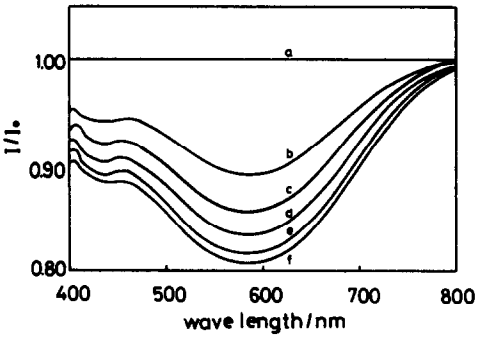

Fig. 6. NH_3 concentration dependence of spectrum in reflection mode for the PEO composite treated with HCl. (a) 0, (b) 1000, (c) 2000, (d) 3000, (e) 4000, (f) 5000 ppm NH_3 in 50% RH air.

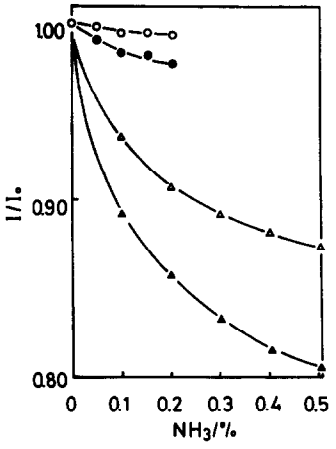

Fig. 7. NH_3 concentration dependence of the optical intensity at 590 nm for the composites treated with HCl. (○) PMMA, in dry air, (●) PMMA, in air with 50% RH, (△) PEO, in dry air, (▲) PEO, in air with 50% RH.

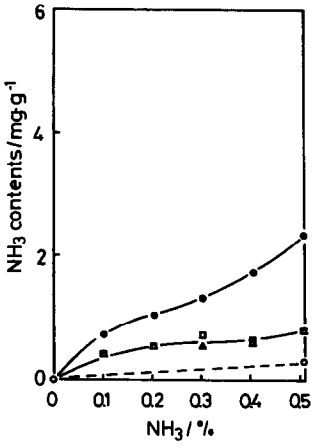

Fig. 9. NH_3 sorption isotherms of PMMA composites. (○) untreated with HCl, in dry air, (△) untreated with HCl, in air with 50% RH, (□) treated with HCL, in dry air, (●) treated with HCl, in air with 50% RH.

cation induced the blue shift (about 10 nm). Furthermore, the exposures to dry air with 5000 ppm ammonia and to 50% RH air with the same concentration of ammonia did not induce the changes of the reflection spectra for the composites untreated with hydrochloric acid. It seems that the active site for ammonia molecules is the phenolic OH group.

Gas sorption characteristics

A water sorption isotherm for PMMA and PEO composites was examined to clarify the sensing mechanism (Fig. 8). For both composites, water content monotonically increased with the humidity. As well known, PEO is soluble in water and is more hydrophilic than PMMA. The water sorption ability of PMMA was about 2-fold less than that of PEO. For Reichardt's dye, a considerable amount of water could be sorbed and the sorption ability for water was higher than that of PMMA and was comparable to PEO alone. When the PMMA composite untreated with hydrochloric acid was exposed to dry air with 5000 ppm ammonia, an increase in the weight was observed to be 0.3 mg/g or less as shown in Fig. 9. The humidification of the test gases enhanced the sorption of ammonia. A weight increase of 0.8 mg/g was observed when ammonia gas (5000 ppm) was introduced in 50% RH air. A weight increase by the exposure to 50% RH air was about 15 mg/g. The amount of sorbed ammonia when 5000 ppm ammonia was introduced, was about 20-fold less than that of the water. The treatment of PMMA composite with hydrochloric acid vapor enhanced the sorption of ammonia and

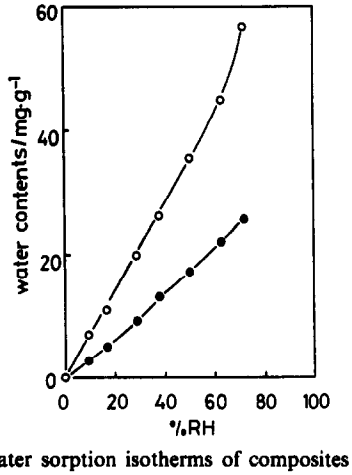

Fig. 8. Water sorption isotherms of composites untreated with HCl. (●) PMMA, (○) PEO.

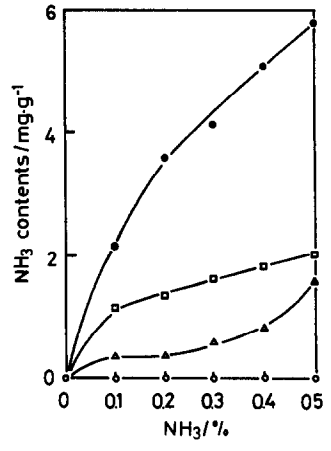

Fig. 10. NH_3 sorption isotherms of PEO composites. (○) untreated with HCl, in dry air, (△) untreated with HCl, in air with 50% RH, (□) treated with HCl, in dry air, (●) treated with HCl, in air with 50% RH.

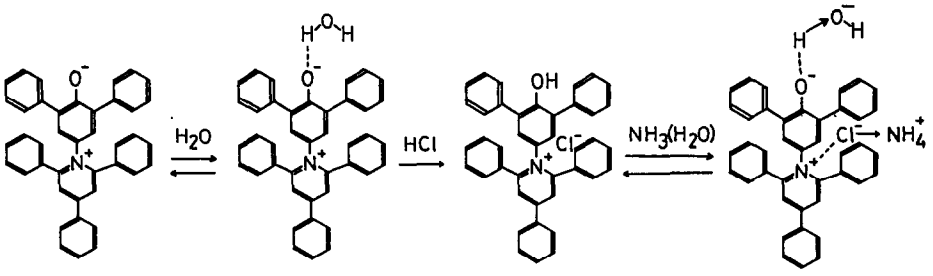

Fig. 11. A proposed sensing mechanism for H_2O and NH_3 detection.

an increase in weight by the exposure to 50% RH air with 5000 ppm ammonia was only about 2 mg/g which was 10-fold less than the water content (20 mg/g) at 50% RH. For the PEO composite untreated with hydrochloric acid, the sorbed water was estimated to be about 35 mg/g in 50% RH air (Fig. 8). The introduction of 5000 ppm ammonia to 50% RH air induced 1.5 mg/g enhancements while no distinguishable enhancements in weight by the sorption of ammonia could be observed for the same in dry air (Fig. 10). The relatively large water uptake suggests that the spectral shifts observed in response to humidity for the composites without hydrochloric acid treatment are due to changes of polarity in the dye environment. The relatively small weight gain for ammonia compared to the weight gain for films exposed to water suggests that this is a chemical effect. A preliminary model based on our experimental results can be expressed as shown in Fig. 11.

CONCLUSIONS

The optical intensity in the reflection mode and the wavelength of maxima observed at 750 nm for Reichardt's betain dye–PMMA composite were very sensitive to the humidity and insensitive to ammonia vapour. The optical intensity monotonically increased with the humidity. Similar behaviour was also observed for the PEO composite while the sensitivity was considerably less than that for PMMA composite. The hydrogen bonding of sorbed water to phenoxide oxygen should stabilize the ground state and results in the negative chromism (hypso-chromic). By using the composite treated with hydrochloric acid, the reflection spectra with a peak at 600 nm became sensitive to ammonia vapor especially for PEO composite. Sensitivity for ammonia was accelerated by the coexistence of water. The treatment with hydrochloric acid induced the formation of phenolic group, -OH and N^+–Cl^- in the dye. The sorption of ammonia forming ammonium cation and hydroxyl anion, decreases the bond strength of O^-–H^+ and N^+–Cl^-.

Acknowledgements—This work was partially supported by the Mazda Foundation's Research Grant.

REFERENCES

1. Q. Zhou, M. R. Shahriari, D. Kritz and G. H. Sigel, Jr., *Anal. Chem.*, 1988, **60**, 2317.
2. K. Ogawa, S. Tsuchiya, H. Kawakami and T. Tsutsui, *Electron. Lett.*, 1988, **24**, 42.
3. H. E. Posch and O. S. Wolfbeis, *Sens. Actuators*, 1988, **15**, 77.
4. Y. Sadaoka, M. Matsuguchi, Y. Sakai and Y. Murata, *Chemistry Lett.*, 1991, 1825.
5. Y. Sadaoka, M. Matsuguchi and Y. Sakai, *J. Electrochem. Soc.*, 1991, **138**, 614.
6. J. F. Giuliani, H. Wohltjin and N. L. Jaruvis, *Optics Lett.*, 1983, **8**, 54.
7. M. R. Shahriari, Q. Zhou and G. H. Sigel Jr., *ibid.*, 1988, **13**, 407.
8. *Aldrichimica Acta*, 1987, **20**, 59.
9. B. P. Johnson, M. G. Khaledi and J. G. Dorsey, *Anal. Chem*, 1986, **58**, 2354.
10. R. W. Taft and M. J. Kamlet, *J. Amer. Chem. Soc.*, 1976, **98**, 2886.
11. M. S. Paley, R. A. McGill, S. C. Haward, S. E. Wallace and J. M. Harris, *Macromolecules*, 1990, **23**, 4557.

Aims and Scope

Talanta, published monthly, provides a forum for the publication of *original research papers*, *preliminary communications*, *annotations* and *reviews* in all branches of pure and applied analytical chemistry. Other features are *analytical data* (stability constants,, etc.) and *letters to the editors*. Papers on fundamental studies and novel instrumentation development are especially encouraged. The latter include physical, inorganic and organic chemistry measurement instrumentations that are unique. New electronic developments are welcome. Novel applications in areas such as clinical chemistry, environmental analysis, geochemistry, materials science and engineering, pharmaceutical and drug analysis, etc. are welcome. Since classical spectrophotometric measurements and applications, titrimetry, *etc.*, are well established, studies in such areas should demonstrate a unique and substantial advantage over presently known systems (with respect to reagents or a particular application). Contributions will be expected to be of the high standard set and maintained by *Talanta* and to make a definite and useful contribution to analytical chemistry: they must be new publications. Papers must be written in English. *Reviews* of rapidly expanding fields or of hitherto widely scattered material are welcome but should be critical. *Original papers* and *reviews* are refereed in the usual way. *Preliminary communications* (intended for the rapid publication of novel ideas and lines of research) are refereed urgently and published direct from typescript to give utmost speed of publication. *Correspondence* of interest to analytical chemists is published at the discretion of the Editors-in-Chief.

TALANTA: CHEMICAL SENSORS

Talanta: Chemical Sensors is a new section of *Talanta*, for presenting significant experimental and theoretical research results relevant to chemical sensing.

This section has been created in recognition of the growing need to perform chemical analysis *in situ* with sensing devices. Original research articles either as *full papers* or as *preliminary communications* will be published. In addition, occasional short reviews of topics of interest to sensor scientists will be considered.

Topics relevant to *Talanta: Chemical Sensors* include: experimental characterization of new sensing devices, theory to describe the response properties of sensing devices, significant and timely applications of sensors to important analytical problems, molecular recognition chemistry of potential value for chemical sensing, interfacing biological catalysts and receptors to physical readouts, and instrumentation development, particularly miniaturization, of potential value for chemical sensing.

Manuscript Submission. Instructions for authors are given at the end of this issue. Please **submit three copies** of the manuscript to the appropriate Editor-in-Chief. Manuscripts from North and South America, Japan, China, Australia, India and other countries in that half of the world should be sent to Gary Christian. Manuscripts from Europe, the Middle East and Africa should be sent to Elo Hansen.

Publishing Office.
Pergamon Press plc, Headington Hill Hall, Headington, Oxford OX3 0BW [*Tel.* (0865) 794141; *Fax* (0865) 743948].

Subscription and Advertising Offices.
North America: Pergamon Press Inc., 395 Saw Mill River Road, Elmsford, NY 10523, U.S.A.
Rest of the World: Pergamon Press plc, Headington Hill Hall, Oxford OX3 0BW, England [*Tel.* Oxford (0865) 794141].

Published Monthly. Annual Subscription Rates (1992).
Annual institutional subscription rate (1992): £480.00 (US$770.00). Two-year institutional rate (1992/93): £912.00 (US$1389.00). Sterling prices are definitive. US dollar prices are quoted for convenience only, and are subject to exchange rate fluctuation. Prices include postage and insurance and are subject to change without notice. Subscription rates for Japan are available on request. Personal subscription rate for those whose library subscribes at the regular rate is also available on request.

Back Issues. Back issues of all previously published volumes, in both hard copy and in microform are available direct from Pergamon Press offices.

Talanta, Vol. 39, No. 10, p. i, 1992
Pergamon Press Ltd. Printed in Great Britain

ERRATA

In the article "Determination of sulfide with chloranilic acid by biamperometric and automatic potentiometric end-point detection with a lead chloranilate selective electrode" by Raba *et al.* (*Talanta*, 1992, **39**, 1007) references 17 and 19 should have read

17. H. A. Flaschka, *EDTA Titrations*, 2nd Ed., p. 80. Pergamon Press, Oxford, 1964.

19. O. H. Müller, *Polarography*, in A. Weissberger (ed.), Physical Methods of Organic Chemistry, 3rd Ed., Vol. I, Part IV, p. 3155. Interscience, New York, 1060.

Talanta, Vol. 39, No. 9, p. i, 1992
Printed in Great Britain

0039-9140/92 $5.00 + 0.00
Pergamon Press Ltd

NOTICE

REGISTRATION FORM

Federation of Analytical Chemistry & Spectroscopy Societies
Nineteenth Annual Conference -- Philadelphia, Pennsylvania
September 20-25, 1992

Date: _____

Last Name (Please print legibly) _____ First Name _____ Middle Initial _____

Affiliation _____

Address _____

City _____ State _____ Zip _____ Phone Number _____

Registration Fees

- ☐ 1. Preregistration (check, MC, VISA only) $125
- ☐ 2. Registration at conference (cash, check, MC, VISA)....$140
- ☐ 3. Single day registration.....$100 for _____ (day)
- ☐ 4. Friday registration only $50
- ☐ 5. Student, full time.....$30
- ☐ 6. Workshops (see fees below).$___
- ☐ 7. Spouse and Tour Program, *To Be Announced*
- ☐ 8. FACSS Wednesday Dinner (Call FACSS Office 301-846-4797)
- ☐ 9. Exhibits Only.....$20

Memberships

- ☐ 1. ACS Analytical Div.
- ☐ 2. SAS
- ☐ 3. ANACHEM
- ☐ 4. ISA
- ☐ 5. DVCF
- ☐ 6. Coblentz
- ☐ 7. Royal Society of Chemistry

Technical Interests

- ☐ 1. NMR
- ☐ 2. Molecular Spectroscopy
- ☐ 3. Atomic Spectroscopy
- ☐ 4. Mass Spectrometry
- ☐ 5. Spectroscopy, Other
- ☐ 6. Chromatography
- ☐ 7. Process/Control
- ☐ 8. Electrochemistry
- ☐ 9. Clinical
- ☐ 10. Other _____

Advertising

From which source did you learn of FACSS

- ☐ 1. Spectroscopy
- ☐ 2. Applied Spectroscopy
- ☐ 3. American Laboratory
- ☐ 4. The Bulletin Spectroscopy
- ☐ 5. Analytical Chemistry
- ☐ 6. FACSS Direct Mailer
- ☐ 7. Other_____

Total $_____ Make checks payable to FACSS

☐ VISA (13 or 16 numbers)
☐ Master Card (16 numbers)
Credit Card Number ☐☐☐☐☐☐☐☐☐☐☐☐☐☐☐☐

Signature _____ ☐☐ ☐☐
Printed name as appears on card _____ expiration date required

FACSS WORKSHOPS

- ☐ A. Monday, September 21, Half Day .....$60 **Sample Preparation**
- ☐ B. Monday, September 21, Full Day .....$90 **Basic Statistics**
- ☐ C. Monday, September 21, Half Day .....$60 **Lasers in Analysis**
- ☐ D. Tuesday, September 22, Full Day ..... free **Professional Chemists in Industry**
- ☐ E. Tuesday, September 22, Half Day .....$60 **Size Exclusion Chromatography**
- ☐ F. Tuesday, September 22, Half Day .....$60 **Supercritical Fluid Chromatography**
- ☐ G. Wednesday, September 23, Full Day.....$90 **Chemometrics**
- ☐ H. Wednesday, September 23, Half Day.....$60 **LC/Mass Spectrometry**
- ☐ I. Wednesday, September 23, Half Day.....$60 **Robotics**
- ☐ J. Thursday, September 24, Full Day.....$90 **Analytical GC**
- ☐ K. Thursday, September 24, Half Day.....$60 **ICP/MS**
- ☐ L. Thursday, September 24, Half Day.....$60 **Optical Standardization**

Deadline for Preregistration is **August 16, 1992**, Mail to:

FACSS
P.O. Box 278
Manhattan, KS 66502-0003

Talanta, Vol. 39, No. 8, p. i, 1992
Printed in Great Britain

0039-9140/92 $5.00 + 0.00
Pergamon Press Ltd

NOTICE

FOURTH INTERNATIONAL SYMPOSIUM ON PHARMACEUTICAL AND BIOMEDICAL ANALYSIS

Baltimore, Maryland, U.S.A.
April 18–22, 1993

The Fourth International Symposium on Pharmaceutical and Biomedical Analysis (PBA '93) will be held in April 1993 in the historic port city of Baltimore. This meeting will follow the highly successful Symposia held in Barcelona, Spain (PBA '87), York, U.K. (PBA '90) and Boston, U.S.A. (PBA '91). All those involved in the analysis of drugs, related materials and endogenous compounds, in all areas of the pharmaceutical and biomedical sciences, are cordially invited to attend.

The principal scientific themes include:

- Advances in Separation Techniques—LC, CE, SFC, GC
- Analysis of Bulk Substances and Formulations
- Analysis of Enantiomers
- Analytical Biotechnology
- Analytical Considerations in Performulation and Drug Delivery Studies
- Assay Validation
- Bioanalysis in Clinical and Preclinical Drug Development
- Pharmaceutical Quality Control
- Sample Preparation and Derivatization Techniques
- Spectroscopy and Spectroscopic Methods, NMR, MS, UV, FL

The scientific program will feature invited keynote speakers, submitted lectures and posters. As in previous Symposia in this series, poster discussion sessions will be organized around specific topics to allow exchange of ideas and research results in a more relaxed and less formal atmosphere. The Scientific Sessions will be preceded on the Sunday morning and afternoon by a series of workshops on a number of topical themes, presented by internationally recognized scientists in their respective fields.

All papers submitted will be published after reviewing in a special issue of the *Journal of Pharmaceutical and Biomedical Analysis*. Registered participants will receive a complimentary copy of the Proceedings, the Book of Abstracts, and entry to the Exhibition.

For further information please contact: Shirley Schlessinger, PBA '93, Suite 1015, 400 East Randolph Drive, Chicago, IL 60601, U.S.A. Phone: 312 527-2011

Talanta, Vol. 39, No. 5, p. i, 1992
Printed in Great Britain

0039-9140/92 $5.00 + 0.00
Pergamon Press plc

NOTICE

1992 CPAC SUMMER INSTITUTE ON PROCESS ANALYSIS AND CONTROL

The Center for Process Analytical Chemistry (CPAC) at the University of Washington will sponsor the 1992 CPAC Summer Institute, to be held July 6–16, 1992, in Seattle. A series of one and two-day modules on selected topics in process analysis and control will be presented by CPAC investigators.

The Center is a National Science Foundation Industry/University Cooperative Research Center sponsored by about fifty sponsors from the chemical industries. The Institute is designed for industrial and academic scientists and engineers who would like an intensive course on research and applications in this rapidly evolving field. Participants will come away with the fundamentals of process monitoring and control technologies as well as applications to industrial and environmental problems. The courses will provide attendees with a better understanding of how to implement sensing, data processing, and control methods in their own organisation. The power of multivariate methods of data analysis to enhance process monitoring, modeling and control is a common theme to be explored in the Institute. Topics to be covered include the following:

July 6	Flow Injection Analysis *Gary Christian and Jarda Ruzicka (Chemistry)*
July 7–8	Sensors and Sensor Systems: Optical, Mass, Electrochemical, and Thermal *Lloyd Burgess (Chemistry), Sinclair Yee and Pat Carey (Electrical Engineering)*
July 9–10	Signal Processor Integrated Circuitry for Sensor Applications *Mani Soma (Electrical Engineering)*
July 13	Chemometrics *Bruce Kowalski (Chemistry)*
July 14	NIR Spectroscopy *James Callis (Chemistry)*
July 15–16	Model–Predictive Control *Larry Ricker (Chemical Engineering)*

Participants may register for one or more modules, in any combination. For further information and registration details, please contact: Dr. Deborah L. Illman, Associate Director, CPAC, BG-10, University of Washington, Seattle, WA 98195, U.S.A. [Tel: (1 206) 685 2326].

Talanta, Vol. 39, No. 3, pp. i–iii, 1992
Printed in Great Britain

0039-9140/92 $5.00 + 0.00
Pergamon Press plc

NOTICES

NATO ASI ON MULTIFUNCTIONAL MESOPOROUS INORGANIC SOLIDS

Hotel Tivoli Sintra, Sintra, Portugal
5–17 April 1992

Call for Papers

Mesoporous materials have pore diameters in the range 20–150Å. There is an urgent need to understand the fundamental aspects regarding the synthesis, characterization and application of such materials which may be used for separation processes with or without membranes, catalysis, non-linear optics, corrosion-resistant coatings, sensors and battery electrodes and electrolytes. Three types of inorganic materials will be discussed:

(1) Mesoporous materials from layered compounds such as phosphates, phosphonates, layered double hydroxides and clays.
(2) Sol gel derived mesoporous oxides such as zirconia and titania.
(3) Hydrothermally derived mesoporous zeolites.

It is believed that there is a common theme between these three classes in that the requirements of pore size, methods of characterization and applications are similar. Consequently, the ASI will allow experts from the various fields to explore the fundamental aspects.

Potential participants are invited to apply as early as possible to:

Prof. César A C Sequeira
Instituto Superior Técnico
Av. Rovisco Pais
1096 Lisboa Codex
Portugal

ANNUAL CHEMICAL CONGRESS

MANCHESTER (UMIST)
13–16 April 1992

FIRST CIRCULAR

The 1992 Annual Chemical Congress of the Royal Society of Chemistry will take place at Manchester during 13–16 April 1992.

In addition to the symposia, the Congress will include the following principal lectures:

The Royal Society of Chemistry Presidential Address	Sir Rex Richards President, The Royal Society of Chemistry
Robert Robinson Lecture	Professor G Stork Columbia University, New York, U.S.A.
Theophilus Redwood Lecture	Professor A Hulanicki University of Warsaw, Poland

SCIENTIFIC PROGRAMME

Analytical

New directions in chromatography

Dalton

Developments in the chemistry of the main group elements

Invited lecturers: A Cheetham, J Dwyer, E. Flanigan, Z Gabelica, J C Vedrine, A Julbe, J F Nixon, F Mathey. O Stelzer, O J Scherer, J D Woollins, P P Power, N Burford, A Sullivan, F J Feher, R Househalter

It is planned to arrange a poster session in association with this symposium.

Education

From secondary school to honours degree: the formation of tomorrow's professional chemists.

Faraday *jointly with* **Analytical**

Characterization of solids and surfaces

Industrial

Surface analysis techniques and applications

Invited lecturers: C D Battich, J A Busby, J E Castle, J Comyn, J A Creighton, M Davies, K Delargy, R McIntyre, C G Pantano, J B Pethica, A Swift, R Wild and J Yarwood

Perkin

Asymmetric processes

Invited lecturers: D H G Crout, S G Davies, C Gennari, H Kagan, W Oppolzer, I Paterson, M T Reetz, W R Rousch, S M Roberts, N S Simpkins, H Yamamoto & others to be announced

Professional Affairs Board *jointly with* **Younger Chemists Committee**

Chemists, careers and changes

Historical

Manchester chemists

Invited lecturers: R Bud, D Cardwell, W Cocker, J H S Green, K Magee, J W Nicholson, P N Reed, C A Russell, K Schofield, A S Travis, T I Williams

Interdivisional, *organized by the Sonochemistry Group*

Sonochemistry

It is planned to arrange a poster session in association with this symposium.

Interdivisional, *organized by the Chemical Information Group in association with the Institution of Chemical Engineers*

Data for chemists and chemical engineers

Invited lecturers: Dr Ruttledge, D. L Baulch, S Goodwin, A Johns, D Ilton, W A Wakeham B Edmond

External Relations/Women Chemists

Food additives (provisional)

Water Chemistry Forum, *jointly with* **Analytical**

Title to be announced

For further information contact:

Dr John F Gibson
Secretary (Scientific)
The Royal Society of Chemistry
Burlington House
London W1V 0BN
Tel: (071) 437 8656
Fax: (071) 437 8883

FOURTH INTERNATIONAL SYMPOSIUM ON SUPERCRITICAL FLUID CHROMATOGRAPHY AND EXTRACTION

20–22 May 1992
Sheraton-Springdale Hotel, Cincinnati, Ohio, U.S.A.

First Circular
Call for Papers

The symposium will include oral, poster and discussion sessions. Plenary lectures by leading authorities in SFC and SFE will also be included.
The scientific program will include:

Multidimensional SFC and SFE
Off-line and on-line SFE
Physicochemical applications of SFC
Preparative SFC and SFE
Stationary phase and column packing
Optimization studies in SFE and SFC
Applications in regulatory analysis
Microextraction and analysis
Fluid purification
Quantitation in SFE
Matrix effects in SFE
Coupled techniques with SFC and SFE

Scientific and Organizing Committee

Keith Bartle (University of Leeds)
Thomas Chester (Procter & Gamble)
Jerry King (NCAUR-ARS/USDA)
Larry Taylor (VPI & SU)

Submission of Presentation Titles

Authors intending to submit papers for the symposium are encouraged to submit a tentative title as soon as possible. Abstract deadline will be 1 March, 1992. Abstracts (1000 words) will be printed in the symposium proceedings.

Application for a limited number of student scholarships can be made by submitting a poster abstract along with a supporting letter from the mentor to the organizing committee.

For further information please contact:

Larry T. Taylor
Department of Chemistry
Virginia Polytechnic Institute and State University
Blacksburg VA 24061-0212
U.S.A.

Talanta, Vol. 39, No. 2, pp. i–ii, 1992
Pergamon Press plc. Printed in Great Britain

NOTICES

2nd FECHEM CONFERENCE ON EDUCATION IN ANALYTICAL CHEMISTRY ANALYTICAL CHEMISTRY—A KEY FOR A SAFER FUTURE FOR MANKIND

will be organized by
the Czechoslovak Chemical Society
on behalf of the Working Party on Analytical Chemistry of the
Federation of European Chemical Societies
at Charles University, Prague
on August 31–September 1, 1992

The Conference will deal with all aspects of education in analytical chemistry and will consist of invited plenary lectures, contributed oral and poster presentations, a panel discussion and a section devoted to audiovisual aids and the use of computers for education in analytical chemistry.

Contact address:

Dr. J. Barek, Department of Analytical Chemistry, Charles University, Albertov 2030,
12840 Prague 2, Czechoslovakia
FAX: +42-2-291958
Phone: +42-2-292051; +42-2-297541
E-mail: NEMEC AT CSEARN

ANABIOTEC '92

4th International Symposium on Analytical Methods, Systems and Strategies
in Biotechnology Noordwijkerhout, The Netherlands 21–23 September 1992

Call for Papers

Analytical methods, systems and strategies are an integral part of academic and industrial research in biotechnology. Scientists working in this broad field, ranging from biodetection to advanced instrumental analysis, share a common interest in the interdisciplinary approach required to be successful in analysis in biotechnology; and they have a common interest in sharing this knowledge at ANABIOTEC.
Topics planned include:

- Chromatography; HPLC, GC, preparative and displacement chromatography, sample preparation
- Spectroscopy; NMR, IR, MS.
- Separation techniques, such as capillary zone electrophoresis (CZE), field flow fractionation (FFF).
- Flow Injection Analysis (FIA).
- Biodetection (such as DNA/RNA probes, immuno-analysis).
- Hyphenated techniques.
- Kinetic methods.
- New developments.

More detailed information can be obtained from:

Symposium Secretariat: ANABIOTEC
c/o CAOS, W.G. Plein 475, 1054 SH Amsterdam, The Netherlands
Tel.: (20)616 5151, Fax (20)689 0981

Announcement and Call for Papers

NINETEENTH ANNUAL MEETING OF THE FEDERATION OF ANALYTICAL CHEMISTRY AND SPECTROSCOPY SOCIETIES

20–25 September, 1992
Adams Mark Hotel, Philadelphia, Pennsylvania, U.S.A.

The nineteenth annual meeting of the Federation of Analytical Chemistry and Spectroscopy Societies (FACSS) will be held at the Adams Mark Hotel. FACSS is considered by many to be the premier annual technical analytical meeting. This year's conference will provide an expanded technical program with an emphasis on emerging technologies in analytical, spectroscopic and chromatographic sciences.

The deadline for submission of your title and a preliminary 100 word brief is **4 March, 1992.** A title submission form appears on the next page.

For information concerning the scientific program, please contact **Barry Lavine, Program Chairman**, Dept. of Chemistry, Clarkson University, Potsdam, NY 13676.

Nominations are requested for the **Tomas Hirschfeld Student Awards,** which will be presented at the conference for the most outstanding papers submitted by graduate students. The student nominees will give their papers at the FACSS conference. To be considered for these awards, students must submit the title of their paper, two letters of nomination including one from their graduate advisor, any preprints/reprints, and a 250-word abstract to the FACSS National Office by 4 March, 1992.

Contributed papers are solicited in all areas of analytical chemistry including atomic and molecular spectroscopy, chromatography, laser spectroscopy, mass spectrometry, nuclear magnetic resonance, process analysis, computers and software, environmental analysis, and biotechnology. The scientific program will also include various award symposia.

For general information please contact: **Matthew Klee, General Chairman,** Hewlett Packard Corp., P.O. Box 800, Avondale, PA 19311.

For other information please contact the FACSS National Office: FACSS, P.O. Box 278, Manhattan, KS 66502 or phone (301)-846-4797.

Talanta, Vol. 39, No. 4, pp. i–vi, 1992
Printed in Great Britain

0039-9140/92 $5.00 + 0.00
Pergamon Press plc

NOTICES

NATO ASI ON MULTIFUNCTIONAL MESOPOROUS INORGANIC SOLIDS

Hotel Tivoli Sintra, Sintra, Portugal
5–17 April 1992

Call for Papers

Mesoporous materials have pore diameters in the range 20–150Å. There is an urgent need to understand the fundamental aspects regarding the synthesis, characterisation and application of such materials which may be used for separation processes with or without membranes, catalysis, non-linear optics, corrosion-resistant coatings, sensors and battery electrodes and electrolytes. Three types of inorganic materials will be discussed.

(1) Mesoporous Materials from layered compounds such as phosphates, phosphonates, layered double hydroxides and clays.
(2) Sol gel derived mesoporous oxides such as zirconia and titania.
(3) Hydrothermally derived mesoporous zeolites.

It is believed that there is a common theme between these three classes in that the requirements of pore size, methods of characterisation and applications are similar. Consequently, the ASI will allow experts from the various fields to explore the fundamental aspects.

Potential participants are invited to apply as early as possible to:

Prof. César A C Sequeira
Instituto Superior Técnico
Av. Rovisco Pais
1096 Lisboa Codex
PORTUGAL

ANNUAL CHEMICAL CONGRESS

MANCHESTER (UMIST)
13–16 April 1992

FIRST CIRCULAR

The 1992 Annual Chemical Congress of the Royal Society of Chemistry will take place at Manchester during 13–16 April 1992.

In addition to the symposia, the Congress will include the following principal lectures:

The Royal Society of Chemistry Presidential Address	Sir Rex Richards President, The Royal Society of Chemistry
Robert Robinson Lecture	Professor G Stork Columbia University, New York, USA
Theophilus Redwood Lecture	Professor A Hulanicki University of Warsaw, Poland

SCIENTIFIC PROGRAMME

Analytical

New directions in chromatography

Dalton

Developments in the chemistry of the main group elements

Invited Lecturers: A Cheetham, J Dwyer, E Flanigan, Z Gabelica, J C Vedrine, A Julbe, J F Nixon, F Mathey, O Stelzer, O J Scherer, J D Woollins, P P Power, N Burford, A Sullivan, F J Feher, R Househalter

It is planned to arrange a poster session in association with this symposium.

Education

From secondary school to honours degree:
The formation of tomorrow's professional chemists.

Faraday *jointly with* **Analytical**

Characterisation of solids and surfaces

Industrial

Surface analysis techniques and applications

Invited Lecturers: C D Battich, J A Busby, J E Castle, J Comyn, J A Creighton, M Davies, K Delargy, R McIntyre, C G Pantano, J B Pethica, A Swift, R Wild and J Yarwood

Perkin

Asymmetric processes

Invited Lecturers: D H G Crout, S G Davies, C Gennari, H Kagan, W Oppolzer, I Paterson, M T Reetz, W R Rousch, S M Roberts, N S Simpkins, H Yamamoto & others to be announced

Professional Affairs Board *jointly with* **Younger Chemists Committee**

Chemists, careers and changes

Historical

Manchester chemists

Invited Lecturers: R Bud, D Cardwell, W Cocker, J H S Green, K Magee, J W Nicholson, P N Reed, C A Russell, K Schofield, A S Travis, T I Williams

Interdivisional, *organised by the Sonochemistry Group*

Sonochemistry

It is planned to arrange a poster session in association with this symposium.

Interdivisional, *organised by the Chemical Information Group in association with the Institution of Chemical Engineers*

Data for chemists and chemical engineers

Invited Lecturers: Dr Ruttledge, D L Baulch, S Goodwin, A Johns, D Ilton, W A Wakeham B Edmond

External Relations/Women Chemists

Food additives (Provisional)

Water Chemistry Forum, *jointly with* **Analytical**

Title to be announced

For further information contact:

Dr John F Gibson
Secretary (Scientific)
The Royal Society of Chemistry
Burlington House
London W1V 0BN
Tel: (071) 437 8656
Fax: (071) 437 8883

FOURTH INTERNATIONAL SYMPOSIUM ON SUPERCRITICAL FLUID CHROMATOGRAPHY AND EXTRACTION

20–22 May 1992
Sheraton-Springdale Hotel, Cincinnati, Ohio, U.S.A.

First Circular
Call for Papers

The symposium will include oral, poster, and discussion sessions. Plenary lectures by leading authorities in SFC and SFE will also be included.
The scientific program will include:

Multidimensional SFC and SFE
Off-line and On-line SFE
Physicochemical Applications of SFC
Preparative SFC and SFE
Stationary Phase and Column Packing
Optimization Studies in SFE and SFC
Applications in Regulatory Analysis
Microextraction and Analysis
Fluid Purification
Quantitation in SFE
Matrix Effects in SFE
Coupled Techniques with SFC and SFE

Scientific and Organizing Committee

Keith Bartle (University of Leeds)
Thomas Chester (Procter & Gamble)
Jerry King (NCAUR-ARS/USDA)
Larry Taylor (VPI & SU)

Submission of Presentation Titles

Authors intending to submit papers for the symposium are encouraged to submit a tentative title as soon as possible. Abstract deadline will be 1 March, 1992. Abstracts (1000 words) will be printed in the symposium proceedings.

Application for a limited number of student scholarships can be made by submitting a poster abstract along with a supporting letter from the mentor to the organizing committee.

For further information please contact:

Larry T Taylor
Department of Chemistry
Virginia Polytechnic Institute and State University
Blacksburg VA 24061-0212
U.S.A.

12th INTERNATIONAL SYMPOSIUM ON MICROCHEMICAL TECHNIQUES

CORDOBA, SPAIN
7–12 September 1992

The Symposium will be held from September 7 to 12, 1992 at Córdoba (Spain) in the Palacio de Congresos, 10 m from the Mosque in the old quarter.

Topics

ISM-92 will cover both pure and applied aspects of analytical chemistry related to micro- and trace-analysis. Special attention will be paid to the application of modern instrumental techniques in the field of trace-analysis.

Scientific Programme

Plenary and keynote lectures will be presented by invited speakers. For the general sessions, contributions are requested for presentation in either oral or poster sessions.

Scientific Committee

F. Adams (Antwerp)
A. Genninghoven (Munster)
G. den Boef (Amsterdam)
F. Camoes (Lisbon)
S. Caroli (Rome)
J. Cazaux (Reims)
K. Dittich (Leipzig)
W. Fresenius (Taunusstein)
F. Frimmel (Karlsruhe)
R. Giljbels (Antwerp)
M. Grasserbauer (Vienna)
B. Griepink (Brussels)
G. Giochon (Oak Ridge)
E. Hansen (Lyebig)
D. Hercules (Pittsburg)
K. Heumann (Regensburg)
A. Hulanicki (Warsaw)
S. Ikeda (Osaka)
D. Klockow (Dortmund)
G. Knapp (Graz)
V. Krivan (Ulm)
D. Massart (Brussels)
J. Mermet (Lyon)
W. Mertz (Lundwigshafen)
H. Muntau (Ispra)
R. Niessner (Munchen)
M. Otto (Freiberg)
H. Pardue (West Lafayette)
D. Pérez Bendito (Cordoba)
E. Pungor (Budapest)
G. Rauret (Barcelona)
A. Sanz Medel (Oviedo)
W. Simon (Zürich)
H. Ruzicka (Seattle)
H. Thomas (Cardiff)
G. Tölg (Dortmund)
A. Townshend (Hull)
M. Valcárcel (Cordoba)
Y. Zolotov (Moscow)

For further information contact:

Departamento de Química Analítica
Facultad de Ciencias
E-14004 Córdoba
Spain
Tel: 34-57-234453
Fax: 34-57-452285

Papers

All delegates will be offered to submit a full paper for publication in a 1992 special conference issue of Analytica Chimica Acta. All invited and submitted papers will be reviewed by ACA in the normal way. All registered participants will receive a copy of the ACA conference issue.

Abstracts

An abstract of 200–350 words (1 page) should be submitted as soon as possible but no later than 1 December 1991 for consideration by the Scientific Committee. The deadline for abstracts is 15 January 1992. All registered participants will receive the book of abstracts.

Abstracts are to be submitted on good quality white paper (A4). The abstract itself must be typed, single spaced in English within an area equivalent to 13 cm wide by 19 cm high.

Main Topics

- Electrochemical Detection in FIA/CFA/HPLC
- Developments in Stripping Analysis
- Pharmaceutical and Biomedical Applications of ElectroAnalysis
- (Bio)sensors and Chemically Modified Electrodes
- New ElectroAnalytical Techniques and instrumentation
- Environment Applications of ElectroAnalysis

Invited Speakers

K. Stulik, Czechoslovakia
C. M. G. van den Berg, United Kingdom
J.-M. Kauffmann, Belgium
L. Gorton, Sweden
H. P. van Leeuwen, The Netherlands

Exhibition

An exhibition will be arranged in conjunction with the Conference.

For more information contact:

ESEAC'92/W. P. van Bennekom
P.O. Box 80.082
3508 TB UTRECHT
THE NETHERLANDS
tel + 31 30 537305
fax + 31 30 515114

4th EUROPEAN CONFERENCE ON ELECTROANALYSIS

Noordwijkerhout
The Netherlands
31 May–3 June 1992

The 4th European Conference on ElectroAnalysis will be held in Noordwijkerhout, The Netherlands, during the period 31 May–3 June 1992.

Scope

The conference is entirely devoted to modern electroanalytical subjects. The current status of electroanalytical techniques including theoretical developments and instrumental applications will be discussed.

Scientific Committee

W. E. van der Linden (chairman), The Netherlands
C. M. G. van den Berg, United Kingdom
G. den Boef, The Netherlands
M. Branica, Yugoslavia
A. Ivaska, Finland
R. Kalvoda, Czechoslovakia
K. Tóth, Hungary
M. R. Smyth, Ireland
P. Tuñon-Blanco, Spain

FOURTH INTERNATIONAL SYMPOSIUM ON PHARMACEUTICAL AND BIOMEDICAL ANALYSIS

Baltimore, Maryland, U.S.A.
April 18–22, 1993

The Fourth International Symposium on Pharmaceutical and Biomedical Analysis (PBA '93) will be held in April 1993 in the historic port city of Baltimore. This meeting will follow the highly successful Symposia held in Barcelona, Spain (PBA '87), York, U.K. (PBA '90) and Boston, U.S.A. (PBA '91). All those involved in the analysis of drugs, related materials and endogenous compounds, in all areas of the pharmaceutical and biomedical sciences, are cordially invited to attend.

The principal scientific themes include:

- Advances in Separation Techniques—LC, CE, SFC, GC
- Analysis of Bulk Substances and Formulations
- Analysis of Enantiomers
- Analytical Biotechnology
- Analytical Considerations in Performulation and Drug Delivery Studies
- Assay Validation
- Bioanalysis in Clinical and Preclinical Drug Development
- Pharmaceutical Quality Control
- Sample Preparation and Derivatization Techniques
- Spectroscopy and Spectroscopic Methods, NMR, MS, UV, FL

The scientific program will feature invited keynote speakers, submitted lectures and posters. As in previous Symposia in this series, poster discussion sessions will be organized around specific topics to allow exchange of ideas and research results in a more relaxed and less formal atmosphere. The Scientific Sessions will be preceded on the Sunday morning and afternoon by a series of workshops on a number of topical themes, presented by internationally recognized scientists in their respective fields.

All papers submitted will be published after reviewing in a special issue of the *Journal of Pharmaceutical and Biomedical Analysis*. Registered participants will receive a complimentary copy of the Proceedings, the Book of Abstracts, and entry to the Exhibition.

For further information please contact: Shirley Schlessinger, PBA '93, Suite 1015, 400 East Randolph Drive, Chicago, IL 60601, U.S.A. Phone: 312 527-2011

LIST OF CONTENTS

JANUARY

FEBRUARY

MARCH

APRIL

MAY

JUNE

JULY

AUGUST

SEPTEMBER

OCTOBER

NOVEMBER

TOM S. WEST HONOUR ISSUE

Talanta, Vol. 39, No. 2, p. v, 1992
Pergamon Press plc. Printed in Great Britain

ERRATUM

Arrhenius Plots for Activation Energy of Atomization in Graphite-Furnace Atomic-Absorption Spectrometry

C. L. Chakrabarti and S. J. Cathum

(*Talanta*, 1991, **38**, pp. 157–166)

Printing corrections for Table 3 were omitted by the printer, and the correct table is as follows:

Table 3. Activation energy values for atomization of copper obtained using equation (25)

E_a, *kJ/mole* Test number 1	2	3	Average E_a, *kJ/mole*	Location of the data points on the absorbance signal profile used for calculation of E_a
355	325	344	341	At or immediately after the appearance
349	343	325	339	temperature, i.e., at "low" temperatures.
328	355	338	340	
337	343	343	341	
338	311	343	336	
304	284	321	303	From the "transition region" temperature, *i.e.*, between the "low" and the "high" temperature.
271	254	296	274	At longer times after the appearance temperature,
242	230	268	247	*i.e.*, when temperature is "high". The temperature
217	210	220	216	increases as one descends the columns of Table 3.

The following corrections were also omitted:

p. 157 (right-hand column), $-Ea/R$ should be $-E_a/R$

p. 161, after equation (32): $X = \ln(k_{1\infty}/k_{2\infty})$

p. 161, *Standard solutions*. The phrase "containing 5.00 ng/ml copper" should have been deleted in the sentence "Test solutions containing 5.00 ng/ml copper were prepared by serial dilution of the stock solution just before use".

p. 163 (left-hand column), (third horizontal row) should be (second horizontal row from the top).

Talanta, Vol. 39, No. 11, pp. V–VI, 1992
Printed in Great Britain.

0039-9140/92 $5.00 + 0.00

FOREWORD

Professor Tom S. West

This special issue of *Talanta* is in honour of the sixty-fifth birthday of Professor Tom West.

Professor West is an analytical chemist of high international standing, who has also contributed significantly to other aspects of national and international science.

The papers for the honour issue are contributed by his former colleagues and research students at University of Birmingham, Imperial College London, and the Macaulay Institute Aberdeen, as well as by some colleagues from the time when he was Secretary General of IUPAC. The coordinating editors are Jack Betteridge and Mo Williams, who were amongst his first research students in Birmingham, and both of whom were involved in the editorial team of *Talanta* in the early 1960s. Professor West was himself a member of the Editorial Advisory Board of the journal for several years, and much of his research work has been published therein.

We all wish him good health in the coming years and success in his continuing scientific efforts.

* * *

TRIBUTE TO TOM WEST

During the 1960s and 1970s, Tom West and I competed as scientists in the field of atomic spectroscopy. This was a healthy and wonderful time for both of our groups. I had great respect for the energy, innovation, and wonderful publications which came forth from the Tom West group

at Imperial College. After Tom went to Aberdeen, he continued his fine research although at a lesser rate. Tom West has been a major player in the past 30 years or more in analytical chemistry. His contributions are enormous in number and excellent in substance. This special issue of TALANTA honours Tom West as a teacher, scholar, administrator, researcher, innovator, friend, and colleague. Thanks Tom for leading the way for so many of us.

J. D. WINEFORDNER

Talanta, Vol. 39, No. 10, pp. V–VI, 1992
Pergamon Press Ltd. Printed in Great Britain

TALANTA ADVISORY BOARD

The Editorial Board and the Publisher of *Talanta* take pleasure in welcoming the following as members of the Advisory Board of the Journal.

A. BERTHOD R. J. HURTUBISE
J. F. VAN STADEN Z. FANG
B. KARLBERG

Alain Berthod, born in 1950, graduated in Chemistry in 1974. He received his Ph.D. degree in 1979 from the Chemistry Department of the University of Lyon, France. Since then, he has been appointed as Researcher by the French National Research Institution (C.N.R.S., Centre National de la Recherche Scientifique). He obtained the French State Doctorate in 1983. He is currently Professeur Agrégé in the Laboratoire des Sciences Analytiques at Lyon University, team CNRS # 435, directed by J. M. Mermet. His research interests include the use of liquid ordered media (micellar solutions, emulsions and microemulsions) in analytical science: electroanalysis in ordered media, micellar liquid chromatography and emulsion formulation. In 1986 and 1987, he spent 18 months as a sabbatical visiting scientist in Professor J. D. Winefordner's Group in Gainesville, Florida, U.S.A. where he developed hyphenated laser-chromatography techniques. He is currently working on new methods of separation: micellar chromatography, countercurrent chromatography and enantiomer separations. He authored or co-authored more than 80 papers on these topics. He serves as a paper reviewer for most international analytical chemistry journals and is a member of the editorial board of the Journal of Liquid Chromatography.

Zhaolun Fang graduated from Beijing (Peking) University, People's Republic of China in 1957. He became a Research Associate in 1965, an Associate Professor in 1977, and a full Professor in 1986 at the Institute of Applied Ecology (formerly Institute of Forestry and Soil Science) of the Chinese Academy of Sciences (Academia Sinica), Shenyang, People's Republic of China. He is currently Director of Flow-Injection Analysis Research Centre of the Institute, with concurrent posts as Director of Instrumental Analysis Centre of the Chinese Academy of Sciences (Shenyang Branch), Member of the Board of Directors of the Chinese Chemical Society, Chairman of the Committee on Flow-Injection Analysis of the Chinese Instrument Society, and Professor at the Shenyang College of Pharmacy. He received awards from the Chinese Academy of Sciences in 1981, 1982 and 1990. His research interests include flow-injection analysis atomic spectrometry with applications in environmental and biological fields, and has published over 120 research papers and co-authored three books in these areas.

Robert J. Hurtubise is Professor of Chemistry at the University of Wyoming in Laramie, Wyoming, U.S.A. He received his B.S. and M.S. degrees in chemistry from Xavier University, Cincinnati, Ohio, U.S.A. and his Ph.D. degree in analytical chemistry from Ohio University, Athens, Ohio, U.S.A. In addition to holding academic positions, Dr. Hurtubise has also worked in the pharmaceutical industry. Professor Hurtubise's research interests include the theoretical and practical aspects of solid-matrix luminescence analysis, the solid-matrix and solution luminescence of DNA adducts and related biological samples, and the theoretical and applied aspects of high-performance liquid chromatography and capillary electrophoresis. He has lectured widely and has published over a hundred research papers, numerous review articles, five chapters, and two books. His most recent book is entitled *Phosphorimetry: Theory, Instrumentation and Applications.* In addition to his association with *Talanta*, he serves on the Editorial Advisory Board for *Analytical Instrumentation.*

Bo Karlberg received his B.S. degree in chemistry and mathematics from the University of Lund in 1967 and his Ph.D. degree in analytical chemistry from the University of Umeå in 1973. Since then he has been working as a research chemist at Astra Pharmaceuticals, Södertälje, in 1973–1979 and later at Bifok/Tecator, Sollentuna, where he still holds a part-time position. In 1991 he was appointed Associate Professor at Stockholm University. He was among the early researchers on response mechanisms of glass electrodes and other ion-selective electrodes but later directed his research towards automation of wet chemistry procedures based on the continuous flow approach (FIA in particular). His current research interests lie in environmental analysis and monitoring. He has organized several international meetings including the Flow Analysis II meeting in Lund in 1982.

Jacobus (Koos) F van Staden joined SASOL in the early sixties after his matriculation examinations, whereafter he went on study leave in 1966 to the University of the Orange Free State where he received his B.Sc. (1968), B.Sc. Honours (1969) and M.Sc. (1970) degrees. He returned to SASOL with main responsibility for gas chromatography, mass spectrometry,

corrosion and wet chemistry. Hereafter he moved to the University of Zululand (1973), Pretoria Technikon, South Africa (1975) before joining the University of Pretoria, South Africa (1976) where he is now full Professor and Head of Analytical Chemistry. He obtained a D.Sc. degree from the University of Pretoria in 1978. He received the Robertson award (1967–1970) and the D F du Toit Malherbe award (1980) for his research on flow-injection analysis. Koos is a fellow of the Royal Society of Chemistry, member of the South African Chemical Institute (currently Chairman of the Publicity committee and member of Council), member of the South African Council for Natural Scientists and currently Chairman of the Chemistry Section of the South African Academy for Science and Art. He was the Chairman of the first national symposium on Analytical Science in South Africa and is currently National Representative for South Africa of the Commission on General Aspects of Analytical Chemistry of IUPAC. His main interests are in automatic methods and process control (continuous flow systems and flow injection analysis), separation techniques and chromatography, electrochemical sensors, spectrometric detectors and water- and environmental-pollution analysis. Koos is also active in Chemical Education and is currently Subject Editor (Chemistry) of *Spectrum*, the journal for Teachers of Mathematics, Physical Science and Technology. He is the (co)-author of over 130 scientific publications (full length articles in specialist journals and popular scientific articles), 12 books (of which one has a chapter in flow injection atomic spectroscopy), over 25 internal research reports and over 90 representations at conferences, symposiums, seminars and work-shops in North-America, Europe, Britain, Japan and Africa. He serves on the Advisory Editorial Boards of some international journals.

Talanta, Vol. 39, No. 4, pp. V–VI, 1992
Pergamon Press plc. Printed in Great Britain

EDITORIAL

The Editorial Board and the Publisher of *Talanta* take pleasure in welcoming Dr. Lars Kryger as the new Review Editor for the journal, and also in welcoming Professor Totaro Imasaka and Dr. Milan Meloun as new members of the Advisory Board.

Lars Kryger received his M.Sc. degree in 1971 after specializing in inorganic and structural chemistry in the group of S. E. Rasmussen, Aarhus University, Denmark. In 1975, after studying under D. Jagner (now Göteborg, Sweden), he received his Ph.D. in analytical chemistry. Following one year as a post doctoral fellow with S. P. Perone, Purdue University, Indiana, he returned to Aarhus University where he is now employed as a lecturer. His current research interests include the development of computerized electroanalytical instruments and electrochemical trace analysis. Furthermore, he collaborates with R. P. Baldwin's group (Louisville, Kentucky) on the construction and characterization of modified electrodes. In 1981 he received the Louis Gordon Memorial award for a *Talanta* review on Pattern Recognition methods. In addition to his association with *Talanta*, he serves as a member of the Advisory Board for *Mikrochimica Acta*. For two years during his early career Lars Kryger worked as a science teacher in Tanzania. He is married, has a son and a daughter, and enjoys sailing, cooking and social winter bathing.

Totaro Imasaka received his B.S., M.S., and Ph.D (Dr. of Engineering) degrees from the Department of Applied Chemistry, Faculty of Engineering, Kyushu University, graduating in 1978. After one-year of postdoctoral studies at Stanford University, he returned as a research associate to Kyushu University. From 1979 to 1980 he worked as a lecturer at Kyushu University. He was appointed associate professor in 1981 and Professor in 1991. He was a recipient of the 1984 Young Chemist Award presented by The Chemical Society of Japan. Professor Imasaka's current research interest is trace analysis using laser spectroscopy, and for ten years he has studied time-resolved fluorescence spectrometry and thermal lens spectrophotometry. Recently, he has focused his attention on supersonic jet spectrometry combined with fluorescence spectrometry and multiphoton ionization mass spectrometry. He also invented semiconductor laser spectrometry for practical trace analysis. More recently he has concentrated his attention on developing a multi-color laser based on four-wave mixing for analytical applications. He has published over 100 original papers and 50 review articles, he has also served as the organizer of several international meetings in Japan.

Milan Meloun was born in 1943 in Czechoslovakia, graduated in physical chemistry in 1965 from Purkyne University Brno, received a Ph.D. degree in analytical chemistry in 1973 from the University of Chemical Technology Pardubice, a RNDr degree in chemometrics from Charles University, Prague in 1975 and most recently a D.Sc. degree in chemometrics and analytical chemistry from the Technical University of Prague in 1990. For more than 20 years he has read Instrumental Methods of Analytical Chemistry at the University of Chemical Technology in Pardubice. He is also Secretary of the Chemometrics section of the Czechoslovakia Chemical Society. From 1979 to 1981 he introduced courses of Statistical Data Treatment, Chemometrics and Data Processing in instrumental Analytical Chemistry during his visiting Professorship at the University of Baghdad. In 1988–1990 he gave courses of Chemometrics at the Department of Inorganic Chemistry, The Royal Institute of Technology, Stockholm. Dr. Meloun's research interests lie in the computer-assisted interpretation of solution composition and complex-forming equilibria, and regression analysis of potentiometric, spectrophotometric and extraction data. He has published over 70 papers, and has given 75 lectures at scientific conferences. He has also co-authored 10 books and 7 textbooks. A critical survey of up-to-date algorithms demonstrated by a detailed solution of 50 analytical equilibria problems is featured in his book *Computation of Solution Equilibria* (Horwood, 1988) and a methodology and programs in two chapters in

Computational Methods for the Determination of Formation Constants (Plenum Press, 1986). During the last 10 years he has been concerned with developing statistical software for chemometrics and results are demonstrated on 400 solved problems in his two-volume textbook *Chemometrics in Instrumental Analysis* (Horwood, 1991).

Talanta, Vol. 39, No. 2, pp. V–VI, 1992
Pergamon Press plc. Printed in Great Britain

OBITUARY

Professor Nobuhiko Ishibashi, 1928–1991

It was with great shock that we learned during the "Flow Analysis V" conference in Kumamoto, Japan that its principal organizer and General Secretary, Professor Nobuhiko Ishibashi, suddenly and unexpectedly had passed away on August 23, 1991. At the reception of the event, held in the evening prior to the opening of the conference, Professor Ishibashi was his ever enjoyable self, obviously taking pleasure in the secured success of the imminent conference, which had assembled more than 160 participants from 28 different countries from all continents. Although noting that he had a slight flu, Professor Ishibashi was determined to engage in the full programme of the conference, and was looking forward to his own presentation on the last day of the meeting. He died in the evening before that. It thus befell a deeply moved Professor Keihei Ueno instead to give a eulogy on his old friend and colleague at the very same time all participants had been expecting to listen to another of Professor Ishibashi's always interesting and informative presentations.

Professor Ishibashi received a bachelor's degree in engineering from Kyushu University in 1951. Following a short period in industry, he returned to his *Alma Mater* the same year as a research associate at the Department of Applied Chemistry. In 1956 he became Assistant Professor, then Associate Professor in 1957, and finally, after having earned his D.Eng. degree in applied chemistry in 1961, he was in 1966 appointed to Professor of the newly established chair in applied analytical chemistry at the university. Professor Ishibashi stayed at Kyushu University until March of this year when he, in accordance with the laws of his country, retired, yet only to transfer his vitality and enthusiasm to the private University of Kiniki.

Professor Ishibashi's early research interest was focused on electrochemistry, a subject which despite his later diversification into other research areas, continued to have his special attention throughout his academic career. Thus, in addition to publishing numerous papers on electrochemistry, he was the inventor of several ion-selective electrodes now commercially available. In this context, it should be emphasized that his theory on the intrinsic selectivity coefficient (Jyo–Ishibashi theory) has been most useful for the understanding of the selectivity and sensitivity of ion-selective electrodes. He has made valuable contributions in absorptiometry and fluorometry, where his work on lasers as light sources in high-sensitivity spectrometry in 1977 earned him the distinction of attaining the lowest detection limit for fluorescein recorded thus far (0.02 ppt). He was a pioneer in using diode lasers in analytical spectrometry methods such as thermal lensing, photoacustics and fluorometry. In the last field he promoted the combination of the supersonic jet and synchronous scan techniques to extend the selectivity of laser fluorometry of aromatic compounds. Yet to many analytical chemists in Japan, but particularly in the international scientific community, he will most likely be remembered as the *avant-garde* of Flow Injection Analysis in his native country. He not only took the initiative to introduce this novel concept of continuous flow analysis into Japan, but was a most active practitioner of FIA himself, producing a long array of papers dealing with a variety of applications. As its principal inspirator and orator, his was the founding father of the Japanese Association of Flow Injection Analysis in 1983 and the vital nucleus behind its promotion of the very first periodical devoted entirely to FIA, that is, the Journal of Flow Injection Analysis. Professor Ishibashi was instrumental in the later transformation of the journal, which originated as a national journal where all articles were published in Japanese, into a truly international outlet, attracting authors from all over the world.

As a result of his advanced and visional research activities Professor Ishibashi was bestowed with several national awards over the years: The Sano Award from the Electrochemical Society of Japan (1962), the Analytical Award from the Japanese Society for Analytical Chemistry (1974), the Shimadzu Award from the Shimadzu Foundation (1988) and the Chemical Society Award from the Chemical Society of Japan (1990). During his research career he was the author of more than 250 scientific papers, served on the editorial advisory board of several international periodicals (notably Analytica Chimica Acta, Analytical Chemistry and Mikrochimica Acta), and was Vice-President of the Japanese Society for Analytical Chemistry (1980–81) and of the Electrochemical Society of Japan (1987–88).

But what Professor Ishibashi very likely will be remembered for, at least for a non-Japanese who never had the privilege to be his student, coworker or colleague, was his always contagious enthusiasm, open mind, unbound energy and passion for science. It was always a pleasure to meet and talk with him at international meetings, and he will be dearly missed by his many friends in the international scientific community.

We mourn the departure of a genuine and good colleague, and express our sympathy to his wife who often accompanied him at international events. Although taken away much too early, we take comfort in the fact that Professor Ishibashi died in the midst of what he truly appreciated and amongst those who truly appreciated him.

Elo H. Hansen Gary D. Christian

Talanta, Vol. 39, No. 10, pp. VII, 1992
Pergamon Press Ltd. Printed in Great Britain

RONALD BELCHER MEMORIAL AWARD 1992

Dr. Mian Jiang

The third Ronald Belcher Memorial Award has been awarded to Dr. Mian Jiang of Wuhan University, Peoples' Republic of China. Dr. Mian is particularly interested in Electroanalytical Chemistry and Chemically Modified Electrodes and intends using the award in a visit to European research workers in the field.

The Belcher award is made in Commemoration of the late Professor Belcher's outstanding contributions to analytical chemistry, international relations and understanding, and his interest in student welfare. The award is made in alternate years in the form of a grant to enable a young analytical scientist to travel abroad.

Talanta, Vol. 39, No. 4, pp. VII–VIII, 1992
Printed in Great Britain

0039-9140/92 $5.00 + 0.00
Pergamon Press plc

OBITUARY

Professor Jiri Stary

Throughout the Summer and early Fall of 1991, Professor Jiri Stary fought a losing battle with an illness which gradually weakened him until he died on October 3rd. It is hard to believe that he is gone, leaving his many friends, colleagues, students and family mourning. His qualities as a researcher and a teacher made him loved by all. Though a man of soft words and a friendly smile, he was an uncompromising believer in personal freedom, human rights and decent behavior. Thus on every occasion throughout his entire life, he scrupulously avoided advancing himself by political means, an attitude many people in his position did not, or did not dare, to adopt. Even in the most difficult times he remained firm, and with his unpretentious style, sought refuge in his research. He was a true scholar who pursued his work, driven by curiosity and a joy of discovery.

Jiri Stary was born in the Czech village of Zbizuby on the 26th of July, 1933. He obtained his M.S. degree at the Charles University in Prague, and his Ph.D. degree at the Moscow State University in 1958. Following his studies at the Joint Institute of Nuclear Science in Dubna and Moscow State University, he obtained the prestigious title of Doctor of Sciences in 1965, perhaps as the youngest Czechoslovakian scientist ever to obtain this degree. He spent his professional career at the Department of Nuclear Chemistry of the Technical University in Prague, where he became a full Professor in 1980. Since 1969 he was a member of the Analytical Division of the IUPAC and ultimately became the National Representative. Professor Stary was Associate Editor of the *Journal of Radioanalytical and Nuclear Chemistry* and he was a member of the editorial boards of several journals. His own publications comprise over 120 papers, 20 reviews and 4 monographs.

His work in the area of radiochemical separations, his discovery of substoichiometric separations and his studies on solvent extraction equilibria, published in many international journals, including *Talanta*, comprise knowledge of a lasting value. His monograph, "*Solvent Extraction of Metal Chelates*" (Pergamon Press, Oxford), is as useful today as it was when it was first published in 1965. Though never honored by prestigious international awards (which he never sought), Jiri Stary was indeed in the league of the giants of the Czech School of Chemistry, as Jaroslav Heyrovsky or Rudolf Pribyl were.

I was blessed to join him as a junior colleague soon after he was hired in 1958 at the Department of Nuclear Chemistry in Prague by a famous polar explorer, Professor Behounek. We worked together for a number of years in the early sixties, and I was swept by his enthusiasm and impressed by his deep knowledge of complex chemistry. It was not unusual for him at that time to spend days and nights in a row in a dingy antiquated basement laboratory at the Chemical Institute of the Charles University in Albertov in order to learn as much as possible about how to separate short-lived radioisotopes. It is conceivable that his extensive work in radiochemistry, especially during his early years in the Soviet Union, planted the seed for the illness which ultimately killed him.

To those who have known him, it is hard to accept that he has gone so early. It would perhaps be easier to believe that he continues his calculations and experiments somewhere in the Universe in a Laboratory where administrative paperwork cannot reach him. If that is so, we all may hope to join him one day, and to enjoy research and life as he indeed did.

Jaromir Růžička

AUTHOR INDEX

Typeset in Great Britain by BPCC Techset Ltd, Exeter. Printed in Great Britain by BPCC Wheatons Ltd, Exeter.

SUBJECT INDEX

Typeset in Great Britain by BPCC Techset Ltd, Exeter. Printed by BPCC Wheatons Ltd, Exeter.